INTERMAG 2022

January 10-14 2022

Abstract Book

Session TU
TUTORIAL: QUANTUM MAGNONICS

Sara Majetich, Chair
Carnegie Mellon University, Pittsburgh, PA, United States

INVITED PAPERS

TU-01. Quantum Magnonics with a Superconducting Qubit.
Y. Nakamura[1,2] 1. RIKEN Center for Quantum Computing, Saitama, Japan; 2. Research Center for Advanced Science and Technology, The University of Tokyo, Tokyo, Japan

Magnons are quanta of collective spin excitations, such as in magnetostatic modes and spin waves, ubiquitously found in magnetic materials. While conventional experimental techniques in magnetic resonance and spintronics can only detect large amplitude signals, either coherent or incoherent, the recent progress in quantum magnonics has enabled us to investigate the single magnon limit [1]. In this tutorial, we discuss how we can control and detect single magnons in a macroscopic-scale ferromagnetic crystal. We strongly couple a superconducting qubit, an artificial two-level system realized in a superconducting circuit, to a magnon via a virtual excitation of photon in a microwave cavity. The interaction allows us to generate entanglemen

[1] D. Lachance-Quirion et al., Appl. Phys. Express 12, 070101 (2019). [2] Entanglement-based single-shot detection of a single magnon with a superconducting qubit, D. Lachance-Quirion et al., Science 367, 425 (2020). [3] Dissipation-based quantum sensing of magnons with a superconducting qubit, S.P. Wolski et al., Phys. Rev. Lett. 125, 117701 (2020).

TU-02. Cavity Magnoncs. *S. Viola Kusminskiy[1] 1. Max Planck Institute for the Science of Light, Erlangen, Germany*

In the last years, a new field has emerged at the intersection between Condensed Matter and Quantum Optics, denominated "Quantum Magnonics". This field strives to control the elementary excitations of magnetic materials, denominated magnons, to the level of the single quanta, and to interface them coherently to other elementary excitations such as photons or phonons. The recent developments in this field, with proof of concept experiments such as a single-magnon detector, have opened the door for hybrid quantum systems based on magnetic materials. This can allow us to explore magnetism in new ways and regimes, has the potential of unraveling quantum phenomena at unprecedented scales, and could lead to breakthroughs for quantum technologies. A predominant role in these developments is played by cavity magnonic systems, where an electromagnetic cavity, either in the optical or microwave regime, is used to enhance and control the interaction between photons and magnons. This Tutorial Session will cover the basic concepts behind Quantum Magnonics, as well as the most recent developments in the field.

TU-03. Emerging Opportunities for Coherent Information Processing at the Intersection of Superconductivity and Magnetism. *Y. Li[1] 1. Materials Science Division, Argonne National Laboratory, Argonne, IL, United States*

Hybrid magnonic systems incorporating superconducting systems have recently emerged as a new promising direction for coherent information processing by exploiting magnon excitations and high quality factor superconducting resonators [1]. Magnons are fundamental excitations of magnetic systems with a frequency band which can be adapted in microwave superconducting quantum circuits. In particular, magnons possess large dipolar magnon-photon coupling and wide frequency tunability, which may find new potentials in quantum information. Superconducting resonators serve as coherent data buses of many quantum circuits with long microwave coherence time. Superconducting-circuit-based cavity magnonics may provide a convenient circuit platform that bridges magnonics and quantum information. In this tutorial, we will discuss recent progresses of cavity magnonics built on superconducting circuits. We will start from the original idea of coupling spin ensembles with superconducting resonators, and how magnetic spins are involved to replace spin ensembles. Then we will examine different magnetic materials and superconducting resonator designs for building superconducting cavity magnonics. Last, we will discuss future opportunities and challenges in scaling up such hybrid magnonic systems on superconducting circuits, with an emphasis on maintaining coherence time of magnons and photons, as well as utilizing superconducting properties such as vortices for empowering magnonics.

[1] Y. Li *et al.*, Hybrid magnonics: Physics, circuits, and applications for coherent information processing, *J. Appl. Phys.*, 128, 130902 (2020)

Session PL
PLENARY AND IEEE AWARDS CEREMONY

Juergen Fassbender, Co-Chair
HZDR, Dresden, Germany
Victorino Franco, Co-Chair
University of Seville, Seville, Spain

INVITED PAPER

PL-01. Nanoscale Magnetoelasticity, An Overlooked Opportunity.
G. Carman[1,2] 1. Mechanical & Aerospace Engineering, UCLA, Los Angeles, CA, United States; 2. Translational Applications of Nanoscale Multiferroic Systems TANMS, Los Angeles, CA, United States

The magnetoelastic coupling between magnetic and mechanical phenomenon in materials has been well understood for decades. This coupling, however, continues to be perceived as a nuisance rather than a unique opportunity for controlling magnetic physical states and related material parameters in the nanoscale. To explore this topic in more detail researchers have begun to evaluate nanoscale magnetoelastic materials for microelectronic applications. Efforts in this area are partially motivated by growing issues stemming from the increasing power consumption of traditional devices leading to the demise of Moore's law. Specifically, researchers have shown large energy efficiency improvements (>3 order of magnitude) in strain powered magnetic bit writing (magnetoelectric/multiferroic) and spin waves propagation when compared to conventional electrical current based magnetic approaches. While this illustrates a primary benefit of magnetoelastic materials, there are a large number of additional applications that would benefit from increased efficiency in controlling nanoscale magnetic behavior. The purpose of this presentation is to provide an overview of recent advancements in strain powered magnetoelastic devices and in doing so, showcase their advantages over existing technologies to motivate increased research activities and cross collaborations. One major challenge facing magnetoelastic control of magnetism in the small scale is the need for advanced multi-physics approaches representing different length scales. Several recent advancements include the implementation of fully coupled continuum models (micromagnetics + elastodynamics) for device design as well as the exploration of fundamental magnetoelastic and associated properties with Density Functional Theory DFT. These modeling approaches represent a driving engine enabling exponential growth in research and development in contrast to the traditional "make it and test it" philosophy. During the last few years, theoreticians have also begun to incorporate magnetoelastic phenomena in bridging codes like Molecular Dynamic Simulations to explore more specific local interactions at the intersection between continuum and DFT modeling representing an exciting new opportunity for the community. These modeling capabilities provide critical insights into new approaches, properties, and materials to design and understand various magnetoelastic dynamic operations. These models are enabling novel applications beyond the historical sonar community and microelectronic interests, such as magnetic sensors, motors, and wireless energy transfer to name a few. For example, research shows strain-powered magnetoelastic devices provide a new form of contactless communications in highly cluttered dielectric environments (e.g. mammalian tissues or seawater) using electrically small magnetoelastic antenna. These advances highlight the possibility of future chip-to-chip communication platforms. Additionally, our society has become reliant on electromagnetic motors to power locomotion in everything from cars to robots to conveyor belts at the macro level. These electromagnetic motors, however, largely fail when the dimensions decrease below the sub-millimeter regime due to energy inefficiencies and increased volumetric power consumption. This is no longer the situation as recently demonstrated when strain powered magnetoelastics have operationally captured and released T-cells using a magnetoelastic motor like platform. Therefore, magnetoelastic behavior, while fundamentally understood, has not yet been adequately explored by the research community considering the many opportunities available in the "micro/nano scale". As this presentation illustrates, magnetoelasticity is a research area poised for significant expansion over the next decade.

Session SA
APPLICATION OF SYMMETRY BREAKING IN CORRELATED AND QUANTUM MAGNETIC MATERIALS

Thomas Zac Ward, Chair
Oak Ridge National Laboratory, Oak Ridge, TN, United States

INVITED PAPERS

SA-01. Tuning Spin Excitations in Magnetic Films by Confinement.
V. Bisogni[1] *1. NSLS II, Brookhaven National Laboratory, Upton, NY, United States*

The past years have witnessed an increasing interest in the field of quantum materials (QM), not only thanks to their fascinating properties as a macroscopic manifestation of quantum mechanics (high-temperature superconductivity, quantum Hall effect, giant magnetoelectric effect, etc...), but also for the opportunities that these materials can offer towards the next generation of electronic devices. Understanding the physics behind quantum materials is thus a primary goal of condensed matter physics, both from a fundamental point of view as well for gaining control over the QM functional properties. Among all the experimental observables, excitations in QMs can provide unique information about the key-interactions at play in the system (magnetic interactions, electron-phonon coupling, spin-orbit coupling, topology, multiferroicity, etc...) and the nature of the excitations themselves (magnon, phonon, intra-band electronic excitations, orbiton, exotic modes, etc...). In this talk, I will focus on soft Resonant Inelastic X-ray Scattering (RIXS), as an emergent technique for the study of excitations and their momentum dependence. I will present recent results achieved on ferromagnetic thin films to investigate the evolution of the spin dynamics as a function of thickness [1]. Our work reveals an asymmetric evolution of the spin dynamics between the in-plane and out-of-plane directions: while the spin excitations remain invariant along the in-plane direction, in the out-of-plane direction a dampening is observed as a function of thickness. Such result is interpreted as an effect of confinement, enabling the use of the thickness as a "knob" to control the spin excitation energies.

[1] J. Pelliciari, S. Lee, K. Gilmore, J. Li, Y. Gu, A. Barbour, I. Jarrige, C. H. Ahn, F. J. Walker, V. Bisogni, Nature Materials, 20, 188 (2021).

SA-02. Controlling the Stripe Order in a Diluted Frustrated Magnet.
T. Vojta[1], X. Ye[1] and R. Narayanan[2] *1. Physics, Missouri University of Science and Technology, Rolla, MO, United States; 2. Physics, Indian Institute of Technology Madras, Chennai, India*

Significant attention has recently been attracted by phases that spontaneously break real-space symmetries in addition to spin, phase, or gauge symmetries. These phases include, for example, the charge-density wave or stripe phases in the cuprate superconductors, the Ising-nematic phases in the iron pnictides, and the valence-bond-solids in certain quantum magnets. We discuss the interplay between the broken real-space symmetries and vacancies, impurities and other types of quenched disorder that are inevitable in real materials. Specifically, we demonstrate that spinless impurities in a frustrated Ising magnet give rise to a random-field mechanism that can destroy the stripe-ordered phase. The strength of the emerging random fields is governed by the spatial impurity distribution. Moreover, the mechanism can be tuned very efficiently by weak exchange anisotropies that explicitly break the real-space symmetry, providing a way of controlling the phase diagram of this many-particle system. This work was supported in part by the National Science Foundation under Grant Nos. DMR-1828489 and OAC-1919789.

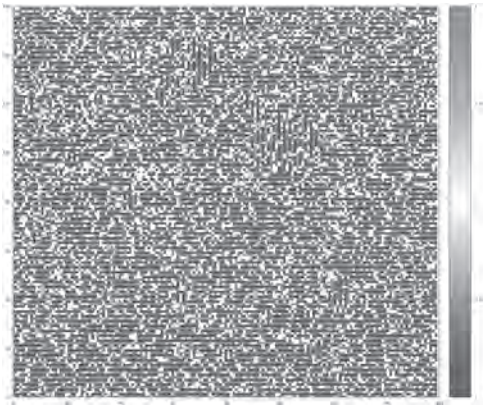

Domains of horizontal and vertical stripes in the diluted J_1-J_2 Ising model.

SA-03. Compositional disorder in the extreme limit: A novel route to the design and manipulation of dynamic and frustrated magnetic systems.
A.R. Mazza[1] and T.Z. Ward[1] *1. Oak Ridge National Laboratory, Oak Ridge, TN, United States*

The limited number of available spin-active elements makes the design of new magnetic materials a challenge. By focusing on maximizing disorder of the spin and exchange interaction landscape, new and highly tunable magnetic behaviors – from macroscopically ordered states to degenerate and frustration-driven dynamic systems – can be explored. Magnetic order classically relies on uniformity, with disorder resulting in lower ordering temperatures and prevention of percolation. However, in a chaotic limit, disorder can be treated as a parameter which can manipulate the local microstates towards a global response from long-range order to phase degeneracy. A classical Heisenberg model is found to be sufficient to describe how compositionally disordered systems drive continuous control over ordering types and critical temperatures. Theory then guides the design and growth of high entropy perovskite oxide films demonstrating the utility of this predictive materials approach. From this, we design the near degeneracy of macroscopic magnetic phase percolation between antiferromagnetic and ferromagnetic states. This leads to the discovery that manipulating the local spin disorder can be used to drive monolithic exchange bias behaviors in the single crystal films similar to that observed in AFM-FM bilayer heterojunctions, providing important new insights into recent proposals that spin and exchange disorder can be the dominating factor in generating exchange bias responses.

SA-04. Emergent magnetic states in transition metal nitride heterostructures. *E. Guo*[1] *1. Institute of Physics, Chinese Academy of Sciences, Beijing, China*

Transition metal nitrides (TMN) is a large group of materials which exhibit excellent mechanical properties, exceptional good thermal conductivity, and corrosion resistance. Among their intriguing physical properties, magnetism in TMNs had not been extensively studied in the past. In this talk, we firstly take CrN as a prototype system to investigate its high conductivity and unique antiferromagnetism as a response to the epitaxial strain. [1, 2] By shrinking the film thickness to a critical value of ≈30 unit cells, a profound conductivity reduction accompanied by unexpected volume expansion is observed in CrN films. The electrical conductivity is observed surprisingly when the CrN layer is as thin as a single unit cell thick, which is far below the critical thickness of most metallic films. Both first-principles calculations and linear dichroism measurements reveal that the strain-mediated orbital splitting effectively customizes the relatively small bandgap at the Fermi level, leading to an exotic phase transition in CrN. In the second part of talk, we demonstrate the first synthesis of chromium oxide (Cr_2O_3)–chromium nitride (CrN) superlattices with atomically sharp interfaces.[3] The ferromagnetic spin ordering was achieved at interfaces comprising two antiferromagnets and decays by increasing interlayer thickness. Combined multiple magnetic probes (XMCD, PNR, NV-center) and DFT calculations, we attribute the unexpected ferromagnetism to the spin canting at the interfaces, thus yielding the lowest stable energy.

References [1] Q. Jin et al., Advanced Materials 33, 2005920 (2021). [2] Q. Jin et al., Phys. Rev. Mater. 5, 023604 (2021). [3] Q. Jin et al., to be submitted.

SA-05. Designing Spin Textures through Local Control of Magnetocrystalline Anisotropy. *Y. Takamura*[1], M.S. Lee[1], R.V. Chopdekar[2], P. Lyu[1], T. Wynn[5], E. Folven[6], J. Grepstad[6], S.T. Retterer[3], P. Shafer[2] and E. Arenholz[4] *1. Materials Science and Engineering, University of California, Davis, Davis, CA, United States; 2. Advanced Light Source, Lawrence Berkeley National Laboratory, Berkeley, CA, United States; 3. Center for Nanophase Materials Sciences, Oak Ridge National Laboratory, Oak Ridge, TN, United States; 4. Oak Ridge National Laboratory, Oak Ridge, TN, United States; 5. Stanford Synchrotron Radiation Lightsource, SLAC National Accelerator Laboratory, Menlo Park, CA, United States; 6. Norwegian Institute of Science and Technology, Trondheim, Norway*

The development of spintronic devices based on ferromagnetic (FM) and antiferromagnetic (AF) materials requires the ability to design spin textures such as artificial magnetic skyrmions, which are characterized by adjacent FM regions of a thin film with both in-plane and out-of-plane moments. In particular, AF spin textures have received significant interest in recent years due to their promising characteristics including fast operating speeds, nanoscalability, and stability against magnetic stray fields. Due to their strong interactions between charge, spin, lattice, and orbital degrees of freedom, strongly correlated electron systems such as FM $La_{0.7}Sr_{0.3}MnO_3$ (LSMO) and AF $La_{1-x}Sr_xFeO_3$ (LSFO) provide an ideal platform for the design of magnetic spin textures. In this work, an ion implantation-based patterning process was used to define magnetic islands – also referred to as micromagnets - embedded within a non-magnetic matrix.[1] This patterning process gives rise to a complex 3D strain state within the magnetic islands due to the combined strains imposed from the underlying substrate and surrounding amorphous matrix, allowing for control of the local magnetocrystalline anisotropy by varying the ion implantation dose and epitaxial strain.[2] X-ray diffraction experiments and simulations show that as a function of increasing implant dose, a uniaxial expansion of the *c*-axis of the unit cell leads to a transition from in-plane easy axis toward perpendicular magnetic anisotropy. Above a critical dose of 3 x 10^{13} Ar^+/cm^2 significant crystalline disorder results, leading to a decrease in the average Mn valence state and near complete suppression of magnetization. X-ray photoemission electron microscopy (X-PEEM) imaging was performed on patterned micromagnets in LSMO and LSFO thin films as well as LSMO/LSFO heterostructures (Figure 1). The FM and AF spin textures demonstrate that an intricate interplay exists between shape and magnetocrystalline anisotropy energies as well as exchange coupling interactions at LSMO/LSFO interfaces.[3,4] These magnetic spin textures can be controlled using parameters such as the LSMO and LSFO layer thicknesses, micromagnet shape, and temperature.[4] In the limit of ultrathin LSFO layers in an LSMO/LSFO heterostructure, shape anisotropy effects dominate such that the AF spin axes lie perpendicular to micromagnet edges and can be oriented along any in-plane crystallographic direction. These studies demonstrate that strongly correlated and quantum materials provide a unique platform for engineering FM and AF spin textures for spintronics applications.

[1] Y. Takamura *et al., Nano Letters,* 6 1287 (2006) [2] M.S. Lee *et al., AIP Adv*., 10, 045306 (2020) [3] M.S. Lee *et al., ACS Nano,* 10, 8545 (2016) [4] M.S. Lee *et al., JAP,* 127, 204901 (2020)

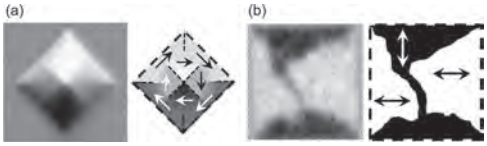

Fig. 1: X-PEEM images and domain schematics for (a) FM spin textures in LSMO micromagnets and (b) AF spin textures in LSFO micromagnets in an LSMO/LSFO heterostructure.

Session SB
SPINTRONIC DIODES: CHALLENGES AND NEW DIRECTIONS

Riccardo Tomasello, Co-Chair
Politecnico di Bari, Bari, Italy
Mario Carpentieri, Co-Chair
Politecnico of Bari, Bari, Italy

INVITED PAPERS

SB-01. Challenges in microwave and THz spintronic diodes.
G. Finocchio[1] 1. University of Messina, Messina, Italy

Microwave detectors based on the spin-torque diode effect are among the key emerging spintronic devices (see ref.[1] and references therein). By utilizing the spin of electrons in addition to their charge, they have the potential to overcome the theoretical performance limits of their semiconductor (Schottky) counterparts. Those devices realized with magnetic tunnel junctions and in active regime exhibit high-detection sensitivity >200kV/W at room temperature and zero bias field, thanks to the injection locking mechanism, and for low-input power (micro-Watts or lower). Those performance can be improved with the bolometric effect or when coupled properly in arrays. Here, I will discuss our recent results in the field of microwave detectors based on spin diodes and possible implementations of THz detectors based on antiferromagnets working in linear and parametric excitation regime. I will point out how those devices can impact the IoT market and can be used for implement hardware multiplication by using the concept of degree of rectification and as dual band detectors in frequency shifting keying demodulation schemes in which the information is coded in two discrete values of the frequency in a carrier signal. In particular, the frequency response of spin-torque diodes and their current tunability can be also used as building blocks of the hardware realization of neurons and synapses in neuromorphic applications. Another application of spintronic diodes, when they have a broadband frequency response, is as electromagnetic energy harvesting, which offers an attractive energy source for applications in self-powered portable electronics in the "internet of things" era. Here I will show the development of a bias-field-free spin-torque diodes based on a magnetic tunnel junction having a canted magnetization in the free layer, and demonstrate that those devices could be an efficient harvester of broadband ambient RF radiation, capable to efficiently harvest microwave powers of microWatt and below and to power a black phosphorous nanodevice. I will also review recent idea on spintronic detectors in presence of nonuniform ground states such as skyrmions.

[1] G. Finocchio, et al. Perspectives on spintronic diodes, Appl. Phys. Lett. 118, 160502 (2021);

SB-02. WiFi Band Energy Harvesting using Spin-Torque Diode and Nonlinear Hall Effects.
H. Yang[1] 1. National University of Singapore, Singapore

There is a great interest to generate electricity using ambient RF energy. We addressed this using two different approaches. We first use the intrinsic quantum property of the Weyl semimetal to convert the RF energy into electricity [1]. The nonlinear Hall effect (NLHE) can produce a dc transverse voltage in zero magnetic field. However, it requires NLHE to be detected at room temperature. Despite of several studies of NLHE in topological materials and 2D materials, the room-temperature NLHE has not yet been achieved. We find the room-temperature NLHE in a type-II Weyl semimetal $TaIrTe_4$, which hosts a robust NLHE due to broken inversion symmetry and large band overlapping at the Fermi level. The NLHE is present only when the electric field is applied along the axis of the mirror plane (a-axis of the crystal). Based on the observed room-temperature NLHE in $TaIrTe_4$ we demonstrate the wireless RF rectification with zero external bias and magnetic field. An incident electric field along the a-axis (E_a) generates a rectified voltage along the b-axis (V_b), whereas, there is no rectification when the incident electric field is along the b-axis (E_b) in consistent with the symmetry constraints of NLHE. This work opens a door to realizing room temperature rectification applications based on the NLHE in Weyl semimetals. The other approach is to use the spin-torque diode effect of spin-torque oscillators (STOs) [2]. For the application in rectification and energy harvesting, the spin-diode effect is demonstrated by measuring the rectified dc voltage. Due to the canted anisotropy, the free layer of the individual STOs shows a large RF sensitivity as a result of non-linear dynamics. We demonstrate series connections have an advantage for rectification due to the additive effect of the diode voltages from STOs. Using eight oscillators in series, the rectified voltage is enhanced and we have achieved a rectification efficiency of 6% at -20 dBm, which outperforms the Schottky diode capability at sub μW power. By integrating the electrically connected eight STOs with conventional electronics, we demonstrate the battery-free energy-harvesting system by utilizing the wireless RF energy to power electronic devices such as LEDs. We also demonstrate the capability of this energy harvesting system in holding dc power using a time-varying signal, which is useful in harvesting energy from discrete commercial sources such as a WiFi router. Our results highlight the significance of electrical topology (series vs. parallel) while designing an on-chip STOs system.

[1] D. Kumar et al., Nat. Nanotechnol. 16, 421 (2021) [2] R. Sharma et al., Nat. Commun. 12, 2924 (2021)

SB-03. Radio-Frequency Spintronic Neural Networks.
N. Leroux[1], A. Ross[1], D. Markovic[1], D. Sanz Hernandez[1], J. Trastoy[1], P. Bortolotti[1], D. Querlioz[2], L. Martins[3], A. Jenkins[3], R. Ferreira[3], A. Mizrahi[1] and *J. Grollier[1] 1. CNRS/Thales, Palaiseau, France; 2. C2N, Université Paris Saclay, Palaiseau, France; 3. INL, Braga, Portugal*

A key challenge of neuromorphic computing is to build hardware neural networks with dense connectivity between nanoscale synapses and neurons, approaching the brain's thousands of synapses per neuron (*1*). In this talk, I will show that spin diodes are microwave nano-synapses that naturally and densely interface with neurons made of spin-torque nano-oscillators (*2*). I will describe the principle of these novel synapses and explain how their microwave features can be harnessed to achieve the multiply-and-accumulate operations at the core of neural networks, with over 500 synapses/neuron. I will show that they implement all-to-all connections as well as convolutional operations in a fully parallel way with high density and speed. I will describe our experiments highlighting these functionalities (*3*), and show that they open the path to radio-frequency deep learning.

1. J. Grollier *et al.*, *Nat. Electron.*, 1–11 (2020). 2. N. Leroux *et al.*, *Phys. Rev. Appl.* 15, 034067 (2021). 3. N. Leroux *et al.*, *Neuromorphic Comput. Eng.* (2021), doi:10.1088/2634-4386/abfca6.

SB-04. Antiferromagnetic Spin-torque Oscillators: Ultrafast Dynamics and Possible Applications. *O. Gomonay*[1] *1. Institute of Physics, Johanes Gutenberg University, Mainz, Germany*

Antiferromagnets are prospective materials for spintronic applications due to their internal ultrafast dynamics, robustness with respect to the external magnetic fields, and high sensitivity to spin-torques of different nature. Moreover, in contrast to ferromagnets, spin-torques can induce steady precession of the Néel vector at THz frequencies whose values can be controlled by the current. Hence, antiferromagnets can be considered as tunable current controlled auto-oscillators, which is the main component of phase-controlling devices. An auto-oscillation regime is supported solely by antidamping torques that compensate the internal energy losses. However, the frequency of the precession, threshold value, the type of dynamics etc can be effectively manipulated by applying the field-like torques. In this presentation we review recent developments in the field of antiferromagnetic spin-torque oscillators and discuss new functionalities stemming from the combining effect of the field-like and antidamping-like torques. To demonstrate the effects of different torques we start from the dynamics of ultrafast switching and discuss various mechanisms including the Néel spin-orbit torques [1], thermomagnetoelastic mechanism [2], and optically-induced spin-transfer torques [3]. We illustrate possible applications of nontrivial antiferromagnetic dynamics for the detection and emission of teraherz radiation in altermagnets CuMnAs and Mn2Au in which electrical current can induce simultaneously the ac Néel spin-orbit torque and dc spin-orbit torque [1]. Using NiO antiferromagnet as an example, we discuss and compare various scenarios of ultrafast dynamics, such as: i) reorientation of the Néel vector due to the field-like torques of magnetoelastic nature and spin-orbit torques due to spin-pumping [4]; ii) fast switching and stable precession induced by the ac spin-transfer torques whose frequency coinsides with the frequency of antiferromagnetic resonance. We also analyse the chaotic regimes of an antiferromagnetic oscillator that appear at certain combination of field-like and damping-like torques (see Fig.1) and and discuss possible applications for neuromorphic computations [5]. As an outline of future development, we discuss influence of the magnetoelastic and thermal effects and combination of different stimulus for the effective control and manipulation of the antiferromagnet-based devices.

[1] O. Gomonay, T. Jungwirth, and J. Sinova. Narrow-band tunable terahertz detector in antiferromagnets via staggered-field and antidamping torques. Phys. Rev. B, 98, 104430 (2018) [2] H. Meer, F. Schreiber, C. Schmitt, R. Ramos, E. Saitoh, O. Gomonay, J. Sinova, L. Baldrati, and M. Kläui. Direct imaging of current-induced antiferromagnetic switching revealing a pure thermomagnetoelastic switching mechanism. Nano Lett., 21,114 (2021). [3] Th. Chirac, J.-Y. Chauleau, P. Thibaudeau, O. Gomonay, and M. Viret. Ultrafast antiferromagnetic switching in NiO induced by spin transfer torques. Phys. Rev. B 102, 134415 (2020). [4] L. Baldrati, O. Gomonay, A. Ross, M. Filianina, R. Lebrun, et al. Mechanism of Néel Order Switching in Antiferromagnetic Thin Films Revealed by Magnetotransport and Direct Imaging. Phys. Rev. Lett., *123*, 177201 (2019). [5] B. Wolba, O. Gomonay, and V. P. Kravchuk. Chaotic Antiferromagnetic Nano-Oscillator driven by Spin-Torque. Phys. Rev. B, 104, 024407 (2021).

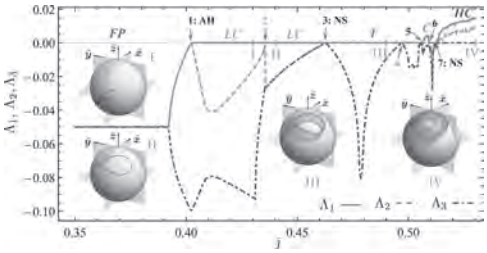

Current-induced transition to chaos traced by variation of the largest of three Lyapunov's exponents. Red lines on the spheres show trajectories of the Neel vector. From [5].

SB-05. Signal Detector and RF Energy Harvester Based On A Spintronic Diode With Perpendicular Anisotropy. P. Artemchuk[1,2], O. Prokopenko[2], V. Tyberkevych[1] and *A.N. Slavin*[1] *1. Physics, Oakland University, Rochester, MI, United States; 2. Radio Physics, Electronics and Computer Systems, Taras Shevchenko National University of Kyiv, Kyiv, Ukraine*

The spin-torque magnetic diode (STMD) effect [1] is a quadratic rectification effect of the input microwave current $I_{RF}(t)$ in a magnetoresistive nanojunction, which is commonly observed in the traditional regime of operation of an STMD, when the magnetization of the "free" layer (FL) lies in-plane, and when the frequency f_s of the current $I_{RF}(t)$ is close to the ferromagnetic resonance (FMR) frequency f_0 of the junction. In this case, the induced resonance oscillations of the junction resistance $R(t)$ can mix with the oscillations of the input microwave current $I_{RF}(t)$, and produce an output DC voltage $U_{DC} = \langle I_{RF}(t)R(t) \rangle$ (where "<>" denotes time averaging) across the junction. It was demonstrated theoretically in [2] that in an STMD, biased by an out-of-plane static magnetic field, a different dynamical regime of the STMD operation characterized by large-angle out-of-plane magnetization precession can be realized. The excitation of the large-angle precession has a threshold character, and is possible only for input microwave currents exceeding a certain frequency-dependent critical value, and sufficiently low frequency. In this regime of the out-of-plane precession the output DC voltage of an STMD increases with the frequency of the input signal, but is virtually independent of its power. An STMD working in the regime of large-amplitude out-of-plane precession functions as a *non-resonant threshold detector* of low frequency microwave signals, due to the large nonlinear shift of its operating frequency. Therefore, this precession regime is particularly suitable for applications in the microwave energy harvesting. It was demonstrated experimentally in [3] that the out-of-plane magnetization precession regime in an STMD operation predicted in [2] can be realized without *any bias magnetic field*, if an STMD FL has a perpendicular magnetic anisotropy. In such a regime an STMD has the rectification properties that are independent of the input microwave frequency, and the performance of the STMD-based energy harvesting device is comparable to the performance of the state-of-the-art Schottky diode for low-power rectification. It was further shown in [3] that the developed bias-free STMD provides sufficient dc voltage to power a practical nanodevice – a black phosphorus photosensor. Here we present an analytical and numerical theory explaining the performance of a bias-free STMD with perpendicular magnetic anisotropy [4]. We show that in an STMD, having a magnetic FL with perpendicular magnetic anisotropy of the first and second order, and no external bias magnetic field, the out-of-plane regime of magnetization precession can be excited by sufficiently large (exceeding a certain threshold) RF signals with the frequencies smaller than 250 MHz. We also show that such a device can operate as a broadband energy harvester capable of converting incident RF power into a DC power

with a conversion efficiency of ~5%. The developed analytical theory of the bias-free STMD operation can be used for the optimization of high-efficiency RF detectors and energy harvesters based on STMDs. Our results are paving a way for use of spintronic detectors and harvesters as building blocks for self-powered nano-systems, such as implantable biomedical devices, wireless sensors, and portable electronics.

[1] A. Tulapurkar, Y. Suzuki, A. Fukushima et al., Nature., Vol.438, p.339 (2005). [2] V. Prokopenko, I. N. Krivorotov, E. Bankowski et al., J. Appl. Phys., Vol. 111, p.123904 (2012). [3] B. Fang, M. Carpentieri, S. Louis et al., Phys. Rev. Appl., Vol. 11, p.014022 (2019). [4] P. Yu. Artemchuk, O. V. Prokopenko, E. N. Bankowski *et al.*, AIP Advances., Vol. 11, p. 025234 (2021).

Session SC
EXPLORING MAGNETISM AT THE NANOSCALE WITH SCANNING NV MAGNETOMETRY

Patrick Maletinsky, Chair
University of Basel, Basel, Switzerland

INVITED PAPERS

SC-01. Magnetic Domains and Moire Magnetism in atomically thin $CrBr_3$ and CrI_3. *J. Wrachtrup[1,2] 1. Physics, University of Stuttgart, Stuttgart, Germany; 2. Max Planck Institute for Solid State Science, Stuttgart, Germany*

The emergence of atomically thin van der Waals magnets provides a new platform for the studies of two-dimensional magnetism and its applications. However, the widely used measurement methods in recent studies cannot provide quantitative information of the magnetization nor achieve nanoscale spatial resolution. These capabilities are essential to explore the rich properties of magnetic domains and spin textures. In this talk, we will present our recent results using cryogenic scanning NV magnetometry to unambiguously prove the existence of magnetic domains and study their dynamics in atomically thin CrBr3 [1]. We also measured Moire magnetisation patterns in twisted thin films of CrI3. Owing to the high spatial resolution of our technique, we were able to determine a periodic pattern consisting of antiferromagnetically and ferromagnetically ordered domains in twisterd layers of this material [2].

[1] Qi-Chao Sun et al. Magnetic domains and domain wall pinning in atomically thin CrBr3 revealed by nanoscale imaging, Nature Commun. 12, 1989 (2921) [2] Tiancheng Song et al. Direct visualization of magnetic and moire magnetism in tiwsted 2D magnets, Science, in press (2021)

SC-02. Exploring antiferromagnetic order at the nanoscale with a single spin microscope. *V. Jacques[1] 1. Laboratoire Charles Coulomb, CNRS and Université de Montpellier, Montpellier, France*

Experimental methods allowing for the detection of single spins in the solid-state, which were initially developed for quantum information science, open new avenues for the development of highly sensitive quantum sensors [1]. In that context, the electronic spin of a single nitrogen-vacancy (NV) defect in diamond can be used as an atomic-sized magnetometer, providing an unprecedented combination of spatial resolution and magnetic sensitivity under ambient conditions [2]. In this talk, I will illustrate how scanning-NV magnetometry can be used as a powerful tool for exploring condensed-matter physics, focusing on chiral spin textures in antiferromagnetic materials [3-5].

[1] C. Degen et al., *Rev. Mod. Phys.* 89, 035002 (2017) [2] L. Rondin et al., *Rep. Prog. Phys.* 77, 056503 (2014) [3] I. Gross et al., *Nature* 549, 252 (2017) [4] A. Haykal et al., *Nat. Comm.* 11, 1704 (2020) [5] A. Finco et al., *Nat. Comm.* 12, 767 (2021)

SC-03. Optimizing color center-based nano-sensing. N. Oshnik[1], L. Mehmel[1], O. Opaluch[1], A. Damm[1], S. Shradha[2], F. Eilenberger[2] and *E. Neu[1] 1. University of Kaiserslautern, Kaiserslautern, Germany; 2. University of Jena, Jena, Germany*

Individual color centers offer unique capabilities as versatile, nanoscale sensors. Most of these sensing capabilities employ the electronic spins of the color centers. A central advantage here is the optical state read-out of individual electronic spins. To fully harness the sensing capabilities, it is of high importance to efficiently collect the fluorescence of the centers. For scanning probe-based sensing and imaging, we incorporate the color centers into conically shaped nanopillars. The color centers are embedded close to the apex of the nanopillar. These nanostructures, manufactured in sophisticated top-down processes [1], thus enable scanning color centers near a sample and enhance fluorescence collection [2]. We also investigate the coupling of excitation laser light with different laser wavelengths into various nanopillar types and find significant enhancements of the excitation fields in the nanopillars [3], thus witnessing optimal excitation in the nanostructures. Besides incorporating centers in scanning probe nanostructures, we optimize color center-based sensing via optimal control approaches [4]: Using numerical methods, we identify optimal shapes for the microwave pulses used for spin manipulation. Simultaneously, we optimize the laser pulses that initialize the color center spin state especially their duration and intensity. While magnetic sensing is the main application field of color centers, novel approaches to color center-based sensing are evolving as color centers enable sensing via near field processes such as Förster resonance energy transfer (FRET). We recently realized FRET between nitrogen vacancy (NV) centers and a luminescent two-dimensional material, namely WSe_2 [5]. We will discuss recent advances in this field including approaches to manufacture hybrid nanostructures consisting of diamond and two-dimensional materials and potential applications.

[1] M. Radtke et al. Micromachines, 10, 718 (2019) [2] P. Fuchs et al., New Journal of Physics, 20, 125001 (2018) [3] A. Hochstetter and E. Neu, AIP Advances, 11, 065006 (2021) [4] P. Rembold et al., AVS Quantum Science 2, 024701 (2020) [5] R. Nelz et al. Adv. Quantum Techn. 3, 1900088 (2019)

SC-04. Imaging hydrodynamic flow in WTe2 with cryogenic quantum magnetometry. *U. Vool[1] 1. Harvard University, Cambridge, MA, United States*

Hydrodynamic electron flow, where electrons in a conductor flow collectively - akin to a fluid, is a unique signature of strong electron interactions in a material. This effect has been observed in 2D materials, but observations in bulk materials are intriguing as high-carrier density should screen the interactions. In this talk, I will discuss a recent measurement of hydrodynamic flow in the semimetal WTe2, allowing us to gain insight into the microscopic origin of its electron interactions. We image the spatial profile of the electric current by using a nitrogen-vacancy scanning tip. Using coherent quantum sensing, we obtain magnetic field resolution of ~10nT and spatial resolution of ~100nm. The current pattern we observe differs substantially from the flat profile of a normal metal, and indicates correlated flow through the semimetal. The pattern also shows non-monotonic temperature dependence, with hydrodynamic effects peaking at ~20 K. We compare our results to a model which combines ab initio electron scattering rates and the electronic Boltzmann transport equation. The model shows quantitative agreement with our measurement, allowing us to extract the strength of electron-electron interactions in our material. Furthermore, we conclude that electron interactions are phonon-mediated. This result opens a path for hydrodynamic flow and strong interactions in a variety of new materials.

U. Vool, A. Hamo, G. Varnavides, Y. Wang et. al. Nature Physics (2021)

SC-05. Extending Quantum Coherence of Quantum Sensors.
A. Bleszynski Jayich[1], S. Meynell[1], D. Yang[1] and M. Joos[1] *1. Physics, UC Santa Barbara, Santa Barbara, CA, United States*

The nitrogen vacancy (NV) center in diamond is an atomic-scale defect in diamond that is highly sensitive to a wide variety of fields: magnetic, electric, thermal, and strain. A versatile quantum sensor, the NV center holds particular promise for nanometer-scale imaging. Here I discuss an NV-based imaging platform where we have incorporated an NV center into a scanning probe microscope and used it to image a variety of condensed matter systems, including skyrmions, nanoscale topological spin textures, as well as current flow patterns in graphene. I also discuss recent experiments that utilize the NV center's sensitivity to fluctuating magnetic fields to image conductivity with nanoscale spatial resolution. A grand challenge to improving the spatial resolution and magnetic sensitivity of the NV is mitigating surface-induced quantum decoherence, which I will discuss in the second part of this talk. Decoherence at interfaces is a universal problem that affects many quantum technologies, but the microscopic origins are as yet unclear. Our studies guide the ongoing development of quantum control and materials control, pushing towards the ultimate goal of NV-based single nuclear spin imaging.

Session SD
FRONTIERS OF ORBITAL PHYSICS: STATICS, DYNAMICS, AND TRANSPORT OF ORBITAL ANGULAR MOMENTUM

Olena Gomonay, Chair
Johannes Gutenberg University Mainz, Mainz, Germany

INVITED PAPERS

SD-01. Theory of Orbital Hall Effect and Current-Induced Torques by Orbital Current. *D. Go*[1,4], D. Jo[2], K. Kim[3], H. Lee[2] and Y. Mokrousov[1,4]
1. Forschungszentrum Jülich, Jülich, Germany; 2. Pohang University of Science and Technology, Pohang, The Republic of Korea; 3. Korea Institute of Science and Technology, Seoul, The Republic of Korea; 4. Johannes Gutenberg University Mainz, Mainz, Germany

The current-induced torque is one of the most important phenomena in spintronics as it provides a way to control magnetic order parameters by electrical means. So far, most studies on the microscopic mechanisms of the current-induced torque have focused on the role of spin current carried by conduction electrons, which exerts spin-transfer torque on the magnetization upon the injection into a ferromagnet. In solids, however, electronic Bloch states originate from the atomic orbitals of the constituent atoms. Thus, while it is natural to expect that such orbital information may be used to control the magnetization because the orbital degree of freedom carries the angular momentum as the spin degree of freedom does, the role of orbitals in the physics of the current-induced torque has been barely investigated. In recent years, we uncovered mechanisms of generating the electronic current carrying finite orbital angular momentum such as the orbital Hall effect (OHE) [1] and proposed to utilize the orbital current for controlling the magnetization [2]. The latter is shortly denoted by "orbital torque" (OT) nowadays. In this talk, I review recent theoretical progress in the mechanisms of the OHE and the OT. In the first part, I will explain that the OHE arises in various metals regardless of their strength of the spin-orbit coupling, whose magnitude is typically an order of magnitude larger than that of the spin Hall effect (SHE) in heavy metals [3]. In fact, the SHE is a concomitant effect of the OHE, whose hierarchical relation will be explained. In the second part, I will discuss the mechanisms of the OT. The main problem is that it is hard to distinguish the orbital contribution and the spin contribution to the torque on the magnetization in most torque measurements. This is one of the main difficulties to quantify the OT. Theoretically, we recently developed a general theoretical formalism that tracks the transfer of the angular momentum in solids between the lattice, the local magnetic moment, and the electron's spin and orbital, and successfully implemented it within the density functional theory framework [4]. This enables us to understand the microscopic nature of the OT and quantify different competing contributions. Finally, I will also discuss unique qualitative features of the OT mechanisms: significant dependence of the interface orbital transparency on the crystallinity and long-range transport and dephasing in a ferromagnet [5].

[1] D. Go, D. Jo, C. Kim, and H.-W. Lee, Phys. Rev. Lett. 121, 086602 (2018). [2] D. Go and H.-W. Lee, Phys. Rev. Res. 2, 013177 (2020). [3] D. Jo, D. Go, and H.-W. Lee, Phys. Rev. B 98, 214405 (2018). [4] D. Go, F. Freimuth, J.-P. Hanke, F. Xue, O. Gomonay, K.-J. Lee, S. Blügel, P. M. Haney, H.-W. Lee, and Y. Mokrousov, Phys. Rev. Res. 2, 033401 (2020). [5] D. Go, D. Jo, K.-W. Kim, S. Lee, M.-G. Kang, B.-G. Park, S. Blügel, H.-W. Lee, and Y. Mokrousov, arXiv:2106.07928.

SD-02. Ferroelectric control of Rashba states: towards non-volatile spintronics driven by ferroelectricity. *M. Bibes*[1] *1. Unité Mixte de Physique CNRS/Thales, Palaiseau, France*

After 50 years of exponential increase in computing efficiency, the technology of today's electronics is approaching its physical limits, with feature sizes smaller than 10 nm. New schemes must be devised to contain the ever-increasing power consumption of information and communication systems, which requires the introduction of non-traditional materials and new state variables. As recently highlighted, the remanence associated with collective switching in ferroic systems is appealing to reduce power consumption[1]. A particularly promising approach is spintronics, which relies on ferromagnets to provide non-volatility and to generate and detect spin currents. However, magnetization reversal by spin transfer torques is a power consuming process. This is driving research on multiferroics to achieve a low-power electric-field control of magnetization, but practical materials are scarce and magnetoelectric switching remains difficult to control. In this talk, we will propose an alternative strategy to achieve low-power spin detection and generation, in non-magnetic systems combining ferroelectricity and Rashba spin-orbit coupling[2]. We will describe various materials strategies based on single materials, multilayers and two-dimensional electron gases. In particular we will show results on $SrTiO_3$-based electron gases in which a large electric field induces a ferroelectric-like state that enables a non-volatile control of its spin-orbit properties and spin-charge conversion capabilities[3]. These observation open the way to the electric-field control of spin currents and to ultralow-power spintronics, in which non-volatility would be provided by ferroelectricity rather than by ferromagnetism. This work received support from the ERC Advanced grant n° 833973 "FRESCO".

1. Manipatruni, S. Beyond CMOS computing with spin and polarization. *Nature Physics* 14, 338 (2018). 2. Varignon, J., Vila, L., Barthélémy, A. & Bibes, M. A new spin for oxide interfaces. *Nature Phys* 14, 322–325 (2018). 3. Noël, P. *et al.* Non-volatile electric control of spin–charge conversion in a SrTiO3 Rashba system. *Nature* 580, 483–486 (2020).

SD-03. Ultra-efficient spin manipulation by orbital currents. *M. Kläui*[1] *1. Physics, Johannes Gutenberg University Mainz, Mainz, Germany*

While so far the focus has been on spin currents, effects of orbital currents, i.e. the flow of the electrons with finite orbital angular momentum, can outperform conventional spin current effects. As shown, orbital currents can even play a pivotal role in generating spin currents thus leading to torques with unprecedented amplitude to manipulate magnetization. Experimentally, orbital currents for efficient manipulation of magnetization have only recently started to be explored. In order to generate orbital currents, materials with orbital Hall effects can be used that can be light metals and thus cheap, abundant and environmentally friendly. In our work we studied spin orbit torques generated in TmIG/Pt/(Cu(O)x) heterostructures. We observed that the torques exerted on the TmIG are enhanced by a factor up to 16 if the CuOx is added on top of the Pt compared to the conventional TmIG/Pt stack [1]. Such an enhancement is extremely surprising if one considers only conventional spin-charge interconversion based on spin orbit coupling

effects and given the low spin-orbit coupling of Cu and Cu(O)x one does not expect large torques. However the results can be naturally explained as Cu(O)x can generate large orbital currents that are then converted to spin currents in the Pt layer, which then manipulate the TmIG extremely efficiently. More recently we studied magnetoresistance effects in systems with layers that generate orbital currents. We found that the Orbital Rashba-Edelstein Magnetoresistance can be observed in Py/Cu(O)x, which is an orbital magnetoresistance effect related to the conventional spin Hall magnetoresistance [2]. In particular in this work, the length scale of the orbital to spin current conversion in Py could be identified as a key step to harnessing orbital currents efficiently even without a heavy metal based orbital to spin conversion layer.

[1] S. Ding et al., Phys. Rev. Lett. 125, 177201 (2020) [2] S. Ding et al., arxiv:2105.04495 (2021)

SD-04. Competition between orbital and spin angular momenta of the THz beams at the antiferromagnetic resonances and Landau level transitions. *A. Sirenko[1] 1. Physics, NJIT, Newark, NJ, United States*

Circularly polarized light with spin angular momentum is one of the most valuable probes of magnetism. Recently we demonstrated that light beams with orbital angular momentum (OAM), or vortex beams, can also couple to magnetism exhibiting dichroisms in a magnetized medium [1.2]. Terahertz (THz) vortex beams with various combinations of the orbital angular momentum l=±1, ±2, ±3, and ±4 and spin angular momentum s = ±1, or conventional circular polarization, were used for studies of the magnon spectra at the antiferromagnetic resonance conditions in $TbFe_3(BO_3)_4$ and Ni_3TeO_6 single crystals. In both materials we observed strong vortex beam dichroism for the magnon doublet, which is split in an external magnetic field applied along the spin ordering direction. The absorption conditions at the magnon frequencies depend on the total angular momentum of light j that is determined by the combination of the spin and orbital angular momenta: j=s+l. For the higher orders of l, the selection rules for AFM resonances dictated by l completely dominate over that for conventional circular polarization. Our results demonstrate the high potential of the vortex beams with OAM as a new spectroscopic probe of magnetism in matter. In addition to the results for AFM materials, we will also present our recent experiments with vortex beam spectroscopy of the Landau level resonances in 2DEG semiconductor heterostructures in high magnetic field. Various parts of this work was performed in collaboration with T. N. Stanislavchuk[1], P. Marsik [2], L. Bugnon[2], M. Soulier[2], C. Bernhard[2], V. Kiryukhin[3], and S.-W. Cheong[3] [1] Department of Physics, New Jersey Institute of Technology, Newark, New Jersey 07102, USA [2] Department of Physics, University of Fribourg, CH-1700 Fribourg, Switzerland [3] Rutgers Center for Emergent Materials and Department of Physics and Astronomy, Rutgers University, Piscataway, New Jersey 08854, USA.

[1] https://journals.aps.org/prl/abstract/10.1103/PhysRevLett.126.157401 [2] https://journals.aps.org/prl/abstract/10.1103/PhysRevLett.122.237401

SD-05. Theory of Spin and Orbital Edelstein Effects. *A. Johansson[1,2]*, B. Göbel[2,1], J. Henk[2], M. Bibes[3] and I. Mertig[2] *1. Max Planck Institute of Microstructure Physics, Halle (Saale), Germany; 2. Martin Luther University Halle-Wittenberg, Halle (Saale), Germany; 3. Unité Mixte de Physique, CNRS, Thales, Université Paris-Saclay, Palaiseau, France*

The (spin) Edelstein effect, also known as current-induced spin polarization, provides charge-spin interconversion in nonmagnetic systems with broken inversion symmetry [1,2]: An external electric field generates a charge current as well as a homogeneous spin density. Thus, a finite magnetization can be generated and tuned exclusively electrically. In addition to this conventionally discussed spin Edelstein effect, the electrons' orbital moments are also expected to provide a current-induced magnetization, which is called the orbital Edelstein effect [3-5]. Thus, the magnetization induced electrically by the Edelstein effect can comprise contributions from both the spin and the orbital moments, as sketched in Fig. 1. In this talk the spin and orbital Edelstein effects are discussed within a semiclassical Boltzmann approach. The theory is applied to a simple Rashba system as well as the topologically nontrivial two-dimensional electron gas at $SrTiO_3$ interfaces [6]. In this particular system the orbital Edelstein effect is predicted to exceed its spin counterpart by at least one order of magnitude. This finding can be understood by a band-resolved analysis of the spin and orbital Edelstein effects.

[1] A. G. Aronov and Y. B. Lyanda-Geller, JETP Lett., Vol. 50, p. 431 (1989) [2] V. M. Edelstein, Solid State Commun., Vol. 73, p. 233 (1990) [3] T. Yoda, T. Yokoyama and S. Murakami, Sci. Rep., Vol. 5, p. 12024 (2015) [4] T. Yoda, T. Yokoyama and S. Murakami, Nano Lett., Vol. 18, p. 916 (2018) [5] L. Salemi *et al.*, Nat. Commun., Vol. 10, p. 5381 (2019) [6] A. Johansson *et al.*, Phys. Rev. Research, Vol. 3, p. 013275 (2021)

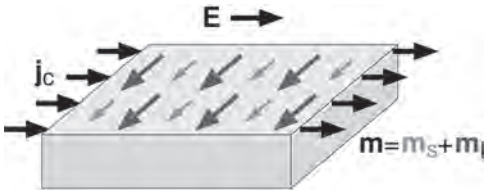

Fig.1: Spin and orbital Edelstein effects in a Rashba system. The external electric field E generates a charge current j_c (black arrows) and a homogeneous magnetization m, which comprises spin (m_s, red) and orbital (m_l, blue) contributions.

Session SE
FREESTANDING COMPLEX OXIDE FILMS: A NEW PARADIGM FOR MAGNETIC HETEROSTRUCTURES

Alexander J. Grutter, Chair
National Institute of Standards and Technology, Gaithersburg, MD, United States

INVITED PAPERS

SE-01. Extreme Tensile Strain States in $La_{0.7}Ca_{0.3}MnO_3$ Membranes. *H. Hwang*[1,2] *1. Stanford University, Stanford, CA, United States; 2. SLAC National Accelerator Laboratory, Menlo Park, CA, United States*

A defining feature of emergent phenomena in complex oxides is the competition and cooperation between ground states, which can be sensitively tuned by the lattice. This has been explored using hydrostatic pressure, epitaxial lattice-mismatch in films, and uniaxial strain. Manganites provide canonical examples where various metallic and insulating phases, and associated magnetic and orbital ordering, are delicately balanced. Extending the range of lattice control would enhance the ability to access and investigate new phases. Here we stabilize extreme tensile strain in nanoscale $La_{0.7}Ca_{0.3}MnO_3$ membranes[1], exceeding 8% uniaxially and 5% biaxially[2]. Biaxial strain suppresses the ferromagnetic metal, inducing an insulating ground state that can be extinguished by magnetic field. Electronic structure calculations indicate that the insulator consists of charge-ordered Mn^{4+} and Mn^{3+} with staggered strain-enhanced Jahn-Teller distortions within the membrane plane. This highly-tunable strained membrane approach provides a broad opportunity to design and manipulate correlated states in transition metal compounds.

1. D. Lu, D. J. Baek, S. S. Hong, L. F. Kourkoutis, Y. Hikita, and H. Y. Hwang. *Nature Mater.* 15, 1255 (2016). 2. S. S. Hong, M. Q. Gu, M. Verma, V. Harbola, B. Y. Wang, D. Lu, A. Vailionis, Y. Hikita, R. Pentcheva, J. M. Rondinelli, and H. Y. Hwang, *Science* 368, 71 (2020).

SE-02. Multiferroic Membranes in the Ultrathin Limit. *Y. Nie*[1] *1. Nanjing University, Nanjing, China*

Two-dimensional (2D) materials such as graphene and transition metal dichalcogenides (TMD) have demonstrated how the new electronic phases emerge when a bulk crystal is thinned down to a mono-layer. As transition metal oxide perovskites host a variety of correlated phases, realizing the analogs with transition metal oxide perovskite materials would open the door to a rich spectrum of exotic 2D correlated phases that have not yet been explored. Here we report on the fabrication of freestanding perovskite films with high crystalline quality down to a single unit cell. Using the water-soluble $Sr_3Al_2O_6$ as the sacrificial buffer layer[1] and recently improved growth methods based on molecular beam epitaxy[2-5], we synthesize freestanding $SrTiO_3$ and multiferroic $BiFeO_3$ ultrathin films by reactive molecular beam epitaxy and transfer them to different substrates such as crystalline silicon wafers[2]. We find that $BiFeO_3$ membranes exhibit an unexpected giant tetragonality and polarization when approaching the ultimate 2D limit. Our results demonstrate the absence of critical thickness for stabilizing the crystalline order in the ultrathin oxide membranes. Moreover, recent progress in the strain engineering and integration of oxide membranes with silicon and semiconductor will also be discussed[6,7].

[1] D. Lu, et al., *Nat. Mater.* 15, 1255 (2016) [2] D.X. Ji, *et al.*, *Nature* 570 87–90 (2019) [3] T.W. Zhang, *et al.*, *Appl. Phys. Lett.* 111, 011601 (2017) [4] H.Y. Sun, *et al.*, *Nat. Commun.* 9.1, 2965 (2018) [5] H.Y. Sun, *et al.*,*Thin Solid Films* 697, 137815 (2020) [6] H. Lu, *et al.*, *Adv. Mater. Interfaces* 1901604 (2020) [7] H. Lu, *et al.*, *under review* (2021)

SE-03. Freestanding Single-Crystalline Complex-Oxide Membranes by Remote Epitaxy. *H.S. Kum*[1] *1. Electrical and Electronics Engineering, Yonsei University, Seoul, The Republic of Korea*

The ordered structure of crystalline thin films offers a multitude of technologically important emerging properties and an exceptional playground to explore the fundamental properties of matter. In particular, complex-oxide materials exhibit many physical properties that is desirable to advance conventional electronics, photonics, and quantum devices, such as ferromagnetism, ferroelectricity, piezoelectricty, pyroelectricty etc. These properties may be apparent in bulk form or thin-film form and may also be created or enhanced by application of strain. Typically, strain is applied to a crystalline material by growing the material on top of another substrate material with difference lattice constants. However, there are only a few choices of substrate materials available, and thus the design space for heteroepitaxial systems are severely limited as the strain states is fixed by pseudomorphic conditions between the epitaxial layer and the substrate [1]. To solve these restrictions, we developed a method, termed remote epitaxy, to produce freestading single-crystalline complex-oxide membranes of any cyrstalline structure such as pervoskite spinel and garnet [2]. In this method, monolayer or bilayer of graphene is transferred on top of single-crystalline complex-oxide substrates before proceeding with epitaxial growth. Due to the extreme thiness of graphene, the epitaxial growth proceeds as if the graphene is not present well aligned to the substrate underneath. However, after growth, due to the slippery van der Waals nature of graphene, one can easily exfoliate the epitaxial film off of the substrate using a thin support layer such as Ni and tape. Using this method, we demonstrate freestanding single-crystalline perovskite $SrTiO_3$ (STO), spinel $CoFe_2O_4$ (CFO), and garnet $Y_3Fe_5O_{12}$ (YIG) membranes which can be freely bent and stacked to create artificial heterostructures. Furthermore, we demonstrate artificial heterostructures using these freestanding single-crystalline membranes. As a demonstration, we show a CFO/PMN-PT heterostructure made artificially as a strain-mediated magnetoelectric composite, where the magnetic properties of CFO can be tuned via voltage across the PMN-PT, or generate voltage across the PMN-PT by applying a magnetic field across the CFO. We also show magnetostatic and magnetoelastic coupling by stacking CFO/YIG membranes. Finally, we show that it is possible to tune the Fermi-level of graphene by sandwiching it between YIG and CFO. We hope such demonstration of artificial 3D-3D and 2D-3D heterostructures will open up a new playground for material scientists, physicist, and device engineers to explore these materials with unrestricted manipulation and integration possibilities.

1. H. S. Kum, D. Lee, W. Kong et al. Nature Electronics Vol. 2, p. 439-450 (2019). 2. H. S. Kum, H. Lee, S. Kim, S. Lindemann et al. Nature Vol. 578, p. 75–81 (2020). 3. S.-H. Bae, H. Kum, W. Kong et al. Nature Materials Vol. 18, p. 550-560 (2019).

Fig. 1 Schematic illustration of remote epitaxy process of single-crystalline complex-oxide materials.

SE-04. Magnetic Depth Profiling of Freestanding Oxide Films.
P.P. Balakrishnan[1] *1. NIST Center for Neutron Research, National Institute of Standards and Technology, Gaithersburg, MD, United States*

Complex oxide thin films have highly tunable magnetic properties, not only due to the correlated degrees of freedom within these materials, but also due to the constraints imposed by limited choice of substrate material. For example, the magnetic properties of manganites depend heavily on subtle changes to crystallographic structure, resulting in a dead layer at the substrate/film interface which can inhibit technological applications [1,2,3]. Recently, exciting new techniques have been developed to separate oxide thin films from the substrate after growth, decoupling structural and chemical degrees of freedom at the interface [4]. This technique may enable both development of more magnetically uniform films as well as enable their integration with previously incompatible materials, such as with existing silicon-based technologies or more exotic structures. Thin films of (001)-oriented $LaMnO_{3+\delta}$ (LMO) are grown using pulsed laser deposition on a water-soluble $Sr_3Al_2O_6$ (SAO) film on top of a (001) $SrTiO_3$ substrate. After coating the film with a 1 μm thick support layer of PMMA polymer, the SAO is dissolved in water, allowing the film to be separated from the substrate; this freestanding film can then be transferred to a different substrate. In this work, we investigate the effects of film thickness, choice of substrate, as well as film processing on the magnetic and chemical uniformity of the films. X-ray diffraction measurements show that after the transfer process, freestanding films remain highly crystalline and oriented, but are no longer strained to the substrate. Magnetometry indicates similar Curie temperature, magnetic anisotropy, and saturation magnetization for both freestanding and epitaxial films, but cannot discern any differences in magnetic uniformity. Therefore, we turn to polarized neutron reflectometry (PNR) to provide a detailed understanding of both the chemical composition – with particular sensitivity to light elements such as hydrogen – and in-plane magnetization as a function of depth. As shown in Fig. 1, an LMO film transferred onto an LSAT substrate is smooth and uniform. Between the substrate and freestanding film is a thin region with slightly different nuclear scattering length density (SLD) but significantly reduced magnetic SLD. STEM and EELS measurements suggest that this region is an amorphous layer of residue caused by the transfer procedure; however, there does not appear to be a magnetically dead layer at the film interface. In contrast, films transferred onto oxidized silicon substrates are much more complicated (Fig. 2). First, the same interfacial region exhibits a very low SLD, indicating the presence of air or water, trapped at the interface due to long-range corrugation of the film or absorbed into the film during processing. The interpretation of the PNR data is supplemented with other depth-sensitive measurement techniques, such as secondary ion mass spectroscopy (SIMS), which is indicative of significant water incorporation into the LMO film, concentrated at both surfaces. Additionally, the films are no longer magnetically uniform. In particular, the top surface of the LMO films have a reduced in-plane magnetization. We find that despite elimination of chemical bonds with the substrate surface, the choice of substrate can still affect the magnetic properties of freestanding films through chemical effects, which may have implications for the integration of these freestanding films into silicon-based devices.

[1] Zhai, X., Cheng, L., Liu, Y., *et al.* Nat. Commun. 5, 4283 (2014). [2] Moon, E. J., Balachandran, P. V., *et al.* Nano Lett. 14, 2509-2514 (2014). [3] Liao, Z., Zhang, J. Appl. Sci. 9, 144 (2019). [4] Lu, D., Baek, D. J., Hong, S. S., *et al.* Nat. Mater. 15, 1255–1260 (2016).

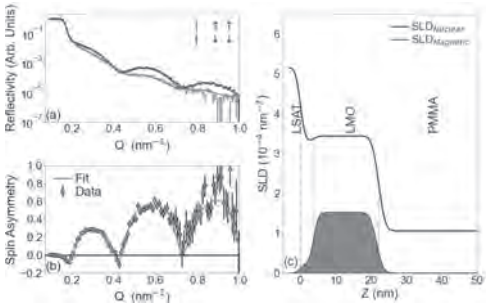

Fig. 1. (a) PNR data and (b) spin asymmetry of a 20 nm LMO free-standing film transferred onto an LSAT substrate, taken at 50 K in an in-plane magnetic field of 3 T. (c) The nuclear and magnetic depth-profile used to generate the best-fit model.

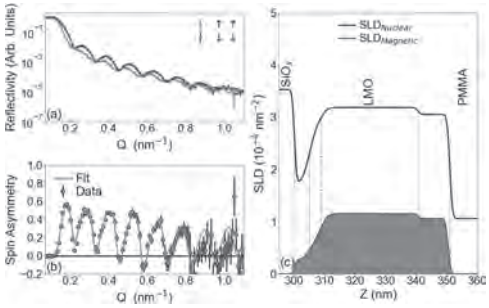

Fig. 2. (a) PNR data and (b) spin asymmetry of a 50 nm LMO free-standing film transferred onto a Si/SiO_x substrate, taken at 7 K in an in-plane magnetic field of 1.5 T. (c) The nuclear and magnetic depth-profile used to generate the best-fit model.

SE-05. Free-standing Ferroelectric and Magnetoelectric single crystal Membranes with super-elasticity.
M. Liu[1] *1. School of Electrical Engineering, Xi'an Jiaotong University, Xian, China*

Ferroelectrics are usually inflexible oxides that undergo brittle deformation. We synthesized freestanding single crystalline ferroelectric BTO($BaTiO_3$), BFO($BiFeO_3$) and BTO/LSMO bi-layer membranes and with a damage-free lifting-off process. Our ferroelectric membranes can undergo a nearly 180° folding during in-situ bending test, demonstrating a super-elasticity and ultra-flexibility[1]. We found that the origin of the super-elasticity was from the dynamic evolution of ferroelectric nanodomains in BTO and phase change in BFO. High stresses modulate the energy landscape dramatically and allow the dipoles to rotate continuously. A continuous transition zone is formed to accommodate the variant strain and avoid high mismatch stress usually causing fracture. BTO/LSMO shows a self-assembled spring shape due to the lattice mismatch as free-standing in the air. Such spring can undergo up 50% of the length change upon a mechanic forced is loaded. The phenomenon should be possible in other ferroelectrics systems through domain engineering. The ultra-flexible epitaxial ferroelectric membranes could enable many magnetoelectric applications such as flexible sensors, memories and electronic skins.

Dong, *et al.*, Science 366, 475-479 (2019)

Session SF
SOFT MAGNETIC COMPONENTS AND MATERIALS FOR EMERGING POWER CONVERSION APPLICATIONS

Paul Ohodnicki, Co-Chair
University of Pittsburgh, Pittsburgh, PA, United States
Kiyonori Suzuki, Co-Chair
Monash University, Clayton, VIC, Australia

INVITED PAPERS

SF-01. Power Dense Inductors Based Upon Co-Based Nanocrystalline Alloys. *P. Ohodnicki*[1], A. Talaat[1], S. Kernion[2], K. Byerly[2] and A. Leary[3] *1. University of Pitsburgh, Pittsburgh, PA, United States; 2. CorePower Magnetics, Pittsburgh, PA, United States; 3. NASA Glenn Research Center, Cleveland, OH, United States*

There exist needs for advanced inductors that are (1) power dense, (2) highly efficient, and (3) high temperature stable for a range of power electronics applications which include on-board converters and off-board charging systems for electric vehicles. Nanocrystalline soft magnetic alloys are of great interest for medium frequency and medium to high power applications due to their large saturation flux density relative to ferrites, as well as their improved losses and reduced magnetostriction relative to amorphous alloys. However, state-of-art commercial Fe-based nanocrystalline alloys display inherently large permeabilities and consequently they require gapping for high power inductor applications and suffer from inherent limitations of mechanical brittleness and relatively poor temperature stability (rated at 150C). Recent advances in Co-based nanocrystalline alloys have enabled a new class of highly scalable inductors which overcome the limitations of existing Fe-based nanocrystalline alloys through in-line tension anneal processing to enable a new level of control for large-scale inductor designs not previously possible without the requirement for core gapping. Local permeability control (i.e. permeability engineering) is made possible through real-time controls of applied tension and controlled thermal processing during the in-line processing step, of particular interest for reduced peak temperature rise and highly power dense inductor designs by engineering the distribution of magnetic flux throughout the core. Advanced thermal processing techniques can also be applied during the in-line processing stage to tailor the characteristic spatial length-scale and distribution of the spatially varied permeability profile, and after the in-line processing to tailor domain structure and optimize losses. Temperature stability of magnetic properties are also far superior to traditional Fe-based alloys, with current experiments showing the potential for stability of structure and magnetic properties as high as 400C and even approaching 500C. The presentation will address the latest advances in Co-based nanocrystalline strain annealed gapless inductors for power dense inductor applications. Topics to be addressed will include: 1) Phase identity and magnetic property variation as a function of chemistry in Co-based nanocrystalline alloys; 2) The latest in tension annealing at scale and spatially tuned permeability engineering methods; 3) Demonstrations of engineered permeabilities as well as optimized domain structures for taliored magnetic properties; 4) Development of tailored multi-objective optimization tools specifically for permeability engineered gapless core inductors; 5) Application of advanced lmulti-objective optimization tools for inductor design and benchmarking in both electric vehicle and medium voltage power electronics applications; The presentation will conclude with recent experimental results as well as emerging ideas and future perspectives for highly optimized thermal processing methods and techniques, including spatial optimization of the crystallization process and consequently the magnetic properties through spatially tailored rapid thermal processing with electromagnetic field-assisted methods and techniques.

[1] K. Byerly et al., JOM 70 (6), 879-891 (2018). [2] A. Leary et al., US Patent #10168392 (2019). [3] A. Leary et al., Journal of Materials Research 31, 3089-3107 (2016). [4] R. Beddingfield et al., Journal of Materials Research 33, 2189-2206 (2018). [5] A. Talaat, Journal of Alloys and Compounds 854, 156480 (2021).

SF-02. Application of FeNi-based Metal Amorphous Nanocomposites (MANCs) in Axial High Speed Motors. *M. McHenry*[1], K. Byerly[1], Y. Krimer[1], J. Egbu[1] and S. Simizu[1] *1. Materials Science and Engineering, Carnegie Mellon University, Pittsburgh, PA, United States*

FeNi-based metal amorphous nanocomposite (MANC) alloys are soft magnetic materials (SMMs) with promise for high-speed motor (HSM) applications [1]. This talk will review synthesis, structure, properties and performance relationships in FeNi-based MANCs. This will include (1) synthesis by planar flow casting, strain annealing and stress relief annealing; (2) structural studies by x-ray diffraction (XRD), high resolution TEM, and XPS; (3) DC and AC magnetometry and loss measurements (Fig. 1) and performance metrics for 2.5 kW and 20 kW flux switching with permanent magnet (FSWPM) axial motors [2]. In particular, magnetic core loss, W_L, coercivity, H_c, squareness ratio, K_r, and permeability, μ_r, are reported as a function of (stress relief) re-annealing temperature to optimally achieve $W_{1T,400Hz}$ = 0.51 W/kg, H_c = 2.42 A/m, K_r = 0.22, losses comparable to the commercial alloy FINEMET [3]. The steps in manufacturing a 2.5 kW FSWPM motor from tape wound cores: (1) tape winding; (2) water jet cutting; (3) stator and rotor parts assembly; (4) stator assembly; (5) rotor assembly; and (6) motor assembly will be described. Scaling to >20 kW will be discussed for DOE VTO applcations.

[1] N. Aronhime, V. DeGeorge, V. Keylin, P. Ohodnicki, and M. E. McHenry, "The Effects of Strain-Annealing on Tuning Permeability and Lowering Losses in Fe-Ni-based Metal Amorphous Nanocomposites." J. Materials 69(11), 2164-70, (2017). 10.1007/s11837-017-2480-x. [2] S. Simizu, P. R. Ohodnicki and M. E. McHenry; Metal Amorphous Nanocomposite (MANC) Soft Magnetic Material (SMM) Enabled High Power Density, Rare Earth Free Rotational Machines. IEEE Trans. Mag. 54(5), 1-5, (2018). 10.1109/TMAG.2018.2794390. [3] K. Byerly, Y. Krimer, Charudatta Phatak, E. Theisen, and M. E. McHenry, Optimization of Frequency Dependent Magnetic Losses in an FeNi-based Metal Amorphous Nanocomposite (MANC) Alloy for High-Speed Motor Applications, J. Mat. Res. Published on-line, June 22, 2021.

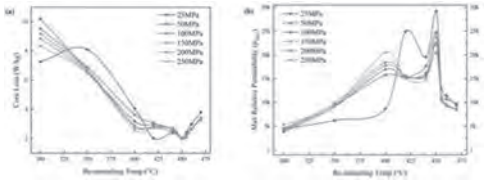

Fig. I (a) Power loss (1.1 T, 2000 A/m and 400Hz) and (b) maximum permeability for Fe-Ni-based MANC core samples (25-250 MPa) as a function of re-annealing temperature.

SF-03. Soft magnetic composites for intracellular pulse electric field tumor treatment using DSRD-based nanosecond high power pulse generators. *P. Andalib*[1], C. Yu[1], A. Kaltashov[2] and V.G. Harris[1]
1. Department of Electrical and Computer Engineering, Northeastern University, Boston, MA, United States; 2. Department of Chemical Engineering, Northeastern University, Boston, MA, United States

High repetition nanosecond high power pulse generation (HPPG) has become a fascinating and valuable technology for penetrating intracellular membranes, among which tumor treatment based on the intracellular electroeffect has shown promising results and attracted much attention from the medical community [1]. This technology, however, faces many unresolved technical challenges. One of the most important barriers to the effective development of efficient HPPGs is the lack of suitable magnetic materials to serve as inductor cores for energy storage. Here, we define efficiency and thermal management challenges posed by existing HPPG systems from limitations imposed by available technologies and their impact upon overall performance of such generators. The scale of these limitations will be discussed using time and frequency domain analyses of a nanosecond kV DSRD-based high power pulse generator. These entail systematic studies of commercial-off-the-shelf magnetic materials and inductors by PSPICE simulations performed using generated magnetic material models that support interdependent nonlinear magnetic phenomena. These investigations provide for the first time accurate estimations and valuable insights into the dissipation of higher energy harmonics and consequent untenable thermal rise from the DSRD's energy storage inductors for a variety of applications including those in the health sciences.

[1] K. H. Schoenbach *et al.*, "Ultrashort electrical pulses open a new gateway into biological cells," *Proc. IEEE*, vol. 92, no. 7, pp. 1122–1137, Jul. 2004.

SF-04. Solid State Transformer Technology Based on Advanced Materials and Design Concepts. *S. Bhattacharya*[1] and R.B. Beddingfield[1]
1. ECE, NC State University, Raleigh, NC, United States

This presentation will focus on the applications of Soft Magnetic Components and Materials for Emerging Power Conversion Applications such as Solid State Transformer [SST] Technology and several power conversion systems at both Medium-Voltage [MV] and Low-Voltage [LV]. The re-evaluation of conventional magnetics solutions has become important and essential due to the emergence and adoption of WBG [Wide-Band Gap] power devices such as SiC and GaN devices. These devices not only enable co-design of MV and higher switching frequency, but also enable higher temperature operations requiring characterization of magnetics for such specifications. This presentation will cover advances in medium frequency magnetics for WBG devices based power converters and especially for high power converters. It will highlight the latest advances in soft magnetic material qualification and characterization under non-sinusoidal waveforms. It will provide an overview of magnetic core loss models and implications for thermal modeling. It will also address novel techniques for understanding leakage inductance and anomalous losses due to leakage flux. The novel concept of strain annealing for permeability engineering and design opportunities for heterogeneously tuned permeability cores in high power converter applications will be addressed.

SF-05. Recent Advances and Remaining Challenges in Manufacturing of Amorphous and Nanocrystalline Alloys. *E. Theisen*[1] *1. Metglas Inc., Conway, SC, United States*

A review of soft magnetic amorphous and nanocrystalline alloys currently used in the market al.ng their primary industrial applications will be discussed. The distribution transformer market continues to be the largest volume application of Fe-based amorphous foil with higher efficiency standards globally helping to drive the growth of amorphous-based transformers. High permeability grades of amorphous foil have largely supplanted the convention grades due to the higher induction levels (1.63T) and increased stacking factor (>90%). Magnetic domain refinement of amorphous foil, further reducing the core losses, is now commercially available. Amorphous foil has long been envisioned for high efficiency electric motors. The emerging trends with electric vehicles have revitalized the efforts to incorporate amorphous and nanocrystalline foils as the motor lamination materials. There are many approaches to fabricate these motor components and we will discuss the methods that have been industrially adopted. FeCo based amorphous alloys further enhance the induction levels (1.8T) and can be viable in these applications. Nanocrystalline alloys of the FeBSiNbCu composition have now become an industry standard for ultra-low loss, high frequency and high permeability applications. Advanced processing methods have produced higher induction nanocrystalline alloys with higher Fe and lower Nb content. There are also new FeCo and FeNi nanocrystalline alloys being developed specifically suited towards gapless inductor and motor applications that will be discussed.

Session SG
NEXT GENERATION ELECTRICAL MACHINES

Jonathan Bird, Co-Chair
Portland State University, Portland, OR, United States
Yacine Amara, Co-Chair
University of Le Havre, Le Havre, France

INVITED PAPERS

SG-01. Energy Conversion for a Sustainable Future: Role of Advanced Magnetic Materials and Advanced Manufacturing. *A. El-Refaie*[1]
1. Electrical and Computer Engineering, Marquette University, Milwaukee, WI, United States

Energy sustainability is arguably one of the most critical challenges for a sustainable future. With predictions showing future scarcity and/or higher degree of extraction difficulty of traditional sources of energy for example coal, oil and natural gas, the shift to sustainable clean sources of energy is a must. Another key reason is the increasing detrimental impact of using fossil fuels. Over the last few decades, there has been serious effort to replace mechanical and hydraulic systems with electrical systems. This effort also includes replacing fixed-speed and old electrical drives with higher performance variable-speed drives. This is mainly due to the higher reliability, efficiency and robustness of electrical systems. This trend of "more electric" systems could be seen across a wide range of applications. These include traction, aerospace, actuation, mining, oil & gas, and industrial applications as examples. This push for electrification posed a lot of challenges to develop electrical systems that meet the demanding requirements of the various applications including harsh environments, high power density, high efficiency and fault tolerance in safety-critical applications. At the heart of the electrification effort is the development of advanced electrical machines and drives. This presentation will provide an overview of the various applications where electrification is taking place. The presentation will focus on electrical machines and drives that have been developed or are currently under development with special focus on permanent magnet machines. The presentation will also cover some general trends in electrical machines and potential areas of research including advanced magnetic materials and advanced manufacturing.

SG-02. Flux Modulation Machines – Innovation & Beyond. *R. Qu*[1,2] and D. Li[1,2] *1. State Key Laboratory of Advanced Electromagnetic Engineering and Technology, Huazhong University of Science and Technology, Wuhan, China; 2. School of Electrical and Electronic Engineering, Huazhong University of Science and Technology, Wuhan, China*

For the regular machines, the pole-pairs of machine stators and rotors are identical, where the torque is produced by the single working harmonic from the rotor and stator magnetic fields. During the last hundred years, numerous studies have been done to enhance the working harmonics and weaken the non-working harmonics, so as to acquire the sinusoidal air-gap magnetic fields and improve the quality of torque. The presentation will provide a view on electrical machines from the third eye –Flux Modulation point of view. As a new type of machine, the flux modulation PM machines, have drawn more and more attention due to their great torque density capability. Compared with regular PM machines, the pole-pairs of armature windings and rotor PMs in flux modulation machines are different, where the torque is generated by multiple working harmonics of PM magnetic fields and armature magnetic fields. Under the same electric and magnetic loadings, the flux modulation machines can acquire nearly double torque density of regular PM machines. This presentation will introduce flux modulation fundamental operation principles, machine main features, and topologies including multiple magnetomotive force harmonic machines, multiple permeance harmonics machines and double-modulation machines. Applications, challenges, and research opportunities will be discussed as well.

SG-03. Withdrawn

SG-04. Formula E: Electric Machines and Drives Strategy. *J. Paulides*[1] and L. Encica[1] *1. R&D, AE Group, Waalwijk, Netherlands*

Arguably the pinnacle of motorsport are race cars and therefore an excellent showcase for new technologies from the different areas of automotive systems. Racing "should" utilize components that are beyond the state-of-the-art and within the Advanced Electromagnetics Group (www.ae-grp.nl) we are providing powertrains and test systems for the design, testing, and validation of high-tech and innovative race car powertrains for all-electric racing championships. These e-racing championships are not something that is started in the 21st century. No, already in 1899 Belgian driver and engineer Camille Jenatzy drove flat out in his torpedo-shaped 'La Jamais Contente' ('never satisfied') in a sparsely populated area to the northwest of Paris and became the first person to reach more than 100 km/h in a car [1]. Even though the electric powertrain failed to dominate the car industry in the twentieth century, 115 years later in 2014, Formula E appeared with its first-ever race in Beijing, China. Founded in 2011, this is an all-electric championship that showcases around the world a combination of sustainability claims, entrepreneurial spirit and commercial savviness. In Formula E all cars are aerodynamically similar but have some technological differences. Formula E was helped by the automotive world entering the 'Dieselgate' or 'Emissionsgate' in 2015. Despite these achievements, Formula E still struggles to showcase the technology to the public. Manufacturers are accumulating ever more know-how on electric cars, where Formula E may even turn out to be a hindrance in terms of innovative solutions. As such, the rulebook has to keep track of what is in it for the OEMs that participate. As an example, the Porsche Taycan model has a peak charging capacity of 270 kW and is one the fastest electric vehicles currently on the market. However, Formula E 2020 vehicles charge at a peak rate of 100 kW. Some motorsport fans have mocked the city based racetracks, and Formula E cars were nicknamed 'hairdryers' for not having the classic racing sound. In the beginning drivers had to change vehicles during the race because of the batteries. Especially discussed was the 'Fanboost' (an e-voting service providing your favourite driver with extra power in the race). However, what ever is said it is a racing class that is on the move and aim to adapt new technologies. For example, in the FIA Formula E season 3, the VENTURI team used an inverter with insulated-gate bipolar transistors/ Silicon Carbide Schottky Barrier Diode module. It reported a 2 kg weight reduction and 19% size reduction compared season 2 inverter with IGBT module [2]. In the next season a full Silicon Carbide module was used, where the inverter is capable of operating at 150°C junction temperature with a reduced switching losses of 75% compared to the IGBT solution. This opens the path for integrated

motor that will use the high power density of SiC devices, and their high efficiency and cooling loop simplification thanks to the high temperature operation capability of SiC devices [3]. These electrical machines and drives not only have to withstand large forces, but also need to be designed to account for many advanced innovations. High-torque densities are a key requirement in traction machines. Using a multiple air gap design can achieve up to 60 percent higher torque density relative to single airgap machine. This talk will provide an overview of advanced powertrain technologies that aided to progress vehicle racing. By a careful choice and sizing of powertrain components coupled with an optimal energy management strategy from the batteries, attractive racing will be here to stay.

1. H.E. Næss, A. Tjønndal (2021) "The Case of Formula E", Innovation, Sustainability and Management in Motorsports pp 1-16, https://doi.org/10.1007/978-3-030-74221-8_1 2. ROHM Semiconductor. ROHM supplies Full SiC Power Modules to Formula E racing team Ven-turi. Accessed: June. 16th, 2021. [Online]. Available:https://www.rohm.com/news-detail?news-title=rohm-supplies-full-sic-power-modules-to-formula-e-racing-team-venturi&defaultGroupId=false 3. T. M. Jahns and H. Dai, ''The past, present, and future of power electronics integration technologyin motor drives,'' CPSS Transactions on Power Electronics and Applications, vol. 2, no. 3, pp.197-216, Sept. 2017.

SG-05. Analyse of the flux density and iron loss distributions in segmented magnetic circuits made with mixed electrical steel grades.

A. Rebhaoui[1,2], S. Randi[3,2], *J. Lecointe*[1] and C. Demian[1] *1. Université Artois, Laboratoire Systèmes Electrotechniques et Environnement (LSEE), Béthune, France; 2. VEDECOM, Versailles, France; 3. Renault Technocenter, Guyancourt, France*

Reducing the rate of CO2 emissions for hybrid electric vehicles (HEV) and improving the autonomy for full battery electric vehicle (BEV) constitute major challenges for motor manufacturers. That can be done by losses reduction in each part of the electric powertrains. In the electric motors, using high grades magnetic material and optimal design allows reducing iron losses in the important area of the Torque-Speed plane. That is why segmented stator cores mixing grain oriented electrical steel (GOES) and non-oriented electrical steel (NOES) constitute a serious way of improvement. The goal of the paper is to present the existing structures with, for instance GOES teeth and NOES yoke, and to analyze the contribution of the high grade steel in the automotive motor improvement, in terms of efficiency, masse and volume. GOES has strong advantages in terms of iron losses and flux density at saturation, when it is magnetized in the Rolling Direction (RD). GOES has the drawback of being very anisotropic and the performance is not so interesting in the Transverse Direction, compared to NOES, especially in term of iron losses at high induction and high operational frequencies [1]. That implies to adapt the machine geometry to the specificities of this steel [2] [3] [4]. Another disadvantage of GOES is the sensitivity to the manufacturing processes: bending, cutting, compacting… [3]. From a micro-structural point of view, cutting the sheets causes a destruction of the grains close to the cutting border. At a macroscopic scale, that reduces the magnetic performance, depending not only on the cutting technique but also the dimensions of the sheet [5]. First, in the full paper, the authors present the existing magnetic circuit structures and how the constraints linked to the high anisotropy ratio has been taken into account. The electric motor analyzed mixes GOES teeth and NOES yoke, as shown in Fig.1. Second, the question of the modelling is posed. The full analytic simulation of the motor is not really adapted taking into account the complexity of the anisotropy. The Finite Element software applications integrate now both anisotropy and saturation, but not always in 3D. The strong difficulty is that the magnetic characteristics differ as a function of the magnetization angle. As a result, the results are not enough accurate in term of flux density distribution. The loss models, when they are implemented for GOES, are not reliable when the sheet is magnetized in multiple directions. Third, in order to analyse the contribution of the elements constituting the magnetic circuit, the authors propose a device, shown in Fig. 2, for numerical and experimental tests. It is designed in order to reproduce the phenomena occurring in the electrical motors, especially in the region between the teeth and the yoke. To do that, it combines two Epstein frames modified to magnetize different magnetic structures. The goal is to analyse the flux densities in the magnetic circuit and the iron losses, depending on several parameters as different geometries of junctions between the segments. The angle and the depth of insertion of the teeth into the yoke will be analysed. It allows also to evaluate the effect of the flux passing not directly in a teeth, but only the yoke. That happens in fractional slot permanent magnet machines and, in that case, the TD is fully solicited. Then, the nature and the grades of the materials will be tested with 0,20mm GOES and NOES. Effect of manufacturing will also be shown with experimental test made with cut laminations. Fourth, an existing full NO steel reference motor will be numerically compared with an improved machine made with mixed NOES and GOES. The comparison will be made on local quantities (flux density, etc) as well as on integral quantities (Flux, EMF, Electromagnetic torque and losses). The authors will also present simulation results showing the efficiency improved by the use of GOES.

[1] T. Tomida, N. Sano, S. Hinotani, F. Fujiwara, H. Kotera, N. Nishiyama et Y. Illai, *IEEE Trans. on Mag.,* 41 (110), pp. 4063 - 4065, 2005. [2] R. Pei, L. Zeng, S. Li et T. Coombs, IEEE, Int. conf. on electrical machines & systems, 2017. [3] R. Aydoun, G. Parent, A. Tounzi et J. P. Lecointe, *Open Physics,* pp. 1 - 8, 2020. [4] S. Lopez, B. Cassoret, J. F. Brudny, L. Lefebvre; J. N. Vincent, *IEEE Trans. on Mag,* pp. 4161 - 4164, 2009. [5] R. Sundaria, A. Daem, A. Hemeida, P. Sergeant, A. Arkkio et A. Belahcen, *IEEE annual conf. of the IEEE ind. el. society,* pp. 1022 - 1027, 2019.

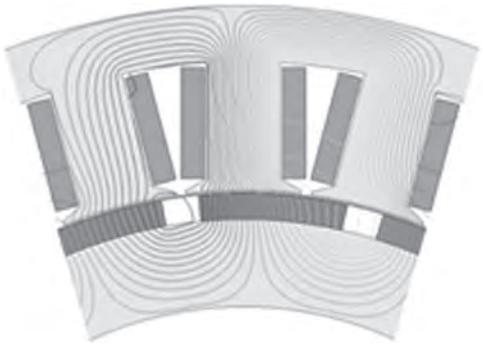

Fig.1

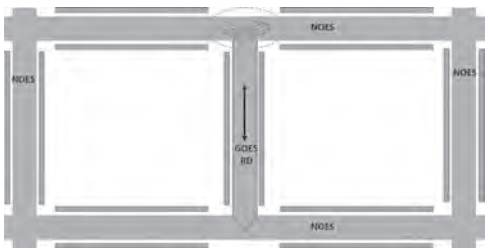

Fig. 2

Session AOA
FUNDAMENTAL PROPERTIES AND COOPERATIVE PHENOMENA I

Durga Paudyal, Chair
Ames Laboratory, Ames, IA, United States

CONTRIBUTED PAPERS

AOA-01. Topological Boundary Constraints in Artificial Colloidal Ice. C. Rodríguez-Gallo[1], A. Ortiz[1] and *P. Tierno*[1] *1. Condensed Matter Physics Department, University of Barcelona, Barcelona, Spain*

The effect of boundaries and how these can be used to influence the bulk behavior in geometrically frustrated systems are both long-standing puzzles, often relegated to a secondary role. In this talk, I will investigate boundary effects in a geometrically frustrated system, namely an artificial colloidal ice, a microscale soft matter analog of a frustrated nanoscale spin ice system. The artificial colloidal ice is realized by confining interacting paramagnetic colloids to a lattice of gravitational double wells [2]. With this system, both via numerical simulations and "proof of concept" experiments, I will demonstrate that boundaries can be engineered to control the bulk behavior in a colloidal artificial ice [3]. I will also show that an antiferromagnetic frontier forces the system to rapidly reach the ground state (GS), as opposed to the commonly implemented open or periodic boundary conditions. Further, strategically placing defects at the corners may be used to generate novel bistable states, or topological strings, which result from competing GS regions in the bulk. The presented results could be generalized to other frustrated micro- and nanostructures where boundary conditions may be engineered with lithographic techniques.

[1] A. Ortiz-Ambriz and P. Tierno, Nat. Commun. 7, 10575 (2016). [2] A. Ortiz-Ambriz, C. Nisoli, C. Reichhardt, C. J. O. Reichhardt, and P. Tierno, Rev. Mod. Phys. 91, 041003 (2019). [3] Carolina Rodríguez-Gallo, Antonio Ortiz-Ambriz, and Pietro Tierno, Phys. Rev. Lett. 126, 188001 (2021)

AOA-02. Artificial Out-of-Plane Ising Antiferromagnet on the Kagome Lattice with Very Small Further-Neighbour Couplings. *J. Colbois*[1], K. Hofhuis[2,3], Z. Luo[2,3], X. Wang[2,3], A. Hrabec[2,3], L. Heyderman[2,3] and F. Mila[1] *1. Institute of Physics, Ecole Polytechnique Fédérale de Lausanne, Lausanne, Switzerland; 2. Laboratory for Mesoscopic Systems, Department of Materials, ETH Zurich, Zurich, Switzerland; 3. Laboratory for Multiscale Materials Experiments, Paul Scherrer Institute, Villigen PSI, Switzerland*

Short-range classical antiferromagnetic Ising models on frustrated lattices give rise to exotic phases of matter, in particular due to their macroscopic ground-state degeneracy [1, 2]. Recent experiments on artificial spin systems comprising arrays of chirally coupled nanomagnets [3] provide a significant strengthening of the nearest-neighbour couplings compared to systems with dipolar-coupled nanomagnets. Following Ref. [4], I will present the results of an extensive investigation with tensor network [5] and Monte Carlo [6] simulations of the nearest- and further-neighbour (J1–J2–J3||) kagome lattice Ising antiferromagnet, and compare them with the experimental spin-spin correlations of a kagome lattice of chirally coupled nanomagnets (Fig. 1). I will show that, even though the ratios between the further-neighbour couplings and the nearest-neighbour coupling estimated from micromagnetic simulations are much smaller than for dipolar-coupled nanomagnets, they still play an essential role in the selection of the correlations (Fig. 2).

[1] C. Lacroix, P. Mendels, and F. Mila, Vol. 164 (Springer Science and Business Media, 2011) [2] C. L. Henley, Ann. Rev. Cond. Mat. Physics, Vol. 1, pp. 179–210 (2010) [3] Z. Luo, T. P. Dao, A. Hrabec, et al., Science, Vol. 363, pp. 1435–1439 (2019) [4] J. Colbois, K. Hofhuis, Z. Luo, et al., Phys. Rev. B., Vol. 104, p. 024418 (2021) [5] B. Vanhecke, J. Colbois, L. Vanderstraeten, et al., Phys. Rev. Research, Vol. 3, p. 013041 (2021) [6] G. Rakala and K. Damle, Phys. Rev. E, Vol. 96, 023304 (2017)

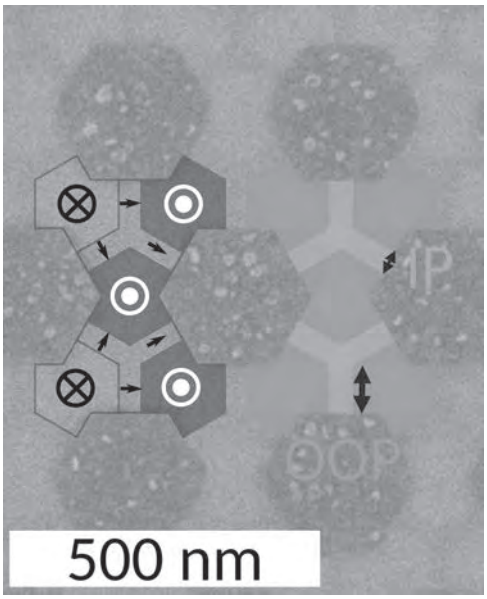

Fig. 1. Scanning electron microscopy image of our samples consisting of extended kagome lattices etched from Pt(6 nm)/Co(1.6 nm)/Al(2 nm) films, and comprising chirally coupled regions with out-of-plane (OOP) and in-plane (IP) anisotropy. The OOP regions take on the role of Ising spins in our model. The interactions through the IP regions create effective antiferromagnetic couplings between the OOP regions, with very strong nearest-neighbour couplings and much smaller further-neighbour couplings. An example OOP-IP configuration is indicated on the left of the Figure.

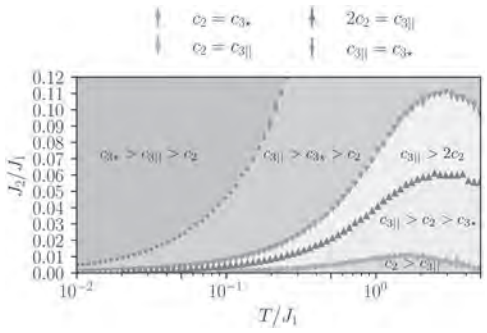

Fig. 2 Monte Carlo map of the descending order of the spin-spin correlations in the J1-J2 model (nearest- and next-nearest neighbour couplings) as a function of the values of the temperature T/J1 and the ratio J2/J1. c1, c2, c3* and c3|| stand for nearest-, next-nearest- and two types of third-nearest-neighbour correlations. In the experiment, the correlations satisfy c3|| > c2 > c3*, with c3|| > 2c2 (light green region). For small enough J2, there is a temperature region with c2 > c3|| (orange region), compatible with the nearest-neighbour physics in terms of the descending order of the correlations.

AOA-03. Order and disorder : The magnetic and crystalline electric field skyline of $NdCu_2$ nanoparticles. *E.M. Jefremovas*[1], M. De la Fuente Rodríguez[1], F. Damay[4], D. Alba-Venero[6], B. Fåk[3], P. Bender[7], A. Michels[2], J.A. Blanco[5] and L. Fernández Barquín[1] *1. Ciencias de la Tierra y Física de la Materia Condensada, Universidad de Cantabria, Santander, Spain; 2. Department of Physics and Material Science, Université du Luxembourg, Luxembourg, Luxembourg; 3. Institut Laue-Langevin, Grenoble, France; 4. Laboratoire Léon Brillouin, Gif sur Yvette, France; 5. Física, Universidad de Oviedo, Oviedo, Spain; 6. ISIS, STFC, Rutherford Appleton Lab, Didcot, United Kingdom; 7. Heinz Maier-Leibnitz Zentrum (MLZ), Technische Universität München, Garching, Germany*

In recent years we have been focused on the understanding of magnetism in ensembles of 4f metallic nanoparticles (NPs) (R = Tb,Nd, Gd-M = Cu, Al, Y, La). As a result, we have reported that the existence of an ordered magnetic core and a disordered magnetic shell is regularly found in those ensembles. Depending on the stoichiometry (in our case, RX_2) it is possible to easily tune the RKKY interactions to provoke the appearance of ferromagnetic or antiferromagnetic (AF) order within the NPs. Moreover, the fact that we are dealing only with thousand of moments per particle leads to use the super- prefix to define correctly the magnetic behaviour [1]. Besides, it is an upsetting fact that both the collective moment dynamics and the role of the crystalline electric field (CEF) in ensembles of NPs have barely been unearthed. To fill in this gap, we are reporting here a complete neutron-based study (Neutron Diffraction, ND, Small-Angle Neutron Scattering, SANS, and INS) on $NdCu_2$ NPs (<D>≈13nm) to depict the skyline of order and disorder at the nanoscale. ND measurements (LLB) point to that the bulk commensurate AF structure is retained within the core. SANS confirms the survival of the AF within the nanoscale, together with a strong emergence of disorder, in the form of a rise in the low-Q region (Q<0.665 $Å^{-1}$). Magnetic measurements indicate the interactions among the surface moments strong enough to establish a Spin Glass behaviour, leading therefore to a Superantiferromagnetic state. Regarding the CEF panorama, macroscopic specific heat analyses anticipate a broad Schottky contribution, with a maximum located at T~25 K. Then, microscopic INS measurements (ILL) performed at T=10K (paramagnetic) and T=1.5K (magnetic state) reveal that the splitting of the CEF levels, as well as the spin–wave excitations that emerged below the Néel transition ($T_N \approx 6$ K) in polycrystalline $NdCu_2$ [2] are maintained in the NPs. Furthermore, we have been able to isolate the INS from the surface, which has allowed us to unravel the role of finite–size effects and microstrain. These two effects lead to a partial inhibition of the transitions from the ground state to the first excited level, as well as a stiffening of the magnon modes [3].

[1] E. M. Jefremovas et al., Nanomaterials 10, 6 (2020); E. M. Jefremovas et al., Nanomaterials 10, 11 (2020); C. Echevarría-Bonet et al. PRB 87, 18 (2013). [2] E. Gratz et al. J. Phys: Condens. Matter 3, 9297 (1991) [3] E. M. Jefremovas et al., (submitted to Phys. Rev. B, 2021).

AOA-04. Long-range Magnetic Ordering in Artificial Kagome Spin Ice. *K. Hofhuis*[1,2], A. Hrabec[1,2], H. Arava[1,2], N. Leo[3], S.H. Skjærvø[1,2], Y. Huang[4], R.V. Chopdekar[4], S. Parchenko[1,2], A. Kleibert[5], S. Koraltan[6], C. Abert[6], C. Vogler[6], D. Suess[6], P.M. Derlet[7,1] and L. Heyderman[1,2] *1. Laboratory for Mesoscopic Systems, ETH Zurich, Zurich, Switzerland; 2. Laboratory for Multiscale Materials Experiments, Paul Scherrer Institute, Villigen PSI, Switzerland; 3. CIC nanoGune, Donostia-San Sebastian, Spain; 4. Lawrence Berkeley National Laboratory, Berkeley, CA, United States; 5. Swiss Light Source, Paul Scherrer Institute, Villigen PSI, Switzerland; 6. Physics of Functional Materials, University of Vienna, Vienna, Austria; 7. Condensed Matter Theory Group, Paul Scherrer Institute, Villigen PSI, Switzerland*

The extent of magnetic ordering in highly-frustrated thermally active artificial kagome spin ice is limited by the lowest achievable blocking temperature, as the moments freeze before ordering is achieved [1]. A more substantial degree of magnetic ordering can be achieved by either lowering the blocking temperature of the individual nanomagnets or by increasing the critical transition temperature of the system. First, we pursue an approach of introducing interfacial Dzyaloshinskii-Moriya interactions (DMI), which lowers the blocking temperature by a factor of five, while keeping the transition temperature unchanged [2]. We demonstrate that a seven-ring kagome structure consisting of 30 nanomagnets with DMI can be thermally annealed into its ground state. Furthermore, the spin-ice correlations extracted from extended kagome lattices are found to exhibit the quantitative signatures of long-range charge-order, thereby giving experimental evidence for the theoretically predicted continuous transition to a charge-ordered state. Second, we find that slight modifications of the nanomagnets at the vertices in the artificial kagome ice allow us to control the energy landscape which leads to an increase of the critical temperatures [3]. These results provide paths for the tuning of magnetic ordering in artificial spin systems.

[1] S.H. Skjærvø, C.H. Marrows, R.L. Stamps, and L.J. Heyderman. *"Advances in artificial spin ice."* Nature Reviews Physics 2, 13-28 (2020). [2] K. Hofhuis, A. Hrabec, H. Arava, N. Leo, Y.L. Huang, R.V. Chopdekar, S. Parchenko, A. Kleibert, S. Koraltan, C. Abert, C. Vogler, D. Suess, P.M. Derlet, and L.J. Heyderman., *"Thermally superactive artificial kagome spin ice structures obtained with the interfacial Dzyaloshinskii-Moriya interaction."* Physical Review B 102, 180405(R) (2020). [3] K. Hofhuis *et al.* manuscript in preparation.

AOA-05. Properties of 3 Dimensional Co and Py Bi-Material Artificial Spin Ice. *B. Myint*[1] and V. Ng[1] *1. Electrical and Computer Engineering, National University of Singapore, Singapore*

Different types of artificial spin ice systems (ASI) ranging from 2D to 3D arrays of nanostructures have been reported due to their potential applications in computation and memory [1]. Magnetic domain states representing different energy levels of ASI systems are controlled by varying shape, size and spacing of the nanoislands. We report the behavior of bi-material 3D ASI created with two magnetic materials. Fig 1 shows the bi-material ASI formed by overlapping Co nanowires (NWs) on a Py antidot lattice using self-aligned stepwise nanosphere lithography [2,3]. The schematic shows how zigzag Co NWs (in red) run over and above Py antidots (in blue). Fig 1(c) shows overlap regions created a thickness variation along the structure. The magnetization reversal study of bi-material ASI along its hard-axis direction is conducted using MFM. Fig 2 shows the remnant magnetic domain images at different field values. The magnetic moment directions of Co NWs and Py antidots are represented by yellow and green arrows respectively. At saturation (2500 Oe), domains of both Co NWs and Py anti-

dots point along the field direction, as in Fig 2 (a). As the field is reversed to -400 Oe in Fig 2 (b), Py antidot domains switched completely whereas Co domains started to reorientate along the length of NWs. The complete reversal for Co NWs occurred at -1200 Oe in Fig 2 (c). The difference between the switching fields of Co and Py is due to shape and material dependent anisotropy. At the intersections and vertices, Co and Py are in contact even though they are displaced vertically. Their magnetic moments interact with each other as shown in Fig 2(b), resulting in competition and thus various frustrations in the ASI. The unique magnetic switching behavior of the bi-material ASI at different magnetization conditions will be discussed and compared with single material ASI via MFM, MOKE and 3D OOMMF [4] simulations. This study aims to understand the magnetic behavior of bi-material ASI to unlock their potential for future applications.

[1] S.H. Skjærvø, C.H. Marrows, R.L. Stamps, et al. Nature Reviews Physics, no. 2, p. 13 (2020). [2] B. Myint, D.S.F. Yap and V. Ng, Nano Express, no. 1, p. 020029 (2020) [3] B. Myint and V. Ng, physica status solidi (RRL) - Rapid Research Letters, 2100197 (2021) [4] M.J. Donahue and D.G. Porter, OOMMF User's Guide, Version 1.0 Interagency Report NISTIR 6376

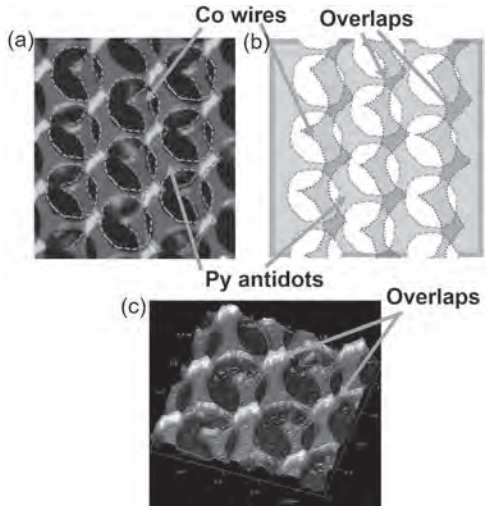

Fig 1. (a) AFM image, (b) schematic and (c) tilted 3D view of Co and Py ASI

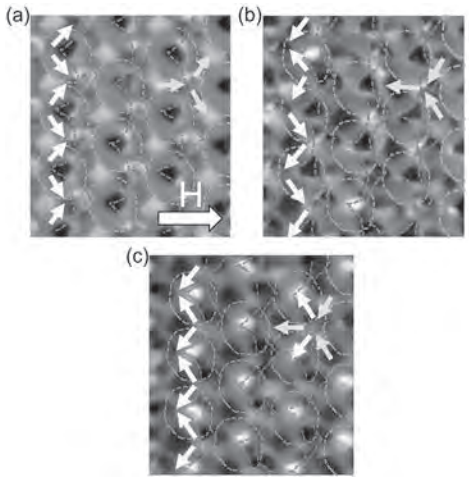

Fig 2. Remnant MFM magnetic domain images of Co and Py ASI system at different fields (a) 2500 Oe (b) -400 Oe and (c) -1200 Oe.

AOA-06. Dipolar Artificial Spin Ice on a Cairo Lattice. *K.V. Nefedev*[1,2], V. Strongin[1,2], A. Farhan[3,4] and A. Makarov[1] *1. Theoretical Physics and Intelligent Technologies, Far Eastern Federal University, Vladivostok, Russian Federation; 2. Applied Mathematics, Far East Branch of Academia of Science of Russia, Vladivostok, Russian Federation; 3. Laboratory for Multiscale Materials Experiments, Paul Scherrer Institute, Villigen, Switzerland; 4. Physics Department, University of California, Santa Cruz, CA, United States*

To investigate the influence of geometric frustration on the properties of low-energy configurations of systems of ferromagnetic nanoislands located on the edges of the Cairo lattice, the model of interacting Ising-like magnetic dipoles is used. By the method of complete enumeration, the densities of states of the Cairo pentagonal lattices of a finite number of Ising-like point dipoles are calculated. The calculated ground and low-energy states for systems with a small number of dipoles can be used to solve the problem of searching for the ground states in a system with a relatively large number of dipoles. It is shown that the ground-state energy of the Cairo pentagonal lattices exhibits nonmonotonic behavior on one of the lattice parameters. The lattice parameters can be used to control the degree of geometric frustration. For the studied lattices of a finite number of Ising dipoles on the Cairo lattice in the ground-state configurations, a number of closed pentagons is observed, which are different from the obtained maximum closed pentagons. The magnetic order in the ground-state configurations obeys the ice rule and the quasi-ice rules. Comparison of the theoretically predicted ground state and the experimentally obtained low-energy states showed that in the experiment, clusters of the ground state are observed Fig 1, [1]. Artificial spin ice systems on the Cairo lattice can exhibit exotic thermodynamic properties that would be interesting to study for the development of the theory of phase transitions. We investigated the problem of the configuration of the ground state in a zero external magnetic field. It is of interest to study the behavior of the magnetic susceptibility as a function of temperature, calculate the blocking temperature and Curie temperature, energy, spin excess, and degeneracy of the ground-state configurations in a nonzero external magnetic field.

Makarova K., Strongin V., ... & Nefedev K. (2021). Low-energy states, ground states, and variable frustrations of the finite-size dipolar Cairo lattices. *Physical Review E*, *103*(4), 042129.

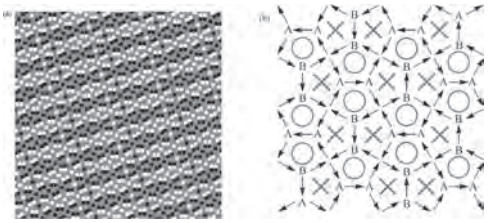

FIG. 1. (a) Calculated XMCD image for the candidate for the ground state of the dipole Cairo lattice. (b) One of four possible ground-state configurations for a system of 80 dipoles, c = 376 nm.

AOA-07. Magnetization Plateau of the Distorted Diamond Spin Chain with Anisotropic Ferromagnetic Interactions. *T. Sakai*[1,2], K. Okamoto[1], R. Furuuchi[1] and H. Nakano[1] *1. Graduate School of Science, University of Hyogo, Kamigori, Japan; 2. SPring-8, National Institutes for Quantum and Radiological Science and Technology, Sayo, Japan*

The frustrated quantum spin systems exhibit various exotic magnetic phenomena. One of interesting phenomena is the magnetization plateau, which corresponds to the quantization of the magnetization. The S=1/2 distorted diamond spin chain is a typical one-dimensional frustrated systems. The previous theoretical study, using the numerical diagonalization of finite-size culsters and the level spectroscopy analysis[1], indicated the S=1/2 distorted diamond spin chain can exhibit the 1/3 magnetization plateau due to two different mechanisms, depending on the ratio of the exchange interactions. Azurite $Cu_3(OH)_2(CO_3)_2$ is a good candidate

material of the distorted diamond spin chain. The high-field magnetization measurement successfully revealed that azurite exhibits the 1/3 magnetization plateau[2]. Recently as another good candidate material alumokluchevskite $K_3Cu_3AlO_2(SO_4)_4$ was discovered[3]. In this compound ferromagnetic exchange interactions exist as well as antiferromagnetic ones, while azurite has only antiferromagnetic ones. On the other hand, if the anisotropic ferromagnetic interaction is introduced to the distorted diamond spin chain, another mechanism of the 1/3 magnetization plateau would be expected, based on the previous theoretical study on the mixed spin chain[4]. Thus it would be interesting to study the model of the distorted diamond spin chain with the anisotropic ferromagnetic interaction, to consider the magnetization plateau. In the present work, we investigated this model using the numerical diagonalization and the level spectroscopy analysis and obtained the phase diagram at 1/3 of the saturation magnetization, which includes the plateau phase due to a new mechanism for the distorted diamond spin chain.

[1] K. Okamoto, T. Tonegawa and M. Kaburagi, J. Phys.: Condens. Matter 15, 5979 (2003). [2] H. Kikuchi, Y. Fujii, M. Chiba, S. Mitsudo, T. Idehara, T. Tonegawa,K. Okamoto, T. Sakai, T. Kuwai and H. Ohta, Phys. Rev. Lett. 94, 227201 (2005). [3] K. Morita, M. Fujihara, H. Koorikawa, T. Sugimoto, S. Sota, S. Mitsuda and T. Tohyama, Phys. Rev. B 95, 184412 (2017). [4] T. Sakai and K. Okamoto, Phys. Rev. B 65, 214403 (2002).

AOA-08. Tension-free Dirac Strings and Steered Magnetic Charges in 3D Artificial Spin Ice. *S. Koraltan*[1], F. Slanovc[1], F. Bruckner[1], C. Nisoli[2], A. Chumak[3], O. Dobrovolskiy[3], C. Abert[1] and D. Suess[1] *1. Physics of Functional Materials, Faculty of Physics, University of Vienna, Vienna, Austria; 2. Theoretical Division, Los Alamos National Laboratory, Los Alamos, NM, United States; 3. Nanomagnetism and Magnonics, Faculty of Physics, University of Vienna, Vienna, Austria*

Dipolar Spin Ices (DSI) are geometrically frustrated magnetic materials, where the moments are arranged on the sites of a pyrochlore lattice [1]. The ground-state obeys the ice-rule, where two magnetic moments point to the center of the tetrahedral unit cell and two point out. If the rule is broken, i.e. one moment is switched, a net magnetic charge is observed at the center of the tetrahedron, referred to as magnetic monopoles. The trace of the switched magnetic moments is referred to as a Dirac string, which has magnetic monopoles at its ends. However, these materials require cryogenic conditions for the stability of monopoles. To study the magnetic monopoles on more suitable platform, artificial spin ices (ASI) consisting of elongated magnetic islands were considered [2]. Their 2D nature lifts the degeneracy of the ground state, as not all ice-rule obeying vertices have equal energies. Due to this differentiation between energetic states of the vertices, the Dirac strings bind the monopoles and store energy, limiting the mobility within the lattice. Here, we combine the advantages of DSI and 2D ASI, and present a 3D ASI lattice [3], where 3D ellipsoids with nearly perfect ising behavior are arranged on an Ice Ih crystal, where the angle between the ellipsoids is always $\theta = 109.5°$, see Fig. 1. This symmetry recovers the lifted degeneracy of the ground state and enables tension-free Dirac strings. Based on the definitions of unbound magnetic monopoles [4], we show that the mobility threshold for magnetic charges is by 2 eV lower than their unbinding energy, while the propagation barrier is constant. The energy of the system does not increase with the length of the Dirac string, showing its tension-free nature. Furthermore, we apply external global fields and steer one magnetic monopole in the desired direction without creating additional magnetic charges, see Fig. 2. Finite temperature micromagnetic analysis reveals that the magnetic monopoles within the 3D ASI lattice are stable and steerable at room temperature.

[1] - Bramwell, S. T. & Harris, M. J. The history of spin ice. *J. Phys.: Condens. Matter* 32, 374010 (2020). [2] - Skjærvø, S. H., Marrows, C. H., Stamps, R. L. & Heyderman, L. J. Advances in artificial spin ice. *Nat Rev Phys* 2, 13–28 (2020). [3] - Koraltan, S. *et al.* Tension-free Dirac strings and steered magnetic charges in 3D artificial spin ice. NPJ Comput. Mater. (2021) - In press [4] - Mól, L. A. S., Moura-Melo, W. A. & Pereira, A. R. Conditions for free magnetic monopoles in nanoscale square arrays of dipolar spin ice. *Phys. Rev. B* 82, 054434 (2010).

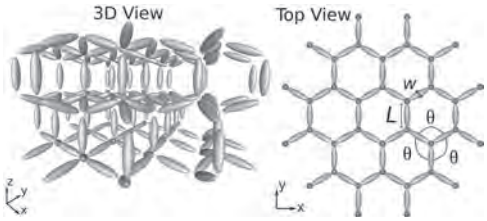

Fig.1: 3DASI lattice with 3D and top view.

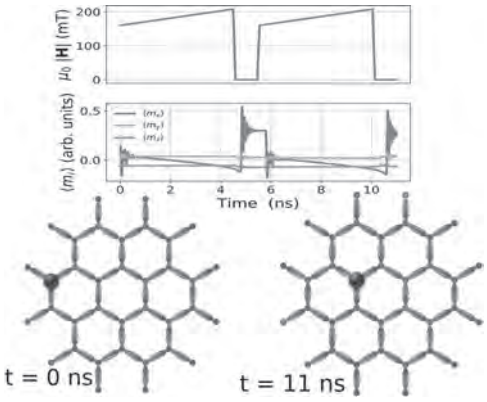

Fig. 2: Averaged magnetization and applied field with respect to time, and the schematic magnetic configurations before and after propagation of monopole.

AOA-09. Withdrawn

AOA-10. Correlated Disorder in a Molecular Assembly: A New Artificial Spin System. *M. Alfonso Moro*[1], J. Coraux[1], B. Canals[1] and N. Rougemaille[1] *1. Néel Institute, CNRS, Grenoble, France*

Artificially designed systems provide a powerful experimental platform to probe, model and challenge the properties of matter [1]. Artificial systems are also fabricated to explore intriguing or exotic effects, which do not exist in nature or which would be too difficult to study otherwise. In that context, lattices of nanomagnets have provided a remarkable playground for studying lattice spin models and investigating cooperative magnetic phenomena associated with frustrated magnetism [2, 3]. This approach complements what can be done using other artificial systems [4-6]. Here, we explore the physics of a non-magnetic highly frustrated magnet: a molecular assembly of fullerenes (C_{60}) deposited on a Cu surface, in which the molecules can take two heights (comparable to an Ising variable) with respect to the metal surface (see Fig. 1). Scanning tunneling microscopy (STM) reveals that five distinct phases coexist (see Fig. 2). We will discuss the properties of a phase exhibiting strong disorder in the height pattern of “low” and “high” C_{60}. This phase has been proposed as a potential realization of the Ising triangular antiferromagnet (TIAF) [7], a model known to remain disordered at all temperatures and have a zero point entropy [8]. We determine whether this disorder is random or correlated, i.e., if the patterns we image in real space follow certain local rules, similar to those found in ice-like systems. To account for the experimental observations, we propose an original approach which links the structural properties of the molecular assembly to an emergent magnetic description of the C_{60} pattern. Our analysis not only explains the properties of the disordered phase, but also successfully describes all the other imaged phases, offering new opportunities to bridge concepts used in frustrated magnetism to those employed in surface science, even in a truly non-magnetic system.

[1] N. Rougemaille, B. Canals, The European Physical Journal, B Vol. 92, p.62 (2009) [2] R. F. Wang, C. Nisoli, R. S. Freitas. et al., Nature, Vol. 439, p.303 (2006) [3] S. H. Skjaervo, C. H. Marrows, R. L. Stamps et al.,

Nature Review Physics, Vol. 2, p.13 (2019) [4] K. Runge, B. Pannetier, Europhysics Letters, Vol. 24, p.737 (1993) [5] E. Ganz, F. Xiong, I.-S. Hwang et al. Physical Review B, Vol. 43, p.7316 (1991) [6] A. Ortiz-Ambriz, P. Tierno, Nature Communications, Vol. 7, p.10575 (2016) [7] W. W. Pai, C.-L. Hsu, M. C. Lin et al., Physical Review B, Vol. 69, p.125405 (2004) [8] G. H. Wannier, Physical Review, Vol. 79, p.357 (1950)

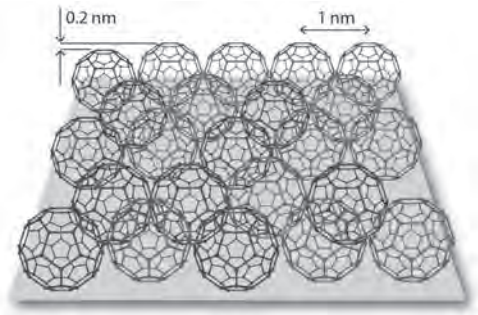

Fig.1. Assembly of C_{60} (football-like structures) on a Cu surface (grey). The molecules take two heights with respect to Cu, "high" (red) and "low" (blue).

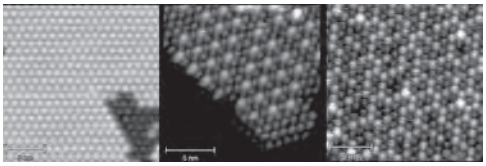

Fig.2. STM images of C_{60} on Cu(111). "High" and "low"molecules appear as yellow and blue dots, respectively. From left to right: uniform-height, periodic and disordered phases.

AOA-11. Arctic Circle Phenomenon and magnetic fragmentation in a square lattice based frustrated spin system. *L. Reneuve*[1,2], B. Canals[3] and N. Rougemaille[3] *1. Université Grenoble Alpes, Grenoble, France; 2. Institut Néel, Grenoble, France; 3. Institut Néel, CNRS, Grenoble, France*

In frustrated spin systems, the ground state manifold (i.e., the family of states of lowest energy), is often defined by local constrains inherited both from the frustrated nature of spin interactions and the local topology. These constraints (e.g., an analogue of the Gauss law in electromagnetism) give rise to exotic phases at low temperature, for instance spin liquids hosting very peculiar dynamics: magnetic monopoles, loop-like excitations, etc. In some precise cases, a phenomenon called magnetic fragmentation can arise, where each individual spin splits into two parts: one contributing to an ordered phase and the other to a highly fluctuating one. The phase arising from such phenomenon then displays both a mean ordered background and structured liquid-like fluctuations [1]. While frustrated spin systems have been studied widely under open or periodic boundaries conditions, recent interest has been given to a specific kind of boundaries in 2D: Domain Wall Boundary Conditions. By fixing the spins on the borders of the system in a controlled way and thus adding another set of constraints to the system, the collective organisation unexpectedly propagates very far from the border and into the system's bulk. This careful choice of the border constraints spectacularly results in a spontaneous phase separation of the system: an extensive part located in the corners freezes while a central circular one is partially polarized and fluctuates. This phenomenon is known as the Arctic Circle Phenomenon [2]. In this work we propose a new carefully designed frustrated spin model on the square lattice and some associated Domain Wall Boundary Conditions. Thanks to a Monte Carlo approach we show that it both exhibits magnetic fragmentation and an Arctic Circle Phenomenon at low temperature.

[1] M E Brooks-Bartlett, S T Banks, L D Jaubert *et al.,* Physical Review X (2014) [2] W Jockusch, J Propp & P Shor, arXiv:math.CO/9801088 (1995)

AOA-12. Is a field demagnetization protocol applied to an a priori athermal, artificial square ice magnet, a stochastic process? *O. Brunn*[1,2], B. Canals[1] and N. Rougemaille[1] *1. CNRS - Institut NEEL, Grenoble, France; 2. Institute of Scientific Instruments of the Czech Academy of Sciences, Brno, Czechia*

Lithographically patterned arrays of magnetostatically interacting nanostructures are now well-established tools for investigating the physics of frustrated magnets [1]. Reaching a low-energy manifold where intriguing phenomena occur is challenging experimentally, and the effective temperature of the system under study must be lowered efficiently. So far, two main approaches were used in practice. Either the artificial systems are rotated in a decaying magnetic field [2], or their magnetization dynamics are activated by a thermal treatment [3]. Even though both protocols were employed successfully in previous works, there is a fundamental difference between them. If one can intuitively understand that thermal fluctuations may be a source of stochasticity, one might wonder whether field demagnetization protocols are not instead a source of determinism, especially when the experiments are conducted well below the blocking or Curie temperature of the nanomagnets. The main purpose of this presentation is to answer the following questions: What happens if the very same athermal lattice is field demagnetized several times? Would we get the same arrested state repeatedly and deterministically, or are the successive arrested configurations statistically decorrelated because stochasticity drives the physics? Here we investigate the response of an athermal, artificial square ice [4] submitted to successive field demagnetization protocols. We show that each resulting magnetic state differs substantially from the previous one, but not entirely. Analyzing these states via spin and vertex density maps, we find that the field demagnetization protocol we apply is essentially a stochastic process, despite quenched disorder, which is unambiguously present in our arrays, acts as a source of determinism. We also provide a comparison with conventional two-dimensional square spin system [2] submitted to the very same field history and show that quenched disorder plays a less important role. Finally, we demonstrate that the spin and vertex density maps are a convenient tool to probe and reveal quenched disorder in an artificial spin system, as they allow to spot the regions that remain unaffected between successive field protocols.

[1] N. Rougemaille, B. Canals, Eur. Phys. J. B, Vol. 92, p. 62 (2019) [2] R. F. Wang, C. Nisoli, R. S. Freitas, Nature, Vol. 439, p. 303 (2006) [3] J. P. Morgan, A. Stein, S. Langridge, Nat. Phys., Vol. 7, p. 75 (2011) [4] Y. Perrin, B. Canals, N. Rougemaille, Nature, Vol. 540, p. 410 (2016)

AOA-13. Approximates of the Square Ice and F-model Using Two-dimensional Artificial Lattices of Nanomagnets. *V. Schánilec*[1,2], O. Brunn[1,3], B. Canals[1], M. Horáček[3], S. Krátký[3], P. Meluzín[3], T. Šikola[4,2] and N. Rougemaille[1] *1. Univ. Grenoble Alpes, CNRS, Grenoble INP, Institut NEEL, Grenoble, France; 2. Central European Institute of Technology, CEITEC BUT, Brno University of Technology, Brno, Czechia; 3. Institute of Scientific Instruments of the Czech Academy of Sciences, Brno, Czechia; 4. Institute of Physical Engieneeering, Faculty of Mechanical Engieneering, Brno University of Technology, Brno, Czechia*

Artificially fabricated systems of interacting nanomagnets are a powerful platform for investigating the exotic many-body physics of frustrated spin models [1,2]. Here we show that a proper design of the lithographically patterned systems usually employed in artificial spin ice studies allows exploring the physics of vertex models as well. We focus our work on the celebrated six-vertex model. We provide experimental results on its three possible variants (the Rys F-model, the square ice and the Slater-KDP model) using purely two-dimensional lattices. With Magnetic Force Microscopy, we visualise the low-energy spin configurations of these variants, as exemplified in Figure 1 for the F-model. Based on our magnetic images, we investigate the properties of the Faraday loops (see Figure 2, where their parity and chirality are highlighted) as the square ice energy constraint is detuned to force the system to approach the pure F-model condition. Our findings [3] will be compared to recent theoretical predictions [4,5]. The key element of our approach is to replace the spin degree of freedom in

conventional artificial spin systems with a micromagnetic knob, which allows fine control of the vertex energy. Besides, the design we propose permits reducing the density of topological defects drastically after a field demagnetisation protocol. The advantages and limitations of our strategy will be discussed in this presentation.

[1] R. F. Wang, *et al.*, Nature 439, 303 (2006) [2] Y. Perrin, B. Canals, and N. Rougemaille, Nature 540, 410 (2016) [3] V. Schánilec *et al.*, unpublished [4] C. Nisoli, Eur. Phys. Lett. 132, 47005 (2020) [5] D. M. Arroo and S. T. Bramwell, Phys. Rev. B 102, 214427 (2020)

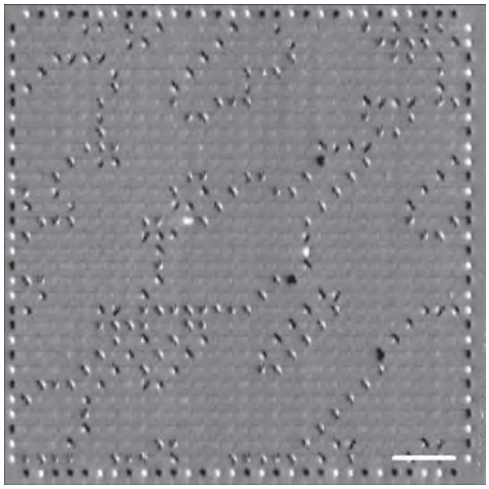

Fig. 1: Magnetic image of a two-dimensional square lattice fabricated to approximate the low-energy manifold of the F-model. Only the type II domain walls and a few type III topological defects are visible in the image. The scale bar is 2 microns.

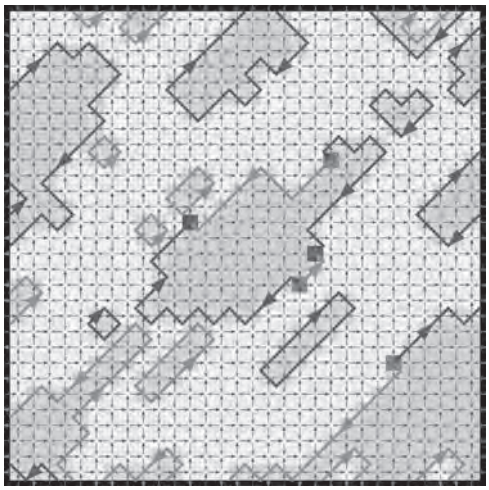

Fig. 2: Spin configuration of the lattice shown in Figure 1. Green and blue areas are type I domains (ground state of the F-model). Type II and type III vertices are shown in red and dark green/purple, respectively. Blue and red lines show the Faraday loops according to their parity (blue vs. red). The head of the large arrows indicates the chirality of the Faraday loops.

AOA-14. Magnetic and thermoelectric properties of Bi, Cu double-substituted $La_{1-x}Sr_xCoO_3$. *D.P. Dubey*[1] and R. Chatterjee[1] *1. Physics Department, Indian Institute of Technology- Delhi, New Delhi, India*

Recycling of waste heat and the search for renewable energy sources is a contemporary issue of the interest for the world in general [1-3]. Oxides thermoelectric materials (TEs) have advantage over other well-known alloy based TEs, due to their chemical and thermal robustness, high thermal stability and excellent oxidation resistance. Among all oxides, the perovskite transition metal oxides like cobaltite, exhibit rich physical properties for a good thermoelectric figure of merit. In this work, a detailed magnetic and thermoelectric properties are investigated for Bi, Cu co-doped cobaltite sample. The polycrystalline samples of $La_{0.95-x}Bi_xSr_{0.05}Co_{0.5}Cu_{0.5}O_{3,}$, have been synthesized through Solid State Reaction route. The X-ray diffraction (XRD) data shows a distorted rhombohedral phase (space group) and the scanning electron microscopy (SEM) data on bulk shows optimal grain growth with grain size ~1-3μm. The electron dispersive analysis of X-ray (EDAX) with elemental mapping, confirms the existence of stoichiometric and homogeneous compositions for all prepared samples. The ZFC-FC and (M-H) plots shows the spin glass behavior at low temperature (~10K). The specific heat capacity C_p measurement was carried out on PPMS, where an anomaly observed around room temperature. The data of specific heat used to calculate the thermal conductivity from the values of thermal diffusivity by Discovery DXF-900. The electrical conductivity and Seebeck measurement performed by ZEM-3 Advanced Riko Inc. It was found that, with increasing the Bi-substitution for samples, the thermal conductivity (decreases, while the Seebeck voltage (*S*) increases. The decrease of and increase of *S*, is desirable for good thermoelectric properties. The power factor (*PF*) and *ZT* values were extracted from the derived parameters and the results (*ZT*~ 0.016, *PF*~ 80μW/mK^2) shows the co-doping system of $La_{0.95-x}Bi_xSr_{0.05}Co_{0.5}Cu_{0.5}O_3$ have enough potential for efficient thermoelectric performance.

[1]. Jian He and Terry M. Tritt, Science 357, eaak9997 (2017). [2]. Christopher J. Vineis, Ali Shakouri, Arun Majumdar, and Mercouri G. Kanatzidis Adv. Mater. 22, 3970–3980 (2010). [3]. J. Ravichandran J. Mater. Res. 32(1), 183-203 (2017).

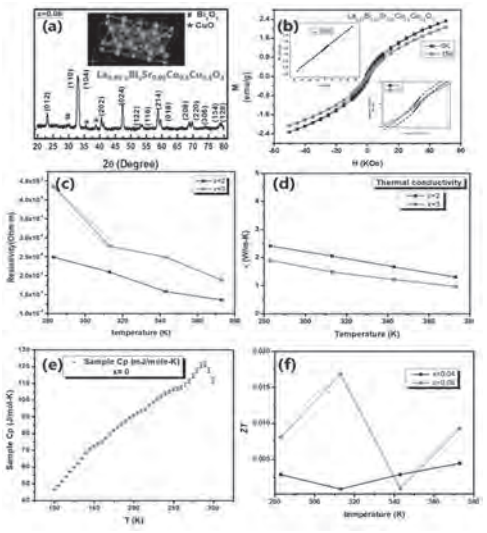

Fig. 1: (a) XRD diffractogram, (b) M-H plot for *x*= 0.06 sample, (c), (d) electrical resistivity and thermal conductivity variation with temperature respectively, (e) variation of specific heat with temperature, (f) *ZT* vs temperature for *x*= 0.04 & 0.06 samples.

AOA-15. Static and Dynamic Magnetic Properties of Cu-Based Organic-Inorganic Hybrid Perovskite Single Crystals. E. Vetter[1], H. Lu[2], R. Song[3], *A. Comstock*[1], V. Blum[3], W. Zhang[4], M. Beard[2] and D. Sun[1] *1. Department of Physics, North Carolina State University, Raleigh, NC, United States; 2. Chemistry and Nanoscience Center, National Renewable Energy Laboratory, Golden, CO, United States; 3. Department of Mechanical Engineering and Material Science, Duke University, Durham, NC, United States; 4. Department of Physics, Oakland University, Rochester, MI, United States*

Cu-based hybrid organic-inorganic perovskites represent an intriguing class of quasi-two-dimensional layered materials. They are well known to behave as nearly ideal two-dimensional (2D) Heisenberg magnets, making them potentially suited for spintronic applications. However, the nature of spin wave propagation in these materials and how it is affected by the presence of various anisotropic exchange contributions warrants further investigation. Here we examine the static and dynamic magnetic properties of $(C_6H_5CH_3CH_2NH_3)_2CuCl_4$, $(S\text{-}C_6H_5CH_3CH_2NH_3)_2CuCl_4$, $(C_8H_9NH_3)_2CuCl_4$, and $(C_6H_5CH_3CH_2NH_3)_2CuBr_4$ single crystals using SQUID magnetometry and ferromagnetic resonance (FMR) spectroscopy, respectively. Static magnetization and susceptibility measurements reveal the effects of organic cation and halide substitution on critical ordering behavior. Dynamic FMR measurements show spin wave propagation in the paramagnetic region above the critical temperature as a result of strong intra-layer exchange coupling.

INVITED PAPER

AOA-16. Self-induced spin glass phase in dhcp Nd. *A. Bergman*[1] *1. Dept. of Physics and Astronomy, Uppsala University, Uppsala, Sweden*

One of the most intriguing phases of magnetic order is manifested by the spin glass state. In these systems, the magnetization exhibit glassy dynamics, including ageing and memory effects. Their peculiar dynamics can be explained by having an energy landscape with several local minima combined with larger energy barriers, which result in non-ergodic behavior. Such energy landscapes have historically been associated with disorder and thus spin glass dynamics have been expected to only occur in chemically disordered materials, such as certain transition metal alloys. Bulk Nd crystallizes in the dhcp structure and across its phase diagram, a number of complex non-collinear magnetic states have been observed in earlier experimental studies. Here we will present our recent theoretical and experimental findings [1] that thick films of elemental crystalline Nd does in fact exhibit glassy dynamics at low temperatures. Since the disorder in the system is limited, the glassy behaviour can not have the same origin as conventional spin glasses. In this talk we will discuss how the magnetic behaviour of the low temperature state of dhcp Nd can in fact be described as a self-induced spin glass. Furthermore we will highligt differences between self-induced and conventional spin glasses and also discuss and how the exchange interactions in the material cause the energy landscape that drives the glassy dynamics.

[1] U. Kamber, A. Bergman, A. Eich, D. Iusan, M. Steinbrecher, N. Hauptmann, L. Nordström, M. I. Katsnelson, D. Wegner, O. Eriksson, and A. A. Khajetoorians, Science 6757 368 (2020)

Session AOB
FUNDAMENTAL PROPERTIES AND COOPERATIVE PHENOMENA II

Eleanor M Clements, Co-Chair
National Institute of Standards and Technology, Gaithersburg, MD, United States
Roberto Zivieri, Co-Chair
University of Ferrara, Ferrara, Italy

INVITED PAPER

AOB-01. Recent developments of magnetism in flatland: Discovery of Intrinsic 2D-XY Ferromagnetism in a van der Waals Monolayer.
A. Bedoya Pinto[1], J. Ji[1], A. Pandeya[1], P. Gargiani[2], M. Valvidares[2], P. Sessi[1], J. Taylor[3], F. Radu[3], K. Chang[1] and S. Parkin[1] *1. Max-Planck Institute of Microstructure Physics, Halle, Germany; 2. ALBA Sincrotro, Barcelona, Spain; 3. Helmholtz Zentrum für Materialien und Energie, Berlin, Germany*

Long before the recent fascination with 2D materials, the critical behavior and universality scaling of phase transitions in low-dimensional systems was a topic of great interest. Particularly intriguing is the case of magnetic order in two dimensions, once excluded in systems with continuous symmetry by the Hohenberg-Mermin-Wagner theorem. While an out-of-plane anisotropy has been shown to lift this restriction and stabilize magnetic order in van der Waals monolayers -as demonstrated in CrI3, CrBr3 and Fe3GeTe2- [1], this proof has remained elusive for a 2D magnet with in-plane rotational symmetry. In this presentation, we highlight the discovery of such an atomically-thin easy-plane system, namely a $CrCl_3$ monolayer on Graphene/6H-SiC (0001) grown by molecular-beam epitaxy. Employing *in-situ* X-ray magnetic circular dichroism, we demonstrate intrinsic ferromagnetic ordering in the monolayer with a critical scaling characteristic of a 2D-XY system [2]. We highlight the role of the in-plane hexagonal crystalline symmetry and negligible substrate interaction to attain an ideal easy-plane (XY) instead of the more ubiquitous easy-axis (Ising) behaviour. These observations point towards the first realization of a finite-size Berezinskii-Kosterlitz-Thouless (BKT) phase transition in a large-area, quasi-freestanding monolayer magnet with a XY universality class; and further constitutes a suitable platform to study exotic phenomena inherent of easy-plane magnets, like superfluid spin transport or in-plane topological spin textures such as merons.

[1] B. Huang, et.al. *Nat. Mater.* 19, 1276–1289 (2020). [2] A. Bedoya-Pinto et.al. arXiv:2006.07605, Science (under review), 2021.

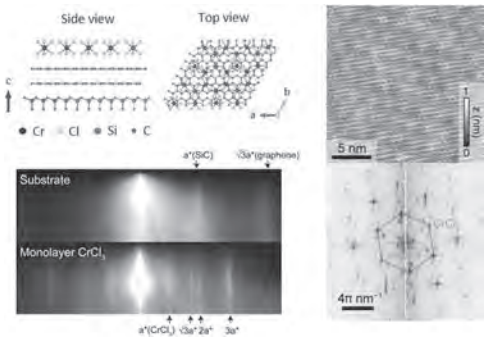

Fig. 1 Schematic crystal structure of $CrCl_3$/Graphene/6H-SiC layers in top view and cross-section configurations, along with the in-situ RHEED pattern of monolayer $CrCl_3$ grown by on the Graphene substrate, along Γ-M direction. On the right, the atomically resolved STM image of the CrCl3 monolayer results in a moiré pattern from the superposition of hexagonal unit cells of $CrCl_3$ and graphene. The Fourier-transformed image yields a twist angle of 23.8 degree.

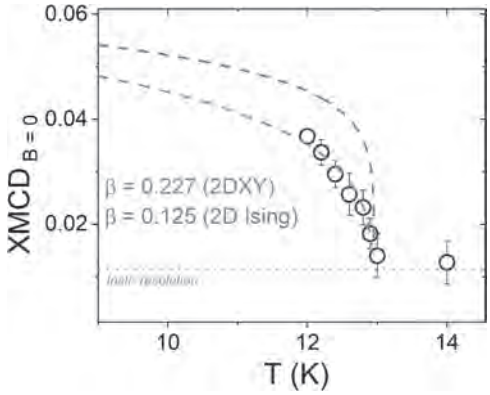

Fig. 2 XMCD values at zero magnetic field (remanence) as a function of temperature. The critical scaling fit close to the phase transition is shown, determining the exponent β=0.227, consistent with a 2DXY magnetic universality class.

CONTRIBUTED PAPERS

AOB-02. Failure of the mean-field description of magnetic fluctuations in the superconducting quantum dot.
V. Janiš[1] and J. Yan[1] *1. Institute of Physics, The Czech Academy of Sciences, Praha, Czechia*

The quantum dot with electron correlations attached to superconducting leads displays a local quantum phase transition from a spin-singlet (zero phase) to a spin-doublet (pi phase) ground state. We recently showed that one needs to apply an external magnetic field to distinguish the physical properties of the two phases [1]. Most of the properties of the superconducting quantum dot, including the zero-pi transition, can be qualitatively correctly described

by a mean-field theory with a two-particle self-consistency [1]. The mean-field description of magnetic fluctuations with static self-energy fails, however, at non-zero temperatures. Linear response theory in the external magnetic field is broken with field-induced poles in the mean-field dynamical transversal susceptibility. Poles in the dynamical susceptibility generate, however, non-analytic singular contributions to the self-energy when going beyond the mean-field approximation. The renormalization of the electron propagators must hence be made dynamical and in the spin-polarized state in order to smooth the singularities in the perturbation expansion and to keep the self-energy and Green functions analytic. The dynamical renormalization due to the electron correlations leads to the broadening of the energies of the in-gap states into bands filling the superconducting gap with increasing temperature even in the limit to zero magnetic field. We demonstrate this behavior on a single impurity Anderson model attached to superconducting leads.

[1] V. Janiš and J. Yan, Phys. Rev. B 103, 235163 (2021)

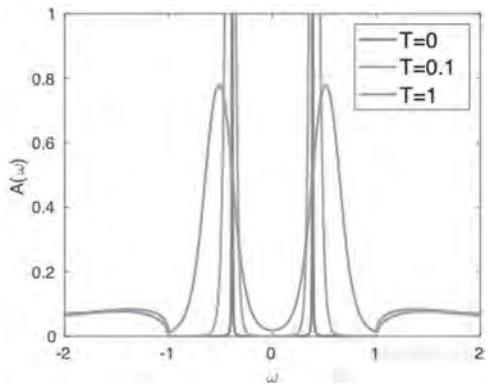

Thermodynamically induced broadening of the energies of the in-gap states of the superconducting single-impurity Anderson model with the Coulomb repulsion U=Δ, the strength of the hybridization of the dot to the superconducting leads Γ=Δ, and the superconducting gap of the dot (-Δ,Δ) at different temperatures T and zero magnetic field in the energy scale Δ =1.

AOB-03. Spin Reorientation in Antiferromagnet-ferromagnet Phase Transitions. *A. Buzdakov*[1,2], K. Zvezdin[3], A. Kimel[4] and A.K. Zvezdin[3]
1. Moscow Institute of Physics and Technology, Moscow, Russian Federation; 2. I-FEVS, Torino, Italy; 3. Prokhorov General Physics Institute, Moscow, Russian Federation; 4. Radboud Universiteit, Nijmegen, Netherlands

A model of an antiferromagnet-ferromagnet phase transition is considered, the prototype of which is the FeRh compound with a phase transition temperature of ~ 300-400 K. The model includes Kittel's idea [1] on the dependence of the exchange interaction between ions in a metal on the deformation in a crystal - u. The second ingredient in the model is the Jahn-Teller magnetic effect [2] for paramagnetic ions (like Rh in FeRh). The thermodynamic potential of the model in an external magnetic field B can be represented as: $F = Eu^2/2 + E_x(u,T)\cos2\psi - MB\cos\psi + K_A(\cos^2\theta - \cos^2\psi \cos2\theta) - T\ln(2\cosh(\Delta/T))$, where E is Young's modulus, E_x is the exchange energy, $M = (M1 + M2)/2$ is the ferromagnetic order parameter, K_A is the anisotropy parameter, T is the temperature of the system, $\Delta(\psi,B)$ is the distance between singlet levels of a paramagnetic ion. The order parameter in this model is the angle ψ between the sublattices, which undergoes changes with increasing temperature and external magnetic field, and changes from π/2 in the antiferromagnetic phase to 0 in the ferromagnetic phase. The phase diagram is shown in Fig. 1: in weak fields B < B* - a first-order phase transition occurs, in strong fields B > B* - a second-order phase transition with a tricritical point occurs. The spin reorientation resembles that observed at the Morin point, for example, in DyFeO3 [3].

[1] C. Kittel, Physical Review., Vol.120, pp.335-342 (1960) [2] A.K. Zvezdin, A.A.Mukhin, A.I. Popov, Journal of Experimental and Theoretical Physics., Vol.45, p.573 (1977) [3] K.P. Belov, A.K.Zvezdin, A.M. Kadomtseva, Orientatsionnye perekhody v redkozemel'nykh magnetikakh, Moskva: Nauka (1979)

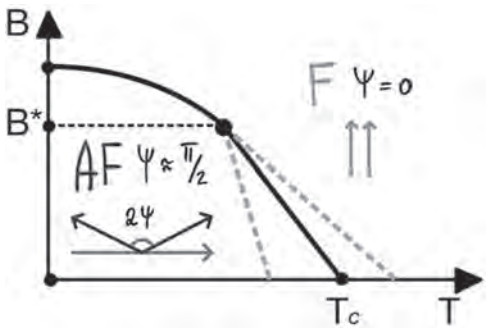

Fig.1. B-T phase diagram: dependence of the magnetic state on the magnitude of the external magnetic field and temperature.

AOB-04. Depinning transition of domain walls with internal degrees of freedom. A. Skaugen[1] and *L. Laurson*[1] *1. Computational Physics Laboratory, Tampere University, Tampere, Finland*

Domain wall dynamics in ferromagnets is complicated by internal degrees of freedom, e.g., Bloch lines within the domain walls. We develop a reduced model of domain walls in disordered thin films with perpendicular magnetic anisotropy capturing such features, able to reach two orders of magnitude larger system sizes than full micromagnetic simulations [1], and use the model to study the depinning transition of domain walls. For weak disorder, excitations of the domain wall internal magnetization are rare, and the depinning transition takes on exponent values of the quenched Edwards-Wilkinson equation. Stronger disorder results in disorder-dependent exponents concurrently with nucleation of an increasing density of Bloch lines within the domain wall [2].

[1] T. Herranen and L. Laurson, Phys. Rev. Lett. 122, 117205 (2019). [2] A. Skaugen and L. Laurson, submitted (2021).

AOB-05. N-th Root Topological Lattices. *H. Sahin*[1,2], S. Rafi-Ul-Islam[1], Z. Siu[1], J. Kong[2], C. Lee[3] and M.B. Jalil[1] *1. Electrical and Computer Engineering, National University of Singapore, Singapore; 2. Institute of High Performance Computing, A*STAR, Singapore, Singapore; 3. Department of Physics, National University of Singapore, Singapore*

Square root topological lattice models such as the non-Hermitian 1D Su-Schrieffer-Heeger (SSH) model [1] and the 2D honeycomb lattice [2, 3] have recently been introduced and realised in several platforms [4, 6]. The recipe for the square root construction has paved the way for 2^n root models [7], in which the transition from higher to lower roots can be readily made due to the arborescent structure of the resultant lattice by taking the n-th power of the corresponding Hamiltonian ($(H_{root})^n$) and subtracting a constant energy. The present method is only applicable for the square root operation. Here, we introduce a new procedure which enables us to realise any arbitrary n-th root of the lattice, including prime number roots, by simply adding $n-1$ new sites between two parental sites such that the new directional couplings create a closed loop in either the clockwise or anti-clockwise directions (Fig. 1a). While the Hermiticity is preserved in square root operations, the non-reciprocal couplings in the n-th root method require breaking the Hermiticity so that the arborescent construction can be followed to form $(H_{root})^n$ as the direct sum of $H_{parental}$ and $H_{residual}$ where $H_{parental}$ is the original lattice Hamiltonian, which is topologically non-trivial [8], and $H_{residual}$ represents the direct sum of all the residual parts. This form allows us to transition between roots (Fig. 1b) without the need for a constant energy

shift in every operation (Fig. 2). Every root operation results in a multiplication of the energy band structure, which depends on the degree of the root. This multiplication in energy also results in the multiplication of the topological states. In contrast to conventional TIs, the *n*-th root version of the topological lattices possesses multiple topological mid-gap states with finite energy as well as non-Hermitian phenomenon such as the non-Hermitian skin effect, which may be useful for various potential applications such as magnetic sensing due to the extensive sensitivity and robustness of the topological states.

[1] M. Ezawa, *Phys. Rev. Research*, vol. 2, no. 3, p. 033397, Sep. 2020. [2] T. Mizoguchi, Y. Kuno, and Y. Hatsugai, Physical Review A102, 033527 (2020). [3] T. Mizoguchi, T. Yoshida, and Y. Hatsugai, Physical Review B103, 045136 (2021). [4] M. Yan, X. Huang, L. Luo, et al. Physical Review B102,180102 (2020). [5] M. Kremer, I. Petrides, E. Meyer, et al. Nature Communications11, 907 (2020). [6] L. Song, H. Yang, Y. Cao, et al. Nano Letters20, 7566 (2020). [7] A. M. Marques, L. Madail, and R. G. Dias, Physical Review B103, 235425 (2021). [8] J. Arkinstall, M. H. Teimourpour, L. Feng, et al. Physical Review B95, 165109 (2017).

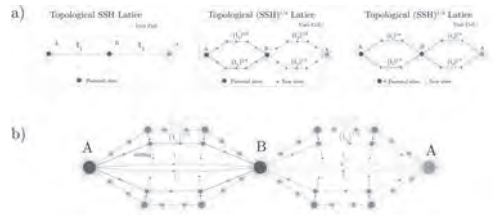

Fig. 1 Illustration of systematic shifting between (SSH)$^{1/n}$ lattices.

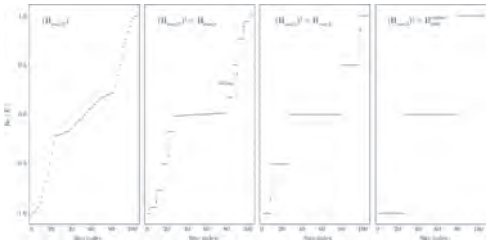

Fig. 2 Real energy spectrum as a function of site index of cubic root (*3^n)* SSH model with 1 unit cell, the transition from *n=3* to *n=0*.

AOB-06. Critical Behavior of the Classical Spin-1 Ising Model for Magnetic Systems. *R. Zivieri*[1,2] *1. National Institute of High Matematics, Rome, Italy; 2. Department of Physics and Earth Sciences, University of Ferrara, Ferrara, Italy*

The spin-1 Ising model was developed in the 70s to describe the critical phase transitions of physical systems characterized by three states such as the λ fluid-superfluid transition and phase separation in He^3-He^4 [1]. In the latest decades, efforts were made to study special cases of the spin-1 Ising Hamiltonian for 2D and 3D physical systems by using approximate methods. In this work, we investigate the statistical thermodynamic properties and the critical behavior predicted by the spin-1 Ising classical Hamiltonian for magnetic systems [2]: $H_{\text{Ising-1}} = -J\sum_{<ij>} s_i s_j - K\sum_{<ij>} s_i^2 s_j^2 + D\sum_i s_i^2 - L\sum_{<ij>} (s_i^2 s_j + s_i s_j^2) - H\sum_i s_i$ (1) *J*, *K* and *L* are the bilinear, the biquadratic and the bicubic exchange coefficients, respectively, *D* is the anisotropy coefficient, *H* is the external magnetic field and $s_i = -1,+1,0$. The spin-1 Ising Hamiltonian is mapped onto the spin-1/2 Ising Hamiltonian by means of the variable transformation $t_i = 2s_i^2 - 1$ used for some special cases of Eq.(1) with $t_i = -1,+1$ [3,4]. As a result of the mapping, we determine, in the parameter space, the critical surface $R(D,H,T) = 0$ as a function of the exchange coefficients. The $R = 0$ critical surface has the role of a vanishing "magnetic field" in analogy to the usual spin-1/2 Ising Hamiltonian [2]. For a magnetic system, due to the breaking of the time-reversal symmetry of the bicubic term, we set $L = 0$ in Eq.(1). In Fig.1 the surface $R = 0$ for a 2D square magnetic lattice of spins in the special case $J = L = 0$ is shown. The first-order and critical phase transitions occurring across the $H = 0$ critical line are classified by calculating, per each spin, the free energy and its derivatives. The free energy corresponding to the Hamiltonian of Eq.(1) is computed on the surface $R = 0$ starting from an empirical partition function written for the spin-1/2 Ising model [5]. The theoretical predictions are confirmed by Metropolis Monte Carlo simulations [6].

[1] M. Blume, V.J. Emery and R.B. Griffiths, Physical Review A, Vol.4, p.1071 (1971). [2] R. Zivieri, Statistical Thermodynamics of the Spin-1 Ising Model, in preparation. [3] R.B. Griffiths, Physica, Vol. 33, p. 690 (1967). [4] F.Y. Wu, Chinese Journal of Physics, Vol.16, p.153 (1978). [5] H.Q. Wei, arXiv: 1905.04295v2, 25 August 2019. [6] N. Metropolis, A.W. Rosenbluth, M.N. Rosenbluth, A.H.Teller and E. Teller, Journal of Chemical Physics, Vol. 21, p. 1087 (1953).

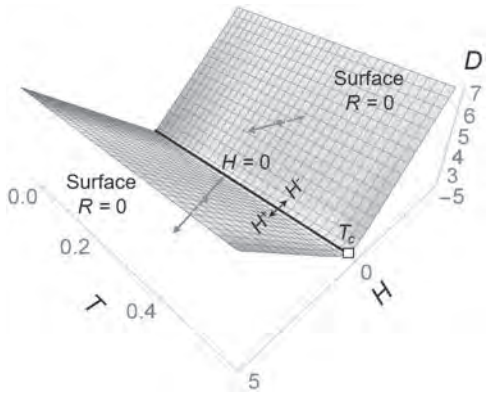

Critical surface $R = 0$ in the (T, D, H) parameter space setting the biquadratic coefficient $K = 1$ for a 2D magnetic square lattice. T_c is the critical temperature and H^+ and H^- indicate the positive and negative magnetic field amplitudes.

AOB-07. Withdrawn

AOB-08. AC Frequency Modulated Phase Transitions in Topolectrical Circuits. S. Rafi-Ul-Islam[1], *H. Sahin*[1,2], C. Sun[1], Z. Siu[1] and M.B. Jalil[1]
*1. Electrical and Computer Engineering, National University of Singapore, Singapore; 2. Institute of High Performance Computing, A*STAR, Singapore, Singapore*

Topolectrical (TE) circuits have not only bridged the seemingly different disciplines of electrical circuits and topological condensed matter but also allowed the realization of highly tunable lattice systems with desired topological properties based on the parameters of the corresponding TE circuit lattices [1, 2]. The frequency dependence of the electrical inter-node couplings (i.e., the admittance of capacitors and inductors) suggests that the circuits can be switched between the insulating, semimetallic, and Chern insulator phases by varying the frequency of the alternating signal [3]. Here, we propose a TE circuit lattice that exhibits this switching within a single circuit set-up. We consider a 2-dimensional (2D) TE circuit containing two types of nodes A and B (Fig. 1a) with complex nearest-neighbor couplings (combination of capacitive and resistive) realized via negative impedance converters (NICs) (Fig. 1b) and capacitive next-nearest neighbor (NNN) couplings. The critical frequency of the circuit depends only on the grounding inductor and NNN capacitor (Fig. 1c). In the absence of resistive coupling, the TE circuit respects time-reversal symmetry (TRS) and hosts insulating and semimetallic phases when the frequency is less than, and greater or equal to the critical frequency, respectively. Furthermore, the 2D Weyl points in the semimetallic phase are connected by topological edge states in the admittance spectra (Fig. 2b,e). However, a non-zero R_d breaks TRS and a bulk bandgap appears. Chiral edge states emerge under

open boundary conditions and the circuit exhibits the quantum anomalous Hall effect at $\omega > \omega_c$ (Fig. 2f). Moreover, the Chern number of the system changes signs when the frequency crosses the critical value.

[1] T. Hofmann, T. Helbig, C. H. Lee, et al. Phys. Rev. Lett.122, 247702 (2019). [2] S. Rafi-Ul-Islam, Z. B. Siu, C. Sun, et al. New J.Phys.22, 023025 (2020). [3] J.-M. Hou, Phys. Rev. Lett.111, 130403 (2013).

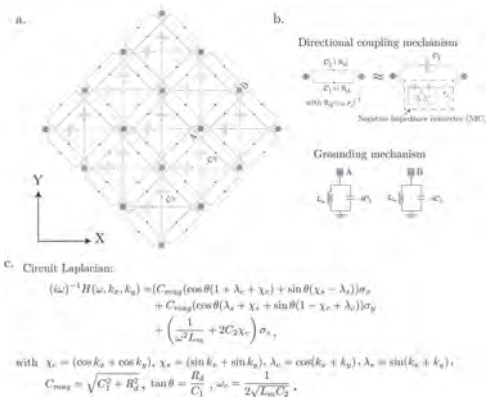

Fig. 1 a. Schematic of frequency-dependent Chern circuit. b. NIC and grounding connections. c. System Hamiltonian and critical frequency.

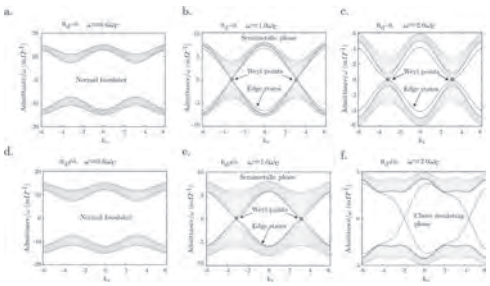

Fig. 2 a-f. Admittance dispersion of a finite system at different frequencies. The top and bottom rows correspond to zero and non-zero resistive couplings, respectively. Common parameters: C_1=1.5 mF, C_2=1 mF and L_m=1 nH.

AOB-09. Effect of Calcium Doping on Magnetocaloric Properties and Critical Behaviour of $La_{0.55}Ca_xSr_{0.45-x}MnO_3$ around FM-PM Phase Transition. *M.A. Bally*[1] and D.A. Khan[1] *1. Physics, Bangladesh University of Engineering and Technology, Dhaka, Bangladesh*

Effect of calcium doping on magnetocaloric properties and critical behaviour of $La_{0.55}Ca_xSr_{0.45-x}MnO_3$ (x = 0.00, 0.05, 0.1, 0.2 and 0.25) prepared by solid state reaction technique has been reported here. XRD measurements reveal rhombohedral structure for all the samples. Lattice parameters as well as Mn-O-Mn bond angle decreases with increasing Ca content. These structural changes control ferromagnetism in the materials via the double-exchange mechanism [1]. Temperature dependent magnetization measurement reveals a reduction of saturation magnetization and decrease in Curie temperature (T_C) from 354 K to 311 K with increase in Ca content. A second order ferromagnetic (FM) to paramagnetic (PM) phase transition of all the samples is confirmed by Arrott plots. The magnetocaloric effect is calculated from the isothermal magnetization measurements using Maxwell's thermodynamic relations. The maximum entropy change ($(-\Delta S_m)_{max}$) and relative cooling power (RCP) are observed to decrease while T_C shifted toward the room temperature with increase in Ca content. Therefore the sample $La_{0.55}Ca_xSr_{0.45-x}MnO_3$ could be used as good solid state refrigerant for magnetic refrigerator near room temperature. Critical behaviour around PM-FM phase transition has been investigated using various methods including modified Arrott plots (MAP) [2], Kouvel–Fisher (KF) [3] method and critical isotherm analysis. The M-H data taken around T_C was investigated in the framework of the mean field model, the 3D–Heisenberg model, the 3D–Ising model and tricritical mean field model [2]. The well agreement between MAP and KF methods confirms that the calculated values of the critical exponents are reliable. Calculated critical exponents reveal that the samples with x=0.00, 0.05, 0.1 possess a long-range ferromagnetic interaction belonging to the mean-field model, and x=0.2, 0.25 possess ferromagnetic short-range interactions belonging to the 3D Heisenberg model. Chemical pressure due to substitution of larger Sr ions with smaller Ca ions, cooperative Jahn–Teller distortions, and presence of ferromagnetic clusters all have significant influence on the nature of the FM-PM phase transition in the studied samples.

[1] C. Zener, "Interaction between the d-Shells in the Transition Metals III: Calculation of the Weiss Factors in Fe, Co, and Ni", Phys. Rev., Vol. 83, pp. 299, (1951). [2] H. E. Stanley, Introduction to Phase Transitions and Critical Phenomena, Oxford University Press, London, 1971. [3] J. S. Kouvel and M. E. Fisher, Phys. Rev. vol.136, p.1626, (1964).

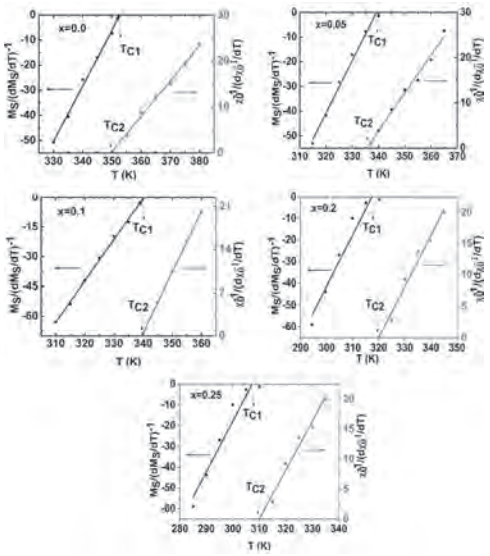

Fig. 1 K-F plot

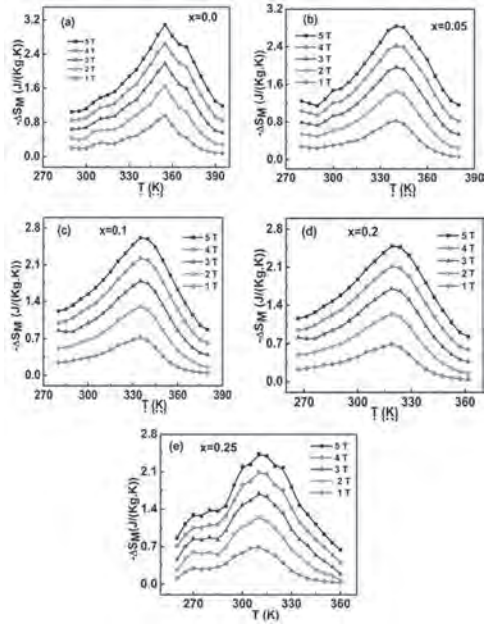

Fig. 2 Entropy chang vs. T

AOB-10. Effects of Random Fields on the Phase Transition of a Two-Dimensional Ferromagnet. *E. Ibrahim*[1], P. Tang[2] and S. Zhang[1]
1. Physics, University of Arizona, Tucson, AZ, United States; 2. Institute of Physics, Beijing National Laboratory for Condensed Matter Physics, Beijing, China

The long-range ordering of two-dimensional magnets with the isotropic short-ranged exchange interaction is destroyed by the fundamentally strong thermal fluctuation of low dimensional systems. We show that the spatial fluctuation, modeled by a random field at the lattice sites, significantly suppresses the long-range ordering as well. By using the random phase approximation along with the quantum statistics of low-energy magnon excitations, we have derived, from the anisotropic Heisenberg model, the magnetization as a function of the temperature in the presence of the random field. We found that the random field effectively decreases the energy gap of the magnon excitations. Since the energy gap is essential for 2D magnetic ordering, the random field would significantly reduce the transition temperature. Another finding is that the phase transition between the ferromagnet and the paramagnet becomes first-order, namely, the magnetization jumps from a finite value in the ferromagnetic phase to nearly zero at the paramagnetic phase. We will present the quantitative relations of above findings with the strength of the random field, and we estimate how these predictions could be experimentally realized. This work is supported by NSF-ECCS-2011331.

AOB-11. Withdrawn

AOB-12. Withdrawn

AOB-13. Exchange Interactions in Mixed-Rare-Earth Transition-Metal Compounds. *R. Skomski*[1], D. Paudyal[3], B. Balasubramanian[1], A. Ullah[1], A. Laraoui[2] and D. Sellmyer[1] *1. Physics and Astronomy & NCMN, University of Nebraska, Lincoln, NE, United States; 2. Electrical Engineering, University of Nebraska, Lincoln, NE, United States; 3. Ames Laboratory, Ames, IA, United States*

Many-sublattice effects in rare-earth transition-metal (RE-TM) oxides and alloys are investigated by model calculations. The considered materials, which are of interest in optics, rare-earth quantum-information processing, permanent magnetism, and magnetic refrigeration, include RE-iron garnets ($R_3Fe_5O_{12}$) and 2:17/1:5 RE-cobalt alloys [1-4]. The exchange behavior of these compounds is dominated by the TM sublattice interactions (J_{TT}), complemented by substantial corrections due to the RE-TM intersublattice interactions (J_{RT}), whereas RE-RE interactions (J_{RR}) are usually negligible [5]. J_{RT} is largest for the elements in the middle of the lanthanide series, and the question arises about the situation for mixture of RE elements. For example, misch metal (mainly Ce-Pr-Nd) is readily available, because it does not need to undergo expensive RE element separation. RE atoms have similar sizes and similar chemical properties, which leads to a large degree of solid-solution miscibility, but many physical properties of the mixed compounds do not superpose. For example, the mean-field Curie temperature T_c is obtained by diagonalizing the intersublattice interaction matrix [5, 6] and therefore a nonlinear function of the exchange constants J_{RT}. The diagonalization can be performed easily for two sublattices and, with some labor, for three sublattices, but no general solutions exist for four or more sublattices, $\{T, R_\mu\} = \{T, R, R', R'', ...\}$. However, an exact diagonalization is possible once the weak RE-RE interactions (J_{RR}, $J_{RR'}$, $J_{R'R}$, *etc.*) are ignored. An analytical formula is obtained that predicts T_c as a function of the exchange constants and of the individual concentrations c_μ of the rare-earth elements. The RE elements with the highest J_{RT} yield a disproportionally strong T_c contribution, even for relatively small concentrations c_μ. Our diagonalization approach can also be used for some quantum-mechanical problems involving interatomic hopping, many-electron interactions, and quantum entanglement. The work in Nebraska is supported by NSF-DMREF (No. 1729288), NSF-EQUATE (OIA-2044049), the NU Collaborative Initiative, and NCMN, whereas the research at Ames is funded by DOE.

[1] O. Gutfleisch, M. A. Willard, E. Brück, C. H. Chen, S. G. Sankar, and J. P. Liu, Adv. Mater. 23, 821-842 (2011). [2] R. Skomski and J. M. D. Coey, Permanent Magnetism, Institute of Physics, Bristol 1999. [3] Y. Zhydachevskyy, I. I. Syvorotka, V. Tsiumra, M. Baran, L. Lipinska, A. Wierzbicka, and A. Suchocki, Sol. Energy Mater Sol. Cells 185, 240-251 (2018). [4] K. Mandal, A. Yan, P. Kerschl, A. Handstein, O. Gut?eisch and K.-H. Müller, J. Phys. D: Appl. Phys. 37, 2628-2631 (2004). [5] N. H. Duc, T. D. Hien, D. Givord, J. J. M. Franse, and F. R. de Boer, J. Magn. Magn. Mater. 124, 305-311 (1993).

Session AOC
FUNDAMENTAL PROPERTIES AND COOPERATIVE PHENOMENA III

Amilcar Bedoya Pinto, Co-Chair
Max Planck Institute of Microstructure Physics, Halle, Germany
Aurelian Rotaru, Co-Chair
Stefan cel Mare University, Suceava, Romania

INVITED PAPERS

AOC-01. Weyl-Kondo Semimetal – How Strong Correlations Intersect with Electronic Topology. *Q. Si*[1] *1. Department of Physics and Astronomy, Rice Center for Quantum Materials, Rice University, Houston, TX, United States*

Strong correlations in metals are known to yield a rich variety of quantum phases [1]. Whether and how they also drive electronic topology is of considerable current interest and, yet, a largely open question. A promising setting arises in heavy fermion systems, which may feature not only strong correlations but also a large spin-orbit coupling. Recently, a Weyl-Kondo semimetal phase has been concurrently discovered in theoretical [2] and experimental [3] studies. The theoretical work was carried out in a Kondo lattice model that is time-reversal invariant but inversion-symmetry breaking. In this talk, I will i) describe the basic characteristics of the Weyl-Kondo semimetal phase, with a particular emphasis on how strong correlations not only produce the Weyl nodes but also pin them near to the Fermi energy, and its experimental signatures, as has been advanced in the material Ce3Bi4Pd3; ii) discuss the extreme topological control of the correlation-driven Weyl nodes [4,5]; and iii) present a design principle – via the cooperation of strong correlations with space-group symmetry--for new Weyl-Kondo semimetal materials [6]. Finally, I will discuss the enrichment of our results for the strong correlation physics, in the form of a global phase diagram, of heavy fermion metals [1]. *This work was done with Sarah Grefe, Hsin-Hua Lai, Lei Chen, Chandan Setty and Haoyu Hu at Rice University and with Silke Paschen, Sami Dzsaber, Andrey Prokofiev, Jennifer Cano and Maia G. Vergniory. It was supported by the Air Force Office of Scientific Research Grant No. FA9550-21-1-0356, the National Science Foundation Grant No. DMR-1920740, and the Robert A. Welch Foundation Grant No. C-1411.

[1] S. Paschen and Q. Si, Nat. Rev. Phys. 3, 9 (2021). [2] H.-H. Lai et al. PNAS 115, 93 (2018); S. E. Grefe et al., Phys. Rev. B101, 075138 (2020) [3] S. Dzsaber et al. Phys. Rev. Lett. 118, 246601 (2017); ibid, PNAS 118, e2013386118 (2021). [4] S. Dzsaber et al. arXiv:1906.01182 [5] S. E. Grefe et al. arXiv:2012.15841 [6] L. Chen et al., arXiv:2107.10837.

AOC-02. Magnetoelectric effect in Dipolar Clusters. *P. Mellado*[1], S. Rica[1] and A. Concha[1] *1. Engineering and Sciences, Universidad Adolfo Ibanez, Santiago, Chile*

We combine the anisotropy of magnetic interactions and the point symmetry of finite solids in the study of dipolar clusters as new basic units for multiferroics metamaterials. The hamiltonian of magnetic dipoles with an easy plane at the vertices of polygons and polyhedra maps exactly into a hamiltonian with symmetric and antisymmetric exchange couplings. The last one gives rise to a Dzyaloshinskii-Moriya contribution responsible for the magnetic modes of the systems and their symmetry groups, which coincide with those of a particle in a crystal field with spin-orbit interaction. We find that the clusters carry spin current and that they manifest the magnetoelectric effect. We expect our results to pave the way for the rational design of magnetoelectric devices at room temperature.

Paula Mellado, Andres Concha, and Sergio Rica, Phys. Rev. Lett. 125, 237602 (2020)

CONTRIBUTED PAPERS

AOC-03. Quantum-confined charge transfer that enhances magnetic anisotropy in lanthanum M-type hexaferrites. C. Bhandari[1], M.E. Flatté[2] and *D. Paudyal*[1] *1. Ames Laboratory, Ames, IA, United States; 2. University of Iowa, Iowa City, IA, United States*

Iron-based hexaferrites are critical-element-free permanent magnet components of magnetic devices. Of particular interest is electron-doped M-type hexaferrite i.e., $LaFe_{12}O_{19}$ (LaM) in which extra electrons introduced by lanthanum substitution of barium/strontium play a key role in uplifting the magnetocrystalline anisotropy. We investigate the electronic structure of lanthanum hexaferrite using a localized density functional theory which reproduces semiconducting behavior and identifies the origin of the very large magnetocrystalline anisotropy. Localized charge transfer from lanthanum to the iron at the crystal's 2a site produces a narrow $3d_z^2$ valence band strongly locking the magnetization along the c-axis. The calculated uniaxial magnetic anisotropy energies from fully self-consistent calculations are nearly double the single-shot values, and agree well with available experiments. The chemical similarity of lanthanum to other rare earths suggests that LaM can host for other rare earths possessing non-trivial 4f electronic states for e.g., microwave-optical quantum transduction.

Churna Bhandari, Michael E. Flatté, Durga Paudyal, https://arxiv.org/pdf/2106.11947.pdf

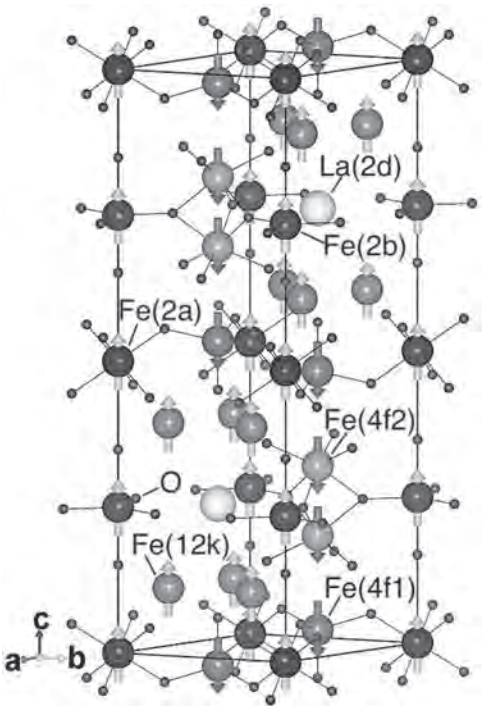

Fig. 1 Crystal structure of M-type hexaferrite ($LaFe_{12}O_{19}$) with Gorter's-type spin configurations of the dif-ferent Fe sublattices. Violet, brown, and purple balls are Fe(2a), Fe (12k), and Fe (2b) with spin-↑(green) and dark greenand magenta balls are Fe (4f1) and Fe (4f2) with spin-↓(red), respectively. Yellow and black balls are La and O atoms.

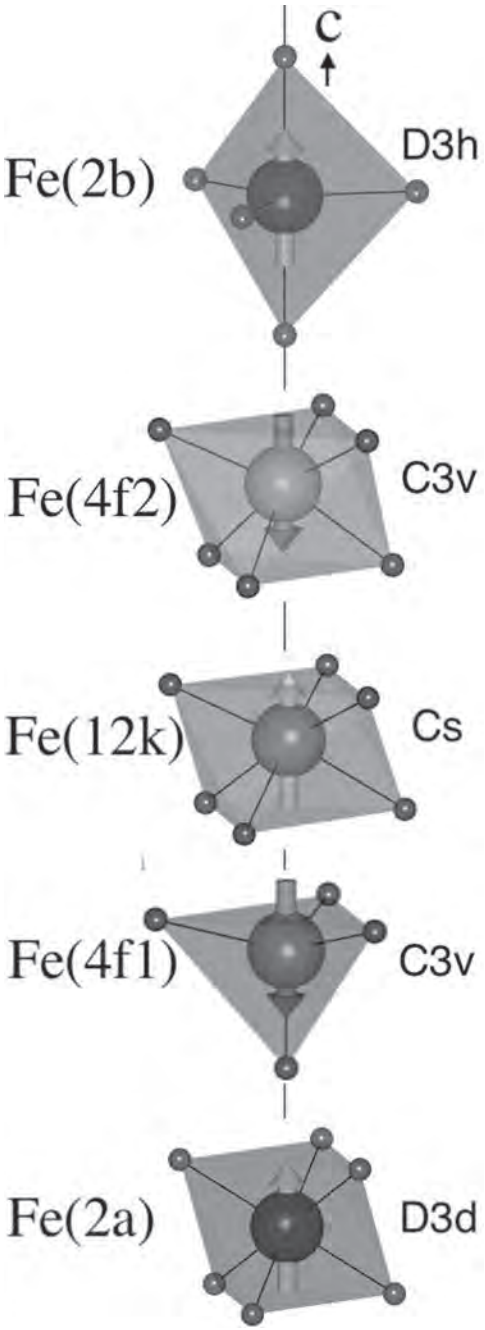

Fig. 2 The polyhedra of each Fe-sublattice based on their nearest O atoms are shown with the site symmetries.

AOC-04. A J_1-J_3 Heisenberg kagome lattice with an order by disorder induced Potts order. V. Grison[1], B. Bernu[1], L. Pierre[2] and *L. Messio*[1,3]
1. LPTMC, Sorbonne Université, Paris, France; 2. Université Nanterre, Nanterre, France; 3. Institut Universitaire de France, Paris, France

Motivated by the physical properties of Vesignieite $BaCu_3V_2O_8(OH)_2$ [1], we study the J_1-J_3 Heisenberg model on the kagome lattice [2], that is proposed to describe this compound for $J_1<0$ and $J_3>>|J_1|$. The nature of the classical ground state and the possible phase transitions are investigated through analytical calculations and parallel tempering Monte Carlo simulations. For $J_1 < 0$ and $J3 > (1+\sqrt{5})*|J_1|/4$, the ground states are not all related by an Hamiltonian symmetry. Order appears at low temperature via the order by disorder mechanism, favoring collinear configurations and leading to an

emergent q=4 Potts parameter to a finite temperature phase transition. For J_3 between $|J_1|/4$ and $(1+\sqrt{5})*|J_1|/4$, the ground state goes through a succession of semi-spiral states, possibly giving rise to multiple phase transitions at low temperatures. Effect of quantum fluctuations are studied through linear spin wave approximation and high temperature expansions of the S=1/2 model.

[1] D. Boldrin et al. Phys. Rev. Lett. 121, 107203 (2018) [2] V. Grison, et al. Phys. Rev. B 102, 214424 (2020).

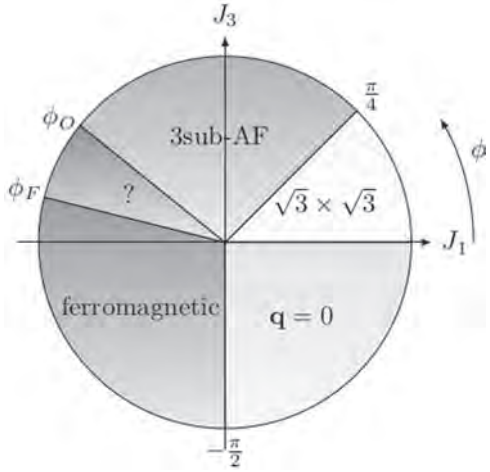

Fig. 1 Zero temperature phase diagram of the J_1-J_3 Heisenberg model on the kagome lattice. Vesignieite is in the *3subAF* phase.

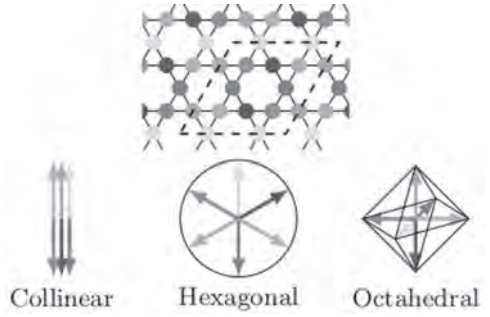

Fig. 2 States in the *3subAF* phase include the three specific states represented here. The collinear state is favored by the order by disorder mechanism.

AOC-05. $Ba_3Co_2O_6(CO_3)_{0.7}$: Candidate Spin-Liquid on the Honeycomb-Lattice. *A.S. Padgett*[1,2] and Y. Takano[2] *1. High Voltage Sciences, Sandia National Laboratories, Albuquerque, NM, United States; 2. Physics, University of Florida, Gainesville, FL, United States*

Since P.W. Anderson *et al.*proposed the theoretical existence of the quantum spin liquid ground state in 1973, antiferromagnetic spin-1/2 systems exhibiting large quantum fluctuations have attracted significant interest as spin liquid candidates. The experimental verification of the spin liquid ground state would not only advance fundamental condensed matter physics, but also provide a path forward to discovering new, exotic spin system ground states. If only nearest neighbor interactions are considered, the spin-1/2 Heisenberg antiferromagnet on a honeycomb lattice should order in a Néel ground state. However, sufficiently strong next nearest neighbor interactions combined with a small coordination number and low dimensionality, which increase the role of quantum fluctuations, such as those exhibited in $Ba_3Co_2O_6(CO_3)_{0.7}$, could result in a quantum spin liquid ground state. For this reason, we have investigated the low temperature specific heat and magnetization of $Ba_3Co_2O_6(CO_3)_{0.7}$, a nonstoichiometric compound with the CoO_6 chains forming a honeycomb lattice. The magnetization exhibits an anomalous decrease in slope with increasing field beyond 10 T when the field is applied parallel to the *c* axis of the sample, indicating that randomness plays an important role in $Ba_3Co_2O_6(CO_3)_{0.7}$. Specific heat measurements conducted on $Ba_3Co_2O_6(CO_3)_{0.7}$ failed to show any sign of ordering down to 160 mK in fields between zero and 18 T. This corroborates earlier measurements made at higher temperatures over a narrower field range by Igarashi *et al.* Further, the specific heat behaves linearly at temperatures below 700 mK. Perhaps most interestingly, $Ba_3Co_2O_6(CO_3)_{0.7}$ has a very large Wilson ratio. Although this is not a theoretical prediction of any quantum spin liquid models, all known spin liquid candidates exhibit Wilson ratios greater than 1, often times greater by an order of magnitude. Herein we discuss our motivation, experiments, and results which advance strong evidence that $Ba_3Co_2O_6(CO_3)_{0.7}$ hosts a spin liquid ground state.

Supported by the Laboratory Directed Research and Development program at Sandia National Laboratories, a multi-mission laboratory managed and operated by NTESS LLC, a wholly owned subsidiary of Honeywell International Inc. for the U.S. Department of Energy's NNSA under contract DE-NA0003525. Any subjective views or opinions that might be expressed in the paper do not necessarily represent the views of the U.S. Department of Energy or the United States Government.

AOC-06. Effect of manganese doping and magneto-photocurrent in organo-metal halide perovskites. T.A. Fasasi[1], S.W. Tsang[1] and *A. Ruotolo*[2] *1. City University of Hong Kong, Kowloon, Hong Kong; 2. Florida Polytechnic University, Lakeland, FL, United States*

Organo-metal halide perovskites have attracted great attention in the solar cell industry and in the research community because of their excellent opto-electronic characteristics [1]. It has recently been reported that the opto-electronic properties of these materials can be tuned by applying an external magnetic field or by introducing an internal magnetic moment via doping with magnetic elements [2,3]. In this work, hybrid perovskite films with formula $MAPb_{1-x}Mn_xI_3$, where x = 0, 1%, 5% and 10% were prepared. The effect of an externally applied magnetic field on devices fabricated with these films were studied by magneto-photocurrent and magneto-photoluminescence [4]. In devices fabricated from pristine $MAPbI_3$, we found a negative magneto-photocurrent and a positive magneto-photoluminescence. The magnetic field favors parallel spin-alignment, which results in an increase of the population of triplets at the expenses of the population of singlets. Since the dissociation rate of triplets is lower, the application of a magnetic field leads to a reduction of the photocurrent. At the same time, since the radiative recombination of triplets is faster, this leads to a positive magneto-photoluminescence. Surprisingly, the magneto-photocurrent changes polarity according to the excitation wavelength (see Fig. 1). Using green-yellow light reduces the contribution of lattice vibration. This favors long-range exchange interaction. When long-range exchange interaction dominates, magneto-photocurrent changes polarity to become positive. Long-range exchange interaction can also be tuned by partially substituting Pb with Mn ions. Mn increases short-range spin-exchange interaction because of the formation of localized magnetic polarons. The application of a magnetic field increases the size of the polarons, which results in an enhanced magneto-photocurrent (see Fig. 2). Unfortunately, the effect was observed only for very low concentrations of Mn. In fact, increasing Mn concentration leads to an increase of the film granularity and, therefore, an increase of the recombination rate along the grain boundaries.

[1] G. Xing et al., Scienc, 342, 344 (2013). [2] C. Zhang et al., Nat. Phys. 11, 427 (2015). [3] P. A. Bobbert et al., Phys. Rev. Lett., 99, 216801 (2007). [4] T. A. Fasasi et al., under review (2021).

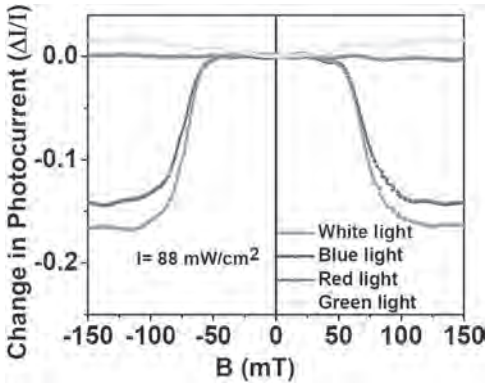

Fig. 1: Magneto-photocurrent under different light wavelengths.

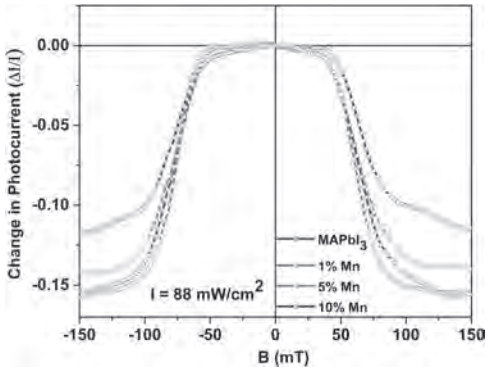

Fig. 2: Magneto-photo current at different Mn concentrations.

AOC-07. Magnetic properties of S = 1 spin chain in $Sr_2Ni(SeO_3)_2Cl_2$: XY-antiferromagnet at Sakai-Takahashi phase diagram.
E. Kozlyakova[1,2], A. Moskin[2], P. Berdonosov[2], V. Gapontsev[3,4], S. Streltsov[3,4], M. Uhlarz[5], S. Spachmann[6], A. ElGhandour[6], R. Klingeler[6,7] and A. Vasiliev[2,1] *1. National University of Science and Technology "MISIS", Moscow, Russian Federation; 2. Lomonosov Moscow State University, Moscow, Russian Federation; 3. Ural Federal University, Ekaterinburg, Russian Federation; 4. Institute of Metal Physics RAS, Ekaterinburg, Russian Federation; 5. Hochfeld-Magnetlabor Dresden (HLD-EMFL), Dresden, Germany; 6. Kirchhoff Institute of Physics, Heidelberg University, Heidelberg, Germany; 7. Centre for Advanced Materials, Heidelberg University, Heidelberg, Germany*

An experimental realization of the Haldane conjecture of a gapped spin liquid is of great interested among condensed matter scientists. The conjecture is implemented in the chains of Heisenberg integer spins bounded by identical intrachain exchange interactions *J* and could be realized in uniform quasi-one-dimensional integer spin compounds [1]. The Haldane phase has to compete with magnetic anisotropy and long-range ordered phases, depending on the ratio of interchain *J*′ and intrachain *J* exchange interactions and uniaxial *D* and rhombic *E* single-ion anisotropy. The critical ratios J′/J and D/J for Haldane phase, easy axis long ordered AFM and easy plane long ordered XY-AFM were first discovered by Sakai and Takahashi [2]. Many compounds, both organic and inorganic, have been studied to verify this idea, some of them have been identified as belonging to the Haldane sector of the Sakai-Takahashi phase diagram. In this work, the position on Sakai-Takahashi phase diagram was determined for the novel integer spin S = 1 chain compound, strontium nickel selenite chloride $Sr_2Ni(SeO_3)_2Cl_2$. XRD measurements showed that the crystal structure of the compound contains the NiO_4Cl_2-octahedra bridged by the SeO_3-pyramids into uniform spin chains. These chains are well separated by strontium cations and cavities of selenium's lone pair of electrons that could lead to 1D-dimensionality of magnetic subsystem. In magnetic measurements it was determined that strontium nickel selenite chloride, $Sr_2Ni(SeO_3)_2Cl_2$, is a spin S = 1 chain system which passes through a correlations regime at $T_{max} \sim 12$ K to long-range order at $T_N = 6$ K. The values of $J'/J = 0.083$ and $D/J = 0.357$ place this compound into a hitherto unoccupied XY-AFM sector of the Sakai-Takahashi phase diagram. The results was recently published in Scientific reports journal [3]. Support by the P220 program of Government of Russia through the project 075-15-2021-604 is acknowledged. We also acknowledge the support of the HLD-HZDR, member of the European Magnetic Field Laboratory (EMFL).

[1] F.D.M. Haldane, PRL 50, 1153-1156 (1983) [2] T. Sakai & M. Takahashi, PRB 42, 4537-4543 (1990) [3] E.S Kozlyakova, A.V. Moskin, P.S. Berdonosov et al. Quasi-1D XY antiferromagnet Sr2Ni(SeO3)2Cl2 at Sakai-Takahashi phase diagram. Sci Rep 11, 15002 (2021)

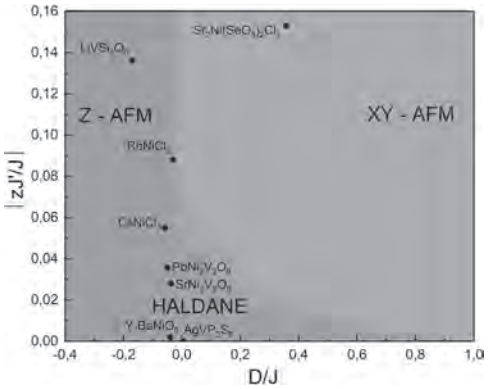

Sakai-Takahashi phase diagram for uniform spin-1 chain compounds, novel compound $Sr_2Ni(SeO_3)_2Cl_2$ is also marked.

AOC-08. Pressure effect on spin-crossover materials: Experiment vs theory.
A. Rotaru[1] *1. Electrical Engineering and Computer Science, Stefan cel Mare University, Suceava, Romania*

Spin-crossover (SCO) complexes form an interesting class of switchable materials that can exist in two different spin states, known as the low-spin (LS) and high-spin (HS) states. These complexes may be switched between the two spin states under various stimuli including temperature, pressure, light, magnetic and electrical fields [1]. Among these stimuli, pressure is one of the most appealing thermodynamic parameters used to probe the spin transition properties of spin-crossover materials since it allows for tuning both the crystal field as well as the interactions between SCO centers. Since the pioneering works of Drickamer [2], Konig [3] and Gutlich[4], the pressure effect has continuously attracted the interest of the scientific community, being intensively studied until nowadays. In general, the application of an external pressure induces a transformation of the SCO complex to the low-spin state, i.e. to the state of lower molecular volume, and has the effect of shifting the switching temperatures towards higher values. However, the interpretation of the pressure effect on molecular SCO phenomena has been, in some cases, compromised by the relatively poor or incomplete information resulted from experimental difficulties related to the need for hydrostatic conditions at low temperatures. In this work I will talk on both hydrostatic [5, 6] and non-hydrostatic [7] pressure effects on the spin transition properties of molecular spin crossover complexes in terms of major thermal hysteresis loop and FORC diagram methods. We have shown that for high pressure gradients, the thermal hysteresis loop becomes asymmetric. Remarkably, the FORC diagram method has been proved to be much more sensitive to local changes than the "bulk" parameters, which characterize the major hysteresis loop. This makes the FORC diagram method a suitable technique to characterize the hydrostaticity degree of a pressure cell. Acknowledgements. This work was partially funded by UEFISCDI, project number PN-III-P1-1.1-TE-2019-2194 (Contract No: TE 123/2020)

[1] A. Bousseksou, et al. *Chem. Soc. Rev.*, 40 (2011) 3313-3335. [2] C.P. Slichter, H.G. Drickamer, *J. Chem. Phys.*, 56 (1972) 2142-2160 [3] E. Konig, et al. *Journal of Chemical Physics*, 83 (1985) 3055-3061 [4] V.

Ksenofontov, et al. Chem. Phys. Lett., 294 (1998) 545-553. [5] A. Rotaru, et al. *Phys. Rev. B*, 83 (2011) 224107. [6] A. Rotaru, et al. *J. Phys. Chem. Lett.*, 8 (2017) 3147-3151. [7] A. Rotaru, *J. Appl. Phys.* 129 (2021) 064501.

AOC-09. Chiral edge conduction induced by large anisotropic exchange interactions. *S. Sayed*[1,2], P. Brahma[1], C. Hsu[1] and S. Salahuddin[1,2] *1. Electrical Engineering and Computer Sciences, University of California, Berkeley, Berkeley, CA, United States; 2. Materials Sciences Division, Lawrence Berkeley National Laboratory, Berkeley, CA, United States*

Recently, 5d and 4d oxides and halides with honeycomb lattice structures are of great interest [1-2] for exhibiting an interplay between an isotropic Heisenberg-type exchange interaction (*J*) and an anisotropic Kitaev-type exchange interaction (*K*), see Fig. 1a. We predict that such an interplay can lead to topological edge states with chiral conduction when the anisotropic interaction is at least twice the strength of the isotropic interaction (i.e. $K \geq 2J$), see Figs. 1b-c. We show that these interactions give rise to new types of antiferromagnetic orders, which determine the chirality of the edge atomic chain. We show calculations for sodium iridate and alpha-ruthenium chloride, both known to exhibit a zigzag antiferromagnetic order at low temperatures, and discuss the chiral edge conduction in the context of the relative strength between *J* and *K*. The edge conduction in the presence of a zigzag antiferromagnetic order will be manifested as a quantized Hall conductance when the number of zigzag atomic chains is odd (see Fig. 1b) since both edges will have the same magnetic orders. On the other hand, the Hall conductance will be zero when the number of zigzag atomic chains is even (see Fig. 1c) since the edges will have opposite magnetic orders. These signatures of the exchange interaction induced chiral edge conductions in odd and even numbers of two-dimensional atomic chains are similar to the well-known signatures of a quantum anomalous Hall insulator and an axion insulator states typically observed in a three-dimensional magnetic topological insulator [3-4], respectively. We further use a widely used model for two-dimensional topological materials to analyze the underlying mechanisms of the predicted phenomena.

[1] Reports on Progress in Physics 80, 016502 (2016). [2] Journal of Physics: Condensed Matter 29, 493002 (2017). [3] Phys. Rev. Lett. 120, 056801 (2018). [4] Science Advances 3, eaao1669 (2017)

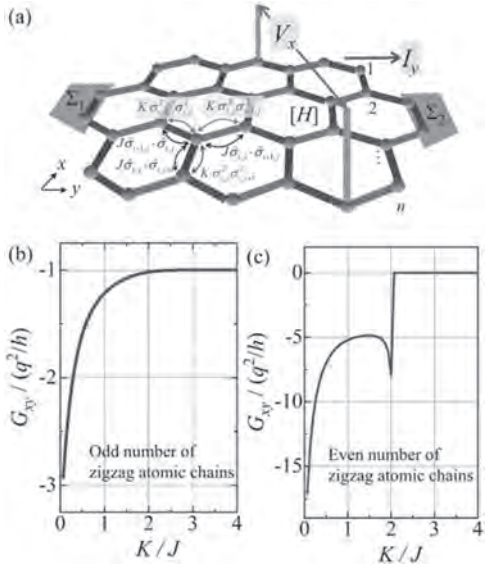

(a) Honeycomb lattice with isotropic (*J*) and anisotropic (*K*) exchange interactions. Hall conductance $G_{xy} = V_x / I_y$ is calculated when the number of zigzag atomic chains is (b) odd and (c) even, as a function of *K* / *J*.

AOC-10. Magneto-Raman study of magnon and spin-orbit exciton in $CoTiO_3$. *T.T. Mai*[1], K. Garrity[2], J.R. Simpson[3], R. Valdes Aguilar[4], K. Ross[5] and A.R. Hight Walker[1] *1. Physical Measurement Laboratory, NIST, Gaithersburg, MD, United States; 2. Material Measurement Laboratory, NIST, Gaithersburg, MD, United States; 3. Physics, Astronomy, and Geosciences, Towson University, Towson, MD, United States; 4. Physics, Ohio State University, Columbus, OH, United States; 5. Physics, Colorado State University, Fort Collins, CO, United States*

CoTiO3 is a semiconductor with a band gap of ~2.25 eV. The Co2+ in edge-sharing octahedra form a stacked honeycomb lattice along the c-axis, with an easy-plane antiferromagnetic ordering below 38 K. The spins in each honeycomb plane, which is perpendicular to the c-axis, are ferromagnetically aligned, while the planes are antiferromagnetically aligned with each other. With a J_eff=1/2 ground state of Co2+ ions in a stacked honeycomb lattice, CoTiO3 has recently been in the spotlight due to its promise of exotic magnetic behavior. Specifically, the magnon spectrum was measured by two different groups via inelastic neutron scattering [1,2]. This spectrum displays a linear crossing at the Dirac point, as well as higher energy spin-orbit excitons, coming from the J=5/2 multiplets. Thus, CoTiO3 is a promising material to explore the properties of topological magnons. We are reporting on our recent work on CoTiO3 using temperature dependent magneto-Raman scattering. First, we follow the evolution of the Brillouin Zone center excitations of not only the optical magnon, but also several spin-orbit excitations across the magnetic transition. Our experiment provides a high-resolution measurement of these magnetic modes at k=0. Second, by applying the external magnetic field along the c-axis and along a hexagonal axis, we revealed the highly anisotropic g-factor of these magnetic excitations. Surprisingly, we measured the beginning of a magnetically induced crossing between the acoustic and optical magnon (see Figure). We use a spin wave model based on previous studied to support our data.

[1] Yuan, B. et al. Dirac Magnons in a Honeycomb Lattice Quantum XY Magnet CoTiO3. Phys. Rev. X 10, 011062 (2020). [2] Elliot, M. et al. Order-by-disorder from bond-dependent exchange and intensity signature of nodal quasiparticles in a honeycomb cobaltate. Nat Commun 12, 3936 (2021).

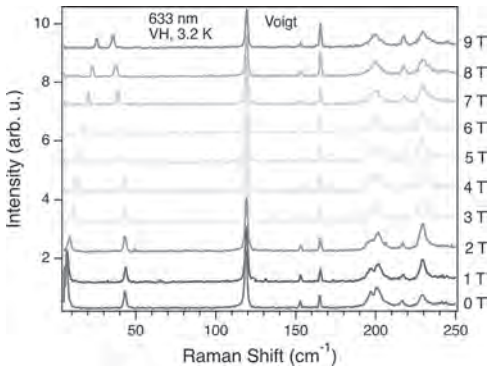

Magnetic field dependent of the Raman spectrum of CoTiO3 in crossed polarizations at 3.2 K, in the antiferromagnetic phase. The two magnon modes at 6 cm-1 and 43 cm-1 can be seen moving closer to each other as the external field, which is perpendicular to the c-axis, goes from 0 to 9 T.

Session APA
FUNDAMENTAL PROPERTIES AND COOPERATIVE PHENOMENA IV
(Poster Session)

Amilcar Bedoya Pinto, Chair
Max Planck Institute of Microstructure Physics, Halle, Germany

APA-01. Quasi-one dimensional magnetism in $Mn_xCo_{1-x}Nb_2O_6$ compounds. *M.L. Hneda*[1,2], J.M. da Cunha[3] and O. Isnard[4,5] *1. Instituto Latino-Americano de Ciências da Vida e da Natureza, Universidade Federal da Integração Latino-Americana, Foz do Iguaçu, Brazil; 2. Instituto de Engenharia, Ciência e Tecnologia, Universidade Federal dos Vales do Jequitinhonha e Mucuri, Janaúba, Brazil; 3. Instituto de Física, Universidade Federal do Rio Grande do Sul, Porto Alegre, Brazil; 4. Institut Néel, CNRS, Grenoble, France; 5. Université Grenoble Alpes, Saint-Martin-d'Hères, France*

The orthorhombic *Pbcn* $Mn_xCo_{1-x}Nb_2O_6$ series of compounds ($0 \le x \le 1$) exhibit the presence of weakly coupled magnetic chains. The cation chains are Heisenberg type (weak anisotropy) for Mn rich side and Ising chains (strong anisotropy) for Co rich side. All samples are investigated by both X-ray and neutron powder diffraction as well as magnetic measurements. Specific heat measurements down to 1.8 K are also presented and discussed in the light of magnetic measurements and compared to neutron diffraction data. In addition, opposite behavior occurs in the extreme compounds since for $MnNb_2O_6$ it is observed a negative Curie-Weiss temperature θ_{CW} indicating dominant antiferromagnetic interactions. On the contrary, $CoNb_2O_6$ shows a positive θ_{CW}, characteristic of dominating ferromagnetism coupling. Mn compound presents a magnetic structure characterized by a propagation vector $k = (0,0,0)$ and Co one by $k = (0,½,0)$ and $(½,±½,0)$. Due to competing interactions between the magnetic ions, different magnetic structures and frustration can be observed. We thus use the substitution of magnetic cations to change the interatomic distances and modify the exchange interactions between the magnetic ions both intra and inter magnetic chains. For Mn rich sample $Mn_{0.8}Co_{0.2}Nb_2O_6$ it is observed an ordered state characterized by $k = (0,0,0)$ propagation vector. Intermediate concentrations samples present short range correlations and analyses from neutron diffuse scattering showed an antiferromagnetic interaction with first neighbors and ferromagnetic with the second ones in the same chain for $Mn_{0.6}Co_{0.4}Nb_2O_6$, and ferromagnetic interaction with first neighbors and ferromagnetic with the second ones for $Mn_{0.4}Co_{0.6}Nb_2O_6$. These results also indicate antiferromagnetic coupling between neighboring chains for both cases.

APA-02. Withdrawn

APA-03. Phase transitions in lightly doped Mott insulators in the presence of magnetic field. *L.B. Dubovskiy*[1] *1. Theoretical Division, NRC "Kurchatov Institute", Moscow, Russian Federation*

It is supposed that high-temperature superconductivity in the cuprates emerges from doped insulators [1]. When extra carriers are inserted into the parent state, the electrons become mobile and the superconductivity appears due to strong correlations in the electron system in the vicinity of the Mott state. The authors of [2] have created (Sr(1-x) La(x))^2 Ir O(4) samples with a range of different lanthanum doping concentrations x, 0<x<6%. This material can be seen as a quasi-two-dimensional electron-doped Mott insulator similar to the cuprates. The authors have investigated how the Mott state reacts when dopant atoms are inserted with various doping concentrations. The pure Mott state is not sustained at doping levels above ~5%. At that point, the authors have discovered an abrupt transition to a strikingly inhomogeneous electronic structure. We considered the above system on the basis of the phenomenological phase transition theory analogous to [3]. We have found that the surface tension between insulating and metal phases in this system is very sensitive to the value of the external magnetic field and moves the value of the critical value doped impurities concentration.

1. B. Keimer, S.A. Kivelson, J. Zaanen et al. Nature 518, 179-186, 2015. 2. I. Battisti, K.M. Bastiaans, M.P. Allan et al. Nature Physics, 13, 21, 2017. 3. L.B. Dubovskii, Physica B 536 469-473, 2018

APA-04. A Circuit Lattice Representation of a Second-Order Dirac Semimetal. S. Rafi-Ul-Islam[1], *H. Sahin*[1,2], Z. Siu[1] and M.B. Jalil[1] *1. Electrical and Computer Engineering, National University of Singapore, Singapore; 2. Institute of High Performance Computing, A*STAR, Singapore, Singapore*

d-dimensional higher-order topological systems (TS) possess boundary states on (*d*−*n*)-dimensional interfaces where $n \ge 2$ [1, 2]. Here, we demonstrate a highly tunable 3-D second-order Dirac semimetal (SODSM) phase on a topolectrical (TE) circuit lattice comprising inductors and capacitors (Fig. 1) [3]. We first construct a 2-D second-order TS on the *x*–*y* plane with four types of sublattice nodes (Fig. 1a). Electrical couplings with negative signs are achieved via a negative impedance converter (NIC) (Fig. 1d). To induce SODSMs, we extend the TE lattice along the *z*-direction by stacking the circuit layers in the *x*–*y* plane via the interlayer capacitor C_z, which modifies the effective intercell hopping and hence the locations of the gapless points. The presence of both inversion and time-reversal symmetries ensures the existence of pairs of gapless points. The admittance band dispersion at resonant frequency hosts a pair of Dirac points (DPs) along the k_z axis under periodic boundary conditions (PBC) along all directions (Fig. 2a). Moreover, two first-order DPs connected by Fermi arc surface edge states emerge under open-boundary conditions (OBC) in the *x*-direction and PBC in the *y* and *z* directions. Interestingly, second-order flat hinge-like states appear in the admittance bandgap and connect the two DPs in the SODSM when PBC is imposed in the *z*-direction and OBC in the *x* and *y* directions (Fig. 2c). Furthermore, the density of states (DOS) vanishes in the vicinity of the DPs. The DPs can be traced via the impedance readout between two terminal nodes. Large impedance peaks exist only near the locations of the DPs, and the impedance falls sharply to nearly zero at other points with finite DOS (Fig. 2d).

[1] S. A. A. Ghorashi, T. Li, and T. L. Hughes, Phys. Rev. Lett.125, 266804 (2020). [2] F. Schindler, A. M. Cook, M. G. Vergniory, et al. Sci. Adv.4, eaat0346 (2018). [3] S. Rafi-Ul-Islam, Z. B. Siu, and M. B. Jalil, Commun. Phys.3, 1 (2020).

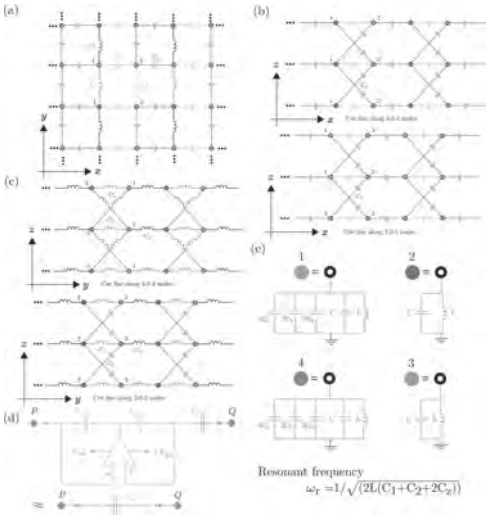

Fig. 1 Schematic of SODSM TE circuit. Cross-section of TE circuit on a. *x-y* plane, b. *x-z* plane, c. *y-z* plane. d. Schematic of NIC using an op-amp. e. Grounding mechanisms.

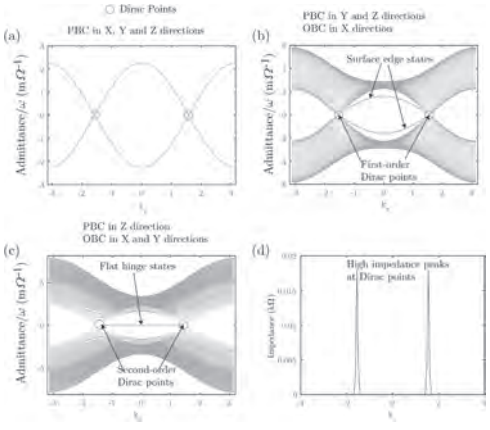

Fig. 2 a. Admittance dispersion under PBC in all directions. b. First-order DPs under PBC in *y* and *z* directions and OBC in the *z*-direction. c. SODSM under PBC in *z*-direction and OBC in the *x* and *y* directions. d. Impedance reading of SODSM.

APA-05. Experimental Study of Emergent Ground State Behaviour in $Gd_{1-x}Ce_xNi_5$ (x=0; 0.2; 0.5; 0.8 and 1) Melt-Spun Ribbons. *A. Dzubinska*[1], J.R. Fernandez[2], M. Reiffers[3], J. Espeso[2], R. Varga[1], K. Arun[4] and J.G. Sal[2] *1. CPM TIP, University of Pavol Jozef Safarik, Kosice, Slovakia; 2. CITIMAC, University of Cantabria, Santander, Spain; 3. Faculty of Humanities and Natural Sciences, Presov University, Presov, Slovakia; 4. Intermetallics and Non-linear Optics Laboratory, Department of Physics, National Institute of Technology, Tiruchirappalli, India*

To see the competition between effect of spin fluctuations, e.g. [1] and magnetic ordering the $Gd_{1-x}Ce_xNi_5$ (x=0; 0.2; 0.5; 0.8 and 1) system in a ribbon form was prepared. The XRD results display with the increase of the Ce content, and the unit cell is expanding. The shoulder obtained from the magnetic susceptibility for $CeNi_5$ measured in zero-field cooling and field cooling mode between T = 100 K and T = 150 K corresponds with a maximum presence in polycrystalline $CeNi_5$ compound [2]. The origin of spin fluctuations is possible explained in several ways. The authors of [3, 4] publications suppose that it is an intrinsic material feature. Moreover, the previous study did not show a low-temperature change [5, 6]. The temperature dependencies of the magnetic properties from the rest of the samples besides $GdNi_5$ have a character typical for antiferromagnetic materials. However, the study of other physical properties does not confirm antiferromagnetic ordering. An effective paramagnetic moment for $CeNi_5$ is 3.52 μ_B/f.u, slightly higher than for free Ce^{3+} ion and for $GdNi_5$ is 7.52 μ_B/f.u. The magnetic properties studies show that only a tiny percentage of Gd creates transition temperature in dopped material. This conclusion is partially supported by a negative value of paramagnetic Curie temperature. The paramagnetic region of the *M(T)* curve under the applied magnetic field fitted with a Curie-Weiss fit. The heat capacity was measured by the 2-τ method in the temperature range from 2 K to 300 K with DC applied magnetic fields from 0 T to 9 T. The obtained results of this method support magnetic measurements analyses. In summary, we will present the preparation, structural, morphological and physical properties analysis of single-phase ribbons of the $Gd_{1-x}Ce_xNi_5$ (x=0; 0.2; 0.5; 0.8 and 1) melt-spun ribbons. The obtained results can bring new knowledge to a group of advanced materials in condensed matter physics. The prepared samples belong to advanced materials and potential magnetic actuators due to their interesting physical properties. *This research work was supported partially by VEGA 1/0404/21; VEGA 1/0705/20; VEGA 1/0053/19, and APVV-16-0079.*

[1] M. Reiffers et al., *J. Magn. Magn. Mat.* 272-276, 605 – 607 (2004) [2] M. Zapotokova et al., *European Physical Journal B*, 86, 4 (2013) [3] S. Nasu, et. al, *J. Phys. Chem. Solids* 52, 2779 – 2783 (1971) [4] J. Tang et al., *J. Alloys and Compounds* 207/208, 241 (1994) [5] O. Musil et al., *J. Phys.* 54, D311 (2004) [6] M. Coldea et al., *J. Magn. Magn. Mat.* 157, 627 (1996)

APA-06. Inducing Fe moment in LaFeSi with p-block elements substitution. *R.K. Chouhan*[1], T. Del Rose[1,2], Y. Mudryk[1] and V. Pecharsky[1,2] *1. Ames Laboratory, Ames, IA, United States; 2. Department of Materials Science and Engineering, Iowa State University, Ames, IA, United States*

Ternary silicide LaFeSi with tetragonal CeFeSi-type structure (space group, P4/nmm) has been known for more than three decades [1-3]. However, the weak Pauli paramagnetic behavior [4] indicating zero Fe moment makes it unusable for any magnetic applications. A recent study [5, 6] has reported two transitions in a $LaFe_2Si$ composite alloy containing two phases, $LaFe_{13-x}Si_x$ (magnetically active) and $LaFeSi_{0.95}$ (magnetically inactive), with a high dTc/dH = 0.85 K/kOe and large positive magnetoresistance near Tc for the first transition while the second transition does not respond to the applied magnetic field. These emergent phenomena cannot be explained by a simple combination of pure $LaFe_{13-x}Si_x$ and LaFeSi phase properties. In order to explore the role that non-magnetic LaFeSi plays in increasing the magnetoresistance and magnetocaloric effect, we studied the LaFeSi phase using density functional theory based full-potential linearized augmented plane wave (FP-LAPW) [7, 8]. Specifically, we examined the effect of p-element substitution on the electronic and magnetic properties focusing on pathways to induce Fe magnetic moments. Surprisingly, we found that the substitution of p-block elements partially or completely at the Si (2c-sites) of the LaFeSi compound leads to non-zero Fe moments. Our theoretical study confirms that the small atomic radii elements "C and Al" are better substitutes compared to the large atomic radii elements "Ga and Ge", and lead to moments 3 – 4 times higher. In addition, this theoretical simulation gives a clear picture to the understanding of the quenched Fe-moments with the LaFeSi phase and will also help in advancing the magnetic functionality of the LaFeSi compound.

[1] O. I. Bodak, E, I. Gladyshevskii and P. I. Kripyakevich, Zh. Struct. Khim., 11, 283 (1970). [2] R. Welter, G. Venturini and B. Malaman, Journal of Alloys and Compounds, 189, 49-58 (1992). [3] M. Noorafshan, Z. Nourbakhsh, Journal of Superconductivity and Novel Magnetism 31 (1), 209-216 (2018). [4] G. Venturini, B. Malaman, M. Meot-Meyer, D. Fruchart, G. Le Caer, D. Malterre and B. Roques, Rev. Chim. Mingr., 23, 162 (1986). [5] A. K. Pathak, Y. Mudryk, N. A. Zarkevich, Dominic H. Ryan, D. D. Johnson, V. K. Pecharsky, Acta Materialia, 215,117083 (2021). [6] D. J. García, V. Vildosola, P. S. Cornaglia, Journal of Physics-Condensed Matter 32(28), 285803 (2020). [7] P. Blaha, K. Schwarz, F. Tran, R. Laskowski, G.K.H. Madsen and L.D. Marks, J. Chem. Phys. 152, 074101 (2020). [8] P. Blaha, K. Schwarz, P. Sorantin, and S. B. Trickey, Comput. Phys. Commun. 59, 399 (1990).

APA-07. Neutron diffraction study of incommensurate magnetism in square-lattice magnet $EuGa_2Al_2$. *E.M. Clements*[1], J.W. Lynn[1], S. Chi[3], J. Moya[2], S. Lei[2], K. Allen[2] and E. Morosan[2] *1. NIST Center for Neutron Research, Gaithersburg, MD, United States; 2. Physics and Astronomy, Rice University, Houston, TX, United States; 3. Neutron Scattering Division, Oak Ridge National Laboratory, Oak Ridge, TN, United States*

$EuGa_2Al_2$ belongs to a class of intermetallic compounds with the $ThCr_2Si_2$-type structure (space group *I4/mmm*) marked by a rich variety of charge- and spin-ordered ground states. [1] The Eu^{2+} local moments (S = 7/2) order antiferromagnetically below the Néel temperature, T_N = 19.5 K, with low magnetic anisotropy, and possible charge density wave ordering along *c* appears below T^* = 51 K. [2] Bulk magnetic susceptibility measurements reveal transitions between three distinct phase regimes on cooling in zero field and metamagnetic transitions bordering a pocket of reduced susceptibility for elevated magnetic fields ($B_{||c} \sim 1$ T). The complex magnetic phase diagram mirrors that of isostructural $GdRu_2Si_2$, where a topological Hall effect was associated with a rare square skyrmion lattice stabilized by higher order spin interactions. [3] Here, we investigate the zero-field magnetic structures of a $EuGa_2Al_2$ single crystal via magnetic neutron diffraction from T_N = 19.5 K down to base temperature of 5 K. Below T_N, magnetic satellites emerge with incommensurate wavevector $q_{inc,1}$ = (~0.2,0,0), revealing a modulated spin structure that propagates along a*. The intensities at 17 K can be modeled by a helix with moments lying in the b-c plane. Near 16 K, we observe a sudden broadening in the magnetic scattering which can be fit with two resolution limited peaks. Here, a new wavevector, $q_{inc,2}$, emerges in a first-order transition yielding a mixed phase regime that persists down to 11 K. In the ground state, satellites at $q_{inc,2}$ can be described by a spin cycloid model that again propagates along a* with moments in the a-c plane. In light of our results, $EuGa_2Al_2$ provides an intriguing platform to explore the interplay of modulated magnetism and charge order in centrosymmetric rare-earth magnets.

1. K. Wang et al., *npj Quantum Mater.* 6, 28 (2021). 2. N. D. Khanh et al., *Nat. Nanotechnol.* 15, 444 (2020). 3. M. Stavinoha et al., *Phys. Rev. B* 97, 195146 (2018).

APA-08. Magnetic Interplay Between Gd and Pr in the CeScSi-type Layered Structure. *T. Del Rose*[1,2], D. Haskel[3], R. Choudhary[1], A. Pathak[4], Y. Mudryk[1], D. Johnson[1,2] and V. Pecharsky[1,2] *1. Ames Lab, U.S. Department of Energy, Ames, IA, United States; 2. Materials Science and Engineering, Iowa State University, Ames, IA, United States; 3. Advanced Photon Source, Argonne National Laboratory, Argonne, IL, United States; 4. Department of Physics, SUNY Buffalo State, Buffalo, NY, United States*

Ternary RScGe intermetallics (R = Rare earth) crystallizing in a layered CeScSi-type structure (space group I4/mmm) demonstrate rich physics and a range of diverse magnetic phenomena. For example, PrScGe exhibits multiple magnetic transitions: paramagnetic (PM) to antiferromagnetic (AFM), then AFM to ferrimagnetic (FIM), and finally FiM-I to FiM-II upon cooling.[1] GdScGe, in contrast, remains ferromagnetic below its Curie temperature (T_C) of 350 K, which is notably higher than the T_C (= 293 K) of its only magnetic constituent, Gd.[2] These RScGe systems become even more interesting with substitutional alloying or additions of interstitials. Thus, $Sm_{1-x}Nd_xScGe$ shows an extraordinary large exchange bias[3] and GdScGeH exhibits a loss of dimensionality and magnetic order.[4] Here, through x-ray magnetic circular dichroism (XMCD) measurements, we report the interplay between Gd and Pr atoms in representatives of pseudo-ternary $Pr_{1-x}Gd_xScGe$. We present direct evidence of antiparallel coupling between heavy and light lanthanide ions that occupy the same sublattice resulting in near zero magnetization. We explain how coupling magnetic compensation with small cooling fields can create magnetic memory – possibly opening up a new avenue for magneto-thermal memory devices. Lastly, we discuss the addition of hydrogen and its effects on dimensionality and electronic structure. This work was supported by the Office of Science of the U.S. Department of Energy (DOE), Division of Materials Sciences and Engineering, Office of Basic Energy Sciences. The Ames Laboratory is operated for the U.S. Department of Energy (DOE) by Iowa State University of Science and Technology under contract No. DE-AC02-07CH11358. XMCD research at the Advanced Photon Source was supported by the U.S. Department of Energy, Office of Science, Office of Basic Energy Science, under contract DE-AC02-06CH11357.

1. Manfrinetti, P., *et al. J. Alloys Compd.* 450, 86–91 (2008). 2. Guillou, F., *et al. J. Phys. Condens. Matter* 29, 485802 (2017). 3. Kulkarni, P. D., *et al. J. Phys. D. Appl. Phys.* 42, 082001 (2009). 4. Mahon, T. *et al. Inorg. Chem.* 57, 14230–14239 (2018).

APA-09. Ferromagnetic Spin Glass State Behaviour in Pr_2AgSi_3. *R. Djoumessi*[1], B. Sahu[1] and A. Strydom[1] *1. Highly Correlated Matter Research Group, Physics Department, University of Johannesburg, Johannesburg, South Africa*

The R_2TX_3 (R = rare-earth, T = transition and X = s and p block element) series of compounds are interesting owing to their fascinating structural and magnetic properties [1-3]. In this present work, we have studied the magnetic properties of the new Pr_2AgSi_3 polycrystalline compound. The sample was synthesized by arc-melting method and confirmed to crystallize in the tetragonal α-$ThSi_2$ structure with space group I4/*amd*. The Pr atoms are arranged on a triangular lattice in this crystal structure. The sample was studied by dc– and ac–magnetic susceptibility and specific heat measurements. A ferromagnetic transition was observed at $T_c \approx 15$ K which is slightly above the spin freezing temperature $T_f \approx 13$ K. The high-temperature dc-magnetic susceptibility exhibit ferromagnetic exchange. The irreversibility observed between zero-field cooled (ZFC) and field cooled (FC) dc-susceptibility data suggests a spin-glass behaviour in the compound. The characteristics of spin-glass behaviour were further confirmed in ac-magnetic susceptibility, aging and memory effect measurements in both ZFC and FC modes. An asymmetric response during heating and cooling of the system is observed in the magnetic relaxation measurement with a positive heating cycle in both ZFC and FC mode. It therefore follows the hierarchical model of spin glass systems. The existence of frustrated moments due to the triangular arrangements of Pr atoms is discussed in terms of the magnetic cluster model observed in Pr_2AgSi_3.

[1] Santanu Pakhira, Chandan Mazumdar and R Ranganathan, Scientific Reports 7, 1 (2017) [2] Santanu Pakhira, Chandan Mazumdar and R Ranganathan, Physical Review B 94, 104414 (2016) [3] D.X. Li, S. Nimori and Y. Shiokawa, Physical Review B 68, 012413 (2003)

APA-10. Anomalous Behaviour in the Seebeck Coefficient of $Cr_{100-z}Os_z$ Alloy System. P.R. Fernando[1,2], A.R. Prinsloo[1] and *C.J. Sheppard*[1] *1. Physics, University of Johannesburg, Johannesburg, South Africa; 2. Eastern University, Vantharumoolai, Sri Lanka*

The magnetic phase diagram (MPD) of the $Cr_{100-z}Os_z$ alloy system exhibits possible quantum critical behavior (QCB), with the commensurate spin-density-wave to paramagnetic (CSDW-PM) phase line terminating at $z \approx 14$ in a superconducting dome emerging at $z \approx 12$ [1]. The co-existence of SDW antiferromagnetism (AFM) and superconductivity (SC) is also reported for the z = 12.2 sample with bcc structure [1]. Considering the unique behavior in the $Cr_{100-z}Os_z$ system [1], the present study reports on the temperature dependence of the thermoelectric power or Seebeck coefficient, $S(T)$, for this system. In general, $S(T)$ is sensitive to changes in the electronic structure as well as to various scattering mechanisms, and can be used to probe the presence of phonon and magnon drag effects [2,3], making it the perfect tool to investigate the magnetic behavior in the mentioned system. $S(T)$ measurements were performed on polycrystalline $Cr_{100-z}Os_z$ ($2.1 \leq z \leq 14.1$) samples prepared using arc-melting techniques. Only primary bcc reflections were observed in the x-ray diffraction results. For a magnetic material the absolute thermoelectric power can be approximated as [4]: $S = S_{pd} + S_{mag} + S_{diff}$, where S_{pd} and S_{mag} is the phonon and magnon drag terms and S_{diff} is due to the diffusion of electrons. The first two terms dominate at low T and the latter at elavated T. The low-temperature thermoelectric power of Cr and

its alloys can be written in the simplified form of [2]: $S = aT + bT^3$, where a and b are constants. Thus, at low T a plot of S/T as a function of T^2 should be linear and can be used to obtain a and b. Resulting plots of $a(z)$ and $b(z)$ show anomalies associated with three crucial points in the $Cr_{100-z}Os_z$ MPD: (i) $z \approx 7$ is associated with the destabilization of the CSDW phase, (ii) $z \approx 12$ where SC manifest and (iii) $z \approx 14$ linked to QCB [1]. Considering dS/dT where T approaches 0 K, $dS/dT\big|_{T\to 0}$, as function of z, anomalies are also observed at $z \approx 12$ and 14, linked to the onset of SC and QCB in this system. Thus, as was previously suggested for selected Cr based alloy systems [5], S can be a decisive parameter that can be utilized in characterizing and understanding the critical behavior reflected in the MPD of $Cr_{100-z}Os_z$.

[1] A.R.E. Prinsloo, C.J. Sheppard, P.R. Fernando, Acta Physica Polonica A, Vol. 131 (4), p.1132, (2016) [2] E. Fawcett, H.L. Alberts, V. Yu. Galkin, D.R. Noakes, and J.V. Yakhmi, Rev. Mod. Phys., Vol. 66(1), p.25, (1994) [3] A.L. Trego and A.R. Mackintosh, Phys. Rev., Vol. 166, p.495 (1968) [4] S. Arajs, E.E. Anderson and K.V. Rao, J. Less-Common Metals, Vol. 26, p.157 (1971) [5] L. Reddy, A.R.E. Prinsloo, C.J. Sheppard, and A.M. Strydom, J. Korn. Phys. Soc, Vol. 63(3), p.756 (2013)

APA-11. Strategies for monopole current control in Artificial Spin Ice Systems. E. Berganza Eguiarte[1], *G. López-Polín*[2] and R.M. Corona[3] *1. Karlsruhe Institute of Technology, Karlsruhe, Germany; 2. Consejo Superior de Investigaciones Científicas, Madrid, Spain; 3. Universidad de Santiago de Chile, Santiago de Chile, Chile*

Artificial Spin Ice systems[1,2] (ASI) constitute materials-by-design where nanometer scale ferromagnetic structures are arranged in close proximity to each other in such a way that their interacting magnetic moments, lead to complex phenomena. As a result of their collective behavior, monopole-antimonopole pairs can be created by thermal activation or through the application of magnetic field. These soliton pairs, which are connected forming dimensional strings of reversed magnetization (see red stripes in the Figure 1), are envisioned to be implemented in devices, analogously to electric currents. However, their application in real devices requires controlling monopole currents which is still challenging.[3] In this work, we are exploring novel methods to achieve control over the propagation of monopole currents, proposing new fabrication methods based on Scanning Probe Lithography and finding new reliable ways to nucleate Dirac strings, which are then assessed by Magnetic Force Microscopy and micromagnetic simulations.

1 R. F. Wang, C. Nisoli, R. S. Freitas, J. Li, W. McConville, B. J. Cooley, M. S. Lund, N. Samarth, C. Leighton, V. H. Crespi, P. Schiffer. Artificial 'spin ice' in a geometrically frustrated lattice of nanoscale ferromagnetic islands. *Nature* 439, 303–306 (2006). 2 S. H. Skjærvø, C. H. Marrows, R. L. Stamps & L. J. Heyderman. Advances in artificial spin ice. *Nat. Rev. Phys*. 2, 13–28 (2020). 3 R. P. Loreto, L. A. Morais, C. I. L. de Araujo, W. A. Moura-Melo, A. R. Pereira, R. C. Silva, F. S. Nascimento, L. A. S. Mól. Emergence and mobility of monopoles in a unidirectional arrangement of magnetic nanoislands. *Nanotech*. 26, 295303 (2015).

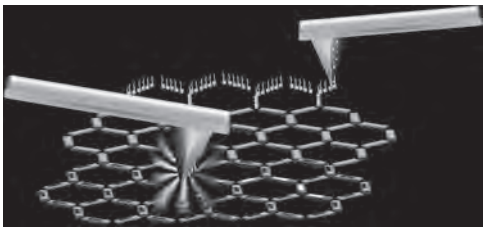

APA-12. Static and dynamic critical behaviour of spin glass transition in ordered h-$DyMnO_3$ system. *P. Singh*[1] and D. Pandey[1] *1. School of Materials Science and Technology, Indian Institute of Technology (Banaras Hindu University), Varanasi, India*

Experimental observation of spin glass transition in chemically ordered compounds is an unconventional phenomenon and a matter of debate as 'disorder' is considered to be the 'main ingredient' for a spin glass transition to occur [1-2]. $DyMnO_3$ is one such chemically ordered and geometrically frustrated system which has gained lots of attention due to its type-I multiferroic behaviour [4]. Recently, this compound has been reported to undergo a reentrant type cluster SG transition at T~6.6 K possibly originating due to magnetoelastic strains generated infinitesimal disorder [4]. However, it needs to be properly established whether this transition is a true equilibrium thermodynamic phase transition like the conventional spin glass transitions in disordered systems or not. To address this problem, scaling of non-linear static and dynamic susceptibilities has been proved to be an efficient method near the critical point. It gives an accurate determination of the critical exponents and thus helps in establishing the universality class of the system [1]. In the present work, we have tested the thermodynamics of the spin-glass transition in ordered h-$DyMnO_3$ system and attempted to establish its universality class using scaling hypothesis. For this, field-cooled DC magnetization data at different magnetic fields and AC susceptibility data at various frequencies were collected using the single crystal sample. Using these, the linear (χ_1) and third order (χ_3) DC magnetic susceptibilities were determined using polynomial fitting. The χ_3 versus temperature plot shows a clear divergence near T_{SG}. Further, we first demonstrate the static and dynamic scaling in both temperature (T) and field (H) for this system. The scaling establishes the reported spin glass transition as an equilibrium thermodynamic phenomenon and also supports the survival of the phase transition in presence of an externally applied field.

[1] K. Binder and A. P. Young, Rev. Mod. Phys. 58, 801 (1986). [2] D. K. Singh and Y. S. Lee, Phys. Rev. Lett. 109, 247201 (2012); M. J. P. Gingras, C.V. Stager, N. P. Raju, B. D. Gaulin, and J. E. Greedan, Phys. Rev. Lett. 78, 947 (1997). [3] Keshav Kumar, et al. Chemical Communications 56(94), 14897 (2020) [4] P. Aravinth Kumar, et al. The Journal of Physical Chemistry C 123.50, 30499 (2019).

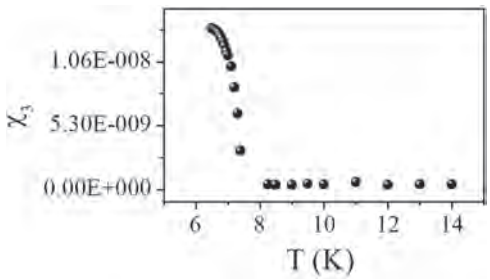

χ_3 versus temperature plot showing divergence near T_{SG}

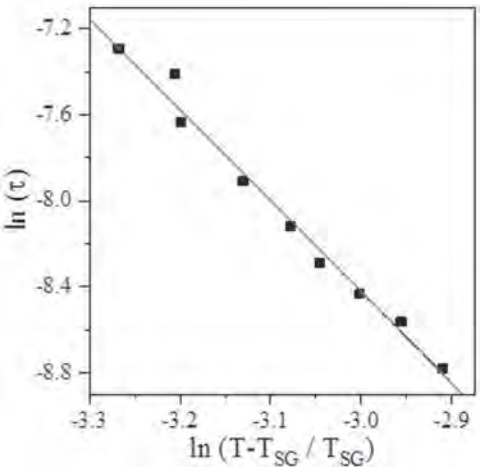

Power law fitting using the AC-χ data

APA-13. Magnetic susceptibility of spin crossover monodisperse particles. *A. Diaconu*[1] *1. Electrical Engineering and Computer Science, "Stefan cel Mare" University of Suceava, Suceava, Romania*

Spin crossover is a phenomenon by which a material can switch between two electronic states, called high spin (HS) and low spin (LS) states, which contain alternate representations of binary information. Accordingly, this spin transition can be explored by various technique: magnetic, dielectric/ electric, optical, spectroscopic, structural, calorimetric, etc. [1]. The two spin states can then be distinguished by their different magnetic, dielectric/ electric, optical, mechanical, spectroscopic and structural properties. We report on the investigation of the magnetic susceptibility of spin crossover (SCO) monodisperse particles. To this date there are no studies involving such structures. Moreover, it was shown that particles under a certain size do not show hysteresis when classical methods are used for testing [2]. This is particularly important for memory applications where nanoparticles are implemented. By constructing planar coils of nanometric scales, monodisperse particles can be arranged by either electrophoresis or direct deposition in between the inductor's windings [3]. By measuring small changes in the inductance, informations about the magnetic suscetibility of nanoparticles can be extracted. We present the temperature and magnetic field dependece of magnetic susceptibility of SCO nanoparticles and the properties of such systems as infered from our results.

G. Molnar. S. Rat, L. Salmon, Adv. Mater., 30,17003862 (2018) A. Rotaru, F. Varret, A. Gindulescu. Eur. Phys. J. B 84: 439 (2011) A. Rotaru, J. Dugay, R.P. Tan, Advanced Materials, 25,1745-1749 (2013)

APA-14. Single crystal growth and low temperature physical properties of triangular lattice antiferromagnet - $Ca_3NiNb_2O_9$. *D. Rout*[1], S. Singh[3,2], M. Jonak[3,4] and R. Klingeler[3,4] *1. Physics, Indian Institute of Science Education and Research Pune, Pune, India; 2. Centre for Energy Science, Indian Institute of Science Education and Research Pune, Pune, India; 3. Physics, Kirchhoff Institute of Physics, Heidelberg, Germany; 4. Centre for Advanced Materials, Kirchhoff Institute of Physics, Heidelberg, Germany*

Single crystals of the triangular lattice Heisenberg antiferromagnet (TLHAF) $Ca_3NiNb_2O_9$ and its non – magnetic analogue $Ca_3MgNb_2O_9$ were grown using the four - mirror optical float zone furnace. Here we have studied the influence of various growth atmospheres and pulling rates on the crystal quality and phase homogeneity. Both the compounds melt congruently and the grown crystal specimens suffer from cracks when the crystal boule is cooled, thus making it difficult to obtain large single crystalline pieces. To overcome this difficulty, an after – heater was used to reduce the formation of cracks. Interestingly, the crystal boule of $Ca_3NiNb_2O_9$ exhibits two regions of distinct colours and optical opacities i.e. opaque black and translucent green. Further, the as - grown, opaque, black specimen was subjected to air annealing at 1200°C for 24hrs, wherein its appearance changed from black to translucent green, without any change of weight. Low temperature specific heat and magnetization measurements carried out on the as - grown black sample (AGO) and the air annealed sample (ANT) revealed contrasting ground state properties. While the as - grown specimen exhibits a broad hump close to 10 K in specific heat measurement, the air annealed sample showcases two transitions at T_{N1} = 4.6 K and T_{N2} = 4.3 K, in agreement with the previous reports by J Ma *et al.*[1]. Moreover, room temperature synchrotron XRD further revealed that AGO specimen crystallizes in a higher symmetry orthorhombic space group while the ANT specimen crystallizes in the reported monoclinic space group. Thus, the ground state of this triangular lattice system is very sensitive to the growth conditions and annealing experiments help recover the properties reported for the polycrystalline sample.

1. Z. Lu, L. Ge and J. Ma, PHYSICAL REVIEW B 98, 094412 (2018) 2. Hwang, J. et al. PhysRevLett.109.257205, 109, 1–5 (2012) 3. Shirata, Y. et al, Journal of the Physical Society of Japan 80, 093702-093702 (2011) 4. M Lee et al.2016 J. Phys.: Condens. Matter 28 476004 (2016) 5. N. A. Fortune, Q. Huang and H. D. Zhou Phys. Rev. B 103, 184425 (2021)

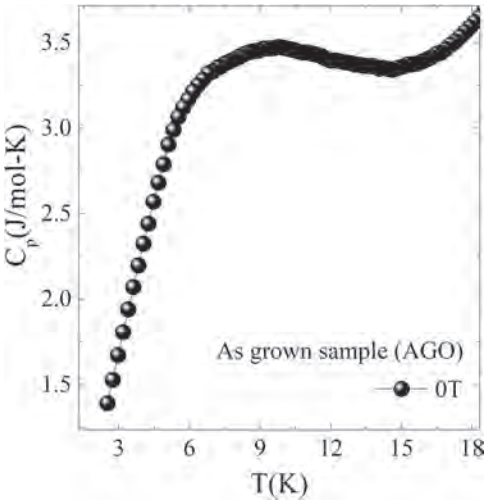

Fig. 1 Temperature variation of specific heat of the as - grown sample (AGO) at zero field exhibiting a broad hump close to 10 K

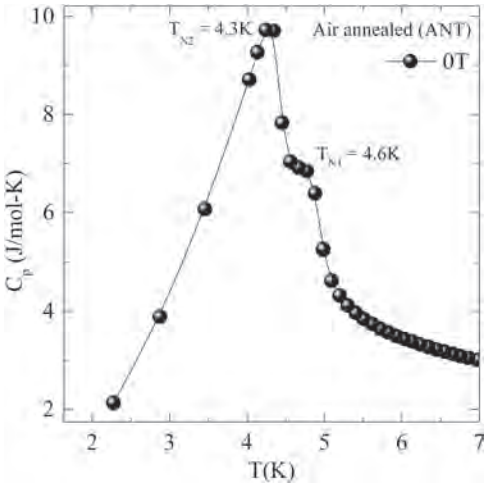

Fig. 2 Temperature variation of specific heat of the air annealed (ANT) sample exhibiting two distinct transitions at T_{N1} = 4.6 K and T_{N2} = 4.3 K

APA-15. Magnetization process of cubic Fe_3O_4 submicron particles studied by small-angle polarized neutron scattering. *E. Nomura*[1], M. Chiba[1], S. Matsuo[1], S. Kobayashi[1], J. Manjanna[2], Y. Kawamura[3], J. Suzuki[3], K. Ohishi[3] and K. Hiroi[4] *1. Iwate Univ., Iwate, Japan; 2. Rani Channamma Univ., Belagavi, India; 3. CROSS, Tokai, Japan; 4. JAEA, Tokai, Japan*

Ferromagnetic particles showing a spin vortex (SV) structure have received considerable attentions for biomedical applications due to their higher efficient heating properties [1] and higher magneto-mechanical effects [2]. Understanding the formation process of the SV structure is extremely important for improving their biomedical performance. In this study, we have performed small-angle polarized neutron scattering (SANS) experiments to understand the SV structure under magnetic fields for cubic Fe_3O_4 submicron particles, where complex SV formation is expected [3]. We conducted SANS experiments at the small and wide-angle neutron scattering instrument TAIKAN in MLF, J-PARC [4] for cubic Fe_3O_4 submicron particles with a side length of 265 ± 34 nm at T = 10 and 300 K. A magnetic field H was applied to the particles perpendicular to the incident neutron beam in the range of -10 kOe to 10 kOe. From the SANS intensities, we obtained $|M_z(q)|^2$ and $|M_x(q)|^2+|M_y(q)|^2$, consisting of the Fourier components of the magnetization [5], where x and z denote directions of the incident neutron beam and the magnetic field, respectively. Figs. 1(a) and 1(b) show the intensity of $|M_z(q)|^2$ and $|M_x(q)|^2+|M_y(q)|^2$ at T = 10 K under several magnetic fields, respectively. The magnetic field dependences of the integrated intensity at T = 10 and 300 K are also shown in the insets of both figures. At T = 10 K, as the magnetic field is reduced from 10 kOe, the intensity of $|M_z(q)|^2$ decreases and takes a minimum value at H ~ -450 Oe, while the intensity of $|M_x(q)|^2+|M_y(q)|^2$ increases and take a maximum value at H ~ -150 Oe. The magnetic field dependence of these intensities can be explained by the SV formation and the gradual tilting of the vortex axis away from the magnetic field direction due to the increase in magnetocrystalline anisotropy energy at low magnetic fields.

[1] N. A. Usov, *et al.*, Scientific Reports, vol. 8, p. 1224 (2018). [2] L. Peixoto *et al.*, Appl. Phys. Rev., vol. 7, p. 011310 (2020). [3] W. William *et al.,* J. GeoPhys. Res., vol. 111, p. B12S13 (2006). [4] S. Takata *et al.*, JPS Conf. Proc., vol. 8, p. 036020 (2015). [5] A. Michels, J. Phys.: Condens. Matter, vol. 26, p. 383201 (2014).

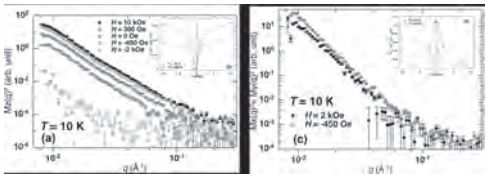

Fig. 1 (a) $|M_z(q)|^2$ and (b) $|M_x(q)|^2+|M_y(q)|^2$ under magnetic fields at T = 10 K. The insets in Figs. (a) and (b) show the magnetic field dependences of the integrated intensities of $|M_z(q)|^2$ and $|M_x(q)|^2+|M_y(q)|^2$ at T = 10 and 300 K, respectively.

Session BOA
MAGNETOELECTRONIC MATERIALS AND PHENOMENA: HEUSLERS AND RELATED MATERIALS

Atsufumi Hirohata, Chair
University of York, York, United Kingdom

CONTRIBUTED PAPERS

BOA-01. Electronic transport and optical properties of Mn_2*Me*Al (*Me* = Ti, V, Cr, Mn, Fe, Co, Ni) Heusler compounds. *A. Semiannikova*[1], Y.A. Perevozchikova[1], E.I. Shreder[1], A.A. Makhnev[1], A.V. Lukoyanov[1,2], E.B. Marchenkova[1], P.S. Korenistov[1], V.Y. Irkhin[1] and V.V. Marchenkov[1,2] *1. M.N. Mikheev Institute of Metal Physics, UB RAS, Ekaterinburg, Russian Federation; 2. Ural Federal University, Ekaterinburg, Russian Federation*

Among the large number of Heusler alloys, a special place is occupied by of half-metallic ferromagnets (HMF) and spin gapless semiconductors (SGS). These materials have the same unique feature for spin down, namely, a gap is observed in the electronic band structure. Therefore, a high degree of charge carriers spin polarization may be reached. Thus, using of these materials is possible in spintronics. However, in the case the opposite spin direction electronic structure has a significant difference. There is no energy gap near the Fermi level current carriers in HMF, whereas the top of the valence band touches the bottom of the conduction band in the point in SGS [1,2]. Since Mn_2*Me*Al Heusler alloys contain 3d-transition metals [3], it is of great interest to follow experimentally the changes when varying *Me*-component in a sequence Ti, V, Cr, Mn, Fe, Co, Ni. The aim was to compare changes in the experimental electronic transport and optical properties with the electronic band structure calculations. The temperature dependences of the electrical resistivity were measured. The dispersion of the real $\varepsilon_1(\omega)$ and imaginary $\varepsilon_2(\omega)$ parts of the dielectric constant were determined, which indicate the mechanisms of intraband acceleration of electrons by the field of a light wave and contribution from the interband absorption, respectively. The calculations of the electronic structure and spin polarization were performed in GGA within the Quantum-Espresso software package [4]. It was found that the energy gap parameters and the current carrier spin polarization vary significantly depending on the number of valence electrons, which is reflected in the change of their electronic and optical characteristics. Some features in the electronic and optical properties allows us to suggest the possible proximity to HMF- and/or SGS-states in the Mn_2*Me*Al system. The work was performed within the framework of the state assignment of the Ministry of Science and High Education of Russia (the themes "Spin", No. AAAA-A18-118020290104-2 and "Electron" No. AAAA-A18-118020190098-5) with partial support from the RFBR (project No.20-32-90065), and the Government of the Russian Federation (Decree No. 211, Contract No. 02.A03.21.0006).

[1] M.I. Katsnelson, V.Yu. Irkhin, L. Chioncel et al., Rev. Mod. Phys., Vol. 80, p. 315 (2008). [2] X. L. Wang, Phys. Rev. Lett. Vol. 100, p. 156404 (2008). [3] T. Graf, C. Felser, and S.S.P. Parkin, Prog. Solid State Chem., Vol. 39, p. 1 (2011) [4] P. Giannozzi, O. Andreussi, T. Brumme et al., J. Phys.: Condens. Matter, Vol. 29, p. 465901 (2017).

BOA-02. Experimental and theoretical investigation of FeCrVAl and related compounds. *P. Kharel*[1], G. Baker[1], M. Flesche[1], L. Stuelke[2], P. Shand[2] and P. Lukashev[2] *1. Physics, South Dakota State University, Brookings, SD, United States; 2. Physics, University of Northern Iowa, Cedar Falls, IA, United States*

Materials exhibiting high degree of spin polarization such as half-metals or spin-gapless semiconductors are in demand for spin-transport-based devices. Especially, half metallic Heusler compounds have attracted much attention because they have tunable magnetic properties and exhibit high Curie temperature much above room temperature. We have synthesized one such predicted half metal, FeCrVAl, using arc melting and annealing. The vacuum annealing was done at 600ºC for 48 hours. In addition, we also studied the effect of Mn substitution on the structural, magnetic, and electronic band properties of FeCrVAl synthesizing samples with compositions $FeCr_{0.5}Mn_{0.5}VAl$ and $FeCrV_{0.5}Mn_{0.5}Al$. The room temperature, x-ray diffraction patterns indicate that FeCrVAl and $FeCrV_{0.5}Mn_{0.5}Al$ are cubic in structure with A2 type disorder, whereas $FeCr_{0.5}Mn_{0.5}Val$ is more ordered as evidenced by the presence of superlattice peaks. All samples show small saturation magnetizations at room temperature and the thermomagnetic curves M(T) are similar to that of a paramagnetic material. However, as shown in Fig.1 below, the M(T) of $FeCr_{0.5}Mn_{0.5}VAl$ is different and shows a slow magnetic transitionat 800 K similar to that of a ferrimagnetic material. In this presentation, we will discuss the structural, magnetic and electron band properties of the synthesized materials and the effect of disorder on the properties of FeCrVAl. This research is supported by the *National Science Foundation* (NSF) under Grant Numbers 2003828 and 2003856 via DMR and EPSCoR.

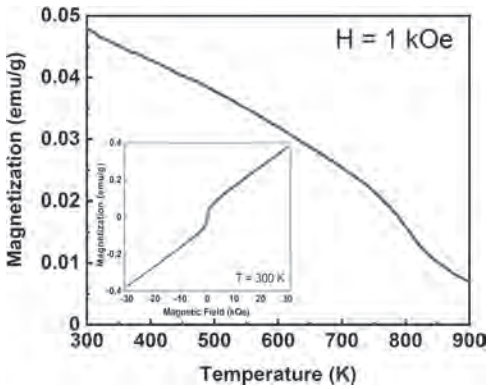

Figure 1: Thermomagnetic curve M(T) of $FeCr_{0.5}Mn_{0.5}VAl$ alloy. The inset shows the M (H) curve recorded at 300 K.

BOA-03. Growth and Electronic Properties of Heusler Alloys Predicted to be Topological Insulator: Toward Spin/Charge Conversion Devices. *V. Palin*[1,2], Y. Fagot-Revurat[1], C. de Melo[1], C. Guillemard[1,2], A. Anadon[1], S. Petit-Watelot[1], J. Rojas-Sanchez[1], P. Le Fèvre[2], F. Bertran[2] and S. Andrieu[1] *1. Institut Jean Lamour, Université de Lorraine, Nancy, France; 2. Synchrotron SOLEIL, Gif-sur-Yvette, France*

Due to their large spin orbit coupling, 3D topological insulators (TI) have been widely studied in the last decade for spinorbitronics related applications. Thanks to their spin momentum locking property [1], they are predicted to generate huge spin-orbit-induced torques on an adjacent ferromagnet which make them suitable for magnetization switching devices. Therefore, their properties should fit perfectly to a new kind of magnetic random access memory (MRAM) using spin-orbit torque switching [2]. A lot of studies done on 3D topological insulators have been made on the Bi based compounds Bi_2Se_3, Bi_2Te_3 and BiSb. However, other kind of

materials were also predicted to possess topological behaviors such as several Heusler compounds [3]. Some encouraging results were obtained on some bulk half-Heusler [4] that should be reproduced in thin films. This study is thus dedicated to PdYBi and PtYBi half-Heusler thin films deposited by molecular beam epitaxy. The $C1_b$ half-Heusler structure was checked by combination of *in situ* electron diffraction (RHEED and LEED), x-ray diffraction (XRD) and high-angle annular dark-field scanning transmission electron microscopy (HAADF-STEM) (Fig. 1). Angle resolved photoemission spectroscopy (ARPES) was also performed to determine their band structure and identify the presence of topological surface states with linear dispersion, the so called Dirac cones (Fig. 2). Finally, we pattern spin torque and spin pumping devices by standard UV-lithography. Transport measurement were thus performed using spin torque ferromagnetic resonance (ST-FMR) [5,6] and spin pumping ferromagnetic resonance (SP-FMR) [7]. The spin to charge interconversion [8] has been measured showing a larger efficiency on TIs than for reference samples made with Pt.

[1] M.Z. Hasan, C.L. Kane, Rev. Mod. Phys., Vol. 82, 3045 (2010) [2] A. Manchon *et al.*, Rev. Mod. Phys, Vol. 91, 035004 (2019) [3] F. Casper *et al*., Semicond. Sci. Technol., Vol. 27, 063001 (2012) [4] Z.K. Liu *et al.*, Nat. Commun., Vol. 7, 12924 (2016) [5] C. Guillemard *et al.*, App. Phys. Lett., Vol. 113, 262404 (2018) [6] D. Céspedes-Berrocal *et al.*, Adv. Mater., Vol. 33, 2007047 (2021) [7] T. Fache *et al.*, Phys. Rev. B, Vol. 102, 064425 (2020) [8] J.C. Rojas-Sánchez, A. Fert, Phys. Rev. Applied, Vol 11, 054049 (2019)

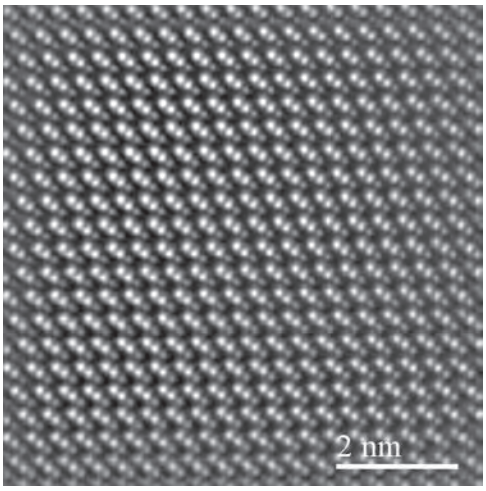

Fig. 1. HAADF-STEM micrograph of the PtYBi layer along the [1-10] zone axis.

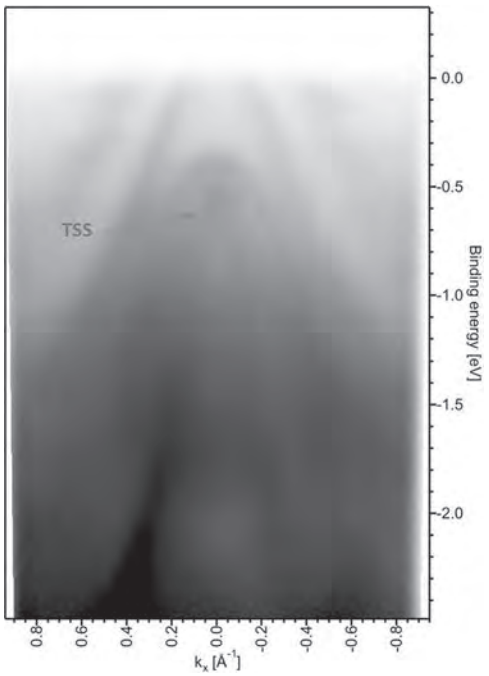

Fig. 2. ARPES spectrum of PtYBi centred at the Γ point of the Brillouin zone. Topological surface state (TSS) identified with [4].

BOA-04. Perpendicular Anisotropy Controlled by Seed and Capping Layers of Heusler Alloy Films. W. Frost[1], M. Samiepour[1] and *A. Hirohata*[1] *1. Department of Electronic Engineering, University of York, York, United Kingdom*

Heusler alloys have been investigated intensively as a potential spin source with 100% spin polarisation at room temperature [1,2]. Theey can be used in magnetoresistive junctions for a next generation read head and a magnetic memory cell [3]. We have recently reduced their crystallisation temperature by growing on the (110) plane [4]. This can be achieved by growing on a body-centred cubic seed layer [5],[6]. In this study, we systematically investigate the effect of seed and capping layers on $Co_2FeAl_{0.5}Si_{0.5}$ (CFAS) Heusler-alloy films. Heusler alloy films were grown on a thermally oxidised Si substrate in the form of Cr (0 and 3)/W (10)/CF(A)S (10)/*X* (5)/Ru (3) (thickness in nm, *X*: W, Ta, V, Ag and Pt) using a high target utilisation sputtering system at room temperature. These films were annealed at 300~350°C for 1~3 hours. The structural and magnetic properties were characterised by X-ray diffraction (XRD) and vibrating sample magnetometry. The magnetisation reversal process was also imaged using magnetic force microscope. Figure 1(a) confirms all films show W crystallisation along the (110) surface orientation, promoting the CFAS crystallisation as confirmed by the CFAS(220) peak. As shown in Fig. 1(b), all CFAS films exhibit perpendicular magnetic anisotropy but with clear deviations under the influence of top-interfaces. The magnetisation curve of the W cap exhibits the highest squareness. In-plane magnetisation measurements also confirm the CFAS/W top interface shows single-step reversal. This means that the sample consisting of a W/CFAS/W trilayer shows the ideal magnetic properties for junction applications. As listed in Fig. 1(d), all films show M_S within the range of 650~850 emu/cm^3, which is almost 30% smaller than the bulk value. This work was partially supported by EPSRC (EP/M02458X/1 and EP/V007211/1) and JST CREST (No. JPMJCR17J5).

[1] C. Felser and A. Hirohata (Eds.), *Heusler Alloys* (Springer, Berlin, Germany, 2016). [2] K. Elphick, W. Frost, M. Samiepour, T. Kubota, K. Takanashi, H. Sukegawa, S. Mitani and A. Hirohata, *Sci. Technol. Adv. Mater.* 22, 235 (2020). [3] A. Hirohata, H. Sukegawa, H. Yanagihara, I. Zutić, T. Seki, S. Mizukami and R. Swaminathan, *IEEE Trans. Magn.* 51, 0800511 (2015). [4] J. Sagar, L. R. Fleet, M. Walsh, L. Lari, E. D. Boyes, O.

Whear, T. Huminiuc, A. Vick and A. Hirohata, *Appl. Phys. Lett.*105, 032401 (2014). [5] W. Frost and A. Hirohata, *IEEE Trans. Magn.* 52, 4400604 (2016). [6] W. Frost and A. Hirohata, *J. Magn. Magn. Mater.* 453, 182 (2018).

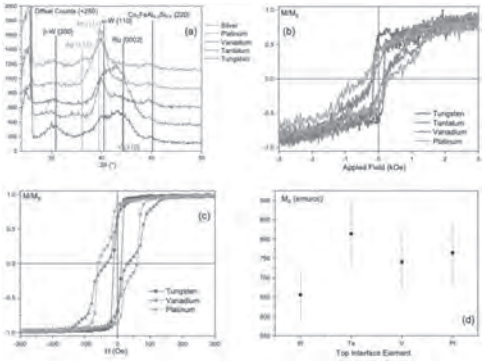

(a) XRD θ-2θ scans and (b) out-of-plane and (c) in-plane magnetisation curves of Si/SiO_2//W (10)/CFAS (10)/*Y* (5)/Ru (3) (thickness in nm, *Y*: W, Ta, V, Ag and Pt). (d) Saturation magnetisation of these films calculated from (c).

BOA-05. Thickness dependent study of magnetization dynamics and transport properties of half-metallic Co_2MnSi Heusler epitaxial thin films. *A. Friedel*[1,2], C. de Melo[1,3], C. Guillemard[1,4], V. Palin[1,4], J. Rojas-Sanchez[1], P. Pirro[2], S. Petit-Watelot[1] and S. Andrieu[1] *1. Institut Jean Lamour, Université de Lorraine, Nancy, France; 2. Fachbereich Physik and Landesforschungszentrum OPTIMAS, Technische Universität Kaiserslautern, Kaiserslautern, Germany; 3. LMOPS EA 4423 Laboratory, CentraleSupélec, Université de Lorraine, Metz, France; 4. Synchrotron SOLEIL-CNRS, L'Orme des Merisiers, Gif-sur-Yvette, France*

Co_2Mn-based Heusler compounds form a family of promising candidates for spintronic and magnonic applications combining desirable properties such as a high saturation magnetization, low Gilbert damping coefficients and high Curie temperatures. By a decent control of the stoichiometry [1], the electronic and magnetic properties of the Heusler compounds can be tuned, especially regarding the spin polarization and the associated Gilbert damping parameter [2]. Epitaxial Co_2MnSi thin films are of particular interest since they have been shown to exhibit half-metal magnetism, i.e. a 100% spin polarization at the Fermi energy [3-5] and an associated ultralow Gilbert damping in the 10^{-4} range [5]. Yet, downscaling towards ultrathin films or microstructures is a critical necessity for applications known to impact the properties of magnetic materials. In this contribution, we report on the magnetisation dynamics and transport properties of epitaxially grown Co_2MnSi thin films [1] with thicknesses in the range of 4-44 nm [6]. Chemical ordering was checked by scanning transmission electron measurements (STEM) as shown in the enclosed figure (Fig.1). The magnetization dynamics were investigated by ferromagnetic resonance measurements, revealing a low Gilbert damping parameter in the 10^{-3}-10^{-4} range for the whole thickness series. Anisotropic magnetoresistance (AMR) measurements confirmed the half-metallicity of the Co_2MnSi thin films (Fig.2). The study of the film resistivity as a function of the film thickness allowed to estimate the electron mean free path in Co_2MnSi. From the evolution of the resistivity with temperature, we extracted the Debye temperature, residual resistivity and the distance between the Fermi energy and the minimum of the minority spin conduction band [6]. These results show the feasibility of transport measurements for the confirmation of half-metallicity in the Co_2MnSi Heusler compound.

[1] C. Guillemard *et al.*, J. Appl. Phys. 128, 241102 (2020) [2] C. Guillemard *et al.*, Adv. Mater. 32, 1908357 (2020) [3] M. Jourdan *et al.*, Nat. Commun. 5, 3974 (2014) [4] C. Guillemard *et al.*, Phys. Rev. Applied 11, 064009 (2019) [5] S. Andrieu *et al.*, Phys. Rev. B 93, 094417 (2016) [6] C. de Melo, C. Guillemard, A. M. Friedel, V. Palin, J. C. Rojas-Sanchez, S. Petit-Watelot, S. Andrieu: *Unveiling transport properties of Co_2MnSi Heusler epitaxial thin films with ultra-low magnetic damping* (under revision)

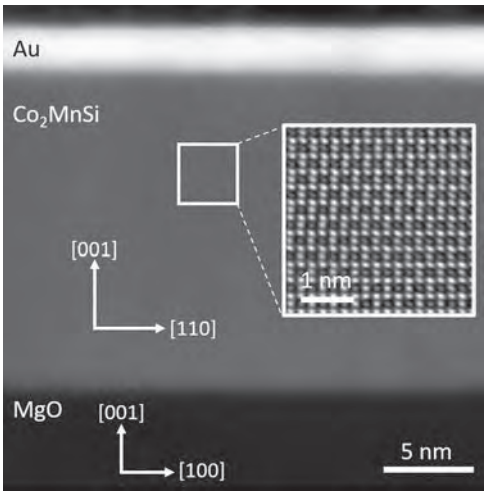

Fig.1: STEM micrograph of the Co_2MnSi film with 17 nm thickness, taken along the [110] axis. The inset shows a filtered STEM-HAADF micrograph that was performed in the region indicated by the yellow frame, where an intensity analysis of the atomic columns revealed $L2_1$ ordering.

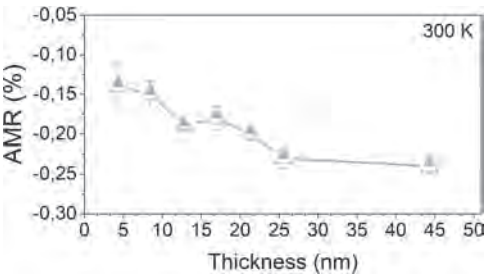

Fig.2: AMR ratio vs. Co_2MnSi film thickness

BOA-06. Weak ferromagnetism and electronic properties of half-metallic Co_2HfSn and Co_2ZrSn Heusler alloys. *P. Tiberto*[1], G. Barrera[1], P. Allia[1], A. Difalco[2], A. Castellero[2], M. Palumbo[2] and M. Baricco[2] *1. Advanced Materials and Life sciences, INRIM, Torino, Italy; 2. Chemistry Dept., Università di Torino, Torino, Italy*

Co-based Heusler alloys are currently exploited in several interesting spintronics applications, such as magnetic electrodes in spin-valve and magnetic tunnel junction devices, due to their half-metallic ferromagnetic properties [1]. Their magnetic and electronic transport behavior at room temperature are intensely studied and tuned to meet several applications demands. In particular, the electronic transport properties display an unusual trend of Seebeck coefficient and electrical conductivity proving the half-metallic ferromagnetic behavior of these compounds [2]. In this work, Co_2HfSn and Co_2ZrSn bulk alloys are synthetized by arc-furnace in which the melt contains pure elements in the appropriate stoichiometric quantities; subsequent, annealing at 800 °C for 6 days is performed to release stress and reach the equilibrium phase. Magnetic properties were investigated in the wide temperature range from 2 to 500 K by SQUID and VSM magnetometers; isothermal hysteresis loops *M(H)* and magnetization as a function of temperature curves *M(T)* have been measured. Magnetic results are in excellent agreement with the mean-field model of itinerant ferromagnetism (Stoner model) in the limit of very weak ferromagnetism. The linear relationship between M^2 and H/M (i.e. Arrott plot) is maintained at all studied temperatures, both well below

and above the Curie temperature (see Fig. 1a). The weak itinerant ferromagnetism model, by means of its temperature-dependent coefficients, is successfully used to determine the Curie temperature resulting at 432 K and 458 K for the Co_2HfSn and Co_2ZrSn alloy, respectively. In addition, the extrapolation of the experimental M(T) curve at T = 0 K reveals a magnetic moment of 2.0 μ_B/f.u. 1.81 μ_B/f.u. for the Co_2HfSn and Co_2ZrSn samples, respectively. Electric and magnetic experimental results are compared with the *ab-initio* calculation, which provides the spin-polarized density of states (DOS) confirming that Co_2HfSn and Co_2ZrSn alloys are half-metallic compounds with a majority-spin channel across the Fermi surface, whereas the minority-spin channel shows a small band gap (see Fig. 1b).

[1] *Spintronics: from Materials to Devices*, C. Felser and H. F. Gerhard eds., Springer (2013). [2] A. Difalco et al., Metals, vol. 10, p. 624 (2020)

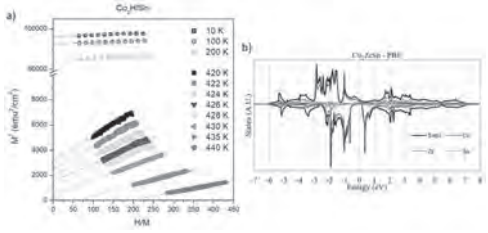

a) Arrott plot for the Co_2HfSn sample; b) DOS by *ab-initio* calculation for the Co_2ZrSn sample

BOA-07. Stabilizing an hexagonal phase of a ternary full Heusler alloy $Fe_2MnSi_{1-x}Ge_x$. B.M. Pimentel[1], V.M. Andrade[2], *V.G. de Paula*[1], K. Pirota[3], F. Beron[3], M. Cardoso[4], J.N. Gonçalves[4], J.S. Amaral[4], A.M. dos Santos[5] and M.S. Reis[1] *1. Institute of Physics, Federal Fluminense University, Niterói, Brazil; 2. IFIMUP - Institute of Physics for Advanced Materials, Nanotechnology and Photonics, University of Porto, Porto, Portugal; 3. 'Gleb Wataghin' Physics Institute, University of Campinas (UNICAMP), Campinas, Brazil; 4. Department of Physics and CICECO, University of Aveiro, Aveiro, Portugal; 5. Neutron Scattering Division, Oak Ridge National Laboratory, Oak Ridge, TN, United States*

Although Heusler alloys are typically found as cubic ($L2_1$) or distorted tetragonal structures, these materials can crystallize in alternative configurations, such as hexagonal (DO_{19}) under some conditions. Understanding the stabilization conditions of these structures is critical for proper design. The competition between cubic and hexagonal full Heusler alloys and the consequences concerning their magnetic properties were systematically studied through a structural and magnetic characterization of the $Fe_2Mn(Si,Ge)$ system. This system was specifically chosen and the parent compositions are cubic (x=0) and hexagonal (x=1). We have found that for x≤0.4, the parent cubic Fe_2MnSi phase accommodates Ge in Si site. This change of occupation sites leads to an increase of the unit cell volume caused by the larger Ge ionic radius (figure 1 top). Interestingly, the cubic phase, both saturation of magnetization (M_S) and Curie temperature (T_C) are insensitive to Ge content (x). For x>0.4, the cubic unit cell exceeds a critical volume of about 11.61 Å^3/atom above which the hexagonal phase forms, reaching 100% of hexagonal for x=1 (figure 1 bot). The change in structure results in high sensitiveness of both the M_S and T_C with x values (figure 2), related to a strong magnetocrystalline anisotropy of the hexagonal phase. Both cubic and hexagonal magnetic features were qualitatively reproduced by Density Functional Theory (DFT) calculations. The hexagonal structure reaches a Tc of 438 K and 5.5 μB/f.u. for x=1, while x=0 shows T_c=220 K and $M_{S=}$ 2.3 μB/f.u. The deformation promoted by Ge in these compounds is necessary to the hexagonal structure stabilization, which, allied with high magnetocrystalline anisotropy, can give rise to novel functionalities.

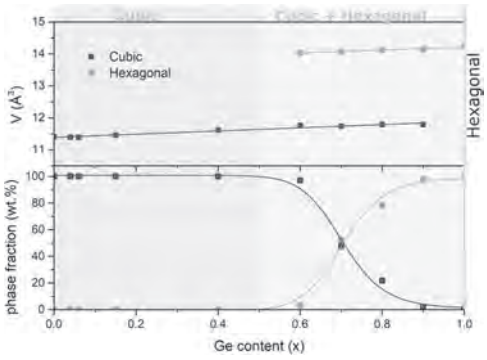

Fig. 1 Dependence of unit cell volume as function of x at top, which shows a linear increase to both phases. The bottom displays the fraction of cubic and hexagonal phases of the samples.

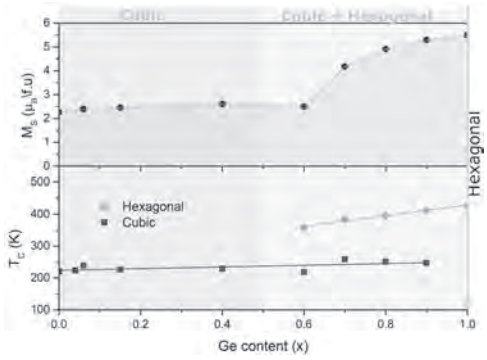

Fig. 2 M_s as function of x at top shows an enhance of 197% due to the changing of structure. The bottom figure shows the dependence of T_C as function of x. It is possible to observe a constant value related to the cubic T_C, while the hexagonal T_C shows a linear increasing with x.

BOA-08. Possible half-metallic and spin-gapless semiconducting behavior in quaternary Heusler compounds $Co_{2-x}Y_xFeGa$ (Y = Ti, V, Cr, Mn, Fe, and Co, x = 0.50). *R. Mahat*[1], K. Shambhu[1], U. Karki[1], S. Regmi[1], J. Law[3], V. Franco[3], I. Galanakis[2], A. Gupta[4] and P. LeClair[1] *1. Physics and Astronomy, University of Alabama, Tuscaloosa, AL, United States; 2. Department of Materials Science, School of Natural Sciences, University of Patras, Patras, Greece; 3. Departmento de Fisica de la Materia Condensada ICMSE-CSIC, Universidad de Sevilla, Sevilla, Spain; 4. Department of Chemistry and Biochemistry, University of Alabama, Tuscaloosa, AL, United States*

Exceptional tunability in the electronic and magnetic properties makes Heusler compounds very promising from both the fundamental and applied perspectives. Half-metallic ferromagnetism, half-metallic fully-compensated ferrimagnetism, spin-gapless semiconducting behavior, and fully-compensated ferrimagnetic spin-gapless semiconducting behavior have been predicted or demonstrated experimentally in Heusler compounds which makes them suitable for applications in a number of novel spintronic devices[1,2,3,4,5]. Half-metallic Co-based Heusler alloys are among the most attractive systems due to their high Curie temperatures, high spin polarization and the structural similarity to binary semiconductors[6,7,8]. Spin-gapless semiconductors can be regarded as a combination of gapless semiconductors and half-metallic ferromagnets where the conducting electrons or holes are not only 100% spin polarized but also easily excited. The realization of spin-gapless semiconducting behavior in Heusler alloys is expected to fulfill the needs for semiconductor spintronics. In this work, we have introduced the substitution of low valence transition metal atoms Y = Ti, V, Cr, Mn, and Fe to Co atoms in the parent Co_2FeGa system, and examined the properties of quaternary Heusler compounds $Co_{2-x}Y_xFeGa$ (x = 0.50), both

experimentally and theoretically to get a global overview of the electronic, magnetic, electron transport and mechanical properties. All single-phase alloys exhibit Heusler like $L2_1$ ordering, as corroborated by X-ray diffraction. The low-temperature saturation magnetic moments agree fairly well with the values expected from a Slater-Pauling rule for half metals (Fig.1). Electrical transport measurements are performed to explain the electronic structure of the alloys. The temperature dependence of electrical resistivity for Mn substituted alloy shows semiconducting nature in the complete temperature regime (5-400)K (Fig.2). *Ab initio* calculations are also performed to understand the experimental findings.

1. R. A. de Groot, F. M. Mueller, P. G. Van Engen and K. H. J. Buschow, *Phys. Rev. Lett.*, 50, 2024–2027 (1983). 2. O. Siham, G. H. Fecher, C. Felser, and J. Kübler, *Phys. Rev. Lett.,* 110, 100401 (2013). 3. S. Wurmehl, H. C. Kandpal, G. H. Fecher and C. Felser, *J. Phys.: Condens. Matter*, 18, 6171–6182 (2006). 4. X. L. Wang, *Phys. Rev. Lett.*, 100, 156404 (2008). 5. Y. J. Zhang, Z. H. Liu, E. K. Liu, G. D. Liu, X. Q. Ma and G. H. Wu, *EPL*, 111, 37009(2015). 6. C. Felser, G. H. Fecher, and B. Balke, Angewandte Chemie International Edition, 46, 668 (2007). 7. I. Galanakis, P. Dederichs and N. Papanikolao, Physical Review B, 66, 174429 (2002). 8. R. Mahat, S.KC, U. Karki, J.Y., Law, V. Franco, I. Galanakis, A. Gupta, and P. LeClair, Physical Review B (2021).

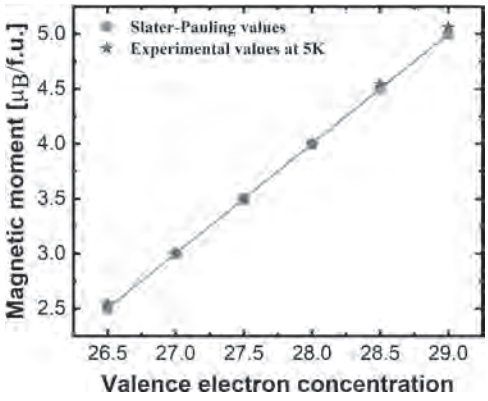

Fig. 1 The variation of saturation magnetic moment with valence electron counts per formula units with element Y.

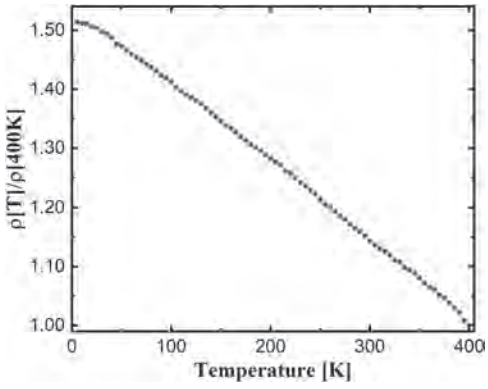

Fig. 2 Temperature dependence of electrical resistivity in $Co_{1.50}Mn_{0.50}$ FeGa at zero magnetic field showing semiconducting behavior.

BOA-09. Withdrawn

BOA-10. High Moment and Curie Temperature in Co_2FeZ Heusler alloys. K. Shambhu[1], R. Mahat[1], J. Law[2], V. Franco[2], W. Butler[1], A. Gupta[3] and *P. LeClair*[1] *1. Physics and Astronomy, The University of Alabama, Tuscaloosa, AL, United States; 2. Departmento de Fisica de la Materia Condensada, Universidad de Sevilla, Sevilla, Spain; 3. Chemistry, The University of Alabama, Tuscaloosa, AL, United States*

Materials with high saturation magnetization (M_S) and high Curie temperature (T_C) are root of many applications such as magnetic recording, magnetic resonance imaging, spintronics, electric motors, and generators[1]. Having a very high M_S and a T_C that is well above the device's operating temperature is helpful in mitigating the thermal induced effects. The transition metal binary alloys such as FeCo[2], FeNi[3] are among the few examples that have been investigated to exhibit very high values of M_S and T_C. Heusler alloys, an intermetallic mixture of transition metals and the main group elements, is another promising family that has promise of possessing high M_S and T_C, with added benefit of high spin polarization, and excellent tunability over the binary alloys. For instance, in Heusler alloys M_S and T_C exhibit a seemingly linear dependence on the total number of valence electrons (N_V), allowing a pathway to tune both M_S and T_C. In this talk, we will discuss how the partial substitution of transition element by a main group element is helpful in enhancing the M_S and T_C values. We will present our experimental finding on the two systems viz. Co_2FeGe and Co_2FeSi – both of which have $N_V = 30$ and the partial substitution as in series $Co_2Fe_{1+x}Z_{1-x}$ (Z = Ge, Si) then increases the N_V leading to enhanced M_S and T_C values, as shown in figure below. The values shown in figure are the highest reported values, to our knowledge among the cubic Heusler alloys. We will also discuss the added benefit of our substitution scheme in stabilizing a single-phase compound without having to add fourth element, especially in case of $Co2Fe_{1+x}Ge_{1-x}$ where the parent Co_2FeGe alloy decomposes into multiple phases[4].

1. G. Scheunert *et al.*, Applied Physics Reviews 3, 011301 (2016). 2. M. T. Kief *et al.*, IEEE Transactions on Magnetics 44, 1 (2008). 3. B. Glaubitz *et al.,* J. Physics: Condens. Matter 23, 254210 (2011). 4. S. KC *et al.*, To be published.

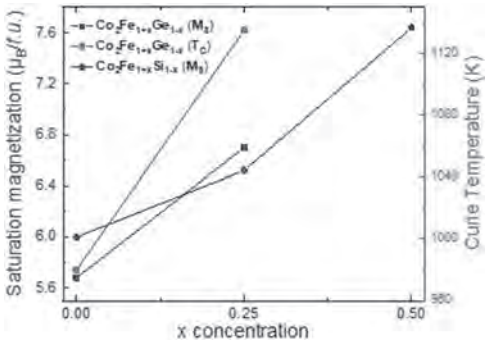

Fig: Enhancement of M_S and T_C as a result of partially substituting main group element (Si or Ge) by Fe in Co_2FeZ (Z = Si, Ge).

BOA-11. Withdrawn

Session BOB
MAGNETOELECTRONIC MATERIALS AND PHENOMENA: 2D AND TOPOLOGICAL MATERIALS

Yu-hang Li, Co-Chair
University of California, Riverside, Riverside, CA, United States
Jiawei Jiang, Co-Chair
Tianjin University, Tianjin, China

CONTRIBUTED PAPERS

BOB-01. Features of the Electronic Properties of Topological Semimetal $PtSn_4$ and WTe_2 Single Crystals. *A. Perevalova*[1], S. Naumov[1], A.A. Makhnev[1], E.I. Shreder[1], S.M. Podgornykh[1], E.B. Marchenkova[1], V. Chistyakov[1], J. Huang[2] and V.V. Marchenkov[1,3] *1. M.N. Mikheev Institute of Metal Physics, UB RAS, Yekaterinburg, Russian Federation; 2. National Cheng Kung University, Tainan, Taiwan; 3. Ural Federal University, Yekaterinburg, Russian Federation*

Topological materials attract a lot of attention due to their unique electronic properties and are considered to be promising for nanoelectronics and spintronics. Relatively recently, Dirac node arc structure in $PtSn_4$ [1] and type-II Weyl semimetal properties in WTe_2 were discovered [2]. At present, there are works devoted to the study of transport and optical properties of these materials. However, the reasons leading to some peculiarities of the electronic properties of $PtSn_4$ and WTe_2 are not always clear, in addition, the results of determining the mean free path l of current carriers in these materials are reported extremely rarely. The purpose of this work is to study the features of electronic properties of $PtSn_4$ and WTe_2, including the estimation of l. $PtSn_4$ and WTe_2 single crystals were grown according techniques described in [3] and [4], respectively. Electrical resistivity, magnetoresistivity and Hall Effect were measured by the four-contact technique in the temperature range from 4.2 K to 300 K in magnetic fields of up to 10 T. Optical properties were measured using a Beattie method. In zero field, temperature dependences of the electrical resistivity $\rho(T)$ of $PtSn_4$ and WTe_2 have a "metallic" type. Whereas the applied magnetic field causes a minimum in the dependence $\rho_{xx}(T)$. One of the possible explanation for the minimum is the transition from high to weak effective magnetic fields [5], which is observed for compensated conductors with a closed Fermi surface. At this minimum, it is assumed that the mean free path l of current carriers is equal to the Larmor radius r_H, that allow us to estimate the value of l in $PtSn_4$ and WTe_2. The concentration of current carriers and their mobility were determined from Hall Effect measurements. Optical characteristics are in good agreement with the data on electronic transport at room temperature. The research was carried out within the state assignment of the Ministry of Education and Science of the Russian Federation (theme "Spin", No. AAAA-A18-118020290104-2), supported in part by RFBR (project No. 20-32-90069) and the Government of Russian Federation (Decree No. 211, Contract No. 02.A03.21.0006).

1. Y. Wu, L.-L. Wang, E. Mun et al., Nat. Phys., Vol. 12, p. 667-671 (2016). 2. C. Wang, Y. Zhang, J. Huang et al., Phys. Rev. B, Vol. 94, p. 241119(R) (2016). 3. E. Mun, H. Ko, G.J. Miller et al., Phys. Rev. B, Vol. 85, p. 035135 (2012). 4. A.N. Domozhirova, S.V. Naumov, S.M. Podgornykh et al., J. Phys.: Conf. Ser., Vol. 1851, p. 012023 (2021). 5. I. M. Lifshitz, M. Ya. Azbel, M. I. Kaganov, Electronic Theory of Metals, Nauka, Moscow, 1971.

BOB-02. Spin Fluctuations in Quantized Transport of Magnetic Topological Insulators. *Y. Li*[1] and R. Cheng[1] *1. UC, Riverside, Riverside, CA, United States*

Quantized electronic transport in magnetic topological insulators is intertwined with spontaneous magnetic ordering, as magnetization controls band topology through the exchange interaction. We show that considering the exchange gaps at the mean-field level is inadequate to predict phase transitions between electronic states of distinct topology. Thermal spin fluctuations that disturb the magnetization can act as frozen disorders, which strongly scatter electrons and thus reduce the onset temperature of quantized transport appreciably even in the absence of structural impurities. This effect, which has hitherto been overlooked, provides an alternative explanation of recent experiments on magnetic topological insulators.

Yu-Hang Li, and Ran Cheng, Phys. Rev. Lett. 126, 026601 (2021)

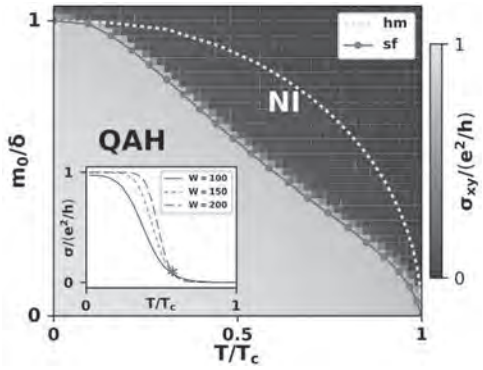

Phase diagram of the two-terminal conductance on the m_0–T plane where m_0 describes the coupling between the top and bottom surfaces of a topological insulator thin film and T is the temperature. The inset illustrates how T_{SF} is obtained from finite-size scaling. The red dots plot T_{SF} and the red curve is a guide to the eye that marks the phase boundary in the presence of spin fluctuations. The dashed lime curve marks T_{hm}, which is the phase boundary in the absence of spin fluctuations. The background color shows the Hall conductance calculated independently for a system of L=W=50, which conforms with T_{SF}.

BOB-03. Sign Reversal and Large Anisotropy in the Magnetoresistance of Oriented Thin Films of $Ag_{2+\delta}Te$. *Z. Hua*[1] and P. Xiong[1] *1. Physics, Florida State University, Tallahassee, FL, United States*

Inorganic chiral crystals have attracted much recent interest for their potential topological quantum properties[1]. In particular, β-Ag_2Te was shown to be a bulk insulator hosting a topological surface state (TSS) of highly anisotropic Dirac dispersion[2]. On the other hand, in chiral materials, an electric current along the helical axis produces a collinear spin polarization; this is known as chirality-induced spin selectivity (CISS)[3]. This raises the intriguing possibility

that Ag_2Te may be a material that simultaneously exhibits TSS and CISS. Here we report on electrical transport measurements on oriented films of nonmagnetic $Ag_{2+\delta}Te$. The films were grown by electron-beam evaporation on quartz, which were shown to be highly textured by XRD. With decreasing temperature, the film resistivity shows semiconducting behavior at high temperatures, and plateaus below ~50 K, consistent with the predominance of a TSS (Fig. 1). The in-plane field magnetoresistance (MR) of the samples exhibits qualitatively different behavior for the longitudinal and transverse configurations. The transverse MR is positive and of a similar magnitude to polycrystalline Ag_2Te samples[4]. In contrast, the longitudinal MR is negative in the semiconducting temperature range, and remains substantial at 300 K. At lower temperatures, the longitudinal MR shows a non-monotonic behavior, with sign reversals for the slope and even magnitude with increasing field (Fig. 2). The unusual MR in the oriented films of $Ag_{2+\delta}Te$ implies two competing mechanisms behind the magnetotransport properties of $Ag_{2+\delta}Te$, possibly reflecting the coexistence of a TSS on the surface and CISS in the bulk. *Work supported by NSF grant DMR-1905843

[1] G. Chang *et al.*, Nature Materials 17, 978 (2018). [2] A. Sulaev *et al.*, AIP Advances 3, 032123 (2013). [3] R. Naaman, *et al.*, Nat. Rev. Chem. 3, 250 (2019). [4] R. Xu *et al.*, Nature 390, 57 (1997).

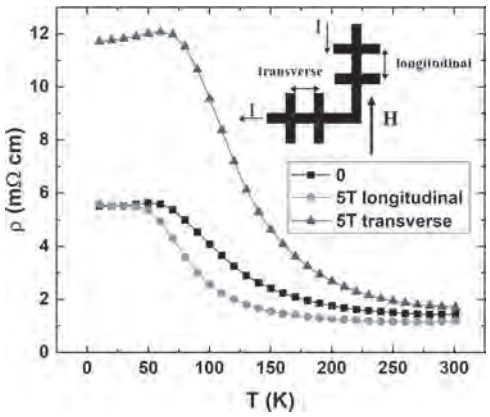

Fig.1 Resistivity as a function of temperature for a $Ag_{2.19}Te$ film (S1) in 0, and 5 T of in-plane magnetic field for longitudinal and transverse configurations.

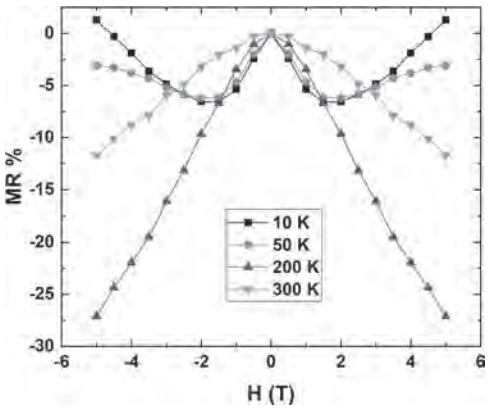

Fig.2 Longitudinal MR at different temperatures for a $Ag_{2.19}Te$ sample (S2).

BOB-04. Ab initio study on the possible magnetic topological semimetallic state in $MnMg_2O_4$. *S. Tomita*[1], D. Yao[2], H. Tsuchiura[1,4] and K. Nomura[3] *1. Department of Applied Physics, Tohoku University, Sendai, Japan; 2. Department of Physics, Tokyo Institute of Technology, Meguro-ku, Tokyo, Japan; 3. Institute for Materials Research, Tohoku University, Sendai, Japan; 4. Center for Spintronics Research Network, Tohoku University, Sendai, Japan*

The search for magnetic topological semimetals has been one of the most intriguing issues in the field of spintronics because they exhibit anomalous transport properties that can be utilized for novel spintronic devices. Quite recently, it was theoretically predicted that an inverse spinel compound VMg_2O_4 is a good magnetic Weyl semimetal [1,2]. The Weyl points are found just above the Fermi energy in the eg-band formed by the 3d-orbitals of the tetravalent V on the diamond lattice. Stimulated by these previous works, here we study the electronic states and transport properties of another spinel compound $MnMg_2O_4$, in which V is totally substituted for Mn with a smaller ionic radius. The significant difference between V and Mn is that, if they maintain the nominal tetravalent configuration, V has one electron in the eg-orbital while Mn also has one hole in the eg-orbital in the low-spin state or one electron in the t_{2g} orbital in the high-spin state. Here we focus on how the topological properties found in VMg_2O_4 can be affected by the orbital symmetry by first-principles calculations using WIEN2k code. The band structure and the density of states of $MnMg_2O_4$ are shown in Figure 1 (a) and (b), respectively. We find that the Fermi energy lies at the t_{2g} band and high-spin state is realized in the 3d electrons of Mn. The resulting band structure is half-metallic with the minority band gap is found to be 3eV. We note that, unlike the eg-band lies around 1eV below the Fermi level, there is no obvious linear crossing in the t_{2g} band. We also compute the intrinsic anomalous Hall conductivity (AHC) within the linear-response theory in the clean limit, and the energy dependence of the AHC is shown in Fig. 2. As expected from the band structure in Fig. 1(a), the AHC is very small at the Fermi energy, shown with black line. We also examine the effects of the compressive strain on the electronic structures and AHC of the systems. Lifting the degeneracy of the t_{2g} band, the Weyl points appears slightly above the Fermi energy, resulting in a large AHC (-144 S/cm).

[1] W. Jiang et al., Phys. Rev. B 101, 121113(R) (2020). [2] H. Zhang et al., Phys. Rev. B 102, 155116 (2020).

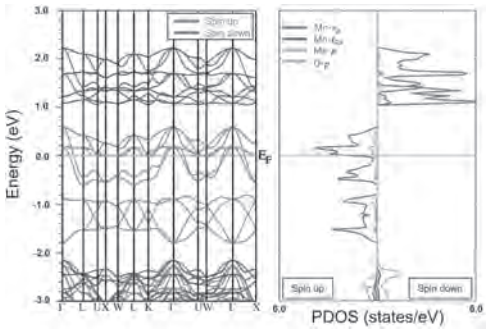

Fig.1 (a) The band structure and (b) the density of states of $MnMg_2O_4$.

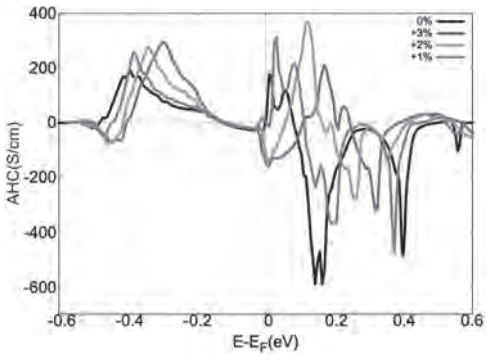

Fig.2 The energy dependences of the anomalous Hall conductivity with several compressive strains.

BOB-05. Threshold behaviors of direct and Hall currents in topological spin-Hall effect. *A. Zadorozhnyi*[1] and Y. Dahnovsky[1] *1. Physics and Astronomy, University of Wyoming, Laramie, WY, United States*

We study spin-dependent direct and Hall conductivities in the threshold region of Fermi energy, $\varepsilon_F = 2J$, where J is the exchange integral between the conduction electron spins and the skyrmion spin texture. For ε_F at the threshold value and above the spin-down electrons are allowed to exist (sse Fig. 1). We find the two in the direct and four narrow peaks in the Hall conductivities for Fermi energies slightly below the threshold value. The found effects are dramatic because the electric current changes by approximately eight times in the narrow range of gate voltages (4 me). The values of the peaks strongly depend on skyrmion size. For small and very large skyrmion sizes the peak amplitudes are small compared to the conductivity absolute values. At the skyrmion radius *a=6 nm* and very light conduction electrons, $m^* = 10^{-2}m_e$, the extrema are the most pronounced (see Fig. 2). The temperature evolution reveals the strong smearing effect where the peak-wise behavior completely disappears at room temperatures. Spin transistor could be considered for possible applications where in the narrow region of gate voltage the sharp conductivity change occurs.

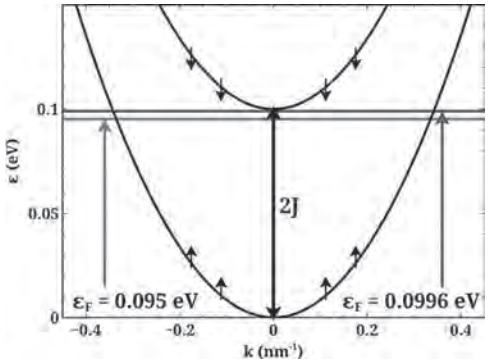

Fig. 1. Band structure for the spin-up (lower) and spin-down (upper) electrons. The splitting between the bands is equal to *2J*. The positions of ε_F are shown by blue and red lines

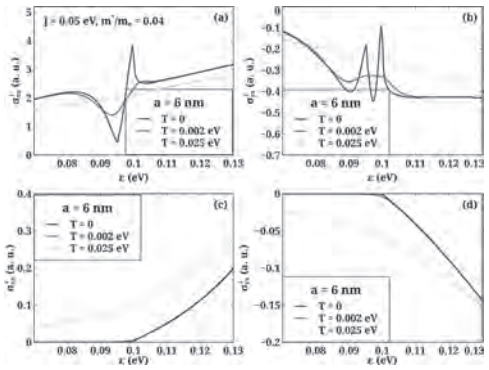

Fig. 2. Direct ((a) and (c)) and Hall ((b) and (d)) conductivities for spin-up ((a) and (b)) and spin-down ((c) and (d)) components for the various temperatures, $k_BT = 0$ eV (the blue line), $k_BT = 0.002$ eV (the red line), and $k_BT = 0.025$ eV (the green line) with respect to ε_F for the skyrmion size a=6.0 nm.

BOB-06. Charge Carrier Mass Discrepancy in $In_{1-x}Mn_xAs/GaSb$ Quantum Wells by Shubnikov de Haas Oscillations and Cyclotron Resonance. *L. Riney*[1], X. Liu[1], J. Ortiz[4], R. Winkler[2,3], S. Bac[1], J. Wang[1], L. DeVaulchier[4], Y. Guldner[4], T. Orlova[5], M. Zhukovskyi[5], M. Dobrowolska[1], J.K. Furdyna[1] and B. Assaf[1] *1. University of Notre Dame, Notre Dame, IN, United States; 2. Northern Illinois University, DeKalb, IL, United States; 3. Materials Science Division, Argonne National Laboratory, Argonne, IL, United States; 4. Laboratoire de Physique, Ecole Normale Supérieure, Paris, France; 5. Notre Dame Integrated Imaging Facility, University of Notre Dame, Notre Dame, IN, United States*

At the interface of InAs/GaSb, the broken gap alignment leads to an anti-crossing between the InAs s-like conduction levels and the GaSb p-like valence levels. The hybridization of these levels cause a topological gap to open. The observation of the quantum anomalous Hall effect (QAHE) is expected to occur if the s-p ordering is inverted (non-trivial) for one spin species and trivial for the other, which can be achieved through the introduction of magnetism into system. In this work, we characterize a series of Mn doped InAs/GaSb type-II quantum wells using fields up to 16T for magneto-transport and magneto-optics. We report an n to p type transition with increasing Mn concentration, as well as, robust quantum oscillations from 1.5K to 70K. We also find a discrepancy between the charge carrier mass calculated from SdH oscillations and cyclotron resonance. Upon observing the manifestation of paramagnetic ordering in this system, we hypothesize that it's an ideal platform for measuring the magnetic exchange interaction which is a crucial step to realizing the quantum anomalous Hall effect. We would like to acknowledge NSF-DMR-1905277 for supporting this research

BOB-07. Electric-Field Switching of Dzyaloshinskii-Moriya Interaction and Skyrmionic Chirality in Two-Dimensional Multiferroics. *J. Jiang*[1] and W. Mi[1] *1. Department of Applied Physics, Tianjin University, Tianjin, China*

Realizing topological spin textures and its electric control are widely attractive for their promising applications in information and communications technology [1-3]. Using first-principles calculations, we show that a strong Dzyaloshinskii-Moriya interaction (DMI) can be induced in two-dimensional (2D) magnetoelectric multiferroics with vertical electric polarization. Atomistic spin simulations verify that such a significant DMI can promote the stabilization of skyrmions in 2D multiferroics. Moreover, the presence of electric polarization in 2D multiferroics provides the unique opportunity for the electric control of DMI chirality and thereby the topological magnetism. Our results provide a promising route toward the highly desired electric field control of topological magnetism. This work was supported by the National Natural Science Foundation of China (51871161 and 52071233).

[1] A. Fert, N. Reyren, and V. Cros, Magnetic skyrmions: advances in physics and potential applications. Nat. Rev. Mater. 2, 17031 (2017). [2] L. Wang, Q. Feng, Y. Kim, R. Kim, K. H. Lee, S. D. Pollard, Y. J. Shin, H. Zhou, W. Peng, D. Lee, W. Meng, H. Yang, J. H. Han, M. Kim, Q. Lu, and T. W. Noh, Ferroelectrically tunable magnetic skyrmions in ultrathin oxide heterostructures. Nat. Mater. 17, 1087 (2018). [3] C. Xu, P. Chen, H. Tan, Y. Yang, H. Xiang, and L. Bellaiche, Electric-field switching of magnetic topological charge in type-I multiferroics. Phys. Rev. Lett. 125, 037203 (2020).

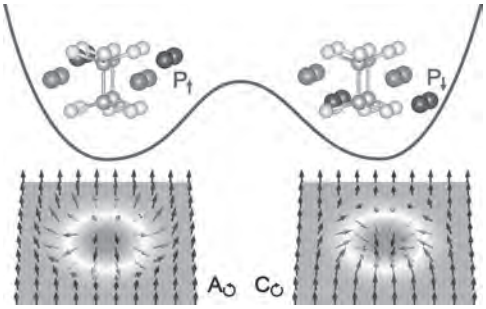

Fig. 1. Reversible chirality of skyrmion in 2D magnetoelectric multiferroics

BOB-08. Structural and Electronic Properties of Mn Implanted MoS_2.
H. Bana[1], P. Lin[1], R. Villarreal[1], Z. Zarkua[1], M. Auge[2], H. Hofsäss[2], A. Tajeda[3], G. Di Santo[4], L. Petaccia[4], E. Tosi[4], P. Lacovig[4], S. Lizzit[4], M. Nissen[5], I. Baev[5], M. Martins[5], F. Tumino[6], A. Li Bassi[6] and *L.M. Pereira[1] 1. Quantum Solid-State Physics, KU Leuven, Heverlee, Belgium; 2. Institute of Physics, University of Göttingen, Göttingen, Germany; 3. Laboratoire de Physique des Solides, CNRS, Univ. Paris-Sud, Orsay, France; 4. Elettra Sincrotrone Trieste, Trieste, Italy; 5. Universität Hamburg, Institut für Experimentalphysik, Hamburg, Germany; 6. Department of Energy, Politecnico di Milano, Milan, Italy*

2-dimensional molybdenum disulfide (MoS_2) is an intrinsically non-magnetic semiconductor. Introducing and controlling magnetism is critical in order to explore MoS_2 in spintronic and quantum technologies [1]. Various transition metal dopants have been predicted to induce robust ferromagnetic coupling [2] in MoS_2, with Mn and V identified as the most promising candidates [1,2]. Various approaches to magnetically dope MoS_2 have arguably been limited in terms of reproducibility, scalability and control over the doping process (dopant concentration and incorporation configuration). Here, we present an in-depth study of the effects of Mn doping using ultra-low energy (ULE) ion implantation [3] on the structural and electronic properties of single-layer MoS_2 (supported on Au(111)[4]). Our ULE implantation approach allows precise tuning of the kinetic energy of Mn ions, providing control over the form of incorporation and concentration while preserving the structural and electronic properties. Samples spanning different implantation parameters (fluence, energy and temperature) were studied via synchrotron-based X-ray photoelectron spectroscopy (XPS), angle-resolved photoelectron spectroscopy, X-ray absorption near edge spectroscopy and Raman spectroscopy. Mn implantation results in an increase in surface defects, however, the electronic structure of MoS_2 is preserved. A significant fraction of the implanted Mn atoms pass through (rather than being incorporated in the MoS_2 layer) and get trapped at the MoS_2-Au interface thus modifying the charge transfer from Au to MoS_2 and resulting in Fermi-level unpinning. This work forms the basis for further studies on the magnetic and spintronic properties of magnetically doped MoS_2.

[1] X.-L. Fan, Y.-R. An, and W.-J. Guo, Nanoscale Research Letters, 11(1), 12 (2016) [2] A. Ramasubramaniam and D. Naveh, Physical Review B, 87, 195201 (2013) [3] P.-C. Lin, R. Villarreal, and H. Bana, ACS Nano, 15, 5449 (2021) [4] F. Tumino, C.S. Casari, and M. Passoni, Nanoscale Advances, 1, 643 (2019)

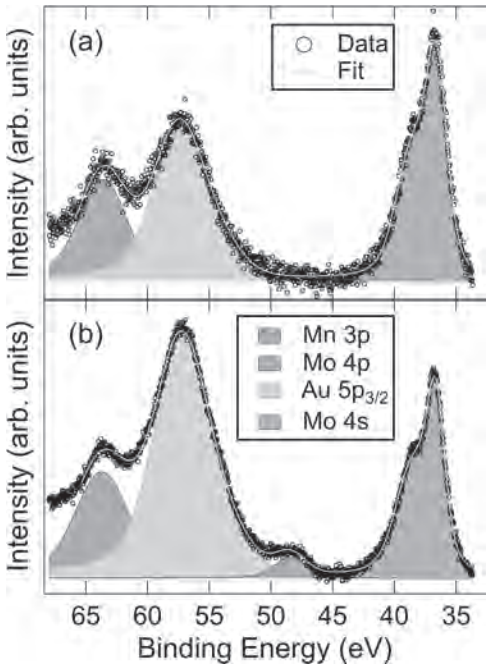

Fig. 1 High-resolution XPS measurement performed at 400 eV photon energy along with the resulting fit (line) and the deconvoluted components (solid areas) for (a) pristine MoS_2 and (b) ULE Mn implanted MoS_2 showing the Mn 3p core level.

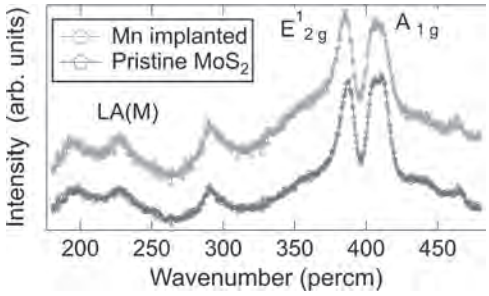

Fig. 2 Raman spectra (shifted vertically) acquired for pristine and Mn implanted single-layer MoS_2 acquired using 532 nm excitation laser showing an increase in the intensity of LA(M) defect-induced peak as a result of Mn ULE implantation.

BOB-09. $ZrTe_2/CrTe_2$: an epitaxial van der Waals platform for spintronics.
Y. Ou[1], W. Yanez[1], R. Xiao[1], M. Stanley[1], S. Ghosh[2], B. Zheng[1], Y. Huang[1], T. Pillsbury[1], A. Richardella[1], C. Liu[1], V. Crespi[1], K. Mkhoyan[2] and N. Samarth[1] *1. Physics, The Pennsylvania State University, State College, PA, United States; 2. Chemical Engineering and Materials Science, University of Minnesota, Minneapolis, MN, United States*

The rapid discovery of two-dimensional (2D) van der Waals (vdW) quantum materials has led to heterostructures that integrate diverse quantum functionalities such as topological phases, magnetism, and superconductivity. While much of the attention in this context has been centered on the heterogeneous stacking of exfoliated flakes, the epitaxial synthesis of vdW heterostructures with well-controlled interfaces is developing as an attractive route towards wafer-scale platforms for systematically exploring fundamental properties and fashioning proof-of-concept devices. Here, we use molecular beam epitaxy (MBE) to synthesize a vdW heterostructure that interfaces two material systems of contemporary interest: a 2D ferromagnet (1T-$CrTe_2$) and a topological semimetal ($ZrTe_2$).[1] We characterize the crystal structure and stoichiometry of our MBE-grown thin

films via scanning transmission electron microscopy, x-ray diffraction, and x-ray photoelectron spectroscopy. We also carry out *in-vacuo* angle-resolved photoemission spectroscopy to determine the band structure of the 1T-$CrTe_2$ films and find good agreement with first-principles band structure calculations. Temperature-dependent anomalous Hall measurements reveal that robust ferromagnetic order persists in the true 2D limit of one unit-cell (u.c.) thick 1T-$CrTe_2$ grown epitaxially on $ZrTe_2$. In thicker samples (12 u.c. thick $CrTe_2$), the anomalous Hall effect exhibits a magnetic field dependence that may arise from real-space Berry curvature. Finally, in ultrathin $CrTe_2$ (3 u.c. thickness), we demonstrate current-driven magnetization switching in a full vdW topological semimetal/2D ferromagnet heterostructure device. This work was supported by NSF Grant Nos. DMR-1539916, DMR-2011401, ECCS-2025124, DOE EFRC grant DE-SC0019331, and SMART, one of seven centers of nCORE, a Semiconductor Research Corporation program, sponsored by NIST.

1. Y. Ou *et al.*, arXiv : 2107.08599

BOB-10. Room-temperature Ferromagnetism in 0D/2D Hybrid Systems. *N.A. Kapuruge*[1], T. Alba[1], K. Lasek[1], F. Nugera[1], V.O. Jimenez[1], M. Phan[1] and H. Gutierrez[1] *1. Physics, University of South Florida, Tampa, FL, United States*

In recent years, spintronics has gained increasing interest due the possibility of storing and processing information through the manipulation of both the charge and the spin of electrons. Dilute magnetic semiconductors are ideal for fabrication of such spintronic devices as they display a carrier mediated ferromagnetism which allows the electronic control of magnetism. In this work, we propose a materials system composed of 2D TMD materials, particularly $MoSe_2$; decorated with nanoparticles containing magnetic elements such as oxides of Mn, V and Fe. The 2D materials were synthesized by chemical vapor deposition (CVD) and the nanoparticles were deposited in a thermal evaporator under a high vacuum. Micro-Raman and PL spectroscopy were used to study their optical properties; while the morphology, and thickness of the samples were characterized via SEM, and AFM, respectively. Magnetic measurements performed on $MoSe_2$ films, without the nanoparticles, reveal a weak ferromagnetic response probably arising from the presence of selenium vacancies. Similarly, weak ferromagnetism is observed for the nanoparticles deposited directly on a SiO_2 substrate, without the TMD films. However, when the nanoparticles are deposited on 2D $MoSe_2$, the hybrid nanoparticle/$MoSe_2$ system displays enhanced room-temperature ferromagnetism, suggesting a strong magnetic exchange coupling between the two material components. Temperature dependent measurements of saturation magnetization and coercive field indicates stronger magnetic coupling at lower temperatures. A Raman red shift was observed on $MoSe_2$ films after depositing the nanoparticles. The PL peak also red shifts and develops an asymmetric tail toward lower energies as the thickness of the nanoparticles film is increased. Here we discuss the possible origin of these changes in the Raman and PL spectra of $MoSe_2$, for instance, electronic doping and/or strain. The 0D/2D hybrid system proposed here, provide an alternative route to induce room-temperature ferromagnetism in 2D materials, which could impact the future development of a new generation of spintronic devices.

BOB-11. Electronic, magnetic, and structural properties of Ni/MoS_2 and Ni/WSe_2 interfaces. *T.E. Kidd*[1], A. Stollenwerk[1], C. Gorgen[1], L. Stuelke[1], Y. Moua[1], P. Shand[1] and P. Lukashev[1] *1. Physics, University of Northern Iowa, Cedar Falls, IA, United States*

The transition metal dichalcogenides are a class of layered materials with a van der Waals terminated surface that provides novel bonding characteristics for the preparation of nanometer scale metallic films. Furthermore, in single layer form, systems such as MoS_2 act as a semiconducting analog to graphene, making it of interest to understand the formation of metal contacts on MoS_2 for developing optoelectronic and spintronic device structures. We have investigated the electronic, magnetic, and structural properties of the Ni/MoS_2 and Ni/WSe_2 interfaces for nanometer scale films using a combination of scanning probe microscopy and density functional calculations. Our experiments show that Ni grows in a very different manner than other FCC metals like Au, Ag, and Pd. Despite a very large lattice mismatch, these three metals form quantized nanostructures with atomically flat surfaces. Nanometer scale Ni films show no signs of such quantized features, instead forming grains as might be expected for metallic growth on an inert system with poor lattice matching. The difference in growth patterns arises from a significantly larger bonding energy at the Ni/dichalcogenide interface. While the enhanced bonding also increases the impact of strain on film growth, it also leads to stronger hybridization between the Ni and dichalcogenide molecules. According to our calculations, this induces spin-polarized metallic behavior in the uppermost molecular layer of the otherwise semiconducting dichalcognide substrate. This confinement to the uppermost molecular layer creates an atomically abrupt magnetic interface within the dichalcogenide substrate. At the same time, the electronic and magnetic properties of Ni are nearly unaffected by the presence of WSe_2 and MoS_2, except a small reduction of magnetic moment at the interfacial Ni atoms. This research is supported by Grant No. DE-SC0020334 funded by the U.S. Department of Energy, Office of Science.

BOB-12. Magnetization evolution in room-temperature van der Waals magnet $CrTe_2$. C. Tang[1], Q. Lu[2], L. Alahmed[1], *M. Mahdi*[1], A. Shah[1], V. Gupta[1], R. Cheng[8], N. Rush[1], S. Ambhire[3], P. Khanal[6], Y. Xiong[7], T. Liu[4,9], P. Li[1], S. Urazhdin[5], W. Wang[6], W. Zhang[7], M. Hamilton[1], S. Zhang[3] and G. Bian[2] *1. Electrical and Computer Engineering, Auburn University, Auburn, AL, United States; 2. Physics and Astronomy, University of Missouri, Columbia, MO, United States; 3. Physics, Case Western Reserve University, Cleveland, OH, United States; 4. Materials Science & Engineering, University of California, Los Angeles, Los Angeles, CA, United States; 5. Physics, Emory University, Atlanta, GA, United States; 6. Physics, University of Arizona, Tucson, AZ, United States; 7. Physics, Oakland University, Rochester, MI, United States; 8. Electrical and Computer Engineering, University of California, Riverside, Riverside, CA, United States; 9. Physics, Florida State Unversity, Tallahassee, FL, United States*

Magnetic two-dimensional (2D) van der Waals (vdW) materials show promising magnetic properties, which can be utilized to build spintronic devices with improved performance and new functionalities. However, most vdW magnets have Curie temperatures below 300 K. With molecular beam epitaxy (MBE) [1], we recently synthesized 1T-phase single-crystal $CrTe_2$ thin films [2], which show ferromagnetism and strong perpendicular magnetic anisotropy at room temperature. We have also studied the magnetic domain evolutions and the anomalous Hall effect (AHE) in these samples at different temperatures and magnetic fields. As shown in Fig. 1, MFM has revealed clear magnetic stripe domains with out-of-plane polarization in the 16 ML $CrTe_2$ film at room temperature. The magnetic stripe domains still exist upon applying an out-of-plane magnetic field, but the width becomes narrower at +1.2 kOe and wider at -1.2 kOe, respectively. We have patterned the samples into Hall bars and measured electron transport properties at different temperatures. Both the 8 ML and 16 ML $CrTe_2$ films show AHE up to room temperature. However, the AHE changes sign between 100 K and 150 K. This indicates intriguing magnetic domain evolution at lower temperatures. Further work has been carried out toward a deeper understanding of the magnetization in $CrTe_2$. Our study has highlighted $CrTe_2$ as a unique platform for studying vdW magnetism and opened a new avenue for developing large-scale 2D magnet-based spintronics devices.

[1] Zhang X, Lu Q, Liu W, Nature communications, 12(1), p. 1-9 (2021) [2] Meng L, Zhou Z, Xu M, Nature communications, 12(1): p. 1-8 (2021)

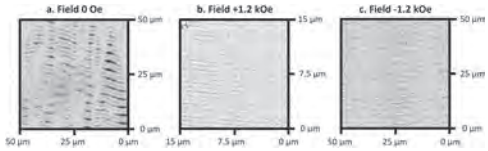

Fig.1: MFM images showing stripe domains for the 16 ML $CrTe_2$ at H = 0 (a), +1.2 kOe (b) and -1.2 kOe (c), respectively.

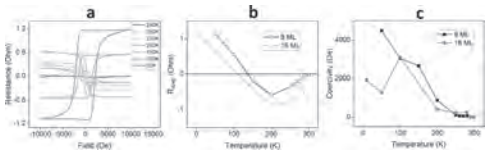

Fig.2: a. Anomalous Hall resistance vs. H at different temperatures for 8 ML $CrTe_2$. b, c. Dependence of anomalous hall resistance (R_{AHE}) (b) and coercivity (c) vs. temperature for 8 ML and 16 ML $CrTe_2$.

BOB-13. Large-Scale Epitaxy of the van der Waals Room Temperature Ferromagnet Fe_5GeTe_2. M. Ribeiro[1], G. Gentile[1], A. Marty[1], D. Dosenovic[2], H. Okuno[2], C. Vergnaud[1], J. Jacquot[3], D. Jalabert[2], D. Longo[4], P. Ohresser[4], A. Hallal[1], M. Chshiev[1,5], O. Boulle[1], *F. Bonell*[1] and M. Jamet[1] *1. University Grenoble Alpes, CNRS, CEA, IRIG-Spintec, Grenoble, France; 2. University Grenoble Alpes, CEA, IRIG-MEM, Grenoble, France; 3. University Grenoble Alpes, CEA, IRIG-SYMMES, Grenoble, France; 4. Synchrotron SOLEIL, L'Orme des Merisiers, Saint-Aubin, Gif-sur-Yvette, France; 5. Institut Universitaire de France (IUF), Paris, France*

Two-dimensional van der Waals (vdW) materials have emerged as a platform for the observation of long-range magnetic order in atomically thin layers [1]. New heterostructures based on them can be conceived to harness a wide range of magneto-optical and magneto-electrical properties. Layered Fe-Ge-Te compounds particularly stand out due to their itinerant ferromagnetism and Curie temperature (T_C) above 200K [2,3]. They host noticeable magnetic effects such as a large anomalous Hall effect of topological origin [4], magnetic skyrmions [5] and giant tunneling magnetoresistance [6]. Fe-Ge-Te alloys have mostly been studied in the form of thin flakes exfoliated from bulk crystals. However, technologically relevant applications require the ability to grow films over large areas with an accurate control of the thickness and a T_C at or above room temperature (RT). Here, we demonstrate the large-area growth of single-crystal Fe_5GeTe_2 on insulating Al_2O_3(0001) using molecular beam epitaxy (MBE) [7]. SQUID measurements show the persistence of soft ferromagnetism up to RT, with a T_C of 293K. The orbital and spin moments determined by X-ray magnetic circular dichroism are in good agreement with our first principles calculations. Structural characterization by RHEED electron diffraction, X-ray diffraction and scanning transmission electron microscopy (STEM) confirm the layer-by-layer growth and the single-crystalline character of the films. The stoichiometric 5:2:1 Fe:Ge:Te elementary composition is ascertained by Rutherford backscattering spectroscopy (RBS). In contrast to reports on bulk crystals, virtually no Fe deficiency is observed in MBE-grown films. Characterization is complemented by atomic force microscopy to assess the surface morphology and by energy-dispersive X-ray spectroscopy to demonstrate the chemical uniformity of the layers. We further investigate ultrathin Fe_5GeTe_2 and show that the T_C remains high (240K) in 2-monolayers-thick films. These results open important perspectives for the large-scale fabrication of high-T_C layered ferromagnets and for the realization of ultracompact vdW heterostructures for spintronics.

[1] C. Gong and X. Zhang, *Science* Vol. 363, eaav4450 (2019) [2] Z. Fei *et al.*, *Nature Materials* Vol. 17, p.778 (2018) [3] A. F. May *et al.*, *ACS Nano* Vol. 13, p.4436 (2019) [4] K. Kim *et al.*, *Nature Materials* Vol. 17, p.794 (2018) [5] B. Ding *et al.*, *Nano Lett.* Vol. 20, p.868 (2020); T.-E. Park *et al.*, *Phys. Rev. B* Vol. 103, p.104410 (2021) [6] Z. Wang *et al.*, *Nano Lett.* Vol. 18, p.4303 (2018) [7] M. Ribeiro *et al.*, arXiv:2106.12808 (2021)

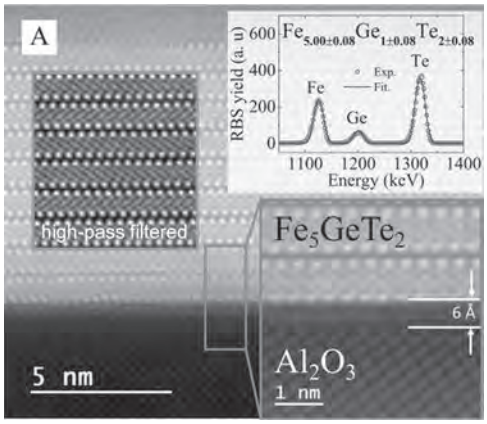

Fig. 1: STEM cross section of Fe_5GeTe_2 grown by MBE. Inset: Composition determined by RBS.

BOB-14. Withdrawn

BOB-15. Magneto-Raman Spectroscopy of Antiferromagntic $FePS_3$ and Ferromagnetic V-Doped WS_2. *J.R. Simpson*[1,2], T.T. Mai[2], R. Valdes Aguilar[4], A.R. Hight Walker[2], M. Liu[3], D. Zhou[3] and M. Terrones[3] *1. Dept. of Physics, Astronomy, and Geosciences, Towson University, Towson, MD, United States; 2. Physical Measurement Laboratory, National Institute of Standards & Technology, Gaithersburg, MD, United States; 3. Dept. of Materials Science and Engineering, The Pennsylvania State University, University Park, PA, United States; 4. Physics, The Ohio State University, Columbus, OH, United States*

The recent discovery that van der Waals-bonded magnetic materials retain long range magnetic ordering down to a single layer[1,2] stimulates a thorough Raman spectroscopic study of such materials, including $FePS_3$ and V-doped WS_2. Bulk $FePS_3$ was shown to be a quasi-2D Ising antiferromagnet, with additional features in the Raman spectra emerging below the Neel temperature (T_N ~ 120 K). Using temperature- and magnetic field-dependent Raman spectroscopy as an optical probe of magnetic structure, we demonstrate[3] that one of these Raman-active modes (ψ_4) below T_N is a magnon with a frequency of ~ 3.7 THz (~122 cm^{-1}). Contrary to previous work[4], which interpreted this feature as a phonon, our Raman data[3] shows the expected frequency shifting and splitting of the magnon as a function of temperature and magnetic field, respectively, were we find the *g*-factor ~2. Other Raman-active modes emerging below T_N are attributed to zone-folded phonons in the antiferromagnetic state. The anomalous temperature dependence of these modes along with an analysis of temperature-dependent magnetization data, suggests a persistence of short-range magnetic order above T_N. In contrast to antiferromagnetic FePS3, the transition metal dichalcogenide WS_2 doped is found to be ferromagnetic when doped with vanadium down to the monolayer.[5] We compare our magneto-Raman measurements on V-doped WS_2 to circularly polarized magneto-PL measurements.

[1] C. Gong, L. Li, Z. Li, *et al.*, Nature 546, 265 (2017). [2] B. Huang, G. Clark, E. Navarro-Moratalla, *et al.*, Nature 546, 270 (2017). [3] A. McCreary, J. R. Simpson, T. T. Mai, *et al.*, Phys. Rev. B 101, 064416 (2020). [4] J.-U. Lee, S. Lee, S. H. Ryoo, *et al.*, Nano Lett. 16, 7433 (2016). [5] F. Zhang, *et al.*, Adv. Sci. 7, 2001174 (2020).

Session BOC
MAGNETOELECTRONIC MATERIALS AND PHENOMENA: COMPLEX OXIDES

Jing Wang, Chair
The Institute of Physics, Chinese Academy of Sciences, Beijing, China

INVITED PAPER

BOC-01. Superconductivity at $LaAlO_3/KTaO_3$ interfaces. *Y. Xie*[1]
1. Physics, Zhejiang University, Hangzhou, China

Very recently superconductivity with a transition temperature (T_c) up to 2.2 K was discovered at $KTaO_3$-based interfaces [1-3]. In this talk I will present our progresses in this newly discovered superconducting oxide interface. We confirmed that the superconductivity depends strongly on the orientation of the interface and discovered a T_c ~0.9 K superconductivity at (110)-orientated interface [2]. We controlled the superconductivity of (111)-orientated interface with electric field, achieving a superconductor-to-insulator quantum phase transition [3]. Strikingly, we found that the tuning effect was achieved by change in the spatial profile of the carriers in the interface and hence, effective disorder, rather than carrier density. A few interesting quantum phenomena (i.e. quantum metal) that are related to the interplay between disorders and two-dimensional superconductivity were observed. We also observed a critical thickness of $LaAlO_3$, ~3 nm [4]. The interface is conducting (insulating) when $LaAlO_3$ is thicker (thinner) than this thickness. Our further study on this critical thickness suggests that the determinant mechanism of the interface conduction is the electron transfer from oxygen vacancies in the $LaAlO_3$ film to the $KTaO_3$ substrate.

[1] Changjiang Liu, Xi Yan, Dafei Jin, Yang Ma, Haw-wen Hsiao, Yulin Lin, Terence M. Bretz-Sullivan, Xianjing Zhou, John Pearson, Brandon Fisher, J. Samuel Jiang, Wei Han, Jian-Min Zuo, Jianguo Wen, Dillon D. Fong, Jirong Sun, Hua Zhou, and Anand Bhattacharya, *Science* 371, 716-721 (2021). [2] Zheng Chen, Zhongran Liu, Yanqiu Sun, Xiaoxin Chen, Yuan Liu, Hui Zhang, Hekang Li, Meng Zhang, Siyuan Hong, Tianshuang Ren, Chao Zhang, He Tian, Yi Zhou, Jirong Sun, and Yanwu Xie, *Phys. Rev. Lett.* 126, 026802 (2021). [3] Zheng Chen, Yuan Liu, Hui Zhang, Zhongran Liu, He Tian, Yanqiu Sun, Meng Zhang, Yi Zhou, Jirong Sun, and Yanwu Xie, *Science* 372, 721-724 (2021). [4] Yanqiu Sun, Yuan Liu, Siyuang Hong, Zheng Chen, Meng Zhang, and Yanwu Xie, "Critical thickness in superconducting $LaAlO_3/KTaO_3$(111) heterostructures", *Phys. Rev. Lett.* online.

CONTRIBUTED PAPERS

BOC-02. Anomalous Nernst effect in perovskite $La_{0.5}Ca_{0.5}CoO_3$. *A. Ghosh*[1], M. Manikandan[1] and R. Mahendiran[1] *1. Physics, National University of Singapore, Singapore*

Anomalous Nernst effect (ANE) has drawn special attention during the last few years because of its possibility in thermal energy harvesting and fundamental physics involved [1]. Reports on ANE in perovskite oxides are relatively few compared to ferromagnetic metallic alloys. The ANE was previously reported in Sr substituted $LaCoO_3$ [2]. Because of the smaller size of Ca^{2+} cation compared to Sr^{2+}, magnetic interactions are expected to be modified. Hence, we studied the ANE in $La_{0.5}Ca_{0.5}CoO_3$ for the first time, which shows ferromagnetic ordering at 147 K (Fig. 1(a)). The non-saturating nature of the field dependence of magnetization and its smaller value shown in the inset of Fig. 1(a) indicates the existence of competitive FM-AFM interactions that largely depends on the spin states of the Co^{3+} and Co^{4+} ions[2-4]. Such a system can be very interesting to study ANE as the aforementioned competitive effect may dramatically affect the spin-dependent deflection of thermally driven charge carriers. The presence of the ANE in $La_{0.5}Ca_{0.5}CoO_3$ is confirmed from the field dependences of the Nernst thermopower (S_{xy}) as shown in Fig. 1(b), which shows hysteresis like the magnetization. In this preliminary work, we have carried out ANE measurements only at four selected temperatures. S_{xy} nearly saturates above 20 kOe at 40 K but not at 100 K, where it has a maximum value at the highest field. The S_{xy} shows behavior similar to superparamagnetic at 160 K and linear behavior at 200 K with much-reduced values. Magnetic, electrical transport, thermoelectric measurements, and ANE at multiple temperatures will be carried out to realize the mutual effects of magnetism, charge, and heat currents to establish a better relationship between them. This work was supported by the Ministry of Education, Singapore (Grant no. R144-000-422-114 and R144-000-442-114).

[1] M. Mizuguchi and S. Nakatsuji, Sci. Technol. Adv. Mater. 20, 262 (2019). [2] T. Miyasato *et al.*, Phys. Rev. Lett. 99, 086602 (2007); M. Soroka *et al.*, Phys. Rev. Mater. 5, 035401 (2021). [3] J. C. Debnath *et al.*, J. Alloys Compd. 510, 125 (2012). [4] I. Fita *et al.*, Phys. Rev. B 71, 214404 (2005).

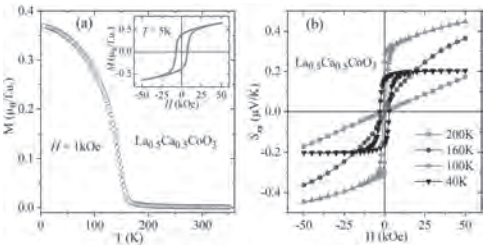

Fig. 1: (a) Temperature dependence of magnetization (M) in $La_{0.5}Ca_{0.5}CoO_3$. Inset: Field dependence of (b) M at 5 K. and (b) Nernst thermopower (S_{xy}) measured at T = 40, 100, 160 and 200 K.

BOC-03. Withdrawn

BOC-04. Oxygen ion migration regulates magnetism in $La_{0.5}Sr_{0.5}CoO_3$ film. *Z. Yin*[1,2], C. Zhang[1,2], H. Zhou[1,2], Z. Yu[1,2], Y. Wang[1,2], Y. Gao[1,2], J. Wang[1,2], F. Hu[1,2], S. Jirong[1,2] and B. Shen[1,2] *1. Beijing National Laboratory for Condensed Matter Physics & State Key Laboratory of Magnetism, Institute of Physics, Chinese Academy of Sciences, Beijing, China; 2. School of Physical Sciences, University of Chinese Academy of Sciences, Beijing, China*

Controlling ion migration of transition metal oxide(TMO) to recast crystal structure and macroscopic properties is current research emphasis [1, 2], which has potential applications in solid fuel cells, resistance switching etc. Among cobalt-based TMO, B-site atom determines functionality, but oxygen atom is hard to ignored. Electronic structure of B-site atom is profoundly affected by oxygen content due to coupling of lattice, charge, orbit, and spin. Vacuum annealing is a stable method to extract O^{2-}-ions [3, 4]. 40nm $La_{0.5}Sr_{0.5}CoO_3$(P-LSCO) film are grown on LSAT(100) substrate. Then films are respectively annealed at 400 centigrade for 2 hours(B-LSCO) and 500 centigrade for 35 hours(S-LSCO) to extract O^{2-}-ions. Fig. 1a shows soft X-ray absorption spectrum(XAS) for cobalt L-edge, and an obvious peak

shift to low energy (L_3-peak of S, B and P-LSCO appear at 782.2eV, 781.5eV and 780.4eV respectively) indicates continuous decrease in average valence states of Co and oxygen content during O^{2-}-ions extracting process. For XAS of oxygen *K*-edge (Fig. 1b), the A and C peaks, representing hybridization of Co-2p/3d and O-2p orbital, gradually decrease in three samples. While B-peak, which represents content of oxygen vacancy, exhibits an increasing trend, consistent with above results. As a result, dramatic magnetism transformation was observed in film upon annealing. Fig. 1c and 1d show magnetic moment-temperature(*M-T*) curves and magnetic moment-magnetic field (*M-H*) curves for three samples, demonstrating ferromagnetism(FM) with Tc~220K, antiferromagnetism(AFM) and ferromagnetism with Tc>300K in P-LSCO, B-LSCO and S-LSCO, respectively. In sum, we achieved giant magnetic transformation from FM to AFM to FM accompanying with O^{2-}-ion migration in LSCO film by vacuum annealing, which provides idea for regulating physics properties by ion migration engineering.

1. Y. D. Gu, et al. *ACS Appl. Mater. Interfaces* 2019, 11, 19584−19595. 2. N. P. Lu, et al. *Nature* 546, 124–128 (2017). 3. J. Li, et al. *Nano Energy* 78 (2020) 105215. 4. H. l. Huang, *J. Phys. D: Appl. Phys.* 53 (2020) 155003 (6pp).

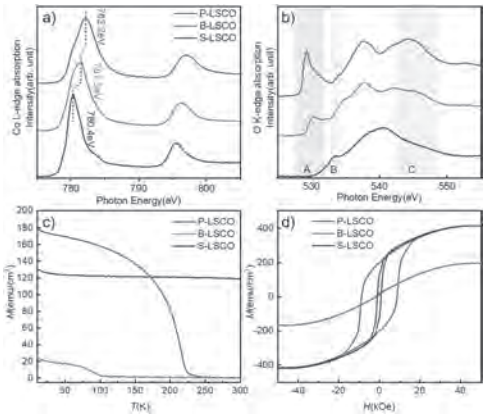

Fig. 1 XAS for a) cobalt *L*-edge, b) oxygen *K*-edge, c) *M-T* curve, d) *M-H* curve

BOC-05. Tunnel magnetoresistance effect of $NiCo_2O_4$/MgO/Fe magnetic tunnel junctions. *T. Nagahama*[1], Y. Hara[2], A. Ysujie[2] and T. Shimada[1] *1. Graduate School of Engineering, Hokkaido University, Sapporo, Japan; 2. CSE, Hokkaido University, Sapporo, Japan*

$NiCo_2O_4$(NCO), an inverse spinel structure, is expected to be highly potential spintronics materials as a magnetic oxide thin film with metallic electric conductivity, ferrimagnetism, and perpendicular magnetic anisotropy [1]. In addition, half metallicity (spin polarizability: -100%), which is similar to Fe_3O_4, has been predicted theoretically, so that it is expected that a large TMR ratio can be obtained by using NCO as an electrode material for magnetic tunnel junctions (MTJs). More recently, large TMR ratios greater than 200% in MTJs with NCO electrodes were observed experimentally, indicating a large spin polarization of NCO [2]. On the other hand, the direct evidence of negative spin polarization like an inverse TMR effect has not been observed yet. In this study, we investigated the TMR effect of MTJs using NCO and evaluated the spin polarization of NCO. The composition of the film was MgO (001)// NiO/$NiCo_2O_4$ (24 nm)/MgO (2.1 nm)/Fe (10 nm)/ Au, and the film was formed by a reactive MBE method. The NCO film was transferred to a load lock chamber after the deposition and annealed in an oxygen atmosphere (300 Pa, 623K). The MTJs were fabricated by conventional microfabrication method (photolithography, sputtering, milling), and temperature dependence and bias dependence of TMR ratios were investigated. We confirmed the epitaxial growth of films by RHEED. The RHEED patterns of NCO film changed from rock salt-type crystal structure to spinel-type by annealing under an oxygen atmosphere. FIG. 1 shows the MR curve of MTJ with NCO at 20 K with the in-plane magnetic field. An inverse TMR effect was observed, which is the direct evidence of negative spin polarization of NCO. As the bias voltage increased, the absolute value of the TMR ratio decreased monotonically. FIG. 2 shows the temperature dependence of the TMR ratio. The TMR ratio was -25% at 10 K, and the absolute value of the TMR ratio decreased with increasing temperature and was less than -1.0% at 100 K. The behavior could be attributed to the temperature dependence of magnetization of NCO.

[1] X. Chen et al., Adv. Mater. 31 1805260 (2019) [2] D. Kan et al., Appl. Phys. Lett. 117, 042408 (2020)

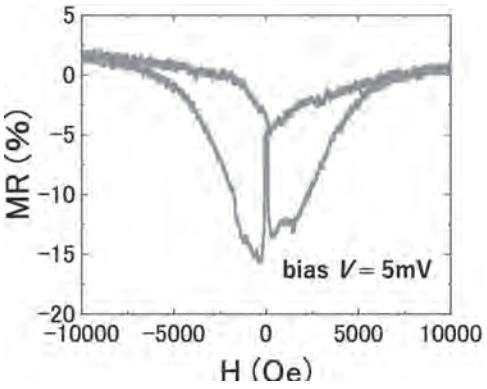

Fig 1. MR curve for $NiCo_2O_4$/MgO/Fe at 20 K.

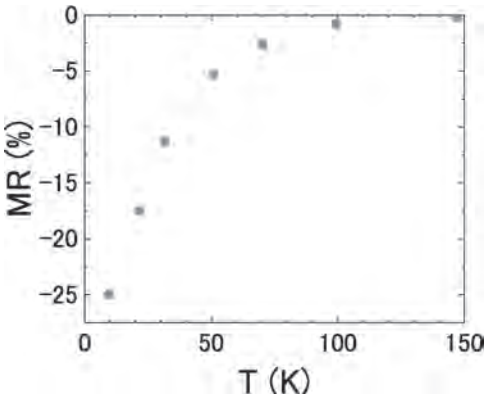

Fig 2. Temperature dependence of TMR ratio at 2mV.

BOC-06. Hysteresis Across the Voltage-Driven Perovskite-Brownmillerite Topotactic Phase Transformation in Epitaxial $La_{0.5}Sr_{0.5}CoO_{3-\delta}$. *W.M. Postiglione*[1], V. Chaturvedi[1], R. Chakraborty[1], B. Yu[2], W. Tabis[2,3], S. Hameed[2], N. Biniskos[2], A. Jacobson[1], Z. Zhang[4], H. Zhou[4], M. Greven[2], V.E. Ferry[1] and C. Leighton[1] *1. Chemical Engineering & Materials Science, University of Minnesota, Minneapolis, MN, United States; 2. Physics and Astronomy, University of Minnesota, Minneapolis, MN, United States; 3. Faculty of Physics and Applied Computer Science, AGH University of Science and Technology, Krakow, Poland; 4. Advanced Photon Source, Argonne National Laboratory, Lemont, IL, United States*

Electrochemical control of magnetic materials, *e.g.*, *via* electrolyte gating, has drawn much interest for magnetoionics [1]. Cobaltite oxides are particularly exciting in this context as materials such as $La_{1-x}Sr_xCoO_{3-\delta}$ can be reversibly transformed between ferromagnetic (F) metallic perovskite (P) and antiferromagnetic (AF) insulating brownmillerite (BM) phases by gate voltage (Fig. 1) [1,2]. The majority of prior work focused on $SrCoO_{3-\delta}$, and the F P and AF BM *endpoints*. Here, we study these phenomena across the entire $La_{1-x}Sr_xCoO_{3-\delta}$ phase diagram [2], additionally emphasizing the rich hysteretic phenomena accompanying the transitions [3]. Electronic transport, *operando* synchrotron X-ray diffraction, optical spectroscopy, and

magnetometry techniques are combined to provide new insights into the mechanisms of this transformation. As illustrated in Fig. 2, for example, hysteretic transport measurements (*e.g*., the prominent peaks in Fig. 2(b)) reveal clear signatures of phase pure P, P-BM coexistence, and BM regimes (evidencing a 1st order transformation), confirmed by X-ray, optics, and magnetometry. V_g hysteresis loops are also highly asymmetric (*e.g*., Fig. 2(a)), further enabling determination of the optimal maximum voltages to maximize reversibility, endurance, *etc*., as is essential for applications. The results demonstrate reversible control of Curie temperature, magnetization, and resistivity over large windows, reaching 220 K, 2 m_B/Co, and 10^5, respectively. Such V_g hysteresis loop studies thus significantly advance the understanding of this system, and are of broad relevance in magnetoionics.

C. Leighton, *Nat. Mater.*, 18, 13–18 (2019) V. Chaturvedi *et al.*, *ACS Appl. Mater. Interfaces*, submitted (2021) W. M. Postiglione *et al.*, in preparation (2021)

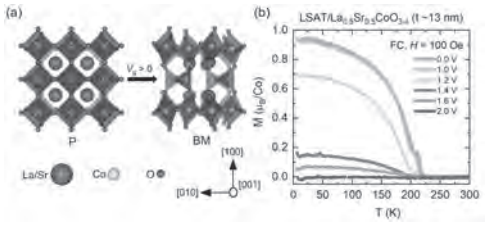

Fig. 1: (a) Perovskite (P) and brownmillerite (BM) crystal structure. (b) Magnetization (*M*) *vs*. temperature (*T*) for a 13 nm $La_{0.5}Sr_{0.5}CoO_{3-\delta}$ film on LSAT(001) *vs*. gate voltage V_g.

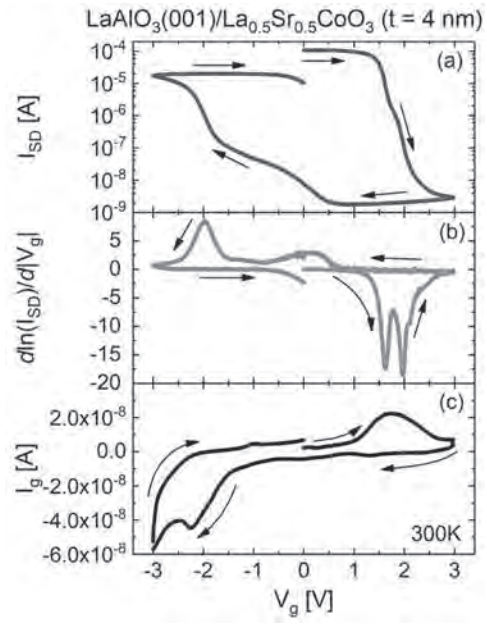

Fig. 2: Gate voltage (V_g) dependence of (a) the source-drain current I_{SD}, (b) $d\ln(I_{SD})/d|V_g|$, and (c) the gate current I_g, for a 4-nm-thick $La_{0.5}Sr_{0.5}CoO_{3-\delta}$ film on $LaAlO_3$(001). Arrows indicate the sweep direction.

BOC-07. Incommensurate Magnetic Phases of the Multiferroic Compound $MnCr_2O_4$ Described with the Superspace Formalism.

M. Pardo-Sainz[1,2], A. Toshima[3], G. André[4], J. Basbus[5], G. Cuello[6], T. Honda[7], T. Otomo[7], K. Inoue[3], Y. Kousaka[2] and J. Campo[1] *1. Instituto de Nanociencia y Materiales de Aragón (INMA), CSIC, Zaragoza, Spain; 2. Osaka Prefecture University, Osaka, Japan; 3. Chirality Research Center and Institute for Advanced Materials Research, Hiroshima University, Hiroshima, Japan; 4. Laboratoire Léon Brillouin (LLB), Saclay, France; 5. Centro Atómico Bariloche, INN - CNEA - CONICET, S. C. de Bariloche, Argentina; 6. Institut Laue-Langevin (ILL), Grenoble, France; 7. Institute of Materials Structure Science, High Energy Accelerator Research Organization (KEK), Tsukuba, Japan*

Nowadays, chromium-based normal spinel oxides ACr_2O_4 are one of the most studied materials in the condensed matter community due to the interplay between its magnetic, electric and structural properties as well as to its potential application to different key industry sectors. In these compounds, several physical effects have been observed, which include magnetostriction, colossal magnetoresistance, multiferroic, spin frustration and more [1-3]. In particular, for $MnCr_2O_4$, the ground state magnetic structure is still controversial because the magnetic structures reported by different groups and investigated by independent techniques are inconsistent [1-6]. The magnetic structure of this compound was reinvestigated by magnetization, specific heat and neutron diffraction experiments at different temperatures. The results suggested that a new magnetic phase, not previously reported, is developed under 18 K when the sample is synthesized under a reductive atmosphere. The magnetic phases present in this sample were: long-range ferrimagnetic order below T_C = 45 K; incommensurate conical spin order with propagation vector k_{S1} = (0.62(1), 0.62(1), 0) below T_{S1} = 20 K; and incommensurate conical spin order with propagation vector k_{S2} = (0.660(3), 0.600(1), 0.200(1)) below T_{S2} = 18 K. Using the superspace group formalism [7, 8], the symmetry of the nuclear and magnetic structures is described. The presence of transverse conical magnetic structures in the lower-temperature phases implies the existence of multiferroicity. Using simple theoretical calculations, we derive the directions along which the electric polarization lies for each magnetic phase.

[1] K. Dey et al., Journal of Magnetism and Magnetic Materials, Vol. 435, p. 15 (2017) [2] K. Tomiyasu, J. Fukunaga, and H. Suzuki, Physical Review B, Vol. 70, p. 214434 (2004) [3] N. Mufti et al., Journal of Physics: Condensed Matter, Vol. 22, p. 075902 (2010) [4] J. M. Hastings and L. M. Corliss, Physical Review, Vol. 126, p. 556 (1962) [5] G. T. Lin et al., Physical Review B, Vol. 97, p. 064405 (2018) [6] D. Tobia et al., Journal of Physics: Condensed Matter, Vol. 27, p. 016003 (2015) [7] J. M. Perez-Mato et al., Journal of Physics: Condensed Matter, Vol. 24, p. 163201 (2012) [8] J. Rodríguez-Carvajal and J. Villain, Comptes Rendus Physique, Vol. 20, p. 770 (2019)

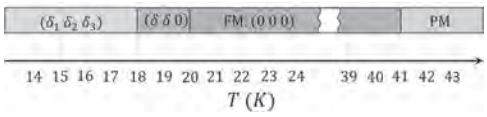

Fig. 1: Phases present in $MnCr_2O_4$ together with their phase transition temperatures. Green: paramagnetic, purple: ferrimagnetic, pink: conical with k_{S1} = (0.62(1), 0.62(1), 0), blue: conical with k_{S2} = (0.660(3), 0.600(1), 0.200(1)).

BOC-08. Dynamic Electric-Field-Induced Magnetic Effects in Cobalt Oxide Thin Films: towards Magneto-Ionic Synapses. *S. Martins*[1], J. de Rojas[1], Z. Tan[1], M. Cialone[2], A. Lopeandia[1,3], J.H. Martín[4], J. Costa-Kramer[5], E. Menéndez[1] and J. Sort[1,6] *1. Physics Department, Autonomous University of Barcelona, Cerdanyola del Vallès, Spain; 2. CNR-SPIN Genova, Genova, Italy; 3. Catalan Institute of Nanoscience and Nanotechnology (ICN2), Barcelona, Spain; 4. ALBA Synchrotron Light Source, Cerdanyola del Vallès, Spain; 5. IMN-Instituto de Micro y Nanotecnología (CNM-CSIC), Tres Cantos, Spain; 6. Institució Catalana de Recerca i Estudis Avançats (ICREA), Barcelona, Spain*

Voltage control of magnetism via electric-field-driven ion migration (magneto-ionics) has generated intense interest due to its potential to greatly reduce heat dissipation in a wide range of information technology devices, such as magnetic memories, spintronic systems or artificial neural networks. Oxygen ion migration in transition-metal-oxide thin films (Fig. 1) can lead to, among other effects, either the generation or full suppression of controlled amounts of ferromagnetism ('ON-OFF' magnetic transitions) in a non-volatile and fully reversible manner (Fig. 2). However, oxygen magneto-ionic rates at room temperature have generally been considered too slow for industrial applications. Here, we demonstrate that sub-second ON-OFF transitions in electrolyte-gated paramagnetic cobalt oxide films can be achieved by drastically reducing the film thickness from > 200 nm down to 5 nm. Remarkably, cumulative effects at 100 Hz indicate that activation times are on the order of 10^{-2} s in the thinner films, among the fastest reported so far in magneto-ionic systems relying on O^{2-} ion migration. Neuromorphic-like dynamic effects occur at these frequencies, including potentiation (cumulative increase of magnetization), depression (*i.e.*, partial recovery of magnetization with time), threshold activation, and spike time-dependent magnetic plasticity (learning and forgetting capabilities), mimicking many of the main biological synapse functions. The systems under investigation show features (including the operational dynamic range) that could be useful for the design of artificial neural networks whose magnetic properties would be governed with applied voltage (*i.e.*, magneto-ionic neuromorphic-like computing applications).

Fig. 1 Schematic view of the electric double layer formed upon gating at the interface between the Co_3O_4 film and the liquid electrolyte.

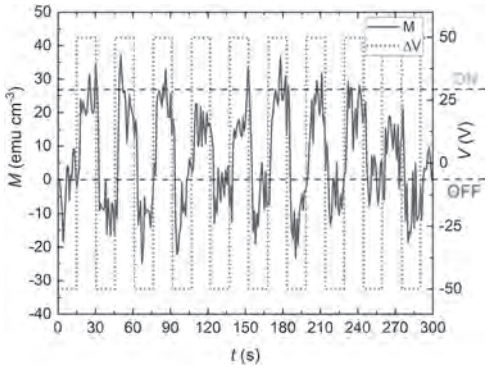

Fig. 2 Magneto-ionic cyclability of the 5 nm-thick cobalt oxide film taken upon applying –50 V/+50 V voltage cycles with a period of 30 s, assessed from time-dependent in-plane magnetic measurements under a magnetic field of 10 kOe: applied voltage (red discontinuous curve) and magnetization (blue line).

BOC-09. Magnetic and transport properties of $SrRuO_3$/ $La_{0.85}Ca_{0.15}MnO_3$ epitaxial bilayer thin films. D. Kumar[1], A.A. Tulapurkar[2] and *C.V. Tomy*[1] *1. Physics, Indian Institute of Technology Bombay, Mumbai, India; 2. Electrical Engineering, Indian Institute of Technology Bombay, Mumbai, India*

The effect of interfaces in heterostructures of manganites with other compatible oxides has been widely investigated due to the emergence of exotic phenomenon like charge, spin, orbital, lattice, and electronic reconstruction at the interface [1, 2]. These effects can give rise to promising technological applications in spintronic devices, sensors, etc. We have studied the interface effects using a bilayer of $SrRuO_3$(SRO)/$La_{0.85}Ca_{0.15}MnO_3$(LCMO) grown on $SrTiO_3$(STO) substrates, which gives an interface of ferromagnetic metal (FMM)/ferromagnetic insulator (FMI). We have also studied the effect of stacking order of the bilayer by depositing SRO as the top layer or LCMO as the top layer. The magnetic as well as the transport properties of the films were indeed found to be dependent on the stacking order in the bilayers. We could also observe both the conventional exchange bias (CEB) as well as the spontaneous exchange bias (SEB) in these bilayers with clear dependence on the stacking arrangement of the layers, even though these effects are generally observed in FM-AFM interfaces [3]. The exchange bias effect in ferromagnetic layers is attributed to the antiferromagnetic coupling (superexchange interaction between Ru and Mn ions) between the SRO and LCMO layer at the interface [4]. The stacking order dependence of magnetic and transport properties are explained on the basis of interfacial strains experienced by the thin films.

[1]. H. Y. Hwang, Y. Iwasa, M. Kawasaki, B. Keimer, N. Na-gaosa, and Y. Tokura, Nature Materials 11, 103 (2012). [2]. P. Padhan, W. Prellier, and B. Mercey, Phys. Rev. B 70, 184419 (2004). [3]. N. Moutis, C. Christides, I. Panagiotopoulos, and D. Niarchos, Phys. Rev. B 64, 094429 (2001). [4]. X. Ke, M. S. Rzchowski, L. J. Belenky, and C. B. Eom, Applied Physics Letters 84, 5458 (2004)

BOC-10. A DFT+*U* study of point defects in spinel ferrites. *K. Sharma*[1,2], D. Li[1,2], L. Calmels[1,2] and R. Arras[1,2] *1. CEMES-CNRS, Toulouse, France; 2. University of Toulouse, Toulouse, France*

Spinel ferrites MFe_2O_4 (M = Co, Ni) are insulating ferrimagnets with high saturation magnetizations and Curie temperatures well above room temperature, making these materials suitable for various spintronic applications [1-3]. These compounds possess a so-called inverse spinel structure, in which half of the Fe^{3+} cations are located in tetrahedral sites, while the remaining cations are located in octahedral sites formed by the distorted face-centered cubic lattice of oxygen atoms. Manipulating the cation distribution in these compounds could help to tune the magnetic and electronic conduction properties [4] and even lead to the appearance of a multiferroic ordering for perfectly ordered structures [5]. We performed *ab initio* calculations based on the density functional theory, to investigate the changes induced in the properties of the Co and Ni spinel ferrites, due to the presence of structural defects, ranging from cation disorder to oxygen and cation vacancies. The obtained results will be discussed in regard to their bulk thermodynamical stability, which will then be extended to surface reconstructions and supported by nudged elastic band calculations of the energy barrier separating two metastable defective structures. We will finally describe in detail the resulting variations of the magnetic moments and orderings, as well as the calculated changes of band gap widths and the possible appearance of gap states at the Fermi level, which would undoubtedly modify the electronic conductivity. Such study will pave the way for a general understanding of the magnetoelectric and resistive behavior of spinel ferrites.

1. R. Valenzuela, Phys. Res. Int. 2012, 591839 (2012) 2. J.-B. Moussy, J. Phys. D: Appl. Phys. 46 143001 (2013) 3. A. Hirohata, H. Sukegawa and H. Yanagihara, IEEE Trans. Mag. 51, 0800511 (2015) 4. X. Chen, X. Zhu and W. Xiao, ACS Nano 9, 4210 (2015) 5. J. K. Dey, A. Chatterjee and S. Majumdar, Phys. Rev. B 99, 144412 (2019)

BOC-11. Defect mechanism for ferroelectricity in orthoferrites.
S. Ning[1,2], A. Kumar[1], K. Klyukin[1], J. LeBeau[1], B. Yildiz[1,3] and C. Ross[1]
1. Department of Materials Science and Engineering, MIT, Cambridge, MA, United States; 2. School of Materials Science and Engineering, Nankai University, Tianjin, China; 3. Department of Nuclear Science and Engineering, Massachusetts Institute of Technology, Cambridge, MA, United States

Single-phase multiferroic materials that allow the coexistence of ferroelectric and magnetic ordering above room temperature are highly desirable, motivating an ongoing search for mechanisms for unconventional ferroelectricity in magnetic oxides. Here, we report an antisite defect mechanism for room temperature ferroelectricity in epitaxial thin films of yttrium orthoferrite, $YFeO_3$, a perovskite-structured canted antiferromagnet [1]. A combination of piezoresponse force microscopy, atomically resolved elemental mapping with aberration corrected scanning transmission electron microscopy and density functional theory calculations reveals that the presence of Y_{Fe} antisite defects facilitates a non-centrosymmetric distortion promoting ferroelectricity. This mechanism is predicted to work analogously for other rare earth orthoferrites, with a dependence of the polarization on the radius of the rare earth cation. Furthermore, a vertically aligned nanocomposite consisting of pillars of a magnetoelastic oxide $CoFe_2O_4$ embedded epitaxially in the $YFeO_3$ matrix exhibits both robust ferroelectricity and ferrimagnetism at room temperature, as well as a noticeable strain-mediated magnetoelectric coupling effect [2]. Our work uncovers the distinctive role of antisite defects in providing a novel mechanism for ferroelectricity in a range of magnetic orthoferrites and further augments the functionality of this family of complex oxides for multiferroic applications.

1. S. Ning, A. Kumar and C. A. Ross et al. Nat. Commun.12, 4298 (2021) 2. S. Ning, A. Kumar and C. A. Ross et al. (in preparation)

BOC-12. Magnetic Characterization of Ru-doped $BaSnO_3$ Thin Films.
E.R. Lindgren[1,2] and Y. Suzuki[2,3] *1. Materials Science & Engineering, Stanford University, Stanford, CA, United States; 2. Geballe Laboratory for Advanced Materials, Stanford University, Stanford, CA, United States; 3. Applied Physics, Stanford University, Stanford, CA, United States*

La-doped $BaSnO_3$ thin films have been identified as a promising high mobility transparent semiconducting oxide, which could play an important role in the development of an all-oxide power electronics platform. In order to incorporate spin functionality into these materials, we explore magnetic doping of the perovskite stannates. Using pulsed laser deposition we have fabricated Ru doped $BaSnO_3$ films on (001) $SrTiO_3$ substrates. X-ray diffraction (XRD) was used to verify epitaxial growth and confirm high crystalline quality. Here we report the magnetic characterization of the Ru doped $BaSnO_3$ films. We have studied 4% and 8% Ru doping of the Sn site in $BaSnO_3$ thin films and compared them to undoped $BaSnO_3$ films. Ru doped films show paramagnetic responses at 5K. For samples with 4% Ru doping, we observe a paramagnetic signal that saturates at ~1.7μ_B/Ru atom consistent with the low spin state of Ru^{4+} ions. Films with 8% doping show a lower saturation value, which is attributed to lower than expected dopant incorporation. All Ru doped $BaSnO_3$ films show a magnetic susceptibility that is inversely proportional to temperature consistent with Curie's law. UV-vis spectroscopy measurements show above 80% transmission in the 500-1800nm range, and above 50% between 380-500nm. When we combine 8% Ru doping on the Sn site with 4% La doping on the Ba site, we find insulating behavior. However when we combine individual layers of conducting 4% La:$BaSnO_3$ and paramagnetic 4% Ru:$BaSnO_3$, we find paramagnetic conducting behavior with mobilities of up to 80cm^2/Vs. *We acknowledge support from the National Science Foundation under grant #1762971 and #2037652.

BOC-13. Withdrawn

BOC-14. Universal magnetic domain wall creep driven by magnetoelectric effect.
J. Shen[1], K. Toyoki[1], Y. Kotani[2], T. Tada[1], R. Nakatani[1,3] and Y. Shiratsuchi[1,3] *1. Department of Materials Science and Engineering, Graduate School of Engineering, Osaka University, Osaka, Japan; 2. JASRI/SPring-8, Hyogo, Japan; 3. Center of Spintronics Research Network, Graduate School of Engineering Science, Osaka University, Osaka, Japan*

The recent development of spintronics enabled us to control antiferromagnetic (AFM) moments/domains. We have been reported that the AFM domain state of the Cr_2O_3 thin film in the Pt/Co/Au/Cr_2O_3/Pt thin film could be controlled by using the magneto-electric (ME) effect including the ME-induced AFM domain wall (AFM-DW) velocity [1]. In this scheme, the driving force of the DW motion is analogous to the Zeeman energy in the ferromagnetic (FM) film. Hence, it is expected that the AFM domain wall creep follows the universal law which has been confirmed in the DW creep induced by magnetic field, current and electric field. In this paper, we investigated the universality of the AFM DW creep driven by the ME effect using Pt/Co/Au/ME Cr_2O_3/Pt thin film. Pt(2 nm)/Co(0.5 nm)/Au(0.7 nm)/Cr_2O_3(90 nm)/Pt(20 nm) thin film was prepared by using the DC magnetron sputtering system. The film was patterned into the micro-dot with a diameter of 30 mm using photolithography and Ar ion milling. The AFM-DW velocity was evaluated based on the magnetic domain observation using the scanning soft X-ray magnetic circular dichroism (XMCD) microscope at BL25SU, SPring-8. The magnetic domain observations were done at remanent state, i.e. m_0H = 0 T and E = 0 V/m, after the pulsed ME field, m_0H = 2.5, 2.75 and 3 T and E = -43 – -207 MV/m with 10-100 ns pulse width, was applied. The observation temperature was 270 K. Figure 1 shows the changes of DW velocity with applying the pulsed ME field increasingly which is a good illustration of different dynamical regimes. In a relatively low pulsed field, the energy is not enough to overcome the pinning barrier and cause a slow-motion which is the creep. With the increase of the pulsed-field, when it is higher than the pinning field, DW motion changes to the depinning regime. The DW mobility increases with the pulse field, from which we will discuss the depinning energy, the depinning velocity at the depinning field in the Pt/Co/Au/Cr_2O_3/Pt thin film. Based on these values, we show that the universality is persisted for the ME-driven AFM DW motion.

[1] Y. Shiratsuchi *et al.*, J. Phys.: Condens. Matter 33, 243001 (2021).

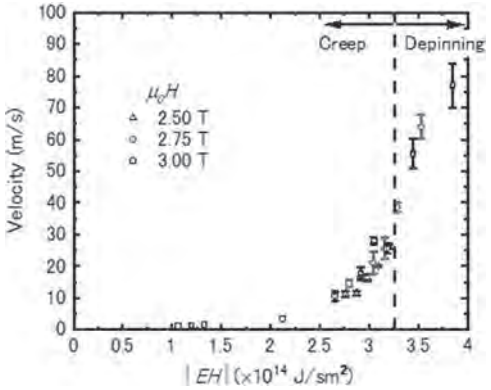

Fig.1 Domain wall motion driven by pulsed ME field. The creep and depinning regimes are divided by a dashed line.

BOC-15. First Principles Calculation of Oxygen Vacancy Effects on the Magnetic Properties of the Perovskite $SrNiO_3$. *E. Cho*[1], K. Klyukin[1], S. Ning[1,2], J. Li[3], R. Comin[3], R. Green[5,6], B. Yildiz[4] and C. Ross[1]
1. Department of Materials Science and Engineering, Massachusetts Institute of Technology, Cambridge, MA, United States; 2. School of Materials Science and Engineering, Nankai University, Tianjin, China; 3. Department of Physics, Massachusetts Institute of Technology, Cambridge, MA, United States; 4. Department of Nuclear Science and Engineering, Massachusetts Institute of Technology, Cambridge, MA, United States; 5. Department of Physics and Engineering Physics, University of Saskatchewan, Saskatoon, SK, Canada; 6. Stewart Blusson Quantum Matter Institute, University of British Columbia, Vancouver, BC, Canada

Nickelates have been studied extensively due to their intriguing physical properties [1], but less attention has been paid to the properties of divalent A-site cation perovskite nickelates with a formal valence state of 4+ for Ni. Here, we study the electronic and magnetic properties of perovskite $SrNiO_{3-\delta}$ with an oxygen deficiency δ up to 0.375 using density functional theory. Because of the strong covalency and negative charge transfer energetics, the structure is predicted to exhibit ligand holes $\underline{L}$, with Ni present as $d^8\underline{L}^2$ or $d^7\underline{L}$ and significant magnetic moment at the oxygen sites (Fig. 1). The ground state for δ = 0 to 0.375 consists of ferromagnetically ordered Ni with the Ni and O moments coupled antiferromagnetically, and the removal of oxygen increases the net magnetization (Fig. 2). These behaviors are also predicted for other A-site cations such as Ca and Ba. This work demonstrates the importance of ligand holes in oxides with formally high valence Ni, including their influence on the magnetic properties, and motivates further experimental study of the electronic and magnetic properties of nickelates with divalent A-site cations.

[1] S. J. Catalano, M. Gilbert and J. Kreisel, Reports Prog. Phys., Vol. 81, 046501 (2018)

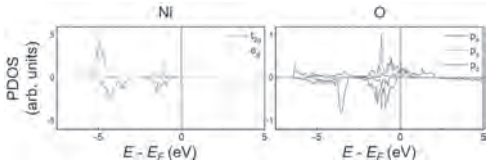

Fig. 1. Projected density of states (PDOS) of Ni and O bonded along the c axis of Ni in ferromagnetic $SrNiO_3$ (δ = 0). Because the selected O is bonded in the z direction, the p_z orbital participates in σ bonding, and p_x and p_y orbitals participate in π bonding. The p_x and p_y PDOS overlap.

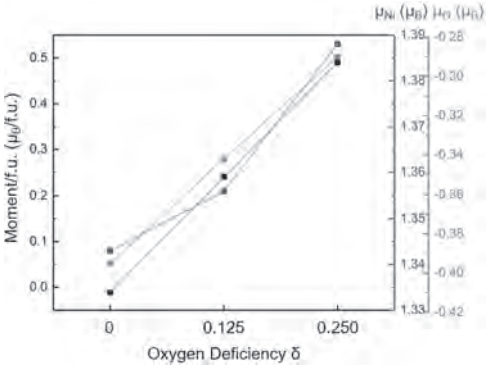

Fig. 2. Total, Ni, and O magnetic moment dependence on δ. δ = 0.250 Ni moments were averaged over all possible vacancy positions.

Session BOD
MAGNETOELECTRONIC MATERIALS AND PHENOMENA: MAGNETIC SEMICONDUCTORS AND MULTIFERROICS

Karin Leistner, Chair
IFW Dresden, Dresden, Germany

CONTRIBUTED PAPERS

BOD-01. Converse magnetoelectric effect in $Co_2MnSi/Pb(Mg_{1/3}Nb_{2/3})O_3$-$PbTiO_3$ interfacial multiferroic heterostructures. *T. Usami*[1], S. Fujii[2], S. Yamada[1,2], Y. Shiratsuchi[3,1], R. Nakatani[3,1] and K. Hamaya[1,2]
1. Center for Spintronics Research Network, Osaka University, Toyonaka, Japan; 2. Graduate School of Engineering Science, Osaka University, Toyonaka, Japan; 3. Graduate School of Engineering, Osaka University, Suita, Japan

Ferromagnetic/ferroelectric interfacial multiferroic heterostructures have attracted much attention since the magnetism can be controlled by an electric field (E) [1]. From the viewpoint of spintronic applications, it is important to implement half-metallic Heusler alloys such as Co_2MnSi (CMS) [2] and Co_2FeSi [3] into the multiferroic heterostructures. In addition, since the half-metallic characteristics of the Heusler alloys depend generally on the structural order parameter, understanding of the correlation between the converse magnetoelectric (CME) effect and the structural ordering in the Heusler alloy/ferroelectric heterostructures is needed. Here, we experimentally examine multiferroic heterostructures composed of CMS films with different structural order parameters grown on ferroelectric $Pb(Mg_{1/3}Nb_{2/3})O_3$-$PbTiO_3$ (PMN-PT) substrates. Two different CMS thin films (30 nm) were grown on PMN–PT(001) substrates by molecular beam epitaxy at 350 or 80°C. During the growth, both films showed clear streak patterns in *in-situ* reflection high-energy electron diffraction measurements. After the growth, we confirmed the epitaxial relationship of the CMS[100](001)||PMN-PT[110](001) from X-ray diffraction measurements. In addition, we found that $L2_1$-ordered phase is formed in the 350°C-grown CMS film while $B2$-ordered phase is formed in the 80°C-grown one. In this study, the former and the latter are referred to as $L2_1$-CMS and $B2$-CMS, respectively. To study the CME effect, we perform in-plane magneto-optical Kerr effect measurements at room temperature with applying E. Figure 1 shows hysteresis loops of the Kerr rotation angle (θ_K) for (a) $L2_1$-CMS and (b) $B2$ -CMS heterostructures under E of ± 8 kV/cm. Only for the $L2_1$-CMS, the shape of the Kerr hysteresis loop is modulated by changing E. This result shows that the formation of $L2_1$-ordered phase plays an important role for achieving the effective CME effect in the CMS/PMN-PT heterostructure. Further systematic investigations will be given in the presentation.

[1] T. Taniyama, J. Phys. Condens. Matter 27, 504001 (2015). [2] Y. Sakuraba *et al.*, Appl. Phys. Lett. 88, 192508 (2006). [3] K. Hamaya *et al.*, Phys. Rev. B 85, 100404(R) (2012).

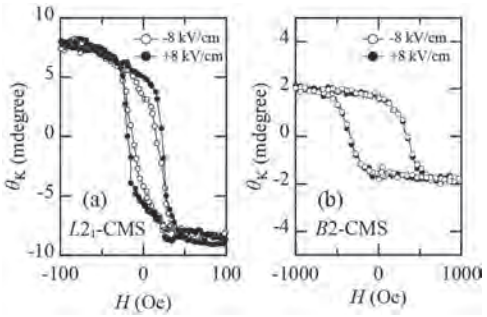

Fig.1. Magneto-optical Kerr loops for the $L2_1$-CMS (a) and $B2$-CMS (b) under E=±8 kV/cm at room temperature. The electric field is applied along the PMN-PT[001] direction.

BOD-02. Magnetic Constitution of PbTe:Cr - Experimental Aspects. *K. Gas*[1], A. Królicka[1], S. Kret[1], K. Dybko[1,2], T. Story[1,2] and M. Sawicki[1]
1. Institute of Physics, Polish Academy of Sciences, Warsaw, Poland; 2. International Research Centre MagTop, Institute of Physics, Polish Academy of Sciences, Warsaw, Poland

One of the most promising ways of improvement of thermoelectric energy conversion leads via band gap engineering towards the enlargement of the density of states at the Fermi level, e.g. via a co-doping to induce a resonant level in the electric transport relevant band [1]. Cr in PbTe is a particularly interesting example since Cr atoms form mixed valence $Cr^{2+/3+}$ donor centers resonant with the PbTe conduction band [2]. We report on detailed temperature and magnetic field dependence of magnetization of PbTe doped with transition metal $Cr^{2+/3+}$. The material is studied by a SQUID magnetometer in order to quantitatively determine the contribution of single substitutional $Cr^{2+/3+}$ as well as of various Cr-Te magnetic nanocrystals, including their identification. The applied experimental procedure reveals the presence of about 10^{19} cm^{-3} paramagnetic Cr ions, of which 2/3 are the Cr^{3+} ions formed via self-ionization of Cr^{2+} resonant donors. The magnetic finding agrees with previous Hall effect studies thus providing a new experimental support for the proposed electronic structure model of PbTe:Cr system with resonant $Cr^{2+/3+}$ state located (at low temperatures) about 100 meV above the bottom of the conduction band. Below room temperature a ferromagnetic-like signal points to the presence of Cr-rich nanocrystalline precipitates. Two most likely candidates, namely: Cr_2Te_3 and Cr_5Te_8 are identified upon dedicated temperature cycling of the sample at the remnant state. As an ensemble, the nanocrystals exhibit (blocked) superparamagnetic properties. Also HR-TEM confirmed the presence of numerous single nanometer size precipitates of Cr-Te compounds. The magnetic susceptibility of both n- and p-type PbTe in the temperature range $100 < T < 400$ K has been established. These magnitudes are essential to properly account for the high temperature magnetic susceptibility of PbTe:Cr [3]. This study has been supported by the National Science Centre (Poland) through project OPUS (UMO - 2017/27/B/ST3/02470) and by the National Science Centre for Development (Poland) through grant TERMOD No TECHMATSTRATEG2/408569/5/NCBR/2019 and by the Foundation of Polish Science through the IRA Programme co-financed by EU within SG OP.

[1] J. P. Heremans *et al.*, *Science* 321, 554 (2008). [2] T. Story *et al.*, *Acta Phys. Pol*. 82, 879 (1992); W. Mac *et al.*, *ibid* 87, 492 (1995). [3] K. Gas, A. Królicka, K. Dybko, P. Nowicki, Z. Khosravizadeh, T. Story, M. Sawicki, J. Magn. Magn. Mater, 537, 168154 (2021).

BOD-03. Multiferroic Behavior in $NH_4Al(SO_4)_2$-$12H_2O$: Magnetism and Ferroelectricity Based on Proton Orbital Degeneracies. *L. Meng*[1], C. Peng[1], C. He[1] and F. Yen[1] *1. Harbin Institute of Technology, Shenzhen, Shenzhen, China*

We find the magnetic susceptibility of $NH_4Al(SO_4)_2$-$12H_2O$ below its ferroelectric Curie temperature of T_C = 58 K can be tuned to become positive or negative simply by controlling the cooling speed. We explain this by taking into consideration that reorienting NH_4^+ ions possess weak magnetic moments that are linearly coupled to dipole moments which in turn are aligned by the crystal field with cooling but at the same time experiencing competition from geometric frustration. With fast cooling such as a rate of 1.0 K/min, the magnetic moments are not able to become ordered in time so the system remains mostly diamagnetic. In contrast, with a slow cooling rate of 0.1 K/min, the magnetic moments are allowed to access a more ordered state so the magnetic susceptibility becomes positive. From such, four -ferroic states can be accessed below T_C by applying either a positive or negative bias field and cooling the sample slow or fast to obtain polarization and magnetization of different polarities. Specific heat and dielectric constant measurements near T_C indicate the origin of multiferroic behavior as originating from proton orbital degeneracies. Our findings identify an entire new class of multiferroic materials in the ammonium alums and possibly other hydrogen-bonding compounds.

F. Yen, Z. Z. Zhao, S. X. Hu, et al., *Angew. Chem. Int. Ed.,* 56, 13675–13678 (2017). L. Meng, C. He and F. Yen, *J. Phys. Chem. C*., 124, 17255-17261 (2020). L. Meng, C. He, W. Ji, et al., *J. Phys. Chem. Lett*., 11, 8297-8301 (2020).

BOD-04. Voltage control of thin films with in-plane and perpendicular exchange bias. *J. Zehner*[1,3], R. Huhnstock[2], D. Wolf[3], M. Hasan[4], M. Huang[4], D. Bono[4], K. Nielsch[3], A. Ehresmann[2], G.S. Beach[4] and K. Leistner[1] *1. Faculty of Natural Sciences, Chemnitz University of Technology, Chemnitz, Germany; 2. Institute of Physics, Kassel University, Kassel, Germany; 3. Leibniz Institute for Solid State and Materials Research, Dresden, Germany; 4. Department of Materials Science and Engineering, Massachusetts Institute of Technology, Cambridge, MA, United States*

Voltage control of magnetism could be a key technology towards future energy efficient nanomagnetic devices. Voltage gating of 3d ferromagnetic metals via a liquid or solid state electrolyte is a versatile route to large reversible changes in the magnetic anisotropy due to ionic changes. Such magneto-ionic control offers the non-volatile setting of magnetic properties, which is especially desirable for low energy consumption. [1] So far, research on magneto-ionic control focused on ferromagnetic systems. Further functionalization towards exchange bias (EB) systems, composed of a ferromagnet adjacent to an antiferromagnet (AFM), is exciting to broaden the possible application areas towards tunable magnetic field sensors and magnetophoretic devices. In our work, we present magneto-ionic changes of in-plane and perpendicular EB systems. For the in-plane system we chose IrMn/Fe/FeO_x gated in an alkaline electrolyte. In this case, the voltage induces a reversible electrochemical transformation of interfacial iron-oxide to metallic iron. TEM and XPS measurements reveal an associated thickness change of the Fe layer as origin for the non-volatile changes of the EB and the coercivity, which agrees well with a simple EB model. Such a non-volatile voltage-setting of the EB can be exploited, e.g., for patterned magnetophoretic devices. [2] As a second system, we studied the voltage control of perpendicular exchange bias (PEB) thin films, which could be beneficial for the development of modern spintronic devices. For this, we first fabricated a NiO/Pd/Co based thin film system. We show that the thin Pd interlayer (0.2 nm) is crucial for the occurrence of PEB. When gating this structure via a solid state GdO_x layer, hydrogen ion migration leads to a reversible on and off switching of PEB (Fig. 1). After the first hydrogen gating step, the coercivity increases, while the magnitude of the EB decreases. This inverse correlation is traced back to the crystallization of the initial amorphous ferromagnetic layer. [3] Transferring the hydrogen gating mechanism to a ferrimagnetic (GdCo) based PEB system enables a voltage induced sign change of the EB.[4]

[1] A. J. Tan, M. Huang, C. O. Avci, F. Büttner, M. Mann, W. Hu, C. Mazzoli, S. Wilkins, H. L. Tuller, and G. S. D. Beach, *Magneto-Ionic Control of Magnetism Using a Solid-State Proton Pump*, Nat. Mater. 18, 35 (2019). [2] J. Zehner, R. Huhnstock, S. Oswald, U. Wolff, I. Soldatov, A. Ehresmann, K. Nielsch, D. Holzinger, and K. Leistner, *Nonvolatile Electric Control of Exchange Bias by a Redox Transformation of the Ferromagnetic Layer*, Adv. Electron. Mater. 5, 1900296 (2019). [3] J. Zehner, D. Wolf, M. U. Hasan, M. Huang, D. Bono, K. Nielsch, K. Leistner, and G. S. D. Beach, *Magnetoionic Control of Perpendicular Exchange Bias*, Phys. Rev. Mater. 5, L061401 (2021). [4] M. Huang, M. U. Hasan, K. Klyukin, D. Zhang, D. Lyu, P. Gargiani, M.l Valvidares, S. Sheffels, A. Churikova, F. Büttner, J. Zehner, L.Caretta, K. Y. Lee, J. Chang, J. P. Wang, K. Leistner, B. Yildiz and G. S. D. Beach, *Voltage control of ferrimagnetic order and voltage-assisted writing of ferrimagnetic spin textures*, Nature Nanotechnology 2021 – *accepted for publication* –

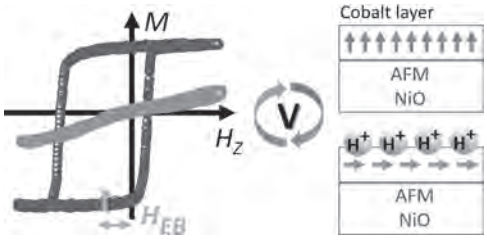

Fig. 1: Voltage induced switching between PEB and in-plane anisotropy.[3]

BOD-05. Noncollinear antiferromagnetic textures in confined geometries. *O. Pylypovskyi*[1,2], N. Hedrich[3], K. Wagner[3], A.V. Tomilo[4], B.J. Shields[3], T. Kosub[1], D.D. Sheka[4], J. Fassbender[1], P. Maletinsky[3] and D. Makarov[1] *1. Helmholtz-Zentrum Dresden-Rossendorf e.V., Dresden, Germany; 2. Kyiv Academic University, Kyiv, Ukraine; 3. Universitat Basel, Basel, Switzerland; 4. Taras Shevchenko National University of Kyiv, Kyiv, Ukraine*

In comparison with ferromagnetic domain walls and skyrmions, their counterparts in antiferromagnets (AFMs) demonstrate appealing properties in their control and dynamics, e.g., absence of Walker limit and Magnus force [1]. The complex intrinsic magnetic structure of AFMs leads to special properties such as negligibly small stray fields, exchange-enhanced resonance frequencies up to THz range, and the presence of staggered spin-orbit torques. Together they render AFMs as prospective materials for spintronic and spin-orbitronic applications [2]. Here, we consider bipartite, easy-axis AFM samples of finite size. We derive the boundary conditions for the Neel order parameter in the presence of Dzyaloshinskii-Moriya interactions (DMI) of Bloch type in addition to exchange (see Fig. 1), and apply them to describe domain walls and skyrmions. DMI leads to the deformation of the uniform ground state at the side faces, with the twist angle proportional to the DMI coefficient. Both domain walls and skyrmions become wider and change their type to the mixed Bloch-Neel one when approaching the top (bottom) surface of the sample. The characteristic depth where the influence of the boundary on magnetic texture is significant is about 5 magnetic lengths [3]. In the absence of the intrinsic DMI, the exchange-driven boundary conditions determine the behavior of domain walls in AFMs with a patterned surface. Imaging the domain wall in a single crystal Cr_2O_3 using nitrogen vacancy (NV) magnetometry, we show that it mimics the behavior of an elastic ribbon deformed by the effective pinning sites created by mesas. Crossing the mesa at an angle, the domain wall shape experiences an additional

bend, determined by the aspect ratio of the mesa A=t/w with t and w being its thickness and width, see Fig. 2. This deformation can be described by the effective Snell's law as $\sin\theta_i/\sin\theta_r \approx 1 + 3.1\,A$ with θ_i and θ_r being incidence and refraction angles at the top surface [4].

[1] O. Gomonay, V. Baltz, A. Brataas et al. Nat. Phys. Vol. 14, P. 213 (2018). [2] V. Baltz, A. Manchon, M. Tsoi et al. Rev. Mod. Phys. Vol. 90, P. 015005 (2018), H. Yan, Z. Feng, P. Qin et al. Avd. Mat. Vol. 32, P. 1905603 (2020). [3] O. V. Pylypovskyi, A. V. Tomilo, D. D. Sheka et al. Phys. Rev. B, Vol. 103, P. 134413 (2021) [4] N. Hedrich, K. Wagner, O. V. Pylypovskyi et al. Nat. Phys. Vol. 17, P. 574 (2021)

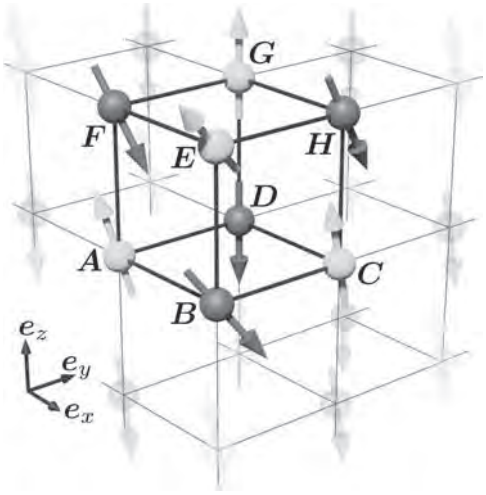

Fig. 1 Tilt of the boundary spins in G-type chiral AFM [3]. The highlighted octamer with spins A...H is represented by a single Neel vector.

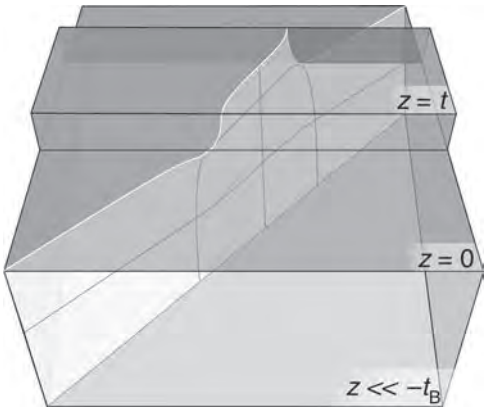

Fig. 2 Deformation of the domain wall crossing the mesa of thickness *t* (simulations) [4].

BOD-06. Acoustically Actuated Antennas Induced by Magnon-Phonon Coupling. *Y. Ji*[1] and T. Nan[1] *1. School of Integrated Circuits, Tsinghua University, Beijing, China*

Recently, acoustically actuated antennas based on the thin-film magnetoelectric heterostructures have been demonstrated with 1-2 orders of magnitude miniaturization over the conventional counterparts. However, it remains challenging to improve their radiation efficiency and develop the high quality antenna modulation technique. Here, we computationally demonstrate a fully coupled model describing the radiation mechanism, including Newton, Maxwell and Landau-Lifshitz-Gilbert (LLG) equations, together with piezoelectric and magnetostrictive constitutive relations. We theoretically propose that magnons, the quanta of spin waves, can be utilized to strongly enhance the radiation efficiency of acoustically actuated antennas when magnon and phonon modes are coupled. In the strong coupling region, our model shows that the radiation efficiency can be 100-time enhanced, and antenna modulation can be substantially simplified. Additionally, a right-hand circular polarization (RHCP) radiation field can be observed.

[1] T. Nan, H. Lin, Y. Gao et al., "Acoustically actuated ultra-compact NEMS magnetoelectric antennas," Nat. Commun., vol. 8, no. 296, 2017. [2] Z. Yao, S. Tiwari, T. Lu et al., "Modeling of Multiple Dynamics in the Radiation of Bulk Acoustic Wave Antennas," IEEE J. Multiscale Multiphys. Comput. Tech., vol. 5, pp. 7–20, 2019. [3] C. Berk, M. Jaris, W. Yang et al., "Strongly coupled magnon–phonon dynamics in a single nanomagnet," Nat. Commun., vol. 10, no. 2652, 2019.

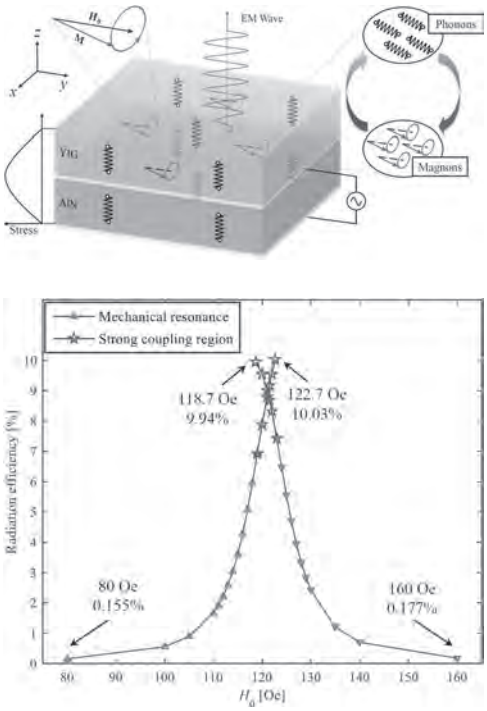

BOD-07. Proton switching molecular magnetoelectricity. *Y. Hu*[1*] and S. Ren[1] *1. The State University of New York, Buffalo, Buffalo, NY, United States*

Molecular magnets and ferroelectrics alone have reached a record high critical temperature.[1-4] The van-der-Waals-bonded molecular magnets and ferroelectrics become a major challenge for the strain or Coulomb screen mediated magnetoelectric coupling, due to the weak strictive effect and limited Coulomb screening of molecular insulating building blocks.[1-4] Molecular materials benefit from their synthetic versatility that results from local coordination and proton chemistries, as well as their large lattice and vacancy network structures that allow precise tailoring and stimuli-dependent modulation of their properties.[1-7] The convergence of proton conduction and multiferroics is generating a compelling opportunity to achieve strong magnetoelectric coupling and magneto-ionics, offering a versatile platform to realize molecular magnetoelectrics.[1-3] In the work, we describe machine learning coupled with additive manufacturing to accelerate the design strategy for hydrogen-bonded multiferroic macromolecules accompanied by strong proton dependence of magnetic properties. The heterogeneous macromolecules studied here are grown in aqueous solution at room temperature, with the capability of additive manufacturing, and present an extraordinarily proton-compatible low driving field (Fig. 1). The proton switching magnetoelectricity occurs in three-dimensional molecular heterogeneous solids (Fig. 2). It consists of a molecular magnet network as proton reservoir to modulate ferroelectric polarization, while molecular ferroelectrics charging proton transfer to reversibly manipulate magnetism. The magnetoelectric coupling induces a reversible 29% magnetization control at ferroelectric

phase transition with a broad thermal hysteresis width of 160 K (192 K to 352 K), while a room-temperature reversible magnetic modulation is realized at a low electric field stimulus of 1 kV cm^{-1}. The findings of electrostatic proton transfer provide a pathway of proton-mediated magnetization control in hierarchical molecular multiferroics.

1. Y. Hu et al., Nat. Commun., (2021) (In press). 2. Y. Hu, S. Ren, APL Materials, Vol.8, p.080702 (2020). 3. Y. Hu et al., Proc. Natl. Acad. Sci. U.S.A., Vol.117, p.27204 (2020). 4. P. Perlepe et al., Science, Vol.370, p.587 (2020). 5. Y. Hu et al., Adv. Mater., Vol.31, p.1807178 (2019). 6. Y.Hu et al., Small, Vol.15, p.1900299 (2019). 7. Y. Hu et al., Adv. Mater., (2021) (In press).

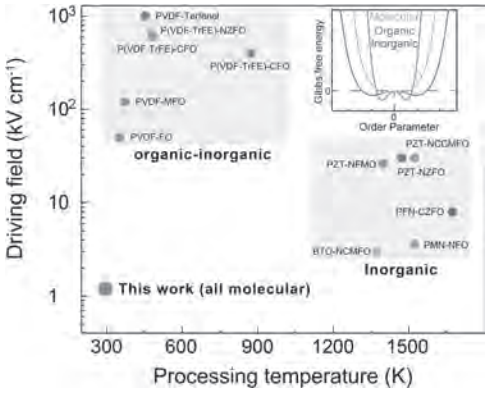

Fig.1. Selected multiferroic composites. Inset shows the free energies.

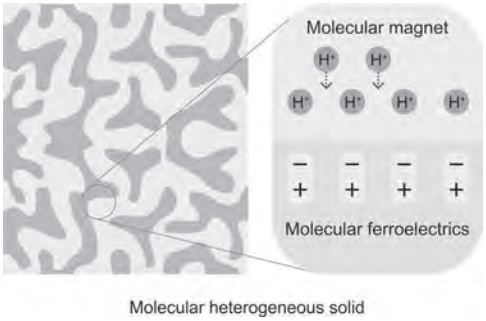

Fig. 2. Schematic diagram for the proposed proton mediated ME coupling in molecular heterogeneous solid.

BOD-08. Effect of Exchange Coupled Magnetic Structures on Magnetization Switching of Strain-Mediated Magnetoelectric Heterostructures. *P. Pathak*[1] and D. Mallick[1] *1. Electrical Engineering, Indian Institute of Technology Delhi, New Delhi, India*

Strain-mediated magnetoelectric (ME) heterostructures comprising ferromagnetic and piezoelectric materials have received substantial importance due to their energy efficiency[1]. A large number of works on ME devices are reported in the literature, comprise of a single ferromagnetic layer[2]. However, the ME properties can be enhanced efficiently by using multi-layered ferromagnetic structures exchange-coupled at the interface. By dimensionally varying the individual ferromagnetic layer, the ME properties can be tuned also. In this work, we investigated the ME properties of exchange coupled Ni/FeGaB (ferromagnets) on single-crystal PMN-PT (piezoelectric) substrate using the finite difference method (Fig 1). Elliptical ferromagnets of bilayer Ni/FeGaB having different aspect ratios (AR=Major axis: Minor axis) are simulated. For equal thicknesses of Ni and FeGaB, in-plane rotation towards tensile stress direction is observed once an external voltage is applied across PMN-PT. This shows that the larger magnetostrictive coefficient material contributes more due to dominant stress anisotropy energy when the equal thickness of bilayer ferromagnets is considered. Secondly, unequal thicknesses of Ni and FeGaB are considered. It is observed that in-plane rotation is predicted by the magnetic layer having a larger thickness once an external voltage is applied. Thick FeGaB ferromagnet showed in-plane rotation towards tensile stress, while thick Ni ferromagnet showed in-plane rotation towards compressive stress direction. This is predicted because the dominant stress anisotropy energy lies along the tensile and compressive stress direction for FeGaB and Ni respectively. In all cases, it is observed that in-plane rotation reduces towards principal stress direction when AR is increased. This is because the stress anisotropy energy reduces and demagnetization energy rises with increasing AR. This work confirms the tunability of ME properties in exchange-coupled strain-mediated ME structures.

[1] P.Pathak and D.Mallick, "Size-Dependent Magnetization Switching in Magnetoelectric Heterostructures for Self-Biased MRAM Applications," in IEEE Transactions on Electron Devices, doi: 10.1109/TED.2021.3088079. [2] I. M. Miron et al., "Perpendicular switching of a single ferromagnetic 371 layer induced by in-plane current injection," Nature, vol. 476, no. 7359, 372 pp. 189–193, Aug. 2011, doi: 10.1038/nature10309.

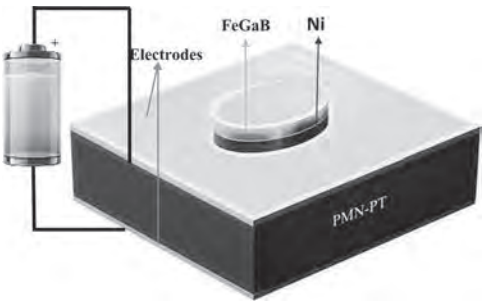

Prototype schematic investigated.

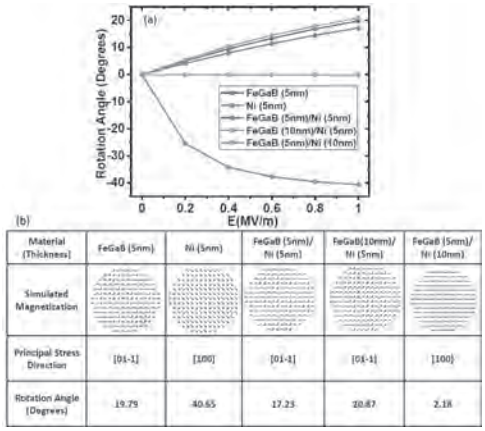

(a) Electric field controlled magnetic rotation for elliptical ferromagnet of AR 1.1:1 and corresponding (b) Simulated magnetization and calculated rotation angle at E=1MV/m.

BOD-09. Voltage Controlled Superparamagnetic Ensembles for Low Power Reservoir Computing. *A. Welbourne*[1], A.L. Levy[2], M.O. Ellis[1], H. Chen[1], M.J. Thompson[1], E. Vasilaki[1], D. Allwood[1] and T. Hayward[1] *1. University of Sheffield, Sheffield, United Kingdom; 2. École Polytechnique, Paris, France*

Reservoir computing is gaining traction as a bio-inspired, novel-hardware, machine-learning approach to solving the computational problems fundamental to modern technology [1]. Magnetic systems fulfill the requirements of reservoirs: non-linearity, fading memory, and a reproducible response. When subject to a temporal input sequence they can replace algorithms on complex networks of transistors [2]. This offers the potential for compact devices, with reduced energy costs. Here, we propose voltage-controlled superparamagnetic ensembles as ideal candidates for ultra-low-energy reservoirs.

In these devices thermal noise is utilised to drive dynamics and data input is provided by strain-mediated voltage inputs [3]. Using an analytical model (confirmed by micromagnetics) of the response of the system [4], we simulate the physical reservoir (Fig. 1). By inputting a temporal sequence and training a single layer of output weights, we have performed standard machine learning benchmarks with competitive performance: spoken digit recognition with 95 % accuracy, and chaotic time series prediction with error comparable to current reservoir approaches [1,2]. We also explore how the use of delayed feedback can provide substantial error reductions in chaotic time series prediction tasks. Fig. 2 illustrates how high performance on the NARMA10 task can be maintained on timescales from τ = 1.4 μs (KV/K_BT = 20) to τ = 66 ms (KV/K_BT = 50) by tuning the strength of the delayed feedback. We suggest that the low energy consumption expected for these voltage controlled and thermally driven, devices makes them ideal candidates for edge computing applications where high performance is needed at very low latency and power.

[1] L. Appeltant, et al., Nature Communications, Vol. 2, p.468 (2011) [2] J. Grollier, et al., Nature Electronics, Vol. 3, p.360-370 (2020) [3] A. Welbourne, et al., Applied Physics Letters, Vol. 118, p.202402 (2021) [4] O. Hovorka, et al., Applied Physics Letters, Vol.97, p.062504 (2010)

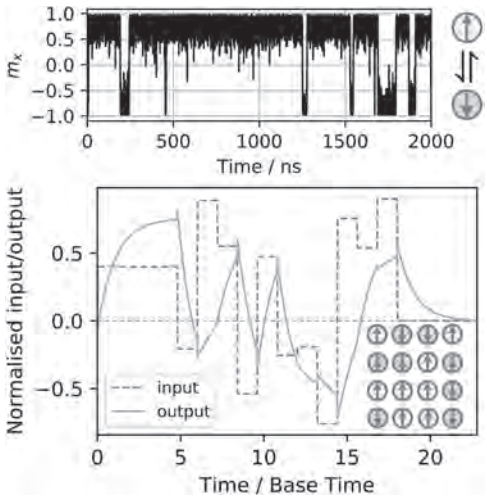

Fig. 1 Superparamagnetic ensemble. Applied strain biases dwell times of individual dots in up versus down states. A reproducible non-linear response with fading memory emerges from the ensemble average of many stochastic nanodots subject to the same temporal input.

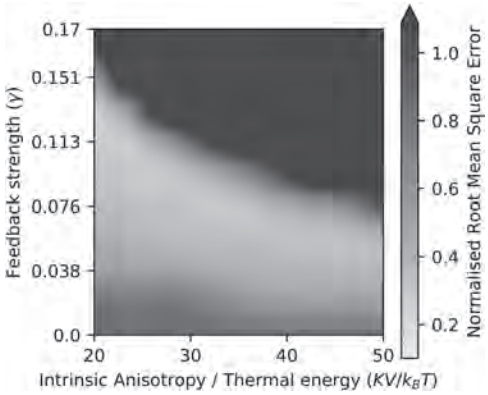

Fig. 2 Performance in chaotic time series prediction (NARMA10) as a function of uniaxial anisotropy strength (normalized by thermal energy). Performance is maintained across a range of timescales by tuning the strength of delayed feedback into the reservoir.

BOD-10. Laser-Controlled Real and Reciprocal Space Topology in Multiferroic Insulators. T. Hirosawa[1], J. Klinovaja[1], D. Loss[1] and *S.A. Diaz*[2] *1. University of Basel, Basel, Switzerland; 2. University of Duisburg-Essen, Duisburg, Germany*

Magnetic materials in which it is possible to control the topology of their magnetic order in real space or the topology of their magnetic excitations in reciprocal space are highly sought-after as platforms for alternative data storage and computing architectures. Here we show that multiferroic insulators, owing to their magneto-electric coupling, offer a natural and advantageous way to address these two different topologies using laser fields. We demonstrate that via a delicate balance between the energy injection from a high-frequency laser and dissipation, single skyrmions—archetypical topological magnetic textures—can be set into motion with a velocity and propagation direction that can be tuned by the laser field amplitude and polarization, respectively. Moreover, we uncover an ultrafast Floquet magnonic topological phase transition in a laser-driven skyrmion crystal and we propose a new diagnostic tool to reveal it using the magnonic thermal Hall conductivity.

T. Hirosawa, J. Klinovaja, D. Loss, and S. A. Díaz, "Laser-controlled real- and reciprocal-space topology in multiferroic insulators," arXiv:2108.06535.

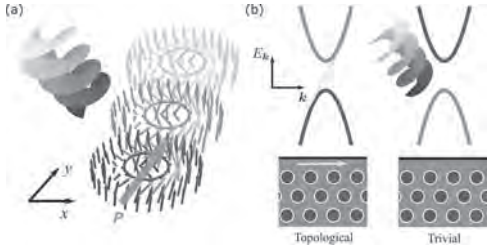

Real- and reciprocal-space topology can be controlled by lasers. (a) The topological spin structure of a skyrmion carrying in-plane electric polarization P undergoes translational motion under a circularly polarized laser. (b) An ultrafast topological phase transition occurs in the Floquet magnon band structure of skyrmion crystals due to the effective magnetic field induced by circularly polarized laser irradiation.

BOD-11. Lattice dynamics and trimeron order of the Verwey transition in magnetite - theory vs. experiment. *D. Legut*[1] and P. Piekarz[2] *1. IT4Innovations, VSB Technical University of Ostrava, Ostrava, Czechia; 2. Institute of Nuclear Physics, Polish Academy of Sciences, Cracow, Poland*

In this talk, we shed a light on hidden quantum properties in magnetite, the oldest magnetic material known to mankind. The study reveals the existence of low-energy waves that indicate the important role of electronic interactions with the crystal lattice as well as the lattice vibrations in both high-temperature cubic as well low-temperature monoclinic phases. This is another step to fully understand the metal-insulator phase transition mechanism in magnetite, and in particular to learn about the dynamical properties and critical behavior of this material in the vicinity of the transition temperature. The attention of physicists in magnetite was attracted by the fact that at a temperature of 125 K it shows an exotic phase transition, named after the Dutch chemist Verwey. This Verwey transition was also the first phase metal-to-insulator transformation observed historically. During this extremely complex process, the electrical conductivity changes by as much as two orders of magnitude and a rearrangement of the crystal structure take place. Verwey proposed a transformation mechanism based on the location of electrons on iron ions, which leads to the appearance of a periodic spatial distribution of Fe^{2+} and Fe^{3+} charges at low temperatures as well as the orbital order. In this talk, we confirm the fundamental components of this charge-orbital ordering are polarons – quasiparticles formed as a result of

local deformation of the crystal lattice caused by the electrostatic interaction of a charged particle (electron or hole) moving in the crystal. In the case of magnetite, the polarons take the form of trimerons, complexes made of three iron ions, where the inner atom has more electrons than the two outer atoms. Our study reveals a very accurate model of lattice vibrations for the high-temperature phase as well as confirm the effect of the charge-orbital (trimeron) order on phonon energies and mean square displacements in the monoclinic(low-temperature) phase and hence to contribute to shed a light at the complexity of the Verwey transition. The work was published [1-3] and acknowledges Path to Exascale project, No.CZ.02.1.01/0.0/0.0/16_013 /0001791.

1. E. Baldini, C.A.. Belvin, M. Rodriguez-Vega, I. O. Ozel, D. Legut, A. Kozlowski, A. M. Oles, K.Parlinski, P. Piekarz, J. Lorenzana, G. A. Fiete, and N. Gedik, *Discovery of the soft electronic modes of the trimeron order in magnetite*, Nature Physics 16, 541 (2020). 2. S. Borroni, E. Baldini, V. M. Katukuri, A. Mann, K. Parlinski, D. Legut, C. Arrell, F. van Mourik, J. Teyssier, A. Kozlowski, P. Piekarz, O. V. Yazyev, A. M. Oles, J. Lorenzana, and F. Carbone, *Coherent generation of symmetry-forbidden phonons by light-induced electron-phonon interactions in magnetite*, Phys. Rev. B 96, 104308 (2017). 3. P. Piekarz, D. Legut, E. Baldini, C. A. Belvin, T. Kolodziej, W. Tabi,A. Kozlowski, Z. Kakol, Z. Tarnawski, J. Lorenzana, N. Gedik, A. M. Oles, J. M. Honig, and K. Parlinski, *Trimeron-phonon coupling in magnetite*, Phys. Rev. B 103, 104303 (2021).

BOD-12. Withdrawn

BOD-13. Cross-linking and charging molecular magnetoelectronics.

Y. Huang[1], Y. Chen[2], Y. Hu[1], T. Mitchell[1], L. An[1], Z. Li[1], J. Benedict[1], H. Li[2] and S. Ren[1] *1. University at Buffalo, Buffalo, NY, United States; 2. Sun Yat-Sen University, Guangzhou, China*

Magnetoelectrics are witnessing an ever-growing success towards the voltage-controlled magnetism derived from inorganic materials. However, these have predominantly focused on the ferroelectromagnetism at solid-to-solid interfaces suffering several drawbacks, including the interface-sensitive coupling mediators, high-power electric field, and limited chemical tunability. Here we report a promising design strategy to shift the paradigm of next-generation molecular magnetoelectrics, which relies on the integration between molecular magnetism and electric conductivity though an in-situ cross-linking strategy. Following this approach, we demonstrate a versatile and efficient synthesis of flexible molecular-based magnetoelectronics by cross-linking of magnetic coordination networks that incorporate conducting chain building blocks. The as-grown compounds feature an improved critical temperature up to 337 K and a room-temperature magnetism control of low-power electric field. It is envisaged that the cross-linking of molecular interfaces is a feasible method to couple and modulate magnetism and electron conducting systems.

[1] Y.L. Huang, et al., *Nano Lett.*, 21, 9, 4099–4105 (2021). [2] Y.L. Huang, and S.Q. Ren, *Appl. Mater. Today* 22, 100886 (2021).

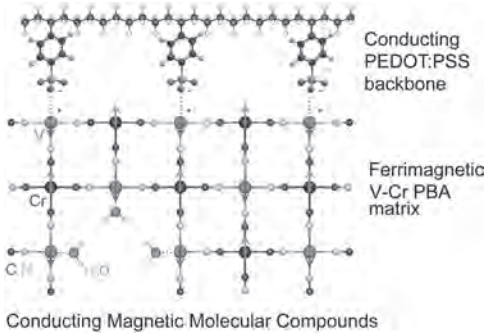

The proposed schematic structure of conducting magnetic molecular compounds (MCs). The room-temperature ferrimagnetically ordered V-Cr PBA matrix is cross-linked with conducting PEDOT:PSS backbones. The most promising model is that a negative SO_3^- anion is cross-linked (dash red line) to a positive vanadium cation to compensate for the vacancy of $[Cr(CN)_6]^{3-}$ anion.

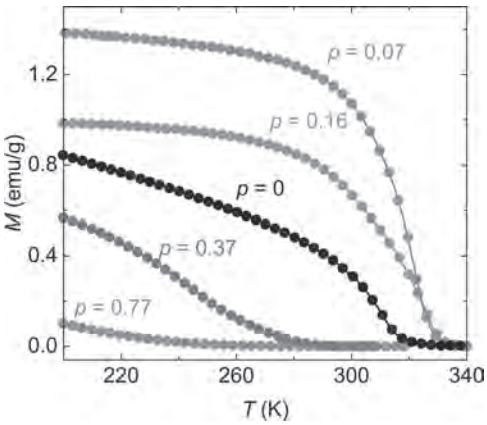

Temperature dependent magnetization of MCs with p (the atomic ratio of sulfur and vanadium in synthesized MCs) varying from 0 to 0.77 under a magnetic field of 10 Oe indicate a tunable the ferrimagnetic transition T_c that is enhanced from 320 K ($p = 0$) to 337 K ($p = 0.07$), then is reduced ($p > 0.16$) to below room temperature.

Session BPA
MAGNETOELECTRONIC MATERIALS AND PHENOMENA
(Poster Session)

Luis M. Moreno-Ramírez, Chair
Universidad de Sevilla, Seville, Spain

BPA-01. Electronic band structure and magnetism of $CoFeV_{0.5}Mn_{0.5}Si$. *G. Baker*[1], M. Flesche[1], A. Ramker[2], P. Shand[2], P. Lukashev[2] and P. Kharel[1]
1. Physics, South Dakota State University, Brookings, SD, United States; 2. Physics, University of Northern Iowa, Cedar Falls, IA, United States

Half-metallic Heusler alloys have attracted much attention due to their potential application in spin-transport-based devices. We have synthesized one such alloy, $CoFeV_{0.5}Mn_{0.5}Si$, using arc melting and high-vacuum annealing. The vacuum annealing was done at 600°C for 24 hours. First principles calculation indicates that $CoFeV_{0.5}Mn_{0.5}Si$ shows nearly half-metallic band structure with the degree of spin polarization of about 93%. The room temperature x-ray diffraction patterns are indexed with the cubic crystal structure without disorder and secondary phases. The annealed sample show ferromagnetic order with the Curie temperature well above room temperature (Tc = 657 K) and the high-field (3T) magnetization at room temperature of about 83 emu/g. Figure 1 below shows the magnetization as a function of temperature of $CoFeV_{0.5}Mn_{0.5}Si$ measured at 1 kOe which shows a smooth magnetic transition at the Curie temperature. The observed structural and magnetic properties are consistent with the theoretical results and these results indicate that $CoFeV_{0.5}Mn_{0.5}Si$ has a potential for room temperature spin-transport-based devices. This research is supported by the *National Science Foundation* (NSF) under Grant Numbers 2003828 and 2003856 via DMR and EPSCoR.

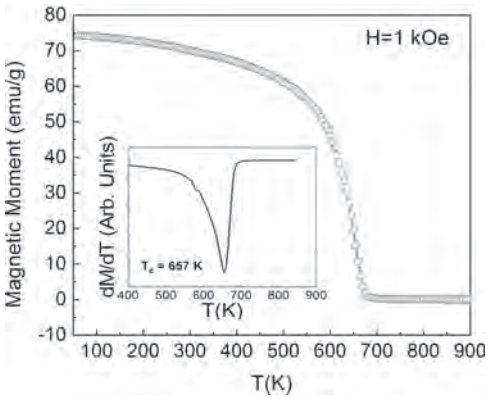

Figure 1: Thermomagnetic curve M(T) of $CoFeV_{0.5}Mn_{0.5}Si$ alloy. The inset shows the dM/dT versus T curve.

BPA-02. Antiferromagnetic Phase in Sputtered Topological Insulator/Ferromagnetic Heterostructure Interface. *N. Bhattacharjee*[1], A. Fedorko[1], V. Lauter[2], M. Matzelle[1], B. Singh[3], A.J. Grutter[4], A.R. Will-Cole[1], R. Markiewicz[1], A. Bansil[1], D. Heiman[1] and N.X. Sun[1]
1. Northeastern University, Boston, MA, United States; 2. Oak Ridge National Laboratory, Oak Ridge, TN, United States; 3. Tata Institute of Fundamental Research, Mumbai, India; 4. National Institute of Standards and Technology, Gaithersburg, MD, United States

A gap opening in the surface state bands via breaking of TRS in topological insulators (TI) is needed for realization of dissipationless Quantum Anomalous Hall Effect (QAH) and other fascinating topological properties [1-5]. Here, we report formation of an antiferromagnetic (AFM) phase at the interface of sputter grown crystalline textured TI, Bi_2Te_3 when coupled with ferromagnetic metal (FM), $Ni_{80}Fe_{20}$ (Permalloy, Py). We grew samples of 40 nm c-axis oriented Bi_2Te_3 at 250 degC followed by 20 nm of Py at room temperature. Diffusion of Ni from Py and formation of distinct Ni-doped Bi2Te3 interfacial phase was observed. Zero Field Cooled (ZFC) magnetic hysteresis loop measurements at low temperatures showed a large spontaneous exchange bias of ~80 Oe at 6 K which suggests presence of strong FM/AFM coupling in the samples (Figure. 1). Location of the antiferromagnetic phase at Ni intercalated Bi_2Te_3 interfacial layer was identified using Polarized Neutron Reflectometry (PNR) (Figure 2) at 7 K. The magnetic scattering length density (MSLD) has a value of ~0.26 at 1T saturation field but is ~0 at a low field of 50 Oe when the magnetic moments in the interfacial layer are antiferromagnetically ordered. The large exchange bias in the Ni intercalated Bi_2Te_3 interfacial layer clearly suggests a large exchange energy which is characteristic of super-exchange mediated coupling of moments in Ni, Bi and Te based Van der Waals (VdW) MTI compounds [8]. This large exchange bias raises the possibility of formation of topologically nontrivial magnetic material at the interface. The observation of magnetic phase at the interface layer further raises the possibility of QAH state and paves the way for further exploration of TI/FM based heterostructures and applications for energy efficient spintronic devices which are compatible with industrial CMOS processes.

1. Y. L. Chen, J. G Anaytis and J.H. Chu et al., Science Vol. 325, p. 5937 (2009). 2. J. Wang, B. Liang and S.C. Zhang et al., Phys. Rev. B 92, 081107(R) (2015). 3. D. Xiao, J. Jiang and C. Z. Chang et al., Phys. Rev. Lett. 120, 056801 (2018). 4. J. Li, Y. Li and Y. Xu et al., Sci. Adv. 5: eaaw5685 (2019). 5. Y. Deng, Y. Yu and Y.Zhang et al., Science Vol. 367, Issue 6480, pp. 895-900 (2020).

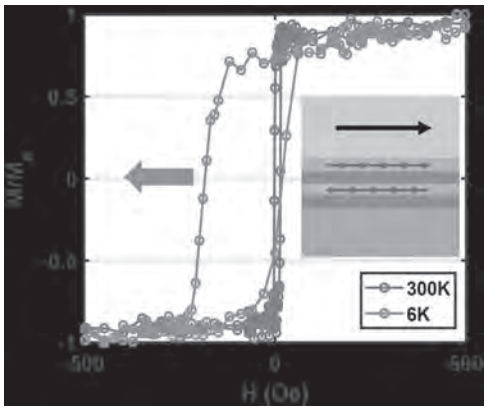

Fig. 1 ZFC hysteresis loop measured at 300 K and 6 K. At 6 K a large exchange bias of ~80 Oe emerges because of coupling of AFM interface layer with FM Py layer.

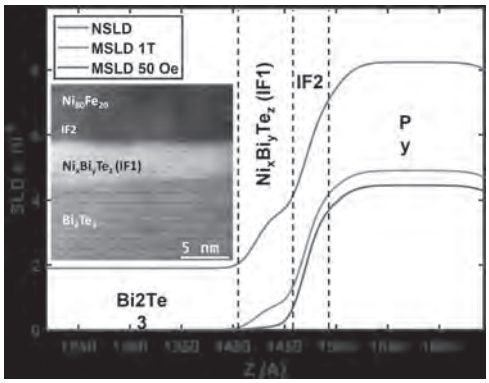

Fig. 2 PNR measurement at 7 K showing finite moments at 1 T saturation and AFM ordering at the Ni intercalated interface at 50 Oe. Inset: STEM-HAADF image with clear indication of the AFM Ni-intercalated Bi2Te3 layer.

BPA-03. Determining critical and Curie temperature of Heusler superconducting ferromagnets *Ni_2NbSnZ* (*Z = Ga*, *Ge,* and *Sb*).
S. Nalevanko[1,2], L. Galdun[2,3], M. Varga[2], A. Dzubinska[2], M. Reiffers[4], J. Kacmarcik[5] and R. Varga[2,3] *1. Institute of Physics, Univerzita Pavla Jozefa Safarika v Kosiciach, Kosice, Slovakia; 2. CPM - TIP, Univerzita Pavla Jozefa Safarika v Kosiciach, Kosice, Slovakia; 3. RVmagnetics, a. s., Kosice, Slovakia; 4. Fac. Hum. and Nat. Sci., Presovska Univerzita v Presove, Presov, Slovakia; 5. Centre of Low Temperature Physics, Ustav experimentalnej fyziky Slovenskej akademie vied, Kosice, Slovakia*

Superconductor science is rapidly progressing, and new superconducting materials are being explored, such as ferromagnetic superconductors. Heusler alloys with the stoichiometry X_2YZ, where *X* and *Y* are transition metals and *Z* is the p-element [1], show several physical properties depending on their chemical composition. Besides spin polarisation, magnetocaloric, or shape memory effect, they may also exhibit the mentioned coexistence of ferromagnetism and superconductivity. *Ni_2NbSn* represents such a superconducting Heusler alloy with a ferromagnetic ordering under the critical temperature of superconductivity. The critical temperature of the alloy is 3.4 K [2] at zero external magnetic field, which is still insufficient for practical use. One of the solutions to increase the alloy's critical temperature may consist of doping with p-elements, which modifies the lattice constant and the pressure inside the crystal lattice. The characteristics of the alloys in the series *$Ni_{50}Nb_{25}Sn_{24}Z_1$*, where *Z* is *Ga*, *Ge*, or *Sb* have been determined by structural, magnetic, and transport measurements. It has been shown that even the 1 % doping has modified the magnetic and superconducting properties of the alloys. The measurements showed that Curie and superconducting temperature are always close to each other, which means that superconductivity correlates with ferromagnetism.

[1] T. Klimczuk, C. H. Wang and K. Gofryk, PHYSICAL REVIEW B, Vol. 85, p.174505 (2012) [2] T. Graf, C. Felser and S. S.P. Parkin, Progress in Solid State Chemistry, Vol. 39, p.1-50 (2011)

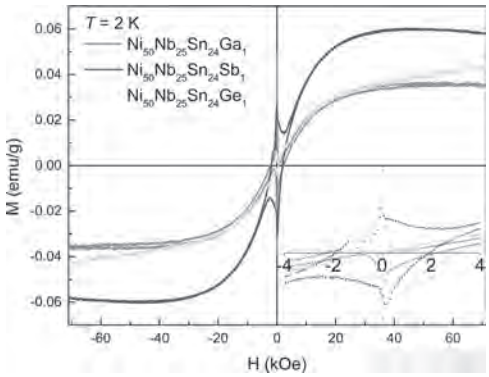

Hysteresis loop measurements of the doped alloys at the temperature of 2 K.

BPA-04. Growth of ferromagnetic Kagome metal Fe_3Sn_2 using Pt buffer layer.
K. Khan[1], H. Bangar[1], R.S. Yadav[1] and P.K. Muduli[1] *1. Physics, Indian Institute of Technology Delhi, New Delhi, India*

Fe_3Sn_2 is a ferromagnetic (FM) kagome metal that shows many interesting properties such as large anomalous Hall effect (AHE) [1], spin re-orientation with temperature [2], and formation of magnetic skyrmions without requiring DMi [3]. In this work, we demonstrate the growth of ferromagnetic Fe_3Sn_2 thin films by using a platinum (Pt) buffer layer. We deposited Fe_3Sn_2 thin film on two different buffer layers (Ta, Pt) as 1) Sample 1(color: blue): Subs.Si-SiO_2/Ta(3nm)/Fe_3Sn_2(60 nm) and, 2) Sample 2(color: red): Subs.Si-SiO_2/Pt(3nm) /Fe_3Sn_2(60 nm) grown at room temperature using RF-magnetron sputtering with a working pressure of 2 mTorr. Subsequently, the samples were annealed at 500 ^oC for 1 hr. In Fig.1, X-ray diffraction measurements have been performed, sample 1 shows peak (2θ) at 28, 33.9, 39.8, and 44.6^o corresponding to (011), (110), (111), and (021) reflection of AFM phase (FeSn) and peak (2θ) at 30, 40.6, and 43 correspond to (015), (002) and (024) reflection of ferromagnetic (Fe_3Sn_2). Thus sample 1 has both FM (Fe_3Sn_2) as well as AFM (FeSn) phases present. In sample 2, all peaks of the AFM phase are almost completely suppressed and only observed an enhanced peak (2θ) at 30 and 43 corresponds to (015) and (024) reflection of FM (Fe_3Sn_2) phase. As shown in inset Fig 2, sample 1 we obtained a large value of coercive field ($H_c \approx 275$ Oe) and a low value of saturation magnetization ($M_s \approx 240$ emu/cc). Whereas for sample 2, we found a low ($H_c \approx 100$ Oe) and large ($M_s \approx 464$ emu/cc). The value of M_s for sample 1 is low due to the small FM domain embedded inside AFM domains, while the M_s for sample 2 is almost comparable to the bulk value due to a single FM phase [4]. We have also performed the M-T measurement on these samples as shown in Fig 2. We observed more than two times enhancement of M_s for sample 1 in which Fe_3Sn_2 was grown on Pt buffer layer as compared to Ta buffer layer. Since, Pt buffer layer provides a good lattice matching with Fe_3Sn_2 and increases the crystallinity of Fe_3Sn_2 film, leading to higher M_s.

[1] T. Kida *et.* al, J. Phys.: Condens. Matter, 23, 112205 (2011). [2] L. Fenner, A. Dee, and A. Wills, J. Phys.: Condens. Matter, 21, 452202 (2009). [3] Z. Hou *et*. al., Adv. Mat,. 29, 1701144 (2017). [4] L.Ye., M. Kang, J. Liu *et al.*, Nature, 555, 638 (2018)

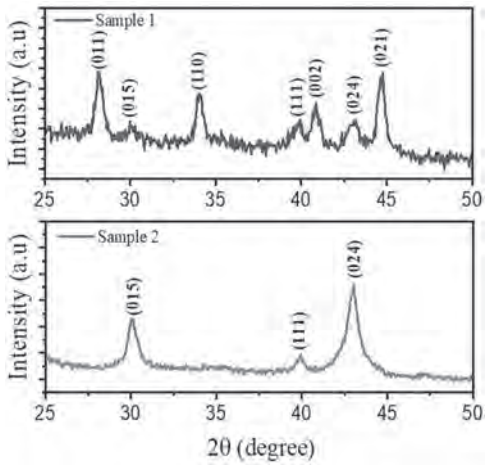

Fig. 1. XRD pattern of sample 1 and sample 2.

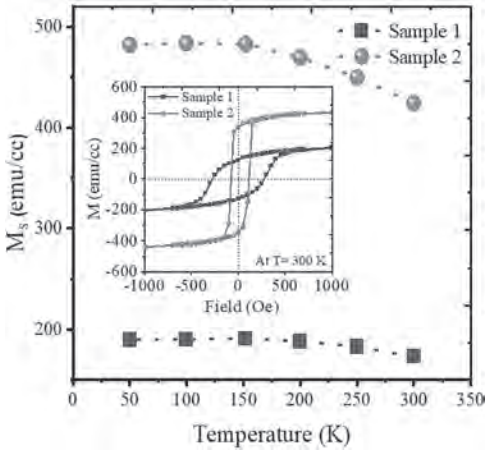

Fig. 2. M-T measurement of sample 1 and sample 2 with buffer layers of Ta and Pt, respectively, and the inset shows the room temperature magnetization curve.

BPA-05. Spin-gapless semiconducting behavior and sublattice spin cross-over in magnetically compensated half-Heusler compound ($Co_{0.5}Mn_{0.5}$)MnAl. *R. Harikrishnan*[1] and N. Harish Kumar[1] *1. Advanced Magnetic Materials Laboratory, Department of Physics, Indian Institute of Technology, Madras, Chennai, India*

Spin gapless semiconductors (SGSs) are an alternative for dilute magnetic semiconductors in magnetic multilayer devices. Though many Heusler-based SGSs exist, their high magnetic moment can reduce the efficiency of spintronic devices. A fully compensated ferrimagnetic SGS (FCF-SGS) with high spin polarisation will be an ideal choice for efficient spin transport. The FCF-SGS state has been reported in some full-Heusler and Quaternary Heusler systems[1][2]. But the experimental studies on half-Heusler compounds have received relatively less attention. Though the FCF-SGS state has been predicted in a number of half-Heusler compounds, none of them crystallized in the $C1_b$ structure [3][4]. Jianhua Ma *et al.*predicted the coexistence of a pseudogap near the Fermi energy and ferrimagnetism in CoMnAl, with a magnetic moment of 1 μ_B/f.u [5]. As per the Slater-Pauling (S-P) rule, magnetic moment compensation in CoMnAl can be achieved by replacing half of the Co atoms with Mn. The structural properties, magnetic moment compensation, and SGS properties of the polycrystalline ($Co_{0.5}Mn_{0.5}$)MnAl prepared by Arc-melting were investigated in detail. The sample crystallized in $C1_b$ structure with lattice parameter 5.85 Å. The magnetic moment at 5 K was found to be 0.09 μ_B/f.u, in agreement with the S-P rule and indicates fully compensated ferrimagnetism. The sublattice-spin cross-over is revealed by the change in sign observed in the magnetization and anomalous Hall effect measurement across the compensation point. The high Curie temperature (613 K) suggests strong exchange interaction between Mn and Co atoms (Fig.1). In the temperature range 2-400 K, the sample exhibits an unusual semiconducting behavior with less temperature dependence of resistivity (Fig.2), nearly constant carrier concentration, a very small Seebeck coefficient, and low density of state, as seen in other previously reported spin-gapless semiconductors [6].

[1] W. Feng, X. Fu and C. Wan, Phys. Status Solidi - Rapid Res. Lett. 9, 641–645,(2015). [2] Y. Venkateswara, S. Gupta, and S.S. Samatham, Phys. Rev. B. 97 1–8, (2018). [3] Y.J. Zhang, Z.H. Liu and E.K. Liu, Epl. 111, (2015). [4] Y.J. Zhang, Z.H. Liu, and Z.G. Wu, IUCrJ. 6, 610–618, (2019). [5] J. Ma, V.I. Hegde and K. Munira, Phys. Rev. B. 95,1–25, (2017). [6] S. Ouardi, G.H. Fecher, C. Felser, Phys Rev Lett, 100401, 2–6, (2013).

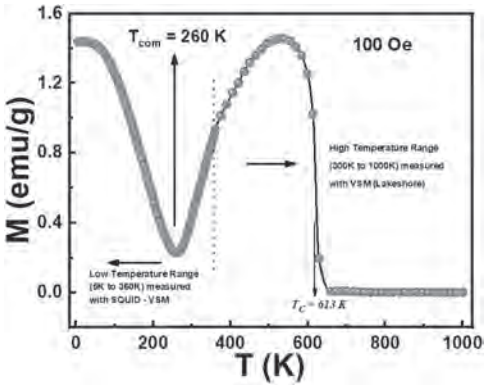

Fig. 1. Magnetic compensation and Ferrimagnetic transition in ($Co_{0.5}Mn_{0.5}$)MnAl

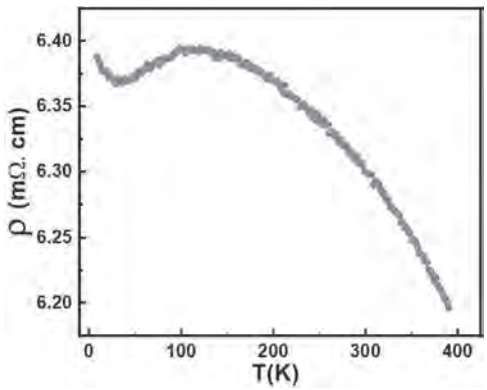

Fig. 2. Variation of electrical resistivity in ($Co_{0.5}Mn_{0.5}$)MnAl with temperature in the range 2-400 K

BPA-06. Enhancement of Anomalous Hall Effect in Magnetic Weyl Semimetal Co_2TiSi Heusler Alloy Thin Films with V doping. *M. Liu*[1], M. Oogane[1,2], M. Tsunoda[1,3] and Y. Ando[1,2] *1. Tohoku University, Sendai, Japan; 2. Center for Science and Innovation in Spintronics (Core Research Cluster) Organization for Advanced Studies, Sendai, Japan; 3. Center for Spintronics Research Network, Sendai, Japan*

Recently, Co_2TiSi Heusler alloy is theoretically predicted that is one of the Weyl semimetal (WSM) candidates, and also the half-metal [1, 2, 3]. Since it is expected that a large anomalous Hall effect (AHE) can be observed in the WSM materials, Co_2TiSi is an attractive material showing both a large AHE and a large spin polarization. And it is also expected that the AHE can be enhanced by the Fermi level tuning in Co_2TiSi with V doping [4, 5]. In this research, we optimized the fabrication conditions for producing $Co_2Ti_{1-x}V_xSi$ thin films, and investigated their AHE. The ultra-high vacuum magnetron co-sputtering method was used for the preparation of thin films using Co_2TiSi and Co_2VSi targets. The structure of the

sample was MgO (001) sub. / $Co_2Ti_{1-x}V_xSi$ (50 nm) / Ta (5 nm). For the preparation of $Co_2Ti_{1-x}V_xSi$ films, we changed the doping amount of x, and the post annealing temperature (T_a) was changed in the range of 300 to 700°C. We characterized the crystal structure, magnetic properties, and anomalous Hall effect by XRD, SQUID, and PPMS, respectively. Four-hold symmetric (111) superlattice diffractions from Co_2TiSi and $Co_2Ti_{0.84}V_{0.16}Si$ are observed, shown in Fig.1, meaning that the $L2_1$ ordered epitaxial films were successfully fabricated. High magnitude of saturation magnetization was also confirmed at low measurement temperature for both films. By the plot of anomalous Hall conductivity vs electric conductivity, all samples show that the intrinsic mechanism dominates over the extrinsic mechanism which is also expected in WSM. The anomalous Hall conductivity of Co_2TiSi sample was only 53 S/cm at low temperature and it was enhanced to 98 S/cm by the Fermi level tuning in $Co_2Ti_{0.84}V_{0.16}Si$, shown in Fig.2. We infer that the Fermi level for the prepared Co_2TiSi is not cross the Weyl points and it is expected that the AHE can be huge enhanced by the Fermi level tuning in $Co_2Ti_{0.61}V_{0.39}Si$. This research was conducted by participating in the GP-Spin, Tohoku University, and supported by CSIS Organization for Advanced Studies and the CSRN.

[1] A. Bernevig, H. M. Weng, Z. Fang et al., J. Phys. Soc. Jpn., 87, 041001 (2018). [2] G. Q. Chang, S. Y. Xu, H. Zheng et al., Sci. Rep. 6. 38839 (2016). [3] J. Barth, G. H. Fecher, B. Balke et al., Phys. Rev. B 81, 064404 (2010). [4] J. Zou, Z. He, and G. Xu, Npj Computational Materials, 5(1) (2019). [5] I. Galanakis, P. H. Dederichs, and N. Papanikolaou, Phys. Rev. B 66, 174429 (2002).

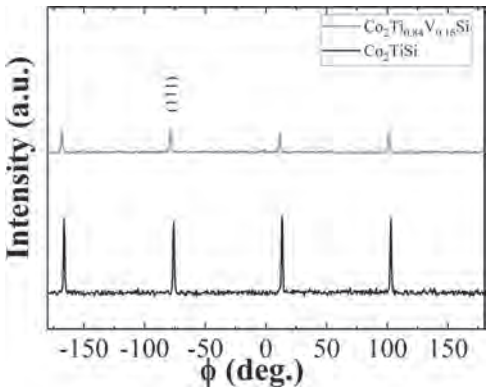

Fig. 1 The XRD profile of phi-scan for (111)-peaks in $Co_2Ti_{1-x}V_xSi$ films

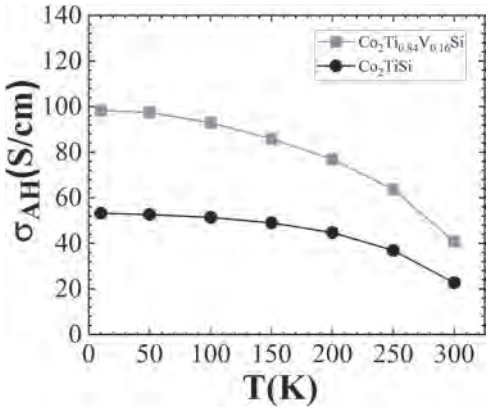

Fig. 2 Measurement temperature dependence of anomalous Hall conductivities in $Co_2Ti_{1-x}V_xSi$ films

BPA-07. Quantum Phase Transition in Partially Cu-Doped $ZrNi_{2-x}Cu_xGa$ Heusler Alloys. *K.M. Stillwell*[1], M. Khan[1], S. Bhatt[1] and A. Pathak[2]
1. Physics, Miami University, Oxford, OH, United States; 2. Physics, SUNY Buffalo State College, Buffalo, NY, United States

Quantum phase transition (QPT) is a 2nd order solid state phase transition that starts at a quantum critical point (QCP) and continues to 0 K. Since all thermal fluctuations are absent at 0 K, QPT is caused by strong quantum fluctuations[1]. Since the lowest measuring temperature that can be experimentally reached in a research laboratory is between 20 mK and 50 mK, the QCP is generally determined by performing an extrapolation of the experimental data points (to 0 K) in the p vs. T (p is the control parameter and T is the temperature) phase diagram. $ZrNi_2Ga$ is a superconductor and belongs to the Ni-based Heusler family. The material exhibits a superconducting phase transition at ~2.9 K.[2] When Ni is partially replaced by Cu in $ZrNi_{2-x}Cu_xGa$ the transition temperature linearly decreased to 1.85 K for $x = 0.25$.[3] This is indicative of QPT in the system. Here, we have studied the magneto-transport properties of $ZrNi_{2-x}Cu_xGa$ ($0.25 < 0 \leq 0.5$) to further explore the possible QPT in the system. The samples were prepared by arc melting and the transport measurements were done on a Physical Property Measurement system with Helium-3 attachment. All samples exhibited the $L2_1$ cubic structure at room temperature. A superconducting phase transition temperature of as low as ~1 K was observed in the system, which nearly confirms the possibility of QPT in the $ZrNi_{2-x}Cu_xGa$ system. The experimental results will be presented in details.

[1] P. Gegenwart, Q. Si, F. Steglich, Quantum criticality in heavy-fermion metals, Nat. Phys. 4, 186 (2008). [2] J. Winterlik, G. H. Fecher, C. Felser, M. Jourdan, K. Grube, F. Hardy, H. von Löhneysen, K. L. Holman, and R. J. Cava, Phys. Rev. B 78, 184506 (2008). [3] D. R. Basaula, J. Brock, and M. Khan, AIP Advances 8, 055704 (2018).

BPA-08. A comparative study of the martensitic phase transitions in Fe doped $Ni_2Mn_{0.4-x}Fe_xCr_{0.6}Ga$ and $Ni_2Mn_{0.4}Fe_xCr_{0.6-x}Ga$ Heusler alloy systems. *A. Schaeffer*[1], C. Kerr[1], A. Pathak[2] and M. Khan[1] *1. Physics, Miami University, Oxford, OH, United States; 2. Physics, SUNY Buffalo State College, Buffalo, NY, United States*

Ni_2MnGa is an exemplary Heusler alloy to exhibit the martensitic phase transformation (MPT) from the high-temperature austenite phase to a lower temperature martensite phase.[1] The martensitic transformation occurs at $T_M \approx 202$ K followed by a ferromagnetic phase transition at $T_C^A \approx 380$ K. When Mn is partially substituted by Cr in $Ni_2Mn_{1-x}Cr_xGa$ T_M increased while T_C decreased, such that the two transitions overlapped at ~260 K for $x = 0.50$. [2] Additionally, the alloys exhibited resistivity drops of 2.5 - 18 % at the MPT. The largest magnitude drop occurred in materials exhibiting $T_M > T_C$. Here, we present an experimental study on the transport and magnetic properties of Fe doped $Ni_2Mn_{0.4-x}Fe_xCr_{0.6}Ga$ and $Ni_2Mn_{0.4}Fe_xCr_{0.6-x}Ga$ Heusler alloy systems. The goal was to compare the magnetic and transport properties of the two systems where Mn is replaced by Fe in one system and Cr is replaced by Fe in the other. All compounds were prepared by arc melting and annealing techniques. The samples were subjected to x-ray diffraction, electrical resistivity, and dc magnetization measurements. The diffraction data showed the samples were either tetragonal or Cubic at room temperature. For both systems T_M and T_C decreased with increasing x. However, T_M decreased much rapidly for the $Ni_2Mn_{0.4}Fe_xCr_{0.6-x}Ga$ system while the rate of decrease of T_C was slower. The experimental results will be presented and discussed taking the valence electron concentration, e/a, and the structural disorder into consideration.

1. P. J. Webster, K. R. A. Ziebeck, S. L. Town, and M. S. Peak, Philos. Mag. B 49, 295 (1984). 2. M. Khan, J. Brock and I. Sugerman, Phys. Rev. B 93, 054419 (2016).

BPA-09. Withdrawn

Session BPB
MAGNETOELECTRONIC MATERIALS AND MULTIFERROIC PHENOMENA
(Poster Session)

Xiufeng Han, Co-Chair
Institute of Physics, Chinese Academy of Sciences, Beijing, China
Lambert Alff, Co-Chair
TU Darmstadt, Darmstadt, Germany

BPB-01. Magnetostriction in microwave synthesized $La_{0.5}Ba_{0.5}CoO_3$.
M. Manikandan[1], *A. Ghosh*[1] and R. Mahendiran[1] *1. Physics, National University of Singapore, Singapore*

$La_{1-x}Sr_xCoO_3$ (LSCO) changes from a paramagnetic semiconductor for x= 0 to a ferromagnetic metal for x≥ 0.2. Magnetoelastic property of these oxides has been overlooked so far despite it showed giant anisotropic magnetostriction (1000-3000 ppm at 14.2 T) for x = 0.3 and 0.5 [1]. Its origin was suggested to the field-induced spin-state transition [low (S= 0) to intermediate (S= 3/2) spin] of Co^{3+} ions, and the creation of spin-orbit coupling. Subias et al.[2] report the atomic-scale origin of the magnetostriction in $La_{0.5}Sr_{0.5}CoO_3$ by measuring local changes in Co-O bond length by analyzing the differential X-ray absorption data. Magnetic interactions among Co^{3+}/Co^{4+} ions and their spin states are sensitive to the crystal field effect and average ionic radius of the rare earth and alkaline earth cations. We successfully synthesized the polycrystalline $La_{0.5}Ba_{0.5}CoO_3$ by microwave irradiation with short-time irradiation of 20 minutes at 1200°C, and measured its magnetization (M) and Joule magnetostriction λ_{par} whose field dependence at 10 K are shown in Fig.1(a). M shows hysteresis at low fields and increases without saturation up to H = 50 kOe. The M value at 50 kOe is much smaller than $La_{0.5}Sr_{0.5}CoO_3$ for which M = 2 μ_B/f.u.which suggests the lack of long-range ferromagnetic order in this sample. λ_{par} smoothly increases with H without showing a saturation. The value of λ_{par} at 50 kOe is 265 ppm, which is smaller than in LSCO but yet a significant value among most transition metal perovskite oxides. λ_{par} for 50 kOe has the maximum value at 10 K and decreases smoothly as the ferromagnetic -paramagnetic transition is approached (T_C = 177 K) and becomes negligible above T_C. (see Fig. 1(b)). Work is in progress to correlate the magnetostriction, spin state of Co ions, electronic phase separation, and negative thermal expansion proposed in this compound[3,4] R.M. thanks the Ministry of Education, Singapore (Grant no. R144-000-422-114 and R144-000-442-114).

[1] M. R. Ibarra et al. Phys. Rev.B 57, R317 (1998). [2] G. Subias et al., Phys. Rev. B. 100, 104420 (2019). [3] D. Kumar et al. J. Phys. Cond.Matter. 25, 216005 (2013). [4] Z. Tan et al. J. Phys. Chem. Lett..11, 6785 (2020).

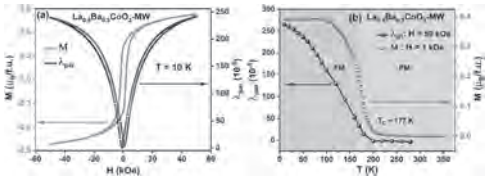

Fig 1: (a) Field dependence of magnetization (M) on left y-axis and parallel magnetostriction (λ_{par}) on right y-axis of $La_{0.5}Ba_{0.5}CoO_3$ at 10 K. (b) Temperature dependence of the maximum value of λ_{par} at H = 50 kOe on left-yaxis and M for H = 1 kOe on right y-axis.

BPB-02. Enhanced performance of magnetoelectric laminated composites by geometry engineering for high frequency applications.
A. Lasheras[1], P. G. Saiz[2], J. Porro[2,3], I. Quintana[4], C. Polak[5] and A. Lopes[6,3] *1. University of the Basque Country, Leioa, Spain; 2. BCMaterials, Basque Center for Materials, Applications and Nanostructures, Leioa, Spain; 3. KERBASQUE, Basque Foundation for Science, Bilbao, Spain; 4. Tekniker, Basque Research and Technology Alliance (BRTA), Eibar, Spain; 5. Vacuumschmelze GmbH & Co. KG, Hanau, Germany; 6. Centre for Cooperative Research on Alternative Energies (CIC energiGUNE), Basque Research and Technology Alliance (BRTA), Vitoria-Gasteiz, Spain*

The development of new materials with tunable properties are in demand for different applications in novel technologies and devices. In this regard, magnetoelectric laminated composites based on the coupling between magnetostrictive and piezoelectric phases have emerged over the last years due to their high induced electric response at the electromechanical resonance frequencies [1][2]. However, their application in areas requiring high working frequencies requires further development of these materials due to the difficult compromise between the increase of the frequency (obtained with shorter samples) and the high ME response (higher for larger areas of ME laminates). This work presents novel geometrically modified magnetoelectric laminates based on the $Fe_{64}Co_{17}Si_{6.6}B_{12.4}$ metallic glass and the polyvinylidene fluoride (PVDF) piezoelectric polymer. Laminates with rectangular, triangular and rhombic shapes with an area of 25 mm^2 have been fabricated. The induced ME responses of the laminates under an applied DC magnetic field and as a function of the frequency have been analyzed. The results evidence that, at the electromechanical resonance frequency, the triangular and rhombic shaped laminates show an improved induced ME response (102 mV and 103 mV, respectively) in comparison with the common rectangular shaped one (98 mV). Furthermore, the working frequencies of the triangular and rhombic laminates significantly increase up to 83 kHz and 102 kHz, respectively, with respect to the rectangular one (67 kHz). Going a step forward, the novel geometries have been compared with that of rectangular magnetoelectric laminates of equivalent EMR frequencies (19 mm and 17 mm long laminates for 83 kHz and 102 kHz, respectively). These rectangular laminates show a drastic drop of their induced ME responses (29 mV and 6.7 mV, respectively), due to the quality factor impair caused by the demagnetizing effects in these shorter samples. This study represents a critical advance in the performance of magnetoelectric laminated composites through geometry modification, opening the door to their implementation in enhanced high frequency devices.

[1] C.M. Leung, J. Li, D. Viehland, X. Zhuang, J. Phys. D. Appl. Phys., vol. 51, 263002 (2018) [2] J. Gutiérrez, A. Lasheras, P. Martins, N. Pereira, J.M. Barandiarán, S. Lanceros-Mendez, Sensors, vol. 17, 1251 (2017)

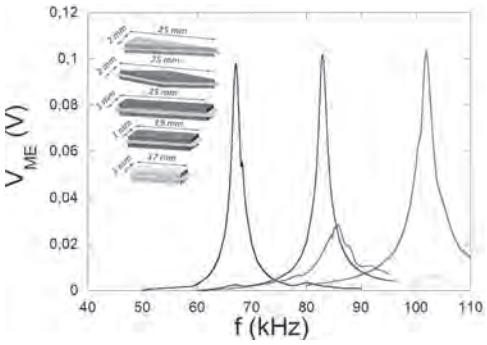

BPB-03. Investigation of Room Temperature Multiferroicity in Chemical Vapor Deposited Aurivillius Phase Thin Films for Next Generation Data Storage Technologies. *L. Colfer*[1], M. Bansal[2], B. Shaw[3], J. Halpin[1], T.S. Maity[2] and L. Keeney[1] *1. Tyndall National Institute, Cork, Ireland; 2. Indian Institute of Science Education and Research, Thiruvananthapuram, Trivandrum, India; 3. University of Cambridge, Cambridge, United Kingdom*

Multiferroics (MF) intertwine ferroelectric (FE) and ferromagnetic (FM) properties, allowing for novel ways of manipulating data and storing information. The Aurivillius phase $Bi_6Ti_XFe_YMn_ZO_{18}$ (B6TFMO), is a rare example of a single-phase room temperature MF system displaying magnetoelectric switching[1]. Earlier work on non-epitaxial, 100 nm-thick Aurivillius films have displayed saturation magnetization (M_S) values of up to 215 emu/cm^3 and in-plane saturation polarization (P_S) values of >26 μC/cm^2[2]. However, for Aurivillius phase materials to be useful for applications, their functional properties must be enhanced in epitaxially grown thin films, ensuring correct orientation and strain-induced enhancement of MF properties in devices[3]. Here, we report a single step direct liquid injection chemical vapor deposition process (DLI-CVD) which is being developed for the growth of epitaxial films[4]. Density functional theory (DFT) predicts that FE polarisation is enhanced (diminished) with increase in tensile (compressive) strain. Furthermore, it predicts that tensile strain optimises magnetic cation ordering within Aurivillius phase structures[5]. In this contribution, the magnetic properties of ~40 nm thick $Bi_5Ti_xFe_yMn_zO_{15}$ (BTFMO) films synthesised by DLI-CVD on substrates imposing tensile and compressive strain, $SrTiO_3$ (STO) and $La_{0.26}Sr_{0.76}Al_{0.61}$ $Ta_{0.37}O_3$ (LSAT), respectively, were investigated. X-ray diffraction (XRD) confirms the epitaxial relationship between film and substrate (Fig. 1). The piezo-response force microscopy measurements found the films were naturally self-polarized. Further, the magnetization measurements were performed to assess the key drivers responsible for the enhancement of FM response of the sample. Magnetization vs. field (*MH*) measurements depict the increase of remanence (REM) and coercivity as temperature is decreased showing FM behaviour (Fig. 2). A temperature dependent study has also been performed for zero field cooling, field cooling as well as REM magnetization measurements. This work will optimize this MF material to exploit it in future energy storage applications. (L Colfer, M Bansal: equal contribution)

1. L. Keeney, T. Maity, M. Schmidt, *et al.*, *J. Am. Ceram. Soc.*, 96, 2339 (2013) 2. A. Faraz, T. Maity, M. Schmidt, *et al., J Am Ceram Soc.*, 100, 975 (2017) 3. M. Tyunina, J. Narkilahti, M. Plekh, *et al. Physical review letters*, 104.22, 227601 (2010) 4. L. Keeney, Z. Saghi, M. O'Sullivan, *et al., Chem. Mater.*, 32, 10511 (2020) 5. Birenbaum, A.Y., C. Ederer, *Appl. Phys. Lett.,* 108, 082903 (2016)

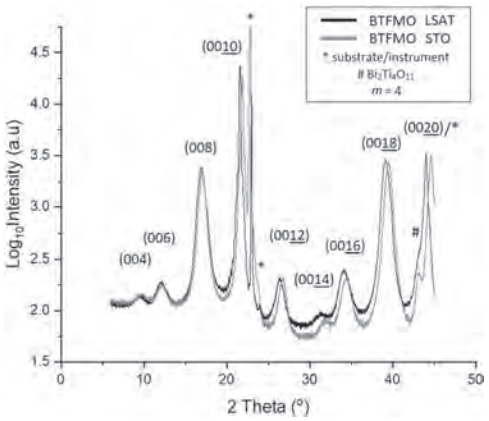

Fig. 1 XRD analysis of BTFMO on LSAT and STO

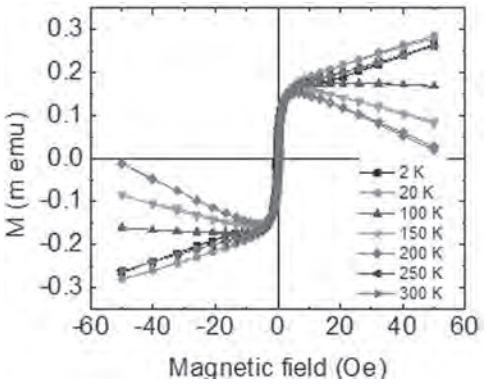

Fig. 2 *MH* measurements of BTFMO on LSAT

BPB-04. Structural, dielectric and electrocaloric properties of $Ba(Ti,Zr)O_3$-$(La,Sr)MnO_3$ composite multiferroic. *A. Gaur*[1] and S. Srinath[1] *1. School of Physics, University of Hyderabad, Hyderabad, India*

We report the dielectric and electrocaloric (EC) properties of sol-gel synthesized $BaTi_{0.84}Zr_{0.16}O_3$ (BTZ) and BTZ-$La_{0.78}Sr_{0.22}MnO_3$ (LSM) composite in 80:20 molar ratio. The dielectric properties $\in'$ and $\in''$ of mechanically mixed ferroelectric (FE)-ferromagnetic (FM) composites are often influenced by the interface, especially at low frequencies. Other side, ferromagnets that possess a decent conductivity turn liable for concentrating the electric field over the FE-domains and thus enhancing the overall polarization. It is important to separate the dipolar contribution to the composite permittivity from the interfacial/carrier one to truly assess the dielectric materials, suited for energy storage and EC application. We discuss the dielectric analysis based on modulus $M^*(=1/\in^*)$ with the aim to discriminate the dipolar and interfacial contribution and to establish their temperature and frequency dependence. M''-ω graph of the composite exhibits a broad relaxation peak in MHz range (Fig. 1) while $\in''$-ω graph is typical of interface dominated: $\in''$ as high as 39,313 (6,643) at 20 Hz, decreasing to 642 (260) at 2 MHz measured at 100°C (25°C). M''-max shifts to higher frequencies with the increase in temperature. The M''-peak, associated with BTZ-dipoles, is fitted using Cole-Davidson (CD) equation, $M''=[(\in_s-\in_\infty)(\cos\Phi)^\gamma \sin(\Phi\gamma)]$ $\in_\infty{}^2+(\in_s-\in_\infty)^2(\cos\Phi)^{2\gamma}+2\in_\infty(\in_s-\in_\infty)(\cos\Phi)^\gamma\cos(\Phi\gamma)]^{-1}$ with $\Phi=\tan^{-1}(\omega\zeta)$, to estimate the dielectric parameters: static and high-frequency dielectric constants $\in_s$ and $\in_\infty$ respectively, relaxation time, ζ, corresponding to the M''-peak (Fig. 1(a)) and the CD parameter, γ, which is related to the distribution of relaxation time ($0\le\gamma\le1$ and $\gamma=1$ for a system with uniquely defined ζ). The fit parameters $\in_s$ and ζ obtained at different temperatures are shown in Fig. 2(b, c). $\in_s$ goes through a peak, correlated with BTZ phase (Fig. 2(a), whereas, ζ decreased systematically with increasing in temperature. These analyses indicate that M* is more suitable parameter to consider for the dielectric-ferromagnetic composites.

Qian Yang, Wei Zhang, Meiling Yuan, Limin Kang, Junxiao Feng, Wei Pan and Jun Ouyang, Preparation and characterization of self-assembled percolative $BaTiO_3$–$CoFe_2O_4$ nanocomposites via magnetron co-sputtering, Sci. Technol. Adv. Mater. 15 (2014) 025003. Zhi Yu and Chen Ang, Maxwell–Wagner polarization in ceramic composites $BaTiO_3$–$(Ni_{0.3}Zn_{0.7})Fe_{2.1}O_4$, J. Appl. Phys. 91, 794 (2002). D. W. Davidson, Dielectric relaxation in liquids: I. The representation of relaxation behavior, Canadian Journal of Chemistry, vol. 39, 571-594, (1961) Sandeep Mahajan, O P Thakur, Chandra Prakash, and K Sreenivas, Effect of Zr on dielectric, ferroelectric and impedance properties of $BaTiO_3$ ceramic, Bulletin of Materials Science, Vol. 34, 1483–1489 (2011).

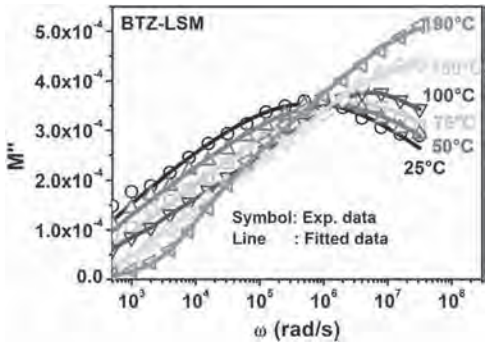

Fig. 1 M″(ω)

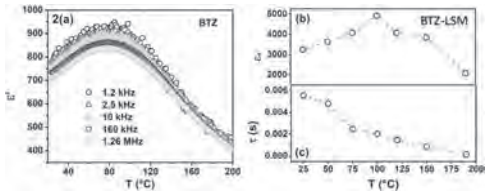

Fig. 2 a) ∈′(T), b) ∈″(T), c) ζ(T)

BPB-05. Detection of antiferromagnetic order parameter based on Hall measurements for Pt/Cr_2O_3/Pt trilayer. *X. Wang*[1], K. Toyoki[1], R. Nakatani[1,2] and Y. Shiratsuchi[1,2] *1. Department of Materials Science and Engineering, Osaka University, Suita, Japan; 2. Center of Spintronics Research Network, Osaka University, Toyonaka, Japan*

Magnetoelectric (ME)-controlled antiferromagnet (AFM) based random access memory has outstanding energy efficiency and excellent robustness to magnetic disturbances, but how to read out the data is a topic of research. Conventionally, it can be read out by the magnetization of the adjacent ferromagnetic layer coupled with the ME AFM layer via exchange bias [1,2]. However, the interfacial exchange coupling with the ferromagnetic layer has a non-negligible effect on the switching of AFM order-parameter causing excess energy. In this paper, we use the spinning-current anomalous Hall magnetometry [3] to access to the AFM order parameter of ME AFM of 40-nm-thick Cr_2O_3 thin film. In this technique, the AFM order parameter (interfacial AFM moment) manifests as the remanent Hall resistance R_{H_Rem}. Pt(2 nm)/Cr_2O_3(40 nm)/Pt(20 nm) thin film was prepared on α-Al_2O_3(0001) substrate by using the DC magnetron sputtering system. Structural characterizations were carried out using reflection high-energy electron diffraction (RHEED), X-ray diffraction, and X-ray reflectivity. R_{H_Rem} was evaluated as a function of temperature after cooling the film from 320 K (above the Néel temperature T_N). Magnetic-field dependence of Hall resistance, i.e. anomalous Hall effect (AHE) were also measured. For the Hall measurements, a micro-fabricated Hall device (width: 2 μm and length: 50 μm) were used. Figure 1 shows the temperature dependence of R_{H_Rem} for the difference cooling field. The finite R_{H_Rem} is observed and the sign of R_{H_Rem} reverses by the cooling field. With increasing temperature, R_{H_Rem} slightly increases, reaches maximum around 225 K and decreases again. Finally, R_{H_Rem} becomes zero around 290 K which is near T_N of the Cr_2O_3 thin film characterized by the spin Hall magnetoresistance measurements [4]. Hence, R_{H_Rem} is emerged by the AFM order parameter. We also found that the magnetic-field dependence of Hall resistance exhibits the hysteresis, which is a signature of the spin-flip transition of the Cr_2O_3 thin film.

[1] P. Borisov *et al.*, Phys. Rev. Lett. 94, 117203 (2005). [2] Y. Shiratsuchi *et al.*, J. Phys. Condensed Matter. 33, 243001 (2021). [3] T. Kosub *et al.*, Phys. Rev. Let. 115, 097201 (2015). [4] T. Iino, Y. Shiratsuchi *et al.*, Appl. Phys. Lett. 114, 022402 (2019).

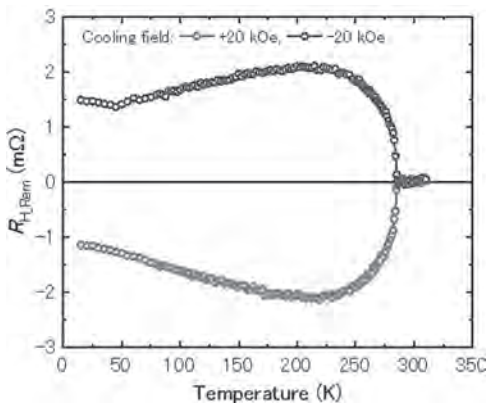

Figure 1 Temperature dependence of anomalous Hall effect resistances under different cooling fields of -20 kOe (blue), +20 kOe (red).

BPB-06. Anomalous Nernst effect in Fe-Si alloy films. *Y. Hamada*[1], Y. Kurokawa[1], T. Yamauchi[1] and H. Yuasa[1] *1. Information Science and Electrical Engineering, Kyushu University, Fukuoka, Japan*

The anomalous Nernst effect (ANE), one of the long-studied thermomagnetic effects, has been regarded as a promising next-generation energy harvesting technology for large-area and flexible devices. However, since the ANE power is too short for practical use, it is necessary to enhance ANE and many ferromagnetic materials have been widely investigated [1]. We experimentally investigated the anomalous Nernst effect (ANE) in an Fe_3Si film whose ANE was predicted to be large, based on the topological band structure [2]. We also measured the Seebeck and anomalous Hall effects to separate the ANE term from the Hall effect of the carrier flow induced by the Seebeck effect. The sample structure and measurement system are shown in Fig. 1. In addition to Fe_3Si, Fe_2Si, FeSi, and $FeSi_2$ 50nm films were fabricated on SiO_2 substrate by co-sputtering and annealed in vacuum at 1123K for 1 hour. Figure 2 shows the ANE coefficient as a function of Si composition in Fe-Si compounds. The ANE coefficients were estimated as 1.0 and 0.5 μVK^{-1} for the Fe_3Si and Fe_2Si samples, respectively. These values are much larger than the ANE coefficient of film Fe, whereas Fe_3Si and Fe_2Si both have a smaller saturation magnetization than Fe. In general, the Nernst coefficient can be decomposed into two terms: $S_{yx} = \rho_{xx}\alpha_{yx} - \tan\theta_{AHE}S_{xx}$. Here, the first term S_1 exhibits the intrinsic ANE term that converts heat flow into a transverse voltage, and the second term S_2 reflects the voltage originating from the Hall effect of the carrier flow induced by the Seebeck effect during the anomalous Nernst effect. From Fig. 2, it was found that the first term S_1 was dominant in the ANE improvement of Fe_3Si, suggesting that the ANE of Fe_3Si is enhanced because of its band structure, as expected from the theoretical calculation. Fig.1 Schematics of the sample structure and ANE measurement configuration. Fig.2 Negative value of the ANE coefficient S_{xy}, the first term S_1, and the second term S_2 as a function of Si composition in Fe-Si compounds.

[1] M. Mizuguchi, S. Nakatsuji, Sci, Technol. Adv. Mater. 20, 264 (2019) [2] A. Sakai, S. Minami, and T. Koretsune, Nature 581, 53-57 (2020)

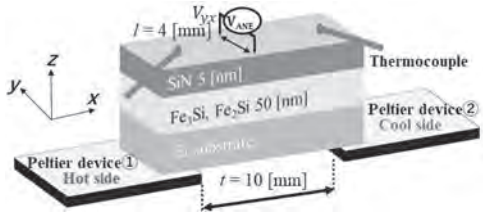

Fig.1 Schematics of the sample structure and ANE measurement configuration.

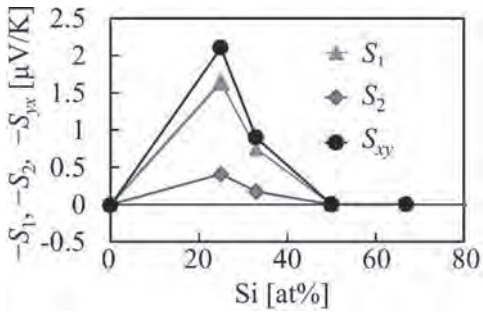

Fig.2 Negative value of the ANE coefficient S_{xy}, the first term S_1, and the second term S_2 as a function of Si composition in Fe-Si compounds.

BPB-07. Electromagnetic evaluation method for both air-gap distance of non-contact sensor and cementite content inside spheroidal graphite cast iron. *K. Kawada*[1], M. Kuromizu[2], Y. Ono[2] and Y. Gotoh[1] *1. Innovative Engineering, Oita University, Oita, Japan; 2. Graduate School of Engneering, Oita University, Oita, Japan*

The Spheroidal graphite cast iron is used for high-strength parts of large heavy machinery. The cementite (Fe_3C) may be contained in cast iron during the casting process. Since the strength is reduced if the cemenite is contained in the cast iron, the evaluation of the cementite content is important. The permeability and conductivity of the cementite domain are less than that of the domain in the cast iron without cementite. It is possible to evaluate the cemenite content using an electromagnetic field. However, the flux density is also influenced by the changing distance (lift-off: L_o) between the cast iron and the inspection sensor. Since the surface of the cast iron may be coated with rust preventive, it may not be possible to determine the exact L_o. In this paper, the inspection method for estimating the cementite content and L_o at the same time is proposed. Fig.1 shows the inspection model. The sensor is composed of an AC excition coil with 10 kHz and 2A, a mangetic yoke and a detection coil. The *B-H* curves of the cast iron with and without cementite are shown in Fig.2. The conductivities of the cast iron with and without cementite are 1.9 x 10^6 S/m and 1.63 x 10^6 S/m, respectively. The permeability and conductivity of the cast iron with cementite are smaller than those of cast iron without cementite. Fig.3 shows a complex plane of the output voltage in a detection coil by changing the L_o and the cementite content. This figure shows the real V_{Re} and imaginary V_{Im} components of the output voltage. The output voltage due to the changes of the L_o and the cementite content is distinguished even if the ampulitude output voltage is the same value. In this resarch, when both cementite content and L_o are unknown, these values are estimated by the linear interpolation using this complex plane in Fig.3. Table 1 shows the estimation results of both unknown cementite content and L_o. This table shows that the actual cementite content and L_o are mostly estimated.

M.Kurosawa, T.Ushimoto, T.Abe, T.Takagi, T.Sato, H.Kage, T.Noguchi, "Detection of Cementite in Spheroidal Graphite Cast Irons Using Eddy Current Method", J.JFS, vol.77, no.12, pp. 826-832, 2005

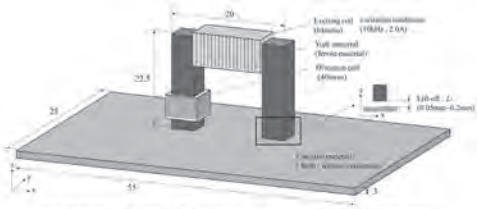

Fig.1 Electromagnetic sensor and the spheroidal graphite cast iron with and without cementite

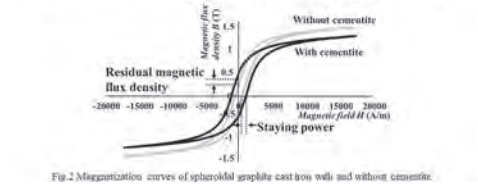

Fig.2 Magnetization curves of spheroidal graphite cast iron with and without cementite

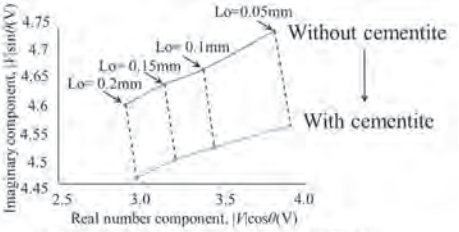

Fig.3 Complex plane of output voltage in a search coil(10kHz,2.0A)

Table.1 Estimated results of cementite content and lift-off, L_o

cementite		True value	Estimated value	error
With	Content rate(%)	100.0	97.0	3.0
	Lift-off: L_o (mm)	0.08	0.075	0.005
Without	Content rate(%)	0.0	5.0	5.0
	Lift-off: L_o (mm)	0.08	0.074	0.006

BPB-08. Giant Ferroelectric Modulation of Barrier Height and Width in Multiferroic Tunnel Junctions. *L. Jiang*[1], Y. Wang[2], W. Chen[1] and X. Han[1] *1. Institute of Physics, Chinese Academy of Sciences, Beijing, China; 2. Central South University, Changsha, China*

The high tunneling electroresistance (TER) effect, generally caused by ferroelectric (FE)-modulated barrier height or width, is essential for the applications of multiferroic tunnel junctions in data storage. It is traditionally obtained by distinct electrical screening lengths of electrodes. Interface engineering can enhance the TER effect further. In this work, taking Co-$(TiO_2$-$BaO)_N$-Co tunnel junctions as examples, we demonstrate a distinct principle than the screening lengths for designing extraordinary TER effect. We reveal that when the interfacial FE displacement is much larger than that of the FE bulk, it will bend the barrier band near the interface violently, and the interfacial polarization direction pointing to or away from the interface determines whether the energy band rises or falls. The large interfacial Ba-O displacement and its corresponding polarization direction in Co-$BaTiO_3$-Co tunnel junctions can be significantly modulated by the direction of FE polarization, resulting in a metallic-insulating transition of the entire thin $BaTiO_3$ barrier. For thick $BaTiO_3$ barrier (N = 25, ~10 nm), the effective tunnel barrier width shifts between about 2 nm and 6.5 nm as the polarization of $BaTiO_3$ switches direction, which can dramatically modulate the tunneling efficiency. This effect shed light on a novel route for enhancing TER through the interface engineering.

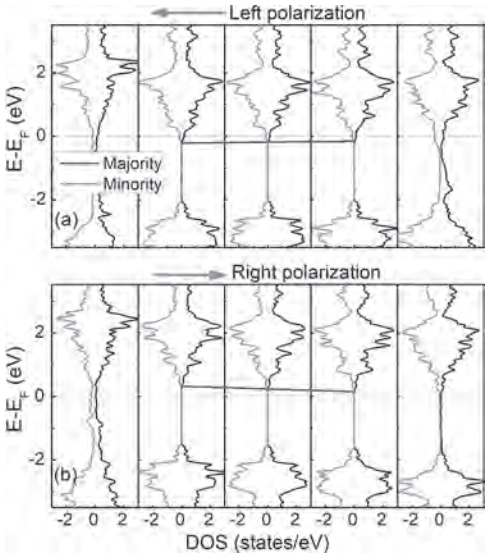

Density of states for each BTO unit cell in Co-(TiO_2-BaO)$_5$-Co MFTJ with (a) left-polarized and (b) right-polarized state. Black (red) line is DOS of majority (minority). From left to right, the DOS figures correspond to the BTO unit cell near the Co-TiO_2 interface to near the BaO-Co interface. The dotted line indicates the Fermi level position. The blue solid line connects the CBM of each BTO unit cell.

BPB-09. Withdrawn

BPB-10. Withdrawn

BPB-11. Nonlinear magnetoelectric effects excited by magnetic field pulses. *D.V. Savelev*[1], D.V. Chashin[1], Y.K. Fetisov[1], D.A. Burdin[1], L.Y. Fetisov[1] and V.O. Belan[1] *1. MIREA - Russian Technological University, Moscow, Russian Federation*

Magnetoelectric (ME) effect in composite structures consisting of ferromagnetic (FM) and piezoelectric (PE) layers manifests itself as the polarization of the sample in an external magnetic field. The effect arises from a combination of the magnetostriction of the FM layer and the piezoelectric effect in the PE layer [1]. In this work, for the first time, nonlinear effects in an ME structure excited by magnetic field pulses are investigated. The inset in Fig. 1 schematically shows the investigated structure. The structure contained a layer of PE lead zirconate-titanate (PZT) with dimensions of 20 mm × 6 mm and a thickness of d = 1.5 mm, located between two layers of an amorphous magnetic alloy Metglas 2605SA1 with a thickness of 23 μm. The structure is placed in a solenoid that creates magnetic field pulses with a duration of 1-40 μs and an amplitude of up to h = 7.4 Oe and in a constant magnetic field H = 0-100 Oe. The dependences of the ME voltage at the frequency of the acoustic resonance of the structure 77 kHz, generated by the PZT layer, on pulse duration and its amplitude, and field H were measured. Figure 1 shows the dependence of the magnitude of the ME voltage u on the field H when the structure is excited by pulses with a duration of 13 μs. The shape of the curve repeats the field dependence of the second derivative of the magnetostriction with respect to the field. The efficiency of nonlinear frequency doubling was $\alpha = u/(d \times h^2) \approx 3.3$ mV/(cm×Oe^2). Nonlinear ME effects were also observed with simultaneous excitation of the structure by pulsed and harmonic magnetic fields. The observed effects can be used to create sensors for pulsed magnetic fields. The work was supported by the Russian Science Foundation, grant 19-79-10128.

[1] F. Kreitmeier, D.V. Chashin, Y.K. Fetisov et al., Sensors, Vol. 12(11), p. 14821-14837 (2012).

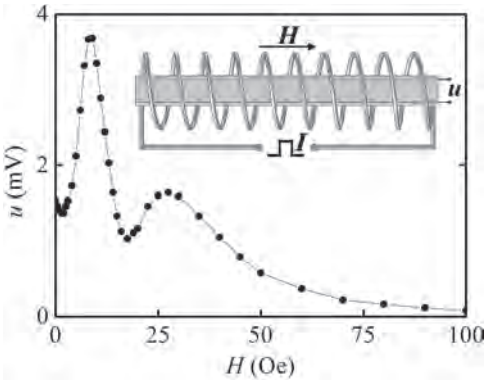

Figure. 1. Second harmonic of ME voltage *u* vs. magnetic field *H*.

BPB-12. Low-temperature crystal and magnetic structure of the multiferroic material $Fe_4Ta_2O_9$. *M. Sen*[1], S. Panja[1], L. Harnagea[1], A. Cervellino[2], V. Pomjakushin[3] and S. Nair[1] *1. Department of Physics, Indian Institute of Science Education and Research (IISER), Pune, India; 2. Materials Science, Paul Scherrer Institute, Forschungsstrasse, Switzerland; 3. Laboratory for Neutron Scattering and imaging, Paul Scherrer Institute, Villigen PSI, Switzerland*

$Fe_4Ta_2O_9$ belongs to the family of tantalates and niobates of the form $A_4X_2O_9$ (where A =Mn, Fe or Co and X =Ta or Nb) which has recently attracted extensive attention owing to its magnetoelectric properties. It crystalizes in centrosymmetric space group P3c1 where the A ions occupy two non-equivalent crystallographic sites on (2/3, 1/3, z) and (1/3, 2/3, z) contributing to magnetoelectric effect. A recent study from our group has reported that it shows a series of low temperature magnetic transitions, many of which are associated with emergence of a polar order, thus making it a true multiferroic. In this work, for the first time we report the existence of a structural phase transition in $Fe_4Ta_2O_9$ with the help of synchrotron X-ray diffraction and powder neutron diffraction study. Upon cooling below T1 80 K, the symmetry of crystal structure is lowered from trigonal P-3c1 to monoclinic C2/c. For this space group the decomposition of the magnetic representation for both the Fe1 and Fe2 located in general sites (x,y,z) reads as mag= 3Γ1⊙ 3Γ2⊙ 3Γ3⊙3Γ4 In the antiferromagnetically ordered state below T1, Fe1 and Fe2 magnetic moments are found to be lying in the ab plane, and are arranged antiferromagnetically inside the planes. For every Fe atom in either the weakly or strongly buckled honeycomb layers, the moments of the three nearest-neighbour Fe atoms in the same layer are directed oppositely. Along the c axis, the moments of Fe1 and Fe2 atoms are coupled ferromagnetically. The moment at Fe1 and Fe2 site are found to be 1.052 and 1.496 μB respectively. Fig.1 Neutron Diffraction pattern obtained at room temperature using a wavelength of λ = 1.886 Å on HRPT and associated crystal structure of $Fe_4Ta_2O_9$ at (top panel, P-3c1) 100 K and 70 K (bottom panel, C2/c). Fe1 atoms are plotted in blue, Fe2 are in pink, Ta atoms in green. The observed, calculated intensities and their difference are plotted in black circles, and red and blue lines, respectively. The vertical bars in dark yellow mark the Bragg positions for the structural (upper) phases and magnetic (lower) phases respectively.

1. N. Narayanan, A. Senyshyn, D. Mikhailova *et al.* Physical Review B 98, 134438 (2018) 2. N. D. Khanh, N. Abe, H. Sagayama *et al.* Physical Review B 93, 075117 (2016) 3. S. Chaudhary, P. Srivastava, S.D. Kaushik *et al.,* Journal of Magnetism and Magnetic Materials 475, 508–513 (2019) 4. Rajesh Jana, Denis Sheptyakov, Xiaoyan Ma *et al.,* Physical Review B 100, 094109 (2019) 5. Soumendra Nath Panja, Luminita Harnagea, Sunil Nair, *et al.,* Physical Review B 98, 024410 (2018) 6. Hadi Papi, 1, 2 Virgile Yves Favre, 2 Hossein Ahmadvand, *et al.,* Physical Review B 100, 134408 (2019)

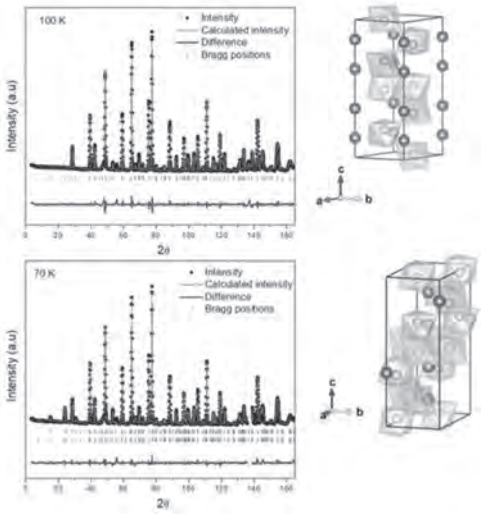

BPB-13. The effect of high pressure on the electrical and transport properties of the InSb-MnSb magnetic eutectic composition. *A. Kochura*[3], R.G. Dzhamamedov[2], A.B. Davydov[1], T.R. Arslanov[2], V.V. Rodionov[3], M. Alam[4], A.P. Kuzmenko[3] and B.A. Aronzon[1] *1. P.N. Lebedev Physical Institute, Russian Academy of Sciences, Moscow, Russian Federation; 2. Daghestan Scientific Center, Amirkhanov Institute of Physics, Russian Academy of Sciences, Makhachkala, Russian Federation; 3. Regional Centre of Nanotechnology, South-West State University, Kursk, Russian Federation; 4. Bangamata Sheikh Fojilatunnesa Mujib Science and Technology University, Jamalpur, Bangladesh*

Ferromagnet/semiconductor magnetic composites are interesting in connection with the possibility to implement the control by the spin subsystem using electric fields. A directionally crystallized eutectic consisting of an InSb semiconductor matrix and MnSb needles demonstrates ferromagnetism with a critical temperature of about 600 K and negative magnetoresistance with pronounced anisotropy. Figure shows the pressure dependences of the electrical resistivity (*r(P)*) and the effective Hall coefficient for the InSb-MnSb eutectic alloy. With an increase in pressure, the dependence *r(P)* increases almost twofold, reaching a maximum at 3.4 GPa and then demonstrates a sharp decrease by almost fourfold. Hall effect measurements $R_H(P)$ indicate that p-type conductivity is maintained over the entire pressure range. When the pressure is decreased, both the *r(P)* and $R_H(P)$ dependences exhibit hysteresis, which may indicate a pressure-induced phase transformation associated with the InSb structure, which is confirmed by studies of Raman scattering of light before and after the application of pressure. An increase in the mobility of the majority charge carriers is observed below the region of structural transformation (when the crystal is still in the zinc blende phase), which can occur due to a sharp decrease in scattering by valence electrons and indicates a smearing of the charge of localized valence electrons. After applying pressure at low temperatures, a giant magnetoresistance was discovered. In the region of low fields, it has a small peak. If we assume that its presence is associated with quantum corrections, then the experimental curves are well approximated by the Hikami-Larkin-Nagaoki formula for three-dimensional structures. The low-temperature magnetotransport studies were supported by the Russian Sciences Foundation, Grant No. 21-12-00254 (https://rscf.ru/en/project/21-12-00254/). The rest measurements was supported by the Ministry of Science and Higher Education of the Russian Federation (Grant No. 0851-2020-0035).

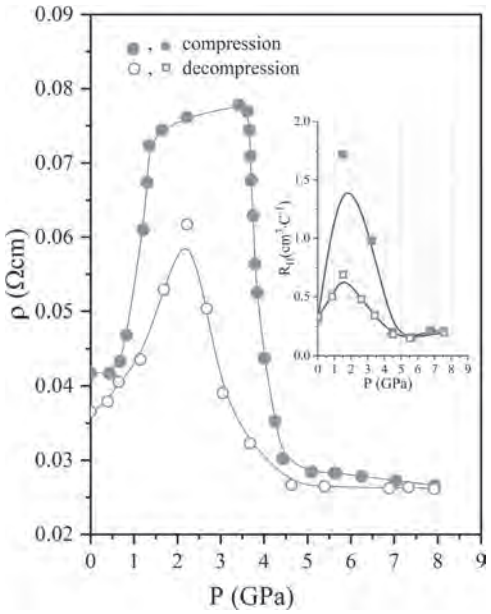

Figure. Dependences of resistivity and Hall coefficient (inserts) on pressure at 293 K for InSb-MnSb with the orientation of the MnSb needles along the current contacts

BPB-14. Oxygen Defect Engineered Magnetism of La_2NiMnO_6 Thin Films. *J.P. Palakkal*[1], T. Schneider[1] and L. Alff[1] *1. Institute of Materials Science, Technische Universität Darmstadt, Darmstadt, Germany*

The magnetism of double perovskite (DP) is interesting due to its complex nature. A near room-temperature magnetic transition (T_C) and a magneto-dielectric coupling in the vicinity of T_C make the DP La_2NiMnO_6 (LNMO) interesting [1]. The bulk LNMO has a high-temperature magnetic transition near T_{C1} = 270 K and a low-temperature transition near T_{C2} = 150 K [2,3]. T_{C1} is originating from the orthorhombic phase containing Ni^{2+} and Mn^{4+} cations and the T_{C2} is originating from the rhombohedral phase with Ni^{3+} and Mn^{3+} cations [2]. Recently, this material has got even more attention due to its oxygen-reduction/evolution reactions caused by its favorable electronic structure [4]. Here, we present a careful study of oxygen defect engineered LNMO thin films and the control of its magnetic transitions. The LNMO thin films were deposited on $SrTiO_3$ substrates by using pulsed laser deposition (PLD). The thin films were subjected to in-situ annealing after deposition. The oxygen defect concentration got reduced with the in-situ annealing at 900 ^oC, in a partial oxygen atmosphere of 500 mTorr. The samples S5, S30, and S60 were prepared by annealing 5, 30, and 60 minutes, respectively. The out-of-plane lattice constant and the thickness of the films got decreased with an increase in the density when the annealing time was increased. All the films are in-plane locked to the substrate. The saturation magnetization at 10 K is around 3.80 μ_B/f.u. for all films, with a corresponding anti-site disorder ~15%. All the films are showing a superstructure ordering peak of the double perovskite lattice around 19.7^o, indicating that the Ni and Mn cations are ordered in the lattice. The derivative plot of the field cooled (FC) curve gives three distinct transitions for all the samples. The sample S5 has a lower temperature transition at 62 K, with a spin-glass behavior, which is absent for the S30 and S60. A higher temperature transition at 265 K appears for the S30 and S60. Oxygen annealing leads to an enhanced magnetic transition temperature in the reported LNMO films.

[1] D. Choudhury *et al.*, Phys. Rev. Lett. 108, 127201 (2012). [2] V. L. J. Joly, P. A. Joy, S. K. Date, and C. S. Gopinath, Phys. Rev. B 65, 184416 (2002). [3] R. I. Dass, J. Q. Yan, and J. B. Goodenough, Phys. Rev. B 68, 064415 (2003). [4] M. Qu *et al.*, Chem. Mater. 33, 2062 (2021).

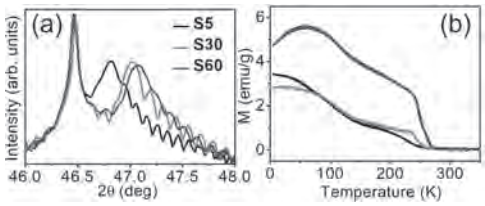

Fig. 1 (a) The XRD pattern and (b) the FC magnetic moment as a function of temperature at 100 Oe, of LNMO films. The sample numbers represent the annealing time in minutes.

BPB-15. Synthesis, characterization and experimental investigation of hyperfine interactions in $HoMnO_3$. *N.P. Lima*[1], A.P. Souza[1], A. Burimova[1] and A.W. Carbonari[1] *1. CERPQ, Nuclear and Energy Research Institute, São Paulo, Brazil*

During the last two decades, great attention has been attracted to the study of ferromagnetic materials due to their potential application in technology. Ferromagnetics are defined to be materials that possess two or more primary ferroic characteristics i.e. ferroelasticity, ferromagnetism or ferroelectricity. In the literature, a considerable part of studies explores materials with both ferromagnetic and ferroelectric properties, since these systems usually demonstrate a strong coupling between electric and magnetic ordering. Such coupling allows an additional degree of freedom in designing devices, as it is possible to switch the magnetization by an applied electric field and switch electrical polarization by applying a magnetic field. Although the description of conceptual devices based on multiferroics is present in the literature, none of the materials described are directly suitable for practical applications because the transitions occur at low temperatures only. Most of the multiferroics whose properties come from strongly correlated electrons in the d (or the f) orbital, are complex oxides. Considering applications and economic aspects, in this work we report the synthesis of $HoMnO_3$ via a Pechini route with its crystalline structure controlled using X-ray diffraction. Time differential perturbed angular correlation (TDPAC) spectroscopy was applied to study the peculiarities and temperature evolution of local magnetic and electric structures and the centrosymmetric break of this compound. The probe parents employed in TDPAC studies included ^{111}In and ^{140}La. We compare the local magnetic and electrical interactions in these systems in order to spot the correlations between those. Additionally, we investigate the role of doping with lower and higher valence elements, i.e. the eventual TDPAC probes $^{2+}$Cd and $^{4+}$Ce, in structural peculiarities.

Session COA
SOFT MAGNETIC MATERIALS I: AMORPHOUS AND NANOCRYSTALLINE

Ahmed Talaat, Chair
University of Pittsburgh, Pittsburgh, PA, United States

CONTRIBUTED PAPERS

COA-01. On the modelling of the anhysteretic magnetization of soft magnetic materials. *J.M. Silveyra*[1] and J.M. Conde Garrido[1]
1. Laboratorio de Sólidos Amorfos, Instituto de Tecnologías y Ciencias de la Ingeniería (INTECIN), Universidad de Buenos Aires – CONICET, Buenos Aires, Argentina

Soft magnetic materials play a key role in the conversion of energy [1]. The analysis and optimization of devices with soft magnetic cores, such as inductive sensors and electric machines, rely on a simple and precise modelling of their nonlinear anhysteretic magnetization. The Langevin-Weiss equation is physically-based and accurate for homogeneous isotropic materials. In fact, it has even been adopted as the backbone of the popular Jiles-Atherton model to describe magnetic hysteresis. However, many studies show the difficulty of retrieving the modelling parameters given an experimental anhysteretic curve, for which stochastic optimization methods are generally used. We present a simple and deterministic method for finding the modelling parameters of the single and even the double-Langevin-Weiss function. Contrary to what has previously been assumed, the single-Langevin-Weiss function can provide a good description of any homogeneous material, even nanocrystalline alloys with strong transverse uniaxial anisotropy (Fig. 1). The overlooked key is to allow the Weiss molecular field to be negative. For non-homogeneous soft magnets, we show that the anhysteretic magnetization can accurately be described by the double-Langevin-Weiss function, corresponding to two sets of magnetic moments. The model is accurate not only for materials exhibiting a double-peak semi-log magnetization derivative curve (such as in grain-oriented steels in their rolling direction), but even for materials with a double-peak differential susceptibility curve (such as in silicon steels under compressive stress, Fig. 2). The overlooked key for the latter case, is to allow an antiferromagnetic arrangement of both sets of moments.

[1] JM Silveyra, E Ferrara, DL Huber, and TC Monson, "Soft magnetic materials for a sustainable and electrified world", Science, Vol. 362 (2018). doi: 10.1126/science.aao0195 [2] R Szewczyk, "Jiles–Atherton model for Octave/MATLAB" (2021). https://www.github.com/romanszewczyk/JAmodel/ [3] A Raghunathan, P Klimczyk, and Y Melikhov, "Application of Jiles-Atherton model to stress induced magnetic two-phase hysteresis", IEEE Transactions on Magnetics, Vol. 49, pp. 3187-3190 (2013). doi: 10.1109/TMAG.2013.2243823

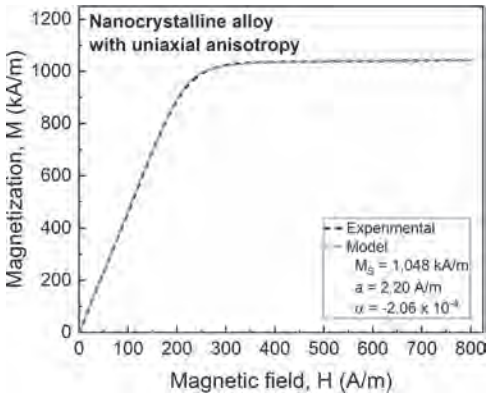

Fig. 1. Anhysteretic curve of a nanocrystalline alloy [2] with induced uniaxial transverse anisotropy fitted with our method based on the single-Langevin-Weiss model.

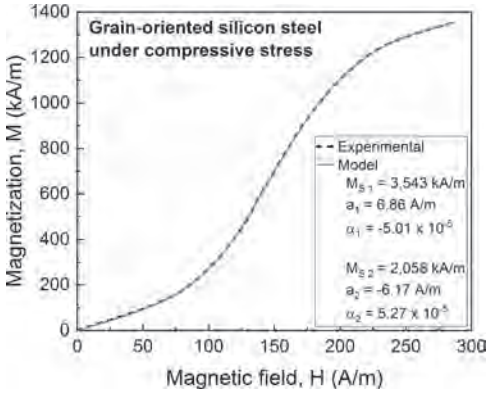

Fig. 2. Anhysteretic curve of a Goss steel under compressive stress [3] fitted with our method based on the double-Langevin-Weiss model.

COA-02. Fabrication of soft magnetic composite containing amorphous Fe-Co-B-Si magnetic flakes with good magnetic and mechanical properties. *N. Sanada*[1], T. Suetsuna[1] and H. Kinouchi[1]
1. Functional Materials Laboratory, Nano Materials & Frontier Research Laboratories, Corporate Research & Development Center, Toshiba Corporation, Kawasaki, Japan

We have developed a soft magnetic composite (SMC) containing amorphous magnetic flakes with magnetic anisotropy [1, 2]. In general, not only good magnetic properties but also good mechanical properties are required for practical use. In this research, we optimized the molding condition in the SMC containing amorphous Fe-Co-B-Si magnetic flakes and insulating matrix to realize both good magnetic and mechanical properties. The scanning electron microscope (SEM) image of the fabricated SMC is shown in Fig. 1. The mechanical property was greatly improved without deteriorating the magnetic properties after optimizing the molding condition. Table

1 shows the properties of the fabricated SMCs with those of the conventional SMC. After optimizing the molding condition, the saturation magnetization of the SMC was increased from 0.85 T to 0.99 T, and the flexural strength was significantly increased from 190 MPa to 420 MPa. The porosity of the SMC was measured, and it was decreased from 16 vol% to 9 vol%, which was thought to be one of the reasons of the improvement of both saturation magnetization and flexural strength after optimizing the molding condition. The coercivity of the SMC was as low as that of the conventional SMC, although it was slightly increased from 1.3 Oe to 1.7 Oe. It was found that the fabricated SMC had relatively low coercivity and significantly high flexural strength compared to the conventional SMC, although the saturation magnetization of it was lower than that of the conventional SMC because of relatively low saturation magnetization of the amorphous Fe-Co-B-Si magnetic flakes (1.43 T).

[1] T. Suetsuna, H. Kinouchi, T. Kawamoto, and N. Sanada, J. Magn. Magn. Mater., Vol. 473, p.416 (2019) [2] T. Suetsuna, H. Kinouchi, and N. Sanada, J. Magn. Magn. Mater., Vol. 519, p.167475 (2021)

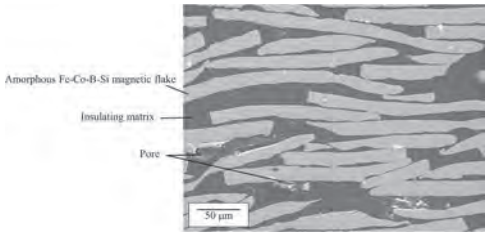

Fig. 1. SEM image of the fabricated SMC after optimizing the molding condition.

	Before optimizing the molding condition	After optimizing the molding condition	Conventional SMC*
Saturation magnetization (T)	0.85	0.99	2.0
Coercivity (Oe)	1.3	1.7	1.2 ~ 1.7
Flexural strength (MPa)**	190	420	40 ~ 90

* The SMC is commercial one, and the properties of saturation magnetization, coercivity, and flexural strength were measured in our group.
** The flexural strength was measured after molding without machining.

Tab. 1. Saturation magnetization, coercivity, and flexural strength of the fabricated SMCs with those of the conventional SMC.

COA-03. Evaluation of three-dimensional electromagnetic properties of the soft magnetic composite containing amorphous Fe-Co-B-Si magnetic flakes with magnetic anisotropy. *H. Kinouchi*[1], N. Sanada[1] and T. Suetsuna[1] *1. Toshiba Corporation, Kawasaki, Japan*

We have developed a soft magnetic composite (SMC) containing magnetic flakes with magnetic anisotropy to realize quite low magnetic loss [1]. The developed SMC is a material with layered structure of amorphous Fe-Co-B-Si magnetic flakes, and in-plane uniaxial magnetic anisotropy is induced by heat treatment under a magnetic field, as shown in Fig. 1. However, its three-dimensional electromagnetic properties had not been investigated in detail. In this research, the magnetic permeability and electrical resistivity were investigated in each of three axial directions. First, a cubic sample with a side of approximately 6 mm was set to a measuring system of permeability with coil and yoke, and permeability in each of three axial orthogonal directions of the sample was measured. Figure 1 shows the case when the permeability in in-plane easy axis (*X* axis) direction is measured. The permeability in in-plane hard axis (*Y* axis) direction and out-of-plane hard axis (*Z* axis) direction are also measured by rotating the sample by 90 degrees. Figure 2 shows the permeability of the fabricated SMC. It was found that the permeability in each of three axial directions is quite different (permeability in *X* axis direction > permeability in *Y* axis direction > permeability in *Z* axis direction) in the range of from 0.1 T to 0.7 T. Next, the electrical resistivity in each of three axial directions was measured by DC four-probe method. It was found that the electrical resistivity of the fabricated SMC in each of three axial directions was significantly higher than that of the conventional silicon steel sheet, and almost at the same level as that of the conventional SMC. Therefore, eddy-current loss can be suppressed effectively in each of three axial directions, similar to the case of the conventional SMC. In conclusion, the fabricated SMC is quite a unique material which can control magnetic flux with low eddy-current loss three-dimensionally by different permeability in each of three axial directions. The AC iron loss of the fabricated SMC has been under measurement.

[1] T. Suetsuna, H. Kinouchi, T. Kawamoto, and N. Sanada, J. Magn. Magn. Mater., Vol. 473, p.416 (2019).

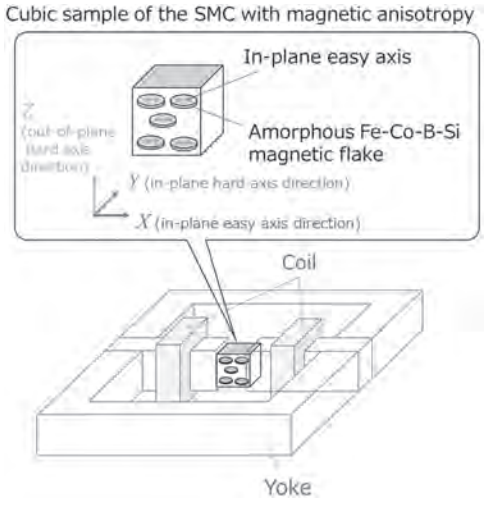

Fig.1 Schematic of the measuring system of permeability.

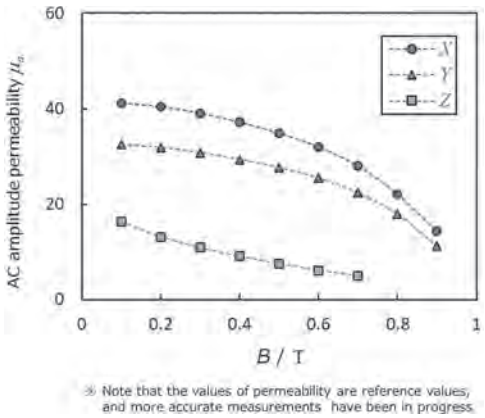

Fig. 2 Dependence of magnetic flux density on permeability of the fabricated SMC.

COA-04. Scalable Synthesis of CoFe and NiFe Nanoparticles from Ferrite Precursors with Tailored Magneto-Thermal Properties by a Combined Co-precipitation, Milling and Reduction Process. *D. Casaleiz*[1], M. Villanueva[1], A.J. Campos[1], J. Castillo[2], J. Camarero[1,3], E.M. Palmero[1], A. Espinosa[1,2], G. Salas[1] and A. Bollero[1] *1. IMDEA Nanociencia, Madrid, Spain; 2. Nanobiotecnología (IMDEA Nanociencia), Unidad Asociada al Centro Nacional de Biotecnología (CSIC), Madrid, Spain; 3. Dept. de Física de la Materia Condensada and Instituto Nicolás Cabrera, Universidad Autónoma de Madrid, Madrid, Spain*

Ferrites and magnetic nanoparticles (NPs) are widely used in sectors such as energy, electronics and biomedicine [1,2]. This work shows an optimum combination of co-precipitation, milling and reduction process of ferrite precursors ($CoFe_2O_4$ and $NiFe_2O_4$) to obtain CoFe and NiFe NPs, respectively, with tailored magnetic properties and improved heat generation for magneto-thermal applications. Ferrite precursor powders have been

synthesized by co-precipitation [3] followed by nanostructuring through self-developed ultrafast milling (24 min). Reduction at different temperatures under Ar+H_2 has led to NPs with a tuneable composition going from pure ferrite to CoFe and NiFe NPs, with core-shell nanostructures ($CoFe_2O_4$-CoFe and $NiFe_2O_4$-NiFe) at intermediate reduction stages. An optimized temperature has resulted in CoFe and NiFe NPs with a high saturation magnetization of 235 and 149 emu/g, respectively. Milling has allowed for diminishing the reduction temperature in 100 °C compared to that required for non-milled particles, which is of relevance in view of upscaling (Fig. 1) [4]. The magneto-thermal response of the NPs has been studied by exposure to alternating magnetic fields at 103 kHz for 5 min. Remarkably, an increase of 28% in the heat generated (under an applied field of 20 mT) has been obtained for the reduced milled CoFe NPs in comparison to the non-milled NPs (Fig. 2), due to particle refinement and high saturation magnetization. The milled NiFe NPs has shown a lower heat generation due to agglomeration effects. This cost-efficient and scalable approach eases the synthesis of NiFe and CoFe NPs for magneto-thermal applications. Acknowledgments. Authors acknowledge financial support from EU M-ERA.NET through COSMAG project (PCI2020-112143); from MICINN through NEXUS project (PID2020-115215RB-C21); and from CM through NanoMagCOST project (P2018/NMT-4321). A.J.C.-H. acknowledges support from "La Caixa" by the Doctoral INPhINIT Incoming program (LCF/BQ/DI20/1178002).

1. A. Bollero *et al., ACS Sustainable Chem. Eng*., Vol. 5, p.3243 (2017). 2. G. Salas *et al., J. Phys. Chem. C*., Vol. 118, p.19985 (2014). 3. F.J. Pedrosa *et al. RSC Adv*., Vol. 6, p.87282 (2016). 4. D. Casaleiz *et al.*, submitted for publication.

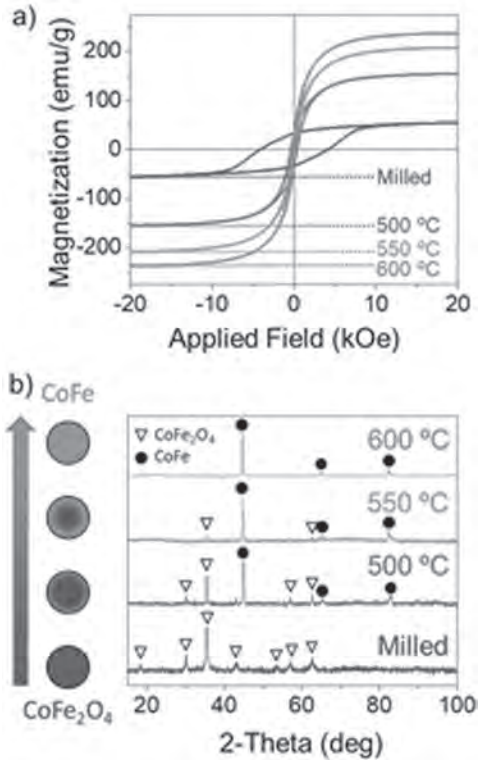

Fig.1. (a) Room temperature hysteresis loops and (b) XRD patterns of milled cobalt ferrite NPs reduced at different temperatures.

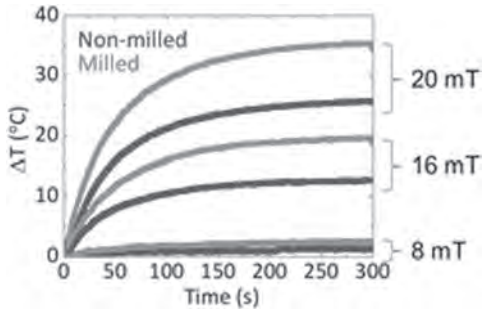

Fig.2. Magneto-thermal measurements of milled and non-milled CoFe NPs.

COA-05. Structural and magnetic characterization of Co-based soft magnetic amorphous nanocomposite films. *P. Nakarmi*[1], D. Tweddle[2], A. Koenig[2], K. Cole-Piepke[2], A. Leary[3], R. Noebe[3], G. Thompson[2], C. Mewes[1] and T. Mewes[1] *1. Department of Physics and Astronomy, The University of Alabama, Tuscaloosa, AL, United States; 2. Metallurgical and Materials Engineering, The University of Alabama, Tuscaloosa, AL, United States; 3. NASA Glenn Research Center, Cleveland, OH, United States*

Metal Amorphous Nanocomposites (MANCs) are an evolving class of soft magnetic materials consisting of an Fe- or Co-based crystalline phase embedded in an amorphous matrix. In thin-film form, they possess highly tunable magnetic properties, low eddy current and hysteresis losses, and are capable of performing under high-frequency magnetic field reversal. Therefore they are good candidates for a range of applications including use in power electronics, transformers, and electric motors[1, 2]. We investigated the structural, static and dynamic properties of magnetron sputtered and vacuum annealed (5 minutes and 20 minutes at 520°C) films of CoFeMnNbSiB using Transmission Electron Microscopy (TEM), Atom Probe Tomography (APT), Vibrating Sample Magnetometry (VSM) and Ferro-Magnetic Resonance (FMR). The sputtered films did not show crystallinity, however, an Mn-rich columnar structure that spanned the thickness of the film parallel to the growth direction was observed. After annealing for 5 minutes and 20 minutes, the columnar structure transformed to a partially crystallized microstructure with Co and Fe enriched crystallized phases with ~7nm grain size enclosed by an amorphous intergranular region as shown in Fig. 1. The magnetization dynamics of the films were measured using a custom-built instrument with a frequency range of 1-65 GHz and fields up to 1.6 T. The FMR spectrum of annealed samples shows two overlapping resonances (Fig. 2) due to the two phases present in the samples whereas the as-sputtered sample shows only one resonance. The effective magnetization remained constant whereas the linewidth increased from 13 to 55 Oe after annealing. The magnetic coercivity was observed to be (~26 Oe) independent of annealing while the saturation magnetization increased from 828 to 953 emu/cm^3. The observed changes in magnetic properties with annealing indicate that short-time annealing can be useful in optimizing the performance of these MANCs and tailoring properties for various applications.

1. Silveyra, J.M., et al., *Amorphous and nanocomposite materials for energy-efficient electric motors.* Journal of electronic materials, 2016. 45(1): p. 219-225. 2. McHenry, M.E., M.A. Willard, and D.E. Laughlin, *Amorphous and nanocrystalline materials for applications as soft magnets.* Progress in materials Science, 1999. 44(4): p. 291-433.

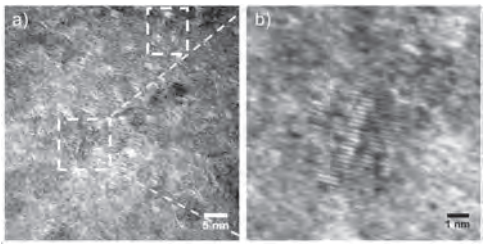

Fig. 1.a) TEM image of 20 minutes annealed sample b) Magnified section of a crystalline region

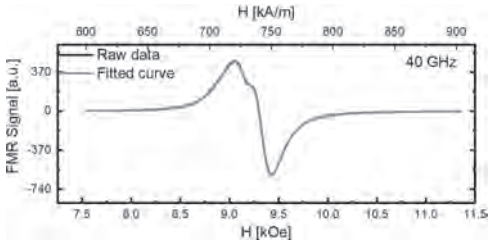

Fig. 2. FMR spectrum of 20 minutes annealed sample at 40 GHz reflecting two overlapping peaks due to dual-phase in the sample

COA-06. Graded magnetic anisotropy in Co-rich microwires.
P. Corte-Leon[1,2], V. Zhukova[1,2], J. Blanco[2], A. Irigaray[2], M. Ipatov[1,2] and A. Zhukov[1,2] *1. Advanced Polymers and Materials: Physics, Chemistry and Technology, University of the Basque Country, San Sebastián, Spain; 2. Applied Physics I, University of the Basque Country, San Sebastián, Spain*

Magnetic wires can present outstanding magnetic properties such as giant magnetoimpedance (GMI) or magnetic bistability and related single domain wall (DW) propagation. Magnetically soft glass-coated magnetic microwires prepared by the Taylor-Ulitovsky technique with metallic nucleus covered by flexible, insulating and biocompatible glass are quite demanded for a great number of applications [1]. Recenly, we showed that stress-annealing allows magnetic softening, GMI effect improvement and even grading the magnetic anisotropy in Fe-rich microwires [2]. Although generally thinner wires present certain advantages related to the industrial application, for some applications (like non-contact stress monitoring or magnetic tags) thicker wires are highly requested. Recently, preparation of thicker (above 50 μm in diameter, d) glass-coated Fe-rich microwires is reported [3]. In this paper, we present our recent experimental results on preparation and processing of "thick" Co-rich magnetic microwires (d = 94 μm) with graded magnetic anisotropy. From previous publications related to the effect of stress-annealing on magnetic anisotropy of Fe-rich microwires, is known that the stress-annealing induced anisotropy depends on the annealing temperature, T_{ann} [2]. Such graded magnetic anisotropy has been obtained by stress-annealing of Co-rich microwire at variable annealing temperature. The hysteresis loops for different sections of the microwire have been evaluated using a short (2 mm long) movable pick-up coil. A gradual change in the hysteresis loop (measured by the short pick-up coil) of the sample stress-annealed at variable T_{ann} is observed (see Fig.1). Such microwire, presents also variable squareness ratio, M_r/M_0, along the microwire length, L (see Fig.1). Obtained graded anisotropy has been attributed to a gradual modification of the domain structure along the microwire. Previously, for preparation of thin films with a graded magnetic anisotropy, rather sophisticated methods were used, including a change in the chemical composition during the deposition of thin films [4]. Accordingly, we propose a rather simple route to design graded magnetic anisotropy in a magnetic microwire.

[1] V. Zhukova et.al., Sensors, Vol. 19, p.4767 (2019). [2] V. Zhukova et.al., Acta Mater., Vol. 155, 279 (2018). [3] P. Corte-Leon et.al., J. Alloys Compd. Vol. 831, p.150992 (2020). [4] C.L. Zha et.al., Appl. Phys. Lett. Vol. 97, p.182504 (2010).

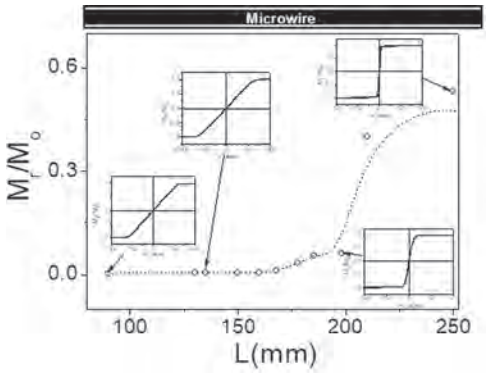

INVITED PAPER

COA-07. Effects of magnetostriction on excess loss in nanocrystalline soft magnetic materials.
H. Tsukahara[1,2], H. Imamura[2], C. Mitsumata[3], K. Suzuki[4] and K. Ono[5,1] *1. KEK, Tsukuba, Japan; 2. AIST, Tsukuba, Japan; 3. NIMS, Tsukuba, Japan; 4. Monash University, Melbourne, VIC, Australia; 5. Osaka University, Suita, Japan*

Magnetostriction is one of the governing factors for core loss at high frequencies. Nanocrystalline soft magnetic materials (NSMMs) are promising candidates for low magnetostriction because of the exchange coupling of nanocrystallites. Since a large resistance of this material inhibits eddy current, excess losses govern energy efficiency. However, it is still unclear how the magnetostriction affects the excess loss in NSMM because the random orientation of the crystal axis complicates the distribution of the magnetostriction. We formulate a micromagnetic simulation model for NSMMs, including the effective field of the magnetostriction. The simulation model of size 2048×2048×2 nm^3 consists of nanocrystallites whose mean diameter is 12.7 nm, and motions of stripe domains are simulated based on the Landau-Lifshitz-Gilbert equation. We choose α-Fe material parameters for the nanocrystallites, except for the magnetostriction constant which is variable. We assume that the magnetocrystalline anisotropy energy, which is suppressed by nano-crystallization, is negligibly small. The simulation predicts that the mean magnetostriction vanishes when λ_{111}=-0.36λ_{100} stands. However, even when this relationship stands, local magnetostrictions remain in the nanocrystallites (Fig. 1(a)). We simulated the domain wall dynamics for the two cases where the magnetostriction is isotropic and the mean magnetostriction vanishes. The domain wall oscillates due to an external magnetic field with a frequency of 100 MHz. Figure 1(b) shows the excess losses as a function of the magnetostriction constant, λ_{100}. When the magnetostriction is isotropic, the excess loss increases dramatically as λ_{100} increases because the magnetic energy of the wall is transferred to the elastic energy through the magnetostriction. Although the excess loss is considerably lowered when the mean magnetostriction vanishes, it shows a positive correlation with λ_{100}, indicating that the local magnetostriction still generates the excess loss in the nanostructure.

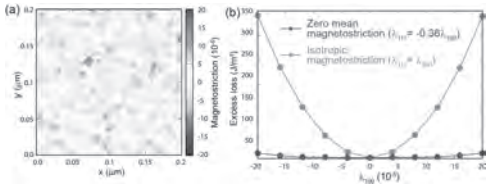

Figure 1: (a) Magnetostriction distribution in NSMM when the mean magnetostriction vanishes. (b) Excess losses as a function of the magnetostriction constant.

CONTRIBUTED PAPERS

COA-08. Epoxy Wetting of FeNi-based Metal Amorphous Nanocomposite. *J. Egbu*[1], O. Burnett[2], K. Byerly[1], P. Ohodnicki[3] and M. McHenry[1] *1. Materials Science & Engineering, Carnegie Mellon University, Pittsburgh, PA, United States; 2. Physics, Carnegie Mellon University, Pittsburgh, PA, United States; 3. Mechanical Engineering and Materials Science, University of Pittsburgh, Pittsburgh, PA, United States*

The trend towards electrification in transportation and aviation, and emerging high-frequency applications, e.g., axial high-speed motors (HSMs) has been enhanced by recent high-performance soft magnetic materials (SMMs). SMMs used in high switching frequency (> 1kHz) devices have been shown to lower core losses, have increased saturation induction, and have the capability of tunable permeability.[1-3] However, traditional SMMs like electric steels and Fe-based metal amorphous nanocomposites (MANCs) dominated by eddy current losses also show brittle mechanical properties at high frequencies. Recently developed FeNi-based MANCs[4] used in HSM exhibit significantly reduced eddy current losses while maintaining good mechanical properties and glass-forming abilities. A protective native surface oxide layer on FeNi-MANCs provides sufficient electrical insulation to reduce interlaminate eddy current losses. Since sufficient adhesion is required to maintain mechanical integrity in manufacturing HSM stator and rotor components, by techniques such as water jet cutting, epoxy resins are used in vacuum impregnation bonding of MANC cores. This work presents a detailed characterization of the surface oxide layer responsible for reducing interlaminate eddy current losses in magnetic cores and the wetting of these oxides by epoxies used in the vacuum impregnation process. X-ray diffraction, X-ray photoelectron spectroscopy (XPS), atomic force microscopy, and scanning electron microscopy were used to characterize surface oxides present in $(Fe_{70}Ni_{30})_{80}Nb_4B_{14}Si_2$ alloy. Fig. 1 (a) shows the XPS depth profile of a heat treated $(Fe_{70}Ni_{30})_{80}Nb_4B_{14}Si_2$ alloy showing ~11 nm thick Fe-rich surface oxide. Wetting experiments were performed to determine contact angle as a function of pre-applied stress and annealing temperature. Fig. 1(b) shows the contact angle measurement of an epoxy droplet compared to a water droplet on a FeNi-MANC alloy (with native oxide) surface. Anisotropy in wetting angle correlation with the strain-induced magnetic anisotropy will be discussed.

1. M.E. McHenry, M.A. Willard, and D.E. Laughlin, Prog. Mater. Sci. 44, 291 (1999) 2. S. Simizu, P.R. Ohodnicki, and M.E. McHenry, IEEE Trans. Magn. 54, (2018) 3. J.M. Slveyra, A. Leary, and M.E. McHenry, J. Electron. Mater. 45, 219 (2016) 4. N. Aronhime, V. DeGeorge, V. Keylin, P. Ohodnicki, and M. E. McHenry, J. Materials 69(11), 2164-70, (2017).

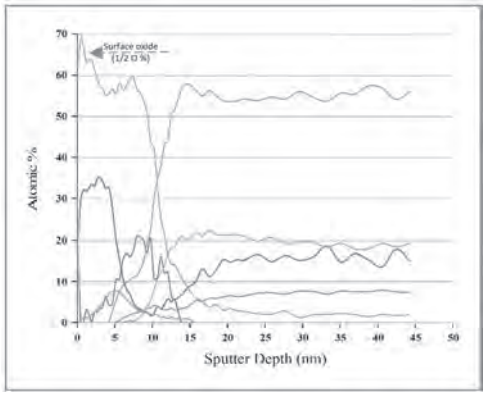

Figure 1. (a) XPS depth profile of $(Fe_{70}Ni_{30})_{80}Nb_4B_{14}Si_2$ alloy sample.

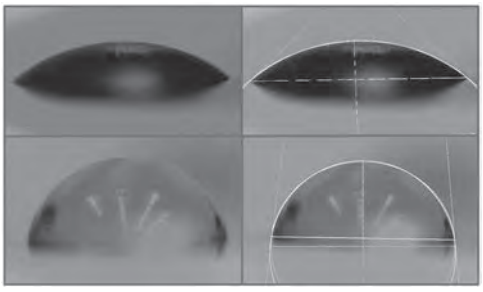

Figure 1. (b) (top) epoxy and (bottom) water droplets on $(Fe_{70}Ni_{30})_{80}Nb_4B_{14}Si_2$ alloy

COA-09. Influence of wet and dry milling conditions on the evolution of microstructure and T_C of Fe-Cr-Nb-B glassy powders. M. Lostun[1], M. Grigoras[1], G. Stoian[1], G. Ababei[1], H. Chiriac[1] and *N. Lupu*[1] *1. Magnetic Materials and Devices Department, National Institute of Research and Development for Technical Physics, Iasi, Romania*

Fe-Nb-Cr-B rapidly quenched melt-spun ribbons (MSRs) show glassy structures in the as-quenched state and Curie temperatures (T_C) of 290-330 K depending on the Cr content [1]. The medical applications are usually requiring submicron powders, which can be easily targeted to the sick body organs by means of the external magnetic field [2]. The present work focusses on the preparation of $Fe_{67.2}Nb_{0.3}Cr_{12.5}B_{20}$ submicron powders by high-energy ball milling from MSRs precursors, using different milling agents: oleic acid (OA), sodium oleate (NAOL) and stearic acid (SA). The main challenge is to preserve the glassy structure from MSRs through the milling process, because only the glassy structure guarantees the low T_C. MSRs were annealed at 400°C for 1 h to facilitate the milling. The ratio stainless steel balls:powder was of 50:1. The powders milled in OA and NAOL in the ratio of 1:1 have been washed in n-heptane and dried at 70°C in vacuum, while for the ones milled in SA, in the ratio of 5:1, trichloroethylene was used for removing the surfactant. After 150 h of milling in OA the powders have ~100 nm, XRD and UHR-TEM investigations indicating the presence of only the glassy structure and the absence of precipitating crystalline phases. The milling up to 250 h reduces the size of the powders to < 50 nm, while the glassy structure is preserved, as confirmed also by the same T_C value (~45°C) as for the precursor MSRs. The milling in NAOL keeps the powders in the range of 800÷900 nm, while T_C remains ~45°C. The milling over 100 h in NAOL results in an increase of T_C to 65°C and of M_s to 45 Am^2/kg, compared with MSRs powders milled in OA (M_s = 35 Am^2/kg). The increase of T_C and M_s is even more obvious for the powders milled in SA (110°C and 112 Am^2/kg, respectively). Moreover, the powders milled in SA are not changing their size even after 50 h of milling, i.e. ~5 μm, comparable with the ones of the precursor MSRs. However, the HR-SEM images indicate round shaped powders after milling in SA, compared with the starting lamellar pieces of MSRs, while the XRD and SAED patterns emphasize similar glassy structures for powders and MSRs. *Financial support by the NUCLEU Program (PN 19 28 01 01) is gratefully acknowledged.*

[1] H. Chiriac, L. Whitmore, M. Grigoras, G. Ababei, G. Stoian, N. Lupu, J. Appl. Phys. 117 (17) (2015) 17B522. [2] H. Chiriac, E. Radu, M. Tibu, G. Stoian, G. Ababei, L. Labusca, D.D. Herea, N. Lupu, Sci. Rep. 8 (2018) 11538.

Session COB
SOFT MAGNETIC MATERIALS II: AMORPHOUS AND NANOCRYSTALLINE

Ivan Skorvanek, Chair
Institute of Experimental Physics SAS, Košice, Slovakia

CONTRIBUTED PAPERS

COB-01. Stress-engineering of Structural and Magnetic Properties in Fe-Si-B Amorphous Microwires and Ribbons. *X. Zhang*[1], E. Rinko[2,3], A. Valeriano Inchausti[4], I. Anderson[2,3], M. Vázquez[4] and L. Lewis[1,5]
1. Mechanical and Industrial Engineering, Northeastern University, Boston, MA, United States; 2. Materials Science and Engineering, Iowa State University, Ames, IA, United States; 3. Ames Laboratory, Ames, IA, United States; 4. Instituto de Ciencia de Materiales de Madrid, CSIC, Madrid, Spain; 5. Chemical Engineering, Northeastern University, Boston, MA, United States

Modern electric machines with improved efficiency and performance require soft and hard ferromagnets with optimized structures and properties; these aspects are often governed by solid-state phase transformations that are sensitive to processing variables such as temperature and stress [1]. Here, we present results that the partial devitrification process and the resulting structural and magnetic features of the Fe-Si-B metallic glass system are altered by tensile stress annealing, with effects that are influenced by specific quenching conditions of the rapid solidification process. Metallic glass samples of composition $Fe_{79}Si_{11}B_{10}$ were fabricated into two distinct forms: 1) water-quenched microwires [2] (cross-sectional area ~0.018 mm^2) and 2) melt-spun ribbons (cross-sectional area ~0.038 mm^2). These samples have been confirmed to undergo a partial devitrification in the range of 400 – 500°C and form Fe(Si) crystals embedded in an amorphous matrix. The microwires and ribbons were separately annealed at temperature T_{ann} immediately below the devitrification onset temperature T_{onset} (T_{ann}/T_{onset} ~ 0.98) under a tensile stress of up to 200 MPa. While the resultant Fe(Si) crystallites in all samples after annealing (both with and without tensile stress) possess a $D0_3$ type chemically ordered crystal structure and {110}-type surface texture, as confirmed by X-ray diffraction, the stress annealed samples exhibit a reduced average grain size (by up to ~40%) relative to the stress-free counterparts. In addition, the magnetic responses measured on sample segments along their long axes are altered by stress annealing. In specific, the stress-annealed ribbons exhibit a three-fold reduction in initial susceptibility relative to that of the stress-free ribbon counterpart, while the microwires exhibit an increased susceptibility, Fig. 1. These differences are attributed to the different residual stress profiles and microstructural features that are correlated to their unique initial glassy state derived from the quenching methods. Acknowledgments: IEEE MagSoc Educational Seed Funding, Northeastern University

[1] M. A. Willard and M. Daniil, Handbook of Magnetic Materials, 173-342 (2013) [2] M. Vázquez, Handbook of Magnetism and Advanced Magnetic Materials, John Wiley, vol.4, p.2192-2222 (2007)

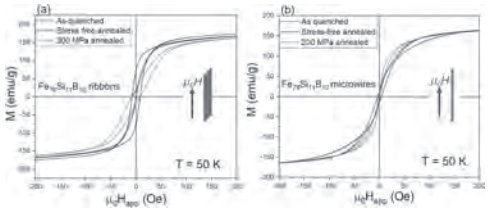

Fig.1. M-H curves of (a) ribbons and (b) microwires in as-quenched, stress-free, and 200 MPa stress annealed state

COB-02. Development of Novel Fe Based Nanocrystalline FeBNbPSi Alloy Powder with High B_s of 1.41T. H. Matsumoto[1], *Y. Kajiura*[1], M. Hosono[1], A. Hasegawa[1], H. Kumaoka[1], K. Yoshidome[1] and S. Mori[1]
1. Material Research Center, TDK Corporation, Narita, Japan

The possibility of the powderization of the precursor with a single amorphous phase was investigated in the FeBNbP and the FeBNbPSi nanocrystalline alloy powders. The $Fe_{90-X}B_xNb_7P_3$ (x=9, 10), the $Fe_{79.5}B_{9.5}Nb_7P_3Si_1$ and the $Fe_{82-x}B_9Nb_6P_3Si_x$ (x=2, 3) powders were prepared by the gas atomization method using high pressure water for rapid quenching. The crystallization by abnormal grain growth was shown by cross sectional images and SAED pattern in the as-atomized $Fe_{81}B_9Nb_7P_3$ particle. On the other hand, the as-atomized particle as a precursor exhibiting low H_c of 141 A/m with single amorphous phase was observed from a cross sectional image and SAED pattern in the $Fe_{80}B_{10}Nb_7P_3$ nanocrystalline alloy powder. In addition, the stability of amorphous phase in the FeBNbP nanocrystalline alloy powder was also significantly improved by the addition of Si. The as-atomized $Fe_{79.5}B_{9.5}Nb_7P_3Si_1$ nanocrystalline alloy powder with Si of 1 at% was decreased the crystallization peak compared with the $Fe_{80}B_{10}Nb_7P_3$ nanocrystalline alloy powder without Si. In particular, the as-atomized $Fe_{79}B_9Nb_6P_3Si_3$ alloy powder with Si of 3% as a precursor powder of nanocrystalline alloy exhibited the excellent magnetic softness of low H_c of 53 A/m compared to ordinary $Fe_{73}Si_{11}B_{11}Cr_3C_2$ amorphous and $Fe_{73.5}Si_{13.5}B_9Nb_3Cu_1$ nanocrystalline alloy powders. Furthermore, the nanocrystallized $Fe_{79}B_9Nb_6P_3Si_3$ powder at 873K achieved both high B_s of 1.41T and low H_c of 37A/m compared to ordinary amorphous, and nanocrystalline alloys. Therefore, we concluded that the novel FeBNbPSi nanocrystalline alloy powder with both high B_s and low H_c was developed for magnetic core of inductor products.

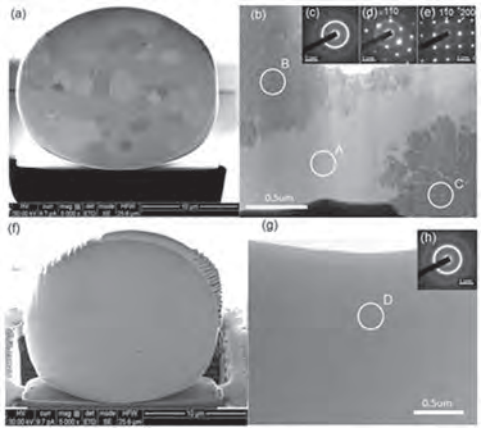

Fig.1 (a) SEM image of the particle cross section with the $Fe_{81}Nb_7B_9P_3$, (b) TEM bright field image of amorphous and crystallization region with the $Fe_{81}B_9Nb_7P_3$, (c), (d), (e) SAED pattern of a region with A, B and C, (f) SEM image of the particle cross section with the $Fe_{80}B_{10}Nb_7P_3$, (g) TEM bright field image of amorphous region with the $Fe_{80}B_{10}Nb_7P_3$, (h) SAED pattern of D region.

Composition / at%	Average particle size / μm	As-atomized H_c / A/m	As-atomized $\lambda_s \times 10^6$	After crystallization B_s / T	After crystallization H_c / A/m	Crystallization temperature / K
$Fe_{81}B_9Nb_7P_3$	28.4	2808	2.8	1.50	2578	873
$Fe_{80}B_{10}Nb_7P_3$	24.7	1249	6.0	1.48	1281	873
$Fe_{79}B_{11}Nb_7P_3$	17.9	141	8.0	1.49	1101	873
$Fe_{79.5}B_{9.5}Nb_7P_3Si_1$	14.6	95	8.4	1.46	153	873
$Fe_{80}B_9Nb_7P_3Si_1$	14.1	113	6.8	1.49	207	873
$Fe_{78}B_9Nb_7P_3Si_3$	32.3	53	7.6	1.41	37	873
$Fe_{77}Si_{12}B_9Nb_7Cr_2$	22.0	88	27.4	1.30	None	None
$Fe_{77.5}Si_{12}B_9Nb_1Cu_1$	23.1	81	5.0	1.22	28	798

Table. 1 Average particle size and magnetic characteristics of $Fe_{90-X}BxNb_7P_3$ (x=9, 10), $Fe_{79.5}$ $B_{9.5}Nb_7P_3Si_1$ and $Fe_{82-x}B_9Nb_6P_3Si_x$ (x=2, 3) powders with ordinary FeSiBCCr and FeSiBNbCu powders.

COB-03. Effect of Joule Heating on GMI and Magnetic Properties of Fe-rich Glass-Coated Microwires. A. Gonzalez Villegas[1,2], V. Zhukova[1,2], M. Ipatov[1,2], P. Corte-Leon[1,2], *A. Zhukov*[1,2] and J. Blanco[2]
1. Advanced Polymers and Materials: Physics, Chemistry and Technology, Universidad del País Vasco, San Sebastian, Spain; 2. Dpto. de Fisica Aplicada, EIG, Universidad del País Vasco, San Sebastian, Spain

Amorphous ferromagnetic glass-coated microwires present various properties suitable for technological applications, such as great magnetic softness, ultra-fast magnetization switching and domain wall propagation, inductive heating capabilities or Giant Magnetoimpedance, GMI, effect [1, 2]. Thus, they have been widely studied in the past few years [1]. As-prepared Fe and Co based microwires differ in some of these properties. Fe microwires are observed to present magnetic bistability and rather low GMI values, while Co ones possess nearly non-hysteretic magnetization curves and higher GMI [1], making the latter a more attractive candidate for GMI related technologies. However, Co is a critical raw material, making Fe-based microwires preferable for large scale applications. Thus, search of appropriate postprocessing for magnetic softness and GMI improvement is essentially relevant. Among the prospective methods allowing these goals are stress-annealing and Joule heating. As the latter is more effective for tuning of GMI in Co-rich microwires [1], systematic studies of Joule heating on magnetic properties and GMI of Fe-rich ones are scarce. Accordingly, influence of Joule heating on magnetic properties and GMI effect of $Fe_{75}B_9Si_{12}C_4$ glass-coated microwires was studied. The GMI ratio, $\Delta Z/Z$, is defined as: $\Delta Z/Z = [Z(H) - Z(Hmax)] / Z(Hmax)$ A decrease in coercivity of Joule heated samples is observed, while hysteresis loop maintain rectangular shape (Fig 1). However, a remarkable increase in $\Delta Z/Z$ is observed (Fig 2). Observed GMI ratio improvement has been discussed considering magnetic anisotropy by induced magnetic field during Joule heating and internal stress relaxation. Remarkable GMI effect improvement observed in Joule heated Fe-rich microwires, along the fact that Fe is a more common, cheap metal than Co, makes them suitable for magnetic sensor applications.

[1] A. Zhukov, J.M. Blanco, V. Zhukova et al. *Giant magnetoimpedance in rapidly quenched materials*. J. Alloys Compd. 814, 2020 [2] I. Morales, D. Archilla, P. de la Presa et al. *Colossal heating efficiency via eddy currents in amorphous microwires with nearly zero magnetostriction*. Sci Rep 10, 602, 2020

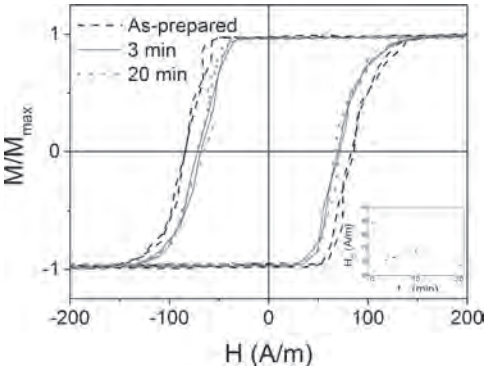

Fig. 1. Hysteresis loops of $Fe_{75}B_9Si_{12}C_4$ microwires Joule heated at 20mA for different times. Inset: coercivity dependence on annealing time.

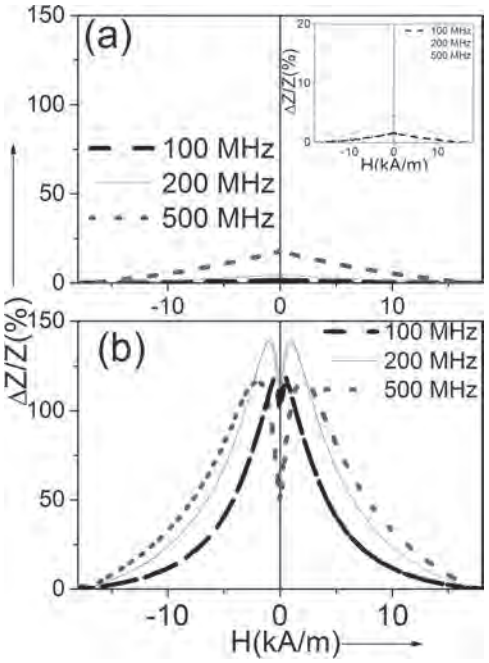

Fig. 2. GMI ratio of as-prepared (a) and Joule heated for 3min (b) $Fe_{75}B_9Si_{12}C_4$ microwires measured at different AC frequencies.

COB-04. Revealing defect-induced spin disorder in nanocrystalline. *M. Bersweiler*[1], E. Pratami Sinaga[1], I. Peral[1], N. Adachi[2], P. Bender[3], N. Steinke[4], E. Gilbert[5], Y. Todaka[2], Y. Oba[6] and A. Michels[1]
1. Department of Physics and Materials Science, University of Luxembourg, Luxembourg, Luxembourg; 2. Department of Mechanical Engineering, Toyohashi University of Technology, Toyohashi, Japan; 3. Heinz Maier-Leibnitz Zentrum, Technische Universität München, Garching, Germany; 4. Institut Laue-Langevin, Grenoble, France; 5. Australian Centre for Neutron Scattering, Technology Australian Nuclear Science and Organization, Kirrawee DC, NSW, Australia; 6. Materials Sciences Research Center, Japan Atomic Energy Agency, Tokai, Japan

In the present work, we combine magnetometry and magnetic small-angle neutron scattering to study the influence of the microstructure on the macroscopic magnetic properties of a nanocrystalline Ni bulk sample, which was prepared by straining via high-pressure torsion. As seen by magnetometry, the mechanical deformation leads to a significant increase of the coercivity compared to nondeformed polycrystalline Ni. The neutron data reveal a significant spin-misalignment scattering caused by the high density of crystal defects inside the sample, which were created by the severe plastic

deformation during the sample preparation. The corresponding magnetic correlation length, which characterizes the spatial magnetization fluctuations in real space, indicates an average defect size of 11 nm, which is smaller than the average crystallite size of 60 nm. In the remanent state, the strain fields around the defects cause spin disorder in the surrounding ferromagnetic bulk, with a penetration depth of around 22 nm. The range and amplitude of the disorder is systematically suppressed by an increasing external magnetic field. Under certain assumptions, the analysis of the penetration depth allows one to determine the magnitude of the effective magnetic anisotropy. For HPT Ni, we find an increased anisotropy (factor of 4), presumably due to magnetoelastic interactions, relative to the single-crystalline ground state. Our findings are supported and illustrated by micromagnetic simulations, which, for the particular case of nonmagnetic defects (holes) embedded in a ferromagnetic Ni phase, further highlight the role of localized spin perturbations for the magnetic microstructure of defect-rich magnets such as high-pressure torsion materials. This work was supported by the financial support from the National Research Fund of Luxembourg (Pride MASSENA Grant No. 10935404 and CORE SANS4NCC Grant), from KAKENHI (Grant No. 19K05102) and from the Japan Science and Technology Agency (Grant No. JPMJSK1511).

[1] M. Bersweiler, E.P. Sinaga, I. Peral, N. Adachi, P. Bender, N.J. Steinke, E.P. Gilbert, Y. Todaka, A. Michels, and Y. Oba, Physical Review Materials, 5 (2021) 044409.

COB-05. Magnetostructural Phase Transition in $Fe_{60}V_{40}$ Alloy Thin Films. *M.S. Anwar*[1,8], H. Cansever[1], B. Böhm[2], R. Gallardo[3], R. Hübner[4], U. kentsch[4], S. Zhou[5], B. Eggert[6], H. Wende[6], K. Potzger[1], J. Fassbender[7], K. Lenz[1], J. Lindner[1], O. Hellwig[1,2] and R. Bali[1] *1. Magnetism, Helmholtz-Zentrum Dresden-Rossendorf, Dresden, Germany; 2. Physics, Technische Universität Chemnitz, Chemnitz, Germany; 3. Physics, Universidad Técnica Federico Santa María, Santa Maria, Chile; 4. Ion Beam Center, Helmholtz-Zentrum Dresden-Rossendorf, Dresden, Germany; 5. Semiconductor Materials, Helmholtz-Zentrum Dresden-Rossendorf, Dresden, Germany; 6. Faculty of Physics and Center for Nanointegration Duisburg-Essen (CENIDE), Universität Duisburg-Essen, Duisburg, Germany; 7. Helmholtz-Zentrum Dresden-Rossendorf, Dresden, Germany; 8. Physics, Technische Universität Dresden, Dresden, Germany*

The tuning and control over the intrinsic magnetic properties, such as saturation magnetization (M_s) and Gilbert damping (α), can be obtained via systematic rearrangement of the lattice at the nanoscale. In certain binary alloys such as B2 $Fe_{60}Al_{40}$ [1] and B2 $Fe_{50}Rh_{50}$ [2], the M_s can be tuned by inducing chemical disorder. The disorder caused by the randomization of site occupancies of the atoms can be achieved by ion-irradiation. Here we explore a magnetic phase transition in $Fe_{60}V_{40}$ thin films caused by ordering of the lattice structure from short-range order to the crystalline state. $Fe_{60}V_{40}$ films (~ 40 nm) were grown onto SiO_2/Si substrate. The as-grown films are weakly ferromagnetic with low M_s of 17 kA/m; whereas irradiation with 25 keV Ne^+ - ions at fluences of ~ 5 × 10^{15} ions/cm^2 leads to a drastic increase of M_s to ~ 750 kA/m, as shown in Fig. 1. X-ray diffraction as well as transmission electron microscopy reveal a structural short-range order in the as-grown films, that transform to A2 $Fe_{60}V_{40}$ with increasing Ne^+ - fluence. The A2 region appears to nucleate at the film top surface and with increasing fluence, it propagates deeper down into the film. The effect of the phase transition on the dynamic behaviour has been investigated using ferromagnetic resonance (Fig. 2). The low value of Gilbert damping (~ 0.002) has been obtained from the frequency dependence of the resonance spectra. Furthermore, the transition can be tracked using Conversion electron Mössbauer spectroscopy to shed light on the variation of local magnetic ordering during the transition. The tunable film structure as well as low damping form the basis for further investigations on nanomagnets embedded within $Fe_{60}V_{40}$ thin films. Funding by the DFG - 322462997 (BA 5656/1-2 | WE 2623/14-2) is acknowledged. Ion-irradiation was performed at the Ion Beam Centre of the HZDR.

[1] J. Ehrler, *et al., New J. Phys.*, 22, 073004 (2020). [2] B. Eggert, *et al., RSC Adv.*,10, 14386 (2020).

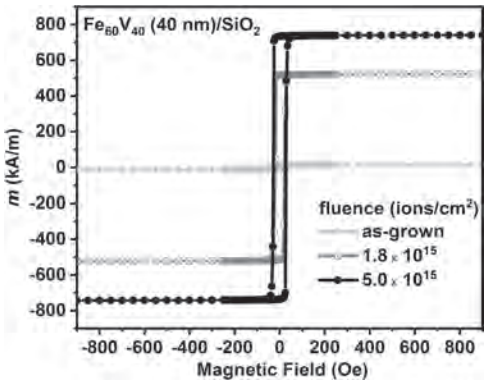

Fig. 1: The effect of 25 keV Ne^+ - irradiation at various fluences, on the magnetization vs. field behaviour of $Fe_{60}V_{40}$ thin films.

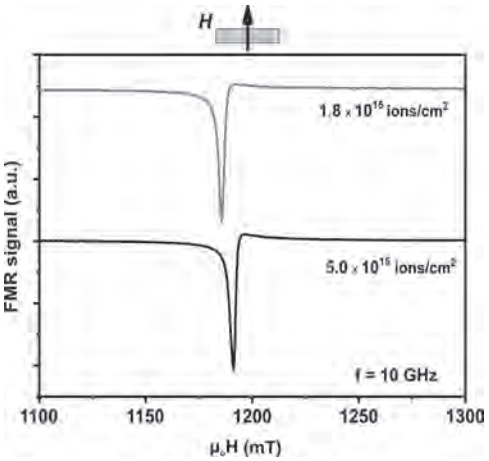

Fig. 2: Variation of FMR spectra in out-of-plane configuration.

COB-06. Domain wall propagation in Fe-rich magnetic microwires with graded magnetic anisotropy. *P. Corte-Leon*[1,3], V. Zhukova[1,3], J. Blanco[3], M. Ipatov[1,3] and A. Zhukov[1,2] *1. Dept. Advanced Polymers and Materials: Physics, Chemistry and Technology, Faculty of Chemistry, University of Basque Country, San Sebastian, Spain; 2. Ikerbasque, Bilbao, Spain; 3. Department Applied Physics, University of Basque Country, San Sebastian, Spain*

Magnetic wires are one of the most convenient materials allowing to study domain wall, DW, propagation. From the viewpoint of technological applications, fast, reliable, and controllable DW propagation is essential [1]. Therefore, great efforts have been made to control the single DW propagation [1]. Amorphous perfectly cylindrical microwires with positive magnetostriction coefficient can present a fast (DW velocity, v, of the order of 1 km/s) single DW propagation [2]. In viscous regime below the Walker breakdown field a uniform v is usually assumed if magnetic fielf, H is constant. We observed that in $Fe_{75}B_9Si_{12}C_4$ magnetic microwire stress-annealing at variable annealing temperature, T, rather different hysteresis loops for different sections of such microwire are observed (Fig. 1a). In as-prepared microwires DW propagation with the same velocity is observed in different section of the microwire (see Fig. 1b). However, in a media with graded magnetic anisotropy v is essentially non-uniform (Fig. 1c): faster DW propagation is observed in the region with moderate stress-annealing induced magnetic anisotropy (see Fig. 1c). Such character of induced anisotropy is evidenced by the dependence of the inner axially magnetized core radius, R_c. on sample length, L (see Fig. 1d). Evaluated $R_c(L)$ dependence and its correlation with $T(L)$ reflects graded magnetic anisotropy obtained by stress-annealing at variable T_{ann}. Higher DW velocity in the region with induced magnetic anisotropy is explained by the transverse character of

stress-annealing induced magnetic anisotropy which affects the travelling domain wall in a similar way as application of transversal bias magnetic field. Obtained graded magnetic anisotropy allows engineering the DW dynamics of Fe-rich microwires and observation of essentially non-uniform singe DW propagation in media with graded magnetic anisotropy.

[1] S.S.P. Parkin, M. Hayashi, L. Thomas, *Science* 320 (2008) 190. [2] V. Zhukova, et.al., *Nanomaterials* 10 (2020) 2407

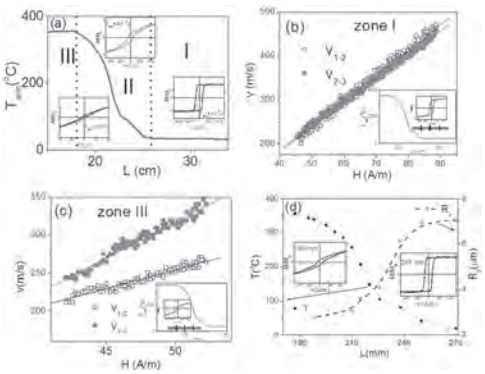

Graded magnetic anisotropy appearing as a modification of hysteresis loop character over the microwire length, *L*, obtained by stress-annealing at variable *T* (a), v(H) dependencies in as-prepared microwire (b) and in the region with graded magnetic anisotropy (c) and R_c *(L)* dependence in microwire with graded anisotropy.

COB-07. Development of an (Fe, Sn)-based Nanocrystalline Soft Magnetic Alloy. *P. Wang*[1] and M. Willard[1] *1. Materials Science and Engineering, Case Western Reserve University, Cleveland, OH, United States*

The $D0_3$ Fe_3Sn phase shows higher magnetization and smaller magnetocrystalline anisotropy compared to Fe_3Si based on the comprehensive first principles calculations [1]. A new computation-based alloy design method, motivated by the work of Villars [2], was used to design a new alloy system $(Fe_{1-x-y}Co_xSn_y)_{87}Nb_3B_9Cu_1$ ($4<x<27$, $5<y<15$) to achieve $D0_3$ Fe_3Sn phase with the help of the melt-spinning process. Differential scanning calorimetry was used to determine the primary crystallization temperatures of the $Fe_{79-x}Co_xSn_8Nb_3B_9Cu_1$ alloys (x=4, 9, 14, 19 and 24), which have peak temperatures from 405°C to 420°C at a heating rate of 10°C /min. The amorphous ribbons were encapsulated in fused quartz ampoules and annealed in tube furnace at 450°C, 500°C, or 550 °C for 3600 seconds. X-Ray Diffraction (XRD) has been used to analyze structural properties of as-spun and heat-treated ribbons of all alloy compositions. Partial crystalline exists during the melt-spinning process for these series alloys except the $Fe_{60}Co_{20}Sn_7Nb_3B_9Cu_1$ as-spun ribbons, which has a single broad scattering peak of XRD diffractograms indicating an amorphous phase. XRD diffractogram of the heat-treated ribbons are comprised of a B2 phase, which has a primitive cubic structure. The crystallite sizes for each heat-treated sample were estimated by Scherrer broadening to have values between 6 and 11 nm. The magnetic properties of as-spun and heat-treated ribbons were studied by vibrating sample magnetometry. Saturation magnetization and coercivity were determined from room temperature magnetic hysteresis loops. The highest magnetization value 171.4 Am^2/kg was achieved by $Fe_{60}Co_{22}Sn_5Nb_3B_9Cu_1$ alloy annealed at 500°C while the coercivity value is 67.3A/m.

[1] A. Singh, A. Stebner, and C. Ciobanu, "Binary and ternary metallic compounds with soft magnetic properties: predictions from density functional theory calculations," *Bull. Am. Phys. Soc.*, 2020. [2] P. Villars, "A three-dimensional structural stability diagram for 998 binary AB intermetallic compounds," *J. Less-Common Met.*, vol. 92, pp. 215–238, 1983, doi: 10.1016/0022-5088(84)90333-3.

COB-08. Nanocrystalline soft magnetic materials produced by Continuous Ultra-Rapid Annealing (CURA). *R. Parsons*[1] and K. Suzuki[1] *1. Materials Science and Engineering, Monash University, Clayton, VIC, Australia*

Ultra-Rapid Annealing (URA) has been demonstrated as a viable means of producing nanocrystalline soft magnetic materials with a saturation magnetic polarization comparable to that of Fe-Si steels (1.85 to 2.02 T) while also maintaining low coercivity (2.5 to 9.3 A/m)[1–3]. However, the high heating rates ($> 10^4$ K/s) and short annealing times (< 3 s) utilized by URA compared to conventional annealing techniques, along with the effect of latent heating during primary crystallization [4], has created new material production challenges. Specifically, the requirement for batch processing by URA places a limit on the commercial viability of this technique. In this work, a Continuous Ultra-Rapid Annealing (CURA) process has been demonstrated whereby a ribbon undergoes URA in a reel-to-reel continuous process. Annealing time (0.1 to 10 s) and tension (5-40 MPa) utilized by CURA are carefully controlled to allow for the processing of brittle nanocrystalline alloys. The microstructural and magnetic properties of nanocrystalline $(Fe_{0.8}Co_{0.2})_{86}B_{14}$ produced by CURA have been characterized. Figure 1 shows DC hysteresis loops acquired from nanocrystalline $(Fe_{0.8}Co_{0.2})_{86}B_{14}$ produced by the batch URA [1,2] and the newly developed CURA processes. The coercivity was reduced from 14.9 A/m to 8.8 A/m and the core loss at 1.5 T and 50 Hz was reduced from 0.62 W/kg to 0.50 W/kg by applying the CURA process. The CURA process has also been utilized to produce a nanocrystalline $(Fe_{0.8}Co_{0.2})_{86}B_{14}$ toroidal core weighing 0.16 kg. This core was machined to produce a stator core for a commercially available 220 W electric motor which demonstrated a 10-25% relative improvement in efficiency over an unmodified motor with a conventional Fe-Si steel stator core [5].

1. Suzuki, K. et al. Appl. Phys. Lett. 110, 012407 (2017). 2. Parsons, R. et al. J. Alloys Compd. 723, 408–417 (2017). 3. Parsons, R., Li, Z. & Suzuki, K. J. Magn. Magn. Mater. (2019). 4. Parsons, R. et al. AIP Adv. 10, 015105 (2020). 5. Scorpion Power Systems SII-2215-1127 Motor Datasheet. (2021).

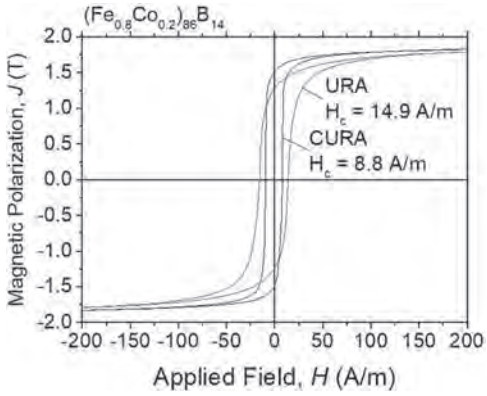

Fig. 1 DC hysteresis loops acquired from nanocrystalline $(Fe_{0.8}Co_{0.2})_{86}B_{14}$ produced by conventional Ultra-Rapid Annealing (URA) and the newly developed Continuous Ultra-Rapid Annealing (CURA) process.

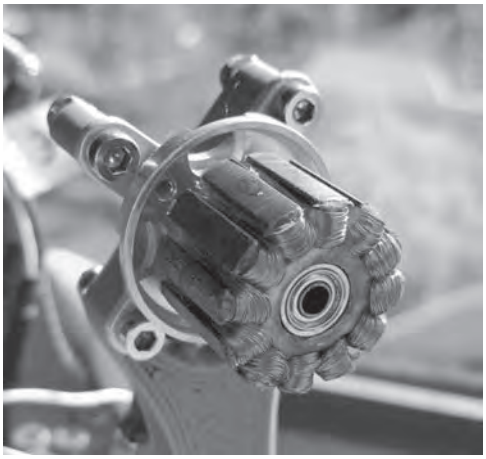

Fig. 2 A photo of the nanocrystalline $(Fe_{0.8}Co_{0.2})_{86}B_{14}$ electric motor stator core produced by CURA after winding of the excitation coils and mounting to a commercially available 220 W motor frame.

COB-09. Laser Patterning Assisted Devitrification and Induced Anisotropies in Soft Magnetic Nanocrystalline Alloys. *A. Talaat*[1], A. Leary[2], D. Greve[3,4], Y. Liu[1], J. Wiezorek[1] and P. Ohodnicki[1,5]
1. Mechanical Engineering & Materials Science, University of Pittsburgh, Pittsburgh, PA, United States; 2. NASA Glenn Research Center, Cleveland, OH, United States; 3. DWGreve Consulting, Sedona, AZ, United States; 4. Electrical &Computer Engineering, Carnegie Mellon University, Pittsburgh, PA, United States; 5. Electrical & Computer Engineering, University of Pittsburgh, Pittsburgh, PA, United States

Macroscopic anisotropies relevant to amorphous and nanocrystalline soft magnetic alloys arise from the coupling between magnetostriction coefficients and mechanical stresses induced during quenching process. Induced magnetoelastic anisotropies by means of local laser annealing associated with both compressive and tensile stresses allow for dramatic changes in the volume of irradiated areas and hence non-uniform stress distributions. In this work, we investigate laser patterning devitrification as a novel method to realize emergent properties in modified regions at the ribbon surface consisting of periodic localized single- and / or multi- laser spots thermally treated under rapid heating and cooling conditions for magnetostrictive (FeNi-rich) and near-zero magnetostrictive (Co-rich) alloys in terms of domain structure. Electromagnetic simulations of the laser patterning process and impacts of heat transients were performed along with results of structural and magnetic property characterization including magnetic domain imaging.

Session COC
SOFT MAGNETIC MATERIALS III: FERRITES

Paul Ohodnicki, Chair
University of Pittsburgh, Pittsburgh, PA, United States

CONTRIBUTED PAPERS

COC-01. Growth-Induced Perpendicular Magnetic Anisotropy in Thin Film Rare Earth Iron Garnets. *A. Kaczmarek*[1], E.R. Rosenberg[1], S. Ngo[1], G.S. Beach[1] and C. Ross[1] *1. Materials Science and Engineering, Massachusetts Institute of Technology, Cambridge, MA, United States*

Perpendicular magnetic anisotropy (PMA) is a property of magnetic films which allows for high-density data storage in spintronic applications. In rare earth iron garnets, PMA typically originates from magnetoelastic anisotropy either as a result of film strain due to lattice mismatch with a single crystal garnet substrate or from thermal mismatch upon annealing[1]. However, PMA derived from magnetoelastic anisotropy requires specific combinations of strain state and magnetostriction coefficients, so there is interest in finding new ways to control PMA in thin films. In this study we demonstrate that PMA can also be obtained from a dominant growth-induced anisotropy (GIA) using europium thulium iron garnet (EuTmIG) as a model material. By varying the ratio of Eu to Tm, the lattice parameter of the garnet can be changed, resulting in films which are under compression or tension on a gadolinium gallium garnet (GGG) substrate, as shown in Fig. 1 with high resolution x-ray diffraction (HRXRD) analysis. Vibrating sample magnetometry (VSM), shown in Fig. 2, indicates that PMA is present in all films regardless of strain state. We propose that PMA in the zero-strain film is attributed to GIA due to the preferential ordering of different rare earth ions on inequivalent lattice sites within the garnet[2]. Additionally, we quantify GIA and spin transport in the films with spin hall magnetoresistance measurements on Pt/EuTmIG hall crosses. This work shows that precise engineering of the structure of these high quality films creates new methods for control of garnet thin film properties for spintronic applications.

(1) Rosenberg, E. R.; Beran, L.; Avci, C. O.; Zeledon, C.; Song, B.; Gonzalez-Fuentes, C.; Mendil, J.; Gambardella, P.; Veis, M.; Garcia, C.; Beach, G. S. D.; Ross, C. A. Magnetism and Spin Transport in Rare-Earth-Rich Epitaxial Terbium and Europium Iron Garnet Films. *Phys. Rev. Mater.* 2018, *2* (9), 094405. https://doi.org/10.1103/PhysRevMaterials.2.094405. (2) Tabor, W. J.; Vella-Coleiro, G. P.; Hagedorn, F. B.; Van Uitert, L. G. Bubble Dynamics and Growth-Induced Anisotropy in $(Y,Eu,Tm)_3(Ga,Fe)_5O_{12}$. *J. Appl. Phys.* 1974, *45* (8), 3617–3620. https://doi.org/10.1063/1.1663826.

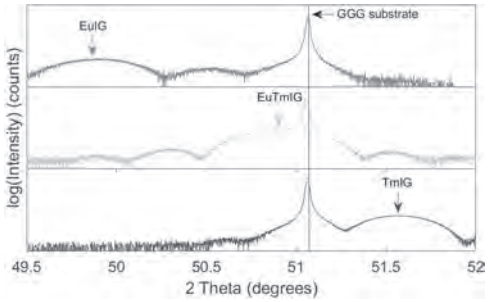

Fig. 1. HRXRD of the (444) symmetric reflection of ~25 nm EuIG, TmIG and $Eu_{0.7}Tm_{2.3}Fe_5O_{12}$ films on (111) GGG substrates show tensile, compressive, and near zero strain states, respectivley, as shown by the relative position of the film and substrate peaks.

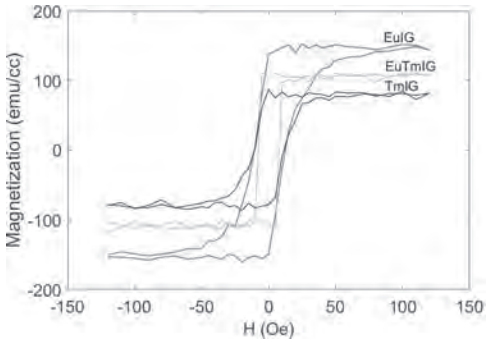

Fig 2. PMA is evident in out-of-plane VSM of all films, regardless of the magnitude of magnetoelastic anisotropy.

COC-02. Gadolinium and Thulium Iron Garnet Thin Films with Perpendicular Magnetic Anisotropy. *C. Holzmann*[1], O. Ciubotariu[1] and M. Albrecht[1] *1. Institute of Physics, University of Augsburg, Augsburg, Germany*

Rare earth iron garnet thin films are ferrimagnetic insulators and as such of great interest for spintronic research, including the spin-Seebeck or spin-Hall effect. Yttrium iron garnet is well known for its ultra-low Gilbert damping parameter, but recently other rare earth garnets with more complex magnetic structures gained interest. Perpendicular magnetic anisotropy (PMA) is often beneficial for spintronic effects, but in thin films an in-plane magnetic easy axis is favored by the magnetic shape anisotropy. However, our simulations based on bulk parameters predict PMA in garnet thin films caused by the strain-induced magnetoelastic anisotropy (fig. 1) [1,2]. Thulium (TmIG) and gadolinium iron garnet (GdIG) thin films were grown epitaxially on different substrates by pulsed laser deposition, including on GGG and GSGG. Single-crystalline films with smooth interfaces are ensured by depositions at elevated temperatures (around 600°C) at low deposition rates (0.01-0.02 nm/s) under an oxygen atmosphere ($p_{O2} \approx 0.02$ mbar). PMA is achieved at room temperature for the garnet thin films grown under tensile in-plane strain on GSGG. While TmIG thin films show a strain relaxation with increasing film thickness and a subsequent transition to an in-plane magnetic easy axis [3], the GdIG films exhibit PMA from 10 to 220 nm thickness. Furthermore, GdIG has a bulk compensation temperature around 286 K. With increasing film strain, a decreasing compensation temperature is found. A tunable magnetic easy axis in the thin films, dependent on the film strain as well as temperature is shown (fig. 2), enabling further research in the field of spintronics.

[1] Quindeau A. *et al.,* Advanced Electronic Materials 3, 1600376 (2017). [2] Zanjani S. and Onbasli M., AIP Advances 9, 035024 (2019). [3] Ciubotariu O. *et al.,* Scientific Reports 9, 17474 (2019).

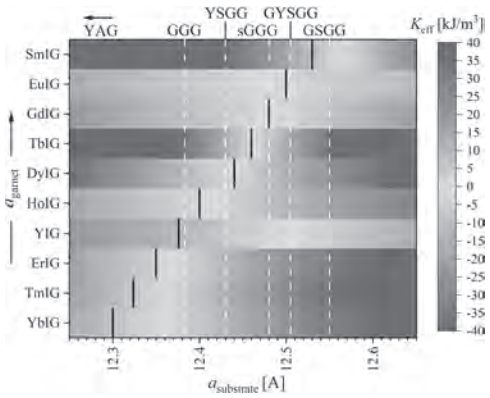

Fig. 1 Simulation of the effective magnetic anisotropy K_{eff} for strained rare earth iron garnet thin films. For $K_{eff} > 0$ (red areas), an out-of-plane magnetic easy axis is predicted, while $K_{eff} < 0$ (blue) marks an in-plane magnetic easy axis.

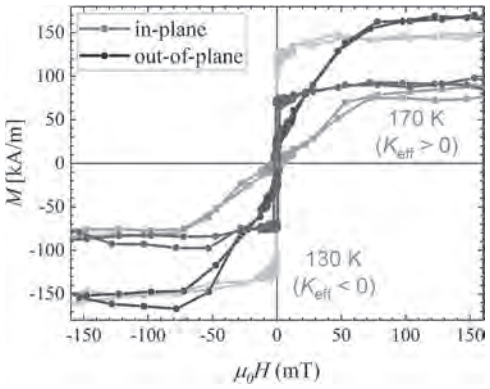

Fig. 2 Hysteresis loops for a 23 nm thick GdIG film grown on GSGG in in-plane (light squares) and out-of-plane (dark circles) geometry, recorded by SQUID-VSM. At a temperature of 130°C (marked in blue) an in-plane magnetic easy axis is visible, while a spin reorientation transition towards an out-of-plane magnetic easy axis at 170°C (red) is observed.

COC-03. Magnetic Coupling in Ferrimagnetic Bilayers. S. Becker[1], Z. Ren[1,2], *F. Fuhrmann*[1], A. Ross[1,3], S. Lord[1,2], S. Ding[1,2], R. Wu[1,4], J. Yang[5], J. Miao[6], M. Kläui[1,2] and G. Jakob[1,2] *1. Institute of Physics, Johannes Gutenberg-University Mainz, Mainz, Germany; 2. Graduate School of Excellence "Materials Science in Mainz" (MAINZ), Mainz, Germany; 3. Unité Mixte de Physique CNRS, Thales, Université Paris-Saclay, Palaiseau, France; 4. Center for Quantum Spintronics, Norwegian University of Science and Technology, Trondheim, Norway; 5. State Key Laboratory for Mesoscopic Physics, Peking University, Beijing, China; 6. School of Materials and Engineering, University of Science and Technology, Beijing, China*

With growing demands for faster and more energy efficient information technology, the utilization of magnons as information carriers is envisioned to be a major step forward [1]. To successfully develop magnon-based devices, there are several requirements for the applied materials to meet. The insulating ferrimagnet Yttrium Iron Garnet ($Y_3Fe_5O_{12}$, YIG) and other garnets are good candidates with an outstanding low damping and large magnon propagation length [1]. Here, we investigate heterostructures of YIG and the insulating ferrimagnet Gadolinium Iron Garnet ($Gd_3Fe_5O_{12}$, GIG) [3, 4] grown by pulsed laser deposition. In contrast to YIG, the Gadolinium replaces the non-magnetic Yttrium and adds with its magnetic moment to the net magnetization of GIG. In heterostructures of YIG/GIG, we observe a ferromagnetic coupling between the Fe sublattices of the two layers leading to complex behavior in response to external magnetic fields and a nontrivial temperature dependence [2]. This observation is supported by measurements of the bulk sensitive SQUID magnetometry (Fig. 1) and surface sensitive spin Hall magnetoresistance [5, 6] and spin Seebeck effect measurements [6, 7]. These techniques enable us to determine the relative alignment of the magnetic sublattices of the layers, as a function of temperature and external magnetic field. The coupled bilayer shows a critical temperature at which its total magnetization is fully compensated. We show that the relative thickness of the YIG and GIG layers can be used to tune this critical temperature. So we can control the magnetic properties to tune magnonic spin current propagation and magnonic properties and could help to switch magnon transport analogously to the giant magnetoresistance effect [8].

[1] A. Chumak, V. I. Vasyuchka, A. Serga et al., Nat. Phys, Vol. 11, p. 453–461 (2015) [2] S. Becker, Z. Ren, F. Fuhrmann et al., Phys. Rev. Appl., 16, 014047 (2021) [3] A. Brooks Harris, Phys. Rev. 132, 2398 (1963) [4] T. Yamagishi, J. Awaka,Y. Kawashima et al., Philos. Mag. 85,1819 (2005) [5] H. Nakayama, M. Althammer, Y.-T. Chen et al., Phys. Rev. Lett.110, 206601 (2013) [6] M. U. Fayaz, M. S. Saleem, Y. Gu et al., J. Appl. Phys.126, 183901 (2019) [7] J. Cramer, E.-J. Guo, S. Geprägs et al., Nano Lett.17, 3334 (2017) [8] J. Cramer, F. Fuhrmann, U. Ritzmann et al., Nat. Commun. 9, 1089 (2018)

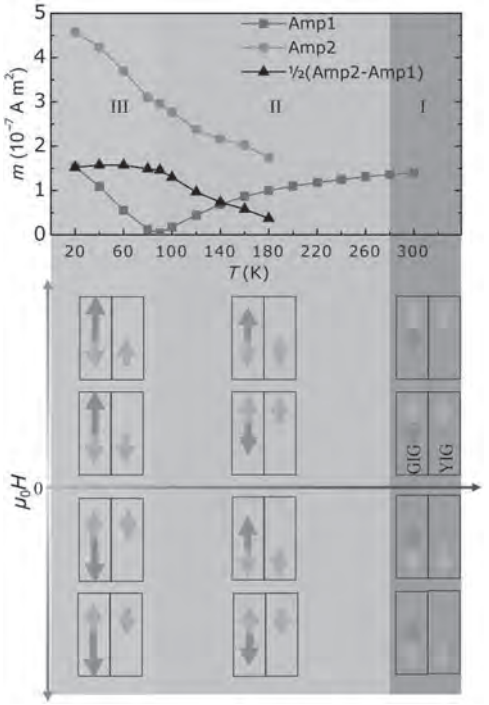

Fig. 1: Temperature dependent SQUID magnetometry measurements of a YIG (36 nm)/GIG (30 nm) bilayer. The alignment of the GIG and YIG films are illustrated below, dependent on Temperature and external magnetic field [2].

COC-04. Role of Magnetic Inhomogeneities and Interdiffusion in Compensated Gadolinium Iron Garnet Thin Films. *K. Srinivasan*[1], P. Quarterman[2], T. Gage[3], C.J. Kinane[4], A.J. Caruana[4], J.G. Barriocanal[5] and B. Stadler[1] *1. Electrical and Computer Engineering, University of Minnesota, Minneapolis, MN, United States; 2. NIST Center for Neutron Research, National Institute of Standards and Technology, Gaithersburg, MD, United States; 3. Center for Nanoscale Materials, Argonne National Laboratory, Lemont, IL, United States; 4. ISIS-Neutron and Muon Source, STFC Rutherford Appleton Laboratory, Didcot, United Kingdom; 5. Characterization Facility, College of Science and Engineering, University of Minnesota, Minneapolis, MN, United States*

Magnetic materials with low total angular momentum are an emerging choice for storage layers in spin-based magnetic random-access memory (MRAM) as they allow for faster switching (read/write) over short pulses <10 ns.[1] Specifically, gadolinium iron garnet ($Gd_3Fe_5O_{12}$; GdIG) is preferred due to antiferromagnetically coupled magnetic sublattices and a compensation temperature near room temperature (280-297 K), which allows current-induced switching in a technologically desirable temperature regime. While the discussion around magnetization switching and related measurements assume uniform compensation temperature, thin films grown using physical vapor deposition techniques can have depth-dependent inhomogeneities in their structural, compositional, and magnetic properties [2], [3]. Here, GdIG is reactively sputtered on gadolinium gallium garnet (GGG) and silicon substrates. Reciprocal space maps from X-ray diffraction show that single-crystalline GdIG/GGG thin films are highly epitaxial with a lattice mismatch of only ~0.6% with respect to the substrate, Figure 1. Temperature-dependent magnetometry using a SQUID shows that the compensation temperature is 287.5±2.5 K for GdIG/GGG and 265±5 K for GdIG/Si. Furthermore, depth-dependence of the composition and in-plane magnetization are characterized using x-ray reflectometry (XRR) and polarized neutron reflectivity (PNR). The magnetic scattering length depth (SLD) profiles measured at saturation/remnant fields reveal a reduced magnetic SLD and interdiffusion layer at the substrate interface, Figure 2. Complementary characterization using cross-section scanning transmission electron microscopy (STEM) shows that GdIG films on GGG and Si have an estimated porosity of 30-35%, which is commensurate with the lower-than-expected nuclear SLD of GdIG from PNR. The results shown here elucidate the inhomogeneities in magnetic and structural characteristics of compensated ferrimagnets crucial for their realization as magnetic free-layers.

[1] J. Finley and L. Liu, *Appl. Phys. Lett.*, vol. 116, no. 11, p. 110501 (2020).
[2] R. Ramos *et al.*, *Nature Communications*, vol. 10, no. 1, pp. 1–8 (2019).
[3] K. Shen, *Physical Review B*, vol. 99, no. 2 (2019).

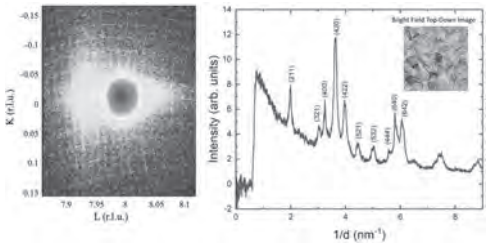

Figure 1. Reciprocal space KL projection of GdIG/GGG (100) and select area electron diffraction of GdIG on SiO2 TEM grids.

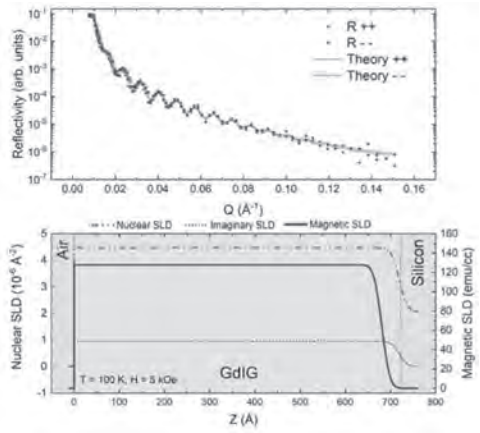

Figure 2. PNR for spin-polarized channels (top) and structural and magnetic SLD profiles for GdIG/Si (bottom).

COC-05. Withdrawn

COC-06. Low Damping Bismuth Substituted Iron Garnet Thin Films for Spintronics. *T. Fakhrul*[1], B. Khurana[1], H. Nembach[2], J.M. Shaw[2], Y. Fan[3], S. Huang[1], B. Lee[1], G.A. Riley[2], Z. Chen[4], D. A. Muller[4], G.S. Beach[1], L. Liu[3] and C. Ross[1] *1. Materials Science and Engineering, MIT, Cambridge, MA, United States; 2. NIST, BOULDER, CO, United States; 3. EECS, MIT, Cambridge, MA, United States; 4. Cornell, Ithaca, NY, United States*

Magnetic materials with perpendicular magnetic anisotropy (PMA) and low Gilbert damping (a) hold great promise towards faster and smaller memory and logic devices. Ferrimagnetic rare earth iron garnets with PMA have recently attracted a great deal of attention for spintronic applications. However, a major drawback for most rare earth iron garnets is their large Gilbert damping. Bi-substituted yttrium iron garnet (BiYIG) has been shown to have both PMA and low damping,[1] and spin-orbit torque-driven domain wall velocities of 4.5 km/s [2] have been observed in BiYIG/Pt. In this work we report the growth, magnetic and spintronic transport properties of single layers and heterostructures consisting of PMA BiYIG and thulium iron garnet (TmIG) grown epitaxially on substituted $Gd_3Ga_5O_{12}$ (GSGG, SGGG) and $Nd_3Ga_5O_{12}$ (NGG) by pulsed laser deposition. BiYIG films with thickness as low as 2.4 nm (2 unit cells) showed magnetic hysteresis loops with PMA, and magnetization vs. thickness shows a non-magnetic layer of only 1.4 nm at the BiYIG/substrate interface, attributed to interdiffusion, and a magnetization of 115 kA/m. The PMA in these films can be fine-tuned by the lattice mismatch between the film and garnet substrate. We find that the magnetoelastic anisotropy is too weak to account for the PMA in these films and the major contributor to PMA is growth induced anisotropy. Ferromagnetic Resonance (FMR) measurements in the out-of-plane configuration demonstrate that BiYIG films have Gilbert damping as low as 1.3×10^{-4} and linewidth as small as 3.4 mT as shown in Fig.1. Brillouin Light Scattering (BLS) measurements reveal the absence of Dzyaloshinskii-Moriya interaction (DMI) in the pure BiYIG films, whereas BiTmYIG exhibits DMI as high as 0.018 mJ/m^2. Furthermore, Spin Hall magnetoresistance (SMR) measurements were also performed to characterize the efficiency of spin transport in Pt/BiYIG and Pt/(Bi,Tm)YIG heterostructures.

[1] Soumah, L., Beaulieu, N., Qassym, L., Carrétéro, C., Jacquet, E., Lebourgeois, R., Youssef, J.B., Bortolotti, P., Cros, V. and Anane, A., 2018. Ultra-low damping insulating magnetic thin films get perpendicular. Nature communications, 9(1), pp.1-6. [2] Caretta, L., Oh, S.H., Fakhrul, T., Lee, D.K., Lee, B.H., Kim, S.K., Ross, C.A., Lee, K.J. and Beach, G.S., 2020. Relativistic kinematics of a magnetic soliton. Science, 370(6523), pp.1438-1442.

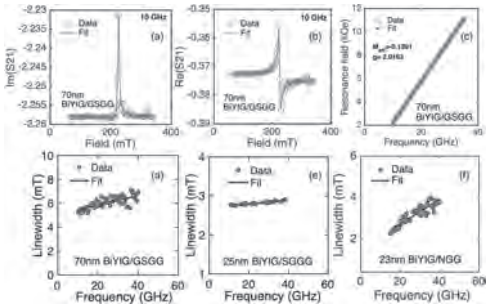

Figure. 1: FMR spectra showing the (a) imaginary and (b) real part of the complex transmission parameter (S_{21}) for a 70nm BiYIG/GSGG film. (c) Representative fit of the resonant field versus frequency for BiYIG/GSGG. FMR linewidth versus frequency for (d) BiYIG/GSGG, (e) BiYIG/SGGG and (f) BiYIG/NGG.

COC-07. Designing Magnetic Metal Oxide Colloidal Nanoparticles for Spatially Resolved Thermometry. A.J. Biacchi[1], F. Abel[1], T.Q. Bui[1], E.L. Correa[1], C. Dennis[1], S. Woods[1] and *A.R. Hight Walker*[1]
1. National Institute of Standards and Technology (NIST), Gaithersburg, MD, United States

Colloidal magnetic nanoparticles (MNPs) of metal oxides are increasingly important for applications such as biomedical imaging, sensing, drug delivery, and hyperthermia. These exploit the very soft magnetism found in nanoscale ferrimagnets, often ferrites, which yield a strong collective response to applied alternating (AC) magnetic fields while remaining dispersed in media. Their synthesis relies on reproducible, scalable, colloidal solution chemistry routes. Further, the size, shape, structure, and composition are tunable, serving as levers to design and manipulate the magnetic behavior of these functional MNPs. Here, we report colloidal MNPs specifically designed for remote 3D thermometry; a technique that employs MNPs to measure and image temperature remotely with high spatial resolution throughout a three-dimensional volume. This metrology is based on the temperature-dependent nature of the particles' magnetization, their dispersibility throughout a liquid or solid of interest, and the ability of applied AC magnetic fields to penetrate through many materials. A series of shape- and size-controlled colloidal MNPs based on ferrites were synthesized *via* the thermal decomposition of organometallic precursors. Further, we exploited compositional doping of transition metal elements and exchange coupling between core-shell magnetic heterostructures to generate improved temperature-dependent magnetization (200-400 K at <0.001 T applied AC field). Extensive structural characterization was performed to better understand the underlying factors influencing the magnetic response. Results collected from X-ray photoelectron and Raman spectroscopies, and high-resolution electron microscopies revealed correlations between the nanoscale atomic structure of these particles with their magnetic performance. Finally, we used a home-built AC magnetic particle spectrometer to determine the magnetization-dependence of these nanothermometers as a function of temperature, frequency, and field amplitude. We show that designed complex metal oxide MNPs display tunable thermosensitivity and AC field signal response, which represents a potential pathway to the implementation of a practical 3D thermal imaging platform based on magnetometry.

COC-08. Withdrawn

COC-09. Magnetic characterization of self-assembled nanostructures in cobalt ferrites using first order reversal curves. S.V. Mullurkara[1], *A. Talaat*[1], B.C. Dodrill[2] and P. Ohodnicki[1,3] *1. Mechanical Engineering and Material Science, University of Pittsburgh, Pittsburgh, PA, United States; 2. Lake Shore Cryotronics, Westerville, OH, United States; 3. Electrical Engineering and Computer Science, University of Pittsburgh, Pittsburgh, PA, United States*

Bulk and thin film Cobalt ferrites have been shown to undergo spinodal decomposition resulting in uniform periodic composition fluctuations with a characteristic wavelength in the microstructure. Fine tuning of the self-assembled microstructure can also be easily achieved by changing relevant thermodynamic parameters. Although decomposition has been shown to manifest itself as an increase in coercivity of the material, the nature of exchange interactions, reversal mechanisms and domain wall motion upon decomposition remains to be investigated. In this work, we systematically investigate the effect of decomposition on magnetic properties using first order reversal curve (FORC) analysis. Bulk powder processing routes combined with heat treatments are used for sample preparation. Room temperature magnetization and FORC measurements have been performed using a vibrating sample magnetometry in fields up to 1T. The distribution of switching and interaction fields have been compiled through a set of minor loops and the magnetization reversal mechanisms and exchange coupling are investigated. Further, various heat treatments at multiple temperatures and varying annealing times will be used to generate self-assembled microstructures with distinct characteristic decomposition wavelengths. The effects of decomposition wavelength on magnetic properties and FORC distributions will also be investigated.

TAKAHASHI, M. and FINE, M.E,Journal of the American Ceramic Society, Vol: 53: Page :633-634.

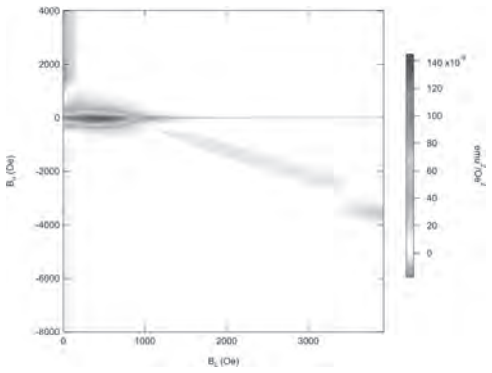

Fig. 1 FORC diagram of the powder after milling (mixture of Co_3O_4 and Fe_3O_4)

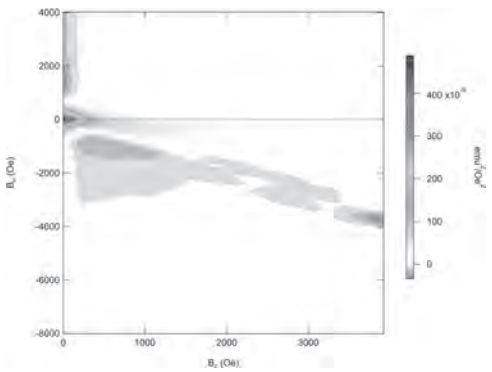

Fig. 2 FORC diagram of spinodal decomposed cobalt ferrite

COC-10. Effect of Particle Size and Insulation Coating Technique on the Core Loss, Relative Magnetic Permeability, and Saturation Magnetization of Insulated Powder Cores. *W. Burgess*[1,2], J. Devkota[1,2] and B. Howard[1] *1. National Energy Technology Laboratory, Pittsburgh, PA, United States; 2. NETL Support Contractor, Pittsburgh, PA, United States*

In this study, powder cores were synthesized by compaction of ferrite and other Fe-based substrates. Relative magnetic permeability and core loss were measured at excitation frequencies to above 1000 kHz. A ferrite coating such as $NiFe_2O_4$ was applied to an Fe-based substrate via precipitation coating techniques. Saturation magnetization values greater than 140 emu/g were recorded for $NiFe_2O_4$-coated Fe. Chemical coating techniques involving the application of either a phosphate or ferrite layer to an Fe-based powder substrate were also studied, and the effect of these coating techniques on core loss and relative permeability was examined. XRD and SEM were used to observe the particle coatings and to determine the effect of temperature on the integrity/chemical makeup of the powder. The effect of annealing/sintering on the core loss properties and relative magnetic permeability was studied. Finally, the effect of particle size on the core loss and relative magnetic permeability properties was examined.

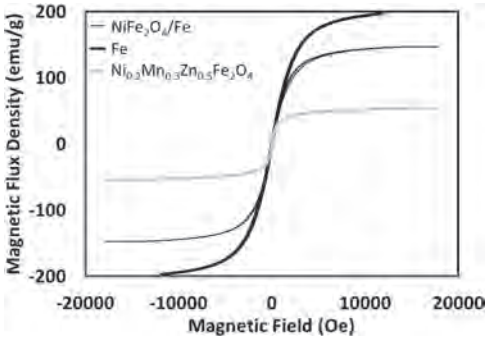

Figure 1. Magnetic properties comparison for powders of $NiFe_2O_4$-coated Fe, Fe, and $Ni_{0.2}Mn_{0.3}Zn_{0.5}Fe_2O_4$.

COC-11. Enhancement of electromagnetic wave absorption in ferrite hetero-hollow spheres. *D. Mandal*[1] and K. Mandal[1] *1. Dept. Condensed Matter Physics and Material Sciences, SN Bose National Centre for Basic Sciences, Burdwan, India*

In order to obtain a light-weight, stable, and cost-effective yet efficient electromagnetic (EM) wave absorbing material, here, we presented tuning of EM wave attenuation properties of as-synthesized low-density ferrite hetero-hollow spheres (HHS) in-detail within a widely used frequency range of 1–20 GHz. Interestingly, in this context, low density nano hollow spheres (NHS) with dual interface are found to be superior than their bulk and solid counterparts. The divalent cation, M^{2+} [M = Mn, Co, Ni, Cu, Zn] substitution in Fe_3O_4 NHS displays $MnFe_2O_4$ NHS to exhibit an optimal reflection loss (*RL*) of about - 32.7 dB, total shielding efficiency (SE_{Total}) ~ -42 dB and a high attenuation constant (α) ~ 196 Np/m. With increase in filler concentration (in epoxy resin matrix) from 0 wt% to 50 wt%, $MnFe_2O_4$ NHS shows a gradual increase in *RL* values and an excellent *RL* of about -45.6 dB at thickness ~4.2 mm. Further, tuning of MnFe2O4 NHS, varying their sizes [mean diameter (in nm) of sample sets = 100, 220, 300, 450, and 550] is demonstrated as an effective strategy to achieve an excellent microwave absorber, and $MnFe_2O_4$ (MnFO) NHS of diameter ~450 nm is found to exhibit a maximum RL of approximately −52.6 dB, SE_{Total} of approximately −39.5 dB, and a high α of ~285 Np/m due to best impedance matching, $|Z_{in}/Z_0|$ ~ 1, along with significant dielectric and magnetic losses. Finally, MnFO@CFO bilayered HHSs exhibit an excellent RL of −47.0 dB at only 20 wt% filler content larger interfacial polarization, additional pairs of dipole, higher magnetic anisotropy, internal reflections and scattering from NHSs become responsible. Analysis from the $\lambda/4$ model for best matching thickness (tm) displays a good agreement between experimental and simulated tm values. This study demonstrates optimized MnFO@CFO NHS as a highly promising low-cost and lightweight EM wave absorber suitable for practical high-frequency applications.

1. D. Mandal* and K. Mandal, 'Electromagnetic wave attenuation properties of MFe2O4 (M = Mn, Fe, Co, Ni, Cu, Zn) Nano-Hollow spheres in search of an Efficient Microwave Absorber', J. Magn. Magn. Mater. 536 (2021) 168127 2. A. Gorai, D. Mandal*, K. Mandal*, 'Multi-Layered Nano-hollow Spheres for Efficient Electromagnetic wave absorption', Nanotechnology 32 (2021) 345707 3. D. Mandal* and K. Mandal, 'Enhancement of Electromagnetic Wave Absorption in MnFe2O4Nano-hollow spheres', J. Appl. Phys. 129 (2021) 074902

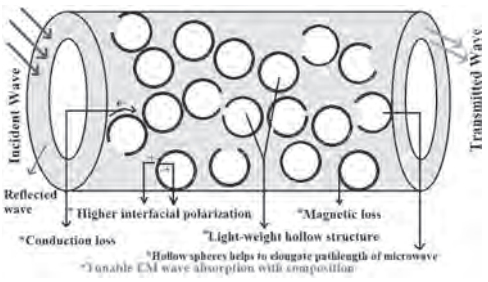

A schematic approach showing a toroidal shaped sample and effectiveness of NHSs toward EM wave absorption.

COC-12. Withdrawn

COC-13. Evidence for Temperature Independent Ferromagnetic Resonance Frequency in Bismuth Substituted Iron Garnets. *D. Gouéré*[1], H. Merbouche[1], C. Carrétéro[1], J. Ben Youssef[2], R. Lebrun[1], P. Bortolotti[1], V. Cros[1] and A. Anane[1] *1. Unité Mixte de Physique CNRS, Thales, Université Paris-Saclay, Palaiseau, France; 2. LabSTICC, Université de Bretagne Occidentale, Brest, France*

Yttrium Iron Garnet is the benchmark material for ferromagnetic resonance; it is up to today the only magnetic material that is being integrated in on-shell electronic devices for its radiofrequency properties that combine high resonance quality factor (10^4) and frequency tunability. It is the goal of YIG magnonics to make use of this potential for a large variety of applications ranging from beyond CMOS computation to radiofrequency front-end and back-end analog signal processing. YIG devices have however a sever drawback that is that they should include thermal stabilization. This is a necessity since YIG has a relatively low Curie temperature (~550K) which results in a high sensitivity of its magnetization to temperature (~0.4 mT /Kelvin). In the present study we show a novel approach to solve this long standing issue by engineering the magnetic anisotropy in Bi substituted YIG. We evidence for those films that vanishing effective magnetization yields high thermal stability over very wide temperature range: from 260K to 400K, where the frequency thermal drift is 50 times smaller than that of YIG while keeping the extremely low damping and insulating character of YIG [1] For instance, we show that this was instrumental to the excitation of coherent spin-waves using SOT described in Ref. 2. FMR frequency can be written for a thin film in the in-plane magnetization configuration as: $f = \gamma\sqrt{(H_a+(M_s-H_u))}$. Where γ is the gyromagnetic factor, H_a is the applied magnetic field, M_s is the saturation magnetization and H_u is the out-of-plane magnetic anisotropy field. The effective magnetization is defined as $M_{eff}=M_s-H_u$. It arises from this equation that the only temperature dependent terms are $M_s(T)$ and $H_u(T)$. Our observation show that here those term can be engeniered to have identical temperature dependences yielding a vanishing effective magnetization. This observation is unexpected as in most magnetic material the magnetic anisotropy has a much steeper temperature dependence than the magnetization. We anticipate that fabricating a material whose FMR frequency is temperature independent open new opportunities for the field of spintronics.

[1] L. Soumah et al. Nat. Commun. 9, 3355 (2018) [2] M. Evelt et al. Phys. Rev. Appl. 10, 041002 (2018)

Session COD
SOFT MAGNETIC MATERIALS IV: BULK CRYSTALLINE

Natan Aronhime, Chair
Carpenter Technology Corporation, Reading, PA, United States

CONTRIBUTED PAPERS

COD-01. Magnetization Reversal Behavior in Electrodeposited FeCoNi Thin Films. *K. Dev*[1], R. Kaur[1], G. Vashisht[1] and S. Annapoorni[1]
1. Department of Physics and Astrophysics, University of Delhi, Delhi, India

In alloy based soft magnetic materials various factors such as alloy composition, phase, synthesis process and annealing conditions affect their magnetic properties. Co, Fe and Ni based alloy thin films exhibit high magnetic moment and high permeability which mark their importance in memory devices and MEMS. The magnetization reversal mechanism in thin films plays a significant role for such technological applications. Here, binary FeCo and ternary $(FeCo)_{(100-x)}$ Ni_x alloy thin films were deposited on Indium Tin Oxide coated glass substrate by electrochemical deposition. The composition of as deposited alloy was confirmed by EDAX. The surface morphology analysed by SEM, confirmed uniformly dispersed flakes all over the substrate in FeCo films. The increasing content of Ni in the alloy results in the formation of irregular shaped granular structure. Bulk magnetic properties were characterized by VSM hysteresis. As the Ni content increases the coercivity as well as remanence decreases (fig.1) and this is probably due to decrease in anisotropy with added Ni content. The ternary alloy tends to exhibit permalloy like properties but with higher magnetization. The decrease in remanence for higher Ni content marks the change in easy axis orientation from film-plane direction in FeCo to an added minor fraction of out-plane orientation in $(FeCo)_{75}Ni_{25}$. The plot of coercivity versus angle (θ) between easy axis of magnetization (film plane) and applied field along with the appropriate fitting model to the magnetization reversal is shown in fig.2. It is clear that for lower Ni content, a good fit to the experimental data for angular variation of coercivity is obtained using Kondorsky model, indicating domain reversal mechanism arising due to domain wall depinning from a local defect. The origin of these pinning centres could be the presence of an oxide layer on top of the film surface or at the ITO-alloy film interface. The magnetization reversal mechanism in FeCoNi alloy is predominantly influenced by the Ni concentration. A deeper understanding of this behaviour would be provided by micromagnetic simulation.

1. F. Schumacher, *Journal of Applied Physics,* 70(6), 3184-3187(1991). 2. T. Hysen, S. Al-Harthi, M.R. Anantharaman, Journal of Magnetism and Magnetic Materials, *341,* 165-172(2013). 3. R. Goyal, R. Gupta, S. Annapoorni, P*hysica Status Solidi (a)*, *215*(14), 1800141(2018). 4. G.Vashisht, V.Kumar, S. Annapoorni, Journal of Magnetism and Magnetic Materials, 497, 166064 (2020).

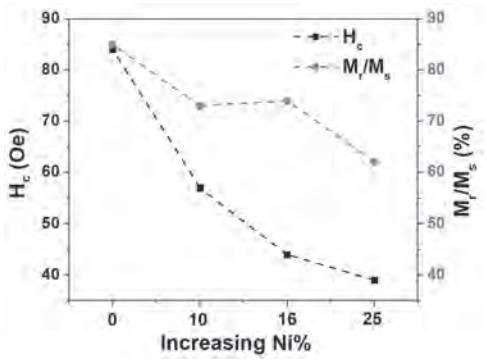

Fig. 1 Change in H_c and M_r/M_s with increasing concentration of Ni

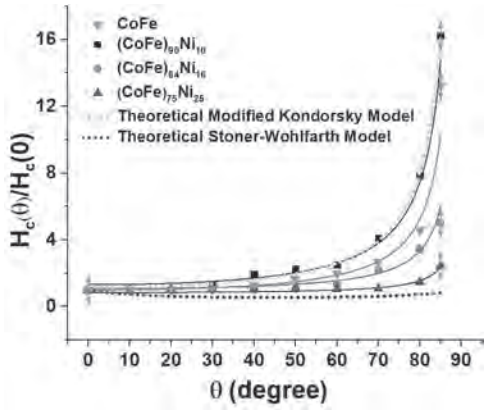

Fig. 2 Angular variation in H_c fitted with modified Kondorsky Model

COD-02. Modelling of magnetic anisotropy in electrical steel sheet by means of cumulative distribution functions of Gaussians. *G.C. Tolentino*[1], J.V. Leite[2], M. Rossi[1], O. Ninet[1], G. Parent[1] and J. Blaszkowski[3] *1. Université Artois, Laboratoire Systèmes Electrotechniques et Environnement (LSEE), Béthune, France; 2. Universidade Federal de Santa Catarina, GRUCAD, Santa Catarina, Florianòpolis, Brazil; 3. Thyssenkrupp Electrical Steel, Isbergues, France*

Developing a model of magnetic materials, such as electrical steel, that allows to account for both their nonlinear and anisotropic behavior remains a challenge. The approach presented in this paper is based on the use of a Gaussian function whose cumulative distribution function's shape is very similar to that of a first magnetization curve. This approach has been introduced in the 90s for the study of isothermal remanent magnetization acquired by rock samples containing magnetic minerals [1,2,3]. The main drawback of this approach lies in the fact that a given magnetization curve is derived from one Gaussian function only, which is itself defined by three fixed parameters only [1], leading to non-negligible differences when compared to experimental data. Moreover, this approach has never been adapted to account for the anisotropic behavior of electrical steel. In this paper, we

propose to enhance this method by using a function which results from the sum of four Gaussian functions, as illustrated in Fig. 1. To account for the anisotropy, all the parameters used to define the Gaussian functions depend on the angle between the magnetic field H and the rolling direction of the steel, denoted θ. Fig. 2 shows the comparison between first magnetization curves for three different magnetization directions (θ) obtained from experimental data (M530-50A electrical steel), from the original model based on the use of one Gaussian function only and from the proposed enhanced model. The work presented in this paper shows multiple originalities and improvements. Firstly, it shows that using more than one Gaussian function allows for a better approximation of first magnetization curves (Fig. 2). Secondly, it shows that considering θ-dependent parameters to define the Gaussian function allows the method to account for magnetic anisotropy (Fig. 2). Thirdly, it highlights that those parameters follow a polynomial trendline.

[1] D. J. Robertson and D. E. France, Physics of the Earth and Planetary Interiors, vol. 82, no. 3–4, pp. 223–234 (1994) [2] H. Stockhausen, Geophysical Research Letters, vol. 25, no. 12, pp. 2217–2220 (1998) [3] D. Heslop, G. McIntosh, and M. J. Dekkers, Geophysical Journal International, vol. 157, no. 1, pp. 55–63 (2004)

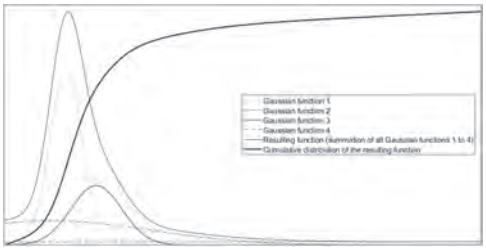

Fig. 1 First magnetization curve derived from a Gaussian function defined as the sum of four subfunctions.

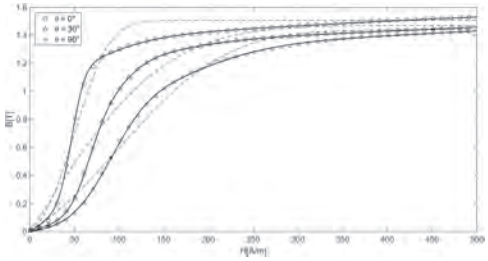

Fig. 2 Comparison between curves obtained from experimental data (markers), from the original model (dashed) and from the enhanced proposed model (solid).

COD-03. Loss Parameter Identification after Cutting for different non-oriented Electrical Steel Grades. *N. Leuning*[1], B. Schauerte[1], S. Schweren[1] and K. Hameyer[1] *1. Institute of Electrical Machines (IEM), RWTH Aachen University, Aachen, Germany*

The magnetic properties of NO electrical steel sheets are very sensitive to cutting. The deterioration of the magnetic properties due to different cutting techniques and processing parameters has been studied for many years [1-3]. Besides the cutting technique, the material properties, e.g., grain size or alloying, have an effect on the deterioration as well [2,4]. The deterioration is caused by residual stress and plastic deformation that remain in the sheet after cutting. As both are induced in the vicinity of the cut edge, the effect is local. In [5] a review on the local distribution is presented, that summarizes the extend of the penetration depths from various research. Although the effect can be measured on Single-Sheet-Tester (SST), Epstein-frame or ring core samples with the approach presented in [1], the quantification and interpretation from global to local information is more complex [5,6]. Consequently, the incorporation of the cutting effect to the design and calculation of electrical machines is challenging. The main requirement is to model the magnetic properties locally. A local material model is presented in [7], where the permeability is modeled with respect to the distance to the cut edge. The model is parametrized with SST samples. The acquisition of data for the parametrization is cumbersome. If the effect of cutting is better understood, less measurements for the parametrization are required and a material-based estimation can be enabled. In this paper, the permeability and loss parameter courses are identified and evaluated for ten NO grades between 0.1- and 0.5-mm sheet thickness, as exemplarily shown in Fig. 1. Measurements are performed on a 120 x 120 mm SST with guillotine cut sample widths between 4 and 120 mm. The magnetizing frequency is varied between 5 Hz and 5000 Hz at sinusoidal flux density. The loss parameters are identified according to [8] and evaluated with regard to [7]. The courses of loss parameters are analyzed in order to identify a possible description with analytical functions and the courses for all ten materials are compared and linked to their differences in grain size, silicon content and sheet thickness.

[1] A. Schoppa, A., J. Schneider and J.-O. Roth, JMMM vol. 215-216, p. 100-102 (2000) [2] R. Rygal, A. J. Moses, N. Derebasi, J. Schneider and A. Schoppa, JMMM, vol. 215-216, p. 687689 (2000) [3] H.A. Weiss, N. Leuning, S. Steentjes, K. Hameyer, T. Andorfer, S. Jenner and W. Volk, W, JMMM vol. 421, p. 250-259 (2017) [4] N. Leuning, S. Steentjes and K. Hameyer, JMMM vol. 497, S. 166080 (2020) [5] M. Bali and A. Muetze, IEEE Trans. on Ind. Applicat. vol. 55 (1), p. 366–375 (2019) [6] T. P. Holopainen, P. Rasilo and A. Arkkio, IEEE Trans. on Ind. Applicat. vol. 53 (2), p. 1049-1053 (2017) [7] S. Elfgen, S. Steentjes, S. Bohmer, D. Franck and K. Hameyer, IEEE Trans. Magn. vol. 52 (5), p. 1–4 (2016) [8] S. Steentjes, M. Leßmann and K. Hameyer, Journal of Applied Physics vol. 113 (17), p. 17A319 (2013)

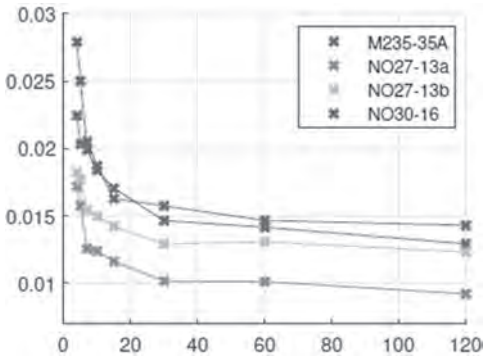

Figure 1 Hysteresis and excess loss parameters of four NO grades.

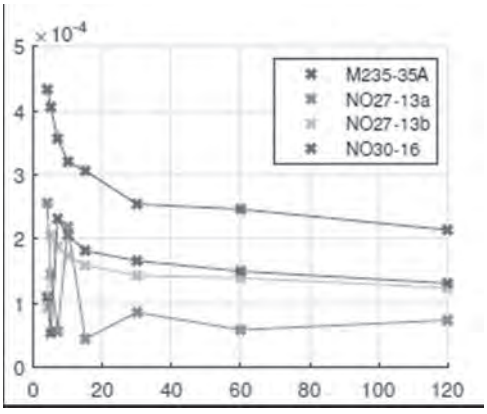

COD-04. Investigation and development of a power loss separation model in Grain-Oriented Electrical Steels combining 1-D alternating and rotational behaviors. *P. Dupont*[1,2], T. Etifier[3,2], O. Maloberti[3,2], M. Ployard[1], D. Laloy[1] and J. Fortin[3,2] *1. Jeumont Electric, Jeumont, France; 2. Laboratoire des Technologies Innovantes (LTI), Amiens, France; 3. UniLaSalle Campus d'Amiens, Amiens, France*

Grain-Oriented Electrical Steels (GOES) are mostly used in transformers but also in specific designs of rotating electrical machines. In both applications, and especially the second, the flux is not always parallel to the easy magnetic axis of GOES usually close to the Rolling Direction (RD) as flux lines can make an angle with the RD (teeth) and can also rotate (yoke, at the vicinity of teeth) [1]. Manufacturers are taking as much benefit as possible from the RD but some areas show reduced performances that are difficult to quantify. This may be explained by the fact that ROTational (ROT) behavior is still not part of classical characterizations [2]. In recent years, besides the development of apparatuses to measure accurately material properties under rotating fields [3], the development of models and methods to calculate ROT losses have been accelerating [4-6]. Efforts to understand and explain them physically is consequent but only few works investigate the relationship between ROT and 1-directional ALTernating (ALT) behaviors which often concerns Non-Grain-Oriented Electrical Steels [7]. In this work supported by experimental results, the authors investigate an original separation loss model that involves not only quasi-static and dynamic components but also ALT and ROT contributions. The work is focused on a coupling term P_{CPLG} combining ROT and ALT losses [8] (see Fig.1) which are known to behave differently when varying the polarization [3]. From measurements, P_{CPLG} is approached by an expression depending on flux density, magnetic field and frequency, similarly to loss separation models. Loss coefficients will be related to the evolution of the magnetic domain structure properties through the various magnetization processes. Thus, physical origins of loss contributions will be discussed. Two kinds of samples of one GO grade have been used for the experiments: 150x150mm^2 samples for measurements under unidirectional excitation fields parallel to the RD or to the Transverse Direction (TD) with a Single Sheet Tester and 60x60mm^2 samples for measurements under ROT excitation fields performed with Rotational Single Sheet Tester.

[1] A. J. Moses, Journal of Materials Engineering and Performance, Vol. 1, pp. 235–244 (1992) [2] J. Sievert, H. Ahlers, M. Birkfeld, et al., Journal of Magnetism and Magnetic Materials, Vol. 160, pp. 115–118 (1996) [3] Y. Guo, J. G. Zhu, J. Zhong, et al., IEEE Transactions on Magnetics, Vol. 44, pp. 279–291 (2008) [4] H. Shimoji and M. Enokizono, Journal of Magnetism and Magnetic Materials, Vol. 254-255, pp. 290–292 (2003) [5] C. Appino, E. Ferrara, F. Fiorillo, et al., Journal of Magnetism and Magnetic Materials, Vol. 500, pp. 166281 (2020) [6] B. Koprivica and S. Zurek, IEEE Transactions on Magnetics, Vol. 57, pp. 1–12 (2021) [7] T. Okubo, G. Shilyashki, H. Pfützner, et al., IEEE Transactions on Magnetics, Vol. 54, pp. 1–6 (2018) [8] P. Dupont, M. Nesser, O. Maloberti et al., April 26-30, 2021, INTERMAG 2021 Conference, Lyon, France

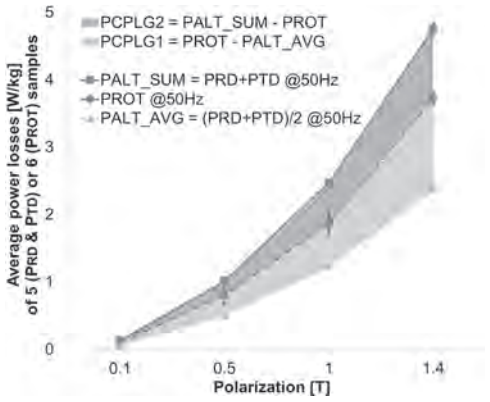

Fig.1 Various power losses contributions against polarization at 50Hz

COD-05. Manufacturing and Characterization of Soft Magnetic Composite Filaments for Additive Manufacturing. *Á. Díaz-García*[1], J. Law[1], M. Félix[2], A. Guerrero[2] and V. Franco[1] *1. Condensed Matter Physics, University of Seville, Seville, Spain; 2. Chemical Engineering, University of Seville, Seville, Spain*

Additive manufacturing (AM) is becoming an alternative to traditional manufacturing methods [1]. In the most extended AM method (fused deposition modeling, FDM), a polymeric filament is extruded above its melting point for its deposition into thin layers. There is a high interest in the use of composite filaments, formed by a polymeric matrix with functional fillers, for the AM of functional parts [2]. The quality of the FDM printed parts is highly dependent on the uniformity of the filament diameter. In the case of composite filaments, a homogeneous distribution of the fillers is also crucial to have a reproducible and uniform functionality. Homogeneous soft magnetic PLA composite filaments for FDM have been recently reported, in which a customized feedstock of polymeric capsules filled with the functional fillers is employed [3]. Fig. 1 shows that composite filaments exhibit a soft magnetic behavior. Additionally, they all have a demagnetizing factor of ~ 1/3 (spheres, according to the shape of the gas atomized powders) regardless of the concentrations of fillers (up to 52 wt. %, corresponding to 12 vol. %). The addition of the fillers causes a remarkable shift in the thermal degradation temperature of the polymer. Increasing filler content produces an abrupt drop in the complex modulus of the polymer above its glass transition, which shifts to lower temperatures according to the peak of tan(δ) (Fig. 2). A decrease in the viscosity in liquid state is also observed, which causes a reduction of the extrudability and printability of the filaments for filler contents above 30 wt. %. The reduction of the viscosity of the composites requires the lowering of the temperatures for their extrusion and printing with respect to the typical ones for PLA. Work supported by AEI/FEDER-UE (grant PID2019-105720RB-I00), US/JUNTA/FEDER-UE (grant US-1260179), Consejería de Economía, Conocimiento, Empresas y Universidad de la Junta de Andalucía (grant P18-RT-746), and Army Research Laboratory under Cooperative Agreement Number W911NF-19-2-0212.

[1] T.D. Ngo, A. Kashani, G. Imbalzano, K.T.Q. Nguyen, D. Hui, Additive manufacturing (3D printing): A review of materials, methods, applications and challenges, Compos. Part B Eng. 143, 172–196 (2018). [2] X. Wang, M. Jiang, Z. Zhou, J. Gou, D. Hui, 3D printing of polymer matrix composites: A review and prospective, Compos. Part B Eng. 110, 442–458 (2017). [3] Á. Díaz-García, J.Y. Law, A. Cota, A. Bellido-Correa, J. Ramírez-Rico, R. Schäfer, V. Franco, "Novel procedure for laboratory scale production of composite functional filaments for additive manufacturing," Mater. Today Commun. 24, 101049 (2020).

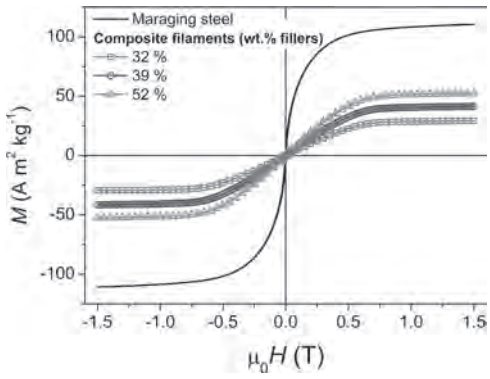

Fig. 1. Magnetization vs. magnetic field for the raw maraging steel powder and composite filaments.

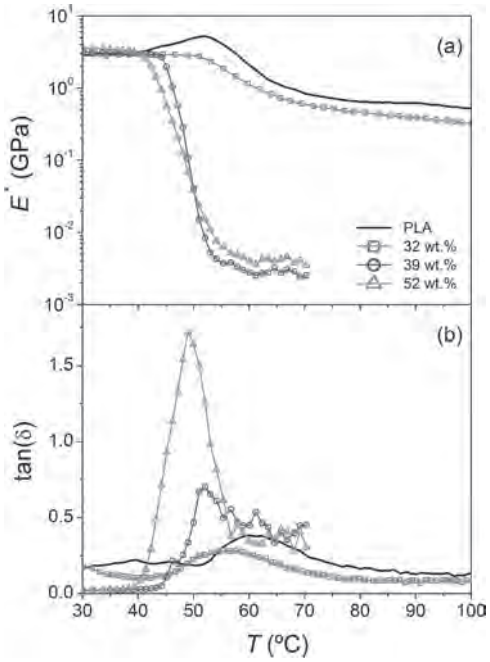

Fig. 2. (a) Complex modulus and (b) tan(δ) of raw PLA and composite filaments.

COD-06. Enhancement of magnetostriction in Fe-Co alloy single-crystal film by group-13 element addition. *Y. Nakamura*[1], M. Ohtake[1], T. Kawai[1], M. Futamoto[1], F. Kirino[2] and N. Inaba[3] *1. Faculty of Engineering, Yokohama National University, Yokohama, Japan; 2. Graduate School of Fine Arts, Tokyo University of the Arts, Tokyo, Japan; 3. Graduate School of Science and Engineering, Yamagata University, Yonezawa, Japan*

Soft magnetic films with large magnetostriction have been investigated for applications like strain sensors, vibration energy harvesting devices, etc. It is reported that Fe-Co alloy films prepared by annealing at high temperatures followed by quenching show large magnetostriction values of 150×10^{-6} – $+250\times10^{-6}$ [1]. The enhancement of magnetostriction is interpreted to be due to strain of bcc-*A*2 lattice caused by inclusion of bcc-*B*2 or fcc-*A*1 nanocrystals [2]. Addition of third element also may cause the lattice strain and enhance the magnetostriction. In the present study, $Fe_{70}Co_{30}$ and $(Fe_{0.7}Co_{0.3})_{95}X_5$ (at. %, X = B, Al, Ga) films are prepared on VN(001) single-crystal underlayers by UHV sputtering. The effect of third element addition on the magnetostrictive property is investigated. The result of Fe-Co-B film is shown below while comparing that of Fe-Co film. Figs. 1(a) and (b) show the RHEED and out-of-plane XRD patterns of Fe-Co and Fe-Co-B films. Reflections from bcc(001) single-crystal surface are observed. Fe-Co and Fe-Co-B(001) single-crystal films are obtained on VN(001) underlayers. The crystallographic orientation relationship is determined as shown in Fig. 1(d). The ratio of out-of-plane to in-plane lattice constant, c/a, measured for Fe-Co(001) film is nearly 1, whereas the lattice of Fe-Co-B(001) film is slightly deformed along the perpendicular direction (c-axis). Fig. 1(c) shows the magnetization curves. An in-plane magnetic anisotropy with the easy magnetization direction of bcc[100] is observed for the Fe-Co film, whereas the Fe-Co-B film shows nearly isotropic in-plane magnetization properties due to influence of lattice deformation along the perpendicular direction. The magnetostriction is evaluated by using a cantilever method under in-plane rotating magnetic fields up to 1200 Oe. Fig. 2 summarizes the magnetostrictive properties. The magnetostriction coefficients, (λ_{100}, λ_{111}), of Fe-Co and Fe-Co-B films are estimated to be ($+200\times10^{-6}$, -10×10^{-6}), and ($+320\times10^{-6}$, $+20\times10^{-6}$), respectively. Addition of B atom is apparently effective in enhancing λ_{100} value. Fe-Co-Al and Fe-Co-Ga single-crystal films are also obtained on VN underlayers and similar enhancement of magnetostriction is recognized.

[1] D. Hunter, W. Osborn, K. Wang, N. Kazantseva, J. Hattrick-Simpers, R. Suchoski, R. Takahashi, M. L. Young, A. Mehta, L. A. Bendersky, S. E. Lofland, M. Wuttig, and I. Takeuchi, *Nat. Commun.*, **2**, 518 (2011). [2] Y. Han, H. Wang, T. Zhang, Y. He, J.M.D. Coey, and C. Jiang, *J. Alloys Compd.*, **699**, 200 (2017).

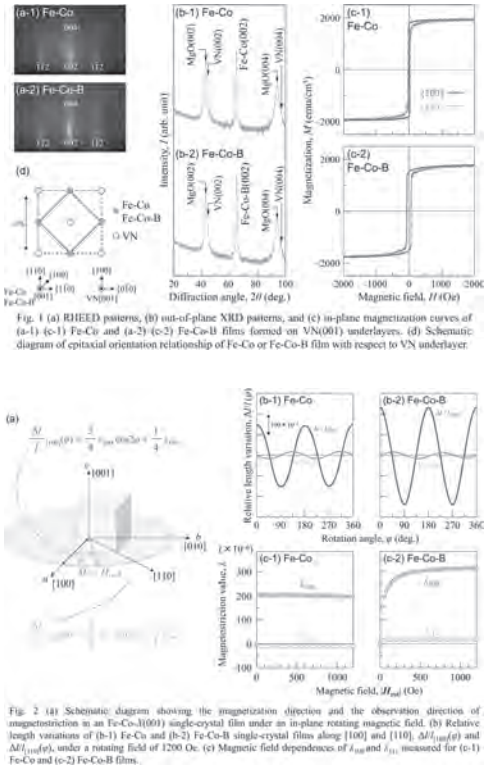

Fig. 1 (a) RHEED patterns, (b) out-of-plane XRD patterns, and (c) in-plane magnetization curves of (a-1) (c-1) Fe-Co and (a-2) (c-2) Fe-Co-B films formed on VN(001) underlayers. (d) Schematic diagram of epitaxial orientation relationship of Fe-Co or Fe-Co-B film with respect to VN underlayer.

Fig. 2 (a) Schematic diagram showing the magnetization direction and the observation direction of magnetostriction in an Fe-Co-3(001) single-crystal film under an in-plane rotating magnetic field. (b) Relative length variations of (b-1) Fe-Co and (b-2) Fe-Co-B single-crystal films along [100] and [110], $\Delta l/l_{100}(\varphi)$ and $\Delta l/l_{110}(\varphi)$, under a rotating field of 1200 Oe. (c) Magnetic field dependences of λ_{100} and λ_{111} measured for (c-1) Fe-Co and (c-2) Fe-Co-B films.

COD-07. High throughput methods to uncover new soft magnetic compositions in the CoFeNiMn-A (A= Al, Si, Cu, V or Ti) high entropy alloy system. *R. Rowan-Robinson*[1], Z. Leong[1] and N. Morley[1] *1. Department of Material Science and Engineering, University of Sheffield, Sheffield, United Kingdom*

High entropy alloys (HEAs) are well suited to high throughput (HiTp) studies, as they typically consist of five or more constituent elements, mixed in near equal quantities. The high configurational entropy of HEAs contributes to stabilising simple FCC and BCC solid solutions, and HEAs have demonstrated promising soft magnetic properties such as high saturation magnetisation alongside high electrical resistivity[1,2]. Here, the HEA system CoFeNiMn-A is studied, where A is either Al, Si, Cu, V, or Ti. Typically Mn has antiferromagnetic ordering, but can exhibit strong ferromagnetism when alloyed, providing opportunities for magnetic HEAs with high saturation magnetisation[3]. Furthermore, the vast chemical freedom provided by the fifth element presents opportunities to tune the magnetic properties and material texture. Here, HiTp methods are critical to enable exploration of the large composition space still available with this fifth alloy element. This work utilises combinatorial sputtering to fabricate sample libraries containing composition variations of up to 35 at.% on a single Silicon wafer (Fig. 1a). A program was developed to model the composition variation across a 3″ Silicon wafer with three sputter sources at different incidence angles with concurrent deposition (Fig. 1b). The resulting sample library is characterised using a HiTp magneto-optical Kerr effect magnetometer which automatically measures the hysteresis loop at each point across this sample library with varying HEA composition (Fig. 1c). These can then be combined to achieve magnetic property mapping within the chemical composition space (Fig. 1d). Following this, XRD, SQUID magnetometry, FMR and magneto-transport are used to generate a complete structural and functional property description of promising compositions. The resulting

methodology not only provides a scalable process for magnetic HEA fabrication and characterisation, but can also be paired with data driven AI material discovery. The large datasets required for this are costly and so far lacking in functional magnetic properties for which these high-throughput methods could provide.

1. Zhang, Y., Zuo, T., Cheng, Y. & Liaw, P. K. *Sci. Rep.* 3, 1455 (2013). 2. Zuo, T. *et al. Acta Mater.* 130, 10–18 (2017). 3. Zhang, B. *et al. J. Mater. Sci. Technol.* 68, 124–131 (2021).

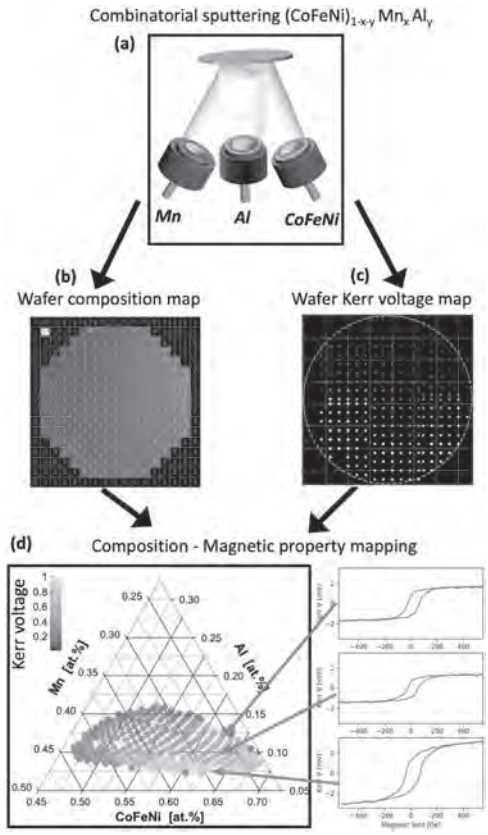

The HiTp thin film methodology as applied to the CoFeNiMnAl magnetic HEA.

COD-08. Experimental identification and physical interpretations of 2D tensor magnetic properties of a grain-oriented electrical steel magnetized between the rolling and the transverse directions.

T. Etifier[2,1], P. Dupont[3,1], *O. Maloberti*[2,1], E. Salloum[2], P. Dassonvalle[2,1], S. Panier[4,1] and J. Fortin[2,1] *1. LTI, Amiens, France; 2. UniLaSalle, Amiens, France; 3. Jeumont Electric, Jeumont, France; 4. Université Picardie Jules Vernes, Amiens, France*

Grain Oriented steels are widely used in transformers and inductors. The materials texture shows an easy magnetization direction adapted to columns and yokes but, at corners when the flux is tilted, the anisotropy must be taken into account. At the quasi-static level, the anisotropy is driven by the crystal grains, demagnetizing field and mechanical stresses, and determines the permeability, the quasi-static hysteresis and the domains orientation at the equilibrium. At the dynamic level, distinct magnetization mechanisms depend on the various domains and walls orientations. It controls the iron losses in any magnetization direction. Numerous scalar models and experimental tools can already describe mainly the unidirectional behavior [1-4]. The extension of scalar models towards tensor models is confronted to unknowns that remain about non-diagonal components and their microscopic physical interpretation explaining the hysteresis cycles in various directions. A dynamic hysteresis model [5] has been chosen. It allows the description of the magnetic behavior related to the anisotropic magnetic structure at equilibrium in quasi-static operating conditions and the anisotropic magnetization mechanisms within domains and walls in dynamic operating conditions. The goal of this work is to identify and determine the tensor properties of an electrical steel, which is necessary to use an anisotropic behavioral model according to two directions of the excitation field, making an angle between 0° (Rolling Direction RD) and 90° (Transverse Direction TD) with RD. The results will be physically discussed considering the main energies that govern the quasi-static domain structure responsible for the slope of the cycles, and those inducing the magnetization mechanisms responsible for the losses, *i.e.* the cycles area [6]. The experiment uses a conventional GO FeSi steel (R120-27) with a thickness of 0.27mm. Several samples with dimensions 150x150mm^2 were laser cut following an accurate angle of respectively 0°, 15°, 30°, 45°, 60°, 75° and 90° with the RD. Measurements were carried out with a Single Sheet Tester which provides data for the magnetic field H and the flux density B in the two directions of the sample's cut edges.

[1] G.Berotti, «*Journal of Magnetism and Magnetic Materials,* vol. 41, p. 253-260 (1984). [2] R.Pry and C.Bean, *Journal of Applied Physics*, vol. 29, n° 3, p. 532-533 (1958). [3] D.C. Jiles and D.L. Atherton, J. Magn. Magn. Mater., North-Holland, Amsterdam (1986). [4] M.-A. Raulet, B. Du Charne, J.P. Masson, and G.Bayada,*IEEE Transactions on Magnetics*, vol. 42, n°2, p. 872-875 (2004). [5] O. Maloberti, G. Meunier, A. Kedous-Lebouc, V. Mazauric and O.Geoffroy, la RIGE, conférence MGE, Lyon (2005). [6] D.-X.Chen and J.L.Munoz, *IEEE Transactions on Magnetics*, vol. 33, n° 3, p. 2229-2244 (1997).

COD-09. Large Magnetostriction in γ′-Fe_4N Single-Crystal Thin Film.

Y. Maeda[1], K. Imamura[1], M. Ohtake[1], T. Kawai[1], M. Futamoto[1], F. Kirino[2] and N. Inaba[3] *1. Faculty of Engineering, Yokohama National University, Yokohama, Japan; 2. Graduate School of Fine Arts, Tokyo University of the Arts, Tokyo, Japan; 3. Graduate School of Science and Engineering, Yamagata University, Yonezawa, Japan*

Soft magnetic materials with large magnetostriction have been studied for applications such as sensors, actuators, vibration energy harvesting devices, etc. Rare-metal free materials are desirable from the viewpoints of natural resource and cost, though RFe_2 (R = Tb, Sm, etc.) [1,2] and Fe-X (X = Ga, Co) [3,4] alloys have been used as magnetostrictive materials. γ′-Fe_4N with perovskite structure is a soft magnetic material with high saturation magnetization (1,440 emu/cm^3), high Curie temperature (490 °C), and high negative spin polarization (nearly –100%). Furthermore, a theoretical calculation predicts that it shows large magnetostriction of $\lambda_{100} = -143\times10^{-6}$ [5]. However, experimental investigation of magnetostriction has not been carried out yet. In order to determine the magnetostriction coefficients along [100] and [111], λ_{100} and λ_{111}, it is useful to employ an epitaxial single-crystal film. In the present study, γ′-Fe_4N single-crystal film is tried to be prepared on MgO(110) substrate by reactive sputtering and the magnetostrictive property is investigated. Fig. 1(a) shows the RHEED pattern observed for an Fe-N film formed on MgO(110) substrate. Clear diffraction spots from (110) single-crystal with perovskite structure are recognized. A γ′-Fe_4N(110) single-crystal film is epitaxially grown in the orientation relationship of Fig. 1(b). Fig. 1(c) shows the XRD pattern. γ′-Fe_4N(110) superlattice reflection is observed. The lattice parameter agrees with the bulk value within small difference less than 0.1% and the order degree is almost 1.0. Therefore, γ′-Fe_4N single-crystal film with high crystallographic quality is successfully obtained. Fig. 1(d) shows the magnetization curves. The film shows a soft magnetic property reflecting the magnetocrystalline anisotropy of Fe_4N crystal. The magnetostriction is evaluated by using a cantilever method under rotating magnetic fields. Fig. 2 summarizes the magnetostrictive properties. The film shows a large negative λ_{100} value of -75×10^{-6}, as suggested by theoretical calculation. Remarkably, a larger λ_{111} value of $+210\times10^{-6}$ is obtained. The present study has shown that γ′-Fe_4N is one of the strong candidates for future rare-metal free magnetostrictive materials.

[1] A. E. Clark and H. S. Belson, *Phys. Rev. B*, **5**, 3642 (1972). [2] H. Samata, N. Fujiwara, Y. Nagata, T. Uchida, and M. D. Lan, *J. Magn. Magn. Mater.*, **195**, 376 (1999). [3] A. E. Clark, K. B. Hathaway, M. Wun-Fogle, J. B. Restorff, T. A. Lograsso, V. M. Keppens, G. Petculescu, and R. A. Taylor,

J. Appl. Phys., **93**, 8621 (2003). [4] D. Hunter, W. Osborn, K. Wang, N. Kazantseva, J. Hattrick-Simpers, R. Suchoski, R. Takahashi, M. L. Young, A. Mehta, L. A. Bendersky, S. E. Lofland, M. Wuttig, and I. Takeuchi, *Nat. Commun.*, **2**, 518 (2011). [5] Y. Zhang, Z. Wang and J. Cao, *Comput. Mater. Sci*, **92**, 464 (2014).

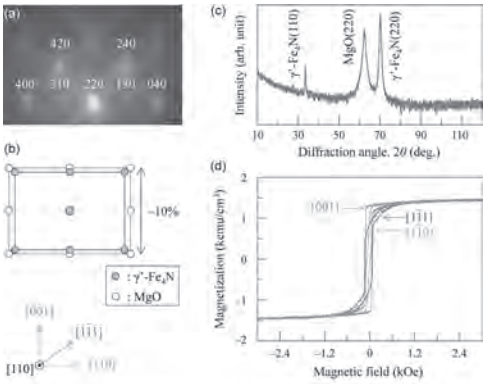

Fig. 1 (a) RHEED pattern, (c) out-of-plane XRD pattern, and (d) magnetization curves of an Fe-N film formed on MgO(110) substrate. (b) Epitaxial orientation relationship between γ'-Fe_4N(110) film and MgO(110) substrate.

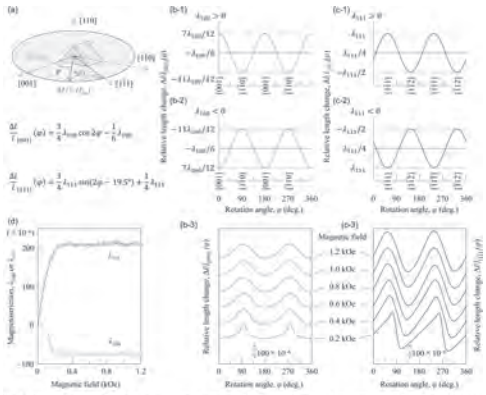

Fig. 2 (a) Schematic diagram showing the magnetization direction and the observation direction of magnetostriction with respect to the typical crystallographic directions. [(b-1), (b-2)] $\Delta\lambda/\lambda_{100}(\varphi)$ and [(c-1), (c-2)] $\Delta\lambda/\lambda_{111}(\varphi)$ calculated for (110) single-crystal films with (b-1) $\lambda_{100} > 0$, (b-2) $\lambda_{100} < 0$, (c-1) $\lambda_{111} > 0$, and (c-2) $\lambda_{111} < 0$. (b-3) $\Delta\lambda/\lambda_{100}(\varphi)$ and (c-3) $\Delta\lambda/\lambda_{111}(\varphi)$ measured for a γ'-Fe_4N(110) single-crystal film. (d) Magnetic field dependences of λ_{100} and λ_{111}.

COD-10. Impact of Ultra-Short Pulsed Laser (USPL) Ablation Process on Separated Loss Coefficients of Grain Oriented Electrical Steels (GOES). M. Nesser[1], *O. Maloberti*[2], E. Salloum[2], J. Dupuy[3], M. Lamblin[3], S. Panier[1], P. Dassonvalle[2], J. Fortin[2], C. Pineau[4] and J. Birat[4] *1. Laboratoire des technologies Innovantes, Amiens, France; 2. ESIEE-Amiens UniLaSalle, Amiens, France; 3. Multitel, Mons, Belgium; 4. IRT M2P, Metz, France*

Pulsed Laser (PL) technology is a recent technique used to optimize the electromagnetic properties of Grain Oriented Electrical Steels (GOES) forming the cores of transformers and chokes [1]. Like the Continuous Wave process, the long and Short Pulsed Laser (SPL) processes have been largely studied [2, 3]. The Ultra-Short Pulsed Laser ablation technique remains unfamiliar for these electrical steels and its deterministic impact on the performance of these materials requires deep investigations. In this paper, the influence of surface laser treatments with ultra-short pulses (Femtosecond laser) on the magnetic properties of GOES was studied using the two-temperature model for the ablation process [4,5,6] and Bertotti's model for magnetic losses [7]. The aim is to understand and identify the origins of the changes in magnetic properties following laser treatment. We showed that the hysteresis and excess loss coefficients behave differently depending on the type of laser treatment and its pulse duration (long, short and ultra-short pulse). First, we presented adjusted models to estimate the impact of the USPL on the sheet surface in terms of laser energetic quantities; more precisely the groove depth [5], the plasma maximum temperature [4], and the peak surface wave pressure [8] were estimated, relative to an optimum. The latter physical impacts of laser pulses were then correlated to Bertotti's loss coefficients: the static hysteresis loss coefficient and the excess loss coefficient. The laser process is not always able to reduce simultaneously both loss contributions. Thus, a compromise must be found to optimize the process. The variation of the flux density level as a function of the applied magnetic field was measured with a single sheet tester SST under a one-directional field parallel to the rolling direction. From these measurements, we deduced the whole power loss contributions and the apparent permeability. Results showed that an optimization of the laser's parameters ensured an iron loss reduction at 50 Hz up to -30% for an induction below 0.5T, and a percentage close to -15% for an induction above 1.5T. At higher frequencies and for 0.1T, the reduction percentage can exceed -30%.

[1] Petryshynets, F. Kováč and V. Puchý, AIP Adv., vol. 8, p. 047604, 2018 [2] J. Dupuy, M. Nesser and O. Maloberti, Proc SPIE 10911 High-Power Laser Mater. Process. Appl. Diagn. Syst. VIII, vol. 10911, p. 1091104, 2019 [3] M. Nesser, O. Maloberti and J. Dupuy, Journal of Magnetism and Magnetic Materials, Vol. 504, p. 166696, 2020 [4] B. N. Chichkov, C. Momma and S. Nolte, Appl. Phys. Mater. Sci. Process., vol. 63, p. 109, 1996 [5] K. H. Leitz, B. Redlingshöfer and Y. Reg, Phys. Procedia, vol. 12, p. 230, 2011 [6] A. H. Hamdani, W. Ahmed and A. Ansar, Key Eng. Mater., vol. 442, p. 172, 2010 [7] G. Bertotti, J. Appl. Phys., vol. 57, p. 2110, 1985 [8] P. Peyre and R. Fabro, Opt. Quantum Electron., vol. 27, p. 1213, 1995

COD-11. Additively manufactured Fe-3Si stator for high performance electrical motor. *T. Lamichhane*[1], C. Chinnasamy[2], B. Andrew[1], J. Yan[3], Z. Gai[4] and M. Paranthaman[1] *1. Chemical Sciences Division, Oak Ridge National Lab, Oak Ridge, TN, United States; 2. Carpenter Technology, Philadelphia, PA, United States; 3. Materials Science and Engineering, Oak Ridge National Lab, Oak Ridge, TN, United States; 4. CNMS, Oak Ridge National Lab, Oak Ridge, TN, United States*

Additive manufacturing carries its potential to develop novel high-performance electrical machines enabling direct printing of complex shapes and simultaneous processing of multiple feedstocks in a single build to optimize the required parameters such as low weight, cost, eddy current loss, and high mechanical strength and corrosion resistance. We printed a Fe-3%Si stator core using selective laser melting and machined it down to thin laminates to assemble a prototype brushless permanent magnet electric motor. The magnetic, mechanical, and electrical properties of the as printed and various heat-treated thin laminates and back emf of the electrical motors are studied. The thin laminates exhibit maximum relative permeability of 7494 with approximate 0.8 Oe applied field and core-loss of about 44 watts/kg at 60 Hz with maximum induction of 15000 Gauss. The designed machine is analyzed using finite element analysis and compared with measured electrical parameters.

COD-12. Mixed magnetic phases in $FeCoCrNiAl_x$ high entropy alloys. *C.S. Jorgensen*[1], L. Santodonato[1], N. Tang[1], N.C. Liyanage[2], L.J. Quigley[1], P. Liaw[1], D.A. Gilbert[1] and L. Debeer-Schmitt[3] *1. Material Science and Engineering, University of Tennessee, Knoxville, TN, United States; 2. Physics, University of Tennessee, Knoxville, TN, United States; 3. Neutron Scattering Division, Oak Ridge National Laboratory, Oak Ridge, TN, United States*

The large distribution in atomic sizes and masses in high-entropy alloys results in extreme local environments, which manifests strongly in the thermal and magnetic properties. In this work, high-entropy alloys of (Fe,Co,Cr,Ni)Al_x, $0 < x < 2$, are prepared and their temperature-dependent magnetic and electronic properties determined. Magnetometry results show that all the samples are ferromagnetic, with a high-temperature phase, T_C >200 K, and a second low-temperature phase with $T_C \approx 20$ K. However, the high-temperature phase is not associated with an open hysteresis loop, suggesting superparamagnetic behavior. The closed hysteresis loop suggests the ferromagnetism appears as small clusters, a theory explored with small-angle

neutron scattering (SANS). The samples also show downturn in the magnetization at T<10 K which can be associated with an antiferromagnetic phase. Recent works have suggested that extreme strain distributions can induce antiferromagnetic ordering. This research used resources at the High Flux Isotope Reactor and the Spallation Neutron Source, as appropriate, a DOE Office of Science User Facility operated by the Oak Ridge National Laboratory, and was funded by the DOE DE-SC0021344.

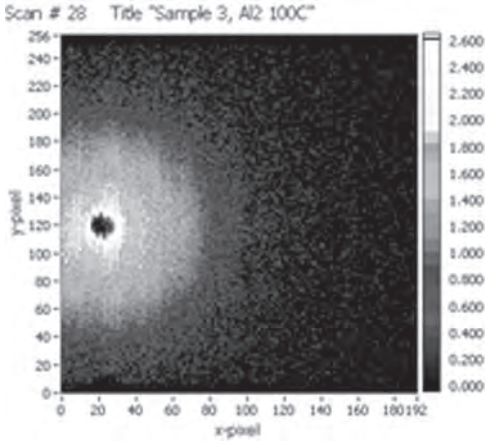

Fig. 1 2D SANS image from an HEA

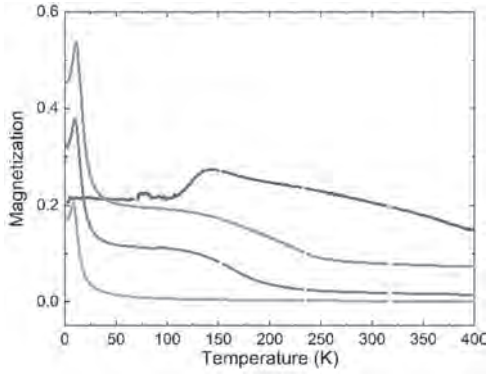

Fig. 2 M vs T data for HEA.

Session CPA
SOFT MAGNETIC MATERIALS V: FERRITES AND BULK CRYSTALLINE (Poster Session)

Arcady Zhukov, Co-Chair
University of Basque Country and Ikerbasque, San Sebastian, Spain
Samuel Kernion, Co-Chair
CorePower Magnetics, Pittsburgh, PA, United States

CPA-01. Investigation of Mg doped Y-type Barium hexaferrite using Mössbauer spectroscopy. *J. Baik*[1] and C. Kim[1] *1. Department of Physics, Kookmin University, Seoul, The Republic of Korea*

Recently, studies on the Y-type hexaferrites are being actively conducted because they exhibit multiferroic properties. Y-type hexaferrite is being used to high-density memories, wireless communication devices, etc. Therefore, to utilize it in these various fields, research on various characteristic changes through ion substitution is attracting attention [1]. Sr substituted Y-type Barium hexaferrite increased the saturation magnetization (M_s) and coercivity (H_c) [2]. Nonmagnetic Al ion substitution at $BaSrCo_2Fe_{12}O_{22}$ stabilized the spin structure [3]. This study, we have investigated the various effect of nonmagnetic Mg ion doping at $Ba_2Co_2Fe_{12}O_{22}$. Polycrystaline $Ba_2Co_{2-x}Mg_xFe_{12}O_{22}$ (x = 0.0, 0.1, 0.3, 0.5) was synthesized by solid state reaction method. We used XRD to analyze the crystal structure of the sample and analyzed the patterns with Rietveld refinement using the Fullprof. To measure magnetic properties, we used VSM and Mössbauer spectroscopy. We measured *M-T* and *M-H* values using VSM. The *M-T* experiments and Mössbauer experiments were conducted from 4.2 to 295 K. The Mössbauer spectra were fitted the six Lorentzian sextets. The $Ba_2Co_{2-x}Mg_xFe_{12}O_{22}$ were analyzed as hexagonal in the R-3m space group. We observed that the lattice constants a_0 and c_0 decreased as the concentration of Mg increased. This is because the ionic radius Mg (0.72 Å) is smaller than that of Co (0.745 Å). In the result of *M-T* experiment, we found the spin reorientation temperature (T_s). T_s were 215, 212, 209 and 202 K at x = 0.0, 0.1, 0.3 and 0.5, respectively. The Mössbauer spectra were analyzed by six sites of Fe. Each lines represented the six different sites of Fe ($3b_{VI}$, $6c^*_{IV}$, $6c_{VI}$, $18h_{VI}$, $6c_{IV}$, and $3a_{VI}$). The result of the analysis, the magnetic hyperfine field (H_{hf}) of $3b_{VI}$ site was largest. H_{hf} and the quadrupole splitting values showed abrupt changes at T_s. The isomer shift values were maintained between 0.1 ~ 0.4 mm/s, indicating that Fe exhibited the Fe^{3+} ion state at all temperatures. The H_{hf} values decreased with increasing Mg doping. Along with the decrease of M_s and H_c in the M-H experiment, these results can be explained by the substitution of nonmagnetic Mg ion for magnetic Co ion.

[1] S.H. Mahmood, F.S. Jaradat, A.F. Lehlooh, Ceram. Int. 40, 5231 (2014). [2] K. L. Cho and C. S. Kim, *IEEE Trans. Magn*, vol. 49, no. 7, p. 4291 (2013). [3] S. hirose, D. Urushihara, and T. Kimura, Appl. Phys. Lett. 118, 062407 (2021).

CPA-02. Fe-site Dopant Tailored Microwave Magnetodielectric Effect in $Y_3Fe_{5-x}Si_xO_{12}$ Garnet. *F. Chen*[1], S. Zhang[1], H. Luo[1] and Y. Cheng[1] *1. Wuhan University of Science and Technology, Wuhan, China*

In recent decades, the well-known magnetoelectric (ME) and magnetodielectric (MD) effects have attracted lots of attentions for both their unique physical connotations and potential applications [1]. Nevertheless, the ME and MD effects are still restricted from the practical microwave applications due to some obvious drawbacks, such as extreme external conditions (large bias magnetic field and ultralow temperature), low operating frequency and significant microwave loss etc. As one of the most important low-loss microwave materials, YIG ferrite has been widely applied in traditional and modern microwave devices. Thus, it can be reasonably speculated that the YIG garnets with ME/MD in microwave ranges might guide a new path to the development of multi-regulation microwave devices. In this work, the influence of Fe-site dopant on the static magnetic, dynamic electromagnetic and microwave MD effect of silicon doped YIG garnet have been investigated. In this work, the $Y_3Fe_{5-x}Si_xO_{12}$ ferrites, where x=0.05, 0.1, 0.15 and 0.2 (denoted as Si-YIG-1 to Si-YIG-4), have been prepared by traditional solid-state reaction. According to the XPS results, it can be confirmed that the Fe^{2+}/Fe^{3+} ratio in Si-YIG gradually increases from 0.369 to 0.876 with the continuous doping of non-magnetic quadrivalent Si^{4+} ions, and consequently introduce the decline of saturation magnetization from 24.586 to 15.424 emu/g due to the obvious reduce of total magnetic moments in the garnet (in Fig. 1). The maximum MD response was detected to be +1.8%~-1.31% in the Si-YIG-2 sample at 2~8 GHz under a DC magnetic field of 1650 Oe (in Fig. 2). Compared with our previous works focused on the microwave MD effect in Ce^{4+} doped YIG [2], it can be concluded that the substitution of Fe-site dopants exhibits a contrary influence on the MD effect of YIG in microwave frequency, which might to be originated from the complex competitive interplay between the enhancing reorientation effect of Fe^{2+}-Fe^{3+} dipoles and reducing total magnetic moments in the Si-YIG samples.

[1] Eerenstein W, Mathur N D, Scott J F. Nature, 442(7104), 759-765 (2006). [2] Chen F, Wang X, Nie Y, et al. Scientific reports, 6(1): 1-8 (2016).

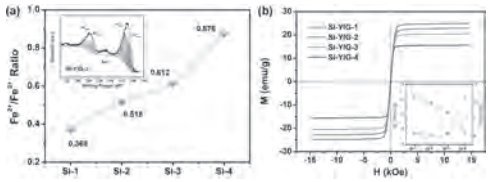

Fig. 1 (a) The dependence of Fe^{2+}/Fe^{3+} ratio and (b) static magnetic properties on the Si substitution.

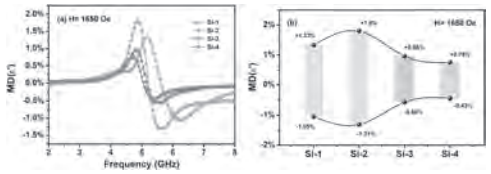

Fig. 2 The magnetodielectric effect of Si-YIG samples.

CPA-03. Withdrawn

CPA-04. Finite size effect on Structural, optical, elastic and spin resonance properties of oleic acid coated $Zn_xFe_{3-x}O_4$ ($0.4 \le x \le 0$) ferrite nanofluids. *P. Kumar*[1,3], S. Pathak[2], K. Jain[1], K. Deep[1,3], H. Khanduri[1], G. Basheed[1,3] and R. Pant[1,3] *1. Indian Reference Materials Division, CSIR-NPL, New Delhi, India; 2. Department of Mechanical Engineering, University of Melbourne, Parkville, Melbourne, VIC, Australia; 3. Academy of Scientific and Innovative Research, Ghaziabad, CSIR-NPL Campus, New Delhi, New Delhi, India*

Microwave spin resonance behaviour of these mixed ferrites are of key consideration for various applications. Mixed ferrites based magnetic nanofluids have a potential candidature in various biomedical and spintronics filed like magnetic fluid hyperthermia, MRI, optical sensor, switches and targeted drug delivery. In this work, a series of zinc doped Fe_3O_4 magnetic nano-fluids with different Zn concentrations represented as $Zn_xFe_{3-x}O_4$ (x=0,0.1,0.2,0.3 & 0.4)were synthesized by the wet chemical co-precipitated techniqueand oleic acid is used as surfactant to prevent the agglomeration of magnetic nanoparticles. Structural, optical, elastic and spin dynamics properties of these ferrofluids have been investigated using different sophisticated characterization techniques such as XRD, HRTEM, SEM, FTIR, UV and EPR etc. The structural and Rietveld refinement was carried out by the XRD data and the result confirms that single cubic spinel phase belongs to Fd3m (227) space group and the average crystallite size calculated from the XRD data varies from 12 to 15 nm. HRTEMstudies revealed that the particles are spherical in nature and mean particle size varies from 15 to 20 nm and all samples are polycrystalline in nature. SEM result was also demonstrated the surface morphology of magnetic particle is spherical in shape with slight agglomeration. FTIR spectroscopy showed the molecular dynamics and the formation of cubic spinel phase of frequency peaks at 535 cm^{-1} and 420 cm^{-1} respectively and also other different functional group which gives the evidences that oleic acid are present on the surface of MNPs. The UV-Visible measurement gives the estimate of the band gap of the materials which lies between(2.2 to 2.8, 3.1 and 3.8 e V) of the all the sample obtained from optical absorption spectra fitting by Tauc plot method. The room temperature microwave spins resonance studies was carried out by using X-band (9.8GHz) EPR spectrometer and calculated various spin resonance parameters[1,2]. In sample compositions the broad resonance signal is observed and enhancement of peak to peak line width is perceived due to the strong super-exchange interaction between the magnetic ions through oxygen ions[1-3].

1. C. Yao, Q. Zeng, G. F. Goya, T. Torres, J. Liu, H. Wu, M. Ge, Y. Zeng, Y. Wang, J. Z. Jiang, J. Phys. Chem. C 111 2007 12274–12278. 2. M. Mozaffari, S. Manouchehri, M. H. Yousefi, J. Amighian, J. Magn. Magn. Mater., 322 2010 383–388. 3. Jun Liu, Yuezhen Bin, and Masaru Matsuo- J. Phys. Chem. C 2012, 116, 134–143.

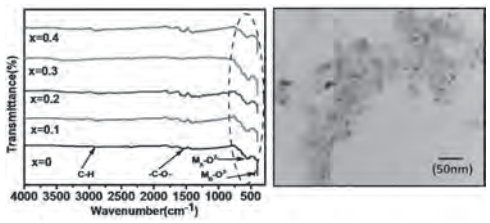

CPA-05. The Effect of Rosensweig Instability of a Ferrofluid Droplet on the Electromagnetic Wave Scattering. *Y. Li*[1,2] and K. Huang[1] *1. Mechanical and Aerospace Engineering, National Defense University, Taoyuan, Taiwan; 2. Mechanical Engineering, National Yan Ming Chiao Tung University, Hsinchu, Taiwan*

Ferrofluids that are colloidal suspensions of ferromagnetic particles suspended in oil or water can be manipulated by an external magnetic field. The ferrofluid droplet would break up into numerous subscale droplets, which is referred to as Rosensweig instability, whose pattern depends on the field conditions. Fig. 1 shows an oil-based ferrofluid (EMG905) droplet breaks up into various patterns of subdroplets in the different field strengths. Fig.1(a) shows a ferrofluid droplet splits up into a few subdroplets under a field strength of 17428 A/m. When an EM wave generated by a 200 mw power laser pointer transmits to the surface of a ferrofluid droplet with an incident angle of θ_i=30°, the reflection of the EM wave remains significant. When the incident angle increases to of θ_i=45° and θ_i=60°, the reflection energy of the EM wave are eliminated and diminished, respectively, due to the scattering effect. The same scenario is seen in the case shown in Fig.1(b), when the field strength is increased to 34300A/m, which results in more numbers of subdroples. It is noted that all the reflections of EW wave are weakened. Fig.1(c) shows the reflection waves for the incident angle of θ_i=30° and θ_i=60° decay when the field strength is increased to 45360 A/m and much more subdroples are created. However, the reflection energy of EM wave for the θ_i=45° increases slightly compared to the cases shown in Figs. 1(a) and 1(b). The experimental results show that ferrofluid droplet subjected to an external magnetic field is applicable to be a smart shield that can absorb and scatter the energy of EM wave and reduce the EM pollution effectively. The effects of roughness, diameter, and composition of ferrofluid droplets on the EM wave energy loss will be discussed in the full manuscript. The quantitative measurement of the reflection loss will be demonstrated as well.

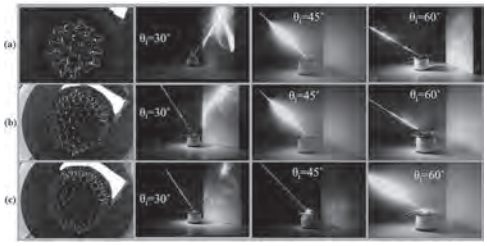

Fig.1 Magnetic-field-induced ferrofluid droplet breaks up into various numbers of subdroplets under a magnetic field strength of (a) H=17428 A/m (b)H=34300 A/m (c)H=45360 A/m. The number of the ferrofluid subdroplets increases with the field strength. The reflection energy of the EM wave varies with the patterns of the ferrofluid subdroplets and the incident angles.

CPA-06. Effect of Sr-doping on Structural and Magnetic Properties of LSMO nanoparticles Prepared by Sol-Gel Auto Combustion Method. *Y. Kaur*[1] and B. Chudasama[1] *1. School of Physics and Materials Science, Thapar Institute of Engineering and Technology, Patiala, India*

Polycrystalline lanthanum strontium manganese oxide (LSMO), $La_{1-x}Sr_xMnO_3$ (x = 0.1–0.4) nanoparticles (NPs) exhibit interesting size dependent structural and magnetic. They find interesting applications in catalysis, biomedicine and data storage [1]. LSMO NPs have attracted considerable attention in recent years because of their tunable novel magnetic properties [2], single domain superparamagnetic structure with near room temperature Curie point (T_c) [3]. Properties of LSMO NPs are strongly correlated with the extent of Sr-doping at La site, their particle size and extent to which different crystallographic phases (rhombohedral / orthorhombic) present. The aim of this study is to understand the effect of Sr-doping on structural and magnetic properties of LSMO NPs synthesized via sol-gel auto combustion route. Their structural and magnetic properties were investigated by X-Ray diffraction coupled with Rietveld refinement and vibrating sample magnetometer. The Rietveld refinement of diffractograms revealed that irrespective of Sr-doping, LSMO NPs were crystallized in rhombohedral (R-3c) and orthorhombic (Pbnm) mixed phases. The rhombohedral phase appears to be the dominant crystalline phase. VSM of Sr-doping LSMO NPs exhibits single domain superparamagnetic structure. With the decrease in Sr-doping, the saturation magnetization (M_s) of LSMO NPs also decreases (Fig. 1), while their T_c remained constant at 360 ± 10 K. In order to establish the correlation between the structural and magnetic properties of LSMO NPs, M-H curves were fitted with the modified Langevin function [4, 5]. From the

best fits, M_s, d_m (magnetic particle size) and s (polydispersity index) were determined. It was observed that with decrease in Sr-doping, both d_m, and s decreased also resulting in reduction in their M_s. The changes in their magnetic properties are in good correlation with the relative changes in the rhombohedral and orthorhombic phases. Thus, through Sr-doping, magnetic properties of LSMO NPs can be tuned by controlling the crystallographic phase fractions.

[1] Vaishnavi M. Kulkarni, Dhananjay Bodas and Kishore M. Paknikar, RSC Advances, 5, 60254-60263 (2015). [2] Soumik Mukhopadhyay and I. Das, EPL, 83, 27003 (2008). [3] Harinarayan Dasa, Akihiro Inukaia, Nipa Debnatha, Journal of Physics and Chemistry of Solids, 112,179-184 (2017). [4] M. Knobel, W.C. Nunes, A.L. Brandl, Physica B, 354, 80 (2004). [5] N. Kaur, B. Chudasama, *J. Magn. Magn. Mater*, 451, 647 (2018).

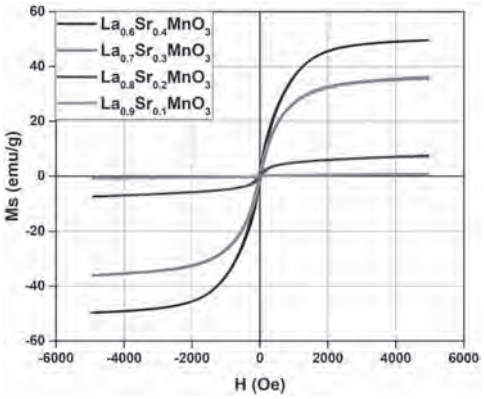

Fig. 1 Effect of Sr-doping on the M_s of $La_{1-x}Sr_xMnO_3$ (x = 0.1 -0.4) nanoparticles

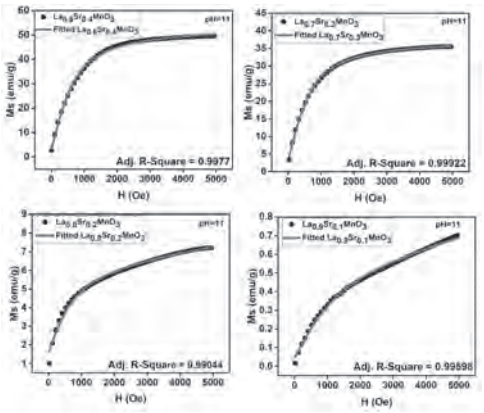

Fig. 2 M_s–H of $La_{1-x}Sr_xMnO_3$ (x = 0.1 -0.4) nanoparticles fitted with modified Langevin function

CPA-07. Effect of Ga-substitution on magnetic and dielectric properties of nanosized yttrium iron garnet ferrites. P. Tsai[1], *J. Zou*[1] and T. Han[1] *1. Department of Applied Physics, National University of Kaohsiung, Kaohsiung, Taiwan*

Yttrium iron garnet ferrites, $Y_3Fe_5O_{12}$ (YIG), have been attracted considerable attention due to its technological importance in various applications such as high quality filters and magneto-optical devices [1]. It is well known that the nanoferrites may exhibit unique structural, magnetic and optical properties far different from those of their bulk counterparts because of low dimensionality and quantum confinement effect [2]. In addition, the correlation of the doping and grain size effects on functional behavior of YIG system has not yet been completely established. In this work, therefore, we prepare a series of $Y_3Fe_{5-x}Ga_xO_{12}$ ($0 \le x \le 2$) nanoparticles by the sol-gel method to systematically study the effect of Ga-substitution on their magnetic and dielectric properties. The crystallographic phase of each sample was confirmed by observing the XRD patterns. Ga substitutions slightly modify the value of the lattice parameters. This could be ascribed to the smaller ionic radius of Ga^{3+} than that of Fe^{3+}, which confirms that the Ga is successfully substituted in the lattice of YIG. The grain size of these samples was found in the nano regime. In addition, the non-linear change of structure parameters for $Y_3Fe_{3.5}Ga_{1.5}O_{12}$ sample has been observed. This behavior may be due to the existence of oxygen vacancies in garnet structure. The oxygen vacancies would induce Fe^{2+} ions then give rising on the value of the lattice constants. It was also found that the dielectric constant increases with increasing Ga-content. Furthermore, the saturation magnetization was decreased whereas coercivity increased with the Ga substitution in YIG nanoferrite. The magnetization decreased at the lattice sites and this is due to Ga^{3+} substitution instead of Fe^{3+} in the tetrahedral position. Another reason for the decrease in magnetization is due to the substitution of smaller ionic radius of Ga in nanosized YIG. It is noticed that the coercivity increased with Ga substitution in YIG nanoferrite. This characteristic could be attributed to the decrease in the grain size close to single domain. The soft character of the Ga-substituted YIG nanoferrites with moderate magnetization suggested the use of these nanoferrites for future applications.

[1] R. J. Joseyphus, A. Narayanasamy, A. K. Nigam, R. Krishnan, J. Magn. Magn. Mater. 296 (2006) 57. [2] L. Li, X. Zhong, R. Wang, X. Tu, L. Peng, J. Magn. Magn. Mater. 433 (2017) 98.

CPA-08. Analysis of the Influence of Grain-Oriented Silicon Steel Splicing Mode of Stator on the Motor Performance. *X. Zhang*[1], H. Zhang[1] and R. Pei[1] *1. Electrical Engineering, Shenyang University of Technology, Shenyang, China*

Due to the high power density requirements of the new energy vehicle drive motor, the saturation degree of magnetic density of motor stator tooth is higher, which brings great difficulties to further improve the performance of the motor. Authors developed a segment type switched reluctance motor (SRM) as a rare earth less motor was developed to reduce the acoustic noise and vibration as well as improve the torque characteristics by using grain-oriented electric steel as the segment core[1]. Oriented silicon steel has high permeability and low loss in the rolling direction, so it is used in the design and application of motor tooth. This paper is based on a 20000rpm300kW drive motor to optimize the design. According to the magnetic properties of the motor, the motor teeth replace the grain-oriented silicon steel (GO) with the original non-grain-oriented silicon steel sheet (NGO). The magnetic circuit of the tooth of the motor was analyzed by finite element simulation software, and the output torque difference of NGO motor, GO material motor and different splicing clearance was compared. In view of the difference in motor performance caused by the splicing of the GO silicon steel core, the measurement system of the ring test specimen of NGO materials is carried out using normal voltmeter-ammeter methods. The types of stator cores tested were NGO silicon steel integral core, NGO tooth yoke spliced iron core, and GO and NGO steel tooth yoke spliced iron core. According to the test results, the performance of the motor is checked, and the feasibility of the design of grain-oriented stator core splicing is analyzed. In this paper, the motor tooth uses GO material to replace the conventional NGO material, the maximum output of the motor increases by 1%, the motor maximum efficiency increases by 1.2%.

[1] Kaneki O, Higuchi T, Yokoi Y, et al. Performance of segment type switched reluctance motor using grain-oriented[C]// International Conference on Electrical Machines and Systems. IEEE, 2012:1-4. [2] Sugawara Y, Kan A. Characteristics of a Switched Reluctance Motor using Grain-Oriented electric steel sheet[C]// Ecce Asia Downunder. IEEE, 2013:1105-1110. [3] Matsuo Y, Higuchi T, Abe T, et al. Characteristics of a novel segment type switched reluctance motor using grain-oriented electric steel[C]// International Conference on Electrical Machines and Systems. IEEE, 2011:1-4.

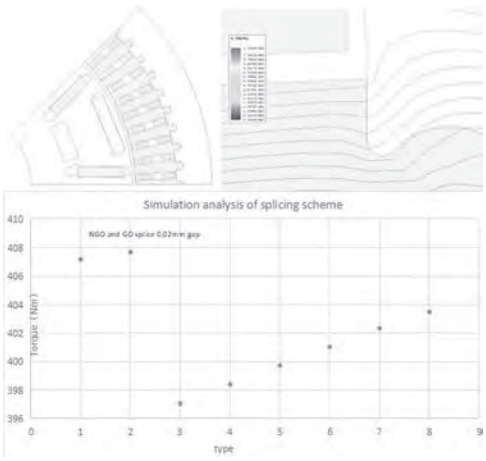

Fig. 1 Design and Analysis

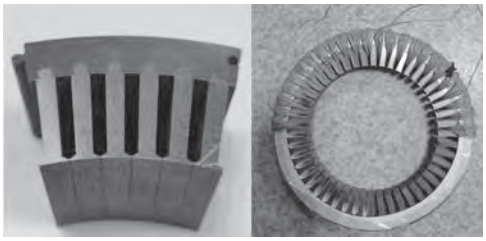

Fig. 2 Iron Core Loss Measurement of the Stator Yoke

CPA-09. Investigation of the Influence of the Anisotropic Magnetic Performance of the Grain-Oriented Silicon Steel on the Motor Design.
H. Zhang[1], *A. Hu*[1] and R. Pei[1] *1. Electrical Engineering, Shenyang University of Technology, Shenyang, China*

Due to the high permeability and low iron loss properties of Grain-Oriented(GO) silicon steel along the rolling direction, many researchers have tried to optimize traction motors by using this materials[1]. It is known that during the work process of the motor, there is a rotating magnetic field in the yoke and a pulsating magnetic field in the tooth of the stator, so that a segmented structure could be applied to take advantage of the GO material[2]. The rolling direction of the GO material is consistent with the direction of the applied magnetic field. Most of the magnetic domains in the GO sheet are in the same direction as magnetic field. The expansion of the magnetic domain will cause the increase of flux density, but because there are fewer non-zero magnetic domains, the magnetic domains rotate. The increment of flux density caused is small, and the energy consumed is not much. It will eventually rotate to the rolling direction and reach the saturation state, thereby reaching the maximum magnetic induction value [3]. However, even if the magnetic field in the tooth part is pulsating, the flux is not always along the rolling direction of the GO material strictly throughout the work process, which will affect the design and the final performance of the motor fabricated. So the magnetic properties of the GO material along the direction different from the rolling direction are still needed to be studied. In our experiment, we test the magnetic properties of the GO material B23R080 with different deflection angle along the rolling direction by Epstein method [4]. And a strange behavior of the BH curves we obtained appeared. This paper will consist of 5 parts: part I is the introduction; in part II we will present our test results of B23R080; part III will be the explanation of the strange performance of the test results; part IV will introduce the influence and our advices to the motor design and the part V will be the conclusion.

[1] G. Paltanea, V. M. Paltanea, I. V. Nemoianu, H. Gavrilă and P. C. Andrei, "Influence of cutting technologies on the magnetic anisotropy of grain oriented electrical steel," 2017 Electric Vehicles International Conference (EV), 2017, pp. 1-4, doi: 10.1109/EV.2017.8242088. [2] R. Pei, L. Zeng, S. Li and T. Coombs, "Studies on grain-oriented silicon steel used in traction motors," 2017 20th International Conference on Electrical Machines and Systems (ICEMS), 2017, pp. 1-5, doi: 10.1109/ICEMS.2017.8056324. [3] M. Emura, M.F. de Campos, F.J.G. Landgraf, J.C. Teixeira, Angular dependence of magnetic properties of 2% silicon electrical steel, Journal of Magnetism and Magnetic Materials, Volumes 226–230, Part 2,2001. [4] Magnetic Materials Part 2: Methods of Measurement of the Magnetic Properties of Electrical Steel Sheet and Strip by Means of an Epstein Frame, IEC International Standard Ref. DIN IEC 60404-2, 2009.

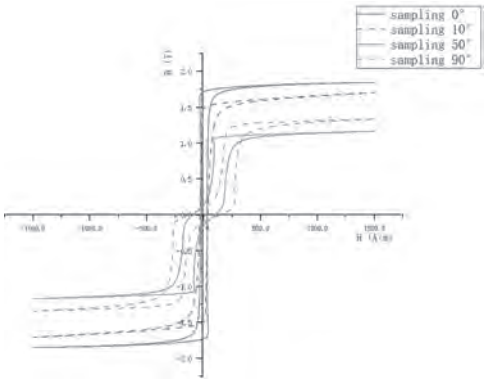

Fig. 1 B-H Curve

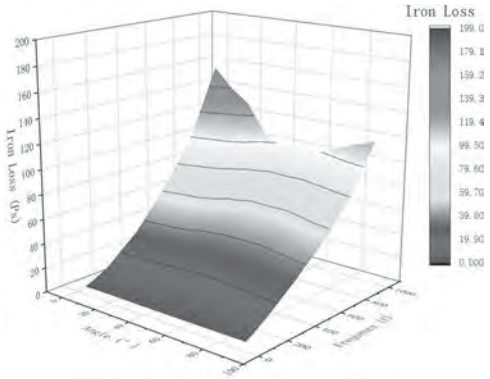

Fig. 2 Iron Loss - Flux Density - Angle

CPA-10. The effect of particle size on core-losses of Fe-Si-Cr soft magnetic composites. *Y. Choi*[1], J. Ahn[1], S. Kim[1], D. Kim[1] and B. Lee[1] *1. Department of Physics and Oxide Research Center, Hankuk University of Foreign Studies, Yongin, The Republic of Korea*

Fe-based soft magnetic composite (SMC) is used as the main raw material for electronic devices such as power inductors. Power inductors should fulfill the requirements, such as stability of magnetic permeability and high-current stability, for frequency bands above 1 MHz. These frequency bands are essential for component integration. [1, 2] Gas-atomized Fe-Si-Cr alloy powders were sieved into five ranges of particle sizes: greater than 63 μm, 53-63 μm, 38-53 μm, 25-38 μm, and less than 25 μm. Particle sizes were named FSC1, FSC2, FSC3, FSC4, and FSC5, respectively. A toroidal core was made by mixing each particle size group with 3.0wt% of epoxy resin. X-ray diffraction, particle size distiribution, vibrating sample magnetometer, and scanning electron mircroscopy were analyzed in order to measure the intrinsic properties of Fe-Si-Cr powders. An impedacne analyzer was used to measure the magnetic permeability of the core, and a B-H analyzer was used to measure the core-loss of fabricated SMCs. Permeability gradually increased, as particle size decreased, except in FSC1. However, samples with larger particle sizes showed rapid decreases in the high-frequency range, limiting them as suitable candidates for electronic devices. [3] Fig.2 shows the core-loss of FSC1, FSC3, and FSC5 samples in order to analyze the particle size dependence. The total core-loss decreased as the particle

size decreased. We separated the eddy-current loss and hysteresis loss from the total core-loss by curve fitting, and proved that the main factor of core-loss reduction was the decrease of eddy-current loss. The eddy-current loss is proportional to the square of particle size. [4] In our study, the smallest FSC5 sample showed the lowest core-loss of 156.27 kW/m^3, which shows that samples with small particle sizes are a good candidate for high-frequency electronic devices applications.

[1] Q. Zhu, L. Li, M.S. Masteller, and G. J. Del Corso, *Appl. Phys. Lett.*, 69, 3917-3915 (1996) [2] A. Makino, *IEEE Trans. Magn.*, 48, 1331-1335 (2012) [3] J.G. Yeo, D.H. Kim, Y.J. Choi, and B.W. Lee, *J. Electron. Mater.*, 48(9), 6018-6023 (2019) [4] A.H. Taghvaei, H. Shokrollahi, K. Janghorban, and H. Abiri, *Mater. Des.*, 30, 3989-3995 (2009)

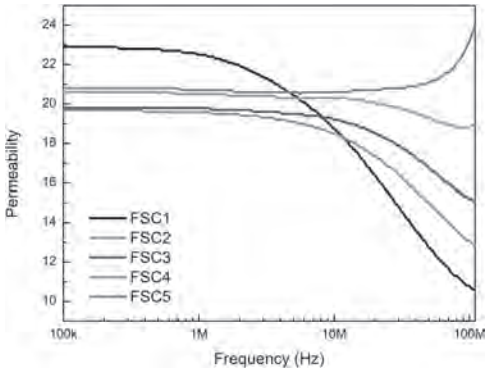

Fig.1. Core permeability of each particle size

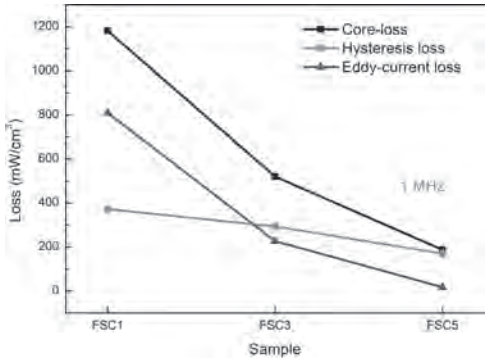

Fig.2. Losses at 1 MHz depending on particle sizes

CPA-11. Proposal of noble co-addition method for α″-Fe_{16}(N, C)$_2$ particles by gas-solid reactions. *M. Tobise*[1], Y. Nomura[2], M. Kodama[2], T. Murakami[1] and S. Saito[1] *1. Electronic Engineering, Tohoku University, Sendai, Japan; 2. Taiyo Nippon Sanso Corporation., Hokuto, Japan*

The metastable α″-$Fe_{16}X_2$ (X= N, C) is known as a unique material having uniaxial anisotropy energy of +1×10^7 erg/cm^3 (X= N) and –6 ×10^6 erg/cm^3 (X= C), respectively, according to the thin film experiment [1]. Therefore, α″-$Fe_{16}X_2$ (X= N and C) particles is very attractive in order to develop new soft magnetic materials because uniaxial anisotropy energy can be changed by N and C concentration. We have been investigating the solid-phase reaction process through the synthesis of α″-phase particles by nitridation or carbonization for reduced α-Fe starting from iron hydroxide or iron oxide [2, 3]. N can be introduced interstitially into α-Fe easily by nitridation using NH_3 gas. On the contrary, it is extremely hard to introduce C interstitially into α-Fe by carbonization using C containing gas such as CO gas since an equilibrium phase Fe_3C is easily generated. Therefore, we examined the reaction route after reduction and the kind of gas used for carbonization to realize α″-Fe_{16}(N, C)$_2$ particles. At first, we tested 3 kinds of route after reduction, Route A; nitridation and carbonization are performed at the same time, Route B; carbonization first and nitridation next, and Route C; nitridation first and carbonization next (Fig. 1). Among these routes, it was only Route C that α″-Fe_{16}(N, C)$_2$ particles were successfully produced, that is, *material route C*; from α-Fe by reduction to α″-$Fe_{16}N_2$ by nitridation, and α″-Fe_{16}(N, C)$_2$ by following carbonization. Fig. 2 are the XRD patterns of particles after nitridation and after carbonization which show α″-phase are produced, respectively. C quantity of particles after carbonization was measured with 0.8 wt% by combustion method. This amount of C is 40 times larger than that of 0.02 wt% as solid solution limit of α-Fe in bulk. This noble gas-solid reaction process based on the concept of utilizing α″-$Fe_{16}N_2$ which is the material expanded α-Fe lattice is highly suggestive as a co-addition method of N and C interstitially.

[1] M. Takahashi et al., J. Magn. Soc. Jpn., 239 (2002) 479. [2] M. Tobise et al., AIP Adv., 9 (2019) 035233. [3] M. Tobise et al., IEEE Trans, Mag., 57 (2021) 2100305.

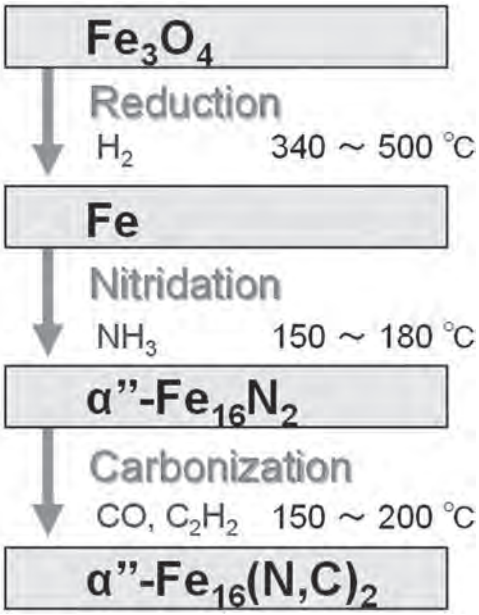

Fig. 1 The route of gas-solid reaction to synthesize α″-Fe_{16}(N,C)$_2$ particles.

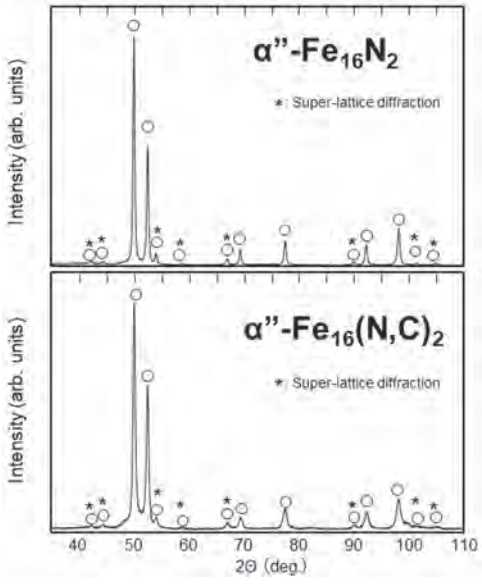

Fig. 2 XRD patterns of α″-$Fe_{16}N_2$ and α″-Fe_{16}(N, C)$_2$ particles. Open circle represents α″-phase.

CPA-12. Synthesis and printing of $Fe_{50}Rh_{50}$ nanoparticle inks– a laser-based route to generate magnetocaloric structures. *S. Tahir*[1], C. Donate-Buendia[1], R. Nadarajah[2] and B. Gökce[1] *1. Materials Science and Additive Manufacturing, Bergische University Wuppertal, Wuppertal, Germany; 2. Technical Chemistry 1, University of Duisburg-Essen, Essen, Germany*

Magnetocaloric refrigeration has emerged as an attractive candidate to replace conventional compression-based refrigeration systems in virtue of its higher Carnot efficiency and eco-friendlier refrigeration thereby replacing potent CFCs. This solid-state refrigeration can be exploited mainly for compact devices such as micro refrigerators, thermal diodes, regulators, and electronics where heat extraction is challenging. To facilitate the usage of magnetocalorics for such applications, 2D printing of magnetocaloric nanoparticle inks is versatile approach to generate custom structures. Among magnetocaloric materials, the FeRh alloy system demonstrates the largest magnetocaloric effect at first order (AFM-FM) phase transition at near-to-equimolar composition. Previous studies reveal that the synthesis of FeRh nanoparticles using conventional processes leads to undesired Fe/Rh core-shell structures and for a magnetocaloric response, a uniform near-to-equiatomic distribution of Fe and Rh within nanoparticles is critical. Here, we demonstrate a laser-based approach for the synthesis of FeRh nanoparticles[1] and 2D sintering of a developed ink[2]. A $Fe_{50}Rh_{50}$ bulk target was ablated using an infrared picosecond-pulsed laser in organic solvents (acetone, acetonitrile, and ethanol) leading to the formation of paramagnetic solid solution $Fe_{50}Rh_{50}$ nanoparticles with reduced oxygen content (up to 5 at. %).[1] The generated nanoparticles were used to formulate an ink (up to 1 wt.%) in ethanol and dispersed on PVP-coated glass substrates and were patterned using 532 nm CW laser. The 2D laser sintering facilitates the formation of pore-free custom structures and induces ultrafast partial phase transition from paramagnetic to ferromagnetic and antiferromagnetic phases.[2]

1. Nadarajah, R.; Tahir, S.; Landers, J.; Koch, D.; Semisalova, A. S.; Wiemeler, J.; El-Zoka, A.; Kim, S.-H.; Utzat, D.; Möller, R.; Gault, B.; Wende, H.; Farle, M.; Gökce, B., Controlling the Oxidation of Magnetic and Electrically Conductive Solid-Solution Iron-Rhodium Nanoparticles Synthesized by Laser Ablation in Liquids. *Nanomaterials* 2020, *10* (12), 2362 2. Nadarajah, R.; Landers, J.; Salamon, S.; Koch, D.; Tahir, S.; Doñate-Buendía, C.; Zingsem, B.; Dunin-Borkowski, R. E.; Donner, W.; Farle, M.; Wende, H.; Gökce, B., Towards laser printing of magnetocaloric structures by inducing a magnetic phase transition in iron-rhodium nanoparticles. *Scientific Reports* 2021, *11* (1), 13719

CPA-13. Morphological evolution of Fe_xCo_{100-x} alloy nanoparticles and their correlation to magnetic behaviour. *Moditma*[1], R. Malik[2], V.R. Reddy[3] and S. Annapoorni[1] *1. Department of Physics and Astrophysics, University of Delhi, Delhi, India; 2. ARSD College, University of Delhi, Delhi, India; 3. UGC-DAE Consortium for Scientific Research, University Campus, Khandwa Road, Indore, India*

Among soft ferromagnetic materials, FeCo alloys are known to possess the highest values of saturation magnetization (M_s), about 15% greater than iron. In order to gain insight into the magnetic behaviour, composition dependent studies of long-term stable Fe_xCo_{100-x} (x=0, 30, 40, 50, 60, 70, 100) alloy nanoparticles, prepared by instantaneous polyol reduction [1], have been performed. Using appropriate molar concentration of precursor salts, desired alloy compositions were prepared. X-ray diffraction studies revealed a consistent decrease of lattice parameters with increasing Co content, ranging from 2.866 Å in Fe nanoparticles to 2.847 Å for $Fe_{30}Co_{70}$ nanoparticles, suggesting alloy formation in the desired composition range. Morphologically, an evolution from cubical to spherical shaped nanoparticles is observed when going from the Fe-rich to Co-rich side. Intermediate compositions like those of $Fe_{50}Co_{50}$ accordingly form ~ 200 nm spherical structures, with sharp cubical edges. Effect on magnetic properties with alloy composition was assessed by room temperature M-H curves and ^{57}Fe Mössbauer spectroscopy. An increase of M_s values was observed with increasing Co content, reaching upto ~ 200 emu/g at 30% Co. At the microscopic scale, hyperfine fields (BHF) correspondingly increased, as depicted in Figure 1, reaching a maximum of 36.7 T at 40% Co. This has been associated to the increase of Fe moment from 2.2 μ_B to 3 μ_B upon Co addition, resulting in an increase of the average moment per atom [2]. Annealing resulted in a decrease of BHF values and Mössbauer line widths, with a corresponding increase of M_s values, suggesting increased magnetic ordering and approach to bulk behaviour [3]. Thus, highly crystalline Fe_xCo_{100-x} alloy nanoparticles, with good stability, composition control and desired magnetic properties have been prepared by a facile synthesis process. The present study thus paves the way to investigate further interesting aspects of the evolution of antibacterial behaviour of the magnetic nanoparticles with varying alloy compositions, as done previously for equiatomic nanoparticles [4].

[1] Moditma et al. *J Supercond Nov Magn* 33, 1653 (2020). [2] J.M. MacLaren et al. *J App. Phys* 85, 4833 (1999). [3] B. deMayo et al. *J. App. Phys* 41, 1319 (1970). [4] Moditma et al. *Nanotechnology* 32, 335101 (2021).

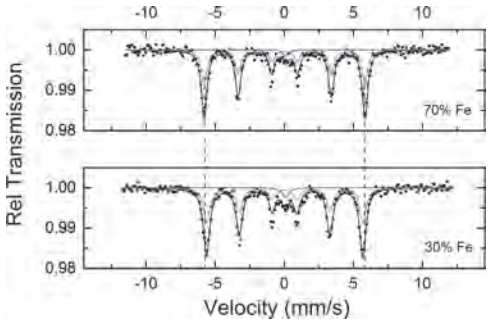

Typical Mössbauer spectra of two extreme alloy compositions. Dashed lines are used to indicate change in BHF values.

CPA-14. Fe-Ni-Mn alloy produced by mechanical alloying and spark plasma sintering. K. Zaara[1], M. Chemingui[3], *J. Suñol*[1], Y. Gallard[4] and V. Optasanu[2] *1. University of Girona, Girona, Spain; 2. Université Bourgogne, Dijon, France; 3. Université Sfax, Sfax, Tunisia; 4. Université de Bourgogne, Besançon, France*

In recent decades, one of the methods used to produce magnetic alloys is the combination of mechanical alloying (MA)and spark plasma sintering (SPS). In this way, the magnetic particles produced by mechanical alloying are obtained as bulk specimens. Obviously, the production conditions affect the microstructure of the alloys produced and their functional response. In this work, the influence on the magnetic response of an Fe-Ni-Mn alloy when subjected to treatment at different temperatures and pressures is shown. The figure shows the hysteresis magnetic cycle of three specimens. From microstructural analysis carried out by means of X-ray diffraction, it is found that excessive pressure favors the formation of precipitates of a minority phase and that high temperatures favor the formation of intermetallic compounds and oxides. Crystallographic phases that directly affect the magnetic response. Similar studies have been conducted on samples of Fe-Co-Ni and Fe-Co-Ni-B-Si [1].

[1] K. Zaara, M. Cheminghi, J.J. suñol et al. Crystals 2020, 10, 919.

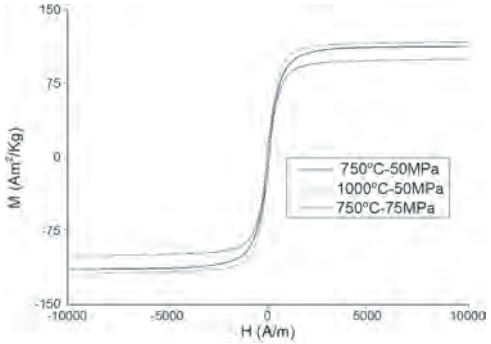

CPA-15. Research and Application of the Fe-Co-V Soft Magnetic Alloy to The High Torque Density Electric Machine. H. Zhang[1], *L. Wang*[1] and R. Pei[1] *1. Electrical Engineering, Shenyang University of Technology, Shenyang, China*

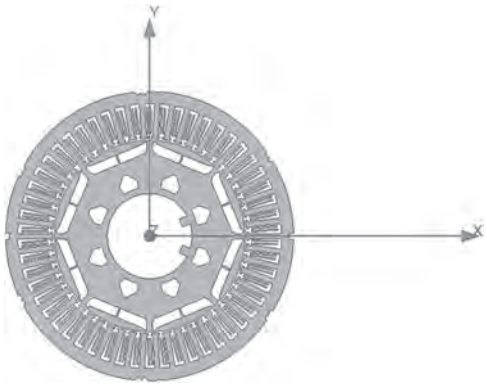

The development of the electric vehicle makes a higher requirement to the torque/power density of the traction motors. It has been difficult to meet the requirements by using conventional silicon steels. Therefore, the application of "new" materials could become a breakthrough. In this paper, we research the properties and the application in traction motors of the Fe-Co-V alloy 1J22. Compared with conventional silicon steels, 1J22 has a higher saturation flux density, which enables the motor to have a higher torque density. However, the impact of stamping and shear stress during the processing progress greatly reduces the magnetic properties, which means the annealing processes is necessary and will change the magnetic performance significantly[1]. According to the Fe-Co binary alloy phase diagram[2], it can be seen that the annealing temperature cannot be higher than 910 degrees. For our experiment, the annealing temperature of 850 degrees is adopted. At the same time, hydrogen protection is applied to avoid the oxidation reaction. R. S. Sundar found that the magnetic performance with a holding time of 4 hours can reach an excellent level and when the temperature is above 750 degrees during cooling, slowly lower the temperature at a rate of 50 degrees/hour. At 730 degrees, an ordered phase will be produced [3], the short-range order in the disordered phase will grow up to form a long-range order which makes the dislocations difficult and leads to the poor ductility and the brittleness of the alloy. The saturated flux density (Bs) of Fe-Co binary alloy increases with the increase of Co content. When the Co content is 35%, Bs is 2.45T. When the Fe-Co atom ratio is close to 1:1, the magnetocrystalline anisotropy constant is about 0, which has the highest magnetic permeability. Dr. White's team [2] added 2% V to the alloy to improve its brittleness. We use 1J22 material to develop a prototype with a rated power of 6kW and a rated speed of 4500rpm. The torque density of the prototype is increased by 14% compared with the conventional motor used silicon steel. This paper is divided into 4 parts: Magnetic properties test and metallographic observation; Motor design; Prototype manufacturing and test and conclusion.

[1] Galenko, P.P. Influence of the annealing temperature and holding time on the stability of magnetic properties of a Fe-Co alloy. Journal of Engineering Physics 45, 1433–1436 (1983). [2] Binary Alloy Phase Diagrams, Alloy Phase Diagrams, Vol 3, ASM Handbook, Edited By H. Okamoto, M.E. Schlesinger, E.M. Mueller, ASM International, 2016, p 89. [3] R. S. Sundar & S. C. Deevi (2005) Soft magnetic FeCo alloys: alloy development, processing, and properties, International Materials Reviews, 50:3, 157-192. [4] JH. White, C.V. Wahl, U.S. Patent 1,86,2599.(1932)

Session CPB
SOFT MAGNETIC MATERIALS VI: AMORPHOUS AND NANOCRYSTALLINE (Poster Session)

Naoki Ito, Chair
Hitachi Metals, Ltd., Yasugi, Japan

CPB-01. Relationship between morphology and soft-magnetic properties of Co-Sr-F nano-granular films. *C. Wang*[1], Y. Endo[2], Y. Cao[1], H. Kijima-Aoki[1], N. Kobayashi[3], S. Ohnuma[1,3] and H. Masumoto[1] *1. Frontier Research Institute for Interdisciplinary Sciences, Tohoku University, Sendai, Japan; 2. Department of Electrical Engineering, Graduate School of Engineering, Tohoku University, Sendai, Japan; 3. Research Institute for Electromagnetic Materials, Sendai, Japan*

With the rapid improvement of electromagnetic (EM) equipment, the high-frequency (HF) soft magnetic films have been studied intensively as HF components such as a film type inductor, an electromagnetic noise suppressor sheet, and so on.[1, 2] In particular, the nano-granular films are well-known as one of the best choices as HF components, which can prevent the ensuing plunge in electrical resistivity as ferromagnetic resonance frequency (f_{FMR}) increases. Herein, we select Co-Sr-F nano-granular films as the material of HF components and investigate their structure and magnetic properties in detail. The structure is nanocomposite, that is, Co nano-granules are evenly dispersed in a ceramic matrix. TEM observations indicate Co nano-granules change from a spherical to a columnar shape as the Co content increases. The electrical resistivity decreases from 10^9 to 10^4 μΩ*cm with a steep around 50~55 at.% of Co content as the Co content increases because of the change in the morphology of the film. In the range of Co content above 50 at.%, their coercivities are obtained and their saturation magnetizations (Ms) increase linearly(Fig.1). These results indicate that the films are ferromagnetic in the range of Co content above 50 at.%. To clarify f_{FMR} of these films, the change in permeability of these films with frequency is measured, and the observed f_{FMR} is summarized in Fig. 2 as a function of Co content. For Co content between 51~55 at.% (stage I), f_{FMR} remains constant around 4.8 GHz, while, for Co content above 55 at.% (stage II), f_{FMR} increases to 12 GHz monotonically. These behaviors can be explained by the change in the morphology of Co nano-granules. Namely, in stage I, as Co nano-granules are spherical, Kittel formula[3] is expressed as $f_{FMR}=\gamma H_z$ (γ is the gyromagnetic ratio). In stage II, as Co nano-granules are columnar, Kittel formula is described as $f_{FMR}=\gamma(H_z+1/2M_S)$ and f_{FMR} increases linearly with the increase of Ms. Therefore, these results demonstrate f_{FMR} and film morphology correlates each other apparently, and suggest that Co-Sr-F nano-granular films are one of the candidates for HF components.

[1] S.X. Wang, Nature, 407 (2000) 150-151. [2] S. Ge, Journal of Physics D: Applied Physics, 40 (2007) 3660-3664. [3] C. Kittel, Physical Review, 73 (1948) 155-161.

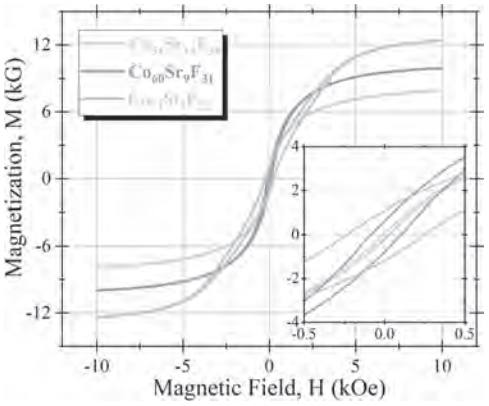

Fig. 1 Magnetization curves of Co-Sr-F nano-granular thin film.

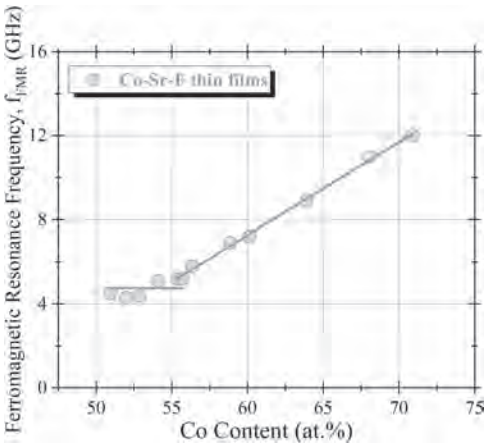

Fig. 2 The dependence of f_{FMR} on Co content.

CPB-02. Micromagnetic study of anisotropy in cylindrical amorphous nanowires. *C. Rotarescu*[1], H. Chiriac[1], N. Lupu[1] and T. Óvári[1] *1. National Institute of Research and Development for Technical Physics, Iasi, Romania*

The magnetization switching in glass-coated amorphous nanowires with cylindrical symmetry is presented and discussed. We studied the coercive field dependence of the nanowires dimensions in order to understand the main aspects of the magnetization reversal processes in amorphous nanowires with cylindrical symmetry. The considered samples were two alloys with representative compositions: (1) the alloy $(Co_{0,94}Fe_{0,06})_{72,5}Si_{12,5}B_{15}$, with very small negative magnetostriction, considered, from this reason, almost zero; and (2) the alloy $Fe_{77,5}Si_{7,5}B_{15}$, with a positive magnetostriction. In order to substantiate the approach taken, we simulated the axial hysteresis loops for amorphous nanowires with various diameters, whilst keeping a constant sample length. The results, illustrated in Figure 1, reveal the fact that the coercive field decreases when the diameter is larger. This dependence is related to the value of the shape anisotropy, which increases with the ratio between length and diameter. The simulated loops allowed us to understand the effect of anisotropy on coercivity. For the magnetoelastic contribution,

we used a simple anisotropy distribution to calculate the axial hysteresis loops in the case of glass-coated $Fe_{77.5}Si_{7.5}B_{15}$ amorphous nanowires. The results, for different magnitudes of the magnetoelastic anisotropy, are shown in Fig.2. One observes that the magnetoelastic contribution clearly affects the remanence of the axial hysteresis loops. A smaller squareness also shows an easier nucleation of a domain with reversed magnetization. The use of such cylindrical nanowires in magnetic logic gates is straightforward, given their bistable behavior which paves the way for application in new miniaturized devices [1]. Acknowledgement: Work supported by the Executive Unit for Financing Higher Education, Research, Development and Innovation (UEFISCDI) under the project PN-III-P4-ID-PCE-2020-1856 (contract no. PCE 1/2021).

References: [1] C. Rotarescu, H. Chiriac, N. Lupu, T.-A. Óvári, AIP Advances 9 105316 (2019).

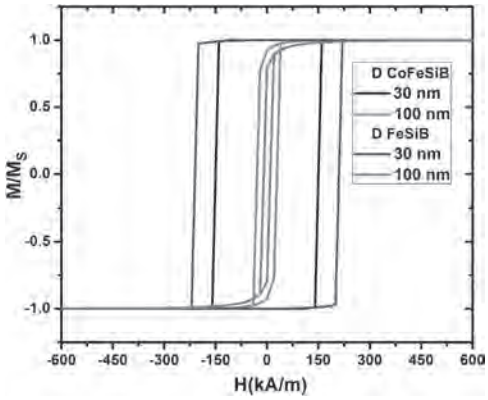

Fig. 1 Hysteresis loops of cylindrical amorphous nanowires with different diameters and compositions.

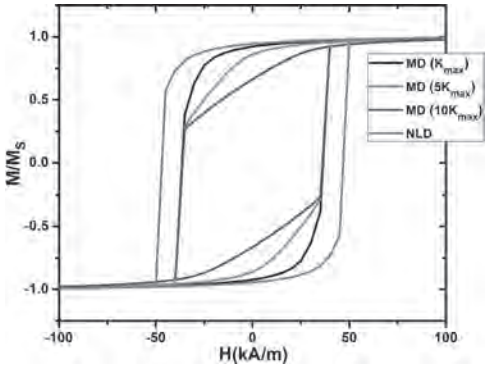

Fig. 2 Hysteresis loops for different anisotropy distributions: (i) monotonous distribution (MD) with various amplitudes; and (ii) nonlinear distribution (NLD).

CPB-03. Withdrawn

CPB-04. Application of Bayesian Optimization and Regression Analysis to Ferromagnetic Materials Development. *A.R. Will-Cole*[3], G. Kusne[1,2], P. Tonner[1], C. Dong[3], X. Liang[3], H. Chen[3] and N.X. Sun[3]
1. National Institute of Standards and Technology, Gaithersburg, MD, United States; 2. University of Maryland, College Park, MD, United States; 3. Electrical Engineering, Northeastern University, Boston, MA, United States

Bayesian optimization is a well-developed machine learning field for black box function optimization. In Bayesian optimization a surrogate predictive model, here a Gaussian process, is used to approximate the black box function. The estimated mean and uncertainty of the surrogate model are paired with an acquisition function to decide where to sample next. Bayesian optimization with Gaussian processes can be used for structure-property relationship optimization in materials systems with second order phase transitions or gradual disordering without a distinct phase transition. In this study we applied this technique to known ferromagnetic thin film materials such as ferromagnetic $(Fe_{100-y}\ Ga_y)_{1-x}B_x$ (x=0–21 & y=9–17) and $(Fe_{100-y}\ Ga_y)_{1-x}C_x$ (x=1–26 and y=2–18) to demonstrate optimization of structure-property relationships, specifically the dopant concentration or stoichiometry effect on magnetostriction and ferromagnetic resonance linewidth. These systems both experience gradual disordering without distinct phase transition with increase in boron and carbon concentration, thus are great case systems for Bayesian optimization with Gaussian processes. We have shown that using simulated Bayesian optimization methods to guide experiments, the number of samples required to statistically determine the optimum was reduced by 50% compared with traditional research methods. Our results suggest that Bayesian optimization can be used to save time and resources to optimize ferromagnetic films. This method is transferrable to other ferromagnetic material structure-property relationships, providing an accessible implementation of machine learning to magnetic materials development.

CPB-05. Study of the magnetic properties of nano-thin permalloy films depending on the grain size. N.A. Djuzhev[1], *G.D. Demin*[1], R.N. Andrushin[1], E.V. Novikov[1], B.K. Medvedev[1] and D.D. Noskova[1,2]
1. R&D Center "MEMSEC", National Research University of Electronic Technology (MIET), Moscow, Zelenograd, Russian Federation; 2. Lebedev Physical Institute of the Russian Academy of Sciences (LPI RAS), Moscow, Russian Federation

Currently, anisotropic magnetoresistive (AMR) sensors are actively used in many promising areas, such as automotive industry, geomagnetic navigation, biomedicine, etc. This is due to the fact that AMR sensors have quite good sensitivity to the magnetic field, high reliability, thermal stability, resistance to harsh environment and low cost. An important role in the fabrication of magnetoresistive elements of AMR sensors is played by the magnetic characteristics of thin ferromagnetic films at the nanoscale, which, in turn, depends on their internal crystal structure, controlled by the parameters of the technological process [1]. In this work, we experimentally analyzed the dependence of the key magnetic properties (coercivity, AMR coefficient, and magnetic anisotropy field) of a 30 nm permalloy ($Ni_{80}Fe_{20}$) thin film on its grain size controlled by the substrate temperature during magnetron sputtering (Figure 1). It was shown that both the AMR coefficient and the magnetic anisotropy field tend to reach a constant level of 2.25% and 5 Oe, respectively, with an increase in the grain size. In turn, the dependence of the permalloy film coercivity on the grain size has a minimum in the region of about 8 nm and sharply increases at a smaller thickness, which corresponds to the assumed behavior of NiFe from previous studies [2]. The results obtained are important for the development of magnetic nanostructures for a new generation of highly sensitive magnetoresistive sensors based on the AMR effect [3]. This work was performed with the financial support of the Foundation for Assistance to Small Innovative Enterprises in Science and Technology (FASIE) (contract No. AAAA-A20-120111290020-5) using the equipment of MIET Core Facilities Center «MEMSEC».

[1] N. Djuzhev, A. Iurov, N. Mazurkin, et al., EPJ Web Conf., Vol. 185, p.01003 (2018) [2] M.A. Akhter, D.J. Mapps and Y.Q. Ma Tan, J. Appl. Phys., Vol. 81, p.4122 (1997) [3] Y.-D. Pan, L.-R. Yu, L. Wang, et al., Rare Metals, Vol. 40, p.2026 (2021)

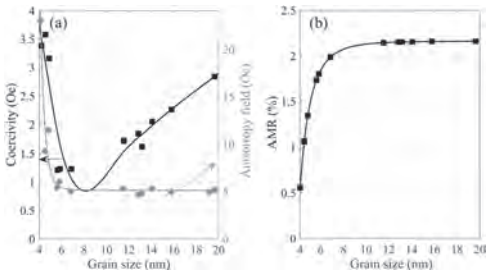

Figure 1. (a) Coercivity (anisotropy field) and (b) AMR coefficient as a function of the grain size of 30 nm permalloy film.

CPB-06. Study on Structural Characteristics and Magnetic Properties of Fe-B Particles with Submicron Sizes Synthesized by A Liquid-phase Reduction Method. *Y. Endo*[1], K. Murata[1], H. Kijima-Aoki[1], T. Miyazaki[1] and H. Masumoto[1] *1. Tohoku University, Sendai, Japan*

Soft magnetic metal particles possess a high potential as high-frequency magnetic cores, owing to their high resistivity and saturation magnetization. These particles with sizes of a few tens of micrometers have been produced by various methods such as water atomizing, mechanical forging, and so on, but the frequency range where they are used as magnetic core is limited to less than a few tens of kHz because of eddy current loss within the particles. In contrast, the particles with sizes less than about 1 um synthesized by chemical reduction of solutions have been studied intensively from scientific point of view. However, little attention has been focused on magnetic softness or high permeability enough for high-frequency applications. Until now, we investigated magnetic softness and permeability of 0.3-um Fe-B-P amorphous particles synthesized by a chemical process [1]. Herein, we investigated structural characteristics and magnetic properties of their composites of Fe-B particles with various submicron sizes synthesized by chemical preparation in an aqueous method, and discussed the effect of median size on their properties. The shape and structure of the particles are spherical and amorphous regardless of median size. As shown in Fig. 1, the coercivity of the particles decreases from about 40 to 10 Oe as the median size increases, whereas the remanece ratio of the particles is independent of the median size and become lower. These results suggest the good magnetic softness with the low hysteresis loss. The saturation magnetization of the particles is independent of the median size. Their values are approximately 135-150 emu/g. Furthermore, as for the dynamic magnetic properties of the particles (Fig. 2), each ferromagnetic resonance (FMR) peak can be observed in the frequency range of approximately several GHz and their line-widths broaden, which might be ascribed to dipole-dipole interaction between particles and/or effective diamagnetic field. Therefore, these results demonstrate that the amorphous Fe-B spherical particles with submicron sizes are one of the candidates as soft magnetic materials for next generation high-frequency applications.

References [1] Y. Shimada, Y. Endo, M. Yamaguchi, S. Okamoto, O. Kitakami, Y. Imano, H. Matsumoto and S. Yoshida : “Synthesis and magnetic softness of sub-micron amorphous particles”, J. Magn. Soc. Jpn., Vol.34, No.3, pp.220-225 (2010). Acknowledgement This work was supported in part by JSPS KAKENHI Grant No. JP19K21952 from MEXT, Japan. This work was also supported in part by CSIS, CSRN, and CIES, Tohoku University.

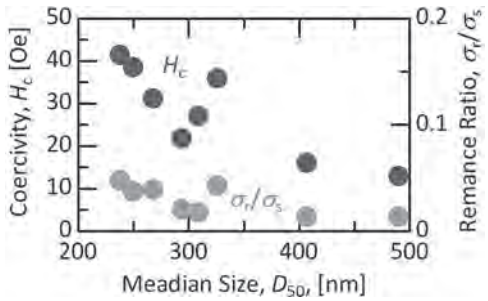

FIG. 1. H_c and σ_r/σ_s vs D_{50}

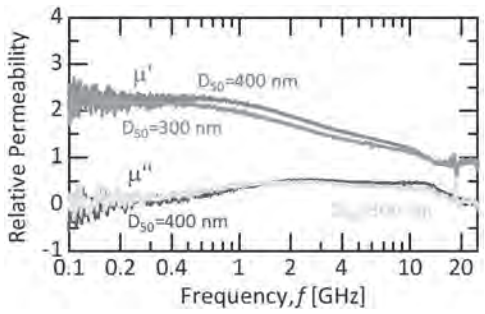

FIG. 2. μ-f properties

CPB-07. Magnetic Property Measurement and Analysis of High-Frequency Soft Magnetic Materials Under Non-sinusoidal Excitation Considering Temperature Effect. Y. Li[1], *C. Jin*[1], M. Yang[1], S. Mu[1] and C. Zhang[1] *1. Hebei University of Technology, Tianjin, China*

Electrical equipment operates under high temperature and non-sinusoidal excitation. The magnetic properties and loss of soft magnetic materials under these conditions are complicated, which are quite different from those under normal temperature and sinusoidal excitation[1-2]. At present, most of the relevant researches separate the temperature dependence of magnetic properties from non-sinusoidal excitation, which is not sufficient to characterize the magnetic properties of soft magnetic materials[3-4]. This paper carried out magnetic property measurement and analysis under various temperatures (25~120°C) of high-frequency magnetic materials ferrite (N87), nanocrystalline (FT-3KL), and ultra-thin silicon steel (GT050) with multi-frequency (1~20kHz), different non-sinusoidal waveform excitation (square and rectangular wave), and multiple excitation states (Duty ratio 0.1~0.9). As shown in Fig.1, a typical non-sinusoidal excitation platform is constructed to generate various non-sinusoidal waveforms, and a thermotank with a real-time temperature controller is used to heat the magnetic ring sample. The data acquisition and processing part is built by LabVIEW with an oscilloscope, which can measure and display the *B-H* loop of the test sample more precisely. Taking ferrite and nanocrystalline for examples. As shown in Fig.2(a), the temperature dependence of ferrite is significant, and its loss is less affected by the excitation state, while nanocrystalline is more sensitive to the excitation waveform. As shown in fig.2(b), the loss of nanocrystalline appears to be a minimal when the duty ratio is 0.5 and exhibits a symmetrical distribution. This work can provide a theoretical basis for the micro-magnetization mechanism of magnetic materials under complex operating conditions. The complete analysis of the magnetic properties of the above materials will be shown in the full-text version.

[1] J. Chen, D. Wang and Y. Jiang, IEEE Transactions on Magnetics, vol. 54, no. 11, pp. 1-7 (2018) [2] S. Li, B. Sarlioglu and S. Jurkovic, IEEE Transactions on Industry Applications, vol. 53, pp. 4923-4933 (2017) [3] Shaoshen Xue et al., IET Science, Measurement & Technology, vol.10, pp. 846-854 (2016) [4] S. Barg, K. Ammous and H. Mejbri, IEEE Transactions on Power Electronics, vol. 32, pp. 2146-2154 (2017)

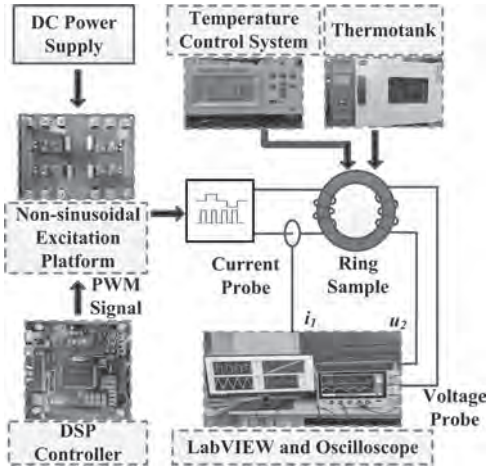

Figure 1 Temperature-dependent Magnetic property measurement system of soft magnetic materials under Non-sinusoidal excitation

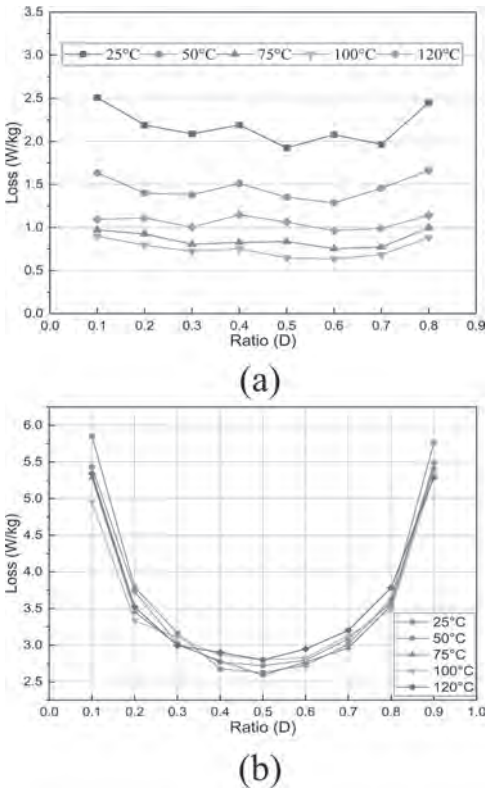

Figure 2 (a) Duty ratio and loss curve of N87 excited by 10KHz square wave, B=0.1T (b) Duty ratio and loss curve of FT-3Kl excited by 10KHz square wave, B=0.5T

CPB-08. Measurement and Analysis of Vibration and Noise Characteristics of Medium-Frequency Transformer Core Under Non-Sinusoidal Voltage Excitation. Y. Li[1], *Z. Yang*[1], C. Zhang[1] and S. Mu[1] *1. Hebei University of Technology, Tianjin, China*

Vibration of the core during the operation of medium-frequency transformer is the main electromagnetic noise source, which will cause environmental noise pollution and even influence the reliability of the transformer [1-2]. At present, the research on vibration and noise of silicon steel under multiple conditions is developing rapidly. However, the measurement of magnetic properties, vibration and noise of ultra-thin oriented silicon steel are not complete [3]. Therefore, a real-time vibration and noise measurement platform based on a triaxial acceleration sensor is built in this paper to measure the magnetic properties, vibration and noise of ultra-thin oriented silicon steel simultaneously, as shown in Fig.1. The vibration and noise of amorphous, GT-050 and GT-100 ultra-thin grain-oriented silicon steel core under sinusoidal, square and rectangular waveforms are compared and analyzed. The calculation formula of the vibration acceleration under non-sinusoidal excitation is also deduced. In addition, the effect of dead time on vibration and noise is analyzed. Part of the results are shown in Fig. 2. It can be seen that the vibration of the core increases with the increase of frequency and magnetic flux density. The vibration and noise under non-sinusoidal excitation are much greater than that under sinusoidal excitation. The vibration amplitude in the lamination direction is larger than other directions. By comparison, ultra-thin oriented silicon steel has higher saturation magnetic flux density, lower loss and lower vibration noise than amorphous alloys. The measurement data in this paper can provide a basis for material selection for medium-frequency electrical equipment designers.

[1] Shuai P, Biela J. Influence of Material Properties and Geometric Shape of Magnetic Cores on Acoustic Noise Emission of Medium Frequency Transformers[J]. IEEE Tran. Power Electronics, 2016, 32(10):7916-7931. [2] Sarker P C, Islam M R, Guo Y, et al. State-of-the-Art Technologies for Development of High Frequency Transformers with Advanced Magnetic Materials[J]. IEEE Trans. Appl. Supercond., 2019, 29(2):1-11. [3] Fang Feng, Yang Jie, Zhang Yuanxiang, et al. Microstructure and magnetic properties of ultra-thin grain-oriented silicon steel: Conventional process versus strip casting[J]. Journal of Magnetism and Magnetic Materials, 2021,535.

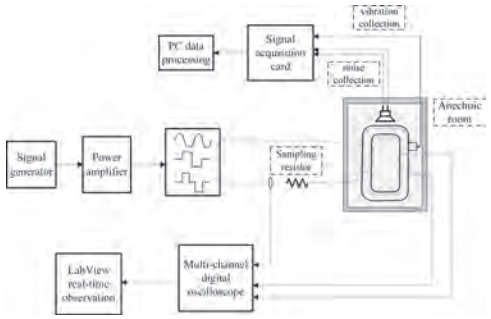

Fig. 1. Real-time measurement platform for transformer core vibration and noise

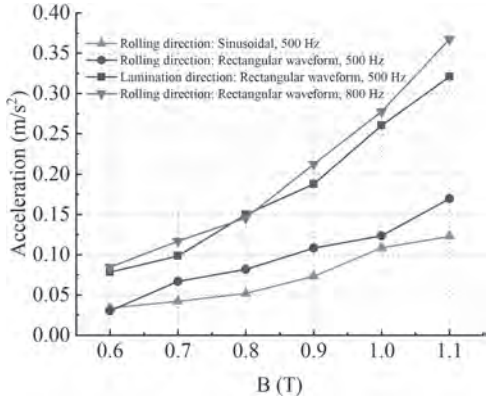

Fig. 2. Vibration acceleration of GT-100 under different excitations and directions

CPB-09. Nonlinear Effects in the Magnetization Switching of Nearly Zero Magnetostrictive Amorphous Submicron Wires. S. Corodeanu[1], C. Hlenschi[1], C. Rotarescu[1], H. Chiriac[1], N. Lupu[1] and *T.A. Ovari*[1] *1. Dept. of Magnetic Materials & Devices, National Institute of R&D for Technical Physics, Iasi, Romania*

Rapidly solidified amorphous wires with diameters below 1 μm have opened up new miniaturization opportunities for sensing devices and created new application possibilities [1]. Here we report on an in-depth study of magnetization

switching in nearly zero magnetostrictive $(Co_{0.94}Fe_{0.06})_{72.5}Si_{12.5}B_{15}$ amorphous wires with diameters between 300 and 450 nm, prepared by an improved variant of glass-coated melt spinning. Hysteresis loops were measured using a method developed specifically for thin wires [2]. All samples were magnetically bistable, exhibiting a rectangular axial loop. Hence, magnetization reversal takes place by depinning and subsequent propagation of a single domain wall when the applied field H reaches the value of the switching field, H^*. We measured the domain wall velocity at various values of H, starting from $H = H^*$ up to the maximum employed value, H_{max} = 10 000 A/m. The most remarkable results are shown in Fig. 1, which illustrates both the switching field and the domain wall velocity vs. sample diameter. Both exhibit strongly nonlinear variations with the diameter. Also, the slopes of the curves are always opposite to one another. The nonlinear shape of wall velocity vs. sample diameter is maintained even at larger fields, up to $H = H_{max}$. The maximum wall velocity at $H = H^*$, i.e. 1450 m/s, was observed for a sample with 410 nm in diameter. Domain wall velocity increases monotonically with applied field for all samples. Fig. 2 shows the field dependence of domain wall velocity for the 410 nm sample, with a maximum of nearly 4000 m/s at $H = H_{max}$. The nonlinear effects have been attributed to the nonlinear distribution of intrinsic frozen-in stresses, that are inherent to the rapid solidification preparation process. The results allow one to accurately control and tailor the magnetic behavior of these ultrathin magnetic wires for specific applications. Work supported by the Romanian Executive Unit for Financing Higher Education, Research, Development and Innovation (UEFISCDI) through project PN-III-P4-ID-PCE-2020-1856 MaDWallS (contract no. PCE1/01.02.2021).

[1] T.-A. Óvári, N. Lupu, H. Chiriac, in Magnetic Nano- and Microwires (2nd Edition), edited by M. Vázquez (Woodhead Publishing, Cambridge), p. 221 (2020). [2] S. Corodeanu, H. Chiriac, N. Lupu, T.-A. Óvári, IEEE Trans Magn, Vol. 47, p. 3513 (2011).

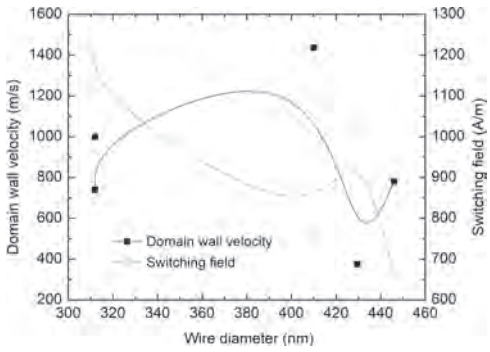

Fig. 1. Switching field & wall velocity vs. sample diameter.

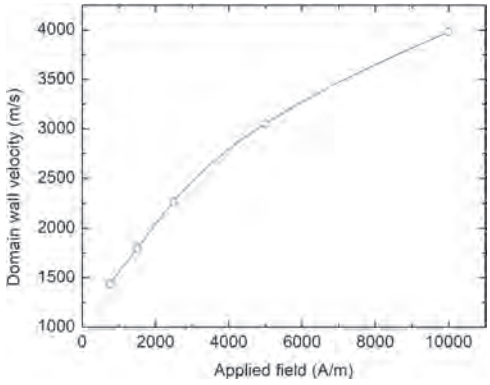

Fig. 2. Domain wall velocity vs. applied field for a 410 nm in diameter sample.

CPB-10. Thickness-dependent Structural and Magnetic Properties of Fe_4N Thin Films. *S. Seema*[1], A. Tayal[2], P. Gupta[3,4], S. Chakravarty[5] and M. Gupta[1] *1. Physics, UGC-DAE Consortium for Scientific Research, University Campus, Khandwa Road, Indore, Indore, India; 2. Deutsches Elektronen-Synchrotron DESY, Notkestrasse 85, D-22607 Hamburg, Germany, Hamburg, Germany; 3. Raja Ramanna Centre for Advanced Technology, Indore, India, Indore, India; 4. Homi Bhabha National Institute, Training School Complex, Anushakti Nagar, Mumbai, India, Mumbai, India; 5. UGC-DAE Consortium for Scientific Research, Kalpakkam Node, India, Kalpakkam Node, India*

Thickness (t) of a thin film modulates several properties and studies show that different magnetic orderings, diverse morphologies, and exchange couplings can be achieved by controlling the film t [1]. Tetra iron nitride (Fe_4N) is a very popular compound well-known for its magnetic properties and is the material of choice for futuristic spintronic devices [2]. A number of literature reports have been focused on the phase and saturation magnetization (M_s) studies of Fe_4N films. Only a handful of reports focus on the dependence of M_s on t of the film [2,3,4]. An extensive literature survey showed that M_s of sputter-deposited Fe_4N thin films varies largely depending on t. However, no specific trend seems to be followed for M_s with t variation. A general observation showed that M_s reduces on increasing t of the film, while the reason behind this variation remains unrevealed. Therefore, we studied the M_s variation with an increase in t of dcMS deposited CrN (111) buffer layered polycrystalline Fe_4N films [5,6]. We characterized structure using x-ray diffraction (XRD) (θ-2θ and grazing), M_s using S-VSM, and x-ray magnetic circular dichroism (XMCD). We correlated local and electronic structure studied using extended x-ray absorption fine structure (EXAFS) with the variations observed in M_s. Fig. 1 shows XRD data of Fe_4N films grown on the CrN buffer layer which are (111) oriented. The M_s of the samples measured using bulk magnetization measurement technique S-VSM (emu/cm^3) and the total magnetic moment (μ_B/Fe atom) calculated by analyzing XMCD data has been plotted in the inset of fig 1. The magnetic moment follows an almost similar trend as M_s measured by S-VSM. For Fe_4N films with t =30nm, the M_s is highest from both bulk and element-specific magnetization measurements. To explore this, we studied local bonding using EXAFS and found variation in Fe-N bond distances as shown in fig. 2. Therefore, the changes in local structure of Fe_4N with t increasing led to reduction in M_s.

[1]. I. Infante, F. Sanchez, J. Fontcuberta, Phys Rev B 76 (22) (2007) 224415 [2]. Y. Takahashi, T. Miyamachi, S. Nakashima, Phys Rev B 95 (22) (2017) 224417 [3]. W. Mi, Z. Guo, X. Feng, Acta Materialia 61 (17) (2013) 6387-6395 [4]. Z. Lai, Z. Li, X. Liu, J. Phys. D: App. Phys. 51 (24) (2018) 245001 [5]. Seema, Niti, M. Gupta, AIP Conf. Proceedings 1942 (1) (2018) 080075 [6]. Seema, M. Gupta, J. Stahn, J. Magn. Magn. Mat. (2020) 166806.

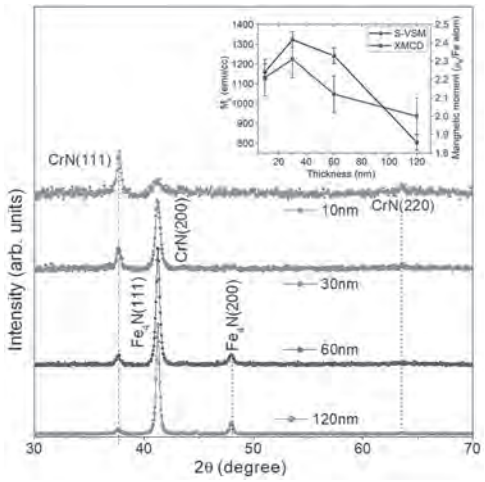

Fig.1 XRD data of Fe_4N films of different t. Inset shows M_s measured using S-VSM (emu/cc) and XMCD (μ_B/Fe atom).

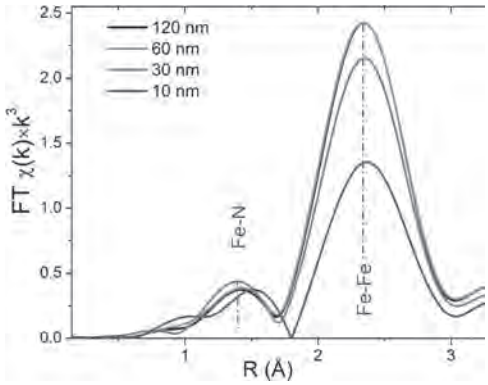

Fig.2 Fourier transform moduli of the Fe K-edge EXAFS (χ(R)) spectra of Fe_4N films with different t.

CPB-11. Transformation of the magnetostriction constant of amorphous microwires by heat treatment. *J. Alam*[1], M.G. Nematov[2] and L. Panina[1,2] *1. Technology of Electronic Materials, National University of Science and Technology, MISIS, Moscow, Russian Federation; 2. Institute of Physics, Immanuel Kant Baltic Federal University, Kaliningrad, Russian Federation*

Thermal treatments of amorphous alloys are known to cause structural relaxation which is followed by an evaluation of the magnetic anisotropy and saturation magnetostriction. In this work, we investigated the effect of annealing with a temperature close to the onset of the crystallization on the magnetic hysteresis properties of glass-coated amorphous microwires of Co-rich compositions with a nearly zero magnetostriction. The annealing process was performed on the wires by two methods: dc current annealing and conventional annealing in finance (at 475-490 °C for 30 min). The current intensities were chosen to ensure similar annealing conditions. The annealing temperatures were higher than the Curie temperature (~360 °C) and slightly lower than the primary crystallization temperature (510 °C). We have demonstrated a sharp change in the shape of the magnetic hysteresis after annealing which is caused by the change in the magnetostriction. It is known that annealing without applied stress can produce short-range order relaxation and consequently releases some frozen-in stresses and improves soft magnetic properties. In the present paper, we propose current and conventional annealing at relatively high temperatures slightly lower than the primary crystallization temperature. Therefore, we proposed a method of controllable change in magnetic anisotropy by changing the sign of magnetostriction. In particular, this results in a change in the shape of magnetic hysteresis and enhances the sensitivity of MI at microwave frequencies. The hysteresis loop of samples are shown in Figures 1, 2. The annealing at temperatures higher than the Curie temperature increases the saturation magnetostriction and induces an axial easy anisotropy. A sharp change in the behavior of the hysteresis loops occurs after annealing with temperatures near the crystallization point, which can be explained by a change in the sign of the magnetostriction constant from small positive to large negative.

[1] M. G. Nematov et al. Journal of Alloys and Compounds 837 (2020) [2] A. Zhukov and V. Zhukova, Nova Science Publishers, New York (2009)

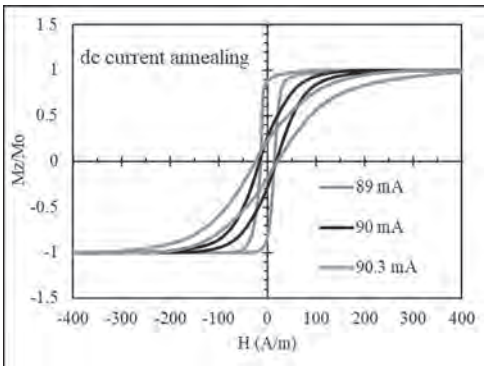

Fig. 1 Hysteresis of $Co_{71}Fe_5B_{11}Si_{10}Cr_3$ (diameter:D/d=29/25 μm) microwire after annealing at I_{an}~90 mA which corresponds to 490 °C

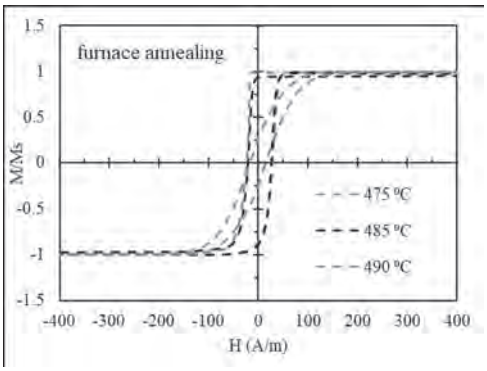

Fig. 2 Hysteresis of $Co_{71}Fe_5B_{11}Si_{10}Cr_3$ (diameter:D/d=29/25 μm) microwire after annealing at (475 °C, 485 °C, 490 °C)

CPB-12. Comprehensive Investigation of Rotational Magnetic Properties for Nanocrystalline Alloy and Ultra-thin Grain-oriented Silicon Steel. *M. Yang*[1], Q. Yang[1], Y. Li[1], Z. Lin[1], S. Yue[1] and C. Zhang[1] *1. Hebei University of Technology, State Key Laboratory of Reliability and Intelligence of Electical Equipment, Tianjin, China*

The developments of electrical equipment require the devices to be miniaturized and used at high frequency and high power. Nanocrystalline magnetic alloys and ultra-thin silicon steel could play a key role in medium and high-frequency electromagnetic energy conversion devices, and integral performance. These two magnetic materials can be used as a core in the medium and high-frequency electrical equipment, in which there is a two-dimension (2-D) circular or elliptical magnetization, and rotational loss at the T-joints structure [1-2]. However, there are relatively few studies in rotational magnetic properties for nanocrystalline magnetic alloys and ultra-thin silicon steel. In order to explore more applications of the above materials in electrical applications, the 2-D rotational magnetic properties at high frequency should be studied [3]. In this paper, the 2-D rotational magnetic properties of nanocrystalline alloy (1k107B) and ultra-thin silicon steel (GT100) are systematically studied. Based on the novel high-frequency 2-D magnetic properties tester and the frequency-domain feedback algorithm with harmonic compensation method, the 2-D circular magnetic properties of 1k107B (1kHz - 20kHz) and GT100 (200 Hz – 2 kHz) are measured. The variations of the *B-H* phase difference are investigated with the change of frequency and magnetic flux density. And the effect of the *B-H* phase difference on the loss is analyzed. The magnetic anisotropy differences between the above two materials are compared. Based on the experimental data, the rotational losses of nanocrystalline alloy and ultra-thin grain-oriented silicon steel have a downward trend at the medium and high flux density. Especially, the 1k107B has the great isotropic feature at low flux density, while it has the

relative anisotropy at high flux density. The magnetic anisotropy of GT100 is very obvious, and when without the feedback, the *B* loci become rhombus shape which is an interesting phenomenon. The conclusion in this paper can provide a theoretical reference for the study of the magnetization mechanism and dynamic hysteresis model.

[1] O. de la Barriere, C. Appino, C. Ragusa, F. Fiorillo, M. LoBue, F. Mazaleyrat, IEEE Transactions on Magnetics., Vol. 54, p.2001415 (2018). [2] S. Yue, Y. Li, Q. Yang, K. Zhang, C. Zhang, IEEE Transactions on Magnetics., Vol. 55, p.6100705 (2019). [3] L. Chen, T. Ben, H. Zhao, C. Fang, Y. Wang, AIP Advances., Vol. 9, p.035316 (2019).

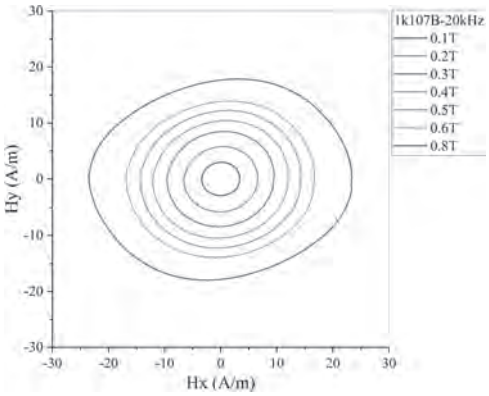

Fig. 1 *H* loci of nanocrystalline alloy 1k107B at 20kHz.

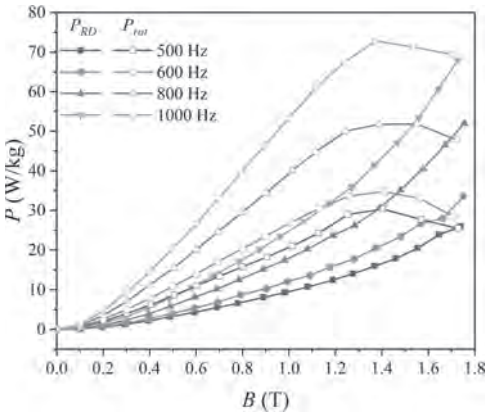

Fig. 2 Comparison of alternating and rotational loss of GT100.

Session DOA
RARE-EARTH HARD MAGNETIC MATERIALS

Hossein Sepehri-Amin, Chair
National Institute for Materials Science, Tsukuba, Japan

CONTRIBUTED PAPERS

DOA-01. High-field magnetization studies and their analysis in $RFe_{11}Ti$ and $RFe_{11}TiH_1$ rare-earth intermetallics. *N. Kostyuchenko*[1], I.S. Tereshina[2], E.A. Tereshina-Chitrova[3], Y. Skourski[4], M. Doerr[5], A.K. Zvezdin[1,6], M. Paukov[7,8] and H. Drulis[9] *1. Moscow Institute of Physics and Technology (National Research University), Dolgoprudny, Russian Federation; 2. Faculty of Physics, Lomonosov Moscow State University, Moscow, Russian Federation; 3. Institute of Physics CAS, Prague, Czechia; 4. Hochfeld-Magnetlabor Dresden (HLD-EMFL), Helmholtz-Zentrum Dresden-Rossendorf, Dresden, Germany; 5. Institut für Festkörper- und Materialphysik, Technische Universität Dresden, Dresden, Germany; 6. Prokhorov General Physics Institute RAS, Moscow, Russian Federation; 7. Faculty of Mathematics and Physics, Charles University, Prague, Czechia; 8. Nuclear Fuel Cycle Department, Centrum Vyzkumu Rez, Husinec-Rez, Czechia; 9. Institute of Low Temperature and Structure Research, Polish Academy of Sciences, Wroclaw, Poland*

Research in magnetism includes the discovery and development of ever more powerful and inexpensive rare-earth – iron intermetallics. This opens a wide range of applications; such is electric motors, smartphones, magnetic recording technology [1,2]. The investigations of iron rich intermetallics $RFe_{11}Ti$ are becoming more and more promising [2,3], including due to the possibility of their modification by light interstitial dopants. The magnetic properties of these intermetallic compounds are determined by the crystal-field and exchange parameters [4-7]. The developed measurement methods of high-field magnetization studies allow us to make experiments in fields up to 100 T. Such experimental studies have demonstrated that the crystal-field parameters were previously determined with the insufficient precision [5,7] and the full magnetization process cannot be described correctly. So, it is necessary to revise the results achieved several decades ago and obtain new ones. We report on the theoretical and experimental high-field magnetization study of the rare-earth intermetallics $RFe_{11}Ti$ and $RFe_{11}TiH_1$, which attract a great interest during the search for resource saving materials [1-3,7]. In the theoretical part of the study we combined well-known crystal-field theory with modern calculations using computer code written by us [5,6]. The magnetization curves were measured in fields up to 60 T and calculated up to 100 T at 4.2 K. This allowed us to study the field-induced transitions taking place in magnetic fields up to 60 T (Fig. 1). Using these high-field magnetization data we calculated the crystal-field and exchange parameters [4-6]. The analysis of the refined parameters obtained creates a chance of deep understanding of rare-earth's impact on the magnetic properties of these materials. This is important to design new hard magnetic materials. Work was supported by the pr. "NANOCENT", pr. no. CZ.02.1.01/0.0/0.0/15_003/0000485, financed by ERDF. Physical properties measurements were performed in the MGML (http://mgml.eu/) supported within the program of Czech Research Infrastructures (pr. no. LM2018096) and by the Hochfeldlabor Dresden, part of the EMFL.

1) R. Skomski, J.M.D. Coey, Scripta Materialia, Vol. 112, p. 3 (2016) 2) G.C. Hadjipanayis, A.M. Gabay, A.M. Schönhöbel, et al., Engineering, Vol. 6, p. 141 (2020) 3) C. Skelland, T. Ostler, S.C. Westmoreland, et al., IEEE Trans. Magnet., Vol. 99, p. 1 (2019). 4) I.S. Tereshina, N.V. Kostyuchenko, et al. Scientific Reports, Vol. 8, p. 3595 (2018) 5) N.V. Kostyuchenko, I.S. Tereshina, et al. Journal of Low Temperature Physics, Vol. 200, p. 164 (2020) 6) N.V. Kostyuchenko, A.K. Zvezdin, et al. Phys. Rev. B, Vol. 92, p. 104423 (2015) 7) J. W. Körner, G. Krugel, C. Elsässer, Scientific Reports, Vol. 6, p. 24686 (2016)

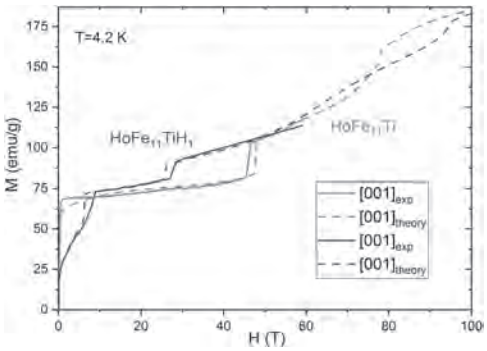

Magnetization curves obtained for $HoFe_{11}Ti$ and $HoFe_{11}TiH_1$.

DOA-02. New potential materials for rare earth lean permanent magnets from computational design and the challenge of the 4f electrons. *H.C. Herper*[1] and O. Eriksson[1,2] *1. Physics and Astronomy, Uppsala University, Uppsala, Sweden; 2. School of Science and Technology, Örebro University, Örebro, Sweden*

Rare earth permanent magnets play a key role in view of the increasing market for green energy applications and new materials which can compete with $Nd_2Fe_{14}B$ but are environmentally less problematic are highly sought after. Fe-based $ThMn_{12}$ phases contain less RE material than the commercially used compounds and have attracted quite some interest. An efficient and resource saving way to identify out of this class new phases which have the potential to become permanent magnets is by computational materials design. However, predicting the magnetic properties of 4f systems is challenging because of the localization of the 4f electrons which determines to a large extend the level of theory needed for a reliable description and prediction. We have shown that the 4f electrons in Sm 1:12 can be viewed as fully localized and can be safely treated as core electrons while for $CeFe_{11}Ti$ the correlation effects are smaller and the 4f states can still be viewed as valence states [1,2]. In the case of $NdFe_{11}Ti$ the 4f electrons are partially localized as can be seen from the hybridization function in Fig. 1. The hybridization function serves as a qualitative measure for the interaction of the 4f electrons with the valence electrons in a system [3]. As a consequence of the partial localization, the cone type magnetocrystalline anisotropy (MCA) of the latter system is only observed in a DFT+U description with an intermediate Hubbard U value, see Fig. 2. Assuming full localization (4f in core) results in a uniaxial MCA which contradicts the experimental findings at low temperatures. Plain DFT also fails. It is also discussed in how far the strong dependence of the MCA and related magnetic properties of $NdFe_{11}Ti$ on the theoretical description influences the prediction of new phases. As test case the quaternary system $Nd_{1-x}Y_xFe_{12-y}Ti_y$ was chosen. Supported by NOVAMAG (EU686056), the Swedish Foundation for Strategic Research (EM16-0039), and SNIC (Swedish National Infrastructure for Computing).

[1] A. Schönhöbel, R. Madugundo, O. Yu. Vekilova, Journal of Alloys and compounds Vol. 786, p. 969 (2019) [2] R. Martinez-Casado, A. Dasmahapatra, M.F. Sgroi et al. Journal of Physics: Condensed Matter Vol. 31, p. 505505 (2019) [3] H. C. Herper, T. Ahmed, J. M. Wills et al., Phys. Rev. Materials, Vol. 1, p. 033802 (2017)

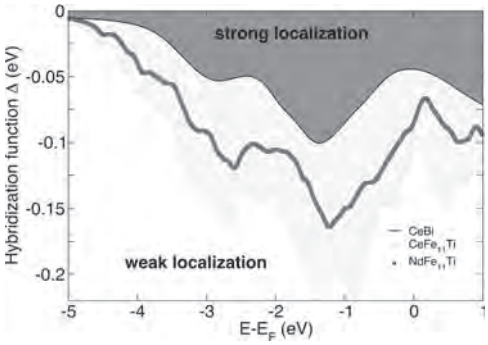

Fig.1: Comparison of the hybridization function of NdFe11Ti, CeFe11Ti and strongly localized CeBi.

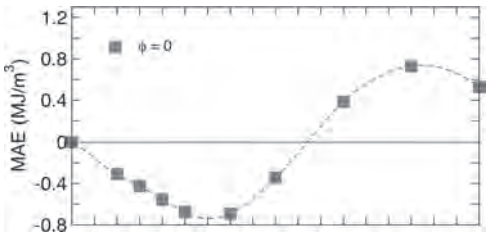

Fig.2: Calculated angular dependent MCA of $NdFe_{11}Ti$ reproducing the cone type behavior observed at low temperatures.

DOA-03. Energy based model for Twin boundary prediction in the Sm-Fe-Co 1:12 phase. *G. Hrkac*[1], C. Skelland[1], J. Fischbacher[2], S. Ener[3], O. Gutfleisch[3] and T. Schrefl[2] *1. EMPS, University of Exeter, Exeyer, United Kingdom; 2. Center for Integrated Sensor Systems, Danube University, Krems, Austria; 3. TU Darmstadt, Darmstadt, Germany*

To be able to investigate the origins and effects of twins in magnetic materials, one has to understand that by introducing twins, one introduces another interface and have to analyse the interface energy of a twin itself. Further one has to identify the most prominent grain boundary neighbors, 1:5, 3:29 or liquid phases. To proof our hypothesis we started to construct an elliptical grain and calculate interfaces between 1:12 phase and the 1:5 phase. It was found that one of the interfaces is coherent below 0.2 J/m2 and the other one is semi-coherent above 0.2 J/m2. This shows that interface can be optimized for one interface but not for two. For the second case, we introduce a twin in our system but keep the orientation of our 1:12 phase the same. The total energy of this system is composed of two interfaces to the 1:5 phase, which are energetically coherent and the twin interface in the 1:12 phase, which is energetically coherent. We start by calculating the total interface energy of surface 1, 1:12 phase to 1:5 phase coherent, 0.175 Jm2, surface two has the configuration 1:12 phase to 1:5 phase semi-coherent, 0.237 J/m2. For case one the surface 3 is zero as there is no twin. For the case 2, the twin surface has an interface energy of 0.175 J/m2. We now vary the aspect ratio. In figure 1, you can see the normailsed energy increase of case 1 (circle) no twin and case 2 (diamond) with twin as function of grain size. On the right axis we have plotted the normailsed energy difference delta E between Case 2 and 1. A positive value means, Case 2 is unfavorable as it needs more energy and Case 1 is preferred. A negative value is that by forming a twin Case 2 becomes more favourable which occurs between 900 and 1200 nm grain size, in aggrement with experiemnts [1]. We have shown that the boundary where twins start to emerge are dependent on the interface energy, hence the boundary and also the shape of the grain plays an important part.

[1] Semih Ener, Konstantin P Skokov, Dhanalakshmi Palanisamy, Thibaut Devillers, Johann Fischbacher, Gabriel Gomez Eslava, Fernando Maccari, Lukas Schäfer, Léopold VB Diop, Iliya Radulov, Baptiste Gault, Gino Hrkac, Nora M Dempsey, Thomas Schrefl, Dierk Raabe, Oliver Gutfleisch, Acta Materialia 214, 116968 (2021)

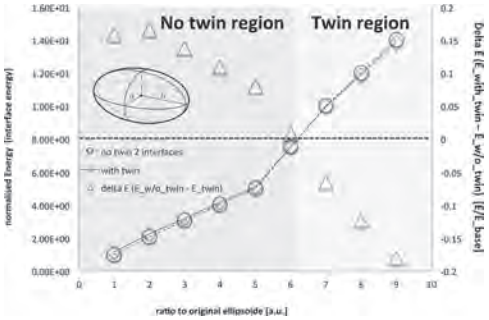

Twin boundary model: total interface energies for ellipsoid as function of ratio of the a-axis.(1=100nm, 2=200nm, 3=300nm, 4=200nm, 5=250nm, 6=375nm, 7=500nm, 8=600nm and 9=700nm).

DOA-04. Cost effective modification of $SmCo_5$-type alloys. C. Sarafidis[1], G. Sempros[1], S. Giaremis[1], J. Kioseoglou[1] and *M. Gjoka*[2] *1. Department of Physics, Aristotle University of Thessaloniki, Thessaloniki, Greece; 2. Institute of Nanoscience and Nanotechnology, N.C.S.R. Demokritos, Agia Paraskevi, Athens, Greece*

Environmental and technological progress in sectors like energy, transportation, robotics requires large amounts of Permanent Magnets (PMs) [1]. However, high demand predictions are difficult to be met by the current supply chain [2]; subsequently there is urgent need for new materials, with less content in critical or expensive resources but compatible with current industrial infrastructure and able to maintain adequate performance. $SmCo_5$ is a well-established PM with excellent properties which come at a high cost and criticality; stoichiometry modification is a path towards improving the overall merit from the applications' scope [3]. In this work the effect of partially substituting Sm and Co in $SmCo_5$ with less expensive constituents is presented. $Sm_{0.5}MM_{0.5}(Co_{1-x-y}Fe_xNi_y)_5$ samples were prepared by arc-melting constituting elements in Ar atmosphere followed by thermal treatment at 1100 - 1200 K in vacuum. Alloys were structurally and magnetically characterized experimentally and DFT calculations were performed within spin polarized rotationally invariant DFT+U framework and the the Perdew-Burke-Ernzerhof derivation of the generalized gradient approximation pseudopontentials by using the VASP code [4-6] confirmed that the desired $CaCu_5$-type phase could be stabilized. Under our experimental conditions single phase hexagonal phase was not formed. X-Ray diffraction plots analyzed with the Rietveld method revealed a three-phase system with the main phase crystallizing in hexagonal $CaCu_5$-type structure (a = b = 0.4877(2) nm, c = 0.4109(2) nm). There were two additional rhombohedral phases, Gd_2Co_7-type (a = b = 0.5037(2) nm, c = 3.6627(1) nm and Th_2Zn_{17}-type (a = b = 0.8449(4) nm, c = 1.2332(3) nm) which are built within the basic hexagonal frame and their main axes are aligned and related ($c/a[1:5] = 0.843$, $c/a[2:7] = 0.808$, $a_{1:5} = a_{2:7} = \sqrt{3} \cdot a_{2:17}$, $c_{1:5} = 3 \cdot c_{2:17} = 9 \cdot c_{2:7}$). This relation is evident in Fig. 1 where powder and epoxy-oriented xrd plots are presented. The materials present fairly large magnetization (Ms = 75-90 Am^2/kg) and retain the large anisotropy and thermal endurance of the $SmCo_5$ material.

[1] O. Gutfleisch, M.A. Willard, E. Brück, C.H. Chen, S.G. Sankar, and J.P. Liu, Adv. Mater. 23, 821 (2011). [2] A. Filippas, G. Sempros, C. Sarafidis, Mater. Today: Proc., 37 (4), 4058 (2021). [3] D.W. Hu, M. Yue, J.H. Zuo, R. Pan, D.T. Zhang, W.Q. Liu, J.X. Zhang, Z.H. Guo, and W. Li, J. Alloys Compds. 538, 173-176 (2012). [4] S. L. Dudarev, G. A. Botton, S. Y. Savrasov, C. J. Humphreys, A. P. Sutton, Phys. Rev. B 57 (1998) 1505. [5] J. P. Perdew, K. Burke, M. Ernzerhof, Phys. Rev. Let. 77 (1996) 3865. [6] G. Kresse, J. Furthmüller, Phys. Rev. B 54 (1996) 11169.

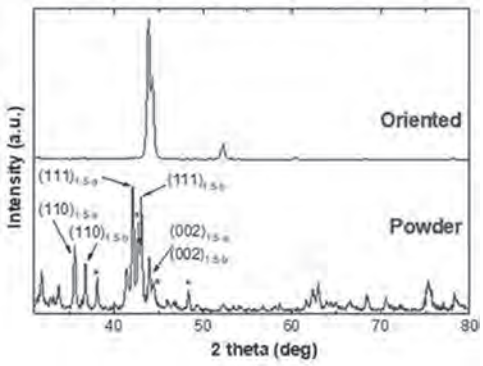

Fig.1: X-ray plots of powder and epoxy-oriented samples of $Sm_{0.5}MM_{0.5}Co_4Ni$ materials.

DOA-05. Epitaxy Induced Highly Ordered Sm_2Co_{17}–$SmCo_5$ Nanoscale Thin Film Magnets. S. Sharma[1,2], G. Gkouzia[1], A. Zintler[1], D. Günzing[3], J. Lill[3], D. Motta Meira[4], R. Eilhardt[1], H. Singh[1], R. Xie[1], M. Major[1], I. Radulov[1], P. Komissinskiy[1], H. Zhang[1], K. Skokov[1], H. Wende[3], K. Ollefs[3], L. Molina-Luna[1] and *L. Alff*[1] *1. Materials Science, TU Darmstadt, Darmstadt, Germany; 2. NIMS, Tsukuba, Japan; 3. Physics, Universität Duisburg-Essen, Duisburg, Germany; 4. Argonne National labs, Argonne, IL, United States*

Using molecular beam epitaxy, a nanoscale thin film magnet of *c*-axis-oriented Sm_2Co_{17} and $SmCo_5$ is stabilized. While typically in the prototype $Sm(Co,Fe,Cu, Zr)_{7.5–8}$ pinning-type magnets, an ordered nanocomposite is formed by complex thermal treatments, here, a one-step approach to induce controlled phase separation in a binary Sm–Co system is shown. A detailed analysis of the extended X-ray absorption fine-structure confirmed the coexistence of Sm_2Co_{17} and $SmCo_5$ with 65% Sm_2Co_{17} and 35% $SmCo_5$. The $SmCo_5$ phase is stabilized directly on an Al_2O_3 substrate up to a thickness of 4 nm followed by a matrix of Sm_2Co_{17} intermixed with $SmCo_5$. This structural transition takes place through coherent atomic layers, as revealed by scanning transmission electron microscopy. Highly crystalline growth of well-aligned Sm_2Co_{17} and $SmCo_5$ with coherent interfaces results in strong exchange interaction, leading to enhanced magnetization and magnetic coupling. The arrangement of Sm_2Co_{17} and $SmCo_5$ phases at the nanoscale is reflected in the observed magneto-crystalline anisotropy and coercivity. As next-generation permanent magnets require designing of materials at an atomic level, this work enhances our understanding of self-assembling and functioning of nanophase magnets and contributes to establishing new concepts to engineer the microstructure for beyond state-of-the-art magnets.

[1] S. Sharma *et al.*, ACS Appl. Mater. Interfaces 13, 32415 (2021). doi: 10.1021/acsami.1c04780

DOA-06. Withdrawn

DOA-07. Challenges of reaching high coercivity in coarse grained $ThMn_{12}$ magnets. *S. Ener*[1], K. Skokov[1], F. Maccari[1], D. Palanisamy[2], L. Schäfer[1], I. Radulov[1], B. Gault[2], D. Raabe[2] and O. Gutfleisch[1] *1. Functional Materials, Materials Science, Technical University of Darmstadt, Darmstadt, Germany; 2. Max-Planck-Institut für Eisenforschung (MPIE) Düsseldorf, Düsseldorf, Germany*

The rare-earth (RE) supply crisis of ten years ago, which led to a drastic increase in prices, revealed the dependency on critical RE elements for the production of high-performance permanent magnets [1]. As a consequence, a great effort has been made in the search for new material systems which present magnetic properties similar or superior to those of benchmark $Nd_2Fe_{14}B$, but which contain less critical elements One of such alternatives are Nd- and Sm-based intermetallic compounds with a tetragonal $ThMn_{12}$-type crystal structure, exhibiting intrinsic magnetic properties comparable to $Nd_2Fe_{14}B$. In this work, we investigated the microstructural features of $ThMn_{12}$-type materials for Ce-, Nd- and Sm-based systems [2-4]. A detailed systematic study was carried out for the $SmFe_{11}Ti$ composition where the length scales from thin films to bulk single- and poly-crystalline samples. The twins were observed at micro- and nano-length scales, and it was found that the twin orientation is approximately 58±2 degrees for each grain. Similar twinning angle is also observed for $ThMn_{12}$-type systems with different rare-earth elements. The twin boundary plane corresponds to a {011}-plane family in the unit cell of $Sm(Fe,Ti)_{12}$. High resolution electron microscopy and atom probe tomography (APT) studies on poly-crystalline bulk samples show an enrichment of Sm and a depletion of Ti at the twin boundary. The composition of the twin boundary is estimated to be $Sm_{9.6}Fe_{84.9}Ti_{5.5}$, matching the composition of the $Sm_3(Fe,Ti)_{29}$ phase, which with a lower anisotropy field. The effect of twins on magnetization reversal was investigated by means of magneto-optical Kerr effect (MOKE) microscopy. It was shown that initial magnetization starts at the twin boundary, indicative of strong magnetic coupling between the neighboring variants across the twin boundary. Micromagnetic simulations were carried out with a microstructure similar to that observed in the bulk samples, and the results show that the formation of twins reduces the estimated coercivity values to 38% of the expected switching field.

[1] O. Gutfleisch, M.A. Willard, E. Brück, C.H. Chen, S.G. Sankar, J.P. Liu, Adv. Mater. vol. 23, p. 821 (2011) [2] F. Maccari, S. Ener, D. Koch, I. Dirba, K.P. Skokov, E. Bruder, L. Schäfer, O. Gutfleisch, J. Alloy. Compd. vol. 867 p.158805 (2021) [3] F. Maccari, L. Schäfer, I. Radulov, L.V.B. Diop, S. Ener, E. Bruder, K.P. Skokov, O. Gutfleisch, Acta Mater. vol. 180 p.15 (2019) [4] S. Ener, K.P. Skokov, D. Palanisamy, T. Devillers, J. Fischbacher, G. Gomez Eslava, F. Maccari, L. Schäfer, L.V.B. Diop, I. Radulov, B. Gault, G. Hrkac, N.M. Dempsey, T. Schrefl, D. Raabe, Oliver Gutfleisch, Acta Mater. vol. 214 p. 116968 (2021)

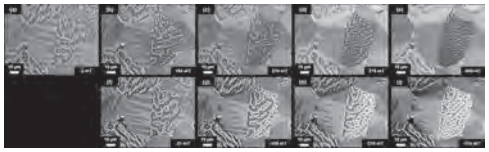

DOA-08. Magnetic property effects in highly grain-refined Dy-free Nd-Fe-B sintered magnets. *I. Anderson*[1], W. Tang[1], K. Dennis[1], M.J. Kramer[1] and J. Cui[1] *1. Ames Laboratory, Ames, IA, United States*

Strong permanent magnets (PMs) are critical for electric vehicle (EV) traction motors to reach high power density levels. Although Nd-Fe-B magnets have superior ambient magnetic strength, Dy additions currently provide thermal stability to enable motor operating temperatures of 150-180C. For sustainable PMs for EV motors, replacement of Dy in Nd-Fe-B magnets is needed since Dy is a scarce heavy rare earth (HRE) and is from (essentially) one source. Fortunately, ultrafine (<4μm) grain size also can improve high temperature magnetic properties and increase ambient temperature coercivity in Dy-free Nd-Fe-B magnets, although not without reduced mechanical properties and only in lab-scale samples [1,2]. Our initial work used commercial Dy-free Nd-Fe-B alloy powders which we ball milled conventionally up to 11h, causing average particle size to decrease to 2.1 μm, but average grain size of resulting sintered magnets grew to 3.8 μm, due to grain growth from high temperature sintering (1080C). Intrinsic coercivity H_{cj} and maximum energy product $(BH)_{max}$ of the ultrafine grained magnets increased up to 13.7 kOe and 43.6 MGOe. While our new work with high energy milling has further refined feedstock powder size, reduction of sintering temperature also is needed to suppress grain growth in magnets and fully exploit ultra-fine grain benefits on magnetics. Thus, an extrinsic transient liquid phase (TLP) sintering aid, Pr-30.2at.%Cu (442C eutectic), was studied for consolidation at reduced sintering temperature with suppression of grain growth.

A reduced sintering temperature with full heat treatment (FHT) raised coercivity (Fig 1), presumably from suppression of grain growth. When the 1045C sintered sample with FHT (from Fig 1) was annealed at 480C, 5h (Fig. 2), coercivity also rose, presumably from increased grain defect "smoothing" by penetration of residual liquid TLP further into the magnet microstructure. These improved magnetic properties will be correlated with microstructural analysis. Supported by USDOE-EERE-VTO-EDT through Ames Lab contract no. DE-AC02-07CH11358.

K. Hono and H. Sepehri-Amin, "Strategy for high-coercivity Nd-Fe-B magnets," *Scripta Materialia*, vol. 67, no. 6, pp. 530–535, Sep. 2012, doi: 10.1016/j.scriptamat.2012.06.038. W. Tang, G. Ouyang, B. Cui, J. Wang, K.W. Dennis, M.J. Kramer, I.E. Anderson, J. Cui, "Magnetic and mechanical properties of grain-refined Dy-free Nd-Fe-B sintered magnets," Journal of Magnetism and Magnetic Materials 521 (2021) 167533.

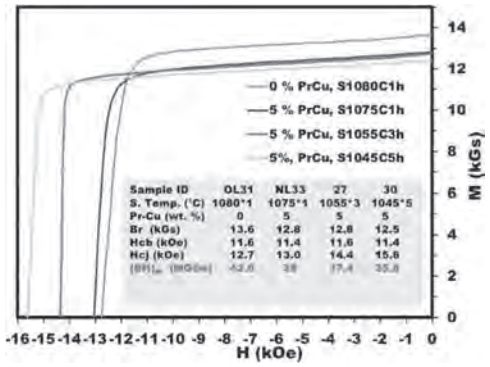

Fig 1. Effect of TLP and sintering temperatures on coercivity.

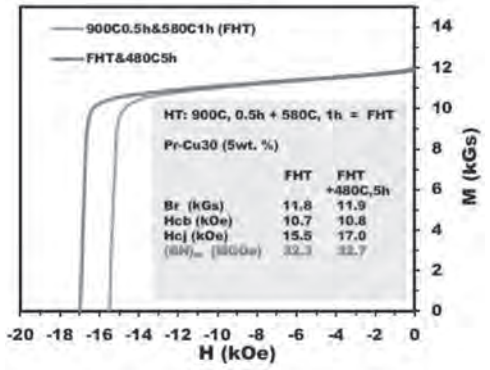

Fig 2. Effect of 480C anneal with TLP on coercivity (sample sintered at 1045C, 5h).

DOA-09. Giant Coercivity and Magnetic Blocking in Molecular Radical-Bridged Lanthanide Compounds. *S. Demir*[1] *1. Chemistry, Michigan State University, East Lansing, MI, United States*

Molecules that possess an energy barrier to spin inversion have intriguing potential applications in areas such as magnetic refrigeration, molecular spintronics and high-density information storage. For these applications, however, key performance characteristics such as large spin–relaxation barriers and high magnetic blocking temperatures are required. Lanthanides have been proven to be particularly well-suited for the design of single-molecule magnets owing to their large magnetic moments and magnetic anisotropy that stem from strong spin-orbit coupling of the 4f orbitals. By using lanthanide ions such as Tb^{3+}, Dy^{3+}, and Er^{3+} which possess intrinsically large orbital angular momentum, significantly higher barriers and blocking temperatures can be achieved. A general methodology to enhance single-molecule magnet properties in mononuclear lanthanide complexes comprises matching the ligand field symmetry with the anisotropic electron density distribution of the maximal M_J state. Employing this methodology, we will present the synthesis of mononuclear rare-earth metallocene complexes that function as new lanthanide-based single-molecule magnets [1-3]. Another particularly successful approach to improve blocking temperatures is to generate strong magnetic exchange between lanthanide centers through the employment of radical bridging ligands. If the magnetic exchange coupling is large enough then quantum tunneling of the magnetization can be attenuated. Here, we will further present the synthesis of multiple bimetallic radical-bridged lanthanide single-molecule magnets and describe effective suppression of quantum tunneling pathways using various organic bridging radical ligands [4-7]. In addition, we combine both methodologies and demonstrate with the first series of N_2^{3-} radical-bridged metallocene complexes that the combination of axial magnetic anisotropy provided by the cyclopentadienyl ligands with the strong magnetic exchange coupling enabled by the inorganic N_2^{3-} radical results in exceptionally large magnetic hysteresis loops which remain open up to high temperatures, Figure 1 [8].

[1] Large Spin–Relaxation Barriers for the Low–Symmetry Organolanthanide Complexes [$Cp^*_2Ln(BPh_4)$] (Cp^*=pentamethylcyclopentadienyl; Ln = Tb, Dy). Demir, S; Zadrozny, J. M.; Long, J. R. *Chemistry A European Journal* 2014, *31*, 9524–9529. [2] Slow Magnetic Relaxation in a Dysprosium Ammonia Metallocene Complex. Demir, S.; Boshart, M. D.; Corbey, J. F., Woen, D. H.; Gonzalez, M. I.; Ziller, J. W.; Meihaus, K. R.; Long, J. R.; Evans, W. J. *Inorganic Chemistry* 2017, *56*, 15049–15056. [3] Slow magnetic relaxation in a neodymium metallocene tetraphenylborate complex. Demir, S., Meihaus, K. R.; Long, J. R. *Journal of Organometallic Chemistry* 2018, *857*, 164–169. [4] Exchange Coupling and Magnetic Blocking in Bipyrimidyl Radical-Bridged Dilanthanide Complexes. Demir, S.; Zadrozny, J. M.; Nippe. M; Long, J. R. *Journal of the American Chemical Society* 2012, *134*, 18546–18549. [5] Exchange coupling and magnetic blocking in dilanthanide complexes bridged by the multi-electron redox-active ligand 2,3,5,6-tetra(2-pyridyl)pyrazine. Demir, S., Nippe, M., Gonzalez, M. I.; Long, J. R. *Chemical Science* 2014, *5*, 4701–4711. [6] Radical ligand-containing single-molecule magnets. Demir, S.; Jeon, I.-R.; Long, J. R., Harris, T. D. *Coordination Chemistry Reviews* 2015, *289–290,* 149–176. [7] Demir, S., *manuscripts in preparation.* [8] Giant coercivity and high magnetic blocking temperatures for N_2^{3-} radical-bridged dilanthanide complexes upon ligand dissociation. Demir, S., Gonzalez, M. I., Darago, L. E., Evans, W. J.; Long, J. R. *Nature Communications* 2017, *8*, 2144.

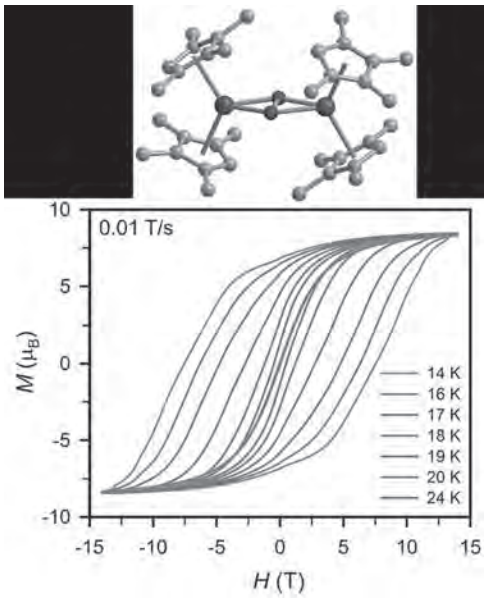

Fig.1 Magnetic hysteresis data and structure for $[(Cp^{Me4H}{}_2Tb)_2(\mu\text{-}N_2^{\bullet})]^{-}$.[8]

DOA-10. Criteria for Permanent-Magnet Materials. *R. Skomski*[1], J. Cui[2], B. Balasubramanian[1], A. Ullah[1] and D. Sellmyer[1] *1. Physics and Astronomy & NCMN, University of Nebraska, Lincoln, NE, United States; 2. Ames Laboratory & Iowa State University, Ames, IA, United States*

The design and discovery of new functional materials has acquired a sense of urgency recently for critical-elements reasons. In the case of permanent magnets, computational and experimental methods are being used synergistically to aid the search for new materials with large values of saturation magnetization M_s, anisotropy K, and Curie temperature T_c [1-3]. Ideally, the materials exhibit $\mu_o M_s > 0.8$ T and $K > 1.5$ MJ/m^3. Another criterion for the evaluation of new permanent-magnet materials before the typically difficult task of synthesis and coercivity development is the hardness parameter $\kappa = (K/\mu_o M_s^2)^{1/2}$ [3]. This parameter can also be written as $\kappa = (H_a/2M_s)^{1/2}$, where $H_a = 2K/\mu_o M_s$ is the anisotropy field, so that each value of κ yields a straight line when H_a is plotted vs. M_s. Ideally, κ is comparable to or larger than one [3, 4]. Figure 1(a) combines the M_s and κ requirements to yield an area of promising permanent magnets (yellow). However, the main figure of merit in permanent magnets energy product. Figure 1(b) plots K against M_s, which has several advantages: (i) the blue isoenergetic curves show the expected maximum energy product, (ii) real-structure factors such a remanence ratio, Kronmüller factor α, packing fraction, and loop shape easily be included in the isoenergetic curves; and (iii) the primary intrinsic properties are K and M_s, not H_a and M_s. If the boundary of the yellow area and blue curves were physically equivalent, the boundary and the blue curves would be approximately parallel. This in not the case for the ascending branch of the boundary, where the curves are almost perpendicular due to the very different natures of hardness and energy product. Aside from helping to identify promising permanent-magnet materials, this work underlines the long-term aspect of permanent-magnet development. The work in Nebraska is supported by NSF-DMREF (No. 1729288), NSF-EQUATE (OIA-2044049), the NU Collaborative Initiative, and NCMN, whereas the research at Ames is funded by DOE.

[1] B. Balasubramanian *et al.*, Mol. Syst. Des. Eng. 5, 1098 (2020). [2] M. Sakurai *et al.*, Phys. Rev. Mater. 4, 114408 (2020). [3] O. Gutfleisch, M. A. Willard, E. Brück, C. H. Chen, S. G. Sankar, and J. P. Liu, Adv. Mater. 23, 821 (2011) [4] R. Skomski and J. M. D. Coey, Scr. Mater. 112, 3 (2016). [5] Y. Hirayama, T Miyake, and K Hono, JOM 67, 1344 (2015).

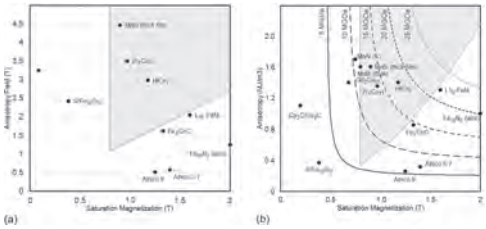

Fig. 1. Permanent-magnet performance plots: (a) H_a-M_s plot and (b) K-M_s plot, the axes showing $\mu_o H$ and $\mu_o M$. The specific model used for the blue curves assume $M_r = M_s$, a straight $M(H)$ line in the second quarter, and $\alpha = 0.4$.

DOA-11. Synthesis of Sm-Fe binary phases at unexplored low temperature by low-temperature reduction-diffusion process with LiCl-KCl molten salts. *J. Kim*[1], S. Okada[1] and K. Takagi[1] *1. Magnetic Powder Metallurgy Research Center, National Institute of Advanced Industrial Science and Technology, Nagoya, Japan*

Sm-Fe based permanent magnets are suggested as next-generation magnets to suppress Nd-Fe-B magnet, e.g. $(Sm,Zr)(Fe,Co)_{10}N_{1.5}$ compound (M_s = 1.7 T, H_A = 77 kOe).[1] Low-temperature reduction-diffusion (LTRD) process was developed by using LiCl molten salt and $TbCu_7$-type Sm-Fe powder was successfully synthesized at 873 K.[2] LiCl was able to decrease LTRD-process temperature to 873 K, but it would be reduced more when using a molten salt with lower melting point such as LiCl-KCl (eutectic m.p.:630 K). Sm-Fe binary phases depending on annealing temperatures have been investigated, but there is no below 873 K.[3, 4] This is presumably because crystallization of amorphous Sm-Fe phase did not occur at lower 873 K when using the non-equilibrium process. In this study, synthesis of Sm-Fe powders was attempted with decreasing temperature to 673 K using LiCl-KCl eutectic molten salts to reveal whether crystallization occurs in LTRD process and explore the Sm-Fe phases in lower synthesis temperature than 873 K. Fe nano particles (NPs) and $SmCl_3$ (25% vs. Fe) were mixed with LiCl, KCl and Ca granules and subjected to LTRD reaction at 673~873 K for 10 h under Ar. The products were washed by water to remove Ca and interstitial hydrogen atoms inserted in Sm-Fe phases during washing process were removed by annealing in vac. at 473 K for 3 h. XRD patterns of Sm-Fe particles are shown in Fig. 1 and the synthesized Sm-Fe phases are summarized in table 1. The crystallization of Sm-Fe phases successfully occurred in LTRD process even 673 K. $SmFe_2$, $SmFe_3$ and $TbCu_7$-type Sm-Fe phases were synthesized at 673, 773 and 823 K, respectively. It is supposed that Fe NPs and the reduced Sm from $SmCl_3$ is better to react than the case of amorphous Sm-Fe of the non-equilibrium process. In this study, LTRD process, which is able to react at 673 K, was developed, but already known Sm-Fe phases were produced in this condition. There is a possibility that new phases synthesized at low temperature will be discovered if using different LTRD-process conditions or other system not only Sm-Fe system.

[1] S. Sakurada, A. Tsutai and T. Hirai, Journal of Applied Physics Vol. 79 p. 4611-4613 (1996) [2] S. Okada and K. Takagi, Journal of Rare Earths (2021), https://doi.org/10.1016/j.jre.2021.05.017 [3] A. Teresiak, M. Kubis and N. Mattern, Journal of Alloys and Compounds, Vol. 274 p.284-293 (1998) [4] Y. Luo, D. Yu and H. Li, Journal of Rare Earths, Vol. 32, No. 10, p 960-964 (2014)

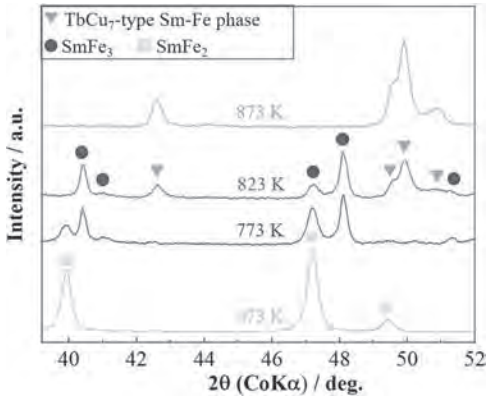

Fig. 1 XRD patterns of Sm-Fe powders synthesized by LTRD process at 673~873 K for 10 h.

Synthesis temperature (K)	Synthesized phases
873	$TbCu_7$-type Sm-Fe
823	$TbCu_7$-type Sm-Fe, $SmFe_3$
773	$SmFe_3$, $SmFe_2$
673	$SmFe_2$

Table 1 Summary of Sm-Fe phases synthesized by LTRD process at 673~873 K.

DOA-12. Effects of Ce–Mn Substitutions on Magnetic Properties of *M*-type Strontium Hexaferrites. *Z. Zi*[1] and Y. Sun[1] *1. Key Laboratory of Materials Physics, Institute of Solid State Physics, Chinese Academy of Sciences, Hefei, China*

M-type strontium hexaferrites of $Sr_{1-x}Ce_xFe_{12-x}Mn_xO_{19}$ ($0.0 \le x \le 0.4$) have been synthesized by the chemical coprecipitation method. X-ray diffraction (XRD) studies indicate that the samples are single-phase with the space group of $P6_3/mmc$. The results of field-emission scanning electronic microscopy

show that the grains are regular hexagonal platelets with sizes from 0.5 to 1.5 μm. It is observed that the value of H_c increases at low substitution ($x \leq 0.1$), reaches a maximum at $x = 0.1$ and then decreases at $x \geq 0.1$, while the value of M_s decreases monotonously with increasing x. The variations of magnetic properties can be tentatively attributed to the effects of Ce–Mn substitutions. The results above indicate that our samples might be promising candidates for permanent magnets in the future.

[1] P.Y. Meng, K. Xiong, L. Wang, S.N. Li, Y.K. Cheng, G.L. Xu, J. Alloys Compd. 628 (2015) 75 [2] S. Zhou, Y.Yang. R.Y. Lei, J.P. Zhou, X.M. Chen, J. Magn. Magn. Mater. Available online 26 July 2021, 168333 https://doi.org/10.1016/j.jmmm.2021.168333 [3] A. Rai, A.K. Thakur, AIP Conf. Proc.1728 (2016) 020491. [4] Y. Wang, Y.L.Liu, J. Li, Q. Liu, H.W. Zhang, V.G. Harris, AIP Advances 6 (2016) 056410. [5] K.S. Martirosyan, E. Galstyan, S.M. Hossain, Y.J Wang, D. Litvinov, Sci. Eng. B 176 (2011) 8. [6] N. Yang, H. Jia, J. Pang, J. Alloys Compd. 438 (2007) 262. [7] H.M. Lee, Y.J. Kim, J.H. Ahn, J. Alloys Compd. 504S (2010) S332. [8] Prabhjyot Kaur, S.K. Chawla, S.S. Meena, S.M. Yusuf, Kunal Pubby, S. Bindra Narang, Ceram. Int. 43 (2017) 590

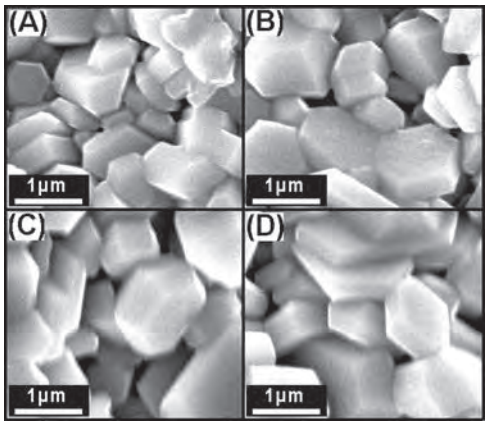

Figure 1. FE-SEM micrographs of SCFMO hexaplatelets

Session DOB
PERMANENT MAGNETS AND PROCESSING I

Wei Tang, Chair
Ames Laboratory, Ames, IA, United States

INVITED PAPER

DOB-01. Selective Laser Melting of Partially Anisotropic Rare Earth-based Permanent Magnets. *D. Goll*[1], F. Trauter[1], R. Loeffler[1] and G. Schneider[1] *1. Materials Research Institute, Aalen University, Aalen, Germany*

Additive manufacturing based on selective laser melting (SLM) promises versatile new opportunities for hard magnetic materials as key materials for electrification. However, SLM technology is challenging, especially for today's strongest permanent magnets based one rare earth (RE) metals. It requires special processing chambers to handle the powders sensitive to oxidation. SLM of RE-based permanent magnet material so far was mainly performed on nanocrystalline Fe-Nd-B powder with overstoichiometric Fe content (e.g. MQP-S from Magnequench). Recently, it has been shown, that due to rapid solidification in SLM, a nanocrystalline microstructure with hard magnetic properties develops in the bulk [1]. In addition, the development of very fine Fe-Nd-B microstructures with directed crystal growth and finely dispersed Nd-rich phase is possible [2]. Material systems such as Co-Sm or Fe-Pr-Cu-B can offer advantages for SLM processing. Due to their solidification process and phase equilibria, they form magnetically advantageous microstructures. Permanent magnet properties can be obtained by annealing, without the need of subsequent powder metallurgical processing or rapid quenching. By a proper choice of processing parameters and post-annealing conditions good permanent magnet properties and partial magnetic anisotropy can be realized for printed parts of both materials. In the case of $(CoCuFeZr)_{17}Sm_2$ a coercivity of 2.77 T, remanence of 0.78 T and maximum energy density of 109 kJ/m^3 have been achieved (Fig. 1). Due to texture of the printed parts the remanence is 24 % higher than for a comparable isotropic sintered magnet. In the case of FePrCuB a coercivity of 0.67 T, remanence of 0.67 T and maximum energy density of 69.8 kJ/m^3 have been obtained (Fig. 2). Due to higher degree of texturing, the printed parts so far exhibit a 26 % higher remanence compared to identically annealed cast material of the same composition. The paper highlights the correlation between microstructure and related magnetic properties for the processing parameter-sets used.

[1] D. Goll, G. Schneider et al., Micromachines, Vol. 12, 538 (2021) [2] D. Goll, G. Schneider et al., Physica Status Solidi RRL, Vol. 13, 1800536 (2019)

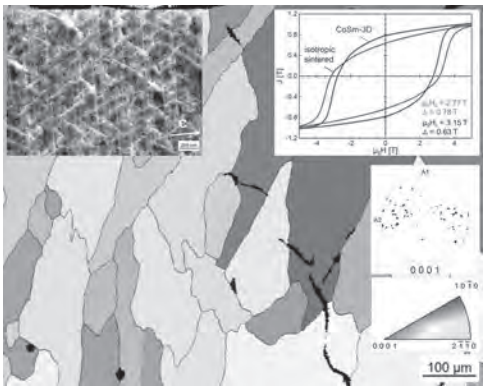

Fig. 1: Microstructural and magnetic properties of $(CoCuFeZr)_{17}Sm_2$ SLM-printed component.

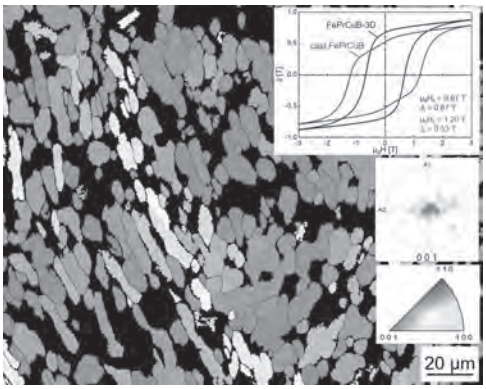

Fig. 2: Microstructural and magnetic properties of FePrCuB SLM-printed component.

CONTRIBUTED PAPERS

DOB-02. Withdrawn

DOB-03. Fe-Ni-Al Heusler Alloys: Phase Stability and Magnetocrystalline Anisotropy. *O.N. Miroshkina*[1,2], M.E. Gruner[1], V. Buchelnikov[2] and V. Sokolovskiy[2] *1. Faculty of Physics, University of Duisburg-Essen, Duisburg, Germany; 2. Condensed Matter Physics Department, Chelyabinsk State University, Chelyabinsk, Russian Federation*

Ferromagnetic shape memory alloys (FSMA) are promising candidates for application as actuators, sensors, magnetomechanical devices, harvesters, and magnetic cooling systems. In their low-temperature, low-symmetry phases they may also possess a considerable magnetocrystalline anisotropy, which is necessary for the FSMA but may render them useful as low-cost permanent magnets as well. Heusler-type $Fe_2Ni_{1-x}Al_x$ and $Co_2Ni_{1-x}Al_x$ alloys

are an interesting subgroup, as these materials are ductile, cheap, and easily synthesized, while possessing a high Curie and martensitic transformation temperature, which can be adapted by changing the composition. One binary end-point of the ternary phase diagrams, FeNi, is of substantial interest for permanent magnet applications since it shows a large magnetocrystalline anisotropy (MAE) in its ordered phase, which is, however difficult to synthesize. However, also in the ternary Heusler-type systems, structure and type of chemical order are still under debate. In this work, we report systematic first-principles investigations of the structural and magnetic properties of the ternary Fe-Ni-Al, Co-Ni-Al, and Fe-Ni-Ga-based Heusler alloys. We calculated the ground state energy and magnetic properties of different structural motives and degree of order. For the most favorable structures, we evaluated magnetocrystalline anisotropy, magnetic exchange coupling, and lattice free energy to assess the equilibrium properties for the compositions under study. We found that for Fe_2NiAl, the layered T^p crystal structure suggested in Ref. [1] is the most favorable ordering motif from the energetic point of view. Moreover, the MAE of T^p-Fe_2NiAl is found to be of the same order, which makes it thus another promising candidate for permanent magnet applications [2]. This work is funded by the German Research Foundation (DFG) – TRR 270, subproject B06 and Russian Science Foundation (RSF) No. 17-72-20022. Calculations were partly performed on the MagnitUDE supercomputer of the University of Duisburg-Essen (DFG INST 20876/209-1 and 20876/243-1 FUGG).

1. P. Neibecker, M. E. Gruner, X. Xu, et al., Phys. Rev. B, Vol. 96, p. 165131 (2017) 2. V. Sokolovskiy, O. Miroshkina, V. Buchelnikov, M.E. Gruner, https://arxiv.org/abs/2107.08804 (2021)

DOB-04. Effects of deformation ratio and temperature on microstructure and properties of NdFeB magnets by one-step hot deformation. *K. Xu*[1], W. Fan[1], B. Zhou[1], J. He[1], H. Yu[1] and Z. Liu[1]
1. School of Materials Science and Engineering, South China University of Technology, Guangzhou City, China

Abstract: Compared with the widely used industrial production process of sintering, hot deformation (HD) process has many advantages and it was once considered as a candidate technology for the fourth generation rare earth permanent magnets. At present, the research of HD Nd-Fe-B magnets mainly focuses on the magnet preparation and microstructure control[1]. One-step HD can shorten the preparation process of bulk anisotropic magnets to the minimum, which highlights the advantages of simple high-definition process. However, there are still many aspects of this method that have not been systematically studied in depth. In this study, the effects of deformation ratio and temperature on the microstructure and properties of NdFeB magnets were studied by adjusting the one-step HD process. The results show that the optimized magnetic properties with H_{cj}, J_r and $(BH)_{max}$ of 960 kA/m, 1.2 T and 33 MGOe are obtained at 750 °C with 80% deformation ratio, which are very close to the performance of ordinary hot pressing/hot deformation (HP/HD) magnets, as shown in Fig. 1 (a). The microstructure and corrosion resistance were studied. The results show that with the increase of HD temperature and deformation rate, the corrosion resistance of the magnet first increases and then decreases, and the platelet grains become more obvious. When the HD temperature exceeds 750 °C and the deformation exceeds 80%, the grain growth is too large and the grain boundary thickness decreases sharply. After 90%, there is no grain boundary phase and the grain shape of the two deformed magnets is basically the same, as shown in Fig. 1 (b). It can be considered that one-step HD can replace HP/HD and achieve the simplest process while maintaining the performance [2]. As shown in Figs. 1 (c) (d), with the increase of deformation rate and HD temperature, the magnetic energy product and remanence first increase and then decrease, and the coercivity monotonously decreases.

References [1] Y. Lee, B. Liao, Y. Wong, H. Chang, W. Chang, IEEE Trans. Magn. 54(2018) 2100605. [2] K. Xu, X. Liao, H. Yu, X. Zhong, Z. Liu, J. Magn. Magn. Mater. 537 (2021) 168193.

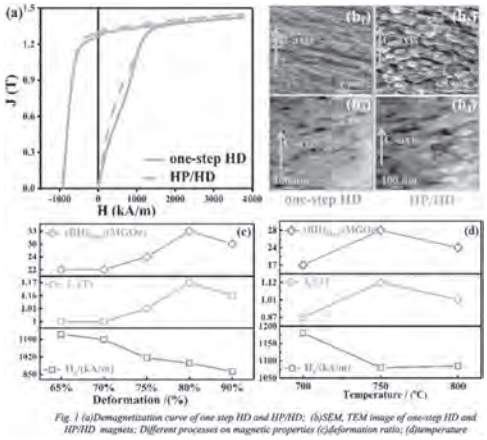

Fig. 1 (a)Demagnetization curve of one step HD and HP/HD; (b)SEM, TEM image of one-step HD and HP/HD magnets; Different processes on magnetic properties (c)deformation ratio; (d)temperature

DOB-05. A strategy to enhance magnetic and service performance of Nd-Fe-B magnets by HRE-free grain boundary diffusion. *J. He*[1], H. Zeng[1], W. Song[1], B. Zhou[1], H. Yu[1], X. Zhong[1] and Z. Liu[1] *1. South China University of Technology, Guangzhou, China*

Abstract Grain boundary diffusion (GBD) provides a promising way for Nd-Fe-B magnets to obtain high coercivity with less consumption of critical rare earths (RE). With the expansion of application field, the mechanical and anti-corrosion properties of Nd-Fe-B magnets has attracted increasing attention except their magnetic properties. Here, we proposed a strategy to simultaneously enhance these properties by GBD without employing heavy rare earths (HRE). The diffusion sources of $Pr_{70}Al_{20}Cu_{10}$ (PrAlCu) and $Al_{75}Cu_{25}$ (AlCu) were prepared by arc melting. The thickness of initial magnet is 4.5 mm. The results show that the coercivity can be enhanced from 1000 to 1346 and 1089 kA/m by diffusion of PrAlCu and AlCu, respectively (Fig. 1(a)). Interestingly, the compression strength of the magnets also increased by 485 and 252 MPa, respectively. In addition, it is found that AlCu diffusion can improve the corrosion resistance of the magnets, which is different from that of PrAlCu [1]. The microstructure analysis showed that PrAlCu diffusion leads to the formation of continuous grain boundary (GB) layers for magnetic decoupling and strong binding between 2:14:1 grains (Fig. 1(b)). Although the non-RE diffusion source of AlCu shows less efficiency in increasing the content of RE-rich GB phases (Fig. 1(c)), it reduces the defects at interfaces, which is helpful for hindering the reversal domain nucleation [2, 3], as shown in Figs. 1(d1) to (d3). The modified GBs by AlCu diffusion also are effective for crack bridging or buffering, and exhibit an enhanced chemical stability. The high-abundance elements La/Ce based diffusion sources are also investigated in this work. The present results indicate that GBD of the HRE-free low-melting alloys can be used to effectively improve both the magnetic and service performance of Nd-Fe-B magnets due to the optimized microstructure.

[1] H.X. Zeng, Z.W. Liu, J.S. Zhang, X.F. Liao, H.Y. Yu, J. Mater. Sci. Technol. 36 (2020) 50-54. [2] J. He, X. Liao, X. Lan, W. Qiu, H. Yu, J. Zhang, W. Fan, X. Zhong, Z. Liu, J. Alloys Compd. 870 (2021) 159229. [3] Z. Liu, J. He, Q. Zhou, Y. Huang, Q. Jiang, J. Mater. Sci. Technol. 98 (2022) 51-61.

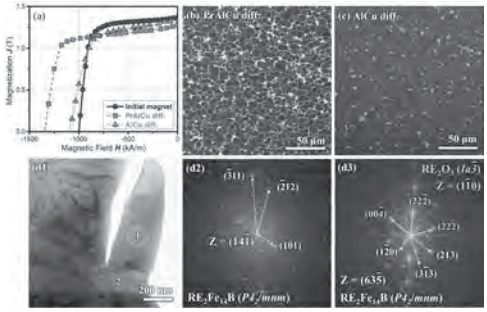

DOB-06. Crystallinity improvement of finely pulverized Sm_2Fe_{17} powder by post-milling annealing and its side-effects. *A. Hosokawa*[1], W. Yamaguchi[1] and K. Takagi[1] *1. Magnetic Powder Metallurgy Research Center, National Institute of Advanced Industrial Science and Technology, Nagoya, Japan*

$Sm_2Fe_{17}N_3$ is an excellent hard magnetic compound, being expected as new generation permanent magnet material that can potentially outperform Nd-Fe-B magnets especially at higher temperature[1]. However, the drawback is that this compound decomposes at 620 °C and thus it was regarded that producing a bulk magnet is extremely difficult [2]. Although several researchers reported that combining a spark plasma sintering apparatus with a cemented carbide die-set enables to produce sintered $Sm_2Fe_{17}N_3$ magnets [3-5], coercivity of the sintered magnet was found to deteriorate upon sintering [5]. To prevent the possible unfavorable effect of the surface oxides on powder particles, our group recently developed a novel low-oxygen powder metallurgy process and succeeded in producing anisotropic $Sm_2Fe_{17}N_3$ sintered magnets from finely pulverized high-performance powder without coercivity degradation, but the achievable maximum energy product of the magnet was disappointingly low compared to the excellent performance of the powder [6, 7]. Detailed microstructural analyses later revealed that the performance degradation seems to be due to high density lattice defects and randomly oriented nanocrystalline grains at the particle surfaces caused by the milling process [8]. Generally speaking, these lattice defects can be reduced/eliminated by annealing but the annealing temperature cannot be raised very much in this case due to the relatively low decomposition temperature of $Sm_2Fe_{17}N_3$. In this study, we focused on Sm_2Fe_{17} fine pulverized powder instead of $Sm_2Fe_{17}N_3$ and explored the possibility of damage recovery to remove those microstructural defects by post-milling annealing/nitridation treatments. This treatment improved crystallinity to some extent, as shown in Fig. 1, but failed to eliminate the randomized nanocrystalline grains completely[9]. In addition, it was found that α-Fe forms upon annealing of stoichiometric Sm_2Fe_{17}, which is inconsistent with the Sm-Fe binary phase diagram at a glance. The mechanism of this unexpected α-Fe formation was investigated by detailed microstructural analyses using transmission electron microscopy and three dimensional atom probe tomography.

[1] T. Iriyama, K. Kobayashi, N. Imaoka, T. Fukuda, H. Kato, Y. Nakagawa, Effect of Nitrogen-Content on Magnetic-Properties of $Sm_2Fe_{17}N_x$ ($0 < x < 6$), IEEE Transactions on Magnetics 28(5) (1992) 2326-2331. [2] C.N. Christodoulou, T. Takeshita, Nitrogenation of Sm_2Fe_{17} - Mechanism, Phases and Stability, Journal of Alloys and Compounds 202 (1993) 173-182. [3] D.T. Zhang, M. Yue, J.X. Zhang, Study on bulk Sm_2Fe_17Nx sintered magnets prepared by spark plasma sintering, Powder Metall 50(3) (2007) 215-218. [4] K. Takagi, H. Nakayama, K. Ozaki, K. Kobayashi, Fabrication of High-performance Sm-Fe-N isotropic bulk magnets by a combination of High-pressure compaction and current sintering, Journal of Magnetism and Magnetic Materials 324(7) (2012) 1337-1341. [5] K. Takagi, H. Nakayama, K. Ozaki, Microstructural behavior on particle surfaces and interfaces in $Sm_2Fe_{17}N_3$ powder compacts during low-temperature sintering, Journal of Magnetism and Magnetic Materials 324(15) (2012) 2336-2341. [6] R. Soda, K. Takagi, M. Jinno, W. Yamaguchi, K. Ozaki, Anisotropic Sm2Fe17N3 sintered magnets without coercivity deterioration, Aip Adv 6(11) (2016). [7] K. Takagi, Y. Hirayama, S. Okada, W. Yamaguchi, K. Ozaki, Novel powder processing technologies for production of rare-earth permanent magnets, Science and Technology of Advanced Materials 22(1) (2021) 150-159. [8] A. Hosokawa, W. Yamaguchi, K. Suzuki, K. Takagi, Influences of microstructure on macroscopic crystallinity and magnetic properties of Sm-Fe-N fine powder produced by jet-milling, Journal of Alloys and Compounds 869 (2021) 159288. [9] A. Hosokawa, K. Suzuki, W. Yamaguchi, K. Takagi, Mechanism of anomalous alpha-Fe formation from stoichiometric Sm2Fe17 jet-milled powder during post-pulverization annealing, Acta Materialia 213 (2021).

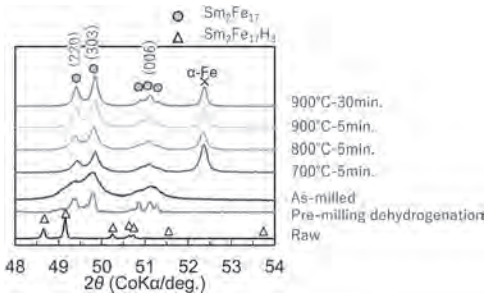

Fig. 1 Change in XRD patterns by annealing

DOB-07. Understanding Grain Morphology Close to the Superparamagnetic Limit. *C. Skelland*[1], T. Schrefl[2] and G. Hrkac[1] *1. College of Engineering, Mathematics, and Physical Sciences, University of Exeter, Exeter, United Kingdom; 2. Center for Modelling and Simulation, Danube University Krems, Wiener Neustadt, Austria*

Reducing the size of magnetic grains puts them close to their superparamagnetic limit, beyond which random thermal fluctuations can flip the magnetic moment of the grain, limiting their use in magnetic applications. Understanding grain properties close to this limit is key to understanding magnetic behaviour. Sepheri-Amin et al.[1] studied Pt surface segregation in FePt $L1_0$ grains: as grain size decreases from 20nm to 5nm, anisotropy reduces from K_u = 10.5 MJ/m^3 to K_u = 6 MJ/m^3, owing to the Pt surface layer making up an increased percentage of the grain. Similarly, preferential grain morphologies dictate granular surfaces which play a significant role in a grains magnetic properties. We studied five different morphologies, shown in Figure 1, for FePt $L1_0$ grains using LAMMPS[2] and MEAM potentials[3]. Our grain size ranged from 3-9nm in diameter, equating to a total number of atoms per grain of 1,000-15,000, in 1,000 atom intervals. To compare the probability of different morphologies we made the grains compositionally identical, and compared them using Boltzmann Factors, given by the equation below: $p_i/p_j = e^{(\xi_j-\xi_i)/(k_B T)}$ Here p_i, p_j is the probability of grain morphology i, and j respectively, ξ_i, ξ_j is the energy of states i, and j respectively, k_B is the Boltzmann constant, and T is the temperature. As can be seen in Figure 2, we found the Octahedron and the Truncated Octahedron were the most probable atomistic structures by hundreds of orders of magnitude at room temperature, a trend continued to higher temperatures. This result is due to these morphologies having predominantly {111} crystal planes on their surfaces, which are by far the most energetically preferable at ~2.2 J/m^2 compared to ~2.7 J/m^2 for the remaining major planes {100}, {110} etc.[4]. This demonstrates that stable FePt $L1_0$ grains will predominantly feature {111} faces, making control of this surface of primary importance for controlling their magnetic properties.

[1] H Sepehri-Amin et al., Scripta Materialia, Vol. 135, pp. 88–91, (2017) [2] Steve Plimpton, Journal of Computational Physics, Vol. 117, pp. 1–19, (2017) [3] Jaesong Kim, Yangmo Koo, and Byeong-Joo Lee, Journal of Materials Research, Vol. 21, pp. 199–208, (2006) [4] Jae-Song Kim et al., Journal of Applied Physics, Vol. 99, p. 53906, (2006)

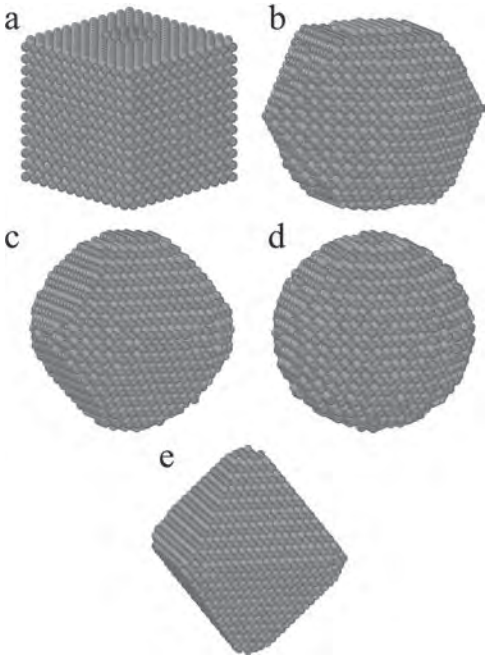

Fig. 1 Grain morphologies at 7,000 atoms, a) Cuboid, b) Truncated Octahedron Major, c) Truncated Octahedron Minor, d) Sphere, e) Octahedron.

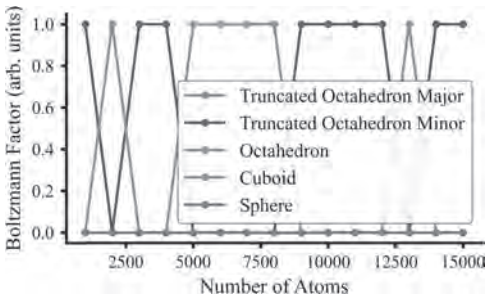

Fig. 2 Boltzmann Factor comparison of grain morphologies at 300K.

DOB-08. Origin of large unidirectional magnetic anisotropy in NiMn and PdMn. *N. Josten*[1], S. Noorzayee[1], M. Acet[1], F. Scheibel[2], A. Çakir[3] and M. Farle[1] *1. Faculty of Physics and Center for Nanointegration (CENIDE), University Duisburg-Essen, Duisburg, Germany; 2. Institute of Material Science, Technische Universität Darmstadt, Darmstadt, Germany; 3. Department of Metallurgical and Materials Engineering, Mugla University, Mugla, Turkey*

$Ni_{50}Mn_{50}$ with $L1_0$ ordering is generally known as an antiferromagnet for exchange bias applications [1]. In slightly off-stoichiometric $Ni_{50+x}Mn_{50-x}$ with excess nickel magnetic annealing leads to strongly pinned magnetic moments pointing in the direction of the annealing field [2]. The result is a large unidirectional magnetic anisotropy and small net magnetization. With $Pd_{50+x}Mn_{50-x}$ another alloy was found showing this effect. To potentially utilize this phenomenon we will discuss how the pinned magnetization can be maximized through variation of composition and annealing procedure. Funded by the Deutsche Forschungsgemeinschaft (DFG, German Research Foundation) – Project-ID 405553726 – TRR 270.

[1] A. E. Berkowitz and K. Takano, J. Magn. Magn. Mater. 200, 552-570 (1999) [2] L. Pál et al., Phys. Stat. Sol. 42, 49-59 (1970).

DOB-09. Tuning Magnetocrystalline Anisotroy of LTP MnBi with Sn. *M. Choi*[1], Y. Hong[1], H. Won[1], J. Lee[2], T. Lee[2], T. Lim[2], F. Yan[3] and X. Han[3] *1. Electrical and Computer Engineering, The University of Alabama, Tuscaloosa, AL, United States; 2. Institute of Fundamental and Advanced Technology (IFAT), Hyundai Motor Company, Uiwang-si, The Republic of Korea; 3. Metallurgical and Materials Engineering, The University of Alabama, Tuscaloosa, AL, United States*

The spin orientation of LTP MnBi can be controlled by partially substituting Bi of MnBi with the third element or temperature. The spin reorientation occurs at about 90 K from *ab*-plane (0-90K) to *c*-axis (T>90K) of LTP MnBi[1]. Sakuma et al. have performed first-principles calculations (FPC) on Sn-doped $Mn(Bi_{1-x}Sn_x)$ and found that magnetocrystalline anisotropy constant (K_u) increases to about 3MJ/m^3 at x=0.1 from -0.5MJ/m^3 at x=0 and then remains unchanged up to x=0.3[2]. The K_u at x=0 is not close enough to -0.15 of experimental K_u[3]. Therefore, the K_u for x>0 in [2] are not convinced. This may be attributed to RT and unrelaxed lattice constants (LC) used in the calculations. In this study, we have performed FPC on LTP $MnBi_{1-x}Sn_x$ (x=0, 0.5) in Fig. 1 to obtain K_u. The LTP MnBi unit cell has two Mn atoms at the 2*a* sites of (0,0,0) and (0,0,1/2) and two Bi atoms at the 2*c* sites of (1/3,2/3,1/4) and (2/3,1/3,3/4)[4]. We have relaxed unit cell to obtain LC *a* and *c*. Doped Sn decreases the *a* and *c* from 4.287 and 6.118 Å for x=0 to 3.954 and 5.456 Å for x=0.5, respectively. These relaxed LC (x=0) are in good agreement with the experimental LC[5]. The WIEN2k package based on density functional theory (DFT) was used to conduct the FPC[6]. We used the DFT within the local-spin-density approximation (LSDA). Figure 2 shows density of states for $MnBi_{1-x}Sn_x$ (x=0, 0.5). The net magnetic moments (MM) per formula unit is 3.613μ_B/*f.u.* for x=0 and 2.517μ_B/*f.u.* for x=0.5. The corresponding saturation magnetization decreases to 0.794 from 0.865T as Sn concentration increases to x=0.5. The calculated MM of 3.613μ_B/*f.u.*, K_u of -0.202 MJ/m^3, and T_C of 711 *K* for x=0 are in good agreement with the previously reported results[7]. The K_u for x = 0.5 is 1.711MJ/m^3. The Sn substitution for Bi changes the out-of-plane anisotropy from the in-plane to the out-of-plane and increases the magnetocrystalline anisotropy energy. The T_C for x=0.5 will be reported. * This work was supported in part by the National Science Foundation (NSF) under Grant No. 1650564.

[1] Michael A. McGuire, Huibo Cao, Bryan C. Chakoumakos, and Brian C. Sales, *Phys. Rev.* B 90, 174425 (2014). [2] Akimasa Sakuma, Yuki Manabe, and Yohei Kota, *Journal of the Physical Society of Japan* 82, 073704 (2013). [3] W.E. Stutius, T. Chen, and T.R. Sandin, AIP Conf. Proc. 18, 1222 (1974) [4] http://materials.springer.com/isp/crystallographic/docs/sd_1823960, 2020 (accessed 11 November 2020). [5] B. W. Roberts, *Phys. Rev*. 104, 607 (1956) [6] P. Blaha, et al., WIEN2K: An Augmented Plane Wave + Local Orbitals Program for Calculating Crystal Properties (Karlheinz Schwarz, Techn. Universitat, Wien, Austria, 2001) [7] J. Köhler et al., *J. Phys.: Condens. Matter* 8, 8681(1996)

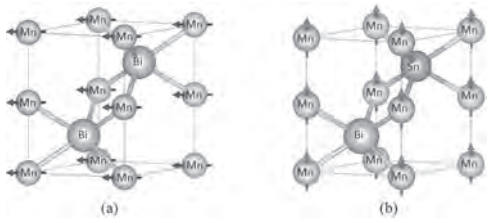

Figure 1. Crystal structure for (a) MnBi (in-plane) and (b) $MnBi_{0.5}Sn_{0.5}$ (out-of-plane)

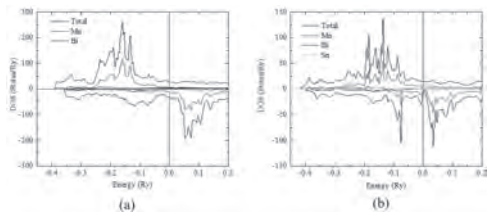

Figure 2. Density of states for (a) MnBi and (b) $MnBi_{0.5}Sn_{0.5}$

DOB-10. Synthesis of single-crystalline $TbCu_7$-type Sm-Fe powders by reducing reduction-diffusion temperature using molten salt. *S. Okada*[1] and K. Takagi[1] *1. Magnetic Powder Metallurgy Research Center, Advanced Industrial Science and Technology (AIST), Nagoya, Japan*

$TbCu_7$-type Sm-Fe-N is one of the candidates for a next-generation magnet because it has high saturation magnetization exceeding that of Nd-Fe-B and an anisotropic magnetic field equivalent to that. However, since $TbCu_7$-type Sm-Fe is a metastable phase, the synthesis method is limited to non-equilibrium processes such as a rapid-quenching method, and therefore only isotropic magnets are available. In this study, we attempted to synthesize a $TbCu_7$-type Sm-Fe single-crystalline fine powder by developing a reduction-diffusion (R-D) method that can synthesize anisotropic magnet powders. Previous studies for synthesis of $TbCu_7$-type Sm-Fe powder have shown that the $TbCu_7$-type Sm-Fe phase is formed at approximately 550-700 °C. Since the conventional R-D process requires high reaction temperature above the Ca melting point (about 850 °C) in order to diffuse Ca throughout the reaction vessel, it is not possible to synthesize $TbCu_7$-type Sm-Fe by the R-D process. Therefore, we newly suggested the use of molten salt as a solvent for Ca to reduce R-D reaction temperature to around 600 °C. LiCl was used as the molten salt, and it was mixed with Fe fine powder, $SmCl_3$, and Ca. The mixture was subjected to R-D reaction and the obtained crude product was washed with water and dried. As a result of XRD patterns of obtained powders shown in Fig. 1, the R-D reaction was revealed to possible even below the Ca melting point by using LiCl molten salt, and the targeted $TbCu_7$-type Sm-Fe was formed below 650 °C. From the EBSD analysis of the obtained powder, it was also verified that the synthesized $TbCu_7$-type Sm-Fe powder was consisted of submicron-sized single-crystalline particles. This study has provided a new route with potentiality to realize a $TbCu_7$-type Sm-Fe-N anisotropic magnetic powder.[1]

[1] S. Okada and K. Takagi, J. Rare Earths, in press (DOI: 10.1016/j.jre.2021.05.017)

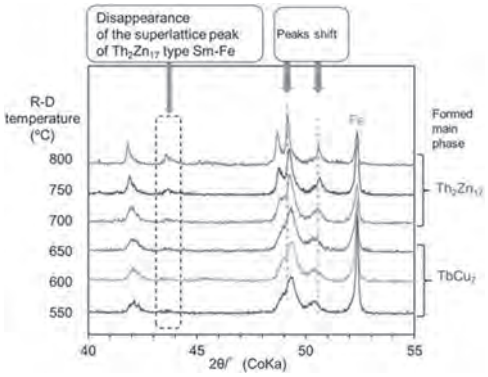

Fig.1 XRD pattens of powders synthesized with different R-D temperature.

Session DOC
NON-RARE EARTH PERMANENT MAGNET MATERIALS AND NANOCOMPOSITES I

Adrian Quesada, Co-Chair
Institute of Ceramics and Glass (CSIC), Madrid, Spain
Alberto Bollero, Co-Chair
IMDEA Nanociencia, Madrid, Spain

CONTRIBUTED PAPERS

DOC-01. Remanence Improvement in Exchange-Decoupled Composites Owing to Dipolar Interactions. *A. Quesada*[1], C. Granados[1], J. Guzmán-Mínguez[1], P. Kuntschke[2], C. de Julián Fernández[3], C. Munuera[4], S. Erohkin[5], D. Berkov[5], T. Schliesch[2] and J. Fernandez[1]
1. Institute of Ceramics and Glass (CSIC), Madrid, Spain; 2. Max Baermann GmbH, Cologne, Germany; 3. IMEM (CNR), Parma, Italy; 4. Institute of Materials Science of Madrid (CSIC, Madrid, Spain; 5. General Numerics Research Lab, Jena, Germany

The theory on exchange spring magnets, published by Kneller and Hawig in 1991, heralded the next big leap forward in the field of advanced permanent magnets. The theory predicted that a magnet prepared by combination of a hard and a soft magnetic phase would exhibit an improved remanent magnetization, M_r, as long as the two phases were mutually exchange coupled [1]. However, accomplishing an actual improvement has proven rather challenging. When large particles of soft phase are strongly exchange coupled to a hard phase, a magnetic softening is induced, instead of the desired hardening [2]. However, moderate M_r enhancements have been detected in exchange-decoupled composites [3]. The dominant magnetic interactions in exchange decoupled systems are magnetodipolar [4]. Therefore, exploiting the dipolar interactions between exchange decoupled hard and soft phases is an alternative strategy to prepare magnetic composites with an enhanced performance [5]. The efficacy of the method relies on controlling the magnitude of the self demagnetizing fields, which strongly depends on the size and shape of the soft phase. Here, exchange decoupled $SrFe_{12}O_{19}$ (hard)/Fe (soft) composites have been prepared, both in powder and injection moulded magnet dense form. The influence of the size of the soft phase has been experimentally studied, covering a range between 25 nm and 11 μm. Micromagnetic simulations have been carried out for the specific system in order to understand the spin dynamics inside the soft grains (see Figure 1). Regardless of the soft phase dimensions, the composites show a larger M_r than predicted by the theory. In fact, we observe and report here for the first time an increase in remanence in hard-soft injection moulded magnets in the absence of exchange coupling. Micromagnetic simulations point at the existence of a vortex like state at the core of the Fe particles, which orients with the internal field created by the ferrite particles, as the reason for this increase in remanence. Figure 1. (a) experiment; (b) micromagnetic simulations at remanence and (c) at coercivity. The authors would like to thank financial support from the European Commission through the project AMPHIBIAN (H2020 NMBP 2016 720853).

References [1] E. F. Kneller, R. Hawig, IEEE Trans. Magn. 27 3588 (1991). [2] A. Quesada, C. Granados-Miralles, A. López-Ortega, S. Erokhin, E. Lottini, J. Pedrosa, A. Bollero, A. M. Aragón, F. Rubio-Marcos, M. Stingaciu, G. Bertoni, C. de Julián Fernández, C. Sangregorio, J. F. Fernández, D. Berkov, M. Christensen, Adv. Electron. Mater. 2 1500365 (2016). [3] A. Aragón Sánchez, M. Pilar Marín Palacios, A. Hernando Grande, S. Deledda, A. Quesada Michelena, J. Francisco Fernández Lozano, A. Bollero Real, F. Javier Pedrosa Ruiz, Patent no: P201600092 [4] M. I. Montero, F. Cebollada, M. P. Morales, J. M. González, A. Hernando, J. Appl. Phys. 83 6277 (1998). [5] http://amphibianproject.eu/

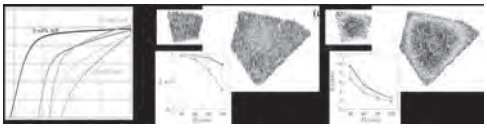

DOC-02. Optimizing magnetic properties and coupling of hard $SrFe_{12}O_{19}$ based nanocomposites. *P. Maltoni*[1], G. Barucca[2], T. Sarkar[1], G. Varvaro[4], D. Peddis[3,4] and R. Mathieu[1] *1. of Materials Science and Engineering, Solid State Physics, Uppsala University, Uppsala, Sweden; 2. SIMAU, Università Politecnica delle Marche, Ancona, Italy; 3. DCCI, Universita di Genova, Genova, Italy; 4. CNR-ISM, Roma, Italy*

Magnetic nanocomposites (NCs) have gained a lot of interest over the last years, due to the possibility to finely control and modify their features at the nanoscale, which allows to extend their applicability in a multitude of energy-related technological areas [1]. In this regard, exchange coupled hard-soft NCs have received significant attention, as a promising strategy to achieve high magnetic performances [2]: the main challenge is to develop systems which simultaneously show a large coercivity (H_C) and high magnetization. Hereby our focus is on the optimization of hard $SrFe_{12}O_{19}$ (SFO) ferrites magnetic performance, in order to be used as building block in bi-magnetic NCs [3]. This work is aimed at extensively studying the role of diamagnetic Al^{3+} in the tuning of the magnetic properties of a series of SFOs obtained by sol-gel self-combustion synthesis ($SrFe_{12-x}Al_xO_{19}$ with x ranging from 0 to 2.4). By means of X-ray powder diffraction (XRPD), transmission electron microscopy (TEM) and SQUID magnetometry we demonstrate that the magnetic behavior of the different samples is closely related to their size, morphology and elemental composition. The resulting partial occupation of diamagnetic Al^{3+} in specific Fe^{3+} sites of the hexagonal ferrite structure affects the magnetic moment as well as the magnetic order (e.g. a sketch of the crystal structure is reported in Fig.1): by increasing its amount, the resulting magnetization is reduced, hinting at the modification of the magnetic collinearity, although the coercivity is hugely enhanced (up to 943 kA/m), as seen in Fig.2. Based on these results, we have designed and prepared bi-magnetic NCs by introducing a magnetically softer $CoFe_2O_4$ phase in different fractions (up to 20 w/w%). We address the sol-gel self-combustion chemical approach as a unique way to develop such NCs, compared to physically mixing [4], and our results clearly show that the synthesis strategy plays a critical role in the extent of magnetic coupling that can be achieved between the hard-soft phases. We thank the Swedish Energy Agency and Swedish Research Council (VR) for financially supporting this work.

[1] R. Skomski, P. Manchanda, P. K. Kumar, B. Balamurugan, A. Kashyap, D. J. Sellmyer, IEEE Trans. Magn., 49, 3215 (2013) [2] F. Sayed, G. Kotnana, G. Muscas, F. Locardi, A. Comite, G. Varvaro, D. Peddis, G. Barucca, R. Mathieu, T. Sarkar, Nanoscale Adv., 2, 851 (2020) [3] P. Maltoni, T. Sarkar, G. Varvaro, G. Barucca, S. Ivanov, D. Peddis, R. Mathieu, J. Phys. D: Appl. Phys., 54, 124004 (2021) [4] P. Maltoni, T. Sarkar, G. Barucca, G. Varvaro, F. Locardi, D. Peddis, R. Mathieu, J. Phys. Chem. C., 125, 10, 5927 (2021)

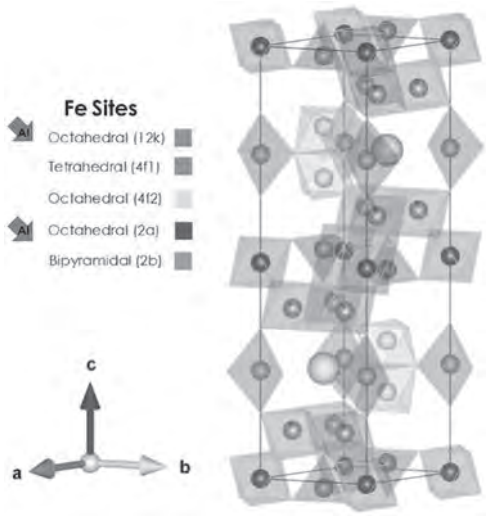

Fig.1 Unit cell of $SrFe_{11}Al_1O_{19}$

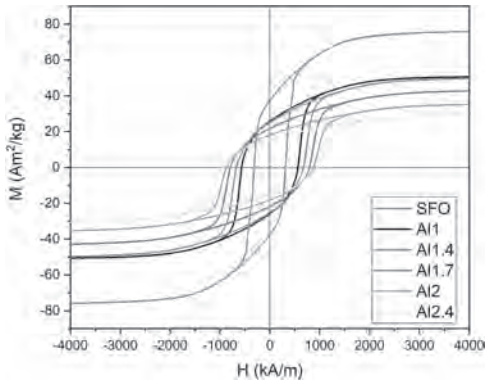

Fig.2 M vs H loops at 300K for $SrFe_{12-x}Al_xO_{19}$ (Al:0, 1, 1.4, 2)

DOC-03. Hybrid FeCo Nanowires– Strontium Ferrite Composites for Rare-Earth-free Magnets. J. Guzmán-Mínguez[1], S. Ruiz Gómez[2], L. Vicente-Arche[1], C. Granados[1], C. Fernandez Gonzalez[3], F. Mompean[4], M. Garcia Hernandez[4], D. Mishra[5,6], J. Fernandez[1], L. Perez[7,3], A. Quesada[1] and *C. de Julián Fernández*[6] *1. Institute of Ceramics and Glass CSIC, Madrid, Spain; 2. University Complutense of Madrid, Madrid, Spain; 3. IMDEA Nanoscience, Madrid, Spain; 4. Institute of Materials Science - CSIC, Madrid, Spain; 5. Institute of Technology Jodhpur, Jodhpur, India; 6. Institute of Materials for Electronics and Magnetism - CNR, Parma, Italy; 7. Unité Mixte de Physique CNRS Thales Univ. Paris-Saclay, Palaiseau, France*

In this work we show the optimization of the microstructure and properties of micrometric FeCo nanowires and micrometric $SrFe_{12}O_{19}$ (SFO) powders to get a composite with improved hard properties for magnets. The work is centred in the research of novel ferrite-based magnets with improved properties respect commercial state-of-art ones. In fact, even if rare-earth magnets constitute those with the most important technological and economical importance, ferrite magnets constitute by far the most widely used by weight [1,2] and any improvement of their performances is expected to have an important impact [3]. The most promising approach to improve the performances of ferrite magnets is the development of nanocomposites formed by magnetically coupled high magnetization and hard magnetic phases [3]. We have investigated the properties of mixtures and of composites containing micrometric FeCo nanowires and micrometric SFO powders [4]. FeCo NWs were prepared by template-assisted electrochemical deposition using nanoporous templates and membranes to obtain NWs with different diameters (30, 50, and 100 nm) and 5 to 10 micron of length. Structural and magnetic studies indicate that the NWs have a CoFe oxide shell that passivates the NWs of further oxidation, and it decreases their total magnetization. Even their large length/diameter ratio, the coercive field of the NWs depends on the diameter, increasing as the diameter decreases. The magnetic properties of the mixtures are dependent on the NW diameter and of the soft-hard ratio. The loops exhibit single and double step shape indicating different regimes of magnetic coupling and decoupling, being the first dominant only with NWs of 50 nm of diameter and a composition below or of 20%wt. The magnetic properties change under the magnetic orientation of the composite. In fact, the oriented bonded composites magnets exhibit a larger energy product up to 40% larger than the corresponding ferrite ones. The magnetic properties of these magnets will be discussed considering the magnetic configuration of the NWs and the SFO particles in the different cases. This research was supported by EU- H2020 AMPHIBIAN Project (H2020-NMBP-2016-720853) and by the JECS Trust.

[1] R. C. Pullar, Progress in Materials Science 57, 1191 (2012). [2] S H Mahmood and I Abu-Aljarayesh Hexaferrite Permanent Magnetic Materials. Materials Research Forum LLC (2016) [3] C. de Julián Fernández et al., J. Applied Phys. D: Applied Physics, 54, 153001 (2021). [4] J. M. Gúzman Mínguez et al. ACS Appl. Nano Mater. 3, 9842 (2020).

DOC-04. Fe-Si and its Nanocrystallization as Soft Phase in SmCo-based Nanocomposites. *Y. Zhang*[1], Y. Li[1], W. Liu[1], M. Yue[1] and D. Zhang[1] *1. Beijing University of Technology, Beijing, China*

Nanocomposite permanent magnets showed theoretical $(BH)_m$ of more than $1MJ/m^3$, saving rare earth resources, good mechanical and corrosion resistance attract the interest of researchers. Good magnetic anisotropy is necessary to achieve high $(BH)_m$, but it is difficult to obtain ideal texture due to the uncoordinated deformation between soft and hard phases. Therefore, in this study, $Fe_{93.5}Si_{6.5}$ was selected as the soft phase because of its higher hardness than α-Fe. By studying its nanocrystallization and magnetic properties of $SmCo_5$/Fe-Si magnet, it can be found that Fe-Si is suitable as the soft phase. Fe-Si particles show Ms of 18.5 kG, and particle size < 5 μm after milling. The demagnetization curves and the corresponding magnetic properties of the hot-pressed $SmCo_5$/Fe-Si magnets with the milling time (t) are showed in Fig. 1. One can see that the obvious kinks in the demagnetization curves with the t < 8 h. When the $t \geq 8$ h, the demagnetization curves show "single-hard-phase" characteristics, indicating that ideal microstructure in the hot-pressed magnet ensuring good intergranular exchange coupling. With the increase of t, the remanence (B_r) of hot-pressed SmCo5/Fe-Si magnet increases first, and peaks at 12 h of 9.9 kG, then decreased. The grain refinement caused by the increase of t is the reason for the increase of B_r, while the partial amorphization caused by too long t is the reason for the decrease of B_r. Coercivity shows the same the same variation as the B_r, and reaches the maximum value of 11.4 kOe when the t = 6 h. Comprehensively, the $(BH)_m$ of the magnet reaches the maximum (14.3 MGOe) with the t of 8 h. When the t is more than 8 hours, the Fe-Si phase is well dispersed into the main phase of $SmCo_5$, and the aggregated Fe region is hardly observed. TEM observation shows that the soft phase grains in hot-pressed SmCo5/Fe-Si magnet milled for 12 hours are fine and evenly distributed. The nanocrystallization process of Fe-Si phase can be summarized that Fe-Si particles first evolve from agglomerated irregular shape to nono-strip, and finally to uniformly dispersed Fe-Si grains.

[1] Yitong Zhuge, Yuqing Li, Xiaochang Xu, Dongtao Zhang, Hongguo Zhang, Weiqiang Liu, Ming Yue. Morphology and magnetic properties of Sm_2Co_7/α-Fe nanocomposite magnets produced by high energy ball milling and spark plasma sintering[J]. Journal of Rare Earths, 2021, 39(03): 312-316.

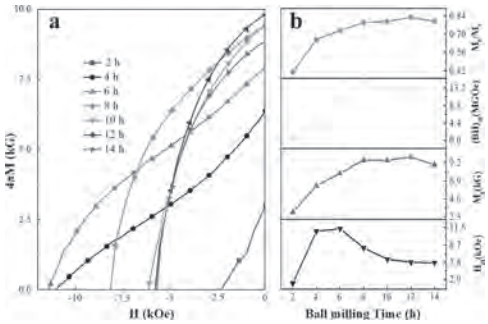

Fig. 1. Demagnetization curves (a) and magnetic properties (b) of $SmCo_5$/Fe-Si magnets with different *t*.

DOC-05. Magnetization reversal in nanofabricated soft-in-hard exchange-spring magnets. *I.G. de Moraes*[1], Y. Hong[1], F.O. Keller[1], C. Naud[1], S. Le Denmat[1], L. Ranno[1], T. Devillers[1] and N. Dempsey[1]
1. Institut Néel, Université Grenoble-Alpes, CNRS, Grenoble, France

Exchange spring hard-soft magnetic nanocomposites (NCs) are proposed as potential high-performance magnets [1,2]. Their relatively poor performance [3-6] compared to predicted values [7] is attributed to insufficient control over the size and distribution of the soft phase. In this work e-beam lithography was used to control the size, shape and position of soft magnetic (FeCo) nano-rods embedded in a micro-patterned hard magnetic matrix (25 nm thick FePt-$L1_0$). We report a study of samples with different nanorod widths (24 and 120 nm) and comparable volume content. Their global M(H) loops have similar H_c values, but that of the sample with wide nanorods is concave (Fig. 2a), and First Order Reversal Curve diagrams reveal that this sample has some uncoupled soft magnetic phase. Uncoupled soft phase reversal is confirmed by MFM imaging in different remanent states, where hard and soft phase switching can be distinguished owing to the different length scales of the patterns (Fig. 1). Micromagnetic modelling (MuMax3) was performed to simulate magnetization reversal and MFM contrast. Good agreement is obtained between the measured (Fig. 2a) and simulated (Fig. 2b) data. Magnetization distribution cross-sections during reversal indicate that the wide soft rods reverse independently of the hard matrix, while the narrower rods are coupled during the entire reversal process (Fig. 2c-e). Convoluting results of stray field distributions at the experimental scan height with an MFM probe modelled as a monopole, we obtained comparable images with periodic patterns with the same length scale as the nanorods (Fig. 2f-g). The use of MFM remanent imaging combined with simulations to study magnetization reversal will be discussed in the framework of a broader study of model soft in hard nanocomposites.

[1] Coehoorn, R., De Mooij, D. B., & de Waard, C. D. J. of Magnetism and Magnetic Materials, 80, 101 (1989). [2]Kneller, E. F., & Hawig, R, IEEE Transactions on Magnetics, 27, 3588 (1991). [3] Li, X. et al. Advanced Materials, 29, 16 (2017). [4] Dai, Z. M., et al. Nanoscale 9, 22, 7385-7390 (2017). [5] I. de Moraes and N. M. Dempsey, Book chapter, Springer International Publishing, pp. 403–433 (2021). [6] Ping, D. et al. Acta materialia 47,18, 4641-4651 (1999). [7] Skomski, R., and J. M. D. Coey, Physical Review B 48.21, 15812 (1993).

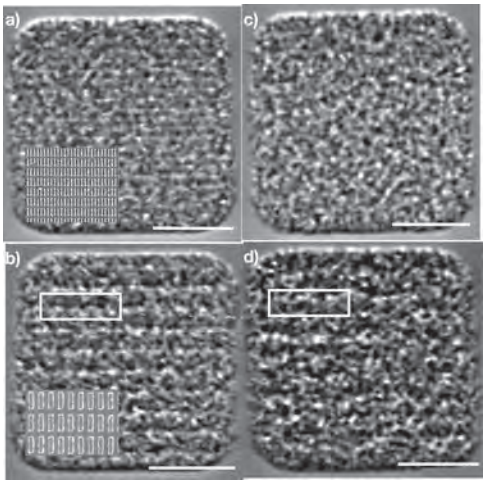

Fig. 1 MFM images of NCs in remanent state, after applied field of 250 mT (left) and 500 mT (right), for rod widths of 24 nm (a,c) and 120 nm (b,d). Inserts - SEM plan view images of the nanorods (1 μm scale bar).

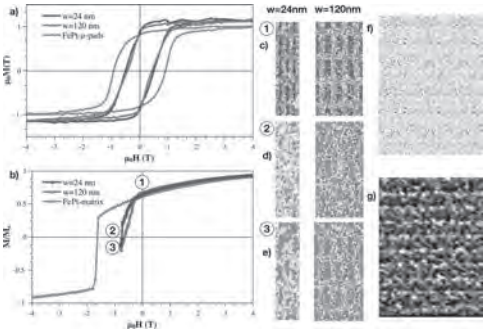

Fig. 2 a) Experimental M(H) loops; b) Simulated demagnetization curves. c-e). Magnetization maps at the height of the rod (numbers indicate position along the demag curve). Simulated (f) and experimental (g) MFM contrast.

DOC-06. High-throughput and Data-mining Search for Novel Rare-Earth-Free Permanent Magnets. *A. Vishina*[1], H.C. Herper[1] and O. Eriksson[1,2] *1. Physics and Astronomy, Uppsala University, Uppsala, Sweden; 2. School of Science and Technology, Örebro University, Örebro, Sweden*

Where the high-performance permanent magnets are needed (e.g. in the area of 'green' energy technology, such as electric vehicles and windmills) rare-earth (RE) magnetic materials dominate. At the same time, the heavier RE elements are quite expensive, some of them are rapidly decreasing in availability, and are often mined with the methods that leave an environmental footprint. Additionally, nowadays, there is a gap between the 'strong' RE-based magnets and their RE-free alternatives. We are using the data-mining approach in the search for high (and medium)-performance RE-free/lean magnetic materials. Filtering through a large number of known structures from ICSD database [1], we are looking for materials with high magnetization M > 1 T, uniaxial MAE > 1 MJ/m^3, and T_c >300 K. Sometimes, additional elements alterations are attempted to tweak the properties that are below the required values or make the material more cost-effective. Two searches have already been performed – a search amongst the materials containing a 3d- and a 5d-elements [3] and the materials that contain at least two 3d- metals [4]. New material was found (that had not been used as a permanent magnet before) and consequently synthesized by our experimental collaborators – Co_3Mn_2Ge [4]. From the ab-initio calculations, the defect-free material was predicted to have the saturation magnetization of 1.71 T, the uniaxial magnetocrystalline anisotropy of 1.44 MJ/m^3, and

the Curie temperature of 700 K. The samples synthesized, however, were found to have a partial disorder of Co and Ge. A saturation polarization of 0.86 T at 10 K was detected, together with a uniaxial magnetocrystalline anisotropy constant of 1.18 MJ/m^3, and the T_C = 359 K. These magnetic properties make Co_3Mn_2Ge a very promising material to be considered as a rare-earth free permanent magnet. Its magnetism depends critically on the amount of disorder of the Co and Ge atoms, a further improvement of the magnetism is possible. The next high-throughput search is being currently performed in collaboration with the experimental colleagues. We would like to acknowledge the financial support of the SSF and SNIC for the computation resources.

1. http://www2.fiz-karlsruhe.de/icsd_home.html 2. John M. Wills *et al.,* arXiv:cond-mat/9912173 (1999) 3. A. Vishina, O. Yu. Vekilova, T. Björkman, A. Bergman, H. C. Herper and O. Eriksson *Phys. Rev. B* 101, 094407 (2020) 4. A. Vishina, D. Hedlund, V. Shtender, E. K. Delczeg-Czirjak,. R. Larsen, O. Yu. Vekilova, S. Huang, L. Vitos, P. Svedlindh, M. Sahlberg, O. Eriksson, Heike C. Herper, Acta Materialia, 212, 116913 (2021)

DOC-07. Effect of Dopants (Mo, Cr, V) on the Magnetic Properties of Mn-Al-C nanostructured by Flash-Milling. *C. Muñoz Rodriguez*[1], J. Soler Morala[1], E.M. Palmero[1], B. Skårman[2], H. Vidarsson[2], P. Larsson[2] and A. Bollero[1] *1. Group of Permanent Magnets and Applications, IMDEA Nanoscience, Madrid, Spain; 2. Höganäs AB., Höganäs, Sweden*

Permanent magnets (PMs) are indispensable in sectors as important as energy and electromobility. MnAlC is an excellent rare earth-free candidate to contribute to fill the gap existing between ferrites and NdFeB magnets, provided a successful development of its PM properties. This will be only possible by combining a high magnetization, through a maximized content of the only ferromagnetic phase in the MnAl system (τ-phase), and an enhanced coercivity, through efficient nanostructuring and phase transformation [1]. We have recently shown the importance of combining the formation of the β-Mn phase and Mn_3AlC to increase coercivity -while maintaining a high remanence- in both powder and bulk MnAlC magnets produced by a simplified hot-pressing method [2]. The choice of specific additives may be a successful route to enhance magnetic properties [3]. This study shows the possibility of reaching a coercivity exceeding 2.5 kOe (200 kA/m) for 1 at.% Mo- and Cr-doped MnAlC powder and 3.3 kOe (263 kA/m) for V-doped MnAlC powder. This has been possible by combining gas-atomization and the self-developed flash-milling method (30-240 s) for efficient nanostructuring and promoting the creation of nanoprecipitates acting as pining centers [4]. A five-fold increase in coercivity has been achieved by comparison with that of the unmilled powder (see Fig. 2 for Mo-doped MnAlC). Furthermore, a proper choice of the milling time followed by an optimized annealing has allowed for combining high coercivity with an enhanced remanence (35 emu/g for a Cr-doped MnAlC sample) [4]. This approach opens a new path for engineering novel MnAlC doped nanostructures with promising PM properties. Acknowledgments. Gas-atomized powder was synthesized by Höganäs AB under the industrial project ECNanoManga between Höganäs and IMDEA Nanociencia. IMDEA acknowledges financial support by NEXUS project (PID2020-115215RB-C21) from MICINN.

[1] J. Rial *et al.*, Acta Mater., 157, 42 (2018); Engineering, 6, 173 (2020). [2] C. Muñoz-Rodríguez *et al.*, J. Alloys Compd., 847, 156361 (2020). [3] V. Shtender *et al.*, Sci. Rep. 11, 14453 (2021). [4] C. Muñoz-Rodríguez *et al.* In preparation (2021).

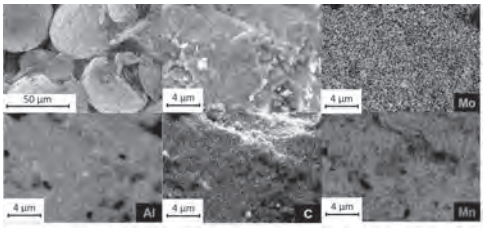

Fig. 1. SEM and EDX elemental maps images for a flash-milled (120 s) Mo-doped MnAlC sample.

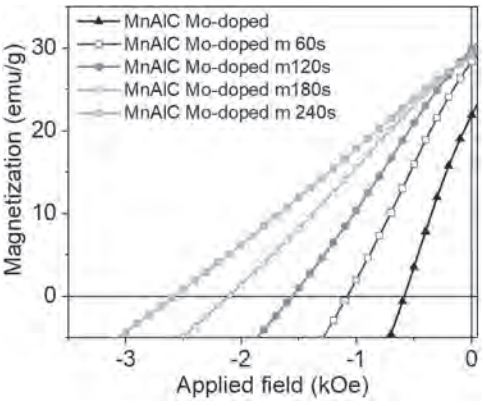

Fig. 2. Second quadrant of the hysteresis loops measured for Mo-doped MnAlC gas-atomized powder and for the same sample after flash-milling powders for different milling times (60 – 240 s).

DOC-08. $Fe_{16}N_2$ Permanent Magnet Production by High-Pressure Consolidation. *O. Zirhli*[2,1], N. Gunduz Akdogan[3,4], D. Le Roy[5], S. Le Floch[5] and O. Akdogan[1,4] *1. Mechatronics Engineering, Bahcesehir University, Istanbul, Turkey; 2. Materials Science and Nano Technology, Sabanci University, Istanbul, Turkey; 3. Piri Reis University, Istanbul, Turkey; 4. Nanoterial Technology Corporation, Istanbul, Turkey; 5. Univ Lyon, Université Claude Bernard Lyon 1, CNRS, Institut Lumière Matière, Lyon, France*

Neodymium-based magnets are used dominantly in the industry due to their exceptional magnetic properties. However, because of regulations and environmental harm on rare earth elements, it is unsustainable to use Nd-Fe-B. $Fe_{16}N_2$ is proposed as an alternative to rare-earth-based magnets, as it shows a giant magnetic energy product and abundance of its elements. Here we demonstrate an improvement to our previously published low-cost synthesis method to produce highly coercive $Fe_{16}N_2$ flakes and a consolidation method to form it into a permanent magnet. The synthesis path begins with deforming iron powder into iron flakes by surfactant-assisted ball milling. Iron flakes are heat treated under air to achieve a porous morphology to increase Fe to $Fe_{16}N_2$ conversion yield. Porous flakes are reduced under Ar/H_2 gas flow, followed by a low-temperature nitridation process under ammonia gas. Synthesized $Fe_{16}N_2$ flakes exhibit saturation magnetization up to 180 emu/g and coercivity up to 1.1 kOe. (Fig. 1) Rietveld analysis of the X-ray diffraction measurement of flakes shows up to 93% volumetric fraction of $Fe_{16}N_2$ phase. To consolidate $Fe_{16}N_2$ cold press method is used. Consolidated flakes do not indicate any trace of phase decomposition, hence a solid $Fe_{16}N_2$ magnet is produced. (Fig.2.) A cost-effective method to bulk produce $Fe_{16}N_2$ magnet could be sustainable for next-generation magnet applications.

Zirhli, O., Gunduz Akdogan, N., Odeh, Y. N., Misirlioglu, I. B., Devlin, E., & Akdogan, O. (2020). Fabrication and Characterization of Fe16N2 Micro-Flake Powders and Their Extrusion-Based 3D Printing into Permanent Magnet Form. In Advanced Engineering Materials (Vol. 22, Issue 11). https://doi.org/10.1002/adem.202000311

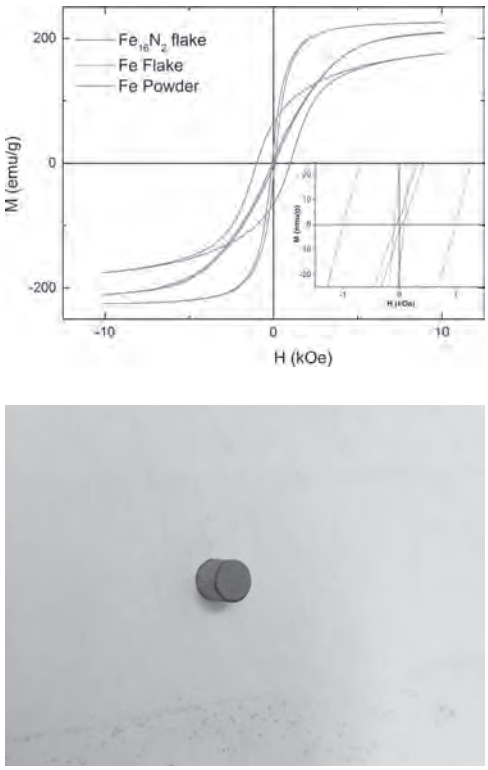

DOC-09. Effects of Tensile Stress during Annealing of Alnico Melt Spun Ribbons. *E. Rinko*[1,2], X. Zhang[3], A. Valeriano Inchausti[4], L. Lewis[3], M. Vázquez[4], W. Tang[2], M.J. Kramer[1,2] and I. Anderson[1,2] *1. Materials Science and Engineering, Iowa State University, Ames, IA, United States; 2. Ames Laboratory, Ames, IA, United States; 3. Mechanical and Industrial Engineering, Northeastern University, Boston, MA, United States; 4. Instituto de Ciencia de Materiales de Madrid (CSIC), Madrid, Spain*

The good high-temperature performance of alnico permanent magnets (PMs), based on Al, Ni, Co, and Fe, make them a potential alternative to critical rare earth (RE) PMs to power electric machines. Synthesis of higher grades of alnico employs an applied magnetic field at elevated temperatures, *i.e.*, magnetic annealing (MA), to bias a spinodal transformation from a partially ordered body centered cubic solid solution to a ferromagnetic Fe-Co phase (α_1) and an Al-Ni matrix phase (α_2) with coherent lattices. To maximize coercivity (H_c), up to ~3900 Oe in theory, α_1 should exist as isolated small (<20 nm), cylindrical "needles" to promote shape anisotropy [1, 2], but MA and subsequent draw anneals have yet to approach this H_c. Upon revisiting the thermodynamic basis of this spinodal transformation [3], a novel opportunity was seen to utilize a tensile stress instead of a magnetic field to bias the formation of α_1 more effectively. Experimental alnico compositions were rapidly solidified into melt-spun ribbons. Ribbon samples (~ 1 mm x 30 μm x 20 mm long) were annealed between 760-860 °C in a controlled atmosphere (N_2) with and without a 10 MPa tensile stress for 5 min and furnace cooled. Initial X-Ray diffraction (XRD) data suggests that stress-annealed (SA) ribbons, regardless of annealing temperature, have a different phase assembly. There is a distinction between the face centered cubic patterns in the annealed (A) vs. SA samples. Additionally, SA samples show larger α_1 and α_2 *d*-spacings differences at 830 °C and 860 °C, which indicates an enhanced α_1 and α_2 composition separation (Figure 1). This enhanced composition separation induced by a tensile stress could lead to improved H_c and magnetic saturation after draw anneals. Further structural (microstructure) and magnetic property characterization should help to more fully define the effect of stress-annealing of alnico, especially observing the final morphology of the α_1 and α_2 phase assemblage. Acknowledgement: This work is supported in part by IEEE MagSoc Educational Seed Funding and KC-NSC through Ames Lab contract no. DE-AC02-07CH11358.

[1] L. Ke, R. Skomski, T.D. Hoffmann, L. Zhou, W. Tang, D.D. Johnson, M.J. Kramer, I.E. Anderson, C.Z. Wang, Simulation of alnico coercivity, Applied Physics Letters, 111, 022403-1 - 022403-5, (2017) [2] L. Zhou, M.K. Miller, P. Lu, L. Ke, R. Skomski, H. Dillon, Q. Xing, A. Palasyuk, M.R. McCartney, D.J. Smith, S. Constantinides, R.W. McCallum, I.E. Anderson, V. Antropov, M.J. Kramer, Architecture and magnetism of alnico, Acta Materialia, 74, 224-233 (2014) [3] J.W. Cahn, Magnetic Aging of Spinodal Alloys, Journal of Applied Physics, 34, 3581-3586, (1963)

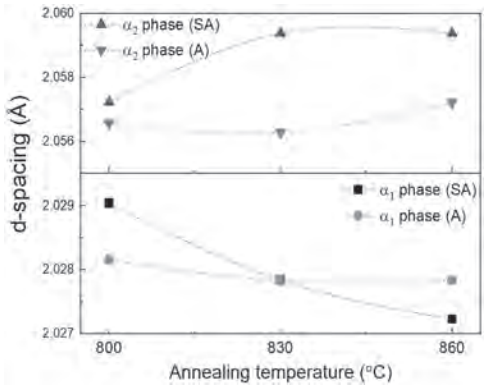

Figure 1: d-spacing of the highest resolved hk0 α1 and α2 peaks in SA and (A) XRD patterns.

DOC-10. Indications for Novel L1′ Ordering in Fe-Pt Alloys Near the Fe-rich Eutectoid Composition. *A. Savovici*[1], W.A. Soffa[1] and J.A. Floro[1] *1. Materials Science, University of Virginia, Charlottesville, VA, United States*

Magnetic properties and phase transformations in the archetypal binary alloys Fe-Pt, Co-Pt, and Fe-Pd are typically studied at near-equimolar compositions, due to the high magnetocrystalline anisotropy of the ordered $L1_0$ intermetallic. But these systems also possess eutectoid triple points, and proper thermal treatments at these compositions can create fascinating two-phase microstructures, e.g., nanochessboards in Co-Pt. Phase transformation behavior in the Fe-Pt system associated with the Fe-rich A1-> $L1_2$+$L1_0$ eutectoid has barely been examined. We have produced an Fe-Pt arc melt with 34 at% Pt, nominally in the $L1_2$+$L1_0$ coexistence region. Continuous cooling of this sample through the eutectoid at various rates decomposes the high-temperature A1 phase into two *tetragonal* phases with different c/a ratios, rather than forming a cubic and tetragonal phase as suggested by the equilibrium phase diagram. Analysis of the Bragg-Williams long-range order parameter leads us to hypothesize the coexistence of $L1_0$ (Fig. 1) with the L1' (Fig. 2) phase that was proposed by Shockley[1] in 1938. Subsequently, L1' has been shown using computational approaches to be a stable low-temperature ordering of off-stoichiometry $L1_0$. L1' is a specially decorated L10 lattice that accommodates off-stoichiometric compositions only on the basal-plane center atom. Until recent work by our group in Fe-Pd thin films, L1' had not been observed experimentally. This research will examine the ordering mechanisms and phase evolution in bulk Fe-Pt, and the effect of ordering kinetics and lengthscales on the magnetic properties in and near the two-phase region. Support of the National Science Foundation through grant DMR-1709914 is gratefully acknowledged.

1. Shockley W. *J Chem Phys*. 1938;6(3):130-144.

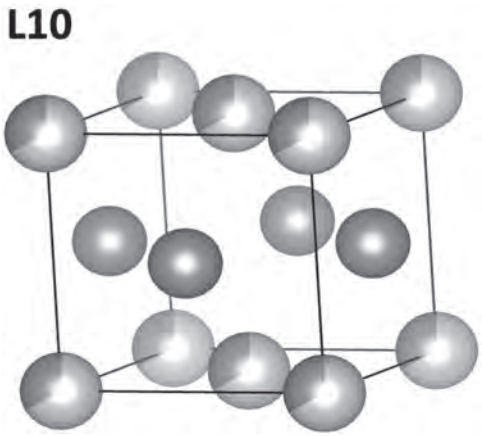

Fig 1. In these unit cell illustrations, Fe is orange and Pt is gray. L10 and L1′ are both tetragonal phases that share the P4/mmm space group, however, the two structures accommodate (off-stoichiometric) excess iron differently. In our Fe- 34 at% Pt composition sample, fully ordered L10 distributes excess Fe-atoms equally across all Pt sites.

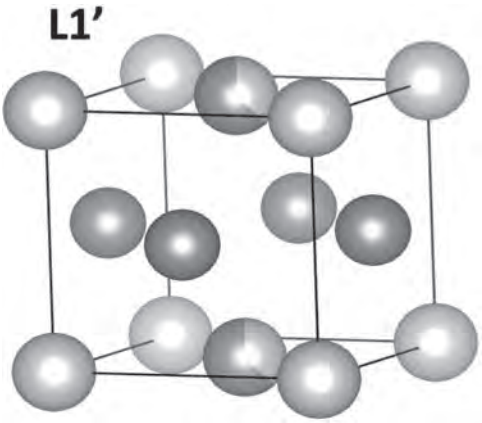

Fig 2. For the same composition, fully ordered L1′ places excess Fe-atoms only on the basal-plane center atom, while the corner Pt-site remains undisturbed.

DOC-11. The Formation of a Nanoscale Hard Magnetic Ferrite from Prussian Blue Nanocrystals. *J.G. MacDougall*[1], A. Namai[1], M. Yoshikiyo[1] and S. Ohkoshi[1] *1. School of Science, Chemistry, The University of Tokyo, Tokyo, Japan*

Epsilon iron oxide (ε-Fe_2O_3) is a nanoscale iron oxide polymorph with a large coercive field value (> 20 kOe at room temperature). High yield ε-Fe_2O_3 syntheses involve the use of a SiO_2 matrix to prevent agglomeration during high temperature sintering (> 900°C).[1-3] Herein, we present a new synthesis method of ε-Fe_2O_3 at low temperature and ambient pressure which uses no protective matrix, via a precursor of Prussian blue with a small amount of embedded ε-Fe_2O_3 nanoparticles. Core ε-Fe_2O_3 nanoparticles, prepared using a standard method,[4] were sonicated in $K_4[Fe(CN)_6]_{(aq)}$ solution before 2M $HCl_{(aq)}$ was added. The obtained sample (denoted core-shell) was sintered in air at 300°C, 400°C and 500°C for 2 hours. Fig. 1a shows TEM images of the core-shell, 300°C, 400°C and 500°C sintered samples. ε-Fe_2O_3 nanoparticles are shown to have spherical morphology, d_{TEM} = 23 ± 7 nm, whereas Prussian blue nanocrystals are larger cubic or spherical particles. The sintered samples at 300°C, 400°C and 500°C show aggregations of spherical and cubic nanoparticles which become more distinct as the temperature increases. Fig. 1b shows the XRD spectra with Rietveld analysis. The core-shell sample shows peaks assigned to ε-Fe_2O_3 (24%, orthorhombic, $Pna2_1$) and Prussian blue (76%, cubic, Fm3m). In the sintered samples, Prussian blue peaks are not present, though the peaks corresponding to the core ε-Fe_2O_3 remain with the particle size calculated via the first principles method consistent in all samples, ca. 25 nm. At 300°C, a second phase of ε-Fe_2O_3 and γ-Fe_2O_3 with particle sizes ca. 3 nm are present, alongside a small amount of α-Fe_2O_3. At 400°C, the proportion of small size Fe_2O_3 nanoparticles decreases, and the proportion of ca. 25 nm ε-Fe_2O_3 and α-Fe_2O_3 increases. At 500°C, the only phases present are ca. 25 nm ε-Fe_2O_3 (92%) with a small amount of macroscale α-Fe_2O_3 (8%). Prussian blue was shown to convert to ε-Fe_2O_3 at high yield when sintered at 500°C in the presence of ε-Fe_2O_3 core nanoparticles. This is the lowest temperature ε-Fe_2O_3 has been reportedly prepared at in ambient pressures and may pave the way to a lower energy synthesis method for this hard magnetic ferrite.

1. J. Jin, S. Ohkoshi and K. Hashimoto, Adv. Mater., Vol. 16,. 48 (2004) 2. S. Sakurai, A. Namai, K. Hashimoto et al., J. Am. Chem. Soc., Vol. 131, p. 18299 (2009) 3. H. Tokoro, W. Tarora, A. Namai et al., Chem. Mater, Vol. 30, p. 2888-2894 (2018) 4. S. Ohkoshi, A. Namai, K.Imoto et al., Sci. Rep., Vol. 5, p. 14414 (2015)

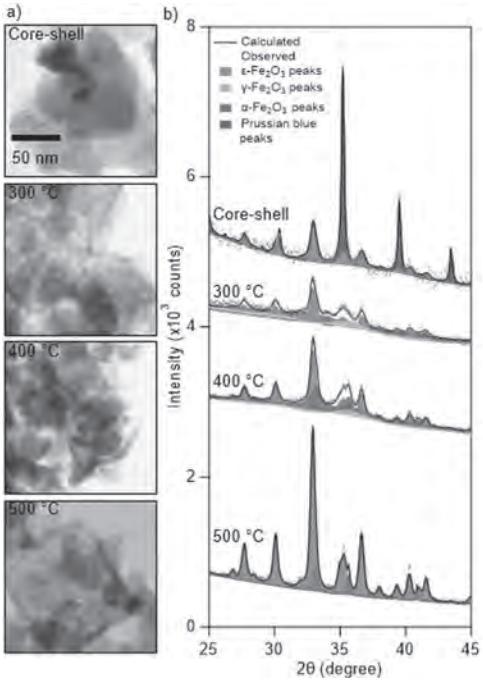

Fig. 1 a) TEM images and b) XRD spectra of respective samples

DOC-12. Submicron particles of Ga-substituted strontium hexaferrite obtained by citrate auto-combustion method. *E. Gorbachev*[1], L. Trusov[1] and P. Kazin[2] *1. Department of Materials Science, Lomonosov Moscow State University, Moscow, Russian Federation; 2. Department of Chemistry, Lomonosov Moscow State University, Moscow, Russian Federation*

M-type hexaferrites is known to be sensitive to thier chemical composition, which can be an effective instrument to preciesly control magnetic properties of the materials. In this study, we demonstrate the synthesis and the investigation of the magnetostatic and magnetodynamic properties of single-domain gallium substituted strontium M-type hexaferrite particles $SrFe_{12-x}Ga_xO_{19}$ (x = 1 - 6). The synthetic approach is based on a precursor preparation *via* a facile citrate-nitrate auto-combusion method followed by thermal treatment at 1200 °C. The annealing of the porous precursor led to the formation of single-domain hexaferrite particles with mean sizes of 360 – 560 nm. Introduction of Ga^{3+} ions up to x = 4 into the hexaferrite structure resulted in a growth of coercivity from 5.1 to 6.4 kOe, and further increase in gallium concentration led to a decrease in the coercivity. The samples display natural ferromagnetic resonance frequency in the range of 49 – 57 GHz. Crystal structure refinement reveals, that Ga^{3+} ions preferably occupy

2*a,* 4f_1, 12*k,* and 2b sites and cause a decrease in the magnetic anisotropy and a modest decrease in the saturation magnetization. The research was supported by RFBR grant no 21-53-12002.

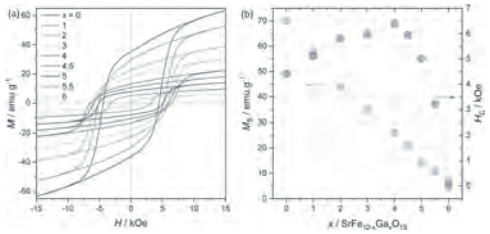

a) Magnetic hysteresis loops of $SrFe_{12-x}Ga_xO_{19}$ (x = 0 – 6) samples; b) The dependencies on the substitution degree (x) of coercivity (H_C) and saturation magnetization (M_S).

Session DOD
ADVANCED PROCESSING OF PERMANENT MAGNETS

Isabelle de Moraes, Co-Chair
Institut Jean Lamour, Université de Lorraine, Vandoeuvre-lès-Nancy, France
Jeffrey Shield, Co-Chair
University of Nebraska-Lincoln, Lincoln, NE, United States

CONTRIBUTED PAPERS

DOD-01. A Sustainable Route for Permanent Magnets Fabrication: Additive Manufacturing Applied to Recycled Ferrite Residues.

D. Casaleiz[1*], E.M. Palmero[1], J. de Vicente[1], A. Seoane[2], R. Altimira[2] and A. Bollero[1] *1. Group of Permanent Magnets and Applications, IMDEA Nanociencia, Madrid, Spain; 2. Ingeniería Magnética Aplicada, IMA S.L.U., Barcelona, Spain*

Ferrites are the most used permanent magnets (PMs) due to their availability and low cost, being an alternative to PMs based on critical rare-earths in new applications such as electromobility [1]. In this work we will show the possibility of 3D-printing objects using strontium ferrite powder obtained by successful recycling of the residue generated from manufacturing commercial ferrite magnets. Tuning the morphology and microstructure of the Sr-ferrite residue by post-processing made possible to end with Sr-ferrite powder with PM properties superior, not only to the residue precursor, but to those of the brand new commercial powder (3.5 fold increase in coercivity and a 25% increase in remanence) [2]. The recycled ferrite was used as precursor for synthesizing composites by the solution casting method [3], and extruding filaments for advanced manufacturing of magnets (with a particle content up to 65 wt%) by Fused Filament Fabrication. Magnetic characterization of composites, filaments and printed objects was performed by Vibrating Sample Magnetometer (VSM), showing that the magnetization scales accordingly to the content of ferrite particles and that there is no deterioration of the PM properties of the starting particles along processing (Fig. 1). Scanning Electron Microscopy (SEM) analysis showed a homogeneous distribution of the particles in the polymer matrix (Fig. 2) [4]. This work has shown an efficient path for developing new and alternative PMs by the combination of recycling and 3D-printing. Acknowledgements. Authors acknowledge financial support from MICINN by NEXUS project (PID2020-115215RB-C21), industrial collaboration PLASMAG with IMA S.L.U. and from the Regional Government of Madrid by NanoMagCOST project (P2018/NMT-4321).

1. A. Bollero and E. M. Palmero, Recent Advances in Hard Ferrite Magnets. In: J.J. Croat and J. Ormerod (eds.) *Modern Permanent Magnets*. Elsevier. In press. 2. A. Bollero, *et al. ACS Sustain. Chem. Eng.* Vol. 5, p.3243-3249 (2017). 3. E.M. Palmero, *et al. Sci. Technol. Adv. Mater*. Vol. 19, p.465 (2018); *Addit. Manuf*. Vol. 33, p.101179 (2020). 4. D. Casaleiz, *et al.* In preparation (2021).

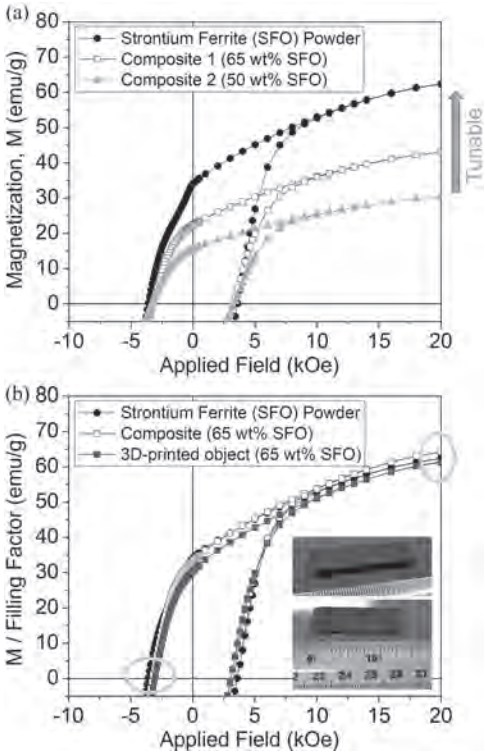

Fig. 1. (a) First and second quadrants of the hysteresis loops of starting powder and composites with different content of ferrite. (b) Normalized hysteresis loops of the starting powder, composite and 3D-printed object. Insets show a 3D-printed piece based on ferrite particles.

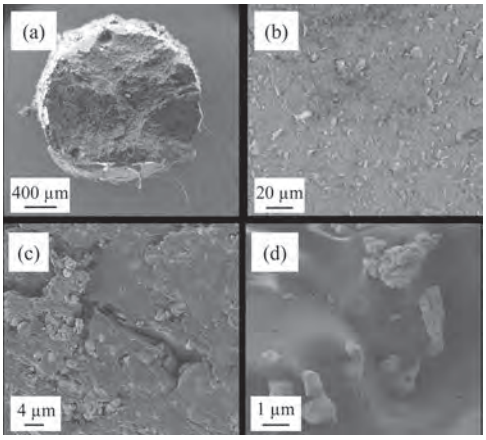

Fig. 2. SEM images of: (a) cross section and (b) closer view of a magnetic filament with a 50 wt% of ferrite; and (c) and (d) inner morphology of a 3D-printed object with a particle content of 65 wt%.

DOD-02. Optimizing the Particle Size Distribution in Permanent Magnet Composites to Extrude Flexible Filaments for Additive Manufacturing. *E.M. Palmero*[1], D. Casaleiz[1], J. de Vicente[1] and A. Bollero[1] *1. Permanent Magnets and Applications, IMDEA Nanociencia, Madrid, Spain*

Additive manufacturing (AM) of composites is attracting much interest in high-tech sectors for fabricating complex high-performance objects with tailored properties [1]. For permanent magnets (PMs), the challenge is to develop magnets by AM with no geometrical restrictions, high filling factor (FF), and non-deteriorated PM properties [2], together with finding alternatives (e.g., improved ferrites and promising MnAlC-based alloys) to rare earth-based magnets [3]. Composites (PM particles/polymer) were synthesized by solution casting, followed by extrusion of filaments for 3D-printing, being reported for the very first time (Fig. 1). Several alternative PM materials were studied (gas-atomized τ-MnAlC, Sr-ferrite and hybrids —Sr-ferrite/NdFeB). Particle size and fine-to-coarse particles ratio (FP/CP) play a key role on the flexibility and powder loading of MnAlC filaments (length>10 m), reaching FF>80% and non-deteriorated PMs properties (Fig. 1) [4]. These results will be compared to the obtained for filaments based on Sr-ferrite (Hc=239 kA/m, FF=92%), NdFeB (Hc=812 kA/m, FF=93%) and hybrids (Hc=629 kA/m, FF=90%) (Fig. 2). MnAlC-based objects were 3D-printed under controlled temperature, proving that alternative PM materials can be efficiently synthesized and processed to develop novel PMs by AM (Fig. 1) [4]. Acknowledgements. Authors acknowledge collaborations with B. Skårman, H. Vidarsson and P.-O. Larsson (Höganäs, Sweden) by the industrial contract *GAMMA,* and A. Nieto and R. Altimira (IMA, Spain), and financial support from: EU M-ERA.NET by *COSMAG* project (PCI2020-112143); MICINN by *NEXUS* project (PID2020-115215RB-C21); CM by *NanoMagCOST* project (P2018/NMT-4321).

[1] L.E. Murr, J. Mater. Sci. Technol. 32, 987 (2016). [2] C. Huber et al., Appl. Phys. Lett. 109, 162401 (2016); J. Jaćimović et al., Adv. Eng. Mater. 19, 1700098 (2017). [3] A. Bollero et al., ACS Sustainable Chem. Eng. 5, 3243 (2017); J. Rial et al., Acta Mater. 157, 42 (2018); J. Rial et al. Engineering, 6, 173 (2020); C. Muñoz-Rodríguez et al., J. Alloys Compd., 847, 156361 (2020). [4] E.M. Palmero et al., Sci. Technol. Adv. Mater. 19, 465 (2018); IEEE Trans. Magn. 55, 2101004 (2019); Addit. Manuf. 33, 101179 (2020).

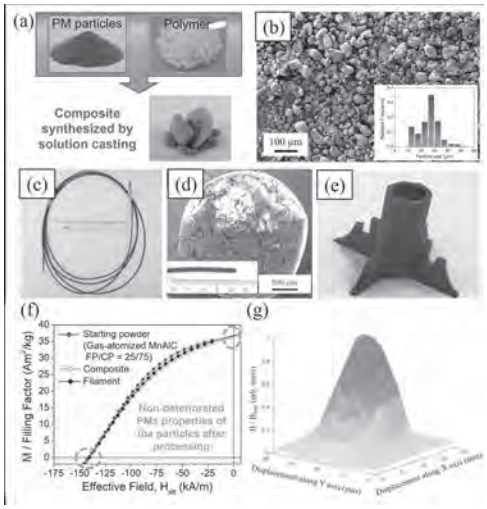

Fig. 1. (a) Gas-atomized MnAlC, polymer, and composite; (b) SEM image of MnAlC particles and size distribution; (c), (d) image and SEM cross section of a MnAlC/ABS filament; (e) MnAlC-based 3D-printed object; (f) normalized magnetic response of MnAlC-based samples; and (g) magnetic flux density of a 3D-printed MnAlC-based disc.

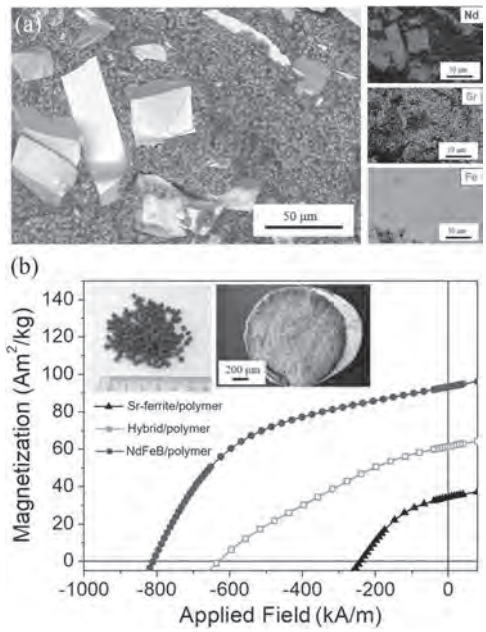

Fig. 2. (a) SEM and EDX of a hybrid composite; (b) second quadrant of the hysteresis loops for the hybrid, Sr ferrite- and NdFeB-based materials. Insets show composite pellets and SEM cross section of a Sr ferrite-based filament.

INVITED PAPER

DOD-03. In-situ alignment of anisotropic hard magnets of 3D printed magnets. M. Suppan[1], K. Mathauer[1], C. Huber[1], S. Kobe[5], S. Schuschnigg[2], B. Saje[3], I. Teliban[4], M. Groenefeld[4] and *D. Suess*[1]
1. University of Vienna, Vienna, Austria; 2. Montanuniversitaet Leoben, Leoben, Austria; 3. Kolektor Magnet Technology GmbH, Essen, Germany; 4. Magnetfabrik Bonn GmbH, Bonn, Germany; 5. Jozef Stefan Institute, Ljubljana, Slovenia

3D printing of permanent magnets has recently received considerable attention [1,2]. In previous work the realization of isotropic magnets was demonstrated using fused filament fabrication, which results in the fabrication of polymer bonded magnets, with properties very similar to state-of-the-art magnets fabricated by injection molding [1]. In Ref [3] the easy axis of the printed magnet was aligned by printing the magnetic filament on magnetized hard magnets. Within this talk we will present a significant step forward by producing magnets where the easy axis can be locally aligned in-situ during the printing process. This is realized by redesigning the printer nozzle of a fused filament fabrication printer (FFF) so that permanent magnets can be placed next to the nozzle. The magnetic strayfield of the permanent magnets is optimized so that it aligns the easy axis of anisotropic ferromagnetic particles inside a paste-like compound material when it is in the melted state. Two different magnetic materials are investigated: (i) Strontium hexaferrite inside a PA6 matrix (Sprox® 10/20p), fill grade: 49 vol% and (ii) $Sm_2Fe_{17}N_3$ inside a PA12 matrix, fill grade: 44 vol%. In the presence of the external alignment field, the Sr ferrite particles inside the PA6 matrix can be well aligned as shown in Fig. 1, where the hard axis hysteresis loop (blue) and easy axis hysteresis loop (orange) is shown. The ratio of the remanence of the hard axis loop and the easy axis hysteresis loop is 2.2, which shows a significant alignment. No significant alignment for $Sm_2Fe_{17}N_3$ could be achieved, where the ratio of the easy and hard axis remanence is just 1.15. The results show the feasibility to fabricate magnets with arbitrary and locally defined easy axis, since the permanent magnets (or alternatively electromagnet) can be mounted on a rotatable platform. Hence, highly optimized magnets can be produced such as Hallbach arrays which can not be produced by any other method.

[1] C. Huber et al., Appl. Phys. Lett.,. 109 162401 (2016). [2] L. Li et al., Scientific reports 6.1 1-7 (2016) [3] K. Sonnleitner et al., Applied Physics Letters, 116.9 092403 (2020).

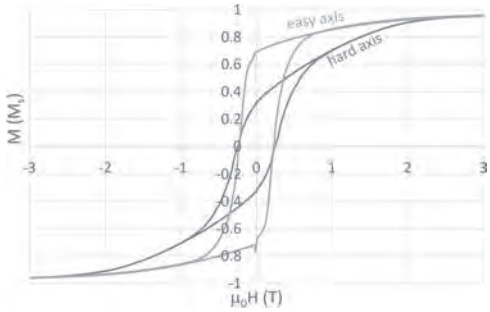

Hysteresis loops in hard and easy axes of a hard magnetic ferrite (Sprox) measured with the VSM. The 3d printed magnetic material is aligned in-situ during the print process by permanent magnets next to the printer nozzle.

CONTRIBUTED PAPERS

DOD-04. Modeling in-situ magnetic alignment during magnetic 3D printing. *A. Sarkar*[1], M. Paranthaman[2] and C.I. Nlebedim[1] *1. Ames Laboratory, Ames, IA, United States; 2. Oak Ridge National Laboratory, Oak Ridge, TN, United States*

Additive manufacturing (AM) via 3D printing technologies have become a frontier in materials research, including its application in the development and recycling of permanent magnets[1,2]. The limited availability of the rare earth elements (REEs) for magnets present a demanding challenge and necessitates reduction in the losses of REEs from conventional or subtractive manufacturing. AM allows for a minimal waste production and re-utilization of recovered rare earths in the magnet processing. I*n-situ* alignment during 3D printing of magnetic materials has opened new horizons for manufacturing of complex permanent magnets[3,4]. The introduction of functionalized magnetic 3D printing as an AM process allows rapid prototyping of multi-directionally aligned magnetic systems, and reduced energy requirement due to the elimination of post-production alignment[3]. In this work, we have developed a robust multiphysics model to simulate the alignment of magnetic particles in a polymer matrix, during 3D printing. Magnetization vs. field measurements of extruded and printed Sm-Co bonded in PLA (15 vol.%) and Nd-Fe-B+Sm-Fe-N bonded in Nylon 12 (65 vol.%), with and without alignment, confirmed the alignment of magnetic particles. A parametric analysis was performed to understand the effect of process variables, like alignment field, loading fraction, printing speed and particle size, on the degree of alignment of the samples (Fig.1)[5]. The model is upgraded to consider variable particle size distributions, non-homogenous particle spacing and different printing temperature. The model predicts a competing behavior between particle-fluid and particle-particle interactions under magnetic field. The model provides a framework to efficiently predict the DoA in tandem with a functionalized-magnetic 3D printer and allows the user to adjust the operating parameters according to the desired DoA. This work is supported by the Critical Materials Institute (CMI), an Energy Innovation Hub funded by the U.S. Department of Energy (DOE), Office of Energy Efficiency and Renewable Energy, Advanced Manufacturing Office. Ames Laboratory is operated for the U.S. DOE by Iowa State University of Science and Technology under Contract No. DE-AC02-07CH11358.

[1] C. Huber, C. Abert, F. Bruckner, M. Groenefeld, O. Muthsam, S. Schuschnigg, K. Sirak, R. Thanhoffer, I. Teliban, C. Vogler, R. Windl, and D. Suess, Appl. Phys. Lett. 109, 162401 (2016). [2] L. Li, B. Post, V. Kunc, A.M. Elliott, and M.P. Paranthaman, Scr. Mater. (2017). [3] A. Sarkar, M.A. Somashekara, M.P. Paranthaman, M. Kramer, C. Haase, and I.C. Nlebedim, Addit. Manuf. 34, 101289 (2020). [4] Y. Kim, H. Yuk, R. Zhao, S.A. Chester, and X. Zhao, Nature 558, 274 (2018). [5] A. Sarkar, M.P. Paranthaman, and I.C. Nlebedim, Addit. Manuf. 46, 102096 (2021).

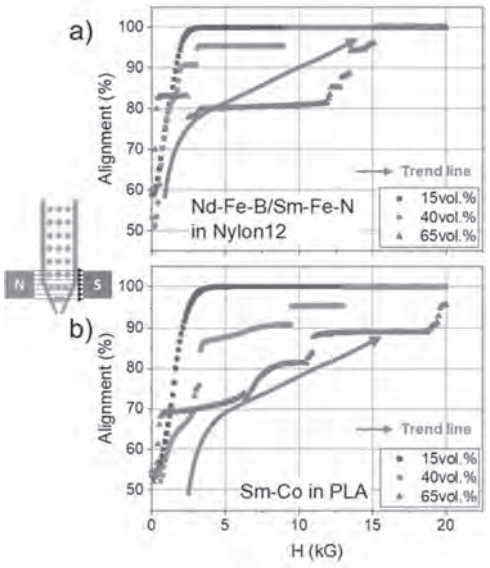

DOD-05. Time Dependence Analysis as a Function of the Temperature of Magnetic Polymer Composite Filaments. *T. Ahmed*[1], C. Belduque[2], M.Y. Chen[1,4], J.S. Tate[1,2] and W.J. Geerts[1,3] *1. Materials Science, Engineering and Commercialization, Texas State University, San Marcos, TX, United States; 2. Mechanical and Manufacturing Engineering, Texas State University, San Marcos, TX, United States; 3. Department of Physics, Texas State University, San Marcos, TX, United States; 4. Electrical Engineering, Texas State University, San Marcos, TX, United States*

Strontium ferrite/polyamide12 (PA12) magnetic composite fused deposition modeling filaments made using a twin-screw extruder are being studied to be used for Magnetic Field Assisted Additive Manufacturing (MFAAM) of permanent magnets. A previous study shows that the magnetic viscosity (MV) varies with field and field angle. The M_x MV is maximum in the easy plane (1.1%) and decreases with a factor of two along the filament's macroscopic hard axis [1]. The M_y MV is nearly zero along the hard axis and in the easy plane but maximum for intermediate angles. Here we study the time dependence as a function of temperature using a MicroSense EZ9 biaxial VSM to determine the melt viscosity. Samples were made by loading ~14 mg of $SrO(Fe_2O_3)_6$/PA12 (26 or 40 wt%) cylindrical-shaped filament parts in pyrex glass tubes. The filament is compacted with PEEK stoppers on both sides to secure its position and avoid direct exposure to the atmosphere while heating. Our aim is to study the rotation of the magnetic particles in the molten PA12 matrix. We first heat the sample to 200 °C to orient all the particles in the y-direction using a field of 22 kOe. Then the sample temperature is lowered to the target temperature after which the field is lowered to zero. Finally, a field step is applied in the x-direction and M_x and M_y are monitored as a function of the time. The rotation of the moment vector with time is calculated from the data. Measurements are done for the fields of 500 and 2000 Oe, and at the temperatures of 120, 124, 128, 132, and 136°C. Up to 128°C, no strong time dependence was observed. Between 128 and 132°C, the magnetic particles orientations are no longer fixed in the matrix, but they can rotate and line up along the field direction. The time dependence of the rotation of the magnetic particles in the PA12 matrix is calculated from M_x and M_y (Fig. 1 and Fig. 2). The time constant decreases with temperature and field. The melt viscosity of the molten PA12 matrix at 136 °C is determined from the data is 1.4E5 Pa.s at 500 Oe field.

[1] Tanjina N. Ahmed et al., AIP Adv.,11, 015048 (2021) This work was supported by an NSF DMR-MRI grant (Award 1726970) and a TxState Research Enhancement grant.

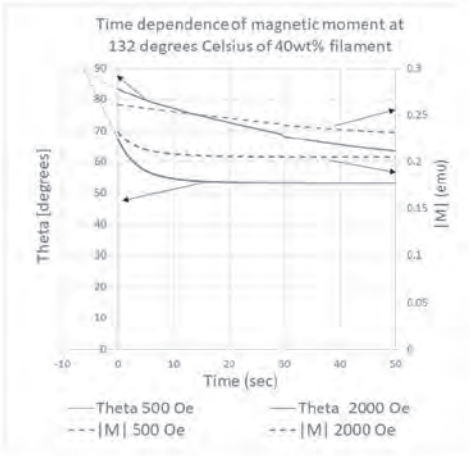

Fig 1. Time dependence of magnetic moment at 132 °C of 40wt% filament

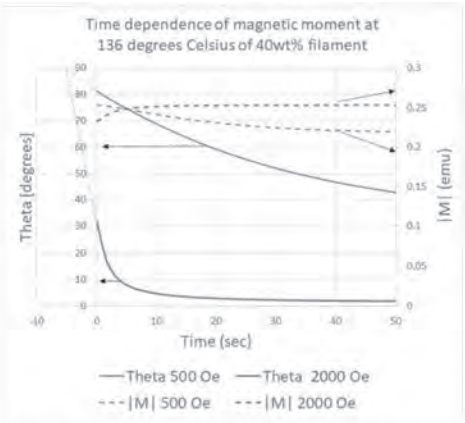

Fig 2. Time dependence of magnetic moment at 136 °C of 40wt% filament

DOD-06. Magnetic Properties of PDMS Embedded with Strotium Ferrite Particles Cured Under Different Magnetic Field Conditions. *A. Oliveira*[1], M. Hasan Kashem[2], D. Luna[3], W.J. Geerts[3], W. Li[2] and J. Yang[1] *1. Mechanical Engineering, Texas Tech University, Lubbock, TX, United States; 2. Chemical Engineering, Texas Tech University, Lubbock, TX, United States; 3. Department of Physics, Texas State University, San Marcos, TX, United States*

Soft materials embedded with hard magnetic particles have recently gained widespread recognition as small-scale actuators due to their capacity to be a rapid and precise shape-shifting material[1, 2]. Strontium ferrite ($SrFe_{12}O_{19}$) particles have been shown to be a great candidate for such applications, since it is an inert hard magnetic material [3]. The study of magnetic properties of hard-magnetic soft materials is a critical step to better design these upcoming actuators. The preparation of such material is done by mixing the particles into the uncured elastomer (PDMS), in liquid form, and then pouring the mixture in a mold for curing. If the samples are subjected to a magnetic field during the curing process, chains of particles are formed in the direction of the applied field (see Fig 1). We expect that the individual particles rotate in the fluid such that their easy axes becomes parallel to the curing field, thus creating an easy axis in the composite in this same direction. The magnetic properties of such types of composites, or for any other soft matrix, cannot yet be found in literature. In this study, we analyzed three concentrations of strontium ferrite particles in PDMS under three field configurations, resulting in 9 different samples. The concentrations used were 1:1, 2:1 and 4:1 ratios of PDMS to strontium ferrite per weight. All three samples of each concentration were cured either in a zero magnetic field, or over the north

pole of a permanent magnet, or over the side of said magnet (see Fig 2). A biaxial vibrating sample magnetometer (VSM) was used to measure torque curves and the hysteresis curves parallel and perpendicular to the curing field. The samples cured in a field show a squareness ratio of up to 0.94 while the samples cured in zero field, only close to 0.5. The samples cured in a field show a magnetic anisotropy with an easy axis parallel to the curing field. Anisotropy values are compared to the crystal anisotropy of strontium ferrite to determine the shape anisotropy contribution due to the observed chaining.

[1] W. Hu, G.Z. Lum, M. Mastrangeli and M. Sitti, Nature, Vol. 554, pp.81 (2018). [2] Z. Ren, W. Hu, X. Dong and M. Sitti, Nature Communications, Vol. 10, Art. No 2703, (2019). [3] C. Belduque, R. Robinson, A. Medina, T. Ahmed, R. Kala, W. Geerts and J. Tate, SAMPE Conference Proceedings (2021).

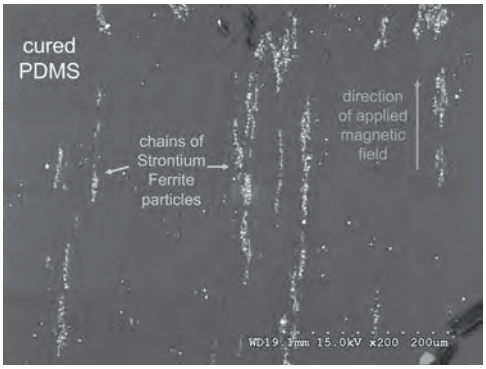

Fig. 1 PDMS/strontium ferrite composite showing alignment of particles when cured under magnetic field.

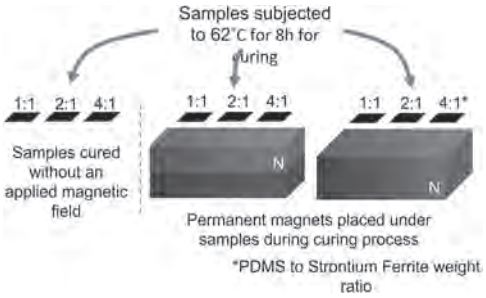

Fig. 2 Curing process of samples

DOD-07. Preparation of Fe-Pt thin-sheet magnets using exfoliation behavior. *M. Nakano*[1], Y. Miyahara[1], A. Tsuruoka[1], A. Yamashita[1], T. Yanai[1], T. Honda[2], T. Shinshi[3] and H. Fukunaga[1] *1. Nagasaki University, Nagasaki, Japan; 2. Kyushu Institute of Technology, Kitakyushu, Japan; 3. Tokyo Institute of Technology, Yokohama, Japan*

Since miniaturization of Fe-Pt magnets with excellent biocompatibility is a hopeful material to develop the performance of small medical devices [1], a lot of researchers prepared isotropic Fe-Pt thick-film magnets with the thickness above several microns by a sputtering, electrodeposition, and laser ablation technique [2-4]. Moreover, isotropic Fe-Pt thin-sheet magnets with a thickness range from 10 to 100 microns were prepared using a cold rolling and a rapidly quenching [5-6]. The use of Fe-Pt thin sheets does not need to optimize a substrate for each application. However, it is generally hard to improve the magnetic properties by controlling the microstructure compared with Fe-Pt films prepared by the deposition methods mentioned above. J. P. Liu reported a nano-composite Fe-Pt/α-Fe film with excellent magnetic properties by using a sputtering [7]. Here, a laser ablation technique was adopted to obtain Fe-Pt thin sheets by peeling Fe-Pt thick films from a Si substrate. As future work, we pay attention to the preparation of nano-composite Fe-Pt/α-Fe multilayered thin sheets because we have demonstrated rare-earth nano-composite films such as Nd-Fe-B/α-Fe and Sm-Co/α-Fe using the laser ablation technique [8]. In this research, Fe-Pt thin sheets thicker than 10 microns with Fe contents range from 50 to 60 at. % were prepared. Isotropic Fe-Pt thin sheets could be obtained by taking advantage of the exfoliation behavior after depositing Fe-Pt films on Si substrates using a laser ablation technique. (see Figure) A post-annealing process was used to obtain the L_{10} phase, and the (BH)max value of Fe-Pt thin sheets showed approximately 70 kJ/m^3. Moreover, the test of a cantilever containing the obtained Fe-Pt thin sheets showed good mechanical characteristics.

[1] A. Yamazaki, *et al.*, J. Magn. Magn. Mater. 272-276(2004)e1741-1742. [2] W. F. Liu, *et al.*, J. Magn. Magn. Mater. 302(2006) 201-205. [3] M. Nakano, *et al.*, J. Appl. Phys. 103(2008)#07E110. [4] T. Yanai, *et al.*, AIP advances, 10(2020)#015149. [5] N.H. Hai, *et al.*, J. Magn. Magn. Mater. 262(2003)353-360. [6] T. Bitoh, *et al.*, Scripta Materialia, 53(2005)429–434. [7] Liu, J. P., *et al.*, Appl. Phys. Lett. 72(1998) 483–485. H. Fukunaga, *et al.*, IEEE Trans. Magn. 50(2014)#2101504.

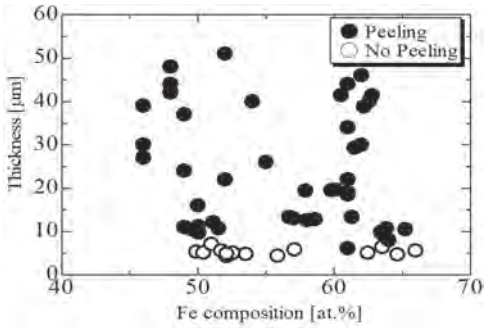

Figure Conditions of obtaining Fe-Pt thin sheet magnets through a peeling process using a laser ablation technique. When thickness exceeded approximately 7 μm, exfoliation behavior tended to occur.

Session DPA
PERMANENT MAGNETS AND PROCESSING II
(Poster Session)

Xubo Liu, Co-Chair
Ames Laboratory, Ames, IA, United States
Jeotikanta Mohapatra, Co-Chair
University of Texas at Arlington, Arlington, TX, United States

DPA-01. The effect of C addition on the magnetic properties and microstructures of nanocrystalline $SmFe_{11}Ti$ alloy. *H. Lee*[1], M. Kang[1] and J. Kim[1] *1. Hanyang University, Ansan, The Republic of Korea*

Recently, $SmFe_{11}Ti$-based compounds with the $ThMn_{12}$ crystal structure have been widely studied as a candidate for new permanent magnets due to their excellent intrinsic magnetic properties. Although those compounds have a high anisotropy field (12 T), the actual coercivity is less than 10% of their anisotropy field [1]. In general, it is well known that fine precipitates corresponding to the size of the domain wall (several nm to several tens of nm) increase the coercivity of hard magnetic materials by acting as the domain wall pinning site. The addition of C to the $SmFe_{11}Ti$ alloy may result in TiC precipitates in the matrix, and subsequent changes in the coercivity can be expected. In this study, $SmFe_{11}Ti$ alloys containing different amount of C atoms were fabricated by the melt-spinning method to investigate the effects of C atoms on the microstructures and magnetic properties. $SmFe_{11}Ti_{1+x}C_x$ (x = 0, 0.05, 0.1, 0.2) alloys with the $ThMn_{12}$ crystal structure was successfully fabricated by the melt-spinning method and subsequent heat treatment. The optimum heat treatment condition was found to be 850°C for 15 minutes, and the coercivity was shown to be about 6.2 kOe regardless of the C content (Fig. 1). In order to understand these results, the microstructural analysis was performed. It was found that the matrix had the $ThMn_{12}$ crystal structure and the average grain size was about 30 nm in all samples regardless of the C content (Fig. 2). In these samples, coarse TiC grains (>100 nm) instead of TiC nano-precipitates were formed independently from the matrix. This result explains the reason why the coercivity did not change. Thus, the experimental conditions for obtaining the precipitates are under investigation.

1 A. K. Srinithi and K. Hono, Journal of Magnetism and Magnetic Materials, Vol. 529, 167866 (2021)

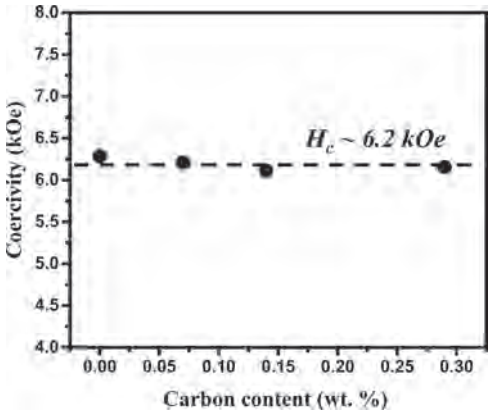

Fig. 1 Coercivity measured at 2.5 T of $SmFe_{11}Ti_{1+x}C_x$ (x = 0, 0.5, 0.1, 0.2) alloys heat treated at 850°C for 15 minutes.

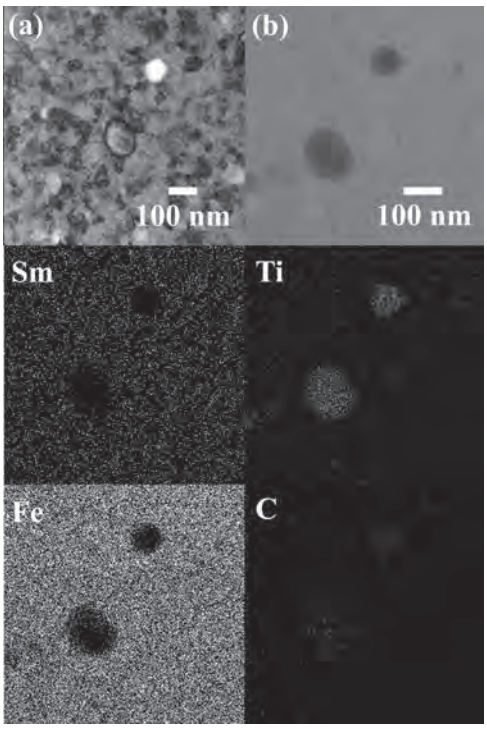

Fig. 2 Microstructures of $SmFe_{11}Ti_{1.2}C_{0.2}$ sample heat treated at 850°C for 15 minutes. (a)Bright field image using Transmission Electron Microscopy. (b)Dark field image and corresponding EDS mapping image using Scanning Transmission Electron Microscopy. The grains which was shown in dark contrast on the image was region that Ti and C was concentrated.

DPA-02. Modifying magnetic properties of MnBi with Carbon: An experimental and theoretical study. *M. Flesche*[1], Z. Mehlgerg[1], B. Lamsal[2], B. Lama[3], S. Valloppilly[4], Y. Zhou[2], T. Paudel[3], D. Sellmyer[5] and P. Kharel[1] *1. Physics, South Dakota State University, Brookings, SD, United States; 2. Electrical Engineering and Computer Science, South Dakota State University, Brookings, SD, United States; 3. Physics, South Dakota School of Mines and Technology, Rapid City, SD, United States; 4. Nebraska Center for Materials and Nanoscience, University of Nebraska-Lincoln, Lincoln, NE, United States; 5. Physics and Astronomy, University of Nebraska-Lincoln, Lincoln, NE, United States*

Research on rare-earth-free permanent magnet materials have attracted much attention due to the limited supply and high price of the rare-earth metals used in current state-of-the-art permanent magnets. MnBi and MnBi-based magnets have been investigated as prospective rare-earth-free magnets because the magnetic anisotropy of MnBi increases with increasing temperature reaching a maximum value at 590 K. However, segregation of Bi during synthesis of MnBi is one of the issues which reduces the saturation magnetization. We have found that MnBi synthesized in carbon environment

substantially reduces the amount of Bi segregation improving its saturation magnetization. We have synthesized $Mn_{55}Bi_{45}$ and $Mn_{55}Bi_{45}C$ samples using arc melting and high vacuum annealing. The room temperature x-ray diffraction patterns indicate that both $Mn_{55}Bi_{45}$ and $Mn_{55}Bi_{45}C$ crystallize in the hexagonal NiAs crystal structure (Low temperature phase, LTP). The X-ray diffraction pattern also indicates that the amount of Bi segregation in $Mn_{55}Bi_{45}C$ is less than that in MnBi. As shown in Fig. 1 below, the high field (3T) magnetization measured at room temperature are 61 emu/g and 66 emu/g for $Mn_{55}Bi_{45}$ and $Mn_{55}Bi_{45}C$, respectively. There is small increase in the value of anisotropy constant due to carbon doping. In order to find the possibility of carbon occupying the MnBi lattice, we have carried out first principles calculations of MnBi alloy as well. The conclusions of the first principles calculation and experimental data on structural and magnetic properties of $Mn_{55}Bi_{45}$ and $Mn_{55}Bi_{45}C$ will be presented. This research is supported by South Dakota-NASA EPSCoR Research Initiation Grant no 80NSSC19M0063.

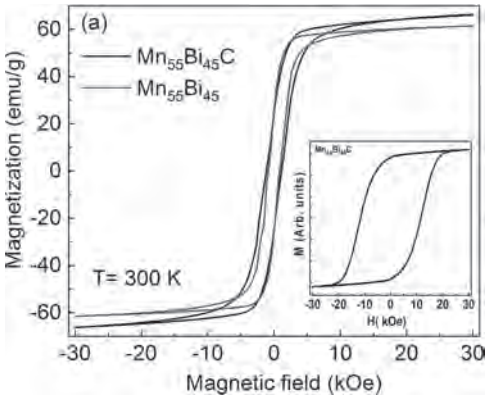

Fig. 1: Isothermal magnetization curves M(H) for $Mn_{55}Bi_{45}$ and $Mn_{55}Bi_{45}C$ measured at 300 K. Inset shows the M(H) curve for $Mn_{55}Bi_{45}C$ after aligning in magnetic field.

DPA-03. First-principles study of rare earth permanent magnets with point defects created by radiation. *R. Suzuki*[1], T. Yayama[1] and F. Akagi[1]
1. Kogakuin University, Yokohama, Japan

1. Background Rare earth permanent magnets, i.e., $Nd_2Fe_{14}B$ and Sm_2Co_{17}, have been used in spacecraft motors. However, the direct atomic displacement in the rare earth permanent magnets' so-called knock-on damage occurs via cosmic rays [1]. If the knock-on atom does not return to a normal lattice position, the empty lattice point becomes atomic vacancy, so-called a point defect. As a result, the rare earth permanent magnets degrade in magnetic properties and demagnetize, and it could also cause cascade damages. We studied $Nd_2Fe_{14}B$ with point defects by first-principle calculation to show how the point defect affects its magnetic properties. 2. Calculation method and models Formation energies and magnetic properties were calculated by the first-principles calculations based on density functional theory, which is implemented in the VASP code with GGA + U method (U = 6 eV) [2]. The cut-off energy was 700 eV, k-point mesh was set to and lattice constants were determined based on the experimental values [3]. A point defect of Nd was assumed to be generated when the interatomic bond in the $Nd_2Fe_{14}B$ crystal was cut by the collision of radiation particles with Nd atoms (Fig. 1). The generation processes of point defects of B and Fe were assumed to be the same as Nd. Thus the point defect formation energy was defined as the energy difference before and after the collision as shown in Eq. 1. $E_{form}=(E_{def}+E_{iso})-E_{perfect}$ (1) where E_{per}, E_{def} and E_{iso} are the total energies of electrons in a perfect crystal, a crystal with a point defect, and an isolated atom, respectively. 3. Results First, we confirmed that the magnetic moments of the calculation for the perfect crystal and experiment were similar (Table I). Subsequrntly, we found that only the crystal with the point defect of B increased the magnetic moment. We also found that the point defect formation energies of Fe were lower than those of B and Nd and the point defect formation energies of B and Nd were similar.

[1] A. Samin, M. Kurth, L. R. Cao, *Nucl. Instrum. Methods in Phys. Res.* B, 342, pp. 200-205 (2015). [2] G. Kresse, J. Futhmuller, *Comp. Mater. Sci.,* 6, pp. 15-50 (1996). [3] H. S. Li, R. C. Mohanty, C. G. Grenier, *J. Magn. Magn. Mater.*, 162, pp. 301-306 (1996). [4] M. Yan, L. Q. Yu, J. M. Wu, X. G. Cui, *J. Magn. Magn. Mater.*, 306, pp. 176-180 (2006).

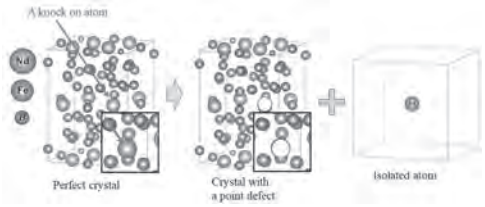

Fig.1 Calculation models for point defect formation energy of Nd in $Nd_2Fe_{14}B$.

	Perfect crystal	Exp.[4]	Crystal with a point defect		
			B	Fe	Nd
Magnetic moment (μ_B)	148.6	149.2	150.5	146.5	147.0
Point defect formation energy (eV)	-	-	9.2	7.1	9.3

Table I. Magnetic moments and point defect formation energies

DPA-04. Non-contact Magnetic Screw by Additive Manufacturing Fabrication. T. Chang[1], P. Huang[1], S. Kung[2], C. Shih[1], M. Tsai[3], *C.U. Ubadigha*[3], W. Chang[4] and C. Huang[5] *1. Electrical Motor Technology Research Center, National Cheng Kung University, Tainan, Taiwan; 2. Electrical Engineering, National Cheng Kung University, Tainan, Taiwan; 3. Mechanical Engineering, National Cheng Kung University, Tainan, Taiwan; 4. Physics, National Chung Cheng University, Chia-Yi, Taiwan; 5. Mechanical Engineering, National Kaohsiung University of Science and Technology, Kaohsiung, Taiwan*

INTRODUCTION This paper presents the design and fabrication of magnetic screws using 3D printing with magnetic materials. Magnetic screws possess the characteristics of non-contact magnetic transmission and eliminates the disadvantage of friction loss inherent in traditional screws. Using commercially available magnets and arranging them into spiral shape would cause spiral segment differences [1]. Either way, these will cause discontinuous magnetic flux, high cost and reduced efficiency [2-5]. In this work, finite element analysis is adopted to simulate and validate the fabricated magnetic screw. Prototypes and experiment results for the magnetic screw fabricated using PDM (Pellet deposit melting) and hybrid soft magnet SLM (Selective Laser Melting) with commercial sintered NdFeB magnet were provided; and furthermore, the 3D printed magnets as compared to the arranged magnets were analyzed. SIMULATION and PROTOTYPE FABRICATION A magnet powders mixed plastic pellet extrusion 3D printer PDM (Pellet Deposition Melting) in this study is developed and then applied to fabricate isotropic NdFeB bonded magnet segments, the simulation results of magnets fabricated to form a continuous spiral shape as shown in Figure 1(a), which prototype is fabricated as shown in Figure 2(a). Another the simulation results and prototype are fabricated via SLM and commercial sintered NdFeB magnet as shown in Figure 1(b)(c) and Figure 2(b). The spiral shape is divided into several small segments of inclined arc magnets, and each small segment is assembled by a commercial magnet and SLM soft magnet. Two kinds of magnetic screw can be spliced into a continuous spiral. CONCLUSION This work proposed two methods of 3D printing for making continuous spiral magnets to form non-contact magnetic screws that can be closely formed and generate continuous magnetic flux, thereby avoiding the need for molds and reducing costs.

[1] S. Pakdelian, N. W. Frank and H. A. Toliyat, "Magnetic Design Aspects of the Trans-Rotary Magnetic Gear," in IEEE Transactions on Energy Conversion, vol. 30, no. 1, pp. 41-50, March 2015, doi: 10.1109/TEC.2014.2361289. [2] K. Jenney and S. Pakdelian, "Design and Fabrication of the Trans-Rotary Magnetic Gear Using Quasi-Halbach Arrays," IECON 2018 - 44th Annual Conference of the IEEE Industrial Electronics

Society, 2018, pp. 450-455, doi: 10.1109/IECON.2018.8592701. [3] N. I. Berg, R. K. Holm and P. O. Rasmussen, "Design and test of a novel magnetic lead screw for active suspension system in a vehicle," 2014 International Conference on Electrical Machines (ICEM), 2014, pp. 470-477, doi: 10.1109/ICELMACH.2014.6960222. [4] M. Cirolini, A. F. Flores Filho, Y. C. Wu and D. G. Dorrell, "Design Aspects of a Reluctance-Based Magnetic Lead Screw," in IEEE Transactions on Magnetics, vol. 55, no. 7, pp. 1-6, July 2019, Art no. 8001906, doi: 10.1109/TMAG.2019.2895681. [5] F. Gao, Q. Wang and J. Zou, "Analytical Modeling of 3-D Magnetic Field and Performance in Magnetic Lead Screws Accounting for Magnetization Pattern," in IEEE Transactions on Industrial Electronics, vol. 67, no. 6, pp. 4785-4796, June 2020, doi: 10.1109/TIE.2019.2931241.

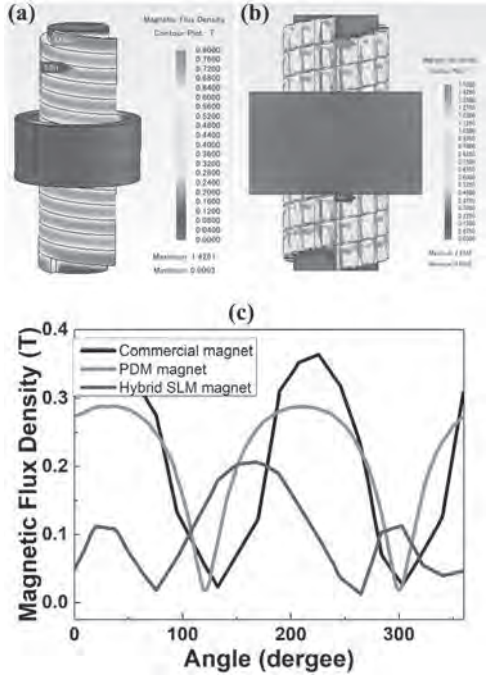

Figure 1. Finite element analysis of magnetic screw on (a) PDM, (b) hybrid, (c) the magnetic flux density of different process magnetic screws.

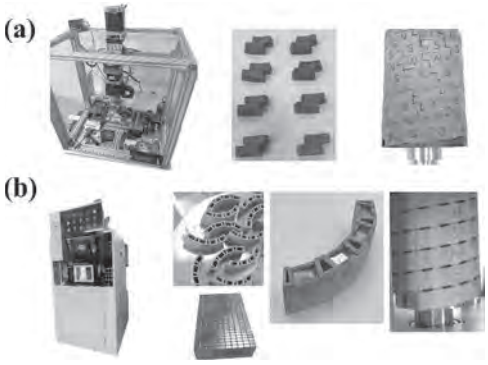

Figure 2. Magnetic screw sample: (a)by PDM (b) by hybrid magnets.

DPA-05. Robustness of magneto-crystalline anisotropy and its effect on coercivity in $(Fe_{0.7}Co_{0.3})_2B$. *X. Liu*[1] and C.I. Nlebedim[1] *1. Ames Laboratory, Ames, IA, United States*

Recently, more attention has been paid to developing rare earth free permanent magnets. $(Fe_{0.7}Co_{0.3})_2B$ with tetragonal structure shows good intrinsic hard magnetic properties. It has a large saturation magnetization (Js=13 kGs), a high Curie temperature (Tc=940 K), and a moderate uniaxial magneto-crystalline anisotropy (MCA) field (H_A= 7.7 kOe) [1-4]. In addition to the good intrinsic properties, the hard magnetic properties such as coercivity are also sensitive to microstructure. In particular, the coercivity reduces sharply upon the existence of the low MCA regions in microstructure, which favors the nucleation of the magnetic domain for the magnetization reversal. There always exist some local structural defects in real magnets, such as chemical composition fluctuation, local strain, and even the second impurity phase. In this work, the sensitivity of MCA to composition fluctuation and structural defects has been studied by a first-principles DFT calculation. The calculated MCA energy (E_{mca}) of $(Fe_{0.7}Co_{0.3})_2B$ with perfect structure is 0.125 meV/f.u. A fluctuation of cobalt content of 10%, or 1% isotropic lattice strain (Fig.1), or 2% tetragonal distortion will cause a reduction of E_{mca} up to 30% in $(Fe_{0.7}Co_{0.3})_2B$. The spin-resolved MCA analysis indicates that spin-up and spin-down electrons contribute positively to E_{mca} while the spin mixing has a negative contribution (Fig.1). The interplay of these different contributions results in optimized chemical composition or geometrical structure to maximize MCA. Micromagnetic simulation indicates that the coercivity decrease from 2.2 kOe to 1.0 kOe in an isotropic magnet of $(Fe_{0.7}Co_{0.3})_2B$ with an average grain size of 30nm by considering the existence of randomly distributed local reduction of MCA energy up to 30%. This work is supported by the Critical Materials Institute (CMI), an Energy Innovation Hub funded by the U.S. Department of Energy (DOE), Office of Energy Efficiency and Renewable Energy, Advanced Manufacturing Office. Ames Laboratory is operated for the U.S. DOE by Iowa State University under Contract No. DE-AC02-07CH11358.

[1] W. Coene, F. Hakkens, R. Coehoorn, D.B. de Mooij, C. de Waard, J. Fidler and R. Griissinger, J. Magn. Magn. Mater. 96, 189-196 (1991) [2] K.D. Belashchenko, et. al. Appl. Phys. Lett. 106, 062408 (2015) [3] A. Edstrom, M. Werwinski, D. Iusan, J. Rusz, O. Eriksson, K. P. Skokov, I. A. Radulov, S. Ener, M. D. Kuzmin, J. Hong, M. Fries, D. Yu. Karpenkov, and O. Gutfleisch, Phys. Rev. B 92, 174413 (2015) [4] Tej Nath Lamichhane, Olena Palasyuk, Vladimir P. Antropov, Ivan A. Zhuravlev, Kirill D. Belashchenko, Ikenna C. Nlebedim, Kevin W. Dennisb, Anton Jesche, Matthew J. Kramer, Sergey L. Bud'ko, R. William McCallumb, Paul C. Canfield, Valentin Taufour, J. Magn. Magn. Mater., 513 (2020) 167214

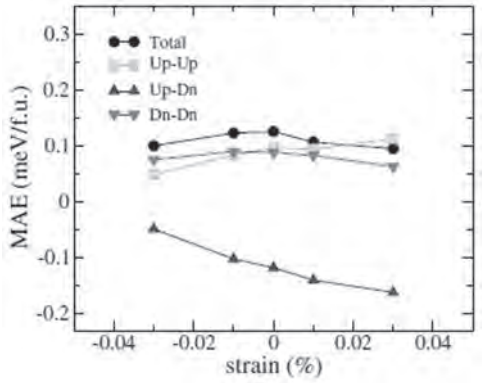

Calculated spin-resolved- and total- magnetocrystalline anisotropy energy as a function of lattice strain in $(Fe_{0.7}Co_{0.3})_2B$.

DPA-06. Hard magnetic properties of $(Sm,Zr)(Fe,Co)_3$ magnets. *T. Saito*[1] *1. Chiba Institute of Technology, Narashino, Japan*

It is known that the $SmFe_3$ phase is a ferromagnetic phase with a rhombohedral structure and that specimens with the $SmFe_3$-type phase exhibited coercivity [1-3]. In order to improve the magnetic properties of the $SmFe_3$ phase, several $(Sm,Zr)(Fe,Co)_3$ melt-spun ribbons were prepared in this study. The relationships between the structures and magnetic properties of the $(Sm,Zr)(Fe,Co)_3$ melt-spun ribbons are examined. Sm-Fe alloy ingots with nominal compositions of $(Sm_{1-x}Zr_x)(Fe_{0.75}Co_{0.25})_3$ (x = 0–0.4) were prepared by induction melting under an argon atmosphere. The Sm-Fe melt-spun specimens were produced from the alloy ingots by melt-spinning technique. Heat treatment of the as-quenched specimens was performed

in an argon atmosphere for 1 hour at different temperatures of 773–1173 K. The structures and magnetic properties of $(Sm,Zr)(Fe,Co)_3$ melt-spun ribbons were investigated in the as-quenched condition and after annealing. The $(Sm,Zr)(Fe,Co)_3$ melt-spun ribbons consisted of the amorphous phase. These as-quenched melt-spun ribbons showed low coercivity. Annealing of the melt-spun ribbons resulted in the formation of the $SmFe_3$-type phase. Figure 1 shows the dependence of the coercivity of the $(Sm,Zr)(Fe,Co)_3$ melt-spun ribbons on the annealing temperature. Annealing of the melt-spun ribbons resulted in a drastic increase in coercivity. It was found that the coercivity of the $(Sm,Zr)(Fe,Co)_3$ melt-spun ribbons reached its maximum when annealed at 973 K. The highest coercivity, H_c = 7.8 kOe, was obtained in the $(Sm_{0.8}Zr_{0.2})(Fe_{0.75}Co_{0.25})_3$ specimen after annealing at 973 K.

[1] K. H. J. Buschow, J. Less-Common Metals 25, 131 (1971). [2] J. F. Herbst and J. J. Croat, J. Appl. Phys. 53, 4304 (1982). [3] H. Samata, et al. Jpn. J. Appl. Phys. 36, 3492 (1997).

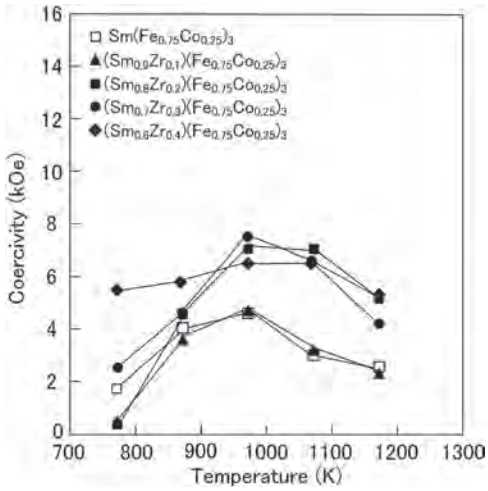

Fig.1 Dependence of the coercivity of the $(Sm,Zr)(Fe,Co)_3$ melt-spun ribbons on the annealing temperature.

DPA-07. Magnetic properties of $Ce_{85}Al_{15}$ doped NdFeB sintered magnet by grain boundary diffusion of $Tb_{70}Cu_{30}$ powders. *Y. Wong*[1], H. Chang[1], Y. Lee[1], W. Chang[1], C. Chiu[2] and C. Mo[3] *1. Department of Physics, National Chung Cheng University, Chia-Yi 621, Taiwan; 2. New Materials Research & Development Dept., China Steel Corp., Kaohsiung, Taiwan; 3. R& D Department, Himag Magnetic Corporation, Pingtung, Taiwan*

NdFeB sintered magnet shows the highest energy product ($(BH)_{max}$) at room temperature of all developed magnetic materials, but the drastic decrease in magnetic anisotropy field (H_A) of $Nd_2Fe_{14}B$ (2:14:1) phase with rising temperature limits its application at high temperature [1]. In recent years, the grain boundary diffusion (GBD) has been reported to be an effective method to significantly enhance coercivity ($_iH_c$) with minor sacrificing remanence (B_r), and also to reduce the usage of heavy rare earth (HRE) elements simultaneously [2]. The formation of core-shell structure, the distribution of HRE only at the surface of 2:14:1 phase, through GBD of HRE-containing alloys, could inhibit the nucleation of reverse domain, and thus enhance $_iH_c$ [3]. In this work, the dual-alloy (DA) sintering method together with GBD treatment are adopted to further enhance coercivity and modify the magnetic properties of NdFeB sintered magnets. $(BH)_{max}$ of 51.4 MGOe and $_iH_c$ of 14.9 kOe are obtained for the original NdFeB magnet made by sintering $Ce_{85}Al_{15}$ doped NdFeB powders. Magnetic isolation due to the distribution of Ce and Al at grain boundary increases of the coercivity effectively, yet few Ce entering into grain interior decreases B_r, $(BH)_{max}$, and Curie temperature slightly. In addition, coercivity of the above magnets can be further enhanced to 22.7-25.1 kOe by GBD with different amount of $Tb_{70}Cu_{30}$ powders. The clear core-shell structure, which consists of $(Nd, Tb)_2Fe_{14}B$ phase with higher H_A as the shell and $Nd_2Fe_{14}B$ phase as the core, is observed. CeAl helps to form continuous and smooth grain boundary. The diffusion source of TbCu could infiltrate into the magnet al.ng such smooth grain boundary and form homogeneous core-shell structure. As a result, coercivity are remarkably enhanced from 14.9 kOe for DA sintered magnet with 2 wt.% CeAl to 25.1 kOe for the magnet GBD with TbCu. Most importantly, various levels of the NdFeB magnets, such as 52M, 35-50SH, and 45UH, could be attained by simply modifying the amounts of CeAl for DA sintered magnets and/or GBD with TbCu powders.

[1] S. Hirosawa et al., J. Appl. Phys. 59 (1986) 873. [2] K. Hirota et al., IEEE, 2006. 42(10): p.2909-2911. [3] Marko Soderznik et al. Acta Mater. 115 (2016) 278-284.

DPA-08. Withdrawn

DPA-09. Effect of heat treatment on the properties of NdFeB films grown by sputtering. *A.C. Krohling*[1], J.D. Ardisson[1] and W.A. Macedo[1] *1. Physics, CDTN, Belo Horizonte, Brazil*

NdFeB rare earth permanent magnets have gained great interest due to their numerous applications, for example in electric motors, wind turbines, among others, recently the manufacture of these magnets in microchips has gained notoriety[1,2]. One of the techniques for deposition of these magnets in micrometre thickness is the deposition by magnetron sputtering[3]. In this work we present results of NdFeB films prepared by magnetron sputtering with targets of different stoichiometry, $Nd_{13}Fe_{70}B_{17}$(1000nm) and $Nd_{17}Fe_{75}B_8$(1000nm) both films were produced with seed and protective layer of Ta(60nm). The NdFeB films were deposited at a temperature of T_0=20°C, and then heated in an ex-situ oven at a temperature of T_A=600°C, with a base pressure of 10^{-7}mbar, for 8h for the $Nd_{13}Fe_{70}B_{17}$ film and 4h for the $Nd_{17}Fe_{75}B_8$. In Fig.1, we observe the diffractograms of the NdFeB samples deposited at T_0=20°C, we verified the diffraction of several planes characterizing the polycrystallinity of these materials, without a preferential orientation of the c axis, typical of $Nd_2Fe_{14}B$ films, an interesting fact is that the heat treatment for both films gives rise to broad peaks in the region of the Φ(311) and Φ(105) planes, due to the interdiffusion process of the samples. The magnetic behavior is shown in Fig.2, for the $Nd_{17}Fe_{75}B_8$ sample deposited at T_0=20°C with the H field parallel (//) to the sample plane, this sample show a signal similar to a soft magnet material with Hc=10Oe, which indicates that the T_0 growth temperature does not establish a high anisotropy perpendicular to the plane. The heat treatment for 4h for $Nd_{17}Fe_{75}B_8$ sample considerably increases the coercivity to 660Oe and its magnetization, we can notice in the hysteresis curve a strangulation in the low field region, which indicates a magnetic coupling competition between the richer phases of Nd/Fe, which contributes to a coercive field distribution in this region[3-5].

[1] O Gutfleisch 2000 J. Phys. D: Appl. Phys. 33 R157 [2] J.M.D. Coey, Perspective and Prospects for Rare Earth Permanent Magnets, Engineering, Volume 6, Issue 2, 2020, Pages 119-131 [3] S. N. Piramanayagam, M. Matsumoto, and A. Morisako, "Perpendicular magnetic anisotropy in NdFeB thin films", Journal of Applied Physics 85, 5898-5900 (1999) [4] N. M. Dempsey, A. Walther, F. May, and D. Givord, K. Khlopkov and O. Gutfleisch IFW Dresden, Institute of Metallic Materials, Helmholtzstr. 20, 01069 Dresden, Germany, "High performance hard magnetic NdFeB thick films for integration into micro-electro-mechanical systems", Applied Physics Letters 90, 092509 (2007) [5] Wenfeng Liu, Mingang Zhang, Kewei Zhang, Yuesheng Chai, "Microstructure and Magnetic Properties of NdFeB Films through Nd Surface Diffusion Process", Advances in Condensed Matter Physics, vol. 2017, Article ID 4296243, 5 pages, 2017.

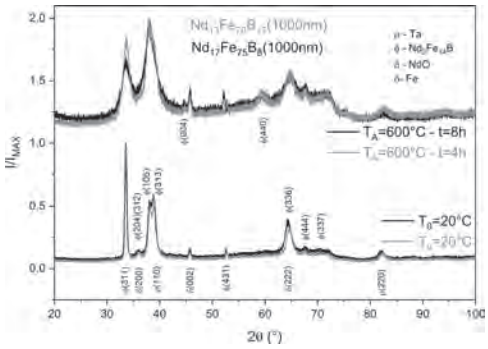

Fig.1 - Diffractograms of samples of $Nd_{13}Fe_{70}B_17$(1000nm) and $Nd_{17}Fe_{75}B_8$(1000nm) deposited at T_0=20°C and heated for 4h and 8h respectively.

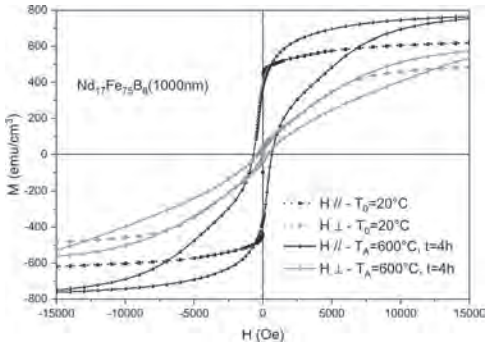

Fig.2 - Magnetic hysteresis of the $Nd_{17}Fe_{75}B_8$(1000nm) film deposited at T_0=20°C and heated in T_A=600°C for 4h.

DPA-10. Substitution effect of light elements on magnetic anisotropy in α″-$Fe_{16}X_2$ (X=B,C,N,O,F). *Y. Kota*[1] and A. Sakuma[2] *1. National Institute of Technology, Fukushima College, Iwaki, Japan; 2. Department of Applied Physics, Tohoku University, Sendai, Japan*

We theoretically studied the substitution effect of light elements X (B,C,N,O,F) on magnetocrystalline anisotropy energy in α″-$Fe_{16}X_2$ shown in Fig. 1(a). In recent, an iron-nitride, α″-$Fe_{16}N_2$, is considered as a candidate of rare-earth-free permanent magnet, since the uniaxial magnetic anisotropy constant (K_u) was expected on the order of 10^5 J/m^3 by a theoretical computation [1]. Furthermore, the substitution effect of transition elements has been studied to find a larger K_u material [2,3]. In the present study, in contrast, we focus on the substitution effect of typical elements and performed first-principles calculations of electronic structure and magnetic properties using the Vienna ab-initio simulation package. The exchange-correlation functional was described by the general gradient approximation based on the Perdew-Burke-Ernzerhof scheme. The cutoff energy of the plane wave bases was set to 520 eV, and the k-point mesh for the Brillouin zone integration was set to 10×10×9. The magnetocrystalline anisotropy energy was evaluated within the magnetic force theorem. Figure 1(b) shows the calculation result of K_u in $Fe_{16}X_2$ (X=B,C,N,O,F) in addition to K_u in $Fe_{16}X_0$. Note that, in the calculation of $Fe_{16}X_0$, we used the lattice parameters (lattice constants and Fe-atom positions) of $Fe_{16}X_2$ determined by the structural optimization and removed X-atoms from the unit cell. In Fig. 1(b), the K_u value strongly depends on the species of X. Also, the comparison of the K_u values of $Fe_{16}X_2$ and $Fe_{16}X_0$ clearly reveals that the chemical effect between Fe- and X-atoms has an important role to yield the uniaxial magnetic anisotropy in $Fe_{16}X_2$. The light elements seem to be not related with magnetism; however, these elements assist the appearance of magnetic anisotropy in Fe indirectly. In the presentation, we will discuss the X-dependent electronic structure of Fe and the magnetic anisotropy.

[1] L. Ke et al., Phys. Rev. B 88, 024404 (2013). [2] M. H. Han et al., J. Phys: Condens. Matter 32, 035801 (2020). [3] R. Islam et al., J. Appl. Phys. 128, 114902 (2020).

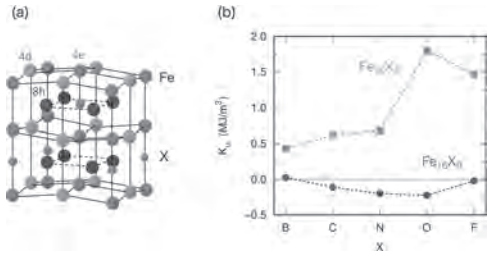

Fig. 1 (a) Crystal structure of α″-$Fe_{16}X_2$. (b) Calculation result of K_u in $Fe_{16}X_2$ and $Fe_{16}X_0$. Positive value of K_u indicates that the magnetic easy axis coincides along the [001] direction.

DPA-11. Magnetic Domain Structure and Remanence Losses of NdFeB Magnets Under the Influence of Demagnetization Factors. *Y. Ma*[1], J. Cao[1] and L. Li[1] *1. Harbin Institute of Technology, Harbin, China*

In order to reveal the demagnetization mechanism of NdFeB magnets and establish the relationship between microstructure and magnetic property, this paper focuses on the structural change of magnetic domain and the demagnetization behavior of NdFeB magnets under various demagnetization factors. Temperature, constant demagnetizing field and alternating demagnetizing field are applied to NdFeB magnets by high and low temperature alternating test chamber, demagnetization test device, programmable DC power supply and programmable AC power supply. Demagnetization test device is made up of 2000 turns copper winding winded on a laminated hollow rectangular steel core. Magnetic properties of the studied material are determined by magnetic domain size, amplitude and open-circuit remanence. The magnetic domain structure and open-circuit remanence are measured by atomic force microscope and Tesla meter. When the sample is demagnetized, the open-circuit remanence of the measuring point in the magnetization direction decreases, and the open-circuit remanence of the measuring point perpendicular to the magnetization direction increases. In the domain imaging, the domain size in the magnetization direction becomes fine and the amplitude decreases, while the domain size perpendicular to the magnetization direction expands and the amplitude increases. The change of magnetic domain structure is consistent with the macroscopic demagnetization law. As the domain size decreases, the number of domains increases and the area of domain wall increases. As a transition region with weak magnetism, the increase of domain wall area will lead to the decrease of macro magnetic properties. When the alternating demagnetizing field is 1000Hz at 140 °C, the remanence losses in the magnetization direction reaches 47.9%, and the domain size increases from 2.35 μm reduced to 1.15 μm. This work is helpful to understand the demagnetization mechanism of NdFeB magnets.

S. Hamidizadeh, N. Alatawneh and R. R. Chromik, IEEE Transactions on Magnetics, Vol. 52, p.1-4 (2016) P. Peng, J. Zhang and W. Li, IEEE Transactions on Magnetics, Vol. 56, p.1-10 (2020) M. Haavisto, S. Tuominen and H. Kankaanpää, IEEE Transactions on Magnetics, Vol. 46, p.3582-3584 (2010) P. Zhou, D. Lin and Y. Xiao, IEEE Transactions on Magnetics, Vol. 48, p.1031-1034 (2012) M. Haavisto and M. Paju, IEEE Transactions on Magnetics, Vol. 45, p.5277-5280 (2009) M. Soderznik, H. Sepehri-Amin and T.T. Sasaki, Acta Materialia, Vol. 135, p.68-76 (2017)

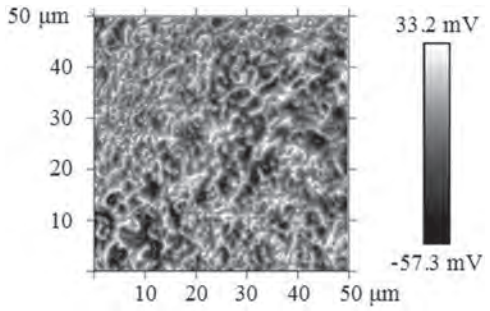

Fig. 1 Magnetic domain of NdFeB magnet demagnetized by an alternating magnetic field with frequency of 1000Hz at 140 °C.

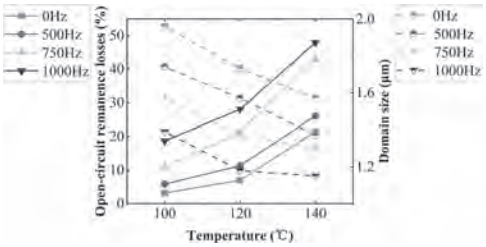

Fig. 2 Open-circuit remanence losses and domain size of NdFeB magnets demagnetized by multiple levels of alternating fields and temperatures.

DPA-12. Magnetic and structural transition in the martensitic transformation of the GdCu compound. *B. Bosch-Santos*[1,2], G.A. Cabrera-Pasca[3], O. Silveira Leite Neto[1], A.A. Miranda-Filho[1], E.L. Correa[2], C. Dennis[2] and A.W. Carbonari[1] *1. Centro do Reator de Pesquisa, Instituto de Pesquisas Energéticas e Nucleares - IPEN, São Paulo, Brazil; 2. Material Measurement Laboratory, National Institute of Standards and Technology - NIST, Gaithersburg, MD, United States; 3. Universidade Federal do Pará, Abaitetuba, Brazil*

The GdCu compound has a martensitic transformation from the cubic CsCl-type to the orthorhombic FeB-type structure, beginning around 250K and finishing about 120K. Furthermore, this compound has two antiferromagnetic transitions, with Néel temperatures around 150K (CsCl) and around 50 K (FeB) [1, 2]. To study the magnetic and structural behavior in the GdCu compound we have used x-ray diffraction, dc magnetization measurements and perturbed gamma-gamma angular correlation (PAC) spectroscopy. Samples of GdCu (Gd = 99.9 % and Cu = 99.999% pure) were prepared by arc-melting the constituent elements in stoichiometric proportions in a pure argon atmosphere. The crystal structure of the synthesized compounds was determined by x-ray diffraction and the results analyzed by the Rietveld method, which showed a single phase corresponding to the cubic structure at room temperature. PAC spectroscopy measurements at different temperatures using ^{111}Cd as the probe nuclei at Cu sites show the martensitic transformation. At 220 K the PAC spectrum has probe nuclei in two different environments with a population of 62% and 38% in the cubic and orthorhombic structures, respectively. No magnetic hyperfine field was observed around 145 K as previously reported [2]. These findings are consistent with the antiferromagnetic structure (π, π, 0)-type [2] and with the symmetry considerations of the Gd spin-up and spin-down around the Cu site in this cubic phase. Below 51 K an antiferromagnetic transition (helimagnetic structure) [2] is observed in the orthorhombic structure. Below this temperature, a temperature dependent hyperfine field can be fitted to the PAC spectra with corresponding Larmor frequencies following a Brillouin function (J_{Gd} = 7/2) and yielding a magnetic hyperfine field of 15.7 T. At 40 K, the PAC spectrum presents probe nuclei occupying site fractions with populations of 20% and 80%, corresponding to CsCl- and FeB-type structures, respectively. Therefore, the PAC results show that after cooling and warming cycle, the sample remains a mixture of the orthorhombic and cubic phases.

[1] P. Sharma, J. Brar, M. Bharath and R. Bindu. J. Phys.: Condens. Matter 32, 305603 (2020). [2] J. A. Blanco, J. I. Espeso, J. Garcia Soldevilla, J. C. Gomez Sal, M. R. Ibarra, C. Marquina and H. E. Fischer. Phys. Rev. B 59 512 (1999).

DPA-13. Deep Learning-based Estimation Method of Magnetization Distribution in Permanent Magnet. *D. Takasu*[1], H. Sasaki[1], N. Nakamura[1] and Y. Okamoto[1] *1. Department of Electrical and Electronic Engineering, Hosei University, Koganei, Japan*

Because the degree of vibration in the permanent magnet synchronous motor (PMSM) is dependent on the magnetization distribution in the permanent magnet. The accurate estimation of magnetization distribution at the previous stage of the practical design eliminates the manufacturing of PMSM with poor performance. To nondestructively estimate the magnetization distribution in the permanent magnet, some numerical methods using the magnetic flux density measured on the outside region of the permanent magnet have been proposed [1], [2]. Because there are countless combinations of magnetization distribution in the permanent magnet, these methods can effectively remove the non-physical distributions. However, since those performances depend on the parameter tunings, the non-physical distributions cannot be completely removed. Then, the deep learning-based estimation method is proposed. In this paper, the deep feedforward neural network is applied to the estimation method. The network is configured by the framework of Keras [3], which is the python-based library of deep learning. The number of network layers is set to 9 layers. The number of neurons in the input layer is set to 344, which is identical to the summation of *x*- and *y*- direction of magnetic flux density on 172 measuring points on the outside of the 2-D permanent magnet model. The number of neurons in the output layer is set to 816, which is identical to the number of cells for the magnetization. The target distribution of magnetization is focused on the parallel orientation. The training data are generated by changing the angle of parallel direction every 0.01 degree within [0, 360] with the uniform intensity of magnetization. The weighted coefficients are determined by AdaGrad [4]. The input data (magnetic flux density) is generated by Biot-Savart law, and the 5 % error of the magnetization intensity is superposed on all data, as shown in Fig. 1. While the non-physical distribution tends to be estimated using the conventional methods [1], [2], the practical distribution is estimated using the proposed deep learning system, as shown in Fig. 2. The complicated magnetization distributions in 3D field will be estimated in the full paper.

[1] H. Igarashi, T. Honma, and A. Kost, *IEEE Trans. Magn.,* vol. 36, no. 4, pp. 1168-1171 (2000). [2] L. Arbenz, et al., *IEEE Trans. Magn.,* vol. 53, no. 11, Art. no. 8109504 (2017). [3] https://keras.io/ja/ [4] J. Duchi, et al., *Journal of machine learning research*, vol. 12, no. 7, pp. 2121-2159 (2011).

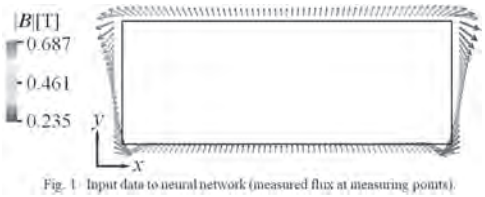

Fig. 1 Input data to neural network (measured flux at measuring points).

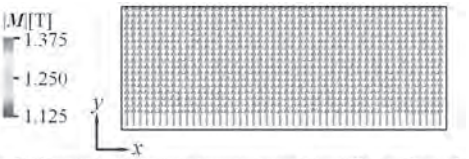

Fig. 2. Magnetization distribution in permanent magnet estimated by neural network.

DPA-14. The Phase Structure and Properties of Fe-riched 2:17-type Sm-Co Sintered Magnets. *J. Jia*[1], D. Zhang[1], J. Yang[1,2], Z. Xie[1], Y. Li[1], H. Zhang[1], W. Liu[1] and M. Yue[1] *1. Faculty of Materials and Manufacturing, Key Laboratory of Advanced Functional Materials, Ministry of Education of China, Beijing University of Technology, Beijing, China; 2. School of Mechanical Engineering, Anyang Institute of Technology, Anyang, China*

The 2:17-type Sm-Co sintered magnet has excellent magnetic properties, which is widely used in aviation modern high-tech fields [1-2]. It was reported that the cell size increased with increasing isothermal aging time [3]. The effect of Fe-rich content on the phase structure and element distribution was rarely discussed. In this study, the phase structure, elementals distribution and magnetic properties of Fe-rich magnets were studied. The magnets with nominal composition $Sm(Co_{0.91-x}Fe_xCu_{0.07}Zr_{0.02})_{7.6}$ (x=0.22, 0.30, 0.35) were prepared, and the corresponding final magnets were named $Fe_{0.22}$, $Fe_{0.30}$ and $Fe_{0.35}$. At the solid solution, the 2:17H phase, 2:17R phase and Zr-rich(1:3R) phase diffraction peaks are detected in the $Fe_{0.30}$ and $Fe_{0.35}$ magnet, while the $Fe_{0.22}$ magnet bears typic 1:7H phase. Furthermore, the characteristic peaks [Fig. 1(a)] of 2:17H, 2:17R and 1:3R phases enhanced with the increase of Fe content, indicating that the high Fe content is not conducive to obtain homogeneous solid solution resulting in poor magnetic properties. The powder XRD patterns [Fig. 1 (b)] of three final magnets are almost the same, except the 1:3R phase can be detected in the $Fe_{0.30}$ and $Fe_{0.35}$ magnets. Fig. 2 shows the elemental distribution of the $Fe_{0.22}$ and $Fe_{0.35}$ magnets. Compared with the uniform element distribution of $Fe_{0.22}$ magnet [Fig. 2(a-e)], there are large-sized Sm and Cu enrichment in $Fe_{0.35}$ magnet, as marked in Fig. 2 (g) and (f). The enrichment regions in $Fe_{0.35}$ magnet consumes a lot of Sm and Cu, leading to the destruction of the continuity of the cell wall and incomplete cellular structure which is revealed by TEM results. The poor cellular structure should be the main reason for the low coercivity of the $Fe_{0.35}$ magnet. Our results confirmed that the 1:7H main phase in the solid solution was destroyed with too large Fe content. In addition, enrichment of Cu and Sm elements and incomplete cell structure formed for the large Fe content magnet, resulting in poor magnetic properties.

[1] J.F. Liu et al., J. Appl. Phys., vol. 85, p. 2800–2804(1999). [2] C. X. Wang et al., IEEE Trans., vol. 53, p. 2102004(2017). [3] Kuikui Song et al., J. Magn. Magn. Mater., vol. 465, p. 569-577(2018).

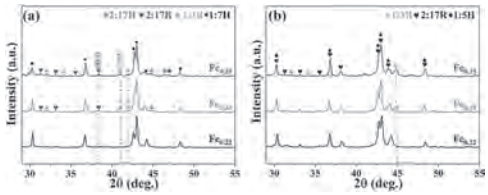

Fig. 1 (a) and (b) the powder XRD patterns of final magnets and solid solution magnets with different Fe contents

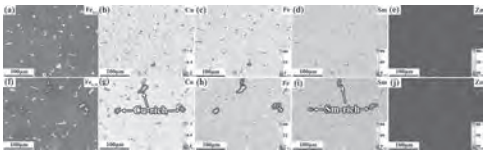

Fig. 2 Element distribution of (a)-(e) $Fe_{0.22}$ and (f)-(j) $Fe_{0.35}$ magnet

DPA-15. Effects of 3D-Seeds on Microstructure and Magnetic Properties of Nd-Fe-B thin films. *K. Koike*[1], K. Furusawa[1], H. Nakajima[1], N. Inaba[1], H. Kato[1], S. Hara[2], Y. Saito[2], S. Okubo[2], H. Ohta[2] and M. Itakura[3] *1. Yamagata University, Yonezawa, Japan; 2. Kobe University, Kobe, Japan; 3. Kyushu University, Kasuga, Japan*

The addition of HREs such as Dy and Tb is extremely effective in improving the heat resistance of NdFeB magnets. However, HREs are strategic elements with extremely high risk. Since the anisotropic NdFeB magnet film is an ideal model for bulk magnets, it has played an important role in studies aimed at elucidating the coercivity mechanism to avoid the utilization of HREs in NdFeB magnets [1]. On the other hand, anisotropic NdFeB thick films with high orientation and high coercivity, which can obtain higher $(BH)_{max}$ than isotropic thick films, have been developed by a nanocrystal formation process called the two-step method using post-annealing for amorphous of NdFeB [2, 3]. The introduction of nanocrystal seeds is expected to improve the crystallinity and magnetic properties of NdFeB thin films, which have the simple structure compared to those thick films. We reports effects of 3D seeds on microstructure and magnetic properties of NdFeB thin films prepared using two-step method. The Mo(20 nm)/NdFeB(1 nm)/NdFeB(150 nm)/Mo(10 nm) thin films made by using UHV sputtering on MgO(001). The 3D islands of the NdFeB seeds which have 25 nm in diameter and about 2.5 nm hight, was formed on Mo underlayer heated at 660°C. The Nd-Fe-B layer was deposited on the seeds during heating at 350-450°C. As-deposited films of amorphous state were treated by multi-step annealing using halogen ramp heater in UHV chamber. Fig. 1 shows demagnetization curves of the optimization annealed NdFeB films with and w/o 3D seeds. Perpendicular magnetic anisotropy, coercivity and residual magnetization of the NdFeB films with seeds were improved by introduction of seeds. The microstructural evolution of the NdFeB films with seeds consists of an amorphous NdFeB phase separated by a thin NdO in an as-deposited state, and the formation of textured $Nd_2Fe_{14}B$ grain on the seeds/Mo underlayer after annealing was observed by cross-sectional TEM. This results show that the 3D seeds is advantageous to obtain perpendicular magnetic anisotropy and coercivity by improving the texture structure of the NdFeB thin films.

[1] K. Koike et al., Nanoscale Res. Lett. 11 (2016) 33. [2] T. Okuda et al., Jpn. J. Appl. Phys., 42 (2003) 6859. [3] N. M. Dempsey et al., Appl. Phys. Lett. 90 (2007) 092509.

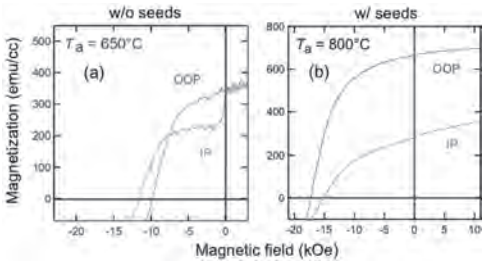

Demagnetization curves of the optimization annealed NdFeB films (a) with and (b) w/o 3D seeds.

DPA-16. Magnetic properties of nanocrystalline $Sm_1Fe_{10.5-x}Co_xMo_{1.5}$ alloys with x =0,1,2. *Y. Xu*[1] and G. Hadjipanayis[1] *1. University of Delaware, Newark, DE, United States*

RT_{12} compounds with the $ThMn_{12}$ crystal structure have been recently studied as potential candidates for high-performance magnets, due to their low rare-earth content which are considered as critical elements. These compounds with high Fe content, are expected to be strong magnets, because of their large magnetization, high Curie temperature as well as strong uniaxial magnetocrystalline anisotropy when R=Sm. Arc-melted alloys with composition $Sm_1Fe_{10.5-x}Co_xMo_{1.5}$($x$ =0,1,2) were prepared with the tetragonal $ThMn_{12}$ structure. The cast samples were first high-energy-ball-milled followed by hot-compaction at 650 degree celsius under 275 MPa. Annealing of compacted samples was done from 700 to 1000 degree celsius to optimize the magnetic properties. The effects of Co on the magnetic properties, including the Curie temperature, saturation magnetization, anisotropy field, and energy product, have been investigated. It was found that the Curie temperature shows a linear relationship with the Co substitution; an increasing Co content increases Ms but decreases H_c, The $Sm_1Fe_{10.5-x}Co_xMo_{1.5}$ alloy with x =1 has an Hc=2782 Oe and shows the highest energy product(2.63 MGOe) after annealing at 750 degree celsius for 48 h. This work was supported by the U.S. Department of Energy under Grant DE-FG02-90ER45413.

[1] K.H.J. Buschow. Permanent magnet materials based on tetragonal rareearth compounds of the type rfe12xmx. Journal of Magnetism and MagneticMaterials, 100(1):79 – 89, 1991. [2] A.M. Gabay and G.C. Hadjipanayis. Recent developments in rfe12-typecompounds for permanent magnets. Scripta Materialia, 154:284 – 288, 2018. [3] X.C. Kou, E.H.C.P. Sinnecker, R. Grossinger, G. Wiesinger, T. Zhao, J.P.Liu, and F.R. de Boer. Magnetocrystalline anisotropy of smfe12 xmoxcompounds with x = 0.5, 1.0, 1.5, 2.0 or 3.0. Journal of Magnetism andMagnetic Materials, 140-144:1025 – 1026, 1995. International Conference on Magnetism.19 [4] A. Muller. Magnetic material R,Fe,Mo,(Co) with $ThMn_{12}$ structure. Journalof Applied Physics, 64:249–251, July 1988. [5] L. Schultz, K. Schnitzke, and J. Wecker. Magnetic hardening of sm-fe-mo, sm-fe-v and sm-fe-ti magnets. Journal of Magnetism and MagneticMaterials, 83(1):254 – 256, 1990. [6] L. Schultz and J. Wecker. Coercivity in ThMn12-type magnets. Journal ofApplied Physics, 64:5711–5713, November 1988. [7] A.M. Schonhobel, R. Madugundo, A.M. Gabay, J.M. Barandiaran, and G.C.Hadjipanayis. The sm-fe-v based 1:12 bulk magnets. Journal of Alloys andCompounds, 791:1122 – 1127, 2019.

x	a(nm)	c(nm)	c/a	H_a(T)	M_S(emu/g)
0	0.8567	0.4788	0.559	9.4	101.9
1	0.8570	0.4788	0.559	8.3	99.6
2	0.8568	0.4785	0.558	7.5	103.5

Table 2: Lattice parameters and magnetic properties of arc-melted alloys $Sm_1Fe_{10.5-x}Co_xMo_{1.5}$ at 300K, with x =0, 1, 2

x	H_c(Oe)	T_c(°C)	$(BH)_{max}$(MGOe)	M_S(emu/g)	M_R(emu/g)
0	3428	182	2.38	94.17	44.02
1	2782.2	241	2.63	97.02	47.21
2	1635.4	322	2.34	99.37	50.33

Table 2: Magnetic properties of hot compacted nanocrystalline $Sm_1Fe_{10.5-x}Co_xMo_{1.5}$ magnets, with x =0, 1, 2, annealed at 750 degree celsius

Session DPB
NON-RARE EARTH PERMANENT MAGNET MATERIALS AND NANOCOMPOSITES II (Poster Session)

Emily Rinko, Co-Chair
Iowa State University, Ames, IA, United States
Parashu Kharel, Co-Chair
South Dakota State University, Brookings, SD, United States

DPB-01. Ordering Mechanism of $L1_0$-FePt Nanoparticles Synthesized by Ag Addition. D. Zhao[1,2], *W. Pei*[1,2], Z. Sun[1,2], L. Chang[3,4], Q. Wang[1,2] and Q. Wang[3,4] *1. School of Materials Science and Engineering, Northeastern University, Shenyang, China; 2. Key Laboratory of Anisotropy and Texture of Materials (Ministry of Education), Northeastern University, Shenyang, China; 3. School of Metallurgy, Northeastern University, Shenyang, China; 4. Key Laboratory of Electromagnetic Processing of Materials (Ministry of Education), Northeastern University, Shenyang, China*

FePt nanoparticles (NPs) with fct ($L1_0$) structures have a wide promising application in high-density magnetic storage media, catalysis, and biomedicine [1, 2], because of their high magnetocrystalline anisotropy, catalytic activity, and good biocompatibility. Ag addition can promote ordering transition and directly obtain $L1_0$-FePt NPs with high structural ordering [3-5]. However, the ordering mechanism of the NPs by Ag addition and the ordering transition process are rarely reported. Herein, we report the direct synthesis of $L1_0$-FePt NPs by Ag addition. The ordering transition process was investigated, and the ordering mechanism was discussed. The metal precursors $Pt(acac)_2$, $Fe(acac)_3$, and AgAc were dissolved in HDA in the presence of HDD as reductant. And then the mixed solution was heated to 360 °C for 180 min. Finally, the product was collected by centrifugation with ethanol. The phase structure and magnetic properties of a series of products sampled at 360 °C for different reaction times (from 0 min to 180 min) are shown in Fig. 1 and Fig. 2, respectively. The precursors of Ag and Pt were firstly reduced, and form AgPt phase at beginning of the reaction. With reacting for 10 min, the precursor of Fe was reduced, and the FePt NPs were obtained. The products were mainly combined of elemental Ag and $L1_0$-FePt phases. The magnetic properties of the products changed from diamagnetic to ferromagnetic. With extending the reaction time, the both content of Ag and $L1_0$-FePt phases continuously increased. The coercivity of products enhanced from 0.9 kOe to 6.3 kOe with increasing the reaction time from 10 min to 180 min. These results indicate that Ag atoms are easy to migrate and enrich because of their low surface energy and high mobility. The Ag migration helps the formation of a large number of defects and vacancies in the crystal lattice, which can promote the rearrangement of atoms, and reduce the ordering transition barrier. Therefore, Ag addition can result into improvement of structural ordering of the FePt NPs.

[1] S. Sun, C. B. Murray, D. Weller, L. Folks and A. Moser, Science, 287 1989-1992 (2000). [2] S. H. Sun, Adv. Mater., 18 393-403 (2006). [3] H. Wang, P. Shang, J. Zhang, M. Guo, Y. Mu, Q. Li and H. Wang, Chem. Mater., 25 2450-2454 (2013). [4] W. C. Wen, R. V. Chepulskii, L. W. Wang, S. Curtarolo and C. H. Lai, Acta Mater., 60 7258-7264 (2012). [5] X. Chen, Y. Wang, H. Wang, D. Shu, J. Zhang, P. Ruterana and H. Wang, J. Mater. Chem. C, 5 5316-5322 (2017).

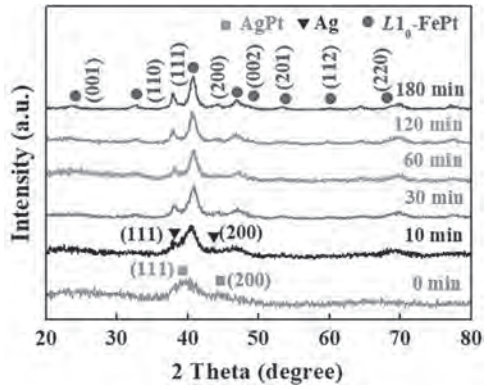

Fig.1 The XRD patterns of products obtained at 360 °C for different reaction times

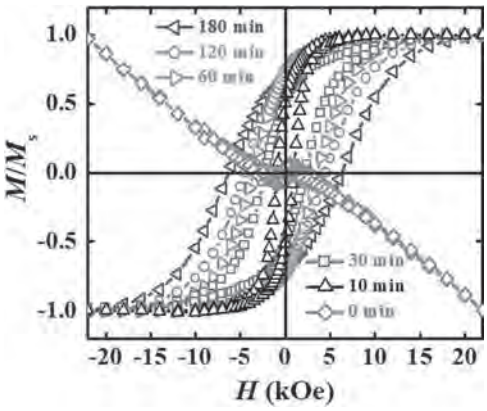

Fig. 2 The hysteresis loop of products obtained at 360 °C for different reaction times

DPB-02. One-step synthesis of $L1_0$-FePt@$PtBi_2$/Bi core-shell nanoparticles with high structral ordering. L. Chang[1,2], D. Zhao[3], T. Li[3], C. Wu[4], K. Wang[1,3], *W. Pei*[3] and Q. Wang[1] *1. Key Laboratory of Electromagnetic Processing of Materials (Ministry of Education), Northeastern University, Shenyang, China; 2. School of Metallurgy, Northeastern University, Shenyang, China; 3. School of Materials Science and Engineering, Northeastern University, Shenyang, China; 4. School of Materials Science and Engineering, Liaoning Technical University, Shenyang, China*

$L1_0$-FePt nanomaterials have widespread promosing applications in magnetic device, and catalysis[1,2]. In recent years, the one-step synthesis of $L1_0$-FePt nanoparticles (NPs) with doping third element has attracted much attention[3,4], because the method is simple and efficient. Previous work showed the element Bi with large atomic radius, low melting point and low surface energy[5] can obviously improve ordering degree of $L1_0$-FePt NPs. However, the effect of Bi element on the structral ordering and morphology of the FePt NPs are unclear. In this work, $L1_0$-FePt@$PtBi_2$/Bi core-shell NPs with high

structural ordering were successfully synthesized. The effect of Bi content on the core-shell structure of the NPs and ordering degree were detailedly investigated. With increase of Bi content, the morphology of FePt NPs have obviously difference. When the Bi content is 23at.%~32at.%, the NPs form a core-shell structure as shown in Figure 1. The core is composed of $L1_0$-FePt phase, and the shell is distributed by hcp-Bi and fcc-$PtBi_2$ phases as seen Fig.1(d1) and (d2). Bi has low melting point and low surface energy, which makes Bi diffuse to the particle surface. Thus the core-shell structure is formed. The investigation of magnetic properties indicated that the coercivity of core-shell NPs increases firstly and then decreases with the increase of Bi content (Figure 2). When the Bi content is 34at.%, the coercivity reaches the maximum of 1.6 T. This is because of the improve of ordering degree and the enlarge of $L1_0$-FePt core. Bi has a large atomic radius, which makes it produce vacancies and defects in the FePtBi particles. In addition, the Bi diffusion out of the particles can further enchance the vacancies, which is benefit to ordering transition of FePt. In conclusion, we can regulate the ordering degree, magnetic properties and core-shell morphology of $L1_0$-FePt@$PtBi_2$/Bi by controlling the Bi content.

[1] B. Shen, S. Sun, *Chem. Eur.J.*, Vol. 26, p. 6757-6766 (2020) [2] J. Li, Z. Xi, and Y. Pan, *J. Am. Chem. Soc.*, Vol. 140, p. 2926-2932 (2018) [3] Y. Yu, P. Mukherjee and Y. Tian, *Nanoscale*, Vol. 6(20), p. 12050-12055 (2014) [4] W. Pei, D. Zhao and C. Wu, *ACS Appl. Nano Mater.*, Vol. 3, p. 1098-1103 (2020) [5] F. M. Abel, V. Tzitzios and E. Devlin, *ACS Appl. Nano Mater.*, Vol. 2, p. 3146-3153 (2019)

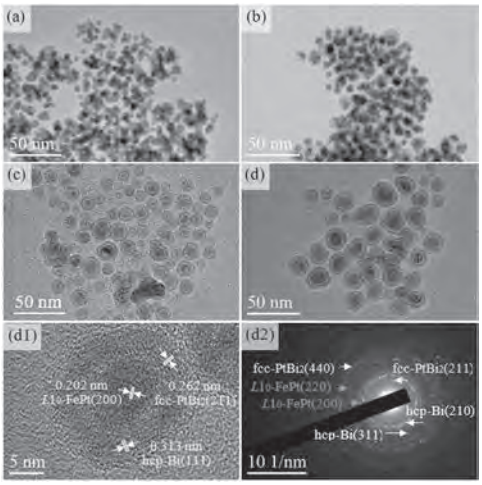

Figure 1. TEM images of $L1_0$-FePt@$PtBi_2$/Bi with Bi content is (a) 0at.%; (b) 13at.%; (c) 23at.%; (d) 32at.%; HRTEM image (d1) and diffraction pattern (d2) of 32at.% Bi

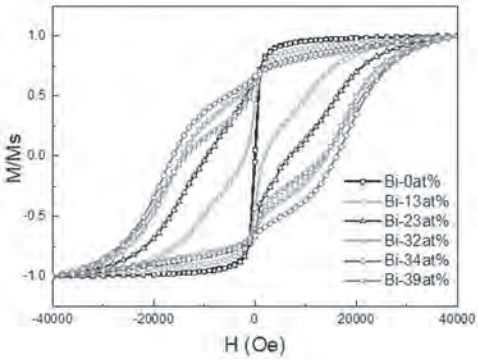

Figure 2. M-H curves of $L1_0$-FePt@$PtBi_2$/Bi with different Bi content

DPB-03. Effect of Structural Transformation (fcc to $L1_0$) on the Magnetic Properties of FePt, CoPt and $PtFe_{0.5}Co_{0.5}$ Nanoparticles. *V. Deepchand*[1] and G. Hadjipanayis[1] *1. Physics and Astronomy, University of Delaware, Newark, DE, United States*

FePt and CoPt nanoparticles exhibit hard magnetic properties in the ordered face-centered tetragonal (fct/$L1_0$) structure. FePt nanoparticles attract a lot of interest because of their many potential applications such as high density recording media, biomedicine and catalysis [1-3]. In the fct state, FePt has a high magnetocrystalline anisotropy of about 70 Merg/cm^3 and a high coercivity making it ideal for use in high density recording media [4]. Various chemical techniques have been used to enhance the coercivity of $L1_0$ FePt particles such as using a halide intermediary [5] or a Bi additive [6]. Usually, the as-made particles have the fcc structure and low coercivity. In most cases, the simplest way to obtain the $L1_0$ structure after synthesis is by performing heat treatment under an inert environment above 550°C. The drawback of post annealing is an increase in grain size and sintering, which reduces the suitability of the nanoparticles in applications such as catalysts. In the first part of this work, we studied the different stages of the $L1_0$ state transformation in FePt nanoparticles after annealing under various conditions, and then used a simplistic model to describe the temperature dependence of coercivity of selected FePt samples into different stages of the fcc to fct transformation. In the second part, we studied the properties of chemically synthesized CoPt nanoparticles. CoPt nanoparticles are chemically stable and have a high magnetocrystalline anisotropy of the order of 4×10^7 erg/cm^3, making them suitable as a stable permanent magnetic material [7] and for applications in ultrahigh density magnetic recording [8]. In our work, we mainly studied the magnetic properties of CoPt which were annealed at 700°C for 4 hours and applied a model to describe its temperature dependence of coercivity. We also synthesized a ternary system of Pt-Fe-Co, $PtFe_{0.5}Co_{0.5}$, and studied the evolution of its structure from fcc to fct after heat treatment under different conditions, and compared its magnetic properties to those of FePt and CoPt.

[1] S. Sun, Adv. Mater. 18, 393 (2006). [2] Q. Li et al., Nano Lett. 15, 2468 (2015). [3] Y. Shi et al., J. Nanomater. 2015, (2015). [4] D. Weller et al., J. Vac. Sci. Technol. B 34, 060801 (2016). [5] W. Lei et al., Nano Lett. 18, 7839 (2018). [6] F. M. Abel et al., ACS Appl. Nano Mater. 2, 3146 (2019). [7] J. A. Christodoulides et al., IEEE Trans. Magn. 36, 2333 (2000). [8] D. Weller and M. F. Doerner, Annu. Rev. Mater. Sci. 30, 611 (2000).

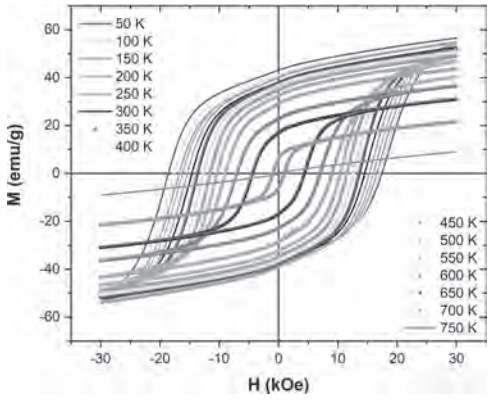

Fig. 1. Hysteresis loops of FePt annealed at 600°C for 1 hour at different temperatures.

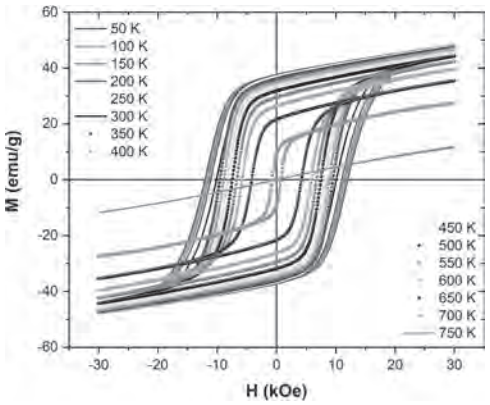

Fig. 2. Hysteresis loops of FePt annealed at 800°C for 1 hour at different temperatures.

DPB-04. Infrared Laser Annealing of Nanocomposite Nd-Fe-B/Mo/FeCo Multilayered Magnet Films. *K. Koike*[1], T. Uchida[1], K. Sakurai[1], N. Inaba[1], H. Kato[1], S. Hara[2], Y. Saito[2], S. Okubo[2], H. Ohta[2] and M. Itakura[3] *1. Yamagata University, Yonezawa, Japan; 2. Kobe University, Kobe, Japan; 3. Kyushu University, Kasuga, Japan*

Nanocomposite magnets composed of $Nd_2Fe_{14}B$ and α-Fe nanoparticles are not only expected to increase the $(BH)_{max}$ compared to Nd-Fe-B magnets [1], but also effective in reducing the use of HREs [2]. Recently, we have reported on NdFeB/Mo/FeCo multilayered magnet films formed by a two-step method [3]. However, long-time multi-step annealing (MSA) using a halogen lamp was necessary to realize this magnet film. It is well known that method using a laser is an excellent technique that can significantly reduce the process time and is expected to improve the magnetic properties. In this study, we report the formation of nanocomposite NdFeB/Mo/FeCo magnet films using infrared laser annealing (iLA) technique. The Nanocomposite [NdFeB(30 nm)/Mo(0.3 nm)/FeCo(5 nm)/Mo(0.3 nm)]$_5$ multilayered magnet films were prepared by UHV sputtering [3] followed by iLA processing. It is equipped with a CW semiconductor laser with a wave length of 939.8 nm and a spot size of about 5 mm in diameter on surface of films. Fig. 1 shows in-plane magnetization curves of the multilayered films as-deposited and iLA processed at 760°C. Both films with and w/o Mo interlayer before iLA processing showed soft magnetism with small coercivity and weak perpendicular magnetic anisotropy (PMA). The PMA of the film with the Mo interlayer is larger than that of the film without the Mo interlayer. Magnetic properties of both films were drastic changed from soft magnetism with PMA to hard magnetism with in-plane magnetic anisotropy after iLA processed at 760°C. Coercivity of in-plane of iLA processed film with Mo interlayer was 10 kOe which was double of the film w/o Mo interlayer. After iLA process, we can see that the squareness of film was improved by the introduction of Mo interlayer. These results show that the iLA process is effective in forming in-plane anisotropic nanocomposite NdFeB/Mo/FeCo magnet films even though the processing time of the iLA process is 1/100 of the processing time of the MSA process [3].

[1] E. F. Kneller and R. Hawig: IEEE Trans. Magn. 27 (1991) 3588. [2] S. Hirosawa, et al., J. Alloys Com. 408 (2006) 260. [3] K. Koike, et al., AIP Adv. 11 (2021) 015134-1.

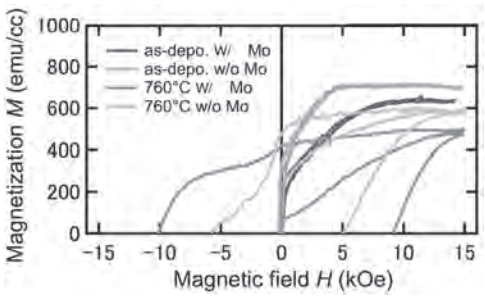

An in-plane magnetization curves of [Nd-Fe-B/Mo(t_{Mo} = 0 nm, 0.3 nm)/FeCo]$_5$ multilayered films as-deposited state and iLA processed at 760°C.

DPB-05. Influence of low sintering temperature of substituted M-type barium hexaferrite on its static and high-frequency magnetic properties. *K. Rana*[3], S. Thakur[4], M. Tomar[1] and A. Thakur[2] *1. Physics and Astrophysics, University of Delhi, New Delhi, India; 2. Physics, Centre of Nanotechnology, Amity University, Gurugram, India; 3. Electronic Materials Device Laboratory, University of Delhi, New Delhi, India; 4. Instituto de Alta Investigación, Universidad de Tarapacá, Arica, Chile*

Cobalt substituted M-type barium hexaferrite with nominal composition $BaCo_xFe_{12-x}O_{19}$ ($0.0 \leq x \leq 1.0$) in the steps of 0.2 were prepared via the chemical co-precipitation method. Thermal analysis was performed on pure BaM sample before undergoing thermal treatments to extract the beneficial information about their crystallization point. From TGA/DTA analysis it was confirmed that 900°C was an ideal sintering temperature for the pure BaM ferrite sample. On that basis, all six samples were sintered at the same temperature. XRD confirmed the formation of the M phase in all the samples whereas the morphology of all the samples was investigated by using the FESEM technique. Magnetic parameters like saturation magnetization (M_s), coercivity (H_c), and squareness ratio (SQR) were examined by using VSM. The value of M_s was found to decrease from 65.74 emu/g to 54.30 emu/g at the very initial stage (x=0.2) due to the small amount of dopant but after that with an increase in the dopant content, M_s value was found to increase up to x=0.8 and reached 65.39 emu/g. Moderate M_s value with a higher coercivity of 3784 Oe was obtained for x=0.8. On the other hand, the variation of complex permittivity and complex permeability with composition was investigated over the X-band frequency range (8.2GHz-12.4GHz). Excellent and sustainable values of permittivity (more than10) and magnetic loss $Tan\delta_\mu$ (at x=0.021) at x=0.8 makes this composition suitable for high-frequency application as well as electromagnetic shielding.

1. S Kumar, S Supriya and R Pandey, Journal of Magnetism and Magnetic Materials., 458, 30.38 (2018) 2. R Meena, S Bhattacharya and R Chatterjee, Materials Science and Engineering B., 171, 133-138 (2010)

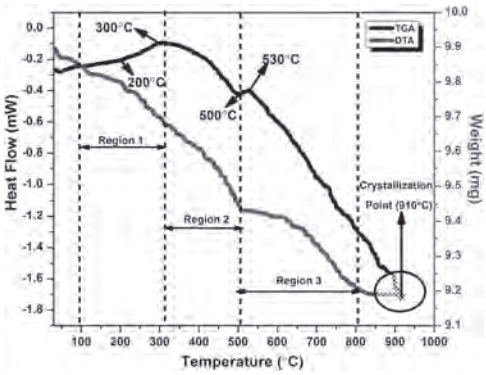

Fig.1 TGA/DTA analysis of pure BaM hexaferrite before undergoing appropriate heat treatments.

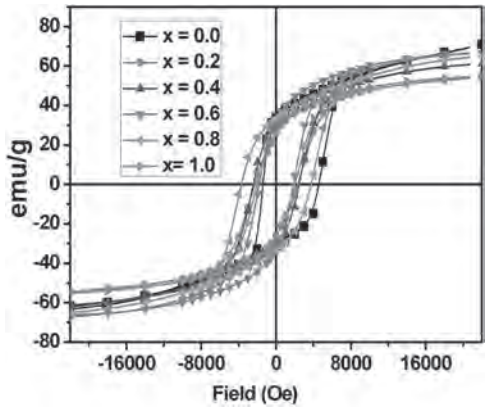

Fig.2 M-H loops of $BaCo_xFe_{12-x}O_{19}$ (0.0≤x≤1.0) sintered at 900°C

DPB-06. Structural, Magnetic, and Mössbauer Spectroscopic Study of La^{3+} and Cu^{1+} Co-doped M-type Strontium Hexaferrite. H. Kim[2] and *S. Yoon[1] 1. Department of Physics, Gunsan National University, Gunsan, The Republic of Korea; 2. Basic Materials & Chemicals R&D Center, LG Chem Research Park, Daejeon, The Republic of Korea*

Effects of La^{3+} and Cu^{1+} co-doping on structural and magnetic properties of M-type strontium hexaferrite have been studied by using crystallographic and magnetic measurements. Stoichiometric $Sr_{1-x}La_xFe_{12-x/2}Cu_{x/2}O_{19}$ (x=0, 0.25, 0.5, 0.65) samples have been prepared by the conventional ceramic method using La_2O_3, $SrCO_3$, Fe_2O_3, and CuO powders with repeated sintering at 1300 °C for 24 hours. EDS analysis showed that the ratios of metal elements were in good agreement with compositions of the samples. XRD patterns showed that when x ≥ 0.7, $LaFeO_3$, $SrFeO_{3-\delta}$, and $CuFe_2O_4$ coexisted along with the M-type hexaferrite. Lattice parameters deduced from the GSAS refinement shows that *a* slightly increases while *c* decreases with increasing *x* (Table 1). Variations of the saturation magnetization M_S and the coercivity H_C with *x* was obtained from room temperature VSM measurement as in Table 1. Whereas the H_C decreases monotonically with *x*, the M_S increases with the La^{3+} - Cu^{1+} co-doping throughout the doping range examined. Effective magnetic anisotropy constants *K* are calculated as well from the hysteresis curves using the law of approach to saturation method. *K* shows gradual increase with increasing *x* as listed in Table 1. XPS Cu2p scan shows that dominant valence state of Cu is +1. There were no trace observed for Cu^{2+} or metallic Cu (Fig. 1(a)). Apparently, monovalent Cu^{1+} has no spin magnetic moment. In view of the fact that diamagnetic substitution of either $4f_1$ or $4f_2$ site give rise to positive contribution to M_S, this behavior strongly suggests that Cu^{1+} ions preferentially replace Fe^{3+} ions at those sites. Finally, Mössbauer spectra show gradual decrease in $4f_2$ intensity, in support of the octahedral $4f_2$ site preference of Cu^{1+}. In addition, one extra sextet with H_{hf} ≈ 341 kOe was detected from the Mössbauer spectra, which were explained by the 12*k* site Fe^{3+} that have more than one $4f_2$ Cu^{1+} neighbors (Fig. 1(b)).

x	a (Å)	c (Å)	M_S (emu/g)	H_C (Oe)	K (J/m^3)
0	5.8776	23.0374	55.2	3862	3.82×10^5
0.25	5.8822	23.0080	52.8	3366	4.86×10^5
0.5	5.8830	22.9759	63.9	1487	4.90×10^5
0.65	5.8845	22.9575	70.7	328	5.17×10^5

Table I Various parameters of $Sr_{1-x}La_xFe_{12-x/2}Cu_{x/2}O_{19}$ (x=0, 0.25, 0.5, 0.65)

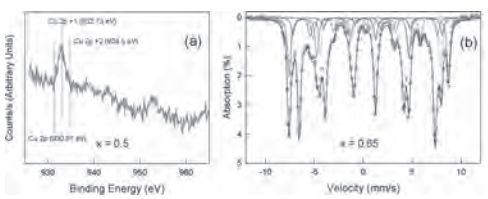

Fig. 1 (a) XPS Cu 2p scan for $Sr_{0.5}La_{0.5}Fe_{11.75}Cu_{0.25}O_{19}$ and (b) room temperature Mössbauer spectra of $Sr_{0.35}La_{0.65}Fe_{11.675}Cu_{0.325}O_{19}$

DPB-07. Sandwiched $CoFe_2O_4/SrFe_{11.5}Al_{0.5}O_{19}/CoFe_2O_4$ nanoparticles with exchange-coupling effect. *E. Gorbachev*[1], L. Trusov[1] and P. Kazin[2] *1. Department of Materials Science, Lomonosov Moscow State University, Moscow, Russian Federation; 2. Department of Chemistry, Lomonosov Moscow State University, Moscow, Russian Federation*

Exchange-coupled hard/soft ferrite nanoparticles are prospective to squeeze out a part of expensive magnets based on rare-earth elements. However, known exchange-coupled composite ferrite nanoparticles often suffer from a lack of a powerful enough hard-magnetic core, a high defectivity of magnetic phases, and a poor interface between them. Herein we demonstrate the first efficient synthesis of sandwiched nanomagnets, which exhibit the pronounced exchange-coupling effect. This work is featured by using individual high-coercive strontium hexaferrite nanoplates prepared by a borate glass crystallization method as cores for the composite particles. High crystal quality of the hexaferrite cores as a substrate provides an epitaxial growth of $CoFe_2O_4$ layers on the 001 facets from the organic high-boiling solvent and results in enhancing the remanence magnetization and the maximum energy product of the composite material. The obtained composite nanoparticles are characterized by well-defined epitaxial interfaces between the constituent phases. The exchange coupling results in strongly different magnetic properties compared to ones expected for a mechanical mixture of hexaferrite and cobalt ferrite. At room temperature, the magnetic properties are determined by the uniaxial magnetocrystalline anisotropy of the hexaferrite, while upon cooling the situation changes to the triaxial magnetocrystalline anisotropy typical for the spinel cobalt oxide. In the temperature range 5 – 300 K the composite shows significant improvement of the $(BH)_{max}$ values of both initial phases. The results of this work open new prospects for fabrication of multilayer oxide heterostructures with a synergetic performance which expands applications of exchange-coupled composites. The research was supported by Russian Science Foundation grant no 20-73-10129

DPB-08. Magnetic properties of Mn-Ga-B melt-spun ribbons. *T. Saito*[1] and D. Nishio-Hamane[2] *1. Chiba Institute of Technology, Narashino, Japan; 2. Institute for Solid State Physics, The University of Tokyo, Kashiwa, Japan*

In recent years, large coercivity has been reported in Mn-based compounds such as MnBi and MnGa. [1-3] In this study, Mn-Ga-B system alloys were produced by melt-spinning technique. This paper discusses the structures and magnetic properties of these alloys. Mn-Ga and Mn-Ga-B alloy ingots were prepared by arc melting in an argon atmosphere. The alloy ingots were placed in a quartz crucible with an orifice of 0.6 mm at the bottom. The alloy ingots were induction melted in an argon atmosphere and then ejected through the orifice with argon onto a chromium-plated copper wheel rotating at a surface velocity of 50 ms^{-1}. Heat treatments were performed in an argon atmosphere at temperatures between 673 K and 1073 K for 1h. The structures of the specimens were examined by X-ray diffraction and transmission electron microscope (TEM). The magnetic properties of the specimens were examined by a vibrating sample magnetometer (VSM). Figure 1 shows the hysteresis loops of the Mn-Ga melt-spun ribbons and the annealed specimens. Although the Mn-Ga melt-spun ribbons showed low coercivity, annealing of the ribbons resulted in an increase in the coercivity value. The annealed $Mn_{65}Ga_{35}$ melt-spun ribbon exhibited a coercivity of 4.8 kOe with a remanence of 43 emu/g. It was found that the addition of boron into $Mn_{65}Ga_{35}$ alloys resulted in the further increase in the coercivity value. TEM studies revealed that these melt-spun ribbons consisted of the Mn_3Ga phase with very fine grains.

[1] K. Wang, E. Lu, J. W. Knepper, F. Yang, and A. R. Smith, Appl. Phys. Lett. 98, 162507 (2011). [2] T. J. Nummy, S. P. Bennett, T. Cardinal, and D. Heiman, Appl. Phys. Lett. 99, 252506 (2011). [3] Y. B. Yang, X. G. Chen, R. Wu, J. Z. Wei, X. B. Ma, J. Z. Han, H. L. Du, S. Q. Liu, C. S. Wang, Y. C. Tang, Y. Zhang, and J. B. Yang, J. Appl. Phys. 111, 07F312 (2012).

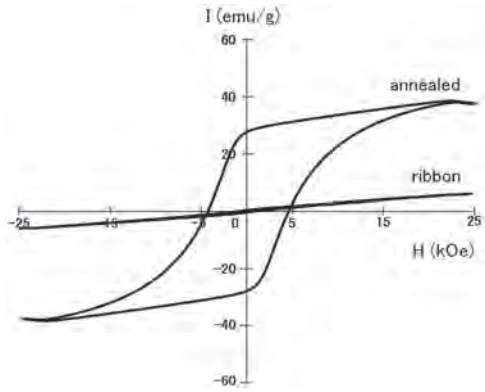

Fig.1 Hysteresis loops of the Mn-Ga melt-spun ribbons and the annealed specimens.

DPB-09. Magnetocrystalline Anisotropy in V– and Cu–doped $Fe_{16}N_2$ under DFT+*U*. *P. Stoeckl*[1], P. Swatek[2] and J. Wang[2] *1. Physics, University of Minnesota Twin Cities, Minneapolis, MN, United States; 2. Electrical and Computer Engineering, University of Minnesota Twin Cities, Minneapolis, MN, United States*

While giant saturation magnetization has been observed in α''–$Fe_{16}N_2$, its magnetic anisotropy and structural stability leave room for improvement. Several recent studies have investigated the effect of substitution to improve its magnetic properties and/or its stability; among these, substitution of Fe with V or Cu has shown promise. We thus compare the magnetic properties of such alloys in some more detail using first-principles electronic-structure calculations: The magnetocrystalline anisotropy (MCA) energies of ordered $Fe_{16-n}V_nN_2$ and $Fe_{16-n}Cu_nN_2$ alloys (n=1, 2) are obtained within the plane-wave density-functional theory (DFT) code Quantum ESPRESSO. Both the generalized-gradient approximation (GGA) and GGA+U method are considered, with particular focus on the effect of Hubbard parameters U, J, including a calculation via the linear-response method.

N. Ji, M. S. Osofsky, V. Lauter, L. F. Allard, X. Li, K. L. Jensen, H. Ambaye, E. Lara-Curzio, and J.-P. Wang, *Phys. Rev. B* 84, 245310 (2011). P. Stoeckl, P. Swatek, & J.-P. Wang *AIP Advances* 11(1), 015039 (2021). M. H. Han, W. J. Kim, E. K. Lee, H. Kim, S. Lebègue, and J. J. Kozak, J. Phys.: Condens. Matter 32, 035801 (2020).

DPB-10. Microwave-assisted Development of Nanostructured Cobalt-based Magnetic Materials. *C.I. Nlebedim*[1] and K. Gandha[1] *1. Critical Materials Institute, Ames Laboratory, Ames, IA, United States*

We will present our recent work on the development of cobalt-based magnetic materials with nanowire and nanochain structures synthesized via microwave technique. Cobalt is widely used and nearly indispensable in permanent magnets and soft magnetic materials due to the remarkable properties of its alloys. For example, Fe-Co soft magnetic alloys have the highest saturation magnetization and high Curie temperature needed for motors, generators, etc. Also, cobalt and iron enable rare-earth elements (REE) and non-REE permanent magnets such as $Sm_2(Co,Fe,Cu,Zr)_{17}$ and Alnico magnets, respectively. More recently, $(Fe_xCo_{1-x})_3B$ has been proposed as potential non-RE permanent magnets [1]. Nanostructured magnetic cobalt and iron nanoparticles can enable the development of non-REE magnets, capable of filling the "gap" between hard ferrites and magnets with critical REE [2,3]. Magnetic nanoparticles (MNPs) exhibit unique shape and size-dependent magnetic properties compared to traditional bulk magnets, making it possible to control and improve their magnetic performance for specific applications. In recent years, solution-phase reactions synthesis of MNPs with desired size, morphology, structure, and magnetic controls has been explored [4.5]. We will present our recent work in developing iron and cobalt nanostructured materials in view of both hard and soft magnetic applications. Fig. 1(a) shows anisotropic 1-D Co nanostructures synthesized by microwave-assisted chemical approach and Fig. 1(b) shows the microstructure of Fe-Co magnetic nanochains. Magnetic properties of the nanostructures are shown in Fig. 2. We will also present the stabilization of orthorhombic and hexagonal nanostructures in Fe-Co-B alloys based on which hard magnetic properties can be developed. ACKNOWLEDGMENT This research was supported by the Critical Materials Institute, an Energy Innovation Hub funded by the U.S. Department of Energy, Office of Energy Efficiency and Renewable Energy, Advanced Manufacturing Office.

1. S. K. Pal, K. P. Skokov, T. Groeb, S. Ener, and O. Gutfleisch, Journal of Alloys and Compounds 696, 543 (2017). 2. J. Cui, M. Kramer, L. Zhou, F. Liu, A. Gabay, G. Hadjipanayis, B. Balasubramanian, and D. Sellmyer, Acta Materialia 158, 118 (2018). 3. J. Mohapatra, M. Xing, J. Elkins, J. Beatty, and J. P. Liu, Advanced Functional Materials 31, 2010157 (2021). 4. K. Gandha, K. Elkins, N. Poudyal, X. Liu, and J. P. Liu, Scientific Reports 4, 5345 (2014). 5. M. A. Bousnina, A. Dakhlaoui-Omrani, F. Schoenstein, Y. Soumare, A. H. Barry, J.-Y. Piquemal, G. Viau, S. Mercone, and N. Jouini, Nanomaterials 10, 334 (2020).

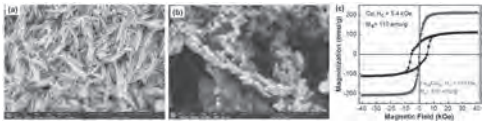

Fig. 1. Morphology of microwave-assisted synthesized (a) Co nanowires and (b) Fe-Co nanochains. (c) Room temperature magnetic properties of Co nanowires, and Fe-Co.

DPB-11. Recycling of Alnico Magnets by Ultrasonic Atomization and 3D Printing. *R. Wroblewski*[1], W. Bojarski[1], L. Zrodowski[1,2], B. Moronczyk[1] and M. Leonowicz[1] *1. Faculty of Materials Science and Engineering, Warsaw University of Technology, Warsaw, Poland; 2. AMAZEMET, Warsaw, Poland*

Refrigeration devices utilizing the magnetocaloric effect require not only Active Magnetic Regenerators (AMRs) but also efficient magnetic field sources. Of course, permanent magnets based on neodymium are best suited for this purpose, but Nd is a critical raw material, and possible problems with its availability have to be considered. A potential solution to the problem could be Alnico magnets, which can provide good flux density at very economical prices. In our work, we recycled an Alnico 8 magnet via ultrasonic atomization and subsequent 3D printing, thus obtained powders using the Selective Laser Melting (SLM) method. The printouts exhibited a uniform elemental distribution and a single-phase iron-based solid solution structure. This enabled to omit the homogenization annealing, generally conducted at 1250 °C, which seems to be economically advantageous. The magnetic properties of the as-printed samples were low - Hci ~ 26 emu/g and Ms ~140 emu/g. The printouts were subjected to thermo-magnetic treatment according to the parameters described in Refs. [1 & 2]. The results obtained - Hci ~ 240-280 emu/g and Ms ~140 emu/g - are not yet comparable to commercially available magnets but seem to be promising regarding the possibility of near-net shaping of the Alnico magnets using 3D printing.

[1] M. Stanek, L.Wierzbicki and M. Leonowicz, Investigations of Thermo-Magnetic Treatment of Alnico 8 Alloy, Archives of Metallurgy and Materials, Vol. 55, pp. 571-577, Poland (2010) [2] H. M. Dillon, Effects of heat treatment and processing modifications on microstructure in alnico 8H permanent magnet al.oys for high temperature applications, Graduate Theses and Dissertations, Iowa State University, USA (2014)

DPB-12. Residual stress tuned magnetic properties of thick CoMnP/Cu multilayers. Y. Chen[1], *C. Lin*[1], T. Chin[1,2], J. Chang[3] and C. Sung[3]
1. Department of Materials Science and Engineering, Feng Chia University, Taichung, Taiwan; 2. High Entropy Materials Center, National Tsing Hua University, Hsinchu, Taiwan; 3. Department of Power Mechanical Engineering, National Tsing Hua University, Hsinchu, Taiwan

Hard magnetic thick films by electrodeposition have a vast application in the field of sensors, energy harvesting, MEMS, etc. Yet the very large residual stress (σ_r) built-up in mono-layered thick magnetic films leads to cracks, dimensional changes and deteriorated magnetic properties. Here, we explored a strategy to tune σ_r by inserting a soft Cu interlayer in between very hard CoMnP magnetic layers, and to facilitate magnetic properties. The electrodeposited film structure is an alternating CoMnP/Cu on Cu-substrate. We kept a sum of all magnetic layers at ~20 μm to compare with a mono-layered CoMnP. The thickness of Cu interlayer was kept at 1.4 μm. The magnetic layers are 94 wt.% Co and possess highly textured (002) HCP microstructures (Fig. 1(a)). Insertion of Cu interlayers effectively reduces σ_r. Higher layer number results in lower fill factor, while the out-of-plane (OP) hard magnetic properties approximate to the 19.4 μm mono-layer (Fig. 1(b) and Table 1). The apparent internal stresses of the crystallites characterized through XRD $\sin^2\psi$ method clearly illustrate the coupling of macroscopic and microscopic stresses. Details of the XRD $\sin^2\psi$ analysis can be seen in our other publication. Magnetic properties are found highly correlated with the measured internal and residual stresses, hence layer structures. We explain in a quantitative measure the evolution of the intrinsic magnetocrystalline and stress-induced anisotropy in mono- and multilayered structures. This manifests the optimal design of layer structure through the tuned residual/internal stresses and anisotropy. The highly reduced σ_r is beneficial to maintain dimension during MEMS process and enhance long term stability. Our findings provide not only insights into the effect of layer residual stresses on hard magnetic properties, but also an excellent demonstration of the feasibility for further improvement in hard magnets by this manner.

[1] S. Roy, D. Mallick and K. Paul, "MEMS-Based Vibrational Energy Harvesting and Conversion Employing Micro-/Nano-Magnetics," in *IEEE Transactions on Magnetics*, vol. 55, no. 7, pp. 1-15, July 2019. [2] Y. Wang, J. Ewing and D. P. Arnold, "Ultra-Thick Electroplated CoPt Magnets for MEMS," in *Journal of Microelectromechanical Systems*, vol. 28, no. 2, pp. 311-320, April 2019. [3] Y. Li, J. Kim, M. Kim, A. Armutlulu and M. G. Allen, "Thick Multilayered Micromachined Permanent Magnets with Preserved Magnetic Properties," in *Journal of Microelectromechanical Systems*, vol. 25, no. 3, pp. 498-507, June 2016. [4] C.-W. Wu, C.-C. Lin, T.-S. Chin, J.-Y. Chang and C.-K. Sung, "Effects of Cathode Rotation and Substrate Materials on Electrodeposited CoMnP Thick Films," in *Materials Research Express*, vol. 8, pp. 016103, January 2021. [5] Y.-S. Chen, C.-C. Lin, T.-S. Chin, J.-Y. Chang and C.-K. Sung, "Residual Stress Analysis of Electrodeposited CoMnP Monolayers and Thick CoMnP/Cu Multilayers," submitted to *the TACT 2021 International Thin Films Conference*, 2021.

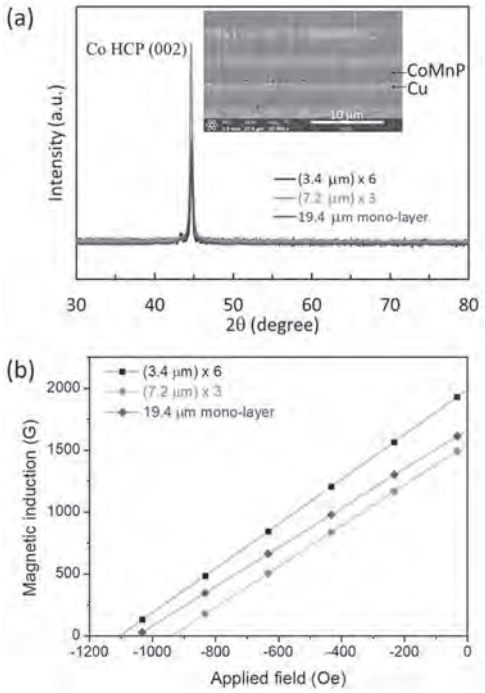

Fig. 1 (a) XRD patterns (θ-2θ scan). Inset showing the cross-sectional micrograph of the multilayer. (b) OP demagnetization curves.

CoMnP layer structure	σ_r (kPa)	Fill factor (γ)	$\gamma*(BH)_m$ (kGOe)	Apparent internal stress (N/m)	$\gamma*\sigma_r$ (kPa)	% reduced in internal stress
(3.4 μm) X 6	-5.35	0.74	393 ± 19	-3.2 ± 0.4	-3.96	33%
(7.2 μm) x 3	-5.93	0.89	334 ± 18	-3.6 ± 0.2	-5.28	25%
19.4 μm	-6.99	1.0	392 ± 36	-4.8 ± 0.1	-6.99	--

Table 1 Comparison of mechanical and magnetic properties. Fill factor is the ratio of the summed thickness of individual CoMnP layers to the total structure thickness in multilayer.

Session EOA
3D NANOMAGNETISM AND NANOWIRE ARRAYS
Pavel Ripka, Chair
Czech Technical University, Prague, Czechia

INVITED PAPER

EOA-01. 3D Nanomagnetism in Interconnected Magnetic Nanowire Networks. E. Burks[2], D.A. Gilbert[2,3], J. Malloy[1,2], A. Quintana[1], C.J. Jensen[1], P. Murray[2], C. Flores[2], T. Felter[4], S. Charnvanichborikarn[5], S. Kucheyev[5], J. Colvin[5], G. Yin[1] and *K. Liu*[1,2] *1. Georgetown University, Washington, DC, United States; 2. University of California, Davis, Davis, CA, United States; 3. University of Tennessee, Knoxville, TN, United States; 4. Sandia National Laboratories, Livermore, CA, United States; 5. Lawrence Livermore National Laboratory, Livermore, CA, United States*

Networks of interconnected magnetic nanowires offer an exciting platform to explore 3-dimensional (3D) nanomagnetism, where their structure, topology and frustration may be used as additional degrees of freedom to tailor the materials properties. We have achieved quasi-ordered metallic networks over cm-scale areas. Using a cost-effective multiple azimuthal angle ion-tracking and etching method with suitable fluence, interconnected nanoporous polycarbonate membranes were first fabricated. A subsequent electrochemical deposition process led to interconnected metallic nanowire networks, with density as low as 40 mg/cm^3 (Fig. 1) [1]. New magnetization reversal mechanisms in cobalt networks (Fig. 1d) are captured by the first-order reversal curve (FORC) method, which demonstrate the evolution from strong demagnetizing dipolar interactions to intersections-mediated domain wall pinning and propagation, and eventually to shape-anisotropy dominated magnetization reversal (Fig. 2). By varying the applied magnetic field strength, orientation, and sequence, it is in principle possible to selectively address a certain subset of the nanowire networks, encode digital information into their magnetic state, and propagate it through the networks for potential 3D magnetic memory and logic applications. Such network of magnetic nanowires also has the potential to implement repeatable multistate memristors in neuromorphic circuits, due to the expected discrete nature of domain wall motion through the intersecting networks. Interestingly, another random configuration of metallic nanowire networks has found applications in deep-submicron particulate filtration, relevant to combatting COVID-19 and air pollution, due to the extremely large surface areas and the excellent mechanical strength [2]. This work has been supported by the NSF (ECCS-1611424 and ECCS-1933527), SRC/NIST nCORE SMART center, DTRA, U.C. Davis and Georgetown University.

[1] E. C. Burks, D. A. Gilbert, P. D. Murray, C. Flores, T. E. Felter, S. Charnvanichborikarn, S. O. Kucheyev, J. Colvin, G. Yin and Kai Liu, *Nano Letters*, 21, 716 (2021). [2] J. Malloy, A. Quintana, C. J. Jensen, and Kai Liu, *Nano Letters*, 21, 2968 (2021).

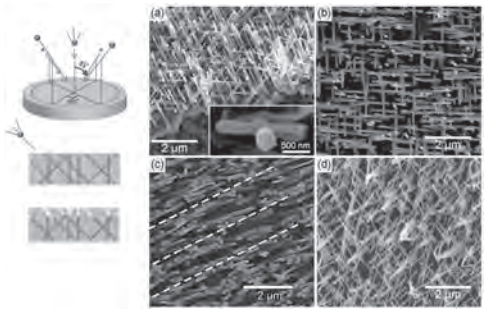

Figure 1: (a) Side-view and (b) top-view SEM images of an interconnected copper network, tracked at five angles as illustrated by the schematics. Inset in (a) shows that at an intersection the wires are physically connected. Top-view SEM images of (c) a copper network and (d) a cobalt network, tracked at three angles. This produces intersections in planes that contain the three irradiated angles (which are highlighted with white dashed lines).

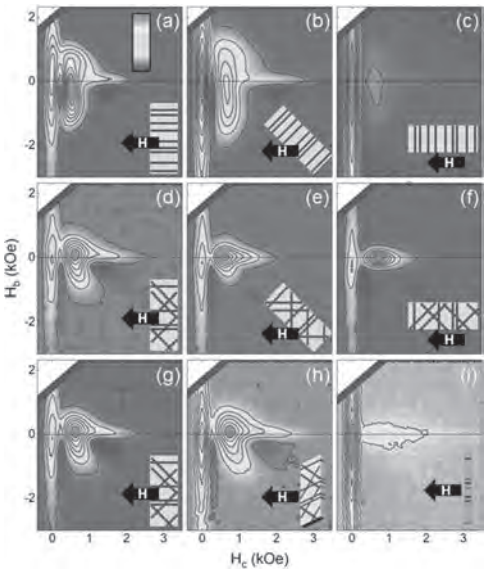

Figure 2. FORC diagrams shown in 2D contour plots for (a-c) a single-angle irradiated sample, and (d-i) three-angle irradiated sample. The schematic diagrams in the lower right corner of panels (a-i) indicate the orientation of the wires (black lines) and membrane (blue box) relative to the applied field shown by the large black arrow.

CONTRIBUTED PAPERS

EOA-02. Nanostructured magnets prepared by magnetophoresis-assisted capillary assembly of Co nanorods. *L. Lacroix*[1], G. Viau[1], A. Gonon[1], T. Blon[1], I. Lecerf[1], T. Leichlé[2] and T. Ondarcuhu[3] *1. LPCNO, Université Toulouse, Toulouse, France; 2. LAAS, Toulouse, France; 3. IMFT, Toulouse, France*

The fabrication of micrometric magnetic materials and their integration into portable devices reveal great interests for telecommunications, automotive, biomedical and space applications, but still remain highly challenging. The bottom-up approach for nanostructured magnets is an interesting alternative route to the classical rare earth metallurgy or thin film deposition. Indeed, the recent progresses in the magnetic nanoparticle synthesis allow a good control of the particle size, shape and chemical composition. Single-crystalline Co nanorods (NRs), which combine a high magnetization and a large magnetic anisotropy, can be prepared by the polyol process [1]. These anisotropic particles constitute building blocks of primary choice for permanent magnet applications. [2] We reported recently a versatile approach for the fabrication and direct integration of nanostructured magnetic materials of controlled shaped at specific locations onto silicon substrates [3]. The magnetophoresis-assisted capillary assembly of magnetic nanoparticles leads to the fabrication of high-performance Co-based permanent magnets (Figure 1). Integrated submillimeter magnets as well as millimetric self-standing magnets exhibiting magnetic properties competing with NdFeB-based composited were obtained through this cost- and time-efficient process. The proof-of-concept of electromagnetic actuation of a MEMS cantilever by means of these supercrystals highlights their potentiality as efficient integrated magnetic materials within nomadic devices.

[1] E. Anagnostopoulou et al., Nanoscale 8, 4020 (2016) [2] S. Ener et al., Acta. Mater. 145, 290 (2018) [3] P. Moritz et al., ACS Nano 15, 5096 (2021)

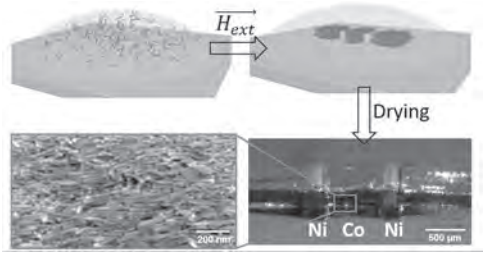

Figure 1. Schematic view of the magnetophoresis-driven capillary assembly of Co nanorods. Scanning Electron Microscopy of the integrated Co magnet in between the Ni blocks which served as flux concentrator to drive the assembly and the enlarged view evidencing the proper nanorod alignment.

EOA-03. Magnetic Texture Fluctuations in Coupled Mesospin Systems. *S. Slöetjes*[1], A. Ciuciulkaite[1], B. Hjörvarsson[1] and V. Kapaklis[1] *1. Department of Physics and Astronomy, Uppsala University, Uppsala, Sweden*

We study the effect of thermal fluctuations on dipole coupled mesospins, the building blocks of artificial spin ice (ASI), in a micromagnetic framework. Taking into account the internal magnetic texture, we focus specifically on the fluctuations at the edges, which have previously shown to exhibit a temperature dependent switching between two states that are essentially half of a C- or S-state [1]. We study two different systems, the first being a system of two coupled magnets and the second being a fourfold coordinated ASI vertex. For the two mesospin system with parallel magnetization, we find magnonic mode splitting at the edges, which is relatively unaffected by temperature. When the magnetization in the two mesospins is opposite, we find the appearance of an asymmetric potential, which can be quantified through the magnetic texture correlations. The Arrhenius law is used to find the attempt frequency and the energy barriers associated with switching, the latter are found to be inversely proportional to the spacing. We find a logarithmic dependence of the attempt frequency on the energy barrier, which is indicative of entropy-energy compensation at small spacings (large barriers). The temperature dependent edge dynamics for the ASI vertex is evaluated for the four different types (Type I-IV), each displaying their own characteristic dynamics. An example of such dynamics is the collective switching of the handedness associated with the perpendicular edge magnetization in a type IV vertex configuration. These results indicate the presence of rich texture dynamics, even at the level of the individual building blocks of the ASI.

[1] S. D. Slöetjes, B. Hjörvarsson, and V. Kapaklis, *Applied Physics Letters* 118, 142407 (2021)

INVITED PAPER

EOA-04. Magnetic charge propagation upon a 3D artificial spin-ice. A. May[1], M.D. Saccone[2], A. van den Berg[1], J. Askey[1], M. Hunt[1] and *S. Ladak*[1] *1. School of Physics and Astronomy, Cardiff University, Cardiff, United Kingdom; 2. Theoretical Division, Los Alamos National Laboratory, Los Alamos, NM, United States*

Artificial spin-ice systems (ASI) have been studied for 15 years, allowing detailed studies to examine the frustration, ordering and monopole transport in a variety of two-dimensional geometries [1]. The nanostructuring of magnetic materials in three-dimensions presents a new paradigm in condensed matter physics and allows access to a wide range of new physical phenomena [2]. With respect to ASI systems, there are several reasons why 3D geometries are interesting. This includes the realisation of a degenerate ice-rule, mimicking of bulk spin-ice geometries and studying the influence of surfaces upon ordering. In this talk, I will outline the realisation of a 3D artificial spin-ice system [3] which takes the geometry of a diamond-bond lattice (Fig. 1), capturing the arrangement of spins in bulk pyrochlore systems. By using magnetic force microscopy (Fig. 2), I will show that the vertex states upon the surface can be determined, and the global switching of the lattice can be measured. We find very different magnetic charge dynamics along two principal directions upon the lattice. For a field applied along the surface termination, local energetics force magnetic charges to nucleate over a larger characteristic distance, reducing their magnetic Coulomb interaction and producing lone, uncorrelated monopoles. In contrast, applying a field transverse to the surface termination yields large numbers of highly correlated monopole-antimonopole pairs. A combination of micromagnetic and Monte-Carlo simulations are used to understand the results. These suggest it is the difference in effective chemical potential that yields the striking differences in monopole transport. We anticipate that our study will inspire a new generation in artificial spin-ice research whereby the ground states in complex 3D frustrated lattices are explored.

[1] S. H. Skjærvø et al., Nature Reviews Physics 2, 13–28 (2020) [2] A. Fernandez-Pacheco, et al., Nature Communications, Vol. 8, p. 15756 (2017) [3] A. May et al. Nature Communications 12, 3217 (2021)

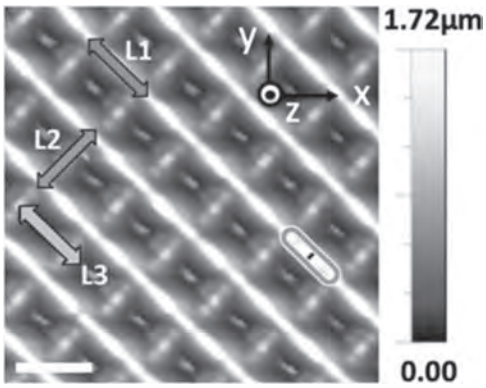

Fig 1. Atomic force microscopy image of the 3DASI system. Distinct layers within the system are labelled L1 - L3.

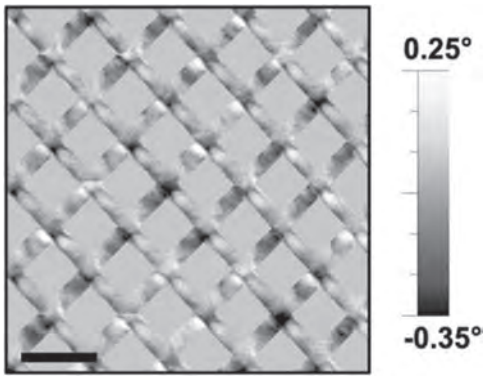

Fig 2. Magnetic force microscopy of the 3DASI surface, showing a number of ice-rule and monopole states.

CONTRIBUTED PAPERS

EOA-05. Magnetization reversal in individual core/shell cylindrical nanowires with non-magnetic interlayer. M. Méndez[1], J. García[1], J. Fernandez-Roldan[1], V. Vega[1], A. Gonzalez[1] and *V.M. Prida*[1]
1. University of Oviedo, Oviedo, Spain

Three-dimensional core-shell magnetic nanostructures are appealing for novel applications in magnetic recording, biotechnology, nanoelectronics, and spintronics devices [1-6]. While few works report on three-layered core/shell cylindrical nanowires (NWs) systems recently investigated, the magnetization switching processes in these nanostructures remain yet unexplored [7-8]. In this study we investigate the switching process of an individual FM/NM/FM core/shell NW made of $Fe_{50}Co_{50}$(core)/ SiO_2 (interlayer)/ Fe_3O_4(shell) that were experimentally synthesized by atomic layer deposition coupled with electrochemical deposition technique. Magneto-optical Kerr effect measurements allow to access the switching process of individual NWs and its contrast with micromagnetic modelling of the reversal process in order to determine the switching of each layer, either the external shell or the inner core of the whole NW. Analysis of magnetization reversal curves through First Order Curves (FORC) were performed for the FeCo NW (Fig. 1a), the core/shell NW (Fig.1b) and the shell magnetite Nanotube (NT) (Fig. 1c), respectively, where it can be clearly distinguished the stronger magnetostatic interactions among the NWs. From micromagnetic modelling, we have found the conditions to select the first switching layer under the applied magnetic field by tailoring the thickness of the non-magnetic interspacing layers. Our results show that the magnetizations of the the FeCo core and the magnetite shell may switch either simultaneously, or at different switching fields during the reversal of the NW/NT structure. The elimination of the non-magnetic layer in micromagnetic simulations confirms that the reversal mechanism of our experimental core/shell NWs is uniquely promoted by magnetostatic dipolar coupling between the ferromagnetic layers with a direct exchange decoupling between both magnetic layers. These results set an appealing strategy for the design of novel 3D magnetic storage and spintronic devices based on core/shell cylindrical NWs that has not been envisaged up to know.

[1] C.-L. Li et al., Sensors & Actuators B: Chemical, Vol. 210, pp. 46-55, (2015). [2] F. Wang et al., Carbon, Vol. 145, pp. 701-711, (2019). [3] G. A. Jacob, R. J. Joseyphus, Appl. Phys. A, Vol. 127, pp. 33, (2021). [4] M. Gong et al., Small, Vol. 10, pp. 4118-4122, (2014). [5] S.H. Moon et al., Nano Lett., Vol. 17, pp. 800-804, (2017). [6] W. Zhang et al., Chem. Commun., Vol. 54, pp. 11005-11008, (2018). [7] Y.T. Chong et al., Adv. Mater., Vol. 22, pp. 2435-2439, (2010). [8] M. Takahashi et al., Langmuir, Vol. 31, pp. 2228-2236, (2015).

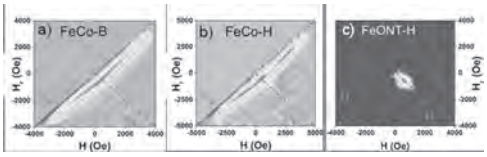

FORC images for the FeCo nanowire (a), the core/shell nanowire (b) and the shell magnetite nanotube (c), respectively

EOA-06. Effects of growth kinetics on structural and magnetic properties of Co nanowires. *J. Mohapatra*[1], J. Elkins[1], M. Xing[1] and J. Liu[1] *1. Department of Physics, The University of Texas at Arlington, Arlington, TX, United States*

The synthesis of single-crystalline and single-domain ferromagnetic nanowire materials has been an area of intense research,[1-3] however the control of geometric parameters (diameter, lengths, tip morphology and uniformity) in nanowire syntheses is mostly empirical. Here, we demonstrate a simple method for precise control of geometric parameters in nanowire synthesis by establishing both steady-state growth conditions and a uniform rate of particle growth through the continuous and controlled additions of precursors. To prepare Co nanowires, we used both the 'LaMer' and 'extended LaMer' processes, which allows us to fine control over diameter, aspect ratio, and morphology uniformity of the nanowires with reproducibility. Meanwhile, the structural property analysis of a series of nanowires revealed both qualitative and quantitative information on the growth kinetics of the nanowires. It has been demonstrated how the precursor flow rate, metal precursor mole ratio and the reducing ability of long-chain amine affect the nanowire morphology. We then show how such fine geometric control affects the magnetic coercivity of nanowire assemblies. Based on the shape anisotropy and orientation of the nanowire assemblies, a record high room-temperature coercivity exceeding 10 kOe has been measured in Co nanowires with a diameter of 8 nm.

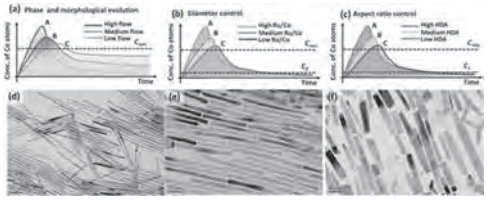

Fig. 1 Schematic illustration of the effect of (a) flow rate of Co-precursor, (b) mole ratio of $RuCl_3$ to Co-precursor and (c) long-chain amine content on the growth kinetic of Co nanowires. (d-f) The TEM images of Co nanowires prepared through the continuous flow of Co-precursor at various decreasing flow rates.

EOA-07. Giant Magnetoresistance and Magneto-Thermopower in 3D Interconnected Multilayer Nanowire Networks. *N. Marchal*[1], T. da Câmara Santa Clara Gomes[1], F. Abreu Araujo[1] and L. Piraux[1] *1. Institute of Condensed Matter and Nanosciences, Université Catholique de Louvain, Louvain-la-Neuve, Belgium*

Template-assisted electrodeposition of interconnected nanowire networks revealed to be a promising technique to develop flexible macroscopic spin caloritronic devices [1-3]. This versatile process allows to stack ferromagnetic and non-magnetic metallic layers with controlled morphology and material composition. The interconnected multilayer nanowire networks embedded in a flexible polymer film exhibit large magnetoresistance and magneto-thermoelectric effects, easily characterized thanks to the current-perpendicular-to-plane configuration in such structure. The coupling between heat and spin currents is analyzed through the extraction of the spin-dependent Seebeck coefficients from experimental characterizations of transport properties in the macroscopic in-plane direction of the film. This complex architecture paves the way to flexible magnetically controlled thermoelectric devices. Various multilayer nanowire networks made of FM/Cu stacks (FM = Co, $Ni_{50}Co_{50}$ and Ni_xFe_{100-x} with $60 < x < 97$) were fabricated by direct electrodeposition inside 3D nanoporous templates. The multilayer structure keeps large thermopower compared to those of their corresponding ferromagnetic metals while providing large variations of the Seebeck coefficients under an external magnetic field [1-5]. Such magneto-thermoelectric effects were observed to be comparable and even larger than the magnetoresistance effects, reaching a ratio up to 7 for the $Ni_{97}Fe_3$/Cu nanowire network. This enhancement of the magneto-thermopower is related to the significant spin-dependence of the Seebeck coefficient for Ni-rich NiFe alloys compared to Co and $Ni_{50}Co_{50}$. The spin-dependent Seebeck coefficient $S_\uparrow - S_\downarrow$ for Co/Cu, $Ni_{50}Co_{50}$/Cu, and $Ni_{97}Fe_3$/Cu nanowire networks were determined around -8.5, -10 and -21 μV/K at room temperature, respectively [3, 5]. The observation of such large spin-dependence of the thermoelectric power holds promise for the development of magnetically modulated flexible thermoelectric devices.

[1] T. da Câmara Santa Clara Gomes, F. Abreu Araujo and L. Piraux, *Science Advances* 5(3), eaav2782(2019). [2] F. Abreu Araujo, T. da Câmara Santa Clara Gomes and L. Piraux, *Advanced Electronic Materials* 5, 1800819 (2019). [3] T. da Câmara Santa Clara Gomes, N. Marchal, F. Abreu Araujo and L. Piraux, *Nanomaterials* 10, 2092 (2020). [4] N. Marchal, T. da Câmara Santa Clara Gomes, F. Abreu Araujo and L. Piraux, *Nanoscale Research Letters* 15, 137 (2020). [5] N. Marchal, T. da Câmara Santa Clara Gomes, F. Abreu Araujo and L. Piraux, *Nanomaterials* 11, 1133 (2021).

EOA-08. Apparent permeability of ordered magnetically soft nanowire and microwire arrays. *P. Ripka*[1], D. Hrakova[1], M. Mirzaei[1], V. Grim[1], M. Butta[1] and O. Kaman[2] *1. Fac. of Electrical Engineering, Dept. of Measurement, Czech Technical University, Prague, Czechia; 2. Department of Magnetics and Superconductors, Institute of Physics of the Czech Academy of Sciences, Prague, Czechia*

Arrays of magnetically soft nanowires and microwires have potential sensor applications [1, 2]. We have reported nanowire array manufactured by electrodeposition of permalloy into polycarbonate membranes [3]. In this paper we report permalloy nanowire and microwire arrays produced using alumina and silicon membranes with hexagonally ordered pores with constant pitch. These membranes allow to optimize the nanowire array properties such as coercivity, apparent permeability and amplification factor. Finite element modelling of nanowire arrays is demanding due to the computational complexity. In [4] we calculated apparent permeability and demagnetization factor of single wire and small wire arrays. We have also proposed simplified 2D equivalent model allowing to calculate properties of wire arrays very efficiently [5] and verified the validity of this model by full 3D simulations and also experimentally on arrays of up to 91 permalloy microwires. In this paper we apply this model to manufactured arrays of 3 mm diameter containing 100 000 to 40 million wires with diameters between 180 nm and 2.5 μm and compare simulation results to measurements by SQUID. Figs. 1 and 2 show examples of the measured hysteresis loops with red line showing the slope corresponding to apparent amplitude permeability. The values calculated by FEM using constant permeability model show significant deviations especially at low density arrays. We will show that this difference is caused by the nonlinear shielding effect: the field in the outermost wires is much stronger and thus they are saturated first. Because of that the saturation process propagates fast from the periphery towards inside array which can be shown on non-linear model.

[1] M. Vázquez, Magnetic Nano- and Microwires: Design, Synthesis, Properties and Applications: Elsevier Science, 2015. [2] J. A. Moreno, C. Bran, M. Vazquez and J. Kosel, "Cylindrical Magnetic Nanowires Applications," in IEEE Transactions on Magnetics, vol. 57, no. 4, pp. 1-17, April 2021, Art no. 800317 [3] P. Ripka, V. Grim, M. Mirzaei, D. Hrakova, J. Uhrig, F. Emmerich, C. Thielemann, J. Hejtmanek, O. Kaman, and R. Tesar: Modelling and measurement of magnetically soft nanowire arrays for sensor applications, Sensors 2021, 21(1), 3, [4] P. Ripka, V. Grim, M. Mirzaei: The apparent permeability and the amplification factor of magnetic wires and wire arrays JMMM 527, 2021, 167726 [5] M. Mirzaei, P. Ripka. V. Grim: A Simplified 2D Equivalent Model for Magnetic Wire Array, IEEE Trans Magn. early access 10.1109/TMAG.2021.3085485

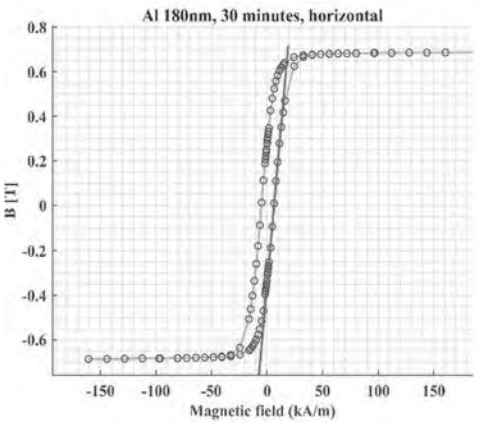

Fig. 1 Hysteresis loop of the array of 180 nm diameter 100 μm long wires with 480 nm pitch. Measured apparent amplitude permeability $\mu_a = 45$, calculated incremental $\mu_{ai} = 8.6$.

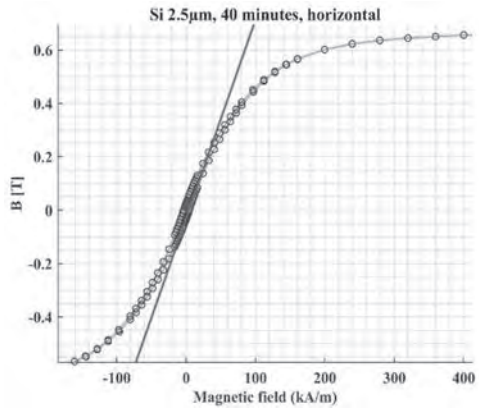

Fig. 2 Hysteresis loop of the array of 2.5 μm diameter 200 μm long wires with 4.2 μm nominal pitch. Measured apparent amplitude permeability $\mu_a = 5.5$, calculated incremental $\mu_{ai} = 3.8$.

EOA-09. Feasibility of Using NiCu/FeCo Coupled Bi-segmented Nanowires as In-line Writing Heads for 3D Racetrack Storage Devices.
V.M. Andrade[1], S. Caspani[1], A. Rivelles[2], S. Bunyaev[1], V.O. Golub[3], J.P. Araujo[1], G.N. Kakazei[1], C. Sousa[1] and *M.P. Proenca*[1,2] *1. IFIMUP - Institute of Physics for Advanced Materials, Nanotechnology and Photonics, Department of Physics and Astronomy, Faculty of Sciences, University of Porto, Porto, Portugal; 2. ISOM, Universidad Politécnica de Madrid, Madrid, Spain; 3. Institute of Magnetism NAS of Ukraine and MES of Ukraine, Kyiv, Ukraine*

Multi-segmented nanowire (NW) arrays are strong candidates to improve the memory storage capacity due to their lower magnetic bit area [1]. But writing/reading information on such devices is still a challenge. Recently, micromagnetic simulations revealed that the integration of a soft magnetic segment (with lower coercivity) along the racetrack could ease the writing process by using external magnetic fields [2]. Here, we demonstrate the feasibility of using NiCu/FeCo magnetic NWs as in-line writing components in 3D racetrack memory devices. Using template-assisted DC electrodeposition [3-5], 4 samples of NW hexagonal arrays (50 nm-diameter, 100 nm of inter-wire distance) were produced: i) $Ni_{90}Cu_{10}$; ii) $Fe_{20}Co_{80}$; iii) bi-segmented NiCu/FeCo; and iv) multi-segmented NiCu/$[FeCo/Au]_3$. Morphological, chemical and structural characterization revealed the formation of single, bi- and multi-segmented NW arrays with tuned dimensions and uniform compositions (Fig. 1). Magnetic hysteresis loops, ferromagnetic resonance (FMR) measurements and first-order reversal curve (FORC) diagram analysis confirmed the hard and soft magnetic properties of the FeCo and NiCu single arrays, respectively. In the interacting NiCu/FeCo bi- and multi-segmented systems, a significant reduction of the parallel coercivity occurred, while keeping the magnetization easy axis lying parallel to the NWs' axis. FORC diagrams also demonstrated a two-step reversal process in systems (Fig. 2), illustrating a FORC fingerprint typically present in soft/hard magnetic interacting bi-layered NWs [6]. Micromagnetic simulations confirmed such a two-step reversal process, revealing the presence of strong interactions at the soft/hard interface [7]. This work was supported by projects POCI-01-0145-FEDER-028676, POCI-01-0145-FEDER-031302, UIDB/04968/2020, EXPL/IF/00541/2015 and contract IF/01159/2015 from Portuguese FCT and COMPETE 2020 (FEDER); grant 02.2020/0261 from the National Research Foundation of Ukraine; and project PID2020-117024GB-C42 from the Spanish *Ministerio de Ciencia e Innovacíon*.

[1] S. Parkin and S.-H. Yang, Nature Nanotechnology, Vol. 10, p. 195–198 (2015) [2] J. Rial and M. P. Proenca, Nanomaterials, Vol. 10, p. 2403 (2020) [3] C. Sousa et al., Applied Physics Reviews, Vol. 1, p. 031102 (2014) [4] C. Bran et al., Journal of Physics D: Applied Physics, Vol. 48, p. 145304 (2015) [5] E. M. Palmero et al., Journal of Applied Physics, Vol. 116, p. 033908 (2014) [6] J. Garcia Fernandez et al., Nanomaterials, Vol. 8, p. 548 (2018) [7] V. M. Andrade et al. "NiCu/FeCo Bi-segmented Nanowires as Writing Elements in 3D Racetrack Memories", *in preparation* (2021)

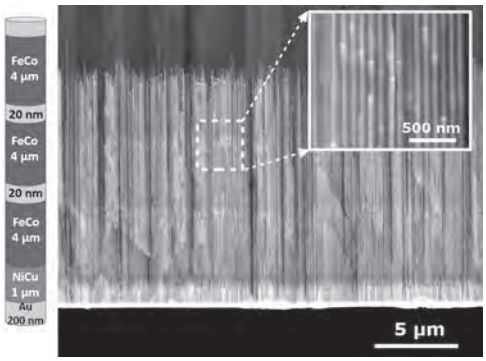

Fig. 1. Scanning electron microscopy images of the electrodeposited multi-segmented NWs.

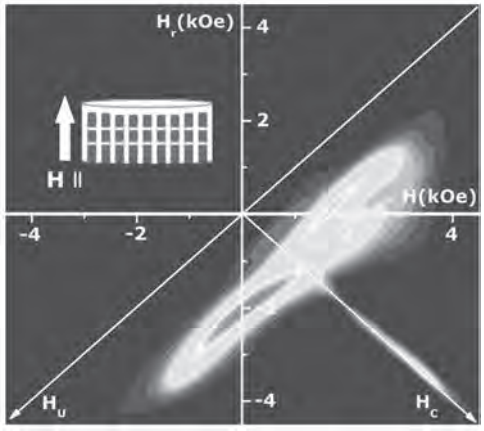

Fig. 2. FORC diagram of the multi-segmented sample along the parallel direction.

EOA-10. Intersection-Mediated Magnetoresistance in 3D Nanowire Networks.
D. Bhattacharya[1], C.J. Jensen[1], Z. Chen[1], L. Debeer-Schmitt[3], A.J. Grutter[2], K. Krycka[2], J.A. Borchers[2], E. Burks[5], D.A. Gilbert[4], G. Yin[1] and K. Liu[1] *1. Physics, Georgetown University, Washington, DC, United States; 2. Center for Neutron Research, NIST, Gaithersburg, MD, United States; 3. Oak Ridge National Laboratory, Oak Ridge, TN, United States; 4. Material Science and Engineering, University Of Tennessee, Knoxville, TN, United States; 5. UC Davis, Davis, CA, United States*

Three-dimensional (3D) magnetic assemblies can accommodate unique topological features and exotic spin textures, along with embedded magnetic frustrations [1]. Recently, we have realized interconnected cobalt nanowire networks using multiple angle ion-tracking and electrodeposition; such networks exhibit new magnetization reversal behaviors, offering an interesting platform for 3D information storage [2]. Here we report magnetoresistance (MR) studies of such interconnected networks, to explore how the magnetic configurations can be correlated with spin transport. When a sizable collection of connected nanowires is measured, typical anisotropic magnetoresistance behavior with sharp minima near the coercive fields is found, suggesting that the current is largely bypassing the high resistance intersections. However, when only a few interconnected nanowires are measured, the MR curve exhibits multiple kinks and local minima, indicative of domain wall pinning by the intersections (Fig. 1). More interestingly, during the positive to negative field sweep, a significant MR minimum is observed at positive field, which is the largest among all the MR minima. These features are not seen in parallel nanowires and are a direct consequence of the intersections. Micromagnetic simulations using an equivalent resistor model based on two intersecting nanowires reproduces the experimental observations, including the multiple kinks and a large MR minimum in positive field. Furthermore, small angle neutron scattering has been used to characterize magnetic correlations in the networks under different applied magnetic field configurations. These results show that the intersections in the networks play an important role in pinning / depinning of domain walls, which may be utilized for 3D magnetic memory and memristive devices. Work supported by the SRC/NIST nCORE SMART center and NSF.

[1] A. Fernandez-Pacheco, et al. Nat. Commun., 8, 15756 (2017). [2] E. Burks et al. Nano Lett., 21, 716–722 (2021).

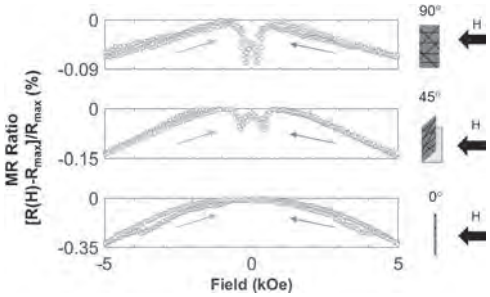

Figure 1: Magnetoresistance of a few interconnected Co nanowires showing multiple kinks, indicative of domain wall pinning and depinning during magnetization reversal.

EOA-11. Reservoir computing in an artificial spin-vortex ice.

K.D. Stenning[1], J.C. Gartside[1], A. Vanstone[1] and W.R. Branford[1]
1. Imperial College London, London, United Kingdom

Sparked by the limitations of the Von-Neumann architecture, the burgeoning field of neuromorphic computation aims to develop systems that process information both 'in-memory' and in a brain-like manner. Neural networks comprise three types of layers – an input layer, hidden layers and an output layer each connected by numeric weights. Training such networks requires continuous updating of each weight requiring both time and energy. Reservoir computing (RC)[1] is a subset of neuromorphic computation where training occurs only on the output layer, reducing time and energy cost significantly compared to traditional neural networks, while competing with traditional approaches for time-series classification / prediction task accuracy. Artificial spin networks comprising patterned nanomagnets serve as promising computational substrates for such applications, information can be stored in a single nanomagnet spin (i.e. a nanomagnetic 'bit') or the magnetic configuration (microstate) of the entire network. Strong dipolar coupling enables a highly non-linear history-dependent collective response to external stimuli, a key property for RC[1]. Artificial spin ice (ASI) is one such network where geometric frustration gives rise to a rich microstate space and emergent collective behaviour[2] highly promising for RC[3,4]. However, in these systems individual nanomagnets are constrained to Ising-like states, severely limiting microstate richness. We have previously shown in simulation that combining Ising-like and vortex states allows powerful reconfigurable functionality[5]. Modifying a subset of bars[6,7] in an ASI such that the Ising and vortex states are bistable gives rise to highly non-linear responses to global- and RF-fields allowing multiple reservoir readouts, detectable by the recently developed 'spectral fingerprinting' technique[8]. Here, we explore ASVI-based RC for forecasting and classifying time-series with varying complexity and assess the strengths and limitations of such systems compared against traditional ASI and competing neuromorphic hardware platforms.

Tanaka, Gouhei, et al. *Neural Networks* 115 (2019): 100-123. Skjærvø, Sandra H., et al. *Nature Reviews Physics* 2.1 (2020): 13-28. Hon, Kwan, et al. *Applied Physics Express* 14.3 (2021): 033001. Jensen, Johannes H., and Gunnar Tufte. *Artificial Life Conference Proceedings*. MIT Press, 2020. Stenning, Kilian D., et al. *ACS nano* 15.1 (2020): 674-685. Gartside, Jack C., et al. *Nature Communications* 12.1 (2021): 1-9. Gartside, Jack C., et al. *arXiv preprint arXiv:2107.08941*(2021). Vanstone, Alex, et al. *arXiv preprint arXiv:2106.04406* (2021).

Session EOB
MAGNETIC NANOSTRUCTURES AND EXCHANGE BIAS

Lise-Marie Lacroix, Chair
Université de Toulouse, Toulouse, France

CONTRIBUTED PAPERS

EOB-01. Predicting the Crossover from Individual to Collective Magnetism in Dense Nanoparticle Systems: Local Anisotropy *vs* Dipolar Interactions. *E. H. Sánchez*[1], M. Vasilakaki[2], S. Lee[3], P.S. Normile[1], M. Andersson[4], R. Mathieu[4], A. López-Ortega[5], B. Pichon[6], D. Peddis[7], C. Binns[1], P. Nordblad[4], K.N. Trohidou[2], J. Nogues[8] and J.A. De Toro[1] *1. Applied Physics & IRICA, Universidad de Castilla-La Mancha, Ciudad Real, Spain; 2. Institute of Nanoscience and Nanotechnology, Agia Paraskevi, Greece; 3. Institute of Materials Research and Engineering (IMRE), Singapore, Singapore; 4. Department of Materials Science and Engineering, Uppsala University, Uppsala, Sweden; 5. Universidad Pública de Navarra, Pamplona, Spain; 6. Institut de Physique et Chimie des Matériaux de Strasbourg, Université de Strasbourg - CNRS, Strasbourg, France; 7. Dipartimento di Chimica e Chimica Industriale, Università degli Studi di Genova, Genova, Italy; 8. Catalan Institute of Nanoscience and Nanotechnology, CSIC and BIST, Barcelona, Spain*

It has been known for decades that strongly dipolarly-interacting nanoparticle (NP) systems may exhibit collective behavior.[1] However, two fundamental questions remain unsolved: (i) whether the phase transition temperature may be significantly affected by the NPs anisotropy or it is essentially determined by the intensity of the interNP dipolar interactions, and (ii) what is the minimum ratio of dipole-dipole interaction (E_{dd}) to NP anisotropy ($K_{ef}V$, anisotropy×volume) energies necessary to crossover from individual to collective behavior. To shed light on these questions, we have studied a series of NP assemblies where, in contrast with the common approach of varying the NP concentration, dipolar interactions are similarly intense, but the NP anisotropy widely varies across the series. This parameter has been tuned through four different degrees of cobalt-doping in maghemite NPs with diameter ~ 6.8 nm, resulting in a variation of nearly an order of magnitude. All the compacts made of bare NPs display a collective freezing transition to a low temperature superspin glass state, except the one with the highest anisotropy NPs, which presents a "marginal" behavior. This result unambiguously establishes that the NP anisotropy is a crucial factor in determining the existence and the value of the phase transition temperature. Additionally, a threshold of $K_{ef}V/E_{dd} \sim 130$ to suppress collective behavior has been found, corroborated by Monte Carlo simulations. This translates into a simple crossover value based on the maxima of the zero-field cooled magnetization of counterpart non-interacting and interacting NP systems, T_{MAX}(interacting)/T_{MAX}(non-interacting) ~ 1.7, to predict the individual-like/collective behavior of any interacting NP assembly. This value is supported by a literature survey (see Figure 1, where the line marks the estimated crossover). Size-independent threshold NP concentrations are also calculated for common materials.

1. Elena H. Sánchez, Marianna Vasilakaki, Su Seong Lee *et al.*, *Chem. Mater.* 32, 969 (2020).

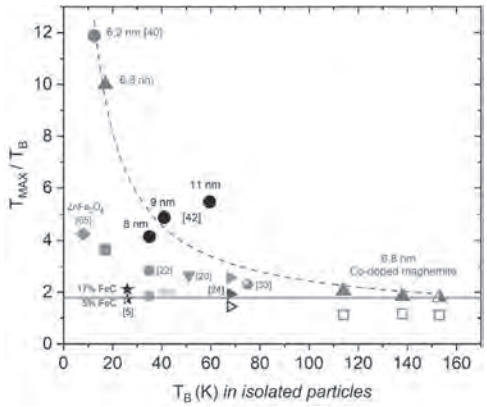

Fig. 1. Phase diagram of dipolarly interacting NP systems. The solid (hollow) symbols correspond to systems with reported superspin glass (individual-like) behavior. The solid line is the proposed threshold for collective behavior. The NPs are maghemite unless otherwise noted.

EOB-02. Nanoscale magnetic correlations and fluctuations in assemblies of Fe_3O_4 nanoparticles. *K. Chesnel*[1], J. Rackham[1], D. McPhearson[1], C. Hawkins[1], D. Griner[1], D. Smith[1], R. Harrison[2], A. Reid[3] and M. Transtrum[1] *1. Physics, BYU, Provo, UT, United States; 2. Chemistry, BYU, Provo, UT, United States; 3. SSRL, SLAC, Stanford, CA, United States*

Magnetic nanoparticles are increasingly used in biomedical applications such as drug-delivery, gene delivery, hyperthermia, or contrast agents for MRI. Magnetite (Fe3O4) nanoparticles are good candidates for these applications due to their non-toxicity and long-life in the bloodstream. While the structural and magnetic properties of bulk Fe3O4 has been widely studied [1], knowledge is still lacking regarding the magnetic behaviour of collections of Fe3O4 nanoparticles. In particular, when the particles are small and the assembly is superparamagnetic, it is useful to understand the nature of the magnetic correlations within the assemblies. Here we show how inter-particle magnetic correlations can be probed at the nanoscale via x-ray resonant magnetic scattering (XRMS) [2] as illustrated in Fig.1a. By tuning the energy of the x-rays to resonant edges of Fe and comparing opposite polarization helicities, we extract information about the local inter-particle magnetic orders within the nanoparticle assemblies. We show the dependence on particle size, varying from 5 to 11 nm, suggesting an enhancement of magnetic couplings for bigger particles. [3] Additionally, we show model based on chains of nanoparticles, which we use to fit the XRMS data. The data fitting suggests the occurrence of a mix of antiferromagnetic ordering and randomness near remanence at high temperature and near the coercive region at low temperature, for larger particles. [4] Finally we will show preliminary photon correlation (XPCS) (see Fig.1b) and muon sin resonance data obtained on 5 nm Fe3O4 nanoparticles revealing temperature dependence on the dynamics of magnetic fluctuation. [5,6]

[1] Verwey, Nature 144, 327 (1939); Fleet, Acta Cryst. B 37, 919-929 (1981) [2] Kortright *et al.*, Phys. Rev. B 71, 012402 (2005) [3] Chesnel

et al., Magnetochemistry 4, 42-58 (2018) [4] Rackham *et al.*, AIP Advances 9 (3), 035033 (2019) [5] Klomp *et al.* IEEE Trans. Mag. 56 (11) 2300109 (2020) [6] Frandsen *et al.* Phys Rev. Mater. 5 (5), 054411 (2021)

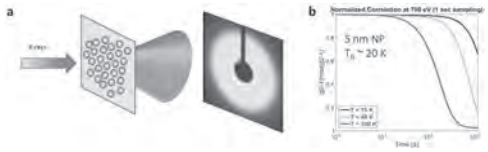

EOB-03. Magnetic and Transport Properties of Shell-ferromagnetically Precipitated Spin-Polarized Co_2TiGe in a CoTi matrix. A. Çakir[1], N. Josten[2], S. Noorzayee[2], M. Farle[2] and *M. Acet*[2]
1. Metallurgical and Materials Engineering, Mugla Sitki Kocman University, Mugla, Turkey; 2. Physics, University of Duisburg-Essen, Duisburg, Germany

When temper-annealed around 650 K in the presence of a magnetic-field, off-stoichiometric Heusler alloys in the form $Ni_{50}Mn_{45}X_5$ (*X*: Al, Ga, In Sn, Sb) decompose and form 2-5 nm full Heusler precipitates which become embedded in a surrounding NiMn neighborhood. The precipitates are cubic and ferromagnetic (FM) whereas the matrix is tetragonal and antiferromagnetic (AF) with a high anisotropy. This spinodal decomposition progresses according to the reaction $5Ni_{50}Mn_{45}X_5 \rightarrow Ni_{50}Mn_{25}X_{25} + 4Ni_{50}Mn_{50}$. The AF/FM interface becomes so strongly pinned in the applied annealing-field direction that a magnetization reversal is not observed in fields up to 20 T. Such materials are relevant to non-volatile magnetic memory applications. In a similar manner, it is possible to temper anneal other Heusler-based materials to obtain precipitation. We adopt this method to prepare spin-polarized FM $Co_{50}Ti_{25}Ge_{25}$ precipitates in a Pauli paramagnet (PM) $Co_{50}Ti_{50}$ matrix. The decomposition progresses according to $5Co_{50}Ti_{45}Ge_5 \rightarrow Co_{50}Ti_{25}Ge_{25} + 4Co_{50}Ti_{50}$. The aim is to understand the influence of the spin polarized state on the magnetic and transport properties at reduced dimensions. For this purpose, we carry out x-ray diffraction (XRD), microprobe analysis, magnetization, and resistivity studies. Time-, field-, and temperature-dependent magnetization studies along with XRD show the presence of decomposition into $Co_{50}Ti_{25}Ge_{25}$ precipitates becoming embedded in a PM matrix. Field-dependent resistivity measurements show asymmetric field-dependence and suggest the preservation of spin-polarization over macroscopic dimensions.

EOB-04. Investigation of magnetic domain nucleation in exchange-biased nanostructures. *S. Akhundzada*[1], U. Karki[2], M. Reginka[1], M. Merkel[1], C. Mewes[2], T. Mewes[2], A. Ehresmann[1] and M. Vogel[1]
1. Institute of Physics and Center for Interdisciplinary Nanostructure Science and Technology (CINSaT), University of Kassel, Kassel, Germany; 2. Department of Physics and Astronomy, University of Alabama, Tuscaloosa, AL, United States

The interface driven exchange bias effect (EB) is a well-studied phenomenon observed in ferromagnetic (FM)/antiferromagnetic (AFM) thin film systems resulting from the interfacial exchange coupling between the F and AF spins [1]. In numerous studies, asymmetrically shaped hysteresis loops have been reported mainly described by coherent rotation of the magnetic domains on the one hysteresis branch and rapid nucleation and domain wall propagation on the other one [2, 3]. Romanens et al. were able to correlate these asymmetries in perpendicular magnetized thin film systems to higher domain nucleation densities when the applied field is aligned antiparallel to the EB field compared to the parallel orientation [4]. Here the statistics of magnetic domain nucleation during the magnetization reversal process in exchange-biased magnetic nano-stripes is investigated by high-resolution optical Kerr microscopy. In such structures the magnetization dynamics are governed by the exchange bias field, the shape anisotropy and stray field interactions between the stripes. The dependency of the nucleation on these parameters is investigated systematically by variation of the lateral dimensions of the stripes and the orientation of the exchange bias fields relative to the stripe axis. Understanding the nucleation behavior of magnetic domains in nanostructures is an important step in the development of spintronic devices.

[1] W. H. Meiklejohn, J. Appl. Phys. 33, 1328 (1962) [2] J. McCord, R. Schäfer and R. Mattheis, J. Appl. Phys. 93, 5491 (2003) [3] P. Blomqvist, K. M. Krishnan and H. Ohldag, Phys. Rev. Letters 94, 107203 (2005) [4] F. Romanens, S. Pizzini and F. Yokaichiya, Phys. Rev. B 72, 134410 (2005)

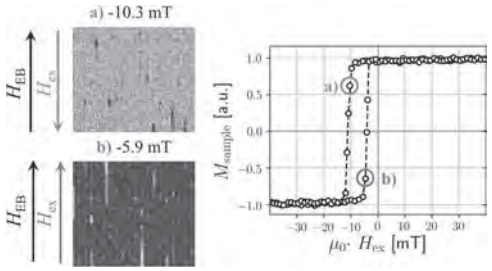

Fig 1. Magnetization reversal measured for a nano-stripe array with 2 µm wire width consisting of [Cu(5nm)/IrMn(30nm)/NiFe(10nm)/Al(4nm)]. The Kerr microscopic snapshot shows the domain nucleation along a) the decreasing and b) increasing hysteresis branch. In the parallel configuration of the external magnetic field H_{ex} and unidirectional anisotropy H_{EB} more domains are formed than in the antiparallel configuration, as observed in the Kerr images by the corresponding dark and white dots.

EOB-05. Nanoscale Spin Helices Stabilised by a Hierarchy of Magnetic Interactions in Exchange-Modulated Heterostructures. *G. Causer*[1], D. Cortie[2], B.R. McGrath[5], J. Zeng[3], K. Lin[3] and K. Livesey[4]
1. Physics Department, Technical University of Munich, Munich, Germany; 2. Australian Centre for Neutron Scattering, Australian Nuclear Science and Technology Organisation, Lucas Heights, NSW, Australia; 3. Department of Materials Science and Engineering, National Chung Hsing University, Taichung, Taiwan; 4. School of Mathematical and Physical Sciences, The University of Newcastle, Callaghan, NSW, Australia; 5. Department of Physics, University of Colorado, Colorado Springs, Colorado Springs, CO, United States

Chiral spin helices, which are analogous to Bloch domain walls and form the ground state of topological skyrmions phases [1], find application in spin-valve and logic devices [2]. In this work, we investigate chiral spin helices prepared in $Ni_{80}Fe_{20}/\alpha\text{-}Fe_2O_3$ bilayers by external magnetic fields, to gain a microscopic understanding of spin helices, and the magnetic interactions which lead to their stability. Thin film characterisation by means of X-ray reflectivity and diffraction, atomic force and transmission electron microscopy, and magnetometry establishes polycrystalline bilayers, with sharp structural interfaces, and blocking temperatures around 75 K [3]. Polarised neutron reflectometry data, acquired after following a specialised selection of magnetic field and cooling procedures [4], is used to depth-profile the magnitude and direction of the in-plane helical moments across the thickness of the film. Depending on the distance from the $Ni_{80}Fe_{20}/\alpha\text{-}Fe_2O_3$ interface, magnetic frustration causes the spins of the $Ni_{80}Fe_{20}$ layer to form an out-of-plane propagating spin texture which takes the mathematical form of a one-dimensional anharmonic helix. Micromagnetic simulations reveal the competition between the external magnetic field, interface localised exchange bias field and thin film anisotropy are responsible for the resultant chiral spin structure. Furthermore, our analytical calculations predict these metastable helices to unwind after a critical number of turns, emitting pulsed microwave energy, founding interesting dynamical applications. This work contributes crucial understanding to the hierarchy of magnetic interactions responsible for the stability of helical spin arrays in thin films for future information storage and logic devices.

[1] S. Mühlbauer et al., Science 323, 915 (2009) [2] K. O'Grady et al., J. Magn. Magn. Mater. 322, 883 (2010) [3] G. L. Causer et al., J. Appl. Phys. 59, SAAC03 (2020) [4] D. L. Cortie, PhD thesis, University of Wollongong (2013)

EOB-06. Three-axis torque investigation of exchange bias in a micromagnetic disk. M. Dunsmore[1], *J.A. Thibault*[1], K. Fast[1], V.T. Sauer[1], J.E. Losby[2], Z. Diao[3], E.J. Luber[4], M. Belov[5] and M.R. Freeman[1]
1. Physics, University of Alberta, Edmonton, AB, Canada; 2. Physics and Astronomy, University of Calgary, Calgary, AB, Canada; 3. Physics, Florida Agricultural and Mechanical University, Tallahassee, FL, United States; 4. Chemistry, University of Alberta, Edmonton, AB, Canada; 5. Nanotechnology Research Centre (NANO), National Research Council (NRC), Edmonton, AB, Canada

Micrometer diameter bilayers of 20 nm Permalloy/20 nm Cobalt Oxide deposited on nanomechanical resonators were used to investigate exchange bias effects. The mechanical compliances of two resonator axes were enhanced by severing one torsion arm, Figure 1, resulting in a unique three-axis resonator that responds resonantly to torques generated by a three-axis RF field [1]. Our technique permits simultaneous measurement of three orthogonal torque components. Measurements of the anisotropies associated with exchange bias effects have been made. First, at cryogenic temperatures, observations of shifted linear hysteresis loops confirm the presence of a positive exchange bias at the Py/CoO interface. A rotating DC bias field was used to probe in-plane anisotropies through the out-of-plane torque, as shown in Figure 2 (open circles). Training effects in both the linear and rotating hysteresis data were observed and show that most of the training occurs during the first half of the first loop, consistent with an athermal training mechanism [2]. The data from the rotating hysteresis loops were fit with parameters from a macrospin solution to the Landau-Lifshitz-Gilbert equation. In order to reproduce our observations standard anisotropy terms, a spin-flop coupling term [3], and a rotatable anisotropy axis [3,4] are introduced to the model. Each parameter of the exchange bias model accounts for specific features of the rotational loop. A unidirectional anisotropy asymmeterizes the extrema magnitudes. The orientation of the rotatable anisotropy axis with respect to the ferromagnetic magnetization introduces a one-fold rotational symmetry that would otherwise be at least two-fold. The spin-flop term influences the angular positions of the peaks in the torque curve.

[1] K.R. Fast et al., AIP Advances 11, 015119, 2021. [2] Sarah Jenkins, Roy W. Chantrell and Richard F.L. Evans, Phys Rev B 103, 104419 (2021). [3] M.D. Stiles and R.D. McMichael, Phys Rev B 59, 3722 (1999). [4] O.E. da Silva et al., JMMM 451, 507 (2018).

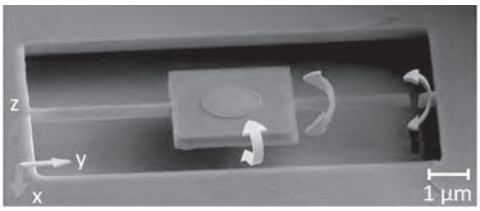

Figure 1: Electron micrograph of a micromechanical device used for demonstration of the three-axis torque measurement technique. The arrows indicate the three orthogonal torsional displacements.

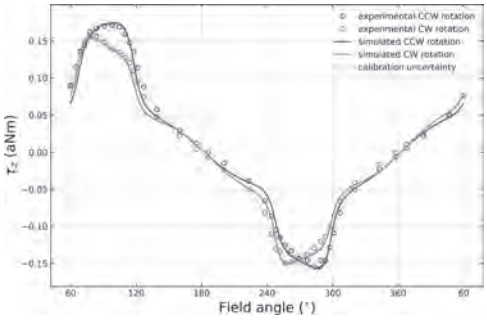

Figure 2: Thermomechanically calibrated experimental data of the z torque component (resonator at liquid nitrogen temperature). Data were recorded during a rotational hysteresis loop. Fits from macrospin solutions to the LLG equation are shown.

EOB-07. Unravelling exchange bias phenomena in V_2O_3/Co bilayers. *J.M. Diez*[1], J.L. Fernandez Cuñado[2], P. Perna[2], P.N. Lapa[3], A. Bollero[2], R. Miranda[1,2], I.K. Schuller[3] and J. Camarero[1,2] *1. Universidad Autónoma de Madrid, Madrid, Spain; 2. IMDEA Nanoscience, Madrid, Spain; 3. University of California San Diego, San Diego, CA, United States*

The research on hybrid systems combining dissimilar materials with artificial interfaces is among the major challenges of the nanotechnology during the last decades. Bilayers composed of a ferromagnetic (FM) layer interfaced with a transition-metal-oxide (TMO) layer can be consider as model hybrid systems. V_2O_3 is a archetypical TMO system exhibiting a first-order metal insulator transition (MIT) when the temperature is decreased below T_{MIT}= 170 K [1], from a paramagnetic metallic state to an antiferromagnetic (AFM) insulating phase, accompanied simultaneously by a structural phase transition [2]. Below T_{MIT}, several interfacial exchange-coupling effects have already been found in similar FM/V_2O_3 bilayers [3]. Here we present a detailed angular and temperature dependent angle-resolved vector magnetometry study of the system mentioned across the MIT. This provides fundamental insights on how to tailor and control the interfacial exchange effects. More specifically, we investigated the magnetic anisotropy landscape of Co/V_2O_3 bilayers, where the Co layer has a well-defined uniaxial magnetic anisotropy at room temperature (Fig.1a1 and Fig.1b1). We have studied the effects using different magnetic anisotropy configurations by setting a magnetic orientation of the FM layer across the MIT transition by means of different field cooling (FC) procedures. Just after the FC, the low temperature (50 K) loops display strong interfacial exchange coupling effects (Fig.1a2 and Fig.1b2), i.e., enhanced coercive field, clear exchange bias, and asymmetric magnetization reversal. In general, depending on the FC procedure, different angle-dependent and temperature evolutions are found, which are ascribed to the modifications of the anisotropy configuration. Our findings demonstrate that we have an effective control of the interfacial exchange phenomena in the FM/TMO heterostructures, especially across the MIT, which enables the development of novel magnetic devices with specific functionalities.

[1] Imada, M., Fujimori, A. and Tokura, Y. Rev. Mod. Phys. 70, 1039-1263 (1998). [2] Y. Kalcheim, et al. Phys.Rev. Lett. 122, 057601 (2019). [3] De La Venta, J., Wang, S., Ramirez, J. G., and Schuller, I. K. Appl. Phys. Lett., 102(12), 122404 (2013).

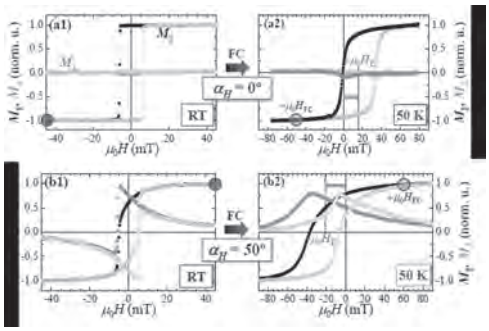

Figure 1. Representative v-MOKE loops of a V_2O_3 (100 nm)/Co (15nm) structure above (a1,b1) and below (a2,b2) the MIT transition using different field coolings: a) Negative-FC along the easy axis and b) Positive-FC around 50° off the easy axis

EOB-08. Withdrawn

EOB-09. Exchange Coupled Magnetic Nanoheterostructures with Enhanced Energy Product. B. Muzzi[5,2], A. López-Ortega[4], M. Albino[3], M. Petrecca[3], C. Innocenti[1,3], G. Bertoni[1], C. de Julián Fernández[6] and *C. Sangregorio*[5,3] *1. CNR National Research Council, Nano, Modena, Italy; 2. Dept. of Biotechnology, Chemistry and Pharmacy, Univ. of Siena, Siena, Italy; 3. Dept of Chemistry, INSTM & Univ. of Florence, Sesto Fiorentino, Italy; 4. Departamento de Ciencias, Universidad de Navarra, Pamplona, Spain; 5. CNR National Research Council, ICCOM, Sesto Fiorentino, Italy; 6. CNR National Research Council, IMEM, Parma, Italy*

Magnetic hybrid nanostructures have been largely investigated in the recent past. The combination at the nanoscale of components endowed with different magnetic properties, indeed, enable the emergence of novel intriguing phenomena, the most prominent being exchange bias and exchange spring magnet. These phenomena have been proposed in the recent past as efficient strategies to enhance the performance of magnetic materials employed in several applications, and particularly to increase the energy storage capability of permanent magnets. [1,2] The CoFe/$Co_{1-x}Fe_xO$/Cobalt ferrite system is particularly suited to investigate such exchange phenomena, as it comprises a soft material with the highest saturation magnetization, (245 Am^2kg^{-1} for $CoFe_2$), an antiferromagnet with tuneable ordering temperature in the 205 K - 295 K range, and a highly anisotropic hard magnet, which can convert one into each other by simple oxidation/reduction processes. In this contribution we present the synthesis and investigation of the structural, morphological and magnetic properties of a series of nanoparticles with complex architecture and variable composition, belonging to the CoFe/$Co_{1-x}Fe_xO$/Cobalt ferrite family. the study was aimed at investigating the possibility to exploit exchange coupling to enhance the energy product, BH_{max}, of magnetic nanoparticles. The magnetic nanoheterostructures were prepared by thermal decomposition of metal-organic precursors (Co,Fe mixed oleate) in high-boiling solvent containing oleic acid and sodium oleate as stabilizing surfactants, and their size, shape and composition was tuned by fine control of the synthesis parameters, namely, the boiling temperature of the solvent and oleic acid to sodium oleate ratio.[3] The effect of the introduction of Ni^{2+} ion in the spinel lattice on the magnetic properties is also discussed. This research was supported by EU- H2020 AMPHIBIAN Projects (n. 720853).

[1] E. Lottini, A. Lopez-Ortega, G. Bertoni, et al. Chem. Mater. Vol. 28 p. 4214 (2016). [2] A. López-Ortega, E. Lottini, G. Bertoni, et al. Chem. Mater. Vol. 29 p. 1279 (2017). [3] B. Muzzi, M. Albino, C. Innocenti, et al. Nanoscale, Vol. 12, p. 14076 (2020).

EOB-10. The effect of x-ray illumination on magnetic domain memory in [Co/Pd] / IrMn multilayers. *C.S. Walker*[1], M. Parkes[1], C. Olsson[1], D. Keavney[3], E. Fullerton[2] and K. Chesnel[1] *1. Physics, Brigham Young University, Provo, UT, United States; 2. Center for Memory and Recording research, San Diego, CA, United States; 3. Advanced Photon Source, Argonne National Laboratory, IL, United States*

Thin ferromagnetic films with perpendicular anisotropy exhibit nano-sized magnetic domains forming various patterns. When an external magnetic field is applied and cycled, the domains pattern is usually lost. However, if the ferromagnetic layer is coupled with an underlying antiferromagnetic layer, it may show magnetic domain memory (MDM). [1-3] MDM is the ability of the magnetic domains to retain their exact same domain topology upon field cycling. We are studying the effect that illumination by coherent resonant x-rays may have on MDM in a [Co / Pd] / IrMn multilayers. Our x-ray resonant magnetic scattering (XRMS) data suggests that under high dose of x-ray illumination, the material may lose its existing MDM. To investigate this possible effect we have used magneto-transport measurements [4,5] to track the exchange bias while the sample is illuminated by x-rays, using synchrotron radiation (see Fig.1a). Magneto-transport is here used to measure the magnetization loop from which we can extract a bias field. A loss of exchange bias would indicate that the x-rays illumination dose may alter the strength of the exchange couplings and ultimately the amount of MDM. Knowing if a loss of exchange bias has occurred requires collecting magneto-transport data (Fig.1b) as well as XRMS data (Fig.1c) and correlating the observed changes under various dose of x-ray illumination. These measurements include Hall effect signal and as well as magnetoresistance signal, collected both on inner contacts and on outer contacts. For the outer contacts, the spacing between wire bonds is ~1cm, whereas for the inner contacts, the spacing between wire bonds is ~100. These measurements help us understand the shape of the magneto-transport data collected under x-ray illumination and determine if x-ray illumination has an effect on exchange couplings, and ultimately MDM.

[1] K. Chesnel, A. Safsten, M. Rytting, and E.E. Fullerton, Nature Communications 7, (2016). [2] K. Chesnel, B. Wilcken, M. Rytting, S.D. Kevan, and E.E. Fullerton, New Journal of Physics 15, 023016 (2013). [3] K. Chesnel, J. Nelson, B. Wilcken, and S.D. Kevan, Journal of Synchrotron Radiation 19, 293 (2012). [4] C. Hurd, *Hall Effect in Metals and Alloys* (Springer, 2012). [5] L.J. van der Pauw, A Method of Measuring Specific Resistivity and Hall Effect of Discs of Arbitrary Shape (1958).

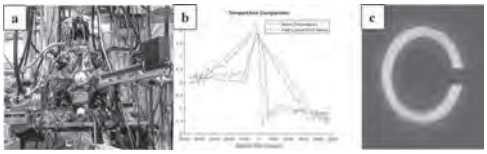

a) Instrument used for our x-ray resonant magnetic scattering (XRMS) experiment at the APS, showing the vacuum scattering chamber and the octupolar magnet to apply a field in any direction. b) Magneto-transport measurement taken while [Co/Pd] / IrMn multilayers was illuminated with x-rays. c) XRMS speckle pattern from the [Co/Pd] / IrMn film, measured at the Co L_3 edge.

Session EOC
MAGNETIC NANOSTRUCTURES

Victor M. Prida, Chair
University of Oviedo, Oviedo, Spain

CONTRIBUTED PAPERS

EOC-01. Chemically-induced Magnetic Dead Shells in Superparamagnetic Ni Nanoparticles from Polarized Small-Angle Neutron Scattering. *B. Das*[1], J. Batley[1], C. Korostynski[1], M. Nguyen[1], I. Kamboj[1], K. Krycka[2], P. Quarterman[2], J.A. Borchers[2], E. Aydil[3] and C. Leighton[1] *1. Chemical Engineering and Materials Science, University of Minnesota, Minneapolis, MN, United States; 2. NIST Center for Neutron Research, National Institute for Standards and Technology, Gaithersburg, MD, United States; 3. Chemical and Biomolecular Engineering, New York University Tandon School of Engineering, Brooklyn, NY, United States*

Advances in synthesis and characterization of magnetic nanoparticles (NPs) have yielded great gains in the understanding of their complex magnetic behaviour, with implications for numerous applications. Recent work using Ni NPs as a model soft ferromagnetic (FM) system achieved *quantitative* understanding of the superparamagnetic blocking temperature-particle diameter relationship[1]. This hinged, however, on the assumption of an FM NP volume lower than the chemical volume due to a non-FM surface dead shell, indirectly deduced from magnetometry. Here, we completely determine both the chemical and magnetic internal structure of such Ni NPs, *via* unpolarized, half-polarized, and fully-polarized small-angle neutron scattering (SANS) measurements and analyses, coupled with X-ray diffraction and magnetometry. The postulated magnetic dead shell is not only detected but conclusively identified as a Ni phosphide, derived from the trioctylphosphine commonly used in hot-injection syntheses. The shell thickness (t^*) can be controlled by synthesis temperature (T_s), falling to as little as 0.5 nm at 170 °C (Fig. 1). Polarized SANS further reveals bulk-like ferromagnetism in the Ni core, the magnetic scattering length density (SLD) being in ideal agreement with magnetometry (Fig. 2), quantitatively supporting prior modeling of superparamagnetism. These findings advance the understanding of synthesis-structure-property relationships in metallic magnetic NPs, point to a route to ligand-free stabilization, and highlight the power of polarized SANS measurement and analysis capabilities for magnetic NP science and technology. Work supported by the UMN DOE Center for Quantum Materials.

[1] J.T. Batley, M. Nguyen, I. Kamboj, C. Korostynski, E.S. Aydil and C. Leighton, *Chem. Mater.* 32, 6494 (2020).

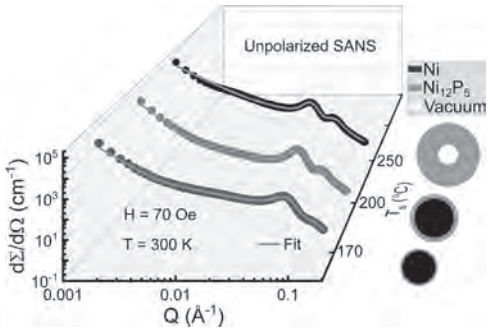

Fig. 1. Unpolarized SANS cross-section ($d\Sigma/d\Omega$) *vs*. wave vector (Q) (circles), fitted with a core-shell model (lines) yielding t^* = 0.5, 8.5 and 1.2 nm and total average diameter $\langle D \rangle$ = 8.5, 11.7 and 15.4 nm, for T_s = 170 (blue), 200 (green) and 250 °C (black) respectively. The schematics on the right summarize the fitting results.

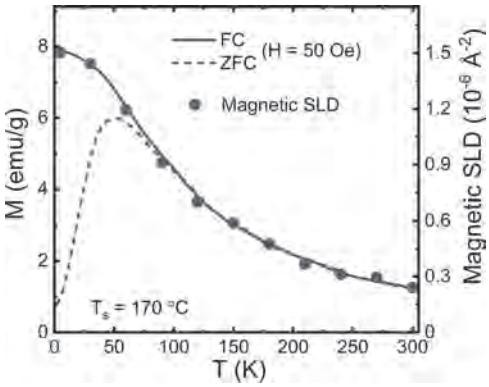

Fig. 2. Ni core magnetic SLD vs. T (circles) from half-polarized SANS for the NPs at T_s = 170 °C, superimposed on magnetometry field-cooled (FC) (solid line) and zero field-cooled (ZFC) (dashed line) data measured at 50 Oe.

EOC-02. Decreasing the magnetic anisotropy of Fe_3O_4 by Co-doping? *D. Serantes*[1], D. Faílde[1], A.O. Fumega[1], V. Pardo Castro[1], D. Baldomir[1], B. Pelaz[2], P. del Pino[2] and R.W. Chantrell[3] *1. Applied Physics, Universidade de Santiago de Compostela, Santiago de Compostela, Spain; 2. CiQUS, Universidade de Santiago de Compostela, Santiago de Compostela, Spain; 3. Physics, University of York, York, United Kingdom*

Doping magnetite with Co is usually regarded as an effective method to largely increase its anisotropy constant, K. In the present work we discuss the existence of a region with a decreased K value, at about 4% to 7% Co-doping, where a transition from positive to negative K occurs. Our approach simply assumes that the effective K is directly proportional to the doping fraction, which can have a different magnitude and symmetry than the parent phase. As a representative example, we focus here on the so-called *macrospin* model (i.e., up to dozens of nm in size, with coherent rotation of

the constituent atomic magnetic moments) of $Co_xFe_{3-x}O_4$ ($0<x<1$) magnetic nanoparticles case due to its importance for a variety of applications, ranging from magnetic recording to biomedicine. Remarkably, the predicted unexpected trend is confirmed by *ab initio* electronic structure calculations. The comparison between theoretical and published experimental results is extremely good, thus supporting the assumed approach as suitable to describe such type of magnetic alloys. Lastly, it is worth to mention that while we have focused on Co-doping of magnetite as a significant example for applications, our model and predictions apply could be extended to other types of alloys with anisotropy-type change in the series, and not necessarily on nanosized dimensions.

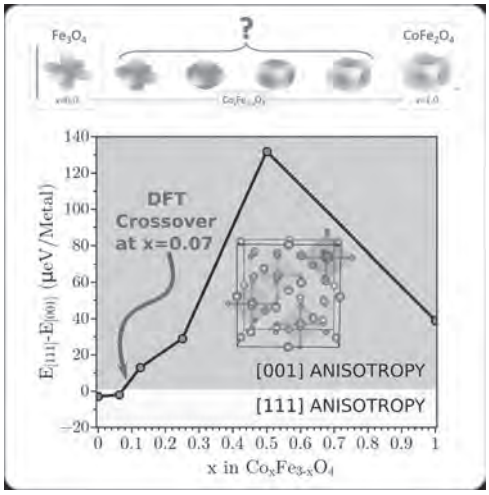

Illustrative sketch of the symmetry change of the anisotropy upon Co-doping (top panel), and magnetic anisotropy energy difference with Co-doping along the [111] or [001] directions (bottom panel).

EOC-03. Disentangling Atom- and Site- Selective Spin Canting in Co-ferrite Nanoparticles with Tunable Structural Disorder. *A. Fraile Rodríguez*[1,2], C. Moya[1,3], M. Escoda-Torroella[1,2], M. García del Muro[1,2], C. Piamonteze[4], S.R. Avula[4], X. Batlle[1,2] and A. Labarta[1,2] *1. Física de la Matèria Condensada, Universitat de Barcelona, Barcelona, Spain; 2. Institut de Nanociència i Nanotecnologia (IN2UB), Universitat de Barcelona, Barcelona, Spain; 3. Université Libre de Bruxelles, Brussels, Belgium; 4. Swiss Light Source, Paul Scherrer Institut, Villigen PSI, Switzerland*

Cobalt ferrite nanoparticles (NP) are competitive systems in technological and biomedical applications due to a suitable combination of excellent chemical and magnetic characteristics, such as a high chemical stability, surface active sites, and ease of synthesis and functionalization, together with a high anisotropy constant, a high coercivity, and a moderate saturation magnetization. However, in order to control the functional response of Co-ferrite NP, one of the biggest challenges is to quantitatively disentangle the dependence of the overall magnetic response on the composition, structure, or surface chemistry. In this work, we address the key role of the structural defects on the magnetic properties of Co-ferrite NP investigated by element- and site-specific X-ray magnetic circular dichroism (XMCD) combined with high-resolution transmission electron microscopy of individual NP [1]. We studied a series of samples of monodisperse 8 nm NP, prepared by chemical routes [2,3], with similar stoichiometry and cation distribution but with a tunable number of structural defects. Element- specific XAS and XMCD spectra and hysteresis loops reveal that the collinear alignment of Co^{2+} (O_h) cations is much more affected by the structural disorder than that of the Fe^{3+} cations. This is because structural defects give rise to effective local anisotropy axes, causing a prevalent Co^{2+} spin canting through the spin–orbit coupling due to the relatively large value of the partially unquenched moment of these cations. As the structural disorder is further increased, the rest of the cations in the two sublattices are progressively dragged off the ferromagnetic alignment, being Fe^{3+}(Td) cations the least sensitive to defects due to the smaller number of next-nearest neighbors in the T_d-sublattice. Our work highlights the importance of combining advanced synthesis with the use of complementary local probes with element, valence, site, and structural sensitivity to enhance the performance of nanoscale magnetic materials.

[1] C. Moya, A. Fraile Rodríguez, et al., J. Phys. Chem. C, 125, 691 (2021). [2] C. Moya et al., M.D.P. Morales, et al. Phys. Chem. Chem. Phys. 17, 13143 (2015). [3] C. Moya, G. Salas, M.D.P. Morales et al., J. Mater. Chem. C 3, 4522 (2015).

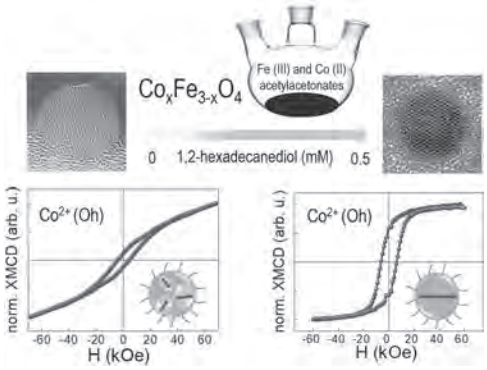

HRTEM images for Co-ferriteNP with increasing crystalline quality. Bottom panel: XMCD hysteresis loops measured at 2 K for Co^{2+} cations in Oh sites for highly-defective (left) and highly-crystalline (right) NP.

EOC-04. Effect of the Applied Field on the Brown and Neel Relaxation Times for Magnetite Nanoparticles Subjected to High Frequency Fields. *P. de la Presa*[1] and I. Morales Casero[1] *1. Complutense University of Madrid, Madrid, Spain*

When a magnetic field is applied, the magnetization is reversed by means of two mechanisms: a) Neel rotation that corresponds to the reversal of the magnetic moment within the magnetic domain and b) Brownian rotation in which the particle rotates towards the field due to the magnetic torque. In most of the literature, the analysis of Brownian or Neel relaxation is considered at zero applied field; however, as the field decreases the energy barrier, the Brownian and Neel relaxation times also decrease, i.e, the relaxations become fasters with the applied field. We analyse here the case of 34 nm Fe_3O_4 nanoparticles (MNPs) subjected to a radiofrecuency field of 50 kHz and different field amplitudes, which has been reported by several authors to present chain formation [1,2]. We calculate that for μ_0H = 22 mT, all the MNPs within the size distribution relax by Brown and this is relevant for chain formation because it is the only mechanism that governs the translations and rotations of the MNPs. As field increases, the Neel relaxation time shortens becoming smaller than Brownian relaxation and, consequenly, the smaller particles within the size distribution relax by Neel: the higher the field, the larger the size of the particles that change from Brown to Neel relaxation. Moreover, both mechanisms can take place at the same MNPs depending of the applied field. For example, for the most frequent particle size (d= 34 nm), the Néel relaxation becomes dominant for fields higher than 45 mT: if the maximum applied field is 60 mT, Brownian relaxation takes place for $|\mu_0H|<45$ mT, whereas the Neel magnetic reversal occurs for 45 mT < $|\mu_0H|<60$ mT. Therefore, in a single field cycle, both mechanisms could be present in the same MNPs. Considering the sinusoidal variation of the field with a period of 20 ms, $\tau_B<\tau_N$ during 80% of the field period, in a rough estimation. These findings have important consequences when defining protocols for magnetic hyperthermia since MNPs in a solid tumour can release more heat than expected because the Neel relaxation time become faster than the Brownian one due to the high applied field.

[1] Nemati et al., *J Phys Chem C*, 2018, 122, 2367-2381 [2] Morales et al., *Nanomaterials*, 2018, 8, 970

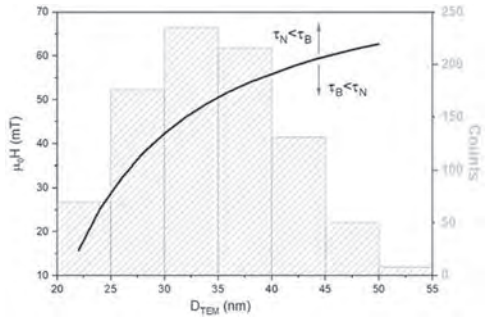

The black curve shows the applied field for which $\tau_N = \tau_B$ as a function of particle size for 34 nm MNPs.

EOC-05. Exploring the Single Domain Limit of High Magnetization Nanoparticles: A Combined Theoretical and Experimental Study.
Y. Chen[1], C. Adebi[2] and A. El-Ghazaly[2] *1. Materials Science and Engineering, Cornell University, Ithaca, NY, United States; 2. Electrical and Computer Engineering, Cornell University, Ithaca, NY, United States*

Developments in the design and fabrication of the high saturation magnetization nanoparticles in the single-domain size regime are highly desirable due to their extensive applications in biomedicine, magnetic resonance imaging, microelectromechanical systems, radio frequency electronics, and soft robotics. In this work, we present for the first time an in-depth investigation of different-sized iron cobalt ($Fe_{65}Co_{35}$) nanoparticles covering magnetization configurations from flower to vortex to multi-domain states. A finite element micromagnetic model was used to predict magnetic properties of $Fe_{65}Co_{35}$ nanoparticles ranging in size from 10 to 100 nm. The simulation results reveal that the flower-to-vortex transition of the $Fe_{65}Co_{35}$ nanoparticles occurs at around 20 nm, corresponding to the particle size with the highest coercivity. A decrease in remanence is expected for larger particle sizes, where simulations showed the most dramatic drop for particles between 40 and 60 nm. Furthermore, the simulated behaviors were verified experimentally. By systematically varying the reaction parameters, $Fe_{65}Co_{35}$ nanocubes with tunable edge lengths were synthesized. Scanning electron microscope (SEM) images of as-synthesized samples indicate a narrow size distribution. The measured hysteresis loops confirmed the maximum coercive field for cubes of size 17 nm and the sudden decrease in remanence for samples within the range of 40–60 nm. By combining chemical synthesis and micromagnetic calculations, we have experimentally unveiled the size-dependent spin configurations in $Fe_{65}Co_{35}$ nanoparticles. These results open the door to a more accurate design and control of spin texture, remanence, and coercivity in high magnetization nanoparticles which are vital building blocks of new biomedical and electronic materials.

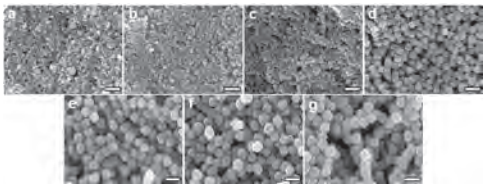

Fig. 1 SEM images of $Fe_{65}Co_{35}$ nanocubes with various edge lengths, (a) 17 nm, (b) 34 nm, (c) 40 nm, (d) 62 nm, (e) 77 nm, (f) 92 nm, and (g) 97 nm. The scale bars are 200 nm.

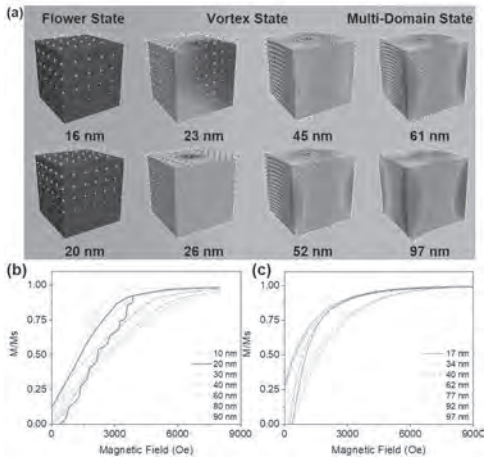

Fig. 2 (a) The simulated spin configuration for a cube of each respective size. (b) Simulated hysteresis loops of a 5×5×5 sphere array with different sizes. (c) Measured hysteresis loops of as-synthesized $Fe_{65}Co_{35}$ nanocubes at 300 K.

EOC-06. Fluorescent detection of dipicolinic acid as a biomarker for anthrax using Tb ion-coordinated Fe_3O_4 nanoparticles.
T. Koo[1], M. Ko[1], B. Park[1], M. Kim[1] and Y. Kim[1] *1. Materials Science and Engineering, Korea University, Seoul, The Republic of Korea*

Anthrax is a fatal disease caused by bacteria called bacillus anthracis. The bacteria can be used as a bioterror agent due to its high toxicity and resistance to the external environment of its spore. Dipicolinic acid (DPA) is released when the spore germinates; therefore, sensitively detecting DPA as a biomarker of the spores is focused on by many researchers [1]. Among them, nano-sensors including trivalent lanthanide ions have been used to detect DPA sensitively and promptly because the trivalent lanthanide ion such as europium (Eu^{3+}) and terbium (Tb^{3+}) shows unique fluorescent properties originated from their energy levels, and the intensity can be enhanced by chelating with DPA called antenna effect [2]. However, nanomaterials such as polymers or inorganic nanoparticles containing fluorescent substances usually quench the fluorescence by absorbing the excitation and emission light concurrently [3]. Therefore it is necessary to separate the fluorescent signal from the nanomaterials to improve its sensitivity. Herein, we develop terbium ion-coordinated iron oxide (Fe_3O_4-Tb) nanoparticles and detect DPA via measuring fluorescent signals from the Tb-DPA complexes [4]. The Fe_3O_4-Tb nanoparticles have a magnetite (Fe_3O_4) core and the surface is enveloped by Tb^{3+} that is coordinated with polyacrylate. Because of the small crystallite size of the Fe_3O_4-Tb nanoparticle, it has a trivial coercivity; therefore, Fe_3O_4-Tb nanoparticles do not agglomerate each other and reacts DPA with high reproducibility [5]. When the Fe_3O_4-Tb nanoparticles contact with DPA, Tb^{3+} is disassociated from the nanoparticle surface and chelated with DPA. The formed Tb-DPA complexes have a green fluorescence under certain ultraviolet (UV) wavelengths. We separate the iron oxide core via a permanent magnet to prevent quenching of the nanoparticles, then the clear signal shows a lower detection limit (5.1 nM) than the infectious dosage of anthrax (60 μM) [6]. The detecting method also has a high selectivity when compared with other aromatic carboxylic acids, which have a molecular structure similar to DPA.

[1] X. R. Bai *et al.*, *Anal. Chem.* 89, 10335 (2017) [2] M. Donmerz *et al., J. Hazard. Mater.* 324, 593 (2017) [3] D. Kim *et al., ACS Nano* 11, 8448 (2017) [4] T. M. Koo *et al., J. Hazard. Mater.* 408, 124870 (2021) [5] B. C. Park *et al., Nat. Commun.* 11, 298 (2020) [6] P. M. Pellegrino *et al. Anal. Chem.* 70, 1755 (1998)

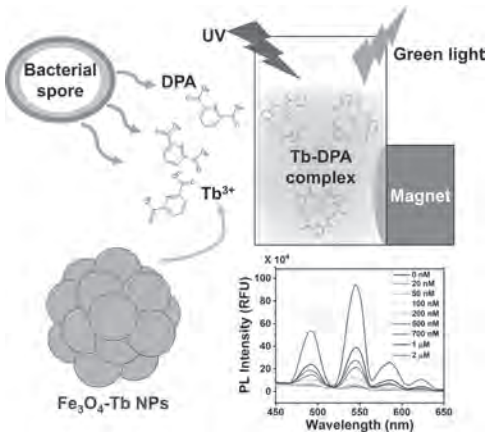

Fig.1. Detection mechanism for DPA with Fe_3O_4-Tb nanoparticles and the fluorescent intensity dependent on the concentration of DPA.

EOC-07. Withdrawn

EOC-08. Intraparticle and interparticle extended magnetic structures in chemically homogeneous manganese ferrite nanoparticle assemblies. *Y. Ijiri*[1], K. Krycka[3], A. Khelil[1], H. Chen[2], E. Everhart[1], J.A. Borchers[3], J. Rhyne[3] and S. Majetich[2] *1. Department of Physics and Astronomy, Oberlin College, Oberlin, OH, United States; 2. Department of Physics, Carnegie Mellon University, Pittsburgh, PA, United States; 3. NIST Center for Neutron Research, National Institute of Standards and Technology, Gaithersburg, MD, United States*

Magnetic nanoparticles are key to many important biomedical and sensor applications, but it is difficult to identify the governing intraparticle and interparticle interactions that dictate their behavior. In earlier work, we have shown that dense core-shell $Fe_3O_4/Mn_xFe_{3-x}O_4$ (x ~1) nanoparticle assemblies can display not only an interesting canted spin structure within a particle but one which is correlated from nanoparticle to nanoparticle [1,2]. Here, we discuss results on ordered assemblies of 7.6 nm diameter chemically homogeneous $MnFe_2O_4$ nanoparticles, where special care has been taken to assure phase uniformity. The particle assemblies have been investigated using polarization-analyzed small angle neutron scattering (PASANS) methods to allow for clean separation of magnetic vs. structural features over a range of temperatures (10-400 K) and magnetic fields (0 to 1.4 T). As shown in Fig. 1, while the magnetic behavior in remanence mostly follows a single particle form factor at high temperature, the scattering deviates as the sample is cooled and grows maximally at intermediate temperatures (~50-100 K). In addition, intermediate field values display a magnetic structure canted from field alignment as depicted in Fig 2. The data are interpreted through models ranging from a simple modified Guinier-Porod to a Lorentzian-squared correlation to a micromagnetic simulation approach; in any case, the formation of magnetically-coupled clusters of nanoparticles is highlighted. These results illustrate the ability of PASANS to extract important magnetic features in nanoscale systems. We acknowledge support from grants DE-SC0019237 (Department of Energy), DMR-1606887 (National Science Foundation) and DMR-2010792. (National Science Foundation in support of the Center for High Resolution Neutron Scattering).

[1] S.D. Oberdick et al. *Sci. Rep.* 8, 3245 (2018) [2] Y. Ijiri et al. *Phys. Rev. B* 99, 094421 (2019).

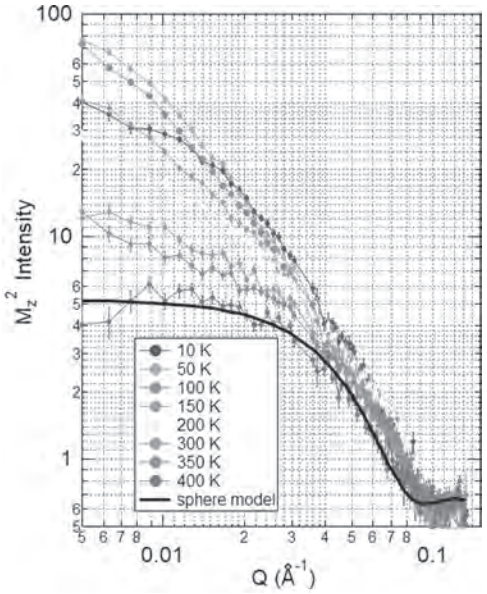

Fig.1: Remanent field magnetic scattering intensity as a function of scattering vector Q for T=10-400 K. Solid black line is the scattering form factor expected for a simple ~8 nm sphere.

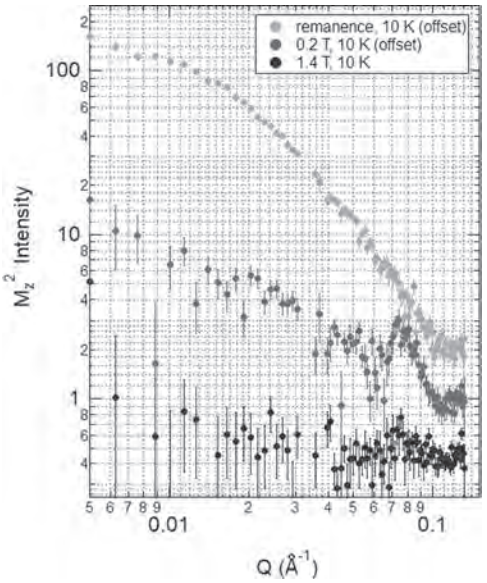

Fig. 2: Perpendicular magnetic scattering component at 10 K for fields of remanence, 0.2 T and 1.4 T, showing development of a canted ordering peak in 0.2 T.

EOC-09. Magnetic Correlations of Iron Oxide Nanoparticles as Probed by PASANS in Stretched Magnetogel Composites. *S. Oberdick*[1,2], J.A. Borchers[3] and K. Krycka[3] *1. CU Boulder, Boulder, CO, United States; 2. NIST, Boulder, CO, United States; 3. NCNR/NIST, Gaithersburg, MD, United States*

Ensemble magnetization of magnetic nanoparticles (NPs) has a sensitive dependence on the structural arrangement of particles. To better understand the correlation between spatial positions of NPs and ensemble magnetization, an experimental system is needed where particle position can be adjusted while simultaneously probing nanoscale magnetization. Here, we describe experiments using polarization analyzed small angle neutron scattering (PASANS) to study the change in magnetic correlations of ~7 nm iron oxide (Fe_3O_4) NPs embedded in stretched silicone rubber. PASANS is

a powerful tool for mapping both the inter- and intra- particle magnetization of NPs on length scales ranging from 0.1 – 100 nm. The magnetic NP polymer gel, or magnetogel, can be stretched on the neutron beamline during an experiment. The macroscopic stretching is accompanied by nanoscale deformations, where polymer chains move to accommodate a new equilibrium configuration. NPs embedded in the gel change their configuration as a function of applied stress, providing a method to adjust the average center-to-center spacing between particles. The scattering data from the unstretched gel in a 1 T applied magnetic field can be modelled by 7.4 nm iron oxide NPs assembled in a hard sphere packing with 30% volume fraction. When the sample is stretched 3x its original size in a direction parallel to the applied field, the morphology changes dramatically. Specifically, the data can be described using a cluster model where NP dimers have emerged (Figures 1a and 1b). Stretching causes the particles to morph from semi-close packed, but individual, 7.4 nm diameter NPs into dimer-like clusters that are 15 nm long, as viewed perpendicular to the applied field (Figures 2a and 2b). These PASANS experiments clearly demonstrate that stretching the magnetogel modulates the structural characteristics of magnetic NPs in a pronounced, controllable manner.

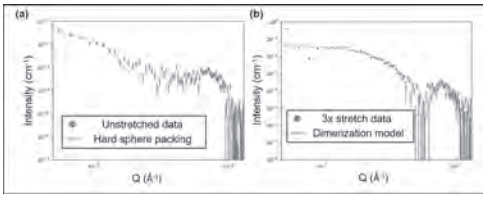

Fig. 1: Magnetic scattering from (a) unstretched and (b) 3x stretched gel in a 1 T field. The data set in (a) is fit to a hard sphere-like packing and (b) is fit to a model containing dimers

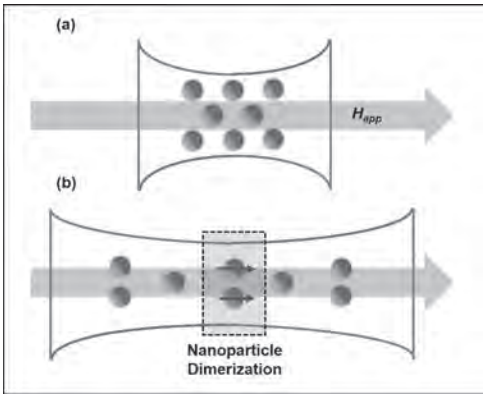

Fig. 2: Schematic showing rearrangement of NPs in (a) unstretched and (b) 3x stretched configurations.

EOC-10. Withdrawn

EOC-11. Substrate Conformal Imprint Lithography Defined Synthetic Antiferromagnetic Nanoplatelets for Torque Related Applications.

J. Li[1], W. Sijtsma[1], M.A. Verschuuren[2], B. Koopmans[1] and R. Lavrijsen[1]
1. Applied Physics, Eindhoven University of Technology, Eindhoven, Netherlands; 2. SCIL Nanoimprint Solutions, Philips Group Innovation, Eindhoven, Netherlands

The utilization of magnetic torques at the nano and microscale induced via an externally applied magnetic field is of particular interest for applications such as micromixing [1] and mechanical cancer cell destruction [2]. Over the past several years, synthetic antiferromagnetic (SAF) nanoplatelets with perpendicular magnetic anisotropy (PMA) have been identified as one of the most promising vehicles due to their high tunability, easy-axis/hard-plane PMA efficiently transferring the full magnetic torque to their environment [3]. However, the fabrication of these nanoplatelets, especially in the submicron regime with a high yield is still a challenge and efficient characterization methods of the magnetic properties and mechanical behavior in a fluid environment are still lacking. In this work, we present a novel fabrication method based on substrate conformal imprint lithography (SCIL) [4] and discuss the size effect on the magnetic properties. The basic thin film stack is shown in the insert of Fig. 1. Platelets with 1.89 ± 0.02 μm dimeter (Fig. 1) and 102 ± 1 nm diameter were successfully produced with a yield of ~10^8 and ~ 10^{10} particles per 2 inch wafer. MOKE and SQUID were used to measure the hysteresis loop. A dramatically increase of the coercivity (Hc) after patterning is observed (see Fig. 2) rendering the particles ferromagnetic at zero applied field destroying their favorable properties. To define where the increase comes from, a systematic size study is conducted on PMA-SAF nanoplatelets fabricated through electron beam lithography (EBL). We find that Hc and its distribution increase with decreasing size (see Fig. 2). A model based on local anisotropy distribution and thermal activation was established to fit the data [5]. The fit can accurately describe the Hc behavior giving insight on how to engineer the particles. In this talk we will discuss the physics, our current methods to circumvent the Hc issue and give an outlook on single-platelet mechanical behavior characterization methods [6].

[1] Kitenbergs, G., et al. Journal of Magnetism and Magnetic Materials (2015), 380, 227-230. [2] Mansell, R., et al. Scientific reports 7.1 (2017): 1-7. [3] Vemulkar, T., et al. Applied Physics Letters 107.1 (2015): 012403. [4] Verschuuren, M. A., et al. Advanced Optical Technologies 6.3-4 (2017): 243-264. [5] Thomson, T., et al. Physical review letters 96.25 (2006): 257204. [6] Li, J., et al. In preparation (2021).

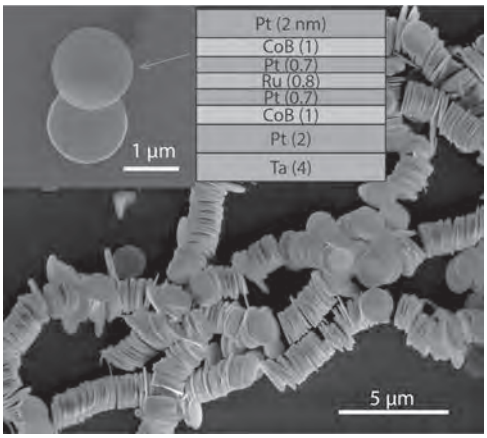

Fig.1. SEM images of released PMA-SAF nanoplatelets. The insert is the basic stack of the nanoplatelets

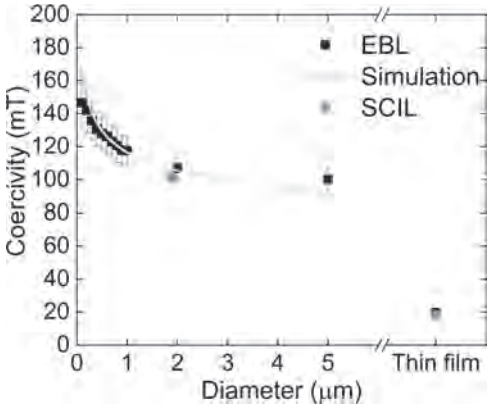

Fig.2. Coercivity as a function of the diameter of PMA-SAF nanoplatelets.

EOC-12. Inclusion of Field Dependent Magnetic Relaxation Time In Zero-Field-Cooled Magnetization Models Provides Better Characterization of Magnetic Nanoparticles. *A.R. Chalifour*[1], S.L. FitzGerald[2], T.M. Crawford[2] and K. Livesey[1,3] *1. UCCS Biofrontiers Center and Department of Physics, University of Colorado - Colorado Springs, Colorado Springs, CO, United States; 2. Department of Physics and Astronomy, SmartState Center for Experimental Nanoscale Physics, University of South Carolina, Columbia, SC, United States; 3. School of Mathematical and Physical Sciences, The University of Newcastle, Callaghan, NSW, Australia*

One of the most commonly utilized methods of MNP characterization is by analysis of the zero-field-cooled (ZFC) magnetization curve and one of its defining features, the blocking temperature [1]. Commonly thought to be at the inflection point of the curve (magenta diamond), it represents the transition of a system from a ferromagnetic to superparamagnetic state [1,2]. Conventionally, the Néel-Arrhenius equation, an estimate of the average time for a moment to flip over the energy barrier, is rearranged to the form $K = kT_B\ ln(\tau_m/\tau_o)\ /\ V$ to approximate the anisotropy K. The expression is formed from the thermal barrier at the blocking region kT_B, the mean MNP volume V, and a ratio of the measurement time τ_m to a *constant* characteristic attempt time τ_o. However, a paper by Brown [3] showed that the attempt time and barrier height depend on the applied field strength and other fundamental characteristics of the system. He also developed an expression for the relaxation time, but it is only valid when all the MNPs have easy anisotropy axes *parallel* to the external applied field. To rectify this, we have developed a new magnetic relaxation time expression in the framework created by Brown which is *field-dependent* and models the case of *randomly* oriented particles well. To show that this new expression provides better characterization of MNPs, we have fit the experimental data for a system of 8.5 nm diameter magnetite Fe3O4 nanoparticles (black dots) subject to various field strengths using both the field-independent and -dependent expressions with the ZFC model given in [2]. A weighted average of the anisotropy values yields 13,909 J/m^3 (dashed red line) for the Néel-Arrhenius equation and 15,608 J/m^3 (solid blue line) for the new theory. The accepted value of the material is 16,000 J/m^3 [1,2]. The theory also predicts a blocking temperature (green star) which is higher than the one provided by the inflection point.

[1] I.J. Bruvera *et al.* J. Appl. Phys. 118, 184384 (2015) [2] K.L. Livesey et al. Sci. Rep. 8, 11166 (2018) [3] W.F. Brown, Jr. Phys. Rev. 130, 1677-1686 (1963) Funding is acknowledged from National Science Foundation awards DMR 1808412 and 1808426.

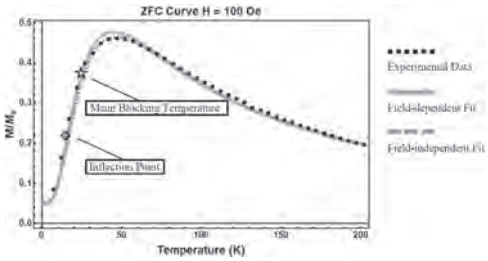

The fit curves for a field-independent (dashed red) and field-dependent (solid blue) zero-field-cooled model using experimental data (black dots) from 8.5 nm diameter magnetite Fe3O4 nanoparticles. The inflection point (magenta diamond) and correct blocking temperature (green star) are shown for comparison.

EOC-13. Modeling magnetic correlations in magnetite nanoparticle assemblines using x-ray magnetic scattering data. *J. Rackham*[1], K. Chesnel[1], M. Transtrum[1], R. Harrison[2] and A. Reid[3] *1. Physics, Brigham Young University, Provo, UT, United States; 2. Chemistry, Brigham Young University, Provo, UT, United States; 3. SLAC National Accelerator Laboratory, Menlo Park, CA, United States*

Magnetic nanoparticles are used in nanotechnologies and biomedical applications, such as drug targeting, MRI, bio-separation [1-4]. Magnetite (Fe3O4) nanoparticles stand to be effective in these roles due to the non-toxic nature of magnetite and its ease of manufacture [5]. To this end, a greater understanding of the magnetic behavior of the individual magnetite nanoparticles is needed when a collection of them is used. This research seeks to discover the local magnetic ordering of ensembles of magnetite nanoparticles (Fig.1a) occurring at various stages of the magnetization process at temperatures above and below their blocking temperature for various particle sizes [6]. We use x-ray circular dichroism (XMCD)[7] and x-ray resonant magnetic scattering (XRMS)[8] (see Fig.1b), which provides information about the spatial magnetic orders in the material. Here we discuss the modeling of the XRMS data (Fig.1c,d) using a one-dimensional chain of nanoparticles in real space [9] (see Fig.1e) as well as an empirical Gaussian packet model in q-space [9]. We find that at low temperature and and the coercive point, inter-particle magnetic correlations emerge, including a combination of ferromagnetic, and antiferromagnetic alignments of nanospins.

[1] Frey N.A.; Peng S.; Cheng K.; Sun S. Chem. Soc. Rev. 38, 2532-2542 (2009) [2] S. Mornet et al., J. Mater. Chem. 14, 2161 (2004) [3] E. Duguet et al., Nanomedicine 1(2), 157 (2006) [4] J. H. Gau et al., Acc. Chem. Res. 42(8),1097 (2009) [5] A. Ito et al., J. Biosci. Bioeng. 100, 1 (2005) [6] K. Chesnel et al. Journal of Physics: Conference Series, Volume 521, 8th International Conference on Fine Particle Magnetism (ICFPM2013) 24–27 June 2013, Perpignan, France [7] Y. P. Cai et al. J. Appl. Phys. 115 (17), 17B537 (2014) [8] K. Chesnel, et al., Magnetochemistry 4 (4), 42 (2018) [9] J. Rackham et al. AIP Advances 9, 035033 (2019)

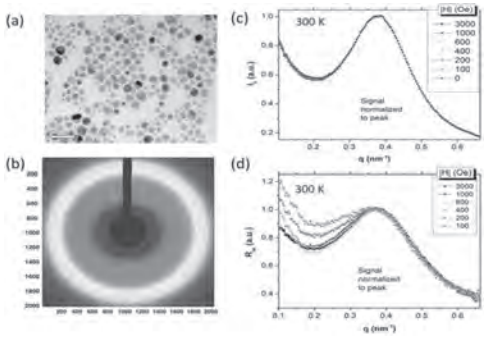

Fig.1 (a) TEM image of the Fe3O4 NP assembly, (b) 2D XRMS pattern, (c) 1D integrated charge scattering signal, (d) associated magnetic ratio signal.

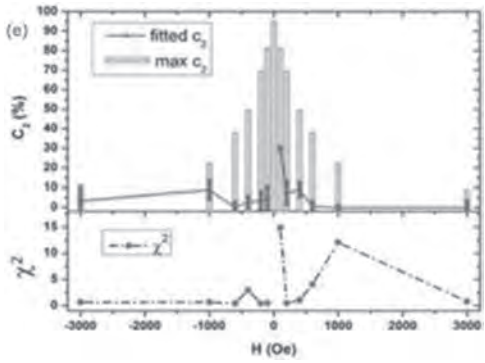

Fig.2 (e) Top: fitted antiferromagnetic coverage (c2) including error bars at 95% confidence intervals for range of magnetic fields. The blue bars indicate the possible range for c2. Bottom: Fitting residual.

Session EOD
THIN FILMS I

Ricardo Ferreira, Co-Chair
INL - International Iberian Nanotechnology Laboratory, Braga, Portugal
Akinobu Yamaguchi, Co-Chair
University of Hyogo, Hyogo, Japan

INVITED PAPER

EOD-01. Local and Non-local Curvature-induced Chiral Effects in Nanomagnetism. *O.M. Volkov[1] 1. Institute of Ion Beam Physics and Materials Research, Helmholtz-Zentrum Dresden-Rossendorf, Dresden, Germany*

The structural inversion symmetry plays an important role in low-dimensional nanomagnets, due to its strong influence on magnetic and electrical properties. It can lead to the appearance of chiral effects, such as the topological Hall effect [1], or to the formation of chiral noncollinear magnetic textures, as skyrmions [2] and chiral domain walls (DWs) [3]. These chiral structures are envisioned to be the key components for realizing novel concepts for magnonics [4], antiferromagnetic spintronics [5], spin-orbitronics [6], and oxitronics [7]. The main magnetic interaction being responsible for the stabilization of chiral magnetic textures is the intrinsic Dzyaloshinskii-Moriya interaction (DMI) [8,9]. It originate in certain magnetic crystals in which the unit cell lacks inversion symmetry, such as the gyrotropic magnetic crystals, or appear typically in ultrathin films or bilayers due to the inversion symmetry breaking on the film interface [3]. At present, tailoring of DMI is done by optimizing materials, either doping a bulk single crystal or adjusting interface properties of thin films and multilayers. A viable alternative to the conventional material screening approach can be the exploration of the interplay between geometry and topology. This interplay is of fundamental interest throughout many disciplines in condensed matter physics, including thin layers of superconductors [10] and superfluids [11], nematic liquid crystals [12], cell membranes [13], semiconductors [14]. In the emergent field of curvilinear magnetism chiral effects are associated to the geometrically broken inversion symmetries [15]. Those appear in curvilinear architectures of even conventional materials. There are numerous exciting theoretical predictions of exchange- and magnetostatically-driven curvature effects, which do not rely on any specific modification of the intrinsic magnetic properties, but allow to create non-collinear magnetic textures in a controlled manner by tailoring local curvatures and shapes [16,17]. Until now the predicted chiral effects due to curvatures remained a neat theoretical abstraction. Recently, we provided the very first experimental confirmation of the existence of the curvature-induced chiral interaction with exchange origin in a conventional soft ferromagnetic material. It is experimentally explored the theoretical predictions, that the magnetisation reversal of flat parabolic stripes shows a two step process [18,19]. At the first switching event, a domain wall pinned by the curvature induced exchange-driven DMI is expelled leading to a magnetisation state homogeneous along the parabola's long axis. Measuring the depinning field enables to quantify the effective exchange-driven DMI interaction constant. The magnitude of the effect can be tuned by the parabola's curvature. It is found that the strength of the exchange-induced DMI interaction for the experimentally realised geometries is remarkably strong, namely ~0.4 mJ/m^2, compared the surface induced DMI. The presented study legitimates the predictive power of full-scale micromagnetic simulations to design the properties of ferromagnets through their geometry, thus stabilising chiral textures. We explore these curvilinear magnetic thin films for the realization of novel artificial magnetoelectric materials based on curvilinear helimagnets embedded in piezoelectric matrix [20], to enable the geometrical tuning of the magnetochirality in curvilinear 1D architectures [21], tailoring of magnetic states in flat nanospirals [22] and as components of shapeable magnetoelectronics for interactive wearables [23].

[1] N. Nagaosa, et al., Nature Nanotech. 8, 899 (2013) [2] U. K. Rößler, et al., Nature 442, 797 (2006) [3] A. Fert, et al., Nature Rev. Mat. 2, 17031 (2017) [4] A. V. Chumak, et al., Nature Physics 11, 453 (2015) [5] T. Jungwirth, et al., Nature Nanotech. 11, 231 (2016) [6] I. M. Miron, et al., Nature 476, 189 (2011) [7] V. Garcia, et al., Nature 460, 81 (2009) [8] I. Dzyaloshinsky, J. Phys. Chem. Solids 4, 241 (1958). [9] T. Moriya, Phys. Rev. Lett. 4, 228 (1960). [10] J. Tempere, et al., Phys. Rev. B 79, 134516 (2009) [11] H. Kuratsuji, Phys. Rev. E 85, 031150 (2012) [12] T. Lopez-Leon, et al., Nature Physics 7, 391 (2011) [13] H. T. McMahon, et al., Nature 438, 590 (2005) [14] C. Ortix, Phys. Rev. B 91, 245412 (2015) [15] Y. Gaididei, et al., Phys. Rev. Lett. 112, 257203 (2014) [16] J. A. Otálora, et al., Phys. Rev. Lett. 117, 227203 (2016) [17] V. P. Kravchuk, et al., Phys. Rev. Lett. 120, 067201 (2018) [18] O. Volkov et al., PRL 123, 077201 (2019). [19] O. Volkov et al., PSS-RRL 13, 1800309 (2019). [20] O. Volkov et al., J. Phys. D: Appl. Phys. 52, 345001 (2019). [21] O. Volkov et al., Scientific Reports 8, 866 (2018). [22] M. Nord, et al., Small 1904738 (2019). [23] J. Ge, et al., Nature Comm. 10, 4405 (2019).

CONTRIBUTED PAPERS

EOD-02. Magnetization reversal and domain structure in epitaxial W/Co/Pt multilayers with various basic stack repetition number. *S.K. Jena[1,2], R. Islam[3], E. Milinska[1], M.M. Jakubowski[1], R. Roman Minikayev[1], S. Lewinska[1], A. Lynnyk[1], P. Aleszkiewicz[1], A. Pietruczik[1], C. Autieri[3,4] and A. Wawro[1] 1. Institute of Physics, Polish Academy of Sciences, Warsaw, Poland; 2. Jerzy Haber Institute of Catalysis and Surface Chemistry, Polish Academy of Sciences, Kraków, Poland; 3. International Research Centre for Interfacing Magnetism and Superconductivity with Topological Matter, Institute of Physics Polish Academy of Sciences, Warsaw, Poland; 4. Consiglio Nazionale delle Ricerche CNR-SPIN, Fisciano, Italy*

Magnetization reversal and domain structure in epitaxial asymmetric layered system W/Co/Pt with perpendicular magnetization (PMA) and Dzialoshinskii-Moriya interaction (DMI) are discussed. Two types of stacks: (i) W/Co(1.0 nm)/Pt(dPt)/W(dW)/Co(1.0 nm)/Pt with pronounced antiferromagnetic interlayer coupling and (ii) (W/Co/Pt)n, n = 10 and 20, multilayers with stripe or bubble domain structure are investigated. In the double Co layer system the interlayer coupling depends on the double layer spacer paremeters. For dPt = dW its strength decreases from 0.083 mJ/m^2 to 0.012 mJ/m^2 while individual spacer layer thickness increases from 0.7 nm to 1.2 nm. For dW ≠ dPt the coupling strength is getting weaker. Particularly, the single spacer systems (with dPt or dW kept in the same range from 1.4 nm to 2.0 nm) do not exhibit such feature, indicating a crucial role of the complex spacer structure (double layer spacer, asymmetrical interfaces and associated DMI) affecting both the RKKY coupling and PMA (Fig. 1). The multilayer structures W(1.0 nm)/Co(0.6 < dCo < 1.0 nm)/Pt at the remanent state exhibit typical labyrinth domain structure with tendency towards lattice skyrmion formation with diameter of around 75 nm (Fig. 2). DMI strength

determined from the aligned domain structure reaches the value of D = 2.49 mJ/m^2 (surface DMI parameter D_S = 1.83 pJ/m)[1], which was reproduced in and DFT and micromagnetic calculations. Such high value of D is a result of high quality crystalline structure characteristic for epitaxial systems and additive contribution to DMI from asymmetric well-defined interfaces. The IEEE educational seed funding 2020, the European Regional Development Fund – Program REINTEGRATION 2017 OPIE 14-20 (Foundation for Polish Science) and the projects no: 2016/23/G/ST3/04196 and 2020/37/B/ST5/02299 (National Science Centre in Poland) are acknowledged.

[1] S.K. Jena, R. Islam, E. Milinska, *et al. Nanoscale* 13, 7685, (2021).

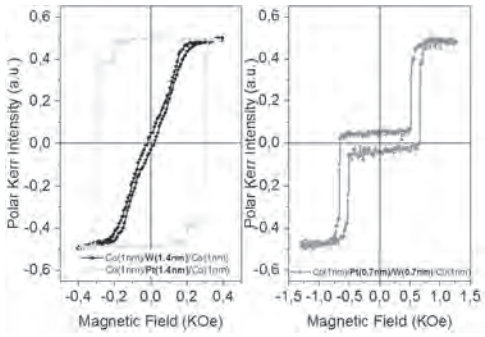

Fig.1 PMOKE hysteresis loop from the W/Co/Pt(dPt)/W(dW)/Co/Pt layered structures: dW = dPt = 0.7 nm (red); dW = 0 nm, dPt = 1.4 nm (green); and dW = 1.4 nm dPt =0 nm (black)

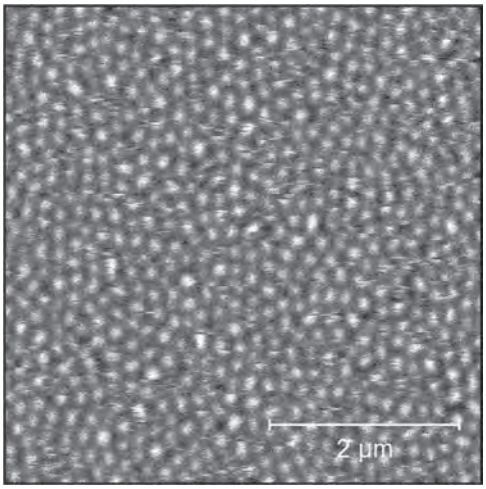

Fig. 2. Magnetic force microscopy image of (W/Co/Pt)20 multilayer at the applied field of 200 Oe.

EOD-03. Study of As-deposited and Annealed Ta/CoFeB/TaO_x Heterostructures Using X-Ray Photoelectron Spectroscopy. *S. Syamlal*[1], S. Kalal[2], H. Perumal[1], D. Kumar[2], M. Gupta[2] and J. Sinha[1] *1. Department of Physics and Nanotechnology, SRM Institute of Science and Technology, Kattankulathur, Chennai, India; 2. UGC DAE Consortium for Scientific Research, University Campus, Khandwa Road, Indore, India*

In-depth investigation of structural and magnetic property correlation in technologically important heavy metal/ferromagnet/oxide heterostructures are crucial for the development of spintronics based devices [1]. In recent times, in Ta/CoFeB/TaO_x heterostructures, zero-field magnetization switching, reasonably large Dzyaloshinskii-Moriya interaction, and stabilization of skyrmions have been reported [2-4]. Here, we study the change in magnetic and structural properties of sputter deposited (1 nm) Ta/(1.5 nm) CoFeB/(0.5 nm) TaO_x heterostructures induced by post-deposition annealing at 300 °C. Both as-deposited and annealed film stacks possess in-plane magnetic anisotropy and we observe nearly two times increase in the saturation magnetization (M_s) of annealed film stack (~ 800 emu/cc) in comparison to the as-deposited one (~ 400 emu/cc). The surface topography study suggests reduced surface roughness for the annealed film stack as compared to the as-deposited stack. Using, x-ray photoelectron spectroscopy we analyze the B 1s, Ta 4f and Fe 2p spectra for both as-deposited and annealed heterostructures. Interestingly, the analysis of Ta spectra revealed that B has intermixed with Ta layers in the annealed stack, thus forming new chemical states such as TaB and TaOB (cf. Fig.1). Boron 1s peak analysis suggests that the annealing causes B diffusion out of the CoFeB layer and subsequent exposure to the atmosphere results in the formation of BO_x. Analysis of Fe 2p spectra in the annealed stack shows an additional signature of metallic Fe^0 $2p_{1/2}$ peak, which likely plays a critical role in enhancing the M_s (cf. Fig.2). These XPS results are crucial in thorough understanding of the mechanism that governs M_s and ultimately, spin-orbit coupling induced effects in ferromagnetic thin film heterostructures.

[1] F. Hellman, A. Hoffmann, Y. Tserkovnyak *et al.*, Rev. Mod. Phys., Vol.89, p.025006 (2017) [2] G. Yu, P. Upadhyaya, Y. Fan *et al.*, Nat. Nanotech., Vol.9, p.548 (2014) [3] A.K. Chaurasiya, S. Choudhury, J. Sinha *et al*., Phys. Rev. Appl., Vol. 9, p.014008 (2018) [4] W. Jiang, P. Upadhyaya, W. Zhang *et al.*, Science, Vol.349, p.283 (2015) [5] Syamlal S K, Shailesh Kalal, Hari Prasanth Perumal *et al.*, Mater. Sci. Eng. B, Vol.272, p.115367 (2021)

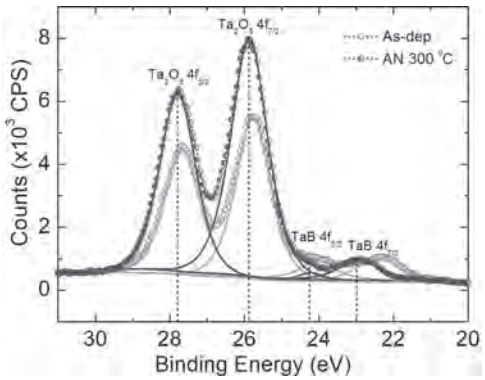

Fig. 1. XPS spectra of Ta 4f core levels of as-deposited and annealed films. The binding energy shift in the annealed spectra are due to formation of new chemical state such as TaB.

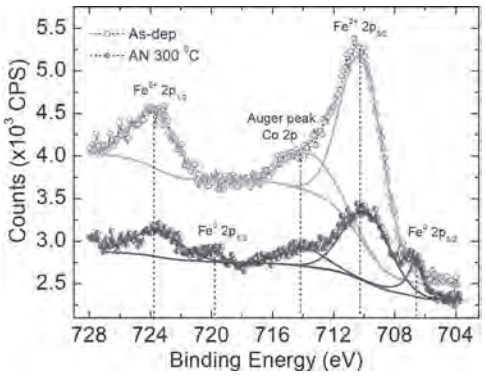

Fig. 2. XPS spectra of Fe 2p core levels of as-deposited and annealed films. An additional peak Fe^0 $2p_{1/2}$ is observed in the annealed film stack.

EOD-04. X-ray investigation of long-range antiferromagnetic ordering in FeRh. *M.T. Grimes*[1,2], N. Gurung[1,3], H. Ueda[1], B.F. Pedrini[1], D. Porter[4], V. Scagnoli[1,3], L. Heyderman[1,3] and T. Thomson[2] *1. Paul Scherrer Institut, Villigen, Switzerland; 2. University of Manchester, Manchester, United Kingdom; 3. ETH Zurich, Zurich, Switzerland; 4. Diamond Light Source, Didcot, United Kingdom*

The meta-magnetic phase transition of equiatomic FeRh allows the 3 temperature model of phase transitions to be probed as it undergoes: (i) a lattice expansion, (ii) an antiferromagnetic (AF) to ferromagnetic (FM) transition [1], and (iii) a change in electronic structure. A spin canting model has been used to describe a spin re-orientation pathway [2], where a feedback loop with induced Rh moments promotes FM order. To investigate such behaviour, a probe of the AF spins is required [3]. In general, the zero-stray field of anti-ferromagnetic materials means that it is hard to detect and perform such measurements. Here, we demonstrate a probe of long-range AF order using non-resonant x-ray scattering. The G2-type order of FeRh in the AF state provides a probe of AF order using 'magnetic' Bragg peaks [4]. We demonstrate that these peaks can be measured using x-rays at energies below the Fe K edge. Due to the low efficiency of the magnetic scattering in this material, we describe a grazing incidence geometry to optimise the intensity (see Fig. 1). Based on Scherrer analysis we estimate a coherence length of 40-80 nm, smaller than previous reports in XMLD experiments [5], indicating we are limited by structural defects. The temperature dependent behaviour of the AF order shows an inverse correlation to the emergence of FM moment as seen in Fig. 2. The AF-FM transition as determined by the ordering appears later indicating a mixed phase [6]. Long-range AF order appears to persist when FM moment is already established. Time resolved experiments based on this technique may determine the existence of a metastable AF state on time scales where the FM band structure has already formed [7]. It has been shown that the lattice expansion occurs in ≈ 30 ps [8], but it is not known how the long range AF order evolves on such timescales. X-ray diffraction can therefore be used to ascertain if how and if the AF structure is related to lattice expansion occurring at the phase transition.

[1] J. S. Kouvel and C. C. Hartelius, J. Appl. Phys., 33, no. 3, (1962). [2] L. M. Sandratskii and P. Mavropoulos, Phys. Rev. B - Condens. Matter Mater. Phys., 83, no. 17, 174408, (May 2011). [3] E. Kren, L. Pal, and P. Szabo, Phys. Lett., 9, no. 4, 297–298, (May 1964). [4] M. Blume and D. Gibbs, Phys. Rev. B, 37, no. 4, 1779–1789, (Feb. 1988). [5] C. Baldasseroni, C. Bordel, C. Antonakos, *et al.*, J. Phys. Condens. Matter, 27, no. 25, 256001, (Jun. 2015). [6] J. R. Massey, K. Matsumoto, M. Strungaru, *et al.*, Phys. Rev. Mater., 4, no. 2, 024403, (Feb. 2020). [7] F. Pressacco, V. Uhlír, M. Gatti, *et al.*, Struct. Dyn., 5, no. 3, 034501, (May 2018). [8] S. O. Mariager, F. Pressacco, G. Ingold, *et al.*, Phys. Rev. Lett., 108, no. 8, 087201, (Feb. 2012).

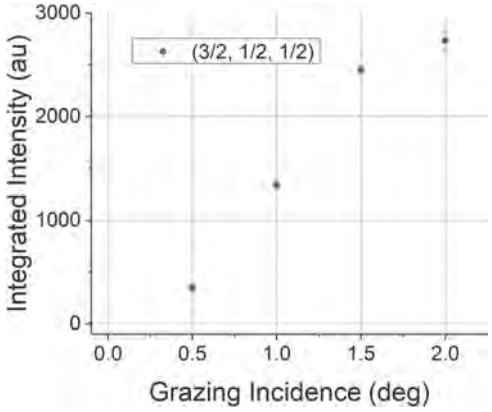

Fig. 1 Dependence of the (3/2,1/2,1/2) peak intensity upon grazing incidence angle (E=4.95 keV)

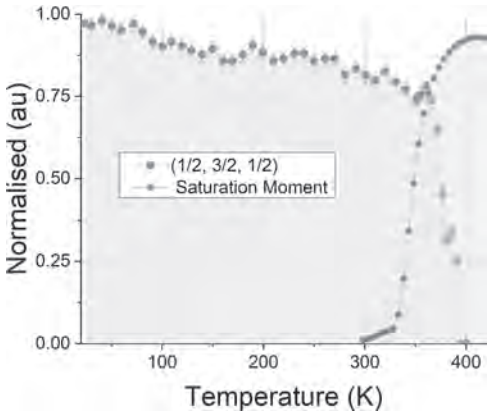

Fig. 2 The inverse correlation between the intensity of the FeRh (1/2, 3/2, 1/2) magnetic peak, and the saturation moment of the FeRh film

INVITED PAPER

EOD-05. Tuning Room Temperature Compensation in Synthetic Co/Gd Ferrimagnetic Quadlayers for Advanced Spintronics Devices. *T. Kools*[1], B. Koopmans[1] and R. Lavrijsen[1] *1. Department of Applied Physics, Eindhoven University of Technology, Eindhoven, Netherlands*

Flexibility for interface engineering, and access to all-optical switching of the magnetization, make synthetic ferrimagnets (SFiMs) an interesting candidate for advanced spintronic devices like racetrack memory [1,2]. However, the absence of compensation at room temperature (RT) in Co/Gd bilayers has hampered the efficiency with which their magnetic order can be manipulated, as the highest efficiency of spin-orbit torques and current induced domain wall motion (CIDWM) are generally achieved under compensation [3,4]. In order to combine the favourable properties of SFiMs with compensation at RT, Co/Gd/Co/Gd quadlayer structures are investigated. We present a systematic study of the conditions for magnetization compensation and perpendicular magnetic anisotropy (PMA) in Co/Gd/Co/Gd quadlayers. These conditions were investigated on a sample with the middle Co and Gd films wedged orthogonally with respect to each other, as shown in Fig. 1a. By scanning the polar magneto-optical Kerr effect (MOKE), a magnetostatic phase diagram like in Fig. 1b can be obtained. Three regimes are distinguished: In-plane magnetization (teal), and out-of-plane (OOP) Co (red) and Gd (blue) dominated. The boundaries between these regimes provide valuable insight into the balance between shape anisotropy and PMA, and the conditions for compensation. A simple model based on partial intermixing at Co/Gd interfaces has been developed which explains the experiments well, and provides a tool to qualitatively and quantitatively understand these phase diagrams. This work provides a simple framework to experimentally characterise, and describe basic magnetostatic properties in these promising heterostructures. The compensated SFiMs investigated in this research, carry the promise of breaking the elusive 1000 m/s barrier for CIDWM, and exhibiting ultrafast exchange-driven dynamics, both relevant properties for future spintronic devices.

[1]: M. Lalieu, R. Lavrijsen and B. Koopmans, Nature communications., Vol. 10.1, p.1 (2019) [2]: M. Beens, M. Lalieu and B. Koopmans, Physical Review B, Vol. 100(22), p.220409 (2019) [3]: R. Bläsing, K. Liu and S. Parkin, Nature communications, Vol. 9(1), p.1 (2018) [4]: L. Caretta, M. Schneider and D. Engel, Nature nanotechnology, Vol. 13(12), p.1154. (2018) [5] : T. Kools et al., In-Prep (2021)

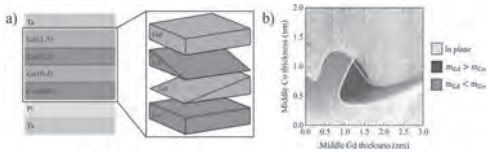

Characterization of double wedge Co(0.65)/Gd(0-3)/Co(0-2)/Gd(1.5) SFiMs. a): Schematic of wedge orientations in the multilayer. b): Magnetostatic phase diagram measured with polar MOKE. Yellow dashed line indicates compensation at RT. Green lines indicate a toy model fit to the boundaries between the three regimes.

CONTRIBUTED PAPERS

EOD-06. Anisotropy-Induced Spin Reorientation in Chemically Modulated Amorphous Ferrimagnetic Films. E. Kirk[1,2], *C. Bull*[3], S. Finizio[2], H. Sepehri-Amin[4], S. Wintz[2], A. Suszka[1,2], N. Bingham[1,2], P. Warnicke[2], K. Hono[4], P.W. Nutter[3], J. Raabe[2], G. Hrkac[5], T. Thomson[3] and L. Heyderman[1,2] *1. Laboratory for Mesoscopic Systems, Department of Materials, ETH Zurich, Zurich, Switzerland; 2. Paul Scherrer Institute, Switzerland, Switzerland; 3. Nano Engineering and Spintronic Technologies Group, Department of Computer Science, University of Manchester, Manchester, United Kingdom; 4. Research Center for Magnetic and Spintronic Materials, National Institute for Materials Science, Tsukuba, Japan; 5. College of Engineering, Mathematics and Physical Sciences, University of Exeter, Exeter, United Kingdom*

The intricate magnetic structure of rare-earth transition-metal (RE-TM) alloys makes these materials suitable for application in all-optical magnetic switching [1], spin-orbit torque devices [2] and topologically isolated systems such as Skyrmions [3]. This is due to their high perpendicular magnetic anisotropy and lack of grain boundaries [4]. Most interesting is the ability to design RE-TM thin films where temperature can be used to control spin reorientation [5,6], saturation magnetization [7] and magnetic anisotropy [8]. However, to control this ability sufficiently for use in devices such as thermal sensors, a detailed understanding of the relationship between the spin reorientation with temperature and the thickness-dependent nanoscale compositional structure is required. We have observed such a tuneable, temperature-driven spin reorientation in ferrimagnetic FeGd films using magnetometry and scanning transmission X-ray microscopy (STXM) [9]. FeGd (*t*)/Ta (8nm) films, where t = 20nm and 40nm, were sputtered onto Si(100) substrates, coated with a 95nm Si_3N_4 layer. FeGd layers were co-sputtered from Fe and Gd targets, resulting in an average composition of $Fe_{0.69}Gd_{0.31}$. Temperature-dependent M(H) loops show an abrupt reorientation of M along the in-plane (IP) easy axis at a temperature of 180K (250K) for the t = 40nm (t = 20nm) film [Fig.1]. The nature of this reorientation can be explained by a nonequilibrium modulation of the chemical composition of the films. This leads to a magnetic domain pattern of nanoscale speckles, superimposed on a background of IP domains that form Landau configurations in μm-scale patterned elements [Fig.1(b)]. This speckle magnetic structure gives rise to a sharp two-step reversal mechanism [Fig.2] that is temperature dependent. The possibility to balance competing anisotropies through the temperature provides opportunities to manipulate topological spin textures.

[1] C.-H. Lambert, S. Mangin, B.S.D.C.S. Varaprasad, *et al.*, Science 345,1337 (2014); [2] N. Roschewsky, T. Matsumura, S. Cheema, *et al.*, Appl. Phys. Lett. 109, 112403 (2016); [3] L. Caretta, M. Mann, F. Büttner, *et al.*, Nat. Nanotechnol. 13,1154 (2018); [4] T.A. Ostler, R.F.L. Evans, R.W. Chantrell, *et al.*, Phys. Rev. B 84, 024407 (2011); [5] E. Stavrou, R. Sbiaa, & T. Suzuki, J. Appl. Phys. 87, 6893 (2000); [6] C.E. Graves, A. H. Reid, T. Wang, *et al.*, Nat. Mater. 12, 293 (2013); [7] P. Hansen, C. Clausen, G. Much, *et al.*, J. Appl. Phys. 66, 756 (1989); [8] F. Radu, R. Abrudan, I. Radu, *et al.*, Nat. Commun. 3, 715 (2012); [9] E. Kirk, C. Bull, S. Finizio, *et al.*, Phys. Rev. Mater. 4, 074403 (2020).

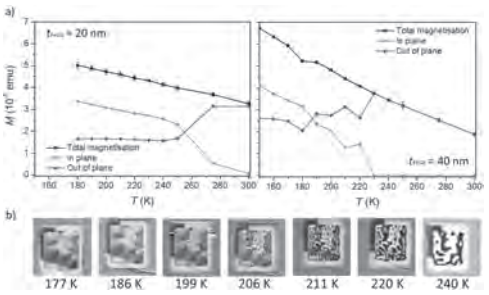

Fig.1: a) Magnetization vs temperature loops for 20nm and 40nm-thick FeGd films. b) STXM images of a 40nm-thick, 5 x 5μm² FeGd structure on a membrane substrate, showing IP to OOP transition.

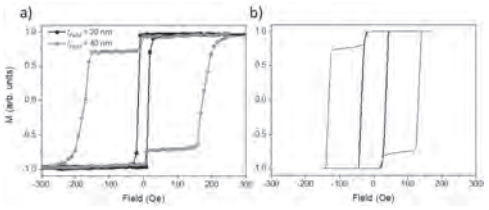

Fig.2: Measured a) and simulated b) hysteresis loops for 20nm and 40nm FeGd films, showing single and two-step reversal mechanisms.

EOD-07. Modified Magnetic Interface in Compositionally Modulated Ferrimagnetic $Fe_{1-x}Gd_x$ Multilayers. *J.E. Shoup*[1], P. Quarterman[2], T. Charlton[3], B. Kirby[2], J.A. Borchers[2] and D. Arena[1] *1. Physics, University of South Florida, Tampa, FL, United States; 2. NIST, National Institute of Standards and Technology, Gaithersburg, MD, United States; 3. Spallation Neutron Source, Oak Ridge National Laboratory, Oak Ridge, TN, United States*

Metallic ferrimagnets consisting of rare earth (RE) / transition metal (TM) alloys exhibit an intriguing magnetic compensation of the RE/TM magnetic sublattices as a function of composition and temperature. We are developing compositionally modulated RE/TM alloy films that exploit the large change in $T_{MagComp}$ as the RE content is varied. We grow $Fe_{1-x}Gd_x$ films where the Gd content x is modulated throughout the depth of the film and key question in such structures is the interface length between two $Fe_{1-x}Gd_x$ layers with different Gd content; this will establish the minimum modulation length of RE/TM structures with varying composition. We examine a series of bilayer structures [Si/ SiO_2(3nm)/Ta(10nm)/$Fe_{1-x}Gd_x$(50nm)/ $Fe_{1-y}Gd_y$(50nm)/ Ta(8nm)] where the Gd content (x or y) is varied. To investigate the magnetic profile of these films, we utilize polarized neutron reflectometry (PNR) as a function of temperature. PNR is an ideal technique to examine these structures as it probes the magnetization parallel to the field as a function of depth and the magnetic scattering length density (mSLD) is modified significantly as the temperature is tuned through $T_{MagComp}$ of a particular layer. We examine samples where $T_{MagComp}$ of a particular layer is > 300 K, ~100 K and ~50 K. A sample that has $T_{MagComp}$ >300K and ~100K for the bottom and top layers respectively exhibits strong modifications to the spin asymmetry [SA: (↑↑- ↓↓)/(↑↑+↓↓)] of the PNR. The SA develops a pronounced dip at Q~0.045 Å^{-1} and reduced broadening of the peak at Q~0.28 Å^{-1} as the temperature decreases (Fig 1). Similar variations to the SA are observed in samples with different compensation temperatures. To extract the magnetic behavior of the samples while emphasizing the interfacial region, we fit the mSLD for each temperature while keeping the structural properties the same. The fitting suggests that the evolution of the magnetic interface is nontrivial.

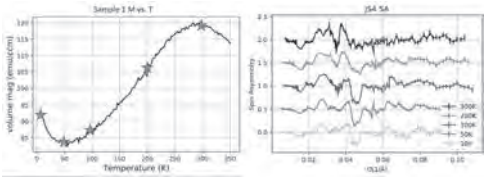

1-A: High field (1 T) magnetometry vs. temperature for a magnetic bilayer. PNR measurements performed at selected temperatures, denoted by stars, across the complicated temperature profile. 1-B: Spin Asymmetry for the bi-layer samples performed at the 5 temperatures from 1-a.

EOD-08. Adjustable exchange springs in ferrimagnetic multilayers with stripe domain patterns visualized by X-ray vector tomography.
J. Hermosa[1,2], A. Hierro-Rodriguez[1,2], A. Sorrentino[3], J. Martín[1,2], L. Alvarez Prado[1,2], E. Pereiro[3], C. Quiros[1,2], *M. Velez*[1,2] and S. Ferrer[3]
1. Physics Dept., University of Oviedo, Oviedo, Spain; 2. CINN (CSIC-UO), El Entrego, Spain; 3. Alba Synchrotron, Cerdanyola del Vallès, Spain

Exchange springs are versatile systems in which domain walls can be tailored by the different magnetic properties of exchange coupled layers such as in ferrimagnetic GdCo/GdCo' multilayers [1]. We present here an experimental study by soft X-ray magnetic vector tomography [2] of $Gd_{12}Co_{88}/Nd_{17}Co_{83}/Gd_{24}Co_{76}$ multilayers with weak stripe domains (induced by NdCo) and in which the competition between exchange and magnetostatic coupling can be tuned by the composition of the ferrimagnetic GdCo layers (as sketched in Fig. 1) [3]. The 3D analysis of the vector magnetic configuration of the Gd sublattice m(Gd) in a demagnetized state shows a complex configuration that includes stripe domains with a distorted closure domain structure across the thickness, exchange spring walls with out-of-plane magnetization reversal and modulated ripple patterns (Fig. 2). An analytical model, proposed to describe global coupling across the exchange spring boundary between NdCo and GdCo layers, shows that the strength of effective interlayer coupling can be finely tuned playing with the averaging of lateral and in-depth competing interactions so that it can be externally adjusted by magnetic history. Work supported by Spanish MICINN under grant PID2019-104604RB/AEI/10.13039/501100011033.

[1] C. Blanco-Roldán, Y. Choi, C. Quirós, et al. Phys. Rev. B 92, 224433 (2015) [2] A. Hierro-Rodriguez, C. Quirós, A. Sorrentino, et al. Nature Comm. 11, 6382 (2020) [3] J. Hermosa, A. Hierro-Rodríguez, C. Quirós, et al, J. Magn. Magn. Mater. (in press)

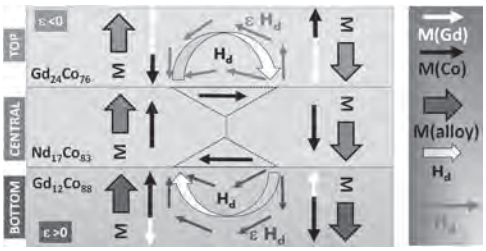

Fig. 1 Sketch of GdCo/NdCo/GdCo' ferrimagnetic multilayer with competing interactions. Exchange at the interface favors parallel alignment of M(Co) in all the layers. However, at top layer $Gd_{24}Co_{76}$ layer, net magnetization is aligned with M(Gd) and antiparallel with M(Co). Magnetostatic interactions, represented by an effective stray field εH_d, favor an antiparallel alignment of M(Co) at both sides of the interface. These competing interactions create an exchange spring near the top of the multilayer.

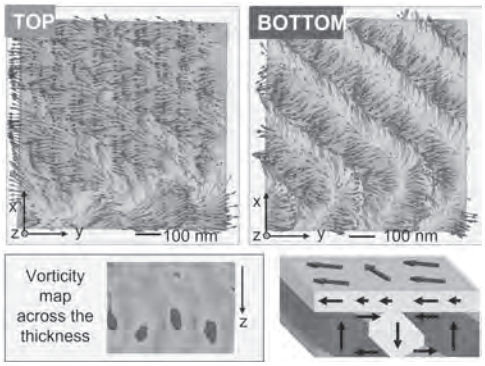

Fig 2. Tomographic reconstruction of m(Gd) (m_y contrast): At top $Gd_{24}Co_{76}$, there is a ripple pattern around easy anisotropy axis; At bottom $Gd_{12}Co_{88}$, there is a distorted closure domain structure. Across the thickness, closure vortex cores are arranged in a zig-zag. Sketch shows the exchange spring between stripe domains at NdCo/GdCo layers and in-plane domain with ripple at top $Gd_{24}Co_{76}$ layer.

EOD-09. Proximity induced magnetism in Pt layered with rare-earth:transition metal ferrimagnetic alloys.
C. Swindells[1,2], B. Nicholson[2], O.A. Inyang[2], Y. Choi[3], T. Hase[4] and D. Atkinson[2]
1. Department of Materials Science and Engineering, University of Sheffield, Sheffield, United Kingdom; 2. Department of Physics, Durham University, Durham, United Kingdom; 3. Advanced Photon Source, Argonne National Laboratory, Argonne, IL, United States; 4. Department of Physics, University of Warwick, Coventry, United Kingdom

Interfacial phenomena in magnetic thin film systems are key to future spintronic applications. For materials close to the Stoner criterion, such as Pt, electronic hybridisation at the interface with a magnetic material results in a proximity induced moment (PIM), with debate ongoing regarding the role of the induced moment with regards to interfacial spin transport [1,2]. Recently, rare-earth:transition metal (RE:TM) ferrimagnetic alloys have shown promise in spintronic applications, due to the net zero magnetisation at the compensation point of the two competing magnetic sub-lattices. This compensation, which occurs as a function of both temperature and alloy composition, enhances domain wall motion [3], thermal switching [4] and leads to vanishing skyrmion Hall angles [5]. However, in multilayered systems, it has not been experimentally shown whether the induced moment in a Pt at the interface with a RE:TM ferrimagnet will align with the net moment, or one of the magnetic sublattices. Here we present the results of a recently published study [6] investigating the magnetic moments in ferrimagnetic / Pt systems, using Co77Gd23 and (Co50Fe50)77Gd23 ferrimagnetic alloys to vary the dominant magnetic sublattice. Temperature dependent SQUID measurements, combined with element specific resonant x-ray measurements at the APS, Argonne Lab on the Pt and Gd L3 edges, allowed for the determination of the alignment of the Gd moments and induced Pt moments on either side of the compensation transition. In both cases, the PIM was found to be parallel to the TM sublattice rather than the RE or the net moment. Our results highlight the prominence of the d–d mediated interactions between the Pt and the constituents of the ferrimagnetic RE:TM alloys over the net macroscopic moment.

[1] M. Caminale, et al., Phys. Rev. B, 94 014414 (2016) [2] L. J. Zhu, D. C. Ralph, and R. A. Buhrman, Phys. Rev. B, 98, 164406 (2018) [3] K. Kim et al., Nat. Mater. 16 1187 (2017) [4] R. Evans et al., Appl. Phys. Lett 104 082410 (2014) [5] Y. Hirata et al., Nat. Nanotechnol 14 232 (2019) [6] C. Swindells et al., Phys. Rev. Res 2 033280 (2020)

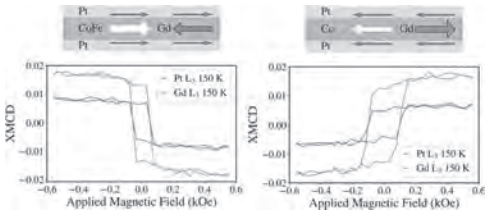

Fig 1: Element specific hysteresis loops taken at the Pt and Gd L3 edges for CoGd/Pt (Gd dominated) and CoFeGd/Pt (CoFe dominated)

Session EOE
THIN FILMS II

Melissa Loving, Co-Chair
Northrop Grumman Corporation, College Park, MD, United States
Susana Cardoso de Freitas, Co-Chair
INESC-MN, Lisbon, Portugal

INVITED PAPER

EOE-01. Controlling the Angle Between Magnetic Moments of Adjacent Ferromagnetic Layers. *E. Girt*[1], J. Besler[1], P. Omelchenko[1], Z. Nunn[1], S. Farhoosh[1], B. Heinrich[1], C. Abert[2] and D. Seuss[2] *1. Physics, Simon Fraser University, Burnaby, BC, Canada; 2. Physics, University of Vienna, Vienna, Austria*

Interlayer exchange coupling in transition metal multilayers has been intensively studied for over three decades and is incorporated into almost all spintronic devices. Unfortunately, this phenomenon has not been used to its full potential, as the current spacer layers only allow for the control of collinear orientation of magnetic moments of ferromagnetic layers. Recently, a class of spacer layers was discovered, which, when inserted between two ferromagnetic layers, can control the angle between the magnetic moments of these ferromagnetic layers; this allows the access of not only two ground states, antiferromagnetic (180°) and ferromagnetic (0°), but any state between 0° and 180°. These spacer layers consist of a nonmagnetic material (Ru), used to achieve a large antiferromagnetic interlayer exchange coupling between ferromagnetic layers, alloyed with a ferromagnetic material (Fe or Co). Shown in Fig.1 are the bilinear (J_1) and biquadratic (J_2) coupling constants and zero field coupling angle (θ) between the magnetic moments of the ferromagnetic layers of Co|$Ru_{100-x}Fe_x$(d)|Co as a function of RuFe thickness, d, and Fe atomic concentration, x. The noncollinear coupling in Co|RuFe|Co occurs for x between 62 and 82. In this RuFe composition range, J_1 strongly decreases while J_2 increases with increasing Fe concentration, satisfying the condition required for noncollinear alignment between the magnetic moments of Co layers ($J_2 > |J_1|/2$). The largest measured J_2 in Co|RuFe|Co, $J_2 = 3.8$ mJ/m^2, is larger than any J_2 value previously reported. For the thickness region $0.5 \le d \le 0.8$ nm, θ remains constant with d for most of the RuFe alloys. However, varying the concentration of Fe in Ru allows for precise control of θ between 180° and 90°. From a fabrication point of view, it is very important that a single parameter controls θ. Shown in Fig. 2 are θ and the saturation magnetization (M_s) of Co|$Ru_{100-x}Fe_x$(0.7 nm)|Co and Co|$Ru_{100-x}Co_x$(0.7 nm)|Co. The transition from antiferromagnetic to ferromagnetic coupling in Co|RuFe(0.7 nm)|Co occurs for x between 66 and 82 and in Co|RuCo(0.7 nm)|Co for x between 50 and 62. In both structures, the transition from antiferromagnetic to noncollinear coupling coincides with a sharp increase in M_s. This increase in M_s is attributed to a magnetic order in the spacer layer, which was found to be responsible for the large observed noncollinear coupling. In this talk, we will also show that noncollinear coupling can be achieved in Fe|RuFe|Fe structures, where the Co ferromagnetic layers are substituted with Fe. Micromagnetic simulations reveal that the biquadratic coupling originates from spatial fluctuations of the bilinear coupling between ferromagnetic layers across the novel spacer layer. The size of spatial fluctuations is determined to be below 2 nm, ensuring that noncollinear alignment will be preserved even if device size approaches 10 nm. These new spacer layers have the potential to be used in most spintronic devices, as the optimal design of these devices almost always requires noncollinear alignment between at least two adjacent ferromagnetic layers.

Z. Nunn, C. Abert, D. Suess and E. Girt, Sci. Adv., Vol. 6, p.1 (2020)

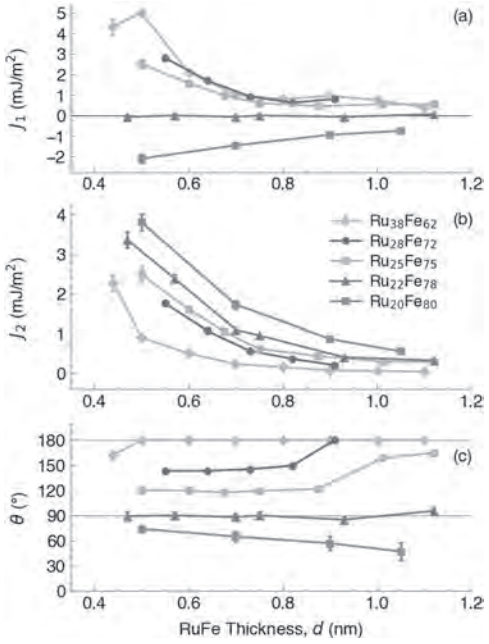

Fig.1 (a) J_1, (b) J_2, and (c) θ of Co|$Ru_{100-x}Fe_x$(d)|Co for $0.4 \le d \le 1.2$ nm. Data were collected at room temperature (298 K).

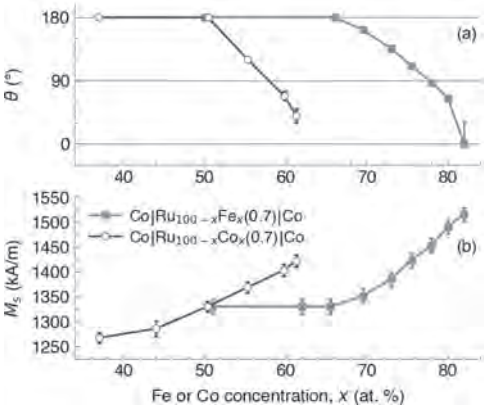

Fig.2 (a) θ and (b) M_s of Co|$Ru_{100-x}Fe_x$(0.7 nm)|Co and Co|$Ru_{100-x}Co_x$(0.7 nm)|Co at 298 K.

CONTRIBUTED PAPERS

EOE-02. First principles study of perpendicular magnetic anisotropy in thin-film Co_2MnSi. L. Stuelke[1], P. Kharel[2], P. Shand[1] and *P. Lukashev*[1]
1. Physics, University of Northern Iowa, Cedar Falls, IA, United States;
2. Physics, South Dakota State University, Brookings, SD, United States

Combining perpendicular magnetic anisotropy (PMA) with half-metallicity (HM) in thin-film geometry may provide additional functionalities for spintronic devices. However, such combination may be a challenging task, since HM is usually destroyed in thin-film geometry (e.g., due to the emergence of surface states), while PMA is most pronounced in reduced geometry, because of the contribution from surface anisotropy. Here, we explore the nature of PMA in thin-film full Heusler alloy Co_2MnSi. This material is one of the first compounds for which half-metallic electronic structure was experimentally confirmed. In addition, it has been reported that this alloy may exhibit PMA in thin-film geometry. Here, by analyzing site-projected magnetocrystalline anisotropy energy (MAE), we confirm that both PMA and surface half-metallicity are very sensitive to the termination surface and mechanical strain. In particular, while MnSi-termination under compressive strain may retain both 100% spin-polarization and out-of-plane magnetization orientation, Co-termination has a detrimental impact on both. These results may serve as a guide for practical nano-device applications in the field of spintronics. This research is supported by the *National Science Foundation* (NSF) under Grant Numbers 2003828 and 2003856 via DMR and EPSCoR.

EOE-03. Magnetocrystalline Anisotropy of Fe and FeCo Thin Films. *J.N. Rychly*[1], H. Glowinski[1], J. Snarski-Adamski[1], P. Kuswik[1] and M. Werwinski[1] *1. Institute of Molecular Physics Polish Academy of Sciences, Poznan, Poland*

In the race for the miniaturization of electronic devices, modern science reached the ultimate level of monoatomic layers. Whereas, magnetic tunnel junctions with perpendicular magnetic anisotropy reached the limit of about twenty atomic monolayers [1]. In our work, we systematically study the magnetic anisotropy of Fe and FeCo thin films of size from one to twenty atomic monolayers. Theoretical studies are based on calculations using the full-potential local-orbital electronic structure code FPLO [2] and generalized gradient approximation (GGA). The chemical disorder in FeCo layers was modeled using virtual crystal approximation (VCA). A set of layers with different thicknesses formed based on the bcc structure was subjected to full geometry optimization. The set of equilibrium structures was then recalculated using a fully relativistic approach for two orthogonal magnetization directions (in-plane and out-of-plane). The results of calculations allow the interpretation of parallel experimental studies in which FeCo layers on Au substrate are analyzed. The result of ab-initio calculations is a series of dependences of structural and magnetic parameters on layer thickness. Fig. 1 shows an example of the dependence of the optimized lattice constant on the Fe layer thickness. For few-atom-thick Fe layers there is a large reduction of the lattice parameter with respect to the value for bulk bcc Fe, to which the parameters determined for thicker layers converge. Fig. 2 presents the dependence of the magnetocrystalline anisotropy energy (MAE) on the Fe layer thickness. Positive values denote perpendicular magnetic anisotropy, negative values denote anisotropy in-plane. The calculated value of MAE for Fe monolayer equal to 0.58 meV/atom is in good agreement with the previous GGA result equal to 0.50 meV/atom [3]. These results were compared with measurements of the ratio of orbital to spin magnetic moment using VNA-FMR. We found that the contribution of surface anisotropy to the effective anisotropy is strong enough to overcome the shape anisotropy in Au/CoFe/Au systems.

[1] K. Watanabe, et al., Nat. Commun. 9, 663 (2018) [2] K. Koepernik, H. Eschrig, Phys. Rev. B. 59, 1743 (1999) [3] R. Wu, A.J. Freeman, J. Magn. Magn. Mater. 200, 498 (1999)

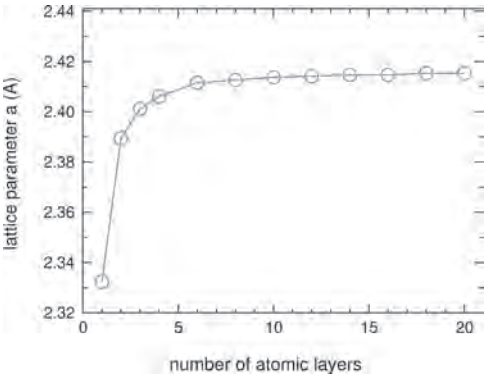

Fig.1 Dependence of the lattice parameter on the Fe layer thickness.

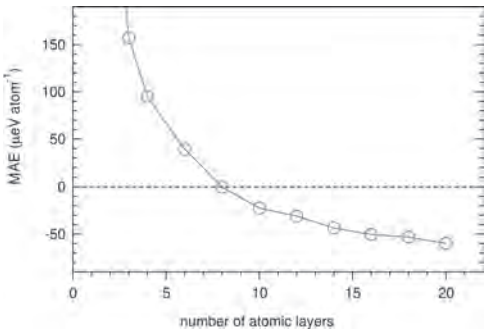

Fig.2 Dependence of MAE on Fe layer thickness.

EOE-04. Magnetostrictive properties of Co-Fe alloy epitaxial thin films with Co-rich composition. *S. Noro*[1], M. Ohtake[1], T. Kawai[1], M. Futamoto[1], F. Kirino[2] and N. Inaba[3] *1. Faculty of Engineering, Yokohama National University, Yokohama, Japan; 2. Graduate School of Fine Arts, Tokyo University of the Arts, Tokyo, Japan; 3. Graduate School of Science and Engineering, Yamagata University, Yonezawa, Japan*

Co-Fe alloys have recently attracted much attention as one of magnetostrictive materials and have been investigated for applications such as sensors, vibration energy harvesting devices, etc. Large magnetostriction of 150×10^{-6} – 250×10^{-6} is observed for Co-Fe alloys with Co-rich compositions [1,2], where bcc lattice is locally deformed by inclusion of fcc nanocrystals [2]. In order to clarify the intrinsic magnetostriction property, it is important to understand the magnetostriction coefficients, λ_{100} and λ_{111}. However, the magnetostriction coefficients of Co-Fe alloys with Co-rich compositions have not yet been made clear. In the present study, epitaxial $Co_{70}Fe_{30}$ (at. %) films are prepared on MgO substrates of (001) and (110) orientations by UHV sputtering to determine the λ_{100} and λ_{111}. Figs. 1(a) and (c) respectively show the RHEED patterns observed for $Co_{70}Fe_{30}$ films prepared on MgO(001) and (110) substrates. A diffraction pattern from bcc(001) single-crystal surface is recognized for the film formed on MgO(001) substrate, whereas reflections from two types of bcc(211) crystal are overlapped as shown by the spots, A and B, in the RHEED pattern observed for the film formed on MgO(110) substrate. (001) single- and (211) bi-crystalline $Co_{70}Fe_{30}$ films are epitaxially grown in the orientation relationships of Figs. 1(b) and (d), respectively. The lattice spacings estimated by XRD agree with the values of bulk $Co_{70}Fe_{30}$ crystal within small differences less than ±0.5%. Single- and bi-crystalline $Co_{70}Fe_{30}$ films with high crystallographic quality are successfully prepared. The magnetostriction is evaluated by using a cantilever method under rotating magnetic fields. Fig. 2 summarizes the magnetostrictive properties. The (λ_{100}, λ_{111}) of single- and bi-crystalline $Co_{70}Fe_{30}$ films are estimated to be ($+60\times10^{-6}$, $+150\times10^{-6}$) and ($+55\times10^{-6}$, $+185\times10^{-6}$), respectively. As the Co composition increases beyond 50 at. %,

the λ_{100} drastically decreases, whereas the λ_{111} further increases, as shown in Fig. 2(k). The present study has revealed the magnetostriction coefficients, λ_{100} and λ_{111}, of Co-Fe alloy with Co-rich composition and these values will be employed for study on the mechanism of magnetostriction in Co-Fe alloy system.

[1] D. Hunter, W. Osborn, K. Wang, N. Kazantseva, J. H.-Simpers, R. Suchoski, R. Takahashi, M. L. Young, A. Mehta, L. A. Bendersky, S. E. Lofland, M. Wuttig, and I. Takeuchi, *Nat. Commun.*, **2**, 518 (2011). [2] Y. Han, H. Wang, T. Zhang, Y. He, J. M. D. Coey, and C. Jiang, *J. Alloys Compd.*, **699**, 200 (2017).

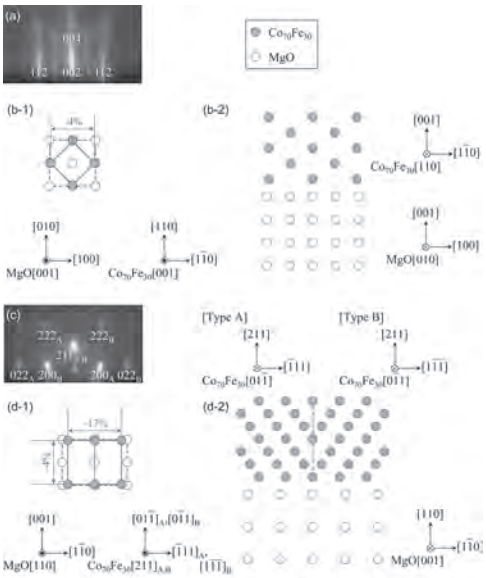

Fig. 1 [(a), (c)] RHEED patterns observed for $Co_{70}Fe_{30}$ films formed on (a) MgO(001) and (c) MgO(110) substrates. [(b), (d)] Planer and cross-sectional view schematic diagrams of epitaxial orientation relationships of $Co_{70}Fe_{30}$ films with respect to (b) MgO(001) and (d) MgO(110) substrates.

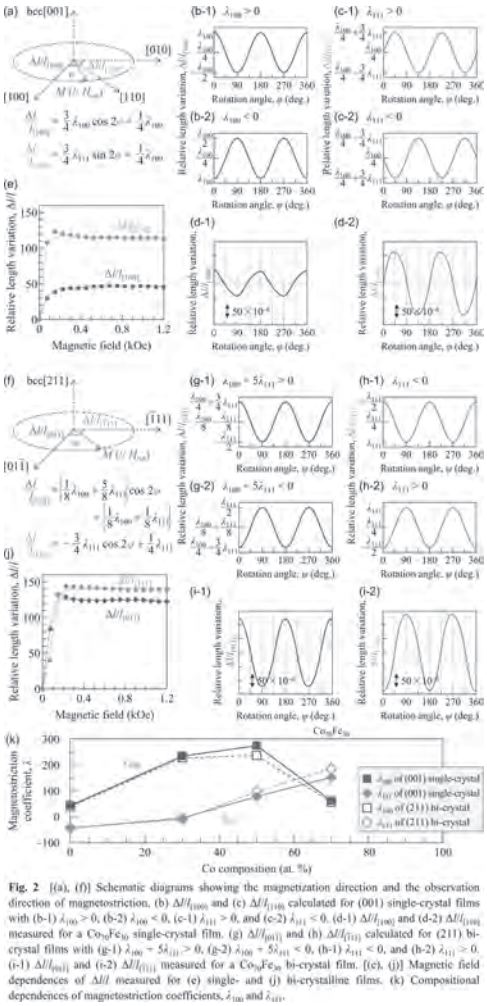

Fig. 2 [(a), (f)] Schematic diagrams showing the magnetization direction and the observation direction of magnetostriction, (b) $\Delta l/l_{[100]}$ and (c) $\Delta l/l_{[110]}$ calculated for (001) single-crystal films with (b-1) $\lambda_{100} > 0$, (b-2) $\lambda_{100} < 0$, (c-1) $\lambda_{111} > 0$, and (c-2) $\lambda_{111} < 0$. (d-1) $\Delta l/l_{[100]}$ and (d-2) $\Delta l/l_{[110]}$ measured for a $Co_{70}Fe_{30}$ single-crystal film. (g) $\Delta l/l_{[011]}$ and (h) $\Delta l/l_{[\bar{1}11]}$ calculated for (211) bi-crystal films with (g-1) $\lambda_{100} = 5\lambda_{111} > 0$, (g-2) $\lambda_{100} = 5\lambda_{111} < 0$, (h-1) $\lambda_{111} < 0$, and (h-2) $\lambda_{111} > 0$. (i-1) $\Delta l/l_{[011]}$ and (i-2) $\Delta l/l_{[\bar{1}11]}$ measured for a $Co_{70}Fe_{30}$ bi-crystal film. [(e), (j)] Magnetic field dependences of $\Delta l/l$ measured for (e) single- and (j) bi-crystalline films. (k) Compositional dependences of magnetostriction coefficients, λ_{100} and λ_{111}.

EOE-05. Effect of site disorder on the resonant microwave absorption in $Co_2Fe_{0.5}Ti_{0.5}Si$ Heusler alloy thin films. *M. Rahaman*[1], S.K. Sahoo[2], A. Haldar[2], M. Raja[3], S. Kaul[1] and S. Srinath[1] *1. School of Physics, University of Hyderabad, Hyderabad, India; 2. Department of Physics, Indian Institute of Technology Hyderabad, Kandi, India; 3. Defence Metallurgical Research Laboratory, Hyderabad, India*

Motivated by immense scientific interest in Co-based Heusler compounds [1 - 3] Co_2FeSi and Co_2TiSi as promising candidates for spintronics applications, 100 nm thick $Co_2Fe_{0.5}Ti_{0.5}Si$ (CFTS) thin films were grown on Si(100) substrates at substrate temperatures (TS) ranging from 200°C to 550°C by ultra-high vacuum magnetron sputtering. The deposited films were annealed in-situ at TS for 30 min. Energy-dispersive X-ray absorption spectroscopy yielded the actual alloy composition as $Co_{2.01}Fe_{0.51}Ti_{0.24}Si_{1.24}$. X-ray diffraction (XRD) patterns, shown in figure 1, reveal no Bragg peaks for TS200 film, broad fundamental peak (220) for TS350 film, and three sharp peaks (111), (220), and (422) for the remaining films. Thus, the crystalline structure gradually evolves from amorphous to ordered $L2_1$ structure as the TS increases; the TS500 film has the highest $L2_1$ order. Ferromagnetic resonance (FMR) spectra were recorded at various polar ('out-of-plane', OP) field angles, θ_H, at a fixed frequency of 9.45 GHz. A typical FMR spectrum, taken at $\theta_H = 0$ for the TS500 film, shown in figure 2(a), demonstrates that besides the uniform precession q = 0 spin wave (SW) mode, the SW modes with $q \neq 0$ exist. A detailed analysis [4 - 6] of the resonance field, H_{res}, versus θ_H plots (see Fig.2(a) inset) reveals a dominant OP uniaxial anisotropy. Fig.2(b) bears out that the frequency (f) vs. H_{res} plots, obtained using the broad-band (3–17 GHz) FMR setup, are well described by the Kittel resonance condition [7] (the curves through the data points):

$f=\gamma/2\pi[(H_r+H_k)\times(H_r+H_K+4\pi M_{eff})]^{1/2}$, where $\gamma=(2\pi g\mu_B)/h$ is the gyromagnetic ratio, M_{eff}, effective magnetization while H_K, g, and μ_B are the in-plane (IP) anisotropy field, Lande g-factor and Bohr magneton. We find that the IP anisotropy is very weak, and g has the minimum value of 2.02 for the TS500 film with the highest $L2_1$ order. The Gilbert damping constant (α) is determined from the linear fits (straight lines) to the frequency-dependent 'peak-to-peak' FMR linewidth (ΔH) data (symbols), shown in Fig.2(b) inset, based on the relation [8] $\Delta H=\Delta H_{inhomo}+(2/\sqrt{3})2\pi\alpha f/\gamma$. The TS500 film has the lowest value of $\alpha = 0.0032$.

1. Y. Sakuraba, et al. Appl. Phys. Lett. 104, 172407 (2014). 2. D. Bombor, et al. Phys. Rev. Lett. 110, 066601 (2013). 3. Y. Miura, et al. J. Appl. Phys. 99, 08J112 (2006). 4. V. Siruguri, et al. J. Phys.: Condens. Matter 8, 4567 (1996). 5. G. A. Basheed, et al. J. Appl. Phys. 109, 07A321 (2011). 6. B. K. Hazra, et al. J. Phys. D: Appl. Phys. 52 325002 (2019). 7. C. Kittel, Phys. Rev. 73, 155 (1948). 8. M. Belmeguenai, et al. Phys. Rev. B 87, 184431 (2013).

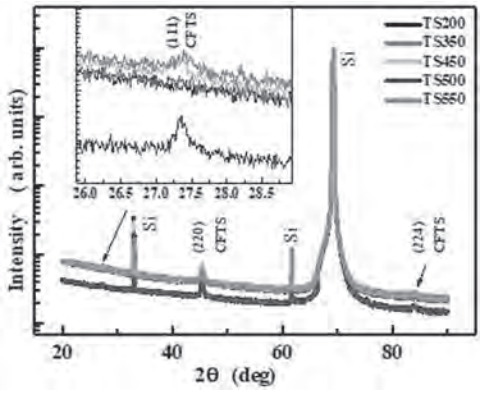

Fig.1:XRD patterns.

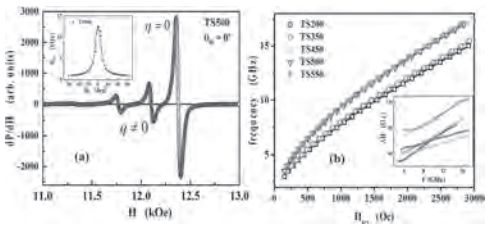

Fig.2(a) FMR spectrum; inset: $H_{res}(\theta_H)$. (b) $f(H_{res})$; inset: $\Delta H(f)$.

EOE-06. Effect of Fullerence on magnetization relaxation and domain wall dynamics in a perpendicularly magnetized Pt/Co/C_{60}/Pt system.
P. Sharangi[1], A. Mukhopadhyaya[2], S. Mallik[1], M. Ali[2] and S. Bedanta[1]
1. Physical Science, National Institute of Science Education and Research, Bhubaneswar, India; 2. Institute of Nano Science and Technology, Mohali, India

Buckminsterfullerene (C_{60}) can exhibit ferromagnetism at the interface (called as a spinterface) when it is placed next to a ferromagnet (FM). The formation of spinterface can influence the domain size and dynamics of the organic/ferromagnetic heterostructure [1-3]. Perpendicular magnetic anisotropic (PMA) systems are the most suitable candidates for data storage devices due to their high intrinsic anisotropy [4]. It has been demonstrated that with increasing thickness of the OSC layer on a Co ultrathin film one can tune the anisotropy of the system from in-plane to out-of-plane geometry [5]. However, FM-OSC systems with PMA have not been studied extensively. In this context, we have studied the tunability of magnetization relaxation and domain structure for Pt/Co/C_{60}/Pt system with perpendicular anisotropy. We have prepared thin films of Pt/Co/Pt [sample 1] and Pt/Co/C_{60}/Pt [sample 2]. Fig.1 show the hysteresis loops and domain images measured using polar MOKE for both the samples. It has been observed that the size of the bubbles shrinks for sample 2 in comparison to sample 1. The possible explanation may be the formation of spinterface at Co-C_{60} interface, which increases the overall anisotropy of the system and decreases the domain size. However, the overall shape of the bubble domains remains same to its parent Pt/Co/Pt thin film. To calculate the relaxation time of a system we have performed magnetic relaxation measurements at different sub-coercive fields (0.93, 0.95, 097 *Hc*). For both the samples relaxation time decrease with increasing the applied magnetic field, which is expected. However, for Pt/Co/C_{60}/Pt (sample 2) the relaxation time is reduced by ~ 50% as compared to Pt/Co/Pt (sample 1). Therefore, it is inferred that by introducing a C_{60} layer the switching speed of a system can be tuned which is a promising way to build device applications. Further, we have performed DFT calculation to understand the underneath mechanism of the Co/C_{60} spinterface.

1. S Mallick, *et al., Sci. Rep.* 8, (2018) 11648. 2. S. Mallik, *et al., Nanotechnology* 30, (2019) 435705. 3. S. Mallik, *et al. Appl. Phys. Lett*. 115 (2019), 242405. 4. N. Nishimura, *et al., J. Appl. Phys*. 91, (2002) 5246–5249. 5. K. Bairagi, *et al., Phys. Rev. B 98*, (2018) 085432.

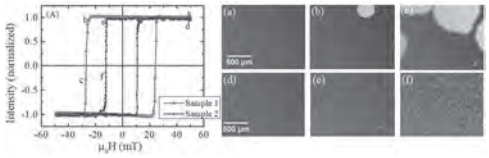

Figure 1: (A) Hysteresis loops for sample 1(red) and 2 (blue). (a–c) and (d–f) are the domain images at different field marked in (A) for samples 1 and 2, respectively.

EOE-07. Drastic enhancement of the magnetic anisotropy of thin Co films by Fullerene overlayers.
M. Benini[3,1], A. Sahoo[1], R.K. Rakshit[2], M. Singh[2], A. Riminucci[1], P. Graziosi[1], G. Varvaro[4], S. Sanna[3], V.A. Dediu[1] and I. Bergenti[1] *1. ISMN, CNR, Bologna, Italy; 2. CSIR - National Physical Laboratory, New Delhi, India; 3. Physics and Astronomy, University of Bologna, Bologna, Italy; 4. Consiglio Nazionale delle Ricerche, Institute of Structure of Matter, Rome, Italy*

The modification of the magnetic anisotropy of thin ferromagnetic films caused by the interfacing with molecular layers was reported for the first time for the Co/ZMP interface [1] and has become subject of active research [2] [3][4]. The nature of such modifications is supposed to be governed by the hybridization between organic molecules and d-orbitals of the ferromagnetic material, leading to modifications of the crystal fields and magneto-crystalline anisotropy for thin ferromagnetic layers [3]. We report on the strong enhancement of the magnetic anisotropy of polycrystalline Co films interfaced with C_{60} molecular layers. The Co films of 3, 5 and 10 nm were grown at RT by e-beam deposition in UHV conditions (10^{-9} mbar); fullerene layers were deposited in similar conditions by thermal evaporation, without breaking the vacuum. While it is expected that the effect is fully established at the Co/C_{60} interface, 25 nm of fullerene were deposited to avoid Cobalt oxidation. For comparison, Al capped cobalt films were grown in the same conditions (Al capping of 3nm). Ex-situ AFM characterization of 3, 5 and 10 nm Co films shows an atomically flat, granular surface (RMS of (0.3 ± 0.1) nm). The in-plane magnetic anisotropy was measured by L-MOKE and AMR and exhibited a drastic enhancement for the Co/C_{60} case. The RT coercive fields (Fig. 1) are a factor of two higher for the Co/C_{60} systems. Moreover, for 5 nm thick Co the coercive fields achieved the extraordinary enhancement by a factor of 20 at 100K. The in-plane vs out-of-plane behavior was measured by VSM magnetometry and a significative increase in magnitude of the effective anisotropy constant for the Co/C_{60} systems was detected. We will also report on various additional characterizations and simulations and will present a phenomenological model describing the observed effects. We believe these results may have a strong impact in various device applications, such as magnetic sensors or memories, where polycrystalline Co films represent a major player.

[1] K. V. Raman, A. M. Kamerbeek, A. Mukherjee, Nature, Vol. 493, p.509 (2016) [2] T. Moorsom, M. Wheeler, T. M. Khan, Physical Review B, Vol. 90, p.6 (2014) [3] K. Bairagi, A. Bellec, V. Repain, Physical Review Letters, Vol. 114, p. 247203 (2015) [4] M. Cinchetti, L. Hueso, V. A. Dediu, Nature Materials, Vol. 16, p.507 (2017)

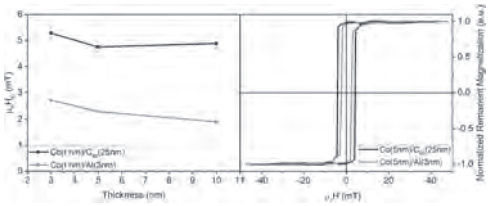

Fig.1 Left: RT coercive fields as a function of Co thickness. Right: Hysteresis loops for 5 nm Co with C_{60} and Al capping

EOE-08. Easy-cone magnetic anisotropy in tetragonally distorted $NiCo_2O_4$ epitaxial film. *H. Koizumi*[1] and H. Yanagihara[1] *1. University of Tsukuba, Tsukuba, Japan*

$NiCo_2O_4$ (NCO) is a conductive inverse spinel oxide which shows ferrimagnetism with a Néel temperature as high as $T_C \approx 400$ K [1]. In addition, NCO(001) films grown on $MgAl_2O_4$ (MAO) substrates exhibited perpendicular magnetic anisotropy (PMA) at room temperature. Recently, semi-quantitative explanation that the origin of PMA is due to the magnetoelastic effect to the compressive strain for Co at the tetrahedral site is proposed [2]. However, the detail properties of magnetic anisotropy (MA) of NCO film, such as temperature dependence, are not yet well understood. In this study, we report on the temperature dependence of the MA and on the change of MA from PMA to easy-cone magnetic anisotropy (ECMA). Figure 1 shows the temperature dependence of the magneto-torque curves at various temperatures of the NCO(001) films. The torque curve at room temperature is mainly composed of a twofold component, indicating that the MA of NCO film is PMA. However, the fourfold components emerge in the torque curves with decreasing temperature. This result indicates that the magnetically preferential direction is neither perpendicular nor parallel to the film but ECMA in the low temperatures. Anomalous Hall (AHE) measurements with magnetic field tilted from normal to the film were also performed to estimate the cone angle. Figure 2 shows field-angle dependence of squareness ratio (SR) determined from AHE results. One can see that SR exceeds 1 at certain angles. The cone angle estimated from the SR of AHE is consistent with the one from the conventional magneto-torque analysis. This result supports NCO film exhibits ECMA in low temperatures. The observed spin reorientation from PMA to ECMA seems to occur continuously at a temperature around 70 K. We have succeeded in demonstrating the method to estimate the cone angle from AHE measurements with tilted field angular dependence.

[1] X. Chen, *et al.*, Adv. Mater. 31, 1805260 (2019). [2] C. Mellinger, *et al.*, Phys. Rev. B 101, 014413 (2020).

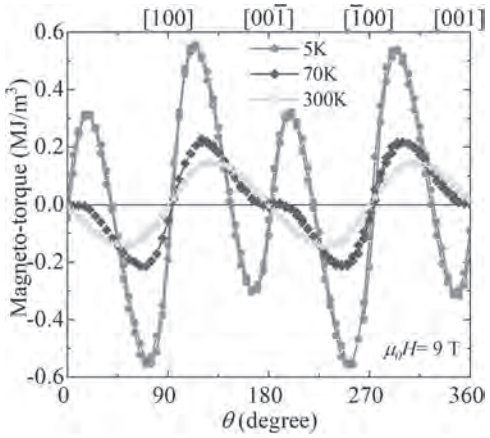

Fig. 1 Temperature dependence of the magneto-torque curve.

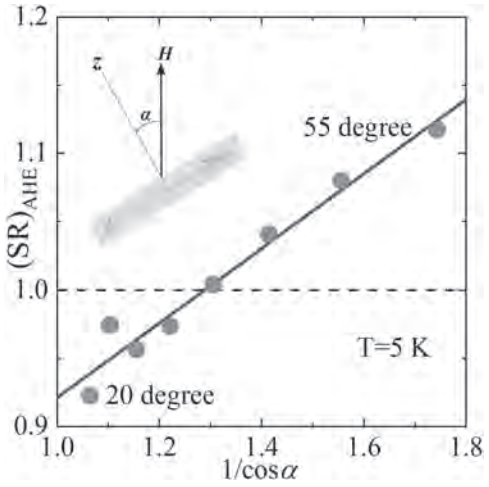

Fig. 2 Tilted field angle (α) dependence of SR of AHE.

EOE-09. Structural and Magnetic Study of Single Nano-Hetero-Structured Co-Rich CoP Magnetic Thin Films. *A. Samanta*[1,2] and S. Roy[1,2] *1. Micropower Devices/Systems and Nanomagnetics Group, Tyndall National Institute, Cork, Ireland; 2. Department of Physics, University College Cork, Cork, Ireland*

Though nano-hetero-structured (NHS) magnetic materials preparation using sputtering, electron beam lithography/ evaporation (EBL/EBE) have inspired a wealth of experimental results, to date, there is a very limited experimental understanding of preparing *in situ* NHS magnetic material using electrodeposition technique and the elucidation of their magnetic behavior. Towards this end, using pulse reverse [1] electrodeposition technique with a modified and stable acidic bath chemistry at room temperature, we have prepared *in situ* NHS magnetic cobalt phosphorus (CoP) thin film and investigated its characteristics structurally and magnetically combined with micromagnetic simulation utilizing MuMax^3 [2]. Despite the availability of various techniques, the electrodeposition technique [1,3–5] has been chosen due to its relatively higher deposition rate and low cost. Here, CoP thin films with ultralow coercivity to moderate coercivity have been prepared from a single starting material from the same bath. The crossover from the ultralow coercivity to a comparatively higher coercivity has been demonstrated by the manipulation of the time width of the current (shown in FIG. 1) in a single amorphous system of CoP nanomagnetic thin film. We have characterized the developed smooth, stress-free, and shiny electroplated samples structurally by SEM, TEM, and magnetically by the hysteresis loop tracer (ShB Instruments, USA). The SEM micrographs confirm the fine-grain surface morphology of the cobalt phosphorous nanomagnetic thin films. The elemental analysis by energy dispersive X-Ray (EDX) yields the stoichiometry of the electrodeposited cobalt phosphorous. This pulse reverse plating technique could be an ideal option to tune the spin configuration with respect to the multi-nano layer thicknesses to obtain an optimum exchange coupling. The static in-plane magnetic measurement by the hysteresis loop tracer is shown in FIG. 2(c)-(d) reveals different hysteresis loops of electrodeposited CoP thin film.

Acknowledgment: AS gratefully acknowledges the financial support for this work from EU-H-2020 project "EnABLES-JRA", Project ID: 730957.
References: [1] S. Roy, A. Connell, M. Ludwig, N. Wang, T. O'Donnell, M. Brunet, P. McCloskey, C. ÓMathúna, A. Barman, and R. J. Hicken, J. Magn. Magn. Mater. 290–291, 1524 (2005). [2] A. Vansteenkiste, J. Leliaert, M. Dvornik, M. Helsen, F. Garcia-Sanchez, and B. Van Waeyenberge, AIP Adv. 4, 107133 (2014). [3] P. McCloskey, B. Jamieson, T. O'Donnell, D. Gardner, M. A. Morris, and S. Roy, J. Magn. Magn. Mater. 320, 2509 (2008). [4] P. McCloskey, B. Jamieson, T. O'Donnell, D. Gardner, M. A. Morris, and S. Roy, J. Magn. Magn. Mater. 322, 1536 (2010). [5] P. McCloskey, T. O'Donnell, B. Jamieson, D. Gardner, M. A. Morris, and S. Roy, in *Handb. Nanoelectrochemistry Electrochem. Synth. Methods, Prop. Charact. Tech.*, edited by M. Aliofkhazraei and A. S. H. Makhlouf (Springer International Publishing, Cham, 2016), pp. 1–27.

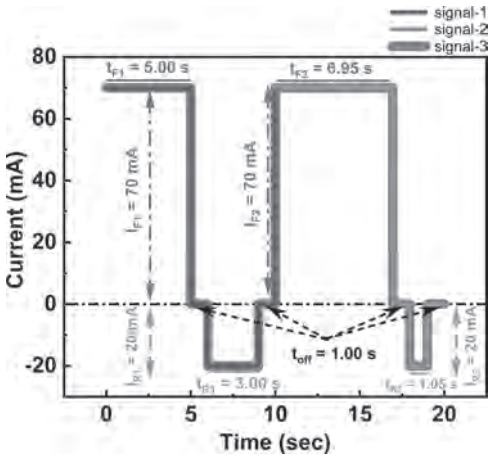

Fig. 1 Waveform and timing diagram for PR electroplating to develop nanomaterials from a single bath.

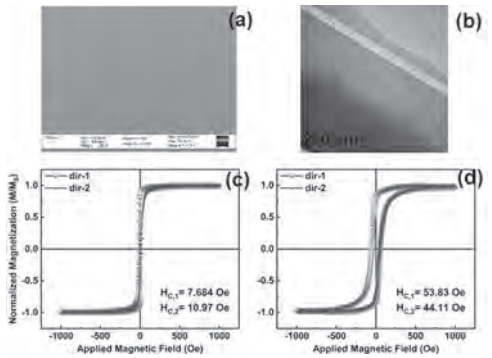

Fig. 2 (a) An SEM and (b) a cross-sectional TEM image of CoP thin film. Hysteresis loop of (c) ultralow CoP, and (d) comparatively higher CoP

EOE-10. γ′ phase formation in Fe-N thin films prepared on MgO(001) substrates by reactive sputtering. *K. Imamura*[1], Y. Maeda[1], M. Ohtake[1], M. Futamoto[1], T. Kawai[1], F. Kirino[2] and N. Inaba[3] *1. Faculty of Engineering, Yokohama National University, Yokohama, Japan; 2. Graduate School of Fine Arts, Tokyo University of the Arts, Tokyo, Japan; 3. Graduate School of Science and Engineering, Yamagata University, Yonezawa, Japan*

Fe_4N with γ′ phase shows high negative spin polarization [1] and the thin films have been recently attracted much attention to spintronics applications. In order to extract the basic magnetic properties, it is required to prepare Fe-N films consisting of only γ′ phase. The phase formation in Fe-N film is delicately influenced by the preparation method and the deposition conditions. Although various methods such as MBE [2–4] have been used, sputtering [5–7] is more suitable for practical applications. However, there are few reports on the systematical investigation of sputtering condition for γ′-Fe_4N film formation. In the present study, Fe-N films are prepared on single-crystal MgO(001) substrates by reactive sputtering. The substrate temperature is varied from RT to 600 °C. The total pressure of Ar and N_2 gases is kept constant at 0.67 Pa and the N_2 partial pressure ratio is varied from 0 to 5%. The influences of substrate temperature and N_2 partial pressure ratio on the phase formation are investigated in detail. Fig. 1(a) summarizes the crystallographic phases of Fe-N films prepared under different conditions, which are determined by RHEED and XRD as shown for example in Figs. 1(b)–(d). Only α phase (bcc phase) is formed in the films prepared at RT under N_2 partial ratios of 2.5–5% as well as in the films prepared under N_2 pressure ratio of 0%. Low substrate temperature does not promote the nitriding of Fe. When the N_2 pressure ratio increases to 2.5%, the films prepared at 200–400 °C involve γ′ phase in addition to α phase. With further increasing the N_2 pressure ratio up to 5%, single γ′ phase is successfully stabilized. However when the substrate temperature is increased to 600 °C, the films consist of only α phase for all the investigated N_2 pressure ratios. High temperature prevents the formation of Fe_4N compound, similar to the case of bulk material. The amount of N atom included in the film and the chemical bonding state are carefully investigated by XPS (not shown here). Fig. 2 shows the magnetic properties of films consisting of α, α+γ′, and γ′ phases. These films show soft magnetic properties reflecting the magnetocrystalline anisotropies and the saturation magnetizations of Fe and Fe_4N crystals.

[1] S. Kokado, N. Fujima, K. Harigaya, H. Shimizu and A. Sakuma, *Phys. Rev. B*, **73**, 172410, (2006). [2] D. Gölden, E. Hildebrandt and L. Alff, *J. Magn. Magn. Mater.*, **422**, 407, (2017). [3] A. Narahara, K. Ito, T. Suemasu, Y. K. Takahashi, A. Ranajikanth, and K. Hono, *Appl. Phys. Lett.*, **94**, 202502, (2009). [4] K. Ito, S. Higashikozono, F. Takata, T. Gushi, K. Toko and T. Suemasu, *J. Cryst. Growth*, **455**, 66, (2016). [5] H. Li, X. Li, D. Kim, G. Zhao, D. Zhang, Z. Diao, T. Chen and J. P. Wang, *Appl. Phys. Lett.*, **112**, 162407, (2018). [6] Q. Lu, M. Xie, G. Han, B. Zheng, Y. Song, J. Qiang, X. Wang, Z. Wu, P. Yan and W. Liu, *J. Magn. Magn. Mater.*, **474**, 76, (2019). [7] M. Takahashi, H. Shoji, M. Abe, H. Komaba and T. Wakiyama, *IEEE Transl. J. Magn. Jpn.*, **6**, 102, (1991).

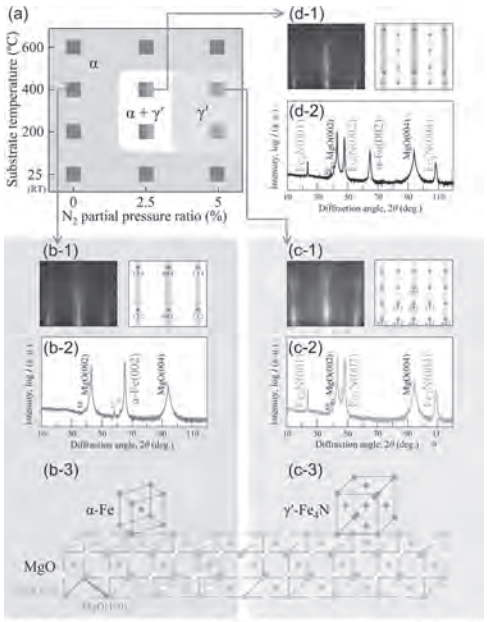

Fig. 1 (a) Phase diagram of Fe-N film prepared on MgO(001) substrate by reactive sputtering. (b-1)–(d-1) RHEED and (b-2)–(d-2) XRD patterns of Fe-N films consisting of [(b-1), (b-2)] α, [(c-1), (c-2)] γ′, and [(d-1), (d-2)] α+γ′ phases. [(b-3), (c-3)] Crystallographic orientation relationships of Fe-N(001) films composed of (b-3) α and (c-3) γ′ phases with respect to MgO(001) substrate.

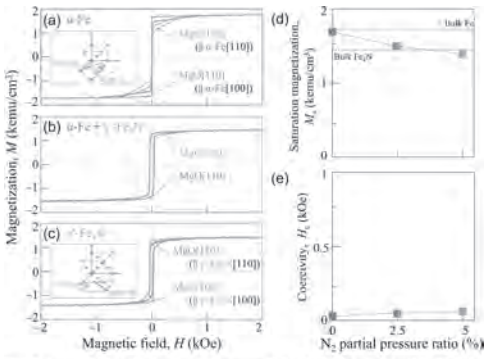

Fig. 2 (a)–(c) Magnetization curves measured for Fe-N films consisting of (a) α, (b) α+γ′, and (c) γ′ phases. Dependences of (d) saturation magnetization and (e) coercivity of Fe-N film prepared at 400 °C on N_2 partial pressure ratio.

EOE-11. Flexible strain-free $La_{0.7}Sr_{0.3}MnO_3$ membranes. *C. Zhang*[1], Z. Yin[1], J. Wang[1], F. Hu[1], S. Jirong[1] and B. Shen[1] *1. Institute of Physics, Chinese Academy of Sciences, Beijing, China*

The charge, spin and orbital degrees of freedom in strong correlation oxide materials, such as $La_{0.7}Sr_{0.3}MnO_3$ (LSMO), are tightly coupled to the lattice. Therefore, utilizing the local entanglement of the charge, orbital and spin, strain can be used to manipulate the quantum states of the materials, which further modifies the physical properties of the LSMO.[1,2] However, non-essential strains are usually introduced to the film during the growth process of LSMO, which makes it difficult for us to explore the intrinsic properties of LSMO films. In the present research, we fabricated unconstrained LSMO films on a flexible substrate of mica via van der Waals (vdW) epitaxy, which eliminates tight lattice matching of the LSMO film and substrate and results in an oriented strain-free film. What's more, we further developed a room-temperature exfoliation-transfer method to transfer the LSMO film away from mica substrate;[3] getting flexible strain-free films. Besides flexibility, the strain-free LSMO films exhibited excellent magnetoresistance properties and mechanical stability. Our strategy may pave the way for future design of correlated electron states of complex oxides. This work was supported by the National Key Research and Development Program of China (2017YFA0303601, 2019YFA0704900, 2020YFA0711502, 2018YFA0305704, 2017YFA0206300), the National Natural Sciences Foundation of China (52088101, 11934016, U1832219, 51971240, 51771223, 11921004), the Strategic Priority Research Program (B, XDB33030200), and the Key Program of the Chinese Academy of Sciences (CAS).

1. Aymeric Sadoc et al., *Phys. Rev. Lett.* 2010, *104* (4), 046804. 2. Er-Jia Guo et al., *Adv. Funct. Mater.* 2018, 28, 1800922 3. Cheng Zhang et al., *ACS Applied Materials & Interfaces* 2021 *13* (24), 28442-28450

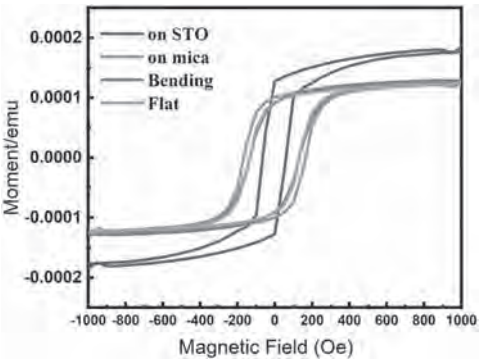

fig. 1 M–H loop of LSMO under bending modes.

EOE-12. Withdrawn

EOE-13. Withdrawn

EOE-14. Theoretical study of Yu-Shiba-Rusinov states and Shiba bands for Fe dimers and chains on Au/Nb(110). *B. Nyári*[1], A. Lászlóffy[2], L. Szunyogh[1] and B. Ujfalussy[2] *1. Department of Theoretical Physics, Budapest University of Technology and Economics, Budapest, Hungary; 2. Wigner Research Centre for Physics, Budapest, Hungary*

One of the main goals of quantum computing is to find stable quantum bit realizations. Magnetic chains on superconducting surfaces manifest topologically protected Majorana quasiparticles as zero-energy modes located at the ends of the chain makeing them possible candidates for such fault-tolerant quantum computing. The rapid development of scanning tunneling microscopy measurements in the past decade provided an effective way to study these system in experiments with a high energy resolution turning not only the experimental but the theoretical interest to this way. In the present work we introduce an ab initio approach employing multiple scattering theory and Green's function embedding for the calculation of the spectral properties of magnetic impurities embedded onto the surface of a superconducting host. We consider different Fe clusters separated by a single Au overlayer on Nb(110) which is highly motivated by experiments. We perform systematic calculations for dimers and chains along different crystallographic directions, with different distances of the Fe atoms and in different magnetic configurations. Based on the local density of states (LDOS) we study the conditions under which Majorana zero modes might appear.

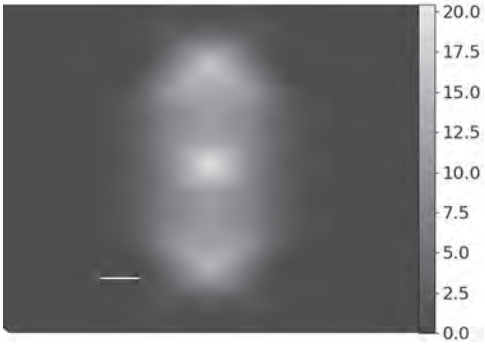

Fig.1 The spatial distribution of a YSR state for an Fe dimer on Au/Nb(110)

Session EOF
PATTERNED FILMS

Tom Thomson, Co-Chair
University of Manchester, Manchester, United Kingdom
Hikaru Nomura, Co-Chair
Osaka University, Toyonaka, Japan

INVITED PAPERS

EOF-01. Magnetic noise measurements and demonstration of a field-induced magnetic monopole plasma in artificial spin ice.
M. Goryca[1,2], X. Zhang[3], J. Li[2], A. Balk[2], J.D. Watts[4], C. Leighton[4], C. Nisoli[2], P. Schiffer[3] and S. Crooker[2] *1. University of Warsaw, Warsaw, Poland; 2. Los Alamos National Laboratory, Los Alamos, NM, United States; 3. Yale University, New Haven, CT, United States; 4. University of Minnesota, Minneapolis, MN, United States*

Arrays of interacting nanomagnets known as Artificial Spin Ice (ASI) have allowed the design of geometrically frustrated exotic collective states not found in natural magnets. A key emergent description of fundamental excitations in ASIs and in natural pyrochlore spin ices is that of magnetic monopoles - mobile quasiparticles that carry an effective magnetic charge. These charge excitations can interact with each other and with applied magnetic fields via the magnetic analog of the electronic Coulomb interaction, representing the emergence of a range of novel phenomena, including the possibility of "magnetricity". While the presence of monopoles in ASI has been observed in pioneering imaging measurements [1-3], dynamical studies of monopole kinetics, and (especially) the ability to tune continuously through monopole-rich regimes in thermal equilibrium, remain at an early stage. In this work we use a high-bandwidth magneto-optical noise spectrometer (Fig. 1(b)) to passively "listen" to spontaneous magnetization fluctuations in archetypal, thermally active square ASI. The noise reveals specific regions in the magnetic field-dependent phase diagram (Fig. 1(a),(c)) where the density of mobile monopoles increases well over an order of magnitude compared with neighboring regimes, a consequence of the field-tunable tension on the Dirac strings connecting mobile monopoles. Moreover, detailed noise spectra demonstrate that monopole kinetics are minimally correlated (*i.e.*, most diffusive) in this plasma-like regime [4]. Experiments and Monte-Carlo simulations of more complex ASIs (including quadrupolar and vertex-frustrated Shakti and Tetris lattices) show similarly fascinating behavior, revealing surprisingly rich field-dependent phase diagrams of these systems. The discovery of on-demand monopole regimes with tunable kinetic properties opens the door to new probes of magnetic charge dynamics and provides a new paradigm for the studies of magnetricity in artificial magnetic materials.

[1] S. Ladak *et al.*, Nat. Phys. 6, 359 (2010). [2] E. Mengotti *et al.*, Nat. Phys. 7, 68 (2011). [3] C. Phatak *et al.*, Phys. Rev. B 83, 174431 (2011). [4] M. Goryca *et al.*, Phys. Rev. X 11, 011042 (2021).

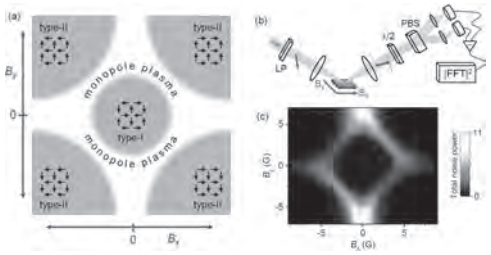

Fig. 1. (a) Notional schematic of the anticipated field-dependent phase diagram of square ASI. Between antiferromagnetic ordering at small magnetic field (blue) and fully polarized order at large field (red), a monopole-rich regime is expected. (b) Schematic of experimental setup for optical detection of magnetization fluctuations in ASI. (c) Measured map of the total magnetization noise power from square ASI versus applied in-plane magnetic fields B_x and B_y. The diamond-shaped feature indeed reveal a plasma-like regime, with the high density of mobile magnetic monopoles.

EOF-02. Reconfigurable magnetism in a bi-stable nanomagnetic array: Artificial Spin-Vortex Ice. J.C. Gartside[1], A. Vanstone[1], K. Stenning[1], H.H. Holder[1], T. Dion[2], D.M. Arroo[3], H. Kurebayashi[2] and *W.R. Branford*[1] *1. Physics, Imperial College London, London, United Kingdom; 2. London Centre for Nanotechnology, University College London, London, United Kingdom; 3. Materials, Imperial College London, London, United Kingdom*

Artificial spin ices (ASI) are magnetic metamaterials comprising geometrically-tiled interacting nanomagnets. Typically each nanoisland is magnetized along its long axis giving an Ising 'macrospin'. There has been significant recent interest in these systems for functional magnonics due to their large reconfigurable dipolar field landscape. Here we present recent advances using a width modification scheme where artificial spin ice is modified by widening a subset of bars relative to the rest of the array. There are two principal benefits to the width modification. Firstly, Increasing width decreases the coercive field of the macrospins, so certain geometric tilings of the wide bars allow preparation of any ordered macrospin vertex state via simple global-field protocols[1]. Secondly at a certain width the macrospin spin state will be energetically equivalent with the vortex state so the wide bars can be tuned to be metastable in the macrospin and vortex states, yielding Artificial Spin-Vortex Ice (ASVI)[2]. The precise control of both nanoisland magnetism and vertex configuration by the width modification enables us to demonstrate the efficacy of zero-field ferromagnetic resonance measurements of the spin-wave spectrum as a fingerprint of the local dipolar field environment and vertex populations in magnetic nanostructures[3]. Artificial Spin-Vortex Ice allows a cross over experimentally from the classic 2-state Ising ASI to a 4-state Potts model system where the macrospins can convert into closed vortices. Unlike in a 'clock model' Potts system, the dipolar interactions are almost completely eliminated in the vortex state.[4] The enhanced bi-texture microstate space gives rise to emergent

physical memory phenomena, with ratchet-like vortex training and history-dependent nonlinear training dynamics. We observe vortex-domain formation alongside MFM tip vortex-writing. Tip-written vortices dramatically alter local reversal and memory dynamics. The precise control and the dramatic differences in local dipolar environment are very promising for reconfigurable magnonics. In the width modified macrospin ASI, we obtain shifts in ferromagnetic resonance frequency of the order of hundreds of MHz and access states with mode hybridization. ASVI yield much stronger contrast in dipolar environment such that the gap between the macrospin and the vortex peak is around 3.8 GHz.

[1]Gartside, J. C., Vanstone, A., Dion, T., Stenning, K. D., Arroo, D. M., Kurebayashi, H. & Branford, W. R. *Nature Communications* 12, 2488 (2021). [2]Gartside, J. C., Stenning, K. D., Vanstone, A., Dion, T., Holder, H. H., Arroo, D. M., Kurebayashi, H. & Branford, W. R. *Arxiv 2107.08941* (2021). [3]Vanstone, A., Gartside, J. C., Stenning, K. D., Dion, T., Arroo, D. M. & Branford, W. R. *Arxiv 2106.04406* (2021). [4]Stenning, K. D., Gartside, J. C., Dion, T., Vanstone, A., Arroo, D. M. & Branford, W. R. *Acs Nano* 15, 674–685 (2021).

CONTRIBUTED PAPERS

EOF-03. Artificial Spin Ice with Y-shaped Nanomagnets. *X. Zhang*[1], G. Fitez[1], J. Ramberger[2], C. Leighton[2] and P. Schiffer[1,3] *1. Applied Physics, Yale University, New Haven, CT, United States; 2. Department of Chemical Engineering and Materials Science, University of Minnesota, Minneapolis, MN, United States; 3. Physics, Yale University, New Haven, CT, United States*

Artificial spin ice (ASI) [1] systems are two-dimensional arrays of single-domain nanomagnetic islands that are designed to study collective behavior of interacting magnetic systems. These nanoislands usually have a stadium shape so that the magnetization orients along the longer axis, i.e., the moments are Ising-like. Most research on ASI systems focuses on different arrangements of nanoisland arrays [2], but, recently, some studies have focused on modifying the shapes of nanoislands [3,4]. Here, we introduce a new design of nanoislands, the Y-shape island, which has three equal-length arms joining at the center, with 120° separation. This island has six possible moment configurations in which the magnetization on each arm points either toward the center or away from it. We fabricated such nanoislands from permalloy, arranged in a hexagonal lattice geometry (Fig 1). Since permalloy has little magnetocrystalline anisotropy, the magnetization of the nanoislands can be well-controlled by utilizing shape anisotropy. We annealed such samples above the Curie temperature and examined the moment configurations using magnetic force microscopy after the samples cooled back to room temperature. We find strong correlations among the complex moment arrangements of these islands, suggesting the possibility of new types of moment ordering and new phenomenological ways of describing these novel magnetic objects associated with their unusual symmetry. Work at Yale University was funded by the US Department of Energy, Office of Basic Energy Sciences, Materials Sciences and Engineering Division under Grant No. DE-SC0020162. Work at the University of Minnesota was supported by NSF through Grants No. DMR-1807124 and DMR-2103711.

[1] R. F. Wang, *et al. Nature* 439, 303–306 (2006) [2] S.H. Skjærvø, *et al. Nat. Rev. Phys*. 2, 13–28 (2020). [3] D. Louis, *et al. Nat. Mat*. 17, 1076-1080 (2018). [4] R. Streubel, *et al. Nano Lett*. 18, 7428-7434 (2018).

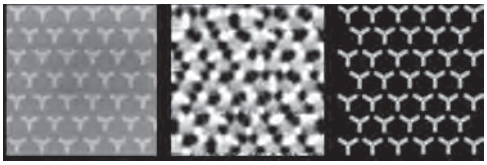

Figure 1. (a) A scanning electron microscopy image of Y-shape nanoislands in hexagonal geometry. (b) A magnetic force microscopy image taken after annealing at 550 degree C. The white and black dots correspond to the poles of the island moments. (c) The corresponding moment schematic.

EOF-04. Energetics of complex spin textures in LSMO artificial spin ice structures. *D.Y. Sasaki*[1], R.V. Chopdekar[2], S.T. Retterer[3], D.Y. Jiang[4], J.K. Mason[1], M.S. Lee[1] and Y. Takamura[1] *1. Department of Materials Science and Engineering, University of California, Davis, Davis, CA, United States; 2. Advanced Light Source, Lawrence Berkeley National Laboratory, Berkeley, CA, United States; 3. Center for Nanophase Materials Science, Oak Ridge National Laboratory, Oak Ridge, TN, United States; 4. Department of Chemical Engineering, University of California, Davis, Davis, CA, United States*

The fundamental building blocks of artificial spin ice (ASI) systems are magnetic nanoislands designed for Ising-like single domain configurations magnetized along the nanoisland length due to shape anisotropy. The dipolar interaction between these macrospins serve as the basis for investigating geometric frustration in ASIs with a variety of array geometries ranging from square-like arrangements to quasicrystals. Using X-ray photoemission electron microscopy (X-PEEM) to perform magnetic domain imaging, we studied thermally demagnetized $La_{0.7}Sr_{0.3}MnO_3$-based brickwork ASIs and showed that non-Ising domains, which we call complex spin textures (CSTs), can be stabilized through appropriate selection of nanoisland width, W, and ASI lattice parameter, a. While W-dependent formation of CSTs can be explained due to the dominance of shape anisotropy, the a-dependence was unexpected for nanoislands possessing identical W, suggesting that inter-island effects play an important role. MuMax[3] micromagnetic simulations indicated that an intermediate range of 100 nm $\leq W <$ 150 nm and 600 nm $\leq a \leq$ 700 nm exists where the formation of Ising states are preferred over CSTs as shown in Fig. 1. For larger values of W and a that reside above the black border in the energy diagram of Fig. 1, CST formation becomes energetically favorable over an arrangement of Ising states in higher energy vertex configurations. Energy analysis suggests that while magnetostatic energy dominates the energetics, the small contribution from exchange energy determines whether nanoislands can exist in Ising or CST states. The nanoisland magnetic state changes the magnetostatics arising from both *intra*-island shape anisotropy and *inter*-island dipolar interaction. These results suggest the potential to create tunable nanoisland domain states, providing a new direction in the development of ASI systems with exotic phase transitions as well as novel nanomagnetic logic architectures.

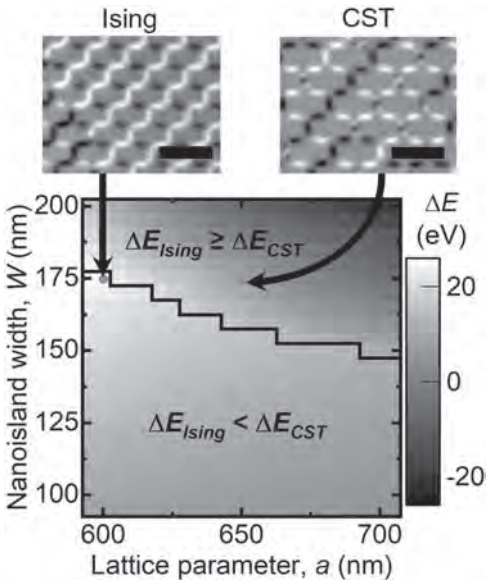

Fig. 1: PEEM images (top) of brickwork ASI with W = 175 nm and a set to 600 nm (left) and 650 nm (right). MuMax³ simulations of the minimum energy surface (bottom) with gray points corresponding to configurations from PEEM images. Scale bars are 2 µm.

EOF-05. Role of Chiral Switching Barriers on Relaxation Kinetics in Artificial Square Ice. *N. Leo*[1], M. Menniti[1], P. Vilalba Gonzales[1], M. Pancaldi[2] and P. Vavassori[1,3] *1. CIC nanoGUNE BRTA, Donostia - San Sebastián, Spain; 2. Elettra Sincrotrone, Trieste, Italy; 3. Ikerbasque, Bilbao, Spain*

Collective dynamics in lithographically-defined artificial spin ices offer insights into emergent correlations and phase transitions of geometrically-frustrated Ising spin systems. Their temporal and spatial evolution observed in experiments are also often simulated using kinetic Monte Carlo (kMC) simulations. As we recently showed, simplified models that describe the switching barriers, which are necessary to obtain predictive simulations results, overlooked a chiral contribution that leads to a splitting of barrier energies and results in faster relaxation [1,2]. As consequence of the chiral barrier splitting, the relaxation pathways are modified. In this work, we study the evolution from the field-saturated state to the ground-state order of artificial square ice with kMC simulations; and compare the effect of commonly-used mean-field barriers to the chiral split-barrier description at different interaction strengths and temperatures. We assess general measures that describe the dynamic evolution, such as vertex populations and net magnetisation as well as spatial correlations. By taking into account the chiral barrier splitting we observe faster and more efficient evolution to the ground state. Compared to the mean-field barrier model, for which the demagnetisation is mainly dominated by the nucleation and propagation of ground-state strings (for strong interactions) or random events (for weak interactions), the chiral barrier splitting promotes a richer diversity of switching events. This leads to a variety of behaviours, such as breaking up strings without the generation of charged defect vertices, the formation of coral-like domain walls, and efficient annihilation of domain walls in the later stages of the evolution to the ground state. Our results demonstrate that the rich demagnetisation dynamics of artificial square ice, as is also observed experimentally, can be partially explained even in the absence of additional disorder.

[1] S. Koraltan, M. Pancaldi, N. Leo *et al.*, Physical Review B 102, 064410 (2020). [2] N. Leo, M. Pancaldi, S. Koraltan *et al.*, New Journal of Physics 23, 033024 (2021).

EOF-06. Computational Study of Artificial Spin Systems Emulating the Random Bond Ising Model. *J. Latessa*[1], Z. Huang[2], L. Schwiebert[1] and J. Sklenar[2] *1. Computer Science, Wayne State University, Detroit, MI, United States; 2. Physics, Wayne State University, Detroit, MI, United States*

Artificial spin ice (ASI) systems are traditionally used to emulate artificial materials such as spin ice [1]. In general, ASI are structurally ordered magnetic nanostructures that have magnetically disordered ground states caused by frustration in the geometry of the system. Artificial spin systems deliberately engineered to have structural disorder effects are less frequently studied, but some examples exist [2,3]. In this work we have implemented a Monte Carlo simulation to study a specific type of ASI, the quadrupolar lattice, which has been structurally disordered to emulate a Random Bond Ising Model. The quadrupolar lattice has been observed to have both ferroquadrupolar and antiferroquadrupolar ordered phases [4], and in our work structural disorder is used to create competition between these two ordered states. The application we have developed can create square quadrupolar lattice systems of any size in which structural disorder is achieved by randomly removing a percentage of individual spins in the lattice. The remaining spins can be initialized in a random, magnetized, ferroquadrupolar, or antiferroquadrupolar configuration in either the presence or absence of an external field. We are able to show how the ferro quadrupolar ordering of the lattice vanishes as the percentage of removed islands increases due to competing antiferro interactions. At each time step, the energy of noninteracting spins can be calculated in parallel, and a parameter can be preset to specify the range of interacting islands. Several copies of a given lattice are generated and executed in parallel to derive a correlation value among the several lattices which will be used to help us investigate disorder-driven phase transitions within the quadrupolar lattice.

[1] Wang et al. Nature 439, 303-306 (2006). [2] Drisko et al. Nature Comm. 8, 14009 (2017). [3] Frotanpour et al. Phys. Rev. B 102, 224435 (2020). [4] Sklenar et al. Nature Physics 15, 191-195 (2019).

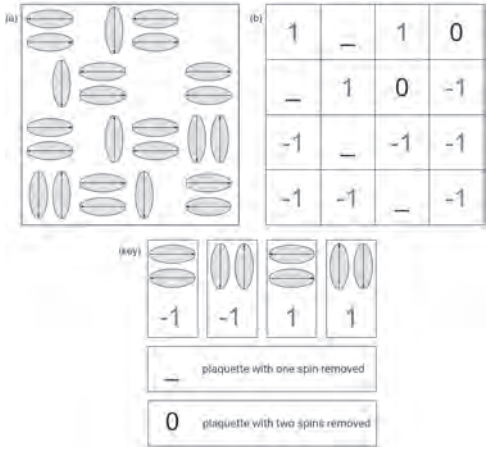

Panel (a) shows the final state of a qualitative 4x4 region of a 12x12 Potts representation [4] of a lattice with 30% disorder. Panel (b) shows how the qualitative 4x4 region is displayed as generated output. The ferroquadrupolar ordered phase, which would be indicated by all 1's or all -1's, is disrupted by the disorder. When only a small percentage of spins are removed (not shown), the ferroquadrupolar order of the system is maintained.

EOF-07. Static Magnetic Properties of Bi-component Nanotriangles in Hexagonal Arrangement Fabricated by Stepwise Nanosphere Lithography. *H. Su*[1] and V. Ng[1] *1. Department of Electrical and Computer Engineering, National University of Singapore, Singapore*

Bi-component magnonic crystals have shown promising applications in magnonics and spintronics [1,2]. Arrays of two-dimensional exchange and magnetostatically coupled bi-component nanotriangles (BNTs) comprising

of alternating permalloy (Py) and cobalt (Co) in hexagonal arrangement were fabricated by self-aligned stepwise nanosphere lithography [3]. The separation (S) between constituent NTs was varied to investigate the effects of exchange and magnetostatic interaction. Static magnetic properties of BNTs were investigated by OOMMF simulations and compared to homogeneous Py NTs [4]. Fig 1(a) shows simulated M-H loops for BNTs during hard axis magnetization with different S values. The loops exhibit distinct two-step switching corresponding to magnetization reversal of Py and Co NTs at different fields. Py NTs are observed to switch at a lower field shown in Fig 1(d) for S=0 nm. For homogeneous Py NTs in Fig 1(b), multiple kinks were also observed for S=0 & -60 nm (overlapping NTs) but these represent the domain changes in individual NTs. For S= -60nm, antiparallel alignment was displayed in each NT pair during reversal. For S=60nm, the NTs react independently due to the lack of strong exchange coupling. Hence switching is random and independent of location. For S=0, the NTs within the inner ring switched at a lower field, as shown in Fig 1(e). Fig 2 shows MFM images of BNTs with S=0 during hard axis field reversal. The magnetic domains of BNTs at remanence after saturation is in good agreement with simulation in Fig 1(c). In contrast to Fig 1(d), Co NTs were observed to reverse at a lower field. This is attributed to the smaller fabricated Co size compared to Py NTs. We will discuss the effect of material difference and separation between constituent NTs in detail via OOMMF simulation and field reversal study.

[1] M Krawczyk and D Grundler, Journal of Physics: Condensed Matter, vol. 26, No. 12 (2014) [2] A. O. Adeyeye, S. Jain, and Y. Ren, IEEE TRANSACTIONS ON MAGNETICS, VOL. 47, NO. 6, P. 1639 - 1643 (2011) [3] B. Myint, D. S. F. Yap and V. Ng, Nano Express, 1, No. 2 (2020) [4] M. J. Donahue and D. G. Porter, OOMMF User's Guide, Version 1.0 Interagency Report NISTIR 6376 (1999)

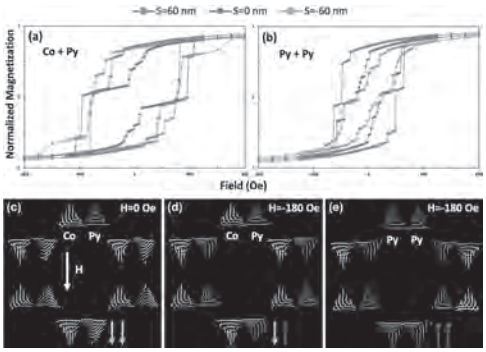

Fig. 1 Simulated M-H loops for S= -60, 0, +60 nm for (a) Co/Py NTs; (b) Py/Py NTs. Simulated spin states for (c-d) BNTs; (e) Py/Py NTs at different fields. Colored arrows indicate spin orientations.

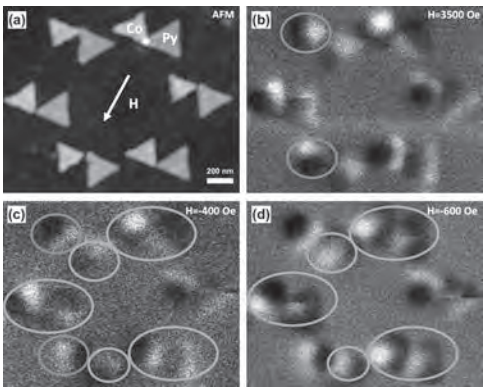

Fig. 2 (a) AFM; (b-d) MFM of BNTs with S=0 nm at remanence after applying field of 3500, -400 and -600 Oe. White arrow indicates the applied field direction. Colored circles indicate a change in magnetic domain.

EOF-08. FORC Analysis of Nanopatterned vs. Unpatterned Films: Coercivity and Switching Mechanisms. *A.D. Mshar*[1], D.D. Arnold[1], P.B. Visscher[2], R.K. Dumas[3] and S. Gupta[1] *1. Metallurgy and Materials Engineering, University of Alabama, Tuscaloosa, AL, United States; 2. Physics and Astronomy, University of Alabama, Tuscaloosa, AL, United States; 3. Quantum Design, San Diego, CA, United States*

We have studied the use of self-assembled block copolymers to pattern multilayers of Co and Pd on silicon wafers. Stacks ranging from 4 to 12 bilayers of Co(0.3 nm)/Pd(0.8 nm) were sputtered onto Ta/Pd seed layers and capped with 3 nm of Ta, and were found to have perpendicular magnetic anisotropy as-deposited. The block copolymer, PS-PFS, was dissolved in toluene and spun onto the wafers. After heat treatment to phase-separate the polymers, the PS was removed by oxygen plasma ashing. The remaining polymer, PFS, formed self-assembled spheres that were used as masks to ion-mill the Co/Pd multilayers into nanopillars [1]. To study the effect of etch time and etch angle on the coercivity distribution, we synthesized samples in a "design of experiments" grid in these two variables. Scanning electron micrographs showed nanopillars ranging from 10 to 30 nm in diameter, depending primarily on etch time (Fig. 1). M-H loops measured on both patterned and unpatterned wafers showed an increase of up to 113% in coercivity upon patterning. First Order Reversal Curves (FORC) were measured, and the resulting FORC distributions showed different features for the nanopatterned vs. unpatterned films. Fig. 2 shows the FORC curves and the resulting FORC distribution for an unpatterned multilayer [Co/Pd] plotted by (1) FORC+ (MagVis.org), which shows the exact measured FORC density without averaging and (2) the more often used averaged color map, in which information is lost. Both displays show a large positive peak with coercivity (H_c) about 500 Oe, with a "dipole tail" characteristic of switching by domain nucleation and wall motion [2]. In the FORC+ plot, the tail consists of a string of negative (blue, on the left) and positive (orange, on the right) pixels – the variation of density along the tail is smaller in the averaged curve, but this comes at the expense of greatly overestimating the separation between the positive and negative tails.

[1] A. G. Owen, Hao Su, A. Montgomery and S. Gupta, J. Vac. Sci. Technol. B 35, 061801(2017). [2] E. Davies, O. Hellwig, E. E. Fullerton, et al, "Magnetization reversal of Co/Pt multilayers: Microscopic origin of high-field magnetic irreversibility," Phys. Rev. B 70(22), 224434 (2004).

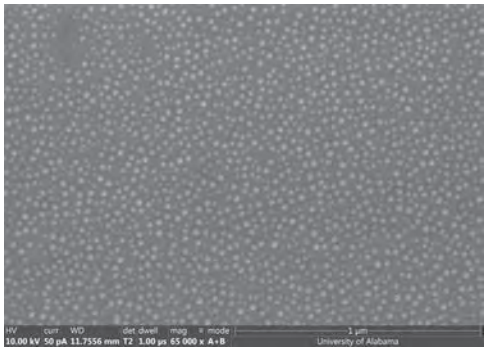

Fig. 1. SEM image of a patterned [Co(0.3 nm)/Pd(0.8 nm)]$_{12}$ film: 20 nm diameter pillars.

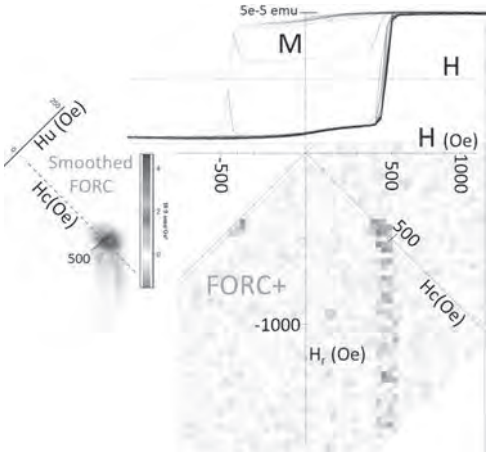

Fig. 2. Top: FORC curves M(H). Bottom right: FORC+ distribution. Orange is positive, blue negative Left: Smoothed FORC distribution, on the same scale but displaced to left, with color legend.

EOF-09. Development of Dy μ-disks for imaging of helimagnetic domains. *I. de Moraes*[1], G. Beutier[2], L. Badie[1], D. Wermeille[3,4] and K. Dumesnil[1] *1. Institut Jean Lamour, Université de Lorraine-CNRS, Nancy, France; 2. SIMaP, CNRS-Grenoble INP-Université Grenoble Alpes, Grenoble, France; 3. XMaS, The UK Materials Science CRG, The ESRF, Grenoble, France; 4. Department of Physics, University of Liverpool, Liverpool, United Kingdom*

Non-collinear antiferromagnetic orders are of strong interest in the fields of spintronics, topological magnetism and multiferroicity [1]. However, the magnetic imaging of these materials is particularly challenging due to their zero net magnetization. Dy epitaxial films exhibit an antiferromagnetic helical phase and strong X-ray magnetic scattering at the Dy L_3 edge [2] These characteristics make it a perfect candidate to fully vectorial reconstruction of a non-collinear magnetic order, enabled by the new combination of Resonant X-ray Magnetic Scattering (RXMS) [3] and Coherent Diffraction Imaging (CDI) [4]. In order to implement this technique, micro-objects are required as model samples. The micropatterning of Dy nanofilms (top-down approach) is however particularly challenging due to the high reactiveness of Dy. In this work, we present the results of this microfabrication process, from the growth of Dy epitaxial nanofilms to the patterning and full characterization of the μ-disks. The high crystalline quality of the Dy(0001) films, grown on A-plane sapphire/(110) Nb templates, is kept after the optical lithography followed by Ion Beam Etching. X-ray diffraction (Fig.1) indicates a moderate decrease in coherence length (10%) and an increase in mosaicity (17%) in 2 mm disks compared with continuous films. However, an FCC phase is formed, likely due to hydrogenation during the patterning process [5] SQUID measurements and RXMS (BM28-ESRF) confirm the occurrence of the helical phase in the Dy μ-disks, with similar Néel and Curie temperatures as in continuous films, but with a slight increase in critical fields. The temperature dependence of (002-t) magnetic satellites reveals that helical turn angles in the patterned samples do not differ significantly from those observed in epitaxial films [6](Fig. 2). The effect of the buffer layer (Nb or Nb/Y) is also studied and correlated to the role of epitaxial strains.

[1] S.-W. Cheong, M. Fiebig, W. Wu, L. Chapon, V. Kiryukhin, Npj Quantum Mater. 5 (2020) 3. [2] K. Dumesnil, C. Dufour, Ph. Mangin, G. Marchal, Phys Rev B. 53 (1996) 11218–11221. [3] L. Paolasini, F. de Bergevin, Cr Phys. 9 (2008) 550–569. [4] J. Miao, T. Ishikawa, I.K. Robinson, M.M. Murnane, Science. 348 (2015) 530–535. [5] E.J. Grier et al., J Phys D Appl Phys. 33 (2000) 894. [6] K. Dumesnil et al.l, Phys Rev B. 58 (1998) 3172–3179.

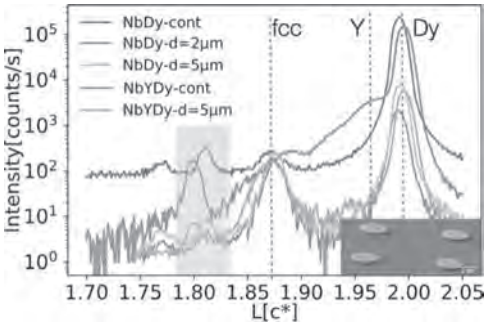

Fig. 1 *(0 0 L)* scans at the Dy L_3 edge at 130 K measured for Nb/Dy (green), Nb/Y/Dy (orange) and their respective μ-disks. Grey region indicates the magnetic satellites. Insert: SEM tilted view of Dy μ-disks.

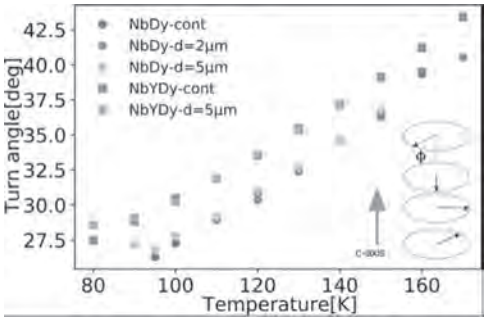

Fig. 2 Turn angle of the Dy helical phase as a function of temperature (same samples as in Fig.1).

EOF-10. Direct observation of a Dynamical Glass Transition in a Nanomagnetic Artificial Hopfield Network. *M.D. Saccone*[1,2], F. Caravelli[1], K. Hofhuis[4,3], S. Parchenko[4,3], S. Dhuey[5], A. Kleibert[6], C. Nisoli[1] and A. Farhan[3] *1. T4, Los Alamos National Lab, Los Alamos, NM, United States; 2. CNLS, Los Alamos National Lab, Los Alamos, NM, United States; 3. Laboratory for Multiscale Materials Experiments (LMX), Paul Scherrer Institute, Villigen PSI, Switzerland; 4. Laboratory for Mesoscopic Systems, Department of Materials, ETH Zurich, Zurich, Switzerland; 5. Molecular Foundry, Lawrence Berkeley National Laboratory, Berkeley, CA, United States; 6. Swiss Light Source, Paul Scherrer Institute, Villigen PSI, Switzerland*

Spin glasses, generally defined as disordered systems with randomized competing interactions that result in an extensively degenerate ground state[1, 2], are a widely investigated complex system. Theoretical models describing spin glasses are broadly used in other complex systems, such as those describing brain function[3], error-correcting codes[4], or stock-market dynamics[5]. This wide interest in spin glasses provides strong motivation to generate an artificial spin glass within the framework of artificial spin ice systems[6]. Here, we present the first experimental realization of an artificial spin glass, consisting of dipolar coupled single-domain Ising-type nanomagnets arranged onto an interaction network that replicates the aspects of a Hopfield neural network[7]. Using cryogenic x-ray photoemission electron microscopy (XPEEM), we performed temperature dependent imaging of thermally driven moment fluctuations within these networks and observed characteristic features of a two-dimensional Ising spin glass. Specifically, the temperature dependence of the spin glass correlation function follows a power law trend predicted from theoretical models on two-dimensional spin glasses. Furthermore, we observe clear signatures of the hard to observe rugged spin glass free energy[1] in the form of sub-aging, out of equilibrium autocorrelations[1] and a transition from convergent to divergent dynamics[1, 8].

1. J. Mydosh, Reports on Progress in Physics., Vol. 78, p.052501 (2015) 2. K. Binder and A. P. Young, Reviews of Modern physics., Vol. 58, p.801-976 (1986) 3. A. G. Hudetz, C. J. Humphries and J. R. Binder, Frontiers

in Systems Neuroscience., Vol. 8, p.234 (2014) 4. N. Sourlas, Nature., Vol. 339, p.693-695 (1989) 5. J. Maskawa, Empirical Science of Financial Fluctuations., pp.153-158 (2002) 6. S. H. Skjærvø, C. H. Marrows, R. L. Stamps and L. J. Heyderman, Nature Reviews Physics., Vol. 2, pp.13-28 (2020) 7. J. J. Hopfield, Proceedings of the national academy of sciences., Vol. 79, pp.2554 (1982) 8. A. J. Bray and M. A. Moore, Physical Review Letters., Vol. 58, pp.57-60 (1987)

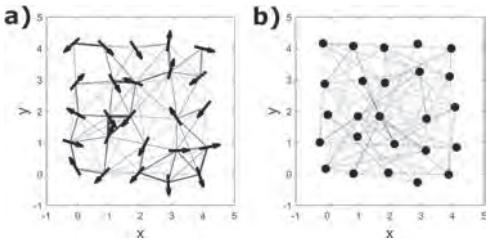

EOF-11. Control of Macroscopic Properties by Tuning Microscopic Interactions in Artificial Ferroic Crystals. *J. Lehmann*[1], A. Bortis[1], P.M. Derlet[2], C. Donnelly[3,2], N. Leo[4,2], L. Heyderman[2,1] and M. Fiebig[1] *1. Department of Materials, ETH Zurich, Zurich, Switzerland; 2. Paul Scherrer Institute, Villigen, Switzerland; 3. Cavendish Laboratory, University of Cambridge, Cambridge, United Kingdom; 4. CIC nanoGUNE BRTA, Donostia-San Sebastián, Spain*

Ferroic materials, i.e., materials with a spontaneous spin, charge or structural order are invaluable for solid-state research and industrial applications. The technologically most relevant feature of ferroics is the formation of domains. The size and switchability of these determine the applicability of a ferroic material for data storage, energy conversion, its use as a sensor, and much more. Unfortunately, the macroscopic properties of ferroics, such as the size and morphology of the domains or the mobility of the domain walls, are in a largely unknown relationship with the interplay of the underlying microscopic interactions. In order to identify the influence of such intrinsic interactions and separate these from extrinsic factors like impurities, grains or mechanical strain, we transfer magnetically-ordered ferroic systems to mesoscopic length scales. Accordingly, the quantum-mechanical spins are substituted by sub-micrometer-sized bar magnets as their classical analogon, which provides an unparalleled experimental accessibility of our systems. We use periodic arrays of planar nanomagnets as artificial ferroic model systems to enable the implementation and tuning of a well-defined set of microscopic interactions, while avoiding any type of extrinsic perturbation. Moreover, our design is based on uniformly ordered magnetic whirls with zero net magnetization, which excludes any influence from the otherwise all-determining demagnetization field. We study domain- and domain-wall configurations in our model systems by magnetic force microscopy and Monte Carlo simulations and show how the domain size, morphology and stability are controlled across orders of magnitude by changing the ratio of just two geometrically tunable intrinsic coupling parameters. Furthermore, we find that their ratio determines the density of topological magnetic defects that form inside the domain walls. Our results not only deepen the knowledge about ferroics as such, but they show the capabilities of magnetic metamaterials for modelling and accessing further complex ordered phases of matter.

J. Lehmann, A. Bortis, P. M. Derlet, C. Donnelly, N. Leo, L. J. Heyderman and M. Fiebig, Nature Nanotechnology, Vol. 15, p. 896 (2020).

EOF-12. Local magnetization reversal in FeGa magnetic nanostructures. *G. Pradhan*[1], F. Celegato[1], G. Barrera[1], M. Coisson[1] and P. Tiberto[1] *1. Istituto Nazionale di Ricerca Metrologica, Turin, Italy*

The recent advances in nanofabrication techniques have given a boost to the study of artificially patterned nanostructures for smart multifunctional systems. In case of magnetic nanostructures, the quest of the last two decades was to gain advances in high density magnetic storage, sensor technology and magneto-logic devices [1,2]. Large-area arrays of nanostructures are fabricated by several methods, either top-down or bottom-up techniques. Conventional top-down methods lead to highly ordered, small area patterns together with the high equipment cost, limits widespread applications. Alternative bottom-up techniques generate large-area patterned structures despite being less-ordered [3,4]. Among the important properties that need to be investigated, magnetization processes as a function of the applied magnetic field in patterned magnetic structures are of utmost importance. In this work, patterned FeGa nanodots have been produced exploiting either Laser writing lithography (top-down) [5] or self-assembling nanospheres (bottom-up) [6]. Nanodots fabricated using laser writing have a diameter between 1 μm to 2 μm (Fig 1(b)) as observed by scanning electron microscopy (SEM). With nanosphere lithography, we obtained lower dimensions of dots (d ~350-400 nm) shown in (e). The magnetic hysteresis behaviour changes significantly with the dot dimensions ((c) and (f)). The magnetic states of $Fe_{80}Ga_{20}$ and $Fe_{70}Ga_{30}$ nanodots (for different dimensions) are studied by magnetic force microscopy (MFM) as a function of magnetic field along the film plane (Fig 2). Vortex-type domain structure was obtained for $Fe_{80}Ga_{20}$ nanodots at demagnetized states. Single domain states are recorded at saturated states with opposite contrast. Further, compositional change of FeGa reports change in crystal phase and magnetostriction of the nanodots.

[1] S. Tehrani, E. Chen, M. Durlam, et al. Journal of Applied Physics, 85.8, 5822-5827 (1999) [2] S. D. Bader, Reviews of modern physics, 78, 1 (2006) [3] P. Tiberto, G. Barrera, L. Boarino, et al. Journal of Applied Physics, 113.17, 17B516 (2013) [4] P. Tiberto, L. Boarino, F. Celegato, et al. Journal of Nanoparticle Research, 13.9, 4211-4218 (2011) [5] Z. L. Wu, Y. N. Qi, X. J. Yin, et al. Polymers, 11.3, 553 (2019) [6] T. R. Albrecht, D. Bedau, E. Dobisz, et al. IEEE transactions on magnetics, 49.2, 773-778 (2013)

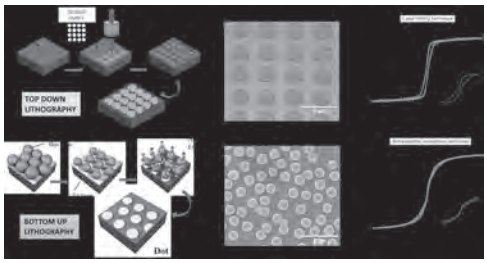

Fig. 1: Schematic, SEM images and magnetic hysteresis of nanodots are represented by (a), (b) and (c) for laser writing and by (d), (e) and (f) for nanosphere lithography, respectively.

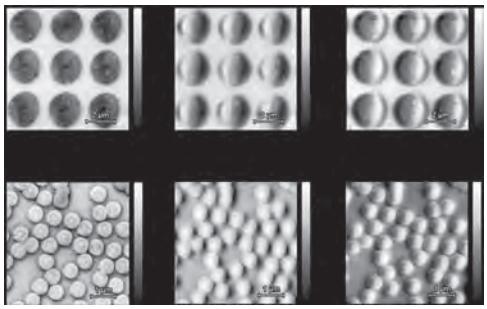

Fig. 2: MFM recordings at demagnetized state, positive and negative saturated state are shown in (a), (b) and (c) for nanodots fabricated by Laser writing, and in (d), (e) and (f) by nanosphere lithography, respectively.

Session EPA
STRUCTURED MATERIALS: NANOPARTICLES AND NANOWIRES
(Poster Session)

Paola Tiberto, Co-Chair
INRIM, Torino, Italy
Claudio Sangregorio, Co-Chair
ICCOM - Institute for OrganoMetallic Chemistry, Sesto Fiorentino, Italy

EPA-01. Motion Synchronicity of a Micro-magnetic-particle Chain in a Rotating Field. J. Cheng[1], C. Li[1] and *C. Chen*[1] *1. Mechanical Engineering Department, National Yang Ming Chiao Tung University, Hsin-Chu City, Taiwan*

Manipulations of micro-sized magnetic particles by an external field have been widely studied for the applications in MEMS and biofluidics. A popular way of manipulation is forming a microchain containing several particles in a liquid environment. The chain can be well controlled by a designated external field to perform rotation [1] or oscillation [2] for desired purposes. Nevertheless, the induced hydrodynamic drag would affect the formation and motion of the chain, such as the well studied chain rupture in a dynamic field. In the present paper, study of motion synchronicity of a micro-magnetic-particle chain in a rotating field is focused. To achieve synchronous rotation with the external field, force balance acting on the chain is required. Experiments are performed firstly to identify actual rotating frequency of an un-ruptured chain, denoted as fc, subjected to various field frequency fH. As the results shown in figure, for a 3-particle chain, motion synchronicity can only preserved up to a critical field frequency. Beyond this critical field frequency, the average rotating frequency of the chain starts to decay. The critical field frequency increases if magnetic field strength H is raised. The mechanism of this asynchronous motion can be understood by the competition of magnetic torque and hydrodynamic torque. The predicted critical frequencies, based on two approximations reported in the literatures [3,4], i.e., fc1 and fc2 shown in the figure, agree well with the experiments. In addition, temporal dynamical motion is also presented to illustrate the asynchronous motion.

[1] J.-H. Cheng, C.-R. Lin, C.-Y. Chen, AIP Advances, 10, 015201 (2020) [2] Y.-H. Li, H.-C. Lin, C.-Y. Chen, IEEE Transactions on Magnetics, 49, 7, 4120-4123 (2013) [3] C. Wilhelm, J. Browaeys, A. Ponton, J.-C. Bacri, PRE 67, 011504 (2003) [4] Y. Gao, M. A. Hulsen, T. G. Kang, J. M. J. den Toonder, PRE 86, 041503 (2012)

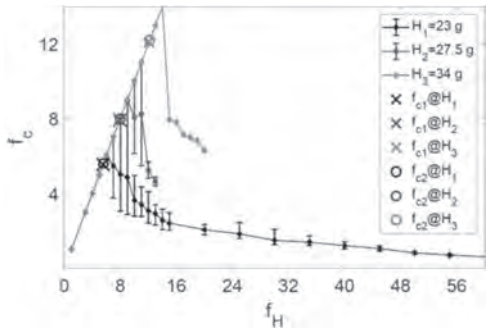

Actual rotating frequency of a 3-particle chains fc subjected to various field frequency fH. Marks of circle (O) and cross (X) are the predicted critical frequency for correspondent field strength H. The linear lines inductae synchronous motion of the chain and external field. Beyond a critical frequency, the actual rotating frqeuency of chain fc starts to drop. The predicted critical frquencies for different field strength H agree well with the experiments.

EPA-02. Magnetite Nanoparticles: A Detailed Analysis of the Low Temperature Magnetic Transitions. P. Ortega[1], E.M. Jefremovas[1], R. Das[3,4], Z. Nemati[5], M. Phan[5], H. Srikanth[5], M. Fdez-Gubieda[7], A. Muela[2], C. Grüttner[6], *L. Fernández Barquín*[1] and J. Alonso[1] *1. CITIMAC, Universidad de Cantabria, Santander, Spain; 2. Inmunología, Microbiología y Parasitolgía, Universidad del País Vasco, Leioa, Spain; 3. Phenikaa University, Hanoi, Vietnam; 4. Phenikaa Research and Technology Institute, Hanoi, Vietnam; 5. Physics, University of South Florida, Tampa, FL, United States; 6. Micromod Partikeltechnologie GmbH, Rostock, Germany; 7. Electricidad y Electrónica, Universidad del País Vasco, Leioa, Spain*

Magnetite is one of the oldest known magnetic materials. At room temperature, magnetite exhibits an inverse spinel structure with Fe^{3+} ions split between tetrahedral and octahedral sites, and Fe^{2+} ions occupying only octahedral sites. As it is well known, with decreasing temperature, magnetite undergoes a first order magnetic transition accompanied by a metal-insulator transition: the so-called Verwey transition (~120 K) [1]. However, there is another magnetic transition taking place at even lower temperatures (< 50 K), whose underlaying nature is still not well understood. In bulk magnetite, a few studies have attributed this transition to different causes, such as the freezing of conduction electrons or rearrangement of electrons within domain walls [2,3]. Of particular interest is the case of magnetite nanoparticles, whose magnetic properties have been extensively studied in the last decades due to their multiple applications, especially in biomedicine [4]. However, a clear understanding on the presence of this transition in these nanoparticles has remained elusive [5]. Therefore, this work has been focused on the study of the low T transition in several types of magnetite nanoparticles, with different sizes, shapes, and purities. These nanoparticles have been structurally and morphologically characterized by using a combination of X-ray Diffraction and Transmission Electron Microscopy. Different oxidation states of the nanoparticles (i.e., into maghemite) have been revealed. Their magnetic response has been analyzed both as a function of the temperature (M vs. T, 5-300 K) and the magnetic field (M vs. H, up to 5 T). Some of these nanoparticles have exhibited a magnetic response close to the bulk, with saturation magnetization ~90 Am^2/kg (300 K) and a clear Verwey transition. The low T transitions have been studied by AC susceptibility. In all cases, we have observed 1 or 2 magnetic transitions below 50 K, even for single domain nanoparticles. The nature of these transitions has been further investigated by using different spin relaxation models. Arrhenius law fittings suggest electron hopping freezing ($\tau_0 = 10^{-8} – 10^{-9}$ s, and E_B/k_B = 200-300 K) for the nanoparticles with magnetic behavior closer to the bulk.

[1] F. Walz*, J. Phys. Condens. Matter* 14, R285 (2002) [2] H. Kronmüller, *J. Magn. Magn. Mater.* 4, 280-286 (1977) [3] V. Skumryev, H. J. Blythe, J. Cullen, and J. M. D. Coey, *J. Magn. Magn. Mater.* 196–197, 515–517 (1999) [4] D. González-Alonso, J. I. Espeso, H. Gavilán, et al., *Nanoscale Adv.* 3, 3491 (2021) [5] R. Das, V. Kalappattil, M. H. Phan, and H. Srikanth *J. Magn. Magn. Mater.* 522, 167564 (2021)

EPA-03. Coexistence of Verwey and Morin transitions and emerging magnetic phenomena in iron oxide core/shell nanorods. *S.B. Attanayake*[1], A. Chanda[1], R. Das[2], M. Phan[1] and H. Srikanth[1] *1. Physics, University of South Florida, Tampa, FL, United States; 2. Phenikaa Research and Technology Institute, Phenikaa University, Hanoi, Vietnam*

Over the past few years, the outstanding magnetic properties of highly crystalline iron oxide (Fe_3O_4) nanorods (NRs) have been extensively investigated by us for advanced magnetic hyperthermia [1], as well as spintronics applications [2]. Building upon this success, we propose an effective thermal treatment approach to creating a novel class of iron oxide core/shell structured nanorods. In this study, we demonstrate how Fe_3O_4/α-Fe_2O_3 core/shell structures can be formed in these nanorods through a controlled annealing process. The highly crystalline Fe_3O_4 nanorods were hydrothermally grown first and then annealed at 250° C for different periods of time (1, 3, 5, 7, and 9 h) to form Fe_3O_4/α-Fe_2O_3 core/shell structures, which are characterized by XRD and TEM. Magnetometry measurements indicate that the Verwey transition becomes sharper with increasing the annealing duration, which is attributed to the improved crystallinity of the Fe_3O_4 phase. Relative to the as-synthesized NRs, the saturation magnetization of the annealed NRs is reduced considerably, which is resulted from the reduced volume fraction of the Fe_3O_4 core and the formation of the antiferromagnetic α-Fe_2O_3 shell. When the annealing duration is extended to 5 h, a sharp drop in magnetization is observed in the temperature-dependent magnetization around 260 K which is associated with the Morin transition of the α-Fe_2O_3 layer. Interestingly, zero-field-cooled and field-cooled magnetic hysteresis loops show a negligible horizontal shift but a significantly large enhancement in magnetization was observed when the core/shell NRs are cooled down in a magnetic field of 1T from the room temperature, suggesting the presence of an intermediate layer composed of canted/disordered spins in between the core and shell. These findings indicate that the Fe_3O_4/α-Fe_2O_3 core/shell nanorods would be an excellent model system for probing interfacial magnetism at the nanoscale [3].

[1] R. Das, J. Alonso, Z. Nemati Porshokouh, V. Kalappattil, D. Torres, M. Phan, E. Garaio, J. García, J. Sanchez Llamazares, and H. Srikanth, Tunable High Aspect Ratio Iron Oxide Nanorods for Enhanced Hyperthermia. *The Journal of Physical Chemistry C* 120, 10086 (2016) [2] S. Chandra, R. Das, V. Kalappattil, C. Harnegea, R. Nechache, M.H. Phan, F. Rosei, and H. Srikanth, Epitaxial Magnetite Nanorods with Enhanced Room Temperature Magnetic Anisotropy, Nanoscale 9, 7858 (2017) [3] C. Kons, M.H. Phan, H. Srikanth, and D.A. Arena, Z.N. Porshokouh, J.A. Borchers, and K. L. Krycka, Investigating spin coupling across a three-dimensional interface in core/shell magnetic nanoparticles, *Physical Review Materials* 4, 034408 (2020)

EPA-04. Magnetocaloric Effect and Ferromagnetic Shape Memory Behavior of Electrodeposited Nanowires Array. *M. Varga*[1,2], L. Galdun[1], K. Saksl[3] and R. Varga[1] *1. Center for Progressive Materials, Technology and Innovation Park, P.J. Safarik University in Kosice, Košice, Slovakia; 2. Department of Condensed Matter Physics, Institute of Physics, Faculty of Sciences, UPJS, Kosice, Košice, Slovakia; 3. Institute of Materials Research, Slovak Academy of Sciences, Košice, Slovakia*

Multifunctional nanomaterials are an essential requirement to prepare smart sensor- or actuator-based devices [1]. Some of multifunctional materials can be found in the large group of Heusler alloys. Ni_2FeGa and Ni_2MnGa-based Heusler alloys are well known for their magnetocaloric and shape memory behavior [2], [3]. Moreover, their properties depend on the overall chemical composition, which makes them tunable [4]. Fabrication of magnetocaloric and shape memory Heusler alloys-based nanowires might be the next step to prepare a nanodimensional sensing and actuation device. Furthermore, these materials show a multifunctional behavior. It makes them suitable for preparation of a simultaneous sensing and actuation device. This research aims to describe the magnetocaloric and ferromagnetic shape memory behavior of electrochemically fabricated Heusler alloy-based nanowires with the chemical composition of Ni-Fe-Ga and Ni-Mn-Ga (Figure 1). Preparation of the Ni-Fe-Ga and Ni-Mn-Ga nanowires in an array introduces a magnetostatic interaction between the adjacent nanowires into the system. Combined with their shape anisotropy, it is possible to prepare nanowires with a highly efficient magnetocaloric behavior. The magnetic entropy change of >0.2 J/kg.K was observed for the Ni-Fe-Ga nanowires (Figure 2). The Ni-Mn-Ga nanowires show an inverse magnetocaloric effect with the magnetic entropy change of even higher values. The magnetic field with the strength of up to 2 T was applied in the parallel direction with respect to the individual nanowires' longitudinal axes for both the Ni-Fe-Ga and Ni-Mn-Ga nanowires. Moreover, the structural transformation region associated with the magnetocaloric and shape memory processes of the Ni-Fe-Ga and Ni-Mn-Ga nanowires was observed above room temperature. Therefore, application of the prepared nanowires can be found in the temperature region of the human body or at the working temperatures of the majority of electrotechnical devices.

[1] C. Gonçalves, A. F. da Silva, J. Gomes, et. al., Inventions, vol. 3, pp. 1–13 (2018) [2] L. Frolova, J. Mino, T. Ryba et al., J. Alloys Compd., vol. 747, pp. 21–25 (2018) [3] Y. C. Zhang, F. X. Qin, et. Al. J. Magn. Magn. Mater., vol. 513, p. 167100 (2020) [4] M. Hennel, L. Galdun, T. Ryba, et. al., J. Magn. Magn. Mater., vol. 511, p. 166973 (2020)

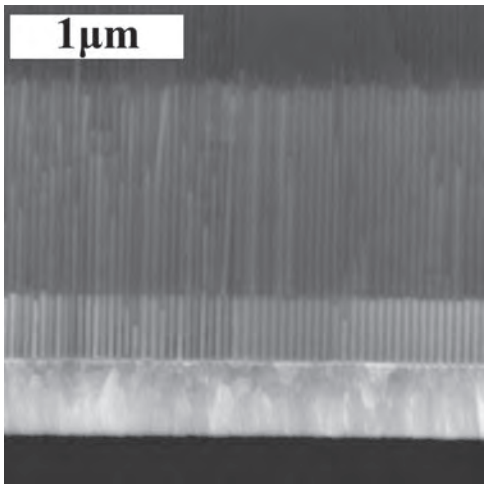

Fig.1: SEM micrograph of the electrochemically prepared Ni-Mn-Ga nanowires

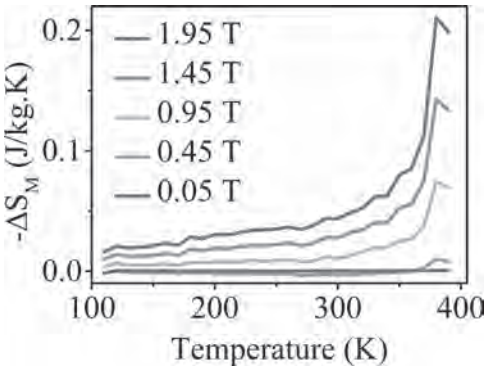

Fig.2: Magnetic entropy change of the magnetocaloric Ni-Fe-Ga nanowires at different applied magnetic fields

EPA-05. Analysis of Exchange Bias training effect in Exchange coupled $LaFeO_3$/NiO nanocomposites. *P. Sharma*[1] and R. Chatterjee[1] *1. Physics, Indian Institute of Technology Delhi, Hauz Khas, India*

Interaction between an antiferromagnetic (AFM) material with a ferromagnetic (FM) material can establish a directional coupling at the interface, referred as an exchange bias (EB) phenomenon [1]. This phenomenon is characterized by the horizontal shift of the magnetic hysteresis loop when the system is cooled through Neel's temperature in the presence of the

external magnetic field. In addition, a simultaneous hysteresis loop shift along the magnetization axis has also been observed frequently in the literature and is termed as "vertical magnetization shift" (VMS) [2]. EB is the backbone of designing magnetic storage devices and is among the modern approaches to spintronics. One of the interesting characteristics of EB is the training effect. A reduction of EB field and the coercivity upon consecutive measurement of magnetic hysteresis loop is defined as training effect [3]. In this work, we report the study of EB training effect in nanocomposites of antiferromagnetic/antiferromagnetic $LaFeO_3$-NiO oxides, synthesized through complex propylene glycol gel chemical technique. The value of the exchange field decreases significantly between the first and second cycles and after the second loop, a monotonous decrease is observed (Fig. 2). The typical experimentally observed trend between EB field and n (number of cycles) is explained by power law and the experimental data points fits well for loop index and the fitting parameter obtained is 1253 Oe. Furthermore, we have interpreted the observed training effect in $LaFeO_3$/NiO nanocomposite using Benik's recursive relation and the obtained parameters are Oe & $(Oe)^{-2}$. Both, the power law and recursive relation points accord well with experimental data points (Fig. 2). These elaborated analytic approaches have definitely helped us to understand origin of EB training effect in composites of AFM nanoparticles.

[1] M. Kiwi, Exchange bias theory, Journal of Magnetism and Magnetic Materials, 234 (2001) 584-595. [2] H. Ohldag, H. Shi, E. Arenholz, J. Stohr, D. Lederman, Parallel versus antiparallel interfacial coupling in exchange biased Co/FeF_2, Phys Rev Lett, 96 (2006) 027203. [3] C. Binek, Physical Review B 70 (1), 014421 (2004).

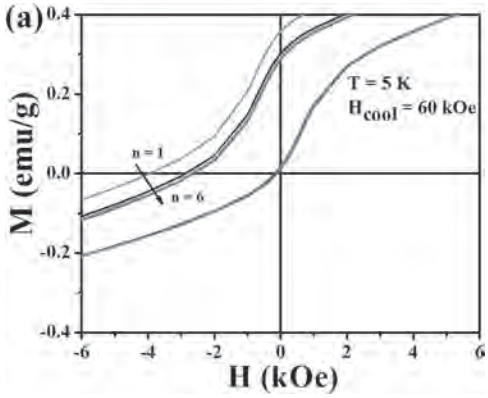

Fig. 1 Enlarged view of six consecutive M-H loop cycles in cooling field of 60 kOe measured at 5 K for $LaFeO_3$/NiO nanocomposite.

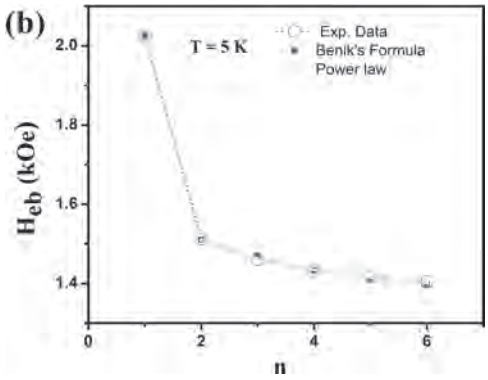

Fig. 2 Solid squares represent the data points calculated by using Benik's recursive relation, solid line corresponds to Power law fitted data and experimental data is represented by using the circular symbol.

EPA-06. Bias field mediated tunable vertical hysteresis loop shift in $Ni_{80}Fe_{20}$/$SrRuO_3$ heterostructure. *M. Bansal*[1], S. Giri[2], W. Li[2], J. L. Macmanus-Driscoll[2] and T.S. Maity[1,2] *1. Indian Institute of Science Education and Research Thiruvananthapuram (IISER TVM), Trivandrum, India; 2. University of Cambridge, Cambridge, United Kingdom*

Conventional horizontal exchange bias (EB) has earned huge popularity since 70 years of its discovery due to its numerous applications in various material systems[1]. Researchers have been curious to find a shift along the vertical axis of the magnetic hysteresis (*MH*) loop, i.e., magnetization axis but are unable to provide any significant result yet[2,3]. In this work, we show a novel vertical *MH* shift or vertical bias (VB) in $Ni_{80}Fe_{20}$/SrRuO3 heterostructure of thin film with 1:2 thickness ratio. Thin film of 13 unit cells (t = 5nm) of SrRuO3 (SRO) was grown epitaxially on $SrTiO_3$ (100) substrate by pulsed laser deposition. A polycrystalline $Ni_{80}Fe_{20}$ thin film (t = 2 nm) was deposited on it by DC/RF sputtering. We observe a significant VB (~33%) at 2 K after field cooled measurement similar to conventional EB measurement done (Fig.1). There is no VB observed for zero field cooling. Applying a bias field of 1 T (-1 T) shifts the loop in positive (negative) moment direction. Importantly, the shift is only observed for low loop tracing field range, i.e., ±0.5 T (< SRO's saturation field). Temperature dependent *MH* measurements depict that the vertical shifts are only observed below Curie temperature (T_C) of SRO (~125 K) and further increases on decreasing the temperature. Moreover, OOMMF micromagnetic simulations results agree with the experimental findings(Fig.2)[4]. With assistance of simulations and theoretical data analysis, a trend for change of VB with thickness ratio and anisotropy of the two films is found to be governed by Spring thickness law and Imperial law, respectively. A generalised model is proposed to incorporate experimentally extracted temperature data with computationally realized laws of thickness and anisotropy. The model is tuneable, controllable and reproducible to other material combinations and hence opens up new pathway to extraordinary spintronic applications in future[5-7].

[1] Maniv, Eran, et al. *Nature Physics* 17.4 (2021): 525-530. [2] Buchner, Martin, et al. *Physical Review B* 99.6 (2019): 064409. [3] R. Rana et al., Scientific reports, vol. 4, no. 1, pp. 1–8, 2014. [4] M. J. Donahue and M. Donahue. US Department of Commerce, National Institute of Standards and Technology, 1999. [5] Ming Zheng and Wei Wang., ACS Applied Materials Interfaces, 8(22):14012{14018, 2016. [6] F Tian et al., Materials, 13(21):4701, 2020. [7] Can Onur Avci et al., Applied Physics Letters, 110(20):203506, 2017.

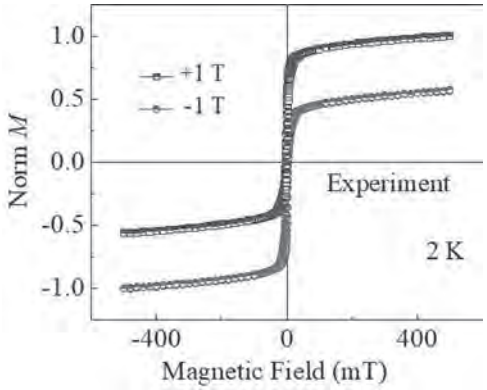

Fig. 1 VB for $Ni_{80}Fe_{20}$/SRO (at 2 K) with 7 T bias field/±7 T field range and ±1 T bias field/±0.5 T field range of *MH* loop (experimental)

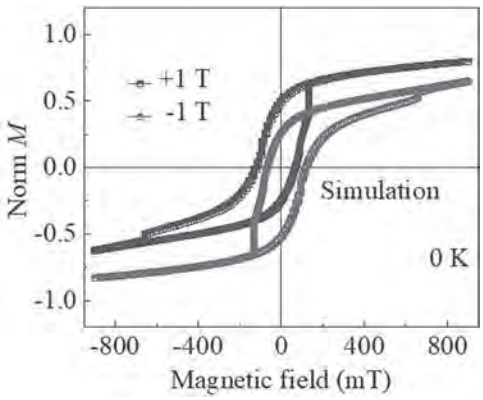

Fig. 2 VB for $Ni_{80}Fe_{20}$/SRO with ±7 T loop tracing field range and high pulse with ±1 T field range (simulation)

EPA-07. Withdrawn

EPA-08. Withdrawn

EPA-09. Topological effect of interface texture on the exchange bias in ferro-antiferromagnetic thin films grown on hybrid seed layers. *A.D. Talantsev*[1,2], A. Elzwawy[3], M. Bakhmetiev[1] and C. Kim[4] *1. Group of Magnetic and Spin Logical Processes and Devices, Institute of Problems of Chemical Physics, Moscow, Russian Federation; 2. Laboratory of Robotized Sensor Systems, Tyumen State University, Tyumen, Russian Federation; 3. Ceramics Department, Inorganic Chemistry Industries and Mineral Resources Division, National Research Centre, Cairo, Egypt; 4. Department of Emerging Materials Science, Daegu Gyeongbuk Institute of Science and Technology, Daegu, The Republic of Korea*

An exchange bias in NiFe/IrMn bilayer has been tailored by modification of the ferromagnetic/antiferromagnetic (F/AF) interface texture through the thickness variations of Au and Cu layers in Ta/Au and Ta/Cu hybrid seed layer stacks. The revealed variations of exchange bias with Au and Cu seed layer thicknesses t_{Au} and t_{Cu} are gradual, but have opposite signs. For the Ta/Cu seed layer, the increase of t_{Cu} from 1 nm to 5 nm results in enhancement of exchange bias by 10 percent. For the Ta/Au seed layer, the similar variation of t_{Au} reduces the exchange bias by more than 30 percent. The effect correlates with the modifications of interface texture. The selection between Cu and Au in the seed layer stack defines this texture, as well as alignment of NiFe and IrMn crystallographic planes. The NiFe/IrMn films, grown on Ta/Cu seed layers, are of multigrain structure, with the dominance of (001) textured grains, having wide angular distribution for orientations of crystallographic planes in respect to the interface plane. For the NiFe/IrMn thin films, grown on Ta/Au hybrid seed layer stack, both NiFe and IrMn layers have (111) texture with horizontally aligned (111) crystallographic planes. The effects of F/AF interface texture on exchange bias are simulated by a first principle model, considering the exchange bias to be proportional to the amount of F-AF atomic coupled pairs. The simulation reveals topological origin of the observed correlation between the exchange bias and the interface texture. Instead of defining the exchange bias value, the texture defines topological possibility for exchange bias enhancement by roughness, as well as the range, within which the exchange bias can be tailored by substitutional defects. This work was performed in accordance with the program of Institute of Problems of Chemical Physics AAAA-A19-119092390079-8, grant of president of Russian Federation 2644.2020.2, and partly supported by the National Research Foundation of Korea (NRF) grant funded by the Korea government (MSIT) (No. NRF-2018R1A5A1025511).

EPA-10. Ferromagnetic resonance of superparamagnetic iron-oxide nanoparticles: quantification of dipole-dipole interactions. *D.W. Slay*[1] and M. Charilaou[1] *1. Physics, University of Louisiana at Lafayette, Lafayette, LA, United States*

As the number of biomedical applications of superparamagnetic iron-oxide nanoparticles (SPION) grows, having a detailed understanding of their magnetic state is increasingly important. It is commonly assumed that dipole-dipole interactions are not relevant for superparamagnetic nanoparticles because of thermal fluctuations. Here we show evidence that dipole-dipole interactions do indeed affect the collective magnetic state of a SPION sample. Ferromagnetic resonance spectroscopy of iron-oxide nanoparticles with a diameter of 10 nm reveals that the configuration of the particles has a strong effect on their effective magnetic anisotropy on short time scales. Fitting the experimental spectra using a theoretical model [1] enables the quantification of these anisotropy fields. Nanoparticles in suspension with a surfactant exhibit an easy-axis anisotropy due to field-induced alignment, whereas condensed dry nanoparticles (which no longer have the surfactant) exhibit an easy-plane anisotropy due to agglomeration. The difference between the effective uniaxial anisotropies in suspension versus the dry state is on the order of 0.1 T. The effective uniaxial anisotropies exhibited by the nanoparticles in these configurations are an order of magnitude larger than the intrinsic magneto-crystalline anisotropy. This suggests that dipole-dipole interactions can be important to the collective magnetic state of superparamagnetic systems despite thermal fluctuations and should be considered for high-frequency applications.

[1] M. Charilaou, Journal of Applied Physics, Vol. 122, p. 063903 (2017)

EPA-11. Compositional dependence of magnetic properties of multiferroic $Ga_{2-x}Fe_xO_3$ nanoparticles. T. Han[1], P. Tsai[1], *J. Wang*[1], J. Zou[1] and T. Chen[1] *1. Department of Applied Physics, National University of Kaohsiung, Kaohsiung, Taiwan*

The $Ga_{2-x}Fe_xO_3$ (GF_xO) compound, is a quite interesting material due to simultaneous exhibit magnetic and electric orderings [1,2]. However, the physical properties of GF_xO at reduced grain sizes remain underexplored due to the challenges associated with their synthesis with a proper control over the crystalline phase. In addition, the effect of the Fe/Ga ratio on the magnetic properties of the nanosized GF_xO system has not yet been completely established. In this work, therefore, we prepare a series of GF_xO nanoparticles with $0.8 \le x \le 1.2$ using the sol-gel method to systematically study the effect of the Fe/Ga ratio on their structural and magnetic properties. All the samples of GF_xO with $0.8 \le x \le 1.2$ have been characterized by the powder XRD measurements and Rietveld refinements. All the observed peaks can be indexed by reflections of the $Pc2_1n$ orthorhombic structure of GF_xO, and no impurity phase was found. The determined lattice parameters are found to display a monotonic increase with the Fe content x. Composition of the GF_xO nanoparticles was confirmed by energy dispersive X-ray spectra. The evolution of the Néel temperature (T_N) of GF_xO samples versus their Fe-content (x). It is found that with increasing Fe-content, up to 1.2, the T_N increases from 279 to 350 K. Moreover, the magnetic hysteresis curves measured below T_N exhibit two-phase-like magnetic behavior consisting of soft and hard magnetic phases. The results could be explained by the site-disorder of the cations in GF_xO nanoparticles.

[1]. T. Arima, D. Higashiyama, Y. Kaneko, J. P. He, T. Goto, S. Miyasaka, T. Kimura, K. Oikawa, T. Kamiyama, R. Kumai, and Y. Tokura, Phys. Rev. B 70, 064426 (2004). [2]. B. Srimathy, Indranil Bhaumik, S. Ganesamoorthy, R. Bhatt, A. K. Karnal, and J. Kumar, J. Alloys Compd. 590, 459 (2014).

EPA-12. The Magnetic and Exchange Bias Properties of Phase Segregated $Mn_{2-x}Fe_xNi_{1.6}Ga_{0.4}$. *B.L. Reese*[1], X. Liu[1], Y. Zhu[1], A. Pathak[2] and M. Khan[1] *1. Physics, Miami University - Oxford, Oxford, OH, United States; 2. Physics, Buffalo State College, Buffalo, NY, United States*

The exchange bias (EB) phenomenon, generally quantified by the shift of the hysteresis loop along the magnetic field axis, has been observed in several Mn-rich Heusler alloys [1, 2, 3]. The fundamental science that drives EB and its technological impact are both of great interest [4, 5]. The EB effect in Mn-rich Heusler alloys is primarily related to the coexisting ferromagnetic (FM) and antiferromagnetic (AFM) interactions. Interestingly, the Mn atoms are responsible for both the FM and AFM interactions in these materials. In the Heusler alloy Mn(2)NiGa, both FM and AFM interactions are present. However, the material does not exhibit any EB effect. Interestingly, a strong EB was observed in Ga-deficient/Ni-rich Mn(2)Ni(1.4)Ga(0.6), which demonstrated the importance of crystalline site occupancies of the Mn atoms in driving EB [6]. Here, we have performed an experimental study on the effect of Fe doping on the magnetic and EB properties of Mn(2-x) Fe(x)Ni(1.6)Ga(0.4) ($0 \leq x \leq 0.35$). The goal of the study was to explore the effect of Fe doping on the FM and AFM interactions in the system. The samples were fabricated by arc melting, drop-casting, and annealing techniques. X-ray diffraction measurements and the scanning electron microscopy images showed that the alloys were phase segregated with two different lower symmetry structures. For all values of x, EB was observed in the materials. An EB field of as large as ~4000 Oe and a coercive field of ~14 kOe were observed in the materials. The structural, magnetic, and EB properties of all the alloys in the Mn(2.x)Fe(x)Ni(1.6)Ga(0.4) system will be presented.

[1] M. Khan, I. Dubenko, and S. Stadler, and N. Ali, Appl. Phys. Lett., Vol.91, 072510 (2007) [2] B. M. Wang, Y. Liu, and P. Ren, Phys. Rev. Lett., Vol.106, 077203 (2011) [3] Z. D. Han, B. Qian, and D. H. Wang, Appl. Phys. Lett., Vol.103, 172403 (2013) [4] J. Nogués and I. K. Schuller, J. Magn. Magn. Mater., Vol.192, p.203 (1999) [5] Manuel Bibes, Javier E. Villegas, and AgnèsBarthélémy, Adv. Phys., Vol.60, p.5 (2011) [6] M. Khan and A. Albagami, J. Alloy Comp., Vol.727, p.100 (2017)

EPA-13. Withdrawn

EPA-14. Self-Assembled Magnetite Nanoparticles above a hard drive: the effect of the Soft Underlayer and Changing the Separation of Reversed Magnetic Regions. *J. Davidson*[1], A.R. Mohtasebzadeh[2], T. Crawford[2] and K. Livesey[3] *1. Department of Physics, University of Colorado Colorado Springs, Colorado Springs, CO, United States; 2. Smart State Center for Experimental Nanoscale Physics and Department of Physics and Astronomy, University of South Carolina, Columbia, SC, United States; 3. School of Mathematical and Physical Sciences, The University of Newcastle, Callaghan, NSW, Australia*

Self-Assembled Magnetic Nanoparticle (MNP) structures have a wide range of applications in industry, chemistry, and medicine[1]. It has been shown through experiments and computational simulation that various patterns of MNPs can be deposited on a substrate [2,3]. One mechanism for self-assembly is the gradient of an applied field exerting a force on the MNPs. For example, a single perpendicular transition of magnetization (from up alignment to down) in a computer hard drive can produce a gradient sufficient to promote a single line with a width of multiple MNPs assembling on the substrate. Therefore, the chosen magnetic structure of the substrate is a determining factor in creating the desired end structure. While simulations have been performed to understand this assembly, they lack key features found in experimental systems. This work builds upon existing computational models [3] by including small reversed regions in the magnetization, multiple transition regions in the simulated area, and changes to the total magnetic field created by the addition of a soft underlayer found in hard disk drives, as seen in Fig. 1. Along with new geometry, we also investigate the effect of varying the transition separation (distance d in Fig. 1) on the final structure. Our simulations investigate the trajectories of 27 nm diameter magnetite nanoparticles using a model based on Langevin dynamics including translation and rotation. The simulation results match those found experimentally both qualitatively and also in quantitative measures of the hexagonal ordering of assembled MNPs.

[1] M. Grzelczak, J. Vermant, E. M. Furst, et al., *ACS Nano Vol. 4*, p. 3591-3605 (2010) [2] Ye, L., Pearson, T., Cordeau, Y. *et al. Sci Rep* 6, 23145 (2016). [3] Zhao, Zhiyuan, et al. *The Journal of Physical Chemistry C* Vol.121 p. 801-810. (2017) JD and KL acknowledge funding from DMR-1808412. RM and TC acknowledge funding from DMR-1808426 and NSF EPSCoR OIA-1655740 Made in SC.

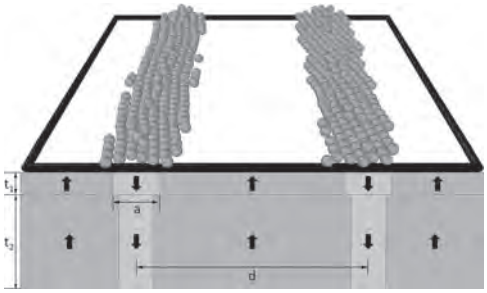

Fig. 1. The magnetic profile of the hard and soft layers of the hard drive. With constants t_1, t_2, a, and d being the hard layer thickness, soft layer thickness, width of reversed magnetization, and separation of regions respectively. Above the substrate is the deposited nanoparticle structure found through simulation results using this geometry.

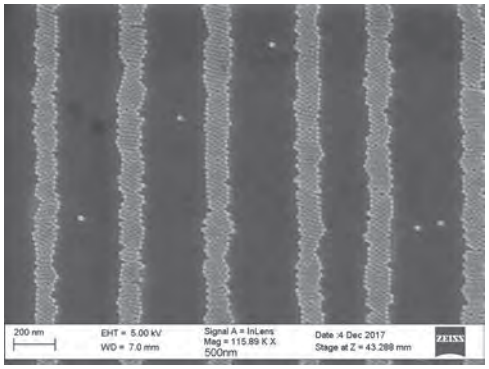

Fig. 2. Scanning Electron Microscope image of magnetic nanoparticles assembled on substrate with spacing of 500 nm between the center of the reversed magnetized regions.

Session EPB
THIN FILMS AND PATTERNED FILMS (Poster Session)

Joao Ventura, Co-Chair
IFIMUP-IN, Universidade do Porto, Porto, Portugal
Tomoyuki Ogawa, Co-Chair
Tohoku University, Sendai, Japan

EPB-01. Investigation of the dynamics of twisted bilayer artificial spin ice structure. *R.B. Popy*[1], J. Frank[1], G. Macauley[2] and R. Stamps[1]
1. Physics and Astronomy, University of Manitoba, Winnipeg, MB, Canada; 2. ETH Zurich-Paul Scherrer Institute, Villigen, Switzerland

Geometrical frustration arises in systems whose structures support multiple degenerate ground states. Artificial spin ice (ASI), have been built in diverse configurations which allow us to control frustration by experimentally tuning suitable parameters[1]. We present computational results on ASI systems consisting of planar arrays of nanosized elongated ferromagnetic islands where geometrical frustration takes place at the vertices due to interactions between elements. To date, most studies have employed two-dimensional geometries in order to study magnetic charge dynamics, phase transitions, vertex-based frustration, and other interesting effects[2]. Recently, there has been a surge of interest in realizing three-dimensional artificial spin ice[3]. The work mentioned here concerns the non-equilibrium dynamics of a bilayer artificial spin ice (BASI) structure consisting of two identical arrays separated by some distance and rotated at an angle between the two array axes. Introducing an angle between the layers enables the observation of novel, emergent phenomena as it changes the nature of the interactions between the spins. We consider both square and pinwheel ice geometry for each array[4]. Using different Monte Carlo techniques, we examine avalanche processes and ground state ordering as a function of the interaction strength between layers for different non-collinear orientations between the arrays.

[1] RF Wang, C Nisoli, RS Freitas, J Li, et al. Nature, 439(7074):303{306, 2006. [2] Cristiano Nisoli, Vassilios Kapaklis, and Peter Schiffer. Nature Physics, 13(3):200{203, 2017. [3] Gia-Wei Chern, Charles Reichhardt, and Cristiano Nisoli. Applied Physics Letters, 104(1):013101, 2014. [4] R. Mac^edo, G. M. Macauley, F. S. Nascimento, and Robert L. Stamps. Physical Review B, 98(1):014437, 2018.

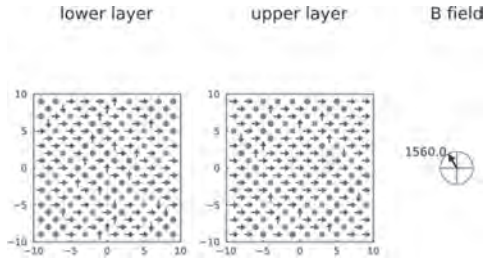

Fig.1: Snapshot of vertex configurations for a square BASI structure consisting of two identical arrays (each with a size of 20x20). The layers are in close proximity with a spacing of 15% of the lattice constant (to make the inter-array coupling the strongest) along with a relative angle of 38 degrees between them. The structure is subjected to a rotating applied field (represented in degrees) of strength B = 10.25 in reduced units. The symbols used are green circles for type 1 vertices, blue arrows indicating the net moment of type 2 vertices, and red crosses for type 3 vertices.

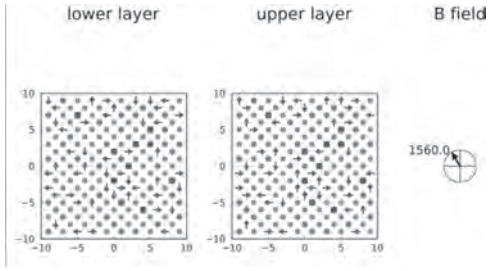

Fig.2: Same as fig.1 but now there is no relative angle between the layers. The additional purple squares represent type 4 vertices.

EPB-02. Magnetic properties of high (110)-oriented Co-Fe-Ga alloy films prepared by chemical co-precipitatiton. *Y. Ohno*[1], K. Yamada[1] and M. Shima[1] *1. Department of Materials Science and Processing, Graduate School of Natural Science and Technology, Gifu University, Gifu, Japan*

Topotactic transformation (TT) is a transition in which the crystal lattice of a newly formed phase has one or more crystallographically equivalent, orientational relationships to that of the original phase [1]. Since thin films with high crystal orientation can be easily fabricated via TT [2], and it is expected to be further developed in the field of functional thin film materials because it is possible to control physical properties such as magnetic anisotropy by crystal orientation [3]. In this study, we have investigated the TT growth and magnetic properties of Co-Fe-Ga (CFG) alloy films via chemical synthesis from the initial precursor and the subsequent oxide. CFG alloy films were made by co-precipitation, spin-coating, and annealing processes. Low-temperature heat treatment (LTHT) was applied to the precipitate at 333 K for 3 days, it was then dissolved in ethanol to prepare a precursor solution. The solution was spin-coated onto a (100) Si substrate and annealed in air at 973 K for 30 minutes to form an oxide film. Finally, the oxide film was annealed at 973 K for 3 hours in a gas mixture of N_2:H_2 = 4:1 to obtain an alloy film. Figure 1 shows X-ray diffraction (XRD) patterns of the CFG alloy films. It made from the precursor with LTHT exhibits 110 and 220 peaks of the bcc proving that it is a highly (110)-oriented alloy. The ionic/atomic arrangement of the (001) plane in the precursor is similar to those of the (111) plane in the spinel oxide and the (110) plane in the alloy, suggesting that a highly (110)-oriented film was grown via TT. Figure 2 shows the magnetic hysteresis loops of the CFG alloy films at 300 K by vibrating sample magnetometry. The squareness R_s for the in-plane direction of the film is 0.59. This value is nearly twice as large as that of the non-oriented film (R_s = 0.30), suggesting that the magnetocrystalline anisotropy helps promote the in-plane anisotropy in the (110)-oriented film because it's likely that the easy magnetization axis of CFG alloy films is the [-110] crystallographic directions as well as that of Co-based Heusler alloys [4-5].

[1] J. B. Clark, J. W. Hastie, L. H. E. Kihlborg, R. Metselaar, M. M. Thackeray, *Pure Appl. Chem.* 66, 577 (1994). [2] T. Mairoser et al. *Nat. Commun.* 6, 7716 (2015). [3] D. H. Kim et al., *Adv. Mater.* 29, 1606831 (2017). [4] S. Trudel, O. Gaier, J. Hamrle, and B. Hillebrands, *J. Phys. D: Appl. Phys.*43, 193001 (2010). [4] M. S. Gabor, T. Petrisor Jr., C. Tiusan, M. Hehn, and T. Petrisor, *Phys.Rev. B* 84, 134413 (2011).

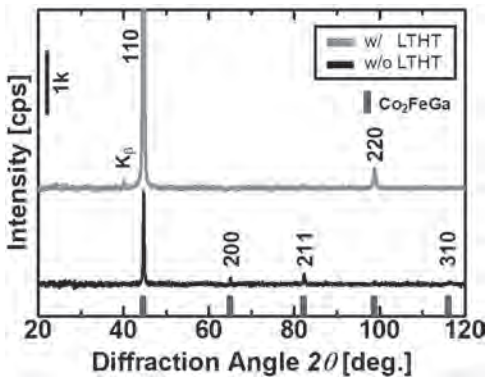

Fig.1 XRD patterns of CFG alloy films.

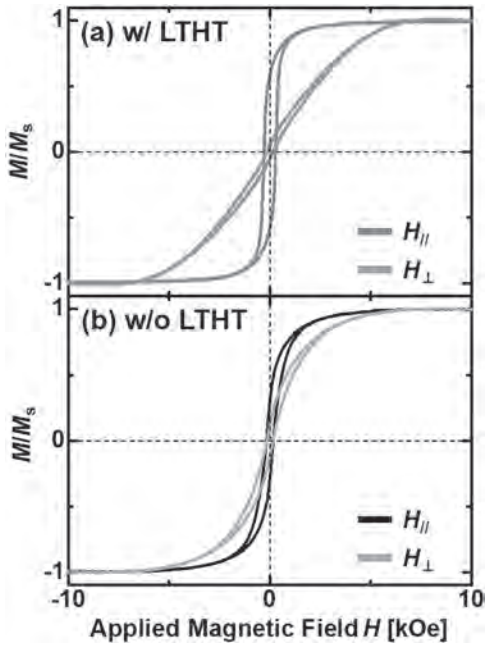

Fig.2 Magnetic hysteresis loops of (a) highly (110)-orientated and (b) non-oriented CFG alloy films.

EPB-03. Withdrawn

EPB-04. Influence of growth conditions and ion bombardment on the perpendicular magnetic anisotropy in Co/Pd multilayered systems.
E. Sebastiani[1], *A. Parente*[1,2], G. Caballero[1], E. González[1,2], O. Rodriguez[1], M. Menghini[2] and A. Muñoz[1,2] *1. Universidad Complutense de Madrid, Madrid, Spain; 2. IMDEA Nanoscience, Madrid, Spain*

Magnetic multilayered systems grown under specific conditions show perpendicular magnetic anisotropy, PMA. The PMA provides several advantages over in-plane magnetization in media storage and spintronic devices[1-2]. Systems with PMA usually have higher thermal stability, smaller domain wall widths, lower threshold current for spin transfer switching[3] and can be used for current induced domain wall motion[4]. The final goal of this work is to tailor magnetic properties of Co/Pd multilayered systems by controling growth conditions (Fig. 1) and modifying the films by ion bombardment (Fig. 2). The PMA of the magnetic multilayers has been studied by combining structural, magnetic, and electrical characterization techniques. The magnetic characterization is complemented with a complete structural and compositional analysis of the multilayers and a characterization of the anomalous Hall effect as a function of temperature for different irradiation doses. This study allows determining the correlation between structural and electrical properties and the PMA. Different samples were grown varying plasma power and Ar partial pressure. We have observed a correlation between interfacial roughness in the heterostructures and the growth conditions. Ion bombardment also affects interfacial roughness, induces intermixing, favors clustering and alloying resulting in a decrease of the PMA as the irradiation dose increases. In conclusion, these two different approaches allow to control PMA of Co/Pd multilayers.

[1] J. E. Davies, Physical Review B. 70 (2004). [2] Hellman, F., Hoffmann, A., Tserkovnyak, Reviews of Modern Physics. 89, 025006 (2017) [3] L. Liu, T. Moriyama, D. C. Ralph, Applied Physics Letters. 94, 122508 (2009). [4] Franken JH, Swagten HJM, Koopmans B, Nat Nanotechnology 7, 499 (2012).

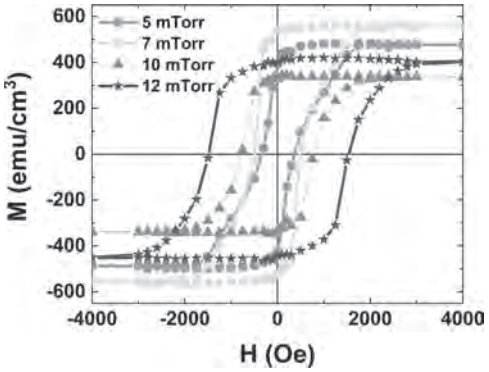

Fig.1 Effect of the growth conditions on the PMA of Co/Pd multilayers. SQUID hysteresis loops meassurements for samples grown by sputtering at different Ar partial pressures.

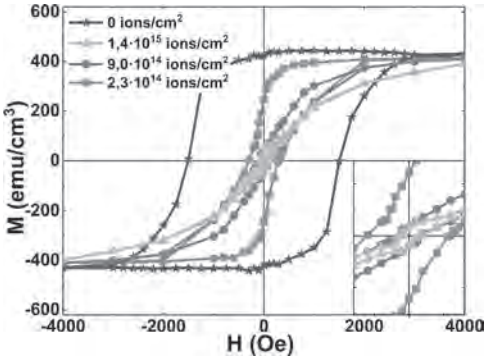

Fig. 2 Effect of the ion bombardment dose on the PMA of Co/Pd multilayers. SQUID hysteresis loops meassurements for samples grown by sputtering at 12 mTorr and irradiated with different ion doses.

EPB-05. Perpendicular Magnetic Anisotropy, Interlayer Exchange Coupling and Annealing Stability in Krypton-sputtered Pt/Co/Ir Synthetic Antiferromagnets.
C. Taylor[1,2], J. Eckert[1], M. Savadkoohi[3,2] and D.B. Gopman[2] *1. Physics, Harvey Mudd College, Claremont, CA, United States; 2. Materials Science and Engineering Division, National Institute of Standards and Technology, Gaithersburg, MD, United States; 3. Mechanical Engineering, University of the District of Columbia, Washington, DC, United States*

Pt/Co/Ir-based synthetic antiferromagnets (SAFs) are key building blocks in high performance magnetic memory devices due to their large perpendicular magnetic anisotropy (PMA) and interlayer exchange coupling (IEC) energies, respectively, and tolerance to thermal processing [1-2]. Fortuitously, the IEC field and PMA field both can be enhanced significantly via judicious tuning of the Ir thickness [3]. Further gains in IEC and PMA may be required in emerging memory devices. And while the materials system may appear to be well optimized, additional refinement could be realized through the exploration of alternative processing approaches. In particular, the replacement of Argon with a heavier gas during sputtering (e.g. Krypton) is known

to enhance the PMA of Co/Pt multilayers due to reduced bombardment of the growing film from gas species during deposition, reduced intermixing of layers and improved columnar film growth, overall enhancing the PMA [4]. To the best of our knowledge, this remains an unexplored approach for SAFs in general, and particularly not for the Pt/Co/Ir system. We investigated the role of sputter gas in the properties of a SAF structure grown by DC magnetron sputtering in an ultrahigh vacuum chamber (base pressure < 10^{-7} Pa) on a thermally oxidized Si wafer with the following film stacking structure (thicknesses in parentheses in nm): Ta(5)/Pt(5)/$[Co(0.4)/Pt(0.6)]_{x5}$ /Co(0.4)/Ir(t Ir)/$[Co(0.4)/Pt(0.6)]_{x3}$ /Ru(2)/Ta(3). We varied the Ir spacer thickness between 0.3 nm and 0.7 nm to cover the first IEC peak around 0.5 nm. The sample sputtered in an 6 mTorr Kr environment exhibited a peak IEC field of 1.7 T, exceeding its Ar counterpart by over 35% (see Figure 1). This same thickness is also associated with the largest PMA ($\mu_0 H_K$ = 5.4 T), which exceeded the Ar-sputtered counterpart by over 30% (see Figure 2). A 400°C post-annealing treatment in vacuum (< 4 x 10^{-6} Pa) only causes a moderate reduction in the IEC field to 1.5 T. These results suggest that using Krypton as the sputtering gas could lead to superior performing SAFs for emerging memory devices.

[1] Y. Huai, H. Gan, Z. Wang, Applied Physics Letters, Vol. 112, p.1 (2018) [2] K. Yakushiji, A Sugihara, A. Fukushima, Applied Physics Letters, Vol. 110, p.1 (2017) [3] Y. Lau, Z. Chi, T. Taniguchi, Physical Review Materials, Vol. 3, p.1 (2019) [4] G. Bertero, R. Sinclair, IEEE Transactions on Magnetics, Vol. 31, p.1 (1995)

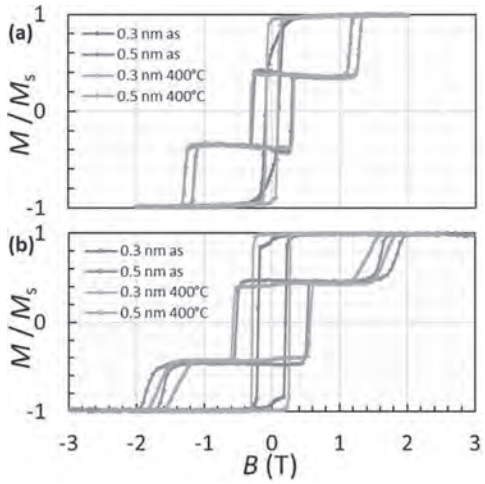

Fig. 1 Out-of-plane magnetic hysteresis curves for Pt/Co/Ir SAF sputtered in 6 mTorr (a) Ar or (b) Kr

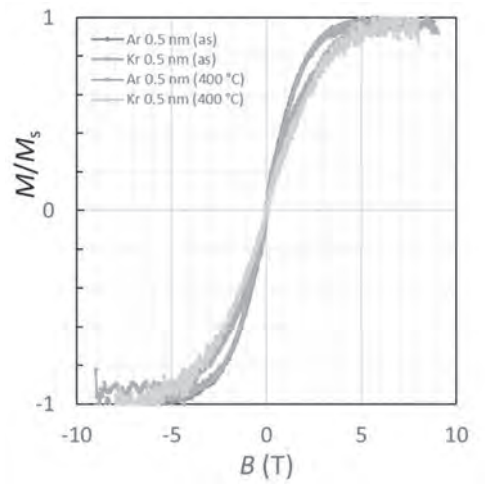

Fig. 2 In-plane magnetic hysteresis loops for Pt/Co/Ir SAF

EPB-06. Shape effect of cobalt nano-particles on magnetic properties of Co-SiO_2 nano-granular films. *H. Kijima-Aoki*[1], Y. Endo[1], T. Miyazaki[1], T. Nojima[1], K. Ikeda[2], N. Kobayashi[2], S. Ohnuma[1,2] and H. Masumoto[1] *1. Tohoku University, Sendai, Japan; 2. Research Institute for Electromagnetic Materials, Sendai, Japan*

Magnetic-dielectric nano-granular films are of great interest to electromagnetic device applications such as thin-film inductors, magnetic sensors, and magneto-optical devices. In general, nano-granular films of metal content are less than 40at.% exhibit superparamagnetic because nm-size magnetic metal granules are the sphere and randomly dispersed in a matrix. It is known that the shape of magnetic nano-particle affects a lot of magnetic anisotropy (*e.g.,* Large perpendicular magnetic anisotropy realized in soft magnetic Co-SiO_2 nano-granular films with prolate-shaped cobalt nano-particles[1]). However, the shape effect from "oblate" to "prolate" spheroid on magnetic properties has not been fully understood. Here, we present successful particle shape modulation in nano-granular films by an optimized tandem sputtering method. To change the nano-particle shape of Co-SiO_2 films, Co and SiO_2 were alternately sputtered with the substrate rotating speeds controlled from 2 to 5 rpm. In Fig. 1, the ferromagnetic properties are found in Co-SiO_2 nano-granular films. The particle shapes were changed from (a) oblate to (c)prolate spheroid even though Co and SiO_2 atomic ratios are kept constant to be 3:7. As a result of shape change from oblate to prolate, the magnetic anisotropy field (see saturation magnetization field H_s) reversed (a)in-plane to (c)out-of-plane. From the temperature dependence of coercive field H_c(bottom right), prolate-shaped cobalt particles remark the highest out-of-plane magnetic anisotropy enhancement. Nano-particle shape effect significantly appears to surface anisotropy enhancement at low temperature. The in-plane electrical resistivity (ρ) of the film decreased with increasing vertical length of the prolate particle, whereas optical transmittance increased even though the metal content was unchanged. The shape-controlled nano-granular composite materials potentially apply to high-frequency inductors, magnetoelectric sensors, and optical devices.

[1] H. Kijima-Aoki, S. Takeda, S. Ohnuma and H. Masumoto, *IEEE Magn. Lett.* 9, (2018) 1-5

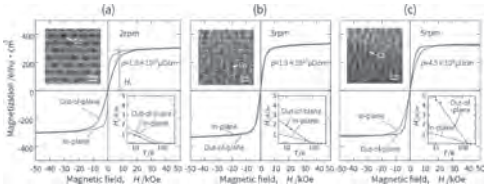

Fig.1 The in-plane(red) and out-of-plane(blue) magnetization curves of Co-SiO_2 films prepared with a substrate rotation speed of (a)2, (b)3, and (c)5 rpm. Inset shows cross-sectional TEM image and temperature dependence of coercive field H_c.

EPB-07. Identifying the Origin of Reduced Magnetization in Buried Thin Layers. *S.E. Ilse*[1], G. Schütz[1] and E. Goering[1] *1. Modern Magnetic Systems, Max Planck Institute for Intelligent Systems, Stuttgart, Germany*

Magnetic tunnel Junctions (MTJ) are important building blocks in spintronics and essential for modern data storage devices. Precise knowledge and control of the magnetic properties of the thin magnetic layers building up an MTJ and the interface between magnetic layer and the insulating oxide are crucial for the functionality. By combining X-ray reflectometry (XRR) with X-ray magnetic circular dichroism (XMCD) we are sensitive to magnetic layers and the corresponding magnetic depth profile. Hence, with X-ray resonant reflectometry (XRMR) we combine the strength of XRR and XMCD and are able to determine chemical and magnetic depth profiles with great precision and the element specific roughnesses of the corresponding interfaces [1,2]. To determine those depth profiles we simulate XRMR measurements using ReMagX [1-3] and fit the simulations to match actual measurements. In our current project, we study samples with a 2 nm magnetic layer in contact with an electric insulator at one and with chromium at the other interface. A schematic of the sample design can be

seen in Fig. 1. We choose the three magnetic transition metals Fe, Co, Ni as magnetic layers and SiO_2 as insulator since it is available with well-defined structural properties. The detailed chemical and magnetic depth profile obtained by ReMagX fits for a sample with Ni as magnetic layer is shown in Fig. 2. A general reduction of the saturation magnetization compared to the respective bulk material can be seen for all samples in the XRMR measurements. Additionally, the magnetic depth profiles reveal a thin magnetic dead layer at the interface between magnetic layer and chromium. Since the interfaces is rough, and the elements intermix with each other, the magnetic dead layer can be attributed to the formation of an alloy between chromium and the magnetic transition metal due to intermixing. At the oxide/magnet interface no reduced magnetization is observable. With field and temperature dependent SQUID measurements a reduced Curie temperature could be determined which leads to a reduced magnetization at room temperature.

[1] S. Macke and E. Goering, J. Phys.: Condens. Matter 26.36 (2014) 363201. [2] S. Macke, et al., Adv. Mater. 26.38 (2014): 6554-6559. [3] S. Macke, www.remagx.org

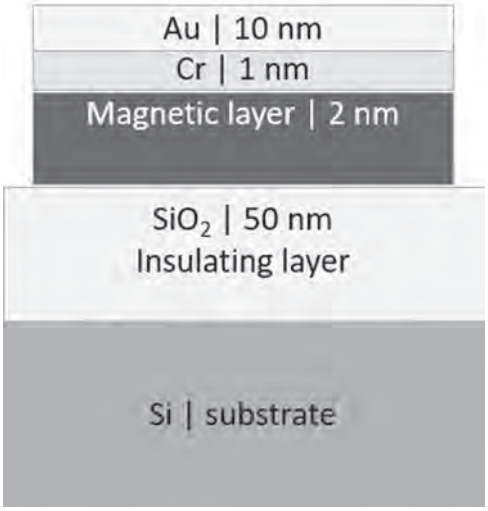

Fig. 1 Schematic of the sample design.

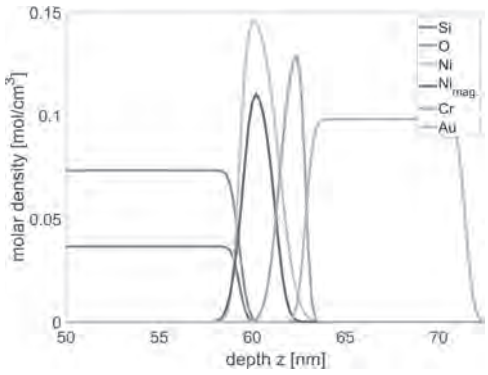

Fig. 2 Chemical and magnetic depth profile of a sample with Ni as magnetic layer obtained by XRMR measurements.

EPB-08. Asymmetric modification of the magnetic proximity effect in Pt/Co/Pt trilayers by the insertion of a Ta buffer layer and a Cu spacer layer. *A. Mukhopadhyay*[1], S.K. Vayalil[1], D. Graulich[2], I. Ahamed[3], S. Francoual[4], A. Kashyap[3], T. Kuschel[2] and P. Kumar[1] *1. Department of Physics, Indian Institute of Science, Bangalore, Bangalore, India; 2. Center for Spinelectronic Materials and Devices, Bielefeld University, Bielefeld, Germany; 3. School of Basic Sciences & School of Computing and Electrical Engineering, Indian Institute of Technology, Mandi, Mandi, India; 4. Deutsches Elektronen-Synchrotron DESY, Hamburg, Germany*

A static magnetic moment in the heavy metal can be induced by the adjacent ferromagnet in certain systems (e.g., Fe/Pd, Fe/Pt) [1,2]. The phenomenon of a nominally paramagnetic material getting spin-polarized in the presence of an adjacent ferromagnet by the exchange interaction is known as the magnetic proximity effect (MPE) [3,4]. The MPE in the top and bottom Pt layers induced by Co in Ta/Pt/Co/Cu(*c*)/Pt and Ta(*t*)/Pt/Co/Pt multilayers, respectively, has been studied by interface-sensitive, element-specific x-ray resonant magnetic reflectivity. The asymmetry ratio for circularly polarized x-rays of left and right helicity has been measured at the Pt L_3 absorption edge (11567 eV) with an in-plane magnetic field (± 158 mT) to verify its magnetic origin. The proximity-induced magnetic moment in the bottom Pt layer decreases with the thickness of the Ta buffer layer (shown in Fig.1). Grazing incidence x-ray diffraction has been carried out to show that the Ta buffer layer induces the growth of Pt(011) rather than Pt(111), which in turn reduces the induced moment. A detailed density functional theory study shows that an adjacent Co layer induces more magnetic moments in Pt(111) than in Pt(011). Hence, the increasing Ta buffer layer thickness diminishes the growth of Pt(111) which in turn reduces the proximity-induced magnetic moment in the bottom Pt layer [5]. Whereas, with the increasing Cu spacer layer, the proximity-induced magnetic moment in the top Pt layer decreases (shown in Fig.2) due to the hindrance to the direct interaction between the top Pt layer and the Co layer. However, interestingly, a non-zero moment in the top Pt layer still has been found with a non-zero Cu spacer layer. The manipulation of the magnetism in Pt by the insertion of a Ta buffer layer or a Cu spacer layer provides a way to control the magnetic proximity effect, which is of huge importance in spin-transport experiments across similar kinds of interfaces.

[1] J. Vogel, A. Fontaine and J. Goulon, Phys. Rev. B, Vol. 55, p.3663 (1997). [2] T. Kuschel, C. Klewe and G. Reiss, Phys. Rev. Lett., Vol. 115, p.097401 (2015). [3] P. K. Manna and S. M. Yusuf, Phys. Rep., Vol. 535, p.61 (2014). [4] C. Klewe, T. Kuschel and G. Reiss, Phys. Rev. B, Vol. 93, p.214440 (2016). [5] A. Mukhopadhyay, Sarathlal KV and PS Anil Kumar, Phys. Rev. B, Vol. 102, p.144435 (2020).

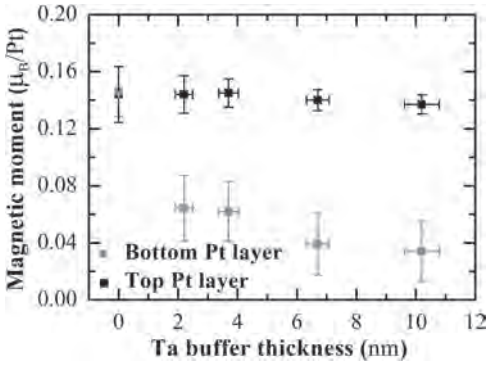

Fig.1: Dependence of magnetic moment in the top and bottom Pt layers on the Ta buffer thickness.

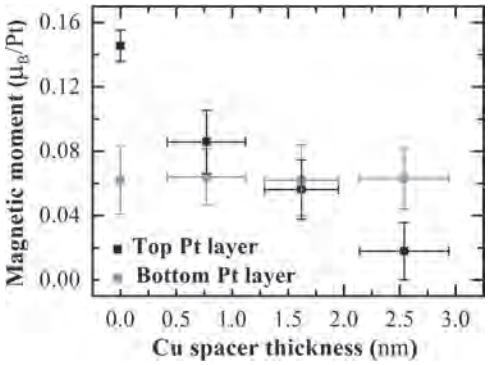

Fig.2: Dependence of magnetic moment in the top and bottom Pt layers on the Cu spacer thickness.

EPB-09. Magnetotransport of $SrIrO_3$ based symmetric heterostructure. *A. Jaiswal*[1], R. Schneider[1], M. Le Tacon[1] and D. Fuchs[1] *1. Institute for Quantum Materials and Technologies, Karlsruhe Institute of Technology, Karlsruhe, Germany*

Transition-metal oxide (TMO) based heterostructures are the fertile playground to explore or functionalize novel quantum states. In this regard, the combination of 3*d* and 5*d* TMOs have gained special interest because of the strong competition between strong spin-orbit coupling and electron correlation at the interface of those heterostructures. Additionally, the inversion symmetry breaking may result in a distinct interfacial Dzyaloshinskii-Moriya interaction (DMI) and the formation of non-collinear magnetic texture in case of magnetic TMOs. Among the 5*d* TMOs, $SrIrO_3$ (SIO) has gained significant attention in recent years. It displays large spin-orbit coupling and the semi-metallic ground state is highly susceptible to structural distortions. In this study, we have grown crystalline trilayer structures consisting of SIO and a 3*d* ferromagnetic insulator (FMI), i. e., (SIO/FMI/SIO or FMI/SIO/FMI). In-situ observation of RHEED oscillations and x-ray diffraction indicate layer-by-layer epitaxial growth. We will report in detail on the electronic transport and magnetic properties of the these heterostructures.

EPB-10. Dzyaloshinskii-Moriya Interaction and exchange bias in epitaxial Pd/Co/CoO films. *A. Kozlov*[1], G.S. Suslin[1], V. Shatilov[1], E. Tarasov[1,2], A. Davydenko[1] and I. Tkachenko[2] *1. Institute of Science-Intensive Technologies and Advanced Materials, Far Eastern Federal University, Vladivostok, Russian Federation; 2. Institute of Chemistry, Far Eastern Branch Russian Academy of Sciences, Vladivostok, Russian Federation*

In this work we study the influence of interface parameters on the perpendicular magnetic anisotropy (PMA) and the interfacial Dzyaloshinskii-Moriya interaction (DMI) of Pd(111)/Co/CoO/Pd thin epitaxial films with different oxidation depths. Epitaxial Si(111)/Cu(2 nm)/Pd(2 nm)/Co(1 nm) films were grown by molecular beam epitaxy in ultrahigh vacuum chamber. After deposition of ferromagnetic layer, films were exposed the procedure of artificial oxidation with dry oxygen. We varied the oxide thickness and this way we changed the remanent ferromagnetic thickness. Determination of the thickness of the magnetic layers carried out by measuring the saturation magnetic moment with vibrating samples magnetometry. We also used SQUID-magnetometer for low-temperature measurements. Magnetic structure was investigated by a magneto-optical Kerr effect (MOKE) microscope which was equipped with a hand-made coil applying out-of-plane magnetic fields and an in-plane electromagnet. Significant elastic strains appear on Pd/Co interface lead to induce strong perpendicular magnetic anisotropy [1]. Artificial oxidation of magnetic layer leads to symmetry breaking on the bottom and top magnetic interfaces in epitaxial films, which reduces compensation of interfacial DMI. It should be noted that including of oxide layer is eliminate the asymmetrical contribution of chiral dumping in comparing with symmetrical Pd/Co/Pd [2] structures, it following from symmetrical parabolic shape of domain walls velocity curves as shown on figure 1(a) and allow determine the DMI field by minimal velocity field H_{min}[3]. Moreover, Pd/Co/CoO thin films demonstrate strong exchange bias in out-of-plane magnetic field at a low temperature, as shown on figure 1(b). The reported study was partially funded by Council for Grants of the President of the Russian Federation (project - MK-1384.2021.1.2), the Russian Ministry of Science and Higher Education (the state task 0657-2020-0013) and grant of the Government of the Russian Federation (Project Proposal No.2020-220-08-4899) .

[1] A. V. Davydenko, et al., Phys. Rev. B, Vol. 95, 064430 (2017) [2] A. V. Davydenko, et al., Phys. Rev. B, Vol.103, 094435 (2021) [3]S.-G. Je, D.-H. Kim and S.-C. You, Phys. Rev. B, Vol. 88, 214401 (2013)

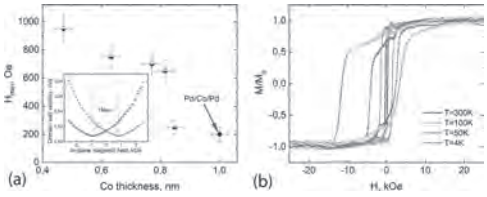

Fig. 1 a) H_{min} as a function of Co thickness and axample of domain wall velocity curves (on the inset); b) Hysteresis loops of Pd/Co/CoO measured with different temperatures

EPB-11. Interface dependence of NMR spectra of ^{59}Co with different molecular overlayers. *M. Benini*[1,3], R.K. Rakshit[2], M. Singh[2], G. Allodi[4], S. Sanna[1], V.A. Dediu[3] and I. Bergenti[3] *1. Physics and Astronomy, University of Bologna, Bologna, Italy; 2. CSIR - National Physical Laboratory, New Delhi, India; 3. ISMN, CNR, Bologna, Italy; 4. Physics and Earth Sciences, University of Parma, Parma, Italy*

The formation of hybrid ferromagnetic/molecule heterostructures can lead to strong modifications of the magnetic properties of the ferromagnetic layer[1]. Such modifications, like magnetic anisotropy easy axis reorientation[2, 3] and magnetic hardening[4] are linked to the hybridization at the interface between the molecules p-orbitals and the ferromagnetic surface d-orbitals[1][2]. Here we report a novel finding: an interface dependent of NMR spectra of 7 nm polycrystalline Co thin films capped with two different organic molecules, Fullerene C_{60} and Gallium-quinoline Gaq_3. Cobalt layers are grown simultaneously on two Al_2O_3(0001) substrates at RT and UHV by e-beam evaporation. The molecular layers are then grown without breaking the vacuum, by thermal evaporation at similar conditions. The molecular layer thickness is 25 nm, in order to guarantee a uniform coverage of the metallic surface. Cobalt surface characterization is performed by ex-situ AFM on a bare 7nm Co ultra-thin film (Fig. 1), showing a uniform, atomically flat and granular surface (RMS of (0.3 ± 0.1) nm). Ex-situ AFM characterization of the molecular layers shows a complete coverage, and RMS less than 1nm. NMR characterization is performed at T=77°K in zero external applied field. ^{59}Co spectra where taken in the frequency range 190-235 MHz. For each sample, different spectra were acquired with different transmitted RF power, in order to obtain the enhancement factor [5]. We obtain an enhancement factor ratio of 2 between the Co/Gaq_3 and the Co/C_{60} systems. This is in agreement with L-MOKE characterization at T= 77°K, showing that the Co/Gaq_3 system is magnetically harder than the Co/C_{60}. The corrected NMR spectra, (Fig. 2), show the presence of both FCC and HCP phases. Remarkably, their spectral weights is different for the two samples, depending on the molecular species deposited over the Cobalt surface. These results can be explained as due to an interface-induced modification of the hyperfine field felt by the ^{59}Co nuclei, implying a profound impact of the interface on the magnetic properties of a significant portion of the ferromagnetic structure.

[1] M. Cinchetti, V.A. Dediu, L.E. Hueso, Nature Materials, Vol. 16 p.507 (2017) [2] K. Bairagi, A. Bellec, V. Repain, Physical Review Letters, Vol. 114, p. 247203 (2015) [3] K. Bairagi, A. Bellec, V. Repain, Physical Review B, Vol. 98, p.085432 (2018) [4] K. V. Raman, A. M. Kamerbeek, A. Mukherjee, Nature, Vol. 493, p.509 (2016) [5] P. Panissod, Frontiers in Magnetism of Reduced Dimension Systems, Vol. 49, p.225 (1998)

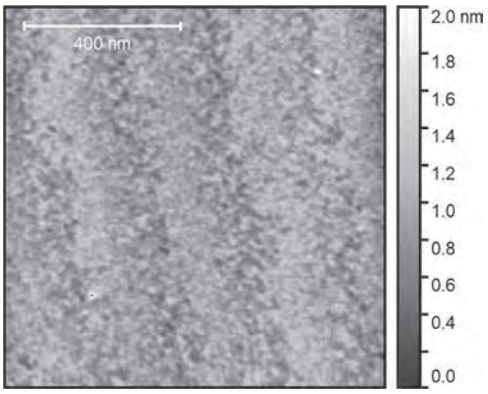

Fig.1 AFM image of 7 nm Co on Al_2O_3(0001).

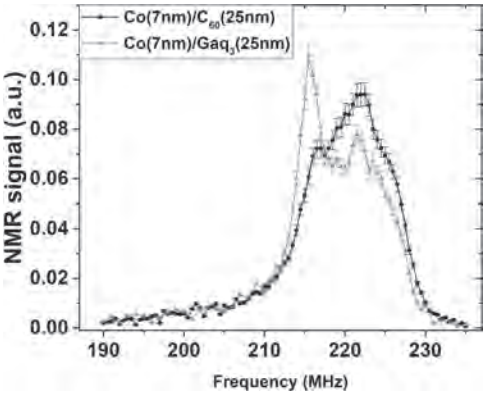

Fig.2 NMR spectra of Co(7nm)/C_{60} and Co(7nm)/Gaq_3.

EPB-12. Anisotropy Enhancement in Co / C_{60} Fullerene Bi-Layers Determined by Ferromagnetic Resonance. J.E. Shoup[1], M.D. Rogers[2], O. Cespedes[2] and *D. Arena*[1] *1. Physics, University of South Florida, Tampa, FL, United States; 2. Condensed Matter, Universtiy of Leeds, Leeds, United Kingdom*

Modification and control of magnetic anisotropy is crucial for the development of new permanent magnet materials, high density information storage, and many advanced spintronic applications. Enhanced anisotropy is often achieved via shape modification, stabilization of non-cubic crystal structures, or proximity effects such as exchange bias. An unusual proximity effect occurs at the interfaces of thin Co films adjacent to π-conjugated C_{60} fullerene films where initial field hysteresis loops exhibit a substantial asymmetry and considerable broadening at reduced temperatures [1]. We investigate these effects with temperature-dependent broadband ferromagnetic resonance (FMR). A key question in these studies is whether the C_{60}-derived anisotropy affects the dynamical properties of the Co / C_{60} system including resonant fields, damping, and spectroscopic *g*-factors. We examine the magnetometry and FMR response of a Co [12 nm] / C_{60} [35 nm] / Nb [16 nm] sample as a function of temperature and field history. Conventional field hysteresis loops identify two main effects: the asymmetry is present only for the initial loop and the enhanced coercive field increases monotonically for temperatures below 200 K. Temperature-dependent FMR from 4 – 35 GHz confirm these observations. The effective magnetization ($\mu_0 M_{eff}$) tracks the increased anisotropy of the Co / C_{60} upon cooling, but following field cycling $\mu_0 M_{eff}$ is reduced. The difference ($\Delta\mu_0 M_{eff}$) is as large as 26 mT at 10 K and $\Delta\mu_0 M_{eff}$ drops to zero above 200 K. These effects are not observed in control samples with a Cu spacer layer inserted between the Co and C_{60} layers. Gilbert-type damping is slightly increased in the Co / C_{60} system at all temperatures, however, the enhanced anisotropy prior to field cycling has little effect on damping.

[1] T. Moorsom, O. Cespedes *et al.*, π-anisotropy: A nanocarbon route to hard magnetism *Physical Review B* 101, 060408 (2020).

Session FOA
MAGNETOCALORICS I

Tino Gottschall, Co-Chair
Helmholtz-Zentrum Dresden-Rossendorf, Dresden, Germany
Jiazheng Hao, Co-Chair
Institute of High Energy Physics, Dongguan, China

INVITED PAPER

FOA-01. Developments in magnetocaloric devices. *N.J. Wilson*[1], P. Burdett[1], E. Lovell[1], R. Bettles[1] and D. Sanderson[1] *1. Camfridge Ltd., Cambridge, United Kingdom*

The field of caloric materials has seen immense development over the last twenty years, with magnetocalorics competing alongside electrocaloric, elastocaloric, barocaloric and multi-caloric materials in an endeavour to create new energy-efficient and low-GWP cooling and heating devices at a competitive price. Among the array of caloric materials, magnetocalorics show neither the largest temperature nor entropy changes (at least under practical magnetic fields), but devices based on the magnetocaloric effect retain two distinct advantages – the magnetic field can be produced using a permanent magnet (so with perfect efficiency) and magnetocaloric devices can readily implement highly-effective work recovery strategies for efficient thermodynamic cycling. These competitive features have resulted in two recent active magnetic regenerative (AMR [1]) demonstration systems with good thermodynamic efficiencies (in the 40%-50% of Carnot range [2,3)] which is almost comparable to a conventional vapour compressor. However, both these magnetocaloric systems use gadolinium (a relatively expensive and somewhat critical raw material[4]) as a magnetocaloric refrigerant. Huge efforts have been focused on developing lower-cost (2nd generation alloys such as $La(FeCoSi)_{13}$ [5]) and higher-performing (3rd generation alloys like $(MnFe)_2P$ [6] and $La(FeMnSi)_{13}$-H [7]) magnetic refrigerants to enhance both power density and efficiency, and thus to increase competitiveness and surpass the performance of the vapour compressor. However, third generation alloys have largely underperformed gadolinium in devices [8]. The challenges in working with third generation alloys are formidable. $La(FeMnSi)_{13}$-H is a brittle metal (even before hydrogenation) that readily oxidises during processing and once manufactured the material is hard to shape into optimised heat exchange geometries, can be prone to corrosion and both thermal and field cycling can induce part fatigue. To achieve high-efficiency and good power-density in an AMR, the cyclic operating frequency needs to be maximised (for power density) whilst minimising exchange fluid operating pressure (for efficiency). This necessitates the use of regular geometry regenerators, with high surface areas and small conductive length scales. Such geometries require high tolerances otherwise efficiency rapidly degrades [9]. Using mass production methods, high-tolerance multi-material cascaded $La(FeMnSi)_{13}$-H AMRs have been successfully fabricated, which show robustness against fatigue and resistance against corrosion. Benchmarking of these new AMR structures shows a doubling of power density and enhanced efficiency of $La(FeMnSi)_{13}$-H multi-material cascades over equivalent multi-material GdDy-alloy cascades in magnetocaloric devices. We will outline how the twin operational challenges of corrosion (through corrosion inhibitors) and material fatigue (material optimisation) in $La(FeMnSi)_{13}$-H have been overcome. This will lead into a discussion of how magnetic heat-technologies can be brought closer to market.

[1] Barclay JA, Steyert WA, U.S. Patent No. 4,332,135 (1982) [2] Bahl C et al., Thermag IX, 9th IIR/IIF Int. Conf. on Caloric Cooling (2021) [3] Chaudron, JB et al., Proc. of Thermag VIII, 8th IIR/IIF Int. Conf. on Caloric Cooling (2018) [4] Gottschall T, Skokov K, Fries M et al., Adv. Energy Materials, Volume 9, Issue 34 (2019) [5] Katter M, Zellmann V, Reppel GW, et al., IEEE Trans. Magn.44, 3044 (2008) [6] Tegus O, Bruck E, Buschow KHJ et al., Nature 415, 150–152 (2002) [7] Barcza A, Katter M, Zellmann V et al., IEEE Trans. Magn.47, 3391 (2011). [8] Masche, M, et al., IIR Thermag IX, 9th IIR/IIF Int. Conf. on Caloric Cooling (2021) [9] Lei T, Engelbrecht K, Nielsen K, Applied Thermal Engineering, Volume 111 (2017)

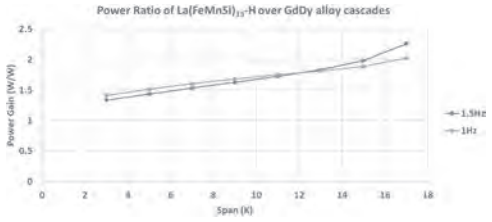

CONTRIBUTED PAPERS

FOA-02. Giant Magnetocaloric Effect in the $(Mn,Fe)_2(P,Si)$ System: From Bulk to Nano. *F. Zhang*[1], C. Taake[2], I. Dugulan[1], I. Caron[2], N. Van Dijk[1] and E. Brück[1] *1. Faculty of Applied Sciences, Delft University of Technology, Delft, Netherlands; 2. Department of Physics, Bielefeld University, Bielefeld, Germany*

In the field of nanoscale magnetocaloric materials (MCMs), novel concepts including microrefrigerators, thermal switches, microfluidic pumps, energy harvesting devices and biomedical applications have been proposed[1-3]. However, reports on nano-scale $(Mn,Fe)_2(P,Si)$-based materials, which are one of the most promising bulk materials for solid-state magnetic refrigeration, are rare[4]. We have synthesized nano-scale $(Mn,Fe)_2(P,Si)$-based nanoparticles, and systematically investigated the influence of the grain size and microstructure on the magnetocaloric effect (MCE) by using XRD, DSC, high-resolution TEM, SQUID and Mössbauer spectra. The results show that the decreased saturation magnetization (M_s) is mainly attributed to an atomically disordered shell at the surface of the nanoparticles. With a decreased particle size both the thermal hysteresis and T_C are reduced. In addition, we determined an optimal temperature window for annealing after synthesis of 300-600 °C and found that a post-treatment strategy can enhance M_s from 120 to 148 Am^2kg^{-1} and the magnetic entropy change ($|\Delta S_m|$) from 0.8 to 1.2 $Jkg^{-1}K^{-1}$ for a magnetic field change of $\Delta\mu_0 H = 1$ T, while the grain size is kept almost constant, which demonstrates competitive MCE characteristics among the reported nano MCMs systems (e.g nano Gd). This improvement can be attributed to the synergetic effect of annealing and nitration, which effectively removes part of the defects (e.g. dislocations) inside the particles. For comparison, in a control experiment under Ar atmosphere M_s slightly improves from 120 to 131 Am^2kg^{-1}, while ΔS_m decreased from 0.8 to 0.5 $Jkg^{-1}K^{-1}$ due to the appearance of an MnP impurity phase. The produced superparamagnetic particles have been probed by high-resolution TEM, Mössbauer spectroscopy and magnetic measurements. Our results provide important insight into the performance of nanoscale giant magnetocaloric materials.

1. J. Li *et.al*, Magnetocaloric effect in magnetothermally-responsive nanocarriers for hyperthermia-triggered drug release. *Nanotechnology.,* 23, 1-10 (2012). 2. J. Wu *et.al*, A novel cascade micro-unit regeneration cycle for solid state magnetic refrigeration. *Appl. Therm. Eng.,* 137, 836-847 (2018). 3. J. Puga *et.al*, Novel thermal switch based on magnetic nanofluids with remote activation. *Nano Energy*., 31, 278-285 (2017). 4. F. Guillou *et.al*, Taming the first-order transition in giant magnetocaloric materials. *Adv. Mater*., 26, 2671-2675 (2014).

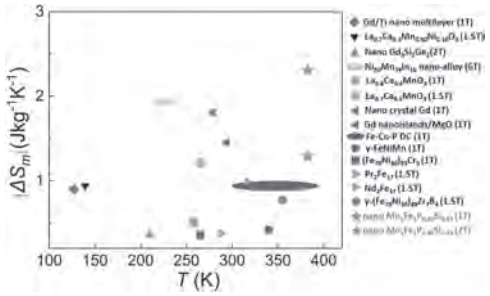

Figure 1. Map of the absolute magnetic entropy change $|\Delta S_m|$ for different field changes $\mu_0\Delta H$ as a function of the magnetic transition temperature for nano MCMs. The stars correspond to the present data for the nano $(Mn,Fe)_2(P,Si)$-based sample.

FOA-03. Giant Magnetocaloric effect near room temperature in low-cost $(MnNiSi)_{1-x}(FeCoGa)_x$ alloys. *S. Ghosh*[1], A. Ghosh[2], P. Sen[3] and K. Mandal[1] *1. S. N. Bose National Centre for Basic Sciences, Kolkata, India; 2. Saha Institute of Nuclear Physics, Kolkata, India; 3. Variable Energy Cyclotron Centre, Kolkata, India*

Magnetic and structural transitions are found to couple in the vicinity of room-temperature in transition metal-based (MnNiSi)1-x(FeCoGa)$_x$ (x = 0.15 - 0.17) alloys which essentially leads to a coupled first-order magnetostructural transition (MST) from high-temperature paramagnetic hexagonal structure (Ni_2In-type) to a low-temperature ferromagnetic orthorhombic structure (TiNiSi-type) and as a result, giant magnetocaloric effect (MCE) is observed in these alloys [1]. The alloys with x = 0.15, 0.16, and 0.17 exhibit isothermal magnetic entropy change (ΔS_M) as large as ~25 Jkg^{-1}K^{-1} at 323 K, ~31.1 Jkg^{-1}K^{-1} at 281 K, and ~23.8 Jkg^{-1}K^{-1} at 213 K respectively due to field change of ΔH = 50 kOe which is shown in Fig. 1. The giant magnetocaloric response with significantly large relative cooling power (RCP = 191.8, 209.6 and 139.2 J/kg respectively for x = 0.15, 0.16, and 0.17 due to ΔH = 50 kOe) enable these materials as potential candidates for magnetic refrigeration. The magnetocaloric response has been analyzed using Maxwell relation following both heating and cooling protocols and we observed that cooling mode is preferred to determine the ΔS_M precisely which is confirmed by the measured ΔS_M value using the Clausius-Clapeyron equation, from the analysis of universal scaling behavior of the calculated ΔS_M data and the calorimetry study of MCE.

[1] Ghosh, S., Ghosh, A., Sen, P., and Mandal, K., 2020, Giant Room-Temperature Magnetocaloric Effect Across the Magnetostructural Transition in $(MnNiSi)_{1-x}(FeCoGa)_x$ Alloys, Phys. Rev. Appl., 14(1), 014016.

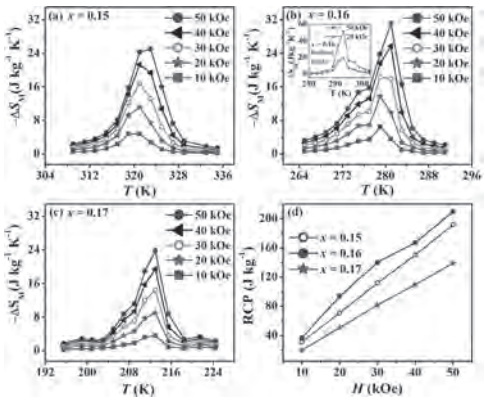

ΔS_M as a function of temperature for the for the different field variation, estimated using Maxwell relation from isothermal *M-H* curves following cooling protocol, for the alloy with (a) x = 0.15, (b) x = 0.16 [inset: ΔS_M – T measured form isothermal *M-H* curves during heating cycle] and (c) x = 0.17. (d) RCP as a function of field changes for all the alloys.

FOA-04. The variation of Fe/Ni concentration and its effect on the magnetic and magnetocaloric properties of $Mn_{0.5}Fe_{0.5-x}Ni_{1+x}Si_{0.94}Al_{0.06}$. *J.F. Casey*[1], B. Akintunde[2], R.C. Das[2], M. Khan[2] and A. Pathak[1] *1. Department of Physics, State University of New York, Buffalo State, Buffalo, NY, United States; 2. Department of Physics, Miami University, Oxford, OH, United States*

The MnTX (T = Ni, Co; X = p-block elements) compounds have received considerable attention due to the coupled first-order magnetic and structural phase transitions (MST) they exhibit. Large magnetocaloric effects are often associated with these phase transitions. The $Mn_{1-x}Fe_xNiSi_{1-y}Al_y$ system is a member of the MnTX family for which a large magnetic entropy change of 23 J kg^{-1} K^{-1} has been reported at T= 210K, ΔH = 2T. This value was reported for x = 0.5, y = 0.07 and for x = 0.5, y = 0.05 the peak value decreased to 17 J kg^{-1} K^{-1} (T = 315K, ΔH = 2T) (Biswas et. al. Acta Mat. 180 (2019) 341). For x = 0.4, y = 0.7, a peak magnetic entropy change of 9.3 J kg^{-1} K^{-1} was recently observed near 247 K (Ghosh et. al. JMMM 500 (2020) 166345). These studies suggested that the $Mn_{1-x}Fe_xNiSi_{1-y}Al_y$ system exhibits the maximum entropy change for x = 0.5. It is interesting to study the effect of Fe and Ni concentration variation on the magnetocaloric properties of the $Mn_{0.5}Fe_{0.5-x}Ni_{1-x}Si_{1-y}Al_y$, which has not been reported yet. Therefore, in this work, we present an experimental study on the effects of partially replacing Fe with Ni on the structural, magnetic, and magnetocaloric properties of $Mn_{0.5}Fe_{0.5-x}Ni_{1+x}Si_{0.94}Al_{0.06}$ ($0.025 \le x \le 0.10$). The results of x-ray diffraction and scanning electron microscopy (SEM) showed that the samples exhibited a single-phase and energy dispersive spectroscopy analysis showed that the resulting compositions were close to the nominal compositions. Maximum magnetic entropy changes of – ΔS_M = 22 and 57 J kg^{-1}K^{-1} for ΔH = 2 and 5 T, respectively have been realized for x = 0.1 around 322 K. The observed large MCEs are due to the MST exhibited by the materials from low-temperature FM orthorhombic phase to high-temperature PM hexagonal phase. Work at SUNY, Buffalo State was supported by the startup fund from SUNY Buffalo State College and Undergraduate Summer Research Fellowship award, Undergraduate Research Office, Buffalo State.

FOA-05. Magnetocaloric Properties of a New Type of Magnetocaloric Materials - M_5XB_2 System. *H. Ojiyed*[1] and E. Brück[1] *1. Applied Sciences, Delft University of Technology, Delft, Netherlands*

The M_5XB_2 materials system has been widely studied as permanent magnetic materials[1] [2]. As permanent magnetic materials, their coercivity and magnetic energy product are lower than those of the mainstream permanent magnetic materials. Xie *et al.*[3] and Cedervall *et al.*[4] proposed that the Mn_5PB_2 and $(Fe_{1-x}Co_x)_5PB_2$ compounds have the prospect of being

applied as magnetocaloric materials due to their near room temperature Curie temperature. In this work, the structure and magnetocaloric properties of the $Mn_5(SiP)B_2$ compounds of the M_5XB_2 material system were studied. According to a refinement of the XRD data the $Mn_5(Si_{1-x}P_x)B_2$ compounds all crystallize in the Cr_5B_3–type body-centered tetragonal structure, with a small amount of Mn_2P as a secondary phase (less than 7%). The lattice parameters and the unit-cell volume of the compounds change linearly with the increase in P content. These experimental results are consistent with calculated DFT results. The Curie temperature of the compounds can continuously be adjusted between 305 and 411 K by changing the Si/P ratio. The introduction of P also caused a decrease in saturation magnetization. The magnetic phase transition of these compounds was determined using Arrot plots and the field exponent *n* for the magnetic entropy change based on Landau's theory. The studied compounds all show a second-order magnetic phase transition. Since the compounds show a second-order phase transition, the magnetic entropy change caused by the phase transition was not large: 1.9 and 1.4 J/kgK for Mn_5SiB_2 and Mn_5PB_2, respectively. However, the advantage of this series of compounds is that the Curie temperature can be adjusted continuously around room temperature.

1. M. Kasaya, Sci. Rep. Tohoku Univ. LVIII (Supp. 2/37) (1975) 2. R. Wäppling, *et al.* J. Phys. Supp. 12/37 (1976) (C6-591-593) 3. Z. G. Xie *et al.* Appl. Phys. Lett. 97, 202504 (2010) 4. J. Cedervall. *et al.* Inorg. Chem. 57, 777−784(2018)

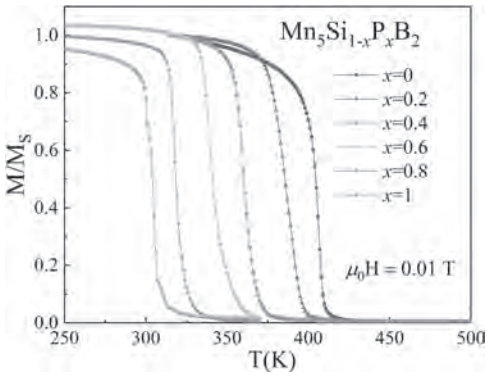

Fig. 1. Temperature dependence of magnetization of $Mn_5(Si_{1-x}P_x)B_2(0 \le x \le 1)$ in a field of 0.01T.

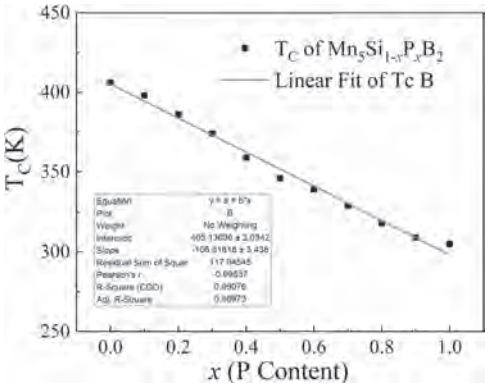

Fig. 2. T_C as a function of P content for $Mn_5(Si_{1-x}P_x)B_2$ ($0 \le x \le 1$).

FOA-06. Nonlinear influence of excess Mn on the magnetoelastic transition in $(Mn,Cr)_2Sb$. *Q. Shen*[1], N. Van Dijk[1] and E. Brück[1]
1. Fundamental Aspects of Materials and Energy, TU Delft, Delft, Netherlands

Mn_2Sb is a ferrimagnet with T_C around 550 K crystallizing in the tetragonal Cu_2Sb-type structure [1]. By doping other elements into the system, an Antiferromagnetic-Ferrimagnetic (AFM-FIM) transition can be induced in Mn_2Sb. Tuneable transition temperature and small thermal hysteresis make Mn_2Sb-based compounds extremely attractive for heat recovery applications [2]. Regularly, researchers add excess Mn to compensate for the evaporation of Mn for preparing Mn_2Sb-based alloys. Here we report that the fraction of excess Mn cannot only influence the fraction of secondary phase MnSb but also the magnetoelastic transition in $(Mn,Cr)_2Sb$ compounds. Table 1 gives the composition of main phase $(Mn,Cr)_2Sb$ as determined by Energy Dispersive X-ray Spectroscopy. X-ray patterns in Fig.1(a) show a strong reduction of secondary phase MnSb with increasing excess Mn, while the magnetoelastic transition temperature (T_t) in Fig.1(b) initially increases then decreases with excess Mn. By Electron Probe Micro Analysis we find with increasing excess Mn a higher Cr content in the MnSb second phase in comparison to the matrix. This competition for Cr leads to a nonlinear dependence of T_t with nominal Cr content. However, as shown in Fig.1(c) we observe a linear relation of T_t and *c/a* ratio for a wide range of temperatures 170 K-370 K and in Fig.1(d) a corresponding composition diagram of *c/a* is established to give guidance to prepare $(Mn,Cr)_2Sb$ alloys with desirable transition temperature for waste heat recovery applications.

[1] C. Kittel, Physical Review, Vol. 120, p. 335 (1960). [2] L. Caron, X. F. Miao, J. C. P. Klaasse, Applied Physics Letters, Vol. 103, p. 112404 (2013).

	Cr1Mn0	Cr1Mn2	Cr1Mn8	Cr2Mn0	Cr2Mn2	Cr2Mn8	Cr3Mn0	Cr3Mn2	Cr4Mn0	Cr4Mn2	Cr5Mn2	Cr5Mn8	Cr6Mn2
Cr(±0.4)	1.1	1.1	1.1	1.2	1.7	1.3	2.2	1.7	2.6	2.9	2.9	2.3	3.0
Mn(±1.5)	64.6	64.8	65.1	64.2	63.7	64.4	63.2	64.3	63.5	62.3	62.5	62.9	61.5
Sb(±0.9)	34.3	34.1	33.7	34.6	34.6	34.3	34.6	34	33.9	34.8	34.6	34.8	35.

Table 1 Main-phase composition in atom percent determined by Energy Dispersive X-ray Spectroscopy (EDS) for various $(Mn,Cr)_2Sb$ alloys. The starting composition is coded with Cr*x*Mn*y* where *x* and *y* give the increasing Cr addition and excess Mn in weight percent, respectively.

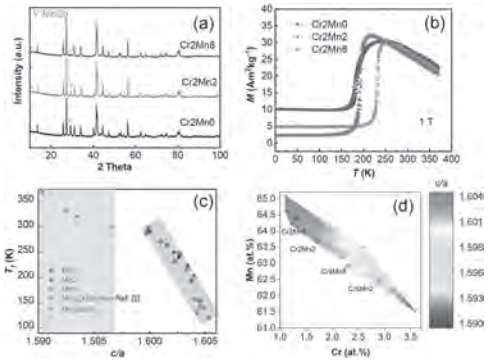

Fig.1(a) XRD patterns at room temperature (RT) (b) *M-T* curves of Cr2 with different excess Mn contents. (c) *c/a* ratio (derived from RT XRD data) dependence of the transition temperature T_t. The shadow area indicates *c/a* of antiferromagnetic samples at RT. (d) Composition dependence of the *c/a* ratio. Black dots correspond to experimental data.

FOA-07. Observing variations of the local iron moment and charge symmetries in $La(Fe,Si)_{13}$ for Mn- and rare earth doping through nuclear resonant spectroscopy. *J. Lill*[1], B. Eggert[1], B. Beckmann[2], O.N. Miroshkina[1], I. Radulov[2], K. Skokov[2], R. Brand[1], K. Ollefs[1], M.E. Gruner[1], O. Gutfleisch[2] and H. Wende[1] *1. Faculty of Physics and Center for Nanointegration Duisburg-Essen (CENIDE), University of Duisburg-Essen, Duisburg, Germany; 2. Materials Science, TU Darmstadt, Darmstadt, Germany*

Magnetocaloric materials are characterised by a significant adiabatic temperature change ΔT_{ad} induced by an external magnetic field and accompanied by a sizeable isothermal entropy change ΔS_{iso} [1]. At the characteristic transition temperature T_{tr}, an isostructural first-order phase transition from the ferromagnetic to the paramagnetic phase is associated either by a drastic volume change or a crystal symmetry change. Among others, $La(Fe,Si)_{13}$ based compounds are outstanding materials of current interest with their large magnetocaloric effect [2], providing both a large ΔS_{iso} and high ΔT_{ad},

accompanied by an isostructural phase transition. Thereby, $La(Fe,Si)_{13}$ condensates in a cubic $NaZn_{13}$ structure with two non-equivalent Fe sites. Fe_I occupies the highly symmetrical 8a sites, while Fe_{II} and Si both occupy the low symmetrical 96i sites [3]. Magnetocaloric materials are highly discussed candidates for a new type of environmentally friendly cooling devices, using the magnetocaloric effect. Therefore, it is crucial to deepen the understanding of how to taylor the magnetic properties of these materials to optimize their hysteresis and therefore the efficiency of the system. Especially the phase transition temperature T_{tr}, around 200 K for the undoped $La(Fe,Si)_{13}$ system, as well as the width of the thermal hystersis, the adiabatic temperature change ΔT_{ad}, and the order of the phase transition can be adjusted by the partial substitution of Fe with Mn, or by substituting La with either Ce, Pr or Nd. Here, we present element specific investigations of the ferromagnetic and paramagnetic phase as well as along the thermal driven phase transition, focussing on the magnetic moment changes and charge symmetries of the Fe sites under doping of $La(Fe,Si)_{13}$. The results obtained using nuclear resonant spectroscopy will be accompanied by magnetometry results which represent the macroscopic magnetic moment of $La(Fe,Si)_{13}$. Financial support by DFG (CRC/TRR270, "HoMMage").

[1] T. Gottschall et al. Adv. Energy. Mater. 9, 1901322 (2019) [2] F. Scheibel et al. Energy Technol. 6 (8) 1397-1428 [3] M. E. Gruner Phys. Rev Lett. 114, 057202 (2015)

FOA-08. Compositionally graded La-Fe-Si films. *E. Fontana*[1], T. Devillers[1] and N. Dempsey[1] *1. Université Grenoble Alpes, CNRS, Grenoble INP, Institut Néel, Grenoble, France*

$La(Fe, Si)_{13}$ is a promising candidate for magnetocaloric based technology such as magnetic refrigeration or energy harvesting [1-3]. This alloy family consists of a low content of rare earth (7.1 at. %) and high content of iron, resulting in a cheap and non-toxic compound. $La(Fe, Si)_{13}$ based alloys exhibit a large magnetocaloric effect (MCE) at the transition between ferromagnetic and paramagnetic states, which occurs at Curie temperatures (T_c) ranging between 200-259K [4]. The magnetic properties (T_c, magnetization, MCE), the crystal structure (cubic or tetragonal) and the type of transition can be tuned by adjusting the Si content. Furthermore, the Curie temperature can be increased to above room temperature by doping and hydrogenation [5]. Recently our group reported for the first time the possibility to fabricate thick films of $La(Fe, Si)_{13}$ [6]. Here we present a study on compositionally graded films of La-Fe-Si. The films were fabricated by triode co-sputtering of three targets (La-Fe, Fe, Si-Fe) onto thermally oxidised stationary Si substrates (100 mm in diameter). The composition of the as-deposited films was mapped by EDX, as shown in Fig. 1. The films were annealed ex-situ in a rapid thermal annealing furnace at 900°C. For each film, we selected samples from specific regions for characterization using optical and scanning electron microscopy, VSM-SQUID magnetometry and X-ray spectroscopy. Fig. 2 displays M(T) measurements on four La-Fe-Si samples of 5 µm thickness, taken from the regions specified in Fig. 1. The presentation will report results from films of nominal thickness ranging between 150nm – 5µm. The presentation will give details about how the structural and magnetic properties vary as a function of film composition, thickness and annealing conditions. Prospects for further developments and possible applications will also be discussed. Acknowledgement: This research has received funding from the French National Research Agency under the HiPerTherMag project (ANR-18-CE05-0019).

[1] R. Gauß, G. Homm and O. Gutfleisch, J. Ind. Ecol., Vol. 21, p. 1291 (2017) [2] J. Liu, J.D. Moore, K.P. Skokov, et al., Scr. Mater., Vol. 67, p. 584, (2012) [3] A. Ahmim, M. Almanza, V. Loyau, et al., IEEE Trans. Magn., Vol. 57, p. 2500205 (2020) [4] K. Niitsu, S. Fujieda, A. Fujita, et al., J. Alloys Compd., Vol. 578, p. 220 (2013) [5] B. G. Shen, J. R. Sun, F. X. Hu, et al., Adv. Mater., Vol. 21, p. 4545 (2009) [6] N. H. Dung, N. B. Doan, P. De Rango et al. J. Appl. Phys., Vol. 127, p. 215103 (2020)

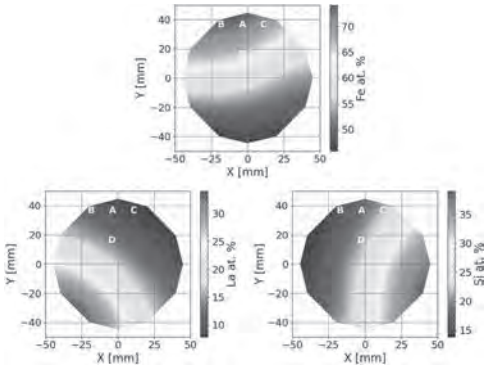

Fig. 1: Composition maps of La-Fe-Si film of nominal thickness 5 µm.

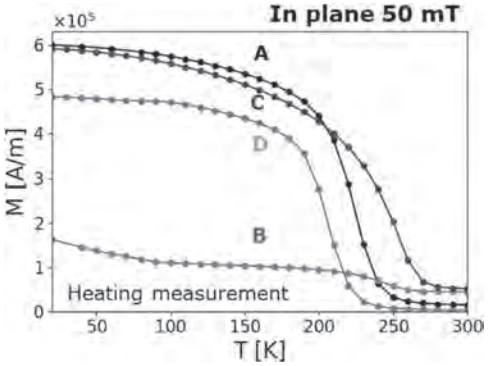

Fig. 2: M(T) measured in-plane under an applied field of 50 mT of La-Fe-Si film of nominal thickness 5 µm for the positions marked in Fig. 1.

FOA-09. Withdrawn

FOA-10. Unusual magnetic, magnetocaloric, and transport properties in phase-separated $LaFe_2Si$. *A. Pathak*[1], J.F. Casey[1], T. Del Rose[4,5], Y. Mudryk[5], D.H. Ryan[2], N.A. Zarkevich[3], D. Johnson[4,5] and V. Pecharsky[4,5] *1. Department of Physics, State University of New York, Buffalo State, Buffalo, NY, United States; 2. Department of Physics, McGill University, Montreal, QC, Canada; 3. NASA Ames Research Center, Moffett Field, CA, United States; 4. Department of Materials Science and Engineering, Iowa State University, Ames, IA, United States; 5. Ames Laboratory, U. S. Department of Energy, Ames, IA, United States*

The $LaFe_{13-x}Si_x$ compounds have been studied for nearly two decades for their potential to serve as materials for magnetocaloric cooling. They exhibit either first- or second-order phase transitions depending on x(Si). Here we present the discovery of a naturally formed two-phase composite at the $LaFe_2Si$ stoichiometry, which exhibits strongly responsive behaviors without mechanical degradation that can be exploited in weak magnetic fields. Some of the unusual properties include a two-step, nearly anhysteretic first-order phase transformation between ferromagnetic (FM) and paramagnetic (PM) states, instead of a singular phase change present in conventional $LaFe_{13-x}Si_x$, that is preserved in magnetic fields as high as 100 kOe. In addition to the giant magnetocaloric effect, the title material exhibits large, plateau-like positive magnetoresistance, both extending over a much wider temperature range when compared to phase-pure $LaFe_{13-x}Si_x$. Finally, the composite also shows a Griffiths-like phase associated with short-range FM clustering in the PM state (Pathak et. al., Acta Mat. 215 (2021) 117083). We will also discuss the effect of impurities on magnetic, magnetocaloric, and transport behaviors of $LaFe_2Si$. The work at Ames Laboratory was supported by the Division of Materials Science and Engineering, the Office of Basic Energy

Sciences of the DOE. Ames Laboratory is operated for the U.S DOE by Iowa State University under Contract No. DE-AC02-07CH11358. Work at SUNY, Buffalo State was supported by the startup fund from SUNY Buffalo State College and the Undergraduate Research Office, Buffalo State.

FOA-11. Tuning conventional alloys towards the high-entropy space: thermomagnetic and magnetocaloric behavior. *J. Law*[1], Á. Díaz-García[1], L.M. Moreno-Ramírez[1] and V. Franco[1] *1. Department of Condensed Matter Physics, ICMS-CSIC, University of Seville, Seville, Spain*

High-entropy alloys (HEAs), based on the design concept of mixing five or more principal elements to yield high entropy of mixing (ΔS_{mix}), expands the compositional space of multicomponent materials when compared to conventional materials, which are mainly based on one or two main constituents. HEAs, thus, form compositions without dominant elements, in which new materials with excellent properties, some of them being superior or unique compared to the conventional materials, have been found [1]. These advantages prompted a large surge in studying HEAs, with the explored compositions evolving from first-generation single phase equiatomic to second-generation multiphase non-equiatomic HEAs. The latter are recently reported with properties that outdo those of the first-generation HEAs, such as excellent strength-ductility combination, surpassing the low temperature limit, or enhanced magnetocaloric properties of rare-earth-free high-entropy alloys owing to a first-order magnetic phase transition [1-3]. Here, we present, when tuning CoCrMnNiTi alloys from conventional to the high-entropy region (i.e. ΔS_{mix} > 1.5 R, where R is the gas contstant, 8.314 J mol^{-1} K^{-1}), the evolution of their thermomagnetic and magnetocaloric behavior. The obtained HEA has a martensitic temperature tuned nearer to room temperature and a 10% increase in the entropy change (Fig. 1). This work demonstrates the recently proposed claim [1-3] that it is possible to obtain high-performance magnetocaloric materials within the HEA compositional space. Work supported by AEI/FEDER-UE (grant PID2019-105720RB-I00), US/JUNTA/FEDER-UE (grant US- 1260179), Consejería de Economía, Conocimiento, Empresas y Universidad de la Junta de Andalucía (grant P18-RT-746), Army Research Laboratory under Cooperative Agreement Number W911NF-19-2-0212 and Sevilla University under VI PPIT-US program.

[1] J. Y. Law, V. Franco, "Pushing the limits of magnetocaloric high entropy alloys", To be published. [2] J.Y. Law, L.M. Moreno-Ramírez, Á. Díaz-García, A. Martín-Cid, S. Kobayashi, S. Kawaguchi, T. Nakamura, and V. Franco, "MnFeNiGeSi high-entropy alloy with large magnetocaloric effect", Journal of Alloys and Compounds 855, 157424 (2021). [3] J.Y. Law, Á. Díaz-García, L.M. Moreno-Ramírez, and V. Franco, "Increased magnetocaloric response of FeMnNiGeSi high-entropy alloys", Acta Materialia 212, 116931 (2021).

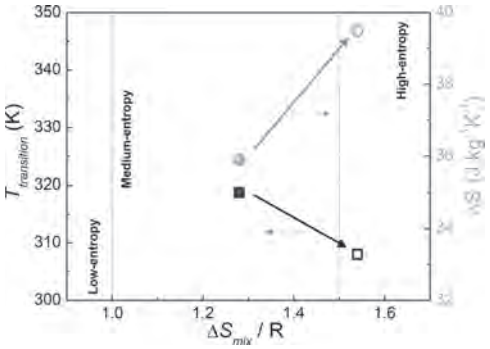

Fig 1. The variation of martensitic transition temperatures (square symbols) and entropy change at the transition (circular symbols) after tuning a conventional alloy towards the high-entropy region (ΔS_{mix} > 1.5 R).

FOA-12. Giant magnetocaloric effect in 2D cobalt hydroxide nanosheets. *J. Mohapatra*[1], J. Elkins[1], M. Xing[1], H. Zeng[2] and J. Liu[1] *1. Department of Physics, The University of Texas at Arlington, Arlington, TX, United States; 2. Department of Physics, University at Buffalo, The State University of New York, Buffalo, NY, United States*

In this study, a soft-chemical exfoliation procedure[1] was used to produce 2D cobalt hydroxide nanosheets with a giant magnetocaloric effect and isothermal magnetic entropy change (ΔS_M) exceeding 50 J.kg^{-1} at $\mu_0 H$ = 5 T. The large ΔS_M value is considered to be correlated with the enhanced uncompensated spin canting on the surfaces. The temperature-dependent field-cooled magnetization curve exhibits a paramagnetic-ferromagnetic phase transition at a temperature (T_f) around 35 K. Unlike the as-synthesized bulk cobalt hydroxide materials which exhibit low saturation magnetization of 65 emu/g, the 2D nanosheets show enhanced saturation magnetization below the T_f, resulting in the largest magnetic entropy change $-\Delta S_M$ near T_f. The findings suggest that the 2D cobalt hydroxide is a promising candidate for magnetic refrigeration in low-temperature regions.

1. Mohapatra, J.; Ramos, A.; Elkins, J.; Beatty, J.; Xing, M.; Singh, D.; La Plante, E. C.; Liu, J. Ping, Ferromagnetism in 2D α-Fe_2O_3 nanosheets. *Appl. Phys. Lett.* 2021, 118, (18), 183102.

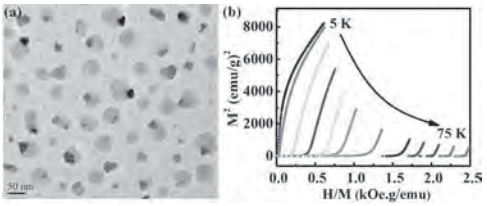

Fig. 1 (a) Transmission electron microscopy (TEM) image of 2D layered structure of cobalt hydroxide and (b) the Arrott plots for the corresponding sample.

FOA-13. A high-throughput search of magnetocaloric materials using first-principles calculations. *R. Vieira*[1,2], O. Eriksson[1,3], T. Björkman[2] and H.C. Herper[1] *1. Uppsala University, Uppsala, Sweden; 2. Åbo Akademi, Turku, Finland; 3. Örebro University, Örebro, Sweden*

The concept of domestic magnetic cooling devices has gained momentum since the early 2000s, motivated mainly by the benefits in energy efficiency compared to the current standard devices. However, the application of this technology for domestic usage raises technical challenges on the choice of magnetocaloric materials. For instance, domestic magnetic cooling devices must operate around room temperature and with limited magnetic fields (< 2T), which reduces the pool of functional magnetocaloric materials available drastically [1]. As a result, a significant part of the research on the magnetic refrigeration field focuses on searching for new magnetocaloric materials with a better performance-cost ratio. High-throughput (HT) studies based on first-principles calculations can play a crucial role to detect new magnetocaloric materials and help to estimate trends for material tuning. However, to identify systems of interest from a large body of data, it is necessary to carefully choose the screening parameters such that the accuracy and costs of the calculations are balanced. A key quantity to characterize the performance of these systems is the entropy variation between two magnetic phases. In this previous, we studied the electronic, structural and magnetic properties of bulk FeRh [2] and Gd from first principles aiming to find a reliable non-tailored approach to determine the entropy variation of the magnetocaloric effect. The calculated entropy values are in good agreement with experimental results for the total entropy [1,3], inspiring the development of an HT workflow. In this work, we discuss the developed workflow and the initial results of its application in an initial small search space of approximately 50 structures with potential magnetostructural transitions. Ee identified potential magnetocaloric materials and well-known magnetocaloric Heusler alloys, which attest to the efficiency of our approach.

[1] - T. Gottschall, K. P. Skokov, O. Gutfleisch, *Advanced Energy Materials*, Vol. *9*(34), p.1901322 (2019) [2] - R. M. Vieira, O. Eriksson, H. C. Herper, *Journal of Alloys and Compounds*, Vol. *857*, p.157811 (2021) [3] - D. W. Cooke, F. Hellman, C. Baldasseroni, *Physical Review Letters*, Vol. *109*(25), p.255901 (2012)

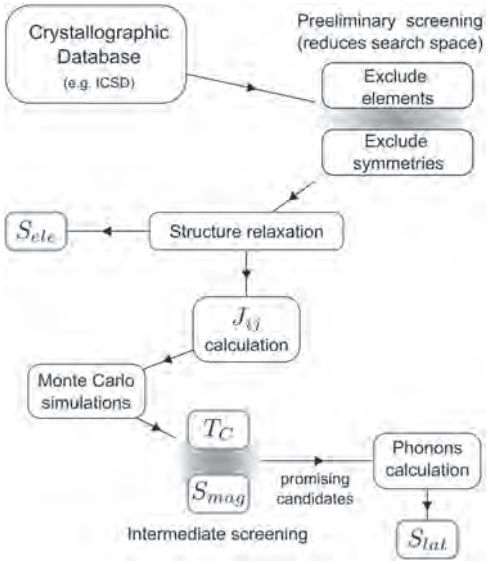

Fig. 1 - Workflow for HT-compatible entropy calculations with intermediate screening processes.

Session FOB
MAGNETOCALORICS II

Fengxia Hu, Co-Chair
Institute of Physics, Chinese Academy of Sciences, Beijing, China
Jia-Yan Law, Co-Chair
University of Seville, Seville, Spain

CONTRIBUTED PAPERS

FOB-01. All-d-metal full Heusler alloys for caloric and spintronic applications. *V.G. de Paula*[1] and M.S. Reis[1] *1. Physics, UFF, Niterói, Brazil*

Heusler alloys are important magnetic materials firstly discovered by Friedrich Heusler more than 100 years ago; and, nowadays, remain a subject of intense research. For this class of materials, p-d orbital hybridization among transition metals and metalloids plays an essential role, rising caloric effects and half-metallicity. However, it also originates mechanical brittleness, undermining its technological exploration. In the last years, the suppression of p-d type hybridization by removal of metalloid atoms and its replacement by other transition metals came up as an efficient approach to overcome this limitation. Here we discuss our recently published review paper [1], covering the recent theoretical and experimental advances in the matter. We address essential questions that arise upon the absence of the metalloids, such as the occurrence of martensitic transition, crystallographic structures, mechanocaloric effects, and spin polarization. Stable Heusler phases are formed based on d-d type hybridizations, combining intense caloric effects with high mechanical ductility. We also highlight some open questions, such as atomic site occupation rule and prediction of half-metallicity, that deserve further attention. Finally, we offer some perspectives that may help guide future research on the subject.

[1] V. G. de Paula and M. S. Reis. All-d-metal full heusler alloys: A novel classof functional materials. Chemistry of Materials, 2021.

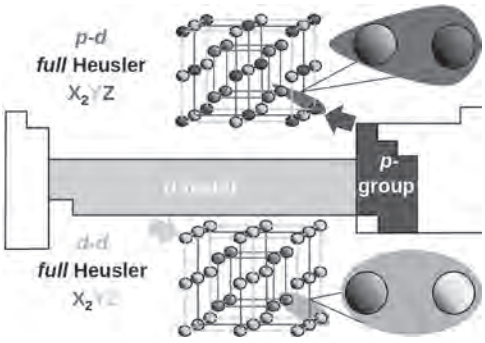

Figure 1: Schematic representation of conventional (p-d) and all-d-metal (d-d) full Heusler alloys. For conventional Heusler, the presence of a metalloid(blue atom) establishes a p-d covalent bonding with the transition metals (green atoms). On the other hand, the replacement by a third transition metal (yellow atoms) originates a more metallic d-d bonding, deeply affecting both mechanical and functional properties of full Heuler compounds.

FOB-02. The local magnetic moment and vibrational properties of Sn in NiMnSn-Heusler alloys during magnetostructural phase transition. *B. Eggert*[1], B. Beckmann[2], J. Lill[1], T. Lojewski[1], S. Rauls[1], F. Scheibel[2], A. Taubel[2], O.N. Miroshkina[1], K. Ollefs[1], R. Brand[1], M. Hu[3], M.E. Gruner[1], O. Gutfleisch[2] and H. Wende[2] *1. Faculty of Physics and Center for Nanointegration Duisburg-Essen (CENIDE), University of Duisburg-Essen, Duisburg, Germany; 2. Materials Science, TU Darmstadt, Darmstadt, Germany; 3. Advanced Photon Source, Argonne National Laboratory, Lemont, IL, United States*

Materials with first-order magnetostructural phase transition exhibit a large magnetocaloric effect and may lead to environmentally friendly and more energy efficient alternatives to conventional vapor compression refrigeration [1]. Here, materials like FeRh [2], La(Fe,Si)13 [3,4] or NiMn-based Heusler alloys exhibit a sizeable magnetocaloric effect, characterized by large adiabatic temperature change ΔT_{ad} and isothermal entropy change ΔS_{iso} at the phase transition temperature [5]. The investigated off-stochiometric NiMnSn Heusler alloy exhibits a first-order phase transition from low temperature ferrimagnetic martensite to high temperature ferromagnetic austenite phase. To identify the driving force of the magnetostructural phase transition, we performed ^{119}Sn nuclear resonant inelastic X-ray scattering (NRIXS) experiments and ^{119}Sn Mössbauer spectroscopy, along the phase transition, to follow the evolution of lattice dynamics, charge density around the Sn-nuclei and the local magnetic moment, respectively, during this transition. In addition to the element-specific investigations, we tracked changes in the electric resistivity and lattice expansion by strain measurements to compare changes in the macroscopic and microscopic electronic and lattice degrees of freedom. Such an investigation is crucial for a deep understanding of the phase transition to maximise the magnetocaloric effect - necessary for future applications at room temperature. ^{119}Sn-NRIXS measurements indicate variations in the Sn-selective phonon density of states that lead to a reduction of the Sn-partial vibrational entropy and a softening of the lattice in the austenite phase. On the other hand, ^{119}Sn-Mössbauer spectroscopy indicates an increase of the transferred hyperfine field of Sn, showing that the local surrounding of the Sn-nuclei varries. We acknowledge the financial support through the DFG (CRC/TRR270, “HoMMage”). This research used resources of the Advanced Photon Source, a U.S. Department of Energy (DOE) Office of Science User Facility operated for the DOE Office of Science by Argonne National Laboratory under Contract No. DE-AC02-06CH11357.

[1] F. Scheibel et al. Energy Technol. 6, 1397-1428 (2018) [2] M. Wolloch et al. Phys. Rev. B 94, 174435 (2016) [3] M. Gruner et al. Phys. Rev. Lett. 114, 057202 (2015) [4] A. Terwey et al. Phys. Rev. B 101, 064415 (2020) [5] T. Gottschall et al. Adv. Energy Mater. 9, 1901322 (2019)

FOB-03. Designing multicaloric materials for a novel multi-stimuli cooling cycle utilizing thermal hysteresis. *A. Taubel*[1], F. Scheibel[1], L. Pfeuffer[1], B. Beckmann[1], W. Liu[1], J. Lemke[1], M. Töllner[1], T. Gottschall[2], S. Ener[1], K. Skokov[1] and O. Gutfleisch[1] *1. Materials Science, Technical University of Darmstadt, Darmstadt, Germany; 2. Dresden High Magnetic Field Lab, Helmholtz-Zentrum Dresden-Rossendorf, Dresden, Germany*

Magneotaloric (MC) refrigeration can be more energy efficient and environmentally friendly than current vapor compression technology [1]. A novel solution has been proposed to enhance the cyclic performance, which benefits from the thermal hysteresis by using two stimuli to trigger the phase transition in a multicaloric material [2]. As a result, higher temperature changes can be achieved for fully reversible phase transitions by the application of magnetic field and uniaxial stress. This approach reduces the amount of permanent magnet material and allows for higher field strengths. In this work, we present the challenges and progress for the multicaloric material development by methods to enhance the functional and mechanical properties. The main objective is adopting the properties for a classical MC cycle towards the extended needs of the multi-stimuli cycle (Fig. 1) and tailoring the desired properties by intrinsic and extrinsic means. One approach is to enhance the mechanical properties of multicaloric Ni-Mn-In [3] Heusler alloys by producing near-net-shape suction cast rods with fine grain sizes (Fig. 2). To tailor the caloric response, we analyzed the influence of the microstructure on the field- and stress induced phase transition as well as the time dependence for different field application rates [4]. We also show that novel all-d Ni-Co-Mn-Ti Heusler alloys [5] have a superior mechanical stability and that introducing secondary phases in Ni-Mn-In by doping can lead to an increase in mechanical stability while maintaining the caloric response for magnetic field changes of 2 T. In a next step, the developed materials are analyzed for their multicaloric performance in a unique test bed, which allows to apply a 9 T magnetic field pulse and a uniaxial stress in one setup. This allows us to assess the cyclic temperature changes that can be achieved for the suitable material systems. This work was supported by the ERC Advanced Grant “CoolInnov” (No 743116), and the CRC/TRR 270 “HoMMage” (DFG).

[1] O. Gutfleisch et al., Adv. Mater. 23, 821-842 (2011) [2] T. Gottschall et al., Nature Mat. 17, 929–934 (2018) [3] A. Gracia-Condal et al., Applied Physics Reviews 7, 041406 (2020) [4] L. Pfeuffer et al., Acta Mater. 217, 117157 (2021) [5] A. Taubel et al., Acta Mater. 201, 425-434 (2020)

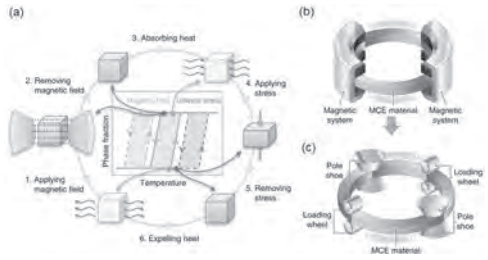

Fig. 1 Schematic of the multi-stimuli cycle utilizing a large thermal hysteresis. [2]

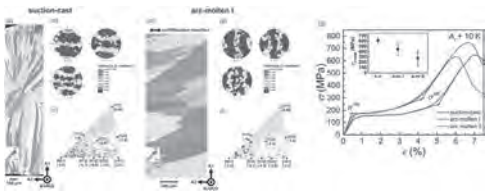

Fig. 2 Microstructure analysis by EBSD of suction-cast (a-c) and arc-molten (d-f) Ni-Mn-In and the correlation with mechanical properties (g). [4]

FOB-04. Micromagnetic phase-field model for magnetostructural transitions in Heusler alloys. *D. Ohmer*[1], M. Yi[2], O. Gutfleisch[1] and B. Xu[1] *1. Materials Science, TU Darmstadt, Darmstadt, Germany; 2. State Key Lab of Mechanics and Control of Mechanical Structures & Key Lab for Intelligent Nano Materials and Devices of Ministry of Education & College of Aerospace Engineering, Nanjing University of Aeronautics and Astronautics, Nanjing, China*

With the increasing standards of living across the world and continuously increasing population, the global energy demand is growing fast, especially for cooling. Magnetocaloric cooling systems have gained attention as promising alternatives to conventional gas compression systems.v[1–3] Heusler alloys show a large magnetocaloric effect due to a magnetostructural transition, resulting in adiabatic temperature changes ΔT_{ad} of up to 8 K,[4] and are promising candidates for magnetocaloric cooling devices.v[5,6] We propose a micromagnetic and multicaloric phase-field model capable of simulating the magnetostructural transition in Heusler alloys. Micromagnetics are used to describe the magnetic subsystem. The magnetic transition is considered by scaling of the magnetic energy terms with the phase order parameter. In this work, the ferromagnetic martensite to paramagnetic austenite and paramagnetic martensite to ferromagnetic austenite transitions are simulated. This model can be used to simulate the field- and pressure dependence of the phase transition temperature T_t, which is of high interest for the multi-stimuli concept proposed by Gottschall et al. [7] For the ferromagnetic martensite and paramagnetic austenite, application of uniaxial pressure and magnetic field shifts T_t towards higher temperatures (Fig. 1a). For the paramagnetic martensite and ferromagnetic austenite (Fig. 1b), the magnetic field shifts T_t to lower temperatures. With the proposed model, stresses and fields needed to fully induce a phase transition can be simulated and support experimental efforts. In addition, due to the implementation of the model in the finite-element (FE) framework MOOSE, [8,9] multi-grain structures can be simulated in the future, to calculate internal stresses during the phase transition. The authors acknowledge the support from the European Research Council (ERC) under the European Unions Horizon 2020 research and innovation programme (Grant agreement No 743116, project CoolInnov) and DFG CRC/TRR270.

[1] C Zimm, A Jastrab, A Sternberg, V Pecharsky, K Gschneidner, M Osborne, and I Anderson. Description and Performance of a Near-Room Temperature Magnetic Refrigerator. In Peter Kittel, editor, Advances in cryogenic engineering, pages 1759–1766. Springer US, Boston, MA, 1998. [2] Oliver Gutfleisch, Matthew A. Willard, Ekkes Brück, Christina H. Chen, S. G. Sankar, and J. Ping Liu. Magnetic materials and devices for the 21st century: Stronger, lighter, and more energy efficient. Advanced Materials, 23(7):821–842, 2011. [3] V. Franco, J.S. S Blázquez, B. Ingale, and A. Conde. The Magnetocaloric Effect and Magnetic Refrigeration Near Room Temperature: Materials and Models. Annual Review of Materials Research, 42(1):305–342, 2012. [4] Tino Gottschall, Konstantin P. Skokov, Bianca Frincu, and Oliver Gutfleisch. Large reversible magnetocaloric effect in Ni-Mn-In-Co. Applied Physics Letters, 106(2):21901, jan 2015. [5] Jian Liu, Tino Gottschall, Konstantin P Skokov, James D Moore, and Oliver Gutfleisch. Giant magnetocaloric effect driven by structural transitions. Nature Materials, 11(7):620–626, 2012. [6] Tino Gottschall, Konstantin P. Skokov, Dimitri Benke, Markus E. Gruner, and Oliver Gutfleisch. Contradictory role of the magnetic contribution in inverse magnetocaloric Heusler materials. Physical Review B, 93(18):2–7, 2016. [7] Tino Gottschall, Adrià Gràcia-Condal, Maximilian Fries, Andreas Taubel, Lukas Pfeuffer, Lluís Mañosa, Antoni Planes, Konstantin P. Skokov, and Oliver Gutfleisch. A multicaloric cooling cycle that exploits thermal hysteresis. Nature Materials, 17(10):929–934, 2018. [8] Brian Alger, David Andrš, Robert W. Carlsen, Derek R. Gaston, Fande Kong, Alexander D. Lindsay, Jason M. Miller, Cody J. Permann, John W. Peterson, Andrew E. Slaughter, and Roy Stogner. MOOSE Web page. https://mooseframework.org, 2019. [9] Derek R. Gaston, Cody J. Permann, John W. Peterson, Andrew E. Slaughter, David Andrš, Yaqi Wang, Michael P. Short, Danielle M. Perez, Michael R. Tonks, Javier Ortensi, Ling Zou, and Richard C. Martineau. Physics-based multiscale coupling for full core nuclear reactor simulation. Annals of Nuclear Energy, 84:45–54, 2015.

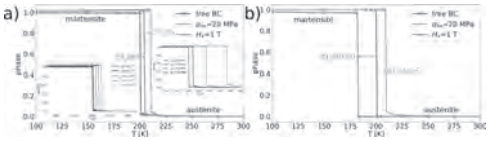

Phase order parameters as a function of temperature, magnetic field and pressure, for a ferromagnetic martensite and paramagnetic austenite on the left, and for a paramagnetic martensite and ferromagnetic austenite on the right.

FOB-05. On the impact of additive manufacturing processes on the microstructure and magnetic properties of Co-Ni-Ga shape memory Heusler alloys. *F. Scheibel*[1], C. Lauhoff[2], S. Riegg[1], P. Krooß[2], E. Bruder[1], E. Adabifiroozjaei[1], L. Molina-Luna[1], S. Böhm[3], T. Niendorf[2] and O. Gutfleisch[1] *1. Material Science, Technical University of Darmstadt, Darmstadt, Germany; 2. Institute of Materials Engineering, University of Kassel, Kassel, Germany; 3. Institute for Production Technologies and Logistics, University of Kassel, Kassel, Germany*

High-temperature shape memory alloys (HT-SMAs) are required in automotive and aerospace applications [1]. HT-SMA Co-Ni-Ga undergo a first-order magneto-structural transformation (FOMST) from *B*2 austenite to $L1_0$ martensite. A fully reversible superelastic response up to 500 °C as well as excellent cyclic stability have been reported for single crystals (SC) [2]. However, polycrystalline Co-Ni-Ga suffers from intergranular cracking and a premature failure after several cycles due to the anisotropic volume change of randomly orientated grains [3]. Additive manufacturing can be used to design SMA with columnar grain or even textured microstructure, preferred for structural integrity. In this study Co-Ni-Ga has been processed using direct energy deposition (DED) and laser powder bed fusion (L-PBF) [4]. A columnar grain structure is established by using both DED and L-PBF (Fig 1). The FOMST and magnetization properties are studied and compared with those of a SC and the as-cast material. A 0.7 at. % and 1.9 at. % loss of Ga is observed for DED and L-PBF processing, respectively. This loss directly effects the saturation magnetization (M_{sat}) and transition temperatures. The L-PBF processed alloy shows a broad FOMST and large thermal hysteresis, while the DED manufactured alloy shows a behaviour being similar to its SC counterpart (Fig 2). The broad FOMST and large hysteresis of the L-PBF sample are attributed to the formation of Co-rich γ′-phase (Fig 1) reducing the Co-content in the surrounding matrix eventually reducing M_{sat} and the Curie-temperature. In addition to the sharp FOMST, the DED manufactured sample provides a columnar grain structure and ⟨001⟩texture along the building direction (BD) (Fig 1). This enables DED processed Co-Ni-Ga alloys to become an alternative for SC or other cost intensive SMAs. This work was supported by the ERC Adv. Grant "CoolInnov", and the CRC/TRR 270 "HoMMage" (DFG) and the DFG grant 398899207.

[1] J. Mohd Jani, M. Leary, A. Subic, M.A. Gibson, Mater. Des. 1980-2015 56, 1078-1113 (2014) [2] P. Krooß, T. Niendorf, P.M. Kadletz, C. Somsen, M.J. Gutmann, Y.I. Chumlyakov, W.W. Schmahl, G. Eggeler, H.J. Maier, Shape Mem. Superelasticity. 1, 6-17 (2015) [3] C. Lauhoff, M. Vollmer, P. Krooß, I. Kireeva, Y.I. Chumlyakov, T. Niendorf, Shape Mem. Superelasticity. 5, 73-83 (2019) [4] F. Scheibel, C. Lauhoff, S. Riegg, P. Krooß, E. Bruder, S. Böhm, T. Niendorf, O. Gutfleisch, "On the impact of additive manufacturing processes on the microstructure and magnetic properties of Co-Ni-Ga shape memory Heusler alloys", submitted to Materials & Design, under review

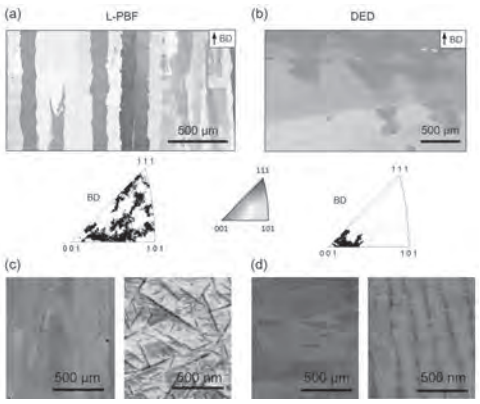

Fig 1. EBSD IPF mapping of (a) L-PBF and (b) DED processed, with respect to the BD. HR-SEM shows γ′-phase in the L-PBF sample (c), no γ′-phase in observed after DED (d).

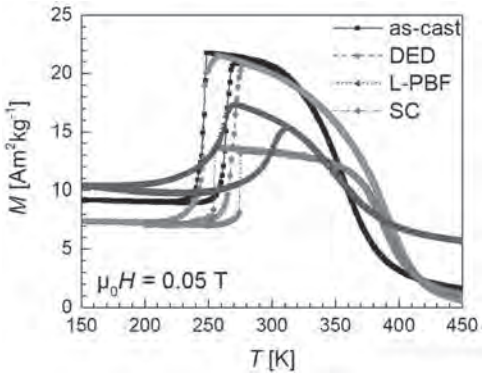

Fig 2. Temperature dependent magnetization Co49Ni21Ga30 SC, L-PBF and DED processed well as an as-cast alloy.

FOB-06. Extrusion-Based 3D Printing of Magnetocaloric Structures. *V. Sharma*[1], L. Balderson[2], R. Heo[3], C. Hunt[2], H. Zhao[1], R.L. Hadimani[1] and R. Barua[1] *1. Mechanical and Nuclear Engineering, Virginia Commonwealth University, Richmond, VA, United States; 2. Department of Chemistry, Viriginia Commonwealth University, Richmond, VA, United States; 3. Department of Biomedical Engineering, Virginia Commonwealth University, Richmond, VA, United States*

Magnetic refrigeration is an energy-efficient, environmentally-friendly alternative to conventional vapor-compression cooling technology. There are several magnetic cooling device designs in existence today that are potentially commercially viable, on condition that that suitable working materials can be developed. This challenge is unresolved due to issues associated with shaping the mostly brittle magnetocaloric alloys into thin-walled channeled regenerator structures to facilitate efficient heat transfer between the solid refrigerant and the heat exchange fluid in an active magnetic regenerator (AMR) cooling device. To address these challenges, we have developed an extrusion-based additive manufacturing (AM) method to 3D print porous magnetocaloric structures.[1] This AM technique's novelty lies in the initial material feedstock comprising of magnetic particles (upto ~ 85 wt%) and sacrificial polymer binders dispersed in a multi-solvent system. While the solvents control the ink rheology, the polymers bind the magnetic particles, enabling retention of the regenerator architecture. Next, a two-step sintering process removes the binder and subsequently promotes grain growth and densification of the final finished part. Research efforts involving $La_{0.6}Ca_{0.4}MnO_3$ nanoparticles will be presented. Figure 1 shows that the magnetocaloric response (indicated by the magnetic entropy change) of the 3D printed test scaffold is only ~17% lower than that of the precursor particles. Spatially designed structures with channel dimensions of 150 µm

were obtained to exhibit the effectiveness of this fabrication process. The microstructures and porosity of the as-printed and sintered samples will be discussed in the context of results obtained via 3D X-ray computed tomography. Overall, this study provides strategies for realizing low-cost magnetic regenerators, thus potentially eliminating one of the main barriers to commercialization of magnetic cooling technology.

[1]H. Zhao, R. Barua and R. Hadimani, "3D Printed Magnetocaloric Devices with Controlled Micro-channels and Magnetic Anisotropy and Methods of Making the Same", Application (#69/928, 002).

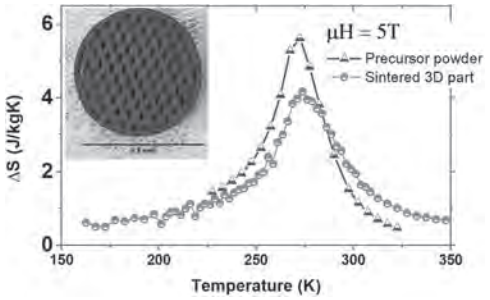

Fig 1. Magnetic entropy change curves of $La_{0.6}Ca_{0.4}MnO_3$ powders and corresponding 3D printed structure. Inset shows a printed sample with channeled structure.

FOB-07. Multifunctional magnetic composites based in meta-magnetic shape memory alloys for 3D printing applications. *D. Khanna*[1,2], V.S. Alarcos[1,2], V.R. Callardo[1,2] and J. Pérez-Landazábal[1,2] *1. Sciences, Public University Of Navarra, Pamplona, Spain; 2. Institute for Advanced Materials and Mathematics INAMAT2, Pamplona, Spain*

The possibility of inducing a structural martensitic transformation by applying a magnetic field in meta-magnetic shape memory alloys gives rise to interesting properties such as magnetic actuation, giant magnetoresistance, or giant inverse magneto-caloric effect, which make these alloys very attractive for practical applications in sensing and magnetic refrigeration. Composites made from polymer matrix with meta-magnetic shape memory powder have been recently proposed to overcome the intrinsic brittleness of the bulk alloys. This, in fact, opens the possibility of the use of particles for additive manufacturing purposes. The production, characterization, and optimization of the properties of powder particles are therefore milestones to get valuable functional composites. In the present work, the martensitic transformation and the magnetic properties of $Ni_{45}Co_5Mn_{37}In_{13}$ powder microparticles obtained by ball milling have been studied. Even for very large milling times, a considerable dispersion in the particle size is observed in all the samples. Nevertheless, it is found that the characteristic of the transformation and the magnetic response is exactly the same in those particles with the same particle size, irrespective of the milling time. A direct correlation between size and deformation can be then established, from which the effect of mechanically induced microstructural defects on the magnetism is analyzed. The effect of mechanically induced defects on the magnetocaloric effect and the viability of the use of the studied microparticles for composite elaboration are also analyzed. Polymer composites have been elaborated by embedding the micro/nanoparticles in a mixture of polylactic acid(PLA) and poly-caprolactone(PCL). In order to get 3D printable wires with optimum mechanical properties and good magnetic response, the particles size, polymers fractions, and particles concentration have been varied. The magnetic response and printability of the obtained filaments have also been studied.

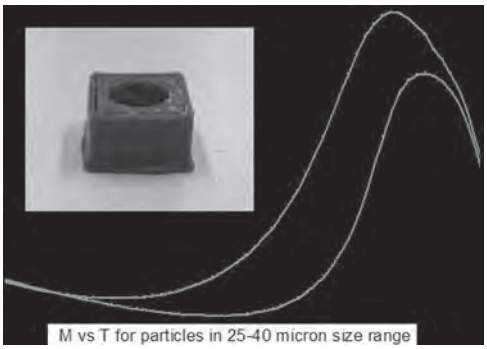

Magnetization values at 100 Oe magnetic field for annealed particles in the size range of 25-40 microns (inset- 3D printed composite with the corresponding particles)

FOB-08. Magnetocaloric Heusler Alloy Composites for Fused Deposition Modeling. *Á. Díaz-García*[1], J. Law[1], L. Zrodowski[2], B. Moronczyk[3], R. Wroblewski[3] and V. Franco[1] *1. Condensed Matter Physics, University of Seville, Seville, Spain; 2. AMAZEMET, Warsaw, Poland; 3. Faculty of Materials Science and Engineering, Warsaw University of Technology, Warsaw, Poland*

The use of composites combining a thermoplastic and functional fillers for additive manufacturing (AM), as in fused deposition modeling, FDM, provides a path for low cost development of functional parts with complicated geometries [1]. Magnetic refrigeration requires refrigeration beds with intricate geometries for the passage of the heat transfer fluid. Heusler alloys exhibiting magneto-structural transformation (MST) are attracting enormous attention as they can show a large response without relying on critical elements [2]. However, machinability of these alloys is compromised, making AM attractive for the fabrication of the refrigerator beds. Off-stoichiometry Ni_2MnGa Heusler powder has been obtained by ultrasonic atomization, resulting in spheric particles subsequently sieved at 100 μm (Fig. 1). Differential scanning calorimetry (DSC) enabled to identify the MST in the atomized Heusler alloy (Fig. 2(a)). This powder was used to fill customized PLA capsules that were used as the feedstock for the extrusion of composite filaments for FDM according to the method showed in Ref. [3]. Composite filaments were manufactured with different concentrations of fillers ranging from 30 to 64 wt. %, determined by thermogravimetric analysis, TGA, (Fig. 2(b)). As the particles were not subjected to high temperatures during the extrusion of the filaments (less than 200 °C), the phases present in the alloy do not change. The AM of magnetocaloric parts can avoid the shape limitation and, in this case, the polymer matrix would prevent the weakening of the structure due to the successive volume changes taking place with the cyclical occurrence of an MST. Work supported by AEI/FEDER-UE (grant PID2019-105720RB-I00), US/JUNTA/FEDER-UE (grant US-1260179), Consejería de Economía, Conocimiento, Empresas y Universidad de la Junta de Andalucía (grant P18-RT-746), Army Research Laboratory under Cooperative Agreement Number W911NF-19-2-0212 and POB "Technologie Materialowe" of Warsaw University of Technology within the Excellence Initiative: Research University (IDUB) program.

[1] X. Wang, M. Jiang, Z. Zhou, J. Gou, D. Hui, 3D printing of polymer matrix composites: A review and prospective, Compos. Part B Eng. 110, 442–458 (2017). [2] V. Franco, J.S. Blázquez, J.J. Ipus, J.Y. Law, L.M. Moreno-Ramírez, A. Conde, Magnetocaloric effect: from materials research to refrigeration devices, Prog. Mater. Sci. 93, 112–232 (2018). [3] Á. Díaz-García, J.Y. Law, A. Cota, A. Bellido-Correa, J. Ramírez-Rico, R. Schäfer, V. Franco, "Novel procedure for laboratory scale production of composite functional filaments for additive manufacturing," Mater. Today Commun. 24, 101049 (2020).

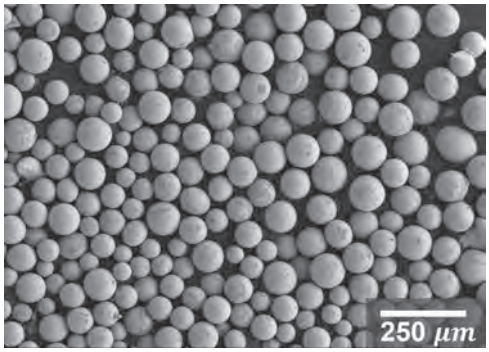

Fig. 1. Scanning electron micrograph of Ni_2MnGa powder.

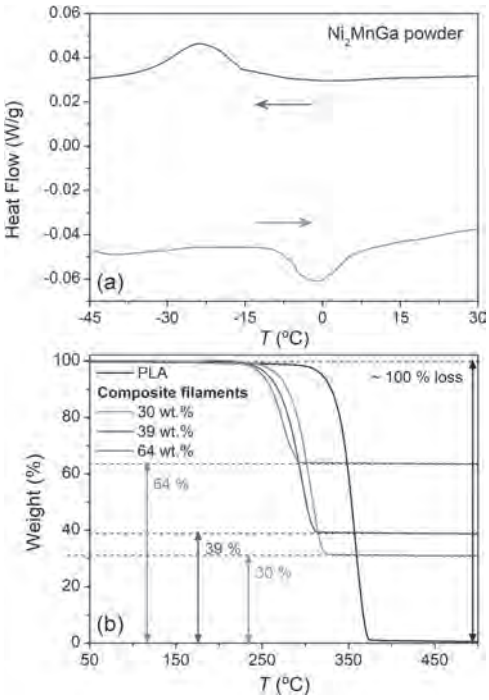

Fig. 2. (a) DSC results of Heusler powder and (b) TGA curves of raw PLA and PLA-based composite filaments.

FOB-09. Temperature First Order Reversal Curves (TFORC) distributions and their relation to magnetocaloric performance.
L.M. Moreno-Ramírez[1] and V. Franco[1] *1. University of Seville, Seville, Spain*

Temperature First Order Reversal Curve (TFORC) distributions of thermal hysteresis is a novel technique to characterize first-order phase transition of magnetocaloric materials (MCM) [1]. At this early stage the theory supporting the interpretation of the diagrams is still under development [2]. Based on simple phenomenological models, we were able to interpret some distinct features of the distributions in terms of the characteristics of the transformations, in agreement with those obtained experimentally [3]. In order to search for new tools for the optimization of MCM, we extended the analyses in order to correlate TFORC distributions and magnetocaloric performance of the materials as both are directly linked to the characteristics of the transformations. Magnetostructural transformations have been modeled using Brillouin function for describing the magnetic behavior of the different phases, with the addition of skew-normal distributions for simulating the phase transformations. The different parameters of the skew-normal distribution have been modified without variation of the transformation width and the thermal hysteresis in order to stablish a fair comparison among the different transformations. Figure 1 shows a set of symmetric and right and left skewed magnetic transformations (a), their corresponding TFORC distribution (contour line at 0.5) (b) and the reversible magnetocaloric performance (c). We conclude that the most favorable case for moderately large fields is the one having left skewed transformations (e.g. 15 % larger than right skewed case), which corresponds with a triangular TFORC distribution with the symmetry axis parallel to T_h axis and its vertex pointing to the right.

[1] V. Franco et al. IEEE Magnetics Letters, 2016, 7, 6602904. [2] L.M. Moreno-Ramírez et al. Metals, 2020, 10, 1039 [3] Á. Díaz-García et al. Journal of Alloys and Compounds, 2021, 867, 159184

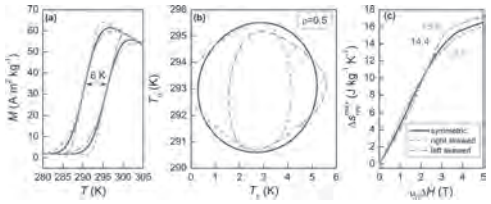

Figure 1. Magnetic transition (a), contour line of the TFORC distribution at 0.5 (b) and reversible isothermal entropy change (c) for a set of symmetric and right and left skewed transformations.

FOB-10. Enhanced Magnetocaloric Response of High-Entropy Alloy Microwires due to Induced Nanocrystals by Current Annealing.
H. Yin[1,2], J. Law[2], Y. Huang[1], H. Shen[1], S. Jiang[3], S. Guo[1] and V. Franco[2]
1. School of Materials Science and Engineering, Harbin Institute of Technology, Harbin, China; 2. Condensed Matter Physics, University of Seville, Sevilla, Spain; 3. Space Environment Simulation Research Infrastructure, Harbin Institute of Technology, Harbin, China

High-entropy alloys (HEAs), whose new alloy design concept with multiple principal elements, attracted a lot of attention for structural application and functional aspects. Since their first report in 2004, their compositions have developed from first generation with quinary equiatomic single-phase to second-generation multi-phase structure with non-equiatomic compositions. For magnetocaloric HEAs, their limitations have been recently found to be overcome by using non-equiatomic HEA compositions: GdTbCoAlFe (with Curie temperatures up to 108 K) overcomes the low temperature limit of the rare-earth-containing HEAs (typically saturates around < 60 K) [1,2] and the first-order magnetostructural phase transition in FeMnNiGeSi surpasses the smeared out magnetocaloric effect (MCE) of rare-earth-free HEAs [3,4]. In this work, we further enhance the MCE of non-equiatomic $Gd_{34.9}Tb_{19.4}Co_{19}Al_{23.3}Fe_3$ HEA through microstructural control, in which the alloy microwires are annealed using the current density annealing technique. Induced nanocrystals in the amorphous matrix observed from transmission electron microscopy (TEM) are found to increase and grow with the current density magnitude (Fig. 1). This leads to an increase in the working temperature span of the HEA microwires and at the same time offers a relative cooling power (*RCP*) comparable to many reported amorphous MCE alloys, both conventional alloys and HEAs (Fig. 2). Our findings pave a pathway for further optimizing MCE through appropriate processing methods on top of careful alloy design selection.

[1] H. Yin, Y. Huang and Y. Bao, Journal of Alloys and Compounds, vol. 815, p. 150983 (2020) [2] H. Yin, J. Law and Y. Huang, Materials & Design, vol. 206, p. 109824 (2021) [3] J. Law, L. Moreno-Ramírez and Á Díaz-García, Journal of Alloys and Compounds, vol. 855, p. 157424 (2021) [4] J. Law, Á Díaz-García and L. Moreno-Ramírez, Acta Materialia, vol. 212, p. 116931 (2021)

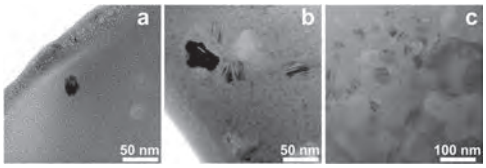

Fig. 1 TEM results of the (a) as-cast and annealed $Gd_{34.9}Tb_{19.4}Co_{19}Al_{23.3}Fe_3$ microwires using current density values of (b) 50 and (c) 100 x 10^6 A m^{-2}.

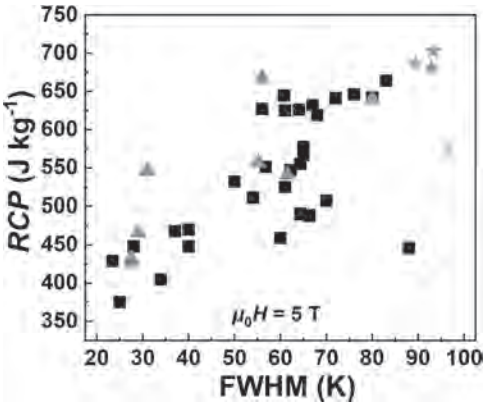

Fig. 2 Literature comparison of *RCP* as a function of full-width at half maximum (FWHM) for studied microwires (star symbols) versus amorphous conventional alloys (triangles) and HEAs (squares).

FOB-11. Shape Memory Effect in Ni_2FeGa Heusler Glass-Coating Microwire. L. Frolova[1], M. Hennel[1], P. Sarkar[1], L. Nulandaya[1,3], L. Galdun[1,2], T. Ryba[2] and *R. Varga[1,2] 1. Center of Progressive Materials, TIP UPJS, Kosice, Slovakia; 2. RVmagnetics, Kosice, Slovakia; 3. Inst. Exp. Phys., Slovak Academy of Sciences, Kosice, Slovakia*

Miniaturization of materials with shape memory effect allows for their applications in small devices. Heusler-based glass-coated microwires belongs to such a group of materials as they offer easy production of large amount of microwires within short time (up to kilometer of microwire can be produced from 1 gram of master alloy within 10 minutes) [1]. One of the best Heusler composition for shape memory application is based on Ni_2MnGa [2]. However, the Taylor Ulitovski method of microwires production bring some disadvantages as it prevents from production of manganese-based microwires due to the evaporation of manganese during production. Therefore, analogical composition are necessary. One of example is Ni_2FeGa based alloy (fig.1). It allows easy and repeatable production of large amount of shape memory microwires, offering also reduced (comparing to NiMnGa-based one), but still significant magnetocaloric effect and also barocaloric effect. In the given contribution, we show how the martensitic transformation can be easily tailored by properly selecting the chemical composition (controlling the valence electron density) of Ni_2FeGa based microwire in order to obtain such transformation just above the room temperature. We also show, how the Curie temperature can be adjusted to be close to structural transformation temperature by alloying 4 at.% of Al, B, In, enhancing thus the performance of shape memory microwires. Microwire's shape offer another advantage of change of easy axis during the phase transition, which allows for precise monitoring of transformation stage through the measurement of permeability (which shows over 1200% change with 2 % contraction due to transformation – fig.2) or magnetoimpedance. Such a feature transforms microwires to SMART miniaturized actuators that can monitor by itself their stage of actuation.

[1] M. Vazquez, Magnetic nano-and microwires, Elsevier, 2015. [2] O. Heczko, P. Vertat, M. Vronka, V. Kopecky, O. Perevertov, *Shape memory superelasticity* 2 (2016) 272.

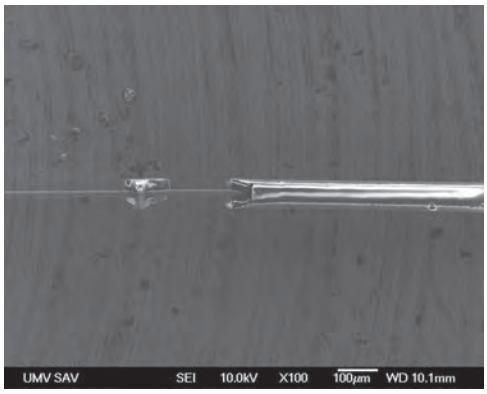

Figure 1: SEM image of glass-coated Ni_2FeGa microwire.

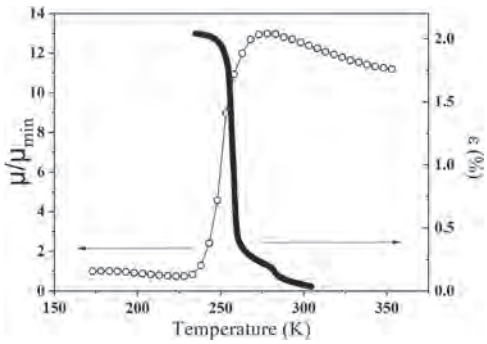

Figure 2: Temperature dependence of strain and permeability of Ni_2FeGa glass-coated microwires.

FOB-12. Withdrawn

Session FOC
MAGNETOELASTICS AND MAGNETOOPTICS

SN Piramanayagam, Co-Chair
Nanyang Technological University, Singapore, Singapore
Radhika Barua, Co-Chair
Virginia Commonwealth University, Richmond, VA, United States

INVITED PAPER

FOC-01. Conditions for effective coupling between surface acoustic waves and spin waves. N.K. Babu[1], A. Trzaskowska[1], P. Graczyk[2], G. Centala[1], S. Mieszczak[1], H. Glowinski[2], M. Zdunek[1], S. Mielcarek[1] and *J.W. Klos*[1] *1. ISQI, Faculty of Physics, Adam Mickiewicz University in Poznan, Poznan, Poland; 2. Institute of Molecular Physics, Polish Academy of Sciences, Poznan, Poland*

The frequencies and wave vectors of dipolar dominated spin waves (SW) and surface acoustic waves (SAW) cover the same ranges. Therefore, the propagating waves of both kinds can potentially scatter each other - in other words, the necessary condition for the interaction in a linear regime can be satisfied. The simplest structure in which the magnetoelastic coupling between SW and SAW can be observed is the magnetostrictive layer deposited on the substrate. The confinement of SWs in the magnetic layer is necessary to induce the dipolar interaction and surface localization of SAW ensures the co-existence of both kinds of waves in the magnetostrictive layer deposited on the surface. The strength of the magnetoelastic interaction depends on the orientation of the wave vector concerning the direction of the static magnetic field[1]. Moreover, this interaction is different for different types of SAWs, specifically, Rayleigh-SAWs (R-SAW) and Love-SAWs (L-SAW)[1,4] – see Fig.1. Thus, the coupling is strongly anisotropic and cannot be observed for arbitrary selected SAWs and SWs, even if their frequencies and wave vectors match. This effect is well-known and broadly discussed in the literature[1]. Our study shows an additional factor limiting the interaction between SAWs and SWs. The SAW/SW coupling proves to require an appropriate profile of the elastic wave near the surface of the magnetostrictive structure, at distances much smaller than the wavelength. For R-SAWs the tangential component of displacement u_x can have nodes within the magnetic layer, resulting in a reduction of the net strength of magnetoelastic interaction even if the strain ε_{xx} is locally significant. In an L-SAW the displacement u_y does not have any nodes (u_y changes monotonously in the normal direction). We have shown that this additional factor plays a role for some types of surface acoustic waves (R-SAWs), while other types (L-SAWs) are insensitive to it. We think that the studies on magnon-phonon interaction in confined geometries (surfaces, cavities) are very promising and can reveal unusual interaction mechanisms. *Sample* We studied $[Co_{20}Fe_{60}B_{20}/Au]_{20}$ multilayer of the thickness 60 nm as a magnetostrictive medium. In $Co_{20}Fe_{60}B_{20}$ layers (2.1 nm) the magnetization is oriented in-plane and the presence of Au layers (0.9 nm) reduces the SWs' frequencies due to out-of-plane anisotropy. The multilayer was deposited on top of a 4 nm titanium (Ti) and a 15 nm gold (Au), which buffers the naturally oxidized (001) silicon substrate. *Method* We measured the dispersion relations of thermally excited SAWs and magnetostatic SWs using a six-pass tandem Brillouin spectrometer (Scientific Instrumentsc©TFP2-HC), which ensures a contrast of 10^{15}. A frequency-stabilized diode-pumped solid-state laser (Coherentc©VERDI V5) operating at λ_0= 532 nm was used as a source of incident light. The measurements were performed in the 180° backscattering geometry with crossed (p-s)polarization of the incident and scattered light for SWs and non-crossed (p-p) polarization for SAWs. Using the finite element method in COMSOL Multiphysics©, we solve numerically the coupled equations of motion for magnetization and mechanic displacement. *Acknowledgement* The authors hereby acknowledge the financial support from the National Science Centre, Poland, project No. UMO-2016/21/B/ST3/00452. S. Mies. would like to additionally acknowledge the support from the National Science Centre, Poland, project No. UMO-2020/36/T/ST3/00542.

[1] L. Dreher, M. Weiler, M. Pernpeintner, et al., Phys. Rev. B, Vol. 86, p. 134415 (2012) [2] N. K. P. Babu, A. Trzaskowska, P. Graczyk, et al., Nano Lett., Vol. 21, p.946 (2020) [3] Y. Hashimoto, D. Bossini, T. H. Johansen, et al., Phys. Rev., Vol. 97, p.14040 (2016) [4] M. Geilen, F. Kohl, A. Nicoloiu, et al., Appl. Phys. Lett., Vol. 117, p. 213501 (2020) [5] N.E. Khokhlov, P.I. Gerevenkov, L.A. Shelukhin, et al., Phys. Rev. Applied, Vol. 12, p. 044044 (2019)

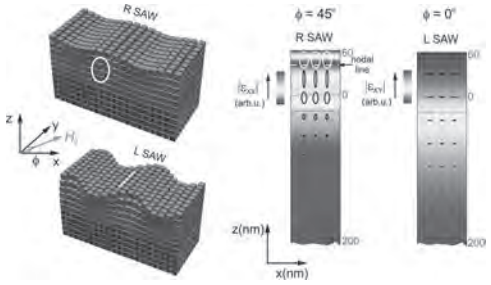

Fig.1 (left) - the illustration of the Rayleigh and Love surface acoustic waves (R SAW and L SAW). (right) -the numerically calculated profiles of the strain tensor playing the most significant role for magnetoelastic interaction of spin waves with R SAW (magnetic field applied the 45 deg) and L SAW (magnetic field applied at 0 deg). Please note that the interaction with R SAW can be canceled due to the nodal line.

CONTRIBUTED PAPERS

FOC-02. Enhanced Magnetic Actuation of Magnetorheological Elastomers Using Nano-Magnetic Particles. *L. Cestarollo*[1], S. Smolenski[3] and A. El-Ghazaly[2] *1. Materials Science and Engineering, Cornell University, Ithaca, NY, United States; 2. Electrical and Computer Engineering, Cornell University, Ithaca, NY, United States; 3. Physics, Bowdoin College, Brunswick, ME, United States*

Magnetorheological elastomers (MREs) constitute ideal candidates for enabling magnetic control and reconfigurability of soft, integrated interfaces, such as valves for microfluidics, tactile displays for haptics, or actuators for flexible electronics or robotics [1-2]. MREs are composite materials made of a soft elastomeric matrix and magnetic micro- or nanoparticles. Just a few studies have focused on the actuation of MREs, which can undergo very large and rapid deformations upon application of magnetic fields [3–5]. Additionally, prior studies primarily fabricated MREs utilizing relatively large particles with sizes on the micron scale [2–8], which prevent these materials from being utilized to recreate shapes requiring sharp film curvatures in small spaces. We fabricated films with isotropic and anisotropic particle arrangements with different compositions. Anisotropic films present a steeper magnetization curve with larger remanent magnetization than their isotropic counterparts (Fig. 1a). Also, the stiffness of the films

increases at a faster rate than the magnetization as a function of nanoparticle content (Fig. 1b). Therefore, for concentrations larger than 6 vol%, even if a film contains more nanoparticles (determining a larger actuation force), the film will not be able to stretch significantly more due to its stiffer nature (Fig. 2). Our isotropic films exhibit drastically higher deflections compared to other studies [3–5], up to 17x the deflections reported in Marchi et al. [5]. Our optimal film is able to deform up to 734 μm upon application of ~100 mT, and up to 1.59 mm at ~290 mT (the highest field measured). Finally, we implemented our optimized MRE films in a programmable and real-time reconfigurable tactile display for the visually impaired.

[1] H. Böse, T. Gerlach, and J. Ehrlich, Journal of Intelligent Material Systems and Structures, vol. 0, no. 0, pp. 1–15, 2021. [2] N. Lazarus, C. D. Meyer and S. S. Bedair, vol. 7, no. 19, pp. 10080–10084, 2015. [3] F. Pirmoradi, L. Cheng, and M. Chiao, Journal of Micromechanics and Microengineering, vol. 20, no. 1, p. 015032, 2009. [4] W. Wang, Z. Yao and J. C. Chen, vol. 14, no. 10, pp. 1321–1327, 2004. [5] S. Marchi, A. Casu and F. Bertora, ACS Appl. Mater. Interfaces, vol. 7, no. 34, pp. 19112–19118, 2015. [6] S. R. Mishra, M. D. Dickey and O. D. Velev, Nanoscale, vol. 8, no. 3, pp. 1309–1313, 2016. [7] M. Ashjari, A. R. Mahdavian and N. G. Ebrahimi, Journal of Inorganic and Organometallic Polymers and Materials, vol. 20, no. 2, pp. 213–219, 2010. [8] Y. Tong, X. Dong, and M. Qi, Soft Matter, vol. 14, no. 18, pp. 3504–3509, 2018.

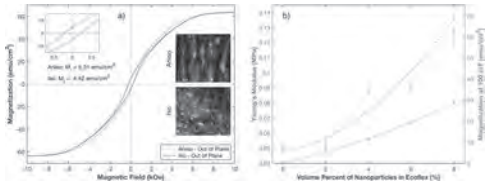

Fig. 1: a) M vs H hysteresis loops for isotropic and anisotropic 6 vol% films and their cross-sectional structure imaged via cryo-SEM. b) Young's moduli of the isotropic samples along with the respective magnetization values measured in the out-of-plane direction at an applied field of about 100 mT.

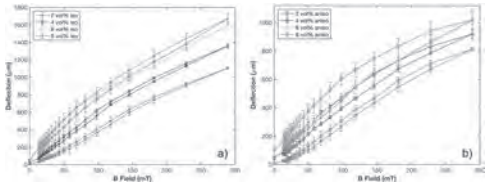

Fig. 2: Deflection measurements with hysteresis loops for a) isotropic, and b) anisotropic samples at different nanoparticle loadings.

FOC-03. Enhanced Magnetostriction in Galfenol Through Dilute Ce-Doping. *A. Baker*[1], H. Henderson[1], E.E. Moore[1], M. Islam[2], Y. Ijiri[3], M. Willard[2] and S.K. McCall[1] *1. LLNL, Livermore, CA, United States; 2. Case Western Reserve University, Cleveland, OH, United States; 3. Oberlin College and Conservatory, Oberlin, OH, United States*

Magnetostrictive materials such as FeGa (Galfenol) provide high precision solid-state sensing capabilities, with applications in magnetic field sensing, load cells, or tunable inductor circuits. The magnetostrictive coefficient in Galfenol can be enhanced by doping rare earth elements, with recent reports showing that light rare earths such as Ce or La are particularly effective. Work by He *et al.*[1] studying trace doping across the RE series ascribed this improvement to distortions of the lattice and the quadrupole moment of the dopant. Further, it was observed that the ideal doping of La is around 0.2 at. %. Here we demonstrate that significant enhancements can be achieved with much lower levels of Ce (see Fig. 1), motivated by CALPHAD studies of the Fe-Ga-Ce phase diagram, which identified the solubility limit of Ce in FeGa. Higher Ce levels lead to the formation of a deleterious CeGa2 phase, which can be suppressed by quenching from elevated temperatures. Experimental results confirm that additional Ce does not further enhance performance. A comprehensive study of Ce additions will be presented, identifying the conditions required to achieve optimal properties. Prepared by LLNL under Contract DE-AC52-07NA2

[1] Yangkun He, Chengbao Jiang, Wei Wu, Bin Wang, Huiping Duan, Hui Wang, Tianli Zhang, Jingmin Wang, Jinghua Liu, Zaoli Zhang, Plamen Stamenov, J.M.D. Coey, Huibin Xu, *"Giant heterogeneous magnetostriction in Fe–Ga alloys: Effect of trace element doping"*, Acta. Mat. 109, 177 (2016)

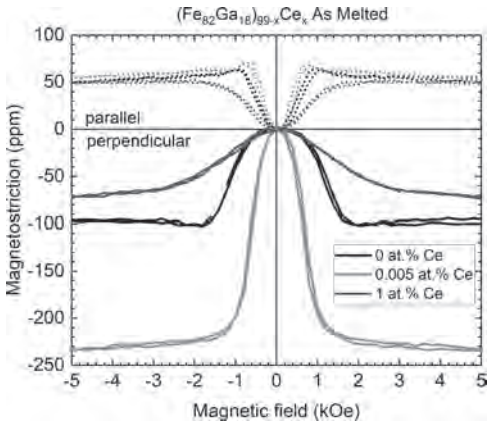

Figure 1 Magnetostriction of polycrystalline FeGa samples measured with applied field in the plane of the sample, aligned parallel and perpendicular to the surface-mounted strain gauge, yield positive and negative length change, respectively. Dilute Ce doping leads to a significantly enhanced magnetostriction relative to the pristine or over-doped sample.

FOC-04. Evolution of magnetic order under high fields and external pressure in metallic Fe_3Ga_4. *B. Wilfong*[1], V. Sharma[2], A. Fedorko[3], O. Bishop[2], X. Zhou[5], G.M. Stephen[4], A.L. Friedman[4], D. Heiman[3], R. Barua[2] and M.E. Jamer[1] *1. Physics, United States Naval Academy, Annapolis, MD, United States; 2. Mechanical and Nuclear Engineering, Virginia Commonwealth University, Richmond, VA, United States; 3. Physics, Northeastern University, Boston, MA, United States; 4. Laboratory for Physical Science, College Park, MD, United States; 5. Argonne National Laboratory, Lemont, IL, United States*

Magnetic ordering and magnetic phase transitions near room-temperature in metallic systems are of key interest fundamentally and for possible device implementation. A system of recent interest is the intermetallic Fe_3Ga_4 which crystallizes in a complex monoclinic unit cell which houses many significant nearest and next-nearest neighbor interactions that dictate the magnetic ordering in the system. Single crystal Fe_3Ga_4 was synthesized through a chemical vapor transport method to yield needle-like single crystals. Magnetic measurements at ambient pressure reveal similar behavior to previous work with complex magnetic ordering evolution where a ferromagnetic (FM) ground state is supplanted by an intermediate antiferromagnetic (AFM) state before transitioning back to an FM state, shown in Figure 1. Importantly, the nature of the intermediate AFM state which exists at room temperature is unknown but displays elaborate evolution with applied field and applied pressure. High applied field within the AFM state shows anisotropic behavior depending on applied field direction but metamagnetic behavior is observed in all field directions. With high enough applied field, the AFM state transitions to a fully field-polarized FM state which systematically increases the magnetic saturation of the FM state down to base temperature. Electrical resistivity measurements reveal metallic behavior across the entire temperature range below 400 K with no observable anomalous behavior but confirms the metallic antiferromagnetic nature of Fe_3Ga_4 at room temperature (Figure 1). Applied pressure has a robust effect on the magnetic ordering in this system whereby increased external pressure drives the FM-AFM transition to higher temperatures and

the FM-AFM transition to lower temperatures shown in Figure 2. These measurements position Fe_3Ga_4 as metallic and antiferromagnetic material at room temperature for which the magnetic state has been shown to be tunable with temperature, pressure, and magnetic field. This has important implications for exploiting the room temperature properties for applications as well as to understand the fundamental physics which drives the exotic intermediate AFM phase.

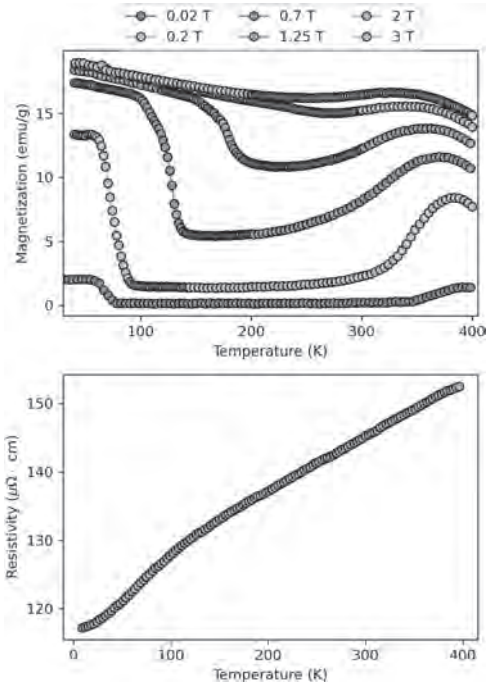

Figure 1

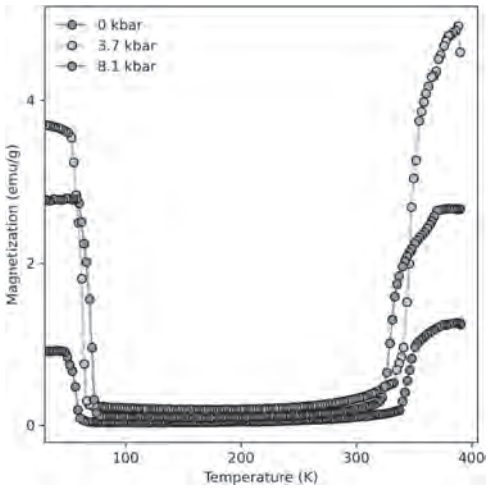

Figure 2

FOC-05. Large room-temperature reversible barocaloric effect in $MnCoGe_{0.99}In_{0.01}$ alloys at low pressure. *Z. Yu*[1,2], F. Hu[1,2], J. Wang[1,2], S. Jirong[1,2] and B. Shen[1,2] *1. Beijing National Laboratory for Condensed Matter Physics & State Key Laboratory of Magnetism, Institute of Physics, Chinese Academy of Sciences, Beijing, China; 2. School of Physical Sciences, University of Chinese Academy of Sciences, Beijing, China*

Solid-state refrigeration materials have various thermal effects, among which the hydrostatic pressure is an economical and practical method to drive the barocaloric effect (BCE) of brittle materials[1,2]. The BCE is ubiquitous in first-order phase transition materials, and its packaging technology is not limited to the shape of the materials[3,4]. In the brittle magnetocaloric materials $MnCoGe_{0.99}In_{0.01}$, there is a low-pressure induced large reversible BCE near room temperature, which avoids part of the refrigeration capacity reduction caused by hysteresis loss[5]. Here, we report the BCE of $MnCoGe_{0.99}In_{0.01}$ at hydrostatic pressure of 1kbar by variable-pressure calorimetry. Fig.1a shows the temperature dependence of the heat capacity dQ/dT of $MnCoGe_{0.99}In_{0.01}$ at different hydrostatic pressures after baseline subtraction, it can be found that the thermal hysteresis (ΔT_{hys}) at 1bar is 8.8K and the phase transition temperature moves to lower temperature with the increase of pressure. The linear fitting relationship between the transformation temperature shifts with the pressure (dT/dP) is obtained according to the heating and cooling transformation temperature under different pressures, as shown in the inset of Fig. 1b. The dT/dP is -10.6K/kbar in the heating process and is -8.7K/kbar in the cooling process. The entropy curve S(T,P) of $MnCoGe_{0.99}In_{0.01}$ during heating and cooling process was obtained by the calorimetric curves(Fig. 1a) through the pressure-dependent integrations across the phase transition, as shown in Fig.1b. We evaluated the reversible parts (ΔS_{rev} and ΔT_{rev}) of entropy change ΔS and adiabatic temperature change ΔT at 1kbar from the overlapping of the irreversible ΔS and ΔT during application and removal of pressure, as shown in Fig.1c and 1d, where the shaded areas represent the ΔS_{rev} and ΔT_{rev}, respectively. The relative narrow ΔT_{hys} and high driving rate dT/dP under pressure are more conducive to achieve large ΔS_{rev} and ΔT_{rev}. The ΔS_{rev} of 19J/kg K and ΔT_{rev} of 2.9K within a temperature span of 56K at 1kbar have been achieved. The refrigeration capacity of $MnCoGe_{0.99}In_{0.01}$ at 1kbar is as high as 373J/kg K.

1. Araceli Aznar, Pol Lloveras, et al., *Advanced Materials, 31, 1903577(2019).* 2. Jiazheng Hao, Fengxia Hu, Zibing Yu, et al., *Chem. Mater.*, 32, 1807(2020). 3. F.B. Li, M. Li, et al.,*Nat. Commun.*, 11, 4190 (2020). 4. Hongwei Liu, Zhe Li, et al.,*Scripta Mater.*, 177 (2020). 5. Rong-Rong Wu, Li-Fu Bao, Feng-Xia Hu, et al., *Scientific Reports,* 5, 18027(2015).

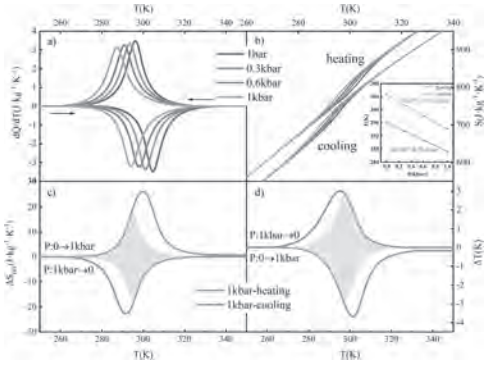

Fig.1. For $MnCoGe_{0.99}In_{0.01}$, a)dQ/dT, b)S, c) ΔS_{rev}, d)ΔT_{rev}.

FOC-06. Hydrostatic Pressure Induced Giant Enhancement of the Solid-state Caloric Effect in the Rare-earth-based Giant Magnetocaloric Materials. *J. Hao*[1], F. Hu[2], J. Wang[2], F. Shen[2], Z. Yu[2], H. Zhou[2], H. Wu[3], Q. Huang[3], J. Wang[2], J. He[4], L. He[2], S. Jirong[2] and B. Shen[2] *1. Spallation Neutron Source Science Center, Institute of High Energy Physics,Chinese Academy of Sciences, Dongguan, China; 2. Institute of Physics, Chinese Academy of Sciences, Beijing, China; 3. NIST Center for Neutron Research, National Institute of Standards and Technology, Gaithersburg, MD, United States; 4. Division of Functional Material Research, Central Iron and Steel Research Institute, Beijing, China*

Conventional vapor compression refrigeration encounters environmental problems. As an alternative, solid-state refrigeration based on magnetocaloric effect (MCE) or barocaloric effect (BCE) has attracted tremendous attentions for its environmental-friendly and energy-saving superiority. The core of solid-state refrigeration lies in the magnitude of the caloric effect of

refrigerants. Increasing the caloric effect as much as possible is a long-term pursuit [1-5]. Here, we report a large enhancement of MCE and BCE by hydrostatic pressure in Co-doped $La(Fe,Si)_{13}$, which has been regarded to be promising refrigerants since its discovery in 2000[1]. The maximal entropy change S_{MCE} almost doubled under 11.31kbar while the S_{BCE} under 9kbar increases more than three times (Figure 1c and 1d). To disclose the essence from the atomic level, neutron powder diffractions were performed (Figure 1a). The results reveal that hydrostatic pressure sharpens the magnetoelastic transition and enlarges the volume change wherein through impacting the intra-icosahedral Fe-Fe bonds (B1, B2, B3) rather than the inter-icosahedral ones (B4, B5) in the $NaZn_{13}$-type structure [1]. Such result is distinct from the case introducing chemical pressure by H atoms in the $La(Fe,Si)_{13}$-based compounds, which can adjust phase transition temperature, but not the sharpness of phase transition and the MCE. To understand the mechanism, first-principles calculations are performed (Figure 1b), which offers a theoretical support for the hydrostatic pressure enhanced magnetovolume effect and the evolution from second-order to first-order transition [1]. The present study proves the enormous potential of enhancing caloric effect through influencing the specific atomic environments by pressure, which is also useful to achieve other pressure-related effects, such as controllable negative thermal expansion.

[1] J. Z. Hao, F. X. Hu, J. T. Wang, et. al, Chemistry of Materials, 2020. 32(5):1807-1818. [2] J.Z. Hao, F.X. Hu, B.G. Shen, et. al, Journal of Magnetism and Magnetic Materials, 2020. 512. [3] J.Z. Hao, F.X. Hu, B.G. Shen, et. al, Scripta Materialia, 2020. 186:84-88. [4] J.Z. Hao, F.X. Liang, F.X. Hu, et. al, Journal of Alloys and Compounds, 2018. 744:426-431. [5] J.Z. Hao, F.X. Hu, B.G. Shen, et. al, Chinese Physics B, 2020. 29(4). [6] L. Manosa, D. Gonzalez-Alonso, A. Planes, et. al, Nature Communication, 2011. 2:595.

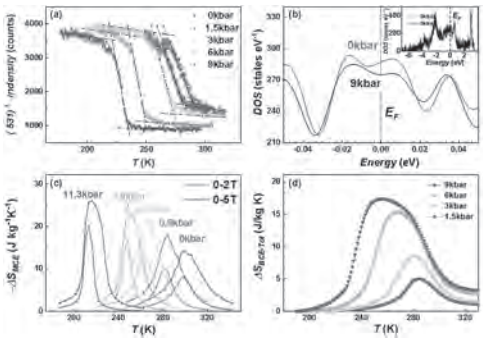

Figure 1 (a)Neutron intensity of the (531) reflection under different pressures for $La(Fe_{0.92}Co_{0.08})_{11.9}Si_{1.1}$ compound. (b) The total density of states near the Fermi level E_F in the nonmagnetic state under pressures 0 and 9kbar. The inset shows the total DOS in the nonmagnetic state. (c) The magnetocaloric and(d) barocaloric effect under different pressures.

FOC-07. Magneto-mechanical properties of thin films on stretchable substrate measured by in situ MOKE. *H. Ben Mahmoud*[1], D. Faurie[1], P. Renault[2] and F. Zighem[1] *1. LSPM-CNRS, Villetaneuse, France; 2. Pprime Institute, Poitiers, France*

Flexible/Stretchable electronics has been a rapidly growing field for several years. In particular, magnetic systems realized on flexible/stretchable substrates are of increasing interest for their potential applications (flexible and stretchable sensors, spintronic and magnonic devices, etc) [1,2]. However, these systems will be subjected to large strains during their use. It is therefore important to understand the different phenomena involved at very large strains in order to estimate the durability of their functional (magnetic) properties, through the study of elementary magnetomechanical phenomena [3]. In this context, we have developed a new experiment coupling a MOKE (Magneto-Optical Kerr Effect) magnetometer (see attached image) and uniaxial tensile tests in order to follow the evolution of magnetic properties at different mechanical regimes. This device has been used to study model thin films of Cobalt (50 nm) deposited on Kapton polymer substrate at high strains (up to 20%). The evolution of the magnetization curves as a function of the applied strain was analyzed in order to estimate the evolution of the coercive field, the remanent magnetization and the saturation field. This analysis has been correlated to the different deformation mechanisms (in particular the elastic domain, plasticity and the multi-cracking of the Cobalt film). Moreover, we have studied the influence of (brittle) W overlayer (14 nm) on the magnetomechanical properties. Through this presentation, we will show the instrumental development of the device (traction machine coupled to the magnetometer) and the mechanisms underlying the measured properties. The perspectives of this early work will also be discussed. In particular, we will show a new MOKE magnetometer combined with a biaxial device. First results obtained from this original set-up will be showed.

[1] F. Zighem, D. Faurie, "A review on nanostructured thin films on flexible substrates: links between strains and magnetic properties", Journal of Physics: Condensed Matter 33, 233002 (2021) [2] M. Ha, G. S. C. Bermúdez, T. Kosub, I. Mönch, Y. Zabila, E. S. O. Mata, R. Illing, Y. Wang, J. Fassbender, D. Makarov, "Printable and Stretchable Giant Magnetoresistive Sensors for Highly Compliant and Skin Conformal Electronics", Advanced Materials 33, 2005521 (2021) [3] S. Merabtine, F. Zighem, D. Faurie, A. Garcia-Sanchez, P. Lupo, A. Adeyeye. "Multicracking and Magnetic Behavior of $Ni_{80}Fe_{20}$ Nanowires Deposited onto a Polymer Substrate", NanoLetters 18, 3199 (2018)

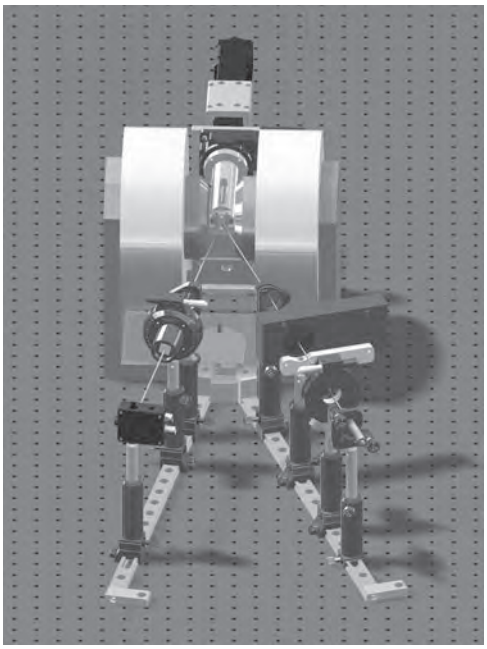

Sketch of the MOKE magnetometer combined with in situ tensile tester (able to deform samples from 0% to 100% of strain)

FOC-08. Withdrawn

FOC-09. Withdrawn

FOC-10. Observation of optical gyromagnetic properties in a magneto-plasmonic metamaterial. *W. Yang*[1], H. Duan[2] and L. Bi[1] *1. National Engineering Center of Electromagnetic Radiation Control Materials, University of Electronic Science and Technology of China, Chengdu, China; 2. College of Mechanical and Vehicle Engineering, Hunan University, Changsha, China*

Metamaterials with artificial optical properties have attracted great research interest in the past two decades. In particular, artificial magnetic resonances have been reported in metamaterials, leading to non-unity permeability tensor at optical frequencies. However, only non-unity diagonal elements of the permeability tensor have been demonstrated so far. A gyromagnetic permeability tensor with non-zero off-diagonal elements have not been achieved at optical frequencies. Here, we report the observation of gyromagnetic properties at near infrared wavelength range in a magneto-plasmonic metamaterial. The non-zero off-diagonal permeability tensor element is approved by transverse magneto-optical Kerr effect (TMOKE) under s-polarized incidence, which should have been otherwise vanished if the permeability tensor were not gyromagnetic. By applying the Nicolson-Ross-Weir (NRW) method, we show the effective off-diagonal permeability tensor elements reach 10^{-3} level at the resonance frequencies of the SRR, which is at least two orders of magnitude higher than magneto-optical materials at the same wavelengths. The local electric field introduced in the structure is the reason for its creation. Our work demonstrates the possibility to engineer the full permeability and permittivity tensors in metamaterials at optical frequencies, which may lead to a variety of applications of the next generation nonreciprocal photonic devices, magneto-plasmonic sensors and active metamaterials

Pendry, J. B., Holden, A., Stewart, W. & Youngs, I. *Phys. Rev. Lett.* Vol. 76, p.4773 (1996). Ignatyeva, D. O. *et al. Nat. Commun.* Vol. 11, p.5487 (2020).

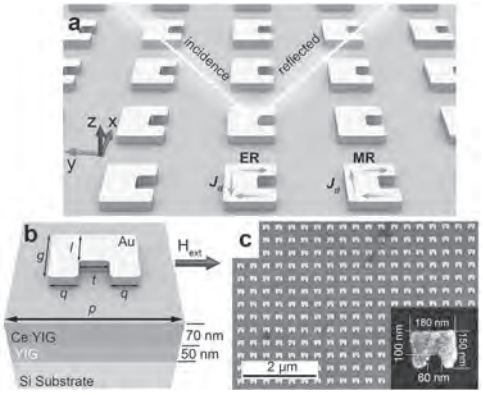

Figure. 1 a, Schematic diagram of the MO-SRR metamaterial. b, Schematic of a unit cell of the MO-SRR metamaterial with an Au-SRR on top of Ce:YIG film (blue), YIG film (gray) and the silicon substrate (Orange). c, SEM image of the MO-SRR metamaterial.

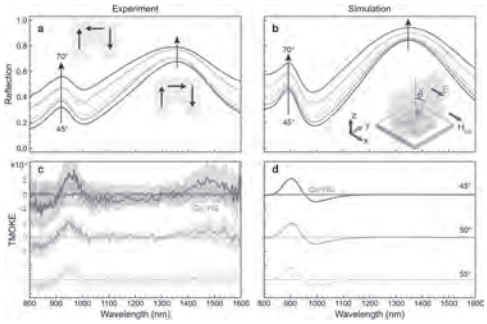

Figure. 2 a, Measured and b simulated reflection spectra of the MO-SRR metamaterial for incident angles ranging from 45° to 70° under S-polarized incidence. The inset of a shows the electric field directions for the electric and magnetic resonances. The inset of b shows the schematic of the incident plane and polarization. c, Measured and d simulated TMOKE spectra of the MO-SRR metamaterial and the Ce:YIG thin film for different incident angles under S-polarized incidence.

FOC-11. Strain-controlled ferromagnetic domains induced by interfacial proximity to Mott insulator V_2O_3. *A. Fraile Rodríguez*[1,2], I. Valmianski[3], J. Rodríguez-Álvarez[1,2], M. García del Muro[1,2], J. Ramirez[4], C. Wolowiec[3], F. Kronast[5], I.K. Schuller[3], A. Labarta[1,2] and X. Batlle[1,2] *1. Física de la Matèria Condensada, Universitat de Barcelona, Barcelona, Spain; 2. Institut de Nanociència i Nanotecnologia (IN2UB), Universitat de Barcelona, Barcelona, Spain; 3. Physics, University of California San Diego (UCSD), La Jolla, CA, United States; 4. Physics, Universidad de Los Andes, Bogotá, Colombia; 5. Helmholtz Zentrum Berlin, Berlin, Germany*

Coupling between lattice degrees of freedom and the spin systems without the use of magnetic fields allows for efficient spintronic devices. A promising alternative to produce large effects uses materials which exhibit a first order structural phase transition (SPT). In particular, for Ni/V_2O_3 bilayers, changes in the coercive field of up to 500% have been reported due to interfacial proximity to an archetypal Mott insulator V_2O_3 layer across its SPT [1]. In this work [2], using photoemission electron microscopy (PEEM) combined with X-ray magnetic circular dichroism (XMCD) we find an abrupt temperature-driven reorientation of the Ni magnetic domains. Angular dependent ferromagnetic resonance (FMR) shows a remarkable change in the magnetic anisotropy of the Ni film across the SPT of V_2O_3. Direct measurements of the lateral correlation length of the Ni domains from XMCD images show an increase of almost one order of magnitude at the SPT compared to room temperature and a broad spatial distribution of the local transition temperatures. Micromagnetic simulations based on these results are in quantitative agreement with the PEEM data, thereby corroborating the phase coexistence of Ni anisotropies caused by the V_2O_3 SPT. In summary, we show that the rearrangement of the Ni domains is due to the strain induced by the oxide layers' structural domains across the SPT [2]. Our results illustrate the use of alternative hybrid systems to manipulate magnetic domains at the nanoscale, which allows for engineering of coercive fields for novel data storage architectures. The work was supported by Spanish MCIU and AEI (MAT2015-68772-P; PGC2018-097789-B-I00) and European Union FEDER funds. Some of this work was supported by by DOE-BES grant number DE-FG02-87ER45332.

[1] J. De La Venta, S. Wang, T. Saerbeck, et al.Appl. Phys. Lett., 104, 062410 (2014). [2] I. Valmianski, A. Fraile Rodríguez, J. Rodríguez-Álvarez et al.Nanoscale 13, 4985 (2021).

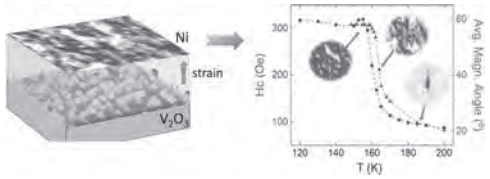

Temperature-driven reorientation of magnetic domains in a thin Ni film across the structural phase transition of a prximity-coupled V_2O_3 layer, giving rise to large changes in the magnetic anisotropy of the Ni film.

FOC-12. Maximizing Strong Magnon-Phonon Coupling in a Single CoFe Nanomagnet. *S. Kim*[1*], W. Yang[1], C. Berk[2], S. Dhuey[3], S. Cabrini[3] and H. Schmidt[1] *1. School of Engineering, University of California Santa Cruz, Santa Cruz, CA, United States; 2. Lawrence Berkeley National Laboratory, Berkeley, CA, United States; 3. Molecular Foundry, University of California Berkeley, Berkeley, CA, United States*

Understanding and controlling the interactions between mechanical (phonon) and magnetic (magnon) modes has received growing attention over the past few years [1]. In particular, strong coupling between degenerate magnon and phonon modes was recently reported in single nickel nanomagnets [2] and GaFe nanogratings [3]. These findings open new pathways towards quantum engineering in hybrid magnonic systems [4] and other applications. A critical next step is to maximize and control the strong coupling effect in individual magnets. Here, we report more than 6x enhanced coherent coupling in a 2.7x smaller element along with control over the effect via the nanomagnet shape. This was accomplished by working with CoFe which has much higher magnetostriction coefficients than nickel [5,6] and is of broad interest for spintronic applications. Polycrystalline CoFe nanomagnets of varying shapes were fabricated by e-beam lithography, CoFe evaporation, and liftoff (see insets to Fig. 1a and 1b). The samples were excited and probed using a two-color pump TR-MOKE setup, which allows for the measurement of the full system dynamics [7]. Fig. 1a shows the field-dependent magnetic and non-magnetic dynamics of a 200 nm square CoFe nanomagnet. The characteristic anticrossing which is a hallmark of strong coupling, is observed and shows a very large minimum splitting of 4.57 GHz at an applied field of 3.5 kOe in agreement with theoretical expectations. In contrast, the non-magnetic channel does not exhibit any vibrational modes for a circular nanomagnet of the same size (Fig. 1b), and consequently, the magnetic channel shows only the standard Kittel mode (blue dots). These results indicate further control of coherent coupling in magnon-phonon systems with careful design of material and geometric parameters.

[1] Yang, W. and Schmidt, H., *Appl. Phys. Rev.,* Vol. 8, p. 021304 (2021) [2] Berk, C. et al., *Nat. Commun*., Vol. 10, p. 2652 (2019) [3] F. Godejohann, et al., *Phys. Rev. B*, Vol. 102, p. 144438 (2020) [4] D.D. Awschalom et al., *IEEE Trans. Quant. Eng.,* arXiv:2102.03222 [5] Gontarz, R. et al., *P. Phys. Stat. Sol.,* Vol. 6, p. 909 (1964) [6] Hunter, D., Osborn, W., Wang, K. et al., *Nat. Commun.,* Vol. 2, p. 518 (2011) [7] Yahagi, Y. et al., *Phys. Rev. B*, Vol. 90, p. 140405 (2014)

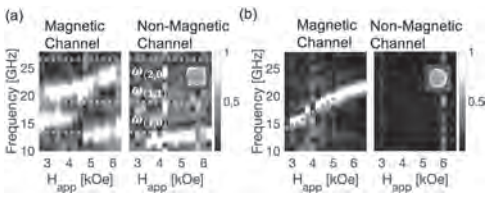

Fig. 1: Fourier spectra of the magnetic and non-magnetic field scans of a square (a) and circular (b) CoFe nanomagnet, respectively. Green dotted lines: phonon modes (ω_{nx}, ω_{ny}); blue circles: OOMMF simulation of Kittel mode. Fourier amplitudes are normalized at each magnetic field. Insets: SEM images of the 30 nm thick nanomagnets (200nm edge length / diameter).

FOC-13. Optimizing Magnetostriction in Fe-Ga-Zr Nanocrystalline Alloys. *M. Islam*[1], R. Nandwana[1], J. Healy[1], J.K. Jaklich[1], B. Dong[1], M. Willard[1], A. Yu[2], Y. Ijiri[2], E.E. Moore[3] and S.K. McCall[3] *1. Department of Materials Science and Engineering, Case Western Reserve University, Cleveland, OH, United States; 2. Department of Physics and Astronomy, Oberlin College, Oberlin, OH, United States; 3. Materials Science Division, Lawrence Livermore Laboratory, Livermore, CA, United States*

The iron-rich alloy Galfenol (Fe_{1-x}-Ga_x, 10%<x<30%) has been of significant interest for sensor technologies due to the sizeable magnetostriction coefficient found in single-crystal and polycrystalline films. [1,2] However, it is necessary to improve the magnetic softness of the material for many applications. To do so, we have explored the use of Zr and other glass formers and additives, rapid solidification approaches, and subsequent annealing to produce a nanocrystalline (Fe,Ga)-based alloy with the desired magnetostrictive and structural properties. We report studies on a series of 11 melt-spun and annealed $(Fe_{1-x}$-$Ga_x)_{92}Zr_8$ alloy ribbons where the Ga concentration (x) has been varied from 15% to 36%. As illustrated in Fig. 1, in contrast to single-crystal and polycrystalline films, the ribbons exhibit the dominant bcc-like phase for Galfenol over a more extensive concentration range with fewer other ordered phases. Analysis of the x-ray peak locations reveals a deviation in lattice parameter from bulk behavior for alloy with similar x, suggesting that the surrounding amorphous phase matrix for the nanocrystallites within the ribbons is Ga-rich. Beginning at x=26%, x-ray diffraction scans exhibit signs of the formation of the ternary $ZrFe_6Ga_6$, consistent with CALPHAD-type database calculations. Magnetization measurements reveal a maximum saturation magnetization for the alloy with x=15% and coercivity values increase rapidly on formation of the ternary intermetallic phase. Fig. 2 illustrates the in-plane magnetostriction coefficient for the series of samples, displaying a peak value for x=24-26% which differs from the values observed in single crystalline sample x=18-20%. Acknowledgment: Prepared by LLNL under Contract DE-AC52-07NA2.

[1] B. Stadler, M. Reddy, R. Basantkumar, Galfenol Thin Films and Nanowires, Sensors, Vol. 18(8), P. 2643 (2018). [2] J. Atulasimha, A. B. Flatau, A review of magnetostrictive iron–gallium alloys, Smart Mater. Struct., Vol 20(4), P. 043001 (2011).

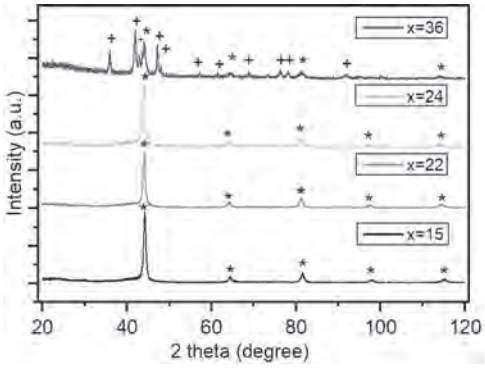

Fig. 1: X-ray diffraction of $(Fe_{1-x}$-$Ga_x)_{92}Zr_8$ alloy ribbons for x=15-36% after annealing for 1 hour at 550 °C. (*) peaks indicate the bcc-like phase, with (+) symbols denoting those associated with $ZrFe_6Ga_6$.

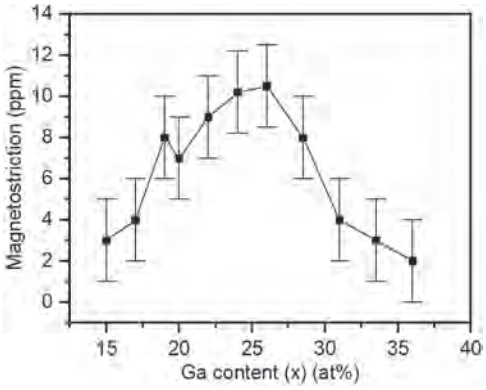

Fig. 2: Magnetostriction coefficient vs composition for annealed $(Fe_{1-x}\text{-}Ga_x)_{92}Zr_8$ alloy ribbons for x=15-36%.

FOC-14. Harnessing Magnetic and Optical Properties in Atomically Thin Alloy Mo-WS_2/W-MoS_2 Semiconductors. *M. Trinh*[1], Y.T. Pham[1], D. Zhou[2], M. Liu[2], V.O. Jimenez[1], S. Ambardar[1], D. Voronine[1], M. Terrones[2] and M. Phan[1] *1. Physics, University of South Florida, Tampa, FL, United States; 2. Materials Science and Engineering, Pennsylvania State University, University Park, PA, United States*

Two-dimensional (2D) transition metal dichalcogenide (TMD) semiconducting monolayers possess exotic physical properties useful for optoelectronic applications owing to their direct bandgap, high carrier mobility, and strong spin-orbit coupling, among many others. The recent discovery of room-temperature magnetism in magnet-doped TMDs has triggered a new surge on these materials. It has been reported that V-doped WSe_2 and WS_2 monolayers exhibit tunable ferromagnetism at room-temperature up to 8 at.% dopants [1,2]. However, the optical properties of these materials substantially suffer from these dopants; e.g. excitonic emission is completely quenched at high dopant levels. Therefore, combining magnetic and optical properties within a TMD monolayer represents a challenging task. In this work, we propose a non-magnetic transition metal cross-doping approach as a possible solution to the problem. We show that a CVD-grown heterostructure consisting of monolayer TMDs, Mo-WS_2/W-MoS_2, where the Mo-WS_2 stands for Mo-doped WS_2 and vice versa, possesses enhanced ferromagnetism at room temperature while preserving the excellent optical property of the individual layer. The origin of magnetism in this 2D material likely arises from the presence of vacancy defects and local strain induced by doping of TMDs with various radii. When introducing vanadium magnetic dopant to this heterostructure at a low concentration (e.g., 0.5 at.% V), the dopant-spins antiferromagnetically couple with the pre-existing magnetic moments, resulting in a lower net magnetization. Further increase of the V concentration, however, leads to an increase of the total magnetization, highlighting the dominant ferromagnetic interactions between the magnetic dopant-spins. The optical properties of these samples were investigated by tip-enhanced photoluminescence using a gold nano-tip. We also observed a clear sharp in-plane heterostructure with tens of nanometers resolution which preserved the excitonic properties of each layer in the pristine and in low V-doped samples. For the high dopant level sample, the PL was quenched almost completely. This finding has shown the possibility of harnessing magnetic and optical properties in TMD monolayers.

1. Zhang, et al. Monolayer Vanadium-doped Tungsten Disulfide: An Emerging Room-Temperature Diluted Magnetic Semiconductor. *Advanced Science*, 7, 2001174 (2020). 2. Pham, et al. Tunable Ferromagnetism and Thermally Induced Spin Flip in Vanadium-doped Tungsten Diselenide Monolayers at Room Temperature. *Advanced Materials,* 32, 2003607 (2020).

FOC-15. Low-cost Processing of $AlFe_2B_2$ Feedstock Powders for Additive Manufacturing of Magnetocaloric Structures. *A.R. Duong*[1], V. Sharma[1], M. Dey[2], S. Javaid[2], S. Gupta[2] and R. Barua[1] *1. Mechanical & Nuclear Engineering, Virginia Commonwealth University, Richmond, VA, United States; 2. Mechanical Engineering, University of North Dakota, Grand Forks, ND, United States*

High temperatures and inert atmospheres are required to produce borides due to the covalent character of their chemical bonds and, consequently, their high melting temperatures. Solid and melt state processing of borides from the primary reactants typically results in dense samples, which are crushed, milled, and sieved laboriously into fine powder for further processing. The size reduction process introduces numerous complications that hinder large-scale powder production. Against this backdrop, Molten Salt Infiltration and Encapsulation Method (MSIEM) is a sustainable energy-efficient process that uses no inert gas, relatively low temperatures, and moderately short reaction times to synthesize powders with uniform chemical composition and high-phase purity. In this study, fine particles of the promising magnetocaloric boride $AlFe_2B_2$ were prepared by sintering a green compact composed of the constituent elements Al, Fe, and B encapsulated within a layer of KBr molten salt at 1000 °C for 12 hours in the open air. Results indicate that the Al/Fe loading ratio in the precursor compacts strongly influences the phase purity, structural properties, and magnetofunctional response of the samples. It is observed that Curie temperature (T_c), saturation magnetization (M_s), and magnetic entropy change (ΔS_{mag}) of the powders increase with the decrease in the Al/Fe ratio – a feature attributed to the change in the Al/Fe antisite disorder. Powders of nominal composition $Al_{1.2}Fe_2B_2$ were found to be nearly single-phase stoichiometric Fe_2AlB_2 materials containing only 3% Al_2O_3 as the impurity phase. These powders exhibit an irregular polyhedral morphology with particle sizes in the range 2-5 m and demonstrate a promising magnetocaloric effect corresponding to a ΔS_{mag} = 4.2 J $kg^{-1}K^{-1}$ at a magnetic field of $\mu_0 H_{app}$ = 2 T near room temperature, Figure 1. Research efforts centered on 3D printing magnetocaloric structures using the low-cost feedstock $AlFe_2B_2$ powders produced via MISEM will be presented and discussed.

References: M. Dey, S. Javaid, D. Clifford, V. Sharma, R. Barua and S. Gupta, "Synthesis of Nanolayered Ternary Borides Powders (MAB Phases) by Sustainable Molten Salt Infiltration and Encapsulation Method", ACS Sustain. Chem. Eng. (Under Review)

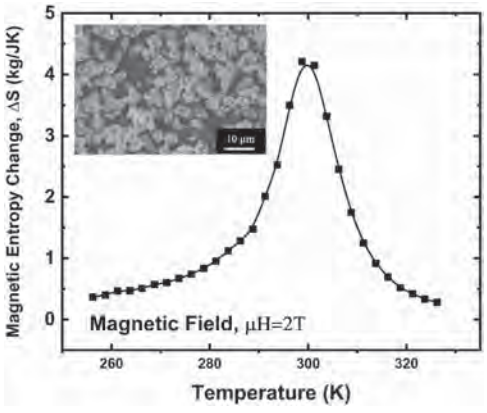

Fig 1. Magnetic entropy change curves of powders of composition $Al_{1.2}Fe_2B_2$ synthesized via MISEM using KBr salt. Inset shows the morphology of the sintered powders.

Session FOD
THERMOELECTRICS AND MAGNETOCALORICS

Ramanathan Mahendiran, Co-Chair
National University of Singapore, Singapore
Sunil Nair, Co-Chair
IISER, Pune, India

INVITED PAPER

FOD-01. Exploring Transverse Thermoelectric Generation in Magnetic Systems Toward Applications. *W. Zhou*[1], K. Uchida[1] and Y. Sakuraba[1] *1. Research Center for Magnetic and Spintronic Materials, National Institute for Materials Science, Tsukuba, Japan*

The transverse thermoelectric effect refers to the generation of a charge current perpendicular to the applied temperature gradient, with a good example being the anomalous Nernst effect (ANE) in magnetic materials. This is different from the Seebeck effect (SE) in traditional thermoelectric generation, where the charge current is parallel to the temperature gradient. Hence, it is possible to convert thermal energy from a heat source to electrical energy by simply forming a material onto the heat source surface. The output voltage can be enhanced by elongating the length of the material within the surface, instead of constructing three-dimensional serial junctions as seen in current thermoelectric generators. As a result, the transverse thermoelectric generation allows different device design principles, which could enable efficient waste heat harvesting, reduce the cost of modules, and improve on durability and flexibility [1]. Meanwhile, recent reports of large anomalous Nernst thermopower in materials with topological band structures [2-4] have attracted increasing interests to investigate the transverse thermoelectric generation in various material systems, from the viewpoints of fundamental physics as well as thermoelectric applications. In this talk, we discuss the transverse thermoelectric generation in various magnetic systems [5,6], and show that a simple planar structure of them responds linearly to the out-of-plane heat flux. This feature could be especially suitable for creating a heat flux sensor with low thermal resistance. We also propose and demonstrate a conceptually different effect called the Seebeck-driven transverse thermoelectric generation (STTG) [7,8]. By creating a system that consists of thermoelectric and magnetic materials, the artificial hybridization of SE of the thermoelectric material into the anomalous Hall effect of the magnetic material enables transverse thermoelectric generation with a similar symmetry to the ANE, while could realize a significant enhancement in transverse thermopower.

[1] K. Uchida, W. Zhou, and Y. Sakuraba, *Appl. Phys. Lett.*, Vol. 118, p.140504 (2021). [2] A. Sakai, Y. P. Mizuta, A. A. Nugroho *et al.*, *Nat. Phys.*, Vol. 14, p.1119 (2018). [3] S. N. Guin, K. Manna, J. Noky *et al.*, *NPG Asia Mater.*, Vol. 11, p.16 (2019). [4] K, Sumida, Y. Sakuraba, K. Masuda *et al.*, *Commun. Mater.*, Vol. 1, p.89 (2020). [5] W. Zhou, and Y. Sakuraba, *Appl. Phys. Express*, Vol. 13, p.043001 (2020). [6] W. Zhou, K. Masuda, and Y. Sakuraba, *Appl. Phys. Lett.*, Vol. 118, p.152406 (2021). [7] W. Zhou, K. Yamamoto, A. Miura *et al.*, *Nat. Mater.*, Vol. 20, p.463 (2021). [8] K. Yamamoto, R. Iguchi, A. Miura *et al.*, *J. Appl. Phys.*, Vol. 129, p.223908 (2021).

CONTRIBUTED PAPERS

FOD-02. Flexible Thermoelectric Magnetic Switches based on Interconnected Nanowire Networks. *T. da Câmara Santa Clara Gomes*[1], N. Marchal[1], F. Abreu Araujo[1] and L. Piraux[1] *1. Université Catholique de Louvain, Louvain-La-neuve, Belgium*

The development of sensors and logic devices powered by waste heat would address the rapid development of miniature wearable devices and is clearly in line with sustainable development. Making these devices flexible so that they can conform to complex hot surfaces or the human body is a key advantage. Unfortunately, the performance of devices based on conventional thermal and thermoelectric technologies is relatively poor. In this context, the functionalities offered by the spin degree of freedom in Spin Caloritronics, an emerging field at the intersection of Thermoelectrics and Spintronics, holds promising perspectives. Here, we designed a new concept of planar flexible thermoelectric magnetic switches made of thermocouples formed from two dissimilar arrays of crossed magnetic nanowires (NWs) embedded in a single polymer film (Fig. 1). One leg is formed by homogeneous NWs and the other leg is formed by multilayer NWs showing giant magneto-Seebeck effects [1-3]. By fine-tuning their respective compositions, an ideal on/off ratio in the switching of the thermoelectric output voltage (from 0 to few tens of μV, Fig. 2), or a sign reversal can be achieved in the presence of a magnetic field. These actions can be performed quickly, reversibly and without cycle limitation, resulting in no device degradation. By comparison, the magnetically activated thermal switches developed to date only allow a modest change in heat flow (a factor of 2-3 at most on the thermal conductivity variation). This paves the way to the development of thermally activated sensors and logic devices, exploiting the residual thermal energy of hot surfaces with complex geometry. Our light-weight devices resist repeated bending and stretching, have low toxicity, can be easily shaped with no lateral dimensional limitations, and allow the replication of traditional thermoelectric generator architectures where individual modules are connected electrically in series and thermally in parallel (Fig. 1).

[1] T. da Câmara Santa Clara Gomes, F. Abreu Araujo and L. Piraux, *Science Advances* 5(3), eaav2782 (2019). [2] F. Abreu Araujo, T. da Câmara Santa Clara Gomes and L. Piraux, *Advanced Electronic Materials* 5, 1800819 (2019). [3] N. Marchal, T. da Câmara Santa Clara Gomes, F. Abreu Araujo and L. Piraux, *Nanoscale Research Letters* 15, 137 (2020).

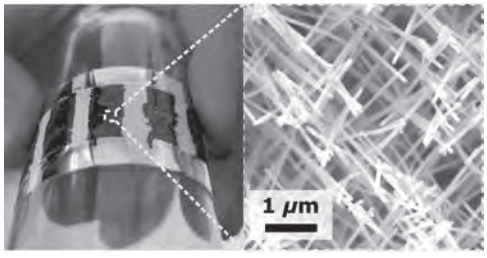

Fig 1. Flexible thermoelectric magnetic switch based on thermocouples made of dissimilar crossed magnetic NWs networks.

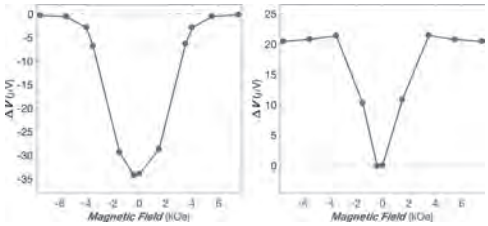

Fig 2. Ideal switches where the "on" and "off" states can be reach at zero or saturation magnetic field (left) or vice-versa (right).

FOD-03. Large magnetic entropy change in Nd_2In near the boiling temperature of natural gas. *W. Liu*[1], F. Scheibel[1], T. Gottschall[2], E. Bykov[2], I. Dirba[1], K. Skokov[1] and O. Gutfleisch[1] *1. Materials Science, Technische Universität Darmstadt, Darmstadt, Germany; 2. High Magnetic Field Laboratory, Helmholtz-Zentrum Dresden-Rossendorf, Dresden, Germany*

In the great transformation from fossil fuels to CO_2-neutral renewable energies, the woldwide comsumption of liquid natural gas (LNG) is rising to facilitate the transition and the demand of LNG is predicted to double by 2040 [1]. As an emerging and energy-saving technology, magnetocaloric gas liquefaction could be an alternative to the tranditional gas-compression refrigeration. Here we report a new firtst-order magnetocaloric material Nd_2In with a negligible thermal hysteresis. Nd_2In shows a maximum magnetic entropy change of 7.42 J/kg K in fields of 2 T at 109 K, which is close to the boiling temperature of natural gas. A fully reversible adiabatic temperature change of 1.13 K under a magnetic field change of 1.95 T is reached. Studying thermal expansion and magnetostriction, a two-stage magnetic transition with a negligible volume change is observed. The longitudinal strain increases with magnetic fields and then decreases. This phenomenon may be a result of a pure electromic mechanism which may be the reason for the negligible thermal hysteresis. These interesting properties are useful for the practical design of a magnetocaloric natural gas liquefaction system and for the fundamental understanding of the phase transitions in other RE_2In intermetallics. [2]

[1] See https://igu.org/resources/global-gas-report-2020/ [2] W. Liu et al., Appl. Phys. Lett. 119, 022408 (2021)

FOD-04. Tuning the magnetic and magnetocaloric properties in $Dy_6(Fe,Mn)X_2$ intermetallics (X=Sb, Te, Bi). A. Herrero[1], *A. Oleaga*[1], I.R. Aseguinolaza[1], A.J. Garcia-Adeva[1], E. Apiñaniz[1], A.V. Garshev[2], V.O. Yapaskurt[3] and A.V. Morozkin[2] *1. Department of Applied Physics, University of the Basque Country, Bilbao, Spain; 2. Department of Chemistry, Moscow State University, Moscow, Russian Federation; 3. Geological Faculty, Moscow State University, Moscow, Russian Federation*

A thorough study of seven members of the intermetallic $Dy_6(Fe,Mn)X_2$ family with X=Sb, Te, Bi, has been performed over a broad temperature range in order to explore the possibility of tuning their magnetic and magnetocaloric properties by modifying their composition. These intermetallics present a paramagnetic to ferromagnetic transition (in the range 129-370 K), followed, as temperature decreases, by a spin-reorientation one (from 52 to 170 K) and a ground magnetic state at 2 K with antiferromagnetic components. This state turns into a ferromagnetic state when a magnetic field is applied. This complexity gives rise to two direct magnetocaloric effect (DMCE) and one inverse magnetocaloric effect (IMCE) in all compounds, creating a table-like region between the two DMCE, a requirement for improving the efficiency of an Ericsson refrigeration cycle. The position and height of this region can be efficiently tuned varying the composition, finding that the alloys with Sb (Dy_6FeSb_2 and $Dy_6FeSbTe$) have the best magnetocaloric properties among the studied compounds, including an especially relevant IMCE. The critical behavior of the PM-FM transitions has been studied obtaining the magnetic critical exponents β,γ, δ, which suggest long-range order interactions, though in some cases there is an unconventional critical behavior. The magnetocaloric scaling laws were checked reinforcing the obtained critical exponents, and the universal curves for the magnetocaloric effect were also found for the seven cases.

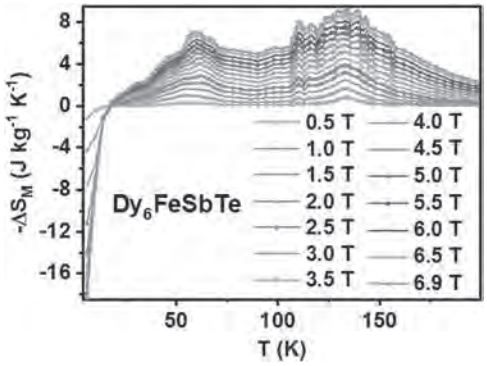

Fig. 1: MCE for $Dy_6FeSbTe$

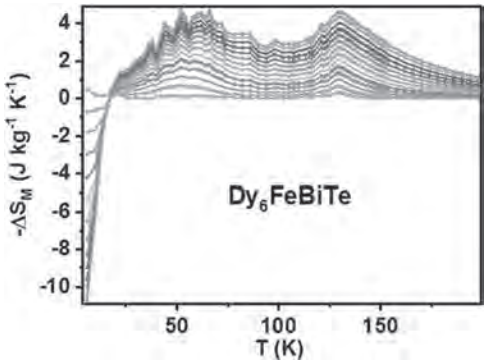

Fig. 2: MCE for $Dy_6FeBiTe$

FOD-05. Magnetocaloric properties of rare earths in pulsed magnetic fields. *T. Gottschall*[1], E. Bykov[1], M. Kuz'min[2], A. Amirov[3,4], A. Aliev[3,4], A.M. Tishin[6], D. Schlagel[5], Y. Mudryk[5], V. Pecharsky[5], C. Salazar-Mejia[1], Y. Skourski[1] and J. Wosnitza[1] *1. Helmholtz-Zentrum Dresden-Rossendorf, Dresden, Germany; 2. Aix-Marseille Université, Marseille, France; 3. Immanuel Kant Baltic Federal University, Kaliningrad, Russian Federation; 4. Amirkhanov Institute of Physics of Dagestan Federal Research Center, Makhachkala, Russian Federation; 5. Ames Laboratory, U.S. Department of Energy, Ames, IA, United States; 6. M.V. Lomonosov Moscow State University, Moscow, Russian Federation*

The direct determination of the adiabatic temperature change, ΔT_{ad}, as a function of the magnetic field and the starting temperature is of central importance for a profound characterization of magnetocaloric materials [1]. Recently, we developed a technique to measure the temperature change in pulsed magnetic fields by using ultra-thin thermocouples attached to the sample [2]. This enables the investigation of different phenoma, such as the scaling behavior of the magnetocaloric effect in high magnetic fields [3], the dynamics of first-order phase transitions in dependence of the sweeping rate [2], thermal transport properties of composite structures, and more. In this work, we give an overview of the most recent results that have been obtained in pulsed magnetic fields at the Dresden High Magnetic Field Laboratory for several different rare-earth elements. Figure 1 shows the adiabatic temperature change of a gadolinium single crystal as a function of the magnetic field for different initial temperatures. The inset illustrates the temporal progression of the pulsed magnetic field. We could demonstrate that the usual $H^{2/3}$ power law of the magnetocaloric effect fails in fields beyond 10 T. For that reason, the position of the maximum ΔT_{ad} shifts towards higher temperatures and is, therefore, no longer observed at the Curie point. Terbium behaves similar to gadolinium in high magnetic fields, but even

outperforms in terms of the maximum adiabatic temperature change. In addition, it has to be considered that terbium exhibits a large magnetic anisotropy and as a consequence also the magnetocaloric effect strongly depends on the crystal orientation. This allows a large temperature change to be generated even in the static fields, namely by rotation of the crystal.

[1] T. Gottschall et al. Adv. Energy Mater. 9, 1901322 (2019). [2] T. Gottschall et al. Phys. Rev. Applied 5, 024013 (2016). [3] T. Gottschall et al. Phys. Rev. B 99, 134429 (2019).

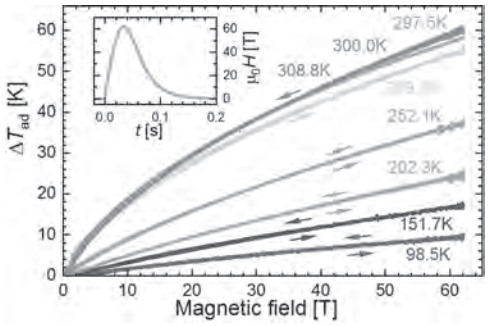

Fig. 1: Adiabatic temperature change ΔT_{ad} of a gadolinium single crystal in pulsed magnetic fields up to 62 T at different initial temperatures T_0. For all curves, both the magnetization and the demagnetization branches are plotted. Experimental data presented in this and other figures are measured with the magnetic field vector along the [0001] direction. The inset shows the temporal profile of the magnetic field pulse. The rise time amounts to 33ms.

FOD-06. Cryogenic magnetocaloric effect and thermomagnetic transitions in RE_6Co_2Ga (*RE* = Ho, Dy or Gd) compounds. *D. Guo*[1,2], L.M. Moreno-Ramírez[2], C. Romero-Muñiz[3,4], Y. Zhang[1], J. Law[2], V. Franco[2], J. Wang[1] and Z. Ren[1] *1. School of Materials Science and Engineering, Shanghai University, Shanghai, China; 2. Departamento de Física de la Materia Condensada, Universidad de Sevilla, Sevilla, Spain; 3. Department of Physical, Chemical and Natural Systems, Universidad Pablo de Olavide, Sevilla, Spain; 4. Departamento de Física Aplicada I, Universidad de Sevilla, Sevilla, Spain*

Gas liquefaction is an essential aspect for gas storage and transport and its demand will significantly increase as the use of gases such as natural gas as well as H_2, He, N_2, and O_2 become prominent in the development of new technologies (e.g. hydrogen based ones). Systems based on the magnetocaloric effect (MCE) are attracting the interest of the scientific community as they can overcome some of the issues of conventional liquefaction systems [1, 2]. In this work, we studied a series of rare-earth rich RE_6Co_2Ga (*RE* = Ho, Dy or Gd) compounds, which shows excellent MCE in the range of H_2 and N_2 liquefaction temperatures [3]. All the samples crystallize in the Ho_6Co_2Ga-type crystal structure (*Immm* space group) without significant presence of impurity phases. The nature of the thermomagnetic transition depends on the rare-earth element, showing metamagnetic anti-to-paramagnetic (AF to PM) transitions for Ho and Dy while a ferro-to-paramagnetic (FM to PM) transition is obtained for Gd. Novel MCE field dependence method [4] and conventional Banerjee's criterion have been used for distinguishing the order of the transition: samples with Ho and Dy are found to undergo first-order phase transition whereas a second order phase transition is observed for the one with Gd. Fig.1 depicts the temperature dependence of the isothermal entropy change (ΔS_{iso}) for a magnetic field change of 0-5 T for Ho and Gd samples. The two compounds show significant values of 10.1 and 9.1 J kg^{-1} K^{-1} at 26 and 75 K, close to the liquefaction temperatures of H_2 and N_2, respectively.

[1] V. Franco, J.S. Blázquez and J.J. Ipus, Prog. Mater. Sci., Vol. 93, p. 112 (2018) [2] Y.K. Zhang, J. Alloy. Compd., Vol. 787, p. 1173 (2019) [3] D. Guo, L.M. Moreno-Ramírez and C. Romero-Muñiz, Sci. China Mater., (2021) http://engine.scichina.com/doi/10.1007/s40843-021-1711-5 [4] J.Y. Law, V. Franco and L.M. Moreno-Ramírez, Nat. Commun., Vol. 9, p. 2680 (2018)

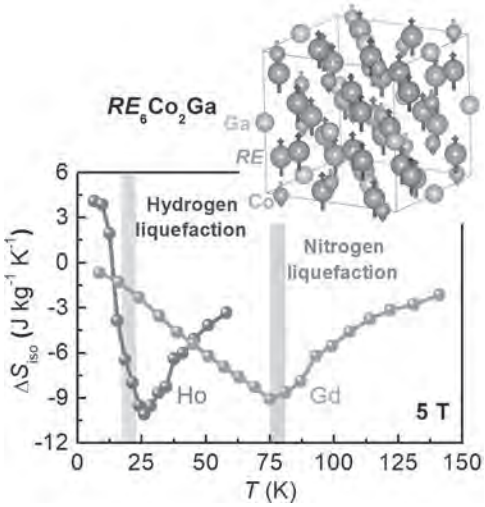

The temperature dependence of isothermal entropy change for Ho_6Co_2Ga and Gd_6Co_2Ga compounds whose crystal structures belong to Ho_6Co_2Ga-type.

FOD-07. Large cryogenic magnetocaloric effect in $GdNi_{1-x}Co_x$ ($0 \leq x \leq 0.15$). A. Biswas[1], T. Del Rose[1,2], *Y. Mudryk*[1] and V. Pecharsky[1,2] *1. Ames Laboratory of US DOE, Iowa State University, Ames, IA, United States; 2. Department of Materials Science and Engineering, Iowa State University, Ames, IA, United States*

Materials for magnetocaloric refrigeration near room temperature attract main attention, but compounds exhibiting large magnetocaloric effects (MCE) in the cryogenic regime are also of importance.[1,2] In particular, MCE materials that can support liquefaction of certain gases, from hydrogen (boils at 20 K) to natural gas (~110 K), are of interest for diversification of energy supplies.[2] Here we report a large MCE in $GdNi_{1-x}Co_x$ series in the temperature range between 70 and 115 K that can be controlled by varying x(Co) between 0 and 0.15. The compounds undergo second-order magneto-elastic transformations where the transitions from paramagnetic to ferromagnetic states are coupled with anisotropic changes in lattice parameters without significant changes in phase volume.[3,4] Lattice symmetry also remains unperturbed across the transitions.[3,4] While the transition temperatures increase nearly linearly with x(Co), doping with Co slightly reduces the maximum magnetic entropy changes: from -14 J/ Kg K at 71 K when x(Co) = 0 to -10 J/Kg K at 115 K when x(Co) = 0.15 (all values are quoted for a 50 kOe magnetic field change). The calculated temperature-averaged-entropy changes (TECs), one of the important figures of merit for assessing the potential of magnetic refrigerants,[5] are comparable with the best known potential magnetocaloric materials exhibiting second-order phase transition. Our detailed analysis of the magnetic field dependence of the magnetic entropy changes along with critical exponent analysis explore the role of magneto-elastic coupling on the magnetocaloric properties of $GdNi_{1-x}Co_x$ alloys. Acknowledgement: This work was performed at Ames Laboratory and was supported by the Division of Materials Science and Engineering of the Office of Basic Energy Sciences of the U.S. Department of Energy (DOE). Ames Laboratory is operated for the U.S. DOE by Iowa State University under Contract No. DE-AC02-07CH11358.

1. K.A. Gschneidner, Jr., V.K. Pecharsky, Ann. Rev Mater. Sci. V-30, 387 (2000). 2. L. Li, M. Yan, J. Alloy. Comp. V-823, 153810 (2020) 3. D. Paudyal, Y. Mudryk, Y. B. Lee, V. K. Pecharsky, K. A. Gschneidner, Jr., and B. N. Harmon, Phys. Rev. B V-78, 184436 (2008). 4. Y. Mudryk, D. Paudyal, T. Prost, L.S. Chumbley, V.K. Pecharsky, and K.A. Gschneidner, Jr., Acta Mater. V- 92, 18-24 (2015). 5. L.D. Griffith, Y. Mudryk, J. Slaughter, V.K. Pecharsky, J. Appl. Phys. V-123, 034902 (2018).

Session FPA
MAGNETOCALORICS III
(Poster Session)

R. Nirmala, Co-Chair
Indian Institute of Technology, Chennai, India
Franziska Scheibel, Co-Chair
Technische University Darmstadt, Darmstadt, Germany

FPA-01. Enhanced refrigerant capacity in Mn_5Ge_3 melt spun ribbon near room temperature. *L. Bachhraj*[1,3], Y. Bitla[2], A. Patra[2], R. Pant[1,3] and G. Basheed[1,3] *1. CSIR - National Physical Laboratory (NPL), Dr. K. S. Krishnan Marg, New Delhi, India; 2. Department of Physics, Central University of Rajasthan, Ajmer, India; 3. Academy of Scientific and Innovative Research (AcSIR), Ghaziabad, India*

Magnetic refrigeration (MR), exploiting the adiabatic demagnetization phenomena, is preferable over conventional gas-compression based technology due to its low cost and high efficiency along with environment-friendly method [1-3]. Recently, earth-abundant Mn-based alloy, Mn_5Ge_3 has emerged as a potential alternative with reasonably high relative cooling power (RCP) which is the centre of the present study [4]. Concerning the technological applications, the role played by the size-reduction (macro to micro-scale) on the engineering of innovative devices is still in its early age. In this context, Mn_5Ge_3 ribbons are synthesized using the melt spinning technique. The temperature and field-dependent dc magnetization are measured with physical properties measurement system (Quantum design, 8T). The M (T) curve at 1 kOe shows a sharp ferromagnetic ordering at $T_C \sim 304$ K. Furthermore, the M (H) hysteresis loop at 5 K reveal the typical soft ferromagnetic behaviour with saturation magnetisation (M_S) of 136 emu/g with approximately zero hysteresis loss which is highly preferential for MR technology. From magnetic isotherms, the magneto-caloric effect is studied in the wide temperature range of 250-360 K. Using the Maxwell equation, Isothermal magnetic entropy change (ΔS_M) is calculated as 5 J/Kg-K at 5 T applied field [See Fig 1]. From inset of Fig. 1, It is quite apparent that all the normalized entropy curves with various ΔH values collapse into a single curve, confirms second order magnetic phase transition. Next, we calculate another parameter such as $RCP = \Delta S_m|_{max} \times \delta T_{FWHM}$, where δT_{FWHM} is the span for half to maxima of ΔS_m (T) curve around a magnetic transition for practical utilization in MR. The RCP value is obtained as 295 (600) J/kg for a field change of 3 (5) T which is significantly larger than 201.3 J/kg (3 T) as observed in an earlier Mn_5Ge_3 study [5]. Hence, a large RC value makes the Mn_5Ge_3 ribbon highly promising for magnetic refrigeration application near room temperature.

1. V. Franco, J. Bluez, J. Ipus, J. Law, L. Moreno - Ramz, A. Conde, Prog. Mater. Sci. 93, 112–232 (2018). 2. V.K. Pecharsky, K.A. Gschneidner Jr, J. Magn. Magn. Mater. 200 (1), 44–56 (1999). 3. V. Franco, J. Blazquez, B. Ingale, A. Conde, Annu. Rev. Mater. Res. 42 305–342 (2012). 4. Songlin, Dagula, O. Tegus, E. Bruck, F.R. de Boer, K.H.J. Buschow, J. Alloy. Compd. 337, 269–271 (2002). 5. T.F. Zheng, Y.G. Shi, C.C. Hu, J.Y. Fan, D.N. Shi, S.L. Tang, Y.W. Du, J. Magn. Magn. Mater. 324, 4102–4105 (2012).

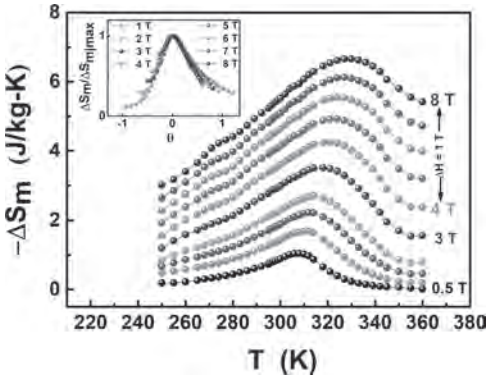

The temperature dependence of $-\Delta S_m$ in field range of 0.5 - 3T ($\Delta H = 0.5$ T) and 4 - 8T ($\Delta H = 1$ T). The inset shows normalized $-\Delta S_m$ as a function of the rescaled temperature (θ).

FPA-02. Improving the Magnetocaloric Response of Fe-rich $(Mn,Fe)_2(P,Si)$ Alloys. *A. Kiecana*[1], I. Batashev[1], K. Kwakernaak[2], N. Van Dijk[1] and E. Brück[1] *1. Radiation, Science and Technology, TU Delft, Delft, Netherlands; 2. Materials Science and Engineering, TU Delft, Delft, Netherlands*

Magnetic cooling, based on the magnetocaloric effect (MCE), offers many advantages over traditional compressor-based refrigeration. Among many promising materials, the $(Mn,Fe)_2(P,Si)$ family of compounds attracts broad attention due to the non-toxic composition, large magnetocaloric effect, tunable Curie Temperature (T_c) and limited thermal hysteresis (ΔT_{hys}). The stoichiometry of the quaternary alloy $(Mn,Fe)_2(P,Si)$ has a significant impact on the magnetocaloric performance. Additionally, the magnetocaloric response of the $(Mn,Fe)_x(P,Si)$ system is highly sensitive to the heat treatment conditions. For the Fe-rich $(Mn,Fe)_x(P,Si)$ ($2.00 \geq x \geq 1.80$) melt-spun ribbons, we investigated the phase purity as a function of starting composition and annealing temperature. For a first batch, annealed for 2h at 1373 K, we found with decreasing M/NM ratio from 2.00/1 to 1.90/1 an increase in T_c from 251.3 to 310.1 K and a decrease in ΔT_{hys} from 33.3 to 8.3 K. These changes were accompanied by a decreasing amount of the metal-rich $(Mn,Fe)_3Si$ impurity phase. A further decrease of the M/NM ratio leads to a rapid reduction of T_c to 178.5 K and an increase in hysteresis to 75.7 K. Along with these changes, the formation of the non-metal (Mn,Fe)Si impurity phase was observed. In order to investigate the effect of the heat treatment, ribbons were annealed at 1313 and 1433 K. The magnetic entropy change (ΔS_m) and ΔT_{hys} increase with increasing annealing temperature, indicating the enhancement of the First Order Magnetic Transition (FOMT). The formation and composition of the $(Mn,Fe)_3Si$ impurity strongly depend on the annealing conditions, as evidenced by SEM/EDS analysis. The change in the annealing temperature caused a significant change in the composition and amount of the $(Mn,Fe)_3Si$ impurity phase. These changes were accompanied by the enlargement of grains and grain boundaries. The (Mn,Fe)Si impurity phase segregated in the form of micro-sized inclusions. Unlike $(Mn,Fe)_3Si$, the (Mn,Fe)Si impurity appeared stable and remained strongly Fe and Si-rich for all annealing temperatures.

FPA-03. Structural, magnetic and mechanical properties of Gd films. *E. Fontana*[1], T. Devillers[1], M. Salaün[1], J. Motte[1], A. Bosseboeuf[2], M. Verdier[3] and N. Dempsey[1] *1. Université Grenoble Alpes, CNRS, Grenoble INP, Institut Néel, Grenoble, France; 2. C2N, CNRS, University Paris Saclay, Palaiseau, France; 3. University Grenoble Alpes, CNRS, Grenoble INP, SIMaP, Grenoble, France*

Gadolinium is the simplest material with a strong magnetocaloric effect close to room temperature (T_c = 293 K) and no thermal hysteresis [1], making it an ideal test-bench material for magnetic refrigeration and energy harvesting prototypes [2,3]. Gd ribbons of thickness 36-215 μm were prepared by cold-rolling [4] while films of thickness 20-150 μm were deposited by evaporation onto dimpled Hastelloy substrates [5]. More recently, films of thickness in the μm range were made by magnetron sputtering [6,7]. Here we present a study of Gd films of thickness in the range 3.5 - 40 μm, deposited by triode sputtering onto Si substrates at RT or 400°C, with Ta buffer and capping layers. As has been reported in magnetron sputtered films [7], our triode sputtered films can be removed from the substrate to produce free-standing films, and peel-off is easiest for films deposited at elevated temperature. Films were characterized structurally (optical and Scanning Electron Microscopy, XRD), magnetically (VSM-SQUID, extraction magnetometer) and mechanically (interferometer, nanoindenter). An SEM image of the fractured cross section of a 20 μm thick film deposited at 400°C is shown in Fig. 1, together with θ-2θ XRD patterns from the upper and lower surfaces of the film. It can be seen that the film texture changes from (00l) at the lower surface to (103) at the upper surface. A spin-reorientation transition is clearly seen in the M(T) curve of a 3.5 μm thick film, while it becomes smeared in thicker films (Fig. 2), owing to the evolution in crystallographic texture. In this presentation we will report on the influence of film thickness and deposition temperature on the structural, magnetic and mechanical properties of Gd films, which are being developed for integration into micro-scaled thermal energy harvesting devices [3]. Acknowledgement: This research has received funding from the French National Research Agency under the HiPerTherMag project (ANR-18-CE05-0019).

[1] K. A. McEwen, "Handbook on the Physics and Chemistry of Rare Earths", K. A. Gschneider et al. (eds), Vol. 1, p 411 (1979) [2] K. A. Gschneidner, Jr. and V. K. Pecharsky, Annu. Rev. Mater. Sci., Vol. 30, p.387, (2000) [3] M. Almanza et al., digest submitted to this conference [4] S. Taskaev, K. Skokov, V. Khovaylo, et al., J. Appl. Phys., Vol. 117, p. 123914, (2015) [5] K. P. Shinde, B. B. Sinha, S. S. Oh, et al., J. Magn. Magn. Mater., Vol. 374, p. 144 (2015) [6] D. Nguyen Ba, L. Becerra, N. Casaretto, et al., AIP Adv., Vol. 10, p. 035110 (2020) [7] D. Nguyen Ba, Y. Zheng, L. Becerra, et al., Phys. Rev. Appl., Vol.15, p. 064045 (2021)

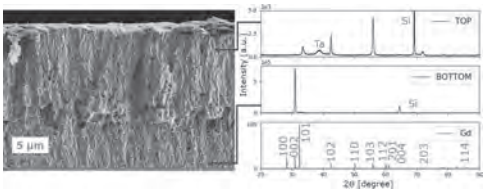

Fig. 1 Left: SEM image of a 20 μm thick Gd film deposited at 400 °C. Right: θ-2θ XRD spectra from the upper and lower surfaces of the film, following peel-off from the substrate.

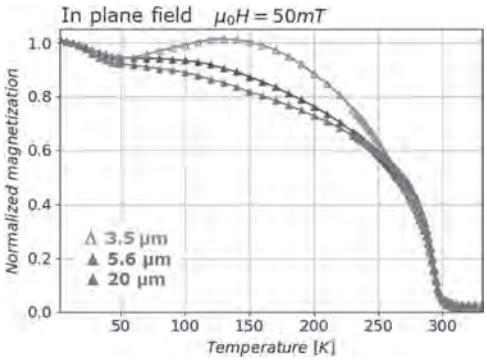

Fig. 2 Magnetization vs temperature, measured under 50 mT, of Gd films deposited at 400°C.

FPA-04. Substitution effects on the magnetic phase transition and magnetocaloric effects in nanolaminated $AlFe_2B_2$ alloys. S. Wang[1], P. Liu[1], *J. Chen*[2] and W. Cui[1] *1. Northeastern University, Shenyang, China; 2. State Key Laboratory of Transducer Technology, Aerospace Information Research Institute, CAS, Beijing, China*

Recently, a kind of novel transition-metal boride, called as MAB phase, possesses a general formulae of $(MB_2)_nMAl$ (n = 1, 2, 3) and layered crystal structure. M can be Cr, Mn, Co elements. But only for M = Fe, $AlFe_2B_2$ is ferromagnetic with phase transition temperature ranged between 280 ~ 320 K[1]. Due to the second-order nature, no hysteresis is desired and some attentions are paid to explore it as emerging magnetocaloric materials. In this work, the substitution effects of C for B and Ti, V for Fe have been studied. All alloys were prepared by arc-melting. The as-prepared ingots were annealed at 1073 K for 4 days followed by quenching into iced water. Structures and magnetic properties are studied by Bruker diffractometer and cryogenic VSM. The XRD patterns of $AlFe_2B_{2-x}C_x$, $AlFe_{2-y}Ti_yB_2$ and $AlFe_{2-z}V_zB_2$ show that the single-phase can be formed for $x \leq 0.1$, $y \leq 0.1$ and $z \leq 0.1$. More substitution leads into the impurities. The thermal magnetization curves of $AlFe_2B_{2-x}C_x$ alloys are shown in Fig. 1. The FM-PM phase transition occurs at 283K. With increased C substitution, the Tc is gradually increased. However, the almost flat M-T curve is observed for x=0.3 due to the decomposition of main $AlFe_2(B,C)_2$ phase. By minor Ti and V substitution for Fe, the T_c is decreased to 280 K due to magnetic dilution. Increased substitution does not further lead into decreased T_c due to the possible substitution limitation. All isothermal magnetization curves are reversible, indicating the second-order nature. The ΔS is maximized at their respective T_c. Under the field of 7 T, ΔS^{max} is 6.4 $Jkg^{-1}K^{-1}$. More C substitution leads into decreased ΔS^{max} to 4 $Jkg^{-1}K^{-1}$ in $AlFe_2B_{1.9}C_{0.1}$, 4.8 $Jkg^{-1}K^{-1}$ in $AlFe_{1.9}Ti_{0.1}B_2$ and 5 $Jkg^{-1}K^{-1}$ in $AlFe_{1.9}V_{0.1}B_2$, due to the decreased magnetization.

1 Z. H. Zhang et al.J. Magn. Magn. Mater., 484 154-158 (2019)

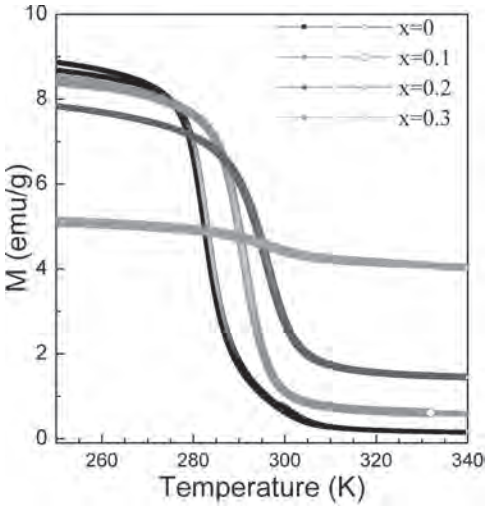

Fig.1 The M-T curves of $AlFe_2B_{2-x}C_x$ (x=0, 0,1 and 0.2) alloys measured under 0.05 T. The solid and open symbols stands for the heating and cooling process respectively.

FPA-05. Study the magnetocaloric properties of shape-dependent nanostructured Gd_2O_3: Nanoplates, Nanorods, and Nanospheres. *D. Neupane*[1], J.F. Casey[2], A. Pathak[2] and S. Mishra[1] *1. Physics and Materials Science, The University of Memphis, Memphis, TN, United States; 2. Physics, SUNY, Buffalo State, Buffalo, NY, United States*

A recent study shows that the magnetic entropy changes of Gd_2O_3 nanostructure depend on the morphology and it varies from - 8.7 J kg^{-1} K^{-1} for nanotubes to - 20 J kg^{-1} K^{-1} for the rod. Several attempts have been made to study the magnetocaloric effect (MCE) on different morphology but comparative study on morphology dependent MCE is missing. Here we investigate the MCE of Gd_2O_3 nanoparticles of different morphology. Single-phase Gd_2O_3 nanoparticles were synthesized via the hydrothermal method and a homogeneous precipitation method followed by heat-treated in the air at $1100^{O}C$ for 12h. Four Gd_2O_3 nanoparticles of different shapes viz. bulk, rod, spheres, and plate were prepared. The morphology of the samples was analyzed using a scanning electron microscope (SEM). The SEM images of synthesized Gd_2O_3 showed fine 1D nano-rods, 2D nano-plates-like architecture prepared via hydrothermal method while hollow nanosphere morphology was achieved with a homogeneous precipitation method. The phase identification and lattice parameter of the powders were performed using x-ray diffraction which showed the presence of a highly crystalline single phase cubic crystal structure. Magnetic measurements were performed from 5 to 100K and magnetic field up to 50kOe. The material demonstrated typical paramagnetic behavior in the whole measured temperature region. The M-H data in the temperature range of 3–30 K is used to calculate the isothermal magnetic entropy change. The maximum value of ΔSm for 50 kOe field change at 5K is 11.2 J kg^{-1} K^{-1} for the nanoplate sample, 9.4 J kg^{-1} K^{-1} for the nano-rod, and 9.2 J kg^{-1} K^{-1} for the nano-sphere, and 10.7 J kg^{-1} K^{-1} for Bulk. The large ΔSm could be attributed to the surface area and surface geometry of the sample. More surface area indicates more surface spins that enhanced magnetization value. These results show the Gd_2O_3 nanoplates are promising materials for low-temperature application. Work at SUNY, Buffalo State was supported by the startup fund from SUNY Buffalo State College and the Undergraduate Research Office, Buffalo State.

1. Phan, M. H., & Yu, S. C. (2007). Review of the magnetocaloric effect in manganite materials. *Journal of Magnetism and Magnetic Materials*, *308*(2), 325-340. 2. Ram, N. R., Prakash, M., Naresh, U., Kumar, N. S., Sarmash, T. S., Subbarao, T., ... & Naidu, K. C. B. (2018). Review on magnetocaloric effect and materials. *Journal of Superconductivity and Novel Magnetism*, *31*(7), 1971-1979. 3. Hazarika, S., Behera, P. S., Mohanta, D., & Nirmala, R. (2019). Magnetocaloric effect of Gd2O3 nanorods with 5% Eu-substitution. *Applied Surface Science*, *491*, 779-783. 4. Tian, G., Gu, Z., Liu, X., Zhou, L., Yin, W., Yan, L., ... & Zhao, Y. (2011). Facile fabrication of rare-earth-doped Gd2O3 hollow spheres with upconversion luminescence, magnetic resonance, and drug delivery properties. *The Journal of Physical Chemistry C*, *115*(48), 23790-23796

FPA-06. An Efficient Strategy for the Discovery of Novel Magnetocaloric Materials. *I. Batashev*[1,2], G. de Wijs[2], E. Brück[1], N. Van Dijk[1] and M. Maschek[1] *1. TU Delft, Delft, Netherlands; 2. Radboud University, Nijmegen, Netherlands*

The interest in the magnetic cooling devices has led to an intensive search for suitable well-performing magnetocaloric materials over the last 25 years. However, to this date only a few material systems have been found to be suitable for commercial applications. Computational screening makes possible sieving through thousands of known compounds without the need to perform time-consuming measurements and therefore can play an important role in detecting novel magnetocaloric materials. To identify such systems of interest we selected several screening parameters using properties of various well-known MCE materials as a reference. Along with magnetic properties, other factors important for practical applications were taken into consideration including price, availability, and toxicity of candidate materials. Combining these criteria, we implemented an algorithm for the screening process as a set of automated computational tools. It relies on information readily available in the structural databases to perform detailed modelling via *ab-initio* calculations. Two computational databases (Aflowlib and Materials Project) and two experimental databases (COD and ICSD) are used as initial source of information totaling to 800k candidate compositions. As a main metric to predict the magnetocaloric performance we use the magneto-elastic response of the candidate. This is done by computing magnetic moment of the material across a range of deformations, both volumetric and uniaxial. This parameter shows good correlation with ΔS_M measured in known magnetocaloric materials. A step-by-step application of initial screening parameters to sort out unsuitable materials before performing more computationally heavy assessments allows us to quickly process large number of candidates. This resulted in a shortlist of promising compounds to serve as a guide for experimental research. The flexibility of the computational toolset makes it possible to easily build in additional screening parameters to further adjust or refine the search process.

FPA-07. Large plateau-like Magnetic entropy change in Sn doped Ni-Co-Mn-Ti all *d* metal Heusler alloy. *S. Samanta*[1], S. Ghosh[1] and K. Mandal[1] *1. Magnetism Laboratory, Department of Condensed Matter Physics and Material Sciences, S. N. Bose National Centre for Basic Sciences, Kolkata, India*

In recent years, magnetic refrigeration (MR) has gained much attention, rather than conventional gas refrigeration, being an energy efficient and eco-friendly technology. For that purpose, the current research for exploring potential magnetocaloric material is focused on the material exhibiting first-order magnetostructural transition (MST) along with large change in magnetization and hence large magnetocaloric effect (MCE) [1]–[3]. Recently, Ni-Co-Mn-Ti-based all d-metal Heusler alloy is found to be an excellent candidate for magnetic refrigeration which exhibits multicaloric properties such as MCE [4], elastocaloric effect [5], and giant barocaloric effect [6]. In the present work, we explore the effect of Sn doping at Ti-site and also heat treatment condition on MCE properties of $Ni_{35}Co_{15}Mn_{37}Ti_{13-x}Sn_x$ (x = 0,1 and 2) alloys through thermal and magnetic measurements. The observed MST temperature (T_M) shifts toward lower temperature with Sn doping whereas, the sharpness of the transition enhances with annealing time which effectively increases the MCE response as shown in fig.1 (a)). The sample with $x = 1$ exhibits a plateau-like magnetic entropy change (ΔS_M) with a maximum peak value of $\Delta S_M \sim 5.7$ $Jkg^{-1}K^{-1}$ due to a magnetic field change of 50 kOe. It is interesting to note that ΔS_M value remains almost the same with value ~ 4 $Jkg^{-1}K^{-1}$ for a temperature region of 300 K-350 K shown in fig.1 (b). Large ΔS_M in a wide temperature interval is attributed to the existence of inter-martensite transition along with MST. The large ΔS_M value with wide tunable operating temperature region in the

vicinity of room temperature and the estimated large relative cooling power (RCP) of ~ 384 J/kg enable the material a suitable candidate for solid-state MR technology.

[1] J. Liu, T. Gottschall, K. P. Skokov, J. D. Moore, and O. Gutfleisch, "Giant magnetocaloric effect driven by structural transitions," *Nat. Mater.*, vol. 11, no. 7, pp. 620–626, 2012. [2] V. Franco, J. S. Blázquez, J. J. Ipus, J. Y. Law, L. M. Moreno-Ramírez, and A. Conde, "Magnetocaloric effect: From materials research to refrigeration devices," *Prog. Mater. Sci.*, vol. 93, pp. 112–232, 2018. [3] S. Ghosh, A. Ghosh, P. Sen, and K. Mandal, "Giant Room-Temperature Magnetocaloric Effect across the Magnetostructural Transition in (MnNiSi)1-x (FeCoGa)x Alloys," *Phys. Rev. Appl.*, vol. 14, no. 1, p. 1, 2020. [4] H. Neves Bez *et al.*, "Giant enhancement of the magnetocaloric response in Ni–Co–Mn–Ti by rapid solidification," *Acta Mater.*, vol. 173, pp. 225–230, 2019. [5] D. Cong *et al.*, "Colossal Elastocaloric Effect in Ferroelastic Ni-Mn-Ti Alloys," *Phys. Rev. Lett.*, vol. 122, no. 25, p. 255703, Jun. 2019. [6] A. Aznar *et al.*, "Giant barocaloric effect in all-d-metal Heusler shape memory alloys," *Phys. Rev. Mater.*, vol. 3, no. 4, p. 044406, Apr. 2019.

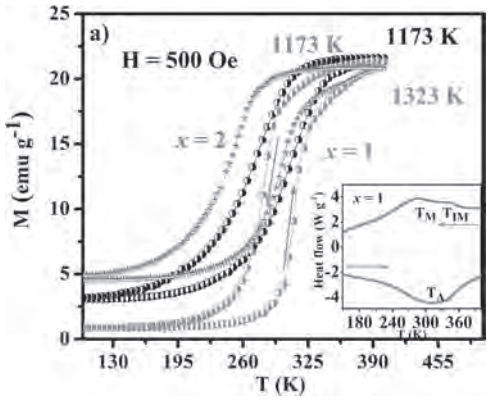

Figure 1: (a) Magnetization vs. T for x = 1 and 2alloys under different annealing temperatures. Inset shows DSC heat-flow vs. T with a ramp rate of 10 K/m of x = 1 sample.

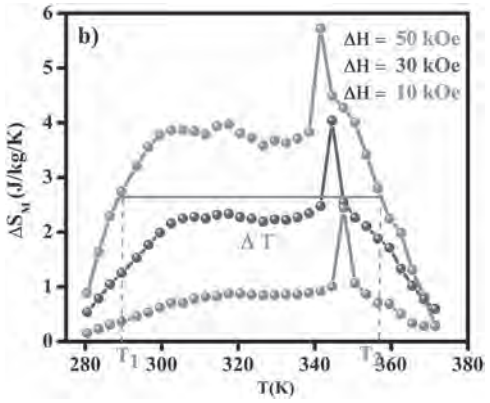

Figure 1: (b) ΔS_M vs. T at different magnetic field for x = 1 alloy.

FPA-08. Magnetocaloric Effect in Fe-Mn based High Entropy Alloys.
M. Ghahremani[1] and A. Aslani[2] *1. Computer Science, Mathematics and Engineering, Shepherd University, Shepherdstown, WV, United States; 2. Electrical and Computer Engineering, George Washington University, Washington, DC, United States*

During the past decade, the magnetic properties of high-entropy alloys have been studied, motivated in part by the observation of large magnetocaloric effects (MCE) displayed by these alloys near room temperature. In this paper, we present new data to illustrate the enhanced magnetic and magnetocaloric properties of FeMnGeNiSi alloys which were synthesized through vacuum arc melting technique under an argon atmosphere. The magnetization of these samples was measured, and their Curie temperatures were determined. The magnetocaloric effect temperature change of these samples was measured directly using an advanced direct MCE measurement apparatus. The result shows different magnetocaloric temperature changes for various compositions. The magnetization of these alloys is characterized by two critical temperatures. Below the lower critical temperature, the alloys are ferrimagnetic martensite. Between the two critical temperatures, the alloys are ferromagnetic martensite and above the higher critical temperature, they are paramagnetic austenite. The transitions at both critical temperatures are first order. The ferri-to-ferromagnetic transition and the crystallographic martensite-to-austenite transition explain the various facets observed in the ZFC and FC versus temperature plots and their variations with an increasing magnetic field. In addition, in this research, the latent heat of the FeMnGeNiSi alloys linked with the first-order transformation has been studied through direct measurements of the adiabatic temperature change during the magnetization process. The experimental procedure used guarantees independent data points and negates any contribution of hysteretic losses to the magnetocaloric effect. Thus, the differences between the magnitudes of the adiabatic temperature (ΔT_{ad}) measurements during the magnetization with the initial temperature change directions from low-to-high and high-to-low are solely attributed to the latent heat exchange, which accompanies the irreversible structural first-order transformation. The amount of the latent heat varies with the amount of iron and manganese in the alloys which is discussed in this paper.

FPA-09. Producing gadolinium free-standing and flexible films, with high quality surface for energy applications: the role of thickness and growth temperature.
D. Nguyen Ba[1,2], L. Becerra[2], M. Marangolo[2], M. Almanza[1] and M. LoBue[1] *1. Université Paris-Saclay, ENS Paris-Saclay, CNRS, SATIE, Gif-sur-Yvette, France; 2. Sorbonne Université, CNRS, Institut des NanoSciences de Paris, Paris, France*

Gadolinium (Gd) films have been considered for micro and nano-scale application, because of their high magnetic moment and a Curie point close to room temperature (RT) [1]. Recently, free-standing thick films have been pointed out as promising active substance in energy conversion micro-devices [2] due to their magnetocaloric properties (MC). Indeed, as put in [2], good MC properties, surface quality, absence of substrate, and flexibility are the main features to get a caloric membrane to be deployed in a micro-electromechanical system (MEMS). Unfortunately, a systematic study of the optimal preparation parameters to obtain the aforementioned properties, is still lacking. Actually, film thickness, growth temperature, and the choice of the buffer layer, are all key features affecting the final result after substrate removal. Here, polycrystalline Gd films are prepared by sputtering on a silicon substrate with a thermally oxidized layer. Thickness of the film is varied from 100 nm to 17 μm, exploring growth temperatures in an interval between RT up to 666 K. Buffer layers of tungsten (W) and tantalum (Ta) are used. More than 45 Gd thick films with various growth temperatures, thicknesses and buffer layers have been prepared. The first result is that notwithstanding the growth temperature and thickness, tungsten buffer makes the substrate removal more difficult, particularly over large film surfaces (e.g. tens millimetres size). Increasing the growth temperature improves the magnetic properties [3] and changes the surface morphology. For instance, surface roughness is 10 nm and 121 nm for films prepared at 543 K and 666 K, respectively. Using tantalum, wide area free-standing films of various thicknesses from 5 to 17 μm have been obtained, with a flexibility depending on the growth temperature. Thinner free-standing films, namely 3 μm Ta/Gd/Ta have also been obtained showing smaller sizes (i.e. few millimeters size). In summary, the main result here is the identification of optimal preparation conditions (buffer layer, growth temperature and thickness) to obtain large, smooth and flexible Gd films to be used in MEMS device as a magnetocaloric membrane.

[1] G. Scheunert, O. Heinonen, R. Hardeman, A. Lapicki, M. Gubbins, and R. M. Bowman, A review of high magnetic moment thin films for microscale and nanotechnology applications, Appl. Phys. Rev. 3, 011301 (2016). [2] N. B. Doan, Y. Zheng, L. Becerra, M. Marangolo, M. Almanza,

and M. LoBue, Magnetocaloric Effect in Flexible, Free-Standing Gadolinium Thick Films for Energy Conversion Applications, Phys. Rev. Applied 15, 064045 (2021). [3] N. B. Doan, L. Becerra, N. Casaretto, J. -E. Duvauchelle, M. Marangolo, S. Ahmim, M. Almanza, and M. LoBue, Magnetocaloric gadolinium thick films for energy harvesting applications, AIP Adv. 10, 035110 (2020).

FPA-10. Magneto-structural phase transition in the *B*-site disordered $Sr(Fe_{1/2}Nb_{1/2})O_3$ perovskite: A combined dc magnetization and x-ray diffraction study. *A. Kumar*[1,2], S. Nair[1] and D. Pandey[2] *1. Department of Physics, Indian Institute of Science Education and Research (IISER), Pune, India; 2. School of Materials Science and Technology, Indian Institute of Technology (BHU), Varanasi, India*

ABO_3 type compounds with perovskite structure are known to exhibit a very rich variety of phase transitions ranging from ferroelectric, antiferroelectric, ferrielectric, antiferrodistortive octahedral tilt, ferromagnetic, antiferromagnetic, ferrimagnetic, John-Teller, metal-insulator and superconducting transitions [1]. The richness of these phenomena is further enhanced by introducing substitutional disorder at the A or B sites leading to relaxor ferroelectricity, dipole-glass, spin-glass and quantum phase transitions [2]. The technological applications of these perovskites is due to the functional properties imported by such phase transitions. In this context, the B-site disordered iron-niobate family has evinced considerable interest due to the temperature stable giant dielectric constant and multiferroicity. The low temperature magnetic transitions and the ground state of these complex perovskites is now fully understood [3,4]. However, understanding of the high temperature behaviour is still lacking. In the present investigation, we report high temperature phase transitions in $Sr(Fe_{1/2}Nb_{1/2})O_3$ (SFN) using dc magnetization and x-ray diffraction measurements. Our dc magnetization M (T) study reveals two magnetic transitions around 620 K and 700 K for the first time. The magnetic transition occurring around 620 K is linked with the structural phase transition as confirmed by temperature dependent x-ray diffraction studies. The integrated intensity of the strongest superlattice reflection (I_{SL}) and the octahedral tilt angle (φ) decrease continuously with increasing temperature and vanishes across the structural phase transition. We have fitted temperature variation of both I_{SL} and φ using the expressions $B(T_C-T)^{\beta}$ and $B(T_C-T)^{2\beta}$, respectively, where B is constant, T_C is the structural phase transition temperature and β is critical exponent. The value of β comes out to be 0.24 which suggests the tricritical nature of the phase transition. Another transition around 700 K in the M (T) plot occurs close to the peak temperature in the loss tangent (tanδ). We believe that this transition is most likely driven by oxygen vacancies.

[1] R. J. D. Tilley, Perovskites: Structure property relationships (John Wiley & Sons, Ltd, United Kingdom) (2016). [2] S. Vasala and M. Karppinen, Prog. Solid State Chem. 43, 1-36 (2015). [3] A. Kumar et al., Phys. Rev. B 99, 214425 (2019). [4] A. Kumar et al., J. Alloys and Compds 859, 157779 (2020).

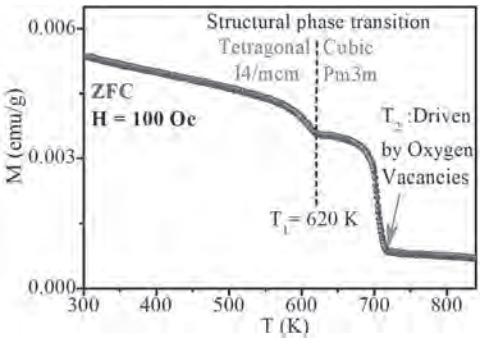

DC magnetization versus temperature plot of $Sr(Fe_{1/2}Nb_{1/2})O_3$ at 100 Oe field

FPA-11. Magnetocaloric Effect Study on Heusler Based Glass-Coated Microwires. *M. Hennel*[1,2], L. Galdun[1] and R. Varga[1] *1. CPM-TIP, UPJS, Kosice, Slovakia; 2. UFV, PF UPJS, Kosice, Slovakia*

Magnetocaloric effect is a new nonconventional method that can be used to provide cooling power with several benefits compared to conventional gas-compression based cooling. Heusler alloys are promising candidates for micro-magnetic cooling applications thank their desirable behaviour. Preparation of Heulser alloys in a form of glass-coated microwires by the Taylor-Ulitovsky technique allows easy and fast production of microwires with protective glass coating and many additional advantages such as scalability of the size of cooling material. Previous works show the possibility of tuning the structural and magnetic transformation temperature of glass coated Heusler microwires by changing the chemical composition and valence electron concentration ratio *e/a*. This is one of the most favourable properties of glass coated Heusler microwires. Combining structural and magnetic transformation may enhance the amplitude of the magnetocaloric effect when both transformations overlap, the evaluation of their contribution may become complicated. Therefore, we would like to present the possible analyses which can provide information about the magnetocaloric effect or the transformation temperatures including both structural and magnetic transitions. Direct measurements of magnetocaloric effect, indirect measurement of magnetocaloric effect, resistivity measurements, Arrott plot method, universal curves, method of critical exponent *n*, Kouvel-Fisher method with Arrott-Noakes plots and many others can be used to study the magnetocaloric effect and transformations on a presented group of alloys. This research was supported by Slovak Grant Agency VEGA 1/0053/19, Slovak Grant Agency grant number APVV-16-0079.

[1] V. Franco and A. Conde, International Journal of Refrigeration, Vol. 33(3), p. 465–473 (2010) [2] A. Kharrat and W. Boujelben, Journal of Low Temperature Physics, Vol. 197, p. 357–378 (2019) [3] M. Hennel, L. Galdun, T. Ryba, R. Varga, Journal of Magnetism and Magnetic Materials, 511, 166973 (2020)

FPA-12. Near room temperature magnetocaloric properties in Ni deficient $Mn_{0.525}Fe_{0.5}Ni_{0.975}Si_{0.95}Al_{0.05}$. *M. Khan*[1], R.C. Das[1], B. Akintunde[1], J.F. Casey[2] and A. Pathak[2] *1. Physics, Miami University, Oxford, OH, United States; 2. Physics, SUNY Buffalo State College, Buffalo, OH, United States*

$Mn_{0.5}Fe_{0.5}NiSi_{0.95}Al_{0.05}$ is a member of the MnTX (T = Ni, Co; X = p-block elements) family of intermetallic compounds. It exhibits a first-order ferromagnetic transition coupled with a structural phase transition at 315 K. Near this transition a large magnetic entropy changes of ~17 J kg^{-1} K^{-1}, for a field change of ΔH = 2 T, has been reported for $Mn_{0.5}Fe_{0.5}NiSi_{0.95}Al_{0.05}$.[1] In this work, we present an experimental study on the crystalline, magnetic, and magnetocaloric properties of Ni deficient (Mn-rich) $Mn_{0.525}Fe_{0.5}Ni_{0.975}Si_{0.95}Al_{0.05}$. The study has been performed by x-ray diffraction, scanning electron microscopy, and dc magnetization measurements. X-ray diffraction measurements showed that the sample simultaneously exhibited the orthorhombic and hexagonal structures at room temperature. The ferromagnetic transition temperature occurred at ~338 K, which is significantly larger than 315 K observed in $Mn_{0.5}Fe_{0.5}NiSi_{0.95}Al_{0.05}$. A maximum magnetic entropy changes of ΔS_M = -9.5 and 25 J $kg^{-1}K^{-1}$ for ΔH = 2 T and 5 T, respectively, has been observed. Reasonably large refrigeration capacity of 60 J /kg and 160 J/kg for field changes of ΔH = 2 T and 5 T, respectively, has also been observed. The experimental results and related discussions will be presented in detail. Work at SUNY, Buffalo State was supported by the startup fund from SUNY Buffalo State College and Undergraduate Summer Research Fellowship award, Undergraduate Research Office, Buffalo State.

[1] Biswas et. al. Acta Mat. 180, 341 (2019).

FPA-13. Observation of large magnetocaloric effect in rare-earth substituted Gd_2O_3 nanorods. *S. Hazarika*[1], A.V. Morozkin[2], G. Karanam[3], R. Nama[3], K. Pradeep[3] and R. Nirmala[1] *1. Physics, Indian Institute of Technology Madras, Chennai, India; 2. Chemistry, Moscow Lomonosov State University, Moscow, Russian Federation; 3. Department of Metallurgical and Materials Engineering, Indian Institute of Technology Madras, Chennai, India*

Recent studies on nanostructures of pure and rare earth substituted Gd_2O_3 reveal large low temperature magnetocaloric effect [1, 2]. In the present work, nanorods of Gd_2O_3 with 5 at.% Nd^{3+} and 5 at.% Er^{3+} ion substitution at Gd-site have been synthesized using a template-free and surfactant-free hydrothermal method [Fig. 1]. The samples have $MnFeO_3$-type cubic crystal structure (space group *Ia*-3, *N* 206, *cI*80) at 300 K. From the powder X-ray diffraction data, using the Scherrer formula, a crystallite size of ~ 25 nm and ~ 20 nm is estimated for the Nd-substituted and Er-substituted Gd_2O_3 nanorod samples. Raman spectra also confirm the cubic structure of the samples at 300 K. Both samples show paramagnetic behaviour in the temperature range of 300 K to 5 K. From the magnetization vs field data measured in the temperature range of 5 K to 31 K, the isothermal magnetic entropy change (ΔS_m) is calculated. The maximum ΔS_m value at 6 K for 70 kOe field change is about -19.8 $Jkg^{-1}K^{-1}$ and -23.5 $Jkg^{-1}K^{-1}$ respectively for 5 at.% Nd- and Er- substituted Gd_2O_3 nanorods. The magnetocaloric effect is of the same order as in the pure and other rare-earth-substituted Gd_2O_3 nanostructures. Thus the mixed rare-earth oxide nanostructures are found to be potential candidates for low temperature magnetic cooling applications.

[1] A. Zelenakova, P. Hrubovcak, O. Kapusta, V. Zelenak, and V. Franco, Appl. Phys. Lett. 109 (2016) 122412 [2] S. Hazarika, P. S. Behera, D. Mohanta and R. Nirmala, Appl. Surf. Science 491 (2019) 779

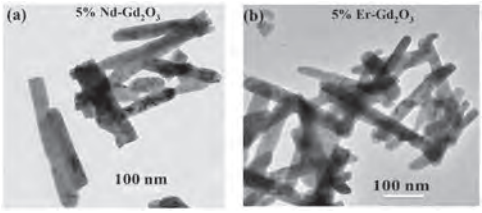

High-resolution Transmission Electron Microscopy images of Nd- and Er-substituted Gd_2O_3 nanorolds

FPA-14. Anomalous Magnetic Properties of $GdCrTiO_5$ Nanoparticles. *B. Bharati*[1,2], P. Mohanty[2], C.J. Sheppard[2] and A.R. Prinsloo[2] *1. Spectrum Analytical Facility, University of Johannesburg, Johannesburg, South Africa; 2. Chromium Research Group, Department of Physics, University of Johannesburg, Johannesburg, South Africa*

Magnetic cooling obtained from magnetocaloric (MC) effect can be used as a substitute to usual refrigeration [1]. Recently, few reports illustrated the MC effect in Gd based compounds [1-2]. Das *et al.* [2], found the MC effect in exchange frustrated bulk magnet, $GdCrTiO_5$, where the origin of strong frustration is due to exchange interaction of Gd^{3+} and Cr^{3+} sublattices. There are limited reports on the magnetic properties of bulk $GdCrTiO_5$ [2-4], but none focused on the nano-dimension. Therefore, in the present case, the structural and magnetic properties of sol-gel synthesized and subsequent calcined (at 800 °C) $GdCrTiO_5$ nanoparticles were explored. The synthesized $GdCrTiO_5$ nanoparticles stabilizes in a orthorhombic crystal structure with space group *Pbam*, with lattice parameters, *a*, *b*, *c* of 7.381(2), 8.679(2), 5.862(2) Å, respectively, as confirmed from the x-ray diffraction measurements. The transmission electron microscopy shows the particle size as 37 ± 1 nm. The temperature dependence of dc magnetization, $M(T)$, was measured for $GdCrTiO_5$ nanoparticles and the Néel temperature, $T_N = 190 \pm 2$ K, obtained. At low fields, the spins of the Cr and Gd align in opposite directions to each other and the net moment align in the opposite direction to the applied field, in the temperature range 10 to 108 K. Additionally, spin reorientation is observed at temperature of $T_{SR} =$ 17 ± 3 K. Irreversibility appeared in field-cool-cooling (FCC) and field-cool-warming (FCW) curves at low temperatures, indicating a ferromagnetic-antiferromagnetic (FM-AFM) transition. This FM-AFM transition and T_{SR} was not observed in bulk $GdCrTiO_5$ [2-4]. Both FM nature and exchange bias effect is further established from the field-dependent magnetization measurements. Furthermore, a change in isothermal magnetic entropy ($-\Delta S_m$) of 22 ± 3 $J.kg^{-1}.K^{-1}$ is found below 10 K, for a 7 T change in field. The obtained magnetic properties in this report are discussed in terms of exchange frustration originating from the competing interactions of the magnetic sublattices of the Cr^{3+} and Gd^{3+} in the $GdCrTiO_5$ nanoparticles.

[1] J. Shi, T. Sauyet and Y. Dang,. J. Phys.: Condens. Matter. Vol. 33, p.205801 (2021). [2] M. Das, S. Roy and N. Khan, Phys. Rev. B Vol. 98, p.104420 (2018). [3] T. Basu, K. Singh and S. Gohil. J. Appl. Phys. Vol. 118, p. 234103 (2015). [4] T. Basu, D.T. Adroja and F. Kolb, Phys. Rev. B Vol. 96, p.184431 (2017).

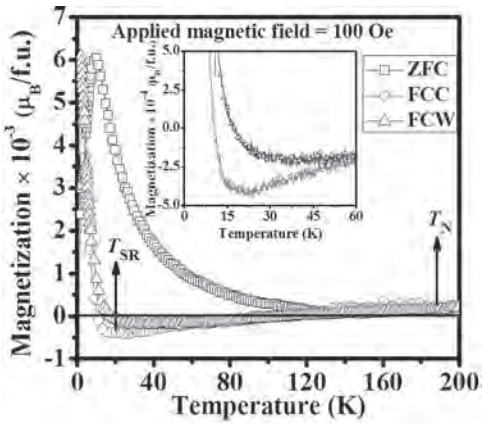

Fig. 1. $M(T)$ data for $GdCrTiO_5$ nanoparticles.

FPA-15. The Effect of Thickness Induced 3D Strain on Magnetocaloric Properties of Epitaxial $La_{0.8}Ca_{0.2}MnO_3$. *W. Akram*[1], S. Giri[2], M. Bansal[1] and T.S. Maity[1] *1. School of Physics, Indian Institute of Science Education and Research Thiruvananthapuram, Thiruvananthapuram, India; 2. Physics Department, Kharagpur College, Kharagpur, Paschim Medinipur, India*

The magnetic refrigeration, based on magnetocaloric effect (MCE) has gradually emerged to be the alternative to vapour-based refrigeration and promised to sustain the nature by reducing the need for greenhouse and ozone depleting chemicals [1]. Decades of research have been invested to increase the efficiency of such magnetic refrigerants either by recombining various materials or by applying strain [2-4]. Here, we varied the thickness (t) of epitaxially grown $La_{0.8}Ca_{0.2}MnO_3$ (LCMO) on two types of substrates $SrTiO_3$ (STO) and $LaAlO_3$ (LAO) in the range of 25 – 300 nm and investigated the thickness induced 3-D strain effects on MCE. STO and LAO apply in-plane biaxial tensile and compressive strain, respectively on LCMO. But, for both the LCMO/STO and LCMO/LAO, the maximum entropy change (ΔS_{max}) (~12.1 J/Kg-K and ~3.2 J/Kg-K, respectively at 6 T magnetic field) can be seen at t ~75 nm (Fig. 1). The temperature dependent magnetization for all LCMO/STO films shows clear hysteresis whilst for LCMO/LAO, it shows a broader transition region compared to the former with no hysteresis. These indicate the first order magnetic phase transition in LCMO/STO but the second order magnetic phase transition in LCMO/LAO. To compare the viability of these epitaxial films with different order of phase transitions as the efficient refrigerants, we calculated Relative Cooling Power (RCP). They show maximum RCP at t ~75 nm (~361 J/Kg for LCMO/STO and ~339 J/Kg for LCMO/LAO) (Fig. 2). The Curie temperature (T_C) also varies with t for both the films showing maxima at ~75 nm. This anomalous behaviour of MCE and T_C bellow 100 nm thickness is explained by considering two well-known effects simultaneously- Double Exchange interaction and $3d_{x^2-y^2}$ orbital stabilization [5,6]. These two effects can determine the strength of the ferromagnetic interaction and hence T_C as well as MCE. Moreover, a generalized model of thickness optimization for maximum MCE is proposed

here by fitting the ΔS_{max} vs t curve with the Lorentz function. The fitted curves give maxima for ΔS_{max} at t ~66±5nm for both films. This model can be used to optimize the thickness in other magnetocaloric devices for large MCE.

1. Pecharsky, V. K., et al. "Massive Magnetic-Field-Induced Structural Transformation in G d 5 G e 4 and the Nature of the Giant Magnetocaloric Effect." *Physical review letters* 91.19 (2003): 197204. 2. Krenke, Thorsten, et al. "Inverse magnetocaloric effect in ferromagnetic Ni–Mn–Sn alloys." *Nature materials* 4.6 (2005): 450-454. 3. Moya, X., et al. "Giant and reversible extrinsic magnetocaloric effects in La 0.7 Ca 0.3 MnO 3 films due to strain." *Nature materials* 12.1 (2013): 52-58. 4. Giri, S. K., et al. "Strain induced extrinsic magnetocaloric effects in La0. 67Sr0. 33MnO3 thin films, controlled by magnetic field." *Journal of Physics D: Applied Physics* 52.16 (2019): 165302. 5. Zhang, Jun, et al. "Anomalous strain effect on magnetic properties of La1− xBaxMnO3 epitaxial thin films." *Surface and Interface Analysis* 32.1 (2001): 62-65. 6. Zarifi, Mehdi, et al. "The consequences of growth modes on the magnetotransport properties of La0. 4Pr0. 3Ca0. 3MnO3/LAO films." *AIP Advances* 8.11 (2018): 115206.

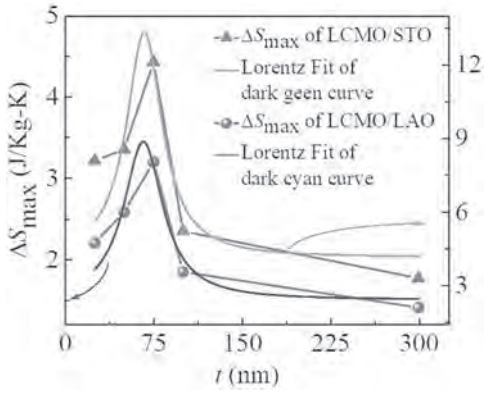

Figure 1 ΔS_{max} vs t plot showing maxima at t ~66±5nm

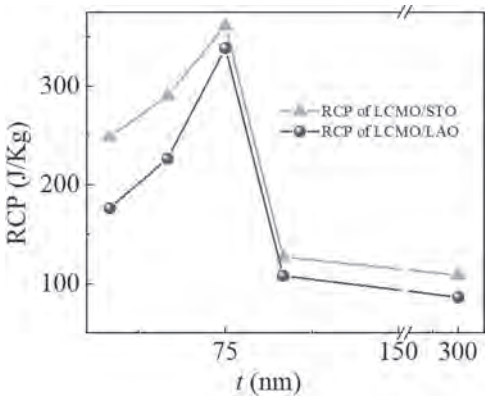

Figure 2 RCP vs t plot

Session FPB
MAGNETOCALORICS IV
(Poster Session)

Feiran Shen, Chair
Institute of Physics, Chinese Academy of Sciences, Beijing, China

FPB-01. Modifications in the magnetocaloric effect owing to composition changes in $Gd_2In_{1-x}Ge_x$ ($0 \le x \le 0.2$) system of compounds.
S. Sharma[1] and P. Kumar[1] *1. Department of Applied Sciences, Indian Institute of Information Technology Allahabad, Prayagraj, India*

In this paper, we report the variations observed in magnetothermal, magnetocaloric, and magnetic properties of the $Gd_2In_{1-x}Ge_x$ ($0 \le x \le 0.2$) system of compounds concerning the changes in substitution of *Ge*. Changes have been recorded in a temperature sweeping range of 2-300 K while the magnetic field was increased from 0 to a maximum of 5 T. All the compositions set into the *Ni_2In*-type hexagonal structure and no structural changes are observed with the change in the value of *x*. Though the transition temperature values, which are $T_C \approx 191$ K and $T_N \approx 100$ K in case of $x = 0$, have only subtle shifts with the *Ge* substitution yet promising changes have been observed in the magnetocaloric effect. At $x = 0.2$ the isothermal magnetic entropy variation peak touches the value of ~ 2.5 J/kg.K in a field change from 0 to 5 T. This showcases that the compounds reported can meet the challenge of the influential applicants in the race of magnetocaloric compounds.

1. S. V. Taskaev, et al., Letters on Materials, 11.1, 104-108 (2021). 2. M. I. Ilyn, A. M Tishin, K. A. Gschneidner, Cryocoolers, 11, pp. 457-464 (2002). 3. R. Liu, S. Sun, G. Yao, Journal of Magnetism and Magnetic Materials, 168305 (2021). 4. Y. Yang, Y. Xie, X. Zhou, AIP Advances, 8, 056406 (2018).

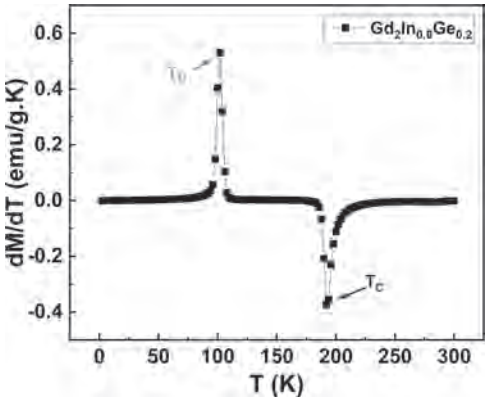

Fig. 1 First derivative of the magnetization curve of the compound $Gd_2In_{0.8}Ge_{0.2}$ revealing the transition temperature clearly. The T_N (Néel temperature) is the antiferromagnetic transition temperature while T_C (Curie temperature) is the ferromagnetic transition temperature.

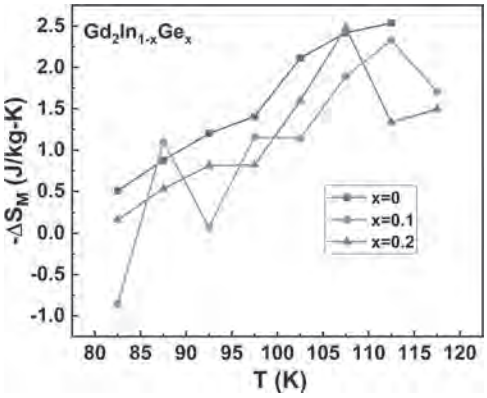

Fig. 2 Change in isothermal magnetic entropy vs. temperature for the $Gd_2In_{1-x}Ge_x$ ($0 \le x \le 0.2$) system of compounds in the vicinity of T_N.

FPB-02. Magnetocaloric effect in melt-spun rare earth intermetallic compound $ErAl_2$.
M.M. Prusty[1], C. Arout[4], A.V. Morozkin[5], G. Karanam[2], K. Pradeep[2], P. Paulose[3] and R. Nirmala[1] *1. Physics, Indian Institute of Technology Madras, Chennai, India; 2. Department of Metallurgical and Materials Engineering, Indian Institute of Technology Madras, Chennai, India; 3. Tata Institute of Fundamental Research, Mumbai, India; 4. Defence Metallurgical Research Laboratory, Hyderabad, India; 5. Chemistry, Moscow State University, Moscow, Russian Federation*

Rare earth intermetallic compound $ErAl_2$ has been prepared by a rapid solidification process namely melt-spinning. The primary motivation for this work is the observation of substantial magnetocaloric effect and relative cooling power values in the neighbourhood of the ferromagnetic transition of several melt-spun rare earth intermetallic compounds and alloys [1, 2], Melt-spun $ErAl_2$ crystallizes in cubic Laves phase structure (Space group *Fd-3m*) as that of the regular arc-melted sample. The average crystallite size calculated from powder X-ray diffraction data is ~ 54 nm and the particle size obtained from high resolution transmission electron microscopy is about ~70 nm. Melt-spun $ErAl_2$ orders ferromagnetically at ~ 10 K (T_C) which is very close to the T_C of the arc-melted sample (14 K). The hysteresis is negligible and the saturation magnetization value at 5 K is about 7.5 μ_B/f.u. Isothermal magnetic entropy change, ΔS_m, calculated from the magnetization vs field data shows a maximum of --34 $Jkg^{-1}K^{-1}$ at 14 K for 70 kOe field change [Fig. 1]. This value is of the same order as that in the arc-melted sample (-42 $Jkg^{-1}K^{-1}$ near T_C). The presence of large magnetocaloric effect in the nanostructured $ErAl_2$ asserts melt-spinning technique as an efficient alternative for the synthesis of magnetocaloric intermetallic materials. The magnetic field dependence of magnetocaloric effect is studied by fitting the maximum isothermal magnetic entropy change (ΔS_m^{max}) values for a given field change (ΔH) to a power law i.e. $\Delta S_m^{max} \propto \Delta H^n$. The value of 'n' is found to be 0.65 for melt-spun $ErAl_2$ at 14 K whereas a value of n = 0.63 is obtained for arc-melted $ErAl_2$ at 14 K. This is close to the value expected for a For a mean-field ferromagnet.

1. J. Lyubina, R. Schäfer, N. Martin, L. Schultz and O. Gutfleisch, Adv. Mater. 22 (2010) 3735 2. R. Rajivgandhi, J. Arout Chelvane, S. Quezado, S.K. Malik and R. Nirmala, J. Magn. Magn. Mater. 433 (2017) 169

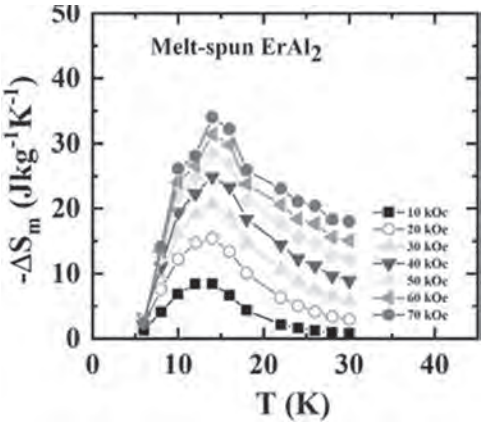

FPB-03. Rare-earth chromite $DyCrO_3$: Structural and magnetic properties. *E.T. Sibanda*[1], A.R. Prinsloo[1], C.J. Sheppard[1] and P. Mohanty[1] *1. Department of Physics, University of Johannesburg, Johannesburg, South Africa*

Rare-earth orthochromites ($RCrO_3$, R = rare-earth element) with a distorted perovskite structure have attracted attention due to their unusual physical properties, including temperature-induced magnetization reversal, spin-reorientation, spin-flipping, Magneto-caloric effect (MCE), and exchange-bias [1]. These materials represent a new class of multiferroic, which exhibit the coexistence of ferroelectric and magnetic orders below the Néel temperature (T_N) [2]. It has been found that the magnetic behavior of $RCrO_3$ compounds is strongly influenced by the Cr^{3+}–Cr^{3+} super-exchange interaction rather than the R^{3+}–Cr^{3+} and R^{3+}–R^{3+} super-exchange interactions [1, 3]. In this contribution, the structural and magnetic properties of magneto-caloric $DyCrO_3$ are studied. The sample was prepared by sol-gel method and calcined at 900 °C to yield an average particle size of 175 ± 10 nm with an average crystallite size of 65.07 ± 0.06 nm and lattice strain of 0.0038 ± 0.0006, as determined from transmission electron microscopy (TEM) and Williamson-Hall analysis of x-ray diffraction patterns, respectively. Rietveld refinement of the powder x-ray diffraction patterns was performed using GSAS software (Fig. 1), based on centro-symmetric space group *Pbnm*. Magnetization measurements as a function of temperature, with different probing magnetic fields, were carried out to determine the various magnetic transitions in the sample under zero field cooled (ZFC) and field cooled (FC) modes (Fig. 2). $DyCrO_3$ orders AFM ascribed to the Cr magnetic order at $T_N^{Cr} \approx 147$ K. The magnetization increases for $T < T_N^{Cr}$. This is the paramagnetic response of Dy^{3+} ions, as these continuously rotate to align with the Cr^{3+}, before the Dy^{3+} order at T_N^{Dy} at about 5 K [4]. This magnetic transition contributes to the MCE of $DyCrO_3$. This behavior is in agreement with previously reported values [5]. The transition temperatures observed in the curves are validated with measurements. The cause of observed anomalies in magnetic transition will be discussed considering the magnetic interactions and structural changes.

[1] S. Mahana, U. Manju, and D. Topwal, J. Phys. D: Appl. Phys., 51, p.305002. (2018) [2] J.R. Sahu, C.R. Serrao, and N. Ray, J. Mater. Chem., 17(1), p.42-44. (2007) [3] E. Bousquet, and A. Cano, J. Condens. Matter Phys., 28(12), p.123001. (2016) [4] P. SujathaáDevi, J. Mater. Chem., 3(4), p.373-379. (1993) [5] A. McDannald, L. Kuna, and M. Jain, J. Appl. Phys., 114(11), p.113904. (2013)

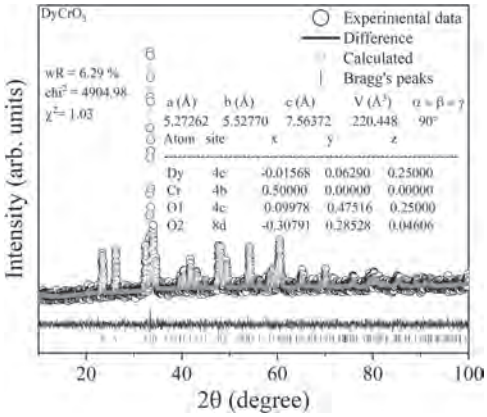

Fig. 1

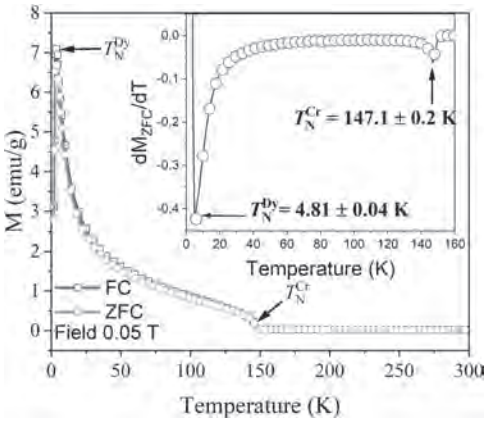

Fig. 2

FPB-04. Peculiar magnetic phase transition and large magnetocaloric effect in Nd_2In. *A. Biswas*[1], A. Thayer[1,2], Y. Mudryk[1], I. Hlova[1], O. Dolotko[1] and V. Pecharsky[1,2] *1. Ames Laboratory, Ames, IA, United States; 2. Department of Materials Science and Engineering, Iowa State University, Ames, IA, United States*

First-order magnetic phase transitions (FOMPTs) generally occur due to concurrent discontinuous changes in magnetic and crystallographic sublattices. FOMPTs that involve changes in crystallographic symmetry are known as magneto-structural (MSTs), and they are commonly known as magneto-elastic (METs) when lattice symmetry remains invariant across the transition. Both MSTs and METs can give rise to plethora of functionalities. Here we report a peculiar magnetic phase transition in a lanthanide-based compound – Nd_2In – which is neither MST nor MET, but it has handful of features generally observed across FOMPTs. Nd_2In shows a non-hysteric paramagnetic-ferromagnetic transition with a nearly discontinuous change in magnetization at $T_C \sim 109$ K, a typical FOMPT feature, and a broad second-order transition at ~52 K. The transition at T_C is also manifested as a sharp peak in heat capacity around T_C and much larger than recently reported[1] magnetocaloric effect with the maximum calculated entropy change (ΔS) of -13 J/ Kg K in a 2 T magnetic field change. This behavior is qualitatively similar to other R_2In compounds where magnetoelastic FOMPTs are well established.[2,3] Further, the temperature and magnetic field dependence of ΔS can be expressed as $\Delta S \sim H^n$, where the local exponent, n, varies with both magnetic field and temperature, showing clear maxima with $n > 2$, a characteristic feature of FOMPT.[4] The temperature-dependent X-ray powder diffraction study, on the other hand, shows no evidence of lattice volume discontinuity or change of crystal symmetry across T_C.

Acknowledgement: This work was performed at Ames Laboratory and was supported by the Division of Materials Science and Engineering of the Office of Basic Energy Sciences of the U.S. Department of Energy (DOE).

Ames Laboratory is operated for the U.S DOE by Iowa State University under Contract No. DE-AC02-07CH11358.

1. W. Liu, F. Scheibel, T. Gottschall, E. Bykov, I. Dirba, K. Skokov, and O. Gutfleisch, Applied Physics Letters, V-119, 022408 (2021). 2. F. Guillou, A. K. Pathak, D. Paudyal, Y. Mudryk, F. Wilhelm, A. Rogalev, and V. K. Pecharsky, Nature Communications, V- 9, 2925 (2018) 3. A. Biswas, N.A. Zarkervich, A. K. Pathak, O. Dolotko, I. Z. Hlova, A.V. Smirnov, Y. Mudryk, D. D. Johnson, and V. K. Pecharsky, Physical Review B, V-101, 224402 (2020) 4. J. Law, V. Franco, L. Moreno-Ramirez, A. Conde, D. Karpenkov, I. Radulov, K. P. Skokov, and O. Gutfleisch, Nature Communication, V- 9, 2680 (2018).

FPB-05. Magnetic and magnetocaloric properties of $Tm_xDy_{1-x}Al_2$ (x = 0.25, 0.50 and 0.75). *P.d. Ribeiro*[1], B.d. Alho[1], R. Soares[1], E. Nobrega[1], V. de Sousa[1], P. von Ranke[1], Y. Mudryk[2] and V. Pecharsky[2,3] *1. Rio de Janeiro State University, Rio de Janeiro, Brazil; 2. Ames Laboratory, Ames, IA, United States; 3. Department of Materials Science and Engineering, Iowa State University, Ames, IA, United States*

We investigate magnetic, thermal, and magnetocaloric properties of rare earth intermetallic compounds with 0.25, 0.5 and 0.75, through a theoretical model Hamiltonian that considers contributions of the crystalline electric field anisotropy in both Tm and Dy magnetic sublattices, disorder in exchange interactions among Tm-Tm, Dy-Dy and Tm-Dy magnetic ions, and the Zeeman effect. Employing earlier reported [1] and new experimental measurements, we first determine a single free variable, the intersublattice magnetic exchange parameter, to properly model the temperature and magnetic field dependencies of heat capacity and magnetization. Then we used the modeling results to explain the emergence of an anomalous spin reorientation transition and its influence on the magnetocaloric effect in the title compounds. Theoretical results agree with experimental data reasonably well.

[1] A. K. Pathak *et. al.*, J. Alloys Comp., 774, 321 (2019). [2] P. O. Ribeiro et. al, J. magn. magn. mater., 442, 265 (2017).

FPB-06. Investigating the structural and magnetic properties of $CoFeNi_{0.5}AlCr_x$. M. Anis[1], R. Osman[1], J. Harris[1], A. Quinata-Nedelcos[2], Y. Azakli[1] and *N. Morley*[1] *1. University of Sheffield, Sheffield, United Kingdom; 2. New Model Institute for Technology and Engineering, Hereford, United Kingdom*

Multi-component alloys contain more than 4 elements in percentages between 12 to 35%, this can lead to single or dual phase alloys. These dual phase alloys have been shown to have promising magnetic properties [1,2], therefore further investigation is required. Two studies were carried out on the $CoFeNi_{0.5}AlCr_x$ alloy to investigate how the structural and magnetic properties change as a function of Cr concentration and post-synthesis heat treatment. The addition of Cr to $CoFeNi_{0.5}Al$ changed the alloy from single phase BCC to dual phase BCC, due to the formation of nanoparticles within a matrix (Fig 1a). The Cr also reduced the saturation magnetisation at 300K. The dual phases gave rise to 2 different magnetic phases: i. high Curie temperature (T_c) almost independent of Cr, ii. low T_c decreasing with increasing Cr (Fig 1b). For $CoFeNi_{0.5}Cr_{0.5}Al$, four post heat treatments were investigated, these were either heated at 1423K for 5 or 10hrs, then either furnace cooled or water quenched. All the samples were BCC, with the water quenched 10hrs (WQ10) and furnace cooled 5 and 10hrs (FC5 and FC10) alloys all having nanoparticles within a matrix, while the water quenched 5hrs (WQ5) alloy had no clear separation of phases. These differences were observed in the T_c, as for WQ10, FC5 and FC10 alloys there were 2 distinct transition in the M-T curves (Fig 1c), while for WQ5 the transition appear as one broad change. The magnetocaloric properties were studied for all the $CoFeNi_{0.5}AlCr_x$ alloys. It was found that Cr decreased the change in entropy (ΔS) for both T_c (Fig 1d). For all alloys, the low T_c had a smaller ΔS compared to the high T_c but a larger refrigerant capacity due to a wider temperature transition. For $CoFeNi_{0.5}AlCr_{0.25}$, the two T_c were within 100K of each other, such that the ΔS curves overlapped giving a wider temperature range, and a refrigerant capacity of 150J/K. Thus tuning the two transitions to be <100K of each other increases the refrigerant capacity.

[1] N. A. Morley, C. R. B. Lim, J. Xi, A. Quintana-Nedelcos, Z. Leong," *Scientific Reports*, 10, 14506, (2020) [2] A Quintana-Nedelcos, Z Leong, N. A. Morley, *Materials Today Energy* 100621 (2021)

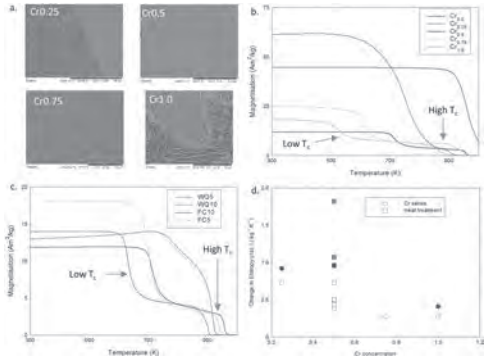

Figure 1a. SEM images of $CoFeNi_{0.5}AlCr_x$, Magnetisation as a function of temperature at 20 kA/m for 1b. $CoFeNi_{0.5}AlCr_x$ and 1c. $CoFeNi_{0.5}AlCr_{0.5}$ and 1d. Change in entropy as a function of Cr concentration (open shapes = low T_c, and solid shapes = high T_c)

FPB-07. A new spin structure and giant baromagnetic effect in $Mn_{0.87}Fe_{0.13}NiGe$ alloy. *F. Shen*[1], H. Zhou[2], J. Hao[1], L. He[1], F. Hu[2], H. Wu[3], Q. Huang[3], S. Deng[1], T. Liang[1] and B. Shen[2] *1. Spallation Neutron Source Science Center, Dongguan, China; 2. Chinese Academy of Sciences, Institute of Physics, Beijing, China; 3. National Institute of Standards and Technology, NIST Center for Neutron Research, Gaithersburg, MD, United States*

Pressure sensor (PS) has important application in artificial intelligence and modern industries. Baromagnetic effect (BME), i.e., pressure-induced magnetic moment change, is regarded as the candidate technology for new PS. The reported large BME in $Mn_3Ga_{0.95}N_{0.94}$[1] has gained great attention. The origin comes from the pressure-induced spin re-orientation from Γ^{5g} antiferromagnetic (AFM) to M-1 ferrimagnetic phase. Recently, the ternary metallic compounds MM′X (M, M′ = transition metals, X = main elements) have attracted renewed attention due to their barocaloric effect[2], and giant negative thermal expansion[3]. In the MM'X family, previous research indicated that the AFM coupling of the stoichiometric MnNiGe is very robust. The substitution of Mn with Fe introduces Fe-Mn ferromagnetic (FM) coupling, which can help to establish a cone-spiral magnetic coupling[4]. Hence, a new cycloidal spiral AFM structure (CyS-AFM^b) was discovered in $Mn_{0.87}Fe_{0.13}NiGe$[5], which is sensitive to magnetic field and stress. As a result, a giant BME was achieved. The employed $Mn_{0.87}Fe_{0.13}NiGe$ alloy were prepared by arc-melting technique. The CyS-AFM^b was discovered in $Mn_{0.87}Fe_{0.13}NiGe$ below 150 K. A low magnetic field can make the CyS-AFM^b transform to a conical spiral FM with angle 70°(70°-CoS-FM^b), accompanied by a step rise of magnetization (Fig.1). More importantly, the new CyS-AFM^b is no longer insensitive to stress compared to the MnNiGe without Fe-doping. A pressure higher than 4kbar induces abnormal change of Mn(Fe)-Mn(Fe) distances hence transform the CyS-AFM^b into a conical spiral ferromagnetic configuration(45°-CoS-FM^a) with easily magnetized but much shortened magnetic moment (Fig.2). As a result, giant BME was observed under either a low magnetic field or a field of 2T~5T. The maximal BMC appears to be ~5.34 emu/g*kbar under 0.35T while ~9.03emu/g*kbar under 2.2T in a wide temperature range, which all far exceed those of the previous reported $Mn_3Ga_{0.95}N_{0.94}$.

1. K. W. Shi, Y. Sun, J. Yan, et al., Adv. Mater., Vol. 28, p.3761-3767 (2016) 2. R. R. Wu, L. F. Bao, F. X. Hu, et al., Sci. Rep., Vol. 5, p.18027 (2015) 3. Y. Y. Zhao, F. X. Fu, L. F. Bao, et al., J. Am. Chem. Soc., Vol. 137, p.1746-1749 (2015) 4. F. R. Shen, H. B. Zhou, F. X. Hu, et al., Mater. Horiz., Vol. 7, p.804-810 (2020) 5. F. R. Shen, H. B. Zhou, F. X. Hu, et al., J. Am. Chem. Soc., Vol. 143, p.6798–6804 (2021)

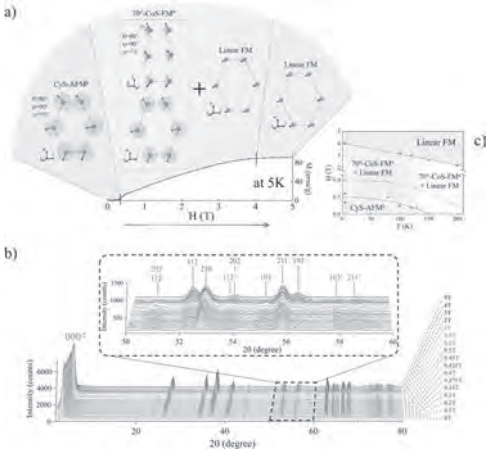

Fig.1. a)M-H curve at 5K with the sketch of spin structure evolution with H, b)Variable magnetic field NPD patterns at 5K, and c)phase diagram.

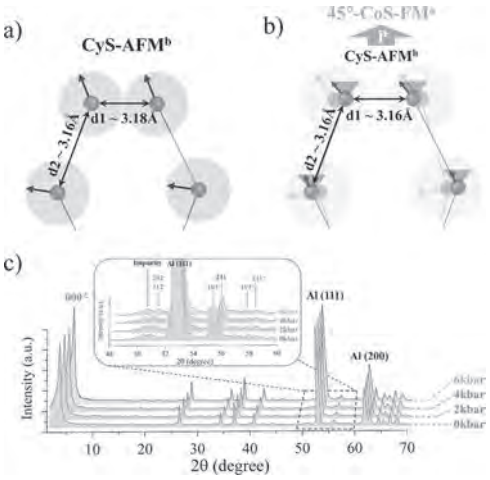

Fig.2. The sketch of a)the CyS-AFM^{b} andb)the 45°-CoS-FM^{a}, and the variable pressure NPD patterns at 120K.

Session FPC
MAGNETOELASTICS II
(Poster Session)

Wei He, Chair
Institute of Physics, Chinese Academy of Sciences, Beijing, China

FPC-01. Magnetostriction and heat-capacity study on the metamagnetic phase transition of $Dy_2In_{1-x}Al_x$ alloys. S. Wang[1], P. Liu[1], *J. Chen*[2] and W. Cui[1] *1. Northeastern University, Shenyang, China; 2. State Key Laboratory of Transducer Technology, Aerospace Information Research Institute, CAS, Beijing, China*

Compared with the conventional vapor compression refrigeration, the magnetic refrigeration technique is promising, which is based on the giant magnetocaloric effect occured during the magnetic phase transition. To enhance MCE in the SOMP system is always intriguing because of no hysteresis. Recently, by Al substituting for In in $Dy_2In_{1-x}Al_x$ system[1], weak metamagnetic phase transitions and resultant enhanced MCE were observed. However, the mechanism underlying the metamagnetism is still unclear. In this work, the magnetostriction and heat-capacity were studied during the metamagnetic phase transition. The $Dy_2In_{1-x}Al_x$ (x=0~0.4) ingots were prepared by arc-melting and annealed at 1023 K for 4 days. The phase constituent and magnetic properties have been examined by X-ray powder diffraction (XRD) and cryogenic PPMS. The alloys are formed in the hexagonal structure with FM for $x \leq 0.3$ and in orthorhombic structure with AFM for $x = 0.4$. The T_c is gradually decreased with increased Al content. Near T_c of Dy_2In alloy, with increased external field, the magetostriction $\lambda_{//}$ is also positively increased and saturated to be ~ 120 ppm. As comparison, the saturation magetostriction $\lambda_{//}^S$ is negative and increased to be ~ -200 ppm. In $Dy_2In_{0.7}Al_{0.3}$ alloy with the critical composition, the maximum of magnetic entropy change is obtain. From Fig.1, the highest $\lambda_{//}^S$ of ~ -1000 ppm is achieved near 60 K, which is the Tc for $Dy_2In_{0.7}Al_{0.3}$ alloy. From the temperature-dependent heat-capacity measurement, when the magnetic phase transition occurs, a peak is observed on the C_p-T curve for all alloys. Due to the concurrence of maximized ΔS_{max} and $\lambda_{//}^S$, it is concluded that enhanced ΔS_{max} is mainly caused by strong magnetoelastic coupling.

1. G. Q. Yao, F. L. Wei, J. S. Zhang, Scripta Mater., 167 37 (2019)

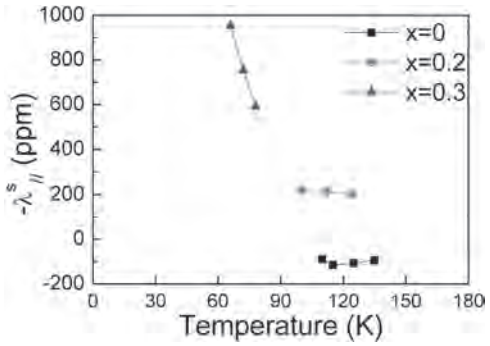

Fig.1 The temperature-dependent saturation magnetostriction ($\lambda_{//}^S$) for $Dy2In_{1-x}Al_x$ (x = 0, 0.2, 0.3)

FPC-02. Analysis and Experimental Research on High Frequency Magnetic Properties of Different Magnetostrictive Materials Considering Temperature Effect. *W. Huang*[1], Z. Xia[1] and P. Guo[1] *1. Hebei University of Technology, Tianjin, China*

Magnetostrictive materials represented by Terfenol-D, Galfenol and Fe-Co have the advantages of high energy density, fast response speed, control accuracy and high displacement resolution,and have been widely used in the fields of precision machining, ultrasonic cleaning, actuator. Under the condition of high frequency excitation, there are more hysteresis loss, eddy current loss, copper loss of excitation winding in the magnetostrictive device. The existence of various losses will change the temperature value and distribution of the material. Due to the temperature-sensitive properties, the material exhibits different magnetic and mechanical properties at different temperatures. If only the magnetic properties at room temperature are used to analyze the various performance of the magnetostrictive device in actual work, the analysis results will appear large deviations from the actual phenomenon. Therefore, it is necessary to accurately analyze the magnetic properties of magnetostrictive materials at different temperatures. Reference [1] tested the high frequency characteristics of Terfenol-D and improved the traditional loss separation formula based on the loss test data. Reference [2] measured and analyzed the magnetic and loss characteristics of ferrite, nanocrystal and amorphous alloy. On this basis, a temperature-controllable high-frequency magnetic characteristic test system is built based on the AMH-1M-S dynamic magnetic characteristic tester and a thermostat. The high-frequency magnetic properties of Terfenol-D, Galfenol and Fe-Co at different temperatures (10-80°C) were measured, and a comparative analysis was made from the magnetic domain rotation and mechanism. The results show that the three samples have the same change trend affected by temperature, but the degree of change is obviously different. Among them, Terfenol-D has the strongest temperature sensitivity and the largest magnetic energy loss. Figure 1 shows the hysteresis loops of the three materials. Figure 2 shows the loss trend of the three samples at different temperatures.

[1] Wenmei Huang, Xiaoqing Wu, Pingping Guo. Variable Coefficient Magnetic Energy Losses Calculation Model for Giant Magnetostrictive Materials, IEEE Transaction on Magnetics, 2021, 57(2):6300505. [2] Ming Yang, Yonjian Li, Qingxin Yang. Magnetic Properties Measurement and Analysis of High Frequency Core Materials Considering Temperature Effect. IEEE Transactions on Applied Superconductivity 2020, 30(4): 5900905.

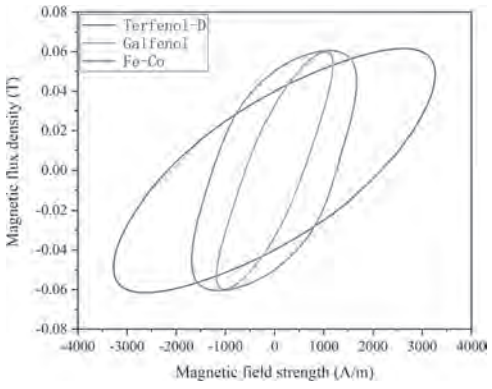

Fig.1. The hysteresis loop of three materials (f=10 kHz, B_m=0.06 T, ΔT= 20°C)

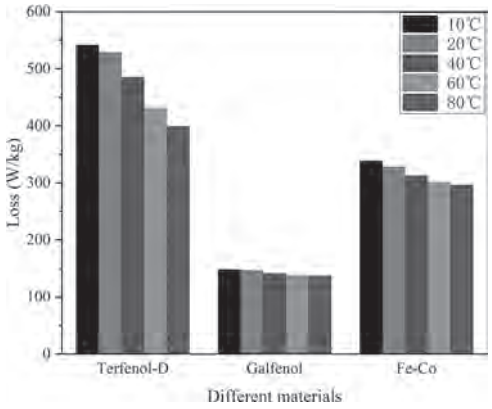

Fig.2. The loss trends of three materials at different temperatures (f=10 kHz, B_m=0.06 T)

FPC-03. Controlling Piezoelectric Love Waves in Magnetoacoustic Devices. *O. Latcham*[1], Y. Au[1], A. Shytov[1], S. Horsley[1] and V. Kruglyak[1] *1. University of Exeter, Exeter, United Kingdom*

We study the scattering of piezoelectric Love waves from isolated magnetic stripes and arrays of those. Typically these surface acoustic waves (SAWs) have long lifetimes and can be coupled – via magnetostrictive effects - to the magnetization dynamics within a thin magnetic stripe, as shown in Fig.1. The coupling is enhanced in the vicinity of the Kittel resonance of the stripe, which can be tuned via the externally applied magnetic field. We analyze the reflection, transmission and losses, including radiation into the bulk, for the Love waves. The reflection and transmission spectra have asymmetric (Fano) lineshapes. When the stripes are arranged into periodic arrays these effects are resonantly enhanced due to Bragg scattering, which would also result in magnetoelastic Borrmann and induced transparency effects [1]. We identify a non-leaky branch at the first phononic band gap (see Fig.2) that is protected from Brekhovskikh attenuation [2]. This vindicates treating magnetoelastic arrays within the 1D approximation and will prove useful when probing and exploiting these waves. We also find that the scattering from the magnetic stripes could be non-reciprocal, with the degree of non-reciprocity enhanced when the precession is circular. Our analytical results are validated with numerical simulations using COMSOL multiphysics.

[1] O. S. Latcham, Y. I. Gusieva, A. V. Shytov, O. Y. Gorobets, and V. V. Kruglyak, Appl. Phys. Lett. 117, 102402 (2020) [2] A. A. Maznev, Phys. Rev. B 78, 155323 (2008)

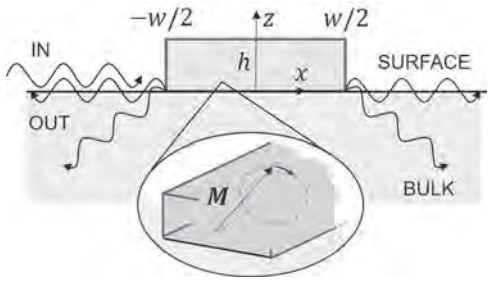

Fig.1: A magnetic stripe, with precessing magnetization M, thickness h, and width w, is situated atop a piezoelectric substrate. Incident surface acoustic waves ('IN') are scattered into surface and bulk modes.

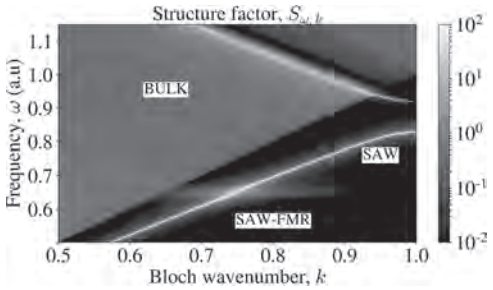

Fig.2: Elastic structure factor $S_{\omega,k}$ of an infinite array of stripes. The lowest surface branch ('SAW') is separated from the bulk continuum ('BULK') at k=π/a. The magnetic anti-crossing is labeled 'SAW-FMR'.

FPC-04. Theoretical investigation of the nonhysteretic first-order phase transition of Eu_2In through free-energy analysis. *B.d. Alho*[1], P.d. Ribeiro[1], P. von Ranke[1], F. Guillou[2], Y. Mudryk[3] and V. Pecharsky[3,4] *1. DEQ, UERJ, Rio de Janeiro, Brazil; 2. Inner Mongolia Key Laboratory for Physics and Chemistry of Functional Materials, Inner Mongolia Normal University, Hohhot, China; 3. Ames Laboratory, Ames, IA, United States; 4. Iowa State University, Ames, IA, United States*

Eu_2In was recently reported to exhibit a giant nonhysteretic magnetocaloric effect due to a first-order magnetic phase transition with a small phase volume change of approximately 0.1% around T_C = 55 K [1]. We present magnetic and compute magnetocaloric properties of a Eu_2In compound using a microscopic description based on a model Hamiltonian that takes into account magnetic exchange and magnetoelastic interactions [2]. In the model the thermodynamic nature of the transition is conveniently represented by a single magnetoelastic interaction parameter. A good agreement between the theoretical results and earlier published experimental data confirms the effectiveness of our approach. Keywords: Hysteresis; magnetocaloric effect; intermetallic compounds; magnetoelastic.

[1] F. Guillou *et. al.*, Nature Comm., 9, 2925, 2018. [2] B. P. Alho *et. al.*, Solid State Comm., 152, 951, 2012.

FPC-05. Static and dynamic magneto-elastic sensing properties of Fe-Al alloy powder-epoxy composite patches. *S. Na*[1], B. Yoo[2], D.J. Pines[2], J. Yoo[1] and N.J. Jones[1] *1. Physical Metallurgy and Fire Performance Branch, Naval Surface Warfare Center Carderock Division, Bethesda, MD, United States; 2. Aerospace Engineering, University of Maryland, College Park, MD, United States*

Hybrid magneto-elasto-optical systems have the potential to translate surface strain into a color change for structural health monitoring (SHM), mediated by the magnetic coupling between two different functional materials, specifically magnetostrictive and magnetochromatic materials. This hybrid system has the potential to be applied as a paint to large structures, therefore small particle sizes are needed to allow the particles to stay suspended in solution. In this work, polymer-matrix composites with magnetostrictive Fe-Al alloy particles are evaluated to determine the magneto-elastic coupling properties in composite patches attached to a surface prior to understanding the hybrid magneto-elasto-optical interaction. Fe-Ga alloy (Galfenol) powders are usually considered for use in magnetorheological (MR) fluids, MR elastomers for tactile sensors, and SHM systems as composite patches to detect ultrasonic guided waves [1-5]. Figure 1 shows changes of magnetic properties as functions of Alfenol particle fraction and shape, associated with the magneto-elastic coupling effect under compressive stress along the out-of-plane direction. A tension apparatus was also designed to control applied stress precisely to the composite patches attached on dog-bone specimens in a solenoid coil. Flake-shaped particles are more sensitive to increases in applied stress than spherical particles. In addition to the static state, Alfenol MPCs with flake-type powders exhibited better sensing performance than Galfenol ones at frequencies of 120 kHz using ultrasonic guided wave techniques.

[1] R. Elhajjar *et al.*, *Progress in Materials Science.* 97, 204 (2018). [2] S. W. Or *et al.*, *IEEE Trans. Magn.* 40, 71 (2004). [3] B. Yoo *et al.*, *J. Appl. Phys.* 117, 17A916 (2015). [4] S. H. Kwon *et al.*, *J. Indust. Eng. Chem.* 82, 433 (2020). [5] B. Yoo *et al.*, *IEEE Trans. Magn.* 52, 2501104 (2016).

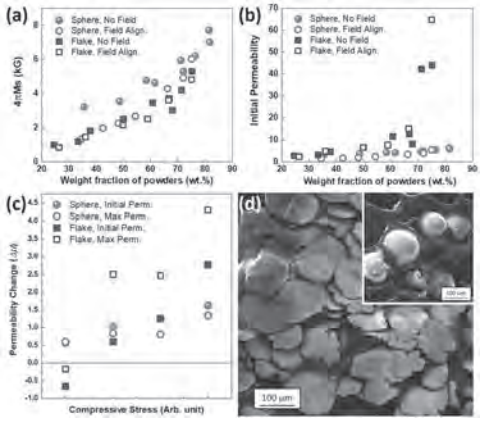

Figure 1. Magnetic properties of composites and particle images; (a)-(b) magnetization and initial permeability as functions of particle shape and weight fraction, where average particle size in diameter was 80 μm and magnetic field was applied out of the plane of the composite patch during curing, (c) permeability changes as a function of compressive stress using a clamping shaft collar to squeeze disc patch on a vertical VSM sample holder, and (d) SEM images of flake and spherical type Alfenol powders with a size of 106-150 μm in diameter, where flake powders were prepared from gas-atomized powders using a wet ball milling process.

FPC-06. Study of Effective Particle Shape-Dependent Magnetization Behavior of Soft Magnetic Polymeric Composites. W.M. Kiarie[1], *D. Sitarski*[2] and D. Jiles[3,1] *1. Materials Science and Engineering, Iowa State University, Ames, IA, United States; 2. Aerospace Engineering, Iowa State University, Ames, IA, United States; 3. Electrical and Computer Engineering, Iowa State University, Ames, IA, United States*

In this work, an investigation of the effect of magnetic particles with different aspect ratios on the effective magnetization response of magnetorheological elastomers (MREs) was carried out. MREs are composites that consist of magnetically permeable particles dispersed in a nonmagnetic polymeric matrix [1]. These materials are well known due to their tunability property. When subjected to an externally applied magnetic field, changes occur in their mechanical properties leading to the so-called magnetorheological (MR) effect [2]. This is often attributed to the magnetic interaction among the magnetic filler particles [3]. Several factors significantly influence the MR effect such as the polymer matrix, particles-volume fraction, size, and shape of the magnetic particles [4]. In this study, based on continuum formulation theory, microscale modeling using a finite element analysis (FEA) was used to determine the effect of the latter on the macroscopic magnetization of MREs. Using Jiles-Atherton hysteresis model parameters, the hysteresis loops of MRE were numerically resolved in the FEA software, COMSOL Multiphysics [5]. The simulations were performed for randomly oriented (unaligned) and aligned microstructures with a constant particle-volume fraction (φ= ~20%) and varying particle-aspect ratios (AR=1, 2.5, 5, and 7.5). A computational homogenization scheme is used to relate the microscopic behavior to the macroscopic properties of these composites. From the analysis, it was found that for unaligned MRE the effective magnetization increased with an increase in the particle-aspect ratio particularly in the linear region, the saturation magnetization is seen to be independent of the particle shape (see Fig. 1a). This effect is much more noticeable for particles aligned with the applied field (see Fig. 1b). While for particles aligned perpendicular to the applied field, an opposite effect is seen where increasing aspect ratio resulted in decreasing of magnetization relative to the applied field.

[1] H. Wu *et al.*, "Chain Formation Mechanism of Magnetic Particles in Magnetorheological Elastomers during Pre-Structure," *J. Magn. Magn. Mater.*, no. 2021, p. 167693, 2020. [2] S. Sun *et al.*, "An adaptive tuned vibration absorber based on multilayered MR elastomers," *Smart Mater. Struct.*, vol. 24, no. 4, 2015. [3] M. R. Jolly, J. D. Carlson, and B. C. Muñoz, "A model of the behaviour of magnetorheological materials," *Smart Mater. Struct.*, vol. 5, no. 5, pp. 607–614, 1996. [4] E. Galipeau and P. Ponte Castañeda, "The effect of particle shape and distribution on the macroscopic behavior of magnetoelastic composites," *Int. J. Solids Struct.*, vol. 49, no. 1, pp. 1–17, 2012. [5] W. M. Kiarie, E. J. Barron, A. P. S. Baghel, *et al.*, "Modeling of Magnetic Properties of Magnetorheological Elastomers using JA Hysteresis Model," *IEEE Trans. Magn.*, vol. 9464, no. c, pp. 1–1, 2020.

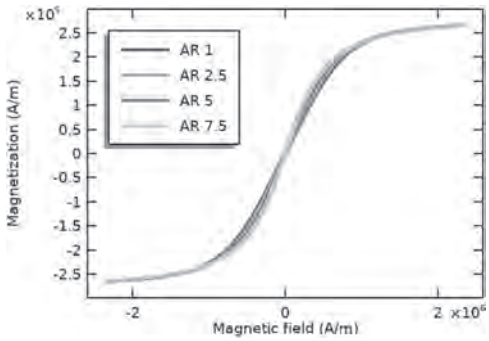

Fig. 1 Effective magnetization behavior for a) unaligned MRE with varying particle-aspect ratios

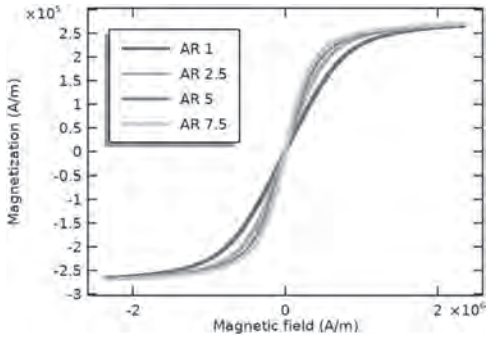

Fig. 2 Effective magnetization behavior for b) aligned MRE with different particle-aspect ratios

Session FPD
MAGNETOOPTICS II
(Poster Session)

Shawn Pollard, Chair
The University of Memphis, Memphis, TN, United States

FPD-01. Circular Displacement Current induced Novel Magneto-Optical Effects in All-dielectric Metasurfaces. *S. Xia*[1], D. Ignatyeva[2], Q. Liu[3], Y. Chen[3], J. Qin[1], V.I. Belotelov[2], M. Veis[4] and L. Bi[1] *1. University of Electronic Science and Technology of China, Chengdu, Chile; 2. Lomonosov Moscow State University, Leninskie Gory, Moscow, Russian Federation; 3. College of Mechanical and Vehicle Engineering National Engineering Research Center for High Efficiency Grinding, Hunan University Changsha, Hunan, China; 4. Charles University of Prague, Faculty of Mathematics and Physics, Prague, Czechia*

In recent years, various methods have been reported to boost the magneto-optical (MO) response. Several works have reported the enhancements of the MO response relying on the plasmonic effects attributed to the strongly confined electromagnetic field in the structures[1-3]. However, the nonnegligible disadvantage of this approach is the optical losses due to the high absorption coefficient of the metal materials[1]. Therefore, combining the all-dielectric metasurfaces which have high-refractive-index and low intrinsic loss with planar photonic structures offers an alternative route to these problems[4,5]. But most of the observations so far are focused on enhancement of existing magneto-optical effects in planar MO thin films. A high index contrast, all dielectric magneto-optical metasurface featuring strong Mie resonance modes have not been fabricated. Here, we report observation of circular displacement current induced novel magneto-optical effects in a high index contrast Si/Ce:YIG/YIG/SiO2 all dielectric metasurface. We observe giant transverse magneto-optical Kerr effect (TMOKE) up to 7 % under s-polarized incidence, which is non-existent in planar magneto-optical thin films. This phenomenon is essentially originated from the unique circular displacement current when exciting the magnetic resonance modes, which changes the incident electric field direction locally. These results indicate promising potential of controlling light propagation by utilizing the complex Mie resonance modes in magneto-optical all dielectric metasurfaces. Our work may inspire the development of novel magneto-nanophotonic devices such as vectoral magnetic field sensing, free space non-reciprocal photonic devices and magneto-optical imaging.

1. Belotelov, V.I. et al. Enhanced magneto-optical effects in magnetoplasmonic crystals. Nat Nanotechnol 6, 370-376 (2011). 2. Grunin, A.A., Zhdanov, A.G., Ezhov, A.A., Ganshina, E.A. & Fedyanin, A.A. Surface-plasmon-induced enhancement of magneto-optical Kerr effect in all-nickel subwavelength nanogratings. Applied Physics Letters 97, 261908 (2010). 3. Jain, P.K., Xiao, Y., Walsworth, R. & Cohen, A.E. Surface Plasmon Resonance Enhanced Magneto-Optics (SuPREMO): Faraday Rotation Enhancement in Gold-Coated Iron Oxide Nanocrystals. Nano Letters 9, 1644-1650 (2009). 4. Kuznetsov, A.I., Miroshnichenko, A.E., Brongersma, M.L., Kivshar, Y.S. & Luk'yanchuk, B. Optically resonant dielectric nanostructures. Science 354, aag2472 (2016). 5. Yang, Y., Kravchenko, II, Briggs, D.P. & Valentine, J. All-dielectric metasurface analogue

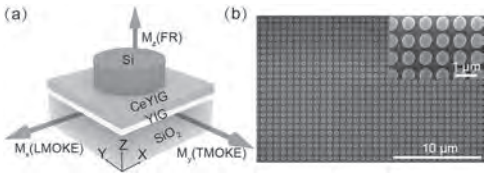

Figure 1. (a) Schematic diagram of the metasurface. (b) Scanning electron microscope image of a fabricated device.

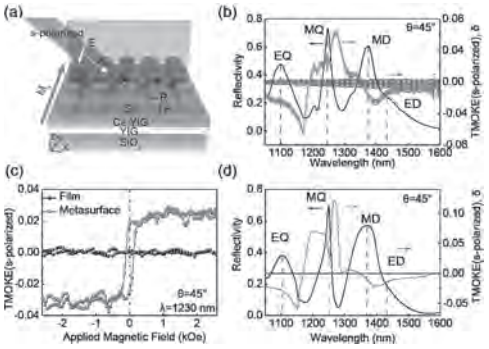

Figure 2. (a) Schematic diagram of s-polarized TMOKE characterization set-up. (b)Measured s-polarized TMOKE and reflection spectra of the metasurface compared with bare Ce:YIG/YIG thin films. (c) Measured TMOKE hysteresis for the metasurface and the bare MO films at 1230 nm wavelength. (d) Simulated reflection spectra and TMOKE responses of the metasurface for s-polarized light.

FPD-02. Light diffraction in rotating magnetic emulsions in a magnetic field. *C.V. Yerin*[1] and S.S. Belykh[1] *1. Physical and Technical Faculty, North-Caucasian Federal University, Stavropol, Russian Federation*

Recently, the range of applications of magnetic emulsions has significantly expanded due to the development of microfluidics [1] and biomedical technologies [2]. Using magnetically sensitive emulsions, methods have been proposed for measuring the viscosity and surface tension of liquids [3] and even for determining the content of methyl alcohol [4]. In this work, we present the results of a study of the effect of diffraction scattering of light in magnetic emulsions with low interfacial tension, synthesized based on AMG-10 hydraulic oil. Magnetic emulsions were produced by mixing kerosene-based magnetic fluid in AMG-10 hydraulic oil. The size of microdroplets could vary from 1000 to 7000 nm. To study the effect of diffraction scattering of light, an optical setup was used, which consisted of a helium-neon laser with a radiation wavelength of 633 nm, a cylindrical cuvette, and a screen. The image of the diffraction pattern was recorded by the CMOS matrix of a camera. Image processing was performed using specialized software ImageJ. The sample cuvette was a glass cylinder, fixed on a fluoroplastic tube driven by a DC motor with a belt drive. The range of rotation frequencies was 9–200 rpm. The diffraction pattern is oriented in the direction perpendicular to the long axes of the elongated microdroplets. When the cell is rotated, the droplet axes deviate from the direction of the magnetic field along the direction of rotation, which leads to a rotation of the diffraction band relative to the initial direction. The deflection angle depends

on the cell rotation speed and the magnetic field strength (Fig. 1 and Fig. 2). The interpretation of the effect of diffraction scattering in magnetic emulsions is based on considering the diffraction of light by an irregular structure of elongated microdroplets of various sizes, located randomly. Calculations give a result that is in complete agreement with the experiment. This work was financially supported by the Ministry of Science and Higher Education of Russia (project no. 0795-2020-007).

1. I. Torres-Diaz and C. Rinaldi, Soft Matter., V. 10. p. 8584, (2014). 2. Q.A. Pankhurst, N.T.K. Thanh, S.K. Jones, and J.J. Dobson, Phys. D: Appl. Phys., V. 42. 224001 (2009). 3. V. Mahendran, J. Philip, Sens. Actuators. V.B 185. p. 488, (2013).

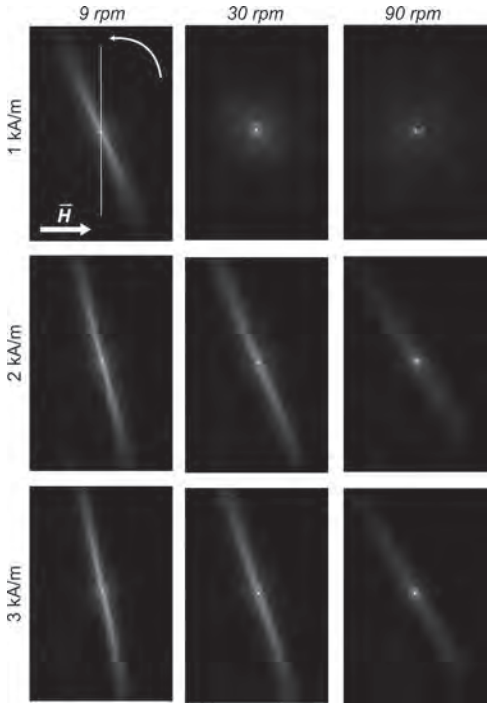

Fig. 1 Photographs of the diffraction pattern at the various magnetic fields and rotation speeds

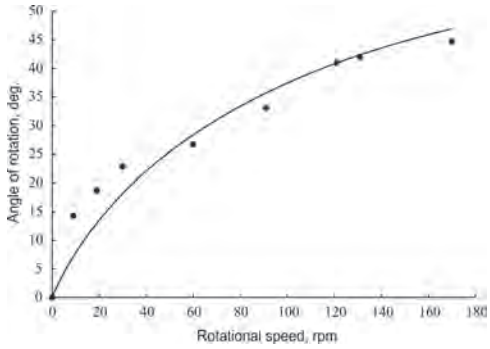

Fig. 2 Dependence of the angle of rotation on the rotation speed (magnetic field is *H*=2 kA/m)

FPD-03. Crystallization of magneto-optical bismuth terbium iron garnet films. *K. Hayashi*[1], Q. Du[1], T. Fakhrul[1], J. Hu[1] and C. Ross[1] *1. Department of Materials Science and Engineering, Massachusetts Institute of Technology, Cambridge, MA, United States*

Iron-based garnet films that have large magneto-optical (MO) effect are a promising material for MO device applications. In particular, terbium iron garnet (TbIG) can crystallize directly on a Si substrate without garnet seed layers [1-4] and, therefore, recent investigations show quite practical optical isolators taking advantage of TbIG [1,2]. However, crystallization for TbIG requires high temperatures and it is desirable to limit the heating to those regions of the chip where devices are formed. In this study, we compare the structure, magnetic and MO properties of TbIG and Bi doped TbIG (Bi-TbIG) films processed by rapid thermal annealing (RTA) to those annealed locally using an embedded resistor with 40-μm-square area. TbIG ($Tb_{2.77}Fe_5O_{12}$) and Bi-TbIG ($Bi_{0.02}Tb_{2.82}Fe_5O_{12}$) films are made by pulsed laser deposition at room temperature, which allows for liftoff patterning using a photoresist mask. The crystal structure for the films is characterized by micro-Raman spectroscopy and X-ray diffraction (XRD) and the magnetic properties by vibrating sample magnetometry. XRD shows single phase garnet after RTA 1073 – 1273 K. Raman spectra for Bi-TbIG film before/after 1173 K annealing and for the Si substrate are shown in Fig. 1. The Raman spectrum for the as deposited film is almost the same as that of the Si substrate while a Raman peak corresponding to the strongest peak of TbIG (E_g) is observed around 261 cm^{-1} in the annealed film. Raman spectroscopy enables detection of local crystallization in Bi-TbIG on embedded resistors. Figure 2 shows room temperature in-plane M-H loops of the annealed TbIG and Bi-TbIG films. The TbIG film is not saturated at 1 T while the Bi-TbIG is saturated at 0.7 T. Coercivity in TbIG rapidly increases in the vicinity of the compensation temperature (T_{comp}) [3] which is ~250 K for bulk TbIG, and slightly lower for thin film TbIG with Tb deficiency [4]. Bi doping lowers (T_{comp}) further [4] explaining the easier saturation of the Bi-TbIG film. The high figure of merit of Bi-TbIG and its higher remanence make this material attractive for integrated photonic devices.

1: P. Dulal, A. D. Block and T. E. Gage, *ACS Photonics*, 3, 1818 (2016). 2: K. Srinivasan, C. Zhang and P. Dulal, *ACS Photonics*, 6, 2455 (2019). 3: K. Srinivasan, C. Radu and D. Bilardello, *Adv. Funct. Mater*. 30, 2000409, (2020). 4: T. Fakhrul, S. Tazlaru and B. Khurana, *Adv. Optical Mater*. 2100512, (2021).

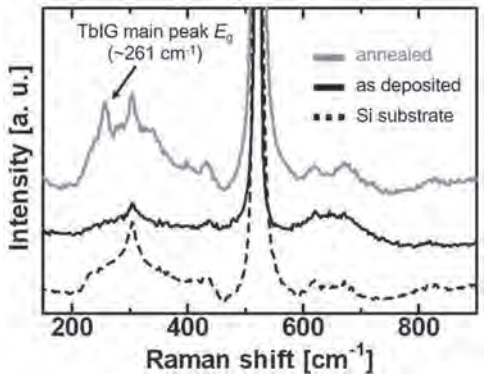

Figure 1; Raman spectra of Bi-TbIG samples and Si substrate

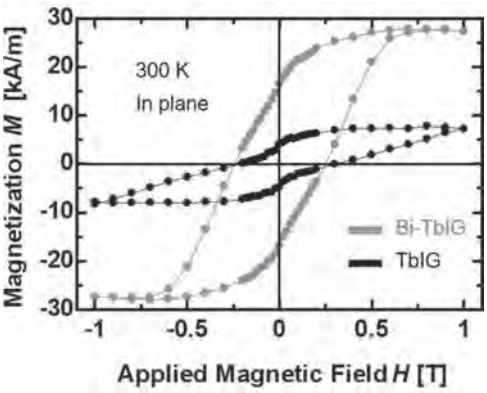

Figure 2; M-H loops of annealed Bi-TbIG and TbIG films at 300 K

FPD-04. *d*-zero Magnetism induced by Optical Excitation in Single Crystal $SrTiO_3$. *L. Prendeville*[1], M. Coey[1], E. Roy[1] and J. Besbas[1]
1. School of Physics and CRANN, Trinity College Dublin, Dublin, Ireland

Strontium titanate (STO) is an amazing oxide. A transparent, diamagnetic insulator, STO has been shown to display a small superposed ferromagnetic-like response that is temperature-independent, at least up to 400 K [1]. The effect is strongest for (110) single-crystal slices and it has been interpreted in terms of mesoscopic, defect-related *d*-zero orbital paramagnetism [2]. Crooker *et al.* reported optically-induced spin magnetism in oxygen-deficient STO below 18 K using magnetic circular dichroism spectroscopy [3]. We thus wanted to re-examine the magnetic properties of STO by optical means to see if there is a response to polarised light that might support the unusual paramagnetism. By performing polar time-resolved magneto-optical Kerr effect (TR-MOKE) measurements on (110) STO using a 400/800 nm pump-probe setup in the absence of a magnetic field, we found that the crystal exhibits a response that depends on the polarisation of the ~100 fs pump pulses, Fig 1. By rotating a quarter waveplate to smoothly vary the polarisation, the MOKE signal is maximised/minimised when the pump is right/left circularly polarised, Fig. 1 insert. We suggest that this is evidence for orbital-related paramagnetism. The circularly polarised pump electric field acts like an effective magnetic field causing electrons to rotate in plane so that their induced orbital magnetisation is detected by the probe pulse. After the pump excitation we observe a tail in the signal with a decay time of ~0.2 ps. This is evident in Fig. 2 where the response is fitted with a Gaussian and the tail with an exponential decay. Another interesting observation is that the tail depends on the pump polarisation, Fig. 2 insert. This seems to be a second effect, separated from the pump-induced orbital paramagnetic response; it may be evidence for spin polarised electrons, possibly related to oxygen vacancies. This indicates that a short but lasting optically-induced spin orientation occurs in bulk STO at room temperature.

1. Coey, J. M. D., Venkatesan, M. and Stamenov, P., Surface magnetism of strontium titanate, J. Phys. Condens. Matter., 28, 485001 (2016) 2. Sen, S., Prendeville, L. and Coey, J. M. D., Mesoscopic orbital paramagnetism: The role of zero-point energy, J. Magn. Magn. Mater., 520, 167366 (2021) 3. Rice, W., Ambwani, P., Bombeck, M., Thompson, J. D., Haugstad, G., Leighton, C. and Crooker, S. A., Persistent optically induced magnetism in oxygen-deficient strontium titanate, Nat. Mater., 13, 481 (2014)

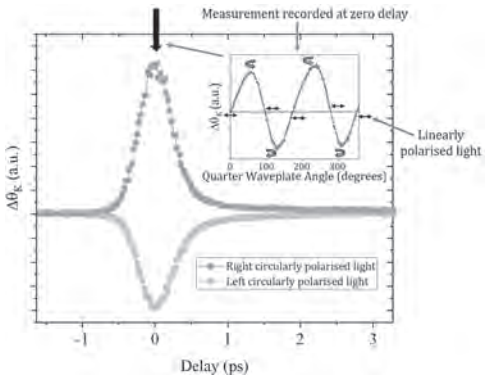

Fig. 1 The TR-MOKE response of a (110) STO crystal depends on the pump polarisation

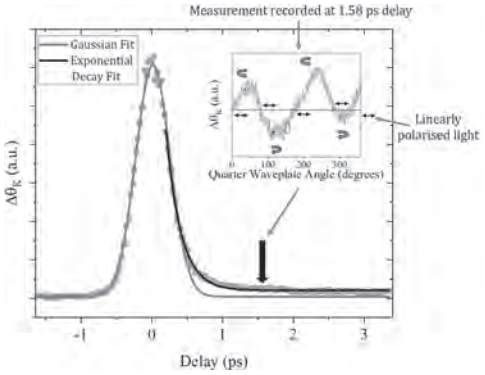

Fig. 2 The TR-MOKE signal at a delay of 1.58 ps also varies sinusoidally with the pump polarisation

FPD-05. Proximity and Charge-Transfer Mediated Magnetism at Nickel Ferrite Interfaces with Graphene and Hexagonal Boron Nitride Monolayers. *N. Schulz*[1], A. Chanda[1], G. Dutt[2], T. Sarkar[2], M. Kamalakar[3], M. Phan[1] and H. Srikanth[1] *1. Physics, University of South Florida, Tampa, FL, United States; 2. Department of Materials Science and Engineering, Uppsala University, Uppsala, Sweden; 3. Department of Physics and Astronomy, Uppsala University, Uppsala, Sweden*

Graphene (Gr) is a particularly interesting material for spintronic and technological applications due to its low intrinsic spin orbit coupling and hyperfine interaction, which lead to high spin lifetimes and coherence lengths [1]. Furthermore, it is common in spintronic applications to introduce a structural isomorph to Gr, hexagonal Boron Nitride (hBN) to improve lattice matching in heterostructure engineering[2]. Specifically for spintronic and spin-caloritronic applications, a ferrimagnetic (FM) layer is often used as a magnon source. Therefore, it is important to understand the interfacial properties of FM/Gr(hBN) interfaces. Here, we explore the change in magnetic anisotropy in the FM insulator Nickel Ferrite (NFO) due to the inclusion of monolayer Gr and hBN. This was done by performing radio frequency transverse susceptibility measurements utilizing a tunnel diode oscillator technique, which is a sensitive probe of the system's effective anisotropy[3]. Specifically, in-plane (IP) and out-of-plane (OOP) measurements were taken for bare NFO, NFO/Gr, NFO/hBN samples. We find that the inclusion of the Gr layer reduces the overall anisotropy for both IP and OOP drastically, by a factor of 2, in the entire temperature of 20 – 300 K. On the other hand, the inclusion of the hBN layer slightly reduces the in-plane anisotropy at low temperature ($T < 180$ K) but increases it at high temperature ($T > 180$ K). Since NFO is an insulator and Gr is a semimetal there is a large conductivity difference at the interface which likely leads to charge transfer reducing the overall anisotropy[4]. This is further supported by the less drastic change with the inclusion of monolayer hBN, a semiconductor. Relative to NFO, magnetometry measurements show an enhancement of the saturation magnetization in NFO/Gr and NFO/hBN, highlighting an additional role played by the magnetic proximity effect.

[1] Panda, J., Ramu, M., Karis, O., Sarkar, T., & Kamalakar, M. V. (2020). Ultimate Spin Currents in Commercial Chemical Vapor Deposited Graphene. *ACS Nano*, *14*(10), 12771–12780. https://doi.org/10.1021/acsnano.0c03376 [2] Zomer, P. J., Guimarães, M. H., Tombros, N., & van Wees, B. J. (2012). Long-distance spin transport in high-mobility graphene on hexagonal boron nitride. *Physical Review B*, *86*(16). https://doi.org/10.1103/physrevb.86.161416 [3] Srikanth, H., Wiggins, J., & Rees, H. (1999). Radio-frequency impedance measurements using a tunnel-diode oscillator technique. *Review of Scientific Instruments*, *70*(7). https://doi.org/10.1063/1.1149892 [4] Zhou, B., Balgley, J., Lampen-Kelley, P., Yan, J.-Q., Mandrus, D. G., & Henriksen, E. A. (2019). Evidence for charge transfer and proximate magnetism in graphene–α–RuCl3 heterostructures. *Physical Review B*, *100*(16). https://doi.org/10.1103/physrevb.100.165426

FPD-06. Magnetic proximity effect on the helimagnetic state of highly crystalline manganese phosphide films. *N.W. Mudiyanselage*[1], D. DeTellem[1], R. Pokharel Madhogaria[1], A. Chanda[1], J.E. Shoup[1], A.T. Duong[2], M. Trinh[1], D. Arena[1], H. Srikanth[1], S. Witanachchi[1] and M. Phan[1] *1. Physics, University of South Florida, Tampa, FL, United States; 2. Phenikaa University, Hanoi, Vietnam*

Over the past few years, the magnetic proximity effect (MPE) has gained intense attention of the magnetic community.[1] Despite the fact that the influence of MPE in bilayers of ferromagnetic (FM) and antiferromagnetic (AFM) materials has been extensively investigated, studies on MPE in bilayers of a FM and a non-collinear magnet are rather limited. Manganese Phosphide (MnP) is a well-known metallic magnet with helical spin configurations at low temperatures.[2-3] Our recent study on highly crystalline MnP thin films has shown the presence of strain-mediated magnetism with two magnetic transitions: a paramagnetic (PM) to FM transition at T_C ~ 279 K and a FM to helimagnetic transition at T_N ~ 110 K.[2] This finding has motivated us to investigate how the helimagnetic spin texture of the MnP film is influenced when another FM layer is placed in its close proximity. To address this, we sputtered a 5 nm Fe film on the 100 nm MnP film, with a 2 nm-thick capping layer of Ta, at room temperature. Magnetometry measurements show a large increase in T_C and a large decrease in T_N for the Fe/MnP bilayer (T_C ~ 300 K and T_N ~ 75 K) relative to the MnP sample (T_C ~ 279 K and T_N ~ 110 K), indicating the presence of strong MPE. The M-H data indicate that in the helimagnetic regime (T < 75 K), the coercive field (H_C) of the Fe/MnP sample ($H_C^{Fe/MnP}$ ~ 1367 Oe) has nearly doubled when compared to the average value of the individual H_C of MnP and Fe reference samples (((H_C^{Fe} + H_C^{MnP})/2) = 780 Oe). Interestingly, the interfacial magnetic coupling strength, defined as $\Delta H_C = |((H_C^{Fe} + H_C^{MnP})/2) - H_C^{Fe/MnP}|$, decreases significantly with decreasing temperature in the helimagnetic regime. Furthermore, the ratio of remanence magnetization (M_r) to saturation magnetization (M_s) of Fe/MnP is higher than the average value of individual M_r/M_s ratios of MnP and Fe. Overall, the observed shapes of the *M-H* loops of the Fe/MnP bilayer deviate remarkably from those of the reference samples. Since the exchange bias effect is negligible in the Fe/MnP system, these observations consistently validate the presence of the MPE.

[1] Lenz, K., Zander, S. and Kuch, W., Magnetic Proximity Effects in Antiferromagnet/Ferromagnet Bilayers: The Impact on the Néel Temperature. *Phys. Rev. Lett.* 98, 237201 (2007). [2] Madhogaria, R., Hung, C., Muchharla, B., Duong, A., Das, R., Huy, P., Cho, S., Witanachchi, S., Srikanth, H. and Phan, M.H., Strain-modulated helimagnetism and emergent magnetic phase diagrams in highly crystalline MnP nanorod films. *Phys. Rev. B* 103, 184423 (2021). [3] Zhigadlo, N., Barbero, N. and Shiroka, T., Growth of bulk single-crystal MnP helimagnet and its structural and NMR characterization. *J. Alloys and Compounds*, 725, 1027 (2017)

FPD-07. Ultra-short Pulsed Laser Ablation Process on a GO FeSi Electrical Single Sheet: Impact on the Static/Dynamic Magneto-mechanical Behavior and Optimization. *E. Salloum*[1,2], O. Maloberti[1,2], S. Panier[2], M. Nesser[2], J. Dupuy[3], M. Lamblin[3] and J. Fortin[1,2] *1. R&D, Unilasalle, Amiens, France; 2. LTI, UPJV, Amiens, France; 3. Multitel, Mons, Belgium*

Ultra-Short Pulsed Laser Ablation process performed on the surface of a Grain-Oriented Electrical Steel (GOES) has shown a significant decrease in the iron losses up to 20%. This is due to a modification of the domain structure that is re-organized using a total energy minimization. Therefore, this leads to a change in the permeability and in the magneto-mechanical behavior also known as the magnetostriction. These modifications are respectively due to the modification of the magnetostatic and the magnetoelastic energy contributions. In this study, the effect of the ablation on the magnetic and the magneto-mechanical properties is revealed and compared to classical irradiation and scribing processes in the static and the dynamic working conditions. Synchronous real time magnetic and mechanical measurements are performed using a dedicated test bench: the Single Sheet Tester with a mechanical adaptation using a fixed-free sample with a piezoelectric accelerometer. GOES samples are measured and compared before and after treatment for different optimal laser parameters. Results have shown that different performances can be simultaneously obtained: - Magnetostriction reduction up to 50% - Permeability increase at low induction up to 20% Physical origins of the change in both static and dynamic magneto-mechanical properties due a laser process will be discussed and proposed to orientate the optimization of laser process parameters towards the best compromise between iron loss reduction, permeability increase and magnetic induced vibrations.

[1] A. Allwardt L. Lahn, C. Wang, T. Belgrand, and J. Blaszkowski. Impoved Transformer Noise Behavior by Optimized Laser Domain Refinement at ThyssenKrupp Electrical Steel. (48(4)):1453–1456, 2012. [2] M. Enokizono T. Kajiwara. Effect of Laser Stress on Vector Magnetic Properties of Electrical Steel Sheets. (50(4)):2002404, 2014. [3] Identification of Magnetic Induced Strain of Electrical Steels Using Non-Destructive Acceleration Measurement and Inverse Vibration Modeling, E. Salloum, O. Maloberti, S. Panier, M. Nesser, P. Klimczyk and J. Fortin, J. Sound Vib, 492(February 2020), 115806. [4] Correlation between laser energetic parameters and magnetic properties of GO laminations under surface treatments with long and short pulsed lasers, M. Nesser, O. Maloberti, E. Salloum, J. Dupuy, J. Fortin, S. Panier and P. Dassonvalle, J. Magn. Magn. Mater., 503(June 2020), 166696.

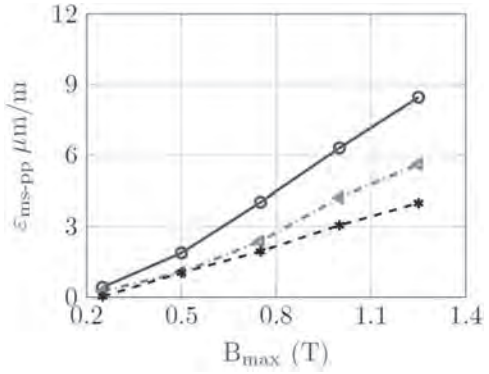

Fig. 1: Peak-to-Peak Magnetostriction: Ref (Blue), ablation 1 (Red), ablation 2 (Black)

Session GOA
SPINS IN 2D MATERIALS AND GRAPHENE

Josep Ingla-Aynés, Chair
Delft University of Technology, Delft, Netherlands

CONTRIBUTED PAPERS

GOA-01. Magnetic Ordering in 2D van der Waals Halide VI_3.
K. Carva[1], A. Koriki[1], J. Pospisil[1] and M. Kratochvílová[1] *1. DCMP, Charles University, Prague, Czechia*

Magnetic van der Waals (vdW) materials composed of weakly bonded two-dimensional (2D) layers exhibit promising potential for high-tech magnetic, magneto-electric and magneto-optic applications in nanostructures. Due to their intrinsic magnetocrystalline anisotropy, several vdW magnets could be thinned down to nanoscale thickness, while still maintaining magnetism. A prominent example of such materials are transition metal trihalides, in particular CrI_3, a first atomically thin ferromagnet, realized in 2017 [1]. VI_3 also belongs among 2D ferromagnets at low enough temperatures. It is a semiconductor undergoing subtle structural phase transition at 78K. Furthermore, its magnetic anisotropy exhibits rather unusual features, foremost a deviation of its easy exis from the normal to the layers [2]. We have studied its properties by first principles calculations and reproduced the unusual magnetic anisotropy. Its properties have been linked to lattice distortions present at some of its low temperature phases (Fig. 1). The calculations also revealed an unusually large orbital momentum on V atoms, noncollinear to the spin momentum [3]. We have studied spin dynamics of this system for finite temperatures. We have shown how is the Curie temperature affected by the layered structure with a weak coupling between layers. Notably the Curie temperature in this system increases with applied pressure. Our calculations allow us to ascribe this effect to an increase of interlayer exchange interactions [4]. We also predict possibility of unusal magnetic order with spins aligned inside magnetically decoupled layers.

[1] B. Huang, et al., Nature, Vol. 546, p. 270 (2017) [2] A. Koriki et al., Phys. Rev. B, Vol. 103, p. 174401 (2021) [3] L. M. Sandratskii and K. Carva, Phys. Rev. B, Vol. 103, p. 214451 (2021) [4] J. Valenta et al., Phys. Rev. B, Vol. 103, p. 054424 (2021)

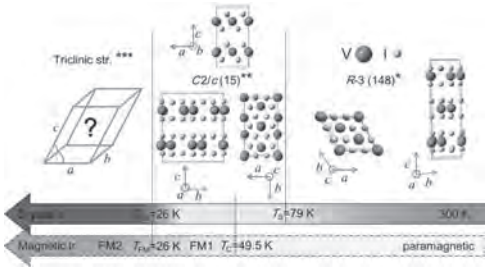

The evolution of crystal and magnetic transitions in VI_3 below room temperature

GOA-02. FeClBr: A Two-dimensional Intrinsic Magnetic Material with Spontaneous Valley Polarization at Room Temperature.
R. Li[1] and W. Mi[1] *1. Department of Applied Physics, Tianjin University, Tianjin, China*

Valley degree of freedom in two-dimensional (2D) materials is fertile ground for the fundamental science, and also has great application prospects in the field of information processing and storage.[1-2] The great challenge of valley application is to achieve the spontaneous valley polarization. The discovery of 2D magnetic materials provides an opportunity to achieve spontaneous valley polarization due to the broken of time-reversal symmetry. In this work, we report a 2D intrinsic ferromagnetic semiconductor FeClBr monolayer with spontaneous valley polarization based on the first-principles calculations. FeClBr monolayer shows high Curie temperature of 651 K, perpendicular magnetic anisotropy and large valley splitting of 188 meV, which is beneficial for the practical application in valleytronics. Besides, FeClBr monolayer can realize the anomalous valley Hall effect not only by the hole doping and circularly polarized light, but also can response to the linear light. FeClBr monolayer is a promote candidate to study the spintronics and valleytronics. This work was supported by the National Natural Science Foundation of China (51871161 and 52071233).

[1] Z. Zhu, A. Collaudin, B. Fauqué, W. Kang and K. Behnia, Field-induced polarization of Dirac valleys in bismuth. Nat. Phys. 8, 89-94 (2012). [2] J. R. Schaibley, H. Y u, G. Clark, P. Rivera, J. S. Ross, K. L. Seyler, W. Y ao and X. Xu, Valleytronics in 2D materials. Nat. Rev. Mater. 1, 16055 (2016).

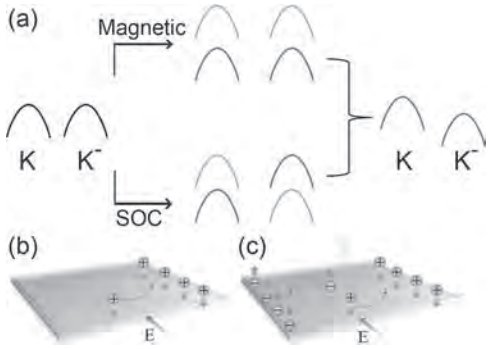

Fig. 1. (a) Schematic diagram of underlying mechanisms of the spontaneous polarization. (b) and (c) are diagrams of the anomalous valley Hall effect in FeClBr monolayer under hole doping and light irradiation.

GOA-03. Two-dimensional Magnetic Order in Cr-based Transition Metal Chalcogenides.
J. Phillips[1] and V. Pardo Castro[1] *1. Física Aplicada, Universidade de Santiago de Compostela, Santiago de Compostela, Spain*

Long-range ferr*f*omagnetic order in the single-layer limit appears to be possible in several chromium-based chalcogenides and halides with layered structure. Ab initio calculations based on the density functional theory of different Cr-based chalcogenides are analyzed approaching the twodimensional limit. The focus will be on magneto-crystalline anisotropy and how to obtain an out-of-plane magnetic polarization that would help circumvent the restrictions of the Mermin-Wagner theorem. This will be studied through various means like strain, pressure, the stability of charge density waves (CDW)[1], stoichiometry and other different structural details. The electronic structure of these compounds will be discussed as an approach to the understanding of the magnetic properties of the transition metal chalcogenide family in general.

Adolfo O. Fumega, Jan Phillips, Victor Pardo, J. Phys. Chem. C 124, 21047 (2020).

GOA-04. Towards Large Scale Quantum Engineering of band structure Spin-Filtering in TMDC-based Magnetic Tunnel Junctions.
V. Zatko[1], S. Dubois[2], J. Peiro[1], M. Galbiati[1], M. Och[3], C. Mattevii[3], P. Brus[4], B. Servet[4], F. Godel[1], F. Petroff[1], A. Fert[1], J. Charlier[2], M. Martin[1], B. Dlubak[1] and P. Seneor[1] *1. Unité Mixte de Physique CNRS Thales Université Paris Saclay, Palaiseau, France; 2. Institute of Condensed Matter and Nanosciences (IMCN), Université Catholique de Louvain, Louvain-la-Neuve, Belgium; 3. Department of Materials, Imperial College, London, United Kingdom; 4. Thales Research and Technology, Palaiseau, France*

Introducing 2D materials in spintronics structures is foreseen to increase control over spin properties and extracted spin signals.[1] Graphene and h-BN have been the first 2D materials to show spin filtering properties in Magnetic Tunnel Junctions (MTJs). Recently, advances within the Transition Metal Dichalcogenides (TMDs) family of 2D semiconductors opened new possibilities to further tailor spintronics properties. We will start by presenting a detailed process to integrate chemical vapor deposited WS_2, with step-by-step characterizations (photoluminescence, Raman spectroscopy,…) to ensure the high quality of the interfaces. The TMD is integrated in a hybrid spin-valve $Co/Al_2O_3/WS_2/Co$. The Co/Al_2O_3 is used here as a spin analyzer in order to probe the spin-polarized current from the 2D/Co interface. We further validate the protocol by measuring magnetoresistance signals above the state of the art concerning MTJs based on 2D semi-conductors. Our main result is the study of a highly thickness dependent spin polarization of the WS_2/Co interface. We show that depending on the number of WS_2 layers stacked in contact with the cobalt electrode, we can tune the sign and amplitude of the extracted spin polarization. This unique behavior is further discussed with ab-initio calculations in support highlighting the band structure dependence of WS_2 and its influence on the spin transport in such MTJs[2]. Leveraging on this results, we will show how a large-scale pulsed laser deposition process of 2D semiconductors[3] carried at CMOS compatible temperatures, allows to engineer the band-gap landscape in these junctions, toward a fine control of 2D semiconductor based MTJ spin transport properties.[4] We will finally discuss how our work unveils the potential of WS_2 for tunable band-gap spin filtering and compatibility to large-scale devices. As this band structure evolution is common to many other TMDs, our work also opens the way to the integration of many other members of this very large 2D materials family, in order to reveal their spin transport properties in MTJs.

[1] Review: M. Piquemal-Banci *et al.* J. Phys. D: Appl. Phys. 50, 203002 (2017) [2] V. Zatko *et al.* ACS Nano 13, 14468 (2019) [3] F. Godel, VZ *et al.* ACS Appl. Nano Matter 3, 7908 (2020) [4] V. Zatko *et al.* ACS Nano 15, 7279 (2021)

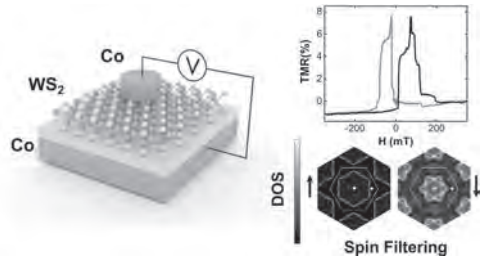

Figure 1: Schematic of the $Co/Al_2O_3/WS_2/Co$ MTJ (left). TMR of a monolayer based MTJ (top right). Ab-initio calculation of the cobalt Fermi Surface.

GOA-05. Intrinsic spin-orbit torque in van der Waals magnetic materials.
F. Xue[1,2] and P.M. Haney[1] *1. Physical Measurement Laboratory, National Institute of Standards and Technology, Gaithersburg, MD, United States; 2. Institute for Research in Electronics and Applied Physics, University of Maryland College Park, College Park, MD, United States*

Spin-orbit torque enables electrical control of the magnetic state of ferromagnets or antiferromagnets. The quintessential system exhibiting spin-orbit torque is a bilayer composed of a heavy metal and a ferromagnet. The heterostructure bilayer geometry breaks the inversion symmetry and allows the spin-orbit torque arising from the spin current flow from the heavy metal layer to the ferromagnetic layer. In this work, we consider the intrinsic spin-orbit torque generated in inversion symmetry breaking magnetic materials directly without stacking with other materials. In the first example of ferromagnetic monolayer Fe3GeTe2, we calculate the intrinsic spin-orbit torque which arises due to the global inversion symmetry breaking. In addition, spin-orbit torque in Fe3GeTe2 has the unique property that the lowest order contribution is fieldlike and time-reversal even because of the C3z rotation symmetry. This is in contrast to the conventional case in which the lowest order is time-reversal odd and fieldlike and the next lowest-order is time-reversal even and dampinglike. We next show that the next lowest-order spin-orbit torque in Fe3GeTe2 is time-reversal odd and dampinglike which can play a more important role in switching the magnetization in the ensuring dynamics, as described by the Landau-Lifshitz-Gilbert equation. In the second example of antiferromagnetic bilayer CrI3, we find staggered dampinglike (time-reversal even) torque and uniform fieldlike (time-reversal odd) torque due to local inversion symmetry breaking and global inversion plus time-reversal symmetry. This is similar to the previous studies of CuMnAs and Mn2Au, where the Neel order switching is demonstrated using uniform fieldlike torque. However, CrI3 has a unique property in that the anisotropy energies and exchange energies are similar in magnitude. This leads to qualitatively different results in the switching dynamics: the staggered dampinglike torque is the dominant switching mechanism. The primary role of staggered dampinglike torque applies to other antiferromagnets in which the product of Gilbert damping and exchange field is smaller than the anisotropy field.

GOA-06. Emergent Ferromagnetism in Fe-doped WS_2 Monolayers at Room Temperature: Experimental and First-Principles Studies.
Y.T. Pham[1], K.C. Nguyen[1], T. Zhang[2], M. Liu[2], V.O. Jimenez[1], V. Kalappattil[1], F. Zhang[2], K. Fujisawa[2], A. Elias[2], M. Trinh[1], I.I. Oleynik[1], M. Terrones[2] and M. Phan[1] *1. Physics, University of South Florida, Tampa, FL, United States; 2. The Pennsylvania State University, University Park, PA, United States*

Two-dimensional (2D) transition metal dichalcogenides (TMDs) hold big promise towards perspective ultralow-power and ultracompact nanodevice applications due to their outstanding optoelectronic and valleytronic properties. The recent observations of room temperature ferromagnetism in 2D-TMDs doped with magnetic metals (e.g., V, Fe, Co) have drawn a great deal of attention in the scientific community.[1-3] However, the origin of ferromagnetism in these systems has remained elusive.[3] In this study, we perform a liquid-phase precursor-assisted approach for *in situ* substitutional Fe doping to exploit magnetic functionality in WS_2 monolayers.[4] Magnetometry measurements indicate that while pristine WS_2 monolayers possess a weak ferromagnetic ordering on the diamagnetic background, Fe-doped WS_2 monolayers exhibit enhanced ferromagnetism at room temperature. The sharp increase in saturation magnetization (M_s) of low Fe-doping (~0.7 at.%) followed by the reduction of M_s for high Fe-doping (~2.8 at%) shows the tunability of ferromagnetism by controlling the Fe concentration. High-resolution STEM images of Fe-doped WS_2 monolayers reveal two major dopant configurations, including the single Fe substitution at a W-site (Fe_W) and the cluster-like triple Fe substitution with an S vacancy ($3Fe_W+V_S$). The cluster form is more dominant in WS_2 monolayers with higher Fe concentrations. First-principles calculations based on density functional theory for Fe-doped WS_2 monolayers with (Fe_W) and ($3Fe_W+V_S$) configurations reveal coexisting ferromagnetic and antiferromagnetic

couplings, depending on the dopants' distance and location, consistent with the experimentally observed non-monotonous temperature dependence of M_s. The spatial-dependent ferromagnetic configurations can be stabilized with total magnetic moments up to 4.0 μ_B and 2.0 μ_B for double Fe_W and ($3Fe_W$+V_S), respectively. These findings shed light on the complexity of ferromagnetism in Fe-doped 2D-TMD systems.

1. Y. T. H. Pham, M. Z. Liu, V. J. Ortiz., Z. Yu, V. Kalappattil, F. Zhang, K. Wang, T. William, M. Terrones, M. H. Phan, *Adv. Mater.* 32, 2003607 (2020). 2. F. Zhang, B. Y. Zheng, A. Sebastian, H. Olson, M. Z. Liu, K. Fujisawa, Y. T. H. Pham, V. J. Ortiz, V. Kalappattil, T. Zhang, R. Pendurthi, Y. Lei, A. Laura Elias, Y. Wang, P. E. Hopkins, S. Das, V. H Crespi, M. H. Phan, M. Terrones, *Adv. Sci.* 7, 2001174 (2020). 3. S. Fu, K. Kang, K. Shayan, A. Yoshimura, S. Dadras, X. Wang, L. Zhang, S. Chen, N. Liu, A. Jindal, X. Li, A. N. Pasupathy, A. N. Vamivakas, V. Meunier, S. Strauf, E.-H. Yang, *Nat. Commun.* 11, 2034 (2020). 4. T. Zhang, K. Fujisawa, F. Zhang, M. Liu, M. C. Lucking, R. N. Gontijo, Y. Lei, H. Liu, K. Crust, T. G. Nakajima, H. Terrones, A. Laura Elías, M. Terrones, *ACS Nano* 14, 4326 (2020).

GOA-07. Magnetic proximity effects induced in MoS_2 by Fe(001)/MgO(*n*MLs) bilayers: A first-principles study. *P. Marcon*[1,2], D. Li[1,2], Y. Lu[3,4], R. Arras[1,2] and L. Calmels[1,2] *1. CEMES-CNRS, Toulouse, France; 2. Université de Toulouse, Toulouse, France; 3. Institut Jean Lamour, Nancy, France; 4. Université de Lorraine, Nancy, France*

Transition metal dichalcogenide (TMD) monolayers (MLs) such as MoS_2 are direct band-gap semiconductors [1] that can be used to design innovative (opto)electronic and spintronic devices provided that the density and spin-polarization of charge carriers can be tuned in these two-dimensional crystals. In particular, spin-injection in a TMD monolayer could be controlled without applying a strong external magnetic field if one is able to design a device in which the TMD monolayer is very close to the surface of a ferromagnetic layer with perpendicular magnetic anisotropy. We used first-principles methods based on the density functional theory to investigate the spin-dependent electronic properties of Fe(001)/MgO(*n*MLs)/MoS_2 metal-insulator-semiconductor (MIS) stacking, in which a MgO spacer with an adjustable thickness (*n*=2 to 7 MLs) is inserted between a thin (7MLs) Fe ferromagnetic layer with perpendicular magnetic anisotropy and a MoS_2 monolayer [2]. Our calculations show that MoS_2 is bound by weak Van-der-Waals interactions to the rest of the stacking and that an electron transfer occurs from the Fe/MgO interface to the MoS_2 monolayer due to the difference between the work functions of Fe and MoS_2. This charge transfer, which increases with the thickness of the MgO layer, is responsible for the existence of an internal electric field in MgO. We describe the modification of the electronic structure and spin texture of MoS_2, when the MgO thickness is reduced from 7 to 2 MLs: this thickness reduction enhances the Fe magnetic proximity effects and lowers the density of electrons transferred to MoS_2. We give information on the occupation of the MoS_2 conduction bands, on the local spin-polarization of the electron states at the Fermi level and on the splitting between the spin-up and spin-down valence and conduction bands at the K and K' valleys, as a function of the MgO thickness. We also discuss the splitting of the valence bands and the spin texture near Γ, which can be explained in terms of the Rashba effect and magnetic proximity.

[1] K. F. Mak et al., Phys. Rev. Lett. 105, 136805 (2010). [2] Z. Zhou, P. Marcon *et al.* ACS Appl. Mater. Interfaces 13, 32579 (2021).

INVITED PAPER

GOA-08. Large Exchange Splitting in Monolayer Graphene Magnetized by an Antiferromagnet. Y. Wu[6], *G. Yin*[1,6], L. Pan[6], A.J. Grutter[2], Q. Pan[6], A. Lee[6], D.A. Gilbert[3], J.A. Borchers[2], W. Ratcliff II[2], A. Li[4], X. Han[4] and K.L. Wang[6,5] *1. Department of Physics, Georgetown University, Washington, DC, United States; 2. NIST Center for Neutron Research, National Institute of Standards and Technology, Gaithersburg, MD, United States; 3. Department of Materials Science and Engineering, University of Tennessee, Knoxville, TN, United States; 4. Department of Physics and Astronomy, Beijing University of Technology, Beijing, China; 5. Department of Physics and Astronomy, University of California, Los Angeles, CA, United States; 6. Department of Electrical and Computer Engineering, University of California, Los Angeles, CA, United States*

Due to the long spin diffusion length and the high mobility, monolayer graphene is an intriguing material element for spintronic applications [1]. For example, if a monolayer graphene can be magnetized, Dirac electrons and holes will carry opposite spins, leading to a good spin filter or a convenient generator of pure spin currents. However, a prestine monolayer graphene does not have net magnetization. Previous experiments have demonstrated that when a monolayer graphene is transferred to the surface of a magnet, the p orbitals on the carbon atoms can overlap with the magnetic atoms in the adjacent layer, leading to an induced magnetization in the graphene layer [2]. This is known as the proximity effect, and has been reported in different types of ferromagnetic heterostructures. Compared to ferromagnets, antiferromagents are better candidates to magnetize graphene. Due to the zero net magnetization, an antiferromagnet does not respond to external magnetic noise, and therefore devices using antiferromagnetic heterostructures have good scalbility and stability. Also, antiferromagents can switch almost three orders of magnitude faster than conventional ferromagnets, which may lead to high-speed information processing. Here, we show that a monolayer graphene can indeed be magnetized through the proximity effect provided by a thin film of hexagonal chromium selenide (Fig. 1), a semiconducting antiferromagnet [3]. The induced spin splitting energy is experimentally measured to be 134meV at 2K. Such exchange splitting is experimentally confirmed by the shift of quantum oscillations in the graphene layer. The magnitude of the splitting energy is obtained by its modulation through field cooling, with the exchange splitting energy increasing driven by positive cooling fields and decreasing by negative cooling fields (Fig. 2). The magnitude of the exchange coupling and the Laudau-level indices are confirmed by a machine-learning search for the best fit in a large parameter space. Such spin splitting is also supported by polarized neutron reflectometry and magneto-optic Kerr measurements. Acknowledgements: The transport measurement and theoretical modelling in this work were supported by Spins and Heat in Nanoscale Electronic Systems (SHINES), an Energy Frontier Research Center funded by the US Department of Energy (DOE), Office of Science, Basic Energy Sciences (BES) under award #SC0012670. We are also grateful for support from the National Science Foundation (NSF) (DMR-1411085 and DMR-1810163) and the ARO programme (contract no. W911NF-15-1-10561). Research was performed in part at the NIST Center for Nanoscale Science and Technology. This work used the Extreme Science and Engineering Discovery Environment (XSEDE), which is supported by NSF grant no. OCI-1053575. Specifically, it used the Bridges system (supported by NSF award no.ACI-1445606) at the Pittsburgh Supercomputing Center (PSC). Certain commercial equipment, instruments or materials are identified in this paper to foster understanding. Such identification does not imply recommendation or endorsement by the National Institute of Standards and Technology, nor does it imply that the materials or equipment identified are necessarily the best available for the purpose.

[1] W. Han, R. K. Kawakami, *et al.* and J. Fabian, Nature Nanotechnology, Vol 9, p.794 (2014) [2] Z. Wang, C. Tang *et al.* and J. Shi, Physical Review Letters, Vol. 114, p.016603 (2015) [3] Y. Wu, G. Yin, *et al.* and K. L. Wang, Nature Electronics, Vol 3, p.604 (2020)

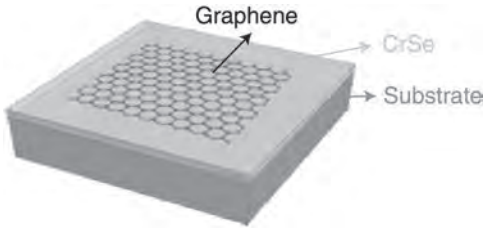

Fig. 1. The schematic of the graphene/CrSe heterostructure. Hexagonal CrSe has a layered AFM structure. Each layer contains a non-colinear spin texture with a non-zero magnetization along z. Adjacent layers cancel the moments of each other, resulting in a net antiferromagnet.

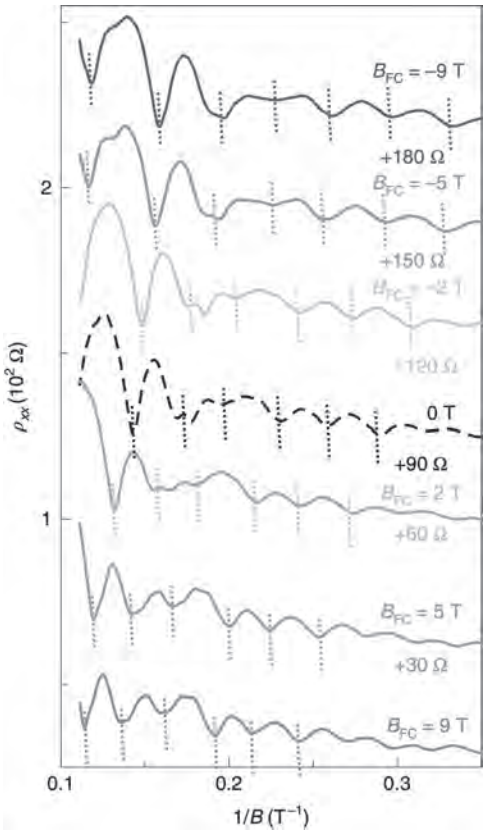

Fig. 2. Quantum oscillations are shifted by field cooling in the heterostructure. The dips corresponding to each Landau level are denoted by dashed lines.

CONTRIBUTED PAPERS

GOA-09. Electrical control of spin-orbit coupling-induced spin precession and spin-to-charge conversion in graphene proximitized by WSe_2. *F. Herling*[1], J. Ingla-Aynes[1], S. Chenattukuzhiyil[1], N. Ontoso[1], J. Fabian[2], L.E. Hueso[1,3] and F. Casanova[1,3] *1. Nanodevices, CIC nanoGUNE BRTA, San Sebastian-Donostia, Spain; 2. Institute for Theoretical Physics, University of Regensburg, Regensburg, Germany; 3. IKERBASQUE, Basque Foundation for Science, Bilbao, Spain*

Two-dimensional materials are an exciting new material family that has the capability to advance toward the implementation of novel spin-based devices. For these atomically-thin layers, the proximity effect is especially important and opens ways to transfer properties from one material into another. In van der Waals heterostructures, transition metal dichalcogenides (TMD) can be used to enhance the spin-orbit coupling of graphene, resulting in strong spin anisotropy [1] and long, gate tunable spin diffusion. These properties provide unique control knobs to manipulate coherent spin precession in the absence of an external magnetic field. Remarkably, we observe in graphene/WSe_2 devices that the sign of the precessing spin polarization can be tuned electrically by a back gate voltage and by a drift current [2]. This realization of a spin field-effect transistor at room temperature in a diffusive system, a long-awaited goal of spintronics, could be a cornerstone for the implementation of energy efficient spin-based logic. Another notable consequence of transferring TMD flakes onto graphene and increasing the spin-orbit coupling by proximity effect is the occurrence of gate controllable spin-to-charge conversion (SCC) due to the Rashba-Edelstein effect and the spin Hall effect (SHE) [3,4], even with unconventional symmetries [5,6]. To quantify the SCC, the significant figure of merit is the SCC length given by the ratio between the charge current and spin current densities. In case of the SHE it can also be calculated by the product of spin Hall angle, θ_{SH}, and the spin diffusion length, λ_s. We report an unprecedented SCC length of up to 41 nm solely due to spin Hall effect in graphene proximitized with WSe_2. Such highly efficient SCC up to room temperature will play a crucial role for the future integration of spintronic devices into existing electronic infrastructure.

[1] T. S. Ghiasi *et al., Nano Lett.,* 17, 7528, 2017. [2] J. Ingla-Aynes *et al.*, *Phys. Rev. Lett.,* 127, 047202, 2021. [3] C. K. Safeer, *et al.*, *Nano Lett.,* 19, 1074, 2019. [4] L. A. Benítez, *et al.*, *Nat. Mater.,* 19, 170, 2020. [5] C. K. Safeer, *et al.*, *Nano Lett.,* 19, 8758, 2019. [6] A. M. Hoque, *et al.*, *Commun Phys*, 4, 124, 2021. [7] F. Herling *et al.*, *APL Mater.*, 8, 071103, 2020.

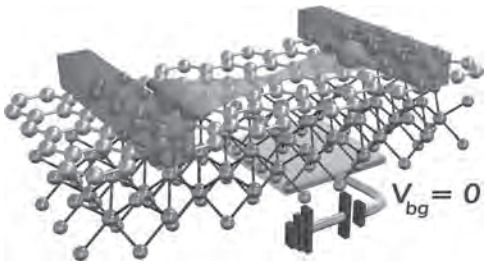

Fig. 1 Sketch of a graphene/TMD-based spin field-effect transistor operating at the strong spin-orbit coupling regime, where the valley-Zeeman SOC induces coherent spin precession.

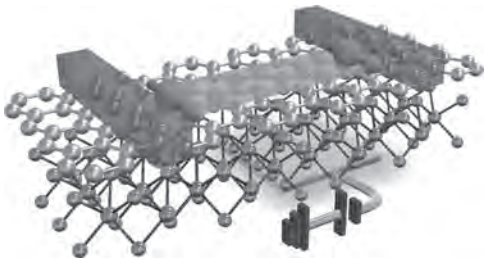

Fig. 2 Turning on a back gate voltage or a dc drift current (not pictured) modulates the diffusivity of the channel to control the spin precession.

GOA-10. Tuning Spin-Orbit Coupling in Graphene-based Heterostructure with Cobalt Dusting Effects. *T. Do*[1,2], S. Lee[3], Y. Jang[4], C. Hwang[3] and T. Kim[1,2] *1. IBS Center for Quantum Nanoscience, Ewha Womans University, Seoul, The Republic of Korea; 2. Department of Physics, Ewha Womans University, Seoul, The Republic of Korea; 3. Korea Research Institute of Standards and Science, Daejeon, The Republic of Korea; 4. Department of Physics, Incheon National University, Incheon, The Republic of Korea*

Spin-orbit coupling (SOC) is a crucial effect that plays a key role in manipulating the degree of freedom of electrons to be used for information process of next generation 2D spintronic devices. The tunability of SOC in spintronic materials, especially in 2D materials such as graphene, becomes very important for realization of innovative quantum devices.[1] However, tuning

SOC in graphene-based heterostructures has still remained the non-trivial task as well as difficulties in control this phenomenon at industrial scale. In this work, we have systematically investigated the effects of Co (x = 0.05-2.5 nm) insertion on graphene\3.0 nm Pt heterostructures. Co and Pt were deposited using Ultra-High-Vacuum (UHV)-Molecular Beam Epitaxy (MBE) technique on top of the large-scale CVD-grown graphene films. To observe the spin transport modulation by Co-dusting effects, Pt Hall bar devices were provided beyond Si\$SiO_2$\ graphene\Co heterostructures using *in-situ* shadow mask patterning technique. A comparative study of spin transport was carried out for the Si\$SiO_2$\ graphene\Pt hetero devices with and without 2.5-nm-thick Co layer. Surprisingly, the perpendicular magnetoresistance (MR) results clearly showed that the co-existence of weak localization (WL) as well as weak antilocalization (WAL) effects for the device without Co film. In addition, we observed the enhanced WAL effect at 77K as the Co thickness decreases down to 0.05 nm at the large applied perpendicular magnetic field. The microstructural characterization of the interfaces of the heterostructures was performed using atomic force microscope (AFM), HR-TEM as well. Additionally, theoretical analysis[2] was performed to understand the Co-dusting effects at the graphene\Pt interface. The competition between the localization and the antilocalization effects on the magnetotransport properties was observed by adjusting the insertion of Co. The dominant magnetotransport mechanism changes from WL to WAL. Our results indicate that the spin-orbit coupling strength can be modulated by the Co-dusting at the graphene\Pt interface.

[1] D. Pesin, D. & A. MacDonald, *Spintronics and pseudospintronics in graphene and topological insulators*. Nature Mater. 11, 409–416 (2012) [2] F. Tikhonenko, A. Kozikov, A. Savchenko, and R. Gorbachev, *Transition between electron localization and antilocalization in graphene*, Physical Review Letters 103, 226801 (2009).

GOA-11. Engineering functional graphene-based systems by thermally assisted metal intercalation. *I. Arnay*[1], A. Gudín[1], A. Guedeja-Marron Gil[1,2], J.M. Diez[1,3], A. Anadón[1], R. Guerrero[1], M. Varela[2], J. Camarero[1,3], R. Miranda[1,3] and P. Perna[1] *1. IMDEA Nanociencia, Madrid, Spain; 2. Departamento de Física de Materiales & Instituto Pluridisciplinar, Universidad Complutense de Madrid, Madrid, Spain; 3. Departamento de Física de la Materia Condensada, Instituto Nicolás Cabrera, and Condensed Matter Physics Center (IFIMAC), Universidad Autónoma de Madrid, Madrid, Spain*

Controlled tuning of interfacial Dzyaloshinskii-Moritya interaction (DMI) in thin multilayers films opens exciting opportunities to push forward current spintronic technologies. Skyrmion magnetic structures have been stabilized in ferromagnetic (FM) ultrathin films [1] as well as in analogous multilayers [2] due to the DMI generated between FM layers and metals with strong orbit-coupling, and in combination with the presence of perpendicular magnetic anisotropy (PMA). We have recently demonstrated the formation of stable chiral spin textures in Gr/Co/Pt(111) structures with enhanced PMA [3,4]. Interestingly, we have observed a diminished effective DMI in the heterostructure due to the appearance of a Rashba type contribution in the gr/Co interface. DMI at the Gr interface can be tunnd by the introduction of different FM materials, openning new ways towards the creation of stable chiral spin textures by enhancing the effective DMI value such as in the Ir/Fe/Co/Pt system [5]. Thus the successful intercalation of Fe under graphene would be an important handle to tune the DMI in spinorbitronics devices based on graphene. However PMA would be desired, which requires a homogeneous growth of Fe films as thin as 1 MLs, according to previous studies [6]. In this work we have optimized the growth of Gr/Fe/Pt heterostructures. The quality of the Pt buffer has been corroborated by x-ray diffraction and low energy electron diffraction probing single oriented growth and low roughness prior to Fe and Gr deposition. We have achieved the successful intercalation of Fe films in a thickness range of 1-5 MLs, confirmed by x-ray photoelectron spectroscopy. The study of the C1s core level spectra showed an energy shifting by 0.4 eV due to the transition from p-doped to n-doped graphene when going from Pt to Fe. We asses high interface quality and good chemical contrast in the final heterostructures by high resolution transmission electron microscopy (Fig.1). Atomic resolution images prove the epitaxial growth of Fe with ABC stacking characteristic of fcc structure as well as elemental mapping corroborates the presence of chemically abrupt interfaces.

[1] S.Heinze et al. Nat. Phys. 7, 713-718 (2011) [2] S. Woo et al. Nat. Nanotech. 11, 444-448 (2016) [3] F.Ajejas et al. Nano Lett 18, 5364-5372 (2018) [4] F. Ajejas et al. Appl. Mat & Inter. 12, 4088-4096 (2020) [5] A. Soumyanarayanan et al. Nat. Mat. 16, 898-904 (2017) [6] W. Q. Liu et al. Sci. Rep. 5, 11911 (2015)

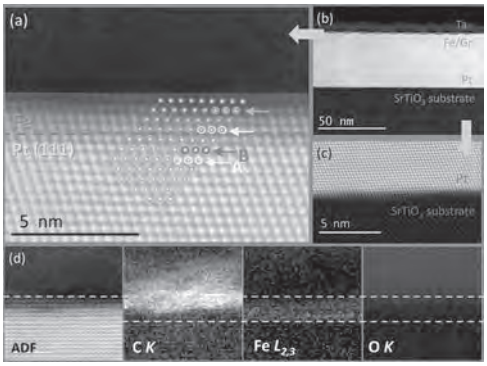

Fig.1: HR-TEM and EELS characterization of Gr/Fe/Pt/STO multilayers

GOA-12. Substitutional Magnetic Dopants in Graphene: Kondo Screening or RKKY Interactions. *R. Villarreal*[1], P. Lin[1], H. Bana[1], Z. Zarkua[1], V. Hendriks[1], M. Nair[2], K. Verguts[1,3], S. Brems[3], S. de Gendt[1,3], S. Achilli[4], G. Fratesi[4], M. Auge[5], F. Junge[5], H. Hofsäss[5], S. De Feyter[1], G. Di Santo[6], L. Petaccia[6], M. Nissen[7], I. Baev[7], M. Martins[7] and L.M. Pereira[1] *1. KU Leuven, Leuven, Belgium; 2. CUNY Advanced Science Research Centre, New York, NY, United States; 3. imec vzw, Leuven, Belgium; 4. Università degli Studi di Milano, Milano, Italy; 5. University of Göttingen, Göttingen, Germany; 6. Elettra Sincrotrone Trieste, Trieste, Italy; 7. Universität Hamburg, Hamburg, Germany*

Imprinting magnetism in graphene has been an important challenge since its discovery. In the dilute regime, magnetic impurities are expected to couple to the Dirac electrons via the Kondo effect in a paramagnetic phase. In the less dilute regime, magnetic impurities in graphene may develop long-range magnetic order mediated by the conduction electrons via the Ruderman-Kittel-Kasuya-Yoshida (RKKY) interaction. Today, the Kondo and RKKY-exchange physics of Dirac electrons in graphene is still elusive while theory predicts competition between a non-trivial Kondo unscreened phase against a RKKY-coupled phase. Considerable experimental efforts have been devoted in this context, with the local magnetic moments originating from carbon vacancies, from adsorption and intercalation (of atoms, clusters or molecules), and from substitutional foreign atoms. Here, we report the incorporation of substitutional manganese (Mn) atoms into graphene as a model case of magnetic doping with transition metals. Ultra-low energy (ULE) ion implantation allows us to precisely tune the kinetic energy of Mn ions, providing control over the form of incorporation and concentration while preserving the structural and electronic properties of graphene [1]. Using low-temperature scanning tunneling microscopy (LT-STM) together with density functional theory (DFT), we identified and characterized point defects that are associated with substitutional Mn in a carbon single vacancy (Fig.1). Based on an x-ray magnetic circular dichroism (XMCD) study, we demonstrate an overscreened Kondo phase in the system of graphene with dilute (up to 1%) substitutional Mn. These results are complemented by synchrotron-based X-ray photoelectron spectroscopy (XPS),

angle-resolved photoemission spectroscopy (ARPES), Raman spectroscopy, among others. The new insights provided by our work establish a framework for the controlled incorporation of magnetic dopants in graphene and other 2D materials, using ULE ion implantation.

[1] P.-C. Lin, R. Villarreal, S. Achilli *et al.*, ACS Nano, 15 (3), 5449 (2021)

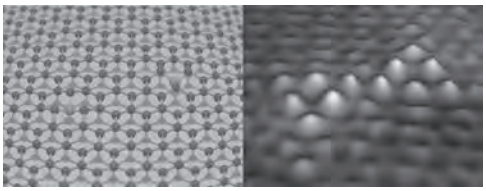

Fig 1. (Left) Cartoon of the atomic structure of graphene with two substitutional Mn atoms. (Right) STM topography of graphene on Cu(111) with two substitutional Mn atoms.

Session GOB
SPINS AND SPIN ORBIT TORQUE IN TOPOLOGICAL INSULATORS

Olaf Van't Erve, Chair
Naval Research Laboratory, Washington, DC, United States

CONTRIBUTED PAPERS

GOB-01. Room-temperature ferromagnetism in 2D vdW Fe_3GeTe_2 and its potential application. H. Wang[1] and *T. Nie[1] 1. Beihang University, Beijing, China*

Since the discovery of single-layer graphene in 2004, two-dimensional (2D) van der Waals (vdW) materials represented by it have demonstrated excellent electrical, magnetic, mechanical and optical physical properties under the structure of one or several layers of atomic thickness[1]. Based on these superior properties, 2D-layered vdW ferromagnetic materials have become the basis for constructing low-dimensional spintronics devices[2], in which Fe_3GeTe_2 (FGT)[3], $Cr_2Ge_2Te_6$[4] and CrI_3[5] as the main representative materials exhibit strong perpendicular magnetic anisotropy and other important characteristics in single layer. However, the Curie temperature (T_c) of above materials has not reached room temperature yet, which has greatly hinderer the subsequent development for device application. Therefore, recently researchers have been committed to explore 2D vdW ferromagnetic materials for room-temperature T_c in both theory and experiment. Here, we experimentally report that the interfacial engineering effect could effectively increase the T_c of the 2D vdW ferromagnetic material FGT from 230 K to 400 K, through heteroepitaxy with topological insulator of Bi_2Te_3. Furthermore, we realize the SOT switching of Bi_2Te_3(8)|FGT(4) at room temperature with a write current density of 2.2×10^6 A/cm^2 through electrical transports. The high SOT efficiency displays that the nontrivial origin of topological materials. In particular, the thermal effect in the heterostructure can be reduced by varying the thickness of FGT, which originates from the large anomalous Nernst effect of FGT. Moreover, we report the oxidation process of FGT films exposed to the atmospheric air, which was studied by X-ray photoelectron spectroscopy measurements. The conclusion provides information for the subsequent growth and protection of FGT films, which facilitates the in-depth study of other properties. Our results may open up a new door to benefit the magnetic order in the 2D limit and realize spintronic devices based on 2D-layered vdW ferromagnetic materials with room temperature performances towards industrialization.

1. A. K. Geim, K. S. Novoselov, Nat. Mater., Vol. 6, p. 183–191 (2007). 2. X. Lin, W. Yang, K. L. Wang, W. Zhao, Nat. Electron., Vol. 2, p. 274–283 (2019). 3. S. Liu, X. Yuan, Y. Zou, Y. Sheng, C. Huang, E. Zhang, J. Ling, Y. Liu, W. Wang, C. Zhang, J. Zou, K. Wang, F. Xiu, npj 2D Mater. Appl., Vol. 1, p. 30 (2017). 4. C. Gong, L. Li, Z. Li, H. Ji, A. Stern, Y. Xia, T. Cao, W. Bao, C. Wang, Z. Q. Wang, Z. Q. Qiu, R. J. Cava, S. G. Louie, J. Xia, X. Zhang, Nature, Vol. 546, p. 265–269 (2017). 5. B. Huang, G. Clark, E. Navarro-Moratalla, D. R. Klein, R. Cheng, K. L. Seyler, D. Zhong, E. Schmidgall, M. A. McGuire, D. H. Cobden, W. Yao, D. Xiao, P. Jarillo-Herrero, X. Xu, Nature, Vol. 546, p. 270–273 (2017).

GOB-02. Large bulk spin-orbit torques in van der Waals ferromagnet Fe_3GeTe_2. *K. Lee*[1,2], F. Martin[2], M. Schmitt[2], A. Liedtke[2], A. Shahee[2], H.T. Simensen[3], T. Scholz[4], T. Saunderson[2], D. Go[5], M. Gradhand[6], Y. Mokrousov[5], T. Denneulin[7], A. Kovacs[7], B. Lotsch[4], A. Brataas[3] and M. Kläui[2] *1. Division of Display and Semiconductor Physics, Korea University, Sejong, The Republic of Korea; 2. Institute of Physics, Johannes Gutenberg University Mainz, Mainz, Germany; 3. Centre for quantum spintronics, Norwegian University of Science and Technology, Trondheim, Norway; 4. Max Planck Institute for Solid State Research, Stuttgart, Germany; 5. Peter Grünberg Institut and Institute for Advanced Simulation, Forschungszentrum Jülich and JARA, Juelich, Germany; 6. University of Bristol, Bristol, United Kingdom; 7. Ernst Ruska-Centre for Microscopy and Spectroscopy with Electrons and Peter Grünberg Institute, Forschungszentrum Jülich, Juelich, Germany*

The emergence of magnetic van der Waals materials opens a new variety of material systems to investigate the current induced magnetization manipulation in two dimensional materials. Especially by utilizing spin-orbit torques in combination with the magnetic van der Waals materials the efficient current induced magnetization manipulation can be achieved. In the unique system of Fe_3GeTe_2, there have been theoretical predictions of the presence of a unique bulk spin-orbit torque due to its crystal structure [1]. Thus, we quantify the spin-orbit torque induced effective fields using the harmonic analysis and from the symmetry of the measured torques we find a dominant bulk spin-orbit torque that arise from the symmetry in the crystal structure. Additionally, we have measured the temperature dependence of the bulk spin-orbit torques which show a peculiar behavior which could imply an additional component of the spin-orbit torque [2]. The results show that Fe_3GeTe_2 exhibits a unique bulk spin-orbit torque in addition to the conventional interfacial spin-orbit torque enabling magnetization manipulation in single layers without the need for multilayer engineering.

[1] Ø. Johansen et al. Phys. Rev. Lett. 122, 217203 (2019) [2] F. Martin et al. arXiv: 2107.09420

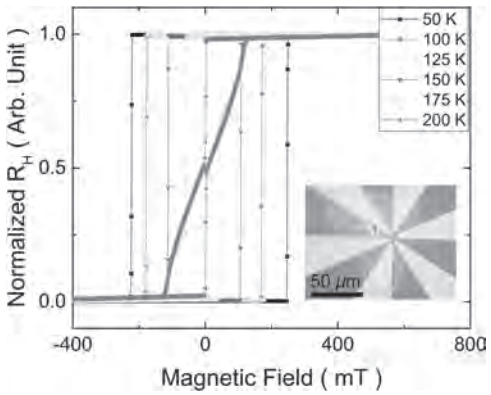

Fig. 1 The hysteresis loops of Fe_3GeTe_2 at different temperatures with the magnetic field applied in the z direction. In the inset an optical microscope image of the final device is depicted.

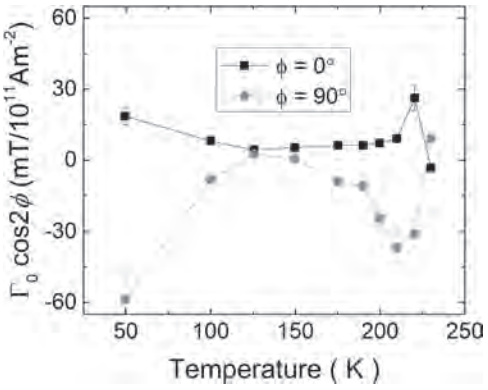

Fig. 2 The extracted bulk spin-orbit torque parameter Γ_0 * cos(2Φ) as a function of the temperature showing the opposite sign for the Φ = 0° and Φ = 90° data over the full temperature range.

GOB-03. Spin-orbit torques in topological insulator - two-dimensional ferromagnet heterostructures. *T. Guillet*[1], G. Gentile[2], R. Galceran[1], J.F. Sierra[1], M. Costache[1], M. Jamet[2], F. Bonell[2] and S.O. Valenzuela[1] *1. Catalan Institute of Nanoscience and Nanotechnology (ICN2), Bellaterra, Barcelona, Spain; 2. IRIG-SPINTEC, CEA Grenoble, Grenoble, France*

Topological insulators (TI) have gained much interest in the field of spintronics for the generation of pure spin currents. Indeed, three-dimensional TIs are predicted to host exotic properties like topologically protected surface states (TSS), which show Dirac-like band dispersion and spin-momentum locking [1]. One of the main strategies is to take advantages of the spin polarization of the TSSs to manipulate the magnetization of an adjacent ferromagnetic thin film (FM) using the spin-orbit torque (SOT) mechanism [2]. In the past few years, the community attempted to replace the traditional heavy metals by a TI in order to enhance the SOT efficiency with limited success. It now appears that the interface sharpness and the high chemical affinity between Bi-based TIs and classical *3d* FMs is a major hurdle to reach the predicted breakthrough in magnetization switching power-efficiency [3]. The emergence of ferromagnetism in two dimensions in 2017, which started a new field in condensed matter physics, could bring a solution to this issue. The van der Waals (vdW) nature of the interaction between the TI and the 2D-FM should limit chemical reactions, interface intermixing and hybridization of state between the two layers. Our approach focuses on stacking and growing 2D-FM (Fe_3GeTe_2) onto high-quality compensated TIs ($(Bi_{0.4}Sb_{0.6})_2Te_3$) grown by molecular beam epitaxy. We use both low and high field second harmonic magnetotransport measurement to characterize the SOT generation, finding a strong temperature dependence of the harmonic signals. We also reports the SOT current-induced magnetization switching operation at low critical current density ($J_c < 10^{10}$ A/m^2) in the vdW heterostructure.

[1] Hasan et al., Rev. Mod. Phys. 82, 3045 (2010) [2] Manchon et al. Rev. Mod. Phys. 91, 035004 (2019) [3] Bonell et al., Nano Lett. 8, 5893 (2020) [4] Huang et al.,Nature 546, 270 (2017)

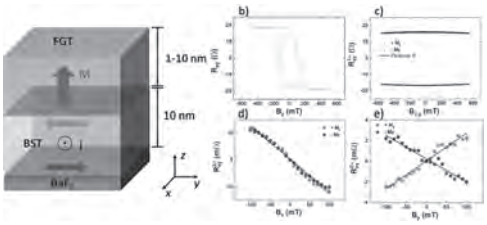

Fig.1: Second harmonic spin-orbit torque measurement in BST/FGT bilayers. a) Measurement geometry. b) Anomalous Hall effect (AHE) recorded by applying the magnetic field along *z*. c) AHE recorded by sweeping the field along *y*. d) Damping-like torque second harmonic measurements. e) Field-like torque second harmonic measurements. The sample temperature is 70 K and the applied current density is 1.3 × 10^{10} A.m^{-2}.

GOB-04. Spin-Orbit Torques in Topological-Insulator/2D-Ferromagnet Heterostructures. *N. Figueiredo Prestes*[1], P. Tsipas[2], P. Pappas[2], J. Peiro[1], V. Zatko[1], S. Krishnia[1], N. Reyren[1], H. Jaffrès[1], A. Dimoulas[2] and J. George[1] *1. Unité Mixte de Physique, CNRS, Thales, Université Paris-Saclay, Palaiseau, France; 2. NCSR DEMOKRITOS, Athens, Greece*

The search for multifunctionality in materials for technological applications has led to the observation of several interesting phenomena [1]. From the topological magnetic textures of skyrmions to the spin-polarized surfaces states of topological insulators (TI), various exotic states of matter are being predicted and reported in the literature [2]. In this work, we report recent results on systems resulting from the integration of TI's and 2D-ferromagnets (2D-FM). Due to the higher resistivity of 2D-FM's, these systems could represent a suitable framework to probe the spin-current generation efficiency of the topological insulator interface [1]. Magnetic and electric properties of MBE grown Bi_2T_3/Cr_xTe_y and Bi_2T_3/FGT bilayers have been characterized through the use of SQUID magnetometry and low-temperature transport measurements. Furthermore, second-harmonic techniques were used to investigate the Spin-to-Charge conversion at the TI/2D-FM interfaces. These measurements revealed the occurrence of current-induced magnetic torques with large contributions from the field-like torque component, figure 1. In fact, the damping-like (DL) to field-like (FL) torque ratio for Bi_2T_3/Cr_xTe_y was found to be about 0.1. Such a large value of the FL component is compatible with the expected results from charge-to-spin conversion induced by the Rashba-effect at the TI/2D-FM interface [3]. Magnetization switching experiments induced by pulsed current were conducted in the Bi_2Te_3/FGT bilayer and resulted in partial but consistent reversal of the magnetization, figure 2. We acknowledge the Horizon 2020 FETPROAC Project No. SKYTOP-824123 "Skyrmion —Topological Insulator and Weyl Semimetal Technology,"

[1] Mogi, M., Yasuda, K., Fujimura, R. *et al.* Current-induced switching of proximity-induced ferromagnetic surface states in a topological insulator. Nature Communications 12, 1404 (2021). [2] Deng, H., Chen, Z., Wolos, A. *et al.* High-temperature quantum anomalous Hall regime in a $MnBi_2Te_4$/Bi_2Te_3 superlattice. Nature Physics. 17, 36–42 (2021). [3] Haney, P. M., Lee, H-W., Lee, K-J. *et al.* Current induced torques and interfacial spin-orbit coupling: Semiclassical modeling. Physical Review B. 87, 174411 (2013).

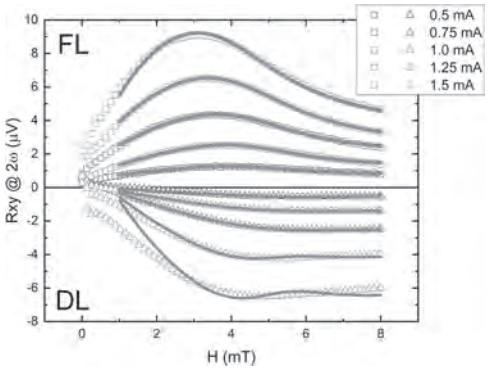

Fig. 1: Second-harmonic component of the transversal voltage in the Field-Like and Damping-Like configuration at 160K for the Bi_2Te_3/Cr_xTe_y bilayer patterned in 5μm Hall Bar.

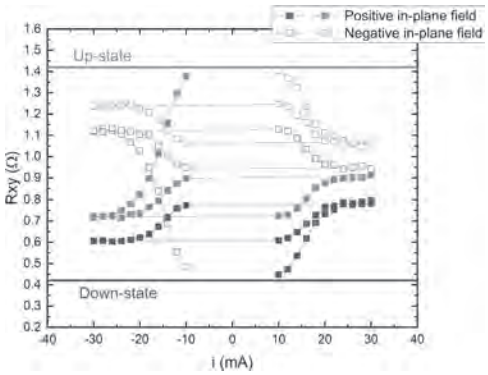

Fig. 2: Current induced magnetic reversal probed via anomalous Hall effect at 150K for the Bi_2Te_3/FGT bilayer. Starting from either up (red curves) or down (blue curves) magnetic states, the application of 100μs current pulses leads to a hysteric behavior of the anomalous Hall voltage independently of the polarity of the 7kOe in-plane field (open or filled points).

GOB-05. Bilinear magnetoresistance in HgTe topological insulator: opposite signs at opposite surfaces demonstrated by gate control.
F. Yu[1], J. Li[1], P. Noël[1], M. Cosset-Chéneau[1], P. Ballet[1], T. Meunier[1], J. Attané[1], A. Fert[2] and *L. Vila*[1] *1. Spintec, Université Grenoble Alpes, Grenoble, France; 2. UMphy, Palsaiseau, France*

Spin-orbit effects appearing in topological insulators (TI) and at Rashba interfaces are currently revolutionizing how we can manipulate spins and have led to several newly discovered effects, from spin-charge interconversion and spin-orbit torques to novel magnetoresistance phenomena. In particular, a puzzling magnetoresistance has been evidenced, bilinear in electric and magnetic fields. Here, we report the observation of bilinear magnetoresistance (BMR) in strained HgTe, a prototypical TI. From magneto-transport measurements we show that the magnetoresistance is composed of a linear and quadratic term with respect to magnetic field intensity in the plane of the sample and transverse to the current direction. The linear term in field is also linear with the current. We show that both the amplitude and sign of this BMR can be tuned by controling, with an electric gate, the relative proportions of the opposite contributions of opposite surfaces. The BMR show three sign changes according to the gate voltage value. At magnetic fields of 1 T, the magnetoresistance is of the order of 1 % and has a larger figure of merit than previously measured TIs. We propose a theoretical model giving a quantitative account of our experimental data. The cubic symmetry of HgTe rules out the explanation of BMR by the hexagonal warping put forward in the previous example of BMR in the TI Bi2Se3 [1]. On the contrary, we show that our results can be explained by the model of Dyrdal et al.[2], in which the BMR is induced by the combination of the spin-momentum locking of the surface states of a TI and the scattering by inhomogeneities of this locking. The separation of the opposite BMRs coming from the top and bottom surface of the HgTe layer has been obtained by varying a top gate voltage to shift differently the Fermi levels of the top and bottom surface states with respect to their Dirac point. Depending on the gate voltage, the dominant contribution to the BMR parameter (for $I > 0$) comes from the top surface and is positive, or is due to the bottom surface and is negative. This phenomenon, unique to TI, offer novel opportunities to tune the electrical response of surface states for spintronics.

[1] P. He, S. S. L. Zhang, D. Zhu, Y. Liu, Y. Wang, J. Yu, G. Vignale, and H. Yang, Nature Physics 14, 495 (2018). [2] A. Dyrdal, J. Barnas, and A. Fert, Physical Review Letters 124, 046802 (2020).

GOB-06. Topological and trivial gaps in graphene-based van der Waals heterostructures under strain and disorder.
L. Oroszlany[1,2] *1. Department of Physics of Complex Systems, Eötvös Loránd University, Budapest, Hungary; 2. Lendulet Topology and Correlation Research Grou, MTA-BME, Budapest, Hungary*

We explore the electronic structure and topological phase diagram[1,2] of heterostructures formed of graphene and ternary bismuth tellurohalide layers[3] and adatoms capable of inducing strong spin-orbit coupling. We show that both mechanical strain inherently present in fabricated samples, and disorder due to thermal fluctuations could induce a topological phase transition in these heterostructures. We construct an effective tight-binding description for low energy excitations and fit the model's parameters to ab initio band structures. We propose a simple approach for predicting phase boundaries as a function of mechanical distortions and disorder and hence gain a deeper understanding of how the topological phase in the considered system may be engineered.

[1] Z Tajkov, J Koltai, J Cserti, L Oroszlány Physical Review B 101, 235146 (2020) [2] Z Tajkov, D Visontai, L Oroszlány, J Koltai Nanoscale 11, 12704 (2019) [3] B. Fülöp, Z. Tajkov, J. Peto, P. Kun, J. Koltai, L. Oroszlány, E. Tóvári, H. Murakawa, Y. Tokura, S. Bordács, L. Tapasztó, Sz. Csonka 2D Materials 5, 031013 (2018)

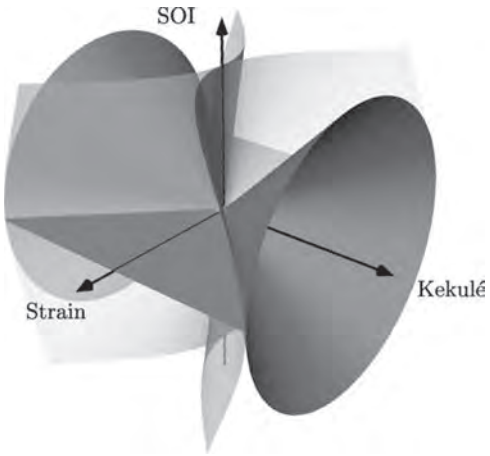

Topological phase diagram of graphene-based heterostructures under strain as a function of proximity induced spin-orbit coupling and mechanical distortions.

GOB-07. Observation of a superconducting state of possible Ising-type topological superconductor $FeTe_{0.6}Se_{0.4}$, equipping ferromagnetic electrodes with perpendicular magnetic anisotropy. *K. Ohnishi*[1], S. Gupta[2], S. Kasahara[3], Y. Kasahara[4], Y. Matsuda[4], E. Shigematsu[1], R. Ohshima[1], Y. Ando[1] and M. Shiraishi[1] *1. Electronic Science and Engineering, Kyoto Univ., Kyoto City, Japan; 2. School of Physics and Astronomy, Univ. Leeds, Leeds, United Kingdom; 3. Research Institute for Interdisciplinary Science, Okayama Univ., Okayama city, Japan; 4. Physics, Kyoto University, Kyoto City, Japan*

Iron selenide telluride, FeTeSe is a family of Fe-chalcogenide and Fe-based superconductor. This material is a compound material and possesses an in-plane symmetry breaking. From spintronic viewpoints, FeTeSe allows Ising-type superconductivity, which enables the locking of spin in out-of-plane directions. In addition, FeTeSe can be a great candidate for topological superconductor which can arise the S=1 spin-triplet Cooper pairs at the surface. To detect possible perpendicular spin-triplet states in FeTeSe electrically, ferromagnetic electrodes with perpendicular magnetic anisotropy (PMA) is necessary. However, an interplay of ferromagnetism of the electrodes and superconductivity of FeTeSe has not been sufficiently explored. We prepared exfoliated thin $FeTe_{0.6}Se_{0.4}$ (FTS) flakes and deposited PMA electrodes on the FTS, which is made of $[Pt/Co]_{10}$ multilayer ("10" denotes a stacking number). The conventional four-terminal measurement was implemented as the in-plane and perpendicular external magnetic field (H_{ext}) was applied up to 9 T. The superconducting transition is observed at T = 15 K. More importantly, the upper critical field of the FTS is anisotropic and the in-plane upper critical field is measured to be 145 T [1]. Y. Saito *et al.* reported the enhancement of the in-plane upper critical field of a member of Ising-type superconductivity, MoS_2 [2]. Therefore, these results show that the superconductivity of exfoliated thin film FTS is robust and FTS is a potential material for Ising-type superconductor, which can open a new pathway to super-spintronics. More detailed discussion will be given in the presentation.

[1] K. Ohnishi *et al.*, to be submitted. [2] Y. Saito *et al.*, Nature Phys. 12, 144 (2016).

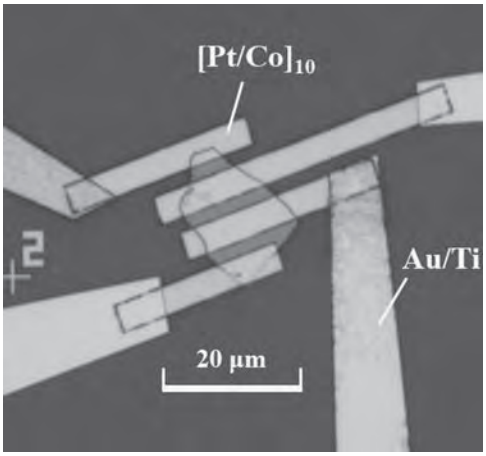

Fig. 1: An optical microscopy image of the mechanically exfoliated FTS single crystal.

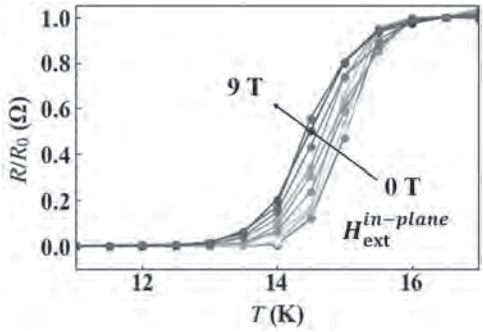

Fig. 2: Temperature dependence of the normalized resistance of the FTS with PMA electrodes, when in-plane magnetic field is applied. The normalization was carried out using the normal-state resistance R_0 at 16 K.

GOB-08. Laser induced spin injection to [GeTe / Sb_2Te_3] supperlattice through a TbFeCo film. *S. Sumi*[1], H. Awano[1] and J. Tominaga[2] *1. Toyota Technological Institute, Nagoya, Japan; 2. National Institute of Advanced Industrial Science and Technology, Tsukuba, Japan*

A [GeTe/Sb_2Te_3] superlattice is known as a topological insulator and it shows magnetic responses such as magneto-optical effect although it does not contain any magnetic elements [1]. We reported the superlattice have a topologically protected spin diffusion length more than 100 μm at room temperature [2]. In this paper, we show a laser induced spin injection to the superlattice through a TbFeCo film. Figure 1 shows measurement setup for a laser induced spin injection. The [GeTe/Sb_2Te_3] superlattice is deposited on a sapphire substrate. The blue laser (405 nm) spot with a diameter of 0.6 um is irradiated on a TbFeCo (50 nm) wire with a width of 80 μm, where a domain wall was introduced along to the wire. The injected spins are detected by a Pt (70 nm) wire with a width of 80um. Distance between the TbCoFe wire and the Pt is 100 μm. A detail preparation method is described in the reference [2]. Laser induced spin injection results are shown in Fig. 2. Figure 2 (a) shows a polarized microscope image of the TbFeCo wire. The laser is scanned to wall direction. Detected signal of the Pt wire as a function of the laser position are shown in Fig. 2 (b). The signals change clearly at the wall position and show a maximum value of 0.06 μV with a laser power of 1.0 mW. We can get spin injection signal from the TbFeCo to the Pt through the superlattice without current. The laser induced spin injection method is one of the useful methods for low-energy spinttronics device. This work was partly supported by a Grant-in-Aid for Science research of JST-CREST (No. JPMJCR14F1), and JSPS Grant-in-Aids for Scientific Research (20H02185).

[1] Bang, D., et al., Sci. Rep. 4, 5727 (2014). [2] Tominaga, J., et al., npj 2D Mater. Appl. 4, 22 (2020).

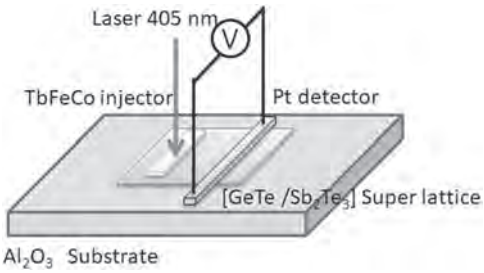

Fig. 1 Measurement setup for a laser induced spin injection.

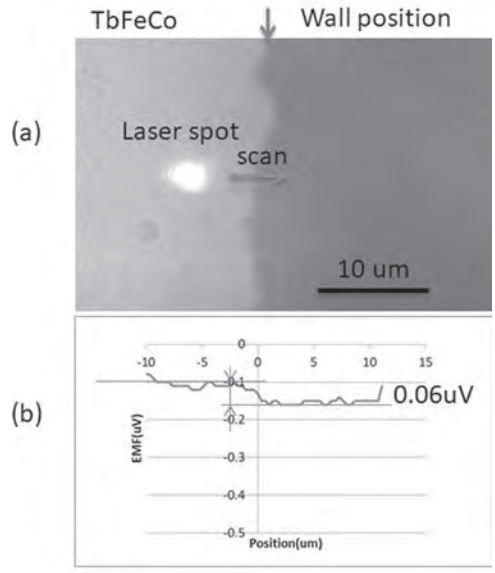

Fig. 2 Laser induced spin injection results.

GOB-09. Large Spin to Charge Conversion Efficiency in Polycrystalline Topological Insulator. *B.B. Singh*[1], S.K. Jena[1], M. Samanta[2], K. Biswas[2] and S. Bedanta[1] *1. Physics, NISER, Bhubaneswar, India; 2. JNCASR, Bangalore, India*

Topological insulators (TIs) are new state of quantum materials due to unique band topology [1]. Presence of spin momentum locked Dirac surface states and insulating ground states of TIs have drawn attention of fundamental research in last decade [2–5]. Such a spin momentum locked surface states are protected by time reversal symmetry which makes them immune to any spin flip back scattering [6]. These surface states due to high spin orbit coupling (SOC) have been exploited for efficient spin to charge conversion or vice versa [7–12]. Recently, TIs are used to switch the magnetization by spin orbit torque (SOT) [8,13,14] and magnon current detection [15]. The fundamental mechanism for efficient spin to charge conversion in TIs are mainly inverse spin Hall effect (ISHE) [11] and inverse Rashba Edelstein effect (IREE) [16–21]. Bi_2Se_3 is a well-established topological insulator (TI) having spin momentum locked Dirac surface states at room temperature and predicted to exhibit high spin to charge conversion efficiency (SCCE) for spintronics applications. The SCCE in TI is characterized by an inverse Edelstein effect length (λ_{IREE}). We report $\lambda_{IREE.} \sim 0.36$ nm, which is highest ever observed in Bi_2Se_3. Here, we performed spin pumping and inverse spin Hall effect (ISHE) in polycrystalline Bi_2Se_3/CoFeB bilayer. The Bi_2Se_3 thickness dependence of $l_{IREE,}$ perpendicular surface anisotropy (K_S), spin mixing conductance and spin Hall angle confirmed that spin to charge conversion is due to spin momentum locked Dirac surface states (see figure 1). We propose that the role of surface states in SCCE can be understood by the evaluation of K_S. The SCCE is found to be high when the value of K_S is small.

[1] X.-L. Qi and S.-C. Zhang, Rev. Mod. Phys. 83, 1057 (2011). [2] X.-L. Qi, T.L. Hughes, and S.-C. Zhang, Phys. Rev. B 78, 195424 (2008). [3] X.-L. Qi, R. Li, J. Zang, and S.-C. Zhang, Science 323, 1184 (2009). [4] D. Hsieh, Y. Xia, D. Qian, L. Wray, J.H. Dil, F. Meier, J. Osterwalder, L. Patthey, J.G. Checkelsky, N.P. Ong, A.V. Fedorov, H. Lin, A. Bansil, D. Grauer, Y.S. Hor, R.J. Cava, and M.Z. Hasan, Nature 460, 1101 (2009). [5] C.-Z. Chang, J. Zhang, X. Feng, J. Shen, Z. Zhang, M. Guo, K. Li, Y. Ou, P. Wei, L.-L. Wang, Z.-Q. Ji, Y. Feng, S. Ji, X. Chen, J. Jia, X. Dai, Z. Fang, S.-C. Zhang, K. He, Y. Wang, L. Lu, X.-C. Ma, and Q.-K. Xue, Science 340, 167 (2013). [6] M.Z. Hasan and C.L. Kane, Rev. Mod. Phys. 82, 3045 (2010). [7] M. Jamali, J.S. Lee, J.S. Jeong, F. Mahfouzi, Y. Lv, Z. Zhao, B.K. Nikolić, K.A. Mkhoyan, N. Samarth, and J.-P. Wang, Nano Lett. 15, 7126 (2015). [8] M. Dc, R. Grassi, J.-Y. Chen, M. Jamali, D. Reifsnyder Hickey, D. Zhang, Z. Zhao, H. Li, P. Quarterman, Y. Lv, M. Li, A. Manchon, K.A. Mkhoyan, T. Low, and J.-P. Wang, Nature Materials 17, 800 (2018). [9] K. Kondou, R. Yoshimi, A. Tsukazaki, Y. Fukuma, J. Matsuno, K.S. Takahashi, M. Kawasaki, Y. Tokura, and Y. Otani, Nature Physics 12, 1027 (2016). [10] S. Zhang and A. Fert, Phys. Rev. B 94, 184423 (2016). [11] P. Deorani, J. Son, K. Banerjee, N. Koirala, M. Brahlek, S. Oh, and H. Yang, Phys. Rev. B 90, 094403 (2014). [12] C.H. Li, O.M.J. van 't Erve, J.T. Robinson, Y. Liu, L. Li, and B.T. Jonker, Nature Nanotechnology 9, 218 (2014). [13] J. Han, A. Richardella, S.A. Siddiqui, J. Finley, N. Samarth, and L. Liu, Phys. Rev. Lett. 119, 077702 (2017). [14] Y. Wang, D. Zhu, Y. Wu, Y. Yang, J. Yu, R. Ramaswamy, R. Mishra, S. Shi, M. Elyasi, K.-L. Teo, Y. Wu, and H. Yang, Nature Communications 8, 1364 (2017). [15] Y. Wang, D. Zhu, Y. Yang, K. Lee, R. Mishra, G. Go, S.-H. Oh, D.-H. Kim, K. Cai, E. Liu, S.D. Pollard, S. Shi, J. Lee, K.L. Teo, Y. Wu, K.-J. Lee, and H. Yang, Science 366, 1125 (2019). [16] M. DC, J.-Y. Chen, T. Peterson, P. Sahu, B. Ma, N. Mousavi, R. Harjani, and J.-P. Wang, Nano Lett. 19, 4836 (2019). [17] R. Sun, S. Yang, X. Yang, E. Vetter, D. Sun, N. Li, L. Su, Y. Li, Y. Li, Z. Gong, Z. Xie, K. Hou, Q. Gul, W. He, X. Zhang, and Z. Cheng, Nano Lett. 19, 4420 (2019). [18] H. Wang, J. Kally, J.S. Lee, T. Liu, H. Chang, D.R. Hickey, K.A. Mkhoyan, M. Wu, A. Richardella, and N. Samarth, Phys. Rev. Lett. 117, 076601 (2016). [19] J.-C. Rojas-Sánchez, S. Oyarzún, Y. Fu, A. Marty, C. Vergnaud, S. Gambarelli, L. Vila, M. Jamet, Y. Ohtsubo, A. Taleb-Ibrahimi, P. Le Fèvre, F. Bertran, N. Reyren, J.-M. George, and A. Fert, Phys. Rev. Lett. 116, 096602 (2016). [20] Y. Shiomi, K. Nomura, Y. Kajiwara, K. Eto, M. Novak, K. Segawa, Y. Ando, and E. Saitoh, Phys. Rev. Lett. 113, 196601 (2014). [21] P. Noel, C. Thomas, Y. Fu, L. Vila, B. Haas, P.-H. Jouneau, S. Gambarelli, T. Meunier, P. Ballet, and J.P. Attané, Phys. Rev. Lett. 120, 167201 (2018).

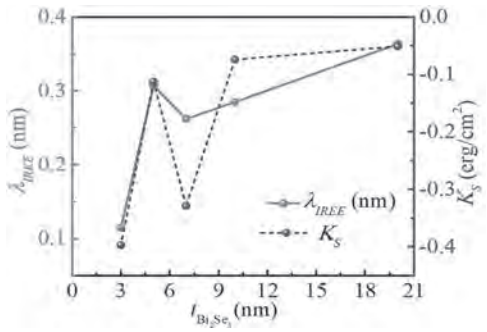

Figure 1 Schematics of the measurement of inverse spin Hall effect (ISHE) (b) Bi_2Se_3 thickness dependence of 2D spin to charge conversion efficiency (λ_{IREE}).

GOB-10. Elemental Topological Dirac Semimetal α-Sn with High Quantum Mobility. *L. Anh*[1,2], K. Takase[1], T. Chiba[3], Y. Kota[3], K. Takiguchi[1] and M. Tanaka[1,4] *1. Department of Electrical Engineering and Information Systems, The university of Tokyo, Tokyo, Japan; 2. PRESTO, Japan Science and Technology Agency, Saitama, Japan; 3. National Institute of Technology, Fukushima College, Fukushima, Japan; 4. Center for Spintronics Research Network, The University of Tokyo, Tokyo, Japan*

Among many topological materials, α-Sn stands out as a unique and promising candidate: It is the only elemental material that shows multiple topological phases, which can be controlled by various means such as applying strain, varying the thickness, incorporating magnetism and applying electric fields (see Fig. 1a) [1]. However, thus far, only a few studies have accurately captured the nontrivial features of α-Sn, especially its quantum transport properties. The main reason is the insufficient crystal quality of α-Sn, which can easily transform into the more stable trivial β-Sn phase or be impaired by the interface roughness. In this work, we demonstrate epitaxial growth of very high-quality α-Sn thin films on InSb (001) substrates using molecular beam epitaxy. A cross-sectional scanning transmission electron microscopy (STEM) lattice image clearly indicates a high-quality diamond-type crystal structure of α-Sn without any other precipitates, and a perfectly flat interface with the InSb buffer layer (Fig. 1b). As shown in Fig 1c, the longitudinal

conductance G_{xx} exhibits strong and clear Shubnikov-de Haas (SdH) oscillations, which appear at a magnetic field B as small as 0.3 T at 2 K and persist up to 20 K, manifesting the high sample quality. These components correspond to a topological surface state (TSS) band and a heavy hole band (HH) of α-Sn. By fitting the Lifshitz-Kosevich (LK) theory to G_{xx}, we estimate unprecedentedly high quantum mobilities of both the TSS (30000 cm^2/Vs), which is ten times higher than the reported values [2], and the bulk heavy-hole (HH) state (1808 cm^2/Vs), which has never been obtained experimentally. Remarkably, both the TSS and the HH bands have nontrivial phase shift γ = 0.81 and 0.71, respectively, which unambiguously indicate that our α-Sn samples are in a topological Dirac semimetal (TDS) phase. [3]. Our results prove that high-quality crystal growth of α-Sn is the key to unlocking its rich potential for topological physics and device applications.

[1] D. Zhang, H. Wang, J. Ruan, G. Yao, H. Zhang, *Phys. Rev. B* 97, 195139 (2018). [2] Q. Barbedienne et al., *Phys. Rev. B* 98, 195445 (2018). [3] L. D. Anh et al., arXiv:2105.13884.

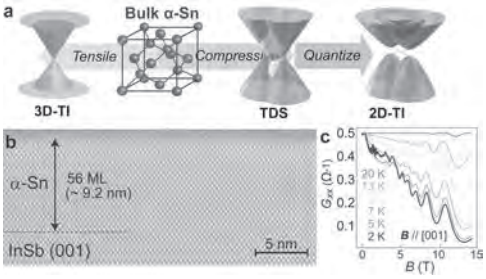

a, Various topological phases that can be realized in the α-Sn platform. b, STEM lattice image of our α-Sn thin film grown on an InSb (001) substrate. c, Strong SdH oscillations observed under a perpendicular magnetic field.

GOB-11. Room Temperature Spin Transport in Cd_3As_2. *G.M. Stephen*[1], A.T. Hanbicki[1], T. Schumann[2], J.T. Robinson[3], M. Goyal[2], S. Stemmer[2] and A.L. Friedman[1] *1. Laboratory for Physical Sciences, College Park, MD, United States; 2. Materials Department, University of California, Santa Barbara, Santa Babara, CA, United States; 3. Electronics Science and Technology, Naval Research Laboratory, Washington, DC, United States*

As the physical limits of CMOS loom closer, alternative state variable paradigms become increasingly important. Devices utilizing the electron spin as a state variable are especially promising due to their intrinsic non-volatility, speed, and versatility. Fully incorporating spintronic devices into next-generation computing systems requires optimized architectures and materials capable of efficiently harnessing the electron spin. One particularly promising class of materials are topological Dirac semimetals (TDS), exemplified by Cd_3As_2. TDS materials have high mobilities, 3D Dirac cones, and can exist in multiple quantum phases. We demonstrate the function of Cd_3As_2 as a channel for the flow of spin currents by incorporating it with hybrid graphene/MgO tunnel barriers as a non-local spin valve, the basic unit of spintronic devices for logic operations. We show that the spin valves operate at least up to room temperature.[1] We quantify the spintronic transport in the devices by measuring the spin Hall effect/inverse spin Hall effect, observing spin Hall angles up to θ_{SH} = 1.5 and spin diffusion lengths of 10-40 μm. Long spin-coherence lengths with efficient charge-to-spin conversion rates and coherent spin transport up to room temperature, as we show here in Cd_3As_2, are enabling steps toward realizing practical spintronic-based computing systems.

[1] G. M. Stephen *et al.* ACS Nano 15, 5459 (2021).

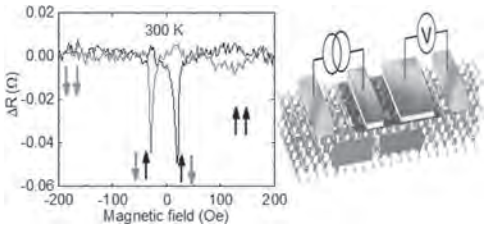

Session GOC
SKYRMION DYNAMICS
Sadamichi Maekawa, Chair
RIKEN, Wako, Japan

INVITED PAPER

GOC-01. Electrical manipulation of skyrmioninc textures in chiral magnets. *H. Du*[1], J. Tang[1], W. Wang[2], D. Song[2], J. Zang[3] and M. Tian[1] *1. High Magnetic Field Laboratory, Chinese Academy of Sciences, Hefei, China; 2. Institutes of Physical Science and Information Technology, Anhui University, Hefei, China; 3. Department of Physics and Astronomy, University of New Hampshire, Durham, Durham, NH, United States*

Chiral magnets that can host magnetic skyrmions with compact texture, uniform size and high mobility are promising informational functional materials for an emerging class of spintronic devices. Creating, deleting, and driving skyrmions are crucial for this purpose. In this talk, we will report these operations in chiral magnets. We will first introduce the techniques of nanostructured devices fabrication and in-situ electrical Lorentz TEM observations [1-2]. Based on the techniques, we show magnetic skyrmions can be deterministically shifted step-by-step, created and deleted by a geometry notch using nanosecond current pulses with a low a current density about 10^{10}A/m^2 at room temperature. We further report the creation, and manipulation of a type of multi-*Q* three-dimensional skyrmionic texture, characterized by a circular spin spiral ties a bunch of skyrmion tubes and then defined as skyrmion bundles [3].

1 J. Tang *et al.*, Natl. Sci. Rev. 8, nwaa200 (2021) 2. J. Tang *et al.*, ACS Nano 14, 10986 (2020) 3. J. Tang *et al.*, Nature Nanotechnology (2021, doi.org/10.1038/s41565-021-00954-9)

CONTRIBUTED PAPERS

GOC-02. Current-driven single-skyrmion motion in a room-temperature chiral-lattice magnet. *L. Peng*[1], K. Karube[1], Y. Taguchi[1], N. Nagaosa[1,2], Y. Tokura[1,2] and X. Yu[1] *1. RIKEN Center for Emergent Matter Science (CEMS), Wako, Japan; 2. Department of Applied Physics, University of Tokyo, Tokyo, Japan*

Nanometric skyrmions are promising candidates of information carriers in energy-efficient spintronic devices. The electric current-induced Néel-type-skyrmion Hall motion, which is caused by the spin-orbit torque (SOT), has been demonstrated in thin-film heterostructures with interfacial Dzyaloshinskii-Moriya interaction[1]. In this talk[2], I will present the spin-transfer torque (STT)-induced single-skyrmion motion at room temperature in a chiral-lattice magnet $Co_9Zn_9Mn_2$. We have directly tracked and controlled a single-skyrmion trace using nanosecond-duration current pulses. We have directly observed the directional reversal of the current-induced skyrmion Hall motion by flipping the external magnetic field. Systematical measurements of the single-skyrmion dynamics with tuning electric current reveal the dynamic transition of the skyrmion motion from a pinned-static state to the flow motion by way of a creep motion. Our experimental observations of skyrmion flow motion qualitatively coincide with numerical calculations in the disorder system, suggesting the pinning effect on the skyrmion dynamics. We have also evaluated the intrinsic skyrmion Hall angle and the skyrmion velocity in the skyrmion flow regime.

[1] Jiang, W. J. *et al. Nat. Phys.* 13, 162–169 (2017). [2] L. C. Peng, K. Karube, Y. Taguchi, N. Nagaosa, Y. Tokura & X. Z. Yu. (submitted) (2021)

GOC-03. Current-driven deformation of isolated magnetic skyrmions. *F.S. Yasin*[1], K. Karube[1], A. Kikkawa[1], Y. Taguchi[1], Y. Tokura[1,2] and X. Yu[1] *1. Center for Emergent Matter Science (CEMS), RIKEN, Wako, Japan; 2. Applied Physics, University of Tokyo, Bunkyo, Japan*

The ability to manipulate magnetic skyrmions [1,2] within microdevices by means of external stimuli such as an electric current or magnetic field is integral to both spintronics and our understanding of spin-current dynamics [3]. While several studies have reported successful current-induced translation of individual skyrmions [4], the skyrmions are usually treated as rigid bodies. Recently, isolated skyrmions have been theorized to deform under current application [5,6], but such deformation has yet to be experimentally identified. Here we report the current-driven deformation of isolated, pinned magnetic skyrmions within a thin plate composed of the chiral magnet $Co_{10}Zn_{10}$ measured using defocussed Lorentz transmission electron microscopy (LTEM). We stabilized isolated skyrmions at room temperature with an external magnetic field of 40 mT applied normal to the thin plate. Using live video recording, we acquired images of several isolated skyrmions during application of 1 s long electrical current pulses over a range of current densities, order $j = 10^9$ A/m^2. Figure 1 depicts the skyrmion's elliptical deformation during current application, which occurs at an angle relative to the current direction. The skyrmion returns to its original shape upon pulse termination. We determine that the eccentricity, or severity of the deformation, increases from $e = 0.39 \pm 0.06$ to $e = 0.5 \pm 0.05$ for increasing j, shown in Figure 2, where the reported values are the mean and standard error. This deformation agrees with recent predictions and helps paint a clearer picture of the spin-current interaction, which promises to be an essential part of future spintronic devices.

1. Mühlbauer, S., Binz, B., Jonietz, F., et al., Science Vol. 323, p. 915-19 (2009). 2. Yu, X., Onose, Y., Kanazawa, N., et al., Nature Vol. 465, p. 901-4 (2010). 3. Nagaosa, N. and Tokura, Y., Nature Nanotechnology Vol. 8, p. 899-911 (2013). 4. Yu, X., Morikawa, D., Nakajima, K., et al., Science Advances Vol. 6, no. 25, eaaz9744 (2020). 5. Masell, J., Rodrigues, D. R., McKeever, B. F., et al., Phys. Rev. B Vol. 101, 214428 (2020). 6. Liu, L., Chen, W., and Zheng, Y., Phys. Rev. Appl. Vol. 14, 024077 (2020).

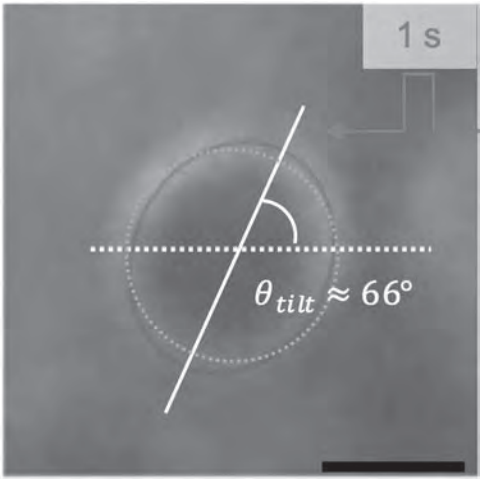

Fig. 1 Lorentz transmission electron micrograph of a pinned isolated skyrmion during a 1 s electric current pulse (j = 4.36×10^9 A/m^2). The solid dark line is a conic function fit via the least squares method, compared with the dashed green line, which is the j = 0 A/m^2 fit. The deformation axis tilt angle is measured from the dashed white line. Scale bar 100 nm.

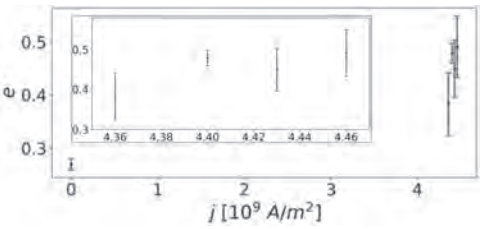

Fig. 2 Eccentricity e versus current density j of isolated skyrmions over several current densities. Inset outlined in green excludes j = 0 A/m^2.

GOC-04. Deterministic Bloch Chirality in Interfacial DMI Systems: An Astroid for DW Switching. *M.D. Kitcher*[1], N. Pandey[1], M.D. Graef[1] and V.M. Sokalski[1] *1. Materials Science & Engineering, Carnegie Mellon University, Pittsburgh, PA, United States*

The interfacial Dzyaloshinskii–Moriya interaction (DMI) emerges in ferromagnet/heavy metal thin films with broken z-mirror symmetry, stabilizing Néel domain walls and skyrmions of one chirality as dictated by its Rashba-type field. On the other hand, both Bloch chiralities remain energetically degenerate at static equilibrium for mixed domain walls in films with a moderate DMI. Multiple research groups have nevertheless independently reported significant Bloch chirality asymmetries in the B_z-stabilized domain microstructures of different interfacial DMI systems [1, 2]. In this work, we demonstrate how the asymmetric wall energy landscape in such systems can produce a deterministic Bloch chirality when domain walls are driven away from static equilibrium. For $D < D_c$, the two ground state domain walls—having Bloch components of opposite chiralities—exhibit different restoring torques and steady state configurations. As dictated by the driving field's direction and sign of DMI, one wall, which we term the lax wall, becomes labile at a lower B_z prior to the Walker field. At this lability point, the wall lies at an inflection point in its energy landscape and the domain wall susceptibility ($\chi_{dw} \propto (\sigma_{\Phi\Phi})^{-1}$) diverges. The lax wall therefore reorients at higher fields to the steady state configuration of its counterpart, which we call the locked wall (Fig. 1). Using the Slonczewski equations and the 1D wall energy model, we analytically derived a DMI–B_z phase diagram of steady state domain wall Bloch chirality (Fig. 2), which includes an astroid analogous to the Stoner–Wohlfarth domain switching model. While these equations predict that locked walls precess beyond the Walker field, it was observed that they can instead persist due to DMI-induced asymmetries in vertical Bloch line (VBL) evolution—extending the Bloch monochirality regimes [3]. Here, we generalize these Bloch chirality preferences to arbitrary VBL behavior in these systems, before discussing how the theory of horizontal Bloch line evolution could similarly mediate Bloch chirality preferences [4].

1. J.J. Chess, S.A. Montoya, E.E. Fullerton et al., AIP Advances, Vol. 7, p.056807 (2017) 2. S.D. Pollard, J.A. Garlow, K.-W. Kim et al., Physical Review Letters, Vol. 125, p.227203 (2020) 3. Y. Yoshimura, K.-J. Kim, T. Taniguchi et al., Nature Physics, Vol. 12, p.157–161 (2016) 4. J.C. Slonczewski, Journal of Applied Physics, Vol. 44, p.1759 (1973)

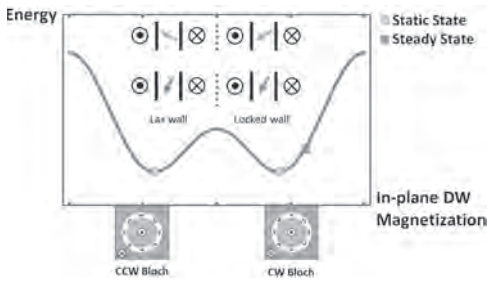

Fig. 1 Steady state Bloch monochirality via DMI-induced asymmetric evolution of lax & locked walls.

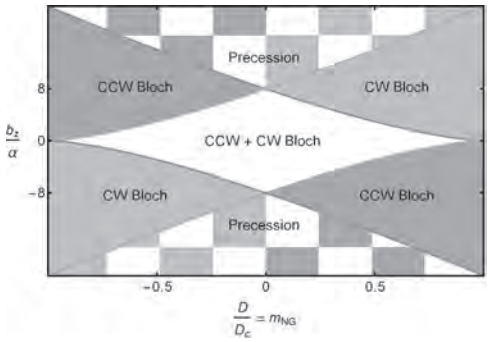

Fig. 2 DMI–B_z phase diagram of steady state domain wall Bloch chirality

GOC-05. Scaling law of current-driven magnetic skyrmion creep. *M. Song*[1], M. Yoo[1], S. Yang[2], M. Park[1] and K. Kim[1] *1. Korea Advanced Institute of Science and Technology, Daejeon, The Republic of Korea; 2. Korea Research Institute of Standards and Science, Daejeon, The Republic of Korea*

Magnetic skyrmion, a topological defect that carries a topological charge, has attracted considerable interest due to its potential application in future memory and logic devices [1, 2]. Recent studies have shown that the skyrmion moves with a fast speed in a controllable manner at a low current [2, 3]. Despite the advances in knowledge, the fundamental understanding of skyrmion motion in a real system is still far from satisfactory because of the lack of studies on the interaction between the skyrmion and pinnings. In general, the interaction between the pinnings and a moving object produces a scaling law, which depends on the symmetry and dimension [4, 5]. In this regard, exploring the scaling behavior of skyrmion motion is fundamentally important. In this work, we investigate the skyrmion creep motion in a W/CoFeB/Ta/MgO system where the skyrmions move along the medium by thermal activation while interacting with pinnings. We nucleate numerous skyrmionic bubbles by magnetic field manipulation technique [6], and observe the skyrmion creep motion by applying an electric current. Using MOKE microscopy and software-based image processing, we track more than 650,000 current-driven skyrmion motions to analyze the scaling law of skyrmion creep motion. A wide range of current density from 7 x 10^7 A/m^2 to 1.6 x 10^9 A/m^2 was applied to obtain skyrmion speed ranging from 1 μm/s to 150 μm/s. The result shows that the skyrmion does not follow the conventional scaling law valid in the domain wall creep motion but

follows the scaling law of stochastic hopping motion. This indicates that the skyrmion motion should be understood differently from the motion of the magnetic domain wall. Our work provides the direct statistical measurement and analysis of the thermally activated skyrmion creep motion, which paves the way toward the complete understanding of skyrmion dynamics.

[1] A. Fert *et al., Nat. Nanotechnol.* 8, 152 (2013) [2] M. Song *et al., IEEE Trans. Electron. Dev.* 68, 1939 (2021) [3] S. Luo *et al., Nano Lett.* 18, 1180 (2018) [4] S. Lemerle *et al., Phys. Rev. Lett.* 80, 849 (1998) [5] K. -J. Kim *et al., Nature* 458, 740 (2009) [6] K. -W. Moon *et al., NPG Asia Mater.* 13, 20 (2021)

GOC-06. Helitronics: Electrical Manipulation of Helimagnetic Phases.
J. Masell[1,2] and N. Nagaosa[1,3] *1. CEMS, RIKEN, Wako, Japan; 2. TFP, Karlsruhe Institute of Technology, Karlsruhe, Germany; 3. Department of Applied Physics, University of Tokyo, Tokyo, Japan*

Frustrated magnetic systems can establish one-dimensionally modulated helical/spiral textures as the ground state, see Fig.1. For example, in chiral materials the dominant ferromagnetic exchange interaction competes with a Dzyaloshinskii-Moriya interaction, or in centrosymmetric systems the sign of the exchange interaction can alternate as function of distance between atoms. Upon application of an external magnetic field, the spirals/helices often collapse and form skyrmions. Skyrmion lattices and isolated skyrmions can be easily manipulated by electric currents and therefore are a celebrated new candidate for spintronics/skyrmionics applications. In contrast, the long-ranged helical phase is usually pinned and its translational dynamics is of little interest in spintronics. I will present our recent studies on the current-driven dynamics of the helical phase and its defects. Recently, experiments have shown that electric current pulses can unpin and move the helical phase in a thin FeGe film [1]. Our simulations predict different reorientation mechanisms due to defects deep in the bulk or due to edges, respectively, which is consistent with experimental observations. Moreover, we predict a series of instabilities from incremental to large current densities, showing that the dynamics of the helical phase are much more diverse than expected [1,2]. Conversely, once the helical phase is set in motion, it can induce both an electrical current and a spin current [3]. We have also investigated defects in the helical phase. Isolated skyrmions can be stabilized in the helical background, where they are naturally confined to lanes [4]. After suppressing the intrinsic instability of the helical phase, we theoretically analyzed the dynamics of such skyrmions and proposed a protocol for creating them on demand by current pulses at defects [5]. By studying other defects such as dislocations and topological domain walls [6], we found that they can exhibit a large susceptibility contrast, which could be a key to efficient defect detection despite the small scale and small stray field [7].

[1] J. Masell, X.Z. Yu, N. Kanazawa, *et al.*, Phys. Rev. B 102, 180402(R) (2020) [2] J. Masell and N. Nagaosa, in preparation [3] D. Kurebayashi, Y. Liu, J. Masell, and N. Nagaosa, in preparation [4] J. Müller, J. Rajeswari, P. Huang, *et al.,* Phys. Rev. Lett. 119, 137201 (2017) [5] R. Knapman, D.R. Rodrigues, J. Masell, *et al.*, J. Phys. D 54, 404003 (2021) [6] P. Schoenherr, J. Müller, L. Köhler, et al., Nat. Phys. 14, 465-468 (2018) [7] M. Stepanova, J. Masell, E. Lysne, *et al.*, arXiv:2103.14449

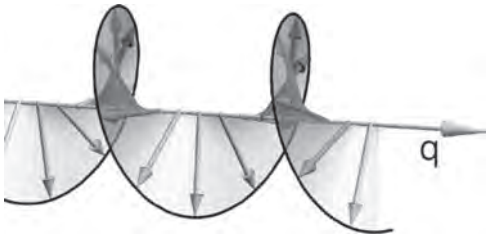

Fig.1: Schematic representation of the magnetization (colored arrows) in the helical phase. Taken from [1].

GOC-07. Withdrawn

GOC-08. Evolution of Novel Chiral Spin Textures in Fe/Gd Based Multilayers.
W. Parker[1], S. Montoya[2], E. Fullerton[3], R. Moraski[1] and B. McMorran[1] *1. Physics, University of Oregon, Eugene, OR, United States; 2. Naval Information Warfare Systems Command, San Diego, CA, United States; 3. Center for Memory and Recording Research, University of California San Diego, La Jolla, CA, United States*

Research into magnetic skyrmions and their spintronics applications has revealed complex chiral spin textures. However, direct characterizations of the structure of skyrmion and related spin textures pose an experimental challenge. To better understand their structure, we use Lorentz transmission electron microscopy (LTEM) to track their evolution from well-studied domain walls (DWs) into skyrmion and biskyrmion phases. Magnetic skyrmions were first predicted as a result of the Dzyaloshinskii-Moriya interaction (DMI) found in materials with broken inversion symmetry[1]. However, topologically equivalent chiral bubbles, or dipole skyrmions, can be stabilized in achiral thin films by competing long-range dipole and short-range DW energies[2]. Recently, a novel skyrmion phase consisting of bound skyrmion pairs with opposite helicities was reported in achiral Fe/Gd multilayers[3] (Fig. 1). However, the primary magnetic imaging techniques for thin films are LTEM, which yields projected in-plane magnetic field, and resonant X-ray techniques, which yield projected out-of-plane magnetization. This complicates identification of complex magnetic spin textures, as multiple spin textures can yield qualitatively similar projected magnetic fields, and there has been subsequent debate over the structure of the reported skyrmion phases[4,5]. By tracking the field-dependent evolution of magnetic spin textures from the well-studied magnetic stripes to the novel skyrmion phases, we can identify key components of these spin textures. First, by applying an out-of-plane magnetic field with a small in-plane component, stripe DWs form, alternatingly aligned and anti-aligned with the in-plane component, matching previous results[2]. As the field is further increased, the stripe DWs split, and the aligned DWs form the center of the novel texture, while the anti-aligned form closure loops (Fig. 2), supporting that the magnetization is a pair of contour-rotating vortices. Fully understanding these textures will require knowledge of the 3D structure, so surface sensitive techniques like SEMPA, SPLEEM, and MFM will be vital moving forward.

1. Jiang et al., Physics Reports., Vol. 704, p.1-49 (2017) 2. Montoya et al., Physical Review B., Vol. 95, no. 2, p.024415 (2017) 3. Lee et al., Applied Physics Letters., Vol. 109, no. 2, p.022402 (2016) 4. Loudon et al., Advanced Materials., Vol. 31, no. 16, p.1806598 (2019) 5. Streubel et al., Advanced Materials., Vol. 33, no. 8, p.2004830 (2021)

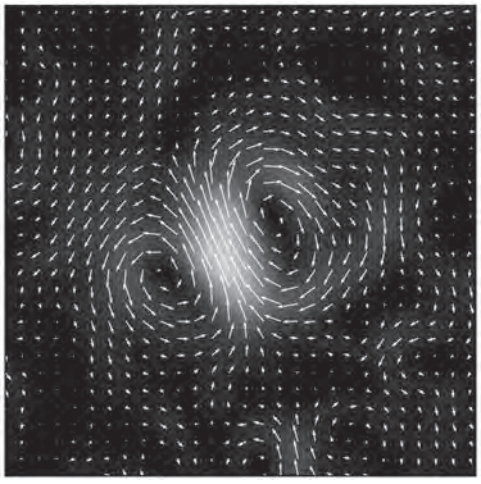

Fig. 1. The projected in-plane field of the novel texture.

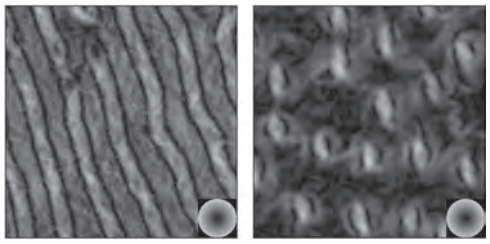

Fig. 2. Stripe domains breaking into the novel phase.

GOC-09. Angle-dependent Magnetotransport Properties of Skyrmions in Amorphous Fe/Gd Multilayers. *S. Montoya*[1], M. Lubarda[3], V. Lomakin[2,1] and E. Fullerton[1,2] *1. Center for Memory and Recording Research, University of California San Diego, La Jolla, CA, United States; 2. Electrical and Computer Engineering, University of California San Diego, La Jolla, CA, United States; 3. Mechanical and Aerospace Engineering, University of California San Diego, La Jolla, CA, United States*

Skyrmions, particle-like chiral magnetic spin textures, have attracted extensive research interest due to their novel electromagnetic properties and potential application to memory technologies [1]. Primarily, these spin textures have been shown to result from competing Heisenberg and Dzyaloshinskii-Moriya interactions (DMI) in bulk and thin-films. However, skyrmions can be stabilized by magnetostatics, which results in the coexistence of equally populated left and right-helicity spin textures [2]. Dipole-stabilized magnets can exhibit spin textures that are locally chiral and globally (on average) achiral. In Fe/Gd multilayers, hybrid skyrmions are stabilized that exhibit a complex 3-dimensional structure with opposite helicity Neel-like magnetic spin arrangements near the surfaces of the film, and a Bloch-like spin arrangement near the center of the film. Here we report field-dependent magnetotransport measurements of patterned wires of an Fe/Gd multilayers which exhibits magnetic phases ranging from disordered stripes, coexisting stripes and skyrmions, skyrmion lattice, and disordered skyrmions (Fig. 1). First, we will describe the coexistence of two helicity chiral spin textures results in Bloch-line rearrangement as a function of applied perpendicular fields, a feature not anticipated in DMI chiral magnets given their single helicity. Furthermore, we demonstrate how the application of in-plane and perpendicular fields can locally modify the chiral spin texture population in dipole magnets, as well as other unexpected features. Our results show how dipole-stabilized magnetic stripes and skyrmions provide a platform to investigate the interplay between local and global chirality effects.

[1] A. Fert, N. Reyren, and V. Cros, *Nat. Rev. Mater*. 2, 17031 (2017). [2] S. A. Montoya, *et. al. Phys. Rev. B* 95, 024415 (2017).

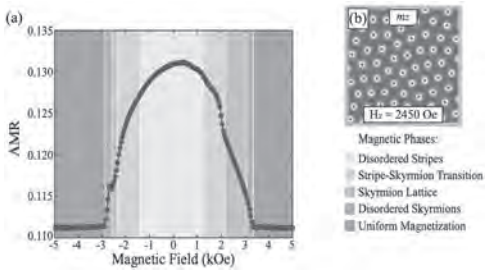

Figure 1. (a) Micromagnetic modeling of anisotropic magnetoresistance (AMR) as a magnetic field is applied from negative to positive saturation [M_S = 400 emu/cm3, $K_U = 4 \times 105$ erg/cm3, $A = 5 \times 10{-}7$ erg/cm, 10µm x 10µm x 80nm slab]. Field-regions where different magnetic phases are formed are overlaid on the AMR curve. (b) Image depicts the top-side view of the magnetization along the z-axis for an equilibrium state (*i.e.,* skyrmion lattice) that forms under H_z = 2450 Oe.

GOC-10. Sub-monolayer capping induced switching of magnetic chirality. *G. Chen*[1], C. Ophus[2], R. Lo Conte[3,4], R. Wiesendanger[3], A. Schmid[2] and K. Liu[1] *1. Georgetown University, Washington, DC, United States; 2. Lawrence Berkeley National Laboratory, Berkeley, CA, United States; 3. University of Hamburg, Hamburg, Germany; 4. University of California, Berkeley, Berkeley, CA, United States*

Chiral spin textures such as skyrmions and chiral domain walls are fundamentally interesting, with promise for device applications [1][2]. In thin film systems, inversion symmetry breaking of atoms at the interface gives rise to the Dzyaloshinskii-Moriya interaction (DMI), which stabilizes magnetic chirality with preferred handedness. Experimentally, controlling the handedness is crucial to tune the efficiency of current-induced manipulation of spin texture, a key feature in new spintronic devices. This is conventionally achieved by stacking asymmetric multilayers where the thickness of each layer is at least a few monolayer [3]. Here we report a full chirality switching of chiral Néel walls in $[Ni/Co]_n$ multilayer induced by capping only 0.2 monolayer of Pd at room temperature (Fig. 1). We systematically monitor the domain wall type using spin-polarized low energy electron microscopy (SPLEEM) during the switching with increasing Pd thickness. The gradual evolution of domain walls from left-handed to right-handed Néel walls allows us to quantify the DMI induced by the capping Pd sub-monolayer. We also observe the evolution of a skyrmion structure during the DMI switching, where no significant topological protection of the skyrmion winding number was found (see mixed Néel-component in Fig. 1d). Our results demonstrate the detailed chirality evolution within skyrmions during the DMI sign switching, which is relevant to the topological property of skyrmions. Work supported by the NSF (DMR-2005108), SRC/NIST nCORE SMART center and DOE (DE-AC02-05CH11231).

[1] R. Wiesendanger, Nat. Rev. Mater. 1, 16044 (2016). [2] A. Fert, et al. Nat. Rev. Mater. 2, 17031 (2017). [3] W. Jiang, et al. Phys. Rep. 704, 1-49 (2017).

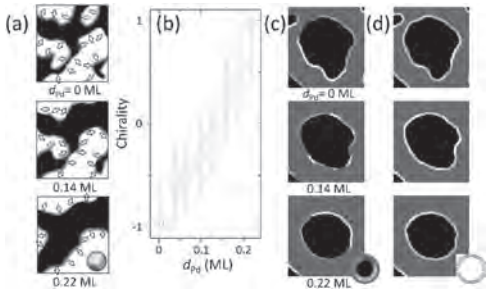

Figure 1. The spin structure and chirality evolution as a function of the Pd capping layer thickness. (a) Compound SPLEEM images of Ni/Co/Pd/W(110) with various Pd thickness, showing chirality switching from left-handedness to right-handedness. (b) The quantified chirality varies as a function of the Pd thickness. (c) The compound SPLEEM images highlighting the chirality evolution of a skyrmion bubble, showing the change of the Néel-component (panel d), where the blue and orange regions illustrate the left/right-handed chirality, respectively.

GOC-11. Frustration of coupled helices in weakly perpendicular magnetic thin films. *S.A. Morley*[1], J. Li[2], R. Tumbleson[1,3], S. Montoya[4], E. Fullerton[4], D. Lederman[3], S.D. Kevan[1] and S. Roy[1] *1. Advanced Light Source, Lawrence Berkeley National Laboratory, Berkeley, CA, United States; 2. Department of Materials Science and Engineering, University of California Davis, Davis, CA, United States; 3. Department of Physics, University of California Santa Cruz, Santa Cruz, CA, United States; 4. Center for Memory and Recording Research, University of California San Diego, La Jolla, CA, United States*

Anti-symmetric exchange, or the Dzyaloshinskii–Moriya interaction (DMI), is responsible for non-collinear spin textures such as canting, helices and skyrmions in bulk systems or films with asymmetric structure [1]. Analogously,

thin films without DMI can have competing anisotropies which stabilise non-collinear magnetic textures. Using resonant soft x-ray scattering, we study the rigid stripe rotation in an Fe/Gd multilayer which accompanies the transition from the stripe phase to the six-fold dipole skyrmion lattice. The sample was measured in transmission and the small-angle diffraction gave the average period and in-plane orientation, **Φ**, of the perpendicular stripes. By changing the sample tilt, ω, we control the resultant field vector which changes the threshold, H_{onset}, and abruptness of the observed rotation (Fig. 1a). We used micromagnetic simulation software MuMax3 [2] to model the system using similar parameters to previous work [3]. By carefully setting the initial state and polarity of the Bloch center of the helical domain wall we reproduce the rotational behaviour observed experimentally (Fig. 1a(inset), 1b). We show on inspection of the simulated 3D spin structure that as the magnetic field is increased the helical domain wall region tries to unwind before rotation and then reverts back to a more wound structure in the rotated state before transitioning into the skyrmion/bubble lattice and finally saturating.

[1] Back, C. *et al. J. Phys. D: Appl. Phys.* 53 363001 (2020). [2] Vansteenkiste, A., & Van de Wiele, B. *Journal of Magnetism and Magnetic Materials*, 323, 2585 (2011). [3] Montoya, S. A. *et al. Physical Review B* 95, 024415 (2017).

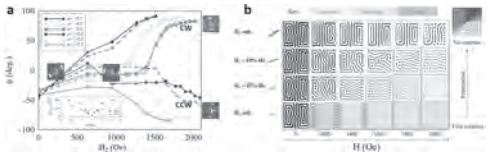

(a) The Φ angle of the diffracted peaks is plotted for different values of ω as a function of the modulus of applied field where solid symbols are H_z and open symbols are $-H_z$. Increasing Φ shows clockwise (CW) motion for ω>1 and counter clockwise (CCW) motion for ω>1. (Inset) The experimental in-plane (IP) component of $H_{onset\ al}$ng with the corresponding values from the simulations. (b) Micromagnetically simulated rotation of the stripe domains for combined IP and OOP magnetic field. *H* is indicated at the bottom and is in the *z* direction for all panels except the bottom row where it denotes an in-plane field along the *x* direction. Simulated area was 2x2 μm², color wheel indicates direction of in-plane magnetisation and white and black are up and down perpendicular magnetisation, respectively.

GOC-12. Electrical discrimination of magnetic-skyrmion chirality via spin-orbit and -transfer torques in a branched nanowire.

K. Yamada[1], A. Hirohata[2] and Y. Nakatani[3] *1. Chemistry and Biomolecular Science, Gifu University, Gifu City, Japan; 2. Department of Electronic Engineering, University of York, York, United Kingdom; 3. Graduate School of Informatics and Engineering, University of Electro-Communications, Chofu, Japan*

Recently many works on magnetic memories and logic circuits, which use a magnetic skyrmion, have been reported [1,2]. Previously we demonstrated by simulation that skyrmions with opposite chiralities of a Néel skyrmion can be formed in the same magnetic thin film, and their chiralities can be switched by introducing a single heat pulse [3]. To date the chirality has been measured by imaging a skyrmion using magnetic force microscopy and X-ray photoemission electron microscopy [4,5]. However, to realize such a memory, an electrical method to discriminate the chiralities is essential. In this presentation, we demonstrate an electrical method to discriminate the chirality (*i.e.*, counter clockwise (CCW) or clockwise (CW)) of a skyrmion in a branched nanowire by using spin-orbit torque (SOT) and spin-transfer torque (STT) by using simulation (see Fig.1) [6]. The simulated results show that the motion changes depending on the chirality when additional SOT is applied on a skyrmion moving in a branched wire by STT. In our simulations, we investigated the values of a current density and a spin Hall angle for discrimination of the chirality, and a branch angle of branched nanowires. Figure 2 shows the phase diagram of the branch and current density at the spin Hall angle $\theta^H = 0.1$. Shaded area shows the angle and current ranges of the main branch to discriminate both chirality types of skyrmions, where the magnitude of the current density is 0.2-0.4 TA/m² regardless the branched angle in the range between 15° and 90°. The results confirm that the material/physical parameters can be within the experimentally achievable range. Our method can be used as a fundamental building block for fully electrical detection in memory and logic devices using the chirality of skyrmions as a data bit in addition to the presence of the skyrmions as conventionally used. This can lead to multiple-valued operation [6].

[1] J. Iwasaki, et al. *Nat. Nanotech.* 8, 742-747 (2013). [2] J. Sampaio, et al. *Nat. Nanotech.* 8, 839-844 (2013). [3] Y. Nakatani, et al. *Sci. Rep.* 9, 13475 (2019). [4] W. Legrand, et al. *Nano Lett.* 17, 2703-2712 (2017). [5] S. Zhang, et al. *Nano Lett.* 18, 1057-1063 (2018). [6] Y. Nakatani, et al. *Sci. Rep.* 11, 8415 (2021).

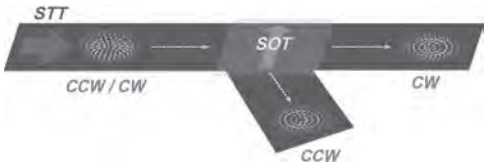

Figure 1. Illustration of a nanowire with a branch to discriminate a skyrmion chirality.

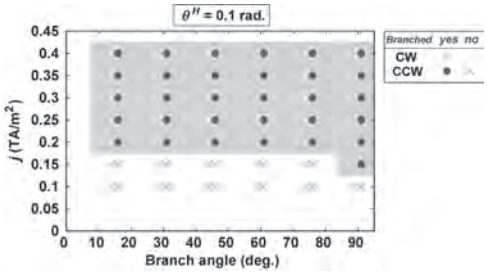

Figure 2. Phase diagram of the branch and current density at the spin Hall angle $\theta^H = 0.1$. Shaded area shows the angle and current ranges of the main branch to discriminate both chirality types of skyrmions.

GOC-13. Gauge Theory Applied to Chiral Magnets.

P. Ansalone[1], E.S. Olivetti[1], A. Magni[1], A. Sola[1] and V. Basso[1] *1. Istituto Nazionale di Ricerca Metrologica, Torino, Italy*

Compounds such as MnSi, FeCoSi, FeGe and MnGe, crystallising in the B20 structure type, exhibit non-trivial magnetisation configurations, including helical states and skyrmions [1-4]. The interest in such magnetic states lies in the possibility to manipulate the skyrmions as logic bits through the spin-transfer torque effect driven by a low electric current density [5, 6]. The chiral magnetic states are described, in the literature, by introducing an energy term of the Dzyaloshinskii-Moriya (DM) type. However, the non-centrosymmetry provides only the necessary condition for a non-vanishing DM interaction; for this reason, the connection through the DM term and the underlying crystal structure is not always evident [7, 8]. In this paper, we propose a local gauge approach to address the problem. The method relies on exploiting the local gauge invariance of the micromagnetic energy under the action of a local rotation [9, 10]. We show that in the presence of non-centrosymmetric local crystal symmetry, the local gauge invariance provides two additional terms in the micromagnetic energy: the first one is a DM-type term, and the second one is an additional anisotropy energy contribution. We apply the theory to specific crystals of the B20 type to highlight the physical aspects directly emerging from the point group symmetries.

[1] S. A. Meynell, M. N. Wilson, K. L. Krycka, B. J. Kirby, H. Fritzsche, and T. L. Monchesky, "Neutron study of in-plane skyrmions in MnSi thin films," Physical Review B, vol. 96, no. 5, Aug. 2017, DOI: 10.1103/physrevb.96.054402. [2] S. A. Meynell, M. N. Wilson, H. Fritzsche, A. N. Bogdanov, and T. L. Monchesky, "Surface twist instabilities and

skyrmion states in chiral ferromagnets," Physical Review B, vol. 90, no. 1, Jul. 2014, DOI: 10.1103/physrevb.90.014406. [3]A. Bauer and C. Pfleiderer, "Generic Aspects of Skyrmion Lattices in Chiral Magnets," in Topological Structures in Ferroic Materials, Cham: Springer International Publishing, 2016, pp. 1–28. [4]N. Nagaosa and Y. Tokura, "Topological properties and dynamics of magnetic skyrmions," Nature Nanotechnology, vol. 8, no. 12, pp. 899–911, Dec. 2013, DOI: 10.1038/nnano.2013.243. [5] F. Jonietz et al., "Spin Transfer Torques in MnSi at Ultralow Current Densities," Science, vol. 330, no. 6011, pp. 1648–1651, Dec. 2010, DOI: 10.1126/science.1195709. [6] X. Zhang, M. Ezawa, and Y. Zhou, "Magnetic skyrmion logic gates: conversion, duplication and merging of skyrmions," Scientific Reports, vol. 5, no. 1, Mar. 2015, DOI: 10.1038/srep09400. [7] A. Ullah et al., "Crystal Structure and Dzyaloshinski–Moriya Micromagnetics," IEEE Transactions on Magnetics, vol. 55, no. 7, pp. 1–5, Jul. 2019, DOI: 10.1109/tmag.2018.2890028. [8] X. S. Wang, H. Y. Yuan, and X. R. Wang, "A theory on skyrmion size," Communications Physics, vol. 1, no. 1, Jul. 2018, DOI: 10.1038/s42005-018-0029-0. [9] V. Basso and P. Ansalone, "Electric field effect on spin waves: Role of magnetic moment current," EPL (Europhysics Letters), vol. 130, no. 1, p. 17008, Apr. 2020, DOI: 10.1209/0295-5075/130/17008. [10] P. Ansalone, S. Perna, M. d'Aquino, V. Scalera, C. Serpico, and V. Basso, "A Local Gauge Description of the Interaction between Magnetization and Electric Field in a Ferromagnet," IEEE Transactions on Magnetics, pp. 1–1, 2021, DOI: 10.1109/tmag.2021.3086357.

Session GOD
SKYRMION STABILIZATION, VOLTAGE CONTROL, AND NEUROMORPHIC APPLICATIONS

Jan Masell, Chair
RIKEN, Karlsruhe, Germany

INVITED PAPER

GOD-01. Skyrmion Creation and Annihilation by Electric Current Vorticity. *J. Fujimoto*[1], H. Funaki[2], W. Koshibae[2], M. Matsuo[3,2] and S. Maekawa[2,3] *1. University of Tokyo, Hongo, Japan; 2. RIKEN Center for Emergent Matter Science, Wako, Japan; 3. Kavli Institute for Theoretical Sciences, University of Chinese Academy of Sciences, Beijing, China*

A recent experiment showed that magnetic skyrmions are created in FeGe films by electric current without a magnetic field [1]. This experiment also showed that the skyrmions are annihilated just by reversing the electric current direction. For the non-reciprocal phenomena, the sample geometry is of crucial importance, i.e., the sample has a notch structure, and the skyrmion creation/annihilation does not occur in the sample without the notch structure. Motivated by this experiment, we propose a theory that the electric current vorticity plays an essential role in magnetic phenomena [2]. The notch structure arises the vortical structure in electric current profile; the current vortex has angular momentum and couples with electron spin angular momentum. Through the exchange interaction between the conduction electron and localized spins, the electric current vortex induces the Dzyaloshinskii-Moriya (DM) interaction as well as the effective Zeeman coupling for the localized spins. The vorticity-induced Zeeman field changes its direction by reversing the electric current direction, as shown in Fig.1, which is responsible for the skyrmion creation and annihilation. The vorticity-induced DM interaction has the DM vector which depends on the electric current direction and gives rise to the distortion of the magnetic skyrmions. We also find that the electric current vortex induces a spin current that carries the magnetic skyrmions far from the notch structure. In the talk, we first introduce the spin-vorticity coupling, which is derived originally from the relativistic quantum mechanics in curved spaces [3] and extended into the interaction between the electric current vorticity and electron spin [4,5]. Secondly, we briefly show the experimental results by Yu et al.[1], and then we present the theory mentioned above for explaining the experiment. We will discuss the spatial profile of electric current based on the hydrodynamic equation with frictional force and the dynamics of the magnetic textures.

[1] X. Z. Yu, et al., Sci. Adv. 6, eaaz9744 (2020). [2] J. Fujimoto, W. Koshibae, M. Matsuo, and S. Maekawa, Phys. Rev. B 103, L220402 (2021). [3] M. Matsuo, Y. Ohnuma, and S. Maekawa, Phys. Rev. B 96, 020401(R) (2017). [4] G. Okano, M. Matsuo, Y. Ohnuma, S. Maekawa, and Y. Nozaki, Phys. Rev. Lett. 122, 217701 (2019). [5] J. Fujimoto, et al., in preparation.

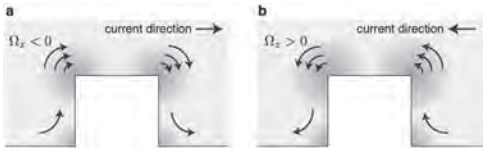

The current-direction dependence of the vorticity near the notch structure. (a) the current direction is from left to right, and (b) the inverse. The current vorticity is reversed by reversing the current direction.

CONTRIBUTED PAPERS

GOD-02. Fast current-induced domain wall and skyrmion motion in a nearly compensated amorphous ferrimagnetic alloy. *Y. Quessab*[1], J. Xu[1] and A. Kent[1] *1. Department of Physics, New York University, New York, NY, United States*

Magnetic racetrack memories offer the possibility of increasing the density and speed of data storage. Yet, achieving fast current-induced motion of domain walls (DWs) and skyrmions at room temperature remains a challenge. We study nearly compensated ferrimagnetic CoGd alloys inserted between two heavy metals for which we have already demonstrated the optimization of spin-orbit torques (SOTs)[1] and interfacial Dzyaloshinskii-Moriya interactions[2]. Ferrimagnets are attractive materials for their low stray field and fast spin dynamics which has been theoretically predicted to enable formation of ultrasmall[3] and fast skyrmions. However, so far, the reported skyrmion velocities[4] are much lower than of DWs[3]. Here, we investigate the nucleation and dynamics of chiral magnetic textures induced by current pulses in Pt/CoGd(5 nm)/(W or Ta) films. First, we demonstrate fast motion of DWs driven by SOTs *at room temperature*. We observe a maximum DW velocity of about 460 m s^{-1} (Fig. 1). Hence, we confirm that our ferrimagnetic materials have a very low DW pinning and density of defects, which is ideal for fast current-induced motion of DWs and skyrmions. Most literature studies focus on materials with a skyrmionic ground state. Here, our CoGd films have a sharp magnetic hysteresis loop and skyrmions are metastable. In Fig. 2a, we show that we can achieve field free nucleation of skyrmion bubbles with a single 5-ns current pulse and with a density of 2.7 $x10^{12}$ A m^{-2}. In addition, sequential magneto-optical Kerr (MOKE) imaging (Fig. 2b-f) after applying a single 5-ns current pulse with a density of 1.5 $x10^{12}$ A m^{-2} reveals fast skyrmion motion with a velocity of about 400 m s^{-1}. A small out-of-plane magnetic field of -5.7 mT is applied to stabilize the skyrmion bubble. In this study, we demonstrate that our low pinning ferrimagnetic films enable one of the fastest skyrmion motion thus far reported[5]. Our results could pave the way for ultrafast racetrack memory operations. This research was supported by DARPA award No. D18AP00009.

[1]Y. Quessab *et al.*, Advanced Science, 2100481 (2021) [2] Y. Quessab *et al.*, Scientific Reports 10, 7447 (2020) [3]L. Caretta *et al.*, Nature Nanotechnology 13, 1154 (2018) [4]S. Woo *et al.*, Nature Communications 9, 959 (2018). [5]R. Juge *et al.*, Physical Review Applied 12, 044007 (2019).

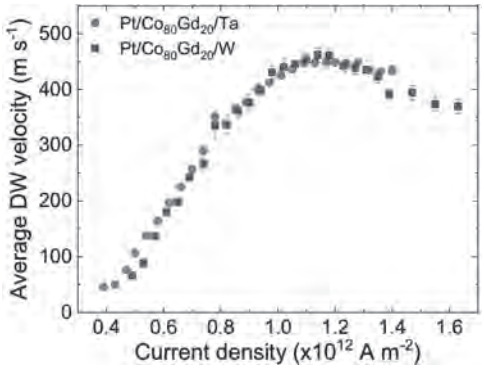

Fig. 1 Average DW velocity driven by SOTs in Pt/CoGd/(W or Ta).

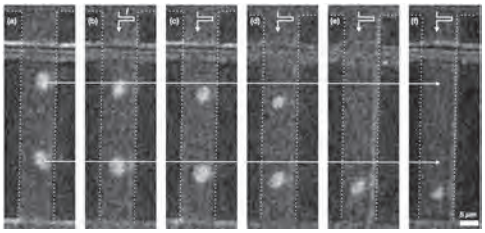

Fig. 2 Field free current-induced nucleation (a) and motion (b-f) of skyrmion bubbles by a single 5-ns current pulse.

GOD-03. Stabilizing skyrmions in ferri/ferromagnet heterostructure towards efficient motion. *S. Mallick*[1], H. Damas[2], M. Hehn[2], N. Reyren[1], K. Bouzehouane[1], J. Rojas-Sanchez[2], V. Cros[1] and A. Fert[1] *1. Unité Mixte de Physique, CNRS, Thales, Université Paris-Saclay, Palaiseau, France; 2. Université de Lorraine, CNRS, Institute Jean Lamour, Nancy, France*

In this study, we have considered hybrid multilayer systems integrating layers of ferrimagnetic alloys of rare earth and transition metal [1] with cobalt-based multilayers accommodating skyrmions. The objective is to leverage the large emitted spin currents [2] from the ferrimagnet (GdFeCo), that we recently evidenced, to drive the skyrmions more efficiently in the ferromagnet. It has been observed that the global spin Hall angle (due to the coexistence of SHE and SAHE type spin currents) in GdFeCo is 0.8, which is significantly larger than the values observed in Pt/Co based heterostructures [2]. Hence, we use in-plane magnetized GdFeCo as a source of large spin current to drive the skyrmions in a Pt/Co/Cu heterostructure. The sample prepared by sputtering deposition have the following structure: $Si/SiO_2//Gd_{20}FeCo(4\ nm)/Cu(2.5\ nm)/[Pt(1\ nm)/Co(t_{Co})/Cu(1\ nm)]_{x4}/Al(3\ nm)$, where t_{Co} is varied between 1.2 to 1.8 nm. Fig. 1(a) shows typical hysteresis loop for the samples. The inset of fig. 1(a) confirms the in-plane magnetization of the GdFeCo layer with a saturation field ~350 mT, whereas, the Pt/Co/Cu heterostructure presents a typical loop to host the skyrmions. Wormlike stripe domains are observed in the demagnetized state (fig. 1(b)) indicating that the ground state is 1D textures. By applying perpendicular field of ~60 mT, isolated skyrmions are observed by MFM with an average size ~100 nm (fig. 1(c)). We further note that the skyrmions are easily perturbed even by the stray field of a low moment magnetic tip, indicating the presence of low pinning landscape. One of the forthcoming objectives will be to evaluate the respective effective torque contributions i.e. from the ferrimagnetic films and/or from more standard SHE. Finally, the purpose is to observe some gain in efficiency on the skyrmion displacement generated by the spin emission from GdFeCo. Acknowledgement: French ANR grant TOPSKY (ANR-17-CE24-0025) and DARPA TEE program grant (MIPR#HR0011831554) for their financial support.

1. L. Caretta *et al.*, *Nature Nanotechnology* 13, 1154 (2018) 2. D Céspedes-Berrocal *et al.*, *Advanced Materials* 33, 2007047 (2021).

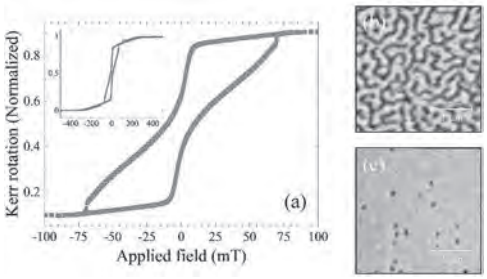

Fig. 1: (a) Polar MOKE loop for GdFeCo/Pt/Co/Cu heterostructure with t_{Co} = 1.5 nm. The inset image shows the complete hysteresis cycle. (b) and (c) MFM images measured in demagnetized state and at $\mu_0 H_{out}$ = 60 mT, respectively.

GOD-04. Controlling generation position and motion path of magnetic skyrmions. M. Im[1], S. Je[2], *H. Han*[1], D. Jung[3], S. Jeong[3], A. Soumyanarayanan4[4], D. Vasudevan[1] and K. Lee[3] *1. Lawrence Berkeley National Laboratory, Berkeley, CA, United States; 2. Chonnam National University, Chonnam, The Republic of Korea; 3. UNIST, Ulsan, The Republic of Korea; 4. Institute of Materials Research and Engineering, Singapore, Singapore*

Magnetic skyrmions are topologically stable particle-like spin textures, which have attracted massive interest not only due to their fascinating features for understanding the fundamental physics of nanospin behavior but also their potentials in a wealth of technological applications for high efficient storage/memory and computing devices [1]. Skyrmions also offers the dual functions of data storage and data transfer, which is an extremely beneficial and unique feature for highly efficient multifunctional operations, and therefore, they are promising building blocks for future spintronic devices. To realize the skyrmion-based logic, memory, computing devices, generating and deleting skyrmions in the desired position of systems, controlling route of skyrmion motions and consequently compatible with conventional semiconductor manufacturing processes and integrated circuits are essential. However, those issues haven't been addressed yet. We demonstrated a framework for writing and deleting skyrmions in a targeted area of a system by a reliable yet simple method [2]. We found that Joule heating and the Oersted field induced by the injected current through the device are key ingredients for writing and deleting skyrmions with spatial and temporal selectivity. We also studied controlling the path of skyrmion motion by optimizing the design of devices. The route of skyrmion motion was found to considerably rely on the skyrmion-skyrmion and skyrmion-edge interactions [3]. Based on this study, we tried to design skyrmion-based fundamental building blocks of computing that can be used as computational primitives to compute logic and dense memory and investigate efficient computational models that best make use of our primitives to implement computational functions relevant to microelectronic applications.

[1] A. Fert, N. Reyren, V. Cros, Nature Rev. Mat. 2, 17031 (2017). [2] S.-G. Je et al., Nano Letters, 21, 3, 1253 (2021). [3] S. Jeong et al., to be submitted (2022).

GOD-05. Confinement and Protection of Magnetic Skyrmions. K. Ohara[1], X. Zhang[1], Y. Chen[1], Z. Wei[3], Y. Ma[4], J. Xia[2], Y. Zhou[2] and *X. Liu*[1] *1. Department of Electrical and Computer Engineering, Shinshu University, Nagano, Japan; 2. School of Science and Engineering, The Chinese University of Hong Kong, Shenzhen, China; 3. School of Mechanics and Engineering Science, Zhengzhou University, Zhengzhou, China; 4. College of Optical Science and Engineering, Zhejiang University, Hangzhou, China*

Topological spin textures, such as magnetic skyrmions, are promising building blocks for future spintronic applications [1]. To use skyrmions as information carriers, it is vital to find effective ways to control the skyrmion

dynamics [1]. Directional motion of skyrmions can be achieved by applying a suitable electric field [2], which paves the way for practical applications of skyrmions for low-power consumption memory and logical circuits. However, the confinement and control of the skyrmion position have been remaining as a challenge due to the skyrmion Hall effect. In this talk, we will present an effective method to confine and control skyrmions in a magnetic multilayer thin film by locally modifying magnetic properties, such as the perpendicular magnetic anisotropy (PMA) and Dzyaloshinskii-Moriya interaction (DMI) [3]. Our theoretical and experimental findings suggest that the boundary between two regions of different magnetic properties may create a confining potential in the sample, which can effectively protect skyrmions from being destroyed at the sample edge. We will also point out that such a confining potential can be used to guide the skyrmion motion in principle. The confinement, protection, and guide of skyrmions in magnetic films are critical techniques for both fundamental and advanced applications based on skyrmions, such as the racetrack memories and artificial neurons. Our results provide a way to give skyrmions extra endurance and robust retention to work as information carriers.

[1] Nat. Rev. Phys. 2, 492 (2020); J. Phys. D: Appl. Phys. 53, 363001 (2020); J. Phys.: Condens. Matter 32, 143001 (2020); J. Appl. Phys. 124, 240901 (2018); Nat. Rev. Mats. 2, 17031 (2017); Adv. Mater. 29, 1603227 (2017); Phys. Rep. 704, 1 (2017); J. Phys. D: Appl. Phys. 49, 423001 (2016); Proc. IEEE 104, 2040 (2016); Nat. Rev. Mats. 1, 16044 (2016); J. Phys.: Condens. Matter 27, 503001 (2015); Nat. Nanotech. 8, 899 (2013). [2] C. Ma, et. al, Nano Lett. 19, 353-361 (2019). [3] K. Ohara, et al., Nano Lett. 21, 4320-4326 (2021).

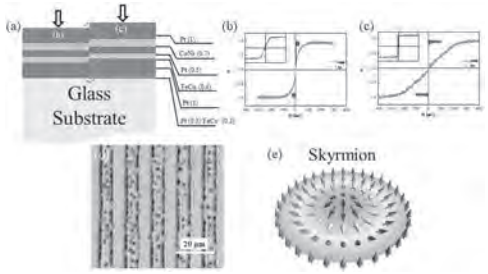

Fig.1 (a) Schematic of the experimental sample configuration. The enhanced PMA and DMI is realized by fabricating an additional Pt/FeCo layer as indicated by the red layer. The boundary between areas with different PMA and DMI is indicated by the blue circle. The unit of thickness is nm. (b) Hysteresis loops of default PMA and DMI measured by VSM and polar-Kerr. (c) Hysteresis loops of enhanced PMA and DMI measured by VSM and polar-Kerr. (d) Experimental observation of room temperature stable skyrmions in default PMA and DMI which confined in parallel narrow channels formed by boundaries of stripe patterns with enhanced PMA and DMI. (e) Illustration of a Néel-type magnetic skyrmion stabilized by interfacial DMI.

GOD-06. Creation and Annihilation of Magnetic Skyrmions in Confined Geometry using Voltage Control of Magnetic Anisotropy.

M. Rajib[1], D. Bhattacharya[1], B. Dai[2], S.A. Razavi[2], H. Wu[2], K.L. Wang[2] and *J. Atulasimha*[1] *1. Mechanical and Nuclear Engineering Department, Virginia Commonwealth University, Richmond, VA, United States; 2. Electrical and Computer Engineering, University of California, Los Angeles, CA, United States*

Skyrmions are typically manipulated by driving them with an electrical current in a racetrack and have been proven to be advantageous, due to their high mobility, energy efficient drivability and potential in overcoming edge roughness-related pinning occurring in domain wall (DW)- based racetrack devices [1]-[3]. However, to have high density skyrmion based memory devices, it is essential to create and manipulate skyrmions in magnetic tunnel junctions (MTJs). Previously, it has been shown with micromagnetic simulations that voltage-controlled magnetic anisotropy (VCMA) can be used in perpendicular MTJs to create an intermediate skyrmion starting from a ferromagnetic up/down state and subsequently annihilating it to form a ferromagnetic down/up state [4] and thus energy efficient electrical field switching robust to defects and thermal noise can be achieved. Towards the experimental realization of this switching strategy, skyrmions have to be created and manipulated with VCMA in a confined geometry where the skyrmion lateral dimension equals the lateral dimension of a nanodot. However, so far creation and annihilation of fixed magnetic skyrmions using VCMA has only been experimentally observed through magnetic force microscopy (MFM) imaging in thin ferromagnetic films where the skyrmions are much smaller in lateral dimension compared to the thin films and the imaging was performed after withdrawal of the applied electric field (Fig.1) [5]. Here, we will study experimental creation and annihilation of skyrmions using VCMA in a confined geometry of <1μm lateral dimension with in-situ application of voltage while imaging. This will enable visualization of the skyrmion/ferromagnet state as a function of the applied electric field and the mechanism through which skyrmions can be manipulated with VCMA induced change in PMA in the presence of interactions with the boundary of the patterned nanodot. Fig. 2 shows an example of a nanostructure in which such experiments will be carried out. Acknowledgement: NSF grant CCF #1909030

[1] A. Fert, V. Cros, and J. Sampaio, Skyrmions on the track, Nature Nanotechnol. 8, no. 3, p. 152-156 (2013). [2] J. Iwasaki, M. Mochizuki and N. Nagaosa, Current-induced skyrmion dynamics in constricted geometries, Nature Nanotechnology, 8, p. 742–747 (2013). [3] W. Kang, X. Zhang, and W. Zhao, Skyrmion-electronics: an overview and outlook, Proceedings of the IEEE, vol. 104, no. 10 (2016). [4] D. Bhattacharya and J. Atulasimha, Skyrmion-mediated voltage controlled switching of ferromagnets for reliable and energy-efficient two-terminal memory, ACS Appl. Mater. Interface, vol. 10, no. 20, p. 17455–17462 (2018). [5] D. Bhattacharya, S. A. Razavi, H. Wu, B. Dai, K. L. Wang, and J. Atulasimha, Creation and annihilation of non-volatile fixed magnetic skyrmions using voltage control of magnetic anisotropy, Nature Electronics, 3, p. 539-545 (2020).

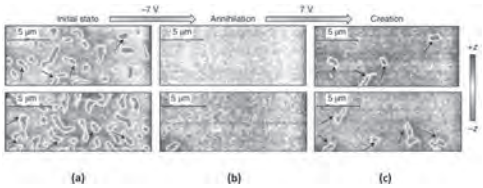

Fig. 1. Magnetization state before application of any electric field (a) and after application of negative (b), positive (c) voltage pulse [5]

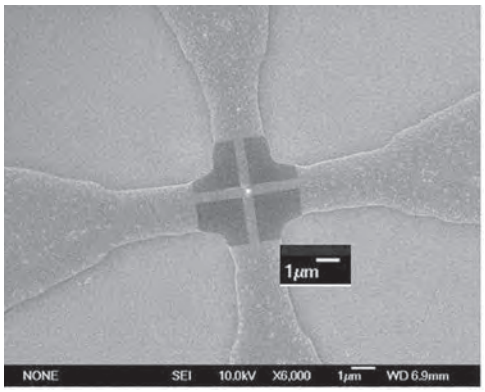

Fig. 2. Skyrmions to be studied in confined geometries

GOD-07. Get skyrmions back on track : Suppressing skyrmion Hall angle by material engineering or gate voltage. *C. Fillion*[1], R. Kumar[1,2], J. Fischer[1], L. Monnier[1], M. Belmeguenai[4], A. Fassatoui[3], S. Pizzini[3], L. Ranno[3], S. Auffret[1], I. Joumard[1], O. Boulle[1], G. Gaudin[1], L.D. Buda-Prejbeanu[1], C. Baraduc[1] and H. Béa[1] *1. SPINTEC, Grenoble, France; 2. Antaios, Meylan, France; 3. Institut NEEL, Grenoble, France; 4. Université Sorbonne Paris Nord, LSPM, CNRS, Villetaneuse, France*

In magnetic trilayers composed of heavy-metal/ferromagnet/oxide (HM/FM/MOx), the structural inversion asymmetry gives rise to the so-called interfacial Dzyaloshinskii-Moriya interaction (iDMI) [1]. This antisymmetric exchange interaction is at the origin of non-collinear spin textures, such as spin spirals or magnetic skyrmions [2] with chiral Néel domain-walls (DWs). Their dynamics is directly related to their chirality, imposed by the iDMI sign [3]. Thus, controlling their current-induced motion (CIM) driven by spin-orbit torques can be achieved by controlling the iDMI. In this study, we propose techniques to control the skyrmion motion in a Ta/FeCoB/TaOx trilayer, through the control of the iDMI sign and amplitude. The skyrmion motion can be controlled, or even reversed, either by modulation of deposition parameters or dynamically by applying a gate voltage. We have found that modulation of the oxidation state at the FeCoB/TaOx interface (Fig. 1(a-b)) leads to an inversion of the iDMI sign, as measured by Brillouin light scattering. This iDMI sign crossover is accompanied by an inversion of the skyrmion CIM direction. Skyrmion motion reversal can also be triggered by a gate voltage through the control of iDMI sign (Fig. 1(c-d)). Moreover, our micromagnetic simulations show that a fine control of the iDMI amplitude and sign is feasible on individual nanometer-size magnetic skyrmion without annihilating it (Fig. 2(a-c)). The dipolar energy prevents the spin texture from annihilation when iDMI is close to zero, leading to a stable Bloch skyrmion (Fig 2b). The angle of the moments inside the DWs (Fig. 2d) evolves continuously from 0° to 180° when varying the iDMI value. This allows a fine tuning of the skyrmion CIM direction (Fig. 2e), allowing to suppress the skyrmion Hall angle, otherwise detrimental for device applications.

[1] I. E. Dzyaloshinskii, J. Exptl. Theoret. Phys., (U.S.S.R.), vol. 46, p 960 (1964) [2] A. Fert, N. Reyren and V. Cros, Nature Review Materials, vol. 46, p. 6 (2017) [3] A. Thiaville, S. Rohart, É. Jué et al., EPL (Europhysics Letters), vol. 100, p. 57002 (2012)

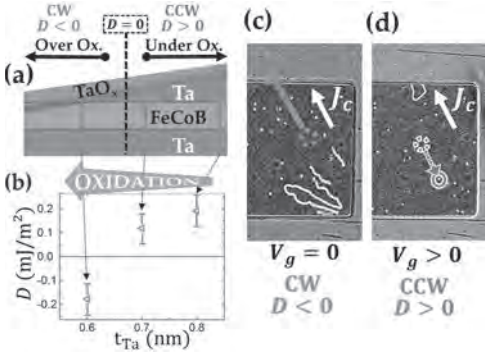

Figure 1: Control of iDMI sign: (a-b) Modulation of the FeCoB/TaOx interface oxidation and (c) Gate-controlled skyrmion motion (Magneto-Optical Kerr Effect images)

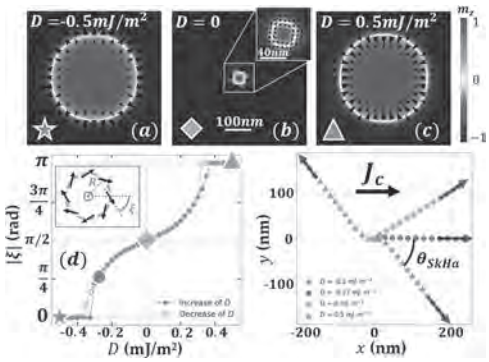

Figure 2: (a-c) Micromagnetic simulations: Adiabatic iDMI reversal on a nm-size magnetic skyrmion leading to (d) continuous transformation from CW (D>0) to CCW chirality (D>0). (e) Skyrmion's trajectory controlled by iDMI value

GOD-08. Nucleating Magnetic Skyrmions in Gr/Co/Pt Patterned Nanodots via the Voltage Controlled Magnetic Anisotropy. *P. Olleros-Rodríguez*[1], O. Chubykalo-Fesenko[2] and P. Perna[1] *1. IMDEA Nanoscience Institute, Madrid, Spain; 2. Materials Science Institute of Madrid (ICMM), Madrid, Spain*

Topologically protected chiral spin textures with dimensions in the nanometer scale, namely magnetic skyrmions, have been proposed as information carriers in the development of next-generation computational- and in non-traditional computing-devices. [1] In the recent years, the use of electric fields has gained a large interest due to the possibility of designing simple and low-consuming magnetoelectronic devices, based on the magnetolectric effect, that can be easily implemented in nowadays electronics enhancing its capabilities. [2] Here, we explore the possibility of nucleating magnetic skyrmions in HfO2/Gr/Co/Pt patterned nanodots by modifying the uniaxial anisotropy of the system via the voltage-controlled magnetic anisotropy (VCMA). [3] We conduct micromagnetic simulations in which the effect of the electric field is introduced by modifying the uniaxial anisotropy of the system as it is found for the VCMA case. The results reveals that there exists a dynamical path in which a magnetic skyrmion can be nucleated starting from an initial saturated state. This path requires the nucleation of an intermediate magnetic vortex state, obtained due to the reduction of the uniaxial anisotropy via the VCMA. Under proper conditions, the recovery of the anisotropy leads to a topological phase transition so the system does not recover its initial saturated configuration and evolves towards a final magnetic skyrmion. We show that this picture is valid for metastable and stable magnetic skyrmions, and that the nucleation probability is maximized when the variation of the anisotropy takes place in timescales large enough so that the system evolves in a quasi-equilibrium path in the configuration space. Moreover, we show that the use of a small magnetic field of a few mT pointing along the out-of-plane direction of the dot allows to increase largely the nucleation probability.

[1] Fert, A., Reyren, N. and Cros, V., 2017. Magnetic skyrmions: advances in physics and potential applications. *Nature Reviews Materials*, *2*(7), pp.1-15. [2] Song, C., Cui, B., Li, F., Zhou, X. and Pan, F., 2017. Recent progress in voltage control of magnetism: Materials, mechanisms, and performance. *Progress in Materials Science*, *87*, pp.33-82. [3] Amiri, P.K. and Wang, K.L., 2012, September. Voltage-controlled magnetic anisotropy in spintronic devices. In *Spin* (Vol. 2, No. 03, p. 1240002). World Scientific Publishing Company.

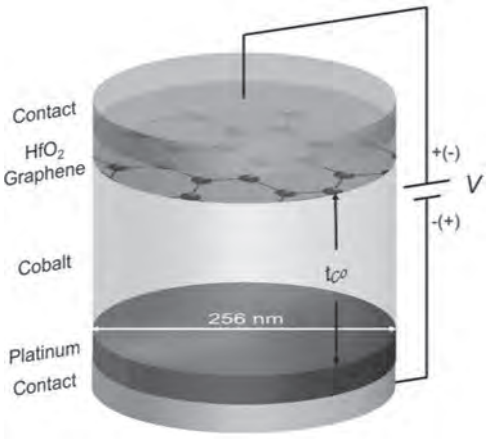

Fig. 1 Modelled HfO2/Gr/Co/Pt nanodot

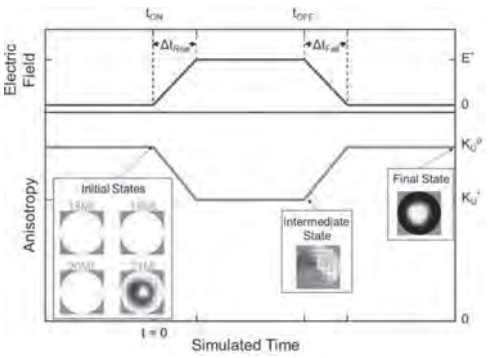

Fig. 2 Modelled electric field pulse (Blue line in the upper panel). The effect of the electric field is introduced in the model as a linear response of the magnetic anisotropy of the system (Red line in the bottom panel).

GOD-09. Creation and Annihilation of Skyrmions for Neuromorphic Computing Applications. A.H. Lone[1], A. Ganguly[2], D. Divyanshu[1], *S. Amara*[1] and H. Fariborzi[1] *1. CEMSE, King Abdullah University of Science and Technology, Jeddah, Saudi Arabia; 2. Khalifa University of Science and Technology, Abu Dhabi, United Arab Emirates*

Magnetic Skyrmions are topologically protected swirling structures induced by chiral interactions in non-centrosymmetric magnetic compounds or thin films with broken inversion symmetry [1]. The spintronic devices based on these textures promise increased density and energy efficient data storage due to small nanometric size and topological protection [2][3]. In this work we present the effect of DMI, surface anisotropy, magnetic field and spin orbit torque (SOT) on the creation and annihilation of the skyrmions. Fig.1 (a) shows that the skyrmion density is increased as we increase the magnitude of DMI coefficient from 1mJ/m^2 to 3mJ/m^2. But with increasing the surface anisotropy the density is reduced and skyrmions are annihilated at some threshold anisotropy K_{th} which is proportional to the magnitude of the DMI coefficient. Furthermore, the size of skyrmion decreases with increasing anisotropy as shown in Fig. 1(b). In Fig. 1 (c-d) we study the effect of external magnetic field on the skyrmions. Fig. 1 (c) shows the MOKE images of the fabricated sample depicting the transition of magnetic texture from Labriynth domains to skyrmions around 8 Oe. The skyrmion density increases proportionally with field till 20 Oe and begins to roll off after 20 Oe. These results are supported by MuMax simulations as shown in Fig. 1(d). These results suggest that by proper optimization of material parameters and stack geometry we can tweak the skyrmion density for its application in memory and logic. In Fig. 2(a) we show MTJ with skyrmions in the free layer, using SOT control we propose this device for its application in neuromorphic computing. The SOT manipulation of skyrmion size, density and motion is shown in Fig. 2 (b). Increasing current Ic via the heavy metal increases the skyrmion density from 21μm^{-2} (at 2×10^{11} A/m^2) to 40 21μm^{-2} (at 8×10^{11} A/m^2). Further increase in Ic results in decrease of the skyrmion density. Finally, we implement a simple neuromorphic circuit using the proposed device.

[1]. Albert Fert, Nicolas Reyren and Vincent Cros, "Magnetic Skyrmions: Advances in Physics and Potential Applications," *Nature Reviews Materials*, Vol. 2, No. 17031, June 2017. [2] Seonghoon Woo et.al, "Deterministic creation and annihilation of single magnetic skyrmion observed by direct time resolved X-ray microscopy," *Nature Electronics*, Vol.1, 288-296, May-2018. [3] K. Everschore et.al, "Perespective: Magnetic Skyrmions: Over of recent progress in an active research field," *Journal of App. Phy*, 124-240901, 2018.

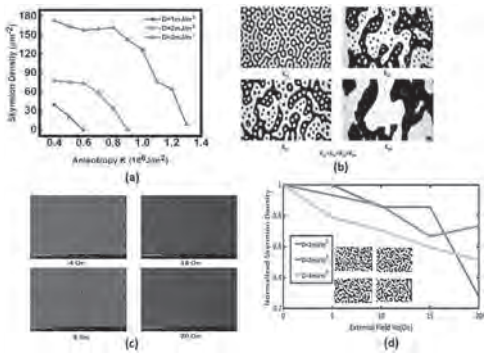

Fig. 1: (a) Skyrmion density vs anisotropy and DMI coefficient. (b) Density and size of skyrmion vs anisotropy. (c) MOKE images (d) MuMax simulations.

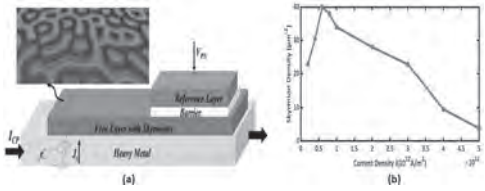

(a) Skyrmion-MTJ neuromorphic device. (b) Skyrmion density vs current density

GOD-10. Nanoscale room-temperature skyrmionic synapse for deep spiking neural networks. *R. Chen*[1], C. Li[1], Y. Li[1], J.J. Miles[1], G. Indiveri[2], S. Furber[1], V.F. Pavlidis[1] and C. Moutafis[1] *1. The University of Manchester, Manchester, United Kingdom; 2. University of Zurich and ETH Zurich, Zurich, Switzerland*

Skyrmion-based devices have been proposed as candidates for future low-power, ultra-dense nanocomputing and neuromorphic systems enabled by the characteristic properties (nanoscale size, non-volatility, robustness, low current density of propagation) of magnetic skyrmions, arising from their topology [1-2]. This is more pressing especially since the recent experimental demonstrations at room temperature (e.g., in technologically relevant magnetic multilayers (MMLs) [3-4]). At the same time, skyrmions have attracted extensive interest in CMOS-compatible nanodevices that can emulate biological synapses. Specifically, a multi-bit storage device using skyrmions as information carriers (bits) has been proposed in ideal conditions [5-6]. However, room temperature operation is required to integrate skyrmionic synapses in practical future devices. In our recent work [7], we propose a nanoscale skyrmionic synapse composed of MMLs that enables room temperature device operation (Fig. 1). We demonstrate that when embedding such MML skyrmionic synapses in a simple spiking neural network (SNN) with the spike-timing-dependent plasticity (STDP) learning rule, we can achieve only a ~75% classification accuracy in the MNIST handwritten data set. We propose that this performance can be significantly improved to ~98.61% by using a deep SNN with supervised learning

rules. Our results illustrate that the proposed skyrmionic synapse can be a competitive candidate for future energy-efficient neuromorphic computing and edge computing.

[1] A. Fert, et al., Nat. Nanotechnol., Vol. 8, p.152 (2013) [2] J. Sampaio, et al., Nat. Nanotechnol., Vol. 8, p.839, (2013) [3] C. Moreau, et al. Nat. Nanotechnol., Vol. 11, p.444 (2016) [4] O. Boulle, et al. Nat. Nanotechnol., Vol. 11, p.449 (2016) [5] S. Li, et al., Nanotechnology, Vol. 28, p.31LT01 (2017) [6] T. Bhattacharya, et al., IEEE Access, Vol. 7, p.5034 (2018) [7] R. Chen, et al., Phys. Rev. Appl. Vol. 14, p.014096 (2020)

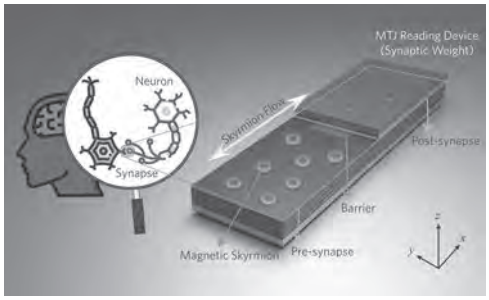

Fig. 1. Schematic of biological neurons connected with a synapse, and the proposed nanoscale multilayer skyrmionic synapse device. The multilayer structure enables room-temperature operations.

GOD-11. Topology-Driven Spin-Diode Reversal Effect: a New Degree of Freedom Towards Vortex-Based Spin-Torque Oscillators in Neuromorphic Computing. *C. Chopin*[1], L. Martins[2], L. Benetti[2], S. de Wergifosse[1], A. Jenkins[2], R. Ferreira[2] and F. Abreu Araujo[1] *1. IMCN / BSMA, Université Catholique de Louvain, Louvain-la-Neuve, Belgium; 2. International Iberian Nanotechnology Laboratory, Braga, Portugal*

It has been recently shown that spin-torque vortex oscillators (STVOs) can be functionalized as nano-neurons and solve complex neuromorphic computing tasks [1-4]. While the different studies show that STVOs are performing very well on cognitive tasks like speech recognition, none of the studies explains the added value of the vortex-based nano oscillators in a rigorous theoretical way (some show a comparison to a simulated phenomenological oscillator). Here we propose a semi-analytical model [5] that fully describes the vortex dynamics with its detailed non-linearities that compares quantitatively with the well established tools performing micromagnetic simulations. The advantage of this technique is that the vortex dynamics is computed much faster than with micromagnetic simulation, namely by a factor of about 2.4 million. When an AC current is passing through a magnetic tunnel junction (MTJ) for instance, it may give rise to an oscillation of the magnetization due to the spin-transfer torque effect. This oscillation results in the variation of the resistance due to the magneto-resistance effect. The combination of this oscillating resistance and an external excitation (RF signal) giving rise to an additional AC current leads to a DC voltage component, and this rectification is called the spin-diode effect [6]. With our semi-analytical model, we were able to simulate the spin-diode effect in seconds instead of months or years and discover a new degree of freedom for the functionalization of our STVOs. The degree of freedom that interests us is related to one of the topological charges of the magnetic vortex, i.e. the vortex chirality. This topological charge corresponds to the magnetization in-plane curling direction of the vortex and can be either +1 (counter-clock-wise) or -1 (clock-wise). Combining the relative orientation of the chirality with the Amp'ere-Oersted field generated by the excitation current, it's possible to perform a spin-diode reversal effect as shown in Fig. 1. Finally, as seen in Fig. 1, the reversal effect is confirmed experimentally using a magnetic tunnel junction for which the magnetic ground state is a magnetic vortex

[1] J. Torrejon, *et al.*, Nature, vol. 547, p. 428–431 (2017) [2] M. Romera, *et al.*, Nature, vol. 563, p. 230–234 (2018) [3] M. Riou, *et al.*, *Phys. Rev. Applied*, vol. 12, p. 024049, (2019) [4] F. Abreu Araujo, *et al.*, Scientific Reports, vol. 10, p. 1-11 (2020) [5] F. Abreu Araujo, C. Chopin, S. de Wergifosse, submitted to Scientific Reports (2021) [6] A. Tulapurkar, *et al.* Nature, vol. 438, p. 339–342 (2005)

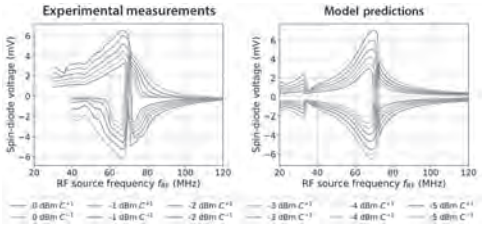

Comparison between experimental measurements and model predictions.

GOD-12. Skyrmionic Interconnect Device. *R. Chen*[1], Y. Li[1], V.F. Pavlidis[1] and C. Moutafis[1] *1. The University of Manchester, Manchester, United Kingdom*

Skyrmionic devices show potential for low-power-low-heat nanocomputing with multiple information carriers, enabled by quasi-particles with a topological charge N, including skyrmions (N=±1) [1] and skyrmioniums (N=0) [2-3]. This is more pressing since the co-existence of stable and high-degree skyrmionic configurations with arbitrary value and sign of N has been experimentally demonstrated in liquid crystals and numerically predicted in ferromagnetic systems [4-5]. Hitherto, skyrmionic on-site memory, nanocomputing, and neuromorphic components have increasingly been investigated [6-7]. However, the "missing component" in skyrmionics so far has been an all-magnetic skyrmion-based interconnect, which may be relevant to future spintronic neuromorphic computing and quantum computing hardware. Our recent work investigates the dynamics of magnetic skyrmionic quasi-particles for a new concept for skyrmionic nanodevices, i.e., skyrmionic interconnect device [8]. We propose encoding sequences of information by using distinct skyrmionic quasi-particles as information carriers in a single device, such that we exploit topological filtering in order to enable automatic signal multiplexing (Fig. 1), circumventing the need for control signals. This results in saving signal routing by 50%, a major benefit compared to modern CMOS devices. We then propose to strategically etch notches in the device to introduce pipelining, which significantly boosts the signal throughput of the device. Our proposal widens the possibilities for spintronics-based nanocomputing.

[1] A. Fert et al., Nat. Nanotechnol., Vol. 8, p.152 (2013) [2] A. N. Bogdanov, et al. J. Magn. Magn. Mater. Vol. 195, p.182 (1999) [3] B. Göbel et al., Sci. Rep., Vol. 9, p.12119 (2019) [4] D. Foster, et al., Nat. Phys., Vol. 15, p.655 (2019) [5] F. N. Rybakov, et al., Phys. Rev. B, Vol. 99, p.064437 (2019) [6] X. Zhang, et al. J. Phys. Condens. Matter Vol. 32, p.143001 (2020) [7] R. Chen, et al., Phys. Rev. Appl., Vol. 14, p.014096 (2020) [8] R. Chen, et al., Phys. Rev. Research, Vol. 2, p.043312 (2020)

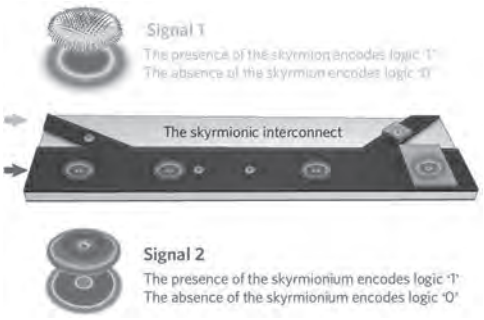

Fig. 1. Schematic drawing of the proposed skyrmionic interconnect device, and spin texture of a Néel skyrmion and a skyrmionium.

Session GOE
SKYRMIONS IN ANTIFERROMAGNETS AND FERRIMAGNETS

Steven P Bennett, Chair
U.S. Naval Research Laboratory, Washington, DC, United States

CONTRIBUTED PAPERS

GOE-01. Phase Coexistence and Transitions between Anti- and Ferromagnetic States in a Synthetic Antiferromagnet. *C.E. Barker*[1], C. Barton[2], E. Haltz[1], O. Kazakova[2], T. Moore[1] and C. Marrows[1] *1. School of Physics and Astronomy, University of Leeds, Leeds, United Kingdom; 2. Quantum Technologies, National Physical Laboratory, Teddington, United Kingdom*

Skyrmions—topologically protected vortex-like spin structures—have been proposed as the new information carriers in racetrack memory devices [1]. In order to realise such devices a small size, high speed of propagation, and minimal deflection angle are required. Modelling has shown that synthetic antiferromagnets (SAFs) present the ideal materials system to realise these aims [2]. However, their magnetic compensation makes observation of skyrmions difficult and indeed this was only recently achieved [3]. There is thus significantly more to understand about the behaviour of synthetic antiferromagnets and the skyrmions therein. Here we present a comprehensive magnetic force microscopy (MFM) study of a SAF multilayer composed of 20 magnetic layers alternating between CoB and CoFeB each coupled antiferromagnetically with a Ru spacer layer to the one above and below. As shown in the hysteresis loop presented in Fig. 1 the SAF undergoes a phase transition between the compensated antiferromagnetic state and its field-polarised ferromagnetic state as a field is applied. MFM shows that in our samples this is as a result of defect-driven bubble nucleation where FM ordered regions nucleate and then expand to cover the entire film. Once the FM regions exceed a critical size they collapse into a skyrmion/stripe domain pattern and so retain a net zero magnetisation. At a narrow range of fields, e.g. as shown in Fig. 2 we observe a phase coexistence between the compensated AF state and the net-zero magnetisation FM state. As the magnetic field is increased we go on to observe isolated skyrmions at fields below saturation as expected in a FM system. These results give perspective on the ferromagnetic nature of skyrmions observed in systems at fields just below saturation and can help to inform the observation of true antiferromagnetic skyrmions.

[1] S. P. Parkin *et al.*, Science, 320, 190 (2008) [2] X. Zhang *et al.*, Nature Communications, 7, 10293 (2016) [3] W. Legrand *et al.*, Nature Materials, 19, 34 (2020)

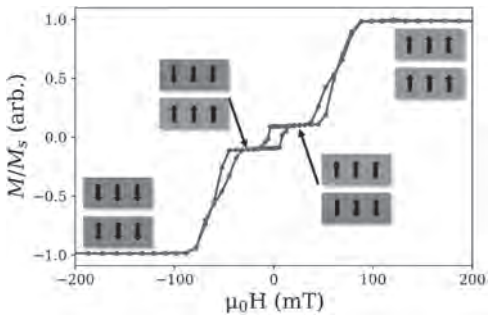

Fig. 1. Hysteresis loop of our SAF system along with depiction of the magnetic configuration of a pair of layers at each of the steps.

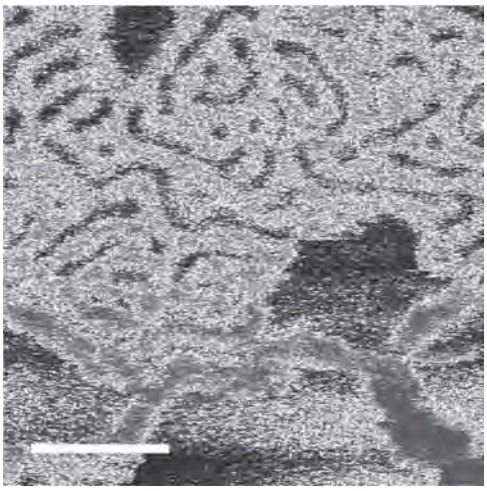

Fig. 2. Mixed phase state of our SAF system acquired at 43 mT, where red/blue texture is FM domain structure that has expanded from nucleated bubbles and the regions of uniform blue are the remaining SAF areas. Scale bar is 1 μm.

GOE-02. Observation of skyrmion and stripe domain phases in synthetic antiferromagnetic coupled multilayer systems using Lorentz transmission electron microscopy. *K. Fallon*[1], D. McGrouther[1], A. Silinga[1], E. Haltz[2], C.E. Barker[2], T. Moore[2], G. Burnell[2], C. Marrows[2] and S. McVitie[1] *1. SUPA, School of Physics and Astronomy, University of Glasgow, Glasgow, United Kingdom; 2. School of Physics and Astronomy, University of Leeds, Leeds, United Kingdom*

Skyrmions in ferromagnetic multilayer systems show promise for numerous technological applications, however skyrmions in synthetic antiferromagnetic systems (SAF) are; i) smaller than their ferromagnetic counterparts and ii) have no skyrmion Hall effect. Lorentz transmission electron microscopy (TEM) images magnetic textures with contrast arising from the thickness-projected magnetic induction of the sample [1]. A balanced SAF results in complete cancellation of the oppositely magnetised layers. We have performed micromagnetic simulations of SAF skyrmions that show this to be true with no contrast predicted at zero applied field. However application of a field perpendicular to the stack results in a size differential of the skyrmions in the oppositely magnetised layers. This reflects the circular symmetry of the skyrmion and a donut-like region remains as a signature of the skyrmion in projection. The simulations demonstrate that it should be possible to study SAF skyrmions with TEM. SAF skyrmions have been previously been imaged with magnetic force microscopy due to the cancelling effect of the AF coupled layers [2]. The sample studied has composition (Ångstrom thickness): Ta(50)/[Ru(7)/Pt(8)/CoFeB(10)/Ru(7)/Pt(8)/CoB(16)]x10/Ru(7)/Pt(20) with the CoFeB/CoB layers designed to have equal moment. Fresnel images (defocused TEM) of this system are presented in Figs 1 and 2. As the material is magnetised principally out of plane, the sample is tilted by 25° to generate contrast. No contrast is observed at zero applied field (not shown). Only when the field in increased to 35 mT, as

seen in Fig. 1, do we see a dense array of round features appearing (~ 90 nm diameter). SQUID-VSM measurements indicate the AF coupling is dominant at this field. Hence we believe these are SAF skyrmions. As the field is increased further, 125 mT in Fig. 2, the contrast level increases and we observe the magnetic state evolving into a stripe domain phase which is typical of the SAF in the ferromagnetic phase at higher fields. The domain periodicity is 200 nm.

[1] Fallon, K., Hughes, S., Zeissler, K. et al. Controlled Individual Skyrmion Nucleation at Artificial Defects Formed by Ion Irradiation. Small, 16, 1907450, (2020). [2] Legrand, W., Maccariello, D., Ajejas, F. et al. Room-temperature stabilization of antiferromagnetic skyrmions in synthetic antiferromagnets. Nat. Mater. 19, 34–42 (2020).

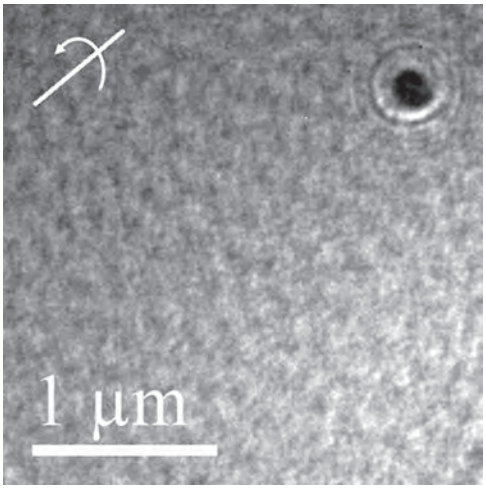

Fig. 1. Fresnel image of SAF skyrmions in field of 35 mT. The line shows the tilt axis, tilt angle is 25°.

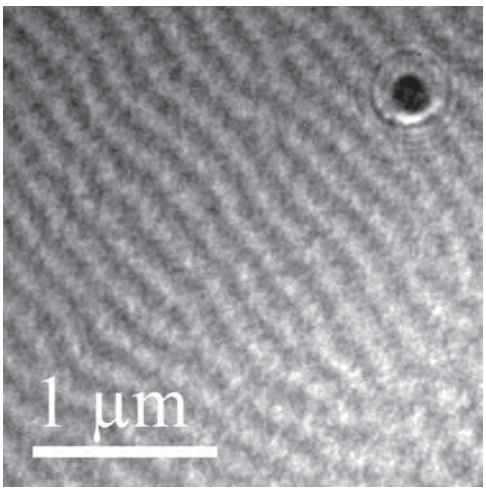

Fig. 2. Fresnel image of stripe domains at 125 mT. (Same tilt as Fig. 1).

GOE-03. Synthetic antiferromagnet with built-in planar asymmetry.
K. Wang[1] and G. Xiao[1] *1. Department of Physics, Brown University, Providence, RI, United States*

Inversion symmetry breaking (ISB) is of great significance in governing many interesting physics. For example, the interfacial Dzyaloshinskii-Moriya interaction (DMI) exists at the heavy metal/ferromagnet (HM/FM) interface with the ISB along the sample normal direction, which holds promises for design and control of chiral spin textures in low-dimensional magnets with efficient current-driven dynamics [1,2]. In this talk, we discuss about a synthetic antiferromagnet (SAF) with built-in planar asymmetry which is attributed to both variable ferromagnetic-layer thickness and the spacer thickness. First we show how the sign and strength of the interlayer exchange coupling (IEC) and magnetic configurations depend on the ferromagnetic-layer thicknesses and the spacer thickness [3]. Interestingly, the IEC can be efficiently modified via changing the ferromagnetic-layer thickness which is essential to advancing magnetic memory and sensing [4] applications with efficient controls. Furthermore, we show the demonstration of the existence of interlayer DMI in our SAF with the built-in planar asymmetry, which supports a chiral magnetization across the SAF. We present the study of current-induced spin-orbit torque (SOT) switching of the chiral magnetization across the SAF and analyse the interlayer DMI's effects on magnetization and its switching through a combination of experimental and numerical studies [5]. Based on our studies, we will give an outlook of potential applications of our findings in future SOT and domain wall-based devices.

[1] K. Wang, L. Qian, W. Chen, S.-C. Ying, G. Xiao, and X. Wu, Spin torque effect on topological defects and transitions of magnetic domain phases in Ta/CoFeB/MgO, Phys. Rev. B 99, 184410 (2019). [2] K. Wang, L. Qian, S.-C. Ying, G. Xiao, and X. Wu, Controlled modification of skyrmion information in a three-terminal racetrack memory, Nanoscale 11, 6952 (2019). [3] K. Wang, L. Qian, S.-C. Ying, and G. Xiao, Manipulation of the interlayer exchange coupling in perpendicular magnetized thin films via tunable magnetic-layer and spacer thicknesses, Phys. Rev. B 102, 144430 (2020). [4] K. Wang, Y. Zhang, and G. Xiao, Anomalous Hall sensors with high sensitivity and stability based on interlayer exchange-coupled magnetic thin films, Phys. Rev. Appl. 13, 064009 (2020). [5] K. Wang, L. Qian, S.-C. Ying, and G. Xiao, Spin-orbit torque switching of chiral magnetization across a synthetic antiferromagnet, Commun. Phys. 4, 1 (2021).

GOE-04. Skyrmions in synthetic antiferromagnets and their nucleation using electrical current and ultrafast laser illumination.
R. Juge[1], N. Sisodia[1], J. Urrestarazu Larrañaga[1], Q. Zhang[1], V. Pham[1], R. Belkhou[2], N. Mille[2], N. Novakovic[3], F. Kronast[3], S. Wintz[6], M. Weigand[3], J. Gräfe[6], M. Belmeguenai[4], L.D. Buda-Prejbeanu[1], L. Ranno[5], G. Gaudin[1] and *O. Boulle*[1] *1. Spintec, Grenoble, France; 2. Soleil Synchrotron, Saint-Aubin, France; 3. Helmholtz-Zentrum Berlin für Materialien und Energie, Berlin, Germany; 4. Laboratoire des Sciences des Procedés et des Matériaux, Université Paris 13, Villetaneuse, France; 5. Institut Néel, Grenoble, France; 6. Max Planck Institute for Intelligent Systems, Stuttgart, Germany*

Magnetic skyrmions are topological spin textures which hold great promise as nanometer scale information carriers in memory and logic devices. While room temperature magnetic skyrmions and their current induced manipulation were recently demonstrated [1–5], the stray field resulting from their magnetic moment as well as their topological charge limit their minimal size and reliable motion in tracks. Antiferromagnetic (AF) skyrmions allow to lift these limitations owing to their vanishing magnetic moment and canceled topological charge, promising room temperature ultrasmall skyrmions, fast dynamics and insensitivity to external magnetic fields. While room temperature AF spin textures have been recently demonstrated [6–9], the observation and controlled nucleation of AF skyrmions operable at room temperature in industry compatible AF material systems is still lacking. Here we demonstrate that isolated skyrmions can be stabilized at zero field and room temperature in a fully compensated SAF. SAF based on (Pt/Co/Ru/Pt/Co/NiFe) multilayers with vanishing magnetization were grown using magnetron sputtering. Using X-ray microscopy XMCD-PEEM and STXM, we observe chiral Néel domain walls as well as SAF skyrmions at zero external field and room temperature, with average diameters of 200 nm. By employing the corresponding X-ray energy, we are able to resolve the skyrmions in the different SAF layers and demonstrate their AF alignment. Magnetic microscopy, micromagnetic simulations and an analytical model confirm the SAF skyrmion homochirality and allow the identification of the physical parameters controlling their size and stability. We also show that the SAF skyrmions can be nucleated at zero magnetic field using local current injection as well as ultrafast laser excitations. These results pave the way for the use of SAF skyrmions in skyrmion based devices.

[1] O. Boulle *et al.*, Nat Nano 11, 449 (2016). [2] R. Juge *et al.*, Phys. Rev. Applied 12, 044007 (2019). [3] S. Woo *et al.*, Nat Mater 15, 501 (2016). [4] W. Jiang *et al.*, Nature Physics (2016). [5] C. Moreau-Luchaire *et al.*, Nat Nano 11, 444 (2016). [6] S. Gao *et al.*, Nature 586, 37 (2020). [7] H. Jani *et al.*, Nature 590, 74 (2021). [8] W. Legrand *et al.*, Nat. Mater. 1 (2019). [9] T. Dohi *et al.*, Nat Commun 10, 1 (2019). [10] Juge et al., submitted

GOE-05. Magnetic states in a triangular antiferromagnet – a model for $CoNb_3S_6$. *O. Heinonen*[1], R.A. Heinonen[2], I. Martin[1] and H. Park[1]
1. Argonne National Laboratory, Lemont, IL, United States; 2. University of Rome Tor Vergata, Rome, Italy

Triangular and kagome antiferromagnets (AFMs) provide for interesting and rich magnetic structures because of geometric frustration. Recently, a number of triangular and kagome AFMs have also been shown to exhibit a large anomalous Hall effect (AHE). This is attributed to Berry curvature effects connected to non-trivial topology of the electronic structure. $CoNb_3S_6$ (CNS) is a stacked triangular antiferromagnet with triangular planes of Co intercalated with NbS_2 planes. The crystallographic unit cell breaks inversion symmetry with consecutive Co planes offset by half a lattice vector. The broken inversion symmetry allows for a Dzyaloshinskii-Moriya interaction (DMI) that by symmetry must have its vector in the Co plane, not perpendicular to it as is the case in kagome AFMs. It was recently shown [1, 2] that CNS exhibits a large AHE and a very small uniform magnetic out-of-plane moment below the Neel temperature; the magnetic susceptibility was also found to be very small, both in-plane and out-of-plane. It is clear that the magnetic structure cannot be collinear AFM because of the large AHE, and the small out-of-plane moment cannot explain the AHE. However, the combination of form of the DMI and the crystallographic unit cell leads to another potential source of frustration and potentially incommensurate magnetic structures that may contribute to AHE. We have constructed a simple model of CNS, consisting of near-neighbor AFM, DMI interactions and biquadratic exchange, and single-ion anisotropy. We used finite-temperature atomistic modeling as well as a reduced 2D model to study the 0 T phase diagram. Increasing DMI drives an in-plane spin spiral with an out-of-plane magnetic component. The in-plane wave vector is typically incommensurate with the lattice spacing for non-zero D and moves inward from the Brillouin zone boundary with increasing D. Both in-plane and out-of-plane susceptibilities are very small until a large applied field drives a first-order transition to a fully polarized state.

[1] N. Ghimire et al. Nature Comm. 9, 1 (2018). [2] G. Tenasini et al., Phys. Rev. Research 2, 023051 (2020)

GOE-06. Direct imaging of chiral domain walls in ferrimagnetic alloys. *B. Seng*[1,2], D. Schönke[1], J. Yeste[1], R.M. Reeve[1], N. Kerber[1], J. Bello[2], F. Kammerbauer[1], M. Bhukta[1], N. Bergeard[3], T. Ferté[3], C. Boeglin[3], F. Radu[4], R. Abrudan[4], T. Kachel[4], D. Lacour[2], S. Mangin[2], M. Hehn[2] and M. Kläui[1] *1. Institut für Physik, Johannes Gutenberg Universität, Mainz, Germany; 2. Institut Jean Lamour, Nancy, France; 3. Institut de Physique et Chimie des Matériaux de Strasbourg, Strasbourg, France; 4. Helmholtz-Zentrum Berlin für Materialien und Energie, Berlin, Germany*

Magnetic skyrmions are topological spin textures that can be stabilized by the Dzyaloshinskii-Moriya interaction [1,2]. There are particularly suitable for next generation spintronics devices, like the skyrmion-based racetrack memory [3]. Recent studies confirmed their current-driven skyrmion dynamics in ultrathin ferromagnets via spin-orbit torques [4], where the chirality and spin texture of the skyrmions are key. However, the topological Magnus effect leads to a transverse motion of ferromagnetic skyrmions due to their non-zero topological charge [5], which is disadvantageous for devices. Antiferromagnetically exchange-coupled skyrmions or compensated ferrimagnets could suppress this effect owing to an overall zero topological charge [6]. Here we explore a GdFeCo-based ferrimagnet system with perpendicular magnetic anisotropy. We demonstrate that in this system the chirality of worm domains as well as a magnetic skyrmionium can be observed using scanning electron microscopy with polarization analysis (SEMPA) (Figure) [7]. The high spatial resolution magnetic imaging technique reveals the domain wall (DW) spin structure as a function of temperature, with the observed structures found to be pure Néel-type spin textures, which is promising for devices. From the images we extract the DW width as a function of the temperature and we calculate the exchange stiffness for the system. Figure: Determination of the magnetization direction inside the DW of different ferrimagnetic chiral spin textures. a) The direction of the in-plane magnetization in the DW is displayed, as defined by the color wheel in the bottom left corner of the image. Scale bar in a): 1 μm. b) Distribution of the direction of the in-plane magnetization in the DW with respect to the local tangent at RT: angle Ψ (see inset where a clockwise angle is defined as negative following the usual convention). A Gaussian fit indicates a central value around −90°. c) Absolute in-plane magnetization intensity with the DW skeleton displayed in white and d) direction of the in-plane magnetization in the DW of a ferrimagnetic skyrmionium at 320 K. Scale bars in c,d): 500 nm. Extracted from [7].

[1] I. Dzyaloshinskii, J. Phys. Chem. Solids 4, 241 (1958). [2] T. Moriya, Phys. Rev. 120, 91 (1960). [3] R. Tomasello *et al.*, Sci. Rep. 4, 6784 (2015). [4] S. Woo *et al.*, Nat. Mater. 15, 501 (2016). [5] K. Litzius *et al.*, Nat. Phys. 13, 170 (2017). [6] Y. Hirata *et al.*, Nat. Nanotechnol. 14, 232 (2019). [7] B. Seng *et al.*, Adv. Funct. Mater., 202102307 (2021).

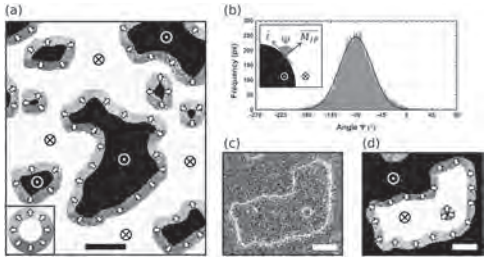

GOE-07. Role of rare-earth element on the Dzyaloshinskii-Moriya Interaction in amorphous ferrimagnets. *D.H. Suzuki*[1] and G.S. Beach[1]
1. Materials Science and Engineering, Massachusetts Institute of Technology, Cambridge, MA, United States

Many spintronic devices require chiral spin textures such as skyrmions or homochiral domain walls. Chiral spin textures are stabilized by the Dzyaloshinskii-Moriya Interaction (DMI), an indirect exchange interaction arising from broken inversion symmetry and by high spin-orbit coupling in an adjacent heavy metal layer. As a result, control of DMI is critical to engineering spintronic devices. Amorphous rare-earth transition-metal ferrimagnets are a technologically interesting class of spintronic materials due to their small stray fields relative to ferromagnets, resulting in smaller skyrmions, and high domain wall velocities in films near their angular momentum compensation point.[1] Previous work has measured the DMI using different heavy metal layers in ferro- and ferrimagnetic systems[2-3], however, the DMI resulting from ferrimagnet/heavy metal interfaces has yet to be fully explored. In particular, the rare-earth element's contribution to DMI is not well understood in rare-earth transition-metal ferrimagnets. In this study, we measure the DMI as a function of Gd content in Pt/GdCo thin films. Films were prepared by DC magnetron sputter deposition on Si wafers with layer structure: Ta(4nm)/Pt(4nm)/GdCo(3nm)/Ta(4nm)/Pt(2nm). The top Ta(4nm)/Pt(2nm) serves as an anti-oxidation cap. The composition of the films range from 27 – 47 at.% Gd. The DMI is determined by a combination of Brillouin light scattering and domain wall motion experiments. We find that the DMI strength monotonically decreases with increasing Gd content. Additionally, the magnitude of the DMI strength is significantly reduced compared to previous measurements of DMI in ultrathin Pt/Co systems, even accounting for the increased thickness of the GdCo layer in our films.[4] This suggests that Gd does not contribute to the DMI but rather dilutes the effective DMI arising from the Pt/GdCo interface and that the DMI primarily arises from the Pt-Co interaction in Pt/GdCo systems.

[1] L. Caretta, M. Mann, F. Buttner et al., Nature Nanotechnology, Vol. 13, p.1154-1160 (2018) [2] A. Hrabec, N. Porter, A. Wells et al., Physical Review B, Vol. 90, p.20402 (2014) [3] Y. Quessab, J. Xu, C. Ma et al., Scientific Reports, Vol. 10, p.1-8 (2020) [4] M. Belmeguenai, J. Adam, Y. Roussigné et al., Physical Review B, Vol. 91, p.180405 (2015)

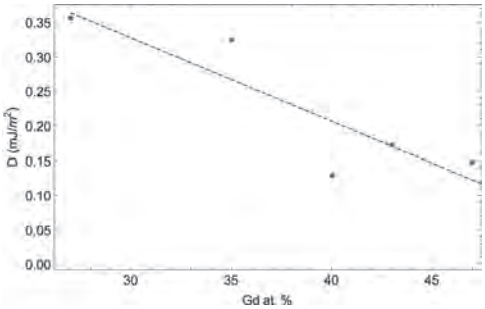

Fig. 1. Measured DMI versus Gd content in 3nm GdCo films, demonstrating the strong dependence of DMI on Gd content.

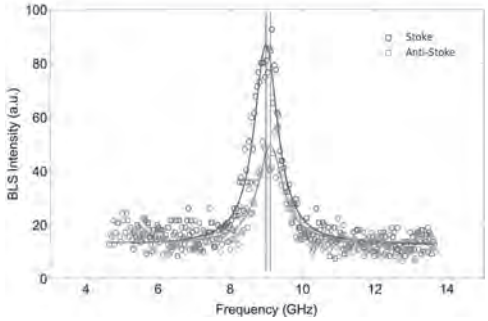

Fig. 2. BLS spectrum of GdCo showing Stokes/Anti Stokes frequency splitting, indicating the presence of DMI in the film.

GOE-08. Robust and tunable rare-earth ferrimagnetic systems for dense, small and high-mobility skyrmions at room temperature.

T. Dutta[2], A. Mandru[2], O. Yildirim[2] and *H.J. Hug*[2,1] *1. University of Basel, Basel, Switzerland; 2. Empa, Swiss Federal Laboratories for Materials Science and Technology, Dübendorf, Switzerland*

Skyrmions are excellent candidates for racetrack memory and synaptic devices[1,2]. However, their movement in ferromagnets (FM) is hindered by their transverse movement (skyrmions Hall effect, SkHE) and pinning at defects[3]. Ferrimagnetic (FiM) systems are proposed to overcome the transverse movement, while amorphous ferromagnets systems such as CoFeB have already shown significant reduction in pinning[4,5] but yield skyrmions with larger diameters. Therefore, we propose a robust amorphous-ferrimagnetic system to bring forth the best of the two. So far, skyrmions have been generated in amorphous ferrimagnetic systems such as Pt/GdFeCo/MgO[5] and Pt/CoGd/TaO[6] where SkHE and pinning were considerably mitigated. However, these systems lack a certain robustness owing to the rapidly diminishing DMI at the FiM/Heavy metal (HM) interface with increase in rare-earth (RE) content. This hinders the concurrent attainment of small size, desired density, room temperature (RT) stability and high–mobility in skyrmions. To overcome this we followed a strategy previously used to generate dense, small skyrmions in FM[7]- employing two DMI generating interfaces of Ir/Fe-FiM and Co-FiM/Pt. The two DMIs at the interfaces being additive, strengthens the total DMI and provides a robust, tunable FiM system capable of addressing the above-mentioned challenges. Figure 1 shows the schematic, hysteresis loops and MFM images of a few of these multilayers. By tuning the rare-earth/3d transition magnetic material ratio and thicknesses in both the FiM layers, along with systematic change in the Tb/Gd ratio (tunes anisotropy) we were able to achieve a robust multilayer FiM system, with small (~50 nm), high-density skyrmions, and up to 88% reduction in the necessary energy to nucleate them. For instance, in 1c we show a considerably high-density of skyrmions, around ~72 nm in diameter, while the magnetization and nucleation fields are reduced by 70% and 88% respectively. Our multilayer system serves as a suitable template for designing desired skyrmion densities, sizes and reduced SkHE along with lower energy requirements for nucleation and possibly movement.

[1] A. Fert, V. Cros, and J. Sampaio, Nat Nanotechnol 8 (3), 152 (2013). [2] J. Grollier, D. Querlioz, and M. D. Stiles, Proc IEEE Inst Electr Electron Eng 104 (10), 2024 (2016). [3] M. Bacani, M. A. Marioni, J. Schwenk et al., Sci Rep 9 (1), 3114 (2019). [4] K. Everschor-Sitte, J. Masell, R. M. Reeve et al., J Appl Phys 124 (24) (2018). [5] S. Woo, K. M. Song, X. Zhang et al., Nat Commun 9 (1), 959 (2018). [6] L. Caretta, M. Mann, F. Buttner et al., Nat Nanotechnol 13 (12), 1154 (2018). [7] A. Soumyanarayanan, M. Raju, A. L. Gonzalez Oyarce et al., Nat Mater 16 (9), 898 (2017).

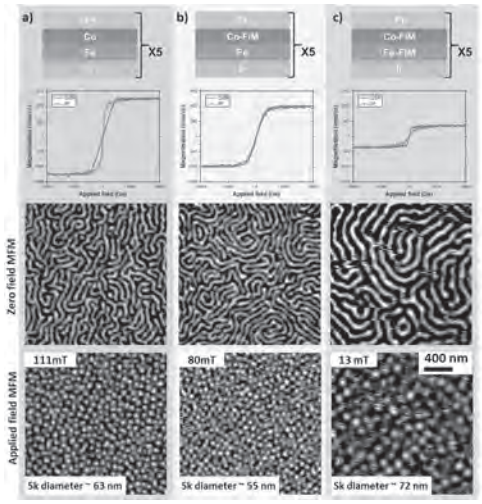

Figure 1: Schematic, hysteresis loops, MFM (same scale in all images) of a) FM and b)-c) FiM

Session GOF
SKYRMIONS, ANTISKYRMIONS AND TOPOLOGY

Max Hirschberger, Chair
The University of Tokyo, Tokyo, Japan

CONTRIBUTED PAPERS

GOF-01. Dipolar-Stabilized First and Second-Order Antiskyrmions in Ferrimagnetic Multilayers. *M. Heigl*[1], S. Koraltan[2], M. Vanatka[3], C. Abert[2,4], M. Urbanek[3], D. Suess[2,4] and M. Albrecht[1] *1. Institute of Physics, University of Augsburg, Augsburg, Germany; 2. Faculty of Physics, University of Vienna, Vienna, Austria; 3. CEITEC BUT, Brno University of Technology, Brno, Czechia; 4. Research Platform MMM Mathematics - Magnetism - Materials, University of Vienna, Vienna, Austria*

Skyrmions and antiskyrmions are topologically protected spin structures with opposite vorticities. Particularly in coexisting phases, these two types of magnetic quasiparticles may show fascinating physics and potential for spintronic devices. While skyrmions are observed in a wide range of materials until now antiskyrmions were exclusive to materials with D_{2d} symmetry [1]. In our recent work, we have shown first and second-order antiskyrmions stabilized by magnetic dipole-dipole interaction in Fe/Gd-based multilayers [2]. Using Lorentz transmission electron microscopy imaging, we observed coexisting first and second-order antiskyrmions, Bloch skyrmions, and type-2 bubbles (Fig. 1) and determine the range of material properties and magnetic fields where the different spin objects form and dissipate. Phase diagrams of the spin objects were created in dependence on the magnetic out-of-plane field, temperature, saturation magnetization, and uniaxial magnetic anisotropy. We performed micromagnetic simulations to obtain more insight into the studied system and conclude that low values of saturation magnetization and uniaxial magnetic anisotropy lead to the existence of this zoo of different spin objects and that they are primarily stabilized by dipole-dipole interaction. Further, we investigated the nucleation process of antiskyrmions experimentally and theoretically revealing the necessity of a crossing point of three magnetic stripe domains to form an isolated antiskyrmion with an out-of-plane magnetic field. The previous unobserved second-order antiskyrmions and the disclosed coexistence of antiskyrmions and skyrmions potentially reachable for a whole range of different materials provide great potential for further studies on quasi-particle interactions, spin dynamics as well as for possible future applications in spintronics.

[1] A. K. Nayak, V. Kumar, T. Ma et al., Nature, Vol. 548, p.561 (2017)
[2] M. Heigl, S. Koraltan, M. Vanatka et al., Nat. Commun., Vol. 12, p.2611 (2021)

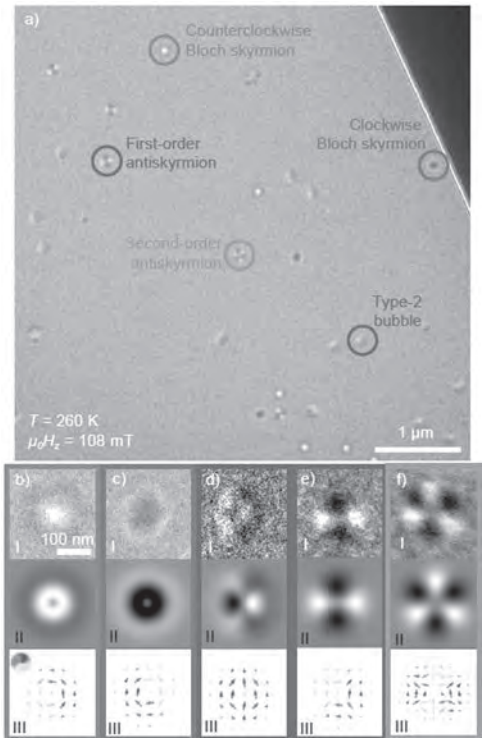

Fig. 1. Underfocused LTEM image of $[Fe/Ir/Gd]_2/[Fe/Gd]_{76}/[Fe/Ir/Gd]_2$ showing five different coexisting spin objects (a). Bloch skyrmion with counter- (b) and with clockwise rotation (c), type-2 bubble (d), first-order antiskyrmion (e), and second-order antiskyrmion (f). Zoomed-in spin objects (b-f, I) and simulated LTEM contrast (b-f, II) caused by the theoretical spin textures (b-f, III).

GOF-02. Real-space imaging of topological skyrmions/antiskyrmions and their transformation. *L. Peng*[1], R. Takagi[1,2], K. Karube[1], W. Koshibae[1], J. Masell[1], K. Shibata[1,3], F. Kagawa[1,4], S. Seki[1,2], N. Nagaosa[1,4], Y. Tokura[1,4], Y. Taguchi[1] and X. Yu[1] *1. RIKEN Center for Emergent Matter Science (CEMS), Wako, Japan; 2. Department of Applied Physics and Institute of Engineering Innovation, University of Tokyo, Tokyo, Japan; 3. Institute of Industrial Science, University of Tokyo, Tokyo, Japan; 4. Department of Applied Physics, University of Tokyo, Tokyo, Japan*

Magnetic skyrmions with vortex-like spin textures have been extensively studied in fields of fundamental physics and spintronics. Recently, antiskyrmions have attracted much more attention because of their unique spin configurations with Bloch- and Néel-type domain walls arising from an anisotropic Dzyaloshinskii–Moriya interaction (DMI). In this talk, I will present our real-space imaging of room-temperature antiskyrmions forming a square lattice in a Heusler compound with D_{2d} symmetry. We use in-plane magnetic fields to control the topological nature of skyrmions/antiskyrmions,

including the topological number, helicity, and lattice form, paving the route to controlling topological spin textures with spintronic functions. Our experimental observations coincide well with our micromagnetic simulations for magnets exhibiting D_{2d} symmetry and anisotropic DMI[1]. I will then show our recent discovery of an antiskyrmion-hosting material with S_4 symmetry, in which antiskyrmions exist over a wide temperature range beyond room temperature. The transformation of antiskyrmions to skyrmions occurs upon changing magnetic field and lamella thickness[2].

[1] L. C. Peng, R. Takagi, W. Koshibae, K. Shibata, K. Nakajima, T. Arima, N. Nagaosa, S. Seki, X. Z. Yu & Y. Tokura. *Nat. Nanotech.* 15, 181-186 (2020) [2] K. Karube†, L. C. Peng†, J. Masell, X. Z. Yu, F. Kagawa, Y. Tokura & Y. Taguchi. *Nat. Mater.* 20, 335-340 (2021)

GOF-03. Coexistence of topologically distinct spin textures.
B. Göbel[1], J. Jena[2], I. Mertig[1] and S. Parkin[2] *1. Martin-Luther-Universität Halle-Wittenberg, Halle, Germany; 2. Max-Planck-Institut für Mikrostrukturphysik, Halle, Germany*

Over the last decade, the field of skyrmionics has attracted great research interest, as skyrmions (small, whirl-like spin textures) possess a topologically-induced stability that allows to consider them as the carriers of information in future data storage devices. However, due to their topological charge of $N_{Sk} = \pm 1$ there are two major shortcomings of skyrmion-based racetrack storages: The skyrmions do not move parallel to a current and multiple skyrmions interact with each other potentially altering the bit sequence of present and absent skyrmions in the device. A solution to these problems is the utilization of alternative magnetic nano-objects that go beyond conventional skyrmions; see review [1]. We have identified Heusler materials as particularly relevant, since here multiple topologically distinct nano-object can even coexist. In this talk, we show via Lorentz transmission electron microscopy measurements [2] and Hall transport measurements [3] that arrays of skyrmions can be stabilized in tetragonal inverse Heusler materials by long-range dipole-dipole interactions. The material's D_{2d} symmetry gives rise to an anisotropic Dzyaloshinskii-Moriya interaction (DMI) that otherwise supports antiskyrmions. The skyrmions and antiskyrmions are extremely stable so that they can coexist and can even appear fractionally near the sample's edges [4]. An advanced version of the racetrack memory data storage is proposed [5], where a bit sequence could be encoded by skyrmions and antiskyrmions ('1' and '0' bits as shown in Figure 1). Such a concept is more reliable than single-particle-based racetracks in which a sequence of bits is encoded by the presence or absence of a single type of nano-object at certain positions along the racetrack. As another possibility we present the coexistence of 4 distinct types of magnetic bubbles. They are very stable and can be written and read based on their distinct in-plane magnetization [6]. A quaternary-digital data storage would have a drastically increased storage capacity.

[1] B. Göbel, I. Mertig, O. Tretiakov. "Beyond skyrmions: Review and perspectives of alternative magnetic quasiparticles" *Physics Reports* 895, 1-28 (2021). [2] J. Jena*, B. Göbel*, T. Ma, V. Kumar, R. Saha, I. Mertig, C. Felser, S. Parkin. "Elliptical Bloch skyrmion chiral twins in an antiskyrmion system" *Nature Communications* 11, 1115 (2020). [3] P. Sivakumar, B. Göbel, I. Mertig, S. Parkin. *et al.* " Topological Hall Signatures of Two Chiral Spin Textures Hosted in a Single Tetragonal Inverse Heusler Thin Film". *ACS Nano* 14, 13463 (2020). [4] J. Jena, B. Göbel, D. Loss, S. Parkin *et al.* "Observation of fractional spin textures and bulk-boundary correspondence" pre-print DOI: 10.21203/rs.3.rs-136696/v1 [5] J. Jena*, B. Göbel*, S. Parkin. *et al.* "Evolution and competition between chiral spin textures in nanostripes with D_{2d} symmetry". *Science Advances* 6, eabc0723 (2020). [6] B. Göbel, I. Mertig. "Quaternary-Digital Data Storage Based on Magnetic Bubbles in Anisotropic Materials" Physical Review Applied 15, 064052 (2021).

Fig. 1 In Heusler materials, the anisotropic DMI stabilizes antiskyrmions (red) and elliptically deformed skyrmions (blue).

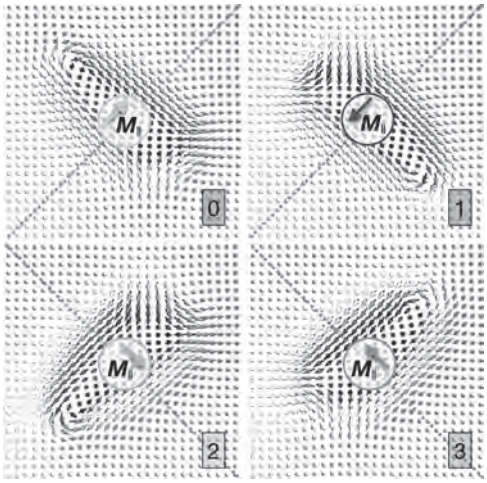

Fig. 2 Four distinct bubbles (bits of '0', '1', '2' and '3') with distinct inplane magnetizations.

GOF-04. Observation of Increasing Topological Hall Resistivity with Temperature in Skyrmion Hosting Magnetic Multilayers with $[Pt|CoB|Ir]_{xN}$ Structure.
A.J. Huxtable[1], J. Gretton[1], M. Ali[1], G. Burnell[1], C. Marrows[1] and K. Zeissler[1] *1. University of Leeds, Leeds, United Kingdom*

It has been predicted and measured that topologically non-trivial magnetisations can provide an extra contribution to the Hall resistivity (R_{xy}), called the topological Hall effect (THE)[1]. Skyrmions have a topology defined by the winding number, S, which takes an integer value dependent upon the number of total 'twists' in their magnetisation. The THE has been shown to be present in many B20 materials with bulk Dzyaloshinkii-Moriya Interaction (DMI) hosting skyrmions but the picture is less clear for multilayers with interfacial DMI. Observations by Maccariello et al. saw resistivity effects that could be accounted for by only the ordinary and anomalous Hall effects (OHE & AHE)[2]. In contrast, work by Zeissler et al. saw an extra contribution beyond the OHE and AHE that was larger than the THE predicted by theory[3]. In this work, Hall transport measurements combined with imaging of the magnetic texture were used to identify such contributions to understand discrepancies between the predicted[1], and observed[2,3], magnitudes of the topological contribution. Measurements of $R_{xy}(B)$ were performed in $[Pt|CoB|Ir]_{xN}$ multilayers with different repeat numbers, N, over a range of temperatures from 290 K to 2 K. Figure 1 shows the temperature dependence of the anomalous Hall resistivity at saturation, ρ_A, with an increase in size at T < 20 K, for a sample with N=4. The R_{xy} measurements for the same sample were analysed in combination with SQUIDVSM magnetometry data to produce Figure 2. The maximum excess Hall resistivity, ρ_{excess}, is observed to increase with temperature and cannot be accounted for by the ordinary and anomalous Hall effects alone. This implies an extra Hall effect that may be topological in nature suggesting that the maximum density of topological magnetisation textures increases with temperature.

[1] P. Bruno, V. K. Dugaev, M. Taillefumier, Physical Review Letters, 93, 9 (2004) [2] D. Maccariello, W. Legrand, N. Reyren et al., Nature Nanotechnology, 13, 233–237 (2018) [3] K. Zeissler, S.Finizio, K. Shahbazi et al., Nature Nanotechnology, 13, 1161 – 1166 (2018)

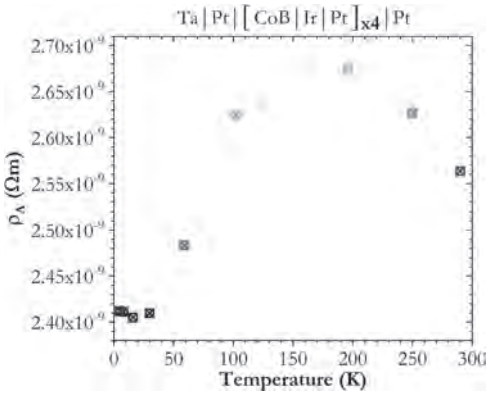

Fig. 1 Anomalous Hall resistivity at saturation, ρ_A, vs T showing an increase in size for T > 20 K, in samples of Ta|Pt|[CoB|Ir|Pt]$_{x4}$ Pt multilayers.

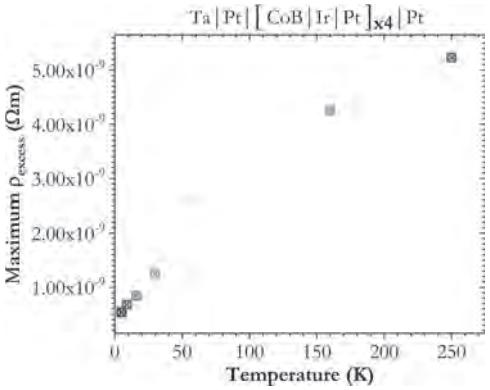

Fig. 2 Excess Hall resistivity (possibly topological in nature) that cannot be accounted for by ordinary or anomalous Hall effects, ρ_{excess}, vs T, showing an increase in the height of the maximum peak as temperature increases.

GOF-05. Study on the topology-relevant stability of vortex-antivortex pair in a permalloy element. *H. Han*[1,2], S. Lee[2], M. Jung[3], N. Kim[2], W. Chao[1], Y. Yu[4], J. Hong[3], K. Lee[2] and M. Im[1] *1. Center for X-ray Optics, Lawrence Berkeley National Laboratory, Berkeley, CA, United States; 2. Department of Materials Science and Engineering, Ulsan National Institute of Science and Engineering (UNIST), Ulsan, The Republic of Korea; 3. Department of Emerging Materials Science, Daegu Gyeongbuk Institute of Science and Technology (DGIST), Daegu, The Republic of Korea; 4. Advanced Light Source, Lawrence Berkeley National Laboratory, Berkeley, CA, United States*

The spin structure with the non-trivial topology has attracted intense attention in nanomagnetism community since the non-trivial topology of spin structure was claimed to provide high stability and high defect tolerance to spin structures [1]. The magnetic vortices and antivortices are topological spin structures, which are characterized by a half-integer skyrmion number q ($|q| = 1/2$), and the sign of q is determined by the orientation of the core polarization, $p = +1$ or -1. Depending on the core polarization of a vortex and an antivortex, the vortex-antivortex (V-AV) pair can be topologically trivial ($|q| = 0$) or non-trivial ($|q| = 1$) [2, 3]. Although the stability of V-AV pairs is a scientifically and technologically critical issue, the stability of V-AV pairs, particularly relevant to the topological properties of V-AV structures has been rarely addressed experimentally due to the difficulty of establishing stably formed topologically different V-AV pair within an identical magnetic nanostructure. In this work, we investigate the stability of stably generated topologically different V-AV pairs in a permalloy rectangular element through a study on their field-driven motions by magnetic transmission x-ray microscopy [4]. We found that the topologically trivial V-AV pair is easily annihilated when the vortex and antivortex get close to each other. In contrast, the topologically non-trivial V-AV pair stably remains even they get very close. Our work experimentally demonstrates that the non-trivial topology indeed contributes to higher stability of the topologically non-trivial V-AV pair and proves that topological stability is valid in V-AV pair systems.

[1] N. Nagaosa and Y. Tokura, *Nat. Nanotech* 8, 899-911 (2013) [2] N. Gao *et al., Nat. Commun.* 10 (1), 5603 (2019) [3] S. Zhang *et al., Sci. Rep.* 5 (1), 15773 (2015) [4] H.-S. Han *et al., Appl. Phys. Lett.* 118, 212407 (2021).

GOF-06. Interplay of Weyl electronic structure with long-range magnetic structure in Co_xFe_{1-x} Ge alloy. *B. Sabir*[1] and J.D. Gayles[1] *1. Physics, University of South Florida, Tampa, FL, United States*

The interplay between magnetism and topology plays a revolutionary role in material research, providing an additional means to control the symmetries exhibited by materials and opening the possibility for next-generation electronic devices. In this work, we study alloys of the B20 Chiral crystals $Co_xFe_{1-x}Ge$ for x=0.1, 0.2, via density functional theory by investigating the electronic structure and topological properties by symmetry analysis of the multiplicity of the bands, degenerate. Our results reveal that our alloys stabilize as skyrmionic crystals and their magnetization increases smoothly from nonmagnetic CoGe to ferromagnetic $Co_xFe_{1-x}Ge$ when x=0.1,0.2. The effect of Spin-orbit coupling (SOC) is systematically varied simultaneously with the magnetic structure to investigate the topological Weyl crossing points. Giant open Fermi arcs are created at the fermi surfaces that confirm Weyl fermionic behavior. Lastly, magnetic structure and SOC determine the shape, size, and seemingly the chirality of Fermi arcs. Thus, our results reveal the importance of the interplay between the magnetic structure and Weyl semimetals (WSMs), in addition to providing insight into the SOC effect on topological properties.

1. Wilde et al., *Nature* 594, no. 7863 pp 374–79 (2021). 2. Spencer C., Gayles J., Porter N. et al. Physical Review B 97(21) (2018)

GOF-07. Hall Effect and Topological Phase Transition in Exchange-Coupled Nanomagnets. *A. Ullah*[1,2], B. Balasubramanian[1,2], R. Pahari[1,2], D. Sellmyer[1,2] and R. Skomski[1,2] *1. Physics and Astronomy, University of Nebraska Lincoln, Lincoln, NE, United States; 2. Nebraska Center for Materials and Nanoscience, Lincoln, NE, United States*

The real-space Berry phase associated with conduction carriers has recently attracted much attention from the viewpoints of fundamental science and spin-electronics applications. The noncoplanar spin textures responsible for the Berry phase usually appear during the magnetization reversal, often occur in systems with Dzyaloshinskii-Moriya interactions (DMI) due to, broken inversion symmetry, and yield skyrmions in specific temperature and magnetic-field ranges [1, 2]. One key aim in skyrmion research is to realize small feature sizes, which lead to a pronounced topological Hall effect (THE), at high temperatures. Confined geometries such as nanoparticles or clusters are potential systems for this purpose because the competing exchange and magnetocrystalline anisotropy of nanoparticles are expected to cause substantially noncoplanar noncollinear spin structures even in the absence of DMI. Here, we use experiments and micromagnetic simulations to investigate spin textures in exchange-coupled Co nanoclusters produced by inert-gas condensation-type cluster deposition. The nanoclusters have an average size of 14 nm and exhibit a significant topological Hall effect (THE), as shown in the experimental Hall data of Fig. 1(a). The micromagnetic THE simulations, Fig. 1(b), predict the skyrmion number Q by integration over the skyrmion density and are in good agreement with the experimental data. THE is caused by the noncoplanar noncollinear spin

structure of the Co nanoclusters, visualized in Fig. 1(c). A characteristic feature of both experimental THE and theoretical prediction (skyrmion number Q) is a drastic change over a relatively small field range, which we interpret as a topological phase transition analogous to the Lifshitz transition in metals. This work is supported by NSF-DMREF (No. 1729288), NSF-EQUATE (OIA-2044049), the NU Collaborative Initiative, and NCMN

[1] N. Nagaosa and Y. Tokura, *Nature Nanotech*. 8, 899 (2013). [2] B. Balasubramanian, P. Manchanda, R. Pahari, Z. Chen, W. Zhang, S.R. Valloppilly, X. Li, A. Sarella, L. Yue, A. Ullah, P. Dev, D. A. Muller, R. Skomski, G. C. Hadjipanayis, and D.J. Sellmyer, *Phys. Rev. Lett.* 124, 057201 (2020).

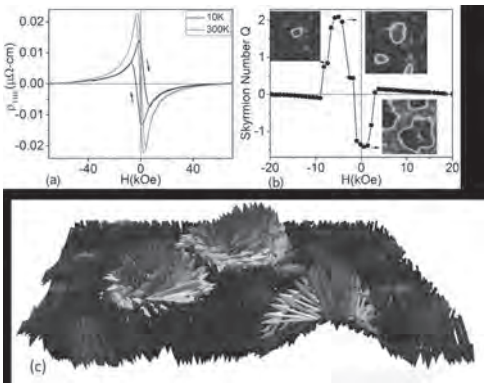

Fig. 1. Topological Hall effect (THE) in Co nanoclusters: (a) measured THE at 300 K and 10 K, (b) calculated Q as a function magnetic field and (c) simulated spin structure. The insets in (b) show the simulated spin textures at different fields. Red and blue colors represent spin-up and spin-down magnetization directions, respectively.

GOF-08. Topological Hall effect in epitaxial thin films of tetragonal Heusler compounds. *A. Markou*[1], P. Swekis[1], J.D. Gayles[2], S. Parkin[3] and C. Felser[1] *1. Solid State Chemistry, Max Planck Institute for Chemical Physics of Solids, Dresden, Germany; 2. Physics, University of South Florida, Tampa, FL, United States; 3. NISE, Max Planck Institute for Microstructure Physics, Halle, Germany*

Magnetic materials that host chiral spin textures have come to the forefront of condensed matter physics as potential candidates for future spintronic applications. Of these spin textures, skyrmions and antiskyrmions are mesoscale whirling objects with distinct chiral magnetic boundaries and opposite topological charges. Recently, the tetragonal Heusler compounds with D_{2d} symmetry show to host elliptical Bloch skyrmions and antiskyrmions [1]. This phenomenon, to host multiple topological spin textures, is especially interesting for applications when observed through real-space imaging techniques, such as magnetic force microscopy (MFM), and transport signatures. One such transport signature is the topological Hall effect (THE), which is a transverse response to an applied current, and it is distinct for each topological texture. In this work, we present the magnetic and magnetotransport properties in epitaxial thin films of the tetragonal Heusler compounds Mn_xPtSn and Mn_2RhSn. We show that the Mn_xPtSn displays two magnetic regions, a collinear state above the spin reorientation and noncoplanar below [2]. Further, we tune the Mn content (x) [3], which allows for microscopic control of the magnetic exchange parameters (Fig. 1). We show a microscopic control of the exchange parameters that influence the size of the magnetic textures and thereby the transport signatures. In Mn_2RhSn films, we observe two peaks in the THE, which allow us to determine the existence of two distinct topological objects over a wide range of temperature and magnetic fields [4]. In particular, we find skyrmions to be stable at low temperatures and antiskyrmions at higher temperatures. MFMstudies further support the coexistence of two topological objects in our films [5]. AM and CF acknowledge the European Union's Horizon 2020 research and innovation programme, under FET-Proactive grant agreement no. 824123 (SKYTOP).

[1] A. K. Nayak et al., Nature 548, 561-566 (2017). [2] P. Swekis et al., Phys. Rev. Materials 3, 013001(R) (2019). [3] P. Swekis et al., ACS Appl. Electron. Mater. 3, 1323 (2021). [4] P. K. Sivakumar et al., ACS Nano 14, 13463 (2020). [5] A. K. Sharma et al., Adv. Mater. 2101323 (2021).

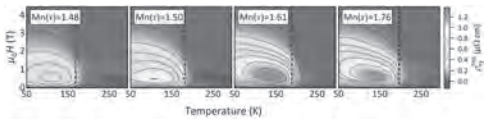

Topological Hall resistivity as a function of applied magnetic field and temperature for Mn_xPtSn films with different Mn content (x).

GOF-09. Withdrawn

GOF-10. Direct control of antiferromagnetic topological textures at room temperature. *H. Jani*[1] *1. Physics, National University of Singapore, Singapore*

Ferromagnetic topological textures have shown great promise for implementation in beyond-CMOS computing paradigms, such as racetrack or neuromorphic applications. However, the presence of dipolar-field limitations and the deleterious skyrmion Hall effect, have so far inhibited their practical exploitation in devices. Alternatively, antiferromagnetic (AFM) analogues, made from topological winding of the staggered magnetization, are predicted to exhibit relativistic dynamics, deflection-free motion, and size scaling. Discovery and control of such textures has remained elusive, until recently, due to sub-lattice compensation in natural AFMs. In this talk, I will present a general field-free approach we used to realize a wide family of topological AFM textures, including exotic Bloch and Néel merons or antimerons (half-skyrmions) and bimerons [1]. In the earth-abundant oxide – hematite, in both epitaxial thin films and free-standing membranes – these textures can be nucleated and stabilized at room temperature, with characteristic size ~100 nm. I will discuss how texture chirality and dimension may be controlled by tuning exchange, anisotropy and interfacial interactions [2,3,4], and present the possibility of realizing hitherto unreported AFM skyrmions in this system [5]. Lastly, I will outline how our results point to the discovery of these AFM topological textures in a variety of AFM materials [2], which can be directly addressed by current-based spin-orbit torques, paving the way towards the construction of low-energy AFM spintronic applications.

[1] Jani H* et al.Nature 590, 74 (2021) [2] Jani H* et al.Nat Commun 12, 1668 (2021) [3] Chmiel FP et al.Nat Mater 17, 581 (2018) [4] Radaelli PG et al.Phy Rev B 101, 144420 (2020) [5] Harrison J et al.(to be submitted)

GOF-11. Magnetic Skyrmions Probed by Spin-polarized Scanning Tunneling Microscopy: Topology Imprinted on the Charge Current and Spin Transfer Torque. *K. Palotas*[1,2], L. Rozsa[3] and L. Szunyogh[2] *1. Wigner Research Center for Physics, Budapest, Hungary; 2. Budapest University of Technology and Economics, Budapest, Hungary; 3. University of Konstanz, Konstanz, Germany*

The controlled creation and annihilation of individual magnetic skyrmions have been demonstrated by using spin-polarized scanning tunneling microscopy (SP-STM) [1], where the spin-polarized current exerts a torque on the spin moments of the sample. This is a promising step towards future technological applications using skyrmions for carrying or storing information. However, the detailed microscopic mechanisms of these processes are presently unknown. Our work contributes to this understanding by a theoretical investigation of the tunneling electron charge and spin transport probing magnetic skyrmions. The spin-polarized charge current (I) and tunneling spin transport vector quantities, the longitudinal spin current and the spin transfer torque (STT), are consistently calculated within a simple electron

transport theory [2]. The electron tunneling model is extended to SP-STM in high spatial resolution, and applied to magnetic skyrmions [3,4]. Besides the vector spin transport characteristics, the relationships among conventional charge current SP-STM images [5], the magnitudes of the spin transport quantities [3], and the topology of various skyrmionic objects [6] are analyzed. It is also shown (Figure 1) that at specific SP-STM tip positions the STT efficiency (*STT/I*) can reach very high values close to the theoretical maximum, *h/e* [7]. Thus, a theoretical prediction for a possibly highly efficient localized magnetic switching is also provided. Funding Acknowledgments: National Research Development and Innovation Office (NRDIO) of Hungary (FK124100, K131938, TKP2020-IES-BME-IE-NAT), Ministry of Innovation and Technology (New National Talents Program, Bolyai+) and the NRDIO within the Quantum Information National Laboratory of Hungary, and the János Bolyai Research Scholarship of the Hungarian Academy of Sciences.

[1] N. Romming et al., Science, Vol. 341, 636 (2013) [2] K. Palotás et al., Physical Review B, Vol. 94, 064434 (2016) [3] K. Palotás et al., Physical Review B, Vol. 97, 174402 (2018) [4] K. Palotás, Physical Review B, Vol. 98, 094409 (2018) [5] K. Palotás et al., Physical Review B, Vol. 96, 024410 (2017) [6] L. Rózsa et al., Physical Review B, Vol. 95, 094423 (2017) [7] K. Palotás et al., Journal of Magnetism and Magnetic Materials, Vol. 519, 167440 (2021)

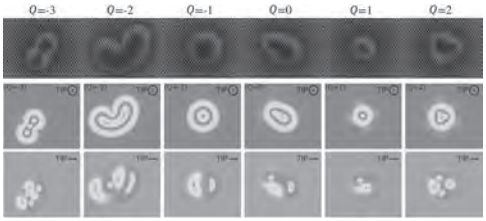

Real-space skyrmionic spin structures with various topological charges (Q), and the calculated STT efficiency depending on the SP-STM tip position (blue...red: 0...0.97 *h/e*) [7].

GOF-12. Reversible writing/deleting of magnetic skyrmions through hydrogen adsorption/desorption. *G. Chen*[1,3], C. Ophus[2], A. Quintana[1], H. Kwon[4], C. Won[5], H. Ding[7], Y. Wu[6], A. Schmid[2] and K. Liu[1,3]
1. Georgetown University, Washington, DC, United States; 2. Lawrence Berkeley National Laboratory, Berkeley, CA, United States; 3. University of California, Davis, Davis, CA, United States; 4. Korea Institute of Science and Technology, Seoul, The Republic of Korea; 5. Kyung Hee University, Seoul, The Republic of Korea; 6. Fudan University, Shanghai, China; 7. Nanjing University, Nanjing, China

Magnetic skyrmions are topologically nontrivial spin textures with envisioned applications in energy-efficient magnetic information storage. Toggling the presence of magnetic skyrmions via writing/deleting processes is essential for spintronics applications, which usually require the application of a magnetic or electric field or an electric current [1]. Here we report reversible field-free hydrogen-driven writing/deleting of skyrmions in Ni/Co/Pd/W(110) multilayers at room temperature [2]. Using spin polarized low energy electron microscopy (SPLEEM), skyrmion creation and annihilation is observed during hydrogen chemisorption / desorption cycles. We show that the adsorption of hydrogen on the surface of Ni/Co/Pd/W(110) multilayers changes the balance of magnetic energy contributions, particularly the magnetic anisotropy, which in turn drives the skyrmion creation/annihilation. Using SPLEEM for magnetization vector mapping we resolve the spin structure of the written skyrmions and show that they are left-handed hedgehog Néel-type. Monte-Carlo simulations support our interpretation attributing the reversible skyrmion writing and deleting to anisotropy changes. The roles of hydrogen and oxygen on magnetic anisotropy and skyrmion deletion on other magnetic surfaces are also demonstrated. Such ambient temperature reversible skyrmion operations in the absence of magnetic, electric field or electric current provide new paths for the design of skyrmion-based spintronics and magneto-ionic devices. Work supported by the NSF (DMR-2005108), SRC/NIST nCORE SMART center and DOE (DE-AC02-05CH11231).

[1] W. Jiang, G. Chen, K. Liu, J. Zang, S. G. E. te Velthuis, and A. Hoffmann, Skyrmions in magnetic multilayers. Phys. Rep. 704, 1 (2017). [2] G. Chen, *et al.* Reversible writing/deleting of magnetic skyrmions through hydrogen adsorption/desorption. DOI:10.21203/rs.3.rs-575830/v1 (2021).

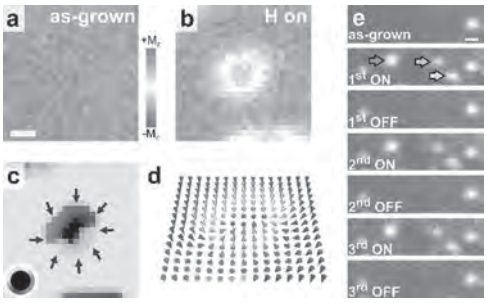

Figure 1. (a,b) SPLEEM image of Ni/Co/Pd/W(110) on a local -M_z domain, before/after the hydrogen exposure. Scale bar is 100 nm. (c) Compound SPLEEM image resolving the bubble-like domain in panel b as a skyrmion. (d) Arrow-array representation of panel c. (e) SPLEEM images showing reversible skyrmion writing/deleting over three hydrogen on/off cycles (indicated by the red, orange and yellow arrows), scale bar is 200 nm.

Session GOG
FUNDAMENTAL INTERACTIONS IN SKYRMIONS AND NOVEL PHASES

Aisha Aqeel, Chair
University of Munich, Munich, Germany

CONTRIBUTED PAPERS

GOG-01. First-principles study of exchange interactions at the atomic scale. *S. Haldar*[1] and S. Heinze[1] *1. Institute of Theoretical Physics and Astrophysics, University of Kiel, Kiel, Germany*

The development of spin-polarized scanning tunneling microscopy (STM) [1] has opened the route towards exploring the magnetic properties of nanostructures on surfaces on the atomic scale. It has also become experimentally feasible to measure not only the spin-polarized current but also the exchange forces between a magnetic scanning probe tip and a magnetic nanostructure, a technique which has been coined magnetic exchange force microscopy (MExFM) [2]. Recently, the first simultaneous measurements of spin-polarized tunneling currents and exchange forces have been performed [3]. Here, we use first-principles calculations based on density functional theory (DFT) to study the properties of magnetic adatoms on Mn/W(110) as well as the exchange interaction with a ferromagnetic tip. For Co and Ir adatoms on Mn/W(110), we find that the canted spin structure of the Mn surface layer is encoded into different orbitals of the adatoms which thus display intra-atomic noncollinear magnetism [4]. Our calculations can explain the puzzling asymmetric shape of Co adatoms on the spin spiral of Mn/W(110) observed in spin-polarized STM measurements [5]. Surprisingly, the spin polarization of the clean Mn/W(110) surface is relatively weak and the exchange force field is more sensitive to atomic-scale variations in the magnetization [6]. For the exchange force calculations, we have used Co, Mn, and Ir adatoms on Mn/W(110). Mn has been chosen since it exhibits a much larger magnetic moment than Co and possesses a half-filled *3d* shell as a free atom. Ir is a *5d* transition-metal atom which thus shows large spin-orbit coupling related effects such as tunneling anisotropic magnetoresistance [7]. First-principles calculations also reveal that the measured atomic-scale variations in the exchange force originate from different contributions of direct and indirect (Zener type) exchange mechanisms, depending on the chemical tip termination. Our conclusions apply in general to adatoms on surfaces with a noncollinear magnetic structure e.g. spin spirals, skyrmions, or domain walls, and explain recent experimental results of spin-polarized scanning tunneling microscopy experiments [5].

[1] M. Bode, Rep. Prog. Phys. Vol. 66, p.523 (2003). [2] U. Kaiser, A. Schwarz, and R. Wiesendanger, Nature Vol. 446, p.522 (2007). [3] N. Hauptmann, J. W. Gerritsen, D. Wegner, A. A. Khajetoorians, Nano Lett., Vol. 17, p.5660 (2017) [4] S. Haldar and S. Heinze, Phys. Rev. B Vol. 98, p.220401(R) (2018) [5] D. Serrate et al., Phys. Rev. B Vol. 93, p.125424 (2016) [6] N. Hauptmann, S. Haldar et al. Nat. Commun. Vol. 11, p.1197 (2020) [7] N. Caffrey, et al., J. Phys.: Condens. Matter Vol. 26, p.394010 (2014)

GOG-02. Ruderman-Kittel-Kasuya-Yosida-type interfacial Dzyaloshinskii-Moriya interaction in heavy metal/ferromagnet heterostructures. *T. Kim*[1], I. Cha[1], Y. Kim[1], G. Kim[1], A. Stashkevich[2], Y. Roussigné[2], M. Belmeguenai[2], S.M. Chérif[2], A.S. Samardak[3] and Y. Kim[1] *1. Korea University, Seoul, The Republic of Korea; 2. Université Sorbonne Paris Nord, Villetaneuse, France; 3. Far Eastern Federal University, Vladivostok, Russian Federation*

The interfacial phenomena have been recently revisited and experimentally illustrated because of their huge potential to explore novel magnetic behaviors such as Skyrmions, chiral domain wall dynamics, and spin-Hall effects [1,2]. Among various interfacial effects, interfacial Dzyaloshinskii-Moriya interaction (iDMI) is drawing attention [3]. Here, we have experimentally shown that iDMI can also be derived from FM/oxide interface by inserting the MgO spacer layer between heavy metal and ferromagnetic metal. We fabricated sample structure of Ta (3)/Pt (5)/MgO (t_{MgO})/CoFeSiB (0.9)/MgO (1.0)/Ta (2). Using Brillouin Light Scattering (BLS) spectroscopy, iDMI energy density is calculated. The most pronounced iDMI value (D_{eff} = -0.70 ± 0.06 mJ/m^2) occurred when there was no MgO spacer layer. As the t_{MgO} increases, iDMI energy density shows an oscillating-like behavior. To qualitatively understand the experimental results, a toy model based on RKKY exchange coupling was introduced. From the numerical simulation, we confirmed that the oscillation of the iDMI was the result of the RKKY-type interaction between itinerant electrons through the spacer. Such behavior could be achieved with the help of a reduction in MgO bandgap energy due to oxygen deficiency. The structural analysis is conducted using X-ray Diffraction (XRD), Transmission Electron Microscope (TEM), and Secondary Ion Mass Spectroscopy (SIMS). Reduced MgO bandgap energy was confirmed using Reflective Electron Energy Loss Spectroscopy (REELS). This study confirmed that the origin of the iDMI is an exchange mechanism linking the two ferromagnetic metal atoms via a spin-orbit coupling heavy metal atom and the RKKY-type interaction could be used to explain. Hence, the magnitude of iDMI could be modified through spacer layer thickness between heavy metal and ferromagnetic metal engineering.

References [1] A. Soumyanarayanan *et al.*, Nat. 539, 509 (2016). [2] S. Woo *et al.*, Nat. Mater. 15, 501 (2016). [3] J. Cho *et al.*, Nat. Commun. 6, 7635 (2015).

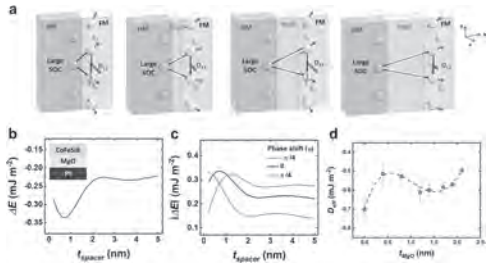

Fig. 1 Summary of experimental and calculated iDMI energy density changes according to the MgO thickness. a, Schematic of MgO spacer layer thickness change. b, Calculated iDMI energy with respect to the MgO spacer thickness. c, Calculated iDMI energy density with different phases. d, experimentally obtained iDMI energy density changes.

GOG-03. Phase transitions of skyrmion lattices. J. Zazvorka[2], F. Dittrich[3], Y. Ge[3], N. Kerber[3], K. Raab[3], T.B. Winkler[3], K. Litzius[1], M. Veis[2], *P. Virnau*[3] and M. Kläui[3] *1. MPI for Intelligent Systems, Stuttgart, Germany; 2. Physics, Charles University, Prague, Czechia; 3. Physics, University of Mainz, Mainz, Germany*

Magnetic skyrmions are whirls of magnetization with many exciting properties. As quasi-particles, they exhibit two-dimensional phase transition behavior [1,2], which allowed us to drive a skyrmion lattice from a liquid phase to the onset of a hexatic phase as shown by the analysis of hexagonal

order [1] (figure). From the liquid structure of the lattice, we derived coarse-grained interaction potentials directly from experiments with which the phase behavior can be reproduced. This demonstrates that not only static properties are well-described in terms of a simple computational model, but that skyrmions are indeed an ideal, tunable system to investigate phase transitions in reduced dimensions with simulations and experiments.

[1] J. Zázvorka, F. Dittrich, Y. Ge, N. Kerber, K. Raab, T. Winkler, K. Litzius, M. Veis, P. Virnau, M. Kläui, Skyrmion lattice phases in thin film multilayer, *Adv. Funct. Mat.* 30, 2004037 (2020). [2] M. Kläui, Freezing and melting skyrmions in 2D, *Nature Nanotechnology* 15, 726-727 (2020).

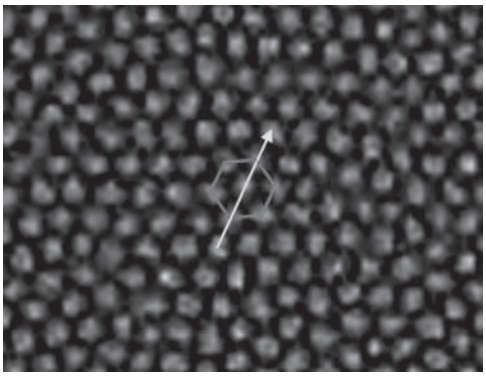

GOG-04. Theory of Néel-Bloch transition for compact magnetic skyrmions. *A. Bernand-Mantel*[1], C. Muratov[2] and T. Simon[3]
1. Laboratoire de Physique et Chimie des Nano-Objets, Université de Toulouse-CNRS, Toulouse, France; 2. Department of Mathematical Sciences, NJIT, Newark, NJ, United States; 3. Institute for Applied Mathematics, University of Bonn, Bonn, Germany

Magnetic skyrmions are a prime example of topologically non-trivial spin textures observed in a variety of magnetic materials. They emerge when the exchange and anisotropy energies promoting parallel alignment of spins in a ferromagnet enter in competition with energies favoring non-collinear alignment of spins such as the Dzyaloshinskii-Moriya interaction (DMI), the long-range dipolar interaction or higher-order exchange interactions. The orthodox theory of skyrmions in ultrathin ferromagnetic layers with interfacial DMI relies on a model that accounts for the dipolar interaction through an effective anisotropy term, neglecting long-range effects. At the same time, in single ferromagnetic layers with interfacial DMI, large chiral skyrmions, also called skyrmionic bubbles have been observed, suggesting a non-trivial interplay between DMI and long-range dipolar effects[1]. The competition between these two energies also leads to the formation of skyrmions exhibiting spin rotations with intermediate angles between Neel and Bloch, a phenomenon also present in domain walls. In addition, there is a growing body of theoretical evidence that points to a need to take into account the long-range dipolar energy in the models describing magnetic skyrmions. The above considerations put into question the validity of the commonly used assumption that the long-range contribution of the dipolar interaction is negligible. Here we use rigorous mathematical analysis to develop a skyrmion theory that takes into account the full dipolar energy in the thin film regime and provides analytical formulas for compact skyrmion radius, rotation angle and energy[2,3]. We demonstrate that the DMI threshold at which a compact skyrmion loses its Néel character is a factor of 3 higher than that for a single domain wall. A reorientation of the skyrmion rotation angle from Néel to intermediate Néel-Bloch angles is predicted as the layer thickness is increased in the low DMI regime, which is confirmed by micromagnetic simulations. We will also present an extension of our model which includes applied magnetic field.

[1] A. Bernand-Mantel et al. Scipost 4, 27 (2018) [2] A. Bernand-Mantel, C. Muratov, T. Simon, Physical Rev. B101, 045416 (2020) [3] A. Bernand-Mantel, C. Muratov, T. Simon, Archive for Rational Mechanics and Analysis 239 219 (2021)

GOG-05. Resonant tender x-ray scattering from Ru-4d conduction electrons in the skyrmion host $Gd_3Ru_4Al_{12}$. *M. Hirschberger*[6,5], L. Spitz[1,5], J. Bertinshaw[2], S. Francoual[3], B. Keimer[2], T. Arima[4,5] and Y. Tokura[6,5] *1. Paul-Scherrer-Insitut, Villigen, Switzerland; 2. Max-Planck-Institute for Solid State Research, Stuttgart, Germany; 3. Deutsches Elektronen-Synchrotron (DESY), Hamburg, Germany; 4. Department of Advanced Materials Science, The University of Tokyo, Kashiwa, Japan; 5. Center for Emergent Matter Science, RIKEN, Wako, Japan; 6. Quantum-Phase Electronics Center and Department of Applied Physics, The University of Tokyo, Bunkyo, Japan*

The spin and orbital texture of conducting electronic states in magnetic solids is a focus of intense scrutiny, being relevant to a multitude of emergent phenomena. These include novel optical responses, nonlinear transport properties, as well as spin current generation and control. Complex magnets with sizable local moments and intermediate spin-orbit coupling, e.g. in Ruthenium-based oxides and intermetallics, are believed to be suitable targets in this regard. Here, we report on the spiral ordering of Ruthenium spins, as driven by their interaction with local rare earth moments in the centrosymmetric skyrmion host $Gd_3Ru_4Al_{12}$. Resonant elastic scattering of tender x-rays was carried out at beamline P09 of the PETRA-III synchrotron at DESY in Hamburg, Germany. A specialized all-in vacuum beam path suppresses absorption of x-rays in air (E = 2.8-3 keV). We exploit the resonant x-ray scattering process (Fig. 1) as an element-specific probe, targeting the spin texture of the Ru-4d electrons directly. Through comparison of scattering signals at the Ru-L_2 and L_3 absorption edges, we disentangle the spin and orbital textures in real space. Our analysis converges on a picture of a distorted spiral texture for Ru-4d, which results from a competition between Ruderman-Kittel-Kasuya-Yosida (RKKY) interactions and spin-orbit coupling. The experimental result is discussed in the framework of the Kondo Hamiltonian. We highlight the relevance of our findings for the topological Hall effect in the field-induced skyrmion lattice phase of $Gd_3Ru_4Al_{12}$ [1], and for the mechanism underlying the novel emergent (or quantum) inductance response in the spiral phase [2].

[1] M. Hirschberger *et al.*, Nature Communications 10, 5831 (2019) [2] T. Yokouchi *et al.*, Nature 586, 232–236 (2020) [3] M. Hirschberger *et al.*, manuscript in preparation

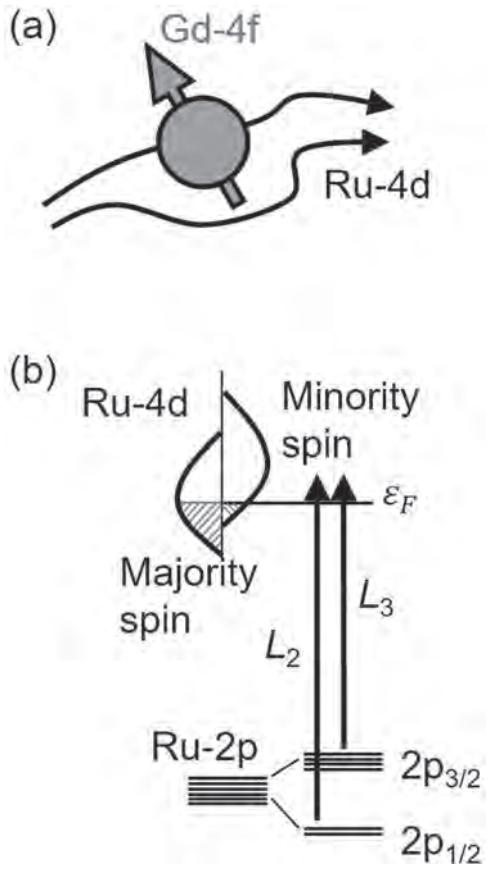

Fig. 1: (a) Illustration of coupled local moments (Gd^{3+} local 4f-spin) and Ruthenium 4d conduction electrons in $Gd_3Ru_4Al_{12}$. (b) Resonant elastic scattering process at the Ru-*L* absorption edge, with L_2 and L_3 resonances indicated separately.

GOG-06. A New Magnetic Intermediate State, "*B-Phase*", in MnSi Probed by Small-Angle Neutron Scattering and Muon Spin Rotation. M. Pardo-Sainz[3], M. Ohkuma[2], S. Iwasaki[4], K. Ohishi[1], M. Mito[2], J. Akimitsu[4], Y. Cai[5,6], K. Kojima[5,6], Y. Kousaka[4,7], K. Inoue[8], V. Laliena[9] and *J. Campo*[3,8] *1. Neutron Science and Technology Center, Comprehensive Research Organization for Science and Society (CROSS), Ibaraki, Japan; 2. Graduate School of Engineering, Kyushu Institute of Technology, Kitakyushu, Japan; 3. Aragonese Nanoscience and Materials Institute, Spanish National Research Council (CSIC), Zaragoza, Spain; 4. Research Institute for Interdisciplinary Science, Okayama University, Okayama, Japan; 5. TRIUMF, Vancouver, BC, Canada; 6. University of British Columbia, Vancouver, BC, Canada; 7. Department of Physics and Electronics, Osaka Prefecture University, Osaka, Japan; 8. Chirality Research Center, Hiroshima University, Higashihiroshima, Japan; 9. Applied Mathematics Department, University of Zaragoza, Zaragoza, Spain*

A violation of space-inversion symmetry entails a Dzyaloshinskii-Moriya interaction originating from the spin-orbit interaction, which stabilizes a chiral helimagnetic spin alignment. The chiral helimagnetic structures, forming only one-handed screw magnetic structures, have attracted attention because of the emergence of unique topological magnetic textures such as magnetic skyrmion lattices (SkL) [1] and chiral magnetic soliton lattices [2]. Recently, we suggested theoretically, that at low T the conical (CH) and forced-ferromagnetic (FFM) phases in cubic helimagnets, are not connected but are separated by another SkL, which could be metastable, and a new phase of unknown nature (*B-phase*) just below the critical field H_c at low T [3]. The theoretical predictions at low T are in good agreement with the experiments reported in ref [4,5]. On the other hand, by using careful ac susceptibility at low temperature, we determined the magnetic phase diagrams of oriented crystals of MnSi [6]. It is consistent with the theoretical prediction for the new unknown low temperature phase. In order to clarify the nature of this new phase at low T near critical field, we performed SANS measurements at TAIKAN in J-PARC and muon spin rotation (μSR) measurements at M15 in TRIUMF. At both 0.3 T (CH phase) and 0.5 T (*B-phase*), the SANS patterns show two peaks along the horizontal axis for $H \perp$ incoming neutron beam wave vector k_i. These are the magnetic Bragg peaks of the conical state [7]. On the other hand, no diffraction peaks were observed for $H // k_i$, in which, for example, a six-fold-symmetric diffraction pattern due to a formation of SkL is observed in *A*-phase (SkL). These results suggest the CH phase exists in *B-phase* and it is different from *A*-phase near T_c. According to the μSR results, we found the internal magnetic field distribution in *B-phase* is apparently different from that in CH and FFM phases, consistent with the SANS results. In the presentation, we will talk about the theory and the results of both SANS and μSR in detail, and discuss a spin texture in *B-phase*

[1] S. Muhlbauer *et al.*, Science 323, 915 (2009). [2] T. Togawa *et al.*, Phys. Rev. Lett. 108, 107202 (2012).. [3] V. Laliena and J. Campo, Phys. Rev. B 96, 134420 (2017). [4] H. Oike *et al.,* Nat. Phys. 10, 62 (2016). [5] T. Nakajima *et al.,* Phys. Rev. B 98, 014424 (2018). [6] M. Ohkuma *et al.,* in preparation. [7] K. Ohishi *et al.,* JPS Conf. Proc. 33, 011060 (2021).

GOG-07. Non-Collinear Three-Dimensional Textures In Magnetic Multilayers: Hatching of Skyrmionic Cocoons. *M. Grelier*[1], F. Ajejas[1], Y. Sassi[1], K. Bouzehouane[1], A. Vecchiola[1], S. Collin[1], A. Fert[1], V. Cros[1] and N. Reyren[1] *1. Unité Mixte de Physique CNRS/Thales, Palaiseau, France*

In nanomagnetism and spintronics, magnetic multilayers continue to thrive as pivotal structures to engineer complex non-trivial spin textures thanks to the tunability of their composition and their properties. Two-dimensional magnetic textures such as skyrmions or chiral domain walls were mostly under focus for the last decade, but recently interest has surged for more complex objects which display an inhomogeneous behavior over the vertical dimension [1,2]. Interesting examples include bobbers which could become remarkable assets for the development of logic devices [3] or the recently observed hopfions [4] or even different skyrmions phases [5]. Our own efforts to engineer and explore three-dimensional textures in Pt/Co based multilayers allows us to observe the signature of new textures, which we name skyrmionic cocoons. At low magnetic field, they resemble tubular skyrmions but upon an increase of the out-of-plane field, they shrink and disappear in the outer layers (Fig 1.b,c), becoming elongated ellipsoids. To observe such textures, we grew multilayers displaying variable thicknesses of a ferromagnetic material, thereby introducing a non-uniform effective anisotropy. By carefully tuning the thickness of each magnetic layer, it was possible to observe in a single sample two distinct types of objects, as shown by the strong difference in the Magnetic Force Microscopy (MFM) contrasts (Fig 1.a). With the support of micromagnetic simulations (Fig 1.b), we identify them as two vertically coupled cocoons (large contrast) and single cocoons only present in half of the layers (weak contrast). The existence and field-dependent behavior of such textures could represent interesting possibilities for potential applications.

[1] W. Legrand, et al. Sci. Adv. 4, eaat0415 (2018) [2] Donnelly, Claire, et al. *Nature* 547.7663 (2017): 328-331. [3] Zheng, Fengshan, et al. Nature Nanotechnology volume 13, pages 451–455 (2018) [4] Kent, Noah, et al. *Nature communications* 12.1 (2021): 1-7. [5] Mandru, Andrada-Oana, et al. *Nature communications* 11.1 (2020): 1-7.

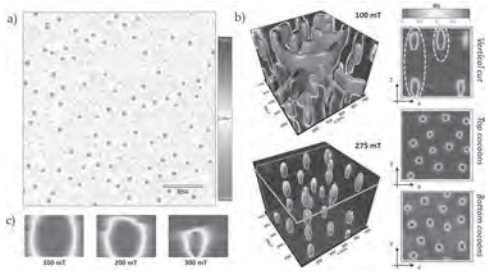

Fig 1. a) MFM measurement at 265 mT on a multilayer with variable thickness of Co. b) Corresponding micromagnetic simulations at different fields displayed with isosurfaces, mz=0 (white) and mz=-0.8 (red), with plane cuts identified by the coloured lines. The yellow dotted ellipses evidence the two kinds of objects correlated with the MFM image: coupled cocoons (left) and single cocoons (right). c) Simulated vertical cuts showing the evolution of a cocoon at different out-of-plane magnetic fields.

GOG-08. Brillouin Light Scattering from Quantized Spin Waves in Nanowires with Antisymmetric Exchange Interactions. J. Xu[1], G.A. Riley[2,3], J.M. Shaw[2], H. Nembach[2,4] and *A. Kent*[1] *1. Department of Physics, New York University, New York, NY, United States; 2. Quantum Electromagnetics Division, NIST, Boulder, CO, United States; 3. Center for Memory and Recording Research, University of California – San Diego, La Jolla, CA, United States; 4. Department of Physics, University of Colorado, Boulder, CO, United States*

Antisymmetric exchange interactions are used to stabilize magnetic textures and lead to non-reciprocal spin-wave propagation [1-2]. As a result, left and right propagating waves at the same energy have different wavelengths. Thus, interference between counter-propagating spin waves does not lead to standing waves; instead, confined modes have a time-dependent phase, i.e., their phase is modulated at a rate determined by the Dzyaloshinskii–Moriya interactions (DMI) [3]. We report on a Brillouin light scattering (BLS) study of confined spin waves in Co/Pt nanowires with strong DMI, whose widths range from 100 to 400 nm [4]. Two different scattering geometries were used: a transverse geometry where the incident light is perpendicular to the nanowire, as illustrated in Fig. 1(a), and a longitudinal geometry, where the incident light is parallel to the nanowire. Fig. 1(b) shows a SEM image of a nanowire array. Fig. 2(a-d) show sample BLS spectra for both scattering geometries. Fig. 2(e) shows spin-wave quantization in narrow (<200nm width) wires dramatically reduces the frequency shift between BLS Stokes and anti-Stokes lines in the transverse geometry. In contrast, the frequency shift associated with the longitudinal geometry is independent of nanowire width. A model that considers phase-modulated confined modes captures this physics and predicts a dramatic reduction in frequency shift of light scattered from higher energy spin waves in narrow wires, which is confirmed by our experiments. Our results show that, in contrast to the BLS frequency shift in the longitudinal scattering geometry, which enables direct determination of the DMI, the BLS frequency shift in the transverse scattering geometry is not directly related to the DMI.

[1] J.-H. Moon *et al.*, PRB 88, 184404 (2013) [2] H. T. Nembach *et al.*, Nature Physics, 11, 825 (2015) [3] B. W. Zingsem *et al.*, PRB, 99, 214429 (2019) [4] J-W. Xu *et al.*, arXiv 2107.10303 (2021)

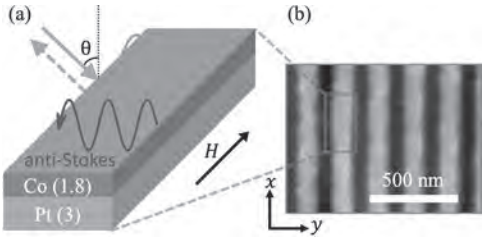

Fig. 1 (a) Schematic of spin waves in a confined geometry with chiral magnetic interactions. (b) A SEM image of the nanowire array consisting of 100 nm width Co/Pt nanowires with 100 nm spacing.

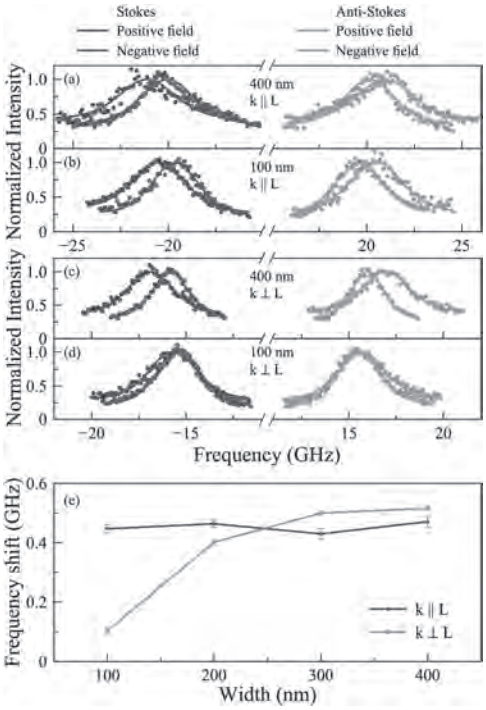

Fig. 2 (a)-(d) BLS spectra for Stokes and anti-Stokes processes for both positive and negative fields on nanowire arrays with different widths. (e) The absolute value of the frequency shift on nanowire arrays with different widths in the longitudinal (k∥L) and transverse (k⊥L) scattering geometries.

GOG-09. The 3-dimensional depth profile of magnetic skyrmion tubes. *N.C. Liyanage*[1], L.J. Quigley[2], S. Montoya[5], N. Tang[2], T. Liu[6], M.R. Fitzsimmons[1,7], S.K. Sinha[3], R. Kawakami[6], J.A. Borchers[4], E. Fullerton[5], B.B. Maranville[4], L. Debeer-Schmitt[7], A.J. Grutter[4] and D.A. Gilbert[2,1] *1. Department of Physics and Astronomy, University of Tennessee, Knoxville, TN, United States; 2. Materials Science Department, University of Tennessee, Knoxville, TN, United States; 3. Physics Department, University of California, San Diego, CA, United States; 4. NIST Center for Neutron Research, National Institute of Standards and Technology, Gaithersburg, MD, United States; 5. CMRR, University of California, San Diego, CA, United States; 6. The Department of Physics, The Ohio State University, Columbus, OH, United States; 7. Neutron Scattering Division, Oak Ridge National Laboratory, Oak Ridge, TN, United States*

Magnetic skyrmions have been the focus of intense research due to their topologically protected properties and potential applications to next-generation spintronic devices. These chiral spin textures are frequently presented as a 2D projection, inherently ignoring their three-dimensional tube-like structure. Recently, we have demonstrated the realization of skyrmions stable

at room temperature and zero applied magnetic field in Gd/Fe multilayers. These skyrmions are stabilized by magnetic dipolar interactions, rather than Dzyaloshinskii–Moriya interactions (DMI). [1-3]. Given the Fe/Gd multilayers possess low magnetization, low anisotropy, and are relatively thick (~80-nm), flux-closure domains are favored at the top and bottom surfaces of the film; TEM results reveal an azimuthal winding along the center of the film. The dipole skyrmions exhibit a hybrid structure with Neel-type spin structure on the top and bottom, with chirality defined by the dipole fields, and a Bloch-type structure around the equatorial belt. In this work, we use grazing-incidence small-angle neutron scattering (GISANS) (Fig. 1) and polarized neutron reflectometry (PNR), both performed on a single Fe/Gd specimen, to determine the depth-dependent profile of the hybrid skyrmion. Specifically, in the GISANS and PNR patterns, the specular data captures the depth-dependent structure of the skyrmions, which averages to zero across the sample plane since the structure is highly symmetric. While the off-specular GISANS data (Fig 1(c)) captures the in-plane periodic structure. Together, these datasets provide a full depth-dependent profile of the hybrid skyrmions. To interpret the data, micromagnetic simulations of the hybrid skyrmions were performed using the object-oriented micromagnetic framework (OOMMF), then the specular and off-specular patterns were calculated and compared to the experimental results. Through iterative modification of the model, a simulated pattern is generated which accurately reproduces our experiments. This work was supported by U.S. DOE, Office of Science. Award DE- SC0021344.

[1]. S. A. Montoya et al., Phys. Rev. B 95, 224405 (2017) [2]. S. A. Montoya et al., Phys. Rev. B 95, 024415 (2017) [3]. R. D. Desautels et al., arXiv:1904.13274

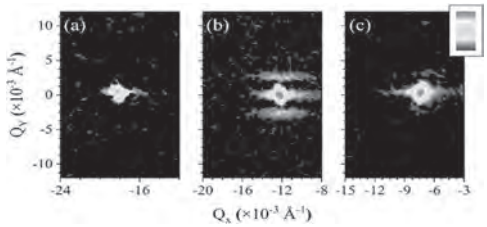

Fig 1. GISANS patterns for (a) Saturated. (b) Stripe domains. (c) Skyrmion state.

GOG-10. Unravelling the details of the magnetic texture of skyrmion tubes in three dimensions. S. Schneider[1], D. Wolf[2], A. Lubk[2] and *B.F. Rellinghaus[1] 1. Dresden Center for Nanoanalysis, TU Dresden, Dresden, Germany; 2. IFW Dresden, Dresden, Germany*

Skyrmions exhibit topologically nontrivial spin textures [1] and can be motioned by comparably small spin-polarized currents [2]. This renders them promising for the use as information carriers in future magnetic data storage and processing technologies, referred to as Skyrmionics. To better understand the physics of Skyrmions, a detailed knowledge of the real space magnetic structure of these spin solitons is mandatory. We have therefore studied the 3D magnetic textures of Skyrmion tubes (SkTs) using in-line and off-axis electron holography (EH). While the orientation of the in-plane magnetic induction B obtained from a $Fe_{0.95}Co_{0.05}Ge$ nanoplate using in-line EH shows the expected hexagonal vortex-like pattern (Fig. 1), a thorough quantitative analysis implies that the underlying 3D texture deviates from that of homogeneously extended Bloch Skyrmions [3]. Low temperature holographic vector field electron tomography (VFET [4]) in an external magnetic field was therefore used to quantitatively reconstruct the full 3D magnetic texture of SkTs in an FeGe needle [5]. The resulting high-resolution 3D magnetic images (Fig. 2) reveal various previously unseen details of the SkTs. Our findings include the occurrence of local deviations from a homogeneous Bloch character within the tubes. They highlight the collapse of the Skyrmion texture upon approaching the surfaces of the needle, provide evidence for the coexistence of longitudinal and transverse Skyrmion textures, and reveal an axial modulation of the SkTs that is found to be strongly correlated among neighboring tubes in the needle. Based on the quantitative 3D magnetic induction data, we have calculated spatially resolved energy density maps across the SkTs that provide experimental evidence for the energetic stabilization of these magnetic solitons through an energy gain due to the Dzyaloshinskii-Moryia interaction, which overcompensates the exchange energy in the tube centers.

Financial support by the German Research Foundation (DFG) through SPP2137 (#LU-2261/2-1, #RE-1164/6) and by the European Research Council (ERC, grant #715620) is gratefully acknowledged. [1] A.N. Bogdanov and A. Hubert, J. Magn. Magn. Mater. 138, 225 (1994). DOI: 10.1016/0304-8853(94)90046-9 [2] N. Nagaosa and Y. Tokura, Nat. Nanotechnol. 8, 899 (2013). DOI: 10.1038/nnano.2013.243 [3] S. Schneider et al., Phys. Rev. Lett. 120, 217201 (2018). DOI: 10.1103/PhysRevLett.120.217201 [4] D. Wolf et al., Commun. Phys. 2, 87 (2019). DOI: 0.1038/s42005-019-0187-8 [5] D. Wolf et al., arXiv:2101.12630 [cond-mat.mtrl-sci]

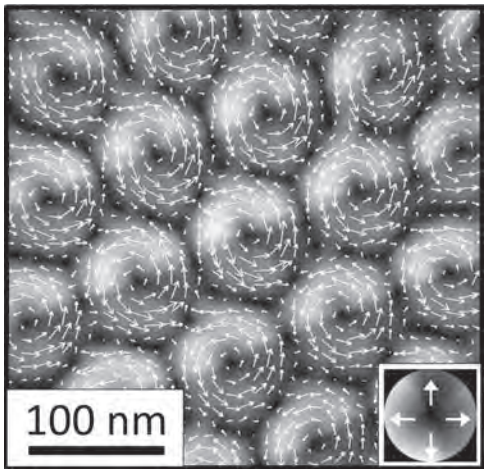

Fig. 1 Orientation map of the projected in-plane component of the magnetic induction in the hexagonal Skyrmion lattice of a $Fe_{0.95}Co_{0.05}Ge$ nanoplate.

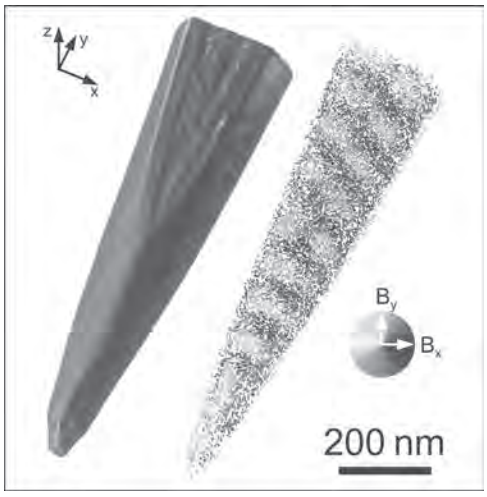

Fig. 2 Morphology of an FeGe needle (left) and direction of the 3D magnetic induction <u>B</u> (right) as determined from holographic VFET experiments.

GOG-11. Tuning of the Dzyaloshinskii-Moriya interaction by He^+ ion irradiation. *H. Nembach*[1,2], E. Jué[1,2], K. Potzger[3], J. Fassbender[3], T. Silva[1] and J.M. Shaw[1] *1. NIST, Boulder, CO, United States; 2. Department of Physics, University of Colorado, Boulder, CO, United States; 3. Institute of Ion Beam Physics and Materials Research, Helmholtz-Zentrum Dresden - Rossendorf, Dresden, Germany*

Skyrmions have received significant attention over the last years mostly motivated by their potential for future non-volatile memories, where the individual bits are represented by skyrmions The Dzyaloshinskii-Moriya Interaction (DMI) stabilizes skyrmions and determines their chirality. Here, we demonstrate, that the DMI can be increased by approximately 20% using by He^+ ion irradiation[1]. This underlines the importance of interface roughness and intermixing for the DMI and provides the opportunity for local modification of the DMI. We prepared a Ta(3 nm)/$Co_{20}Fe_{60}B_{20}$(1.9 nm)/Pt(3.5 nm)/MgO sample, which was diced in multiple coupons for irradiation with 40 keV He^+ ions with a fluence up to 10^{16} ions/cm^2. We measured the spin-wave frequencies for both field polarities in the Damon-Eshbach geometry post ion-irradiation with Brillouin Light Scattering (BLS) to determine the DMI magnitude at the interface, h is Planck's constant, g the spectroscopic splitting factor, the Bohr magneton, mm^{-1} the wavevector of the spinwaves and m_A the magnetic moment per area. m_A is readily obtainable from SQUID measurements without any assumptions about the thickness of the ferromagnet, which potentially changes during ion-irradiation due to intermixing. D_{int} increases from its initial magnitude before it decreases for the highest fluence, see Fig. 1. In order to get a better understanding of the role of the anisotropic FM-Pt-FM triplets, where FM stands for Co or Fe, we carried out Monte-Carlo simulations to determine how the number of these triplets evolves with ion-irradiation. First the displacement of the atoms with increasing fluence was calculated and based on these results the number of triplets was determined, see Fig. 2. Even though, the triplets are the fundamental building block for the DMI, the number decreases montonically in contrast to D_{int}. We conclude that the increase in DMI cannot be explained by a simple increase in the effective number of anisotropic triplets near a more diffuse Co/Pt interface and more subtle details in the electronic structure need to be considered.

[1] H.T. Nembach et al., arXiv:2008.06762v1

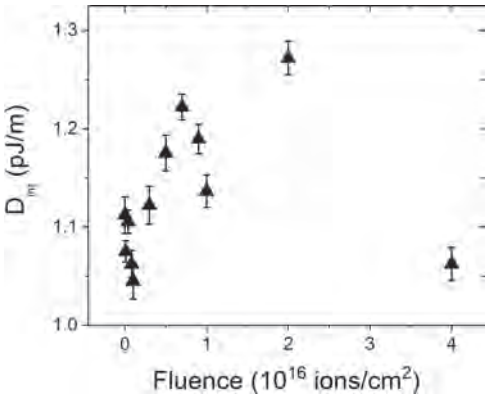

Fig.1: Evolution of D_{int} with increasing fluence.

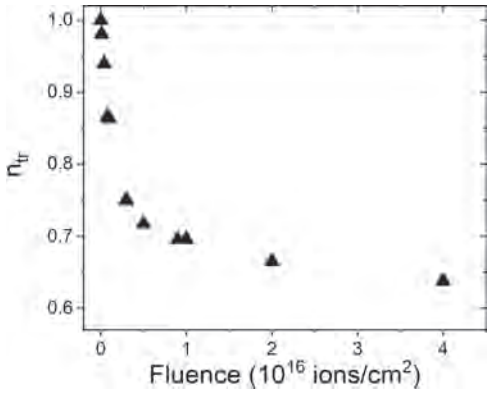

Fig. 2: Decrease of the anisotropic FM-Pt-FM triplets with ion-irradiation.

GOG-12. Influence of Ga+ Ion Irradiation on Skyrmion Motion. *V. Ahrens*[1], L. Gnoli[2], D. Giuliano[2], S. Mendisch[1,3], M. Kiechle[1], F. Riente[2] and M. Becherer[1] *1. Department of Electrical and Computer Engineering, Technical University of Munich, Munich, Germany; 2. Department of Electronics and Telecommunications, Politecnico di Torino, Torino, Italy; 3. Infineon Technologies AG, Neubiberg, Germany*

Focused ion beam (FIB) irradiation is a versatile means to tune magnetic thin films on the nanoscale [1]. Ion irradiation can create nucleation sites for Skyrmions [2] and even establish Skyrmion-tracks [3]. In this work, we present statistical data of Skyrmion motion driven by 50 ns long current pulses in a sputtered W/CoFeB/MgO trilayer. In this layers a Skyrmion phase can be stabilized by a an oop-field in the low single digit mT regime. Furthermore, we elaborate on how Skyrmion motion can be tuned and directed by non-destructive Ga^+ Ion irradiation with ultra-low doses (<1e13 Ions/cm^2) and high dose resolution of < 1e12 Ions/cm^2. First, we will give an overview of how the magnetic properties of the thin film are affected by ion irradiation. Here we analyze the average domain size, film coercivity (H_c) and relative decrease of saturation magnetization (M_s) and effective magnetization (M_{eff}), over different irradiation steps and compare this data to stepwise annealing of the samples. Next, we track the motion of at least 50 Skyrmions for various current densities in magnetic wires, utilizing wide-field magneto-optical measurements, as depicted in Figure 1. Hereby half of the wire is treated with Ga^+ ions. We show that ion irradiation can be used to adjust the motion of Skyrmions towards lower velocities. While the Skyrmion velocity is very similar in the pristine parts of the wires, the velocity in the irradiated region is heavily dependent on the ion dose (see Figure 2). This lower velocity is accompanied by a significantly reduced Skyrmion Hall angle in the irradiated part, which leads to a nearly straight motion in the direction of the current flow. Beyond that, also stochastical motion due to thermal effects is largely supressed in the irradiated parts.

[1] Fassbender, J., & McCord, J. *Journal of Magnetism and Magnetic Materials*, Vol. *320*(3-4), p. 579-596 (2008) [2] Fallon, Kayla, et al. *Small* Vol. 16(13), p.1907450 (2020) [3] Juge, Roméo, et al., *Nano Letters*, Vol. 21(7), p. 2989-2996 (2021)

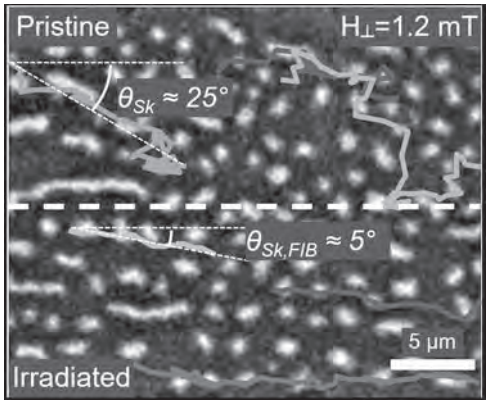

Fig. 1 Frame of a WMOKE movie at a constant 1.2 mT oop-field to stabilize Skyrmions. Exemplary Skyrmion tracks are shown as an overlay. The mean Skyrmion Hall angle θ_{Sk} is given for both the upper unirradiated and the lower irradiated part.

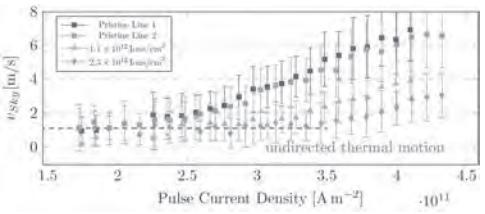

Fig. 2 Plot of the Skyrmion velocity over the current density of the driving pulses for the two pristine parts of wires (light and dark blue), one irradiated with 1e12 Ions/cm² (green), and one with 2e12 Ions/cm² (orange).

GOG-13. Facilitating Skyrmion Nucleation in Ir/Co/Pt Multilayers With Ga⁺ Ion Irradiation. *M.C. de Jong*[1], B.H. Smit[1], M.J. Meijer[1], J. Lucassen[1], J. van Liempt[1], H. Swagten[1], B. Koopmans[1] and R. Lavrijsen[1]
1. Department of Applied Physics, Eindhoven University of Technology, Eindhoven, Netherlands

Skyrmions are topologically protected chiral spin textures that have shown promise as data carriers in future spintronic applications. They can be stabilized by the interfacial Dzyaloshinskii-Moriya interaction (iDMI) in material systems with inversion asymmetry and spin-orbit coupling, such as Ir/Co/Pt multilayers [1]. The ability to locally (at the nanoscale) tune such interface interactions, and hence the skyrmion energy, could lead to novel ways to optimise the nucleation and control of skyrmions. In this contribution we investigate the local tuning of the iDMI and the perpendicular magnetic anisotropy (PMA) using Ga⁺ ion irradiation, as well as its effect on skyrmion nucleation. Ga⁺ ion irradiation affects the coordination of atoms at the interfaces (Fig. 1a), which is expected to decrease both PMA and iDMI [2]. From Fig. 1b, we find that the reduction in PMA and iDMI are correlated, suggesting that both effects depend similarly on the interface quality. This reduces the energy cost of domain walls but does not affect their chirality. Hence, we expect that this will also facilitate the nucleation of more complicated chiral textures, such as skyrmions. To confirm this, we studied for the first time the current driven nucleation of skyrmions [3] in identical devices with and without Ga⁺ ion irradiation. We find that the ion irradiation indeed affects skyrmion nucleation, see Fig. 2. The critical current density required for nucleation is reduced by almost 30% and the number of skyrmions is doubled by irradiation. Thus, we argue that ion irradiation can be used to facilitate and control the nucleation of skyrmions in novel devices.

[1] C. Moreau-Luchaire, C. Moutafis, N. Reyren, et al., *Nature Nanotechnology*, Vol. 11, p. 444-448 (2016) [2] X. Zhao, B. Zhang, N. Vernier, et al., *Applied Physics Letters,* Vol. 115, 122404 (2019) [3] W. Legrand, D. Maccariello, N. Reyren, et al., *Nano Letters*, Vol. 17, p. 2703-2712 (2017)

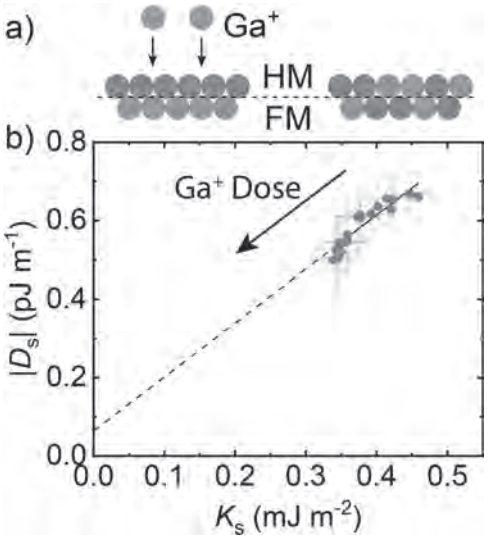

Fig. 1 a) Illustration: Ion irradiation causes intermixing at interfaces (left to right). b) Plot of the strength of the iDMI D_s against the strength of the interface PMA K_s, both D_s and K_s decrease when the Ga⁺ dose is increased, as indicated by the arrow.

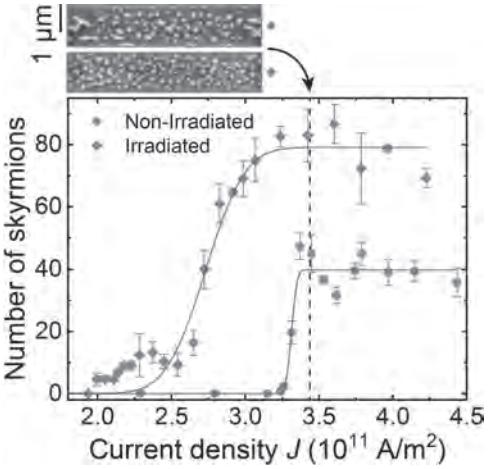

Fig. 2 Number of skyrmions nucleated in our devices after applying 1000 50 ns pulses with current density *J*. In an irradiated device the number of skyrmions is increased and the current density required for nucleation is lowered. Black lines are fits to the data with the error function. Top: MFM scans of the devices.

Session GOH
SPIN DYNAMICS
Jun'ichi Ieda, Chair
Japan Atomic Energy Agency, Tokai, Japan

INVITED PAPER

GOH-01. Latest Strides on Magnon-Phonon Coupling (acoustic): Spin current, Nonreciprocity and Nonlinearity. *J. Puebla*[1], M. Xu[2,1], Y. Hwang[2,1], K. Yamamoto[3,1], S. Maekawa[1,4] and Y. Otani[2,1] *1. Center for Emergent Matter Science, RIKEN, Wako, Japan; 2. Institute for Solid State Physics, University of Tokyo, Kashiwa, Japan; 3. Advanced Science Research Center, Japan Atomic Energy Agency, Tokai, Japan; 4. Kavli Institute for Theoretical Sciences, University of Chinese Academy of Sciences, Beijing, China*

In this contribution, I present our most recent research on magnon-phonon coupling. A fundamental form of magnon-phonon interaction is an intrinsic property of magnetic materials, the "magnetoelastic coupling." This form of interaction has been the basis for describing magnetostrictive materials and their applications, where strain induces changes of internal magnetic fields. Different from the magnetoelastic coupling, more than 40 years ago, it was proposed that surface acoustic waves may induce surface magnons via rotational motion of the lattice in anisotropic magnets [1]. However, a signature of this magnon-phonon coupling mechanism, termed magneto-rotation coupling, has been elusive. We recently demonstrated a nonreciprocal acoustic wave attenuation with an unprecedented ratio of up to 100% rectification, which is understood as consequence of the magneto-rotation coupling [2,3]. Figure 1 illustrates the concept of magneto-rotation coupling. Considering the wide application of the general acoustic device in sensing, filtering, and information transportation, the intriguing nonreciprocal features of our magneto-rotation devices suggest an extraordinary versatility of acousto-magnetic applications. Regarding spin current. As it is well-known, the coupling of surface acoustic waves with a ferromagnet acts as a method of spin current generation via acoustic ferromagnetic resonance [4,5]. An intriguing scenario to explore is the spin current generation when the strength of magnon-phonon coupling is enhanced. We have carefully engineered an acoustic wave device in the presence of acoustic cavity. An acoustic cavity is formed by placing two acoustic reflectors separated by a distance equal to a multiple of the acoustic wavelength of our device. In our acoustic cavity device, we observed enhancements of up to two times in acoustic ferromagnetic resonance and up to three times more spin current generation compared with a non-cavity reference device [6]. Figure two shows the comparison of output voltage obtained with (blue circles) and without (red squares) acoustic cavity. The apparent discrepancy between the enhancements of energy absorption in acoustic ferromagnetic resonance (two times) and the enhancements of spin current generation (three times), is an open question. Beyond the enhancement of spin current generation, improvements of magnon-phonon coupling towards the strong coupling regime can have important consequences such as early on-sets of nonlinear effects, enhancement of magnon propagation length, condensation and transfer of coherent phase information.

[1] S. Maekawa and M. Tachiki, AIP Conference Proceedings 29, 542 (1976) [2] M. Xu, K. Yamamoto, J. Puebla, Science Advances 6 (32), eabb1724 (2020) [3] K. Yamamoto, W. Yu, T. Yu, Journal of the Physical Society of Japan 89 (11), 113702 (2020) [4] J. Puebla, M. Xu, B. Rana, Journal of Physics D: Applied Physics 53 (26), 264002 (2020) [5] M. Xu, J. Puebla, F. Auvray, Phys. Rev. B 97, 180301(R), Rapid Communications (2018) [6] Y. Hwang, J. Puebla, M. Xu, Applied Physics Letters 116, 252404, Editors Choice (2020)

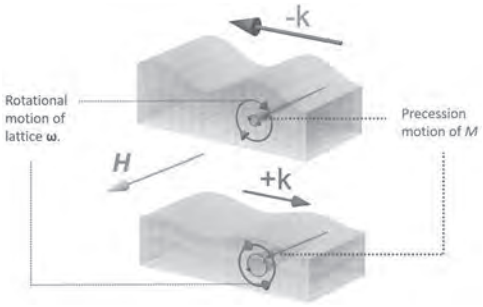

Fig. 1 Schematics of the magneto-rotation coupling. Depending on the propagation direction, SAWs rotate the lattice in opposite directions (as indicted by the blue and red oriented cycles in the figure). This rotational motion couples with the magnetization via magnetic anisotropies, giving rise to a circularly polarized effective field, which either suppresses or enhances the magnetization precession (purple cone), and, in turn, induces a nonreciprocal attenuation on the SAWs.

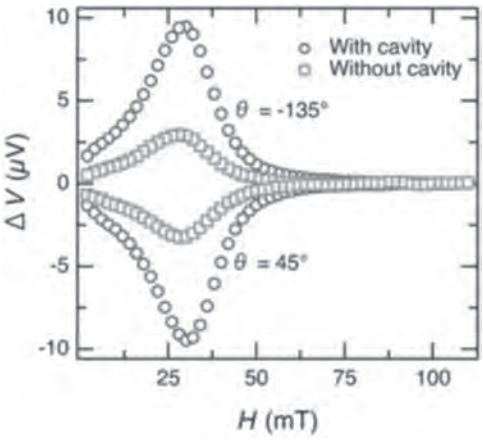

Fig. 2 Enhancement of spin current by an acoustic cavity. Detected electric voltage when a 10 mW of RF power is applied to generate surface acoustic waves (SAW) and an external in-plane magnetic field θ= 45° and 135° is applied with respect to the SAW wavevector. Data are taken from samples with acoustic cavity (blue circles), and without (red squares) acoustic cavity.

CONTRIBUTED PAPERS

GOH-02. Broadband terahertz spectroscopy of anisotropic magnetoresistance reveals intrinsic contributions. *L. Nadvornik*[1,2], M. Borchert[2,3], L. Brandt[4], R. Schlitz[5], K. de Mare[6,7], K. Výborný[6], I. Mertig[4], G. Jakob[8], M. Kläui[8], S.T. Goennenwein[5], M. Wolf[3], G. Woltersdorf[4] and T. Kampfrath[2,3] *1. Faculty of Mathematics and Physics, Charles University, Prague, Czechia; 2. Department of Physics, Freie Universität Berlin, Berlin, Germany; 3. Department of Physical Chemistry, Fritz Haber Institute of the Max Planck Society, Berlin, Germany; 4. Institut für Physik, Martin-Luther-Universität, Halle, Germany; 5. Institut für Festkörper- und Materialphysik, Technische Universität Dresden, Dresden, Germany; 6. Institute of Physics, Academy of Sciences of the Czech Republic, v.v.i., Prague, Czechia; 7. Department of Applied Physics, Eindhoven University of Technology, Eindhoven, Netherlands; 8. Institut für Physik, Johannes Gutenberg-Universität Mainz, Mainz, Germany*

Anisotropic magnetoresistance (AMR) is a ubiquitous and versatile probe of magnetic order in contemporary spintronics research [1]. It arises from the dependence of the resistance of a magnetically ordered solid on the relative angle between the applied electric field and the magnetization vector independent of their polarity. The origins of the AMR are usually ascribed to extrinsic effects (i.e. spin-dependent electron scattering), whereas intrinsic (i.e. scattering-independent) contributions are neglected [2]. Here, we perform a broadband measurement of the AMR of prototypical ferromagnets such as Co, Ni or NiFe alloys in a frequency range from DC to 28 THz [3]. The large bandwidth covers the regimes of both diffusive and ballistic intraband electron transport and, thus, allows us to separate extrinsic and intrinsic AMR components. Analysis of the THz response based on Boltzmann transport theory reveals that the AMR of the Ni and NiFe alloys is of predominantly extrinsic nature. However, the Co thin film exhibits a sizeable intrinsic, frequency-independent AMR contribution, which amounts to more than 2/3 of the DC AMR contrast of 1%. These features are attributed to the lower symmetry of the hexagonal structure of Co crystallites which allows for larger anisotropies in their bandstructure. The new insight into the nature of AMR is not only relevant for the fundamental understanding of the magnetotransport but might also advance the ultrafast probing techniques in spintronic devices.

[1] T. Jungwirth, X. Marti, P. Wadley, and J. Wunderlich, Nature Nanotech. 11, 231 (2016). [2] T. R. McGuire and R. I. Potter, IEEE Trans. Mag. 11, 1018 (1975). [3] L. Nádvorník, M. Borchert, L. Brandt et al., Phys. Rev. X 11, 021030 (2021).

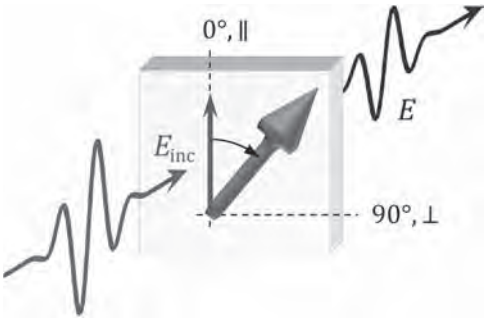

Fig. 1. THz detection of the AMR. The incident THz pulse applies transient electric field in the direction of polarization, in which, as a consequence of the AMR, the electrical resistance and the transmission of the THz pulse depend on the angle of the magnetization. Variations in transmitted amplitude allow us to calculate the AMR contrast.

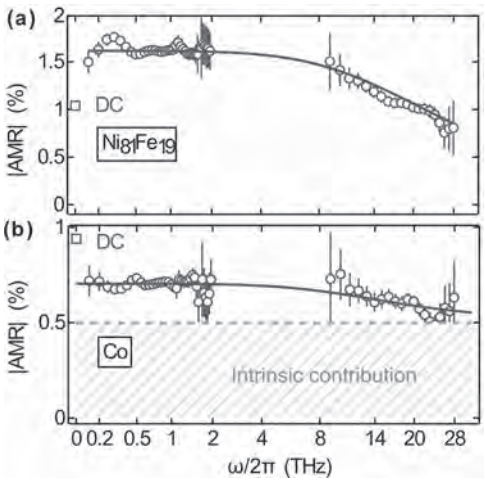

Fig. 2. Spectral composition of the AMR in different metals. (a) The absolute value of the AMR contrast in permalloy versus frequency is well described within the Drude formalism (curve) assuming only magnetization-dependent electron scattering rates. (b) The same measurement for a cobalt sample shows a scalable frequency-independent offset which witnesses the intrinsic contribution to the AMR.

GOH-03. Magnetically switchable ultrafast spintronic THz emitters. *M. Fix*[1], R. Schneider[2], J. Bensmann[2], S. Michaelis de Vasconcellos[2], R. Bratschitsch[2] and M. Albrecht[1] *1. Institute of Physics, University of Augsburg, Augsburg, Germany; 2. Institute of Physics and Center for Nanotechnology, University of Münster, Münster, Germany*

The recent discovery of ultrafast spintronic THz emitters has attracted a lot of attention due to their high power and broadband emission as well as easy fabrication [1,2]. They are based on nanometer-thin bilayers of a ferro-/ferrimagnetic (FM) and a nonmagnetic (NM) metal layer and rely on the inverse spin Hall effect. The THz emission properties can be tuned by using different FM and NM materials, tailoring the magnetic properties [3], or building functional layer stacks [4]. Here, we present a spin valve THz emitter (see fig. 1), which allows for switching of the THz emission amplitude by a small magnetic field [5]. The operation of the switchable THz emitter is based on a magnetically soft free Fe layer and a pinned Fe layer, which is exchange biased by an antiferromagnetic $Ir_{0.23}Mn_{0.77}$ film. The Fe layers are magnetically decoupled from each other by thin NM spacer layers of Pt or W that exhibit a large spin Hall angle. Excitation of the structure with ultrashort optical laser pulses leads to the creation of spin currents from the two Fe layers into the sandwiched NM film. There, the spin currents are converted into ultrafast charge currents by the inverse spin Hall effect. Depending on the relative magnetization direction of the two Fe layers, and hence the polarization of the spin currents, these charge currents add up (fig. 1a) or cancel each other out (fig. 1b), leading to a high or vanishing THz emission. The relative magnetization alignment can be controlled by switching the free Fe layer with applied magnetic fields on the order of 10 mT, while the magnetization direction of the pinned Fe layer remains constant due to the exchange bias. Therefore, the system allows the switching from the low to the high amplitude THz emission state by small applied magnetic fields, enabling easy implementation and high switching rates. Thus, our study combines the high power and broadband emission of ultrafast spintronic THz emitters with an easy-to-use switching mechanism.

[1] T. Seifert, S. Jaiswal, U. Martens *et al.*, Nat. Photonics 10, 483 (2016) [2] D. Yang, J. Liang, C. Zhou *et al.*, Adv. Opt. Mater. 4, 1944 (2016) [3] R. Schneider, M. Fix, J. Bensmann *et al.*, Appl. Phys. Lett. 115, 152401 (2019) [4] M. Fix, R. Schneider, J. Bensmann *et al.*, Appl. Phys. Lett. 116, 012402 (2020) [5] M. Fix, R. Schneider, S. Michaelis de Vasconcellos *et al.*, Appl. Phys. Lett. 117, 132407 (2020)

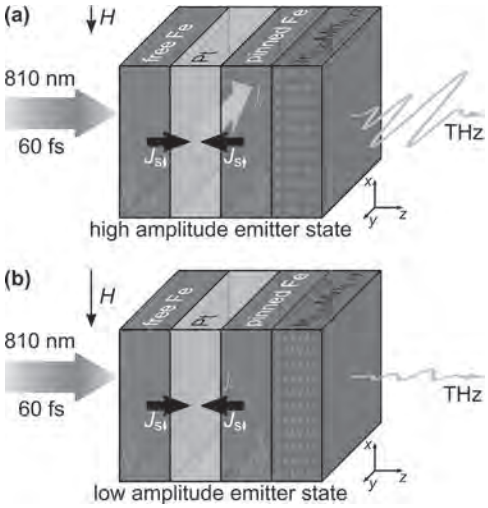

Fig. 1: Schematic illustration of the switchable spintronic spin-valve THz emitter for (a) the high and (b) the low amplitude THz emitting state, with the magnetization directions (red arrows), the spin currents J_S and the charge currents J_C.

GOH-04. Ferromagnetic resonance as a spectroscopic tool for investigating topological surface states. *L. Pietanesi*[1], R. Diaz-Pardo[1], T. Mayer[2], D. Bougeard[2], M. Kronseder[2] and C.H. Back[1] *1. Technical University Munich, Munich, Germany; 2. University of Regensburg, Regensburg, Germany*

Topological Insulators (TIs) [1,2] are characterized by a bulk bandgap and metallic surface states (TSSs) that exhibit spin-momentum locking, and therefore are predicted to be very efficient in spin-to-charge interconversion phenomena. A very challenging task when using Bi-based TIs for spintronic devices is to disentangle bulk and surface contributions, due to unintentional bulk doping effects [3]. In this work, following the p-n junction approach proposed in [4], we use ferromagnetic resonance (FMR) as a spectroscopic tool to selectively probe spin-pumping into TSSs. The samples investigated are $SrTiO_3/Bi_2Se_3(1)/(Bi_{1-x}Sb_x)_2(Te_{1-y}Se_y)_3(10)/NiFe(10)$ hetorostructures, where the numbers in parenthesis indicate the thickness in nm. We vary the Sb concentration x: for low x, BSTS is n-type; for x>0.55, the Fermi level (E_F) in the p-n junction moves from the bulk conduction band (CB) into the gap at the top surface. We perform frequency dependent FMR measurements, and extract the Gilbert damping parameter α at different temperatures. The result is shown in Fig.1: α shows almost constant behavior above 150K, and increases at lower temperatures, where the bulk states contribution becomes less important and the TSSs conduction is dominant, revealing the higher spin-pumping efficiency of TSSs compared to the bulk states. We measure FMR while back-gating the p-n junction on samples with x values such that E_F is placed in the bulk bandgap. The behavior of α versus applied voltage is shown in Fig.2 for two different x. α is minimum when E_F reaches the Dirac point, and it increases away from this point due to a higher in TSS's DOS. The spectra for the two samples are shifted in voltage, confirming that for lower concentrations E_F lies closer to the CB. When the applied back-gate voltage is large enough to shift E_F inside the bulk bands, α saturates, due to the high bulk conductivity of the structure screening the electric field. In conclusion, we showed that we can use FMR as a spectroscopic tool to selectively probe spin-pumping from a ferromagnet into the TSSs of a TI, drastically reducing bulk contributions.

[1] L. Fu, CL Keane, Phys. Rev. B, Vol 76, pp. 045302 (2007) [2] J.E. Moore, Nature, Vol 464, pp. 194-198, (2010) [3] D. O. Scanlon, P. D. C. King et al., Adv. Mater., Vol 24, pp. 2154 (2012). [4] T. Mayer, H. Werner, F.Schmidt et al., Phys. Rev. Mat., Vol 5, pp. 014202 (2021)

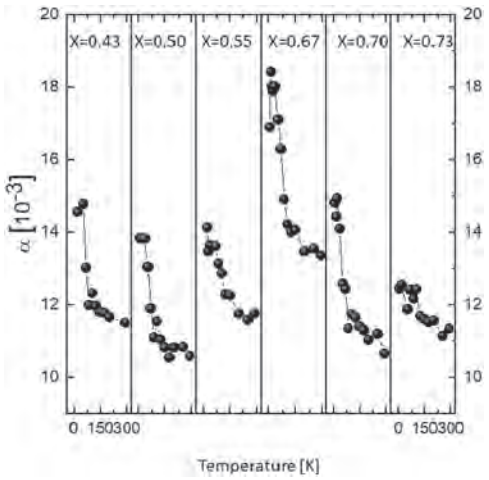

Fig. 1 Temperature dependence of α for different concentrations

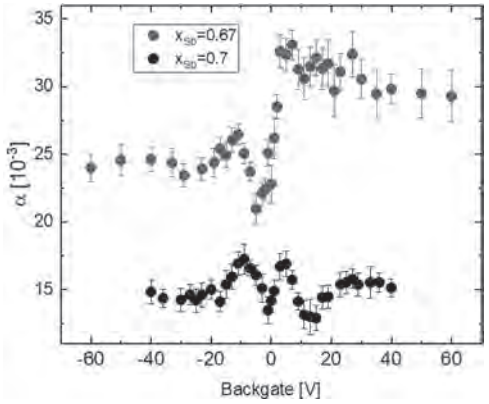

Fig. 2 Backgate dependence of α for two different Sb concentrations

GOH-05. Simultaneous electrical and optical detections of spin-torque ferromagnetic resonance. *Y. Shiota*[1], R. Hisatomi[1], T. Moriyama[1] and T. Ono[1] *1. Institute for Chemical Research, Kyoto University, Uji, Japan*

Spin-torque ferromagnetic resonance (ST-FMR) by means of an electrical homodyne detection has widely been used to study the magnetic properties and spin-torque efficiency. By exerting an oscillating spin-torque (*e.g.* spin-transfer-torque [1], spin-orbit-torque [2], and voltage-torque [3]) on the magnetic moment at the resonance conditions, a rectified dc voltage is generated as a result of mixing between the microwave current and resentence oscillation. In this study, we performed the ST-FMR measurement in Pt/Py bilayer structures with the electrical homodyne detection and optical heterodyne detection simultaneously, and investigated the spatially-resolved spin precession dynamics. We prepared Py(5 nm) / Pt(6 nm) films grown on a thermally oxidized Si substrate by magnetron sputtering. The film was patterned into a 5-μm-wide strip with a coplanar waveguide. Figure 1(a) shows the device and the measurement setup used in this study. In addition to the optical heterodyne detection path reported in our previous studies [4], the electrical homodyne detection path was incorporated. The electrical signal from the rectified voltage V_{dc} and the optical signal from the magneto-optical Kerr effect in the polar configuration S_{21} were recorded by sweeping the external magnetic field with fixed microwave frequency. Figures 1(b) and 1(c) show the simultaneously measured FMR spectra at various microwave frequencies. From the line-shape analysis, we found slightly different linewidths between electrical and optical signals, as shown in Fig. 2. From the spatial-resolved FMR measurements in the optical signal, we also found that the inhomogeneous broadening and the Gilbert damping constant depend on the position in the transverse direction. Our study shows that the ferromag-

netic resonance measurement based on the heterodyne-MOKE technique is a powerful tool for characterizing static and dynamic magnetic properties of magnetic thin films with a sub-micron spatial resolution.

[1] A.A. Tulapurkar *et al., Nature* 438, 339 (2005). [2] L. Liu *et al., Phys. Rev. Lett.* 106, 036601 (2011). [3] T. Nozaki *et al., Nat. Phys.* 8, 491 (2012). [4] Y. Shiota *et al., Appl. Phys. Lett.* 116, 192411 (2020), Y. Shiota *et al., Phys. Rev. B* 102, 214440 (2020)

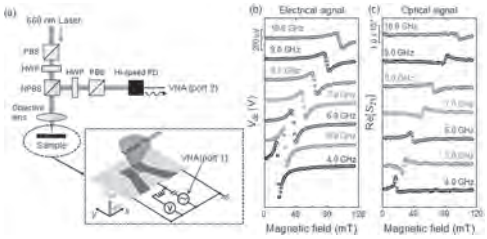

Fig. 1 (a) Measurement setup (b)(c) Electrical and optical signals of ST-FMR spectra.

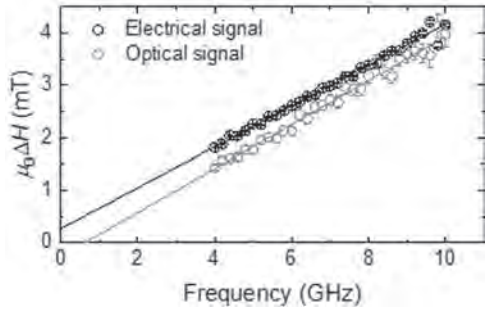

Fig. 2 (a) Microwave frequency dependence of linewidth obtained from electrical (square) and optical (circle) signals.

GOH-06. DC voltage generated by the unidirectional spin Hall magnetoresistance in the spin torque ferromagnetic resonance spectrum. *M. Aoki*[1], Y. Ando[1], E. Shigematsu[1], R. Ohshima[1], T. Shinjo[1] and M. Shiraishi[1] *1. Electronic Science and Engineering, Kyoto University, Kyoto, Japan*

Spin torque ferromagnetic resonance (ST-FMR)[1] has widely been used for evaluation of the spin Hall effect (SHE) of the nonmagnetic metal (NM) in an NM/ferromagnetic metal (FM) bilayer structure. Figure 1 shows a schematic of the measurement setup of the ST-FMR. DC voltage, V_{DC}, is monitored under a microwave irradiation with sweeping the external magnetic field, B_{ext}. V_{DC}-B_{ext} curve in the ST-FMR measurement is composed of symmetric and anti-symmetric Lorentzian functions. In the simplest case, efficiency of the SHE, which is especially called spin Hall angle (SHA), can be estimated by taking the amplitude ratio between two Lorentzian functions. However, unwanted effects such as the spin pumping, the anomalous Nernst effect, and non-uniform flow of the charge current impede a precise estimation of SHA. Therefore, a cross-check of the obtained SHA by using another methodology is desired. In this study, we found an additional signal related to the SHA in the ST-FMR spectrum[2]. Figure 2 shows the ST-FMR spectrum of a tantalum (Ta)/cobalt (Co) sample, where the microwave frequency, f, was 12 GHz and the microwave power, P, was 5 dBm. l, w, and q defined as shown in Fig. 1 were 5 μm, 5 μm, and 45°, respectively. In addition to the conventional Lorentzian functions which correspond to the ST-FMR, a magnetization-dependent background (BG) signal was also observed. From the B_{ext}, P, f, temperature and NM material dependences, we conclude that the BG signal is mainly generated by the spin-dependent unidirectional spin Hall magnetoresistance (SD-USMR)[3], the origin of which is the spin-dependent electron mobility in the FM. From the magnitude of the BG signal, SHA of Ta was estimated to be -0.042±0.006, which is consistent with the previous works. The ST-FMR spectrum is produced by the spin orbit torque, whereas the BG signal is produced by the spin accumulation. Therefore, our finding provides an effective cross-check of the SHA, which are obtained from two different physical origins by using only one ST-FMR spectrum.

[1] L. Liu, T. Moriyama, D. C. Ralph and R. A. Buhrman, Phys. Rev. Lett. 106, 036601 (2011). [2] M. Aoki, E. Shigematsu, R. Ohshima, T. Shinjo, M. Shiraishi and Y. Ando, Phys. Rev. B, submitted. [3] C. O. Avci, K. Garello, A. Ghosh, M. Gabureac, S. F. Alvarado and P. Gambardella, Nat. Phys. 11, 570 (2015).

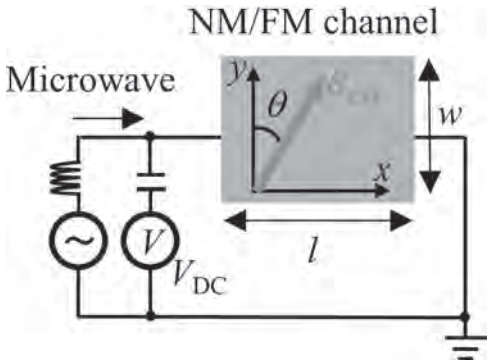

Fig. 1 A schematic of the device and the electrical circuit used in the ST-FMR measurement

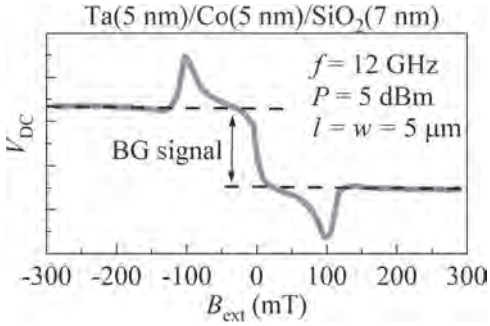

Fig. 2 ST-FMR spectra with the BG signal originating from the SD-USMR for Ta/Co.

GOH-07. Alloying effect on auto-oscillation properties of $W_{100-x}Ta_x$/CoFeB/MgO spin Hall nano-oscillators. *N. Behera*[1], H. Fulara[1], M. Zahedinejad[1], A. Houshang[1] and J. Åkerman[1] *1. Physics, University of Gothenburg, Gothenburg, Sweden*

Pure spin currents produced by the spin Hall effect(SHE) in a nonmagnetic heavy metal has the potential to drive ultra-fast, energy-efficient spintronic devices such as spin Hall nano-oscillators(SHNOs)[1-3], spin-orbit torque based magnetic random access memory(SOT-MRAM), and spin logic devices[4,5]. One key challenge in such emerging devices remains to reduce their high current densities(J_c) and energy consumption to drive magnetization switching and auto oscillations in the adjacent ferromagnets. Efforts have been made to increase the SOT efficiency(ζ_{SOT}) by choosing suitable material combinations and/or use oxygen incorporation[6]. However, the increased ζ_{SOT} is observed at the expense of an equivalent increase in the longitudinal resistivity(ρ), which essentially cancels out any reduction in the power consumption. A more successful direction is instead to alloy elements, which are in themselves already good SOT material[7]. Here, we demonstrate such alloying of W with Ta to obtain a simultaneous increase of both the ζ_{SOT} and the spin Hall conductivity(σ_{SH}), which in turn substantially reduces the J_c in $W_{100-x}Ta_x$(5nm)/CoFeB(t_{CFB}=1.4 to 2 nm)/MgO(2nm) SHNOs. First, we performed STFMR measurements on microbars (6 ×18 μm^2, 6 ×12 μm^2) to determine their magnetodynamical properties such as current induced ζ_{SOT} and σ_{SH}. The ζ_{SOT} varies from maximum ~ -0.57(x=10%) to ~-0.18(x = 50%) as compared to pure β-W, ~-0.36(x=0). Thanks to a reduced resistivity of

$W_{100-x}Ta_x$, the increased ζ_{SOT} is accompanied with a significant increase of the σ_{SH} of about ~140% as compared to pure β-W. Finally, we investigated the alloying effect on the auto-oscillation threshold current(I_{th}) densities by fabricating SHNOs of different widths varying from 10nm to 150nm on a 4 × 14 μm^2 mesa[1] and observed about 40% reduction in I_{th} (at x=12%) as compared to pure β-W measured. The trade-off between ζ_{SOT}, ρ, and σ_{SH} demonstrates the promising aspects of a W-Ta alloying approach for energy-efficient operation of emerging spintronic devices.

1. H Mazraati, S Chung, and J. Åkerman, Appl. Phys. Lett. Vol. 109, p. 242402 (2016). 2. H. Fulara, M. Zahedinejad, and J. Åkerman, Sci. Adv. Vol. 5, p. eaax8467 (2019). 3. M. Zahedinejad, A. A. Awad and J. Åkerman, Nat. Nanotechnol. Vol. 15, p.47–52 (2020). 4. K. Garello, C. O. Avci, and P. Gambardella, Appl. Phys. Lett. Vol. 105, p. 212402 (2014). 5. M. Cubukcu, O. Boulle and G. Gaudin, Appl. Phys. Lett. Vol. 104, p. 042406 (2014). 6. K. Demasius, T. Phung, and S. S. Parkin, Nat. Commun. Vol. 7, p. 10644 (2016). 7. J. Kim, D. Han, and M. Kläui, Appl. Phys. Lett. Vol. 117, p. 142403 (2020).

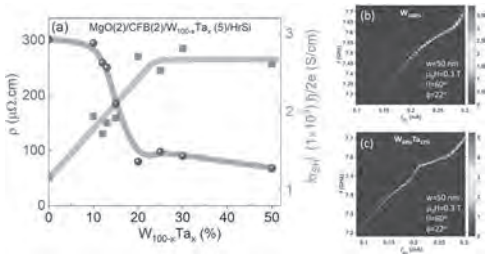

Fig.1: (a) Variation of ρ(blue) and σ_{SH}(red) vs. $W_{100-x}Ta_x$ alloy composition. (b-c) Power spectral densities showing a 40% reduction in the SHNO I_{th} for two SHNOs with identical constriction width of 50nm.

GOH-08. Study of Spin-Orbit Interactions and Multilevel Switching in Co/Pt/Co trilayer. *K. Grochot*[1,2], P. Ogrodnik[1,3], L. Karwacki[4,5], P. Mazalski[6,7], J. Kanak[1], J. Checinski[1], W. Skowronski[1], S. Zietek[1] and T. Stobiecki[1,2] *1. Institute of Electronics, AGH University of Science and Technology, Cracow, Poland; 2. Faculty of Physics and Applied Computer Science, AGH University of Science and Technology, Cracow, Poland; 3. Faculty of Physics, Warsaw University of Technology, Warsaw, Poland; 4. Institute for Theoretical Physics, Utrecht University, Utrecht, Netherlands; 5. Institute of Molecular Physics, Polish Academy of Sciences, Poznan, Poland; 6. Jerzy Haber Institute of Catalysis and Surface Chemistry of the Polish Academy of Sciences, Cracow, Poland; 7. Faculty of Physics, University of Bialystok, Bialystok, Poland*

The magnetization dynamics of Co layers, magnetostatic features, and spin-orbit interactions within the multilayer system Ti(2)/Co(1)/Pt(0-4)/Co(1)/MgO(2)/Ti(2) (thicknesses in nanometers) patterned on micrometre-sized devices have been studied. Here, the Pt is used as a source of the spin current, and as a non-magnetic spacer whose variable thickness enables the magnitude of the ferromagnetic interlayer exchange coupling (IEC) to be effectively tuned [1]. From anomalous Hall effect (AHE), anisotropic magnetoresistance (AMR) and spin Hall magnetoresistance (SMR) measurements, we found that the increase in Pt thickness (t_{Pt}) leads to the reorientation of Co-magnetizations from the in-plane to the perpendicular direction at $t_{Pt} \approx 1.3$ nm. The further increase in Pt thickness, above 3 nm, reduces ferromagnetic coupling and, consequently, two weakly coupled Co layers become magnetized orthogonally to each other. The relevant simulations reproduced experimental results, whereas the provided diffusive model explained the SMR and AMR magnitudes to a satisfactory extent [2]. Next, the effective SOT field (field-like (HFL) and damping-like (HDL)) and the effective spin Hall angle were determined and analyzed as a function of Pt thickness (Fig.1). The experimental results were compared with the predictions of the spin diffusive model extended with the Rashba-Edelstein charge-to-spin conversion effect at interfaces. The results were discussed in terms of differences in Pt/Co and Co/Pt interfaces, also revealed by the structural characterization. Finally, we show that the asymmetry of both interfaces, the IEC and the domain structure, enable multi-level current (Fig.2) and field-free magnetization switching. This work was supported by NCS Poland, Grants No.: 2016/23/B/ST3/01430 and 2016/23/G/ST3/04196. KG acknowledge support for conference participation by the EU Project POWR.03.02.00-00-I004/16.

[1] S.Lazarski et al., Phys. Rev. Applied. Vol. 12, p.014006 (2019) [2] P.Ogrodnik et al., arXiv:2106.10103 (2021)

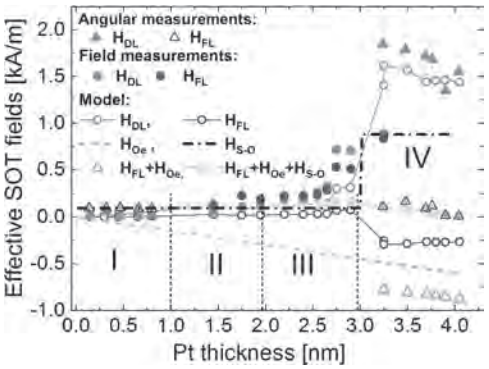

Fig.1 H_{DL} and H_{FL} determined from harmonics measurements and theoretical values from the spin diffusive model.

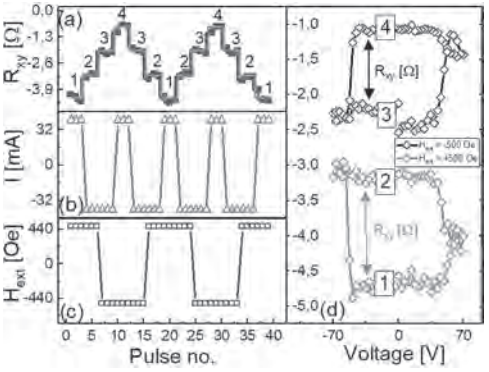

Fig.2 Multi-level current switching in Co/Pt(1.55)/Co (a) driven by combination of current (b) and magnetic field (c) between four stable resistance states (d).

GOH-09. Field-free Spin-orbit Torque-driven Multistate Switching of Canted GdCo Moments. *C. Hsu*[1], M. Alawein[1], S. Sayed[1,2] and S. Salahuddin[1,2] *1. Electrical Engineering and Computer Science, University of California, Berkeley, Berkeley, CA, United States; 2. Materials Sciences Division, Lawrence Berkeley National Laboratory, Berkeley, CA, United States*

Rare earth-transition metal (RETM)-based ferrimagnets are known to exhibit strong bulk perpendicular magnetic anisotropy and bulk Dzyaloshinskii-Moriya interaction [1]. These properties make RETM ferrimagnets a model system to study exciting magnetic phenomena such as magnetic skyrmion [2,3], chiral domain wall [3], all-optical switching [4], spin-orbit torque switching [5] and canted magnetic moments. Here, we demonstrate a field-free spin-orbit torque-driven multistate switching of a nearly compensated GdCo ferrimagnet sandwiched between Ta and Pt. We show that our GdCo film exhibits a strong canting of magnetic moments, and the canted moments can be deterministically switched among three stable states using a current-driven spin-orbit torque, even in the absence of a magnetic field. We further show that the three states persist in the presence of an in-plane magnetic field and the levels of the three states can be tuned with the magnitude of the magnetic field. We consider various possible origins of the canting, including concentration gradient, Dzyaloshinskii - Moriya

interaction, and balanced pair-correlations of unlike atoms versus like atoms in the growth direction, and discuss various methods to differentiate among these mechanisms. Furthermore, we discuss the possibility of domain formations to explain the observed multistate. Our results provide a new perspective to study the competing magnetic interaction in RETM-based ferrimagnetic alloys at the near-compensation point, and enable a new pathway to achieve multistate spin-orbit torque devices.

[1] D.H. Kim, M. Haruta, H.W. Ko, et al. Nature Materials., Vol. 18, p. 685–690 (2019) [2] L. Caretta, M. Mann, F. Büttner, et al. Nature Nanotechnology., Vol. 13, p.1154–1160 (2018) [3] A. Singh, J. C.T. Lee, K.E. Avila, et al. Nature Communications., Vol. 10, p.1988 (2019) [4] C.D. Stanciu, F. Hansteen, A. V. Kimel, et al. Physical Review Letters, Vol. 99, p.047601 (2007) [5] N. Roschewsky, C.H Lambert, S. Salahuddin. Physical Review B, Vol. 96(6), p. 1–5 (2017)

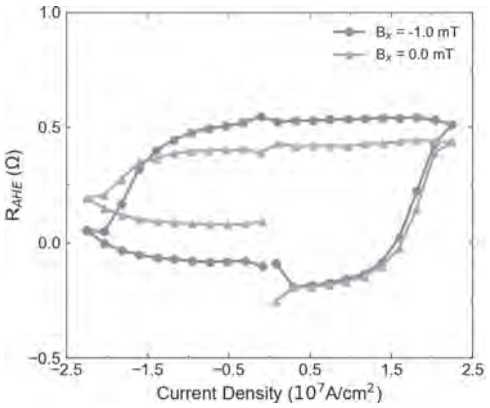

Multistate switching of canted GdCo moments via spin-orbit torque with zero in-plane symmetry breaking field.

GOH-10. Low power spin-orbit torque magnetization switching in all-sputtered BiSb topological insulator / perpendicularly magnetized CoPt / MgO multilayers on Si substrate. *F. Tuo*[1], N.H. Khang[1] and P. Nam Hai[1,2] *1. Tokyo Institute of Technology, Tokyo, Japan; 2. The University of Tokyo, Tokyo, Japan*

BiSb topological insulator is a promising candidate for spin-orbit-torque (SOT) magnetoresistive random-access memory (MRAM). A giant spin Hall angle θ_{SH} up to 52 and 10.7 has been observed for BiSb deposited by MBE on GaAs(111) [1] and by sputtering on c-plane Al_2O_3 [2] substrates, respectively. In realistic MRAM, however, magnetic tunnel junctions whose core structure includes an MgO barrier layer and a free ferromagnetic layer on top have to be deposited on Si/SiO_x substrates. In this work, we demonstrate the large θ_{SH} = 2.4 of BiSb in all-sputtered BiSb/CoPt/MgO multilayers on Si/SiO_x substrates, and investigate the SOT magnetization switching behaviors. Low power and fast switching is attained, demonstrating the robustness and reliability of BiSb as a spin current source. We deposited BiSb(10)/Pt(0.8)/Co(0.6)/Pt(0.8)/MgO(10) (Fig. 1(a)), from top to bottom on Si/SiO_x substrates at room temperature (thickness in nm). The Pt/Co/Pt trilayers are perpendicularly magnetized with a large anisotropy field of 4.5 kOe (Fig. 1 (b)(c)). Fig. 1(d) shows 2nd harmonic Hall resistance $R_2\omega$ - field H_x characteristics at different current density J^{BiSb}, and a representative fitting curve (dashed) for evaluation of the antidamping-like field H_{AD}. Fig. 1(e) shows the estimated H_{AD} at various J^{BiSb}, which yields θ_{SH} = 2.4. Fig. 2(a) shows the pulse width τ dependence SOT switching loop. The magnetization of CoPt trilayers can be efficiently switched by a small threshold current density J_{th}^{BiSb} = 2.3 MAcm^{-2} at pulse width of 50 ms. The J_{th}^{BiSb} - τ characteristics yields the thermal stability factor Δ = 32 (Fig. 2(b)). We also demonstrate robust switching by consecutive pulses (Fig. 2(c)) and fast switching down to 100 ns (Fig. 2(d)). Our work shows that it is possible to implement ultralow power SOT-MRAM using BiSb on Si/SiO_x substrates.

[1] N. H. D. Khang *et al.*, Nat. Mater. 17, 808 (2018). [2] T. Fan *et al.*, arXiv:2007.02264 (2020).

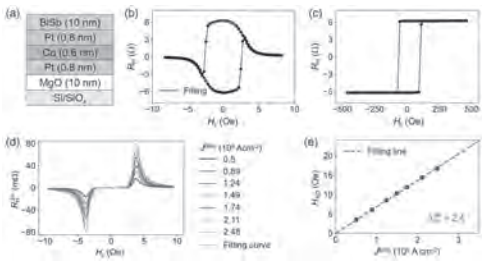

Fig. 1 (a) Schematic structure. (b)(c) Hall resistance measured with magnetic field perpendicular to the film plane and in-plane along the current direction. (d) $R_{2\omega}$ as a function of H_x at different J^{BiSb}. (e) H_{AD} as a function of J^{BiSb}.

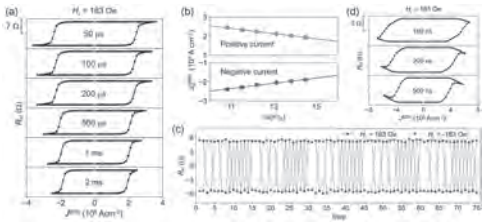

Fig. 2 (a) SOT switching loops at different τ. (b) J_{th}^{BiSb} as a function of τ. (c) Robust switching by 100 μs pulse currents. (d) Switching loops by short pulses.

GOH-11. Development of an Optically-Gated Fe/*n*-GaAs Spin-Polarised Transistor. J. Kim[1], M. Samiepour[2], E. Jackson[2], J. Ryu[3], D. Iizasa[3], T. Saito[3], M. Kohda[3,4], J. Nitta[3,4], H. Beere[5], D. Ritchie[5] and *A. Hirohata*[2] *1. Physics, University of York, York, United Kingdom; 2. Electronic Engineering, University of York, York, United Kingdom; 3. Materials Science, Tohoku University, Sendai, Japan; 4. Spintronics Research Network, Tohoku University, Sendai, Japan; 5. Physics, University of Cambridge, Cambridge, United Kingdom*

Efficient modulation of electrically-injected spin signals that is suitable for modern-day transistor functionality is yet to be established. In this work, we demonstrate in detail the fabrication of Fe/*n*-GaAs spin injection device and the experimental setup for an optical gating of the non-local spin transport signal. Three- and four-terminal Hanle measurements confirm successful spin injection into *n*-GaAs, with strong interfacial spin dephasing at high magnetic fields. Tunable-wavelength, time-resolved pump-probe Kerr rotation [1] was used to verify the strongest photoexcitation signal with 822 nm and the long spin relaxation time of ~ 2.4 ns in the channel *n*-GaAs layer. As seen in Figure 1, changes in the non-local spin transport signal, $V_{3\text{-}4}$, were measured with the modulation light with opposite helicity illuminated in the region of pure spin current. The helicity-dependent optical modulation efficiency, calculated as the ratio between the difference and the sum of the signals at the opposite helicity, of (0.4 ± 0.3)% was obtained at 30 K at the maximum available laser power of 7 mW. Furthermore, *in-situ* scanning electron microscope interface imaging, developed by authors [2], was used to reveal the correlation between the contrast inhomogeneity of the Fe/*n*-GaAs injector interface and the injection current, as displayed in Figure 2. The larger contrast inhomogeneity observed at lower injection currents suggest “pin-hole” type charge transport at bias voltage lower than the Schottky barrier height.

[1] D. Iizasa, A. Aoki, T. Saito *et al.*, Phys. Rev. B, Vol. 103, p. 024427 (2021) [2] A. Hirohata, Y. Yamamoto, B. A. Murphy *et al.*, Nat. Commun., Vol. 7, p. 12701 (2016)

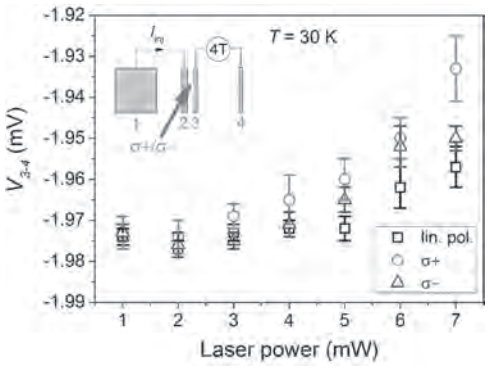

Figure 1: Non-local voltage V_{3-4} measured at 30 K against the optical modulation laser power with the linear (black square), clockwise (red circle) and the anticlockwise (blue triangle) circular polarisation. Inset: measurement geometry of optical modulation of non-local spin valve.

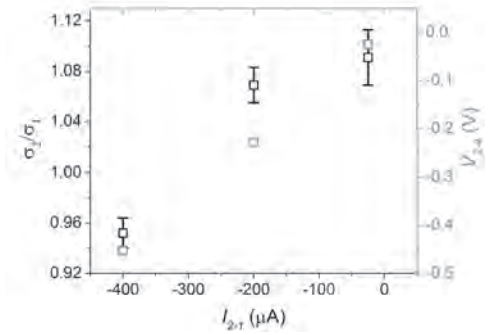

Figure 2: The injection current I_{2-1} dependence of the ratio of interface SEM contrast deviations between the injector (inset, 2) and the drain (inset, 1) contact, s_2/s_1, and the interface voltage V_{2-4}. Inset: subtracted SEM images at 2.5 keV and 3.0 keV with I_{2-1} of -400 μA

GOH-12. Terahertz Emission from CoFeB/Pt Spintronic Structures Controlled by In-Plane Uniaxial Anisotropy. *S.M. Hewett*[1], C. Bull[1,2], P.W. Nutter[2], T. Thomson[2] and D.M. Graham[1,3] *1. Department of Physics and Astronomy, The University of Manchester, Manchester, United Kingdom; 2. Department of Computer Science, The University of Manchester, Manchester, United Kingdom; 3. The Cockcroft Institute, Daresbury, Warrington, United Kingdom*

Terahertz (THz) frequency radiation finds wide application [1-4] due to the abundance of THz frequency transitions in nature. Of the many available methods for THz generation, only spintronic THz emitters (STEs), consisting of multilayer ferromagnetic (FM)/non-magnetic (NM) thin films, have shown the ability to offer wide gapless bandwidth [5] and high electric field [6], from modest nJ femtosecond laser excitation. The amplitude of the emitted THz radiation has been shown to scale with laser fluence and the external magnetic field, H_{app}, before saturating [7]. The resulting THz pulse is polarized perpendicular to the magnetization, M, of the STE [5,7]. This opens up huge potential for devices in which THz amplitude and polarization are controlled at source through magnetic manipulation. Recently emerging field shaping schemes [8, 9] may create regions of low resultant H_{app} where THz emission is controlled by the remanent magnetization, M_r. We explore the THz emission characteristics of CoFeB/Pt structures in this below-saturation regime and reveal their anisotropic behavior with orthogonal in-plane (IP) easy and hard axes. We show that the H_{app} required for saturation is orientation dependent (Fig.1) with respect to the plane of the sample. With the EA aligned to H_{app}, at subsequent zero field the THz emission from the STE remains close to that achieved at magnetic saturation (Fig.2), effectively providing a field free emitter. Further, we explore the impact of oblique sputtering deposition parameters known to give rise to IP magnetic anisotropy in FM thin films [10]. We show that the THz emission behavior is sensitive to the resulting variation in magnetic anisotropy, and correlates closely to IP angle-dependent vibrating sample magnetometry measurements, demonstrating the potential applicability of STEs as a tool for the interrogation of static magnetic behavior in spintronic systems.

[1] P.Uhd Jepsen et al., Laser Photonics Rev., Vol. 5(1), p.124 (2011); [2] H. Y. Hwang et al., J. Mod.Opt., Vol. 62(18), p.1447 (2015); [3] J. A. Spies et al., J. Phys. Chem. C, Vol. 124, p.22335 (2020); [4] M. Naftaly et al., Sensors, Vol. 19, p.4203 (2019); [5] T. Seifert et al., Nat. Photonics, Vol. 10, p.483 (2016); [6] T. Seifert et al., Appl. Phys. Lett., Vol. 110, p.252402 (2017); [7] R. Adam et al., Appl. Phys. Lett., Vol. 114, p.212405 (2019); [8] M. T. Hibberd et al., Appl. Phys. Lett., Vol. 114, p.031101 (2019); [9] H. Niwa et al., Opt. Express, Vol. 29, p.13331 (2021); [10] A. T. Hindmarch et al., Phys. Rev. B, Vol. 83, p.212404 (2011)

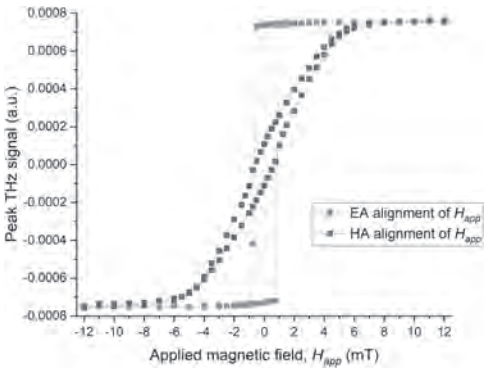

Fig.1 Hysteresis behavior in the THz emission from a CoFeB/Pt STE for EA and HA alignment of H_{app}.

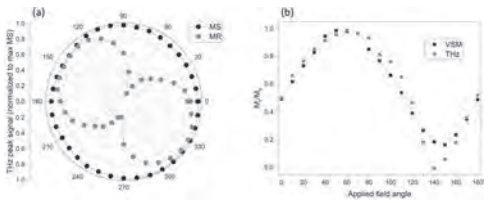

Fig.2 (a) Peak THz amplitude as a function of sample angle with respect to IP H_{app} of 20 mT (M_S) and 0 mT (M_R); (b) VSM and THz comparatives for the remanence magnetization and THz emission normalized to saturation values.

GOH-13. Magnonic Contribution to Unidirectional Spin Hall Magnetoresistance in Epitaxial Cr/Fe Bilayer. *T.T. Nguyen*[1], V. Nguyen[2], S. Jeong[2], E. Park[2], H. Jang[2], N. Lee[2], S. Lee[3], B. Park[3], S. Cho[2], H. Lee[4], J. Hong[1] and S. Kim[2] *1. Emerging Materials Science, Daegu Gyeongbuk Institute of Science and Technology, Daegu, The Republic of Korea; 2. Department of Physics, University of Ulsan, Ulsan, The Republic of Korea; 3. Department of Materials Science and Engineering, Korea Advanced Institute of Science and Technology, Daejeon, The Republic of Korea; 4. Department of Physics, Pohang University of Science and Technology, Pohang, The Republic of Korea*

Magnon refers to the spin-wave quantum associated with the flip of a single spin which gives rise to exotic phenomena such as quantum Bose-Einstein condensation [1], spin pumping [2], spin Seebeck effect [3], and magnon-related transports [4]. Recently, it has been reported that a non-linear magnetoresistance, namely unidirectional magnetoresistance (UMR), can be observed in ferromagnet (FM)/non-magnet (NM) bilayers and has magnon contribution in addition to spin dependent scattering origin [5]. In this study, we systematically investigate the UMR in epitaxial Cr/Fe bilayers and find that the UMR is significantly enhanced when the Fe

magnetization is aligned to a particular crystallographic direction. Magnon magnetoresistance (MMR) driven by the electron-magnon scattering is also larger than other directions. We find that this result is attributed to the Ising-type character of the Cr/Fe. This suggests a strategic route to boost magnon generation efficiency in the magnonic devices.

[1] Serga, A. A. et al. *Nat Commun* 5, 3452 (2014). [2] Sandweg, C. W. et al. Phys. Rev. Lett. 106, 216601 (2011). [3] Uchida, K. et al. *Appl. Phys. Lett.* 97, 172505 (2010). [4] Mihai, A. P. et al. *Phys. Rev. B* 77, 060401 (2008). [5] Kim, K.-J. et al. *Appl. Phys. Express* 12, 063001 (2019).

GOH-14. Interface driven spin pumping and inverse Rashba–Edelstein effect in FeGaB/Ag/BiSb multilayers. *V. Sharma*[1], P. Bajracharya[1], A. Johnson[1] and R. Budhani[1] *1. Department of Physics, Morgan State University, Baltimore, MD, United States*

Spin-to-charge conversion (SCC) mechanism has been extensively demonstrated in normal metal (NM) interface with ferromagnets using inverse spin Hall effect (ISHE) [1].Recently, a new mechanism of charge-spin interconversion at inversion symmetry breaking interfaces between topological insulators (TIs) and magnetically ordered materials has been introduced [2]. It is driven by the inverse Rashba-Edelstein effect (IREE) [3]. In this work, we have investigated the Inverse Rashba Edelstein effect (IREE) of a simple binary three-dimensional topological insulator $Bi_{85}Sb_{15}$ (BiSb) in the trilayer system of FeGaB/Ag/BiSb with different Ag thickness. Figure 1(a) shows the variation of resonance field (H_r) with microwave frequency while Fig. 1(b) shows the FMR linewidth (ΔH) calculated from the LLG model of magnetization precession showing the enhancement due to spin pumping from FeGaB into the BiSb layer. Fig. 2(a) shows the results of field-dependence charge current (I_c) generation in the TI at FMR and the FMR lineshape at 10 GHz. It is interesting to note that the I_c increases with Ag thickness, shows that the IREE process at the Ag/BiSb interface dominates over ISHE in the bulk of BiSb film. The conversion efficiency of IREE is determined by calculating the IREE length (λ_{IREE}) [3-5], which is shown in Figure 2(b). These findings offer a method to generate and detect the IREE in a room temperature deposited heterostructure using simple coplanar waveguide setup (Inset of Figure 2(b)).

[1] Hellman, Frances, et al. "Interface-induced phenomena in magnetism." *Reviews of modern physics* 89.2 (2017): 025006. [2] Bercioux, Dario, and Procolo Lucignano. "Quantum transport in Rashba spin–orbit materials: a review." *Reports on Progress in Physics* 78.10 (2015): 106001. [3] Sánchez, JC Rojas, et al. "Spin-to-charge conversion using Rashba coupling at the interface between non-magnetic materials." *Nature communications* 4.1 (2013): 1-7. [4] Zhang, Wei, et al. "Spin pumping and inverse Rashba-Edelstein effect in NiFe/Ag/Bi and NiFe/Ag/Sb." *Journal of Applied Physics* 117.17 (2015): 17C727. [5] Rojas-Sánchez, J-C., et al. "Spin to charge conversion at room temperature by spin pumping into a new type of topological insulator: α-Sn films." *Physical review letters* 116.9 (2016): 096602. .

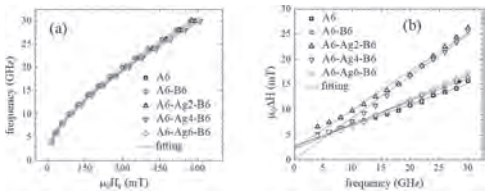

Figure 1 (a) Variation of FMR resonance field (H_r) as a function of excitation frequency. (b) Variation of FMR linewidth with the microwave frequency. Red line shows the fitting using LLG model. A6, A6-B6 and A6-Ag(x)-B6 mean the FeGaB(6nm), FeGaB(6nm)/BiSb(6nm) and FeGaB(6nm)/Ag (2-6nm)/BiSb(6nm) respectively.

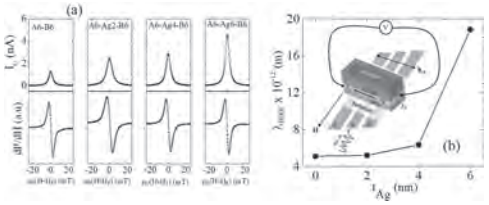

Figure 2 (a) (top) Field dependence current I_C derived from the voltage measured at FMR driven by 10 GHz excitation, (bottom) FMR spectrum measured at 10 GHz. Red line shows the Lorentzian fitting. (b) Variation of λ_{IREE} as a function of the Ag layer thickness. Inset shows the experimental setup used for the measurements.

GOH-15. Nonlinear planar Hall effect from spin-momentum locking inhomogeneities in topological insulator Bi_2Se_3. *Y. Wang*[1], V. Mambakkam[2], Y. Wang[2], S.A. Law[2] and J.Q. Xiao[1] *1. Department of Physics and Astronomy, University of Delaware, Newark, DE, United States; 2. Department of Materials Science and Engineering, University of Delaware, Newark, DE, United States*

Nonreciprocal electrical transport responses arise in materials with broken inversion and time-reversal symmetries [1]. Although these nonlinear magnetoresistance or Hall effects are typically weak compared with their linear analogs, they can be used to probe exotic properties like spin-orbit interaction, spin textures and superconductivity. At the surface of the 3D topological insulator (TI) Bi_2Se_3, a nonlinear planar Hall effect (NPHE) was reported to exist due to the hexagonally warped spin structures [2]. This NPHE is expected to be small at low carrier densities because the hexagonal warping effect is negligible at the Dirac point. In this study, we observed a similar NPHE in Bi_2Se_3/CoFeB and magnetic insulator/Bi_2Se_3 heterostructures. Though with a lower carrier density, the NPHE in these systems is two orders of magnitude larger than the previously reported one. Moreover, the strength of this NPHE scales inversely with carrier density. This suggests that the intrinsic hexagonal warping is not the dominant mechanism for the observed NPHE. Instead, we attribute this large NPHE to the recently proposed extrinsic mechanism based on the interplay between current-induced spin-polarization and scattering from spin-momentum locking inhomogeneities [3]. Our results provide experimental evidence for this new mechanism and show that the NPHE can be enhanced by disorder engineering.

[1] Y. Tokura and N. Nagaosa, Nat. Commun. 9, 3740 (2018). [2] P. He, S. S.-L. Zhang, D. Zhu, S. Shi, O. G. Heinonen, G. Vignale, and H. Yang, Phys. Rev. Lett. 123, 016801 (2019). [3] A. Dyrdal, J. Barnas, and A. Fert, Phys. Rev. Lett. 124, 046802 (2020).

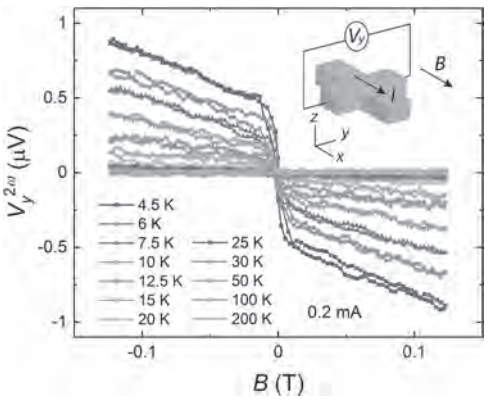

Fig. 1 Nonlinear planar Hall effect in a YIG(2.46m)/Bi_2Se_3(8nm) sample.

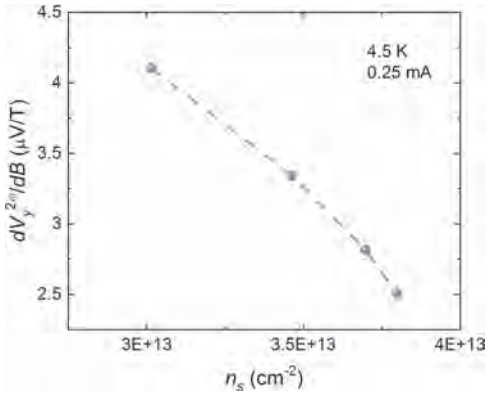

Fig. 2 Carrier density dependence of the nonlinear planar Hall effect.

Session GOI
MAGNETIZATION CONTROL

Chuanpu Liu, Chair
Colorado State University, Fort Collins, CO, United States

INVITED PAPER

GOI-01. Control of Magnetism Using Surface States in Topological Dirac Semimetal α-Sn. J. Ding[1], C. Liu[1], V. Kalappattil[4], Y. Zhang[1,2], O. Mosendz[3], U. Erugu[4], R. Yu[1,5], J. Tian[4], A. DeMann[1], S.B. Field[1], X. Yang[2], H. Ding[5], J. Tang[4], B. Terris[3], A. Fert[6], H. Chen[1] and *M. Wu*[1] *1. Department of Physics, Colorado State University, Fort Collins, CO, United States; 2. School of Optical and Electronic Information, Huazhong University of Science and Technology, Wuhan, China; 3. Western Digital Research Center, Western Digital Corporation, San Jose, CA, United States; 4. Department of Physics and Astronomy, University of Wyoming, Laramie, WY, United States; 5. National Laboratory of Solid State Microstructures and Department of Physics, Nanjing University, Nanjing, China; 6. Unité Mixte de Physique, CNRS, Thales, Université Paris-Saclay, Palaiseau, France*

Topological Dirac semimetals represent a relatively newly-discovered topological quantum phase. In comparison with other topological Dirac semimetals, α-Sn is much more attractive because (1) it is a single-element material and is therefore relatively easy to grow and (2) it can transform to other topological phases, such as a topological insulator or a Weyl semimetal, under certain strain and field conditions. This talk will discuss about the use of topological surface states in α-Sn to control magnetization in ferromagnets. The first half of the talk will be on large damping enhancement in a NiFe thin film due to topological surface states in an adjacent α-Sn thin film [1]. It will be shown that an α-Sn film separated from a NiFe film by a Ag spacer can cause an extra damping in the NiFe film that is three times bigger than the intrinsic damping. The second half of the talk will be on current-induced magnetization switching in an α-Sn/Ag/CoFeB trilayer [2]. It will be shown that thanks to the surface states in the α-Sn film, the magnetization in the CoFeB film can be switched by a charge current at room temperature, without the need of an external magnetic field. The switching efficiency is as high as in topological insulator-based systems. Taken together, these results suggest that, like topological insulators, the topological Dirac semimetal α-Sn may have promising applications in spintronics.

[1] "Large damping enhancement in Dirac-semimetal – ferromagnetic-metal layered structures caused by topological surface states," Jinjun Ding, Chuanpu Liu, Yuejie Zhang, Vijaysankar Kalappattil, Rui Yu, Uppalaiah Erugu, Jinke Tang, Haifeng Ding, Hua Chen, and Mingzhong Wu, Advanced Functional Materials, 2008411 (2021). [2] "Switching of a magnet by spin-orbit torque from a topological Dirac semimetal," Jinjun Ding, Chuanpu Liu, Vijaysankar Kalappattil, Yuejie Zhang, Oleksandr Mosendz, Uppalaiah Erugu, Rui Yu, Jifa Tian, August DeMann, Stuart B. Field, Xiaofei Yang, Haifeng Ding, Jinke Tang, Bruce Terris, Albert Fert, Hua Chen, and Mingzhong Wu, Advanced Materials, 2005909 (2021).

CONTRIBUTED PAPERS

GOI-02. Magnetization-Dependent Spin Hall Effect in a Perpendicularly Magnetized Film. *D. Qu*[1,2], T. Chuang[3], S. Lee[1] and S. Huang[3] *1. Institute of Physics, Academia Sinica, Taipei, Taiwan; 2. Center for Condensed Matter Sciences, National Taiwan University, Taipei, Taiwan; 3. Department of Physics, National Taiwan University, Taipei, Taiwan*

The spin Hall effect (SHE) converts a charge current into a transverse spin current through spin-orbit scatterings. In the SHE, the charge current, the spin current, and the spin polarization are mutually orthogonal. As a result, an in-plane charge current generates a spin current with a fixed in-plane spin orientation at the film surface, and the out-of-plane spin orientation is strictly prohibited. Recently, this restriction has been lifted in the magnetization-dependent spin Hall effect (MDSHE) in magnetic materials [1, 2], where the charge-induced spin polarization can be additionally manipulated by the magnetization directions, opening new perspectives for spintronics. Nevertheless, the existing reports of the MDSHE have various competing contributions and artifacts due to their all metallic heterostructures. As a result, experimentally, the MDSHE remains unequivocally established, not to mention the quantitative analyses. In this work [3], we unambiguously established the MDSHE in a ferromagnet. We utilize the magnetic insulator YIG to thermally inject the pure spin current into a perpendicular magnetized Pt/Co/Pt layer (PML). With the experimental geometry as shown in Fig. 1, by switching the Pt/Co/Pt magnetization, we obtained opposite spin-to-charge conversion signals as shown in Fig 2. We excluded any possible artifact and demonstrated that the origin of the observed signal is entirely due to the MDSHE. Thus, the spin polarization induced by the MDSHE could be arbitrarily and independently controlled by the magnetization direction. Furthermore, by comparing with the conventional SHE, we explicitly identified the strength of the MDSHE and further estimated the magnetic spin Hall angle to be -0.36%. Our approach provides a versatile and controllable route to explore the unconventional spin and charge conversions in magnetic materials and benefit next-generation spintronic applications.

[1] A. M. Humphries, et al., Nat. Commun. 8, 911 (2017) [2] M. Kimata, et al., Nature 565, 627 (2019) [3] T. C. Chuang, et al., Phys. Rev. Research 2, 032053(R) (2020)

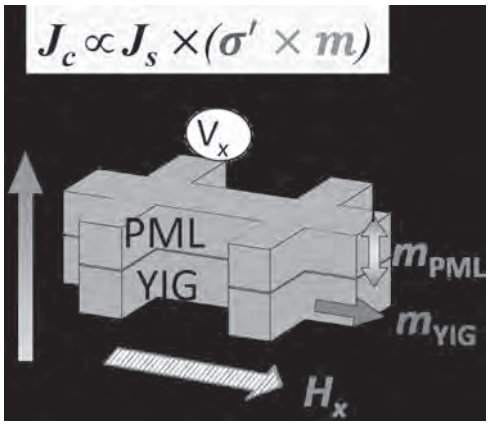

Fig. 1 Illustration of the experimental geometry

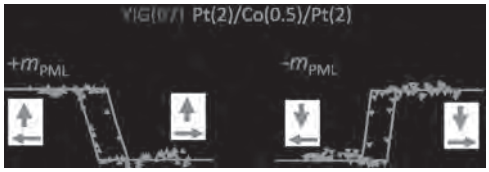

Fig. 2 MDSHE voltages observed for opposite PML magnetizations

GOI-03. Spin diode effect in magnetic garnets. *R. Kohno*[1], K. An[1], N. Thiery[1], V. Naletov[1,2], L. Vila[1], J. Ben Youssef[3], H. Merbouche[4], V. Cros[4], A. Anane[4], T. Hauet[5], V.E. Demidov[6], S. Demokritov[6], G. de Loubens[7] and O. Klein[1] *1. Université Grenoble Alpes, CEA, CNRS, Grenoble INP, Spintec, Grenoble, France; 2. Institute of Physics, Kazan Federal University, Kazan, Russian Federation; 3. LabSTICC, CNRS, Université de Bretagne Occidentale, Brest, France; 4. Unité Mixte de Physique, CNRS, Thales, Université Paris-Sud, Université Paris Saclay, Palaiseau, France; 5. Institut Jean Lamour, CNRS, Université de Lorraine, Nancy, France; 6. Department of Physics, University of Muenster, Muenster, Germany; 7. SPEC, CEA-Saclay, CNRS, Université Paris-Saclay, Gif-sur-Yvette, France*

Diodes are a key component in electronics with their nature of asymmetric conduction enabling rectification in circuits. Non-linear response is one criterion to have such effects and spin waves, or the quanta magnons are known to be highly nonlinear with respect to input power or spin transfer torques (STT), which leads to microwave rectification in spin torque nano oscillators[1,2]. While non linear dynamics of magnons due to STT in confined geometry has been well studied thanks to the macrospin nature, its nonlinear nature has been so far elusive in extended films. We measure non-linear spin transport behavior of magnetic garnet thin films by spin orbit torques (SOT) in non-local geometry (Fig.1) [3] and report spin diode effect marked by a strong asymmetric conductance at large current density. Namely higher spin conductance is obtained for the polarity increasing spin fluctuations than for the opposite polarity. We demonstrate that spin diode effects are determined by the collective dynamics of magnetostatic magnons and emergence of the asymmetry requires to work in the long-range regime (large separation between the 2 electrodes > 2μm) to efficiently filter out the spurious symmetric contribution of the rapidly decaying thermal magnons[3]. As the intensity of the spin current increases, the transport properties of magnetostatic magnons crosses 3 different regimes. i) At low currents, it is ballistic set by the film thickness. ii) Close to the damping compensation threshold, it switches to a highly correlated dynamical regime limited by spin-spin relaxation and shows a sharp increase of the non-local conductance. iii) As the temperature of the magnons approaches the Curie temperature, it switches to a diffusive regime, where the propagation length is reduced by collisions with thermal magnons, showing negative differential spin conductance (Fig.2).

[1] M. Tsoi, A. G. M. Jansen, J. Bass et. al., Nature 406 46 (2000) [2] A. A. Tulapurkar, Y. Suzuki, A. Fukushima et. al., Nature 438 339 (2005) [3] L. J. Cornelissen, J. Liu, R. A. Duine et. al., Nature Physics 11 1022 (2015) [4] K. An, R. Kohno, N. Thiery, et. al., Phys. Rev. B 103 174432 (2021)

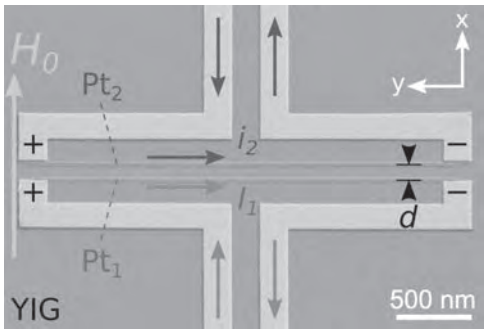

Fig.1. Schematics of the four-terminal diode device which consists of two Pt electrodes (Pt_1 and Pt_2) separated by distance *d* on a Yttrium Iron Garnet thin film.

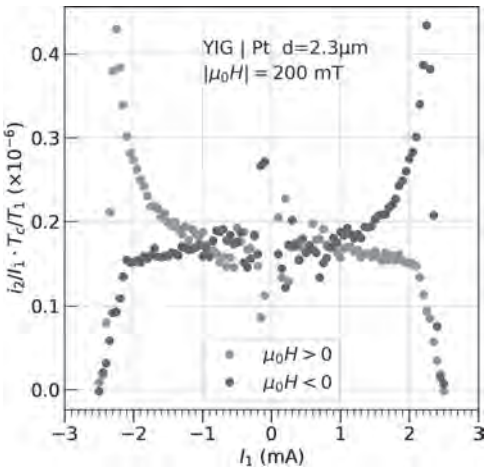

Fig.2. Renormalized SOT contribution of the spin conduction i_2 detected in Pt_2 as a function of I_1, the current injected in Pt_1. Here T_1 is the temperature of the Pt_1 and T_c is the Curie temperature.

GOI-04. Giant spin-charge conversion in an all-epitaxial $LaTiO_{3+\delta}$/$SrTiO_3$ heterostructure. *S. Kaneta-Takada*[1], M. Kitamura[2], S. Arai[1], R. Okano[1], L. Anh[1,3], T. Endo[1], K. Horiba[2], H. Kumigashira[2,4], M. Kobayashi[1,5], M. Seki[1,5], H. Tabata[1,5], M. Tanaka[1,5] and S. Ohya[3,5] *1. Department of Electrical Engineering and Information Systems, The University of Tokyo, Bunkyo-ku, Japan; 2. Photon Factory, High Energy Accelerator Research Organization (KEK), Tsukuba, Japan; 3. Institute of Engineering Innovation, The University of Tokyo, Bunkyo-ku, Japan; 4. Institute of Multidisciplinary Research for Advanced Materials (IMRAM), Tohoku University, Sendai, Japan; 5. Center for Spintronics Research Network (CSRN), The University of Tokyo, Bunkyo-ku, Japan*

Realizing highly efficient spin-charge conversion is essential for developing low-power-consumption spin-orbitronics devices, such as spin-orbit-torque magnetoresistive random access memory and spin-Seebeck power generators. Especially, spin-charge conversion at two-dimensional interfaces, the so-called Rashba-Edelstein effect, has attracted much attention because of its large conversion efficiency (λ_{IEE}). In particular, two-dimensional electron gas (2DEG) formed at oxide interfaces, such as $LaAlO_3/SrTiO_3$ (LAO/STO) and AlO_x/STO, has been reported to have extremely large λ_{IEE} [1–4]. Meanwhile, a non-zero Berry phase with a giant Rashba coefficient up to 1.8×10^{-11} eVm has been recently found in the 2DEG at the $LaTiO_{3+\delta}$ (LTO)/STO interface [5], offering a new attractive platform for generating a more efficient

spin-charge conversion. For spin-pumping experiments, we have grown an all-epitaxial $La_{0.67}Sr_{0.33}MnO_3$ (LSMO) [30 unit cells (u.c.)]/LTO (3 u.c.) heterostructure on an STO (001) substrate (Fig. 1) by molecular beam epitaxy, for which we precisely controlled each layer thickness using oscillation of reflection high-energy electron diffraction and a shuttered growth technique. The 2D carrier confinement at the LTO/STO interface was confirmed by the band-structure characterization using angle-resolved photoemission spectroscopy (ARPES). Our spin-pumping measurements showed that the electromotive force (EMF) drastically increases with decreasing temperature (Fig. 1). The estimated λ_{IEE} reaches 167.7 nm at 15 K (Fig. 2), which is the highest value among those reported for all materials including metals, semiconductors, and topological systems so far. An intrinsic spin-charge conversion model can quantitatively explain the temperature dependence of λ_{IEE} based on a tight-binding band-structure calculation with the band parameters that are optimized to reproduce the ARPES result. This work was partly supported by Grants-in-Aid for Scientific Research, CREST of JST, and the Spintronics Research Network of Japan (Spin-RNJ).

[1] E. Lesne *et al.*, Nat. Mater. 15, 1261 (2016). [2] S. Ohya *et al.*, Phys. Rev. Res. 2, 012014 (2020). [3] D. C. Vaz *et al.*, Nat. Mater. 15, 1187 (2019). [4] P. Noël *et al.*, Nature 580, 483 (2020). [5] M. J. Veit *et al.*, Nat. Commun. 9, 1458 (2018). [6] J. -Y. Chauleau *et al.*, Europhys. Lett. 116, 17006 (2016).

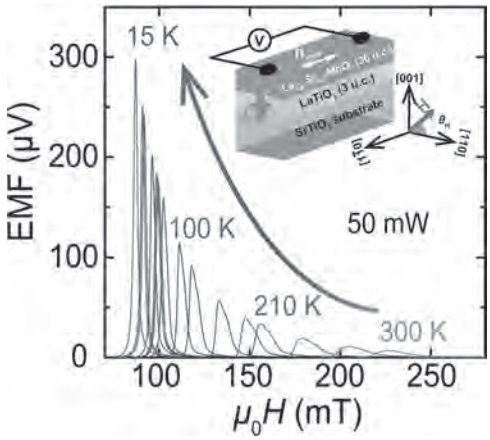

Fig. 1 Magnetic-field dependence of the EMF measured at various temperatures ranging from 15 to 300 K.

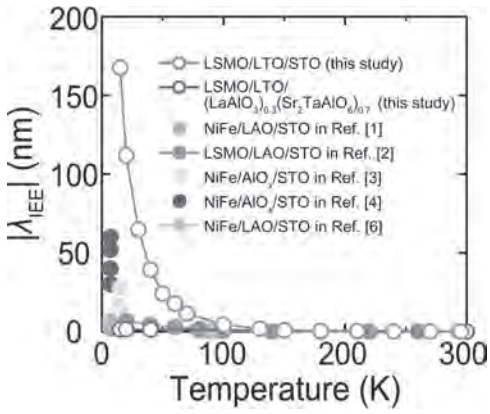

Fig. 2 Temperature dependences of the inverse Edelstein length λ_{IEE} in various material systems.

GOI-05. Universal scaling of the temperature dependence of longitudinal spin Seebeck effect in compensated ferrimagnets.
A. Chanda[1], N. Schulz[1], C. Holzmann[2], J. Seyd[2], M. Albrecht[2], M. Phan[1] and H. Srikanth[1] *1. Physics, University of South Florida, Tampa, FL, United States; 2. Institute of Physics, University of Augsburg, Augsburg, Germany*

The longitudinal spin Seebeck effect (LSSE) is an efficient method for generating incoherent magnon excitations by applying a vertical temperature gradient across a magnetic material. To avoid the contamination of the thermally generated "pure" spin current by the electronic degrees of freedom, magnetic insulators are exclusively preferred for LSSE. Although the ferrimagnetic insulator $Y_3Fe_5O_{12}$ (YIG) is known as the hallmark system for LSSE because of its ultra-low Gilbert damping,[1] other members of the insulating iron garnet family, including the compensated ferrimagnet $Gd_3Fe_5O_{12}$ (GdIG), have recently attracted considerable interest due to their unique compensated spin configurations.[2] In particular, the fascinating observation of the change in sign of the LSSE signal in a GdIG/Pt bilayer around the magnetic compensation temperature due to reorientation of sublattice magnetizations has motived us to address to an emerging fundamental question: "*Is there a general trend for the temperature dependence of LSSE in compensated ferrimagnets*?" Therefore, we have performed a comprehensive investigation of LSSE in GGG/GdIG(*t*)/Pt(5nm) bilayers with 5 different thicknesses ranging between 31 and 272 nm. We find that all the GdIG films possess an in-plane magnetic easy axis, and the compensation temperature decreases from 270 to 220 K with decreasing film-thickness from 272 to 31 nm. Using a proposed rescaling method, we have demonstrated, for the first time, a "universal scaling" behavior for the temperature dependence of LSSE signal for our GdIG films with different compensation temperatures, which, we believe, holds true for other compensated ferrimagnetic systems as well. In addition, we have performed the LSSE study on a 31 nm GdIG film grown on lattice-mismatched GSGG substrate that exhibits an out-of-plane magnetic easy axis and observed a clear distinction in the magnetic field dependent LSSE signal, relative to the 31 nm GGG/GdIG film showing an in-plane magnetic easy axis. This highlights a strong correlation between the LSSE signal and the magnetic anisotropy in compensated ferrimagnets. Our findings will pave the way to explore LSSE in other novel compensated ferrimagnets.

[1] V. Kalappattil, R. Das, M.-H. Phan, and H. Srikanth, Scientific reports 7, 1 (2017). [2] S. Geprägs, A. Kehlberger, F. Della Coletta, Z. Qiu, E.-J. Guo, T. Schulz, C. Mix, S. Meyer, A. Kamra, and M. Althammer, Nature communications 7, 1 (2016).

GOI-06. Coherent ac spin current transmission across an antiferromagnetic CoO insulator.
Q. Li[1,2], M. Yang[3,2], C. Klewe[4], P. Shafer[4], A.T. N'Diaye[4], D. Hou[5], T. Wang[2], N. Gao[2], E. Saitoh[6], C. Hwang[7], R.J. Hicken[8], J. Li[9], E. Arenholz[4] and Z.Q. Qiu[2] *1. National Synchrotron Radiation Laboratory, University of Science and Technology of China, Hefei, China; 2. Physics department, UC Berkeley, Berkeley, CA, United States; 3. Anhui University, Hefei, China; 4. Advanced Light Source, Lawerence Berkeley National Laboratory, Berkeley, CA, United States; 5. University of Science and Technology of China, Hefei, China; 6. University of Tokyo, Tokyo, Japan; 7. Korea Research Institute of Standards and Science, Yuseong, The Republic of Korea; 8. Department of Physics and Astronomy, University of Exeter, Exter, United Kingdom; 9. International Center for Quantum Materials, Peking University, Beijing, China*

The recent discovery of spin current transmission through antiferromagnetic insulating materials opens up vast opportunities for fundamental physics and spintronics applications. The question currently surrounding this topic is: whether and how could THz antiferromagnetic magnons mediate a GHz spin current? This mismatch of frequencies becomes particularly critical for the case of coherent ac spin current, raising the fundamental question of whether a GHz ac spin current can ever keep its coherence inside an antiferromagnetic insulator and so drive the spin precession of another ferromagnet

layer coherently? Utilizing element- and time-resolved x-ray pump-probe measurements on Py/Ag/CoO/Ag/ $Fe_{75}Co_{25}$/MgO(001) heterostructures, here we demonstrate that a coherent GHz ac spin current pumped by the Py ferromagnetic resonance can transmit coherently across an antiferromagnetic CoO insulating layer to drive a coherent spin precession of the $Fe_{75}Co_{25}$ layer [1]. Moreover, by determining the CoO Néel vector orientation using XMLD spectroscopy and separating the interlayer coupling effect from the spin-current effect, we demonstrate the absence of anisotropic spin current for parallel and perpendicular alignment of the Fe and CoO spin axes [2].

[1] Q. Li, M. Yang, C. Klewe, P. Shafer, A.T. N'Diaye, D. Hou, T.Y. Wang, N. Gao, E. Saitoh, C. Hwang, R. J. Hicken, J. Li, E. Arenholz and Z. Q. Qiu, Coherent ac spin current transmission across an antiferromagnetic CoO insulator, Nat. Commun. 10, 5265 (2019). [2] M. Yang, Q. Li, D. Hou, P. Shafer, A. T. N'Diaye, C. Klewe, T. Y. Wang, Xixiang Zhang, C. Hwang, and Z. Q. Qiu, Independence of the spin current from the Néel vector orientation in antiferromagnet CoO, Phys. Rev. B 101, 224418 (2020).

GOI-07. Auto-oscillations in Two-magnet Heterostructures Driven by Thermal Spin Currents in Perpendicular Geometry. *S. Regmi*[1], B. Arkook[1], C. Safranski[2], R. Rodriguez[1], J. Shi[1] and I. Barsukov[1] *1. Physics and Astronomy, University of California Riverside, Riverside, CA, United States; 2. IBM T.J. Watson Research Center, Yorktown, NY, United States*

Combining insulating and metallic ferromagnets in hybrid heterostructures adds novel functionalities to such devices by harnessing the virtues of both material systems. Here, we utilize bilayers of yttrium iron garnet (YIG) and nickel (Ni) and fabricate (200 nm x 3 um) nanowire devices using e-beam lithography and ion-milling. The magnetoresistive phenomena of Ni allow us to access static and dynamic states of the heterostructure. Using spin-torque ferromagnetic resonance technique, we investigate coupled spin waves in the geometry with magnetic field applied perpendicular to the device plane and identify aligned and nonaligned modes. Then, by supplying mA-large currents to the nanowire, we observe microwave emission from the nanowire, corresponding to auto-oscillations of the nonaligned mode. We find the signal to be symmetric in both field and current polarity, indicating that the excitation is driven by thermal spin currents. This observation of thermally-driven auto-oscillations in heterostructures with noncollinear magnetization opens avenues for further functionalization of spin dynamics of hybrid magnetic systems. This work was supported by the National Science Foundation through Grant No. ECCS-1810541.

1. Chris Safranski, Igor Barsukov, Han Kyu Lee, et al., Nat. Commun. 8, 117 (2017) 2. Bassim Arkook, Christopher Safranski, Rodolfo Rodriguez, et al., arXiv:1909.12445

GOI-08. Spin superfluidity in noncollinear antiferromagnets. A.A. Kovalev[1] and *B. Li*[1] *1. University of Nebraska - Lincoln, Lincoln, NE, United States*

We explore the spin superfluid transport in exchange interaction-dominated three-sublattice antiferromagnets. The system in the long-wavelength regime is described by an SO(3) invariant field theory. Additional corrections from Dzyaloshinskii-Moriya interactions or anisotropies can break the symmetry; however, the system still approximately holds a U(1)-rotation symmetry. Thus, the power-law spatial decay signature of spin superfluidity is identified in a nonlocal-measurement setup where the spin injection is described by the generalized spin-mixing conductance [1]. We suggest to explore iron jarosites as promising material candidates for realizing our proposal.

[1] Bo Li and Alexey A. Kovalev, Phys. Rev. B 103, L060406 (2021)

GOI-09. Thermal spin current generation in the multifunctional ferrimagnet $Ga_{0.6}Fe_{1.4}O_3$. *A. Anadón*[1], S. Homkar[2], E. Martin[1], B. Meunier[2], C. Dubs[3], D. Preziosi[2], S. Petit-Watelot[1], N. Viart[2] and J. Rojas-Sanchez[1] *1. Institut Jean Lamour, Nancy, France, France; 2. IPCMS, Strasbourg, France; 3. INNOVENT e.V. Technologieentwicklung, Jena, Germany*

The seach for ferromagnetic insulating materials with multifunctional properties is currently a highly sought after objective in spintronics. In current spintronics, functional devices are typically made of a bilayer composed of a material with large spin-orbit coupling (NM) and a ferromagnet (FM). These type of devices allow functionalities like the manipulation of the FM magnetization by the spin Hall effect (SHE)[1] in the NM or energy harvesting by means of its inverse counterpart the inverse spin Hall effect.[2] Insulating ferrimagnets are preferred for this purpose to pave the way towards low dissipation spintronics devices.[3] Additional functionalities like the possibility of the electric field control of the magnetic properties of such systems could be given to these heterostructures through the introduction of multifunctional ferromagnets opening the possibility of having more efficient and versatile devices.[4] In this work we have studied the thermo-spin current generation in bilayers composed of Pt and the multifunctional magnetoelectric $Ga_{0.6}Fe_{1.4}O_3$ (GFO).[5] We compare the performance of the system with the widely used yttrium iron garnet obtaining a similar value of the spin Seebeck effect, likewise to what was observed previously in spin Hall magnetoresistance. We also rule out the possibility of a dominant proximity effect in the thermo-spin voltage by exploring the different magnetoresistive effects in the bilayer. In addition, by fabrication of thermo-spin devices with controlled dimensions we are able to accurately quantify the relevant parameters of the thermal effects, obtaining more accurate and comparable values for the spin Seebeck coefficient. These results pave the way for the use of the magnetoelectric multiferroic GFO with a view to control the spin current production of NM/FM heterostructures by an electric field.

1. Anadon, A. *et al. ACS Appl. Nano Mater.* 4, 1, 487–492 (2021) 2. Ramos, R. *et al. APL Materials* 4, 104802 (2016) 3. Avci, C. O. *et al. Nat. Mater.* 16, 309–314 (2017). 4. Ramesh, R. *Nature* 461, 1218–1219 (2009). 5. Roy, A. *et al. Ferroelectrics* 473, 154–170 (2014).

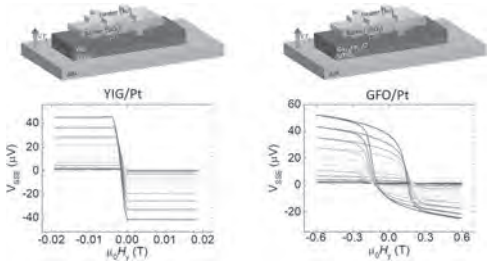

Fig. 1. Thermo-spin current generation in YIG and GFO. The thermo-spin voltage is comparable in both systems.

GOI-10. Towards the development of $Tm_3Fe_5O_{12}$ magnetic insulator and Bi_2Se_3 topological insulator for charge-spin interconversion.

S. Husain[1], M. Ribeiro[2], S. Krishnia[1], N. Figueiredo Prestes[1], A. Marty[2], F. Bonell[2], N. Reyren[1], O. Boulle[2], M. Jamet[2], V. Cros[1] and J. George[1]
1. Unité Mixte de Physique, CNRS, Thales, Université Paris-Saclay, Palaiseu, France; 2. CEA, CNRS, Grenoble INP, IRIG-SPINTEC, Univ. Grenoble Alpes, Grenoble, France

Charge-spin interconversion using large Spin Orbit (SO) material has been intensively studies thanks to potential spintronic application in information and communication technology. It has been demonstrated that the interface between heavy metal and both metallic and insulating ferromagnetic layers could lead to spin current absorption and manipulation of the magnetization driven by electrical pulse[1][2]. More recently Rashba surface states and Topological insulator (TI) have been reported like a good candidate for the spin to charge interconversion[3]. Nevertheless, current shunting by metallic ferromagnet at the interface with TI makes hard to address unambiguously the charge to spin conversion from surface states. As a supplementary effect, the role of proximity effect and exchange interaction in between ferromagnetic material and TI needs to be clarified. To comprehend this issue, we first grow a thin film of magnetic insulator $Tm_3Fe_5O_{12}$(TmIG) by off-axis sputtering and demonstrated the high quality of the film in the thickness range of 5 to 15 nm (Figure. 1(a)). We achieved to demonstrate, as a reference experiment, spin current absorption at the interface in between Pt and TmIG by 2nd harmonic experiment to extract torque and magnetization reversal driven by pulse current experiment. The high quality of the film makes possible to growth by MBE Bi_2Se_3 TI on top of it as illustrated in Figure 1(b). The TmIG films exhibit perpendicular magnetic anisotropy (Figure 1 (c)) with nearly bulk magnetization. We will address a comparative study of the interfacial effect when using SHE material (Pt) or TI (Bi2Se3) with ferromagnetic insulator TmIG. This work has been supported by the Defense Advanced Research ProjectsAgency (DARPA) Topological Excitations in Electronics (TEE) program, through Grant MIPR No. HR0011831554.

[1] A. Manchon, J. zelezný, I.M. Miron, T. Jungwirth, J. Sinova, A. Thiaville, K. Garello, P. Gambardella, Rev. Mod. Phys. 91 (2019) 035004. [2] C.O. Avci, A. Quindeau, C.F. Pai, M. Mann, L. Caretta, A.S. Tang, M.C. Onbasli, C.A. Ross, G.S.D. Beach, Nat. Mater. 16 (2017) 309–314. [3] J.C. Rojas-Sánchez, S. Oyarzún, Y. Fu, A. Marty, C. Vergnaud, S. Gambarelli, L. Vila, M. Jamet, Y. Ohtsubo, A. Taleb-Ibrahimi, P. Le Fèvre, F. Bertran, N. Reyren, J.M. George, A. Fert, Phys. Rev. Lett. 116 (2016) 096602.

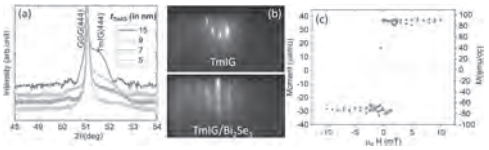

Figure 1 (a) X-Ray (θ-2θ) diffraction patterns recorded on TmIG(5-15nm) thin films grown on GGG substrate. (b) RHEED patterns recorded before (on TmIG surface) and after Bi_2Se_3 growth. (c) Magnetization hysteresis recorded in out-of-plane field on TmIG(15nm) sample.

GOI-11. Spin Current Rectifier Based on the Kitaev Spin Model.

O. Kanehira[1], H. Tsuchiura[1,2] and A. Koga[3] *1. Department of Applied Physics, Tohoku University, Sendai, Japan; 2. Center for Spintronics Research Network, Tohoku University, Sendai, Japan; 3. Department of Physics, Tokyo Institute of Technology, Meguro-ku, Japan*

There has been a growing interest in magnon-based spintronics where magnon-mediated spin current is utilized for information processing and computing applications. Quite recently, one of the authors and his coworkers have shown that novel spin transport phenomena can be realized in the Kitaev spin model [1]. The ground state of the Kitaev spin model is known to be a quantum spin liquid (QSL) state, and the spin degrees of freedom in the model are fractionalized into the itinerant and localized Majorana fermions [2]. Minakawa et al. have shown that, when a magnetic-field pulse is applied to one end of the system, then spin excitations appear at the opposite end without inducing magnetic excitations in the bulk QSL state [1]. They have also found that this novel spin transport is carried by the current of the itinerant Majorana fermions. Stimulated by this work, we theoretically investigate the possibility of constructing a spin current rectifier using the Kitaev spin model. The basic idea is as follows (Fig. 1): it is known that applying a magnetic field along the [111] direction drives the system into the topological phase with chiral Majorana edge currents [2]. Then we can expect that the itinerant Majorana fermions entering the topological phase can interact with the chiral edge current, and then could be redirected along it. We analyze the dynamics of the system schematically shown in Fig. 1 using the time-dependent mean-field theory [3], and the calculated time evolution of the itinerant Majorana mean-field is shown in Fig. 2. It should be noted here that the coupling between the regions I and II is assumed to be weak. We can clearly see that the Majorana current penetrate into the region II in the absence of the magnetic field (Fig. 2 (a)), but not when the region II is in the topological phase (Fig. 2(b)), implying the redirection of the itinerant Majorana current.

[1] T. Minakawa *et al.*, Phys. Rev. Lett., Vol. 125, p.047204 (2020) [2] A. Kitaev, Ann. Phys., Vol. 321, p.2 (2006) [3] J. Nasu and Y. Motome, Phys. Rev. Research, Vol. 1, p.033007 (2019)

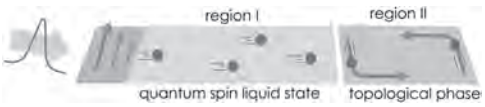

Fig. 1: The schematic diagram of the spin current rectifier using the Kitaev spin model.

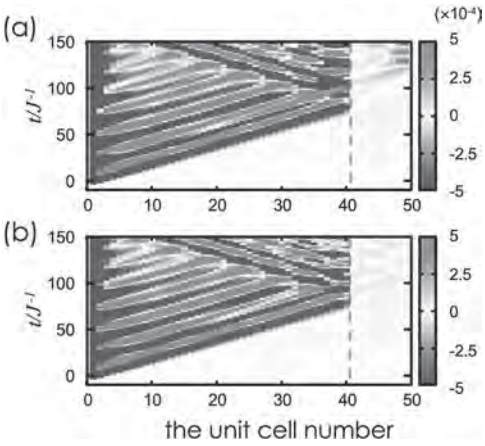

Fig. 2: Real-time evolution of the Kitaev spin system shown in Fig. 1. The contour plot of the itinerant Majorana mean-field on the plane of the time t and the space x in the system (a) without and (b) with the magnetic field in the region II.

GOI-12. The damage analysis for irradiation tolerant spin-driven thermoelectric device based on $Y_3Fe_5O_{12}$/Pt heterostructures.

J. Ieda[1], S. Okayasu[1], K. Harii[2], M. Kobata[3], K. Yoshii[3], T. Fukuda[3], M. Ishida[4] and E. Saitoh[5,1] *1. Advanced Science Research Center, Japan Atomic Energy Agency, Tokai, Japan; 2. Department of Functional Materials Research, National Institutes for Quantum and Radiological Science and Technology, Takasaki, Japan; 3. Materials Sciences Research Center, Japan Atomic Energy Agency, Hyogo, Japan; 4. System Platform Research Laboratories, NEC, Kawasaki, Japan; 5. Department of Applied Physics, University of Tokyo, Tokyo, Japan*

The combination of spin-driven thermoelectric (STE) devices based on spin Seebeck effect (SSE), and radioactive isotopes as heat sources, has potential as a next-generation method of power generation in applications such

as power supplies for space probes. However, there has been very limited knowledge available [1] indicating the irradiation tolerance of spin thermoelectric devices. Through analysis using a heavy ion-beam accelerator and the hard X-ray photoemission spectroscopy (HAXPES) measurements, we show that a prototypical STE device based on $Y_3Fe_5O_{12}$/Pt heterostructures has tolerance to irradiation of high-energy heavy-ion beams [2]. We used 320 MeV gold ion beams modeling cumulative damages due to fission products emitted from the surface of spent nuclear fuels. By varying the dose level, we confirmed that the thermoelectric and magnetic properties of the SSE elements are not affected by the ion-irradiation dose up to 10^{10} ions/cm^2 fluence and that the SSE signal is extinguished around 10^{12} ions/cm^2, in which the ion tracks almost fully cover the sample surface. In addition, the HAXPES measurements were performed to understand the effects at the interface of $Y_3Fe_5O_{12}$/Pt. The HAXPES measurements suggest that the chemical reaction that diminishes the SSE signals [3] is enhanced with the increase of the irradiation dose. We share the current understandings of the damage analysis in $Y_3Fe_5O_{12}$/Pt for developing better STE devices applicable to harsh environmental usages. This work was supported by MEXT Innovative Nuclear Research and Development Program Grant Number JPMXD0212345678.

[1] A. Yagmur *et al.*, "Gamma radiation resistance of spin Seebeck devices," Appl. Phys. Lett. 109, 243902 (2016). [2] S. Okayasu *et al.*, "Tolerance of spin-Seebeck thermoelectricity against irradiation by swift heavy ions," J. Appl. Phys. 128, 083902 (2020). [3] M. Kobata *et al.*, "Hard X-ray Photoelectron Spectroscopy Study of Pt/$Y_3Fe_5O_{12}$," JPS Conference Proceedings 30, 011192 (2020).

GOI-13. Interface and bulk induced spin-to-charge conversion at TbCo/Pt/YIG spin valve structure. *A. Yagmur*[1], S. Sumi[1], H. Awano[1] and K. Tanabe[1] *1. Toyota Technological Institute, Nagoya, Japan*

In this study, we demonstrate the conventional inverse spin Hall effect (ISHE) and magnetization-dependent ISHE (MD-ISHE) in TbCo/Pt/$Y_3Fe_5O_{12}$ devices using the spin Seebeck effect [1,2]. It was found that a thermally injected spin current is converted into two charge currents: (1) dependent on the magnetization direction of TbCo (MD-ISHE) and (2) independent on the magnetization direction of TbCo (ISHE). Here, we investigate the effect of Pt and TbCo thicknesses on the ISHE and MD-ISHE. We found that the MD-ISHE is originated by the TbCo/Pt interface, whereas the conventional ISHE is dominated by the bulk Pt and TbCo. Our findings demonstrate that perpendicularly magnetized TbCo supplies additional symmetry to the ISHE and provides advantages in terms of tailoring the spin-current polarization. This work was partially supported by a Grant-in-Aid for Scientific Research(C) (Grant No. 20K05307) from JSPS and the Tokai Foundation of Technology.

[1] A. Yagmur, S. Sumi, H. Awano, and K. Tanabe, Large Inverse Spin Hall Effect in CoTb Alloys due to Spin Seebeck Effect, Phys. Rev. Appl. 14, 064025 (2020). [2] A. Yagmur, S. Sumi, H. Awano, and K. Tanabe, Magnetization-dependent inverse spin Hall effect in compensated ferrimagnet TbCo alloys, Phys. Rev. B 103, 214408 (2021).

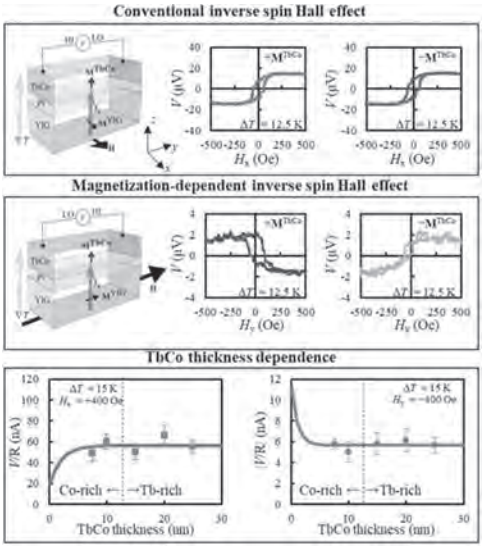

Session GOJ
METAL SPINTRONICS

Mingzhong Wu, Chair
Colorado State University, Fort Collins, CO, United States

INVITED PAPER

GOJ-01. Theory of emergent inductance with spin-orbit effects. *Y. Yamane*[1,2] and J. Ieda[3] *1. Frontier Research Institute for Interdisciplinary Sciences, Tohoku Universirty, Sendai, Japan; 2. Research Institute of Electrical Communication, Tohoku University, Sendai, Japan; 3. Advanced Science Research Center, Japan Atomic Energy Agency, Tokai, Japan*

Inductors are one of the most vital electronic components in today's technology for electric voltage transformation, electric noise filtering, and so on. Its working principle, however, has been essentially the same ever since its earliest inventions in 19th century; a conducting coil stores the energy in a magnetic field when an electric current flows through it, leading to the induction of an electromotive force that opposes the change in the current. Recently, an inductance of quantum mechanical origin was predicted [1] and experimentally demonstrated [2,3] to arise in spiral magnets, and coined as emergent inductance. The spiral-based emergent inductance can be formulated based on a dynamical Berry phase originating from the exchange coupling, where the role of the electromagnetic potential in the classical counterpart is played by a spin-dependent Berry connection generated by the spatial variation of the magnetization. More recent theoretical works [4,5] have shown that two excitation modes of a spiral magnetic texture, namely its translational displacement and rotation of the spiral plane, contribute to the emergent inductance with opposite signs, allowing a negative indutance [2,3]. The discovery of the emergent inductance in spiral magnets has reopened the textbook of electronics, and we are at the beginning of a new chapter exploring quantum mechanical mechanisms of electromagnetic inductance. In this work, we extend the theory of emergent inductance by taking into account spin-orbit coupling effects. We propose an emergent inductance originating from a dynamical Aharonov-Casher (AC) phase of an electron in ferromagnets. This emergent inductance of AC phase origin turns out to universally arise when magnetism and a spin-orbit coupling coexist, even with spatially-uniform magnetization. Revisiting the widely studied systems, such as heavy metal/ferromagnet heterostructures, with the new perspective of emergent inductance will lead to realization and exploration of new physical implications of an AC phase, as well as to an innovative advance in spintronics and inductor technologies.

[1] N. Nagaosa Jpn. J. Appl. Phys. 58, 120909 (2019). [2] T. Yokouchi et al., Nature 586, 232 (2020). [3] A. Kitaori et al., arXiv:2103.02814. [4] J. Ieda and Y. Yamane, Phys. Rev. B 103, L100402 (2021). [5] D. Kurebayashi and N. Nagaosa, arXiv:2103.11317.

CONTRIBUTED PAPERS

GOJ-02. Bulk spin-orbit torques in centrosymmetric magnetic single layers. *L. Zhu*[1], D.C. Ralph[2] and R.A. Buhrman[2] *1. Institute of Semiconductors, Chinese Academy of Sciences, Beijing, China; 2. Cornell University, Ithaca, NY, United States*

Recent discovery of "unexpected" spin-orbit torques (SOTs) within magnetic single layers has attracted attention. However, it has remained elusive as to how to understand and how to tune the SOTs. In this talk, we will first show a strong bulk dampinglike SOT and its characteristics in composition-uniform ferromagnetic CoPt that is polycrystalline and chemically disordered. We find that the bulk dampinglike SOT arises from the interplay of a strong bulk spin Hall effect of CoPt (an imbalanced internal spin current that is transversely polarized and independent of the magnetization orientation) with a "hidden" inversion symmetry-breaking (not a gradient in composition, magnetism, electron scattering, or grain shapes). In the second part, utilizing the single layers of chemically disordered Fe_xPt_{1-x}, we unveil the mechanism of the bulk SOTs by studying their dependence on the introduction of a controlled vertical composition gradient and on temperature. We find that the associated "hidden" inversion symmetry-breaking that allows for a non-zero net torque is most likely a strain non-uniformity that can arise from a composition gradient and/or the substrate. The findings point to the possibility of developing low-power single-layer SOT devices by strain engineering.

[1] L. Zhu, X. S. Zhang, D. A. Muller, D. C. Ralph, R. A. Buhrman, Adv. Funct. Mater. 30, 2005201 (2020). [2] L. Zhu, D. C. Ralph, R. A. Buhrman, Adv. Funct. Mater. DOI: 10.1002/adfm.202103898 (2021).

GOJ-03. Spin-Orbit Torques beyond the Spin-Diffusion Model in Ferromagnet/Normal-Metal/Ferromagnet Trilayers. *K. Belashchenko*[1], G.G. Baez Flores[1], A.A. Kovalev[1] and V. Amin[2] *1. Department of Physics and Astronomy and Nebraska Center for Materials and Nanoscience, University of Nebraska-Lincoln, Lincoln, NE, United States; 2. Department of Physics, Indiana University-Purdue University, Indianapolis, Indianapolis, IN, United States*

Spin-orbit torques in Co/Cu/Co, Co/Pt/Co, and Py/Cu/Py trilayers are studied using the first-principles non-equilibrium Green's function method with supercell disorder averaging. The trilayers with the Cu spacer exhibit strong current-in-plane giant magnetoresistance, and the calculated torques also exhibit features that can not be captured by the spin-diffusion model. For trilayers in the parallel configuration we find strong disorder-dependent dampinglike torque which can greatly exceed the torque in bilayers with Pt. This torque is strongly suppressed in the antiparallel configuration, suggesting the key role of interlayer scattering processes. We also consider the torques arising when the magnetizations in the two ferromagnetic layers are orthogonal to each other. In addition to the known dampinglike and fieldlike torque components, we find a new torque with the angular dependence $(s\bullet m_2)m_1$ where $s=E\times z$ while m_1 and m_2 are the magnetizations in the spin-orbit source and detector layer, respectively. For further insight, we develop a semiclassical model of spin torques in trilayers based on the spin-dependent Boltzmann equation. Numerical calculations reveal that spin torques on one ferromagnetic layer are modulated by the other ferromagnetic layer through interlayer scattering. Our results suggest that in contrast to ferromagnet/heavy-metal bilayers where the spin-diffusion model has been extensively used in the description of spin-orbit torques, ferromagnetic trilayers with strong current-in-plane giant magnetoresistance can exhibit unconventional torques that can not be captured by this model.

GOJ-04. Direct X-ray detection of the spin Hall effect in CuBi. S. Ruiz Gómez[1], R. Guerrero[3], W. Khaliq[1], C. Fernandez-Gonzalez[2,3], S. Finizio[4], P. Perna[3], J. Camarero[3], L. Perez[2,3], L. Aballe[1] and *M. Foerster*[1] *1. ALBA synchrotron, Barcelona, Spain; 2. Fisica de Materiales, Universidad Complutense de Madrid, Madrid, Spain; 3. IMDEA Nanoscience, Madrid, Spain; 4. Swiss Light Source, Zurich, Switzerland*

The spin Hall effect, and its inverse, are important spin-charge conversion mechanisms widely investigated due to their fundamental importance in the development of spintronics devices. Its measurement has been mostly related to electrical detection schemes involving an interface with another magnetic material and thus, a combination of the properties of both materials as well as the interface are measured. The large scattering of reported results from these methods for the same material and temperature call out for a more direct and interface-free approach. Optical detection schemes have been successfully used for the determination of SHE in semiconductor. However, this approach has proven challenging for metallic systems, due to their considerably shorter spin diffusion lengths. Only recently, optical measurements for Pt and W have been reported [1]. Considering that magnetic circular dichroism (XMCD) has become a reference tool for precision measurements of small or diluted magnetic signals, We propose the use of XMCD-PEEM microscopy for direct, interface-free determination of SHE in metals. In particular, we report the observation of spin separation due to SHE in a single layer of Bi-doped Cu (Cu95Bi5), a material in which giant SHE has been already reported [2,3]. We have performed interface free x-ray spectroscopy measurements at the Cu L3,2 absorption edges while applying electrical current to the sample. The sign of spin accumulation depends on the direction of the current and the amplitude of the X-ray magnetic circular dichroism (XMCD) signal scales with the density current and have different sign when measuring in the L2 or L3 absorption edges, as expected for SHE. We have measured an induced magnetic moment of (2.7 ± 0.5) x 10-12μB A-1 cm2 per Cu atom averaged over the probing depth, which is of the same order as for Pt measured by magneto-optics. Our results constitute the proof of concept for the direct, interface free and element-selective measurement of the SHE in a single material by means of X-ray spectromicroscopy and highlight the potential of CuBi for spin-charge conversion applications [4].

[1] C. Stamm et al. Phys. Rev. Lett. 119, 087203 (2017). [2] Y. Niimi et al. Phys. Rev. Lett. 109, 156602 (2012). [3] S. Ruiz-Gómez et al. APL Materials 6, 101107 (2018) [4] S. Ruiz Gómez et al. arXiv:2107.02620 (2021).

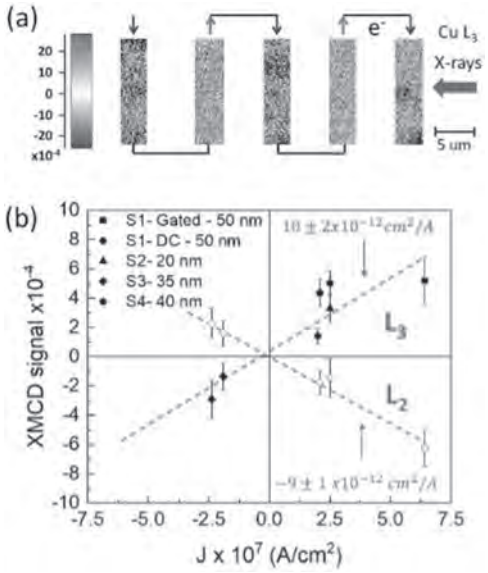

Fig. 1 (a) Visualization of the spin accumulation in a $Cu_{95}Bi_5$ electrode. (b) XMCD signal.

GOJ-05. Large Exotic Spin Torques in Antiferromagnetic Iron Rhodium. *J. Gibbons*[1,2], T. Dohi[3], V. Amin[4], F. Xue[5,6], H. Ren[7,8], J. Xu[7], H. Arava[2,9], S. Shim[10,11], H. Saglam[12,2], Y. Liu[13], J.E. Pearson[2], N. Mason[10,11], A.K. Petford-Long[2,9], P.M. Haney[5], M. Stiles[14], E. Fullerton[8], A. Kent[7], S. Fukami[3] and A. Hoffmann[1,11] *1. Materials Science and Engineering, University of Illinois at Urbana-Champaign, Urbana, IL, United States; 2. Materials Science Division, Argonne National Laboratory, Lemont, IL, United States; 3. Laboratory for Nanoelectronics and Spintronics, Research Institute of Electrical Communications, Tohoku University, Sendai, Japan; 4. Physics, Indiana University - Purdue University Indianapolis, Indianapolis, IN, United States; 5. Nanoscale Processes and Measurements Group, National Institute of Standards and Technology, Gaithersburg, MD, United States; 6. Institute for Research in Electronics and Applied Physics & Maryland Nanocenter, University of Maryland, College Park, MD, United States; 7. Center for Quantum Phenomena, New York University, New York, NY, United States; 8. Center for Memory and Recording Research, University of California San Diego, La Jolla, CA, United States; 9. Materials Science and Engineering, Northwestern University, Evanston, IL, United States; 10. Physics, University of Illinois at Urbana-Champaign, Urbana, IL, United States; 11. Materials Research Laboratory, University of Illinois at Urbana-Champaign, Urbana, IL, United States; 12. Applied Physics, Yale University, New Haven, CT, United States; 13. Center for Nanoscale Materials, Argonne National Laboratory, Lemont, IL, United States; 14. Alternative Computing Group, National Institute of Standards and Technology, Gaithersburg, MD, United States*

Precise control of magnetic dynamics can enable many novel computing applications, including magnetic random access memory and spin torque oscillator-based neuromorphic computing. Spin torques stand out as an excellent tool for efficiently manipulating magnetic states, and can be easily produced via spin-orbit effects in a spin source layer. Unfortunately, underlying crystal symmetries in the spin source material often restrict the geometry of the spin torques, making them poorly suited to practical applications. Magnetic ordering can break the symmetries of a spin source material and allows the generation of versatile spin torques with controllable geometries tailored to applications. Antiferromagnetic materials in particular have robust magnetic ordering that makes them ideal as spin sources. We present spin torque ferromagnetic resonance measurements (Fig. 1) and second harmonic Hall measurements characterizing the geometry and efficiency of spin torques generated in antiferromagnetic iron rhodium alloy. We find highly temperature-dependent spin torques with spin torque efficiencies above 90% at room temperature and above 300% at 170K, much higher than most competing materials. Further, these torques do not show the angular dependence expected for ordinary spin Hall torques. Instead, it appears that the torque derives from a spin current with spin polarization parallel to the FeRh magnetic order, which makes these torques useful for exciting dynamics in a variety of samples. This makes iron rhodium a compelling option for the development of spin torque technology. This work was supported as part of Quantum Materials for Energy Efficient Neuromorphic Computing, an Energy Frontier Research Center funded by the U.S. DOE, Office of Science.

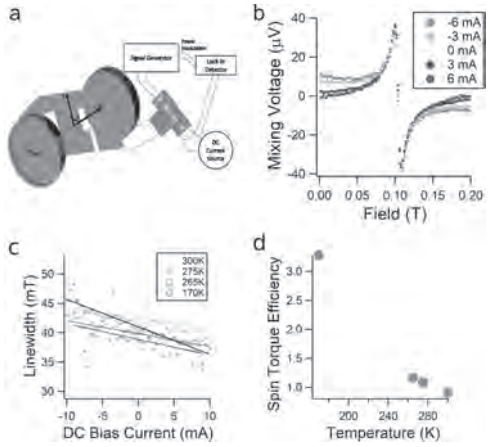

Fig. 1 DC Biased Spin Torque Ferromagnetic Resonance. (a) Diagram of the measurement setup. (b) Characteristic resonance scans. (c) Linewidth over a range of DC currents. Increasing current increases the spin current, modifying the effective damping linearly. Shown at 300K, 275K, 260K, and 170K. (d) Spin torque efficiency is huge and grows by a factor of 3.5 between 300K and 170K.

GOJ-06. Spin absorption anisotropy in lateral spin valves. *M. Cosset-Cheneau*[1], V. Pham[1], D. Gusakova[1], G. Zahnd[1], C. Grezes[1], X. Waintal[2], A. Marty[1], H. Jaffrès[3], L. Vila[1] and J. Attané[1] *1. Spintec, Grenoble, France; 2. Pheliqs, Grenoble, France; 3. CNRS-THALES, Palaiseau, France*

While classical electronics focuses on the control of the charge current, spintronics aims at using a spin current, e.g. a flow of angular momentum for logical and memory applications. One of the main use of such a spin current is magnetization switching used for writing in memory devices. Indeed, when a spin current enters into a ferromagnet, its angular momentum (or polarization) is transmitted to the magnetization, and possibly changes its orientation. The transfer of angular momentum from the spin current to the magnetization can be done in two ways depending on the relative orientation between the polarization and the magnetization direction. If they are collinear, the polarization is absorbed by the ferromagnet through diffusive processes originating from the spin switchings during scattering on defects. However, when the magnetization and polarization are transverse, ballistic processes originating from the conduction electron's spin rotation around the exchange field of the ferromagnet drive the polarization absorption. Understanding the mechanisms of the spin current relaxation into a ferromagnet is therefore of crucial interest for spintronics applications, and remain a seldom explored fundamental question. One of the main difficulty in studying spin current relaxation in a ferromagnetic material is the fact that a charge current generates parasitic effects through the anisotropic magnetoresistance and planar Hall effect. We consequently used lateral spin valves, allowing the measurement of the spin relaxation in a ferromagnet with different relative magnetization direction using a pure spin current, e.g. a flow of angular momentum in the absence of charge current. This measurement allowed us to observe the spin-current relaxation anisotropy in a ferromagnet and to extract the spin mixing conductance, an elusive but fundamental parameter of the spin-dependent transport [1]. Finally, these results allows us to move toward the study of magnetization dependent Spin Hall Effect in ferromagnetic materials.

[1] M. Cosset-Chéneau et al. Phys. Rev. Lett. 126, 027201 (2021)

INVITED PAPER

GOJ-07. Chirality-dependent Edelstein effect in elemental Tellurium nanowires. *F. Calavalle*[1], M. Suaréz Rodríguez[1], A. Johansson[2], D.C. Vaz[1], h. yang[1], B. Martin Garcia[1], A. Chuvilin[1,3], I. Mertig[2], M. Gobbi[1,3], L.E. Hueso[1,3] and F. Casanova[1,3] *1. CIC nanoGUNE BRTA, Donostia-San Sebastián, Spain; 2. Max Planck Institute of Microstructure Physics, Halle, Germany; 3. IKERBASQUE, Bilbao, Spain*

Materials with helical crystal structures have been suggested to be a condensed matter analogue of solenoids, where a current flow produces inductive magnetic fields [1]. At the microscopic scale, a finite spin accumulation can be generated in strong spin-orbit coupling and low symmetry systems via the Edelstein effect [2,3]. Recently, chiral non-magnetic materials have received a lot of attention due to their low symmetries and complex radial spin textures, that could be potentially exploited for spintronic device applications [4,5,6]. However, a straightforward magnetotransport study on the relationship between chirality, spin texture and current-induced spin polarization is still missing. Here, we link one-to-one the direction of the spin polarization, induced by a chirality-dependent Edelstein effect, to the handedness of chiral tellurium (Te) nanowires (NWs), through simple angle-dependent magnetotransport experiments. Transmission electron microscopy (TEM) analysis and theoretical calculations corroborate the transport data. Te NWs show a large, chirality-dependent non-reciprocal charge transport when the electrical current and the magnetic field applied are collinear to the chiral axis of the crystal. By applying a gate voltage, we can also manipulate the magnetotransport response, acting on the carrier density and modifying the spin texture at the Fermi surface. The efficiency of the charge-to-spin interconversion process is one order of magnitude larger than what has been reported so far. Our results are a step forward towards the development of chiral spintronics.

[1] T. Yoda et al., *Scientific Report,* 5, 12024, 2015 [2] V. Edelstein, *Solid state communications,* 73, 233, 1990 [3] A. Soumyanarayanan et al., *Nature,* 539, 509, 2016 [4] Sakano et al., *Physical Review Letters,* 124, 136404, 2020 [5] T. Furukawa et al., *Phys. Rev. Research,* 3, 023111, 2021 [6] S. H. Yang et al., *Nature Review Physics,* 3, 328, 2021

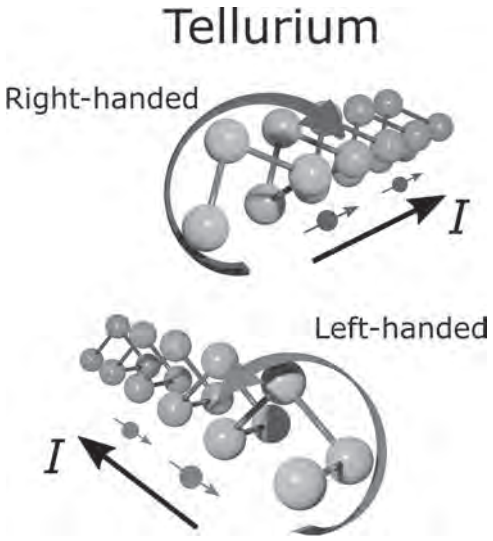

Figure 1: Sketch of the chiral structure of right- and left-handed Te NWs where the current-induced spin polarization depends on the crystal handedness

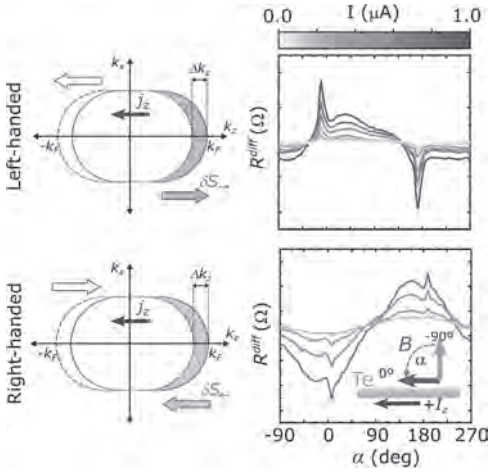

Figure 2: On the leftt, sketch representing the Edelstein effect mechanism. The shift in k_z of the Fermi contours lead to the formation of spin accumulations oriented in opposite directions according to the chirality-dependent radial spin texture of Te. On the right, current-dependent angular dependences of the magnetoresistance $R^{diff}= [R(I_z) - R(-I_z)]/2$ measured at 9 T and 10 K for two Te NWs with opposites handedness. The signals show specular features between left- and right-handed NWs.

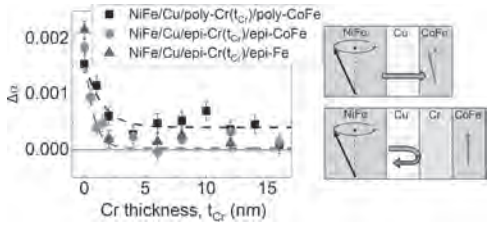

Fig. 1 Δα vs. Cr layer thickness t_{Cr} in NiFe/Cu/Cr(t_{Cr})/(Co)Fe measured at room temperature. Both the epitaxial and polycrystalline series show decaying with t_{Cr}, due to spin reflection at the Cu/Cr interface.

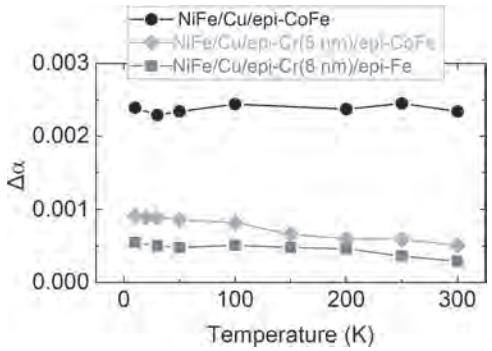

Fig. 2 Δα vs. temperature, showing that spin transport is affected only weakly even as Cr develops stronger antiferromagnetic order at lower temperatures.

CONTRIBUTED PAPERS

GOJ-08. Spin-Reflective Metallic Cu/Cr Interface. *Y. Lim*[1], B. Nepal[2], D.A. Smith[1], S. Wu[1], A. Srivastava[2], P. Nakarmi[2], C. Mewes[2], Z. Jiang[1], A. Gupta[1], D. Viehland[1], C. Klewe[3], P. Shafer[3], J. Heremans[1], T. Mewes[2] and S. Emori[1] *1. Virginia Tech, Blacksburg, VA, United States; 2. University of Alabama, Tuscaloosa, AL, United States; 3. Advanced Light Source, Berkeley, CA, United States*

Electrically conductive metals are typically good transmitters or absorbers of pure spin currents. Here, we report evidence that an interface of two conductive elemental metals – namely, Cu and Cr – constitutes a good spin-current *reflector*. Our study was initially motivated by the question of whether the elemental antiferromagnet Cr acts as a spin transmitter (akin to electrically insulating NiO [1]) or a spin absorber (akin to metallic IrMn [2]). To this end, we have performed ferromagnetic resonance (FMR) spin pumping measurements on spin-valve-like stacks of NiFe(10)/Cu(5)/Cr(t_{Cr})/(Co)Fe(4), where the FMR-driven NiFe layer pumps an AC pure spin current. Any spin current transmitted through the Cu/Cr spacer would be absorbed by the (Co)Fe sink, generating additional Gilbert damping, Δα, for the NiFe source. Thus, Δα is proportional to how much a spin current is transmitted or absorbed across the Cr interlayer. In Figure 1, the sharp decline of Δα with increasing Cr thickness indicates a remarkable trend: The introduction of Cr suppresses spin transmission and absorption – i.e., the spin current is largely reflected by the Cu/Cr spacer. However, our complementary element-selective X-ray FMR measurements confirm that the spin current is transmitted through the Cr spacer in NiFe/Cr/CoFe. We therefore identify the Cu/Cr interface, rather than the Cr bulk, as the source of the strong spin reflection. Figure 2 shows that Δα varies only weakly with decreasing temperature (increasing antiferromagnetic order in Cr), which suggests that antiferromagnetism in Cr is not responsible for the spin-reflective behavior. Our finding points to the possibility that other electrically conductive metals can form effective spin reflectors, thereby offering new avenues in the fundamental studies and engineering of pure spin currents across interfaces.

[1] M. Dabrowski et al. Phys. Rev. Lett. 124, 217201 (2020) [2] W. Zhang et al. Phys. Rev. Lett. 113, 196602 (2014)

GOJ-09. Superimposed contributions to two-terminal and nonlocal spin signals in lateral spin-transport devices. *A.M. Spiesser*[1], R. Jansen[1], Y. Fujita[1,2], H. Saito[1], S. Yamada[2], K. Hamaya[2] and S. Yuasa[1] *1. Research Center for Emerging Computing Technologies, National Institute of Advanced Industrial Science and Technology (AIST), Tsukuba, Japan; 2. Center for Spintronics Research Network, Graduate School of Engineering Science, Osaka University, Toyonaka, Japan*

Lateral spin-transport devices have been instrumental for the study of spin currents in non-magnetic (NM) materials. Such devices typically consist of a lateral NM channel contacted by two ferromagnetic (FM) electrodes and by some additional NM electrodes. The FM contacts enable the injection of a spin current into the channel, as well as the detection of the induced spin accumulation in the channel. These lateral spin-transport devices are operated in two distinct modes. The first is the nonlocal (NL) geometry[1-2], which uses four electrodes (two FM and two normal metal ones), thereby allowing the separation of the electrical charge and spin current. The second is the two-terminal (2T) geometry[3-8], which uses only the two FM contacts to apply the current and detect the spin voltage. Here, we probed the NL and 2T spin signals in a lateral spin-transport device with a Si channel and Fe/MgO tunnel contacts under the application of magnetic fields up to 20 kOe (Fig. 1). This wide range of magnetic fields reveals some important new features: the 2T magnetoresistance and the NL spin signals consist of various superimposed contributions. In addition to the spin signals arising from the usual spin transport of mobile carriers through the Si channel from one FM contact to the other, there are two other contributions, namely, (i) spin signals arising from the spin accumulation of mobile carriers in the Si channel, but generated at each of the FM contacts separately, and (ii) spin signals originating from the spin accumulation of carriers that are confined at or near the Si/MgO interface of the magnetic tunnel contacts, with rather different spin precession characteristics. Perhaps surprisingly, in the NL spin signal a clear *broad Hanle signal* from confined electrons is also observed and argued to be mediated by heat flow from the injector to the NL detector. This work provides a comprehensive picture of spin transport in lateral devices that will be of general interest to those working on devices based on semiconductors, metals, or two-dimensional materials.

1. M. Johnson and R. H. Silsbee, Phys. Rev. Lett. 55, 1790 (1985). 2. F. J. Jedema, H. B. Heersche, A. T. Filip, J. J. A. Baselmans, and B. J. van Wees, Nature 416, 713 (2002). 3. T. Sasaki, T. Oikawa, T. Suzuki, M. Shiraishi, Y. Suzuki, and K. Noguchi, Appl. Phys. Lett. 98, 262503 (2011). 4. M. Gurram, S. Omar, and B.J. van Wees, Nat. Commun. 8, 248 (2017). 5. M. Oltscher, F. Eberle, T. Kuczmik, A. Bayer, D. Schuh, D. Bougeard, M. Ciorga, D. Weiss, Nat. Commun. 8, 1807 (2017). 6. M. Ishikawa, M. Tsukahara, M. Yamada, Y. Saito, and K. Hamaya, IEEE Trans. Mag. 54, 1400604 (2018). 7. R. Jansen, A. Spiesser, H. Saito, Y. Fujita, S. Yamada, K. Hamaya, and S. Yuasa, Phys. Rev. Applied 10, 064050 (2018). 8. A. Spiesser, Y. Fujita, H. Saito, S. Yamada, K. Hamaya, S. Yuasa, and R. Jansen, Appl. Phys. Lett. 114, 242401 (2019).

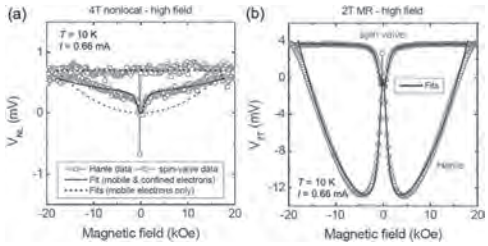

(a) Nonlocal and (b) 2T spin signals (symbols) together with fits (solid and dashed lines) for high magnetic fields up to 20 kOe.

GOJ-10. Nonreciprocal transport of pure spin current at the Au/Pt interface. *P. Omelchenko*[1], E.A. Montoya[2], E. Girt[1] and B. Heinrich[1] *1. Simon Fraser University, Burnaby, BC, Canada; 2. Dep. of Physics and Astronomy, University of California, Irvine, CA, United States*

Asymmetric charge transport at the interface of two materials with dissimilar electrical properties, such as metal/semiconductor and p-n junctions, is the fundamental aspect behind modern diode and transistor technology. Therefore, it is interesting to study pure-spin-current transport at the interface of two materials with different spin transport properties. Here we demonstrate asymmetric transport of pure-spin-currents across an interface of dissimilar non-magnetic materials, Au/Pt. In this work we present a study of spin transport by spin-pumping from either Py ($Ni_{80}Fe_{20}$) or Co in Py/Au/Pt/Co and Py/Au/Pt structures. The thickness of Pt was varied from 0 to 3 nm and the magnetic damping was measured by ferromagnetic resonance. The magnetic damping due to spin-pumping of Py in Py/Au/Pt follows the characteristic thickness dependence of ferromagnet/normal-metal. The typical ferromagnet/normal-metal/spin-sink thickness dependence is reproduced by spin-pumping from Py in the Py/Au/Pt/Co structure. Here the Co layer acts as a spin-sink. However, pumping from Co while Py is the spin-sink in the Py/Au/Pt/Co structure is very uncharacteristic of a spin-sink structure. Instead, this data suggests that very little spin-current makes it to the Py layer, i.e. a reflection of spin-current at the Au/Pt interface. The data could not be self consistently fit with the continuity of spin-accumulation and continuity of spin-current boundary conditions at the Au/Pt interface [1,2]. Including spin-memory-loss also failed to fit the data [3]. We proposed a new boundary condition that assumes that the reflected and transmitted spin-currents at the Au/Pt interface are proportional to the established spin chemical potentials on either side of the interface. This model can self consistently fit all the measured data. It suggests that spin-pumping from Py results in a ~30% reflection and ~70 transmissions of the spin-current across the Au/Pt interface. However, spin pumping from Co results in ~70% reflection and 30% transmission of spin-current at the Au/Pt interface.

[1] Y. Tserkovnyak, A. Brataas, G. E. W. Bauer and B. I. Halperin, Rev. Mod. Phys. Vol. 77 (2005) [2] E. Montoya, B. Heinrich and E. Girt, Phys. Rev. Lett. Vol. 113 (2014) [3] K. Gupta, R. J. H Wesselink, R.Liu, Z. Yuan and P. J. Kelly, Phys. Rev. Lett Vol. 124 (2020)

GOJ-11. Surface states mediated spin-to-charge conversion in $Bi_{1-x}Sb_x$/Co and Bi_2SnTe_4/Co topological insulators probed by THz emission spectroscopy. *E. Rongione*[1,2], L. Baringthon[1,3], S. Fragkos[4], P. Tsipas[4], J. Hawecker[2], T. Dang[1], E. Xenogiannopoulou[4], P. Le Fèvre[3], N. Reyren[1], G. Patriarche[5], A. Lemaître[5], A. Dimoulas[4], R. Lebrun[1], J. George[1], S. Dhillon[2] and H. Jaffrès[1] *1. Unité Mixte de Physique CNRS/Thales, Palaiseau, France; 2. Laboratoire de Physique de l'Ecole Normale Supérieure, Paris, France; 3. Synchrotron SOLEIL, Saint-Aubin, France; 4. Institute of Nanoscience and Nanotechnology, Athens, Greece; 5. Centre de Nanosciences et Nanotechnologies, Palaiseau, France*

Terahertz (THz) spintronic emitters (STE) are promising candidates for covering the THz gap, offering a gapless broadband emission up to 30 THz [1]. They consist in nanometer-thin multilayers composed by a ferromagnetic (FM) layer and a heavy metal (HM) from the 3*d*-5*d* family with a spin-charge conversion (SCC) and THz emission scaling with the spin Hall angle. Recently, efforts have been made to increase the STE output power by layer thickness engineering and interface optimization to reduce THz absorption in metallic layers and spin current absorption in thick FMs [2, 3]. Alternative path now turns to bilayers of FM and topological insulator (TI). TIs present conductive topological surface states (TSS) which allow interfacial SCC via the inverse Rashba-Edelstein effect (IREE). In these systems, enhanced SCC is expected owing to *i*) the large Fermi velocity of related TSS together with *ii*) the insulating behavior of the TI bulk, strongly reducing THz absorption. In this study, we demonstrate large THz emission using the TSS of $Bi_{1-x}Sb_x$ and Bi_2SnTe_4 TIs. We report in Fig. 1a THz emission features from dynamical spin-injection in $Bi_{0.79}Sb_{0.21}$(15nm) and Bi_2SnTe_4(5SL) compared to Co/Pt ISHE STE. Stoichiometry of Bi_2SnTe_4 has been chosen to minimize the presence of bulk bands at the Fermi crossing [4] contrary to other Bi-based TIs such as Bi_2Se_3 [5]. Emission performances of $Bi_{0.79}Sb_{0.21}$ and Bi_2SnTe_4 are about the same order of magnitude as Co/Pt ISHE SCC state-of-the-art STE. Moreover, thickness-independent renormalized emission shown in Fig. 1b on Bi_2SnTe_4 is in favor of an interfacial SCC carried by IREE. Besides, Fig. 1c presents azimuthal crystalline dependence of the THz magnetic contribution which reveals an isotropic emission, expected from an IREE model for SCC. In conclusion, TIs here illustrated by $Bi_{1-x}Sb_x$ and Bi_2SnTe_4 would be suitable candidates for strong STE output power and THz emission spectroscopy allows to explore TSS mediated SCC mechanism.

[1] Seifert T. et al., "Efficient metallic spintronic emitters of ultrabroadband terahertz radiation", Nature Photon 10, 483–488 (2016). [2] Dang T. H. et al., "Ultrafast spin-currents and charge conversion at 3*d*-5*d* interfaces probed by time-domain terahertz spectroscopy", Appl. Phys. Rev. 7, (2020). [3] Hawecker J. et al., "Spin Injection Efficiency at Metallic Interfaces Probed by THz Emission Spectroscopy", Adv. Optical Mater., 2100412, (2021). [4] Fragkos S. et al., "Topological surface states in epitaxial $(SnBi_2Te_4)_n(Bi_2Te_3)_m$ natural van der Waals superlattices", Phys. Rev. Materials 5, 014203 (2021). [5] Wang X. et al., "Ultrafast Spin-to-Charge Conversion at the Surface of Topological Insulator Thin Films", Adv. Mater. 30, 1802356 (2018).

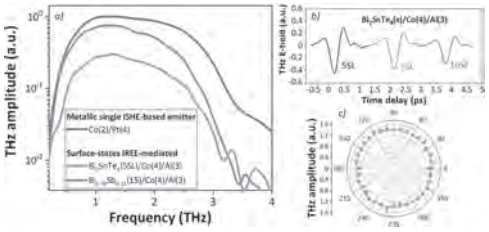

(a) $Bi_{0.79}Sb_{0.21}$/Co and Bi_2SnTe_4/Co THz emission compared to Co/Pt ISHE STE. (b) Absorption renormalized THz emission as a function of Bi_2SnTe_4 thickness. (c) $Bi_{0.79}Sb_{0.21}$/Co isotropic THz emission mapped as a function of the azimuthal crystalline orientation.

GOJ-12. Field-free spin-orbit torque switching driven by facet-induced out-of-plane spin polarization. *T. Chen*[1], W. Liao[1], T. Tsai[1], Y. Huang[1], H. Yen[1] and C. Pai[1] *1. National Taiwan University, Taipei, Taiwan*

Spin-orbit torque (SOT) is realized to be an efficient mechanism to manipulate the magnetization in SOT magnetic device [1]. However, the necessity of external field to achieve deterministic SOT switching in perpendicularly magnetized system has been a great challenge for developing the future SOT technology. Therefore, several methods are promoted to demonstrate the SOT switching in the absence of external field. Most works utilize structural engineering like wedge deposition [2] and adopting antiferromagnet [3] or additional ferromagnetic layer [4]. Recent works suggest that the unconventional SOT with out-of-plane spin polarization observed in low-symmetry material system can induce field-free SOT switching [5]. Unfortunately, the preparation process of these material systems are complicate and challenging. In this work, we show that the out-of-plane spin polarization can be generated in the facet structure prepared by conventional magnetron sputtering. The unconventional SOT is characterized by performing the field-free hysteresis loop shift measurement, More importantly, the demonstration of unidirectional field-free SOT switching further examinates the existence of out-of-plane spin polarization. This work therefore paths a new route for the advanced spintronics technology.

[1] L. Liu, C.-F. Pai, Y. Li, H. Tseng, D. Ralph, and R. Buhrman. *Spin-torque switching with the giant spin Hall effect of tantalum*, Science 336, 555-558 (2012). [2] T.-Y. Chen, H.-I. Chan, W.-B. Liao, and C.-F. Pai. *Current-Induced Spin-Orbit Torque and Field-Free Switching in Mo-Based Magnetic Heterostructures*, Phys Rev Applied 10, 044038 (2018). [3] S. Fukami, C. Zhang, S. DuttaGupta, A. Kurenkov, and H. Ohno. *Magnetization switching by spin–orbit torque in an antiferromagnet–ferromagnet bilayer system*, Nature Mater. 15, 535-541 (2016). [4] S.-h. C. Baek, V. P. Amin, Y.-W. Oh, G. Go, S.-J. Lee *et al. Spin currents and spin–orbit torques in ferromagnetic trilayers*, Nature Mater. 17, 509-513 (2018). [5] I. Kao, R. Muzzio, H. Zhang, M. Zhu, J. Gobbo *et al. Field-free deterministic switching of a perpendicularly polarized magnet using unconventional spin-orbit torques in WTe_2*, arXiv preprint arXiv:2012.12388 (2020).

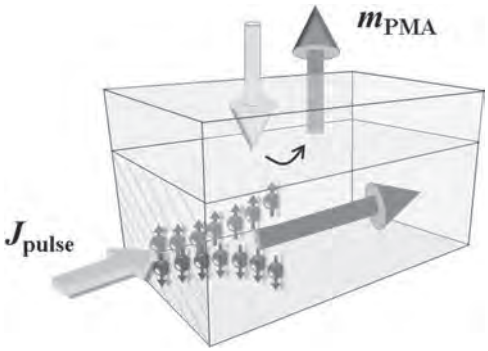

Fig. 1 Illustration of SOT switching induced by out-of-plane spins.

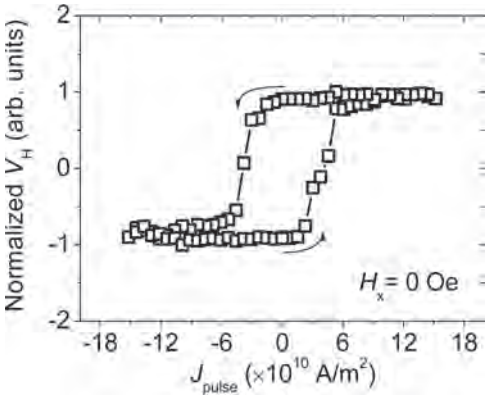

Fig. 2 Field-free SOT switching induced by out-of-plane spin polarization.

GOJ-13. Observation of Large Spin Torques-Related Unidirectional Magnetoresistance in Metallic Heterostructures. T. Zhang[1], C. Cheng[1], C. Huang[1], C. Peng[1], Y. Huang[1], T. Chen[1], *Y. Liu*[1] and C. Pai[1,2] *1. Department of Materials Science and Engineering, National Taiwan University, Taipei, Taiwan; 2. Center of Atomic Initiative for New Materials, National Taiwan University, Taipei, Taiwan*

Spin-related magnetoresistance (MR) from versatile condensed matter systems can be employed as the main mechanism to detect the orientation of magnetization in next generation magnetoresistive random-access memories (MRAM). Recently, novel MR effects such as spin Hall MR (SMR) [1,2] and spin-dependent unidirectional MR (SD-UMR) [3,4] are extensively studied due to the correlation between MR and spin-orbit interactions in both classical and emergent materials systems. In our work, we disentangle the underlying mechanisms of the UMR in W/CoFeB magnetic heterostructures by systematic current-dependent and field-dependent MR measurements at room temperature. As shown in Fig.1, the current-dependent UMR of W/CoFeB heterostructures can be roughly divided into three regimes. In the first and second regimes, UMR increases linearly and then nonlinearly to the applied current density J as J reaches ~5×10^{10} A/m^2, which originates from the SD-UMR [Fig.2(a)] and spin-flip UMR (SF-UMR) [Fig.2 (b)] [4]. In the third regime, as J reaches ~ 10^{11} A/m^2, the UMR ratio will further saturate at 0.36%, which is larger than the typical UMR magnitudes reported previously in metallic system. With the aid of numerical simulations, this large UMR can be attributed to the extra contribution from SMR, which stems from the tilting of magnetization M caused by the competition between the spin Hall effect induced spin torques (STs) from W layer and the external field H_y. This tilting behavior is illustratively shown in Fig.2 (c). Consequently, we define this UMR as the spin-transfer torque UMR (STT-UMR). The damping like-ST (DL-ST) efficiency of W/CoFeB heterostructures can be also roughly estimated by using both the experimental UMR data and the simulation results. Our finding therefore verifies the correlation between the STs and this large room-temperature UMR, thereby providing an alternative approach to determine DL-ST efficiency.

[1] H. Nakayama *et al.*, Phys Rev Lett 110, 206601 (2013). [2] J. Kim, P. Sheng, S. Takahashi, S. Mitani, and M. Hayashi, Phys Rev Lett 116, 097201 (2016). [3] C. O. Avci, K. Garello, A. Ghosh, M. Gabureac, S. F. Alvarado, and P. Gambardella, Nat. Phys. 11, 570 (2015). [4] C. O. Avci, J. Mendil, G. S. D. Beach, and P. Gambardella, Phys. Rev. Lett. 121, 087207 (2018).

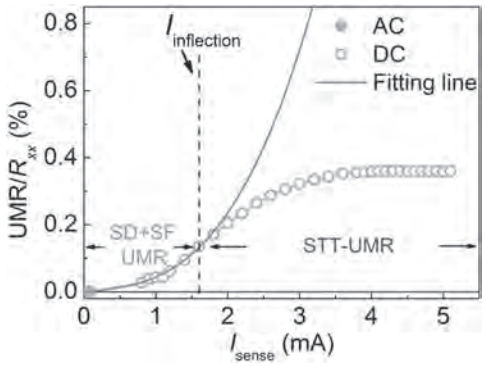

Fig.1 UMR/R_{xx} versus I_{sense} with H_y = 600 Oe for a W(4)/CoFeB(2) sample. When $I_{sense} > I_{inflection}$, the curve can be fitted by $(a+b)I + cI^3$.

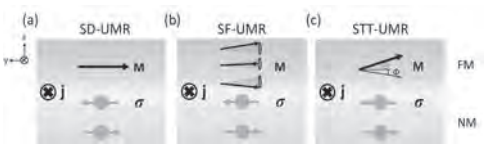

Fig.2 Illustration of (a) spin-dependent UMR (SD-UMR), (b) spin-flip UMR (SF-UMR), and (c) spin-transfer torque UMR (STT-UMR).

GOJ-14. Hard magnet topological semimetals in XPt_3 compounds with the harmony of Berry curvature. *J.D. Gayles*[1], A. Markou[2] and C. Felser[2]
1. Applied Physics, University of South Florida, Tampa, FL, United States; 2. Solid State Phyiscs, Max Planck Institute for Chemical Physics of Solids, Dresden, Germany

Topological magnetic semimetals, like $Co_3Sn_2S_2$ and Co_2MnGa, display exotic transport properties, such as large intrinsic anomalous (AHE) due to uncompensated Berry curvature. The highly symmetric XPt_3 compounds display anti-crossing gapped nodal lines, a driving mechanism in the intrinsic Berry curvature Hall effects. Uniquely, these compounds contain two sets of gapped nodal lines that harmoniously dominate the Berry curvature in this complex multi-band system. We calculate a maximum AHE of 1965 S/cm in the $CrPt_3$ by a state-of-the-art first principle electronic structure. We have grown high-quality thin films by magnetron sputtering and measured a robust AHE of 1750 S/cm for different sputtering growth conditions. Additionally, the cubic films display a hard magnetic axis along [111] direction. The facile and scalable fabrication of these materials makes them ideal candidates for integration into topological devices [1].

[1] Markou, Anastasios, Jacob Gayles, et al. "Hard magnet topological semimetals in X Pt 3 compounds with the harmony of Berry curvature." *Communications Physics* 4.1 (2021): 1-7.

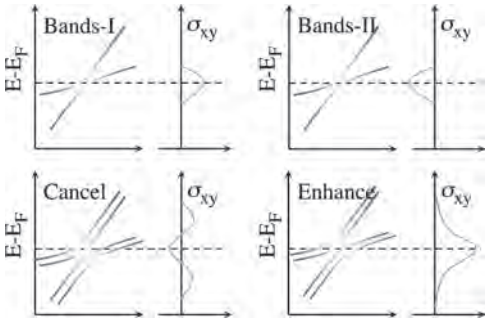

Session GOK
MRAM, MAGNETIC LOGIC AND RELATED DEVICES I

Stephane Mangin, Chair
Université de Lorraine, Vandoeuvre-lès-Nancy, France

INVITED PAPERS

GOK-01. The Impact of the Buhrman Group on MRAM over the Past 25 Years. *J. Katine*[1] *1. Western Digital, San Jose, CA, United States*

Despite having published no papers related to magnetism prior to 1996, In 1996 Prof. Buhrman initiated a new project in his group to explore phenomena relevant to proposed MRAM technologies. Over the next 25 years, his group would make several seminal contributions to this field, and in this talk, I will present a retrospective on the impact Bob Buhrman's group had on MRAM during this timeframe. Twenty-five years ago magnetism played a key role in HDD and tape storage technologies, but magnetism was not exploited in memories that could be integrated with planar semiconductor processing. Today, embedded MRAM is offered at all of the leading foundries, and standalone MRAM memory chips are available at capacities up to 1 Gbit. STT-MRAM is the basis of these of these memories. Many research groups have played key roles in the commercialization of this technology, but Prof. Buhrman's group was responsible for significant advances including the first demonstration of STT switching in lithographically patterned bits [1] and early demonstrations of STT switching in magnetic tunnel junctions [2]. There is considerable effort today on using STT-MRAM as a replacement for embedded SRAM, but it is difficult for STT-MRAM to meet the endurance and speed requirements for these applications. Three-terminal SOT-MRAM technology is a potential alternative to STT-MRAM for such applications. Here again, Prof. Buhrman's group was at the forefront of this research [3], and has subsequently made many important contributions to the understanding of SOT physics.

[1] J.A. Katine, et al., Phys. Rev. Lett. 84 3149 (2000) [2] G.D. Fuchs, et al., Appl. Phys. Lett. 85 1205 (2004) [3] Luqiao Liu, et al., Science 336 pp. 555-8 (2012)

GOK-02. Nanosecond Stochastic Magnetic Tunnel Junctions for Probabilistic Computing - Experiment and Theory. *S. Kanai*[1,2], K. Hayakawa[1,3], K. Kobayashi[1,3], T. Funatsu[1,3], W. Borders[1], J. Igarashi[1], B. Jinnai[4], H. Ohno[1,5] and S. Fukami[1,6] *1. Laboratory for Nanoelectronics and Spintronics, RIEC, Tohoku University, Sendai, Japan; 2. Division for the Establishment of Frontier Sciences, Organization for Advanced Studies, Tohoku University, Sendai, Japan; 3. Graduate School of Engineering, Tohoku University, Sendai, Japan; 4. WPI-Advanced Institute for Materials Research, Tohoku University, Sendai, Japan; 5. Center for Spintronics Research Network, Tohoku University, Sendai, Japan; 6. Center for Innovative Integrated Electronic Systems, Tohoku University, Sendai, Japan*

Probabilistic computing has gathered attention for its ability to efficiently solve nondeterministic polynomial time (NP) problems in polynomial time using established CMOS hardware[1]. A probabilistic computer utilizes stochastic bits called "p-bits", which function as binary stochastic neurons. Recently, magnetic tunnel junctions (MTJs) with a low barrier energy (stochastic MTJs or s-MTJs) have been shown to behave as binary stochastic neurons with 300 times fewer transistors and only one–tenth of the operation energy than purely CMOS-based p-bits, and with this spintronics-based p-bits, integer factorization has been demonstrated as a proof of concept[2]. Performance of the s-MTJ is characterized by its "time-domain response" and "time-averaged response", and in this talk, we summarize the experimental and theoretical investigations on these characteristics. The time-domain response of s-MTJs produces a randomly generated output reflecting the transition between the high and low resistive states. It can be characterized by an average switching event time (the relaxation time), which affects the computation time of the probabilistic computer. Recently, based on an analysis of the time evolution of entropy for the magnetization direction probability distribution, we have proposed that in order for shorter relaxation times, it is necessary not only to reduce the barrier energy but also to increase the precession frequency[3]. We have shown that s-MTJs with in-plane magnetic easy axis have 10- to 1000-fold shorter relaxation times compared to MTJs with perpendicular magnetic easy axis under the same barrier energy, due to the difference of the precessional frequency at reduced barrier energy. According to this design guideline, we have fabricated s-MTJs with in-plane magnetic easy axis, and achieved relaxation times down to 8 ns[4], more than 5 orders of magnitude shorter than that of typical s-MTJs with perpendicular easy axis[2] and about 100 times shorter than other previous reports of s-MTJs with in-plane easy axis. The time-averaged response of the output reflects the ratio of time spent in each state and is characterized by a sigmoidal response to the inputs. We have investigated the sigmoidal characteristics of nanoscale s-MTJ resistance under magnetic field and current. Based on the Néel-Arrhenius law, we have derived an analytical expression of the time-averaged response versus the field and current. The experimental results along with the analysis have clarified new physical insights on the field- and current-induced magnetization switching in nanoscale MTJs[5]. The authors thank to C. Igarashi, R. Ono, M. Musya, I. Morita, T. Hirata, and H. Iwanuma for their technical supports. This work was supported in part by JST-CREST JPMJCR19K3 and JSPS Kakenhi 19H05622, 19KK0130, and 20H02178.

[1] K.Y. Camsari, R. Faria, B. M. Sutton, and S. Datta, *Phys. Rev. X* 7, 031014 (2017). [2] W. A. Borders, A. Z. Pervaiz, S. Fukami, K. Y. Camsari, H. Ohno, and S. Datta, *Nature* 573, 390 (2019). [3] S. Kanai, K. Hayakawa, H. Ohno, and S. Fukami, *Phys. Rev. B* 103, 094423 (2021). [4] K. Hayakawa, S. Kanai, T. Funatsu, J. Igarashi, B. Jinnai, W. A. Borders, H. Ohno, and S. Fukami, *Phys. Rev. Lett.* 126, 117202 (2021). [5] K. Kobayashi, W. A. Borders, S. Kanai, K. Hayakawa, S. Fukami, and H. Ohno, *INTERMAG 2021*, FC-09 (2021).

CONTRIBUTED PAPERS

GOK-03. Withdrawn

GOK-04. Multifunctional Design of Domain Wall-Magnetic Tunnel Junction Artificial Synapses for Accurate Training of Neural Networks. *S. Liu*[1], T.P. Xiao[2], C. Cui[1], J.C. Incorvia[1], C. Bennett[2] and M. Marinella[2] *1. Electrical and Computer Engineering, University of Texas at Austin, Austin, TX, United States; 2. Sandia National Laboratories, Albuquerque, NM, United States*

The processing of artificial neural networks (ANNs) is limited by the memory wall in von Neumann architectures, driving the need for hardware ANNs realized by neuromorphic devices [1]. Previously proposed multi-weight synaptic devices often suffer from a nonlinear and asymmetric update response, limiting their viability for supervised learning [2]. Domain wall-magnetic tunnel junction (DW-MTJ) devices driven by spin transfer torque (STT) and spin orbit torque (SOT) have shown promise in neuromorphic applications, realizing leaky integrate-and-fire neurons in simulation [3-8]. Simulations also show that DW-MTJs can implement synaptic spike-timing dependent plasticity [9]. A type of DW-MTJ with multiple MTJs was demonstrated experimentally [10], and we have recent results on experimental DW-MTJ synapses that are submitted separately for consideration in the conference. Most prior work on DW-MTJ synapses in ANNs do not consider thermal effects and process variation. We evaluate notched DW-MTJ designs shown in Fig. 1a and account for these effects using MuMax3 for device simulation and CrossSim for network simulation [11-13]. Figure 1b shows that excellent linearity, high symmetry, and low thermal noise are maintained at 300 K. High training accuracy was obtained on the Fashion-MNIST task, shown in Fig. 2 [14]. Notably, the greater stochasticity of SOT-driven synapses counters the discretizing effect of notches, boosting accuracy to near ideal. We also implemented short term potentiation for network pruning using shape anisotropy. These results propose a magnetic synapse with tunable plasticity, superior backpropagation performance, and fast updates, a foundational step toward ANNs with fully spintronic matrix operations. *SNL is managed and operated by NTESS under DOE NNSA contract DE-NA0003525*

1) A. Sebastian, M. Le Gallo, R. Khaddam-Aljameh and E. Eleftheriou, Nature Nanotechnology., Vol. 15(7), p. 529–544 (2020) 2) X. Sun and S. Yu, IEEE Journal on Emerging and Selected Topics in Circuits and Systems., Vol. 9(3), p. 570–579 (2019) 3) J. A. Currivan-Incorvia, S. Siddiqui, S. Dutta, E. R. Evarts, J. Zhang, D. Bono, C. A. Ross and M. A. Baldo, Nature Communications., Vol. 7, p. 3–9 (2016) 4) M. Alamdar, T. Leonard, C. Cui, B. P. Rimal, L. Xue, O. G. Akinola, T. P. Xiao, J. S. Friedman, C. H. Bennett, M. J. Marinella and J. A. C. Incorvia, Applied Physics Letters., Vol. 118(11), p. 112401 (2021) 5) W. H. Brigner, X. Hu, N. Hassan, C. H. Bennett, J. A. C. Incorvia, F. Garcia-Sanchez and J. S. Friedman, IEEE Journal on Exploratory Solid-State Computational Devices and Circuits., Vol. 5(1), p. 19–24 (2019) 6) N. Hassan, X. Hu, L. Jiang-Wei, W. H. Brigner, O.G. Akinola, F. Garcia-Sanchez, M. Pasquale, C. H. Bennett, J. A. C. Incorvia and J. S. Friedman, Journal of Applied Physics., Vol. 124(15), p. 152127 (2018) 7) C. Cui, O. G. Akinola, N. Hassan, C. H. Bennett, M. J. Marinella, J. S. Friedman and J. A. C. Incorvia, Nanotechnology., Vol. 31(29), p. 294001 (2020) 8) S. Liu, C. H. Bennett, J. S. Friedman, M. J. Marinella, D. Paydarfar and J. A. C. Incorvia, IEEE Magnetics Letters., Vol. 12, p. 1-5 (2021) 9) O. G. Akinola, X. Hu, C. H. Bennett, M. J. Marinella, J. S. Friedman and J. A. C. Incorvia, Journal of Physics D: Applied Physics., Vol. 52, p. 49LT01 (2019) 10) S. A. Siddiqui, S. Dutta, A. Tang, L. Liu, C. A. Ross and M. A. Baldo, Nano Letters., Vol. 20(2), p. 1033–1040 (2020) 11) A. Vansteenkiste, J. Leliaert, M. Dvornik, M. Helsen. F. Garcia-Sanchez and B. Vann Waeyenberge, AIP Advances., Vol. 4, p. 107133 (2014) 12) S. Agarwal, R. B. Jacobs Gedrim, A. H. Hsia, D. R. Hughart, E. J. Fuller, A. A. Talin, C. D. James, S. J. Plimpton and M.J. Marinella, in IEEE Symposium on VLSI Technology (2018), p. 103-104 13) S. Liu, T. P. Xiao, C. Cui, J. A. C. Incorvia, C. H. Bennett and M. J. Marinella, Applied Physics Letters, Vol. 118(20), p. 202405 (2021) 14) H. Xiao, K. Rasul and R. Vollgraf, arXiv:1708.07747, (2017)

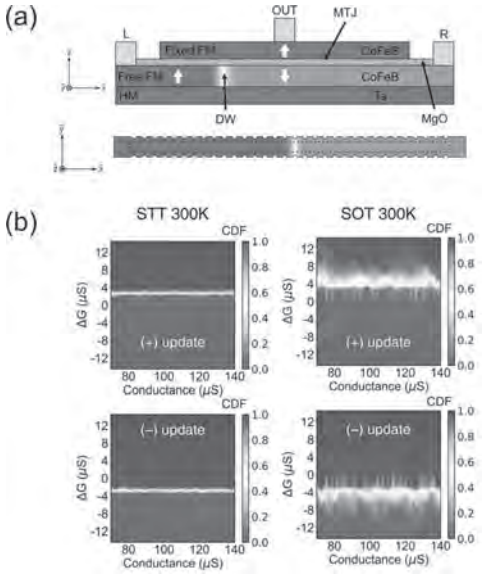

Fig. 1 a) Device diagram b) Conductance G vs dG statistics of a DW-MTJ at 300 K for STT and SOT propagation. Heatmaps are generated from micromagnetic simulations. The CDF represents the probability that a given conductance update is less than the average dG.

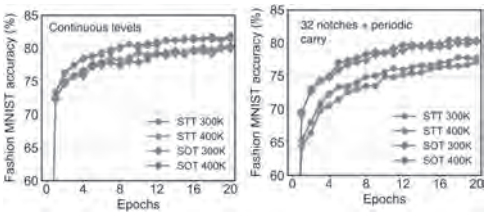

Fig. 2 Validation accuracy of a two-layer perceptron of STT and SOT DW-MTJ synapses at 300 K assuming (a) continuous levels and (b) 32 notches and periodic carry.

GOK-05. Experimental Demonstration of Reservoir Computation using Emergent Domain Wall Dynamics in a Patterned Magnetic Substrate. *I.T. Vidamour*[1], C. Swindells[1], G. Venkat[1], P.W. Fry[3], N. Morley[1], E. Vasilaki[2], D. Allwood[1] and T. Hayward[1] *1. Department of Materials Science and Engineering, The University of Sheffield, Sheffield, United Kingdom; 2. Department of Computer Science, The University of Sheffield, Sheffield, United Kingdom; 3. Nanoscience and Technology Centre, University of Sheffield, Sheffield, United Kingdom*

Reservoir computing (RC) is a machine learning paradigm where computational power is obtained from the intrinsic memory and nonlinearity of a dynamic system. Traditionally, the dynamic system is provided by a recurrent neural network, though many recent studies show this network can be substituted with a physical system. Within the field of magnetism, many systems have been proposed as candidates for RC, such as magnetic tunnel junctions (MTJs) [1], skyrmion textures [2], superparamagnetic arrays [3], and even single domain walls [4]. However, aside from MTJs, few of these proposed systems have been experimentally realised. Recently, we showed that single-layer arrays of interconnected permalloy nanorings exhibit emergent domain wall dynamics suitable for computation [5]. Here, we demonstrate RC *in materio* using a device containing the aforementioned arrays. Data is encoded to the array by modulating the amplitude of a rotating magnetic field. Using two-point resistance measurements, we show that we can extract information on the state of the array through

anisotropic magnetoresistance (AMR). These measurements exhibit nonlinearities between applied field and the measured magnetic state of the system, as well as hysteretic memory. Next, we show how we can control the system's dynamics through scaling of the applied magnetic field, allowing a range of different transfer functions between input and measured magnetic state. These different transfer functions can be exploited to provide improved computational performance on signal, speech, and writing processing tasks. Through optimised scaling of the applied fields, the different computational demands of each task are met on a single device. We believe that the computational versatility, relative simplicity of manufacture, as well as the wide range of available parameter space to further explore makes the ring arrays an exciting platform for neuromorphic computation.

[1] J. Torrejon *et al.*, "Neuromorphic computing with nanoscale spintronic oscillators," *Nature*, vol. 547, no. 7664, pp. 428–431, Jul. 2017, doi: 10.1038/nature23011. [2] D. Pinna, G. Bourianoff, and K. Everschor-Sitte, "Reservoir Computing with Random Skyrmion Textures," *Phys. Rev. Appl.*, vol. 14, no. 5, p. 054020, Nov. 2020, doi: 10.1103/PhysRevApplied.14.054020. [3] A. Welbourne *et al.*, "Voltage-controlled superparamagnetic ensembles for low-power reservoir computing," *Appl. Phys. Lett.*, vol. 118, no. 20, p. 202402, May 2021, doi: 10.1063/5.0048911. [4] R. V Ababei *et al.*, "Neuromorphic computation with a single magnetic domain wall." Sci. Rep. (Accepted July 2021) [5] R. W. Dawidek *et al.*, "Dynamically-Driven Emergence in a Nanomagnetic System," *Adv. Funct. Mater.*, vol. 31, no. 8, 2021.

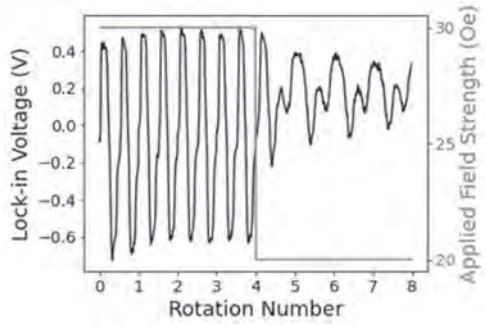

Fig. 1 Measured AMR response for 4 rotations of 30 Oe applied field, followed by 4 rotations of 20 Oe applied field, showing both nonlinear and hysteretic behaviour.

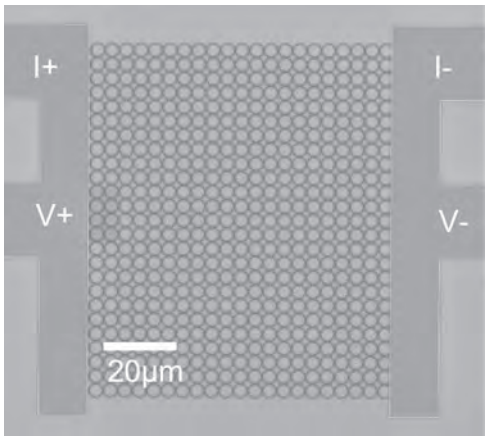

Fig. 2 Micrograph of patterned nanoring array and electric contacts taken from RAITH Voyager electron beam lithography system.

GOK-06. High-Speed CMOS-Free Purely Spintronic Asynchronous Recurrent Neural Network. *C.B. Duffee*[1], P.O. Mathews[1], A. Thayil[2], T. Stovall[3], C. Bennett[4], F. Garcia-Sanchez[6], M. Marinella[4], J.C. Incorvia[5], N. Hassan[1], X. Hu[1] and J.S. Friedman[1] *1. Department of Electrical and Computer Engineering, University of Texas at Dallas, Richardson, TX, United States; 2. Laboratoire de Physique de la Matière Condensée, Ecole Polytechnique, Villeurbanne, France; 3. School of Behavioral & Brain Sciences, University of Texas at Dallas, Richardson, TX, United States; 4. Sandia National Laboratories, Albuquerque, NM, United States; 5. Electrical and Computer Engineering, University of Texas at Austin, Austin, TX, United States; 6. Departamento de Física Aplicada, Universidad de Salamanca, Salamanca, Spain*

Recurrent neural networks (RNN) have proven useful in relational data processing which conventional von Neumann architectures are poorly suited to handle. However, the high energy cost of running RNNs on existing CMOS based devices makes them inefficient for modern applications. This work proposes a low power, fully spintronic RNN architecture as first described in [1]. We propose a biologically inspired neuron composed of domain-wall magnetic tunnel junctions (DW-MTJs) [2][3], as shown in Fig. 1. Inputs to the soma push its domain wall (DW) in the direction of net electron flow, setting the soma either in a high or low resistive state. In a high resistive state, a leaking force acting on the axons' DW overcomes the effects of the small current flow from the soma, rendering the axons in high resistive states. However, in the soma's low resistive state, the axons are pushed into low resistive states, and high currents modulated by synaptic weight voltages are allowed to flow into other neurons. While these neurons can be connected to form all sorts of RNNs, our work focuses on the fully connected Hopfield network [1]. The proposed architecture has performed standard Hopfield network tasks with high accuracy. A 100 neuron network has been trained to recognize three distinct images of letters, as shown in Fig 2. When any letter is distorted up to 30% and applied as an input, the network converges to the undistorted image with a high degree of accuracy [1]. This design also consumes less energy than competing post-CMOS schemes. A 60 neuron network can produce an approximate maxcut solution of a standard 50% connected graph [1][4]. This task completes in 343 ns and consumes 20.5 nJ, comparing favorably to two other works: a memristive network requiring 72 nJ in 600 ns [5], and a SONOS based network that consumes 33 nJ over a timeframe of several microseconds [6].

[1] P. Mathews, C. Duffee and A. Thayil, arXiv e-prints., p. arXiv:2107.02238 (2021) [2] W. Brigner, N. Hassan and X. Hu, arXiv e-prints., p. arXiv:2002.00862 (2020) [3] N. Hassan, X. Hu, and L. Jiang-Wei, Journal of Applied Physics., vol. 124, no. 15 (2018) [4] A. Wiegele, "Biq Mac Library," [online] http://biqmac.uni-klu.ac.at/biqmaclib.html, (2007) [5] A. R. Bevi, P. Monurajan and J. Manjula, Neural Computing and Applications., Vol. 32, no. 13, p. 9443–9452 (2020) [6] S. Yi, S. Kumar, and R. S. Williams, arXiv e-prints., p. arXiv:2104.12288, (2021)

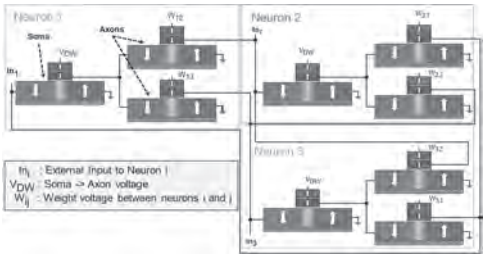

Fig. 1: Schematic of a 3-neuron Hopfield network.

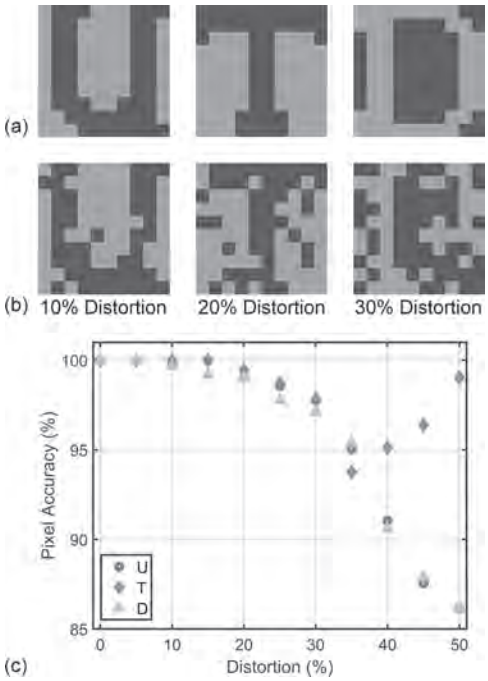

Fig. 2: (a) 10x10 training images. (b) Sample inputs to the network with 10%, 20%, and 30% distortion. (c) Pixel difference (%) between the network output and the undistorted image vs. image distortion (%).

GOK-07. Superparamagnetic tunnel junctions with a synthetic antiferromagnetic free layer. *K. Kobayashi*[1,2], K. Hayakawa[1,2], W.A. Borders[1,2], S. Kanai[1,3], J. Igarashi[1,2], H. Ohno[1,4] and S. Fukami[1,5]
1. Laboratory for Nanoelectronics and Spintronics, Research Institute of Electrical Communication, Tohoku University, Sendai, Japan; 2. Graduate School of Engineering, Tohoku University, Sendai, Japan; 3. Division for the Establishment of Frontier Sciences, Organization for Advanced Studies, Tohoku University, Sendai, Japan; 4. WPI-Advanced Institute for Materials Research, Tohoku University, Sendai, Japan; 5. Center for Innovative Integrated Electronic Systems, Tohoku University, Sendai, Japan

Thermally unstable stochastic magnetic tunnel junction (s-MTJ) constituting a probabilistic bit (p-bit) is a promising building block for probabilistic computers, which is expected to solve computationally hard problems efficiently [1,2]. Each p-bit serves as a binary stochastic neuron [1], where robustness of s-MTJ against external perturbations is required. Previous studies on s-MTJs [2-4] have used a single ferromagnetic free layer, in which the probability to take parallel (P) and antiparallel (AP) configurations significantly change with external magnetic field H along the easy axis due to the Zeeman energy, that is proportional to the net magnetic moment of the free layer [4]. In this work, we investigate s-MTJs with a synthetic antiferromagnetic (SAF) free layer, which has a smaller Zeeman energy leading to high robustness against the external field. A stack structure consisting of a reference layer/ MgO/ CoFeB/ Ru/ CoFeB/ cap layer is deposited by dc/rf magnetron sputtering. CoFeB layers have an in-plane easy axis and are antiferromagnetically coupled to compose a SAF free layer [Fig. 1(a)]. The stack is processed into elliptic MTJs with an averaged diameter of 40-80 nm. In order to compare the robustness of a SAF free layer against H with a single free layer [2-4], we measure their relaxation time through the random telegraph noise signal as a function of H. Figures 1(a) and (b) show the relaxation time τ_P (τ_{AP}) for P (AP) configuration and their ratio τ_{AP}/τ_P against $\mu_0(H\text{-}H_S)$ for typical s-MTJs with a single free layer [4] and a SAF free layer, where H_S is the shift field due to the reference layer and μ_0 the permeability of vacuum, respectively. The SAF free layer has about 8 times smaller slope of the τ_{AP}/τ_P *vs*. H compared to the single free layer, indicating that s-MTJs with a SAF free layer offer a promising pathway for the robust s-MTJs suitable for the p-bit. This work was supported in part by JST-CREST JPMJCR19K3 and JSPS Kakenhi 19H05622, 19KK0130, and 20H02178.

[1] K. Y. Camsari *et al.*, Phys. Rev. X 7, 031014 (2017). [2] W.A. Borders *et al.*, Nature 573, 390 (2019). [3] S. Kanai *et al.*, Phys. Rev. B 103, 094423 (2021). [4] K. Hayakawa *et al.* Phys. Rev. Lett. 126, 117202 (2021).

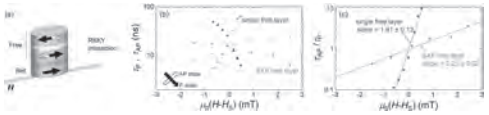

Fig.1 (a) Schematic diagram of MTJ structure with a SAF free layer. (b) Relaxation time for the P (AP) configuration τ_P (τ_{AP}) *vs*. $\mu_0(H\text{-}H_S)$. (c) Ratio of τ_P and τ_{AP} *vs*. $\mu_0(H\text{-}H_S)$.

GOK-08. Synchronous Unsupervised STDP Learning with Stochastic STT-MRAM Switching. *P. Zhou*[1], J. Smith[1], L. Deremo[2], S.K. Heinrich-Barna[2] and J.S. Friedman[1] *1. Department of Electrical and Computer Engineering, The University of Texas at Dallas, Richardson, TX, United States; 2. Texas Instruments Inc., Dallas, TX, United States*

The use of analog resistance states for storing weights in neuromorphic systems is impeded by fabrication imprecision and device stochasticity that limit the precision of synapse weights. This challenge can be resolved by emulating analog behavior with the stochastic switching of the binary states of spin-transfer torque magnetoresistive random-access memory (STT-MRAM) [1]. We propose and design a complete spiking neural network (SNN) system with an electrically-realistic hardware learning circuit that stochastically switches the STT-MRAM synapses [2]. When the fixed and free layers of an STT-MRAM cell have magnetizations in the same direction, the MTJ has low resistance; otherwise the MTJ has high resistance. STT is a stochastic process that switches the MTJ state with a probability dependent on the pulse voltage and duration. The core of the on-chip unsupervised online learning system is shown in Fig. 1(a-b), with STT-MRAM synapses and leaky integrate-and-fire neurons implemented in CMOS. During each clock cycle, the input neurons generate input pulses to the MRAM array, and the output neurons integrate the current from the MRAM array. If a neuron fires, a learning pulse is generated during the next clock cycle and the neuron integration values are reset to zero; if no neuron fires, leaking occurs during the next clock cycle. This synchronous circuit design has been demonstrated via behavioral simulation as shown in Fig. 1(c), Fig. 2. The inference accuracy increases with both increasing numbers of output neurons and increasing numbers of synapses sharing each pixel, and the inference accuracy can reach 90% on MNIST handwritten digits. These results are comparable to simulations of unsupervised single layer SNNs based on multilevel memristors evaluated with a similar size and methodology [3]. The proposed binary STT-MRAM system with stochastic writing will soon be experimentally proven to provide higher accuracies than can be achieved with memristors and phase-change memory. This work is supported by SRC/TxACE.

[1] A. F. Vincent, J. Larroque, N. Locatelli, N. Ben Romdhane, O. Bichler, C.n Gamrat, W. Zhao, J. Klein, S. Galdin-Retailleau, and D. Querlioz. 2015. Spin-transfer torque magnetic memory as a stochastic memristive synapse for neuromorphic systems. IEEE Transactions on Biomedical Circuits and Systems 9, 2 (2015), 166–174. [2] P. Zhou, J. A. Smith, L. Deremo, S. K. Heinrich-Barna, J. S. Friedman, Synchronous Unsupervised STDP Learning with Stochastic STT-MRAM Switching, Government Microcircuit Applications & Critical Technology Conference, Mar. 2021. [3] N. Rathi, P. Panda, and K. Roy, STDP-based pruning of connections and weight quantization in spiking neural networks for energy-efficient recognition. IEEE Transactions on Computer-Aided Design of Integrated Circuits and Systems 38,4 (2018), 668–677.

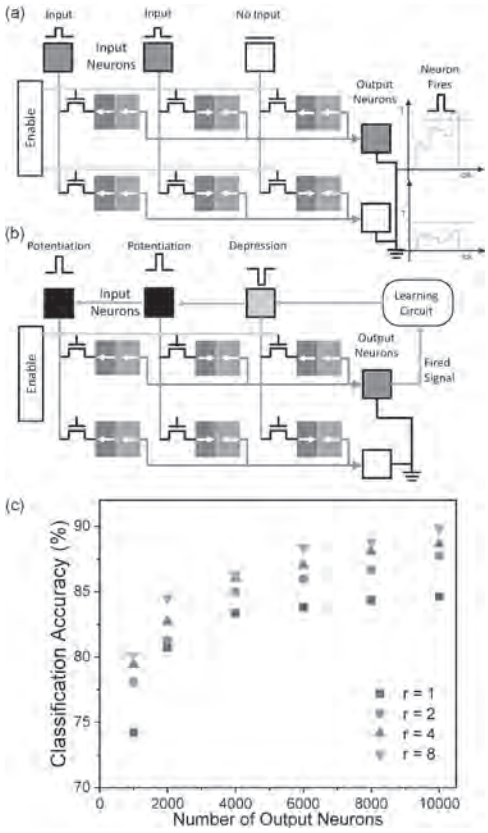

Fig. 1. (a-b) STT-MRAM training and STDP learning circuit. (c) Inference accuracy, where r is the number of synapses representing each pixel.

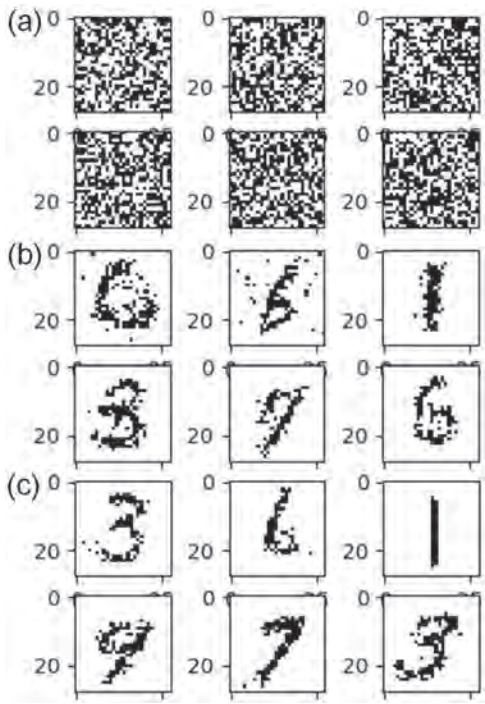

Fig. 2. (a-c) Synapse resistance changing during the training.

GOK-09. Frustrated Arrays of Nanomagnets for Efficient Reservoir Computing. *A.J. Edwards*[1], D. Bhattacharya[2], P. Zhou[1], N.R. McDonald[3], L. Loomis[3], C.D. Thiem[3], J. Atulasimha[2] and J.S. Friedman[1] *1. Electrical and Computer Engineering, The University of Texas at Dallas, Richardson, TX, United States; 2. Department of Mechanical and Nuclear Engineering, Virginia Commonwealth University, Richmond, VA, United States; 3. Information Directorate, Air Force Research Laboratory, Rome, NY, United States*

A reservoir computer (RC) [1] is a powerful machine learning approach, which may be physically implemented by a wide range of complex devices. The advantages of RC greatly reduce the necessary overhead circuitry required for a full hardware realization. In [2], we demonstrated the nanomagnet reservoir computer (NMRC) with micromagnetic simulations. In this work, we present initial experimental results and simulate NMRC solving tasks requiring high memory content, with an area-energy-delay product 10^{10} times lower than conventional RC systems. The complete NMRC system is depicted in Fig. 1. Specific input nanomagnets are written using spin-transfer torque (STT). Reservoir nanomagnets can be comprised of magnetic tunnel junctions (MTJs) used for readout. Output weights are written in a memristor crossbar array output layer. This minimal circuitry enables a low-footprint RC. We manufactured a small nanomagnet reservoir via e-beam lithography [3]. An MFM image of the experiment is shown in Fig. 2. The nanomagnets were in a frustrated state. This is an important step towards fabrication of a full NMRC system. We evaluated the performance of this paradigm on two novel tasks. A 35 node reservoir achieves 100% accuracy for the Boolean function evaluation task. A 200 node reservoir achieved 99.7% accuracy on the elementary cellular automata observer task. These results indicate the reservoir's short-term memory capabilities and ability to integrate information from multiple concurrent inputs. We compared the area, energy, and period of the NMRC to those of a CMOS RC which performed the same tasks with the same accuracy. In the end, our system saw a reduction in area by ~100,000x, in energy by ~1,000x, and in period by ~100x. We demonstrate the applicability of NMRC in SWaP-constrained environments, presenting initial experimental results, showing the NMRC's ability to perform complicated tasks, and describing low-power, low-footprint circuitry to integrate NMRC into a CMOS environment.

[1] H. Jaeger, Germ. Nat. Res. Cent. for Info.Tech., Vol. 148, (2001) [2] P. Zhou, N. R. McDonald and A. J. Edwards, arXiv:2003.10948 [cs.NE], (2020) [3] A. J. Edwards, D. Bhattacharya and P. Zhou, arXiv:2103.09353 [cs.NE], (2021)

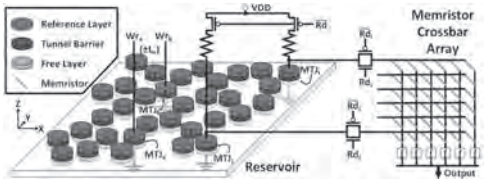

Fig. 1. NMRC system diagram.

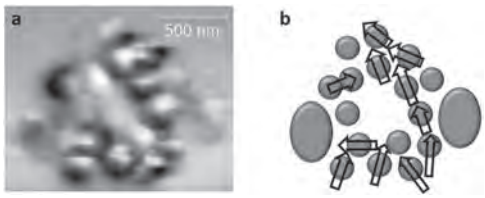

Fig. 2. (a) MFM image of fabricated reservoir. (b) Extracted magnetization directions.

GOK-10. Multi-Weight Artificial Synapses with Straight Notched Geometry for Neuromorphic Computing. *M. Alamdar*[1], T. Leonard[1], S. Liu[1], O.G. Akinola[1], L. Xue[2], J.S. Friedman[3], M. Marinella[4], T.P. Xiao[4], C. Bennett[4] and J.C. Incorvia[1] *1. ECE Dept., University of Texas at Austin, Austin, TX, United States; 2. Applied Materials, Santa Clara, CA, United States; 3. ECE Dept., University of Texas at Dallas, Richardson, TX, United States; 4. Sandia National Laboratories, Albuquerque, NM, United States*

Emulation of neurobiological information processing by artificial neural networks enables new frontiers in efficiency when performing data-intensive and real-time artificial intelligence tasks[1,2]. In this work, we experimentally demonstrate a multi-weight (MW) artificial synapse using a domain wall-magnetic tunnel junction (DW-MTJ) with a straight, notched geometry, depicted in Fig. 1(a). While previous simulations show that DW-MTJ synapses have the necessary characteristics for neuromorphic computing, experimental work has focused on binary DW-MTJs[3], and no experimental works have closely studied the behavior of the MW-DW-MTJ synapse, in contrast with works studying multi-MTJ devices[4]. The heavy metal/ferromagnet/oxide trilayer stack[3] is patterned into a DW track with a single, long output MTJ centered on top of the track. To achieve MW synaptic switching, five notches are fabricated on the track ($n_{1\text{-}5}$). Fig. 1(b) shows the MTJ resistance (R_{MTJ}) vs. out-of-plane magnetic field for a synapse with DW track width w = 350 nm, showing the maximum and minimum R_{MTJ}. To study synaptic switching behaviors, voltage V is applied between the *IN* and *CLK* terminals (50 ns pulses of increasing amplitude, with step size 0.1 V) to move the DW from notch to notch via current driven via spin orbit torque. Fig. 2(a) shows R_{MTJ} vs. V for 10 cycles, showing five resistances each corresponding to the DW in one of the notches. From the spacing dimensions of the notches, we estimate R_{MTJ} when the DW is pinned at each notch, as shown in Fig. 2(b), which are close to the resistances observed in Fig. 2(a). We will show that repeated single-amplitude V pulses also move the DW notch to notch but ramping up the amplitude allows us to observe all switches without tuning the amplitude precisely. We will show how the cycle-to-cycle stochasticity may aid certain online learning tasks when V can be applied repeatably over time to set the synapse weight, allowing for stochastic outer product updates. This work informs essential design parameters using DW-based synapses for future neuromorphic computing.

1. S. Liu *et al.* A domain wall-magnetic tunnel junction artificial synapse with notched geometry for accurate and efficient training of deep neural networks. *Appl. Phys. Lett.* 118, (2021). 2. T. P. Xiao *et al.* Analog architectures for neural network acceleration based on non-volatile memory. *Appl. Phys. Rev.* 7, (2020). 3. M. Alamdar *et al.* Domain wall-magnetic tunnel junction spin orbit torque devices and circuits for in-memory computing. *Appl. Phys. Lett.* 118, 112401 (2021). 4. S. A. Siddiqui *et al.* Magnetic Domain Wall Based Synaptic and Activation Function Generator for Neuromorphic Accelerators. *Nano Lett.* 20, 1033–1040 (2020).

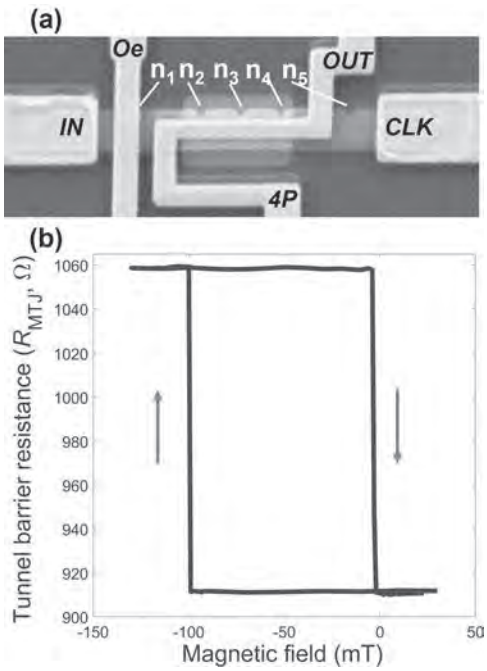

Fig. 1. (a) DW-MTJ synapse. (b) Field loop.

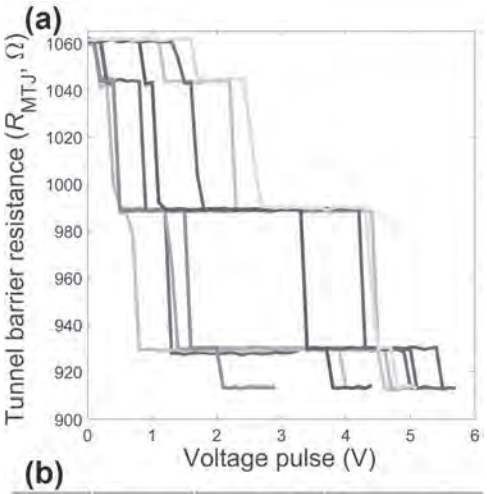

(b)

# Notch	Spacing (nm)	Expected R (Ω)	Measured R_{avg} (Ω)
n_1	0	1060	1060
n_2	180	1040	1043
n_3	680	986	989
n_4	1180	932	930
n_5	1360	913	913

Fig. 2. (a) MW switching for 10 cycles. (b) Expected vs measured R_{MTJ} when the DW is pinned at each notch.

GOK-11. Determination of Attempt Time Using Stochastic Magnetic Tunnel Junctions. *K. Hayakawa*[1,2], S. Kanai[1,3], K. Kobayashi[1,2], W.A. Borders[1,2], J. Igarashi[1,2], B. Jinnai[4], H. Ohno[1,5] and S. Fukami[1,6]
1. RIEC, Tohoku University, Sendai, Japan; 2. Engineering, Tohoku University, Sendai, Japan; 3. DEFS, Tohoku University, Sendai, Japan; 4. WPI-AIMR, Tohoku University, Sendai, Japan; 5. CIES, Tohoku University, Sendai, Japan; 6. CSRN, Tohoku University, Sendai, Japan

Thermally activated phenomena in general are governed by the Arrhenius law $\tau = \tau_0 \exp(\Delta)$, where τ is relaxation time, Δ the thermal stability factor, and τ_0 the attempt time usually assumed to be ~ 1 ns in ferromagnetic systems [1]. Recently, we have revealed that τ_0 can be tuned in in-plane nanomagnets by the effective perpendicular anisotropy field H_K^{eff} in addition to Δ [2,3], playing a crucial role in a computational time of probabilistic computers with stochastic magnetic tunnel junctions (s-MTJs) [4,5]. So far, τ_0 has been experimentally inaccessible at room temperature. Here we quantify τ_0 utilizing in-plane s-MTJ devices with various H_K^{eff}. We prepare s-MTJs with the stack structure of Ta/ PtMn/ Co/ Ru/ CoFeB/ MgO/ CoFeB (t_{CoFeB})/ Ta/ Ru, where the free layer thickness t_{CoFeB} is varied as 1.9, 2.1, and 3.0 nm, showing different $\mu_0 H_K^{\text{eff}}$ of -0.29, -0.48, and -0.72 T (μ_0 is the permeability in free space), respectively. Stacks are processed into elliptic MTJs with an averaged diameter of 90-145 nm. Resistance *vs*. in-plane easy-axis magnetic field curve shows superparamagnetic behavior with zero coercivity. To determine τ_0, we measure τ by the random telegraph noise (RTN) signal under various in-plane magnetic fields along the magnetic hard axis H_y with the circuit in Fig. 1(a). As shown in Figs. 1(b) and (c), H_y changes τ via the energy barrier. Figure 1(d) summarizes τ *vs*. H_y in the MTJ with t_{CoFeB} = 2.1 nm, showing the modulation of τ by more than eight orders of magnitudes from 10 ns to over 1 s. Considering the barrier modulation with H_y, we fit a curve based on the Arrhenius law to the measured τ *vs*. H_y as shown by a dashed line, and determine τ_0 values as 8.9±0.7 ns. We find that larger t_{CoFeB} results in shorter τ_0, consistent with the theoretical prediction [3] that an increase in $|H_K^{\text{eff}}|$ reduces τ_0. This work was supported in part by JST-CREST JPMJCR19K3 and JSPS Kakenhi 19H05622, 19KK0130, and 20H02178.

[1] L. Néel Ann. Geophys. 5, 99 (1949). [2] K. Hayakawa et al., Phys. Rev. Lett. 126, 117202 (2021). [3] S. Kanai et al., Phys. Rev. B 103, 094423 (2021). [4] K.Y. Camsari et al., Phys. Rev. X 7, 031014 (2017). [5] W.A. Borders et al. Nature 573, 390 (2019).

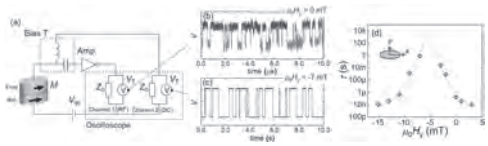

Fig. 1 (a) Measurement circuit for RTN. (b)(c) RTN signals with different $\mu_0 H_y$ for t_{CoFeB} = 2.1 nm. (d) τ *vs*. $\mu_0 H_y$ and the fitting curve based on the Arrhenius law.

GOK-12. Fokker-Planck equation based on normal modes for computing write error rates in magnetic random access memories. *Z. Lin*[1,2] and V. Lomakin[1,2] *1. Department of Electrical and Computer Engineering, University of California San Diego, La Jolla, CA, United States; 2. Center for Memory and Recording Research, La Jolla, CA, United States*

Spin-transfer torque magnetic random access memories (STT-MRAM) are a promising candidate for next generation memory technologies [1]. Because of thermal effects, the switching process is probabilistic, and it is essential to estimate the non-switching probability, which is known as write error rate (WER). To study WER, the general numerical method is to simulate the switching process governing by Landau-Lifshitz-Gilbert (LLG) equation with the stochastic thermal field and spin transfer torque for numerous times and calculate the statistical results, which is time consuming and inefficient. In the single spin approximation, analytical solutions for WER can be obtained based on the Fokker-Plank equation (FPE) [2]. However, no extensions of FP formulations to structures that can have non-uniform switching. Here, we present a FPE constructed based on the eigenfunction expansion of the solutions of the linearized LLG equation, which allows computing WER. In this approach, we first find normal modes and corresponding resonant frequencies of the structure, accounting for all effective magnetic field, including STT. We show that the magnetization dynamics of the linearized LLG equation can be represented in terms of the normal modes and corresponding time dependent coefficients, where a single ground mode in most cases can provide accurate predictions [3]. We then formulate a FPE related to the real and imaginary part of the time dependent modal coefficient. Solving the FPE gives the probability density function (PDF) as a function of time, which can be related to the magnetization and used to calculate the WER. Compared to the stochastic LLG equation simulations in the time domain, the presented approach directly obtains the write error rate by solving FPE only once, and it is scalable to large cases when non-uniform dynamics occurs.

[1] S. Bhatti, et al. *Materials Today* 20.9 (2017): 530-548. [2] W. H. Butler, et al., *IEEE Transactions on Magnetics* 48.12 (2012): 4684-4700. [3] Zhuonan Lin, Iana Volvach, and Vitaliy Lomakin, Resonant states based micromagnetic analysis of magnetic tunnel junctions for spin-transfer torque magnetic random access memory, *in press*.

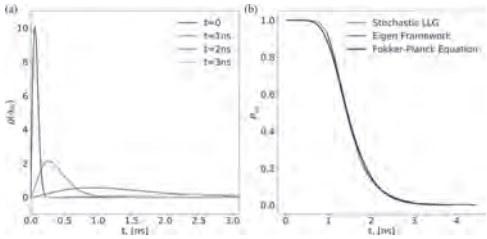

Fig. 1 (a) The PDF of time coefficient magnitude for different times. (b) WER results based on FPE solution, eigenvalue framework simulations [3] and stochastic LLG simulations. The formulated FPE provides accurate results. Magnetic and simulation parameters: D=20nm, Ku = 6.11e6 erg/cc, Ms = 960 emu/cc, Aex = 1e-6 erg/cm, α= 0.01, I = 9.5e-6 A, T=100 K.

GOK-13. High-Speed Switching of FeRh Memristors. *N. Blumenschein*[1], G.M. Stephen[1], C. Cress[2], S.L. LaGasse[2], A.T. Hanbicki[1], S.P. Bennett[3] and A.L. Friedman[1] *1. Laboratory for Physical Sciences, College Park, MD, United States; 2. Electronics Science and Technology Division, United States Naval Research Laboratory, Washington, DC, United States; 3. Materials Science and Technology Division, United States Naval Research Laboratory, Washington, DC, United States*

FeRh is widely studied because of its novel temperature-dependent antiferromagnetic (AFM) to ferromagnetic (FM) phase transition. This AFM-FM phase transition, which is accompanied by a significant change in resistivity, occurs at a critical temperature that can be fine-tuned over a wide range through substitutional doping, strain, and patterning.[1,2] Moreover, the temperature dependence of the transition provides a means to manipulate the state *via* Joule heating. Recent reports, based on ultrafast pump-probe measurements, show the AFM-FM transition occurs on a sub-picosecond timescale, thus devices operating in switching applications have the potential to operate in excess of 100's GHz provided adequate thermal dissipation is achieved. In this work we demonstrate high-speed switching of FeRh wires, giving rise to a dynamic memristive device based on a metamagnetic transition. The thermally-induced AFM-FM transition was evaluated using two-terminal devices consisting of an FeRh wire and Ti/Au contacts. We identified geometrical dependencies in the AFM-FM transition temperature, which scaled with both current density and wire length. Pulsed I-V measurements were used to investigate the dynamic Joule heating effects, including the device switching speed and resulting power switching losses accompanying the AFM-FM transition. The lower bound of our device switching time, measured to be near 300 nanoseconds, was limited by

measurement equipment limitations, not the material system. The performance of this rudimentary device is comparable to other phase change memory technologies with more intricate device architectures. FeRh could be the basis for a very fast, phase-change approach to future computing.

[1] S. P. Bennett, A. Herklotz, C. D. Cress, A. Ievlev, C. M. Rouleau, I. I. Mazin, V. Lauter, Mater. Res. Lett. 6, 106 (2018). [2] C. D. Cress, D. Wickramaratne, M. R. Rosenberger, Z. Hennighausen, P. G. Callahan, S. W. LaGasse, N. Bernstein, O. M. van 't Erve, B. T. Jonker, S. B. Qadri, J. C. Prestigiacomo, M. Currie, I. I. Mazin, S. P. Bennett, ACS Appl. Mater. Interfaces, 13, 836 (2021).

GOK-14. Multi-Weight Directional Artificial Synapses with Trapezoidal Geometry for Neuromorphic Computing. *T. Leonard*[1], M. Alamdar[1], S. Liu[1], C. Cui[1], O.G. Akinola[1], L. Xue[4], T.P. Xiao[3], J.S. Friedman[2], M. Marinella[3], C. Bennett[3] and J.C. Incorvia[1] *1. ECE, University of Texas at Austin, Austin, TX, United States; 2. ECE, The University of Texas at Dallas, Richardson, TX, United States; 3. Sandia National Laboratories, Albuquerque, NM, United States; 4. Applied Materials, Santa Clara, CA, United States*

The development of efficient processing of unstructured information necessitates research into neuromorphic computing. In this work, we report domain wall-magnetic tunnel junction (DW-MTJ) artificial synaptic devices with a trapezoidal geometry that are uniquely suited for neuromorphic computation. DW-MTJ devices are nonvolatile memory-in-logic elements that can be integrated into an artificial neural network[1]. The bottom ferromagnetic layer of the MTJ is a DW track, and the magnetization of that layer is determined by the position of the DW within the track. The device can act as a programmable resistor based on the location of the DW. Simulations have shown that this high level of resistance state control and stability could allow for advanced functionalities for neuromorphic computing[1,2,3]. However, experimental work has focused on binary DW-MTJs[4], and almost no experimental work has been done to understand the behavior of the multi-weight (MW) DW-MTJ synapse, with one paper showing results on a multi-MTJ device[5]. Here, we present a DW-MTJ based MW synapse that is directional, has stable and repeatable resistance states, and uses a single MTJ. The MTJ was lengthened and pinning notches were fabricated along the DW track. This way the DW could rest under the MTJ, opening more resistance states. A trapezoidal DW track was patterned for directional switching, shown in Fig. 1. As the DW is moved from IN to CLK using spin orbit torque switching, the voltage amplitude required to propagate the DW increases as the track widens, which results in MW switching. Going CLK to IN does not exhibit MW switching since depinning from the right-most notch requires the maximum voltage, shown in Fig. 2. We will show how this asymmetry in writing and reset is useful for offline learning to bring the synapse to a resistance state using a particular voltage, and then to reset the device efficiently. We will compare the behavior of the trapezoidal DW-MTJ synapse to the straight DW-MTJ synapse presented separately.

S. Liu, C. Bennett, and J. Friedman, IEEE MAGNETICS LETTERS., Vol. 12, (2021) A. Sengupta, Y. Shim, and K. Roy, IEEE Trans. Biomed. Circuits Syst., Vol. 10, p.1152-1160 (2016) W. H. Brigner, X. Hu, and N. Hassan, IEEE TRANSACTIONS ON ELECTRON DEVICES., Vol. 66, (2019) M. Alamdar, T. Leonard, and C. Cui, Appl. Phys. Lett., Vol. 118, (2021) S. A. Siddiqui, S. Dutta, A. Tang, Nano Lett., Vol. 20, p.1033-1040 (2020) O. Akinola, X. Hu, and C. Bennett, Journal of Physics., Vol. 52, (2019)

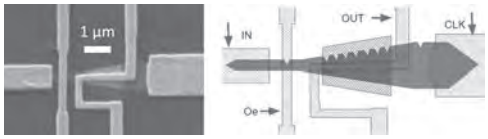

Fig. 1: Trapezoidal Synapse. Left) SEM image. Right) Schematic with DW track in blue, MTJ in red, electrodes in green.

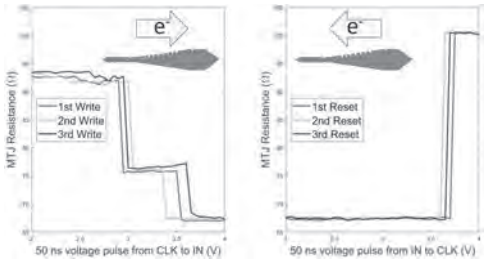

Fig. 2: Three consecutive directional write then reset cycles

Session GOL
MRAM, MAGNETIC LOGIC AND RELATED DEVICES II

Denys Makarov, Chair
Helmholtz-Zentrum Dresden-Rossendorf, Dresden, Germany

INVITED PAPER

GOL-01. Magnon Quantum Effect and Magnonic Devices. *X. Han*[1]
1. State Key Laboratory of Magnetism, Institute of Physics, Chinese Academy of Sciences, Beijing, China

Compared with the electron based spintronic devices, the magnonic devices have many attractive features, including minimization of Joule heating, much longer magnon coherence length and additional phase degree of freedom, etc. It has been expected that the basic magnonic devices, used a core structure of Ferromagnetic insulator/Spacer/Ferromagnetic insulator [FMI/Spacer/FMI], can also be operated by method of magnon current and magnon transfer torque (MTT), which are similar to the classical spin valve (SV) and magnetic tunnel junction (MTJ). Here, we demonstrated a magnon valve (MV, such as YIG/Au/YIG) [1] and magnon junction (MJ, such as YIG/NiO/YIG) [2] which consists of two magnetic insulators (YIG) and a nonmagnetic or antiferromagnetic spacer (S=Au, Pt or NiO, CoO, Cr_2O_3 etc.). Instead of regulating transport of spin-polarized electrons, the magnon valve and magnon junction regulate flow of magnon current. We used the temperature gradient or electric manipulation to excite the magnon current in YIG, and inverse spin Hall effect (ISHE) to detect the magnon current across the magnon valve or magnon junction by the electrical method. Our results show that the magnon current transmission between two magnetic insulating layers (YIG) mediated by the space layer (Au, Pt or NiO, CoO) has high efficiency, and the transmission of the magnon current in a magnon valve and magnon junction becomes high (low) as magnetizations of the two magnetic insulators are parallelly (anti-parallelly) configured. We interpret the magnon valve effect (MVE) and magnon junction effect (MJE) by the angular momentum conversion and propagation between magnons in two YIG layers via the space layer. The temperature dependence of magnon valve ratio (MVR) shows approximately a power law, supporting the above magnon-electron spin conversion mechanism. A large switching on-off ratio can be expected to ±100% in the MJ and MV. Furthermore, novel magnon blocking effect (MBE) in an antiferromagnet spaced MJ and magnonic skin effect (MSE) in an antiferromagnetically coupled heterojunction were suggested respectively [3, 4], and a magnon nonlocal spin Hall magnetoresistance (MNSMR) effect in a platinum layer deposited on an MJ was observed [5]. These works conceptually proves the possibility of using MV and MJ structures to manipulate the magnon current and magnon transfer torque (MTT) in magnetic insulators [6], which has potential applications in magnonic crystals, magnonic devices and circuit in future [7, 8].

[1] H. Wu and X. F. Han *et al. Phys. Rev. Lett.*, Vol. 120, p.097205 (2018). [2] C. Y. Guo, C. H. Wan and X. F. Han *et al. Phys. Rev. B.*, Vol. 98, p.134426 (2018). [3] Z. R. Yan, C. H. Wan and X. F. Han, *Phys. Rev. Applied*, Vol. 13, p.044053 (2020). [4] Z. R. Yan, Y. W. Xing and X. F. Han, *Phys. Rev. B*, DOI: 10.1103/PhysRevB.00.000400, (2021). [5] C. Y. Guo, C. H. Wan and X. F. Han *et al. Nature Electronics*, Vol. 3, p.304 (2020). [6] C. Y. Guo, C. H. Wan and X. F. Han *et al. submitted to Phys. Rev. Lett*., in reviewing. [7] Y. W. Xing, Z. R. Yan, and X. F. Han. *Phys. Rev. B*., Vol. 103, p.054425 (2021). [8] P. Tang and X. F. Han, *Phys. Rev. B*, Vol. 99, p.054401 (2019).

CONTRIBUTED PAPERS

GOL-02. Influence of sputtering conditions on the magnetic properties of Co/Pt-based iridium-synthetic antiferromagnetic coupling reference layer. *H. Honjo*[1], H. Naganuma[1], K. Nishioka[1], T. Nguyen[1], M. Yasuhira[1], S. Ikeda[1] and T. Endoh[1] *1. Center for Innovative Integrated Electronic Systems, Tohoku University, Sendai, Japan*

CoFeB/MgO-based p-MTJs are the de facto standard for current STT-MRAM [1-7]. A Co/Pt-based Ru-synthetic antiferromagnetic (SyF) coupling reference layer is widely used in p-MTJs to compensate the stray magnetic field from the reference layer owing to its high thermal stability [4]. However, to scale down MTJs, a higher stable reference layer is required [8]. To improve the reference layer stability, an Ir-SyF coupling layer has been proposed [9]. To utilize the Ir coupling layer in the Co/Pt-based reference layer, one needs to understand the relationship between MTJ properties and sputtering conditions. In this study, we have investigated the effect of the sputtering conditions on the magnetic and transport properties and also compared them with those of Ru. We prepared two types of stacks with Co/Pt-based Ir- and Ru-SyF coupling layers, as shown in Figs. 1-2. Ir was deposited by two sputtering conditions, denoted as Condition-A and Condition-B. The stacks were annealed at 400°C for 1 h. The magnetic and transport properties of the MTJ stacks were measured using VSM and CIPT method, respectively. The stack with Condition-A exhibits a larger exchange coupling field H_{ex} than that with Condition-B (Fig.1). In the EDX line analysis (Fig.2), Ir profile for Condition-A is wider than that for Condition-B, resulting in lower H_{ex} for Condition-B. A possible reason for the different intermixing degree of Ir and Co seems to be that the atoms for Condition-A recoiled from the Ir sputtering target have a higher energy than the atoms for Condition-A[10]. The stacks with the Ir-SyF show lower TMR ratio (Fig.2), resulting from the Pt diffusion into the MgO barrier. In contrast, the stacks with Ru show high TMR ratio because the Pt diffusion is suppressed. These results indicate that the suppression of Ir and Pt diffusion in the reference layer is crucial to achieving robust MTJs that can withstand annealing. This work was supported by CIES's Industrial Affiliation on the STT MRAM program, CIES Consortium, JST-OPERA, and NEDO.

[1] S. Ikeda *et al.*, Nature Mater. 9, 721 (2010). [2] H. Sato *et al.*, Appl. Phys. Lett. 101, 022414 (2012). [3] H. Sato *et al.*, Appl. Phys. Lett. 105, 062403 (2014). [4] H. Sato *et al.*, Jap. J. Appl. Phys. 53, 04EM02 (2014). [5] T. Y. Lee *et al.*, IEDM 2020. [6] S. H. Han *et al.*, IEDM 2020. [7] C.-Y. Wang *et al.*, VLSI 2019. [8] H. Honjo *et al.*, IEEE Trans. Magn. 52, 25604 (2017). [9] K. Yakushiji, *et al.*, Appl. Phys. Lett. 110, 092406 (2017). [10] S. Iwatsubo *et al.*, J. Appl. Phys. 83, 6667 (1998).

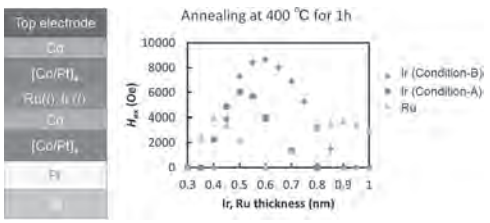

Fig. 1 Coupling layer thickness dependence of H_{ex} for SyF.

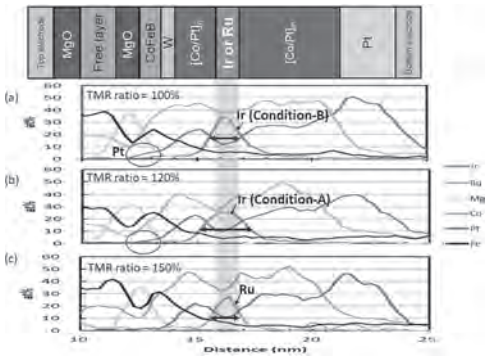

Fig. 2 EDX depth profiles of the stacks with (a) Ir for Condition-B, (b) Ir for Condition-A, and (c) Ru.

GOL-03. Spin-orbit torque magnetization switching in a perpendicularly magnetized full Heusler alloy Co_2FeSi. *M. Jiang*[1], E. Matsushita[2], Y. Takamura[2], L. Anh[1,3], S. Nakagawa[2], S. Ohya[1,3] and M. Tanaka[1,4] *1. Dept. of Electrical Engineering and Information Systems, The University of Tokyo, Tokyo, Japan; 2. Dept. of Electrical and Electronic Engineering, Tokyo Institute of Technology, Tokyo, Japan; 3. Institute of Engineering Innovation, Graduate School of Engineering, The University of Tokyo, Tokyo, Japan; 4. Center for Spintronics Research Network (CSRN), Graduate School of Engineering, The University of Tokyo, Tokyo, Japan*

As one of the next-generation memory technologies, magnetic random access memory (MRAM) is of great interest because of its non-volatility, high access speed, large integration density and low power consumption. Current-induced spin-orbit torque (SOT) magnetization switching has been proposed for improving the writing performance of MRAM. Meanwhile, it has been demonstrated that the Co-based full Heusler alloys show potential for increasing the magnetoresistance ratio and achieving efficient reading due to their relatively large spin polarization[1]. Therefore, achieving the SOT magnetization switching in full Huesler alloys will be promising for optimizing both the reading and writing performance of MRAM devices. Here, we report a successful full SOT magnetization switching in a perpendicularly magnetized full Heusler alloy Co_2FeSi[2] by using Pd as a spin current generating layer. To eliminate the heating effect, a large writing pulse current with a pulse width of 0.1 ms (red columns in Fig. 1) was applied to switch the magnetization, and a small reading current of 1 mA (blue columns in Fig. 1) was applied for 0.5 s to read the Hall resistance. As shown in Fig. 2, with the assistance of the external magnetic field of 500 Oe, the magnetization can be fully switched with a switching current density of 3.7×10^7 A cm^{-2}, which is in the same order of magnitude as that required in the conventional heavy metal (HM)/ferromagnet system even though the Pd shows a relatively smaller spin Hall angle than that of HM[3]. By using harmonic Hall measurements, the damping-like and field-like effective fields per unit current density are estimated to be 56.9 (10^{-7} Oe A^{-1} cm^2) and 39.8 (10^{-7} Oe A^{-1} cm^2), respectively. Our findings will advance the development of SOT-MRAM devices with both better reading and writing performance. This work was partly supported by Grants-in-Aid for Scientific Research (Nos. 18H03860, 20H05650, and 20F20366), CREST Program of JST (JPMJCR1777), Spintronics Research Network of Japan (Spin-RNJ), and Grant-in-Aid for JSPS Fellows (20F20366).

[1] Z. Wen, H. Sukegawa, T. Furubayashi, *et al., Adv. Mater.* 26, 6483 (2014). [2] Y. Takamura, Y. Stutler, E. Matsushita, *et al., J. Magn. Soc. Jpn.* 43, 120 (2019). [3] L. Liu, O J Lee, T J Gudmundsen, et al., *Phys. Rev. Lett.* 109, 096602 (2012).

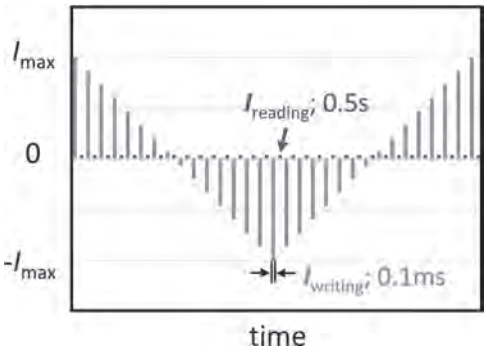

Fig. 1 Pulse current train used for the SOT switching measurements.

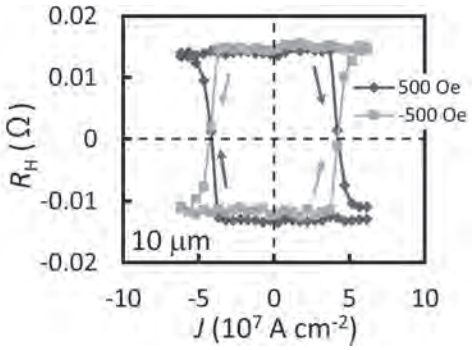

Fig. 2 SOT switching in the $MgO/Co_2FeSi/Pd$ heterostructure at room temperature.

GOL-04. Withdrawn

GOL-05. Complex Hopfield Networks Implemented Using Coupled Spin-Torque Oscillator Arrays. *N. Prasad*[2,1], A. Madhavan[2,3], P. Mukim[2,1] and M. Stiles[2] *1. Dept. of Chemisty and Biochemistry, University of Maryland at College Park, College Park, MD, United States; 2. Physical Measurements Laboratory, National Institute of Standards and Technology, Gaithersburg, MD, United States; 3. Institute for Research in Electronics and Applied Physics, University of Maryland at College Park, College Park, MD, United States*

The rhythmic spiking behavior observed in biological neurons [1] has inspired oscillator based implementations of neural networks [2]. We theoretically investigate the use of synchronized spin-torque nano-oscillators (STNOs) to create an associative memory encoded with synaptic weights as time delays. STNOs frequency lock to external AC drives if the external drive frequency is close to the natural frequency of the STNO [3] but the relative phase varies with the details. Fig. 1 shows the implementation of a complex Hopfield network in which the relative phases between the synchronized STNO oscillations encode quasi-continuously varying information, such as the pixel values of a grayscale image. The synaptic feedback matrix implements a complex weight matrix by taking the AC output voltages from the STNO array and re-injecting weighted and time-delayed superpositions of AC currents back into the STNO array. The feedback matrix is set using one of several training methods. Then, retrieval of a stored pattern in the associative memory proceeds as shown in Fig. 2. The feedback is disconnected and the individual oscillators are injection locked to an array of external AC sources that encode the query image. A schematic evolution of the relative phases of the individual oscillators, starting from a random state, during this preparation phase is plotted in Fig. 2a. Then, the feedback connections are engaged and the network evolves towards one of the patterns stored in the synaptic weights as shown in Fig. 2b. We design CMOS circuitry to implement the synapses and use a compact model for the STNO dynamics to

simulate the circuit with SPICE. These simulations give energy efficiencies and parametric restrictions on the properties of the STNOs and the CMOS circuitry needed for implementing large associative memories.

[1] J. Fell and N. Axmacher, Nat. Rev. Neurosci. 12, 105 (2011). [2] D. E. Nikonov, G. Csaba, W. Porod, et al. IEEE J. Explor. Solid-State Comput. Devices Circuits 1, 85 (2015). [3] S. Kaka, M. R. Pufall, W. H. Rippard, et al. Nature 437, 389 (2005).

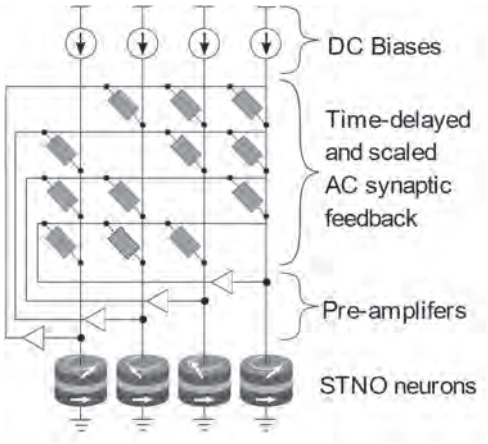

Fig. 1 Schematic of the complex Hopfield network implemented using STNO neurons

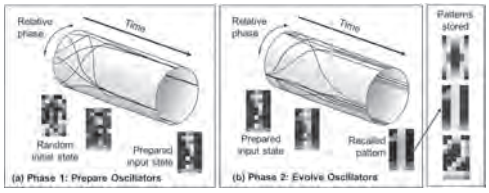

Fig. 2 Steps involved in a typical pattern retrieval operation. (a) The phases of the oscillators are prepared to encode the query image by driving the oscillators with an array of external inputs. (b) The oscillators evolve towards one of the stored images as the feedback is turned on.

GOL-06. Analog multiplication implemented with spin-torque diodes for neural networks applications. *L. Mazza*[1], V. Puliafito[1], E. Raimondo[2], A. Giordano[2], Z. Zeng[3], M. Carpentieri[1] and G. Finocchio[2] *1. Department of Electrical and Information Engineering, Politecnico di Bari, Bari, Italy; 2. Department of Mathematical and Computer Sciences, Physical Sciences and Earth Sciences, University of Messina, Messina, Italy; 3. Suzhou Institute of Nano-tech and Nano-bionics, Chinese Academy of Sciences, Suzhou, China*

Spintronic diodes (STDs) are emerging as a technology for the realization of high-performance microwave detectors [1]. In this paper, we use their rectification properties to perform the analog multiplication between any two numbers. For this purpose, we introduce the concept of degree of rectification (DOR) and we confirm its applicability with micromagnetic and experimental data. The proposed method is suitable for highly integrated implementations and has promising perspectives for neural networks applications [2]. The multiplication can be obtained by measuring the response of a parabolic phenomenon to three well-determined inputs [3][4][5]. Therefore, we analyze the DOR of spintronic diodes, which is the output *dc* voltage measured for a variable input *dc* current in injection-locked devices. This V_{dc}/I_{dc} curve can be well approximated to a parabola as shown in Fig. 1, the experimental data are taken from [6]. The voltage can be approximated by the following equation [6]: $V_{dc}=[(R_{AP}-R_P)/4]\ I_{ac,MAX}\cos(\varphi(I_{dc}))\ \sqrt{p}$ (1) where R_{AP} and R_P are the device resistances in the antiparallel and parallel state, respectively, p is the power of the magnetoresistive signal, $\varphi(I_{dc})$ is the intrinsic phase shift between the *ac* current and the magnetoresistive signal, and the cosine can be well approximated with a parable using Taylor's second-order expansion. Moreover, Eq. 1 can be fully characterized knowing the physical parameters of the device and the values of $I_{dc,MAX}$, $V_{dc,MAX}$ (both represented in Fig. 1) and the second derivative of V_{dc} with respect to I_{dc} evaluated in $I_{dc}=I_{dc,MAX}$. Fig. 2 shows the application of the presented method for 200 cases with random inputs, the red line shows the ideal result; the correlation coefficient found is r=99.83%. We will show how the proposed method can be used to implement the convolution for neural networks applications with excellent results for image recognition.

[1] G. Finocchio et al., "Perspectives on spintronic diodes," Appl. Phys. Lett., vol. 118, no. 16, p. 160502, Apr. 2021, doi: 10.1063/5.0048947. [2] J. Cai et al., "Sparse neuromorphic computing based on spin-torque diodes," Appl. Phys. Lett., vol. 114, no. 19, p. 192402, May 2019, doi: 10.1063/1.5090566. [3] D. M. Chiarulli, B. Jennings, Y. Fang, A. Seel, and S. P. Levitan, "A Computational Primitive for Convolution based on Coupled Oscillator Arrays," in 2015 IEEE Computer Society Annual Symposium on VLSI, Jul. 2015, vol. 07-10-July, pp. 125–130, doi: 10.1109/ISVLSI.2015.77. [4] K. Yogendra, D. Fan, Y. Shim, M. Koo, and K. Roy, "Computing with coupled Spin Torque Nano Oscillators," in 2016 21st Asia and South Pacific Design Automation Conference (ASP-DAC), Jan. 2016, vol. 25-28-Janu, pp. 312–317, doi: 10.1109/ASPDAC.2016.7428030. [5] L. Mazza, V. Puliafito, M. Carpentieri, and G. Finocchio, "Robustness of using Degree Of Match in performing analog multiplication with spin-torque oscillators," Solid. State. Electron., p. 108045, May 2021, doi: 10.1016/j.sse.2021.108045. [6] B. Fang et al., "Giant spin-torque diode sensitivity in the absence of bias magnetic field," Nat. Commun., vol. 7, no. 1, p. 11259, Sep. 2016, doi: 10.1038/ncomms11259.

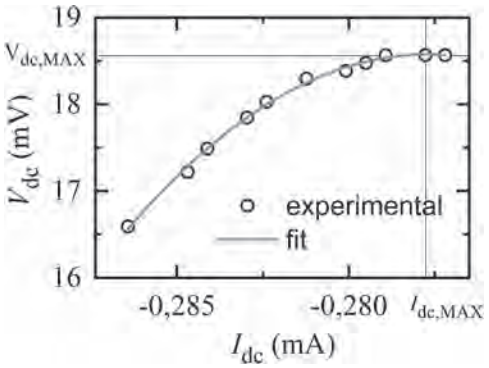

Fig. 1: Output *dc* voltage depending on the input *dc* current (data taken from [4]) for an injection-locked diode (blue circles) and parabolic fit (red line).

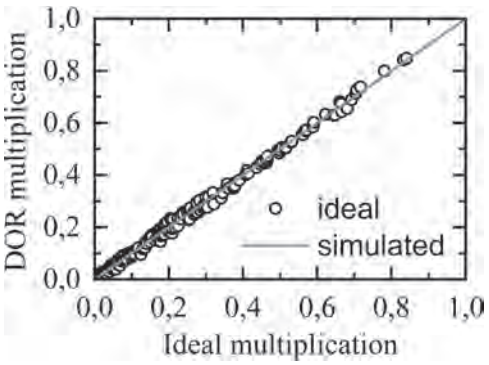

Fig. 2: 200 multiplications obtained with the proposed method (black circles) compared with the ideal result (red line).

GOL-07. Design of a 2-bit Multi-Level Cell with Fully One-Step Writing Mode Based on Spin-Orbit Torque. *M. Wang*[1], Z. Wang[1], A. Du[1], H. Cheng[1], Y. Zhao[2] and W. Zhao[1] *1. School of Integrated Circuit Science and Engineering, Beihang University, Beijing, China; 2. Beijing Microelectronics Technology Institute, Beijing, China*

Magnetic tunnel junction (MTJ) is the basic unit of magnetic random-access memory (MRAM), which is emerging and promising as the next-generation non-volatile memory [1][2]. Recently, multi-level cell (MLC) has drawn attention due to its high density and energy efficiency. However, it is challenging to write two bits of data by applying one current in one step [3][4]. To improve the operationality, we propose a novel design of SOT-based MLC, as shown in Fig. 1. Above the shared heavy metal layer, two MTJs with in-plane magnetization are fabricated with different titled angles. The magnetization vectors of the two reference layers form the acute and obtuse angles, respectively, with +x direction. The current in the ±x or ±y path is applied to the heavy metal layer, achieving the data writing in both MTJs. Following we take the case of applying a current in +y direction ($+I_y$) as an example. The $+I_y$ drives the magnetization of both free layers near the -x direction through the SOT. Then, under the action of shape anisotropy, both magnetizations would move to the direction of the easy axis. Finally, the MTJ is switched to the low or high resistance state according to the relative orientation of the magnetization between the reference layer and the free layer. The snapshots of micromagnetic dynamics shown in Fig. 2 verify the functionality of the proposed MLC cell. In this structure, the final states of both MTJs depend on the direction of the applied SOT currents regardless of initial states. In brief, compared with existing designs, our proposal can use only one current to achieve field-free 2-bits data writing, showing great potential for high-efficiency memory.

[1] B. Dieny, I. L. Prejbeanu, K. Garello, et al., Nature Electronics, vol. 3, no. 8, pp. 446-459 (2020). [2] S. Fukami, T. Anekawa, A. Ohkawara, et al., 2016 IEEE Symposium on VLSI Technology, (2016). [3] S. Das, A. Zaig, M. Schultz, et al., Applied Physics Letters, vol. 117, no. 7, pp. 072404 (2020). [4] K. Ali, F. Li, S. Y. Lua, and C. H. Heng. IEEE Transactions on Magnetics, vol. 54, no. 11, pp. 1-5 (2018).

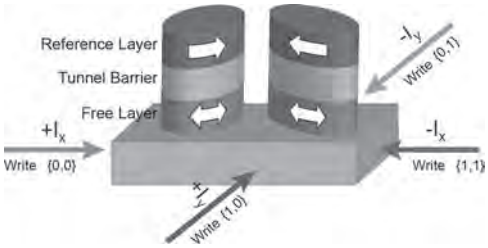

Fig.1 The studied structure in our proposal. The magnetizations of reference layers are along the easy axis of the ellipse layer. "1" and "0" refer to high and low resistance, respectively.

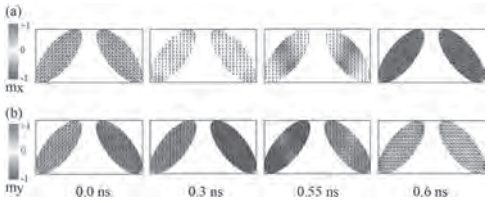

Fig. 2 Snapshots of micromagnetic dynamics when applying $+I_y$. X-axis and y-axis components of magnetization are colored in (a) and (b), respectively.

GOL-08. Time-resolved studies of spin-transfer-torque switching in perpendicular magnetic tunnel junction nanopillars at low temperature. *L. Rehm*[1], G. Wolf[2], B. Kardasz[2], M. Pinarbasi[2] and A. Kent[1] *1. Center for Quantum Phenomena, Department of Physics, New York University, New York, NY, United States; 2. Spin Memory Inc., Fremont, CA, United States*

In perpendicularly magnetized tunnel junctions (pMTJs) operating at or above room temperature, the angle between the layer magnetizations is always nonzero due to thermal fluctuations. Those fluctuations reduce the time required to reverse the magnetization, which has been studied by time-resolved electrical measurements in the thermally assisted [1-3] as well as the dynamic spin-transfer torque regime [4]. However, at low temperature a macrospin model predicts that the switching time would increase substantially [5]. Here we investigate the nanosecond dynamic spin-transfer-torque driven reversal in 40, 50, and 60nm diameter circular state-of-the-art pMTJs by single-shot time-resolved measurements at 4K. We find that the reversal remains highly stochastic even at 4K and there is no significant increase in the switching time. Figure 1 shows the mean switching times (50% point in conductance trace) for antiparallel to parallel switching for the three junction sizes. While we do not observe a correlation between junction size and switching time, we observe a clear correlation for the time it takes to reverse from 25% to 75% of the junction conductance; smaller samples transition faster (see Fig. 2). We also note a clear correlation between pulse amplitude and switching time and find that the spread in switching times as well as transition times is significantly larger for smaller pulse amplitudes ($V/V_0 \leq 1.75$). Hence, the reversal behavior is similar to that found in room temperature studies of alike structures [4]. This is most probably due to junction heating during the voltage pulse, which was recently shown in the thermally assisted spin-transfer switching regime in the same structures at low temperature [6]. In addition, we will discuss our time-resolved conductance traces, which enable a further characterization of the spin-transfer reversal mechanism. This work was supported by Spin Memory Inc. and the NSF.

[1] T. Devolder, A. Le Goff, and V. Nikitin, Phys. Rev. B 93, 224432 (2016). [2] T. Devolder *et al.*, Phys. Rev. B 93, 024420 (2016). [3] P. Bouquin *et al.*, Phys. Rev. B 103, 224431 (2021). [4] C. Hahn *et al.*, Phys. Rev. B 94, 214432 (2016). [5] J. Z. Sun, Phys. Rev. B 62, 570 (2000). [6] L. Rehm *et al.*, Phys. Rev. Appl. 15, 034088 (2021).

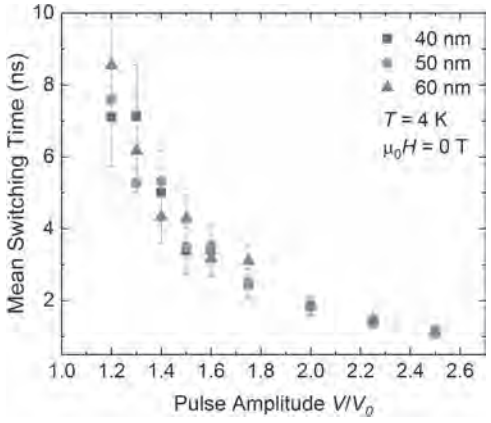

Fig. 1: Mean switching time as a function of pulse amplitude for 40, 50, and 60nm diameter pMTJs at an ambient temperature of 4K and zero magnetic field.

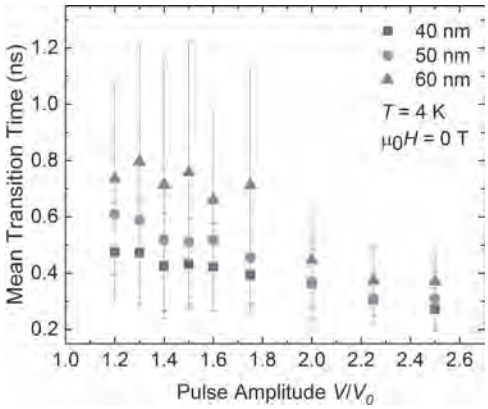

Fig. 2: Mean transition time as a function of pulse amplitude for 40, 50, and 60nm diameter pMTJs at an ambient temperature of 4K and zero magnetic field.

GOL-09. Real time investigation of Double magnetic tunnel junction with switchable assistance layer for high efficiency STT-MRAM.
D. Sanchez Hazen[1], B. da Silva Teixeira[1], D. Salomoni[1], S. Auffret[1], L. Vila[1], R. Sousa[1], L. Prejbeanu[1], L.D. Buda-Prejbeanu[1] and B. Dieny[1]
1. MRAM, SPINTEC, Grenoble, France

Perpendicular Spin Transfer Torque Magnetic Random Access Memory (p-STT-MRAM) needs to combine high speed and low critical switching current at technological nodes below 30 nm. Higher STT write efficiency is therefore required. Double magnetic tunnel junctions (DMTJ) stacks have been proposed to achieve this goal [1-5]. The DMTJ critical switching current is decreased by the combined effect of the STT exerted from two antiparallel polarizers on the storage layer (SL). The retention is increased by doubling the SL/MgO interfaces contributing to the layer's effective perpendicular anisotropy (PMA). Despite the efficiency advantage, the development of p-DMTJ presents several complexities. First, ensuring enough PMA for the top polarizer [6] and second, controlling the stray field compensation of both polarizers acting on the SL. A p-DMTJ structure having a switchable reference layer was recently proposed [7], showing through magnetic simulation similar performance as conventional p-DMTJ with static polarizers. In this work, we report experimental evidence of the working principle for this type of novel p-DMTJ. We fabricated and optimized an ASL-DMTJ structure having a switchable polarizer acting as a switching assistance layer (ASL). Fig.1.(a) and (b) show the two switching sequences, from AP to P and from P to AP states respectively. Both reversals show a transition through an intermediate resistance state (IRS). Differing from the working principles proposed in [7], the ASL is designed to switch its magnetic orientation during the write operation. This maximizes the STT efficiency independently of the switching direction, while also increasing the SL retention, since the assistance layer always aligns parallel to the SL in standby Fig.2(a)-(b). Validation of the switching sequences was possible by performing time-resolved resistance measurements Fig.2.(c)-(b).

[1] G.Hu et al. IEDM, 2156-017X. (2015) [2] B.Rodmacq et al. Patent US8513944B2. (2008) [3] P. Y. Clément et al. IEEE 6th IMW, pp. 1-4. (2014) [4] J. Swerts et al.et al. IEDM, pp. 38.6.1-38.6.4. (2017) [6] Jyotirmoy Chatterjee et al. Applied Physics Express, 063002. (2015) [7] Khvalkovskiy et al. Journal of Applied Physics, 124(13), 133902. (2018)

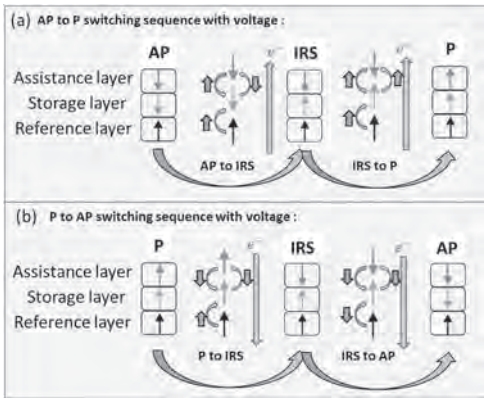

Figure 1. (a) AP→P and (b) P→AP reversal sequence through an intermediated resistance state.

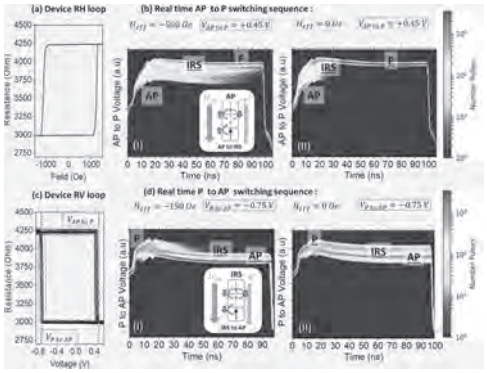

Figure 2. (a) RH of ASL-DMTJ (b) RV loops of ASL-DMTJ. (b) Real time AP→P switching sequence and (d) real time P to AP switching sequence both transiting through the IRS with (I) applied field, (II) at zero field.

GOL-10. Withdrawn

GOL-11. Reduction of power consumption and micromagnetic instabilities associated with domain wall dynamics in perpendicular magnetic tunnel junction nanopillars.
N.N. Statuto[1], A. Lai[1] and A. Kent[1]
1. Center For Quantum Phenomena, New York University, New York, NY, United States

Magnetoresistive random access memories (MRAM) based on spin-transfer torque are a scalable low-power memory solution being actively developed by industry, where the magnetization of a perpendicularly magnetized thin disk is reversed by a spin polarized current. During the switching process domain walls (DWs) can form [1-5] and understanding their dynamics in a disk geometry becomes of great interest. Here we show that DW surface tension always leads to oscillatory DW motion and instabilities that affect the switching dynamics. In a disk, a DW generally takes a circular form to minimize the sum of the surface and volume energies of the reversed domain, with the domain boundary perpendicular to the element boundary [1]. In a collective coordinate model the domain wall has two degrees of freedom, its position relative to the center of the disk q and the angle of the spins relative to the normal to the DW Φ. Here, Φ=0 is a Neel and Φ=90 deg. is a Bloch DW. We analyze the dynamics with micromagnetic and the collective coordinate model. Fig. 1a shows micromagnetic simulations of the evolution of the average perpendicular magnetization (mz) with fixed initial DW position q, such that mz<0, and different initial angles Φ, with no field or current applied. Whereas both Neel and Bloch DWs states relax towards a reversed state (mz=-1), an intermediate initial angle DWs (Φ=45

deg) switches. Fig. 1b shows the (q,Φ) phase diagram indicating that the dynamics of domains close to the disk center is sensitive to small changes in Φ. Moreover, we show that the application of a spin-polarized current (I/Ic~0.2) mitigates the sensitivity of the final state to Φ. This opens a way to reduce the required power for a magnetization switching. The application of a short current pulse to nucleate a DW followed by a significant reduction of the pulse amplitude, well below the critical current, can still reliably switch the nanodisk (Fig. 2, blue curve); in this situation the power, which scales as I^2, can be drastically reduced.

[1] G. Chaves-O'Flynn et al., Phys. Rev. Appl. 4, 024010 (2015) [2] T. Devolder et al., Phys. Rev. B 93, 024420 (2016) [3] P. Bouquin et al., Appl. Phys. Lett. 113, 222408 (2018) [4] J. B. Mohammadi et al., Appl. Phys. Lett. 118, 132407 (2021) [5] N. Statuto et al., Phys. Rev. B 103, 014409

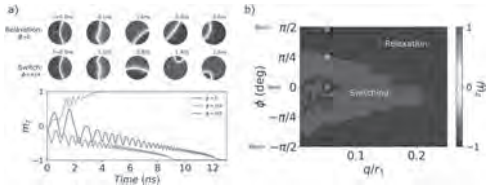

FIG. 1 a) Time evolution of mz for different Φ. b) (q,Φ) Relaxation phase diagram.

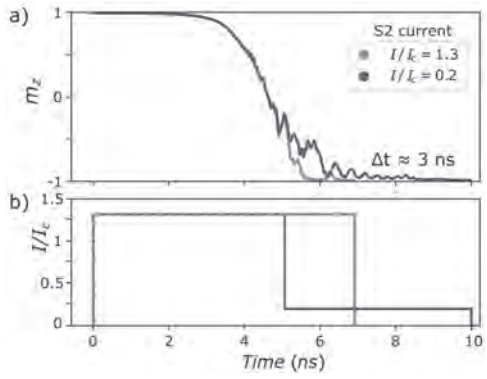

FIG. 2 a) Time evolution of mz for two different currents after 5 ns. b) Spin-current amplitude as a function of the time.

GOL-12. Surface Acoustic Wave Induced Nano-oscillator Based Reservoir Computing. M.F. Chowdhury[1], W. Misba[1], D. Bhattacharya[2], A.J. Edwards[3], J.S. Friedman[3] and *J. Atulasimha*[1] *1. Mechanical and Nuclear Engineering, Virginia Commonwealth University, Richmond, VA, United States; 2. Physics, Georgetown University, District of Columbia, DC, United States; 3. Electrical and Computer Engineering, University of Texas, Dallas, TX, United States*

Reservoir computing (RC) is a computational framework where a fixed, non-linear reservoir maps the inputs into higher-dimensional space and the readout is trained with linear regression and classification [1]. Spintronic nanomagnetic devices are well suited for physical reservoir computing due to their interactive non-linear dynamics, recurrence characteristic, enduring lifetime, and low energy consumption [2-3]. A frustrated nanomagnet layer can also implement physical RC [4]. In this work, we demonstrate via micromagnetic simulation that a nanomagnet array excited by surface acoustic waves (SAW) can be used as a reservoir to classify sine and square waves with high accuracy. The simulated nanomagnet array has an input, 7 outputs (Fig. 1) and a 4 GHz SAW is applied to the input nanomagnet. The SAW amplitude is varied in such a way that its envelope forms a random sequence of sine and square waves of 100 MHz frequency (Fig. 2 (a)). The non-linear responses of the output nanomagnets due to this input are processed by reading the reservoir state every 1 ns while the period of the input is 10 ns. The envelopes of the output magnets' magnetization are shown in Fig. 2 (b) which are used to train the output weights obtained by regression via Moore-Penrose pseudoinverse. For the classification, a random sequence of 100 square and sine wave samples are used. About 80 % of the total samples are trained, and the rest of the samples are used for testing. Various combination of the output nanomagnets exhibit 100 % training accuracy and 100 % testing accuracy which is indicative of the nanomagnet oscillator array being well suited for physical reservoir computing applications. Thus, this proposed strategy to implement reservoir computing could lead to energy efficient neuromorphic devices. Acknowledgment: M.F.F.C, W.A, D.B and J.A are supported in part by the National Science Foundation grant CCF-1815033.

1. Lukoševičius, M. and Jaeger, H., 2009. Reservoir computing approaches to recurrent neural network training. Computer Science Review, 3(3), pp.127-149. 2. Tanaka, G., Yamane, T., Héroux, J.B., Nakane, R., Kanazawa, N., Takeda, S., Numata, H., Nakano, D. and Hirose, A., 2019. Recent advances in physical reservoir computing: A review. Neural Networks, 115, pp.100-123. 3. Torrejon, J., Riou, M., Araujo, F.A., Tsunegi, S., Khalsa, G., Querlioz, D., Bortolotti, P., Cros, V., Yakushiji, K., Fukushima, A. and Kubota, H., 2017. Neuromorphic computing with nanoscale spintronic oscillators. Nature, 547(7664), pp.428-431. 4. Edwards, A.J., Bhattacharya, D., Zhou, P., McDonald, N.R., Loomis, L., Thiem, C.D., Atulasimha, J. and Friedman, J.S., 2021. Frustrated Arrays of Nanomagnets for Efficient Reservoir Computing. arXiv preprint arXiv:2103.09353.

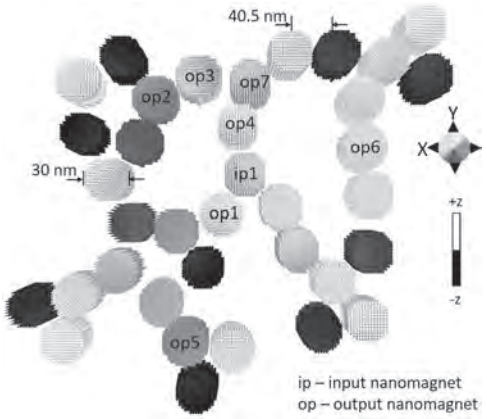

Figure 1: A micro-magnetic snapshot of the input, the reservoir and output nanomagnets.

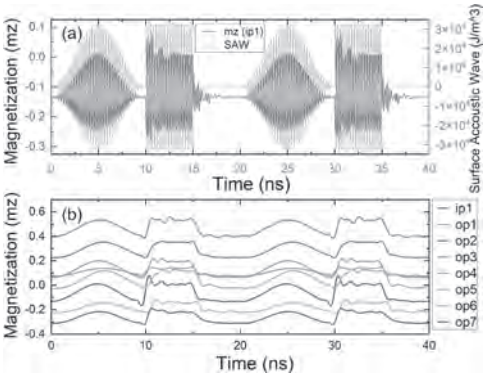

Figure 2: (a) SAW and input response (b) The envelopes of the responses vs. time (ns) of several output nanomagnets.

GOL-13. Current controlled perpendicular superparamagnetic tunnel junctions operating at zero applied magnetic field. *A. Sidi El Valli*[1], G. Lezier[1], J. Langer[2], J. Wrona[2], R. Sousa[1], B. Dieny[1], U. Ebels[1] and P. Talatchian[1] *1. IRIG-Spintec, Univ. Grenoble Alpes, CEA, CNRS, Grenoble INP, Grenoble, France; 2. Singulus Technologies AG, Kahl am Main, Germany*

In superparamagnetic tunnel junctions (SMTJ), the energy barriers that separate the parallel and the antiparallel magnetization configurations are sufficiently small that the thermal noise causes stochastic magnetization fluctuations between the two states. Through magnetoresistance effects, those stochastic fluctuations give rise to telegraphic noise signals with two voltage levels (see Fig.1) [1, 2]. The relative average time spent in each of the two configurations can be controlled by an applied dc current via the spin-transfer torque. Due to their inherent stochastic nature, SMTJs are promising candidates for truly random number generator applications [3, 4], brain-inspired and probabilistic computing [5-10]. However, an external bias magnetic field was always required to fully operate the SMTJ's with current, which represents a drawback to their integration with the required microelectronic circuits. In this work, we report for the first time, SMTJs that are fully controlled by DC current at zero applied magnetic field using perpendicular magnetic tunnel junctions (pMTJ). Stable pMTJs are used in densely magnetic memories [11], nevertheless their thermal stability can be strongly reduced by tuning their free layer thickness, leading to a super-paramagnetic state. Here, we use pMTJ's with a free layer thickness of t=1.6 nm, and with diameters ranging from 150 nm to 80 nm. By applying a DC current in one direction (sign), without any external bias field, we observe stochastic fluctuations in the resistance for dc currents between -0.3 mA and -0.27 mA. As shown in Fig. 2, the average probability in being in high and low resistance state is well controlled by the applied current. In order to obtain good statistics on the extracted probability, we record to stochastic transitions. We extracted the dwell time distribution, which follows an exponential distribution with a mean dwell time that is in agreement with the modified Néel-Brown model. The authors acknowledge partial funding from ERC MAGICAL No 669204, and the Nanoscience Foundation (Grenoble, France).

1. Safranski, Christopher, et al. *Nano Letters* 21.5 (2021): 2040-2045. 2. Rippard, William, et al. *Physical Review B* 84.6 (2011): 064439. 3. Vodenicarevic, Damir, et al. " *Physical Review Applied* 8.5 (2017): 054045. 4. Parks, Bradley, AIP Advances. 8, (2018): 055903 5. Mizrahi, Alice, et al. " *Nature communications* 9.1 (2018): 1-11. 6. W. A. Borders, Nature 573, 390 (2019). 7. Daniels, Matthew W., et al. *Physical review applied* 13.3 (2020): 034016. 8. Chavent, A., et al. *Journal of Magnetism and Magnetic Materials* 505 (2020): 166647.

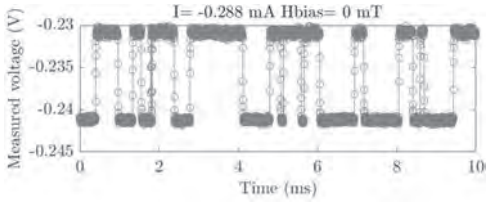

Figure 1 : Experimental voltage time trace of the SMTJ.

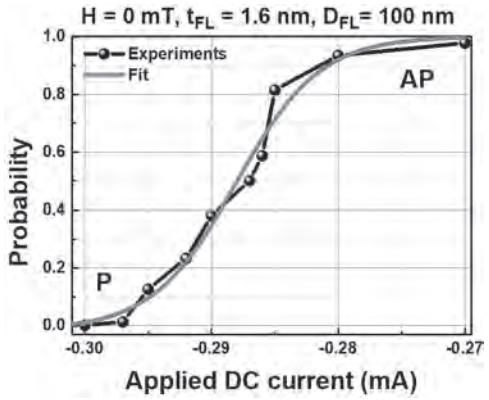

Figure 2 : The probability of occupancy of the high resistance state versus current.

Session GOM
VOLTAGE-CONTROLLED MAGNETIC ANISOTROPY AND SWITCHING

Minori Goto, Chair
Osaka University, Toyonaka, Japan

INVITED PAPER

GOM-01. Voltage-control of magnetic properties in topological-insulator/magnetic-insulator bilayers. *T. Chiba*[1], A. Leon[2] and T. Komine[3] *1. National Institute of Technology, Fukushima College, Iwaki, Japan; 2. Universidad Tecnológica Metropolitana, Santiago, Chile; 3. Ibaraki University, Hitachi, Japan*

Voltage control of magnetic properties in magnets is essential for the next generation of spintronic technologies [1], such as magnetic random-access memories, spin transistors, and spin-wave-based logic gates. For example, the voltage-control of the magnetic anisotropy (VCMA) in ferromagnets promises an energy-efficient reversal of magnetization based on the precessional switching, as demonstrated using a pulsed voltage in a magnetic tunnel junction. On the other hand, magnetic damping is a vital material parameter that governs magnetization dynamics and magnon transport. Therefore, their manipulation by voltages is highly desirable to increase the performance of spintronic devices. However, the voltage-control of those magnetic properties is mainly restricted in ferromagnetic "metals" except for a few experiments with ferro- ferrimagnetic insulators (FIs) [2,3]. In this presentation, we theoretically demonstrate the voltage-control of the (i) magnetic anisotropy and the (ii) magnetic damping in FI/topological insulator (TI) bilayers [4,5]. Three-dimensional TIs, such as Bi_2Se_3, possess an ideally insulating bulk and spin-momentum locked metallic surface states due to a strong spin-orbit interaction. An essential feature of the FI/TI bilayer is that the TI bulk behaves as a semiconductor, enabling the control of the surface carrier density by voltages. Our main results are the following two: (i) We first analytically formulate the uniaxial magnetic anisotropy at the FI/TI interface as a function of the applied voltage. Next, we propose a transistor-like device with nonvolatile magnetic memory functionality, adopting the VCMA writhing method that requires no external magnetic fields. (ii) We also formulate an effective damping torque induced by spin-charge pumping in the FI/ TI bilayer as a gate-voltage function. We find that the effective damping with the out-of-plane magnetization configuration can be modulated by one order of magnitude under the voltage of ~ 0.1 V with realistic material parameters. The voltage control of magnetic anisotropy and damping paves the way for low-power spintronic technologies beyond the current-based control. This work was supported by Grants-in-Aid for Scientific Research (Grant Nos. 20K15163 and 20H02196) from the JSPS and Postdoctorado FONDECYT 2019 Folio No. 3190030.

[1] F. Matsukura, Y. Tokura, and H. Ohno, Nat. Nanotechnol. 10, 209 (2015). [2] Y. Fan et al., Nat. Nanotechnol. 11, 352 (2016). [3] L. Wang et al., Phys. Rev. Appl. 11, 044060 (2019). [4] T. Chiba and T. Komine, Phys. Rev. Appl. 14, 034031 (2020). [5] T. Chiba, A. O. Leon, and T. Komine, Appl. Phys. Lett. 118, 252402 (2021).

CONTRIBUTED PAPERS

GOM-02. A magnetic gain-cell structure for efficient voltage-controlled MRAM. *S. Sayed*[1,2], C. Hsu[1] and S. Salahuddin[1,2] *1. Electrical Engineering and Computer Sciences, University of California, Berkeley, Berkeley, CA, United States; 2. Materials Sciences Division, Lawrence Berkeley National Laboratory, Berkeley, CA, United States*

Spin-transfer torque (STT) based magnetoresistive random-access memory (MRAM) is of great current interest for embedded applications, due to its high speed, high endurance, and long retention time. However, state-of-the-art STT MRAM requires a large switching current that leads to reliability issues, high write energy, and limits the density scaling. In this talk, we will show that a conventional current-controlled MTJ can be changed to a voltage-controlled device if we replace the thin oxide barrier with a resonant tunneling barrier. Such a simple modification will combine two established quantum phenomena: interlayer exchange coupling and resonant tunneling within the scaled magnetic structure to enable a resonant-exchange controlled (REC) magnetization switching [1]. REC-driven magnetization switching can substantially lower the write energy, decouple the energy and speed of operations, eliminate the reliability issues, and enable denser MRAM technologies. A voltage-controlled MTJ has a high baseline resistance, which may cause compatibility issues with standard CMOS. We will discuss a magnetic gain cell structure that consists of a REC MTJ and two transistors for a large separation in the output current for the two memory states while retaining the low power advantages of a voltage-controlled write mechanism [2]. We analyze the REC MTJ using quantum-transport simulations on a CoFeB/MgO/Ru/MgO/CoFeB structure and combine the results with an empirical SPICE model to analyze the magnetic gain cell using 45 nm CMOS models in HSPICE. Our simulation results suggest approximately 10^3 times change in the read current in the gain cell between the two magnetic states. The expected energy and delay are 29.5 fJ/bit and 1.6 ns respectively for a write operation and 7.6 ~ 39 fJ/bit and 0.6 ~ 1 ns respectively for a read operation, thus promising for low energy, fast, and high-density REC MRAM technology.

[1] Sayed et al., Phys. Rev. Applied, 14, 034070, 2020. [2] Sayed et al., IEEE Electron Device Letters, 2021 (to appear).

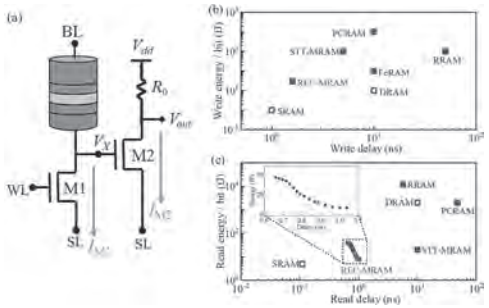

GOM-03. Voltage Modulated RKKY Interaction through Magneto-Ionic Gating. *A.E. Kossak*[1], M. Hasan[1], M. Huang[1], P. Reddy[1], S. Sheffels[1] and G.S. Beach[1] *1. Materials Science and Engineering, Massachusetts Institute of Technology, Cambridge, MA, United States*

The voltage modulation of magnetic properties has been proposed as a solution to the energy efficiency issues with current-controlled methods for spintronic devices. Using a synthetic antiferromagnetic heterostructure, we employ this low-energy solution through magneto-ionic control[1]. The foundation for magneto-ionic control has been demonstrated using oxygen[1], lithium[2], nitrogen[3], and hydrogen[4-6] in rare-earth transition-metal metal-oxide/metal heterostructures. However, a solid-state, reversible approach has not yet been shown for the magneto-ionic voltage-control of the Ruderman–Kittel–Kasuya–Yosida (RKKY) interaction. Our heterostructure is a synthetic antiferromagnet made of two ferrimagnetic gadolinium cobalt layers separated by a ruthenium (Ru) layer. We validate the RKKY interlayer exchange coupling by growing the Ru layer as a wedge and extracting the variation of the exchange field with Ru thickness through polar magneto-optical Kerr effect (MOKE) microscopy. We then demonstrate that the room-temperature pumping of hydrogen into the spacer layer, using the solid-state proton pump platform[4], alters the exchange interaction between the two ferrimagnet layers. We show that the change in magnetic properties is reversible and cyclable. In addition, by harnessing the composition-control of magnetization in ferrimagnetic GdCo, we can demonstrate that the RKKY interlayer exchange coupling can be switched from antiferromagnetic to ferromagnetic and vice versa. The voltage-induced changes in the exchange coupling field can be seen with bias voltages as low as 3V and timescales below 1s. We also demonstrate this effect in Co/Pt and Co/Pd multilayers. This provides a pathway for 180 degrees switching of a free layer with just a gate voltage for the realization of fast, compact, and energy-efficient devices for next-generation spintronic applications.

[1] U. Bauer, L. Yao, A. Tan, *et al.* Nat. Mater., Vol. 14, p.174–181 (2015). [2] S. Dasgupta, B. Das, M. Knapp, *et al.* Adv. Mater., Vol. 26, p.4639–4644 (2014). [3] J. de Rojas, A. Quintana, A. Lopeandía, *et al.* Nat. Commun. Vol. 11, p.5871 (2020). [4] A. J. Tan, M. Huang, C. O. Avci, *et al.* Nat. Mater. Vol. 18, p.35–41 (2018). [5] A. J. Tan, M. Huang, S. Sheffels, *et al.* Phys. Rev. Mat. Vol. 3, p.064408 (2019). [6] M. Huang, A. J. Tan, F. Büttner, *et al.* Nat. Commun. Vol. 10, p.5030 (2019).

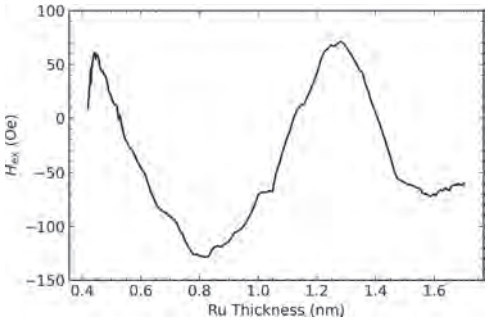

Fig. 1 Interlayer exchange field as a function of ruthenium interlayer thickness in a GdCo/Ru/GdCo heterostructure.

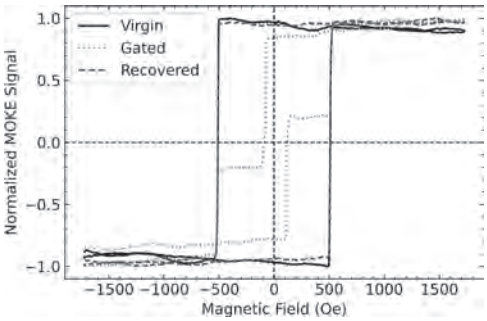

Fig. 2 Solid-state, reversible, voltage-control of RKKY in a GdCo/Ru/GdCo heterostructure using magneto-ionic proton pumping.

GOM-04. Lithium-Ion Battery Technology for Voltage Control of Perpendicular Magnetization. *M. Ameziane*[1], R. Mansell[1] and S. van Dijken[1] *1. Applied Physics, Aalto University, Espoo, Finland*

Voltage control of magnetism provides a promising path toward the development of low-power spintronic devices. Magneto-ionics exploiting voltage-driven ion migration as a control mechanism has attracted interest because it can generate large magnetoelectric effects at low voltage. Here, we demonstrate the use of all-solid-state lithium-ion battery technology for reversible voltage-controlled switching between perpendicular and in-plane magnetization states in a Co/Pt bilayer. The magneto-ionic battery structure consists of a 2 nm Ta/5 nm Pt/20 nm $LiCoO_2$/70 nm LiPON/3 nm Co/5 nm Pt crossbar junction (Fig. 1a,b). Here, the LiPON film functions as a solid-state electrolyte and the $LiCoO_2$ acts as the Li^+ storage layer. Using magneto-optical Kerr effect (MOKE) microscopy, we show that the magnetization of the Co film switches between in-plane and perpendicular directions when voltages of +2.5 V and –2 V are applied (Fig. 1c,d). The magneto-ionic switching effect is reliably reproduced over multiple cycles (Fig. 2a,b) and switching takes less than 0.5 s at room temperature (Fig. 2c). Our structure can be cycled for >500 times without degradation. The magnetoelectric coupling efficiency is estimated to be 7,700 fJ/Vm at room temperature, which is the strongest magnetoelectric effect reported to date. We attribute the effect to changes in the hybridization of electron orbitals at the Co/Pt interface upon voltage-controlled insertion and deinsertion of Li^+ ions. Our work sets a new benchmark for lithium-based magneto-ionics and demonstrates the relevance of battery design principles for the development of low-power spintronic devices.

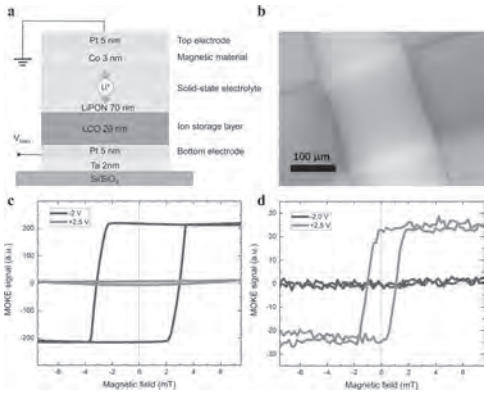

Fig. 1 (a) Schematic of the magneto-ionic battery structure. (b) Optical microscopy image of a single crossbar junction. (c) Polar and (d) longitudinal MOKE hystersis curves recorded at –2.0 and +2.5 V.

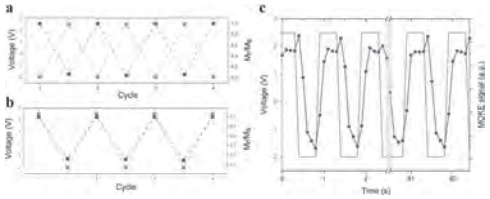

Fig. 2 Reversible voltage-controlled switching of (a) the perpendicular magnetization and (b) the in-plane magnetization in zero magnetic field. (c) Time-resolved modulation of the longitudinal MOKE signal at room temperature recorded while toggling the voltage between –2.0 V and +2.5V in 0.5 s intervals.

GOM-05. Reversible anisotropy manipulation via gate voltages in ferromagnet/oxide multilayers. *A. Di Pietro*[1,2], R. Pachat[4], J.W. van der Jagt[3], L. Herrera-Diez[4], D. Ravelosona[3] and G. Durin[1,2] *1. Magnetism, INRIM, Turin, Italy; 2. Politecnico di Torino, Turin, Italy; 3. C2N - Spin Ion, Paris, France; 4. CNRS, Paris, France*

The application of gate voltages in ferromagnet/Oxide/Heavy metal thin film multilayer has been identified as one possible candidate to manipulate their anisotropy at will [3], [1], [4]. Unfortunately, this method has proven to be unreliable in terms of the reversibility: e.g, the application of a gate voltage onMgO/CoFeB/Ta [3] causes an irreversible change of the magnetic anisotropy axis from in plane to out-of-plane, while HfO_2/CoFeB/Ta stacks display a more complicated behavior, with different regimes characterized by different reversibility behaviors [2]. The microscopic origin of these phenomena remains unclear and is the object of our inquiry. In this work we performed ab-initio simulations on 6 setups comprising Fe/O, HfO2/Fe, MgO/Fe interfaces each one with frontal and interstitial oxygen atomic configurations (fig.1). The pure Fe/O interface prefers interstitial oxygen configurations while the addition of oxides seems to switch this trend around. In particular, HfO2/Fe displays a strong preference for the frontal oxygen arrangement, leading us to identify a possible hypothesis for the phenomenon of the multiple magneto-ionic regimes displayed. In it's as grown form, HfO2/CoFeB is characterized by an underoxidized ferromagnet interface [2]. The application of a gate voltage on HfO2/CoFeB pushes some of the oxygen species in proximity of the interface where they occupy the stable frontal site. Further application of a gate voltage pushes other oxygen atoms toward the still free and more unstable interstitial sites. The occupation of these interstitial sites has the effect of destroying perpendicular magnetic anisotropy as seen both in experiments and simulations [5] [1]. Once these more mobile interstitial sites are occupied, magnetic anisotropy can be switched reversibly by inverting the gate voltage and adjusting the interstitial site occupation (fig.2)

[1] B. Dieny and M. Chshiev,"Reviews of Modern Physics, vol. 89, no. 2, (2017) [2] R. Pachat, D. Ourdani, J. van der Jagt, Phys. Rev. Applied, vol. 15, p. 064 (2021) [3] A. Fassatoui, J. P. Garcia, L. Ranno, PhysicalReview Applied, vol. 14, no. 6, pp. 1–11 (2020) [4] A. Hallal, H. X. Yang, B. Dieny, Physical Review B - Condensed Matter and MaterialsPhysics, vol. 88, no. 18, pp. 1–5 (2013) [5] H. X. Yang, M. Chshiev, A. Kalitsov, Applied Physics Letters, vol. 96,no. 26, pp. 2–4, 2010

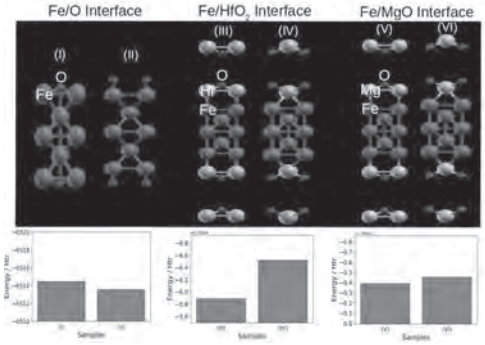

Fig. 1 Comparison of the different interfacial configurations in the differentsamples. The bar plots represent the ground state energies and highlight themore stable configuration

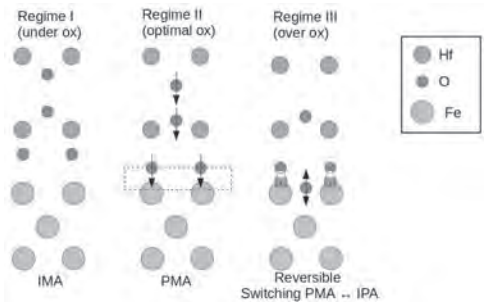

Fig. 2 Hypothesis for the mechanism governing magneto-ionic regimes inHfO2/FM stacks. The text highlights the magnetic properties of the interface under different oxidation conditions.

GOM-06. Gate-controlled giant proximity magnetoresistance and odd-parity magnetoresistance in semiconductor-based nonmagnetic (InAs) / ferromagnetic (GaFeSb) heterostructures. *K. Takiguchi*[1], L. Anh[1,2], T. Chiba[3], K. Okamura[1], H. Shiratani[1], R. Fukuzawa[1,4], T. Takahashi[4,5] and M. Tanaka[1,6] *1. EEIS, University of Tokyo, Bunkyo-ku, Japan; 2. IEI, University of Tokyo, Bunkyo-ku, Japan; 3. National Institute of Technology, Fukushima College, Iwaki-shi, Japan; 4. IIS, University of Tokyo, Meguro-ku, Japan; 5. NanoQuine, University of Tokyo, Meguro-ku, Japan; 6. CSRN, University of Tokyo, Bunkyo-ku, Japan*

The magnetic proximity effect (MPE) induced at the interface of a ferromagnetic (FM) insulator and a nonmagnetic (NM) conducting material with strong spin-orbit coupling is a promising platform for the emergence of novel phenomena [1-4]. Here we present novel magnetotransport phenomena originated from MPE in non-magnetic InAs/ ferromagnetic semiconductor (FMS) (Ga,Fe)Sb heterostructures, where (Ga,Fe)Sb is an FMS with a high Curie temperature over 300 K [5]. In this structure, the two-dimensional electron wavefunction in the InAs quantum well (QW) penetrates into the (Ga,Fe)Sb side so that the strong MPE is realized. In addition, the gate-voltage application can enhance the MPE by pushing the wavefunction towards the FM layer. Firstly, we report a giant and gate-tunable MPE in a NM InAs QW interfaced with (Ga,Fe)Sb, in which a spin splitting Δ (~ 3.8 meV) in the InAs QW is induced and controlled by the gate voltage. This large Δ causes a new giant magnetoresistance that is two or three orders of magnitude larger than previously reported ones [2-4] and has unique angular symmetry (Fig. 1), to which we refer as "proximity magnetroresistance" (PMR) [6]. In addition to PMR, the InAs/(Ga,Fe)Sb system exhibits an extra unusual transport property due to the space inversion symmetry (SIS) breaking and time reversal symmetry (TRS) breaking. The odd-parity magnetoresistance (OMR) in a linear response regime is a novel phenomenon only observed in systems where both TRS and SIS are simultaneously broken [7]–[10]. Even in such rare systems, the OMR magnitude was tiny (the magnitude reported thus far is at most 2%). Here we have found a giant and gate-controllable

OMR as large as 27% in edge transport channels of the InAs QW (Fig. 2)), which is magnetized by an MPE from the underlying (Ga,Fe)Sb layer. We argue that the origin of the large OMR in our system is attributed to TRS breaking and SIS breaking from MPE and from the strong Rashba effect at one-dimensional channel, respectively [11].

[1] I. Vobornik, *et al. Nano Lett.* 11, 4079–4082 (2011). [2] H. Nakayama, *et al. PRL* 110, 206601 (2013). [3] S. Cho, *et al. Sci. Rep.* 5, 14668 (2015). [4] N. Vlietstra, *et al. PRB* 90, 174436 (2014). [5] N. T. Tu, *et al. APL* 108, 192401 (2016). [6] K. Takiguchi, *et al. Nat. Phys*. 15, 1134 (2019). [7] R. Moubah, *et al. JAP* 115, 053911 (2014). [8] Y. Wang, *et al. Nat. Commun.* 11, 216 (2020). [9] T. C. Fujita, *et al. Sci. Rep.* 5, 9711 (2019). [10] S. Albarakati, *et al. Sci. Adv.* 5, eaaw0409 (2019). [11] K. Takiguchi, *et al. arXiv* 2003.11731 (2020).

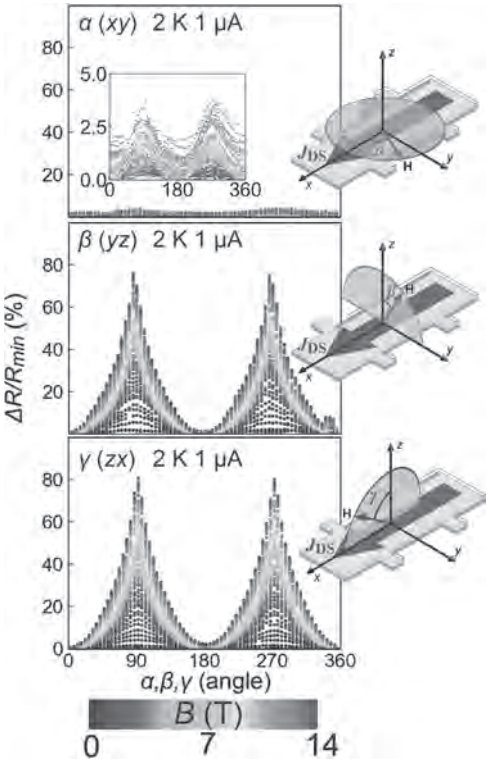

Fig. 1 Magnetic field angle dependence of the resistance at 2 K.

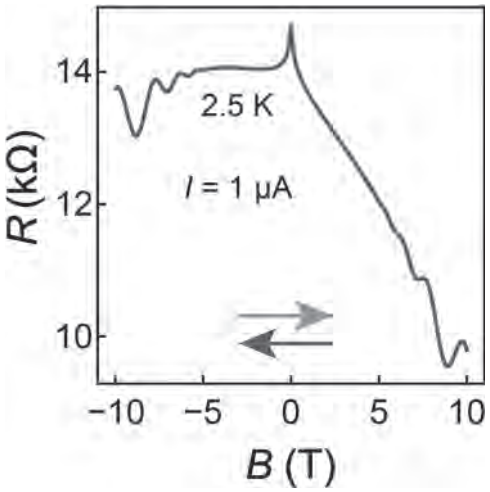

Fig. 2 MR of the InAs/(Ga,Fe)Sb bilayer heterostructure, measured with a DC current of 1 μA and an external magnetic field *B* applied parallel to the *z* axis at 2.5 K.

GOM-07. Magneto-ionic Gating of an Antiferromagnet. *M. Hasan*[1], M. Huang[1] and G.S. Beach[1] *1. Materials Science and Engineering, Massachusetts Institute of Technology, Cambridge, MA, United States*

Electrical manipulation of antiferromagnets (AFM) is a highly desirable functionality and it is currently a heavily investigated research area owing to a number of inherent advantages of AFMs over ferromagnets (FM)[1]. Recently, magneto-ionic gating by hydrogen has been shown to cause large changes in magnetic properties, such as modulation of perpendicular magnetic anisotropy in ultra-thin Co films [2] or switching of the dominant sublattice in a ferrimagnet, GdCo [3]. Here, we present results of magneto-ionically gating the AFM itself in an exchange-biased (EB) heterostructure consisting of Pt/Co/Pt/$Co_{90}Ni_{10}O$/GdO_x/Au on thermally oxidized Si. In this system, EB - a well-known effect that occurs in FM/AFM heterostructures - serves as a means to probe changes occurring in the AFM as well as the entire heterostructure. Our work shows that voltages as low as +3V, can drive hydrogen into the AFM causing local changes to the magnetic properties. Because domain wall creep dynamics is highly sensitive to the local properties of the films, we investigate the effect of gating on EB through measurement of domain wall velocities (in Co) using a wide field MOKE. This ensures that extracted parameters such as the EB, depend only on the local properties of the gated area. Through this method, we have been able to observe a reversible enhancement of the EB by more than 20% upon hydrogenation for a series of AFM thicknesses, suggesting considerable modulation of bulk and or interfacial characteristics of the AFM upon hydrogenation. These early results show that AFMs are susceptible to ionic gating, and we believe our work can pave the way for more robust electrical control of AFMs, pushing the boundaries of the exciting field of AFM spintronics.

[1]. T. Jungwirth et al., Nature Nanotechnology, Vol. 11, p. 231 (2016) [2]. A.J. Tan et al., Nature Materials, Vol. 18, p. 35 (2019) [3]. M. Huang et al., in press., Nature Nanotechnology [4]. A.J. Schellekens et. al., Nature Communications Vol. 3, p. 847 (2012)

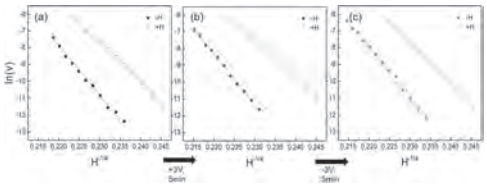

Fig. 1 Linear ln(v) vs $H^{-1/4}$ shows occurrence of domain wall creep [4]. (a) Non-overlapping curves for velocities obtained at +H fields and -H fields reveal the presence of EB in the as deposited condition. (b) After gating the curves move further apart signifying an enhancement of EB field and the enhancement is reversible upon application of a negative voltage as shown in (c).

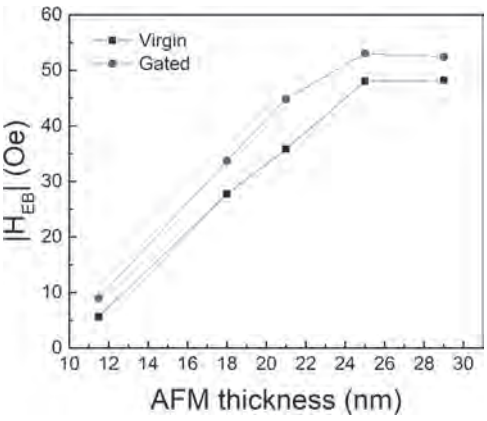

Fig. 2 Enhancement of EB by hydrogen gating for different AFM thicknesses.

GOM-08. All-electrical magnetization switching and reading in ferromagnetic/multiferroic nanodevices at room temperature.

D.C. Vaz[1], C. Lin[2], J. Plombon[2], W. Choi[1], I. Groen[1], I. Arango[1], V. Pham[1], D.E. Nikonov[2], H. Li[2], P. Debashis[2], S.B. Clendenning[2], T.A. Gosavi[2], V. Garcia[3], S. Fusil[3], M. Bibes[3], Y. Huang[4], B. Prasad[4], R. Ramesh[4], F. Casanova[1] and I.A. Young[2] *1. CIC nanoGUNE, Donostia-San Sebastián, Spain; 2. Components Research, Intel Corporation, Hillsboro, OR, United States; 3. Unité Mixte de Physique, CNRS/Thales, Palaiseau, France; 4. Department of Materials Science and Engineering and Department of Physics, University of California, Berkeley, CA, United States*

In recent years, voltage and frequency scaling of CMOS technology has slowed down, accompanied by increasingly larger power requirements. To assure the continuity of Moore's Law, new beyond-CMOS logic devices need to be found. For this purpose, one of the leading options is the magneto-electric spin-orbit (MESO) logic device, where a combination of quantum materials and spin-based phenomena allows for energy-efficient logic and favourable device scaling [1, 2]. Here, we present the first experimental demonstration of a fully operational MESO device. We achieve voltage-driven magnetization switching and reading at room temperature, in Pt/CoFe nanodevices fabricated on a multiferroic $BiFeO_3$ layer. Switching is performed by application of a voltage pulse to the $BiFeO_3$, which magnetoelectrically reverses its ferroelectric and antiferromagnetic state. Through interfacial coupling, the CoFe magnetization is also reversed. Spin-to-charge conversion in the Pt/CoFe nanodevice is used to probe the magnetization direction of the CoFe element [3]. We discuss future strategies for the implementation of cascadable devices and MESO-based logic circuits [4].

[1] S. Manipatruni et al., Nature 565, 35-42, 2019. [2] H. Liu et al., IEEE Journal on Exploratory Solid-State Computational Devices and Circuits 5, 1-9, 2019. [3] V. T. Pham S. et al. Nat. Electron. 3, 309–315, 2020. [4] C. -C. Lin et al., IEEE International Electron Devices Meeting, 37.3.1-37.3.4, 2019.

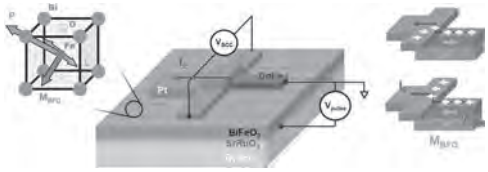

Sketch of the nanostructured Pt/CoFe devices on $BiFeO_3$. Two logic states are given by the magnetization fo the FM direction, switched by reversing the ferroelectric polarization P and antiferromagnetic order L of the $BiFeO_3$, and read through spin-charge conversion in Pt.

GOM-09. Effect of Annealing on Magnetoionics in W/CoFeB/HfO_2.

R. Pachat[1], D. Ourdani[4], M.A. Syskaki[6], A. Di Pietro[3], L. Largeau[1], R. Juge[2], C. Balan[5], J.W. van der Jagt[2], Y. Roussigné[4], M. Gabor[8], S.M. Chérif[4], G. Durin[3], S. Pizzini[5], S. Ono[7], J. Langer[6], M. Belmeguenai[4], D. Ravelosona[2,1] and L. Herrera-Diez[1] *1. C2N, Université Paris-Saclay, Palaiseau, France; 2. Spin-Ion technologies, Palaiseau, France; 3. INRIM, Torino, Italy; 4. Laboratoire des Sciences des Procédés et des Matériaux, Université Paris 13, Villetaneuse, France; 5. Institut Néel, Univ. Grenoble Alpes, Grenoble, France; 6. Singulus Technologies, Kahl am Main, Germany; 7. Central Research Institute of Electric Power Industry, Yokosuka, Japan; 8. Physics and Chemistry Department, Technical University of Cluj-Napoca, Cluj-Napoca, Romania*

Magnetoionics (MI) is a much-in-demand feature for spintronics devices due to its great potential for improving energy efficiency in memory devices. The main feature of MI is to allow for the nonvolatile modulation of magnetic properties [1–5], making MI reversibility a fundamental quality for high device performance. Various studies have addressed issues impacting reversibility such as the presence of different types of ions, oxides and the degree of oxidation at the oxide/ferromagnetic interface [3, 5–8], while the influence of annealing temperature on reversibility has been largely overlooked. Annealing is commonly used to induce crystallization in CoFeB layers leading to the enhancement of perpendicular magnetic anisotropy (PMA), interfacial Dzyaloshinskii-Moriya interaction (iDMI), and tunnel magnetoresistance [9–11], therefore its impact on MI is of great interest. In this study, we show that W/CoFeB/HfO_2 thin films annealed at 350°C and 390°C show a significant but irreversible dependence of PMA and DMI on gate voltage. However, an annealing program using a slow ramp that minimizes the exposure to the highest temperatures allows to induce PMA and iDMI while also showing a MI reversibility of 71% in remanence with respect to PMA. This dependence of MI reversibility on annealing profiles and temperatures could be related to the different degrees of crystallinity obtained under different annealing conditions. Such structural differences, such as size and distribution of crystallites, can greatly impact the ion mobility inside the stack and be responsible for observed modulation of the MI reversibility. Our results therefore show that annealing parameters need to be optimized to obtain enhanced magnetic properties without compromising MI performance.

[1] U. Bauer, S. Emori, and G. S. D. Beach, Nature Nanotechnology 8, 411 (2013), [2] U. Bauer, L. Yao, and G. S. D. Beach, Nature Materials 14, 174 (2015), [3] A. J. Tan, M. Huang, and G. S. D. Beach, Nature Materials 18, 35 (2019), [4] L. Herrera Diez, Y. Liu, and D. Gilbert, Physical Review Applied 12, 034005 (2019), [5] R. Pachat, D. Ourdani, and L. Herrera Diez, Physical Review Applied 15, 064055 (2021), [6] C. Bi, Y. Liu, and W. G. Wang, Physical Review Letters 113, 267202 (2014), [7] J. de Rojas, A. Quintana, and M. Butterling, Nature Communications 11,5871 (2020), [8] A. Fassatoui, J. Vogel and S. Pizzini, Physical Review Applied 14, 064041 (2020), [9] J. Cho, N.-H. Kim, and C.-Y. You, IEEE TRANSACTIONS ON MAGNETICS 54, 1500104 (2018), [10] T. Nagata, M. Haemori, and T. Chikyow, Applied Physics Letters 109, 132404 (2016), [11] W. G. Wang, C. Ni, and G. Miao, Physical Review B 81, 144406 (2010).

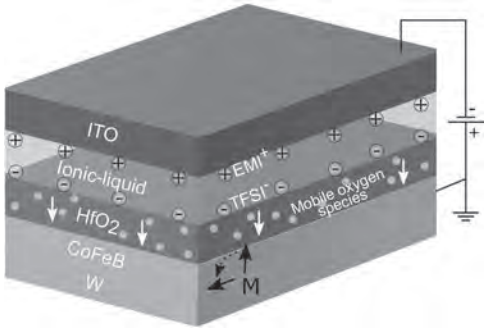

Fig. 1: Schematic of the W/CoFeB/HfO_2 stack with an ionic-liquid [EMI-TFSI] gate showing change in anisotropy with the migration of mobile oxygen species in HfO_2 under an applied EF.

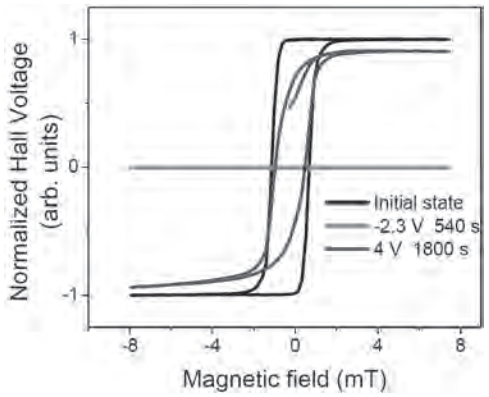

Fig. 2: Hysteresis for reversibility in W/CoFeB/HfO_2 annealed at 350°C with the slow ramp program.

GOM-10. Sub-Volt Switching of Nanoscale Voltage-Controlled Perpendicular Magnetic Tunnel Junctions. *Y. Shao*[1], V. Lopez Dominguez[1], N. Davila[2], N. Kioussis[3], J. Katine[2] and P. Khalili Amiri[1]
1. Department of Electrical and Computer Engineering, Northwestern University, Evanston, IL, United States; 2. Western Digital Corporation, San Jose, CA, United States; 3. Department of Physics and Astronomy, California State University, Northridge, CA, United States

Magnetic random-access memory (MRAM) with perpendicular magnetic tunnel junctions (MTJs) is gaining traction for embedded non-volatile memory and embedded Cache memory applications, due to its low power consumption, relatively high density, small mask count, and compatibility with complementary metal oxide semiconductor (CMOS) processing. One of the requirements of embedded MRAM for Cache applications is to switch the magnetization direction with high speed (~ 3 ns or less for L2 Cache) and with high endurance. The conventional switching mechanism based on current-induced spin-transfer torque (STT) requires significant current density through the MTJ, thus limiting its energy efficiency, endurance, and ability to scale the access transistor size. Voltage-controlled magnetic anisotropy (VCMA) has emerged as an alternative writing mechanism which, owing to its electric-field-based principle, may solve this problem and enable higher bit density and ultra-low power switching [1-6] in advanced CMOS nodes. Previous works on VCMA-induced switching in MTJs achieved write voltages > 2 V in bits with diameter down to 50 nm [7-9]. Here, for the first time, we demonstrate sub- 1 V switching of nanoscale MTJs using VCMA, and demonstrate scaling of this switching mechanism down to 30 nm MTJs. We developed a new voltage-controlled MTJ material stack which simultaneously provides VCMA ~ 100 fJ/Vm, high TMR (> 130% at film level) and thermal anneal stability at 400 Celsius degree for compatibility with embedded CMOS in advanced nodes. We performed VCMA switching on nanoscale perpendicular MTJs with diameters of 30 nm to 70 nm. Switching with higher than 90% probabilities in both directions was obtained on 70 nm MTJs with a voltage pulse amplitude lower than 1 V, as shown in Fig. 1. The switching energy was ~ 15 fJ/bit. The VCMA coefficient obtained from the switching measurements was 102 fJ/Vm, which is in good agreement with the value obtained from DC measurements.

[1] Amiri, P.K., Alzate, J. G., Cai, X. Q., et al., *IEEE Transactions on Magnetics*, 51(11): p. 1-7 (2015) [2] Wang, W.G., Li, M., Hageman, S. et al., Nature materials, 11(1): p. 64-68 (2012) [3] Weisheit, M., Fähler, S., Marty, A., et al., Science, 315(5810): p. 349-351 (2007) [4] Shiota, Y., Nozaki, T., Bonell, F., et al., Nature materials, 11(1): p. 39-43 (2012) [5] Maruyama, T., Shiota, Y., Nozaki, T., et al., Nature nanotechnology, 4(3): p. 158-161 (2009) [6] Kanai, S., Yamanouchi, M., Ikeda, S., et al., Applied Physics Letters, 101(12): p. 122403 (2012) [7] Shiota, Y., Miwa, S., Nozaki, T., et al., Applied Physics Letters, 101(10): p. 102406 (2012) [8] Kanai, S., Nakatani, Y., Yamanouchi, M., et al., Applied Physics Letters, 103(7): p. 072408 (2013) [9] Grezes, C., Ebrahimi, F., Alzate, J.G., et al., Applied Physics Letters, 108(1): p. 012403 (2016)

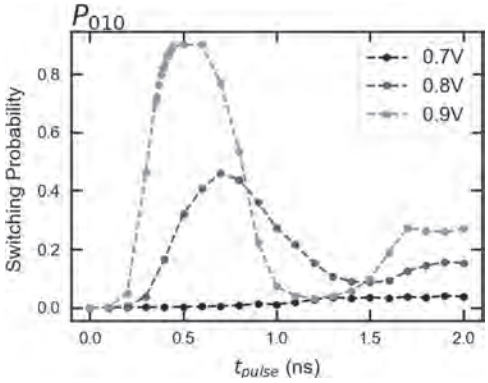

Fig. 1. Probabilities of successive back and forth switching (parallel to antiparallel and back to parallel state) for 70 nm devices under different voltage pulse amplitudes, as a function of pulse width.

GOM-11. Ising Machine Based on Electrically Coupled Spin Hall Nano-Oscillators. *B.C. McGoldrick*[1], J. Sun[2] and L. Liu[1] *1. Electrical Engineering and Computer Science, Massachusetts Institute of Technology, Cambridge, MA, United States; 2. IBM T. J. Watson Research Center, Yorktown Heights, NY, United States*

The Ising machine is an unconventional computing architecture that can be used to solve NP-hard combinatorial optimization problems more efficiently than traditional von Neumann architectures. GHz spin Hall nano-oscillators (SHNOs) are a particularly attractive technology for building fast, energy-efficient, and scalable Ising machines; however, electrical coupling mechanisms which allow for full programmability among different oscillator nodes have not yet been fully demonstrated in such a network. Here, we develop a general analytical framework that can describe injection locking of SHNOs with arbitrary oscillation orbits at both the fundamental frequency and harmonics. With this compact analytical framework, we integrate the SHNO into a Verilog-A device model that can emulate the oscillator's injection locking behavior in circuit simulations, where the dynamics of coupled oscillator networks are simulated together with conventional electronic components (Fig. 1). While our abstract circuit simulations achieve similar accuracy as full micromagnetic simulations, the device model we developed leads to more than 100 times improvement in simulation efficiency and allows us to evaluate the performance using realistic circuits. Using circuit-level simulations, we further study the effects of phase noise and scalability in networks of up to hundreds of coupled oscillators to show that the SHNO-based Ising machine can be operated robustly at room temperature. Compared with existing technologies, SHNO networks exhibit orders of magnitude improvement in time, space, and energy efficiency (Table 1). Our results provide analytical tools and design insights that will be useful for the realization of a CMOS-integrated SHNO Ising machine.

1. S. Dutta, A. Khanna, H. Paik, et al., arXiv preprint arXiv:2007.12331 (2020). 2. A. D. King, W. Bernoudy, J. King, et al., arXiv preprint arXiv:1806.08422 (2018). 3. S. Boixo, T. F. Rønnow, S. V. Isakov, et al., Nature Physics, Vol. 10, p.218 (2014). 4. T. Inagaki, Y. Haribara, K. Igarashi, et al., Science, Vol. 354, p.603 (2016). 5. P. L. McMahon, A. Marandi, Y. Haribara, et al., Science Vol. 354, p.614 (2016). 6. J. Chou, S. Bramhavar, S. Ghosh, et al., Scientific Reports, Vol. 9, p.14786 (2019). 7. F. Chicco, A. Pezzotta, and C. C. Enz, IEEE International Symposium on Circuits and Systems, p.1–4 (2017). 8. S. Dutta, A. Parihar, A. Khanna, et al., Nature Communications, Vol. 10, p.3299 (2019).

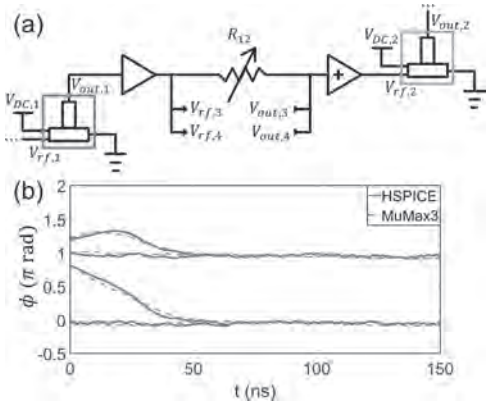

Fig. 1: (a) Electrical coupling circuit linking two SHNOs in the oscillator-based Ising machine. (b) Phases of oscillators in a 4-node coupled network solving the Ising model in circuit simulations (HSPICE) using our abstract device model and in micromagnetic simulations (MuMax3).

	CPU [1]	GPU [2]	D-WAVE [3]	Optical Parametric Oscillator [4, 5]	LC Oscillator [6, 7]	Phase-Transition Nano-Osc. [1, 8]	SHNO [this work]
Solution time	246ms	100μs	30ms	2ms	2.5ms	25.5μs	359ns
Power	60W	≤250W	25kW	-	2.5mW	1.2mW	486μW
Energy to solution	14.8J	≤25mJ	750J	-	6.3μJ	30.6nJ	175pJ
Energy efficiency [sol/s/W]	6.7E-2	≥40	1.3E-3	-	1.6E+5	3.26E+7	5.73E+9
Size [one element)	-	-	-	1km fiber	0.1mm^2	0.2μm^2	0.024μm^2
Room temp.	Y	Y	N	Y	Y	Y	Y

Table 1: Comparison of speed, energy, and space metrics between the SHNO Ising machine and existing technologies. Values are standardized to a 100-node network.

GOM-12. Conservative Skyrmion Logic with Voltage- Controlled Magnetic Anisotropy Synchronization. *B. Walker*[1], C. Cui[2], F. Garcia-Sanchez[3], J.C. Incorvia[2], X. Hu[1] and J.S. Friedman[1] *1. Electrical and Computer Engineering, University of Texas at Dallas, Richardson, TX, United States; 2. Electrical and Computer Engineering, University of Texas at Austin, Austin, TX, United States; 3. Department of Physics, University of Salamanca, Salamanca, Spain*

Magnetic skyrmions have recently been proposed as information carriers due to their topological stability and ease of transport. Recent works demonstrate the feasibility of skyrmions for use in highly cascaded reversible logic structures. [1] However, their use of notches for skyrmion synchronization greatly increases the power consumption and vulnerability to fabrication process variations. To improve this scheme, we propose the use of voltage-controlled magnetic anisotropy (VCMA) for skyrmion synchronization. [2] By simulating the kinetics of skyrmion pinning at perpendicular magnetic anisotropy (PMA) gradients, we quantify the relationship between current density, skyrmion velocity, and synchronizer PMA necessary to pin skyrmions. With this, we propose a VCMA synchronizer with minimized power consumption. We validate the accuracy and efficiency of the VCMA synchronizer by simulating its use in a variety of highly cascaded skyrmion logic circuits, demonstrating the feasibility of large-scale reversible skyrmion computation.

[1] Maverick Chauwin, Xuan Hu, Felipe Garcia-Sanchez, et. al, Skyrmion Logic System for Large-Scale Reversible Computation, Physical Review Applied, Vol. 12, p.064053 (2019) [2] Benjamin W. Walker, Can Cui, Felipe Garcia-Sanchez, et. al, Skyrmion Logic Clocked via Voltage Controlled Magnetic Anisotropy, Applied Physics Letters, Vol. 118, p.192404 (2021)

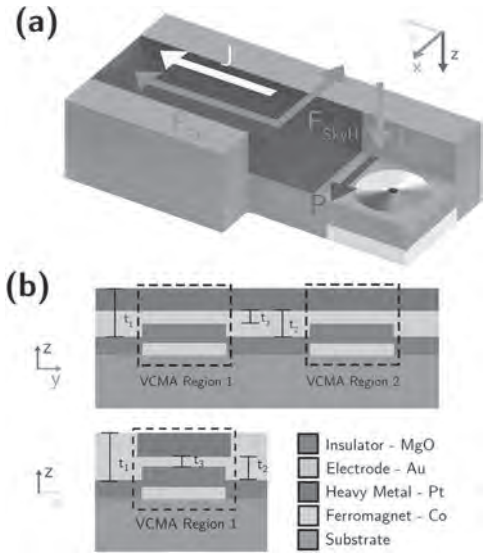

Fig. 1 VCMA-based synchronizer structure. (a) Neel skyrmion (colored circle) exists at heavy metal/ferromagnet interface with polarization (P). Skyrmion propelled in the +y direction due the +y-directed spin- Hall force (F_{SH}). Charge applied to the electrode creates an electric field, reducing the magnetic anisotropy of the interface. (b) Cross sections of synchronizer in the yz and xz planes.

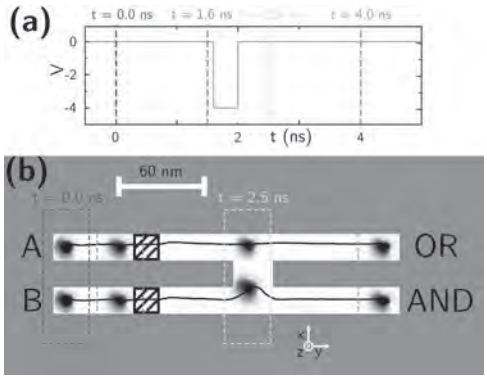

Fig. 2 AND/OR skyrmion logic gate with current density 5×10^{10} J/m^2 in the +y direction. (a) Voltage waveform applied to each VCMA region. (b) Mumax3 micromagnetic simulation results, showing the operation of an AND/OR gate (A=1,B=1), where the presence or absence of a skyrmion represents a logical 1 or 0 respectively. Skyrmion trajectory is represented by the black line and VCMA regions are represented by the dashed squares. At t=1.6 ns, the skyrmions are pinned by the positive anisotropy barrier of the VCMA regions. The clock voltage at t=1.7 ns reduces the anisotropy barrier and the skyrmion depins.

GOM-13. Magneto-ionic Enhancement of Exchange Bias via Electric Fields. *C.J. Jensen*[1], P. Murray[2], A. Quintana-Puebla[1], J. Zhang[3], X. Zhang[3], B. Kirby[4], P. Quarterman[4], A.J. Grutter[4], H. Zhang[5], A. Davydov[5], M. Sall[6,7], L. Herrera Diez[6], D. Ravelosona[6,7] and K. Liu[1,2]
1. Physics, Georgetown University, Washington, DC, United States; 2. University of California, Davis, Davis, CA, United States; 3. King Abdullah University of Science and Technology, Thuwal, Saudi Arabia; 4. Center for Neutron Research, National Institute of Standards and Technology, Gaithersburg, MD, United States; 5. Materials Measurement Laboratory, National Institute of Standards and Technology, Gaithersburg, MD, United States; 6. Centre de Nanosciences et de Nanotechnologies, CNRS, Université Paris-Saclay, Palaiseau, France; 7. Spin-Ion Technologies, Palaiseau, France

Magneto-ionics has shown promise as an effective approach to control magnetic properties via ionic migration, which can be tailored under an electric field.[1] For example, magneto-ionic control of exchange bias (EB), which is prominently used in spin valve type of devices, may lead to energy-efficient switching.[2] Here, we report studies of both oxygen and nitrogen-based magneto-ionic enhancement of EB in the Gd/NiCoO and CoFe/MnN systems, respectively. In the Gd/NiCoO system, where neither of the layers alone is ferromagnetic (FM) at room temperature, EB is established after field cooling (Fig. 1). The EB can be enhanced by up to 35% after a voltage conditioning and subsequently reset with a second field cooling. These effects are caused by the presence of a redox-induced interfacial FM NiCo layer, which further alloys with the Gd layer upon field cooling and voltage application.[3] Ion irradiation is used to alter the interfacial microstructure and in turn the EB.[4] In the CoFe/MnN system, EB is established after field cooling. Under electric gating, EB can be enhanced by up to 19% at 10K (Fig. 2). Polarized neutron reflectometry and electron microscopy reveal that nitrogen moves out of MnN during the field cooling step, and it can be driven back by an electric field, leading to the EB enhancement. These results highlight the viability of the solid-state magneto-ionic approach towards electric control of exchange bias. Work supported by the NSF, SRC/NIST nCORE SMART center, and KAUST.

[1] U. Bauer, L. Yao, A. J. Tan, P. Agrawal, S. Emori, H. L. Tuller, S. van Dijken, and G. S. D. Beach, Nat. Mater. 14, 174 (2015). [2] D. A. Gilbert, J. Olamit, R. K. Dumas, B. J. Kirby, A. J. Grutter, B. B. Maranville, E. Arenholz, J. A. Borchers, and K. Liu, Nat. Commun. 7, 11050 (2016). [3] P. D. Murray, C. J. Jensen, A. Quintana, J. W. Zhang, X. X. Zhang, B. J. Kirby, and K. Liu, ACS Appl. Mater. Interfaces, 13, 38916 (2021). [4]C. J. Jensen, A. Quintana, M. Sall, L. H. Diez, J. Zhang, X. Zhang, D. Ravelosona, and K. Liu, J. Magn. Magn. Mater. 540, 168479 (2021).

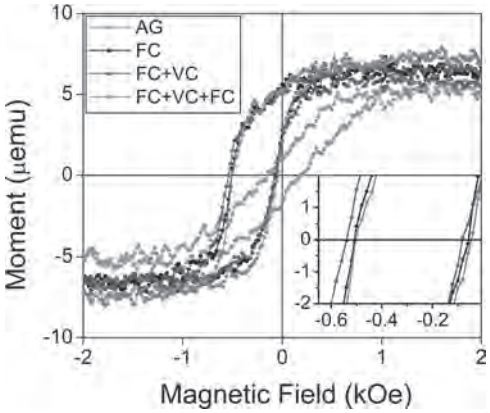

Fig. 1. Room temperature hysteresis loops of a Gd/NiCoO sample in the as-grown (AG) state, after field cooling (FC), after voltage conditioning (FC+VC), and after a second field cooling (FC+VC+FC). Inset shows the zoom-in view near coercive fields.

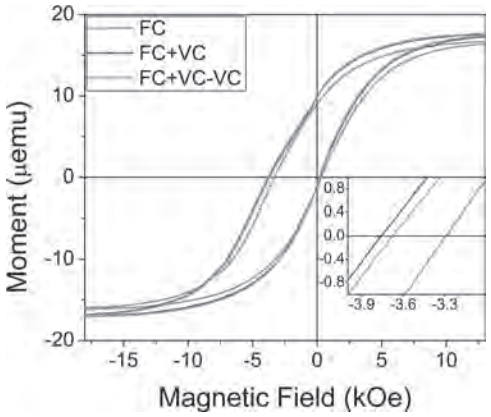

Fig. 2. Hysteresis loops of a CoFe/MnN sample at 10K in the field cooled (FC) state, after voltage conditioning (FC+VC), and after reversing the voltage bias (FC+VC-VC). Inset shows the zoom-in view along the decreasing field branch.

Session GON
MAGNETORESISTANCE IN HETEROSTRUCTURES (GMR, TMR, TAMR)

Gaspare Varvaro, Chair
Consiglio Nazionale delle Ricerche, Monterotondo Scalo (RM), Italy

INVITED PAPERS

GON-01. Computation with Domain Walls and Oscillators in Chirally Coupled Systems. *A. Hrabec[1,2] 1. Department of Materials, ETH Zurich, Zurich, Switzerland; 2. Laboratory for Multiscale Materials Experiments, Paul Scherrer Institute, Villigen, Switzerland*

In order to go beyond the traditional CMOS logic technology, novel spin-based logic architectures are being developed to provide nonvolatile data retention, near-zero leakage, and scalability. In particular, architectures based on magnetic domain walls take the advantage of the fast motion, high density, non-volatility and flexible design of domain walls to process and store information in three dimensions [1,2]. Such logic schemes have so far relied on domain wall manipulation and clocking using an external magnetic field, which hinders their industrial implementation. Here we demonstrate a method for performing all-electric logic operations and cascading using domain wall racetracks [3]. Our concept is based on the recently developed chiral coupling mechanism between adjacent magnets where the magnetic anisotropy competes with the interfacial Dzyaloshinskii–Moriya interaction (DMI) in Pt/Co/AlOx trilayers [4,5]. When a narrow in-plane (IP) magnetized region is incorporated into an out-of-plane (OOP) magnetized track, it couples to its surrounding, leading to the antiferromagnetic alignment of the OOP magnetization on the left and right of the IP region. This is enforced by interfacial DMI favouring a fixed magnetization winding direction, which is left-handed in our Pt/Co/AlOx trilayers. When a current-driven domain wall propagating in the track encounters such a region, the magnetization of the IP regions flips, leading to the annihilation of the incoming domain wall and the nucleation of a new domain wall of opposite polarity on the other side of the IP region (Fig. 1a). The chiral OOP-IP-OOP structure therefore serves as a domain wall inverter, the essential building block for all implementations of Boolean logic. Based on this principle, we fabricated reconfigurable NAND and NOR logic gates, making our concept for current-driven DW logic functionally complete. We also cascaded several NAND gates to build XOR and full adder gates, demonstrating electrical control of magnetic data and device interconnection in logic circuits (Fig. 1b). The functionality of logic circuits can be also expanded by the realization of a domain wall diode based on a geometrically tailored inverter [7]. We also broadened the application of chiral coupling towards dynamic computation with oscillators [8]. By imprinting the magnetic configuration of an IP magnetized disk in an OOP magnetized slab containing sizeable DMI, a chiral polar vortex texture can be established as a ground state in the patterned region (Fig. 2a). By means of micromagnetic calculations, we show that such an oscillator can be driven and manipulated by an injected spin current. We investigated the mutual synchronization of such oscillators via spin wave and dipolar interactions (Fig. 2b) and demonstrated their potential for neuromorphic computing with a neural network of six oscillators.

[1] D. A. Allwood, G. Xiong and C. C. Faulkner, Science, 309, 1688–1692 (2005). [2] S. Parkin and S.-H. Yang, Nat. Nanotechnol., 10, 195–198 (2015). [3] Z. Luo, A. Hrabec and T. P. Dao, Nature, 579, 214-218 (2020). [4] Z. Luo, T. P. Dao and A. Hrabec, Science, 363, 1435 (2019). [5] T. P. Dao, M. Müller and Z. Luo, Nano Lett., 19, 5930-5937 (2019). [6] A. Hrabec, Z. Luo and L. J. Heyderman, Appl. Phys. Lett., 115, 130503 (2020). [7] Z. Luo Z., S. Schären and A. Hrabec, Phys. Rev. Appl., 15, 034077 (2021). [8] Z. Zeng, Z. Luo and L. J. Heyderman, Appl. Phys. Lett., 118, 222405 (2021).

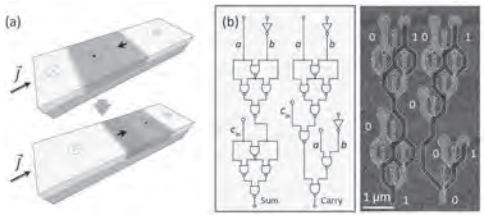

Fig. 1. Current-driven DW logic. (a) Schematic of current-driven DW inversion, occurring as the DW moves across the in-plane region. After selective oxidization, the magnetizations of neighboring OOP and IP regions align with a left-handed chirality in Pt/Co/AlOx. Here a down | up DW is inverted to an up | down DW. (b) Left panel: Schematic of a full adder gate obtained by cascading several NAND gates. Right panel: Full adder gate with "*a*=0" and "*b*=1" inputs resulting in "Sum=1" with a "Carry = 0".

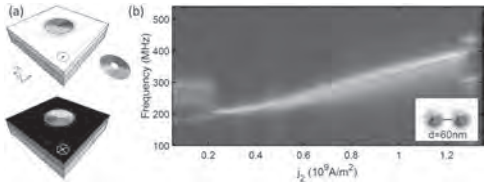

Fig. 2. Computation with chiral oscillators. (a) Equilibrium magnetic texture in the DMI-based nano-oscillator with 100 nm diameter. The oscillator has two equivalent states, depending on the magnetization direction in the OOP region. Magnetization along the +z and –z direction is indicated in white and black, while the IP magnetization direction is given by the color wheel. (b) Synchronization pattern of two oscillators separated by 60 nm distance. The current density in the left oscillator is fixed (j_1=0.8×10^9 A/m2), while the current density of the oscillator on the right (j_2) is swept.

GON-02. Symmetry Dependent Field-free Switching of Perpendicular Magnetization. L. Liu[1], C. Zhou[1], A. Manchon[2] and *J. Chen[1] 1. Materials Science and Engineering, National University of Singapore, Singapore; 2. Physics, Aix-Marseille University, Marseille, France*

Modern magnetic-memory technology requires all-electric control of perpendicular magnetization with low energy consumption. While spin-orbit torque (SOT) in heavy metal/ferromagnet (HM/FM) heterostructures holds promise for applications in magnetic random access memory, till today, it is limited to the in-plane direction. Such in-plane torque can switch perpendicular magnetization only deterministically with the help of additional symmetry breaking, e.g., through the application of an external magnetic field, an interlayer coupling or an asymmetric design. Instead, an out-of-plane spin-orbit torque could directly switch perpendicular magnetization. In current presentation, we report that we observe an out-of-plane spin-orbit torque in an HM/FM bilayer of $L1_1$-ordered CuPt/CoPt and demonstrate field-free switching of the perpendicular magnetization of the CoPt layer.[1] The low symmetry point group (3m1) at the CuPt/CoPt interface gives rise to this spin torque, herein after referred as 3m torque, which strongly

depends on the relative orientation of current flow and crystal symmetry. We observe a 3-fold angular dependence in both the field-free switching and the current-induced out-of-plane effective field as shown in Figure 1. Because of the intrinsic nature of the 3m torque, the field-free switching in CuPt/CoPt shows good endurance in cycling experiments. Experiments with the wide variety of SOT bilayers with low-symmetry point groups at the interface may uncover further unconventional spin-torques in future.

1. Liang Liu et.al. Nature Nanotechnology, 16 (3), 277-282 (2021).

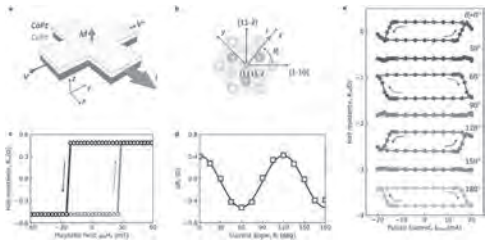

Figure 1| Symmetry-dependent magnetic field-free magnetization switching. a, Schematic of the CuPt/CoPt Hall bar for electrical transport measurement. The red arrow represents the magnetization (*M*). The grey arrow represents the current (*I*) flowing. b, The definition of current flowing direction (θ_I). The current is applied along the Hall bar, which has an azimuth angle of θ_I with respect to the [1-10] direction. c, Anomalous Hall effect of the bilayer for θ_I = 0°. d, Current angle dependence of the SOT induced magnetization switching. The solid line is a cosine fit to the data. e, Current-induced magnetization switching with different θ_I.

CONTRIBUTED PAPERS

GON-03. Stretchable Printed Magnetic Sensors Based on Giant Magnetoresistive Microflakes for On-Skin Electronic Interfaces.
E. Oliveros Mata[1], M. Ha[2], G. Canon Bermudez[1], Y. Zabila[1], J. Fassbender[1] and D. Makarov[1] *1. Institute of Ion Beam Physics and Materials Research, Helmholtz-Zentrum Dresden-Rossendorf, Dresden, Germany; 2. Electronics and Telecomunications Research Institute, Daejeon, The Republic of Korea*

On-demand fabrication of electronic devices is expected to be enabled by high throughput printing technologies[1]. Due to the simplified processing, printing is particularly attractive for flexible and stretchable electronics that are typically fabricated over polymeric soft substrates[2]. Wide research efforts are directed towards the development of conductive pastes with reliable electrical and mechanical properties. Sensing pastes able to detect external stimuli are central for the operation of on-skin electronic interfaces. Among others, magnetic sensors are less prone to mechanical failure due to their touchless nature[3]. Solution processable pastes for magnetic sensing typically consist of composites of magnetoresistive micro- or nanoparticles embedded in polymeric binders[4-7]. Despite the research progress on printable magnetic sensors, until now there were no reports of printed magnetic sensors showing stable response after typical skin deformations: bending and stretching. Here, we will show the fabrication and implementation of skin-compliant printed magnetic field sensors. These rely on microflakes obtained from a giant magnetoresistive (GMR) multilayer $[Py/Cu]_{30}$ stacks. The microflakes were embedded on a poly(styrene-butadiene-styrene) copolymer (SBS) matrix that enables stretchability and high adherence properties. The stretchable printed magnetic sensors were obtained after dispensing the GMR paste over an ultrathin (3-μm-thick) Mylar substrate. We demonstrated stable sensing and mechanical performance even at 100% strain and 16 μm bending deformations, representing two orders of magnitude of performance enhancement with respect to previous works. The obtained sensors showed maximum sensitivity at 0.88 mT, which is compatible with the 40 mT safety threshold established by the World Health Organization. These characteristics enabled a safe and conformal integration of the sensor for on-skin interactive electronics applications. We showed the use of the printed sensor platform for navigating through documents and digital maps. We foresee that the future development of this technology for user-specific fabrication of human-machine touchless interfaces with task-specific capabilities and integration[8].

1 J.S. Chang, A.F. Facchetti and R. Reuss., IEEE Trans. Emerg. Sel. Topics Circuits Syst., Vol. 7, p.7 (2017) 2 Q. Huang and Yong Zhu., Adv Mater. Technol., Vol. 4, p.1800546 (2019) 3 S. Zuo, H. Heidari and D. Farina. Adv Mater. Technol., Vol. 5, p.2000185 (2020) 4 D. Karnaushenko, D. Makarov and M. Stöber, Adv. Mater., Vol.27, p.880 (2015) 5 J. Meyer, T. Rempel and M. Schäfers, Smart Mater. Struct., Vol. 22, p.025032 (2013) 6 B. Cox, D. Davis, N. Crews, Sens. Actuators, A, Vol. 203, p.335 (2013) 7 E.S. Oliveros Mata, G.S. Cañón Bermúdez and M. Ha,. Appl. Phys. A, Vol. 127, p.280 (2021) 8 M. Ha, E.S. Oliveros Mata and G. S. Cañón Bermúdez, Adv. Mater. Vol. 33, p.2005521 (2021)

GON-04. Spin Dependent Transport Properties of Fe_4N/Chiral Methionine/Fe_4N Organic Magnetic Tunnel Junction.
Y. Zhang[1] and W. Mi[1] *1. Department of Applied Physics, Tianjin University, Tianjin, China*

Chiral organic molecules have been paid much attention in spintronics because of chiral-induced spin selectivity effect that shows the relation between spin and chriality.[1]. Here, the tunneling magnetoresistance (TMR) has different values by applying different bias voltage on Fe_4N/chiral Methionine/Fe_4N (Fe_4N/RS-MET/Fe_4N) OMTJs, where TMR is slightly different in the Fe_4N/MET/Fe_4N OMTJs with different chiral METs. In particular, the spin injection efficiency varies with the magnitude and direction of the bias voltage in Fe_4N/R-MET/Fe_4N, which is also related to the magnetization arrangement of the electrodes. Additionally, by applying linearly or circularly polarized light to R-MET molecule in Fe_4N/R-MET/Fe_4N OMTJ, the photocurrent in parallel magnetization configuration (PC) state is fully spin polarized, and the characteristics of spin battery are obtained in both PC and antiparallel magnetization configuration (APC) states. However, the photocurrent can't be obtained by applying light to S-MET of Fe_4N/S-MET/Fe_4N OMTJ, revealing the spin polarized photocurrent selectivity. These results highlight the effect of different chiral molecules on the device performance and lay a theoretical foundation for the realization of chiral organic spintronic devices. This work was supported by the National Natural Science Foundation of China (51871161 and 52071233).

[1] S. H. Yang, R. Naaman, Y. Paltiel, and S. S. P. Parkin, Chiral spintronics. Nat. Rev. Phys. 3, 328–343 (2021).

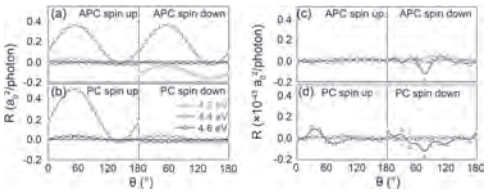

Fig. 1. Calculated photocurrent of Fe_4N/R-MET/Fe_4N (a), (b) and Fe_4N/S-MET/Fe_4N (c), (d) OMTJs under linearly polarized light.

GON-05. Giant tunnel magnetoresistance ratio and oscillation in Fe/MgO/Fe(001) and Fe/MgAlO/Fe(001) magnetic tunnel junctions.
T. Scheike[1], H. Sukegawa[1], Q. Xiang[1], Z. Wen[1], T. Ohkubo[1], K. Hono[1] and S. Mitani[1] *1. National Institute for Materials Science (NIMS), Tsukuba, Japan*

A magnetic tunnel junction (MTJ) is one of the most important device structures in spintronic applications. However, significant improvement in the tunnel magnetoresistance (TMR) ratio at room temperature (RT) is necessary to establish novel spintronic applications. Even in a simple Fe/MgO/Fe(001) MTJ, the experimental TMR ratios (180-220% at RT [1]) are much

smaller than the theoretical values >1,000% [2, 3]. In addition, the origin of TMR oscillation with the barrier thickness in experiments is still an open question [1]. In this study, we revisited Fe/MgO/Fe(001) based structures to bridge the discrepancies between experiments and theories. We deposited Fe/MgO/Fe(001) MTJs on a Cr-buffered MgO(001) single crystal substrate. By combining sputtering and electron-beam evaporation, we improved the barrier interface crystallinity [4]. We further examined an $MgAl_2O_4$ (MAO) based barrier to reduce the lattice mismatch with Fe. An MAO composition of Mg:Al = 4:1 (Mg rich) was selected. Fig. 1 shows TMR ratios of Fe/MgO/Fe and Fe/MAO/Fe MTJs as a function of the barrier thickness at RT. The maximum TMR ratio of Fe/MgO/Fe is 417% at RT (917% at 5 K) [4], which is ~twice (~3 times) of the previous report [1]. The TMR ratio shows significant oscillatory behavior with the MgO thickness. The peak-to-peak of 80% is also much larger (~7 times) than the previous report [1]. A TMR ratio of 496% at RT was observed by CoFe insertion at the bottom Fe/MgO interface [4]. The use of an MAO barrier improved the TMR ratio and oscillation peak-to-peak of Fe/MgO/Fe; the maximum ratio (peak-to-peak) reaches 429% (120%) in Fe/MAO/Fe at RT, which may be due to reduced defects at barrier interfaces. This demonstration will be an important step to achieve much larger TMR ratios for widening the range of spintronic applications. This study was partly supported by the ImPACT Program of the Council for Science, Technology and innovation (Cabinet Office, Government of Japan), JSPS KAKENHI 16H06332, 21H01750, 21H01397, and project JPNP16007, commissioned by the New Energy and Industrial Technology Development Organization (NEDO).

[1] S. Yuasa, T. Nagahama, A. Fukushima, Y. Suzuki and K. Ando, Nat. Mater., Vol. 3, p. 868 (2004) [2] W. Butler, X.-G. Zhang, T. Schulthess and J. MacLaren, Phys. Rev. B, Vol. 63, p. 054416 (2001) [3] J. Mathon and A. Umerski, Phys. Rev. B, Vol. 63, p. 220403(R) (2001) [4] T. Scheike, Q. Xiang, Z. Wen, H. Sukegawa, T. Ohkubo, K. Hono and S. Mitani, Appl. Phys. Lett., Vol. 118, p. 042411 (2021)

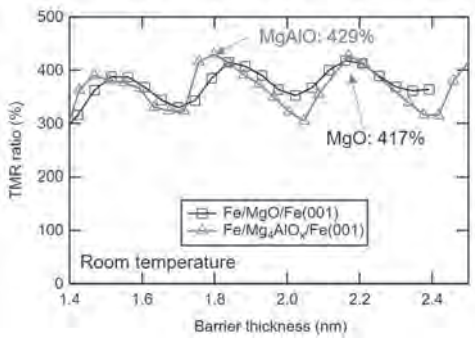

Fig.1 TMR ratio as a function of barrier thickness of Fe/MgO/Fe and Fe/MgAlO/Fe at RT.

GON-06. Spin-dependent Transport Through Photoswitchable Self Assembled Monolayers. *L. Jerro*[1], B. Quinard[1], S. Delprat[1], F. Godel[1], S. Colin[1], A. Sander[1], A. Vecchiola[1], K. Bouzehouane[1], P. Yu[2], T. Mallah[2], F. Petroff[1], P. Seneor[1] and R. Mattana[1] *1. Unité Mixte de Physique CNRS/ Thales, Palaiseau, France; 2. Insitut de Chimie Moléculaire et des Matériaux d'Orsay, Orsay, France*

Magnetic tunnel junctions (MTJs) are known to be one of the main building blocks of spintronics. In these devices, the integration of molecular layers as tunnel barrier is envisioned as an opportunity to allow the engineering of spintronics at the molecular scale. Actually, thanks to the spin-dependent hybridization at ferromagnet/molecule interfaces, it was shown that one could now expect to tailor spin polarization and thus tunnel magnetoresistance(TMR) with molecules (a.k.a. spinterface) [1]. In this direction, among the wealth of molecular systems, self-assembled monolayers (SAMs) appear as one of the most promising tool to tailor the MTJs tunnel barrier. Indeed, as shown in molecular electronics, their properties could be finely tuned at the molecular level. Pioneer experiments have shown that "passive" molecules such as alkane chain could be integrated into MTJs [2,3]. In this talk we will present the first work integrating "active" diarylethene molecules in NiFe/diarylethene/Co MTJs molecular MTJs. As the electron delocalization, energy gap and coupling strength to the electrodes depend on the molecule state, the tunnel resistance and tunnel magnetoresistance (TMR) is expected to be tuned upon switching. We will first present transport properties (I-V, G-V and inelastic electron tunneling spectroscopy) which confirm that these active molecules act as a tunnel barrier in these MTJs. We will then discuss magnetotransport properties. Magnetoresistance curves have been recorded at different bias voltages, temperatures and magnetic field directions. We have obtained magnetoresistance effects (up to 30%, figure 1) in both open and closed formed of diarylethene molecules. The angular dependence of the magnetoresistance reveals that both TMR and tunneling anisotropic magnetoresistance (TAMR) effects coexist and allows us to disentangle them. All these studies demonstrate for the first time that switchable active molecules can be successfully integrated into MTJs to build multifunctional spintronics devices electrically and/or optically controllable. This work is supported by French ANR SPINFUN project (ANR-17-CE24-0004-01)

[1] C. Barraud et al., Nat. Phys. 6, 615 (2010) [2] J. R. Petta et al., Phys. Rev. Lett., 93, 136601 (2004) [3] W. Wang et al., Appl. Phys. Lett. 89, 153105 (2006)

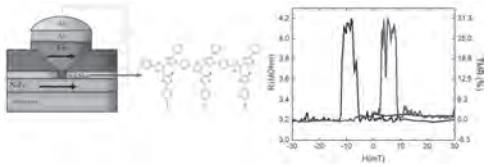

Scheme of the NiFe/diarylethene/Co MTJs studied and example of magnetoresistance curve obtained

GON-07. High bias TMR in ferrimagnetic MTJs based on Mn_3Ga. *M.T. Stamenova*[1] and P.S. Stamenov[1] *1. School of Physics and CRANN, Trinity College Dublin, Dublin, Ireland*

In a recent work [1], we investigated the spin transfer toque (STT) in epitaxial magnetic tunnel junctions (MTJs) based on ferrimagnetic tetragonal Mn_3Ga [2] electrodes and MgO barrier (Fig.1a,b) from first principles ballistic non-collinear spin transport (NEGF + SDFT[LSDA]), using the Smeagol code [3]. We found a long-range spatial oscillation of the in-plane STT (defined as in Ref. [4]) decaying on a length scale of a few nm. We discussed how this STT oscillation can be anticipated from the bulk electronic structure of Mn_3Ga and the spin-filtering properties of the MgO barrier, and it is robust against variations in the stack geometry. This is expected to result in a net in-plane torque which oscillates as a function of the Mn_3Ga thickness, but stabilizes for sufficiently thick layers (>40 MLs) at larger values than the net STT in conventional Fe/MgO/Fe MTJs [1]. We also discussed a novel all-ferrimagnetic MTJ in which the Fe electrode is substituted with Mn_3Ga and found similar STT properties, particularly enhanced in the case of narrow MgO barrier (of 3 MLs), due to resonant interface states. Here we focus on the TMR effect in these MTJ stacks as a function of the applied bias voltage and find a maximum value of over 300%, asymmetry and multiple sign changes in the range ± 2V (Fig.1 c) for the Fe-based junction, in a noteworthy correspondence with experimental observations for similar ferrimagnetic junctions [5]. In the case of the fully symmetric novel ferrimagnetic MTJ, we find a symmetric TMR, peaking at 0 V. This is particularly enhanced for the thin barrier (3 ML) case due to the aforementioned interface resonances. We will discuss effects of geometry optimisation and possible Hubbard U corrections to the LSDA xc-functional on the transport properties, at computed bulk parameters of Mn_3Ga closer to the experimental lattice constant and magnetic moments, as well as the role of different interface terminations. In view of the stronger TMR at finite bias for the Fe-based MTJs, our calculations suggest that further efforts are

justified on the Fermi-level and interface engineering of ferrimagnetic electrodes, by means of both composition and substrate-induced strain, for demanding spintronic applications.

[1] M. Stamenova, P. Stamenov, F. Mahfouzi, et al. Phys. Rev. B, vol. 103, 094403 (2021). [2] K. Rode, N. Baadji, D. Betto, et al. Phys. Rev. B, vol. 87, p. 184429 (2013). [3] A. R. Rocha and S. Sanvito, Phys. Rev. B, vol. 70, p. 094406 (2004). [4] M. Stamenova, I. Rungger, S. Sanvito, et al. Phys. Rev. B, vol. 95, p. 060403(R) (2017); I. Rungger, A. Droghetti and M. Stamenova, Non-equilibrium Green's functions methods for spin transport and dynamics. In: Andreoni W., Yip S. (eds) Handbook of Materials Modeling, Springer (2018). [5] K. Borisov, D. Betto, Y.C. Lau, et al. Appl. Phys. Lett., vol. 108, p. 192407 (2016).

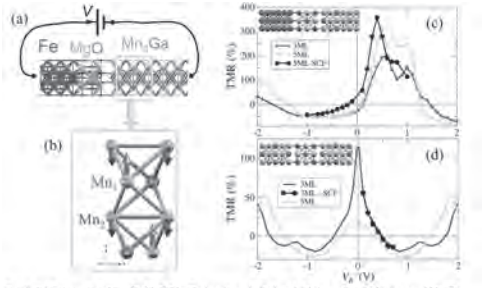

Fig. 1: (a) Schematic of the Fe/MgO/Mn_3Ga junction studied and (b) the unit cell of tetragonal Mn_3Ga depicting also the anti-ferromagnetically coupled magnetic moments at the two inequivalent Mn sites. Calculated TMR ratios as a function of the applied bias voltage for the Fe-based junction (c) and an all-Mn_3Ga junction (d) with different (3 and 5) number of MgO monolayers (the black data correspond to fully self-consistent finite-bias calculations).

GON-08. Perpendicularly Magnetized Co/Pd-based Magneto-resistive Heterostructures on Large-area Flexible Substrates. *M. Hassan*[1,2], S. Laureti[2], C. Rinaldi[3], F. Fagiani[3], S. Varotto[3], G. Barucca[4], N. Schmidt[1], G. Varvaro[2] and M. Albrecht[1] *1. Uni. Augsburg, Institute of Pysics, Augsburg, Germany; 2. CNR-ISM-NM2 Lab, Monterotondo Scalo, Italy; 3. Department of Physics, Polytechnico di Milano, Milano, Italy; 4. SIMAU, Marche Polytechnic University, Ancona, Italy*

Flexible magneto-resistive heterostructures have received a great deal of attention over the past few years as they allow for new product paradigms that are not possible with conventional rigid substrates, such as light-weight, flexibility, shapeability, wearability, and low cost [1]. While the progress and development of longitudinal magnetized devices on non-planar substrates has been remarkable over the last years, perpendicularly magnetized structures on flexible substrates are rather unexplored despite they allow for additional functionality and improved performance that make them of interest for many applications such as wearable electronics [2], soft robotics and biomedicine. To fill this gap, flexible PMA giant magneto-resistive (GMR) spin-valves consisting of a $[Co/Pd]_N$ free layer and a fully compensated $[Co/Pd]_N/Ru/[Co/Pd]_N$ synthetic antiferromagnet reference layer separated by a Cu spacer, were prepared for the first time by using an innovative transfer-and-bonding strategy exploiting the low adhesion of a gold underlayer to SiOx/Si(100) substrates [3]. The approach allows overcoming the limits of the direct deposition on commonly used polymer substrates, whose high surface roughness and low melting temperature could hinder the growth of complex heterostructures with perpendicular magnetic anisotropy. The obtained PMA flexible spin-valves show a sizeable GMR ratio (~1.5%) (fig.1), which is not affected by the transfer process, and a high robustness against bending, thus allowing for their integration on curved surfaces and the development of a novel class of advanced devices based on flexible magneto-resistive structures with perpendicular magnetic anisotropy. Besides endowing the family of flexible electronics with PMA magneto-resistive heterostructures, the exploitation of the results might apply to high temperature growth processes and to the fabrication of other functional and flexible multilayer materials engineered at the nanoscale.

[1] M Melzer et al. J. Phys. D: Appl. Phys. 2020, 53 083002 [2] P. Makushko et al., Adv. Funct. Mater. 2021, 31, 2101089 [3] M Hassan et al., Nanoscale Adv., 2021, 3, 3076-3084

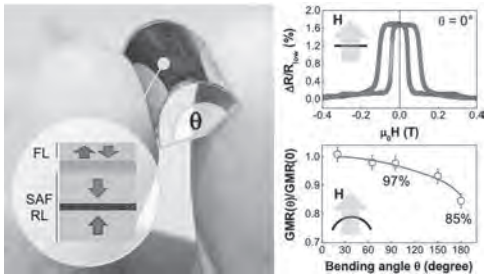

Fig. 1. Flexible GMR spin-valve with perpendicular magnetic anisotropy

GON-09. Flexible magnetoreceptive switch for on-skin touchless human-machine interaction. *P. Makushko*[1,2], E. Oliveros Mata[1], G. Canon Bermudez[1], M. Hassan[3,4], S. Laureti[4], C. Rinaldi[5], F. Fagiani[5], G. Barucca[6], N. Schmidt[3], Y. Zabila[1,7], T. Kosub[1], R. Illing[1], O.M. Volkov[1], I. Vladymyrskyi[2], J. Fassbender[1], M. Albrecht[3], G. Varvaro[4] and D. Makarov[1] *1. Helmholtz-Zentrum Dresden-Rossendorf, Dresden, Germany; 2. National Technical University of Ukraine "Igor Sikorsky Kyiv Polytechnic Institute", Kyiv, Ukraine; 3. University of Augsburg, Augsburg, Germany; 4. Consiglio Nazionale delle Ricerche, Roma, Italy; 5. Politecnico di Milano, Milano, Italy; 6. Università Politecnica delle Marche, Ancona, Italy; 7. The H. Niewodniczanski Institute of Nuclear Physics, Krakow, Poland*

Skin compliant magnetoreceptive electronics is a game changer for prospective human-machine interactions and augmented reality applications [1]. Mechanically flexible magnetoresistive sensors enabled proximity sensing as well as motion and orientation tracking features[2,3] via interaction with magnetic objects. However, current on-skin magnetoreceptors are not yet employed as advanced spintronics-enabled switches and logic elements for skin compliant electronics. The major limitation is the use of in-plane magnetized layer stacks, sensitive mainly to magnetic fields oriented within the sensor plane. Flexible Hall effect sensors[4,5] provide out-of-plane sensitivity but no intrinsic logic, thus requiring more complex electronics. Considering the lower performance of flexible electronics compared to their rigid counterparts[6], full-fledged flexible interactive systems should be based on smart receptors with intrinsic logic functionality. Here we present the first mechanically flexible switch based on spin valves sensitive to out-of-plane magnetic fields[7]. The device is realized on a flexible polyethylene naphthalate (PEN) foil and rely on Co/Pd multilayers with perpendicular magnetic anisotropy and synthetic antiferromagnet as a reference layer. By tuning the magnetic coupling strength between the free and the reference layers, the functionality of the device can be tailored between momentary or permanent (latching) switch. The flexible device retains its performance upon bending down to a bending radius of 3.5 mm and withstand more than 600 bendings. We demonstrate the performance of our device as touchless interactive interface for augmented reality systems, as well as its tolerance to the magnetic field disturbances. We showcase the potential of this new kind of flexible magnetoreceptive functional elements as on-skin human-machine interfaces for virtual and augmented reality applications.

[1] D. Makarov, M. Melzer, D. Karnaushenko, Applied Physics Reviews., Vol 3, p.011101 (2016) [2] M. Melzer, M. Kaltenbrunner, D. Makarov, Nature Communications., Vol 6, p.6080 (2015) [3] G. S. C. Bermúdez, H. Fuchs, D. Makarov, Nature Electronics., Vol 1, p.589 (2018). [4] Z. Wang, M. Shaygan, D. Neumaier, Nanoscale., Vol 8, p.7683 (2016) [5] H. Heidari, E. Bonizzoni, R. Dahiya, IEEE Sensors Journal., Vol 16, p.8736 (2016) [6] G. A. Salvatore, N. Münzenrieder, G. Tröster, Nature Communications., Vol 5, p.2982 (2014). [7] P. Makushko, E. S. O. Mata, D. Makarov, Advanced Functional Materials., Vol 31, p.2101089 (2021).

GON-10. Effect of Counter Electrode on Tunneling Anisotropic Magnetoresistance through Iron Quantum Wells. *M. Al-Mahdawi*[1,2], Q. Xiang[1], Y. Miura[1], M. Belmoubarik[1], K. Masuda[1], S. Kasai[1], H. Sukegawa[1] and S. Mitani[1] *1. National Institute for Materials Science, Tsukuba, Japan; 2. Center for Science and Innovation in Spintronics, Tohoku University, Sendai, Japan*

Utilization of quantum transport is of interest for exploring new functionalities in magnetic tunnel junctions (MTJs). In a recent Letter [1], we showed an anisotropy in resonant tunneling conduction through Fe quantum wells (QWs) in MTJs, with a lattice-matched (001)-oriented stack of: Cr/Fe-QW/$MgAl_2O_4$ [Fig. 1(a)]. The QW confinement is selected for Δ_1-symmetry states by the band-symmetry mismatch between Fe and Cr [2]. We obtained a large tunneling anisotropic magneto-resistance of QWs (QW-TAMR) up to 5% [Fig. 1(b)]. In this work, we experimentally analyze the symmetry of the resonant tunneling conduction states and QW-TAMR. We compare the effect of the counter electrode (X), where we chose three materials having a different Δ_1 band edge level; single-crystal Fe, amorphous CoFeB, and single-crystal Cr [Fig. 1(a)]. Fig. 1(c) shows the bias dependence of differential conductance (G = dI/dV), for an Fe-QW of 6 monolayers (MLs) thickness which has a QW level at the Fermi level. The conductance is high for X = Fe, and it is reduced by an order-of-magnitude for X = Cr, as expected from Δ_1 band mismatching. At X = Fe, FeCoB, the resonant conduction through the QW level is seen at zero bias. When X = Cr, the resonance conduction is suppressed, due to reduction of the tunneling current with a Δ_1 symmetry. In Fig. 1(d), we show the QW-TAMR ratio dependence on bias, extracted from angular dependence of conductance, and defined as $G_{op}/G_{ip} - 1$. For X = Fe or CoFeB, the QW-TAMR spectra are similar in the features, whereas a difference is seen for X = Cr. In single-crystal Fe or amorphous CoFeB, the tunneling through resonant Δ_1 states is allowed, and the anisotropy of resonant conduction is the same. For the Cr electrode, the presence of TAMR at zero bias can be linked to leakage tunneling through non-resonant Δ_5 states coupled to the resonant Δ_1 state by spin-orbit coupling. This work was partly supported by the ImPACT Program of the Council for Science, Technology and Innovation (Cabinet Office, Government of Japan), and the JSPS KAKENHI (JP16H06332).

[1] M. Al-Mahdawi, Q. Xiang, Y. Miura, M. Belmoubarik, K. Masuda, S. Kasai, H. Sukegawa, and S. Mitani, "*Quantum-Well Tunneling Anisotropic Magnetoresistance above Room Temperature*," Phys. Rev. B 103, L180408 (2021). [2] T. Niizeki, N. Tezuka, and K. Inomata, "*Enhanced Tunnel Magnetoresistance Due to Spin Dependent Quantum Well Resonance in Specific Symmetry States of an Ultrathin Ferromagnetic Electrode*," Phys. Rev. Lett. 100, 047207 (2008).

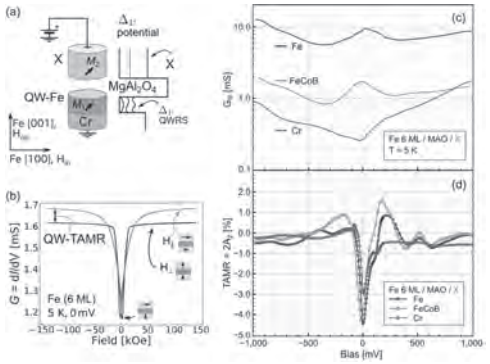

(a) QW-MTJ schematic and potential diagram. (b) Conductance is anisotropic at staturation. The effect of X on (c) conductance spectra, and (d) QW-TAMR spectra.

GON-11. Large spin-scattering asymmetry at half-metallic Co-based Heusler-alloy/ferromagnet interface. *Y. Fujita*[1], Y. Miura[1], T. Sasaki[1], T. Nakatani[1], K. Hono[1] and Y. Sakuraba[1] *1. National Institute for Materials Science, Tsukuba, Japan*

Interface spin-scattering asymmetry (γ) at ferromagnet (FM)/nonmagnet (NM) interfaces has so far been verified with various combinations of FM and NM in current-perpendicular-to-plane giant magnetoresistance (CPP-GMR) devices [1]. Although most of the previous studies pay attention to γ at FM/NM interfaces, spin-dependent scattering occurs even at FM/FM interface [2]; γ at Co/Ni interface was estimated to be quite large value of 0.94 at 4.2 K [1]. Thus, there can be FM/FM interfaces that yields large γ even at room temperature (RT). Half-metallic FM (HMF)/FM interface is expected to generate huge γ at RT because HMFs have a semiconducting gap only in one spin band. The half-metallic Co-based Heusler alloys, e.g., $Co_2Fe_{0.4}Mn_{0.6}Si$ (CFMS), have widely been utilized in the CPP-GMR devices [3]. Here, we show the presence of γ at HMF/FM interface based on CFMS/CoFe interface and its large impact on GMR effect at RT. We fabricated fully epitaxial CoFe(7 – t nm)/CFMS(t nm)/Ag(5 nm)/CFMS(t nm)/CoFe(7 – t nm) CPP-GMR pseudo-spin valves with various t ($0 \le t \le 7$) on Cr(20 nm)/Ag(80 nm) buffer layers grown on MgO(001) substrates. Conventional processes were used to fabricate pillar-type CPP-GMR devices and magnetoresistance (MR) measurements were performed at RT as illustrated in Fig. 1. Figure 2(a) shows the obtained resistance change-area product (ΔRA) as a function of t. ΔRA clearly had a peak at t = 4 nm in its t dependence. This tendency was well reproduced qualitatively by the simulation based on the generalized two current resistor model [4] with considering large γ at CFMS/CoFe interface as shown in Fig. 2(b). Further, the first-principles ballistic transport calculations for (001)-CoFe/CFMS/CoFe also suggested strongly spin-dependent conductance, namely, large γ at CFMS/CoFe interface (not shown here). Thus, the t-dependent behavior of ΔRA in Fig. 2(a) is direct evidence for the large impact of γ at CFMS/CoFe on the GMR effect at RT. This work was partly supported by KAKENHI (Nos. 17H06152, 20H02190, and 20K22487) from JSPS.

[1] J. Bass, J. Magn. Magn. Mater. Vol. 408, 244 (2016). [2] H. Y. T. Nguyen *et al.*, Phys. Rev. B Vol. 82, 220401(R) (2010). [3] Y. Sakuraba *et al.*, Appl. Phys. Lett. Vol. 101, 252408 (2012). [4] N. Strelkov *et al.*, J. Appl. Phys. Vol. 94, 3278 (2003).

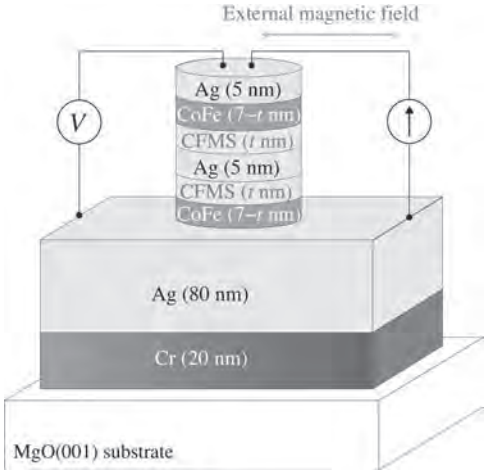

Fig. 1 Schematic of the fabricated CPP-GMR device.

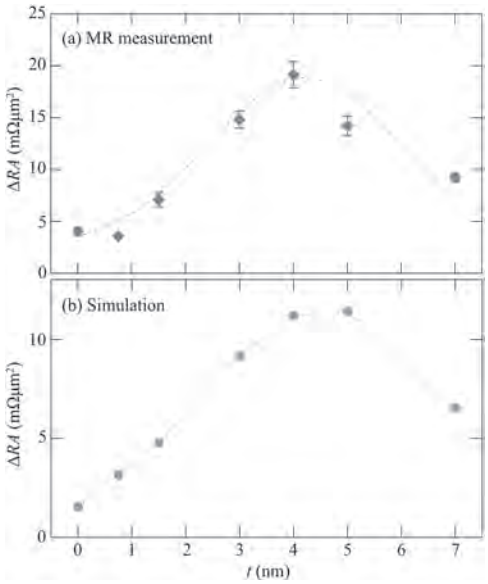

Fig.2 (a) Observed and (b) simulated Δ*RA* as functions of *t*.

Session GOO
ANTIFERROMAGNETIC SPINTRONICS I

Jean Anne C. Incorvia, Co-Chair
University of Texas at Austin, Austin, TX, United States
Vincent Baltz, Co-Chair
Spintec, Grenoble, France

INVITED PAPERS

GOO-01. Coherent Sub-Terahertz Spin Pumping from an Insulating Antiferromagnet. *E. del Barco*[1], P. Vaidya[1], J. van Tol[2], Y. Liu[3], R. Cheng[4], A. Brataas[5] and D. Lederman[6] *1. University of Central Florida, Orlando, FL, United States; 2. NHMFL, Tallahassee, FL, United States; 3. Northeastern University, Shenyang, China; 4. University of California, Riverside, Riverside, CA, United States; 5. Norwegian University of Science and Technology, Trondheim, Norway; 6. University of California Santa Cruz, Santa Cruz, CA, United States*

Emerging phenomena, such as the spin-Hall effect (SHE), spin pumping, and spin-transfer torque (STT), allow for interconversion between charge and spin currents and the generation of magnetization dynamics that could potentially lead to faster, denser, and more energy efficient, non-volatile memory and logic devices. Present STT-based devices rely on ferromagnetic materials as their active constituents. However, the flexibility offered by the intrinsic net magnetization and anisotropy for detecting and manipulating the magnetic state of ferromagnets also translates into limitations in terms of density (neighboring elements can couple through stray fields), speed (frequencies are limited to the GHz range), and frequency tunability (external magnetic fields needed). A new direction in the field of spintronics is to employ antiferromagnetic materials. In contrast to ferromagnets, where magnetic anisotropy dominates spin dynamics, in antiferromagnets spin dynamics are governed by the interatomic exchange interaction energies, which are orders of magnitude larger than the magnetic anisotropy energy, leading to the potential for ultrafast information processing and communication in the THz frequency range, with broadband frequency tunability without the need of external magnetic fields. I will present the first evidence of sub-terahertz coherent spin pumping at the interface of a uniaxial insulating antiferromagnet MnF_2 and a platinum thin film, measured by the ISHE voltage signal arising from spin-charge conversion in the platinum layer. The ISHE signal depends on the chirality of the dynamical modes of the antiferromagnet, which is selectively excited and modulated by the handedness of the circularly polarized sub-THz irradiation. Contrary to the case of ferromagnets, antiferromagnetic spin pumping exhibits a sign dependence on the chirality of dynamical modes, allowing for the unambiguous distinction between coherent spin pumping and the thermally-driven spin Seebeck effect. Our results open the door to the controlled generation of coherent pure spin currents with antiferromagnets at unprecedented high frequencies.

P. Vaidya, *et al.*, Science, (2020).

GOO-02. Out-of-plane spin polarization and antiferromagnetic spin Hall effect. *C. Song*[1], X. Chen[1], H. Bai[1], Y. You[1], F. Pan[1], H. Yang[2] and X. Fan[3] *1. Tsinghua University, Beijing, China; 2. National University of Singapore, Singapore; 3. Lanzhou University, Lanzhou, China*

The spin current with out-of-plane spin polarization (sigma-z) is favorable for the efficient switching of perpendicular magnetized devices, which is required for high-density memories [1,2]. Recently we observed sigma-z both in non-collinear antiferromagnets Mn_3Pt [3] and Mn_3SnN [4], as well as in collinear antiferromagnets Mn_2Au [5,6] and RuO_2 [7] thin films. Strong out-of-plane polarized spin current is generated when the charge current is applied along the magnetic mirror plane of non-collinear antiferromagnet, but tiny when perpendicular. With the aid of strong sigma-z, current induced spin-orbit torque (SOT) switching of adjacent perpendicular ferromagnet is realized without external magnetic field. In Mn_2Au films, sigma-z is generated at two spin sublattices with broken spatial symmetry, and the antiparallel antiferromagnetic moments play an important role. The out-of-plane polarized spin current can be controlled by the current- and electric field-induced Néel vector switching. Thus this Néel vector-dependent spin Hal effect is termed as "antiferromagnetic spin Hall effect", which adds another twist to the atomic-level control of spin currents via the antiferromagnetic spin tructure. RuO_2 is a tetragonal itinerant collinear antiferromagnet with nonmagnetic atoms at noncentrosymmetric positions [8]. This particular crystal structure produces anisotropic band structure,enabling RuO_2 a efficient spin source due to the spin splitting effect. Spin current generated by spin splitting effect do not meet conventional "cross product relationship". The spin current flow direction is related to the crystal structure,while the spin polarization direction is related to the Néel vector. Spin splitting effect has more efficient spin-charge convention and more controllable spin polarization. The role of sigma-z for the field-free SOT switching is theoretically analyzed, and different roles of sigma-z and conventional in-plane spin polarization (sigma-y) are presented with different external magnetic field. Our findings would help to use out-of-plane polarization for efficient SOT-MRAM to combine the advantage of SOT and spin-transfer torque.

[1] C. Song, *et al.* Prog. Mater. Sci. 118, 100761 (2021). [2] D. MacNeill, *et al.* Nat. Phys. 13, 300 (2016). [3] H. Bai, C. Song, *et al.* Phys. Rev. B (under the 2nd review). [4] Y. F. You, C. Song, *et al.* Nat. Commun. (under review). [5] X. Z. Chen, C. Song, *et al.* Nat. Mater. 18, 931(2019). [6] X. Z. Chen, C. Song, et al. Nat. Mater. 20, 800 (2021). [7] H. Bai, C. Song, *et al.* In preparation. [8] R. González-Hernández, *et al.* Phys. Rev. Lett. 126, 127701 (2021).

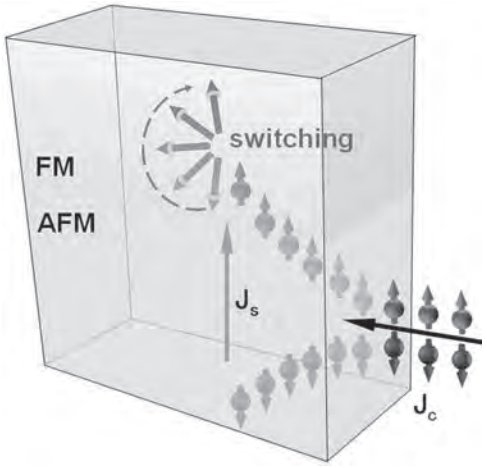

Fig. 1. Schematic of out-of-plane polarized spin current and field-free spin-orbit torque switching.

CONTRIBUTED PAPERS

GOO-03. Observation of unidirectional magnetoresistance in collinear-antiferromagnet/heavy-metal bilayers. *S. Shim*[1,2], M. Mehraeen[3], J. Sklenar[1,4], J. Oh[1,2], J. Gibbons[2,5], H. Saglam[6,7], A. Hoffmann[5,6], S. Zhang[3] and N. Mason[1,2] *1. Physics, University of Illinois at Urbana-Champaign, Urbana, IL, United States; 2. Materials Research Laboratory, University of Illinois at Urbana-Champaign, Urbana, IL, United States; 3. Physics, Case Western Reserve University, Cleveland, OH, United States; 4. Physics and Astronomy, Wayne State University, Detroit, MI, United States; 5. Materials Science and Engineering, University of Illinois at Urbana-Champaign, Urbana, IL, United States; 6. Materials Science Division, Argonne National Laboratory, Lemont, IL, United States; 7. Physics, Yale University, New Haven, CT, United States*

The interplay between electronic transport and the antiferromagnetic order has attracted a surge of interest. Recent studies have shown that a moderate change in the spin orientation of a collinear antiferromagnet may significantly affect the electronic band structure and subsequently manifest itself in transport properties [1]. Among numerous electrical probes to read out such magnetic order, unidirectional magnetoresistance (UMR), where the resistance changes under the reversal of the current direction, can provide rich insights into the transport properties of spin-orbit coupled systems. However, UMR has never been observed in antiferromagnets before, given the absence of intrinsic spin-dependent scattering. Here, we report that a sizable UMR can emerge in an antiferromagnetic system, specifically in a collinear-antiferromagnet/heavy-metal bilayer. The observed UMR in the antiferromagnetic phase of a FeRh/Pt bilayer evolves nonlinearly with increasing magnetic field, persists to large values at high magnetic field and, most notably, exhibits a sign change at a critical field, which is in stark contrast with the UMRs observed in ferromagnetic and non-magnetic systems [2-3]. We attribute this UMR to the strong effective magnetic field due to spin canting in FeRh. Our results can motivate the growing fields of non-centrosymmetric and topological systems, and suggest a route to the development of tunable antiferromagnet-based spintronics devices. This research was primarily supported by the NSF through the University of Illinois at Urbana-Champaign Materials Research Science and Engineering Center DMR-1720633 and was carried out in part in the Materials Research Laboratory Central Research Facilities, University of Illinois. Thin-film growth at Argonne National Laboratory was supported by the U.S. Department of Energy, Office of Science, Materials Science and Engineering Division.

[1] T. Suzuki, R. Chisnell, A. Devarakonda et al., Nature Physics, Vol. 12, p. 1119-1123 (2016). [2] C. O. Avci, K. Garello, A. GhoshAvci et al., Nature Physics, Vol. 11, p. 570-575 (2015). [3] T. Guillet, C. Zucchetti, Q. Barbedienne et al., Phys. Rev. Lett., Vol. 124, 027201 (2020).

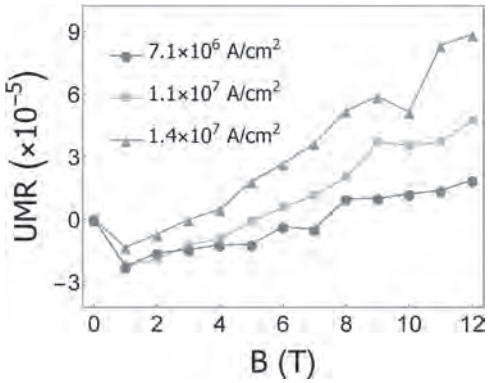

Fig. 1: UMR in the antiferromagnetic phase of FeRh [110]/Pt (T = 10 K), as a function of field B at various current densities J.

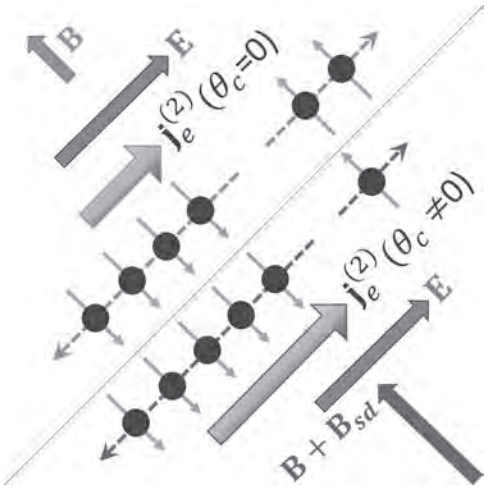

Fig 2: Generation of a nonlinear charge current transverse to the applied B field (top left), which increases considerably in the presence of canting (bottom right).

GOO-04. Suppressing Electrical Switching of Antiferromagnets with High Magnetic Fields. *C. Schippers*[1], M. Grzybowski[1], M. Bal[2], K. Rubi[2], U. Zeitler[2] and H. Swagten[1] *1. Applied Physics, Eindhoven University of Technology, Eindhoven, Netherlands; 2. High Field Magnet Laboratory (HFML - EMFL), Radboud University, Nijmegen, Netherlands*

Antiferromagnetic (AF) spintronics received an enormous impulse after the first demonstrations of electrical switching of the AF order [1]. However, a lot of these observations can equally well be explained by non-magnetic, parasitic effects caused by the same electrical current pulses that are intended to manipulate the magnetic state of the AF [2]. While it is possible to distinguish between magnetic and non-magnetic effects using imaging techniques that can resolve the AF order [3], these techniques are usually very complex. Moreover, since they require access to the AF layer, they are not suitable for systems where the AF is buried beneath other layers. Our approach is to distinguish between the magnetic and non-magnetic effects by suppressing the magnetic effects using high magnetic fields. In this contribution, we study the high magnetic field behavior of the electrical switching of thin-film AFs NiO and CoO, using the devices shown in Fig. 1. We perform switching experiments in magnetic fields up to 16 Tesla (Fig. 2). The measurements show that these high magnetic fields indeed suppress the current-induced switching of the AF order, whereas the thermal effects remain unaffected. Hence, this technique allows to irrefutably separate the magnetic and non-magnetic effects. These results are corroborated by a model accounting for the multi-domain character of the AF. Finally, the experiments with CoO yield an unexpected dependence of the magnetic configuration on the direction of the high magnetic fields. This indicates an unexpectedly complex magnetic anisotropy in CoO that depends on the magnetic field strength and orientation, most likely due to unquenched orbital momentum. These results both demonstrate that combining electrical methods with strong magnetic fields can be a valuable tool for AF spintronics, and give invaluable insight into the interplay of spin-Hall magnetoresistance and thermal effects as well as the domain structure and complex anisotropy of thin-film antiferromagnets.

[1] X. Z. Chen, et al., Physical Review Letters, 120, 207204 (2018) [2] A. Churikova, et al., Applied Physics Letters, 116, 022410 (2020) [3] H. Meer, et al., Nano Letters, 21, 1, 114–119 (2021)

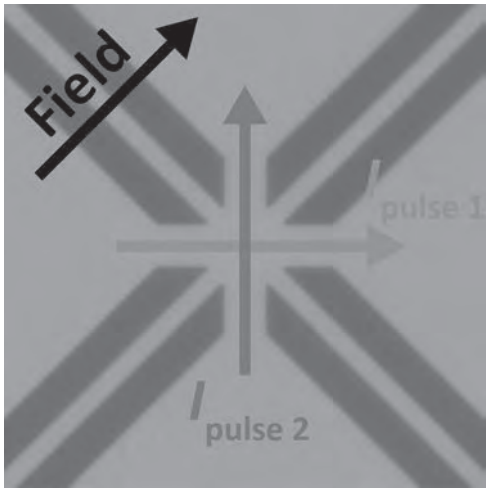

Fig. 1: Micrograph of the device used for the experiments.

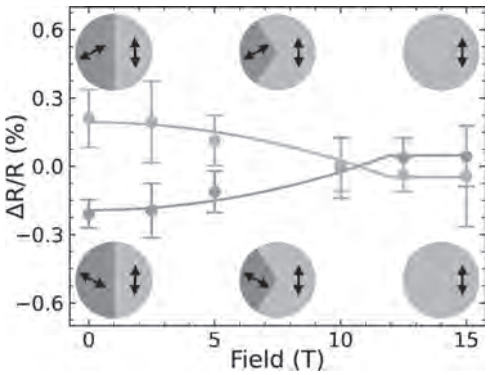

Fig. 2: Switching amplitude as a function of magnetic field. The lines are calculated with the model; the pie charts represent the modeled domain distribution.

GOO-05. Long-range supercurrents through a chiral non-collinear antiferromagnet in lateral Josephson junctions. *K. Jeon*[1], B.K. Hazra[1], K. Cho[1], A. Chakraborty[1], J. Jeon[1], H. Han[1], H. Meyerheim[1], T. Kontos[2] and S. Parkin[1] *1. NISE, Max Planck Institute of Microstructure Physics, Halle (Saale), Germany; 2. Laboratoire de Physique de l'Ecole normale supérieure, ENS, Université PSL, CNRS, Sorbonne Université, Université de Paris, Paris, France*

The proximity-coupling of a chiral non-collinear antiferromagnet (AFM)[1,2] with a singlet superconductor allows spin-unpolarized singlet Cooper pairs to be converted into spin-polarized triplet pairs[3,4], thereby enabling non-dissipative, long-range spin correlations[3,4]. The mechanism of this conversion derives from fictitious magnetic fields that are created by a non-zero Berry phase[5] in AFMs with non-collinear atomic-scale spin arrangements[1,2]. In this talk, I would like to describe our recent achievement of long-ranged lateral Josephson supercurrents through an epitaxial thin film of the triangular chiral AFM Mn_3Ge[6]. The Josephson supercurrents in this chiral AFM decay by approximately 1–2 orders of magnitude slower than would be expected for singlet pair correlations[3,4] and their response to an external magnetic field reflects a clear spatial quantum interference. Given the long-range supercurrents present in both single- and mixed-phase Mn_3Ge, but absent in a collinear AFM IrMn, our results pave a way for the topological generation of spin-polarized triplet pairs[3,4] via Berry phase engineering[5] of the chiral AFMs.

1. Nakatsuji, S. et al. Large anomalous Hall effect in a non-collinear antiferromagnet at room temperature. *Nature* 527, 212–215 (2015). 2. Nayak, A. K. et al. Large anomalous Hall effect driven by a nonvanishing Berry curvature in the noncolinear antiferromagnet Mn_3Ge. *Sci. Adv.* 2, e1501870 (2016). 3. Linder, J. & Robinson, J. W. A. Superconducting spintronics. *Nat. Phys.* 11, 307–315 (2015). 4. Eschrig, M. Spin-polarized supercurrents for spintronics: a review of current progress. *Rep. Prog. Phys.* 78, 104501 (2015). 5. Xiao, D., Chang, M.-C. & Niu, Q. Berry phase effects on electronic properties. *Rev. Mod. Phys.* 82, 1959–2007 (2010). 6. Jeon, K.-R. et al. Long-range supercurrents through a chiral non-collinear antiferromagnet in lateral Josephson junctions. *in press in Nat. Mater.* (2021).

GOO-06. Roles of Destressing and Dzyaloshinskii-Moriya Interaction for Magnetic Reversal in α-Fe_2O_3. *A. Wittmann*[1], K. Litzius[2,1], A. Churikova[1], L. Scipioni[3], A. Shepard[3], T. Newhouse-Illige[3], J. Greer[3], N.O. Birge[4] and G.S. Beach[1] *1. Massachusetts Institute of Technology, Cambridge, MA, United States; 2. Max Planck Institute for Intelligent Systems, Stuttgart, Germany; 3. PVD Products, Wilmington, MA, United States; 4. Michigan State University, East Lansing, MI, United States*

Antiferromagnets are at the forefront of research in spintronics. Recent results demonstrate their high potential for revolutionizing memory technologies. However, many of the underlying phenomena remain to be explored. Here, we study the domain structure and magnetic reversal of the canted antiferromagnet α-Fe_2O_3. Using x-ray magnetic linear dichroism (XMLD) measurements, we observe a strongly field-dependent domain structure of α-Fe_2O_3 (see Fig. 1a). To study the magnetic field control of the Néel order and demagnetization process in more detail, we employ spin Hall magnetoresistance (SMR) measurements in α-Fe_2O_3/Pt bilayer devices. The angle-dependent SMR shows the characteristic saturated negative SMR signal of antiferromagnets (light red curve in Fig. 1b) in agreement with previous findings[1,2]. The dark red curve shows the remanent resistance as a function of the angle of the preceding saturating magnetic field. The data show a simple scaling between the saturated SMR signal and the remanent resistance by a factor of 5. This implies that the internal fields driving the demagnetization do not follow the crystal symmetry of α-Fe_2O_3. Furthermore, the Dzyaloshinskii-Moriya interaction (DMI) induces canting of the two magnetic sublattices giving rise to a ferromagnetic moment at room temperature. The ferromagnetic moment lifts the degeneracy of the sublattices and consequently the orientation of the Néel vector with respect to the applied magnetic field resulting in hysteresis in the SMR signal. The irreversibility upon switching the direction of the magnetic field elucidates the nature and formation of antiferromagnetic as well as ferromagnetic domain walls at low magnetic fields. The insights gained from our work serve as a foundation for further studies of electrical and optical manipulation of the domain structure of canted antiferromagnets.

1. Lebrun, R. *et al.* Anisotropies and magnetic phase transitions in insulating antiferromagnets determined by a Spin-Hall magnetoresistance probe. *Commun. Phys.* 2, 50 (2019). 2. Fischer, J. *et al.* Large Spin Hall Magnetoresistance in Antiferromagnetic a-Fe2O3/Pt Heterostructures. *Phys. Rev. Appl.* 13, 014019 (2020).

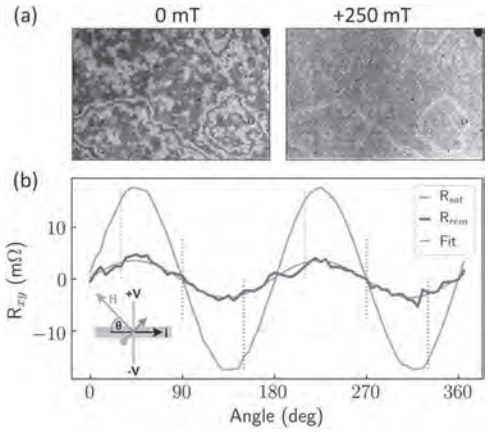

Fig. 1: (a) XMLD image of the domain structure of α-Fe_2O_3 in zero magnetic field (left) and in 250 mT in-plane magnetic field (right). (b) Transverse remanent SMR signal R_{rem} (dark red) of α-Fe_2O_3/Pt Hall cross after H has been reduced from a saturated state R_{sat} (light red) to zero field as a function of angle of the applied magnetic field.

GOO-07. Co/Pt/NS/Pt/Co (NS= Ru, Ir) synthetic antiferromagnetic layers for spin-orbit torque switching originating from the spin-Hall effect. *Y. Saito*[1], S. Ikeda[1,2] and T. Endoh[1,3] *1. Center for Innovative Integrated Electronic Systems, Tohoku University, Sendai, Japan; 2. Center for Science and Innovation in Spintronics, Tohoku University, Sendai, Japan; 3. Department of Electrical Engineering, Tohoku University, Sendai, Japan*

Antiferromagnetic (AF) materials have attracted attention due to their such as fast magnetization dynamics using current-induced spin-orbit torque (SOT) originating from the spin-Hall effect (SHE) [1], low magnetic susceptibility, and lack of magnetic stray field. Bulk AF materials such as CuMnAs and NiO, and metallic superlattices with an AF structure (synthetic AF layer) have investigated as candidate systems for studying AF spintronics using current-induced SOT switching. In this study, we propose the synthetic AF structure with Pt/NS/Pt (NS=Ru, Ir) nonmagnetic spacer materials for the candidate of the systematic investigation of the SOT on the AF structure, and investigate its magnetic and transport properties. Figure 1 shows the schematic diagram for the proposed memory cell for SOT-MRAM. If one can find Pt/NS/Pt (NS= Ru, Ir) spacer layers have exhibiting AF interlayer exchange coupling through relatively thick Pt layers, these multilayer spacer layers would be one of promising materials for the systematic investigation of the SOT on the AF structure, because one can use large SHE in Pt layers and the exchange interaction between the storage and the synthetic AF layers for controlling the magnetization direction of storage layer in the read device shown in Fig. 1. Figures 2(a) and 2(b) show the normalized out-of-plane and in-plane magnetization versus field curves for Co/Pt/NS/Pt/Co (NS=Ru, Ir) films, respectively. The remanence values of the magnetization at $H = 0$ T are nearly zero for both in-plane and out-of-plane magnetization directions for both multilayers, indicating AF interlayer exchange coupling through Pt/NS/Pt (NS= Ru, Ir) spacer layers. In this presentation, we will report the details of Ru and Ir and Pt thickness dependencies of interlayer exchange coupling, SHE and spin diffusion length in Pt/Ru and Pt/Ir multilayers estimated by spin Hall magnetoresistance. This work was supported by the CIES Consortium, the JST OPERA (JPMJOP1611) and JSPS KAKENHI (JP19H00844, JP21K18189).

[1] Y. Saito et al., Appl. Phys. Exp. 12, 053008 (2019), AIP. Advances 9, 125312 (2019), Appl. Phys. Lett. 116, 132401 (2020), AIP. Advances 11, 025007 (2021).

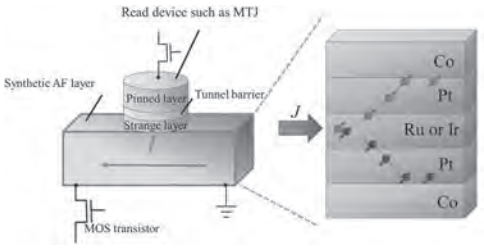

Fig. 1 Schematic diagram for the proposed memory cell of SOT-MRAM.

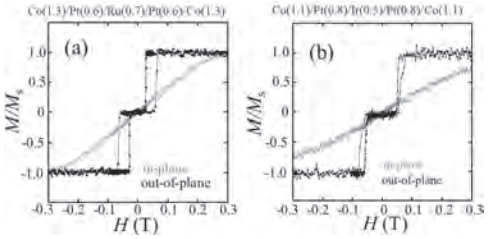

Fig. 2 Normalized out-of-plane and in-plane magnetization versus field curves.

GOO-08. Anisotropic magnetoresistance reversal driven by spin flops in a helical antiferromagnet. *H. Shin*[1], J. Kim[1], J. Hong[1], K. Jeong[1], J. Kim[1], N. Lee[1] and Y. Choi[1] *1. Department of Physics, Yonsei University, Seoul, The Republic of Korea*

A helimagnetic order is a non-collinear spin texture of an antiferromagnet that emerges from competing exchange interactions. While collinear antiferromagnets have been elemental building blocks to establish antiferromagnetic spintronics, manageable factors and origins for anisotropy of non-collinear antiferromagnets have little been examined. Herein, we show that anisotropic magnetoresistance (AMR) is reversed across the spin-flop transition in a helical antiferromagnet, $EuCo_2As_2$. Contrast of the AMR arises from strong 2-dimensional spin nature integrated with spin-flop-driven switching from positive to negative magnetoresistance along an easy axis. Our phenomenological calculations based on molecular field theory reproduce quantitatively experimental data and verifies a crucial role of magnetocrystalline anisotropy in the observed spintronic functionality. We suggest a new type of single-phase antiferromagnetic material revealing changeable sign of memory state, which scheme is applicable to a variety of antiferromagnets.

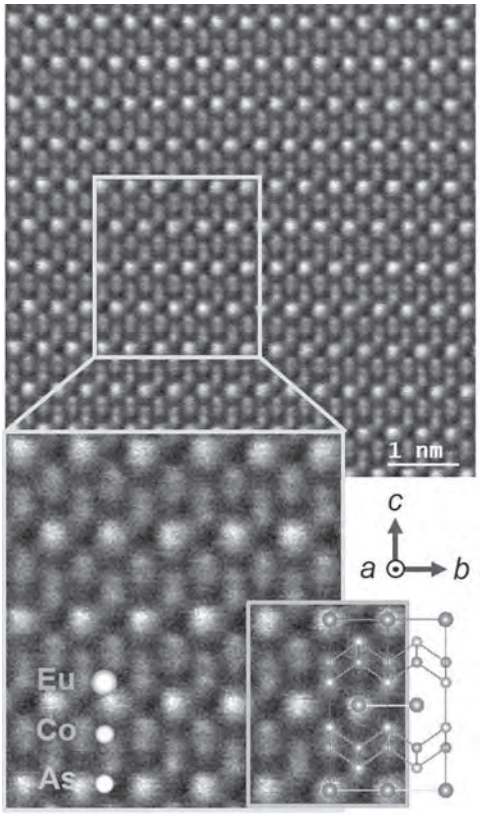

Fig. 1 Scanning Transmission Electron Microscopy (STEM) image of Eu_2Co_2As2 single crystals along [100].

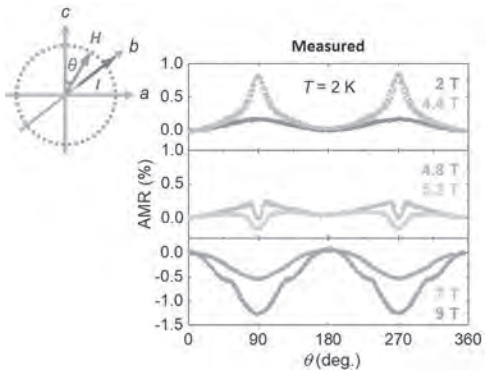

Fig. 2 Plots of the anisotropic magnetoresistance (AMR), measured at T = 2 K by rotating H =2, 4.4, 4.8, 5.2, 7 and 9 T in the *ac* plane with the current along the *b*-axis, $I//b$. Geometry of the AMR measurement is schematically shown. θ = 0° for the *c*-axis and θ = 90° for the *a*-axis.

GOO-09. Toroidal moments: hallmarks of collinear antiferromagnetic order. *R. Winkler*[1] and U. Zülicke[2] *1. Physics, Northern Illinois University, DeKalb, IL, United States; 2. School of Chemical and Physical Sciences, Victoria University of Wellington, Wellington, New Zealand*

A magnetization m is the well-known hallmark of magnetic order in ferromagnets. A counterpart to m describing the magnetic order in antiferromagnets has conspicuously remained absent in the world of magnetism. We derive a Néel operator τ that describes collinear antiferromagnetic order, in the same way a magnetization m signals ferromagnetic order [1]. While m is even under space inversion and odd under time reversal, τ describes a toroidal moment that is odd under both symmetries. Thus m and τ quantify complementary aspects of magnetic order in solids. Orbital ferromagnetic order can be attributed to dipolar equilibrium currents that give rise to a magnetization. We show that, in the same way, antiferromagnetic order arises from quadrupolar equilibrium currents that generate the toroidal moment τ. Considering an antiferromagnetic diamond structure as an example (Fig. 1), we derive explicit analytical expressions for the Néel operator τ and the effects of AFM order on the itinerant electrons in this system [1]. As an example for the efficacy of our approach, we develop a unified theory for magnetoelectricity in quasi-2D paramagnets, ferromagnets and antiferromagnets. In magnetoelectric media, an electric field can induce a magnetization and a magnetic field can induce a polarization, while the system remains in thermal equilibrium [2,3]. This effect appeals to recent efforts to manipulate magnetic order electrically [4]. It requires that both space-inversion and time-reversal symmetry are broken. We present a comprehensive theory [1] for magnetoelectricity in quasi-2D systems, where antiferromagnetic order and toroidal moments play a central role. We obtain quantitative expressions for the magnetoelectric responses due to electric and magnetic fields that reveal explicitly, for the first time, the inherent duality of these responses required by thermodynamics.

[1] R. Winkler and U. Zülicke, Phys. Rev. Research 2, 043060 (2020) [2] L. D. Landau and E. M. Lifshitz, *Electrodynamics of Continuous Media*, (Pergamon, Oxford, 1984) [3] M. Fiebig, J. Phys. D: Appl. Phys. 38, R123 (2005) [4] A. Manchon et al., Rev. Mod. Phys. 91, 035004 (2019)

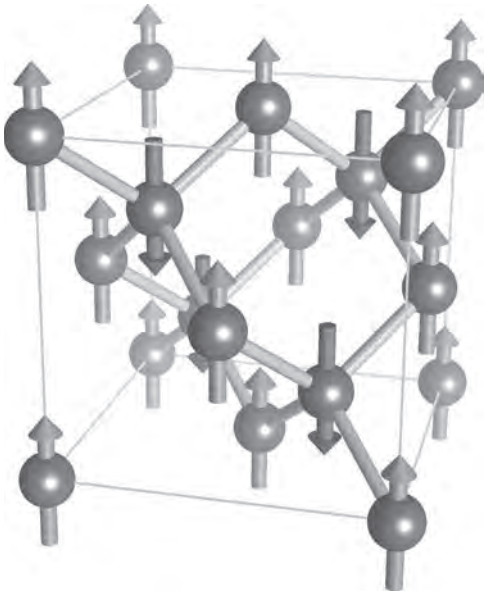

Figure 1: The antiferromagnetic diamond structure breaks time-reversal symmetry θ and inversion symmetry I (though the joint operation θI remains a good symmetry).

GOO-10. Spin transport in a long Josephson junction based on an antiferromagnetic domain wall. *R. Khymyn*[1], R. Ovcharov[1], B. Ivanov[2] and J. Åkerman[1] *1. Department of Physics, University of Gothenburg, Gothenburg, Sweden; 2. Institute of Magnetism of NASU and MESU, Kyiv, Ukraine*

Self-localized spin structures can substantially enrich the scope of the field-free antiferromagnetic spintronics [1]. One of them - the domain wall (DW) is a topological soliton that bridge a connection between two ground states, similar to a link in a Josephson junction (JJ) between two superconductors. JJs are intensively investigated for decades as they promise important advantages for electronics. In particular, JJ-based qubits are already successfully realized and commercialized. We demonstrate that the DW in bi-axial AFM with the easy-axis type of primary anisotropy driven by a spin current is a close analogy of a long Josephson junction (LJJ). Thus, the dynamics of the Neel vector angle inside the DW (Josephson phase Φ) is described by a sine-Gordon type of equation, where applied spin transfer torque (STT) represents a bias current through the junction, anisotropy in a basal plane

defines a plasma frequency, and characteristic speed of magnons, defined by nonhomogeneous exchange energy, corresponds to Swihart velocity. In contrast with a conventional LJJ, a DW has additional degrees of freedom, namely the position of its center X and distribution of the current along a DW. We show by micromagnetic simulations, that when the polarization of the STT is parallel to the easy axis of an AFM, the above allows to nucleate and propel a single kink-type Φ soliton [2], which is Bloch line (Fig.1) that corresponds to the Josephson vortex in LJJ, as well as their series. Withal, a weak alternate current excites Φ-type intrawall spin waves, an analog of plasma waves in LJJ, which spectrum has a bandgap, defined by the anisotropy (Fig.2). STT with a perpendicular polarization allows manipulating the X position, particularly to excite the flexural vibrations of the DW with a gapless spectrum [3] (Fig.2). The variety of possible spin transport regimes together with the possibility of DW movement or bending under the action of applied spin current, offers considerable scope for developing novel spintronics devices.

[1] O. Gomonay et al., Antiferromagnetic spin textures and dynamics, Nature Physics 14, 213–216 (2018) [2] S. K. Kim and Y. Tserkovnyak, Magnetic domain walls as hosts of spin super-fluids and generators of skyrmions, Phys. Rev. Lett., 119, 047202, (2017) [3] H.-K. Park and S.-K. Kim, Channeling of spin waves in antiferromagnetic domain walls, Physical Review B, 103, 214420 (2021)

Fig. 1 Generation of the Bloch line, - an anlog of the Josephson vortex.

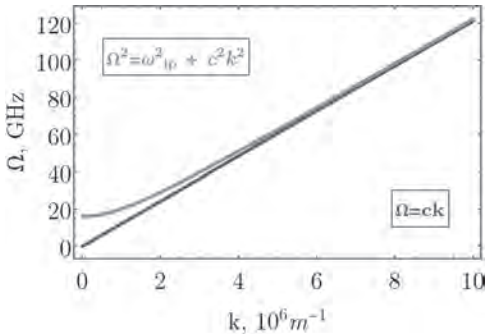

Fig. 2 Dispersion law for Φ (red) and X (blue) intrawall modes in easy-axis Cr2O3 antiferromagnet with the presence of in-plane anisotropy.

GOO-11. Thermal Hall Effect of Magnons in Collinear Antiferromagnetic Insulators: Signatures of Magnetic and Topological Phase Transitions. *R.R. Neumann*[1], A. Mook[2], J. Henk[1] and I. Mertig[1]
1. Institut of Physics, Martin Luther University Halle-Wittenberg, Halle (Saale), Germany; 2. Department of Physics, University of Basel, Basel, Switzerland

The thermal Hall effect, sometimes also called Righi-Leduc effect, appears as transversal heat currents induced by thermal gradients. Magnons, the magnetic excitations in long-ranged ordered systems, transport spin and heat with no charge currents. In this talk I demonstrate that the transversal transport coefficient in a two-dimensional honeycomb antiferromagnet features clear signs of magnetic and topological phase transitions. An external magnetic field drives the system from the antiferromagnetic phase via the noncollinear spin-flop phase into the field-polarized phase. Additionally, topological phase transitions are found in the spin flop phase. Both types of phase transitions manifest themselves in prominent and distinguishing features in the thermal conductivities; depending on the temperature, the conductivity changes by several orders of magnitude, providing a means to identify experimentally these phase transitions.

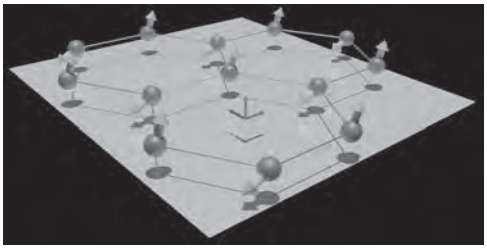

GOO-12. Spectroscopic MOKE and other Berry phased boosted properties of ferrimagnetic and antiferromagnetic Mn_3NiN. *F. Johnson*[1], J. Kimák[2], J. Zazvorka[2], E. Schmoranzerová[2], J. Godinho[2,3], P. Nemec[2], L. Beran[2], M. Veis[2], Z. Soban[3], J. Zemen[4], D. Boldrin[1,5], H. Zhang[6], H. Singh[6], J. Wunderlich[7] and L. Cohen[1] *1. Blackett Laboratory, Imperial College London, London, United Kingdom; 2. Faculty of Mathematics and Physics, Charles University, Prague, Czechia; 3. Institute of Physics, Czech Academy of Sciences, Prague, Czechia; 4. Faculty of Electrical Engineering, Czech Technical University, Prague, Czechia; 5. School of Physics and Astronomy, University of Glasgow, Glasgow, United Kingdom; 6. Institute of Materials Science, TU Darmstadt, Darmstadt, Germany; 7. University of Regensburg, Regensburg, Germany*

The intrinsic anomalous Hall effect (AHE) present in noncollinear Mn_3NiN shows boosted values in spite of the vanishing magnetisation and modest spin-orbit coupling present in the material, while the related anomalous Nernst effect (ANE) has been predicted to be an order of magnitude greater than Mn_3Sn [1,2]. In addition, recent reports suggest an unconventional component in the spin-to-charge conversion process in the related material Mn_3GaN due to the magnetic ordering symmetry [3]. The shared origin of these effects lies in the Berry curvature of the band structure. In this talk I will review our current progress with this system, growth of epitaxial films by pulsed laser deposition on various perovskite substrates and comparison of properties to literature reports. Our recent measurements are taken on Mn_3NiN films grown on STO and BTO substrates, and I will discuss their properties in light of the magnetic-order biaxial in-plane strain phase diagram that we have established previously [4]. I will discuss our recent experimental measurement of spectroscopic MOKE, AHE and ANE compared to the theoretical prediction calculated using spin density functional theory (SDFT) and linear response approximation, highlighting where we find strikingly good agreement. These materials are also predicted to host giant piezomagnetism and strong sensitivity of the Berry phase curvature to strain. These different properties do not necessarily add constructively and I will present our current views on this based on the variation of the AHE in films grown on piezoelectrically controlled BTO.

[1] D. Boldrin, I. Samathrakis, J. Zemen et al., Physical Review Materials 3, 094409 (2019) [2] H. Chen, Q. Niu, and A. H. MacDonald, Physical Review Letters 112, 017205 (2014) [3] T. Nan, C. X. Quintela, J. Irwin et al., Nature Communications 11, 4671 (2020) [4] D. Boldrin, F. Johnson, R. Thompson et al., Advanced Functional Materials 29, 1902502 (2019)

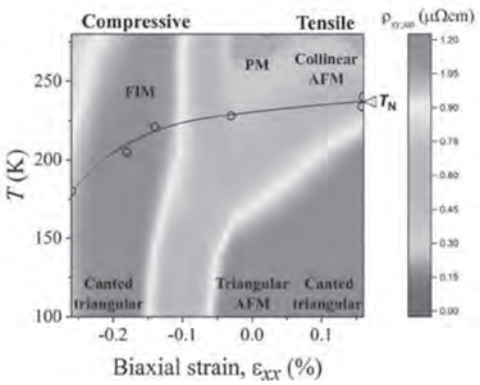

Figure 1: Magnetic phase diagram of Mn_3NiN thin films, showing how the anomalous Hall effect can be used as a probe to investigate the magnetic ordering, which is strongly influenced by strain. Figure taken from reference 4.

GOO-13. Theory of Unidirectional Magnetoresistance in Collinear-Antiferromagnet/Heavy-Metal Bilayers. *M. Mehraeen*[1], S. Shim[2,3], J. Sklenar[2,4], J. Oh[2,3], J. Gibbons[2,3], H. Saglam[5,6], A. Hoffmann[5,7], S. Zhang[1] and N. Mason[2,3] *1. Physics, Case Western Reserve University, Cleveland, OH, United States; 2. Physics, University of Illinois at Urbana-Champaign, Urbana, IL, United States; 3. Materials Research Laboratory, University of Illinois at Urbana-Champaign, Urbana, IL, United States; 4. Physics and Astronomy, Wayne State University, Detroit, MI, United States; 5. Materials Science Division, Argonne National Laboratory, Lemont, IL, United States; 6. Physics, Yale University, New Haven, CT, United States; 7. Materials Science and Engineering, University of illinois at Urbana-Champaign, Urbana, IL, United States*

In recent years, there has been increasing interest in the study of nonlinear magnetotransport phenomena in systems with broken inversion and time-reversal symmetries. One notable example of such effects is the unidirectional magnetoresistance (UMR) -- initially being observed in ferromagnetic-metal and heavy-metal bilayers [1] -- which changes sign when the direction of either the current or in-plane magnetization is reversed. Spin-orbit coupling (SOC) and spin-asymmetry in electron scattering have been demonstrated to play key roles in generating the UMR. A UMR effect was recently detected in an antiferromagnetic FeRh/Pt bilayer [2], despite the lack of intrinsic spin-dependent scattering, when the Neel vector is parallel to the applied current but perpendicular to the external magnetic field. More interestingly, the UMR evolves nonlinearly with the increasing strength of the magnetic field and undergoes a sign change even when the direction of the field remains the same. Based on a tight-binding model that takes into account the interfacial SOC and the exchange coupling between electron spin and the sublattice magnetization, we theoretically examine the physical origin of the unexpected UMR effect, and unveil the connection between the UMR and the antiferromagnetic ordering. We also argue that the characteristic dependence of the UMR on the strength of the magnetic field -- with a sign change in particular -- is unique to antiferromagnetic systems, and hence may be regarded as a magnetotransport signature of antiferromagnetic ordering. The theoretical work is supported by the College of Arts and Sciences, Case Western Reserve University.

[1] Avci, C. O. *et al. Nat. Phys*.11, 570-575 (2015) [2] Shim, S. *et al.* to be published

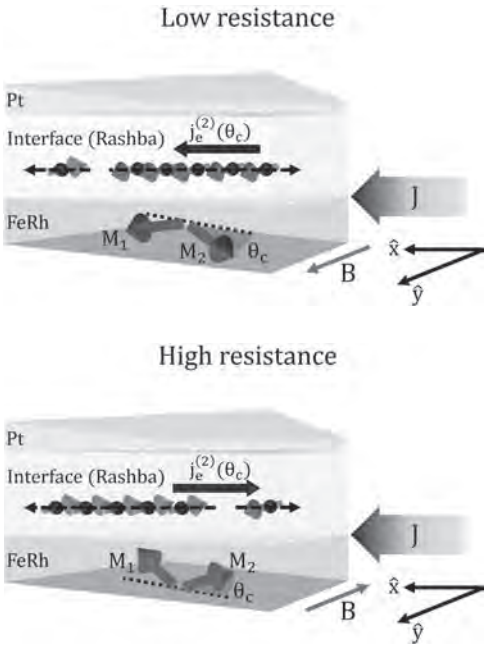

GOO-14. Electrical manipulation of antiferromagnetic order in PtMn and $PtMn_3$ pillars. *J. Shi*[1], V. Lopez Dominguez[1], S. Arpaci[1], F. Garesci[2], C. Wang[1], H. Almasi[1], M. Grayson[1], G. Finocchio[2] and P. Khalili Amiri[1] *1. Northwestern University, Evanston, IL, United States; 2. University of Messina, Messina, Italy*

Antiferromagnets (AFMs) are magnetically ordered materials without a macroscopic magnetization. There is accelerating interest in using them for memory applications, motivated by the possibility for electrically controlling AFM order via spin-orbit torques, and its read-out via magnetoresistive effects [1-2]. Here we show that micrometer-scale bits of the antiferromagnet PtMn, grown on a Ta or Pt heavy metal (HM) layer, can be switched reversibly between different magnetic states by electric currents, with readout through a second harmonic voltage technique [3]. The device exhibits multiple states, which can be set using different current amplitudes and may find application in neuromorphic computing. Micromagnetic simulations suggest that these metastable states consist of vortex and anti-vortex textures that move in response to current. We also demonstrate, using a modified device layout, direct voltage measurements to read out the electrically-induced switching of noncollinear $PtMn_3$. The modified layout and measurement methodology, which was recently demonstrated using the $IrMn_3$/Pt material system [4], is utilized here to distinguish current-induced magnetic and nonmagnetic switching signals in $PtMn_3$/Pt devices. We also realize switching down to 10 μs pulse width, which shows the potential for fast device applications. The effect of temperature and external magnetic field (up to 15 T) are also studied. Our results pave the way towards practical PtMn and $PtMn_3$ antiferromagnetic memories integrated on silicon, and indicate the importance of micromagnetic textures in the static and dynamic behavior of antiferromagnetic devices.

1. MB. Jungfleisch, W. Zhang and A. Hoffmann, Physics Letters A., Vol. 382(13), p.865-871 (2018) 2. P. Wadley, B. Howells and J. Zelezný, Science., Vol. 351(6273), p.587-590 (2016) 3. J. Shi, V. Lopez-Dominguez and F. Garesci, Nature Electronics., Vol. 3(2), p.92-98 (2020) 4. S. Arpaci, V. Lopez-Dominguez and J.Shi, Nature Communications., Vol. 12(1), p.1-10 (2021)

GOO-15. Anomalous Exchange Resonance Driven by Spin-Orbit Torques in Intrinsic Antiferromagnetic Topological Insulator. *J. Tang*[1] and R. Cheng[1] *1. Department of Electrical and Computer Engineering, University of California, Riverside, Riverside, CA, United States*

In antiferromagnetic topological insulator MnBi2Te4, the interplay between topological electrons and magnetization dynamics in the form of spin torques and charge pumping remains an open question. Using the Berry phase theory, we develop a universal formalism to quantify the spin-orbit torques (SOTs) and their reciprocal effects in layered MnBi2Te4, where the symmetry of SOTs exhibits an even-odd layer-number pattern. The dynamical consequences of our finding are demonstrated by the SOT-driven magnetic resonances. In particular, we identify an anomalous exchange (AE) mode in the tri-septuple layer (SL) case, where the magnetic moments from the top and bottom SL rotate with a pi phase difference while those in the middle SL stay static. Unlike the ordinary exchange mode and the acoustic mode, the AE mode does not react to a microwave electromagnetic field. Therefore, the AE resonance can only be excited by the peculiar SOTs we find, providing a unique way to verify the SOTs in MnBi2Te4. Our study lays the theoretical foundation of current-induced spin dynamics in intrinsic antiferromagnetic topological insulators.

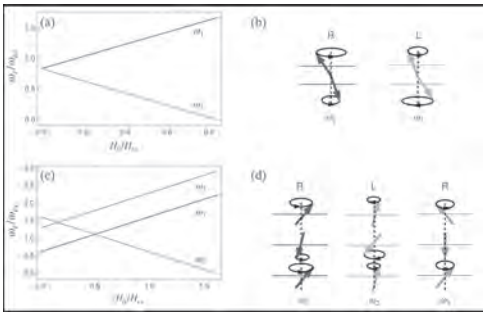

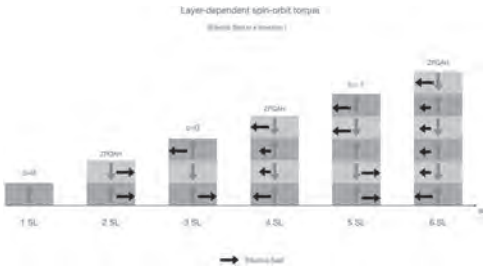

Session GOP
ANTIFERROMAGNETIC SPINTRONICS II
Romain Lebrun, Chair
Unité Mixte de Physique CNRS/Thales, Palaiseau, France

INVITED PAPERS

GOP-01. Chiral-spin rotation of non-collinear antiferromagnetic Mn_3Sn by spin-orbit torque. *Y. Takeuchi*[1], Y. Yamane[2,3], J. Yoon[3,4], R. Itoh[3,4], B. Jinnai[1], S. Kanai[3,5], J. Ieda[3,6], H. Ohno[3,7] and S. Fukami[3,8]
1. WPI-Advanced Institute for Materials Research, Tohoku University, Sendai, Japan; 2. Frontier Research Institute for Interdisciplinary Sciences, Tohoku University, Sendai, Japan; 3. Laboratory for Nanoelectronics and Spintronics, Research Institute of Electrical Communication, Tohoku University, Sendai, Japan; 4. Graduate School of Engineering, Tohoku University, Sendai, Japan; 5. Division for the Establishment of Frontier Sciences, Tohoku University, Sendai, Japan; 6. Advanced Science Research Center, Japan Atomic Energy Agency, Tokai, Japan; 7. Center for Innovative Integrated Electronic Systems, Tohoku University, Sendai, Japan; 8. Center for Spintronics Research Network, Tohoku University, Sendai, Japan

Spin-orbit torque (SOT) is a key ingredient for the electrical manipulation of nanomagnets [1-3]. In addition to ferromagnets, several studies demonstrate the electrical control of antiferromagnets, which have rapidly attracted attention owing to their unique properties such as high-frequency dynamics and robustness against external field noise [4,5]. Among antiferromagnets, non-collinear antiferromagnets exhibit several intriguing phenomena including a large anomalous Hall effect despite their vanishingly small net magnetization [6,7]. A recent study reports a SOT induced reversal of the order parameter (Néel vector) in non-collinear antiferromagnet Mn_3Sn, in the same protocol as SOT switching of ferromagnet [8]. Meanwhile, unique properties and functionalities of non-collinear antiferromagnet have not been unveiled. Here, we report a chiral-spin rotation of the Néel vector in non-collinear antiferromagnet by SOT in epitaxial non-collinear antiferromagnet Mn_3Sn film [9]. We prepare epitaxial heterostructures, consisting of W(3)/Ta(1)/Mn_3Sn(t_{Mn3Sn})/Pt(4) (in nm) on MgO(110) substrate by sputtering [10,11]. Films are annealed at 500 °C for an hour and processed into Hall bar devices. Figure 1 shows the cross-sectional STEM image of Mn_3Sn layer, indicating the epitaxial growth of M-plane oriented Mn_3Sn. SOT can be induced by applying an in-plane current into the heterostructure. Hall resistance (R_H) versus out-of-plane magnetic field (H) is shown in Figure 2(a). To investigate the influence of SOT on Mn_3Sn, we measure R_H as a function of applied current pulse amplitude (I). We examine two kinds of configurations, which are different in the direction of current with respect to the Kagome lattice. Figures 2(b), (c) are summarized R_H-I curves for cases of $I \perp [0001]$ and $I \parallel [0001]$, respectively. We observe a characteristic R_H response, *i.e.*, a transition to an intermediate level of R_H, I-direction dependent critical current of the transition, and larger R_H fluctuation at higher I. Through in-depth experiments and calculations, we find that the observed R_H responses are attributed to a chiral-spin rotation of the Néel vector in Mn_3Sn driven by SOT. Furthermore, we investigate t_{Mn3Sn} dependence of threshold current density and switching field, and find that non-collinear antiferromagnet can be efficiently controlled by SOT, consistent with a study on an antiferromagnetically coupled collinear ferrimagnet [12]. Our results open a way toward a new paradigm of functional spintronics. This work was partly supported by JSPS KAKENHI (Grant No. 19H05622 and No. 20K22409), JSPS Core-to-Core Program, and RIEC Cooperative Research Projects.

[1] I. M. Miron *et al.*, Nature 476, 189 (2011). [2] L. Liu *et al.*, Science 336, 555 (2012). [3] S. Fukami *et al.*, Nat. Nanotechnol. 11, 621 (2016). [4] P. Wadley *et al.*, Science 351, 587 (2016). [5] S. DuttaGupta *et al.*, Nat. Commun. 11, 5715 (2020). [6] S. Nakatsuji *et al.*, Nature 527, 212 (2015). [7] A. K. Nayak *et al.*, Sci. Adv. 2, e1501870 (2016). [8] H. Tsai *et al.*, Nature 580, 608 (2020). [9] Y. Takeuchi *et al.*, Nat. Mater. (2021). https://doi.org/10.1038/s41563-021-01005-3 [10] J.-Y. Yoon *et al.*, Appl. Phys. Express 13, 013001 (2019). [11] J.-Y. Yoon *et al.*, AIP Advances 11, 065318 (2021). [12] J. Yu *et al.*, Nat. Mater. 18, 29 (2019).

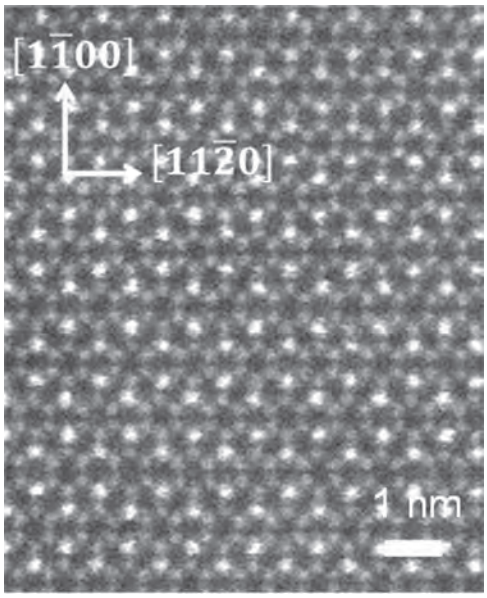

Fig.1 Cross-sectional STEM image of Mn_3Sn layer in prepared stack.

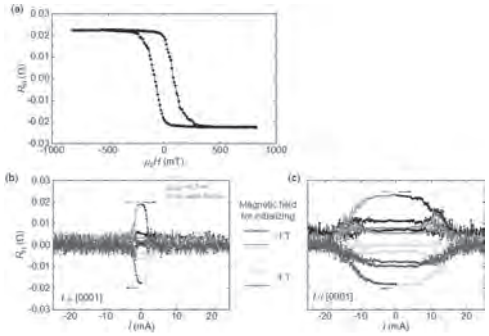

Fig. 2 (a) Hall resistance (R_H) versus out-of-plane magnetic field (H) in W(3 nm)/Ta(1 nm)/Mn_3Sn(8.3 nm)/Pt(4 nm) heterostructure. (b), (c) R_H as a fuction of applied current pulse amplitude (I) for cases of $I \perp [0001]$ and $I \parallel [0001]$, respectively. The duration of current pulse is 100 ms.

GOP-02. Accessing superluminal-like magnon velocity in an antiferromagnetic insulator. *K. Lee*[1], D. Lee[2], D. Yang[1], R. Mishra[1,3], D. Kim[1], S. Kim[4], K. Lee[4] and H. Yang[1] *1. Department of Electrical and Computer Engineering, National University of Singapore, Singapore; 2. Department of Materials Science and Engineering, Korea University, Seoul, The Republic of Korea; 3. Centre for Applied Research in Electronics, Indian Institute of Technology Delhi, New Delhi, India; 4. Department of Physics, Korea Advanced Institute of Science and Technology, Daejeon, The Republic of Korea*

Designing a compact, high-speed and low-dissipation magnetic device is crucial to meet the increasing data processing and storage demands. Antiferromagnets (AFMs) feature benefits over ferromagnets such as dense-packing and high-frequency operation. AFM insulators host magnons to carry spin angular momentum without a charge flow, i.e., Joule-heat-free, which accomplishes low-dissipation. However, accessing these advantages in a single framework remains challenging [1]. In particular, the dense-packing at a nanoscale hinders the readout of the AFM dynamics on (sub-)ps timescales due to the lack of THz-speed probes. Therefore, a direct observation of high-speed propagation of antiferromagnetic magnons at nanoscales is still missing, while the long-distance propagation at microscales has been demonstrated [2]. Here, we show a direct measurement of the magnon propagation time over nanoscales of antiferromagnetic insulator NiO based on optical-driven terahertz emission measurements at Bi_2Te_3 (6 nm)/NiO (≤ 50 nm)/Co (3 nm) [3]. The magnon velocity is found to be gigantic (~650 km/s) (Fig. 1), which far exceeds a bulk magnon group velocity (~40 km/s) estimated from the dispersion of NiO. This superluminal-like magnon velocity is explained by the anomalous magnon dispersion in the presence of damping. This work is relevant to the energy-efficient angular momentum flow in nanoscales, which underlies widespread applications of magnetic devices.

[1] A. V. Chumak et al., B. *Nat. Phys.* 11, 453-461 (2015). [2] R. Lebrun et al., *Nature* 561, 222-225 (2018). [3] K. Lee el al., *Nat. Nanotechnol.* in press (2021).

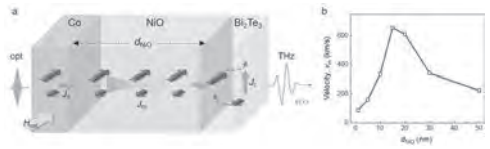

Fig. 1. (a) Schematics of the optical-driven THz emission from Bi_2Te_3 (6 nm)/NiO (d_{NiO})/Co (3 nm) trilayers. (b) Magnon velocities estimated with the magnon propagation times over the different thickness of NiO layer.

CONTRIBUTED PAPERS

GOP-03. Coherent Spin Pumping in Easy-Plane Antiferromagnets. *M. Guo*[1] and R. Cheng[1,2] *1. Physics and Astronomy, University of California, Riverside, Riverside, CA, United States; 2. Electrical and Computer Engineering, University of California, Riverside, Riverside, CA, United States*

Spin pumping has been an efficient way of spin generation, which converts coherent spin precessions in a magnet into pure spin currents in an adjacent metal. Recently, spin pumping has been demonstrated in easy-axis antiferromagnets (AFs) that operate at the terahertz frequency range, opening the exciting possibility of signal generation and processing at ultrafast speed. However, easy-plane AFs which are experimentally easier to prepare than their easy-axis counterparts, were considered to be bad candidates for spin pumping because the N{e}el vector is linearly polarized due to the easy-plane anisotropy, placing a major restriction on the choice of materials for practical applications. Here, using NiO and α-Fe_2O_3 (hematite) as two archetypal easy-plane AFs, we theoretically challenge this seemingly established conclusion by showing that easy-plane AFs can pump DC spin currents with the help of either the Dzyaloshinskii-Moriya interaction or an applied magnetic field without inducing the spin-flop transition. The magnitude of spin pumping turns out to be as strong as that in easy-axis AFs, which significantly broadens the materials pool for antiferromagnetic spintronics. Furthermore, we find that in the presence of a magnetic field, NiO can function as a sub-terahertz spin-torque oscillator at a highly reduced threshold current density.

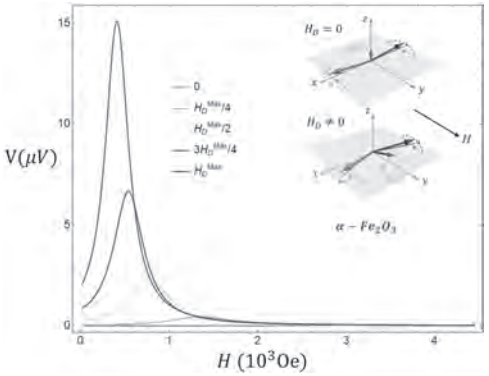

Fig. 1 DC output as a function of the applied magnetic field for different values of DM interaction in α-Fe_2O_3

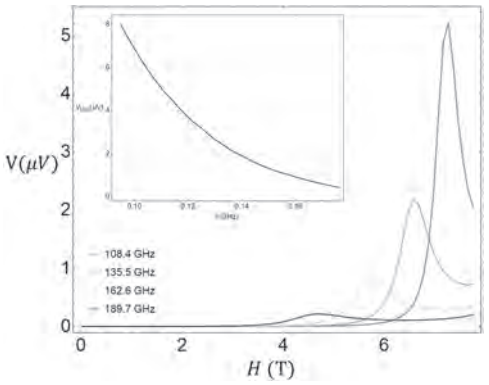

Fig. 2 DC output as a function of the applied magnetic field along the in-plane easy axis direction below the spin-flop transition for different driving frequencies in NiO

GOP-04. Antiferromagnetic Magnon Pseudospin Dynamics and the Magnon Hanle Effect in Hematite Thin Films. J. Gückelhorn[1,2], A. Kamra[3], T. Wimmer[1,2], M. Opel[1], S. Geprägs[1], R. Gross[1,2], H. Huebl[1,2] and *M. Althammer*[1,2] *1. Walther-Meissner-Institut, Garching, Germany; 2. Physik Department, TU Munich, Garching, Germany; 3. IFIMAC - Condensed Matter Physics Center and Department of Theoretical Condensed Matter Physics, Universidad Autónoma de Madrid, Madrid, Spain*

The spin-1/2 of an electron makes it an archetypal two-level system and inspires the description of other two-level systems using an analogous pseudospin. The quantized spin excitations of an ordered antiferromagnet can be viewed as pairs of spin-up and -down magnons and can be characterized by a magnonic pseudospin. The similarity between electronic spin and magnonic pseudospin has triggered the prediction of exciting phenomena like emergent spin-orbit coupling and topological states in antiferromagnetic magnonics. In the last year, first experimental observations of the associated dynamics of antiferromagnetic pseudospin have been reported [1,2]. Based on these findings, we will expand the concept of magnon pseudospin and the description of magnon pseudospin dynamics [3,4] and discuss the influence of dimensionality on the magnon Hanle effect. Additionally, we show our recent experiments demonstrating control of magnon spin transport and

pseudospin dynamics in thin films with varying thickness of the antiferromagnetic insulator hematite (α-Fe_2O_3) utilizing two Pt strips for all-electrical magnon injection and detection [2]. We observe an oscillation in polarity of the magnon spin signal at the detector as a function of the applied magnetic field, which we quantitatively explain in terms of diffusive magnon transport. In particular, we observe a coherent precession of the magnon pseudospin caused by the easy-plane anisotropy and the Dzyaloshinskii-Moriya interaction. Moreover, we find peculiar changes in the magnon spin signal for thicker hematite layers. Our results are paramount in unnlocking the high potential of antiferromagnetic magnonics towards the realization of electronics-inspired phenomena. Financial support from the Deutsche Forschungsgemeinschaft (DFG, German Research Foundation) under Germany's Excellence Strategy - EXC-2111 - 390814868 and project AL2110/2-1, and the Research Council of Norway through its Centers of Excellence funding scheme, project 262633, "QuSpin" is gratefully acknowledged.

[1] T. Wimmer et al., Physical Review Letters 125, 247204 (2020) [2] A. Ross et al., Applied Physics Letters 117, 242405 (2020) [3] A. Kamra et al., Physical Review B 102, 174445 (2020) [4] K. Shen, Journal of Applied Physics 129, 223906 (2021)

GOP-05. Observation of current-induced switching in non-collinear antiferromagnetic $IrMn_3$ by differential voltage measurements.

S. Arpaci[1,2], V. Lopez Dominguez[1], J. Shi[1], L. Sánchez-Tejerina[3], F. Garesci[4], C. Wang[1], X. Yan[1], V. Sangwan[5], M. Grayson[1,2], M. Hersam[1,5], G. Finocchio[3] and P. Khalili Amiri[1,2] *1. Department of Electrical and Computer Engineering, Northwestern University, Evanston, IL, United States; 2. Graduate Program in Applied Physics, Northwestern University, Evanston, IL, United States; 3. Department of Mathematical and Computer Sciences, Physical Sciences and Earth Sciences, University of Messina, Messina, Italy; 4. Department of Engineering, University of Messina, Messina, Italy; 5. Department of Materials Science and Engineering, Northwestern University, Evanston, IL, United States*

Antiferromagnetic materials (AFMs) provide a pathway to overcome the limitations of ferromagnet-based spintronics, enabling fast and high density memory devices, as well as terahertz detectors and sources. This has fueled intensive research on the electrical manipulation of metallic AFMs using interfacial spin-orbit torque (SOT) from a heavy metal (HM) layer [1-4]. However, the threshold current density in HM/AFM bilayers is typically large, thus creating non-magnetic contributions to resistive switching signals, complicating their interpretation. Here, we present a new device structure and measurement protocol based on differential voltage measurements, allowing in situ reference measurements and to systematically separate the switching signals originating in the AFM and HM layers of a HM/AFM heterostructure [5]. The proposed device consists of a double-cross HM structure with six terminals, where the AFM, patterned in a micropillar shape, is placed on one of the two crosses. We successfully use this method in devices formed by Pt and the non-collinear AFM $IrMn_3$. The results provide clear evidence of electrical switching of the AFM order parameter in the $IrMn_3$ pillar by SOT in the range of writing current densities from 36 to 50 MA/cm^2 with no appreciable switching signal from the Pt layer. We discuss the role of different switching configurations (180° and 90° writing currents), as well as the role of thermal activation on the switching characteristics. Control experiments in Pt-only double-cross samples without an AFM pillar reveal HM-dominated switching at higher current densities ~60 MA/cm^2. We discuss active readout of the switching signals using a differential amplifier, with large peak-to-peak output voltage ~100 mV. The structure allows for reliable electrical measurement of resistive signatures of AFM switching induced by SOT, which will be important not only for the fundamental understanding of current-induced AFM domain dynamics, but also as an electrical readout method for practical applications in memory and computing devices.

1. Shi, J., et al., *Electrical manipulation of the magnetic order in antiferromagnetic PtMn pillars.* Nature Electronics, 2020. 3(2): p. 92-98. 2. Dunz, M., T. Matalla-Wagner, and M. Meinert, *Spin-orbit torque induced electrical switching of antiferromagnetic MnN.* Physical Review Research, 2020. 2(1): p. 013347. 3. DuttaGupta, S., et al., *Spin-orbit torque switching of an antiferromagnetic metallic heterostructure.* Nature Communications, 2020. 11(1): p. 5715. 4. Tsai, H., et al., *Electrical manipulation of a topological antiferromagnetic state.* Nature, 2020. 580(7805): p. 608-613. 5. Arpaci, S., et al., *Observation of current-induced switching in non-collinear antiferromagnetic $IrMn_3$ by differential voltage measurements.* Nature Communications, 2021. 12(1): p. 3828

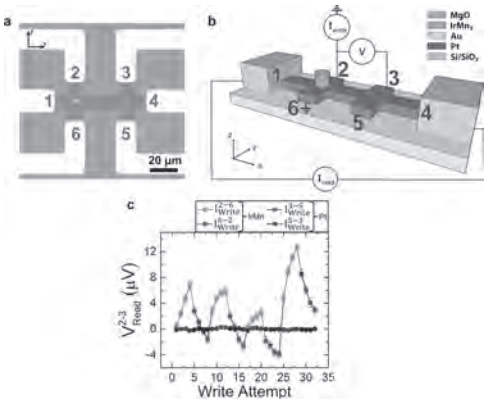

Fig. 1. Design of double-cross device for differential voltage measurements and the measured differential voltage for the 180° switching configuration with 20 mA write pulses.

GOP-06. Spin-Hall Magnetoresistance and Anomalous Hall Effect in Pt/Cr_2O_3 Thin Films.

M. Al-Mahdawi[1], T. Nozaki[2], H. Imamura[2], M. Oogane[1], Y. Ando[1] and M. Sahashi[1] *1. Tohoku University, Sendai, Japan; 2. National Institute of Advanced Industrial Science and Technology (AIST), Tsukuba, Japan*

Similar to ferromagnetic counterparts, various spin-orbit effects in antiferromagnet/heavy metal (AFM/HM) bilayers were demonstrated [1-4]. Cr_2O_3 is an insulating AFM with a collinear spin structure, and a Néel temperature T_N near room temperature. By doping and lattice engineering, we showed that Cr_2O_3 AFM domains can be controlled by low voltages and magnetic fields [5, 6]. This makes Cr_2O_3 promising for understanding spin-orbit effects in AFM/HM interfaces, and voltage/current control of AFM domains. There are a few reports that investigated the anomalous Hall effect (AHE), and spin-Hall magnetoresistance (SMR) in Pt/Cr_2O_3 thin films [7-9]. However, disentangling the two effects is still needed. In this work, we investigate simultaneously AHE and SMR effects. We deposited epitaxial thin films of *c*-Al_2O_3 sub./Pt (25 nm)/Cr_2O_3 (200 nm) /Pt (2 nm) by Molecular-Beam Epitaxy (MBE) method. We measured the transverse and longitudinal resistances in the top Pt layer, after microfabrication into 10-μm wide bars [Fig. 1a]. At sweeping the out-of-plane field, we find a relatively large AHE resistance in the top Pt layer [Fig. 1b]. Furthermore, the AHE has a square-shaped hysteresis loop, due to switching of AFM domains by the switching of the uncompensated magnetization in Cr_2O_3. Above T_N, the AHE resistance flips in sign, and the curve has a Langevin-type character. We extract the SMR magnitude from fittings to the longitudinal resistance, when the applied magnetic field is scanned in the transverse (*yz*) plane [Fig. 1c]. The AHE has a remnant component at zero field that disappears at T_N, whereas the Langevin-type saturation component starts to appear near T_N [Fig. 2a]. Similarly, the SMR shows a large increase commensurate with the Langevin-type AHE [Fig. 2b]. It is likely that the AHE have two mechanisms, proximity-magnetism-induced part dominating below T_N, and a part coming from spin-Hall effect. This work was partly supported by the Center for Science and Innovation in Spintronics (CSIS), Center for Spintronics Research Network (CSRN), Tohoku University.

[1] Seki *et al.*, Phys. Rev. Lett. 115, 266601 (2015). [2] Qiu *et al.*, Nat. Mater. 17, 577 (2018). [3] Fischer *et al.*, Phys. Rev. B 97, 014417 (2018). [4] Cheng *et al.*, Phys. Rev. Lett. 123, 237206 (2019). [5] M. Al-Mahdawi *et al.*, Phys. Rev. B 95, 144423 (2017). [6] T. Nozaki *et al.*, Phys. Status

Solidi (RRL), 1800366 (2018). [7] Kosub *et al.*, Phys. Rev. Lett. 115, 097201 (2015). [8] Schlitz *et al.*, Appl. Phys. Lett. 112, 132401 (2018). [9] Moriyama *et al.*, Phys. Rev. Applied 13, 034052 (2020).

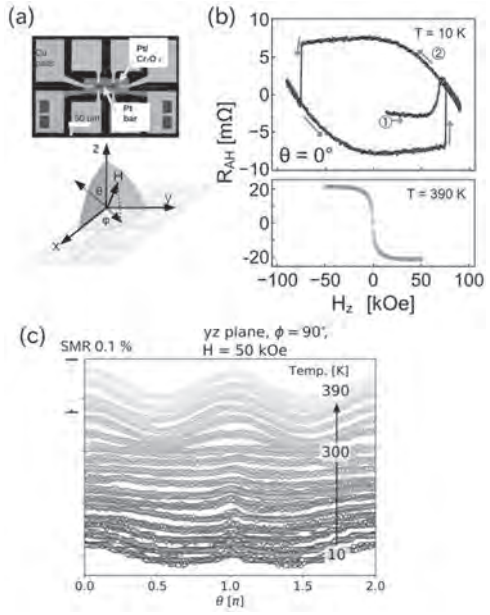

Fig. 1 (a) Microscope image of the device. (b) AHE curves. (c) Angular scans of SMR.

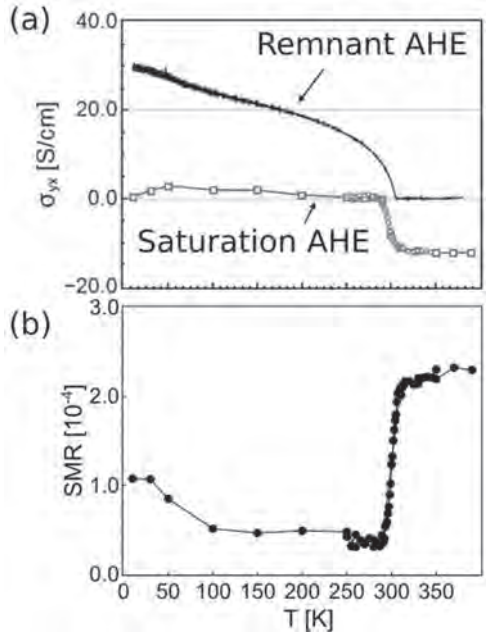

Fig. 2 Temperature dependence of: (a) the two components of AHE conductivity, and (b) SMR.

GOP-07. Voltage-Controlled Dynamic Modulation of Electromagnetic Response in Antiferromagnetic Materials at Terahertz Frequencies. *X. Xu*[1], Y. Semenov[1] and K. Kim[1] *1. North Carolina State University, Raleigh, NC, United States*

Antiferromagnetic materials have recently attracted much interest due to a number of advantages including high resonance frequencies up to the terahertz. Further, the possibility to electrically modulate the magnetic properties such as the anisotropy makes them an excellent candidate for energy-efficient devices at ultra-high frequencies. In this study, we theoretically explored one such application in the dynamic manipulation of electromagnetic responses with a broad tunable spectral range. The materials considered were dielectric antiferromagnets with strong magneto-electric or –elastic coupling which can achieve robust control in the perpendicular magnetic anisotropy. The metallic counterparts were not suitable due to the anticipated large loss. A theoretical analysis based on the Landau-Lifshitz equation was used to derive the frequency-dependent permeability and the resonant frequency of the antiferromagnet for different biaxial anisotropy profiles and incident electromagnetic wave polarizations. Numerical calculations based on typical parameters available in the literature (such as NiO) strongly indicated that the resonance frequency modulation as much as 10's of percent may be possible in the sub-mm wavelength range, along with the corresponding changes in the permeability. Application to specific devices such as a bandpass filter further illustrated the validity of the concept. Funding Acknowledgement This work was supported, in part, by the U.S. Army Research Office (No. W911NF-16-1-0472).

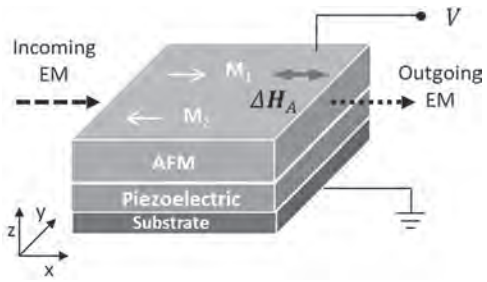

Fig.1 Schematic of the magnetic-piezoelectric composite. Electric field along out-of-plane direction causes magneto-elastic effects and influences eigen-frequency by modifying in-plane magnetic anisotropy. EM wave is incident along x-axis.

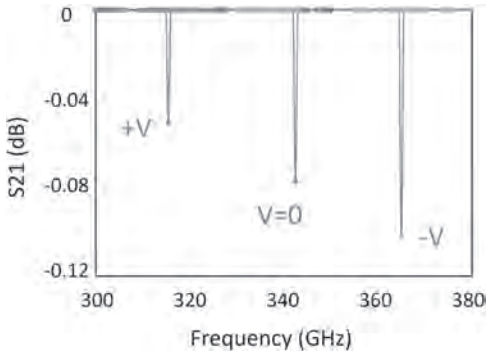

Fig.2 Data showing a high electric field tunable AFMR frequency shift with external voltage at 0, -V, and +V=8kV/cm (Not the final results)

GOP-08. Spin-Hall Diode Based on a Canted Antiferromagnet as a Detector of Microwave Signals. *A. Safin*[1], S. Nikitov[1], V. Tyberkevych[2] and A.N. Slavin[2] *1. Kotel'nikov Institute of Radioengineering of RAS, Moscow, Russian Federation; 2. Oakland University, Rochester Hills, MI, United States*

It is well-known in modern spintronics that magnetic resonance in combination with the inverse spin Hall effect can be used for the detection of microwave-frequency spin currents in ferromagnetic heterostructures [1]. If the detection is necessary in the THz-frequency range, the antiferromagnets (AFM) provide a natural alternative to ferromagnets. A very strong internal magnetic field of the exchange origin existing in AFMs, and keeping the AFM magnetic sublattices antiparallel to each other, provides the so-called "exchange enhancement" to many of the AFM parameters [2]. Thus, the AFM materials demonstrate a great potential for the development of generators and receivers of sub-THz frequency signals [3]. Recently [4],

it has been proposed theoretically that an AFM material having uniaxial anisotropy can be used as a sensitive element for the resonance detection of sub-THz-frequency spin currents. It has been shown that an additional bias DC in the adjacent heavy metal (HM) layer can be used to reduce the effective anisotropy of the AFM layer. In this work, we propose and theoretically describe a concept of a tunable microwave resonance-type quadratic detector based on a heterostructure (Fig.1) comprising a hematite (α-Fe2O3) and a heavy metal (Pt) layers placed on the top of a coplanar waveguide, which provides a linearly polarized AC magnetic field. We show that an external DC magnetic field can be used to the continuously tune the QFMR frequency of the AFM, as shown in Fig.2. We anticipate the above proposed signal detection scheme can quantitatively describe the results of the recent experiments [5,6]. The authors acknowledge a partial financial support from the Government of the Russian Federation under the Project No. 075-15-2019-1874, support from the U.S. National Science Foundation under the grant No. EFMA-1641989, support from the U.S. Air Force Office of Scientific Research under the MURI Grant No. FA9550-19-1-0307, and support from the Oakland University Foundation.

[1] Hellman F., et al. Rev. Mod. Phys. 89, 025006 (2017). [2] Baltz V., et al.// Rev. of Mod. Phys. Vol. 90. 015005 (2018). [3] Khymyn R., et al. // Sci. Rep. Vol. 7. 43705 (2017). [4] Safin A., et al. // APL. Vol.117. 222411 (2020). [5] Boventer I, et al. // Phys. Rev. Lett. Vol.126. 187201 (2021). [6] Wang H., et al. // arXiv:2104.01796 (2021).

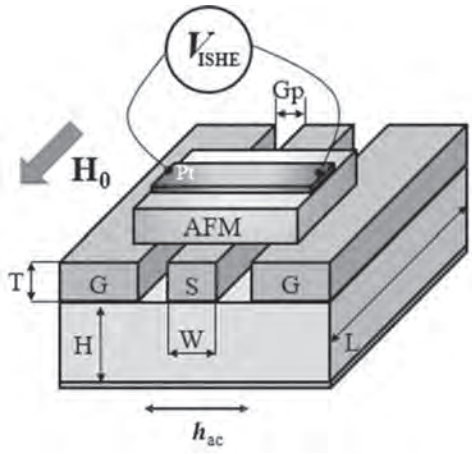

Fig. 1 Schematic view of the microwave detector based on the canted AFM-HM structure

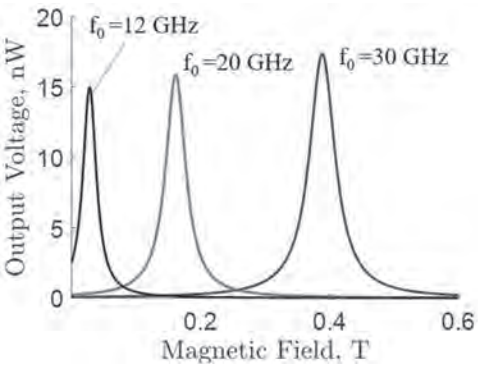

Fig. 2 Resonance curves of the output rectified DC voltage of an AFM-based detector for different input frequencies

GOP-09. Quantifying Spin-Orbit Torques in AFM/HM Heterostructures. *E. Cogulu*[1], H. Zhang[2], N.N. Statuto[1], Y. Cheng[3], F. Yang[3], R. Cheng[2,4] and A. Kent[1] *1. Center for Quantum Phenomena, New York University, New York, NY, United States; 2. Department of Electrical and Computer Engineering, University of California Riverside, Riverside, CA, United States; 3. Department of Physics, The Ohio State University, Columbus, OH, United States; 4. Department of Physics, University of California Riverside, Riverside, CA, United States*

Recently antiferromagnetic materials have been gathering increasing attention from the spintronics community, as detecting and manipulating antiferromagnetic (AFM) order electrically is an important milestone for realizing antiferromagnetic devices. Characterizing the type and amplitude of the spin-orbit torques (SOT) is crucial for understanding and predicting AFM dynamics. One important technique to identify and measure SOTs is to perform harmonic Hall measurements in an AFM/heavy metal (HM) layer. In this study, we report the full angular dependence of 1st and 2nd harmonic voltage measurements in epitaxial c-axis oriented α-Fe_2O_3/Pt bilayer heterostructures (Fig. 1a). By modeling the harmonic resistance signals together with known material parameters such as the exchange field, anisotropy and DMI constant (Fig. 1b), we extract the amplitudes of field-like and anti-damping-like spin-orbit torques from field-dependent measurements in XY, XZ and YZ plane scans (Fig. 1a). Our model suggests a small angle tilt of the easy-plane and indicates that the amplitude of the field-like torques are significantly larger than anti-damping-like torques. Additionally, we show that there is an anomalous Hall-effect contribution in out-of-plane scans and that the Oersted fields are negligible compared to field-like torques. Our work provides a straight-forward way of characterization of spin-orbit torques in AFM/HM heterostructures.

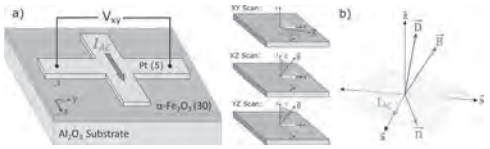

a) Transverse measurement configuration showing the Pt Hall cross with 5 μm channel width on AFM α-Fe_2O_3 layer. An AC current and the transverse voltage is measured with a lock-in amplifier. The thicknesses of α-Fe_2O layer and Pt layers are 30 nm and 5 nm respectively. Next to it, geometry of magnetic field scans in the 3 principal planes (XY, XZ and YZ) is shown. b) Model geometry: D represents both the DMI vector and the hard axis direction. n is the Néel vector which lies in the easy plane. B is the external magnetic field. Alternating current is in x-direction and the spin accumulation in the y-direction. The Néel vector is perpendicular to both D and B.

GOP-10. Dynamics of a ferrimagnetic domain wall by a rotating field. *M. Jin*[1], I. Hong[2], D. Kim[3], K. Lee[1] and S. Kim[1] *1. Department of Physics, KAIST, Daejeon, The Republic of Korea; 2. Korea University, Seoul, The Republic of Korea; 3. KIST, Seoul, The Republic of Korea*

A domain wall has been proposed as central units in spintronic devices such as magnetic domain-wall racetrack memory and domain-wall logic devices [1, 2]. Due to this utility, it is important to find efficient means to drive a domain wall. For example, it has been recently reported that a domain-wall in a ferromagnet can be driven by an AC-field and AC-current and a domain wall in a ferrimagnet can be driven by spin-transfer-torque [3, 4]. Here, we theoretically and numerically study a domain-wall motion in a ferrimagnet by a rotating field. The dynamics of a ferrimagnetic domain wall can be classified into two regimes. First, the stationary solution corresponding to the low frequency can be interpreted to belong to a phase-locking regime, where a domain-wall angle rotates in-phase with an external field. Second, the non-linear solution corresponding to the high frequency can be interpreted as a phase-unlocking regime [5-7], where a domain-wall angle is not synchronous with the applied field. In the phase locking regime, the domain-wall velocity is proportional to the field frequency, which implies

that the velocity of the domain wall can be controlled by the rotating-field frequency. Once the frequency is over the critical frequency (set by the field magnitude), the domain-wall dynamics enters the phase-unlocking regime where the domain wall velocity decreases due to the incoherent precessional motion of a domain wall. Moreover, the sign of the domain-wall velocity is flipped across the angular compensation point where the net spin density of the ferromagnets changes its sign. Considering that there have been experimental demonstrations of the effect of rotating magnetic field on the dynamics of a magnetic vortex domain-wall chirality reversal [8], we believe that our setup is experimentally feasible. Our work reports not only the novel critical phenomenon associated with the dynamics of a ferrimagnetic domain-wall by a rotating field, but also a new way to detect the angular momentum compensation point of ferrimagnets.

[1] D. A. Allwood, G. Xiong, C. Faulkner, D. Atkinson, D. Petit, and R. Cowburn, Science., Vol. 309, p.1688 (2005) [2] S. S. Parkin, M. Hayashi, and L. Thomas, Science., Vol. 320, p.190 (2008) [3] D.-H. Kim, D.-H. Kim, D.-Y. Kim, S.-B. Choe, T. Ono, K.-J. Lee, and S. K. Kim, Physical Review B., Vol. 102, p.184430 (2020) [4] D.-H. Kim, D.-H. Kim, K.-J. Kim, K.-W. Moon, S. Yang, K.-J. Kim, S. K. Kim, Journal of Magnetism and Magnetic Materials., Vol. 514, p.167237 (2020) [5] W. H. Rippard, M. R. Pufall, S. Kaka, T. J. Silva, S. E. Russek, and J. A. Katine, Physical Review Letters., Vol. 95, p.067203 (2005) [6] B. Georges, J. Grollier, M. Darques, V. Cros, C. Deranlot, B. Marcilhac, G. Faini, and A. Fert, Physical Review Letters., Vol. 101, p.017201 (2008) [7] S. Urazhdin, P. Tabor, V. Tiberkevich, and A. Slavin, Physical Review Letters., Vol. 105, p.104101 (2010) [8] A. Bisig, M.-A. Mawass, M. Stark, C. Moutafis, J. Rhen- sius, J. Heidler, S. Gliga, M. Weigand, T. Tyliszczak, B. Van Waeyenberge, et al., Applied Physics Letters., Vol. 106, p.122401 (2015)

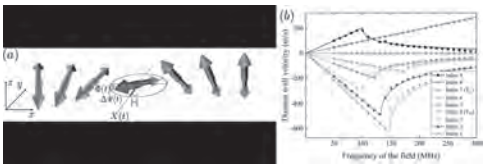

Fig. 1. (a) Schematic of motion of domain wall for a ferrimagnet in a rotating field. (b) Comparison between analytic solutions (lines) and simulation results (dots) at various temperatures.

GOP-11. Spin-pumping and inverse spin-Hall effects in collinear and canted antiferromagnets. *I. Boventer*[1], H.T. Simensen[2], A. Anane[1], M. Kläui[3], A. Brataas[2] and R. Lebrun[1] *1. Unité Mixte de Physique CNRS/ Thales, Palaiseau, France; 2. NTNU, Trondheim, Norway; 3. Johannes Gutenberg Universitat, Mainz, Germany*

Spintronics with antiferromagnets (AFMs) is anticipated to enable enhanced data processing speeds and downscaling for on-chip information processing [1]. However, in compensated AFMs, the absence of a net moment strongly impedes simple access to their ultrafast dynamics, especially in thin films, and the development of ultra-fast AFM based devices [2,3]. Spin to charge conversion mechanisms such as the spin pumping effect could offer a promising avenue to access and manipulate the dynamics of AFM thin films. Nevertheless, spin-pumping in colinear AFMs scales with the dynamical sub-lattice symmetry breaking, which is generally small and was until now only measured in two recent experimental studies [4,5] at low temperature. Here we study theoretically and experimentally the spin pumping signals induced by the resonance of non-collinear AFMs, in which the Dzyaloshinskii-Moriya interaction generates small canted moments[6]. We demonstrate that this sub-class of AFM materials (among which various orthoferrites with sub-THz resonance frequencies) can generate easily observable inverse spin-Hall voltages. The inverse spin-Hall voltage V_{ISHE} is shown to be proportional to the ratio H_D/H_E (H_D : DMI field, H_E : exchange field), whilst it is proportional to H_A/H_E (H_A : anisotropy field) in colinear systems. Using a bilayer of hematite/heavy metal as a model system, we then measure at room temperature the resonance of the low frequency AFM mode and an associated inverse spin-Hall voltage, as large as in collinear AFMs (see Fig. 1). Finally, as expected for coherent spin-pumping, we observe that the sign of the inverse spin-Hall voltage provides direct information about the mode handedness as deduced by comparing hematite, chromium oxide and the ferrimagnet Yttrium-Iron Garnet. Our results open new means to generate and detect spin-currents at terahertz frequencies by functionalizing AFMs with low damping and canted moments.

[1] V. Baltz, A. Manchon, M. Tsoi, T. Moriyama, T. Ono, and Y. Tserkovnyak, *Antiferromagnetic Spintronics*, Rev. Mod. Phys. 90, 015005 (2018). [2] T. Kampfrath, A. Sell, G. Klatt, A. Pashkin, S. Mährlein, T. Dekorsy, M. Wolf, M. Fiebig, A. Leitenstorfer, and R. Huber, *Coherent Terahertz Control of Antiferromagnetic Spin Waves*, Nat. Photonics 5, 31 (2011). [3] S. Foner, *High-Field Antiferromagnetic Resonance in Cr 2 O 3*, Phys. Rev. 130, 183 (1963). [4] P. Vaidya, S. A. Morley, J. van Tol, Y. Liu, R. Cheng, A. Brataas, D. Lederman, and E. del Barco, *Subterahertz Spin Pumping from an Insulating Antiferromagnet*, Science 368, 160 (2020). [5] J. Li, C. B. Wilson, R. Cheng, M. Lohmann, M. Kavand, W. Yuan, M. Aldosary, N. Agladze, P. Wei, M. S. Sherwin, and J. Shi, *Spin Current from Sub-Terahertz-Generated Antiferromagnetic Magnons*, Nature 578, 7793 (2020). [6] I. Boventer, H. T. Simensen, A. Anane, M. Kläui, A. Brataas, and R. Lebrun, *Room-Temperature Antiferromagnetic Resonance and Inverse Spin-Hall Voltage in Canted Antiferromagnets*, Physical Review Letters 126 18, 187201 (2021)

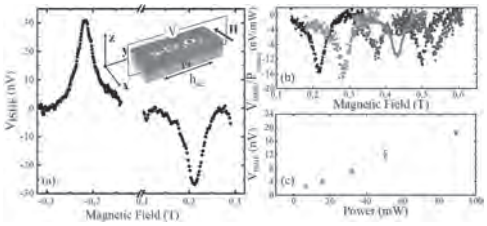

Inverse spin Hall effect voltages V_{ISHE} in the canted easy plane antiferromagnet hematite. (a) ISHE voltage measurement at ± 0.2 T in transverse configuration. (b) V_{ISHE} as a function of the external magnetic field.(c) Dependence of V_{ISHE} with the applied microwave power for a f = 31 GHz.

GOP-12. Strong exchange coupling between Mn_2Au and Permalloy thin films for read-out in antiferromagnetic spintronics. *M. Jourdan*[1], S. Bommanaboyena[1], D. Backes[2], L. Veiga[2], S. Dhesi[2], Y. Niu[3], B. Sarpi[3], T. Denneulin[4], A. Kovacs[4], T. Mashoff[1], O. Gomonay[1], J. Sinova[1], K. Everschor-Sitte[5], D. Schönke[1], R.M. Reeve[1], H. Elmers[1] and M. Kläui[1] *1. Johannes Gutenberg University Mainz, Mainz, Germany; 2. Diamond Light Source, Didcot, United Kingdom; 3. MAX IV Laboratory, Lund, Sweden; 4. Forschungszentrum Jülich, Jülich, Germany; 5. Universität Duisburg Essen, Duisburg, Germany*

With respect to applications, the read-out of the orientation of the staggered magnetization (Néel vector) is one of the major challenges in antiferromagnetic (AFM) spintronics. Here, we present an exceptionally strong exchange coupling of the magnetization of thin (2-10 nm) Permalloy layers and epitaxial antiferromagnetic $Mn_2Au(001)$ (40 nm) thin films [Bom21]. This enables the indirect read-out of the Néel vector orientation via various established methods detecting the orientation of ferromagnetic (FM) magnetization. We demonstrate by photoelectron emission microscopy a perfect imprinting of the AFM domain structure of the Mn_2Au thin film into the domain pattern of the FM. Measuring hysteresis loops of the magnetization, we observed that a magnetic field as large as 0.5 T is required to abruptly align the magnetization of 2 nm of Permalloy parallel with the field. While this happens, the Néel vector and the magnetization do not decouple, but rotate together, as we demonstrate by X-ray magnetic linear and circular dichroism measurements in transmission mode. We show by scanning transmission electron microscopy, that this strong exchange coupling results from a well-defined termination of the $Mn_2Au(001)$ thin films, which is associates with a homogeneous FM terminating layer of the AFM, as shown schematically in the figure.

[Bom21] S. B. Bommanaboyena et al., arXiv:2106.02333 (2021)

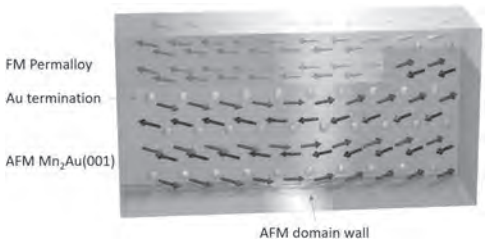

This schematic cut through the Mn_2Au/Py bilayer shows a side view of two 90deg domains and visualizes the morphological origin of the imprinting of the AFM domain pattern into the FM. The magnetization is always aligned parallel with the Néel vector and couples with the same relative orientation, despite the existence of atomic steps.

GOP-13. Anomalous Nernst effect in thin films of non-collinear antiferromagnet Mn_3NiN. F. Johnson[1], *J. Kimak*[2], E. Schmoranzerová[2], H. Reichlova[3], Z. Soban[4], J. Godinho[2,4], K. Olejnik[4], S. Beckert[3], J. Zemen[5], J. Wunderlich[6], P. Nemec[2] and L. Cohen[1] *1. Department of Physics, Imperial College London, London, United Kingdom; 2. Faculty of Mathematics and Physics, Charles University, Prague, Czechia; 3. Institut für Festkörper- und Materialphysik, Technische Universitat Dresden, Dresden, Germany; 4. Institute of Physics of the Czech Academy of Sciences, Prague, Czechia; 5. Faculty of Electrical Engineering, Czech Technical University in Prague, Prague, Czechia; 6. Institute of Experimental and Applied Physics, University of Regensburg, Regensburg, Germany*

Antiferromagnetic materials with non-collinear spin structures (NC-AFMs) offer significant potential for spintronic applications[1]. They have vanishingly small magnetization and ultrafast spin dynamics. In addition, they allow for the presence of important counterparts to the effects considered to be exclusive to materials with net magnetization, such as the anomalous Hall effect (AHE)[2], magneto-optical Kerr effect[3] or anomalous Nernst effect (ANE)[4]. One of the promising candidates of the NC-AFM class are Mn antiperovskites, with a typical representative being Mn_3NiN. In this contribution we present ANE measurements on epitaxial thin films of Mn_3NiN prepared on $SrTiO_3$ substrate with spin structure lying in the (111) plane. Previous theoretical predictions suggest that despite the modest spin-orbit coupling, the magnitude of the ANE in Mn_3NiN ought to exceed that of Mn_3Sn NC-AFM due to the Berry phase boost[5]. We implement two complementary methods to detect the ANE response of the Mn_3NiN films. First, the global Nernst response is measured using a micro-patterned Hall bar device with platinum resistive heaters generating an in-plane thermal gradient. The measured anomalous Nernst data (Fig.1(a)) are in good agreement with the AHE measurements[5], indicating a similar physical origin of the two effects. Second, to add a spatial resolution, scanning thermal gradient microscopy[4] is used. A laser beam incident on a micro-patterned device induces thermal gradients. The method reveals the sample's domain structure. We find a signature of an ANE component that we can control with the external field due to the unsaturated moment present lying in the (111) plane, different from the previously measured Mn_3Sn. This small moment provides a means for manipulating magnetic order, and even writing magnetic domain-like structures (Fig.1(b)). These two methods provide fruitful insight into the magnetic behaviour of NC-AFMs.

[1] J. Zelezný, Y. Zhang, C. Felser, and B. Yan, Phys. Rev. Lett. 119, 187204 (2017) [2] Nakatsuji, S., Kiyohara, N. & Higo, Nature 527, 212–215 (2015) [3] T. Higo, et al. Nature Photon. 12, 73–78 (2018) [4] H. Reichlová et al., Nat. Commun. 10, 5459 (2019) [5] D. Boldrin et al., Phys. Rev. Materials 3, 094409 (2019)

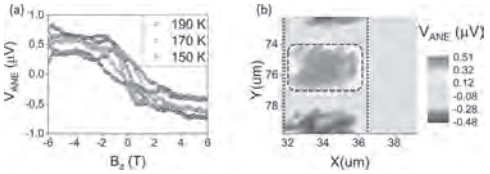

Fig.1. Anomalous Nernst effect in Mn3NiN. (a) Global ANE as a function of the out-of-plane magnetic field at different base temperatures. (b) Scanning thermal gradient microscopy at T = 100 K. The domain-like structure was written by high-intensity laser beam and 500 mT in-plane magnetic field.

GOP-14. Determination of spin-orbit torque efficiency in non-collinear antiferromagnet / heavy metal heterostructures. *K. Kishi*[1,2], Y. Takeuchi[3], Y. Yamane[2,4], J. Yoon[1,2], R. Takechi[1,2], B. Jinnai[3], S. Kanai[1,5], J. Ieda[6], H. Ohno[1,7] and S. Fukami[1,8] *1. Research Institute of Electrical Communication, Tohoku University, Sendai, Japan; 2. Graduate School of Engineering, Tohoku University, Sendai, Japan; 3. Advanced Institute for Materials Research, Tohoku University, Sendai, Japan; 4. The Frontier Research Institute for Interdisciplinary Sciences, Tohoku University, Sendai, Japan; 5. Center for Spintronics Research Network, Tohoku University, Sendai, Japan; 6. Advanced Sciences Research Center, Japan Atomic Energy Agency, Tokai, Japan; 7. Center for Science and Innovation in Spintronics, Tohoku University, Sendai, Japan; 8. Center for Innovative Integrated Electronic Systems, Tohoku University, Sendai, Japan*

Electrical manipulation of antiferromagnetic materials [1-3] is a representative outcome in antiferromagnetic spintronics, a newly established field attracting increasing attention. A recent study showed a novel spintronic phenomenon, that is, the rotation of chiral-spin structure by spin-orbit torque (SOT) in M-plane oriented non-collinear antiferromagnet Mn_3Sn film [4]. Of particular interest in antiferromagnetic spintronics is the efficiency of SOT acting on the antiferromagnetic ordering [5], which has not been well studied so far. In this work, we report the determination of SOT efficiency in non-collinear antiferromagnet Mn_3Sn / heavy metal heterostructures. We deposit W(2)/Ta(3)/Mn_3Sn(15)/MgO(1.3)/Ru(1) (in nm) on MgO(110) substrate by DC/RF magnetron sputtering [6], followed by annealing at 500 °C for an hour. The stack is then patterned into Hall bars, where the angle θ between the channel and kagome plane (0001) of Mn_3Sn is systematically varied. The efficiency of SOT acting on Mn_3Sn is measured by the phase diagram of the switching field (H_C) versus applied current (I). Figure 1 shows a Hall resistance (R_H) as a function of the magnetic field (H) with various applied currents for θ = 0°, i.e., $I \perp$ (0001). decreases with I as was seen in [4]. The switching phase diagrams for each θ are shown in Fig. 2. The linear relationship indicates a dominant contribution of SOT to the reduction of H_C. The slope of H_C-I decreases with increasing θ, which can be understood by considering the reduction of SOT contribution to the rotation of chiral-spin structure [4,7]. From the θ dependence of the slope with a reasonable macrospin approximation, the Slonczewski-like SOT efficiency is determined to be |0.15|, agreeing with previous reports of a system with Ta and ferromagnet [8]. This work was partly supported by JSPS Kakenhi (19H05622, 20K22409, and 21J23061), Iketani Science and Technology Foundation (0331108-A), and RIEC Cooperative Research Projects.

[1] P. Wadley *et al.*, Science 351, 587 (2016). [2] H. Tsai *et al.*, Nature 580, 608 (2020). [3] S. DuttaGupta *et al.*, Nat. Commun. 11, 5715 (2020). [4] Y. Takeuchi *et al.*, Nat. Mater. (2021). https://doi.org/10.1038/s41563-021-01005-3. [5] J. Yu *et al.*, Nat. Mater. 18, 29 (2019). [6] J.-Y. Yoon *et al.*, Appl. Phys. Express 13, 013001 (2019). [7] Y. Yamane *et al.*, Phys. Rev. B 100, 054415 (2019). [8] H. Gamou *et al.*, Phys. Rev. B 99, 184408 (2019).

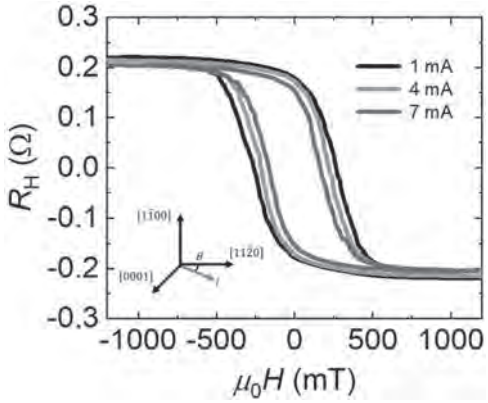

Fig.1 Applied current (*I*) dependence of R_H-*H* curve.

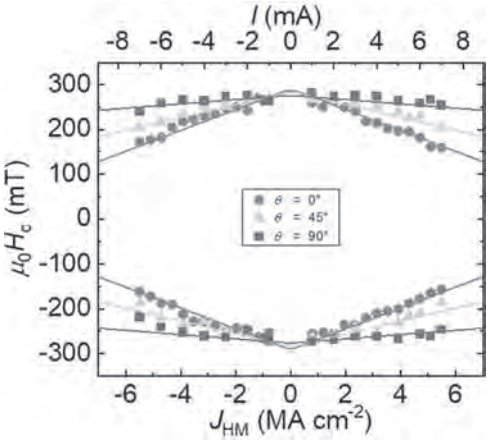

Fig. 2 Switching field (H_C) versus applied current *I* for various θ.

GOP-15. Memory of frozen and rotatable antiferromagnetic spins in epitaxial CoO(111)/Fe and NiO(111)/Fe bilayers. *M. Slezak*[1], H. Nayyef[1], P. Drozdz[1], W. Janus[1], A. Koziol-Rachwal[1], M. Szpytma[1], M. Zajac[2], T. Mentes[3], A. Locatelli[3], F. Genuzio[4] and T. Slezak[1] *1. AGH University of Science and Technology, Krakow, Poland; 2. National Synchrotron Radiation Centre SOLARIS, Jagiellonian University, Krakow, Poland; 3. Elettra - Sincrotrone Trieste, Basovizza, Trieste, Italy; 4. CERIC-ERIC, Basovizza, Trieste, Italy*

We combined XMLD, XMCD and MOKE measurements in order to follow the magnetic properties of epitaxial CoO(111)/Fe(110) [1] and NiO(111)/Fe(110) [2] bilayers. We find that in both studied cases FM sublayer plays a dominant role and determines the magnetic state of the neighboring AFM, however completely different interaction mechanisms are involved. In CoO/Fe bilayers the AFM spins are frozen and their orientation is imprinted by magnetization of Fe layer when the system passes the Neel temperature of CoO. Once the Fe layer grafts the particular magnetic anisotropy (MA) into the CoO overlayer, it later remains frozen and insensitive to external factors like external magnetic field or Fe magnetization direction [3]. Specifically, choice of particular magnetic state of Fe sublayer, when passing Néel temperature of CoO, determines both the axis and direction of interfacial antiferromagnetic spins after the sample is cooled and allows for imprinting their +/- 90° and 0/180° alignment within the sample plane. For example, particular direction of frozen AFM spins determines the corresponding sign of the shift field of exchange biased magnetic hysteresis loop (Fig.1). For NiO/Fe bilayers, due to the weak intrinsic MA of NiO, the AFM spins are rotatable and always follow the reorientation of Fe magnetization that can be controlled by external magnetic field or via the temperature and thickness driven SRT of Fe(110). Recently we showed that in a uniform thickness NiO(111)/Fe(110) system, two magnetic states with orthogonal spin orientations can be stabilized in antiferromagnetic NiO [2]. Field-free, reversible switching between these AFM states was demonstrated. Here we present results of systematic investigations of such field-free, temperature induced switching of AFM NiO spins. Fig. 2 shows temperature dependence of R_{L2} ratio for various thicknesses of Fe. Critical temperature of SRT in AFM NiO can be tuned in wide temperature window ~ (250 – 380 K) for field-free, reversible switching of AFM spins. XML(C)D-PEEM results obtained on individual self-organized NiO/Fe nanostripes will be also presented.

[1] M. Slezak et al., Scientific Reports 9 889 (2019) [2] M. Slezak et al., Nanoscale, 12, 18091 (2020) [3] M. Slezak et al., submitted to JMMM [4] M. Slezak et al., in preparation

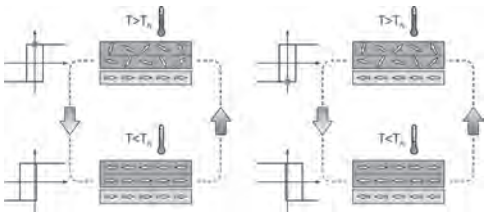

Fig.1. Memory of frozen AFM spins in CoO(111)/Fe bilayer.

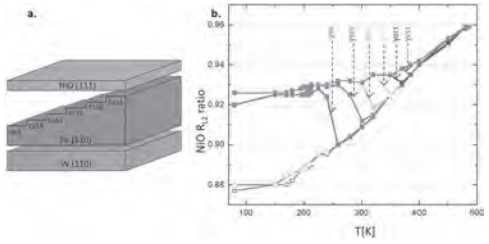

Fig.2. Temperature dependence of XMLD (R_{L2} ratio) for NiO/Fe [4].

Session GOQ
SPIN INJECTION AND SPIN TRANSFER TORQUES

Hélène Béa, Co-Chair
Université Grenoble Alpes, Spintec, Grenoble, France
Emilie Jué, Co-Chair
National Institute of Standards and Technology, Boulder, CO, United States

INVITED PAPERS

GOQ-01. Memristor-controlled mutual synchronization of spin Hall nano-oscillator arrays for neuromorphic computing and spintronic Ising machines. *J. Åkerman[1] 1. Department of Physics, University of Gothenburg, Gothenburg, Sweden*

Synchronization of large spin Hall nano-oscillators (SHNO) arrays is an appealing approach toward ultra-fast non-conventional computing based on nanoscale coupled oscillator networks [1]. However, for large arrays, interfacing to the network, tuning its individual oscillators, their coupling, and providing built-in memory units for training purposes, remain substantial challenges. Here, we address all these challenges using memristive gating of W/CoFeB/MgO/AlOx based SHNOs. We use this type of stack as their substantial perpendicular magnetic anisotropy (PMA) can generate both localized and propagating spin waves [2]. In its high resistance state (HRS), the memristor modulates the perpendicular magnetic anisotropy (PMA) at the CoFeB/MgO interface purely by the applied electric field, which leads to both a voltage-controlled SHNO frequency and a voltage-controlled threshold current [3]. In its low resistance state (LRS), and depending on the voltage polarity, the memristor adds/subtracts a current I_m to/from the SHNO drive. The operation in this LRS also affects the SHNO auto-oscillation mode and frequency, which can be tuned up to 28~MHz/V. This tuning allows us to reversibly turn on/off mutual synchronization in chains of four SHNOs and turn the chain into different partially synchronized states [4]. Memristor gating is, therefore, an efficient approach to input, tune, and store the state of the SHNO array for any non-conventional computing paradigm, all in one platform. Examples include SHNO based Ising Machines [5,6] and pattern recognition using memristive-controlled SHNO chains [4], which will both be discussed in detail in the presentation.

[1] M. Zahedinejad *et al.* Nature Nanotechnology 15, 47 (2020) [2] H. Fulara *et al.* Science Advances 5, eaax8467 (2019) [3] H. Fulara *et al.* Nature Communications 11, 4006 (2020) [4] M. Zahedinejad *et al.* arXiv:2009.06594 [5] D. I. Albertsson *et al.* Appl. Phys. Lett. 118, 112404 (2021) [6] A. Houshang *et al.* arXiv:2006.02236

GOQ-02. Theory of Spin Torques Emerging from Band Topology. *Y. Araki[1] 1. Advanced Science Research Center, Japan Atomic Energy Agency, Tokai, Japan*

Band inversion of electrons due to strong spin-orbit coupling (SOC) is commonly seen in magnetic materials. It characteristically appears in topological insulators (TIs) with inverted bandgaps [1] and Weyl semimetals (WSMs) with pointlike band crossings [2], while metallic systems are also capable of having band inversion. In momentum space around the SOC-induced band inversion, the electron spin is often correlated to its momentum, known as spin-momentum locking (SML). Moreover, the electron system acquires nontrivial band topology characterized by the Berry curvature, which serves as an effective magnetic field in momentum space. It is well understood that the band topology gives a substantial contribution to anomalous transport phenomena, such as the anomalous Hall effect (AHE) and the spin Hall effect (SHE), due to the anomalous velocity of electrons triggered by the Berry curvature. Recent experimental attempts have been successful in synthesizing materials having both nontrivial band topology and magnetism (magnetic TIs, WSMs, etc.), and it is an important question if their magnetic functionalities are also governed by their band topology. In this talk, I show from theoretical aspect that the current-induced spin torques in such magnetic topological materials are influenced and occasionally enhanced due to their band topology. After reviewing the current status of theoretical and experimental studies on magnetic topological materials, I will introduce some of my recent works. From the general point of view, I first propose that the momentum-space topology gives rise to an "intrinsic" contribution to the spin torques, which is robust against disorder and thermal fluctuation similarly to the intrinsic AHE and SHE [3]. This intrinsic torque originates from electron spin polarization converted from the anomalous velocity by SML, and is distinct from the conventional spin-transfer torque (STT) and the spin-orbit torque (SOT) driven by electron spins in transport current. In particular, I point out the intrinsic torque exerting on magnetic textures, such as domain walls (DWs), which we call the "topological Hall torque (THT)". The THT is induced by the cooperation of the real-space magnetic texture and the momentum-space Berry curvature, and can emerge dominantly in bulk crystals without building any complex heterostructures. As a typical example, I show our microscopic calculation result of current-induced torques with the low-energy effective model of magnetic WSM [4]. The band crossing points, called "Weyl points", serve as source and sink of the Berry curvature in momentum space, accompanied with SML of electrons around them (see Fig. 1). The Weyl electrons are therefore capable of generating a strong intrinsic torque. From the microscopic calculation in response to an externally applied electric field, we have derived the SOT, the STT, and the THT exerted by the Weyl electrons. The THT gets enhanced at a sharp magnetic DW, due to the localized states of Weyl electrons formed at the DW [5,6]. For more realistic situations, I also show the phenomenological calculation of the THT in a metallic ferromagnet with band inversion [3]. In response to an external electric field applied to a DW (see Fig. 2), we have obtained a large THT. The THT acts on a DW in the same form as the conventional nonadiabatic STT, but with the unusual size of the nonadiabaticity parameter $\beta \approx 2$, which will enable an efficient control of DW motion by electric field. Experimental measurability of the THT in the metallic ferromagnet $SrRuO_3$, in connection with the temperature dependence in its AHE [7], will also be mentioned.

[1] M. Z. Hasan and C. L. Kane, Rev. Mod. Phys. 82, 3045 (2010). [2] N. P. Armitage, E. J. Mele, and A. Vishwanath, Rev. Mod. Phys. 90, 015001 (2018). [3] Y. Araki and J. Ieda, arXiv:2105.14922. [4] D. Kurebayashi, Y. Araki, and K. Nomura, J. Phys. Soc. Jpn. 90, 084702 (2021). [5] Y. Araki, A. Yoshida, and K. Nomura, Phys. Rev. B 94, 115312 (2016). [6] Y. Araki, Ann. Phys. (Berlin) 532, 1900287 (2019). [7] Z. Fang, N. Nagaosa, K. S. Takahashi, *et al.*, Science 302, 92 (2003).

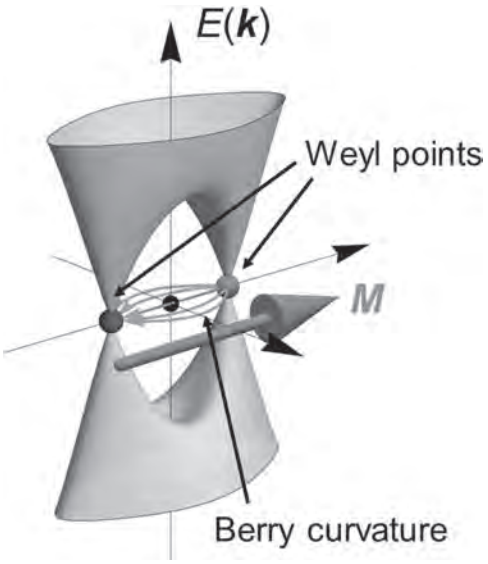

Fig. 1 Schematic image of Weyl points emerging from band inversion. The Berry curvature (magenta curves) emerges in the vicinity of the Weyl points.

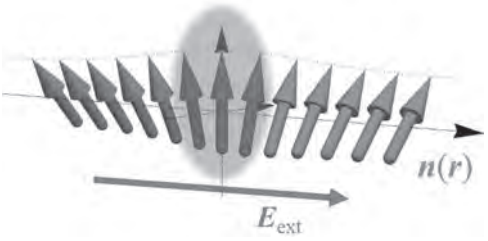

Fig. 2 Schematic image of the setup of magnetic DW in our calculations [3]. We consider an external electric field E_{ext} applied across the DW, and calculate the torque in response to E_{ext}.

CONTRIBUTED PAPERS

GOQ-03. Enhancement of heat controlled magnetic anisotropy by improving a thermal design of magnetic tunnel junctions. *M. Goto*[1,2], R. Kobayashi[1], R. Okuno[1], Y. Yamada[1], T. Mizuno[3], T. Yamane[3], N. Degawa[3], T. Suzuki[3], A. Shimura[3], S. Aoki[3], J. Urabe[3], S. Hara[3], H. Nomura[1,2] and Y. Suzuki[1,2] *1. Osaka University, Toyonaka, Japan; 2. CSRN-Osaka, Toyonaka, Japan; 3. TDK corporation, Chuo-ku, Japan*

Magnetic tunnel junctions (MTJs) have been a promissing devices as a next-generation microwave devices. To obtain higher microwave properties, large spin-torque is significant. Recently, the large spin-torque has been obtained by a temperature change thanks to a heat controlled magnetic anisotropy (HCMA) effect [1]. The temperature change is enhanced by the suppression of heat dissipation due to high interfacial thermal resistance at a metal | insulator interface [2]. However, there has been little study on thermal design in MTJs. Here, we have investigated a HCMA of MTJs with various capping layers to understand the effect of junction structures. Film stack is buffer layer | Ir-Mn | Co-Fe | Ru | Co-Fe-B pinned layer | MgO barrier (1 nm) | Fe-B free layer (2 nm) | capping layer | metal electrode. We prepared two types of the capping layer: MgO (with thickness of 0.3 nm, 0.4 nm, 0.5 nm) and a composite of MgO (0.3 nm) | W (2 nm) | MgO (0.4 nm). Here, the high interfacial thermal resistance is expected at the (Co-)Fe-B|MgO and W|MgO interfaces [3, 4]. The perpendicular magnetic anisotropy and its change were measured through the spin-torque ferromagnetic resonance measurement [5]. Figure 1 shows the magnitude of HCMA defined as the magnetic anisotropy energy change by DC power per unit area. HCMA increases as the total MgO thickness in capping layers increases [6]. The increase in the interfacial thermal resistance may be attributed to roughness at the Fe-B | MgO capping layer interface. This project was supported by JSPS and VAST under the JSPS-VAST Joint Research Program, JSPS KAKENHI Grant Number JP19K15435, JP20H05666, and CREST (Non-classical Spin project, JPMJCR20C1) of the Japan Science and Technology Agency.

[1] M. Goto *et al.*, Nat. Nanotechnol. 14 40 (2019), [2] T. Böhnert *et al.*, Phys. Rev. B 95 104441 (2017), [3] J. Zhang *et al.*, Phys. Rev. Lett, 115, 037203 (2015), [4] H. Wang *et al.*, Mater. Trans, 48, 2349 (2007), [5] A. A. Tulapurkar *et al.*, Nature 438 339 (2005), [6] R. Okuno *et al.*, J. Phys. Condens. Matter, 32, 384001 (2020)

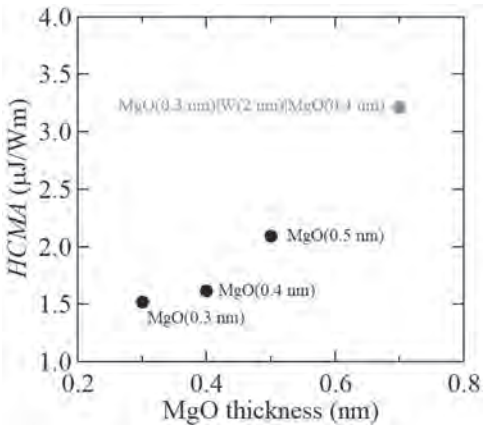

Figure 1 MgO capping thickness dependence of HCMA.

GOQ-04. Ohmic contact on n-type Si using an Iron-based alloy. *N. Yamashita*[1], E. Shigematsu[1], S. Honda[2], R. Ohshima[1], M. Shiraishi[1] and Y. Ando[1] *1. Electronic Science and Engineering, Kyoto University, Kyoto, Japan; 2. Department of Pure and Applied Physics, Kansai University, Suita, Japan*

There are only three transition elements having Curie temperatures (T_c) higher than a room temperature (RT) due to the Stoner criterion: cobalt, nickel, and iron (Fe).[1)] An obstacle for the application of semiconductor-based spin devices is their little variation of the Fermi energy, E_F: they locate at within only 0.7 eV (ranging from −4.5 to −5.2 eV below the vacuum level), which must arise the Schottky barriers at the metal/semiconductor interfaces. Spintronics researchers desire new ferromagnetic/ferrimagnetic materials (FMs) satisfying T_c > RT and widely variable E_F. Here we show that an Fe-based alloy, FeGd, satisfies the condition. $Fe_{100-x}Gd_x$ thin films were prepared by the co-evaporation of Fe and Gd. To examine the E_F, ultraviolet photoelectron spectroscopy was carried out to measure the work function, i.e., the difference between E_F and a vacuum level. The total thickness of the sample film was 60 nm, and the deposition rate of each source was changed during the evaporation to make a variety of x in the film. We observed a large change of the work function depending on x (the atomic percent of Gd). Surprisingly, only 20 % of Gd incorporation in Fe raised the E_F largely from −4.8 to −3.0 eV. The large change of the work function is unprecedented and out of the scope of the conventional understanding based on the image force model.[2,3)] The small work function realized an ohmic contact on n-type nondegenerate Si, which was experimentally observed. We confirmed the $Fe_{80}Gd_{20}$ alloy has magnetization and spin polarization at RT: the magnetization was confirmed at RT by using a vibrating sample magnetometer, and the spin polarization was confirmed at 300K by measuring the anomalous Hall effect. Thus, the FeGd alloy provides a small interface resistance for spin injection into Si at RT. The finding provides a new insight for designing spintronic devices combined with semiconductors.

1) E. C. Stoner, Proc. Math. Phys. Eng. Sci. 165, 372 (1938). 2) J. A. Rothschild and M. Eizenberg, Phys. Rev. B 81, 224201 (2010). 3) S. Halas and T. Durakiewicz, J. Phys.: Condens. Matter 10, 10815 (1998).

GOQ-05. Spin mixing conductance at interfaces of TI/FM and HM/FM heterostructures. *O. Van't Erve*[1], X. Zhang[1], C.H. Li[1] and B. Jonker[1]
1. Naval Research Lab, Washington, DC, United States

The spin mixing conductance is an important figure of merit for spin transport across an interface. This is a particularly important number for Spin Orbit Torque Magnetic Random Access Devices, where spin generated in one layer is used to provide the spin torque needed to flip the magnetization in an adjacent layer. Here the spins are generated in either an topological insulator (TI) or an heavy metal (HM). The overall efficiency of such a device depends on both the charge to spin conversion in the spin generation layer and the spin mixing conductance of the interface. Here we are going to show the results on TI/FM and HM/FM interfaces. In the topological insulator the spins are generated by the spin-momentum locked states in the topological surface states, whereas in the heavy metal the spins are generated through the spin Hall effect. We will show the spin mixing conduction of several heterostructures using a variety of measurements, that include MOKE, FMR, ST-FMR, SMR and ISHE measurements.

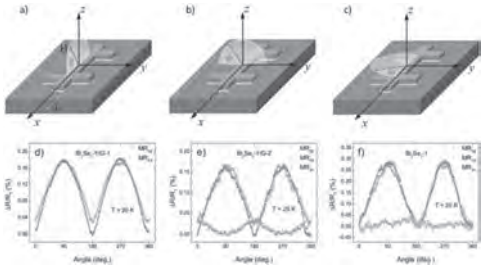

Figure 1 a)-c) schematics for χ rotation, φ rotation, and ω rotation, respectively; d)-f) ADMR of Bi2Se3-YIG-1, Bi2Se3-YIG-2, and Bi2Se3-1 in a magnetic field of 0.5 T, 0.8 T, and 0.8 T, respectively. In e) the in-plane ADMR (ω rotation) follows cosine-squared dependence indicated by an orange curve.

GOQ-06. Splitting of the Nonlinear Spin-Torque Vortex Oscillator Dynamics Originating from the Ampère-Oersted Field Induced by the Excitation Current. *S. de Wergifosse*[1], C. Chopin[1] and F. Abreu Araujo[1]
1. IMCN / BSMA, Université Catholique de Louvain, Louvain-la-Neuve, Belgium

We present the impact of the DC current induced Ampère-Oersted field (AOF) on the dynamics of a spin-torque vortex oscillator (STVO) by comparing results from an analytical model based on the Thiele equation approach (TEA)[1] and from micromagnetic simulations performed using mumax[3] (see Fig. 1). We propose two improvements for the analytical model. The first is the increased precision of the magneto-static contribution [2] by taking into account the aspect ratio of the STVO that increases its validity range. The second enhancement, is the inclusion of a fully analytical description of the AOF contribution [3] to understand its impact on the STVO dynamics. The proposed analytical model describes quantitatively the STVO dynamics in the resonant regime (i.e. when the vortex core position is near the center of the dot and in the damping regime). In addition, the impact of AOF can be clearly seen in the micromagnetic simulations in both the resonant and steady-state regimes (see Fig. 2). as a splitting of the frequency and the vortex core position arises depending on the vortex chirality [4, 5] (anti-clockwise (C^+) or clockwise (C^-)) as shown in Fig. 2. The splitting depends on the relative orientation of the AOF and the vortex chirality as well as the reduced vortex position $s = ||X||/R$ with $X = (x, y)$. The first critical current J_{c1} computed with the model is close to the one extracted from micromagnetic simulations. For a current $J_{dc} > J_{c1}$, the vortex is in the steady-state regime. The second critical current J_{c2} is the critical current where $s > 0.8$ and the vortex becomes unstable, switches polarity, and damps back to the dot center. For $J_{dc} < J_{c1}$ and $J_{dc} > J_{c2}$, the vortex is in the resonant regime. For $J_{dc} > J_{c2}$, the chirality of the vortex can be switched as shown in Fig. 2. In conclusion, the AOF creates a splitting which depends on the vortex chirality. The analytical model describes this phenomenon quantitatively as well as $|f^{STVO}|$ and ω in the resonant regime.

[1] A. Thiele, Physical Review Letters, vol. 30, p. 230 (1973) [2] Y. Gaididei, V. P. Kravchuk, and D. D. Sheka, International Journal of Quantum Chemistry, vol. 110, p. 83–97 (2010) [3] F. Abreu Araujo and J. Grollier, Journal of Applied Physics, vol. 120, p. 103 903 (2016) [4] Y.-S. Choi *et al.* Applied Physics Letters, vol. 93, p. 182 508 (2008) [5] A Dussaux *et al.* Physical Review B, vol. 86, p. 014 402 (2012)

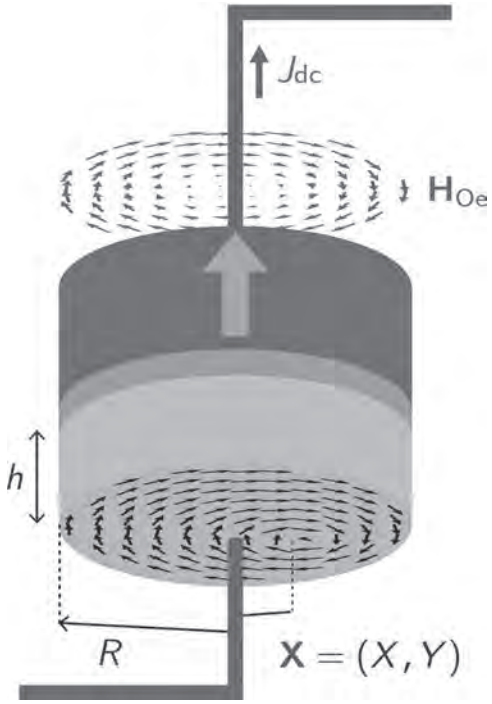

Fig. 1: Scheme of the STVO. The AOF is parallel to the curling magnetization of the vortex (the vortex chirality is C^+).

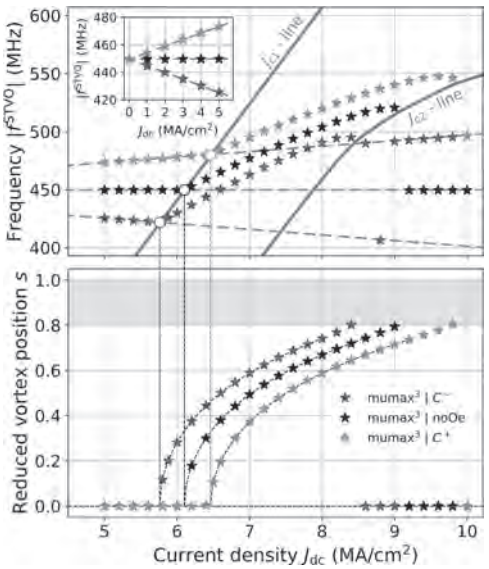

Fig. 2: Vortex dynamical properties (top: absolute frequency of the STVO, bottom: reduced vortex position) vs DC current excitation

GOQ-07. Current driven domain wall dynamics across the angular momentum compensation point in epitaxially grown ferrimagnetic Ni-doped Mn_4N thin films. *S. Ghosh*[1,2], T. Komori[2], A. Hallal[1], J.A. Peña Garcia[3], T. Gushi[1,2], T. Hirose[2], H. Mitarai[2], H. Okuno[4], J. Vogel[3], M. Chshiev[1,5], J. Attané[1], L. Vila[1], T. Suemasu[2] and S. Pizzini[3] *1. Univ. Grenoble Alpes, CEA, CNRS, Grenoble INP, IRIG-Spintec, Grenoble, France; 2. Institute of Applied Physics, Graduate School of Pure and Applied Sciences, University of Tsukuba, Tsukuba, Japan; 3. Univ. Grenoble Alpes, CNRS, Institut Néel, Grenoble, France; 4. Univ. Grenoble Alpes, CEA, IRIG-MEM, Grenoble, France; 5. Institut Universitaire de France, Paris, France*

The motion of domain walls by the use of the magnetic fields as well as spin polarized currents has been a major part of spintronics in the last two decades. The two mechanisms of current induced domain wall motion are Spin transfer torque(STT) and Spin orbit torques(SOT). In the recent years, compensated ferrimagnets have been in focus due to their ability to reach the magnetic and the angular momentum compensation points. At the angular mometum compensation point the precessional motion of the local magnetic moment becomes negligible which has shown to have massively increase the domain wall velocity[1,2]. Here we will focus on a rare-earth free ferrimagentic nitride called Manganese Nitride (Mn_4N). We have previously shown epitaxially grown Mn_4N has a very low magnetization (71 kA/m) and a very high perpedicular magnetic anisotropy (PMA) with mm sized domains[3]. This low magnetization is due to the two different Mn sub-lattices in the anti-perovskite crystal structure. With such a small magnetization and a high spin polarization led us to obtain a very high domain wall velocity of more than 900m/s at $J=1.3*10^{12}$ A/m^2 using pure STT[4]. In this work, we have have shown an even larger domain wall velocity approaching 3000 m/s at $J=1.26*10^{12}$ A/m^2 using pure STT near the magnetic and the angular compensation points in epitaxially grown Ni doped Mn_4N[5]. The magnetic and angular momentum compensation points are obtained by the adjustment of Ni doping in this system at room temperature. These high domain wall velocities are comparable to the best velocities obtained by SOT. Also, in this system there is no requirement for an external in-plane field as shown in some other systems by SOT. Moreover, we also demonstrate a reversal of the domian wall motion direction after crossing the compensation points where the domain walls move in the same direction as the flow of electrons. This phenomenon will be explained with the help of *ab-initio* calculations.

1. K.J. Kim, S.K. Kim, Y Hirata, Nature Materials., Vol 16, p1187 (2017) 2. L. Caretta, M. Mann, F. Buttner, Nature Nanotechnology., Vol 13, p1154 (2018) 3. T. Gushi, L. Vila, O. Fruchart, Jpn J. Appl. Phys., Vol 57, p120310 (2018) 4. T. Gushi, M. J. Klug, J.P. Garcia, Nano Letters., Vol 19, p8716 (2019) 5. S. Ghosh, T. Komori, A. Hallal, Nano Letters., Vol 21,6, p2580–2587 (2021)

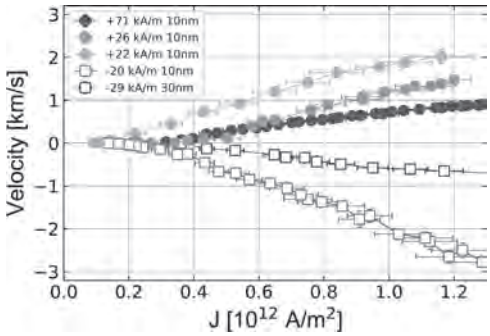

Fig. 1 Current density vs Velocity curves for $Mn_{4-x}Ni_xN$ thin films. Filled symbols show samples before and the open symbols after the compensation point.

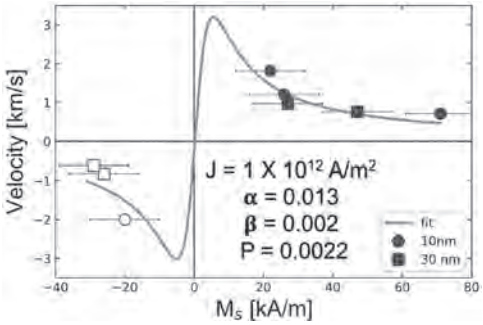

Fig. 2 M_S vs Velocity plot, measured for $J=1*10^{12}$ A/m^2(blacksquares) is compared with the best fit obtained using the q−φmodel.

GOQ-08. Injection locking of edge, bullet, and interior spin wave modes in nano-constriction spin Hall nano-oscillators. *M. Rajabali*[1], A.A. Awad[1,2], J. Yue[1], M. Dvornik[2], R. Khymyn[1], M. Zahedinejad[1], H. Fulara[1], J. Åkerman[1,2] and A. Houshang[1,2] *1. Physics, University of Gothenburg, Gothenburg, Sweden; 2. NanOsc AB, Gothenburg, Sweden*

Injection locking of spin Hall nano-oscillators (SHNOs) via a microwave current has been investigated for applications in novel communication and computation schemes, such as phase shift keying, and neuromorphic computing [1-3]. However, no detailed study has been dedicated to investigate how the different spin wave (SW) modes in nano-constriction SHNOs lock to an external signal as previously done for nano-gap SHNOs [4]. Here, we study the injection locking behavior of three distinctly different SW modes in SHNOs: field-localized edge mode, internal modes, and the self-localized SW bullet, in a Pt(50 Å)/Hf(5Å)/NiFe(50Å) SHNO. The power spectral density (PSD) vs. drive current for a 150nm wide SHNO in two qualitatively different operating regimes has been shown in Fig. 1(a) and (b). As can be seen, three distinct SW modes in the same device are observed merely by changing the field conditions. For an external magnetic field of H_{ext}=7.6 KOe and applied field angle of $\theta = 82^o$ edge and interior modes are detected as shown in Fig. 1(a). Decreasing H_{ext} to 4 KOe and θ to 70^o facilitates the formation of a spin wave (SW) bullet as shown in Fig. 1(b). When subjected to an external microwave signal, these three different modes respond differently to injection locking. SW bullet exhibits a pronounced threshold behavior above which, the locking bandwidth (BW) shows a quadratic dependence on the injected power as shown in Fig.1(c). On the other hand, the other non-solitonic modes, lock readily to the injected signal without requiring a threshold for the injected power. (Fig. 1(c)). However, the locking BW of the non-solitonic modes differ with respect to the injected power; While the internal mode shows the same square dependence on injected power as the bullet, the edge mode exhibits a linear dependence (Fig. 1(d)).

[1] T. Hache, et al. *Appl. Phys. Lett.*, Vol. 114, P. 102403 (2019) [2] T. M. Spicer, et al. *Appl. Phys. Lett.,* Vol. 113, P. 192405 (2018) [3] M. Zahedinejad, et al. *Nature Nanotechnology*, Vol. 15, P. 47–52 (2020) [4] V. E. Demidov, et al. *Nature communication*, Vol. 5, P. 1-6 (2014)

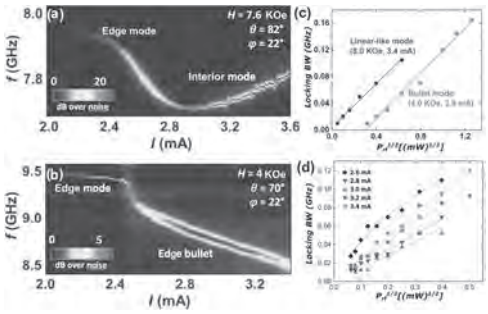

Figure 1. PSD plot of the SHNO at (a) field-localized and (b) self-localized SW modes. Comparing locking bandwidth behavior between (c) bullet and interior modes and (d) non-soliton modes.

GOQ-09. Two-terminal magnetoresistance ratio in Co-based Heusler alloy/germanium lateral spin-valve devices. *M. Yamada*[1,2], K. Sumi[3], T. Naito[3], K. Sawano[4] and K. Hamaya[2] *1. PRESTO, JST, Kawaguchi, Japan; 2. Center for Spintronics Research Network, Osaka University, Toyonaka, Japan; 3. Graduate School of Engineering Science, Osaka University, Toyonaka, Japan; 4. Advanced Research Laboratories, Tokyo City University, Setagaya, Japan*

Enhancement in the magnetoresistance (MR) ratios at room temperature in semiconductor-based structures has been an important topic for realization of spintronic devices. Recently, relatively high MR ratios at room temperature were reported in Si- [1] and Ge- [2] based lateral devices. Although the four-terminal nonlocal spin transport has been clarified from 8 to 300 K in our previous work on Ge [3], there is almost no verification and discussion on the two-terminal MR ratios through the spin transport between two ferromagnetic (FM) electrodes from low temperatures up to room temperature in semiconductor-based devices [4]. Here, we demonstrate the observation of the influence of the thermally excited spin waves in the FM electrodes on the two-terminal MR ratios in Co-based Heusler alloy/Ge lateral spin-valve (LSV) devices. To reliably examine the temperature dependence of two-terminal MR ratios, we fabricated LSV devices with 8-nm-thick $Co_2FeAl_{0.5}Si_{0.5}$ (CFAS)/5~6-atomic-layer-thick Fe (Fe_5)/*n*-Ge Schottky-tunnel contacts [3,5], where the CFAS/Fe_5 is an FM electrode and *n*-Ge is a heavily doped Ge layer (140 nm, $n \sim 10^{19}$ cm^{-3}). As shown in the inset of Fig. 1, evident two-terminal local spin signals (ΔR_S) at 8 K and 297 K are observed. In this study, the two-terminal MR ratio is defined as (ΔR_S /R_P) x 100, where R_P is the resistance in the parallel magnetization state. The decay of the MR ratios with increasing temperature is clearly observed in Fig. 1. Notably, even for the semiconductor-based LSV devices, the decay of the two-terminal MR ratios is roughly explained by a model on the decay of the interface spin polarization of the CFAS/Fe_5 electrodes, as theoretically expected to be an influence of the thermally excited spin waves ($T^{3/2}$ law) on the FM electrodes [6,7]. We will also discuss the influence of FM-electrode species such as Co_2MnSi/Fe_5 and $Co_2Fe_{0.4}Mn_{0.6}Si/Fe_5$ on the decay of the MR ratios with rising temperature.

[1] H. Koike *et al.*, Appl. Phys. Express vol. 13, p.083002 (2020) [2] K. Kudo *et al.*, Appl. Phys. Lett. vol. 118, p.162404 (2021) [3] M. Yamada *et al.*, J. Appl. Phys. vol. 129, p.183901 (2021) [4] Y. Fujita *et al.*, Phys. Rev. B vol. 100, p.024431 (2019) [5] M. Yamada *et al.*, NPG Asia Materials vol. 12, p.47 (2020) [6] A. Fert and H. Jaffres, Phys. Rev. B vol. 64, p.184420 (2001) [7] C. H. Shang *et al.*, Phys. Rev. B vol. 58, p.R2917 (1998)

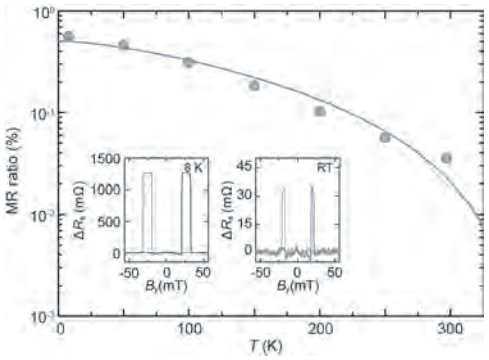

Fig. 1. MR ratio for an LSV device with $Co_2FeAl_{0.5}Si_{0.5}/Fe_5$/Ge Schottky-tunnel contacts. The solid line is guide line based on a $T^{3/2}$ law of the interface spin polarization estimated from the standard theory. The insets show two-terminal local spin signals at 8 K and 297 K.

GOQ-10. Electrically connected spin-torque oscillators array for 2.4 GHz WiFi band transmission. *R. Sharma*[1], R. Mishra[2], T. NgO[1], Y. Guo[1], S. Fukami[3,4], H. Sato[3,4], H. Ohno[3,4] and H. Yang[1] *1. Electrical and Computer Engineering, National University of Singapore, Singapore; 2. Centre for Applied Research in Electronics, Indian Institute of Technology Delhi, New Delhi, India; 3. Center for Science and Innovation in Spintronics, Tohoku University, Sendai, Japan; 4. Center for Spintronics Research Network, Tohoku University, Sendai, Japan*

Spin-torque oscillator (STO) is a class of emerging spintronic devices that can find applications in wireless communication systems in the form of radio frequency (rf) generator[1,2] and rf detector[3]. The STO offers a compatibility with CMOS technology and high frequency tunability[2]. However, the single STO output is not sufficient for the rf applications. In order to overcome this, the mutual synchronization of STOs is critical for communication, energy harvesting and neuromorphic applications. The short range magnetic coupling-based synchronization has spatial restrictions (few μm), whereas the long-range electrical synchronization using vortex STOs has limited frequency responses in hundreds MHz (< 500 MHz), restricting them for on-chip GHz-range applications. Here, we demonstrate electrical synchronization of four non-vortex uniformly-magnetized STOs at 2.4 GHz WiFi band[4], resolving the frequency-area quandary for designing STO based on-chip systems. We use a single dc source to synchronize canted free layer STOs, thereby simplifying the synchronization scheme. Due to mutual synchronization, STOs show a power enhancement and linewidth reduction [Fig. 1a,b]. When injection-locked with an external rf source, the synchronised STOs show a wide locking range around 2.4 GHz [Fig. 1c,d], which can be useful for neuromorphic computing. Under injection locking, synchronized STOs demonstrate an excellent time-domain stability and improved phase noise performance [Fig. 1e,f]. Our results highlight the significance of electrical topology (series vs. parallel) while designing an on-chip STOs system.

1 Kiselev, S. I. *et al.* Microwave oscillations of a nanomagnet driven by a spin-polarized current. *Nature* 425, 380 (2003). 2 Rippard, W. H., Pufall, M. R., Kaka, S., Russek, S. E. & Silva, T. J. Direct-current induced dynamics in $Co_{90}Fe_{10}/Ni_{80}Fe_{20}$ point contacts. *Physical Review Letters* 92, 027201 (2004). 3 Tulapurkar, A. *et al.* Spin-torque diode effect in magnetic tunnel junctions. *Nature* 438, 339 (2005). 4 Sharma, R. *et al.* Electrically connected spin-torque oscillators array for 2.4 GHz WiFi band transmission and energy harvesting. *Nature Communications* 12, 2924 (2021).

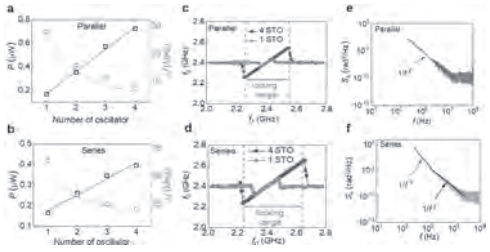

Fig. 1. a,b Oscillation power (P) and linewidth (Δf) versus numbers of oscillators (N) in parallel (a) and series (b), respectively. Solid lines are linear fit and N^{-1} scaling for the power and linewidth, respectively. c,d STO frequency (f_0) versus radio frequency (f_{rf}) response for a single oscillator (red) and four oscillators (blue) at P_{rf} = –20 dBm for the parallel (c) and series (d) connection. The locking range defines the region where $f_0 \sim f_{rf}$. e,f Phase noise for 1 ms time-domain trace in parallel (e) and series (f). The solid black and blue lines in (f) shows the $1/f^2$ and $1/f^3$ phase noise, respectively.

GOQ-11. Spin Torque Oscillation Starting-up Time Dependence on the Initial Magnetization Orientation in Orthogonal Magnetization Disks.
L. Chuhan[1], Y. Kurokawa[1], N. Hashimoto[1], T. Tanaka[1] and H. Yuasa[1]
1. Graduate School and Faculty of Information Science and Electrical Engineering, Kyushu University, Fukuoka, Japan

The spin torque oscillation (STO) in the orthogonal magnetization multilayer, which has the in-plane and perpendicular anisotropy magnetic layers, was studied. It has an advantage of the high spin transfer torque efficiency, on the other hand, the current density range providing the stable STO is limited. Therefore, we introduced the 90° coupling between two magnetic layers and successfully expanded the usable current density range and achieved the STO frequency like dozens GHz [1]. However, the starting-up time for stable STO is relatively long such as several ns to ten ns, that is a remained challenge for STO applications. In this report, we changed the initial orientation from out-of-plane to in-plane, resulting the magnetic orientation became from the vortex structure to the normal domain with mostly aligned spins when the current starts to flow. Generally, the normal domain is less stable than the vortex structure. As a result, the starting-up time of $Co_{90}Fe_{10}$ STO in FePt/Cr/$Co_{90}Fe_{10}$ layers is drastically reduced as shown in Fig. 1. Furthermore, the change of dynamics is more obvious in the case of FePt/Cr/Ni layers. As shown in Fig. 2, not only the starting-up time is shortened, but also the STO amplitude increased about 5 times. The snapshots at 20 ns revealed the reason of the large amplitude. In Fig. 2 (c), the axis of rotation is mostly perpendicular to plane and the angle of rotation is relatively large when the initial orientation is out-of-plane. Compared to this, when the initial orientation is in-plane, the rotation axis is tilted shown in Fig. (d). The average of magnetization affected on the STO amplitude. In summary, we shorten the starting-up time of STO by changing the initial state of the magnetization of the top layer from out-of-plane to in-plane, leading the realization of STO applications.

[1] C. Liu et al., IEEE Transactions on Magnetics, 2021. (in press)

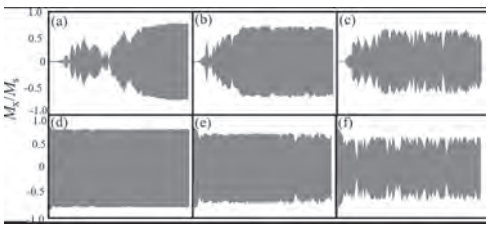

Fig.1. STO of $Co_{90}Fe_{10}$ in FePt/Cr/$Co_{90}Fe_{10}$ when the current density is $1.0x10^8$ A/cm², $1.2x10^8$ A/cm², $1.4x10^8$ A/cm². The initial states are out-of-plane (a)-(c) and in plane (d)-(f).

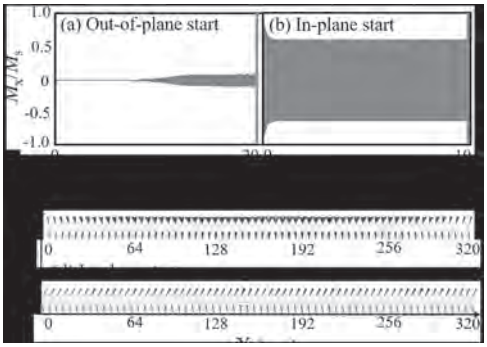

Fig.2. (a)(b) STO of Ni in FePt/Cr/Ni when the current density is $3x10^7$ A/cm². (c)(d) The side views of the magnetization configuration in Ni and FePt. The initial states are out-of-plane (a)(c) and in plane (b)(d).

GOQ-12. All-Optical Spin Injection in Silicon Revealed by Element Specific Time-Resolved Kerr Effect.
S. Laterza[1,2], A. Caretta[2], R. Bhardwaj[2], B. Casarin[1], V. Bonanni[2], A. Simoncig[2], M. Zangrando[2,3], P. Rebernik Ribič[2], G. Penco[2], G. De Ninno[2], L. Giannessi[2], R. Flammini[4], P. Moras[5], P. Rajak[3], M. Mahabul Islam[3], R. Ciancio[3], F. Parmigiani[2,6] and M. Malvestuto[2,3] *1. Physics, University of Trieste, Trieste, Italy; 2. Elettra-Sincrotrone Trieste S.C.p.A., Trieste, Italy; 3. CNR-IOM, Trieste, Italy; 4. ISM-CNR, Roma, Italy; 5. ISM-CNR, Trieste, Italy; 6. International Faculty, University of Cologne, Cologne, Germany*

Understanding how spin currents flow across metal-semiconductor interfaces at femtosecond timescales has impacts on ultrafast spintronics, data processing and storage applications. However, the possibility to directly access the propagation of spin currents on these time scales has been hampered by the simultaneous lack of both ultrafast site selective magnetic sensitive probes and tailored metal-semiconductor interfaces. By means of FEL-based core-resonant Kerr spectroscopy, we report direct experimental evidence of spin currents across a Ni/Si interface in terms of different magnetodynamics at the Ni $M_{2,3}$ and Si $L_{2,3}$ absorption edges. This further allows us to extract the propagation velocity of the spin current in Si as 0.2 nm/fs.

D. D. Awschalom and M. E. Flatté, Nature Physics 3, 153 (2007) M. Battiato and K. Held, Physical Review Letters 116, 196601 (2016), 1604.05882 D. Rudolf, C. La-O-Vorakiat, M. Battiato *et.al.*, Nature Communications 3, 1037 (2012) S. Yamamoto and I. Matsuda, Applied Sciences 7, 662 (2017) H. Ahn, C.-L. Wu, S. Gwo, *et al.,* Physical Review Letters 86, 2818 (2001) C. Svetina, N. Mahne, L. Raimondi *et al.*, Journal of Synchrotron Radiation 23, 98 (2016) A. Caretta, S. Laterza, V. Bonanni *et al.*, Structural Dynamics 8, 034304 (2021) M. Kiziroglou, X. Li, A. Zhukov *et al.*, Solid-State Electronics 52, 1032 (2008)

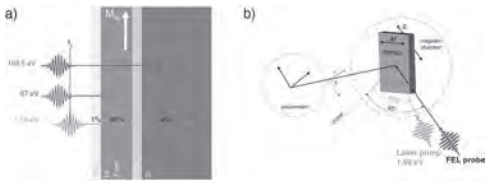

Fig. 1: a) The sample stack consists of a Si substrate (blue), a thin Si_3N_4 passivation layer (grey), 7 nm of Ni film (red) and 2 nm of Ag capping layer (yellow). The white arrow represents the in-plane magnetization of the Ni film. The FEL pulses at the Si $L_{2,3}$ edge (blue arrow) and at the Ni $M_{2,3}$ edge (red arrow) are also depicted. The IR laser pulses at 1.55 eV hit the sample at a time delay t-t0, before the FEL pulses arrival. The penetration depths of the pump and the probes are represented by the length of the arrows. The fraction of the IR laser energy absorbed by each layer is reported above the probe arrow. b) Scheme of the FEL RMOKE set-up at MagneDyn. RMOKE was probed in longitudinal configuration at an angle of incidence of 45°. The polarization ε of the incoming FEL pulses (blue arrow) is in the scattering plane, while the Kerr rotation of the polarization of the reflected pulse is indicated as θ.

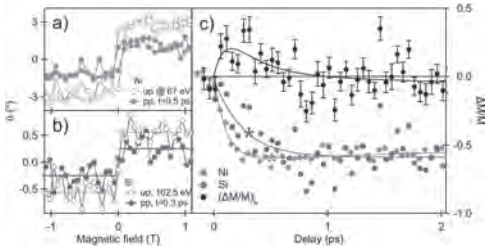

Fig. 2: RMOKE magnetic hysteresis in degrees of Kerr rotation at the Ni $M_{2,3}$ edge (a) and at the Si $L_{2,3}$ edge (b). Empty and filled circles curves represent the unpumped and pumped hysteresis after 0.5 ps (Ni) and 0.3 ps (Si) (colored star markers in c). c) relative change of the site resolved magnetization M (Ni - red and Si - blue dots) as a function of time delay measured in saturation at 550 mT. The solid lines represent the tting results, from which we extract the characteristic times for demagnetization and recovery. The difference $(\Delta M/M)_{js}$ is also shown (gray pentagons).

GOQ-13. Enhanced Torques in Co/Pt Systems via Orbital Current Contribution. *S. Krishnia*[1], F. Leroy[1], J. George[1], S. Collin[1], V. Cros[1] and H. Jaffrès[1] *1. Unité Mixte de Physique, CNRS, Thales, Université Paris-Saclay, Palaiseau, France*

In the last decade, charge to spin conversion and spin-orbit torques have been extensively studied to manipulate the magnetization for efficient data storage devices functionalities. The charge-spin conversion is governed by spin-orbit interactions such as spin Hall effect in the bulk of heavy metals and Rashba effect at their interfaces[1]. Recently, substantial increase in the magnetic torques has been observed with Cu/CuOx or Cu/Al_2O_3 light element interfaces. The observation of magnetic torques in the absence of spin-orbit interaction can be explained in the framework of orbital currents at Cu/CuOx interface[2-3]. Furthermore, as the orbital effects are believed to be one order larger than the spin-orbital coupling effects, we expect larger torques efficiency by utilizing the orbital currents. To aim this, we have measured the damping-like (H_{DL}) and field-like (H_{FL}) effective fields in SiOx/Co(2)/Pt(x)/Cu/CuOx(3) and SiOx/Co2)Pt(x)/AlOx(1) samples (and where x=2-6 nm) using second harmonic Hall measurement technique. Here, all the samples possess an in-plane magnetic anisotropy. As the orbital current does not carry spin (S=0), it is important to convert them into spin-current to interact with magnetization via *s-d* exchange interactions to promote the torques. Therefore, Pt is used to convert the orbital current into the spin current. Although the H_{FL} is found to be negligible in all the samples, one observes that the H_{DL} increases linearly with the current density in Pt, like expected for the current induced torque. Fig. 1 shows H_{DL} for 10^7 A/cm^2 current density in Pt. However, we do not observe significant change for AlOx, a two-fold increase is observed in Co(2)/Pt(4)/Cu/CuOx(3) compared to our reference Co(2)/Pt(4) sample, and where the exact spin current profile has been analyzed. As proposed in the recent literature [2], we attribute this enhancement in torques to the generation of orbital current at Cu/CuOx interface.

[1] A. Manchon *et al.*, *Rev. Mod. Phys.*, 91 (2019). [2] S. Ding *et al.*, *Phys. Rev. Lett.*, vol. 125, 177201 (2020). [3] J. Kim *et al.*, *Phys. Rev. B 103, L020407 (2021)*

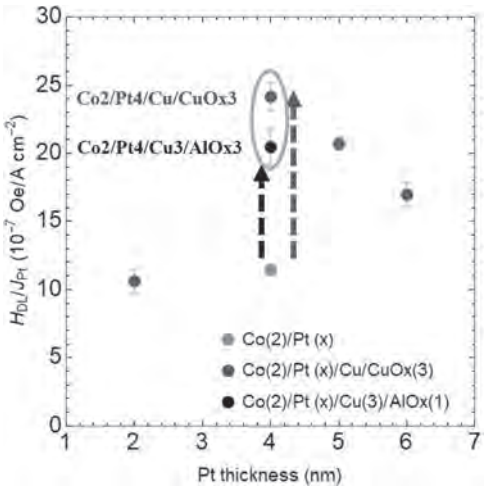

Fig1. Comparison of H_{DL} in various capping layers as a function of Pt thickness. The Blue (Black) arrow shows the increase in H_{DL} in Co/Pt/Cu/CuOx (Co/Pt/Cu/AlOx) samples due to the orbital current at Cu/CuOx (Cu/AlOx) interface.

GOQ-14. Non-linear classification of radio-frequency signals using spintronic hardware in neural networks with hidden layers. *A. Ross*[1], A. Mizrahi[1], A. de Riz[1], N. Leroux[1], L. Martins[2], A. Jenkins[2], R. Ferreira[2] and J. Grollier[1] *1. Unite Mixté de Physique CNRS-Thales, Palaiseau, France; 2. International Iberian Nanotechnology Laboratory, Braga, Portugal*

We demonstrate experimentally a spintronic neural network that communicates with radio-frequency (RF) signals between neurons and synapses, and that natively processes RF signals as inputs. Radio-frequency signals are ubiquitous and are widely employed to convey information. These signals require quick and accurate analysis for diverse applications ranging from medical diagnosis, assessing and issuing warnings of disruptive solar events as well as identification of drones from their RF-ID tags [1,2]. To this end, artificial neural networks are an invaluable tool but suffer from the time and energy consuming digitisation of the analogue inputs. Due to their sensitivity to RF signals, magnetic tunnel junctions are ideal candidates for the implementation of hardware neural networks that intrinsically process radio-frequency waveforms. Spin-torque nano-oscillators implement neurons efficiently. They take DC signals as inputs and broadcast their output in RF form [3]. Meanwhile, chains of spin-diodes achieve synaptic multiply and accumulate functions directly on RF inputs, and produce a DC output [4]. In this work we demonstrate experimentally the principle of a multilayer neural network that performs non-linear operations on RF inputs. We will show that the hardware neural network, composed of an input layer with two neurons, a hidden layer with two neurons and a single neuron as output, can classify complex shapes in a 2D plane with high accuracy. This work opens the path to embedded spintronic neural networks that classify complex RF inputs with high accuracy, high speed and low energy.

[1] N. Chrysaphi, H. A. S. Reid, E. P. Kontar. Astrophys. J. 893, 115 (2020). [2] M. F. Al-Sa'd, A. Al-Ali, A. Mohamed, Future Gener. Comput. Syst. 100, 86–97 (2019). [3] J. Torrejon, M. Riou, F. A. Araujo, Nature 547, 428–431 (2017). [4] N. Leroux, A. Mizrahi, D. Marković. Neuromorphic Comput. Eng. 1, 011001 (2021).

Session GPA
SKYRMIONS AND SPINS IN TOPOLOGICAL INSULATOR AND 2D MATERIALS (Poster Session)

Elton Santos, Chair
The University of Edinburgh, Edinburgh, United Kingdom

GPA-01. Control of a magnetic skyrmionium on a TbFeCo thin film.
S. Kato[1], K. Ohara[1], X. Zhang[1], J. Xia[2] and X. Liu[1] *1. Electrical and Computer Engineering, Shinshu University, Nagano, Japan; 2. Science and Engineering, The Chinese University of Hong Kong, Hong Kong, China*

Topological spin textures on magnetic thin films have attracted much attention in recent years [1]. A typical topological spin texture is called as skyrmion, which has high mobility at ultralow current densities and thus is promising for building future spintronic devices such as racetrack memories and artificial neurons [1]. However, current-driven skyrmions in narrow nanotracks have a serious drawback called the skyrmion Hall effect [1], which is an effect that may lead to the annihilation of skyrmions at sample edges. To overcome the skyrmion Hall effect, one promising approach is the use of magnetic skyrmionium. Magnetic skyrmionium is a skyrmion-like structure carrying a zero net topological charge, which does not show the skyrmion Hall effect during its motion [2]. Therefore, the realization of skyrmioniums in magnetic thin films at room temperature is important for future practical applications based on skyrmioniums. In this work, we will present the experimental observation of a magnetic skyrmionium in TbFeCo thin films and its behaviors under the application of an external magnetic field. The TbFeCo magnetic thin films exhibit perpendicular magnetic anisotropy (PMA) and Dzyaloshinskii-Moriya interaction (DMI) due to their crystal asymmetry [2], which are fundamental for the stabilization of both magnetic skyrmions and skyrmioniums. The images obtained using the magneto-optical Kerr effect (MOKE) suggest that several magnetic skyrmioniums are found in our TbFeCo thin films. We also show the dynamics of a magnetic skyrmionium under an applied magnetic field. Our results are useful for understanding magnetic skyrmionium properties in ferrimagnetic materials and could provide guidelines for the design of spintronic applications based on TbFeCo-type materials.

[1] J. Phys. D: Appl. Phys. 53, 363001 (2020); J. Phys.: Condens. Matter 32, 143001 (2020); J. Appl. Phys. 124, 240901 (2018); Nat. Rev. Mats. 2, 17031 (2017); Phys. Rep. 704, 1 (2017); J. Phys. D: Appl. Phys. 49, 423001 (2016); Proc. IEEE 104, 2040 (2016); J. Phys.: Condens. Matter 27, 503001 (2015). [2]JMMM 195, 182 (1999); Scientific Reports 8, 16966 (2018); Scientific Reports 9, 12119 (2019); Nano Lett. 18, 1057 (2018); PRB, 94, 094420 (2016); PRB, 92, 064412 (2015); Nano Lett. 20, 59 (2020); Nat. Nanotech. 14, 232 (2019); J. Phys. D: Appl. Phys. 50, 293002 (2017); Nat. Nanotech. 13, 1154 (2018); Adv. Funct. Mater. 2102307 (2021); PRL 110, 177205 (2013); PRL 119, 197205 (2017); PRB 95, 054421 (2017); PRB 102, 014458 (2020).

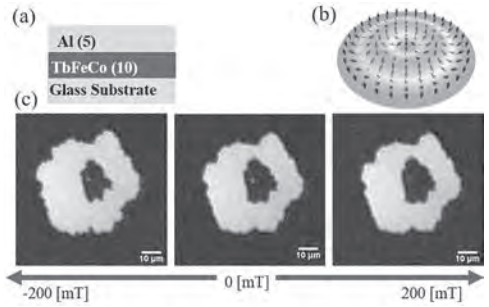

Figure 1. (a) Schematic of experimental sample. (b) Three-dimensional illustration of a magnetic skyrmionium carrying a net topological charge of zero. (c) MOKE images of a skyrmionium observed in the TbFeCo layer, of which the size and shape depend on the applied out-of-plane magnetic field.

GPA-02. Gate-Controlled Skyrmions in Magnetic Trilayer Tracks.
J. Fischer[1], C. Fillion[1], R. Kumar[1,2], L. Monnier[1], A. Fassatoui[3], S. Pizzini[3], L. Ranno[3], L. Cagnon[3], S. Auffret[1], I. Joumard[1], O. Boulle[1], G. Gaudin[1], L.D. Buda-Prejbeanu[1], C. Baraduc[1] and H. Béa[1] *1. SPINTEC, Grenoble, France; 2. Antaios, Meylan, France; 3. Institut NEEL, Grenoble, France*

Structural inversion asymmetry together with spin-orbit coupling can induce interfacial Dzyaloshinskii-Moriya Interaction (iDMI) in Heavy-Metal/Ferromagnet/Metal-Oxide heterostructuctures [1]. In such thin film systems with perpendicular magnetic anisotropy the iDMI combined with dipolar interactions can stabilize non-collinear chiral magnetic spin textures such as Néel Domain Walls (DWs), eventually forming magnetic skyrmion bubbles [2]. The iDMI amplitude and sign determine the spin texture of the DWs and their chirality [3]. Moreover, skyrmions can be moved by a current thanks to spin orbit torques, in a direction depending on their chirality. In this study we report on a deterministic control of their motion related to a chirality switch of magnetic skyrmion bubbles in Ta/FeCoB/TaOx trilayer, covered by a ZrO_2 ionic conductor (Fig. 1a). Monitored under a polar-Magneto-Optical Kerr-Effect (p-MOKE) microscope we apply a gate voltage through a transparent Indium Tin Oxide (ITO) electrode and demonstrate by real space tracking the reversal of their current-induced motion (Fig. 1b). Micromagnetic simulations together with similar measurements on magnetic domain walls confirm the possibility to invert the chirality, eventually leading to versatile spintronic and logic devices. We have furthermore optimized the fabrication of skyrmion Hall-bar tracks (Fig. 2a), containing magnetic skyrmion bubbles (Fig. 2b), with deported ITO top electrodes. These skyrmion racetracks of different shapes and sizes allow to assess the effect of gate voltage and lateral confinement on the skyrmion motion. Eventually, the gate would play the role of a pinning potential and control the skyrmion velocity. In a similar Hall-bar geometry with multiple Hall-contacts we envision to demonstrate the electrical tracking of a moving skyrmion in replacement for the MOKE images that are limited in temporal and spatial resolution.

[1] I. E. Dzyaloshinskii, J. Exptl. Theoret. Phys., (U.S.S.R.), vol. 46, p 960 (1964) [2] A. Fert, N. Reyren and V. Cros, Nature Review Materials, vol. 46, p. 6 (2017) [3] A. Thiaville, S. Rohart, É. Jué et al., EPL (Europhysics Letters), vol. 100, p. 57002 (2012)

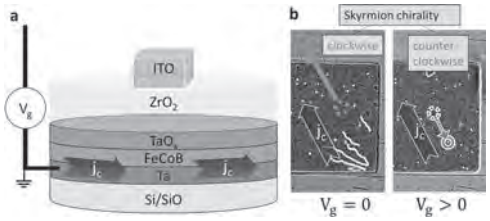

Figure 1: a Ta/FeCoB/TaOx trilayer, covered by ZrO2 ionic conductor and transparent ITO top electrode. b Current-induced and gate-controlled motion of skyrmion bubbles (p-MOKE images).

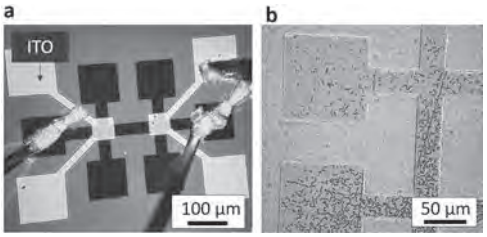

Figure 2: a Microscope and b p-MOKE images of skyrmion Hall-bar tracks with ITO gates, containing magnetic skyrmion bubbles.

GPA-03. Tuning the eccentricity of Bloch skyrmions in $Fe_{1.9}Ni_{0.9}Rh_{0.2}P$. *S. Schneider*[1,2], L. Peng[1], K. Karube[1], Y. Taguchi[1], D. Pohl[2], B.F. Rellinghaus[2], Y. Tokura[1,3] and X. Yu[1] *1. Center for Emergent Matter Science (CEMS), RIKEN, Wako, Japan; 2. Dresden Center for Nanoanalysis, TU Dresden, Dresden, Germany; 3. Department of Applied Physics, University of Tokyo, Bunkyo-ku, Japan*

The experimental discovery of antiskyrmions in $Mn_{1.4}PtSn$ [1] has opened up new pathways towards using microscopically small magnetic whirls as information carriers [2]. For this purpose a thorough understanding of the detailed spin texture of these magnetic solitons, including their stabilization mechanisms is essential. Quite recently, the compound $Fe_{1.9}Ni_{0.9}Pd_{0.2}P$ was found to host antiskyrmions at room temperature, which can be transformed into skyrmions, e.g., by tuning the external magnetic field [3]. Here, we report on an investigation of the skyrmion phase as function of the external magnetic field in a similar material, $Fe_{1.9}Ni_{0.9}Rh_{0.2}P$, where Pd was substituted by Rh, to gain further insight into the formation of topological spin solitons. The occurrence and nature of skyrmions in a $Fe_{1.9}Ni_{0.9}Rh_{0.2}P$ lamella prepared by focused ion beam (FIB) cutting were studied by means of off-axis electron holography that allows for the quantitative determination of the projected in-plane magnetic induction B_{ip}. In Fig. 1 the magnitudes of B_{ip} in the lamella upon exposure to magnetic fields of 170 mT and 330 mT applied along [001] are displayed. In zero field, the skyrmions initially possess an elliptical shape with the semi-major axes parallel to the ⟨110⟩ directions due to dipole–dipole interactions [4, 5]. Increasing the external out-of-plane magnetic field leads to (i) a reduction of the skyrmion size, (ii) an enhancement of B_{ip} and (iii) a deformation of the skyrmions. The initially elliptical skyrmions can be transformed into skyrmions with circular shapes until a critical field is reached, where the system undergoes a transition into the field-polarized phase. The current investigations provide a first insight how the balance between the symmetric and antisymmetric exchange and dipole-dipole interaction can tune the skyrmion structure in $Fe_{1.9}Ni_{0.9}Rh_{0.2}P$. By combining our experimental results with magnetostatic simulations, we aim at shedding light on the complex interplay of these interactions in the stabilization of topological spin textures.

[1] A. K. Nayak et al., Nature 548 (2017), 561 – 566. [2] B. Göbel et al., Physics Reports 895 (2021), 1 – 28. [3] K. Karube et al., Nature Materials 20 (2021), 335 – 340. [4] L. C. Peng et al., Nature Nanotechnology 15 (2020), 181 – 186. [5] J. Jena et al., Nature Communications 11 (2020), 1115.

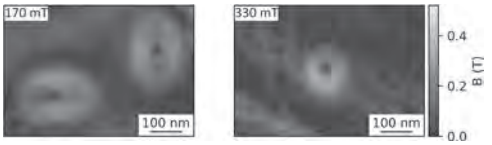

Magnitude of B_{ip} of Bloch skyrmions in $Fe_{1.9}Ni_{0.9}Rh_{0.2}P$ in external fields of 170 mT and 330 mT, respectively.

GPA-04. Room Temperature Skyrmions at Zero Field in Ir/Fe/Co/Pt-based Systems with Antiferromagnetic Coupling. *Y. Feng*[1,2], H.J. Hug[1,2] and A. Mandru[1] *1. Empa, Swiss Federal Laboratories for Materials Science and Technology, Dübendorf, Switzerland; 2. Department of Physics, University of Basel, Basel, Switzerland*

Magnetic skyrmions are localized objects with a non-trivial topology. With their small sizes and stable magnetic properties, skyrmions are of great interest in particular due to their potential applications in future-generation magnetic storage devices. Multilayer ferromagnetic thin-film materials hosting room temperature (RT) skyrmions stabilized by interfacial Dzyaloshinskii-Moriya interactions in [1,2] allow a high tunability in terms of skyrmion size and density, making them very promising platforms for investigating functional skyrmions for future applications. However, several obstacles remain before implementing ferromagnetic skyrmions into applications. One of these problems is that the dipolar interactions in these materials makes it difficult to stabilize small skyrmions without an external field [3,4,5]. Another major difficulty concerns the skyrmion Hall effect which deflects the skyrmions to the device edges [6,7]. Both of these problems could potentially be solved by having skymions in antiferromagnetic (AF) materials, where the dipolar fields are minimized by having the two subsystems aligned antiparallel to each other, and the skyrmion Hall effect is compensated. This has been achieved by Legrand *et al.* in Ref. [5], where RT skyrmions at zero field were generated in a synthetic AF multilayer system and observed by magnetic force microscopy (MFM). Following the same general approach as in Ref. [5], we construct a system that can host high-density skyrmions at zero external field using interlayer exchange coupling and having Ir/Fe/Co/Pt multilayers as starting blocks. These skyrmion-generating layers are coupled with different bias layers that act as an external magnetic field. We will show magnetic characterization and high-resolution MFM imaging results of the impact of various bias layers and coupling strengths on the overall system properties.

[1] C. Moreau-Luchaire, C. Moutafis, N. Reyren *et al.*, Nature Nanotech 11, 444–448 (2016) [2] A. Soumyanarayanan, M. Raju, A. Gonzalez Oyarce *et al.*, Nature Mater 16, 898–904 (2017) [3] C. Moreau-Luchaire, C. Moutafis, N. Reyren *et al.*, Nature Nanotech 11, 444–448 (2016) [4] O. Boulle, J. Vogel, H. Yang *et al.*, Nature Nanotech 11, 449–454 (2016) [5] W. Legrand, D. Maccariello, F. Ajejas *et al.*, Nat. Mater. 19, 34–42 (2020) [6] W. Jiang, X. Zhang, G. Yu *et al.*, Nature Phys 13, 162–169 (2017) [7] K. Litzius, I. Lemesh, B. Krüger *et al.*, Nature Phys 13, 170–175 (2017)

GPA-05. Skyrmion Hosting Multilayers Based on Synthetic Antiferromagnets. *E. Darwin*[1], P. Shepley[1], T. Hase[3], J. Cunningham[2] and B.J. Hickey[1] *1. Condensed Matter, University of Leeds, Leeds, United Kingdom; 2. Electrical Engineering, University of Leeds, Leeds, United Kingdom; 3. University of Warwick, Warwick, United Kingdom*

Heavy metal (HM)/ferromagnet (FM)/HM multilayers became of interest as they can host room temperature skyrmions - chiral, topologically non-trivial spin textures which have an unique set of topological properties leading them to be highly stable [1,2,3]. Recently, attention has been devoted to synthetic antiferromagnet (SAF) multilayers due to their ability to iradicate the problems associated with the skyrmion Hall effect [4,5,6]. However, the current-driven dynamics are far from the theorerical predictions because they are affected by pinning. Here, we report on the properties of $[CoB(6Å)/Ir(4Å)/Pt(6Å)]_{xn}$ multilayers in a SAF state promoted by the Ir spacer. CoB recently became a candidate for skyrmion hosting multilayers as, due to

its amorphous structure, the pinning is reduced [7]. Ir and Pt are used due to their strong interfacial Dzyaloshinskii–Moriya interaction (DMI). The combined effect of the previous features in the investigated multilayer stacks leads to a favorable environment for skyrmions with the perspective of skyrmion electrical transport devices. We performed x-ray reflectivity and magnetometry to extract the saturation magnetisation for the FM, the nature of the FM/HM interfaces, including proximity effects, as well as measurements to determine the DMI. We explored the behaviour of the Ir-induced antiferromagnetic coupling in the stacks by performing hysteresis loops measurements as a function of the number of repeats and temperature. In particular, for the case of two ferromagnetically coupled Pt/CoB/Ir stacks separated by a 4Å Ir layer, where we observed two switches in the hysteresis loop (Fig.2), which is a clear feature of a SAF structure. We also performed magnetic force microscopy (MFM) measurements, and we observed the existence of mixed phase with maze and circular domains, which we identified as SAF skyrmions (Fig.2).

[1] C. Moreau-Luchaire, et al. Nature nanotechnology, Vol.11.5, p444 (2016) [2] A. Soumyanarayanan, et al. Nature materials, Vol.16.9, p898-904 (2017) [3] K. Zeissler, et al. Scientific reports, Vol.7.1, p1-9 (2017) [4] S. Zhou, et al. Journal of Magnetism and Magnetic Materials, Vol.493, p165740 (2020) [5] W. Legrand, et al. Nature materials, Vol.19.1, p34-42 (2020) [6] T. Dohi, et al. Nature communications, Vol.10.1, p1-6 (2019) [7] K. Zeissler, et al. Nature communications, Vol.11.1, p1-11 (2020)

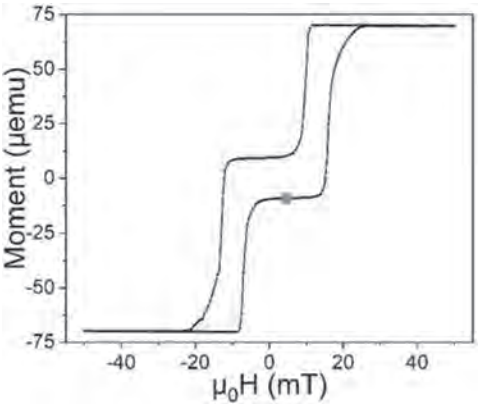

Fig.1 shows the hysteresis loop of the system mentioned. The data was taken by SQUID-VSM and the loop shows two wasp-like switches. The blue dot shows the field at which the MFM image was taken.

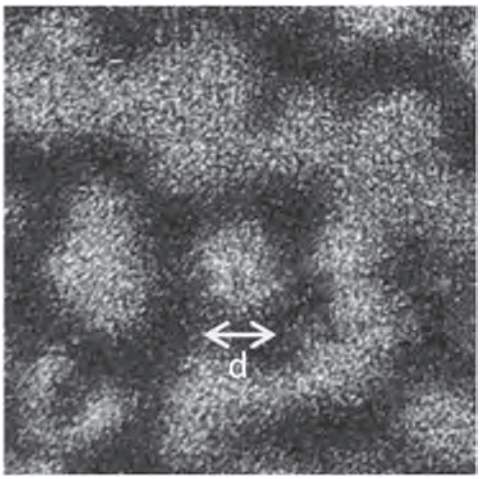

Fig.2 is an MFM image of this system showing a skyrmion of d ≈ 450 nm, surrounded by maze-like domains. It was assumed a field of 5mT was present from the sample holder.

GPA-06. Withdrawn

GPA-07. Tuning the Density of Incomplete and Tubular Skyrmions in Ferro/ferri/ferromagnetic Trilayers. *A. Mandru*[1], O. Yildirim[1], R. Tomasello[2], Y. Feng[1], P. Mirzadeh Vaghehfi[1], T. Dutta[1], G. Carlotti[3], S. Tacchi[4], G. Finocchio[5] and H.J. Hug[1,6] *1. Empa, Swiss Federal Laboratories for Materials Science and Technology, Dubendorf, Switzerland; 2. Dipartimento di Ingegneria Elettrica e dell'Informazione, Politecnico di Bari, Bari, Italy; 3. Dipartimento di Fisica e Geologia, Università di Perugia, Perugia, Italy; 4. Istituto Officina dei Materiali - IOM, Perugia, Italy; 5. Department of Mathematical and Computer Sciences, Physical Sciences and Earth Sciences, University of Messina, Messina, Italy; 6. Department of Physics, University of Basel, Basel, Switzerland*

Room temperature magnetic skyrmions have the potential of enabling compact and energetically-efficient storage such as racetrack memories, albeit with two fundamental challenges: 1) Not being able to restrict their motion along straight paths, leading to skyrmions being lost at the device edge; one possible solution is the use of antiferromagnetically-coupled skyrmions [1]; and 2) Not having stable inter-skyrmion distances, leading to fluctuating distances among bits; a potential solution was revealed with the experimental observation of coexisting skyrmions and chiral bobbers [2], opening the possibility that a chain of binary data bits could be encoded by the two states. However, these observations were in B20-type crystalline materials and at low temperatures. In our previous work [3], we developed a ferro/ferri/ferromagnetic (FM/FI/FM) trilayer system that can host two distinct skyrmions at room temperature and can serve as a solution to the second challenge. The two phases represent a tubular skyrmion (running through the entire trilayer) and an incomplete skyrmion (existing in the FM layers only), as revealed from magnetic force microscopy (MFM) data and micromagnetic simulations. Such a two-skyrmion phase system exists for specific magnetic parameters of the individual sublayers. By exploring this parameter space, in this new study we reveal that the densities of the two skyrmions can be tuned via different routes: either by changing the magnetic properties of the FI or those of the FM. More specifically, we investigate the trilayer system when changing the thickness of the FM multilayers by using a combination of MFM, vibrating sample magnetometry and Brillouin light scattering experiments together with micromagnetic simulations. We show how the competition between different energies allows for the stabilization of either incomplete-only skyrmions, combination of both or mainly tubular skyrmions (Figure 1). Having a good understanding of the interplay between different magnetic properties can lead to better-tailored systems and possibly bring skyrmions a step closer to applications.

[1] W. Legrand et al., *Nat. Mater.* 19, 34–42 (2020) [2] F. Zheng et al., *Nat. Nanotechnol*. 13, 1–7 (2018) [3] A.-O. Mandru et al., *Nat. Commun.* 11, 6365 (2020)

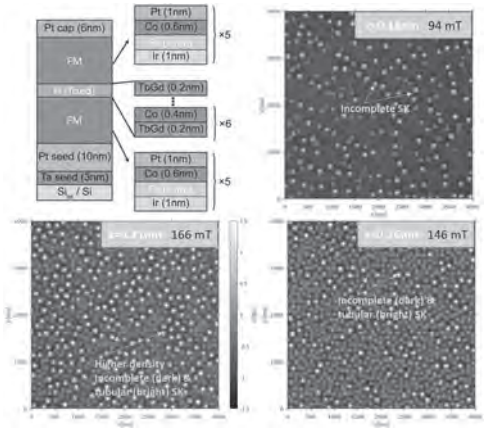

Fig. 1: Sample schematics and MFM images of three FM/FI/FM samples with varying Fe-layer thickness.

GPA-08. A Skyrmion-based Robust Racetrack Device and a Programmable Logic Device with Complete Boolean Logic Gates. *Z. Yan*[1], G. Yu[1] and X. Han[1] *1. Beijing National Laboratory for Condensed Matter Physics, Institute of Physics, Chinese Academy of Sciences, Beijing, China*

Magnetic skyrmions are topologically protected spin structures, offering great promise as information carriers for future spintronic devices. However, a series of challenges, such as unreliable skyrmion motion, pinning effects, and a weak readout signal, prevent the development of skyrmionic applications. The recently demonstrated capability to engineer the local exchange-bias field (LEBF) in an exchange-biased composite, provides solutions to these challenges [1, 2]. By exploiting LEBF, we design and analyze a robust skyrmion shift device[3]. LEBF-induced magnetic domain walls form the boundary of the device channel, and LEBF potential wells are implemented in the channel for positioning skyrmions. Based on simulations with comprehensive models, we demonstrate the proposed device has the advantages of (i) localizing the skyrmions in the absence of current, (ii) suppressing skyrmion annihilation during transport, (iii) promoting steady skyrmion motion, (iv) enhancing the skyrmion velocity, and (v) magnifying the readout signal. On the other hand, a skyrmionic programmable logic device (SkrPLD) with complete Boolean logic functions is proposed and analyzed by micromagnetic simulations [4]. By varying the LEBF, artificial pinning sites are introduced for trapping the skyrmions. Depending on the input currents and the initial position of skyrmions at different pinning sites, different logic functions can be realized. Micromagnetic simulations show that the proposed SkrPLD has robust performance even under thermal fluctuations and inhomogeneity effects. Our results form the basis for the design of robust skyrmion devices through LEBF engineering.

[1] Y. Guang, I. Bykova, Y. Liu, G. Yu, E. Goering, M. Weigand, J. Gräfe, S. K. Kim, J. Zhang, H. Zhang, Z. R. Yan, C. Wan, J. Feng, X. Wang, C. Guo, H. Wei, Y. Peng, Y. Tserkovnyak, X. Han, and G. Schütz, Creating zero-field skyrmions in exchange-biased multilayers through X-ray illumination, *Nat. Commun.* 11, 949 (2020). [2] Y. Guang, Y. Peng, Z. R. Yan, Y. Liu, J. Zhang, X. Zeng, S. Zhang, S. Zhang, D. M. Burn, N. Jaouen, J. Wei, H. Xu, J. Feng, C. Fang, G. van der Laan, T. Hesjedal, B. Cui, X. Zhang, G. Yu, and X. Han, Electron beam lithography of magnetic skyrmions, *Adv. Mater.* 32, 2003003 (2020). [3] Z. R. Yan, Y. Z. Liu, Y. Guang, J. F. Feng, R. K. Lake, G. Q. Yu, and X. F. Han, Robust Skyrmion Shift Device Through Engineering the Local Exchange-Bias Field, *Phys. Rev. Appl.* 14, 044008 (2020). [4] Z. R. Yan, Y. Z. Liu, Y. Guang, K. Yue, J. F. Feng, R. K. Lake, G. Q. Yu, and X. F. Han, Skyrmion-based programmable logic device with complete boolean logic functions, *Phys. Rev. Appl.* 15, 064004 (2021) (Editor's Suggestion).

GPA-09. Large Magneto-Electric Resistance in the Topological Dirac Semimetal α-Sn. *V. Kalappattil*[1], Y. Zhang[1], C. Liu[1], S. Zhang[2], J. Ding[1], U. Erugu[3], J. Tian[3], J. Tang[3] and M. Wu[1] *1. Physics, Colorado State University, Fort Collins, CO, United States; 2. Physics, Case Western Reserve University, Cleveland, OH, United States; 3. Physics, University of Wyoming, Laramie, WY, United States*

The spin-momentum locking of surface states in topological quantum materials can produce a resistance that scales linearly with magnetic and electric fields and also depends on the current direction relative to the crystalline axes[1,2]. Such a bilinear magneto-electric resistance (BMER) effect offers a completely new approach for magnetic storage and magnetic field sensing applications. The effects demonstrated so far, however, are relatively weak or only for low temperatures[1-3]. In this presentation, we report a strong room-temperature BMER effect in topological Dirac semimetal α-Sn thin films[4]. The epitaxial α-Sn films were grown by magnetron sputtering on single-crystal silicon substrates at room temperature. They showed room-temperature BMER responses that are 10^6 times larger than previously reported at room temperature,[2] and also larger than that previously reported at low temperatures.[1,3] These results represent a major advance toward realistic BMER applications. Our experimental data also made possible the first characterization of the three-dimensional, Fermi-level spin texture of topological surface states in α-Sn thin films.

1. P. He et al., *Nat. Phys.* Vol.14, pp. 495–499, Feb. 2018. 2. P. He et al., Nat. Commun. Vol 10, p. 1290, Mar. 2019. 3. P. He et al., *Phys. Rev. Lett*. Vol 120, 266802, June 2018. 4. Y. Zhang, V. Kalappattil et al., arXiv:2107.03472v1, July 2021 (Zhang and Kalappattil are co-first authors.).

GPA-10. Exchange bias and spin-orbit torque in the Fe_3GeTe_2-based heterostructures prepared by vacuum exfoliation approach. *Y. Zhang*[1], H. Xu[1], C. Yi[1], Y. Shi[1], G. Yu[1] and X. Han[1] *1. Institute of Physics, Chinese Academy of Sciences, Beijing, China*

Magnetic two-dimensional (2D) van der Waals (vdWs) materials are receiving increased attention due to their exceptional properties and potential applications in spintronic devices. Because exchange bias and spin-orbit torque (SOT)-driven magnetization switching are basic ingredients for spintronic devices, it is of pivotal importance to demonstrate these effects in the 2D vdWs material-based magnetic heterostructures. In this work, we employ a vacuum exfoliation approach to fabricate Fe_3GeTe_2 (FGT)/$Ir_{22}Mn_{78}$ (IrMn) and FGT/Pt bilayers, which have high-quality interfaces. An out-of-plane exchange bias of up to 895 Oe is obtained in the former bilayer, which is larger than that of the previously studied bilayers. In the latter bilayer, the SOT switching of the perpendicularly magnetized FGT is realized, which exhibits higher SOT-driven switching performance compared to the previously studied FGT/Pt bilayer devices with interfacial oxidation. The minimum of SOT efficiency is further determined to be 0.18 ± 0.04, comparable to the previously reported values for Pt/Co and Pt/CoFeB bilayers. This work highlights the importance of the high-quality interface for the exchange bias and SOT effect and may pave the way for implementing 2D vdWs in spintronic devices.

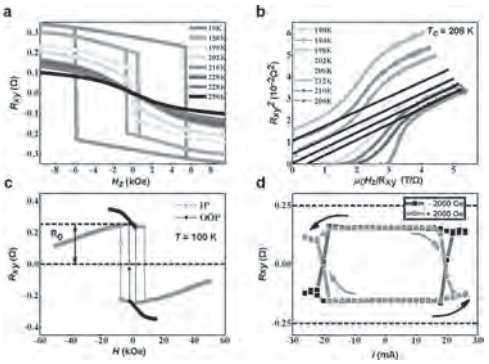

Magnetic properties and SOT-driven perpendicular magnetization switching in the FGT/Pt bilayer device. (a) Hall resistance as a function of the out-of-plane field at different temperatures. (b) Arrott plots of the Hall resistance for the FGT/Pt device. The extracted T_c is about 208 K. (c) R_{AHE} as a function of in-plane (IP) and out-of-plane (OOP) magnetic field at 100 K. (d) Current-driven perpendicular magnetization switching for in-plane magnetic fields of +2000 Oe and –2000 Oe at 100 K with clockwise and anticlockwise switching polarity, respectively. The dashed lines mark the R_{AHE} at saturated magnetization states.

GPA-11. Change in longitudinal spin Seebeck voltage with microstructure in YIG films prepared by sol-gel method. *M. Yamamoto*[1], S. Masaki[1], H. Matsui[1], Y. Shiota[2], T. Moriyama[2], T. Kato[3], T. Ono[2], M. Shima[1] and K. Yamada[1] *1. Department of Materials Science and Processing, Graduate School of Natural Science and Technology, Gifu University, Gifu, Japan; 2. Institute for Chemical Research, Kyoto University, Uji, Japan; 3. Institute of Materials and Systems for Sustainability, Nagoya University, Nagoya, Japan*

Thermoelectric conversion elements utilizing the spin Seebeck effect (SSE) enabled in such a simple structure have recently attracted much attention owing to their unique properties and demands for future practical use [1,2]. We have previously reported the microstructural dependence of longitudinal SSE (LSSE) voltage V_{LSSE} in YIG films consisting of densely

packed nanoparticles prepared by co-precipitation on a Si substrate [3]. The LSSE voltage is found to vary with the film morphology, where V_{LSSE} increases with the smoothness of the film as it enables magnons to propagate more coherently. Hence in order to further enhance V_{LSSE}, the films should be grown with improved smoothness via another chemical route. In this report, we investigate V_{LSSE} in YIG films prepared by the sol-gel method on a substrate including Si and gadolinium gallium garnet (GGG). YIG film samples were made by sol-gel, spin-coating, and annealing at T_a = 1073-1273 K for 2 hours in air. According to the X-ray diffraction (XRD) spectra of the samples, diffraction peaks associated with the garnet phase are readily observed for all of them; the YIG films appear to be a single crystal on GGG, while they are polycrystalline on Si. Figure1 shows surface and cross-sectional scanning electron microscope (SEM) images of the YIG film on Si annealed at 1173 K. The film surface appears to contain cracks and multiple YIG grains, where the areal fractions of voids and surface roughness in the films are, respectively, 58-89% and 36-45% less than those in the films fabricated by co-precipitation [3]. Figure 2 shows the variation of the SSE constant (S) with annealing temperature T_a obtained from YIG/Pt(5 nm) film samples. The value of S for the films on Si apparently decreases with increasing T_a, which is also observed for co-precipitated YIG/Pt(5 nm) films [3]. The values of S for YIG/Pt films on GGG are found to be greater than those on Si presumably because the films on GGG are apparently a single crystal, as shown in the XRD data, that yields a higher efficiency of magnon excitation in the YIG films than those on Si.

[1] K. Uchida et al. *Nature*, 455, 778 (2008). [2] K. Uchida et al. *Nat. Mater*., 9, 894 (2010). [3] K. Yamada et al. *J. Magn. Magn. Mater*., 535, 168093 (2021).

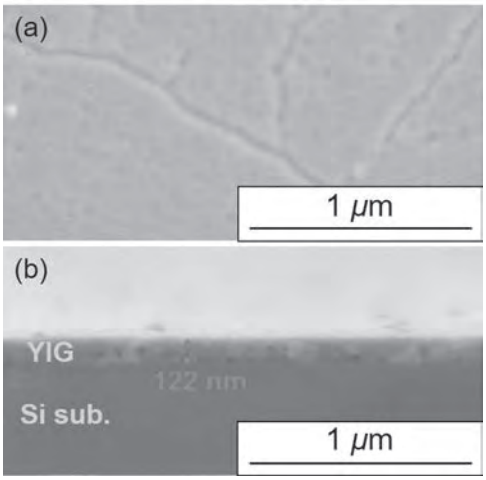

Fig.1 (a) Surface and (b) cross-sectional images of the YIG film measured by SEM.

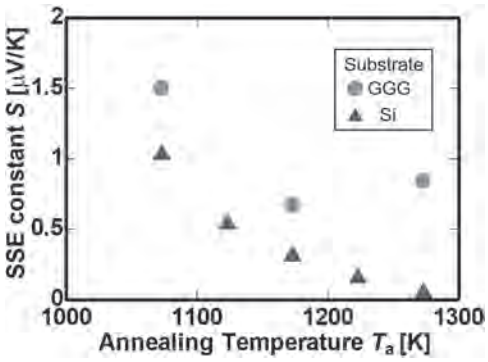

Fig.2 S of YIG/Pt films on a Si or GGG substrate vs T_a.

Session GPB
FUNDAMENTAL SPINTRONICS I
(Poster Session)

Yuta Yamane, Chair
Tohoku University, Sendai, Japan

GPB-01. Non-equilibrium of magnons and phonons in thulium iron garnets. *G. Lee*[1], T. Lee[1], C. Phuoc[2], D. Kim[1], M. Seo[1], Y. Jo[3] and K. Kim[1] *1. Physics, Korea Advanced Institute of Science and Technology (KAIST), Daejeon, The Republic of Korea; 2. Material Science and Engineering, Chungnam National University, Daejeon, The Republic of Korea; 3. Division of Scientific Instrumentation, Korea Basic Science Institute, Daejeon, The Republic of Korea*

The interaction between magnons and phonons is a fundamental subject of research in magnetism [1, 2]. In particular, the non-equilibrium state of magnons and phonons has recently attracted considerable interest because of the technological importance for spin-caloritronic applications [3, 4]. To date, the study of magnon-phonon non-equilibrium was primarily focused on magnetic insulator (MI) yttrium iron garnets (YIGs) [5-7]. However, to fully make use of the phenomena in spin-caloritronic applications, it is required to study the magnon-phonon non-equilibrium in more diverse magnetic systems. In this work, we investigate the magnon-phonon non-equilibrium in an MI-thulium iron garnets (TmIGs) which have recently drawn significant interest due to their unique magnetic properties [8, 9]. We developed optical reflectometry to provide spatial profiles of magnons and phonons subject to the thermal gradient. The spatial gradient of magnons and phonons show exponential decay under the thermal gradient. We found that the characteristic decay length of magnons and phonons are different, indicating the formation of non-equilibrium state between magnons and phonons. Furthermore, we found that the characteristic decay length of magnons is significantly affected by the heating power or magnetic field, whereas that of phonons is almost constant, which we ascribe to the additional non-linear scattering process of magnons. Our work reveals the magnon-phonon non-equilibrium in TmIG, and therefore stimulates further studies towards the spin-caloritronic applications using TmIG.

[1] K. Uchida, H. Adachi, T. An, T. Ota, M. Toda, B. Hillebrands, S. Maekawa and E. Saitoh, Nature Materials 10, 737 (2011) [2] T. Kikkawa, K. Shen, B. Flebus, R. A. Duine, K. Uchida, Z. Qiu, G. E. W. Bauer and E. Saitoh, Physical Review Letters 117, 207203 (2016) [3] K. Uchida, S. Takahashi, K. Harii, J. Ieda, W. Koshibae, K. Ando, S. Maekawa and E. Saitoh, Nature 455, 778 (2008) [4] J. Xiao, G. E. W. Bauer, K. Uchida, E. Saitoh and S. Maekawa, Physical Review B 81, 214418 (2010) [5] M. Agrawal, V. I. Vasyuchka, A. A. Serga, A. D. Karenowska, G. A. Melkov and B. Hillebrands, Physical Review Letters 111, 107204 (2013) [6] K. An, K. S. Olsson, A. Weathers, S. Sullivan, Xi Chen, X. Li, L. G. Marshall, X. Ma, N. Klimovich, J. Zhou, Li Shi and X. Li, Physical Review Letters 117, 107202 (2016) [7] K. S. Olsson, K. An, G. A. Fiete, J. Zhou, Li Shi and X. Li, Physical Review X 10, 021029 (2020) [8] C. O. Avci, E. Rosenberg, L. Caretta, F. Büttner, M. Mann, C. Marcus, D. Bono, C. A. Ross and G. S. D. Beach, Nature Nanotechnology 14, 561 (2019) [9] Q. Shao, Y. Liu, G. Yu, S. K. Kim, X. Che, C. Tang, Q. L. He, Y. Tserkovnyak, J. Shi and K. L. Wang, Nature Electronics 2, 182 (2019)

GPB-02. Laser-induced charge and spin photocurrents in $BiAg_2$ monolayer from first-principles. *T. Adamantopoulos*[1], M. Merte[1,2], F. Freimuth[1,3], D. Go[1,3], S. Blügel[1] and Y. Mokrousov[1,3] *1. Peter Grünberg Institut and Institute for Advanced Simulation, Forschungszentrum Jülich GmbH, Jülich, Germany; 2. Department of Physics, RWTH Aachen University, Aachen, Germany; 3. Institute of Physics, Johannes Gutenberg University Mainz, Mainz, Germany*

The physics of photo-induced effects in interfacial systems is intensively researched these days owing to numerous potential applications. Owing to the complexity of the problem, a comprehensive theoretical picture of photo-galvanic effects taking place at realistic metallic surfaces and interfaces is still lacking. In the past, it was shown that in the ferromagnetic Rashba model with in-plane magnetization charge and spin photocurrents which are of second order in the electric field are allowed by symmetry. Additionally, second order spin photocurrents are allowed by symmetry in the non-magnetic Rashba model. These responses stem from the interfacial spin-orbit interaction (SOI) and can be generated by the application of femtosecond laser pulses [1,2]. Here, we report calculations of laser-induced currents within the Keldysh non-equilibrium formalism combined with the Wannier interpolation scheme which can be applied to metallic and insulating materials of any complexity. We perform our first-principles electronic structure calculations with the DFT code FLEUR [www.flapw.de], and study in detail a $BiAg_2$ monolayer, which is a well-known material realization of the Rashba model. The in-plane magnetization is introduced by the addition of a Zeeman splitting term in the Wannier-interpolated Hamiltonian. We calculate the laser-induced charge photocurrents for the ferromagnetic case and the laser-induced spin photocurrents for both the non-magnetic and the ferromagnetic case. Our results confirm the appearance of in-plane photocurrents as predicted by the Rashba model. The resulting photocurrents satisfy all the predicted symmetry restrictions with respect to the light helicity and the magnetization direction. We provide microscopic insights into the symmetry and magnitude of the computed currents based on the electronic structure of the system. Our work contributes to the study of the role of the interfacial Rashba SOI as a mechanism for the generation of in-plane photocurrents, which are of great interest in the field of ultrafast and terahertz spintronics.

[1] F. Freimuth, S. Blügel, and Y. Mokrousov, Phys. Rev. B, Vol. 103, p. 075428 (2021) [2] F. Freimuth, S. Blügel, and Y. Mokrousov, Phys. Rev. B, Vol. 94, p. 144432 (2016)

GPB-03. Independence of the Inverse Spin Hall Effect with the Magnetic Phase in Thin NiCu Films. *M. Cosset-Chéneau*[1], S. Varotto[2], C. Grezes[1], P. Warin[1], Y. Fu[1], A. Brenac[1], J. Jacquot[3], S. Gambarelli[3], C. Rinaldi[4], V. Baltz[1], J. Attané[1], L. Vila[1] and P. Noël[1] *1. Spintec, Grenoble, France; 2. CNRS-THALES, Palaiseau, France; 3. Pheliqs, Grenoble, France; 4. Politecnico di Milano, Milan, Italy*

The spin to charge interconversion has been intensively studied in 5d materials such as platinum. In these non-magnetic systems, the relation between the charge current, the spin current and its polarization is strongly constrained by symmetries. Recently, a strong spin to charge interconversion efficiency has been obtained in 3d ferromagnets with strong spin orbit interactions such as NiCu. In ferromagnetic materials, the symmetry breaking induced by the presence of the magnetization lifts the geometrical constraints on the relation between charge and spin currents. However, the link between the

ferromagnetic order and spin to charge interconversion remains unclear. By using spin pumping measurements, we injected a spin current from a CoFeB layer into the weak ferromagnets $Ni_{60}Cu_{40}$ and $Ni_{50}Cu_{50}$. The charge current generated by the spin to charge interconversion was subsequently measured across the Curie temperatures (Tc) of these alloys. A change of sign of the generated spin current was observed across the Tc when the CoFeB and NiCu layers are in direct contact. However, this sign change disappears when inserting a copper layer between the two. This indicates that two ferromagnetic materials can be coupled and influence each other at the Ferromagnetic Resonance (FMR), thus questioning the results of studies claiming the observation of spin fluctuation and spin-charge interconversion using FMR measurements. Most importantly, the fact that the generated charge current does not change across the Curie temperature of NiCu alloys indicates that the spin-charge interconversion does not depend on the magnetic phase [1]. The independence of the interconversion on the magnetic phase shows either that the band structure of NiCu is not affected, or that its change across the Tc does not influence the spin-charge interconversion. These results consequently provide an important contribution to both the experimental and theoretical understanding of the spin to charge interconversion in ferromagnetic materials.

[1] S. Varotto et al. Phys. Rev. Lett. 125, 267204 (2020)

GPB-04. Magnon Junction Effect in $Y_3Fe_5O_{12}$/CoO/$Y_3Fe_5O_{12}$ Insulating Heterostructures. *W. He*[1] and X. Han[1] *1. Beijing National Laboratory for Condensed Matter Physics, Institute of Physics, Chinese Academy of Sciences, Beijing, China*

Magnonics is an emergent frontier of magnetism, which aims at using magnons as spin information carriers to avoid the Joule heating and electron scattering in current electron-based spintronics. In general, magnon currents can be excited both thermally and electrically in magnetic insulators, by applying charge currents in an adjacent metallic layer. Here, the magnon junctions (MJs) are studied in the $Y_3Fe_5O_{12}$/CoO/$Y_3Fe_5O_{12}$ heterostructure composed by ferrimagnetic insulator $Y_3Fe_5O_{12}$(YIG) and antiferromagnetic insulator CoO. The temperature gradient driven magnon current transmission could be effectively controlled by the relative orientations of bottom and top YIG layers, i.e., high transmission for the parallel state and low transmission for the antiparallel state, demonstrating the spin transistor-like functions based on magnons. The electrical spin Hall injected magnon current could also be controlled by the MJs, contributing to a magnon junction effect in the magnetoresistance (MR) signals. This work demonstrates the building block of magnonic devices, which sheds light on the future applications of magnon-based memory, logic and computing, etc

[1]W. Q. He et al. Magnon Junction Effect in $Y_3Fe_5O_{12}$/CoO/$Y_3Fe_5O_{12}$ Insulating Heterostructures, Under Review. [2]C. Y. Guo et.al, Physical Review B. 98, 134426 (2018). [3] C. Y. Guo, C. H. Wan, and W. Q. He et.al., Nature Electronics. 3, 304 (2020).

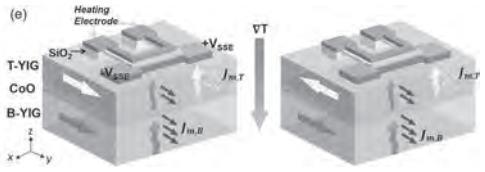

Schematic of magnon junction effect and its measurement steup for MJs, where a temperature gradient is applied to excite the magnon current by spin Seebeck effect.

GPB-05. Spin-Orbit Torques Dependence on the Metal Barrier Thickness in Metal/$SrTiO_3$-based Two-Dimensional Electron Gases Studied by Spin-Torque Ferromagnetic Resonance. *A. Kandazoglou*[1], C. Grezes[1], M. Cosset-Chéneau[1], P. Sgarro[1], P. Noël[1,2], S. Auffret[1], A. Brenac[1], M. Bibes[3], S. Petit-Watelot[4], J. Rojas-Sanchez[4], J. Attané[1] and L. Vila[1] *1. CEA, SPINTEC, Grenoble, France; 2. DMAT, Eidgenossische Technische Hochschule Zurich, Zurich, Switzerland; 3. Unité mixte de Physique CNRS/Thales, Palaiseau, France; 4. Institut Jean-Lamour, Université Lorraine - CNRS, Nancy, France*

Spin-orbitronics exploits the interplay between charge and spin currents enabled by the spin-orbit coupling in non-magnetic systems. This spin-orbit coupling is indeed the phenomenon at the origin of spin-charge interconversions in bulk materials, via the spin Hall effect, and at surfaces presenting a broken inversion symmetry, via the Rashba-Edelstein effect. Recently, spin-to-charge conversion studies in Metal/$SrTiO_3$-based two-dimensional (2D) electron gases have revealed a high conversion efficiency via the inverse Rashba-Edelstein effect [1]. The following demonstration of non-volatile electric-control of the spin-to-charge conversion further brings to light the great potential of these quantum materials for novels ultra-low power spintronics applications [2]. Achieving a metal barrier thickness study is thus desirable to gain insight on the different contributions to the charge-to-spin conversion in metal/$SrTiO_3$-based 2D electron gases. Here, we report spin-orbit torques results obtained by spin-torque ferromagnetic resonance (ST-FMR) in Metal/$SrTiO_3$-based 2D electron gases, for different metal barrier thicknesses. A demonstration of charge-to-spin conversion at the metal/oxide interface is firstly achieved by ST-FMR on both Ta and Mg barrier-based heterostructures. The spin-orbit torques are further investigated for different temperatures, revealing temperature-dependent symmetric and antisymmetric ST-FMR signals. We further achieve the non-volatile electric-control of the sheet resistance of the 2D electron gas in ST-FMR devices, which makes it possible to investigate the gate dependence of the charge-to-spin conversion via ST-FMR techniques. Finally, the dependence of the charge-to-spin conversion with the metallic barrier thickness is discussed, providing routes to improve the spin-orbit torques, and opening the way to optimized spintronics devices based on Metal/$SrTiO_3$ 2D electron gases.

[1] D. C. Vaz et al., Nature Materials, 18, 1187–1193 (2019). [2] P. Noel et al., Nature 580, 483–86 (2020).

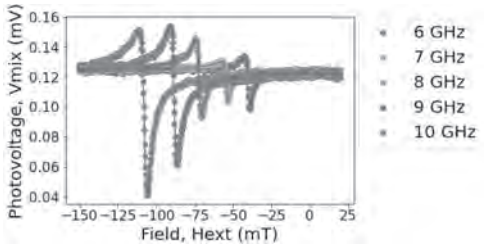

Fig.1: ST-FMR signals in Mg/$SrTiO_3$ heterostructure at 77K

GPB-06. Direct Detection of Transient Spin Pumping during Phase Transition of FeRh. *T. Lee*[1], M. Park[2], S. Kim[1], K. Lee[1], M. Jung[2] and K. Kim[1] *1. Physics, Korea Advanced Institute of Science and Technology, Daejeon, The Republic of Korea; 2. Physics, Sogang University, Seoul, The Republic of Korea*

The dynamics of magnetization generates a spin current, which is referred to as spin pumping [1]. The spin pumping has been intensively studied because it can be utilized in quantifying spin related parameters, such as spin Hall angle, spin diffusion length and spin mixing conductance [2, 3]. In ferromagnet (FM) / heavy metal (HM) layers, which has been a central focus of research during last decade [2-4], the magnetization dynamics of FM generates a spin current in the HM layer, and the spin current is converted into the tangible charge current via inverse spin Hall effect (ISHE) [2-4]. However, the spin pumping efficiency is still low to be used directly for

spintronic applications. Here we demonstrate a giant spin pumping induced by a phase transition of FeRh. FeRh is metallic alloy with CsCl structure which undergoes a phase transition from antiferromagnetic to ferromagnetic phase near 370 K [5]. We measured the transient ISHE voltage in FeRh/Pt bi-layer and found that the spin pumping signal appears during the phase transition of FeRh. Notably, the observed spin pumping signal is at least 2 orders of magnitude larger than those of previous reports [6, 7], suggesting that the spin pumping can be utilized in spintronic applications, e.g., magnetization switching [8]. The large transient spin pumping signal is ascribed to the total angular momentum change between antiferromagnet and ferromagnet during the phase transition, which accompanies the sign change of the exchange interaction. Our work provides a novel method to generate a large spin current, which could be utilized in spintronics application.

[1] Y. Tserkovnyak and A. Brataas, Phys. Rev. B - Condens. Matter Mater. Phys. 66, 1 (2002) [2] O. Mosendz et al. Phys. Rev. B - Condens. Matter Mater. Phys. 82, 1 (2010) [3] W. Zhang et al. Appl. Phys. Lett. 103, (2013) [4] E. Saitoh et al. Appl. Phys. Lett. 88, 15–18 (2006) [5] S. Maat et al. Phys. Rev. B - Condens. Matter Mater. Phys. 72, 1–10 (2005) [6] H. L. Wang et al. Phys. Rev. Lett. 112, 1–5 (2014) [7] Y. Wang et al. Nat. Commun. 11, 1–8 (2020) [8] L. Liu et al. Phys. Rev. Lett. 109, 1–5 (2012)

GPB-07. Magnetization Switching by Spin-Orbit Torque from a Topological Dirac Semimetal. *C. Liu*[1], J. Ding[1], V. Kalappattil[1], Y. Zhang[1,2], O. Mosendz[3], U. Erugu[4], R. Yu[1,5], J. Tian[4], A. DeMann[1], S.B. Field[1], X. Yang[2], H. Ding[5], J. Tang[4], B. Terris[3], A. Fert[6] and H. Chen[1,7] *1. Physics Department, Colorado State University, Fort Collins, CO, United States; 2. Huazhong University of Science and Technology, Wuhan, China; 3. Western Digital Research Center, Western Digital Corporation, San Jose, CA, United States; 4. Department of Physics and Astronomy, University of Wyoming, Laramie, WY, United States; 5. National Laboratory of Solid State Microstructures and Department of Physics, Nanjing University, Nanjing, China; 6. 6Unité Mixte de Physique, CNRS, Thales, Université Paris-Saclay, Palaiseau, France; 7. School of Advanced Materials Discovery, Colorado State University, Fort Collins, CO, United States*

Electrical manipulation of magnetization is of great importance for writing operations in magnetic memory. Recent works show that topological surface states (TSS) in topological insulators, which host highly mobile charge carriers with spin-momentum locking, can be utilized to manipulate magnetization. In principle, there also exist TSS for topological semimetals, but it remains unexplored as to whether such states can also be utilized for magnetization reversal. In this presentation, we report current-induced magnetization switching enabled by TSS in a topological Dirac semimetal α-Sn.[1] Our experiments made use of an α-Sn/Ag/CoFeB tri-layered structure. All the layers were grown by sputtering at room temperature. Field-free current-induced magnetization switching was demonstrated at room temperature. The data show that the switching is driven by the TSS of the α-Sn layer, rather than spin-orbit coupling in the bulk of the α-Sn layer or current-produced Joule heating or Oersted field. The switching efficiency is as high as in topological insulator-based systems. Our work demonstrates that the topological Dirac semimetal α-Sn is as promising as topological insulators in terms of spintronic applications.

[1] J.Ding, C. Liu, and V. Kalappattil, Advanced Materials, 33 (23), 2005909 (2021).

GPB-08. Decoupling anomalous Nernst and longitudinal spin Seebeck effects in Fe_3O_4/Pt thin films around the Verwey transition. *A. Chanda*[1], D. DeTellem[1], Y.T. Pham[1], J.E. Shoup[1], A.T. Duong[2], R. Das[2], S. Cho[3], D.V. Voronine[1], M. Trinh[1], D. Arena[1], S. Witanachchi[1], H. Srikanth[1] and M. Phan[1] *1. Physics, University of South Florida, Tampa, FL, United States; 2. Phenikaa University, Hanoi, Vietnam; 3. University of Ulsan, Ulsan, The Republic of Korea*

Magnetite (Fe_3O_4) is a unique half-metallic magnetic material for longitudinal spin Seebeck effect (LSSE) investigations because of its characteristic Verwey transition ($T_V \approx 125$ K). Since Fe_3O_4 is metallic above T_V, the measured LSSE signal is contaminated by the anomalous Nernst effect (ANE) arising from the Fe_3O_4 layer. Earlier study on the LSSE in Fe_3O_4/Pt [1] did not disentangle the LSSE and ANE signals as a function of temperature above and below T_V. To address this, we have performed a comprehensive study of the temperature dependence of ANE and LSSE in Fe_3O_4 thin films (80 nm) grown on Si and Al_2O_3 substrates. We find that while both effects are present in Fe_3O_4/Pt at $T > T_V$, the ANE signal is much smaller compared to the intrinsic LSSE signal. Below T_V, the total signal across Fe_3O_4/Pt is completely dominated by the LSSE. Through a comprehensive analysis of temperature dependent LSSE and ANE, we decouple their contributions that allow us, for the first time, to observe an anomalous temperature dependence of the intrinsic LSSE signal in Fe_3O_4/Pt around T_V. A comparative study of the intrinsic LSSE in Si/Fe_3O_4/Pt and Al_2O_3/Fe_3O_4/Pt points to the important role of the ordering and density of spins on the Fe_3O_4 surface on the spin transport and spin-charge conversion efficiency [2,3]. The LSSE voltage measured at 300 K in Si/Fe_3O_4/Pt is about two times greater than that of Al_2O_3/Fe_3O_4/Pt. This finding is fully supported by the magnetic force microscopy study that reveals the higher density of magnetic domains on the surface of the Fe_3O_4 film grown on Si compared to the Fe_3O_4 film grown on Al_2O_3. Our study not only provides deeper insights into the LSSE and its temperature evolution in magnetic oxides like Fe_3O_4 but also an effective way for improving the spin-charge conversion efficiency in magnetic films through surface magnetism engineering.

[1] R. Ramos, T. Kikkawa, K. Uchida, H. Adachi, I. Lucas, M. Aguirre, P. Algarabel, L. Morellón, S. Maekawa, and E. Saitoh, Appl. Phys. Lett. 102, 072413 (2013). [2] V. Kalappattil, R. Das, M.H. Phan, and H. Srikanth, Scientific reports 7, 1 (2017). [3] V. Kalappattil, R. Geng, R. Das, M. Pham, H. Luong, T. Nguyen, A. Popescu, L. Woods, M. Kläui, H. Srikanth, and M.H. Phan, Materials Horizons 7, 1413 (2020).

GPB-09. Efficient Spin-Orbit-Torque Switching Assisted by an Effective Perpendicular Field in a Magnetic Trilayer. *T. Ma*[1,2], C. Wan[1], J. Dong[1], C. Guo[1], M. Zhao[1], X. Wang[1], Y. Zhang[1], G. Yu[1] and X. Han[1] *1. Institute of Physics, Chinese Academy of Sciences, Beijing, China; 2. Center of Materials Science and Optoelectronics Engineering, University of Chinese Academy of Sciences, Beijing, China*

Spin-orbit torques (SOTs) provide an electrical way to manipulate the magnetization of magnetic films, which is promising for their application in magnetic random-access memory (MRAM) with high speed and long endurance [1,2]. SOT is usually observed in magnetic-heavy-metal bilayers and casued by the spin Hall effect (SHE) in the heavy metal and as-induced spin current. Restricted by the symmetry of the SHE, the spin current is normally polarized in plane, which can only determinstically switch a magnetic film with in-plane magnetic anisotropy (IMA). To switch a magnetic film with perpendicular magnetic anisotropy (PMA), which is desired for high-density memory applications, an in-plane symmetry-breaking field is indispensable. The field can be provided directly by a sourcing current via the Ostered mechanism or from the exchange-bias or coupling effects [3]. Here, we demonstrate through both theory and experiments that an effective perpendicular field scaling with SOT can inherently result from a magnetic trilayer, which consists of a magnetic film with PMA, another magnetic film with IMA, and a spacer in between to mediate their coupling. More importantly, when the two magnetic films experience two SOTs with the same (opposite) polarity, the effective perpendicular field can favor (hamper) SOT switching of the perpendicular film. This special magentic trilayer can guide the design of efficient and versatile SOT MRAM devices. In our work, a macrospin model is employed to explain the generation of effective perpendicular field. And after a seris of experiments of SOT switching under different in-plane fields, the efficiency to produce the perpendicular field reaches 2.1 $Oe/10^{10}$ Am^{-2}[4].

[1] I. M. Miron, K. Garello and P. Gambardella, Nature, Vol. 476, p. 189 (2011) [2] L. Liu, C.-F. Pai and R. A. Buhrman, Science, Vol. 336, p. 555 (2012) [3] W. J. Kong, C. H. Wan and X. F. Han, Appl. Phys. Lett., Vol. 116, p. 162401 (2020) [4] T. Y. Ma, C. H. Wan and X. F. Han, Phys. Rev. Applied, Vol. 16, p. 014016 (2021)

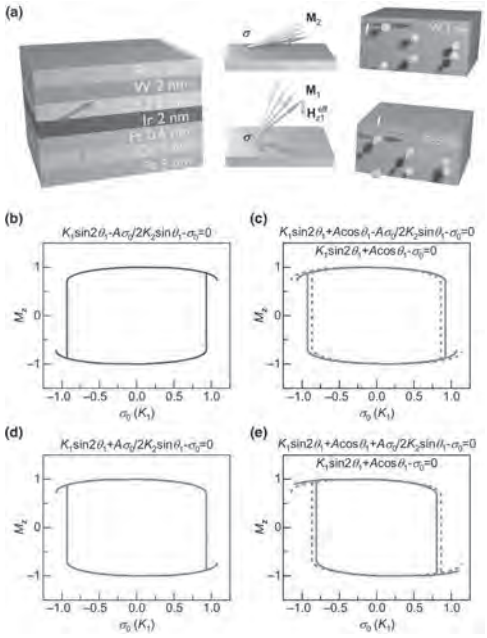

Fig.1. Physics scenario to create H_{z1}^{eff} and predicted dependence of M_z of the perpendicular layer on applied torque.

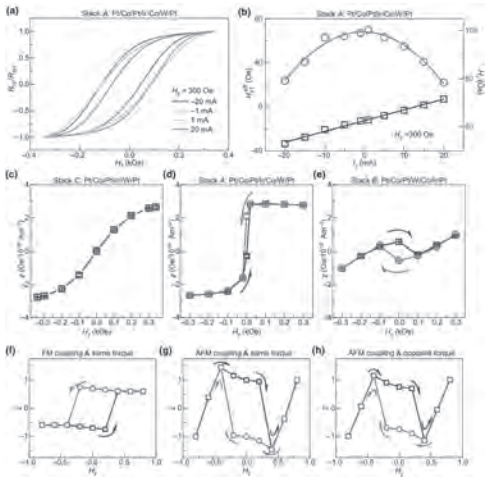

Fig. 2. Direct measurement of H_{z1}^{eff} and dependence of SOT efficiency χ on applied field H_y.

GPB-10. Manipulation of coercivity in GdFeCo/Hf heterostructures by an electrical current. *N. Hai*[1], R.C. Bhatt[2], L. Ye[2], T. Wu[2] and J. Wu[1] *1. Department of Physics, National Changhua University of Education, Changhua, Taiwan; 2. Graduate School of Materials Science, National Yunlin University of Science and Technology, Douliu, Taiwan*

GdFeCo, a rare-earth/transition-metal composition, is a competitive candidate for practical applications on GMR devices [1,2], magneto-optical recording medium [3,4], and ultrafast magnetic switching [5,6]. Particularly, the ability to control magnetic coercivity (H_c) is one of the most important parameters for the advantage in magnetic data storage technologies. It is well known that the coercivity of the GdFeCo compound can be tuned by varying content of Gd or FeCo component [7]. Although these methods can effectively alter the magnetic properties of a sample, the changes are permanent, thus, one may expect a further increase in the flexible ability to manipulate H_c will be explored. Here, we reveal that the coercive field of GdFeCo adjacent to heavy metal Hf can be effectively modulated by electric current. The stack structure of $Gd_{28.5}(Fe_{80}Co_{20})_{71.5}$ (7nm)/Hf(4nm)/MgO(4nm), as illustrated in Fig.1(a), is prepared by means of a RF magnetron co-sputtering, and then characterized by the X-Ray Fluorescence (XRF) spectroscopy technique and the Alternating Gradient Magnetometer (AGM). A 5 μm-width and 100 μm-length Hall bar is fabricated using standard photolithography, E-beam lithography, and Ar ion-beam etching technique. We perform a measurement by injecting a DC current along the Hall channel in the presence of an external magnetic field which is swept perpendicularly to the sample plane, as illustrated in Fig.1(b). Interestingly, we observe that in the early stage of measurement, the H_c reduces drastically while at a higher current level coercivity is able to recover back to its initial value, as shown in Fig. 2. Such dependence of H_c on electric current can be explained by the competing interplay of the spin-orbit torque (SOT) that arises from heavy metal layer Hf and the Joule heating effects. This finding is a supplement for researchers and engineers who are working on spintronics materials

1. B. Dai, Y. Guo, and J. Zhu, J. Phys. D: Appl. Phys. 50, 135005 (2017). 2. C. H. Lai, C. C. Lin, and B. M. Chen, J. Appl. Phys. 89, 7124 (2001). 3. M. koKaneko, Y. Sabi, and I. Ichimura, IEEE Trans. Magn. 29, 3766 (1993). 4. M. Kaneko, J. Magn. Magn. Mater. 148, 351 (1995). 5. R. B. Wilson, J. Gorchon, and Y. Yang, Phys. Rev. B 95, 180409(R) (2017). 6. Y. Yang, R. B. Wilson, and J. Gorchon, Sci. Adv. 3, e1603117 (2017). 7. J. Y. Chen, L. He, and J. P. Wang, Phys. Rev. Appl. 7, 021001 (2017).

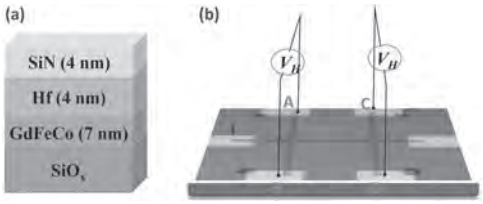

Fig. 1 (a) Schematic illustrations of stacked structure for thin films; (b) Optical microscopy image of the Hall bar device and the schematic of the experimental setup for the magneto-transport measurement.

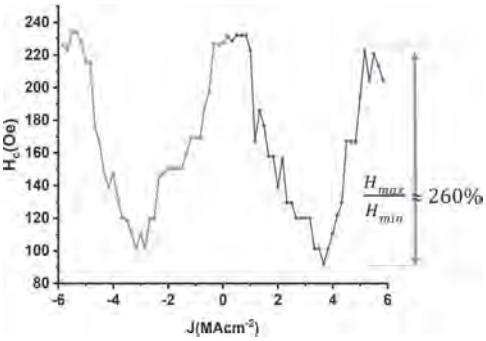

Fig. 2 H_c variation as a function of input DC obtained from the anomalous hall effect (AHE) measurements.

GPB-11. Multi-level resistance switching in high-quality epitaxial FeRh films. *M. Park*[1], S. Ji[1], W. Yoo[1], H. Bang[1], J. Yang[2], K. Kim[2] and M. Jung[1] *1. Physics, Sogang University, Seoul, The Republic of Korea; 2. Korea Advanced Institute of Science and Technology, Daejeon, The Republic of Korea*

FeRh has attracted much interest recently because of its remarkable phase transition from antiferromagnetic to ferromagnetic states just above room temperature[1], which is sensitively modulated by external parameters such as composition and strain[2-3]. In particular, the change in electrical resistance accompanied with the change in magnetization has received more attention for potential applications in spintronics and sensors. Recent studies have shown that FeRh can be used as an antiferromagnetic memory resistor due to the resistance change in the AFM state depending on the field cooled axis[4]. In this study, we precisely control the Rh composition (0.45 £ *x* £ 0.54) in $Fe_{1-x}Rh_x$ phase by adjusting the sputtering power and obtain the high-quality epitaxial films with the orientation relationship of FeRh [100] parallel to MgO [110] substrate (i.e., FeRh [220] parallel to MgO [100]) to

show distinct phase transitions. Surprisingly, we find an anisotropy in the plane; hard [110] and easy [100] magnetization axes, so that the magnetoresistance changes more complicated depending on the directions of external magnetic field and applied current. Our results show a new type of multi-level resistive switching, compared to the previous study of two-level resistance states.

[1] L. Zsoldos, Phys. Status Solidi 20, K25 (1967). [2] K. M. Cher, et al. IEEE Trans. Magn. 47, 4033 (2011). [3] S. Inoue, et al. J. Magn. Magn. Mater. 320, 3113 (2008). [4] X. Marti, et al. Nat. Mater. 13, 367 (2014).

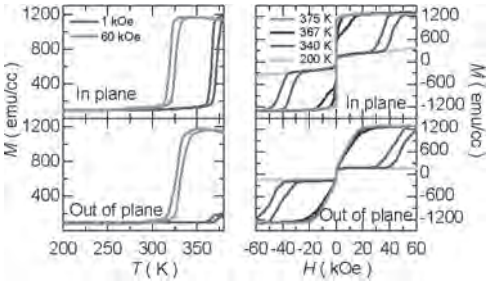

Fig1. Temperature dependent magnetization data and field dependent magnetization curves of high-quality epitaxial FeRh film measured under the magnetic field applied in the film plane and out of the plane.

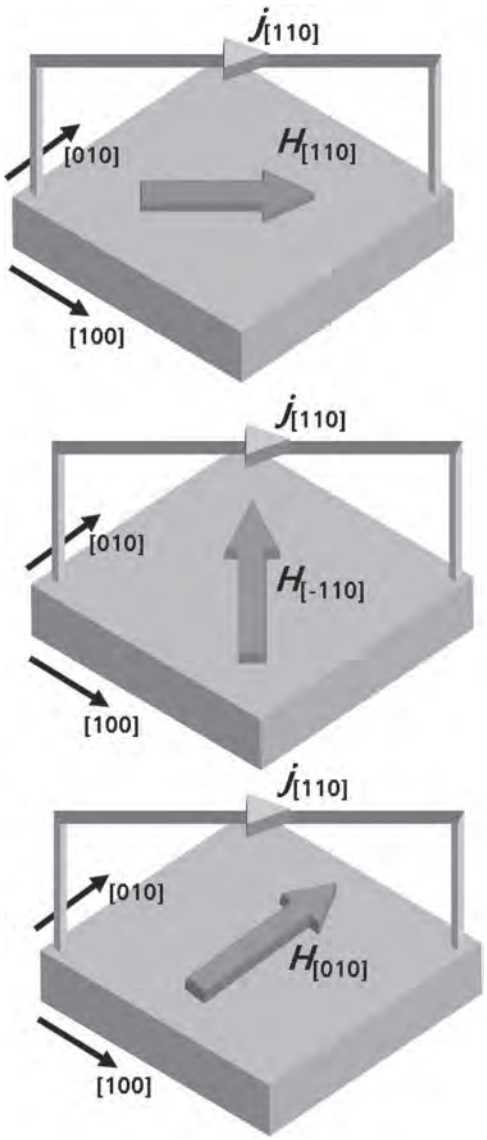

Fig2. Schematic diagram of multi-level resistive switching of epitaxial FeRh film. Directions of applied current and field-cool external magnetic field (red arrows) complicated interact.

GPB-12. Magnonic skin effect and magnon valve effect in an antiferromagnetically coupled heterojunction. *Z. Yan*[1], Y. Xing[1] and X. Han[1]
1. Beijing National Laboratory for Condensed Matter Physics, Institute of Physics, Chinese Academy of Science, Beijing, China

We theoretically study the scattering behavior of spin waves (SWs) at the interface of an antiferromagnetically coupled (AFMC) heterojunction. It is shown that the SWs passing through the interface are evanescent and the incident waves are all reflflected back, demonstrating a magnetization-dependent magnon blocking effect in this structure. We also analytically derive the expressions for the decay length of the evanescent waves (EWs). The theoretical result indicates that with the increase of the spin-wave (SW) frequency, the decay length decreases and the EWs are more concentrated at the interface, showing a magnonic skin effect (MSE) which is similar to the skin effect of electromagnetic waves. Furthermore, a positive magnonic Goos-Hänchen shift (MGHS) of the reflflected waves is also predicted. It can be understood by an effective reflflection interface shift induced by the nonzero decay length of the EWs. The results of micromagnetic simulations are consistent well with all the theoretical fifindings. Based on the above fifindings, we also propose a magnon valve without spacers, which

shows 100% on-off ratio for magnons. Our work provides insights into SW transmissions in the system of AFMC heterostructures and will serve as a promising tool for future magnonic devices.

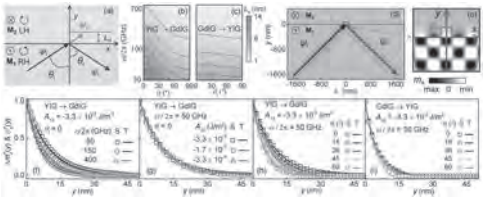

An AFMC FMI bilayer and space dependence of the evanescent spin-wave beam. (a) Illustration of the spin-wave scattering at the interface of bilayer. Bottom layer is FMI1 whose magnetization is along the direction of +z axis accommodating right-handed polarized (RH) spin waves, and magnetization of FMI$_2$ in top layer is along z-axis direction (V) accommodating left-handed polarized (LH,) spin waves. Black, blue and red arrow indicate the propagating direction of the injected spin waves beam, reflected spin waves beam and evanescent spin waves beam. is the decay length of. under various frequency and incident angles for (b) spin waves injected from YIG into GdIG (YIG → GdIG) and (c) GdIG into YIG (GdIG → YIG). (d) Intensity map obtained from micromagnetic simulation of spin-wave scattering at the interface of FMI bilayer.

GPB-13. Spin currents at the interface and spin Hall torque. *V. Basso*[1], A. Magni[1], A. Sola[1] and M. Kuepferling[1] *1. INRIM, Torino, Italy*

The spin orbit torque is one of the most promising effects for inducing magnetization dynamics and switching in a thin ferromagnetic (FM) layer and is at the base of several advancements in the field of spintronic memory devices [1,2]. The effect is caused by the spin current electrically generated by the spin Hall effect in a adjacent heavy metal (HM) layer. The description of the spin orbit torque effects on the magnetization of FM requires the introduction of two torque components in the magnetization dynamic equation: the field-like (FL) and the damping-like (DL), both proportional to intensity of the spin Hall effect [3]. By projecting all the vectors into the plane perpendicular to the magnetization, one finds the DL in the direction of the projected spin current and the FL in the perpendicular direction. The harmonic Hall method permits a detailed characterization of the two components [4] and reveals that the FL is much smaller than the DL and that they both have a non obvious dependence upon the thicknesses of the layers. In the literature, the two torque terms are derived by the introduction of the spin mixing conductance of the interface, whose real and imaginary parts give rise to the two torque terms [3]. However the spin mixing conductance has a difficult physical interpretation and justification. We propose here an alternative approach which is based on the definition of the spin current at the interface of a ferromagnet. To derive the torque terms we allow for the presence of a spin current at the interface of a FM and therefore we extend the boundary conditions of micromagnetism, therefore replacing the classical Brown's boundary conditions. The analysis reveals that by using the continuity of the spin current at the interface between the FM and the HM, one is able to derive two torque components. As a result the ratio between the DL and the FL is proportional to the damping constant of the FM and depends on thicknesses of the two layers. In the present paper we will present the derivation and the properties of the DL and FL torque terms and we will compare the outcome with experimental results from the literature [5].

[1] B. Dieny, I. L. Prejbeanu, K. Garello, P. Gambardella, P. Freitas, R. Lehndorff, W. Raberg, U. Ebels, S. O. Demokritov, J. Akerman et al., Opportunities and challenges for spintronics in the microelectronics industry, Nature Electronics, 3, 446 (2020). [2] A. Manchon, J. Zelezny, I. M. Miron, T. Jungwirth, J. Sinova, A. Thiaville, K. Garello, and P. Gambardella, "Current-induced spin-orbit torques in ferromagnetic and antiferromagnetic systems," Rev. Mod. Phys. 91, 035004 (2019). [3] P.Haney, H. W. Lee, K. J. Lee, A. Manchon and M. D. Stiles, Current induced torques and interfacial spin-orbit coupling: Semiclassical modeling, Phys. Rev. B 87, 174411 (2013). [4] C. O. Avci, K. Garello, M. Gabureac, A. Ghosh, A. Fuhrer, S. F. Alvarado and P. Gambardella, Interplay of spin-orbit torque and thermoelectric effects in ferromagnet/normal-metal bilayers, Phys. Rev. B 90, 224427 (2014). [5] Spin Hall magnetoresistance and spin orbit torque efficiency in Pt/FeCoB bilayers, A. Magni, V. Basso, A. Sola, G. Soares, N. Meggiato, M. Kuepferling, W. Skowronski, S. Lazarski, K. Grochot, M. V. Khanjani, J. Langer and B. Ocker, IEEE Transactions on Magnetics (2021) early access DOI: 10.1109/TMAG.2021.3084866

GPB-14. Towards 100% Spin-Orbit Torque Efficiency in PtCr Alloy with the High Spin Hall Conductivity. *C. Hu*[1], Y. Chiu[1], C. Tsai[1], C. Huang[1], K. Chen[1], C. Peng[1], C. Lee[2], Y. Huang[2], S. Lin[2] and C. Pai[1] *1. National Taiwan University, Taipei, Taiwan; 2. Taiwan Semiconductor Manufacturing, Hsinchu, Taiwan*

To realize a faster and more efficient spin-orbit torque magnetic random-access memory (SOT-MRAM), a conductive spin current source (SCS) possessing large damping-like spin-orbit torque efficiency (ξ_{DL}) than W is an urgent challenge in memories industries. Moreover, the heavy metal/ferromagnet heterostructure is also of great importance to ensure its good thermal stability (Δ) and low magnetic damping constant (α), for the capability of robust data retention and efficient writing process in real applications. In this work, we investigate Pt-Cr/Co(or CoFeB)/MgO heterostructures with perpendicular and in-plane magnetic anisotropy (PMA/IMA), respectively. For PMA and IMA-based devices respectively characterized via anomalous Hall effect hysteresis loop shift measurement and planar Hall effect curve shift measurement, the optimal of Pt-Cr can be up to about 0.89. Comparing to its counterpart (pure Pt) with ξ_{DL}~0.22, this significant enhancement is contributed to the raising resistivity and preserved spin Hall conductivity, leading to the full performance of the large intrinsic Pt spin Hall conductivity. Moreover, the improved in IMA-devices is confirmed via spin-torque ferromagnetic resonance, which is reduced from 0.078 (for pure Pt) to 0.052 (for Pt-Cr). Also, SOT switching in PMA-devices is also performed. The critical switching current density can as low as 9.75×10^5 A cm^{-2} in Pt-Cr layer, almost an order lower than that of pure Pt (1.03×10^7 A cm^{-2} in Pt layer). Moreover, the Δ of PMA devices shows no obvious degradation as alloying. These characteristics demonstrate the potential to utilize Pt-Cr in operating a faster SOT-MRAM with promising data retention ability. The estimated power consumption among other reported SCSs also indicates the best performance in Pt-based SCSs. Considering its larger ξ_{DL}, low resistivity, and reduced α, Pt-Cr accordingly is suggested to be a competitive candidate for the future SOT-MRAM applications.

1. Miron, I.M., et al., Perpendicular switching of a single ferromagnetic layer induced by in-plane current injection. Nature, 2011. 476(7359): p. 189-U88. 2. Liu, L.Q., et al., Current-Induced Switching of Perpendicularly Magnetized Magnetic Layers Using Spin Torque from the Spin Hall Effect. Physical Review Letters, 2012. 109(9). 3. Pai, C.F., et al., Determination of spin torque efficiencies in heterostructures with perpendicular magnetic anisotropy. Physical Review B, 2016. 93(14). 4. C. O. Avci, et al., Interplay of spin-orbit torque and thermoelectric effects in ferromagnet/normal-metal bilayers. Physical Review B, 2016, 90, 224427. 5. Liu, L.Q., et al. Spin-Torque Ferromagnetic Resonance Induced by the Spin Hall Effect. Physical Review Letter, 2011, 106, 036601.

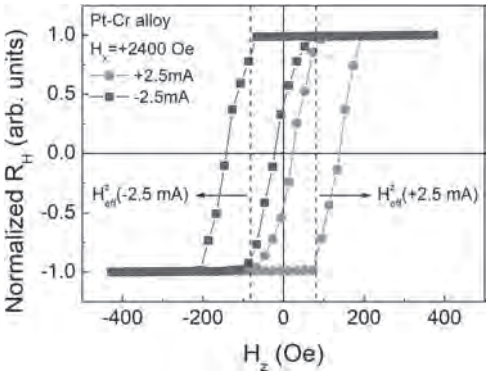

Fig. 1 Representative hysteresis loop shift of Pt-Cr/Co structure

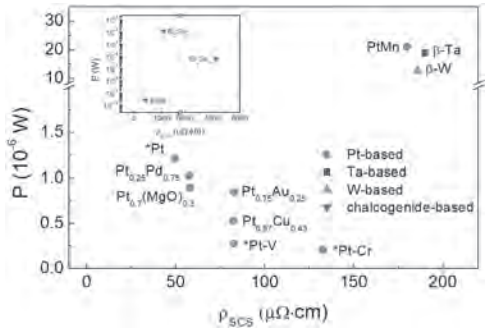

Fig. 2 Summary of calculated power consumption versus resistivities of reported SCSs. The starred points represent the results from this work.

GPB-15. Spin-flop driven anisotropic magnetoresistance in antiferromagnetic spin-valve-like structure. D. Oh[1], *J. Kim*[1], K. Jeong[1], H. Shin[1], J. Hong[1], J. Kim[1], N. Lee[1] and Y. Choi[1] *1. Department of Physics, Yonsei University, Seoul, The Republic of Korea*

A spin-flop transition occurs typically in antiferromagnets, and it induces a significant modification in magnetic anisotropy through a phase conversion. However, the role of spin-flops on anisotropic phenomena has not been investigated in detail. In this study, antiferromagnet-based spintronic functionality on single crystals of $Ca_{0.9}Sr_{0.1}Co_2As_2$ was demonstrated by integrating spin-valve-type structure and large magnetic anisotropy driven by spin-flops. Multiple stacks of 1-nm-thick spin-valve-like unit are intrinsically embedded in the antiferromagnetic spin structure. Along with strong magnetocrystalline anisotropy, the switching operation between low and high resistance states was observed in the presence of a rotating magnetic field. This leads to anisotropic magnetoresistance, which is maximized in the vicinity of the flop transition. Our results observed in a natural antiferromagnet offer the potential of utilizing spin-flop transitions in extensive spintronic applications.

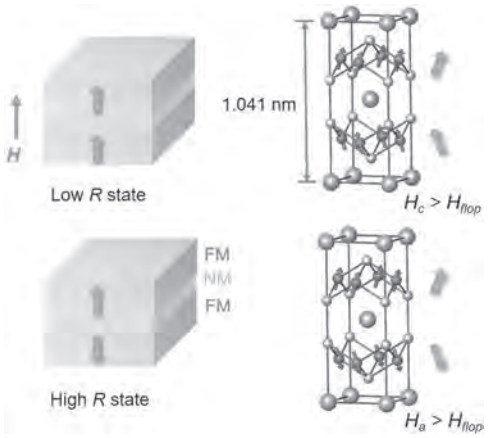

Fig. 1 (Left) Schematic low and high resistance (*R*) states of bilayer GMR-type spin valve structure with out-of-plane magnetizations. Two FM layers are separated by a NM spacer. The arrows within each FM layer denotes the direction of net magnetization. (Right) Spin structures and net magnetic moments in a unit cell at *H* above the H_{flop} for the *c*- and *a*-axes, respectively. The thickness of the naturally formed spin-valve-type unit is approximately 1 nm (*c* = 1.041 nm).

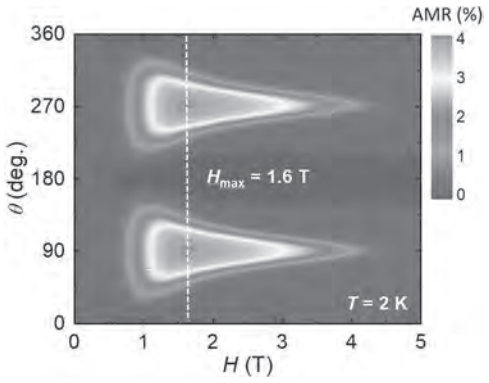

Fig. 2 Contour plots of the AMR taken at *T* = 2 K

Session GPC
FUNDAMENTAL SPINTRONICS II
(Poster Session)

Jorge Puebla, Chair
RIKEN, Wako, Japan

GPC-01. Spin-orbit torque in structures with magnetization-compensated MnGa/Co_2MnSi bilayer. *T. Hara*[1], K. Jono[1], M. Yamanouchi[1] and T. Uemura[1] *1. Grad. School of Information Science and Technology, Hokkaido University, Sapporo, Japan*

Spintronics devices based on spin-orbit torque (SOT) are promising for next generation information technology. Perpendicularly magnetized MnGa/Co_2MnSi (CMS) bilayer [1], in which MnGa and CMS layers are antiferromagnetically coupled to each other, is attractive for a ferromagnetic layer of such devices because of the relatively large perpendicular magnetic anisotropy of MnGa and the half metallicity of CMS. Moreover, previous our study showed that SOT was enhanced by using a MnGa/CMS bilayer structure compared with that in a MnGa single layer structure [2]. Further enhancement of SOT is expected at or near the magnetization-compensation point of MnGa/CMS bilayer because the efficiency of SOT generation is inversely proportional to the magnetization of the ferromagnetic layer. In this work, we systematically investigated SOT in MnGa/CMS/Ta structures with various CMS thicknesses (t_{CMS}) including the compensation point. A wedged structure consisting of, from the substrate side, MgO (10)/NiAl (5)/MnGa (2.5)/CMS (t_{CMS} = 0-1.7)/Ta (5)/MgO (2) was deposited on an MgO(001) substrate (numbers in parentheses are nominal thicknesses in nm). The wedged structure was processed into Hall devices with a 5-μm wide channel to investigate the SOT. We measured the effective magnetic field H_{eff} arising from the interaction between SOT and magnetization in domain walls (DWs) created during the magnetization reversal under current I and in-plane magnetic field H_x along current direction. The magnitude of H_{eff} almost linearly increases with increasing $|H_x|$ at low $|H_x|$ and saturates at large $|H_x|$. The saturated H_{eff} per I ($\mu_0 H_{eff}^*/I$, μ_0 is the permeability in vacuum) is shown as a function of t_{CMS} in Figure. The value of $\mu_0 H_{eff}^*/I$ is increased near the compensation point and reaches about six times that in the device without CMS. These results indicate that magnetization compensation is useful for enhancing the efficiency of SOT generation. This work was supported in part by Japan Society for the Promotion of Science KAKENHI (Grant No. 20H02174 and 20H02598), the Center for Spintronics Research Network.

[1] R. Ranjbar, K. Suzuki, A. Sugihara et al., Mater. Lett. 160, 88-91 (2015)
[2] K. Jono, F. Shimohashi, M. Yamanouchi and T. Uemura, AIP advances. 11, 025205 (2021)

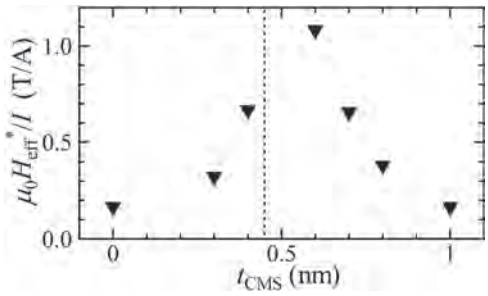

Fig. $\mu_0 H_{eff}^*$ per I as a function of t_{CMS}. The black dotted lines at t_{CMS} = 0.45 nm indicates the magnetization-compensation point.

GPC-02. Composition dependence of in-plane uniaxial magnetic anisotropy and magnetization reversal behavior in Ni-Fe alloy thin films on a single crystal 128° Y-Cut $LiNbO_3$ substrate. *M. Ito*[1], N. Maki[2], A. Yamaguchi[3], M. Shima[1,2] and K. Yamada[1,2] *1. Materials Science and Processing, Gifu University, Gifu, Japan; 2. Chemistry and Biomolecular Science Faculty of Engineering, Gifu University, Gifu, Japan; 3. Laboratory of Advanced Science and Technology for Industry, University of Hyogo, Kamigori, Japan*

Recently, the magnetization reversal using the spin-transfer torque [1] and the spin-orbit torque (SOT) [2] has been actively studied in the field of spintronics to further improve writing speed and power consumption for non-volatile magnetic random access memory [3]. We have previously reported on the magnetization reversal behavior in ferromagnetic (FM) thin films and wires on a single crystal 128° Y-Cut $LiNbO_3$ (LNO) substrates, in which is induced the in-plane uniaxial magnetic anisotropy (K_u) with respect to the (01.2) plane of the LNO substrate [4]. We also have demonstrated that the correlation between the K_u and SOT in the LNO/FM/Pt structure [5]. In this study, we investigate on the magnitude of K_u and the magnetization reversal behavior in Ni-Fe alloy films and wires with various compositions fabricated on a LNO substrate to provide for valuable material designing for the development of spin devices using SOT. The ~30 nm thick samples with various compositions (Ni, $Ni_{74}Fe_{26}$, $Ni_{52}Fe_{48}$, and $Ni_{25}Fe_{75}$) were deposited on a LNO substrate by rf magnetron co-sputtering. The evaluations for the magnitude of Ku and magnetization reversal behavior were conducted by vibrating sample magnetometer and anisotropic magnetoresistance (AMR) effect measurement, respectively. As shown in Fig.1(a), the K_u for $Ni_{52}Fe_{48}$ sample is induced to the direction in the (01.2) plane. Figure 1(b) shows the magnitude of K_u for the samples with various compositions, and that for $Ni_{52}Fe_{48}$ sample is 1.9 kJ/m^3, which is 1.9 times larger than the crystal magnetic anisotropy constant K_1 for that of the polycrystalline bulk (disordered alloy) [6]. In the AMR measurements for $Ni_{52}Fe_{48}$ sample (Fig.2(a)), the magnetization reversal behavior due to the Kondroski model [7] obviously occurs when the longitudinal direction of the $Ni_{52}Fe_{48}$ wire is parallel to the K_u direction at 0 (150) ≤ Φ ≤ 45° (180°) (Fig.2(b)). This result shows the K_u direction and magnitude of K_u are a significant influence on the magnetization reversal behavior.

[1] J.C. Slonczewski, J. Magn. Magn. Mater. 159, L1 (1996). [2] I. M. Miron, et al., Nature 476, 189 (2011). [3] X. Han, et al., Appl. Phys. Lett. 118, 120502 (2021). [4] A. Yamaguchi, et al., J. Magn. Magn. Mater. 453, 107-113 (2018). [5] M. Ito, et al., to be submitted (2021). [6] S. Chikazumi, Physics of Ferromagnetism Ch.12 (Oxford Univ. Press, New York, 1997). [7] E. Kondroski, Phys. Z. Sowjetunion 11, 597 (1937).

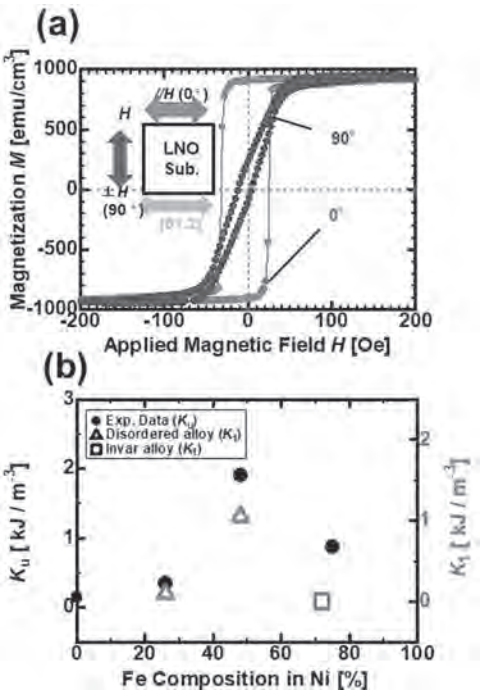

Fig.1 (a) Magnetic hysteresis loops of $Ni_{52}Fe_{48}$ alloy (b) Composition dependence of K_u and K_1 for Ni-Fe alloy

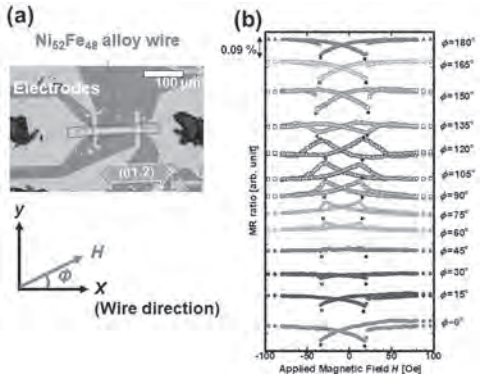

Fig.2 (a) Sample configuration with wire of 10 (100) µm width (length). (b) MR ratio for $Ni_{52}Fe_{48}$ alloy wire

GPC-03. Probing THz emission from spintronic Fe/Pt-emitters with varied interfaces. *L. Scheuer*[1], M. Ruhwedel[1], D. Sokoluk[1], G. Torosyan[2], R. Beigang[1], M. Rahm[1] and E. Papaioannou[3] *1. TUK, Kaiserslautern, Germany; 2. Photonic Center Kaiserslautern, Kaiserslautern, Germany; 3. Institute of Physics, MLU, Halle, Germany*

The field of THz spintronics interlinks the field of ultrafast magnetism and the field of THz optics, raising new fascinating research subjects [1]. While the research in this field advanced quickly, the key technological and scientific challenge of THz spintronic emitters is to increase their intensity and frequency bandwidth. These spintronic emitters, consistent of ferromagnetic (FM)/non-magnetic (NM) heterostructures, generate THz radiation based on spin-to-charge conversion in the metallic layers. Our earlier work covered the optimization of our emitters regarding the film thicknesses [2] and then focused on the electron-defect scattering lifetime and the interface transmission of spin-polarized, non-equilibrium electrons as factors to engineer spintronic Terahertz generation. More precisely, we could clarify the influence of the scattering lifetime on the spectral shape and the interface transmission on the THz amplitude, and how these are linked to structural defects of bilayer emitters [3]. Based on these results we continued our investigation on the role of the FM/NM-interface quality on the THz radiation. A first modification was the blending of the FM and the NM layer into an alloy superseding a sharp interface which resulted in a distinct rise in the THz amplitude (see Fig. 1). Further interface modifications we studied were sharp interfaces FM- and NMwise, but dusted with Au and MgO respectively as an intermediate step during the thin film growth. The Au and, in the second sample set, MgO films were produced with different thicknesses, demonstrating dimensions preventing the formation of homogenous layers. Adding Au to a nonmagnetic heavy metal in small percentages is known to effectively enhance the spin-Hall angle [4] while we know from earlier studies that thin MgO interlayers do not contribute to the spin-to-charge conversion [5]. By comparing these two sample sets we are able to extract the influence of the different scattering center densities onto the spin-Hall effect and thus the THz amplitude.

[1] T. Seifert, M. Münzenberg, T. Kampfrath, Nature Photonics Volume 10, pages 483–488 (2016) [2] G. Torosyan, L. Scheuer, E. Papaioannou, Scientific Reports Volume 8, 1311 (2018) [3] D. Nenno, L. Scheuer, E. Papaioannou, Scientific Reports Volume 9, 13348 (2019) [4] P. Laczkowski et al. Phys. Rev. B 96', 140405(R), (2017) [5] L. Mihalceanu, S. Keller, E. Papaioannou, Appl. Phys. Lett. 110, 252406 (2017)

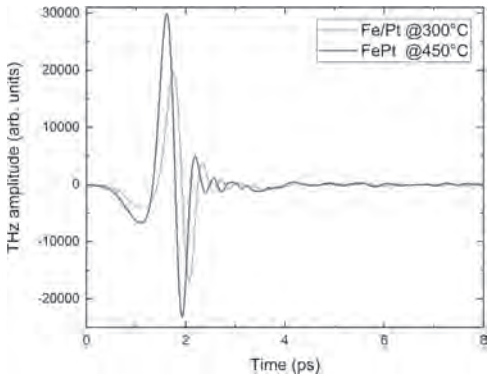

THz pulses from Fe/Pt-bilayers: The emitter grown at 450°C forms an alloy at the interface, yielding a significantly higher amplitude than the emitter with a sharp Fe/Pt-interface grown at 300°C.

GPC-04. Rashba Spin-Orbit Torque in Interface Engineered Ultra-thin Metallic Multilayers. *S. Krishnia*[1], Y. Sassi[1], F. Ajejas[1], S. Collin[1], A. Fert[1], J. George[1], N. Reyren[1], V. Cros[1] and H. Jaffrès[1] *1. Unité Mixte de Physique, CNRS, Thales, Université Paris-Saclay, Palaiseau, France*

Generation of spin-current and its transport across interfaces, as well as its interaction with magnetic moments, are the central themes of spintronic community to enable fast and efficient magnetization dynamics for data storage devices. There are two main mechanisms to produce the spin-current in non-magnetic materials: (a) spin Hall effect (SHE) in heavy metals such as Pt or Ta and (b) Rashba effect (RE) at the interfaces[1]. Irrespective of the origin, the spin-current exerts torques on adjacent ferromagnetic layer with two components: damping-like (DL) & field-like (FL)[2]. However, disentangling properly SHE from RE remains highly challenging. In this experimental study we identify the mechanisms of spin-transport in ultrathin magnetic multilayer whose thicknesses range from less to above the characteristic spin- decoherence length. To this aim, we quantify the different SOT contributions in series of samples Pt8|Cox|Al1.4|Pt3 and P8|Cox|Cu1.4|Pt3 (as a reference) with x varying from 0.4 to 1.4 nm. We extract, in each case, a spin decoherence length to be around 1.1 nm. Surprisingly, SOT investigation in the Pt8|Cox|Al 1.4|Pt 3 reveals a dominating FL torque ($H_{FL}/H_{DL}>1$), which is a signature of a strong Rashba interface in Al-based systems. As a comparison, we find that the Rashba interaction is small in Pt8|Cox|Cu1.4|Pt3 samples. Moreover, we determine the SOTs characteristics in Pt(x)/Co(0.9)/Al(5) by varying the Pt thickness (t_{Pt}). The bulk spin Hall angle of Pt(θ_{SHE}) and ratio of H_{FL} and H_{DL} as a function of t_{Pt} are shown in Figure 1(a) and (b). The increase in H_{FL}/H_{DL} in the range of Pt thickness

where the bulk SHE of Pt started decreasing, strongly favors our argument of the presence of Rashba interface[3], exhibiting thus the specific role of Al insertion layers to enhance spin-orbit effects. Financial support from the Agence Nationale de la Recherche, France, No. ANR-17-CE24-0025 (TOPSKY), the Horizon2020 Framework Programme of the European Commission under FET-Proactive Grant agreement No. 824123 (SKYTOP), FLAGERA SOGRaphMEM and the DARPA TEE programme through grant MIPR no. HR0011831554 are acknowledged

1. Manchon, A. *et al. Rev. Mod. Phys.* 91, (2019). 2. Garello, K. *et al. Nat. Nanotechnol.* 8, 587–593 (2013). 3. S. Krishnia et al. to be submitted

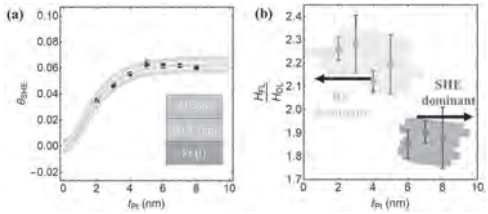

Figure 1(a) θ_{SHE} vs t_{Pt} in Ta(5)/Pt(x)/Co(0.9)/Al(5). (b) Ratio of H_{FL}/H_{DL} as a function of t_{Pt}.

GPC-05. The anomalous Nernst effect in Co_2MnSi thin film. J. Harknett[1], C. Cox[1,2], L. Osborn[1], M.T. Greenaway[1] and *K. Morrison*[1] *1. Physics, Loughborough University, Loughborough, United Kingdom; 2. National Physical Laboratory, Teddington, United Kingdom*

The Anomalous Nernst Effect (ANE) in a magnetic material gives rise to an electric field (E) perpendicular to an applied temperature difference (ΔT), or heat flux (J_Q), and magnetisation vector (M). Recently a wide range of materials, from thin films to bulk single crystals, dilute magnetic semiconductors and topological insulators, have been shown to exhibit an enhanced ANE due to the topological properties of their band structures [1],[2]. In particular these materials exhibit Weyl-like transport phenomena and have large values of the Berry curvature around the Fermi level [3]. The Berry curvature enhances the transverse velocity of the electrons [4] in addition to the statistical force produced by the ΔT, thereby generating a large anomalous thermoelectric response. The family of Heusler alloys contain proposed (and confirmed) magnetic Weyl semimetals most notably Co_2MnGa. However, another Heusler alloy which is of interest, particularly in the magnetic recording field is Co_2MnSi, identified for its 100% spin polarisation [5] and high magnetisation and Curie temperature. Here, we study the ANE and the anomalous Hall effect (AHE) in a series of polycrystalline Co_2MnSi thin films where there is dependence of the lattice ordering upon annealing temperature (T_{Ann}) (Fig. 1)[6]. We find that the fully ordered L21 phase exhibits an ANE with a Seebeck coefficient of S = 0.114 μVK^{-1} but remarkably, for the disordered A2 phase we observe a ~6 times enhancement with S = 0.662 μVK^{-1}. A similar trend with the disorder is seen in the anomalous Hall resistivity (which is expected to scale with the ANE). Whilst Co_2MnSi in the L21 phase does not exhibit any form of non-trivial band structure, the increase in the ANE and AHE (in contrast to the decrease in magnetisation with increasing disorder) seen here suggests a topological origin arising from a subtle difference in the band structures. We compare our measurements with Density Functional Theory (DFT) calculations to reveal the role of band topology on the observed enhancement of the ANE.

[1] H. Reichlova, R. Schlitz, S. Beckert *et. al.*, *Appl. Phys. Lett.* 113, 212405 (2018). [2] S.N. Guin, P. Vir, Y. Zhang *et. al.*, *Adv. Mater.* 31, 1806622 (2019). [3] S.N. Guin *et al.*, *NPG Asia Mater* 11, 16 (2019). [4] D. Xiao *et al.*, *Rev. Mod. Phys.* 82, 1959 (2010). [5] M. Jourdan, J. Minár, J. Braun *et al.*, *Nat. Commun.* 5, 3974 (2014). [6] C.D.W. Cox, A.J. Caruana, *et al.*, *J. Phys. D. Appl. Phys.* 53, 035005 (2020).

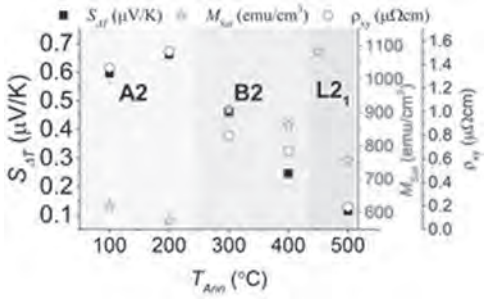

Fig. 1: Dependence of ANE, magnetisation and anomalous Hall resistivity on the ordering of Co_2MnSi thin films.

GPC-06. Investigation of Spin Gapless Semiconducting Behaviour in Quaternary CoFeMnSi Heusler Alloy Thin Films on Si (100). *V. Mishra*[1], V. Barwal[1], L. Pandey[1], N. Gupta[1], S. Hait[1], A. Kumar[1], N. Sharma[1], N. Kumar[1] and S. Chaudhary[1] *1. Physics, Indian Institute of Technology Delhi, New Delhi, India*

Ferromagnetic materials with high spin polarization are highly suitable materials for the spin transfer torque based magnetoresistive random access memories. In this regard, spin gapless semiconductor (SGS) materials such as quaternary Heusler Alloy CoFeMnSi (CFMS) are very promising candidates for the same because of their unique band structure [1]. However, all these exotic properties are susceptible to the microstructure of the grown film. Therefore, optimized growth of a SGS material is a prerequisite for its practical realization in spintronic-based devices. Here, in this study we have tailored the structural ordering in CFMS thin films (~60 nm) grown at different substrate temperatures (T_S) from 150°C to 550°C range over Si(100) substrates using pulsed DC magnetron sputtering. All the grown films were polycrystalline in nature with an enhancement in structural ordering with T_c. Among all the film samples, the film grown at 550°C showed the optimal structure with $L2_1$ ordering. The magnetic measurements revealed that saturation magnetization (M_s) of the sample decreased with the measurement temperature with a value ~3.42 μ_B/f.u. at 5K to 3.11 μ_B/f.u. at 300 K. The Curie temperature (T_C) of the sample was found to be 778±13K. The longitudinal resistivity measurement clearly exhibited a negative temperature coefficient of resistivity, indicating the semiconducting behavior of these CFMS films. The carrier concentration (n) and mobility (μ) were found to be nearly temperature-independent, revealing typical SGS characteristics. The room temperature n and μ values were found to be 3.9 ± 0.04 cm^{-3} and 88.83 ± 1.58 cm^2/V.s, respectively. The temperature-dependent anomalous Hall effect measurements have also been carried out to identify the dominant scattering mechanisms occurring in these films. This measurement suggests the dominance of phonon-induced scattering over impurity-induced scattering.

X.L. Wang, Phys. Rev. Lett. 100 (2008) 1–4.

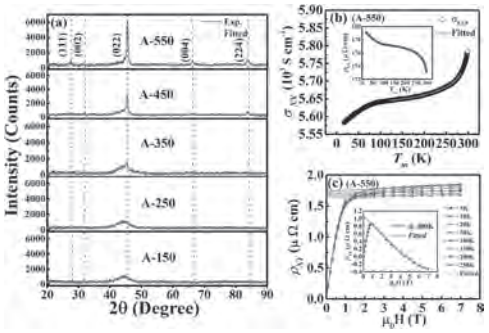

Fig. 1: (a) GIXRD spectra of the samples grown at different T_S, (b) longitudinal resistivity (and/or conductivity at the inset) vs. temperature curve, and (c) Hall resistivity vs. magnetic field recorded at different temperatures (5K to 250K) for A-550 film. Hall resistivity data at 300K is shown in the inset.

GPC-07. Observation of out-of-plane spin polarization in amorphous WTe_2. *W. Liao*[1], C. Peng[1], T. Chen[1] and C. Pai[1] *1. National Taiwan University, Taipei, Taiwan*

Transition metal dichalcogenides (TMDs) has driven lots of attention in spintronics society in recent years due to the tunable conductivity, strong spin-orbit coupling (SOC), and unconventional spin-orbit torque (SOT). One of the TMDs, WTe_2, has been reported to generate the out-of-plane damping-like torque due to the lack of crystal symmetry [1] and possess a sizable bulk SOT efficiency up to 0.5 [2]. Furthermore, the out-of-plane spin polarization-induced field-free deterministic SOT switching is demonstrated in perpendicularly magnetized WTe_2/ferromagnet device [3]. However, most of them require mechanical exfoliation of single-crystalline WTe_2, which is hard to realize in industry applications. Recent work further show that the sputtered WTe_2 thin film can possess sizable SOT with small damping constant [4]. In this work, we present the amorphous WTe_2 prepared by conventional magnetron sputtering can generate the out-of-plane spin polarization. By performing the spin-torque ferromagnetic resonance (ST-FMR) measurement, the out-of-plane spin polarization induced in-plane field-like torque is verified to be preserved in amorphous WTe_2/CoFeB magnetic heterostructure. Our work opens a new path for developing the TMD-spintronics memory technology.

[1] D. MacNeill, G. M. Stiehl, M. H. D. Guimaraes, R. A. Buhrman, J. Park, and D. C. Ralph, Nat. Phys. 13, 300 (2016). [2] S. Shi *et al.*, Nat. Nanotechnol. 14, 945 (2019). [3] I.-H. Kao *et al.*, 2020), p. arXiv:2012.12388. [4] C.-W. Peng, W.-B. Liao, T.-Y. Chen, and C.-F. Pai, ACS Appl. Mater. Interfaces 13, 15950 (2021).

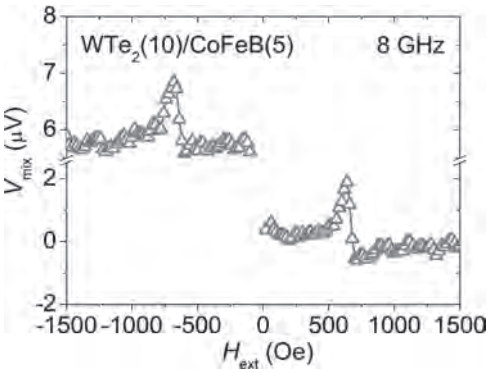

Fig.1 Representative ST-FMR result of WTe_2(10)/CoFeB(5).

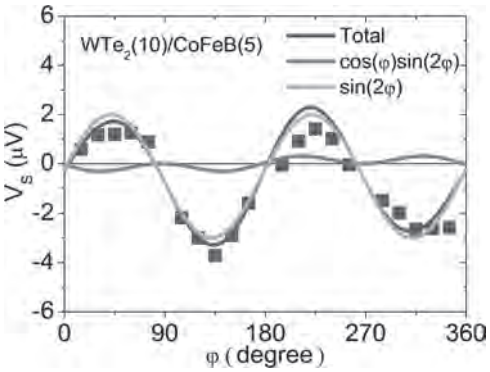

Fig.2 Symmetric ST-FMR components of WTe_2(10)/CoFeB(5) as a function of in-plane magnetic field angle.

GPC-08. Curie temperature dependence of unidirectional spin Hall magnetoresistance in metallic bilayers. *K. Yamanoi*[1], H. Semizu[1] and Y. Nozaki[1,2] *1. Department of Physics, Keio University, Yokohama, Japan; 2. Keio University, Center for Spintronics Research Network, Yokohama, Japan*

The magnetoresistance (MR) effect is one of the most important phenomena to detect the magnetic configuration of any spintronic device. Recently, a novel type of MR called unidirectional spin Hall MR (UMR) has been observed in a bilayer consisting of a ferromagnet (FM) and nonmagnet (NM). The UMR is an odd effect with respect to the reversal of magnetization (M) or current flow. There are two possible origins for UMR: one is spin-dependent (SD)-UMR and another is spin-flip (SF)-UMR. The latter depends on temperature because magnon excitation plays an important role for UMR. In this work, we found the relation between the Curie temperature T_C of FM and the magnitude of SF-UMR. Bilayer films consisting of Pt for NM and NiFe, Ni and NiCu for FM were sputtered on oxidized-Si substrates followed by microfabrication of Hall-bar. T_C for each FM was evaluated by measuring the temperature dependence of M. As shown in Fig. 1, UMR was examined by measuring 2nd-harmonic longitudinal and transverse voltages, i.e. V_{xx} and V_{xy}, with an application of alternating current along *x*-axis. Figure 1(c) shows the typical V_{xx} as a function of the field along *x*-axis. There is a clear difference in the magnitude of V_{xx} measured at positively and negatively saturated states. This is attributed to the change in relative orientation between M and spin polarization of spin current produced via spin Hall effect in Pt. However, a thermoelectromotive force such as anomalous Nernst effect is also superimposed on V_{xx}. Such a parasitic voltage can be separately evaluated from the magnitude of V_{xy}. Figure 2 shows UMR ratio $\Delta R_{UMR}/R_0$ as a function of reciprocal of T_c. The value of UMR ratio increases with decreasing T_c. Moreover, as shown by the broken curve in Fig. 2, we found that $\Delta R_{UMR}/R_0$ is in proportion to the three-halve power of T_0/T_c even though UMR are examined for different FMs. Our result implies that SF-UMR owing to an electron scattering by magnons, whose amplitude shows similar temperature dependence, is independent of FM.

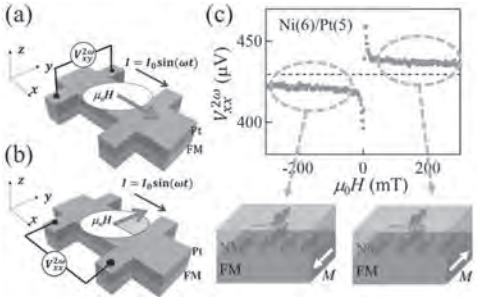

Fig.1 Schematic experimental setup of (a) V_{xx} and (b) V_{xy}. (c) is the field dependence of V_{xx} for Ni/Pt.

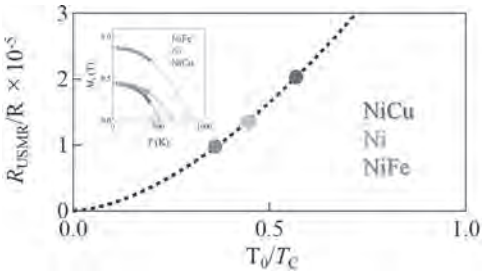

Fig.2 T_C dependence of $\Delta R_{UMR}/R_0$ for each device. T_0 = 300 K. Inset is the temperature dependence of M for each FM.

GPC-09. Thermal Scanning Probe Lithography as a Technique for Fabrication and Local Modification of Non-Local Spin Valves.

A.J. Wright[1], M.J. Erickson[2,3], P.A. Crowell[2], C. Leighton[3] and L. O'Brien[1]
1. Physics, University of Liverpool, Liverpool, United Kingdom; 2. Physics and Astronomy, University of Minnesota, Minneapolis, MN, United States; 3. Chemical Engineering and Materials Science, University of Minnesota, Minneapolis, MN, United States

The non-local spin valve (NLSV) has been widely employed to study spin transport in a variety of materials, owing to its key advantage of complete separation of charge and spin currents.[1,2] Yet, despite their widespread use, there is still an incomplete understanding of the origin of spurious background effects, which can obfuscate and offset the spin signal, for example the high-field spin-Kondo effect[3] and thermoelectric effects in all-metallic NLSVs.[4] In these devices, a non-magnetic metal (NM) channel is contacted by two ferromagnetic (FM) electrodes, a geometry that, to date, has almost exclusively been patterned using electron beam lithography (EBL). Meanwhile, thermal scanning probe lithography (t-SPL) is emerging as an alternative lithographical tool for spintronic devices, with advantages over EBL in cost-effectiveness, resolution and *in situ* imaging. Further, t-SPL can be exploited as a thermal conversion tool, with the potential for manipulation of devices on the nanoscale.[5] In this work, we present the first reported use of t-SPL to lithograph suspended shadow masks for the fabrication of NLSVs (Fig. 1). First, using SEM characterisation and charge and spin transport measurements, we directly compare t-SPL and EBL written devices, validating t-SPL as a viable lithography technique for the fabrication of NLSVs. Through measurements of the non-local resistance, R_{NL}, and the spin-signal, R_{spin}, we then explore how the choice of lithography approach affects spin transport parameters and deleterious background effects such as those mentioned above. By studying the FM separation dependence and thermal evolution of the offset, R_b, we are then able to probe the influence of microstructural and thermoelectric material properties on these background effects, as well as the key role of the choice of FM/NM pairing (Fig. 2).

[1] F.J. Jedema, M.S. Nijboer, A.T. Filip, and B.J. van Wees, Phys. Rev. B 67, p.085319 (2003). [2] I. Zutić, J. Fabian, and S. Das Sarma, Rev. Mod. Phys. 76, p.323 (2004). [3] A.J. Wright, M.J. Erickson, D. Bromley, P.A. Crowell, C. Leighton, and L. O'Brien, Phys. Rev. B 104, p.014423 (2021). [4] F.L. Bakker, A. Slachter, J.-P. Adam, and B.J. van Wees, Phys. Rev. Lett. 105, p.136601 (2010). [5] S.T. Howell, A. Grushina, F. Holzner, and J. Brugger, Microsystems Nanoeng. 6, p.21 (2020).

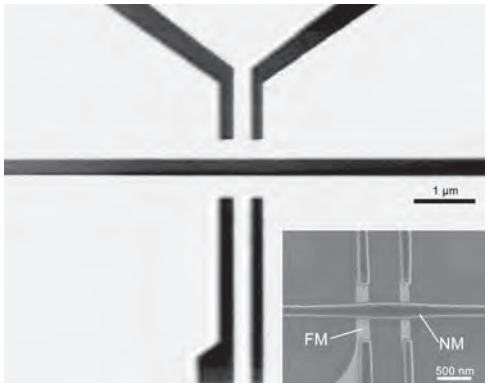

AFM image of a NLSV suspended shadow mask, written using t-SPL. An SEM image (colour added) of a NLSV is shown in the inset, with the FM and NM materials indicated.

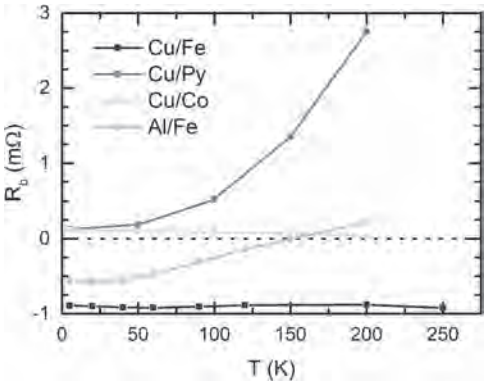

Spin signal background, R_b, as a function of temperature, T, for NLSVs with different material pairings and similar FM separations (400-500 nm).

GPC-10. Large Spin-Current Conversion in Tungsten-based Materials.

R. Xiao[1], J. Zhang[1,2], H. Zhang[1], A. Du[1], J. Yin[1], S. Lu[3], X. Shang[3], C. Zhang[2], B. Man[2], S. Lyu[3], X. Zhou[3], W. Chen[1,2], D. Zhu[1,2], G. Wang[3], W. Zhao[1,2], K. Cao[1,2] and H. Liu[3] *1. Fert Beijing Institute, School of Integrated Science and Engineering, Beihang University, Beijing, China; 2. Beihang-Geortek Joint Microelectronics Institute, Qingdao Research Institute, Beihang University, Qingdao, China; 3. Truth Memory tech. Corporation, Beijing, China*

Magnetic random access memories (MRAMs) driven by current-induced spin-orbit torques (SOTs) become a promising candidate of next generation nonvolatile memory due to the high reliability, ultrafast writing speed, and good compatibility with COMS circuits[1] Pursuing the efficient manipulation of SOT in SOT-MRAM, recent research has focused on sorts of materials with large spin hall angle, like Platinum, β-tungsten, and topological insulators, or on SOT-channels with the special structure like ultrathin insertion layer of Hf or Co in Pt[2-4]. Here we demonstrate a type of SOT channel with large spin hall angle (θ_{SH}) up to 0.62 and relatively low resistivity of about ~200μΩ*cm by oxygen and nitrogen periodically doped in tungsten. As shown in Fig.1(a), our sample stacks from bottom to top are Si/SiO sub./X(t)/CoFeB(1.9)/MgO(1.5)/Ta(1.5)(units in nm). The X layer refers the different SOT channels which include tungsten, oxygen doped tungsten(WO), nitrogen doped tungsten(WN), and oxygen and nitrogen periodically doped in tungsten(WO/WN). The resistivity shows that we obtain a larger β-phase window with oxygen or nitrogen or both two elements incorporation in Fig.1(b), which can provide a more stable deposition condition of β-tungsten. The spin hall angle measurement was carried out by spin-torque ferromagnetic resonance (ST-FMR). The voltage spectra V_{mix} measured by ST-FMR at frequency f = 5 ~ 10 GHz in (WO/WN) sample is displayed in Fig. 2(a). Fig. 2(b) shows the fitting of the measured curve at 7GHz by the Lorentzian function. By analyzing the V_{mix} spectra, we figure out that the damping constant is about 0.01(Fig. 2(c)). While the spin hall angle attains approximately 0.62 which implies its high efficiency to exert spin-orbit torques and a decline of writing current density in SOT-MRAM.

[1] Shao, Q., Li, P., Liu, L., Yang, H., Fukami, S., Razavi, A., ... & Zhang, W. (2021). Roadmap of spin-orbit torques. *IEEE Transactions on Magnetics*. [2] Zhu, L., Zhu, L., Shi, S., Sui, M., Ralph, D. C., & Buhrman, R. A. (2019). Enhancing spin-orbit torque by strong interfacial scattering from ultrathin insertion layers. *Physical Review Applied*, *11*(6), 061004. [3] Demasius, K. U., Phung, T., Zhang, W., Hughes, B. P., Yang, S. H., Kellock, A., ... & Parkin, S. S. (2016). Enhanced spin–orbit torques by oxygen incorporation in tungsten films. *Nature communications*, *7*(1), 1-7. [4] Garello, K., Yasin, F., Couet, S., Souriau, L., Swerts, J., Rao, S., ... & Kar, G. S. (2018, June). SOT-MRAM 300mm integration for low

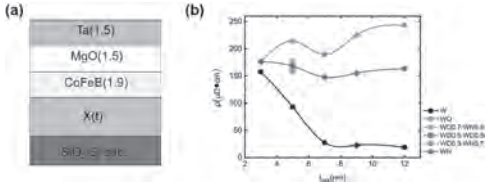

Fig.1 (a). Schematic of samples film stack; (b). The resistivity of samples.

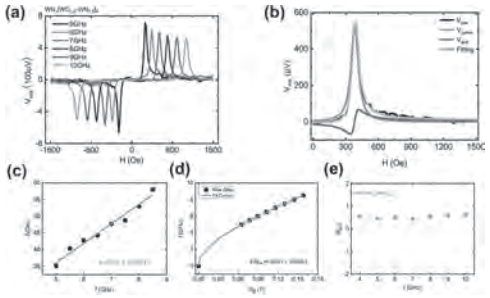

Fig2. (a). Voltage spectra V_{mix} of WN[WO/WN]$_4$ measured by ST-FMR; (b). Fitting of V_{mix} at 7GHz The V_{sym} (V_{asy}) denotes the symmetric (antisymmetric) part of V_{mix}, respectively; (c) The linewidth Δ extracted from the fitting of V_{mix}; (d) The resonant frequency as the function of resonant field; (e) Spin hall angel results.

GPC-11. Non-Volatile Electric-Field Control of Spin-Orbit Torques and Anomalous Hall Effect in Perpendicular Ferromagnet - $SrTiO_3$ System. C. Grezes[1], *A. Kandazoglou*[1], M. Cosset-Chéneau[1], L. Moreno[2], P. Sgarro[1], P. Noël[1,3], S. Auffret[1], K. Garello[1], M. Bibes[2], L. Vila[1] and J. Attané[1] *1. CEA, SPINTEC, Grenoble, France; 2. Unité mixte de Physique CNRS/Thales, Palaiseau, France; 3. DMAT, Eidgenossische Technische Hochschule Zurich, Zurich, Switzerland*

The realization of magnetization switching induced by in-plane current injection in heavy metal/ferromagnetic heterostructures has drawn increasing attention to spin-orbitronics, leading to the advent of spin-orbit torques magnetoresistive random access memories (SOT-MRAM). Compared to heavy metals, oxide 2D electron gases have emerged as alternative spin-orbitronics material systems, which benefit from an efficient spin-charge interconversion through the direct and inverse Edelstein effects. Recently, we have demonstrated an enhancement of the spin-to-charge conversion efficiency by two orders of magnitude in $SrTiO_3$-based 2D gas compared to conventional heavy metals [1], along with a non-volatile electric-control of the spin-to-charge conversion [2]. While the sign and efficiency of the SOTs are fixed by the stack of materials in conventional SOT devices, achieving an electric-control of the mirror charge-to-spin conversion would be of great interest for developing reconfigurable SOT-MRAM and logic gates. Here we report electric-field control of spin orbit torques with electrical remanence in a perpendicular ferromagnet - $SrTiO_3$ system. Non-volatile electric-field control of the sheet resistance is achieved with 1150% contrast, with two switchable and remanent high and low resistivity states of the 2D electron gas. Spin-orbit torques effective fields are further measured using second harmonic Hall methods. A remanent electric-field control of the SOT efficiency is demonstrated, with inversion of the sign of the SOT anti-damping-like effective field. These results are consistent with a combination of both intrinsic modulation of the SOT efficiency together with extrinsic modulation due to the non-volatile electric-control of the current injection in the 2D gas. The non-volatile control of the SOT effective field is further evidenced by reproducible inversion of the SOT torques after initializing with negative or positive voltage pulses of ±130 V, opening the way to reconfigurable spin-orbit torque memory and logic gate architectures.

[1] D. C. Vaz et al., Nature Materials, 18, 1187–1193 (2019). [2] P. Noel et al., Nature 580, 483–86 (2020).

Fig.1: (a) Structure of the sample and measurement geometry. (b) Electric-field control of spin orbit torques with electrical remanence.

Session GPD
MRAM, MAGNETIC LOGIC AND RELATED DEVICES III
(Poster Session)

Manfred Albrecht, Co-Chair
University of Augsburg, Augsburg, Germany
Michal Krupinski, Co-Chair
Polish Academy of Sciences, Kraków, Poland

GPD-01. Design of LUT-Based LDPC Decoders for Spin-Torque Transfer Magnetic Random Access Memory. *C. Duangthong*[1], W. Phakphisut[1] and P. Subniti[1] *1. School of Engineering, King Mongkut's Institute of Technology Ladkrabang, Ladkrabang, Thailand*

STT-MRAM is one of the potential candidates to replace conventional volatile memories [1]. To improve the reliability of STT-MRAM, the LDPC codes have been widely studied in [1 - 3]. While several works focus on the construction of LDPC codes, we aim to design the low-complexity LDPC decoder. However, in STT-MRAM, the required switching time for the P→AP state is greater than the AP→ P state [4, 5]. Thus, the STT-MRAM exhibits a high asymmetry channel. The design method in [6] assumed that the channel was symmetric. Moreover, the quantizer and LUT decoder are designed separately. Therefore, we then propose the design of the LUT decoder using density evolution (DE). The DE offers the joint design between quantizer and LUT decoder while the channel can be either asymmetric or symmetric. Fig. 1 shows the read and write process of STT-MRAM. We employ the channel model of STT-MRAM presented in [7, 8]. Although the proposed design can be applied to the asymmetric channel, we will use the i.i.d channel adaptor to facilitate the performance comparison between the proposed design and the previous design [6]. Due to the process variation and thermal fluctuation, the write and read channels are modeled as the BAC and Z channels. The read decision error is modeled as a Gaussian mixture channel. Since the LDPC decoder requires soft information, the multiple read currents must be applied in the channel quantizer. Here, the read current set needs to be optimized. In the LDPC decoder, the complex computations of the check nodes (CN) and variable nodes (VN) will be replaced by the LUTs. There are 3 steps to design the LUTs: LLR computation, quantization, and integer mapping. The DE is used to approximate the LLR distribution of CN and VN. Then the LLR distribution will be quantized. In this work, the channel quantizer and CN/VN quantizers will be jointly optimized. Next, the computations of CN and VN will be replaced by LUTs which LLR values are mapped to an integer number. Fig. 2 shows the error performance of the proposed LUT decoder outperforms the previous design [6] when 2-bits and 3-bits quantizers are used.

[1] K. Cai, Z. Qin and B. Chen, Channel capacity and soft-decision decoding of LDPC codes for spin-torque transfer magnetic random access memory (STT-MRAM)., pp. 550-554 (2013) [2] B. Li, Y. Pei and W. Wen, Efficient Low-Density Parity-Check (LDPC) Code Decoding for Combating Asymmetric Errors in STT-RAM., pp. 266-271 (2016) [3] Z. Xingwei, K. Cai, P. Chen and Z. Mei, Design of Rate-Compatible Protograph LDPC Codes for Spin-Torque Transfer Magnetic Random Access Memory (STT-MRAM)., Vol. 7, pp. 182425-182432 (2019) [4] T. Na, S. H. Kang and S. -O. Jung, STT-MRAM Sensing: A Review., Vol. 68, pp. 12-18 (2021) [5] J. Yang, B. Geller, M. Li and T. Zhang, An Information Theory Perspective for the Binary STT-MRAM Cell Operation Channel., Vol. 24, pp. 979-991 (2016) [6] J. Lewandowsky and G. Bauch, Information-Optimum LDPC Decoders Based on the Information Bottleneck Method., Vol. 6, pp. 4054-4071 (2018) [7] K. Cai and K. A. S. Immink, Cascaded Channel Model, Analysis, and Hybrid Decoding for Spin-Torque Transfer Magnetic Random Access Memory., Vol. 53, pp. 1-11 (2017) [8] B. Li, Y. Pei and W. Wen, Efficient Low-Density Parity-Check (LDPC) Code Decoding for Combating Asymmetric Errors in STT-RAM., pp. 266-271 (2016)

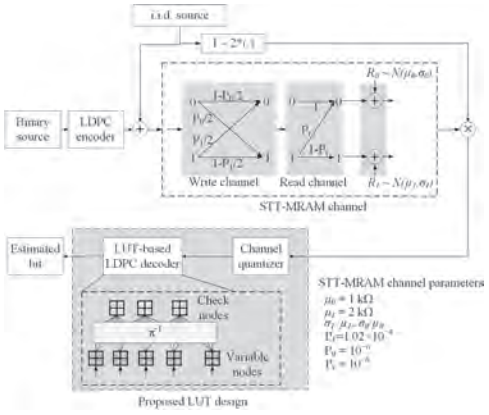

Fig.1 Write and Read Process of STT-MRAM

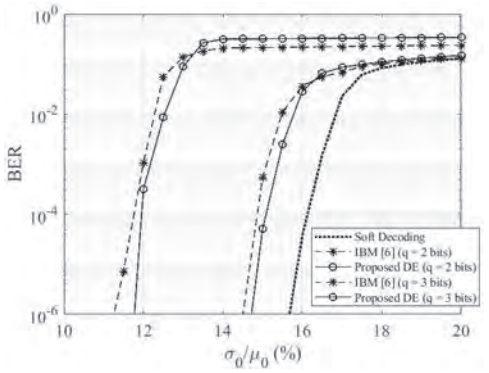

Fig. 2 BER performance of LUT-based LDPC decoder [6]

GPD-02. Spin Orbit Torque Driven Stochastic MTJ Neuron-based Boltzmann Machine for Pattern Classification Application. *D. Divyanshu*[1], A.H. Lone[1], S. Amara[1], S. Srinivasan[2] and H. Fariborzi[1] *1. CEMSE, King Abdullah University of Science and Technology, Jeddah, Saudi Arabia; 2. SCEE, Indian Institute of Technology Mandi, Mandi, India*

The magnetic tunnel junction (MTJ) has gained a lot of interest in neuromorphic computing owing to its tunable switching behavior. Particularly, the stochastic switching behavior of the MTJ provides an intrinsic capability to tackle computationally difficult problems in an energy efficient manner. At the architectural level, the potential associative ability of Boltzmann Machine (BM) allows it to make inference for the input patterns which is not included in the defined input set [1][2]. Motivated by the computational abilities of MTJ and associative abilities of Boltzmann Machine, in this work, we present the spin orbit torque (SOT) driven MTJ based Boltzmann Machine neural network for solving classification problems. We use a fixed learning approach to demonstrate the ability of the BM based topology. Stochastic MTJ neuron model is used in artificial neural network. The sigmoidal response of MTJ switching probability enables us

to utilize the inherent stochastic device characteristic to be implemented as a stochastic unit in BM. Fig. 1(a) shows the sigmoidal switching response of the stochastic MTJ and Fig. 1(b) shows the magnetization dynamics of MTJ. We can clearly observe an SOT tunable stochastic switching behavior. The block diagram of the BM pattern classifier is shown in Fig. 2(a), where each neuron in first layer is connected to output neuron via a fixed weight. To ensure inhibitory connection, the output from each neuron acts as input to rest of the output layer. The average value of the output for all possible outcomes of neurons and for the particular case of specific output to be high (for O2 and O6) is shown in Fig. 2(b). Based on input pattern and synaptic configuration only one output has high value and a winner takes all (WTA) circuit will be able to select the desired output, signifying the proper classification problem. Finally, we conclude by discussing the applicability of these device models and architectures for various other unconventional tasks such as combinatorial optimization and probabilistic inference.

[1] S. Zhang, W. Zhang and K. Kang, "Learning high-level features by deep Boltzmann machines for handwriting digits recogintion," Proceedings of 2nd International Conference on Information Technology and Electronic Commerce, 2014, pp. 243-246, doi: 10.1109/ICITEC.2014.7105611. [2] Emile Aarts and Jan Korst," Simulated Annealing and Boltzmann Machines- A Stochastic Approach to Combinatorial Optimization and Neural Computing".

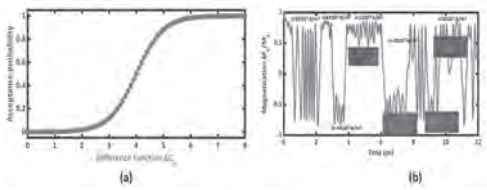

(a): Acceptance probability vs difference function in BM (b) Stochastic switching behavior of SOT driven MTJ.

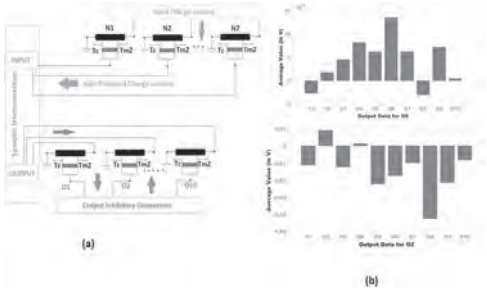

(a): MTJ based BM architecture. (b) Mean value of output neuron layer.

GPD-03. Artificial neuron designed using a spin Josephson oscillator based on a synthetic antiferromagnet. *S. Louis*[1], H. Bradley[2], A.N. Slavin[2] and V. Tyberkevych[2] *1. Electrical and Computer Engineering, Oakland University, Rochester, MI, United States; 2. Physics, Oakland University, Rochester, MI, United States*

Neuromorphic computer architecture based on spiking artificial neurons (for example, Intel's "Loihi" chip [1]) can perform machine-learning tasks more efficiently than traditional computing hardware. It has been proposed in [2] that using spintronic artificial neurons, based on a current-driven antiferromagnetic (AFM) oscillator, will greatly improve the speed and power efficiency of the "spiking neuron" computer architecture. A recent paper [3] presented a theory describing a spin Josephson oscillator (SJO) based on a *synthetic* antiferromagnet. Below, we propose to use an SJO [3] for the development of a new type of an artificial neuron. As shown in Fig. 1, the SJO consists of two anisotropic ferromagnetic (FM) layers (with static magnetization M1, M2 shown by solid arrows) separated by a non-magnetic spacer. Magnetizations M1, M2 are aligned in opposite directions due to the interlayer exchange coupling. Thin Pt layers are placed on the outer edges of the structure (see Fig.1). When a sufficiently large "prompt" pulse of electric current jc (see Fig.2a), exceeding a certain threshold (see dashed line in Fig.2a) flows through the Pt layers, the spin currents caused by the spin-Hall effect in the Pt layers exert spin transfer torques (STT) on M1 and M2, and tilts them, so that the tilted magnetizations start to rotate in the FM easy plane, as shown arrows in Fig. 1. This rotation, after a delay time of 300 ps caused by the internal inertia [2], results in the formation of a short spike of a standard shape and duration (second pulse in Fig.2b), which are independent of the parameters of the "prompt" pulse, and can be used as information carriers in the neuromorphic computing. The advantage of the SJO-based neuron, compared to the AFM neurons described in [2], is in that the SJO can be fabricated using current technologies, has a low power consumption, and the spikes produced by the SJO-based neurons have a short duration of ~ 100 ps.

[1] M. Davies, N. Srinivasa, T.-H. Lin, *et al.,* IEEE Micro Vol. 38, p.82 (2018). [2] R. Khymyn, *et al.,* Scientific reports Vol. 8, p.1 (2018). [3] Liu, Yizhou, et al., Applied Physics Letters Vol.116, p. 132409 (2020).

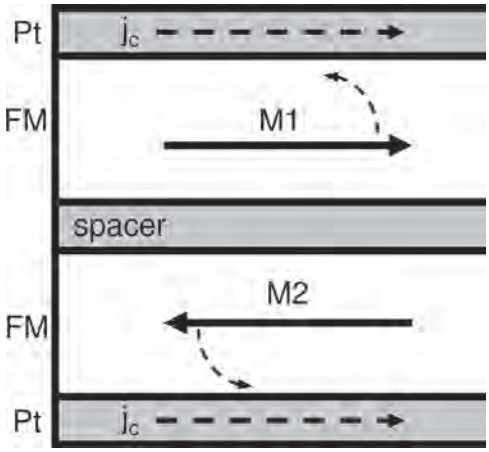

Figure 1: SSJO structure. Two FM layers separated by a non-magnetic spacer. Outer edges are Pt.

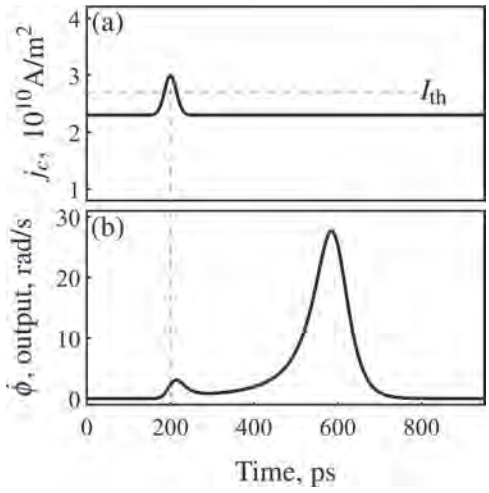

Figure 2: SJO neuron operation. (a) Solid line: input current jc, steady except for a prompt at t = 200 ps. Dashed lined shows threshold current Ith. (b) Output, M1 rotational velocity.

GPD-04. Kuramoto-Model-Based Data Classification Using the Synchronization Dynamics of Uniform-Mode Spin Hall Nano-Oscillators.

N. Garg[1], V. Hemadri Bhotla[1], P.K. Muduli[1] and D. Bhowmik[2,3] *1. Physics, Indian Institute of Technology Delhi, New Delhi, India; 2. Electrical Engineering, Indian Institute of Technology Delhi, New Delhi, India; 3. School of Artificial Intelligence, Indian Institute of Technology Delhi, New Delhi, India*

Oscillator-based data-classification schemes have been proposed recently using the Kuramoto model which predicts synchronization behaviour of coupled oscillators through a general framework neglecting underlying physics [1,2]. Here we propose hardware implementation of a Kuramoto-model-based data-classification scheme through an array of dipole-coupled uniform-mode spin Hall nano-oscillators (SHNOs) [2,3]. Using micromagnetic simulations on 'mumax3' software [4], which actually capture physics of SHNOs, we first study how synchronization range between two uniform-mode SHNOs (150 nm diameter) varies with physical distance between them (Fig. 1b). Thus we correlate the coupling constant in Kuramoto model (Fig. 1a) with dipole-coupling strength between two SHNOs in 'mumax3' (Fig. 1b). Using this correlation, we generate a synchronization map for a two-input-two-output dipole-coupled uniform-mode SHNO system through micromagnetics (Fig. 2a). Red circles show frequency values of input oscillators (F1,F2) for which the two output oscillators are synchronized, and black circles show (F1,F2) for which they are not. These data points coincide with pink region showing sync. and grey region showing de-sync., obtained from Kuramoto model (Fig. 2a). Thus we establish here that synchronization behaviour of SHNOs obtained from physics-based modeling (micromagnetics) is consistent with that obtained from Kuramoto model, where underlying physics of SHNOs is ignored. This shows that a Kuramoto-model-based data classification scheme [2] can indeed be implemented on an array of SHNOs. Next we show, through micromagnetics, classification of data from a popular data set (Fisher's Iris [5]) using an array of uniform-mode SHNOs. While distinguishing flowers in Iris of Setosa type from Virginica type, output oscillators synchronize for Setosa and desynchronize for Virginica (Fig. 2b). The obtained accuracy is 98.67%

1. E. Vassilieva, G. Pinto, G., J. de Barros, and P. Suppes. Learning pattern recognition through quasi-synchronization of phase oscillators. IEEE Transactions on Neural Networks, 22(1), pp.84-95 (2010). 2. D. Vodenicarevic, N. Locatelli, J. Grollier, and D. Querlioz, Nano-oscillator-based classification with a machine learning-compatible architecture. Journal of Applied Physics, 124(15), p.152117 (2018). 3. U. Singh, N. Garg, S. Kumar, P. K. Muduli, and D. Bhowmik, Learning of classification tasks with an array of uniform-mode spin Hall nano-oscillators. AIP Advances, 11(4), p.045117 (2021). 4. A. Vansteenkiste, J. Leliaert, M. Dvornik, *et al.* The design and verification of MuMax3. AIP advances, 4(10), p.107133 (2014). 5. R. A. Fisher, Annals of Eugenics, 7, 179 (1936).

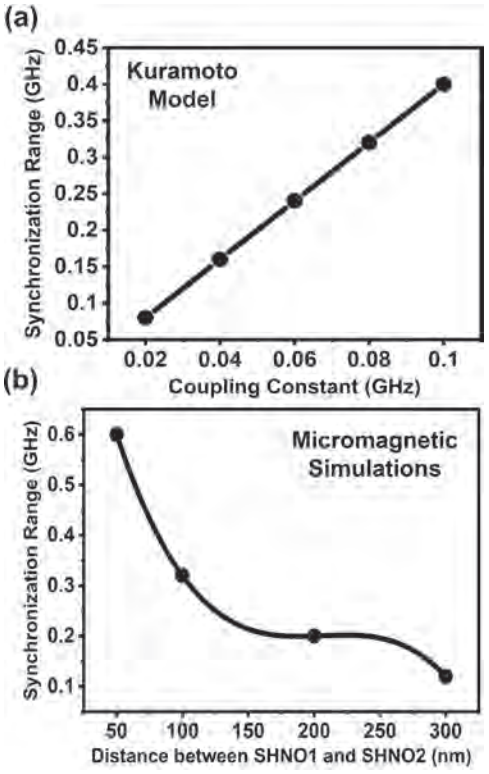

Fig. 1. For a two-oscillator system, coupling constant in Kuramoto model (a) is correlated with distance between two SHNOs in micromagnetics (b) using the synchronization-range values.

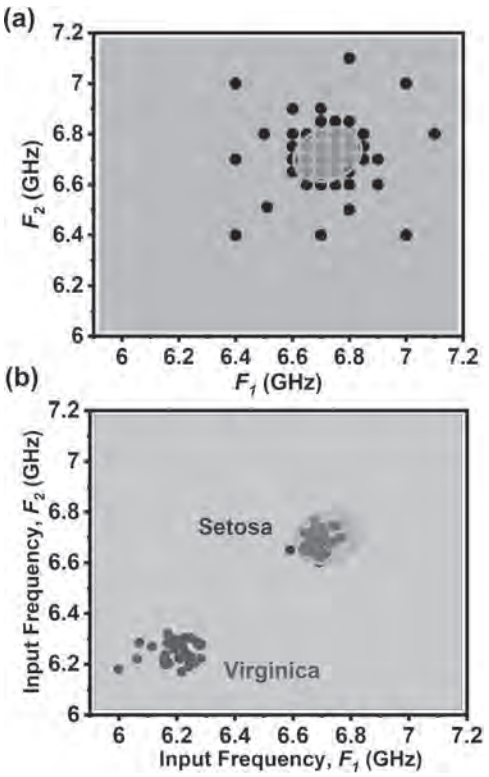

Fig. 2. Synchronization map of the two-input-two-output oscillator system in (a) (details in text) used for data classification from Iris set (b)

GPD-05. Examination of Magnetization Switching Behavior by Bi-directional Read of Spin Orbit Torque MRAM. *A. Yamada*[1], Y. Kishi[1], M. Ke[1] and T. Kawahara[1] *1. Tokyo University of Science, Tokyo, Japan*

In spin orbit torque MRAM, the magnetization of the free layer is erratically switched at the time of reading. We previously proposed a bi-directional read method as a solution to reduce this read disturbance [1]. We examined the size dependence of the effect with this method [2], and the threshold current became constant as the size increased in the short-side direction (Fig. 1(a)). In this study, including the elucidation of this behavior, we compared the size dependence of the movement during magnetization switching between conventional method and our method, and examined the effect of reducing the disturbance. Figures. 1 (c) to (f) are graphs of magnetization switching, and Fig. 2 shows the state during the magnetization switching in the short-side direction. In conventional method, when X was 30 to 60 nm, the magnetization was switched in the monodomain, and when X was 90 to 180 nm, a magnetic domain was formed once and the magnetization was switched due to the movement of the domain wall. Magnetization switching in both directions can suppress magnetization reversal because a spin current in the opposite direction is generated, but when the threshold current is exceeded, the magnetization state becomes unstable. When X is 30 to 60 nm, the monodomain is disrupted and magnetization is switched, and when X is 90 to 180 nm, the magnetization is switched by the movement of the domain wall from the switched magnetic domain. Therefore, the threshold current becomes constant while the size increases in the short-side direction because the magnetization is switched by the generation of the magnetic domain and movement of the domain wall. In the long-side direction, the magnetization is switched by the generation of magnetic domains, because the shape anisotropy strengthens the connection of magnetic domains and the current for switching one magnetic domain increases as the size increases.

[1] H. Kazama and T. Kawahara, "Spin-Orbit Torque MRAM Read Reliability", 2017 IEEE International Magnetics Conference. [2] Y. Kishi, A. Yamada, and T. Kawahara, "Evaluation of Read Disturbance Reduction Effect by Bi-directional Read on Device Size Dependence", 2021 IEEE International Magnetics Conference.

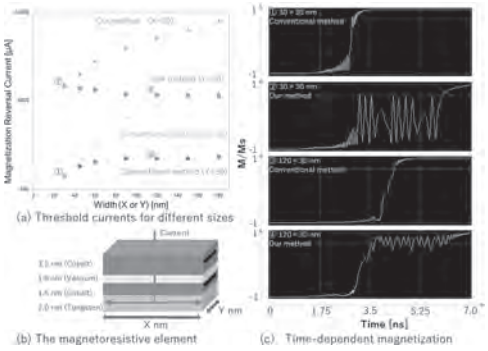

Fig. 1(a) Comparison of conventional and our method threshold currents for different sizes. (b) The magnetoresistive element. (c) Time-dependent magnetization.

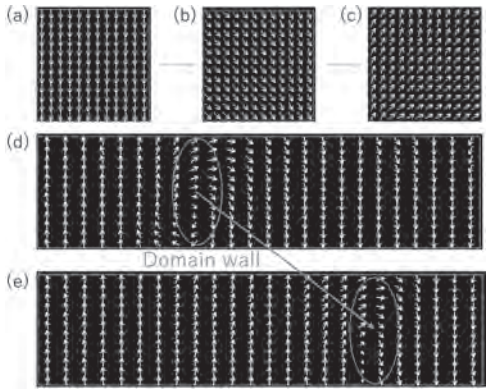

Fig. 2 Magnetization with conventional method. (a) Initial magnetization at 30 × 30 nm. (b), (c) Magnetization switching at 30 × 30 nm. (d), (e) Domain wall movement at 120 × 30 nm.

GPD-06. Atomistic Study of the Thermodynamic Properties and Switching Dynamics of Perpendicular Shape Anisotropy MRAM. *W. Lack*[1], R.F. Evans[1] and S. Jenkins[1] *1. University of York, York, United Kingdom*

MRAM is a non-volatile memory technology that stores a bit as a magnetic state of a ferromagnetic CoFeB free layer which either aligns or anti-aligns with a fixed CoFeB layer, where these two layers sandwich a non-magnetic MgO layer, shown in fig.1a. The modern market is predominantly dynamic and static RAM which are both volatile which requires large amounts of power in high peformance clusters. MRAM is ultrafast and durable while scaling to volumes smaller than the limitations of SRAM and DRAM, attracting significant research and development.[1]To achieve practical applications, MRAM must display high thermal stability, a high tunnel magnetoresistance ratio and a low writing current at competing volumes. A recent development with potential to achieve this scalability is to use tower structures with height greater than the diameter, which allows the perpendicular shape anisotropy and the interfacial perpendicular magnetic anisotropy to favour out-of-plane magnetisation.[2]For reliable MRAM, the switching mechanism at operational temperatures needs to be understood. This study uses atomistic simulations which model the tower structure with varied free layer thicknesses using two anti-ferromagnetically coupled CoPt layers to pin the fixed layer, with a monolayer either side of the MgO with enhanced exchange coupling and uniaxial anisotropy. The system is modelled using a spin Hamiltonian with thermal fluctuations and dipole fields included with the LLG.[3]We have found in fig.1b(i) that the susceptibility of the free layer varies hugely as the volume is increased, but dividing these taller towers into smaller local regions in fig. 1b(ii) we find smaller and correlated curves. This shows the magnetisation is non-uniform throughout the tower, which may suggest a non-uniform magnetisation mode. In fig. 1c(i) we see snapshots of the reversal process at 50K demonstrating nucleated domain wall reversal mode in taller towers, while fig.1c(ii) shows the switching is coherent for smaller towers.

[1] K. Watanabe et al. Nature Communications, 9, article no. 663, 2018 [2] N. Perrissin et al. Nanoscale, issue 25, 2018 [3] R. F. L Evans et al. journal of physics: condensed matter, volume 26, number 10, 2014

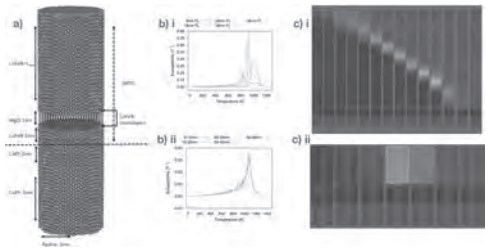

Figure 1 a) The structure of the PSA MRAM b) i) The susceptibility for the whole free layer ii) The susceptibility of 10nm parts of the 48nm tower c) i) Nucleated reversal in the 48nm tower ii) Coherent rotation in the 10nm tower

GPD-07. 3-Terminal Domain Wall Device Based Synapses for Neuromorphic Computing. *D. Kumar*[1], S. Srivastava[1], K. Yamane[2], W. Law[2], G. Rajan[2], V. Naik[2], T. Jin[1], S. Li[1], W. Lew[1], X. Wang[1] and S. Piramanayagam[1] *1. Nanyang Technological University, Singapore, Singapore; 2. GLOBALFOUNDRIES Singapore Pte. Ltd., Singapore, Singapore*

Neuromorphic computing is attracting the attention of researchers for its usefulness in ultra-low-power computing applications[1]. Among the several magnetic and non-magnetic candidates to achieve low-power neuron and synaptic devices, the domain wall magnetic tunnel junctions (DW-MTJ) are the most promising contenders for energy efficiency. However, to realize the synaptic functions in neuromorphic devices, one must achieve multi-resistance states. The pinning sites can aid in achieving the required multi-resistance states[2]. Therefore, we propose meander DW devices, where segments of DW-MTJ wires join at an offset, which alters the energy landscape locally and helps in achieving deterministic DW motion. To study the proposed concept, we optimized the DW-MTJ stack with the perpendicular magnetic anisotropy to achieve a higher tunnel magnetoresistance (TMR) of 169% and a high RA (resistance-area product) of 241 Wmm^2 suitable for DW devices with a large area. Subsequently, we measured the magnetic hysteresis (M-H) loops of the thin films to observe the layer-wise switching along with magnetic field variation (fig. 1 (a)). We have also measured the minor loop (fig. 1 (b)) and found that the coercivity of the free layer is ~21 Oe, which is suitable for energy-efficient DW motion. Next, we optimized the fabrication process for 3-terminal synaptic devices (fig. 1 (c)). We fabricated a sequence of devices with a DW-MTJ wire width w = 10 mm and corresponding offset (d) values ranging from 40% (of w) to 70% in the steps of 10%. Further, we fabricated three types of devices for every offset; (*i*) constant offset, increase in offset by (*ii*) 5%, and (*iii*) 10% over successive pinning sites. Finally, we performed field and current-driven DW motion experiments and witnessed the synaptic functions. Here we present the results of field-driven DW motion in fig. 1 (d). The stack details, process insights, and experimental findings will be presented in detail during the conference.

1. A. Sengupta and K. Roy, Applied Physics Express, 11 (2018) 030101. 2. D. Kumar et al., IEEE Transactions on Magnetics, 55 (2018) 1-8.

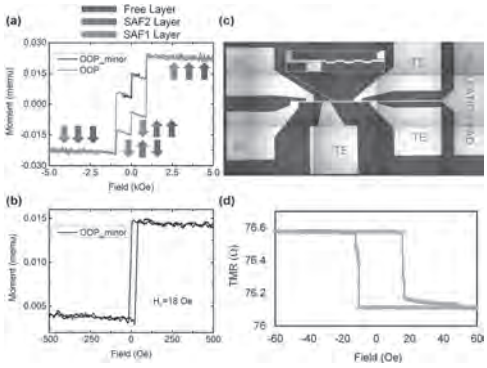

Figure. (a) M-H loop of the full stack, (b) minor loop illustrating the switching of the free layer, (d) micrograph of the 3-terminal synaptic device, and (e) read-out TMR signal of field driven-DW motion.

GPD-08. Coercivity control of thin films with perpendicular magnetic anisotropy by surface acoustic waves. *J. Shuai*[1], M. Ali[1], L. Chen[2], J. Cunningham[2] and T. Moore[1] *1. School of Physics and Astronomy, University of Leeds, Leeds, United Kingdom; 2. School of Electronic and Electrical Engineering, University of Leeds, Leeds, United Kingdom*

Encoding information in thin films with perpendicular magnetic anisotropy (PMA) holds promise for the next generation of data storage and logic operation applications [1]. Thin films with a large coercivity provide high stability of the encoded information but cause a high energy cost of writing data [2]. Therefore, reducing coercivity while writing data is a practical method to decrease the energy cost. Here, we experimentally demonstrated the control of coercivity in a PMA film using surface acoustic waves (SAWs), which can introduce oscillating strain waves in the thin films over millimetric distances. Two interdigitated transducers (IDTs, Fig.1a), whose centre frequency is 93.35 MHz (Fig. 1b), were patterned on opposite ends of a 2-mm-wide stripe of Ta(5.0 nm)/Pt(2.5 nm)/Co(1.1 nm)/Ir(1.5 nm)/Ta(5.0 nm) film. The film was dc magnetron sputtered onto a lithium niobate ($LiNbO_3$) substrate, which supports the SAW propagation. A wide-field Kerr microscope was used to measure the hysteresis loops of the film with SAW both on and off at room temperature. Results showed that the coercivity of the thin films without SAW is 4.93±0.06 mT (Fig. 2a). Owing to the magnetoelastic coupling effect [3,4], the standing SAWs locally reduce the anisotropy and thus the thin film coercivity, which can be controlled by the applied SAW power. Coercivity reduction, which is enhanced by increasing the SAW power, can be up to about 18% for an input SAW power of 28 dBm (4.04±0.09 mT, Fig. 2b). Coercivity reduction only occurs at the centre frequency (Fig. 2c), which rules out the effect of a rising temperature that a SAW potentially can cause. This study indicates the possibility of remote and energy-efficient control of magnetization switching.

[1] B. Tudu et al., Vacuum, 14, 329, (2017) [2] W. Li et al., J. Appl. Phys, 115, 17E307 (2014) [3] P.M. Shepley et al., Sci. Rep. 5, 7921 (2015) [4] L. Thevenard et al., Phys. Rev. B 93, 140405(R) (2016)

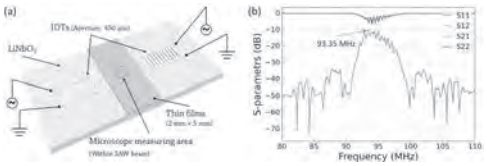

Fig.1 (a) Diagram of experimental setting-up. Interdigitated transducers (IDTs) were patterned by the side of the Ta(5.0)/Pt(2.5)/Co(1.1)/Ir(1.5)/Ta(5.0) film (thickness in nm). Hysteresis loops were taken by a Kerr microscope. (b) S-parameters of the IDTs (centre frequency of 93.35 MHz).

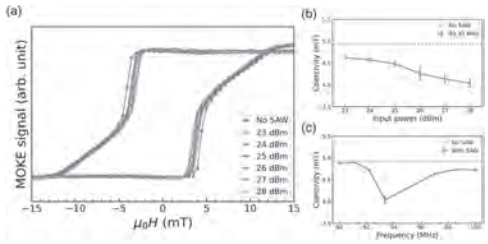

Fig. 2 (a) Hysteresis loops and (b) coercivity of the thin film under various surface acoustic waves (SAW) power (23 to 28 dBm) at 93.35 MHz. (c) Coercivity of the thin films under various frequency at 28 dBm.

GPD-09. Weighted Error Correcting Code (WECC) against Asymmetric Error of STT-MRAM. *Q. Wang*[1] and Y. Jiang[1] *1. School of Internet of Things Engineering, Jiangnan University, Wuxi, China*

As a promising non-volatile memory, Spin Transfer Torque Magnetic Random Access Memory (STT-MRAM) suffers from high error rate due to stochastic switch [1]. Some papers use Error Correcting Code (ECC) with powerful error correction capabilities to suppress high error rate, which lead to high delays and high check bit consumption. According to published reports, the error occurring of STT-MRAM is a serious asymmetry phenomenon [2]. The write error rate of 0 → 1 is much higher than that of 1 → 0 since 0 → 1 transition requires higher energy to ensure reliably commute the value. The traditional ECC approaches for other kinds of memories are designed for symmetric error correcting, which are not suitable for STT-MRAM. A weighted error correction mechanism is proposed and fulfilled in the paper, which can be used for the asymmetric error situation. Firstly, the codewords are weighed by estimating the different probabilities of error in state 0 and 1. In STT-MRAM, the error occurrence rate on state 0 is much higher than that on state 1. Through the check matrix, the words can be preliminarily judged to determine which bits may be wrong. Through the different weights of data 0 and 1, a bit with the highest error probability can be calculated. Then this bit is flipped to get a new codeword, which is substituted into the check matrix again to get a new error situation. The process of WECC is shown in Fig.1. If situation improves, the new codeword can be kept. Otherwise, the previous substitution operation is cancelled. In order to ensure the effectiveness of the error correction mechanism, the assistance of other ECCs such as BCH or LDPC is usually required. The error correction mechanism proposed in the paper can effectively reduce the error correction delay and decrease the check bit consumption. A virtual system in GEM5 is built up to evaluate the proposed WECC mechanism. The simulation results are used for the analysis of the error correction algorithm, showing the effectiveness of the WECC proposed in the paper for STT-MRAM.

[1] Jeehwan Song, Hemant Dixit and Behtash Behin-Aein, IEEE Trans. Magn., Vol.56(12), p.1-11(2020) [2] Bi X, Sun Z and Li H, ICCAD 2012, Vol.2012, p.88-94(2012)

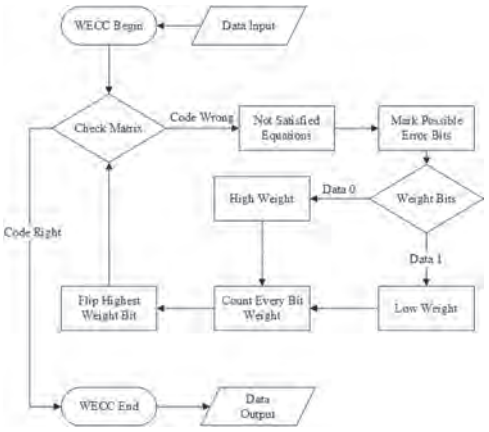

Fig.1 Process of WECC

GPD-10. Nanoscale Thermal Transport Model of Magnetic Tunnel Junction (MTJ) Device for STT-MRAM. *S. Li*[1] and Y. Jiang[1] *1. Department of Electrical Engineering, Jiangnan University, Wuxi, China*

Spin-transfer torque magnetic random access memory (STT-MRAM) based on magnetic tunnel junction (MTJ) device has attracted significant attention due to several features such as high integration density, low power consumption and nearly unlimited endurance [1,2]. Nevertheless, it needs to be noted that the thermal effect generated under bias operation will affect the overall performance and stability of the device [3,4]. To evaluate the thermal phenomenon in MTJ device accurately, the non-equilibrium effect between electrons and phonons near the electrode-barrier interface cannot be ignored [5]. This imbalance leads to additional thermal resistance at the interface which hinders the heat conduction of tunnel junction. Therefore, an effective equivalent model is necessary to represent the heat transport of the device. In the paper, a nanoscale thermal transport model of MTJ device is proposed. In the model, the interface energy balance transport model is used to clarify the non-equilibrium relationship between phonons and electrons at the CoFeB/MgO/CoFeB interface. A parameterization study is carried out to illustrate the temperature distribution of the nanoscale thermal transport model. Furthermore, the phonon-electron coupling distance (δ) estimated based on the thermal conductivity of phonons (κ_p) and electrons (κ_e) of system is implemented to construct the effective equivalent model using finite element simulations, which can realistically reflect the thermal transport under working conditions. The established equivalent model has a guiding role in exploring the thermal transport of nanoscale MTJ device.

[1] X. Fong, Y. Kim and R. Venkatesan, Proc. IEEE, Vol. 104, p.1449 (2016) [2] N. Perrissin, S. Lequeux and S. Nikita, Nanoscale, Vol. 10, p.12187 (2018) [3] W. Boonruesi, J. Chureemart and R. W. Chanterll, Phys. Rev. B, Vol. 102, p.134427 (2020) [4] B. Wu, Y. Q. Cheng and J. L. Yang, IEEE Trans. Reliab., Vol. 65, p.1755 (2016) [5] R. B. Wilson, B. A. Apgar and W. P. Hsieh, Phys. Rev. B, Vol. 91, p.115414 (2015)

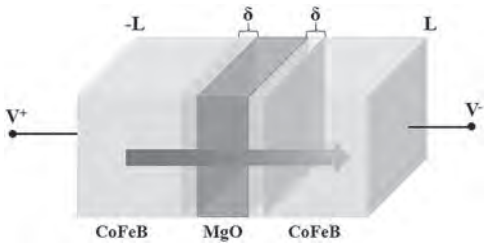

Fig.1. Thermal transport model of MTJ layer stack under applied bias. Note that the light gray square represents the additional thermal resistance area at CoFeB/MgO/CoFeB interface, and δ represents the expanded distance on horizontal axis of additional resistance.

GPD-11. Milli volt class spin motive force due to domain wall motion in GdFeCo magnetic wire. *M. Oikawa*[1], S. Sumi[1], K. Tanabe[1] and H. Awano[1] *1. Toyota Technological Institute, Nagoya, Japan*

Spin transfer torque[1] is an important phenomenon in order to develop of non-volatile magnetic memory. Using this spin transfer torque principle, it was predicted[2] and experimentally confirmed[3] that a voltage could be generated in the magnetic nanostructure. This effect is called spin motive force and is expected for next-generation power sources. It is not clear how the Faraday electromotive force[4] can be separated from the spin motive force, and there are few studies reported and the spin motive force in μV class. It is very small. To greatly increase the value, we fabricated $Gd_{21}(Fe_{75}Co_{25})_{79}$ magnetic wire and succeeded in generating a spin motive force by domain wall motion. We prepared the following film stacks using rf and dc magnetron sputtering: Gd_{21} $(Fe_{75}Co_{25})_{79}$ (20)/SiN (10), the films are grown at the room temperature. The magnetic wires (3 μm wide and 125 μm long) and Hall crosses were micro-fabricated by an Electron-beam lithography (EBL) system and a lift-off method. Next, we prepared two types of samples, a sample with injection of domain wall and a sample without injection of domain wall. A magnetic field was applied to the sample, and the generated voltage was observed by an oscilloscope through a 100x amplifier. Spin motive force is determined by subtracting the induced electromotive force generated in the sample without injection of domain wall. Figure 1 (a) shows the spin motive force measurement system. Figure 1 (b) shows the value of the spin electromotive force by subtracting the induced electromotive force. As a result, a huge spin motive force of 12 mV was obtained. This is financially supported by KAKENHI 918023,918055,918043.

[1] J. C. sloczewski, J. Magn. Magn. Mater. 159, L1 (1996). [2] S. E. Barnes and S. Maekawa, Phys. Rev. Lett. 98, 246601 (2007). [3] S. A. Yaug et al., phys. Rev. Lett. 102, 067201 (2009). [4] M. Hayashi et al., Appl. Phys. Express 3, 113004 (2010).

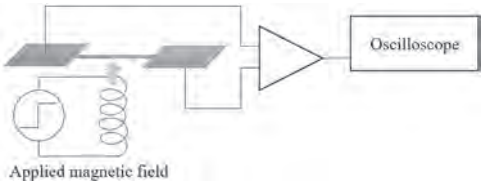

Figure 1a

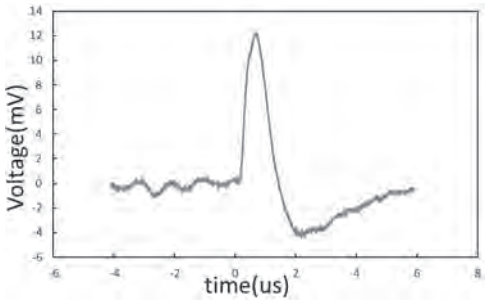

Figure 1b

GPD-12. The fast write strategy of STT-MRAM with pipeline architecture. *G. Zhang*[1] and Y. Jiang[1] *1. Department of Electrical Engineering, Jiangnan University, Wuxi, China*

Spin transfer torque (STT) magnetic RAM (MRAM) is one of the promising emerging memory technologies, which combines endurance, speed and energy efficiency of SRAM and DRAM with non-volatility of flash [1]. However, the write speed and write power consumption is a major challenge for the establishment of STT-based storage devices in universal memory [2]. In the paper, the Early Write Termination (EWT) technology combined with the pipeline architecture is co-designed for the STT-MRAM to improve the write efficiency. In the traditional write operation, the original stored data is directly overwritten by the new data, without concerning on whether the new data is the same as the original data or not. There exists unnecessary operation if the written data is the same as the stored ones, which leads to the write power consumption. To avoid the unnecessary write operation, a pre-charge sense amplifier is used to sense the stored data in advance. Only the new data is allowed to be written into the memory cell when the new data is different from the stored data. Moreover, considering the delay of the additional circuits, the pipeline architecture is also applied on the STT-MRAM. Several latches operating in response to a clock signal to process the data by dividing the write operation into a plurality of stages and carrying out them in pipelining manner [3]. Pipeline technology can process multiple instructions in parallel, greatly increasing the average write speed. The proposed write strategy of STT-MRAM achieves better write efficiency and lower power consumption, which has potential application in STT-MRAM in the future.

[1] K. Huang, R. Zhao, N. Ning, et al., IEEE Trans. Circuits Syst., vol. 61, p. 2614-2623 (2014). [2] Hosomi, M. & Yamagishi, H. & Yamamoto, et al., Tech. Dig. - Int. Electron Devices Meet., p.459-462 (2005). [3] Y. Ma, S. Miura, H. Honjo, et al., Jpn. J. Appl. Phys., vol. 59, p. SG (2020).

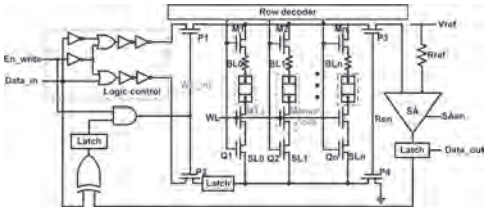

Fig.1 The block diagram of the proposed STT-MRAM architecture using the EWT technology

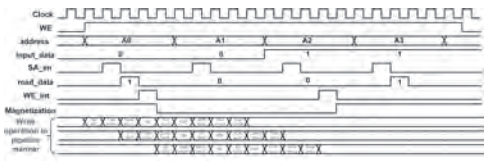

Fig.2 The operation time diagram of the designed write strategy in three-stage pipeline architecture of STT-MRAM.

GPD-13. A RC Thermal Model of 3D-Stacked Stand-alone MRAM. *R. Yong*[1] and Y. Jiang[1] *1. School of Internet of Things Engineering, Jiangnan University, Wuxi, China*

Unlike traditional memories such as SRAM and DRAM, STT-MRAM has many advantages, especially non-volatility, which has attracted the attention of many researchers in recent years. Nowadays, MRAM is one of the most competitive candidates for next-generation memory. However, spintronic devices require large switching current to achieve fast switching speed, which leads to more power consumption and heat fluxes of MRAM. Power budget and thermal issues limit the 3D stacking of MRAM. Therefore, it is necessary to establish a thermal model of the power-related 3D stacked MRAM in the early stage of design. Since in the duality between thermal and electrical phenomena [1], heat flow is analogous to current, temperature is analogous to voltage, thermal conductance is analogous to electrical conductance, and thermal capacity is analogous to electrical capacitance, a RC thermal model can be established, which can avoid using computationally intensive and time-consuming detailed finite-element model [2]. Because 3D stacked MRAM faces cooling problems, it is not only necessary to consider the circuit-level memory layer when analyzing the thermal behavior, but also to take the heat sink responsible for heat dissipation into consideration from the perspective of package level and model together. The content of this paper is organized as follows. Section I is the introduction, which introduces 3D stacking technology and puts forward the thermal issues of 3D memory. Section II presents various thermal modeling approaches. Section III proposes a power and thermal model for 3D-stacked MRAM as shown

in Fig. 1, which also including the simplified memory circuit. In Section IV, the effects of the number of stacked layers, the size of dies, power density, and heat dissipation capacity on temperature are evaluated based on the established RC thermal model. Section IV shows the conclusions. It is demonstrated that this model facilitates the communication between the circuit designer responsible for power consumption and the package designer responsible for heat dissipation in the early stage of MRAM design.

[1]A. Krum, Thermal management, in: F. Kreith (Ed.), The CRC Handbook of Thermal Engineering, CRC Press, Boca Raton, FL, 2000, pp. 2.1–2.92. [2]Floworks: Fluid Flow Analysis for SolidWorks, NIKA GmbH. Website, http://www.floworks.com.

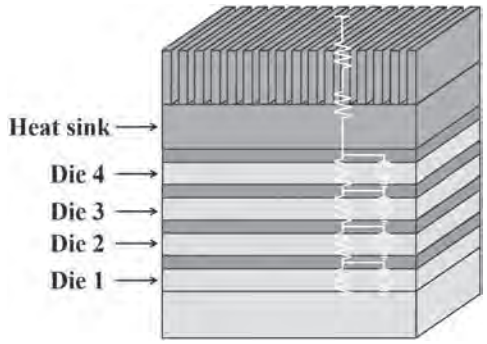

Fig. 1 Thermal model of the 3D-stacked MRAM.

GPD-14. Compact Model of Domain Wall MTJ Device Driven by Spin Orbit Torque and Dzyaloshinskii–Moriya Interaction. *M. Wang*[1] and Y. Jiang[1] *1. Jiangnan University, Wuxi, China*

Current-induced domain wall motion (CIDWM) shows the promising prospect in low-power, high-density, and high-speed circuits application. Recent researches have demonstrated that the MTJ device based on CIDWM has great potential in mimicking a non-volatile artificial neuron and synapse [1, 2]. However, low speed and high-power consumption limit the further development of traditional CIDWM driven by spin transfer torque (STT). By combining the high-speed, low-power advantages of spin orbit torque (SOT) MTJ and the ability of interfacial Dzyaloshinskii–Moriya interaction (DMI) to stabilize the Néel–type domain wall, SOT and DMI-based domain wall (DW) MTJ can achieve low threshold current and high propagation speed. Currently, the corresponding device model is highly required for the circuit design in the field of the artificial neuron and synapse simulation. In the paper, a compact model for CIDWM-MTJ based on SOT and DMI is presented. It integrates SOT mechanism for magnetization reversal and domain wall nucleation, CIDWM behaviors, and tunnel resistance theory of MTJ nanopillar. The micromagnetic simulation and the temporal evolution of the DW position is carried out by solving the LLG equation. Finally, a hybrid MTJ/CMOS circuit is simulated to verify the developed model. The presented model combines the CIDWM dynamics and MTJ magnetic dynamics, showing potential application for the simulation of all-spin artificial neural network. Fig. 1 shows the three terminal device structure for SOT and DMI-based CIDWM-MTJ. I_{write} flows between T2 and T3, generating SOT. DW position in the free layer (FL) is propagated by the SOT and the DMI at the HM/FL interface.

[1] A. Sengupta, Y. Shim, and K. Roy, *IEEE Transactions on Biomedical Circuits and Systems,* vol. 10, no. 6, pp. 1152-1160 (2015). [2] C. H. Bennett, T. P. Xiao et al., in *2020 IEEE International Symposium on Circuits and Systems (ISCAS)*, pp. 1-5 (2020).

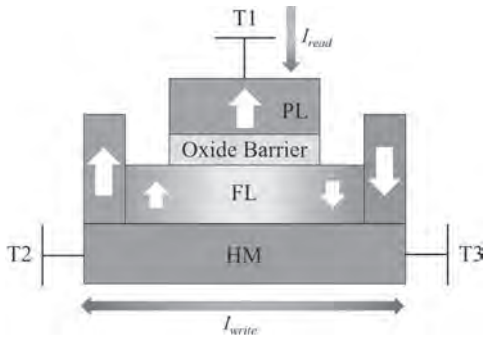

Fig. 1 Three terminal device structure for SOT and DMI-based CIDWM-MTJ.

GPD-15. Nontrivial Relationship Between Current Pulse Width and Spin Torque Switching of Perpendicular Magnetic Tunnel Junctions. J. Beik Mohammadi[1,2], *E. Clay*[1] and J. Andino[1] *1. Loyola University New Orleans, New Orleans, LA, United States; 2. University of New Orleans, New Orleans, LA, United States*

Spin torque switching mechanisms and switching speed of perpendicular magnetic tunnel junctions(pMTJs) free layers are of significant interest for industrial applications and understand the fundamental physics of magnetic material's response to a spin-polarized voltage across it. A voltage pulse, with an amplitude above the critical voltage V_{c0}[1], is applied across the junction to switch the magnetization of the pMTJ free layer. The pulse width must be long enough for guaranteed switching and short enough to avoid unnecessary energy consumption and unwanted heating. We have simulated zero-temperature domain wall mediated spin-torque switching of disk-shaped pMTJs with CoFeB free layer[2] to study the optimum pulse width for successful spin-torque switching. Our data show that 1) below a minimum pulse width(t_{min}), spin-torque switching does not occur, 2) above a maximum pulse width(t_{max}) switching is deterministic, and 3) for $t_{min}<t_{pulse}<t_{max}$, final magnetization state depends on the pulse width (see Figure 1). Previous research has shown that the domain wall structure and position at the beginning of simulation affect the switching dynamics and the final magnetization state[3]. Since the exchange interaction sets the magnetic structure of the domain wall, we varied the exchange interaction strength to investigate its effect on the final magnetization state. Our results confirm that exchange interaction impacts the pulse width required for switching (Figure 2). We will present our results on the effect of the exchange constant of the free layer on pulse width required for switching and discuss the implications of such effects in pMTJ devices.

[1] M. Lavanant, P. Vallobra, S. Petit Watelot, V. Lomakin, A.D. Kent, J. Sun, and S. Mangin, Phys. Rev. Applied 11, 034058 (2019) [2] J. Beik Mohammadi and A. D. Kent, Appl. Phys. Lett 118, 132407 (2021) [3] N. Statuto, J. Beik Mohammadi, A. D. Kent, Phys. Rev. B 103 (1), 014409 (2021)

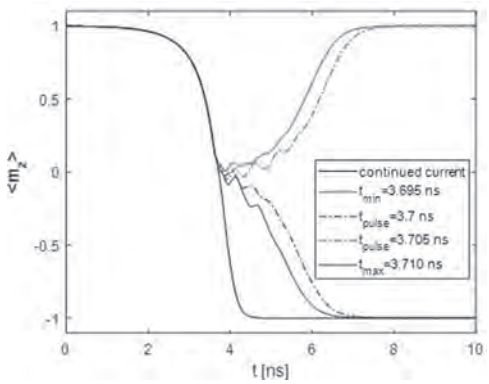

Figure 1: Time evolution of spatially averaged magnetization along the axis perpendicular to a 30nm pMTJ disk when applied pulse voltage is $1.6V_{c0}$. Blue(red) represent (un)successful switching.

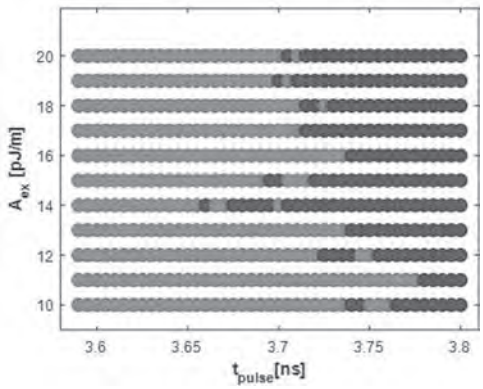

Figure 2: The free layer exchange constant and pulse duration(t_{pulse}) determine the final magnetization state of the junction. When exchange interaction is weaker, longer pulses are needed for switching. Blue(red) represent (un)successful switching.

GPD-16. Withdrawn

GPD-17. Effect of high T_c interface layer in high T_c/ low T_c hybrid memory layer on thermally assisted spin-transfer-torque switching.

W. Zhao[1], T. Kato[2], D. Oshima[1] and S. Iwata[3] *1. Department of Electronics, Nagoya University, Nagoya, Japan; 2. Institute of Materials and Systems for Sustainability, Nagoya Univerisity, Nagoya, Japan; 3. Department of Research, Nagoya Industrial Science Research Institute, Nagoya, Japan*

We have designed hybrid memory for magnetic random-access memory (MRAM) cells, consisting of low Curie temperature (T_c) CoPd/Pd multilayers (ML) and high T_c Co/Pd ML, and confirmed the thermally-assisted (TA) spin-transfer-torque (STT) switching [1-3]. In this study, we fabricated samples with different high T_c Co/Pd interface layer as $[Co(x)/Pd(1.6\text{-}x)]_1$ ML / $[CoPd/Pd]_2$ ML (x = 0.4, 0.6, 0.8 nm), and investigated the temperature dependence of intrinsic critical current density J_{c0} and thermal stability factor Δ. We also measured the magnetization dynamics of the hybrid memory layer by using the time-resolved magneto-optical Kerr effect (TRMOKE), and discussed the effect of the high T_C interface layer on TA-STT switching. Current-perpendicular-to-plane type giant magneto-resistance (CPP-GMR) structures with the hybrid memory and Co/Pt reference layers were fabricated to investigate J_{c0} and Δ, which are estimated from the pulse width dependence of the STT switching current density. The samples without a reference layer were also fabricated to estimate the damping constant α of the hybrid memory layer by the TRMOKE measurements. Figure 1 shows the temperature dependence of J_{c0} of the hybrid memory layer with various of Co thickness x in the interface high T_C layer. J_{c0} decreased by elevating the temperature, and J_{c0} of x = 0.8 drastically decreased compared to the other samples. Figure 2 shows the dependence of α on the Co thickness of the high T_C layer. α of hybrid layers decreased with increasing x, and a drastic decrease was confirmed when x > 0.6 nm. The decrease of α suggests the increase of exchange coupling between high T_c and low T_c MLs. The exchange coupling between high T_c and low T_c MLs is considered to have significant influence on the J_{c0} at room temperature and its temperature dependence as shown in Fig. 1. MuMax[3] simulation also supports the increase of J_{c0} by reducing the exchange coupling between high T_c and low T_c MLs, which will be discussed in the presentation.

[1] Machida et al., IEEE Trans. Magn., 53, 2002205 (2017). [2] W. Zhao et al., IEEE Trans. Magn., 54, 3450405 (2018). [3] W. Zhao et al., J. Magn. Magn. Mater., 493, 165749 (2020).

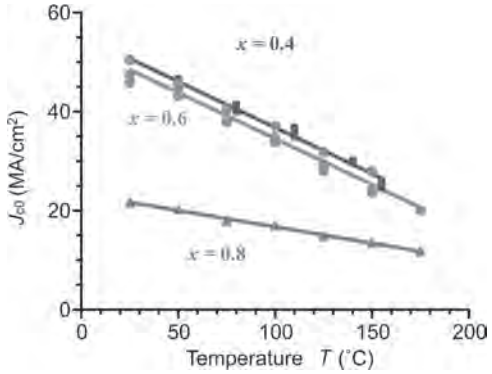

Fig. 1 Temperature dependence of J_{c0} of the hybrid memory layer of $[Co(x)/Pd(1.6\text{-}x)]_1$ / $[CoPd/Pd]_2$.

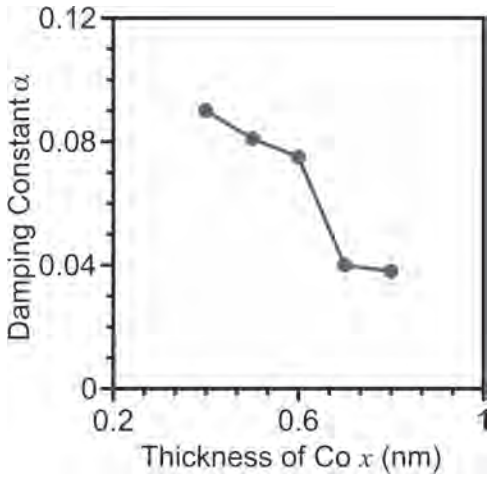

Fig. 2 Dependence of damping constant α of the hybrid memory layer on the thickness of Co x in high T_C Co/Pd layer.

Session GPE
MAGNETORESISTANCE AND VOLTAGE-CONTROLLED MAGNETIC PROPERTIES (Poster Session)

Stephane Mangin, Chair
Université de Lorraine, Vandoeuvre-lès-Nancy, France

GPE-01. Withdrawn

GPE-02. Impact of Magneto-Electric Coupling in Thermally Activated Magnetization Dynamics in Nanomagnets. *S. Perna*[1], P. Ansalone[2], V. Scalera[3], M. d'Aquino[1], C. Serpico[1] and V. Basso[2] *1. DIETI, Università di Napoli Federico II, Naples, Italy; 2. Instituto Nazionale di Ricerca Metrologica, Turin, Italy; 3. Free University of Bozen-Bolzano, Bolzano, Italy*

The magnetization dynamics controlled by an electric field in nanomagnets is one of the most promising ways to achieve energy-efficient unconventional computing based on nanomagnetic devices such as VCMA-MRAM [1], p-bits [2] realized via superparamagnetic particles and spin-logic [3] for ICT applications. The role of the electric field arises naturally when the magnetization dynamics is investigated in a relativistic framework, where the electric field in the laboratory frame is transformed according to Lorentz transformation into a magnetic field in the moving frame interacting with moving magnetic moments [4]. Moreover, the analogous result has been derived as a special case of a non-abelian gauge theory assuming the invariance of the micromagnetic free energy over an arbitrary local rotation applied to the magnetization pattern [5]. As a result, in both cases the micromagnetic energy is modified by the presence of two additional terms in the micromagnetic free energy. The first one has the same structure of the Dzyaloshinskii-Moriya energy [6–8] and the second one is an uniaxial like anisotropy energy term. The presence of an electric field might arise from different physical mechanisms such as an applied electric field or choosing material with non-zero averaged electric crystal field. In such situations, we suggest that a proper way to treat the magnetoelectric coupling is via a phenomenological approach in which the values of the coefficients controlling the additional terms are estimated on the basis of observations. We investigate the impact of the electric field on the magnetic state in confined nanomagnets. We consider thermally activated dynamics in uniformly magnetized samples, where the electric field modifies the free energy barrier and consequently the transition rate between metastable magnetic equilibria. Moreover, we explore the role of the electric field in the stabilization of non-uniform magnetization patterns. In both analyses, we establish a cause-effect relationship between the electric field and the magnetic state, which allows us to define a possible procedure in order to estimate the weighting coefficients for the two additional energy terms due to the magneto-electric interaction.

[1] S. Bhatti, R. Sbiaa, A. Hirohata, H. Ohno, S. Fukami, and S. N. Piramanayagam, "Spintronics based random access memory: A review," Materials Today, vol. 20, no. 9, pp. 530–548, Nov. 2017, doi: 10.1016/j.mattod.2017.07.007. [2] K. Y. Camsari, B. M. Sutton, and S. Datta, "p-bits for probabilistic spin logic," Applied Physics Reviews, vol. 6, no. 1, p. 011305, Mar. 2019, doi: 10.1063/1.5055860. [3] T. Liu and G. Vignale, "Voltage-controlled spin-wave-based logic gate," Jun. 2011, Accessed: Jul. 21, 2021. [Online]. Available: http://dx.doi.org/10.1109/drc.2011.5994464. [4] V. Basso and P. Ansalone, "Electric field effect on spin waves: Role of magnetic moment current," EPL (Europhysics Letters), vol. 130, no. 1, p. 17008, Apr. 2020, doi: 10.1209/0295-5075/130/17008. [5] P. Ansalone, S. Perna, M. d'Aquino, V. Scalera, C. Serpico, and V. Basso, "A Local Gauge Description of the Interaction between Magnetization and Electric Field in a Ferromagnet," IEEE Transactions on Magnetics, pp. 1–1, 2021, doi: 10.1109/tmag.2021.3086357. [6] G. T. Rado and V. J. Folen, "Magnetoelectric Effects in Antiferromagnetics," Journal of Applied Physics, vol. 33, no. 3, pp. 1126–1132, Mar. 1962, doi: 10.1063/1.1728630. [7] I. Dzyaloshinsky, "A thermodynamic theory of 'weak' ferromagnetism of antiferromagnetics," Journal of Physics and Chemistry of Solids, vol. 4, no. 4, pp. 241–255, Jan. 1958, doi: 10.1016/0022-3697(58)90076-3. [8] T. Moriya, "New Mechanism of Anisotropic Superexchange Interaction," Physical Review Letters, vol. 4, no. 5, pp. 228–230, Mar. 1960, doi: 10.1103/physrevlett.4.228.

GPE-03. Reconfigurable spin-logic device via laterally modulated Rashba effect in Pt/Co/AlO_x structures. *M. Kang*[1], J. Choi[1], J. Jeong[1], J. Park[1], H. Park[2], T. Kim[2], T. Lee[1], K. Kim[1], K. Kim[3], J. Oh[2], D. Viet[4], J. Jeong[4], J. Yuk[1], J. Park[2], K. Lee[1] and B. Park[1] *1. Korea Advanced Institute of Science and Technology, Deajeon, The Republic of Korea; 2. Korea University, Seoul, The Republic of Korea; 3. Korea Institute of Science and Technology, Seoul, The Republic of Korea; 4. Chungnam National University, Daejeon, The Republic of Korea*

Spin-orbit coupling effect in structures with broken inversion symmetry, known as the Rashba effect, facilitates spin-orbit torques (SOTs) in heavy metal/ferromagnet/oxide structures, along with the spin Hall effect [1,2]. Electric-field control of the Rashba effect is established for semiconductor interfaces [3], but it is challenging in structures involving metals owing to the screening effect. Here, we report that the Rashba effect in Pt/Co/AlO_x structures is laterally modulated by electric voltages, generating out-of-plane SOTs. This enables field-free switching of the perpendicular magnetization and electrical control of the switching polarity. Changing the gate oxide reverses the sign of out-of-plane SOT while maintaining the same sign of voltage-controlled magnetic anisotropy, which confirms the Rashba effect at the Co/oxide interface is a key ingredient of the electric-field modulation. The electrical control of SOT switching polarity in a reversible and non-volatile manner can be utilized for programmable logic operations in spintronic logic-in-memory devices.

[1] Liu, L. *et al. Science* 336, 555–558 (2012). [2] Miron, I. M. et al. *Nature* 476, 189–193 (2011). [3] Chen, L. *et al. Nat. Electron.* 1, 350–355 (2018)

GPE-04. Enhancement of Voltage Controlled Magnetic Anisotropy (VCMA) Through Electron Depletion. *T. Peterson*[1], A. Hurben[1], D. Zhang[1] and J. Wang[1] *1. University of Minnesota, Minneapolis, MN, United States*

Enhancement of switching perpendicular magnetic tunnel junctions (p-MTJs) with an electric-field has been a milestone for realizing ultra-low energy memory and computing devices. To integrate with current STT-MTJ and SOT-MTJ devices the typical linear fJ/Vm range voltage controlled magnetic anisotropy (VCMA) needs to be enhanced through stack engineering. We have investigated possible non-linear voltage controlled magnetic anisotropy (VCMA) in heavily electron depleted devices, where the magnetic anisotropy could be reduced with positive and negative voltages, differing with the typical linear VCMA voltage behavior. A possible bidirectional and 1.1 pJ/Vm VCMA effect can be realized based on theoretical predictions with heavily electron depleted Fe/MgO interfaces. To improve upon existing VCMA technology we have proposed inserting high work function materials under the magnetic layer which will deplete electrons from the magnetic

layer biasing the gating window into the electron-depleted regime where the pJ/Vm and bidirectional VCMA effect was predicted. We have demonstrated tunable control of the under-layer's work function by utilizing Ta/Pd(x)/Ta trilayers. By modulating the Pd thickness from 0-20 nm we have observed a tunable change in the Ta layer's work function from 4.3eV to 4.8eV. To investigate the extent of the electron depletion as a function of the Pd thickness in the trilayer we have performed DFT calculations on supercells of Ta/Pd (X)/Ta /CoFe /MgO. We are working to improve the quality of our gate dielectric materials to avoid hysteretic ionic effects allowing for a reliable VCMA measurement of the Ta/Pd/Ta samples.

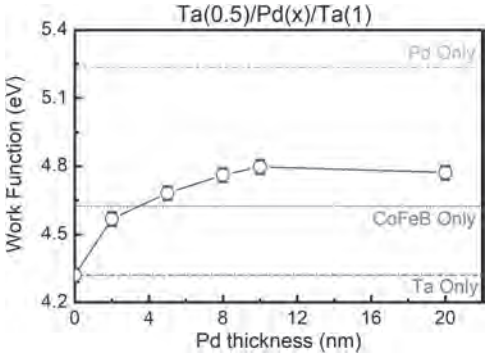

Work function values from UPS measurements of the Ta/Pd/Ta trilayer with a varied Pd thickness. Reference samples of single later Ta, CoFeB, and Pd are shown as horizontal lines.

GPE-05. Improving the spin-orbit torque efficiency in Pt/CoFeB/Pt based perpendicularly magnetized system to decrease the critical current density for current-induced magnetization switching. *S. Kayal*[1], S. Maji[1], A. Mukhopadhyay[1] and P. Kumar[1] *1. Department of Physics, Indian Institute of Science, Bangalore, India*

Controlling and switching magnetization by the process of current-induced torque has a considerable advantage in low power consumption for a memory device and spin logic device applications. For a heavy metal (HM) / ferromagnet(FM) / heavy metal (HM) based perpendicular magnetic anisotropy system with broken normal space inversion symmetry (SIA), current-induced magnetization reversal (CIMR) takes place using spin-orbit torque (SOT) with the assistance of an in-plane (IP) magnetic field. For a similar HM/FM/HM-based PMA system having broken lateral symmetry, also known as the quasi-PMA system, the CIMR occurs without the assistance of the IP field. The lateral SIA [1-4] helps in the CIMR process by producing an effective out-of-plane (OOP) field which does not depend on the direction of the IP field and initial magnetization. Thus, the quasi-PMA system has a massive significance for magnetic field-free CIMR. Pt/CoFeB/Pt based quasi-PMA heterostructure has been chosen for CIMR study with the optimal bottom layer Pt thickness for which the effect of lateral SIA is maximum and consists of a ferromagnetic layer with in-plane magnetic anisotropy (IMA) at the top layer of the heterostructure. The IMA ferromagnetic layer [5] contributes to the CIMR process by producing the stray field. Thus, by designing a heterostructure to combine the SOT originated by spin-Hall effect, the stray field by IMA ferromagnetic layer, and the lateral SIA effect, we have enhanced the SOT efficiency of the system to reduce the critical current density (J_c) for CIMR both under the absence and the presence of the different IP fields. The switching phase diagram (SPD) for this device has been shown in Fig. 1. We have achieved J_c as low as (8.65 ± 0.20) x 10^{10} A/m^2 and (3.35 ± 0.17) x 10^{10} A/m^2 at zero bias and 60 mT, respectively. The device has massive potential in low-power magnetic data storage application.

[1] G. Yu, P. Upadhyaya, Y. Fan, J. Alzate, *Nature Nanotechnology*, vol. 9, pp. 548–554, (2014). [2] G. Yu, M. Akyol, P. Upadhyaya, *Scientific Reports*, vol. 6, pp. 548–554, (2016). [3] V. M. Parakkat, K. R. Ganesh, and P. S. A. Kumar, *Physical Review B*, vol. 96, p. 104412, (2017). [4] S. Guddeti, A. K. Gopi, and P. S. Anil Kumar, *IEEE Transactions on Magnetics*, vol. 54, pp. 1–5, (2018). [5] T. Simsek, *IEEE MAGNETICS LETTERS*, vol. 12, pp. 1–5, (2021).

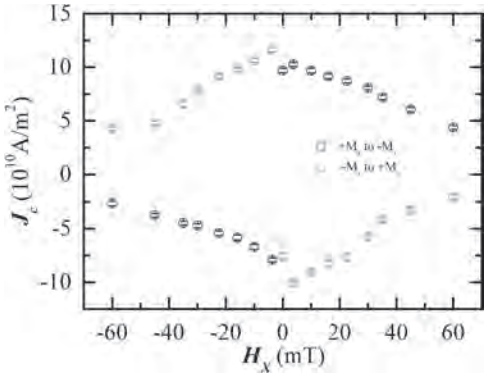

Fig.1. Current-induced switching phase diagram for the device Ta(2)/Pt(3)/CoFeB(0.6)/Pt(0.5)/Ta(1.5)/CoFeB(2.5)/Pt(1)

GPE-06. Spin-orbit torque assisted switching with voltage controlled exchange coupling. *B.R. Zink*[1], Y. Lv[1], D. Zhang[1], D. Lyu[1] and J. Wang[1] *1. Electrical and Computer Engineering, University of Minnesota, Minneapolis, MN, United States*

Application of electric fields (E-fields) on perpendicular magnetic tunnel junctions (p-MTJs) is a promising solution for improving energy efficiency in spintronics based memory and logic systems [1]. Many studies on E-field effects on p-MTJs have focused on voltage-controlled magnetic anisotropy (VCMA) of the p-MTJs free layer to reduce the energy required for p-MTJs to switch magnetization states [2]. In this approach, VCMA temporarily decreases the energy barrier separating the two magnetization states and bidirectional switching is achieved using either an external magnetic field or a spin-polarized current. Another approach is to utilize voltage controlled exchange coupling (VCEC) between two ferromagnetic layers in synthetic antiferromagnetic (SAF) structures. Recently, bidirectional switching through VCEC has been demonstrated on p-MTJs with bottom dual-SAF free layers [3]. Benchmarking on MRAM technologies has shown VCEC-MRAM to have much lower energy dissipation than spin-orbit torque (SOT) MRAM [4]. However, SOT-MRAM has faster write speeds since SOT allows for ultra-fast (≤ 400ps) switching [5]. In this work, we explore the potential for SOT-assisted VCEC switching on p-MTJs with bottom dual-SAF free layers fabricated on bilayer spin hall channels. Fig. 1 shows that the SOT current can tune the coercivity of the p-MTJ, which illustrates that SOT can assist in VCEC switching. Fig. 2 shows that a voltage applied to the MTJ causes either a positive or negative shift in its stray field (center of the field switching curve), which indicates that voltage influences interlayer exchange coupling in the SAF free layer, thus demonstrating VCEC. Since the coercivity of the p-MTJs can be tuned with both VCEC and SOT, dual-biasing of SOT+VCEC can possibly generate stochastic signals for probabilistic-bits. By utilizing the effects of both VCEC and SOT, we introduce a potential solution for low-energy and ultra-fast MRAM technology as well as more novel computing paradigms such as probabilistic spin logic.

[1] P. K. Amiri *et al.*, *IEEE Trans. Magn.*, vol. 51, 3401507 (2015). [2] W. G. Wang, M. Li, S. Hageman, and C. L. Chien, *Nature Materials.*, vol. 11, pp. 64 – 68 (2011). [3] D. Zhang *et al.*, *arXiv:1912.10289v1* (2019). [4] Y. C. Liao, C. Pan, and A. Naeemi, *IEEE J. Explor. Solid-State Computat.*, vol. 6, pp. 9 – 17 (2020). [5] K. Garello *et al.*, *Appl. Phys. Lett.*, vol. 105, 212402 (2014).

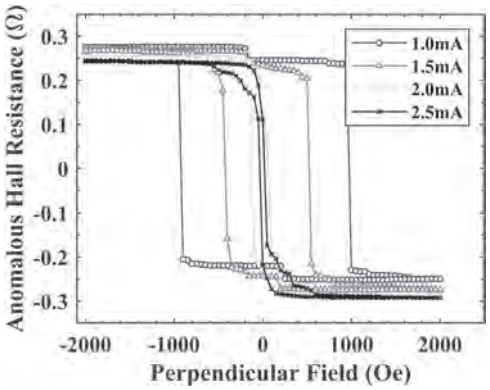

Fig. 1. Anomalous hall resistance versus field measurements at SOT currents ranging from 1mA to 2.25mA.

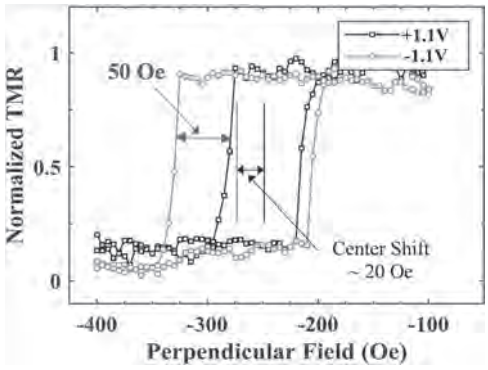

Fig. 2. Tunneling magneto-resistance (TMR) vs. field measurements at VCEC voltages of +1.1V and -1.1V.

GPE-07. Toggling of Exchange Bias in GdCo/NiO Thin Film Heterostructures by Hydrogen Gating. *M. Hasan*[1], J. Zehner[2], M. Huang[1], K. Leistner[2] and G.S. Beach[1] *1. Materials Science and Engineering, Massachusetts Institute of Technology, Cambridge, MA, United States; 2. Leibniz IFW Dresden, Dresden, Germany*

Electrical control of exchange bias in a antiferromagnet/ferro(ferri)magnet heterostructure is highly desirable for spintronic applications, but is very hard to achieve since the effect is related to the spin order in both the antiferromagnet and the ferro(ferri)magnet, which electric fields have little influence over. However, It has been shown that ferrimagnetic order in GdCo metal thin films can be dynamically controlled by voltage through solid-state hydrogen gating [1], via modulation of the relative magnetic moments of the two sublattices that make up GdCo. Here we show that, when a correctly engineered GdCo/NiO bilayer is loaded/unloaded with hydrogen, the expected switching of the dominant sublattice in GdCo is accompanied by a flipping of the effective exchange bias direction as well. We demonstrate cyclical toggling of exchange bias in heterostructures with fully shifted hysteresis loops by application of only modest voltages (<2V). Moreover, by following a specific heating and gating schedule in a heterostructure with the correct properties, we can achieve switching of the EB direction without concurrently toggling the dominant sublattice. Our robust but simple mechanism provides a powerful means of controlling exchange bias that can have broad implications for spintronics.

[1]. M. Huang et al., in press., Nature Nanotechnology

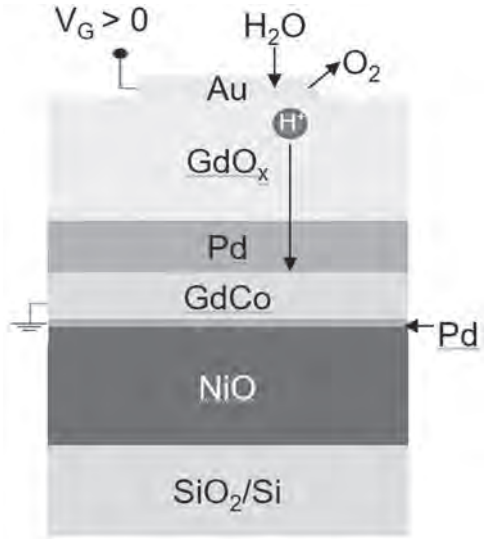

Fig. 1 Schematic device structure showing $+V_G$ splitting atmospheric water and injecting hydrogen into the GdCo layer [1].

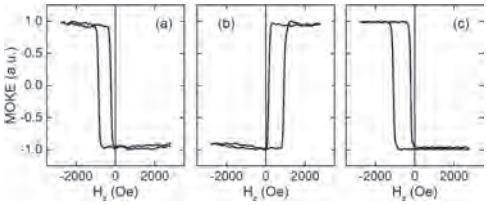

Fig. 2 Polar MOKE hysteresis loops showing (a) Gd-dominant virgin state with -ve EB, (b) Co-dominant state with +ve EB after gating at +1.8V for 240s and (c) Gd-dominant state with -ve EB following application of 0V for 80s.

GPE-08. A Model of Liposomal DDS with Field-Dependent Radical Pair System. *H. Nakagawa*[1], M. Fujimoto[2] and T. Tadokoro[1] *1. Tokyo Denki University, Tokyo, Japan; 2. CPCC, Tokyo, Japan*

So many functional liposomes have been evaluated as biocompatible nanocarriers for drug-delivery systems (DDSs). However, there are no reported studies of the application of radical pair mechanisms (RPMs) to liposomal DDSs under exposures to magnetic fields. We already set about developing a novel DDS *via* intramembranous RPM, using anti-cancer flutamide (FM) as a radical pair-forming drug [1]. In our present research, we considered examining magnetic field effects on intramembranous radical pair mechanisms were examined by measuring the physicochemical changes of liposomal membranes peroxidized by reactive oxygen species—especially, excited singlet oxygen ($^1O_2$). Each dry film composed of various molar ratios of phospholipids, photosensitizers and antenna pigments was hydrated by vortexing them with some appropriate buffer solutions. Each of the dispersions was transferred to a Mini-Extrudor (Avanti Polar Lipids, Inc.) to produce small unilamellar liposomal nanoparticles. Irradiation of the nanoparticles and exposure to magnetic fields were carried out in the same way as in our previous report [2]. ^{1}H- and ^{13}C-NMR spectra of reaction products in methanol-d_4 were obtained with a JEOL JNM A-600 (600.05 MHz) spectrometer at 27°C. Chemical shifts (d) were referred to internal CD_2HOD at 3.35 ppm for ^{1}H-NMR and $^{13}CD_3OD$ at 49.0 ppm for ^{13}C-NMR. FAB mass spectrum was recorded by a JEOL JMS SX-102 mass spectrometer. HPLC was performed using a Shimadzu SCL-10A system controller equipped with a LC-10AS pump and a SPD-10AV detector. As it turned out, we found the possibility that a pulsating field influences the pair mechanism in the process of membrane peroxidations induced by excited singlet oxygen ($^1O_2$). Comparison of our experimental results showed no relationship between lipophilic and hydrophilic radical scavenging activity, suggesting the possibility of the existence of some types

of magnetic field effects on radical pair mechanisms. Accordingly, further studies on the reaction field-dependent radical pair system are now under investigation.

1) H. Nakagawa, AIP Advances 10, 025019 (2020).

GPE-09. Detection of proton NMR by highly sensitive TMR sensor.
M. Oogane[1], K. Fujiwara[2], H. Wagatsuma[1], S. Kumagai[2] and Y. Ando[1]
1. Tohoku University, Sendai, Japan; 2. Spin Sensing Factory Corp., Sendai, Japan

The magnetic tunnel junctions (MTJs)-based sensors (TMR sensor) are promising magnetic field sensor because of room temperature operation, small device size, and the low power consumption. Since the TMR sensors with such features are considered to be widely applicable not only to the magnetic recording, the TMR sensors will be a key device in the ICT and IoT societies. In addition, because of the dramatic increase in sensitivity of TMR sensors in recent years, the realization of the device that can detect the weak magnetic field of pico-Tesla such as bio-magnetic field is expected. We have already reported on the measurement of cardiac magnetic field (magnetocardiography: MCG) and brain magnetic field (magnetoencephalography: MEG) using TMR sensors [1]. In this work, we have obsereved proton NMR signal by using highly sensitive TMR sensor. As shown in Fig. 1, the developed TMR sensor has an extremely low magnetic field detectivity of 0.1 pT / $Hz^{0.5}$ or less in the kHz range by using a magnetic flux concentrator (MFC) (Fig. 1). Protons in the human body generate nuclear magnetic resonance (NMR) at a frequency of 1 to 3 kHz under a weak magnetic field of μT, and we succeeded in measuring the NMR signal for the first time using the TMR sensor (Fig. 2). These results show that the MCG and MEG signal and the magnetic resonance image (MRI) using NMR can be simultaneously measured by the same TMR sensor device. This work was partly supported by JST S-innovation project, the Center for Innovative Integrated Electronic Systems (CIES), the Center for Science and Innovation in Spintronics (CSIS), and the Center for Spintronics Research Network (CSRN).

[1] K. Fujiwara *et al.*, Appl. Phys. Express 11, 023001 (2018).

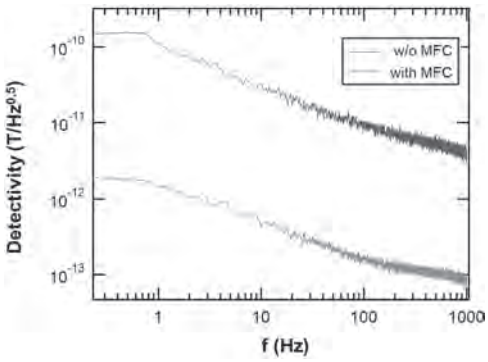

Frequency dependence of detectivity in developed TMR sensors with/ without magnetic flux concentrator (MFC)

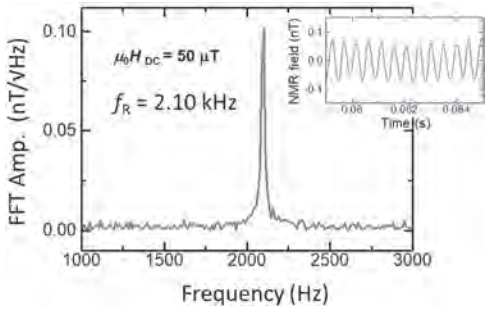

Proton NMR signals under low magnetic field of 50 μT measured by developed TMR sensors with MFC.

GPE-10. Multi-TMR device with a compact footprint for low magnetic field detection at room temperature.
M. Silva[1,2], R. Macedo[1], *S. Cardoso de Freitas*[1,2] and P.P. Freitas[1] *1. Instituto de Engenharia de Sistemas e Computadores - Microsistemas e Nanotecnologias, Lisbon, Portugal; 2. Instituto Superior Tecnico (IST), Universidade de Lisboa, Lisbon, Portugal*

Magnetic tunnel junctions have been implemented in a broad range of applications[1] due to high sensitivity, excellent reliability and low power consumption. This work discusses the implementation of a vertical packed strategy[2] applied to magnetic tunnel junctions. A multi- TMR device was designed to bring higher signal with reduced noise and compact footprint by increasing the number of sensors vertically within a single sensor[fig.1] or an arrays of sensors per level. A CoFeB/MgO/CoFeB based magnetic tunnel junction was selected and the microfabrication process was established to achieve a functional multi-level TMR device, using a 300 nm thick SiN layer to isolate consecutive levels. Then a common electrical contact is created to connect all levels in a parallel configuration to reduce the resistance. The sensor stack presents an initial RxA of 60 kΩ.μm^2 and a TMR=120% deposited by a N3600/N8800 tool at INESC MN. Here we show results for a three-level device microfabricated with a total of 600 sensors within an area of 0.12 mm^2. The impact on the sensor transfer curve of topography and misalignments across levels are discussed. Although accumulated roughness reduces the TMR signals, thus, the sensitivity, the magnetostatic coupling is negligible due to optimized level separation, which successfully mitigates the stray fields. Furthermore, a magnetic field of 71 nT/$Hz^{1/2}$ at 35 Hz was measured on unshielded environment [fig.2]. This value is obtained from converting the voltage output into field units using a sensitivity of 3V/T. Also, the electrical robustness of the multi-TMR devices was evaluated through the breakdown voltage showing similar robustness compared with the arrays in-plane. This work shows an ambitious architecture design for TMR sensor integration in applications requiring small size and low magnetic field detection levels. Comparing with series of sensors achieving 20 nT/$Hz^{1/2}$ at 1 Hz on 10mm^2[3] or 115 pT/$Hz^{1/2}$ at 200 Hz occupying an area of 4.5x5.5 mm^2[4], the proposed geometry is at least 2 orders of magnitude more compact.

[1] C. Zheng *et al.*, *IEEE Trans. Mag.*, vol 55, 1-30 (2019) [2] Silva, M., Franco, F., Leitao, D.C. et al. Sci Rep 11, 215 (2021). [3] R. Guerrero et al. Journal of Applied Physics 105, 113922 (2009) [4] E. Paz et al., Journal of Applied Physics 115, 17E501 (2014)

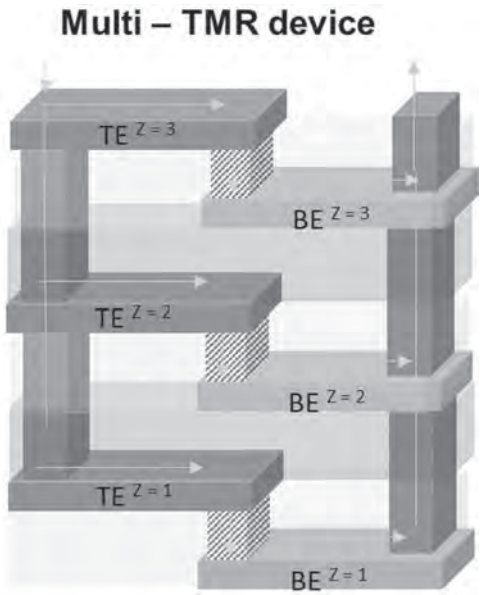

Scheme of vertically packed array (arrows represent current flow).

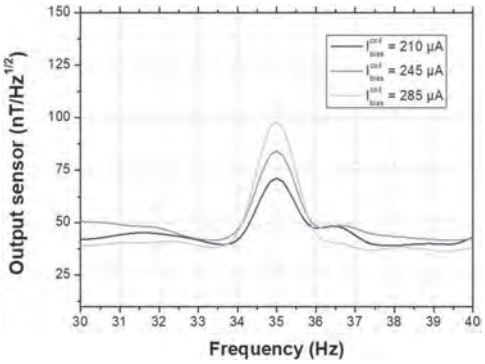

Output of device subjected to variable current amplitude applied to the external coil at 35 Hz.

GPE-11. Giant tunneling magnetoresistance in van derWaals magnetic tunnel junctions formed by interlayer antiferromagnetic bilayer $CoBr_2$. *Y. Zhu*[2,1], X. Guo[2], L. Jiang[1], Z. Yan[1], Y. Yan[2] and X. Han[1] *1. Institute of Physics, Beijing, China; 2. Jilin University, Changchun, China*

The discovery of two-dimensional (2D) van der Waals (vdW) intrinsic magnets has opened a promising avenue to design high-performance magnetic tunnel junctions (MTJs) based on 2D materials. In this work, using first-principles calculations, it is demonstrated that bilayer $CoBr_2$ is intrinsically a magnetic semiconductor with intralayer ferromagnetic (FM) and interlayer antiferromagnetic (AFM) couplings and the interlayer AFM coupling in bilayer $CoBr_2$ is independent on the stacking orders. Moreover, using the nonequilibrium Green's function combined with density functional theory, it is found that due to the large difference between interlayer AFM and FM states of the $CoBr_2$ barrier, the conductance of spin filter (SF) vdW MTJs based on the graphene/bilayer $CoBr_2$/graphene heterostructure for the interlayer FM state of the $CoBr_2$ barrier is about 25 times that for the interlayer AFM state of the $CoBr_2$ barrier. Consequently, a high tunneling magnetoresistance (TMR) ratio of 2420% is achieved in this SF-vdW MTJ at zero bias. In particular, because the current for the interlayer FM state of the $CoBr_2$ barrier rapidly increases with the increase of bias voltage, a giant TMR ratio of up to about 38 000% can be achieved in this SF-vdW MTJ at 0.2-V bias. Our results suggest that SF-vdW MTJs formed by the interlayer AFM barrier with variable conductivity hold great potential for developing vdW MTJs with a high TMR ratio.

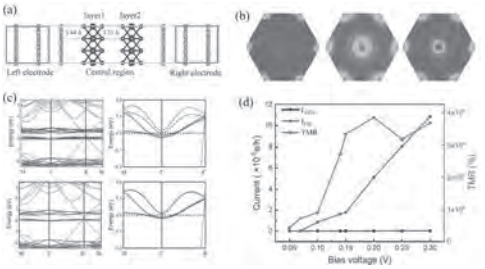

(a) Strucuture of graphene|$CoBr_2$|graphene MTJ. (b) Transmission of MTJ. (c) Band structure of MTJ for AFM and FM. (d) Current and TMR with bias voltage.

GPE-12. Structural and Magnetic Properties of CoIrMnAl Heusler Alloy Epitaxial Films Fabricated with Magnetron Sputtering for Spintronics Applications. *D.C. Lloyd*[1], K. Elphick[1], R. Monma[2,3], T. Roy[4], K. Suzuki[3,5], T. Tsuchiya[5,6], M. Tsujikawa[4,5], S. Mizukami[3,6], M. Shirai[5,6] and A. Hirohata[1] *1. Department Electronic Engineering, University of York, York, United Kingdom; 2. Department of Applied Physics, Graduate School of Engineering, Tohoku University, Sendai, Japan; 3. WPI Advanced Institute for Materials Research (AIMR), Tohoku University, Sendai, Japan; 4. Research Institute of Electrical Communication, Tohoku University, Sendai, Japan; 5. Center for Spintronics Research Network (CSRN), Tohoku University, Sendai, Japan; 6. Center for Science and Innovation in Spintronics (CSIS), Core Research Cluster (CRC), Tohoku University, Sendai, Japan*

A major area of research in the field of spintronics is the development of materials used for the fabrication of magnetic tunnel junctions (MTJ). Current uses for MTJs are data storage read heads and non-volatile memory devices such as MRAM [1]. Emergent computing technologies are already setting the demand for new MTJ electrode materials, namely, extremely high TMR ratios at room temperature [2]. Low temperature TMR ratios in excess of 2600% have been observed experimentally in half-metallic ferromagnetic materials [3]. The reduction in TMR ratio with temperature is thought to be due to loss of spin polarisation and desirable magnetic order at the interface of the electrode and the MgO tunnelling barrier [4]. Therefore, it is critical that any potential electrode material be a close crystallographic match to MgO and present consistent electronic character across a range of interfacial conditions. A potential candidate for MTJ electrodes are quaternary Heusler alloys with equiatomic stoichiometry [5] i.e. having chemical formula XX'YZ. Recent theoretical studies have found that quaternary Heusler alloys of the form CoIrMnZ (Z= Al, Si, Ga, Ge) have near perfect spin polarisation due their half-metallic nature and have Curie temperatures above room temperature [6]. The fully ordered bcc-structure of these alloys is an excellent match to MgO. While swap-disorder within the unit can be used to tune the magnetic properties [7]. Here we have successfully deposited thin films of CoIrMnAl (50nm) at room temperature with B2 crystal ordering using sputter deposition [8]. In-situ annealing at 500-600°C yields a lattice constant approximating the theoretical values (Fig. 1). Magnetic measurements showed ferrimagnetic ordering and a Curie temperature of 400K; which is ~70% of the predicted value. Cross-section scanning transmission electron microscopy reveal that B2 ordering is localised to the interfacial region (~17nm) of the film (Fig. 2). This holds promise for further improvement of the magnetic properties towards the theoretical predictions.

[1] D. Apalkov, B. Dieny, and J.M. Slaughter, Proc. IEEE 104, 1796 (2016). [2] M. Zabihi, et al. IEEE Trans. Comput. 68, 1159 (2019). [3] H. Liu, et al. J. Phys. D. Appl. Phys. 48, 164001 (2015). [4] Y. Miura, K. Abe, and M. Shirai, Phys. Rev. B 83, 214411 (2011). [5] V. Alijani, et al. Phys. Rev. B 84, 224416 (2011). [6] T. Roy, et al. J. Magn. Magn. Mater. 498, 166092 (2020). [7] S. Yamada, et al. Phys. Rev. B 100, 195137 (2019). [8] R. Monma, et al. J. All. Com. 868, 159175 (2021)

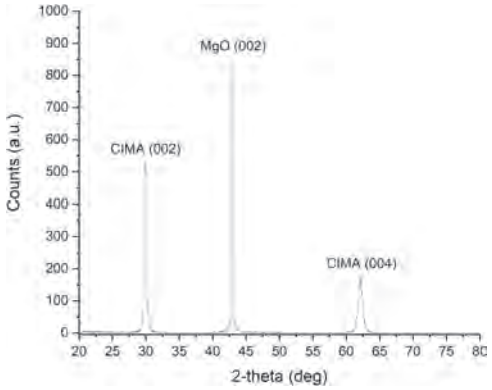

Fig. 1: HRXRD of CIMA film annealed at 500°C (1 hour).

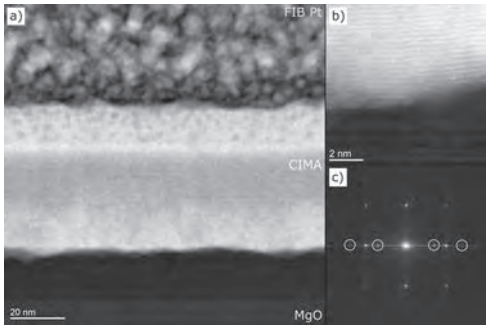

Fig. 2: Cross-section STEM of a) the CIMA layer structure, b) B2 crystal ordering at the interface and c) FFT of the CIMA layer.

GPE-13. Integration of 10 nm thick Dysprosium Iron Garnet Films on Silicon. *M. Gross*[1], J. Bauer[2] and C. Ross[2] *1. Electrical Engineering and Computer Science, Massachusetts Institute of Technology, Cambridge, MA, United States; 2. Material Science and Engineering, Massachusetts Institute of Technology, Cambridge, MA, United States*

Rare earth iron garnets (REIGs) are magnetic insulators that can be grown as nanometer thick films with perpendicular magnetic anisotropy (PMA), making them attractive for studies on ultrafast spin wave dynamics. PMA has been achieved in epitaxial films of several REIG systems on garnet substrates due to magnetoelastic anisotropy from lattice mismatch strain[1-2]. Polycrystalline REIG films as thin as 22nm can also be grown on silicon with PMA due to thermal expansion mismatch between the film and substrate following a high temperature anneal[3]. However, it is of interest to develop ultrathin polycrystalline garnet on silicon with PMA for spintronics devices integrated with CMOS technology. Films below ~20nm thickness crystallize poorly and require a garnet underlayer to provide lattice templating that promotes crystallization. Previous research shows this templating effect still holds when a Pt layer is present between the garnet film and the substrate[4]. Here we report on the growth and properties of 10nm thin polycrystalline dysprosium iron garnet (DyIG) and dysprosium yttrium iron garnet (Y:DyIG) films on Si (100) substates using an underlayer of a non-magnetic garnet, $Gd_3Ga_5O_{12}$, coated with ~1.5nm of Pt to prevent interdiffusion. This enabled the growth of ultrathin polycrystalline DyIG films directly on Si with bulk-like magnetization and PMA. Films were grown by pulsed laser deposition and later crystallized by a rapid thermal anneal (750 °C/5 min). Thermal mismatch creates a tensile strain in the films, which combined with the negative magnetostriction coefficients of DyIG overcomes the shape anisotropy and results in PMA. X-ray diffraction shows single phase pure garnet and atomic force microscopy of the films indicates sub-nanometer surface roughness. Vibrating sample magnetometry (VSM) measurements of a 10nm DyIG/Pt/GGG/Si film showed PMA with a saturation magnetization of 15 emu/cc and a coercivity of ~300 Oe. The spin Hall magnetoresistance and spin mixing conductance of Pt/DyIG/Pt/GGG/Si will be compared with that of Pt/REIG single crystal films.

1. L. Caretta, et al., Science 370 1438 (2020). 2. E. Rosenberg, et al., Phys. Rev. Mater., Vol. 2, 094405 (2018). 3. J. Bauer, et al., APL, Vol. 114, 052403 (2019). 4. M. Aldosary, et al., Appl. Phys. Lett. 108 242401 (2016).

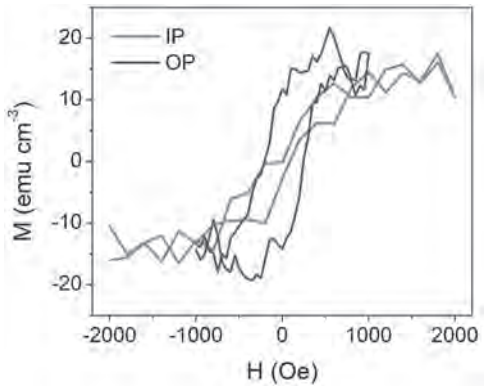

In plane and out of plane VSM hysteresis loops of 10nm DyIG/Pt/GGG/Si film with PMA.

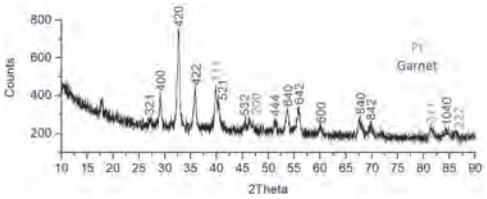

Grazing incidence X-ray diffraction of 10nm/Pt/GGG/Si film.

Session HOA
FERROMAGNETIC RESONANCE
Kyongmo An, Chair
Korea Research Institute of Standards and Science, Daejeon, The Republic of Korea

INVITED PAPER

HOA-01. Magnetoelastic Gilbert Damping in Magnetostrictive $Fe_{0.7}Ga_{0.3}$ Thin Films. *W. Peria*[1], X. Wang[2], H. Yu[2], S. Lee[2,3], I. Takeuchi[2] and P.A. Crowell[1] *1. School of Physics and Astronomy, University of Minnesota, Minneapolis, MN, United States; 2. Department of Materials Science and Engineering, University of Maryland, College Park, MD, United States; 3. Department of Physics, Pukyong National University, Busan, The Republic of Korea*

Gilbert damping remains among the foremost properties impacting the design of spintronic devices. There are many cases where the observed damping is larger than the predicted damping, which is usually based on considerations of electronic structure (such as the Kamberský torque-correlation model [1]). It is therefore of great importance to identify alternative damping mechanisms in order to obtain more accurate results. Two-magnon scattering is one such mechanism, but this can usually be distinguished from Gilbert damping due to its nonlinear dependence on frequency or by orienting the magnetization normal to the film plane [2]. In this talk we discuss how magnetoelastic coupling can cause a substantial enhancement of the overall Gilbert damping in a series of $Fe_{0.7}Ga_{0.3}$ thin films [3]. In our case, the effect is exaggerated due to the exceptionally high magnetostriction found in FeGa alloys (measured in these films as ~100 ppm at room temperature). The effect is based on a model of energy loss through phonon relaxation: Phonons are driven by magnetization dynamics through magnetoelastic coupling, and the relaxation of these phonons leads to a form of Gilbert damping (see Fig. 1) [4]. We show this by presenting the orientational and temperature dependence of the Gilbert damping in total of seven $Fe_{0.7}Ga_{0.3}$ thin films with thicknesses ranging from 17 to 70 nm. The orientation dependence of the Gilbert damping demonstrates that the magnetoelastic Gilbert damping is mitigated for out-of-plane magnetization due to confinement effects from the interfaces of the film, leading to a very large anisotropy (up to a factor of 10 at room temperature). The temperature dependence demonstrates both the effects of the magnetostriction and the phonon viscosity. The damping increases significantly at low temperatures due to the increasing magnetostriction. Importantly, however, we observe a nonmonotonic temperature dependence of the Gilbert damping. As the temperature decreases from ~75 K to 0, the damping decreases due to the reduction in the phonon relaxation rate (main panel of Fig. 2). This is attributed to the influence of the temperature dependence of the phonon viscosity, which increases linearly with temperature (inset of Fig. 2). It is thereby shown that the competing effects of magnetostriction, which decreases with increasing temperature, and phonon relaxation lead to the observed nonmonotonic temperature dependence. We conclude by emphasizing that, in general, the magnetoelastic damping may constitute a significant portion of the total Gilbert damping, particularly in materials with high magnetostriction. This work was supported by SMART, a center funded by nCORE, a Semiconductor Research Corporation program sponsored by NIST.

[1] K. Gilmore, Y. U. Izerda, and M. D. Stiles, Phys. Rev. Lett., Vol. 99, p.027204 (2007) [2] W. K. Peria, X. Wang, H. Yu, S. Lee, I. Takeuchi, and P. A. Crowell, Phys. Rev. B., Vol. 103, p.L220403 (2021) [3] W. K. Peria, T. A. Peterson, A. P. McFadden, T. Qu, C. Liu, C. Palmstrøm, and P. A. Crowell, Phys. Rev. B., Vol. 101, p.134430 (2020) [4] C. Vittoria, S. D. Yoon, and A. Widom, Phys. Rev. B., Vol. 81, p.014412 (2010) [5] A. E. Clark, M. Wun-Fogle, J. B. Restorff, K. W. Dennis, T. A. Lograsso, and R. W. McCallum, J. Appl. Phys., Vol. 97, p.10M316 (2005)

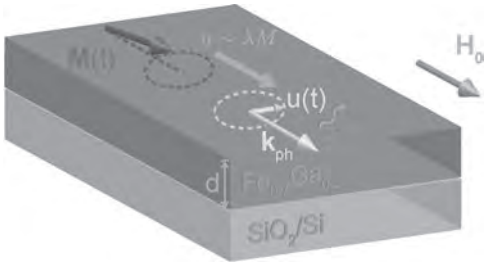

Fig. 1: Schematic diagram of the magnetoelastic damping process with magnetization *M(t)* lying in the film plane. The lattice displacement *u(t)* is driven by the magnetostriction λ, leading to energy loss due to the presence of phonon viscosity (represented by the wavy orange arrows).

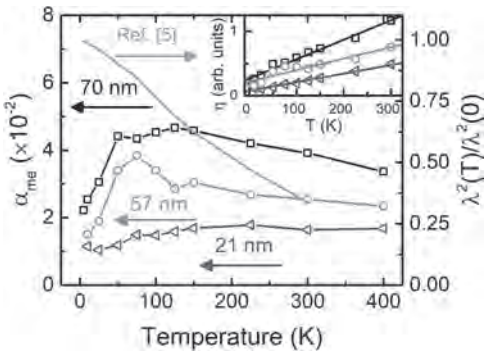

Fig. 2: Main panel, left ordinate: Magneloelastic Gilbert damping as a function of temperature for the 21 nm (blue triangles), 57 nm (red circles), and 70 nm (black squares) $Fe_{0.7}Ga_{0.3}$ films. Main panel, right ordinate: The square of the magnetostriction λ as a function of temperature, interpolated from data given in Ref. [5]. Inset: Phonon viscosity, defined as the ratio of α_{me} to λ^2 shown as a function of temperature for the 21 nm (blue triangles), 57 nm (red circles), and 70 nm (black squares) $Fe_{0.7}Ga_{0.3}$ films.

CONTRIBUTED PAPERS

HOA-02. Quantifying spin-mixed states in ferromagnets. *J.M. Shaw*[1], R. Knut[2], C. Armstrong[3], S. Bhandary[4], Y. Kvashnin[2], D. Thonig[5], E. Delczeg-Czirjak[2], O. Karis[2], T. Silva[1], E. Weschke[6], H. Nembach[1], O. Eriksson[2,5] and D. Arena[3] *1. NIST, Boulder, CO, United States; 2. Uppsala University, Uppsala, Sweden; 3. Univ. South Florida, Tampa, FL, United States; 4. Trinity College, Dublin, Ireland; 5. Örebro University, Örebro, Sweden; 6. Helmholtz Zentrum Berlin Mat & Energie, Berlin, Germany*

We quantify the presence of spin-mixed states in ferromagnetic 3d transition metals by precise measurement of the orbital moment. While central to phenomena such as Elliot-Yafet scattering, quantification of the spin-mixing

parameter has hitherto been confined to theoretical calculations. In this talk we will demonstrate that this information is also available by experimental means. We focus on a series of $Co_{90}Fe_{10}$/Ni multilayers and a $Ni_{80}Fe_{20}$ permalloy thin film. Precise measurement of the orbital to spin moment ratio μ_L/μ_S via ferromagnetic resonance spectroscopy (FMR) and x-ray magnetic circular dichroism (XMCD) show a measurable difference. By accounting for all known experimental artifacts that can give rise to such a discrepancy, we are left to conclude that another factor is giving rise to this effect. We argue that the discrepancy between FMR and XMCD results originate from Kittel's original derivation of the g-factor where the spin-mixing is only considered to first order. [1] However, we show that higher order terms of the spin-mixing parameter produce measurable changes in the g-factor within the precision of modern day broadband FMR. This can lead to an underestimation of μ_L/μ_S in FMR measurements if the spin-mixing parameter $\langle b^2 \rangle$ is neglected. Following Kittel's original derivation, a simple inclusion of second order terms in in the spin mixed states yields the following relation between g and μ_L/μ_S in Eq. 1. where $\langle b^2 \rangle$ is the spin-mixing parameter with the assumption that $\langle b^2 \rangle << 1$. Furthermore, b is defined by the spin-up wavefunction and spin-down wavefunction, while $a^2 + b^2 = 1$. We find values of $\langle b^2 \rangle = 0.022 \pm 0.003$ and $\langle b^2 \rangle = 0.019 \pm 0.001$ for the $Ni_{80}Fe_{20}$ and $Co_{90}Fe_{10}$/Ni samples, respectively. Our results are further supported by ab-initio relativistic electronic structure theory, which agree with experiment.

[1] C. Kittel, *On the Gyromagnetic Ratio and Spectroscopic Splitting Factor of Ferromagnetic Substances*, Phys. Rev. 76, 743 (1949).

$$\left(\frac{\mu_L}{\mu_S}\right)_{FMR} = \frac{g - 2 + 4\langle b^2 \rangle}{2(1 - 2\langle b^2 \rangle)}$$

HOA-03. Anomalous Temperature Dependence of Phonon Pumping by Ferromagnetic Resonance in $[Co/Pd]_n$ Multilayers with Perpendicular Anisotropy. *W. Peria*[1], D. Zhang[2], J. Wang[2] and P.A. Crowell[1] *1. School of Physics and Astronomy, University of Minnesota, Minneapolis, MN, United States; 2. Department of Electrical and Computer Engineering, University of Minnesota, Minneapolis, MN, United States*

The generation of phonons by ferromagnetic resonance in magnetic thin films and subsequent propagation of phonons into the substrate is an effect known as phonon pumping [1-2]. This effect can be utilized in spintronic devices that rely on magnetoelastic coupling for information transfer. The phonon pumping effect is most efficient in the perpendicular configuration, and can therefore be suitably integrated in devices composed of PMA materials. Here we demonstrate the pumping of phonons by ferromagnetic resonance in a series of $[Co(0.8\ nm)/Pd(1.5\ nm)]_n$ multilayers (n = 6, 11, 15, and 20) with large magnetostriction and perpendicular anisotropy. The effect is shown using broadband ferromagnetic resonance over a range of temperatures (10 to 300 K), where a resonant damping enhancement is observed at frequencies corresponding to standing wave phonons across the multilayer. The strength of this effect is strongly dependent on temperature—approximately a factor of 4 larger at 10 K compared to room temperature (see figure). Lastly, we demonstrate that the damping enhancement coincides with a shift in the ferromagnetic resonance field, and further that it is a complementary effect that can be predicted from the resonant damping enhancements. We emphasize that $[Co/Pd]_n$ multilayers are an ideal platform for studying this effect due to their large magnetostriction and perpendicular anisotropy. Importantly, the PMA does not show significant dependence on multilayer thickness, so devices can be engineered that have phonon pumping resonances at zero applied field. This work was supported by SMART, a center funded by nCORE, a Semiconductor Research Corporation program sponsored by NIST.

[1] S. Streib, H. Keshtgar, and G. E. W. Bauer, Damping of Magnetization Dynamics by Phonon Pumping, Phys. Rev. Lett. 121, p.027202 (2018). [2] K. An, A. N. Litvinenko, R. Kohno, A. A. Fuad, V. V. Naletov, L. Vila, U. Ebels, G. de Loubens, H. Hurdequint, N. Beaulieu, J. Ben Youssef, N. Vukadinovic, G. E. W. Bauer, A. N. Slavin, V. S. Tiberkevich, and O. Klein, Coherent long-range transfer of angular momentum between magnon Kittel modes by phonons, Phys. Rev. B 101, p.060407(R) (2020).

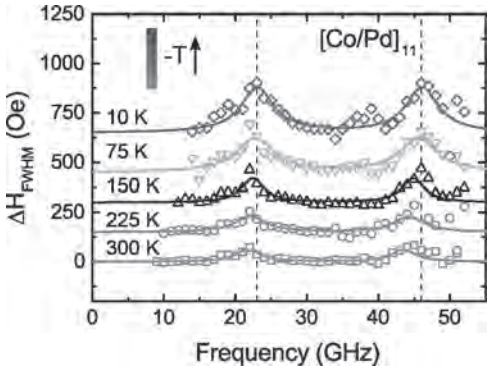

Ferromagnetic resonance linewidth enhancements due to phonon pumping at different temperatures for the $[Co/Pd]_{11}$ multilayer. Linewidth contributions from Gilbert damping and inhomogeneous broadening are excluded. Vertical dashed lines at 23 and 46 GHz show positions of phonon pumping resonances.

HOA-04. Intrinsic and Extrinsic Damping in Polycrystalline Fe Thin Films. *S. Wu*[1], D.A. Smith[1], P. Nakarmi[2], A. Rai[2], M. Clavel[3], M. Hudait[3], J. Zhao[4], F.M. Michel[4], T. Mewes[2] and S. Emori[1] *1. Physics, Virginia Tech, Blacksburg, VA, United States; 2. Physics and Astronomy, The University of Alabama, Tuscaloosa, AL, United States; 3. Electrical and Computer Engineering, Virginia Tech, Blacksburg, VA, United States; 4. Geosciences, Virginia Tech, Blacksburg, VA, United States*

Advancing the understanding of magnetic relaxation, often discussed in terms of "damping," is essential for energy-efficient spintronic memories, oscillators, and spin-wave circuits. BCC Fe is an elemental ferromagnet with attractive properties for these applications. Here, we examine magnetic relaxation – i.e., intrinsic and extrinsic damping – in two series of sputter-grown, polycrystalline Fe thin films with distinct structural properties: (1) strongly textured, smooth Fe films grown on Cu and (2) weakly textured, rough Fe films grown on Ag. Out-of-plane ferromagnetic resonance (FMR) measurements reveal intrinsic Gilbert damping parameters of ≈ 0.0024 for all Fe films thicker than 4 nm, regardless of their structural properties, as shown in Fig. 1. This damping parameter range is in quantitative agreement with that for epitaxial Fe [1]. The remarkable invariance with microstructure strongly suggests that intrinsic Gilbert damping is a local property, averaged over a short length scale of a few nm, with limited impact from grain boundaries and film roughness. The in-plane FMR linewidths of the Fe films exhibit pronounced nonlinear frequency dependencies, indicating the presence of strong extrinsic damping. Figure 2 shows the extrinsic linewidth obtained by subtracting the intrinsic Gilbert contribution ΔH_G (isotropic for Fe [1,2]) from the total in-plane linewidth ΔH_{IP}. To fit our experimental data, we have used a grain-to-grain two-magnon scattering model [3-5] with two types of correlation functions proposed for modeling self-affine and mounded surfaces [6], which capture inhomogeneities in the film. However, neither of the two correlation functions is able to reproduce the data quantitatively. Our finding points to the need to further examine the fundamental impact of film microstructure on extrinsic damping.

[1] B. Khodadadi et al., Phys. Rev. Lett. 124, 157201 (2020) [2] K. Gilmore and M. D. Stiles, Phys. Rev. B, 81, 174414 (2010) [3] R. McMichael et al., IEEE Trans. Mag., 40, 2 (2004) [4] S. Kalarickal et al., Phys. Rev. B, 77, 054427 (2008) [5] W. Peria et al., Phys. Rev. B, 101, 134430 (2020) [6] M. Pelliccione et al., "Evolution of thin film morphology." Springer Series in Materials Science. Vol. 108. Springer-Verlag Berlin, (2008)

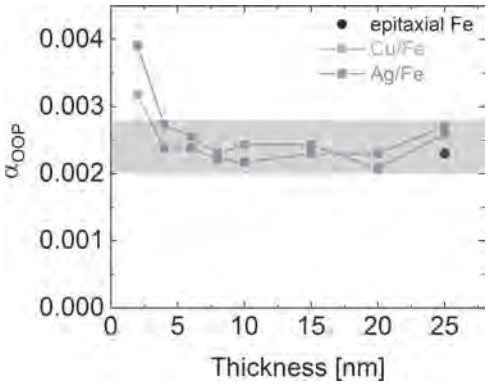

Fig. 1. Out-of-plane Gilbert damping α_{OOP} as a function of film thickness.

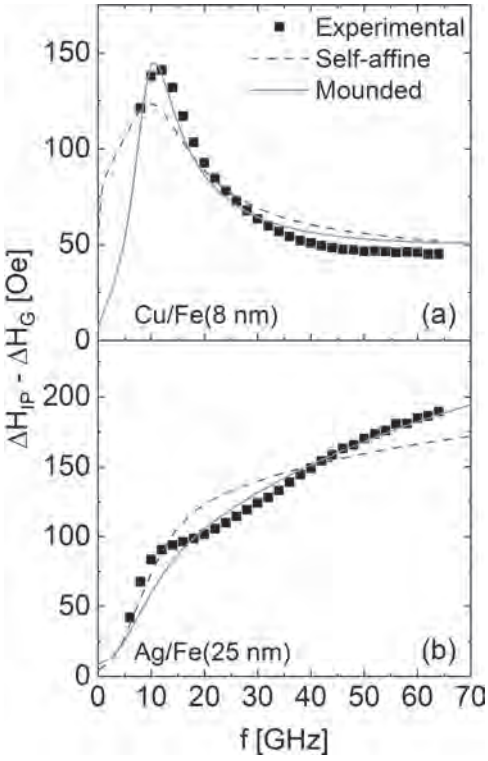

Fig. 2. In-plane extrinsic FMR linewidth vs frequency for (a) Cu/Fe (8 nm) film and (b) Ag/Fe (25 nm) film. Black squares represent experimental linewidth data. Dashed blue and solid red curves represent the fitted curves using correlation functions proposed for modeling self-affine and mounded surfaces, respectively.

HOA-05. The role of proximity induced magnetism on spin transport in multilayered systems. *C. Swindells*[1,2], H. Glowinski[3], Y. Choi[4], D. Haskel[4], P. Michalowski[5], T. Hase[6], P. Kuswik[3] and D. Atkinson[2]
1. Department of Materials Science and Engineering, University of Sheffield, Sheffield, United Kingdom; 2. Department of Physics, Durham University, Durham, United Kingdom; 3. Institute of Molecular Physics, Poznan, Poland; 4. Advanced Photon Source, Argonne National Laboratory, Argonne, IL, United States; 5. Lukasiewicz Research Network, Institute of Microelectronics and Photonics, Warsaw, Poland; 6. Department of Physics, University of Warwick, Coventry, United Kingdom

Spin transport across interfaces is fundamental to many spintronic devices. To fully exploit interfacial phenomena, such as spin-orbit torques and spin-pumping, in ferromagnetic (FM) and heavy metal systems (HM) the properties of both the HM layer and the interface must be considered, particularly in the case of perpendicularly magnetised systems [1]. Previously we showed the evolution of spin transport as a function of FM and HM thicknesses [2] and the role of insulating layers [3]. Debates remains regarding the physical basis of interfacial spin transport and the role of proximity polarisation of the HM layer [4]. A notional 'spin memory loss' term is often used to represent an interfacial contribution, while for Pt in particular, a magnetic polarisation arises in proximity (PIM) to a ferromagnetic material, opens a question about the role that PIM has upon interfacial spin phenomena, with contradictory reports that it has either a profound effect [5] or no effect [6] on spin transport. Here we present the results of a detailed systematic spin transport and PIM study in the same FM/HM samples. Structures with either a constant Pt thickness and a spacer layer thickness wedge, or a constant spacer layer and a Pt wedge were deposited. A combination of dynamic and static magnetic measurements, along with element specific resonant x-ray measurements at the APS, Argonne Lab, were used to address both the interfacial scattering contribution and the role of PIM in Pt on spin transport and to determine their relative contributions. Figs. 1 and 2 show damping and PIM data, with a persisting Pt moment with a 3nm Au layer, and a clear trend observed between the PIM and dynamic behaviour. These results highlight the role of the d-d orbital hybridisation and the induced moment for efficient interfacial transport, which is key for many spintronic applications.

[1] P. Kuswik, H. Glowinski et al., J. Phys.: Condens. Matter 29 (2017) [2] C. Swindells, A. Hindmarch, A. Gallant and D. Atkinson, Phys. Rev. B, 99, 064406 (2019) [3] C. Swindells, A. Hindmarch, A. Gallant and D. Atkinson, Appl. Phys. Lett. 116 (2020) [4] R. Rowan-Robinson et al., Sci. Rep. 7 16835 (2017) [5] M. Caminale, et al., Phys. Rev. B, 94 014414 (2016) [6] L. J. Zhu, D. C. Ralph, and R. A. Buhrman, Phys. Rev. B, 98, 164406 (2018)

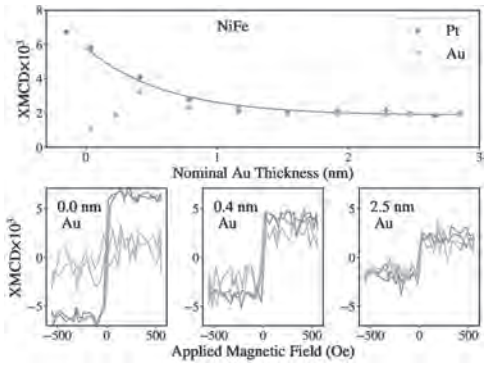

Fig 1: Measured XMCD as a function of Au spacer thickness at both the Pt (blue) and Au (orange) L3 edges for NiFe (7 nm)/ Au / Pt (4 nm)

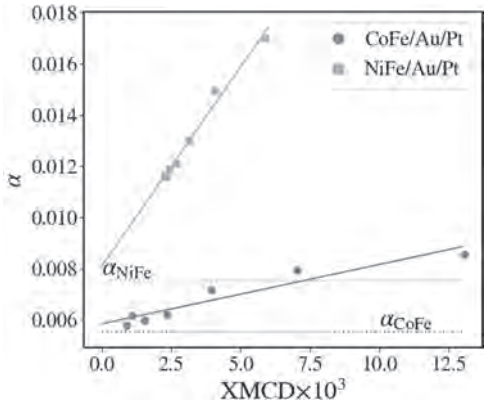

Fig 2: Damping and Pt XMCD for CoFe/Au/Pt and NiFe/Au/Pt. Dotted lines indicate bulk damping contributions.

HOA-06. Ultrathin ferrimagnetic GdFeCo films with very low damping. *L. Bainsla*[1], A.A. Awad[1], M. Zahedinejad[1], A. Kumar[1], N. Behera[1], H. Fulara[1], R. Khymyn[1], A. Houshang[1] and J. Åkerman[1]
1. Physics, University of Gothenburg, Gothenburg, Sweden

Spin-Hall nano oscillators (SHNOs) [1-4] have recently emerged as an alternative for microwave signal generation and bio-inspired oscillatory computing [3,4]. However, the ferromagnetic layer of the SHNO comes with drawbacks: (a) need for strong external magnetic fields, and (b) limited operational frequencies. As a solution, compensated ferrimagnets provide an alternative as they combine the ultrafast magnetization dynamics of antiferromagnets with a ferromagnet-like spin-orbit-torque (SOT) behavior. For use in SHNOs, it is however important to ensure that such films retain their ferrimagnetic behavior also in ultrathin films. In this work, ferrimagnetic $Gd_x(FeCo)_{1-x}$ thin films were grown using co-sputtering of Gd and $Fe_{87.5}Co_{12.5}$ on high resistance (HR) Si (100) substrates, and their magneto-dynamics was studied using ferromagnetic resonance measurements at room temperature. By tuning the stoichiometry of $Gd_x(FeCo)_{1-x}$ films, a nearly compensated behavior is for the first time demonstrated in 2nm thin film (Fig. 1). Values for the effective magnetization and effective Gilbert damping constant (α) of 0.02 Tesla and 0.0078±0.0002 are obtained for 2nm $Gd_{24.4}(FeCo)_{75.6}$ film, where α is comparable to the lowest value obtained in thick films [5]. The vertical red and yellow lines in Fig. 1(c) show literature values [5,6] for the spin angular momentum (x_a) and magnetic momentum (x_m) compensation points in thick films. The stoichiometry for the magnetic moment compensation in this work is very close to those [Fig. 1(c)]. In search of high-frequency auto-oscillations in SHNOs, constrictions with 50-300 nm widths were also prepared using $Gd_x(FeCo)_{1-x}$ (2-10nm)/Pt(5nm) based stacks and promising results using Brillouin Light Scattering show SOT controllable ferromagnetic modes in these devices.

[1]. L. Liu et al., Phys. Rev. Lett. 109, 186602 (2012). [2]. V. E. Demidov et al., Nat. Mater. 11, 1028 (2012). [3]. M. Zahedinejad et al., Nat. Nanotechnol. 15, 47–52 (2020). [4]. J. Grollier et al., Nat. Electron. 3, 360–370 (2020); M. Romera et al., *Nature* 563, 230–234 (2018). [5]. D.H. Kim et al., Phys. Rev. L 122, 127203 (2019). [6]. Y. Hirata et al., Phys. Rev. B 97, 220403 (R) (2018); D. Cespedes-Berrocal et al., Adv. Mat. 33, 2007047 (2021). [7]. C. Kittel, Phys. Rev. 73, 115 (1948). [8]. L. Bainsla et al., Phys. Rev. B 96, 094404 (2017).

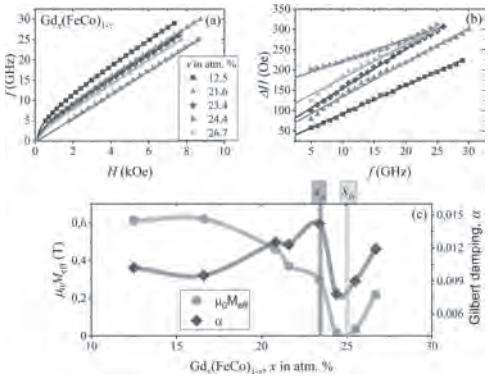

Fig. 1. (a) Frequency (*f*) vs. resonance field and (b) Resonance linewidth vs *f*, of 2 nm thick $Gd_x(FeCo)_{1-x}$ films, with *x* the Gd atomic %. (c) Effective magnetization and effective Gilbert damping constant *vs.* composition of 2 nm $Gd_x(FeCo)_{1-x}$ films; solid symbols represent values obtained by fitting the experimental data to the Kittel's equation [7] and equation (10) in reference [8], while solid lines are a guide to the eye.

HOA-07. Increase of Gilbert Damping in Permalloy Thin Films Due to Heat-Induced Structural Changes. *F. Schulz*[1], R. Lawitzki[2], H. Glowinski[3], F. Lisiecki[3], N. Träger[1], P. Kuswik[3], E. Goering[1], G. Schütz[1] and J. Gräfe[1] *1. Max Planck Institute for Intelligent Systems, Stuttgart, Germany; 2. Department of Materials Science, University of Stuttgart, Stuttgart, Germany; 3. Institute of Molecular Physics, Polish Academy of Sciences, Poznan, Poland*

Materials with low Gilbert damping are crucial for the realization of devices for spin-wave based computing[1,2]. It is necessary for spin-waves to be able to propagate through a material at length scales that are comparable to the device size in order to perform operations such as spin-wave interference[3]. One of the most common materials that is used in contemporary magnonics research is Permalloy (Py, $Ni_{80}Fe_{20}$), which can be deposited on different substrates using several different deposition techniques. This combination of low Gilbert damping and versatility renders Py a perfect candidate for spin-wave based computing. Many magnonic devices require high current densities for operation, which can exacerbate electromigration and cause local phase changes in the material due to Joule heating[4]. In order to investigate how high temperatures affect the magnonic properties of a Py based sample, high resolution transmission electron microscopy, together with energy dispersive x-ray spectroscopy have been deployed on Py thin film samples that have undergone annealing at different temperatures (Fig.1). This structural analysis has been combined with the determination of the Gilbert damping using ferromagnetic resonance measurements (Fig.2). It has been observed that the Gilbert damping parameter increases up to sixfold when the sample was annealed at 350°C, which could be linked to the diffusion of Ni atoms into the Si substrate and the formation of Nickel silicides. These results reveal an unfavourable effect of high temperatures on the magnonic properties of Py based samples and directly link structural changes to the change of the Gilbert damping parameter for the first time in these systems.

[1] S. Neusser and D. Grundler, Adv.Mater. Vol. 21, p. 2927–2932 (2009) [2] A. V. Chumak, V. I. Vasyuchka, A. A. Serga, and B. Hillebrands, Nat. Phys. Vol. 11, p.453–461 (2015) [3] F. Groß, M. Zelent et al., ACS Nano 14, 17184 (2020) [4] I. Zutic, J. Fabian, and S. D. Sarma, Rev. Mod. Phys. Vol. 76, p.323 (2004) [5] F. Schulz, R. Lawitzki et al., Journal of Applied Physics 129.15 (2021)

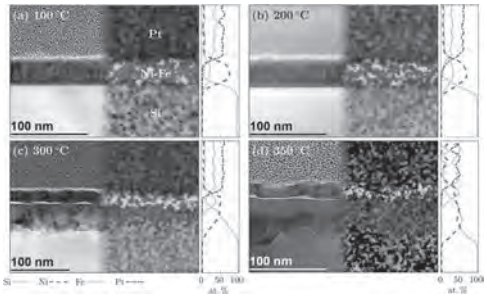

Fig.1: TEM bright field images together with the respective EDX image and the cross section of atomic composition as derived from EDX spectra for samples annealed for 60 min at (a) 100 °C, (b) 200 °C, (c) 300 °C, and (d) 350 °C [5]

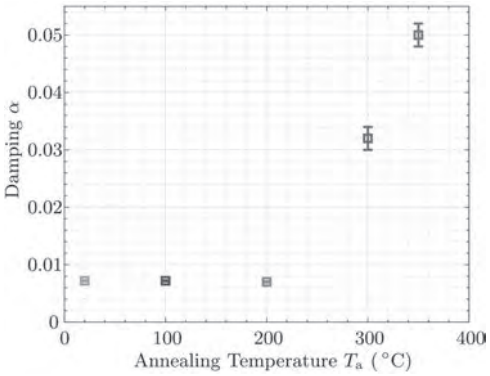

Fig.2: Gilbert damping coefficient α as a function of annealing temperature Ta [5]

HOA-08. New Techniques for Probing the Dynamic Properties of Magnetic Materials. *S.A. Ryan*[1], P.M. Tengdin[1], W. You[1], P. Johnsen[1], C. Gentry[1], A. Grafov[1], A. Blonsky[1], C. Chen[1], D. Zusin[1], X. Shi[1], M. Murnane[1] and H. Kapteyn[1] *1. Department of Physics and JILA, University of Colorado and NIST, Boulder, CO, United States*

We present an overview of new techniques that can probe the properties of magnetic materials on very short time scales. We present a pump-probe spectroscopy method utilizing tabletop extreme UV (EUV) light produced by high harmonic generation. This EUV source allows us to spectroscopically probe ferromagnetism with multi-element specificity and a time resolution on the order of a few-femtoseconds. This made it possible to uncover that surprisingly, it is possible to excite the spin system in pure ferromagnets and alloys on few-femtosecond time scales [1,2]. With the implementation of a flux monitoring reference arm, we are able to remove source instability and improve data quality while reducing acquisition times.

[1] P. Tengdin et al., Science Advances, vol. 4, no. 3, eaap9744, 2018. [2] P. Tengdin et al., Science Advances, vol. 6, no. 3, eaaz1100, 2020.

HOA-09. Low-Damping Vertically Graded Ferromagnetic Films. *R. Maizel*[1], Y. Lim[1], S. Wu[1], D.A. Smith[1], A. Gupta[1], J. Heremans[1] and S. Emori[1] *1. Physics, Virginia Polytechnic Institute and State University, Blacksburg, VA, United States*

Recent studies indicate that ~10-nm-thick ferromagnetic films with vertical compositional gradients can produce strong spin-orbit torques (SOT) [1-3]. Such relatively thick graded films are of technological interest since they are more thermally stable than ultrathin magnetic films in typical SOT devices. However, an important unanswered question is whether graded magnetic films can possess low damping, which is vital for minimizing the input power to drive precessional SOT devices. Here, we show that vertically graded ferromagnetic films exhibit low effective damping, comparable to homogeneous films of low-damping $Co_{25}Fe_{75}$ [4] and $Fe_{80}V_{20}$ [5]. Vertically graded films (thicknesses 5-40 nm) of polycrystalline $Co_{25}Fe_{75}$-$Fe_{80}V_{20}$, sandwiched between Ti/Cu seed and capping layers, were grown by continuously tuning the sputtering powers on $Co_{25}Fe_{75}$ and $Fe_{80}V_{20}$ targets. The effective magnetization differs by a factor of ≈1.7 between $Co_{25}Fe_{75}$ and $Fe_{80}V_{20}$ (Fig. 1), such that the graded films are expected to have highly inhomogeneous magnetic order. Nevertheless, the FMR linewidths of both graded $Co_{25}Fe_{75}$-$Fe_{80}V_{20}$ films are only <25% greater than those of homogeneous $Co_{25}Fe_{75}$ (Fig. 2). Evidently, the intentional inhomogeneity in the graded films does not lead to large linewidth broadening. From the linear fits shown in Fig. 2, we obtain a low effective Gilbert damping parameter of α_{eff} ≈0.003 for both graded $Co_{25}Fe_{75}$-$Fe_{80}V_{20}$ films. However, the data in Fig. 2 exhibit nonlinear behavior likely due to defect-induced two-magnon scattering. This observation suggests that effective damping (FMR linewidth) can be further reduced by optimizing the growth of these graded films. Our results demonstrate vertically graded ferromagnetic films as promising candidates for power-efficient SOT devices.

[1] Liu, L., Yu, J., Gonzalez-Hernandez, R., Phys Rev. B., Vol. 101, p. 220402 (2020) [2] Tang, M., Shen, K., Xu, S., Advanced Materials, Vol. 32, p. 2002607 (2020) [3] Zhu, L., Ralph, D. C., & Buhrman, R. A. Advanced Functional Materials p. 2103898 (2021) [4] Schoen, M. A. W., Thonig, D., Schneider, M. L., Nature Physics p. 839 (2016) [5] Smith, D. A., Rai, A., Lim, Y. Phys. Rev. Appl. Vol. 14, p. 034042 (2020)

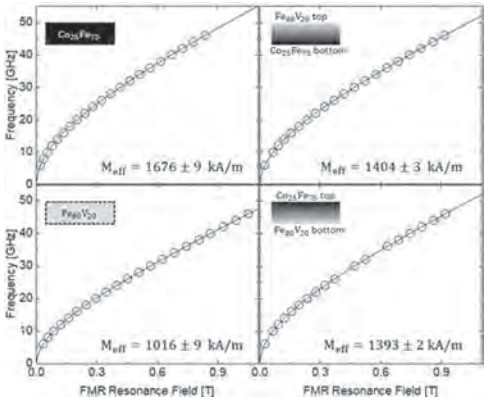

Fig. 1 Frequency vs resonance field for 10-nm-thick homogenous and graded $Co_{25}Fe_{75}$, $Fe_{80}V_{20}$ films. Solid line: Kittel fit

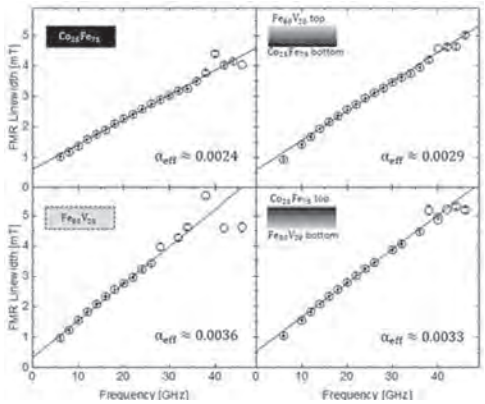

Fig. 2 HWHM Linewidth vs frequency for 10-nm-thick homogeneous and graded $Co_{25}Fe_{75}$, $Fe_{80}V_{20}$ films. Solid lines: linear fit for effective damping.

HOA-10. Dispersion Relation of Nutation Surface Spin Waves in Ferromagnets. *M. Cherkasskii*[1], M. Farle[1,2] and A. Semisalova[1] *1. Faculty of Physics, University of Duisburg-Essen, Duisburg, Germany; 2. Kirensky Institute of Physics, Federal Research Center KSC SB RAS, Krasnoyarsk, Russian Federation*

Recently, it has been theoretically and experimentally demonstrated that the effects of inertia of magnetization should be considered in the full description of spin dynamics at pico- and femtosecond timescales [1-8]. The nutation motion of magnetization is a manifestation of inertia of the magnetic moments. A rigorous derivation including inertia in the Landau-Lifshitz-Gilbert equation was carried out by Mondal et al. in the Dirac-Kohn-Sham framework [6,7]. Here, we show that inertia effect in magnetization dynamics results in a new type of spin waves, i.e. nutation surface spin waves, which propagate at terahertz frequencies in in-plane magnetized ferromagnetic thin films. Considering the magnetostatic limit, i.e. neglecting exchange coupling, we calculate dispersion relation.

In addition, we find that the nutation surface spin waves are backward spin waves [1]. The phase shift between precessing magnetic moments propagates as a spin wave through the ferromagnet because of dipole-dipole or exchange coupling (Fig. 1(a)). Magnetic inertia effects, which are expected to contribute to dynamics of spin waves, originate from spin-orbit coupling. We find that when taking inertia into account one finds that the deviation of alignment of localized moments will propagate through the spin system in the form of *both* precession and nutation motions, i.e. in ferromagnetic materials one needs to add to all "conventional" spin wave modes a high frequency wave-like motion with small amplitude caused by inertia. Moreover, a different type of waves having predominantly inertial nature appears in ferromagnetic thin films, which we call here *nutation surface spin waves*. Since these waves have terahertz frequencies (compared to typically GHz frequencies of other spin wave modes), they can be plotted as a small deviation on top of a "frozen" precession motion (Fig. 1(b)).

[1] M. Cherkasskii, M. Farle, and A. Semisalova, Phys. Rev. B 103, 174435 (2021). [2] M. Cherkasskii, M. Farle, and A. Semisalova, Phys. Rev. B 102, 184432 (2020). [3] M. Fähnle, D. Steiauf, and C. Illg, Phys. Rev. B 84, 172403 (2011). [4] M.-C. Ciornei, J. M. Rubí, and J.-E. Wegrowe, Phys. Rev. B 83, 020410 (2011). [5] E. Olive, Y. Lansac, M. Meyer, M. Hayoun, and J.-E. Wegrowe, J. Appl. Phys. 117, 213904 (2015). [6] R. Mondal, M. Berritta, and P. M. Oppeneer, J. Phys. Condens. Matter 30, 265801 (2018). [7] R. Mondal, M. Berritta, A. K. Nandy, and P. M. Oppeneer, Phys. Rev. B 96, 024425 (2017). [8] K. Neeraj, N. Awari, S. Kovalev, D. Polley, N. Zhou Hagström, S. S. P. K. Arekapudi, A. Semisalova, K. Lenz, B. Green, J. C. Deinert, I. Ilyakov, M. Chen, M. Bawatna, V. Scalera, M. D'Aquino, C. Serpico, O. Hellwig, J. E. Wegrowe, M. Gensch, and S. Bonetti, Nat. Phys. 17, 245 (2021).

Fig. 1. (a) The precession spin wave without inertia (red curve). The blue arrow indicates the motion of the magnetization M. (b) The nutation surface spin wave (purple curve) with a frequency considerably higher than in (a) plotted with small blue circles on top of the "frozen" precession motion.

HOA-11. Nonmonotonic temperature dependence of current-induced effective magnetic field exerted on domain wall in $SrRuO_3$. *M. Yamanouchi*[1], Y. Araki[2], T. Sakai[1], T. Uemura[1], H. Ohta[3] and J. Ieda[2] *1. Graduate School of Information Science and Technology, Hokkaido University, Sapporo, Japan; 2. Advanced Science Research Center, Japan Atomic Energy Agency, Tokai, Japan; 3. Research Institute for Electronic Science, Hokkaido University, Sapporo, Japan*

Current-induced domain wall (DW) motion is one of schemes for electrical manipulation of magnetization direction in spintronics devices. A ferromagnetic oxide $SrRuO_3$ (SRO) is attractive for finding out ways to realize energy efficient DW motion because current density required for the DW motion in SRO is 1-2 orders of magnitude lower than that in ferromagnetic metals [1]. Although we have shown that effective magnetic field H_{eff} exerted on the DW by current (I) could be achieved by assuming the largest nonadiabatic spin transfer torque around a ferromagnetic transition temperature T_C (~147 K) in SRO [2], further systematic studies are necessary to elucidate mechanisms behind the sizable enhancement because Weyl fermions are predicted to exert H_{eff} on the DW in ferromangnets with Weyl points such as SRO [3]. Here, we investigate H_{eff} in wide temperature range. A 21-nm thick SRO film was grown on a miscut (~2°) $SrTiO_3$ (001) substrate by pulsed laser deposition. The film was processed into Hall bar devices with a 2-mm wide channel, a pair of Hall probes, and a 2-mm wide Au/Cr line (Oersted line), which is orthognal to the SRO channel. After preparing a DW in the channel by applying a current pulse to the Oersted line, we measured transverse resistance R_{yx} reflecting perpendicular component of magnetization through the AHE with various Is while sweeping out-of-plane magnetic field H_z at various temperatures. The coercive field H_c for the DW motion varies almost linearly with respect to I, and the slope corresponds to the H_{eff} acting on the DW per I. The ratio of H_{eff} to current density derived from the slope shows nonmonotonic temperature dependence at low temperature and takes larger values around 120 K compared with that arising from conventional field-like spin-transfer torque and spin-orbit torque. Since nonmonotonic temperature dependence of the AHE in SRO is explained by the Berry curvature around Weyl Points [4], and large H_{eff} can be induced by Weyl fermions [3], Weyl fermions can play an important role in the DW motion in SRO. This work was supported in part by JSPS KAKENHI (20H02598, 20H02174, and 19H05622), the Center for Spintronics Research Network. Y.A. is supported by the LEADER.

[1] M. Feigenson *et al.*, Phys. Rev. Lett. 98, 247204 (2007). [2] M. Yamanouchi *et al.*, IEEE Trans. Magn. 55, 1400604 (2019). [3] Y. Araki and J. Ieda, Preprint at https://arxiv.org/abs/2105.14922 [cond-mat.] (2021). [4] Z. Fang *et al.* Science 302, 92 (2003).

HOA-12. Time-resolved Nonlinear Magnetization Dynamics in YIG Thin Films. *A.S. Hamill*[1], T. Qu[2], R. Victora[2] and P.A. Crowell[1] *1. Physics and Astronomy, University of Minnesota, Minneapolis, MN, United States; 2. Electrical and Computer Engineering, University of Minnesota, Minneapolis, MN, United States*

In magnetic thin films, large excitation amplitudes can lead to the onset of the first order Suhl instability, where the driven uniform mode undergoes three magnon scattering to two modes of half the frequency and equal and opposite wavevectors. Although experimental studies of the steady-state behavior are established, a comprehensive study of the nonequilibrium behavior over a large range of excitation powers is lacking. We have developed an experimental technique for sensitive detection of the time evolution of the FMR amplitude over five orders of magnitude in power, which provides a highly comprehensive understanding of the three-magnon scattering process. Applying this technique to patterned 3μm thick YIG thin films, we observe strong agreement with our results from micromagnetic simulations of the Suhl instability. We have developed a semianalytical model to explain the three magnon scattering process. This model shows quantitative agreement with experiment and simulation, including a predicted additional regime corresponding to power-dependent nonlinear oscillatory behavior on the order of 50 MHz. Additional observed effects will also be discussed. *This work was supported by SMART, a center funded by nCORE, a SRC program sponsored by NIST, DARPA under Grant W911NF-17-0100, MINT at Minnesota, and the NSF XSEDE through Allocation No. TG-ECS200001. We acknowledge the use of MSI resources.*

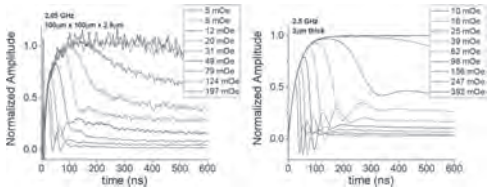

Fig. 1: Experimental and simulated data showing the time-resolved response χ" (normalized to the linear response value) over a wide range of microwave fields *h*. The simulation timescales and microwave fields were rescaled through the phenomenological damping constant $\eta_0=2\pi f\alpha_{Gil}$ to match the damping η_0 from experiment, since large damping was used in simulations to reduce runtime. The curves shown correspond to the same excitation amplitudes relative to the instability threshold in each case. As *h* is increased above the instability threshold, the standard instability is observed (red, blue curves). As *h* is further increased, a nonlinear oscillatory regime and other behavior appear.

HOA-13. Effect of surface treatment on damping constant in Ta-O/Co-Fe-B heterostructures. *T. Nguyen*[1,2], Y. Saito[2], S. Ikeda[1,2], T. Endoh[1,2] and Y. Endo[1,3] *1. Center for Science and Innovation in Spintronics, Tohoku University, Sendai, Japan; 2. Center for Innovative Integrated Electronic Systems, Tohoku University, Sendai, Japan; 3. Graduate School of Engineering, Tohoku University, Sendai, Japan*

Magnetization dynamics have been intensively studied in magnetic heterostructures for the development of spintronic devices such as MRAM and so on [1]. Among different magnetization dynamics parameters, the damping constant is important to understand the strength of the damping torque. A recent report on the magnetization reversal in oxide/ferromagnetic interfaces revealed a high efficiency by tuning the surface oxidization [2]. However, a detail investigation of damping constant is still unclear. Herein we use a broadband ferromagnetic resonance (FMR) measurement with an external magnetic field applied in the film plane and film normal plane to investigate both of in-plane (α_{IP}) and out-of-plane (α_{OP}) damping constants for Ta-O/Co-Fe-B heterostructures, and discuss the influence of oxygen content on $\alpha_{IP,OP}$ in detail. Ta-O (1 nm)/Co-Fe-B (1.2 nm)/MgO (1.3 nm)/Ta (1nm) heterostructures were fabricated on thermally oxidized Si substrates by RF sputtering. Ta-O layer was formed by a surface treatment process for a Ta layer at different oxygen pressure (P_{Oxygen}). Figure 1 (a) shows the P_{Oxygen} dependence of $4\pi M_{s,eff}$. $4\pi M_{s,eff}$ for surface treated samples are higher than that of the non-treated sample (P_{Oxygen}=0). The increase of $4\pi M_{s,eff}$ could be explained by the change in the interfacial anisotropy [3]. Fig. 1 (b) shows the P_{Oxygen} dependence of $\alpha_{IP,OP}$. Both α_{IP} and α_{OP} decrease when P_{Oxygen} increases to 0.03 Pa, and keep almost constant as P_{Oxygen} increases from 0.03 Pa to 0.3 Pa. The decrease of α_{OP} would be attributed to the spin pumping, and/or the magnetic inhomogeneity [4,5], while other contribution such as the two-magnon scattering should be included for a_{IP}. In addition, α_{OP} is smaller than α_{IP}, especially, α_{OP} for surface treated samples (~0.004) are close to the bulk value, indicating the main existence of intrinsic damping in the samples. These results suggest the important role of surface treatment in controlling the damping constant in Ta-O/Co-Fe-B systems. The authors acknowledge Core Research Cluster program, CIES Consortium; JSPS KAKENHI Grants JP19K23583, JP19H00844, JP21K14522; Cooperative Research Project from CSIS, and CSRN, Tohoku Univ. We thank Prof. S. Fukami for his helpful discussion.

[1] H. Honjo et al., IEDM Tech. Dig. 28.5 (2019). [2] H. An et al., Nat. Commun. 7, 13069 (2016). [3] I. Neudecker et al., Jour. Magn. Magn. Mat. 307, 148 (2006). [4] Y. Tserkovnyak et al., Phys. Rev. Lett. 88, 117601 (2002). [5] Y. Endo et al., Jour. Magn. Magn. Mat. 478, 165323 (2019).

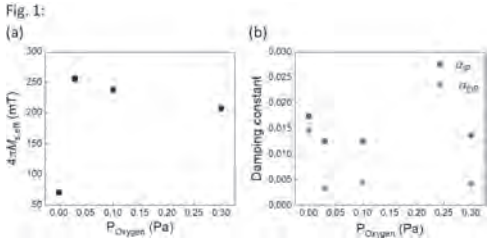

HOA-14. Dynamic instabilitiy in high power FMR of BiYIG nanodisks. *I. Ngouagnia Yemeli*[1], D. Gouéré[2], H. Merbouche[3], T. Srivastava[1], H. Hurdequint[1], V. Cros[2], M. Muñoz[4], S. Sangiao[5], J. de Teresa[5], O. Klein[6], A. Anane[2] and G. de Loubens[1] *1. Université Paris-Saclay, CEA, CNRS, SPEC, Gif-Sur-Yvette, France; 2. Unite Mixte de Physique CNRS/Thales, Palaiseau, France; 3. Institut für Angewandte Physik, University of Münster, Münster, Germany; 4. Instituto de Micro y Nanotecnología (CNM-CSIC), Madrid, Spain; 5. Departamento de Física de la Materia Condensada, Universidad de Zaragoza, Zaragoza, Spain; 6. Université Grenoble Alpes, CEA, CNRS, Spintec, Grenoble, France*

One current goal of spintronics is the development of sustainable information technology based on pure spin currents. One promising way to do this is to use spin waves (SWs) in low damping insulating ferrimagnets like yttrium iron garnet (YIG) where relaxation can be controlled by spin orbit torque (SOT) at a heavy metal interface [1]. However, such metal/insulator hybrid devices exhibit saturation of SW amplification due to nonlinear coupling between modes [2]. Two strategies can be considered to overcome these issues. i) Nanopatterning leads to quantization of SW modes [3], thereby limiting the available nonlinear processes [4]. ii) Tuning the perpendicular magnetic anisotropy (PMA) can be used to control the sign of the nonlinear frequency shift [5]. Recently, the growth of ultra-thin films of bismuth doped YIG (BiYIG) with tunable PMA has been achieved [6], resulting in greatly improved characteristics of SOT emitted SWs [7]. Here, we study the magnetization dynamics in individual nanodisks patterned from such a 30 nm thick BiYIG film with submicron diameters. The static magnetic field is perpendicular to the plane. The in-plane microwave field is produced by an integrated antenna. To detect the FMR, we employ a magnetic resonance force microscope [8]. For the largest disks, the amplitude of the FMR peak quickly saturates as the excitation power is increased, which is accompanied by a strong distortion of the absorption line, that broadens and splits into several peaks (Fig1a). Micromagnetic simulations accurately reproduce these features and reveal that a dynamic instability is responsible for the observed behavior. To experimentally probe this complex dynamics, we apply a second, much weaker excitation field of varying frequency, in addition to the main driving field at high power. The frequency modulation spectrum obtained (Fig1b) reflects the existence of rich low-frequency temporal variations in the magnetization dynamics.

[1] A. Hamadeh et al. Phys. Rev. Lett. 113, 197203 (2014) [2] M. Evelt et al. Appl. Phys. Lett. 108, 172406 (2016) [3] C. Hahn et al. Appl. Phys. Lett. 104, 152410 (2014) [4] Y. Li et al. Phys. Rev. X 9, 041036 (2019) [5] B. Lührmann et al. J. Magn. Magn. Mater. 96, 237 (1991) [6] L. Soumah et al. Nat. Commun. 9, 3355 (2018) [7] M. Evelt et al. Phys. Rev. Appl. 10, 041002 (2018) [8] O. Klein et al. Phys. Rev. B 78, 144410 (2008)

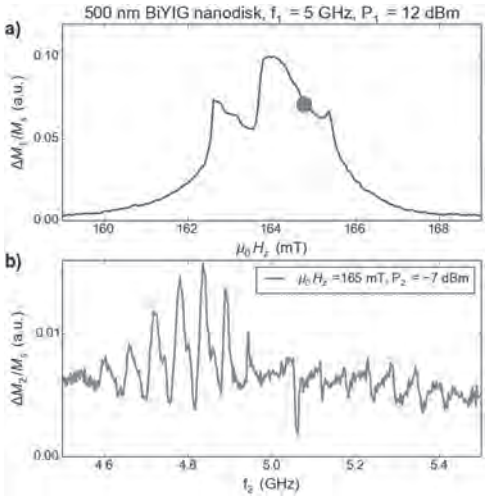

Fig 1. (a) Resonance line in the deeply nonlinear regime. (b) Two-tone spectroscopy performed inside the instability region, at $\mu_0 H_z$ = 165 mT.

HOA-15. High Order Gyromode Observation in Dome-like Nanoparticles. *A. Bondarenko*[1], S. Bunyaev[1], A. Shukla[2], A. Apolinario[1], D. Navas[1,4], N. Singh[3], A. Adeyeye[2,5] and G.N. Kakazei[1] *1. IFIMUP/ Department of Physics and Astronomy, University of Porto, Porto, Portugal; 2. Department of Electrical and Computer Engineering, National University of Singapore, Singapore; 3. Institute of Microelectronics, A*STAR, Singapore, Singapore; 4. Instituto de Ciencia de Materiales de Madrid, Madrid, Spain; 5. Department of Physics, Durham University, Durham, United Kingdom*

An interesting phenomenon occurs in submicron, magnetic vortex ground state particles as their thickness is increased, and the vortex becomes a fully-fledged three dimensional object. Although the ground state remains largely homogeneous through the thickness, one but needs to apply the smallest of excitation to see the emergent shearing of the magnetization texture and resonant modes associated with it [1,2]. Using the nanostencil fabrication technique[3] we obtained planar arrays of increasingly thick (up to 350 nm) magnetic particles, going beyond thicknesses studied previously. Not only do we observe the inversion of intensities of the modes, as high order modes become the most intense, we see also the complete disappearance of the homogeneous G_0 mode, which marks a transition where the 2D dynamic solutions completely cease their existence, see the spectrum presented on Fig. 1. This new effect also goes toward a significant increase of the speed of dynamics in the system. In the course of study we place a special emphasis on taking the real, dome-like particle profiles into account, which, as we show, influence the spectra for thick particles significantly. The profiles used were attained with a help of atomic force microscopy. The realistic boundaries primarily tune the non-radiative standing spin wave modes[4] which in turn affect gyrational modes through hybridization. We observe this through the detailed, microscopic study of mode distributions such as the one on Fig. 2, by matching experimental spectra, and juxtaposing stationary trajectories (in the time domain).

[1]J. Ding, G. N. Kakazei, X. Liu, K. Y. Guslienko, and A. O. Adeyeye, *Sci. Rep.*, Vol. 4, p. 4796(2014) [2]R. V. Verba, A. Hierro-Rodriguez, D. Navas, J. Ding, X. M. Liu, A. O. Adeyeye, K. Y. Guslienko, and G. N. Kakazei, *Phys. Rev. B*, Vol. 93, p. 214437(2016) [3]F. Yesilkoy, V. Flauraud, M. Rüegg, B. J. Kim, and J. Brugger, *Nanoscale*, Vol. 8, p. 4945-50(2016) [4] K. Schultheiss, R. Verba, F. Wehrmann, K. Wagner, L. Körber, T. Hula, T. Hache, A. Kákay, A. A. Awad, V. Tiberkevich, A. N. Slavin, J. Fassbender, and H. Schultheiss, *Phys. Rev. Lett.*, Vol. 122, p. 097202 (2019)

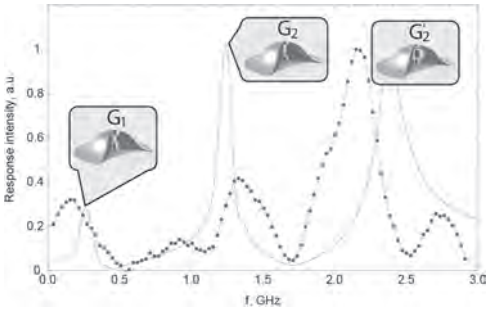

Fig. 1 Microwave absorption spectrum of the 200 nm high particle array (dark red marks and line), and a simulated response of an idealized infinite array of identical particles (solid black line). Peaks are annotated with renders of corresponding simulated resonant mode intensity cross-sections.

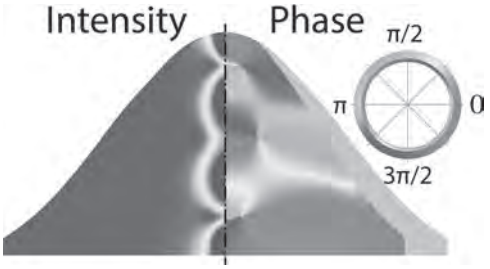

Fig. 2 Intensity and phase distributions of the dominant m_x+im_y contribution of the G_3 mode in a single 350 nm thick particle in the array. Legend on the right shows the connection between a plotted colour and the corresponding value of phase. A smaller inner circle is shifted by π to show out-of-phase colour pairs.

Session HOB
FEMTOSECOND EXCITATION OF MAGNETISM

Gregory Malinowski, Chair
Institut Jean Lamour, Université de Lorraine, Vandoeuvre-lès-Nancy, France

INVITED PAPER

HOB-01. Ultrafast Single Pulse All Optical Magnetization Switching of Ferromagnets. *Q. Remy*[1], J. Igarashi[1,2], S. Iihama[3,4], G. Malinowski[1], M. Hehn[1], J. Gorchon[1], J. Hohlfeld[1], S. Fukami[2,4], H. Ohno[2,4] and S. Mangin[1] *1. Institut Jean Lamour, UMR CNRS, Université de Lorraine, Nancy, France; 2. Laboratory for Nanoelectronics and Spintronics, Research Institute of Electrical Communication, Tohoku University, Sendai, Japan; 3. Frontier Research Institute for Interdisciplinary Sciences, Tohoku University, Sendai, Japan; 4. Center for Spintronics Research Network, Tohoku University, Sendai, Japan*

All Optical Helicity Independent Switching (AO-HIS) of magnetization, using single femtosecond laser pulses, has been demonstrated in GdFeCo ferrimagnetic alloys for various concentrations [1] as well as in other structures with antiferromagnetic coupling, Gd/Co, $[Tb/Co]_n$/Ta/CoFeB and Mn_2Ru_xGa [2,3,4]. Up to now, AO-HIS has never been observed for ferromagnetic layers. However, it was shown that a single pulse magnetization reversal of a ferromagnet could be observed in a spin-valve structure [5]. The switching is then achieved by the ultrashort spin current pulse generated from the ultrafast demagnetization of GdFeCo [5,6]. In this work, we study $Gd_x(FeCo)_{1-x}$/Cu/FM spin-valve structures, where FM can be different ferromagnetic layers [7] and the composition x of the GdFeCo alloy is also changed [8]. By increasing the Gadolinium concentration x, we aim at increasing the spin current injected in the copper layer [6]. We show that this can reduce the laser fluence threshold required to observe the FM magnetization reversal. In particular, no AO-HIS of the GdFeCo layer is required and the threshold fluence for the FM layer is around 1.6 mJ/cm^2 i.e. comparable to GdFeCo and Gd/Co multilayers [1,2] and smaller than what is achieved for Tb/Co/CoFeB [2] and Mn_2Ru_xGa [3]. We also show that by changing the Curie temperature, the laser pulse duration and the Cu/FM interface, one can control the interaction between the spin current and the FM layer and so the laser fluence threshold. Finally, we measured the dynamics of the reversal of the FM layer, which happens in around a picosecond. We show a model, based on a recent theory for the ultrafast magnetization dynamics of ferromagnets [9], that explains this behavior. We thus designed spin-valve structures that could provide technological advantages regarding both speed and energy efficiency of data storage.

[1] Y. Xu *et al.* Adv. Mater., Vol. 29, p.1703474 (2017) [2] M. L. M. Lalieu *et al.* Phys. Rev. B, Vol. 96, p.220411 (2017) [3] L. Avilés-Félix *et al.* Sci. Rep., Vol. 10, p.5211 (2020) [4] C. Banerjee *et al.* Nat. Commun., Vol. 11, p.4444 (2020) [5] S. Iihama *et al.* Adv. Mater., Vol. 30, p.1804004 (2018) [6] G. M. Choi and B. C. Min, Phys. Rev. B, Vol. 97, p.014410 (2018) [7] Q. Remy *et al.* Adv. Sci., Vol. 23, p.2001996 (2020) [8] J. Igarashi, Q. Remy *et al.* Nano Lett., Vol. 20, p.8654 (2020) [9] M. Beens, R. A. Duine and B. Koopmans, Phys. Rev. B, Vol. 102, p.054442 (2020)

CONTRIBUTED PAPERS

HOB-02. Sub-THz spin torque oscillation excited by inverse effective spin torque in ferrimagnetic material at angular momentum compensation composition. *Y. Kurokawa*[1], N. Hashimoto[1], C. Liu[1], T. Tanaka[1] and H. Yuasa[1] *1. Graduate School and Faculty of Information Science and Electrical Engineering, Kyushu University, Fukuoka, Japan*

Magnetization dynamics in transition metal-rare earth (TM-RE) ferrimagnetic metal with angular momentum compensation composition c_A has attracted much attention from the viewpoint of device application, as well as study on its physics because it realizes ultra-fast magnetization dynamics [1]. In this study, we investigate spin torque oscillation excited by spin transfer torque (STT) in the ferrimagnet by using a micromagnetic simulation with antiferromagnetically coupled TM and RE magnetizations [2]. Figure 1 shows the trilayer of ferrimagnet (FiM)/Non-magnet (NM)/ferromagnet (FM) used for the simulation. We assumed $Gd_c(FeCo)_{100-c}$ as the FiM layer and the perpendicular magnetic field H_z = 1.9 T and electric current J were applied to stabilizes an oscillation. Figure 2(a)-2(f) shows the normalized net magnetization of x component M_x/M_S as a function of time. We found that although the vector of STT is the same as that of net magnetization, the spin torque oscillation with frequency of 185 GHz in the FiM layer with c = 19 was excited, which is different from that with c = 15 and 25. The calculated c_A and magnetization compensation composition c_M are 18.8 and 20.3. Here, c = 19 is between the c_A and c_M. The effective gyromagnetic ratio γ_{eff} in the FiM is changed by the c and it becomes negative between c_A and c_M [2]. Because the effective STT is proportional to $1/\gamma_{eff}$, the inverse effective spin torque can be explained by the γ_{eff} inversion between c_A and c_M. These results are important for study on magnetization dynamics in the FiM because we revealed fascinating phenomenon on the spin torque oscillation near angular momentum compensation composition. Acknowledgments This work was financially supported by the MEXT KAKENHI Grant Number 21K14487.

[1] L. Caretta, M. Mann, F. Büttner et al., Nat. Nanotech. Vol.13, p.1154 (2018). [2] H. Oezelt, A. Kovacs, F. Reichel et al., J. Magn. Magn. Mater. Vol. 381, p. 28 (2015).

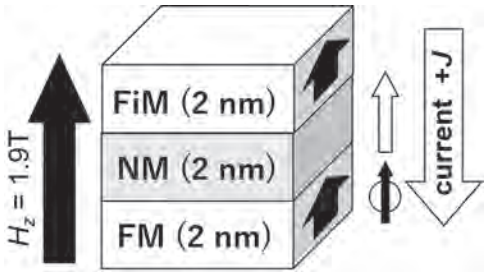

Figure 1. Schematic image of trilayer in the simulation.

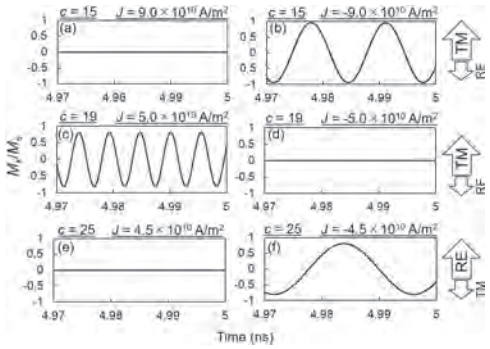

Figure 2. Normalized net magnetization of x component in FiM layer as a function of time.

HOB-03. Probing optically induced spin-currents using THz spin-waves in noncollinear magnetic bilayers. *T. Lichtenberg*[1], M. Beens[1], M.H. Jansen[1], R. Duine[1,2] and B. Koopmans[1] *1. Department of Applied Physics, Eindhoven University of Technology, Eindhoven, Netherlands; 2. Institute for Theoretical Physics, Utrecht University, Utrecht, Netherlands*

Femtosecond (fs) laser-pulse induced spin-currents have proven to be useful ingredients for future spintronics applications, allowing for sub-ps all-optical control of both the magnitude and direction of magnetization [1, 2, 3]. More recently, it was shown that such spin currents can be used to excite THz standing spin-waves (SSWs) [4, 5]. The basic principle of this phenomenon is sketched in the inset of Fig.1. An optically excited spin-current is injected into a noncollinearly magnetized absorption layer, inducing a spin-transfer torque (STT). The spin current is absorbed on a relatively short length scale (≈1 nm). This results in a depth dependence of the STT and thus the magnetization canting, leading to excitation of SSWs. Although spin currents have been studied extensively over the years, the generation mechanism is still heavily debated. In this work, we present a novel measurement technique, where we use spin-current induced THz spin-waves to study the spin current itself [6]. More specifically, we study the laser power dependence of the spin-wave phase to distinguish between two extreme cases: (1) ballistic hot-electron transport, where the temporal shape of the spin current is independent of laser power and (2) angular-moment conservation during demagnetization leading to spin transport. In this case, the demagnetization timescales and thus the temporal profile of the generated spin current is strongly laser-power dependent [7]. We show there is a strong laser pulse energy dependence of the spin wave phase (Fig.2), indicating that the second mechanism is dominant in our experiments. We corroborate these findings using a combination of theory and micromagnetic simulations. We demonstrate our technique is well suited to study optically induced spin-currents in the time domain. Moreover, it can easily be used to study spin current generation in more complex systems in future research.

[1] G. Malinowsk *et al.*, Nature Physics 4, 855 (2008) [2] A.J. Schellekens *et al.*, Nature Communications 5, 1 (2014) [3] G.M. Choi *et al.*, Nature Communications 5, 1 (2014) [4] M. Lalieu, P. Helgers and B. Koopmans, Physical Review B 96, 1 (2017) [5] I. Razdolski *et al.*, Nature communications 8, (2017) [6] Lichtenberg *et al.*, arXiv preprint arXiv:2103.06029 (2021) [7] K. Kuiper *et al.*, Applied Physics Letters 105, 202402 (2014)

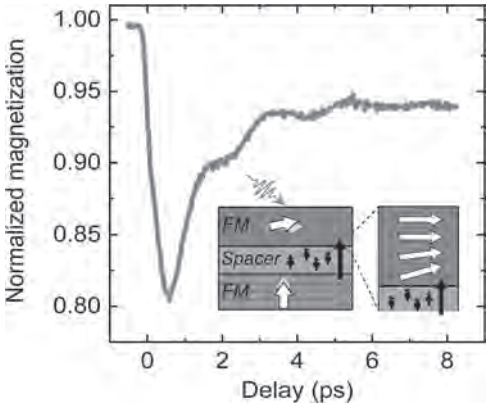

Fig. 1: Out-of-plane magnetization after fs laser-pulse excitation, showcasing the 1st order SSW.

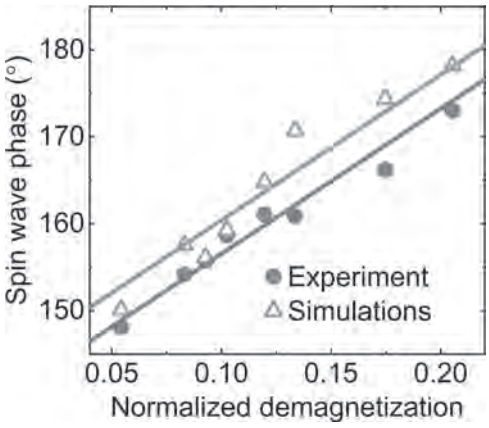

Fig. 2: SSW phase as a function of the normalized demagnetization of the spin-current generation layer –which depends linearly on the laser power– for both the experiment and micromagnetic simulations.

HOB-04. Enhancing All-Optical Magnetization Writing with Spin Currents. *Y. van Hees*[1], M. Peters[1], M. Beens[1], P. van de Meugheuvel[1], B. Koopmans[1] and R. Lavrijsen[1] *1. Applied Physics, Eindhoven University of Technology, Eindhoven, Netherlands*

In recent years, single pulse all-optical switching (AOS) of magnetization with ultrashort laser pulses has garnered much interest due to its potential for future data storage devices [1]. However, a drawback of this mechanism is the fact that the magnetization reverses with each laser pulse. For applications it is desirable to have a deterministic mechanism by which a specific final state can controllably be written. In this contribution, we provide such a mechanism by using spin currents that are optically generated in a ferromagnetic reference layer to influence AOS in an adjacent synthetic ferrimagnetic Co/Gd bilayer (Fig. 1). We find that the relative magnetization orientation of the reference layer and 'free' switching layer determines whether AOS occurs for a certain range of laser pulse energies [2]. Via straightforward engineering of the material stack, this energy gap can already be larger than 25% of the switching threshold energy. We show that this energy gap facilitates writing both states of the free layer deterministically, regardless of the initial state, by using either one or two laser pulses with the proper energies (Fig. 2). The non-local origin of the effect is confirmed by demonstrating the expected dependence on the reference layer composition, as well as a disappearance of the effect when inserting a spin sink between the reference and free layers. Using an s-d model that takes into account non-local transfer of angular momentum [3], we can qualitatively reproduce the behavior. Finally, time-resolved magneto-optical Kerr effect measurements are underway, showing an increased speed of the magnetization dynamics when assisted by

a spin current. These results both provide more insight into elusive optically generated spin currents, and serve as a stepping stone for implementation of AOS in ultrafast and energy efficient future information technologies.

[1] A. Kimel and M. Li, Nature Reviews Materials, 4.3 p189-200 (2019) [2] Y. van Hees et al., Nature Communications, 11, 3835 (2020) [3] M. Beens et al., Physical Review B, 102.5, 054442 (2020)

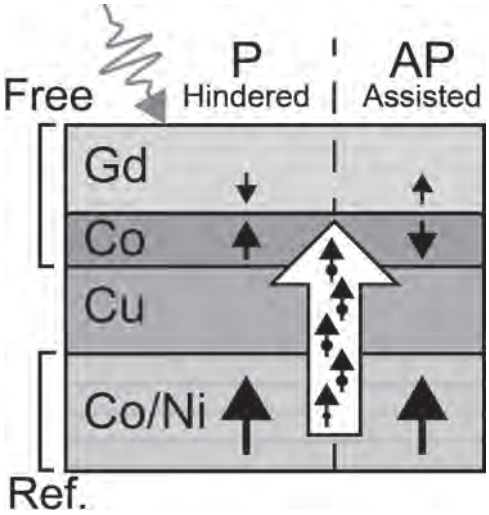

Fig. 1: Sketch of the system, AOS in the free layer is hindered in the parallel (P) and assisted in the anti-parallel (AP) configuration by the spin current from the reference layer.

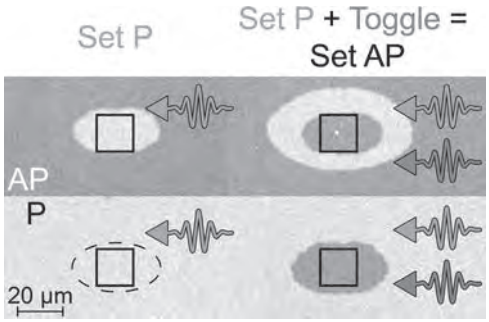

Fig. 2: Kerr microscopy image showing deterministic writing of both free layer states (in black squares) using one or two laser pulses.

HOB-05. Laser-Induced THz-Modes of Lattice Vibrations in Yig:Co Thin Films. *A.I. Frej*[1] and A. Stupakiewicz[1] *1. Physics, University of Bialystok, Bialystok, Poland*

The ferromagnetic garnets have a large scale of the functionality of optical and magnetic phenomena. Our studies respond to fundamental questions of spin-lattice interaction in garnets at sub-picosecond time scale under excitation by ultrashort laser pulses without external magnetic field. Recently, cobalt-doped yttrium iron garnet film (YIG:Co) appeared as a dissipation-free medium that allows for the fastest magnetic recording with the use of a single ultrafast laser pulse at a near-infrared spectral range [1,2]. Investigation of a range of few picoseconds after pumping the sample exposes additional oscillations that correspond to crystal lattice vibrations in a garnet [3]. Here, we demonstrate the excitation and detection of different phonon modes in YIG:Co films using time-resolved pump-probe method. The light pumping of the garnet was introduced in the form of linearly polarized pulses with a duration of about 50 fs. The pump wavelength was set to 1300 nm and the probe to 650 nm. Measurements were conducted in zero magnetic field and at room temperature. Investigation of dependence on the polarization of both pump and probe beams using selection rules [4] give information on the direction and efficiency of the lattice vibrations. At the initial timescale, up to few picoseconds, the optical phonon modes within range 3-11 THz were observed. After the pump pulse, we simultaneously observed the relaxation of different phonon modes and the excitation of a few GHz-frequency ferromagnetic resonance mode. This excitation is consistent with an optically induced magnetic anisotropy change in a garnet film. Our results show the near-infrared pulse-induced phenomena that are usually observed in the far-infrared range at the energy corresponding to the atomic interactions in condensed matter. Thanks to our method, we were able to determine the decay times for different oscillation frequencies. The obtained results indicate the possibility of finding new wavelengths with low photon energy, leading to the all-optical magnetization reversal.

[1] A. Stupakiewicz et al., Nature, Vol. 542, p.71 (2017). [2] A. Frej et al., Appl. Phys. Lett., Vol. 118, p.262401 (2021). [3] E. Cavalli et al., J. Phys.: Condens. Matter, Vol. 12, p.4665 (2000). [4] A. Stupakiewicz et al., Nat. Comm., Vol. 10, p.612 (2019).

HOB-06. Correlation between Femtosecond Laser Induced Spin Current and Spin Dynamics at the Single Layer Graphene/CoFeB Thin Films. *S. Panda*[1], S. Majumder[1], S. Choudhury[1], A. Bhattacharya[1], S. Sinha[1] and A. Barman[1] *1. Department of Condensed Matter Physics and Material Sciences, S. N. Bose National Centre for Basic Sciences, Kolkata, India*

Graphene/ferromagnet interfaces have exhibited various unusual spin-orbit coupling(SOC) related effects despite very small SOC strength of graphene[1-3]. Here we have investigated femtosecond laser induced spin dynamics using an all-optical time-resolved magneto-optical Kerr effect(TR-MOKE) magnetometry in sputter-deposited CoFeB thin films on chemical-vapor-deposition grown single-layer graphene(SLG) by varying the thickness of CoFeB from 1.5 to 6 nm[4]. The ultrafast demagnetization time(τ_m) extracted using three-temperature modelling(Fig. 1(a)) show a monotonic variation with CoFeB thickness(Fig. 1(b)). The Gilbert damping parameter(α) is directly extracted from the decaying amplitude of precessional oscillation(Fig. 1(c)). We have modelled the CoFeB-thickness-dependent α to estimate the effective spin-mixing conductance(G_{eff}) and two-magnon scattering coefficient(β_{TMS}) for SLG/CoFeB interface(Fig. 1(d)) which revealed spin pumping(SP) [4] as the dominant contributor to modulation of α(Fig. 1(e)). Furthermore, we have observed an inverse relationship between τ_m and α for SLG/CoFeB heterostructures(Fig. 1(f)) due to the dominance of SP-induced nonlocal spin-transport mechanism[4]. To disentangle other possible interface contributions to the damping such as spin memory loss(SML), we have inserted a 1-nm-thick Cu spacer layer between the SLG and CoFeB. Negligible damping modulation by the insertion of Cu spacer between SLG and CoFeB confirms that additional effects like SML are absent in our system. In summary, this study has provided a qualitative understanding of different ultrafast spin manipulation mechanisms in a graphene-based heterostructure, which can lead towards the next-generation graphene-based ultrafast spintronics devices. AB acknowledges the financial assistance from S. N. Bose National Centre for Basic Sciences(SNBNCBS), India under Project SNB/AB/11-12/96 and SNB/AB/18-19/211. SNP, SM, SC and ArB acknowledge SNBNCBS for respective fellowship.

[1] H. Yang, A. Duc Vu, A. Hallal et al., Nano Lett. 16, 145–151 (2016). [2] H. Yang, G Chen, A. A. C. Cotta et al., Nat. Mater. 17, 605 (2018). [3] A. K. Chaurasiya, A. Kumar, R. Gupta et al., Phys. Rev. B 99, 035402 (2019). [4] S. N. Panda, S. Majumder, S. Choudhury et al., Nanoscale doi: 10.1039/D1NR03397B (2021).

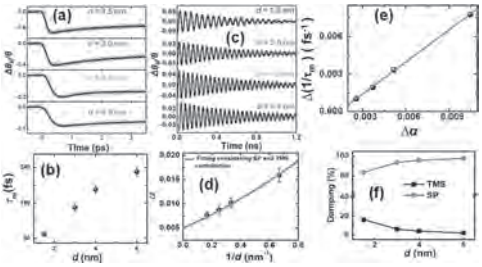

Fig. 1(a) Ultrafast demagnetization in SLG/CoFeB(*d*) (b) Evolution of τ_m with *d* (c) Precessional oscillations at *H*=3.59 kOe (d) Evolution of α fitted with a phenomenological model (e) Variation of $1/\tau_m$ as a function of α (f) Contributions of SP and TMS to α.

HOB-07. Laser-Induced Magnetization Precession in YIG/Metal Thin Film Heterostructures. *E. Schmoranzerová*[1], J. Kimák[1], Z. Soban[2], D. Kriegner[3,2], H. Reichlova[3,2], R. Schlitz[3], M. Munzenberg[5], G. Jakob[4], E. Guo[4], M. Kläui[4] and P. Nemec[1] *1. Faculty of Mathematics and Physics, Charles University, Prague, Czechia; 2. Institute of Physics, Czech Academy of Sciences, Prague, Czechia; 3. Technical University Dresden, Dresden, Germany; 4. Institute of Physics, Johannes Gutenberg University Mainz, Mainz, Germany; 5. Institute of Physics, University of Greifswald, Greifswald, Germany*

Ferrimagnetic insulator Yttrium-Iron Garnet (YIG) is one of the most frequently studied materials owing to its exceptional properties, such as low Gilbert damping and coercive field, which make it suitable for applications in spintronic [1] or magnonic devices [2]. Recently, yttrium garnets have shown their potential for all optical magnetization manipulation and switching [3]. In these systems, the response to laser excitation is usually dominated by inverse magneto-optical (MO) effects which require large energy (mJ) in the laser pulses. Another path to the laser-induced magnetization dynamics is opened by heat-induced modification of magnetic anisotropy. However, this mechanism, though universal across many semiconductor and metallic systems [4][5], is less common in insulating materials. In ferrimagnetic garnets it has so far been detected only in artificially engineered doped systems [6]. In this contribution we demonstrate a possibility to optically induce magnetization precession in epitaxial thin film of pure YIG only by heating of a metallic capping layer. We studied a 50 nm epitaxial YIG film, prepared by PLD on (111) gadolinium gallium garnet (GGG) substrate, parts of which were capped by 8nm metallic layers (Pt, Au). Laser-induced dynamics were detected using two-color pump&probe experiment, with pump wavelength of 800 nm (below bandgap of YIG) and probe wavelengths of 400 nm, maximizing the MO response. Typical time-resolved MO signals at low temperatures (20K) are shown in *Fig 1*. Oscillatory character of the curves is a clear signature of the laser-induced magnetization precession, which is triggered only in presence of the metallic capping. While the precession amplitude depends on the type of the capping layer, its frequency and damping does not, which indicates quasi-equilibrium nature of the magnetization dynamics. We attribute the origin of this effect to the ultrafast heat-induced modification of cubic magnetic anisotropy of the YIG crystal, which is a novel mechanism with possible applications for an efficient magnon generation.

[1]Y. Kajiwara et al.: *Nature* 464, 262-U141 (2010) [2]L. J. Cornelissen, J. Liu, R. A. Duine, J. Ben Youssef, and B. J. van Wees: *Nat. Phys.* 11, 1022 (2015) [3]A. Stupakiewicz, K. Szerenos, D. Afanasiev, A. Kirilyuk, A. V. Kimel: *Nature* 542, 7639 (2017). [4] M. van Kampen et al., Phys. Rev. Lett. 88, 227201 (2002). [5] N. Tesarova et al., Nature Photonics 7, 492-498 (2013) [6] L. A. Shelukhin, et al., Phys. Rev. B 97, 014422 (2018)

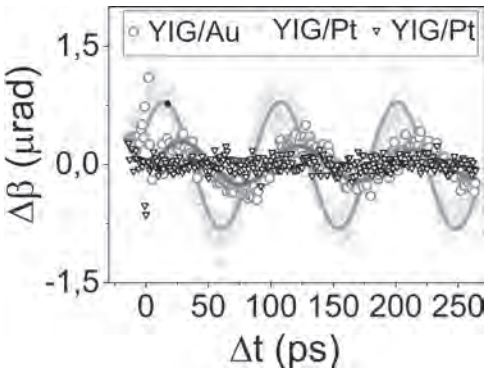

Fig.1: Time-resolved magneto-optical signal of YIG/metal and pure YIG thin films detected at temperature of 20 K and external magnetic field of 300 mT.

HOB-08. Imprinting chirality in collinear magnet with ultrafast laser. *S. Ghosh*[1,2], F. Freimuth[1,2], O. Gomonay[2], S. Blügel[1] and Y. Mokrousov[1,2] *1. PGI - 1, Forschungszentrum Jülich, Jülich, Germany; 2. Institute of Physics, Johannes Gutenberg University, Mainz, Germany*

Ultrafast generation of chiral magnetic order is one of the most sought-after technology for its potential application in next generation magnetic memory devices [1]. Recent experimental demonstration of generation of skyrmions with ultrafast laser pulses [2] has opened new horizons regarding the experimental feasibility of achieving this. In spite of such immense experimental achievement, the theoretical understanding of the underlying physics is still not very clear. Most of the existing studies tries to explain this with classical magnetisation dynamics only and thus completely miss the impact of the electronic interactions which plays crucial role in early sub-picosecond regime. More advanced TD-DFT based approaches are quite successful in explaining the fast dynamics in this regime, however, they are not quite fruitful in explaining the slow magnetisation dynamics which can last for several picoseconds. In this presentation we bridge this gap with the help of a quantum-classical hybrid approach which allows us to reveal the physics with a sub-femtosecond resolution and at the same time look at the steady state after several picoseconds [3]. We have successfully identified both the inherent and emergent interactions which drives the intertwined electronic and magnetic interaction leading to a stable chiral configuration and thus can predict their lifetime as well. We show here that the laser assisted dynamics is inherently different from the predictions of phenomenological two/three temperature model which has been widely used in modelling ultrafast demagnetisation. We show that the thermal re-population leads to formation of multiple domains with higher energy and less stability compared to smooth spiral formed by laser excitation. The final chiral configuration can be tuned both with laser and material parameters and formation can sustain at moderate temperature which makes our findings feasible for experimental realisation and thus would be instrumental in revealing the rich physics of ultrafast optical manipulation of the magnetisation.

[1] K. Gerlinger et al. Appl. Phys. Lett. 118, 192403 (2021). [2] F. Büttner, B. Pfau, M. Böttcher et al. Nat. Mater. 20, 30–37 (2021). [2] S. Ghosh, F. Freimuth, O. Gomonay, S. Blügel, Y. Mokrousov, arXiv:2011.01670.

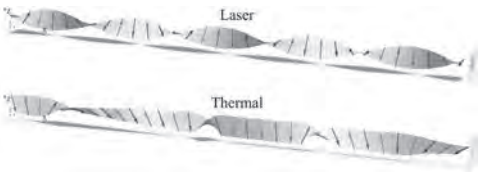

Comparison of magnetisation dynamics excited by laser and thermal repopulation. Thermal excitation forms multiple domain where laser forms a smooth spiral configuration.

HOB-09. Using Spin Waves to Probe Ultrafast Spin Current Generation in Rare Earth Ferromagnets. *Y. van Hees*[1], T. Lichtenberg[1], M. Beens[1], J. Levels[1], B. Koopmans[1] and R. Lavrijsen[1] *1. Applied Physics, Eindhoven University of Technology, Eindhoven, Netherlands*

All-optical switching (AOS) of ferrimagnetic rare earth-transition metal compounds with femtosecond laser pulses shows great promise for technological applications [1]. However, the possibly essential role of spin transport has scarcely been addressed. While it has been claimed that Gd can produce large spin currents [2], these are notoriously difficult to probe, impeding a full understanding of the physics at play. We demonstrate the use of spin waves to probe spin currents generated by ferromagnetic rare earth films. Upon fs laser pulse excitation, spin waves are excited in an in-plane Co layer via an out-of-plane spin current [3, 4] originating from a ferrimagnetic Co/Gd bilayer (Fig. 1). Here, Co stabilizes the antiparallel Gd magnetization, and provides a spin current to compare the effect of Gd to. For increasing Gd thickness, the spin current is expected to shift from Co- to Gd-dominated, reversing its polarization. Using time-resolved MOKE, we find that the homogeneous (FMR) mode experiences a phase rotation of nearly 180° over a small Gd thickness range (Fig. 2), which confirms a large contribution of Gd to the overall spin current. Qualitative modeling supports this interpretation, with efforts underway to better quantify the Gd contribution. Substituting Tb for Gd strongly decreases the amplitude of the FMR mode, implying weaker spin current generation. This might also partly explain the apparent difficulty in achieving AOS in Tb-containing systems. The same spin currents can excite THz frequency standing spin waves in the in-plane layer [5, 6], which appear to be strongly suppressed with increasing rare earth thickness. This is consistent with the relatively slow magnetization dynamics in these materials [7] leading to longer lasting spin currents, which excite high frequency modes less efficiently. This approach for probing optically generated spin currents can elucidate the processes at work in AOS, giving valuable insight for implementation in data storage devices of the future.

[1] A. Kimel and M. Li, Nature Reviews Materials, 4, p189-200 (2019) [2] S. Iihama et al., Advanced Materials, 30.51, 1804004 (2018) [3] A. Schellekens et al., Nature Communications, 5, 4333 (2014) [4] G-M. Choi et al., Nature Communications 5, 4334 (2014) [5] I. Razdolski et al., Nature Communications 8, 15007 (2016) [6] M. Lalieu et al., Physical Review B, 99.18, 184439 (2019) [7] B. Frietsch et al., Science Advances, 6.39, eabb1601 (2020)

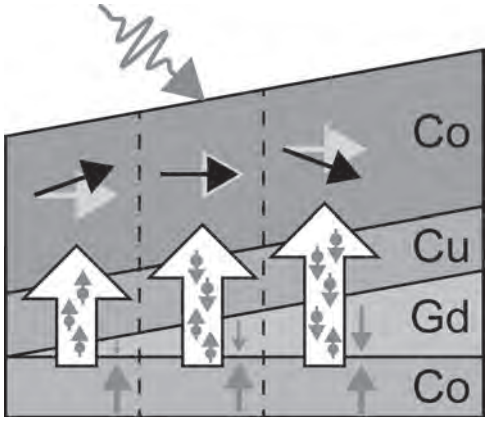

Fig. 1: Sketch of the system. Gray arrows indicate the magnetization state before fs laser excitation.

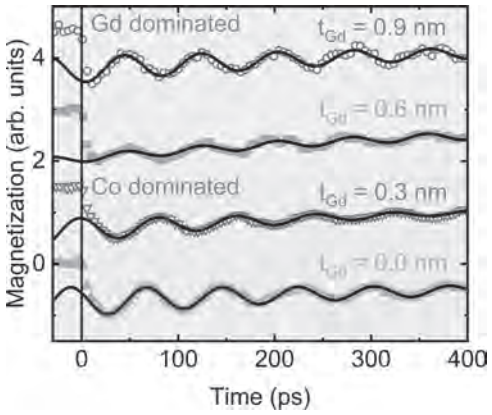

Fig. 2: Homogeneous spin waves in Co as excited by a Co/Gd bilayer (black lines are fits with a damped sine function).

HOB-10. RKKY exchange coupling mediated ultrafast all-optical switching of a ferromagnet. *D. Polley*[1,2], J. Chatterjee[1,4], A. Pattabi[1], H. Jang[1,3], S. Salahuddin[1] and J. Bokor[1,2] *1. EECS, University of California Berkeley, Berkeley, CA, United States; 2. Material Science Department, LBNL, Berkeley, CA, United States; 3. Material Science and Engineering, Seoul National University, Seoul, The Republic of Korea; 4. Fraunhofer Institute for Photonic Microsystems, Dresden, Germany*

The discovery of helicity-independent all-optical switching[1] as well as ps current-pulse driven magnetization reversal[2] of a ferrimagnetic GdFeCo led to a significant development towards ultrafast magnetization reversal of a magnetic tunnel junction (MTJ) based memory element. Ultrafast switching of Co/Pt multilayers coupled with a GdFeCo has been observed within ~ 7 ps which occurs due to RKKY exchange coupling[3]. However, GdFeCo isn't a desirable choice for a MTJ as it does not hold PMA for a patterned dot with a diameter less than a mm[4]. On the other hand, CoGd ferrimagnet can maintain its PMA down to 200 nm diameter[4]. In this work, we have experimentally observed the all-optical time-resolved magnetization dynamics of a "CoGd/Pt spacer (1 to 4 nm)/ [Co/Pt] multilayers" heterostructure. The magnetization of CoGd is reversed after 1.5 ps. The Co/Pt multilayer which has slightly higher demagnetization rate, stays demagnetized as the electron temperature reaches its Currie temperature before getting switched ~ 3 ps due to enough angular-momentum transfer from the CoGd sublattice as shown in Fig. 1(a). We rule out the possibility of Co/Pt swithcing triggered by non-local spin current generated from CoGd as Co/Pt switched for both ferromagnetic and anti-ferromagnetic coupling. We performed analytical calculation to simulate the time-resolved dynamics as shown in Fig. 1(b) using an extended microscopic three temperature model (M3TM) proposed by Beans et al.. Considering inter-sublattice, intra-sublattice and indirect RKKY exchange scatterings, we explain the magnetization reversal dynamics of different magnetic components of ferromagnetically and anti-ferromagnetically coupled as well as decoupled ferromagnet-ferrimagnet heterostructures. We demonstrate that irrespective of the nature of RKKY coupling, ultrafast switching of the Co/Pt multilayers can be achieved, and its switching time strongly depends on the RKKY interaction strength. This work experimentally as well as theoretically establishes the mechanism of all-optical switching in such magnetic heterostructures.

1. I. Radu, K. Vahaplar, C. Stamm, T. Kachel, N. Pontius, H.A. Dürr, T.A. Ostler, J. Barker, R.F.L. Evans, R.W. Chantrell, A. Tsukamoto, A. Itoh, A. Kirilyuk, T. Rasing, and A. V. Kimel, Nature 472, 205 (2011). 2. Y. Yang, R.B. Wilson, J. Gorchon, C.-H. Lambert, S. Salahuddin, and J. Bokor, Sci. Adv. 3, e1603117 (2017). 3. J. Gorchon, C.H. Lambert, Y. Yang, A. Pattabi, R.B. Wilson, S. Salahuddin, and J. Bokor, Appl. Phys. Lett. 111, 042401 (2017). 4. A. El-Ghazaly, B. Tran, A. Ceballos, C.-H. Lambert, A. Pattabi, S. Salahuddin, F. Hellman, and J. Bokor, Appl. Phys. Lett. 114, 232407 (2019). 5. M. Beens, M.L.M. Lalieu, A.J.M. Deenen, R.A. Duine, and B. Koopmans, Phys. Rev. B 100, 1 (2019).

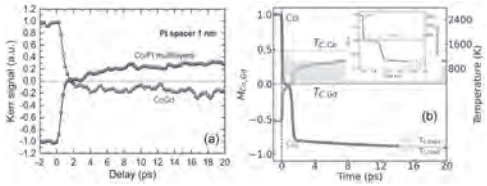

(a) Experimental and (b) theoretical time-resolved magnetization dynamics of a ferromagnetically ([Co/Pt]$_3$/Co/Pt 1 nm/CoGd/cap) coupled stacks.

HOB-11. Modeling ultrafast demagnetization and spin transport: the interplay of spin-polarized electrons and thermal magnons. *M. Beens*[1], R. Duine[2,1] and B. Koopmans[1] *1. Eindhoven University of Technology, Eindhoven, Netherlands; 2. Utrecht University, Utrecht, Netherlands*

Heating magnetic heterostructures with a femtosecond laser pulse generates spin currents on ultrashort time scales [1]. Their unique transient dynamics leads to exciting physics in magnetic multilayers and paves the way towards future spintronic applications. The microscopic origin of laser-induced spin dynamics is still heavily debated. Recent experimental [2] and theoretical [3] studies suggest the important role of electron-magnon scattering, which leads to demagnetization by the generation of thermal magnons, and acts as a source that drives spin transport [2,3,4]. In this work, we model spin transport in rapidly heated magnetic heterostructures, including transport by magnons. We assume that electron-magnon scattering is the driving force of the observed ultrafast spin dynamics and make use of a diffusive description of spin transport that treats itinerant electrons and magnons on an equal footing. We specifically address the relation between the interfacial spin current and the magnetization. In agreement with recent experiments [5,6], we find a direct proportionality between the injected spin current and the temporal derivative of the magnetization, as shown in Fig. 1. Based on an analytical calculation, we discuss that other behavior may arise if the spin current receiving material displays inefficient spin-flip scattering. Furthermore, we investigate the role of magnon transport, and show in what regime it plays a significant role. Fig. 2 shows the amplitude of the spin current as a function of the (dimensionless) bulk e-m scattering rate and the spin-mixing conductance. The latter parametrizes the efficiency of (interfacial) magnon transport. The figure implies that magnon transport cannot be neglected a priori. Whether it plays a significant role strongly depends on the material properties. We discuss the underlying physics for various system parameters and situations.

[1] G. Malinowski, F. Dalla Longa, J.H.H. Rietjens, P.V. Paluskar, R. Huijink, H.J.M. Swagten, and B. Koopmans, Nature Physics 4, 855, (2008) [2] G.-M. Choi, B.-C. Min, K.-J. Lee, and D.G. Cahill, Nature Communications 5, 4334 (2014) [3] E.G. Tveten, A. Brataas, and Y. Tserkovnyak, Physical Review B 92, 180412(R) (2015) [4] M. Beens, R.A. Duine, B. Koopmans, Physical Review B. 102, 054442 (2020) [5] S.M. Rouzegar, L. Brandt, L. Nádvornik, D.A. Reiss, A.L. Chekhov, O. Gueckstock, C. In, M. Wolf, T.S. Seifert, P.W. Brouwer, G. Woltersdorf, and T. Kampfrath, arXiv: 2103.11710 (2021) [6] T. Lichtenberg, M. Beens, M.H. Jansen, R.A. Duine, and B. Koopmans, arXiv: 2103.06029 (2021)

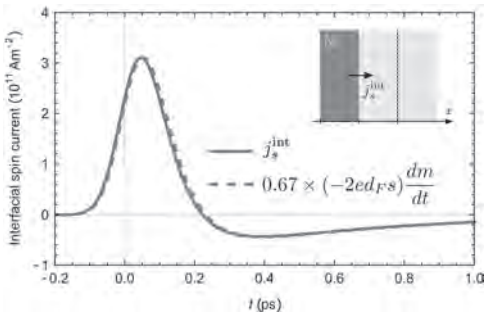

Fig. 1: Interfacial spin current (blue) and the (scaled) temporal derivative of the magnetization (dashed red) as a function of time after laser-pulse excitation.

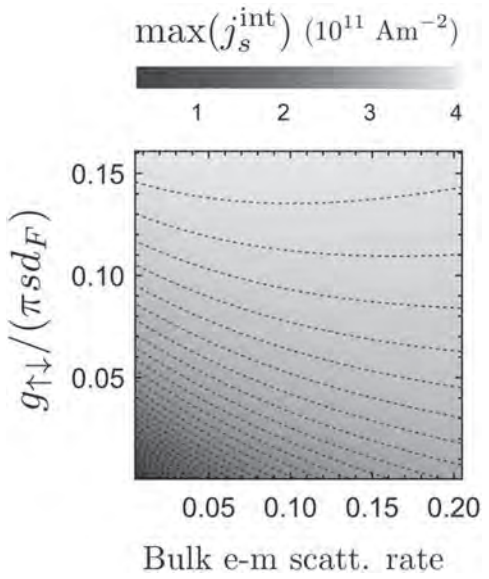

Fig. 2: Phase diagram of the amplitude of the interfacial spin current as a function of the bulk e-m scattering rate and the spin-mixing conductance.

HOB-12. Withdrawn

HOB-13. Ultrafast magnetization dynamics in half-metallic Co_2FeAl Heusler alloy. R. Malik[1], E. Delczeg-Czirjak[1], R. Knut[1], I. Vaskivskyi[1,2], D. Phuyal[1,3], S. Jana[1,4], R. Stefanuik[1], Y. Kvashnin[1], J. Soderstrom[1], D. Thonig[5], R. Gupta[1], A. Kumar[1], P. Svedlindh[1], O. Eriksson[1] and *O. Karis*[1] *1. Uppsala University, Uppsala, Sweden; 2. University of Ljubljana, Ljubljana, Slovenia; 3. KTH, Stockholm, Sweden; 4. Helmholtz-Berlin, Berlin, Germany; 5. Örebro University, Örebro, Sweden*

We report on optically induced, ultrafast magnetization dynamics in the Heusler alloy Co_2FeAl [1], probed by time-resolved magneto-optical Kerr effect. Experimental results are compared to results from electronic structure theory and atomistic spin-dynamics simulations. Heusler alloys offer the possibility to study magnetization dynamics, as a function of structural order, since they normally can be prepared to have a fully ordered $L2_1$ phase, a partially ordered B2 phase, and a completely disordered A2 phase. Experimentally, we find that the demagnetization time (τ_M) in films of Co_2FeAl is almost independent of varying structural order, and that it is similar to that in elemental 3d ferromagnets. In contrast, the slower process of magnetization recovery, specified by τ_R (see Fig. 1), is found to occur on picosecond time scales, and is demonstrated to correlate strongly with the Gilbert damping

parameter (α). This is shown in Fig. 2 where we show the theoretically calculated and FMR derived damping parameter for different B2 orderings on the left axis, and the inverse remagnetization time on the right axis. Our results show that Co_2FeAl is unique, in that it is the first material that clearly demonstrates the importance of the damping parameter in the remagnetization process. Based on these results we argue that for Co_2FeAl the remagnetization process is dominated by magnon dynamics, something which might have general applicability.

1. A. Kumar et al., Phys. Rev. B 96, 224425 (2017).

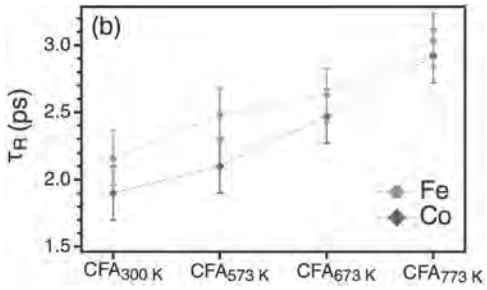

Fig. 1. Measured remagnetization times for the investigated Co_2FeAl alloys. The sample subscripts correspond to the sample growth temperature. Here, an increased temperature corresponds to increased B2 ordering.

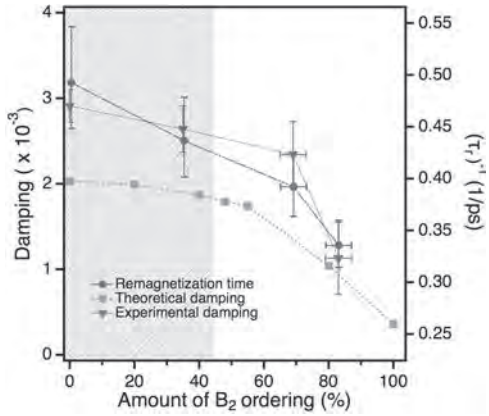

Fig. 2. The relationship of inverse of the measured remagnetization time (right y-axis) and theoretically calculated and experimentally measured Gilbert damping (left y-axis) in Co_2FeAl for varying amount of B2 order along the A2 → B2 path, i.e. 0 corresponds to pure A2 phase while 100 corresponds to pure B2 phase.

HOB-14. Tuneable Ni, Pt, Ir and Co Synthetic Ferrimagnets for All Optical Switching. *J.N. Scott*[1], M. Dabrowski[3], W. Hendren[1], C.M. Forbes[1], A. Frisk[2], D. Burn[2], D.G. Newman[3], P.S. Keatley[3], A.T. N'Diaye[4], T. Hesjedal[5], G. van der Laan[2], R.J. Hicken[3] and R. Bowman[1] *1. Queen's University Belfast, Belfast, United Kingdom; 2. Diamond Light Source, Didcot, United Kingdom; 3. University of Exeter, Exeter, United Kingdom; 4. Lawrence Berkeley National Laboratory, Berkeley, CA, United States; 5. University of Oxford, Oxford, United Kingdom*

Synthetic ferrimagnets (SFM) two ferromagnetic (FM) layers with different magnetic moments, exchange-coupled via the RKKY interaction across a non-magnetic spacer layer, are of particular interest as a feasible media for all optical magnetic switching (AOS). Design of the magnetic properties of these SFM structures requires knowledge and control of the magnetisation, M(T), and anisotropy, K(T), of each FM layer, and the strength of the exchange coupling between them, $J_{ij}(T)$. We have shown it is possible to engineer the magnetic properties of series of compensating Ni_3Pt/Ir/Co SFMs, fabricated by magnetron sputtering and exhibiting perpendicular magnetic anisotropy (PMA). The tuneability of this structure (through variation of the Ni_3Pt deposition temperature and the thickness of each layer) provides an ideal system with which to investigate the effect of M(T), K(T) and $J_{ij}(T)$ on reversal mechanisms within SFMs, with the added benefit of distinct magnetic species allowing element and layer specific characterisation. Initial pump/probe experiments reveal that it is possible to switch these SFMs by application of multiple laser pulses. However, single shot AOS requires stronger antiferromagnetic exchange coupling than can be achieved in Ni_3Pt/Ir/Co SFMs, as a result of the elevated deposition temperatures necessary for PMA in Ni_3Pt. A solution is to replace the Ni_3Pt layer with a Ni/Pt multilayer, in which PMA can be achieved by careful choice of layer thickness. This gives scope for improving the exchange coupling by removing the cooling step during deposition, maintaining element specificity and tuneability of the magnetic properties.

[1] S. Mangin et al. Nature Materials 13, 286 (2014) [2] R. F. L. Evans et al. Appl. Phys. Lett. 104, 082410 (2014)

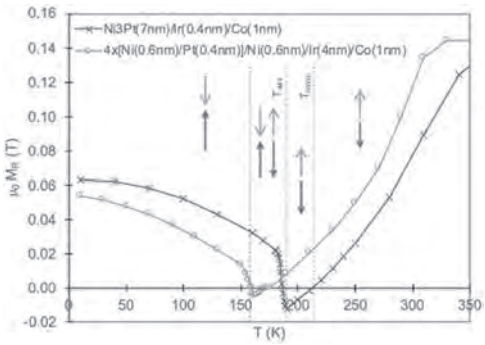

Remanent magnetisation (M_R) versus temperature of a Ni_3Pt based SFM with arrows denoting the layer alignment, Co (green) and Ni_3Pt (red, solid), with the positions of the magnetisation compensation point, T_{comp} and T_{-MR}, the onset temperature of negative M_R, marked. The multilayer sample shows the same temperature dependent behaviour

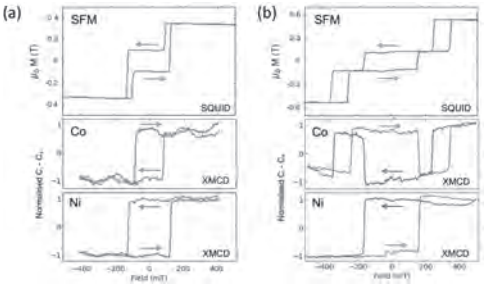

Squid (top) and element specific XMCD hysteresis loops measured at 100K (arrows depict the field sweep direction) of (a) Ta(5nm)/ Ni_3Pt(8.5nm)/Ir(0.5nm)/Co(1nm)/Ir(3nm) and (b) Pt(5nm)/4x-[Ni(0.6nm)/Pt(0.4)]/Ni(0.6nm)/Ir(0.4nm)/Co(0.9nm)/Ir(3nm) SFM

HOB-15. Single pulse all-optical magnetic switching in amorphous $DyCo_x$ and $TbCo_x$. *Z. Hu*[1], J. Besbas[1], R. Smith[1], N. Teichert[1], G. Atcheson[1], P.S. Stamenov[1], K. Rode[1] and M. Coey[1] *1. CRANN, AMBER and School of Physics, Trinity College Dublin, Dublin, Ireland*

Single pulse all-optical switching (SP-AOS) using 40 fs light pulses was discovered in films of the amorphous rare earth-transition metal (RE-TM) alloy a-$Gd(FeCo)_3$ [1]. The switching takes less than 5 ps and relies on the different demagnetisation times of the Gd and Fe,Co subnetworks. Replacing Gd by another RE was expected to yield more materials that exhibit ultrafast switching, but it did not happened. Indeed, amorphous RE-TM alloys other than $Gd(FeCo)_3$ have only been switched transiently by a single pulse [2] or slowly using many polarised pulses [3]. Here, we report stable SP-AOS

in amorphous Dy-Co and Tb-Co films with perpendicular anisotropy. Room-temperature coercivity is 30-50 mT, and compensation temperatures T_{comp} are below 300 K. The example of a-$DyCo_3$ is shown in Fig 1. The behavior is surprising. A single 200 fs pulse creates a non-uniform 40 μm dark spot on a uniformly-magnetized light film. Domain structure on a scale of ~ 3 μm is observed. After two pulses, the darker domains switch back, and the multidomain state will toggle for a few more pulses before leaving the sample in a nonuniform mid-gray state. Images are obtained on a strip of material irradiated with 1-5 pulses, using an off-site Kerr microscope. Other samples show a variety of behavior. The switching of a-$TbCo_4$ shown in Fig. 2 is also granular, but the lighter and darker spots are aggregated into lighter and darker rings with unequal numbers of small dark and light domains. The contrast between rings again disappears after a few pulses, but the small domains persist. This is quite unlike the uniform toggling of large domains, comparable in size to the laser spot, that are seen in SP-AOS of ferrimagnetic a-$Gd(FeCo)_3$ and crystalline Mn_2Ru_xGa. The key difference is probably the random uniaxial anisotropy for the non S-state rare ions and temperature-dependence, which governs that of the coercivity. The influence of stray dipolar fields on a μm scale and possible of radial heat waves in the substrate will be considered in the context of ultra-fast SP-AOS in these a-RE-TM materials.

[1] C. D. Stanciu, F. Hansteen, A. V. Kimel, A. Kirilyuk, A. Tsukamoto, A. Itoh, and Th. Rasing Phys. Rev. Lett. 99, 047601 (2007). [2] S. Alebrand, U. Bierbrauer, M. Hehn, M. Gottwald, O. Schmitt, D. Steil, E. E. Fullerton, S. Mangin, M. Cinchetti, and M. Aeschlimann. Phys. Rev. B 89, 144404 (2014). [3] S. Mangin, M. Gottwald, C-H. Lambert, D. Steil, V. Uhlir, L. Pang, M. Hehn, S. Alebrand, M. Cinchetti, G. Malinowski, Y. Fainman, M. Aeschlimann and E. E. Fullerton Nat. Materials 13, 286–292 (2014).

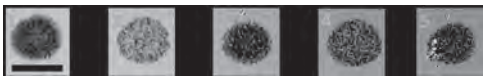

SP-AOS in a 10 nm a-$DyCo_3$ alloy film with perpendicular magnetization. Scale bar 40 μm.

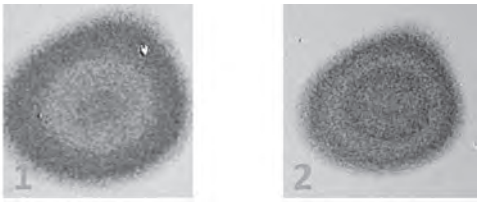

SP-AOS in 20 nm a-$TbCo_4$ with perpendicular magnetic anisotropy.

Session HOC
APPLICATIONS OF MAGNETIZATION DYNAMICS

Kornel Richter, Chair
University P.J. Safarik, Košice, Slovakia

CONTRIBUTED PAPERS

HOC-01. Controlling Magnon Interaction by a Nanoscale Switch.
A. Etesamirad[1], R. Rodriguez[1], J. Bocanegra[1], R. Verba[2], J. Katine[3], I. Krivorotov[4], V. Tyberkevych[5], B. Ivanov[2] and I. Barsukov[1] *1. Physics and Astronomy, University of California, Riverside, Riverside, CA, United States; 2. Institute of Magnetism, Kyiv, Ukraine; 3. Western Digital, San Jose, CA, United States; 4. Physics and Astronomy, University of California, Irvine, Irvine, CA, United States; 5. Department of Physics, Oakland University, Rochester, MI, United States*

The ability to control and tune magnetic dissipation is a key concept of emergent spintronic technologies. Magnon-magnon processes constitute a major dissipation channel in nanomagnets [1-3], redefine their response to spin-torques [4], and hold promise for manipulating magnetic states on the quantum level. Controlling these processes [5,6], while being imperative for many spintronic applications [4], has remained difficult to achieve. We identify two avenues to realize this goal: by breaking the symmetry of the static magnetic state or by breaking the symmetry of the magnon modes. Here we focus on the latter approach due its particular technological relevance. As a vehicle for our study, we employ magnetic tunnel junction nanopillars that consist of a free layer and a synthetic antiferromagnet (SAF) [7]. In the normal state of the SAF, its stray field is small at the position of the free layer – the fields from the two constituent layers of the SAF largely cancel out [8]. However, once we trigger SAF's spin-flop transition, their spins become canted and generate a stray field which is nonuniform at nanoscale – a prerequisite for breaking the symmetry of free layer's magnons. By controllably switching the SAF between its normal and spin-flop states, we achieve to toggle three-magnon processes in the free layer. We tune the magnon interaction by at least one order of magnitude and thus engineer two distinct dissipative states. Our results open up an avenue for manipulating magnon processes by external stimuli at nanoscale, tuning the nonlinear response in magnetic neuromorphic networks, and controlling large excitation regimes in spin-torque devices. They furthermore show promise for engineering coherent magnon coupling in hybrid quantum information systems. This work was supported by the National Science Foundation through Grant No. ECCS-1810541.

[1] H. Schultheiss, K. Vogt, B. Hillebrands, et al., Phy. Rev. B: Condens. Matter Mater. Phys., 86, 054414 (2012) [2] T. Hula, K. Schultheiss, A. Buzdakov, et al., Appl. Phys. Lett., 117, 042404 (2020) [3] A. Navabi, Y. Liu, P. Upadhyaya, et al., Phys. Rev. Appl., 11, 034046 (2019) [4] I. Barsukov, H. K. Lee, A. A. Jara, et al., Sci. Adv., 5, eaav6943 (2019) [5] L. Körber, K. Schultheiss, T. Hula, et al., Phys. Rev. Lett., 125, 207203 (2020) [6] M. Evelt, C. Safranski, M. Aldosary, et al., Sci. Rep., 8, 1269 (2018) [7] A. M. Gonçalves, F. Garcia, H. Lee, et al., Sci. Rep., 8, 1 (2018) [8] J. A. Katine, E. E. Fullerton, J. Magn. Magn. Mater., 320, 1217 (2008)

HOC-02. Enhancing domain wall motion with He^+ irradiation: the role of microscopic pinning parameters.
J.W. van der Jagt[1], M. Sall[1], N. Vernier[2], L. Herrera-Diez[2], M. Belmeguenai[3], Y. Roussigné[3], A. Thiaville[4], V. Jeudy[4], R. Juge[1] and D. Ravelosona[1,2] *1. Spin-Ion Technologies, Palaiseau, France; 2. Centre de Nanosciences et de Nanotechnologies, Palaiseau, France; 3. Laboratoire des Sciences des Procédés et des Matériaux, Villetaneuse, France; 4. Laboratoire de Physique des Solides, Orsay-Cedex, France*

Spintronic devices based on domain wall (DW) motion driven by spin-orbit torque (SOT) offer exciting perspectives for non-volatile memory and logic applications. One of the main issues to overcome is DW pinning at intrinsic material defects. Pinning leads to thermally activated creep and depinning regimes [1], reducing the efficiency of DW motion. W-CoFeB-MgO based structures are archetype materials for SOT-driven DW motion. To get high PMA, crystallization at $T > 350$°C is usually needed, which induces structural inhomogeneities. Here, we investigate DW motion in perpendicularly magnetized W-CoFeB-MgO films crystallized by either annealing at $T = 400$°C, or by He^+ irradiation at reduced temperatures [2]. As we have shown recently, He^+ irradiation is a powerful tool to engineer magnetic materials at the atomic scale [3-6]. Combining a variety of experimental techniques (VSM-SQUID, FMR, BLS, Kerr microscopy) and an analytical model [7] to analyze DW motion, our results reveal that the crystallization process can significantly alter the DW dynamics, even if the macroscopic micromagnetic parameters (K_{eff}, M_s, DMI) are similar. Fig. 1 shows that the DW velocity in the creep regime is significantly different between the two samples. Both the slope and velocity are changed, as well as the occurrence of excess velocity near the depinning field for the irradiated sample. Furthermore, Fig. 2 shows that the roughness of the DW differs significantly between the samples, with the irradiated sample exhibiting much smoother DWs, indicating a greater material homogeneity. The analytical model reveals that a reduction of the depinning temperature T_d and depinning correlation length ξ in the irradiated samples due to a lower defect distribution are the main driving forces behind the drastic change in DW motion. Our results indicate that controlling the crystallization process is a prerequisite for DW-based SOT devices.

[1] V. Jeudy, A. Mougin, S. Bustingorry et al., *Phys. Rev. Lett.*, Vol. 117, p.057201 (2016) [2] J.W. van der Jagt, M. Sall, N. Vernier et al., manuscript in preparation (2021) [3] J. Fassbender. D. Ravelosona and Y. Samson, *J. of Appl. Phys.*, Vol. 37, p.R179 (2004) [4] L. Herrera Diez, M. Voto, A. Casiraghi et al., *Phys. Rev. B*, Vol. 99, p.054431 (2019) [5] X. Zhao, B. Zhang, N. Vernier et al., *Appl. Phys. Lett.*, Vol. 115, p.122404 (2019) [6] T. Devolder, I. Barisic, S. Eimer et al., *J of Appl. Phys.*, Vol. 113, p.203912 (2013) [7] P. Géhanne, S. Rohart, A. Thiaville et al., *Phys. Rev. Res.*, Vol. 2, p.043134 (2020)

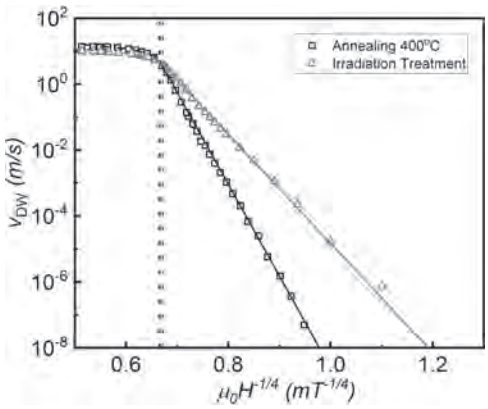

DW velocity in the creep regime for crystallized W-CoFeB-MgO. The solid lines are fits in the creep regime. Dotted lines show the depinning field.

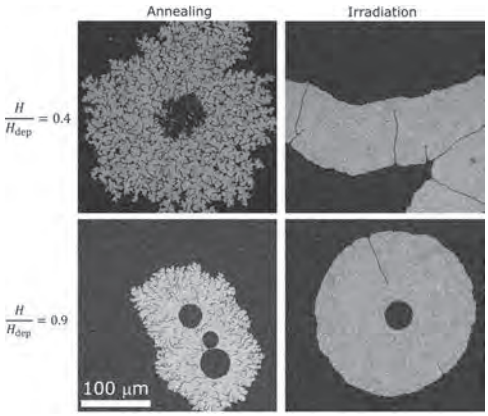

Differential Kerr microscopy images showing DW expansion at zero magnetic field after an OOP field pulse at two different values of H/H_{dep}, with H_{dep} the depinning field.

HOC-03. Tailoring domain wall dynamics and magnetic relaxation in Pd/Co/C_{60}/Pd system at the molecular scale. *E. Pandey*[1], B. Ojha[1], P. Sharangi[1] and S. Bedanta[1] *1. Physical Sciences, National Institute of Science Education and Research (NISER), Bhubaneswar, Khordha, India*

Spin dependent hybridization at the ferromagnet (FM)\organic molecule interface is very promising for fabrication of highly efficient spintronic devices [1-2]. The hybridized interface called as 'spinterface' plays a key role in tuning the interfacial magnetism. A controlled growth of organic molecular layer on the FM helps to achieve desire magnetoresistance, magnetic anisotropy and domain structure in magnetic thin film [3-6]. However, the ability of such spin polarized interface on tailoring the domain wall dynamics, interfacial DMI and magnetic relaxation mechanism is not explored much. In this context, we have fabricated a perpendicularly magnetized Pd/Co/Pd reference sample and studied the effect of spinterface induced modification of magnetic properties in Pd/Co/C_{60}/Pd multilayer. The coercivity and bubble domain size is found to be largely tuneable by varying the thickness of the C_{60} layer. Domains size became significantly smaller for a critical thickness (< 1 monolayer) of C_{60} layer, whereas it again increases until the completion of the formation of spinterface. Interestingly, magnetization relaxation mechanism became much faster in the Pd/Co/C_{60}/Pd sample as compared to the reference one. To ensure the reason behind this, we have performed domain wall (DW) velocity measurements in the creep region by MOKE based microscopy. The samples with C_{60} exhibit one order higher DW velocity than the reference sample. The reduction of magnetic anisotropy in presence of C_{60} inferred as the primary factor for enhanced DW velocity. However, there are other factors e.g. DM interaction, pinning potential, exchange stiffness etc., which may also modify the propagation velocity. As the exchange stiffness constant will be same for all the samples, an evaluation of interfacial DMI has been done by the method of asymmetric DW expansion. A negligible iDMI constant has been observed in the Pd/Co/C_{60}/Pd sample, which rules out the possibility of DMI induced enhancement in DW velocity for our case.

1. S. Delprat et al., J. Phys. D: Appl. Phys. 51, 473001 (2018) 2. M. Sun et al., J. Mater. Chem. C 6, 6619 (2018) 3. M. Gobbi et al. J. Mater. Chem. C 5, 5572 (2017) 4. S. Mallik et al., Scientific Reports 8, 5515 (2018) 5. S. Mallik et al., Appl. Phys. Lett. 115, 242405 (2019) 6. K. Bairagi et al., Phys. Rev. B 98, 085432 (2018)

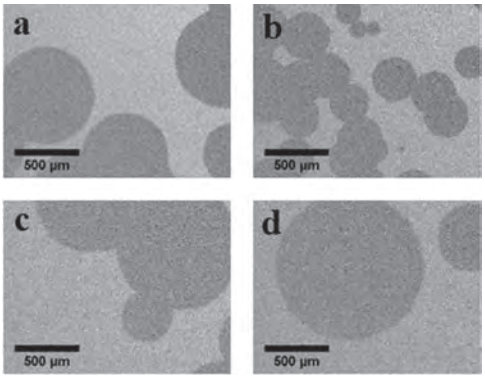

Fig.1. Domain images of Pd/Co/C_{60}/Pd samples with thickness of C_{60} (a) 0 nm (b) 0.7 nm, (c) 2.1 nm and (d) 4.4 nm.

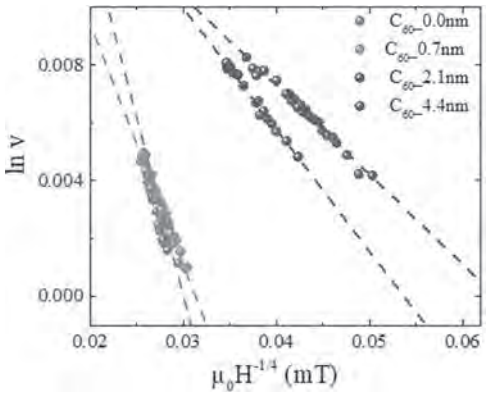

Fig. 2. Plot of ln v versus $\mu_0 H^{-1/4}$ for all the samples.

HOC-04. Tuning the Magnetic Properties of Ferromagnetic [Pt/Co/Mn]$_n$ Multilayers. *M. Lonsky*[1], M. Yoo[1], Y. Huang[1] and A. Hoffmann[1] *1. Materials Science and Engineering, University of Illinois at Urbana-Champaign, Urbana, IL, United States*

Ferromagnetic [Pt/Co]$_n$ multilayers that are composed of n stacked [Pt/Co] bilayers have been widely investigated over the past decades, mainly due to the easy tunability of various magnetic properties such as the potentially strong perpendicular magnetic anisotropy (PMA). More recently, it has been demonstrated that the addition of heavy metals (HM) such as Ir or W can lead to the presence of sizeable chiral exchange interactions in [Pt/Co/HM]$_n$ systems [1]. As a consequence, topological spin textures (e.g., skyrmions) are commonly reported in these material systems even at room temperature, thus making them promising candidates for future spintronics applications [2]. In the present work, we use additional manganese layers to break the spatial inversion symmetry of conventional [Pt/Co]$_n$ stacks and thereby, in combination with spin-orbit interaction, introduce chiral exchange interactions. The investigated [Pt/Co/Mn]$_n$ samples were fabricated by magnetron sputtering. Structural characterization of the multilayer stacks was done by performing X-ray reflectometry (XRR) measurements, while magnetic

hysteresis curves were acquired in a vibrating sample magnetometer (VSM). In addition, real-time imaging of magnetic domains as a function of the external magnetic field was conducted using a home-built magneto-optical Kerr effect (MOKE) microscope. Our results indicate a complex and sensitive dependence of various magnetic energy terms on the individual layer thicknesses, number of multilayer repetitions as well as on deposition parameters. This is particularly reflected in the shape of hysteresis loops or the types of spin textures seen in our magneto-optical imaging experiments. For instance, we discuss that the presence of defects leads to a very slow dynamics of dendritic-type domain groth in some of the investigated multilayers. Finally, we also elaborate on various approaches towards the possible observation of magnetic skyrmions in $[Pt/Co/Mn]_n$ multilayers. This work is supported by the Deutsche Forschungsgemeinschaft (DFG) through the research fellowship LO 2584/1-1 and the NSF through the University of Illinois at Urbana-Champaign Materials Research Science and Engineering Center under Grant No. DMR-1720633.

[1] W. Jiang et al., Physical Review B 99, 104402 (2019) [2] W. Jiang et al., Physics Reports 704, 1-49 (2017)

HOC-05. Temperature dependence static and dynamic properties of soft magnetic thin film FeGaB/Al_2O_3 for microwave applications.
Y. Wang[1], Y. Karampuri[1] and W. Tao[1] *1. School of Information Science and Technology, ShanghaiTech University, Shanghai, China*

The recent reports on magnetodynamic properties of soft magnetic thin films attain the lowest damping factor [1-3]. The damping is required for spin-wave propagation and spin manipulation investigation where the reduced spin-wave dissipation leads to a larger decay length. The low damping thin films are important for microwave applications [4], spin transfer switching devices, and other application in magnon spintronics. In order to achieve the lowest damping, the FeGaB has chosen with Al_2O_3 in this study. Ta(10nm)/FeGaB(15nm)/Al_2O_3(3nm)/Ta(3nm) thin film were deposited on Si/SiO2(190nm) substrate by sputtering and was annealed at 300°C for 3 hours in the Ar gas. The static magnetization results inform that saturation and remanent magnetization has increased for annealed thin film shown in Fig.1 (a). After annealing, the dipolar field influence has reduced, the magnetic moment fluctuation has not observed. Fig. 1 (b) shows the annealed films have monotonously increased. The dynamics properties are studied with temperature variation with 100 K to 300 K and exciting frequency from 2 to 20 GHz. Fig.2 (a) illustrates the absorption spectrum of both films at 100K, the spectrum has shifted to lower fields for annealed films. The unannealed thin film have existed the small hump at higher magnetic films before resonance peak, which may be impurities and surface defects of the thin film. But, the hump has disappeared for annealed films in Fig. 2 (b). The absorption spectrum provides linewidth and resonance fields (H_r) for excitation frequency. The linewidth –frequency plot provides damping factor and inhomogeneous linewidth [5]. The damping factor of both films are decreasing with decreasing temperature as Fig.2 (c). Fig.2 (d) shows the annealed film has larger effective magnetization value than that of unannealed thin film.

References 1. C.L. Jermain et al., Phys. Rev. B 95, 174411 (2017). 2. H. Kurebayashi, et.al, Demokritov, Nat. Mater. 10, 660 (2011). 3. P. Pirro, B. Hillebrands, et.al, Appl. Phys. Lett. 104, 012402 (2014). 4. T. Wu, et.al, Appl. Phys. Lett. 98(1) (2011) 012504. 5. K. Yadagiri, T. Wu, J. Magn. Magn. Mater. 515 (2020) 167277

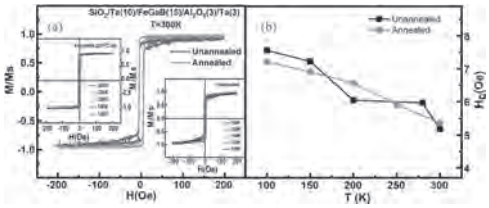

Fig.1 (a) Normalized M-H loop for unannealed and annealed thin films at 300K. Insets shows M-H loop at different temperatures; (b) Coercive fields (Hc) versus temperature.

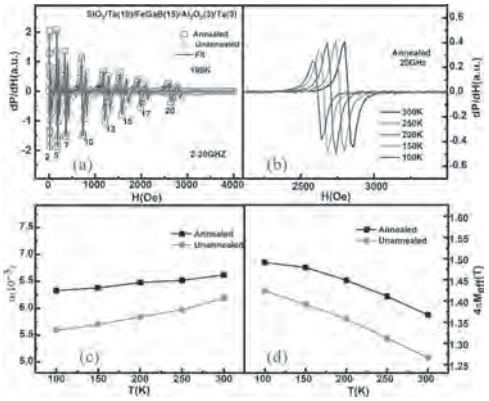

Fig.2 (a) Absorption spectrum of both thin films at 100K, (b) absorption of annealed thin film at 20GHz with different temperatures, (c) damping factor (α) versus temperature, (d) effective magnetization versus temperature.

HOC-06. Magnetization Dynamics of Single and Trilayer Permalloy Nanodots.
M. Kuchibhotla[1], A. Talapatra[2], A. Haldar[1] and A. Adeyeye[2,3] *1. Physics, Indian Institute of Technology Hyderabad, Hyderabad, India; 2. Department of Electrical and Computer Engineering, National University of Singapore, Singapore; 3. Physics, Durham University, Durham, United Kingdom*

Magnetization dynamics in laterally confined nanodots have potential applications in spin-torque nano oscillators,[1] magnetic logic and sensors[2]. The ground state of nanodot shows vortex at remanence and it exhibits rich spin dynamics spectra[3]. With the application of magnetic field, the vortex and saturated magnetization states are observed at low and high field regions respectively[4]. In our present work, we have studied the magnetization dynamics in high aspect ratio single and trilayer nanodots. Circular Permalloy (Py) nanodots (diameter = 120nm) are fabricated over a large area using deep ultraviolet lithography technique. The structures consist of single layer nanodots with thicknesses (L) 20 and 50 nm and a trilayer with two Py layers separated by a non-magnetic layer: Py(20)/Pd(10)/Py(50). Numbers within the brackets are in nm. The dynamic properties are characterized using the ferromagnetic resonance (FMR) technique. The simulated hysteresis loops are shown in Fig. 1(a). The FMR absorptions show rich spectra as a function of magnetic field and thickness. For instance, we discuss the experimental results at an excitation frequency of 10 GHz as shown in Fig. 1(b). We observed two modes for L = 20 nm nanodots at resonance fields 130 and 220 mT and a single mode appears at 210 mT for L = 50 nm nanodots. We performed micromagnetic simulations to understand the experimental results. The simulated mode profiles reveal that the high intense mode corresponds to the center mode (CM) and the low intense mode corresponds to the edge mode (EM) arising due to the inhomogeneous effective field. The CM is found to be sensitive to the thickness of the nanodot. On the other hand, in the FMR spectra of Py(20)/Pd(2)/Py(50), two resonant modes appear at 200 mT and 250 mT. These two center modes arise due to the in-phase and out-of-phase precession of spins in magneto-dynamically coupled layers. These results can be useful for nanoscale magnonic applications.

[1] M. Tarequzzaman, T. Böhnert, M. Decker, J.D. Costa, J. Borme, B. Lacoste, E. Paz, A.S. Jenkins, S. Serrano-Guisan, C.H. Back, R. Ferreira, and P.P. Freitas, Commun. Phys. 2, 1 (2019). [2] R.P. Cowburn, J. Magn. Magn. Mater. 242–245, 505 (2002). [3] K.Y. Guslienko, J. Nanosci. Nanotechnol. 8, 2745 (2008). [4] F.G. Aliev, J.F. Sierra, A.A. Awad, G.N. Kakazei, D.S. Han, S.K. Kim, V. Metlushko, B. Ilic, and K.Y. Guslienko, Phys. Rev. B - Condens. Matter Mater. Phys. 79, 174433 (2009).

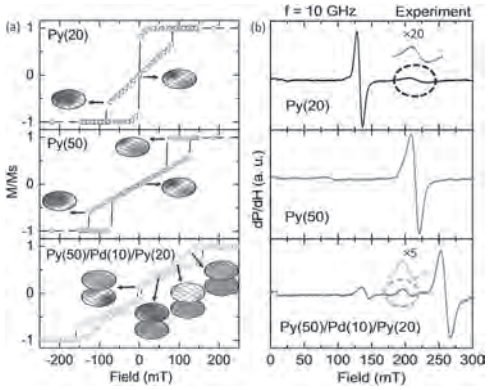

Fig 1: (a) Simulated hysteresis loops for single and trilayer nanodot arrays. The remanent states are shown in the inset. (b) Experimental FMR spectra of single and trilayer nanodot arrays.

HOC-07. Ferromagnetic Resonance of Tuneable Low Magnetostrictive Ni_xFe_{100-x} Superlattice Structures for High Frequency Application. *M.R. McMaster*[1], W. Hendren[1], J. Scott[1] and R. Bowman[1] *1. Mathematics and Physics, Queen's University, Belfast, United Kingdom*

Tailoring and control of electromagnetic properties of synthetic magnetic structures is advantageous for high frequency applications, such as shielding materials in magnetic recording, where characterisation in the gigahertz frequency range is necessary to determine parameters for simulations and aid component design. In such applications it is desirable to have a high saturation magnetisation, low coercivity, high permeability and close to zero magnetostriction. Meeting almost all these requirements, NiFe is the material of choice for many high frequency applications. We present a systematic study of the ferromagnetic resonance (FMR) and spin wave properties of Ni_xFe_{100-x} alloy thin superlattice films of the form $n[Ni_xFe_{100-x}/Ni_yFe_{100-y}]$, where n is the number of bilayers. Films were fabricated by planar magnetron sputtering and the effects of deposition conditions were investigated. Magnetic and material properties were measured using FMR [1], vibrating sample magnetometer and x-ray diffraction, with the aim to determine any relation between microstructure and the static and dynamic magnetic properties. Layer compositions within the bilayers have been chosen with particular interest in fcc/bcc layer combinations such as $Ni_{80}Fe_{20}/Ni_{20}Fe_{80}$, which may have benefits for some static properties such as high magnetisation and low magnetostriction [2]. Studies on single layers have shown dramatic changes in FMR response across the fcc-bcc boundary near x = 40, figure 1. However, for bilayer films it was found that increasing the thickness of the bcc $Ni_{20}Fe_{80}$ layer in the structure increased the resonant frequency but did not significantly reduce the FMR signal, figure 2.

[1] Y. Ding, T.J. Klemmer and T.M Crawford. J. Appl. Phys. 96, 2969 (2004); [2] C.B. Hill. "Manipulation and Magnetostriction of NiFe Films for Advanced Reader Shielding Applications". PhD Thesis. QUB. 2013.

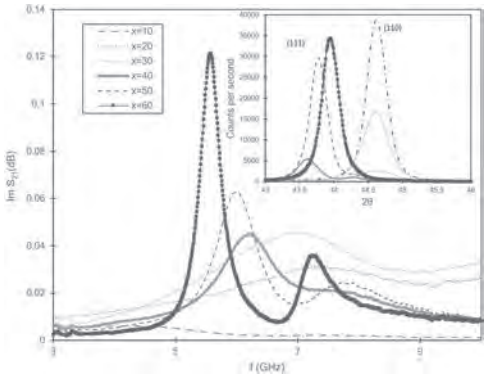

Fig. 1: FMR spectra of 100nm Ni_xFe_{100-x} single layer thin films with x varying from 10 to 60. Note that all measurements were performed at an applied field H=253Oe. XRD is inset.

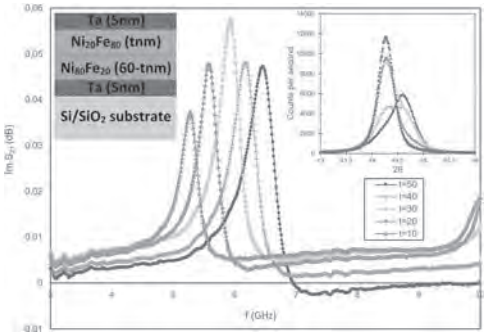

Fig. 2: FMR spectra of $Ni_{80}Fe_{20}$(60-t nm)/$Ni_{20}Fe_{80}$(t nm) thin films with t varying from 50 to 10. Note that all measurements were performed at an applied field of 253Oe. XRD is inset.

HOC-08. Withdrawn

HOC-09. An Improved Eddy Current Loss Model Over Broadband Frequency Range. L. Chen[1,2], *Z. Zhang*[1] and T. Ben[1] *1. College of Electrical Engineering and New Energy, China Three Gorges University, Yichang, China; 2. State Key Laboratory of Reliability and Intelligence of Electrical Equipment, Hebei University of Technology, Tianjin, China*

I Introduction Accurate iron loss prediction is of great significance to the optimal design of electrical equipment[1]. At present, the application of silicon steel lamination in complex excitation greatly increases the difficulty of accurately predicting iron loss, especially eddy current loss. To solve the above problems, various eddy current loss prediction methods have been proposed[2]-[3], but these methods lack the physical background. A physical-based improved parametric magneto-dynamics (IPMD) model is proposed. For the sake of calculating the eddy current loss more accurately, the Tellinen (TLN) hysteresis model is used in the implementation of the IPMD model. II Improved Parametric Magneto-Dynamic Model To solve the problem of inaccurate calculation caused by nonuniform magnetic field distribution of silicon steel lamination at high frequency, the IPMD model based on one-dimensional Maxwell diffusion equation is proposed in this paper. In the IPMD model, the influence of hysteresis on magnetic field distribution is considered by coupling the TLN model, and the influence of skin effect at high frequency is considered by using the nonlinear segmentation method. The segmentation method divides the analysis area of silicon steel lamination into several slices and realizes the uniform expression of the magnetic field on a single slice. According to the characteristics of slow change of magnetic field of inner slice and fast change of magnetic field of outer slice, the thickness of outer slice is appropriately reduced and the thickness

of inner slice is appropriately increased, as shown in Fig.1. By using the piecewise constant function to approximate the magnetic field distribution of silicon steel lamination, the eddy current loss can be accurately predicted by the IPMD model, as shown in Fig.2. III Conclusion The IPMD model proposed in this paper can accurately predict the eddy current loss in a wide frequency range while considering the physical background, which has practical significance for the study of eddy current loss characteristics of soft magnetic materials.

H. Matsumori, T. Shimizu, K. Takano, et al. "Evaluation of Iron Loss of AC Filter Inductor Used in Three-Phase PWM Inverters Based on an Iron Loss Analyzer," IEEE Transactions on Power Electronics, vol. 31, no. 4, pp. 3080-3095, 2016. H. S. Zhao, D. D. Zhang, Y. L. Wang, et al. "Piecewise Variable Parameter Loss Model of Laminated Steel and Its Application in Fine Analysis of Iron Loss of Inverter-Fed Induction Motors," IEEE Transactions on Industry Applications, vol. 54, no. 1, pp. 832-840, Jan-Feb, 2018. R. Liu, and L. Li, "Analytical Prediction Model of Energy Losses in Soft Magnetic Materials Over Broadband Frequency Range," IEEE Transactions on Power Electronics, vol. 36, no. 2, pp. 2009-2017, 2021.

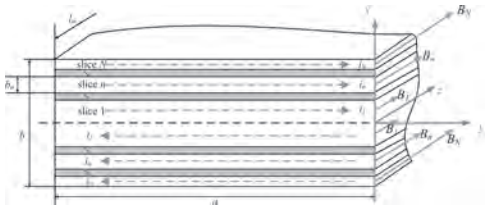

Fig.1. Segmentation method of silicon steel lamination

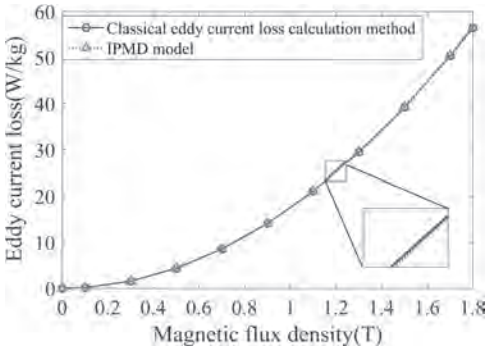

Fig. 2. Comparison between classical eddy current loss calculation method and IPMD model

HOC-10. Magnetic Gilbert Damping at Elevated Temperature: High PMA Ultrathin Film. *R. Mandal*[1,2], Y. Sasaki[2], I. Kurniawan[2], J. Jung[2], Y. Miura[2], Y. Sakuraba[2], K. Hono[2] and Y. Takahashi[2] *1. Advanced Institute for Materials Research, Tohoku University, Sendai, Japan; 2. National Institute for Materials Science, Tsukuba, Japan*

Magnetic Gilbert Damping (α) is an indispensable parameter of ferromagnetic material both from fundamental and application point of view as it controls the dynamical nature of the magnetic system. In communication technology, these spin-relaxation have important contribution for device performance like switching current in spin-transfer torque magnetic random-access memory (STT-MRAM)[1] and controlling the writing speed, bit-error rates in magnetic storage media[2]. Large perpendicular magnetic anisotropy (PMA) is another important parameter for both of them for increasing the capacity. Tetragonally distorted ultrathin $Fe_{50}Co_{50}$ alloy[3,4] is a potential material for STT-MRAM with large PMA and little bit high α. In practical application, as we know the operating temperature of STT-MRAM is far beyond the room temperature (RT), therefore a detailed observation of magnetic parameters at elevated temperature is needed. Particularly here we will discuss about the investigation of α above RT for tetragonally distorted ultrathin $Fe_{50}Co_{50}$ film for better insight of application perspective. The stack of MgO/Rh (50 nm)/$Fe_{50}Co_{50}$ (t =1, 1.5 nm)/Rh (3 nm) was deposited by UHV-magnetron sputtering system. Fig. 1 (a) shows a cross-sectional STEM-HAADF image of 1 nm thick $Fe_{50}Co_{50}$ sample with zone axis of Rh and $Fe_{50}Co_{50}$ are [110], [100], respectively. The tetragonal distortion (c/a) found > 1 as shown in Fig. 1(a). The magnetization curve (fig. 1 (b)) shows out-of-plane anisotropy with large effective PMA of 0.488 MJ/m^3. The high temperature FMR measurement was performed using TRMOKE microscope inside a thermally heated vacuum chamber to evaluate the α. Figure 1 (c) shows the variation of α *vs.* measurement temperature and found the effective α shows very small temperature up to 150°C; which is typically the operating temperature of memory devices. We also performed first-principle calculation to discuss about the origin of such high damping above RT. Judging from the large PMA and a with high thermal stability, this $Fe_{50}Co_{50}$ is a suitable choice for the reference layer in STT-MRAM.

1. J. C. Slonczewski *et al.*, J. Magn. Magn. Mater. 159, L1 (1996). 2. T. Kobayashi *et al.* J. Magn. Soc. Jpn. 41, 52 (2017). 3. R. Mandal *et al.* Appl. Phys. Lett. 113, 232406 (2018) 4. B. Lao et al., *IEEE Transc. Magn.* 50, 2008704 (2014).

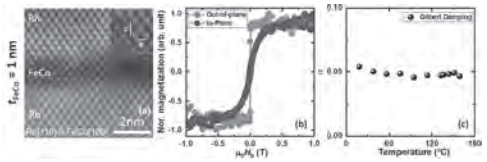

Figure 1: (a) Cross-sectional HADDF image, (b) magnetization curve and (c) α *vs.* operating temperature was shown for 1 nm thick $Fe_{50}Co_{50}$ film.

HOC-11. Bi-stable magnetization switching in a magnetic tunnel junction with thermal isolation. *Y. Kaneda*[1,2], M. Goto[1,2], T. Mizuno[3], T. Yamane[3], N. Degawa[3], T. Suzuki[3], A. Shimura[3], S. Aoki[3], J. Urabe[3], S. Hara[3], H. Nomura[1,2] and Y. Suzuki[1,2] *1. Graduate School of Engineering Science, Osaka University, Toyonaka, Japan; 2. Center for Spintronics Research Network, Osaka University, Toyonaka, Japan; 3. TDK Corporation, Chuo-ku, Japan*

Magnetoresistive random access memory (MRAM) has attracted attention as a next generation memory device because of its high speed and low power consumption properties. Electric magnetization reversal is important for writing a memory. Existing magnetization control technologies such as spin transfer torque [1] can control the magnetization direction more efficiently only in an ultra-thin film. Recently, Joule heat induced magnetic anisotropy change of a free layer in a magnetic tunnel junction (MTJ) was reported [2], which has been expected to be able to control the magnetization direction efficiently even in a thick film. The magnetization switching by this effect is one of the attractive techniques for controlling MRAM, however, sub-nanosecond one has not been observed. In this study, we researched the Joule heat induced magnetization switching in an MTJ. Film structure is buffer layer | IrMn | CoFe | Ru | CoFeB pinned layer | MgO barrier (1 nm) | FeB free layer (2 nm) | MgO (0.3 nm) | W (2 nm) | MgO (0.4 nm) capping layer | metal electrode. Figure 1 shows the measurement set-up. A voltage pulse was applied by an arbitrary waveform generator to the MTJ under a bias magnetic field H_{bias} tilted by angle θ. The pulse width and height are 0.5 ns and 900 mV respectively. After that, the magnetization direction was detected by measuring a resistance change ΔR using a lock-in amplifier. Figure 2 is the result of ΔR with 100 repetitive pulse voltage applications under various $\mu_0 H_{bias}$. We observed uncertain magnetization switching ($\mu_0 H_{bias}$=-15.5 mT, θ=20 °). This research was supported by JSPS Grant-in-Aid for Scientific Research (S) Grant Number JP20H05666.

[1] E. B. Myers *et al.*, Science 285, 867 (1999) [2] M. Goto *et al.*, Nat. Nanotechnol. 14, 40 (2019)

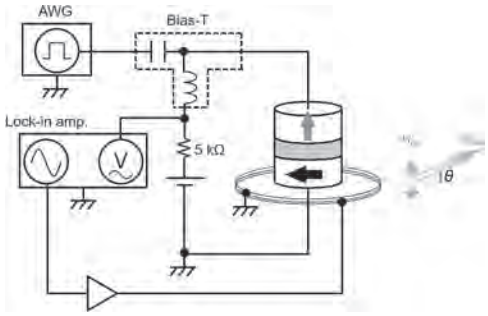

Fig. 1, Schematic of measurement set-up

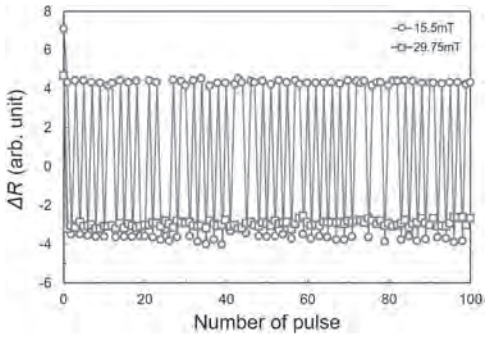

Fig. 2, Δ*R* with 100 repetitive pulse voltages under various bias magnetic fields

HOC-12. Electrically detected ferromagnetic resonance in polycrystalline YIG covered with a layer of Ag paint. *Y. Lee*[1] and R. Mahendiran[1] *1. Physics, National University of Singapore, Singapore*

Recently, ferromagnetic resonance (FMR) in insulating YIG film was shown to be driven by microwave current in the Pt film deposited on the top of YIG film and detected as a dc voltage in the Pt layer due to spin Hall effect and/or spin rectification[1,2]. Here, we demonstrate an alternative method to study FMR in ceramic YIG. A polycrystalline pellet was made from YIG nano-powder by sintering in the air at 900°C for 12 hr. Magnetization at 300K, shown in the main panel of Fig.1(a), affirms the soft ferromagnetic nature of YIG. The upper inset in (a) illustrates the sketch of our experimental setup. Since the resistance of YIG could not be measured by the impedance analyzer, a layer of silver paint was coated on the top surface of the sample and at two ends to allow radio-frequency current to flow. The sample bridges the signal line and the ground plane of the sample stage, which is connected to the impedance analyzer via a rigid coaxial cable. A microwave signal is injected into the Ag paint layer through the signal line. Resistive and reactance of the Ag-paint were measured while sweeping frequency at different values of the dc magnetic field,*H*. The lower inset shows magneto-resistance MR(b) and magnetoreactance MX(c) for five frequencies *(*f) as *H* decreased from 3 kOe to 0 Oe. The MR of the Ag-paint for 3 GHz exhibits a prominent peak at $H = H_r$ around which MX crosses zero. Both the amplitude of the peak in MR and H_r decreases as f decreases. We argue that the peak in MR is caused by FMR. The inset shows the dependence of H_r on *f* and we are able to fit the data with Kittel's relation for in-plane FMR. The observed electrical detection of FMR in YIG with colloidal silver particles having weak spin-orbit coupling than Pt deserves an urgent understanding. R. M. thanks the Ministry of Education, Singapore for support (Grant no. R144-000-442-114).

[1] J. Sklenar et al. Phys. Rev. B. 92,174406 (2015) [2] M. Schreier et al. Phys. Rev. B. 92, 144411 (2015).

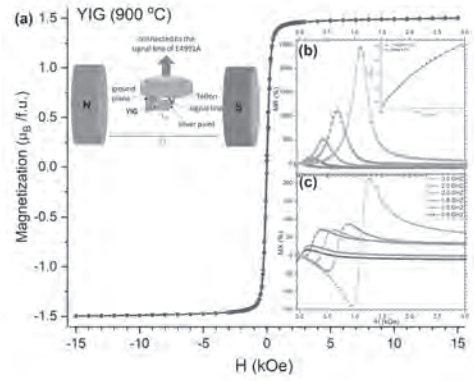

Fig. 1 (a) M-H isotherm of YIG sample at 300 K(main panel) and the schematic diagram of the experimental setup (upper inset). Field dependence of (b) magnetoresistance MR)and (c) magnetoreactance MX at selected frequencies of current excitation (bottom inset). Inset in (b) shows the frequency dependence of the resonance field (symbols) and Kittel's fit for FMR.

HOC-13. Magnetization dynamics of magnetic nanoparticles for thermal and magnetic particle imaging. *T.Q. Bui*[1], A.J. Biacchi[1], K.N. Quelhas[1], M. Henn[1], E.L. Correa[1], W. Tew[1], A.R. Hight Walker[1], C. Dennis[1], M.J. Donahue[1] and S. Woods[1] *1. National Institute of Standards and Technology, Gaithersburg, MD, United States*

The prospect of thermal imaging and control in magnetic particle imaging (MPI) is an important advancement for non-invasive medical diagnostics and therapeutics. Current MPI systems focus mainly on imaging from measurement of nanoparticle concentrations. Accurate derivation of temperature relies on detailed understanding of magnetization dynamics in the presence of AC drive fields and variable temperature [1]. Here, we report measurements of nanosecond magnetization dynamics using both time and frequency domain techniques. It has been reported that the imaging resolution of MPI is critically impacted by nanoparticle relaxation dynamics [2]; specifically, spin relaxation results in image blurring. The dynamic response (e.g. Néel and Brownian relaxation) of magnetic nanoparticles in magnetic fields is intricate, depending strongly on the particles' inherent magnetic and structural properties, inter-particle interactions, and the local environment. We have developed an arbitrary-wave magnetic particle spectrometer with magnetic field amplitude up to 10 mT_{Pk} for characterizing magnetization dynamics over a broad temperature range (200 K to 350 K). We have characterized the dynamic AC susceptibility of nanoparticles ranging in diameter from 10 nm to 70 nm and in composition and observed peaks in the imaginary component (χ'') at frequencies from as low as 50 Hz to 50 MHz. Figure 1 show the χ'' peak frequency for 11.5 nm cobalt-doped ferrite nanoparticles at different temperatures. This peak reveals the effective relaxation timescale ($\tau \sim 1$ μs). Additionally, we used pulsed excitation to characterize the magnetization dynamics with and without magnetic fields. Figure 2 shows a magnetization response of 7.5 nm cobalt-doped ferrites to a magnetic field pulse with 20 ns rise time. Monte Carlo simulations are used for analyzing both time and frequency domain measurements. This knowledge will eventually inform strategies for design and synthesis of magnetic nanoparticles with properties targeted for accurate and sensitive thermal imaging using MPI.

[1] Thinh Q. Bui, Weston L. Tew, Solomon I. Woods. AC magnetometry with active stabilization and harmonic suppression for magnetic nanoparticle spectroscopy and thermometry. *J. Appl. Phys*. 128, 224901 (2020). [2] Zhi Wei Tay, Daniel W Hensley, Erika C Vreeland, Bo Zheng, Steven M Conolly. The Relaxation Wall: Experimental Limits to Improving MPI Spatial Resolution by Increasing Nanoparticle Core size. *Biomed Phys. Eng. Express*, 3 (3), 035003 (2017)

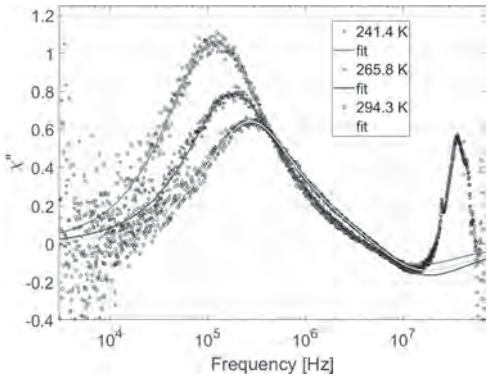

The imaginary component of AC susceptibility for 11.5 nm ferrite nanoparticles

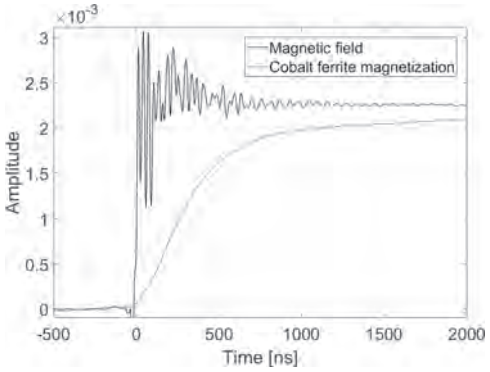

Pulsed magnetic field (black). Magnetization step-response of 7.5 nm cobalt-doped ferrite (red).

Session HOD
DMI, SKYRMIONS AND OTHER TOPOLOGICAL OBJECTS

Stanislas Rohart, Chair
Université Paris-Saclay Faculte des Sciences d'Orsay, Orsay, France

INVITED PAPER

HOD-01. Exploiting excitations of magnetic topological objects.
D.R. Rodrigues[1] 1. Department of Electrical and Information Engineering, Politecnico di Bari, Bari, Italy

New physics emerge from the interplay between spin waves and magnetic topological objects. Excitation modes permit to exploit the full potential of topological objects and increase the range of applications, in particular in the field of insulator-based spintronics. Recently, the number of proposals leveraging excitation modes of topological objects is steadily increasing, such as in microwave generation and detection, spin-wave guides, parametrons and in neuromorphic spintronic devices. In this talk I will present three ways to exploit excitations of magnetic topological objects. First, I will show that domain walls in thin films behave as flexible strings with an extra internal degree of freedom[1]. A direct application is the use of domain walls as spin-wave guides and hosts of magnetic domain wall skyrmions. Moreover, by considering closed domain wall strings, I will derive analytically deformations, instabilities[2,3], and excitation modes of skyrmions[4]. Second, I will propose the use of topological objects as tunable nanoscale in-materio frequency multipliers for spintronic systems[5]. I will show that the excitation of topological objects by fractions of the eigenfrequencies presents advantages compared to the well-known parametric excitation as it requires less energy input and does not generate instabilities away from the excited topological objects. Third, I will discuss a mechanism to controllably manipulate the direction and speed of domain walls in kagome antiferromagnets via a single linearly polarized spin-wave source[6]. In this case, the coupling of spin wave modes inside the non-collinear domain wall allows for a highly tunable spin-wave induced domain wall motion with a frequency dependent domain wall velocity.

[1] Rodrigues, D.R., et al. "Effective description of domain wall strings." *Physical Review B* 97.13 (2018): 134414. [2] Masell, J., Rodrigues, D.R., et al. "Spin-transfer torque driven motion, deformation, and instabilities of magnetic skyrmions at high currents." *Physical Review B* 101.21 (2020): 214428. [3] Litzius, K., Rodrigues, D.R., et al. "The role of temperature and drive current in skyrmion dynamics." *Nature Electronics* 3.1 (2020): 30-36. [4] Kravchuk, V. P., Rodrigues, D.R., et al. "Spin eigenexcitations of an antiferromagnetic skyrmion." *Physical Review B* 99.18 (2019): 184429. [5] Rodrigues, D.R., et al. "Nonlinear dynamics of topological ferromagnetic textures for frequency multiplication." *Physical Review Applied* 16.1 (2021): 014020. [6] Rodrigues, D.R., et al. "Spin-wave driven bidirectional domain wall motion in kagome antiferromagnets." *arXiv preprint arXiv:2104.10460* (2021).

CONTRIBUTED PAPERS

HOD-02. Engineering of intrinsic chiral torques in magnetic thin films based on the Dzyaloshinskii-Moriya interaction.
Z. Liu[1,2], Z. Luo[1,2], S. Rohart[3], L. Heyderman[1,2], P. Gambardella[2] and A. Hrabec[1,2]
1. Laboratory for Multiscale Materials Experiments, Paul Scherrer Institute, Villigen PSI, Switzerland; 2. Department of Materials, ETH Zurich, Zurich, Switzerland; 3. Laboratoire de Physique des Solides, Université Paris-Saclay, Orsay, France

The establishment of chiral coupling in thin magnetic films with inhomogeneous anisotropy has led to the development of novel artificial systems of fundamental and technological interest. The chiral coupling itself is enabled by the Dzyaloshinskii-Moriya interaction (DMI) enforced by the patterned non-collinear magnetization [1-4]. Here, we create a domain wall track with out-of-plane (OOP) magnetization coupled to OOP stripes on each side via narrow parallel strips with in-plane magnetization as shown in Fig.1 (a). Since the chiral coupling prefers antiparallel OOP magnetization configuration over the parallel case, the regions of noncollinear magnetization in a single magnetic layer can be used to bias the domain wall velocity, as shown in series of Kerr images in Fig.1 (b). To tune the chiral torques, the design of the magnetic racetracks can be modified by varying the width of the tracks or the width of the transition region between noncollinear magnetizations, reaching effective chiral magnetic fields of up to 8 mT. Furthermore, we show how the magnitude of the chiral torques can be estimated by measuring asymmetric domain wall velocities. We also demonstrate spontaneous domain wall motion propelled by intrinsic torques even in the absence of any external driving force, which is of high importance for domain wall motion-based neuromorphic devices.

[1] Luo, *et al.* Science 363, 1435 (2019) [2] Luo, *et al.* Nature 579, 214 (2020) [3] Dao *et al.* Nano Lett. 19, 5930 (2019) [4] Hrabec, *et al.* Appl. Phys. Lett. 117, 130503 (2020)

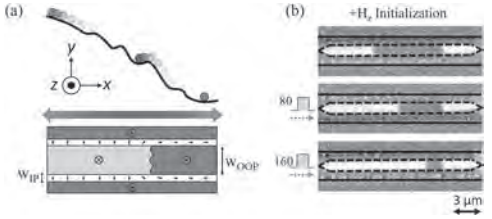

Figure 1: (a) Schematic of a DW racetrack with OOP magnetization delimited by two strips with IP anisotropy. The energy landscape of the DW racetrack is monotonous, except for local DW pinning sites. (b) Sequence of Kerr images of asymmetric DW motion in a racetrack with w_{OOP} = 950 nm. The dashed lines correspond to the position of the IP magnetized strip while the full lines correspond to the boundary of the magnetic track. 80 current pulses are applied between each image; the pulse duration is 50 ns and the current density is 3.6×10^{11} A/m^2.

HOD-03. Magnetization statics and dynamics in Ir/Co/Pt multilayers with Dzyaloshinskii-Moriya interaction. *A.K. Dhiman*[1], R. Gieniusz[1], P. Gruszecki[2], J. Kisielewski[1], M. Matczak[1], Z. Kurant[1], I. Sveklo[1], U. Guzowska[1], M. Tekielak[1], F. Stobiecki[3] and A. Maziewski[1]
1. Laboratory of Magnetism, Faculty of Physics, University of Bialystok, Bialystok, Poland; 2. Faculty of Physics, Adam Mickiewicz University, Poznan, Poland; 3. Institute of Molecular Physics, Polish Academy of Sciences, Poznan, Poland

Magnetic multilayers of Ir/Co/Pt with interfacial Dzyaloshinskii-Moriya interaction (IDMI) [1] were deposited by magnetron sputtering with Co thickness d=1.8nm and repetitions N=6. Ferromagnetic resonance spectroscopy was applied to determine the values of effective magnetic uniaxial anisotropy, H_u = -0.45 T. Exploiting magneto-optical Kerr effect in longitudinal mode microscopy, magnetic force microscopy and vibrating sample magnetometery the magnetic field driven evolution of domain structures and hysteresis loops have been studied. Existence of weak stripe domains structure was deduced – large micrometer size domains with in-plane "core" magnetization modulated by small nano-domains with out-of-plane magnetization. Quantitative evaluation of IDMI was carried out using Brillouin light scattering (BLS) spectroscopy [2,3] from the difference between Stokes and anti-Stokes peak frequencies Δf. Due to the additive nature of IDMI, the asymmetric combination of Ir and Pt covers led to large values of surface DMI energy density D_s. Fig. 1 shows Stokes and anti-Stokes peaks for magnon scattering. It was found that Stokes and anti-Stokes frequencies as well as Δf, measured as a function of in-plane applied magnetic field, show hysteresis. These results are explained under the consideration of the influence of IDMI on the dynamics of in-plane magnetized "core" with weak stripe domains. In order to understand the spatial magnetization distribution and magnetization process, the micro-magnetic simulations were performed. Our findings leverage the impact of IDMI on domain structure. Large values of D_s can be useful for the stabilization of skyrmions [1] and studying the dynamical behavior of magnetic skyrmions in the in-plane magnetized sample [4].

[1] C. Moreau-Luchaire, C. Moutafis, N. Reyren, J. Sampaio, C. A. F. Vaz, N. Van Horne, K. Bouzehouane, K. Garcia, C. Deranlot, P. Warnicke, P. Wohlhüter, J.-M. George, M. Weigand, J. Raabe, V. Cros and A. Fert, Additive interfacial chiral interaction in multilayers for stabilization of small individual skyrmions at room temperature, Nat. Nano. 11, 444-448 (2016) [2] K. Di, V. Li Zhang, H. S. Lim, S. C. Ng, M. H. Kuok, J. Yu, J. Yoon, X. Qiu and H. Yang, Direct observation of the Dzyaloshinskii-Moriya Interaction in a Pt/Co/Ni film, PRL 114, 047201 (2015) [3] A. K. Dhiman, M. Matczak, R. Gieniusz, I. Sveklo, Z. Kurant, U. Guzowska, F. Stobiecki, A. Maziewski, Thickness dependence of interfacial Dzyaloshinskii-Moriya interaction, magnetic anisotropy and spin waves damping in Pt/Co/Ir and Ir/Co/Pt trilayers, Journal of Magnetism and Magnetic Materials 519, 167485 (2021) [4] K. W. Moon, J. Yoon, C. Kim and, C. Hwang, Existence of in-plane magnetic skyrmion and its motion under current flow, Phys. Rev. Appl. 12, 064054 (2019)

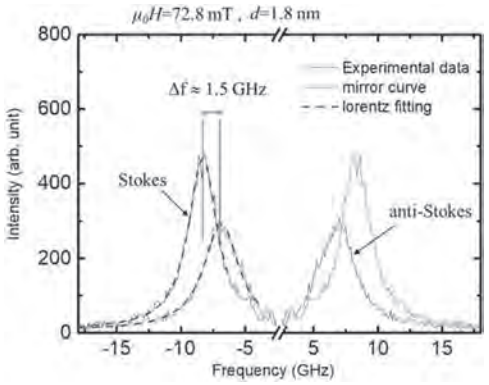

Fig. 1. BLS spectrum for d=1.8 nm where Stokes and anti-Stokes peaks are shown. Measurement was done for wavevector k=11.81 μm^{-1} and applied in-plane magnetic field $\mu_0 H$=72.8 mT. Experimental data (black line) and its mirror curve (red line, for easy comparison) determine the frequency difference Δf ≈1.5 GHz.

HOD-04. Localized and propagating spin-wave modes in thin film multilayers hosting skyrmions. *T. Srivastava*[1,2], I. Ngouagnia Yemeli[1], Y. Sassi[2], F. Ajejas[2], A. Vecchiola[2], K. Bouzehouane[2], N. Reyren[2], V. Cros[2], T. Devolder[3], J. Kim[3] and G. de Loubens[1] *1. SPEC, CEA-Saclay, CNRS, Université Paris-Saclay, Gif-sur-Yvette, France; 2. Unité Mixte de Physique, CNRS, Thales, Univ. Paris-Sud, Université Paris-Saclay, Palaiseau, France; 3. Centre for Nanoscience and Nanotechnology, CNRS, Université Paris-Saclay, Palaiseau, France*

Microwave response of magnetic textures in ferromagnets offers rich physics and has been intensively investigated over the past decades for their potential application in magnonics. Eigenexcitations of films featuring bubble domains [1,2] and stripes [3] have been accounted for, broadly consisting of acoustic, optical and domain wall oscillation modes. Recently, topologically non-trivial chiral magnetic structures called skyrmions [4] have gathered a lot of interest owing to their robust, tiny and particle-like nature. They exhibit unique spectral signatures which have been observed mainly in bulk systems below room temperature [5,6]. The experimental observation and interpretation of their resonant dynamics in thin films remain elusive owing to high damping coefficients. Here we report room temperature investigation of resonant skyrmion dynamics in [Pt/CoFeB/AlOx]×20 multilayers. We optimize our sample by tuning the different layer thicknesses to host magnetic skyrmions at room temperature, along with a fairly low damping parameter α= 0.02. We use magnetic force microscopy to observe the static magnetic domain configuration consisting of randomly distributed skyrmions and dense skyrmion lattice as a function of an out-of-plane magnetic field. Broadband ferromagnetic resonance measurements are performed to study the dynamic response with an in-plane excitation field. Besides the Kittel mode (KM) above saturation, three distinct modes, a low frequency mode (LFM), an intermediate frequency mode (IFM) and a high frequency mode (HFM), appear with unique frequency-field dispersions in the non-saturated state (see Fig). Micromagnetic simulations reveal the characteristics of these modes, where the LFM features a mode localized in the skyrmion edges, while for the IFM skyrmion edge dynamics couples with the uniform background. In the HFM, the precession of skyrmion cores emits omnidirectional spin waves into uniform background, producing interference patterns in the lattice. Our results thus open up new avenues for skyrmion-based magnonic devices.

[1] B. E. Argyle, W. Jantz, and J. C. Slonczewski, J. Appl. Phys., 54, 6 (1983). [2] G. Gubbiotti, G. Carlotti, S. Tacchi *et al.*, Phys. Rev. B, 86, 014401 (2012). [3] U. Ebels, L. Buda, K. Ounadjela *et al.*, Phys. Rev. B, 63, 174437 (2001). [4] A. Fert, N. Reyren and V. Cros, Nat. Rev. Mater., 2, 17031 (2017) [5] M. Mochizuki, Phys. Rev. Lett., 108, 017601 (2012). [6] M. Garst, J. Waizner and D. Grundler, J. Phys. D: Appl. Phys., 50, 29, 293002 (2017)

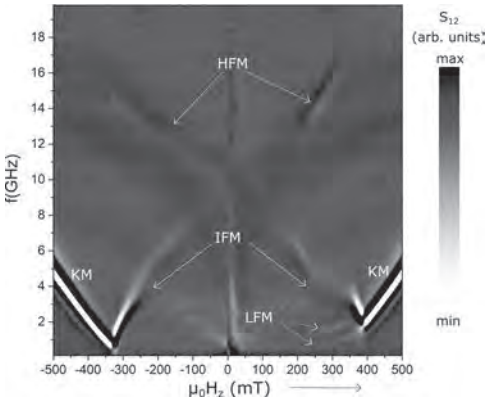

Fig : Frequency-field dispersion map measured by FMR over a frequency range of 0.1 GHz to 20 GHz with an out-of-plane magnetic field swept from -500 mT to 500 mT.

HOD-05. The Bloch Point 3D Topological Charge Induced by the Magnetostatic Interaction. *K. Guslienko*[1,2], F. Tejo[3], R. Hernández Heredero[4] and O. Chubykalo-Fesenko[3] *1. Departamento de Polímeros y Materiales Avanzados, Universidad del País Vasco, UPV/EHU, San Sebastian, Spain; 2. IKERBASQUE, the Basque Foundation for Science, Bilbao, Spain; 3. Instituto de Ciencia de Materiales de Madrid, Madrid, Spain; 4. Departamento de Matemática Aplicada, Universidad Politécnica de Madrid, Madrid, Spain*

A hedgehog or Bloch point is a point-like 3D magnetization configuration in a ferromagnet. Regardless of widely spread treatment of a Bloch point as a topological defect, its 3D topological charge has never been calculated. Here, applying the concepts of the emergent magnetic field and Dirac string, we calculate the 3D topological charge (Hopf index [1]) of the Bloch point in a spherical soft magnetic particle. Using an inhomogeneous helicity γ(r) of the Bloch point magnetization [2] we showed analytically and confirmed by micromagnetic simulations that the Hopf index has some finite, non-integer value determined by the magnetization configuration of the Bloch point, non-localized topological soliton. Thus, Bloch points form a new class of hopfions - 3D topological magnetization configurations, whereas traditional toroidal hopfions (localized topological solitons) considered before have an integer Hopf index [3]. One of the important consequences of our approach, that can be tested experimentally, is a non-zero gyrovector of the Bloch point resulting in its non-trivial dynamics, when the direction of soliton motion is not parallel to a driving force (topological or skyrmion Hall effect). The Bloch points constitute an essential part of the magnetization configurations of the Bloch point domain walls in nanowires. Therefore, the calculations of the Bloch point 3D topological charge and gyrovector can serve as a benchmark for consideration of the complicated Bloch point domain wall dynamics in nanowires.

[1] L. Faddeev, A.J. Niemi, Nature, 387, 58 (1997). [2] E. Feldkeller, Z. Angew. Phys., 19, 530 (1965). [3] B. Göbel, C.A. Akosa, G. Tatara, I. Mertig, Phys. Rev. Res., 2, 013315 (2020).

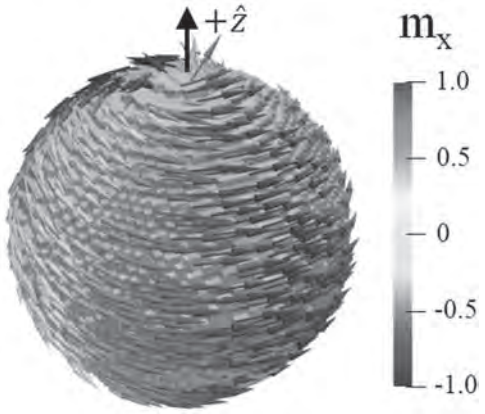

The spiral Bloch point with the inhomogeneous helicity γ(r) in a spherical nanoparticle with radius *R*=50 nm containing a Bloch point in the origin. The magnetization configuration was obtained by micromagnetic simulations using the exchange stiffness A= 21 pJ/m and saturation magnetization M_s=1700 kA/m. The values of the x-component of the reduced magnetization $m_x=M_x/M_s$ are shown by different colors.

HOD-06. Thermally Activated Transitions in Confined Terromagnets with Perpendicular Magnetic Anisotropy as Function of the Interfacial Dzialoshinskii-Moriya Interaction Strength. *G.D. Chaves-O'Flynn*[1], D.L. Stein[2] and P. Kuswik[1] *1. Department of Thin Films, Institute of Molecular Physics, Polish Academy of Sciences, Poznan, Poland; 2. Department of Physics and Courant Institute of Mathematical Sciences, New York University, New York, NY, United States*

The topological number of micromagnetic textures (*Q*) is a useful quantity for information encoding and transport [1,2], and determines the dynamics of magnetic objects such as skyrmions, merons and domain walls. Recent developments allow us to tune the strength of the interfacial Dzyaloshinskii-Moriya interaction, thereby inducing the formation of different states and generating a rich energy landscape for a given physical device, leading to new and potentially useful applications [3]. This energy landscape determines the thermal stability of a given state which is strongly dependent on the barrier that separates neighboring minima [4-6]. In this work we use the String Method for the Study of Rare Events to determine transition states and thermal barriers of a circular nanodisk at different magnitudes of the Dzialoshinskii-Moriya constant (*D*). Low values of *D* are associated with high energies of domain wall formation; in this regime mostly uniform magnetizations with isolated skyrmions correspond to the lowest energy states. The transition between these states occurs by the motion of entire skyrmions across the material's edge. At intermediate values of *D*, domain walls require less energy, skyrmions have large radii and leave the nanodisk via an intermediate minima in which a meron is expelled from the film (Figures 1 and 2). Very large *D* values cause complex textures to form but transtions are still mediated by meron motion across the device's edge. This work emphasizes the importance of considering meron-mediated-transitions to appropriately create the initial path used in methods that use chain-of-states to estimate transition barriers.

[1] J. Sampaio et al. Nature Nanotech. 8, 839 (2013) [2] S. Rohart and A. Thiaville, Phys. Rev. B 88, 184422 (2013) [3] Cortés-Ortuño et al. PRB 99, 214408 (2019) [4] R.L.Novak et al., JMMM 451, 749 (2018) [5] M. Zelent et al. Phys. Status Solidi RRL 11, 1200259 (2017) [6] Felix Büttner, Ivan Lemesh & Geoffrey S. D. Beach, Scientific Reports 8:4464 (2018) *This research was supported in part by the US National Science Foundation Grant No. DMR 1610416, and the National Science Centre Poland under OPUS funding grant No. 2019/33/B/ST5/02013*

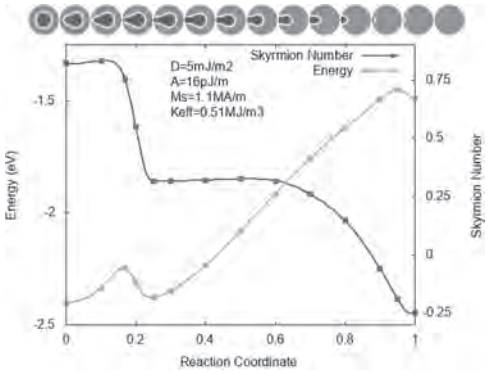

String Method results showing energy and skyrmion number along the transition path. The images above correspond to points indicated in the images. The disk diameter is 80nm and its thickness is 0.4nm.

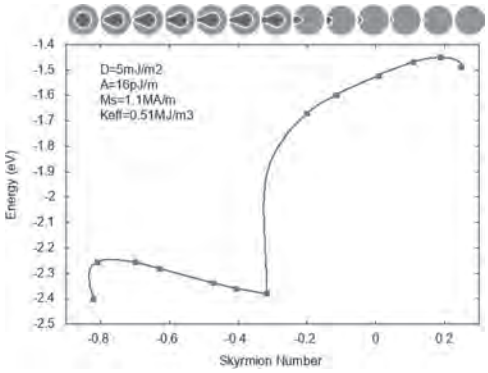

Skyrmion Number vs Energy for the same transition path of Fig.1. The skyrmion numbers of energy minima differ by roughly 1/2, highlighting the importance of meron motion across the edges as a mechanism for switching between energy minima. The values are not half-integer due to magnetization tilting at the sample's edge.

HOD-07. Pinning Behavior of Magnetic Skyrmions in Thin Film.
R. Gruber[1], J. Zazvorka[1,2], *M.A. Brems*[1], D.R. Rodrigues[3], N. Kerber[1], B. Seng[1], K. Everschor-Sitte[3], P. Virnau[1] and M. Kläui[1] *1. Institute of Physics, Johannes Gutenberg-Universität Mainz, Mainz, Germany; 2. Institute of Physics, Faculty of Mathematics and Physics, Charles University, Prague, Czechia; 3. Faculty of Physics, Universität Duisburg-Essen, Duisburg, Germany*

Magnetic skyrmions are magnetic quasi-particles with interesting properties for possible future applications in memory storage devices and non-conventional computing [1-4]. Skyrmions have been found to exhibit thermal diffusion [3], which can be tuned by magnetic fields and temperature [3,5]. This thermally activated stochastic dynamics [3,5-7] is crucial for Brownian token-based computing [4,8] as well as skyrmion-based probabilistic computing [3]. In applications which rely on skyrmion diffusion, pinning effects are of crucial importance as the pinning strength is often comparable to the scales of thermal excitation and thus impacts the operation of skyrmion-based devices. Here, we use skyrmions to probe the energy landscape of a sample by quantifying the spatially-resolved dwell times. To understand the origin of the pinning we image the skyrmion pinning details and find a strong size-dependence (Fig. 1). We observe that the skyrmion is pinned at its domain wall boundary and not as previously considered its core. As a consequence, we find that the size-dependence follows from different favorable overlaps of the skyrmion boundary with the pinning regions. This concept is supported by measurements of stripe domains, whose domain walls coincide with the contours of the averaged skyrmion profiles (Fig. 2), and by micromagnetic simulations which qualitatively show that an arrangement of domain wall pinning regions can introduce size-dependent pinning to a system.

[1] A. Fert *et al.*, *Nat. Nanotechnol*. 8, 152 (2013). [2] D. Prychynenko *et al.*, *Phys. Rev. Appl*. 9, 014034 (2018). [3] J. Zázvorka *et al.*, *Nat. Nanotechnol*. 14, 658 (2019). [4] M. A. Brems et al., arXiv:2107.02097 (2021). [5] N. Kerber *et al.*, *Phys. Rev. Appl.* 15, 044029 (2021). [6] J. Zázvorka *et al.*, *Adv. Funct. Mater*. 30, 2004037 (2020). [7] C. Song *et al., Adv. Funct. Mater*. 31, 2010739 (2021). [8] T. Nozaki *et al.*, *Appl. Phys. Lett*. 114, 012402 (2019).

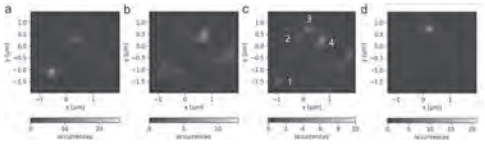

Fig 1. Histograms of occurring skyrmion center positions for external out-of-plane fields of a) -39 µT, b) -37 µT, c) -35 µT and d) -33 µT, which tune the skyrmion size. The color scale represents the number of occurrences of the skyrmion center at a certain position. Even for small field changes, the spatial skyrmion distribution changes drastically.

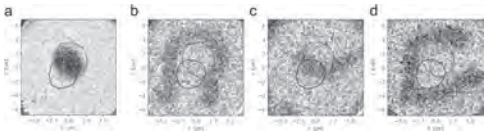

Fig 2. a) Grey-scaled average intensity of Kerr microscope frames for skyrmions pinned at site 2 from Fig. 1c). The colored lines are contour plots representing the skyrmion boundary pathway for the pinning sites 1-4. b-d) Single Kerr microscopy images show arbitrary stripe domains inside the confinement. The colored contour lines are as in Fig. 2a).

HOD-08. Orbital angular momentum of a domain wall and geometrically twisted magnons.
S. Lee[1] and S. Kim[1] *1. Physics, Korea Advanced Institute of Science and Technology, Daejeon, The Republic of Korea*

We theoretically study the dynamics of a domain wall in a ferromagnetic nanotube driven by electrons and magnons by investigating the electron-domain-wall and magnon-domain-wall interactions. Due to the geometry of the sample, domain walls are classified by the Skyrmion charge which counts the winding number of magnetic textures on the domain wall [1]. The domain wall with a non-zero Skyrmion charge generates an emergent magnetic field for interacting particles, which exerts the Lorentz force on moving electrons and magnons and thereby deflects their trajectories. This deflection is manifested as the generation of the finite orbital angular momenta of the electrons and magnons that traverse the domain wall [2,3]. For the case of electrons, we can interpret the exchange of orbital angular momenta between electrons and the domain wall as a current-induced torque. From this peculiar torque, the domain wall with the non-zero Skyrmion charge can be driven by an arbitrary small current without the Walker breakdown. For the case of magnons, we obtain the exact solution for the magnon on the Skyrmion-textured domain wall and also their scattering properties with the domain wall with the aid of supersymmetric quantum mechanics (SUSY QM). We also show that there is a critical wavenumber for the total reflection and it is discretized by the Skyrmion charge of the domain wall. Our results show that the orbital angular momenta of magnetic systems and quasi-particles can be intertwined in a curved geometry.

[1] S. Lee and S. K. Kim, Orbital angular momentum and current-induced motion of a Skyrmion-textured domain wall in a ferromagnetic nanotube, arXiv:2102.08405. [2] C. Jia, D. Ma, A. F. Schäffer, and J. Berakdar, Twisted magnon beams carrying orbital angular momentum, Nat. Commun. 10, 2077 (2019). [3] Y. Jiang, H. Y. Yuan, Z.-X. Li, Z. Wang, H. W. Zhang, Y. Cao, and P. Yan, Twisted Magnon as a Magnetic Tweezer., Phys. Rev. Lett. 124, 217204 (2020).

Fig. 1. A ferromagnetic nanotube with a domain wall possessing a finite Skyrmion charge. The arrows represent magnetizations of spin-wave excitations. The black curve lines the heads of the arrows. The axis of the nanotube is *the z*-axis.

HOD-09. Chiral droplets in ferromagnets, and their current-driven motion. *S. Komineas*[1,2], N. Sisodia[3,4], P.K. Muduli[4] and N. Papanicolaou[5] *1. Institute of Applied and Computational Mathematics, Foundation for Research and Technology - Hellas, Heraklion, Greece; 2. Department of Mathematics and Applied Mathematics, University of Crete, Heraklion, Greece; 3. SPINTEC, CNRS, Grenoble, France; 4. Department of Physics, Indian Institute of Technology Delhi, Delhi, India; 5. Department of Physics, University of Crete, Heraklion, Greece*

We find numerically skyrmionic textures with skyrmion number Q=0 in ferromagnets with the Dzyaloshinskii-Moriya interaction perpendicular anisotropy and the magnetostatic field [1]. The configuration is asymmetric; the largest part has the form of a skyrmion and a smaller part has the form of an antiskyrmion. The texture is topologically trivial (Q=0) and it may be called a chiral droplet. Droplets are stable in an infinite film as well as in disk-shaped magnetic elements. They are stable also in a model without the magnetostatic field [2]. They are found in films for values of the parameters close to the transition from the ferromagnetic to the spiral phase. Chiral droplets are a valuable addition to a short list of skyrmionic textures [3]. The presence of topologically trivial textures (Q=0) along with usual skyrmions (Q=1) in the same magnetic system is rare. It is important because the dynamics of skyrmions is linked to their topology; it depends on the skyrmion number. Under spin-transfer torque (due to an in-plane current), droplets are accelerated in the direction of the current flow and they behave as solitary waves of Newtonian character with no Magnus force effect. This is in stark contrast to the Hall dynamics of the standard Q=1 skyrmion. In the case shown in the figure, the motion is initially complicated, with the droplet making a full π turn while its size is expanded. It is accelerated in the direction of the current and eventually, the velocity acquires a constant value, in very good agreement with the theoretical prediction. The dynamical behavior of a droplet can be compared to that of an axially symmetric skyrmionium [4] in order to show that the global topology rather than the symmetry of the configuration is crucial for skyrmion dynamics. We acknowledge support by the project ThunderSKY, funded by HFRI and GSRT, under Grant No. 871.

[1] N. Sisodia, P. K. Muduli, N. Papanicolaou, and S. Komineas, Phys. Rev. B, 103, 024431 (2021). [2] VV. M. Kuchkin, B. Barton-Singer, F. N. Rybakov, S. Blügel, B. J. Schroers, and N. S. Kiselev, Phys. Rev. B 102, 144422 (2020). [3] B. Göbel, I. Mertig, O. A. Tretiakov, Phys. Rep. 895, 1 (2021). [4] S. Komineas and N. Papanicolaou, Phys. Rev. B 92, 174405 (2015).

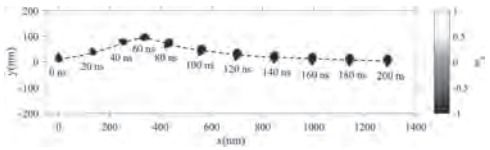

The motion of a chiral droplet when an in-plane current is applied. The droplet is represented via the perpendicular component of the magnetization m_z (color-coded). In the initial stage, the droplet is following a complicated path, it rotates and its shape adjusts to that of a propagating solitary wave. It eventually moves with no Magnus force effect.

HOD-10. Atomistic Simulations of Antiferromagnetic Skyrmions' High-Speed Dynamics and Contrast with Domain Wall Motion. *E.A. Tremsina*[1,2], A. Wittmann[1] and G.S. Beach[1] *1. Department of Materials Science and Engineering, Massachusetts Institute of Technology, Cambridge, MA, United States; 2. Department of Electrical Engineering and Computer Science, Massachusetts Institute of Technology, Cambridge, MA, United States*

Antiferromagnetic skyrmions (AFMSks) have received great interest due to their advantageous properties stemming from the absence of stray fields or Magnus force in antiferromagnetic (AFM) materials. Recent studies revealed that AFM Domain Walls (DWs) can be accelerated to high velocities, where they begin to display relativistic properties, namely velocity saturation to spin wave group velocity v_m and a Lorentz contraction of the DW width[1,2]. AFMSks have been shown to undergo dynamic elliptical elongation[3,4] and were predicted to have a special critical velocity limit v_c, dictated by the Dzyaloshinskii–Moriya interaction (DMI), which also serves to stabilize the skyrmion in the material[5]. However, the exact nature of AFMSk deformations and especially whether they follow Lorentz-invariant solitonic behavior, is not fully understood. Using VAMPIRE[6] atomistic simulations, we show that AFMSks possess fundamentally different dynamic properties than DWs in the same material. AFMSks display a linear velocity-current behavior, but undergo structural deformation which is not linked to relativistic behavior under Lorentz invariance. In addition to the observed dynamic elliptical elongation, we also note an asymmetric stretching(contraction) of the bounding skyrmion domain wall along the perpendicular(parallel) axes to motion. The latter effect has not been addressed previously and does not follow the Lorentz contraction pattern of a single DW. We uncover a universal relationship between the dynamic change in skyrmion size and its velocity relative to the critical limit v_c for a range of material parameters. Lastly, we show that v_c depends on the same material parameters which govern the equilibrium AFMSk structure, and more compact skyrmions (lower radius-to-wall width ratio) can reach higher speeds due to less prominent deformation effects. These results could prove significant for the potential applications of AFMSks for novel logic and memory devices.

1. L. Caretta, S.H. Oh, *et al., Science, 370(6523), 1438–1442 (2020)* 2. T. Shiino, S.H.Oh, *et al.,Phys. Rev. Lett., 117, 087203.* (2016) 3. A. Salimath, *et al.*, Phys. Rev. B 101, 024429 (2020) 4. C. Jin, C.Song, *et al.*, Appl. Phys. Lett. 109, 182404 (2016) 5. S. Komineas, N. Papanicolaou, SciPost Phys*., 8*, 86. (2020) 6. R. Evans, W. Fan, *et al.*, J. Phys.: Condens. Matter 26, 103202 (2014)

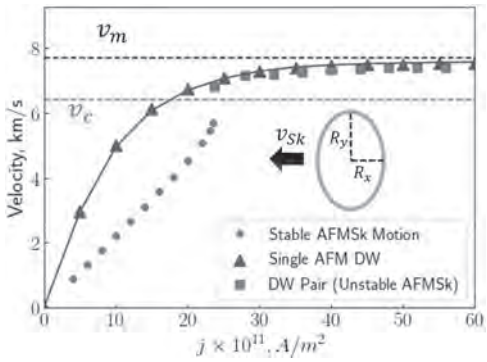

AFMSk vs single DW current-driven dynamics. DWs undergo relativistic velocity saturation to magnon velocity v_m, while AFMSk can only exhibit stable dynamics below a threshold v_c, which is linked to their elliptical deformation and eventual breakdown into a pair of DWs.

HOD-11. Withdrawn

HOD-12. Spin-Wave Resonances of Magnetic Hopfions. *D.W. Raftrey*[1,2] and P. Fischer[1,2] *1. Physics, University of California Santa Cruz, Santa Cruz, CA, United States; 2. Material Science, Lawrence Berkeley National Laboratory, Berkeley, CA, United States*

Spin textures are the foundation of properties of magnetic materials and drive the functionality of magnetic devices. Topological spin textures have led to intense research e.g. in magnetic skyrmions[1] addressing a broad spectrum of challenging scientific and technological questions, including stability, dynamics[2], nucleation, and transport. So far, topological spin textures have been treated foremost as two-dimensional spin textures, however, recent investigations have taken a conceptual leap to three-dimensional nanoscale size magnetic spin textures. Among these spin textures are target skyrmions: double skyrmions that are more stable in three dimensions, Hopfions: linked three dimensional knots[3, 4], and torons: the un-linked pre-images of Hopfions. Here, we report on micromagnetic simulations of fast dynamics in three dimensional spin textures. We focus on the resonant spin wave modes of magnetic Hopfions up to 15 GHz driven by external magnetic fields. A sharp transition is found around 66 mT coinciding with a transition from Hopfions to torons. The modes exhibit characteristic amplitudes in frequency space accompanied by unique localization patterns in real space, and are found to be robust to damping around topological features, particularly vortex lines in Hopfions and Bloch points in torons. Most remarkably, we have identified pronounced differences in spin wave spectra between Hopfions, torons and target skyrmions that can serve as fingerprints in future experimental validation studies of these novel 3d topological spin textures. This work was funded by the U.S. Department of Energy, Office of Science, Office of Basic Energy Sciences, Materials Sciences and Engineering Division under Contract No. DE-AC02-05-CH11231 (NEMM program MSMAG)

[1] Woo, S. et al. Observation of room-temperature magnetic skyrmions and their current-driven dynamics in ultrathin metallic ferromagnets. Nature Materials 15, 501, doi:10.1038/nmat4593 (2016). [2] Büttner, F. et al. Dynamics and inertia of skyrmionic spin structures. Nature Physics 11, 225-228, doi:10.1038/nphys3234 (2015). [3] Wang, X. S., Qaiumzadeh, A. & Brataas, A. Current-Driven Dynamics of Magnetic Hopfions. Physical Review Letters 123, 147203, doi:10.1103/PhysRevLett.123.147203 (2019). [4] Liu, Y., Hou, W., Han, X. & Zang, J. Three-Dimensional Dynamics of a Magnetic Hopfion Driven by Spin Transfer Torque. Physical Review Letters 124, 127204, doi:10.1103/PhysRevLett.124.127204 (2020).

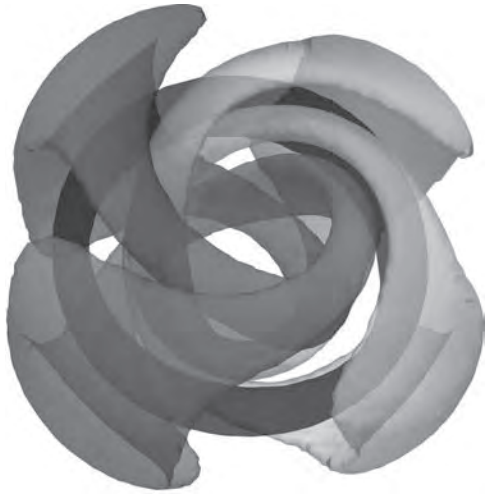

An artistic rendering of a simulated magnetic Hopfion.

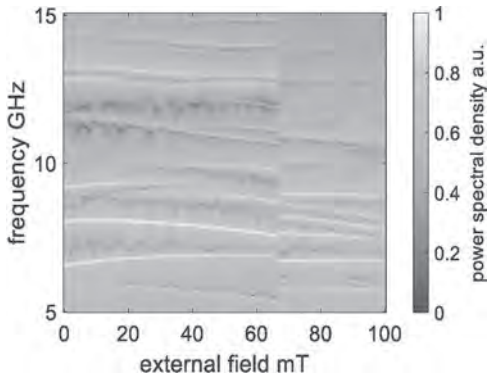

The resonant spin wave mode structure of a Magnetic Hopfion under an applied magnetic field.

HOD-13. Influence of domain wall anisotropy and dimensionality on the current-induced hysteresis loop shift for quantification of the Dzyaloshinskii-Moriya interaction. *T. Dohi*[1,2], S. Fukami[1,3] and H. Ohno[1,3] *1. RIEC, Tohoku University, Sendai, Japan; 2. Institut für Physik, JGU, Mainz, Germany; 3. CSIS, Tohoku University, Sendai, Japan*

The Dzyaloshinskii-Moriya interaction (DMI) is known to stabilize chiral spin textures which add new functionalities in spintronic technologies [1,2]. Some methods to quantify the strength of the DMI have been proposed. In particular, the current-induced hysteresis loop shift [3] is frequently used as it can simultaneously evaluate a spin-orbit torque efficiency χ_{SOT} and does not require any specific apparatus. However, there remain some open questions including a nonlinear behavior of χ_{SOT} against in-plane field $H_{x,y}$ and larger DMI values determined by this method than that by others [4-6]. To address these issues, we systematically investigate the DMI in various systems. Figures 1(a) and (b) show the H_x dependence of χ_{SOT} in small and large DMI systems, respectively. Linear behavior is observed in small DMI systems, whereas the large DMI systems show nonlinear behavior of the χ_{SOT}. Also, we find that for both cases the DMI effective fields (H_{DMI}) derived by the original model [3] are quantitatively different from those obtained by other methods. We revisit the model and find that the domain wall (DW) anisotropy should be considered in the analysis and the corrected value shows a good agreement with that determined by other methods [7]. We also examine the influence of the dimensionality of DW motion, i.e., the direction of DW motion along and perpendicular to the current direction, on the quantification of H_{DMI} with the current-induced hysteresis loop shift. We find that linear behavior could be observed even in large DMI systems unlike Fig. 1(b) if the direction of DW motion is not constrained to the current direction; however, the derived H_{DMI} does not represent the real value [7]. The present findings offer an important insight for reliable quantification of DMI. A portion of this work was supported by the ImPACT Program of CSTI, JSPS Kakenhi No. 19H05622, and RIEC Cooperative Research Projects.

[1] Q. Shao *et al.*, IEEE Trans. Magn. 57, 800439 (2021). [2] S.-H. Yang *et al.*, Appl. Phys. Lett. 116, 120502 (2020). [3] C.-F. Pai *et al.*, Phys. Rev. B 93, 144409 (2016). [4] S. Ding *et al.*, Phys. Rev. B 102, 054425 (2020). [5] Z. Dai *et al.*, ACS Appl. Electron. Mater. 611, 3 (2021). [6] T. Dohi *et al.*, Nat. Commun. 10, 5153 (2019). [7] T. Dohi *et al.*, Phys. Rev. B 103, 214450 (2021).

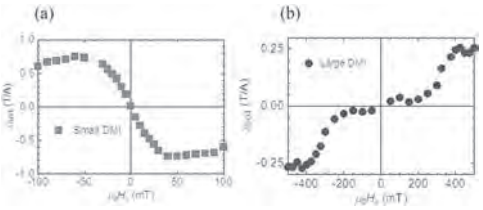

Fig. 1 (a) In-plane field dependence of χ_{SOT} in the small and (b) large DMI systems [7].

HOD-14. Chiral Brownian motion of the magnetic skyrmions.
S. Miki[1,2], Y. Jibiki[1,2], E. Tamura[1,2], M. Goto[1,2], M. Oogane[3], R. Ishikawa[4], H. Nomura[1] and Y. Suzuki[1] *1. Graduate School of Engineering and Science, Osaka University, Toyonaka, Japan; 2. CSRN-Osaka, Osaka University, Toyonaka, Japan; 3. Department of Applied Physics, Tohoku University, Sendai, Japan; 4. ULVAC, Inc., Suita, Japan*

Magnetic skyrmions, which are topologically protected particle-like spin textures, exhibit Brownian motion at ambient temperatures in a ferromagnetic thin film. The skyrmion system can be an ideal platform to design unconventional computers like stochastic/Brownian computers. Therefore, investigation of the Brownian motion of the magnetic skyrmion is now the subject of scientific and technical interest [2-5]. The motion of skyrmions driven by the current [6] and temperature gradient [7] have the chirality depending on the skyrmion number. In this study, we explore the effects of the chiral property of a skyrmion on its Brownian motion experimentally and theoretically. We fabricated the stacking structure as Ta(5)|$Co_{16}Fe_{64}B_{20}$(1.26)|Ta(0.22)|MgO(1.5)|SiO_2(5.0) and observed the position of the skyrmion $\mathbf{x}(t) = (x(t), y(t))$ by using MOKE microscope. Fig. 1 shows the simultaneous velocity-position correlation function $\langle \mathbf{v}(t) \bullet \mathbf{x}(t) \rangle$ and $\langle (\mathbf{v}(t) \times \mathbf{x}(t))_z \rangle$. After enough time has passed, $\langle \mathbf{v}(t) \bullet \mathbf{x}(t) \rangle$ and $\langle (\mathbf{v}(t) \times \mathbf{x}(t))_z \rangle$ correspond to the diffusion coefficient D_{xx} and the angular momentum of the skyrmionic diffusion, respectively, and the latter also has a sizable value. Fig. 2 represents the simulation trajectory in the periodic potential obtained by integrating the Thiele-Langevin eq. [8,9] including the thermal fluctuation and the mass term. The chirality of the Brownian motion is affected by the fluctuated potentials of the samples. This research and development work was supported by ULVAC, Inc., the Ministry of Internal Affairs and Communications, JSPS Grant-in-Aid for Scientific Research (S) Grant Number JP20H05666, Japan and CREST (Non-classical Spin project, JPMJCR20C1) of the Japan Science and Technology Agency.

[1] S. Miki, *et al. J. Phys. Soc. Jpn.* 90, 083601 (2021) [2] E. Tamura & Y. Suzuki, arXiv:1907.06926v1 (2019) [3] Y. Jibiki, S. Miki, *et al. Appl. Phys. Lett*. 117, 082402 (2020) [4] L. Zhao *et al.*, *Phys. Rev. Lett.* 125, 027206 (2020) [5] Y. Suzuki, S. Miki and E. Tamura, arXiv:2104.02345v2 (2021) [6] W. Jiang, *et al. Nat. Phys.* 13, 162 (2017) [7] M. Mochizuki, *et al. Nat. Mater*. 13, 241 (2014) [8] A. Thiele, *Phys. Rev. Lett*. 30, 230 (1973) [9] C. Schuette *et al., Phys. Rev. B* 90, 174434 (2014)

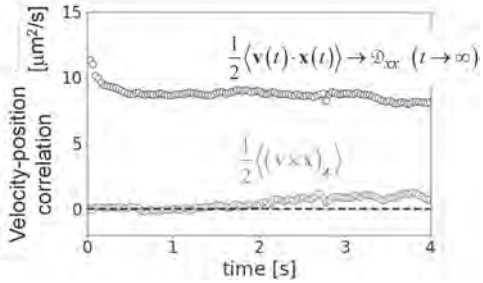

Fig. 1 velocity-position correlation function $\langle \mathbf{v}(t)\, \mathbf{x}(t) \rangle$ and $\langle (\mathbf{v}(t) \times \mathbf{x}(t))_z \rangle$

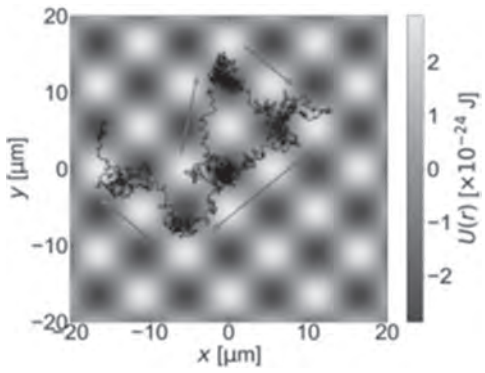

Fig. 2 The simulation result of the motion of the skyrmion in the periodic potential. The red arrows show the direction of the motion.

HOD-15. Anomalous thermal drift of skyrmions in frustrated magnets under spin-orbit torques.
J. Kim[1] *1. Centre de Nanosciences et de Nanotechnologies, CNRS, Université Paris-Saclay, Palaiseau, France*

Skyrmions are topological spin textures that exhibit particle-like dynamics under current-driven forces such as spin-orbit torques (SOT). In frustrated magnets, competing exchange interactions along with the Dzyaloshinskii-Moriya interaction (DMI) can aid in stabilizing textures of different topologies, like skyrmions and antiskyrmions [1], which exhibit different motion under SOT, such as trochoidal trajectories and skyrmion-antiskyrmion pair generation, in addition to the usual rectilinear motion. Such behavior results from a departure from the frozen-core limit, where additional dynamics in the (anti)skyrmion helicity couples to the core position [2]. Here, we discuss the role of thermally driven helicity dynamics in the Brownian motion of skyrmions under weak DMI and SOT. Depending on the magnitude of the DMI, which governs the strength of the restoring force experienced by the helicity, with respect to k_BT, the thermal drift of the skyrmion core under weak SOT can differ greatly from the dynamics at 0 K (Fig. 1). This behavior arises from the thermal drift and diffusion of the helicity under SOT, which is analogous to the well-known problem of Brownian motion in a tilted washboard potential, where the helicity can be assimilated to an oscillator phase in a periodic potential with a linear force term. Under weak SOT or strong DMI, we recover a "phase-locked" solution in which the helicity is pinned, resulting in rectlinear drift. For strong SOT or weak DMI, we find a "free-running" solution, where the helicity varies continuously in time and results in an amplified Brownian diffusion of the skyrmion core. In between these two regimes, thermally-activated hopping of the helicity between energy minima occurs. These results highlight the importance of helicity dynamics and may have bearing on dipole-stabilized bubbles for which drive-dependent skyrmion Hall angles [3] and low drift velocities have been reported [4].

[1] S. Z. Lin and S. Hayami, Physical Review B *93*, 064430 (2016). [2] U. Ritzmann et al. Nature Electronics *1*, 451 (2018). [3] K. Litzius et al. Nature Electronics *3*, 30 (2020). [4] W. Jiang et al. Science *349*, 283 (2015).

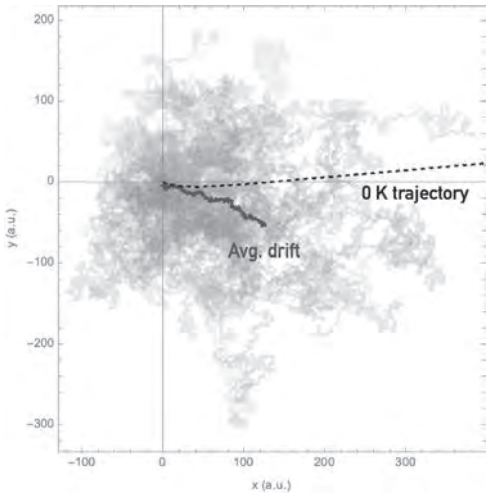

Fig. 1. Comparison between SOT-driven skyrmion motion at 0 K (black line) and 50 different realisations of the Brownian motion at 10 K (colored lines), along with the average thermal drift at 10 K (purple line).

Session HOE
MAGNETIC SKYRMIONS
Olivier Boulle, Chair
SPINTEC, Grenoble, France

CONTRIBUTED PAPERS

HOE-01. Microwave-assisted excitation of a skyrmion lattice. *H. Yang*[1], M. Hervé[2], L. Desplat[3], T. Balashov[4], P. Buhl[5], P.A. Hervieux[3], B. Dupé[6,7] and W. Wulfhekel[1] *1. Karlsruhe Institute of Technology, Karlsruhe, Germany; 2. Institut des NanoSciences de Paris, Sorbonne University, Paris, France; 3. IPCMS, Universite de Strasbourg, Strasbourg, France; 4. RWTH Aachen University, Aachen, Germany; 5. Johannes Gutenberg University Mainz, Mainz, Germany; 6. Fonds de la Recherche Scientifique, Bruxelles, Belgium; 7. University of Liège, Liège, Belgium*

Recent developments of implementing radio-frequency voltage modulation into a scanning tunneling microscope have revealed great insights into the spin dynamics of single atoms. However, up to now most of the observed single-atom electron spin resonance relied on the modulated tip-subject displacements for generating ac magnetic fields. The accessible systems, thereby, are limited to single spins adsorbed on insulating thin films specifically on the MgO surfaces. Here, we demonstrated an alternative utilizing the spin-transfer torque for inducing effective ac magnetic fields and in turn expanding the experiments towards the ferromagnetic resonance regime on a skyrmion lattice.

HOE-02. Configurable Pixelated Skyrmions on Nanoscale Grids. *X. Zhang*[1], J. Xia[1], K. Shirai[1], H. Fujiwara[1], O. Tretiakov[2], M. Ezawa[3], Y. Zhou[4] and X. Liu[1] *1. Shinshu University, Nagano, Japan; 2. University of New South Wales, Sydney, NSW, Australia; 3. University of Tokyo, Tokyo, Japan; 4. The Chinese University of Hong Kong, Shenzhen, China*

The magnetic spin textures with non-trivial topology have been an important topic in the fields of magnetism and spintronics for the last few years [1]. For example, the magnetic skyrmion is a promising topological spin texture, which exists in perpendicularly magnetized systems and can be used as a spintronic information carrier. In this talk, we will show the dynamics of skyrmions on the artificial nanoscale square grid, which can be formed by orthogonal defect lines with reduced perpendicular magnetic anisotropy (PMA) [2]. We find that a skyrmion on the grid is pixelated with a quantized size of the grid. We can store digital information in the position, size, and shape of skyrmions. The center of the skyrmion is quantized to be on the grid and the skyrmion shows a hopping motion instead of a continuous motion. We show that the skyrmion Hall effect is perfectly prohibited due to the pinning effect of the grid. We computationally demonstrate that the position, size, and shape of skyrmions on the square grid are electrically configurable, which may be harnessed to build the programmable racetrack-type memory, multistate memory, and logic computing device. Finally, we will give an outlook on other possible topological spin textures, which can be manipulated on the artificial nanoscale grids. We believe the results presented in this talk could be a basis of future digital computation based on skyrmions on the grid.

[1] Nat. Rev. Phys. 2, 492 (2020); J. Phys. D: Appl. Phys. 53, 363001 (2020); J. Phys.: Condens. Matter 32, 143001 (2020); J. Appl. Phys. 124, 240901 (2018); Nat. Rev. Mats. 2, 17031 (2017); Adv. Mater. 29, 1603227 (2017); Phys. Rep. 704, 1 (2017); J. Phys. D: Appl. Phys. 49, 423001 (2016); Proc. IEEE 104, 2040 (2016); Nat. Rev. Mats. 1, 16044 (2016); J. Phys.: Condens. Matter 27, 503001 (2015); Nat. Nanotech. 8, 899 (2013). [2] Nano Letters 21, 4320 (2021).

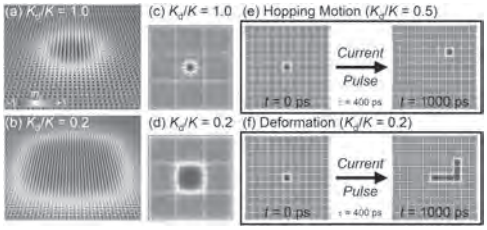

Fig. 1. (a) Illustration of an ordinary skyrmion with a unity topological charge. (b) Illustration of a square-shaped skyrmion with a unity topological charge. (c) Top view of the sample with K_d/K = 1. K_d and K indicate the PMA constants for defect lines and unmodified areas, respectively. Defect lines are indicated by yellow lines. (d) Top view of the sample with K_d/K = 0.2. (e) Hopping motion of a square-shaped skyrmion induced by a current pulse. (f) Deformation of a square-shaped skyrmion induced by a current pulse.

HOE-03. Influence of Geometry on Domain-Wall Pair to Skyrmion Conversion in Typical Magnetic Nanochannel. *H. Perumal*[1], S. Syamlal[1] and J. Sinha[1] *1. Department of Physics and Nanotechnology, SRM Institute of Science and Technology, Kattankulathur, Chennai, India*

In order to develop energy efficient race track memory devices, it is crucial to create and controllably move chiral spin textures, namely, skyrmions in magnetic nanotrack. In recent time, intense efforts have been dedicated to understand the mechanism of domain wall pair to skyrmion conversion in different junction geometry that may fit into the memory applications [1,2]. Here, we study the mechanism of DW pair to skyrmion conversion in a typical junction geometry which consists of the combination of two narrow nanotracks (length – 800 nm, thickness – 1 nm, width varying from 20 nm to 60 nm in steps of 20 nm) and a wide track (width 200 nm). The separation between narrow channels are selected as 10 nm, 30 nm and 50 nm. The micromagnetic simulations have been performed using Ubermag to investigate the magnetization dynamics and the Zhang-Li torque evolver is implemented in Landau Lifshitz Gibert equation to drive the DWs using spin polarized current [3]. For a fixed Gilbert damping parameter (α = 0.3) and different values of non-adiabatic spin torque parameter (β = 0.2, 0.3 and 0.5) we investigate the DW to skyrmion conversion in these nanotracks. Interestingly, under the influence of spin torque, the DW pair gets converted to skyrmion only if the geometrical constraints allow the favorable instability to set in at the junction between optimally separated narrow channels and wide channel (cf. Fig. 1(a-d)) [4]. For certain width and separation between the narrow channels, the DW pair to skyrmion conversion cannot be observed for sufficiently large time scale (cf. Fig. 2(a-d)). We believe these results will be helpful in designing the skyrmion based racetrack memory where the controlled creation of skyrmion is expected to play crucial role.

[1] A. Fert, V. Cross, J. Sampaio Nature Nanotech., Vol. 8, p.152 (2013). [2] Y. Zhou, M. Ezawa, Nat. Commun., Vol. 5, p.4652 (2014). [3] M. Beg, M. Lang, H. Fangohr, IEEE Trans. Magn. p.1 (2021) [4] P. Hari Prasanth, S.K. Syamlal, J. Sinha, In Press, ECS J. Solid State Sci.Technol. (2021).

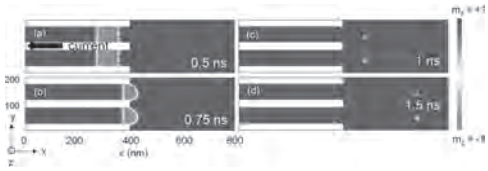

Fig 1: Snapshot of DW pair to skyrmions conversion from two narrow channels for α = β = 0.3, width of the narrow nanochannel = 60 nm, separation between the narrow channel = 30 nm

Fig 2: DW dynamics from two channels for α = β = 0.3, width of the narrow nanochannel = 40 nm, separation between the narrow channel = 10 nm

HOE-04. Current induced skyrmion nucleation at zero field.
S.K. Panigrahy[1], S. Mallick[1], G. Pradhan[1] and S. Rohart[1] *1. Laboratoire de Physique des Solides, Université Paris Saclay, Orsay, France*

For their applications in spintronics, skyrmions need to be controlled one by one, and therefore appear as excitations over a uniform ground state. This is why in most demonstrations, the application of an external field is required. In this study, we show by fine-tuning the micromagnetic parameters, through their control by the ferromagnetic layer thickness, multilayers can be optimized to host zero field skyrmion excitations. We study Pt/Co/Au based heterostructures with varying Co thickness t. Close to the spin reorientation transition (t = 1.6 nm), the domain wall energy vanishes and the ground state is a stripe phase. To favor the uniform state, t is reduced to increase the magnetic anisotropy, until samples show a 100% remanence. Below 1.45 nm, skyrmions could be obtained and stabilized during the magnetization reversal process, and remain stable at zero field. This bistable situation offers a perfect playground to study current-induced nucleation in zero field, which we study in the vicinity of a point contact. Starting from a uniform state, current pulses lead to the formation of magnetic textures. However, to avoid the formation of elongated structures, similar to stripes, Co thickness needs to be further reduced. At 1.2 nm, the magnetic anisotropy is sufficiently large to cut elongated structures into well-defined skyrmions, which could be obtained with good reproducibility. Their topological nature is proven through the observation of the skyrmion Hall effect: depending on the orientation of the initial state, skyrmions are deflected in one or the other directions. Velocities of about 50 m/s induced by SOT, using a current density of 3.7 x 10^{12} A/m^2 in 1μm wide tracks were also observed. This opens an important perspective towards skyrmionic devices at zero field, in particular concerning stacks that are not sensitive to external fields such as ferrimagnets and antiferromagnets. Figure: Zero field MFM images of 3 μm wide magnetic nanotracks, after successive application of 3.7 x 10^{12} A/m^2, 3 ns long current pulses starting from a saturated track. In the first serie (a-c) the sample is initially magnetized downward, in the second one (d-f), it is magnetized upward, evidencing the gyrotropic deflection.

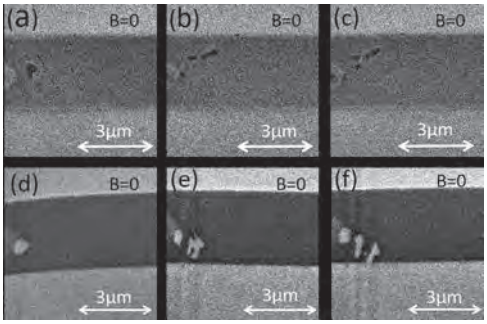

HOE-05. In-situ GHz Dynamics of Skyrmions Probed with SANS.
N. Tang[1], S. Montoya[2], N.C. Liyanage[4], S.K. Patel[2,3], L.J. Quigley[1], A.J. Grutter[5], M.R. Fitzsimmons[4,6], S.K. Sinha[3], J.A. Borchers[5], E. Fullerton[2,7], L. Debeer-Schmitt[8] and D.A. Gilbert[1,4] *1. Material Science Engineering, University Tennessee, Knoxville, Knoxville, TN, United States; 2. Center for Memory and Recording Research, University of California, San Diego, San Diego, CA, United States; 3. Physics Department, University of California, San Diego, San Diego, CA, United States; 4. Department of Physics and Astronomy, University of Tennessee, Knoxville, Knox, TN, United States; 5. NIST Center for Neutron Research, National Institute of Standards and Technology, Gaithersburg, MD, United States; 6. Neutron Scattering Division, Oak Ridge National Laboratory, Oak Ridge, TN, United States; 7. Department of Electrical and Computer Engineering, University of California, San Diego, San Diego, CA, United States; 8. High Flux Isotope Reactor, Oak Ridge National Laboratory, Knoxville, TN, United States*

Magnetic skyrmions present interesting and unique pseudo-particle behaviors which arises from their topological protection [1-2]. Key among these behaviors is their resonant dynamics, under microwave fields, which include both breathing and gyration modes. Due to their small size, and magnetic-only contrast of skyrmions, coupled with high frequency dynamics – in the GHz regime – it is challenging to do *in-situ* measurements on these excitations. This work reports the use of small angle neutron scattering (SANS) to capture the dynamics of hybrid skyrmions stabilized in Fe/Gd multilayers by means of dipolar interactions. Using perpendicular DC fields and in-plane RF fields, we explored the gyration modes of hybrid skyrmions away, below, at, and above resonance [Fig.1(a-d)]. We find the dynamic modes of hybrid skyrmions contribute to the SANS signal in two ways: first, the scattered neutrons incur additional transverse momentum as a result of scattering from a moving source, and second, the gyration skyrmions disrupt ordering of the lattice giving rise to enhancement form-factor scattering. Ferromagnetic resonance measurements confirm the RF and DC field conditions for these gyration modes. Our results offer new insights into the nanoscale dynamics of magnetic skyrmions and present a unique use of SANS to probe magnetization dynamics.

[1] S. A. Montoya *et al.*, Physical Review B 95, 224405 (2017). [2] R. D. Desautels *et al.*, Physical Review Materials 3, 104406 (2019).

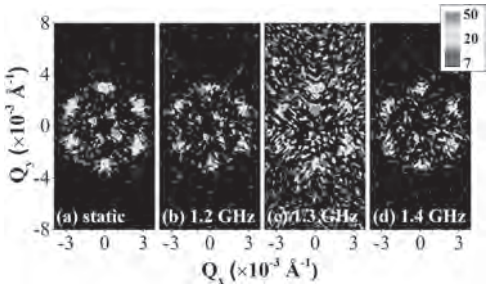

Fig.1 2D SANS pattern of magnetic skyrmions under different magnetic fields and excitation frequencies: (a) Static state (H=0, RF=0), (b) below-resonance state (H=150 mT, RF=1.2 GHz), (c) at-resonance state (H=150 mT, RF=1.3 GHz) and (d) above-resonance state (H=150 mT, RF=1.4 GHz). All 2D images are plotted with the same intensity scale.

HOE-06. Magnetostatic coupling between the skyrmion state in isolated nanodot with saturated ferromagnetic waveguide. *M.K. Zelent*[1], M. Moalic[1] and M. Krawczyk[1] *1. Institute of Spintronics and Quantum Information, Faculty of Physics, Adam Mickiewicz University, Poznan, Poland*

Magnetic skyrmions, the smallest stable magnetization textures, possess intriguing properties and potential applications for information storing, with racetrack 3D memories as an example, and also steering spin waves [1]. However, their stabilization requires special conditions and usually happens in multilayered structures due to interface induced Dzyaloshinskii-Moriya interactions (DMI). The development requires knowledge about the hybrid systems composed of the skyrmion and the other magnetic elements. In this work, using micromagnetic modelling, we propose a concept of symmetry-breaking and show the egg-shape like Néel skyrmion stabilization in the single nanodot dipolary coupled to a thin ferromagnetic waveguide (Fig. 1). We demonstrate this for a system composed of Pt/Co/Ir nanodot and Permalloy waveguide, with an isolated skyrmion in magnetic nanodot located slightly above the in-plane magnetized waveguide. The presence of a nanodot with a magnetization direction perpendicular to the magnetization direction in the waveguide forces a strong imprint, skyrmion-shadow, i.e., a local perturbation of the magnetization in the waveguide. This imprint creates the reactive field, which deforms the skyrmion. We performed systematical micromagnetic simulations for many values of the DMI, which allow us to compare systems with different skyrmion shapes and to explain the source and role of mutual magnetostatic interactions between the waveguide and the skyrmion in the nanodot. Furthermore, we demonstrate that this hybrid magnetic system can be interested in magnonic applications, especially as a source of short wavelengths spin waves, especially with strongly enhanced amplitude of the antisymmetric modes.

[1]. J. Chen, J. Hu, and H. Yu, *ACS Nano* 2021, 15, 3, 4372–4379. The research has received funding from the Polish National Science Centre, project no. UMO-2017/27/N/ST3/00419 and UMO-2018/30/Q/ST3/00416.

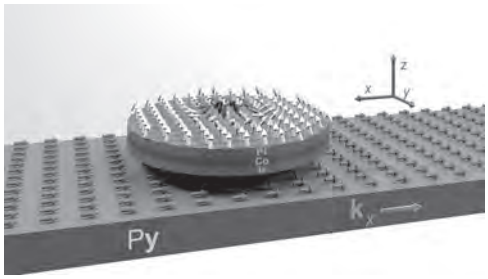

Fig. 1. An artistic visualization of the system under consideration. The Pt/Co/Ir multilayer dot is placed slightly above a Py waveguide. The arrows indicate the direction of magnetization. In the dot we assume a single-domain state or a Néel-type skyrmion state

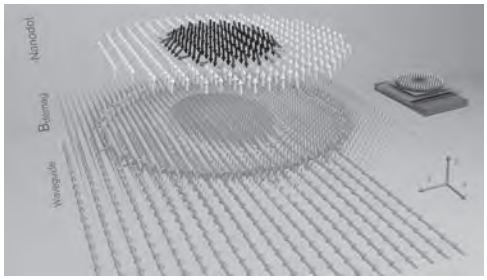

Fig. 2. The 3D plot of the deformed skyrmion in nanodot, the magnetostatic field between the nanodot and imprinted in the waveguide skyrmion-shadow spin texture.

HOE-07. Driving skyrmions with low threshold current density in amorphous CoFeB thin film. *B. Ojha*[1], S. Mallick[2], M. Sharma[1], A. Thiaville[2], S. Rohart[2] and S. Bedanta[1] *1. School of Physical Sciences, National Institute of Science Education and Research (NISER), Jatni, India; 2. Laboratoire de Physique des Solides, Universite Paris-Saclay, Orsay Cedex, France*

Magnetic skyrmions are topologically stable spin swirling particle-like entities which are appealing for next-generation spintronic devices [1]. The expected low critical current density for the motion of skyrmions makes them potential candidates for future energy-efficient electronic devices [1, 2]. In the experimental perspective, there are three major challenges: (i) stabilization of skyrmions at room temperature, (ii) deterministic nucleation of skyrmions, and (iii) efficient motion of skyrmions under spin Hall effect (SHE). Over the last decade, many experimental works have been focused on the aforementioned directions to achieve the ambitious goal of skyrmion-based device applications. However, controlled nucleation and motion of individual skyrmions in nanotracks with low power consumption still remains a challenge. In this context, we have studied Pt/CoFeB/MgO heterostructures in which skyrmions have been stabilized at room temperature (RT). Amorphous CoFeB has been selected as the FM layer since the absence of grain boundaries results in lower pinning in comparison to polycrystalline FM layers (viz., Co, Fe, etc.) [3, 4]. It has been observed that the shape of the skyrmions are perturbed even by the small stray field arising from low moment magnetic tips while performing the magnetic force microscopy (MFM), indicating the presence of a low pinning landscape in the samples. This hypothesis is indeed confirmed by the low threshold current density (0.8×10^{11}A/m^2) to drive the skyrmions in our sample (Fig. 1(b)).

[1] A. Fert *et al.,*Nat. Rev. Mater. 2, 17130 (2017). [2] F. Jonietz *et al.*, Science 330, 1648 (2010). [3] S. Woo *et al.,* Nat. Mater. 15, 501 (2016). [4] B.Ojha *et al.,* arxiv.org/abs/2106.02407 (2021).

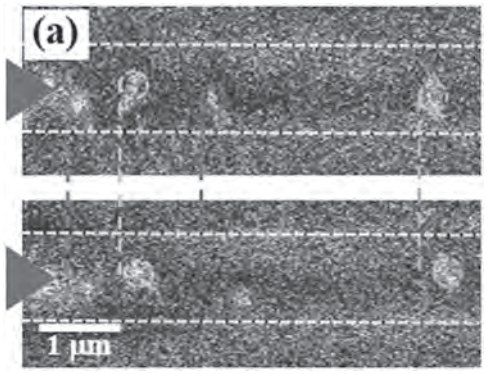

Fig. 1. top and bottom show the position (by coloured circles) and displacement (by coloured lines) of the skyrmions before and after application of one current pulse, respectively.

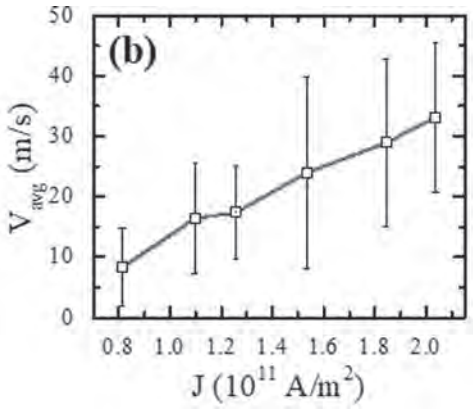

Fig. 2. shows the average skyrmion velocity as a function of different applied current densities.

HOE-08. Concept of current and field-free processing of chiral spin textures in racetrack devices. *A. Schäffer*[1,2], P. Siegl[1], M. Stier[1], J. Berakdar[2], M. Thorwart[1], R. Wiesendanger[1] and E.Y. Vedmedenko[1] *1. University of Hamburg, Hamburg, Germany; 2. Martin-Luther-University, Halle, Germany*

Topologically distinct magnetic structures like skyrmions, domain walls, and the uniformly magnetized state have multiple applications in logic devices, sensors, and as bits of information. One of the most promising concepts for applying these bits is the racetrack architecture controlled by electric currents or magnetic driving fields. In state-of-the-art racetracks, these fields or currents are applied to the whole circuit. Here, we employ micromagnetic and atomistic simulations to establish a concept for racetrack memories free of global driving forces [1,2]. Surprisingly, we realize that mixed sequences of topologically distinct objects can be created and propagated over far distances exclusively by local rotation of magnetization at the sample boundaries. We reveal the dependence between chirality of the rotation and the direction of propagation and define the phase space where the proposed procedure can be realized. The advantages of this approach are the exclusion of high current and field densities as well as its compatibility with an energy-efficient three-dimensional design.

[1] E. Y. Vedmedenko and D. Altwein, Phys. Rev. Lett. 112,017206 (2014) [2] A. F. Schäffer et al. Sci. Reports 10, 20400 (2020)

HOE-09. Engineering of spin-orbit torque in multilayers for efficient skyrmion displacement at zero field. *Y. Sassi*[2], S. Krishnia[1], F. Ajejas[1], D. Sanz Hernandez[1], S. Collin[1], K. Bouzehouane[1], A. Vecchiola[1], A. Fert[1], V. Cros[2] and N. Reyren[2] *1. Université Paris-Saclay, Unité Mixte de Physique, CNRS, Thales, Palaiseau, France; 2. Unité Mixte de Physique, CNRS, Thales, Université Paris-Saclay, Palaiseau, France*

Magnetic skyrmions are localized spin textures in thin magnetic multilayers, which behave as particles and are topologically different from the uniform magnetization state. They have been identified as extremely promising for future applications (racetrack memory, neuromorphic computing, etc), as well as of fundamental interest [1]. In the recent years, numerous efforts have been made to stabilise the sub-10 nm magnetic skyrmions in thin ferromagnetic/heavy metal heterostructures at room temperature [2]. Following these advancements, several groups have investigated current-induced motion of skyrmions by utilizing spin-orbit torques (SOT) generated in adjacent heavy-metal layers [3]. However, efficient current -induced dynamics of isolated skyrmions is still under investigation. In this study, we present SOT motion of skyrmions at room temperature and at zero field measured using MFM and/or MOKE microscopy in various magnetic multilayers. We will compare the following systems: $(Pt/Co/Al)_N$, $(Pt/Co/Ta/Al)_N$ and $(Pt/Co/Al/Ta/Al)_N$, which were designed to increase the SOT, in several device geometries. Pt and Ta exhibiting opposite spin Hall angles, they contribute additively to the net SOT [4]. We will discuss the design of the multi-repeats stacking and then the impact of the geometry regarding the nucleation. The skyrmion density and their size being controlled by tuning the external field, we stabilize states with a high density of skyrmions, as well as states with isolated skyrmions. We can then compare their dynamics as shown in Figure 1 where all the skyrmions are moving with the same velocity. We will show the evolution of the skyrmion velocity and the skyrmion Hall angle as a function of current density and as a function of the external magnetic field. French ANR grant TOPSKY (ANR-17-CE24-0025), DARPA TEE program grant (MIPR#HR0011831554) and EU grant SKYTOP (H2020 FET Proactive 824123) are acknowledged for their financial support.

[1] A. Fert, N. Reyren, V. Cros, Nat. Rev. Mat. 2 (2017), 17031. [2] C. Moreau-Luchaire et al. Nat. Nanotech, 11 (2016), 444 ; S. Woo et al. Nat. Mater. 15 (2016), 501 ; A. Soumyanarayanan et al. Nat. Mater. 16 (2017), 898 ; A. Hrabec et al. Nat. Comm. 8 (2017), 15765. [3] K. Litzius et al. Nat. Phys. 13 (2017), 170 ; S. Woo et al. Nat. Comm. 8 (2017), 15573. [4] S.Woo, M.Mann, A. J. Tan, L. Caretta, G. S. D. Beach, Appl. Phys. Lett. 105, 212404 (2014)

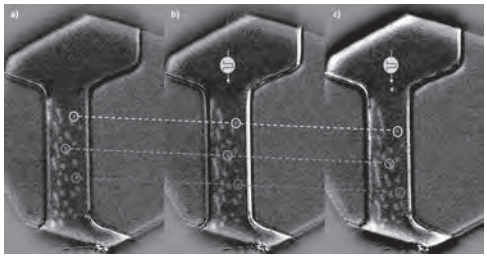

Figure 1: Coherent skyrmion motion observed by MOKE microscopy at zero field. a) Observation after nucleation, b) after 10 pulses, c) and after 20 pulses of 100ns with J = 1.4e^{11} Am^{-2}

HOE-10. Creation and Annihilation of Skyrmion Bubbles by Profile-Programmed Alternating Magnetic Field Pulses. *Y. Chen*[1,2], K. Ohara[1], Z. Xichao[1], J. Xia[1], Z. Wei[2], Y. Zhou[3] and X. Liu[1] *1. Shinshu University, Wakasato, Japan; 2. Zhengzhou University, Zhengzhou, China; 3. The Chinese University of Hong Kong, Shenzhen, China*

Skyrmion bubbles are topologically non-trivial objects in magnetic materials [1], which can be employed as nonvolatile information carriers in advanced functional spintronic devices, such as artificial neurons and synapses [2]. These advanced skyrmion-based applications require effective and controllable creation and annihilation of skyrmion bubbles in nanostructured devices [3]. In this talk, we will present our efforts on the creation and annihilation of skyrmion bubbles by using profile-programmed alternating magnetic field pulses in a micro-sized disk with stacks of [Pt (2 nm)/FeCo (0.8 nm)/Pt (1 nm)/CoNi (1.2 nm)/Pt (1 nm)/CoNi (1.2 nm)/Pt (0.5 nm)]. The magnetic field pulse is generated by a microfabricated single turn coil. By applying an alternating magnetic field with frequency in the range from 10 kHz to 10 MHz, we observe that dynamically stable spin textures are created in the disk. The type of created spin textures is found to depend on the amplitude and frequency of the alternating magnetic field. In addition, the contraction, expansion, and propagation of spin textures are also observed. Most importantly, we find that the creation and annihilation of numerous skyrmion bubbles can be realized by a single profile-programmed magnetic field pulse (see Fig. 1). These experimental observations can be interpreted by micromagnetic simulations. We believe that our results have great potential applications for artificial neural networks and bio-sensors.

[1] Nat. Rev. Phys. 2, 492 (2020); J. Phys. D: Appl. Phys. 53, 363001 (2020); J. Phys.: Condens. Matter 32, 143001 (2020); J. Appl. Phys. 124, 240901 (2018); Nat. Rev. Mats. 2, 17031 (2017); Adv. Mater. 29, 1603227 (2017); Phys. Rep. 704, 1 (2017); J. Phys. D: Appl. Phys. 49, 423001 (2016); Proc. IEEE 104, 2040 (2016); Nat. Rev. Mats. 1, 16044 (2016); J. Phys.: Condens. Matter 27, 503001 (2015); Nat. Nanotech. 8, 899 (2013). [2] Materials

Horizons 8, 854 (2021); Nature Electronics 3, 148 (2020); Nanotechnology 28, 08LT02 (2017); Nanotechnology 28, 31LT01 (2017). [3] Nano Lett. 19, 353-361 (2019); Nano Lett. 21, 4320-4326 (2021).

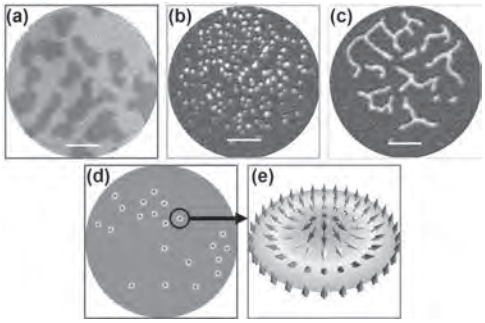

Fig. 1. Experimentally observed creation of (a) large magnetic domains, (b) skyrmion bubbles, and (c) chiral stripe domains induced by the profile-programmed alternating magnetic field pulse. Scale bar, 20μm. (d) Computational illustration of a disk sample with many skyrmions. (e) Schematic of a Neel-type skyrmion in our sample.

HOE-11. Collective Skyrmion Motion Under the Influence of an Additional Interfacial Spin-Transfer Torque. *C.R. MacKinnon*[1], K. Zeissler[2,3], S. Finizio[4], J. Raabe[4], C. Marrows[2,3], T. Mercer[1], P. Bissell[1] and S. Lepadatu[1] *1. Jeremiah Horrocks Institute for Mathematics, Physics and Astronomy, University of Central Lancashire, Preston, United Kingdom; 2. School of Physics and Astronomy, University of Leeds, Leeds, United Kingdom; 3. Bragg Centre for Materials Research, University of Leeds, Leeds, United Kingdom; 4. Swiss Light Source, Paul Scherrer Institut, Villigen, Switzerland*

Skyrmions have clear advantages for future spintronic devices over domain walls in terms of information carrying and storage, however there are still many open questions left and inherent challenges in the transition to applications. Here we study the effect of an additional interfacial spin-transfer torque (ISTT) [1], as well as the well-established spin-orbit torque (SOT), on skyrmion collections [2] – group of skyrmions dense enough that they are not isolated from one another – in magnetic multilayers, by comparing modelling using Boris [3], with experimental results. We show that skyrmion collective motion has additional effects not reproduced when compared to modelled isolated skyrmions [1]. In particular, as the skyrmion collection density increases the effect of local disorder is reduced, leading to reduced threshold current densities, and a sharper dependence of skyrmion Hall Angle (SkHA) on velocity in the depinning regime, in agreement with experimental results. When including both the ISTT and SOT, the small SkHA observed in experiment are in good agreement, also explaining the observed diameter-independent SkHA [4], as seen in Figure 1. Contrary to the model which considers the SOT as the only driving torque, and which predicts a monotonically increasing SkHA with decreasing diameter, inclusion of ISTT results in SkHA closely aligned to experimental results, particularly when the effect of local disorder and skyrmion-skyrmion interactions are taken into account. Our results shed further light on collective current-driven skyrmion motion in magnetic multilayers and highlight the significance of the ISTT in understanding current-driven skyrmion motion in magnetic multilayers.

[1] C. R. MacKinnon, S. Lepadatu, T. Mercer, *et al. Phys. Rev. B* 102, 214408 (2020). [2] C. R. MacKinnon, K. Zeissler, S. Finizio, *et al. arXiv*: 2106.08046 (2021). [3] S. Lepadatu, *J. Appl. Phys*. 128, 243902 (2020). [4] K. Zeissler, S. Finizio, C. Barton, *et al. Nat. Commun.* 11, 428 (2020).

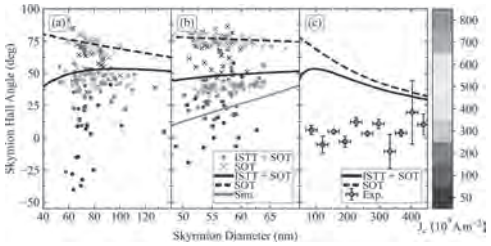

Figure 1. Collective SkHA dependence on skyrmion diameter for (a) $N = 50$ Sk/μm^2 and (b) $N = 100$ Sk/μm^2. (c) Experimentally obtained SkHA from skyrmion collections with a range of diameters with an average current density of 2×10^{11} A/m^2. The overlaid dashed and solid lines show the ideal isolated skyrmion case – independent of current density – for the SOT and ISTT+SOT, respectively. The solid blue line in panel (b) represents a Savitzky-Golay fit to the simulated skyrmion motion, for a current density of $J_c = 2\times10^{11}$ A/m^2.

HOE-12. Dynamics of chiral solitons driven by polarized currents. V. Laliena[1,3], S. Bustingorry[2] and *J. Campo*[3] *1. Applied Mathematics Department, University of Zaragoza, Zaragoza, Spain; 2. Instituto de Nanociencia y Nanotecnología (CNEA-CONICET), Centro Atómico Bariloche, Bariloche, Argentina; 3. Aragon Nanoscience and Materials Institute, Spanish National Research Council (CSIC), Zaragoza, Spain*

Chiral solitons are localized metastable topological magnetic structures whose metastability is greatly enhanced in monoaxial helimagnets by the Dzyaloshinskii-Moriya interaction (DMI) and the uniaxial magnetic anisotropy. Though topological textures in general provide a very interesting playground for new spintronics phenomena, how to properly create and control single chiral solitons is still unclear. We show here that chiral solitons in monoaxial helimagnets, characterized by a uniaxial DMI, can be stabilized with external magnetic fields. We obtain the stability phase diagram. The dynamics of the soliton is governed by the Landau-Lifshitz-Gilbert (LLG) equation. It is shown that a solution of the LLG exists in which the soliton moves steady, i.e. with constant velocity, in response to a polarized electric current, provided the induced spin-transfer torque has a dissipative (nonadiabatic) component, in analogy to what happens with domain walls. The stationary solutions exist only if the applied current density is lower than a critical value, which depends on the applied field and on the DMI strength. We show that the structure of the soliton depends on the applied current density in such a way that steady motion exists only if the applied current density is lower than a critical value, beyond which the soliton is no longer stable [1]. These results are contrasted against micromagnetic simulations. The destruction of the soliton by supercritical currents can be a very useful tool to manipulate information in potential spintronic devices that use the presence or absence of solitons as bits.

[1] V. Laliena, S. Bustingorry and J. Campo, Sci. Rep. 10, 2043 (2020).

HOE-13. Higher Order Skyrmionium Nucleation and Propagation in Insulating, 2D and Metallic Interfaces at Room Temperature. *A.C. Önel*[1,2], A. Mousavi Cheghabouri[3], M. Arıkan[2] and M.C. Onbasli[3] *1. Department of Physics, Gebze Technical University, Kocaeli, Turkey; 2. National Metrology Institute, The Scientific and Technological Research Council of Turkey, Kocaeli, Turkey; 3. Electrical and Electronics Engineering, Koç University, Istanbul, Turkey*

Skyrmions are topologically protected, nanoscale, chiral spin structures which embody rich physics and potential for next generation computation[1]. Skyrmioniums are concentric skyrmions which might enhance the stability of the spin structure and increase information density in memory and logic devices as being immune to topological Hall effect[2] under zero net topological charge (N) conditions. Skyrmionium nucleation and propagation have been reported in Co/Pt[3], Pd/Fe/Ir[4], FeGe[5], however, a comparative investigation

of the effect of insulating, 2D or metallic magnetic interfaces on skyrmionium nucleation characteristics is missing. In this study, we demonstrate and compare spin-orbit torque-driven skyrmionium nucleation at both 0 and 300K in TmIG ($Tm_3Fe_5O_{12}$)/Pt, WTe_2/Py and Co/Pt bilayers. By applying alternating spin-polarized current pulses perpendicular to the film plane, we alternate between concentric skyrmions (N = -1) and concentric skyrmioniums (N = 0). Among the abovementioned materials, their different demagnetizing field terms, saturation magnetizations, exchange, interfacial Dzyaloshinskii-Moriya interaction (DMI), and uniaxial anisotropy constants stabilize skyrmioniums at 300K. Table 1 shows the current density and pulse width requirements for the bilayers. An order of magnitude lower current density has been found to be sufficient for nucleating skyrmioniums along TmIG/Pt interface than for Co/Pt, at 300K. TmIG/Pt requires reduced current for nucleation and growth of skyrmioniums and causes lower Joule heating than Co/Pt. This difference is attributed to the reduced M_s, conductivity, DMI parameter, and an order of magnitude lower A_{ex} of TmIG/Pt interface. The trade-off for TmIG/Pt layer is the reduced room temperature stability of skyrmioniums. We suggest higher K_u in the magnetic layer to improve room temperature stability. The reduced current requirements and minimized thermal drift could help pave the way for integrated skyrmion-based in-memory computing elements.

1. Fert, A., Cros, V. & Sampaio, Nature Nanotechnology 8, 152–156 (2013). 2. Zhang, X. *et al.*, *Phys. Rev. B* 94, 094420 (2016). 3. Göbel, B., Schäffer, A.F., Berakdar, J. *et al.*, *Sci Rep* 9, 12119 (2019). 4. Hagemeister, J. *et al.*, *Phys. Rev. B* 97, 174436 (2018). 5. Zheng, F. *et al.*, *Phys. Rev. Lett.* 119, 197205 (2017).

Material Type	Material Name	K_u ($kJ \cdot m^{-3}$)	M_s ($MA \cdot m^{-1}$)	A_{ex} ($pJ \cdot m^{-1}$)	D_{bd} ($mJ \cdot m^{-2}$)	α	Current Density ($J \cdot m^{-2}$)	Pulse Time (ns)
Ferromagnetic Metal/HM	Co/Pt	800	0.58	15	3.8	0.3	7.6×10^{12}	3.1
Ferrimagnetic Insulator/HM	TmIG/Pt	11.88	0.1	0.84	0.051	0.014	4×10^{11}	9
Semiconductor/FM	WTe_2/Py	50	0.58	10	-1.78	0.0067	2×10^{11}	4.1

Table 1: Comparison of bilayers that stabilize room temperature skyrmioniums in micromagnetic models. Metallic contact size (100 nm diameter) and the geometry (300 × 300 nm^2) are the same for each bilayer.

Session HOF
DYNAMICS IN AF-COUPLED MATERIALS

Jean-Yves Chauleau, Chair
CEA-SPEC, Gif-sur-Yvette, France

CONTRIBUTED PAPERS

HOF-01. Fast Current-Induced Domain Wall Motion in Compensated Co/Gd Quadlayers. *P. Li*[1], T. Kools[1], R. Lavrijsen[1] and B. Koopmans[1]
1. Applied Physics, Eindhoven University of Technology, Eindhoven, Netherlands

Co/Gd based synthetic ferrimagnets have received considerable attention owing to the coexistence of both pronounced spin-orbitronic effects and all-optical switching (AOS), allowing for novel, hybrid devices [1,2]. Previous studies [3,4] have shown that spin-orbit torque (SOT) driven domain wall motion in these 3d-4f ferrimagnets system is most efficient at angular momentum compensation. Following this notion, in this study, we explore the stack engineering of Co/Gd based synthetic ferrimagnets to achieve high SOT driven domain wall motion at room temperature[5]. Here, we experimentally demonstrate that magnetization compensation can be achieved and tuned by varying layer thicknesses in Co/Gd(x)/Co/Gd quadlayer systems (see inset of Fig. 1), which shows AOS in the full range of Gd thickness[5]. Fig. 1 (a) shows the coercivity and polar magneto-optical Kerr effect (MOKE)-signal in such a quadlayer system where the middle Gd layer is wedged. The sign change of the MOKE signal and divergence of the coercivity indicate a compensated system. The CIDWM velocity as a function of Gd thickness of this stack has been investigated, after structuring a series of domain wall conduits from another wedge sample grown in the same batch. In Fig. 1 (b) it can be observed that for low to moderate current densities the optimum in the velocity can be found at compensation. As the current density is increased the optimum in the velocity is found to shift towards larger Gd thicknesses, likely due to the difference in temperature dependence of the magnetization in Co and Gd leading to a shift in the compensation thickness due to joule heating during the applied current pulses. Our study shows a significant improvement of the room temperature domain wall velocity in synthetic ferrimagnetic systems through stack engineering. Further studies to explore the role of the weak exchange link provided by the proximity induced Gd magnetization profile are in progress.

[1] : Lalieu, M.L.M., *et al. Physical Review B* 96.22 (2017): 220411. [2] : van Hees, Youri LW, *et al. Nature communications* 11.1 (2020): 1-7. [3] : Caretta, L. *et al. Nature Nanotechnology* 13.12(2018): 1748-3395 [4] : Blaesing, R. *et al. Nature Communications* 9.1(2018): 2041-1732 [5] : Li *et al. In Progress* (2021).

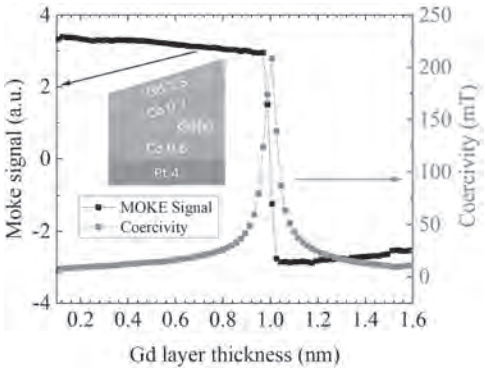

Fig. 1: Coercivity, polar MOKE signal (a) and current-driven domain wall velocity (b) as a function of Gd thickness in a Pt(4)/Co(0.6)/Gd(x)/Co(0.7)/Gd(1.5) multilayer system (thicknesses in nm in parenthesis), and x indicates Gd layer thickness.

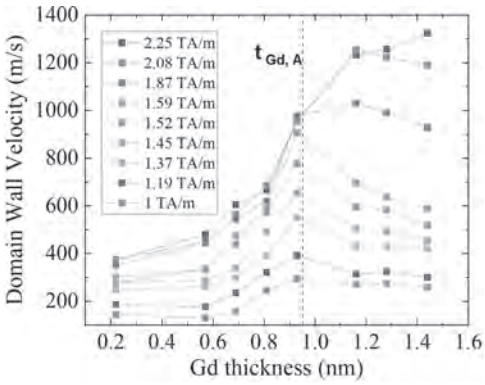

HOF-02. Breathing Modes of Skyrmion Strings in a Synthetic Antiferromagnet. *C.E. Barker*[1], E. Haltz[1], T. Moore[1] and C. Marrows[1]
1. School of Physics and Astronomy, University of Leeds, Leeds, United Kingdom

Skyrmions are topologically protected vortex-like spin structures that have been observed in magnetic multilayers possessing an interfacial Dzyaloshinskii-Moriya interaction [1]. Theoretical studies have suggested a greatly increased velocity of skyrmions propagating in synthetic antiferromagnets (SAFs) when driven by spin-orbit torques [2], and their existence has recently been observed [3]. While Skyrmions have been proposed as potential information carriers in racetrack memory devices, their high frequency excitations also bear interest. It was recently shown that in compensated SAFs the radio frequency breathing mode of a skyrmion splits into in-phase and out of phase modes [4]. In this work we investigate the breathing modes of skyrmion strings in a SAF multilayer where each magnetic layer is coupled antiferromagnetically to the one above and below it by means of numerical simulations using MuMax3 [5]. The extension of the skyrmion string along the z-axis results in further degeneracy of the

breathing modes as shown for a multilayer with four magnetic layers in Fig. 1 and a lowering of the frequency of the first out-of-phase mode. The radius variation of the first two modes is shown in Fig. 2. These features show little variation with applied magnetic field, but similarly to the work in [4] show systematic variation with the strength of the RKKY interaction. The addition of multiple magnetic layers is a better representation of an experimentally realistic stack design, and lowers the frequency of the out-of-phase mode to be more feasibly observable for skyrmion sensing applications.

[1] W. Jiang *et al.*, Physics Reports 704, 1-49 (2017) [2] R Tomasello *et al.*, J. Phys. D: Appl. Phys. 50 325302 (2017) [3] W. Legrand *et al.*, Nature Materials 19, 34 (2020) [4] M. Lonsky *et al.*, Physical Review B 102, 104403 (2020) [5] A. Vansteenkiste *et al.*, AIP Advances 4, 107133 (2014)

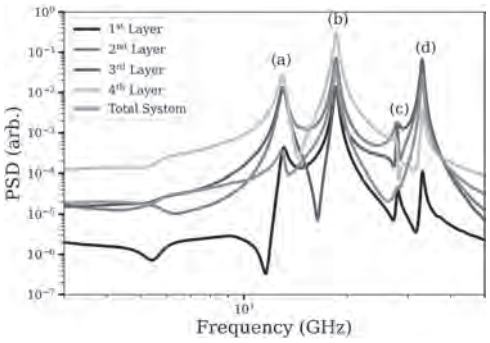

Fig. 1. Frequency response of each individual layer of the SAF along with that of the total system plotted in red.

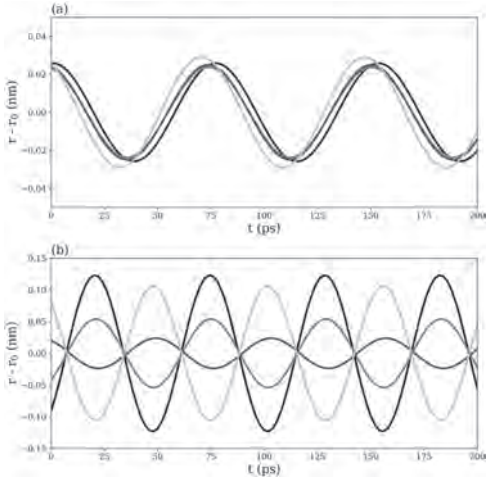

Fig. 2. radius variation of the skyrmions in each layer when driven by a sinusoidal driving field at the frequency of the first two peaks in Fig. 1.

HOF-03. Macromagnetic Simulation of AFM-FM phase transition in FeRh using a modified Landau-Lifshitz-Bloch Equation. *M. Menarini*[1] and V. Lomakin[1] *1. Electrical and Computer Engineering, University of California San Diego, La jolla, CA, United States*

In recent years, there was an increased interest in using antiferromagnetic (AFM) materials for THz frequency sources. The operation of such AFM structures is based on the AFM resonance, which can have THz frequencies, exceeding the frequency ferromagnetic (FM) resonances by order of magnitude [1,2]. Recent experiments showed that it is possible to generate such signal in AFM FeRh/Pt bi-layers by optically exciting them with a sub-picosecond laser pulse [3]. The signal in the AFM state can be originated from a partial phase transition induced by the laser heat from the AF to the FM phase [4]. Such transformation occurs on a sub picosecond time scale [5-7]. Using atomistic simulations, it is possible to reproduce such transition by including both the bilinear and biquadratic exchanges in the Hamiltonian [7,8]. However, to model larger spatial structures, a coarse-grained model for the dynamic of the magnetization is desirable. Here, we present a micromagnetic formulation to model the magnetization dynamics and phase transition in FeRh at low and high temperatures, including the transition near the Curie temperature. The formulation is based on a mean field approximation (MFA), where each macrospin is modeled by two coupled sublattices, including the atomistic biquadratic interactions described as a micromagnetic inter-sublattice molecular field with a cubic dependence of the magnetization. To validate the model, we compare our simulations of the phase transitions in the static and dynamic case with the existing literature. The results show an agreement with the experiments and atomistic modeling, displaying the characteristic hysteretic behavior for the magnetization (Fig. 1), and a similar dynamic response to an external thermal pulse (Fig.2).

1. E. Gomonay and V. Loktev, Low Temperature Physics40, 17 (2014). 2. V. Baltz, A. Manchon, M. Tsoi, T. Moriyama, T. Ono, and Y. Tserkovnyak, Reviews of ModernPhysics90, 015005 (2018). 3. R. Medapalli, G. Li, S. K. Patel, R. Mikhaylovskiy, T. Rasing, A. Kimel, and E. Fullerton, Applied Physics Letters 117, 142406 (2020) 4. M. Menarini, R. Medapalli, E. E. Fullerton, and V. Lomakin, AIP Advances9, 035040 (2019). 5. G. Ju, J. Hohlfeld, B. Bergman, R. J. van de Veerdonk, O. N. Mryasov, J.-Y. Kim, X. Wu,D. Weller, and B. Koopmans, Physical review letters93, 197403 (2004). 6. J.-U. Thiele, M. Buess, and C. H. Back, Applied Physics Letters85, 2857 (2004) 7. J. Barker and R. W. Chantrell, Physical Review B92, 094402 (2015). 8. O. N. Mryasov, Phase Transitions78, 197 (2005)

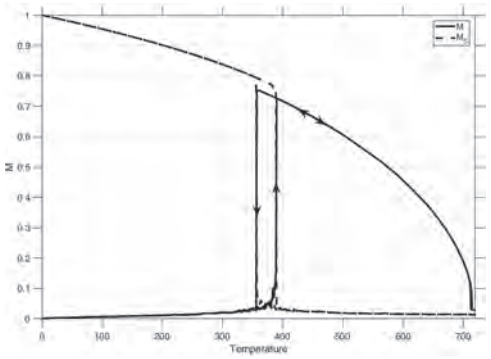

Equilibrium magnetization as a function of temperature.

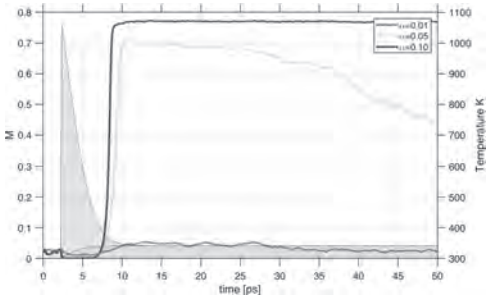

Dynamic response of the magnetization to an optical pulse (shaded area) for different values of the atomistic damping coefficient α

HOF-04. DMI and Cavity Magnonics for Antiferromagnetic Domain Walls. *O.J. Iyaro*[1], I. Proskurin[1,2] and R. Stamps[1] *1. Department of Physics and Astronomy, University of Manitoba, Winnipeg, MB, Canada; 2. Institute of Natural Sciences and Mathematics, Ural Federal University, Ekaterinburg, Russian Federation*

The field of cavity optomagnonics in which cavity-confined photon-magnon interactions are studied has gained great interest in recent years due to its potential applications in quantum information processing and spintronics [1]. In these studies, a number of unique features, notably level repulsion and attraction [2] have been observed in ferromagnetic insulators and simple

topological structures [3]. Here, we report results from an analytical study of the coupling of a pinned antiferromagnetic domain wall to cavity photons via the inverse Faraday effect. We consider spin canting and complex spin textures in antiferromagnetic materials that can arise from Dyzalonshinskii-Moriya interactions (DMI) [4] and analyze the role DMI plays in such systems. We find that the coupling spectrum depends on the DMI, enabling spin interactions with cavity photons in a geometry that otherwise allows no magneto-optical coupling. Since DMI is not easily measurable and is often inferred from other quantities, this result may be used to measure the DMI constant in optomagnonic experiments by measuring the interaction of antiferromagnetic resonances to optical modes in a cavity.

[1] R. Hisatomi, A. Osada and Y. Tabuchi., *Phys. Rev. B. 93, 174427* (2016) [2] M. Harder, Y. Yang and C. M. Hu*., Rev. Lett. 121, 137203* (2018) [3] I. Proskurin, A. S. Ovchinnikov and R. Stamps*., Phys. Rev. B 98, 220411* (2018)

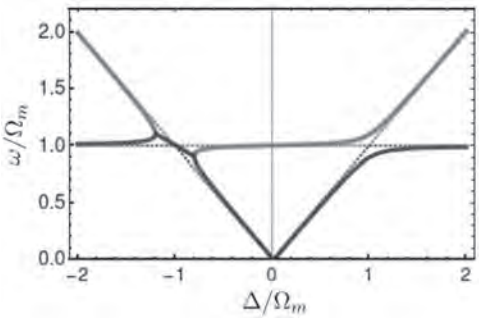

Level attraction (Δ>0) and level repulsion (Δ>0) between magnon and cavity modes as a function of the detuning, Δ. Dotted lines indicate there is no coupling for zero DMI.

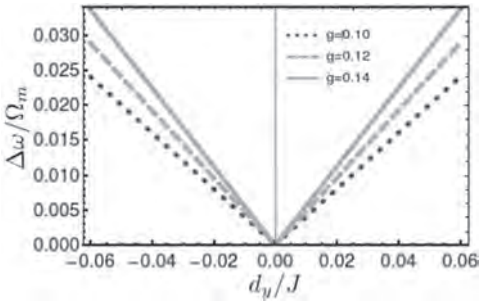

Frequency gap increases linearly with increasing magnitude of DMI strength.

HOF-05. Current-Driven Domain Wall Motion in a Synthetic Antiferromagnet Multilayer. C.E. Barker[1], E. Haltz[1], S. Finizio[2], G. Burnell[1], J. Raabe[2] and *C. Marrows[1] 1. School of Physics and Astronomy, University of Leeds, Leeds, United Kingdom; 2. Swiss Light Source, Paul Scherrer Institute, Villigen, Switzerland*

Synthetic antiferromagnets (SAFs) are of interest in a wide variety of spintronic applications owing to their net zero magnetisation and inherent tunability arising from control over complex stacking sequences [1]. They show very fast domain wall (DW) motion in response to spin torques [2]. Here we describe current-driven DW motion in an SAF with stack structure Ta/[Ru/Pt/CoB/Ru/Pt/CoFeB]×5/Ru/Pt which displays both perpendicular magnetic anisotropy (PMA) and the Dzyaloshinskii-Moriya interaction (DMI). The alternating CoB and CoFeB layers had their thicknesses adjusted to give net zero magnetisation (as determined by SQUID-VSM) for applied fields up to ~500 Oe. They were patterned into 2 μm wide wires with Cu leads attached to each end. These were fabricated on Si_3N_4 membranes to permit imaging of DW motion using scanning x-ray transmission microscopy. The distinct chemical composition of the two sublattices means that we could use the element specificity of this technique to observe the CoFeB separately whilst imaging at the Fe L_3 edge, whilst contrast at the Co L_3 edge is dominated by the other sublattice. Inverted domain structures observed at these two edges, as shown in Fig. 1, confirm the SAF ordering of the layers. Current pulses drive domain wall motion, as shown in Fig. 2, with velocities up to ~ 20 m/s achieved at current densities as low as 4×10^{11} A/m^2.

[1] R. A. Duine et al., Nature Phys. 14, 217 (2018) [2] S.-H. Yang et al., Nature Nanotech. 10, 221 (2015)

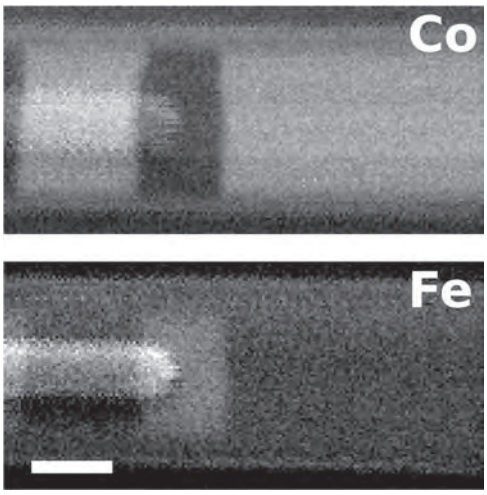

Fig. 1: STXM images acquired at zero field the Co and Fe L_3 edges, which probe different sublattices of the SAF. A finger-shaped Cu lead is visible on the left. 1 μm scale bar.

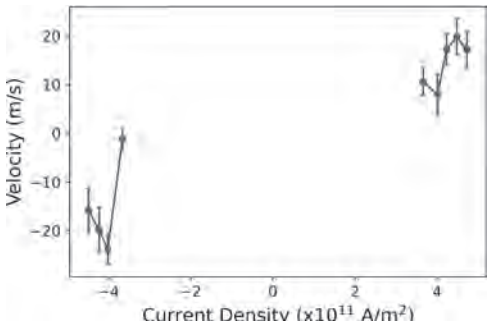

Fig. 2: DW velocity against current density measured using 5 ns current pulses.

HOF-06. Magnetization Dynamics in Synthetic Antiferromagnets (SAFs) with Perpendicular Magnetic Anisotropy (PMA). *D. Huang*[1], D. Zhang[2], D. Lyu[2], J. Wang[2] and X. Wang[1] *1. Mechanical Engineering, University of Minnesota, Minneapolis, MN, United States; 2. Electrical and Computer Engineering, University of Minnesota, Minneapolis, MN, United States*

Synthetic antiferromagnets with perpendicular magnetic anisotropy (p-SAFs) are promising artificial structures for ultrafast spintronics [1]. Owing to the interlayer exchange coupling, p-SAFs contain much richer magnetization dynamics than single layers. Compared with Ferromagnetic Resonance (FMR), femtosecond laser-based techniques have the advantages of manipulating and detecting the magnetization dynamics at high frequencies, and thus are powerful for studying p-SAFs [2]. Here, we present an approach to comprehensively describe the rich physics of magnetization dynamics in p-SAFs initiated by ultrafast laser pulses, including information about the cone angles, directions, and phases of spin precession in each layer for both the high-frequency (HF) and low-frequency (LF) modes. It is found that both the HF and LF modes precess in phase at low external fields.

The theoretical analyses well explain the amplitude and phase of signals obtained from time-resolved magneto-optical Kerr effect (TR-MOKE) measurements under varying magnetic fields. The detailed information of magnetization dynamics provided by this approach can facilitate the design and optimization of SAF-based spintronic devices.

[1] D. Zhang, *et al.*, "$L1_0$ Fe–Pd Synthetic Antiferromagnet through an fcc Ru Spacer Utilized for Perpendicular Magnetic Tunnel Junctions" *Phys. Rev. Appl.* 9(4), 044028 (2018) [2] D. Huang, *et al.*, "Materials Engineering Enabled by Time-Resolved Magneto-Optical Kerr Effect for Spintronic Applications" *ACS Appl. Electron. Mater.* 3(1), 119-127 (2020)

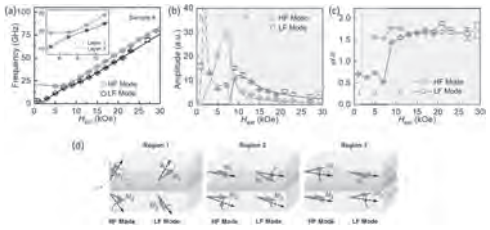

Fig. 1 Magnetization dynamics of one representative sample [Co(0.4)/ Pd(0.7)/Co(0.4)/Ru(0.6)/Ta(0.3)/ CoFeB(1)] in this study: the precession frequencies (a) and amplitudes of TR-MOKE signals (b) of two modes. In (a) and (b), circles are experimental data and curves are theoretical modeling. (c) The phase of TR-MOKE signals for two precession modes. (d) Schematics of precession features at different field regions, defined in (b) and (c). In the low-field region (region 1), both modes precess in phase. While in high-field regions (regions 2 and 3), one precession mode is out-of-phase (optical mode) and the other is in-phase (acoustic mode).

HOF-07. Making ferrimagnetic Mn_4N ferromagnetic by non-magnetic element doping. *T. Yasuda*[1], T. Komori[1], H. Mitarai[1], K. Toko[1], S. Honda[4], S. Ghosh[1,3], L. Vila[3], J. Attané[3], K. Amemiya[2] and T. Suemasu[1] *1. Pure and Applied Sciences, University of Tsukuba, Tsukuba, Japan; 2. KEK, Tsukuba, Japan; 3. Spintec, Grenoble, France; 4. Kansai University, Suita, Japan*

We show that antiperovskite Mn_4N transforms from ferri- to ferromagnetism at room temperature (RT) when the Mn content is decreased by the addition of non-magnetic In atoms. Mn_4N films have attracted increasing attention as candidates for the current induced domain wall motion (CIDWM) devices. They have a small magnetization (Ms ~ 100 kA/m [1]) and perpendicular magnetic anisotropy, contributing to high CIDWM mobility with low threshold current. In addition, $Mn_{4-x}Ni_xN$ [2] and $Mn_{4-x}Co_xN$ [3] epitaxial films have x-dependent magnetic compensation (MC) points at RT, probed by X-ray absorption spectroscopy (XAS) and X-ray magnetic circular dichroism (XMCD) measurements. In $Mn_{4-x}Ni_xN$ nanowires at the vicinity of the MC, we demonstrated ultrafast and efficient CIDWM (3,000 m/s with j=1.2×10^{12} A/m^2) by pure spin transfer torque at RT [4]. In this work, we focused on $Mn_{4-x}In_xN$ epitaxial films as new candidates for such materials [5]. We grew 25nm-thick $Mn_{4-x}In_xN$ films (x=0, 0.15 and 0.27) on MgO(001) by MBE. XAS and XMCD measurements were performed at the twin APPLE II undulator beam line BL16A of KEK-PF in Japan. Figure 1 shows XAS and XMCD spectra of Mn-$L_{2,3}$ absorption edges of the samples. In the XAS spectra of all the samples, distinct shoulders marked by arrows appear at about 2 eV above the main L_3 edges, which are caused by fcc-Mn(II) atoms [3]. In the XMCD spectrum of Mn_4N(x=0), corner-site Mn(I) and fcc-Mn(II) atoms are attributable to peaks α and β, respectively [3]. Their different signs show that the magnetic moments of Mn(I) and Mn(II) are aligned antiparallel. When the In composition x increases up to 0.27, the sign of peak β reverses while that of peak α remains unchanged. It means that the magnetic moment of Mn(II) reverses and now aligns parallel to that of Mn(I), showing a ferri-to-ferromagnetic transition at RT. Figure 2 shows the anomalous Hall effect (AHE) curves at RT. The sign reversal of ρ_{AHE} reconfirms the reversal of the magnetic moment of Mn(II) between x = 0.15 and 0.27 in Fig. 1.

[1] T. Komori *et al.*, J. Cryst. Growth, 507, 163 (2019). [2] T. Komori *et al.*, J. Appl. Phys., 127, 043903 (2020). [3] H. Mitarai *et al.*, Phys. Rev. Mater., 4, 094401 (2020). [4] S. Ghosh *et al.*, Nano Lett., 21, 2580 (2021). [5] M. Mekata, J. Phys. Soc. Jpn., 7, 796 (1962).

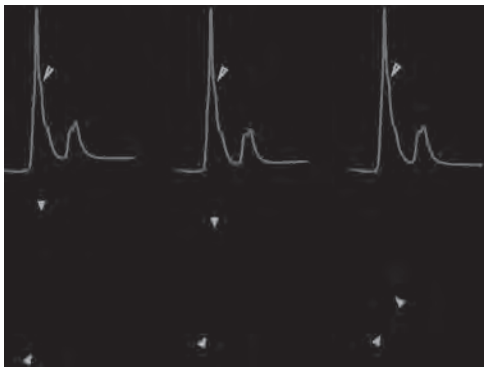

Fig. 1 XAS and XMCD spectra at Mn-L2,3edges in (a) Mn_4N, (b) $Mn_{3.85}In_{0.15}N$ and (c) $Mn_{3.85}In_{0.27}N$.

Fig. 2 Anomalous Hall effect curves of $Mn_{4-x}In_xN$ (x=0.15 and 0.27) films on MgO(001).

HOF-08. Current-Driven Domain Wall Motion in Curved Ferrimagnetic Strips Above and Below the Angular Momentum Compensation. *D. Osuna Ruiz*[1], Ó. Alejos[2], V. Raposo[1] and E. Martínez[1] *1. Department of Applied Physics, University of Salamanca, Salamanca, Spain; 2. Department of Electricity and Electronics, University of Valladolid, Valladolid, Spain*

Magnetic domain walls (DWs) in ferromagnetic nanostrips with perpendicular magnetic anisotropy have widely been a subject of research, not only due to its intrinsic fundamental interest but also to develop spintronic devices where information is coded in domains between walls [1,2]. To that purpose, ferrimagnetic materials (FiM) are recently attracting much attention due to their fast DW dynamics, almost zero interaction with external fields and a wide availability in nature. Controlling the current-driven DW along curved FiMs strips is essential to develop DW-based circuitry, but it faces problems such as DW distortion [3]. A proper design for the strip geometry may overcome these problems, as shape is intimately connected with DW motion via spin currents and interfacial phenomena in the structure. Studying the influence of temperature (or composition) is also key for developing real applications. Therefore, understanding the influence of shape and temperature to fully control the DW motion is nowadays a fundamental topic in spintronics research. In this work we perform a micromagnetic (μm) study on DW motion in ring-like FiM strips, characterising DW terminal velocities and inertial times, as a function of temperature, width, curvature of the strip

(see insets in Fig. 1(a)) and density currents (J). Our full μm model treats spin dynamics in each sublattice separately, which yields results close to 'realistic' FiM. Results show that strips with low width and high curvature give high DW velocities (V_{DW} > 1000 m/s), with ultra-short response times (τ <<0.1 ns, see Fig.1 (b)). This is optimal for developing compact and high-speed tracks for domains since opposite DWs travel at lower but similar speeds, leading to negligible domain distortion. Our results will help to understand curvature effects to develop efficient and reliable DW-based devices.

[1] A. Hubert and R. Schäfer, in Magnetic Domains: The Analysis of Magnetic Microstructures, eds Springer-Verlag Berlin Heidelberg (1998) [2] A. D. Karenowska *et al.,* in Handbook of Spintronics, eds Springer Netherlands, Dordrecht, pp.1505–1549 (2016) [3] O. Alejos *et al.*, in Materials Science and Technology, eds R.W. Cahn, P. Haasen and E.J. Kramer (2020)

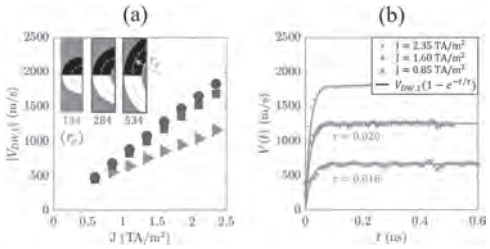

Fig.1. (a) DW velocity as a function of J from sub-lattice i = 1 in a FiM strip of width *w* = 256 nm and different effective radius *re* (nm) at the angular momentum compensation temperature TA = 260 K. (b) Instantaneous DW velocities for three values of J and for a curved strip of *re* = 384 nm and *w* = 256 nm at T = TA. Relaxation times (τ) are extracted from the equation (solid curve) fitted to the data (symbols).

HOF-09. Domain wall dynamics across magnetic and spin compensation points in ferrimagnets. *M. Logunov*[4], S. Safonov[4], A. Fedorov[2,4], A. Fedorova[2,4], N. Moiseev[5], A. Safin[1,4], S. Nikitov[2,4] and A. Kirilyuk[3,4] *1. Moscow Power Engineering Institute, Moscow, Russian Federation; 2. Moscow Institute of Physics and Technology, Dolgoprudny, Russian Federation; 3. FELIX Laboratory, Radboud University, Nijmegen, Netherlands; 4. Kotel'nikov Institute of Radio-Engineering and Electronics of RAS, Moscow, Russian Federation; 5. National Research Mordovia State University, Saransk, Russian Federation*

Recent years have seen an increase of interest in the dynamics of ferrimagnetic materials, in particular in the motion of domain walls [1-4]. Ferrimagnetic materials represent unique systems where the ease of manipulating the spins with applied magnetic fields is combined with exchange-driven acceleration of the internal spin dynamics. Of particular interest is the temperature range around the magnetic and spin compensation points, finely balancing both magnetic moment and angular momentum of the system, and leading to a very particular character of magnetic switching by the domain wall motion. Here we present our studies of the temperature-dependent domain wall dynamics in the temperature range covering both angular momentum and magnetization compensation points in garnet film, and reaching up to the Curie temperature [5]. This is made possible by the very low coercive field of the material, not exceeding 5 mT even in the close vicinity of magnetization compensation temperature. The sample used in our experiments is a single-crystal thin film of magnetic garnet. A very unusual behavior of the domain-wall dynamics is observed, such as extraordinarily high mobility of the domain walls at very low fields. Drastic changes of both domain-wall velocity and mobility by more than 2 orders of magnitude are observed across a relatively small temperature range, related to the delicate balance of magnetization and spins of iron and rare-earth sublattices [5]. Therefore, such fine tuning of the corresponding momenta could be the key for developing ultrafast ferrimagnetic spintronic devices. The work was supported by the Russian Foundation for Basic Research (Projects No. 18-52-16006, 18-29-27020) and the Government of the Russian Federation (Project No. 075-15-2019-1874).

[1] K.-J. Kim, S. K. Kim, Y. Hirata et al., Nature Mater. 16, 1187 (2017). [2] B. A. Ivanov, Low Temp. Phys. 45, 935 (2019). [3] J. Finley and L. Liu, Appl. Phys. Lett. 116, 110501 (2020). [4] E. Haltz, J. Sampaio, S. Krishnia et al., Sci. Rep. 10, 16292 (2020). [5] M. V. Logunov, S. S. Safonov, A. S. Fedorov et al., Phys. Rev. Appl. 15, 064024 (2021).

HOF-10. Nonstationary domain wall dynamics in almost compensated ferrimagnets: a novel scenario. *R. Ovcharov*[1], R. Khymyn[1], B. Ivanov[2] and J. Åkerman[1] *1. Physics Department, University of Gothenburg, Gothenburg, Sweden; 2. Institute of Magnetism of the National Academy of Sciences of Ukraine and the Ministry of Education and Science of Ukraine, Kyiv, Ukraine*

Topological spin structures, such as domain walls (DW) and skyrmions, have intriguing features and can play a key role in spintronics. In both ferromagnets (FM) and antiferromagnets (AFM) a DW, driven by applied torque, behaves like a solid particle, which can be described by collective variables: DW position and the angle of the magnetic order vector, albeit the dynamic properties are dramatically different. For an AFM the DW energy as a function of its momentum is the same as that of a standard relativistic particle (Fig. 1), because of the Lorentz invariance of the AFM dynamics [1]. For FMs the gyrotropic dynamic term couples two degrees of freedom that slows down a FM DW and results in the periodic dependence of the DW energy on momentum (Fig. 1). Thus, the AFM DW is stable up to higher speeds (~10km/s in contrast to ~100m/s for FMs). We demonstrate that the DW dynamics in ferrimagnetic (FiM) materials near the spin compensation point is entirely different from the FM and AFM cases [2]. The dispersion law for FiM DWs exhibits two crossed branches with opposite group velocities (Fig. 1), where each branch contains an endpoint [3]. Driven by a field-like torque, a FiM DW accelerates to a higher speed and momentum than its FM counterpart [4] and can reach the endpoint. Wherein it falls into a region of instability, where the internal dynamics of the DW is excited, and the collective variables approach fails. We show by micromagnetic simulations that the dynamical state of a DW in this case covers a wide frequency range, far beyond the magnon bandgap of a FiM. In this way the FiM DW driven by external field-like torque acts as an efficient source of the spin waves (SW), propagating out of the DW region. We show that by varying the applied torque and spin uncompensation of a FiM one can reach three qualitatively different regimes of the excited SWs: i) frequency-comb spectrum, shown in Fig.2, ii) chaotic behavior of the DW with the broad SW spectrum, iii) double-frequency SW excitation.

[1] V. G. Bar'yakhtar, M. V. Chetkin, B. A. Ivanov, et al., Springer, Vol. 129 (2006). [2] B. Ivanov, E. Galkina, V. Kireev, et al., Low Temperature Physics, Vol. 46, p. 841-850 (2020). [3] E. G. Galkina, C. E. Zaspel, B. A. Ivanov, et al., JETP Letters, Vol. 110, p. 481–486 (2019). [4] KJ. Kim, S. Kim, Y. Hirata, et al., Nature Materials, Vol. 16, p. 1187–1192 (2017).

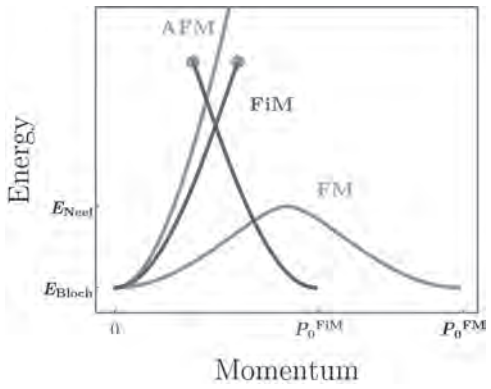

Fig.1 Dependence of the energy on momentum for a DW in FM, AFM (gray), and FiM near compensation point (blue) nano-strips.

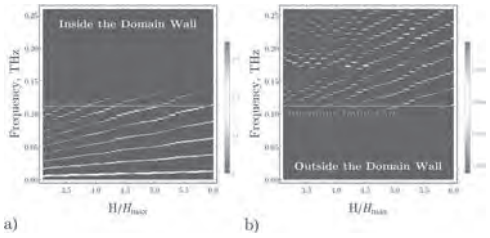

Fig.2 Spectra of the dynamic state inside the DW (a) and magnons emitted outside (b).

HOF-11. Experimental and theoretical approach to magneto-transport properties in $Mn_{4-x}Ni_xN$ with high domain wall mobility. *T. Komori*[1], H. Mitarai[1], T. Yasuda[1], K. Toko[1], S. Honda[2] and T. Suemasu[1] *1. Institute of Applied Physics, University of Tsukuba, Tsukuba, Japan; 2. Kansai University, Osaka, Japan*

In recent years, current-induced domain wall motion (CIDWM) is attractive research field in spintronics because it's expected to enable magnetic non-volatile memory. Our group focuses on Mn_4N and its based nitrides as new candidates for CIDWM application. Especially, $Mn_{4-x}Ni_xN$ nanowire recorded a DW velocity of 3,000 m/s only by spin-transfer torque [1]. We attributed this to the compensation of $Mn_{4-x}Ni_xN$ around x=0.2 [2]. In spite of the excellent CIDWM, magneto-transport properties in $Mn_{4-x}Ni_xN$ have scarcely been reported. In this work, we report both experimental and theoretical investigations of these properties with anisotropic magnetoresistance (AMR) measurement and calculation of PDOS with Vienna Ab initio Simulation Package (VASP). Figure 1 shows Fourier coefficients of AMR measurements in $Mn_{4-x}Ni_xN$ on $SrTiO_3$(001) substrates and energy state of d electrons under various crystal fields. C_2 represents the coefficient of cos2θ component and C_4 does that of cos4θ, where θ is the angle made by the current and the magnetization. Above 100K, small C_2 components dominate AMR while C_4 drastically became large below 100K. This represents the emergence of the tetragonal-like crystal field below 100K because it depends on the difference in PDOS between d_{xy} and d_{yz}, d_{zx} states [3]. However, this trend was weakened by large Ni composition. Figure 2 shows PDOSs of d orbitals in Mn and Ni at corner site (I-site) in $Mn_{4-x}Ni_xN$ (x=0, 0.5). By Ni substitution, spin polarization of d orbitals decreased at Fermi level (E_F). This leads to decrease in both AMR ratio and C_4 components, derived from the theory of s-d scattering [4]. In the previous study, the emergence of C_4 components in Mn_4N was attributable to the possible external effect such as lattice strain caused by the thermal expansion [3,4]. However, since all structures were set to be cubic in our calculation, we expect this is attributable to intrinsic change in PDOS, and dramatically affected by Ni doping. In the talk, we're going to further investigate the modulation of Hall effect in $Mn_{4-x}Ni_xN$ by Ni composiiton.

[1] S. Ghosh, T. Komori, L. Vila *et al.*, Nano Lett., Vol.21, p.2580 (2021). [2] T. Komori, K. Amemiya, T. Suemasu *et al.*, J. Appl. Phys., Vol.127, p.043903 (2020). [3] K. Kabara, M. Tsunoda, S. Kokado, AIP Advances, Vol.7, p.056416 (2017). [4] S. Kokado, M. Tsunoda, J. Phys. Soc. Jpn., Vol.84, p.094710 (2015).

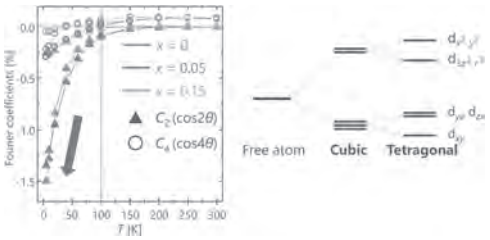

Fig. 1 Fourier coeffcients of AMR in $Mn_{4-x}Ni_xN$ and energy state of d orbitals.

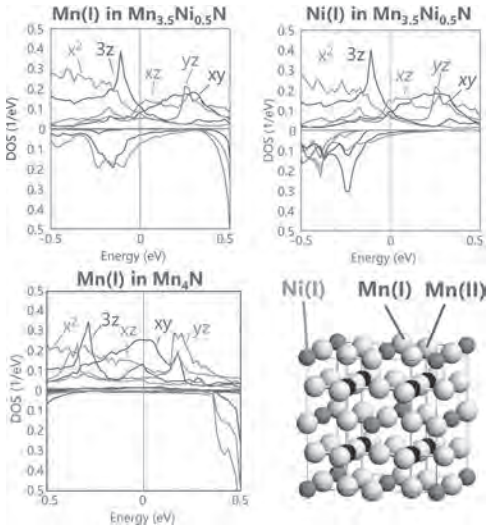

Fig. 2 PDOS of d orbitals of Mn at corner site in $Mn_{4-x}Ni_xN$ (x=0, 0.5)

Session HOG
NEW COMPUTATION SCHEMES

Daniele Pinna, Chair
Forschungszentrum Jülich, Jülich, Germany

CONTRIBUTED PAPERS

HOG-01. Domain Wall Skyrmion Based Artificial Neuron Device.
B. Nepal[1], U. Karki[1], T. Komiyama[2], L. Wang[3], Y. Zhang[4], R. Gunawan[5], M.D. Graef[6], V. Sokalski[6], M. Vogel[7], T. Mewes[1] and C. Mewes[1]
1. Department of Physics and Astronomy, The University of Alabama, Tuscaloosa, AL, United States; 2. Department of Neurosciences, University of California San Diego, La Jolla, CA, United States; 3. Department of Civil and Environmental Engineering, Virginia Tech University, Blacksburg, VA, United States; 4. Department of Cell and Molecular Biology, University of Rhode Island, Kingston, RI, United States; 5. Department of Chemical and Biological Engineering, University at Buffalo - SUNY, Buffalo, NY, United States; 6. Department of Material Science and Engineering, Carnegie Mellon University, Pittsburgh, PA, United States; 7. Institute of Physics and Center for Interdisciplinary Nanostructure Science and Technology, University of Kassel, Kassel, Germany

Biological nervous system inspired neuromorphic computing has attracted considerable attention due to its parallel nature, power efficiency, robustness against variation, and combination of memory and computation. Recently, magnetic skyrmions have been considered as a promising candidate in neuromorphic computing design due to its particle like behaviors, nanoscale size, and low driving current density [1]. A leaky integrate and fire model of a neuron can be achieved by driving skyrmions using spin current along a nanotrack with Dzyaloshinskii-Moriya Interaction (DMI) and perpendicular magnetic anisotropy (PMA) gradient [2]. However, conventional skyrmion motion is very sensitive to the non-adiabaticity parameter. We use a different type of topologically protected magnetic excitation called a domain wall (DW) skyrmion [3] which describes a 360° wind of the DW's internal magnetization along the wall profile and has a topological charge of +/-1. This topological state is confined within a magnetic domain wall and therefore smaller compared to conventional skyrmions and offers a natural nanotrack for the skyrmion along which it can be moved using spin currents. We are able to create a DW skyrmion leaky integrate and fire model of a neuron which operates under a wide range of non-adiabiticity conditions. The figure shows a fully micromagnetic simulation of the DW skyrmion based spintronic neuron. This work is partly supported by MEMONET NSF # 1939999, and the Defense Advanced Research Project Agency (DARPA) program on Topological Excitations in Electronics (TEE) under Grant No. D18AP00011.

1. W. Kang, Y. Q. Huang and W. S. Zhao, Proc. IEEE 104, 2040 (2016). 2. S. Li, W. Kang, Y. Huang and W. Zhao, Nanotechnology 28, 31LT01 (2017). 3. R. Cheng, M. Li, A. and V. Sokalski, Phys. Rev. B 99, 184412 (2019).

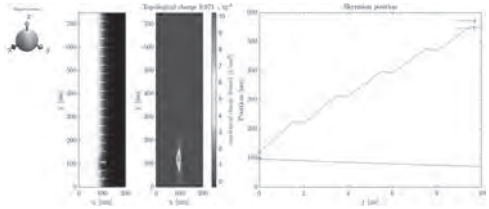

Micromagnetic simulation of proposed DW skyrmion neuron device exhibiting leaky integrate behavior.

HOG-02. Reprogrammable skyrmion-based hybrid demultiplexers for complex computations.
N. Sisodia[1], L.D. Buda-Prejbeanu[1], G. Gaudin[1] and O. Boulle[1] *1. Univ. Grenoble Alpes, CNRS, CEA, Grenoble INP, Spintec, Grenoble, France*

Magnetic skyrmions are promising candidates for logic-in-memory architectures, intrinsically supporting the merging of non-volatile racetrack storage with the capability to perform logic operations. They also have the added advantage of ultralow-power consumption and high speed. Different logic gates based on skyrmions have been proposed in recent years [1][2]. However, in order to perform complex arithmetic computations, several of these elementary gates are required to be cascaded. In many of the proposed designs, cascading inevitably involves the conversion of magnetic information to electrical signals which is detrimental to the device efficiency. In this work, using micromagnetic simulations, we propose two different types of Demultiplexer logic gates based purely on magnetic interactions. These interactions involve repulsive forces between skyrmion-skyrmion and skyrmion-barrier, where the term 'barrier' refers to an energy barrier created by a non-uniform landscape of perpendicular anisotropy which can be achieved experimentally by ion-irradiation as shown recently by Juge *et al.* [3] By combining these demultiplexer logic gates via cascading [4], we further develop a hybrid logic gate akin to a universal gate which is capable of simultaneously producing every possible logical output (XY, X′Y, XY′, X′Y′) from a set of given inputs (X, Y). These outputs can be combined as desired using another proposed logic design producing a fully reconfigurable and conservative logic gate. The developed re-configurable logic gate can significantly reduce the number of elementary logic operations required to perform complex arithmetic computations providing a new pathway for the development of customized skyrmion-based logic gates for task-specific calculations.

[1] S. Luo and L. You, APL Materials, Vol. 9, p.050901 (2021) [2] S. Li, W. Kang, X. Zhang *et al.*, Mater. Horiz., Vol. 8, p.854-868 (2021) [3] R. Juge, K. Bairagi, K. G. Rana *et al.*, Nano Letters, Vol. 7, p.2989–2996 (2021). [4] W. Kluge, Electronics Letters, Vol. 8, p.313 (1972)

HOG-03. Stochastic Computing with Magnetic Domain Wall Devices.
A. Welbourne[1], M. Chambard[1], S. Kyle[1], M. Drouhin[1], L.T. Haigh[1], A.M. Keogh[1], A. Mullen[1], P.W. Fry[1], F. Maccherozzi[2], T. Forest[2], L. Aballe[3], M. Foerster[3], E. Vasilaki[1], D. Allwood[1] and T. Hayward[1]
1. University of Sheffield, Sheffield, United Kingdom; 2. Diamond Light Source, Oxford, United Kingdom; 3. ALBA Synchrotron Light Facility, Barcelona, Spain

Non-volatile logic and memory devices based on domain wall (DW) motion have technological promise [1,2], but stochastic behavior, which typically has to be overcome for proper device functionality, has impeded development [3]. Here, we propose that the intrinsic stochastic behaviors of these devices can be harnessed to perform hardware-based "stochastic computing". Floating-point numbers are encoded as the average value of random bit digital streams, and individual logic gates perform complex mathematical operations that would require extended networks of gates in conventional logic. For example, in stochastic computing multiplication is performed by a single AND gate, whereas, even a 2 bit binary multiplier

would conventionally require eight logic gates. This alternative paradigm also offers the benefit of fast approximation and high error tolerance, but requires the generation of uncorrelated random bitstreams, which is challenging in conventional CMOS devices [4]. Here, we demonstrate the feasibility of creating DW-based stochastic logic architectures. We show that notches in nanowire devices provide pinning sites at which the probability of DW pinning can be tuned via modulating the propagation field (Fig 1). This allows generation of random bit streams (presence or absence of DWs) where their encoded value matches the pinning probability of the defect site. We further demonstrate DW logic gates based on this nanowire architecture that allow computing with the encoded values (Fig 2). Our work demonstrates how the intrinsically stochastic nature of DW pinning allows the realization of the stochastic computing paradigm using devices where random processes occur naturally, thus overcoming one of the challenges of implementing stochastic computing with conventional CMOS architectures.

[1] D. A. Allwood, et al., Science, Vol. 309, p.1688-1692 (2005) [2] S. S. P. Parkin, et al., Science, Vol. 320, p.190-194 (2008) [3] T. J. Hayward and K. A. Omari, J. Phys. D. Appl. Phys., Vol.50, p.084006 (2017) [4] A. Alaghi and J. P. Hayes, IEEE Trans. Comput. Des. Integr. Circuits Syst., Vol.37, p.139-46 (2013)

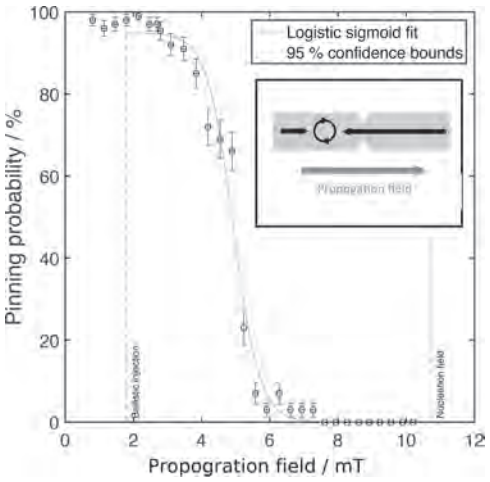

Fig. 1 Notch defects in 400 nm wide (20 nm thick) permalloy nanowires provide sites with tunable pinning probability. DWs arriving at the notch under increasing propagation fields pin with probability following a logistic sigmoid like decrease.

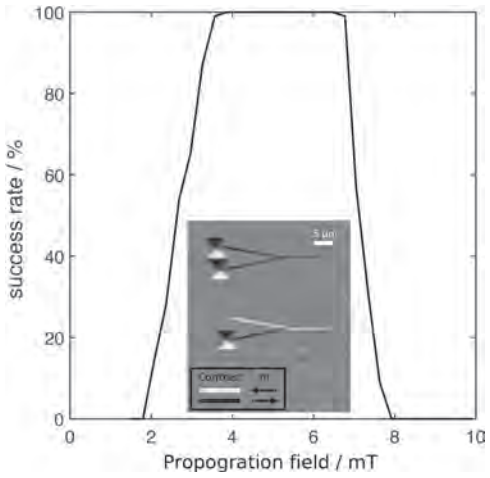

Fig. 2 Operational range of a DW based AND gate. For walls propagated in the range ~4–7 mT the gate behaves deterministically as an AND gate. PEEM data inset illustrates this functionality.

HOG-04. Neuromorphic Learning of a Deep Neural Network with Low Precision and Stochastic Domain Wall Based Memristor. W. Misba[1], M. Lozano[1], D. Querlioz[2] and *J. Atulasimha*[1] *1. Virginia Commonwealth University, Richmond, VA, United States; 2. Université Paris-Saclay, Paris, France*

Spintronic devices are promising for neuromorphic computing due to their greater energy efficiency, high endurance compared to phase change memory and resistive random-access memory [1]. Popular spintronic memristors involve movement of a domain wall (DW) in a perpendicularly anisotropic (PMA) racetrack to achieve variable conductance to implement synaptic weights for deep neural networks (DNNs). However, energy efficient voltage controlled DW devices driven by spin orbit torque with Neel DW stabilized by Dzyaloshinskii-Moriya interaction show stochastic behavior and therefore provide limited states (see Fig.1 [2]). This is modelled rigorously with micromagnetics. To work with these DW devices and achieve high testing accuracy, the DNNs need to be trained with specific algorithms. In this study, we propose both in-situ and ex-situ training algorithms of DNN based on 2-, 3- and 5-state DW synaptic devices. For in-situ training, a mixed precision framework [3] is adopted where low precision synaptic conductances are tuned based on the quantized value of high precision gradients. With our quantized training, the learning is able to tolerate large conductance variation without any considerable accuracy loss as the synaptic state changes only few times during the entire training due to large inter-state interval. Thus, high programming noise intrinsic to DW devices is accommodated in the training which reduces the required number of programming pulses and the energy to train a DNN. The programming energy required for a DNN with 5-state DW synapse is found to be 1.25 pJ/image for MNIST digit classification with ~96.7% accuracy shown in Fig.2. Ex-situ training algorithm is also proposed where the DW devices are characterized based on statistics and then the devices characteristic is inputted to the quantized training algorithm as constraints which shows ~95% accuracy for 5-state synapses for large conductance variation. This work will pave the way to implement high accuracy intelligent future battery powered IoT edge devices using DW devices. Acknowledgement: NSF grant ECCS: #1954589

[1]. H.-S. P. Wong and S. Salahuddin, Nat. Nanotechnol., vol 10, p.191 (2015) [2]. W. A. Misba, T. Kaisar and D. Bhattacharya, arXiv:2010.10076 (2020) [3]. S. R. Nandakumar, M. L. Gallo and C. Piveteau, Frontiers in Neuroscience, Vol. 14, p.406 (2020)

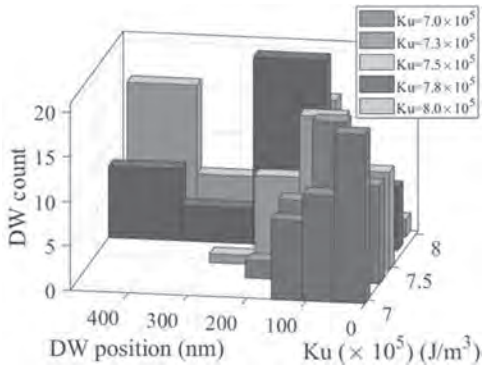

Fig. 1: Stochastic nature of DW devices for voltage control of PMA (Ku) [2]

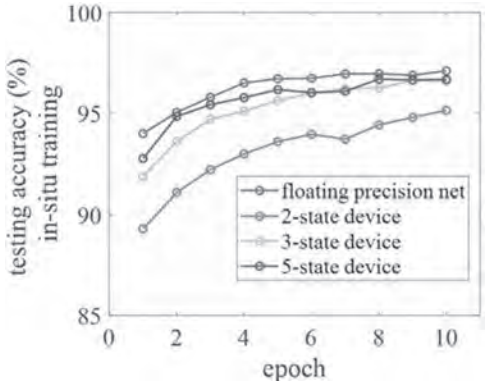

Fig. 2: Testing accuracy comparison with proposed training

HOG-05. Domain Wall-Gated, Cascaded and Low-Power Skyrmion Logic Gates with Robust Operation. *A. Mousavi Cheghabouri*[1] and M.C. Onbasli[1] *1. Electrical and Electronics Engineering, Koc University, Istanbul, Turkey*

Skyrmions hold great promise for next generation computation due to their current-driven control, ultra-low power consumption, non-volatile characteristics, and nanoscale footprint. Any technology candidate for in-memory computing will need to use a universal set of logic gates as its building blocks such as NAND or NOR. Despite previous efforts on all-skyrmion logic gates, the logic inverter that is essential for Boolean logic operations has not yet been addressed under realistic conditions on materials, current drive and device geometries[1-4] with simple current drive and robust operation against geometric defects and Joule heating. Here, we demonstrate a domain wall-gated nanoscale skyrmion logic inverter (NOT) and NOR gates based on Co/Pt bilayer cross junctions. The inverter operation is based on a logic input (0/1: skyrmion absence/presence) applied first along the vertical channel. If there is a skyrmion logic input, this skyrmion is driven by current and converted to a domain wall (DW) to fill the vertical channel. Next, a probing skyrmion is applied[5] horizontally as in Fig. 1. When there is a DW in the vertical channel, the probing pulse coming from the horizontal channel is blocked (output 0, input 1). With no skyrmion in the input, a DW does not form and the horizontal probing skyrmion reaches the gate output (output: 1). A final DC pulse along the vertical channel is applied to clear the inverter for an arbitrary input in the next clock cycle. Our proposed logic inverter has small footprint ($4 \times 240 \times 300$ nm^3), room temperature operation with realistic current drive ($0.4\text{-}1.2 \times 10^{12}$ A m^{-2}), robust operation under imperfect sidewall and notch geometries, and higher temperature effects. The inverter consumes about 1350 k_B per operation at room temperature in addition to Joule heating. Joule heating must be suppressed by using insulating magnetic layers for minimal thermal drift, although we show that the circuit equilibrates at slightly above room temperature due to heat conduction to the substrate. We also present a non-volatile NOR gate that consists of two junctions, which is sufficient to achieve all Boolean logic functionalities.

1. Zhang, X., Ezawa, M. & Zhou, Y. *Scientific Reports* 5, 9400 (2015). 2. Luo, S. *et al.* Reconfigurable Skyrmion Logic Gates. *Nano Letters* 18, 1180 (2018). 3. Zhang, X., Zhou, Y., Ezawa, et al. *Scientific Reports* 5, 11369, (2015). 4. Xing, X., Pong, P. W. T. & Zhou, Y. et al. *Physical Review B* 94, 054408 (2016). 5. Cheghabouri, A. M. & Onbasli, M. C. *Scientific Reports* 9, 9496 (2019).

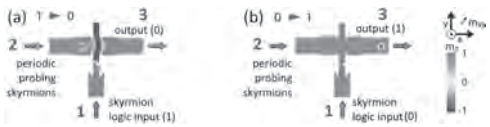

Fig. 1. Inverter logic operation for (a) input 1, (b) input 0 are shown.

HOG-06. Kinematic Domain Wall Model for Large-Scale Neuromorphic Network Simulation. *K. Doleh*[1], C.M. Linseisen[1], L.M. Humphrey[1], F. Garcia-Sanchez[3], X. Hu[1], W.H. Brigner[1], C. Cui[2], J.M. Martin[1], J.C. Incorvia[2], N. Hassan[1], A.J. Edwards[1] and J.S. Friedman[1] *1. Department of Electrical and Computer Engineering, The University of Texas at Dallas, Richardson, TX, United States; 2. Department of Electrical and Computer Engineering, The University of Texas at Austin, Austin, TX, United States; 3. Departamento de Física Aplicida, Universidad de Salamanca, Salamanca, Spain*

As the human brain is extremely computationally efficient, recent attention has gravitated towards biomimetic neuronal and synaptic devices emulating observed neural spiking activity. One promising neuronal device consists of a domain wall magnetic tunnel junction (DW-MTJ), intrinsically performing neuronal integration and thresholding [1, 2]. Landau–Lifshitz–Gilbert (LLG)-based micromagnetic simulations for a single DW-MTJ device are extremely resource heavy [3], and other proposed models are too simplistic to account for many observed magnetic effects like inertia [4]. Thus, there does not exist a reasonably accurate model able to simulate even a medium-scale neuromorphic network (NN) designed with DW-MTJs. Here we propose that classical kinematic phenomena such as inertia and friction are analogous to the physics underlying DW motion, thereby enabling fast, accurate large-scale simulations of DW-MTJ NNs. Our model avoids the time-consuming process of solving the LLG by parameter-fitting kinematic motion based equations to micromagnetic simulations enabling a speedup of ~100,000x. We simulated a 500 nm by 32 nm DW track in mumax3 with randomized perpendicular magnetic anisotropy grains and emulated spin orbit torque (SOT)-driven DW motion (Fig. 1). We extracted the DW position over time for model fitting. We present a preliminary model comprising a second order differential equation solved utilizing Euler's method, which is amenable for low-resource SPICE modeling. Fig. 2 provides a graphical representation of the SOT current and DW position in time juxtaposed against our predictive model demonstrating alignment with simulated dynamics. While the model is not fully accurate, the most important aspects of DW motion for NNs are captured, namely the maximum DW velocity and the stopping location of the DW. This small accuracy loss is traded for a large speedup of ~100,000x. Ultimately, use of this model will enable rapid development of low-power biomimetic NNs with DW-MTJs.

[1] Naimul Hassan, Xuan Hu, Lucian Jiang-Wei, Wesley H. Brigner, Otitoaleke G. Akinola, Felipe Garcia-Sanchez, Massimo Pasquale, Christopher H. Bennett, Jean Anne C. Incorvia, and Joseph S. Friedman, "Magnetic domain wall neuron with lateral inhibition", Journal of Applied Physics 124, 152127 (2018) https://doi.org/10.1063/1.5042452 [2] W. H. Brigner et al., "Graded-Anisotropy-Induced Magnetic Domain Wall Drift for an Artificial Spintronic Leaky Integrate-and-Fire Neuron," in IEEE Journal on Exploratory Solid-State Computational Devices and Circuits, vol. 5, no. 1, pp. 19-24, June 2019, doi: 10.1109/JXCDC.2019.2904191. [3] Junya Shibata et al.2011 J. Phys. D: Appl. Phys. 44 384004 [4] X. Hu, A. Timm, W. H. Brigner, J. A. C. Incorvia and J. S. Friedman, "SPICE-Only Model for Spin-Transfer Torque Domain Wall MTJ Logic," in IEEE Transactions on Electron Devices, vol. 66, no. 6, pp. 2817-2821, June 2019, doi: 10.1109/TED.2019.2912756.

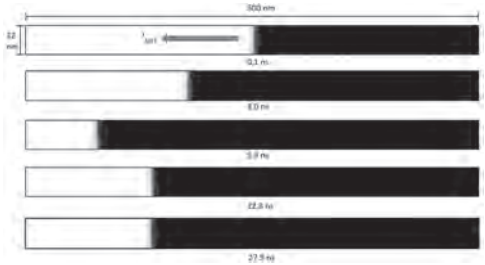

Figure 1: The DW is depicted at various points in the nanowire track. White (black) corresponds to out-of (into)-plane magnetization.

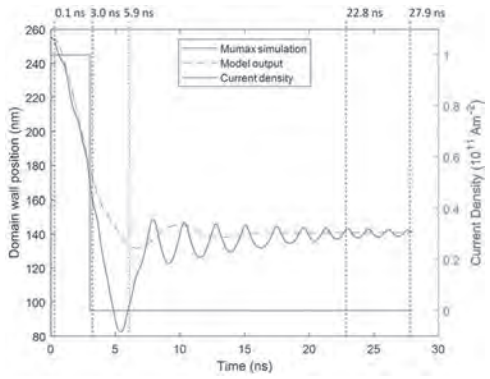

Figure 2: Modeled and simulated DW position vs. time. Dashed lines correspond with the snapshots in Fig. 1.

HOG-07. Machine Learning with Stochastic Magnetic Domain Wall Synapses. *M.O. Ellis*[1], A. Welbourne[2], S. Kyle[2], T. Hayward[2], D. Allwood[2] and E. Vasilaki[1] *1. Department of Computer Science, University of Sheffield, Sheffield, United Kingdom; 2. Department of Materials Science and Engineering, University of Sheffield, Sheffield, United Kingdom*

Despite their importance in a variety of technologies, the high energy cost of many forms of machine learning algorithms is a significant limitation[1]. One solution to this is to employ physical devices that can naturally mimic brain-like behaviour, known as neuromorphic computing [2]. Magnetic domain walls (DWs) are strong candidates for such devices, since they have potential for both data storage and logic operations [3] but stochastic effects limit the feasibility of creating viable devices. Here, we demonstrate how tunable stochastic pinning can be used to emulate synaptic properties for specialised neuromorphic devices. First we show measurements that demonstrate the feasibility of tuning stochastic processes by applying external stimuli. Focused magneto-optic Kerr effect measurements were used to probe the pinning of DWs at notch-shaped defects in 400 nm wide Permalloy nanowires. As shown in Fig 1, by modulating the propagation field (H) by an additional amount (dH) the pinning probability of the DW at the defect site was found to depend sigmoidally on dH and is observed on separate wires. Next, we model these wires as binary stochastic synapses in a neural network with properties based on the experimental measurements. By repeatedly sampling the network the stochastic total output can be converged to an analogue value to improve performance. It is found that for a single cycle of the network it can be trained to recognise handwritten digits with an error rate of 17%. Repeated sampling of the network decreased the error rate to 8% for 128 cycles, close to mean field performance, Fig. 2. We have also found that this performance is only slightly reduced when random individual wire properties are considered and additional neural layers mitigate stochasticity. Our work illustrates how the intrinsic stochasticity of DW devices can be harnessed to provide tunable bespoke hardware for machine learning tasks.

[1] Aly et al. Proc. IEEE 107 (2019) [2] J. Grollier *et al. Nat Electron* 3, 360–370 (2020) [3] D. A. Allwood *et al.*, *Science* 309 (5741), 1688–1692 (2005).

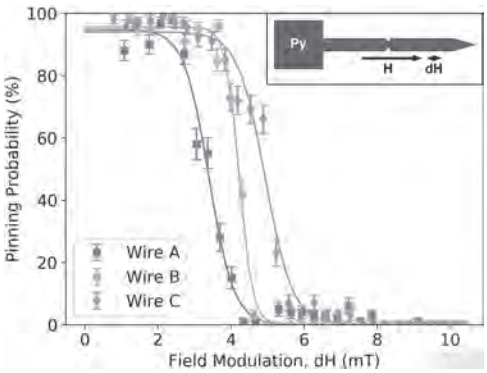

Tuning of domain wall pinning probability in notched magnetic nanowire synapse. Inset shows a schematic of the notched nanowire and applied field direction.

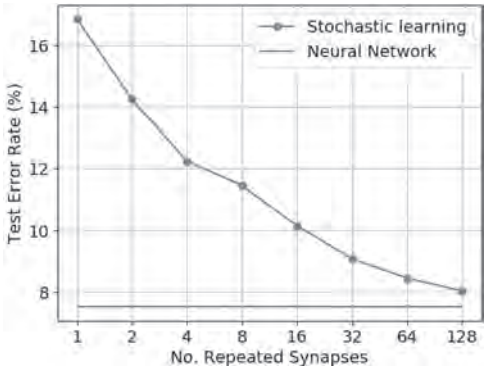

Test error rate of classifying handwritten digits using a single layer stochastic network for varying repeated sampling.

HOG-08. Neuromorphic computation with a single magnetic domain wall. R.V. Ababei[1], *M.O. Ellis*[2], I.T. Vidamour[1], D. Devadasan[1], D. Allwood[1], E. Vasilaki[2] and T. Hayward[1] *1. Department of Materials Science and Engineering, University of Sheffield, Sheffield, United Kingdom; 2. Department of Computer Science, University of Sheffield, Sheffield, United Kingdom*

Classifying or predicting complex time-dependent signals is a challenging computational task. Reservoir computing (RC) is an efficient neuromorphic computing approach that is ideally suited to such tasks, and is typically implemented in software using a recurrent neural network (RNN) with fixed synaptic weights (the reservoir) connected to a single, trainable readout layer. However, more efficient implementations of RC are possible if the software RNN reservoir is substituted with a physical system with the correct properties, such as non-linear response to input signals and inherent memory [1]. In this work, we exploit the chaotic and non-linear dynamics of a single magnetic domain wall (DW) trapped between two anti-notches in a Ni nanostrip as a hardware-based reservoir. We have modelled the structure (inset of Fig. 1) using both a simple 1D model and micromagnetic simulations with an oscillating field. As shown in Fig. 1, complex oscillatory dynamics over a range of field amplitudes are observed. A chaotic and multi-period regime occurs between 0.4 kA/m and 1.2 kA/m and a non-linear regime at higher fields. Thus, the DW oscillator can be used to transform an input magnetic field to the DW position output suitable for RC. A time-multiplexed input signal is injected into the DW oscillator by modulating the applied field magnitude, and we show how this approach allows the device to perform classification tasks as a reservoir. First, we demonstrate how the scaling to convert input data into applied fields affects the classification accuracy of the sine or square wave task, showing that the best recognition rate is obtained at the edge of a chaotic regime of oscillation (Fig.2). We also demonstrate that the DW oscillator can perform complex tasks, such as spoken digit

recognition, and that coupling multiple DWs together enhances the computational capabilities of the reservoir. Our work opens new avenues for research into neuromorphic computing using nanomagnetic hardware.

[1] M. Riou et al., Phys. Review Applied, 2019

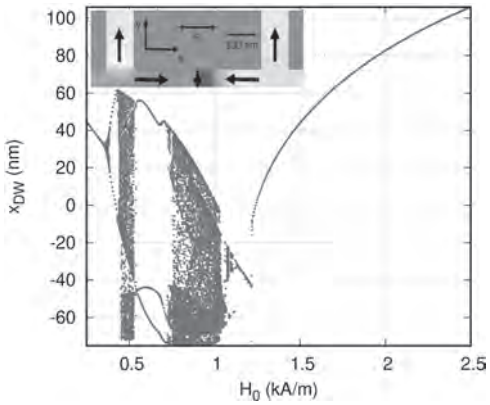

Bifurcation plot showing the DW position once per cycle for a given applied field using the 1D model. Inset: Schematic of the system.

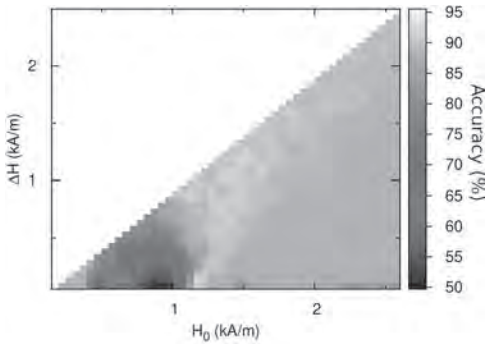

Classification accuracy of the Sine-Square task over a range of field centre (H_0) and field width (ΔH) values.

HOG-09. Skyrmion Based Logic-In-Memory Architecture using Synthetic Antiferromagnets. *N. Sisodia*[1], L.D. Buda-Prejbeanu[1], G. Gaudin[1] and O. Boulle[1] *1. Univ. Grenoble Alpes, CNRS, CEA, Grenoble INP, Spintec, Grenoble, France*

Fast, high-density, and energy-efficient devices are crucial enablers of today's IT technology pushed by the advent of cloud computing, big data, and the internet of things. To face this challenge, the conventional Von Neumann architecture where logic and memory units are separately implemented leads to critical issues: the increase of the length of the global interconnects between the logic and memory units when downscaling results in a critical rise in power and delay. A promising alternative lies in "Logic-In-Memory" (LIM) architectures that merge logic and memory functions in the same device promising non-volatility, ultra-low-power, and high-speed operations. Topological magnetic textures called skyrmions are ideally suited for this purpose due to their nanoscale size, fast motion, and non-volatility. They also repel each other which can be leveraged to perform basic logic operations. Several proposals have been presented in the past for skyrmion-based logic gates [1][2], however, most of these require an intermediate conversion of magnetic information to electrical signals which is inefficient for large-scale computation where several levels of cascading is often required to perform complex operations. In this study, by using micromagnetic simulations, we present a Synthetic Antiferromagnet based LIM architecture that relies purely on magnetic interactions for performing logic operations. We first design a racetrack storage that uses skyrmions as memory bits confined by anisotropy energy barriers and outline simple protocols for "nucleate" and "Shift" operations on skyrmions using current-induced spin-orbit torques. We then combine our racetrack storage with a newly designed 1-bit Full Adder (FA) gate extendable to n-bit FA by cascading. The designed FA is reprogrammable and can also be used to perform AND/OR/NOT/NAND/XOR/XNOR operations. We discuss the performance metrics of the FA gate along with its electrical tolerances and show that the device performs well even with some fluctuations in the amplitude/width of the injected current pulse. The monolithic design of the logic gate and the absence of any complex electrical contacts makes the device ideal for integration with conventional CMOS circuitry.

[1] S. Luo and L. You, APL Materials, Vol. 9, p.050901 (2021) [2] S. Li, W. Kang, X. Zhang *et al.*, Mater. Horiz., Vol. 8, p.854-868 (2021)

HOG-10. Physical Reservoir Computing Using Spin Torque Oscillator with Loop Circuit. *S. Tsunegi*[1,2], T. Taniguchi[1], A. Kamimaki[1], K. Yakushiji[1], A. Fukushima[1], S. Yuasa[1] and H. Kubota[1] *1. AIST, Tsukuba, Japan; 2. JST-PRESTO, Kawaguchi, Japan*

Physical reservoir computing (PRC) utilizing spin-torque oscillator (STO) has been attracting great attention because of its potential applications to time-series data processing such as human voice recognition [1]. In the PRC, magnetization dynamics of the STO is modified by input of the time-series data. The modified dynamics produces fading memory, which is essential to the computing. An amount of fading memory has been investigated by evaluating short-term memory capacity [2]. Large capacity is required for general-purpose processing system. Our previous study showed that the capacity was about 2-4 bits in a vortex STO [3,4]. The value was one order of magnitude smaller than that reported in laser-based physical reservoir computing [5]. In this work, we report a significant improvement of the memory capacity in the vortex STO by utilizing a loop circuit (Fig. 1). The circuit was identical to that used in our previous study [3] except for the loop structure. A self-oscillation of the vortex in the STO was excited by applying direct voltage. The oscillation was modified by radio-frequency (rf) magnetic field, which was generated by applying rf current from an injector to a metal line. The rf field was modulated by the input data, which was homogeneously distributed random time-series data. We inserted a loop structure between the injector and metal line and controlled the loop gain by using an attenuator. Note that the attenuation cannot be less than 14 dB to avoid loop oscillation. The memory capacity was evaluated based on the reproducibility of the input data from the STO waveform [3]. Figure 2 summarizes the memory capacity as a function of the attenuation rate. A large memory capacity of 13 is achieved, which is the highest value achieved in STO-based PRC to date. Since a part of the input data was delayed and looped in the circuit, the magnetization dynamics was influenced by the input many times, resulting in the enhancement. This work was partially supported by NEDO and JST-PRESTO (Grant No. JPMJPR20M5).

[1] J. Torejon *et al.*, Nature 547, 428 (2017). [2] H. Jaeger, GMD Report 152 (2002). [3] S. Tsunegi *et al.*, Jpn. J. Appl. Phys. 57, 120307 (2018). [4] S. Tsunegi *et al.*, Appl. Phys. Lett. 114, 164101 (2019). [5] F. Duport, et al. Opt. Express 20, 22783 (2012)

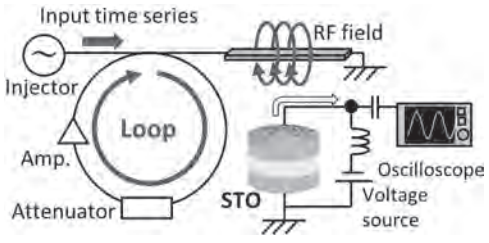

Fig. 1 Schematic illustration of measurement system with loop circuit.

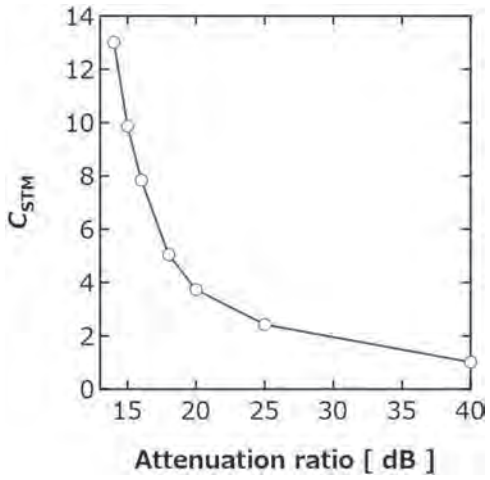

Fig. 2 Attenuation ratio dependence of short-term memory capacity C_{STM}.

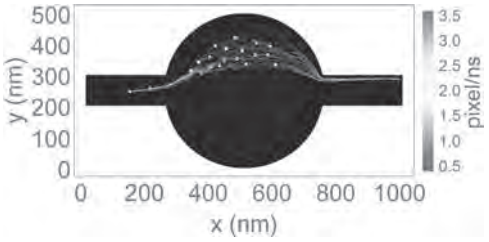

Fig.1

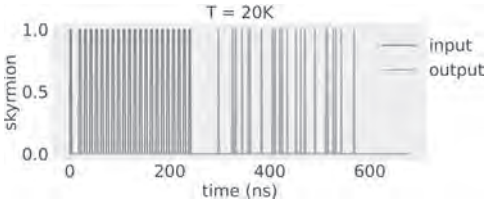

Fig.2

HOG-11. Stochastic Property of Skyrmionic Shuffling Device. *Z. Khodzhaev*[1] and E. Turgut[1] *1. Physics, Oklahoma State University, Stillwater, OK, United States*

Magnetic skyrmions can be transferred from it's position to a desired location using spin torques [1] and there were proposals of skyrmion reacetrack memory and logic gate applications [2]. But, the instabilities and stochastic behavior of Skyrmions due to pinning [3], temperature and applied current, and skyrmion Hall angle (SkHA) [4] makes the realization of these applications challenging. Instead, stochastic skyrmion behaviour can be used to create new computing architectures, e.g., probabilistic and reservoir computing [5,6]. The major aspect of this computation is having a constant uncorrelated signal [5] that results from a reshuffle of the skyrmions. In this study, the stochastic property in a shuffling chamber will be investigated to create uncorrelated signals. The study will guide for the creation of a better probabilistic computing devices. We use the shuffling chamber (Fig. 1) and the current density for the geometry was generated in Mathematica and masking was used to implement it in micromagnetic simulator Mumax3 [7]. At first, the height of the paths were changed to 320, 360, 400 and 520 nm, this resulted in increase on the longevity of the final skyrmion path, and the skyrmion's projectile motion decreased, accordingly. As the height of the rectangle increases, distance between the Skyrmion and the output borderline increases too. At first, the Skyrmion motion was observed under 0 K temperature, and without a grain. The skyrmions had a projectile and predictive motion. Then, the system was run using different temperatures, grain, and different currents to get a stochastic Skyrmion motion. In our simulations, the skyrmion under higher temperature was unstable at the output of the chamber, but by using higher anisotropy constant (Ku) at the output edge of the chamber, the instability was eliminated. The correlation between input and output paths were analyzed using Pearson correlation coefficient (PCC). We vary the temperature from 0 K to 100 K temperatures and find that the PCC changes from -0.055 to -0.04.

[1] Nakatani Y., Yamada K. and Hirohata A., Scientific Reports, 11(1), pp.1-6 (2021) [2] Luo S. and You L., APL Materials, 9(5), p.050901 (2021) [3] Stosic D., Ludermir T.B. and Milošević M.V., Physical Review B, 96(21), p.214403 (2017) [4] Litzius K., Leliaert J., Bassirian P. et al., Nature Electronics, 3(1), pp.30-36 (2020) [5] Pinna D., Araujo F.A., Kim J.V. et al., Physical Review Applied, 9(6), p.064018 (2018) [6] Zázvorka J., Jakobs F., Heinze D., Nature nanotechnology, 14(7), pp.658-661 (2019) [7] Vansteenkiste A., Leliaert J., Dvornik M. et al., AIP advances, 4(10), p.107133 (2014)

HOG-12. Magnetic domain wall stability in stepped wire for multistate storage devices. *R. Sbiaa*[1], S.M. Alrisi[1], T. Jin[2] and S. Piramanayagam[2] *1. Physics, Sultan Qaboos University, Al Khodh, Oman; 2. School of Physical and Mathematical Sciences, Nanyang Technological University, Singapore, Singapore*

Neuromorphic computing is emerging as a potential candidate for Artificial intelligence. In this sense, domain wall (DW) devices play a crucial role in creating synthetic synapses and neurons [1]. In DW devices, controlling DW positions and its motion using an electric current are important challenges. In this study, the devices were fabricated using electron-beam lithography. To stabilize DW at a defined position within the nanowire, staggered design was proposed and fabricated [2]. After making the nanowires, the conductive electrodes for injecting the current were deposited at the edges. Fig. 1, shows an optical image of the fabricated devices. To investigate the motion of DW by a polarized current, we first applied a magnetic field in the direction perpendicular to the device to create a magnetic domain in the nucleation pad. A pulsed voltage was applied to a conventional wire (without steps) of 500 nm width. Even with a very small increment of the voltage amplitude, it was not possible to stabilize the DW within the wire. The critical voltage for releasing the DW from the pad is revealed to be linearly dependent on the pulse width. In this study, (Co/Ni) and (Co/Pt) multilayers with 12 repeats are investigated. For stepped wire, the (Co/Pt) with higher anisotropy did not show a motion of DW by spin-transfer torque effect. There is a need for a high current, which in most cases damages the device. However, a clear control of DW position could be seen by applying a magnetic field as shown in Fig. 2. For the case of (Co/Ni) multilayers with lower anisotropy, it is possible to see a displacement and pinning of DW at different stepped regions within the wire. It is also observed that when only a magnetic field was applied, magnetic domain could randomly be seen in different regions of the nanowire. This randomness could be solved by applying a polarized current along the wire. In this work, we will present the details of the DW dynamics and its stability for different nanowire dimensions and magnetic material properties

[1] D. Bhowmik et al. J. Magn. Magn. Mater. 489, 165434 (2019). [2] M. Bahri et al. Phys. Rev. Applied 11, 024023 (2019).

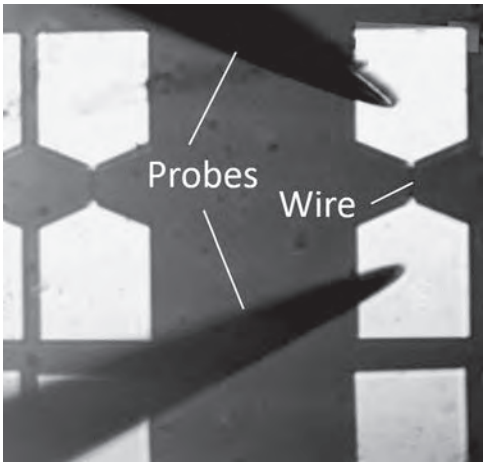

An optical image of the fabricated devices with two pads for applying electric current

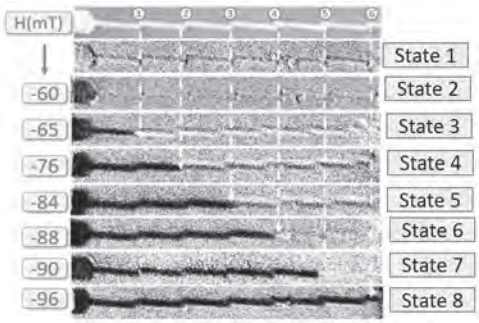

Displacement of DW by a magnetic field at precise positions for (Co/Pt) multilayers

HOG-13. Skyrmion Qubits: A New Class of Quantum Logic Elements Based on Nanoscale Magnetization. *C. Psaroudaki*[1,2] and C. Panagopoulos[3] *1. Institute for Quantum Information and Matter, California Institute of Technology, Pasadena, CA, United States; 2. Department of Physics, California Institute of Technology, Pasadena, CA, United States; 3. Division of Physics and Applied Physics, Nanyang Technological University, Nanyang, Singapore, Singapore*

We introduce a new class of primitive building blocks for realizing quantum logic elements based on nanoscale magnetization textures called skyrmions. In a skyrmion qubit, information is stored in the quantum degree of helicity, and the logical states can be adjusted by electric and magnetic fields, offering a rich operation regime with high anharmonicity. By exploring a large parameter space, we propose two skyrmion qubit variants depending on their quantized state. We discuss appropriate microwave pulses required to generate single-qubit gates for quantum computing, and skyrmion multiqubit schemes for a scalable architecture with tailored couplings. Scalability, controllability by microwave fields, operation time scales, and readout by nonvolatile techniques converge to make the skyrmion qubit highly attractive as a logical element of a quantum processor.

Christina Psaroudaki and Christos Panagopoulos, Phys. Rev. Lett. 2021 (Accepted, in production), Editors' Suggestion

Session HOH
MAGNETIZATION DYNAMICS IN SOFT MATERIALS

Valentine Novosad, Chair
Argonne National Laboratory, Lemont, IL, United States

INVITED PAPER

HOH-01. Magnetic Vortices: into the Third Dimension. *S. Gliga*[1]
1. Swiss Light Source, Paul Scherrer Institute, Villigen, Switzerland

Vortices are familiar phenomena in fluids, distinguishable for example in tornadoes, hurricanes, whirlpools and rings. In ferromagnets, vortices are naturally forming flux-closure states characterized by a curling of the magnetic moments around a very stable and narrow core [1]. The study of vortices is motivated by both fundamental and technological interest. Indeed, their topological properties endow vortices with rich and surprising dynamics, such as the ultrafast reversal of the vortex core [2], making them fascinating objects of study. These properties also establish them as promising candidates for applications in data storage and signal processing. Over the past decades, vortices have been extensively studied in laterally confined thin-film elements, where the magnetization is accessible with two-dimensional imaging methods. Recent developments have enabled non-destructive imaging of three-dimensional magnetic structures at the nanoscale. In particular, using hard X-ray tomography [3], it is now possible to directly image the internal structure within bulk micromagnets. For example, in $GdCo_2$ pillars, we could image the structure surrounding micromagnetic singularities, known as Bloch points, which were predicted over 50 years ago. Recently, we have uncovered three-dimensional structures forming closed vortex loops. The cross-section of these loops consists of a vortex–antivortex pair and, based on magnetic vorticity (a quantity analogous to hydrodynamic vorticity), we identified these configurations as magnetic vortex rings [4]. Such structures have been predicted to exist as transient states in exchange ferromagnets [5]; in contrast, the observed vortex rings exist as static configurations, and we attribute their stability to the dipolar interaction. In addition, we observe stable vortex loops intersected by point singularities at which the magnetization within the vortex and antivortex cores reverses. Such structures can exist because a non-zero divergence of the magnetization is allowed in ferromagnets; they have no analogue in incompressible fluids. Incidentally, it is known since the 1970s that 'Bloch lines' can assume complex structures, but these could only be inferred from surface observations combined with theory. Our results shed new light onto the rich physics of bulk magnets and open possibilities for further studies of complex three-dimensional solitons, enabling the development of applications based on three-dimensional magnetic structures. Thus, the title of this talk could as well be, 'Magnetic Vortices: Back to the Third Dimension'.

[1] A. Wachowiak, J. Wiebe, M. Bode, O. Pietzsch, M. Morgenstern, R. Wiesendanger, Science 298, 577–580 (2002) [2] R. Hertel, S. Gliga, M. Fähnle, and C. M. Schneider, Phys. Rev. Lett. 98, 117201 (2007) [3] C. Donnelly, M. Guizar-Sicairos, V. Scagnoli, S. Gliga, M. Holler, J. Raabe, L. J. Heyderman, Nature 547, 328–331 (2017) [4] C. Donnelly, K. L. Metlov, V. Scagnoli, M. Guizar-Sicairos, M. Holler, N. S. Bingham, J. Raabe, L. J. Heyderman, N. R. Cooper, S. Gliga, Nature Physics 17, 316–321 (2021) [5] N. R. Cooper, Phys. Rev.Lett. 82, 1554 (1999)

CONTRIBUTED PAPERS

HOH-02. Diffusive and Fluid-like Motion of Homochiral Domain Walls in Easy-Plane Magnetic Strips. *D.A. Smith*[1], S. Takei[2,3], B. Brann[1], L. Compton[1], F. Ramos-Diaz[1], M. Simmers[4] and S. Emori[1] *1. Physics, Virginia Tech, Blacksburg, VA, United States; 2. Physics, Queens College, Queens, NY, United States; 3. Physics Doctoral Program, The Graduate Center of the City University of New York, New York, NY, United States; 4. Academy of Integrated Science, Virginia Tech, Blacksburg, VA, United States*

Much effort has focused on achieving micron-scale spin propagation using diffusive spin waves, but their exponential decay with distance makes efficient spin transport challenging. An alternative form of magnetization dynamics – commonly referred to as spin superfluidity [1] or exchange mediated spin transport [2,3] – may enable more efficient transport owing to its topologically-protected easy-plane precession of the magnetization and associated linear decay of spin flow. Our work addresses the open question of how defects impact this easy-plane spin transport at low drive current densities. We performed micromagnetic simulations on easy-plane precessional dynamics in synthetic antiferromagnet nanostrips with and without notch defects. The material parameters were taken from our experimentally measured, low-damping FeV alloys [4]. We view the dynamics as a train of interacting, homochiral domain walls (DWs) rather than as hydrodynamic flow [2]. We observe the transition from (1) isolated, diffusively propagating DWs, which are susceptible to pinning, to (2) a fluid-like flow of a closely packed DW train that is unimpeded by pinning defects. This transition is quantified by computing the superfluid velocity $\nabla\Phi$, where Φ is the in-plane azimuthal angle of the magnetization, at a position beyond the notch defect (see Fig. 1). In Fig. 2, $\nabla\Phi$ differs between the perfect and notched nanostrips as a result of pinning of the DWs at low drive current densities, $J_c < 5 \times 10^{11}$ A/m^2. As J_c increases, $\nabla\Phi$ becomes identical between the two geometries, indicating that the DWs have effectively condensed to form a fluid flowing unaffected by the notch defect. Our findings are promising for future realization of superfluid-like spin transport via easy-plane precession in ferromagnetic metal devices, which are compatible with established fabrication techniques [5].

[1] E. B. Sonin, *Adv. Sci.* 59, 181 (2010) [2] E. Iacocca, T. J. Silva, and M. A. Hoefer, *Phys. Rev. B* 96, 134434 (2017) [3] T. Schenider, D. Hill, A. Kakay, *et al.*, *Phys. Rev. B* 103, 144412 (2021) [4] D. A. Smith, A. Rai, Y. Lim, *et al.*, *Phys. Rev. Appl.* 14, 034042 (2020) [5] D. A. Smith, S. Takei, B. Brann, *et al.,* arXiv:2107.07025

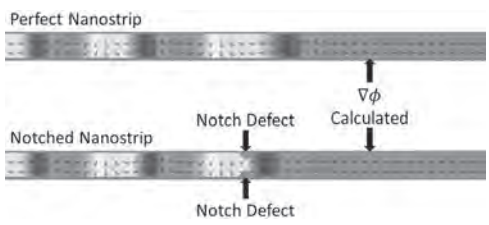

Figure 1: Micromagnetic snapshots of the perfect and notched nanostrips at $J_c = 4 \times 10^{11}$ A/m^2, labeled with location of notch defect at the center and where $\nabla\Phi$ is calculated.

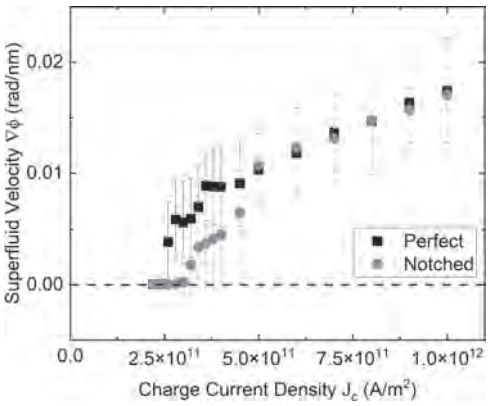

Figure 2: Superfluid velocity ∇Φ as a function of charge current density J_c for the perfect (black squares) and notched (red circle) nanostrips computed at a fixed position beyond the notch defects.

HOH-03. Generation of High Amplitude Microwaves in Nanowires Induced by Domain Wall Motion. *A. Samanta*[1,2] and S. Roy[1,2] *1. Micropower Devices/Systems and Nanomagnetics Group, Tyndall National Institute, Cork, Ireland; 2. Department of Physics, University College Cork, Cork, Ireland*

In emerging applications like telecommunication, radar, microwave generation, etc technology has received keen attention over the conventional voltage-controlled oscillator(VCO) because of their high frequency, strong signal stability, and lower power consumption. Since a substantial amount of power is required to operate the VCOs, the utility of VCOs in the application fields becomes narrower; hence, new technologies are needed to generate microwaves at the cost of lower power. In the recent past, Spin Torque Oscillators(STOs) have been investigated, and, in comparison to the conventional VCOs, small chip size and high tunability have been achieved in the STOs. However, in the real world, the STOs still suffer from a few issues like the generated signals are weak, broad linewidth[1]. Recently, microwave generation through the rotation of a single domain wall in NiFe nanowire has been reported[2]. A theoretical study revealed the idea to generate microwaves from the domain wall oscillation[3]. Previously, in a magnetic nanowire, comparatively high amplitude microwaves (1.7 GHz to 5.8 GHz) were generated using domain wall motion at the lower current densities by simulating a sequence of oppositely magnetized domains (namely upward and downward domains) in one-half of the nanowire[4]. Here, by micromagnetic simulation, we show that approx. 48 GHz microwave (as shown in FIG. 2(b)) could be generated by domain wall motion. A new approach has been introduced to achieve this high amplitude and moderate linewidth of the microwave output signal. Two typical different magnetic materials have been used to define the alternate crosssectional discs along the x-direction, as described in the FIG. 1. To simulate the nanowire, the typical material parameters have been considered. The generated 48 GHz microwave is useful for radar applications.

Acknowledgment: AS gratefully acknowledges the financial support for this work from EU-H-2020 project "EnABLES-JRA", Project ID: 730957. References: [1] J.-S. Kim, M.-A. Mawass, A. Bisig, B. Krüger, R. M. Reeve, T. Schulz, F. Büttner, J. Yoon, C.-Y. You, M. Weigand, H. Stoll, G. Schütz, H. J. M. Swagten, B. Koopmans, S. Eisebitt, and M. Kläui, Nat. Commun. 5, 3429 (2014). [2] T. Ono and Y. Nakatani, Appl. Phys. Express 1, 61301 (2008). [3] R. Sbiaa, M. Al Bahri, and S. N. Piramanayagam, J. Magn. Magn. Mater. 456, 324 (2018). [4] S. Bhatti and S. N. Piramanayagam, Phys. Status Solidi – Rapid Res. Lett. 13, 1800479 (2019).

Fig. 1 Schematic of the nanowire with two different magnetic materials. The red vertical stripe in (1) is NiFe and the gray (2) is CoFe.

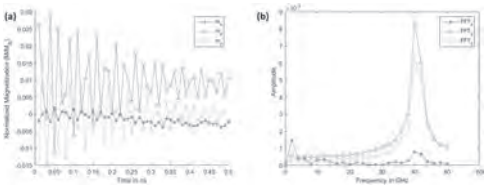

Fig. 2 (a) The simulated oscillating magnetization of the domains along x, y, z direction during the domain wall motion.(b) Corresponding FFT of the oscillating magnetizations in the nanowire. The output signal frequency of 48 GHz was observed.

HOH-04. Dynamics of bi-stable Néel domain wall under spin orbit-torque. K.J. Franke[1], *E. Haltz*[1] and C. Marrows[1] *1. Physics, University of Leeds, Leeds, United Kingdom*

The electrical manipulation of magnetic domain walls (DW) and their potential technological applications for data storage have motivated research in magnetism in the last decades. In particular, the archetypal magnetic layer / heavy metal (FM/HM) stacks are of great interest since the spin-orbit torque (SOT) generated in the HM layer acts on chiral textures in the FM layer such as Néel DW for which the chirality is fixed by the asymmetry of the magnetic layer interfaces [1]. Recently, it has been proposed that Néel DW can also be stabilized under an in-plane magnetic anisotropy, even in the absence of interface asymmetry [2]. The main difference with the classical case is the new bi-stable nature of this texture where the two DW chiralities are energetically degenerate. In this theoretical study, we simulate the dynamics of this bi-stable Néel DW driven by SOT. First, we verify that the DW propagation direction depends on its chirality and then, that the two propagation directions are possible for a given (up-down) DW depending on its initial chirality. We also find the existence of a critical current (Jc) above which the DW is locked in its Bloch state and a maximum of velocity for an intermediate tilted state of the DW (shown in the Fig). We also show that the non-uniformity of the velocity curve around Jc induces an important transient regime and out-of-equilibrium dynamics. Finally, we find that the chirality of the DW, and therefore its propagation direction, can be reversed for a moving DW under certain conditions. By extending the collective coordinate analytical model, we described and reproduced with a very good quantitative agreement the simulated results. All these new dynamics of bi-stable Néel DW open up new possibilities for devices that can mix storage, logic and processing of information.

1. A. Thiaville *et al.*, EPL 100 57002 (2012) 2. K. Franke *et al.*, arXiv:2104.12400 (2021)

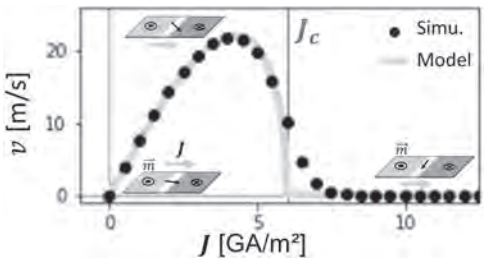

Dynamics of a bi-stable up-down Néel DW driven by SOT in a HM/FM/HM stack. The DW state and the injected current are sketched (J, green arrow). The evolution of the DW velocity versus the current density is shown for the simulation results (points) and our analytic model (solid line).

HOH-05. Reversal modes in perpendicular shape-anisotropy magnetic tunnel junctions: from coherent rotation reversal to vortex formation.
A. Palomino[1], S. Lequeux[1], T. Almeida[2], S. Auffret[1], L.D. Buda-Prejbeanu[1], L. Vila[1], R. Sousa[1], L. Prejbeanu[1], D. Cooper[2] and B. Dieny[1]
1. Univ. Grenoble Alpes, CEA, CNRS, Grenoble INP, IRIG-SPINTEC, Grenoble, France; 2. Univ. Grenoble Alpes, CEA, LETI, Grenoble, France

Coherent magnetization reversal in sub-10nm diameter shape anisotropy magnetic tunnel junctions (MTJs) has recently been reported [1]. That study was limited to MTJs with thinner PSA free layer (up to 15nm) and small diameter, aiming for high retention MRAM below 20nm diameters. Higher aspect ratios will lead to larger thermal stability and therefore larger switching currents, which is unfavorable for memory applications. However, as predicted by Proenca et al. (2021) cylindrical nanostructures with larger diameter and thickness can show other reversal modes such as vortex domain walls (V-DWs). [2]. In this study, we find experimental evidence of coherent reversal for 15 nm thick FeCoB PSA free layer MTJs (Figure 1c) and also transition to V-DW reversal for MTJs with 58 nm NiFe free layer and large diameter sizes (Figure 1g). The behavior was further confirmed by micromagnetic simulations (Figures 1d,h) by using MuMAX3 [3]. Figure 2 shows the calculated magnetic configuration of the vortex DW reversal between perpendicularly saturated states. Although the presence of such vortex state is not desirable for memory devices, the use of a topologically protected vortex state could be used for other devices such as magnetic sensors, currently under investigation in micrometer size spin valve sensors showing reduced noise [4]. In this study, we show how such vortex state with large linear range is also present in MTJs with a thick free layer, with lateral sizes well below 1 micrometer which is highly advantageous in terms of scalability.

1. B.Jinnai et al. Appl. Phys. Lett. 118, 082404 (2021) 2. M.P. Proenca et al. Sci Rep 11, 10100 (2021) 3. A. Vansteenkiste et al. AIP Advances 4, 107133 (2014) 4. D.Suess et al. Nat Electron 1, 362–370 (2018)

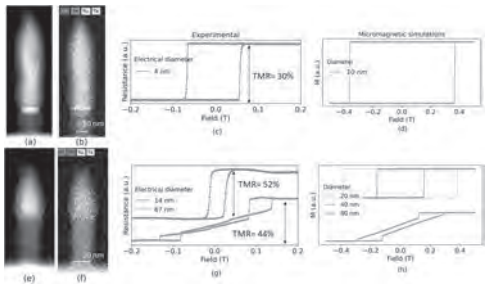

Figure 1. STEM (a,e) and EDX chemical maps (b,f) of MTJs with FeCoB 11nm (b) NiFe 58nm (f) free layers. Experimental R-H loops under perpendicular field show a vortex reversal for thicker NiFe with larger diameter (blue line). Smaller diameters show a coherent reversal (green line) (g). Experimental results are confirmed by micro magnetic simulations using MuMAX3 (d,h) where M-H loops of both materials are shown.

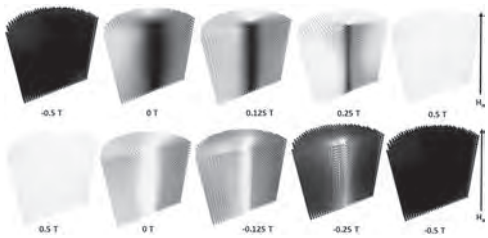

Figure 2. Section view of the magnetization reversal of 60nm thick NiFe layer with 60nm diameter under applied field in the perpendicular direction. A vortex state between both saturated states from negative to positive (top) and vice-versa (bottom) is observed.

HOH-06. Oersted-field- and current- induced Bloch Point domain wall dynamics in cylindrical Ni nanowires.
J. Fernandez-Roldan[1], C. Bran[2], R.P. del Real[2], M. Vázquez[2] and O. Chubykalo-Fesenko[2] *1. University of Oviedo, Oviedo, Spain; 2. Institute of Materials Science of Madrid, Madrid, Spain*

As three-dimensional nanomagnetism evolves, novel non-trivial magnetic textures emerge as appealing information carriers for recording and spintronics based on curved nanosystems, and particularly on Cylindrical Nanowires (NWs) [1,2]. One of the most fascinating candidates that is likely to reach the high velocities required for fast recording technologies is the Bloch Point (BP) domain wall (DW). Recently, theoretical evidence indicated that BPs in NWs could reach high velocities close to 2 km/s in the magnonic regime [3]. While the observation of the BP DW in cylindrical NWs is no longer recent [2], scarce numerical studies that combine both current and Oersted field have been published in NWs [4], despite first attempts to measure DW velocities are in progress [5]. In this work we evaluate the dynamics of the BP DW under both current directions in a Ni NW with 100 nm in diameter. We investigate two cases: i) pre-nucleated BP Wall, and ii) the BP DW originated from the transformation of a Vortex-Antivortex DW. The effects of both spin-polarized current and Oersted field are considered. We discuss in detail the role of the chirality of the BP in relation to the Oersted field, also reported previously in precursors of BPs [4]. We show that while the pre-nucleated DW with the same chirality as that of the Oersted field propagates always against the current direction, the BP originated either from the transformation of the BP with the opposite chirality or from the vortex-antivortex DW can either stop the propagation or propagate parallel to the current. We attribute this effect to the role played by the inertia of the BP in its dynamics. Finally, we provide values of the velocities achieved by the BP in the NW as a function of applied current in Fig. 1. We conclude that BPs with vanishing momentum propagate opposite to the current with velocities that may be suppressed by the Oersted field. Importantly for spintronic applications, both momentum and inertial mass play a major role in the dynamics of BPs that has not been envisaged up to know.

1. A. Fernandez-Pacheco et al., Nat Commun, Vol. 8, p. 15756 (2017) 2. S. Da Col et al., Phys. Rev. B, Vol. 89, p. 180405 (2014) 3. X.-P. Ma et al., Appl. Phys. Lett., Vol. 117, p. 062402 (2020) 4. J.A. Fernandez-Roldan et al., Phys. Rev. B, Vol. 102, p. 024421 (2020) 5. M. Schöbitz et al., Phys. Rev. Lett., Vol. 123, p. 217201 (2019)

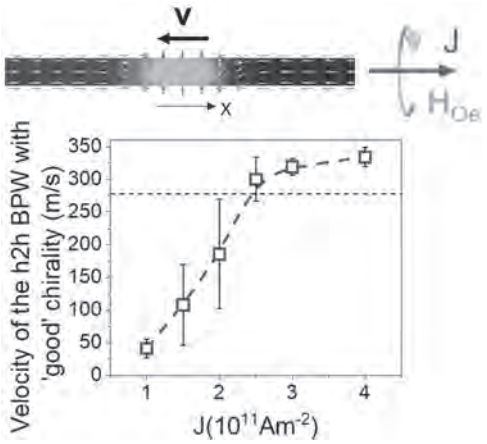

The average velocity of a head-to-head BPW driven by a spin-polarized current in a Ni nanowire, far from the ends of the nanowire, as a function of the current density.

HOH-07. Magnetochiral effect of single domain wall propagation in the Matteucci effect of magnetostrictive microwire. A. Jimenez[1,2], E. Calle[1], J. Fernandez-Roldan[3,1], R.P. del Real[1], R. Varga[2] and *M. Vázquez[1] 1. Institute of Materials Science of Madrid, CSIC, Madrid, Spain; 2. Centre for Progressive Materials, TIP, P.V. Safarik University, Kosiçe, Slovakia; 3. Department of Physics, University of Oviedo, Oviedo, Spain*

Highly-magnetostrictive amorphous microwires show bistable behaviour, i.e. magnetization reverses by depinning/propagation of a single Domain Wall, DW, along the entire wire. This response makes these microwires an ideal system for fundamental studies on DWs dynamics [1,2]. On the other hand, the classical Matteucci effect, ME, consists of the induction of an *emf* voltage at the ends of the microwire under applied axial magnetic field [3], and requires a net azimuthal component of magnetization, M_φ. That *emf* is associated with the DW propagation and its amplitude is proportional to the DW speed, v_{DW}, and the time derivative of M_φ, tailored by the torsion magnetoelastic anisotropy. *emf* has been measured in a bistable FeSiB microwire (12mm-diam, 10cm-long) under torsion (maximum of ξ_{max}=57 πrad/m) and axial driving magnetic field, H_{dr} (square wave). The setup is designed to generate unidirectional motion of the DW that unpins from the same end irrespective of the H_{dr} direction [4], and its speed is quantified by the voltage induced in tiny pickup coils along the microwire. The clockwise/counterclockwise, CW/CCW, torsion dependences of *emf* and v_{DW} are experimentally determined for parallel/antiparallel H_{dr}. Asymmetric behaviour is observed for both, the sense of x and the H_{dr} direction (Fig.1). The DW dynamics is analysed in terms of Landau-Lifschitz-Gilbert eq. considering a bell-like DW (Fig.2). The observed asymmetries are numerically interpreted to derive from the magnetochiral effect related to the DW chirality. The switching of the H_{dr} direction changes the Head-to-Head, H-H, or Tail-to-Tail, T-T, DW character and chirality (i.e., M_φ circulation). As a consequence of this magnetochiral effect, we proof that H-H and T-T DWs propagate at different velocities, v_{DW}, as experimentally observed. Here we provide a first evidence of DWs magnetochiral effects in microwires that offers an opportunity for investigation of topological properties of spin-textures in microwires that has not been envisaged up to now.

1.- M. Vazquez et., Phys. Rev. Lett. 108 (2012) 37201 2.- E. Call et al., J. Magn. Magn. Mater. 498 (2020)166093 3.- M. Vazquez and A. Hernando, J. Phys. D: Appl. Phys. 29 (1996) 4 4.- A. Jimenez et al., IEEE Magn. Lett. 5 (2014) 5000204

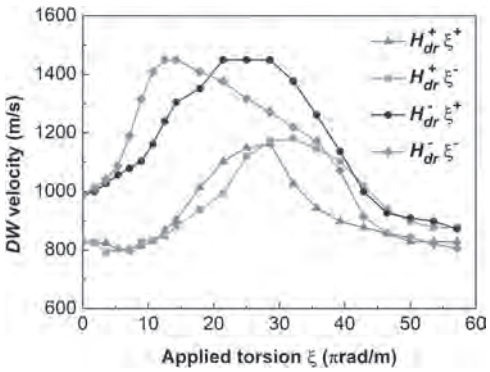

CW, ξ^+, and CCW, ξ^-, torsion dependence of DW speed under H_{dr} = 232 A/m

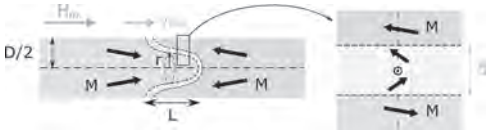

Scheme of a longitudinal slice with a propagating bell-shaped DW. Magnetization in the domains makes a small angle with the microwires axis

HOH-08. Data-Driven Thiele Equation Approach: a New Tool for Vortex Based Spin-Torque Nano Oscillator Dynamics. *F. Abreu Araujo*[1], C. Chopin[1] and S. de Wergifosse[1] *1. IMCN / BSMA, Université catholique de Louvain, Louvain-la-Neuve, Belgium*

In this study we show an original data-driven (semi-analytical) method that takes advantage from an improved analytical model of the spin-torque vortex oscillator (STVO) dynamics based on the Thiele equation approach (TEA) [1]. This approch benefits from the latest improvents in the TEA [2] and absorbs the difference between the analytical model and micromagnetic simulations performed using mumax[3]. The STVO under study is a magnetic tunnel junction (MTJ) with a radius of 100 nm. It is composed of 3 layers, a magnetic polarizer with a spin-polarization p_J of 0.2 and a perpendicular polarization p_z = 1, an insulating barrier (typically MgO), and a magnetic free layer of Permalloy with a thickness of 10 nm leading to a vortex ground state. The simulations are performed for a single geometry and the standard magnetic parameters for Permalloy for different DC current densities (J_{dc}). The Thiele equation approach describes the vortex dynamics as the equilibrium of forces acting on the vortex core. On one side there are the gyrotropic and damping forces and on the other side the spring-like force originating from the spatial derivative of the energy, and the external forces (here the spin-transfer torque). The TEA model [2] describes and improves the energy and the spin-transfer torque terms. As a consequence, this model is valid for a reduced vortex core position s up to s = 0.8 which corresponds to the limit of stability of the vortex. Taking advantage of this model, here we also improved the s-dependence of the gyrotropic $G(s)$ and damping $D(s)$ terms but this time by absorbing the s-dependence using a data-driven approach combining the analytical model and micromagnetic simulations. As shown in the supporting Figure, our semi-analytical TEA leads also to quantitative results in the steady-state oscillating regime compared to the basic TEA [2] that is only quantitative in the resonant regime, i.e. when the vortex core is close to the magnetic dot center.

[1] A. Thiele, "Steady-state motion of magnetic domains", Physical Review Letters, vol. 30, no. 6, p. 230, (1973) [2] F. Abreu Araujo, C. Chopin, S. de Wergifosse, "Ampere-Oersted field splitting of the nonlinear spin-torque vortex oscillator dynamics", submitted to Scientific Reports (2021)

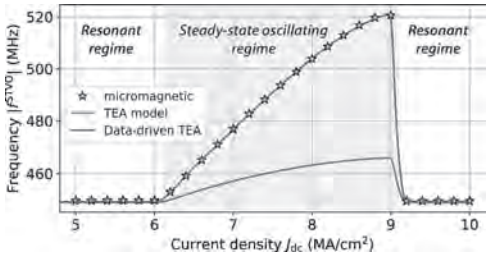

Comparison between the micromagnetic simulation results (stars), the TEA model (red line), and the data-driven TEA method (green line). The gray region in the background corresponds to the steady-state oscillating regime while the the resonant regime appears elsewhere.

HOH-09. Switching between Magnetic Bloch and Néel Domain Walls with Anisotropy Modulations. K.J. Franke[1], C. Ophus[2], A. Schmid[2] and *C. Marrows[1] 1. School of Physics and Astronomy, University of Leeds, Leeds, United Kingdom; 2. National Center for Electron Microscopy, Lawrence Berkeley National Laboratory, Berkeley, CA, United States*

The presence of a Dzyaloshinskii-Moriya interaction (DMI) in perpendicularly magnetised thin films stabilises Néel type domain walls of fixed chirality, as opposed to the Bloch walls that are formed in the absence of a DMI [1]. Néel walls of fixed chirality have been shown to be driven efficiently in the same direction by electric currents through spin-orbit torques [2,3]. Later, a large tuning of the DMI with an applied voltage was demonstrated [4], which can be used e.g. for electric field control of magnetic domain wall motion via the modulation of the DMI [5]. Here, we demonstrate

an alternative mechanism for the control of domain wall type: using micromagnetic simulations and analytical modelling, we show that the presence of a uniaxial in-plane magnetic anisotropy can also lead to the formation of Néel walls in the absence of a DMI. It is possible to abruptly switch between Bloch and Néel walls via a small modulation of both the in-plane, but also the perpendicular magnetic anisotropy [6]. This opens up a route towards efficient electric field control of the domain wall type with tiny applied voltages, as the magnetic anisotropy can be modulated via the direct voltage controlled magnetic anisotropy (VCMA) mechanism [7], or via magneto-elastic anisotropy induced through coupling to a piezoelectric element [8].

[1] A. Thiaville, et al., EPL (Europhysics Letters) 100, 57002 (2012). [2] K.-S. Ryu, et al., Nat. Nanotech. 8, 527–533 (2013) [3] S. Emori, et al., Nat. Mater., 12, 611–616 (2013) [4] T. Srivastava, et al., Nano Letters 18, 4871 (2018) [5] T. Koyama, et al., Science Advances 4 (2018) [6] K. J. A. Franke, et al., arXiv:2104.12400 (2021) [7] T. Maruyama, et al., Nat. Nanotech. 4, 158 (2009) [8] S.Li, et al., J, Appl. Phys. 117, 17D702 (2015)

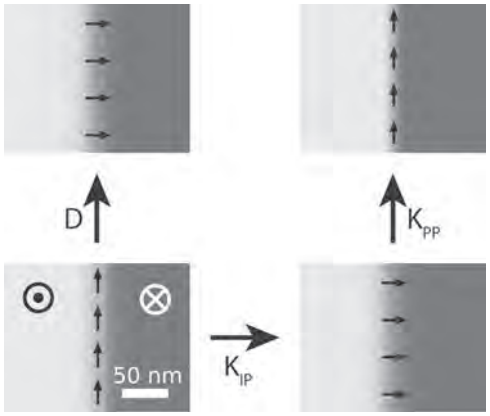

Fig. 1 In a perpendicularly magnetised thin film, domain walls (DWs) are generally of Bloch type (bottom left). The presence of a DMI (top left), stabilises Néel walls. Alternatively, and in-plane magnetic anisotropy can also form Néel walls (bottom right). An increase in the perpendicular magnetic anisotropy switches the DW type back to Bloch (top right).

Session HOI
MAGNONIC CRYSTALS AND MAGNONS

Axel Hoffmann, Chair
University of Illinois at Urbana-Champaign, Urbana, IL, United States

INVITED PAPER

HOI-01. Spin-Wave Induced Spontaneous Symmetry Breaking in Time and Space – Space-Time Magnonic Crystals. *P. Gruszecki*[1], N. Träger[2], J. Gräfe[2] and M. Krawczyk[1] *1. Institute of Spintronics and Quantum Information, Faculty of Physics, Adam Mickiewicz University, Poznan, Poland; 2. Max Planck Institute for Intelligent Systems, Stuttgart, Germany*

Wave propagation in homogeneous media is known and well described by a dispersion relation. The periodic modulation, usually made with some lithography processes, introduces effects predicted by the Bloch theorem, which are widely exploited with photonic crystals and their magnetic counterparts, magnonic crystals. Interestingly, in ferromagnetic materials, space discrete translational symmetry can be introduced also with the periodic magnetization texture, without any structurization. This direction of research promises the formation of magnonic crystals on demand, with a high degree of reconfigurability and offering dynamical tuning. However, the studies of the spin-wave interaction with the periodic stripe domains are at the early stage. In recent years, we investigated the spin-wave-stripe domain interaction and demonstrated the formation of magnonic bands in this type of magnonic crystal [1-2]. Moreover, we analyze the properties of spin waves propagating along domain walls among which we identified spin waves propagating in the form of twisted beams. The concept of symmetry breaking can also be applied to time and the idea of systems with broken translational symmetry in both space and time, so-called space-time crystals, was proposed by F. Wilczek in 2012 [3]. Recently, using scanning transmission X-ray microscopy we experimentally demonstrated and explained with micromagnetic simulations a spontaneous symmetry breaking in space and time in a ferromagnetic thin-film stripe [4]. We achieved this at room temperature by applying to the system a spatially uniform high-amplitude microwave pumping at frequency close to the ferromagnetic resonance. The resulting magnetization texture is periodic in both time and space, see Fig. 1 where is shown space and time dependence of the magnetization in the steady-state. Such a system can be considered as a driven space-time magnonic crystal (STMC). Moreover, we demonstrate an interaction of magnons with this STMC resulting in the appearance of 100 nm long spin waves that are much shorter than the waves expected from the dispersion relation of the uniformly magnetized permalloy stripe at the pumping frequency. In Fig. 2 is shown the spectrum of spin waves with the analytical dispersion relation pointing out the occurrence of this new mode with twice greater wavenumber [5]. We identified that this short wave originates from the second Brillouin zone of the magnonic band structure of the driven STMC. This finding clearly confirms the dynamical formation of the periodicity in space in a homogeneous ferromagnetic element and demonstrates that the dynamical magnetization pattern forms a suitable environment for Brillouin-type scattering of spin waves. *Acknowledgments*. The research has received partially funding from the Polish National Science Centre project No. 2019/35/D/ST3/03729.

[1] C. Banerjee et al., Phys. Rev. B, Vol. 96, pp.024421 (2017). [2] P. Gruszecki et al., Chapter 2, Solid State Physics 70, 1 (2019). [3] F. Wilczek, Phys. Rev. Lett., Vol. 109, pp.160401 (2012). [4] N. Träger et al., Phys. Rev. Lett., Vol. 126, pp.057201 (2021). [5] B. A. Kalinikos and A. N. Slavin, J. Phys. C: Sol. St. Phys., Vol. 19, pp.7013 (1986).

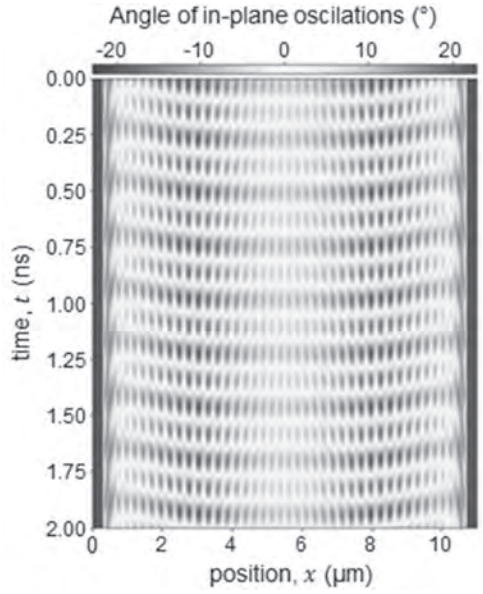

Fig. 1. The simulated space and time dependence of the angle of in-plane oscillations of magnetization in a permalloy stripe upon a high-amplitude spatially uniform in-plane polarized microwave field of amplitude 450 μT and frequency 4.2 GHz.

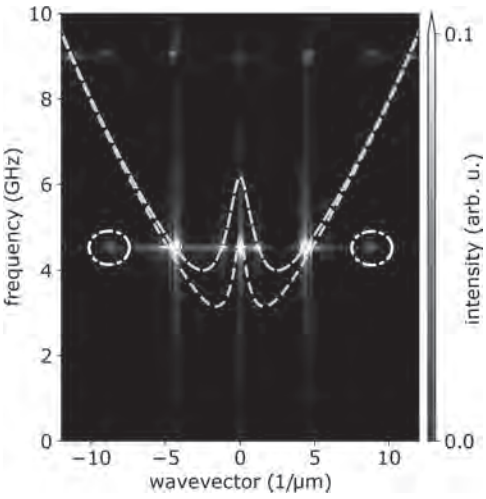

Fig. 2. Spin wave spectra (the colormap in the background) calculated for the same scenario as in Fig. 1. The dashed green lines represent the analytical dispersions for the first two modes. The dash-dotted ellipses indicate the position of new modes resulting from the Brillouin-type scattering of spin waves at the STMC.

CONTRIBUTED PAPERS

HOI-02. Spin-wave rejection efficiency of dynamic magnonic crystal. *M. Iwaba*[1] and K. Sekiguchi[2] *1. Graduate School of Engineering Science, Yokohama National University, Yokohama, Japan; 2. Faculty of Engineering, Yokohama National University, Yokohama, Japan*

Magnonics aims for an ultra-low power signal processing based on spin waves which have a potential to reduce the electric Joule heating. The magnon transistor[1] and psi-shaped interferometer[2] have been fabricated using a magnetic insulator. Recently, the spin-wave switching was demonstrated using dynamic magnonic crystals which can be the key component of magnonic devices[3]. The dynamic magnonic crystals generated a rejection-band against spin waves, and the rejection efficiency was reached up to 75%. However, there was unrevealed factor to obtain 100% rejection efficiency. In this study, we report that the rejection efficiency was greatly changed when the wavenumber of spin waves was modified by a biasing magnetic field. The waveguide was an yttrium iron garnet (YIG) film as shown in Fig. 1(a). An external magnetic field was applied +x direction to the waveguide. A dynamic magnonic crystals (DMCs) generated a rejection band and covered the spin-wave frequency. When the pulse current I = 0.66 A was injected in the DMCs, spin wave packets in time-domain were disappeared perfectly and the intensity of powerspectrum P clearly attenuated as shown in Fig. 1(b). The rejection efficiency is determined by the intensity ratio of $E_{sw} = (P_{off}-P_{on})/P_{off}\times100\%$ and is calculated to be 75%. To obtain the stronger rejection efficiency, we experimented the external magnetic field dependence of rejection efficiency as shown in Fig. 2. Rejection efficiency was greatly changed from 75% to -20%. The maximum of E_{sw} appears when the wavenumber becomes identical to the inverse of spatial period of DMCs at H_{ex} = 955 Oe. The rejection efficiency was fitted by the formula $E\sin((k+\Delta k\times\Delta H)y)$ as shown by the dotted line. The shift of wavenumber was calculated by Δk = 0.11 rad/Oe. This prove that the careful matching between spin-wave wavenumber and DMC's geometry is the significant factor of the spin-wave switching.

[1] A. Chumak, A. Serga, and B. Hillebrands, Nat. Commu., Vol. 5, p.4700 (2014). [2] N. Kanazawa, T. Goto, K. Sekiguchi et al., Sci. Rep., Vol. 7, p.7898 (2017). [3] M. Iwaba, K. Sekiguchi, Appl. Phys. Exp., Vol. 14, p.073002 (2021).

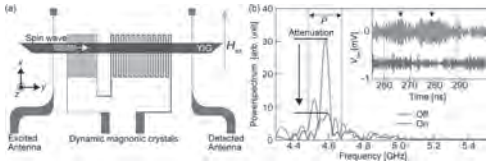

Fig. 1 (a)The spin wave waveguide placed on DMCs between excited and detected antenna. (b) The spin-wave switching using DMCs. The inset shows the realtime waveforms of spin waves with/without DMCs effect. The powerspectrum shows clear attenuation.

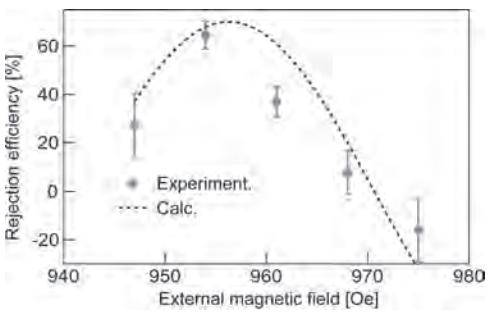

Fig. 2 The external magnetic field dependence of spin-wave rejection efficiency.

HOI-03. Reconfigurable dynamic states in Heusler based magnonic crystals. *S. Mantion*[1] and N. Biziere[1] *1. CEMES-CNRS, Université de Toulouse, Toulouse, France*

Spin waves are promising to develop post-CMOS and/or green technologies due to their sub-micron wavelengths in the GHz range, their frequency tuning with magnetic or electric fields and their small energy dissipation during propagation. Many spin waves based applications have already been demonstrated for data processing and other microwave devices (filters, resonators, delay lines…). To reach these objectives, magnonic crystals (MC) consisting of a periodic modulation of magnetic properties are among the most promising geometries. One key point for applications with MC is to remove the static bias field as most devices operate at zero field. So technological developments imply to find solutions to obtain well-defined spin waves modes at remanence, with the possibility to modify purposely the spin wave spectrum to achieve different functionalities. While several approaches for reconfigurable states have been proposed [1-4], a "material approach" consisting in exploiting the crystal anisotropy of magnetic materials has been poorly explored up to now. Here we show by micromagnetic simulations that materials such as Co_2MnSi Heusler alloy with strong cubic anisotropy can be used to obtain very different spin waves modes at remanence in a simple and classical geometry (Fig. 1 and Fig. 2). In particular, we demonstrate the variation of remanent configuration after saturation with a weak external field H_0 (< 50 Oe) in different directions. This allows to decrease the amplitude, extinct or shift the frequencies of the different modes depending if they correspond to edge or volume modes. We will show the advantage of using cubic anisotropy with respect to isotropic material by comparing the amplitude variation of the different modes. Finally, we will also show that proper design of the crystal with respect to the cubic anisotropy directions can achieve a microwave response very robust against magnetic perturbation.

[1] A. Haldar and A.O. Adeyeye, J. Appl. Phys. 128, 240902 (2020) [2] Qi Wang et al., Science Advances, 4: e1701517 (2018) [3] S. Choudhury et al., Science Advances, 6, 40, eaba5457 (2020) [4] A V Chumak et al., J. Phys. D: Appl. Phys. 42 205005 (2009)

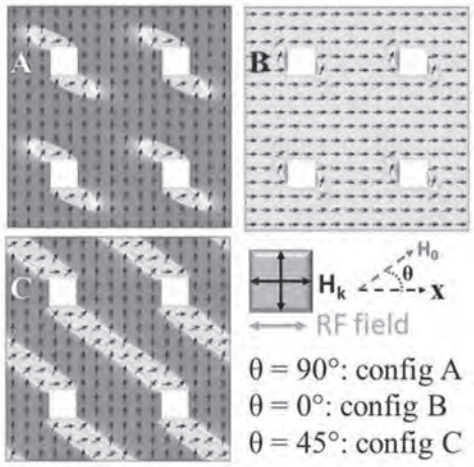

Fig. 1: Remanent magnetic states for different H_0 directions. The dot edge size is 300 nm and the spacing is 900 nm.

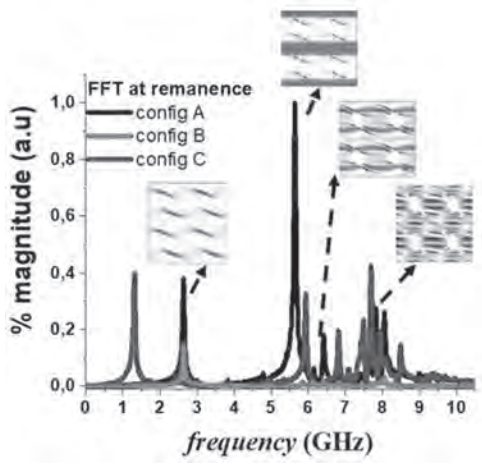

Fig. 2: Corresponding FFT spectrum for a RF field along x. The calculated spatial profiles of the spin waves modes at particular frequencies are shown for the configuration A.

HOI-04. Tuning Interactions in Reconfigurable Kagome Artificial Spin Ices for Magnonics. *V. Bhat*[1] and D. Grundler[2,3] *1. International Research Centre MagTop, Institute of Physics, Polish Academy of Sciences, Warsaw, Poland; 2. Institute of Materials, Laboratory of Nanoscale Magnetic Materials and Magnonics, Ecole Polytechnique Fédérale de Lausanne, Lausanne, Switzerland; 3. Institute of Microengineering, Laboratory of Nanoscale Magnetic Materials and Magnonics, School of Engineering, Ecole Polytechnique Fédérale de Lausanne, Lausanne, Switzerland*

We investigate spin dynamics of a kagome artificial spin ices (KASI) [1,2] consisting of $Ni_{81}Fe_{19}$ (Py) nanomagnets arranged on a disconnected kagome lattice using broadband ferromagnetic resonance (FMR) and micromagnetic simulations. Two KASI samples were prepared using ebeam lithography and lift-off techniques. Each KASI [Fig. 1] covered a writefield area of 120 × 120 μm^2, and was repeated on a 35 × 5 array to increase the signal-to-noise ratio broadband spectroscopy measurements. The nominal length, width, and thickness of a $Ni_{81}Fe_{19}$ (Py) nanobar were kept at 400 nm, 130 nm, and 25 nm, respectively. The shortest distances between two nanobars in samples named Sample-I [Fig. 1(a)] and Sample-II [Fig. 1(b)] was 60 nm and 300 nm, respectively. We observed spin wave spectra that depend characteristically upon the separation between the two nanobars. The obtained spin wave spectra [Figs. 1(d)-1(g)] show distinct changes in resonance frequencies indicating depends upon topological defect configuration [Fig. 1(c)]. We further studied reprogrammable characteristics of spin wave spectra in strongly and weakly dipolarly coupled kagome artificial spin ices. Our work shows disconnected KASIs are promising for reprogrammable spin wave guiding in underlayers. The research was supported by the Swiss National Science Foundation via Grant No. 163016. V.S. Bhat acknowledges support from the foundation for Polish Science through the IRA Programme financed by EU within SG OP Programme.

[1] S. Ladak, D. Read, G. Perkins, L. Cohen, and W. Branford, Nature Physics 6, 359 (2010). [2] E. Mengotti, L. J. Heyderman, A. F. Rodriguez, F. Nolting, R. V. Hugli, and H.B. Braun, Nat. Phys. 7, 68 (2011).

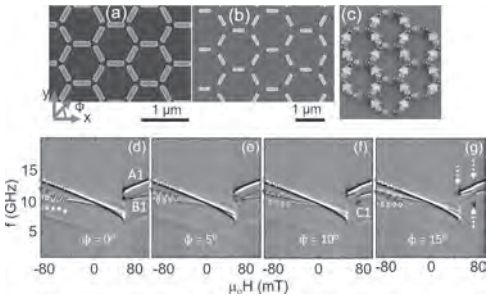

Microscopy images of inner sections of (a) Sample-I and (b) Sample-II. Bright (dark) regions correspond to $Ni_{81}Fe_{19}$ (Si). (c) Cartoon representation of magnetization vectors M (arrows) in the KASI sample when the *T1* (red) and *T2* (cyan) nanobars have undergone switching while *T3* (cyan) nanobars are still aligned with the initial saturating field. The blue and magenta balls represent charges -q and +q, respectively. Spin wave absorption spectra for (a-g) Sample-I (top row for various in-plane angles f. The dashed vertical arrows in (g) define regions in which Type *T1* and *T2* nanobars are switched but *T3* nanobars remain unswitched. The symbols represent simulated resonance frequency values.

HOI-05. Towards observable unidirectional edge modes in topological magnonic crystals. J. Feilhauer[1], M.K. Zelent[3], Z. Zhang[4], J. Christensen[5] and *M. Mruczkiewicz*[1,2] *1. Institute of Electrical Engineering, Slovak Academy of Sciences, Bratislava, Slovakia; 2. Centre For Advanced Materials Application CEMEA, Slovak Academy of Sciences, Bratislava, Slovakia; 3. Faculty of Physics, Adam Mickiewicz University in Poznan, Poznan, Poland; 4. Department of Physics, MOE Key Laboratory of Modern Acoustics, Collaborative Innovation Center of Advanced Microstructures, Nanjing University, Nanjing, China; 5. Department of Physics, Universidad Carlos III de Madrid, Madrid, Spain*

Topological edge states, insensitive to defects, were demonstrated in many wave hosting systems. Topological magnonics is an emerging topic in modern magnetism. Until now, it mainly exploits the analogies of topological waves considered in other wave hosting systems. However, the field of magnonics provides a platform for studying new kinds of phenomena that are specific to spin wave, due to intrinsic nonreciprocal or nonlinear properties of SWs. In spite of several theoretical demonstration of topological magnonics, the experimental confirmation is still missing. The main obstacles preventing experimental observations are: difficulty of nano-fabrication of complex geometry, low coupling between elements, difficulty to control the ground state, low sensitivity of in-plane dynamical field component, high density of modes when scaling up of structures, or high damping in case of DMI-based concepts. One of the designs that is closest to realization is based on perpendicularly magnetized YIG [1], but still requires a complex nano-patterning, high external field and measurements of in-plane field components. Here, we present a numerical demonstration of structure that potentially solves many of the experimental obstacles. Therefore, it is one of the most suitable candidate for realization of unidirectional edge waves in magnonic crystal. Our design is composed of Py squares with side length of 150 nm, cut along diagonals and formed in rectangular lattice (fig 1). The formation of the topological edge state can be realized when each square is in the closed domain state with the same chirality and finite perpendicular component of magnetization (fig 2) [2]. We demonstrate that required magnetic state can be controlled by external magnetic field or MFM tip. Our design shows a potential for scaling up the size of the structure.

[1] Li YM, Xiao J, Chang K., Nano letters, 20;18(5):3032-7. (2018) [2] Shindou R, Ohe JI, Matsumoto R, Murakami S, Saitoh E. Physical Review B.;87(17):174402. (2013)

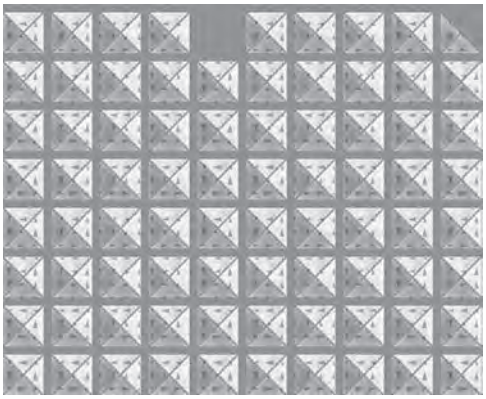

A finite magnonic crystal state stabilized by external magnetic field.

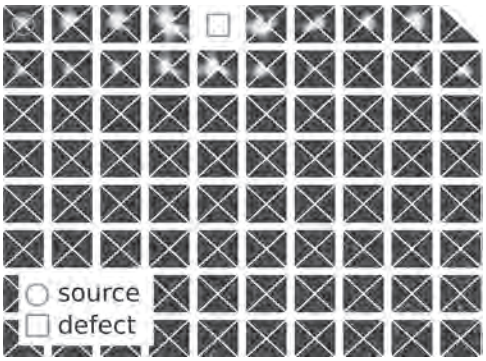

Snapshot of a propagating spin wave in finite magnonic crystal.

HOI-06. Magnonic Frequency Comb Through Nonlinear Magnon-Skyrmion Scattering. Z. Wang[1], *H. Yuan*[2], Y. Cao[1], Z. Li[1], R. Duine[2] and P. Yan[1] *1. University of Electronic Science and Technology of China, Chengdu, China; 2. Utrecht University, Utrecht, Netherlands*

Optical frequency comb is a light source consisting of a series of discrete and equally spaced frequency lines. Since its inception, optical frequency comb has dramatically improved the accuracy of frequency metrology [1] and thus leads to one half of the Nobel Prize in Physics in 2005. Recently, an analogue of optical frequency comb in an acoustic system has been realized in experiment [2], which provides vast opportunities for both fundamental and applied research in phononics. On the other hand, magnons, as elementary excitations in the ordered magnets, are akin to photons and phonons as bosonic quasiparticles. However, the frequency comb of magnons has not been realized to date. The fundamental difficulty is the smallness of nonlinearity in a normal ferromagnet, which hinders the form of frequency comb structure. In this work [3], we realize a novel magnonic frequency comb induced by the nonlinear coupling between magnetic skyrmion and spin waves excited by a microwave field. Here the nonlinear interaction is significantly enhanced by the topological structure of skyrmions and thus leads to the generation of frequency comb through three-magnon process. The mode spacing of frequency combs is equal to the frequency of the skyrmion breathing mode, which can be efficiently tuned by both magnetic and electric means. The essential physics can be further extended to a wide class of magnetic solitons including antiskyrmions, domain walls, and vortices. Our results provide a novel avenue to study frequency comb physics combining the advantages of magnons and general magnetic textures and may further benefit its applications in the spin-wave calibration and metrology.

[1] Th. Udem, R. Holzwarth, and T. W. Hansch, Nature Vol. 416, p.233 (2002). [2] A. Ganesan, C. Do, and A. Seshia, Phys. Rev. Lett. Vol. 118, p. 033903 (2017) [3] Zhenyu Wang, H. Y. Yuan, Yunshan Cao et al., Phys. Rev. Lett. Vol. 127, p. 037202 (2021).

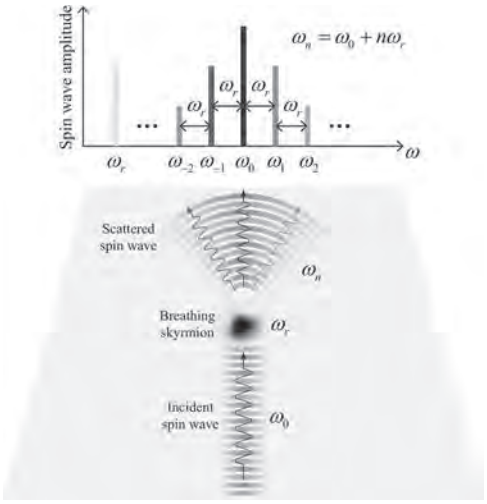

Schematic illustration of nonlinear magnon-skyrmion scattering and the resulting magnonic frequency comb in a magnetic film.

HOI-07. Spin-wave frequency combs. *T. Hula*[1,2], K. Schultheiß[1], F.J. Gonçalves[1], L. Körber[1,3], M. Bejarano[1,4], L. Flacke[5,6], M. Copus[8], A. Kakay[1], M. Weiler[6,7], R. Camley[8], J. Fassbender[1,3] and H. Schultheiss[1] *1. Helmholtz-Zentrum Dresden-Rossendorf, Dresden, Germany; 2. Technische Universität Chemnitz, Chemnitz, Germany; 3. Fakultät Physik, Technische Universität Dresden, Dresden, Germany; 4. Fakultät Elektrotechnik und Informationstechnik, Technische Universität Dresden, Dresden, Germany; 5. Walther-Meißner-Institute, Bayerische Akademie der Wissenschaften, Garching, Germany; 6. Physik-Department, Technische Universität München, Munich, Germany; 7. Fachbereich Physik und Landesforschungszentrum OPTIMAS, Technische Universität Kaiserslautern, Kaiserslautern, Germany; 8. Center for Magnetism and Magnetic Nanostructures, University of Colorado, Colorado Springs, CO, United States*

Optical frequency combs are well established and powerful tools for synchronization, stabilization and frequency conversion in both fundamental science and technological applications. In this work, we present experimental observations on the generation of spin-wave frequency combs. Nonlinear four-magnon scattering is known to cause parasitic losses for a driven spin-wave mode with respect to coherence and amplitude. By means of Brillouin light scattering microscopy, we demonstrate that adding a second microwave frequency causes the scattering to populate well-defined states instead of redistributing energy to the entire spin-wave band. Here, the amplitudes and frequencies of both microwave sources can be utilised in order to tune this behaviour. When reducing the sizes of the magnetic conduits, lateral confinement causes a discretisation of the eigenmode spectrum. Therefore, the formation of frequency combs can be observed even when driving the conduits into the nonlinear regime by just a single pumping frequency. The tunability of multimode spin-wave spectra, as demonstrated in our experiments, offers promising technological applications that allow to bridge the frequency gap between CMOS technology and spin waves.

Hula, T., Schultheiss, K., Goncalves, F. J. T. et al., arXiv:2104.11491, 2021 Marsh, J., & Camley, R. E., Physical Review B - Condensed Matter and Materials Physics, 86(22), 224405, 2012

HOI-08. Magnon straintronics based on the tunable spin-wave propagation in the ensembles of magnonic stripes. *A.V. Sadovnikov*[1], A. Grachev[1] and S. Nikitov[1] *1. Saratov State University, Saratov, Russian Federation*

The recent advances in dielectric magnonics[1-2] push forward the integration of spin-wave computational paradigm towards the integration with CMOS-based materials [3]. In light of this. research has been directed towards the use of spin waves for signal processing at microwave and subterahertz frequencies due to the possibility to carry the information signal without the transmission of a charge current [1,2]. In the present work we demonstrate the experimental observations of the strain-mediated spin-wave coupling phenomena in different magnonic structures based on the asymmetric adjacent magnonic crystals, adjacent magnetic yttrium iron garnet stripes and array of magnetic stripes, which demonstrates the collective spin-wave phenomena. The voltage-controlled spin-wave transport along bilateral magnonic stripes was demonstrated (Fig.1). The model describing the spin-wave transmission response and predicting its value is proposed based on the self-consistent equations [4-6]. We also presents the results of investigation of the spin-wave propagation and spin-resonances formation in the metasurface formed from the meander-shaped ferromagnetic structure. It was demonstrated that the strain can be used to engineer energy-efficient complicated 2D and 3D piezoelectric material and heterostructures [7].

[1] A Barman, G. Gubbiotti, et al. Journal of Physics: Condensed Matter (2021) [2] Nikitov S A, Safin A R, et al. Phys. Usp., 63, 945–974 (2020) [3] A. V. Sadovnikov, et. al., Phys. Rev. B 99, 054424. 2019. [4] Y. K. Fetisov and G. Srinivasan, Appl. Phys. Lett. 88, 143503 (2006). [5] A. V. Sadovnikov, Phys. Rev. Lett. 120, 257203 (2018) [6] B.Rana, Y.Otani, Communications Physics, 2,90 (2019) [7] G. Gubbiotti, A. Sadovnikov, Phys. Rev. Applied, 15, 014061 (2021)

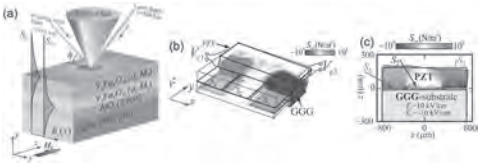

Fig1.(a) Schematic of the BLS experiment (b) Distribution of stress tensor component S_{xx} showing a local deformation of PZT layer; (c) induced stress in the YIG/PZT structures at the applied electric field E_1=10 kV/cm;

HOI-09. Strong Magnon-Magnon Coupling in Two-Dimensional Diamond Shaped Ferromagnetic Nanodots Array. *S. Majumder*[1], S. Choudhury[1], S. Barman[2], Y. Otani[3] and A. Barman[1] *1. CMP&MS, S N Bose National Centre for Basic Sciences, Kolkata, India; 2. Institute for Engineering and Management, Kolkata, India; 3. RIKEN-CEMS, Saitama, Japan*

Strong coupling between magnons and different quantum particles was studied extensively for quantum electrodynamics in the past few years. In this system, magnons in magnetic materials with high spin density are utilized where the "coupling strength" is collectively enhanced by square root of number of spins (N) to overcome the weaker coupling strength between individual spins and the microwave field. However, the strongly magnon-magnon [1] couplings in a confined nanomagnet remains to be revealed which is important for on chief intregration of hybride system. Here, we report the interaction between different magnon modes [2] in a magnetic dot array. The intermodal coupling in the strong coupling regime was approached with a maximum coupling strength of 0.745 GHz and cooperativity of 2.5. Furthermore, it is found that the coupling strength is highly dependent on the orientation of bias field. Micromagnetic simulation reveals that the compitetion between external bias field and inter dot dipolar interaction create a movement of domain in between the dot which results the anticrossing. The tunable coupling strength with the strength and orientation of bias field opens the opportunity of extremely controlled hybrid magnonic devices. This findings could greatly enrich the still evolving field of quantum magnonics.

[1] K. Adhikari, Physical Review B 101, 054406 (2020) [2] C. Dai, J. Appl. Phys. 127, 203902 (2020)

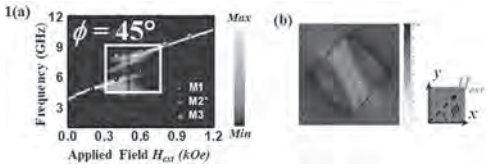

Figure 1: (a) Bias field (Hext) dependent spin wave (SW) absorption spectra of NiFe nanodot lattice are shown at φ = 45°. (b) Distribution of internal at 400 Oe bias field strength along the 45 degree orientation (φ = 45°). The color map for the surface plots and internal field profile with the schematic of the external applied field (Hext) are given at the bottom right corner of the figure.

HOI-10. Influence of the interfacial Dzyaloshinskii-Moriya interaction on the band structure of one-dimensional magnonic crystals. *S. Tacchi*[1], R. Gallardo[2], D. Petti[3], A. Cattoni[4], J. Flores-Farías[2], E. Albisetti[3], G. Carlotti[5] and P. Landeros[2] *1. CNR- Istituto Officina dei Materiali (CNR-IOM), Perugia, Italy; 2. Departamento de Física, Universidad Técnica Federico Santa María, Valparaíso, Chile; 3. Dipartimento di Fisica, Politecnico di Milano, Milano, Italy; 4. Centre de Nanosciences et de Nanotechnologies (C2N), Paris, France; 5. Dipartimento di Fisica e Geologia, Università di Perugia, Perugia, Italy*

In the last years, interfacial Dzyaloshinskii-Moriya interaction (*i*-DMI) in extended films and multilayers, has been the subject of an intense experimental and theoretical research activity. On the contrary only few investigations [1,2] have been devoted to the influence of *i*-DMI on the band diagram of magnonic crystals (MCs). A recent theoretical study of one-dimensional MCs, consisting of a ferromagnetic film in contact with an array of stripes of heavy metal material, indicated that periodic *i*-DMI can lead to the formation of flat bands, due to the appearance of spin wave (SW) modes localized in the sample's areas where *i*-DMI is present [3]. However, experimental evidence of the formation of the flat bands in MCs has been not reported to date. In this work, we have investigated the effect of periodic *i*-DMI on the SW dispersion relation of one-dimensional MCs consisting of an extended CoFeB film 1 nm thick sitting over an array of Pt stripes having a thickness of 7 nm. Two set of samples having a periodicity p=400 nm (with a stripe width w=200 nm) and p=200 nm (with a stripe width in the range between 150 and 170 nm) were analysed. SW dispersion was measured by Brillouin light scattering in the Damon-Eshbach geometry, sweeping the in-plane transferred wave-vector in the direction perpendicular to the external magnetic field applied along the stripe axis. The experimental data were compared to the band diagram calculated by means of the plane wave method. In agreement with theoretical predictions, in all the investigated samples we observe the presence of low-frequency flat bands, due to appearance of SW modes localized in the regions where the Pt stripes are present. The frequency position of the flat band is found to strongly depend on the stripes period. For the samples having smaller periodicity the dispersion curves are characterized by a marked qualitative change. In particular, we observe SWs modes, featuring a strong non-reciprocal intensity, which are present in the SW dispersion only for positive wavevectors. Financial support from the EMPIR programme 17FUN08-TOPS, co-financed by the Participating States and from the European Union's Horizon 2020 research and innovation program, is kindly acknowledged

[1] F. Ma and Y. Zhou, *Interfacial Dzyaloshinskii-Moriya interaction induced nonreciprocity of spin waves in magnonic waveguides*, RSC Adv. 4, 46454 (2014). [2] M. Mruczkiewicz and M. Krawczyk, *Influence of the Dzyaloshinskii-Moriya interaction on the FMR spectrum of magnonic crystals*

and confined structures, Phys. Rev. B 94, 024434 (2016). [3] R. A. Gallardo, D. Cortés-Ortuño, T. Schneider, A. Roldán-Molina, Fusheng Ma, R. E. Troncoso, K. Lenz, H. Fangohr, J. Lindner, and P. Landeros, *Flat bands, indirect gaps, and unconventional spin-wave behavior induced by a periodic Dzyaloshinskii-Moriya interaction*, Phys. Rev. Lett. 122, 067204 (2019).

HOI-11. Heralded parametric single magnon source. *D.A. Bozhko*[1] and R. R. Peroor[1] *1. Department of Physics and Energy Science, University of Colorado Colorado Springs, Colorado Springs, CO, United States*

The creation and detection of single-magnon states constitute an interesting and intriguing challenge for quantum magnonics. An approach using a superconducting qubit paired to a ferromagnet in a volume cavity has been shown [1]. In this work, we present an all-magnon way to construct a single magnon source. If one considers a uniform rf pumping field applied parallel to the magnetization direction of a ferromagnet (we use a single-crystal Yttrium Iron Garnet (YIG) film of 5.1μm thickness), the so-called parallel pumping process could lead to the creation of a pair of magnons at half of the pumping frequency [2]. In a quantum limit, this process is analogous to the spontaneous parametric down-conversion process in quantum optics but offers much more possibilities for control over the generated magnons' frequency and momentum. In our experiments at room temperature, we use an open dielectric resonator (ODR) with a resonant frequency of 13.15GHz to enhance the pumping efficiency (see Fig.1). The width of the pumping area is large compared to the wavelength of the generated magnons, thus they will have equal, but opposite wavevectors and propagate in opposite directions towards two detection antennas. The magnetic field was tuned to 1630Oe to achieve optimum generation conditions. A magnon pair is created spontaneously by a pumping microwave photon. Each magnon from this pair is then coherently amplified by the same microwave pumping signal and result in strong multi-magnon signals containing information about the initial pair of magnons. One can see in Fig.2 the calculated cross-correlation between two detected in a single-shot experiment signals confirming their creation by the same parametric down-conversion process. In the quantum limit, such a device can serve as a single magnon source if one of the outputs will be used for heralding the generated magnon number. The described device could be used together with the recent advancements in theory and fabrication [3,4] to create a variety of devices and circuits, such as all-magnon qubits, quantum gates, and spin-based quantum memory. The possible designs of such elements will be presented and discussed.

[1] Y. Tabuchi, S. Ishino, A. Noguchi et al., Science, Vol. 349, p. 405 (2015). [2] P. Clausen, D.A. Bozhko, V.I. Vasyuchka et al., Phys. Rev. B, Vol. 91, p. 220402 (2015). [3] R. Macêdo, R. C. Holland, P. G. Baity et al., Phys. Rev. Appl. Vol. 15, p. 024065 (2021). [4] P. G. Baity, D. A. Bozhko, R. Macêdo et al., Appl. Phys. Lett. Vol. 119, p. 033502 (2021).

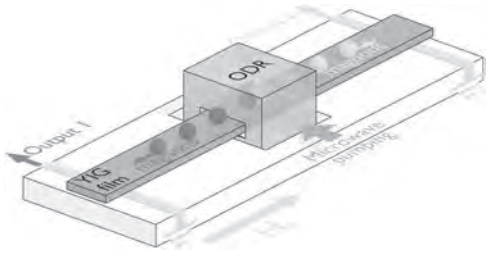

Fig.1. Experimental setup

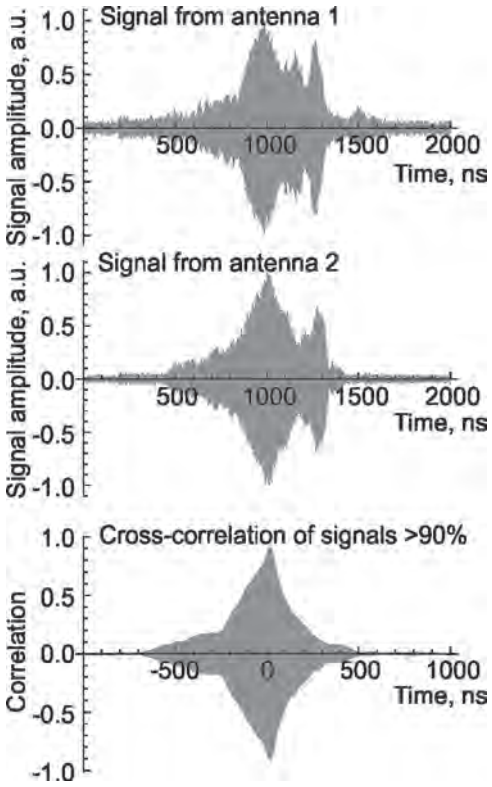

Fig.2. Correlation measurement

HOI-12. Spin wave dynamics in magnonic coupler with antidote interconnection. *A.A. Martyshkin*[1], S. Odintsov[1], E.N. Beginin[1] and A.V. Sadovnikov[1] *1. Saratov State University, Saratov, Russian Federation*

Development of structuring technologies for thin-film magnetic micro- and nanostructures make it possible rapid growing number and variety of studies of mechanisms and methods of excitation and control of spin wave (SW) in magnetic materials [1]. Using of the effects of dipole coupling of spin waves in lateral stripes leads to a periodic transfer of power between the stripes, while the spin-wave coupling can be used to implement the modes of spatial-frequency selection SW [2]. In the regime of multimode propagation of a spin-wave signal in a system of laterally coupled magnetic microwave guides, it turns out to be impossible to completely ensure the transfer of the propagating SW energy from one magnetic microstrip to another. In the same time over the last few years, have become a subject of striking interest structures with periodic changes in magnetic or geometric parameters due to the great potential of the application for signal and information processing devices. Such structures are named magnonic crystals (MC). One of the options for using geometric modulation is the formation of a one-dimensional array of antidots in the magnonic structure of laterally connected magnetic stripes [3]. The disadvantage of MCs with geometric modulation in the form of a one-dimensional array of antidots is the fixed parameters after fabrication of the structure, which implies the difficulty in adjusting the SW propagation. Combining the idea of a magnonic crystal and laterally coupled magnetic waveguides avoids the disadvantages of both types of structures. In this work, we investigated the properties of spin-wave transport in a reconfigurable system of magnetic microwave guides connected laterally by a commutation connection in the form of a one-dimensional antidote array. As a material for microwave guides, we used yttrium iron garnet [$Y_3Fe_5O_{12}$ (111)] with a saturation magnetization M_s = 1750 G due to the low damping of the spin wave. The modes of simultaneous spatial and frequency selection of spin waves by the Brillouin spectroscopy and by the method of micromagnetic simulation are shown. This work was supported by the Russian Science Foundation (Grant 20-79-10191).

A. Barman et al. J. Phys.: Condens. Matter. (2021) S. A. Odintsov, A. V. Sadovnikov, A. A. Grachev, E. N.Beginin, Y. P. Sharaevskii, and S. A. Nikitov. JETP Letters., Vol. 104, p.576. (2016) A. A. Martyshkin, S. A. Odintsov, Y. A. Gubanova, E. N. Beginin, S. E. Sheshukova, S. A. Nikitov, and A. V.Sadovnikov. JETP letters., Vol. 110, p.533. (2019)

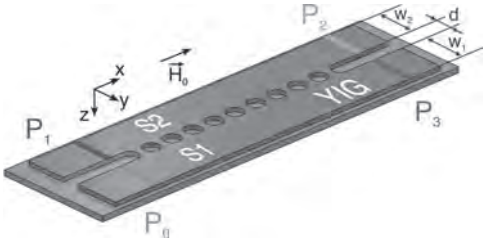

HOI-13. Withdrawn

Session HOJ
MAGNONS AND SPIN WAVES

Yi Li, Chair
Argonne National Laboratory, Westmont, IL, United States

CONTRIBUTED PAPERS

HOJ-01. Chiral Hinge Magnons in Second-Order Topological Magnon Insulators. *A. Mook*[1], S.A. Díaz[2], J. Klinovaja[1] and D. Loss[1] *1. University of Basel, Basel, Switzerland; 2. University of Duisburg-Essen, Duisburg-Essen, Germany*

When interacting spins in condensed matter order ferromagnetically, their ground-state wave function is topologically trivial. Nonetheless, in two dimensions, ferromagnets can support spin excitations with nontrivial topology, an exotic state known as topological magnon insulator (TMI). In Ref. [1], we theoretically unveil and numerically confirm a ferromagnetic state in three dimensions dubbed second-order TMI, whose hallmarks are excitations at its hinges, where facets intersect. Since ferromagnetism naturally comes with broken time-reversal symmetry, the hinge magnons are chiral, rendering backscattering impossible. Hence, as shown in the figure, they trace out three-dimensional paths about the sample unimpeded by defects and are topologically protected by the spectral gap. They are remarkably robust against disorder and highly tunable by atomic-level engineering of the sample termination. We predict that a van der Waals heterostructure built from chromium trihalide and transition metal dichalcogenide monolayers exhibits second-order magnon topology. Our findings empower magnonics, the harnessing of spin waves as information carriers, with the tools of higher-order topology, a promising route to combine low-energy information transfer free of Joule heating with three-dimensional vertical integration.

[1] Alexander Mook, Sebastián A. Díaz, Jelena Klinovaja, and Daniel Loss, Phys. Rev. B 104, 024406 (2021)

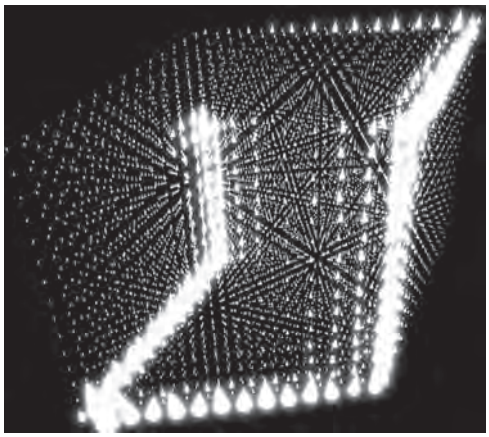

HOJ-02. Generation of Entanglement by Two-Magnon Interference. *C. Trevillian*[1] and V. Tyberkevych[1] *1. Physics, Oakland University, Rochester, MI, United States*

Two-particle interference, i.e., the Hong-Ou-Mandel (HOM) effect [1], is used in many quantum technologies to detect and generate entanglement [2]. HOM has no classical analog and is expressly quantum in nature, making it ideal to study fundamental quantum properties. HOM was first observed with photons in a 50:50 beam splitter (BS) [1] and has been studied in other quantum objects using various interference systems [2], but the effect has not yet been studied in quantum magnonics [3, 4]. Here, we propose a model system for two-magnon interference. The system is an elliptical pillar of 2 antiferromagnetically-coupled ferromagnetic (FM) layers (see Fig. 1 inset) with resonant frequencies ω_1 and ω_2. With no bias magnetic field (B=0) $\omega_1=\omega_2$ and the FM layers are strongly coupled, but they are virtually independent when $B\neq0$. This means that a time-dependent magnetic field $B(t)$ can dynamically tune the system off-resonance ($\omega_1\neq\omega_2$) to excite and detect magnons individually in each FM layer, and on-resonance ($\omega_1=\omega_2$) to allow for interaction of the magnons in two FM layers. The magnonic BS operation is achieved when the system is on-resonance for some time τ such that the probability for single magnon scattering between layers is ½. Our numerical simulations in Fig. 2 show the evolution of the system initially prepared in a two-magnon *unentangled* state $|11\rangle$. After the BS pulse, a *maximally entangled* N00N state ($|20\rangle+|02\rangle)/\sqrt{2}$ is formed. The relative phase between $|20\rangle$ and $|20\rangle$ components of the N00N state can be controlled by shaping the profile of the magnetic field $B(t)$. The magnonic BS is a reversible unitary operation so it can also detect different N00N states. In summary, we found that a dynamically tuned magnon resonance can be used to form a magnonic BS that can generate and detect entanglement by two-magnon interference.

[1] C. K. Hong et al., Phys. Rev. Lett., Vol. 59, pp. 2044–2046 (1987) [2] F. Bouchard et al., Rep. Prog. Phys., Vol. 84, p. 012402 (2021) [3] Y. Li et al., J. Appl. Phys., Vol. 128, p. 130902 (2020) [4] D. D. Awschalom et al., IEEE Trans. Quantum Eng., pp. 1–1 (2021)

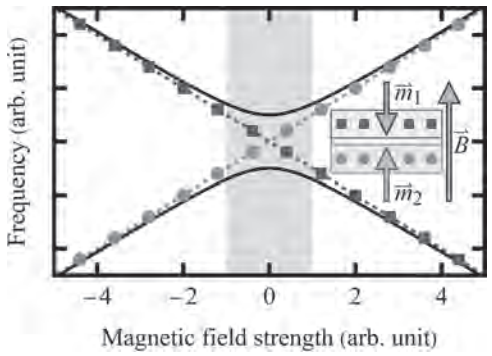

Fig. 1. Dependence of the resonant frequencies on magnetic field B. Solid lines: collective frequencies. Dashed lines and symbols: independent frequencies $\omega_{1,2}$. Gray highlight: strongly coupled region. Inset: elliptical FM/NM/FM pillar geometry.

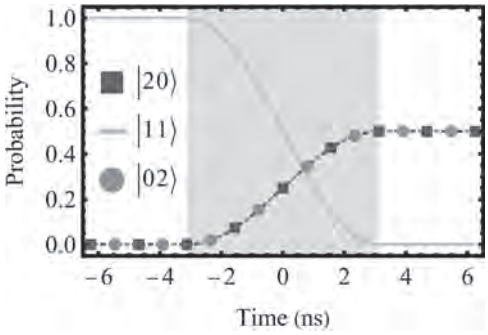

Fig. 2. Evolution of unentangled state $|11\rangle$ into entangled superposition of states $(|20\rangle+|02\rangle)/\sqrt{2}$ under a magnonic beam splitter operation (gray highlight).

HOJ-03. Self-Hybridization of Magnons in Synthetic Antiferromagnetic Tetralayers. *M.M. Subedi*[1], Y. Xiong[2], P.B. Meisenheimer[3], J.T. Heron[3], W. Zhang[2] and J. Sklenar[1] *1. Wayne State University, Detroit, MI, United States; 2. Oakland University, Rochester, MI, United States; 3. University of Michigan, Ann Arbor, MI, United States*

Antiferromagnets carry a huge number of potential applications in magnetic devices due to their high-frequency dynamic properties [1]. In this work, we consider combinations of successive ferromagnetic layers separated by non-magnetic layers of suitable thickness, which creates an antiferromagnetic coupling between adjacent ferromagnets. This type of magnetic heterostructure, or magnetic multilayer, is called a synthetic antiferromagnet [2]. Recently, the magnonic properties of synthetic antiferromagnets have generated intense interest due to their ability to serve as a platform for tuning magnon excitation frequencies by manipulating magnon-magnon interactions. For example, avoided energy crossings between acoustic and optical magnon modes have been observed and tuned by adjusting field orientation and wavenumber in synthetic antiferromagnetic bilayers [3,4]. In this work, we consider permalloy-ruthenium tetralayer structures such as Pt/Py/Ru/Py/Ru/Py/Ru/Py/Pt. Tetralayers were theoretically predicted to have a self-hybridization amongst acoustic or optical magnon pairs [5]. We have experimentally observed self-hybridization effects that are in close agreement with both macrospin model calculations and micromagnetic simulations. This work lays the foundation for electric tunability of magnon-magnon interactions, where avoided energy level crossings can be controlled by modulating the magnetic damping on the surface layers after applying a dc current through the tetralayer structure. Work at Oakland University was supported by U.S. National Science Foundation under Grants No. ECCS-1941426.

[1] S. A. Siddiqui, *et al.* Journal of Applied Physics 128, 040904 (2020). [2] R. A. Duine, *et al.* Nature Physics 14, 217-219 (2018). [3] A. Sud, *et al.* Phys. Rev. B 102, 004403(R) (2020). [4] Y. Shiota, *et al.* Phys. Rev. Lett. 125. 017203 (2020). [5] J. Sklenar and W. Zhang Phys. Rev. Applied 15,044008 (2021).

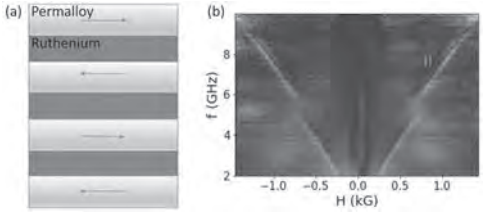

(a) Illustration of a synthetic antiferromagnetic tetralayer structure based upon permalloy and ruthenium. (b) The acoustic magnon spectrum for a tetralayer is measured experimentally as a function of magnetic field. An avoided energy level crossing between two acoustic magnon branches (I & II) is observed near 5.5 GHz and is associated with self-hybridization of the acoustic magnons.

HOJ-04. Spectral-fingerprinting: Microstate readout via remanence ferromagnetic resonance in artificial spin systems. *A. Vanstone*[1,2], J.C. Gartside[1], K. Stenning[1], T. Dion[1,2], D.M. Arroo[1] and W.R. Branford[1] *1. Imperial College London, London, United Kingdom; 2. University College London, London, United Kingdom*

Artificial spin ices are magnetic metamaterials comprising geometrically tiled arrays of interacting nanomagnets. There has been significant recent interest[1,2] in these systems as reconfigurable magnonic crystals due to their vast microstate landscape. Here we measure the spin-wave spectra of square artificial spin systems in zero field and isolate spectral effects arising from the microstate and subtle array imperfections. Crucially remanence FMR allows the study of subtle spectral signatures of the local dipolar field without being dwarfed by the applied field[3]. We examine this in both width-modified, where the microstate may be controlled via global field[4], and normal square ASI comprising identical bars. Width modification allows well-defined transitions between vertex states by switching only selected bars. These controlled states allow the identification of precise frequency shifts and peak amplitude changes associated with specific microstates, verified via a combination of MOKE magnetometry and micromagnetic simulations. Having established the fitting procedure in the ordered states of the width-modified arrays, we apply it to the more challenging problem of disordered microstates in square ASI comprising identical bars. Here reversal is defect-mediated with avalanche-type 1D chain reversal, where a combination of all vertex types appear in intermediate states. We measure remanence FMR and show excellent agreement with micromagnetic simulation and local dipolar field from the pure microstates. We illustrate the great potential of spectral-fingerprinting remanence spin-wave spectroscopy via distinct spectral readout of three microstates with identical (zero) magnetisation. These states are indistinguishable from any magnetometry based technique, but easily discernible via remanence FMR.

[1] S. Gliga, E. Iacocca, and O. G. Heinonen, 'Dynamics of reconfigurable artificial spin ice: Toward magnonic functional materials', *APL Mater.*, vol. 8, no. 4, p. 040911, Apr. 2020, doi: 10.1063/1.5142705. [2] M. T. Kaffash, S. Lendinez, and M. B. Jungfleisch, 'Nanomagnonics with artificial spin ice', *Phys. Lett. A*, vol. 402, p. 127364, 2021. [3] A. Vanstone, *et al.*, 'Spectral-fingerprinting: Microstate readout via remanence ferromagnetic resonance in artificial spin systems', arXiv:2106.04406 [4] J. C. Gartside *et al.*, 'Reconfigurable magnonic mode-hybridisation and spectral control in a bicomponent artificial spin ice', *Nat. Commun.*, vol. 12, no. 1, p. 2488, Dec. 2021, doi: 10.1038/s41467-021-22723-x.

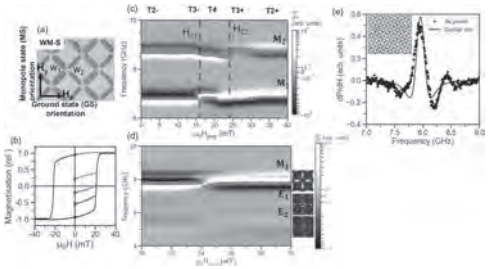

(a) SEM of width-modified square, (b) MOKE magnetometry hysteresis loop showing remanence measurement procedure, (c) Remanence FMR spectral heatmap of width-modified square in monopole orientation showing frequency shift due to local dipolar landscape, (d) Remanence FMR spectral heatmap of normal square sample through reversal, (e) Remanence FMR spectra of as-grown state with MFM of microstate.

HOJ-05. Reconfigurable Training, Vortex Writing and Spin-Wave Fingerprinting in an Artificial Spin-Vortex Ice. *J.C. Gartside*[1], K.D. Stenning[1], A. Vanstone[1], T. Dion[1,2], H.H. Holder[1], D.M. Arroo[1,2], H. Kurebayashi[2] and W.R. Branford[1] *1. Physics, Experimental Solid State, Imperial College London, London, United Kingdom; 2. Physics, University College London, London, United Kingdom*

Strongly-interacting artificial spin systems are moving beyond mimicking naturally-occurring materials to find roles as versatile functional platforms, from reconfigurable magnonics to designer magnetic metamaterials. Typically artificial spin systems comprise nanomagnets with a single magnetisation texture: collinear macrospins or chiral vortices. By tuning nanoarray dimensions we achieve macrospin/vortex bistability and demonstrate a four-state metamaterial spin-system 'Artificial Spin-Vortex Ice' (ASVI). ASVI is capable of adopting Ising-like macrospins with strong ice-like vertex interactions, in addition to weakly-coupled vortices with low stray dipolar-field. The enhanced bi-texture microstate space gives rise to emergent physical memory phenomena, with ratchet-like vortex training and history-dependent nonlinear training dynamics. We observe vortex-domain formation alongside MFM tip vortex-writing. Tip-written vortices dramatically alter local reversal and memory dynamics. Vortices and macrospins exhibit starkly-differing spin-wave spectra with analogue-style mode-amplitude control via vortex training and mode-frequency shifts of df = 3.8 GHz. We leverage spin-wave 'spectral fingerprinting' for rapid, scaleable readout of vortex and macrospin populations over complex training-protocols with applicability for functional magnonics and physical memory.

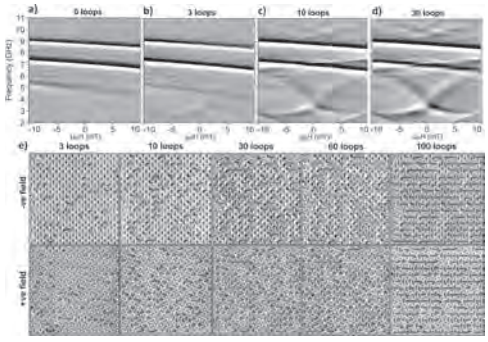

a-d) FMR heatmaps of ASVI taken during 0-30 training loop field-sequence. *x*-shaped vortex modes emerge with increadsing intensity as training progresses. e) Corresponding MFM images showing vortex nucleation and vortex domain growth.

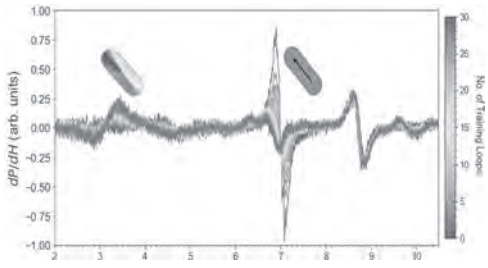

FMR spectra taken at constant -1.2 mT bias field after successive training loops. Macrospin magnon mode-amplitude decreases through training as vortex magnon mode-amplitude increases.

HOJ-06. Comparison of Spin-Wave Modes in Connected and Disconnected Artificial Spin Ice Nanostructures using Brillouin Light Scattering. *A.K. Chaurasiya*[1,5], A.K. Mondal[1], J.C. Gartside[2], K.D. Stenning[2], A. Vanstone[2], S. Barman[3], W.R. Branford[2,4] and A. Barman[1] *1. Condensed Matter Physics and Material Sciences, S N Bose National Centre for Basic Sciences, Kolkata, India; 2. Department of Physics, Imperial College London, London, United Kingdom; 3. Institute of Engineering and Management, Kolkata, India; 4. London Centre for Nanotechnology, Imperial College London, London, United Kingdom; 5. Physics Department, University of Gothenburg, Gothenburg, Sweden*

In recent years, artificial spin ice (ASI) systems have seen burgeoning interest due to their intriguing physics and potential applications in reprogrammable memory, logic and reconfigurable magnonics [1-2]. As the field progresses, direct in-depth comparisons of distinct artificial spin systems are crucial to advancing the field. While studies have investigated the effects of different lattice geometries, little comparison exists between systems comprising continuously connected nanostructures, where spin-waves (SWs) propagate *via* dipole-exchange interaction, and systems with nanobars disconnected at vertices where SW propagation occurs *via* stray dipolar-field. Here, we study the magnonic response of two kagome spin ices, a continuously connected system (c-ASI) and a disconnected system (d-ASI) with vertex gaps *via* Brillouin light scattering (BLS) (see Fig. 1(a) for schematic) and micromagnetic simulation [3]. Array of 25-nm-thick $Ni_{80}Fe_{20}$ (Py) kagome ASI were fabricated using electron-beam lithography and lift-off process. For both samples, the nanobars have length (l) and width (w) of 300 nm and 80 nm, respectively and d-ASI has a 50 nm vertex gap (Figs. 1(b,c)). Bias magnetic field (H) dependent SW spectra (Figs. 1(d,g)) measured by BLS reveal that both c-ASI and d-ASI exhibit frequency minimum, occurring at negative bias magnetic fields, when ramped down from a positive saturation field. A sharp jump in the mode frequencies was observed beyond the minima, linked to bar reversal *via* the switching field observed from the magneto-optical Kerr effect loops and the corresponding mixed magnetization state of nanobars aligned parallel and anti-parallel to the magnetic bias field. Furthermore, we elucidate striking differences in spatial mode-localization and mode quantization between dipole-exchange-mediated c-ASI and dipolar-coupled d-ASI (Figs. 1(e,f) and 1(h,i)). These observations are pertinent for the fundamental understanding of artificial spin systems and broader design and engineering of reconfigurable functional magnonic crystals.

[1] C. Nisoli, R. Wang, J. Li, *et al.*, Phys. Rev. Lett. 98, 217203 (2007). [2] W. R. Branford, S. Ladak, D. E. Read, *et al.*, Science 335, 1597 (2012). [3] A. K. Chaurasiya. A. K. Mondal, J. C. Gartside, *et al.* ACS Nano 15, 11734 (2021).

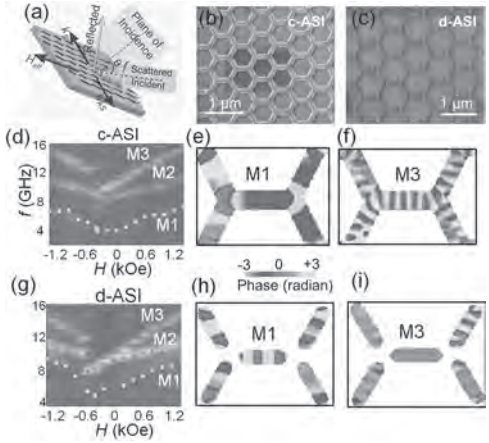

Figure 1(a) Schematic of the BLS measurement geometry. (b,c) SEM images. (d-i) SW mode frequencies as a function of *H* together with the phase profiles for M1 and M3.

HOJ-07. Spin-wave dispersion in magnetic nanotubes: Beyond the thin-shell approximation. *L. Körber*[1,2], G. Quasebarth[1,2], A. Otto[2] and A. Kakay[1] *1. Institute of Ion Beam Physics and Materials Research, Helmholz-Zentrum Dresden - Rossendorf, Dresden, Germany; 2. Fakultät Physik, Technische Universität Dresden, Dresden, Germany*

One of the prospects of magnetic nanotubes in magnetization dynamics is using them as waveguides for spin waves. Recently, we have shown that the spin-wave propagation in thin-shell nanotubes with a vortex-state equilibrium magnetization exhibits strongly nonreciprocal spin-wave transport along the nanotube [1,2]. In particular, spin waves with the same wavelength but opposite propagation direction along the tube inherit different oscillation frequencies. This dispersion asymmetry is of dipolar origin and a consequence of the geometrical magnetic pseudo charges induced by the surface curvature of the nanotube. So far, predictions on the spin-wave dispersion in magnetic nanotubes were only available for tubes with a thin shell (with thicknesses comparable to the exchange length of the material) for which the spatial profile of the spin-wave modes can be assumed to be approximately homogenous in radial direction. With the help of our newly-developed finite-element dynamic-matrix approach for spin waves propagating in waveguides with arbitrary cross section [3], we are now exploring the transition of the spin-wave dispersion and mode profiles as the thickness of the nanotube is increased. To this end, we investigate the emergence of spin-wave modes with a standing-wave character along the nanotube thickness. These modes are shown to be strongly hybridized as long as they share the same azimuthal symmetry. Moreover, they correspond to the radial modes in vortex-state disks or to the perpendicular-standing spin waves in magnetic thin films. We present that the dispersion changes drastically as the nanotube-shell thickness is increased. In particular, the dispersion asymmetry increases to the point where there is an almost completely unidirectional propagation similar to the spin-wave transport reported for exchange-coupled bilayers [4].

[1] Jorge A. Otálora et al., *Physical Review Letters* 2016, *117*, 227203 [2] Jorge A. Otálora et al., *Physical Review B* 2017, *95*, 184415 [3] L. Körber et al., preprint available at arXiv:2104.06943 [4] M. Grassi et al., *Physical Review Applied* 2020, *14*, 024047

HOJ-08. Spin dynamics in a Honeycomb lattice of Permalloy nano-ellipses. *W. Bang*[1], M.T. Kaffash[2], A. Hoffmann[3], J.B. Ketterson[4] and M. Jungfleisch[2] *1. School of Liberal Arts, Koera Tech, Cheonan, The Republic of Korea; 2. Department of Physics and Astronomy, University of Delaware, Newark, DE, United States; 3. Department of Materials Science and Engineering, University of Illinois at Urbana-Champaign, Urbana, IL, United States; 4. Department of Physics and Astronomy, Northwestern University, Evanston, IL, United States*

Artificial Spin Ice (ASI) networks have recently attracted much interest for exploring magnonics-based device applications and information storage concepts [1]. Here, we present experimental and theoretical characterizations of angular-dependent spin dynamics in an ASI which consists of Permalloy nano-ellipses arranged on a honeycomb lattice. We studied two types of networks: 1) those containing contacting nano-ellipses and 2) those with non-contacting nano-ellipses. The lattices were patterned using e-beam lithography, e-beam evaporation, and lift-off. To enhance the sensitivity of the experimental broadband ferromagnetic resonance spectra, the lattices were fabricated on the top of a coplanar waveguide. Theoretical micromagnetic simulations were performed which show excellent agreement with the experimental results. We find the existence of a spin-wave mode localized in the vertex region of the contacting nano-ellipses network [2]. Our finding has important implications when designing an ASI network for potential applications. * This paper was supported by the new professor research program of KOREATECH in 2021.

[1] M.T. Kaffash et al., Phys. Lett. A 402, 127364 (2021). [2] W. Bang et al., Phys. Rev. Appl. 14, 014079 (2020).

HOJ-09. Up-conversion of spin wave modes in Y-shaped Permalloy structures. *J. Liu*[1], A. Guerrero[1], K. Nygren[2], M. Swyt[2] and K. Buchanan[2] *1. Department of Physics and Astronomy, Georgia Southern University, Statesboro, GA, United States; 2. Department of Physics, Colorado State University, Fort Collins, CO, United States*

Methods to controllably generate high wavevector k spin waves are needed for nanomagnonics applications because the efficiency of microstrip antennas is low for high-k spin waves. Strategies involving tapered waveguides [1] and nonlinear effects [2] have been proposed but have limitations. In this work, spin waves were studied in patterned Y-shaped structures made of 2.7-μm wide and 40-nm thick Permalloy microwires using micro-focus Brillouin light scattering (BLS). A microstrip antenna was used to excite spin waves in two legs of the Y-shaped structure, and the generated spin waves propagate into a longer straight wire oriented at 90° with respect to the antenna. An in-plane field B_0 was applied parallel to the antenna (Fig. 1a inset). Frequency scans collected 1 μm from the antenna in the tilted legs each show a single peak between 7.3 GHz and 7.5 GHz (Fig. 1a), whereas two peaks near 6.3 GHz and 7.6 GHz are observed in the straight section (Fig. 1b). A comparison of the data with dispersion relations obtained from micromagnetic simulations (Figs. 2a and 2b) shows that the 6.3 GHz peak corresponds to low-k surface spin waves that are weakly excited by the stray field of the antenna. The higher frequency peak is the signature of up-conversion of low-k spin waves in the legs to the higher k states available at 7.6 GHz. These results represent a new strategy for obtaining higher-k spin waves that may be useful for applications.

[1] V. E. Demidov *et al.*, Appl. Phys. Lett, 99, 082507 (2011) [2] H. Kurebayashi *et al.*, Appl. Phys. Lett, 99, 162502 (2011)

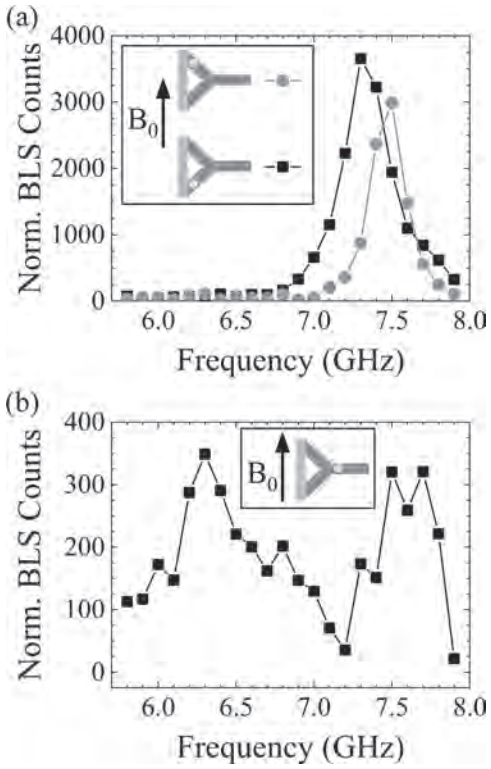

Figure 1: Normalized BLS counts as a function of driving frequency with B_0 = 60 mT for (a) the tilted legs and (b) the straight section of the structure.

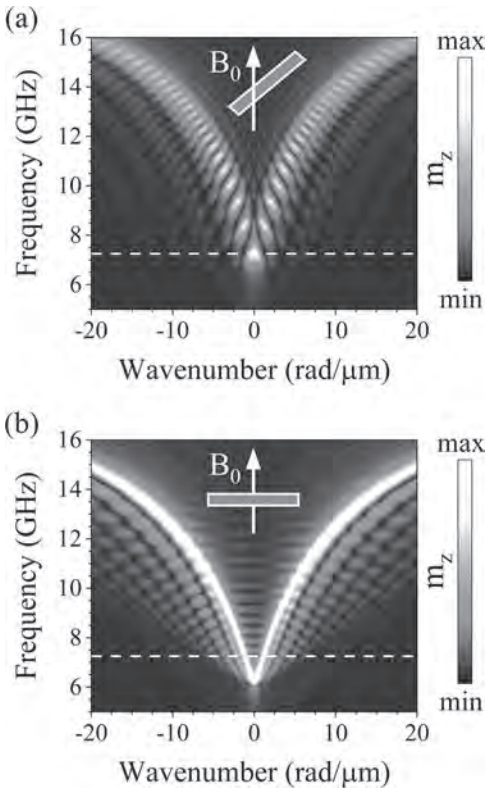

Figure 2: Calculated dispersion relations for (a) the tilted legs and (b) the straight section show that 7.25 GHz (dashed lines) corresponds to $k = 0$ in (a) and $k = \pm 1.1$ rad/μm in (b).

HOJ-10. Withdrawn

HOJ-11. Resonant Spin Transmission Mediated by Magnons in a Magnetic Insulator Multilayer Structure. *Y. Fan*[1], J. Finley[2], J. Han[2], M. Holtz[3], P. Quarterman[3], P. Zhang[2], T. Safi[2], J. Hou[2], A.J. Grutter[3] and L. Liu[2] *1. Department of Materials Science and Engineering, Massachusetts Institute of Technology, Cambridge, MA, United States; 2. EECS, Massachusetts Institute of Technology, Cambridge, MA, United States; 3. NIST Center for Neutron Research, National Institute of Standards and Technology, Gaithersburg, MD, United States*

Magnetic insulators have been utilized in multilayer structures for optimizing spin transport or to form magnon spin valves that can control the magnon spin current. In these studies, it remains an intensively visited topic on what the corresponding roles of coherent and incoherent magnons are in the spin transmission. Meanwhile, understanding the underlying mechanism associated with spin transmission in insulators can help to identify new mechanisms that can further improve the spin transport efficiency. Here, by studying spin transport in a permalloy (Py)/yttrium-iron-garnet (YIG)/Pt multilayer through a non-local spin pumping measurement, we demonstrate that coherent magnons can transfer spins efficiently above the magnon bandgap of the magnetic insulator YIG. Particularly, the perpendicular standing spin-wave (PSSW) mode can greatly enhance the spin flow by inducing a resonant magnon transmission [1]. In Fig. 1(a), we schematically illustrate the spin transmission enhancement effect in the Py/YIG/Pt structure, where the PSSW mode in the YIG layer induces a resonant transmission of magnon spin flow from Py to Pt. In the spin-pumping experiment, as plotted in Fig. 1(b), the inverse spin-Hall effect (ISHE) voltage detected by Pt is increased by more than 1000% at the anti-crossing region between the Py Kittel mode and the YIG PSSW mode, which demonstrates the spin transmission enhancement effect in the structure. In addition, within the magnon bandgap of YIG, we observe a shutdown of spin transmission due to the blocking of coherent magnons. The demonstrated magnon transmission enhancement and filtering effect provides an efficient method for modulating spin current in future magnonic devices.

[1] Y. Fan *et al.*, *Adv. Mater.* 33, 2008555 (2021).

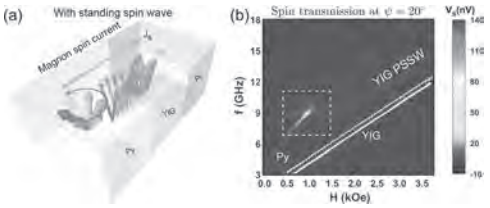

Fig. 1. (a) Schematic of the magnon spin transmission from the Py layer to the Pt layer in the Py/YIG/Pt multilayer structure with the presence of PSSW in YIG. (b) Spin transmission spectrum measured by the ISHE voltage on the Pt underlayer for the GGG/Pt/YIG/Py sample. Dashed rectangular box highlights the Py spin transmission enhancement at the anti-crossing region between the Py Kittel mode and the YIG PSSW mode.

HOJ-12. Electrical Detection of Backward Spin-waves in Epitaxial Fe Films. *S. Nezu*[1], T. Scheike[2], H. Sukegawa[2] and K. Sekiguchi[3] *1. Graduate School of Engineering Science, Yokohama National University, Yokohama, Japan; 2. National Institute for Materials Science, Tsukuba, Japan; 3. Faculty of Engineering, Yokohama National University, Yokohama, Japan*

Magnonics has many advantages in performing logic and nonlinear signal processing with low-power consumption. However, the propagation loss of spin waves prevents a practical application of spin waves[1]. Recently, cubic anisotropy materials were reported to be a promising spin-wave medium[2], because the surface spin-wave minimizes its resonant frequency due to the anisotropic magnetic field. The amplitude, group velocity, and decay length were greatly enhanced, enough to be at a practical application level. In this study, we investigated the electrical detection of backward spin-waves in cubic anisotropic Fe films, which is essential to fabricating two dimensional magnonic devices and has not been reported so far. Micro-scaled spin-wave devices were fabricated as shown in Fig. 1. The device was made of a multilayer stack of Cr(40)/Fe(25)/Mg(0.45)/$Mg_{19}Al_{81}$(1.2)/oxidation (thickness in nanometers) deposited on MgO(001) single crystal substrates, using the magnetron sputtering method. The high-quality epitaxial Fe(001) layer acts as a spin-wave waveguide. The antennas were a pair of asymmetric coplanar strip transmission lines, consisting of Ti (5 nm)/Au (200 nm) bilayer fabricated by electron beam lithography and lift-off method. Spin waves were excited from the antenna connected to Port1 of a vector network analyzer (VNA) and detected from the antenna connected to Port2 of the VNA. Figure 2(a) shows the transmission spectrum ΔS_{21} when an external magnetic field H_{ex} was applied parallel to the hard axis. The magnetic field dependence of the resonant frequency (*f–H* relation) was investigated by resonant spectra and is exhibited in Fig. 2(b). The solid line represents a fitting curve of the *f-H* relation, showing good agreement with the theoretical dispersion. Thus, we succeeded in the electrical detection of backward spin-waves in an epitaxial Fe waveguide and opened the way to design two dimensional magnonic devices.

[1] N. Sato, S.-J. Lee, S.-W. Lee *et al.*, *Applied Physics Express*, Vol. 9, 083001 (2016). [2] K. Sekiguchi, S.-W. Lee, H. Sukegawa *et al.*, *NPG Asia Materials*, Vol. 9, e392 (2017).

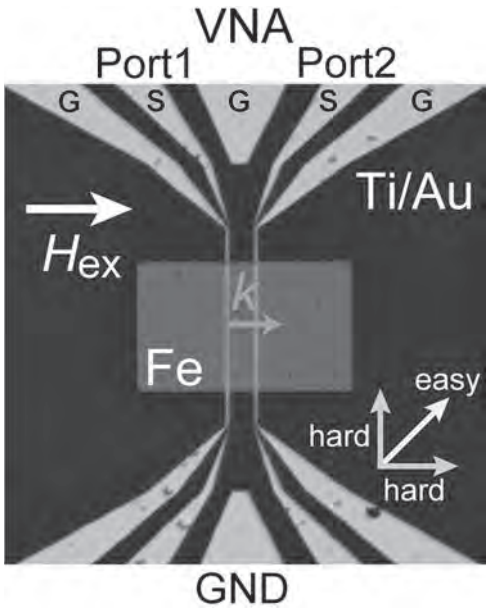

Fig.1 An optical microscope image of a spin-wave device. The antennas are connected to a VNA.

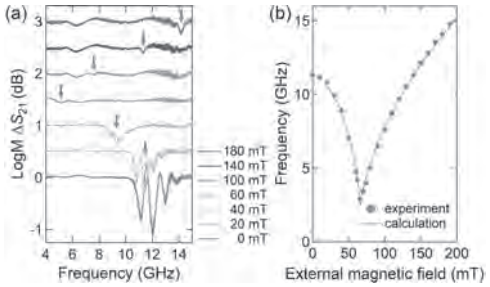

Fig.2 (a)The transmission spectrum ΔS_{21} and (b)f–H relation of backward spin-waves in Fe film. Fitting parameters are M_s = 1600 kA m^{-1}, $\gamma_g = 17.6\times10^6$ s^{-1} Oe^{-1}, k = 0.15 μm^{-1} and α = 0.0026, respectively.

HOJ-13. Nonreciprocal Magnetoacoustic Waves in Dipolar-Coupled Ferromagnetic Bilayers. *M. Küß*[1], M. Heigl[2], L. Flacke[3,4], A. Hörner[1], M. Weiler[5,3], A. Wixforth[1] and M. Albrecht[2] *1. Experimental Physics I, University of Augsburg, Augsburg, Germany; 2. Experimental Physics IV, University of Augsburg, Augsburg, Germany; 3. Walther-Meißner-Institut, Bayerische Akademie der Wissenschaften, Garching, Germany; 4. Physics-Department, Technical University Munich, Garching, Germany; 5. Fachbereich Physik and Landesforschungszentrum OPTIMAS, Technische Universität Kaiserslautern, Kaiserslautern, Germany*

Surface acoustic waves (SAWs) have made their way into many everyday devices, thanks to the greatly reduced wavelength of SAWs compared to free-space microwaves of the same frequency. These "nano earthquakes" can be efficiently launched and detected on piezoelectric substrates with periodic metallic gratings in the MHz- to GHz-range. However, SAWs are in general propagating reciprocally, which means that SAW propagation does not change under inversion of the propagation direction and limits the usage of SAWs for reciprocal devices. Since spin waves (SWs) are known to show a pronounced nonreciprocal behavior, magnetoelastic coupling of SAWs with SWs is a straightforward approach to obtain nonreciprocal magnetoacoustic surface waves (MASWs). Besides the nonreciprocity of the SAW-SW coupling mechanism itself [1, 2], the SW dispersion relation can be nonreciprocal. For example, the Dzyaloshinskii--Moriya interaction (DMI) in an ultrathin ferromagnetic/heavy metal bilayer causes SW nonreciprocity and thus induces nonreciprocal SAW propagation [3]. In our recent study, we experimentally demonstrate the large coupling between SAWs and SWs to obtain highly nonreciprocal MASWs in a dipolar coupled ferromagnetic bilayer [4]. We show that nonreciprocal symmetric and antisymmetric SW modes form in a NiFe/Au/CoFeB magnetic bilayer. Furthermore, we model our results in a phenomenological approach and demonstrate that magnetoacoustic transmission measurements can be used to characterize spin waves.

[1] L. Dreher, M. Weiler, M. Pernpeintner et al., Phys. Rev. B 86, 134415 (2012). [2] M. Küß, M. Heigl, L. Flacke et al., Phys. Rev. Applied 15, 034046 (2021). [3] M. Küß, M. Heigl, L. Flacke et al., Phys. Rev. Lett. 125, 217203 (2020). [4] M. Küß, M. Heigl, L. Flacke et al., Phys. Rev. Applied 15, 034060 (2021).

Illustration of the investigated magnetoacoustic hybrid device. Surface acoustic waves (SAWs) can be excited electrically on a piezoelectric substrate with metallic grating structures (IDTs). Resonant SAW - spin wave coupling in the magnetic thin film gives rise to nonreciprocal transmission of the magnetoacoustic waves.

HOJ-14. Magnonic Goos-Hänchen Effect Induced by One Dimensional Solitons. *V. Laliena*[2] and J. Campo[1] *1. Aragonese Nanoscience and Materials Institute, Spanish National Research Council (CSIC), Zaragoza, Spain; 2. Applied Mathmatics Department, University of Zaragoza, Zaragoza, Spain*

The magnon spectral problem is solved in terms of the spectrum of a diagonalizable operator for a generic class of magnetic states that includes several types of domain walls and the chiral solitons of monoaxial helimagnets. Focusing on the isolated solitons of monoaxial helimagnets, it is shown that the spin waves scattered (reflected and transmitted) by the soliton suffer a lateral displacement analogous to the Goos-Hänchen effect of optics. The displacement is a fraction of the wavelength, but can be greatly enhanced by using an array of well separated solitons. Contrarily to the Goos-Hänchen effect recently studied in some magnetic systems, which takes place at interfaces between different magnetic systems, the effect predicted here takes place at the soliton position, what it is interesting from the point of view of applications since solitons can be created at different places and moved across the material. This kind of Goos-Hänchen displacement is a consequence of the dependence of the phase shift on the transverse component of the wave vector, which does not appear in other known one dimensional systems, as quantum mechanical particles moving in a one dimensional potential. However, it is not particular of the solitons of monoaxial helimagnets, but it is generic for a class of magnetic states, including domain walls in systems with interfacial Dzyaloshinskii-Moriya interaction. The conditions under which the soliton induced Goos-Hänchen effect takes place are discussed [1].

[1] V. Laliena and J. Campo, arXiv:2011.07886

HOJ-15. Measuring the dispersion relations of spin wave bands using time-of-flight spectroscopy. *T. Devolder*[1], G. Talmelli[2], S. Ngom[1], F. Ciubotaru[2], C. Adelmann[2] and C. Chappert[1] *1. Université Paris-Saclay, Palaiseau, France; 2. imec, Leuven, Belgium*

We develop a generic all-inductive procedure to measure the dispersion relation of spin waves in a magnetic stripe. Our method works even if several spin wave branches coexist in the investigated frequency interval, provided that the branches possess sufficiently different group velocities. We first measure the microwave scattering matrix of a network composed of distant antennas inductively coupled to the spin wave bath of a magnetic stripe. The antenna-to-antenna coupling that is independent from the applied magnetic field are suppressed by an appropriate calibration to get the complex spin wave transmission coefficient versus frequency. A comparison with the expected contribution of when a single spin wave mode exists argues for the existence of several spin wave branches in the magnetic conduit (Fig. 1). After a mathematical transformation to the time-domain to get the transmission impulse response, the different spin wave branches are viewed as wavepackets that reach successively the receiving antenna after different travel times (Fig. 2) determined by their group velocities. In analogy with time-of flight spectroscopy, the wavepackets are then separated by time-gating. The time-gated responses are used to recalculate the contribution of each spin wave branch to the frequency domain scattering matrix. The dispersion relation of each branch stems from the absolute phase of the time-gated transmission parameter. The spin wave wavevector can be determined unambiguously if the results for several propagation distances are combined, so as to get the dispersion relations of each band, and in the end the full band structure of the spin waves [1].

[1] T. Devolder et al., Phys. Rev. B, 103, 214431 (2021)

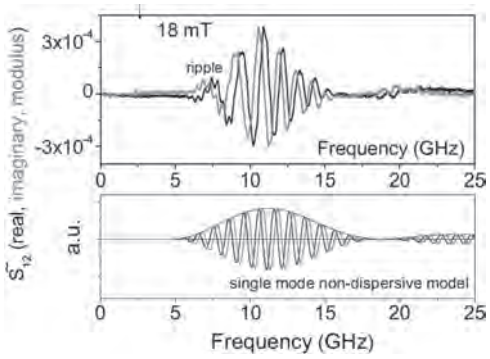

Fig. 1: Top: spin wave transmission coefficient in a 4.7 µm wide CoFeB stripe of thickness 30 nm. The frequency dependence is measured for two sub-micron U-shaped antennas separated by a distance of 6.9 µm at 18 mT of applied field. Bottom: expected contribution of a single spin wave branch.

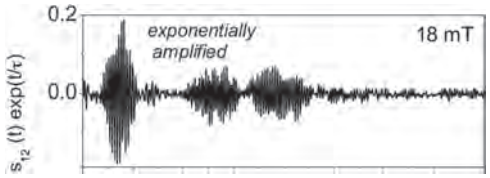

Fig. 2: Time-domain impulse response corresponding the frequency domain data of figure 1. The wavepackets emitted simultaneously at the emitter antenna arrive one after the other at the receiving antenna according to their respective group velocities.

Session HOK
SPIN WAVES AND MAGNETIZATION DYNAMICS I

Jaroslaw W Klos, Chair
Uniwersytet im Adama Mickiewicza w Poznaniu, Poznan, Poland

INVITED PAPER

HOK-01. First Results on Atomically Resolved Spin-Wave Spectroscopy by Transmission Electron Microscopy. *B.W. Zingsem[1,2], V. Migunov[2], T. Feggeler[3], T. Weßels[2], R. Meckenstock[1], T. Denneulin[2], S. Masur[2], M. Winklhofer[4], M. Farle[1] and R. Dunin-Borkowski[2] 1. Physics, University Duisburg-Essen, Duisburg, Germany; 2. Ernst Ruska-Centre, Forschungszentrum Jülich GmbH, Jülich, Germany; 3. Advanced Light Source, Lawrence Berkeley National Laboratory, Berkeley, CA, United States; 4. Research Center Neurosensory Science, University of Oldenburg, Oldenburg, Germany*

Spin-wave spectroscopy methods, such as electron-spin-resonance [1], and ferromagnetic resonance [2], are vital tools for materials characterization and chemical monitoring. Together with momentum-sensitive techniques, such as Brillouin light scattering, they are also central to spintronics experiments and the design of spintronic and magnonic devices. Here, we demonstrate a new technique to spatially resolve spin-waves on the single nanometer scale with the potential for atomic resolution by transmission electron microscopy (TEM). The precessional torque of a spin excitation is coupled to a highly coherent electron beam, which reveals localized resonant spin excitations in transmission electron microscopy. This technique can be applied in-situ and in-operando on its own and together with conventional spectroscopy methods. As a model system, we present first results of magnonic networks comprising ferromagnetic nanoparticles [3,4] and observe the spatial distributions of various spin-resonance modes. Financially supported by the Deutsche Forschungsgemeinschaft (DFG, German Research Foundation) – Project-ID 405553726 – TRR 270 and the European Research Council (ERC) under the European Union's Horizon 2020 research and innovation programme (Grant No. 856538, project "3D MAGiC")

[1] Farle, M., M. Zomack, and K. Baberschke, Surface Science 160(1) 205-216 (1985). [2] Farle, M., Reports on Progress in Physics 61(7) 755-826 (1998). [3] Zingsem, B.W. et al. Nature Communications 10(1) 4345 (2019). [4] A. Barman et al. The 2021 Magnonics Roadmap, Journal of Physics: Condensed Matter (2021)

CONTRIBUTED PAPERS

HOK-02. Element-specific imaging of magnons on the sub 50 nm scale. *T. Feggeler[1], R. Meckenstock[2], D. Spoddig[2], B. Zingsem[2,3], J. Lill[2], D. Günzing[2], S. Wintz[4], M. Weigand[5], H. Wende[2], M. Farle[2,6], M. Winklhofer[7], K. Ollefs[2] and H. Ohldag[1,8] 1. Advanced Light Source, Lawrence Berkeley National Laboratory, Berkeley, CA, United States; 2. University of Duisburg-Essen, Duisburg, Germany; 3. Ernst Ruska Centre for Microscopy and Spectroscopy with Electrons and Peter Grünberg Institute, Forschungszentrum Jülich GmbH, Jülich, Germany; 4. Max Planck Institute for Intelligent Systems, Stuttgart, Germany; 5. Helmholtz Center Berlin, Berlin, Germany; 6. Kirensky Institute of Physics, Federal Research Center KSC SB RAS, Krasnoyarsk, Russian Federation; 7. School of Mathematics and Science, University of Oldenburg, Oldenburg, Germany; 8. Department of Material Sciences and Engineering, Stanford University, Stanford, CA, United States*

Magnonics [1] and spintronics [2] are promising approaches to address the challenges of contemporary information technology, increasing the computation performance by incorporating a higher transistor density, and reducing heat dissipation and power consumption. Magnetic nanoparticle chains have gained interest in this respect offering an easy tailorability of magnonic dispersion controlled by the particle chain arrangement [3, 4]. The comprehensive element-specific characterization of the magnetization dynamics of such systems on the nanoscale is obligatory for future development in this respect. Here we present Time Resolved Scanning Transmission X-ray Microscopy (TR-STXM) as a well-suited technique fulfilling these demands, offering element specific sampling < 30 ps of magnetization dynamics with < 50 nm spatial resolution [5]. We demonstrate the remarkable capabilities TR-STXM on Fe_3O_4 nanoparticle chains naturally grown by biomineralization inside of magnetotactic bacteria *Magnetospirillum Magnetotacticum*, revealing localized non-uniform and uniform resonant responses in terms of amplitude and phase [6].

1. V. V. Kruglyak, S. O. Demokritov, and D. Grundler, Journal of Physics D: Applied Physics, 2010. 43(26). 2. S.A. Wolf, D.D. Awschalom, R.A. Buhrman, et al., Science, 2001. 294(5546): p. 1488-1495. 3. A. Barman, G. Gubbiotti, S. Ladak, et al., J Phys Condens Matter, 2021. 4. B. Zingsem, T. Feggeler, A. Terwey, et al., Nature Communications, 2019. 10: p. 4345. 5. S. Bonetti, R. Kukreja, Z. Chen, et al., Review of Scientific Instruments, 2015. 86(9): p. 093703-1-093703-9. 6. T. Feggeler, R. Meckenstock, D. Spoddig, et al., Physical Review Research, 2021. 3(3).

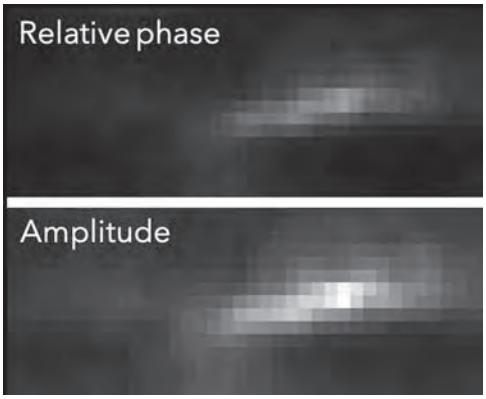

Fig. 1: Amplitude and relative phase of the resonant response of a Fe_3O_4 nanoparticle chain of a magnetotactic bacterium measured by TR-STXM.

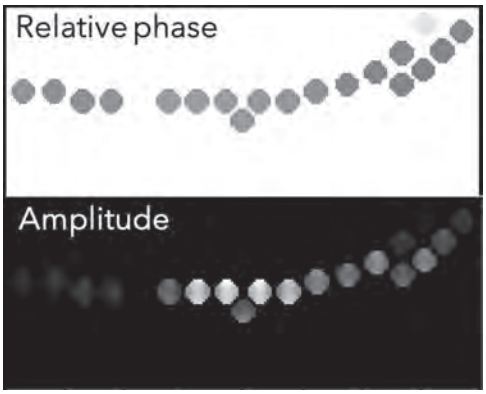

Fig. 2: Amplitude and relative phase of the resonant response of a micromagnetic model of the Fe_3O_4 nanoparticle chain (Fig. 1) obtained from dynamic simulations.

HOK-03. Direct Imaging of Spin-Wave Dynamics in a Low-Damping Ferrimagnet Close to Antiferromagnetic Compensation. *S. Mayr*[1,2], S. Finizio[1], M. Weigand[3], J. Gräfe[4], C. Dubs[5], J. Bailey[1], J. Reuteler[6], H. Stoll[4,7], G. Schütz[4], J. Raabe[1] and S. Wintz[1,4] *1. Paul Scherrer Institut, Villigen PSI, Switzerland; 2. Department of Materials, ETH Zurich, Zürich, Switzerland; 3. Helmholtz-Zentrum Berlin, Berlin, Germany; 4. Max Planck Institute for Intelligent Systems, Stuttgart, Germany; 5. INNOVENT e.V. Technologieentwicklung Jena, Jena, Germany; 6. Scientific Center for Optical and Electron Microscopy, ETH Zurich, Zürich, Switzerland; 7. Institute of Physics, Johannes Gutenberg University Mainz, Mainz, Germany*

Spin waves have been studied extensively during the past years, not only in terms of fundamental research but also in prospect of their potential application as information carriers in future logic or memory devices [1, 2]. For most application scenarios, it will be indispensable to use materials with a low magnetic damping. Here, the ferrimagnetic insulator yttrium iron garnet (YIG) stands out with the highest magnon propagation length observed. At the same time, antiferromagnetic materials have recently become a focus of research, partly due to their ultrafast spin dynamics, thereby providing potential benefits for fast spin-wave signal processing [3]. We aim at combining these two properties by studying sub-micron spin waves in YIG films that are doped with Ga in order to approach antiferromagnetic compensation [4]. Such films were grown on bulk gadolinium gallium garnet (GGG) substrates. We directly imaged spin waves in these films by time-resolved scanning transmission x-ray microscopy (TR-STXM). For that, we developed a thinning process to reach soft x-ray transmissivity, employing a combination of mechanical lapping and Xe plasma focused ion beam (PFIB) etching (Fig. 1a) [5]. Spin waves in the Ga-doped YIG were excited using a microstrip antenna and they exhibited significant propagation lengths (Fig. 1b,c), confirming the low magnetic damping of the material. We observed an almost isotropic spin-wave dispersion, which suggests that the corresponding waves are exchange dominated, even for wavelengths above 100 nm. This can be explained by the large exchange length of the material, due to its low net magnetization. In addition, we observed a strong amplitude nonlinearity in the spin-wave excitation process and exceptionally high spin-wave amplitudes, exceeding precession angles of 20°.

[1] A.G. Gurevich and G.A. Melkov, *Magnetization Oscillations and Waves*. Vol. 1, CRC Press (1996) [2] A.V. Chumak, et al., Nat. Phys. 11 453 (2015). [3] T. Jungwirth, et al., Nat. Nanotechnol. 11 231 (2016). [4] P. Hansen, et al., J. Appl. Phys. 45 6 (1974). [5] S. Mayr, et al., Crystals 11 5 (2021).

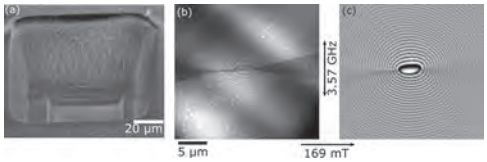

Fig. 1: (a) SEM image depicting a window etched out of a GGG substrate by a PFIB. (b,c) TR-STXM snapshots with out-of-plane magnetic sensitivity displaying spin waves. (b) Absolute absorption image with both magnetic and topographic contrast (GGG thickness variation and microstrip antenna visible). (c) Normalized image showing only the temporal magnetic changes with respect to the time average, highlighting the spin waves.

HOK-04. Probing Spin Waves Through Transient Reflectance Ultrafast Spectroscopy (TRUS) in PLD Grown $Y_3Fe_5O_{12}/Gd_3Ga_5O_{12}$. *S. Satapathy*[1,2], M. Kumar[1,2], R. Kumar[3], Z. Hossain[3], G. Basheed[1,2] and K. Maurya[1,2] *1. CSIR-National Physical Laboratory, New Delhi, India; 2. Academy of Scientific and Innovative Research (AcSIR), Ghaziabad, India; 3. Department of Physics, Indian Institute of Technology, Kanpur, India*

Recent advancements in magnonics based on spin waves (SWs) are one of the best promising alternatives that use coherent collective excitation of spins [1]. Femtosecond (fs) laser pulses have been used as an efficient stimulus to excite a coherent spin precession in magneto-optically active materials such as $Y_3Fe_5O_{12}$ (YIG) [2]. Due to small saturation magnetization, YIG based devices are regarded as incompetent in ultrafast applications as their SW frequencies lie in gigahertz range. In this work, we present room temperature Transient reflectance ultrafast spectroscopy (TRUS) on PLD grown 100nm YIG/GGG (110) thin-film using a 35fs pulsed laser. 2θ-ω scan on a YIG thin-film shows <880> reflection of YIG and GGG (Fig.1); from ω scan, FWHM value of 0.0047^O is obtained that confirms high crystallinity of YIG film. To study the ultrafast photomagnonic phenomena, the film is excited with 2.81eV(440nm) pump energy at a different average power of 0.5,1.0 and 1.5mW. Fig.2 shows the differential reflectance (DR) concerning the probe delay time in the visible region of 600nm and 700nm. The kinetics are fitted using surface xplorer to model the experimental profile by considering two lifetimes; τ_1 is the interband relaxation lifetime and τ_2 is the finalized relocalization of photoexcited carriers and their recombination. A large peak observed during the time overlap between pump and probe is due to the population of excited electronic states in Fe^{3+} ion (d→d transition). These changes are due to modification of the optical bandgap along with incoherent and coherent phonons excitation by the ultrafast laser pulse. Our results are pertinent for all insulating ferrimagnets indicating spin manipulation can be extended into the terahertz frequency range. The above findings reinforce the link between the fields of photonics, magnonics, and femtomagnetism, and open the door for exciting perspectives for photo-induced spin dynamics [3].

1. V. Chumak, V. I.Vasyuchka, A. A. Serga, and B. Hillebrands, Nat. Phys. 11, 453 (2015). 2. S. F. Maehrlein, I. Radu, P. Maldonado, A. Paarmann, M. Gensch, A. M. Kalashnikova, R. V. Pisarev, M. Wolf, P. M. Oppeneer, J. Barker, T. Kampfrath, Sci. Adv. 4, eaar5164 (2018). 3. U. Bovensiepen, Nat. Phys. 5, 461 (2009).

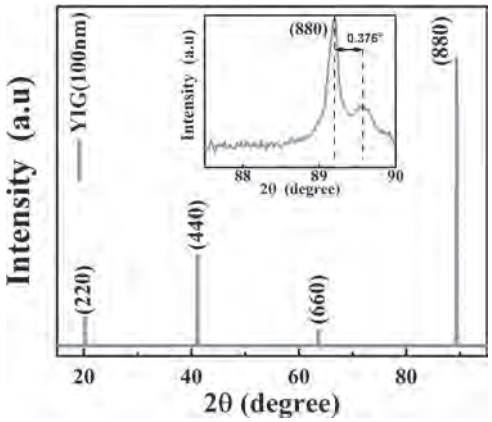

2θ-ω scan of 100nm YIG/GGG(110) sample, inset shows 880 plane reflection of YIG peak.

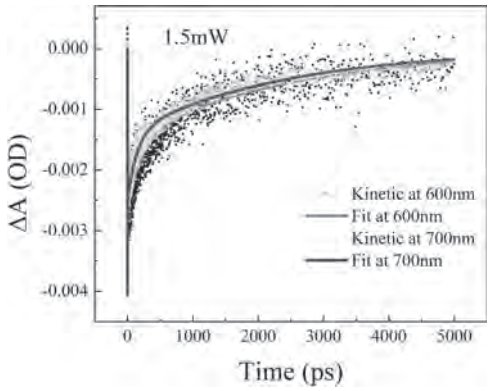

DR spectra vs probe delay time at 600nm and 700nm, excited with an average power of 1.5mW.

HOK-05. Ferromagnetic resonance driven GHz spin dynamics probed by time-resolved dynamic X-ray magnetic linear dichroism.
C. Klewe[1], S. Emori[2], Q. Li[3], M. Yang[4], B.A. Gray[5], H. Jeon[6], B.M. Howe[5], Y. Suzuki[7,8], Z.Q. Qiu[9], P. Shafer[1] and E. Arenholz[10] *1. Advanced Light Source, Lawrence Berkeley National Laboratory, Berkeley, CA, United States; 2. Department of Physics, Virginia Tech, Blacksburg, VA, United States; 3. National Synchrotron Radiation Laboratory, University of Science and Technology of China, Hefei, China; 4. Institute of Physical Science and Information Technology, Anhui University, Hefei, China; 5. Materials and Manufacturing Directorate, Air Force Research Laboratory, Wright-Patterson Air Force Base, Dayton, OH, United States; 6. Sensors Directorate, Air Force Research Laboratory, Wright-Patterson Air Force Base, Dayton, OH, United States; 7. Geballe Laboratory for Advanced Materials, Stanford University, Stanford, CA, United States; 8. Department of Applied Physics, Stanford University, Stanford, CA, United States; 9. Department of Physics, University of California at Berkeley, Berkeley, CA, United States; 10. Cornell High Energy Synchrotron Source, Cornell University, Ithaca, NY, United States*

The birth of antiferromagnetic spintronics has driven extensive research toward understanding spin transport between ferromagnetic (FM) and antiferromagnetic (AFM) materials in FM/AFM heterostructures. Despite the ultrafast THz dynamics in AFMs, multiple studies have found clear evidence for GHz spin current propagation in AFM films. Different mechanisms have been suggested for the observed spin current propagation through an antiferromagnetic insulator.[1-6] Yet, a detailed understanding of the mechanisms behind these effects is lacking, due to the lack of probes that can provide time-resolved studies of GHz spin dynamics in antiferromagnetically ordered systems. In our work, we present the first theoretical and experimental evidence of time-resolved dynamic X-ray magnetic linear dichroism (XMLD) measurements of GHz magnetic precessions driven by ferromagnetic resonance in both metallic and insulating thin films. Our findings show a dynamic XMLD in both ferromagnetic $Ni_{80}Fe_{20}$ and ferrimagnetic $Ni_{0.65}Zn_{0.35}Al_{0.8}Fe_{1.2}O_4$ (NZAFO) for different measurement geometries and linear polarizations. A detailed analysis of the observed signals reveals the importance of separating different harmonic components in the dynamic signal in order to identify the XMLD response without the influence of competing contributions (see Fig.1). In particular, RF magnetic resonance elicits a large dynamic XMLD response at the fundamental frequency under experimental geometries with oblique x-ray polarization. The geometric range and experimental sensitivity can be improved by isolating the 2ω Fourier component of the dynamic response. To account for the effect of crystal-field splitting on the angular dependence of the spin-quantization axis with respect to the crystalline axes, we include crystal-field contributions in the analysis of the dynamic XMLD spectral lineshapes, which yields excellent agreement with the experimental observations. These results illustrate the potential of dynamic XMLD and represent a milestone accomplishment towards the study of GHz spin dynamics in systems beyond ferromagnetic order.

[1] C. Hahn *et al.*, EPL 108, 57005 (2014). [2] H. Wang *et al.*, Phys. Rev. Lett. 113, 097202 (2014). [3] W. Lin *et al.*, Phys. Rev. Lett. 116, 186601 (2016). [4] Z. Qiu *et al.*, Nat. Commun. 7, 12670 (2016). [5] Q. Li *et al.*, Nat. Commun. 10, 5265 (2019). [6] M. Dabrowski *et al.*, Phys. Rev. Lett. 124, 217201 (2020).

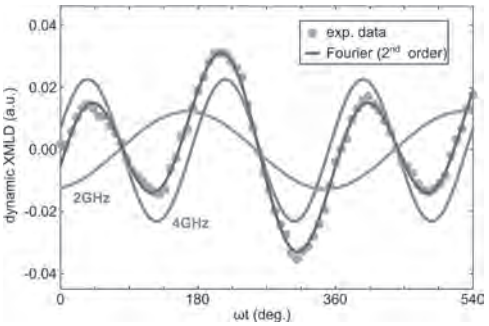

Dynamic XMLD phase delay scan fitted with a Fourier extension to 2nd order and evaluated for 1st and 2nd harmonic components.

HOK-06. Spin-wave optics fabricated by FIB irradiation of YIG films.
M. Kiechle[2], A. Papp[1], S. Mendisch[2], V. Ahrens[2], G. Csaba[1] and M. Becherer[2] *1. Faculty of Information Technology and Bionics, Pázmány Péter Catholic University, Budapest, Hungary; 2. Department of Electrical and Computer Engineering, Technical University of Munich, Munich, Germany*

We present focusing of spin waves with spherical lenses in YIG by creating a magnonic refractive index change via Ga^+ focused ion beam (FIB) irradiation. Direct FIB irradiation in YIG induces an ion-dose-dependent change in the effective magnetization M_{eff} [1], and we use this to locally modify the refractive index. The lenses were designed using the lensmaker's equation where the relative refraction index is estimated from experiments as $n_{rel}=\lambda_0/\lambda_{FIB}= 4.2\mu m/2.5\mu m = 1.68$. In the experiments, we use an in-house sputtered 100 nm thick YIG film on GGG and obtain the largest ΔMeff for a dose of 1×10^{13} ions/cm^2. For larger doses, the change in ΔMeff is reversed and damping increases significantly. The measured spin-wave pattern of two plano-convex spherical lenses is presented in Fig. 1. We use longitudinal time-resolved MOKE microscopy to image the spin-wave patterns in forward volume configuration (isotropic propagation). Bending of the wavefront is visible inside the lenses, as well as the shorter wavelengths. Ion irradiation in thin films to manipulate their magnetic properties has been used in many magnetic materials/compositions but is particularly challenging in insulators. Researchers in our field, to our knowledge, have not FIB irradiated YIG to locally modify the spin-wave dispersion relation, or to pattern YIG without etching. Using spin waves for analog computing (such as

optical signal processing) requires precise local modification of the magnetic properties, and we recently demonstrated the potential of FIB patterning by fabricating a concave grating for spin waves realized with higher ion doses that locally destroy magnetic properties of YIG [2]. Furthermore, gradually changing refractive-index maps can be realized by irradiating a dose-§gradient, giving access to create gradient-index magnonic elements like GRIN lenses [3],[4],[5].

[1] W. Ruane, S. White, J. Brangham, K. Meng, AIP Advances, vol. 8, no. 5, p. 056007 (2018). [2] Á. Papp, M. Kiechle, S. Mendisch, Scientific Reports, vol. 11, no. 1, pp. 1–8, (2021). [3] A. Papp, G. Csaba, and W. Porod, IEEE International Conference on Rebooting Computing (ICRC). IEEE, pp. 1–4 (2016). [4] C. S. Davies, A. Francis, A. V. Sadovnikov, Physical Review B, vol. 92, no. 2, p. 020408 (2015). [5] M. Vogel, P. Pirro, B. Hillebrands, Applied Physics Letters, vol. 116, no. 26, p. 262404 (2020).

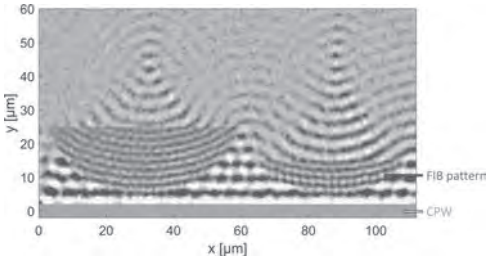

Time-resolved MOKE image of a 20 (left) and a 10 μm (right) thick spin-wave lens fabricated via FIB. The irradiation pattern d-shaped lens is indicated in semitransparent red, the groundline of a coplanar antenna for coherent excitation in gray. The initially applied wavelength is 4.3 μm, and shortened to about 2.5 μm inside the lenses due to the FIB induced M_{eff} increase.

HOK-07. Investigation of magnon absorption from $Y_3Fe_5O_{12}$ into metals. *S. Mae*[1], E. Shigematsu[1], R. Ohshima[1], Y. Ando[1], T. Shinjo[1] and M. Shiraishi[1] *1. Electronic Science and Engineering, Kyoto University, Kyoto, Japan*

Magnon has a potential to be a new information carrier because of its Joule-heating-less and long-distance propagation in ferromagnets [1]. Recently, Das *et al.* demonstrated that magnon in $Y_3Fe_5O_{12}$ (YIG) is absorbed into an adjacent ferromagnet, Ni-Fe alloy (Py), and the absorption can be modulated by the magnetization direction of the Py [2]. Although this study makes progress toward realization of magnonic device, a detailed principle of magnon absorption into metals has not been sufficiently clarified yet. Here, we study magnon propagation with several middle strips (MSs), Py, SiO_2, and metals on SiO_2 to explore the mechanisms of magnon absorption into metals. Figure 1 shows a schematic of the device. Two Ti/Au coplanar waveguides with the center-to-center distance of 300 μm and an MS with a width of 240 μm were fabricated on a YIG substrate (5 μm in thickness). An external magnetic field (B) applied to the device was swept from 50 mT to 140 mT. AC electric current with the power of 0 dBm and frequency of 5 GHz was injected into the antenna using a vector network analyzer and magnons were excited by the induced AC magnetic field. Magnons propagating in the YIG were partially absorbed by the MS and detected by the other antenna as an induced AC magnetic field. We measured the S_{21} parameter and calculated $|S_{21}|$ ($= \int |S_{21}| dB$) to compare the amounts of the detected magnons. To clarify whether the magnon absorption is an interfacial effect between YIG and Py, we measured the samples with Py and SiO_2/Py-MS. Figure 2 shows the comparison of $|S_{21}|$ among the bare YIG, SiO_2-MS, Py-MS, and SiO_2/Py-MS samples. The SiO_2 and Py thicknesses are 10 nm and 16 nm. The magnons detected in the Py and SiO_2/Py-MS samples were less than that in the bare YIG sample, and the decrease of $\Sigma|S_{21}|$ of the sample with the SiO_2/Py-MS was not much different from that of the sample with the Py-MS. These results indicate that the absorption is not originated simply from the interfacial effect between YIG and ferromagnet such as spin exchange interaction. We will discuss a possible mechanism of magnon absorption.

[1] A. V. Chumak V. I. Vasyuchka, A. A. Serga, Nature Physics 11, 453 (2015). [2] K. S. Das, F. Feringa, M. Middlelkamp, Physical Review B 101, 054436 (2020).

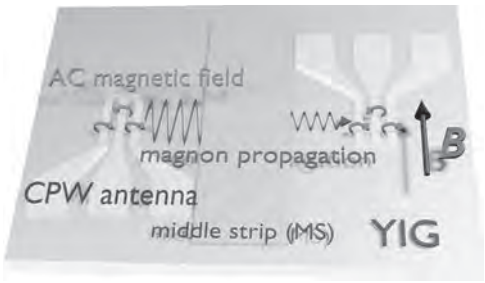

Fig.1 A schematic of device structure.

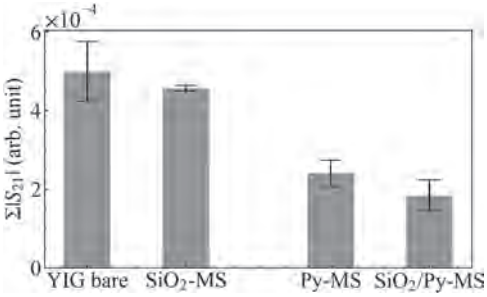

Fig.2 The comparison of $\Sigma|S_{21}|$. The error bars represent the standard error.

HOK-08. Strong magnon-photon coupling with chip-integrated YIG in the zero-temperature limit. *P.G. Baity*[1], D.A. Bozhko[2], R. Macedo[1], W. Smith[3], R. C. Holland[1], S. Danilin[1], V. Seferai[1], J. Barbosa[1], R. R. Peroor[2], S. Goldman[2], U. Nasti[1], J. Paul[1], R.H. Hadfield[1], S. McVitie[3] and M. Weides[1] *1. James Watt School of Engineering, University of Glasgow, Glasgow, United Kingdom; 2. Center for Magnetism and Magnetic Materials, Department of Physics and Energy Science, University of Colorado Colorado Springs, Colorado Springs, CO, United States; 3. SUPA, School of Physics and Astronomy, University of Glasgow, Glasgow, United Kingdom*

The cross-integration of spin-wave and superconducting technologies is a promising method for creating novel hybrid devices for future information processing technologies to store, manipulate, or convert data in both classical and quantum regimes. Such hybrid devices can exhibit interesting properties such as new resonance spectra features induced by the interchange between superconducting microwave lines and ferromagnetic resonance dynamics of yttrium iron garnet ($Y_3Fe_5O_{12}$, YIG) films [1]. On the other hand, hybrid magnon-polariton systems have been typically studied using bulk YIG and three-dimensional microwave photon cavities [2,3]. Limitations in YIG growth have thus far inhibited its incorporation into CMOS compatible technology such as high quality factor superconducting quantum technology. To overcome this impediment, we have used Plasma Focused Ion Beam (PFIB) technology—taking advantage of precision placement down to the micron-scale—to integrate YIG with NbN superconducting microwave devices. Example hybrid devices are shown in Fig.1. Ferromagnetic resonance has been measured at milliKelvin temperatures on PFIB-processed YIG samples using planar microwave circuits. Furthermore, we demonstrate strong coupling between superconducting resonator and YIG ferromagnetic resonance modes by maintaining reasonably low loss while reducing the system down to the micron scale. This achievement of strong coupling on-chip is a crucial step toward fabrication of functional hybrid quantum devices that advantage from spin-wave and superconducting components. For more information, please see our recent publication [4]. This work was supported by the European Research Council under the Grant Agreements 648011 and 648604, the EPSRC through grant EP/M024423/1, the Leverhulme Trust, and the University of Glasgow.

[1] I. A. Golovchanskiy, N. N. Abramov, M. Pfirrmann et al., Phys. Rev. Applied, Vol. 11, p. 044076 (2019). [2] I. Boventer, M. Pfirrmann, J. Krause et al., Phys. Rev. B, Vol. 97, p. 184420 (2018). [3] M. Pfirrmann, I. Boventer, A. Schneider et al., Phys. Rev. Research, Vol. 1, p. 032023(R) (2019). [4] P. G. Baity, D. A. Bozhko, R. Macêdo et al., Appl. Phys. Lett., Vol. 119, p. 033502 (2021).

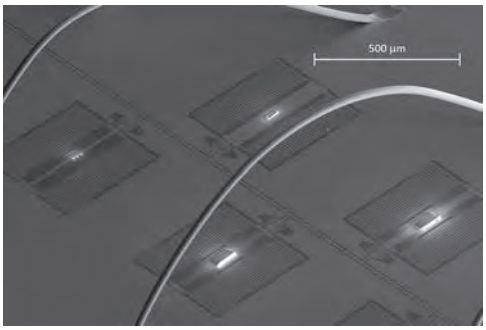

Fig.1 Scanning electron microscope image of YIG samples on superconducting NbN lumped-element resonators. The YIG samples are placed at the position of the resonators' magnetic antinode and fixed in place by Pt deposition. Strong coupling between spin waves and microwave photons has been demonstrated by measuring the transmission spectrum of the resonator-YIG devices as a function of applied external field.

HOK-09. Coherent coupling of two remote magnonic resonators mediated by superconducting circuits. *Y. Li*[1], V.G. Yefremenko[2], M. Lisovenko[2], C. Trevillian[3], T. Polakovich[4], T.W. Cecil[2], P. Barry[2], J.E. Pearson[1], R. Divan[5], V. Tyberkevych[3], C.L. Chang[2], U. Welp[1], W. Kwok[1] and V. Novosad[1] *1. Materials Science Division, Argonne National Laboratory, Lemont, IL, United States; 2. High Energy Physics Division, Argonne National Laboratory, Lemont, IL, United States; 3. Physics, Oakland University, Rochester, MI, United States; 4. Physics Division, Argonne National Laboratory, Lemont, IL, United States; 5. Center for Nanoscale Materials, Argonne National Laboratory, Lemont, IL, United States*

Hybrid magnonic systems incorporating superconductivity have recently emerged as a new promising direction that exploits the advantages of magnon excitations for processing quantum information and high quality factor superconducting resonators [1-3]. However, for designing realistic quantum logic operations with magnonics, an important step is to achieve remote multi-magnon interactions that can be embedded in standard circuit quantum electrodynamics modules such as superconducting quantum circuits. Here, we develop a superconducting circuit platform, incorporating chip-mounted single-crystal YIG spheres, for implementing microwave-mediated distant magnon-magnon interactions. Coherent level repulsion and dissipative level attraction between the magnon modes of the two spheres are demonstrated, with the former mediated by resonant microwave and the latter mediated by propagating microwave. For a single 250-µm-diameter YIG sphere, we achieve a magnon-photon coupling strength of 130 MHz with both the magnon and photon coherence time approaching 1 µs at 1.6 K, corresponding to a cooperativity of 13000. In a two-sphere-one-resonator circuit, we achieve a resonator mediated magnon-magnon coupling strength of 14 MHz in the dispersive coupling regime where the magnon-photon frequency detuning is ten times larger than their coupling strength. We also achieve level attraction of the magnon modes between the two YIG spheres that are integrated on a coplanar waveguide. Our results provide a realistic platform for constructing hybrid magnonic quantum networks at cryogenic temperatures and that can be scaled-up and incorporated into integrated circuits. Work at Argonne was supported by the U.S. Department of Energy, Office of Science, Basic Energy Sciences, Materials Sciences and Engineering Division. Use of the Center for Nanoscale Materials (CNM), an Office of Science user facility, was supported by the U.S. Department of Energy, Office of Science, Office of Basic Energy Sciences, under Contract no. DE-AC02-06CH11357. C.T. and Y.L. acknowledge support from the 2020 IEEE Magnetics Society Educational Seed Funding.

[1] D. Lachance-Quirion, Y. Tabuchi, A. Gloppe, K. Usami, and Y. Nakamura, Hybrid quantum systems based on magnonics, *Appl. Phys. Exp.*, 12, 070101 (2019) [2] Y. Li *et al.*, Hybrid magnonics: Physics, circuits, and applications for coherent information processing, *J. Appl. Phys.*, 128, 130902 (2020) [3] B. Z. Rameshti *et al.*, Cavity Magnonics, *arXiv:*2106.09312

HOK-10. Effects of Spin Wave Dispersion on Surface Acoustic Wave Velocity. *P. Rovillain*[1], J. Duquesne[1], M. Eddrief[1], M. Pini[2], A. Rettori[4,5], S. Tacchi[3] and M. Marangolo[1] *1. Institut des NanoSciences de Paris, Sorbonne Université, CNRS, Paris, France; 2. Istituto dei Sistemi Complessi del CNR (CNR-ISC), Sede Secondaria di Firenze, Sesto Fiorentino, Italy; 3. Istituto Officina dei Materiali del CNR (CNR-IOM), Sede Secondaria di Perugia, c/o Dipartimento di Fisica e Geologia, Universita di Perugia, Perugia, Italy; 4. Dipartimento di Fisica ed Astronomia, Universit_a degli Studi di Firenze, Sesto Fiorentino, Italy; 5. INFN, Sezione di Firenze, Sesto Fiorentino, Italy*

New fascinating phenomena involving coupled spin waves and phonons are observed at the magnetoelastic resonance as acoustically-assisted spin pumping [1, 2] and magnetization swiching [3, 4]. In this context, Surface Acoustic waves (SAW), a mature technology widely used in today's sensors, filters and microwave circuitry trigger efficiently magnetization dynamics: resonant effects are obtained with appropriate intensities and directions of the external magnetic field (B_{ext}). This tunability is an asset for magnonic applications of SAW-FMR (ferromagnetic resonance). Recently, SAW-FMR has been obtained in Fe epitaxially grown on GaAs(001), a spintronic and magnonic compatible magnetoelastic and piezoelectric heterostucture.[5] Here, we show that SAW propagation in Fe thin films is strongly affected by the SWs modes dispersion in the reciprocal space, even at very low K-values. It turns out that the B_{ext}-dependence of the sound velocity depends a lot of the angle between B_{ext} and the SAW vector directions. In particular, the resonant SAW-FMR is possible only in the backward configuration. Furthermore, we give a theoretical description of the observed phenomena by introducing calculated dispersion curves into a phenomenological and approximated approach derived by LLG equations. [6,7] This approach catches the physics of SAW propagation in a Fe thin films, as attested by the comparison with quasi-exact elastic calculations. We give a very good description of the SAW-SW interaction that facilitates the design of magnonic devices where SWs are generated by SAW Interdigital transducers (IDT) and not by much more energy-dissipative inductive antenna.

[1] M. Weiler, et al. PRL 108, 176601, (2012) [2] Uchida, et al., Solid State Comm.198, 26, (2014) [3] L. Thevenard, et al. PRB 93, 134430, (2016) [4] P. Kuszewski, et al. JOP: Cond. Mat. 30, 244003 (2018) [5] J.-Y. Duquesne, et al. PR Applied 12, 024042 (2019) [6] L. Dreher, et al. PRB 86, 134415 (2012) [7] A. Hernandez-Minguez, et al. PR Applied 10, 44018 (2020)

HOK-11. Experimental Observation of the Spin-Wave Talbot Effect. *C. Riedel*[1], T. Taniguchi[1] and C.H. Back[1] *1. Technical University Munich, Garching, Germany*

Interference-based magnonic devices – which exploit eigenmode transportation of ordered spins, *i.e.* spin waves – are potential candidates to overcome the increased power consumption and Joule heating of traditional information storage and transport devices. In this work, we present a custom-made time-resolved magneto-optical Kerr effect (TR-MOKE) microscope for visualizing locally and time-resolved the dynamic magnetization, *i.e.* propagating spin waves. Using femtosecond laser pulses synchronized to the phase of a microwave source, which is used to drive spin-wave dynamics, we demonstrate time-resolved 2D spin-wave images with a spatial resolution < 500 nm. To investigate magnonic interference behaviors, we fabricate

a diffraction grating in a 200 nm thick ferrimagnetic YIG film by argon ion-beam etching. A coplanar waveguide (CPW) located parallel to the grating, is used to coherently excite spin-waves which are imaged by TR-MOKE. Our results represent the experimental realization of a self-imaging phenomenon applied to spin-waves, well-known within the field of linear optics as the Talbot effect [1-3], where it finds several applications in optical measurement techniques. We investigate the spin-wave Talbot effect for different orientations of the external magnetic field with respect to the YIG plane and spin-wave propagation direction. Each geometry displays different interferometric behaviors, in agreement with recent theoretical predictions [2]. Furthermore, as depicted in Fig. 1, we demonstrate that the interference pattern can be tuned through careful selection of the external magnetic field strength. This work contributes to the understanding of spin-wave interference behaviors for enhancing the performance of future magnonic devices.

[1] C. Zhou *et al.*, Optics & Photonics News 15, 46-50 (2004) [2] M. Golebiewski *et al.*, Phys. Rev. B 102, 134402 (2020) [3] S. Mansfeld *et al.,* Phys. Rev. Lett. 108, 047204 (2021)

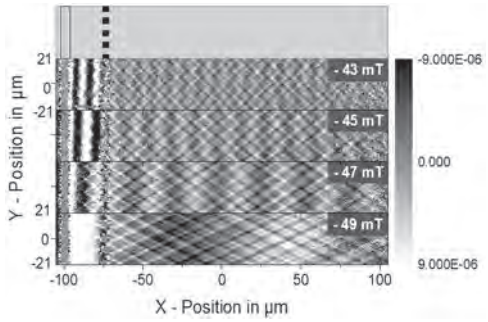

Fig. 1: The top sketch indicates the sample with the ground line of the CPW (yellow stripe) and the diffraction grating (black squares). The lower images display the MOKE signal, which is indicated by the gray scale, at various external magnetic fields. It can be seen that the localization of the interference maxima can be shifted by changing the external magnetic field strength. Here, the magnetic field was applied along the Y-direction.

HOK-12. Dispersion of Magnetostatic Spin Waves in a System of Dipolar Coupled Ferromagnetic Layers. *P. Gerevenkov*[1], V. Bessonov[2], A. Telegin[2], A. Kalashnikova[1] and N. Khokhlov[1] *1. Ioffe Institute, St Petersburg, Russian Federation; 2. M.N. Miheev Institute of Metal Physics, Yekaterinburg, Russian Federation*

Currently, the creation of magnonics elements for the information transfer and processing is an actively developing area of research. A number of recent works have demonstrated an adder [1] and a diode [2] for magnetostatic spin waves (MSW) in coupled waveguide systems. The most important characteristic of these structures for the design of spin-wave logic elements is the dispersion of the MSW. However, obtaining the dispersion in a system of several coupled waveguides is a difficult task. In this work, the dispersion of MSW is studied experimentally and theoretically in the case of two dipolar coupled thin ferromagnetic films. We use multilayered structure of two ferromagnetic layers of galfenol ($Fe_{81}Ga_{19}$) separated by nonmagnetic copper layer FeGa(7 nm)/Cu(5 nm)/FeGa(4 nm) on (100)-GaAs substrate. We choose the galfenol based structures as they exhibit a large values of the magnetization precession lifetime [3] and the MSW propagation length [4] which promises the galfenol as suitable material for magnonic applications. The experimental dispersion of two magnon branches, corresponding to acoustic and optic magnetization dynamics, was obtained by the Brillouin light scattering method [symbols in Fig. 1 (b)]. As a theoretical approach, we use the method presented in [5] [lines in Fig. 1 (b)]. As a result, we experimentally demonstrate the non-reciprocal behavior of the collective magnon modes in the system of two ferromagnetic layers with pure dipolar coupling. The analysis shows the non-reciprocity is determined by the geometrical asymmetry of the structure. The fact paths the way to design of 3D magnonic logic gates based on predicted dispersion of MSW [6].

1. Wang Q. et al., Nat Electron Vol. 3 p.765 (2020). 2. Szulc K. et al., Phys. Rev. Applied Vol. 14 (3) p.034063 (2020). 3. Scherbakov A. V. et al., Phys. Rev. Applied Vol. 11 p.031003 (2019) 4. Khokhlov N. E. et al., Phys. Rev. Applied Vol. 12 p.044044 (2019). 5. Carlotti G. et al., La Rivista del Nuovo Cimento Vol. 22 p.1 (1999) 6. Mahmoud A. et al., J. Appl. Phys. Vol. 128 p.161101 (2020)

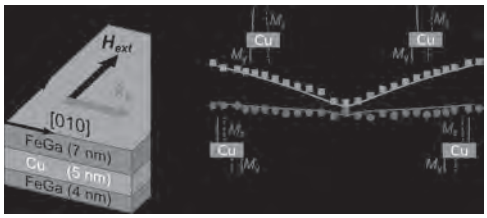

Fig. 1 (a) Structure under the investigation (b) Thermal magnons dispersions for magnetization along easy axis [001]. Acoustic and optic branches shown by red and green symbols, respectively. Lines show the fit from the theoretical model. Insets: distributions of the in-plane and out-of-plane magnetization components M_y, M_z over the thickness of the structure for acoustic and optic branches at $k_z = \pm 22\ 10^4$ rad/cm.

HOK-13. Self-imaging Based Programmable Spin-wave Logic Gates. *M. Golebiewski*[1], P. Gruszecki[1] and M. Krawczyk[1] *1. Faculty of Physics, Adam Mickiewicz University, Poznan, Poland*

The Talbot effect, called also a self-imaging, has been known in linear optics since the 19th century and has found various technological applications. After our demonstration of this effect for spin waves (SWs) using micromagnetic simulations [1], we decided to expand the research for real-size systems with an application potential. I will present how, by using a near diffraction field of a single-mode sources array, we can design a logic gate performing any logical function using self-imaging of SWs at the output. So, this is a proposal to incorporate SWs into computational solutions in order to be able to create ultra-low power magnonic circuits realizing complex operations, without the need for repeated SW and voltage domain conversion. The Talbot effect is well suited to design such reconfigurable logical gates, as this phenomenon depends on many parameters – both static and dynamic. The proposed system is based on phase detection (PD) and threshold detection (TD) techniques. Determining the phase shift $\varphi = \pi/2$ as logical '1' and no shift $\varphi = 0$ as logical '0', we measure an output phase, and define its logical value in the same way. In the case of TD, the SW intensity on the input and/or output is analyzed. The realisation for a thin film of yttrium iron garnet and SW frequency of 40 GHz is shown in Fig. 1 and Table 1. I will discuss selected examples and technical aspects of the proposed solution, drawing the attention of the magnonic community to the self-imaging effect and a potential of SW interference and diffraction in logical functions. The research has received partial support from National Science Centre, Poland from the project OPUS no UMO-2020/37/B/ST3/03936.

[1] M. Golebiewski et al., Phys. Rev. B 102, 134402 (2020)

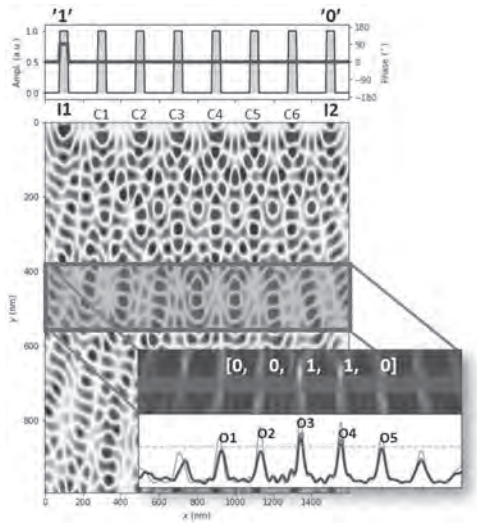

Fig. 1. The design of a 2-in 5-out logic gate. Here, the input I1 is phase-shifted by φ = π/2 (logical '1'), and the I2 is in phase (φ = 0) with the control sources C1-C6 (logical '0'). The outputs O1-O5 visible in the inset, include two self-image intensities greater (red points) than the given threshold (yellow dotted line).

I1	I2	O1	O2	O3	O4	O5
1	1	0	0	1	0	0
1	**0**	**0**	**0**	**1**	**1**	**0**
0	1	0	1	1	0	0
0	0	1	1	1	1	1
Truth funct.		NOR	¬I1	True	¬I2	NOR

Table 1. The truth functions obtainable from this system (the case from Fig. 1 in bold).

Session HOL
SPIN WAVES AND MAGNETIZATION DYNAMICS II

Oleksii M. Volkov, Chair
Helmholtz-Zentrum Dresden-Rossendorf, Dresden, Germany

CONTRIBUTED PAPERS

HOL-01. Mode attraction in Floquet systems with memory: application to cavity magnonics. *I. Proskurin*[1,2], O.J. Iyaro[1] and R. Stamps[1]
1. Department of Physics and Astronomy, University of Manitoba, Winnipeg, MB, Canada; 2. Department of Theoretical and Mathematical Physics, Ural Federal University, Ekaterinburg, Russian Federation

Far from thermodynamic equilibrium, nonlinear systems can be characterized by a stationary regime known as a limit cycle. In magnetic systems with a uniaxial symmetry driven with a circularly polarized field, this regime is referred to as the P-mode [1]. P-modes have been experimentally observed in the non-linear ferromagnetic resonance [2]. Stable P-modes can play a role of the equilibrium state for the elementary excitations around them. We show that these excitations can be used in cavity magnonics to explore unique features of non-Hermitian physics such as mode attraction and exceptional points. Level attraction describes a mode coalescence that can take place in open systems. It indicates development of an instability region in the energy spectrum of the coupled system bounded by exceptional points [3]. This regime has been recently observed in a number of experiments in dissipative cavity magnonics [4]. Here, we present a theory of mode attraction in periodically driven systems. Our theory can be used in conjunction with numerical micromagnetics to describe non-Markovian Floquet systems [5], which allows us to determine the regions of stability and instability and associate them with mode repulsion and attraction. In magnetic systems, our approach works for quantum and semiclassical dynamics, which makes possible to use it in combination with micromagnetic simulations. We apply this approach to demonstrate the level attraction between the excitations around the P-modes and the photons inside a microwave cavity. In a system driven with a circularly polarized field, the excitations around the P-mode form two side bands around the driving frequency (see figure). We show that when the lower side band couples to the cavity mode, it forms a mode attraction spectrum. Finally we discuss possibilities for experimental observation and predicted dependences on driving field amplitude.

[1] G. Bertotti et al. Phys. Rev. Lett. 86, 724 (2001). [2] Y. Li et al. Phys. Rev. X 9, 041036 (2019). [1] N. R. Bernier et al. Phys. Rev. A 98, 023841 (2018). [2] Y.-P. Wang and C.-M. Hu, J. Appl. Phys. 127, 130901 (2020). [5] F. L. Traversa et al. Phys. Rev. Lett. 110, 170602 (2013).

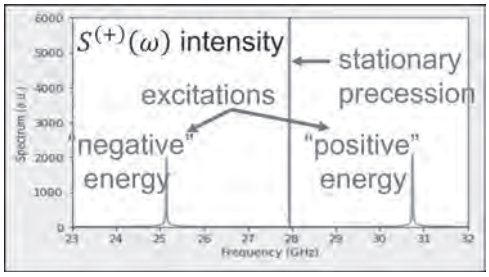

Circular component of the precessing spin driven with the circularly polarized field. The central peak is the P-mode with the frequency of the driving field. Two side bands correspond to the excitation around the P-mode. Coupling to the side band with the negative frequency with respect to the driving field gives mode attraction.

HOL-02. Exchange Constant Determination using Multiple-Mode FMR Perpendicular Standing Spin Waves. *H.J. Waring*[1], Y. Li[1], N. Johansson[1], C. Moutafis[1], I.J. Vera-Marun[2] and T. Thomson[1]
1. Computer Science, University of Manchester, Manchester, United Kingdom; 2. Physics and Astronomy, University of Manchester, Manchester, United Kingdom

The exchange constant (A_{ex}) is recognised as one of the fundamental properties of magnetic materials [1]. However, its accurate experimental determination remains a particular challenge. In thin films, dynamic measurements exploiting Perpendicular Standing Spin Waves (PSSWs) are increasingly used to extract A_{ex}, typically through a measurement of the first order PSSW mode and a subsequent analysis assuming a rigid surface pinning (SP) model initially proposed by Kittel [2–4]. Here we present a systematic study of multiple PSSW modes in NiFe films using Vector Network Analyser-Ferromagnetic Resonance Spectroscopy (VNA-FMR) as a function of thickness (t_{NiFe}) in the range 30 nm to 90 nm and capping layer material (uncapped, Ta, Pt) [6]. An example of a measured PSSW resonance is shown in Fig. 1a. The results show that an analysis of the measured PSSW resonant modes using the SP model provides an A_{ex} that varies with mode number (p), t_{NiFe} and capping layer material (Fig. 1(b-d)). This finding is clearly inconsistent with the physical expectation that the A_{ex} of a material is single valued for a given set of conditions (temperature, pressure etc.). We show through a comprehensive set of micromagnetic simulations that a dynamic pinning model originally proposed by Wigen et al. [5] is able to reproduce the experimental results using a single value of A_{ex}. It is possible to speculate that our data suggest that the layer immediately adjacent to the ferromagnetic layer exerts a small influence on the value of the exchange constant. These findings support the utility of using PSSWs in determining A_{ex} in magnetic thin films but show that the PSSW wavelength and the model used to analyse the measurements must be carefully considered.

[1] J. M. D. Coey, Magnetism and Magnetic Materials, Magnetism and Magnetic Materials, Cambridge University Press (2010) [2] I. S. Maksymov and M. Kostylev, Phys. E Low-Dimensional Syst. Nanostructures, Vol. 69, p. 253 (2015) [3] C. Kittel, Phys. Rev., Vol. 110, p. 1295 (1958) [4] C. F. Kooi, P. E. Wigen, M. R. Shanabarger et al., J. Appl. Phys., Vol. 35, p. 791 (1964) [5] P. E. Wigen, C. F. Kooi, M. R. Shanabarger et al., Phys. Rev. Lett., Vol. 9, p. 206 (1962) [6] H. J. Waring, Y. Li, N.A.B. Johansson et al. (In preparation).

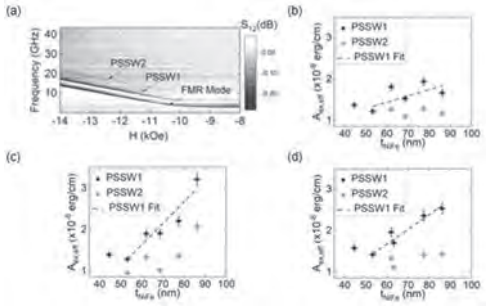

Fig.1 a) The out-of-plane spin-wave spectra of a Ta capped NiFe thin film with thickness 77 nm as a function of applied field and frequency. (b-d) The variation in effective exchange constant ($A_{ex,eff}$) determined using SP model as a function of t_{NiFe} and p for each capping layer case b) Uncapped c) Pt capped d) Ta capped.

HOL-03. Spin-wave spectra of 3D nanovolcanoes fabricated by focused electron beam-induced deposition. O. Dobrovolskiy[1], S. Bunyaev[2], A. Bondarenko[2], S. Lamb-Camarena[1], K. Guslienko[3,4], A. Chumak[1], M. Huth[5] and *G.N. Kakazei*[2] *1. Faculty of Physics, University of Vienna, Vienna, Austria; 2. IFIMUP/Department of Physics and Astronomy, University of Porto, Porto, Portugal; 3. Division de Fisica de Materiales, Depto. Polimeros y Materiales Avanzados: Fisica, Quimica y Tecnologia, Universidad del Pais Vasco, UPV/EHU, San Sebastian, Spain; 4. IKERBASQUE, the Basque Foundation for Science, Bilbao, Spain; 5. Physikalisches Institut, Goethe University, Frankfurt, Germany*

Extending nanostructures into the third dimension has become a major research avenue in modern magnetism and spintronics because of geometry-, curvature-, and topology-induced phenomena. Here, we introduce nanovolcanoes as on-demand engineered nano-architectures for 3D magnon spintronics. 40 nm-thick Co-Fe nanovolcanoes with diameters down to 300 nm were fabricated by the focused electron beam-induced deposition (FEBID) technique (Fig. 1) and studied by perpendicular spin-wave resonance (PSWR) spectroscopy. The spin-wave eigenfrequencies of the nanovolcanoes are notably different from the eigenfrequencies of the nanodisks and nanorings they are built from, because of the strongly non-uniform internal magnetic field. The experimental findings were elucidated with the aid of micromagnetic simulations, which indicate that the rings encircling the volcano craters lead to an effective confinement of the lower-frequency eigenmodes under the volcano crater, while the highest-frequency eigenmodes are confined in the ring area (Fig. 2). Accordingly, extension of 2D nanodisks into 3D nanovolcanoes allows to obtain same response in low frequency part of the spectrum in elements with 30% smaller footprints [1]. The nanovolcanoes can be viewed as multi-mode resonators with potential applications in telecom industry. Also, we demonstrated the engineering of the magnetic properties of CoFe-based nanodisks fabricated by FEBID. The material composition was tuned *in situ* via the e-beam waiting time in the deposition process and their post-growth irradiation with Ga ions. The saturation magnetization M_s of the nanodisks was deduced from PSWR measurements. The achieved variation of M_s in the broad range from 720 to 1430 emu/cm^3 continuously bridges the gap between the M_s values of widely used magnonic materials such as Permalloy and CoFeB [2].

[1] O.V. Dobrovolskiy, N.R. Vovk, A.V. Bondarenko, S.A. Bunyaev, S. Lamb-Camarena, N. Zenbaa, R. Sachser, S. Barth, K.Y. Guslienko, A.V. Chumak, M. Huth, and G.N. Kakazei, *Appl. Phys. Lett.* 118, 132405 (2021). [2] S.A. Bunyaev, B. Budinska, R. Sachser, Q. Wang, K. Levchenko, S. Knauer, A.V. Bondarenko, M. Urbánek, K.Y. Guslienko, A.V. Chumak, M. Huth, G.N. Kakazei, and O.V. Dobrovolskiy, *Appl. Phys. Lett.* 118, 022408 (2021).

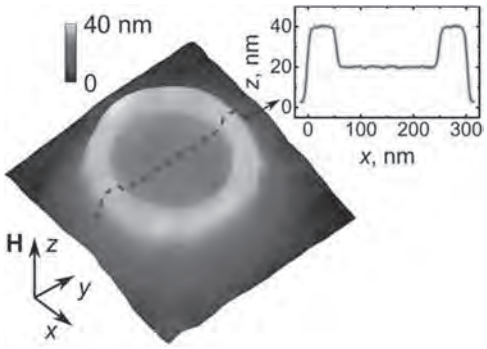

Fig. 1. Atomic force microscopy image of the nanovolcano with the outer diameter of 300 nm and the crater diameter of 200 nm. Inset: cross-sectional line scan.

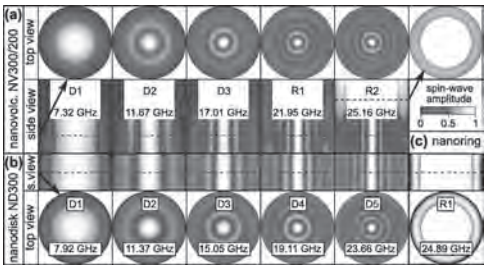

Fig. 2. Calculated spatial dependences of the spin-wave eigenfunctions for (a) 40 nm-thick nanovolcano NV300/200, (b) 20 nm-thick nanodisk ND300, and (c) 20 nm-thick nanoring NR300/200 at the out-of-plane bias magnetic field of 1.2 T.

HOL-04. Exchange-spring enabled high-frequency microwave emission from a spin-torque nano-oscillator. *S. Jiang*[1,2], S. Chung[3,2], Q.T. Le[2], P.J. Wong[1], W. Zhang[1] and J. Åkerman[2,4] *1. School of Microelectronics, Northwestern Polytechnical University, Xi'an, China; 2. Department of Physics, University of Gothenburg, Gothenburg, Sweden; 3. Department of Physics Education, Korea National University of Education, Cheongju, The Republic of Korea; 4. Department of Applied Physics, KTH Royal Institute of Technology, Stockholm, Sweden*

Spin-torque nano-oscillators (STNOs) are nonlinear nanoscale auto-oscillators, utilizing spin torque to generate magnetodynamics, and hold great promise for applications in microwave generators, magnetic memory, and artificial intelligence.[1-3] STNOs, which own free and fixed layers with either in-plane (IMA) [4] or perpendicular magnetic anisotropy (PMA) [5], have been demonstrated up to date. Except for IMA and PMA, an exchange spring can exhibit a tilted magnetic anisotropy by combining IMA and PMA materials through the strong interface exchange coupling.[6] Recent theoretical studies have directed to incorporating the so-called exchange spring structure into STNOs, aiming to achieve a low threshold current and a new degree of freedom on its dynamics. [7] Here, we report the experimental study of STNOs with an exchange spring ([Co/Pd]-Co) reference layer and PMA ([Co/Ni]) free layer as in Fig. 1(a). By intentionally selecting the strength of IMA and PMA in the reference layer, we achieve the following advantages: 1) high-frequency operation (>10GHz) at low-to-zero field regime in Fig. 1(b); 2) wide microwave frequency range at both positive and negative currents, *i.e.* serve as a bipolar STNO in Fig. 1(c), where the free and reference layers are selectively activated by different current polarities; and 3) easy to electrically detect auto-oscillating signals of the free layer, akin to magnetic droplets and ferromagnetic-resonance-like modes. Our findings hence extend the design capability of STNOs for energy-efficient high-frequency spintronics devices.

[1] Zeng, Z. *et. al.* Spin transfer nano-oscillators. Nanoscale 2013, 5, 2219. [2] Chen, T. *et. al.* Spin-torque and spin-Hall nano-oscillators. Proceedings of IEEE 2016, 104, 1919. [3] Romera, M. *et al.* Vowel recognition

with four coupled spin-torque nano-oscillators. Nature 2018, 563, 230. [4] Houshang, A *et al.* Spin transfer torque driven higher-order propagating spin waves in nano-contact magnetic tunnel junctions. Nature Communication 2018, 9, 4374. [5] Chung, S. *et al.* Direct observation of Zhang-Li torque expansion of magnetic droplet solitons. Physical Review Letters 2018, 120, 217204. [6] Nguyen, T. N. A. *et al.* Investigation of the tunability of the spin configuration inside exchange coupled springs of hard/soft magnets. IEEE Transactions on Magnetics 2014, 50, 2004906. [7] Zhou, Y *et al.* J. Spin-torque oscillator with tilted fixed layer magnetization. Applied Physics Letters 2008, 92, 262508.

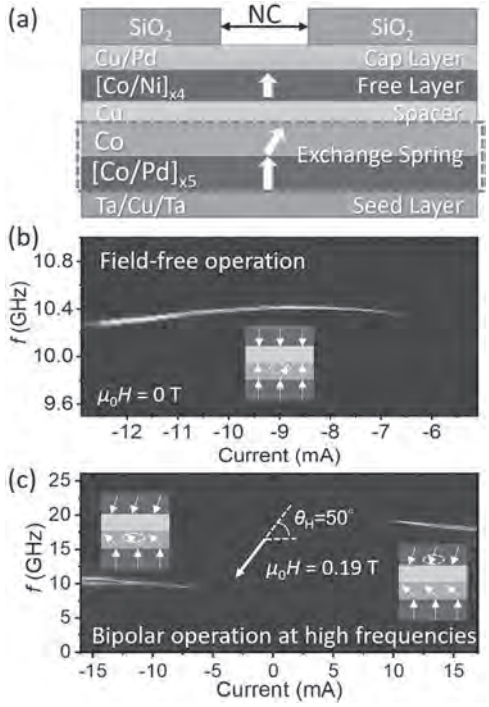

(a) An exchange-spring-based nano contact spin-torque nano oscillator (NC-STNO) with stack information; (b) Power Spectrum Density (PSD) as functions of current at a zero field. The magnetic configuration was initialized to an antiparallel state; (c) PSD as functions of dc current which swept from I_{dc} = +17 to -16 mA measured at θ_H= 50°and $\mu_0 H$ = 0.19 T. The insets are the schematics of magnetodynamics.

HOL-05. Increase of a Bullet Mode Lifetime due to Interaction with a Hot Magnon Gas. *P. Artemchuk*[1], V. Tyberkevych[1] and A.N. Slavin[1]
1. Department of Physics, Oakland University, Rochester, MI, United States

It has been shown [1] that during a rapid cooling process in nanometer thick magnetic films the hot magnon gas undergoes transition to Bose-Einstein condensate of magnons. It has been also demonstrated [2] that during continuous influence of external spin transfer torque (for example, created by spin-Hall effect) formation of a nonlinear bullet mode, having frequency below the minimum of the magnon spectrum, takes place. Due to its nonlinear nature the bullet mode is quite unstable, and quickly decays when the spin transfer torque is switched off [3,4]. Recent experiments, however, have shown that in the presence of a hot magnon gas the bullet mode lifetime (BML) may substantially increase compared to the BML in the state of thermodynamical equilibrium [2]. We developed a simple model of a nonlinear bullet mode interaction with a hot magnon gas undergoing a rapid cooling process. The bullet mode is described as an isolated energy level below the linear spin wave spectrum interacting with a magnon gas through the four-magnon scattering processes. The obtained results show that such an interaction can stabilize the bullet mode due to transfer of magnons from the higher-energy states in a magnon gas to the low-energy bullet mode (see Fig. 1). The BML increases with the increase of the hot magnon gas temperature. A significant increase of the BML is achieved when the temperature of a hot magnon gas exceeds a certain critical value (see Fig. 2). Such a large increase of the BML qualitatively agrees with the experimental results presented in [2]. Our results demonstrate that nonlinear coherent magnon structures, such as the bullet mode, can be stabilized by incoherent interactions with a non-equilibrium magnon gas, which may be important for the future applications in magnonics.

[1] M. Schneider, T. Brächer, D. Breitbach et al., Nat. Nanotechnol., Vol. 15, p. 457 (2020). [2] M. Schneider, D. Breitbach, R. O. Serha et al. arXiv:2106.14710 (2021). [3] A. Slavin and V. Tiberkevich, Phys. Rev. Lett., Vol. 95, no. 237201 (2005). [4] V. E. Demidov, M. Evelt, V. Bessonov et al., Sci. Rep., Vol. 6, no. 32781 (2016).

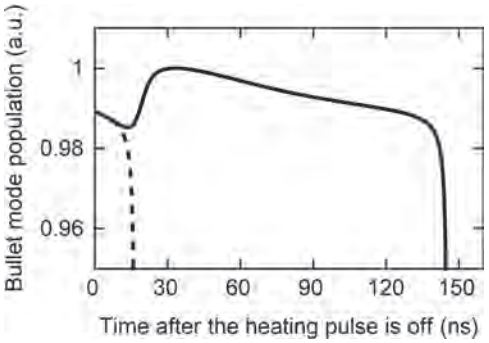

Fig. 1. Normalized magnon population in the bullet mode as a function of time in the absence (dashed line), and in the presence (solid line) of a hot magnon gas with initial temperature T_{heat} = 440 K.

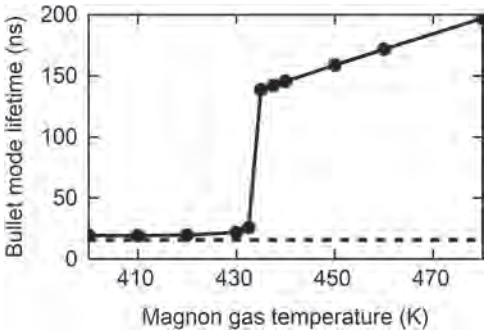

Fig. 2. Dependence of the bullet mode lifetime (BML) on the temperature of the hot magnon gas. Black filled circles connected by solid lines represent the simulation results. Dashed horizontal line marks the BML in the absence of the hot magnon gas.

HOL-06. Evolution of Room-Temperature Magnon Gas toward Coherent Bose–Einstein Condensate. *A.A. Serga*[1], T.B. Noack[1], V.I. Vasyuchka[1], A. Pomyalov[2], V.S. L'vov[2] and B. Hillebrands[1]
1. Fachbereich Physik and Landesforschungszentrum OPTIMAS, Technische Universität Kaiserslautern, Kaiserslautern, Germany;
2. Department of Chemical and Biological Physics, Weizmann Institute of Science, Rehovot, Israel

The appearance of spontaneous coherence is a fundamental feature of a Bose–Einstein condensate (BEC) and an essential requirement for possible applications of the condensates for classical and quantum computing. Using a magnon BEC in a magnetic crystal, such computing can be performed even at room temperature. Using specially shaped bulk samples of yttrium iron garnet crystal, we developed a novel efficient method of BEC investigation by direct detection of microwave radiation emitted by parametrically driven magnon gas (Fig.1a-b). By using this method, we studied the process of coherence formation in a magnon BEC and demonstrated that no

coherent BEC state could be found during the action of a strong magnetic pumping field. At the same time, after the pumping is terminated, the over-populated magnon gas evolves toward BEC and reaches full coherence, with the width of the magnon radiation spectrum decreasing by more than two orders of magnitude (Fig. 1c). The residual bandwidth is mainly determined by the lifetime of magnons, as expected for a fully coherent BEC consisting of a single magnon state. This direct demonstration of the magnon BEC coherence [1] brings the implementation of room temperature BEC-based computing closer. Moreover, the magnon BEC coupling with dynamic stray fields outside the sample is enabled by a proper choice of the sample shape giving direct spectroscopic access to the BEC. Such an approach can function as a convenient tool for integrating magnetic quantum systems into electrical environments.

[1] T. B. Noack, V. I. Vasyuchka, A. Pomyalov, V. S. L'vov, A. A. Serga, and B. Hillebrands, *Evolution of room-temperature magnon gas toward coherent Bose-Einstein condensate*, arXiv 2101.07890 (2021).

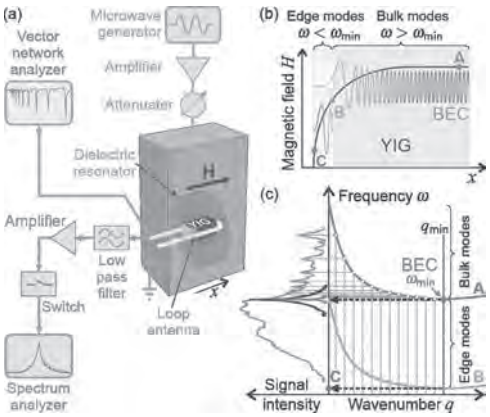

(a) Experimental setup for microwave detection of magnon BEC dynamics. (b) Bulk BEC mode and one of the edge magnon modes in a cuboid YIG sample. The monotonic blue line schematically shows the profile of the static magnetic field *H* within the YIG sample. Letters denote three field values: A – deeply inside the sample, B – at the point where the bulk BEC mode becomes evanescent, C – at the sample edge. (c) Magnon dispersion curves in the middle of the sample (at point A) and near the edge (at point B). The green, blue, and red signal intensity lines show the microwave power spectra registered during 1 μs interval before the end of pumping as well as 2 μs and 4 μs after the pump pulse is turned off.

HOL-07. Double Accumulation and Anisotropic Transport of Magneto-Elastic Bosons in Yttrium Iron Garnet Films. *A.A. Serga*[1], P. Frey[1], D.A. Bozhko[2], V.S. L'vov[3] and B. Hillebrands[1] *1. Fachbereich Physik and Landesforschungszentrum OPTIMAS, Technische Universität Kaiserslautern, Kaiserslautern, Germany; 2. Department of Physics and Energy Science, University of Colorado Colorado Springs, Colorado Springs, CO, United States; 3. Department of Chemical and Biological Physics, Weizmann Institute of Science, Rehovot, Israel*

Interaction between quasiparticles of a different nature, such as magnons and phonons, leads to mixing their properties and forming hybrid quasiparticles—hybrid magnetoelastic bosons, also called magnon polarons—in the areas of intersection of individual spectral branches. In garnet ferrite films, such hybridization results in several new phenomena as the resonant increase in the efficiency of the spin Seebeck effect [1,2] and the spontaneous bottleneck accumulation [3] of the magnetoelastic quasiparticles. Similar to the Bose-Einstein magnon condensation (BEC) [4], the latter phenomenon occurs at the bottom of the magnon spectrum in yttrium iron garnet films exposed to microwaves. However, unlike the BEC, which is a consequence of the equilibrium Bose statistics, the bottleneck accumulation is determined by changing interparticle interactions. Studying the transport properties of accumulated quasiparticles [5], we found that such accumulation occurs in two frequency-distant groups: quasiphonons and quasimagnons. These quasiparticles propagate in the film plane as spatially localized beams with distinctly different directions and velocities. The developed theoretical model describes the double accumulation effect. Parametrically pumped magnons scatter through a step-by-step thermalization process towards the lower energy states. At the magnon-phonon hybridization region, the efficiency of nonlinear scattering decreases, and the downward quasiparticle flux slows down. Owing to the bottleneck effect, quasimagnons form a density peak, in which intensity saturates due to their scattering to the lowest branch of the magnon spectrum. The remaining quasimagnons, scattering to phonon states below the magnon spectrum, transform into quasiphonons with vanishing scattering amplitude. These quasiphonons form the second accumulated group. By considering the 2D magnon-phonon spectrum, we determined the wavevectors and frequencies of each group and concluded about the caustic nature of the quasimagnon beams. Due to nonzero group velocity, the accumulated quasiparticles can be used for data transfer in magnon spintronics. Funded by the ERC Advanced Grant 694709 SuperMagnonics and by the DFG within TRR173 – 268565370 (project B04).

[1] T. Kikkawa, K. Shen, B. Flebus, R. A. Duine, K. Uchida, Z. Qiu, G. E. W. Bauer, and E. Saitoh, *Magnon polarons in the spin Seebeck effect*, Phys. Rev. Lett. 117, 207203 (2016). [2] R. Ramos, T. Hioki, Y. Hashimoto, T. Kikkawa, P. Frey, A.J.E. Kreil, V.I. Vasyuchka, A.A. Serga, B. Hillebrands, and E. Saitoh, *Room temperature and low-field resonant enhancement of spin Seebeck effect in partially compensated magnets*, Nat. Commun. 10, 5162 (2019). [3] D. A. Bozhko, P. Clausen, G. A. Melkov, V. S. L'vov, A. Pomyalov, V. I. Vasyuchka, A. V. Chumak, B. Hillebrands, and A. A. Serga, *Bottleneck Accumulation of Hybrid Magnetoelastic Bosons*, Phys. Rev. Lett. 118, 237201 (2017). [4] S. O. Demokritov, V. E. Demidov, O. Dzyapko, G. A. Melkov, A. A. Serga, B. Hillebrands, and A. N. Slavin, *Bose-Einstein condensation of quasi-equilibrium magnons at room temperature under pumping*, Nature 443, 430 (2006). [5] P. Frey, D.A. Bozhko, V.S. L'vov, B. Hillebrands, and A.A. Serga, *Double accumulation and anisotropic transport of magneto-elastic bosons in yttrium iron garnet films*, Phys. Rev. B 104, 014420 (2021).

HOL-08. Spin Chirality-Mediated Orbital Angular Momentum in Quasi-Two-Dimensional Topological Magnon Insulator Cu(1,3-bdc). *L. Alahmed*[1], J. Wen[4], Y. Xiong[2], L. Zhang[3,5], F. Lux[6], F. Freimuth[6], Y. Mokrousov[6], W. Zhang[2], Y.S. Lee[7] and P. Li[1] *1. Electrical and Computer Engineering, Auburn University, Auburn, AL, United States; 2. Department of Physics, Oakland University, Rochester, MI, United States; 3. Peter Grünberg Institut, Forschungszentrum Jülich, Jülich, Germany; 4. Stanford Institute for Materials and Energy Sciences, SLAC National Accelerator Laboratory, Menlo Park, CA, United States; 5. Institute for Advanced Simulation, JARA, Jülich, Germany; 6. Institute of Physics, Johannes Gutenberg University Mainz, Mainz, Germany; 7. Department of Applied Physics, Stanford University, Stanford, CA, United States*

Cu(1,3-bdc) is a topological magnon insulator where the Cu ions are arranged in a 2D Kagome lattice[1,2]. Here, we study the magnetization dynamics of Cu(1,3-bdc) using vibrating sample magnetometry (VSM, Fig.1a) and ferromagnetic resonance (FMR, Fig.1b,c) spectroscopy. We find that the saturation magnetization M_S values when an external field H is applied out-of-plane (OOP) is less than M_S values when H is applied in-plane (IP) at all tested temperatures. We find similar inequivalence in the g-factor, extracted from the fitted FMR dispersion curves (Fig.2a,b) depending on the direction of H. The g-factor tensor (Fig.2c) points towards orbital momentum contribution to the magnetic moment. As shown in Fig.2d, the temperature dependence of $\Delta M_S = M_{S,\,IP} - M_{S,\,OOP,}$ and $\Delta g = g_{IP} - g_{OOP}$ are closely correlated at T<6K but they diverge at T>6K. Since the g-factor tensor is most likely mediated by orbital magnetism, the deviation of Δg from ΔM_S is unexpected. We propose that this could be a result of thermally-induced non-vanishing spin chirality contributing to the electronic orbital magnetism[3]. Following the approach in Ref.[3],our analysis shows that the symmetry of the system

allows contributions to the orbital magnetization originating from spin excitations for the OOP field, but not the IP field. The prediction of our theoretical assessment is an increase of the g-factor with temperature for OOP field, while it is expected to decay for IP field. The general trend and the change in sign of the g-factor anisotropy observed experimentally at higher temperatures is thus consistent with this theory, which suggests that the spin excitations can renormalize the fundamental quantum mechanical constant conventionally associated with the atomic orbital magnetism. Our findings bring to the forefront a so far not considered mechanism for orbital dynamics in topological magnonic systems.

[1] L. Zhang et al., *Phys. Rev. B* 87, 144101 (2013) [2] R. Chisnell et al., *Phys. Rev. Lett.* 115, 147201 (2015) [3] Lc. Zhang et al., *Commun Phys* 3, 227 (2020)

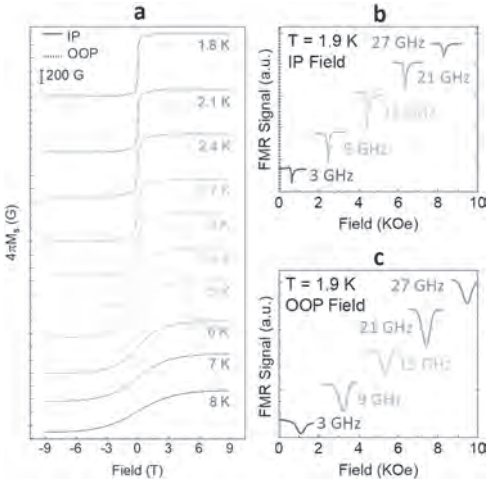

Fig.1:a VSM M vs. H curves at different temperatures. b and c FMR profiles at different microwave frequencies for IP and OOP fields, respectively.

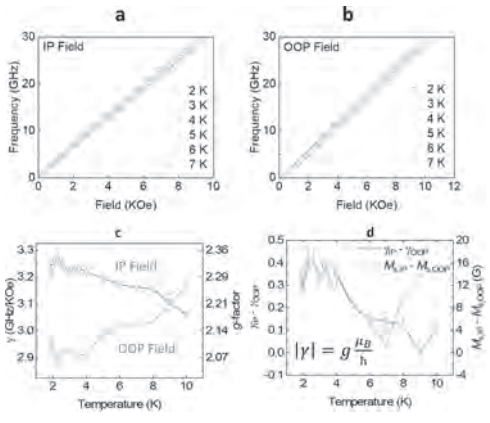

Fig.2: a and b FMR dispersion curves showing Kittel fits for IP and OOP fields, respectively. c Temperature dependence of the gyromagnetic ratio γ and g-factor. d Temperature dependence of Δγ and ΔM_S.

HOL-09. Spin Wave Amplification using Spin-Orbit-Torques, A Micromagnetic Approach. *A. El Kanj*[1], H. Merbouche[1], D. Gouéré[1], I. Boventer[1], R. Lebrun[1], P. Bortolotti[1], V. Cros[1] and A. Anane[1] *1. Unité Mixte de Physique CNRS-Thales, Palaiseau, France*

The investigation of Spin waves (SW) and their quanta, magnons, in thin magnetic films, has emerged as an attractive field of research due to their very short wavelength reaching down to nanometers at GHz frequencies. SWs also have a rich dispersion relation, that depends on their propagation direction with respect to a magnetic field. Hence, SW -based devices are promising candidates for microwave information processing, and eventually for overcoming the limitations encountered with CMOS devices[1]. Yet, a key challenge is to achieve long propagation distances of the spin waves[2]. Recent studies using spin-orbit torques[3] where a Platinum stripe placed on top of a 20 nm thick YIG waveguide (Pt/YIG) showed that SOT could generate a full compensation of the damping, leading to auto-oscillations of the magnetization above a critical injected current density. When excited with a microwave field, spin waves propagation length was increased by a factor of 10 in the bilayer. However, amplification of propagating spin-waves was not observed yet, due to the onset of nonlinear dissipative processes above the critical current. Recently, interests turned towards materials having perpendicular magnetic anisotropy in which one can also achieve a full damping compensation along with SW emission. Here, we propose a new pathway towards SOT-based SW amplification. Using micromagnetic simulations (Mumax3), we demonstrate that pulsed SOT does induce a lossless SWs propagation when the pulse duration is shorter than 200 ns. Remarkably, amplification is achieved when injecting currents exceeding the auto-oscillation threshold (Fig.1). A key condition is however to minimize non-linear coupling. In our case, we achieved this condition in a 20 nm thick Bi-YIG film structure with a vanishing effective magnetization *i.e.* the out-of-plane magnetic anisotropy compensates the demagnetization field[4].

[1] A. V. Chumak, V. I. Vasyuchka, A. A. Serga, and B. Hillebrands, "Magnon spintronics," *Nat. Phys.*, vol. 11, no. 6, pp. 453–461, Jun. 2015 [2] B. Heinz *et al.*, "Long-range spin-wave propagation in transversely magnetized nano-scaled conduits," *Appl. Phys. Lett.*, vol. 118, no. 13, p. 132406, Mar. 2021 [3] M. Evelt *et al.*, "High-efficiency control of spin-wave propagation in ultra-thin yttrium iron garnet by the spin-orbit torque," *Appl. Phys. Lett.*, vol. 108, no. 17, p. 172406, Apr. 2016 [4] L. M. Evelt *et al.*, "Emission of Coherent Propagating Magnons by Insulator-Based Spin-Orbit-Torque Oscillators," *Phys. Rev. Appl.*, vol. 10, no. 4, p. 041002, Oct. 2018

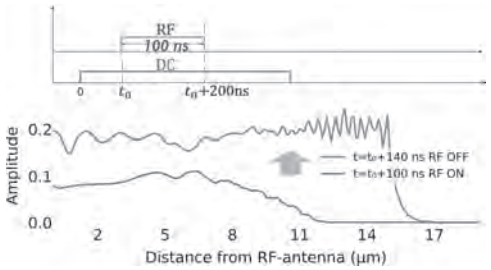

Fig.1: Spin Waves Amplitude evolution in the simulated waveguide when injecting a DC higher than the auto-oscillation threshold. The blue curve is a snapshot at 100 ns after turning on the RF pulse which is turned off after this instant. The red curve is 40 ns later from the blue and shows a clear amplification of the SW's amplitude.

HOL-10. Inner dynamics in ferrimagnetic system across its compensation points. *E. Haltz*[1,2], J. Sampaio[1], S. Krishnia[1], L. Berges[1], A. Mougin[1] and A. Thiaville[1] *1. Solid States Physics Laboratory, Orsay, France; 2. Physics, University of Leeds, Leeds, United Kingdom*

Dynamics in antiferromagnets and ferrimagnets can reach the interesting sub-THz to THz range due to the strong coupling between magnetic sublattices[1]. Unlike antiferromagnets, ferrimagnets have sublattices of different elements, whose balance can be tuned with temperature. In particular, at two distinct temperatures called the magnetic and the angular compensations (TMC and TAC), either the magnetization or the angular moments of the sublattices cancel out[2]. Even if this property makes ferrimagnets ideal to explore the fast AF-like dynamics, the understanding of their inner dynamics requires more study[3]. We have measured the thermal spinwave modes of a GdFeCo thin film, a ferrimagnetic alloy, by Brillouin Light Scattering (BLS)[4], across its magnetic and angular momentum compensation and for various values of applied field. We found that the ferrimagnet presents two spinwave modes for a given wave vector (shown Fig.1), with a complex variation with temperature (shown Fig.2) and field, which arises from its

double-lattice nature. We also observed that the frequencies of these SW modes cross at a characteristic temperature (Tx) which changes with the applied magnetic field. Applying an analytical model with only few parameters, we reproduce with a very good quantitative agreement the SW spectra and their evolution with temperature (shown Fig.2) and field, which validates the underlying energy and dynamical models of the ferrimagnet. We propose that this analysis of extensive spinwave spectra at different conditions provides a powerful characterization of multi-sublattices systems and a test of ferrimagnet energy and dynamics models.

1. Baltz *et al.,* Rev.Mod.Phy. 90 (2018) 2. Hansen *et al.*, JAP 66 (1989) 3. Kim *et al.,* Nat. Mat.19 (2020) 4. Krishnia *et al.,* arXiv:2007.07569 (2020)

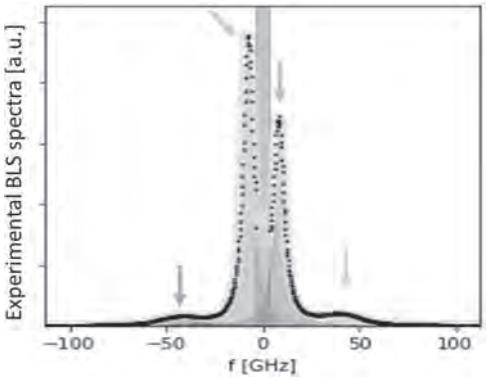

Fig.1 BLS spectra that show the SW modes in GdFeCo close to TAC. The Black points are the experimental BLS spectra. Each filled curve shows the contribution of individual modes and the yellow curve shows the sum of these contributions in the BLS spectrum.

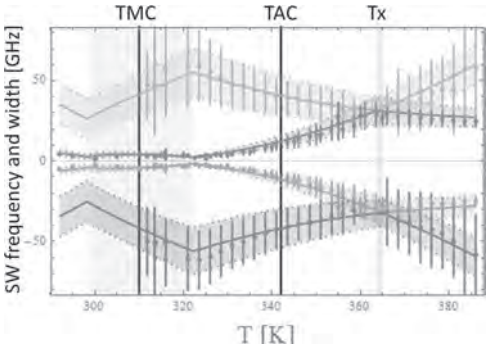

Fig.2 Evolution of the SW modes frequency and width across TMC, TAC and Tx. Points and vertical lines show the measured frequency and width of the modes. The solid lines and the envelopes show the resonance frequency and the width of each modes calculated with our model.

HOL-11. The thermodynamic properties of exchange stiffness.

S. Stansill[1,2] and J. Barker[1,2] *1. University of Leeds, Leeds, United Kingdom; 2. Bragg Centre for Materials Research, Leeds, United Kingdom*

The effective temperature dependence of micromagnetic parameters such as anisotropy (K), exchange stiffness (A) and the Dzyaloshinskii–Moriya interaction (DMI) are usually written as a power law of the magnetisation. For anisotropy this is well founded, based on Callen-Callen theory[1]. For exchange stiffness and DMI the power laws are based on the assumption that they behave the same as anisotropy and from classical numerical models. Recently there has been a lot of interest in the temperature dependence of these properties because their value affects spin textures like skyrmions. Inferring the DMI from experimental measurements often requires first deducing the exchange stiffness by fitting Bloch's law to measurements of magnetisation at finite temperature. The problem is that Bloch's law contains the zero temperature value of exchange stiffness, but is used to fit a finite temperature range over which the value of the exchange stiffness should change significantly. Another issue is that Bloch's law is derived using quantum mechanics with magnons which obey Bose statistics – numerical models typically use classical statistics for the thermal occupation of spin waves. Classical models cannot reproduce Bloch's $T^{3/2}$ law for ferromagnets or the T^2 dependence of sublattice magnetisation in antiferromagnets[2]. So, the classical thermodynamics of exchange is also a poor approximation for real materials in which the quantum distributions of magnons plays a large role. Here we discuss a quantum implementation of atomistic spin dynamics[2], compare with classical results and present the temperature scaling of the micromagnetic exchange stiffness for both ferromagnets and antiferromagnets calculated from magnon spectra. We show antiferromagnets have similar scaling behaviour to ferromagnets and that the results using quantum statistics doesn't follow a power law. Figure 1 presents the thermal behaviour of the exchange stiffness as a function of reduced sublattice magnetisation of the prototypical antiferromagnet NiO used in antiferromagnetic spintronics[3]. At low temperature (high magnetisation) the exchange stiffness is almost temperature independent when using quantum statistics in stark contrast to a power law.

[1] H. Callen and E. Callen, J. Phys. Chem. Solids, 27, 1271 (1966) [2] J. Barker and G. Bauer, Phys. Rev. B, 100, 140401 (2019) [3] V. Baltz, Rev. Mod. Phys., 90, 015005 (2018)

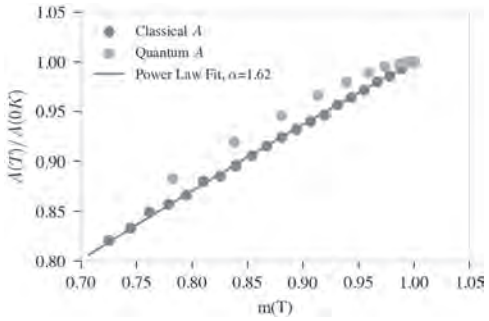

Fig. 1

HOL-12. An Effective Hamiltonian Model for Combined Magnon-Phonon Excitations in Ferrimagnets of the Mn_2RuGa Family.

J. O'Brien[1], M.T. Stamenova[1] and *P.S. Stamenov*[1] *1. School of Physics and CRANN, Trinity College Dublin, Dublin, Ireland*

In the last decade, the low-moment, highly spin-polarized ferrimagnets of the Mn_2RuGa (MRG) family have been investigated as of their potential for application in high-frequency resonance devices [1] relying on either MTJs and CPP transport [2] or Hall bar type structures [3], utilizing STT and/or SOT. Very recently, ultra-fast switching of the magnetisation in a single pulse, all-optical toggle scheme has been shown [4]. The deeper understanding, control and optimisation of any of these approaches, require that an effective model is built, which is computationally much cheaper than, but can be calibrated based on DFT. Here we build such an effective model, starting from a description of generalized Heisenberg Hamiltonian, on the perfectly ordered structure, with two dissimilar magnetic sub-lattices, within the approximation of frozen magnons and phonons. The interactions that are taken into account are the following: isotropic exchange on both sublattices and mutual; two-fold and four-fold anisotropy, with orientation which is different for the different local-symmetry sites; Zeeman coupling to the external field; elastic coupling coefficients for both the magnetic and non-magnetic sites; distance dependencies for the exchange beyond first nearest neighbours and RKKY-type coupling. The main features of the structure and the resulting phonon, magnon and combined excitations are shown on the corresponding panels of Fig. 1. Interestingly, the system exhibits double crossing of the in and out-of-phase magnon branches (for finite k-vectors), potentially allowing for the fast relaxation of the optically

excited magnons and softening of the phonon branches at high momenta. The distance dependent exchange allows for the combined elastic-magnetic excitation of the system and the potential exploitation of phonon-driven ultra-fast magnetisation control schemes.

[1] R. E. Troncoso, K. Rode, P. Stamenov, J. M. D. Coey and Arne Brataas, Phys. Rev. B, 99, 054433 (2019) [2] A. Titova, C. Fowley, E. Clifford, et. al., Sci. Reports, 9, 4020 (2019) [3] N. Thiyagarajah, Y.-C. Lau, D. Betto, et al., Appl. Phys. Lett., 106, 12402 (2015) [4] C. Banerjee, N. Teichert, K. E. Siewierska, et al., Nature Comm. 11 (1), 1-6 (2020)

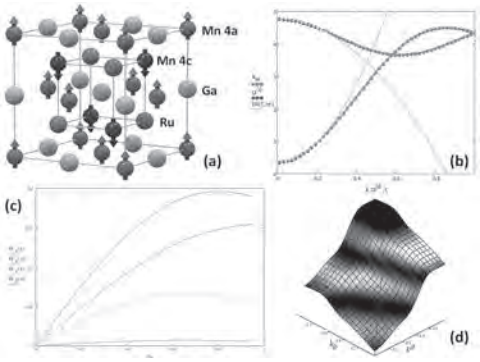

(a) The structure of MRG, with the different magnetic and non-magnetic sites marked. (b) The in-phase (acoustic) and out-of-phase (optical) branches of the primary magnon dispersions along the >001> axis. (c) The main four acoustic phonon modes within the first Brillouin zone. (d) The energy of the combined frozen magnon and phonon excitation for arbitrary momenta.

HOL-13. Adjusting dipolar interactions to control exceptional points in synthetic antiferromagnets. *T. Jeffrey*[1], W. Zhang[2] and J. Sklenar[1]
1. Physics, Wayne State University, Detroit, MI, United States; 2. Physics, Oakland University, Rochester, MI, United States

Synthetic antiferromagnets (S-AFMs) have recently been shown to be ideal systems to search for Exceptional Points (EPs) [1]. In a S-AFM, EPs are the point at which the optical and acoustic magnons coalesce and are indistinguishable from one another. EPs can be reached by varying parameters, such as the exchange coupling between magnetic layers. Once an EP is reached, only a single magnon branch exists in the magnon energy spectrum, and this makes EPs an attractive prospect for controlling magnons in magnetic microstructures. Recently, we have computationally calculated and visualized EPs in S-AFMs using micromagnetic simulations [2]. We determined that dipolar interactions play a pivotal role in determining if and where EPs occur in the parameter space used to describe the S-AFM. Our results are both qualitatively and quantitatively different compared to macrospin models [3], where dipolar interactions are not considered. We are now investigating how the macrospin limit can be recovered in micromagnetic simulations if spacer layers are built into the simulation, or if the shape of the micromagnetic object is changed. By recovering the macrospin limit within micromagnetic simulations, we will demonstrate new geometric parameters that can be used to control EPs and the magnon energy spectrum within S-AFMs. Work at Oakland University was supported by U.S. National Science Foundation under Award No. ECCS-1941426.

[1] H. Liu et al. Science Advances 5, eaax9144 (2019). [2] T. Jeffrey, W. Zhang, and J. Sklenar. App. Phys. Lett. 118, 202401 (2021). [3] J. Lee, T. Kottos, and B. Shapiro. Phys. Rev. B 91, 094416 (2015).

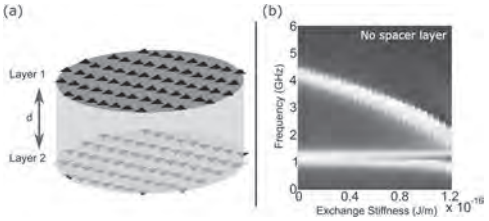

FIG. 1. (a) Illustration of two micromagnetic layers in antiferromagnetic alignment. A nonmagnetic spacer layer is represented by the grey section. (b) Magnon spectra shown when simulating the antiferromagnetic state with ferromagnetic interlayer exchange stiffness. No clear presence of an EP exists in the antiferromagnetic state before it becomes unstable due to the FM exchange stiffness.

Session HOM
MICROMAGNETIC AND HYSTERESIS MODELING

Yasushi Kanai, Chair
Niigata Institute of Technology, Kashiwazaki, Japan

CONTRIBUTED PAPERS

HOM-01. Multi-scale simulations of skyrmion annihilation in disk geometries. *T.B. Winkler*[1], K. Litzius[2], A. De Lucia[1], M. Weißenhofer[3], H. Fangohr[4,5] and M. Kläui[1] *1. Institut für Physik, JGU Mainz, Mainz, Germany; 2. Department of Materials Science and Engineering, MIT, Cambridge, MA, United States; 3. Fachbereich Physik, Universität Konstanz, Konstanz, Germany; 4. Max-Planck Institute for Structure and Dynamics of Matter, Hamburg, Germany; 5. University of Southampton, Southampton, United Kingdom*

Magnetic skyrmions are potential candidates for next-generation data storage and computing devices and therefore of particular interest in the area of nano-magnetism [1-4]. Understanding and controlling skyrmion states is of key importance for future applications. We are investigating the stability of magnetic skyrmions in disk geometries by applying an out-of-plane magnetic field in two ways: on the one hand, the field is aligned against the skyrmion core magnetization direction until the skyrmion annihilates. We call this way of annihilation a *rupture*, since the topological charge has to be ruptured in the center of the disk. Secondly, the field is applied in the skyrmion core magnetization direction, until the skyrmion boundary is pushed out of the sample. The second way of annihilation we are calling the *expulsion* of the skyrmion. We find that the expulsion of the skyrmion needs considerably less energy than the rupture, since the topological charge is eliminated through the boundary and no Bloch point has to be generated to annihilate it [5]. The resulting energy barriers are important technological parameter for skyrmion lifetime calculations [6]. For an infinite sample the rupture field depends on the smallest energy barrier. We find that the expulsion process can be simulated accurately with micromagnetic simulations, while the rupture process needs atomistic resolution. We reduce the computational costs by using a multiscale model [7], that combines a micromagnetic approach for the modeling of the mesoscopic sample, while a Heisenberg model calculation is embedded in the center of the disk, where the rupture takes place.

[1]: D. Pinna, F. A. Araujo, J.-V. Kim, Phys. Rev. Applied, vol. 9, p. 064018, Jun 2018. [2]: J. Zázvorka, F. Jakobs, D. Heinze, Nature nanotechnology, vol. 14, no. 7, pp. 658–661, 2019. [3]: R. Tomasello, E. Martinez, R. Zivieri, Sci. Rep., vol. 4, p. 6784, 2014. [4]: A. Fert, V. Cros, and J. Sampaio, Nat. Nanotechnol., vol. 8, pp. 152–156, 2013. [5]: A. V. Ivanov, D. Dagbartsson, J. Tranchida, Journal of Physics: Condensed Matter, vol. 32, no. 34, p. 345901, 2020. [6]: D. Cortés-Ortuño, W. Wang, M. Beg, Scientific reports, vol. 7, no. 1, pp. 1– 13, 2017. [7]: A. De Lucia, B. Krüger, O. A. Tretiakov, vol. 94, no. 18, p. 184415, 2016

HOM-02. Modelling noncolinear interface coupling in magnetic multilayers. *C. Abert*[1], E. Girt[2] and D. Suess[1] *1. University of Vienna, Vienna, Austria; 2. Simon Fraser University, Burnaby, BC, Canada*

Magnetic multilayer structures are the foundation of numerous magnetic applications including spintronics devices. The coupling of two ferromagnetic layers within such devices is usually achieved by adding a Ru spacer layer, but is restricted to colinear alignment. Recently it has been shown experimentally that adding iron atoms to the ruthenium layer allows for the noncolinear coupling of magnetic layers [1]. Moreover the experiments indicate that both the angle as well as the coupling strength can be precisely controlled by tuning the iron content of the spacer layer. This mechanism opens up a variety of opportunities for the design of novel spintronics devices, e.g. to reduce critical current in STT MRAM devices. While a qualitative understanding of the noncolinear coupling can be gained by the use of a simplified analytical model [2], a micromagnetic or even atomistic treatment of the system offers a detailed and quantitative insight into the coupling mechanism. We present both, a micromagnetic and an atomistic model that resolve the composition of the RuFe spacer layer by considering a random distribution of iron islands in a Ru matrix that mediates antiferromagnetic coupling, see Fig. 1(a). For the micromagnetic model, we perform hysteresis computations and fit the results to a simplified coupling model including a linear and a biquadratic exchange coupling term, see Fig. 2. While the individual islands in the spacer layer introduce a purely colinear coupling of the magnetic layers with different coupling sign, the micromagnetic simulations reveal that configurations of arbitrary angles can be stable due to slight imhomogeneities in the ferromagnetic layers, see Fig. 1(b). While the micromagnetic model already achieves an excellent quantitative agreement of the experimentally determined coupling constants for thin spacer layers, it fails in the detailed description of the inner couplings in the RuFe layer. The atomistic model overcomes this restriction by accounting for (anti-) ferromagnetic couplings of ferromagnetic atoms in all 3 dimensions.

[1] Nunn, Z. R., Abert, C., Suess, D., & Girt, E. Science advances 6(48) eabd8861 (2020) [2] Slonczewski, J. C., Physical review letters, Vol. 67, no. 22, p. 3172 (1991)

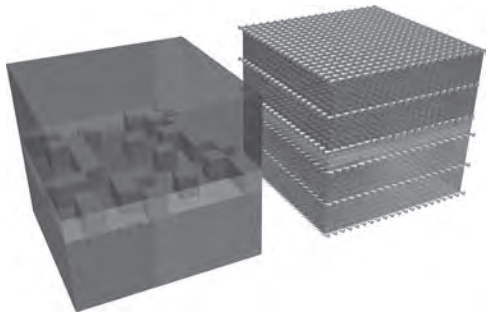

Micromagnetic model of Co/RuFe/Co multiliayer structure with a composite coupling layer.

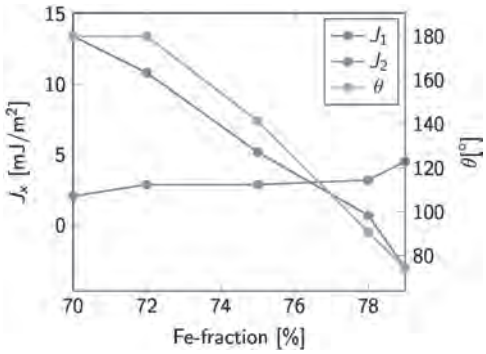

Simulation results for different RuFe-spacer-layer compositions.

HOM-03. Withdrawn

HOM-04. Wave reversal mode: A new magnetization reversal mechanism in magnetic nanotubes. *J. Escrig*[1,2], N. Bajales[3,4], D.M. Arciniegas Jaimes[3], S. Raviolo[3,4] and J.M. Carballo[5] *1. Department of Physics, Universidad de Santiago de Chile, Santiago, Chile; 2. Center for the Development of Nanoscience and Nanotechnology, Santiago, Chile; 3. CONICET, Córdoba, Argentina; 4. Universidad Nacional de Córdoba, Córdoba, Argentina; 5. Universidad Nacional de Río Cuarto, Río Cuarto, Argentina*

The wave reversal mode is a magnetization reversal mechanism that appears in ferromagnetic nanotubes of certain geometric parameters when an external magnetic field is applied perpendicular to their axes. The distinctive feature of this mode is that leads to well-defined S-shaped hysteresis curves [1]. In order to gain insight into the stability of this latter effect, we have performed micromagnetic simulations for permalloy and nickel nanotubes obtaining a non-monotonic behavior for coercivity as well as for remanence as a function of nanotube diameter for both materials. Motivated on these latter intriguing results, we found that measuring the area that encloses the hysteresis curve is a novel and simple strategy to identify the appearance of the wave reversal mode [2]. An additional contribution of this work is the proposal of a new magnetic phase diagram that allows determining the stability of this reversal mechanism as a function of the geometric and magnetic parameters of the tubes [2]. The authors acknowledge the access to Mendieta cluster (CCAD-UNC) and financial support from SECYT-UNC, MINCyT 2019, Fondecyt 1200302, Basal Project AFB180001 and Programa Escala Docente AUGM.

[1] S. Raviolo, D. M. Arciniegas Jaimes, N. Bajales, J. Escrig, J. Magn. Magn. Mater. 497, 165944 (2020). [2] D. M. Arciniegas Jaimes, S. Raviolo, J. M. Carballo, N. Bajales, J. Escrig, J. Magn. Magn. Mater. 523, 167578 (2021).

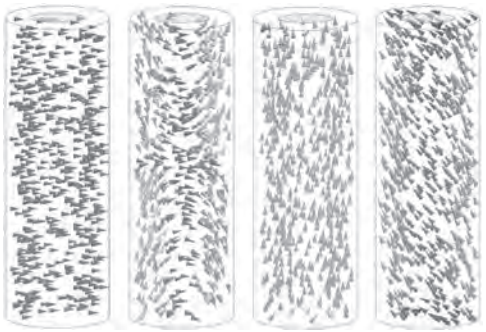

HOM-05. Micromagnetic simulations with realistically-generated sintered microstructures. *A.R. Insinga*[1], E.B. Poulsen[1] and R. Bjørk[1] *1. Energy Conversion and Storage, Technical University of Denmark, Copenhagen, Denmark*

Micromagnetic simulations are used to predict the behavior of permanent magnet materials and compute magnetic hysteresis loops. Using this approach, we investigate the phenomenon of demagnetization and calculate the coercive force for realistically generated microstructures. Instead of employing the well-established but highly idealized approach based on Voronoi diagrams to generate microstructures [1], we generate polycrystalline microstructures using a kinetic Monte Carlo numerical model that simulates the constrained sintering process by including the effect of local stresses arising during the sintering [2]. An example of a microstructure with different colored grains generated using this approach is shown in Fig. 1(a). The micromagnetic simulation is then performed using the micromagnetism and magnetostatic framework MagTense [3, 4]. This framework has the unique capability of handling variable-size meshes by considering the exact analytical expression of the demagnetization field corresponding to the various mesh elements. By taking advantage of this capability, we employ a mesh-refinement procedure [5] that creates meshes that are more refined in the inter-grain soft phase, i.e. where the onset of the demagnetization phenomenon is most likely to occur. An example of variable-size mesh is shown in Fig. 1(b). As shown in the figure, the mesh in this example is composed by blocks of three different sizes. An example of hysteresis loop computed using our approach is shown in Fig. 2. We consider the effect of the statistical misalignment between the easy-axis directions of the different crystal grains. Moreover, we compare out realistic microstructures generation framework with the traditional Voronoi-structures and furthermore investigate the effect of the thickness of the inter-grain region, the effect of inclusions and porosity of the material, and the effect of different grain-size distributions. Our investigation highlights which qualities and features of the microstructure have the most significant impact on the ability of the magnet to resist an opposing field. Therefore, it is an important step towards optimizing the fabrication process and developing new and improved magnetic materials.

[1] J. Fischbacher, A. Kovacs, M. Gusenbauer, H. Oezelt, L. Exl, S. Bance and T. Schrefl, J. Phys. D: Appl. Phys. 51, (19), 193002 1-17, (2018). [2] R. Bjørk, H.L. Frandsen and N. Pryds, Proceedings of the International Conference on SINTERING 2014, (2014). [3] K.K. Nielsen and R. Bjørk, MagTense, https://doi.org/10.11581/DTU:00000071 (2019). [4] R. Bjørk, E.B. Poulsen, K.K. Nielsen and A.R. Insinga, J. Magn. Magn. 535, 168057 1-8, (2021). [5] K.K. Nielsen, C.R.H. Bahl, A. Smith and R. Bjørk, J. Phys. D: Appl. Phys. 50, (41), 414002 1-9, (2017).

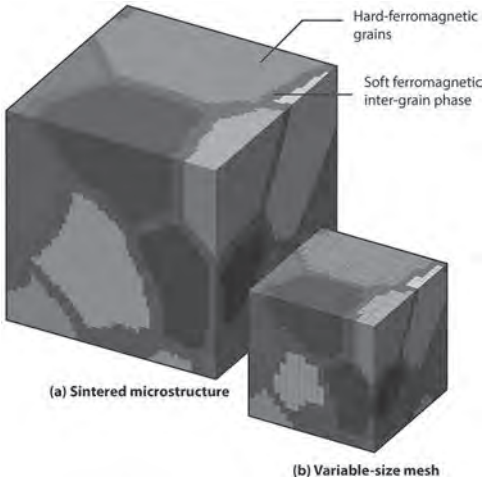

Fig. 1

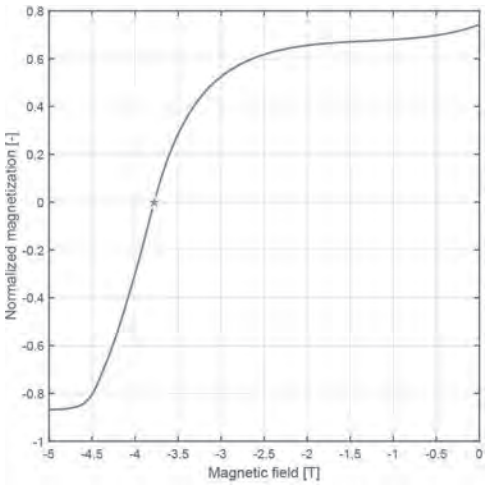

Fig. 2

HOM-06. Normal modes description of nonlinear magnetization dynamics in micromagnetic systems. *S. Perna*[1], F. Bruckner[2], C. Serpico[1], D. Suess[2] and M. d'Aquino[1] *1. DIETI, University of Naples Federico II, Naples, Italy; 2. University of Vienna, Vienna, Austria*

The study of magnetization dynamics is fundamental in the analysis and design of high-speed nanoscale spintronic devices[1]. Recently, ultrafast magnetism also emerged as prolific research field promising magnetic devices working up to the THz range[2,3,4] with low power, scalability and compatibility with CMOS electronics[5]. Magnetization dynamics in such devices is usually studied by solving the Landau-Lifshitz-Gilbert (LLG) equation discretized on a grid of computational cells with edges smaller than the exchange length. This equation is then reduced to a nonlinear many-body evolution problem in which the state variables are magnetization vectors defined on the grid. In this work, a novel approach is adopted where magnetization is expanded in terms of magnetic normal modes which, contrary to classical plane waves, do take into account proper boundary conditions for confined structures[6]. The LLG equation is rewritten as a system of coupled nonlinear ODEs where the unknowns are the amplitudes of the normal modes[7]. Then, nonlinear magnetization dynamics starting from an equilibrium driven by time-varying magnetic fields or spin-torques can be quantitatively described by using a reduced number of normal modes. This is shown to occur in several magnetic systems relevant to applications such as magnetic nanodots and magnonic waveguides. The aforementioned normal modes model (NMM) permits describing spatially-nonuniform and nonlinear magnetization dynamics with a far reduced complexity compared to full micromagnetic simulations. Moreover, for a given magnetic structure, it allows to study far from equilibrium steady-state regimes as function of amplitude, spatial distribution and time-variation of the external excitation without having to repeat full-scale simulations for each set of excitation parameters. As an example, we analyze the ac spin-torque driven nonlinear ferromagnetic resonance (FMR) response of a cylindrical nanodot (50 nm radius, 12 nm thick). The appearance of fold-over effect at frequency 11 GHz higher than that of fundamental mode (3 GHz) is due to the 5th normal mode (see fig. 1).

[1] B. Dieny et al., Opportunities and challenges for spintronics in the microelectronics industry. Nature Electronics 3, 446-459 (2020). [2] Bigot, J.-Y. and Vomir, M. (2013), Ultrafast magnetization dynamics of nanostructures. ANNALEN DER PHYSIK, 525:2-30.https://doi.org/10.1002/andp.2012001992 [3] Zhang, W., Maldonado, P., et al. Ultrafast terahertz magnetometry. NatCommun 11, 4247 (2020). https://doi.org/10.1038/s41467-020-17935-6 [4] Neeraj, K., Awari, N., et al. Inertial spin dynamics in ferromagnets. Nat.Phys. 17, 245–250 (2021). https://doi.org/10.1038/s41567-020-01040-y [5] Makarov, A., Windbacher, T., et al. CMOS-compatible spintronic devices:a review. Semicond. Sci. Technol. 31 113006 (2016). [6] M. d'Aquino, C. Serpico, et al. A novel formulation for the numerical computation of magnetization modes in complex micromagnetic systems, J. Comp.Phys., 228 (2009), 6130-6149. https://doi.org/10.1016/j.jcp.2009.05.026[7] Perna, S., Bruckner, F., et al. Computational Micromagnetics based on Nor-mal Modes: bridging the gap between macrospin and full spatial discretization. arXiv:2105.08829

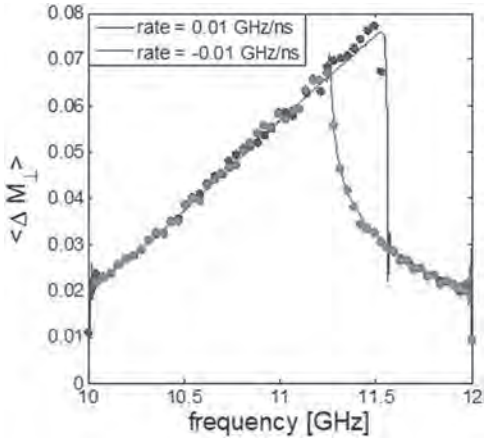

Figure 1: computed FMR response. Solid lines (filled dots) refer to NMM (full micromagnetic simulations).

HOM-07. Physics informed neural networks for computational magnetism. *T. Schrefl*[1,2], A. Kovacs[1,2], J. Fischbacher[1,2], M. Gusenbauer[1,2], M. Hovorka[1,2] and H. Oezelt[2] *1. Christian Doppler Laboratory for Magnet Design through Physics Informed Machine Learning, Wiener Neustadt, Austria; 2. Department for Integrated Sensor Systems, Danube University Krems, Wiener Neustadt, Austria*

With the rise of deep learning, physics informed neural networks [1] became an alternative to finite element simulation in many fields of materials and device design. Physics informed neural networks bring several advantages as compared to traditional numerical methods for solving partial differential equations like finite differences or finite elements: 1. There is no need for mesh generation. 2. Inverse problems may be solved effectively. 3. A whole family of problems may be solved with a single neural network. We demonstrate how physics informed neural networks can be applied in magnetostatics and micromagnetics. The approach is like the Ritz method for computing the magnetic field or the magnetization. However, instead of finite element basis functions [2], we use dense neural networks to approximate the unknowns. The underlying physics is incorporated through the loss function which is minimized during training of the neural network. We first applied physics informed neural network to solve a classical inverse problem in magnetism. We searched for the magnetization in a hollow cylinder that produces a uniform field in the hole and has zero field outside. The mean relative error between the neural network estimate and the analytic solution for the magnetization was 0.27 percent. We computed the demagnetization curve of a $Nd_2Fe_{14}B$ particle. The difference between the finite element solution and the neural network estimate was 0.9 percent. We computed the lowest eigenvalue of Brown's linearized micromagnetic euqation to get the nucleation field for a soft magnetic defect in a hard magnetic matrix. The mean realtive error for the nucleation field of an Fe inclusion in $Sm_2Fe_{17}N_3$ as function of defect size was 0.4 percent as compared to the analytic solution [3]. Because of the ability to solve multiple problems simulateneously, physics informed neural networks have a great potential for optimization and tailoring the magnet's internal structure to achieve a specific demagnetiation curve. The financial support by the Austrian Federal Ministry for Digital and Economic Affairs, the National Foundation for Research, Technology and Development and the Christian Doppler Research Association is gratefully acknowledged.

[1] Karniadakis, G. E., Kevrekidis, I. G., Lu, L., Perdikaris, P., Wang, S., & Yang, L. (2021). Physics-informed machine learning. *Nature Reviews Physics*, *3*(6), 422-440. [2] Fredkin, D., & Koehler, T. (1987). Numerical micromagnetics by the finite element method. *IEEE Transactions on Magnetics*, *23*(5), 3385-3387. [3] Skomski, R., & Coey, J. M. D. (1993). Giant energy product in nanostructured two-phase magnets. *Physical Review B*, *48*(21), 15812.

HOM-08. Berry-Phase Interpretation of Thin-Film Micromagnetism.
R. Skomski[1], B. Balasubramanian[1], *A. Ullah*[1], C. Binek[1] and D. Sellmyer[1]
1. Physics and Astronomy & NCMN, University of Nebraska, Lincoln, NE, United States

The motion of electrons and therefore the topological Hall effect (THE) are governed by the flux density (*B*-field), as contrasted to the applied magnetic field (*H*-field). Maxwell's equations predict that the relevant perpendicular flux density (*B*-field) in laterally homogeneous thin films is $\mu_o H$, independent of the magnetization *M*. However, transport measurements and nonvanishing THEs at $H = 0$ indicate that the motion of the electrons depends on *M*. This paradox is solved by noting that electrons are point-like objects moving in exchange-and-correlation holes. Their magnetostatic interaction with the crystalline environment is realized through Lorentz cavities [1, 2] where $B = \mu_o(H + D_L M)$ with $D_L \sim 1/3$, intermediate between $B = \mu_o H$ and $B = \mu_o(H + M)$. This approximation includes inhomogeneities, because the local magnetization vector $M(r)$ is not necessarily parallel to the volume-averaged magnetization $\langle M \rangle$. The separation of the THE from the magnetization contribution to the anomalous Hall-effect is therefore not straightforward and the use of $\langle M \rangle$ can lead to systematic errors [3-5]. For example, in nanogranular structures (Fig. 1), changes in $\langle M \rangle$ may be dominated by loosely coupled regions (inside the dashed circles) where conductivity, current density $\langle j \rangle$, and Hall-effect contribution are disproportionally small. Another field consideration is that the THE reflects electrons adiabatically exchange-interacting with atomic magnetic moments. The corresponding Berry phase changes the motion of the electrons. The change is formally equivalent to the effect of a fictitious magnetic field, but this field does not obey Maxwell's equations in a micromagnetic sense. This work is supported by NSF-EQUATE (OIA-2044049), NSF-DMREF (No. 1729288), the NU Collaborative Initiative, and NCMN.

[1] S. Chikazumi, *Physics of Magnetism*, Wiley, New York 1964. [2] R. Skomski and J. M. D. Coey, *Permanent Magnetism, Institute of Physics*, Bristol 1999. [3] A. Gerber, Phys. Rev. B 98, 214440-1-4 (2018), [4] L. Wu, F. Wen, Y. Fu, J. H. Wilson, X. Liu, Y. Zh., D. M. Vasiukov, M. S. Kareev, J. H. Pixley, and J. Chakhalian, Phys. Rev. B 102, R220406-1-6 (2020). [5] R. Skomski, A. Ullah, R. Pahari, B. Balasubramanian, and D. J. Sellmyer, APS March Meeting 2021, B40.11.

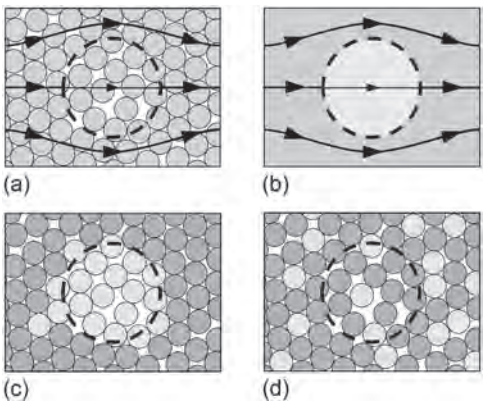

Fig. 1. Effect of structural inhomogeneities on the THE: (a) current density in a nanoparticulate thin film, (b) Bruggeman description of the current, (c) spin-structure in the interaction-domain limit, and (d) spin structure in the non-cooperative limit. The yellow region in (c) fully contributes to the magnetization but only partially to the Hall effect.

HOM-09. Parallel Micromagnetic Monte Carlo Method for Computation of Thermodynamic Equilibrium States in One and Two-Sublattice Systems.
S. Lepadatu[1], G. Mckenzie[1], T. Mercer[1], C.R. MacKinnon[1] and P. Bissell[1] *1. University of Central Lancashire, Preston, United Kingdom*

An efficient method for computing thermodynamic equilibrium states at the micromagnetic length scale is introduced [1], based on the Markov chain Monte Carlo method. Trial moves include not only rotations of spins, but also a change in their magnetization length. The method is parameterized using the longitudinal susceptibility, reproduces the same Maxwell-Boltzmann distribution as the stochastic Landau-Lifshitz-Bloch equation, and is applicable both below and above the Curie temperature. The algorithm has been implemented in Boris [2], is fully parallel [3], can be executed on graphical processing units, and efficiently includes the long range dipolar interaction. Applications to finite-temperature hysteresis loop modelling, chiral magnetic thin films, granular magnetic media, and artificial spin ices are discussed. A typical application is exemplified in relation to Figure 1, where finite-temperature hysteresis loops in a 2 nm thin Co film with interfacial Dzyaloshinsky-Moriya interaction are computed. Simulation of such hysteresis loops in chiral films is problematic with quasi-zero temperature methods such as steepest descent energy minimizer, since the nucleation and annihilation of skyrmions and labyrinth domain structure is principally a thermally activated process. Furthermore, the method is also extended to two-sublattice systems, allowing modelling of ferrimagnetic and antiferromagnetic materials at the micromagnetic length scale. Using a multi-layered computation, which includes both ferromagnetic and antiferromagnetic layers, exchange bias may be simulated in bilayers, as well as more complex multi-layered structures including synthetic antiferromagnetic stacks. Moreover we show the method may also be applied to study of thermal and athermal training effects in exchange bias.

[1] S. Lepadatu, "Micromagnetic Monte Carlo method with variable magnetization length for computation of large-scale thermodynamic equilibrium states" *arXiv:2106.05593 (2021).* [2] S. Lepadatu, "Boris computational spintronics - High performance multi-mesh magnetic and spin transport modeling software" *J. Appl. Phys.* 128, 243902 (2020). [3] S. Lepadatu, G. McKenzie, T. Mercer, C.R. MacKinnon, and P.R. Bissell, "Computation of magnetization, exchange stiffness, anisotropy, and susceptibilities in large-scale systems using GPU-accelerated atomistic parallel Monte Carlo algorithms" arXiv:2103.03517 (2021).

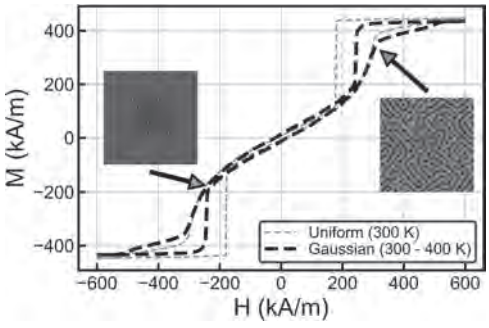

Figure 1 - Hysteresis loops in a 2 nm thin Co film on Pt, using a uniform 300 K temperature (thin dashed line), and a Gaussian temperature profile varying from 300 K at extremities to 400 K at the centre (thick dashed line). The insets show the perpendicular magnetization component on the increasing field sweep, with blue denoting magnetization into the plane, and red out of the plane.

HOM-10. Solving the Standard Micromagnetic Problems using Unstructured Meshes with MagTense. *E.B. Poulsen*[1], A.R. Insinga[1] and R. Bjørk[1] *1. Technological University of Denmark, Copenhagen, Denmark*

Micromagnetics requires calculation of the demagnetization field, anisotropy field, applied field and exchange field. With the MagTense framework, demagnetization is calculated analytically [1] and both anisotropy and applied field are local, leaving only the exchange field in the form of a second order partial derivative. Standard micromagnetics are limited to finite element methods with large, extraneous simulation volumes or finite difference methods with homogeneous simulation grids, as the demagnetization is calculated using a fast Fourier transform [2], but with MagTense, no such limitation exists. However, here an optimal method of calculating second order partial derivatives on arbitrary meshes in micromagnetics must be determined, continuing previous research [3]. We present solutions to the mumag standard micromagnetic problems (mumag) 3[4] and 4[5] using a direct second order partial derivate technique on four different meshes: Prismal, tetrahedral, grained prismal and grained tetrahedral. The grained meshes consist of voronoi generated and Lloyd iterated grain regions with lower resolution towards the center and higher towards the edges, along with high resolution intergrain regions. In fig. 1a) is shown an example of a grained prismal mesh with 9 grains and an intergrain region in gray. Of course, in the mumag standard problems considered, all regions have the same material properties, but it is easy to envision scenarios where they do not. In fig. 1b) is shown the exchange crossover length of mumag 3 as a function of resolution for three different meshes compared to published solutions. All mesh types converge to the correct value, with the tetrahedral meshes converging faster. In fig. 2 is shown the error compared to published solutions of mumag 4 as a function of resolution using regular-, 4 grained- and 9 grained prismal meshes. The unstructured meshes converge to the correct result in a way similar to a regular grid. In both cases it is apparent that while for these problems grained meshes offer few advantages, they are nonetheless correctly implemented and open up a slew of possibilities for accurately simulating complex geometries with far fewer elements in irregular meshes.

[1] R. Bjørk and K. K. Nielsen. Magtense - a micromagnetism and magnetostatic framework,doi.org/10.11581/DTU:00000071, https://www.magtense.org, 2019 [2] A. Vansteenkiste, Ben Van de Wiele, Journal of Magnetism and Magnetic Materials, 323(21):2585–2591, 2011 [3] Emil Poulsen (Nov 03 2020). P3-03 Micromagnetic Exchange Field Calculations for Unstructured Meshes, The 65th Annual Conference on Magnetism and Magnetic Materials, Underline Science Inc. Accessed July 1st, 2021. https://underline.io/3924-p3-03---micromagnetic-exchange-field-calculations-for-unstructured-meshes [4] μMAG Standard Problem 3 Solutions, Accessed on July 1st, 2021. https://www.ctcms.nist.gov/~rdm/results3.html3 [5] μMAG Standard Problem 4 Solutions, Accessed on July 1st, 2021. https://www.ctcms.nist.gov/~rdm/std4/results.html

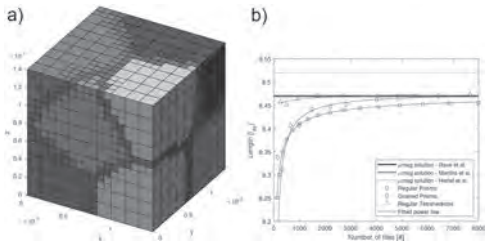

Fig. 1

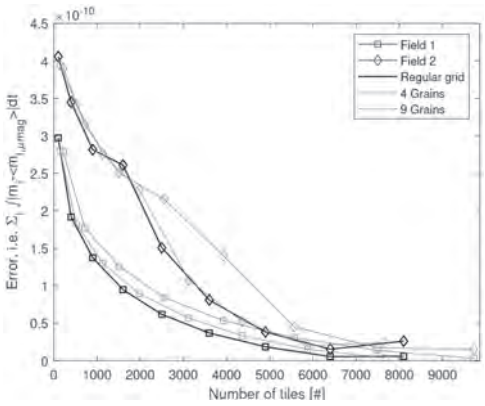

Fig. 2

HOM-11. Effects of α_1-phase Branch Shapes on Coercivity of Rare-earth Free Alnico Permanent Magnet. *H. Won*[1], Y. Hong[1], M. Choi[1], G. Mankey[2], J. Lee[3], T. Lee[3] and T. Lim[3] *1. Department of Electrical and Computer Engineering, The University of Alabama, Tuscaloosa, AL, United States; 2. Department of Physics and Astronomy, The University of Alabama, Tuscaloosa, AL, United States; 3. Institute of Fundamental and Advanced Technology (IFAT), Hyundai Motor Company, Uiwang, The Republic of Korea*

Recently, Ke proposed alnico permanent magnet (PM) model and simulated it using micromagnetic simulation (MS) for magnetic properties [1]. The model is based on the branch (B) on the bottom (U-shaped), the top and bottom (O-shaped), and the middle (H-shaped) on Z-axis. The U-shaped and O-shaped alnico structures showed low coercivity (H_{ci}). However, there is still a lack of comprehensive studies on B dimensions such as B thickness (T_B), width (W_B), and length (L_B) when α_1-phase rods experience coherent rotation and curling [2-4]. Further, the B can be formed as a Y-shaped structure during the thermal magnetic process [3,4]. We have simulated the effects of T_B, W_B, and L_B on H_{ci} for five structures, including H-, U-, O-, YU-, and YH-structures, using LLG micromagnetic simulator v2.63b [5]. Fig. 1 shows the alnico structures used in the simulation. For all structures, α_1-phase rod having a diameter ($D_{\alpha 1}$) of 10 nm was used, representing coherent rotation. The simulation setup used in [1] is adopted. Fig. 2 shows the H_{ci} as a function of T_B, L_B, and W_B for $D_{\alpha 1}$ of 10 nm. As the T_B increases, the H_{ci} first decreases and then remains constant for all the structures. For L_B, a positive linear trend of H_{ci} is found for H- and Y-shaped structures, while there is a negative linear trend for the other two structures. As the W_B increases, nearly constant H_{ci} appears for the H- and Y-shaped structures, but for the U- and O-shaped structures, the H_{ci} shows a positive quadratic trend. As a simulation result, the following dimensions are suggested to realize a high H_{ci} of Alnico PM: thin T_B, long L_B, and W_B with 40 % of $D_{\alpha 1}$ for the H- and Y-shaped structures and thin T_B, short L_B, and W_B with 40-60 % of $D_{\alpha 1}$ for the U- and O-shaped structures. Furthermore, among the five studied structures, the B on the middle location of either H- or YH-shaped is desired to realize a high H_{ci}. We will further discuss the alnico PM rod experiencing curling. This work was supported in part by NSF-I/UCRC for EV-STS under Grant No. 1650564.

[1] L. Ke, R. Skomsi, T. Hoffmann, *Applied Physics Letter*, 111, 022403 (2017). [2] H. Won, Y. K. Hong, M. Choi, *IEEE Magnetic Letters*, 12, 7501505 (2021). [3] S. Zhu, J. Zhao, W. Xia, *Journal of Alloys and Compounds*, 720, 401 (2017). [4] C. Zhang, Y. Li, X. Han, *Journal of Magnetism and Magnetic Materials*, 451, 200 (2018). [5] M. R. Scheinfein, LLG Micromagnetic Simulator™ [Online]. Available: http://llgmicro.home.mindspring.com

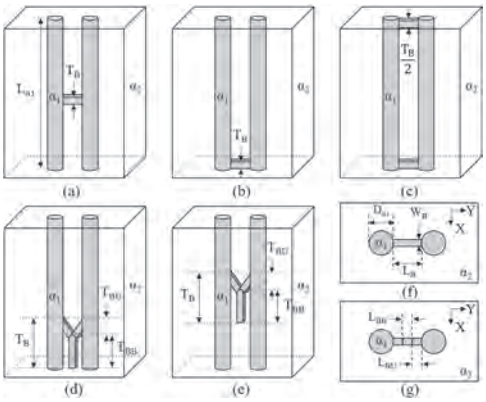

Fig. 1. Alnico structure: Overall view of (a) H-, (b) U-, (c) O-, (d) YU-, and (e) YH-; top view of (f) H-, U-, or O- and (g) YU- or YH-.

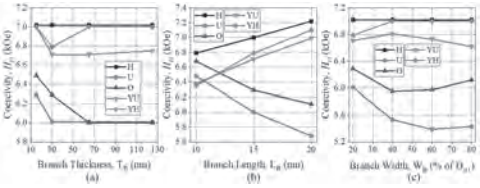

Fig. 2. H_{ci} as a function of (a) T_B, (b) L_B, (c) W_B for $D_{\alpha 1}$ of 10 nm.

HOM-12. A simple scheme for the inversion of a Preisach like hysteresis operator in advanced saturation conditions. *S. Perna*[1], M. Balato[1], C. Petrarca[1] and C. Visone[1] *1. DIETI, University of Naples Federico II, Naples, Italy*

The modeling of rate-independent hysteresis is crucial in the description of many physical phenomena, e.g. nonlinear elasticity in solids, magnetic characterization of ferromagnets, and, more recently, coupled phenomena in smart materials for energy harvesting, sensing actuation purposes, [1]-[3]. The paradigm of hysteresis modeling is represented by the Preisach model, i.e. a weighted sum of ideal relays, able to describe rate-independent phenomena in any system fulfilling wiping out and congruency properties, [4]. Such operator evolved and in many cases assumed the role of a functional unit able to define more complex hysteresis operators, [5], [6]. Despite its complex structure, the Preisach model has been shown to be invertible and under simplified assumptions, the expression of the inverse operator can be expressed in a closed form, [7]. This simplified, invertible formulation of the operator has been extensively deployed in soft ferromagnets for the description of eddy current losses driven by time-varying low magnetic fields, [8]. A similar approach for Villari-induced eddy currents in magnetoelastic alloys has been adopted, [9]. Nevertheless, in conditions with large magnetic fields and strong saturation phenomena, as e.g. in inrush currents, flux density and magnetization differ by the term $\mu_0 H$, which cannot be neglected. The addition of this latter contribution makes the B(H) operator no longer characterized by inverse in closed form, with a consequent increase of the computational cost. This aspect has not been satisfactorily addressed and the aim of this work is to investigate this aspect, namely the inversion of the relationship between flux and current for a nonlinear inductor when hysteresis effects and magnetic saturation cannot be neglected. We show, that it is possible to define an approximate but accurate hysteresis operator, equipped by an inverse in a closed form which can be implemented in a circuit model by a simple numerical scheme. In particular, the exact and approximate models are compared, in terms of computational effort and accuracy through the deployment of suitable experimental data.

[1] P. Krejci, J. Sprekels, Clamped elastic-ideally plastic beams and Prandtl-Ishlinskii hysteresis operators, Discrete & Continuous Dynamical Systems S,1,2, 283-292, (2008). [2] V. Basso, G. Bertotti, Hysteresis in soft magnetic materials, Journal of Magnetism and Magnetic Materials, Volumes 215–216, 2000. [3] A. A. Adly and S. K. Abd-El-Hafiz, An Efficient Vector Hysteresis Model for Unidirectional Magneto-Elastic Interactions, in IEEE Transactions on magnetics, vol. 57, no. 2, pp. 1-5, Feb. 2021, Art no. 7300205, doi:10.1109/TMAG.2020.3024034. [4] I. D. Mayergoyz, Mathematical models of Hysteresis, Springer (1991). [5] C. Serpico and C. Visone, Magnetic hysteresis modeling via feed-forward neural networks, in IEEE Transactions on Magnetics, vol. 34, no. 3, pp.623-628, May 1998, 10.1109/20.668055. [6] D. Davino, P. Krejci, C. Visone, Fully coupled modeling of magneto-mechanical hysteresis through 'thermodynamic' compatibility, Smart Materials and Structures, 22, 9, (2013). [7] C. Visone, M. Sjostrom, Exact invertible hysteresis models based on play operators, Physica B: Condensed Matter, Volume 343, Issues 1–4, 2004. [8] C. Serpico, C. Visone, et. al., Eddy current losses in ferromagnetic laminations, Journal of Applied Physics, 87, 9, (2000). [9] D. Davino, A. Giustiniani, C. Visone and W. Zamboni, Eddy current induced by Villari-effect in magnetostrictive energy harvesting devices, Digests of the2010 14th Biennial IEEE Conference on Electromagnetic Field Computation, 2010, pp. 1-1, doi: 10.1109/CEFC.2010.5481666.

HOM-13. Accurate Small Major Hysteresis Loops Calculation by the Preisach Model With Inverse Switched Hysteresis Operator. L. Chen[1,2], *T. Zhang*[1], T. Ben[1] and P. Wei[1] *1. College of Electrical Engineering and New Energy, China Three Gorges University, Yichang, China; 2. State Key Laboratory of Reliability and Intelligence of Electrical Equipment and the Province-Ministry Joint Key Laboratory of EFEAR, Hebei University of Technology, Tianjin, China*

I Introduction Accurate simulation of hysteresis properties of magnetic materials is of great significance for the optimal design of electromagnetic devices. At the state of the art, the inverse Preisach model are widely used in the FEM procedures as it is easily to implementation [1]. The hysteresis operator of the exist inverse model cannot guarantee the overall positive definiteness of the distribution function on the Preisach plane, which make cause the large errors in calculating the small major hysteresis loop [2]. In this paper, an inverse Preisach model based on inverse switched hysteresis operator is proposed, which only identify the parameters of the limiting hysteresis loop. The limiting hysteresis loop and small major hysteresis loop can be accurately simulated. II Method and Discussion As shown in Fig. 1, an improved inverse Preisach switched hysteresis operator is proposed based on the classical Preisach hysteresis operator. To find the inverse distribution function corresponding to the inverse hysteresis operator, the analytic function is used to approximate the distribution function of the inverse model based on the variation of branches. A hybrid algorithm of velocity control particle swarm optimization and conjugate gradient method (VCPSO-CGM) is used to identify the function's parameters through the data of the limiting hysteresis loop. To achieve efficient numerical calculation, the inverse Preisach plane is discretized into $n \times n$ square grids. The double integral of every unit grid is calculated, and V matrix is formed. To get the output, the F matrix is obtained by accumulating the elements of the V matrix. The input coordinates are obtained by coordinate transformation of the original Preisach plane, and the output can be obtained by interpolating the F matrix. The simulation results are shown in Fig. 2, which are in good agreement with the experimental data. III Conclusion In this paper, an inverse Preisach model based on the inverse switched hysteresis operator is established, which ensures the overall positive definiteness of the distribution function. The results show that the limiting hysteresis loop and small major hysteresis loop can be accurately simulated by inverse Preisach model.

[1] DLALA E, SAITZ J, ARKKIO A. Inverted and forward preisach models for numerical analysis of electromagnetic field problems [J]. IEEE Transactions on Magnetics, 2006, 42(8): 1963-1973. [2] ZIRKA S E, MOROZ Y I, HARRISON R G, et al. Inverse Hysteresis Models for Transient Simulation [J]. IEEE Transactions on Power Delivery, 2014, 29(2): 552-559.

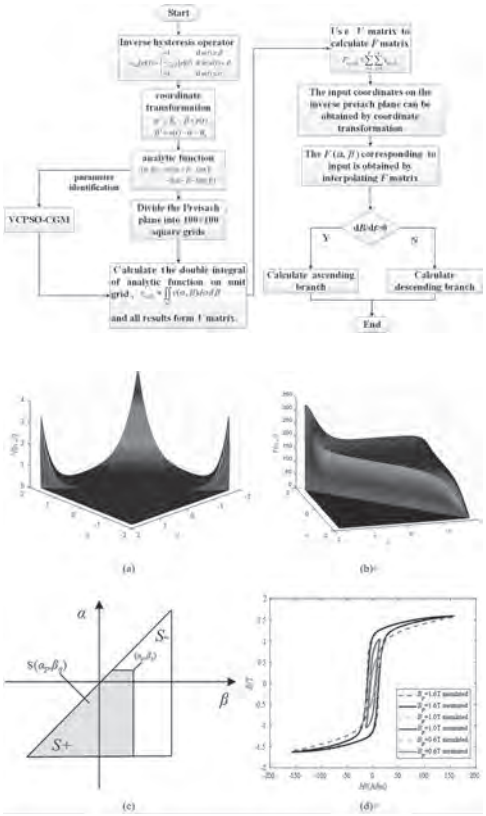
Start
Inverse hysteresis operator
coordinate transformation
analytic function
parameter identification
YCPSO-CGM
Divide the Preisach plane into 100×100 square grids
Calculate the double integral of analytic function on unit grid
and all results form F matrix.
Use F matrix to calculate F matrix
The input coordinates on the inverse preisach plane can be obtained by coordinate transformation
The F (α, β) corresponding to input is obtained by interpolating F matrix
dB/dt>0
Y
N
Calculate ascending branch
Calculate descending branch
End
(a)
(b)
α
β
S+
S-
(c)
(d)

Session HPA
MAGNETIZATION DYNAMICS
(Poster Session)

Liliana D. Buda-Prejbeanu, Co-Chair
SPINtronique et Technologie des Composants, Grenoble, France
Yoshinobu Nakatani, Co-Chair
The University of Electro-Communications, Tokyo, Japan

HPA-01. Domain wall depinning behavior under spin-polarized current in submicron wires with an asymmetric triangle notch. *K. Lai*[1], Z. Gao[1], D. Shiu[1], R. Cao[2] and L. Horng[1] *1. Physics, National Changhua University of Education, Changhua, Taiwan; 2. Electrical Engineering, Feng Chia University, Taichung, Taiwan*

In this study, we investigated domain wall (DW) depinning behavior in 200-nm-wide and 20-nm-thick permalloy wires by mumax[3]. An asymmetric triangle notch was putted at up edge of the wire. Here, we defined the angle from horizontal axis to left side of notch as incoming angle (θ) and the angle from horizontal axis to right side of notch as outgoing angle (Φ). We set θ and depth ratio of notch as 60°and 0.5, respectively. Depth ratio defined notch depth divided by wire width; we changed Φ from 5° to 85°. The head-to-head counterclockwise vortex DW is placed at left side of notch, and then applied 5 *ns*, 20 *ns* and 80 *ns* long spin-polarized current pulse with current density value from 3.0×10^{12} A/m^2 to 7.0×10^{12} A/m^2 to depin the DW. Two DW depinning types have been concluded, one was called bottom nucleation and it's minimum depinning current (J_d) was only dependent on the pinning potential of notch. As $\Phi < 35°$, the pinning potential of left side of notch (E_{left}) > the pinning potential of right side of notch (E_{right}), Φ dominates minimum J_d of bottom nucleation. As $\Phi > 35°$, $E_{left} < E_{right}$, θ dominates. E_{left} is unchanged because of fixed θ, so minimum J_d of bottom nucleation is unchanged. The other was called notch nucleation and its minimum J_d was dependent on the pinning potential of notch and pulse length because of phenomena of nucleation and annihilations under spin-polarized current. The transition point of minimum J_d was between the types of bottom nucleation and notch nucleation. The figure 1 and 2 shows depinning behavior of different pluse length.

A. Vansteenkiste, J. Leliaert, M. Dvornik, M. Helsen, F. Garcia-Sanchez and B. Van Waeyenberge, AIP Advances 4 (10) (2014). J. Leliaert, M. Dvornik, J. Mulkers, J. De Clercq, M. V. Milošević and B. Van Waeyenberge, Journal of Physics D: Applied Physics 51 (12) (2018). S.-H. Huang and C.-H. Lai, Applied Physics Letters 95 (3) (2009). C. Kurniawan, B. Soegijono and D. Djuhana, IOP Conference Series: Materials Science and Engineering 553, 012012 (2019). S. Lepadatu, A. Vanhaverbeke, D. Atkinson, R. Allenspach and C. H. Marrows, Phys Rev Lett 102 (12), 127203 (2009). J. Wang, X. Zhang, X. Lu, J. Zhang, Y. Yan, H. Ling, J. Wu, Y. Zhou and Y. Xu, Applied Physics Letters 111 (7) (2017). G. S. D. Beach, M. Tsoi and J. L. Erskine, Journal of Magnetism and Magnetic Materials 320 (7), 1272-1281 (2008). S. D. Slöetjes, E. Folven and J. K. Grepstad, Physical Review B 101 (1) (2020).

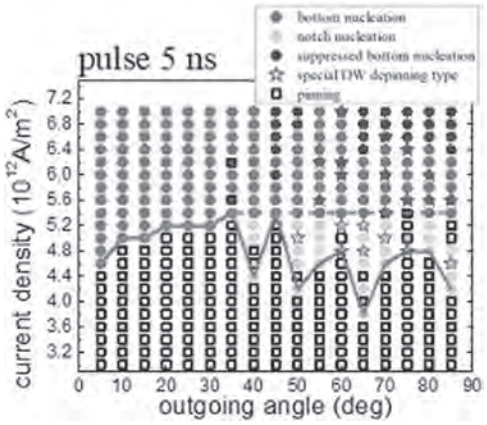

Domain walls depinning phase diagram of pluse = 5 ns

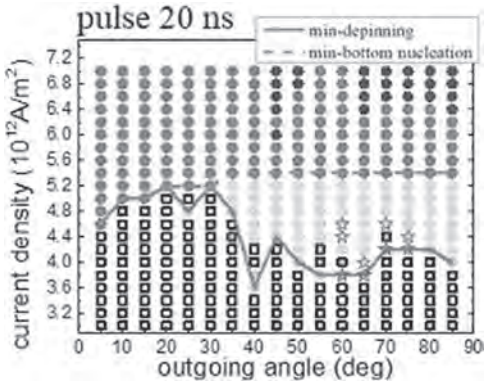

Domain walls depinning phase diagram of pluse = 20 ns

HPA-02. Antiskyrmion excitation modes in antiferromagnetic-exchange coupled disks. *A. Agorou*[1] and T. Trypiniotis[1] *1. Physics, University of Cyprus, Nicosia, Cyprus*

Magnetic antiskyrmions (ASk) are topological magnetic textures that can be stabilized in ultrathin disks by anisotropic Dzyaloshinskii-Moriya interaction (DMI)[1]. In addition to their recent experimental observation[2,3], they have attracted a lot of attention and their dynamic behaviour has been studied in thin nanowires[1] and confined nanodisks[4]. To further our understanding we investigated the resonant modes of magnetic antiskyrmions in antiferromagnetic-exchange coupled thin disks, i.e. in a bilayer SAF, for different microwave excitations. Their response is, as expected, similarly rich to the dynamic behaviour of skyrmions in SAF[5], and the spectra revealed several gyrotropic and breathing modes for in and out of plane excitation, respectively. By analysing the trajectories of the antiskyrmion guiding centre in the two disks as well as the spatial distribution of the spectral power we

have identified a variety of coupled modes in such a system. Furthermore, we show that these modes can be controlled by tuning the strength of the interlayer exchange coupling between the two disks.

1. Huang, Siying and Zhou, et al., "Stabilization and current-induced motion of antiskyrmion in the presence of anisotropic Dzyaloshinskii-Moriya interaction", Phys. Rev. B (96), 144412 (2017) 2. A. K. Nayak, V. Kumar, et al., "Magnetic antiskyrmions above room temperature in tetragonal Heusler materials," Nature 548(7669), 561–566 (2017). 3. L. Camosi, S. Rohart, et al., "Anisotropic Dzyaloshinskii–Moriya interaction in ultrathin epitaxial Au/Co/W(110)," Phys. Rev. B 95(21), 214422 (2017). 4. X. J. Liu, Liqian Guo, Hao Wang, *and* Z. K. Tang, "The internal dynamic modes of an antiskyrmion in ultrathin ferromagnetic nanodisks", AIP Advances (10), 075222 (2020). 5. Lingdi Xing, Dayin Hua, *and* Weiwei Wang, "Magnetic excitations of skyrmions in antiferromagnetic-exchange coupled disks", Journal of Applied Physics 124, 123904 (2018)

HPA-03. Magntic Hopfions in Co/Pt nanostructures and their spin-wave behavior. *Y. Kumar*[1], N. Arora[1] and P. Das[1] *1. Physics, Indian Institute of Technology Delhi, New Delhi, India*

Magnetic Hopfions are three-dimensional topological solitons which are considered as a promising candidate for future spintronics devices and non-volatile magnetic storage. These 3D spin textures are found to be stabilized in frustrated, chiral magnets or materials hosting target skyrmions [1-3]. In this work, we have investigated the stability of Hopfions and their spin-wave behavior in individual nanostructures of thin films of Co/Pt with interfacial DMI. We have performed micro-magnetic simulations to understand in details the process of nucleation and annihilation of Hopfions in nanostrutcures in presence of an external magnetic field. Our results demonstrate a narrow region in the hysteresis loop where Hopfions are stabilized (Fig.1). The spin-wave dynamics in this topological structures were studied by perturbing the system with an external transient square field pulse of duration 60 ps and amplitude of 3 mT applied along the *x*-axis (in the plane of the hopfion). We identified a fundamental spin-wave mode which is excited at about 2 GHz. The nature of this mode is investigated by carrying out fast fourier transform (FFT) at each cell of the discretized geometry. The profile of the mode is investigated by analyzing the image created by plotting the normalized mode-power as well as the phase at the corresponding locations of the nanostructures. Our results suggest that the mode exhibits maximum power in the region of the Hopfions where spins have strong z-components. Furtermore, the excited mode appears to be independent of the external magnetic field.

1. Y. Liu *et al.*, Phys. Rev. Lett. 98, 174437 (2018). 2. Y. Liu *et al.*, Phys. Rev. Lett. 124, 127204 (2020). 3. N. Kent *et al.*, Nat. Commun. 12, 1562 (2021).

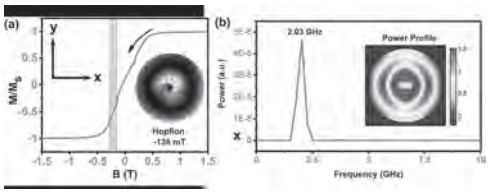

Fig. 1. (a) Field dependece of the normalized magnetization in Co/Pt nanodisc. Inset shows the spin configuration of hopifion stabilized in the highlighted region of the magnetization vs field curve, (b) Spin wave spectra calculated in individual hopfion stabilized in Co/Pt nanodisk exhibiting interfacial DMI. Inset shows the power profile of the excited fundamental mode at 2.03 GHz.

HPA-04. High-frequency ultrafast magnetization dynamics mapped by in-situ Lorentz microscopy. *N. Porwal*[1], J. Weber[1], M. Winklhofer[2] and S. Schaefer[1] *1. Institute of Physics, Carl von Ossietzky Universität Oldenburg, Oldenburg, Germany; 2. Institute for Biology and Environmental Sciences, Carl von Ossietzky Universität Oldenburg, Oldenburg, Germany*

Advancement in in-situ electron microscopy combined with ultrafast time-resolved technique offers a unique access to dynamical processes at the nanoscale. Recently developed ultrafast transmission electron microscopy (UTEM) utilizes ultrashort electron pulses to stroboscopically map the induced dynamics in magnetic nanomaterials [1-3]. Focusing on high-frequency dynamics of chiral magnetic structures, we use radio frequency (RF) electromagnetic field for sample excitation in our Oldenburg UTEM. Here, we report on the development of a resonant RF-cavity compatible with UTEM experiments. For RF-field excitation, a microresonator [4] is designed on printed circuit board which gives localized magnetic-field above 10kA/m at an RF input power of 0.5W within a micro-coil region as shown in Fig. 1(a). The eigen frequency (f = 6.45GHz) of the RF-resonator is measured by using a vector network analyzer (VNA) and the spectral shape of the back-reflected RF power (Fig. 1(b)) matches well with numerical simulations. The RF-resonator is installed on a custom-made sample holder which provides a broadband-electrical connection to an external voltage source and will be used to excite the precessions of the magnetic moments in the sample at GHz frequencies. To account for the strength of the RF-field in the UTEM experiment, we first measure in-situ the polarization state of the RF-fields produced by the RF-resonator and evaluate the local-field distribution using Lorentz TEM. The TEM is operated at an electron energy of 200keV and a VNA, operated at 30 dBm, is used as a source and analyzer of the RF signal. The intensity profile of electron beam deflection at f = 0 and f = 6.45GHz shown in Fig. 1(c) and (d), respectively, allows to retrieve the strength of the RF-field. With this RF-pump/electron probe scheme, we aim to further establish ultrafast-Lorentz microscopy as a powerful tool to characterize magnetization dynamics in chiral magnetic nanostructures.

[1] A. Feist et al., Ultramicroscopy 176, p. 63 (2017). [2] N. Bach et al., Structural Dynamics 6. p. 014301(2019). [3] N. R. da Silva et al. Phys. Rev. X 8, 031052 (2018). [4] B. W. Zingsem et. al., Nature Commun. 10, 4345 (2019).

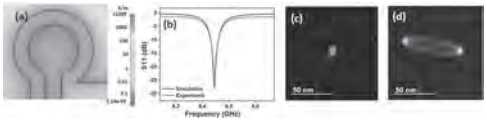

Figure1: (a) Simulated magnetic-field inside the loop. The color bar represents magnetic-field strength. (b) Experimental and simulated tuning curves of microresonator. Intensity profile of electron beam deflection at (c) f = 0 and (d) f = 6.45GHz respectively.

HPA-05. Domain wall depinning from FM/AF interface defects by spin-polarized current. F.A. Andrade[1], F.V. Diniz[1], S.M. Martins Jr[2], L.L. Oliveira[3], *A.L. Dantas*[1,3] and A.S. Carriço[2] *1. Department of Physics, State University of Rio Grande do Norte, Mossoró, Brazil; 2. Department of Physics, Federal University of Rio Grande do Norte, Natal, Brazil; 3. Department of Science and Technology, State University of Rio Grande do Norte, Natal, Brazil*

Sequences of geometrically confined magnetic domain walls (DWs) in micrometer long, flat wires currently hold good promises as a possible system for designing new magnetic memories cell devices. Due to the strong shape anisotropy, narrow and flat rectangular wires (FRW), made of soft ferromagnetic (FM) materials, are prone to have the magnetization oriented along the wire edge. Such wires may turn into possible platforms to hold sequences of DWs, provided a periodic sequence of pinning centers might be created along the wire. A bilayer consisting of an FRW exchange coupled to a two-sublattices vicinal antiferromagnetic (AF) substrate fulfills the main requirements to construct a periodic sequence of pinned DWs.[1,2] This may lead to a corresponding arrangement in the FM film, which may turn structured with

alternating domains separated DWs centered at the step's edges. We presently report a theoretical study of spin-polarized current domain wall (DW) release, considering a vicinal AF substrate with a small miscut angle so that there is no interaction between adjacent DWs. We consider a DW separating two opposite domains in a FM (Py or Fe) nanostrip coupled to a two-sublattice uniaxial AF substrate. In the absence of electric current, the DW center is on the interface step defect. We consider a spin-polarized current applied along the easy axis AF. The spin-transfer torque is restricted to the DW region. Our results indicate that the electric current density threshold value (J*) to detach the interface pinned DWs increases as the interface exchange energy increases. Furthermore, J* is smaller for Py/AF nanostrips than for Fe/AF nanostrips with the same geometrical dimensions. For instance, for an interface field value of 200 Oe, considering a Py nanostrip consisting of 125 nm long, 25 nm wide, and 10 nm thick domains separating the DWs, we have found that, for small values of electric current density, the DW center moves from the interface step defect, contrary to the electric current direction, for around 27.5 nm, until $J^*=29x10^7$ A/cm^2. The corresponding values for an Fe nanostrip with the same dimensions and interface field strength are 15 nm and $J^*=34x10^7$ A/cm^2.

[1] S. S. P. Parkin, M. Hayashi, and L. Thomas, Science 320, 190 2008. [2] M. Klaui, J. Phys.: Condens. Matter 20, 313001 2008.

HPA-06. Magnetostatic coupling between the a ferromagnetic stripe and a nanodot. *M. Moalic*[1], M.K. Zelent[1] and M. Krawczyk[1] *1. Faculty of Physics, Adam Mickiewicz University, Poznan, Poland*

One of the main research directions in magnonics focuses on the excitation of short wavelengthSWs (SWs). Recently, a few approaches have been proposed, but with some limitations like the lack of anefficient source of SWs, which further limits the development of magnonic applications. One promising upcoming solution is to use an inscribed skyrmion in a nanodot but such a system can have a lot of variables, especially with a time-resolved analysis. In this prospect, we will narrow the scope and focus on the static system composed of a nanodot with varying magnetic states on top of an in-plane magnetized stripe. The waveguide ismagnetically saturated along its length and is separated from the nanodot by a spacer of 1.5 nm. It is 384 nmwide and 4.5 nm thick, and a few micrometers long with absorbing boundary conditions at its edge bothextremities to avoid any kind of back-propagating SWs. The nanodot must have a specific geometry and size, as it requires a strong enough interfacial Dzyaloshinskii-Moriya Interaction to allow for the formation of a skyrmion. For this reason, the nanodot is made of Pt/Co/Ir circular layers with a diameter of 300 nm to create a strong shape anisotropy which allows the presence of a metastable state such as a skyrmion in its core. When relaxing this system, a \textit{spin-dot-shadow} is created in the waveguide, meaning the magnetization below the nanodot will deviate from their saturated magnetization along the x axis because of the dipolar coupling with the skyrmion. In the same way, the waveguide will influence the magnetization inside the nanodotand affect the shape of the skyrmion. In our example, the skyrmion's core expends and becomes egg shaped under the influence of the waveguide. In the case of the out-of-plane magnetized nanodot (without an inscribed skyrmion), the induced magnetostatic field can be approximated to the field distribution of the magnetic dipole. *The work was supported by National Science Centre of Poland, Project SHENG No. UMO-2018/30/Q/ST3/00416.* This analysis is repeated for many values of the DMI as it is the principal factor in the resulting texture in the nanodot, which allows us to compare very similar systems with different skyrmions shapes.

HPA-07. Magnetic Properties Affected by the Size and Shape of Magnetic Nanowires. *Y. Chen*[1] and B. Stadler[2] *1. CEMS, University of Minnesota, Minneapolis, MN, United States; 2. ECE, University of Minnesota, Minneapolis, MN, United States*

Magnetic nanowires (MNWs) are increasingly important for applications in memory [1], biolabels [2], and nanowarming of cryopreserved organs [3]. Object Oriented Micromagnetic Framework (OOMMF) was used to visualize moments inside MNWs. The magnetic properties of MNWs were investigated as a function of nanowire shape. Experimental measurements of magnetic nanowires (MNW) often reveal features that are difficult to explain due to statistical shearing of features and interaction fields in large arrays [4]. Measurements of individual nanowires can be used to remove interaction field effects [5], and other measurements such as first-order reversal curves (FORC) [6] and the projection method [7] often attempt to statistically separate bulk effects. For nickel MNWs with fixed length of 3 μm, the coercivity and the remanence are negatively correlated to the diameter of the wire (Fig.1). When the diameter is increased to 200 nm, a 'wasp waist' appeared in the hysteresis loop, Fig.2. (solid line) The reversal process is three-folded. First, since there is a large area for curling in 200nm-diameter nanowires, the magnetic moments at the tips of the MNW fall from pointing along z-axis to aligning in the xy-plane and in the form of vortex. Next, the outer shell of moments turns from in-plane to the negative z-axis. Finally, the axial core of the MNW switches and the wire is fully saturated in the negative z-direction. Interestingly, at H_c, the two vortex walls converged in the center of the MNW and a three-dimensional vortex(hedgehog) [8] was observed using a 2D cross-sectional view, Fig.2 (b). Next, when flat-tipped cylinders were replaced with ellipsoids so that the tips of wire had infinitesimally small areas where vortex was no longer supported, the coercivity of the nanowires significantly increased (Fig.1 and 2, dashed line)

[1] Maqableh, Mazin M., et al. *Nano letters* 12.8 (2012): 4102-4109. [2] Zamani Kouhpanji, MR, et al. *ACS Applied Materials & Interfaces* 13.18 (2021): 21060-21066. [3] Shore, Daniel, et al. *Nanoscale* 11.31 (2019): 14607-14615. [4] Madhukar Reddy, Sai, et al. *Journal of Applied Physics* 111.7 (2012): 07A920. [5] Jin Park, Jung, et al. *Journal of Applied Physics* 113.17 (2013): 17A331. [6] Dobrotă, Costin-Ionut, et al. *Journal of applied physics* 113.4 (2013): 043928. [7] Kouhpanji, Mohammad Reza Zamani, et al. *RSC Advances* 10.22 (2020): 13286-13292. [8] Charilaou, Michalis, et al. *Physical review letters* 121.9 (2018): 097202.

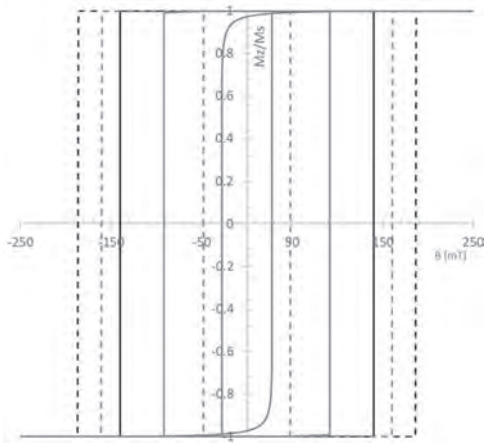

Fig.1 Hysteresis loops for nickel MNWs with diameter of 30 nm(black), 50 nm(red) and 100 nm(blue) in cylinder shape (solid line) and ellipsoid shape (dashed line).

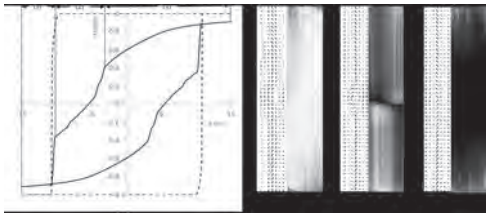

Fig.2 (a) Hysteresis loop for 200 nm nickel MNWs with cylinder shape (solid line) and ellipsoid shape (dashed line). (b) The corresponding 2D and 3D moment map

HPA-08. Analytical approaches to the mutual synchronization of spintorque nano-oscillators. D. Mancilla[1], *M. Castro*[1], S. Allende[1], L.D. Buda-Prejbeanu[2] and U. Ebels[2] *1. Departamento de Fisica, CEDENNA, Universidad de Santiago de Chile, Santiago, Chile; 2. SPINTEC, Univ. Grenoble Alpes, CEA, CNRS, Grenoble INP, Grenoble, France*

Synchronization of spin-torque nano-oscillators (STNOs) via either electrical currents or dipolar interactions is key for many applications such as wireless communication [1] or neuromorphic computing schemes [2]. It will thus be important to have at hand reliable models to predict the synchronization properties for different STNO configurations, as well as for identical and non-identical STNOs. The latter may arise due to variations of material parameters. We present analytical models, based on the spin-wave formalism [3], using two complementary approaches to determine, amongst others, the hysteretic boundaries of the transition from the synchronized (S) to the non-synchronized (NS) state and vice versa. The first is a perturbation approach, providing the transition from the NS to the S state. The phase and power equations are solved considering a small shift in power with respect to the free running power. The second approach, providing the transition from the S to the NS state solves the amplitude and phase equations under the assumption of equal power. The analytical expressions of the boundaries for the NS-to-S and S-to-NS transitions as a function of the current density mismatch are evaluated for the case of synchronization via dipolar interaction of two STNOs that support out-of-plane precession modes using a perpendicular polarizer and an in-plane magnetized free layer [4] under out-of-plane field. The analytical results are in excellent agreement with numerical macrospin simulations, solving the Landau-Lifshitz Gilbert equations, (see Fig. 1). These results can be directly applied to more than two oscillators and will therefore be an important basis to describe coupled STNO arrays. We acknowledge financial support in Chile from FONDECYT 1200867 and 1190727, and Financiamiento Basal para Centros Científicos y Tecnológicos de Excelencia FB 0807 (AFB 180001). D.M.-A. acknowledges Proyecto Postdoc DICYT 042131AP POSTDOC, Vicerrectoría de Investigación, Desarrollo e Innovación. M.A. Castro acknowledges Conicyt-PCHA/Doctorado Nacional/2017-21171016.

[1] T. Chen, et al., Proceedings of the IEEE. 104, 1919-1945(2016). [2] J. Grollier, et al., Nat. Electron. 3, 360 (2020). [3] A. Slavin and V., Tiberkevich, IEEE Trans. Magn, 45,1875(2009). [4] D. Houssameddine et al., Nature Materials 6, 447 (2007)

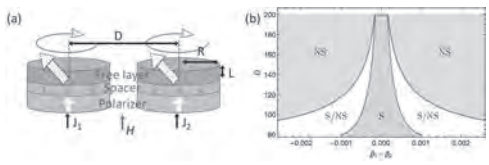

Fig. 1 (a) Schematics of the two coupled STNOs; (b) Arnold tongue as a function of the current density mismatch and the center-to-center distance D between STNOs.

HPA-09. Study on a combined NDT method base on MBN and ACSM. *Z. Wang*[1] and G. Tian[2] *1. College of Automation Engineering, Nanjing University of Aeronautics and Astronautics, Nanjing, China; 2. School of Engineering, Newcastle University, Newcastle upon Tyne, United Kingdom*

Magnetic Barkhausen noise (MBN) plays an essential role in describing the dynamics of domain walls. However, the research on the correlation between Barkhausen effect and magnetostrictive effect in the magnetization process is insufficient. This article synthesizes the Barkhausen effect and the inverse magnetostrictive effect to design a new method combining MBN and Alternating Current Stress Measurement (ACSM). First, we analyzed the relationship between the signal characteristics of the two methods and the microstructure of the magnetic domain from the detection mechanism. Second, we designed a system that can pick up these two different signals on the same coil. Used the hysteresis loop reconstructed by MBN and the incremental conductivity extracted from ACSM to quantitatively analyze the correlation between the microscopic and macroscopic magnetic parameters under different stresses. The final results showed that in the reversible and irreversible magnetic domain change phases, the signal sensitivity of ACSM and MBN were different, and the new method could achieve the complementarity of the two detection mechanisms.

M. Roskosz and K. Fryczowski, Journal of Magnetism and Magnetic Materials., vol. 499, p.166272 (2020) P. Fagan, B. Ducharne, and L. Daniel, Journal of Magnetism and Magnetic Materials., vol. 517, p.167395 (2021) D. C. Jiles and W. Kiarie, IEEE Transactions on Magnetics., vol. 57, p.1–11, (2021) K. Chen, F. P. Brennan, and W. D. Dover, Journal of Strain Analysis for Engineering Design, vol. 35, p.227–233 (2000) F. S. Qiu, M. Jovičević-Klug, and G. Y. Tian, Journal of Magnetism and Magnetic Materials, vol. 523, p.167588 (2020) A. Barrancos, A. Silvestre, and L. S. Rosado, 2021 Telecoms Conference (ConfTELE)., p.1–4 (2021)

HPA-10. The Effect of Asymmetric Notch Pinning and Wire Width on Domain Wall Depinning Behavior in Planar Micron-Size Wires. *D. Shiu*[1], K. Lai[1], R. Cao[2], C. Su[1], Y. Kao[1], J. Wu[1] and L. Horng[1] *1. Physics, National Changhua University of Education, Changhua, Taiwan; 2. Electrical Engineering, Feng Chia University, Taichung, Taiwan*

We study depinning behavior of domain wall (DW) in wide NiFe wires. The wires are 20-nm-thick strips with various micron-size widths and different asymmetric notch. Wire width (W) was designed as widths ranging from 1 μm to 3 μm. The notch has a fixed depth ratio of ~0.5 (notch depth divided by W), various left angles (θ) and fixed right angle (around 60°), as shown in the inset of Fig. 1. The devices were fabricated by e-beam lithography and magnetron-sputtering. We utilized MOKE microscopy to measure depinning field (H_d) of DW. Fig. 1 shown the H_d-θ curves with different W. The H_d-θ curves of 1-μm- and 3-μm-wide wires respectively show increased trend and decreased trend. The H_d-θ curve of 2-μm-wide wire has an unobvious trend. We ran micromagnetic simulation to examine the affections of W and θ. The setup of simulated devices was shown in the inset of Fig. 1. Fig. 2 (a) shows the head to head counter-clockwise (HH-CCW, similar to tail to tail clockwise) H_d-θ curve of narrow wires have dips, but wide wire result is different to the narrow wire. The W affected the structure and pinning potential landscape of DW. The experimental results are quite different to the simulation of narrow wire because W affected pinning potential well (E_w) at the right side of notch. The difference between the measured H_d-θ trend of 1-μm-wide wire and the simulation of 800-nm-wide wire was caused by the different increment step of θ. The E_w is composed by the exchange energy (E_{ex}) and demagnetic energy (E_{dem}) of DW. The E_{ex}-θ curves display a similar trend for all W, as shown in Fig.2 (b). The E_{dem} strongly affected H_d in wide wire, as shown in the blue dashed circle marked region of Fig. 2(a). The DW pinning potential landscape is different in wide wire because of E_{dem}. The simulated results imply that the experimental results were caused by the quite different E_w. The weak shape-anisotropy caused E_{ex} to dominated H_d-θ in 1-μm and 2-μm-wide wires. The H_d-θ trend of the 3-μm-wide wire was caused by the complex DW structure and E_w.

[1]. Y. Gao, B. You, X. Z. Ruan, Sci. Rep. Vol. 6, Article number: 32617 (2016). [2]. V. Estévez, L. Laurson, Phys. Rev. B. Vol. 93, p.064403 (2016) [3]. J. Brandão, R. L. Novak, H. Lozano, J. Appl. Phys. Vol. 116, p.193902 (2014). [4]. L. K. Bogart, D. Atkinson, K. O'Shea, Phys. Rev. B. Vol. 79, p.054414 (2009). [5]. L. K. Bogart, D. S. Eastwood, D. Atkinson, J. Appl, phys. Vol. 104, p.033904 (2008).

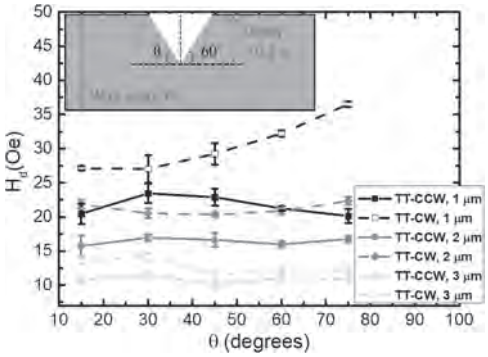

Fig. 1. The measured H_d-θ curve of different widths. Inset is the setup of device.

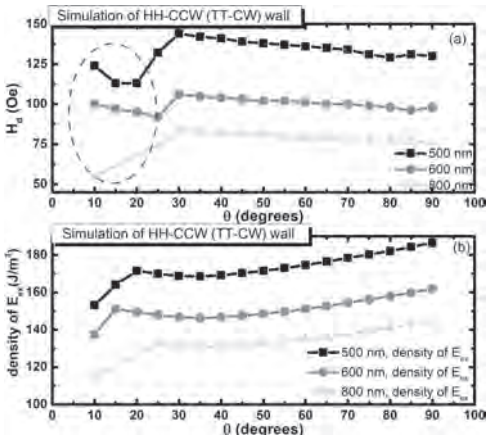

Fig. 2. (a) The simulated H_d-θ curves with different widths. (b) The simulated E_{ex}-θ curves with different widths.

HPA-11. Evaluation of the Magnetization Dynamics in Various Thick YIG Films Using Our Proposed Measurement Technique. T. Nguyen[1] and *Y. Endo[1] 1. Tohoku University, Sendai, Japan*

Recently, much attention has been paid to the study on magnetization dynamics in magnetic thin films from both fundamental and application points of view. The dynamics are described phenomenologically using the Landau-Lifshitz-Gilbert (LLG) equation consisting of both the precession torque of the magnetization and the damping torque. Especially, one of the most dominant parameters to understand the dynamics is the Gilbert damping constant (α) which describes the strength of damping torque in magnetic thin films. Until now, we proposed a new measurement technique which enables simultaneous evaluation of α and satureation magentostriction (λ_s) by measuring correlation between FMR frequency (f_r) and the tensile stress, and clarified a correlation between α and λ_s for Ni-Fe and Fe-Si films[1]. Herein, we investigated the magnetization dynamics of various thick YIG polycrystalline films by our proposed measurement technique, and discussed the correlation between α and λ_s in these films. In case of the 300-nm thick YIG film (Fig. 1), each FMR frequency with tensile stress (f_{rs}) shifted to lower frequency side because of uniaxial magnetostrictive anisotropy. The frequency difference ($\Delta f_r = f_{rs} - f_{r0}$) in external magnetic field (H_{ex}) increased from approximately −70 to −45 MHz with the increase of H_{ex}. λ_s evaluated using the f_{rs}, f_{r0}, and Δf_r was approximately −0.67 ppm. This value was lower than that of polycrystalline YIG (−1.4 ppm), which might be attributed to the structural inhomogeneity such as crystalline orientation, composition and so on. α was evaluated from f_{r0} and half width of the FMR spectra without tensile stress, and was approximately 0.00302. This value is much higher than that of nano-meter thick YIG film deposited on GGG substrate, which may be ascribed to magnetic inhomogeneity such as anisotropy dispersion, two magnon scattering and so on. Moreover, to clarify the correlation between α and λ_s in YIG films, α is summarized in Fig. 2 as a function of λ_s. These parameters do not clearly show a consistent relation, which might be attributed to structural and/or magnetic inhomogeneity.

References [1] Y. Endo et al., APL 112, 252403 (2018); Y. Endo et al., Abstract of 2019 Joint MMM-Intermag Conference (2019). Acknowledgment The authors thank Prof. Satoshi Okamoto, and Associate Prof. Nobuaki Kikuchi at Tohoku University for measuring XRD diffraction patterns, and also thank Dr. S. P. Pati for the film fabrication. This work was supported in part by JSPS KAKENHI Grant No. JP17H03226 from MEXT, Japan. This work was supported in part by CSIS, CSRN, and CIES, Tohoku University. This work was also supported in part by the ASRC in Japan.

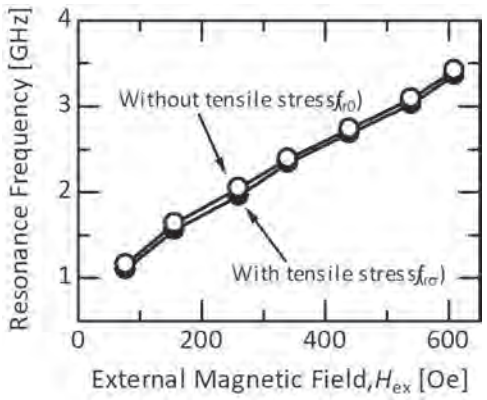

FIG. 1. f_{r0}, $f_{r\sigma}$ vs H_{ex} for the 300-nm thick YIG film.

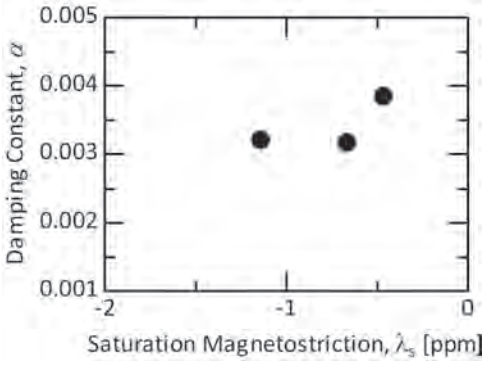

FIG. 2. Relationship between α and λ_s for various thick YIG films.

HPA-12. Resonant spin-wave emission from the moving AFM DW without Lorentz invariance. *X. Ge*[1], F. Chen[1], Z. Li[3], P. Yan[2], H. Piao[4], W. Luo[1], S. Liang[5], X. Yang[1], L. You[1] and Y. Zhang[1] *1. Huazhong University of Science and Technology, Wuhan, China; 2. University of Electronic Science and Technology of China, Chengdu, China; 3. Hebei University of Technology, Tianjin, China; 4. China Three Gorges University, Yichang, China; 5. Hubei University, Wuhan, China*

The antiferromagnetic (AFM) medium is an ideal candidate for emitting terahertz (THz) electromagnetic (EM) waves, which have extraordinary potential application in information technology and biological medicine [1–4]. In this work, we report the theoretical and numerical investigation about the emission of terahertz (THz) spin waves from a moving AFM DW under the magnetic anisotropy energy gradient (dE_a/dx). The DW is accelerated by dE_a/dx that can be generated using the technique displayed in Fig.

1: A DC voltage applied across the wedge-shaped insulating layer generates dE_a/dx, which triggers the AFM DW to move towards the end with a lower magnetic anisotropy energy [5]. Based on an atomistic spin model, we have found that the DW velocity exceeds the relativistic limit and keeps increasing, which is accompanied by the broadening of the DW width. This is different from a traditional relativistic AFM DW motion with an upper limit of the DW velocity and Lorentz contraction [6]. The DW acceleration effectuates the DW precession. When the frequency of the DW precession is greater than the frequency gap of the spin wave propagating in the AFM medium, a continuous THz spin wave is resonantly emitted. The frequency of the spin wave keeps increasing with the decrease of the anisotropy energy constant, which seems to be contrary to the AFM spin wave obeying the relativistic-like dynamics. Our results demonstrate that obeying the relativistic dynamics is not necessary for the spin-wave emission from a moving AFM DW.

[1] B. Ferguson and X.-C. Zhang, "Materials for terahertz science and technology," Nat. Mater., vol. 1, no. 1, pp. 26–33, 2002. [2] Jungwirth T, Marti X, Wadley P, Wunderlich J, "Antiferromagnetic spintronics," Nature Nanotechnology., vol. 11, pp. 231–241, 2016. [3] J. Walowski and M. Münzenberg, "Perspective: Ultrafast magnetism and THz spintronics," J. Appl. Phys., vol. 120, p. 140901, Aug. 2016. [4] V. Baltz, A. Manchon, M. Tsoi, T. Moriyama, T. Ono, and Y. Tserkovnyak, "Antiferromagnetic spintronics," Rev. Mod. Phys., vol. 90, no. 1, p. 015005, 2018. [5] Y. Zhang, S. Luo, X. Yang, and C. Yang, "Spin-orbit-torque-induced magnetic domain wall motion in Ta/CoFe nanowires with sloped perpendicular magnetic anisotropy," Sci. Rep., vol. 7, May. 2017. [6] Shiino T, Oh S-H, Haney P M, Lee S-W, Go G, Park B-G, Lee K-J, "Antiferromagnetic domain wall motion driven by spin-orbit torques," Phys. Rev. Lett., vol. 117, 087203, 2016.

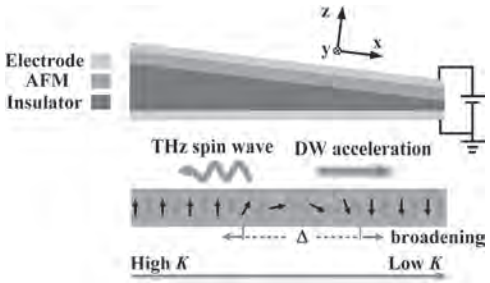

Fig.1. Schematic of calculation model: emission of THz spin wave from a moving DW triggered by a voltage-induced gradient of magnetic anisotropy energy (the emission of the spin wave is accompanied by an increase of the DW width due to the reduction of the magnetic anisotropy energy).

HPA-13. Dynamics of Domain Wall Induced by the Voltage-controlled Strain Field Gradients. *G. Yu*[1], X. He[1], Y. Qiu[1], G. Wu[1], R. Guo[1], M. Zhu[1,2] and H. Zhou[1] *1. Key Laboratory of Electromagnetic Wave Information Technology and Metrology of Zhejiang Province, China Jiliang University, Hangzhou, China; 2. Center for X-Mechanics, Zhejiang University, Hangzhou, China*

Magnetic domain walls (DWs), as a novel information carrier, provide a reliable technique for modern information processing. In previous study, to control the movement of magnetic DWs, different external excitations, such as magnetic field, spin transfer torque, spin-orbit torque, electric field, and spin waves, etc., have been used as the driving force for the DW motion. In this work, we combine electromechanical and micromagnetic simulations to explore a promising way to manipulate the perpendicular magnetic anisotropy (PMA) DW motion in a given direction using voltage-controlled gradient strain. In particular, we show the voltage induced gradient strain driven the DW motion more complicated than simple uniform linear motion, especially for DW motion in a finite length nano-stripe. As shown schematically in Fig. 1(a), the proposed device consists of a ferromagnetic (CoFeB)/heavy metal (FM/HM) nanostrip deposited on a piezoelectric substrate. The initial spin configurations with different i-DMI coefficient are obtained by relax the DW along the y direction. Fig. 1(b) shows the snapshots of magnetization with various i-DMI coefficient when simulated 10 ns after the strain gradient applied. As shown in Fig. 1(b), the direction of the DW will parallel to the x direction due to the i-DMI and form a Neel type DW, while a Bloch type DW formed without i-DMI. From the micromagnetic simulation results shown in Fig. 1(b), along with the DW displacement, DWs are found to tilt away from the y-axis, which agrees with the experimental observations. From these magnetization images, we can also directly see an increment of DW tilting angel as the i-DMI constant increase. These results indicates that strain gradient induced PMA DW motion can be used to develop next generation artificial intelligent memory and logic devices.

1 S. S. P. Parkin, M. Hayashi, and L. Thomas, Science 320, 190 (2008). 2 N. Lei, T. Devolder, and G. Agnus, etc, Nat. Commun. 4, 1378 (2013). 3 J. M. Hu, T. Yang, and K. Momeni, etc, Nano Lett. 16, 2341 (2016). 4 H. Zhou, S. Shi, and D. Nian, etc, Nanoscale. 12, 14479(2020).

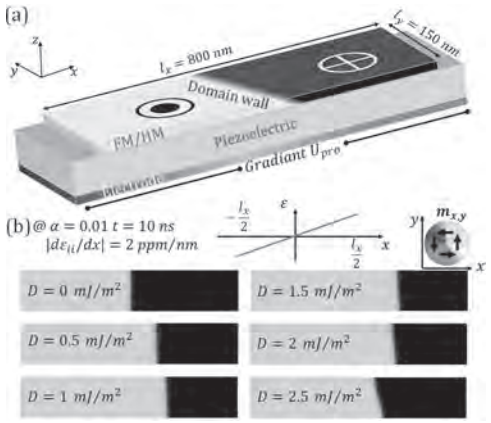

Fig. 1 (a) Schematic view of the investigated strain driven domain wall in a nanostripe with voltage-controlled strain gradient. (b) Snapshots of the magnetization pattern with different i-DMI coefficient.

HPA-14. Domain Wall Pinning with Synthetic Antiferromagnets. *J. Chan*[1], D. Kumar[1], W. Mah[1] and S. Piramanayagam[1] *1. School of Physical and Mathematical Sciences, Nanyang Technological University, Singapore, Singapore*

A recent proposal of a brain-inspired architecture, known as Neuromorphic Computing (NC), has attracted attention from many researchers seeking to achieve low-power processing. The elements of NC include synapses that function as memory with multiple resistance states. Amongst the spin-based neuromorphic elements, the domain wall (DW) device expends the least energy. Nevertheless, the stochastic behaviour of DW motion complicates the position of the domain wall and thus its multi-resistive state. We introduce synthetic anti-ferromagnetic (SAF) pinning sites (Fig. 1(a)) that are embedded within a ferromagnetic wire to control the position of the DW. We simulate pinning (Fig. 1(b)) and de-pinning (Fig. 1(b)) of DWs from the SAF pinning sites with an inter-layer exchange coupling (IEC) of up to -0.3 mJ/m^2. The DWs were driven via Spin Orbit Torque (SOT) and the minimum de-pinning current was estimated for various lengths, DMI and IEC of the pinning site. For longer pinning sites (50 nm), we relate an increased magnitude of IEC with a proportionally larger de-pinning current (Fig. 2(d)) and no dependence established on DMI or further length (Fig. 2(a-c)). However, we report both increasing and decreasing relationships between DMI and de-pinning current (Fig. 2(a-c)) which are distinguished by two stable DW configurations for pinning sites of lesser lengths. We also extend our study to include five pinning sites to demonstrate the various resistive states from which the synaptic properties may be derived.

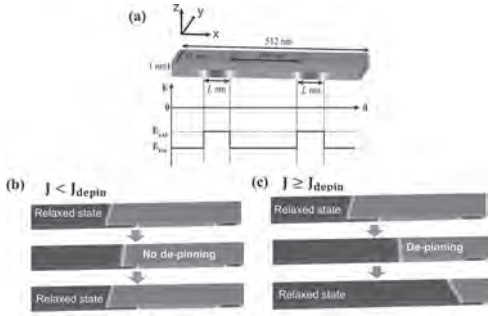

Figure 1. (a) Dimensions of the wire of positive IEC within which two pinning sites of negative IEC are embedded. The difference in the total energy of the SAF and FM regions defines the basis of DW pinning via SAF. (b) Upon establishing a reverse DW at a pinning site, a current is applied which may pin (b) or de-pin (c) the DW from the pinning site.

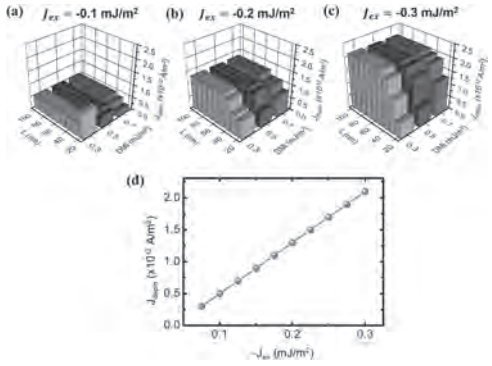

Figure 2. Summary of J_{depin} across various pinning site of lengths, DMI and IEC J_{ex} of (a) -0.1 mJ/m², (b) -0.2 mJ/m² and (c) -0.3 mJ/m². For L ≥ 50 nm, J_{depin} remains a constant irrespective of L and DMI. These constants increase as J_{ex} increases and are plotted in (d) along with several intermediate values of J_{ex} for L = 50 nm and DMI of +0.3 mJ/m².

HPA-15. Depinning Field of Vortex Domain Wall at Triangular Notch with Various Incoming Angles in NiFe Wires. *D. Shiu*[1], K. Lai[1], R. Cao[2], Y. Kao[1] and L. Horng[1] *1. Physics, National Changhua University of Education, Changhua, Taiwan; 2. Electrical Engineering, Feng Chia University, Taichung, Taiwan*

In this research, we studied the depinning behavior and mechanism of vortex domain wall (VDW) in the NiFe wire with an asymmetric triangular notch. We utilized MuMax[3] to investigate the depinning field (H_d) of the notch pinned VDW. We set fixed outgoing angle (Φ = 60 °) and various incoming angles (θ) to explore the impact of the geometry of the notch, as shown in the inset of Fig. 1. The wires are 20-nm-thick strips with various widths. In the simulations, the exchange stiffness, saturation magnetization, crystalline anisotropy constant, damping constant, and cell size of simulation wires are set as 1.3×10^{-6} erg/cm, 860 emu/cm³, 0, 0.01, and 5 nm× 5 nm× 20 nm, respectively. We set the field-driven VDW at left of the notch to observe VDW depin from notch. Fig. 1 shows the H_d-θ curves for the depinning of head-to-head type counter-clockwise (HH-CCW) wall. The θ value corresponding to the maximum H_d is defined as the transition angle (θ_T). The θ_T are 30 ° for all the wires, as shown in Fig. 1. The θ_T values are independent of the wire width because θ_T is determined by the potential well (E_w) at the left side of the notch. The VDW depinning behavior is affected by the potential well (E_w) for our simulated devices. This E_w is affected by the exchange energy (E_{ex}) which can be calculated from the angle (ξ) between the moments at the right side of the VDW and the moments at the left side of the notch, as shown in Fig. 2 (a). E_w decreases as ξ decreases because E_{ex} decreases with ξ. The relation between E_{ex} and ξ can explain the H_d-θ curves in Fig. 1. Fig. 2 (b) shows the direction of simulated magnetic moments of the VDW and the device at θ_T, where the ξ is about zero, the E_w is low and the VDW is not easy to depin from the notch. Our simulation results also confirm that the E_{ex} change can explain the H_d-θ curves at the range of $\theta>\theta_T$. By the way, the H_d-θ curves for the narrow wires have dips because of shape-anisotropy.

[1]. Arne Vansteenkiste, Jonathan Leliaert, Mykola Dvornik., *AIP Advances.,* 4, 107133 (2014). [2]. L. K. Bogart and D. Atkinson., *Phys. Rev. B.,* 79, 054414 (2009). [3]. Y. Gao, B. You, X. Z. Ruan, M. Y. Liu., *Scientific Reports.,* 6, 32617 (2016). [4]. J. Brand~ao, R. L. Novak, H. Lozano., *J. Appl. Phys.*, 116, 193902 (2014).

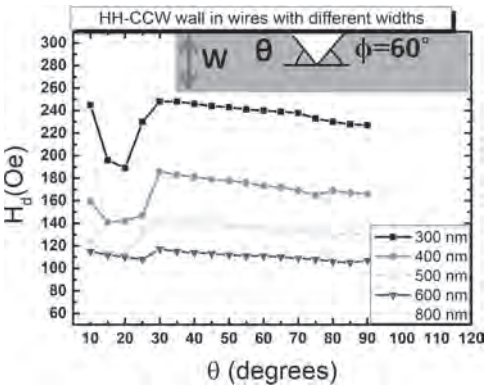

Fig. 1. H_d-θ curves of HH-CCW VDW. The inset is the structure of the devices.

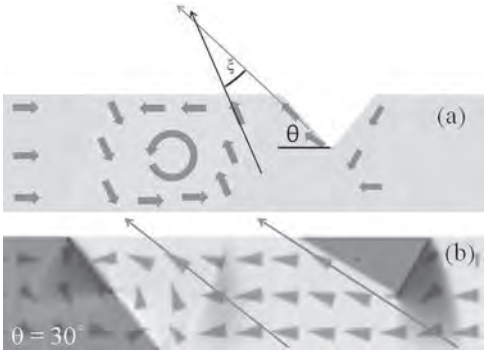

Fig. 2. (a) The interaction between HH-CCW VDW and the left side of the notch. (b) HH-CCW VDW was pinned at the notch with θ = 30°.

HPA-16. Synthetic antiferromagnetic domain wall device as artificial neuron for neuromorphic computing. *W. Mah*[1], D. Kumar[1] and S. Piramanayagam[1] *1. School of Physical and Mathematical Sciences, Nanyang Technological University, Singapore, Singapore*

Spin-based neuromorphic computing (NC) is investigated as a power-efficient enabler for artificial intelligence [1-3]. Hence, magnetic tunnel junction (MTJ) based domain wall devices are investigated as synthetic synapses and neurons to mimic their biological counterparts [2-3]. While a biological neuron resets itself after firing, such a function has not been demonstrated experimentally in spintronic systems [3]. The self-reset feature of neurons reduces the power consumption and the complexity of NC architecture. In this work, we present a domain wall (DW) based artificial neuron that automatically resets without applying a reset pulse. At first, we simulated a synthetic antiferromagnetic (SAF) DW device where the free layer (CoFeB) is driven by spin-transfer-torque (STT) to achieve integrate function. Leakage function was achieved when the antiferromagnetic coupling (AFC) between the free and pinned layers pushes the DW towards the starting position automatically (Fig. 1). The left quarter region of the free layer is ferromagnetically coupled (FC) to the pinned layer so that as DW

returns (during reset), it is stabilized at the initial position (Fig. 2(a) and Fig. 2(b)). Experimentally, the integrate and leakage functions are also achieved as illustrated in Fig. 2(d) and Fig. 2(e), suggesting that an SAF-based neuron is viable for NC.

[1] J. Grollier, D. Querlioz, K. Y. Camsari, K. Everschor-Sitte, S. Fukami, and M. D. Stiles, "Neuromorphic spintronics," *Nat. Electron.*, 2020, doi: 10.1038/s41928-019-0360-9. [2] T. Jin, W. Gan, F. Tan, N. R. Sernicola, W. S. Lew, and S. N. Piramanayagam, "Synaptic element for neuromorphic computing using a magnetic domain wall device with synthetic pinning sites," *J. Phys. D. Appl. Phys.*, vol. 52, no. 44, pp. 0–5, 2019, doi: 10.1088/1361-6463/ab35b7. [3] W. L. Mah, D. Kumar, T. Jin, and S. N. Piramanayagam, "Domain wall dynamics in (Co/Ni)n nanowire with anisotropy energy gradient for neuromorphic computing applications," *J. Magn. Magn. Mater.*, vol. 537, no. October 2020, p. 168131, 2021, doi: 10.1016/j.jmmm.2021.168131.

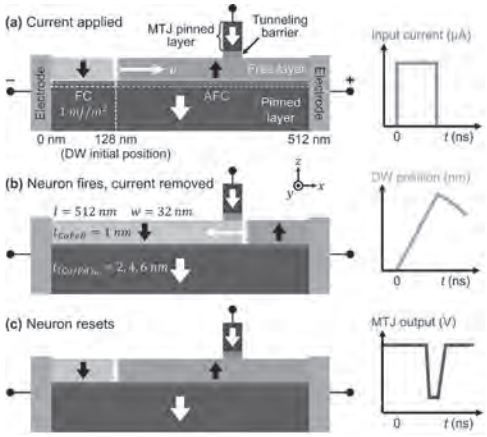

Fig.1 Proposed design of the artificial neuron. Domain wall is moved forward by STT and (after firing), reset backward by SAF coupling.

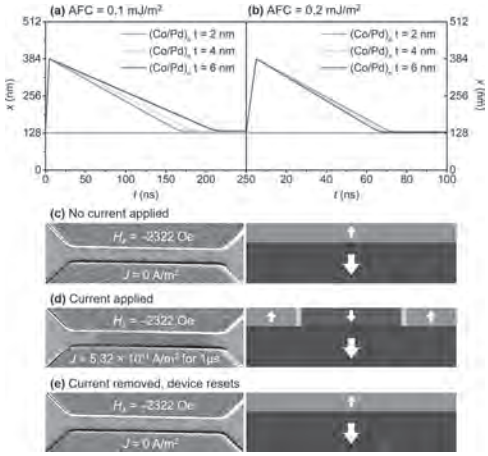

Fig. 2 (a and b) DW position (free layer) vs time graphs for different AFC strength in the simulations. (c, d and e) Kerr images of the fabricated SAF neuron device with magnetic field in the -z direction. (c) No current applied and device is in antiparallel configuration, (d) current is applied, pushing the DW and achieving the integrate function, and (e) current is removed and the device automatically resets, indicating the leakage function.

HPA-17. Fast and Controlled Sequential Nucleation of Narrow Domains in a Ferromagnetic Nano-strip with Non-localised Electrical Currents. *D. Osuna Ruiz*[1], V. Raposo[1], Ó. Alejos[2] and E. Martínez[1]
1. Department of Applied Physics, University of Salamanca, Salamanca, Spain; 2. Department of Electricity and Electronics, University of Valladolid, Valladolid, Spain

Domain wall (DW) dynamics has been intensively studied as the base for novel spintronic devices [1-2]. These dynamics have attracted special attention in ultrathin ferromagnetic strips that show high perpendicular magnetic anisotropy (PMA) since the formation of 'up' or 'down' domains, separated by DWs, can be exploited to store bits. One of the challenges is the initial nucleation of the domains in sequence, typically performed by an Oersted magnetic field from an attached microwave 'bit line' orthogonal to the strip [3]. However, fabrication constraints due to the size of the bit line sets a lower bound for the bits width and, more importantly, the Oersted field that nucleates a DW can annihilate a shifted DW in the strip [3]. Solutions based on a double bit line have been proposed [3], but these still require injecting external currents and a more intricate and multilayer design. In this work, we propose a different approach based on a fluctuating DW as the source. The DW is pinned at one end at the junction of a Y-shaped strip (see red solid circles, Fig. 1) as the DW fluctuates across the strip width (see Fig. 1(b)-(d)). The pinned DW can be originally nucleated by using a bit line. Then, it is forced to oscillate by applying non-localized, pulsed currents (J_{HM}) in the heavy metal (HM) in a controlled manner. Such oscillation injects subsequent DWs that travel along the strip. We characterize the obtained 'domain sequence' as a function of duration (d) and periodicity (T) of the current pulses. Particular combinations result in 'coherent' sequences of domains (see red dashed circles in Fig. 1(e)-(f)) and/or domain reversal, which may be useful to develop DW-based applications.

[1] A. Hubert and R. Schäfer, in Magnetic Domains: The Analysis of Magnetic Microstructures, eds Springer-Verlag Berlin Heidelberg, (1998) [2] A. D. Karenowska *et al.,* in Handbook of Spintronics, eds Springer Netherlands, Dordrecht, pp.1505–1549 (2016) [3] O. Alejos *et al.,* Scientific Reports, 7, 11909 (2017)

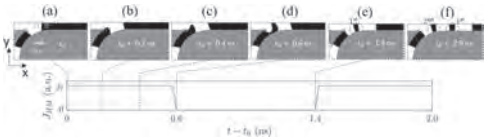

Fig.1. Nucleation of two domains (see red dashed circles in (f)) in the Y-shaped ferromagnetic nanostrip. Black and white are 'down' and 'up' domains, respectively (see green symbols), and grey represents the HM layer beneath the strip. A pulsed current (J_{HM}) is applied in the x-direction over the entire HM. (a)-(d) Snapshots from a full fluctuation of the DW during a pulse of 0.6 ns duration, and (e) after a stabilisation period (J_{HM}=0) of the nucleated domain (~90 nm width) at 1.4 ns. (f) Results after two pulses of period 1.4 ns.

HPA-18. Transient retrograde motion of spin wave-driven skyrmions in multilayer wave guides. *L. Huang*[1], G. Burnell[1] and C. Marrows[1]
1. School of Physics and Astronomy, University of Leeds, Leeds, United Kingdom

One of the tools to move a skyrmion is an injected current[1,2], which gives rise to the risk of producing excessive heat. On the other hand, spin-waves (SW) are a promising way to drive skyrmions without producing such high temperatures and hence affecting the skyrmionic device's performance. Most recent work on SW-driven skyrmion motion is based on micromagnetic simulations on single-layers with either small magnetic track width (W), high SW excitation rf field (A_{rf}), or low Gilbert damping constant α[3,4]. However, to complement the realization of skyrmion motion experimentally, simulations should meet experimentally achievable conditions at the same time: W ≥100nm, A_{rf} ≤100mT and α >0.05. The dataset and characteristic analysis we present concern SW driven skyrmion simulations

by OOMMF[5] with fixed parameters, D=1.5 mJ/m^2, M_S=1004 KA/m, A=3.6 pJ/m, K_u=1 MJ/m^3. We varied the α=0.02-0.06, W=40-100 nm and $A_{rf=}$100-800 mT. The size of the relaxed skyrmion is from 20nm to 23nm when W increases from 40nm to 100nm, so there is more than 5 nm between the skyrmion to each sample edge at initial stage. Fig.1 shows the skyrmion displacement (d_{sky}) with time along the SW propagation direction for various W is shown. When W >50 nm, the skyrmion will initially move opposite to the SW propagation direction before moving forward at longer times. Fig.2 shows that with larger α, the skyrmion will have smaller initial velocity when moving backward. If the leading edge of the skyrmion is regarded as a planar wall on the sample, the domain wall (DW) plane is predicted to rotate when linear momentum transfer between the SW and DW occurs. The angle between the DW wall plane and the out-of-sample direction is defined as DW wall plane angle (Φ_{DW})[6]. Also, the inset shows that Φ_{DW} of skyrmion leading edge has similar behaviour to the d_{sky}, but with an offset. The skyrmion backward motion gives a possible observation result in the future and guidance about finding a balance between W and magnetic properties to have skyrmions with aiming motion type.

1. S. Mühlbauer et al. Science, Vol.330, p1648(2010). 2. K. Everschor et al. Phys. Rev. B, Vol.84, p064401(2011). 3. X. Zhang et al. New J. Phys., Vol.19, p065001(2017). 4. L. Kong et al. Appl. Phys. Lett., Vol.116, p192407(2020). 5. M. Donahue et al. NIST(1999). 6. P. Yan et al. Phys. Rev. B, Vol.88, p144413(2013).

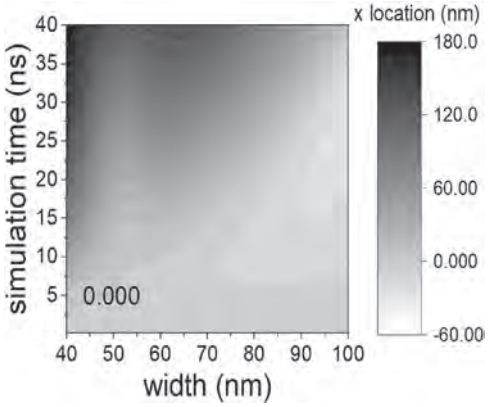

Fig.1 Time-dependent skyrmion displacement in nm for various W.

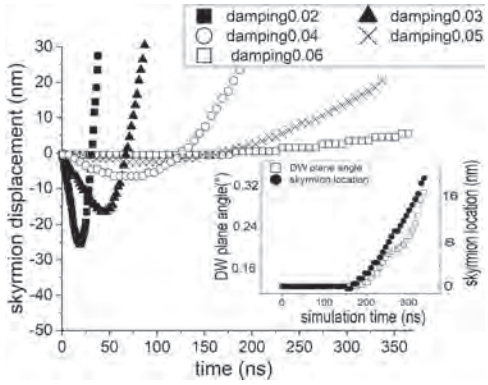

Fig.2 Skyrmion displacement with time for various α. Inset: comparison between Φ_{DW} and skyrmion displacement when α=0.06.

Session HPB
MAGNONS, SPIN DYNAMICS AND MICROMAGNETIC MODELING (Poster Session)

Matthias Benjamin Jungfleisch, Chair
University of Delaware, Newark, DE, United States

HPB-01. Mode selective excitation of spin waves. *T. Taniguchi*[1] and C.H. Back[1] *1. Fakulität für Physik, Technische Universität München, München, Germany*

Magnonic devices are based on the wave properties of spin wave (SW), so that one can transport more information in a single device if modes of SWs are freely controllable. SWs in a narrow waveguide have eigenmodes due to standing waves formed in the width direction and the thickness direction [1, 2]. However, excitation of one specific mode of propagating SW has not been realized, yet. Here, we report that high SW mode can be selectively excited by employing SW conversion. We numerically investigated SW propagation in a T-shaped structure using MuMax3 [3]. A 5-nanometer-thick Py film is assumed as the device and a magnetic field of 70 mT is applied along the y-direction (Fig. 1). By applying an rf field to the cells 1 μm away from the junction, Damon-Eshbach spin waves (DESWs) are excited and travel along the x-direction. The DESWs induce a magnetization precession in the junction, which excites SWs in the magnetostatic backward volume wave configuration (BVSWs). First, we varied the SW resonant frequency (f=12, 18 GHz) using a device having w_1=500 nm and w_2=100 nm. As shown in Fig. 2(a) and (b), the wavelength of the DESW (λ_{DESW}) depends on f which is well known [2]. In addition, the BVSWs clearly change their wave front. To extract the mode number, we applied a Fourier transformation (FT) along the y-direction. The FT results indicate that the 1st mode is dominantly excited at 12 GHz but the 2nd mode is dominant at 18GHz (Fig. 2(d) and (e)). We next changed the device to have w_2=500 nm and repeated the simulation at 18 GHz (Fig. 2(c)). The result indicates the 12th mode was dominant at this condition (Fig.2 (f)). To further understand the high-mode-excitation, we varied the frequency and plotted the FT peak height of each mode as a function of the ratio of the width to λ_{DESW} (Fig.2 (g)). The result implies that modes can be controlled by optimizing a T-shaped waveguide.

[1] H. G. Bauer *et al.*, Appl. Phys. Lett., Vol. 104, p.102404 (2014) [2] B. A. Kalinikos and A. N. Slavin, J. Phys. C, Vol. 19, p.7013 (1986) [3] A. Vansteenkiste *et al.*, AIP Adv., Vol. 4, p.107133 (2014)

Fig.1. Overview of the calculation area. SWs are excited at the orange area.

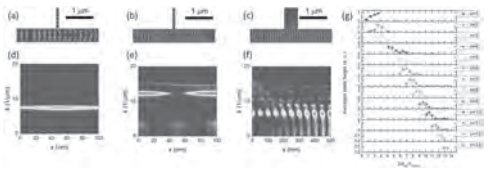

Fig.2. (a)-(c) The z-component of the magnetization and (d)-(f) their corresponding FT of BVSWs. (f, w_2) is (a, d) (12 GHz, 100 nm), (b, e) (18 GHz, 100 nm), and (c, f) (18 GHz, 500 nm). (g) The peak height of FT of each mode obtained from the device with w_2=500 nm.

HPB-02. Arnold tongue of injection locked spin torque nano-oscillators under high and mixed driving signals. *M. Ibarra Gomez*[1], J. Hem[1], P. Talatchian[1], L.D. Buda-Prejbeanu[1] and U. Ebels[1] *1. SPINTEC, Univ. Grenoble Alpes, CEA, CNRS, Grenoble INP, Grenoble, France*

Spin torque nano-oscillators (STNO) generate high frequency output voltage signals upon injection of a spin polarized DC current into a magnetic tunnel junction. For their applications in wireless communications or neuromorphic computing schemes, a central aspect is the control of their phase dynamics via injection locking to an external rf signal [1, 2]. Many interesting, non-linear effects may arise at higher excitation levels that manifest themselves in the Arnold tongue [3, 4]. For the in-plane magnetized STNO (in-plane magnetized polarizer and free layer) [2], we provide here analytical expressions for (i) the asymmetric Arnold tongue boundaries, arising from the dependence of the forcing on the STNO power; (ii) the Takens-Bogdanov bifurcation threshold [4] which leads to a reduced locking range and (iii) the hysteresis boundaries [3,4]. These effects are discussed within a common model for 'pure' rf signals arising from either a spin polarized current or a magnetic field. 'Pure' refers to a well-defined direction u_i (i=x,y,z ; u_x the STNO easy axis) of the spin polarization or a magnetic field [2]. In a further study we also investigate synchronization at harmonic order n=1 (rf signal frequency close to the STNO frequency) for mixed spin polarization with x- and y- components. The important and unexpected finding here is that the STNO phase does not follow an arcsine (Adler-type) behavior [5] within the locking range, but shows a discrete jump that can be as large as Pi/2. Our analysis shows that the phase jump results from a competition between locking to the u_x- and u_y-components of the rf signal, where locking to the u_x-component at n=1 is enabled through the fact that the free running oscillation power is non-constant with frequency components at f. This demonstrates that, for mixed rf signals, injection locking can be more complex, and that the results can be of interest for applications such as the phase jump for phase shift keying concepts [6]. MIG was supported by the French Space Agency (CNES) and the CEA NUMERICS program, which has received funding from the European Union's Horizon 2020 program (No 800945). Partial support was provided by the French National Research Agency (ANR-20-CE24-0002).

[1] W. H. Rippard et al., Phys. Rev. Lett. 95, 067203 (2005) [2] J. Hem et al., Phys. Rev. B 100, 054414 (2019) [3] M. d'Aquino et al., IEEE Magn. Lett. 8, 3504005 (2017) [4] A. Quercia, et al., Physica B: Condensed Matter, 549, 87 (2018) [5] R. Adler, Proc. IEEE, 61, 1380 (1973) [6] A. Litvinenko et al., arXiv:1905.02443

HPB-03. Magnon valve effect and resonant transmission in a one-dimensional magnonic crystal. *Y. Xing*[1], Z. Yan[1] and X. Han[1] *1. Institute of Physics, Chinese Academy of Sciences, Beijing, China*

We theoretically investigate the transmission of exchange-dominated spin waves in a one-dimensional magnonic crystal (MC) with a periodic exchange bias field. By recasting the Landau-Lifshitz-Gilbert equation into an effective Schrödinger equation and establishing spin-wave functions, it is found that MCs with upward (up) and downward (down) magnetization, respectively, correspond to the rectangular N-fold barriers and wells for magnons. The broadband transmission spectra in up and down states are systematically investigated. We show the phenomena of the magnon resonant transmission in both states and calculate the resonant transmission wave

functions, which are related to the magnon density. Our results also show a transmission spectra shift effect (TSSE) between up and down states, which is found to be general in this system. Furthermore, the TSSE is useful to design a type of magnon valve, the magnonic-crystal-based magnon valve (MCMV), which has a large on/off ratio and bandwidth. By high-throughput screening, 125 000 groups of parameters of the MC are calculated, and 1948 parameter groups of high-performance MCMVs are screened out. Our work clarifies the physical details of the exchange-dominated spin-wave transmission in rectangular *N*-fold barriers and wells and also provides a promising route for designing novel magnonic devices.

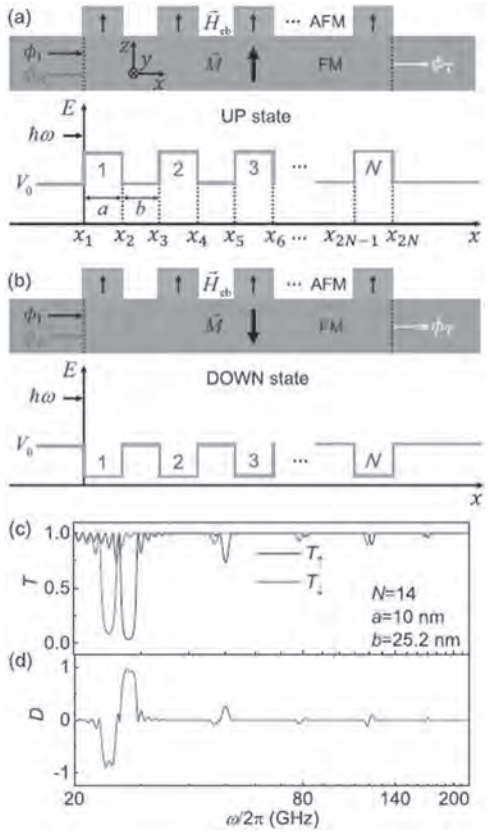

The magnon transmission in a one-dimensional MC. The schematic diagrams of the MC in (a) the up state and (b) the down state. (c) The broadband transmission spectra in up and down states, corresponding to the black curve ($T_\uparrow$) and red curve ($T_\downarrow$) respectively. The parameters of the MC are the following: N = 14, a = 10 nm, and b = 25.2 nm. (d) The difference between $T_\uparrow$ and $T_\downarrow$ as a function of ω/2π. ω/2π is shown in logarithm scale.

HPB-04. Study of Coherent Spin Waves in a Three-Dimensional Artificial Spin Ice Structure. *S. Sahoo*[1], A. May[2], A. van den Berg[2], A.K. Mondal[1], S. Ladak[2] and A. Barman[1] *1. Department of Condensed Matter Physics and Material Sciences, S. N. Bose National Centre for Basic Sciences, Kolkata, India; 2. School of Physics and Astronomy, Cardiff University, Cardiff, United Kingdom*

The study of high-frequency spin dynamics in three-dimensional (3D) magnetic nanostructures may lead to paradigm-shifting, next generation devices including high-density spintronics and neuromorphic systems. Despite remarkable progress in fabrication [1], the measurement and interpretation of spin dynamics in complex 3D magnetic structures remains exceptionally challenging. Here we present the measurement of coherent spin waves within a 3D artificial spin ice (ASI) system using Brillouin light scattering. The 3D-ASI was fabricated by using a combination of two-photon lithography and thermal evaporation. Two spin-wave modes were observed in the experiment whose frequencies showed nearly monotonic variation with the applied magnetic field strength. Numerical simulations qualitatively reproduced the observed spin-wave modes. The simulated mode profiles revealed the collective nature of the modes extending throughout the complex network of nanowires, while showing spatial quantization with varying mode quantization numbers [2]. The study shows a well-defined means to explore high-frequency spin dynamics in complex 3D spintronic and magnonic structures.

[1] A. May et al., Communications Physics 2, 13 (2019). [2] S. Sahoo et al., Nano Lett. 21, 4629 (2021).

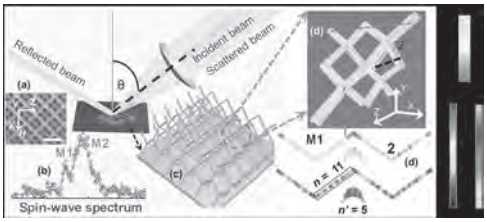

Figure 1: Schematic of BLS measurement geometry. The measurement was performed at θ = 0°. (a) A scanning electron micrograph image of the sample (scale bar: 2 μm) with applied field (*H*) direction, (b) BLS spectra at *H* = 1.8 kOe. (c) Schematic of 3D-ASI network, (d) simulated equilibrium state of magnetisation at *H* = 1.6 kOe and (d) mode profiles of M1 at 1.6 kOe are shown. Respective legends are shown on right side.

HPB-05. Magnonic and phononic dispersion in $Ni_{80}Fe_{20}$ array of antidots. *S. Chiroli*[1], D. Faurie[1], P. Djemia[1], A. Adeyeye[2,3] and F. Zighem[1] *1. CNRS LSPM Université Sorbonne Paris Nord, Villetaneuse, France; 2. Department of Physics, Durham University, Durham, United Kingdom; 3. Information Storage Materials Laboratory Department of Electrical and ComputerEngineering National University of Singapore, Singapore*

Magnonic and phononic crystals are artificial nanostructures with periodic lateral variations in their magnetic and acoustic properties [1,2]. Recently, there has been growing interest in the fundamental understanding of spin waves propagation in magnonic crystals because of their huge potential in a wide range of applications such as microwave resonators, filters and spin wave logic devices [3]. On the other hand, phononic crystal are periodic arrays of nano-objects with alternating elastic properties and mass densities, they have promising applications such as acoustic microsensing or signal processing. Besides these possible applications, the wealthy physics of the acoustic waves is one of the main reasons for the attention to their propagation. Finally, a magphonic crystal is also an artificial crystal that simultaneously presents magnonic and phononic behaviors [4,5]. The phononic and magnonic dispersions of $Ni_{80}Fe_{20}$ antidot arrays deposited on a Si substrate have been investigated by using Brillouin light scattering (BLS) and ferromagnetic resonance (FMR). The periodicity of the arrays is 400 nm with a nanohole diameter of 180 nm and with a thickness of 40 nm. The FMR technique has been employed to first investigate the magnetostatic modes in the center of the first Brillouin zone. We have thus highlighted the presence of several magnetostatic modes and we conducted micromagnetic simulations (OOMMF) that allowed us to determine the spatial location of these different modes. In a second step, we have used BLS to probe the phononic and magnonic features of the magphonic crystal. We have experimentally demonstrated the simultaneous presence of magnonic and phononic bandgaps. The different dispersion curves (both magnonic and phononic) as well as the potential applications of these magphonic crystals will be presented and discussed during the conference.

[1] V. V. Kruglyak, S. O. Demokritov and D. Grundler, J. Phys. D: Appl. Phys. 43, 264001 (2010) [2] T. Gorishnyy, C. K. Ullal, M. Maldovan, G. Fytas and E. L. Thomas, Phys. Rev. Letters 94, 115501 (2005) [3] S. O. Demokritov and A. N. Slavin, "Eds., Magnonics - From Fundamentals to Applications", Springer, Series: Topics in Applied Physics, 125 (2013) [4] V. L. Zhang, F. S. Ma, H. H. Pan, C. S. Lin, H. S. Lim, S. C. Ng, M. H. Kuok, S. Jain and A. O. Adeyeye, Appl. Phys. Lett. 100, 163118 (2012) [5] H. Pan, V. L. Zhang, K. Di, M. H. Kuok, H. S. Lim, S. C. Ng, N. Singh, A.

O. Adeyeye, Nanoscale Res. Lett. 8, 115 (2013) [6] N. Challab, D. Faurie, M. Haboussi, A. O. Adeyeye and F. Zighem, ACS Appl. Mater. Interfaces 13, 25, 29906 (2021)

HPB-06. Collective Hydrodynamic Magnon Transport Study in Magnetically Ordered Insulator Based on Boltzmann Approach. *Y. Li*[1], C. Chen[1] and J. Zhang[1] *1. School of Physics, Tongji University, Shanghai, China*

In recent years, the research of long-distance transport of magnon in magnetic insulator showed a negative voltage in thermal excited magnons signal [1,2]. Subsequent research investigated the negative voltage and find its dependence on the thickness of YIG, which raising a challenge for traditional magnon diffusion model. Similar phenomenon of viscous electrons' backflow in graphene inspired the magnon study. In graphene at low temperature where the scale of electron-electron scattering is much smaller than the scale of electron mean free path, the momentum-conserving process dominated will give make electrons behave as a viscous liquid and exhibit hydrodynamic phenomena as well as classical liquids [3], which could present a negative voltage at two edge of system. In magnons system, same momentum-conserving process would happen, even though magnon as a quasiparticle, people don't emphasize the conservation laws of particular numbers. The conservation of magnon momentum will lead whole system relaxed to an collective equilibrium $N(\lambda)=1/\exp[(\varepsilon_k-k\bullet\lambda)/k_BT]$, which is called displaced Planck distribution [4]. The collective velocity λ of the ordered motion as a function of coordinates must satisfy a Navier-Stokes type hydrodynamic equation. The backflow of viscous magnon naturally produce the negative signal in magnetic insulator system, as similar behaviors in graphene. In this work, based on Boltzmann method and considering momentum-conserving dominated process, we developed a collective hydrodynamic diffusion equation of magnons' viscous fluid, without vanishing k-space scattering. We also found nonlinear properties of hydrodynamics magnon system. Two- dimensional calculations of magnon flux showed the viscosity of magnon fluid created two eddies near the heat source. And our result could not only fit experimental data precisely, but also reconstruct physical scattering process.

[1] Cornelissen L J, Liu J, Duine R A, et al. Long-distance transport of magnon spin information in a magnetic insulator at room temperature[J]. Nature Physics, 2015, 11(12): 1022-1026. [2] Shan J, Cornelissen L J, Vliestra N, et al. Influence of yttrium iron garnet thickness and heater opacity on the nonlocal transport of electrically and thermally excited magnons[J]. Physical Review B, 2016, 94(17): 174437. [3] Bandurin D A, Torre I, Kumar R K, et al. Negative local resistance caused by viscous electron backflow in graphene[J]. Science, 2016, 351(6277): 1055-1058. [4] Callaway J. Model for lattice thermal conductivity at low temperatures[J]. Physical Review, 1959, 113(4): 1046.

HPB-07. Diffusion equation and fractional viscosity-based magneto dynamic model for electrical steel ferromagnetic hysteresis. *B. Ducharne*[1] and G. Sebald[2] *1. INSA Lyon, Villeurbanne, France; 2. ELyTMaX UMI 3757, CNRS – Université de Lyon – Tohoku University, International Joint Unit, Tohoku University, Sendai, Japan*

Magnetic losses in ferromagnetic laminations have been studied for years [1][2]. But, magnetization processes are highly complex, and the ideal model is still in need. Classic methods working in the time domain combine the magnetic diffusion equation solved in 1D (Eq. 1) to a viscosity-based magneto dynamic model (differential equation). This concurrent resolution has already been made through a strong formulation: the diffusion equation temporal term (dB/dt) is replaced by its differential equation expression [3] [4]. This elegant method leads to a fast resolution but unfortunately incorrectly considers the excess losses linked to the domain wall motions kinetic. Improved differential equations have been proposed for a better losses consideration [5], but dB/dt can't be isolated analytically, and the resolution always goes through complex and unstable iterative methods like the fixed point or the Newton-Raphson algorithm [6]. In this study, we propose to use a fractional viscosity-based magneto dynamic differential equation (Eq. 2) [7][8]. Isolation of the dB/dt term is possible by expressing the differential equation remaining terms using a fractional operator. Strong formulation is obtained, which can be solved without an iterative method. This alternative method gives access to local magnetic information (excitation and induction fields)(see Fig. 1). The number of dynamic parameters is limited (ρ a constant and n the fractional order) but large enough to add a degree of freedom in the simulation process and leads to a perfect fit of the experimental results.

[1] C.P. Steinmetz, Introduction by J.E. Brittain, Proc. IEEE, vol. 72, n° 2, pp. 196 – 221, 1984. [2] G. Bertotti, Academic Press, Boston, 1998. [3] M.A. Raulet et al., *IEEE Trans. Mag.*, vol. 40, n° 2, pp. 872 – 875, 2004. [4] B. Ducharne et al., *J. of App. Phys.*, 243907, pp.1-9, 2015. [5] S.E. Zirka et al., *IEEE Trans. Mag.*, vol. 41, n° 3, pp. 1109 – 1111, 2005. [6] S.E. Zirka et al., *IEEE Trans. Mag.*, vol. 42, n° 9, pp. 2121 – 2132, 2006. [7] B. Zhang, IEEE Trans. Mag., Vol. 54, n° 3, pp. 1-4, 2018. [8] B. Zhang, IEEE Trans. Mag., Vol. 54, n° 11, pp. 1-5, 2018.

Simulated local hysteresis cycles, imposed sinus H_{surf}, 150 A/m, 150 Hz

HPB-08. Withdrawn

HPB-09. Optical-helicity induced spin-transfer torque in ferromagnetic multilayers with perpendicular magnetic anisotropy. *S. Iihama*[1,2], K. Ishibashi[3,2] and S. Mizukami[2,4] *1. Frontier Research Institute for Interdisciplinary Sciences (FRIS), Tohoku University, Sendai, Japan; 2. WPI Advanced Institute for Materials Research (AIMR), Tohoku University, Sendai, Japan; 3. Department of Applied Physics, Tohoku University, Sendai, Japan; 4. Center for Spintronics Research Network (CSRN), Tohoku University, Sendai, Japan*

Recently, photon spin injection into heavy metal layers such as Pt attracts attention as a way to manipulate thin film magnetization. Magnetization dynamics in an adjacent ferromagnetic layer can be excited by the spin-transfer torque effect[1,2]. It is expected that photon spins and spin-transfer torques can be generated in ferromagnetic multilayers (MLs) such as [Co/Pt], known as opto-magnetic recording media with perpendicular magnetic anisotropy (PMA). Therefore, it is demanded to study the magnetization dynamics driven by optical-helicity for such MLs towards optically switchable magnetic memory devices[3]. Here, we report the optical-helicity driven magnetization dynamics of [Co/Pt] MLs with PMA. Samples were fabricated by using magnetron sputtering technique. The MLs Pt(3) / $[Co(0.6)/Pt(1)]_N$ / Pt(2) (thickness is in nm) were deposited on thermally oxidized silicon substrates. Laser-induced magnetization dynamics were measured by all-optical pump-probe technique. Figure 1 shows typical optical-helicity induced magnetization dynamics for $[Co/Pt]_4$ samples where in-plane magnetic field was applied. Magnetization precessions were clearly observed and those initial phases were reversed with the helicity of the laser pulse, indicating optical-helicity induced torques on magnetization. To understand the effect of optical-helicity on the magnetization dynamics, the phase of the magnetization precession was analyzed as shown in Fig. 2. It was found that magnetization of MLs was mainly excited by the spin-transfer torque where magnetization is initially tilted towards out-of-plane direction [red broken curve]. Details of photon spin injection into MLs and proposal of optically switchable magnetic memory devices with PMA will be presented.

[1] G. -M. Choi *et al.* Nat. Commun. 11, 1482 (2020). [2] S. Iihama *et al.* Nanophotonics 10, 1169 (2021). [3] H. Becker *et al.* IEEE J. Sel. Top. Quant. 26, 8300408 (2020).

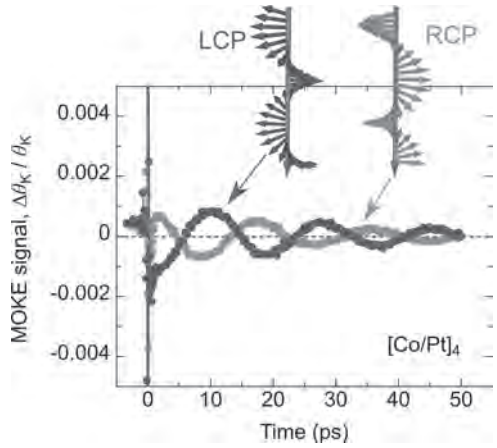

Fig.1 Laser-induced magnetization dynamics for [Co/Pt]$_4$ multilayer thin films with different optical helicity (LCP: left circularly polarized, RCP: right circularly polarized).

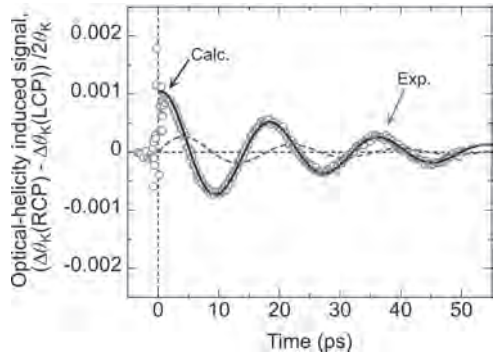

Fig. 2 Subtracting the optical-helicity induced magnetization dynamics by taking difference between signals measured by using RCP and LCP laser pulse. Open symbols are experimental results while solid and broken curves are calculated results.

HPB-10. Current-Induced Magnetization Switching of Exchange-Biased NiO Heterostructures Characterized by Spin-Orbit Torque.

K. Grochot[1,2], L. Karwacki[3,4], S. Lazarski[1], W. Skowronski[1], J. Kanak[1], W. Powroznik[1], P. Kuswik[4], M. Kowacz[4], F. Stobiecki[4,1] and T. Stobiecki[1,2]
1. Institute of Electronics, AGH University of Science and Technology, Cracow, Poland; 2. Faculty of Physics and Applied Computer Science, AGH University of Science and Technology, Cracow, Poland; 3. Institute for Theoretical Physics, Utrecht University, Utrecht, Netherlands; 4. Institute of Molecular Physics, Polish Academy of Sciences, Poznan, Poland

Spin-orbit torque (SOT)-induced magnetization switching provides a potentially efficient alternative to spin-transfer torque switching in spin valves or magnetic tunnel junctions. Current induced SOT-switching of perpendicular magnetization is observed in an external magnetic field collinear with the current (but non-collinear with the magnetization), which, however, is impractical in device applications. In this work, we study magnetization switching induced by spin-orbit torque in W (Pt)/Co/NiO heterostructures with variable thickness of W and Pt heavy-metal layers, a perpendicularly magnetized Co layer, and an antiferromagnetic NiO layer [1]. Using current-driven switching, magnetoresistance and anomalous-Hall-effect (AHE) measurements, we determine the perpendicular and in-plane exchange-bias field. Several Hall-bar devices possessing in-plane exchange bias from both systems are selected and analyzed in relation to our analytical switching model of the critical current density as a function of Pt and W thickness, resulting in an estimation of the effective spin Hall angle and perpendicular effective magnetic anisotropy. We demonstrate in both the W(Pt)/Co/NiO systems deterministic Co magnetization switching without an external magnetic field, which is replaced by an in-plane exchange-bias field. Moreover, we show that due to a higher effective spin Hall angle in the W-based system than in Pt, the relative difference between the resistance states in the magnetization current switching to the difference between the resistance states in magnetic field switching determined by AHE ($\Delta R/\Delta R_{AHE}$) is about twice as high in W-based devices than in Pt, while the critical switching-current density in W-based devices is one order lower than in Pt. The current switching stability and the training process are discussed in detail. This work is funded by National Science Centre, Poland, Grant no. 2016/23/B/ST3/01430 SpinOrbitronics. KG acknowledge support for conference participation by the EU Project POWR.03.02.00-00-I004/16.

[1] K.Grochot et al., Phys. Rev. Appl., Vol. 15, p. 014017 (2021)

Session IOA
MAGNETIC RECORDING TECHNOLOGY I

Chris Rea, Co-Chair
Seagate, Minneapolis, MN, United States
Wei-Heng Hsu, Co-Chair
Seagate, Minneapolis, MN, United States

CONTRIBUTED PAPERS

IOA-01. Multiple spin injection into coupled field generation layers for low current operation of MAMR heads. *Y. Nakagawa*[1], M. Takagishi[1], N. Narita[1], T. Maeda[1] and A. Takeo[2] *1. Corporate Research and Development Center, Toshiba Corporation, Kawasaki, Japan; 2. Toshiba Electronic Devices and Storage Corporation, Yokohama, Japan*

Microwave-assisted magnetic recording (MAMR) is one of the promising techniques for the next generation hard disk drive (HDD) [1]. For MAMR, a spin torque oscillator (STO) embedded in the write head is suitable for microwave generation. Recently, we have proposed a new STO structure with two field generation layers (FGLs) [2]. The magnetizations of dual FGLs oscillate with keeping anti-parallel direction in the in-plane, which provides an ideal microwave profile for MAMR [2,3]. In this talk, we propose another dual FGL structure, which shows substantial oscillation amplitude with a smaller current. In the dual FGL structure, the oscillation of FGLs is driven by the spin-transfer torque (STT) passed to each FGLs from a SIL and one of the poles, respectively [2] (Fig. 1(a)). In the new structure, we insert another SIL between FGLs, forming a dual SIL dual FGL structure (Fig. 1(b)). We simulated the oscillation behavior of the dual FGL structures by solving Landau-Lifshitz-Gilbert (LLG) equation with an STT term. We prepared three simulators; (I) macrospin simulator, (II) micromagnetic simulator for simplified square layers (Fig. 2), and (III) micromagnetic simulator modeling whole write head. In all simulators, the new dual FGL structure showed larger oscillation amplitudes than in the previous structure. Figure 2(a) shows the result in the simulator (II), where FGLs' magnetic thicknesses are 15.6 nmT for both FGLs and for both structures. The cone angle was defined as the angle between the *z*-axis (Fig. 1(a)) and the magnetization. We confirmed the stable antiparallel oscillation (Fig. 2(b)), indicating that the merits of the dual FGL structure [2] are maintained in the new structure. In our presentation, we will further discuss the oscillation behavior, including the dynamics of SILs.

[1] J. -G. Zhu, X. Zhu and Y. Tang, IEEE Trans. Magn. 44, 125 (2008). [2] M. Takagishi et al., IEEE Trans. Magn. 57, 3300106 (2021). [3] T. Olson et al., IEEE Trans. Magn. 51, 3001004 (2015).

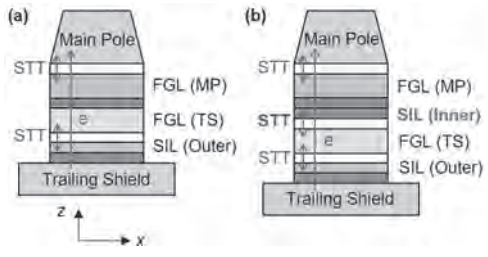

Fig.1 Dual FGL structure embedded in a write pole. (a) Structure in the previous work [2]. (b) SIL-inserted structure. Magnetic layers are separated by non-magnetic spacers whose spin diffusion lengths are long (white) or short (gray).

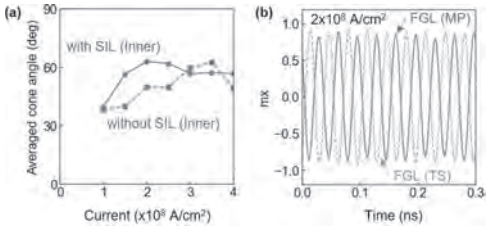

Fig.2 Simulation results in the simulator (II) (a) Current dependence of the cone angle. (b) Time dependence of the normalized in-plane magnetization of FGLs in the SIL-inserted structure.

IOA-02. Spin Transport in an Ultrathin Al Film for Use as a Nonlocal Spin Valve. *Y. Liu*[1] and R. Victora[1,2] *1. School of Physics and Astronomy, University of Minnesota, Minneapolis, MN, United States; 2. Electrical and Computer Engineering, University of Minnesota, Minneapolis, MN, United States*

We present the effect of surface and bulk scattering on electronic and spin transport in aluminum -based ultrathin films in the Laudauer-Buttiker formalism with Green's function technique. Our results potentially widen the application of nonlocal spin valves for read heads that can operate with smaller shield-shield spacing, higher capacity and reliability at room temperature. However, as the overall dimension of the devices scales down, in particular for thickness of the metallic channels smaller than 10nm, the device performance declines substantially due to various spin relaxation mechanisms [1]. It has been suggested that extrinsic effects acting through spin-orbit coupling such as defects, surface roughness, and grain boundary scattering are responsible for the short spin transport in metal. In this work, the combined effects of surface roughness, vacancies, and spin-orbit interaction on the properties of spin transport is investigated in an Al-based NSLV, employing a recursive approach that reduces computation complexity by the square of the number of layers. [2]. Resistivity and spin diffusion length are determined under the assumption that the device is embedded into an insulating surrounding environment. For simplicity, both the leads and the metallic channel are made of Al. Compared with previous work [3,4,5], we extend the calculation from a simple cubic structure with s orbital to a realistic system with fcc crystal structure and multiple orbits. We demonstrate that for thin sputtered films, the scattering due to the vacancies is likely dominant over the surface scatterings as shown in Fig 1 and Fig 2, and can yield reasonable spin diffusion lengths and mean free paths.

[1] S.Rakheja, S.Chang and A. Naeemi, IEEE Trans. Electron Device Vol.60, NO.11(2013). [2] M.L Sancho, J.L Sancho and J.Rubio, J.Phys. F 14, 1205(1984). [3] S.B. Touski and M.Pourfath, Appl. Phys. Lett. 103,143506(2013). [4] S.B. Touski R.Roldan, M.Pourfath and M.L. Sancho, Phys.Rev.B 95,165301(2017). [5] X.Chen and R.H. Victora, Appl.Phys. Lett, 93.162105(2008).

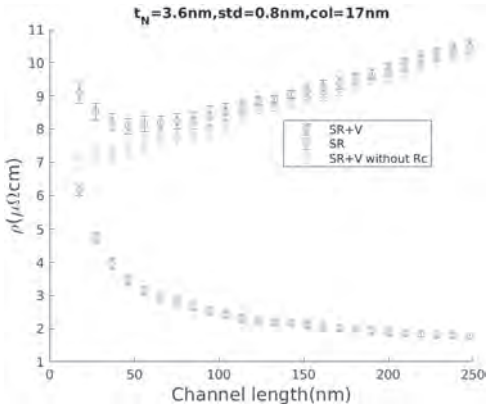

Fig1. Resistivity of 3.6nm thick film changes with channel lengths under different scattering mechanisms at T=0K; SR: surface roughness (standard deviation = 0.8 nm and correlation length = 17 nm). V: 1% vacancies. The yellow curve shows the resistivity variation with contact resistance(Rc) removed.

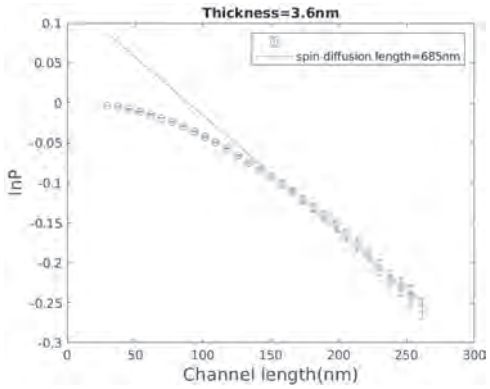

Fig2. Extraction of spin diffusion length for a 3.6nm thick channel under the same conditions as Fig1. P is the spin polarization. SOC = 0.004 Ry. Spin diffusion length = 685 nm.

IOA-03. Stoner-Wohlfarth Model with Standard Deviation of Magnetic Easy Axis. *D. Lee*[1], D. Han[2], S. Jeong[1], N. Lee[1], I. Suzuki[3], Y. Takahashi[3] and S. Kim[1] *1. Department of Physics, University of Ulsan, Ulsan, The Republic of Korea; 2. Department of Materials Science and Engineering, Korea Advanced Institute of Science and Technology (KAIST), Daejeon, The Republic of Korea; 3. National Institute for Materials Science (NIMS), Tsukuba, Japan*

A granular magnetic film is a well-known material system for achieving ultra-high density recording media. This material system consists of small grains on the scale of a few nanometers, typically separated by boundaries a few nanometers thick. FePt-C is the most popular material in the hard disk drive industry. FePt can be deposited as an $L1_0$ structure on MgO (100). [1] C is placed on the MgO layer with surrounding $L1_0$ structured FePt grains. [2] As such, nano-size separation of a magnetic material having excellent thermal stability can be achieved in a thin film. The grain size of the film varies from 7 nm to 20 nm. The Stoner-Wohlfarth model (SW model) is known to be a suitable model for explaining the relationship between the magnetic field and the magnetization direction of a single particle. FePt grains with an $L1_0$ structure have a very high magnetic anisotropy constant, which enables high thermal stability and single particle magnetization behavior. Though the grains should have magnetic single domains due to the small size less than 15 nm, the angular dependence of the switching field does not match the existing SW model for a single particle. In this presentation, we propose the Stoner-Wohlfarth model with standard deviation of the magnetic easy axis to understand the magnetization switching behavior of the FePt-C granular film. In our model, we can quantify the degree of deviation of the magnetic easy axis in the FePt-C granular film.

[1] Wanjiao Zhu et al. J. Phys.: Condens. Matter, 25, 396001 (2013) [2] H. Pandey et al., IEEE Trans. Magn., 52, 3200108 (2016)

IOA-04. A Study of Three-Dimensional Equalization for Reproducing a Double-Layer Magnetic Recording Medium. *Y. Nakamura*[1], M. Nishikawa[1], Y. Kanai[2] and Y. Okamoto[1] *1. Graduate School of Science and Engineering, Ehime University, Matsuyama, Japan; 2. Department of Information and Electronics Engineering, Niigata Institute of Technology, Kashiwazaki, Japan*

The three-dimensional (3D) magnetic recording to multiple recording layers is fascinating with much attention as a next-generation recording method [1]. We have reported that two-dimensional (2D) partial response maximum likelihood (PRML) can achieve good BER performance using the PR channel obtained from the differential-phase bit response in the 3D magnetic recording system with a double recording layer [2]. To further increase the recording density, we study the 3D equalization. In this study, we assume that the writing process is a simple rectangular recording and the areal recording density of each layer is 4 Tbits/inch^2 [2]. We define the magnetic spacing between the bottom of a reader and the top of 1st and 2nd recording layers as $\Delta = 2$ nm and $\Delta = 5$ nm, respectively [2]. In the writing process, the input data sequences are recorded on the respective recording layers. In the reading process, an array head with three magneto-resistive (MR) sensors reads both layers at a time [3]. A channel bit response for the intended track is determined by the read/write channel and the 3D equalizer with 15 taps/reader [3]. We investigated two PR channels based on the in-phase and differential-phase bits on the double recording layers [2]. The PR channel output sequence is fed to the Viterbi detector which decodes the information written in the double recording layers. Figure 1 shows the bit error rate (BER) performances of PRML channels for signal-to-noise ratio (SNR_S) for system noise. The blue and red circles show the BER performances of PRML channels for in-phase and differential-phase responses, respectively. And the open and filled circles show the BER performances using the 2D and 3D equalizers, respectively. As can be seen from the figure, the PRML channel for the differential-phase response shows good BER performance for the SNR_S greater than 24.0 dB.

[1] S. Greaves, Y. Kanai, and H. Muraoka, "Multiple layer microwave-assisted magnetic recording," *IEEE Trans. Magn.*, 53(2) 3000510, (2017). [2] Y. Nakamura, M. Nishikawa, Y. Kanai, and Y. Okamoto, "A study of equalization for reproducing a double-layer magnetic recording medium", *Digest of TMRC 2021*, G3, (2021). [3] R. Suzutou, Y. Nakamura, Y. Okamoto, H. Osawa, Y. Kanai, H. Muraoka, "Performance evaluation of TDMR R/W channel with head skew by LDPC coding and iterative decoding system," *IEEE Trans. Magn.*, 51(11), 3002004, (2015).

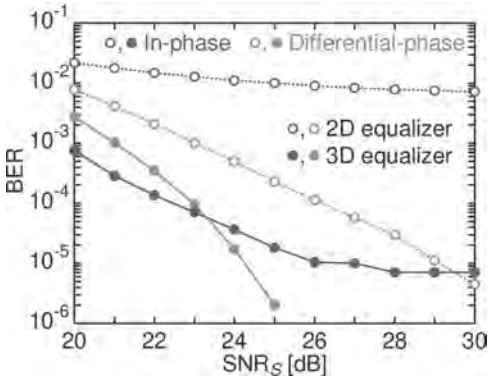

Fig.1 BER performances.

IOA-05. Deep Neural Networks based Soft-Information Improvement for Two-Head/Two-Track Bit-Patterned Magnetic Recording.
N. Rueangnetr[1], K. Kanhunthod[1] and C. Warisarn[1] *1. King Mongkut's Institute of Technology Ladkrabang, Bankok, Thailand*

To increase an areal density (AD) of an ultra-high density bit-patterned magnetic recording (BPMR) system [1], we have proposed track mis-regristration (TMR) correction method combined with the soft information adjustor (SIA) to cope with the effects of TMR and two-dimensional (2D) interference [2]. However, we found that soft information or log-likelihood ratio (LLR) can be improved to earn better bit-error rate (BER) performances. Therefore, we propose to use two deep neural networks (DNNs), e.g., multi-layer perceptron (MLP) [3] and long short-term memory (LSTM) network [4] that are operated together with an early SIA on a two-head/two-track (2H2T) BPMR system as shown in Fig. 1. The user sequences, $x_{l,k} \in \{\pm 1\}$ of the l-th track and k-th bit, are recorded onto the medium. All readback signals are produced using two readers, which are then sent to TMR predictor [2]; meanwhile, they are equalized by the consistent 2D equalizers. Then, the equalized sequences, $z_{l,k}$, are fed into the 2D detectors to output LLRs. The SIA is used to first improve the reliability of each LLR sequence before passing them to our proposed schemes based on DNNs to decide the estimated recorded bits, $x'_{l,k}$. The LLR that is obtained from SIA under various TMR effects is given as an input dataset, while the recorded sequence is fixed as an output dataset of DNNs. All of readback signals that relate to considered datasets are interrupted with several electronic noise levels. Here, we set al. input and output datasets as 5,200 files, each file consists of 2×32,768 bits, which are directly mapped to be as a pair of input and output datasets. Fig. 2 shows BER performances between the proposed and conventional SIA systems [2]. It is clear that the proposed systems yield better BER performances over the conventional system at all TMR levels with and without position jitter. At BER = 10^{-5}, the proposed LSTM gains for about 4.0 and 4.4 dBs over the conventional SIA system for both cases at TMR 0%. We found that LSTM network slightly provides better performance.

[1] H. J. Richter et al., "Recording on bit-patterned media at densities of 1 Tb/in^2 and beyond," IEEE Trans. Magn., vol. 42, no. 10, pp. 2255–2260, Oct. 2006. [2] K. Kankhunthod, W. Busyatras, and C. Warisarn, "Track mis-registration correction method in two-head two-track BPMR systems," ECTI-CON, 2020, pp. 735-738, doi: 10.1109/ECTI-CON49241.2020.9158129. [3] S. Jeong and J. Lee, "Iterative signal detection scheme using multilayer perceptron for a bit-patterned media recording system," Appl. Sci., vol. 10, no. 24: 8819, 2020. [4] S. Hochreiter and J. Schmidhuber, "Long short-term memory," Neural Computation, vol. 9, no. 8, pp. 1735–1780, 1997. [Online]. Available: https://doi.org/10.1162/neco.1997.9.8.1735

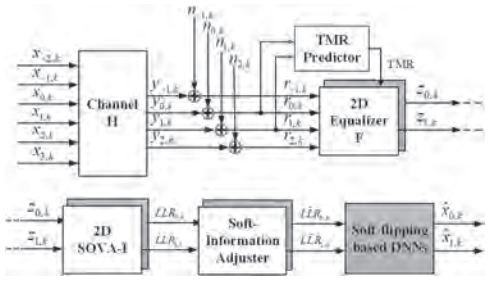

A 2H2T BPMR channel with the DNNs based soft-information improvement.

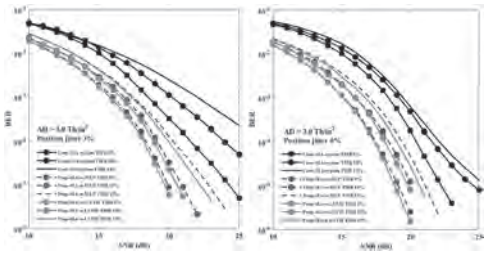

BER performances of the conventional SIA [2] and proposed systems.

IOA-06. Machine Learning Detection Channel Enabling Wide Reader for Bit Patterned Media. *T. Mo*[1,2], D. Laughlin[1,2] and J. Zhu[1,3] *1. Data Storage Systems Center, Carnegie Mellon University, Pittsburgh, PA, United States; 2. Dept. of Materials Science and Engineering, Carnegie Mellon University, Pittsburgh, PA, United States; 3. Dept. of Electrical and Computer Engineering, Carnegie Mellon University, Pittsburgh, PA, United States*

Bit patterned media (BPM) technology is intended to provide ultimate areal recording density for hard disk drives. However, for data read back, if a reader has to only read a single track, the read width might become the limiting factor, rather than that of the technology itself. In this study, a machine learning data detection channel is employed to a relatively wide reader with a read width covering two data tracks, as shown in Fig. 1(a). Adjacent data tracks are staggered by half of the bit separation B, which is also the pitch of patterned bits, in the down-track direction. Perpendicular magnetization is assumed for each patterned bit. The read-back signal consists of equal contributions from both the targeted track and interference tracks and is sampled at equal time intervals as input to the neural network. A convolution neural network (CNN) is applied here. This network has four hidden layers with 40 channels per hidden layer and all the filters in each hidden layer have a kernel size of three. The number of input neurons is determined to cover the entire spread of inter symbol interference. The number of input neurons is 9 in the case shown here, corresponding to the PW50/B=1.4 used. The weights of the filters are determined through the training process. Specifically, the rectified linear unit (ReLU) is used for the taps. Only the corresponding binary data of the target track are used in the training process for the "learning" purpose. The entire network consists of 15,000 learnable parameters or weights. Figure 1(b) shows the detection error rates, as a function of the number of bits used in training. For the case in which the signal is sampled at an interval of B (blue curve), the detection error becomes zero over one million different bit sequences after the network is trained over 50,000 bits. If the sampling frequency doubles (red curve), i.e. sampled at an interval of B/2, the zero error detection can be achieved with just 1,000 training bits. Note that the two cases shown here are noise-free. With noise added, more training bits will be needed. In the talk, results on the detection bit error rates for practical signal-to-noise ratios will be presented.

[1] Barry C. Stipe, et al. "Magnetic recording at 1.5 Pb m-2 using an integrated plasmonic antenna," Nature Photonics, 4, 484-488 (2010).

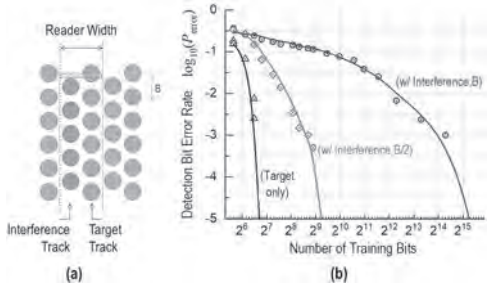

IOA-07. Experimental evolution of two parametric mechanisms of magnetization reversal in FeCoB nanomagnet. *V. Zayets*[1] *1. Platform Photonics Research Center, National Institute of Advanced Industrial Science and Technology (AIST), Tsukuba, Japan*

A new mechanism of recording for a MRAM cell, which is based on a parametric resonance, has been proposed [1] and experimentally studied. The parametric mechanism requires a substantially smaller spin torque for the magnetization reversal due to the resonance nature of this recording mechanism and, therefore, it can be a solution for further reduction of the recording energy for the MRAM operation. Two parametric mechanisms for the magnetization reversal are proposed, studied and experimentally evaluated. The first mechanism is due to a modulation of the magnetic field of the Spin- Orbit Torque. The second mechanism is due to modulation of the anisotropy field. For both mechanisms, a parametric torque is created by a RF modulated current, which resonantly enhances the magnetization precession until a magnetization reversal. Additionally, a parametric mechanism for magnetization reversal by a DC current is proposed and studied. This parametric mechanism may occur in a magneto-resistive structure, in which a magnetization precession modulates an electrical current. It results in a positive feedback loop, in which a magnetization precession creates a torque, which more enhances the precession.

V. Zayets, "Mechanism of parametric pumping of magnetization precession in a nanomagnet. Parametric mechanism of current-induced magnetization reversal.", *arXiv:2104.13008 (2021)*.

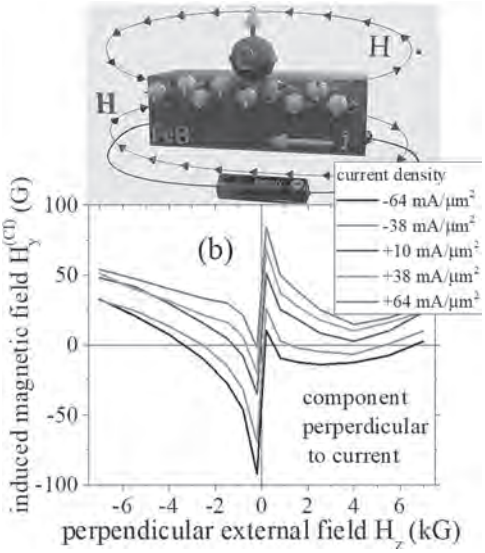

Figure 1. Source of Parametric mechanism 1: current-induced magnetic field directed perpendicularly to magnetization. Top inset shows the magnetic field $H^{(CI)}$, which is induced by spin accumulation (green balls) and directed perpendicularly to the nanomagnet magnetization (blue ball). Figure shows measured current- induced magnetic field $H^{(CI)}$ as a function of current density and external perpendicular-to-plane magnetic field H_z. (a) measured x- and y-components of $H^{(CI)}$. Lines of different color corresponds to a different current density. The magnetic field Hz is used a parameter and scanned from -7 kGauss to +7 kGauss.

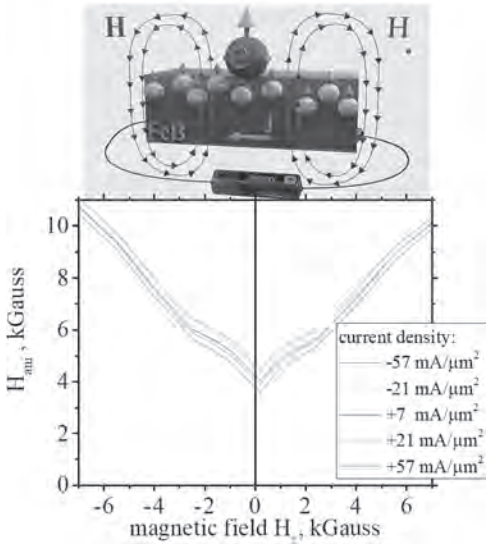

Fig.2 Source of Parametric mechanism 2: current-induced magnetic fielddirected along magnetization, which changes the anisotropy field. Figure shows measured dependence of the anisotropy field H_{ani} in a FeCoB nanomagnet on perpendicular-to- plane magnetic field and current density. H_{ani} vs.H_z. A line of different color correspond to a different current density j.

IOA-08. Master structure dependence of double magnet master on magnetic printing performance onto energy-assisted magnetic recording media. *T. Komine*[1] *1. Ibaraki University, Ibaraki, Japan*

The double magnet master (DMM) magnetic printing onto energy-assisted magnetic recording (EAMR) media with high coercivity is a promising way to write servo-signals with high speed and low cost[1]. The double magnet master media consists of high coercivity and low coercivity magnets separated by non-magnetic insertion. Although the printing performance is expected to be determined by the master structure such as thickness of insertion, master thickness, pattern widths and so on, the influence of the master structure has not been discussed yet. In this study, the magnetic printing by DMM with various master structures was demonstrated by micromagnetic simulation. Figure 1 shows the schematic illustration of DMM medium with various non-magnetic insertion layers. The EAMR media were assumed to be the exchange coupled composite media were utilized as the recording layer. The rectangular grains of the dimension of 5×5×20 nm^3 were assumed in order to confirm magnetic printing characteristics of DMM onto EAMR media. The printed magnetization distributions of the recording layer was solved in the same manner of my previous study[1]. The printing performanes were evaluated by the correlation function for ideal printed magnetization. Figure 2 shows the printing performances for various insertion thickness or L/S pattern width. The inset figures show the printed magnetization distribution in each case. In case of the same L/S pattern widths, the printing performance was not enough because of transition noise under the application of printing field which is almost equal to the recording layer coercivity. Moreover, the stronger printing field leads the wider line width and the printing performance deteriorates. On the other hand, arranging line pattern width can improve the printing performance because of optimizing the recording field with in-plane component. As a result, the optimum insertion layer can improve the printing performance.

[1] T. Komine, "Double magnet master media for magnetic printing onto energy-assisted magnetic recording media", *IEEE Trans. Magn*. (2021) (Early Access).

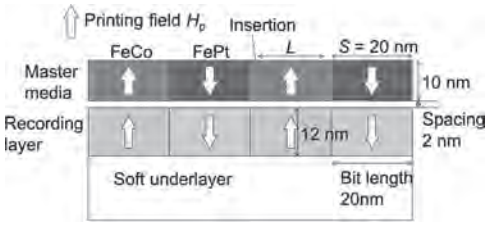

Fig. 1 Schematic illustration of double magnet master media with non-magnetic insertion.

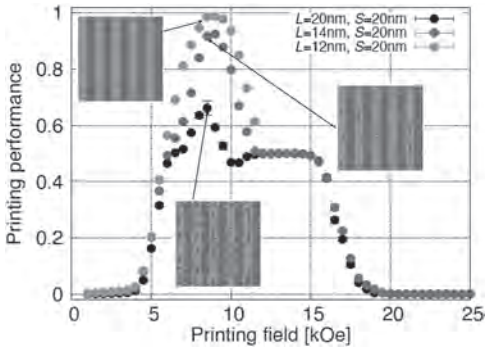

Fig.2 Printing performance of double magnet master media with various insertion thicknesses, and corresponding magnetization distributions.

IOA-09. Higher-order magnetic anisotropy in soft-hard nanocomposite materials. *B.T. Nguyen*[1], S. Jenkins[1,2], R.F. Evans[1] and R.W. Chantrell[1]
1. Physics, University of York, York, United Kingdom; 2. Physics, University of Duisburg-Essen, Duisburg, Germany

Properties of higher-order magnetic anisotropy constants in soft-hard nanocomposite materials still attract much debate [1]. We investigated the magnetic anisotropy in a $L1_0$/A1 FePt system using the VAMPIRE software package [2]. An elongated, faceted cylindrical core-shell was constructed with a $L1_0$-FePt core of varied size surrounded by an A1-FePt shell. The system exchange interaction was 3-dimensional and accounted up to the third-nearest neighbours. A 2-ion Fe-Pt anisotropy component was incorporated to the system Hamiltonian following Mryasov et al. [3]. The angular dependence of the restoring torque was calculated from 0K to 1000K in 5K steps using a constrained Monte-Carlo integrator. Temperature-dependent anisotropy constants were then determined from fitting to the system torque as a function of the constrained angle. We find that the core-shell structure exhibits an unexpected 4th-order anisotropy term of which magnitude depends on the core-size ratio R. The K_2/K_1 ratio, with K_1 and K_2 being the 2nd and 4th-order anisotropy constant respectively, displays a non-monotonic pattern with a peak occurring at $R \sim 0.55$ *[Fig.1]*. We find that K_2 scales with $(M/M_s)^{-2}$ at temperatures below T_c *[Fig.2]* - a remarkable deviation from the established Callen-Callen theory [4] which instead predicts a scaling with $(M/M_s)^{10}$. A simple analytical model shows the 4th-order term to arise from canting of the core and shell magnetisation. Further, the model demonstrates that the magnitude of the 4th-order term is proportional to K_1^2/J, with J the exchange coupling. Given that the 2-ion K_1 term scales approximately with M^2 and J with M^2, the predicted scaling exponent is 2 in agreement with the simulations. Generally, the 4th-order anisotropy constant is shown to exhibit a strong dependence on the system geometry, thus suggesting that the Callen-Callen power law is not universal and valid only for single-ion anisotropies.

[1]: Richter et al., J. Appl. Phys. 109, 07B713 (2011) [2]: Evans et al., Journal of Physics: Condensed Matter, 26, 103202 (2014). More information about VAMPIRE can be found at: http://vampire.york.ac.uk/features/ [3]: Mryasov et al., Europhys. Lett., 69 (5), pp. 805–811 (2005) [4]: Callen et al., J. Phys. Chem. Solids, 16, 310 (1960)

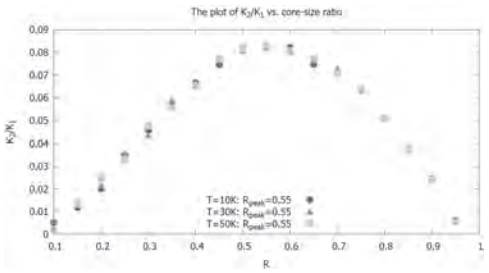

Fig.1: A low temperature scan displays a non-monotonic dependence of K_2/K_1 on core size ratio R with a peak at R ~ 0.55.

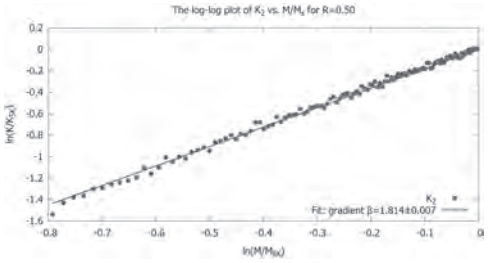

Fig.2: K_2 scaling with M/Ms for R=0.50 results in a scaling exponent β ~ 1.81 not 10 as predicted by Callen-Callen.

IOA-10. Reactive Molecular Dynamic Simulation of Plasma Etching Process of L10-FePt HAMR Media in Embedded Mask Patterning. *J. Zhu*[1] and J. Wang[1] *1. Electrical and Computer Engineering, University of Minnesota, Minneapolis, MN, United States*

Embedded Mask Patterning (EMP) has been demonstrated as a potential HAMR media solution with formation of ultra-fine and highly-ordered L10-phase FePt grains[1]. We used a hybrid model including both reactive and pair-wise interatomic potentials in the classic Molecular Dynamic (MD) simulation to study the methanol-based reactive plasma etching mechanism of the FePt lattice. The major reactive redical etchants in the methanol plasma are identified as Carbon monoxide and Hydrogen spieces[2]. Adsorbed Carbon monoxide molecules reacts with the Fe and Pt atoms and forms caronyl bonds. With assisted ion beams such as Ar+ or He+, we show the chemical etch yield is increased. The ordering change of FePt crystal surface during the etch are also simulated.

[1] H. Wang, H. Zhao, P. Quarterman, and J.-P. Wang, "Embedded mask patterning: A nanopatterning process to fabricate FePt magnetic media," Appl. Phys. Lett., vol. 102, no. 5, p. 052406, 2013. [2] M. Villa et al. "Characterization A Low Pressure of Plasma of Methanol Alcohol", J. Physics: Conference Series 511 (2014) 012019 [3] J. Zhu, P. Quarterman, and J.-P. Wang, "Ion-assisted plasma etch modeling of L10 phase FePt magnetic media fabrication with embedded mask patterning method," IEEE Trans. Magn., vol. 51, no. 11, Nov. 2015, Art. ID 3201605. [4] J. Zhu, P. Quarterman, and J.-P. Wang, "Molecular dynamic simulation study of plasma etching L10 FePt media in embedded mask patterning (EMP) process", AIP Advances 7, 056507 (2017); doi: 10.1063/1.4977223

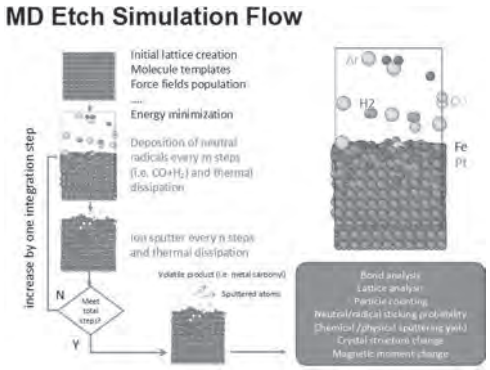

MD Simulation of Plasma Etch of FePt Media

IOA-11. Fabrication of Granular FePt-L1$_0$ HAMR Media with High Grain Aspect Ratio. *C. Xu*[1], B. Zhou[1], T. Du[1], B. Yang[1], B. Varaprasad[1], D. Laughlin[1] and J. Zhu[1] *1. Data Storage Systems Center, Carnegie Mellon University, Pittsburgh, PA, United States*

In granular FePt-L1$_0$ HAMR media. sufficient grain volume is critical for achieving expected areal density capability (ADC) [1][2]. Grain height needs to be increased as the grain size decreases. We present an experimental study on the fabrication of HAMR media with tall/high aspect ratio FePt-L1$_0$ grains. The underlayer stack consists of Ta(5nm)/Cr(40nm)/MgO(8nm) prior to the magnetic layer deposition. A 0.5 nm FePt layer is deposited on the MgO underlayer for initial grain nucleation, followed by the deposition of 2 nm FePt-BN (35% boron nitride) both at 700 ^{o}C. Over the FePt/FePt-BN stack, FePt-SiOx of 10nm thickness is deposited in the following manner: The first 3.5nm are deposited at 600 ^{o}C followed by immediately turning-off of the substrate heating and the rest of the layer is then deposited while the substrate undergoes naturally cooling. The ending temperature is 430 ^{o}C. The volumetric SiOx concentration of the FePt-SiOx layer is also graded from 40% at the bottom to 18% at the top. The L1$_0$ order parameter is S=0.72, calculated based the XRD measurement. Figure 1 shows the plan view HAADF TEM image (left) and cross-section view TEM image (right). The plan view image clearly shows well separated grains with average grain size around 6nm. The cross-section image shows columnar grains with well-defined grain boundaries and a grain aspect ratio ranging from 1.7 to 2. In this film stack, the SiOx grain boundaries are vertically matched with boron-nitride grain boundaries at the interface of the two layers. If the deposition temperature exceeds 650 ^{o}C, the majority of the adjacent FePt grains could become laterally connected over the entire thickness of the FePt-SiOx layer whereas the BN grain boundaries remains intact. While we vary the deposition conditions of the FePt-SiOx layer, the FePt/FePt-BN stack acts as a fixed template layer for the grain growth on top. For the FePt-SiOx layer, the graded SiOx composition combined with the graded deposition temperature serves the key to (1) ensure columnar grains that are well separated by SiOx grain boundaries and (2) avoid the formation of 2nd layer FePt grains.

[1] Y. Kubota, et al. “Heat-Assisted Magnetic Recording’s Extensibility to High Linear and area Density,” IEEE Trans. Magn. vo. 54, 3201206 (2018). [2] Y. Qin and J.-G. Zhu, “Impact of Magnetic Medium Grain Height in Heat-Assisted Magnetic Recording,” IEEE Magnetics Lett. 10, 6502305 (2019).

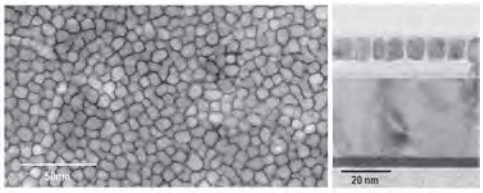

Fig. 1. Planview HAADF (Left) and Cross-section (Right) TEM image of the entire medium stack.

IOA-12. Characterization of the Thermal Time Constants of HAMR Media. *I. Gilbert*[1], C. Rea[2], J. Guzman[2], J. Loven[1] and M. Benakli[2] *1. Seagate Research Group, Seagate Technology, Shakopee, MN, United States; 2. Recording Head Operations, Seagate Technology, Bloomington, MN, United States*

We characterize the thermal rise and fall times in heat-assisted magnetic recording (HAMR) [1,2] media using spin stand measurements under realistic recording conditions as well as simulations. The experimental time constants are inferred from the read signal of a single-frequency tone written while abruptly increasing or decreasing the laser power applied to the near-field transducer (NFT) [3,4]. In addition to changing the peak temperature of the media, the change in laser power also produces a concomitant change in the diameter of the thermal spot in the media, altering the write location relative to the pole. This change in write location is detectable in the read signal as a phase shift. The rise and fall times for these phase shifts, shown in Figure 1, correspond to the thermal time constants of the media temperature. We also used analytical and numerical tools to characterize the transient thermal response of HAMR media. The solution to this problem is greatly simplified by using the NFT as the point of reference for the thermal equation. We also added a convective term (proportional to the disk velocity) to account for the effects of the moving disk. A 3D finite element method is used to calculate the temperature rise in the media in response to an abrupt step in laser power. A typical result is presented in Figure 2. Fitting the media peak temperature vs. time as determined from both experiment and simulation requires two time constants, a fast one and a slow one. The fast one is on the order of 1 ns, while the slow one is on the order of 10 ns. The slow component represents ~15% of the overall temperature rise and can be shown to correspond to the large thermal background, while the fast component corresponds to the central thermal peak. The experimentally-measured thermal rise and fall times differ because the speed at which the thermal spot expands or contracts is convolved with the velocity of the disk relative to the head, a phenomenon analogous to the Doppler effect. These results expand the fundamental understanding of the transient thermal response of HAMR media. They also have particular relevance to the design various pulsed HAMR recording schemes [5-7].

1. M.H. Kryder, E.C. Gage, T.W. McDaniel, W.A. Challener, R.E. Rottmayer, G. Ju, Y. Hsai, and M.F. Erden, “Heat assisted magnetic recording,” *Proc. of the IEEE* 96, 1810 (2008). 2. W.A. Challener *et al.*, Heat-assisted magnetic recording by a near-field transducer with efficient optical energy transfer, *Nat. Photonics* 3, 220 (2009). 3. H.J. Richter, C.C. Poon, G. Parker, M.Staffaroni, O. Mosendz, R. Zakai, and B.C. Stipe, “Direct measurement of the thermal gradient in heat assisted magnetic recording,” *IEEE Trans. Magn.* 49, 5378 (2013). 4. I. Gilbert, Z. Liu, X. Zheng, S. Granz, W. Eppler, and T. Rausch, “Measuring thermal gradient in HAMR using pseudorandom bit sequences,” *IEEE Trans. Magn.* 55, 3001006 (2019). 5. H.J. Richter, G. Parker, M. Staffaroni, M. Grobis, and B.C. Stipe, “Heat assisted magnetic recording with laser pulsing,” *IEEE Trans. Magn.* 50, 3001707 (2014). 6. B.X. Xu, Z.H. Cen, J.H. Goh, J.M. Li, Y.T. Toh, J. Zhang, K.D. Ye, and C.G. Quan, “Performance benefits from pulsed laser heating in heat assisted magnetic recording,” *J. Appl. Phys.* 115, 17B701 (2014). 7. T. Rausch, A.S. Chu, P.-L. Lu, S. Puranam, D. Nagulapally, T. Lammers, J.W. Dykes, and E.C. Gage, “Recording performance of a pulsed HAMR architecture,” *IEEE Trans. Magn.* 51, 3000405 (2015).

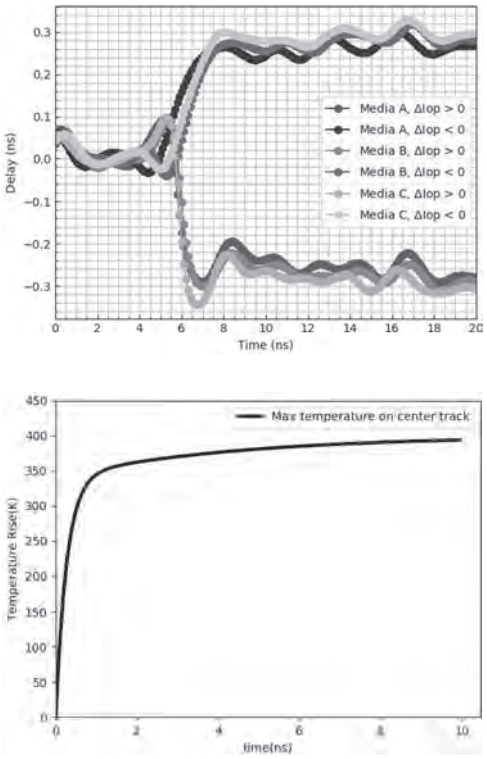

IOA-13. Dependence of Bit Error Rates on HAMR Transition Curvatures. *K. Xue*[1] and R. Victora[1] *1. Electrical and Computer Engineering, University of Minnesota, Minneapolis, MN, United States*

Transition curvature limits the performance of Heat-assisted Magnetic Recording (HAMR), especially when bit length is reduced below 10nm. The dependence of this transition curvature on bit length was obtained micromagnetically in our previous work [1]. In the current study, the dependence of signal-to-noise ratios (SNRs) and bit error rates (BERs) on HAMR transition curvatures is further investigated. More than 20,000 bits are written ideally (with an infinite thermal gradient) with various bit lengths and realistic transition curvatures. A pseudorandom binary sequence is used. The width of the read head is 20nm, shield to shield distance is 22nm, and element thickness is 4nm. Magnetic fly height is 6nm. A Viterbi algorithm is applied to decode the readback signals and calculate BERs. Fig. 1 and 2 show how SNRs and BERs change with transition curvatures (characterized by the coefficient to the quadratic term of the defining parabola) for a minimum bit length of 7.5nm. Clearly, larger transition curvatures result in lower SNRs and higher BERs, thus negatively affecting HAMR performance. Although the results in the figures represent very small bits compared to the readback resolution, our calculations for longer bits and/or narrower shield-shield spacing show similar results, albeit with improved SNR and BER, as will be shown in the presentation.

[1] Xue, Kun, and R. H. Victora. "Dependence of HAMR Transition Curvature on Bit Length." *IEEE Transactions on Magnetics* (2021).

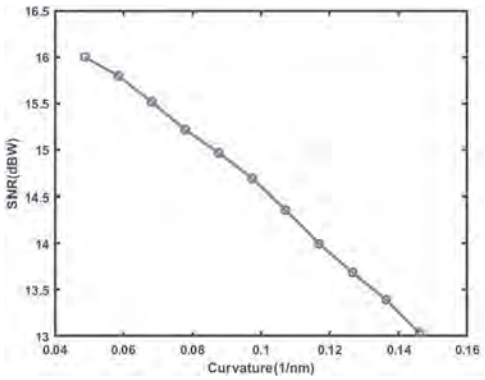

Fig. 1 Dependence of SNRs on HAMR transition curvatures with a bit length of 7.5nm.

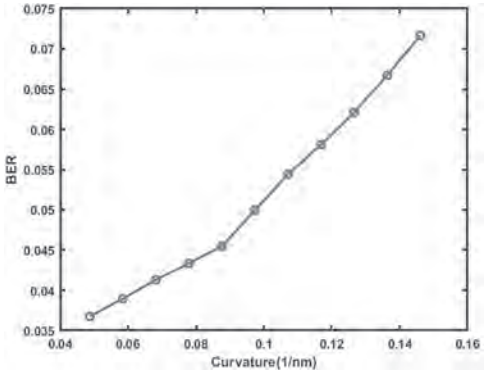

Fig. 2 Dependence of BERs on HAMR transition curvatures with a bit length of 7.5nm.

IOA-14. Enhancing Deterministic All-Optical Switching of Co/Gd Based Synthetic Ferrimagnets by He^+ Irradiation. *P. Li*[1], J.W. van der Jagt[2], R.J. Bruikman[1], R. Juge[2], R. Lavrijsen[1], D. Ravelosona[2,3] and B. Koopmans[1] *1. Applied Physics, Eindhoven University of Technology, Eindhoven, Netherlands; 2. Spin-Ion Technologies, Palaiseau, France; 3. CNRS, Centre de Nanosciences et de Nanotechnologies, Palaiseau, France*

All-Optical Switching (AOS) of the magnetization is seen as the fastest switching mechanism for magnetic materials [1]. Integrating AOS with existing and novel spintronic devices is currently hindered by the relatively large power for switching. Engineering magnetic material at the atomic scale is required to improve AOS efficiency. Previous studies have shown that high temperature annealing of Co/Gd bilayers [2] results in a significant reduction of the AOS threshold fluence due to Co/Gd intermixing [3, 4]. However, this technique is relatively slow, high temperatures are needed and it cannot be applied locally. In this work we study the effect of soft He^+ irradiation on the properties of ultra-thin Co/Gd bilayers [5]. He^+ irradiation is a powerful post-growth process inducing interface intermixing at the atomic scale in thin-film systems, modifying in turn their magnetic properties [6-8]. In addition, local modifications can be engineered using a mask. Here, we use a compact ultra-fast He^+ ion irradiation tool (Helium-S®) [8] to tailor interface intermixing in Co/Gd films. We use polar Kerr microscopy together with fs pulsed laser excitation to investigate the AOS energy as a function of irradiation fluence. As shown in Fig. 1, the switching threshold fluence decreases with increasing irradiation fluence, up to 20% for 6 x 10^{14} ions/cm^2. As seen in Fig. 2, the magneto-static properties measured by VSM-SQUID indicate that with increasing irradiation fluence, the total magnetic moment decreases, and the magnetic moment compensation temperature increases, which is expected from intermixed Co/Gd interfaces[4]. Our work shows that He^+ irradiation is an efficient approach to enhance the energy efficiency of AOS and tune magnetic properties of Co/Gd based systems.

[1] Li., M. and Kimel, A.V. Nature Reviews Materials 4, 189-200 (2019) [2] Lalieu, M.L.M., et al. *Physical Review B* 96.22 (2017): 220411. [3] Beens, M et al. AIP Advances 9, 125133 (2019) [4] Wang, L. et al. *Appl. Phys. Lett.* 112, 022408 (2020) [5] Li, P. et al. Manuscript in preparation (2021) [6] Fassbender, J. et al. *J. of Phys. D.: Appl. Phys.*, Vol. 37, no. 16 (2004) [7] Herrera Diez, L. et al., *Appl. Phys. Lett.*, vol 107, p. 032401 (2015) [8] Zhao, X. et al., *Appl. Phys. Lett.*, vol. 115, p.122404 (2019) [9] www.spin-ion.com

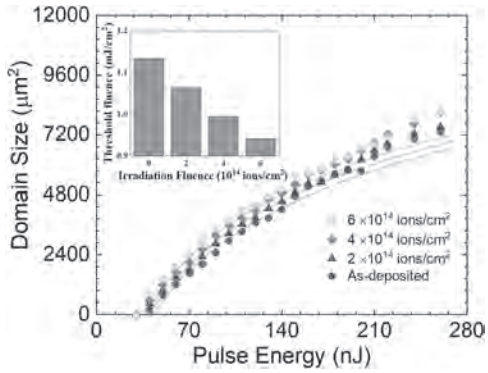

Fig. 1: Measured domain size as a function of pulse energy for four samples with different irradiation fluences. (Inset) The threshold fluence from main plot as a function of irradiation fluence.

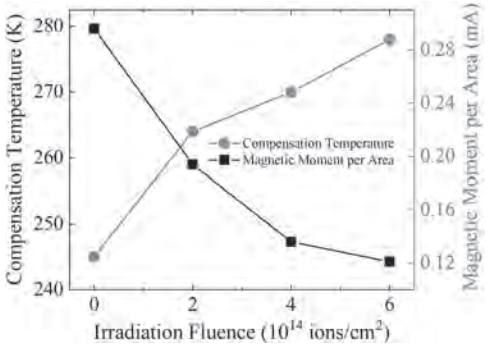

Fig. 2: Compensation temperature and Magnetic moment per area as a function of He^+ irradiation fluence.

Session IOB
MICROWAVE AND MILLIMETER WAVE MATERIALS AND DEVICES

Hanae Kijima-Aoki, Chair
Tohoku University, Sendai, Japan

INVITED PAPER

IOB-01. Uncooled sub-gigahertz spin bolometer. *M. Goto*[1,2], Y. Yamada[1], A. Shimura[3], T. Suzuki[3], N. Degawa[3], T. Yamane[3], S. Aoki[3], J. Urabe[3], S. Hara[3], H. Nomura[1,2] and Y. Suzuki[1,2] *1. Osaka University, Toyonaka, Japan; 2. CSRN-Osaka, Toyonaka, Japan; 3. TDK Corporation, Chuo-ku, Japan*

Bolometer is a highly sensitive rectification device that convert electromagnetic wave into direct current (dc) voltage through a temperature change. A superconducting bolometer has a responsivity of approximately 10^6 — 10^7 V/W under cryogenic temperatures at infrared wavelengths. However, no devices have realized such a high responsivity in the sub-GHz frequency region (Fig 1). Magnetic tunnel junctions (MTJs) have been promising device for such the application. Spin-torque diode effect can convert the sub-GHz microwave into the dc voltage [1]. The recent spin-torque diode has achieved the responsivity of 2×10^5 V/W using a spin-torque auto-oscillation [2]; however, a bolometer level responsivity has not been obtained. In this study, we demonstrate the bolometer-level spin-torque diode effect using an MTJ with a MgO|FeB|MgO structure in which the heat-controlled magnetic anisotropy (HCMA) effect efficiently exerts a spin-torque on the free layer magnetization [3]. The samples, buffer layer | IrMn (7.0) | CoFe | Ru | CoFeB | MgO barrier (1.0) | FeB (2.0) | MgO cap (0.5) | metal cap, were deposited on silicon substrates by the magnetron sputtering. The MTJ with the diameter of 190 nm was fabricated by a photo lithography. The spin-torque diode voltage of dc-biased MTJ was measured by the conventional measurement system of spin-torque diode effect. Figure 1 shows the diode voltage spectrum with an input microwave power of -55 dBm. We obtained the diode voltage of 10.6 mV at the magnetic field of 50 mT applied along the azimuthal angle θ of 11° and in-plane rotation angle φ from pinned layer magnetization of 135°. By considering the insertion loss of 1.16 dB, the responsivity is 4.40×10^6 V/W which is world's best responsivity in the sub-GHz frequency region [4]. This work was supported by JSPS KAKENHI Grant Number JP19K15435 and JP20H05666.

[1] A. A. Tulapurkar *et al.*, Nature, 438, 339 (2005), [2] L. Zhang *et al.*, Appl. Phys. Lett, 113, 102401 (2018), [3] M. Goto *et al.*, Nat. Nanotechnol, 14, 40 (2019), [4] M. Goto *et al.*, Nat. Commun, 12, 536 (2021)

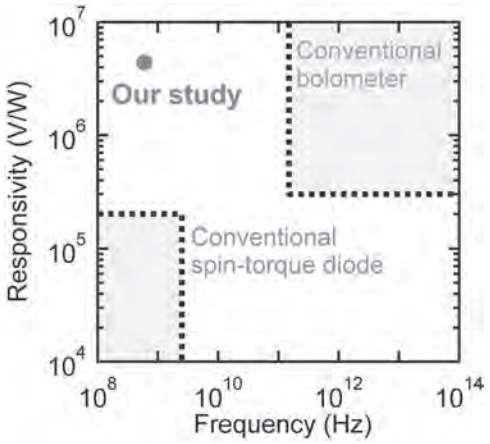

Figure 1 Responsivity of rectification device vs frequency. Blue and orange rectangular regions represent conventional bolometers and spin-torque diodes, respectively.

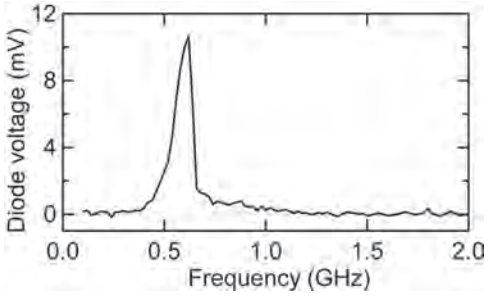

Figure 2 Frequency dependence of diode voltage with an input microwave power of –55 dBm.

CONTRIBUTED PAPERS

IOB-02. Tuning RF Acoustic Waves via Magnetism. *D.A. Bas*[1], P. Shah[1], I. Lisenkov[2], A. Matyushov[3], N.X. Sun[3] and M. Page[1] *1. Materials and Manufacturing, Air Force Research Lab, WPAFB, OH, United States; 2. Independent Researcher, Newton Upper Falls, MA, United States; 3. Electrical and Computer Engineering, Northeastern University, Boston, MA, United States*

Acoustically-driven ferromagnetic resonance (ADFMR) (1,2) is a powerful technique used to transmit RF surface acoustic waves (SAWs) and tune their transmission using a thin magnetic film and a static magnetic field H_{DC}. We explore tunability of ADFMR devices for their potential in agile RF communications applications. Two examples are nonreciprocal ADFMR devices, and devices with curved interdigital transducers (IDTs), which focus SAWs with enhanced intensity in the magnetic film. Nonreciprocity of RF transmission has an important role in critical components like isolators and circulators. We demonstrate that a thin synthetic antiferromagnet using FeGaB (3) can selectively absorb waves travelling in one direction with 48.4 dB isolation-

performance that can compete with state-of-the-art commercial devices despite much smaller package size and power draw. Another tuning knob which can have device impacts is nonlinearity. With curved interdigitated transducers (IDTs), we focus SAW energy to a small, intense region near the center of the magnet. We then study the dependence of the magneto-acoustic interaction on input power. Reaching moderate input powers of 10 dBm or less allows access to a nonlinear regime previously unavailable in these devices. Using a scanning acoustic-wave interferometer, we can observe the change in amplitude of the acoustic waves as they travel across the device surface. The power dependence is studied in depth, and an applied magnetic field modifies the amplitude wherever the magnet is present. Using these tools we gain new insight into how the magnetoelastic coupling works in ADFMR, which guides our understanding in the pursuit of new tunable RF communications device types.

1. L. Dreher, M. Weiler, M. Pernpeintner, et al., "Surface acoustic wave driven ferromagnetic resonance in nickel thin films: Theory and experiment," *Physical Review B,* vol. 86, no. 13, p. 134415 (2012). 2. D. Bas, P. Shah, M. McConney, and M. Page, "Optimization of acoustically-driven ferromagnetic resonance devices," *Journal of Applied Physics,* vol. 126, no. 11, p. 114501 (2019). 3. P. Shah, D. Bas, I. Lisenkov, A. Matyushov, N. Sun, and M. Page, "Giant nonreciprocity of surface acoustic waves enabled by the magnetoelastic interaction," *Science Advances*, vol. 6, no. eabc5648 (2020).

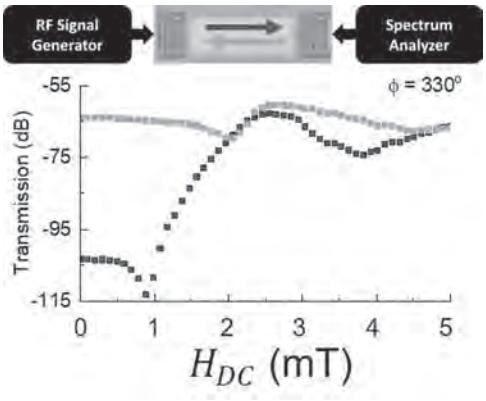

Operation of a magnetoacoustic isolator. With external magnetic field applied in one direction, the device transmits RF unidirectionally with 48.4 dB isolation. Reversing the external field switches the direction of RF transmission.

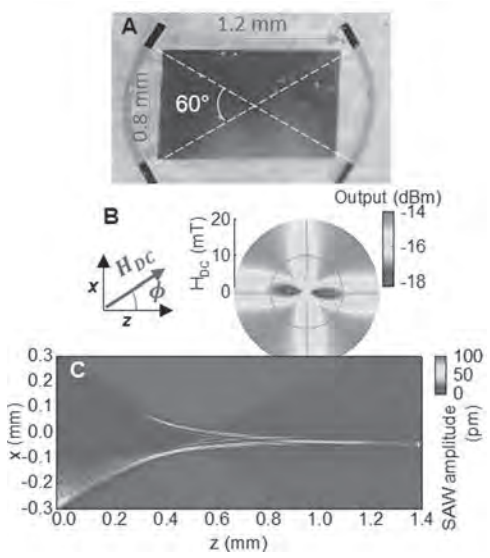

A) Image of a focused IDT ADFMR device. Curved IDTs transmit and receive SAWs, which travel across a 20-nm-thick Ni film on a y-cut $LiNbO_3$ substrate. B) ADFMR pattern showing output with 860-MHz 27-dBm input as a function of H_{DC} angle and magnitude. C) SAW amplitude measured by interferometry.

IOB-03. Phase difference detection in spin-torque nano-oscillators.

M. Jotta Garcia[1], S. Wittrock[1], L. Martins[2], A. Jenkins[2], R. Ferreira[2], U. Ebels[3], P. Bortolotti[1], R. Lebrun[1] and V. Cros[1] *1. Unité Mixte de Physique, CNRS, Thalès, Université Paris-Saclay, Palaiseau, France; 2. International Iberian Nanotechnology Laboratory, Braga, Portugal; 3. Univ. Grenoble Alpes, CEA, CNRS, Grenoble INP, Spintec, Grenoble, France*

In this study, we investigate the simultaneous excitation of the spin transfer dynamics in vortex-based spin-torque nano-oscillators (STNOs) by two separate radio-frequency (rf) signals. STNOs are spintronic devices operating in frequencies that range from less than 100 MHz up to tens of GHz [1], which are promising candidates for future-generation applications, such as rf emission [2], detection [3], neuromorphic computing [4], or as magnetic field sensors [5]. Here, we focus on adding phase sensitivity in the detection functionality of STNOs. For this purpose, we measure the rectification voltage, through the spin-torque diode effect [6], when two different rf signals are applied to the device: one injected directly as an rf current into the STNO, while the other is applied as an in-plane rf-field generated at an inductive line sitting above the device. The objective of this work is to detect the phase difference between the two signals through the measurement of the voltage rectified due to the spin-torque diode effect. As shown in Fig. 1, we find that there is a clear influence of the phase difference between the two rf signals on the rectified voltage, ΔV. When the signals are in-phase, the oscillating magnetic field will act on the magnetization increasing its oscillation amplitude. On the contrary, when out-of-phase, the field will damp the oscillation, thus decreasing the measured rectification voltage, as appears around 120° in Fig. 1. As such, through the rectification voltage we are able to determine the phase difference between the two rf signals. Detection sensitivity can be optimized by fine tuning of the excitation mechanisms (symmetries of spin-orbit torques and geometries of field lines). The work is supported by the French ANR project "SPINNET" ANR-18-CE24-0012.

[1] S. Kiselev et al., Nature Vol. 425, 380 (2003) [2] S. Wittrock et al., Phys. Rev. B Vol. 99, 235135 (2019) [3] A. S. Jenkins et al., Nat. Nanotech., Vol. 11, 360 (2016) [4] M. Romera et al., Nature Vol. 563, 230–234 (2018); D. Marković et al., Appl. Phys. Lett. 114, 012409 (2019) [5] M. Jotta Garcia et al., Appl. Phys. Lett. 118, 122401 (2021) [6] A. A. Tulapurkar et al., Nature 438, 339-342 (2005)

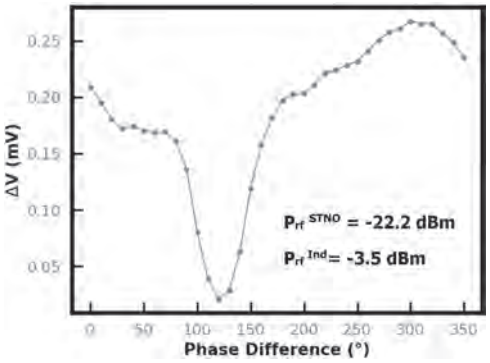

Figure 1 – Evolution of the rectification voltage measured as a function of the phase difference between the two applied rf signals, for zero dc bias and with an applied out-of-plane magnetic field of 250 mT. The rf current injected in the STNO has a power of -22.2 dBm and the rf current injected into the inductive line has a power of -3.5 dBm.

IOB-04. Robust mutual synchronization of spin Hall nano-oscillator chains. *A. Kumar*[1], M. Zahedinejad[1], H. Fulara[1], R. Khymyn[1], A.A. Awad[1], M. Dvornik[2], A. Houshang[1] and J. Åkerman[1] *1. Department of Physics, University of Gothenburg, Gothenburg, Sweden; 2. NanOsc AB, Kista, Sweden*

Since the advent of spin-torque nano-oscillators (STNOs) {1}, mutual synchronization of two or more STNOs has been of intense interest as it not only improves both the microwave signal power and the signal quality factor (Q-factor) appealing to communication technology but can also be used directly for neuromorphic computing due to the tunable magnetic nature of the interaction between STNOs. Thanks to the spin Hall effect, a new class of spintronic oscillators known as spin Hall nano-oscillators (SHNOs) has emerged. Compared to STNOs, they rely on the current flowing in-plane, which makes their fabrication easier and allow for a large number of SHNOs to synchronize in both chains and arrays. {5,6} In this work, we explore mutual synchronization in nano-constriction (NC) based SHNO chains and demonstrate robust synchronization of SHNOs for longer chains with up to 21 Oscillators [Fig. 1(a&b)]. We investigate both NiFe(4 nm)/Pt(5 nm) {6,7} and W(5 mm)/CoFeB(1.4 nm)/MgO(2 nm) {8,9} SHNOs. We report that the robust mutual synchronization can deliver an enhanced output power and significantly lower linewidth (Fig. 2(a&b)). A sub-MHz linewidth [Fig. 2(b), as low as 300 kHz for NiFe/Pt] can be achieved for 21 synchronized oscillators. The high-frequency operation results in a very high quality factor (Q=f/Δf) of >30,000 for NiFe/Pt and >25000 for W/CoFeB/MgO, which is the highest reported in chains. A linear decrease in linewidth and increase in output power (up to in-phase synchronization) is observed with the number of oscillators [Fig. 2(c)]. The low current and low field operation of these oscillators along with wide frequency tunability (2-28 GHz) with both current and magnetic fields, make these oscillators ideal candidates for various spintronic applications.

{1}. S. I. Kiselev, et al. Nature 425, 380 (2003). {2}. A. Houshang, et al., Nat. Nanotechnol. 11, 280 (2016). {3}. R. Lebrun, et al., Nat. Commun.8, 15825 (2017). {4}. R. Sharma, et al., Nat. Commun.12, 2924 (2021). {5}. A. A. Awad, et al., Nat. Phys. 13, 292–299 (2017). {6}. M. Zahedinejad, et., Nat. Nanotechnol. 15, 47–52 (2020). {7}. H. Mazraati, et al., Appl. Phys. Lett. 113, 092401 (2018). {8}. M. Zahedinejad, et al., Appl. Phys. Lett. 112, 132404 (2018). {9}. H. Fulara, et al., Sci. Adv. 5, eaax8467 (2019).

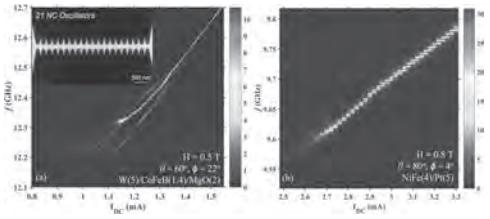

Figure 1 (a) & (b) Power spectral density of mutually synchronized 21 NC SHNOs of W/CoFeB/MgO and NiFe/Pt, respectively. Inset shows SEM image of the NC SHNOs separated by 200 nm.

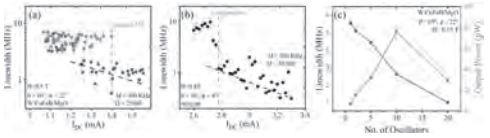

Figure 2 (a) & (b) Linewidth (Δf) vs. I_{DC} for W/CoFeB/MgO and NiFe/Pt, respectively. The dashed brown line represents a complete (brown) mutual synchronization of 21 oscillators. (c) Δf and output power vs. the no. of oscillators under mutual synchronization for W/CoFeB/MgO SHNOs.

IOB-05. Hexagonal Nano-ferrites used on a V-band Self-bias On-chip Circulator for CMOS. W. Quan[1], *M.N. Afsar*[1] and V. Koomson[1] *1. Tufts University, Medford, MA, United States*

Hexagonal ferrite materials such as $BaFe_{12}O_{19}$ and $SrFe_{12}O_{19}$ have strong anisotropic magnetic field and strong remnant magnetism. These properties enable the working frequency of devices such as isolator and circulator, move up to tens of GHz without a strong external bias field and even achieve self-biasing. Other features such as large saturation magnetization, large anisotropy, and low dielectric loss and most importantly, its potential of achieving self-bias, paves the way to fabrication of planar ferrite device that can play a crucial role in a next generation wireless system. Ferrite circulators consume no power and are more suitable for lower-power applications because these are passive, unlike active quasi circulator,. If the fabrication process of aforementioned devices can be integrated into the mature CMOS process flow as an option, it will gain great competiveness as regards the cost. In this work, thin film ferrite material was deposited by employing spin-casting method and patterned with the help of Chemical-Mechanical Polishing (CMP). The spin-casting is a low-temperature process: the nano-sized barium ferrite materials can be processed into composite and spin-casted into thin film layer. This method requires only 120°C baking under external biasing filed. This is advantageous when future integration with CMOS is taken into consideration. In this paper, we present the design, simulation, fabrication and measured results of a self-bias micro-strip line Barium hexagonal Nano-ferrite (BaM) circulator on silicon wafer. This planar Y-junction circulator is 2mm by 2mm by 0.5mm in size, which is capable of future integration with the top three layers of 180nm CMOS technology. Ferrite thin film is deposited and patterned employing composite spin-casting method. Typical characterization techniques are employed together with free-space quasi-optical spectrometry to study complex permittivity and permeability of deposited film up to 120GHz. S parameters of fabricated circulators are characterized by a set of on wafer probes up to 67GHz. We observed over 15dB non-reciprocal phenomenon at 55GHz.

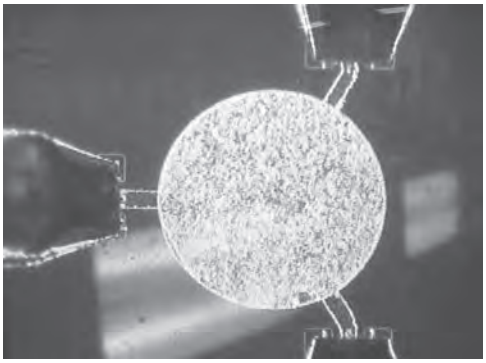

Fig. 1. Three ports probing of fabricated circulator

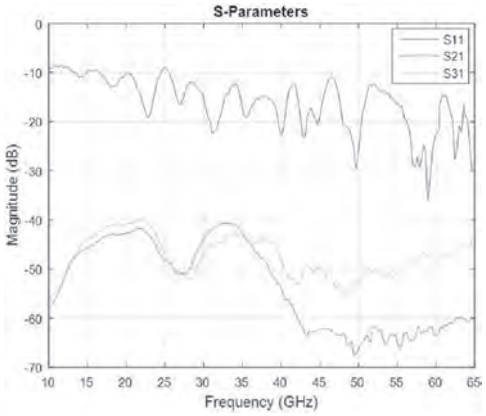

Fig. 2. Measured S-parameter of fabricated ferrite circulator

IOB-06. Multiferroic Lamb Wave Antenna. *R. Zheng*[1], V.M. Estrada[1] and A. Sepulveda[1] *1. MAE, UCLA, Los Angeles, CA, United States*

Conventional antennas such as dipoles and loops rely on electromagnetic resonance, therefore the size of such antennas is constrained by having to be proportional to the free space wavelength of the signal they are designed to radiate (typically greater than λ/10). Electrically small antennas (ESAs) at ultra-high frequency are promising candidates for reducing antenna size, weight, and volume [1][2][3]. However, these ESAs still have several challenges to overcome. For example, ESAs have a significantly reduced radiation efficiency in electrically lossy environments (e.g., the human body [4]). Therefore, a new approach is needed to address both the difficulties in miniaturization of conventional antennas and the reduced efficiency of ESAs in lossy environments. Recently, strain-mediated multiferroic composites have been used to create significant magnetization changes in electrically small form factors. Several publications [5] have demonstrated the potential of using magnetic antennas in replacing current ESAs. However, this approach still faces some challenges, specially at the micron size device level. Currently, the key question surrounding these devices is the amount of magnetic material needed to successfully radiate a detectable signal. The work shown in this report represents our efforts in developing and fabricating a 400MHz strain mediated antenna which has sufficient magnetic material to overcome the ambient noise threshold in medical applications. Our device works by electrically actuating a piezoelectric Aluminum Nitride (AlN) thin film to produce acoustic wave resonance. This film is mechanically coupled to magnetic FeGa/NiFe microelements allowing the dynamic strain produced in the AlN to be transferred to the magnetic elements. Due to the magnetoelastic properties of FeGa/NiFe this results in changes in magnetization, which in turn results in a radiated magnetic field. Optimization of both the design and fabrication process has been conducted to improve yield and ensure the radiation of a detectable signal. This work demonstrates the feasibility of miniaturized strain-mediated multiferroic antennas, which show promising potential for the next generation of ESAs at ultra-high frequency.

[1] S. Perhirin and Y. Auffret, *Microw. Opt. Technol. Lett.*, vol. 55, no. 11, pp. 2562–2568, 2013. [2] E. G. Turitsyna and S. Webb, *Electron. Lett.*, vol. 41, no. 2, pp. 40–41, 2005. [3] R. W. Ziolkowski, *IEEE Antennas Wirel. Propag. Lett.*, vol. 7, pp. 217–220, 2008. [4] F. Rangriz, A. Khaleghi, and I. Balasingham,*14th Eur. Conf. Antennas Propagation, EuCAP 2020*, 2020. [5] M. A. Kemp *et al.*, *Nat. Commun.*, vol. 10, no. 1, pp. 1–7, 2019.

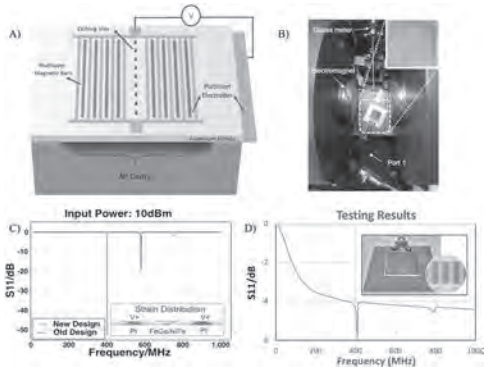

IOB-07. Physical origin of bimodal complex permeability spectrum of a noise-suppression sheet. *T. Igarashi*[1], S. Tamaru[2], N. Kikuchi[3], S. Yoshida[3] and S. Okamoto[3] *1. TOKIN Corporation, Sendai, Japan; 2. Advanced Industrial Science and Technology, Tsukuba, Japan; 3. Tohoku University, Sendai, Japan*

A noise-suppression sheet (NSS), which is composed of very thin soft magnetic flake particles with organic binder, is indispensable to suppress the electromagnetic compatibility problem for recent mobile communication devices. NSS is mounted on the circuit board and absorbs extra-electromagnetic waves inside the mobile device. This absorption property is characterized as a peak of imaginary complex permeability μ″ owing to the ferromagnetic resonance [1]. Although a commercial NSS with flake particles of Sendust (Fe-Si-Al alloy) generally exhibits a bimodal μ″ spectrum, the physical origin of this behavior has not been understood so far. This situation would be a bottleneck for the next generation mobile communication. In this study, we investigated the μ″ spectra of NSSs with various magnetic materials ($Fe_{74.8}Al_{25.2}$, $Fe_{50.2}Co_{47.6}V_{2.2}$, and Fe) and compared with those of constituent single flake particles. μ″ spectrum measurements of single flake particles are realized by means of TC-PERM which is the newly developed complex permeability measurement method with very high sensitivity [2]. Figure 1 shows the complex permeability of NSS of Fe and the constituent single flake grain of 180 μm in diameter and 1 μm in thickness. As well as the commercial NSS of Sendust, the bimodal μ″ spectrum is clearly observed for NSS of Fe. Moreover, quite similar μ″ spectrum is also observed for the single flake grain. This fact strongly indicates that the bimodal μ″ spectrum of NSS is attributed to the nature of a constituent single flake. We found that the magnetic vortex model can reasonably explain this bimodal μ″ spectrum, that is, the low- and high-frequency peaks are owing to the resonances of vortex core gyration motion and flux closure magnetization state, respectively. The calculated low- and high-frequency peaks quantitatively agree with the experimental results as marked in Fig. 1(b). This good agreement can be also confirmed for other materials. This work is supported by MIC SCOPE JP195003002.

[1] S. Yoshida *et al.*, J. Appl. Phys., Vol. 85, No. 8, p.4636 (1999) [2] S. Tamaru *et al.*, J. Magn. Magn. Mater., Vol. 501, p.166434 (2020)

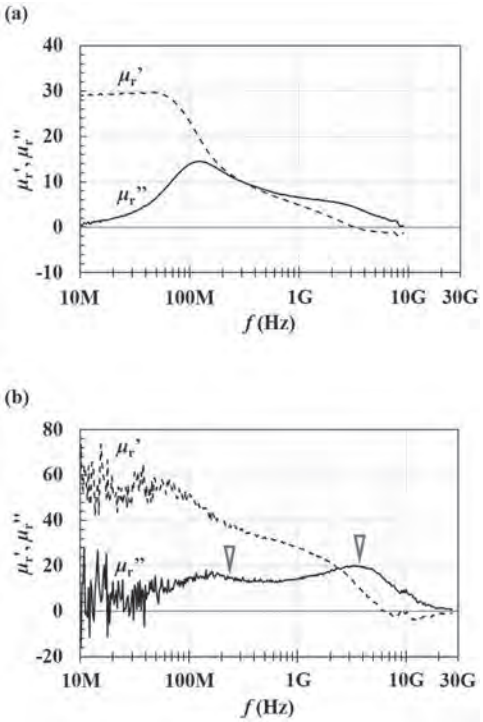

Fig. 1 Complex permeability spectra of (a) NSS and (b) a single constituent flake grain of Fe.

IOB-08. Miniaturizing Patch Antenna with Multi-layer Soft Ferrite and Dielectric Substrate Structure. B. Bryant[1], Y. Hong[1], *H. Won*[1] and M. Choi[1] *1. Department of Electrical and Computer Engineering, The University of Alabama, Tuscaloosa, AL, United States*

The patch antenna is advantageous in many applications because of its simple and inexpensive structure. However, one disadvantage is its large size. One of the methods to reduce the size of an antenna is to utilize ferrite material [1]. While this does effectively miniaturize the antenna, the peak realized gain (PRG) is decreased by 8.3 dBic due to the magnetic loss of the ferrite core. In this paper, we take the multi-layer ferrite and dielectric approach to reduce the patch antenna size. All antennas were simulated using ANSYS HFSS for their performance. Fig. 1 shows the specifications and designs of the patch antennas. The baseline patch antenna has the dimensions given in [2] and uses a 1.4 mm thick FR-4 substrate (permeability (μ_r) = 1, permittivity (ε_r) = 4.4). The dielectric and magnetic loss tangents ($\tan\delta_e$ and $\tan\delta_u$) are 0.02 and 0.00, respectively, at UHF band frequency, and its volume (V) is 9800 mm^3. To realize the multi-layer concept in the antenna size reduction, 0.8 mm thick layers of ferrite (μ_r = 6, ε_r =13, $\tan\delta_u$ = 0.05, $\tan\delta_e$ = 0.02, and V = 2720 mm^3) are inserted into the FR-4 substrate. Three topologies are investigated: one ferrite layer, two ferrite layers, and three ferrite layers. For each topology, the volume of the ferrite remains the same. For the cases with more than one ferrite layer, the inner-most layer has a constant V = 600 mm^3, and the remaining volume is divided equally among the outer layers. Antenna performance results are summarized in Table 1. For one ferrite layer, 16.7% miniaturization is achieved, but the PRG decreases by 14.1 dBi. However, as the number of layers increases to two, 49.8% miniaturization is achieved with a decrease in PRG of 5.6 dBi. For three layers, 49.3% miniaturization is observed with a 5.6 dBi decrease in PRG. Compared to the case with the all-ferrite substrate (V = 9800 mm^3), the patch antenna with two ferrite layers has a 4.4 dBi higher PRG. Ferrite and dielectric substrate contributes remarkably to antenna size reduction.

[1] W. Lee, Y. K. Hong, and H. Won, *IEEE Ant. Wirel. Propag. Lett.* vol. 18, p. 951 (2019). [2] F. Z. Hanin and L. Setti, *2016 5th Intntl. Conf. on Multimedia Comp. and Sys.*, pp. 487-491 (2016).

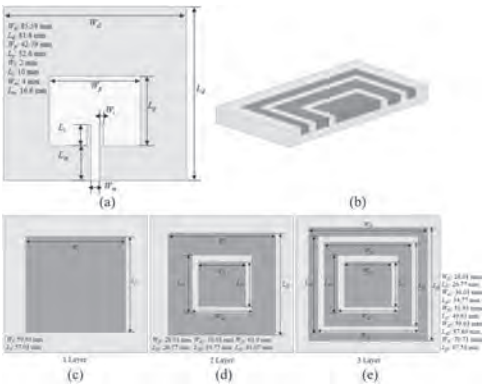

Fig. 1. Design and specifications of (a) baseline patch antenna, (b) ferrite-dielectric layering, and (c) multi-layer patches

Design	Low Freq (GHz)	High Freq (GHz)	Bandwidth (MHz)	Peak Realized Gain (dBi)
Baseline	2.15	2.18	30	2.59
1 Ferrite Layer	1.79	1.84	50	-1.52
2 Ferrite Layer	1.08	1.13	50	-3.04
3 Ferrite Layer	1.09	1.13	40	-2.97
All Ferrite	1.42	3+	1580+	-7.39

Table 1. Comparison of antenna performance results

IOB-09. Composite Right/Left-Handed Metamaterial Lines with Phase-Shifting Nonreciprocity Enhanced by Spoof Surface Plasmon Mode Propagation. K. Okamoto[1], *T. Ueda*[1] and T. Itoh[2] *1. Electrical Engineering and Electronics, Kyoto Institute of Technology, Kyoto, Japan; 2. Electrical Engineering, UCLA, Los Angeles, CA, United States*

Recently, phase-shifting nonreciprocity in normally magnetized ferrite-based metamaterials has been investigated for potential applications to highly efficient beam scanning leaky wave antennas [1]. The magnitude of the nonreciprocity is typically small and may limit the beam scanning angle. Recently, the nonreciprocity has been greatly enhanced by using the slow wave structure with corrugation based on spoof-surface plasmon mode propagation in the metamaterial lines [2],[3]. However, the enhancement technique has not been applied to composite right/left-handed (CRLH) transmission line with Dirac points. In this paper, we propose a new configuration of nonreciprocal CRLH metamaterial lines with a Dirac point having a large nonreciprocity that is enhanced by inserting a corrugation at one of the strip edges of the center microstrip line to excite spoof-surface plasmon mode, as shown in Fig. 1. In the configuration, polycrystalline yttrium iron garnet (YIG) was employed as the ferrite material. In Fig. 2, the simulated and measured results of dispersion curves and phase shifting nonreciprocity $\Delta\beta$ are shown for the case of weakly applied dc magnetic field with effective magnetization of 15 mT and an internal dc magnetic field of 7 mT in the numerical simulation setup and the external dc magnetic field of 26 mT in the experimental setup. It is found from Fig. 2 that experimental results agree well with numerical simulation results. A Dirac point was established near Γ point having the normalized phase-shifting nonreciprocity $\Delta\beta\ p/\pi = 0.025$ corresponding to the beam angle of 15 degrees. Thus, the drastic reduction of the applied dc magnetic field required for the nonreciprocity in the CRLH lines with Dirac points will enable us to use compact electromagnets in the highly efficient beam steering leaky wave antennas.

[1] T. Ueda, S. Yamamoto, Y. Kado, T. Itoh, IEEE Trans. Microw. Theory Tech., 60, 3043. 2012. [2] T. Ueda, K. Okamoto, T. Itoh, IEEE Trans. on Mag., 54, 2502205, 2018. [3] K. Okamoto, T. Ueda, T. Itoh, IEEE MTT-S Int. Microw. Sym. Dig., 28, 2019.

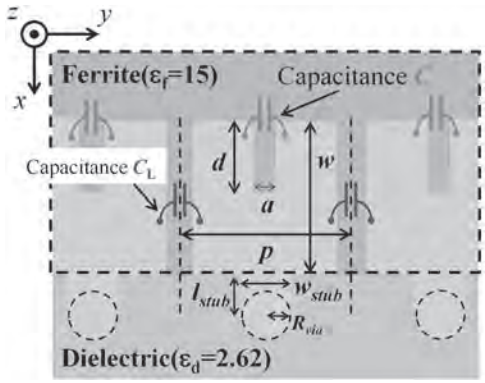

Fig. 1 Top view of the proposed CRLH metamaterial line.

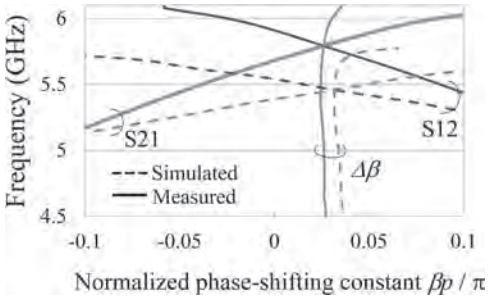

Fig. 2 Simulated and measured results of dispersion curves and phase shifting nonreciprocity Δβ.

IOB-10. New Magnetic Multilayer for Direct On-chip EMI Shielding Layer on Mold Substrate at Sub-100MHz Frequency Range.
A. Kikitsu[1], Y. Kurosaki[1], S. Shirotori[1], A. Fujita[2], H. Nishigaki[2] and S. Matsunaka[2] *1. R&D Center, Toshiba Corp., Kawasaki, Japan; 2. Shibaura Mechatronics Corp., Ebina, Japan*

INTRODUCTION Electromagnetic interference (EMI) in the range of sub-100MHz has attracted attention for the applications of smart phones or EVs [1]. Depositing a shielding layer directly on the semiconductor chips is useful for such densely implemented systems [2]. In addition to a direct-on-chip magnetic multilayer shielding at sub-GHz range [3], it was found that a multilayer of $[Cu(100nm)/NiFeCuMo(100nm)]_{10}$ showed better shielding effect than Cu layer at sub-100MHz range [4]. However, the result was obtained for samples on flat glass substrates, and was not applicable to actual semiconductor chips, that were covered with a mold resin with rough surface. In this paper, a new magnetic multilayer system is investigated. A combination of soft magnetic layers with the above multilayer unit was found to show excellent shielding effect at sub-100MHz even on a rough mold substrate. RESULTS AND DISCUSSION Samples were deposited by magnetron sputtering [4]. A mold substrate with a surface roughness of about 10μm was used. Film stack was $[Cu(100nm)/NiFeCuMo(100nm)]_{10}$/ $[Ta(5nm)/NiFeCuMo(50nm)]_{55}$/$[Ta(5nm)/NiFeCuMo(300nm)]_{10}$. SUS304 was used for underlayer and overcoat. Magnetic property was measured by vibrating sample magnetometer. Magnetic shielding effect (MSE (dB)) was evaluated by a transmitted power (S_{12}) of electromagnetic wave through the sample [3]. Figure 1 shows MSE of the samples on glass and mold substrates. MSE of Cu (8μm) is plotted as a reference. Excellent shielding effect was shown at 20-30 MHz for both substrates. This result seems to be due to a magneto-static coupling between multilayers. Figure 2 shows hysteresis loops. Hysteresis shown at 10-80 Oe comes from SUS layers. The hysteresis loop looks like a single soft magnetic layer even though the samples consist of three different multilayer units. Magneto-static interaction may build up a correlative magnetization motion through multilayer systems, and bring a domain wall resonance at sub-100MHz.

[1] CENELEC technical report CLC/TR 50627 (2015) [2] Y. Shimada et al.: IEEE Trans. Magn., 50, 2801704 (2014) [3] K. Yamada et al.: 2011 IEEE International Symposium on EMC, p.432 (2011) [4] A. Kikitsu et al.: abstract of JEMS 2020, 3238 (2020)

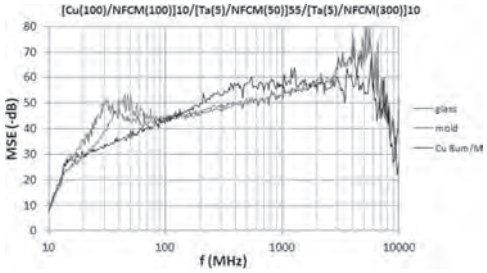

Fig.1 Magnetic shield effects (MSEs) of multilayer samples and Cu

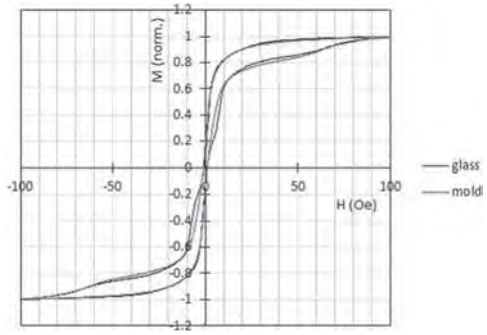

Fig.2 Magnetic hysteresis loops of the sample on glass and mold substrates

IOB-11. Microwave Absorption Performance of M-type Hexagonal Ferrite and MXene Composite.
H. Won[1], Y. Hong[1], M. Choi[1], K. Lee[2], D. Shin[2] and Y. Yoon[2] *1. Department of Electrical and Computer Engineering, The University of Alabama, Tuscaloosa, AL, United States; 2. Semiconductor Materials Division, LG Chem, Ltd., Yeongdeungpo-gu, The Republic of Korea*

Recently, 45 μm thick $Ti_3C_2T_x$ (MXene) showed high total shielding effectiveness (SE) of 92 dB between 8 and 12 GHz [1]. However, MXene mitigates the unwanted EM signal via reflection, and the reflect signal generates another spurious signal, harming neighboring electronic components or systems. This is because the high conductivity and paramagnetic properties of MXene cause impedance mismatch. To improve the impedance matching and absorption intensity, many researchers investigated the MXenes with magnetic material and reported a high SE via absorption but mostly in X-band (8-12 GHz) [2-3]. In this paper, we investigated MXene and M-type hexaferrite ($BaFe_{12}O_{19}$) composite to absorb EM wave occurring in Ka Band (26.5-40 GHz) for mmWave 5G application. We chose $BaFe_{12}O_{19}$ because it possesses a ferrimagnetic resonance (FMR) frequency of 42.5 GHz [4]. MXene was synthesized by the LiF-HCl etching method reported in [2], and $BaFe_{12}O_{19}$ nanopowder, purchased from Sigma Aldrich, was used. The composite was obtained by dispersing 0.25 g of MXene into 50 mL of deionized water and then ultrasonicated with 2.5 g polyvinylpyrrolidone (PVP) for 30 minutes. The sample was mixed with 0.25 g of $BaFe_{12}O_{19}$ powders and stirred for 12 hours. Finally, the composite was centrifuged and dried in an oven for 12 h. First, the phase of the synthesized composite was characterized by X-ray diffraction (XRD: Bruker D8 Discover) using Cu kα radiation, as shown in Fig. 1. Both MXene and $BaFe_{12}O_{19}$ was confirmed in the composite. Fig. 2 shows the static magnetic property of the composite, which is measured by a vibrating sample magnetometer (VSM: MicroSense EV9). Compositing MXene with $BaFe_{12}O_{19}$ increased saturation magnetization (M_s) from 0 for MXene to 10.5 emu/g and intrinsic coercivity (H_{ci}) from 4.8 to 889 Oe. We will discuss the dynamic properties (complex

permittivity, complex permeability, and reflection loss) of the MXene/$BaFe_{12}O_{19}$ composite in the paper. This work was supported in part by NSF-IUCRC under Grant No. 1650564.

[1] C. Koo, F. Shahzad, and A. Choi, *2D Metals Carbides and Nitrides (MXenes)*, (2019). [2] B. Deng, L. Wang, and Z. Xiang, *Materials Letters*, 284, 129029 (2021). [3] H. Yang, J. Dai, and X. Liu, *Materials Chemistry and Physics*, 200, 179 (2017). [4] C. Dong, X. Wang, and P. Zhou, *Journal of Magnetism and Magnetic Materials*, 354, 340 (2014).

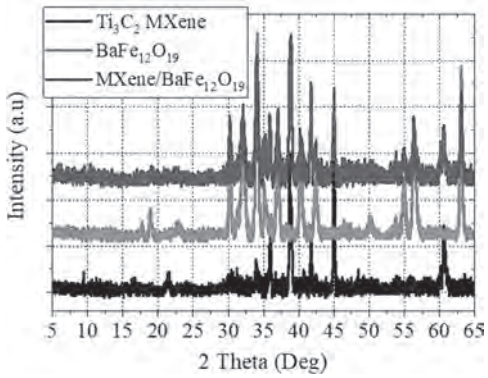

Fig. 1. XRD pattern of MXene, $BaFe_{12}O_{19}$, and MXene/$BaFe_{12}O_{19}$ composite.

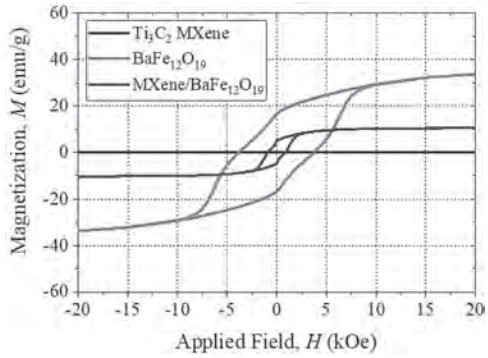

Fig. 2. Magnetic hysteresis loop of MXene, $BaFe_{12}O_{19}$, and MXene/$BaFe_{12}O_{19}$ composite.

IOB-12. NiZn ferrite noise suppressor embedded in IC interposer.
M. Yamaguchi[1,2], A. Takahashi[2], Y. Miyazawa[2] and M. Nagata[3]
1. Departmemt of Electrical Engineering, Tohoku University, Sendai, Japan; 2. New Industory Creation Hachery Center, Tohoku University, Sendai, Japan; 3. Graduate School of Science, Technology and Innovation, Kobe University, Kobe, Japan

This paper discusses magnetic material technology to improve receiver sensitivity in an IC chip. The idea is to use FMR losses to supress conduction noise in receiver circuit. We studied conventional NiZn ferrite particle composite and thin plate. While their materials' FMR frequency is below 1 GHz, strong demagnetization given by the narrowness of current-carrying wires on interposer may shift up the FMR frequency to GHz range and hence useful to suppress electromagnetic noise in the GHz range. While Y and Z-type hexagonal ferrite [1] composite materials are good candidates for this application [2], this idea may widen the range of material selection NiCuZn spinel ferrite particles (commercially available) were embedded in epoxy resin to form composite sheet. Sintered plate was also prepared. Y and Z type hexagonal ferrites [2] are tested for comparison. Average diameter of the particle is 0.1~3.6 μm. The particles are mixed with a polymer binder to form a powder composite. Volume ratio of magnetic particle is nominally 50 %. Thickness of each power composite is about 50 μm to fit the space between interposer and IC chip die, as shown in Fig. 1. Noise suppression performance is proportional to the parameter 2*pai*f* ur", It was 73@ 1 GHz for NiCuZn plate. This peak intensity was doubly higher than hexagonal ferrite composites. The composites and plate was mounted to an IC chip interposer asshown in Fig. 1 A magnetic near field probe (Langer XF-R 3-1) was placed on the IC chip package and measured radiated emission noise from the test IC chip driven by 100-200 MHz clock. The 4.8 GHz component of magnetic near filed was successfully suppressed by the proposed sintered magnetic plate. Degree of suppression counts 4-17 dB, comparing IC only and NiCuZn(17 dBmax), BaZn-Y hexagonal ferrite composite(10 dBmax) at 4.8 GHz, which is higher than material's FMR frequency of NiCuZn ferrite. 3D RF EM simulation (HFSS Ver.14.0) predicts that current crowding at narrow current-carrying wires on chip or interposer could shifted the FMR toward higher frequency and it effected to yield high noise suppression beyond material's FMR frequency.

[1] Vincent G. Harris, IEEE Trans. Magn., 48, 1075 (2012). [2] M. Yamaguchi, et al. "Magnetic Powder Composite Noise Suppressor for Flip Chip Mounted High Speed IC Chip," EMC Sappro & APEMC 2019, MonPM2C.6 (2019). [3] M. Yamaguchi, et al. MMM2020, I2-04 (2020).

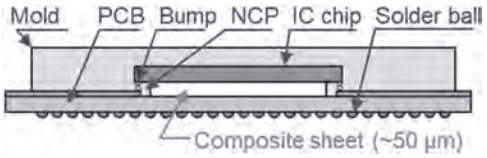

Fig. 1. Cross section of an IC chip interposer.

IOB-13. Enhanced Electromagnetic Wave Absorption by Bi-layered Nano-hollow Spheres.
A. Gorai[1], R. Mandal[2] and D. Mandal[1]
1. Condensed Matter Physics and Material Sciences, Satyendra Nath Bose National Centre for Basic Sciences, Kolkata, India; 2. Electronics and Communications, University of Engineering and Management, Kolkata, India

To cope with the increasingly serious microwave radiation pollution, an extensive search for efficient microwave absorption materials (MAMs) has attracted great attention recently [1-3]. We have already reported the light-weight ferrite nano-hollow spheres (NHS) to exhibit enhanced electromagnetic (EM) wave absorption [4]. Herein, the deposition of the dielectric SiO_2 layer on $MnFe_2O_4$ (MnFO) NHSs is found to be an effective strategy to enhance EM wave attenuation for a larger bandwidth. EM wave absorption properties of as-synthesized bare and SiO_2 coated $MnFe_2O_4$ NHSs with different coating thicknesses are investigated within a widely-used frequency range. Larger interfacial area, higher magnetic anisotropy, internal reflections and scattering from NHSs along with higher magnetic permeability of MnFO are responsible for superior absorption properties of MnFO NHS. The higher dielectric permittivity of SiO_2 coated on the surfaces of MnFO NHSs further improves microwave absorption for a large frequency bandwidth. The MnFO (~ 450 nm)/SiO_2 (~ 68 nm) bi-layered NHSs (TEM micrograph shown in Fig.1) result in a sufficiently high *RL* ~ - 30.0 dB with a composite absorber of thickness only 3mm and filler concentration of 20% as shown in Fig.2. The above study on the variation of SiO_2 thickness over MnFO NHSs helps us to optimize for maximum bandwidth and absorption with minimum composite absorber thickness. Analysis from the λ/4 model for best matching thickness (t_m) displays a good agreement between experimental and simulated t_m values. This study demonstrates the optimized MnFO/SiO_2 NHS as a highly promising low-cost and lightweight EM wave absorber suitable for high-frequency filter applications.

[1] J. Liu, L. Zhang & H. Wu, J. Phys. D: Appl. Phys., Vol. 54, p.203001 (2021) [2] C. Feng, X. Liu, S. W. Or et al. AIP Advances, Vol. 7, p.056403 (2017) [3] D. Mandal & K. Mandal, J. Magn. Magn. Mater., Vol. *536*, p.168127 (2021) [4] D. Mandal & K. Mandal, J. Appl. Phys., Vol. 129(7), p.074902 (2021)

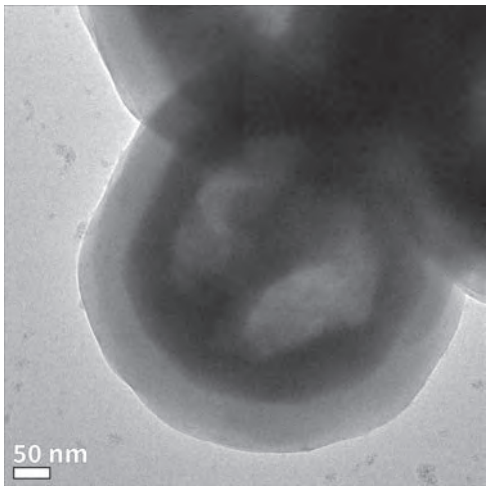

Fig. 1 : Transmission Electron Micrograph of a MnFO/SiO_2 NHS

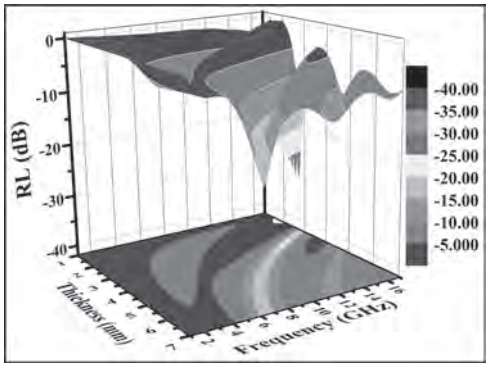

Fig. 2 : Three dimensional plot of reflection loss versus frequency and composite absorber thickness for MnFO (~ 450 nm)/SiO_2 (~ 68 nm) bi-layered NHSs

Session IOC
SENSORS: MATERIALS, DEVICES AND APPLICATIONS I

Shuichiro Hashi, Chair
Tohoku Gakuin University, Tagajo, Japan

INVITED PAPER

IOC-01. Measurement of Bio-magnetic Fields with Tunnel Magneto-resistive Sensors. *M. Oogane*[1], K. Fujiwara[2], S. Kumagai[2], H. Matsuzaki[2] and Y. Ando[1] *1. Tohoku University, Sendai, Japan; 2. Spin Sensing Factory Corp., Sendai, Japan*

The magnetic tunnel junctions (MTJs)-based sensors (TMR sensor) are promising magnetic field sensor because of room temperature operation, small device size, and the low power consumption. Since the TMR sensors with such features are considered to be widely applicable not only to the magnetic recording, the TMR sensors will be a key device in the ICT and IoT societies. In addition, because of the dramatic increase in sensitivity of TMR sensors in recent years, the realization of the device that can detect the weak magnetic field of pico-Tesla such as bio-magnetic field is expected. Magnetoencephalography (MEG) has been applied to brain function research and diagnosis of brain diseases, but unfortunately, the conventional measurement method using a SQUID sensor cannot measure brain field by touching the scalp, the head must be fixed, and maintenance costs are high. The TMR sensors operating at room temperature have the potential to solve these problems. In addition, it has the great advantage that it does not require a special magnetic shielded room, and in principle, it allows measurement while the subject is moving. In addition to bio-magnetic field measurements, the possibility of realizing nuclear magnetic resonance image (MRI) measurements using the same TMR sensor under the low magnetic dc field, such as earth field, is expected. There are various techniques for imaging the shape of a body, such as MRI, ultrasonic waves, blood flow, etc., but techniques for measuring the image of the activity and shape of a body with the same sensor devices have not been reported. We have already reported on the measurement of cardiac magnetic field (magnetocardiography: MCG) and MEG using TMR sensors [1], but, the further improvement in sensitivity and detectivity of TMR sensors is required to realize the actual TMR based-MCG, -MEG and -MRI equipment. We present recent progress in the development of highly sensitive TMR sensors. We have achieved the lowest magnetic field detectivity of 1.0 pT / $Hz^{0.5}$ at 1 Hz in the TMR sensor using a magnetic flux concentrator (MFC) (Fig. 1). By using a TMR sensor with high magnetic field resolution in the low frequency region, we succeeded in measuring MCG at real-time and MEG with a small number of averaging times. Further, as shown in Fig. 1, the developed TMR sensor has an extremely low magnetic field detectivity of 0.1 pT / $Hz^{0.5}$ or less in the kHz band. Protons in the human body generate nuclear magnetic resonance (NMR) at a frequency of 1 to 3 kHz under a weak magnetic field of μT, and we succeeded in measuring the NMR signal for the first time using the TMR sensor (Fig. 2). These results show that the MEG signal and the MRI using NMR can be simultaneously measured by the same TMR sensor device. This work was partly supported by JST S-innovation project, the Center for Innovative Integrated Electronic Systems (CIES), the Center for Science and Innovation in Spintronics (CSIS), and the Center for Spintronics Research Network (CSRN).

[1] K. Fujiwara *et al.*, Appl. Phys. Express 11, 023001 (2018).

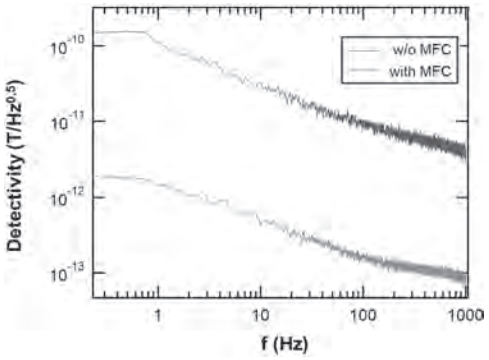

Frequency dependence of detectivity in developed TMR sensors with/ without magnetic flux concentrator (MFC)

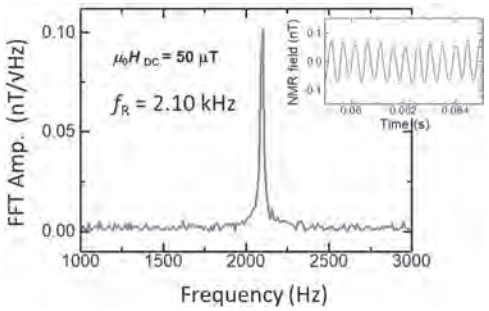

Proton NMR signals under low magnetic field of 50 μT measured by developed TMR sensors with MFC

CONTRIBUTED PAPERS

IOC-02. Adaptive Measurements in Quantum Magnetometry. *R. McMichael*[1], S. Dushenko[1,2] and S.M. Blakley[1] *1. National Institute of Standards and Technology, Gaithersburg, MD, United States; 2. Institute for Research in Electronics and Applied Physics, University of Maryland, College Park, MD, United States*

We present an implementation of sequential Bayesian experiment design[1] for efficient Ramsey sequence magnetometry using NV centers in diamond. In the Ramsey sequence, the magnetic field is encoded as a phase difference between two spin states, where the phase accumulates over a selected precession time τ, and the experimental signal oscillates as a function of τ with precession frequency $\omega = \gamma B$. The challenge is to choose values of τ that make efficient use of measurement time t_m to reduce the field uncertainty σ_B. We use the equivalent noise sensitivity $\eta = \sigma_B t_m^{1/2}$ as a figure of merit. Sequential Bayesian experiment design chooses measurement settings (τ) by forecasting measurement outcomes and the effects they would have on the parameter distributions. The measurement benefit is quantified as the change in the information entropy of the parameter distribution and the measurement cost is the time required. With each measurement, more precise parameter distributions are inferred from new measurement data, improving forecasts and τ choices for later iterations. Results plotted in Fig. 1 compare

the performance of sequential Bayesian experiment design with three other protocols: a non-adaptive variant of the quantum phase estimation algorithm (QPEA) [2], nonadaptive random selection of τ (Random), and an adaptive heuristic that chooses τ inversely proportional to the frequency uncertainty (Tau) [3]. For consistency, all measurement data is interpreted using Bayesian inference. The main figure plots the evolution of η against combined computation time and simulated measurement time. The vertical axis allows comparison of average uncertainty at a fixed measurement time. The inset plots η^2, allowing comparison of time required to achieve a given uncertainty. The SBED protocol is faster than the Tau, Random, and QPEA protocols by factors of 2, 4 and 5, respectively.

[1] R. D. McMichael, S. M. Blakley, and S. Dushenko, J. Res. Natl. Inst. Stan. Vol. 126, p. 126002 (2021). [2] H. T. Dinani, D. W. Berry, R. Gonzalez, et al., Phys. Rev. B Vol. 99, p.125413 (2019) [3] R. Santagati, A. A. Gentile, S. Knauer, et al., Phys. Rev. X Vol. 9, p. 021019 (2019).

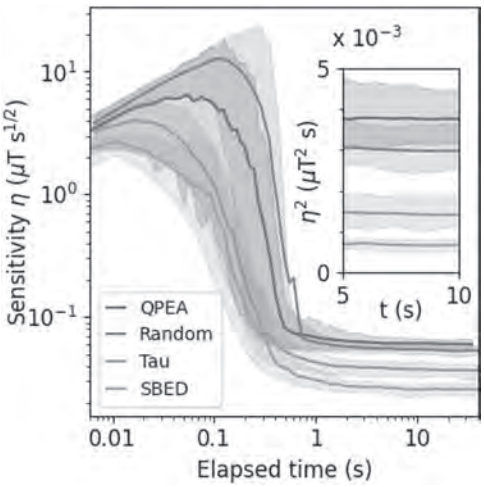

Fig. 1. Comparison of equivalent noise sensitivity $\eta = \sigma_B t_m^{1/2}$ achieved by different measurement protocols. Initial measurements have small effects on the field uncertainty σ_B *as* t_m increases. After 1 s of measurment, all protocols have converged to aymptotic $\sigma_B \propto t_m^{-1/2}$ behavior. The sequential Bayesian experiment design olffers the best performance.

IOC-03. Conductivity Measurement of Nonferrous Plates using a Novel Sensor with Triangular Arrangements of Triple Coils. *M. Mirzaei*[1], P. Ripka[1] and V. Grim[1] *1. Czech Technical University, Prague, Czechia*

The determination of electrical conductivity of the conductive metallic objects in the industrial apparatuses and structures is necessary for health monitoring and maintenance using nondestructive testing and for control purposes in electrical drives [1]. The used Metal parts face corrosion and cracks, which nondestructive testing methods are used for their health monitoring. For example, eddy current nondestructive testing method (ECNDT) is a known method [2]-[8], which needs electrical and magnetic characteristics properties of metals. Electrical conductivity has high influence on the eddy current speed sensor for high-speed transportation using linear drives [1] and [9]-[11]. Eddy current sensors were well developed to measure electrical conductivities of ferrous and nonferrous plates using nondestructive approaches. However, they cannot be integrated with main sensor, for example, eddy current speed sensor or they must be installed separately. A novel eddy current sensor is proposed in this paper, which has one excitation coil and two antiserially pick up coils. The coils arrangement is in equilateral triangular form (Fig. 1). The induced voltage of antiserially connected pick up coils is zero when all coils are far enough from conductive objectives. However, induced voltage is nonzero when one pick up coil is closer to the conductive objects due to the induced eddy currents in the conductive objects and unequal flux linkage in the pick up coils as shown for aluminum plate in Fig. 2. The induced voltage is a function of plate conductivity. The experiments and 2D and 3D finite element method (FEM) analysis are conducted for nonferrous plates at different frequencies to estimate plates conductivities. The accuracy of eddy current sensor was tested and analyzed, which is within 5% error. The full description, analysis and experiments of the proposed sensor will be presented in the full paper.

[1] M. Mirzaei, P. Ripka and V. Grim, IEEE Magnetic Letters, Vol. 11 (2020) [2] W. Yin and K. Xu, IEEE Transactions on Instrumentation and Measurement., Vol. 65, p.164 (2016) [3] M. Lu, R. Huang and W. Yin, IEEE Sensors Journal, Vol. 19, p. 7440 (2019) [4] M. Lu, X. Meng and L. Chen, IEEE Sensors Journal, Vol. 20, p. 2904 (2020) [5] M. Lu, X. Meng and R. Huang, IEEE Transactions on Instrumentation and Measurement., Vol. 70 (2021) [6] M. Lu, Y. Xie and W. Zhu, IEEE Transactions on Industrial Informatics., Vol. 15, p. 4111 (2019) [7] C. Wang, M. Fan, B. Cao, IEEE Sensors Journal, vol. 18, p. 9352, (2018) [8] N. Bowler and Y. Huang, Meas. Sci. Technol., vol. 16 p. 2193, (2005) [9] R. Palka and K. Woronowicz, Energies, vol. 14, (2021) [10] J. K. Noland, IEEE Access, vol. 9, (2021) [11] W.-Y. Ji, G. Jeong and C.-B. Park, IEEE Transactions on Magnetics, vol. 54, (2018)

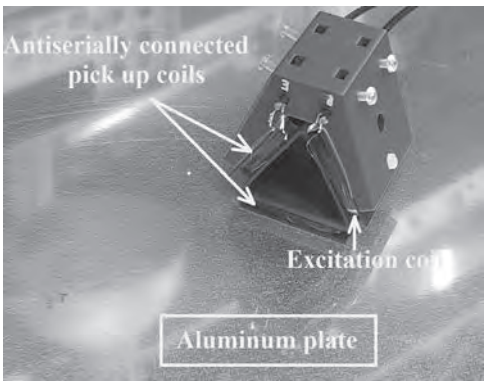

Fig. 1 The sensor with excitation coil and two antiserially connected pick up coils and aluminum plate

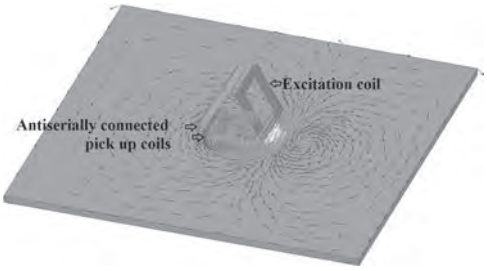

Fig. 2 Eddy current distribution in the aluminum plate using 3D FEM

IOC-04. Resolution Bandwidth of a Spectrum Analyzer Based on a Sweep-Tuned Oscillator. *P.G. Elphick*[1], S. Louis[2], A.N. Slavin[1] and V. Tyberkevych[1] *1. Physics, Oakland University, Rochester, MI, United States; 2. Electrical and Computer Engineering, Oakland University, Rochester, MI, United States*

Spin-torque nano-oscillators (STNOs) generate a microwave signal that can be tuned quickly due to their small size [1]. This fast tuning allows for the time-resolved spectrum analysis of microwave signals [2, 3]. The accuracy of frequency determination, known as resolution bandwidth (RBW), is an important characteristic of spectrum analyzers. In an STNO based spectrum analyzer that uses a matched filter algorithm, three main factors limit the RBW: ΔF_G^2, the STNO generation linewidth determined by thermal noise [1], $\rho = F_\Delta F_s$, the frequency scanning rate where F_Δ is scanning bandwidth and F_s is scanning frequency [2,3], and F_c, the cut-off frequency of the low-pass filter. The analytical expression for the RBW derived in this work is given by the following expression: $2\sigma^2 = \Delta_0^2 (1 + (\Delta_0^2/F_\Delta^2) / (1 + F_s^2 / F_c^2))$, where $\Delta_0^2 = F_G^2 + F_s^2 + F_c^2$. RBW according to this expression is plotted in

Fig. 1 using typical values. The black solid line shows RBW for the case when the cut-off frequency of the low-pass filter is F_c = 10 MHz. It is clear in this case, the RBW at low scan rates is determined by the generation linewidth, which is shown by the gray dotted line. In contrast, the dashed line corresponds to the case when F_c = 100 MHz. With this cutoff frequency, the filter allows more noise from the STNO to pass, thus increasing the RBW. For large scan rates the influence of the generation linewidth and the lowpass filter are not important, and the RBW is fully determined by the inverse scanning period, in agreement with the "bandwidth" theorem (black dotted line). This study provides a new understanding of how F_c impacts STNO based spectrum analysis, and will allow scan to occur at the theoretical limit for low scan rates.

[1] Joo-Von Kim, V. S. Tiberkevich and A.N. Slavin, Phys.Rev.Lett., Vol. 100, p. 017207 (2008). [2] S. Louis, O. Sulymenko, Vasil Tiberkevich, *et al.*, Appl. Phys. Lett. Vol. 113, p.112401 (2018). [3] Litvinenko, Artem, et al. *Nano letters* 20.8 (2020): 6104-6111.

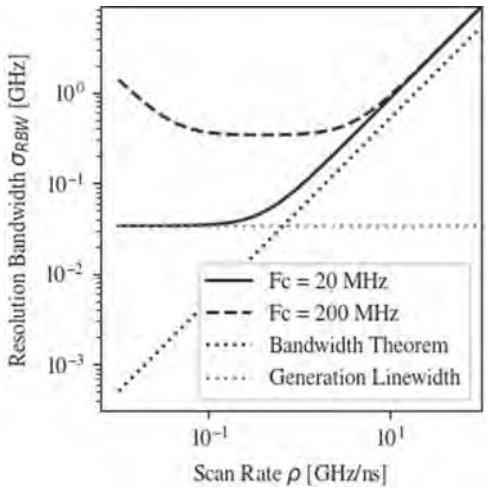

Figure 1: RWB as described by new analytical equation. Black dotted line shows the bandwidth theorem. Black line shows RBW when F_c = 10 MHz, black dashed line shows when F_c = 100 MHz, and grey dotted lines show low scanning rate limit as defined by STNO generation linewidth.

IOC-05. Non-Linear GMI Based Detection Platform for an Enhanced Contactless and Reusable Detection of Magnetic Nanoparticles. *J.J. Beato-López*[4,2], J. Algueta-Miguel[1,3] and C. Gomez-Polo[4,2] *1. Departamento de Ingeniería de Electricidad, Electrónica y Comunicación, Universidad Pública de Navarra, Pamplona, Spain; 2. Institute for Advanced Materials and Mathematics, INAMAT2, Universidad Pública de Navarra, Pamplona, Spain; 3. Institute of Smart Cities, Universidad Pública de Navarra, Pamplona, Spain; 4. Departamento de Ciencias, Universidad Pública de Navarra, Pamplona, Spain*

Magnetic nanoparticles (MNPs) have become a relevant technological topic as a result of their broad use in different fields, biomedicine, environmental applications, 3D printing, etc [1], [2], [3]. This wide use, together with the low MNPs concentrations used in most applications, requires the development of low-cost and high sensitivity detectors. So, this work explores the design of a Giant Magnetoimpedance effect (GMI) based detection platform for *contactless* MNPs detection, enabling its reuse in multiple applications. The GMI effect, based on huge changes in the high-frequency electrical impedance under external magnetic field, has revealed as a useful tool in the design of high sensitivity magnetic sensors [4]. The proposed device is formed by two soft magnetic amorphous wires ($Co_{66}Fe_{12}Si_{13}B_{15}Cr_4$, length 2 cm) placed in parallel and connected electrically in series to increase the effective detection area [5]. Its working principle relies on the GMI response under the effect of the remnant magnetic field generated by Fe_3O_4 MNPs (diameter 140 nm). The detection target (sample) was prepared by depositing different MNPs masses, *m*, from 1 to 15 mg, on different glass substrates. The sample to detect was placed over the sensor surface at different distances, *d*, (0.31 - 13 mm) avoiding physical contact with the sensing wires. Using a voltage divider and a lock-in amplifier (current frequency f = 100 kHz and peak to peak current I = 15 mA.), the changes of the first $V1_f(H)$, and second harmonic $V_{2f}(H)$, components of the GMI voltage were studied as a function of *m* and *d*. The larger detection capacity ($|(V_{if}(x)-V_{if}(x_{max}))/(V_{if}(x_{max}))|$; $i=1,2$; $x=m,d$) under a similar amount of MNPs found for V_{2f} (70%) respecting V_{1f} (10 %), led to the selection of V_{2f} in the final sensor prototype. A homemade electronics for sensor interfacing and signal conditioning was developed to improve both the sensitivity and spatial resolution where MNPs were detectable. The results show how the designed detection platform permits the quantification of low amounts of MNPs at larger distances (order of mm) than other detectors reported in the bibliography under the principles of low-cost, simple design, single-step measurement and reusability.

[1] K. Wu, D. Su, J. Liu, R. Saha, and J.-P. Wang, "Magnetic nanoparticles in nanomedicine: a review of recent advances," *Nanotechnology*, vol. 30, no. 50, p. 502003, Sep. 2019, doi: 10.1088/1361-6528/ab4241. [2] L. Li *et al.*, "Synthesis, Properties, and Environmental Applications of Nanoscale Iron-Based Materials: A Review," *Critical Reviews in Environmental Science and Technology*, vol. 36, no. 5, pp. 405–431, Oct. 2006, doi: 10.1080/10643380600620387. [3] N. Löwa, J.-M. Fabert, D. Gutkelch, H. Paysen, O. Kosch, and F. Wiekhorst, "3D-printing of novel magnetic composites based on magnetic nanoparticles and photopolymers," *Journal of Magnetism and Magnetic Materials*, vol. 469, pp. 456–460, Jan. 2019, doi: 10.1016/j.jmmm.2018.08.073. [4] G. V. Kurlyandskaya, M. L. Sánchez, B. Hernando, V. M. Prida, P. Gorria, and M. Tejedor, "Giant-magnetoimpedance-based sensitive element as a model for biosensors," *Appl. Phys. Lett.*, vol. 82, no. 18, pp. 3053–3055, May 2003, doi: 10.1063/1.1571957. [5] J. J. Beato-López, J. M. Algueta-Miguel, and C. Gómez-Polo, "Contactless magnetic nanoparticle detection platform based on non-linear GMI effect," *Measurement*, vol. 180, p. 109602, Aug. 2021, doi: 10.1016/j.measurement.2021.109602.

IOC-06. Flux Noise Reduction of HTS SQUID Using Josephson Junctions Made by FIB. *K. Hayashi*[1], R. Ohtani[1], Y. Tottori[1], S. Ariyoshi[2] and S. Tanaka[2] *1. Department of Applied Chemistry and Life Science, Toyohashi University of Technology, Toyohashi, Japan; 2. EIIRIS, Toyohashi University of Technology, Toyohashi, Japan*

Superconducting quantum interference devices (SQUIDs), which are the most ultrasensitive magnetic sensors, are generally made by microfabrication of superconducting thin films. The bicrystal junction, which is often used in high-temperature superconducting (HTS) Josephson junctions (JJs), has problems expensive bicrystal substrates, and the fact that JJs can only be arranged in a fixed straight line [1-2]. Because the HTS thin film is a type-II superconductor, magnetic fluxes penetrates the HTS thin film and moves for the Lorentz force, which increases the flux noise at low frequencies. In this study, we investigated a method to fabricate low-noise SQUID magnetic sensors by Ga focused ion beam (FIB) irradiation of high-temperature superconducting thin films. When HTS thin film is irradiated with FIB, point defects are introduced into the HTS crystal structure, which leads to changing into normal conduction. The dependence of the critical current change ratio I_C/I_{C0} on the dose was shown in Fig.1. The dependence of the normal resistance R_N are also depicted. The thickness of the $YBa_2Cu_3O_{7-}\delta$ (YBCO) film was 50 nm and it was protected by a thin Au layer. I_C/I_{C0} decreased with irradiation fluence and changed into normal conduction at 2.0×10^{17} ions/cm^2; after this point R_N increased steeply. HTS nanobridge JJ, were fabricated by FIB irradiation. Figure 2 shows the V-I characteristics of a nanobridge with an HTS film thickness of 50 nm and a bridge width of 120 nm. The critical current was reduced to 264.5 μA and shows a clear Shapiro-steps under microwave irradiation with frequency of 10 GHz. As a method to reduce the magnetic flux noise, we also investigated the introducing of normal conducting pinning sites (anti-dots) into HTS thin films by FIB irradiation. We have confirmed that anti-dots with diameters of several hundred nm can be formed by point irradiation of HTS thin films with FIB.

In the future, we will confirm SQUID operation at a nanobridge JJ with an YBCO film thickness of 50 nm and investigate the improvement of SQUID noise characteristics by introducing anti-dots.

[1] Hsiao-Wen Yu, Ming-Jye Chen, H.C. Yang, S.Y. Yang, and H.E. Horng, "Effect of the grooved $SrTiO_3$ bicrystal line on the $YBa_2Cu_3O_7$ grain boundary,"PhysicaC,vol.333,pp.163–169,2000.[2]K.R.Bukh,C.S.Jacobsen, J. Bindslev Hansen, Y.Q. Shen, and T. Holst, "Observation of distinct, temperature dependent flux noise near bicrystal grain boundaries in $YBa_2Cu_3O_{7-x}$ films," Physica C, vol. 333, pp. 133– 138, 2000.

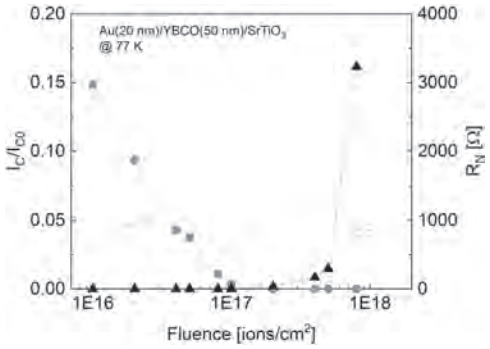

Fig. 1. Dependence of I_C/I_{C0} and R_N on FIB irradiation fluence.

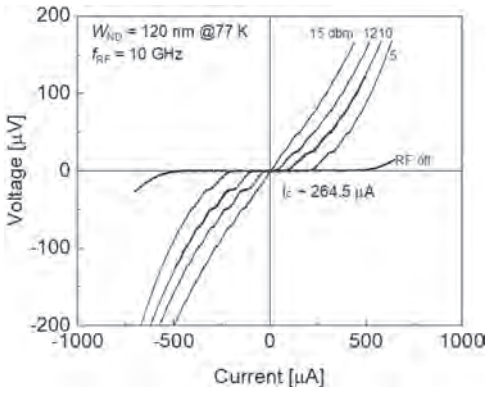

Fig. 2. V-I characteristics of the HTS nanobridge with a width of 120 nm.

IOC-07. Flexible multifunctional sensorics for simultaneous strain and magnetic field measurements. *Y. Zabila*[1,2], A. Maximenko[3], M. Krupinski[2], A. Zarzycki[2], M. Perzanowski[2], P. Horeglad[2], M. Marszalek[2] and D. Makarov[1] *1. Intelligent Materials and Systems, Helmholtz Zentrum Dresden Rossendorf, Dresden, Germany; 2. Department of Magnetic Materials and Nanostructures, The Henryk Niewodniczanski Institute of Nuclear Physics Polish Academy of Sciences, Krakow, Poland; 3. SOLARIS National Synchrotron Radiation Centre, Krakow, Poland*

As an alternative for conventional rigid electronics, there is tremendous progress in the area of mechanically soft electronics [1,2], where functional elements are fabricated on flexible and even elastic membranes that can be bent, folded, or twisted. This technology enables an appealing possibility to adjust the shape of the devices at will after their fabrication and paves the way to their use for smart skin, smart textile applications, where the functional elements should conform to a dynamically varying and curved surface of an object. Flexible magnetic field sensors [3,4] are crucial components of flexible interactive on-skin and wearable electronics as they allow to monitor of any type of motion. Typically, magnetic thin films are used for flexible magnetoelectronics to detect in-plane magnetic fields [5-8]. To acquire the sensitivity to out-of-plane magnetic fields, Bi-based Hall effect sensors have proven their efficiency for smart wearables and electromobility applications. Here, we explore the extreme strain sensitivity of Bi thin films to realise a multifunctional flexible device, which can measure strain and magnetic fields simultaneously. The sensors are fabricated on 12-um-thick polyimide foils capped with Bi thin films of different thicknesses from 20 to 100 nm. They are mechanically stable and withstand severe mechanical bending down to the radii of about 1 mm for 10.000 bending cycles. The fabrication method allows realising ultrathin and flexible Bi-based Hall effect sensors with the sensitivity of 5 Ohm/T, which is a record high for this type of sensor. We propose and validate the measurement sequence relying on the spinning current approach to decouple the signals measured by a single sensor element in transversal and longitudinal resistance channels. Furthermore, we developed a method to analyse the measured transversal and longitudinal resistances to assess the out-of-plane component of the magnetic field (Hall effect) and vector components of the in-plane strain (tensoelectric effect). We apply these sensors as a component of smart skin for soft robotics and human-machine interfaces.

[1] S. Bauer et al., Adv. Mater. 26, 149 (2014). [2] T. Someya et al., MRS Bulletin 42, 124 (2017). [3] D. Makarov, Appl. Phys. Rev. 3, 011101 (2016). [4] G.S. Canon Bermudez et al., Adv. Funct. Mater. (2021). Doi: 10.1002/adfm.202007788 [5] M. Ha et al., Adv. Mater. 33, 2005521 (2021). [6] E.S. Oliveros Mata et al., Applied Physics A 127, 280 (2021). [7] J. Ge et al., Nat. Commun. 10, 4405 (2019). [8] G.S. Canon Bermudez et al., Nat. Electron 1, 589 (2018).

IOC-08. 2D application-ready magnetoelastic cilia tactile sensing device. *P. Ribeiro*[2,3], L. Jamone[1] and S. Cardoso de Freitas[2,3] *1. Advanced Robotics at Queen Mary, Queen Mary University of London, London, United Kingdom; 2. INESC - Microsistemas e Nanotecnologias, Lisbon, Portugal; 3. Department of Physics, Instituto Superior Técnico, Lisbon, Portugal*

The cilium inspired tactile sensor is based on a magnetic sensor located below thin, elongated permanently magnetized elastic pillars. Deformations of the pillar caused by small flows, forces and surface textures change the magnetic field detected by the sensor, thus transducing deformation into an electric signal [1]. In this work, we present a tactile/force sensor based on AlOx tunnel barrier magnetoresistive (TMR) sensors integrated as a monolithic 2D sensitive device [2]. Each sensing direction includes TMR sensors in Wheatstone bridge to minimize noise contamination of the signal [3] and simplifying the signal processing chain. A polydimethylsiloxane matrix with embedded NdFeB particles (at a mass ratio of 65% particles to 35% PDMS) was used to form the cilium on top of the sensor (Fig. 1). The sensor voltage output is connected to a compact electronic interface, allowing it to be easily integrated within another application where sensitive tactile sensing is desired. The fabricated device presents a sensitivity of 3.1 mV/Oe and 3.0 mV/Oe and a bridge offset voltage of 107 mV/V and -13 mV/V in the X and Y sensitive directions, respectively. The characteristic of the cilia sensor, using cilia with and 400 μm diameter by 3 mm height and a magnetic moment of 58 emu cm^{-3} was compared to its simulated response. A good agreement between results and simulation was achieved, with an root mean square error (RMSE) error of 66 μV for each respective cilium dimension (Fig. 2a). Finally, the cilium was manually actuated in both X and Y directions, with a clear distinction between the actuations of each sensitive direction being observed (Fig. 2b).

[1] A. Alfadhel and J. Kosel, "Magnetic nanocomposite cilia tactile sensor", Advanced Materials, vol. 27, pp. 7888-7892, oct 2015 [2] P. Ribeiro, A. V. Silva and S. Cardoso, Simplified process for the monolithic integration of tunnel magnetoresistive sensors in a two-dimensional magnetometer, IEEE Magnetics Letters, vol. 11, mar 2020 [3] J. S. Moreno, D. R. Muñoz, S. Cardoso, S. C. Berga, A. E. N. Antón and P. Freitas, "A non-invasive thermal drift compensation technique applied to a spin-valve magnetoresistive current sensor", Sensors, pp. 71-91, jun 2011

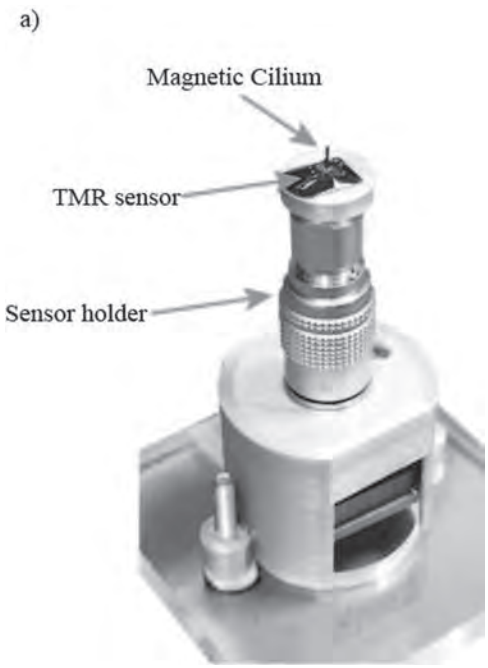

Fig. 1: Photograph of the assembled cilia sensor.

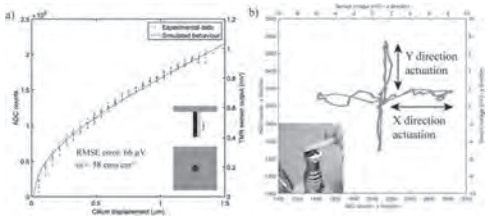

Fig. 2: a) Measured signal vs tip deformation characteristic and simulated results for a sensor with 3 mm height and 400 µm diameter cilium. b) Measured response for manual actuation of the cilium in both X and Y directions.

IOC-09. Wireless Stress Sensor Based on Magnetoelastic Microwires for Biomedical Applications: detection of collagen concentration, pressure and temperature. *P. Marin*[1], M. Vélez[2] and J. López[3,4]
1. Instituto de Magentismo Aplicado, Universidad Complutense de Madrid, Las Rozas, Spain; 2. Instituto de Catálisis, Consejo Superior de Investigaciones Cientificas, Madrid, Spain; 3. Instituto de Magentismo Aplicado, Universidad Complutense de Madrid, Las Rozas, Spain; 4. Spanish CRG BM25-SpLine at The ESRF – The European Synchrotron, Grenoble, France

Hydrogels are networks of very hydrophilic polymeric materials that can be used as scaffolds to organize cells into a three-dimensional architecture, with applications in tissue engineering. The density and alignment of the polymer fibers within the gel determine their mechanical properties that play a crucial role in regulating the interactions between seeded cells [1]. Measurement and interpretation of bulk mechanical properties of hydrogels are difficult. In addition, cells growing inside the scaffold can reorganize the gel fibers and induce local strains and deformations. The ability to record these changes of the mechanical properties inside the hydrogels is important in the quest to engineer functional tissues in vitro [2][3]. It is easy to find literature regarding microwave-related applications of amorphous magnetic microwires (AMW) or AMW-based materials [4]. In the frequency range of GHz, studies of the effect of the magnetization on the scattering properties of a single AMW can be found [5]. This work gives experimental evidence showing that the microwave scattering by a single AMW depends on the magnetic permeability with sufficient strength to be experimentally detected as an effect of the GMI showing the potential of such microwire as a wireless field and/or stress sensor. [6]. Here we present results of a new application of AMW to the wireless measuring of intrinsic local properties of two different types of natural hydrogels. The dipolar resonance frequency of AMW is altered by the dielectric constant of the surrounding medium and due to its magnetostrictive character, the giant magnetoimpedance effect can be modulated in the presence of mechanical stress. This work shows how an AMW allows wireless detecting of hydrogel concentration, as well as changes due to temperature and applied external pressure. Measurements are carried out by inserting a centimeter size AMW into hydrogel solution and recording from a distance the magnetic response by means of GHz antenna and VNA network analyzer. This work demonstrates the potential of using these AMW for sensing and reporting changes in the local internal environment of hydrogel scaffolds due to cell growth.

[1] M. W. Tibbitt and K. S. Anseth, *Biotechnology and Bioengineering*, vol. 103, no. 4. p. 655–663 (2009) [2] M. L. Oyen, *Int. Mater. Rev.*, vol. 59, no. 1, p. 44-59 (2014) [3] J. Lee *et al.*, *Sci. Rep.*, vol. 9, no. 1, 2463 (2019) [4] P. Marín, M. Marcos, and A. Hernando, *Appl. Phys. Lett.*, 262512 (2010) [5] C. Herrero-Gómez, P. Marín, and A. Hernando, *Appl. Phys. Lett.*, vol. 103, no. 14, 142414 (2013) [6] M. Vázquez and A. P. Zhukov*J. Magn. Magn. Mater.*, p 223-228 (1996)

IOC-10. Printing magnetostrictive materials for structural health monitoring of carbon fibre composite. *N. Ahmed*[1], P. Smith[2] and N. Morley[1] *1. Materials Science and Engineering, University of Sheffield, Sheffield, United Kingdom; 2. Mechanical Engineering, University of Sheffield, Sheffield, United Kingdom*

The aerospace industry has become increasingly reliant on carbon fibre composite (CFC) as a structural component in aircraft, due to its strength to weight ratio. One of the disadvantages of CFC are their vulnerability to impact damage and external environment changes during flight, which causes barely visible damage to the structure. One solution to this is structural health monitoring (SHM), which monitors the composite structure to provide early detection for damage. Previous work has found that magnetostrictive ribbons [1] and inkjet printed copper coils used as actuator-sensor pairs have good resolution to detect damage to CFC [2]. This research has focused on inkjet printing magnetic sensors, which can be directly attached to the surface of the composite. JetLab IV (by MicroFab) with piezoelectric print head (60um diameter orifice) was used. The sensor designs were printed using Magnetite (20% in DMF, IPA and water) and nickel (2% in NMP and water) nanoparticle dispersion inks, manufactured by Nanoshel LLC on photo paper (25x25mm) (fig 1). A MPMS3-SQUID magnetometer was used to characterise the ink's magnetisation (fig 2). Magnetite and nickel has saturation magnetisation values of 78 and 27 emu/g respectively. Different designs and printer parameters were explored and their magnetic performance evaluated the magnetic performance of the printed designs using simple mechanical testing such as 3-point bending test and impact testing.

[1] Z. Leong, W. Holmes, J. Clarke, A. Padki, S. Hayes, and N. A. Morley,', *IEEE Trans. Magn.*, 55, 7, 1–6, 2019. [2] A. Gullapalli, V. Beedasy, J. D. S. Vincent, Z. Leong, P. Smith, and N. A. Morley, *Adv. Eng. Mater.*, 2100313, 2021.

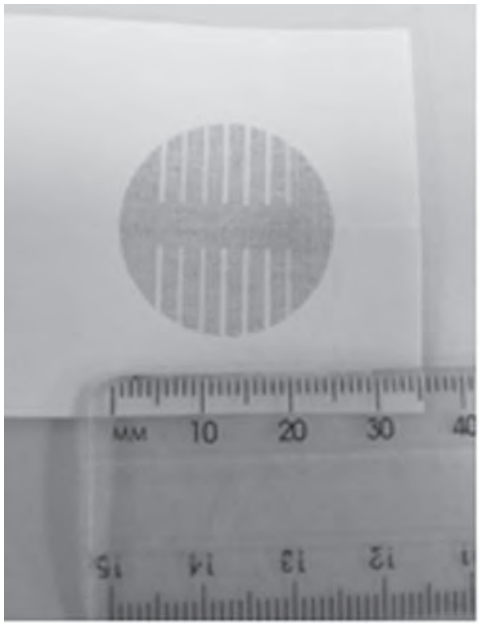

Fig 1. Magnetite printed design on photo paper

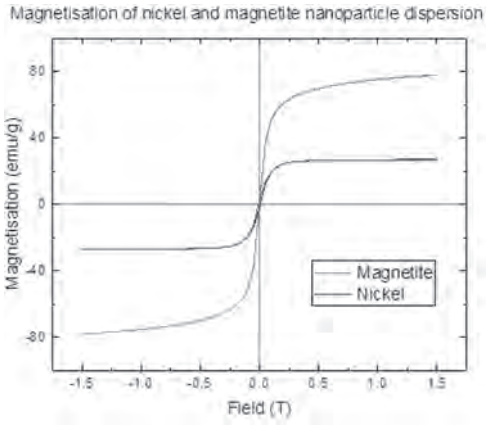

Fig.2 Hysteresis loop of magnetite and nickel ink

IOC-11. The compositional dependence of NiFeCr seed layer on the giant magnetoresistance of [FeCoNi/Cu] multilayers. *P.D. Kulkarni*[1], T. Nakatani[1] and Y. Sakuraba[1] *1. Magnetic Materials Group, Research Center for Magnetic and Spintronic Materials, National Institute for Materials Science, Tsukuba, Japan*

The giant magnetoresistance (GMR) devices are attractive as cost-efficient gradiometers due to a larger magnetoresistance ($\Delta R/R$) in a simple structure [1]. Many studies showed that NiFeCr seed layers promote a strong 111 crystallographic texture of GMR films that gives rise to a large $\Delta R/R$ [2-4]. However, the effect of NiFeCr composition on GMR has not been reported. In this work, we made a systematic study on the structure and GMR effect of $Ni_xFe_yCr_z$ /$Fe_{16}Co_{66}Ni_{18}$ /[Cu /$Fe_{16}Co_{66}Ni_{18}$]$_5$ /Ru films deposited on SiO_x substrate. NiFeCr and FeCoNi layers were deposited by co-sputtering (Ni, Fe, Cr) and ($Co_{80}Fe_{20}$, Ni), respectively. Figure 1 shows a contour of $\Delta R/R$ for various $Ni_xFe_yCr_z$ compositions, with a typical $\Delta R/R$ vs $\mu_0 H$ curve corresponding to $Ni_{55}Cr_{45}$ seed layer. The maximum $\Delta R/R \sim 35\pm2.5\%$ (sensitivity ~ 0.25 %/mT) is observed for the seed layers $(Ni_{0.55}Cr_{0.45})_{100-y}Fe_y$ with $0 \le y \le 47$, indicating that Ni:Cr = 55:45 ratio is critical for large $\Delta R/R$. The estimated bilinear (J_1) and biquadratic (J_2) interlayer exchange coupling in this region show stronger antiparallel coupling ($J_1/J_2 \ge 1$). On the other hand, for Ni:Cr ≥ 62:38 or Ni:Cr ≤ 48:52, $\Delta R/R$ reduces to < 22% as antiparallel coupling reduced ($J_1/J_2 < 1$). XRD θ-2θ profiles confirm that [FeCoNi/Cu] multilayer has fcc 111 texture with the diffraction peaks ($2\theta_{111}$) located between 43.70 and 43.96°. We found a clear correlation between $2\theta_{111}$ and $\Delta R/R$; *i.e.* films with high $\Delta R/R \sim 35\pm2.5\%$ (*i.e.* on seed layers $(Ni_{0.55}Cr_{0.45})_{100-y}Fe_y$ with $0 \le y \le 47$) show $43.88° \le 2\theta_{111} \le 43.96°$, whereas films with $\Delta R/R \le 25\%$ show $2\theta_{111} < 43.82°$. We also calculated the sheet resistance of GMR films at parallel magnetization (R_P in Ω/■). Figure 2 consists a contour of $\Delta R/R$ plotted for corresponding values of $2\theta_{111}$ and R_P, which clearly shows that films with high $\Delta R/R$ consists $43.88° \le 2\theta_{111} \le 43.96°$ and lower R_P. As lower R_P associates to larger grain size [5], these observations indicate that the seed layers of $(Ni_{0.55}Cr_{0.45})_{100-y}Fe_y$ with $0 \le y \le 47$ induce large gain size in the [FeCoNi/Cu] multilayer, thus realizes the large $\Delta R/R$ and sensitivity.

[1] For example, NVE Corporation, see https://www.nve.com/Downloads/intro.pdf. [2] Prabhanjan D. Kulkarni, Tomoya Nakatani, Taisuke Sasaki, Yuya Sakuraba, J. Appl. Phys. 129, 213901 (2021). [3] M. Milyaev, L. Naumova, V. Proglyado, T. Krinitsina, N. Bannikova, and V. Ustinov, IEEE Trans. Magn. 55, 1 (2019). [4] N. S. Bannikova, M. A. Milyaev, L. I. Naumova, V. V. Proglyado, T. P. Krinitsina, I. Yu. Kamenskii, and V. V. Ustinov, Phys. Met. Metallogr. 116, 987 (2015). [5] Luo Wei, Zhu Lin-Li, Zheng Xiao-Jing, Chin. Phys. Lett. 26, 117502 (2009).

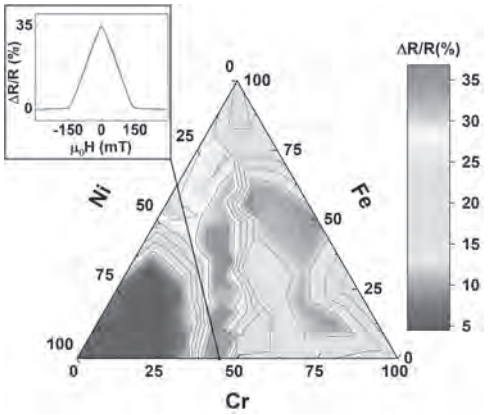

Fig.1: Contour of $\Delta R/R$ for various $Ni_xFe_yCr_z$ seed layers, with a typical $\Delta R/R$ vs $\mu_0 H$.

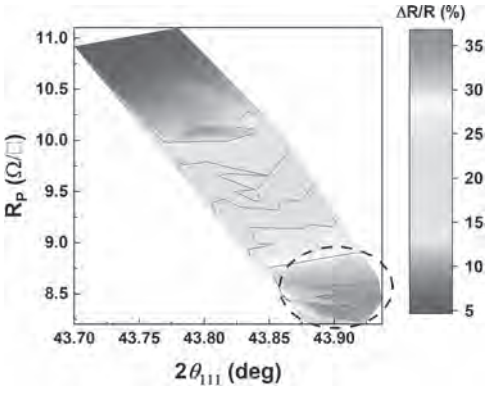

Fig.2: Contour map of $\Delta R/R$ plotted against $2\theta_{111}$ and R_P.

IOC-12. Investigation of noise origin in a symmetric response magnetoresistance (SRMR) sensor using AC modulation. *Y. Higashi*[1], A. Kikitsu[1], Y. Kurosaki[1] and S. Shirotori[1] *1. Toshiba Corporation, Kawasaki, Japan*

High-sensitive Magneto-resistance (MR) sensors, in which it is easy to integrate to system, have attracted much attention as inspection of Li ion battery [1]. Recently 10 pT sensor have been reported [2]. To improve the detectivity, it is effective to adopt an AC modulation system [3]. In the previous

work, we have proposed a new high-sensitive sensor which is referred to a symmetric response magnetoresistance (SRMR) sensor for reducing the 1/f noise [4]. It had higher SNR than its without proposed system, however, we have not reach our goal by an unexpected noise, in which were noise like white noise from 100 Hz to 10kHz (white type noise) and noise like 1/f noise that spread around modulated frequency (1f noise). In this paper, we investigate the dependence of noise characteristics under modulation. To input some different DC voltage to AC modulation voltage makes modulation condition changed. It is found that there is a correlation between 1f noise and noise under 10Hz because of similar dependence that noise magnitude increase in the order of Vdc=+0.5, -0.1 and -0.5V(Fig.1). This result indicates that the 1f noise originated from noise in the low frequency. We investigate whether electronic or magnetic noise in noise in the low frequency is dominant over 1f noise by SPICE simulation. 1/f noise source are added to RH loop and power supply of SRMR as magnetic and electronic noise, respectively. It is found that the magnitude of 1f noise depends on it of magnetic (red line), not electronic noise (blue line) (Fig.2). This result indicate SRMR reduce electronic 1/f noise. This work was supported by the Cabinet Office (CAO), Crossministerial Strategic Innovation Promotion Program (SIP), "An intelligent knowledge processing infrastructure, integrating physical and virtual domains" (funding agency: NEDO).

[1] K. Kimura et al.: *J. Inst. Electr. Eng. Jpn*., vol. 135, no. 7, pp. 437–440, 2015. [2] K. Fujiwara et al., Appl. Phys. Express, 11, 023001, 2018 [3] W.Tian, et al., *IEEE Trans. Magn.,* vol. 52, Issure:2, Feb. 2016, Art. no. 4000306. [4] S. Shirotori et. al., Abstract of MMM2021, 2021

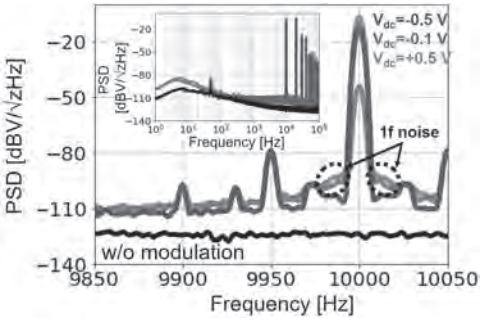

Fig. 1 Each Power Spectral Density (PSD) as a function of frequency at Vdc=-0.5, -0.1 and +0.5V. Modulation frequency is 10kHz and measurement frequency is 70Hz. Some peaks come from the disturbance magnetic field.

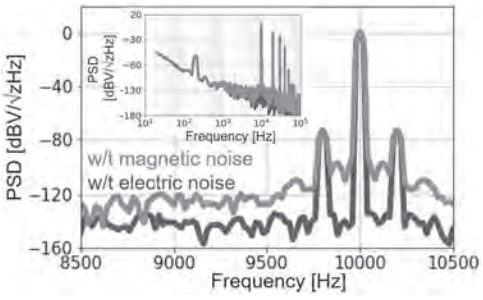

Fig. 2 SPICE simulation results of Power Spectral Density (PSD) with magnetic noise (red line) or electronic noise (blue line). Modulation frequency is 10kHz and measurement frequency is 200Hz.

IOC-13. Detecting Magnetic Ink Barcodes with Magnetoresistive Sensors. *S. Abrunhosa*[1,2], I. Gibb[3], R. Macedo[1], E. Williams[3], N. Muller[3], P.P. Freitas[1,2] and S. Cardoso de Freitas[1,2] *1. INESC MN, Lisbon, Portugal; 2. Instituto Superior Técnico, Lisbon, Portugal; 3. MagVision Ltd, Frome, United Kingdom*

Information encoding in barcodes using magnetic-based technology is a unique strategy to read data buried underneath a non-transparent surface of an object, since a direct line-of-sight between the code and the reader is not required. Usage of magnetic ink character recognition (MICR) [1] is already widespread in the banking industry. Nonetheless, current reading heads need to be placed in contact with the magnetic structures, limiting the possibilities of reading buried information. This is of particular interest in secure labelling and recyclable packaging applications. With the introduction of highly sensitive magnetic readers based on tunnel magnetoresistive sensors (TMR) [2,3], this becomes a reality. These sensors are also known to have good spatial resolution capabilities (few μm) and are capable of high frequency operation, thus enabling high bit density encodings. We have built a reading head capable of detecting signals by scanning barcodes printed with soft and hard ferromagnetic inks. These capabilities extend to depths up to 2 mm and individual structures as thin as 100 μm. To detect soft magnetic codes with a good signal-to-noise ratio, an external magnetic field is required during acquisition, through a permanent magnet included in the reading head. However, when placed in the vicinity of a TMR sensor, this magnet will also affect its transfer curve. Consequently, a fine balance between maximising the magnetisation of the ink during reading and minimising the effect on the transfer curve must be achieved. We have found an optimal configuration using a disc magnet placed behind the TMR sensor, while the surface of the sensor is as close as possible to the barcode. Fig. 1 shows the shows the signal resulting from scanning a soft magnetic barcode using the described configuration.

[1] G. Dimauro et al., International Journal of Pattern Recognition and Artificial Intelligence, 11(04), pp.467-504 (1997) [2] A. Hirohata et al., Journal of Magnetism and Magnetic Materials, 509, p.166711 (2020) [3] S. Cardoso et al., Microsystem Technologies, 20(4-5), pp.793-802 (2014)

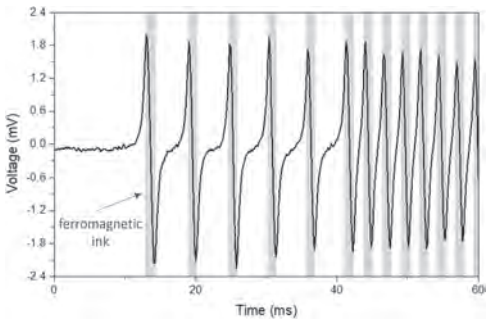

Fig. 1 - Magnetic reading head output after scanning a ferromagnetic barcode, at a reading distance of 200 μm and with a TMR sensor with a sensitivity of 6.1%/mT. Individual barcode stripes (600 μm wide) are represented as grey rectangles under the signal.

Session IOD
POWER DEVICES, INDUCTION
Guijun Li, Chair
Hong Kong University of Science and Technology, Hong Kong, Hong Kong

CONTRIBUTED PAPERS

IOD-01. Large-Signal Characterization Technique for Power Electronics Magnetic Components by Deep Learning with Double Pulse Test Measurement Image. *T. Koga*[2,1], K. Matumoto[1], Y. Ishizuka[1], N. Shigei[3], M. Yamaguchi[4], A. Itagaki[5] and T. Nakamura[5] *1. Nagasaki University, Nagasaki, Japan; 2. Ansys Japan, Shinjuku, Japan; 3. Kagoshima University, Kagoshima, Japan; 4. Tohoku University, Sendai, Japan; 5. Ryowa Electronics Co. Ltd., Sendai, Japan*

Because emerging wide-bandgap devices enable higher frequency switching, modeling of high-frequency magnetic components becomes increasingly important in designing a high-density switching mode power supply. In such difficult situations, the power electronics circuit designers can be helped with obtaining customized and non-linear models for the magnetic components with measurements to reduce their development time and cost [1-5]. Recent studies indicate that the accurate prediction for the model relies on rectangular-voltage-excited measurements [6]. Especially, the double-pulse-test (DPT) is the preferred test method to measure the switching parameters and evaluate the dynamic behaviors of power devices. On the other hand, image classification using deep learning (DL) technology has already been shown to produce results with very high accuracy, in some cases even surpassing human capabilities [7]. Therefore, we propose a large-signal power magnetic components analysis technique combining DPT and DL shown in Fig. 1 for the classification, the non-linear modeling, and the loss estimation. The unique point of the proposed technique is using the measured waveform image data of DPT. The multi-dimension waveform images include the individual characteristics of the measured magnetic components. The project goal is that the power electronics designer can easily have the large-signal characteristics of the magnetic components on their own. In this presentation, the experimental and analysis results applying for the classification of magnetics components with the proposed technique are discussed as our first step for this project. For example, the classification of three different materials and component styles using commonly available inductor whose nominal inductance value is indicated as 100uH. The results are summarized in the table in Fig. 2. And all of the indexes show perfect results, which means the classification is completed. Thus, the results reveal that the large-signal waveforms include very important information for the magnetic characterization, and the image recognition with DL helps the analysis of the waveforms.

[1] Phyo Aung Kyaw, “Deriving Loss Models From Measurements”, PSMA Power Magnetics @ High Frequency Workshop 2020, 2020. [2] Mike Wens, “Triangular Flux Excitation: The Proposed Standard for Measuring Power Inductors,” PSMA Power Magnetics @ High Frequency Workshop 2020, 2020. [3] Steve Sandler, “Accurately Measure Inductance with DC BIAS to 125Amps,” PSMA Power Magnetics @ High Frequency Workshop 2020, 2020. [4] Phyo Aung Kyaw, “Groundbreaking Wireless Charging Performance for Every Application,” PSMA Power Magnetics @ High Frequency Workshop 2020, 2020. [5] B. Wunsch, S. Skibin, T. Christen, “Broadband modeling of magnetic components with saturation and hysteresis for circuit simulations of power converters.,” 2018 IEEE International Magnetics Conference (INTERMAG), pp. 1-2., 2018. [6] J. Wang, X. Yuan and N. Rasekh, “Triple Pulse Test (TPT) for Characterizing Power Loss in Magnetic Components in Analogous to Double Pulse Test (DPT) for Power Electronics Devices,” IECON 2020, 2020, pp. 4717-4724. [7] Russakovsky, O., Deng, J., Su, H. *et al.* ImageNet Large Scale Visual Recognition Challenge. *Int J Comput Vis* 115, 211–252, 2015.

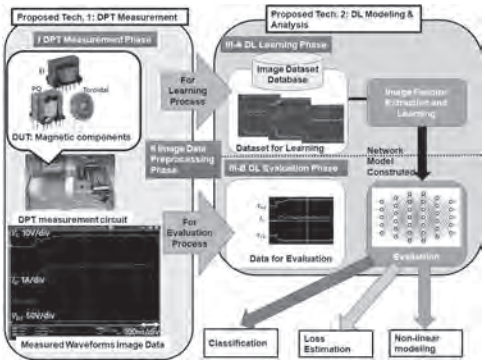

Fig. 1 Proposed Analysis System

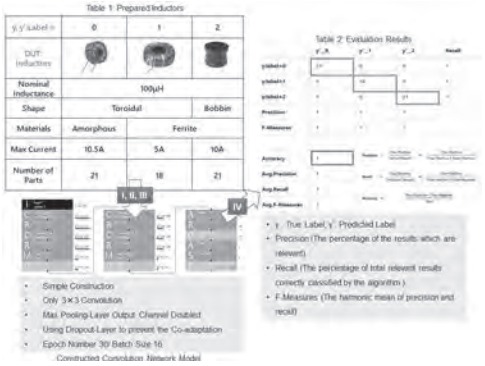

Fig. 2 Evaluated Process and The Results

IOD-02. A Dual-receiver Inductive Charging System for Automated Guided Vehicles. *H. Wang*[1] and K. Cheng[1] *1. The Hong Kong Polytechnic University, Kowloon, Hong Kong*

AUTOMATED guided vehicles (AGVs) are increasingly popular as essential transportation in numerous countries like France, Sweden, and China. Thanks to intrinsic advantages such as low noise and eco-friendliness [1], AGVs become an excellent alternative to conventional petrol vehicles. As a promising charging method, inductive power transfer (IPT) systems are exceptionally suitable for AGVs [2]. These two emerging technologies lead to a win-win situation. Specifically, the high positioning accuracy of self-driving vehicles naturally resolves the misalignment disturbance from IPT systems. The user-friendliness and intelligence of AGVs can also be significantly improved by IPT charging. Inspired by [3], a dual-receiver IPT system is proposed for AGVs. Compared to conventional dual-receiver WPT system. The proposed one can achieve constant current (CC) and constant voltage (CV) simultaneously. Specifically, one receiver can generate CC for charging loads, whereas the other generates CV for loads like control

circuits. Unlike [3], this article utilizes the mutual inductance between receivers to transfer energy. Energy can be transferred step by step from the transmitter coil to the first receiver (RX#1) and then to the second receiver (RX#2), as shown in Fig. 1. Experimental waveforms are shown in Fig. 1 (b). The load changing rate is 33.3% (from 30 to 20 Ω), whereas the variations of voltage and current are null and 4.4%, respectively. Fig.2 shows the key circuit schemes. Fig.2 (b) shows CC can be gained at load R_{L1} and Fig.2 (c) shows CV can be gained at load R_{L2}. Overall, the proposed dual-receiver WPT system shows distinct merits with two different outputs, i.e., CC and CV, simultaneously. By configuring the mutual inductance among coils, such a system avoids additional circuits and complex control systems. The measured dc-dc efficiency is around 86% when delivering a total output power 31.8 W to two loads.

[1] X. Liu, W. Han, C. Liu, and P. Pong, "Marker-free coil-misalignment detection approach using TMR sensor array for dynamic wireless charging system of electric vehicles," in *2018 IEEE International Magnetics Conference (INTERMAG)*, 23-27 April 2018 2018, pp. 1-2, [2] B. Che *et al.*, "Omnidirectional wireless power transfer system supporting mobile devices," in *2015 IEEE International Magnetics Conference (INTERMAG)*, 11-15 May 2015 2015, pp. 1-1, [3] R. Mai, Y. Luo, B. Yang, Y. Song, S. Liu, and Z. He, "Decoupling Circuit for Automated Guided Vehicles IPT Charging Systems With Dual Receivers," *IEEE Transactions on Power Electronics,* vol. 35, no. 7, pp. 6652-6657, 2020.

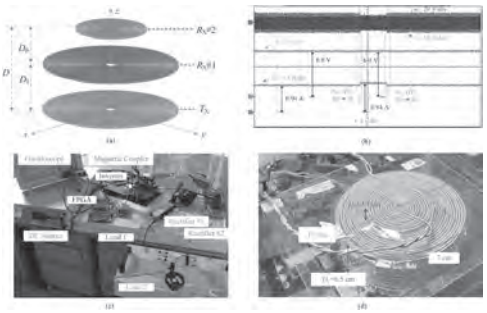

Fig. 1. Key diagrams: (a) Simulated model and (b) Experimental results, (c) Experimental setup, and (d) Magnetic coupler prototype.

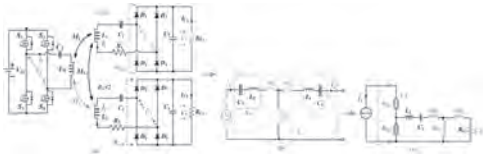

Fig. 2. Key circuit schemes: (a) entire system, (b) equivalent circuit for CC, and (c) equivalent circuit for CV.

IOD-03. A Low-cost Novel Method to Fabricate Integrated Magnetic Core Inductor Embedded in Organic Substrate. *Y. Wu*[1] and H. Yu[1]
1. School of Electrical, Computer and Energy Engineering, Arizona State University, Tempe, AZ, United States

The strong demand for 3D packaging technology has accelerated the miniaturization of passive devices, and inductors are facing challenges because the inductance value will be sacrificed when the size is shrinking. The magnetic core is one of the solutions due to its enhancement of inductance density but it will also add complexity to the fabrication process. Previous research [1-3] shows that the performance enhancement brought by the integration of magnetic will be shadowed by the process complexity. A novel method to fabricate the magnetic core inductors on flexible substrates is proposed in this work. The inductor has a stacking structure of three layers: the Cu trace layer, and the two layers of magnetic core (under and above the Cu). The Cu trace is patterned by the wet etch process on the flexible PCB, and the upper layer magnetic core is directly sputtered on the Cu trace layer with the polyimide layer being planarized on the Cu surface as insulation. A polyimide layer on the carrier wafer is prepared as the substrate for the lower magnetic core layer and the pattern is also created by the liftoff process. Then, the two finished layers are aligned and bonded with a flip-chip bonder with high precision and efficiency. The whole process is shown in Fig.1. Before the whole fabrication process, the device patterns are designed and optimized by the finite element analysis software to extract the parameters for comparison. And finally, the finished devices (shown in Fig.2) are measured with the radiofrequency probe station. The result shows that the inductance density and the quality factor of the magnetic core inductor could be 3.61 nH/mm^2 and 6.22, respectively, with the device size being only 0.95 mm^2. Compare with the air core inductor with the same Cu trace pattern, the magnetic core inductor elevates the inductance by 10% and still keeps the same low profile, of which the thickness of the whole device is within 100 um. These parameters are measured and extracted at 100 MHz and this is the widely used frequency for the power delivery applications such as the in-chip integrated voltage regulators.

[1] G. Wang, H. Liu, H. Qiu, K. Ning, Y. Yang, X. Li, X. Xu, M. Lavanant-Jambert, S. Petit-Watelot, and Y. Lu, Microelectronic Engineering 168, 5–9 (2017). [2] D. Mishra, P. M. Raj, J. Tishler, T. Sun, E. Shipton, and R. Tummala, IEEE Transactions on Magnetics 52(11), 1–5 (2016). [3] T. Wang, Y. Peng, W. Jiang, Y. M. Huang, B. F. Rahman, R. Divan, D. Rosenmann, and G. Wang, IEEE Transactions on Microwave Theory and Techniques 65(2), 504–512 (2016).

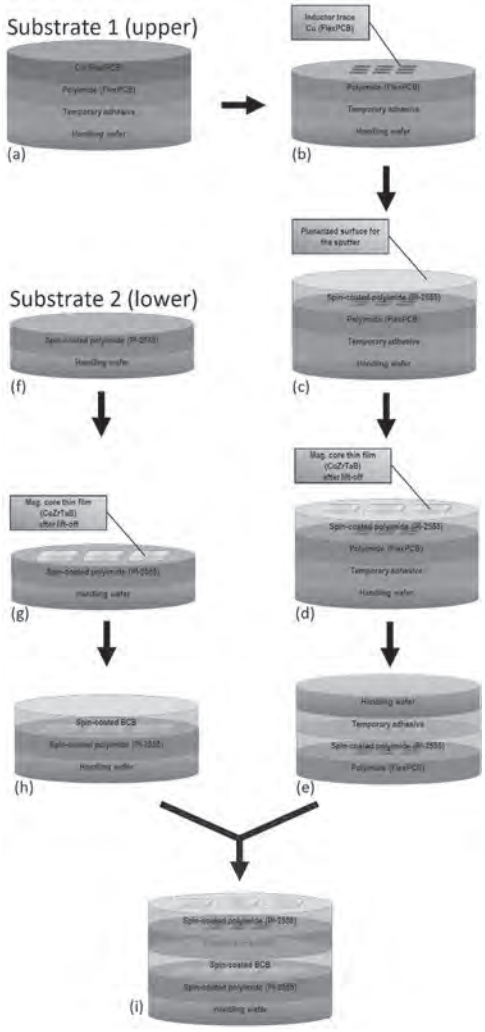

The Fabrication process.

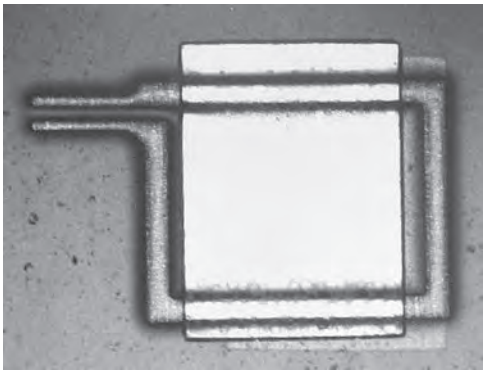

The finished device with the magnetic core on the top and bottom layers.

IOD-04. Fabrication of thick, laminated, electroinfiltrated magnetic nanocomposites to reduce dimensional resonance effects. *S. Amirisetti*[1], C.S. Smith[1], S.C. Mills[2], J. Andrew[2] and D. Arnold[1] *1. Electrical and Computer Engineering, University of Florida, Gainesville, FL, United States; 2. Materials Science and Engineering, University of Florida, Gainesville, FL, United States*

Magnetic nanocomposites have applications in power electronics, where properties such as high permeability, high thickness, high operating frequency, and low loss are desired. Recent work shows that electroinfiltration, where a magnetic composite is formed by electroplating a metal through a deposited nanoparticle layer, produces magnetic composites with high permeabilities and low losses [1]. However, electroinfiltration has a thickness limitation of <4 μm. Attempts to overcome this by fabricating multiple composite layers have been demonstrated, but reveal a trade-off between composite thickness and maximum operating frequency [2]. This trade-off is due to dimensional resonance, caused by the formation of standing waves in the material cross-section. Laminations can be used to overcome this effect, as the resulting laminated layers have smaller cross-sections that increase the frequency at which standing waves begin to form [3]. This work demonstrates a process to create thick magnetic composites by laminating layers of infiltrated magnetic composite with insulating layers of parylene to reduce dimensional resonance effects, as seen in Figure 1. For the magnetic layer, composites made from iron-oxide nanoparticles infiltrated with nickel-metal are used. Four samples are made, containing 1, 2, 3, and 5 layers of magnetic composite, separated from each other by approximately 1-2.5 μm of parylene. Structural characterization of these samples was done using SEM with EDS capabilities, showing that the desired laminated structures were achieved. Next, dc magnetic characterization showed that the magnetic properties of the laminated composites remain nearly constant with the increase in thicknesses. Finally, ac magnetic measurements reveal that these laminated composites have a constant dimensional resonance of ~350 MHz irrespective of an increase in the number of layers, as seen in Figure 2. In conclusion, it is evident that laminating the nanocomposites reduces the effects of dimensional resonance, and a fabrication process for implementing laminations into electroinfiltrated composites has been demonstrated.

1] Connor S. Smith, Shehaab Savliwala, Sara C. Mills, Jennifer S. Andrew, Carlos Rinaldi, David P. Arnold, Electroinfiltrated nickel/iron-oxide and permalloy/iron-oxide nanocomposites for integrated power inductors, Journal of Magnetism and Magnetic Materials, Volume 493, 2020,165718, ISSN 0304-8853. [2] Sara C. Mills, Connor S. Smith, Sai Pranesh Amirisetti, David P. Arnold, Jennifer S. Andrew, Method for the fabrication of thick multi-layered nickel/Iron oxide nanoparticle magnetic composites. * In review [3] S. Lin, T. Brinker, L. Fauth, and J. Friebe, "Review of Dimensional Resonance Effect for High-Frequency Magnetic Components," 2019 21st European Conference on Power Electronics and Applications (EPE '19 ECCE Europe), 2019, pp. P.1-P.10, DOI: 10.23919/EPE.2019.8915152

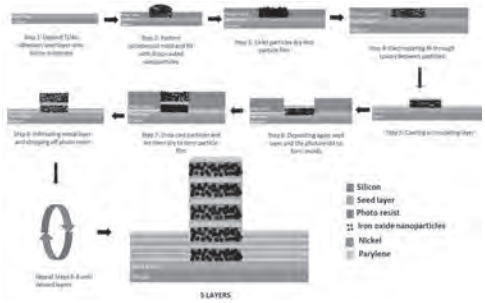

Process flow for laminated electro-infiltration process.

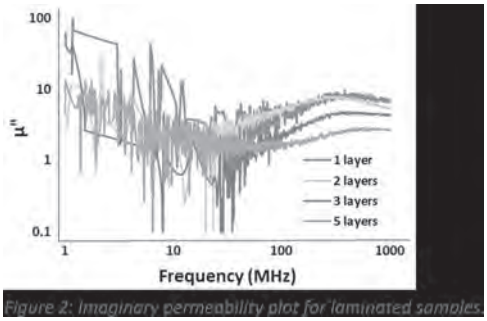

Imaginary permeability plot for laminated samples

IOD-05. Research on electromagnetic transient characteristics and distribution pattern on UHV converter transformer winding. *S. He*[1] and J. Li[1] *1. Xi'an Jiaotong University, Xi'an, China*

The electromagnetic transient distribution characteristics of windings are important for the design and state evaluation of transformer winding insulation structure. A unified electromagnetic transient model for UHV converter winding was established and the electromagnetic transient characteristics of the UHV converter transformer and the temporal and spatial distribution pattern of the electromagnetic transient are obtained. To verify the accuracy of the model, a small-scaled platform for measuring the potential distribution of the transformer is designed and the regularity of the transient characteristics of a large-scale transformer is verified. It is found that for slow wave front overvoltage, the calculation accuracy of this model is greatly improved compared with the pure capacitance network model, and the calculated potential gradient distribution is closer to the actual situation. The basic characteristics of oscillation process in UHV converter winding are as follows: high frequency oscillation with small amplitude is superimposed on the waveform of incident wave. Using the measured voltage data at the converter transformer port to study the potential gradient distribution of UHV converter transformer winding, it can be seen that the maximum potential gradient increases with the increase of pulse steepness. Moreover, a linear relationship can be fitted between the maximum potential gradient of the winding and the steepness of the rising edge, and the distribution of potential gradient at any position of winding can also be fitted with a function. The potential gradient of main insulation and longitudinal insulation at the head end of the winding is the largest, which decreases with the relative position of winding away from the incident end. Through the two fitting functions, the maximum potential gradient and location information in UHV converter transformer can be quickly evaluated, which provides a reference for insulation optimization design and condition evaluation.

[1] He, S., et al., *Transient potential distribution on transformer winding considering the effect of core lamination stack.* Aip Advances, 2020. 10(1): p. 5. [2] Preis, K., et al., *Transient Behavior of Large Transformer Windings Taking Capacitances and Eddy Currents Into Account.* IEEE Transactions on Magnetics, 2018. PP(99): p. 1-4. [3] Smajic, J., et al., *Simulation and Measurement of Lightning-Impulse Voltage Distributions Over Transformer Windings.* IEEE Transactions on Magnetics, 2014. 50(2): p. 553-556.

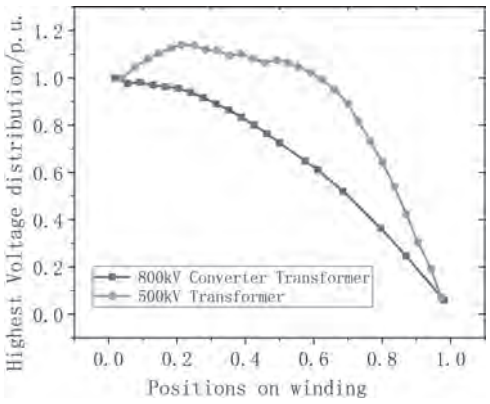

The maximum potential envelope of 800kV converter transformer and 500kV transformer

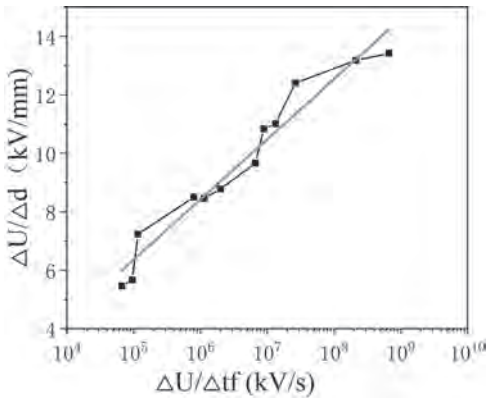

Linear relationship between the maximum potential gradient of the winding and the steepness of the rising edge

IOD-06. Reluctance of Long Solenoids. *A. Sherwali*[1] and W.G. Dunford[1]
1. University of British Columbia, Vancouver, BC, Canada

A long solenoid can be used as the primary of a transformer with an open magnetic circuit. It is then of interest to determine the fairly low magnetizing inductance of the resulting system. The system studied here uses an array of parallel connected, voltage driven coils distributed along the core to control the core flux, as shown in fig 1. The ends of the core are unexcited, so take the form of magnetic poles driving flux through the air return path. When these are spherical and infinitely permeable an analytical expression can be obtained for the effective end return reluctance. This paper considers a more practical example of cylindrical core ends with a known permeability. The total magnetic circuit reluctance consists of the two end return reluctances in series with the core reluctance. As the core becomes longer there is essentially a constant return reluctance in series with a core reluctance proportional to length. It is therefore possible to think in terms of a design criterion such as picking a length where these two reluctances are equal. The final paper will show normalized reluctance results in terms of the core dimensions and permeability. Generally, high permeability cores benefit from having long unexcited ends. The sample results shown in fig 2 are for a constant current density along the core, whereas in the voltage fed system in the final paper the currents will increase towards the ends. Fig 2 does show that as the core becomes long the reluctance is dominated by the core. It also shows that for short cores the return reluctance dominates, so a particular linear current density produces more flux.

Kaplan, B. Z., and U. Suissa. “Evaluation of inductance for various distributions of windings on straight ferromagnetic cores: an unusual approach.” *IEEE transactions on magnetics* 38.1 (2002): 246-249.

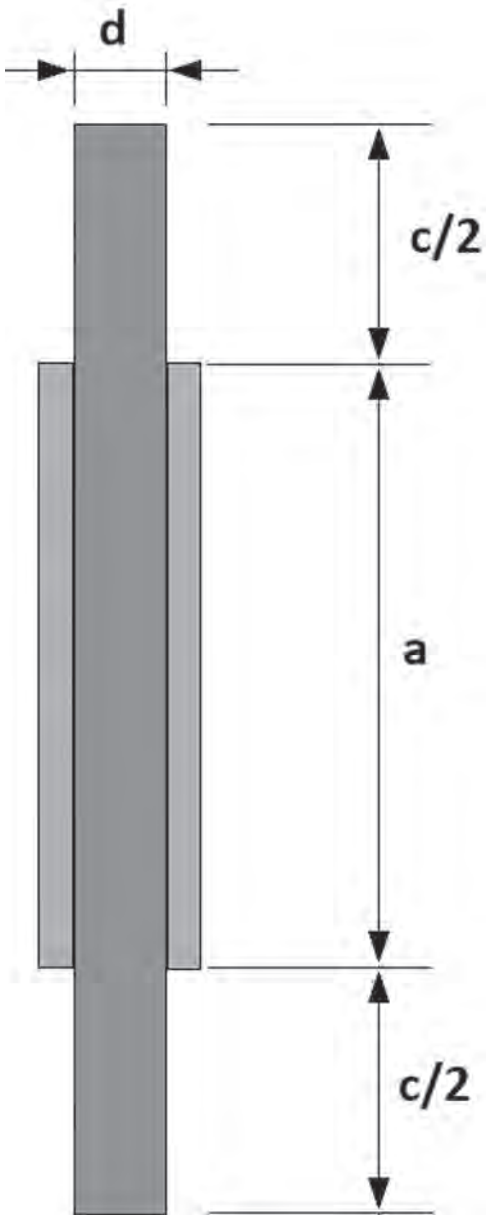

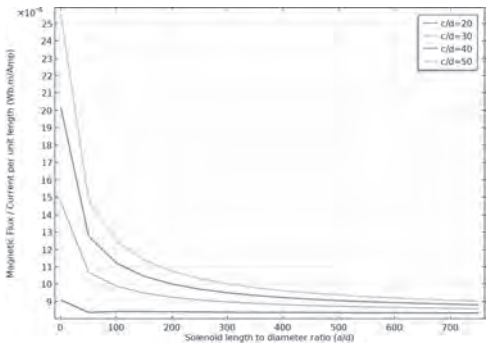

IOD-07. Meter-Range Wireless Motor Drive for Pipeline Transportation. *W. Liu*[1], K. Chau[1], H. Wang[1] and T. Yang[1] *1. Department of Electrical and Electronic Engineering, The University of Hong Kong, Hong Kong, China*

Wireless power transfer (WPT) has brought ever-increasing impacts on the modern technology and human society [1]-[3]. Besides wireless charging, the drive capabilities of wireless power have been recently explored and directly utilized for wireless lighting [4], heating and motoring [5]. The application of wireless motor can promisingly serve for underground pipeline transportations, thus regulating the flow rate. Both the power grid and the control system are deployed deep underground, which may add the construction cost, maintenance difficulty and system complexity. This paper proposes and implements a meter-range wireless motor drive (WMD) system for underground pipeline transportation as shown in Fig. 1. Equipped with one battery bank and one gallium nitride (GaN) inverter, each energy-carrying electric vehicle (EV) can park above the critical node and wirelessly drive the in-pipe pump to accelerate the flow rate. Beneath the earth, a hybrid repeater is configured to enable an efficient meter-range WMD. Also, it facilitates maintaining the load-independent output against the load variances. The system performances of the proposed meter-range WMD system are evaluated as shown in Fig. 2. In Fig. 2(a), the impedance characteristics indicate a stable operating frequency, and thus the meter-range WMD can realize a robust zero-phase-angle operation withstanding various equivalent loads. Additionally, with different compensation networks and parameter designs, the characteristics of transmission efficiencies with respect to the equivalent loads are plotted in Fig. 2(b). After the system optimization, the transmission efficiency can always keep above 90.1% and is usually higher than 94.0% within a wide range. Finally, a prototype has been built and tested accordingly. Theoretical analysis, computational simulation and more experimental results will be given to verify the proposed meter-range WMD system in the full paper. This work was supported by HKU (project no. SFBR 202011159021).

[1] Z. Zhang, H. Pang, A. Georgiadis, et al. *IEEE Trans. Ind. Electron.*, Vol. 66, p.1044–1058 (2019). [2] C. Cheng, Z. Zhou, W. Li, Z. Deng, et al. *IEEE Trans. Ind. Electron.*, Vol. 68, p.1188–1196 (2021). [3] Y. Huang, C. Liu, Y. Zhou, et al. *IEEE Trans. Magnet.*, Vol. 55, p.1–6 (2019). [4] Y. Li, J. Hu, X. Li, et al. *IEEE Trans. Ind. Electron.*, Vol. 67, p.203–213 (2020). [5] C. Jiang, K. T. Chau, T. W. Ching, et al. *IEEE Trans. Magnet.*, Vol. 53, p.1–5 (2017).

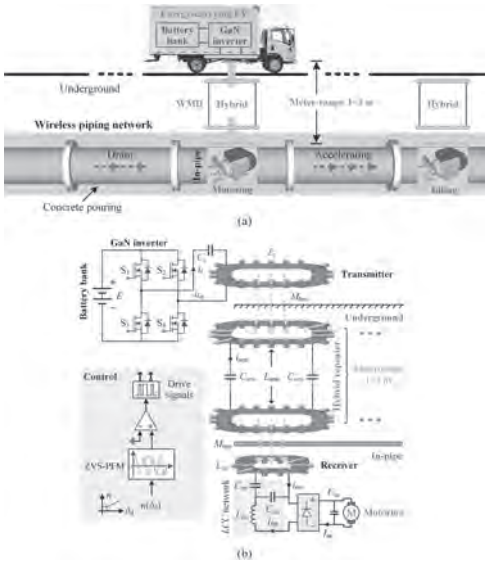

Fig. 1. Proposed meter-range WMD for wireless piping network. (a) Schematic. (b) System configuration.

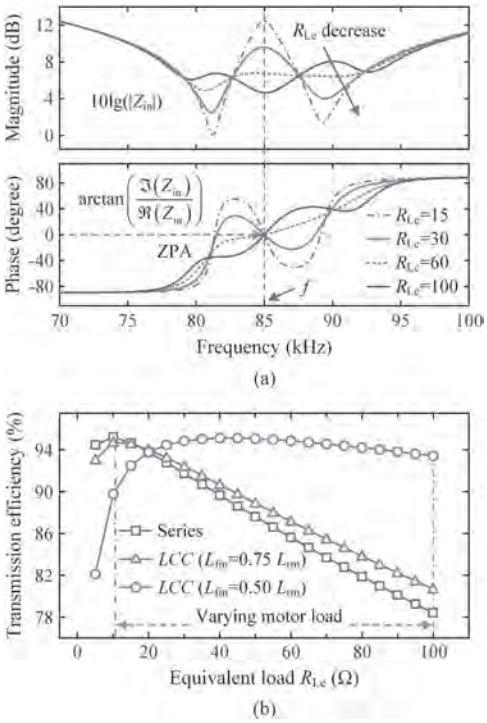

Fig. 2. System performances of proposed meter-range WMD. (a) Impedance characteristics. (b) Transmission efficiency characteristics.

IOD-08. Withdrawn

IOD-09. Modification of transformer coupled permeameter (TC-Perm) for wider bandwidth. *S. Tamaru*[1] *1. Advanced Industrial Science and Technology (AIST), Tsukuba, Japan*

Power electronics is attracting strong attention as one of the key technologies for realizing the carbon neutral society. A higher switching frequency in a power module is sought for making it more compact. However, inductors hinder it because the loss in the magnetic core rapidly increases. Thus, it is crucial to study and eventually suppress the magnetic loss in MF, HF and VHF bands (300 kHz – 300 MHz). Conventional RF permeameters measure mutual or self inductance of the coil wound around the magnetic sample. This method has the following problems, 1) it requires the sample to be the final toroidal shape, and 2) it cannot apply an external magnetic field. It is desirable to measure the RF permeability of a single particle in the powder stage as a function of magnetic field to gain more insight. For this purpose, we developed the transformer coupled permeameter (TC-Perm), and successfully measured a single Sendust particle used in noise suppression sheet over 10 MHz – 20 GHz[1)]. Then we modified it to further expand the bandwidth. In the initial configuration of TC-Perm, the lower bandwidth limit is set by the vector network analyzer (VNA). We replaced it with another VNA covering 100 kHz – 44 GHz. The S_{21} parameter of the jig is proportional to frequency at low frequencies because the two CPWs are inductively coupled. This causes the signal level becoming smaller than the noise floor level of the VNA below a few 10 MHz, making it impossible to measure at low frequencies. We modified the TC-Perm as shown in Fig. 1 to avoid this problem. A low noise amplifier (LNA) with noise figure of 2.4 dB is inserted between the jig and VNA below 100 MHz. Above 100 MHz, the LNA is bypassed by two semiconductor RF analog switches. The Permalloy calibration sample used in Ref. 1 was measured using this system under a bias field of 200 mT. The modified TC-Perm showed approximately

40 times smaller noise level at low frequencies than before modification, which allows it to seamlessly measure the permeability over 300 kHz – 44 GHz. Acknowledgement - This work is supported by MIC SCOPE JP195003002.

S. Tamaru et al., J. Magn. Magn. Matter. 501, 166434 (2020).

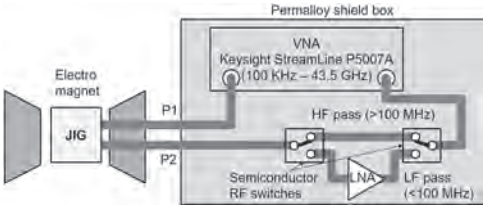

Block diagram of TC-Perm after modification.

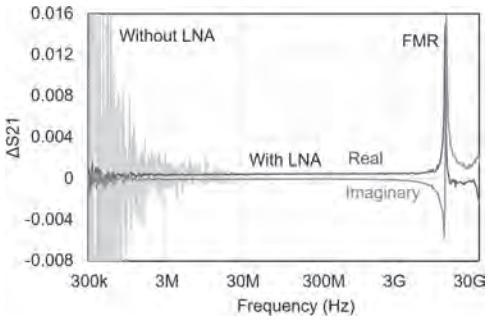

Measurement result of a Py sample with and without LNA.

IOD-10. Pulse Frequency Modulation for Parity-Time-Symmetric Wireless Power Transfer System. *Z. Hua*[1], K. Chau[1], W. Liu[1] and X. Tian[1] *1. The University of Hong Kong, Hong Kong, China*

High-efficiency wireless power transfer (WPT) against the variation of the coupling coefficient is of great significance for many applications, such as dynamic wireless charging for electric vehicles and portable devices. Recently, the concept of parity-time symmetry theory from quantum physics [1] has been applied to a WPT system to solve the problem with the self-oscillating controlled inverter and the series-series topology [2] within a specific range of mutual inductance. However, with traditional self-oscillating controlled inverters, the output power cannot be adjusted despite the high transmission efficiency against transmission distance. Though different modulation schemes [3-5] can be adopted to regulate the output power, the self-oscillated modulation schemes have not been fully investigated. This paper proposes and implements an advanced pulse frequency modulation (PFM) scheme to adjust the output power of the parity-time-symmetric WPT system. Fig. 1(a) shows the circuit topology of the proposed parity-time-symmetric WPT system. Fig. 1(b) is an example of the inverter output voltage and the transmitter-side current waveform, in which the voltage and the current are in phase. Fig. 2(a) presents the self-oscillation frequency against the mutual inductance and Fig. 2(b) shows the efficiency against the mutual inductance. If the mutual inductance is larger than the critical mutual inductance (about 40 μH), the self-oscillating frequency is different from the resonant frequency (200 kHz) of the WPT system, and the transmission efficiency keeps constant and high. Fig. 2(c) presents the normalized output power against different N_1 and N_2 of PFM, showing that by regulating the duty ratio of the PFM, the output power can be regulated. Theoretical analysis, simulation and experimental results will be given to verify the proposed scheme in the full paper. This work was supported by HK RGC (project no. T23-701/20-R).

[1] S. Assawaworrarit, X. Yu, and S. Fan, Nature, vol. 546, p. 387-390 (2017). [2] J. Zhou, B. Zhang, W. Xiao, D. Qiu, et al. IEEE Trans. Ind. Electron., vol. 66, pp. 4097–4107 (2019). [3] W. Liu, K. T. Chau, C. H. T. Lee, et al. IEEE Trans. Power Electron., vol. 35, pp. 6533–6547 (2020). [4] W. Liu, K. T. Chau, C. H. T. Lee, et al. IEEE Trans. Magn., vol. 57, pp. 1–7, Art no. 8201907 (2021). [5] W. Han, K. T. Chau, L. Cao, et al. IEEE Trans. Magn., vol. 57, pp. 1–7, Art no. 8001107 (2021).

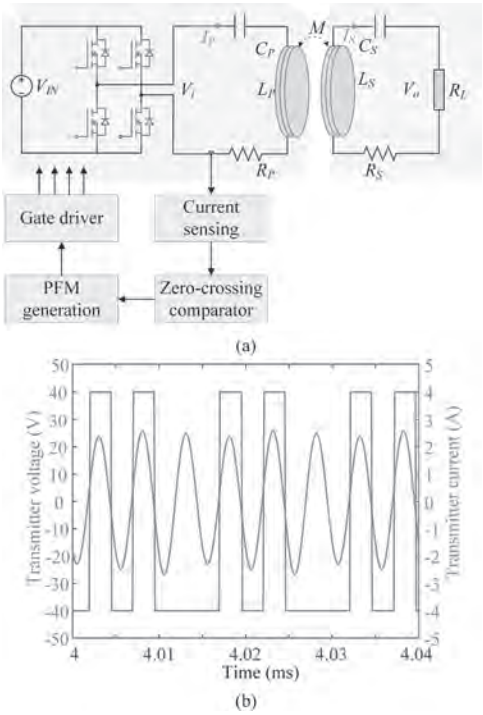

Fig. 1. Proposed parity-time-symmetric WPT system. (a) Topology. (b) An example of transmitter voltage and current.

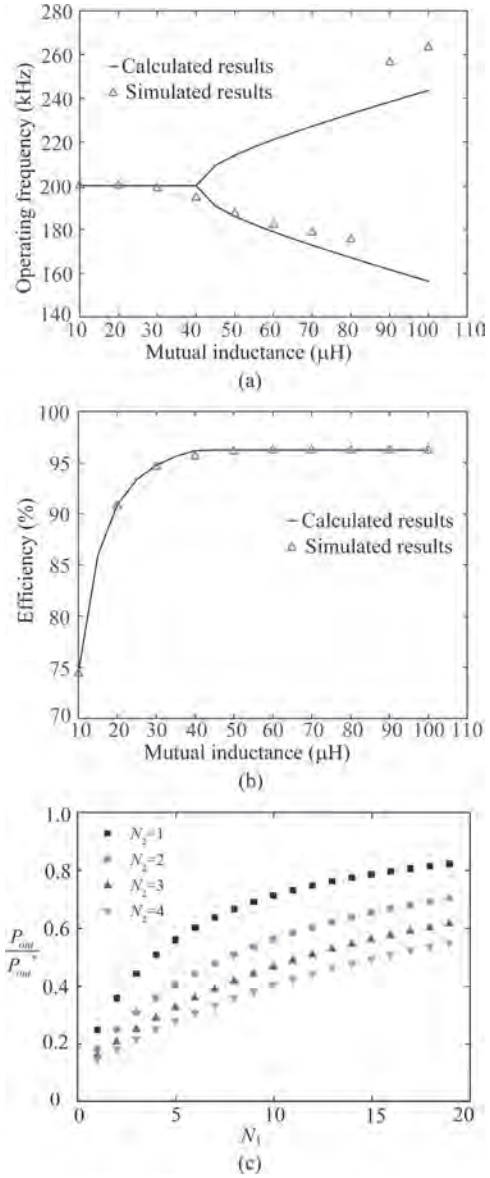

Fig. 2. Simulation results. (a) Operating frequency against mutual inductance. (b) Transmission efficiency against mutual inductance. (c) Normalized output power against N_1 and N_2 of PFM.

IOD-11. Multi-Resonating-Compensation for Multi-Channel Multi-Pickup Wireless Power Transfer. *H. Pang*[1], K. Chau[1], W. Liu[1] and X. Tian[1] *1. The University of Hong Kong, Hong Kong, China*

With the development of wireless power transfer (WPT), numerous applications such as implantable devices [1], consumer electronics [2], and EVs [3] have applied this brand-new technique. Meanwhile, various standards have been put forward along with the popularization of practical niches, which pose challenges and cause inevitable inconvenience. Accordingly, lots of progress has been made for multi-channel multi-pickup (MCMP) WPT [4]-[5]. However, how to randomly transmit multi-frequency power [6] simultaneously using a single transmitting coil becomes a technical concern. In this paper, a multi-resonating-compensation (MRC) topology is proposed for simultaneously satisfying wireless power on-demands as shown in Fig. 1(a). The procedures for selection of parameters are presented, which do not involve solving complex 3rd-degree equations. Also, the proposed system can support randomly three operating frequencies as shown in Fig. 1(b)-(c). Furthermore, the proposed MRC topology can be extended to more operating frequencies by adding parallel-connected LC tanks. Notably, the parameter selection procedures are as simple as selecting three frequencies, which are shown in Fig. 1(d). Regarding the power distribution of the MCMP system, each operating frequency can be modulated flexibly by adopting the proposed amplitude overlay modulation (AOM). Additionally, the operating waveforms and characteristics of the proposed excitation are shown in Fig. 2(a)-(b), involving 100kHz, 300kHz, and 500kHz. Accordingly, the pickup voltages are depicted in Fig. 2(c). Finally, quantitative analysis on the influence of the load variations and harmonic coupling is conducted in Fig. 2(d). Theoretical analysis, simulation, and experimental results will be given to verify the proposed MRC based MCMP WPT system in the full paper. This work was supported by HKU (project no. SFBR 201910159042).

[1] X. Tian, K.T. Chau, W. Han, et al. *IEEE Trans. Magn.*, vol. 57, pp. 5100206:1-6 (2021). [2] Z. Zhang, H. Pang, S. H. K. Eder, et al. *IEEE Trans. Power Electron.*, vol. 36, pp. 958-967 (2021). [3] Z. Zhang, and K.T. Chau, *IEEE Trans. Power Electron.*, vol. 30, pp. 6213-6220 (2015). [4] F. Liu, Y. Yang, Z. Ding, et al. *IEEE Trans. Power Electron.*, vol. 33, pp. 9005-9016 (2018). [5] W. Jin, A. T. L. Lee, S. Li, et al. *IEEE Trans. Power Electron.*, vol. 33, pp. 5016-5028 (2018). [6] W. Liu, K.T. Chau, C.H.T. Lee, et al. *IEEE Trans. Magn.*, vol. 55, pp. 8001609:1-9 (2019).

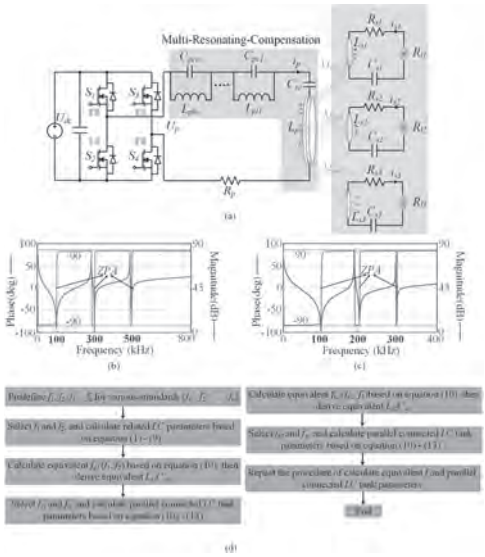

Fig. 1 Proposed MRC based WPT systems. (a) Configuration. (b) Impedance characteristics (100kHz, 300kHz, and 500kHz). (b) Impedance characteristics (100kHz, 200kHz, and 300kHz). (d) Flowchart of parameter design.

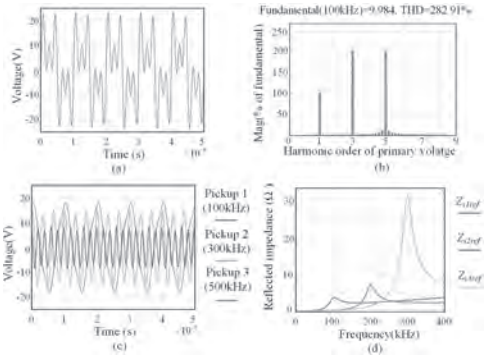

Fig. 2 Operating waveforms and characteristics. (a) Excitation voltage. (b) Harmonic analysis. (c) Pickup voltages. (d) Impedance analysis.

Session IOE
SENSORS, LEVITATION
Xu Li, Chair
Xiamen University, Xiamen, China

CONTRIBUTED PAPERS

IOE-01. Photothermal actuation of levitated pyrolytic graphite revised.
S. Yee[1] and *H. ElBidweihy*[1] *1. Electrical and Computer Engineering, United States Naval Academy, Annapolis, MD, United States*

The significant diamagnetism of pyrolytic graphite allows it to be passively levitated above permanent magnet arrays and translated in the plane of these arrays via incident optical radiation. The translation effect has applications in milliscale robotics for assembly and frictionless manipulation tasks. Previously offered physical explanations for the optically-induced translation effect have cited photothermally induced temperature changes in levitated pyrolytic graphite samples and the thermal dependence of pyrolytic graphite's diamagnetic susceptibility, as observed through measurements at uniform temperatures of bulk samples. In this work, we offer a revision to the theory of photothermal actuation of levitated pyrolytic graphite. Through experiments and simulations, we demonstrate that the gradient of pyrolytic graphite's diamagnetism with temperature - as measured for bulk samples at uniform temperatures - is insufficient to explain the magnitude of forces required by the optically-induced translation phenomenon. We hypothesize that the sufficient contrast in diamagnetism of pyrolytic graphite samples under asymmetric photothermal heating is more than an order of magnitude greater than that expected from measurements where the pyrolytic graphite sample temperature is uniformly varied. We propose that the origin of this enhanced diamagnetic contrast in pyrolytic graphite under asymmetric optical radiation is a photothermoelectric effect on the relative concentrations of electrons in diamagnetically significant orbital states in the graphite. To support this hypothesis, we take qualitative measurements demonstrating the n-type thermoelectricity of pyrolytic graphite samples under optical irradiation. Experimental results presented in this work demonstrated an n-type thermoelectric response in the PyG material under infrared laser irradiation that is consistent with this hypothesis.

[1] Kobayashi, Masayuki, and Jiro Abe. "Optical motion control of maglev graphite." Journal of the American Chemical Society 134.51 (2012): 20593-20596. [2] Ewall-Wice, Miriam, et al. "Optomechanical actuation of diamagnetically levitated pyrolytic graphite." IEEE Transactions on Magnetics 55.7 (2019): 1-6. [3] Young, Jared, et al. "Optical control and manipulation of diamagnetically levitated pyrolytic graphite." AIP Advances 9.12 (2019): 125038. [4] Fujimoto, Manato, and Mikito Koshino. "Diamagnetic levitation and thermal gradient driven motion of graphite." Physical Review B 100.4 (2019): 045405.

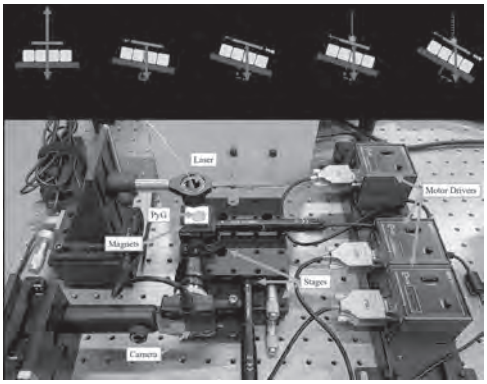

Schematic illustrations of force estimation setup.

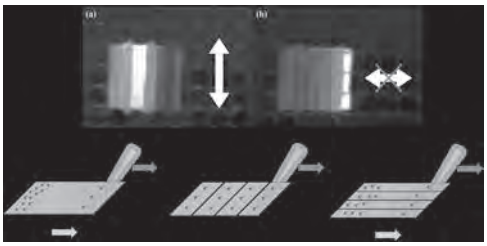

Infrared video image captures and illustrative schematics of the actuation experiments with PyG samples that are modified by scoring their surface to form thermal breaks.

IOE-02. Electromagnetic sensing of the corrosion at different microstructural phases in a medical Ti-Al-4V ELI alloy.
H. Carreon[1] and M. Carreon-Garcidueñas[2] *1. Materiales, Universidad Michoacana, Morelia, Mexico; 2. Biomateriales, Universidad de Navarra, Pamplona, Spain*

Titanium alloys have become increasingly important for biomedical materials due to their high specific strength, good corrosion resistance, and excellent biocompatibility. In this research work, different heat treatments were performed for obtaining equiaxed and Widmanstätten microstructures at the Ti-Al-4V ELI alloy. In order to promote the nucleation of α_2 precipitates (Ti_3Al), an aging process was carried out at 515 ° C and 575 ° C for 2, 288 and 576 hours. The corrosion behaviour was analyzed by double cycle potentiodynamic corrosion tests. Hank's balanced salt solution (HBSS) was used as the electrolyte and the tests were maintained at 37°C. This study uses the eddy current (EC) nondestructive evaluation technique, based on the principle of electromagnetic induction, in an effort to monitor the corrosion damage in the medical Ti-6Al-4V alloy. The experimental results show a significative electrical conductivity variations in EC data of the different Ti-Al-4V ELI alloy microstructures mainly on the equiaxed and Widmanstätten conditions before and after corrosion performance.

IOE-03. Force Analysis of an Electrodynamic Wheel Maglev Drone.
C. Bruce[1] and J. Bird[1] *1. Portland State University, Portland, OR, United States*

When a radial magnetized magnet rotor is rotated over a conductive track, such as aluminum, current is induced that gives rises to both a levitation and a propulsion force simultaneously [1, 2]. When the rotational speed of this electrodynamic wheel (EDW) is greater than the translational speed a thrust force is created, whilst large braking forces are created when the circumferential rotational speed is lower than the translational speed. Both radial [1-5] and axial [6, 7] EDW configurations have been studied, and whilst an axial EDW can interface more effectively with a flat track, due to the field symmetry it is challenging to create large thrust forces when using axial magnets [6, 7]. Most prior published work on EDWs have presented performance results when testing only one EDW [3, 4]. This paper presents simulation and experimental testing results for a new type of wireless controlled, four rotor, EDW maglev drone, as shown in Fig. 1. The EDW maglev is constructed using off-the-shelf components. The proof of principle, radial EDW maglev drone, utilizes 25.4 mm diameter, one pole-pair, diametrically magnetized cylindrical tube NdFeB N42 magnets. It it driven using batteries and is fully contained. All prior published EDW designs utilized multi pole-pair rotors, such as four pole-pairs [1, 3, 4] and two pole-pairs [2, 5]. However, by utilizing a one pole-pair EDW rotor the construction of the EDW is greatly simplified. Furthermore, as the one pole-pair will create the lowest electrical frequency per mechanical revolution the specific power, W/kg, is the lowest [8] therefore improving the lift-to-weight ratio performance. When the airgap is fixed then the rotation of the one pole-pair EDW gives rise to a large oscillation force, as shown in Fig 2(a). This is much larger than seen in higher pole pair EDW rotors [4]. This paper uses both dynamic modelling and experimental air-gap measurements to show that whilst the lift force oscillation is high the percent airgap variation is very small. Fig 2(b) shows a variation in airgap of only 1%.

[1] H. Zhang, K. Kails, P. Machura, and M. Mueller, "Conceptual Design of Electrodynamic Wheels Based on HTS Halbach Array Magnets," *IEEE Transactions on Applied Superconductivity*, vol. 31, no. 5, pp. 1-6, 2021. [2] W. Qin and J. Z. Bird, "Electrodynamic Wheel Magnetic Rolling Resistance," *IEEE Transactions on Magnetics*, vol. 53, no. 8, pp. 1-7, 2017. [3] X. Sang, Z. Deng, J. Chen, L. Jin, Z. Zhang, J. Zhang, *et al.*, "Analysis and Experiment on the Levitation Force and Thrust Force Characteristics of a Permanent Magnet Electrodynamic Wheel for Maglev Car Application," *IEEE Transactions on Applied Superconductivity*, vol. 31, no. 8, pp. 1-4, 2021. [4] J. Bird and T. A. Lipo, "Calculating the forces created by an electrodynamic wheel using a 2D steady-state finite element model," *IEEE Trans. Magn.*, vol. 44, no. 3, pp. 365-372, March 2008. [5] J. Wright and J. Z. Bird, "Analytic Damping and Stiffness Analysis for a 4-DOF Electrodynamic Wheel Maglev Vehicle," in *2018 XIII International Conference on Electrical Machines (ICEM)*, pp. 555-561,3-6 Sept. 2018,2018. [6] K. S. Jung, "Spatial transfer of conductive plate through decoupling of two axial electrodynamic forces generated by magnet wheel," *Mechatronics*, vol. 23, no. 8, pp. 1044-1050, 2013/12/01/ 2013. [7] D. Ogawa, Y. Horiuchi, and N. Fujii, "Calculation of electromagnetic forces for magnet wheels," *IEEE Transactions on Magnetics*, vol. 33, no. 2, pp. 2069-2072, March 1997. [8] C. Bruce, J. Bird, and B. Dechant, "Maglev Lift-to-Drag Ratio and Specific Power Comparison " presented at the Submitted to IEEE/MMM INTERMAG 2022 Conference, New Orleans, 2022.

Fig. 1. The four rotor, one-pole pair, wirelessly controlled proof-of-principle, EDW maglev drone shown placed above a 6061 grade aluminum track that is 9.5mm thick and 152mm wide.

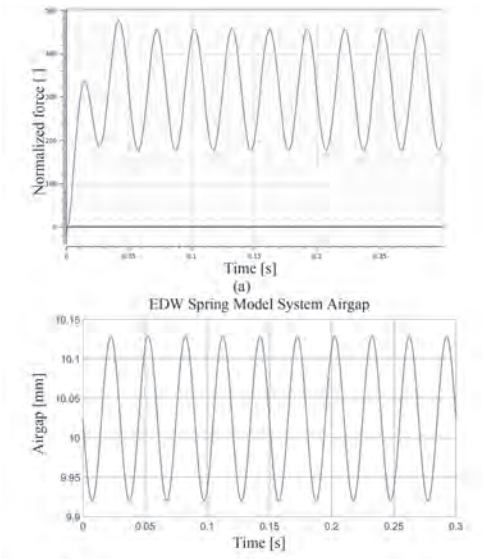

Fig. 2. 3-D Finite element analysis transient simulation showing the normalized lift force as a function of time for a single one pole-pair EDW rotating at ω_m = 1000 r/min. The airgap is maintained fixed at g = 10 mm. (b) Example simulation result for the dynamic airgap model the airgap changes by only 1%.

IOE-04. Withdrawn

IOE-05. Crack detection for welded joint with surface coating using unsaturated AC magnetic flux leakage.
M. Hayashi[1], S. Adachi[1], T. Kawakami[1], Y. Miyamoto[2], J. Wang[1], K. Sakai[1], T. Kiwa[1], K. Tsukada[1], T. Ishikawa[3] and M. Hirohata[2] *1. Graduate School of Interdisciplinary Science in Health Systems, Okayama University, Okayama, Japan; 2. Graduate School of Engineering, Osaka University, Suita, Japan; 3. Faculty of Environmental and Urban Engineering, Kansai University, Suita, Japan*

The welds of steel structures, used in the bridges and roadway steel decks, are stressed areas where fatigue cracks are prone to occur. Once a fatigue crack occurs in a weld, it spreads and becomes larger, increasing the risk of collapse of the structure. Therefore, it is important to detect fatigue cracks in welds at an early stage. However, the surfaces of the structures are coated to protect the structure itself and the landscape. This makes it difficult to detect cracks using the conventional methods of visual inspection and magnetic particle inspection. In this study, a sensor probe adapted to the weld shape of the structure was developed for detecting cracks with the surface coating using the unsaturated AC magnetic flux leakage (USAC-MFL). This method utilizes a small AC magnetic field in the unsaturated region of the initial magnetization for steel and measures the magnetic flux leakage due to the crack. We have previously reported that the crack detection of steel plates was realized with low power and high sensitivity using the USAC-MFL [1]. To evaluate the performance of the developed sensor probe, 20 samples of welded joints with an average coating thickness of 125 and 250 μm were prepared. The slits were located in three positions: in the rib, the weld, and the base (Fig. 1). A total of 70 slits, ranging from 1 mm to 5 mm depth, were measured. The differential signals from the two sensors were recorded and analyzed. The same measurements were performed in the non-slit areas to compare the signals of the slits. Figure 2 shows the result measured at the slits positioned in the weld. The correlation coefficient of slit depth and differential intensity was 0.89, indicating a strong correlation. The same tendency was obtained for the slits in the rib and base. The differential signal intensity of the slit was larger than that of the non-slit area, even 1 mm depth. These results suggest that the USAC-MFL and the developed sensor probe can be used to detect cracks in the welds of steel structures at an early stage with the surface coating.

[1] K. Tsukada, Y. Majima, Y. Nakamura et al., IEEE Trans. Magn., Vol. 53, pp. 1-5 (2017)

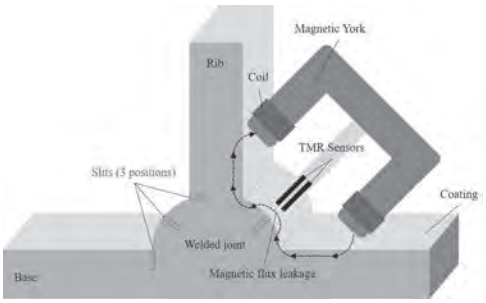

Fig. 1 Welded joint sample with surface coating and the sensor probe.

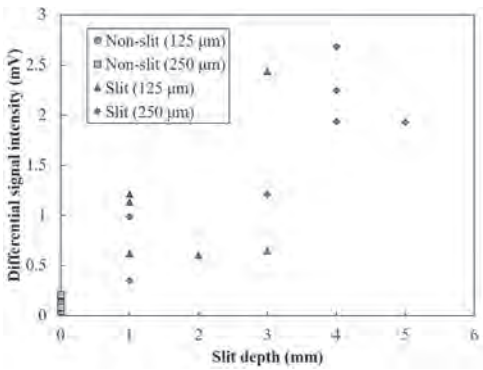

Fig. 2 Dependence of differential signal intensity and slit depth measured in the weld.

IOE-06. Magnetic Permeability Sensor Array Prototype To Evaluate Reservoir Phase Permeability in-Situ Downhole. *R. Adams*[1], J.F. Servin[2], W. Wang[3] and M. Deffenbaugh[1] *1. Sensors Development Team, Aramco Research Center -- Houston, Houston, TX, United States; 2. Reservoir Engineering Technology, EXPEC Advanced Research Center, Dhahran, Saudi Arabia; 3. Reservoir Engineering Technology, Aramco Research Center -- Cambridge, Cambridge, MA, United States*

This work presents a novel system to image formation permeability of the reservoir in situ downhole. Colloidal magnetite fluid with high magnetic permeability is injected from the surface into the subsurface formation. The magnetic fluid permeates through the formation some radial distance ΔR over a given period of time, which is directly related to the formation permeability. A sensor array which measures the radial distribution of magnetic permeability surrounding the tool is deployed downhole during this injection process. By comparing the magnetic permeability radial distribution surrounding the sensor before/during/after fluid injection, the system is able to directly measure phase permeability of the surrounding formation in situ. The sensor array measures the radial magnetic permeability distribution of the formation via mutual inductance between pairs of solenoid coils axially distributed along a downhole tool. As the magnetic permeability of the material surrounding the solenoid coils increases, the mutual inductance between coils increases. Eddy current effects on mutual inductance measurements can be minimized by reducing the interrogation frequency of the measurement such that electrical conductivity and permittivity changes have no effect on the measurement of interest, e.g. the measurement is insensitive to the movement of brine and hydrocarbon and sensitive only to the movement of the magnetic permeability doped fluid. Measuring mutual inductance across the array of solenoid coils distributed along the tool enables the system to map the radial distribution of magnetic permeability surrounding the sensor. A laboratory prototype of this sensor system was built and evaluated for its sensitivity to changes in magnetic permeability distributions surrounding the tool. Results from these laboratory tests are compared to analytical predictions of the tool response. Magnetic permeability doped fluid of various concentrations are measured with the sensor array, and measurement results are compared to the predicted magnetic permeability of the various concentrations of doped fluid.

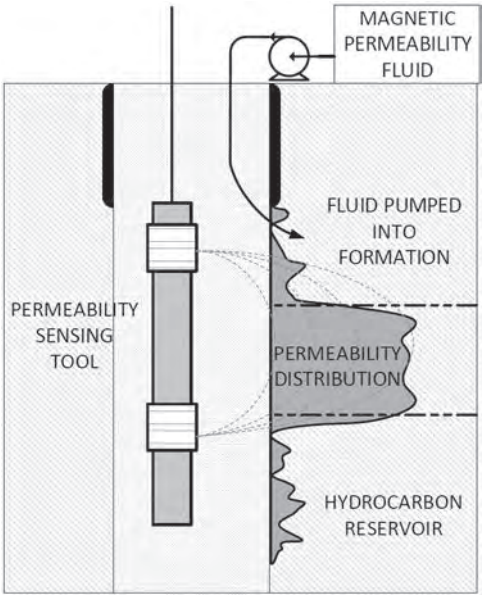

IOE-07. Feedback of magnetic nanoparticles susceptibility to their magnetic dipole interaction with ferromagnetic GMR sensor.
O. Koplak[1], R. Allayarov[1], E. Kunitsyna[1], R. Morgunov[1] and S. Mangin[2]
1. Spintronics, Institute of Problems of Chemical Physics, Chernogolovka, Russian Federation; 2. Spintronics, Institut Jean Lamour, Nancy, France

Effect of individual magnetic nanoparticle on magnetization reversal of ferromagnetic layers is well know [1,2]. Here we present effect of ferromagnetic surface of the magnetoresistive sensor on magnetic susceptibility of nanoparticles (NPs), deposited on the sensor surface. Deposition of $CoFe_2O_4$ nanoparticles on CoFeB/Ta/CoFeB platform, containing two ferromagnetic nanolayers, changes blocking temperature of the NPs. Magnetic dipole interaction between the NPs and the platform effects frequency and field dependences of the blocking temperature of the NPs. Effective barrier of magnetization reversal and blocking temperature of NP, coupled with ferromagnetic platform, are higher, than in NP deposited on diamagnetic substrate. We observed feedback of magnetic susceptibility of cobalt ferrite cubic nanoparticles on magnetic dipole interaction between NPs and ferromagnetic bilaere CoFeB/Ta/CoFeB platform. The main magnetic characteristics of dynamical magnetization reversal in NPs are changed, when they are deposited on the surface of the ferromagnetic platform. Change of the blocking temperature of NPs under the magnetic dipole interaction with platform is caused by increase of the constant of effective magnetic anisotropy of the NPs up to 15-20%. Micromagnetic modeling predicts change of platform magnetization under individual NP up to 10 % that is similar with changes of the blocking temperature, effective magnetic anisotropy and other phenomenological parameters directly determined in experiments (Fig.1). The variations of the magnetizations of the two ferromagnetic layers under alternative magnetic field were visualized by micromagnetic modeling. Obtained results have principal importance for correct data collecting in lab-on-chip devices, where concentration of the NPs or magnetically labeled biology objects should be measured. Change of the AC susceptibility of NPs caused by their magnetic dipole interaction with the platform can valuably affect estimated number of nanoparticles in real devices.

1. RB Morgunov, OV Koplak, RS Allayarov, EI Kunitsyna, S Mangin, Effect of the stray field of Fe/Fe3O4 nanoparticles on the surface of the CoFeB thin films, Applied Surface Science 527, 146836 (2020).

https://doi.org/10.1016/j.apsusc.2020.146836 2. R Morgunov, A Hamadeh, T Fache, G Lvova, O Koplak, A Talantsev, S Mangin, Magnetic field and temperature control over Pt/Co/Ir/Co/Pt multistate magnetic logic device, Superlattices and Microstructures 104, 509-517(2017). https://doi.org/10.1016/j.spmi.2017.02.033

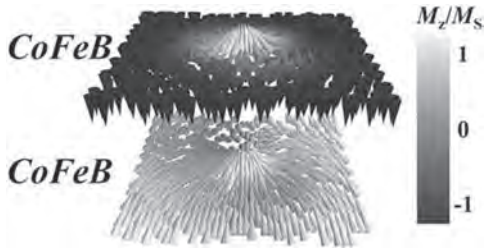

Fig.1. Calculated orientations of local magnetization in top and bottom layers of the CoFeB/Ta/CoFeB platform in presence of ferromagnetic NP on its surface in external magnetic field.

Session IOF
MICROSCOPY, IMAGING AND CHARACTERIZATION I

Amit Chanda, Chair
University of South Florida, Tampa, FL, United States

INVITED PAPER

IOF-01. Multi-modal Microscopy of real-space Antiferromagnetic Topological textures. *H. Jani*[1] *1. Physics, National University of Singapore, Singapore*

Antiferromagnetic (AFM) topological textures have been proposed as promising information vectors that can be deployed in race-track based next-generation computing paradigms. These textures, made from topological whirling of compensated magnetic sub-lattices in natural AFMs, are predicted not only to be very robust and small, but also move at ultra-fast speeds without sideway deflection [1,2]. However, progress in this direction has been restricted by the aforementioned sub-lattice compensation, which makes it very difficult to visualize and control AFM textures via standard magnetic techniques. I will firstly discuss synchrotron-based dichroic spectroscopy [3,4] and microscopy [5,6] which have been the standard work-horses for studying AFMs. Herein, I will present a recently-developed approach of phase-mapping the Néel order parameter, which exploits *angle-dependent dichroic imaging* [7,8]. In the epitaxial and free-standing forms of earth-abundant oxide – hematite (α-Fe_2O_3) – we have been able to generate a family of multi-chiral topological AFM textures including exotic merons/antimerons (half-skyrmions) and bimerons ('in-plane' skyrmions), as well as toplogically-tirivial AFM domain walls [8]. I will discuss how Néel vector phase-mapping can be used to identify the winding sense of these AFM textures. While epitaxial films can be investigated via X-ray *photo-emission electron microscopy*, freestanding membranes can be studied via *scanning transmission microscopy* and *holography*. I will contrast the unique capabilities afforded by each of these techniques, and highlight how the latter allow *in operado* imaging. Lastly, I will discuss recent developements deploying lab-based single-spin *N-vacancy imaging* (NV), sensitive to the weak canted moment in hematite, which allows us to resolve chirality of the topological AFM textures. Availability of such an arsenal of imaging modalities opens up the field of AFM topological spintronics for ready advancements in both fundamental and device physics.

[1] Barker J et al. *Phys Rev Lett* 116, 147203 (2016); Zhang X et al. *Nat Commun* 7, 10293 (2016); [2] Büttner F et al. *Sci Rep* 8, 4464 (2018); [3] van der Laan et al. *Phys Rev B* 34, 6529 (1986); Arenholz E et al. *Phys Rev B* 74, 94407 (2006); [4] Kuiper P et al. *Phys Rev Lett* 70, 1549 (1993); Jani, H* et al. *Nat Commun* 12, 1668 (2021); [5] Scholl A et al. *Science* 287, 1014 (2000); Nolting F et al. *Nature* 405, 767 (2000); [6] van der Laan et al. *Phys Rev B* 83, 064409 (2011); [7] Chmiel, F P et al. *Nat Mater* 17, 581 (2018); [8] Jani, H* et al. *Nature* 590, 74 (2021);

CONTRIBUTED PAPERS

IOF-02. Withdrawn

IOF-03. High-resolution magnetic imaging of magnetic transition region of perpendicular magnetic recording media by alternating magnetic force microscopy with sensitive amorphous FeCoB soft magnetic tip. *H. Saito*[1], H. Tanaka[1] and T. Matsumura[1] *1. Graduate School of Engineering Science, Akita University, Akita, Japan*

The magnetic imaging of zig-zag shaped magnetic transition region of high-density perpendicular magnetic recording media composed by fine granular magnetic grains is one of the ultimate targets of high-resolution magnetic field microscopy. We have developed high-resolution alternating magnetic force microscopy (A-MFM), which enables near-surface imaging of AC & DC magnetic fields [1-2]. A-MFM utilizes the frequency modulation of a cantilever oscillation generated by an off-resonance alternating magnetic force between a magnetic sample and a magnetic tip. For imaging DC magnetic field, A-MFM uses a soft magnetic tip of which magnetic moment is driven by an AC magnetic field to generate the alternating magnetic force. A-MFM can distinguish the zero level and the polarity of perpendicular magnetic field from recording media. The spatial resolution of less than 5 nm was obtained by a sensitive soft magnetic tip coated by amorphous FeCoB thin film with high magnetostriction [3], which has large effective volume of tip magnetization change at the tip-end, which is caused by AC magnetic field driven easy magnetic rotation in magnetic easy plane generated by inverse magnetostrictive effect. The spatial resolution was evaluated in the Fourier spectrum of MFM image by measuring the half of the minimum detectable wave length where MFM signal reaches white noise spectrum. In the present study, we demonstrate high-resolution MFM imaging of the zig-zag transitions in real space. Fig.1(a) and (b) shows the $\partial^2 H_z/\partial z^2$ image and its spatial spectrum for CoCrPt-SiO_2 perpendicular magnetic recording media with a recording density of 500 kfci. The recorded bit boundaries were clearly observed and the MFM spatial resolution was estimated about 3 nm. Fig.(c) is the image of the magnetic transition boundaries, of which signal amplitude is zero in Fig.1(a). Fig.(d) is its magnified image of which pixel size is 2.5 nm square. The zig-zag transition about 5 nm was clearly observed in this study.

[1] W. Lu, Z. Li, K. Hatakeyama, G. Egawa, S.Yoshimura, H. Saito, Appl. Phys. Lett., 96(2010), 143104. [2] Z. Li, X. Li, D. Liu, H. Saito, S. Ishio, Nanoscale 6 (2014), 11163. [3] M. V. Makarova, Y. Akaishi, T. Ikarashi, K. S. Rao, S. Yoshimura, H. Saito, J. Magn. Magn. Mater. 471 (2019), 209.

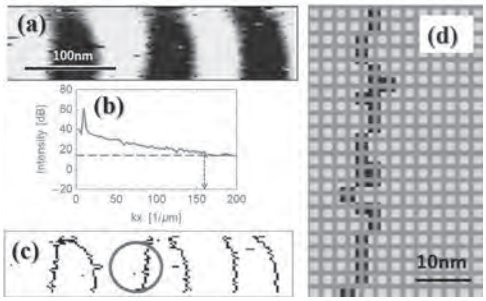

Fig.1 Perpendicular magnetic field gradient image $\partial^2 H_z/\partial z^2$ [(a)] and its spatial spectrum [(b)] for CoCrPt-SiO_2 perpendicular magnetic recording media. Image of magnetic transition boundaries in Fig. (a) [(c)] and its magnified image [(d)].

IOF-04. Field Sensitivity in Magnetic Force Microscopy. H.J. Hug[1,2], *Y. Feng*[1,2], M. Penedo[1,3], P. Kappenberger[1,4], X. Zhao[1,5] and A. Mandru[1]
1. Empa, Swiss Federal Laboratories for Materials Science and Technology, Dübendorf, Switzerland; 2. Department of Physics, University of Basel, Basel, Switzerland; 3. Laboratory for Bio- and Nano-Instrumentation, Lausanne, Switzerland; 4. Condair Group AG, Pfäffikon, Switzerland; 5. Evatec AG, Trübbach, Switzerland

Magnetic force microscopy (MFM) is an established technique for imaging stray fields emanating from a sample with a high spatial resolution and sensitivity. This high resolution and the ease of implementation in existing atomic force microscopy (AFM) tools make the MFM technique particularly desirable for the investigation of magnetic thin films and nanoscale devices. The measured signal in MFM is a change of the dynamic properties of the imaging cantilever arising from the interaction between the magnetic cantilever tip and the sample. Apart from the signals generated by the stray field from the micromagnetic pattern of the sample, the signals measured by an MFM may also contain non-negligible contributions from the sample topography, variations of the surface Kelvin potential and grain-to-grain variations of the areal density of the magnetic moment. As a result, to achieve high spatial resolution of the micromagnetic pattern of the sample, differential imaging techniques have to be employed to disentangle the different contrast contributions: especially when the stray field signals of interest are weak, e.g., in the case of magnetic skyrmion imaging [1,2]. The magnetic part of the MFM signal arises from the interaction of the stray field of the sample with the tip magnetic moment distribution. Methods to calibrate the response of the tip to different spatial wavelengths of the field have been developed [3]. Such a calibration of the MFM tip allows quantitative determination of the magnetic vector field in the plane parallel to the sample surface scanned by the tip. It also permits assessment of the minimally detectable stray field (or the sensitivity) of an MFM. In general, the tip sensitivity becomes weaker for smaller spatial wavelengths (Fig.1). Obtaining a high spatial resolution thus requires a high measurement sensitivity that can be obtained by MFM operation in vacuum and with improved cantilevers In this talk, methods to disentangle different contrast contributions in MFM and evaluate the field sensitivity of the instrument will be discussed.

[1] A. Soumyanarayanan, M. Raju, A. Gonzalez Oyarce *et al.*, Nature Mater 16, 898–904 (2017) [2] K.-Y. Meng, A. S. Ahmed *et al.*, Nano Lett. 19, 5, 3169–3175 (2019) [3] P. J. A. van Schendel, H. J. Hug, B. Stiefel *et al.*, Journal of Applied Physics 88, 435 (2000)

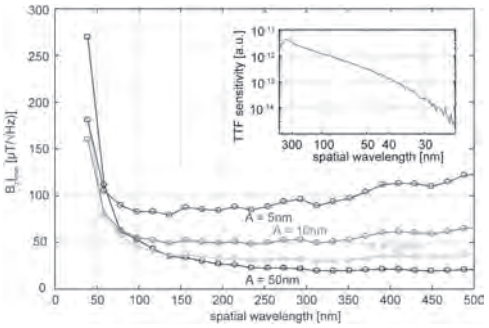

Fig. 1: Dependence of MFM field sensitivity on tip oscillation amplitude and spatial wavelengths.

IOF-05. Quadratic and third-order magneto-optic Kerr effect in Ni(111) thin films with and without twinning. M. Gaerner[1], R. Silber[2], T. Peters[1], J. Hamrle[3] and *T. Kuschel*[1] *1. Bielefeld University, Bielefeld, Germany; 2. VŠB - Technical University of Ostrava, Ostrava, Czechia; 3. Charles University, Praque, Czechia*

The linear magneto-optic Kerr effect (LinMOKE) as well as the quadratic MOKE (QMOKE) are important magneto-optic effects of fundamental physics but also powerful tools for thin-film sample characterization, e.g., to analyze magnetocrystalline anisotropies via vectorial magnetometry [1] or to sense the crystallographic ordering in Heusler compounds [2]. In order to separate and study the dependencies of LinMOKE and QMOKE on the crystallographic direction, the so-called eight-directional method can be used [3]. For each crystallographic in-plane direction, a magnetic field is applied in eight in-plane directions (every 45°) and the responses are added up or subtracted depending on the odd and even nature of LinMOKE and QMOKE with respect to the magnetization. So far, this method or similar ones have been utilized to characterize (001)-and (011)-oriented thin films of cubic crystal structure [4,5]. In addition, new setups for QMOKE spectroscopy have been realized for (001)-oriented thin films [6]. Within this contribution, we apply the eight-directional method to sputter-deposited Ni(111) thin films and report on a strong three-fold anisotropy in longitudinal MOKE (LMOKE), see Fig. 1. This anisotropy can be explained by theory as an optical interplay of elements in the permittivity tensors of first and second order in M, effectively creating cubic MOKE contributions, i.e., MOKE of third order in M. Furthermore, we studied Ni(111) thin films with and without several multiple (111) phases of 60° in-plane rotation (twinning) which have been characterized by off-specular x-ray diffraction texture maps. We observed substantial reduction of QMOKE oscillations in a twinned sample compared to a thin film with almost no twinning. This indicates that the LMOKE anisotropy truly is of crystallographic origin in the ferromagnetic layer and is not due to other, e.g., interface effects.

[1] T. Kuschel et al., J. Phys. D: Appl. Phys. 44, 265003 (2011) [2] R. Silber et al., Appl. Phys. Lett. 116, 262401 (2020) [3] K. Postava et al., J. Appl. Phys. 91, 7293 (2002) [4] R. Silber et al., Phys. Rev. B 100, 064403 (2019) [5] J. H. Liang et al., Appl. Phys. Lett. 108, 082404 (2016) [6] R. Silber et al., Phot. Nano. Fund. Appl. 31, 60 (2018)

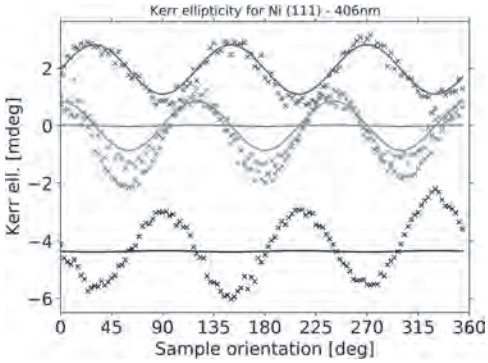

QMOKE anisotropy measurement of a 20-nm thick Ni film on MgO(111) at a wavelength of 406 nm. The threefold anisotropy of longitudinal MOKE (∝ M_L in black), transverse MOKE (∝ M_T in green) and QMOKE (∝ $M_L M_T$ in blue, as well as ∝ M_T^2-M_L^2 in red) are clearly visible.

INVITED PAPER

IOF-06. Table-Top Low-Field MicroMRI for Cell Imaging.
E.B. Buchanan[2], S.E. Russek[1] and K.F. Stupic[1] *1. NIST, Boulder, CO, United States; 2. UT Southwestern Medical Center, Dallas, TX, United States*

Current microMRI uses large superconducting magnets (> 7 T) and can obtain a resolution of approximately 20 μm.[1] However, current microMRI systems cannot resolve cells or compete with optical techniques required for pathology and personalized medicine applications. Point-of-use hyperpolarization systems can provide both enhanced signal and contrast, potentially enabling microMRI of small samples such as tumor biopsies and patient derived organoids used for therapeutic evaluation. Here, we present the development of a novel table-top microMRI system (Fig. 1) that incorporates an integrated point-of-use solid-state water-proton hyperpolarization system that relys on spintronic concepts. The system operates at 135 mT with the NMR and FMR-based hyperpolarization systems running at ~6 MHz and ~10 GHz, respectively. The hyperpolarizer operates at room temperature and low field and is much smaller and simpler than other existing hyperpolarization systems. A set of proton NMR and hyperpolarizer FMR spectra are shown in Fig. 2. The mode structure of the FMR film can be complex and needs to be understood to optimize spin transfer. We discuss spin transport and spin-electrochemistry of ferromagnetic films interacting with proton spins in biologic solutions. The surface spin chemistry and transport are the challenging and essential component of this technology. We present the design of micromagnets, compact gradients, FPGA based console, and compact microwave systems to enable the fabrication of a low-cost small footprint table-top MRI.

1. Lee, C. H. et al. Magnetic Resonance Microscopy (MRM) of Single Mammalian Myofibers and Myonuclei. Sci. Rep. 7, 39496; doi: 10.1038/srep39496 (2017).

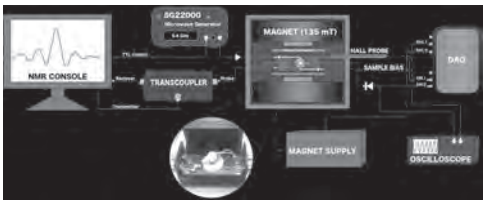

Fig. 1. Schematic of the table-top MRI system showing NMR and hyperpolarizer systems along with a photo of the 3 mm diameter NMR cell and hyperpolarizer, contained in a 25 mm x 50 mm enclosure.

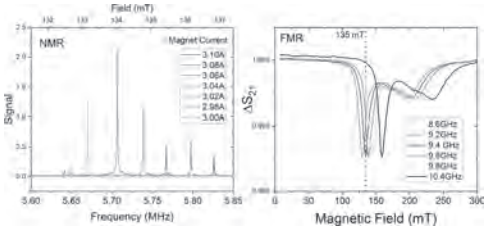

Fig. 2. Proton NMR spectra from microMRI and FMR spectra from the hyperpolarizer near the operation field of 135 mT.

CONTRIBUTED PAPERS

IOF-07. Application of High Sensitive AC Field Modulation GMR Sensor to Magnetic Field Microscope. *A. Kikitsu*[1], Y. Higashi[1], Y. Kurosaki[1], S. Shirotori[1], T. Nagatsuka[2], K. Suzuki[2] and Y. Terui[2]
1. Toshiba Corp., Kawasaki, Japan; 2. Toshiba Nanoanalysis Corp., Kawasaki, Japan

INTRODUCTION A novel high-sensitive Giant Magneto-resistance (GMR) sensor using symmetry MR response and AC field modulation has been developed. It enables high SNR detection of magnetic signal in low frequency range with clear separation of the signal from the modulation field [1]. Its promising application is detecting a magnetic field from small defective leakage current in a semiconductor chip or a Li ion buttery. In this study, the novel sensor was applied to a magnetic field microscope developed for detecting defects [2]. RESULTS AND DISCUSSION Schematic diagram of magnetic field microscope system is shown in Fig.1. Line-shape GMR element with symmetric response (MR~3%) was placed between NiFe yokes (1mm square). AC modulation field (10kHz) was applied from a Cu line under the GMR line. GMR-A and GMR-B in a full bridge circuit were different in the phase of the AC field. A 10kHz component of the output signal was detected by a lock-in amplifier [1]. Objective sample was a printed Cu wire (150μm width) flowing an AC current of 100Hz. Sensor unit was faced to the sample and was scanned two-dimensionally with the spacing of 1mm. A 100Hz component of the output signal was detected by another lock-in amplifier. Detecting time was 100ms per pixel. Magnetic field was also simulated by a finite element method. Figure 2 shows the results. At 4.5mA (a), clear magnetic image similar to the simulated one (e) was observed. The contrast of the image degraded by decreasing the AC current and became unclear at 45μA (c), but it became recognizable by averaging (1 sec/pixel) (d). This means that an ambient magnetic noise brings the detecting limit. These results were comparable to those detected by an MI sensor. Estimated magnetic field detected at 45μA (magnetic noise) was about 4nT. Further reduction in the ambient noise may increase the detecting limit. This work was supported by the Cabinet Office (CAO), Cross-ministerial Strategic Innovation Promotion Program (SIP), "Intelligent Processing Infrastructure of Cyber and Physical Systems" (funding agency: NEDO).

[1] S. Shirotori et. al.: IEEE Trans. Magn., 57, 4000305 (2021) [2] K. Kimura et al.: Electro. Packaging Technol., 28, 16 (2012)

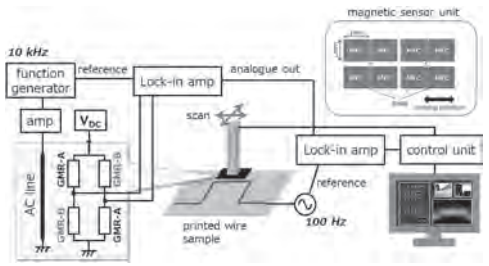

Fig.1 Schematic diagram of magnetic field microscope system

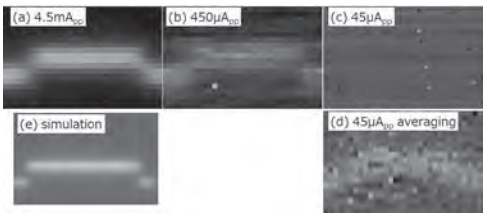

Fig.2 Results of the magnetic imaging

IOF-08. Imaging the Magnetization Vector with Fourier Transform Holography. *M. Di Pietro Martínez*[1], A. Wartelle[1,2], C. Herrero-Martínez[1], F. Fettar[3], J. Motte[3], L. Turnbull[5], F. Ogrin[4], G. van der Laan[6], H. Popescu[7], N. Jaouen[7], F. Yakhou-Harris[2] and G. Beutier[1] *1. SIMaP, Saint-Martin d'Hères, France; 2. ESRF, Grenoble, France; 3. Institut Néel, Grenoble, France; 4. School of Physics and Astronomy, University of Exeter, Exeter, United Kingdom; 5. Centre for Materials Physics, Durham University, Durham, United Kingdom; 6. Diamond Light Source, Oxfordshire, United Kingdom; 7. Synchrotron SOLEIL, Gif-sur-Yvette, France*

Fourier transform holography (FTH) is a lensless imaging technique that uses a known reference in the sample to retrieve the object of interest in one single step of calculation (*i.e.* it does not require an iterative method), overcoming the phase problem inherent to other techniques such as coherent diffraction imaging and ptychography. In the case of an extended reference, a linear differential filter is applied and the object can simply be obtained by calculating the inverse Fourier transform. This approach is known under the name of HERALDO [1]. By exploiting the x-ray magnetic circular dichroism effect, this technique has shown to be useful to image magnetic textures by providing a projection (sometimes two) of the magnetization in 2D layers [2-5]. In this work, we go further and use FTH to image the magnetic structure of a 3D object. To be sensitive to all three components of the magnetization (perpendicular as well as in-plane), we use a sample setup with two perpendicular slits as complementary references (Fig. 1). By tilting the sample around the axes defined by the two slits, we obtain a dual set of projections which gives information about the internal configuration of the sample [6]. We discuss the different problems that can arise in the experiment, such as shadowing effects and a reduced angular range for the tilting of the sample, and how these can be conquered. We test the method in a 1µm thick Fe/Gd multilayer with maze-like magnetic pattern and image a circular window of diameter 5µm. Finally, we use this projection set as input to the tomography algorithm that we developed [7] to reconstruct the vector field structure of the whole object.

[1] M. Guizar-Sicairos and J. R. Fienup, Optics express, Vol. 15, p. 17592-17612 (2007) [2] T. A. Duckworth *et al.,* Optics Express, Vol. 19, p. 16223-16228 (2011) [3] T. A. Duckworth *et al.*, New Journal of Physics, Vol. 15, p. 023045 (2013) [4] L. A. Turnbull *et al.,* ACS nano, Vol. 15, p. 387-395 (2020) [5] M. T. Birch *et al.*, Nature Communications, Vol. 11, p. 1-8 (2020) [6] C. Donnelly *et al.*, Nature, Vol. 547, p. 328-331 (2017) [7] *magtopy* is PyCUDA library which targets the reconstruction of the 3D magnetization using as input a set of projections from tomography measurements: https://gitlab.com/magtopy/magtopy

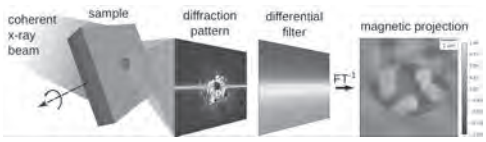

Fig. 1: Fourier transform holography: The coherent x-ray beam illuminates the whole sample. A circular window is milled into the gold layer, which masks the magnetic sample, to allow passing through the x-rays. Two slit references are also milled across the mask and the sample. After filtering the diffraction pattern and applying the inverse Fourier transform, the magnetic projection is recovered (magnetic contrast is obtained by x-ray magnetic circular dichroism). Tilting the sample around two axes allows us to probe all three components of the magnetization.

IOF-09. Depth-resolved magnetization profile of MgO/CoFeB/W perpendicular half magnetic tunnel junctions. *V. Bansal*[1], J. Tonnerre[1,3], F. Fettar[1], E. Mossang[1], J. Chatterjee[2], S. Auffret[2], L. Prejbeanu[2] and B. Dieny[2] *1. Universite Grenoble Alpes, CNRS, Grenoble INP, Institut Neel, Grenoble, France; 2. University Grenoble Alpes, CEA, CNRS, Grenoble-INP, INAC-SPINTEC, Grenoble, France; 3. Syncrotron Soleil, Saint Aubin, Gif-sur-Yvette Cedex, France*

Magnetic tunnel junctions have been a keen focus in spintronics known for their usage in spin-transfer-torque (STT) magnetic random access memories [1] for which MgO/CoFeB/Ta systems with perpendicular magnetic anisotropy (PMA) have proved to be a prime candidate [2]. W insertion between CoFeB and Ta has been shown to improve PMA and tunnel magnetoresistance (TMR) [3,4]. Moreover, TMR and STT excitation are interface sensitive quantities [5]. Probing buried magnetic interfaces in such systems is therefore a major challenge. In this work, soft x-ray magnetic resonant reflectivity (SXRMR) is used to probe the interface magnetization in MgO(1.3nm)/CoFeB(1.4nm)/W(1.9nm) free layer and its change upon annealing. It combines the depth-resolved information of x-ray reflectivity with x-ray magnetic circular dichroism for probing in-plane (*ip*) and out-of-plane (*oop*) magnetization profile of subnanometer resolution[5]. The measurements were performed at the SEXTANTS beamline at SOLEIL. The reflectivity curves are collected at various energies around the L_3 edge for right and left circularly polarized light, from which the average reflectivity (I_{av}) and the magnetic asymmetry $R=(I_{CR}-I_{CL})/(I_{CR}+I_{CL})$, related to the magnetization distribution across the CoFeB layer are derived (Fig. 1). We first investigate the as-deposited sample that shows *ip* anisotropy. The simultaneous fits of R and I_{av} lead to a gradient distribution with no dead layer (Fig.2). This shows an increase of the overall magnetization compared to the one derived for the as-deposited MgO/CoFeB/Ta (Fig. 2), in agreement with magnetometry results. The magnetization profile of the W-capped sample after annealing at 400°C, leads to *oop* anisotropy transition as reflected by R evolving to large (20-80°) angles (Fig.1). The profile is similar with higher magnetization values at both interfaces. The high spin polarization at the bottom interface is in agreement with [6] and the decrease at the top one is ascribed to localized reduction of M_S and T_C as proposed in [7].

[1] H. Ohno, T. Endoh, S. Ikeda et al. *International Electron Devices Meeting*, pp. 9.4.1-9.4.4 (2010) [2] S. Ikeda *et al.*, *Nat. Mater.*, vol. 9, no. 9, pp. 721–724 (2010) [3] J. Chatterjee, R. C. Sousa, B. Dieny et al. *Appl. Phys. Lett.*, vol. 110, no. 20 (2017) [4] Jyotirmoy Chatterjee, Eric Gautier Bernard Dieny et al. A. Phys, vol. 092407 (2019) [5] J.-M. Tonnerre, M. Przybylski, J. Kirschner et al. *Phys. Rev. B - Condens. Matter Mater. Phys.*, vol. 84, no. 10, pp. 1–5 (2011) [6] E. Jal, Jeffrey B. Kortright, Tyler Chase*et al.*, vol. 092404, pp. 5–8 (2015) [7] B. M. S. Teixeira, A. A. Timopheev, N. A. Sobolev, *Phys. Rev. B*, vol. 100, no. 18, p. 184405 (2019)

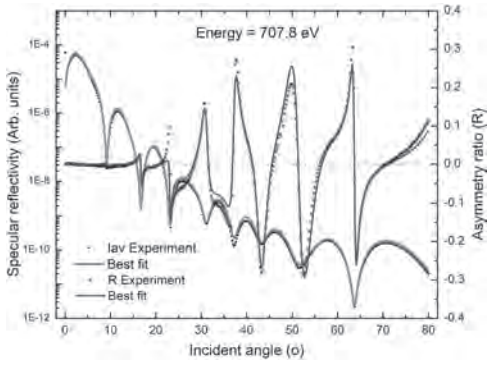

Fig 1. Average reflectivity and magnetic asymmetry measured at 707.8 eV with best fits

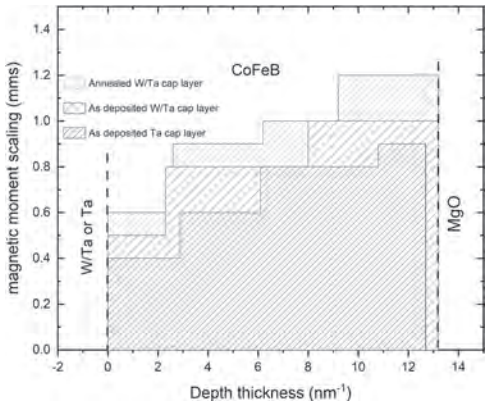

Fig 2. Depth-resolved magnetization profile of studied samples. MMS = 1 corresponds to a Fe magnetic moment of 2.1μ_B

IOF-10. X-ray magnetic linear dichroism for time-resolved imaging of spin axial dynamics. J. Bailey[1,2], S. Finizio[1], J. Förster[3], S. Mayr[1], M. Weigand[4], C. Dubs[5], E. Josten[6], J. Dreiser[1], E. Goering[3], J. Gräfe[3], J. Raabe[1], G. Schütz[3], G. Aeppli[1,2] and *S. Wintz*[1,3] *1. Paul Scherrer Institut, Villigen PSI, Switzerland; 2. EPFL, Lausanne, Switzerland; 3. Max-Planck-Institut für Intelligente Systeme, Stuttgart, Germany; 4. Helmholtz-Zentrum Berlin für Materialien und Energie, Berlin, Germany; 5. Innovent, Jena, Germany; 6. Forschungszentrum Jülich, Jülich, Germany*

Time-resolved scanning transmission x-ray microscopy (TR-STXM) is one of the few techniques that is capable of imaging magnetic systems simultaneously on the ~10 nm length and ~10 ps time scales [1,2]. Up to now, TR-STXM measurements have mainly made use of x-ray magnetic circular dichroism (XMCD) [3] to achieve magnetic contrast. XMCD has the limitation, however, that it is sensitive to the net magnetization of a certain magnetic species, consequentially for some sample systems (such as antiferromagnets) it cannot be used directly. In contrast, x-ray magnetic linear dichroism (XMLD) [4] is sensitive to the axis of magnetization, and as such can be used in different systems [5]. Here we present the use of XMLD for imaging magnetic dynamics with TR-STXM [6]. We utilize this technique to characterise vortex, domain-wall and spin-wave dynamics in the ferrimagnetic insulator yttrium iron garnet (YIG). For that purpose, a lamella of 13x5 μm^2 lateral size was prepared from a YIG film of 185 nm thickness. The Figure shows both the static magnetic state (a-c) and the dynamic response (d,e) of part of this lamella to a local 70 MHz alternating magnetic field excitation. Using XMCD with both light helicities (C+ and C-) as well as XMLD with both linear horizontal (LH) and linear vertical (LV) polarization, it was possible to complementary image the perpendicular magnetization (vortex core) as well as the axes of the in-plane vortex domain configuration of the sample. Normalized image snapshots clearly highlight the dynamic excitation of the sample in XMCD and XMLD (d,e). Our findings demonstrate that TR-STXM using XMCD and XMLD may open the door to the imaging of spin dynamics in antiferromagnetic systems.

[1] M. Kammerer *et al.* Nat. Commun. 2, 279 (2011). [2] S. Bonetti *et al.* Rev. Sci. Instrum. 86, 093703 (2015). [3] G. Schütz *et al.* Phys. Rev. Lett. 58, 737 (1987). [4] G. van der Laan *et al.* Phys. Rev. B 34, 6529 (1986). [5] F. Nolting *et al.* Nature 405, 767 (2000). [6] J. Bailey *et al.* (unpublished).

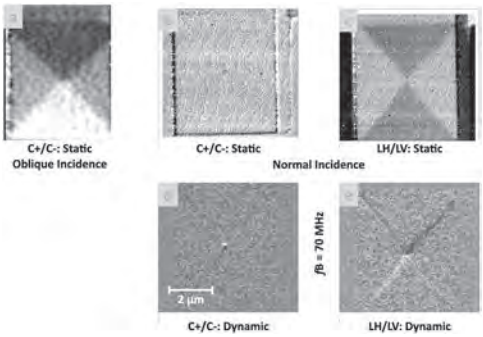

TR-STXM imaging of a YIG vortex structure combining XMCD (a,b,d) and XMLD (c,e). (a) Static XMCD image (C+/C-) with oblique x-ray incidence, mainly showing the in-plane magnetic vortex state. (b-e) Normal x-ray incidence: (b) Static XMCD yielding the central vortex core as black dot. (c) Corresponding XMLD image (LH/LV) revealing the triangular domains of different spin axes. (d) XMCD and (e) XMLD normalized dynamic snapshots with respect to time average, upon alternating magnetic field excitation of 70 MHz.

IOF-11. Soft X-ray Magnetic Laminography Imaging of Magneto-dynamical Processes. *S. Finizio*[1], C. Donnelly[2], S. Mayr[1,3], A. Hrabec[1,3] and J. Raabe[1] *1. Paul Scherrer Institut, Villigen PSI, Switzerland; 2. Cavendish Laboratory, University of Cambridge, Cambridge, United Kingdom; 3. Laboratory for Mesoscopic Systems, ETH Zurich, Zurich, Switzerland*

Until recently, most of the experimental research on magneto-dynamical processes has focused on two-dimensional systems. The extension to the experimental investigation of fully three-dimensional dynamical processes has up to now only been possible through indirect methods and through comparison of two-dimensional data with micromagnetic simulations. One of the main reasons for this is that microscopy techniques that combine three-dimensional magnetic imaging with nanometric resolutions with the possibility to perform time-resolved investigations with sub-ns temporal resolutions are not widely available. A first demonstration of time-resolved three-dimensional imaging was performed with hard X-ray magnetic laminography [1]. However, the technique exhibits limitations both in the sensitivity (due to the use of hard X-rays) and in the selection of accessible frequencies (due to the use of ptychography for imaging the magnetic samples), which has limited its applicability. In this contribution, we present first time-resolved measurements of magnetic vortex and spin-wave dynamics fully resolved in all three spatial dimensions performed at soft X-ray energies, enabling us to obtain strong magnetic contrast from the 3d ferromagnetic elements (L absorption edges) and the rare earth elements (M absorption edges). By combining the laminography imaging technique [1,2] with time-resolved scanning transmission X-ray microscopy to acquire the angular projections, time-resolved three-dimensional imaging with free selection of the frequency of the electrical signals used to excite the dynamical processes is made possible. A spatial resolution of about 40 nm along the plane of the sample was demonstrated, with the possibility to perform measurements with temporal resolutions down to 30 ps if time-of-arrival detection methods are employed [3]. This technique finds direct applicability to the investigation of dynamical processes in 3D magnetic systems such as e.g. nanowires and more complex geometries.

[1] C. Donnelly *et al.*, *Nature Nanotechnology* 15, 356 (2020) [2] K. Witte *et al.*, *Nano Letters* 20, 1305 (2020) [3] S. Finizio *et al.*, *Journal of Synchrotron Radiation* 27, 132 (2020)

IOF-12. Withdrawn

Session IOG
MICROSCOPY, IMAGING AND CHARACTERIZATION II

Koji Sekiguchi, Chair
Yokohama National University, Yokohama, Japan

CONTRIBUTED PAPERS

IOG-01. The Effect of Temperature Variations in Thermal Noise Magnetometry. *K. Everaert*[1,2], B. Van Waeyenberge[2], J. Leliaert[2] and F. Wiekhorst[1] *1. Biosignals, Physikalisch-Technische Bundesanstalt, Berlin, Germany; 2. Department of Solid State Sciences, UGent, Gent, Belgium*

Magnetic nanoparticles are powerful tools in biomedical applications, where they are employed in both diagnosis and therapy. A prerequisite for the efficiency of these applications are precisely characterized particles. Several magnetic measurement techniques are established, which all have in common that they measure the magnetic response of the particles exposed to an externally applied magnetic field, which may change the magnetic state of the particles [1]. Therefore, Thermal Noise Magnetometry (TNM) has been developed, a magnetic nanoparticle characterization technique that does not rely on an external magnetic excitation [2]. It detects amplitude variations in the net magnetic moment of the sample caused by thermal fluctuations. TNM measurements have been proven to be feasible, and complementary to other characterization techniques due to their diminutive impact on the sample [2, 3]. Two mechanisms are responsible for the directional fluctuations of the magnetic moments. Brownian fluctuations occur if the particles are free to move in the sample, i.e. when they are suspended in a solution. The hydrodynamic size of the particles and the viscosity of the fluid influence the Brownian fluctuation rate. In parallel, the magnetization of each particle can also switch in the frame of the particles themselves, called Néel switching. The Néel switching rate is determined by the volume of the particles' magnetic core and anisotropy constant. Additionally, the timescales of both mechanisms also depend on the temperature since the fluctuations are induced by the thermal energy in system. TNM experiments are typically performed at room temperature, but the particles are characterized for biomedical applications at body temperature. From preliminary results, a considerable effect of temperature variations in TNM is visible, influencing the particles' fluctuation rate distributions and noise spectrum. As expected from the theory, the fluctuation rates shift towards higher values for higher temperatures, which leads to a decrease in the noise power in the considered frequency range.

[1] Myrovali, E.et al., Sci. reports, Vol. 6, p. 37934 (2016) [2] Leliaert, J.et al., Appl. Phys. Lett., Vol. 107, p. 222401 (2015) [3] Leliaert, J.et al., J. Phys. D: Appl. Phys., Vol. 50, p. 085004 (2017)

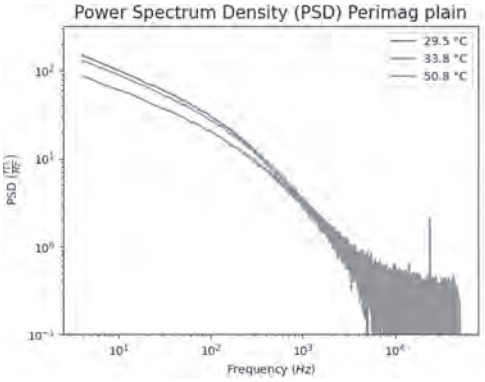

Power spectrum densities for Perimag® particles at different temperatures.

IOG-02. Synthesis and Characterization of Fe-Fe_3O_4 Core-Shell Nanoparticles Dispersed in Carbon Matrix. H. Gyulasaryan[1], E. Papadopoulou[2], N. Tetos[2], G. Chilingaryan[1], E. Myrovali[3], M. Angelakeris[3], M. Farle[2], M. Spasova[2], J. Gray[4], *A.N. Kocharian*[5], O. Bernal[5] and A. Manukyan[1] *1. Institute for Physical Research of National Academy of Sciences, Ashtarak, Armenia; 2. University of Duisburg-Essen, Faculty of Physics and Center of Nanointegration (CENIDE), Duisburg, Germany; 3. Physics Department, Aristotle University of Thessaloniki, Thessaloniki, Greece; 4. Materials Characterization Laboratory, Penn State Materials Research Institute, University Park, PA, United States; 5. Department of Physics and Astronomy, California State University Los Angeles, Los Angeles, CA, United States*

Magnetic metal nanoparticles dispersed in non-magnetic (carbon) matrix are of great importance both from a scientific point of view and in connection with numerous applications in biomedicine, spintronics, catalysis, sensors, etc. [1-3]. Especially promising are synthesis of novel functional nanoparticles with a core-shell architecture for improving their working magnetic characteristics due to the possibility of combining materials with different magnetic properties based on these magnetic nanoparticles [4-5]. The magnetic interactions between the core and the shell provide an additional degree of freedom for tuning the magnetic characteristics [6]. Nanoparticles based on iron and iron oxide with a core-shell architecture are effective intermediaries for heat transfer in an AC magnetic field [7-8]. In current work, Fe-Fe_3O_4 core-shell nanoparticles were synthesized by solid-phase pyrolysis of iron phthalocyanine (FePc), followed by annealing in an oxygen atmosphere. Changing the pyrolysis conditions, it is possible to vary sizes of nanoparticles from 5 to 100 nm and core-shell ratio. The quantitative composition of the core-shell was controlled also by changing the concentration of oxygen. Complex structural analyses of these materials are obtained using HRTEM, STEM, XRD and Raman spectroscopies. Magnetic properties of synthesized materials have been studied with a Quantum Design MPMS XL SQUID magnetometer. To study the structure of the obtained nanoparticles, HAADF-STEM images were taken, confirming the Fe-Fe_3O_4 core-shell architecture of the nanoparticles. Figures 1, and 2 show a HAADF-STEM image with elemental mapping of a single chosen nanoparticle and XRD

pathern of the (Fe-Fe_3O_4)@C sample obtained by synchrotron radiation (λ = 0.98782 Å) correspondingly. This work was supported by European Union's Horizon 2020 research and innovation program under grant No 857502 (MaNaCa). The work at CSULA supported by NSF CREST Grant #HRD-1547723. M. Farle acknowledges support by government of the RF (No 075-15-2019-1886).

1. Kudr, J., Haddad, Y., Richtera, L., Heger, Z., Cernak, M., Adam, V., and Zitka, O., *Nanomaterials,* 2017, vol. 7, p. 243. 2. Gloag, L., Mehdipour, M., Chen, D., Tilley, R.D., and Gooding. J.J., *Adv. Mater.*, 2019, vol. 31, p. 1904385. 3. Gubin, S.P., *Magnetic Nanoparticles*, Weinheim: Wiley, 2009. 4. Nogués, J., Sort, J., Langlais, V., Skumryev, V., Suriñach, S., Muñoz, J.S., and Baró, M.D., *Phys. Rep.*, 2005, vol. 422, p. 65. 5. Manna, P.K. and Yusuf, S.M., *Phys. Rep.*, 2014, vol. 535, p. 61. 6. López-Ortega, A., Estrader, M., Salazar-Alvarez, G., and Roca, A.G., *Phys. Rep.*, 2015, vol. 553, p. 1. 7. Simeonidis, K., Martinez-Boubeta, C., Serantes, D., Ruta, S., Chubykalo-Fesenko, O., Chantrell, R., Oró-Solé, J., Balcells, Ll., Kamzin, A.S., Nazipov, R.A., Makridis, A., and Angelakeris, M., *ACS Appl. Nano Mater.*, 2020, vol. 3, p. 4465. 8. Nemati, Z., Alonso, J., Khurshid, H., Phan, M.H., and Srikanth, H., *RSC Adv.*, 2016, vol. 6, p. 38697.

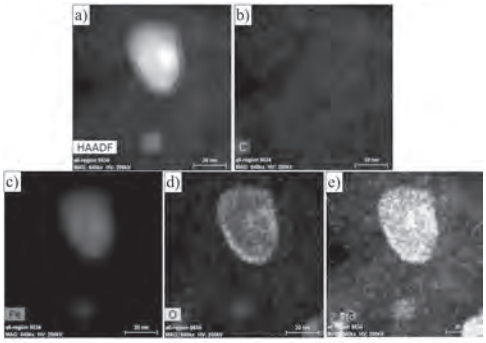

Figure 1. HAADF-STEM image of Fe-Fe3O4 nanoparticles (a) with elemental mapping (b–e).

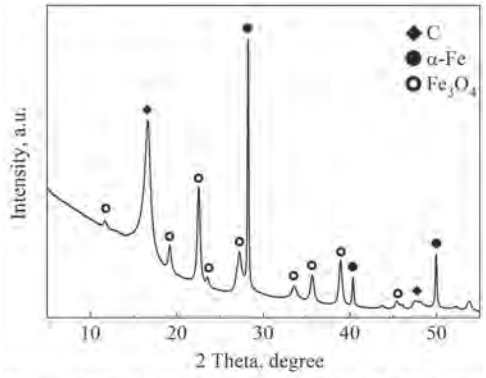

Figure 2. XRD pattern of the sample (Fe-Fe3O4)@C.

IOG-03. Highly Stable Copper–Zinc Ferrite Nanoparticles for MRI Thermometry. D. Lachowicz[1], J. Stroud[2], J. Hankiewicz[2], R. Gassen[2], A. Kmita[1], J. Stepien[1], Z. Celinski[3], M. Sikora[1], J. Zukrowski[1], M. Gajewska[1] and *M. Przybylski*[1,4] *1. Academic Centre for Materials and Nanotechnology, AGH University of Science and Technology, Krakow, Poland; 2. BioFrontiers Center, University of Colorado Colorado Springs, Colorado Springs, CO, United States; 3. Physics Department, University of Colorado Colorado Springs, Colorado Springs, CO, United States; 4. Faculty of Physics and Applied Computer Science, AGH University of Science and Technology, Krakow, Poland*

We demonstrate that water-stable CuZn ferrite nanoparticles can be prepared using one-step thermal decomposition synthesis in poly(ethylene glycol) - PEG. Magnetic properties of obtained nanoparticles were studied using a superconducting quantum interference device magnetometry (SQUID) and a Mössbauer spectroscopy (MS). The results of the MS and the X-Ray Absorption Near Edge Spectroscopy measurements combined with the determined magnetic properties studied using SQUID allowed us to identify the ferrite structure of the studied nanoparticles. Due to strong increase of T_2 with temperature our ultra-small, PEG-coated CuZn ferrite nanoparticles can be used as temperature contrast agents in Magnetic Resonance Imaging (MRI) using a spin-echo sequence. The preliminary MRI experiments at 3.0 T using agar gel phantoms doped with $Cu_{0.08}Zn_{0.54}Fe_{2.38}O_4$ nanoparticles, and exposed to a temperature gradient, show significant changes in the intensity of T_2 weighted spin-echo MR images. The MRI results show a strong correlation between the temperature recorded by external MRI compatible sensors and the image intensity. Thus, we conclude that the spatial maps of phantoms with absolute temperature distribution can be obtained noninvasively from these changes in the MR image intensity (Fig.1). We estimate the uncertainty of the method to be 2.6°C at 20°C. Such a method is limited to known particles with known concentrations, and for practical use, requires one temperature reference point and initial calibration. If our method is used in clinical settings, the well-defined human body temperature of 37°C can be employed as a reference point. Since image intensity also depends on MRI sequence parameters, the calibration must be linked to specific sequence values such as the repetition time and echo time. The simplicity of the synthesis and their auspicious magnetic and biological properties make PEG coated CuZn ferrite nanoparticles a promising contrast agent for MRI thermometry.

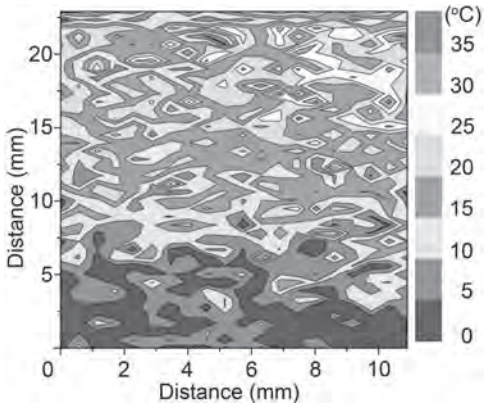

Fig.1. MRI in the presence of a 25°C temperature gradient. Absolute temperature of the map matrix was obtained from converting image pixel intensity to colors using calibration protocol and data four MRI compatible sensors.

IOG-04. *In Situ* Compensation Method for Precise Volume Magnetometry of Biological and Chemical Specimens Requiring Encapsulation. *M. Sawicki*[1] and K. Gas[1] *1. Institute of Physics Polish Academy of Sciences, Warszawa, Poland*

There has been a growing interest in the magnetic characterization of organic compounds aiming at therapeutic purposes. Most frequently these compounds are in the form of powders or solutions of minute volumes, making the magnetometry effort challenging. Practically, the researches have to resort to encapsulation of the specimens in gelatin capsules. Although lightweight, typically of about 30mg, they can outweigh the researched material by a few times, since frequently its weight is in a single mg range. This proportion makes the precise magnetometry challenging and the typical experimental procedure prone to substantial systematic errors. They stem from the technical difficulties in precise *ex situ* compensation of the experimental data for the relevant signal of the capsule. This is predominantly caused either by the non-reproducibility of the magnitudes of the magnetic field in magnetometers operating with superconducting magnets [1,2], or by inadequate centerings of the sample holder for the two sets of measurements. Facing the same problems in a follow up effort of our recent studies of [3], we elaborated a new experimental methodology allowing 10 to 20-fold *in situ* reduction of the signal of capsules, which can be easily incorporated in any magnetometer which can accommodate a straw sample holder (e.g. Quantum Design MPMS and MPMS3 models). The concept is depicted in the Fig. 1. Here, the signal of the center, specimen-carrying capsule, is effectively level off by the signals exerted by the two additional trains of 6 similar capsules abutting the latter. This substantially exposes the signal specific to the contents of the central capsule, making the measurements far less vulnerable to the magnetometer's instabilities and mechanical misalignments, substantially increasing the validity of the studies. Importantly, all of this is accomplished using only the build in functions and data reduction method provided by the manufacturer, eliminating the needs for an elaborate raw data manipulation [4].

[1] M. Sawicki, W. Stefanowicz and A. Ney, Semicond. Sci. Technol. 26, 064006 (2011). [2] K. Gas and M. Sawicki, Meas. Sci. Technol. 30, 085003 (2019). [3] M. Swiatkowski *et al.*, Materials, 14, 2148 (2021). [4] M. J. Coak *et al.*, Rev. Sci. Instrum. 91, 023901 (2020).

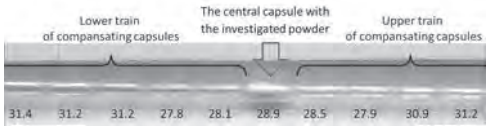

Fig 1. The scheme of the in situ compensation of the signal of the sample-carrying-capsule by two trains of nearly identical capsules (their masses in mg are indicated) placed below and above of the sample in a straw.

IOG-05. Influence of magnetic anisotropy on self-assembly and magnetic properties in binary ferrofluids. *M. Khelfallah*[1], S. Neveu[3], D. Taverna[1], V. Dupuis[3], P. Sainctavit[1,2] and A. Juhin[1] *1. Sorbonne-Université, Institut de Minéralogie, de Physique des Matériaux et de Cosmochimie, Paris, France; 2. Synchrotron SOLEIL, Gif-Sur-Yvette, France; 3. Sorbonne-Université, PHENIX, Paris, France*

Ferrofluids, colloidal solutions of magnetic nanoparticles with unique dipolar moments dispersed in water, present fascinating properties due to the magnetic dipole interactions between particles and their ability to move freely in a liquid. These interactions give rise to exotic shapes, from chain-like structures to complex structures (1). When an external magnetic field is applied, the assemblies turn into microsized chains oriented in the direction of the field (2). Variation of the nanoparticle size, shape and composition changes the magnetic anisotropy, which plays a crucial role in magnetic dipole interactions. This results in a modification of the structuring of ferrofluids as well as their collective magnetic properties like coercivity, magnetic saturation or remanence. Magnetic binary ferrofluids, i.e. those composed of two types of nanoparticles with different magnetic anisotropy, are particularly appealing because they offer an unprecedented interplay of magnetic dipole interactions. Understanding and controlling interparticle interactions could lead to improving the efficiency of known ferrofluids for applications in the biomedical industry (3) and the discovery of novel magnetic responsive materials. On binary ferrofluids mixing a hard ($CoFe_2O_4$) and a soft ($MnFe_2O_4$) magnetic material, chemically selective magnetisation curves were measured by Resonant Inelastic X-ray Scattering spectroscopy combined with X-ray Magnetic Circular Dichroism (4). We show that a soft magnetic material becomes harder under the influence of a hard magnetic material (Fig. 1). At the microscopic and nanoscale, we use Cryogenic Transmission Electron (Cryo-TEM) to image the self-assembly of the ferrofluid (Fig. 2), and Electron Holography to measure the magnetic induction inside an assembly of nanoparticles (5). Combining the information obtained from Cryo-TEM, magnetic measurements and Monte-Carlo simulations (6), our results pave the way for a better understanding of the relationship between magnetic properties and structuring of binary ferrofluids.

(1) S. Kantorovich, A. Ivanov, *Phys.Chem.Chem.Phys.,* 17, 16601, (2015) (2) M. Klokkenburg *et al. J. Phys.: Condens. Matter,* 20, 204113 (2008) (3) U. Ikoba, Q. Wang, *Nanoscale*, 7, 4291-4305 (2015) (4) N. Daffé, *Nanoscale*, 12, 11222 (2020) (5) C. Gatel, E. Snoeck, *Nano Lett.* 8, 12, 4293–4298 (2008) (6) M. Vasilakaki, K. Trohidou, *Phys. Rev. B,* 97, 094413 (2018)

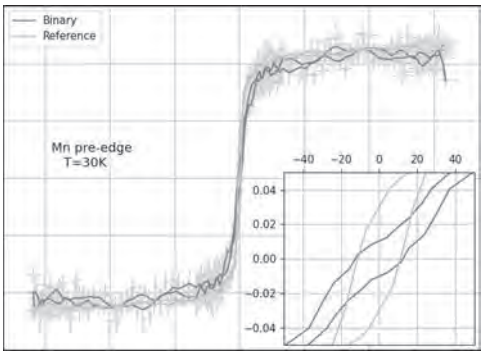

XMCD curve of a binary ferrofluid ($CoFe_2O_4$ + $MnFe_2O_4$ nanoflowers) compared to the reference ferrofluid ($MnFe_2O_4$ only).

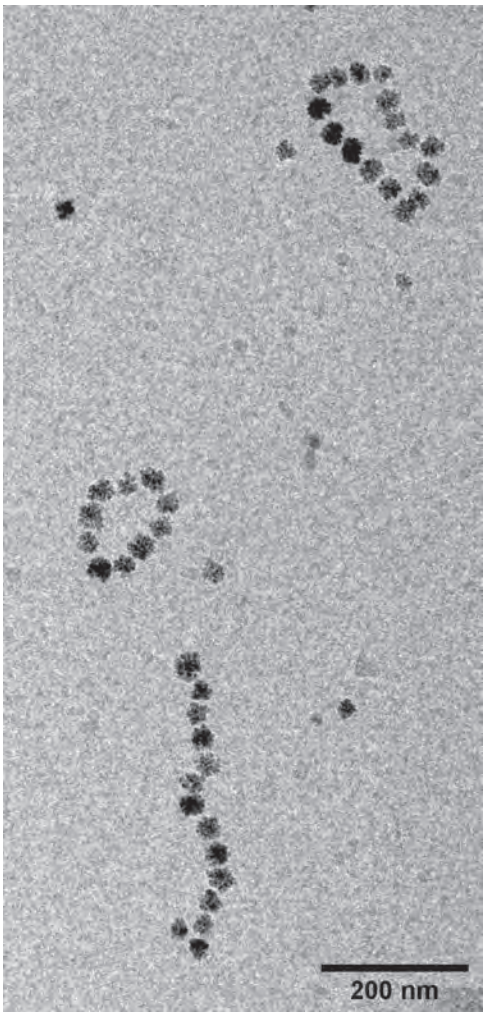

Cryo-TEM image of $CoFe_2O_4$ nanoflowers dispersed in water.

IOG-06. CT Data as A-Priori Information for Multimodal Magnetorelaxometry Imaging. *P. Schier*[1], D. Baumgarten[1,2], M. Kuhlmann[3], F. Wiekhorst[4], U. Ankerhold[3] and M. Liebl[3,4] *1. Institute of Electrical and Biomedical Engineering, UMIT - Private University for Health Sciences, Medical Informatics and Technology, Hall in Tirol, Austria; 2. Institute of Biomedical Engineering and Informatics, Technische Universität Ilmenau, Ilmenau, Germany; 3. Physikalisch-Technische Bundesanstalt (PTB), Braunschweig, Germany; 4. Physikalisch-Technische Bundesanstalt (PTB), Berlin, Germany*

Magnetorelaxometry imaging (MRXI) [1] enables a quantitative and specific localization of magnetic nanoparticles (MNPs) inside living organisms [2] which is required by several novel therapeutic approaches such as magnetic hyperthermia therapy and magnetic drug targeting. MRXI involves aligning the MNPs' magnetic moments using electromagnetic coils and subsequently recording their decaying net magnetization (relaxation). The recorded signals are connected to the MNP iron masses inside the discretized region of interest (ROI) via a system of linear equations [3]. The MNP distribution is recovered by solving the corresponding ill-posed inverse problem. However, the ROI discretization is limited to rather large voxel sizes. Finer voxel grids increase the number of unknowns and aggravate accurate reconstructions of MNP distributions. To date, finer voxel resolutions with reliable reconstruction accuracies are still necessary to obtain clinically relevant MRXI reconstructions. Standard MRXI provides only information about the MNP distributions and every voxel can contain MNPs with equal probability. Obviously, this is not realistic in clinical practice due to the different anatomical structures inside a human body. Accompanying traditional medical imaging techniques such as CT are necessary to gain anatomical information about the ROI. Here, we develop a multimodal reconstruction using CT data as prior for MRXI reconstructions, enabling a distinction between voxels with impossible, improbable and probable MNP occurrences. We test the approach on a cylindrical ROI (see Fig. 1) containing objects that produce different radiographic density (meat, wood, water, etc.) as well as MNPs. CT and MRXI measurements were conducted and the incorporation of the CT data allows us to reconstruct MNP distributions more accurately with half the voxel edge lengths than with mere MRXI (see Fig. 2). Our multimodal approach demonstrates that resolution and quantification accuracy of MRXI substantially benefits from anatomical data provided by alternative techniques such as CT or MRI.

[1] D. Baumgarten, et al., Med. Biol. Eng. Comput., Vol. 46, p.1177-1185 (2008) [2] N. Adolphi, et al., Contrast Media Mol. Imaging, Vol. 7.3, p.308-319 (2012) [3] M. Liebl, et al., Biomed Tech (Berl), Vol. 60.5, p.427-443 (2015)

Fig. 1: MRXI setup inside the CT scanner.

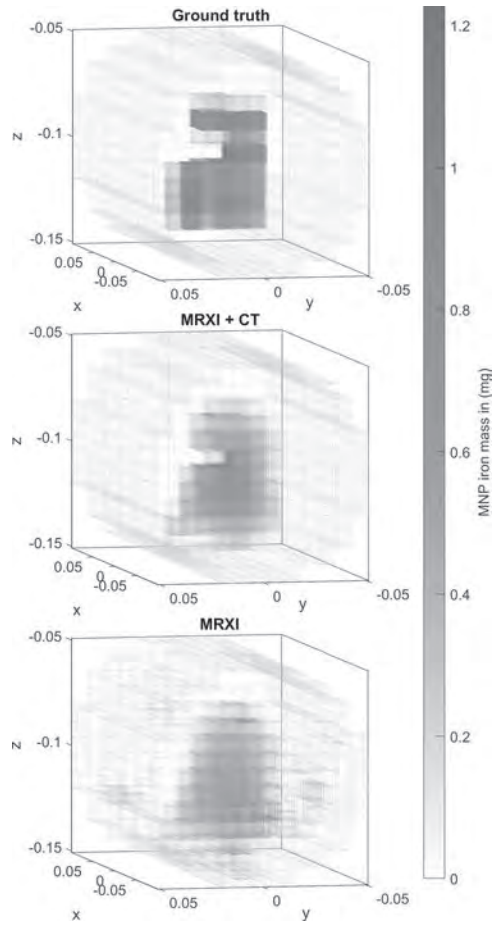

Fig. 2: Top: real MNP distribution. Center: MRXI reconstruction including CT data. Bottom: Mere MRXI reconstruction.

IOG-07. Withdrawn

IOG-08. Atomic Structure and Electron Magnetic Circular Dichroism of Individual Rock Salt Structure Antiphase Boundaries in Spinel Ferrites. *Z. Li*[1,6], J. Lu[2,7], L. Jin[3], J. Rusz[4], V. Kocevski[4,8], H. Yanagihara[5], E. Kita[5], J. Mayer[3,9], R. Dunin-Borkowski[3,9], H. Xiang[2] and X. Zhong[1,6] *1. City University of Hong Kong, Kowloon, Hong Kong; 2. Fudan University, Shanghai, China; 3. Forschungszentrum Jülich GmbH, Juelich, Germany; 4. Uppsala University, Uppsala, Sweden; 5. University of Tsukuba, Tsukuba, Japan; 6. Tsinghua University, Beijing, China; 7. Yancheng Institute of Technology, Yancheng, China; 8. Los Alamos National Laboratory, Los Alamos, NM, United States; 9. RWTH Aachen University, Aachen, Germany*

Functional oxides are ubiquitous and exhibit a wide range of electric, magnetic, optical, and structural properties. Antiphase boundaries are the interfaces between two crystallographically identical regions with shifted phases. Based on previous studies, the correlation between existence of antiphase boundary and decreased saturation magnetization in oxides has been discussed [1, 2]. Due to the resolution limitation of magnetism measurement, it is difficult to investigate the structure-property relationship at high spatial resolution. EMCD, first experimentally verified by Schattchneider et al. [3], is a magnetism measurement method in transmission electron microscope and is confirmed with the ability to reach spatial resolution better than 2 nm using convergent beam [4, 5]. This significant breakthrough enables us to study the magnetic properties of interfaces and boundaries on nanometer scale. In the meanwhile, our group have developed site-specific EMCD [6] and atomic plane resolved EMCD [7] in complex oxides such as spinel and double perovskite. Intensity analysis of antiphase boundary (APB) in HAADF (high angle annular dark-field imaging) STEM (scanning transmission electron microscopy) images suggests that only half of the octahedral interstices are occupied at the rock salt structure interlayer of a new type APB in $NiFe_2O_4$ with a relative translation of (1/4)*a*[011]. High-spatial-resolution EMCD have been used to experimentally demonstrate reductions of ~46.8%±8.2% and ~38.8%±14.5% in the EMCD strengths of Fe and Ni in APB, respectively, compared to perfectly ordered $NiFe_2O_4$ [8]. DFT calculations and dynamical diffraction calculations suggest that the reduced EMCD strengths result from the fact that Fe ions at the APB interlayer are antiferromagnetically coupled with each other, whereas Ni ions show a significant decrease in magnetic moment as a result of the formation of low-spin state Ni^{4+} (d^6) ions. Our combined approach of using element specific EMCD under high-spatial-resolution and first-principles calculations to resolve and identify the atomic structure and magnetic coupling of an individual APB in spinel ferrite is applicable to studies of a broad spectrum of other defects in magnetic materials.

[1] D. T. Margulies *et al.*, *Phys. Rev. Lett.*, vol. 79, no. 25, pp. 5162, 1997. [2] K. P. McKenna *et al.*, Nat. Commun. vol. 5, no. 5740, 2014. [3] P. Schattschneider *et al.*, *Nature*, vol. 441, pp. 486, 2006. [4] P. Schattschneider *et al.*, *Phys. Rev. B*, vol. 78, no. 104413, 2008. [5] L. Jin *et al.*, *Adv. Mater. Inter.*, vol. 3, pp. 1600414, 2016. [6] Z. Q. Wang *et al.*, *Nat. Commun.*, vol. 4, no. 1395, 2013. [7] Z. C. Wang *et al.*, *Nat. Mater.* vol. 17, pp. 221, 2018. [8] Z. Li, *et al.*, *Adv. Funct. Mater.*, vol. 31, no. 21, 2021.

IOG-09. Scanning Tunneling Microscopy and Spectroscopy (STM/S) Reveals Small Energy Gap in $CrBr_3$. *D. Baral*[1], Z. Fu[1], A. Zadorozhnyi[1], R. Dulal[1], A. Wang[1], N. Shrestha[1], U. Erugu[1], J. Tang[1], Y. Dahnovsky[1], J. Tian[1] and T. Chien[1] *1. Physics and Astronomy, University of Wyoming, Laramie, WY, United States*

Since the discovery of monolayer graphene in 2004, immense exploration of 2D materials with the main goal of minimizing electronic devices towards atomic level is in progress. The 2D materials family includes a huge range of materials- from insulators, semiconductors, metals to superconductors. In 2017, two independent groups demonstrated stable magnetic ordering in 2D materials (CrI_3 and $Cr_2Ge_2Te_6$) [1,2] bringing ferromagnetic materials into the 2D family. Since then, 2D magnetism has been discovered in various vdW materials, for example CrX_3 (X= Cl, Br, I) [3,4] among which $CrBr_3$ is the most air stable in the CrX_3 family. Magnetic and optical properties of bulk $CrBr_3$ have been studied since the 1960s. Based on the various optical measurements, it is believed that $CrBr_3$ has an energy gap in the range of 1.68 – 2.1 eV[5,6]. These controversial results have indicated that the electronic properties of $CrBr_3$ are not well explored. In this poster, I will present the STM/S result of both thin and thick $CrBr_3$ flakes with the density fluctuation theory (DFT) calculations to reveal a small energy gap to be 0.57 eV ± 0.04 eV[7]. This uncovering of the small energy gap will solve the controversy and is the key to better understand the electronic properties of $CrBr_3$.

1. Huang, B. *et al. Nature* 546, 270–273 (2017). 2. Gong, C. *et al. Nano Lett.* 546, 265–269 (2017). 3. Kim, M. *et al. Nat. Electron.* 2, 457–463 (2019). 4. Chen, W. *et al. Science.* 366, 983–987 (2019). 5. Wood, D. L. *et al. J. Chem. Phys.* 39, 890–898 (1963). 6. Dillon, J. F. *et al. J. Appl. Phys.* 34, 1240–1245 (1963). 7. Baral, D. *et al. Phys. Chem. Chem. Phys* 23, 3225 (2021).

IOG-10. Magnetic Domains in 2D van der Waals Material Fe_3GeTe_2. *M. Yang*[1,3], Q. Li[2,3] and Z.Q. Qiu[3] *1. Anhui Univeisity, Hefei, China; 2. University of Science and Technology of China, Hefei, China; 3. University of California, Berkeley, Berkeley, CA, United States*

Magnetic van der Waals (vdW) materials have emerged as promising candidates for spintronics applications, especially after the discovery of intrinsic ferromagnetism in monolayer vdW materials. Here, we report a real-space imaging study of itinerant ferromagnet Fe_3GeTe_2 and the enhancement of its Curie temperature well above ambient temperature [1]. We later found

implanting Ga into Fe_3GeTe_2 could greatly enhance the Fe_3GeTe_2 Curie temperature by almost 100% [2]. Magnetic skyrmions are topological spin textures, which usually exist in noncentrosymmetric materials where the crystal inversion symmetry breaking generates the so-called Dzyaloshinskii-Moriya interaction. Using photoemission electron microscopy and Lorentz transmission electron microscopy, we investigated and stabilized Néel-type magnetic skyrmion in vdW ferromagnetic Fe_3GeTe_2 on top of (Co/Pd)n without the need of an external magnetic field.

1. Q. Li, M. Yang, C. Gong, R. V. Chopdekar, A. T. N'Diaye, J. Turner, G. Chen, A. Scholl, P. Shafer, E. Arenholz, A. K. Schmid, S. Wang, K. Liu, N. Gao, A. S. Admasu, S.-W. Cheong, C. Hwang, J. Li, F. Wang, X. Zhang, and Z. Q. Qiu, Nano Lett. 18, 5974 (2018). 2. M. Yang, Q. Li, R. V. Chopdekar, C. Stan, S. Cabrini, J. W. Choi, S. Wang, T. Wang, N. Gao, A. Scholl, N. Tamura, C. Hwang, F. Wang, and Z. Q. Qiu, Adv. Quantum Technol. 3, 2000017 (2020). 3. M. Yang, Q. Li, R. V. Chopdekar, R. Dhall, J. Turner, J. D. Carlström, C. Ophus, C. Klewe, P. Shafer, A. T. N'Diaye, J. W. Choi, G. Chen, Y. Z. Wu, C. Hwang, F. Wang, Z. Q. Qiu, Sci. Adv. 6, eabb5157 (2020).

IOG-11. Characterization of Hybrid Domain Wall Structure and Surface Chirality for Amorphous Fe/Gd Thin Films. *R. Moraski*[1], S. Montoya[2], E. Fullerton[2], W. Parker[1] and B. McMorran[1] *1. Physics, University of Oregon, Eugene, OR, United States; 2. Center for Memory and Recording Research, University of California San Diego, San Diego, CA, United States*

We report on the imaging domain wall structure of amorphous Fe/Gd multilayer thin films with dendritic stripe domains. Micromagnetic calculations suggest in both stripe and skyrmion phases the domain walls have a hybrid structure where the center of the domain wall is Bloch-like with random helicity transitioning to Néel-like walls at the surfaces with fixed helicity. To experimentally probe the domain structure we combine transmission electron microscopy in Lorentz mode (L-TEM) and scanning electron microscopy with polarization analysis (SEMPA). L-TEM images are processed to show the magnetic induction through the bulk of the sample, while SEMPA images show magnetization at the top surface of the sample. In this way, 3-dimensional reconstructions of the surface magnetization can be realized[1]. The SEMPA instrument, based on an Auger microscope, leverages spin-polarized secondary electrons scattered from the top few nanometers of a sample[2]. These secondaries are accelerated through the column and Mott scattered from a gold target in order to reveal the left-right and up-down polarization for both in-plane and out-of-plane electrons. We observe and characterize the the chirality of Néel-like domains closure caps at the surface of Fe/Gd following the convention established by Chen et al.3]. The z-components of magnetization for several domains are shown in Fig. 1. A comparison of the average magnetization vectors in the plane of the sample is shown in Fig. 2, where the difference in L-TEM and SEMPA observations indicate an out-of-plane, twisting component. We have thus confirmed Bloch wall formation in the bulk topped with Néel caps at the surface.

[1] J. Unguris, Experimental Methods in the Physical Sciences, Volume 36, pp. 167-193 (2001) [2] K. Koike and K. Hayakawa, Jpn. J. Appl. Phys. 23 L187 (1984) [3] G.Chen, T. Ma, A. N'Diaye et al. Nat Commun 4, 2671 (2013)

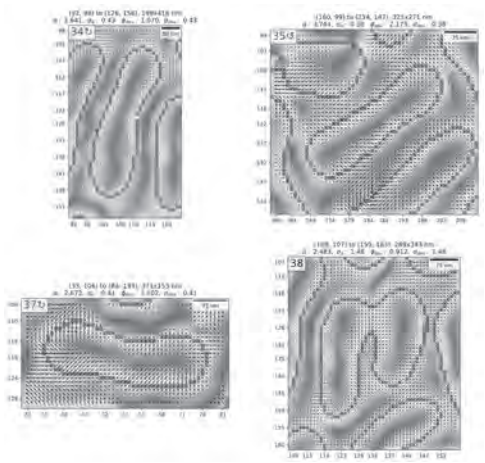

Fig. 1: Hybrid domains in amorphous Fe/Gd with arrows showing reconstructed in-plane and colors showing in- (blue) and out-of-plane (red) magnetization.

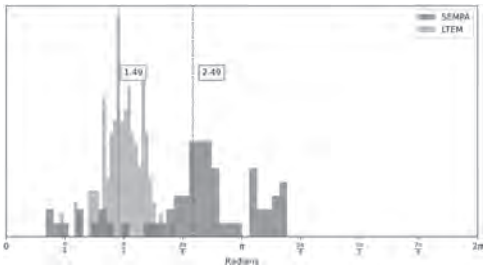

Fig. 2: Angle of in-plane magnetization relative to increasing out-of-plane magnetization (α) showing expected π/2 radians average from L-TEM, indicating Bloch walls, and larger deviations averaging 3π/4 radians from SEMPA, indicating Néel caps.

IOG-12. Curvature-mediated spin textures in magnetic multilayered nanotubes. E. Josten[1], D.W. Raftrey[2,3], A. Hierro-Rodriguez[4], L. Aballe[5], M. Lipinska-Chwalek[6], T. Jansen[6], K. Hoeflich[7], H. Kroencke[7], C. Dubordieu[7,8], D. Buergler[6], J. Mayer[6,9] and *P. Fischer*[2,3] *1. U Zaragoza, Zaragoza, Spain; 2. LBNL, Berkeley, CA, United States; 3. UC Santa Cruz, Santa Cruz, CA, United States; 4. U Oviedo, Oviedo, Spain; 5. ALBA Synchrotron Light Facility, Cerdanyola del Vallès, Spain; 6. FZ Juelich, Juelich, Germany; 7. Helmholtz-Zentrum Berlin für Materialien und Energie, Berlin, Germany; 8. FU Berlin, Berlin, Germany; 9. RWTH Aachen, Aachen, Germany*

The scientific and technological exploration of artificially designed three-dimensional magnetic nanostructures opens the path to exciting novel physical phenomena, originating from the increased complexity in spin textures, topology, and frustration in three dimensions [1,2]. Theory predicts that the equilibrium magnetic ground state of two-dimensional systems which reflects the competition between symmetric (Heisenberg) and antisymmetric (Dzyaloshinskii-Moriya interaction (DMI)) exchange interaction is significantly modified on curved surfaces when the radius of local curvature becomes comparable to fundamental magnetic length scales [3]. Here, we present an experimental study of the spin texture in an 8 nm thin magnetic multilayer with growth-induced in-plane anisotropy and DMI deposited onto the curved surface of a 1.8 μm long non-magnetic carbon nanowire with a 67 nm radius [4]. Using magnetic soft x-ray tomography the three-dmensional spin configuration in this nanotube was retrieved with about 30nm spatial resolution [5,6]. The transition between two vortex configurations on the two ends of the nanotube with opposite circulation occurs through a domain wall that is aligned at an inclined angle relative to the wire axis. Three-dimensional micromagnetic simulations support the experimental observations and represent a visualization of the curvature-mediated

DMI. They also allow a quantitative estimate of the DMI value for the magnetic multilayered nanotube. This work was funded by the U.S. Department of Energy, Office of Science, Office of Basic Energy Sciences, Materials Sciences and Engineering Division under Contract No. DE-AC02-05-CH11231 (Non-equilibrium magnetic materials program MSMAG). This research includes experiments that were performed at MISTRAL beamline at ALBA Synchrotron in collaboration with ALBA staff. AH-R. acknowledges the support from European Union's Horizon 2020 research and innovation program under Marie Sklodowska-Curie grant ref. H2020-MSCA-IF-2016-746958 and from the Spanish AEI under project ref: PID2019–104604RB/AEI/10.13039/501100011033.

[1] A. Fernández-Pacheco, R. Streubel, O. Fruchart, R. Hertel, P. Fischer and R. P. Cowburn, Nature Communications 8, 15756 (2017). [2] R. Streubel, E. Tsymbal, P. Fischer, JAP 129 210902 (2021) [3] D. D. Sheka, O. V. Pylypovskyi, P. Landeros, Y. Gaididei, A. Kákay and D. Makarov, Communications Physics 3 (1), 128 (2020) [4] E. Josten, D. Raftrey, A. Hierro-Rodriguez, A. Sorrentino, L. Aballe, M. Lipinska-Chwalek, T. Jansen, K. Höflich, H. Kröncke, C. Dubourdieu, D. E. Bürgler, J. Mayer, P. Fischer, arXiv:2103.13310v1 [5] R. Streubel, F. Kronast, P. Fischer, D. Parkinson, O.G. Schmidt, D. Makarov, Nature Communication 6 7612 (2015) [6] A. Sorrentino, J. Nicolas, R. Valcarcel, F. J. Chichon, M. Rosanes, J. Avila, A. Tkachuk, J. Irwin, S. Ferrer and E. Pereiro, Journal of Synchrotron Radiation 22 (4), 1112-1117 (2015)

IOG-13. Domain Walls in Magnetic Nanotubes: An Experimental Evidence. *M. Jaber*[2], D. Tiwari[2], J. Hurst[2], M. Schöbitz[2], M. Scheuerlein[1], W. Ensinger[1], D. Gusakova[2], A. Masseboeuf[2] and O. Fruchart[2]
1. Technische Universität Darmstadt, Darmstadt, Germany; 2. SPINTEC, Univ. Grenoble Alpes, CNRS, CEA, Grenoble, France

Ferromagnetic 1D systems are associated with the future paradigm of high-density and low consumption memories. The emergence of curvilinear magnetism [1] came up with the possibility of dealing with 3D geometry such as nanotubes merging on a single structure, the micromagnetism of domain wall and the multi-layered stack needed for spintronic. Unexpected, but technologically ideal, azimuthal curling of magnetization was initially observed in electroless CoNi nanotubes [2] that we attributed to curvature-induced magneto-elastic anisotropy. Here we will present the first experimental evidence of domain wall inner structure in ferromagnetic nanotubes using Electron Holography. Merging various means of characterization ranging from anisotropic magnetoresistance measurement to high-resolution imaging with chemical and magnetic sensitivity including micromagnetic modelling we pave the route for the utilization of such conduits in spintronic devices. Magneto-transport measurements were performed at varying temperatures, applied field magnitude and direction and showed a material resistivity of 2×10^{-6} Ω.m, one order of magnitude higher than in the bulk at 300K, and we extracted an anisotropy field from R(H) loops of the order of K_{eff} = 7.5 kJ.m^{-3}. This has been related to the nanocrystalline nature of the tubes and under the consideration with the non-curvilinear system for magnetostriction considerations. Electron Holography enabled us to locally map and quantify the magnetic flux during magnetic reversal associated with domain wall motion. With the help of micromagnetic modelling, we are able to conclude on the nature and width of domain walls in such tubes as well as analyzing its dynamic in a pseudo-static regime. The ongoing experiments are of fundamental importance to infer the capacities of such a system to experimentally confirm high domain wall velocities and spin-wave propagation that such a system can provide to a technological solution of racetrack memory [3].

[1] Fernández-Pacheco, A. et al., Nature Communications 8,15756 (2017) [2] Michal Stano et al., SciPost Physics 5, 38 (2018) [3] Hertel, R., Condensed Matter 28, 483002 (2016) [4] *http://feellgood.neel.cnrs.fr*

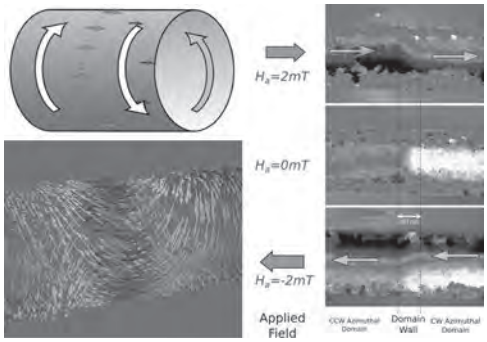

Left: Sketch and micromagnetic model of a Néel wall in azimuthal configuration of a nanotube using our home-built Fellgood [4] code. Right: Phase images at different applied magnetic fields Ha of a domain wall separating by two opposite azimuthal domains.

Session IOH
MAGNETIC BIODETECTION AND THERAPY I

Yuko Ichiyanagi, Co-Chair
Yokohama National University, Yokohama, Japan
César de Julián Fernández, Co-Chair
Istituto dei Materiali per l'Elettronica ed il Magnetismo Consiglio Nazionale delle Ricerche, Parma, Italy
Javier Alonso, Co-Chair
Universidad de Cantabria, Santander, Spain

INVITED PAPER

IOH-01. Bioapplications of magnetic nanowires: barcodes, heaters, biocomposites. *B. Stadler[1] 1. Electrical and Computer Engineering, University of Minnesota, Minneapolis, MN, United States*

Magnetic nanowires can be engineered using composition and shape, and by modulating both of these along their axes (10nm-100um) or their diameters (10-200nm). This talk will discuss applications of both single nanowires and arrays of vertically aligned nanowires in biomedical fields, such as nano-barcodes [1], and biolabels for cells and exosomes [2,3], nano-heaters for hyperthermia therapy and organ preservation [4], and biocomposites [5]. For most of these applications, the reversal mechanism of magnetization can play a critical role. For example, magnetic coercivity and remanence has been used for contact-free readout of nano-barcode signatures, and the motion of domain walls can limit heating. Magnetic reversal typically occurs by uniform precession and coherent rotation or by domain walls that are transverse or vortices. Here, a novel approach to decoding specific reversal signatures will be described via a fast modification of the first order reversal curve (FORC) technique, called the projection method. In addition to decoding, the method elucidates the mechanisms of reversal which is of interest to the fundamental understanding of nanomagnets and can lead to improved future devices, such as decoding using ferromagnetic resonance (FMR) [6]. By understanding the nanomagnetics, these nanowires have been used individually to isolate biospecies, such as cancer cells [2] and tumor-derived exosomes (TEXs) [3] for fundamental studies in medicine. As nanoscale objects, nanowires have also been suspended in cryopreservation agents to provide the rapid, uniform nanowarming needed to restore preserved tissues and organs [4]. The mechanical properties are also found to change in response to magnetic fields which can impact their applications [7]. Finally, by aligning nanowires vertically in bio-friendly polymers, applications such as internal band-aids can be coded or functionalized for personalized health care. This talk will focus on the measurement methods for each of the biomedical applications mentioned, and will relate these measurements back to the fundamental magnetization engineering of the cylindrical nanowires.

[1] MRZ Kouhpanji, BJH Stadler, *Nanoscale Advances* 584 (2020). [2] Sharma, Orlowski, Zhu, Shore, Kim, DiVito, Hubel, Stadler, *Nanotechnology* 135102 (2015). [3] Nemati, Kouhpanji, et al. *Nanomaterials* 1662 (2020). [4] Shore, Ghemes, Dragos, Gao, Shao, Um, Sharma, Tabakovic, Bischof, Stadler, *Nanoscale* 14607 (2019). [5] Kouhpanji, Stadler *ACS Applied Nano Materials* 13286 (2020). [6] Zhou, Um, Zhang, Nelson, Nemati, Modiano, Stadler, Franklin, *IEEE J Electromag, RF, Microwaves in Medicine and Biology* 134 (2019) [7] PR Downey, AB Flatau, PD McGary, BJH Stadler, *Journal of Applied Physics* 103 (7), 07D305 (2008).

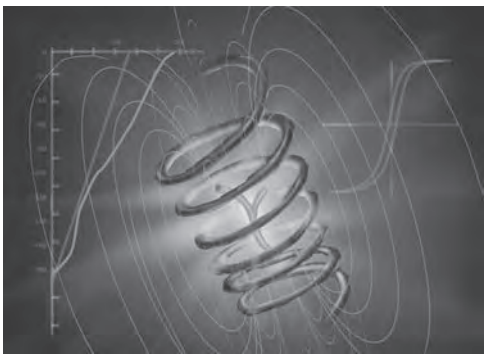

By controlling the reversal behavior of magnetic nanowires, efficient nanowarming can be achieved. One future application is the uniform and rapid warming of cryopreserved tissues and organs, which will ethically extend the viability between donors and recipients.

CONTRIBUTED PAPERS

IOH-02. Optimized Magnetic Drug Delivery with Limited Particle Spreading. *R. Van Durme[1]*, G. Crevecoeur[1,2], L. Dupré[1] and A. Coene[1,2] *1. Electromechanical, Systems & Metal Engineering, Ghent University, Ghent, Belgium; 2. EEDT Decision & Control, Flanders Make, Lommel, Belgium*

In magnetic drug targeting, magnetic micro- or nanoparticles with attached therapeutics are injected into the human body and brought towards diseased regions with magnetic field gradients [1]. The particles in the vascular network undergo blood drag, diffusion, and particle interaction forces which need to be accounted for when guided or steered. In many situations, magnetic forces are overcome by the blood drag force, which may carry particles away from the target with the bloodstream, or are too small to make particles cross bodily membranes into tissue [2]. Moreover, diffusion mechanisms and the direction of the surrounding magnetic forces can cause particles to scatter instead of remaining together. These phenomena inhibit effective targeting. We provide a solution with an optimization algorithm that maximizes as a function of electromagnet currents the particle velocity in a certain direction. The contribution of the magnetic force along a predefined direction is increased compared to other forces, benefiting particle movement. As an additional constraint, a boundary on the magnetic force divergence is set to limit particle spreading. This implies that particles move as a group rather than away from each other (Fig. 1). We also considered a problem in which particles are to be moved from an initial to a final location in a finite time interval with minimized energy dissipation in the coils [3]. For this we used dynamic optimization and added the constraint on the magnetic force divergence. No currently existing targeting strategies have implemented such a directed force maximization or dynamic optimization while taking into account the magnetic force divergence. Simulations of particles in a bifurcated vessel with parabolic flow profile

showed that the magnetic force maximization can increase particle velocities by 20% and move them towards the targeted vessel branch. On the other hand, the dynamic optimization demonstrated that, collections of particles travel uniformly towards a target region with 10 times lower scattering than without divergence constraint, and 10 times more particles at the target.

[1] A. Lübbe, C. Alexiou, and C. Bergemann, Journal of Surgical Research., Vol. 95.2, pp. 200–206 (2001) [2] A. Nacev, C. Beni, O. Bruno, and B. Shapiro, Journal of magnetism and magnetic materials., Vol. 323.6, pp. 651–668 (2011) [3] R. Van Durme, G. Crevecoeur, L. Dupré, and A. Coene, Drug Delivery., Vol. 28.1, pp. 63–76 (2021)

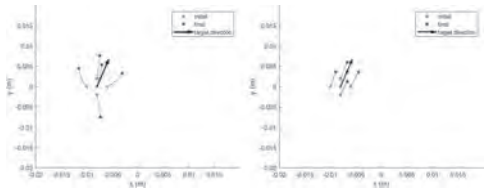

Fig. 1: Particle movement after magnetic force maximization, without and with divergence constraint.

IOH-03. Harmonic Phases of the Nanoparticle Magnetization: an Intrinsic Temperature Probe. *E. Garayo*[2], J. Collantes[1], J. Garcia[3], F. Plazaola[1] and O. Sandre[4] *1. Electricidad y Electronica, UPV/EHU, Leioa, Spain; 2. Ciencias, UPNA, Pamplona/Iruña, Spain; 3. Física Aplicada II, UPV/EHU, Leioa, Spain; 4. Laboratoire de Chimie des Polymères Organiques, Université de Bordeaux, Bordeaux, France*

Magnetic fluid hyperthermia is a promising cancer therapy in which magnetic nanoparticles (MNPs) act as heat sources activated by an external AC magnetic field. The MNPs, located near or inside the tumor, absorb energy from the magnetic field and then heat up the cancerous tissues [1]. However, during a hyperthermia treatment, it is crucial to control the temperature of different tissues: the desired therapeutic effect is not achieved with too low temperature. On the contrary, an excessive temperature increment can produce undesired damage [2]. Nevertheless, the current conventional thermometry in magnetic hyperthermia presents some important technical problems. For example, the widely used optical fiber thermometers only provide the temperature in a discrete. Moreover, surgery is required to locate these probes in the correct place. In this scope, we propose here a non-invasive method to measure the temperature of a MNP sample. The approach is based on the thermal dependence of the high order harmonic phases of the MNP dynamic magnetization. The method is non-invasive and it does not need any additional probe or sensor attached to the MNPs. In addition, this method has the potential to be used to map the spatial distribution of the temperature [3]. In the present work, a previously tested lab-made AC magnetometer [4] was used to study the variation with temperature of high order harmonics (3^{rd}, 5^{th} and 7^{th}) from iron oxide MNPs. These MNP samples are identical to those used in a previous work [5]. External AC magnetic fields typical from magnetic hyperthermia were chosen (40-550 kHz). The actual temperature of the sample (30-50 °C) was measured by optical fiber thermometry. I was observed that the high order harmonic phases vary with temperature in an almost linear manner (see figure 1a). Therefore, we propose here the measurement of the harmonic phases as a non-invasive method to obtain the sample temperature. In this scope, the temperature would be obtained via previous calibration of the harmonic phase with temperature. In order to prove this concept an *in-vitro* experiment has carried out with water dispersed iron oxide MNPs. As it can be observed in figure 2, there is an error less than 0,5 °C.

[1] S. Dutz and R. Hergt, *Int. J. Hyperth.*, vol. 29, no. 8, pp. 790–800 (2013) [2] S. Dutz and R. Hergt, *Nanotechnology*, vol. 25, no. 45, p. 452001 (2014) [3] J. Zhong, M. Schilling, and F. Ludwig, *Nanomaterials*, vol. 8, no. 11, p. 866 (2018) [4] E. Garaio, J. M. Collantes, F. Plazaola, J. A. Garcia, and I. Castellanos-Rubio, *Meas. Sci. Technol.*, vol. 25, no. 11 (2014) [5] E. Garaio *et al.*, *J. Magn. Magn. Mater.*, vol. 368, pp. 432–437 (2014).

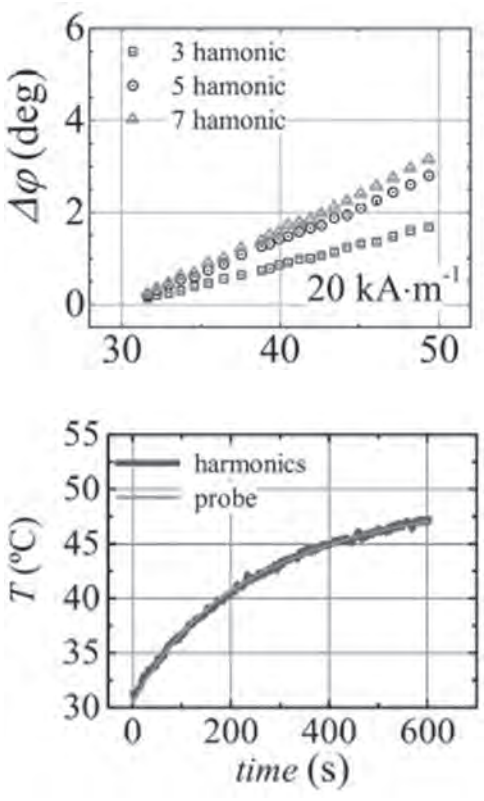

IOH-04. In Silico Safety Analysis of Magnetic Hyperthermia Treatments of Implant-Bearing Patients. *I. Rubia-Rodriguez*[1], L. Zilberti[2], A. Arduino[2], O. Bottauscio[2], M. Chiampi[2] and D. Ortega[3,4] *1. IMDEA Nanoscience, Madrid, Spain; 2. Istituto Nazionale di Ricerca Metrologica (INRiM), Turin, Italy; 3. Condensed Matter Physics, Universidad de Cadiz, Puerto Real, Spain; 4. Institute of Research and Innovation in Biomedical Sciences of the Province of Cádiz (INiBICA), Cádiz, Spain*

Magnetic hyperthermia (MH) is a nanotechnology-driven therapy that seizes the heat release of magnetic nanoparticles when exposed to an alternating magnetic field. It has already been and is currently trialed in clinical settings as adjuvant of chemotherapy and radiotherapy to successfully treat several types of tumors [1, 2]. In silico testing (computer simulations) allows us to mimic several clinical situations and to evaluate the treatment safety in terms of dosimetry and temperature rise, including possible hot spots due to eddy currents, in a cheap and fast way. MH has taken advantages of this virtual testing in its way towards personalized therapy. The versatility of the simulations to evaluate many clinical setups allows us to study the actual risks of the current exclusion criteria [1, 3]. Nowadays, bearing any kind of metallic object, orthopedic implants for example, constitutes a contraindication for the treatment. This is based on the knowledge obtained from MRI related studies, but there is an important lack in the literature about the quantification of these risks in the context of clinical MH. In this work, we use computer simulations to study the actual risks of potential MH patients carrying different orthopedic prosthesis, as well as the influence of the presence of this metallic object in the effective magnetic field reaching the nanoparticles site. We have considered different treatment setups varying tumor locations, implant types and materials to evaluate the temperature increase and the dosimetric values in the major tissue groups. These safety parameters have been included in a multi-criteria decision analysis to asses a risk index for each tissue group in every clinical situation analyzed [4]. Acknowledgements We acknowledge COST Action MyWave (CA 17115), NoCanTher project (grant agreement No 685795), Regional Government of Madrid under contract PEJD-2017-PRE/IND-3663, Spanish

Ministry of Economy and Competitiveness through the grants MAT2017-85617-R, Ramón y Cajal RYC2018-025253-I, the "Severo Ochoa" Program for Centers of Excellence in R&D (SEV-2016-0686) and the support of NVIDIA Corporation through the GPU Grant Program with the donation of the Quadro P6000 GPU used in this work.

[1] M. Johannsen et al. Int. J. Hyperthermia, Vol. 21, p. 637 (2005); M. Johannsen et al. Int. J. Hyperthermia, Vol. 23, p. 315 (2007); D. Ortega, Q. A. Pankhurst. in Nanoscience: Vol. 1: Nanostructures through Chemistry, p. 60 (2013). [2] www.nocanther-project.eu [3] Maier-Hauff et al. J. Neurooncol., Vol. 103, p.317 (2011) [4] I. Rubia-Rodríguez et al. Int. J. Hyperthermia, Vol. 38, p. 846 (2021)

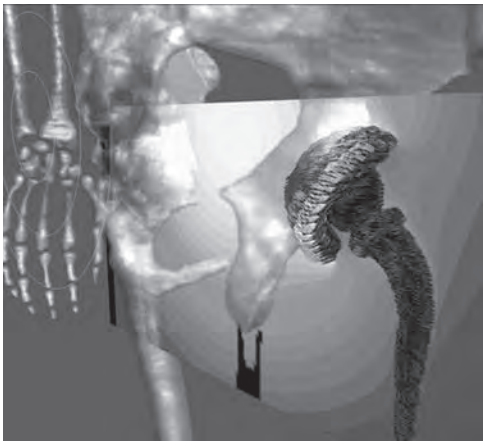

IOH-05. Homogenization of Heating in Magnetic Hyperthermia Through Exploitation of Magnetisation Dynamics of Interacting Particles. J. Leliaert[1], *J. Ortega-Julia*[2] and D. Ortega[3,4] *1. Department of Solid State Sciences, Ghent University, Ghent, Belgium; 2. IMDEA Nanoscience, Madrid, Spain; 3. Condensed Matter Physics, University of Cadiz, Cadiz, Spain; 4. Institute of Research and Innovation in Biomedical Sciences of the Province of Cádiz (INiBICA), University of Cadiz, Cadiz, Spain*

Achieving homogeneous tumour heating is one of the most long-standing challenges in magnetic hyperthermia for cancer therapy. Clinical studies must meet strict safety regulations that require knowledge and control over the physical properties of the chosen magnetic nanoparticles [1]. Whereas it is well-established that the heat released by magnetic nanostructures is influenced by interparticle interactions, as of today there is no method to analyze heat exchange at single-particle level in interacting systems at nonzero temperature. This gap needs to be bridged so to harness nanoparticle magnetization dynamics for the sake of biomedical applications. Building on previous theoretical work [2], we present an equation to estimate the heat dissipation of individual, interacting particles at nonzero temperature that perform both field-induced and thermal switching. After validating this equation, we use the macrospin simulation tool Vinamax [3], to investigate a system of interacting particles with different anisotropies, as we showed in this contribution [4]. Our preliminary results indicate (see figure) that the generated heat becomes more homogeneously distributed at larger fields. We believe that this homogenization of the particle heating will help to achieve a more homogenized heating of tumors during hyperthermia treatments. The use of the proposed equation would simplify the selection process of optimum nanoparticle distributions leading to optimal tumour heating. Its simplicity and flexibility also allow it to be integrated into multi-scale, multi-physics simulations to accurately assess the magnetic hyperthermia therapy without impacting the overall computational time.

1. www.nocanther-project.eu 2. C. Muñoz Menendez, D. Serantes, O. Chubykalo-Fesenko, S. Ruta, O. Hovorka, P. Nieves, K. L. Livesey, D. Baldomir and R. Chantrell, Phys. Rev. B, 2020, 102, 214412. 3. J. Leliaert, A. Vansteenkiste, A. Coene, L. Dupré and B. Van Waeyenberge, Med. Biol. Eng. Comput., 2015, 53, 309–317. 4. J. Leliaert, J. Ortega-Julia, and D. Ortega, Nanoscale, 2021.

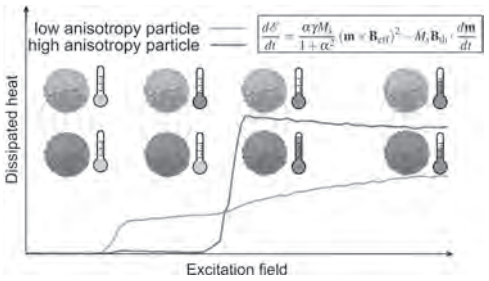

Figure: Heat generated in a system consisting of two interacting nanoparticles with different anisotropies. Both particles show switching behavior as soon as the excitation field amplitude overcomes their anisotropy barrier. The heat generation tends to become more uniform with increasing excitation fields.

IOH-06. Vortex nano-discs: from micromagnetic simulations to cancer cells internalization for magneto-mechanically induced damage applications. *R.P. Magalhães*[1], S. Caspani[1], D. Navas[2], C. Redondo[3], R. Morales[3], S. Lima[4], S. Reis[4], C. Nunes[4], J.P. Araujo[1] and C. Sousa[1] *1. IFIMUP and DFA Faculdade de Ciencias da Universidade do Porto, Porto, Portugal; 2. Instituto de Ciencia de Materiales de Madrid, ICMM-CSIC, Madrid, Spain; 3. Dpto. de Química-Física, Universidad del País Vasco UPV/EHU, Bilbao, Spain; 4. LAQV, REQUIMTE, Faculty of Pharmacy of Porto University, Porto, Portugal*

Novel magnetic nanostructures (MNS) present a unique spin arrangement in the magnetic ground state, namely spin-vortex or synthetic antiferromagnetic state. MNS showed promising results in cell separation, as a contrast enhancing agents in MRI and in magneto-mechanically induced cell annihilation. The main advantages of magneto-mechanically induced cell annihilation are the usage of weaker magnetic fields with lower frequencies, as well as the need for a lower concentration of particles [1,2]. In this work, we developed one subset of biocompatible magnetic nanostructures that exhibit a spin-vortex state. First, micromagnetic simulations, using mumax3 of sub-micron iron discs, were performed for different interdot distance and aspect-ratio (thickness/diameter). By analysing the nucleation and annihilation fields, as well as the magnetic susceptibility, it was found that the (ideal) discs could be considered as isolated for interdot distances greater than twice the radius of the disc (2R) [3]. We also found that discs with an aspect ratio between 5 and 15 should sustain the vortex state in remanence [4]. Iron nano-discs in a vortex state, with a diameter of about 500 nm, were fabricated by electron beam evaporation on a Si substrate pre-patterned by interference lithography. Then, the magnetic vortex nano-discs were released from the substrate by chemical etching of a sacrificial layer. Subsequently, cell viability and uptake assays were performed in a human leukaemia monocyte cell line (THP-1) [5]. Several concentrations of nano-discs were studied by flow cytometry. As a result, the discs were internalized by the cells and found to be innocuous to them, in the absence of an external magnetic field.

[1] L. Peixoto,…C.T. Sousa, Magnetic nanostructures for emerging biomedical applications. Appl. Phys. Rev., 7 (2020) 011310. [2] S. Caspani, R. Magalhães, J. P. Araújo, and C. T. Sousa, Magnetic Nanomaterials as Contrast Agents for MRI. Materials 2020, 13(11), 2586 [3] L. Peixoto, J.P. Araujo and C.T. Sousa. EPJ Web of Conferences 233 (2020) 05002. [4] M. P. Proenca, J. Rial, J. P. Araujo and C. T. Sousa. Magnetic reversal modes in cylindrical nanostructures: from disks to wires. Scientific Reports 11 (2021) 10100. [5] S. Moraes, A. Marinho, S. Lima, A. Granja, J.P. Araújo, S. Reis, C.T. Sousa, C. Nunes, Targeted nanostructured lipid carriers for doxorubicin oral delivery. International Journal of Pharmaceutics 592 (2020) 120029. https://doi.org/10.1016/j.ijpharm.2020.120029

INVITED PAPER

IOH-07. Magnetic Techniques for Rapid Diagnostic Testing for Health Care and Environmental Monitoring. *M. Rivas*[1], M. Salvador[1,2], J. Martinez-Garcia[1], J. Marqués[1], A. Bunge[3], R. Turcu[3], D. Peddis[2,4], M. García[5] and M.D. Cima[5] *1. Physics, University of Oviedo, Gijón, Spain; 2. Istituto di Struttura della Materia, Rome, Italy; 3. National Institute for Research and Development of Isotopic and Molecular Technologies, Cluj-Napoca, Romania; 4. Università degli Studi di Genova, Genova, Italy; 5. Escuela Superior de Ingeniería y Tecnología, Universidad Internacional de la Rioja, Logroño, Spain*

Early detection of disease biomarkers, toxins, and infectious microorganisms is a major goal in modern health care, environmental control, and food safety to help contain and reverse illness or prevent contaminants from entering the food chain. To achieve this, materials scientists develop biosensing platforms whose requirements may differ depending on the application. When biosensing is a tool for screening or point-of-use applications (e.g., at the patient's bedside, in the industrial plant, or harsh environments), it must be fast, low-cost, and easy to use and transport. Lateral flow immunoassays (LFI) meet these requirements. They are paper-based tests, whose best-known example is the home pregnancy test, developed to detect high levels of human chorionic gonadotropin in urine. Thanks to advances in immunology, the method has been extended with great success to a large variety of targets, the most recent the rapid diagnostic tests for SARS-CoV2 [1]. There are some limitations for LFIA expansion, mainly their sensitivity and detection limit, which are not sufficient for some applications. Magnetic nanoparticles and magnetic detectors can be an excellent way to overcome such constraints. LFI (Fig. 1) uses a strip of nitrocellulose along which a liquid sample (urine, saliva, blood, serum, or plasma) can flow by capillary action. The target molecule is selectively captured on the strip by an immunological reaction and tagged by a reporter particle or enzyme that makes it detectable. For this purpose, plasmonic or fluorescent nanoparticles, visible with the naked eye, provide the positive/negative response. Although this is good enough for pregnancy, diagnoses frequently demand quantifying biomarkers, cells, bacteria, viruses, genes, or toxins. Quantification of color reporters involves image analysis, reflectance, or fluorescence measurements. However, these methods are sensitive to ambient light, humidity, and staining of the paper strip, which cause difficulties in calibration and reproducibility, especially in samples with a complex matrix [2]. To improve upon this, ferrite magnetic nanoparticles are now being used as alternative LFI reporters [3]. Although their bio-functionalization can be more challenging than for plasmonic particles, their advantages are clear for many applications. First, iron oxide nanoparticles provide a brownish color that is detectable by the naked eye or on a smartphone camera image. Magnetism can be used for pre-concentration or isolation of the target analyte from the sample matrix, and the magnetic reporters can be relocated closer to the visible membrane surface to increase their visibility. Second, magnetic nanoparticles produce a magnetic perturbation that a magnetic sensor can detect without optical interference [2]. Additionally, magnetic sensors report particles not only from the paper's surface but from the entire cross-section of the strip [4]. Finally, the magnetic signal from the nanotags does not decrease significantly with time. We review the principles and design of magnetic LFI and detail the requirements for magnetic nanoparticles to be used as reporters. We address the current methods used to read their signals that do not sacrifice the simplicity and low cost of the paper-based method. As proof of how magnetic LFI can be a useful analytical tool for biomedicine and food safety applications, we give examples of pneumonia biomarker detection (Fig. 2) and toxin quantification in foods and beverages [2], [4]. We acknowledge support from the Spanish Ministry of Science and Innovation (EIN2020-112354), the Principality of Asturias (IDI/2018/000185), and the Instituto Universitario de Tecnología Industrial de Asturias (SV-20-GIJÓN-1-22).

[1] C. Parolo, C., et al. Nat Protoc 15(12), 3788, 2020 [2] A. Moyano, et al., Anal. Bioanal. Chem. 411 (25), 6615, 2019. [3] A. Moyano, et al., Diagnostics 10(5), 288, 2020 [4] A. Moyano et al., Sensors 21, 3756, 2021.

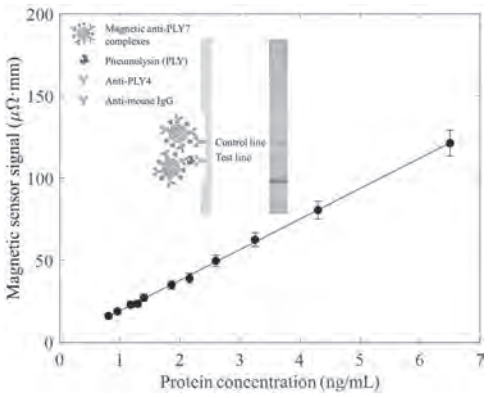

Magnetic sensor reading out of a lateral flow strip for pneumolysin detection. The calibration yields a limit of detection of 0.2 ng of protein per mL of sample. Inset: Scheme (left) and image (right) of a magnetic lateral flow immunoassay.

CONTRIBUTED PAPERS

IOH-08. Imaging of a superparamagnetic iron oxide nanoparticle distribution by a single-sided magnetic particle imaging scanner. *C. McDonough*[1,2], D. Newey[2] and A. Tonyushkin[1,2] *1. Physics, Oakland University, Rochester, MI, United States; 2. Physics, UMass Boston, Boston, MA, United States*

Magnetic Particle Imaging (MPI) is an emerging biomedical imaging modality designed to image distributions of superparamagnetic iron oxide nanoparticles (SPIONs) with high sensitivity[1]. In MPI, the continuous excitation of the SPION is provided by a sinusoidal magnetic field with rf frequencies. The spatial encoding of the signal is produced by selective saturating the SPION with a superimposed magnetic field gradient. Scanning the field-free region across the imaging volume senses the local concentration of SPION that allows a tomographic reconstruction of the tracer distribution inside the volume. SPIONs may serve as tumor markers[2], which would allow the MPI device to be used for in vivo screening of cancer once translated to clinic. Several MPI devices have been developed but to date no translation to human has been done. Our single-sided field-free line (FFL) design, with the hardware to one side of the imaging volume, potentially enables nonrestrictive imaging in larger subjects, promoting utilities such as screening for cancer[3]. In our device, a selection field gradient is generated by a pair of co-planar elongated coils and an excitation magnetic field is generated by a single elongated drive coil[4]. The spatial encoding is provided by dynamical shifting the position of the FFL from altering the relative current between the two selection coils. Pertinent to this unilateral geometry the magnetic field profiles generated by the coils are inhomogeneous thus presenting a challenge to imaging. By implementing an algorithm of selection field compensation by applying a bias current to the drive coil we demonstrate that imaging can be performed. Here, we show the results from imaging simulations by means of specifically tailored filtered backprojection image reconstruction technique. In addition, we present first experimental results from 1D imaging of SPION phantoms (Fig.1) using ony moderate encoding field gradients thus providing proof of concept of our scanner.

[1] B. Gleich and J. Weizenecker, "Tomographic imaging using the nonlinear response of magnetic particles," *Nature*, vol. 435, no. 7046, pp. 1214–1217, (2005). [2] H. Arami, *et al.*, "Tomographic magnetic particle imaging of cancer targeted nanoparticles," *Nanosc.*, vol. 9, no. 47, pp. 18723–18730 (2017). [3] J. Pagan, C. McDonough, T. Vo and A. Tonyushkin, "Single-Sided Magnetic Particle Imaging Device with Field-Free-Line Geometry for *In-Vivo* Imaging Applications," *IEEE Trans. Magnetics,* 57(2): 5300105 (2021). [4] A. Tonyushkin, "Single-Sided Field-Free Line Generator Magnet for Multidimensional Magnetic Particle Imaging", *IEEE Trans. Magnetics,* 53(9):5300506 (2017)

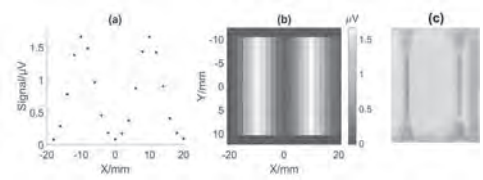

Fig. 1: (a) Projection signal of SPION phantom (gradient of 0.42 T/m); (b) reconstructed image of a phantom using a single projection and knowledge of the phantom's shape; (c) phantom of undiluted Synomag-D SPION (20 mm separation with 1.2 mm diameter).

IOH-09. Magnetometry with diamond nitrogen-vacancy center by using an optical fiber array for two-dimensional imaging.

A. Kuwahata[1,2], Y. Murata[1], H. Tanaka[1], K. Arai[3], R. Katsumi[4], T. Iwasaki[3], M. Hatano[3], R. Igarashi[5], T. Ohshima[5], F. Jelezko[6], M. Kusakabe[2,7], S. Yabukami[1], T. Yatsui[4] and M. Sekino[2] *1. Tohoku University, Sendai, Japan; 2. The University of Tokyo, Tokyo, Japan; 3. Tokyo Institute of Technology, Tokyo, Japan; 4. Toyohashi University of Technology, Toyohashi, Japan; 5. National Institutes for Quantum and Radiological Science and Technology, Chiba, Japan; 6. Ulm University, Ulm, Germany; 7. Matrix Cell Research Institute Inc., Ibaraki, Japan*

Diamond nitrogen-vacancy (NV) centers have been employed in biomedical applications, such as the detection of magnetic nanoparticles by using a magnetometer [1] and magnetocardiography by using a two-dimensional (2D) scanning measurement system with millimeter-scale resolution [2]. To identify the distributions of magnetic nanoparticles in biomedical tissues, in this study, we propose magnetometry with diamond NV center by utilizing an optical fiber array for 2D imaging. Figure 1 shows the fabrication of a fiber array on the surface of a diamond. Nine optical fibers are arranged 3 × 3 on a plane (Fig. 1(a)). The center fiber delivers the excitation light of a green laser and the other eight fibers collect the red fluorescence from the diamond NV. A fiber diameter is 0.25 μm and core diameter is 0.20 μm, and a pitch between each fiber is 0.15 μm, representing the spatial resolution of the sub-millimeter scale (Fig. 1(b)). A head of a fiber array is connected to the surface of the diamond and the other side of the fiber array, FC/PC connectors, emit the red fluorescence generated by the diamond NV (Fig. 1(c)). Figure 2 shows the two-dimensional spatial distribution of red fluorescence variation measured by photodiodes under the application of strong DC magnetic fields. We observed 10-15% of red fluorescence variation for each channel. This result indicates the spatial distribution of the magnetic field on the 2D plane. In conclusion, we have developed the prototype of the fiber array-based magnetometry with diamond NV for 2D measurements of the magnetic fields and observed the red fluorescence variations attributed to the magnetic field variations in the 2D system. Further work is under way to obtain the 2D imaging of the magnetic nanoparticles in biomedical tissues, e.g., the integration of a larger number of fiber arrays (7 × 7) with better spatial resolution. We will pursue this issue in our future research.

[1] A. Kuwahata *et al.*, *Scientific Reports* (2020). [2] K. Arai *et al.*, arXiv:2105.11676. Acknowledgements This work was supported by Tateisi Science and Technology Foundation and MEXT Q-LEAP with the Grant Number JPMXS0118067395.

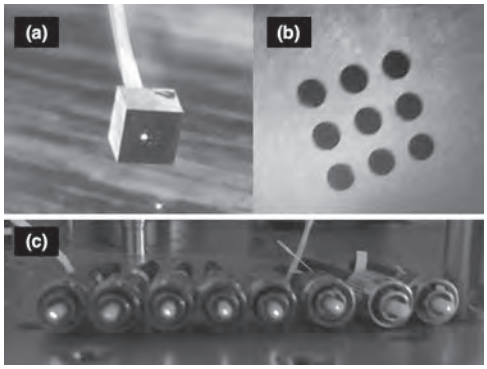

Fabricated fiber array (3 × 3) for diamond NV magnetometry. (a) A head of a fiber array connects a bulk diamond, (b) an enlarged image of a fiber array, and (c) a collection of red fluorescence from diamond NV centers.

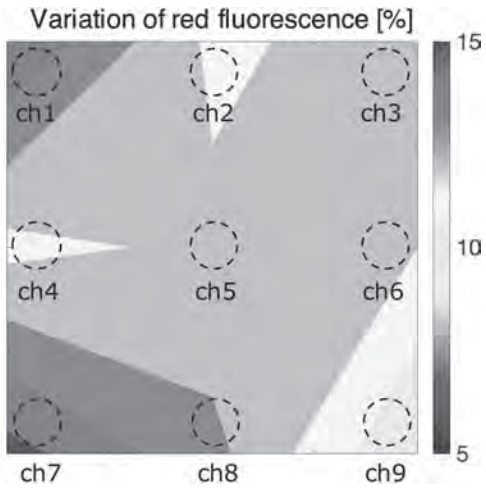

Measured 2D imaging of red fluorescence under strong DC magnetic fields.

IOH-10. Measurement of Sub-Zero Temperatures in Magnetic Resonance Imaging: Applications for MRI-Guided Cryosurgery.

J. Hankiewicz[1], R. Camley[1] and *Z. Celinski*[1] *1. UCCS BioFrontiers Center, University of Colorado at Colorado Springs, Colorado Springs, CO, United States*

Cryoablation surgery guided by magnetic resonance imaging (MRI) is a minimally invasive technology used to treat a wide variety of cancers. During the cryoablation procedure, near real-time temperature information is necessary to monitor changes in tissue temperatures to ensure killing the tumor and leaving the adjacent healthy tissue undamaged. We developed a method that could be used during MRI-guided cryoablation operations. Using both nuclear magnetic resonance spectroscopy and MRI we showed that the nuclear relaxation times of protons have a monotonic dependence on temperature in certain biocompatible polymers. We measured a temperature-dependent brightness of MR images in the temperature range of -55 ^{o}C to +30 ^{o}C. Figure 1 shows example of such measurements in form of temperature map of the phantom. Such images suggest a thermal resolution is better than 3 ^{o}C in 3 mm. To increase signal to noise ratio in our measurements, we studied both experimentally and theoretically the influence of MRI scan parameters on image brightness. We are also doping these silicones with ferrite superparamagnetic nanoparticles to modify their relaxation times in order to speed up acquisition. *Ex-vivo* experiments reveal that silicon rods inserted into tissue can be used to measure its temperature (see Figure 2). We envision that such filaments could provide sufficient information as to allow the creation of 3D temperature maps during MRI-guided surgeries.

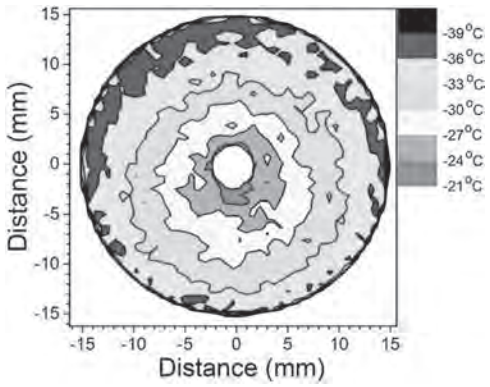

Figure 1. A false color MRI of a phantom with a temperature gradient between the center and outer edge.

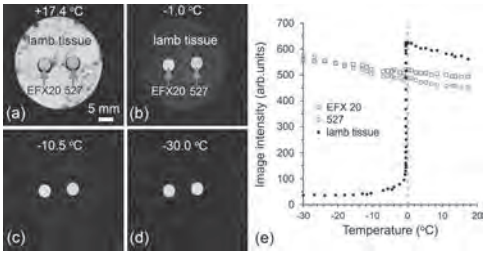

Figure 2. Temperature-dependent MRI results for lamb tissue (ex-vivo) with inserted 4 mm silicone rods. (a-d) show example MR images at different temperatures. (e) shows image intensity as a function of temperature measured in the lamb tissue, and silicones.

IOH-11. Development of Magnetic Particle Imaging (MPI) Scanner for Phantom Image of Tracer Agents. *M. Irfan*[1], N. Dogan[3], O. Mercan Dogan[3] and A. Bingolbali[2] *1. Electronics Engineering, Gebze Technical University, Gebze, Turkey; 2. Bioengineering, Yildiz Technical University, Besiktas, Turkey; 3. Physics, Gebze technical University, Gebze, Turkey*

Magnetic particle imaging (MPI) is an emerging medical imaging technique that utilizes the non-linear magnetization behavior of the superparamagnetic iron oxide nanoparticles (SPIONs) as a tracer agent [1]. Fast image acquisition (low scanning time) rate and high spatial resolution are distinguished properties of MPI. It has no side effects (ionized radiations) as compared to other imaging modalities such as computed tomography (CT) [2]. In this study, an MPI scanner was constructed at 9.3 kHz for the localization of the magnetic nanoparticles and measurement of the spatial resolution as presented in Fig. 1. A selection field of 4.2 T/m for spatial encoding was achieved with two pairs of NdFeB permanent magnets. A three-layer drive coil with a length of 130 mm was designed to achieve a 15 mT (peak) homogeneous magnetic field to excite SPIONs. A receive coil with gradiometric winding was designed to pick up the response of the tracer agents at minimum direct feedthrough. Perimag (Micromod GmbH, Germany) and Vivotrax Plus (Magnetic insight, USA) commercially available tracer agents for MPI applications were utilized for phantom imaging. Nonlinear response of the tracer material was recorded with a data acquisition card (DAQ) and post-processing of the data was performed with x-space (time-based) reconstruction technique. X-space technique relies on the linear and shift-invariant (LSI) property of the received signals [3]. The spatial resolution of 5 mm for Perimag and 6.5 mm for Vivotrax Plus was obtained. The signal strength of the Perimag sample was 4 times higher than the Vivotrax Plus sample as shown in Fig. 2. The tracer material-dependent quantitative aspect (linear) of the MPI has immense application in the early-stage detection of cancer. MPI relaxomter [4] and scanner are key tools to develop and diagnose novel tracer agents [5] for MPI applications.

[1] B. Gleich and J. Weizenecker, "Tomographic imaging using the nonlinear response of magnetic particles," Nature, vol. 435, no. 7046, pp. 1214–1217, Jun. 2005. [2] N. Panagiotopoulos, et al. "Magnetic particle imaging: current developments and future directions." International journal of nanomedicine vol. 10, pp. 3097-114, Apr. 2015. [3] k. Lu, P.W. Goodwill, E.U. Saritas, B. Zheng, and S.M. Conolly, "Linearity and Shift Invariance for Quantitative Magnetic Particle Imaging" IEEE transactions on medical imaging: 32:9, Sep. 2013. [4] M. Irfan, N. Dogan, T. Sapmaz, and A. Bingolbali, "Development of MPI Relaxometer for characterization of Superparamagnetic nanoparticles", J. Magn. Magn. Mater., Article 168082, 2021. [5] M. Irfan, N. Dogan, A. Bingolbali, and F. Aliew, "Synthesis and characterization of $NiFe_2O_4$ magnetic nanoparticles with different coating materials for magnetic particle imaging (MPI)", Journal of Magnetism and Magnetic Materials, Volume 537, Article 168150, 2021.

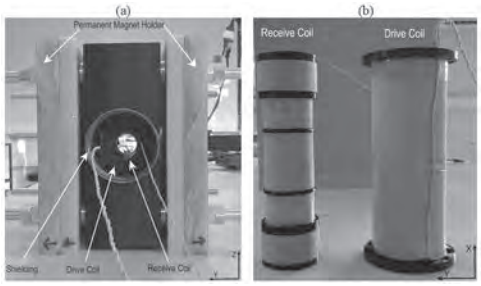

Magnetic particle imaging scanner: (a) Selection field magnets along the y-axis are fixed with epoxy glasses, (b) Drive coil and receive coil along the x-axis used for excitation and signal reception, respectively.

MPI signal intensity and spatial distribution of the commercial MPI tracers: (a) Perimag, (b) Vivotrax Plus.

IOH-12. TMS-like Magnetic Fields Modulate Metabolic Activity of Hepatic and Colorectal Cancer Cells. *A. Guller*[1,2], B. Heng[1] and S. Ahn[1] *1. Macquarie University, Sydney, NSW, Australia; 2. The Institute for Regenerative medicine, Sechenov University, Moscow, Russian Federation*

Transcranial magnetic stimulation (TMS)[1,2] is clinically used in patients with depression[2,3], while the effects of TMS-like magnetic fields on extracranial tissues are almost unknown[4]. Here, we explored effects of TMS-like repetitive magnetic stimulation (RMS) on metabolic activity of human hepatocellular carcinoma (HCC) and colorectal cancer (CRC) cells. The HuH7 (HCC) and HCT116 (CRC) cell cultures were treated using a TMS device "Magstim Rapid2" with an AFC70 coil. Intermittent RMS (iRMS) modes (4 trains of 150 pulses with frequency f=1, 5, 10, 20 or 40 Hz and equal intertrain intervals) and burst RMS (600 pulses delivered in trains, f=40 Hz/bursts, f=3 Hz). The coil power output /magnetic field strength was (100% or 50%, B=0.8 T or 0.4 T, respectively) in burst modes or 100% in iRMS. The activity of SDG, an enzyme essential for energy production, was measured by MTT colorimetric assay in 24 h post-RMS. The control groups included: (1) untreated cells, (2) 20 min room temperature control, and (3) strong metabolic suppression by 100% DMSO solution. The main results are shown in Figures 1 and 2. Dashed red lines are CI95% for mean absorbance in the untreated control group; Abs is MTT assay product absorbance, a.u. In HuH7 cells, the tested protocols of RMS either did not change or stimulated the metabolic activity. However, correlation analysis indicated that the modes with higher frequency, burst pattern, and shorter cycles are more probable as suppressors of the liver cancer cells' metabolism. In HCT116 cells, an iRMS mode 1B100 (f=1 Hz) induced a statistically significant decrease of meta-

bolic activity, while high-frequency iRMS and burst modes stimulated it. In CRC, correlation analysis revealed the opposite to HCC trend of reduction of the metabolic rate at lower frequencies, intermittent PRMS, and the increase of it at high frequencies and burst modes. Our pioneering findings demonstrate the tumour-specific and mode-specific effects of re-purposed TMS technology on hepatic and colorectal cancer cells. The potential of RMS as adjuvant anti-cancer treatment will be discussed. We thank Medilink Australia for providing the "Magstim".

Barker AT, et al.: Neurosurgery 1987, 20:100-9. Rossini PM, et al. U: Clinical neurophysiology 2015, 126:1071-107. Post A, Keck ME: Journal of Psychiatric Research 2001, 35:193-215. Guller A, Clement S, Sowman P, Goldys E: Conference presentation // Intermag-2021.

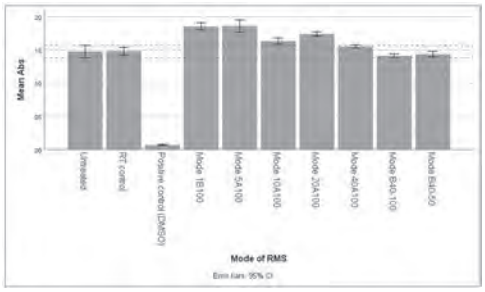

Figure 1. Effect of RMS on HuH7 cells.

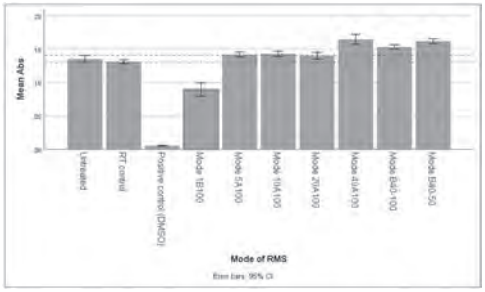

Figure 2. Effect of RMS on HCT116 cells.

IOH-13. Oriented Control of the Stimulation Target During Transcranial Magnetic Stimulation Using Space-varying E-field Vector Modulation with Multi-Core Figure-of-Flower Coil. *I.C. Carmona*[1] and R.L. Hadimani[1,2] *1. Mechanical and Nuclear Engineering, Virginia Commonwealth University, Richmond, VA, United States; 2. Biomedical Engineering, Virginia Commonwealth University, Richmond, VA, United States*

Early in 2021, we presented the *quintuple AISI 1010 steel core coil* (*QCC*) [1], a novel device for transcranial magnetic stimulation (TMS) able to produce focal stimulation in areas as small as 1 mm^2. With it, we introduced the *oriented control of the electric field (E-field) based on the path of the highest current density*. This technique induces groups of peripheral and central charges of the same sign, whose electric repulsion restricts the central charges to propagate vertically below the central coil. As a result, an *oriented central path of the highest current density* is obtained, which focally passes through the target at a certain cortical depth, increasing the *E*-field on it. Now, modifying the elliptical cross-section of the QCC, we created a new figure-of-flower coil (FFC), in which the central coil (*gynoecium*) and peripheral coils (*petals*) are formed by round-cross-section multilayer solenoids with independent AISI 1010 cores. This configuration allowed us to induce controlled gradients in the current densities based on the independent modulation of every coil. This dynamically changes the orientation of the *directional vector* of the *central path of the highest current density and* -therefore- of the *E*-field. The technique, named *Space-varying E-field Vector Modulation (SEVM)*, simultaneously varies amplitude, frequency, and/or phase of the coil currents, in combinations that produce a final direction, translatable to stimulation coordinates. Using ANSYS Maxwell software, we performed finite element simulations of the FFC, varying the number of petals between 4 and 10 (Fig.1). Each coil is made of 50 turns, wire diameter = 1 mm, and AISI 1010 steel cores of similar diameter and saturation at 2 *T*. Coil currents of 5kA at 2.5kHz were used in simulations over a 4-layer homogeneous spherical rat head model of D = 30 mm, with similar electromagnetic properties to those used to investigate TMS in rats [1-2]. The results show dynamic variations in size and position of the stimulated area (Fig.2) (including rotating patterns) with a fixed FFC, eliminating the need for multiple coils for multiple TMS targets. SEVM, QCC, and FCC are efforts towards the next generation of TMS devices with improved controllability.

[1] I. C. Carmona, D. Kumbhare, M. S. Baron, and R. L. Hadimani, "Quintuple AISI 1010 carbon steel core coil for highly focused transcranial magnetic stimulation in small animals," AIP Adv., vol. 11, no. 2, p. 025210, Feb. 2021. [2] P. Rastogi, R. L. Hadimani, and D. C. Jiles, "Investigation of Coil Designs for Transcranial Magnetic Stimulation on Mice," IEEE Trans. Magn., vol. 52, no. 7, Jul. 2016 (and references therein).

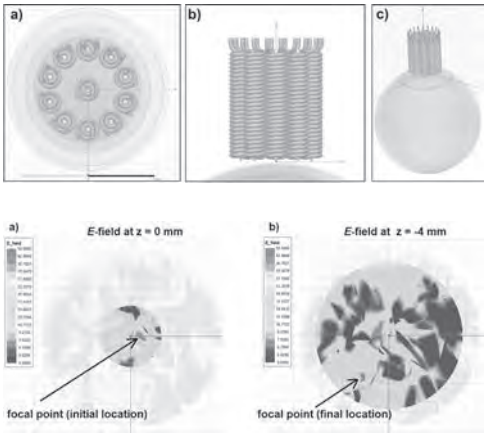

IOH-14. Effect of Neuroanatomy on Motor Evoked Potentials after Intermittent Theta Burst Stimulation. *N. Mittal*[1], B. Thakkar[3], C.B. Hodges[2], Y. Cho[1], C.J. Lewis[1], A. Andrade[4], B. Nevadomski[1], K. Li[1], R.L. Hadimani[1] and C. Peterson[1] *1. College of Engineering, Virginia Commonwealth University, Richmond, VA, United States; 2. Physical Medicine and Rehabilitation, Virginia Commonwealth University, Richmond, VA, United States; 3. Physical Therapy, Virginia Commonwealth University, Richmond, VA, United States; 4. College of Humanities and Sciences, Virginia Commonwealth University, Richmond, VA, United States*

Introduction: Transcranial magnetic stimulation (TMS) can be affected by anatomical features. Therefore, neuroanatomy could influence corticomotor excitability after intermittent theta burst stimulation (iTBS). The relationship between iTBS aftereffects and neuroanatomy was investigated via motor evoked potentials (MEPs) and finite element analysis modeling (FEM) of TMS of MRI-derived head models. Targets were the biceps brachii and first dorsal interosseus (FDI) due to their relevance in activities of daily living. Experimental Details: Ten nonimpaired individuals participated, completing sham-controlled iTBS sessions (one each targeting the biceps and FDI cortical hotspots). MEPs were acquired at an intensity of 120% of resting motor threshold (RMT) while iTBS was delivered at 80% of active motor threshold, both via 70 mm figure-of-eight coils targeting the primary motor cortex. MEPs were recorded with surface electromyography. Each participant underwent an MRI of the head, and models were generated from T1 & T2 weighted images. Fiber tract geometry was extracted from diffusion tensor images for the biceps and FDI corticospinal tracts. Neuroanatomical

parameters established were fiber tract surface area (FTSA), tract fiber count (TFC), and brain scalp distance (BSD) at the point of stimulation. Cortical electric field strength (EFS) was obtained by FEM of TMS of the head models. A linear mixed effects model was used to assess effects of these parameters and RMT on MEPs recorded after iTBS. RMT was included as a metric of the muscle's measured responsiveness to TMS. Results: iTBS targeting the biceps was faciliatory ($p = 0.013$), and dependent on FTSA ($p < 0.001$) and TFC ($p < 0.001$). There was no effect of iTBS on the FDI ($p = 0.223$) but individual changes in corticomotor excitability due to stimulation type scaled with RMT ($p < 0.001$), EFS ($p = 0.001$), BSD ($p = 0.004$), and FTSA ($p = 0.011$). Conclusion: There were unique relationships between neuroanatomical parameters and empirical iTBS response. MRI-based measures of target-specific neuroanatomy impact how the motor system responds to iTBS, making MRI-based modeling potentially useful in selection of motor targets when designing iTBS protocols.

Session IOI
MAGNETIC FLUIDS, ANTIBACTERIAL APPLICATIONS, AND OTHER EMERGING TOPICS

Manh-Huong Phan, Co-Chair
University of South Florida, Tampa, FL, United States
Jungjin Park, Co-Chair
University of Maryland at College Park, College park, MD, United States

CONTRIBUTED PAPERS

IOI-01. Encapsulations of Magnetorheological Fluids using 3D Printed Elastomeric Rectangular Cellular Structures. *J. Park*[1], Y. Choi[1], A. Flatau[1] and N. Wereley[1] *1. University of Maryland, College park, MD, United States*

Magnetorheological fluid (MRF) is a magnetic particle reinforced fluidic material, which is mechanical properties, such as stiffness and damping, can be controlled with the application of a magnetic field.[1] Smart sensor and actuator can be fabricated for adaptive vibration control systems where mechanical properties can be controlled by the application of a magnetic field. Manufacturability of MR fluid systems using the additive manufacturing (AM) process has gained great attention to enable the geometrical design of the MR fluid in an elastic component.[2] In this research, MR fluid was prepared by carbonyl irons which are 6 – 10 μm in diameter with silicon oil (40% volume fraction). Thermoplastic polyurethane (TPU) with shore hardness 60A was used as an elastomeric system. A 3D printer is used to produce cylindrical TPU elastomer with grid structure using 50 % infill (Figure 1a). The MR fluid was added into the TPU elastomer, followed by adding a sealing layer with 3D printing. An external magnetic field (0 and 7 kG) was applied along the sample longitudinal axis at the time of uniaxial dynamic testing with 10% pre-strain. The TPU-MRF samples were characterized via force-displacement tests conducted at 1 Hz under strain amplitudes of 2%. The MR effect on the dynamic stiffness is defined as the ratio of the dynamic stiffness under the maximum magnetic field to the dynamic stiffness in the absence of a magnetic field. Mechanical testing results with the magnetic fields show that the MR effect on the dynamic stiffness is 1.65. (Figure 2a). The area of the force-displacement curve at 7 kG is about 6.5 times larger than the result with 0 kG, indicating a significantly large change in damping property. Frequency was varied from 1 to 10 Hz and the force-displacement curve didn't show significant changes, indicating that the performance of the TPU-MRF system doesn't diminish with increased frequency. (Figure 2b)

1. Ashtiani M, Hashemabadi SH, Ghaffari A. A review on the magnetorheological fluid preparation and stabilization. *Journal of Magnetism and Magnetic Materials*. Jan 2015; 374:716-730. 2. Bastola AK, Paudel M, Li L, Li WH. Recent progress of magnetorheological elastomers: a review. *Smart Materials and Structures*. Dec 2020;29(12)123002

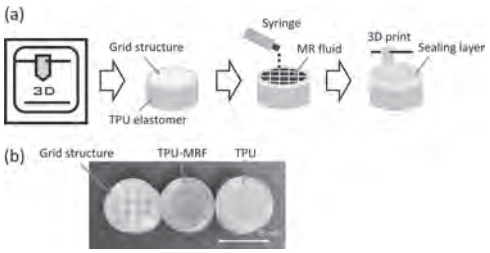

Figure 1 (a) Schematic diagram of a TPU-MRF sample fabrication (b) Image of TPU grid structure, TPU sample with and without MR fluid.

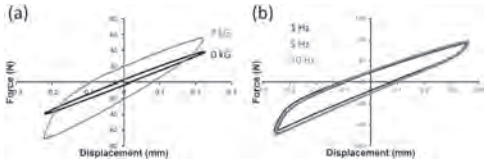

Figure 2 (a) Force-displacement curve of TPU-MRF with 0 and 7 kG. (2% strain) (b) Force-displacement curves of TPU-MRF with a different frequency of vibration at 7 kG. (3% strain)

IOI-02. Fe-C magnetic nanocomposites for removal of emerging pollutants. *L. Cervera-Gabalda*[1] and C. Gomez-Polo[1] *1. Departmento de Ciencias-INAMAT2, Universidad Pública de Navarra, Pamplona, Spain*

Environmental pollution related to the release of phenolic compounds in water resources has become a topic of public concern [1]. Among the conventional water treatment processes, adsorption methods have shown advantages as simplicity, low-cost and high efficiency. Particularly, magnetic carbon based nanocomposites are proposed as highly efficient adsorbers, where the high adsorption capacity of carbon is coupled with the recyclability optimization by the action of a magnetic field. In this work the adsorption of an emergent contaminant as phenol is analyzed employing Fe-C magnetic nanocomposites. The nanocomposites were obtained by the thermal decomposition of fructose, initally mixed with an aqueous solution of $FeCl_3$ (8 wt. %Fe); heated at 180°C and annealed (800°C; 1 hour, Ar atmosphere) [2]. X-ray diffraction, Transmission Microscopy (TEM) and adsorption-desorption curves of nitrogen (BET) show a mesoporous nanostructure, composed by the coexistence of α-Fe and Fe_3C nanoparticles surrounded by a carbon matrix (around 20 and 80% in weight, respectively). The adsorption of phenol was analyzed employing 50 mg of Fe-C, mechanically mixed and stirred in an aqueous solution of 1 mL of phenol (500 mg/L) in 24 mL of H_2O. Phenol concentration of aliquots were analyzed as a function of the mixing time through a UV-Vis spectrometer. A pseudo-second-order-rate model was employed to properly fit the adsorption kinetics, obtaining a phenol adsorption close to 80 % of the initial concentration after 20 min of contact time. The recyclability of the Fe-C adsorbents were checked. Similar adsorption kinetics are found after 3 recycling cycles, slightly decreasing the maximum adsorbed phenol as the Fe-C nanocomposites are reused. Finally, the desorption process was analyzed under an alternating (*ac*) magnetic field (305 kHz, 490 G). The local temperature increase associated to the *ac* magnetization of the Fe-based nanoparticle promotes a more efficient desorption process even in comparison with the equivalent desorption isotherm (at 40ºC) obtained using a conventional muffle.

[1] H. H. Carline de Lima et al. J. Hazard. Mater. 416 (2021) 126167. [2] L. Cervera et al. J. Alloys Compd. 863 (2021)158065.

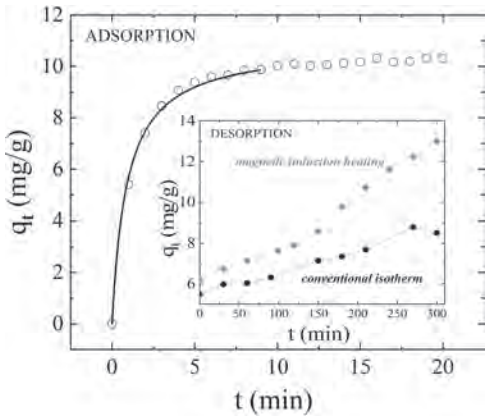

Adsoprtion kinetics of phenol on Fe-C nanocomposites. Inset: phenol desorption under *ac* magnetic field (red) and conventional isotherm (40°C).

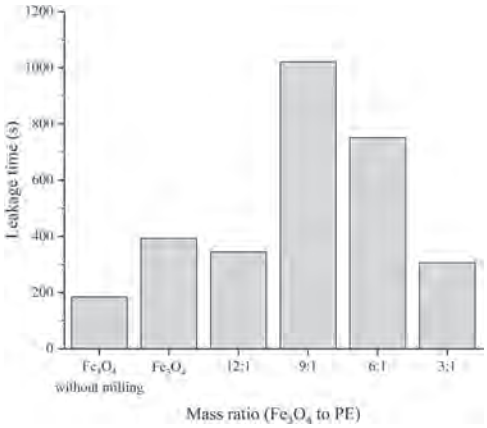

Fig.1 Leakage times from 20 to 10 kPa at different mass ratios of Fe_3O_4 to PE.

IOI-03. Effect of Lubricant Coatings of Magnetic Nanoparticles on the Leakage Rate of Magnetic Powder Sealing. *Z. Li*[1] and D. Li[1] *1. State Key Laboratory of Tribology, Tsinghua University, Beijing, China*

Ferrofluids are a fluid that can be magnetized in a magnetic field. They consist of magnetic nanoparticles, surfactants and a carrier fluid. Sealing with ferrofluid has been a research focus, because of its unique performance compared to traditional sealing methods, including zero leakage, low friction resistance, a simple structure and a long lifetime [1, 2]. However, the magnetic and rheological properties of ferrofluid limit its applications in specific sealing conditions, such as a high pressure difference or extreme temperatures [3]. In previous studies, a novel sealing method using nano- and micro-sized magnetic powders has been raised [4]. It has a higher pressure resistance and can work under a wide range of temperatures [5], but the leakage rate is found to be a critical problem for its engineering application, and particle agglomeration is a major reason. In this research, to control the leakage rate of magnetic powder sealing, Fe_3O_4 magnetic nanoparticles are coated with lubricating materials by high-energy ball milling technique to change the interparticle forces. Magnetic powders with different lubricant coatings and different mass ratios were prepared, such as PEG, MoS_2 and PE. A test bench was set up and sealing experiments with each material were conducted. The leakage rates were compared by the time when the pressure dropped from 20 kPa to 10 kPa. Experimental results showed that lubricant coatings could lower the leakage rate of magnetic powder sealing, but it differed with different materials. Meanwhile, the lowest leakage rate existed with an optimized mass ratio of magnetic particles to lubricating materials. For example, Fe_3O_4 coated with PE showed a decreased leakage rate compared to pure Fe_3O_4 nanoparticles, and the lowest leakage rate occurred at a mass ratio of 9:1. This research provides a simple and effective method to control the leakage rate of magnetic powder sealing, indicating a broad application prospect.

[1] M. Szczech, *Proceedings of the Institution of Mechanical Engineers, Part J: Journal of Engineering Tribology,* Vol. 234, p.274-281 (2020) [2] L. Vékás, D. Bica and M. V. Avdeev, *China Particuology,* Vol. 5, p.43-49 (2007) [3] Y. Chen, D. Li, Y. Zhang, Z. Li and H. Zhou, *IEEE T. Magn.,* Vol. 56, p.1-10 (2020) [4] Z. Li and D. Li, IEEE International Magnetics Conference (2021) [5] V. Yemets, M. Masliany and O. Kostritsyn, *Magnetohydrodynamics,* Vol. 43, p.355-361 (2007)

IOI-04. Self-Assembled Superparamagnetic Structures for Cell Cluster Arrays. *Y. Chen*[1,2], K. Zhou[1], Z. Huang[3], X. Liu[2] and Z. Wei[1] *1. Zhengzhou University, Zhengzhou, China; 2. Shinshu University, Wakasato, Japan; 3. Division of Cardiology, Baltimore, MD, United States*

The fabrication of cell cluster arrays is vital for cancer diagnosis and treatment, which can capture, arrange and aggregate cells quickly into target position [1]. In this talk, we will present a facile and novel method to fabricate cell cluster arrays through size-adjustable self-assembled hexagonal superparamagnetic cone structures. When a strong out-of-plane magnetic field was applied to the ferrofluid on a glass substrate, it will induce the magnetic poles on the upper/lower surfaces of the continuous ferrofluid to increase the magnetostatic energy. The ferrofluid will then experience hydrodynamic instability and be split into small droplets with cone structures because of the compromising surface tension energy and magnetostatic energy to minimize the system's total energy. Furthermore, the ferrofluid cones were orderly self-assembled into hexagonal arrays to reach the lowest energy state. After dehydration of these liquid cones to form solid cones, polydimethylsiloxane was cast to fix the arrangement of hexagonal superparamagnetic cone structures and prevent the leakage of magnetic nanoparticles. The U-343 human neuronal glioblastoma cells were labeled with magnetic nanoparticles through endocytosis in co-culture with a ferrofluid. These magnetically labeled cells were attracted and captured by hexagonal superparamagnetic cone structures to form cell cluster arrays. As a function of the solid cone size, the number of cells captured by each hexagonal superparamagnetic cone structure was increased from 48 to 126 under a 2000 G out-of-plane magnetic field (see fig. 1). The local magnetic field gradient caused by the hexagonal superparamagnetic cones can capture and arrange cells, and restrict the cell growth and migration. The cell cluster array has potential applications in the field of cancer treatment.

[1] Yinling, Chen. et al., ACS Appl. Mater. Interfaces., Vol. 13, p.10667-10673 (2021)

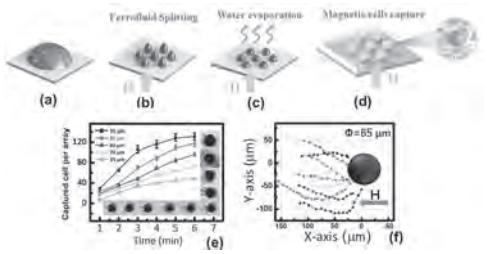

Fig. 1 a-d Process of preparing hexagonal superparamagnetic cone structures and capturing cells, (e) Magnetically labeled cells captured by different sizes of hexagonal superparamagnetic solid cones at different times. (f) Trajectory of cells attracted by a solid cone of 65 mm.

IOI-05. Nd-Fe-B Based Magnetophoretic Microfluidic Device with High Trapping Efficiency. *S. Ozunlu*[1,2], N. Gunduz Akdogan[3,2], H.A. Alshammari[1] and O. Akdogan[1,2] *1. Bahcesehir University, Istanbul, Turkey; 2. NANOTerial Technology Corporation, Istanbul, Turkey; 3. Piri Reis University, Istanbul, Turkey*

The key to a healthy and extended life is the early detection of diseases; abnormal cells, viruses, and bacteria could be detected in the early stages by analyzing various body fluids. To ease the detection and expedite the process, portable test kits that do not require hospitals and/or specialists have been developed. In that matter, biosensors are being developed with the capability of trapping bio-entities inside the microfluidic channels via magnetic field gradients. This work presents an innovative, easy-to-apply, and cost-efficient technique for developing at-home disposable rapid test kits with well-organized patterned arrays of Nd-Fe-B flakes in the PDMS matrix (Fig.1). Nd-Fe-B flakes (H_C = 1.5 kOe) (Fig.2) were synthesized by surfactant-assisted ball milling technique (at 700 rpm for 12 hours) with an average lateral dimension of 10 μm and an average thickness of 100 nm. The ball to powder weight ratio was chosen as 10:1. Dispersant and surfactant were heptane and oleic acid, respectively. Up to 0.1 %, solid content concentration was aligned and decorated to a gingham pattern. The microfluidic channel was prepared by photolithographic method with 3 layers (50 μm each) of UV-sensitive blue dry film which was developed in Na_2CO_3 bath (10% (w/v)). Two individual PDMS pieces (microfluidic channel and Nd-Fe-B/PDMS region) were bonded by a two-part epoxy to finalize the Nd-Fe-B/PDMS patch. In order to test the trapping system, Fe nanoparticles were synthesized. Fe nanoparticles were synthesized by the Y-junction method in the presence of $NaBH_4$ and $FeCl_2$ under Ar/H_2 gas flow. Synthesized particles have an average size of 92 nm. Subsequently, Fe NPs suspended in DMSO or DI water were flown inside the microfluidic channel. A high trapping efficiency (>90%) of Fe nanoparticles was observed. The developed device can be a game-changer for biosensors.

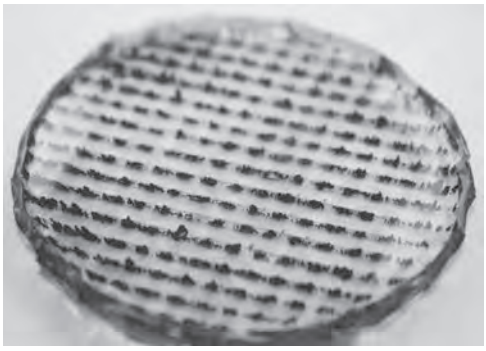

Figure 1. Patterned Nd-Fe-B/PDMS patch.

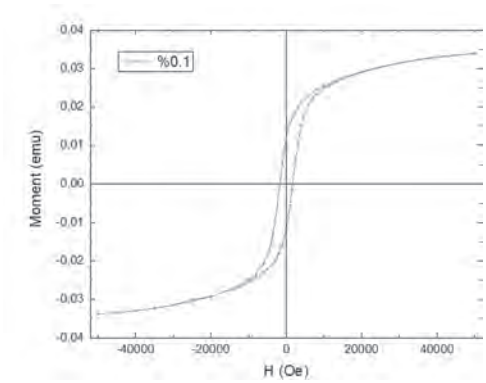

Figure 2. Hysteresis loop of Nd-Fe-B/PDMS patch with 0.1 solid content ratio.

IOI-06. A Green Thermomagnetic Technology for Efficient Passive Cooling by Ferrofluids. *V.B. Varma*[1,2], R. Ramanujan[1,2], S. Cheekati[1,2] and M. Pattanaik[1,2] *1. School of Materials Science and Engineering, Nanyang Technological University, Singapore, Singapore; 2. Singapore-HUJ Alliance for Research and Enterprise (SHARE), Nanomaterials for Energy and Energy-Water Nexus (NEW),), Campus for Research Excellence and Technological Enterprise (CREATE), Singapore, Singapore*

Novel devices are urgently required for better heat transfer of waste heat from a wide variety of industrial, commercial, and residential heat loads. Waste heat is often generated during energy generation, conversion, and utilization. This waste heat can lead to device failure, poor efficiency, lower reliability, and reduced service life. To address this challenge of waste heat transfer, we present an alternative thermomagnetic approach for efficient thermal management of low-grade waste heat. *Thermo-magnetics* employs the temperature-dependent behavior of magnetic materials to remove waste heat by a green, passive method. We have developed several configurations of magnetofluidic cooling (MFC) devices for heat load cooling [1-3], suitable for a broad range of heat load powers (0.5 to 1000 W) and temperatures (45 to 500°C). We have performed dimensionless analysis to quantify and optimize the device performance. We have built a materials selection map and demonstrated the highest passive cooling by 200°C. Our simulations are in excellent quantitative agreement with our experimental results, which we used for simulation-driven system design (SDSD) to obtain predictions and superior performance. It also helped to explain the details of the MFC process, e.g., the role of vorticity, material, and system dimensions on MFC compared to literature. We identified the critical dimensionless numbers and determined their profiles for the whole device. We used our findings to develop MFC devices (Figure 1) to cool a high-power LED @150°C and a solar cell @75°C surface temperature and demonstrated cooling by 100°C for LED and improved solar cell performance by ≈7% by 25°C cooling. *These results will be presented.* Acknowledgments This research is supported by grants from the National Research Foundation, Prime Minister's Office, Singapore, under its Campus of Research Excellence and Technological Enterprise (CREATE) programme.

[1] V. B. Varma, M. S. Pattanaik, S. K. Cheekati, and R. V. Ramanujan, "Superior cooling performance of a single channel hybrid magnetofluidic cooling device," *Energ. Convers. Manage.,* vol. 223, p. 113465, 2020. [2] V. B. Varma, S. K. Cheekati, M. S. Pattanaik, and R. V. Ramanujan, "A Magnetofluidic Device to Cool Light Emitting Diodes," *Joule,* 2021- communicated. [3] M. S. Pattanaik, V. B. Varma, S. K. Cheekati, G. Prasanna, N. M. Sudharsan, and R. V. Ramanujan, "A self-regulating multi-torus magneto-fluidic device for kilowatt level cooling," *Energ. Convers. Manage.,* vol. 198, p. 111819, 2019.

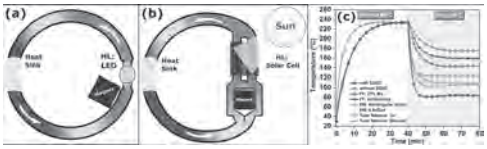

Figure 1. MFC device to cool heat loads (HL) of (a) High Power LEDs and (b) solar cells. (c) Simulation-driven system design (SDSD)[1] provided parameters for superior device performance and elaborated the MFC process and factors affecting it.

IOI-07. Magnetic Nanoparticle Manipulation Using Strain-Mediated FeGaB/PMN-PT Elliptical Ring Structures. *P. Pathak*[1], V. Yadav[1] and D. Mallick[1] *1. Electrical Engineering, Indian Institute of Technology Delhi, New Delhi, India*

In recent years, it is illustrated that the high localized magnetic field (H_{dw}) at magnetic domain walls (DWs) in strain-mediated magnetoelectric (ME) heterostructure can couple to magnetic nanoparticles (MNPs). This characteristic, along with the probability of manipulating DWs have been included in various lab-on-chip applications for precise manipulation of MNPs.

However, this manipulation ability of strain mediated MEs are restricted to magnetostrictive ring structures only where two distinct states, namely onion state and vortex state are observed. Due to the high magnetic energy density in the onion state of these structures, manipulation of MNPs is possible. However, the onion state in these structures is less thermally stable and cannot be obtained easily [1]. Recent studies suggest that an elliptical magnetostrictive ring can easily generate the onion state due to its large shape anisotropy with improved thermal stability [2]. However, MNPs manipulation using elliptical rings on strain-mediated MEs are not investigated to date. In this work, elliptical rings of FeGaB on a single-crystal PMN-PT substrate are analysed (Fig1). Initially, an external magnetic field along the minor axis of magnetic ring is applied and subsequently removed after saturation. The DWs containing onion state is observed at a remanent state up to a certain trackwidth (t_o) as demagnetization energy to flip the magnetization 180^o is higher. After applying an external voltage across PMN- PT, these DWs are rotated at different angles depending on the ring dimension. Also, DW reversibility is analysed after removing an external voltage. For lower trackwidth ($t_o \leq t_{ol}$), maximum in-plane 45^o rotation and reversibility towards initial position are observed because of dominant stress anisotropy (Fig2). For larger trackwidth ($t_o > t_{ol}$) complete in-plane 90^o rotation is observed without DW reversibility because of dominant shape anisotropy energy. The transport dynamics of MNPs is also studied for biological applications.

[1] A. T. Chen and Y. G. Zhao, Research update: Electrical manipulation of magnetism through strain-mediated magnetoelectric coupling in multiferroic heterostruc- tures, APL Mat. 4, 032303 (2016). [2] X.F.Han, Z.C.Wen, Y.Wang, H.F.Liu, H.X.Wei, and D. P. Liu, Nanoelliptic ring-shaped magnetic tunnel junction and its application in mram design with spin- polarized current switching, IEEE Trans. Magn. 47, 2957 (2011).

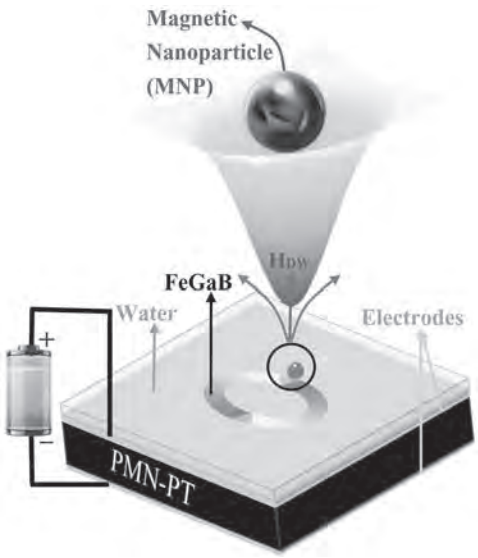

Fig. 1 Prototype geometry investigated for generation of H_{dw} at DW to couple MNP.

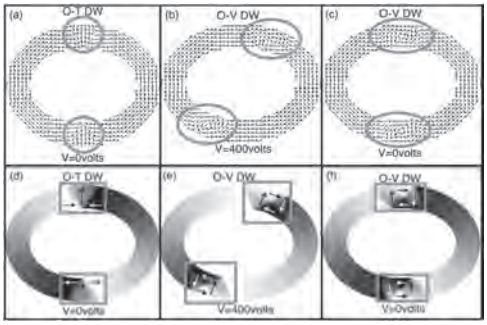

Fig 2 In-plane 45^o DW rotation and reversibility when $t_o \leq t_{ol}$. (a)-(c) Simulated Miromagnetics (d)-(f) corresponding PEEM images.

IOI-08. Antibacterial activity of g-Fe_2O_3/Ag nanocomposites under alternating magnetic fields. Y. Luengo[1], B. Sot[1] and *G. Salas*[1] *1. IMDEA Nanociencia, Madrid, Spain*

The treatment of bacterial infections is becoming a serious global problem due to the increasing bacterial resistance against classical antibiotics (1). To overcome this problem, new antibacterial agents are needed (2). Silver has been known as an antibacterial agent since ancient times and nano-formulated silver has been proved to be a very effective new treatment. However, silver nanoparticles (AgNPs) have limitations related to their low yield for penetrating bacterial biofilms and their concentration-dependent toxicity to human cells. Magnetic nanoparticles based on iron oxides (IONPs) present some special features that can be exploited combining them with AgNPs to enhance the depth of biofilm penetration and to allow removal from the medium by an external magnet (3). Furthermore, the combination of silver bactericidal activity and magnetic hyperthermia is an unexplored and interesting approach. In this work, bifunctional γ-Fe_2O_3-Ag nanocomposites with different silver content and particle sizes, have been synthesized. They have good microbicidal capabilities against the bacterial pathogens *E. coli* (Gram-negative) and *S. aureus* (Gram-positive), which are related to their silver content, the size of the nanoparticles and the release of silver ions. This bactericidal activity can be enhanced by the application of an alternating magnetic field (Fig. 1), which increases the release of silver ions (4).

(1) Prucek, R. et al. Biomaterials 2011, 32, 4704-4713. (2) Gong, P. et al. Nanotechnology 2007, 18, 285604-285611. (3) Ghaseminezhad, S. M.; Shojaosadati, S. A. Carbohydrate Polymers 2016, 144, 454-463. (4) Luengo, Y. et al. Colloids and Surfaces B: Biointerfaces 2020, 194, 111178.

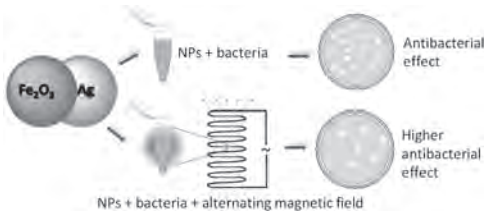

IOI-09. Magnetostrictive nanostructured surfaces for antimicrobial applications. *J. Marqués Marchán*[1], M.M. Fernandes[2,3], J. Fernandez-Roldan[4], M. Méndez[4], V.M. Prida[4], S. Lanceros-Mendez[5,6] and A. Asenjo[1]
1. Instituto de Ciencia de Materiales de Madrid, CSIC, Madrid, Spain; 2. Centre of Physics, University of Minho, Braga, Portugal; 3. Centre of Biological Engineering, University of Minho, Braga, Portugal; 4. Department of Physics, University of Oviedo, Oviedo, Spain; 5. BCMaterials, Leoia, Spain; 6. Ikerbasque, Bilbao, Spain

Medical devices such as laboratory or surgical instruments are extensively used. A common problem that may arise from the use of these tools is the proliferation of microorganisms and biofilms formation on their surface, which leads to nosocomial infections in patients [1]. Novel strategies to prevent the adhesion of microorganisms and thus biofilm formation are being developed using physical methods such as the magnetoelectric stimuli [2-4]. In this work, an array of pillars with submicrometer sizes made of highly magnetostrictive material is employed to control and trigger the antimicrobial activity on its surface by applying a magnetic stimulus. Terfenol-D ($Tb_{0.3}Dy_{0.7}Fe_{1.9}$) was deposited by DC magnetron sputtering over a Si substrate using a hexagonal patterned mask with porous diameter of 450 nm, obtaining magnetic pillars of approximately 300 nm in height (Figure 1). In depth characterization of the structures were performed including their morphological and magnetic characteristics. The antimicrobial activity with Gram-negative (*E. Coli*) bacteria was also assessed by comparing the capability of bacteria killing of Terfenol-D pillars, Terfenol-D thin films and Si substrates. Experiments were performed both under static and dynamic conditions, the latter by applying a varying external magnetic field using a home-made bioreactor [5] to trigger a mechanical stimulus via the magnetostrictive properties of Terfenol-D. Micromagnetic simulations of

the pillars were carried out under the same conditions used in the essays to better understand the magnetization dynamics and magnetostrictive effect. It is shown how the morphology and the application of the magnetic field to the nanostructured surface affects bacteria killing, becoming a proof-of-concept for nanostructured magnetically activated materials for the development of antimicrobial surfaces. The authors acknowledge the IEEE Magnetics Society for the Eductaional Seed Funding.

[1] B. F. Gilmore and L. Carson, Biomaterials and Medical Device – Associated Infections, p. 163-183 (2015) [2] M. M. Fernandes et al., ACS Applied Bio Materials, Vol. 4, p. 559-570 (2021) [3] D. P. Linklater et al., Nature Reviews Microbiology, Vol. 19, p. 8-22 (2021) [4] E. O. Carvalho et al., ACS Appl. Mater. Interfaces, Vol. 11(30), p. 27297-27305 (2019) [5] N. Castro et al., Sensors (Basel, Switzerland), Vol. 20(12), p. 3340 (2020)

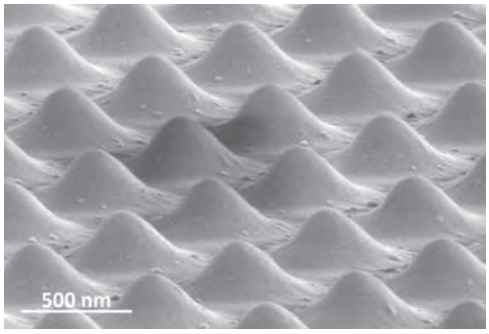

Fig 1. SEM image of the Terfenol-D pillars deposited over a Si substrate.

IOI-10. Green Synthesis and Characterization of Magnetic Fe_3O_4, $CoFe_2O_4$ and $NiFe_2O_4$ from Aloe Vera Extract and its Biomedical Potential. *G.C. Hermosa*[1] and A. Sun[1] *1. Yuan Ze University, Taoyuan, Taiwan*

The magnetic nanoferrites (Fe, Co, Ni) were prepared by an eco-friendly hydrothermal method using an Aloe Vera plant extract solution as both a reducing and stabilizing agent. Magnetic nanoferrites were characterized using XRD, VSM, SEM, TEM and XPS. Cytotoxicity were obtained using the MTT assay. X-ray diffraction analysis also demonstrated that the size range of the nanoferrites exhibited average diameters of 8-29 nm and also exhibiting high crystallinity. Results showed that all the metallic nanoparticles are magnetic with values Fe = 52 emu/g, Co = 33 emu/g and Ni = 7.1 emu/g. The magnetic nanoferrites exhibited high cell viability rate at high concentrations signifying their non-toxic property. From SEM, spherical structure was noticeable and the particle size is also in accordance with XRD. The chemical states for each nanoparticle also confirmed the successful synthesis of each nanoferrite. The magnetic nanoferrites produced in this study by green synthesis methodology from leaf extract of Aloe Vera needs to be further evaluated and could find greater biomedical application.

[1] N. Guijarro, P. Bornoz, M. Prévot, X. Yu, X. Zhu, M. Johnson, X. Jeanbourquin, F. Le Formal and K. Sivula, Sustainable Energy & Fuels 2, (2018). [2] Sun, H. Zeng, D. Robinson, S. Raoux, P. Rice, S. Wang and G. Li, Journal of The American Chemical Society 126, (2004). [3] S. Hazra and N. Ghosh, Journal of Nanoscience and Nanotechnology 14, (2014). [4] M. Irfan Hussain, M. Xia, Xiao-NaRen, K. Akhtar, A. Nawaz, S. Sharma and Y. Javed, Magnetic Nanoheterostructures (2020). [5] S. Bhagyaraj, *Synthesis of Inorganic Nanomaterials* (2018).

IOI-11. Magnetic Field Prediction Using Generative Adversarial Networks. *S. Pollok*[1*], N. Olden-Jørgensen[1], P.S. Jørgensen[1] and R. Bjørk[1] *1. Department of Energy Conversion and Storage, Technical University of Denmark, 2800 Kgs. Lyngby, Denmark*

We present a novel approach to predict magnetic field values at a random point in space from a few point measurements by using deep learning (DL). For this data-driven approach, we produce a large dataset of 20,000 samples with MagTense [1]. Each sample is a magnetic field of resolution 256 × 256 in the center of a 2-D grid, which is surrounded by multiple randomly placed hard magnets with varying magnetization. The DL architecture, inspired by Ref. [2], is depicted in Fig. 1. For the underlying Wasserstein generative adversarial network [3], we train two neural networks: a generator, which predicts the missing field values of a magnetic field, and a critic, which calculates the Wasserstein-1 distance [4] between real and generated field distributions. In addition to minimizing the Wasserstein-1 distance, the network parameters of the generator are updated to lower the L1 reconstruction loss between real and predicted field values. This setup can either be trained on inpainting, where the generator predicts missing field values in a specific region, or in an inverted way, a so-called outpainting task, where small patches across the measurement area are available and the field values around are predicted, as shown in Fig. 2. Given a sample, which was not included in the dataset used for training, the generator has learned to accurately predict the missing field values, which correspond excellently to the real magnetic field. The median reconstruction error of 1,000 test samples on inpainting is 5.09%, while it is 9.58% on outpainting. With this approach, we pave the way to replacing parts of expensive field measurements or calculations by filling the required measurement area with values generated by a trained neural network. Moreover, it can serve as a preprocessing step for the inverse design of magnetic fields [5]. We are currently working on extending the DL architecture for a magnetic field measured in a 3-D volume.

[1] R. Bjørk and K.K. Nielsen. *MagTense*. [Online]. Available: http://www.magtense.org, doi: 10.11581/DTU:00000071 (2019). [2] J. Yu *et al.*, "Generative Image Inpainting With Contextual Attention", *Proc. IEEE Conf. Comput. Vis. Pattern Recognit. (CVPR)*, pp. 5505-5514 (2018). [3] I. Gulrajani *et al.*, "Improved Training of Wasserstein GANs", *arXiv:1704.00028*. [Online]. Available: http://arxiv.org/abs/1704.00028 (2017). [4] C. Villani, "Optimal Transport: Old and New", Springer, Berlin, Heidelberg (2009). [5] S. Pollok, R. Bjørk, and P.S. Jørgensen, "Inverse Design of Magnetic Fields Using Deep Learning", *IEEE Trans. Magn.*, vol. 57, no. 7, Art. no. 2101604 (2021).

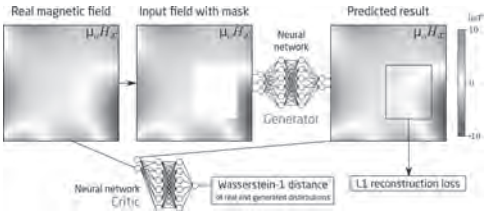

Fig. 1. Novel DL approach for magnetic field prediction. A generator is trained to predict the missing field values, which are subsequently evaluated by a trained critic and the L1 reconstruction loss.

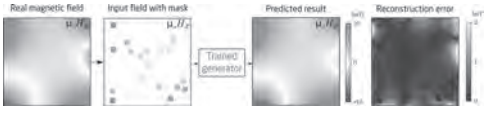

Fig. 2. Qualitative analysis of the trained generator on outpainting with an unseen test sample.

IOI-12. Withdrawn

IOI-13. ^{1}H nuclear relaxation with limited spin diffusion. Development of study model. D. Lachowicz[1], J.A. Stoll[2], M. Gajewska[1], M. Sikora[1], J. Hankiewicz[2], M. Przybylski[1] and *Z. Celinski*[2] *1. Academic Centre for Materials and Nanotechnology, AGH University of Science and Technology, Krakow, Poland; 2. BioFrontiers Institute, UCCS, Colorado Springs, CO, United States*

To study ^{1}H nuclear relaxation without spin diffusion in the presence of superparamagnetic particles we are developing a novel one-step synthesis technique for producing mixed MnZn ferrite particles by thermal degradation of acetylacetonate in the silicone matrix. Iron(III) acetylacetonate, zinc acetylacetonate and manganese(II) acetylacetonate were dissolved in dibenzyl ether and mixed with Dow Corning 7-9600 silicone resin (part A). The mixture was heated to 285 °C to under an argon atmosphere to precipitate nanoparticles. Transmission electron microscopy revealed particles roughly 1 to 7 nm in diameter, embedded in the silicone (see Figure 1). The structure and composition of the particles were checked by Energy-Dispersive X-ray, X-ray Absorption and X-ray Photoelectron spectroscopies. These methods revealed a ferrite structure which incorporates both manganese and zinc and has iron occupying both octahedral and tetrahedral sites. To our knowledge, this represents the first synthesis of ferrite nanoparticles in silicone matrix. Nuclear Magnetic Resonance measurements, especially spin relaxation and diffusion measurements allowed to determine influence of superparamagnetic particles on T_1, T_2 and T_2* relaxation times.

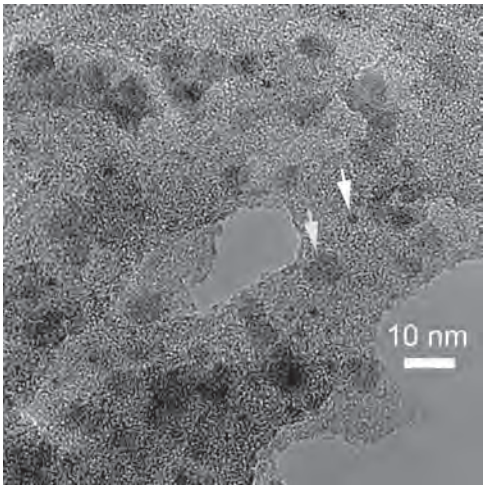

Figure 1. TEM image of synthesized mixed MnZn ferrite nanoparticles in silicone matrix. Arrows point at particles of different sizes: white and green indicate particle approximately 1 nm and 7 nm in diameter, respectively. Gray surrounding mass is the silicone matrix.

Session IPA
MAGNETIC RECORDING TECHNOLOGY II
(Poster Session)

Ganping Ju, Co-Chair
Seagate, Fremont, CA, United States
Yingguo Peng, Co-Chair
Seagate, Fremont, CA, United States

IPA-01. Estimating Interference with Two-Dimensional Viterbi Algorithm for Bit Patterned Media Recording. *T.A. Nguyen*[1] and J. Lee[1]
1. Soongsil University, Seoul, The Republic of Korea

In magnetic recording media, to overcome superparamagnetism, bit patterned media recording (BPMR) is proposed as the potential technology. In BPMR, to increase the areal density (AD), the distance between the islands must be reduced. As the magnetic islands become closer, two-dimensional (2D) interference appears violently. The 2D interference includes inter-symbol interference (ISI) from the down-track direction and inter-track interference (ITI) from the across-track direction. We use detection, which applies the Viterbi algorithm (VA) or the maximum a posteriori (MAP) algorithm, to handle the 2D interference. Because the VA and MAP algorithm are designed to remove the 1D interference, when detecting ISI, we need to remove ITI and vice versa. In this article, we proposed an estimator to predict ITI. This estimator uses the 2D VA with reducing the states. We consider each column of the channel as a symbol like [1]. Our channel is symmetric and has a size of 3x3. Therefore, we have 36 states and 6 input branches for the trellis of the 2D VA. The received signal is feed to the ITI estimator. We detect along the across-track direction to estimate the ITI. Then, we remove the ITI from the received signal and apply the 1D VA to detect along the down-track direction. With the signal is detected by the 1D VA from the down-track direction (horizontal detection), we achieve the estimated original signal. Therefore, we can use the estimated original signal to estimate the interference along the down-track direction (ISI) and remove it from the received signal. Finally, we detect the received signal, which removed the ISI, with 1D VA along the across-track direction (vertical detection). Our proposed model is presented in Fig. 1. In Fig. 1, we use the serial GPR target form in [2]. In the simulation, we compare the serial detection [3], which is designed as the 2D VA, with our proposed model on the BPMR channel at 3 Tb/in^2. The results are presented in Fig. 2. We can see that our proposed model achieves a 1 dB gain compared to serial detection at BER of 10^{-4}.

[1] J. Yao, K. C. Teh and K. H. Li, "Joint Iterative Detection/Decoding Scheme for Discrete Two-Dimensional Interference Channels," IEEE Trans. Comm., vol. 60, no. 12, pp. 3548-3555, 2012. [2] T. A. Nguyen and J. Lee, "One-Dimensional Serial Detection Using New Two-Dimensional Partial Response Target Modeling for Bit-Patterned Media Recording," IEEE Magn. Lett., vol. 11, pp. 1-5, 2020. [3] T. A. Nguyen and J. Lee, "Effective Generalized Partial Response Target and Serial Detector for Two-Dimensional Bit-Patterned Media Recording Channel Including Track Mis-Registration," Appl. Sci., 2020.

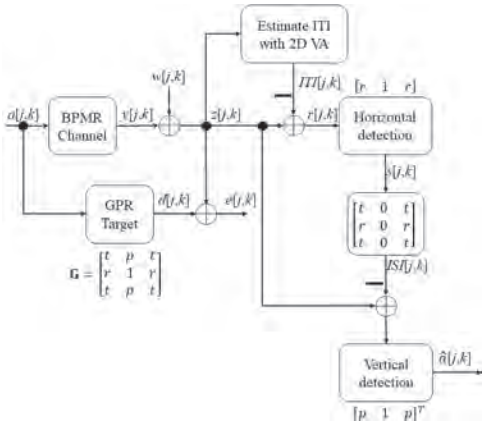

Fig. 1. Our proposed model.

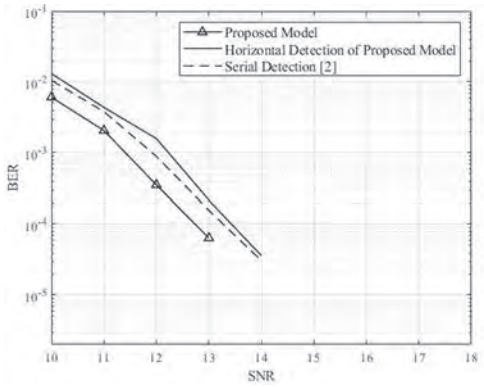

Fig. 2 BER performance of the proposed model.

IPA-02. Improving Serial Detection with MAP Algorithm for Bit Patterned Media Recording. *T.A. Nguyen*[1] and J. Lee[1] *1. Soongsil University, Seoul, The Republic of Korea*

In bit patterned media recording (BPMR), to increase the areal density (AD), we must reduce the distance between the magnetic islands. This leads to severe two-dimensional (2D) interference. The 2D interference includes inter-symbol interference (ISI) and inter-track interference (ITI) from the down- and across-track directions, respectively. To combat the 2D interference, we can decompose the ISI and ITI into the serial model [1]. However, in [1], the authors just use the Viterbi algorithm for detection, the detection lacks prior information from the inner detector to the outer detector. In this article, we use the maximum a posteriori (MAP) algorithm to supply the prior information from the inner detector to the outer detector. Our proposed model is presented in Fig. 1. We use the serial GPR target in [1]. The received signal is feed to the horizontal detection (using MAP algorithm). Each output data of the horizontal detection $r[j,k]$ includes six probability values of 6 symbols, respectively. We use the argmax($r[j,k]$) to

convert the signal $r[j,k]$ into the hard output $b[j,k]$. $b[j,k]$ is used to extract the noise information and create the soft output signal [2] (i.e., $soft(b[j,k])$). The signal $soft(b[j,k])$ is detected by the MAP algorithm in the vertical detection and creates the probability of -1 or +1 in $s[j,k]$. Then, $s[j,k]$ and $r[j,k]$ are entered to the log detection. We calculate the product of the probability of +1 from $s[j,k]$ and the sum of the probability from the symbols, which contains the input +1, in $r[j,k]$. This product is assigned to a numerator. Then, we calculate the product of the probability of -1 from $s[j,k]$ and the sum of the probability from the symbols, which contains the input -1, in $r[j,k]$. This product is assigned to a denominator. Finally, we calculate d = log(numerator/denominator). If $d \geq 0$, $\hat{a}[j,k] = 1$ and if $d < 0$, $\hat{a}[j,k] = 0$. The results of our proposed model are presented in Fig. 2. We compare our model with the serial detection in [2]. Our proposed model improved the bit error rate (BER) performance of the serial detection.

[1] T. A. Nguyen and J. Lee, "One-Dimensional Serial Detection Using New Two-Dimensional Partial Response Target Modeling for Bit-Patterned Media Recording," IEEE Magn. Lett., vol. 11, pp. 1-5, 2020. [2] T. A. Nguyen and J. Lee, "Effective Generalized Partial Response Target and Serial Detector for Two-Dimensional Bit-Patterned Media Recording Channel Including Track Mis-Registration," Appl. Sci., 2020.

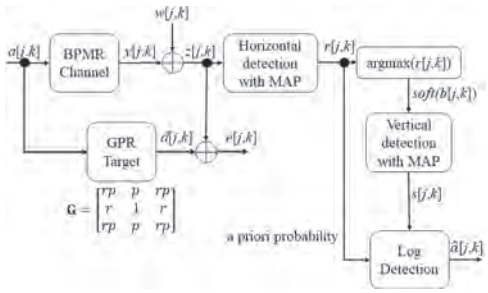

Fig.1 Our proposed model.

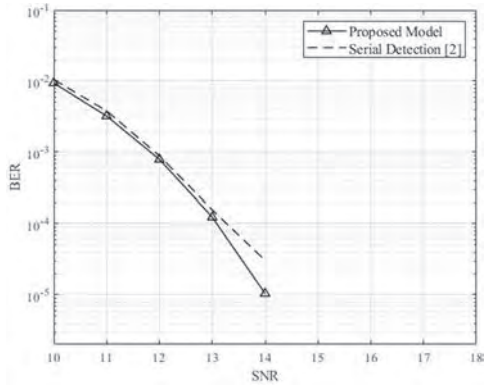

Fig. 2 BER performance of the proposed model.

IPA-03. Bit-Flipping Scheme Using K-Means Algorithm for Bit-Patterned Media Recording. *S. Jeong*[1] and J. Lee[1] *1. School of Electronic Engineering, Soongsil University, Seoul, The Republic of Korea*

Since conventional HDDs that use perpendicular magnetic recording suffer from the problems of thermal stability, superparamagnetic limit, and so on, bit-patterned media recording (BPMR) system is a promising candidate for the next generation of data-storage system to achieve areal density (AD) beyond one terabit per square inch (Tb/in^2) [1]. To increase the AD of the BPMR, the space between islands in both the down- and cross-track directions must be reduced. Consequently, data detection is interrupted by inter-symbol interference (ISI) and inter-track interference (ITI). In this paper, we propose a bit-flipping (BF) scheme using k-means algorithm for BPMR system to improve a bit error rate (BER) performance. A partial response maximum likelihood (PRML) detector which consists of a two-dimensional minimum mean square error (MMSE) equalizer and a one-dimensional PR target soft-output Viterbi algorithm (SOVA) detector is used for equalization and detection, respectively. Fig. 1 shows a block diagram of the proposed BF scheme. We use $s_{j,k} = [s_{j-2}, s_{j-1}, s_j, s_{j+1}, s_{j+2}] = [v_{j-1,k}, v_{j,k-1}, v_{j,k}, v_{j,k+1}, v_{j+1,k}]$ as the input sequence of k-means algorithm in SOVA output sequence $v_{j,k} = [v_{j-1,k-1}, v_{j-1,k}, \ldots, v_{j+1,k}, v_{j+1,k+1}]$ to consider the effect of ISI and ITI and decrease the number of clusters. After k-means algorithm, we compare a sign between p_j of the predicted value in predicted sequence $p_{j,k} = [p_{j-2}, p_{j-1}, p_j, p_{j+1}, p_{j+2}]$ and $v_{j,k}$ in in SOVA output sequence $v_{j,k}$. When the signs are different, we change the sign of $v_{j,k}$. In the simulation, we compare the PRML detector with BF and no BF schemes on the BPMR channel [2]. Fig. 2 shows the BER performance of the PRML detector with BF scheme according to SNR. When the ADs are 2.5Tb/in^2 and 3Tb/in^2, the performance of the proposed scheme is 1.1dB and 2.8dB better than that of one LDPC code at 10^{-4} BER, respectively.

[1] R. L. White, R. M. H. New, and R. F. W. Pease, "Patterned media: A viable route to 50 Gbit/in^2 and up for magnetic recording," IEEE Trans. Magn., vol. 33, no. 1, pp. 990-995, 1997. [2] S. Nabavi, B. V. K.V. Kumar, J. A. Bain, C. Hogg, S. A. Majetich, "Application of image processing to characterize patterning noise in self-assembled nano-masks for bit-patterned media", IEEE Trans. Magn, vol. 45, no. 10, 2009.

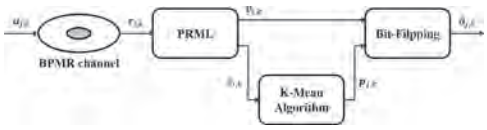

Fig. 1. Block diagram of the proposed bit-flipping scheme.

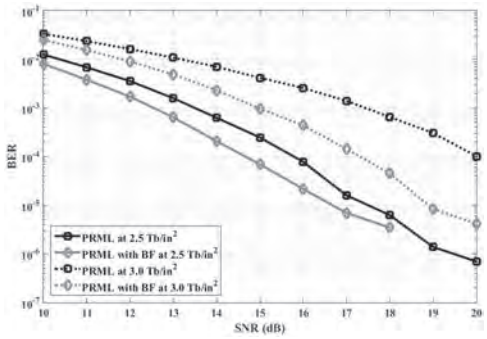

Fig. 2. BER performance of the PRML detector with BF scheme according to SNR.

IPA-04. Optimising Dual Structure Patterned Media for Heat Assisted Magnetic Recording. H. Yamane[1], *S. Greaves*[1] and Y. Tanaka[1] *1. RIEC, Tohoku University, Sendai, Japan*

If hard disc drives were able to store information in more than one recording layer, or structure, their storage capacity should be greatly increased. In recent years microwave-assisted and heat-assisted magnetic recording (HAMR) on dual structure media have been investigated [1][2]. Techniques for deconvoluting the readback signals from two recording structures have also been developed [3]. Here we focus on dual structure, bit patterned media for use with HAMR. Each recording medium dot contained two, discrete storage structures with different Curie temperatures, T_c, allowing data to be written to one, or both structures depending on the maximum temperature to which the dots were heated. The effect of the dot diameter, D, and the thickness of the recording structures, z, was investigated, with the aim of maximising the user areal density (UAD). The Curie temperatures were optimised to maximise the joint switching probability (i.e. $P = P_1 \times P_2$) for D = 6 nm and $z_1 = z_2$ = 5 nm. The switching probability peaked when (T_{c1}, T_{c2}) were around (460 K, 550 K), or (530 K, 460 K). Next, the magnetostatic field distributions from surrounding dots were calculated for a dot pitch of 10 nm. The switching probability as a function of magnetostatic field, H_d, and D is shown in fig. 1. The switching probability increased with D (volume). The switching probability was also calculated as a function of recording

structure thickness, z. Fig. 2 shows P versus K_uV, where K_uV was evaluated at the point where the coercivity, H_c, was equal to the head field H_{head}. In fig. 2 both D and z were varied in each data set. H_c was calculated from M-H loops, whilst H_{head} depended on the distance from the write head to the recording structure. Higher K_uV resulted in higher switching probabilities for both recording structures, but RL1 showed a much greater variation than RL2. To maximise the switching probabilities of both recording structures RL1 should have a larger volume than RL2. The UAD was calculated using Shannon's formula for channel capacity. Values of around 8.6 Tbits/in^2 were predicted for dot areal densities of about 4.5 Tdots/in^2.

[1] S. J. Greaves et al., IEEE Trans. Magn. 55(12), 6701509, (2019). [2] H. Yamane et al., IEEE Trans. Magn. 57(2), 3200706, (2021). [3] A. Aboutaleb et al., IEEE Trans. Magn. 57(3), 3101012, (2021).

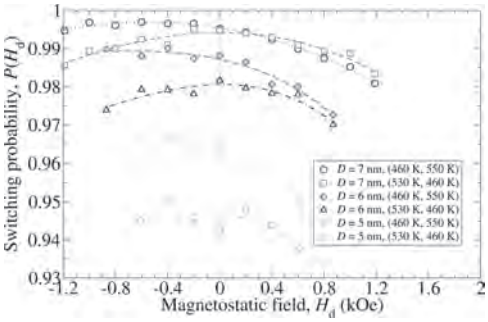

Fig 1 *P* vs. magnetostatic field from surrounding dots and *D*

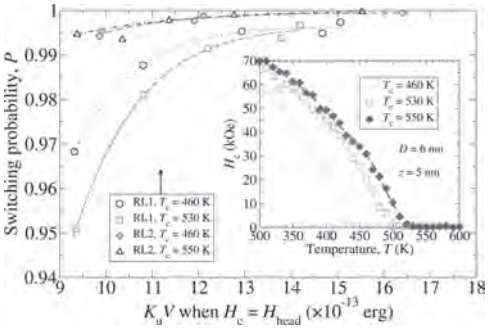

Fig 2 *P* vs. K_uV when $H_c = H_{head}$. Inset: H_c vs. *T*

IPA-05. Micromagnetic Analysis of Dual FGL STO. *R. Itagaki*[1], Y. Kanai[1] and S. Greaves[2] *1. Niigata Institute of Technology, Kasiwazaki, Japan; 2. RIEC, Tohoku University, Sendai, Japan*

Spin-torque oscillators (STO) with two field generation layers (dual FGL), have superior characteristics compared with conventional STOs with a single FGL used for microwave-assisted magnetic recording (MAMR) [1], [2]. As shown in Fig. 1, we used an integrated model with a STO inserted into the gap between the main pole (MP) and the trailing shield (TS) of a write head. The dual FGL STO was composed of two FGLs and one spin injection layer with negative polarization (nSIL). The thicknesses were FGL1 = FGL2 = 5 nm, IL1 = 2 nm, IL2 = IL3 = 1 nm, and nSIL = 3 nm. The STO was tilted by 25° with respect to the x axis. The MP – TS gap = 18.8 nm at the air bearing surface (ABS). We assumed an injected current from MP to TS, and no spin-torque between FGL1 and FGL2. Antiferromagnetic coupling, J_{ex}, was assumed between FGL1 and FGL2. Fig. 2 shows the in-plane component of the magnetization of FGL1 and FGL2 ($M_{in\text{-}plane}/M_s$) averaged over the FGL volume, relative to a unit vector lying in the plane of the FGL. When $M_{in\text{-}plane}/M_s = 1$ the FGL rotates perfectly in the FGL plane. Fig. 2(a) shows $M_{in\text{-}plane}/M_s$ for J_{ex} = -1.33 erg/cm^2 [2] and (b) J_{ex} = -10 erg/cm^2. The average values of $M_{in\text{-}plane}/M_s$ between zero and 16.0 ns were 0.653 for (a) and 0.808 for (b), demonstrating a remarkable improvement in FGL rotation. We also performed calculations for J_{ex} = +1.33, 0, -5, -50, and -100 erg/cm^2. We confirmed that J_{ex} = +1.33 did not work; there was a significant improvement between J_{ex} = 0 and -10; while there was little change from -10 erg/cm^2 for J_{ex} = -50 and -100 erg/cm^2. We also varied some other parameters, e.g., FGL thickness, exchange coupling between nSIL - TS, however, no distinct effect was found. The most dominant factor affecting the FGL rotation was the strength of the antiferromagnetic coupling between FGL1 - FGL2. We acknowledge financial support from ASRC.

[1] J. Zhu, X. Zhu and Y. Tang, *IEEE Trans. on Magn.*, vol. 44, no. 1, pp. 125-131 (Jan. 2008) [2] M. Takagishi, N. Narita, H. Iwasaki, H. Suto, T. Maeda, and A. Takeo: *IEEE Trans. on Magn.,* vol. 57, no. 3, 3300106 (Mar. 2021)

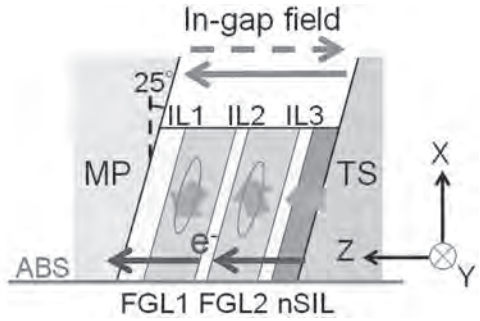

Fig. 1 Schematic of dual FGL STO.

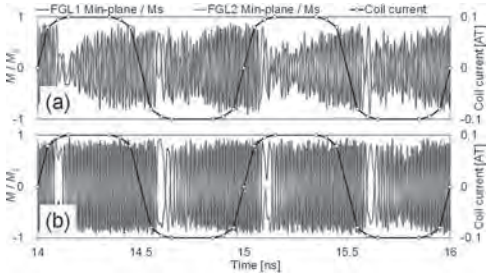

Fig. 2 In-plane component of volume-averaged FGL rotation vs. time. nSIL P_o = -0.3, $J = 4.0\times10^8$ A/cm^2, coil current = 0.2 AT$_{pp}$. (a): J_{ex} = -1.33 erg/cm^2, (b): J_{ex} = -10.0 erg/cm^2. Degauss of write head was carefully done, then STO calculations were performed. Data from 14 – 16 ns are shown.

IPA-06. Influence of pulse width and Joule heating on current-induced domain wall motion. *S. Kambe*[1], S. Ranjbar[1], K. Tanabe[1], S. Sumi[1] and H. Awano[1] *1. Toyota Technological Institute, Nagoya, Japan*

Racetrack memory (RM) is a promising device for a new class of non-volatile memory because of its large storage capacity, fast data access, and low power consumption. Although many studies have been focused on improving the domain wall motion (DWM), only a few studies have been considered the effect of Joule heating on DWM. We first measured the domain wall velocity in the GdFeCo wires by applying single voltage pulses (Picosecond) and then observed the DWM by using a Kerr microscope. Figure 1. (a) shows the DWM in the GdFeCo wire as a function of current density, where the pulse widths of the applied current are 3 ns and 30 ns, respectively. By increasing the current density, DW velocity increases. It is clearly observed that the DW velocity becomes faster as the pulse duration becomes shorter [1][2][3]. In order to clarify the effect of Joule heating on the magnetic wire, we performed a numerical simulation based on the heat diffusion on the surface of the GdFeCo wire when both short and long pulse width currents were applied to the wire. Besides, we found that the temperature of the magnetic wire is higher when the pulse width was longer, as shown in Fig. 1(b). Therefore, the slower DWM in the magnetic wire was observed for a long pulse current of 30 ns due to the higher temperature of the magnetic wire. Consequently, we have experimentally demonstrated and theoretically explained that a short pulse current of 3 ns is faster than a long pulse width of 30 ns. ACKNOWLEDGEMENT This work was supported by the JSPS KAKENHI (grants 918023, 918043,918055)

[1] Caretta, L. *et al.* Fast current-driven domain walls and small skyrmions in a compensated ferrimagnet. *Nat. Nanotechnol.* 13, 1154–1160 (2018). [2] Cai, K. *et al.* Ultrafast and energy-efficient spin–orbit torque switching in compensated ferrimagnets. *Nat. Electron.* 3, 37–42 (2020). [3] Hirata, Y. *et al.* Correlation between compensation temperatures of magnetization and angular momentum in GdFeCo ferrimagnets. *Phys. Rev. B* 97, 1–6 (2018).

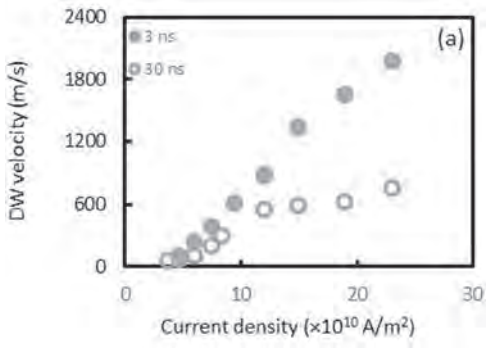

Figure 1.(a) The velocity of the magnetic domain wall in the Pt(5)/ Gd24(Fe88Co22)76(20)/SiN(10) sample as a function of current density

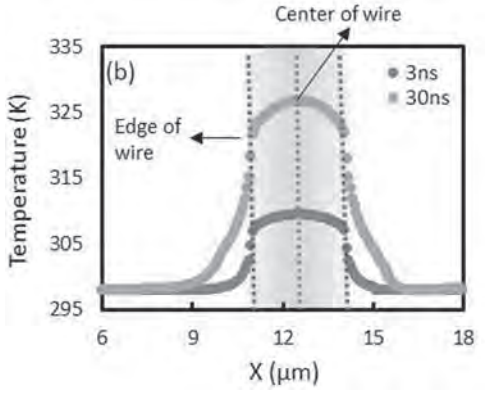

Figure 1.(b) Temperature distribution of GdFeCo magnetic wire in the short hand direction when pulsed current of 3ns and 30ns widths is applied

IPA-07. Dependence of microwave assisted magnetization switching and magnetic recording characteristics on layer anisotropy structure for multilayer media. *K. Kurihara*[1], K. Kawakami[1], X. Ya[1], Y. Kanai[2] and T. Tanaka[1] *1. Kyushu University, Fukuoka, Japan; 2. Niigata Institute of Technology, Niigata, Japan*

Microwave-assisted magnetic recording (MAMR) [1] is a technology which can potentially enable the areal recoding density to further increase. Notched media have been proposed [2] for improving MAMR writability as well as MAMR recording characteristics. In the present study, dependence of microwave assisted magnetization switching (MAS) and magnetic recording characteristics on layer anisotropy structure were investigated by micromagnetic simulations regarding the interlayer exchange constants for notched media. Fig. 1(a) illustrates the layer structure assumed in this study. Recording characteristics were evaluated in terms of signal-to-noise ratios (SNR) derived from the signal power for 200 kbpi and noise power for 1600 kbpi, where a 30-nm-wide single-pole-type head with a spin torque oscillator with the frequency at 22 GHz [3] was assumed in recording process. Fig. 1(b) presents the MAS plots where A_{int12}, A_{int23}, and A_{int34} are 0.5, 0.5, and 0.7 μerg/cm and H_{k4} is 35 kOe, which were estimated under the continuous AC with pulse DC fields. The figure shows that higher switchable max. averaged H_k ($H_{k,ave}$) is obtained when only one of the three layers has large H_k and the other two layers have low H_k. This study found that the MAS properties are sensitive to field durations of DC and AC. In the case when a continuous DC and pulse AC fields, higher switchable max. $H_{k,ave}$ was obtained only when media structure has large H_{k1}, low H_{k2} and low H_{k3}. The calculation also indicated that relatively high A_{int34} (> 0.5 μerg/cm) was preferable. Fig. 2 compares SNRs for three the type of H_k layer structure media where A_{int12}, A_{int23}, and A_{int34} were fixed to 0.5, 0.5, and 0.7 μerg/cm. The figure suggests that SNR for large H_{k1} structure media reaches 16.7 dB around 25 kOe of $H_{k,ave}$. On the other hand, SNRs for large H_{k2} and large H_{k3} structure media decrease with increase in $H_{k,ave}$. The poor SNRs attribute to low signal power for 200kbpi. This may be translated by the MAS properties for multilayer films sensitive to the field durations.

[1] Jian-Gang (jimmy) Zhu et al., IEEE Trans. Magn., Vol. 44, p. 125-131 (2008) [2] X. Bai et al., IEEE Magn. Lett., Vol. 7, p. 4507904 (2016) [3] Y. Kanai et al., IEEE Trans. Magn., Vol. 55, p. 3000613 (2019)

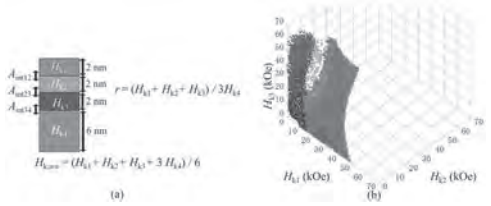

Fig.1. (a) Schematic of medium layer structure and anisotropy fields and (b) MAS plots for a multilayer.

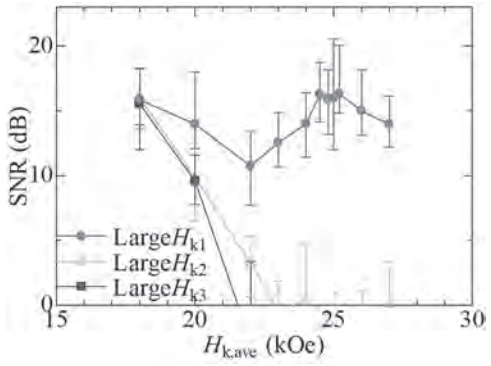

Fig.2. SNRs comparison among three type of layer H_k structure media with r = 0.4.

IPA-08. Estimation of microwave-assisted magnetization switching field by static energy approximation. *K. Kawakami*[1], K. Kurihara[1], X. Ya[1] and T. Tanaka[1] *1. Kyushu University, Fukuoka, Japan*

Microwave-assisted magnetization recording [1] has been attracting intense research interests for ultra-high-density recording. The mechanism of microwave assisted magnetization switching (MAS) under the DC field applied parallel to the anisotropy direction have been theoretically studied so far [2, 3]. According to the references, the effect of microwave assistance is translated by the equivalent field denoted by ω/γ. Whilst, in the case when DC field is applied non-parallel to the anisotropy axis, the estimation of MAS field is quite complex. In this study, we proposed an approximation for estimating the MAS field when the DC field was applied nonparallel to the anisotropy axis. Fig. 1(a) showed the schematic illustrations for approximating magnetization dynamics by a static system. DC magnetic field (H_{DC}) was applied at θ with respect to the anisotropy axis, and circularly polarized field (H_{AC}) in x-y plane. φ stands for the angle between the procession axis and anisotropy axis. Here we extend the theory [2, 3], where the equivalent field lay in the opposite to the magnetization precession axis, hence the z and x-y plane components of the normalized effective magnetic fields are given by $h_{xy}=h_{DC}\sin\theta-(\omega/H_kY)\sin\varphi+h_{AC,}$ $h_z=h_{DC}\cos\theta-(\omega/H_kY)\cos\varphi$ (Eq. 1). Fig. 1(b) showed that the field components obtained by micromagnetic calculation agreed with the asteroid curve, which translated the approximation worked even when DC field has an incident angle. The relation between h_{DC} and φ ($h_{DC}=(0.5\sin2\varphi-h_{AC}\cos\varphi)/\sin(\theta-\varphi)$ Eq. 2) derived from $\partial E/\partial\varphi=0$ and asteroid curve gave approximated DC MAS field. Fig. 2 compared the

approximation and micromagnetic calculation, where h_{SW} were plotted as a function of the DC field incident angles. In the calculation, microwave frequency is lower than critical frequency and h_{AC} is 0.03. The difference between the approximation and micromagnetic simulation were confirmed to be less than 8% and the discrepancy decreased with increase in θ.

[1] Jian-Gang (jimmy), et al., IEEE Trans. Magn., Vol. 44, p.125-131 (2008) [2] G. Bertotti, et al., Phys. Rev. Lett., Vol. 86-4, p. 724-727 (2001) [3] S. Okamoto, et al., J. Appl. Phys., Vol. 107, p. 123914 (2010)

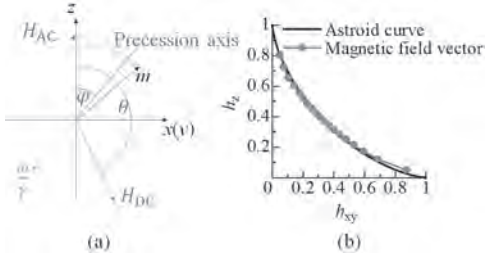

Fig. 1 (a) Schematic illustrations for the stable state of magnetization and magnetic fields. (b) Comparison between the calculated field components and asteroid curve.

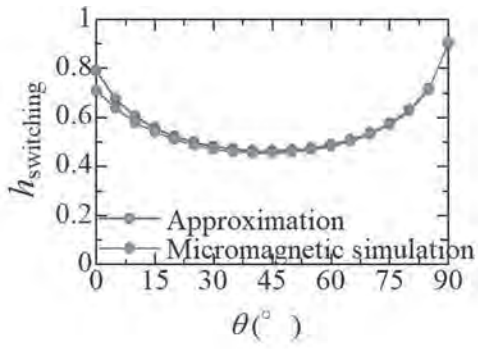

Fig. 2 Comparison between micromagnetic simulation and the approximation.

IPA-09. Curie temperature evaluation for $L1_0$ typed FePt alloy and granular films with various degrees of order by adopting Bloch's $T^{3/2}$ law. *T. Saito*[1], S. Kaneko[1], K. Tham[2], R. Kushibiki[2], T. Ogawa[1] and S. Saito[1] *1. Tohoku University, Sendai, Japan; 2. Tanaka Kikinzoku Kogyo K. K., Tsukuba, Japan*

As a next-generation technology for heat-assisted magnetic recording (HAMR), $L1_0$ typed FePt granular films with moderate Curie temperature (T_c) is a promising candidate [1]. In general, T_c for a FePt granular film is evaluated by high temperature measurement where the saturation magnetization (M_s) becomes 0 [2 - 4]. However, there is still a room for discussion regarding the value of T_c evaluated by such a method for the granular films because of change in the nanostructure by atomic diffusion and blocking phenomenon by thermal magnetization switching during the measurement. Therefore, we evaluated T_c by low temperature measurement through exchange integral (J) utilizing FePt alloy film (300 nm) with negligible nanostructure change and blocking phenomenon. Furthermore, we adopted this method for the granular films and discussed about the correlation between T_c and degree of order. Bloch $T^{3/2}$ law is expressed as the following equation; $M_s(T_{meas})/M_s(0) = 1 - C(k_B/J)^{3/2} T_{meas}^{3/2}$. (1) Here, C, k_B, T_{meas} represent Curie constant, Boltzmann constant, and measurement temperature, respectively. T_c is evaluated from J using mean field approximation as follows; $T_c = 2zS(S+1)J/3k_B$. (2) S shows spin. z is the number of the nearest neighbor atoms and assumed to be 8 since present FePt grains in the films are distorted ($c/a < 1$). Fig. 1 shows the dependence of M_s on $T_{meas}^{3/2}$ for FePt alloy films with various degrees of order (S_{in}). The slopes depended on S_{in}, which showed that J had a correlation with S_{in}. Focusing on the film with $S_{in} = 0.90$, J and T_c was evaluated to be about 2.67×10^{-21} J and 774 K, respectively. On the contrary, the experimentally obtained value of T_c is ~745 K according to the fitting by Brillouin function (see the inset). The evaluated value by adopting Bloch's $T^{3/2}$ law is close to the experimentally obtained one, which shows that the low temperature measurement is effective for the T_c evaluation. Fig. 2 shows (a) J and (b) T_c plotted against S_{in}. J increased monotonously as S_{in} increased. T_c changed from 453 to 774 K (from 180 °C to 501 °C) and had a positive correlation with S_{in}. In the conference, T_c for FePt granular films with various grain boundary materials will also be discussed.

[1] D. Weller et al., *Phys. Status Solidi A*, 210, 1245 (2013). [2] T. Ono et al., *Appl. Phys. Express*, 9, 123002 (2016). [3] T. Bublat et al., *J. Appl. Phys.*, 108, 113910 (2010). [4] C Papusoi et al., *J. Phys. D: Appl. Phys.*, 50, 285003 (2017).

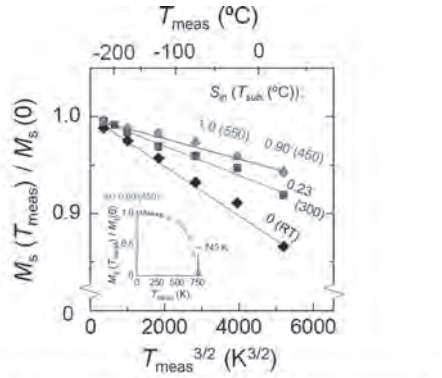

Fig. 1 Dependence of M_s on $T_{meas}^{3/2}$ for FePt alloy films with various degrees of order. An inset shows a typical example of dependence of M_s on T_{meas} for the film with S_{in} = 0.90.

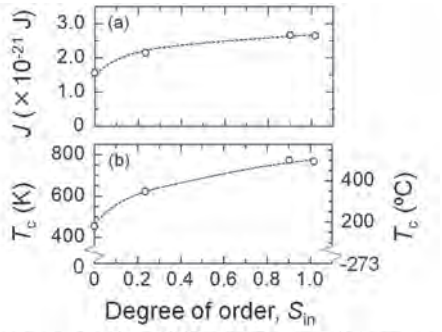

Fig. 2 (a) J and (b) T_c by adopting Bloch's $T^{3/2}$ law plotted against the degree of order for FePt alloy films.

IPA-10. Effect of N_2 gas-addition sputtering on nanostructure and magnetic properties of FePt-BN granular films for heat assisted magnetic recording. *K. Tham*[1], T. Saito[2], R. Kushibiki[1] and S. Saito[2] *1. Tanaka Kikinzoku Kogyo, Tsukuba, Japan; 2. Electronic Engineering, Tohoku University, Sendai, Japan*

Heat assisted magnetic recording (HAMR) is a promising candidate for the next magnetic recording technology. $L1_0$ FePt is an attractive material for HAMR media due to its high magnetocrystalline anisotropy (K_u) of ~5×10^7 erg/cm^3 at room temperature. Realization of columnar small magnetic grains with granular structure and good isolation, strong (001) texture, and high degree of order still remain challenging for its commercial applications. In order to achieve these requirements, many studies to add grain boundary materials (GBMs), such as B_2O_3[1)], SiO_2[2)], TiO_2[3)], BN[4)], and C[5,6)] into the FePt films have been done. According to our previous report, saturation magnetization (M_s) of the media depends on melting point of the GBM[1)], especially in FePt-BN granular film, nitrogen deficiency and B dissolution in FePt magnetic grains may occur simultaneously. Therefore, in order to nitridize B completely, we have carried out an N_2 gas-addition sputtering

to fabricate FePt-BN granular films. In this paper, we will report the evaluation result of nanostructure and magnetic properties of the films. Fig. 1 shows *M-H* loops of FePt-30vol%BN granular films sputtered with N_2 gas addition. The layer structure of the films is shown in the inset. When N_2 of 2% is introduced, hysteresis becomes larger and the gradient at around coercivity (H_c) becomes smaller. The details of magnetic properties are shown in Figure 2. When N_2 is varied from 0 to 2%, M_s slightly increases from around 560 to 600 emu/cm^3. At the same time, a significant increase of H_c from around 12 to 19 kOe can be observed. One reason of the H_c increase is due to the increase of magnetic anisotropy (H_k) from 38 to 58 kOe through the increase of K_u from 1.1×10^7 to 1.7×10^7 emu/cm^3. These results reveal that the complete nitridization of B will lead to the enhancement of M_s, H_k, and K_u of $L1_0$ FePt magnetic grain. In the conference, degree of order and nanostructure of the FePt-BN granular films sputtered with N_2 addition will also be reported.

1) T. Saito et al., *Jpn. J. Appl. Phys*., 59, 045501 (2020). 2) E. Yang et al., *J. Appl. Phys.*, 104, 023904 (2008). 3) Y. F. Ding et al., *Appl. Phys. Lett*., 93, 032506 (2008). 4) B. Zhou et al., *Appl. Phys. Lett.*, 118, 162403 (2021). 5) J. S. Chen et al., *Appl. Phys. Lett.*, 91, 132506 (2007). 6) A. Perumal et al., *J. Appl. Phys.*, 105, 07B732 (2009).

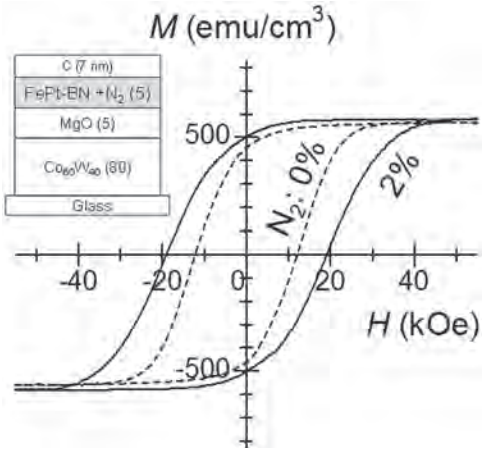

Fig.1 *M-H* loops of FePt-BN granular films sputtered with N_2 gas addition. The layer structure of the films is shown in the inset.

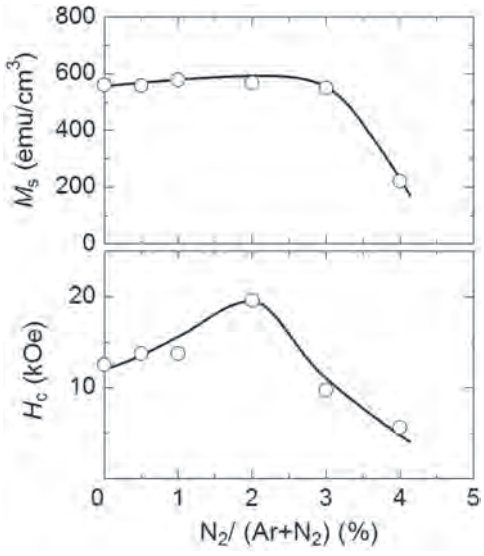

Fig.2 M_s and H_c dependence of FePt-BN granular film on N_2 gas flow ratio during the sputtering.

IPA-11. Humidity effects on the perfluoropolyether lubricants under the operational conditions of the heat-assisted magnetic recording.
H. Son[1], H. Park[1], H. Yang[1] and P. Chung[1] *1. Energy Systems Engineering, Inje University, Gimhae, The Republic of Korea*

Hard disk drives (HDD) with an aerial recording density surpassing terabit level demand a significant breakthrough in the area of magnetic recording technologies. Heat assisted magnetic recording (HAMR) is one of the promising applications of energy-assisted magnetic recording to drastically increase the recording density. During the HAMR process, the system undergoes local laser heating, which needs the layered materials (e.g., lubricant, carbon-overcoat (COC), and magnetic layers) to endure hotspots with temperatures approaching 700 K. Especially, the impact of this extreme heating requirement on the stability of the perfluoropolyether (PFPE) lubricant on the carbon overcoat must be investigated to guarantee the adequate protection of the media from tribological and corrosive damages. Previous experimental studies have investigated the effects of both the mechanical as well as thermal stress on degradation and desorption of PFPE lubricants [1,2]. In the study, we further developed of the previous lubricant depletion models by including the humidity effects on the lubricant layer with responses of thermal stress via the molecular dynamics simulation [3]. To analyze the effects, we explored static and dynamic properties for the various PFPEs with functionalities, humidity conditions and the operational temperature range of the HAMR. In the aspect of film structure, the lubricant film swells while the root-mean square roughness of the lubricant surface representing surface morphology was increased as the humidity increases, which may affect the clearance of the head-disk interface. The changes in the self-diffusion coefficient and the viscosity were also investigated in terms of dynamic properties. To precisely explore the issue of PFPEs under the thermal stresses, we compared the effects of transient versus steady heating to replicate the pulsed heating of the HAMR system. In addition, we constructed the correlation models of operational conditions, which can be utilized by the future researches on thermal stability of the HDI.

[1] Z. Tao and B. Bhushan, *Wear*, 259, 1352–1361 (2005). [2] R. Lei and A. Gellman, *Langmuir*, 16, 6628-6635 (2000). [3] B. Lei, C. H. Wong, and Q. Chen, *Soft Matter*, 9, 700-708 (2013).

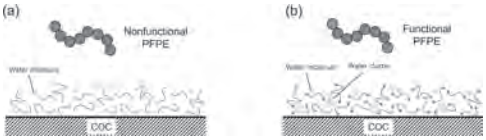

Fig. 1. Schematic descriptions of (a) nonfunctional and (b) functional PFPE lubricants under the humidity condition.

IPA-12. Control of switching time and energy dissipation for ultrafast photo-magnetic recording in dielectrics.
T. Zalewski[1] and A. Stupakiewicz[1] *1. Faculty of Physics, University of Bialystok, Bialystok, Poland*

Recently, it was discovered that without any external magnetic field, only by a single laser pulse, selective and reversible photo-magnetic switching in Co-doped yttrium iron garnet films (YIG:Co) can be obtained. This recording was characterized by an extremely short switching time of about 20 ps at room temperature. Moreover, because of its resonant character the write–read events are accompanied by an unprecedentedly low heat load [1]. Microscopically, in this mechanism incident linearly polarized pump pulse excites strongly anisotropic garnet ions, generating an effective field of photo-induced magnetic anisotropy [2],[3]. Here, we demonstrate the tunability of both magnetocrystalline and photo-induced anisotropies by the engineering of Co-doped thin iron garnet films and temperature variation. All experimental results were obtained using the time-resolved two-color pump and probe setup at Faraday geometry. The setup was tailored to perform the time-resolved femtosecond single-shot imaging on a CCD camera assuring obtain high temporal and spatial sensitivity. Through modifying the pump light fluence we were able to introduce a change in the light-induced anisotropy field. It allowed us to observe the change of

switching times of magnetization and decrease it even more by two times but at the expense of the greater energy required to achieve the switching threshold using a single pump laser pulse. On the other hand, by steering the sample temperatures in the 100-450 K, the range we triggered a change in the magnetocrystalline anisotropy field. Increasing it allowed us to decrease the energy dissipation threshold required for switching over five times. However, decreasing the switching threshold comes at the expense of a longer switching time. Moreover, we demonstrate that the photo-magnetic recording-based garnet medium operates within an extremely large temperature range between -100°C to 100°C. This finding reveals the principles to be employed in achieving cold and ultrafast magnetic recording in dielectrics far beyond today's state-of-the-art.

[1] A. Stupakiewicz, K. Szerenos, and A. V. Kimel, *Nature,* Vol. 542, p. 71 (2017) [2] F. Atoneche, A. M. Kalashnikova and Th Rasing, *Phys. Rev. B,* Vol. 81, p. 3 (2010) [3] K. Szerenos, A. V. Kimel and A. Stupakiewicz, *Phys. Rev. Appl.,* Vol. 12, p. 1 (2019).

Session IPB
SENSORS: MATERIALS, DEVICES AND APPLICATIONS II (Poster Session)

Sho Muroga, Chair
Akita University, Akita, Japan

IPB-01. Non-contact Wideband Current Sensing for High-frequency Power Converters Based on Convection Trace and Out-of-plane Field Sensing with Magnetoresistive Sensors. *X. Qi*[1], W. Miao[3], P. Pong[4] and C. Liu[2] *1. Electrical and Electronic Engineering, The University of Hong Kong, Hong Kong; 2. School of Energy and Environment, City University of Hong Kong, Hong Kong; 3. School of Mechatronic Engineering and Automation, Shanghai University, Shang Hai, China; 4. Electrical and Computer Engineering, New Jersey Institute of Technology, Newark, NJ, United States*

Introduction With demand for high power density and efficiency in power electronics, wide-bandgap power devices have drawn much attention [1] and current frequencies can reach up to megahertz [2]. This can affect adversely the accuracy of resistive-based and electromagnetic-based current sensors [3]. Compared with resistive shunts, current transformers, Rogowski coils, and Hall-effect sensors, magnetoresistive (MR) sensors are more promising due to non-invasiveness, wide bandwidth from DC up to MHz, small size and less vulnerability to drift and noise. Proposed Method and Results When MR sensors measure horizontal magnetic fields (B_x) around a copper trace on a printed circuit board (PCB) in Fig. 1(a), the bandwidth is limited due to the skin effect. At high frequency, the current flow concentrates at edges, leading to drastic change on B_x. The proposed method takes advantage of this phenomenon and focuses on vertical magnetic fields (B_y) instead. By measuring B_y at the right or left side of the trace, B_y variation is alleviated at high frequency because the current flow at both edges produces similar B_y. The concept of flat-bandwidth (FBW) is defined to quantify variations of magnetic fields [4]. FBW gives a maximum current frequency at which the magnetic field magnitude changes by 5% from that at DC. The simulation results of FBW for B_x along y-axis and B_y along x-axis at different distances are shown in Fig. 1(b). B_y offers better frequency response than B_x. At 70 mil, FBW for B_y is over 1 MHz. Furthermore, to increase the signal-to-noise ratio, the trace is designed to be folded on a PCB, and an MR sensor is placed between the trace in Fig. 2(a). Such convection trace can broaden the measurement bandwidth and is less vulnerable to noise. The normalized B_y at center of the convection trace at various frequencies are shown in Fig. 2(b), and FBW is around 5.3 MHz. Even though the frequency reaches 100 MHz, the magnetic field variation is merely slightly over 5%. Thus, the proposed method overcomes the drawback of limited bandwidth for high-frequency current sensing.

[1] J. Millan, P. Godignon, X. Perpina, A. P. Tomas, and J. Rebollo, "A survey of wide bandgap power semiconductor devices," *IEEE Trans. Power Electron.*, vol. 29, no. 5, pp. 2155–2163, May 2014. [2] S. J. Nibir and B. Parkhideh, "Magnetoresistor with planar magnetic concentrator as wideband contactless current sensor for power electronics applications," *IEEE Trans. Ind. Electron.*, vol. 65, no. 3, pp. 2766–2774, Mar. 2018. [3] T. J. Brauhn, M. Sheng, B. A. Dow, H. Nogawa, and R. D. Lorenz, "Module-integrated GMR-based current sensing for closed-loop control of a motor drive," *IEEE Trans. Ind. Appl.*, vol. 53, no. 1, pp. 222–231, Jan./Feb. 2017. [4] M. Sheng, M. H. Alvi, and R. D. Lorenz, "GMR-based Integrated Current Sensing in SiC Power Modules with Phase Shift Error Reduction", *IEEE J. Emerg. Sel. Topics Power Electron.*, DOI: 10.1109/JESTPE.2020.3028275.

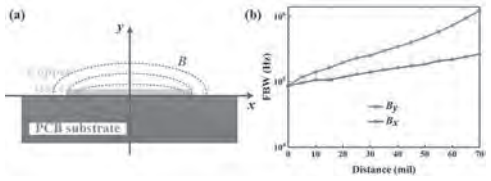

(a) Copper trace on PCB. (b) FBW for B_x along y-axis and B_y along x-axis.

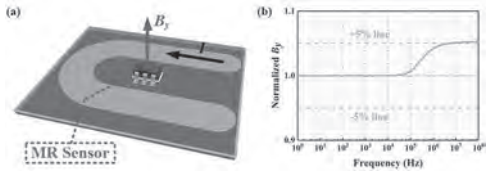

(a) Proposed convection trace. (b) Normalized B_y with respect to frequency.

IPB-02. DC-biased Eddy Current Sensor for Arbitrary Orientation Defects Detection in Ferromagnetic Steel Using Orthogonal DC Magnetic Field and Eddy Current. *D. Um*[1] and G. Park[1] *1. Pusan National Univsersity, Busan, The Republic of Korea*

Many scientists have developed state-of-art EC sensors to overcome difficulties by modifying the configuration of eddy current coil as well as adopting high-sensitive magnetic sensors. Magneto-resistive sensors such as GMR and TMR replace by sensing coils, and they can improve the spatial resolution and SNR with respect to the defect. In addition, multiple exciting coils are used to generate a rotating magnetic field for detecting arbitrary orientation defects. Instead of aforementioned methods, this paper suggests an alternative EC sensor to classify arbitrary orientation defects, which will be coined as 'DC-biased eddy current sensor. This method has originally used to detect opposite surface defects using both dc magnetic field and ac magnetic field [1], [2]. If dc magnetic field is distorted due to the existence of the defect, the magnetic permeability changes depending on the nonlinear characteristics of the ferromagnetic material. Fig.1(a) shows a configuration of DC-biased EC sensor. The permanent magnet is used to excite dc magnetic field, and the focusing coil is used to generate unidirectional eddy current perpendicular to the direction of dc magnetic field. In Fig. 1(b), both magnetic field and electric current make a detour around low permeable and conductive discontinuities. When the defect orientation is perpendicular to the direction of eddy current, only eddy current will be distorted significantly, and large sensitivity of signals can be acquired. In contrast, large perturbation can be observed by permeability changes from large perturbation of dc magnetic field even though the defect orientation is parallel to the direction of eddy current. Fig. 2 compares the normalized eddy current density with and without dc-bias magnetic field, the result can show a clear difference when the defect is oriented parallel to the direction of eddy current so this method can improve both SNR and classification of the defect orientation.

[1] Y. Gotoh and Y. Ishida, IEEE Transactions on Magnetics, vol. 50, pp. 1-4, (2014) [2] J. Wu, J. Zhu, H. Xia, C. Liu, X. Huang, and G. Y. Tian, IEEE Trans. Industrial Informatics., vol. 15, pp. 6252-6259, (2019)

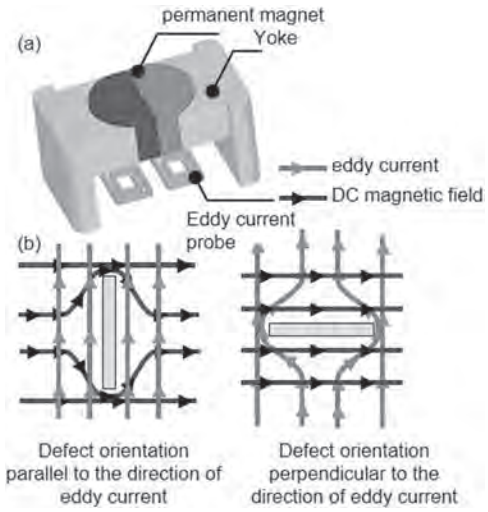

Fig. 1. (a) DC-biasing eddy current sensor and (b) magnetic field and eddy current perturbation with different defect orientations.

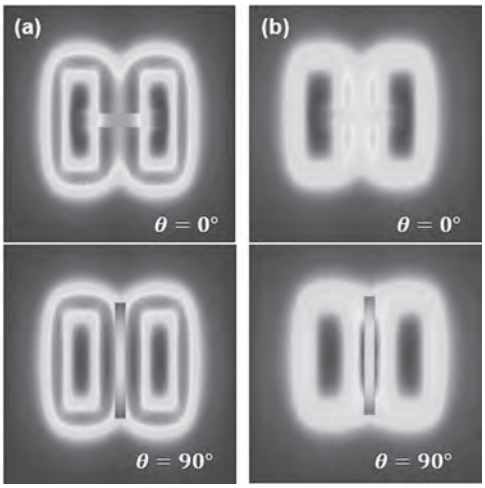

Fig. 2. Comparison of eddy current distribution (a) without (b) with dc bias magnetic field when the defect orientation is θ = 0° and θ = 90°.

IPB-03. Controlling of magnetoimpedance property of thin-film element using Joule-heating. *H. Kikuchi*[1], A. Ueno[1] and M. Tanii[1] *1. Iwate University, Morioka, Japan*

A magnetic field sensor using magnetoimpedance (MI) has a higher sensitivity [1] and MI properties strongly depend on a magnetic anisotropy of a material [2]. Thus, controlling anisotropy is quite important to obtain large impedance changes. In general, an anisotropy can be controlled by a field annealing in vacuum using a furnace. The furnace is a large-scale, and consumes a lot electric power for heating and generating strong field. On the other hand, Joule-heating, a current is directly applied to an element, is a simple way and therefore achieves a compact equipment with a low power consumption. However, there are few reports that Joule-heating applies to ferromagnetic thin-film [3] and no reports that studies controlling anisotropy itself by Joule-heating. Thus, we investigated to controlling magnetoimpedance properties by Joule-heating on a thin-film element as a feasibility study. The amorphous CoNbZr thin-film element with Cu electrode was prepared. Then, a direct DC current of 80-120 mA was applied to the elements using a wafer probe with 1 minute in the atmosphere. In some cases, the element was applied to an external field parallel to the width direction of the elements by magnets during heating. Fig. 1 shows the field dependence of impedance at 100 MHz. Before heating, impedance has maximum at zero field and then decrease with increasing field intensity, which is typical profile when an element has the easy axis along with the longitudinal direction of the element. On the other hand, a double peak appears and its peak height slightly increases with increasing intensity of DC current after Joule-heating with magnets. The field intensity where the impedance has a peak, shifts to higher field with increasing intensity of DC current. Fig. 2 shows the domain structures of the element observed by a Kerr-effect microscopy before and after Joule-heating. Although the element has domains parallel to the length direction of the element before heating, 180° domains parallel to almost width direction appear after heating. This means the easy axis of the thin-film element can be controlled by Joule-heating.

1. L. V. Panina, K. Mohri, "Magneto-impedance effect in amorphous wires," Appl. Phys. Lett. 65 (1994) 1189–1191. 2. H. Kikuchi, M. Takezawa, M. Yamaguchi, K. I. Arai, "Analysis of the high-frequency impedance of micromachined films," *J. Magn. Soc. Jpn*. 21 (1997) 789–792. 3. V. Polewczyk, G. Vinai, F. Motti, S. Santhosh, S. Benedetti, G. Rossi, P. Torelli, "Thermal assisted tailoring of magnetic coercivity in Iron thin films on unstable Lithium Niobate substrate," J. Magn. Magn. Mater. 515 (2020) 167257.

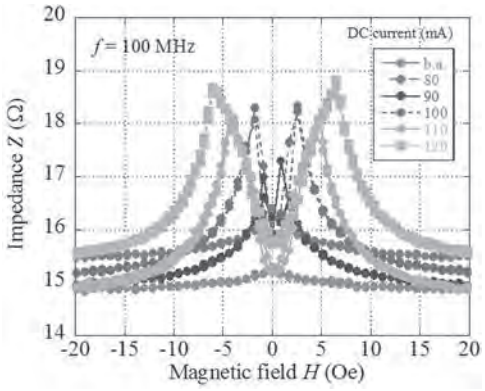

Fig. 1 Field dependence of impedance.

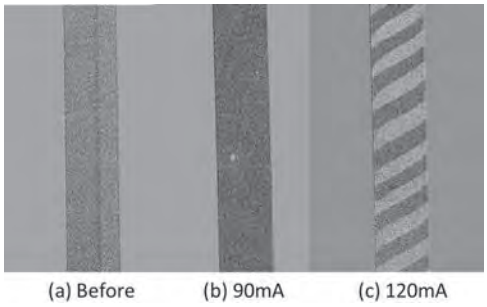

Fig. 2 Changes in domain structures.

IPB-04. Development of magnetic tunnel junctions with symmetric R-H curve for specific sensor application. *S. Manceau*[1,2], V. Pasanisi[1], C. Ducruet[3], P. Sabon[1], C. Cavoit[2], G. Jannet[2], L. Prejbeanu[1], M. Kretzschmar[2] and C. Baraduc[1] *1. Spintec, Grenoble, France; 2. LPC2E, Orléans, France; 3. Crocus, Grenoble, France*

Magnetic Tunnel Junctions (MTJ) are widely used as magnetic sensors but their major disadvantage is their high noise level at low frequency. Some methods to overcome 1/f noise involve adding magnetic modulation [1] or increasing the MTJ area [2]. In order to get a linear response, in-plane MTJ are usually designed with the free layer (FL) set perpendicularly to the reference. However, for a specific application [3], a symmetric R-H characteristic is more suitable to drive a modulation and should be easily obtained by pinning the FL in the same direction as the reference. The aim of this study is to process MTJs with symmetric R-H curve and high sensitivity. The magnetic stack is composed of a pinned synthetic antiferromagnet, MgO tunnel barrier and CoFeB/NiFe free layer. After patterning micron-size junctions of different shapes, we perform a post-process annealing

under magnetic field. In this work, we study different methods to achieve a coherent rotation of the FL magnetization towards the hard axis: i) applying a small external field along the easy axis; ii) using shape anisotropy; iii) using soft pinning by adding an antiferromagnetic layer on the FL separated by a thin Ta spacer [4]. Our measurements highlight the importance of FL pinning on the reversibility and smoothness of the R-H curves. Nevertheless, since pinning reduces sensitivity, an optimum trade-off must be found. We observed that shape anisotropy alone is not sufficient to pin the FL *(fig.1)*, but a coherent rotation is achieved by applying an external field. Moreover, our results show the importance of a good alignment between the reference and the easy axis. Compensating for the process misalignement by tilting the applied field allows to reduce the pinning field to 5 Oe *(fig.2)* with a sensitivity of 3.5%/mT. On the other hand, soft pinning can provide internal pinning ranging from 120 to 0 Oe by increasing the Ta spacer up to 0.25 nm. Choice of the optimum spacer thickness and further process optimizations should reduce hysteresis and improve the sensitivity.

[1] R. C. Chaves, P. P. Freitas and B. Ocker, Appl. Phys. Lett., Vol. 91, p.102504 (2007) [2] E. Paz, S. Serrano-Guisan and R. Ferreira, J. Appl. Phys., Vol. 115, p.17E501 (2014) [3] A. Bocheux, C. Cavoit and M. Mouchel, IEEE (SAS 2016) Proceedings, p.149 (2016) [4] R. Ferreira, E. Paz and P. P. Freitas, IEEE Transactions on Magnetics, Vol. 48, p.3719 (2012)

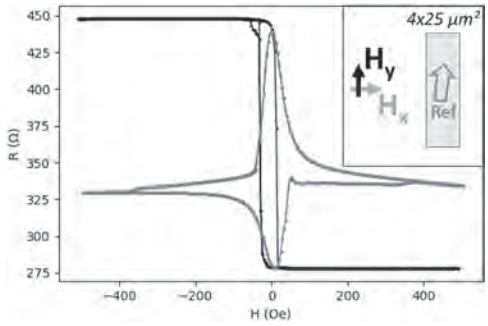

Fig.1: R-H curves measured along easy axis H_y and hard axis H_x

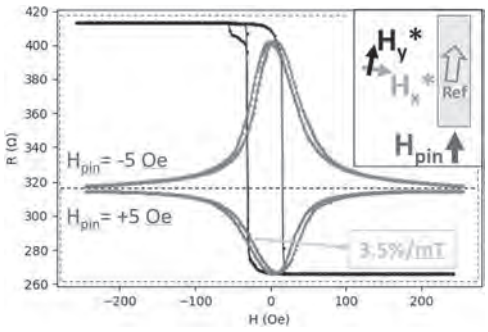

Fig. 2: R-H curves measured with respect to the reference misalignment (1.6°) and pinning fields H_{pin} of 5 and -5 Oe

IPB-05. Specular spin-valve sensors with improved magnetoresistance for polymer-based tubular devices. M. Ferreira[1,2], D.N. Faye[1], *P. Araujo*[1,2], S. Cardoso de Freitas[1,2] and D. Leitao[1,2] *1. INESC MN, Lisboa, Portugal; 2. Tecnico, University of Lisbon, Lisboa, Portugal*

The ability to provide conformable and shapeable devices opened new doors in wearable technologies and biomedical sensors [1]. Depending on the application, the microdevices may be required to retain their initial properties and performance even after being shaped into a particular geometry [2]. To enhance the magnetoresistance of spin-valve (SV) sensors directly grown and patterned on polymeric foils, we have incorporated nano-oxide layers (NOLs) in the multilayer [3]. Specular SVs were directly grown on 25 μm polyimide (PI) foils by ion beam deposition. NOLs were formed in 10min natural oxidation at atmosphere within the load lock. SVs were annealed in vacuum at 250°C for 30min, and cooled under 1T. The thicknesses of $Co_{80}Fe_{20}$ and Ta were tuned to maximize MR, minimize H_f and Hc, and improve the saturation plateau [Fig.1(a)]. The best specular SV on PI was Ta(2)/$Ni_{80}Fe_{20}$(2.5)/$Mn_{74}Ir_{26}$(8)/$Co_{80}Fe_{20}$(2.3)/ NOL/$Co_{80}Fe_{20}$(2)/Cu(2)/ $Co_{80}Fe_{20}$(2.6)/$Ni_{80}Fe_{20}$(2.3)/Ta(5) (nm) with MR=10.8%, H_c<1Oe, Hf~20Oe H_{exc}>400Oe. In rigid substrates the stack Ta/$Ni_{80}Fe_{20}$/$Mn_{74}Ir_{26}$/$Co_{80}Fe_{20}$/ NOL/$Co_{80}Fe_{20}$/Cu/$Co_{80}Fe_{20}$/ $Ni_{80}Fe_{20}$/NOL/$Co_{80}Fe_{20}$/Ta (target compositions in at. %), shows MR=10.3%, H_c<2Oe, H_f<3Oe and H_{exc}>400Oe. Sensors were then micropatterned combining optical lithography, ion milling and lift-off steps, all optimized to minimize damage, and mitigate stress accumulation [4][Fig.1(b,c)]. Linear responses (Fig.2) were obtained with MR up to 9%, $|H_f|$<15Oe, H_c<2Oe, and R_{min}=0.7-1.0kΩ. Samples were then molded for 20min at 140°C in atmosphere, using pre-defined cylindrical casts. To improve mechanical resilience and reduce device failure upon molding [5], samples were encapsulated in 24μm spin-coated SU-8. When in the tubular shape, the embedded specular SV sensors showed a <1% decrease in MR, but an increase in H_c. The concept for magnetic field detection in tubular devices will be demonstrated and discussed (Fig.2).

[1] Ha et al. 2021, *Adv Mat*, *33*, 2005521; Bermúdez et al.2018, Sci Adv 4 [2] Egunov et al.2021 *Small*, 2002549. [3] Veloso et al.2000 *Appl Phys Lett* 77,1020 [4] Ferreira et al.2021 J Magn Mag Mat, 538, 168153 [5] Mouro J, Ferreira M, et al. 2021 Derivation of analytical expressions for the stress and strain distributions, bending plane and curvature radius in multilayer thin-film composites, *under review* Funding: PTDC/NAN-MAT/31688/2017, IF/00713/2015, UID/05367/2020, PD/BD/150390/2019, PD/BD/150391/2019. DCL acknowledges FSE/POPH.

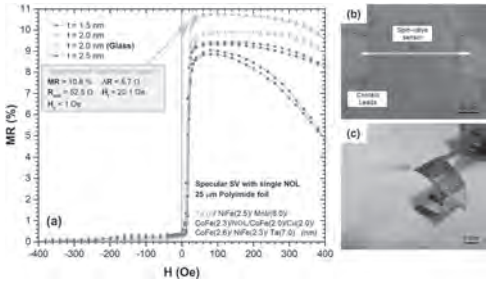

Fig.1: (a) Unpatterned specular SVs on PI foils with different buffer thicknesses. (b) Patterned SV embedded in (c) free-standing PI substrate.

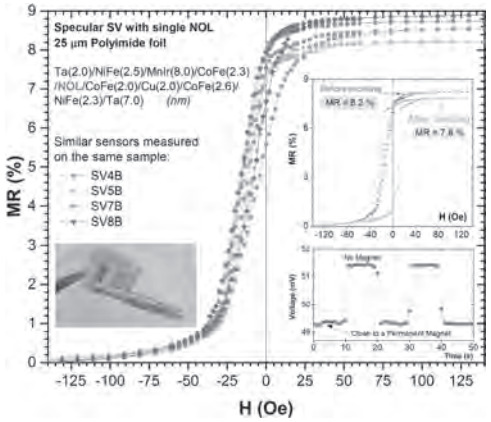

Fig.2: Specular SV sensors output onto 25μm PI foils. The insets show the output before and after molding, a PI tubular device and its response over time to a permanent magnet.

IPB-06. Signal to Noise Ratio Analysis of GMR Line Devices for High Sensitive Magnetic Sensor Applications. *N. Fukatani*[1], M. Ichimura[1] and J. Hayakawa[1] *1. Hitachi Ltd., Kokubunji, Japan*

In recent years, giant magnetoresistance (GMR) devices have been used in many applications due to their small size, high sensitivity, low power consumption, and low cost[1, 2]. For a high sensitive magnetic sensor application, the device resistance is required to be varied linearly over a wide magnetic field range. A high aspect ratio of the GMR line device is useful for the wide range high linearity of the MR curve. However, the high aspect ratio reduces MR ratio and increase signal to noise ratio (SNR) because the exchange bias for minor axis direction in the GMR line is suppressed due to the strong shape anisotropy in the pinned layer. In this study, we investigated the correlation between SNR and MR properties in GMR line devices for magnetic sensor applications. The GMR stack is composed of Si/SiO sub.//seed layer/IrMn(6)/CoFe(1.6)/ Ru(0.85)/CoFe(1.6)/Cu(2.5)/ CoFe(1)/NiFe(3.5)/capping layer (all thickness in nm). The pinned layers were magnetized for minor axis direction in GMR lines. Figures 1(a)-(c) shows a schematic, cross sectional and top view of scanning electron microscope (SEM) images of the GMR device, respectively. The GMR device has ten GMR lines in the parallel configuration. The line length and space width were fixed at 100 μm and 600 nm, respectively. The line width (*W*) was varied from 300 nm to 2 μm. Figure 2(a)-(e) show MR curves of the GMR lines with various *W* with external field of ±20 Oe. The MR curves were measured 100 round trips for evaluating SNR. MR ratio increased as increasing *W* due to the stabilization of antiparallel configuration of free and pinned layers. On the other hand, the linearity of the MR curve decreased at *W* of 2 μm because of the reducton of shape anisotropy. The reduction of MR curve linearity increased device resistance variation. Figure 2(f) shows SNR values calculated from the MR ratio and coefficient of the resistance variatoin. SNR increased as increasing *W*. These results mean that it is important to increase *W* within the range that maintains the linearity of the MR curve.

[1] A. Bernieri, G. Betta, L. Ferrigno, and M. Laracca, IEEE Sens. J. 13, 4513 (2013). [2] L. Jogschies, D. Klaas, R. Kruppe, J. Rittinger, P. Taptimthong, A. Wienecke, L. Rissing, and M. C. Wurz, IEEE Sens. J. 15, 28665 (2015).

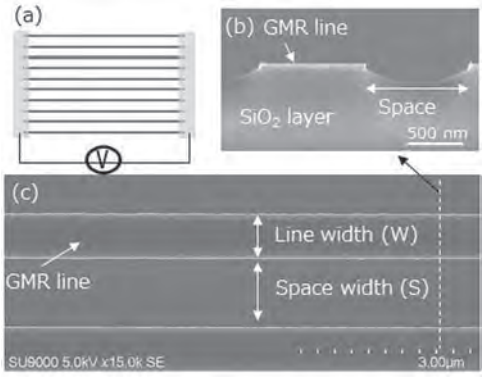

Fig. 1 (a) A schematic, (b) cross-sectional and (c) top view of SEM images of the GMR device.

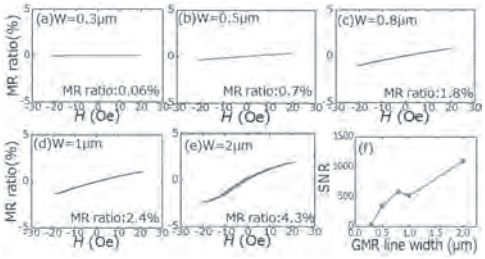

Fig. 2 (a)-(e) MR curves and (f) signal to noise ratios for the various *W* of GMR devices.

IPB-07. Effects of fall times of pulse currents on output voltages for amorphous-wire-based magnetic sensors. *T. Kaneko*[1], Y. Honkura[2], S. Honkura[3] and F. Akagi[1] *1. Kogakuin University, Tokyo, Japan; 2. Magnedesign Co. Ltd., Aichi, Japan; 3. Nanocoil Co. Ltd., Aichi, Japan*

1. Introduction Ultra-high sensitivity and micro-sized magnetic sensors are required in biomagnetic measuring devices. The GigaHertz spin rotation sensor, which is an evolution of the magneto-impedance sensor, has shown high sensitivity while transmitting GHz pulse currents [1]. Detection magnetic fields are sensed via a pickup coil wrapped around the wire when the GHz pulse currents are applied. However, the micro-mechanism in the amorphous wire, which exhibits high sensitivity, has not been characterized. Thus, we investigated the relationship between peak voltages and magnetic fields and the magnetization behavior inside the amorphous wire. 2. Calculation method and conditions The magnetization behavior was calculated using the Landau–Lifshitz–Gilbert equation, which considers eddy currents. The calculation model of the amorphous wire is shown in Fig. 1. The magnetic properties included a saturation magnetization of 1.0 T, a magnetic anisotropy constant of 250 J/m^3, and exchange constants between cells in the plane and the axial direction of 1.0×10^{-11} J/m and 2.0×10^{-11} J/m, respectively. The magnetization easy axis of the amorphous wire from the outer circumference to the inside by 0.75 μm was assumed to be oriented in the circumferential direction because compressive stress is generated in the FeCoSiB amorphous wire, which is induced via rapid quenching during the fabrication processes [2]. 3. Results Fig. 2 shows the relationship between the peak voltages at the fall times of the pulse currents and magnetic fields. When the fall time was 1.0 ns, the calculated and experimental results showed the same tendency. A shorter fall time meant higher absolute values of the peak output voltages and stronger magnetic fields as shown in Fig. 2. At a fall time of 0.385 ns, only the rotations of magnetizations in the outer circumference of the amorphous wire contributed to the output voltages, whereas at a fall time of 5.0 ns, the domain wall motions inside the wire contributed to the output voltages. This was the reason why the output peak voltages increased as the fall time was shortened.

[1] Y. Honkura, S. Honkura, *J. Magn. Magn. Mater.*, 513, 167240, (2020). [2] K. Mohri, F.R Humphrey, K. Kawashima, K. Kimura and M. Mizutani, *IEEE Trans. Mag.*, 26(5), pp.1789-1791 (1990).

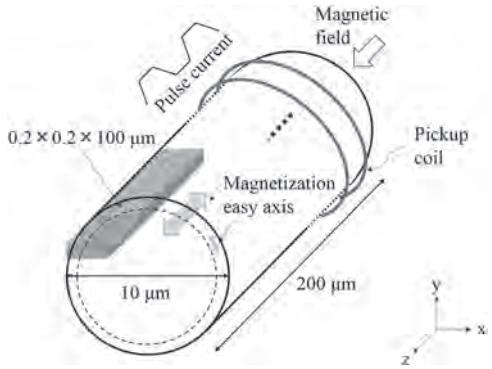

Fig. 1 Model of a magnetic sensor with an amorphous wire

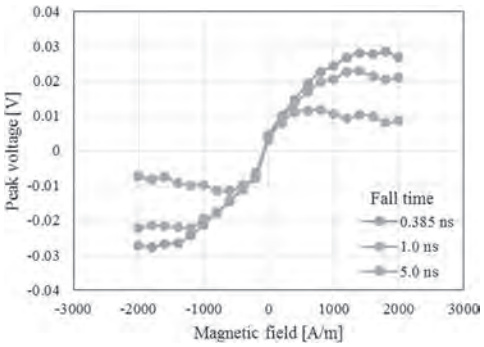

Fig. 2 Relationship between peak voltages and magnetic fields

IPB-08. Vibration Signal Suppression Effect of Dual Induction Eddy Current Probe in Dynamic Environment. *D. Kosaka*[1], T. Shioya[1], Y. Kumakura[2], F. Kojima[3] and H. Yamasaki[2] *1. Polytechnic University, Kodaira, Japan; 2. Tex Riken Co., Ltd., Nishinomiya, Japan; 3. Kobe University, Kobe, Japan*

Background and problem considered Eddy Current Testing (ECT) is one of the Non-Destructive Techniques and is widely used in manufacturing processes of long metal parts for surface inspection of metals. However, ECT creates a bottleneck preventing the speeding up of processes because the vibration of the inspection sample caused by the high speed of the manufacturing processes has a negative impact on ECT [1]. In previous studies, signals caused by vibration are removed from the detection signal by signal processing [2]-[4]. However, these processes are limited in their inspection speed by the speed of the digital signal processors performing the signal processing. We have proposed a new ECT probe that is more effective in suppressing the vibration component in the detection signal than that of the conventional self-induction probe does not require signal processing such as the multi-frequency method [5]. In this paper, the principle and effect of our proposed probe that can suppress vibration signals in detection signals are discussed. The Principle and Vibration Signal Suppression Effect in Dynamic Environment A photo of a used experimental setup is shown in Fig. 1. A brass rod that has two cracks was used as the test specimen. A vibration generator, consisting of a pulley and motor, can apply vibration to the test specimen. The proposed probe is an encircling probe with four coils and three induction modes, the self, mutual and dual induction modes. This probe is characterized by the fact that the vibration signals detected in the self and mutual induction modes cancel each other out, as in noise-canceling headphones when the dual induction mode is used. Fig. 2 shows measured results of the self and dual induction modes when vibration was applied to the brass rod. The amplitude of the dual induction mode was lower than the amplitude of the self induction mode. However, crack signals were not suppressed. The detail of the principle, the experimental method and comparison between the proposed method and the multi frequency method will be presented in our presentation.

[1] C. Reboud, D. Prémel, G. Pichenot, D. Lesselier and B. Bisiaux, “Development and validation of a 3D model dedicated to eddy current non-destructive testing of tubes by encircling probes,” International Journal of Applied Electromagnetics and Mechanics, Vol. 25, No. 1-4, pp. 313-317, 2007. [2] Shu, Li, Huang Songling, and Zhao Wei, “Development of differential probes in pulsed eddy current testing for noise suppression,” Sensors and Actuators A: Physical, Vol. 135, No. 2, pp. 675-679, 2007. [3] D. Kosaka, K. Kakishita, and T. Nara, “Plating thickness evaluation with the radial basis functions,” International Journal of Applied Electromagnetics and Mechanics, Vol. 64, pp. 1081–1089, 2020. [4] Bartels, Keith A., and Jay L. Fisher. “Multifrequency eddy current image processing techniques for nondestructive evaluation,” Proceedings., International Conference on Image Processing. Vol. 1. IEEE, 1995. [5] Daigo Kosaka, Yuji Kumakura, Fumio Kojima, Hiroyuki Yamasaki, “New Eddy Current Probe for Vibration Signal Suppression,” IEEE Transactions on Magnetics, in press.

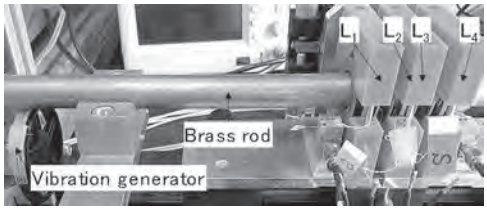

Fig. 1. The experimental setup.

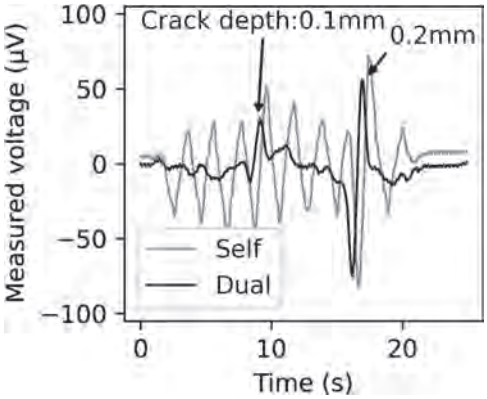

Fig. 2. Measured results in dynamic environment.

IPB-09. Magnetic properties and high frequency characteristic of M-type hexaferrite synthesized by the molten salt method. *M. Kim*[1], M. Gu[2], K. Kim[2] and J. Kim[1] *1. Department of Materials Science and Chemical Engineering, Hanyang University, Ansan, The Republic of Korea; 2. Department of Physics, Yeungnam University, Gyeongsan, The Republic of Korea*

Due to the development of the next generation communication technology, magnetic materials are forced to increase their working frequency. Thus, magnetic materials need to possess high electrical resistivity and anisotropy field. Among them, M-type ferrite, known to have ferromagnetic resonance (FMR) frequency in the GHz range, could be an excellent candidate for the communication devices [1]. Thus, it is required to evaluate the high frequency characteristics of M-type ferrite. In this experiment, $SrFe_{12}O_{19}$ powders were synthesized by the molten salt method using strontium carbonate, hematite, and sodium chloride. These raw materials were mixed by ball milling for 24 hr to form a homogeneous mixture and then annealed in a box furnace with various calcination conditions to synthesize the M-type ferrite phase. In order to control the particle size of $SrFe_{12}O_{19}$ powders, two sizes of hematite powders, 0.3 μm and 1.0 μm, were used. Their magnetic properties were measured by a vibrating sample magnetometer (VSM), and the permeability was measured by a network analyzer. Fig. 1 shows the VSM hysteresis loops and magnetic properties of strontium ferrite powders synthesized by the molten salt method with two different sizes of hematite powders. Since the magnetic saturation is close to the theoretical value (74.3 emu/g) of $SrFe_{12}O_{19}$ at room temperature [2], the M-type ferrite phase is proven to be successfully synthesized. In addition, the difference in the hysteresis loops suggests that the magnetic properties can be controlled by the size of precursor powders. Fig. 2 shows changes in permeability of $SrFe_{12}O_{19}$ sheets with frequency. As shown in Fig. 2, the FMR of the both sheets occurred around 50 GHz, despite the difference in coercivity of the synthesized powders. A more detail on the effects of various M-type ferrite powders on permeability will be discussed.

[1] R. Topkaya, J. Alloys Compd. 725, 1230 (2017) [2] M. Kim, K. Lee, M. Choi, and J. Kim, IEEE Transactions on Magnetics, 54, 1 (2018)

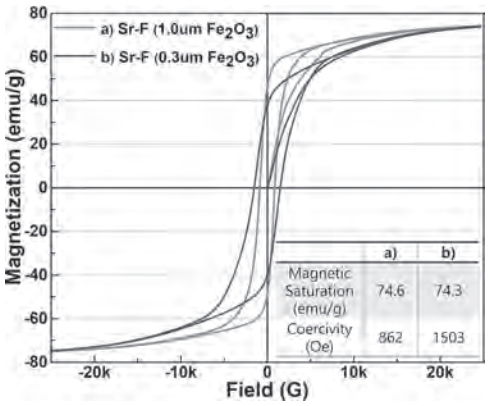

Fig. 1. VSM hysteresis loop and magnetic properties of synthesized $SrFe_{12}O_{19}$ powders

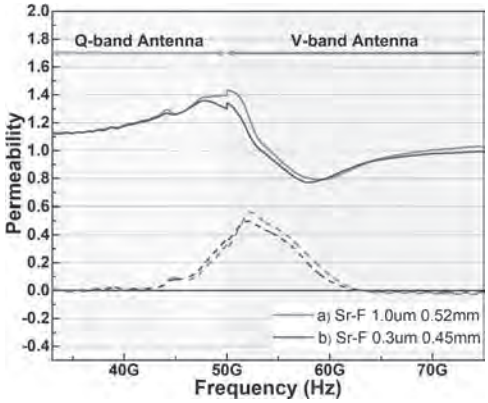

Fig. 2. Permeability of composite sheets of synthesized powders measured by network analyzer

IPB-10. Orienting Receiver to Transmitter in an Inductive Power Transfer System Using Tunnel Magnetoresistance Sensors. *J. Liu*[1], J. Zhou[1], C. Lee[1] and P. Pong[2] *1. Department of Electrical and Computer Engineering, The University of Hong Kong, Hong Kong; 2. Department of Electrical and Computer Engineering, New Jersey Institute of Technology, Newark, NJ, United States*

1. Introduction The distance and orientation between the transmitter and receiver govern the power transfer efficiency of an inductive power transfer (IPT) system [1-2]. Most researches focus on the coupling estimation by the reflected impedance [3-4]. However, the change of reflected impedance is a collection variation of distance, orientation, and load, only providing very limited information of the system behavior. In this paper, a tunnel magnetoresistance (TMR) sensor-based technique is proposed for IPT system to acquire the vectorial magnetic flux density (B-field). The accurate transmitter/receiver location and orientation can be predicted based on the measured B-field. This technique opens a new research direction for autonomous robots wireless charging with the aid of location information. 2. Magnetic Flux Density Acquisition The transmitter and receiver coils are configured in Fig. 1(a). The receiver location is described by the vertical distance between transmitter and receiver P_Z, lateral misalignment P_X, and angular misalignment α. An XY-axis TMR sensor array is placed on the receiver surface, with the center of the sensor array and the receiver coinciding, as shown in Fig. 1(b). The Biot-Savart law describes the B-field surrounding the receiver, which allows us to determine the receiver location and orientation. 3. Preliminary Results First, varying P_X from 0 to 30 mm, the B-field B_z distribution on the X-axis sensor array is depicted in Fig. 2(a). The B_z curves are shifted fairly linearly along with the change of P_X position, as shown in Fig. 2(b). Second, the B-field distribution with 0° and 45° angular misalignment are compared in Fig. 2(c). The α leads to the B-field increase in the center of the Y-axis sensor array. Besides, the α can be evaluated by calculating the arctangent between B_x and B_y on Y-axis sensor array. The linear fit between the reference and calculated α values are plotted in Fig. 2(d), validating the feasibility of the proposed method. 4. Conclusions The TMR sensors acquire the surroundings B-field to determine the location and orientation of the transmitter/receiver in an IPT system. In the full paper, more details of theoretical analysis and experimental results will be presented.

[1] Jadidian, Jouya, and Dina Katabi. "Magnetic MIMO: How to charge your phone in your pocket." Proceedings of the 20th annual international conference on Mobile computing and networking. 2014. [2] Kim, Min-Woo, et al. "High-resolution synthesized magnetic field focusing for RF barcode applications." IEEE Transactions on Industrial Electronics 65.1 (2017): 597-607. [3] Liu, Junwei, et al. "A Parameter Identification Approach with Primary-Side Measurement for DC-DC Wireless-Power-Transfer Converters with Different Resonant Tank Topologies." IEEE Transactions on Transportation Electrification (2020). [4] Guo, Yanjie, et al. "Load Parameter Joint Identification of Wireless Power Transfer System Based on the DC Input Current and Phase-Shift Angle." IEEE Transactions on Power Electronics 35.10 (2020): 10542-10553.

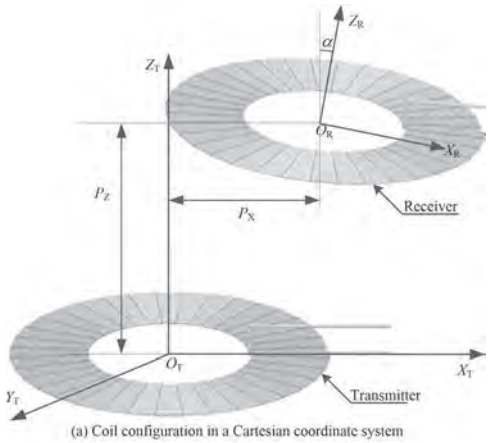

(a) Coil configuration in a Cartesian coordinate system

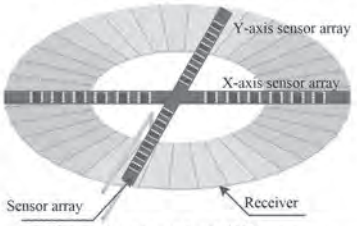

(b) 3D view of receiver coil with TMR sensor array

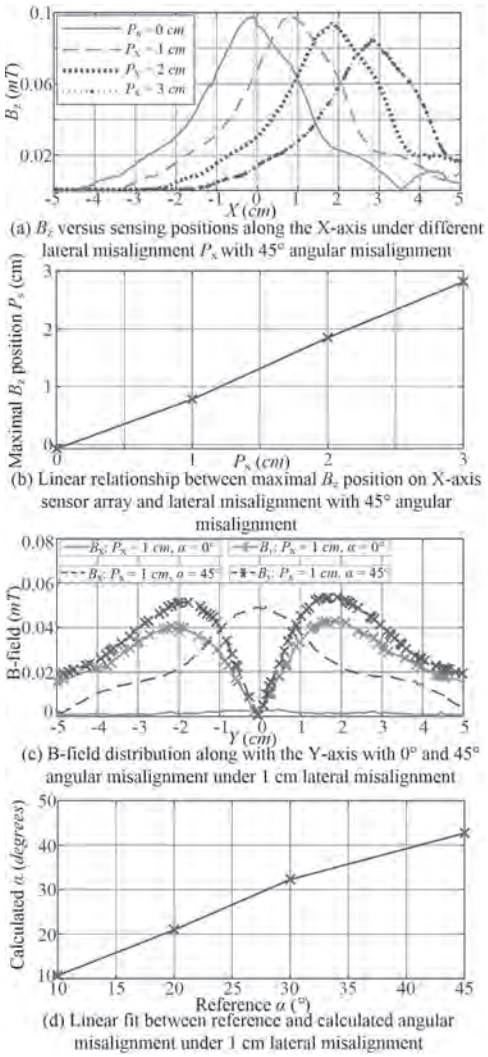

(a) B_z versus sensing positions along the X-axis under different lateral misalignment P_x with 45° angular misalignment

(b) Linear relationship between maximal B_z position on X-axis sensor array and lateral misalignment with 45° angular misalignment

(c) B-field distribution along with the Y-axis with 0° and 45° angular misalignment under 1 cm lateral misalignment

(d) Linear fit between reference and calculated angular misalignment under 1 cm lateral misalignment

IPB-11. Hybrid microfluxgate and current transformer sensor. *C. Lu*[1], Y. Lin[1], Y. Tian[1] and J. Jeng[2] *1. Department of Mechanical Engineering, National Taipei University of Technology, Taipei, Taiwan; 2. Department of Mechanical Engineering, National Kaohsiung University of Science and Technology, Kaohsiung, Taiwan*

The current sensor comprising a ring-core and a magnetic field sensor was shown to be suitable for static and alternating current measurement [1]. Such an architecture is cost-effective and has good isolation for the high-voltage current sensing [2]. In this work, we develop the hybrid current sensor comprising the microfluxgate and the current transformer (CT) technology for wide-bandwidth current measurement. The microfluxgate is consisting of two micro-coil chips 3.5 mm×1.75 mm in dimension made by using the standard CMOS-MEMS 0.35 μm process. The aluminum wire-bonding technique is used to construct the top excitation coil surrounding the amorphous soft magnetic core patterned by photolithography and wet etching techniques. Under the optimal excitation condition, the response of the microfluxgate current sensor becomes linear with the optimized sensitivity. The phase-sensitive second harmonic detection technique is used to drive the microfluxgate sensor. The in-house made current transformer, which is 28 mm in diameter, is combined with the microfluxgate driving system to form the hybrid current sensor by using a summing amplifier. The architecture of the hybrid current sensor is shown in Fig. 1. For non-contact measurement of quasistatic current, the spectral current noise is found to be less than 0.4 μA/√Hz from 0.1 to 10 Hz, and the root-mean-square (RMS) noise is less than 10 μA. The maximum sensing range is ±10 A and the non-linearity is less than 2% within the ±1.5 A range, corresponding to the linear dynamic range of more than 100 dB. Moreover, Fig. 2 reveals the frequency response of the hybrid current sensor. The flat bandwidth is as high as 100 kHz and is capable of accurate measurement of static current. The hybrid microfluxgate and CT sensor has the potential to be the practical miniature device featuring a high-dynamic range, wide bandwidth, and low-temperature drift.

[1] J. T. Jeng, X. T. Trinh, C. H. Hung, and C. C. Lu, Sensors, 19(8), 1882 (2019). [2] Y. Ouyang, J. He, J. Hu, & S. Wang, Sensors, 12(11), 15520-15541 (2012).

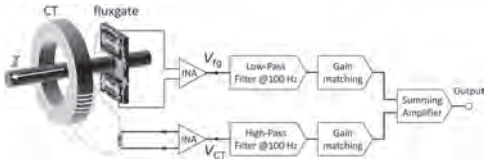

Architecture of the hybrid current sensor.

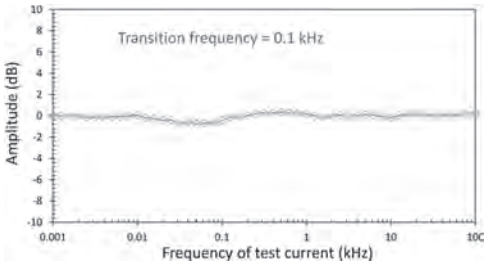

Frequency response of the hybrid current sensor.

IPB-12. Two Sources of Offset Drift in Orthogonal Fluxgates: Thermal and Magnetic. *M. Butta*[1], M. Dressler[1] and M. Janosek[1] *1. Faculty of Electrical Engineering, Czech Technical University in Prague, Prague, Czechia*

In an orthogonal fluxgate with Co-rich amorphous wire [1], the first period after turning it on we observe a large transient of the magnetometer's output towards a stable value. This transient was believed to be a thermal dependence of magnetic properties due to the Joule heating in the core (approx. 0.1 W). To verify this hypothesis, we measured the dependence of the saturation magnetization Bs of the core and verified that Bs drops with a rate of – 0.13%/K, not enough to explain the drift in the output of the magnetometer (up to hundreds of nT). Thus, we run three experiments with a single wire fluxgates: in the first one we had the sensor in a shielding for a long time before turning it on and we measured both the sensor's output and the temperature. The transient of the magnetometer's output seems to follow the one of the temperature. The second experiment shows that this is only an artifact: we let the magnetometer stabilize in the shield, then we changed the temperature by an external heater. The magnetometer's output drifted only by a few nT: the thermal effect cannot entirely explain the drift after turning on (tens of nT). Finally, we let the fluxgate reach a thermal equilibrium while exposing it to a field of 20 μT and then we inserted it in the magnetic shield. In this case, the temperature was almost constant, but there was a large transient. The transient was reversed when the sensor was exposed to the field of -20μT. This proves that the offset drift is caused also by magnetic relaxation of the domains in the core of the fluxgate, after exposing it to a μT-level magnetic field [2]. In order to study this phenomenon, we exposed a similar sensor to a magnetic field of different values, and observed offset relaxation related to that amplitude. We applied pulses of specific amplitude and duration: the transient duration of the offset settling depended on the duration and amplitude of the applied field, confirming the magnetic origin of the transient. This is an important finding for improving the drift of fluxgates without commutating the excitation field [3].

1. I. Sasada, Orthogonal fluxgate mechanism operated with dc biased excitation. *Journal of Applied Physics*, 91 (10 I), pp. 7789-7791 (2002) 2 M. Vazquez and D.-X. Chen, The magnetization reversal process in amorphous wires, IEEE Transactions on Magnetics, Volume: 31, Issue: 2, (1995) 3 M.

Butta M. and I. Coroli, Low Offset Drift-Low-Noise Orthogonal Fluxgate with Synchronized Polarity Flipping, *IEEE Transactions on Magnetics*, 53 (4), art. no. 7779098, (2017)

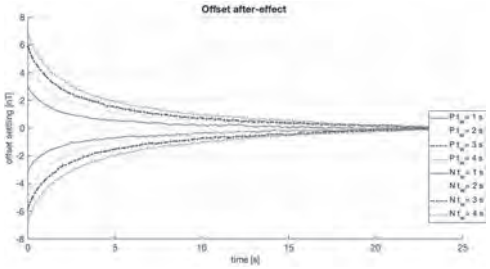

Magnetic after-effect offset settling after a longitudinal field is removed (measured for both field directions and with variable duration)

IPB-13. Withdrawn

IPB-14. Proposal of Inspection Method for Shrinkage Cavity in Spheroidal Graphite Cast Iron Using Differential Vibration Measurement by Electromagnetic Force Vibration. *S. Niwa*[2], A. Hagisaka[2], I. Yamada[2], S. Shiota[1], Y. Gao[1] and Y. Gotoh[1] *1. Department of Innovative Engineering, Faculty of Science and Technology, Ooita University, Ooita, Japan; 2. Graduate School of Engineering, Ooita University, Ooita, Japan*

Introduction It is very important to inspect the shrinkage cavity inside the cast iron, since the spheroidal graphite cast iron (FCD600) may be generated a shrinkage cavity inside it during manufacturing and the strength is extremely reduced. In this research, a new inspection method using differential vibration measurement by electromagnetic force excitation is proposed. In this method, the vibration by the electromagnetic force is generated from the static magnetic field of the permanent magnet and the eddy current inside the cast iron by the alternating excitation coil. Then, the shrinkage cavity is evaluated using the vibration strength of the cast iron surface. In this paper, 3D electromagnetic field analysis and 3D displacement analysis [1] are used to elucidate the test principle and to conduct verification experiments. Inspection Model and Conditions Fig.1 shows the proposed sensor is composed of a permanent magnet with two holes, an AC exciting coil with 500Hz and 2A, and two vibration sensors. The electromagnetic vibration is generated in the steel plate by the static flux density from the permanent magnet and the eddy current from the excitation coil. And, two vibration sensors are measured the vibration strength of the steel plate surface differentially. The shrinkage cavity inside cast iron is estimated by the differential vibration intensity. Calculated and Inspection Results Fig.2(a) shows that the calculated distribution of differential displacements by the two vibration sensors at each position on the cast iron. This figure denotes that the displacement distribution is changed near the shrinkage cavity inside the cast iron. This is because, the density in the cast iron is decreased near the shrinkage cavity in the cast iron. (3) shows the measured differential signal of two vibration sensors at each position on the actual cast iron with the shrinkage cavity. This figure denotes that the differential signal is changed near the shrinkage cavity in the cast iron. Moreover, the measured signal is a tendency similar to the calculated result as shown in Fig.2. The presence of shrinkage cavity inside the cast iron can be confirmed by this change in the differential signal.

[1]Y.Gao, K.Muramatsu and T.Takahata, "Design of a Reactor Driven by Inverter Power Supply to Reduce the Noise Considering Electromagnetism and Magnetostriction", IEEE Transactions on Magnetics, vol. 46, no.6, pp.2179-2182, 2010.

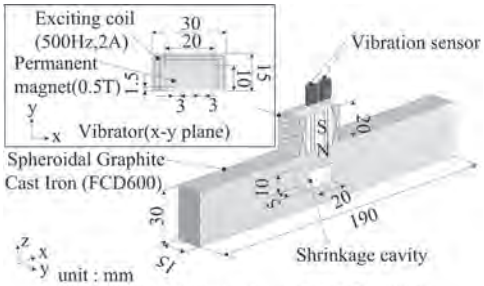

Fig.1 Proposal inspection model (1/2 region).

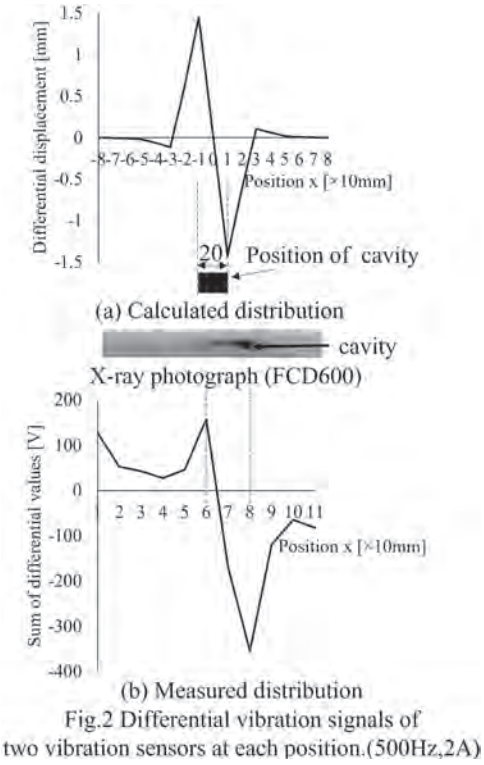

Fig.2 Differential vibration signals of two vibration sensors at each position.(500Hz,2A)

IPB-15. Low-Power AMR Magnetometer Operated in Discontinuous Mode. *D. Novotný*[1], L. Mičan[1] and V. Petrucha[1] *1. Department of Measurement, Czech Technical University in Prague, Prague, Czechia*

In many applications including space missions, Anisotropic Magnetoresistors (AMR) based magnetometers raised their popularity [1,2] as they are solid-state off-the-shelf components with good radiation immunity [3]. One of the issues they suffer is low sensitivity and thus high noise induced by their bridge thermal noise as well as by preamplifier stage noise [4]. To overcome this problem, higher supply voltage of an AMR bridge can be used to raise the sensitivity. This seems to be straightforward but power dissipated on the sensor raises quadratically with bridge voltage and thus it can't be operated in "classical" continuous mode (due to overheating and excessive power consumption). In our research we propose novel method of powering bridge by pulses allowing to obtain better sensitivity and less noise with AMR sensors. During these short pulses (100 us width and 4.5 ms period) we also perform flipping pulses (both S/R) while measuring bridge response with an analog-to-digital converter. Acquired data are then signal-processed on the fly by a microcontroller. In traditional method, 10 V in continuous mode with HMC1021 AMR sensor will dissipate 91 mW of power, while cycling power with a duty cycle of 1:45 means only 2 mW (considering zero overhead power). In mostly used triaxial version it is 273 mW vs 6 mW preserving other main parameters of the magnetometer unchanged. To verify this idea we have developed single axis magnetometer (Fig. 1) with

adjustable both bridge voltage as well as flipping current, with possibility of precise timing of all events. In the first trial/test, we have tried to obtain similar noise with pulsed 10 V bridge as we were able to get in our previous research with continuous supply of 10V [4], (see Fig 2.) After achieving this milestone (solving a lot of technical troubles) we tried 20 V bridge supply to verify expected noise reduction (as sensitivity doubles), but for now without result – at this voltage, AMR's electrical offset saturates the preamplifier. In the near future we aim to tackle this issue and to test the noise drift with temperature in different flipping current configurations.

[1] Leitner, Stefan, et al., IEEE Transactions on Magnetics, Vol. 51, p. 1-4 (2015) [2] P. Brown et al., Review of Scientific Instruments, Vol. 85, p.125117 (2014) [3] Sanz, Ruy, et al., Sensors, Vol. 12, p. 4447-4465 (2012) [4] D. Novotný, V. Petrucha, M. Janošek, IEEE Transactions on Magnetics, Vol. 55, p. 1-5 (2018)

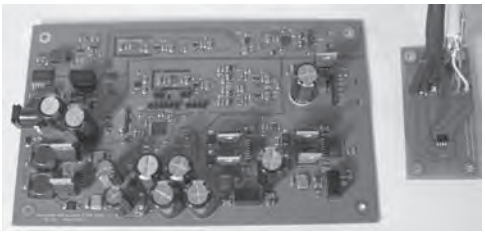

Fig.1 - Photo of the experimental prototype

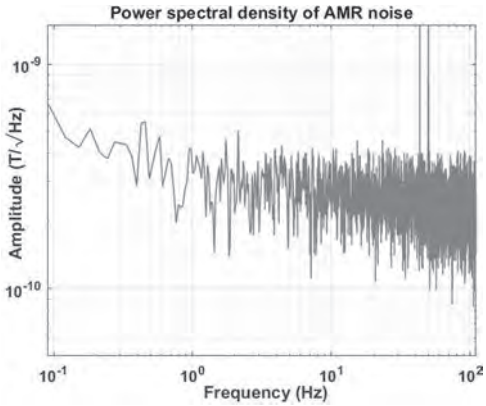

Fig.2 - PSD of noise with pulsed 10 V bridge voltage

IPB-16. Rogowski Coil with Ferromagnetic Powder Core. *V. Grim*[1] and P. Ripka[1] *1. Department of Measurement, Czech Technical University, Prague, Czechia*

Rogowski coil (RC) is a well-known sensor for the measurement of large AC and pulsed [2] current. Their key property is the perfect linearity caused by the absence of any magnetic material in its core [1]. Typically, there is only a single layer of winding because unlike the case of current transformer (CT), in RC the distribution of sensitivity along the circumference and thus rejection of external currents and magnetic fields is given by the winding uniformity [3]. The sensitivity of traditional RCs at powerline frequency is low, which precludes its effective use in energy consumption meters. High sensitivity RCs have to use multiple layers of winding, which is detrimental to its frequency response. Our proposed design adds a low-permeability ferromagnetic core in the form of flakes obtained by grinding a nanocrystalline ribbon. It has very low coercivity compared to silicon steel laminations. The permeability can be adjusted by changing the fill factor, the maximum achieved with this specific material was approximately 20. The increase in permeability causes increase in sensitivity, which would not be possible by increasing the number of turns due to technological limitations. An RC containing the nanocrystalline powder core was manufactured and characterized and the results were compared with a reference design containing no magnetic material. Both samples are wound with 194 turns. In the 50 A range the linearity error is below 0.3 % FS. The sensor is resistant to overload: even at 1000 A the error is only 9 %. Noise was measured at the output of a fluxmeter (Lakeshore 480) preceded by a preamplifier (SR560). The measured values consist mostly of the noise of the instruments and 50 Hz interference. With a 10-fold increase in sensitivity the equivalent primary current noise is therefore reduced with the same ratio. In the full paper we will demonstrate the frequency characteristics of the new sensors and its performance in conjunction with a single-chip power meter containing a digital integrator.

[1] M. H. Samimi, A. Mahari, M. A. Farahnakian, and H. Mohseni, IEEE Sensors Journal, vol. 15, issue 2, pp. 651–658 (2015) [2] J. Zhu, Q. Zhang, J. Jia et al. Plasma Science and Technology, vol. 8, issue 4, pp. 457-460 (2006) [3] J.D. Ramboz, IEEE Trans. Instrum. Meas., vol. 45, no. 2, pp. 511-515 (1996)

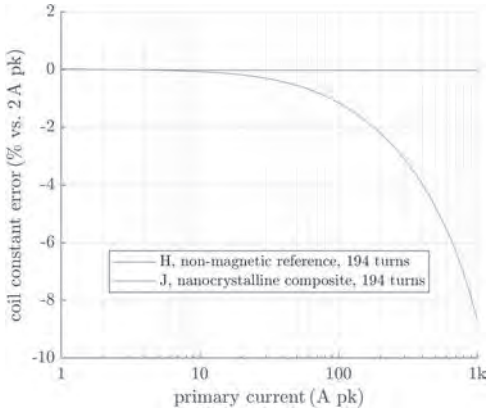

Measured integral nonlinearity

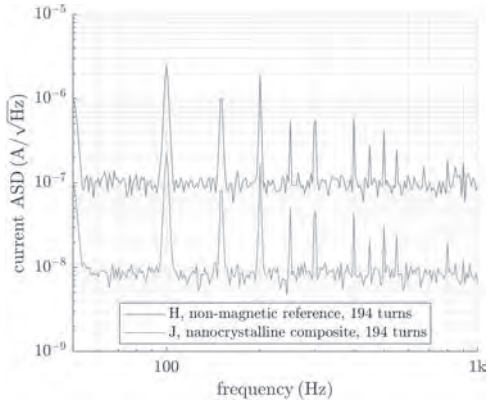

Measured noise spectral density

IPB-17. Evaluation of harmonic signals derived from separately located multiple samples for magnetic particle imaging. *S. Tanaka*[1], H. Hirano[2], M. Futagawa[2], Y. Takemura[3] and S. Ota[2] *1. Electrical and Electronic Engineering Course, Graduate School of Integrated Science and Technology, Shizuoka University, Hamamatsu, Japan; 2. Department of Electrical and Electronic Engineering, Shizuoka University, Hamamatsu, Japan; 3. Department of Electrical and Computer Engineering, Yokohama National University, Yokohama, Japan*

Magnetic particle imaging (MPI) using magnetic nanoparticles (MNPs) as tracers can be used as an early diagnosis technique for diseases such as cancer [1]. The detection signal derived from the MNPs under an alternating current (AC) includes harmonic signals. Both odd and even number of harmonics were measured for MPI [2]. When the MNPs are injected in human body, it is necessary to detect the complex magnetization signal from the MNPs located at different places. In this study, the odd and even number of harmonic signals detected as a complex signal derived from

two separate sample sets were evaluated. γ-Fe_2O_3 nanoparticles used as the measured sample, commercially available as Resovist® from FUJIFILM Toyama Chemical Co., Ltd., were sealed in a cylindrical container of 1 mm diameter and 1 mm height. The AC magnetic field used as a drive field and the direct current (DC) gradient magnetic field used to select a field free point (FFP) for MPI as a selection field were parallel to each other (Fig. 1). The amplitude of the drive field was 10 mT and its frequency was 10 kHz. The magnetic field gradient of the selection field was 0.476 T/m. The FFP was set at the center of a Maxwell-type DC excitation coil in x= 0 mm. Figure 2 shows the intensity of harmonic signals for the samples in x= 2 mm, V_{1+} and x= –2 mm, V_{1-}. The calculated value, $V_{1,\,sum}$, was the sum of the measured V_{1+} and V_{1-}. The harmonic components in V_{1+} and V_{1-} were similar to each other. The odd harmonics in $V_{1,\,sum}$ were equivalent to the sum of the harmonics in V_{1+} and V_{1-}, and the even harmonics in $V_{1,\,sum}$ were equivalent to V_{1+} subtracted from V_{1-}. It is shown that the phases of the even harmonic components of V_{1+} and V_{1-} were opposite when the direction of the DC magnetic field applied to each sample was opposite to each other. In conclusion, when two samples were symmetrically located with respect to the FFP, the even harmonic components in the magnetization signals detected from each sample were cancelled with each other, whereas the odd harmonic components were added.

[1] B. Gleich and J. Weizenecker, Tomographic imaging using the nonlinear response of magnetic particles, Nature 435, 1214 (2005). [2] J. B. Weaver, A. M. Rauwerdink, C. R. Sullivan and Ian Baker, Frequency distribution of the nanoparticle magnetization in the presence of a static as well as a harmonic magnetic field, Medical Physics 35, 1988 (2008).

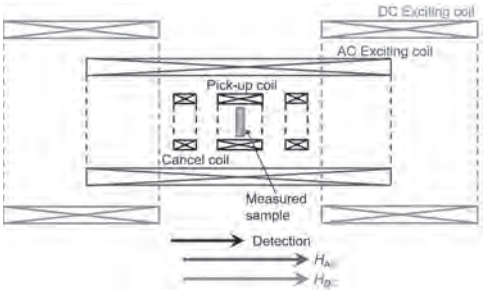

Experimental setup of exciting coils for the DC and AC magnetic field, and detection coil.

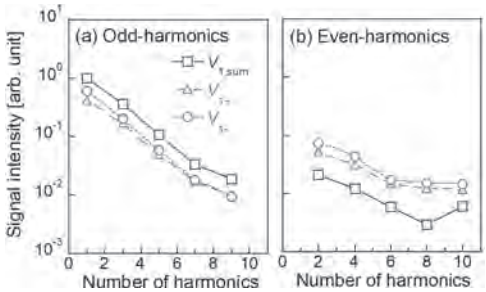

(a) Odd and (b) even harmonics of V_{1+}, V_{1-}, and $V_{1,\,sum}$.

Session IPC
SENSORS, POWER SYSTEM, MACHINES (Poster Session)

Ke Zhu, Chair
HK Electric, Hong Kong, Hong Kong

IPC-01. Effects of the Electromagnetic Structure of the Power Transformer Core on Hysteresis Squareness Ratio, Noise and Vibration Characteristics. *C. Hsu*[3], J. Liu[2] and C. Fung[1] *1. Mechanical Engineering, Oriental Institute of Technology, Banqiao District, Taiwan; 2. Digital Multimedia Design, Kainan University, Lu-Zhou, Taiwan; 3. Asia Eastern University of Science and Technology, New Taipei, Taiwan*

1. Study Objective and Method Transformer magneto-mechanical structure deformation due to lightning impulse effect may cause damage of the transformers in terms of the noise and vibration performance. This study proposed a single-phase transformer with a voltage specification of 345 kV (high voltage)/115 kV (low voltage) and a capacity of 120 MVA [1,2]. The results of the continuous lightning impulse tests revealed that the transformer designed as parameter of K-factor, as shown in Figure 1. After testing results, there is generated significantly low noise (<65 dB) and vibration (<10 μm), which are remarkably lower than the IEEE standard of 85 dB. 2. Experiment Result and Discussion The pattern of the fault currents depends on the fault type and location along the winding length. Figure 2(a)-(b) shows the transformer after the lightning impulse full-wave and chopped wave for high voltage bushing level. The Figure 2(c) shows the thermal imaging results of the transformer after the lightning impulse testing, indicating that high (102 °C) and low (31.2 °C) thermal conduction were obtained at the two sides of the top collier. These thermal imaging measurement results suggest that the transformer can operate effectively because it exhibits satisfactory insulation performance after the lightning impulse and alternating current insulation tests [3,4]. The sweep frequency response analysis is a useful method to detect and diagnosis of the defects for the power transformers. The results of the frequency spectral tests are conducted using SFRA are shown in Figure 2(d). Based on the SFRA theory, the core properties affect the SFRA characteristics only at low frequencies (typically up to 1 kHz). Therefore, the noise results can be considered as correction values between the values obtained before and after the application of the SFRA. The k-factor between 0.4-0.6 for transformer insulation is maintained better performance.

[1] IEEE Standard C57.98, 2011 IEEE Guide for Transformer Impulse Tests. [2] Haize Hu, et. al. Dynamic lightning protection method of electric power systems based on the large data characteristics, *International Journal of Electrical Power and Energy Systems* 2021; 128: 106728-1-14. [3] García B, Burgos JC, Alonso AM. Transformer tank vibration modeling as a method of detecting winding deformations—Part I: Theoretical Foundation. *IEEE Trans. Power Delivery* 2006, 21, 1, 157-163. [4] García B, Burgos JC, Alonso AM, Transformer tank vibration modeling as a method of detecting winding deformations—Part II: Experimental Verification. *IEEE Trans. Power Delivery* 2006, 21, 1, 164-169.

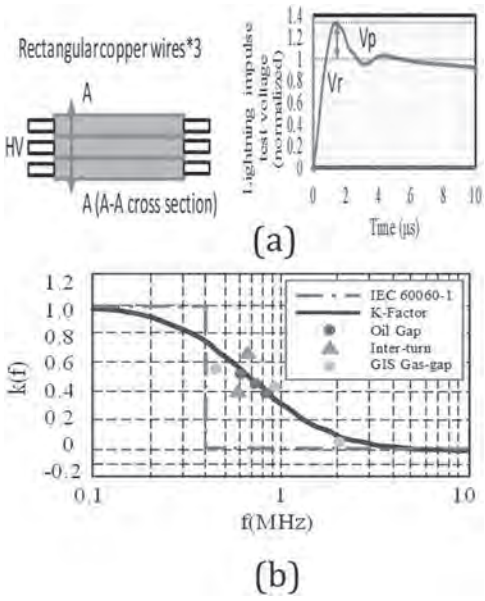

Figure 1 Lightning k-factor: (a) turn-to-turn insulation and overshoot voltage, (b) k-factor distribution.

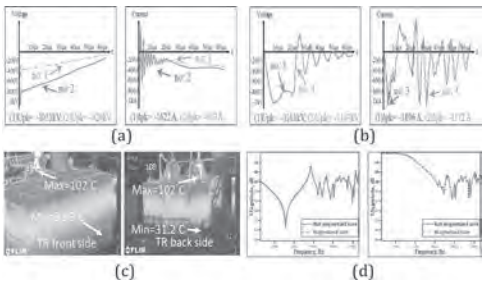

Figure 2. Lightning impulse results: (a)-(b) full wave voltage and current, (c) thermal imaging, front-back side, (d) SFRA at 10 Hz–2 MHz before and after the lightning impulse test.

IPC-02. Optimal Design on the Three-degree-of-freedom Hybrid Magnetic Bearing. *T. Zhang*[1], Z. Wang[1] and X. Ye[1] *1. Faculty of Automation, Huaiyin Institute of Technology, Huaian, China*

Three-degree-of-freedom (3-DOF) hybrid magnetic bearing (HMB) integrated the functions of the radial and axial levitation functions in one unit [1]. With the development of modern industry, the machines develop toward higher speed and higher power. Therefore, it is of great significance to optimize the 3-DOF HMB to reduce the axial length, increase the critical speed and levitation force density of the 5-DOF magnetic levitation motor. Fig. 1 shows the structure and magnetic circuit. In the proposed HMB, the axial inclined air gap is used to reduce the axial length and increase the critical speed. In addition, the rotor is segmented with non-magnetic material to improve the radial levitation performance. It can be seen that the permanent magnet generates a bias flux (shown by the solid lines) to form a closed loop

through the permanent magnet, axial stator, axial air-gap, rotor core, radial air-gap and radial stator. Axial control winding produces the axial control flux (shown by dotted lines) which is closed by the axial stator, two axial air-gaps and rotor core. The radial control flux passes through the radial stator, radial air-gap and rotor. The relationship between levitation force and inclination angle is established based on the equivalent magnetic circuit method. Then the design methods of axial air gap length, inclination angle and radial air gap length are discussed. The magnetic field distributions, air gap flux densities and force-current relationships are calculated by 3D finite element method. The force-current relationships are shown in Fig.2. Finally, the experimental prototype is designed and the experimental platform is established. The suspension performances are tested. The correctness of structure, magnetic circuit and optimization design are proved by theoretical calculations, analyses and experiments.

[1] Y. Le, J. Fang, and K. Wang, "Design and optimization of a radial magnetic bearing for high-speed motor with flexible rotor," *IEEE Trans. Magn.,* vol. 51, no. 6, pp. 1-13, June 2015.

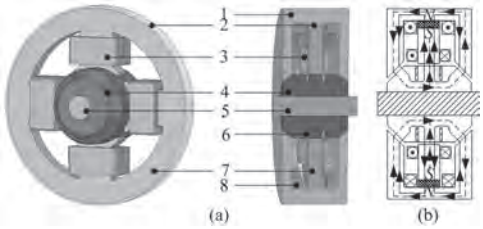

Fig. 1. 3D model and magnetic circuit, (a) 3D model, 1. axial stator, 2. permanent magnet, 3. radial winding, 4. rotor, 5. shaft, 6. non-magnetic material, 7. radial stator, 8. axial winding, (b) magnetic circuit.

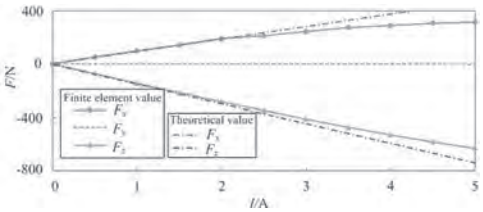

Fig. 2. The relationships of the levitation forces and currents.

IPC-03. XGboost Algorithm on VMD Mode Mixing Suppression for the Motor Bearing Fault Diagnosis. *B. Guan*[2], C. Di[1], Z. Ke[1] and X. Bao[1]
1. School of Electrical Engineering and Automation, Hefei University of Technology, Hefei, China; 2. Department of Electrical and Computer Engineering, The Ohio State University, Columbus, OH, United States

The variational mode decomposition(VMD) method is widely used as a novel tool in the rolling bearing fault diagnosis to extract the fault characteristics of the electric machines. However, with the number of sampling points increasing, the mode mixing effect can be obvious. "Mode mixing" is defined as any intrinsic mode function(IMF) consisting of oscillations of dramatically disparate scales [1]. Mutual information is an indicator which can symbolize the correlation among IMFs. The performance of VMD method specifically depends on the parameters that need to be predetermined [2]. Therefore, based on XGboost algorithm, this article proposed an iterative classification method to find an optimal parameter combination to minimize the orthogonality among IMFs. The most important two parameters can be seen as a combination: (alpha, tau). Given a reasonable range and a large step size, some combinations can be obtained and used as sample training data. Applying these combinations into VMD analysis, finally got the corresponding mutual information values, divided them into several zones by size, and numbered zones as '1','2'…'n'. The number will be used as target training data. Training these two data by XGboost algorithm and got a predictive model, wchih can fill more points in the zones. Finally, finding the zone with the best performance. After several iterations, the optimal combination will be obtained. The corresponding flow chart is shown in Fig.1 The paper's bearing vibration fault signal comes from the Case Western Reserve University[3]. The optimal combination is given as (alpha=930, tau=0.50). The mean mutual information is 0.8523, which is obviously less than the worst value :0.8766. Besides, the impact factors of these two parameters are shown in Fig.2(a), where f1 refers to alpha and f0 refers to tau. The training data for XGboost algorithm in the first iteration is shown in Fig.2(b). The IMFs gotten by using the optimal combination are shown in Fig.3(c). Compared with traditional enumeration method, this method need less computations and can suppress the mode mixing effect.

[1] Wu, Z. & Huang, N. E. Ensemble empirical mode decomposition: A noise-assisted data analysis method. Adv. Adapt. Data Anal. 1, 1–41 (2009). [2] K. Dragomiretskiy and D. Zosso, "Variational Mode Decomposition," in IEEE Transactions on Signal Processing, vol. 62, no. 3, pp. 531-544, Feb.1, 2014, doi: 10.1109/TSP.2013.2288675. [3] C. W. R. University,"https://csegroups.case.edu/bearingdatacenter/pages/12k-drive-end-bearing-fault-data," 2014.

Fig.1 The flow chart.

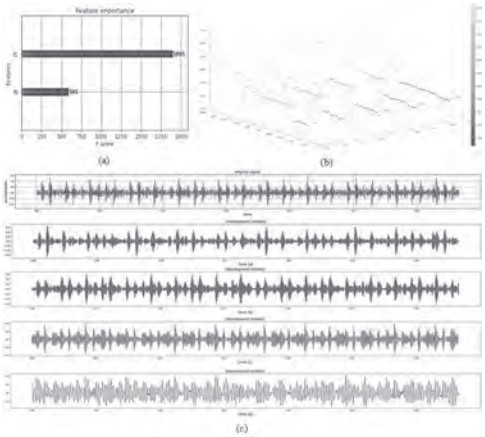

Fig.2 (a) impact factors. (b)Training data for XGboost algorithm. (c) IMFs of the optimal combination.

IPC-04. High-magnetic performance on an H-type dipole electromagnet as a versatile power system. *J. Baena Rodriguez*[1,2] and A.A. Velasquez Torres[2] *1. EECS, Massachusetts Institute of Technology, Cambridge, MA, United States; 2. School of Sciences, Universidad EAFIT, Medellin, Colombia*

We propose a novel H-Type dipole electromagnet as a reliable, versatile, and scalable power system with potential applications in multiple technologies and industries. The device is 33% more power-efficient than commercial proposals and can be used in technologies where magnetostatic high fields with low hysteresis are needed. The efficiency is described by a transfer function that correlates design parameters and materials notating 2.77x10-4 T/(kgW) in terms of the magnetic flux density, weight, and input power. Because of constraints on magnetic materials in the Colombian market and high prices on commercial developments, we proposed constructing a novel H-Type dipole electromagnet to archive 2T of a uniform magnetic field in a 10 mm air gap. We built all electro-mechanical parts and assemblies, including winding two power coils, two low-carbon steel tapered dipoles, embedded systems, and sensors. The uniform magnetic field of 2T achieved showed a 99% linear correlation coefficient and absence of hysteresis effects, evidencing total curve reversibility for sequences of current increments and decreases applied to the coils throughout the characterization range. These electro-mechanical specifications convert the device as a robust tool to generate an intense and uniform magnetic field necessary to perform

a wide range of experiments, including magnetic material characterization, spintronics, and magnetic drug targeting. I. Introduction The measurement of magnetic properties in materials, in micro and nanostructured materials such as micrometric particles, soft magnetic materials, and polycrystalline films [1], defines their potential of application in multiple technologies and industries [2]-[3]. II. Method The design, modeling, and construction are presented. Using a FEM magnetostatic analysis, Fig.2 shows the magnetic flux density, and the distribution of the magnetic field lines was visualized and quantified [4]-[5]. III. Results The magnetic field reached through the column was uniform according to the pole material used, with the option to increase a magnetic field by choosing a suitable cap geometry and introducing a cooling system around the coils with a proper gap adjustment.

[1] T. Furubayashi, "Magnetite films prepared by reactive evaporation", Journal of Magnetism and Magnetic Materials, pp. 272 [2] X. Hu, M. Xu, X. Cui, S. Zhang, "Room effects of Ag-added Fe3O4 films with single Communications", Vol 142 pp.595 [3] H. Zhu, D. Yang, L. Zhu, "Hydrothermal growth and magnetite (Fe3O4) thin films", Surfaces & Coating Technology, Vol 201, pp. 5870 - 5871, December 2006. [4] J. D. Rairán, C. Aguirre, and J. J. Castañeda. finite element method", Tecnura Magazine, Vol 17, pp [5] Z. Markus. "Power Dissipation and Magnetic Forces on Rebars," IEEE transaction on Magnetics 1997.

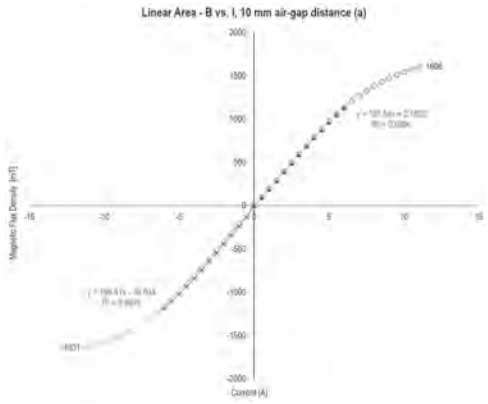

B Vs I with 10mm air-gap

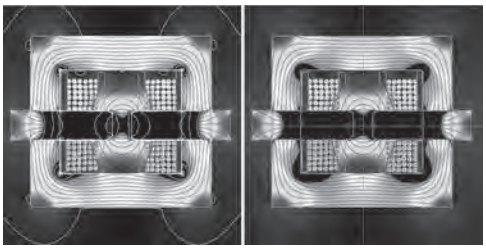

IPC-05. Magnetic Respiratory Monitoring Technology Based Music Therapy for Covid19 Patients: A New Perspective. *K. Hwang*[1], D. Nguyen[1], Y. Rahman[1], V.O. Jimenez[1], B. Muchharla[1] and M. Phan[1]
1. University of South Florida, Tampa, FL, United States

Studies have shown that relaxing music can lower a patient's breathing rate, heart rate, and blood pressure by releasing stress or anxiety and promoting relaxation [1,2]. Based on the successful development of our magnetic respiratory monitoring technology for advanced healthcare [3], in this study we attempt to examine how the breathing pattern of a patient changes when the patient sleeps with and without a favorite music in the background. We observed that during sleep mode with music, the patient breathed more regularly and slowly (11 times per minute) compared to sleep without music (14 times per minute) and wake mode (17 times per minute). This indicated that the relaxing music helped the patient to relax and sleep better. Remarkably, while the abnormal breathing feature was observed at a certain time for all states (wake-up and sleep modes with and without music), the breathing pattern became more regular in the case of sleep with the relaxing music. Furthermore, we designed a musical biofeedback for breathing regulation. In this design, the respiratory motion of the patient was tracked and interpreted as a real-time variable for tempo adjustment to a stored musical file. The patient was able to adjust breathing to synchronize with a separate accompaniment line. When the breathing was regular and at the desired tempo, the resulting sound was synchronous and harmonious. These observations suggest a new possibility of integrating our magnetic respiratory monitoring technology with music to develop an innovative magnetic music therapy for Covid19 patients with breathing difficulty.

1. B. Canga, R. Azoulay, J. Raskin, and J. Loewy, AIR: Advances in Respiration – Music therapy in the treatment of chronic pulmonary disease, *Respiratory Medicine* 109, 1532 (2015) 2. Y. Sakaguchi and E. Aiba, Relationship between Musical Characteristics and Temporal Breathing Pattern in Piano Performance, *Front Hum Neurosci.* 10, 381 (2016) 3. K.Y. Hwang, V.O. Jimenez, B. Muchharla, T. Eggers, A.T. Le, V.D. Lam, and M.H. Phan, *Applied Sciences* 11, 3885 (2021)

IPC-06. Estimation of inductance and resistance of toroidal coils in high temperature environment. *M.D. Noh*[1], T.K. Le[1] and Y. Park[1]
1. Mechatronics Engineering, Chungnam National University, Daejeon, The Republic of Korea

Inductance and resistance of a coil are important parameters for electromagnetic sensors and actuators. If the sensors or actuators are to be operated in high temperature environments, the effect of temperature change on inductance and resistance must be evaluated [1-2]. In this paper, we propose a very simple procedure for estimating the inductance and resistance of toroidal coils operating in high temperature environment. Magnetic stainless steel (SUS430) is used as the core. The ring is wound with ceramic-coated cable. The test specimen is placed inside an oven in which the temperature is controlled up to 500°C. The winding is driven by a linear amplifier (TA330, TRUST Automation) at the command of a function generator (33120A, Agilent). The current is measured by a current probe (80i-110s, Fluke). Fig. 1 illustrates the test setup and shows a picture of the test specimen in the oven. The current through the coil is related to the applied voltage through $V = L (di/dt) + Ri$. Transfer function between the voltage and current can be obtained as $G = 1/(Ls + R)$. Introducing a new operator $\lambda=1/(1+\tau s)$, we can set up a time-domain identification scheme [3]. The inductance and resistance can be estimated through the following recursive least square estimation algorithm. Defining the parameter vector theta = [L R], (1) $\theta(k) = \theta(k-1)+P(k)\varphi(k)e(k)$ (2) $e(k) = y(k) - \varphi(k)\theta(k-1)$ (3) $P(k) = P(k-1) - P(k-1)\varphi(k)\varphi(k)P(k-1)/(1+\varphi(k)P(k-1)\varphi(k))$ The parameter τ determines the convergence speed. In order to validate the method, the resistance of the coil is measured using a precision multimeter (34401A, Agilent) and the inductance is measured with an LCR meter (4263B, Agilent). Fig. 2(a) shows the estimation results compared with the measurements. Fig. 2(b) displays the comparison of resistance estimation with measurements. The estimation for inductance is better than the resistance in terms of agreement with measurements. Since the estimation model is the first order, it is not possible to obtain good estimation quality both for inductance and resistance. Since the resistance is stationary, it may be possible to have another procedure to estimate the resistance, thereby enhancing the quality. This work is supported by National Research Foundation of Korea (NRF-2020R1F1A1067740)

[1] Colmenares, J., Kargarrazi, S., Elahipanah, H., Nee, H. P., & Zetterling, C. M. (2016). High-temperature passive components for extreme environments. 2016 IEEE 4th workshop on wide bandgap power devices and applications (WiPDA) (pp. 271-274). IEEE. [2] Zhao, Z., Liu, Z., Lyu, Y., & Gao, Y. (2019). Experimental investigation of high temperature-resistant inductive sensor for blade tip clearance measurement. Sensors, 19(1), 61. [3] Johansson, R. (1994). Identification of continuous-time models. IEEE Transactions on Signal Processing, 42(4), 887-897.

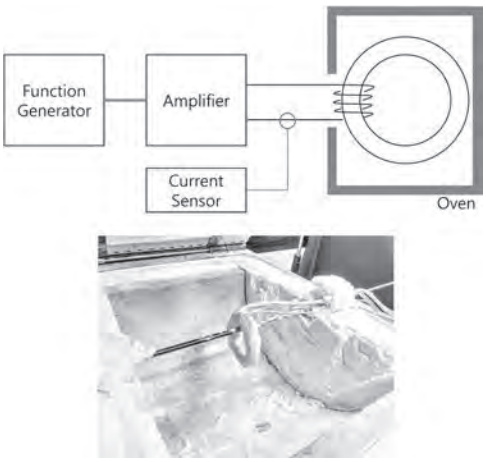

Test setup

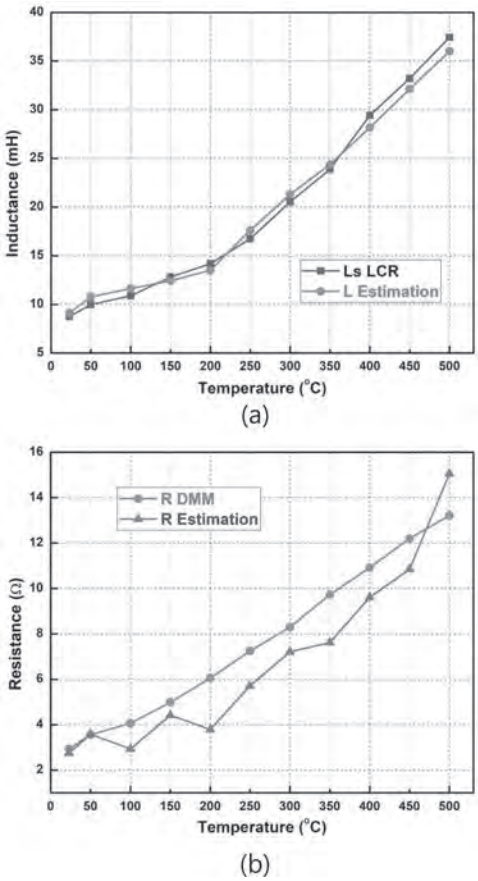

Estimation results

IPC-07. Power Adaption Design for Multifrequency Wireless Power Transfer System. *X. Tian*[1], K. Chau[1], H. Pang[1] and W. Liu[1] *1. Department of EEE, The University of Hong Kong, Hong Kong*

Various industrial applications have put forward higher demands for wireless power transfer systems (WPT) [1]. Using one transmitter to simultaneously power multiple appliances with different electrical requirements is a promising system with the advantages of simplicity and good efficiency [1-2]. One of the key issues of multifrequency transmission is the power adaption and power flow control [3-5]. Most of the traditional work uses the modulation method to solve this problem. However, the signal tracking process can be difficult and complex and will inevitably cause more power losses [2], especially for high operation frequencies. This paper presents a new design scheme to realize the power adaption for multiple receivers. The system can realize a demand-customized output power by adjusting the current harmonics. The system uses only one simple full-bridge inverter, and the redundant modulation process can be cut away. As shown in Fig. 1, the proposed compensation circuit uses a T-type topology. Each branch of the circuit is made of a dual-band component. Based on superposition method, the output voltage of the inverter can be regarded as the combination of the first and third harmonics. Under each operation frequency, the three dual-band components can behave different equivalent impedances and the compensation circuit can thus be regarded as two individual LCC compensation for the accordant frequencies, which guarantees that the system can always operate at zero impedance angle and with adjustable output current harmonics. The simulated operating waveforms of the proposed system are shown in Fig. 2. For two identical resistive loads, the accordant receivers are designed to be resonant at 100 kHz and 300 kHz, respectively. The first and third harmonics of the input current are thus designed to be 3:1 for equivalent output. It can be observed that the compensation circuit successfully controls the output current to the desired values with the inherent harmonics of the input voltage. This work was supported by HK RGC (project no. T23-701/20-R).

[1] W. Liu, K. T. Chau, C. H. T. Lee, C. Jiang, W. Han and W. H. Lam, "Multi-frequency multi-power one-to-many wireless power transfer system," *IEEE Transactions on Magnetics*, vol. 55, no. 7, pp. 1-9, July 2019. [2] Z. Zhang, X. Li, H. Pang, H. Komurcugil, Z. Liang and R. Kennel, "Multiple-frequency resonating compensation for multichannel transmission of wireless power transfer," *IEEE Transactions on Power Electronics*, vol. 36, no. 5, pp. 5169-5180, May 2021. [3] W. Zhong and S. Y. R. Hui, "Auxiliary circuits for power flow control in multifrequency wireless power transfer systems with multiple receivers," *IEEE Transactions on Power Electronics*, vol. 30, no. 10, pp. 5902-5910, Oct. 2015. [4] C. Jiang, K.T. Chau, W. Han, and W. Liu, "Development of multilayer rectangular coils for multiple-receiver multiple-frequency wireless power transfer," *Progress In Electromagnetics Research*, vol. 163, pp. 15-24, July 2018. [5] C. Jiang, K.T. Chau, W. Liu, C. Liu, W. Han, and W.H. Lam, "An LCC compensated multiple-frequency wireless motor system," *IEEE Transactions on Industrial Informatics*, vol. 15, no. 11, pp. 6023-6034, Nov. 2019.

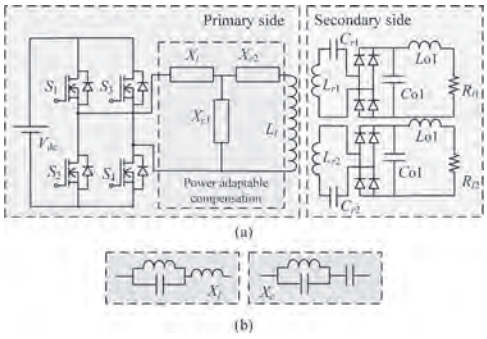

Fig. 1. Proposed system. (a) Topology. (b) Dual-band component.

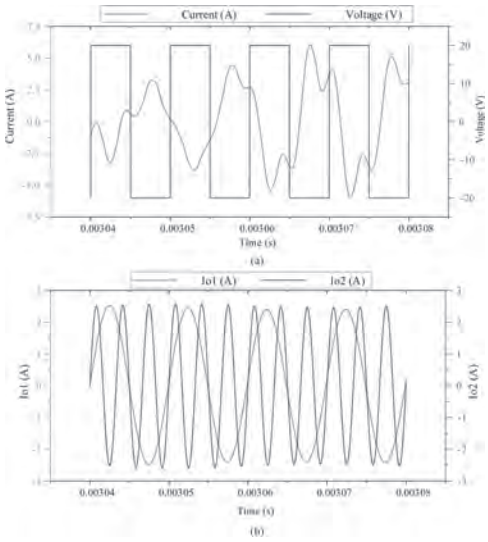

Fig. 2. Simulated waveforms. (a) Input waveforms. (b) Output current.

IPC-08. Withdrawn

IPC-09. Proposal of inspection method for opposite side defect in steel plate using electromagnetic force vibration. *A. Hagisaka*[1], I. Yamada[1], S. Niwa[1], S. Shiota[2], Y. Gao[2] and Y. Gotoh[2] *1. Department of Innovative Engineering, Oita University, Oita, Japan; 2. Department of Mechanical and Energy Systems Engineering, Oita University, Oita, Japan*

Introduction It is important to detect corrosion or defects on the opposite side of steel walls used for structures in petrochemical plants. In this research, the detection method of the opposite side defect in the steel plate by applying vibration due to electromagnetic force and measuring its vibration is proposed. The proposed sensor probe consists of a permanent magnet, an AC excitation coil and a vibration sensor. The defect is evaluated by the excitation frequency component of the measured the vibration intensity. The vibration distribution by the electromagnetic force in the steel plate with and without the defect is evaluated by the electromagnetic nonlinear 3D-FEM and the displacement 3D-FEM analysis. In addition, the verification experiment is also carried out. Inspection model and conditions Fig. 1 shows a proposed sensor using an AC magnetic field of 2A at 700Hz. The alternating current of 700Hz and 2A is passed to the exciting coil. In the proposed sensor, the electromagnetic vibration inside the steel plate is generated by the eddy current from an exciting coil and static flux density from the permanent magnet. Then, a ceramic bar is connected to the vibration sensor, and the vibration on the surface the steel plate is measured. Inspection result and discussions Fig.2 shows the distribution of the displacement at each position on the steel plate when the proposed sensor is moved in the *x*-direction. Fig.2 (a) shows the calculated results, and Fig.2 (b) shows the measured results, respectively. Fig.2 (a) shows the calculated displacement distribution of the vibration sensor inside the proposed sensor by 3D displacement analysis and 3D electromagnetic nonlinear analysis. This figure denotes that the displacement is increased near the defect in the steel plate. This is because, the density of the steel plate is decreased near the defect. Fig. 2(b) denotes that the detection signal is increased near the defect, similar to the analysis result of Fig.2 (a). From these results, the opposite side defect in the steel plate is detected by the vibration intensity of the steady frequency.

[1]Jhang, K. Y., "Applications of Nonlinear Ultrasonics to the NDE of Material Degradation," IEEE-UFFC, Vol. 47, No.3, pp. 540–548, 2000. [2] Jeong, H., Nahm, S. H., Jhang, K. Y. and Nam, Y. H., "A Nondestructive Method for Estimation of the Fracture Toughness of CrMoV Rotor Steels based on Ultrasonic Nonlinearity," Ultrasonics, Vol. 41, No. 7, pp. 543–549, 2003.

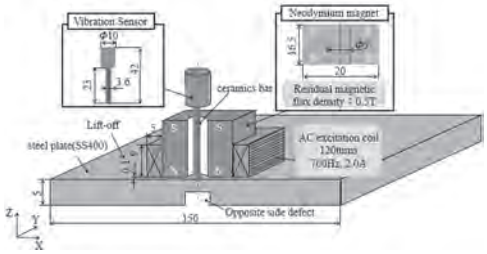

Proposed sensor and Inspection model

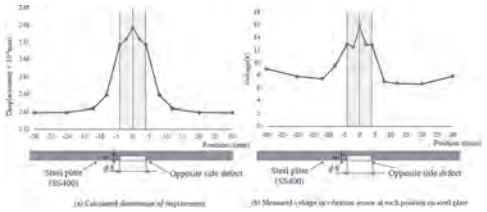

Comparison of analysis results and experimental results

IPC-10. Examination of electromagnetic inspection method for opposite side defect on steel plate using full-wave rectified alternating magnetic field. *R. Ou*[1], Y. Ono[1] and Y. Gotoh[2] *1. Department of Engineering, Oita University, Oita, Japan; 2. Department of Innovative Engineering, Oita University, Oita, Japan*

Introduction It is important to detect an opposite side defect in steel wall in petrochemical plants. As the inspection for the defect, the electromagnetic inspection method using static and alternating magnetic field is examined [1]. However, this method is required two types of power supplies of static and alternating current. On the other hand, when the full-wave rectified magnetic field is expanded by fourier series, it is the combined magnetic field of static and alternating magnetic field. Therefore, in this paper, the inspection method by the full-wave rectified magnetic field using only one power supply is investigated. Since the magnetic property inside the steel plate in this method is minor loop, the flux density is analyzed by 3D nonlinear FEM using the "play model [2]" taking account of minor loop magnetization property. In this research, the usefulness of the inspection method is evaluated by the "play model" and verification experiment. Inspection model and results Fig.1 shows an inspection model using 2 kHz and 1A at a full-wave rectified exciting current. Although the full-wave rectified magnetic field is an AC magnetic field, the flux density is penetrated deep into the steel plate. If there is an opposite side defect, the flux density is distributed around the defect, and leakage flux is generated on the surface of the steel plate. The defect is evaluated by detecting this leakage flux. Fig.2 shows the comparison between calculated and measured results of the detection signal. The vertical axis is the rate of change η_d with respect to the presence or absence of defect in the output voltage, and the horizontal axis is the moving position of the sensor. This figure denotes that the detection signal is increased at the center position of the defect. And, the calculated result is also same tendency as measured result. The inspection of the opposite side defect in the steel plate is possible by impressed the full-wave rectified magnetic field.

[1]Y.Gotoh, and N.Takahashi, *IEEE Trans. Magn.,* vol.44, no.6, pp.2752-2754 (2008). [2] T.Matsuo, Y.Osaka and M.Shimasaki, *IEEE Trans. Magn.,* vol. 36, no.4, pp. 1172-1177, 2000.

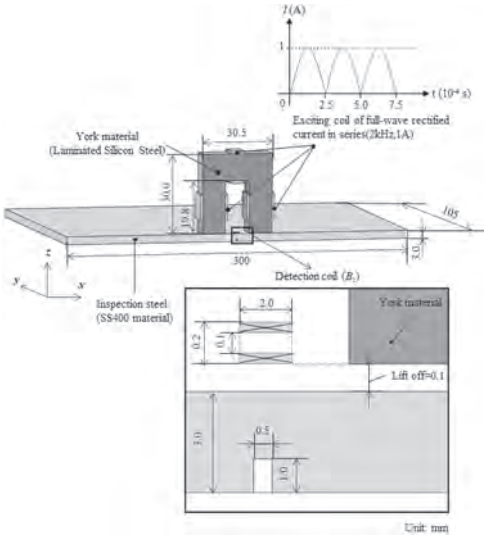

Proposed inspection model using full-wave rectified magnetic field(1/2 model).

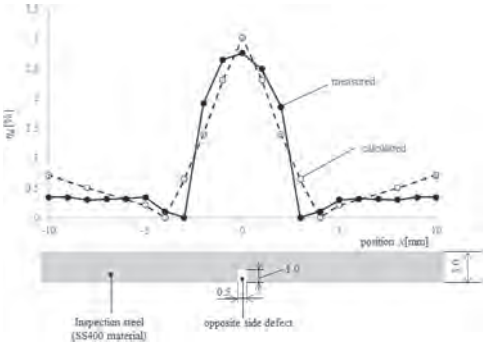

Detection signals of the opposite side defect in the steel plate using the full-wave rectified magnetic field (2kHz, $1A_{0\text{-}p}$).

Session IPD
MICROSCOPY, IMAGING AND CHARACTERIZATION III
(Poster Session)

Spyridon Angelopoulos, Chair
National Technical University of Athens, Zografou, Attiki, Greece

IPD-01. Facile Magneto-optic Detection of Tunable Magnetically-Induced Transparency Spectra in Magnon-Magnon Coupled Bilayers. W. Zhang[1], *J. Inman*[1,2], Y. Xiong[1,2], Y. Li[3], J. Sklenar[4], P. Li[5], S. Louis[2], H. Qu[2], Z. Xiao[3], W. Kwok[3] and V. Novosad[3] *1. Physics Department, Oakland University, Rochester, MI, United States; 2. Electronic and Computer Engineering Department, Oakland University, Rochester, MI, United States; 3. Materials Science Division, Argonne National Laboratory, Lemont, MI, United States; 4. Physics Department, Wayne State University, Detroit, MI, United States; 5. Electronic and Computer Engineering Department, Auburn University, Auburn, AL, United States*

Hybrid magnonic systems host a variety of characteristic quantum phenomena such as the magnetically-induced transparency (MIT) and Purcell effect, which are considered useful for future coherent quantum information processing [1-2]. Here, we experimentally demonstrate a tunable MIT effect in the YIG/Py magnon-magnon coupled system via changing the magnetic field orientations. By probing the magneto-optical Kerr and Faraday effects of Py and YIG, we identify clear features of MIT spectra induced by the mode hybridization between the ferromagnetic resonance of Py and the perpendicular standing spin-wave of YIG. By changing the external magnetic field orientation, we observe a tunable coupling strength between the YIG's spin-wave modes and the Py's uniform mode, upon the application of an out-of-plane magnetic field. Our findings show high promise for investigating tunable coherent phenomena with hybrid magnonic platforms.

[1] Y. Xiong et al. "Detecting Phase-Resolved Magnetization Dynamics by Magneto-Optic Effects at 1550 nm Wavelength", IEEE Trans. Magn. 57, 4300807 (2020). [2] Y. Xiong et al. "Probing magnon–magnon coupling in exchange-coupled YIG/Permalloy bilayers with magneto-optical effects", NPG Sci. Rep. 10, 12548 (2020).

IPD-02. Development of a User-Friendly Time Resolved Scanning Transmission X-ray Microscope at the Advanced Light Source to Study Magnetization Dynamics. T. Feggeler[1], E. Norum[1], A. Butko[3], G. Portman[1], D. Shapiro[1] and *H. Ohldag*[1,2] *1. Advanced Light Source, Lawrence Berkeley National Laboratory, Berkeley, CA, United States; 2. Materials Science and Engineering, Stanford University, Stanford, CA, United States; 3. Computer Sciences, Lawrence Berkeley National Laboratory, Berkeley, CA, United States*

Investigating state of the art material systems and devices that are of importance for magnetism and energy sciences, requires characterization of electronic and magnetic properties on the nanoscale. Scanning probe x-ray spectro-microscopy is an excellent tool for this purpose, since it allows for spatial resolution of the order of 10 nm using soft x-rays at a synchrotron. In addition, the pulsed nature of the source allows to study the temporal behavior of a sample with <100 ps time resolution in a pump probe manner. However, due to the limited ability to normalize the x-ray spectra in these time scales and due to the phase transient of the x-ray pulse the sensitivity for changes in the XAS is limited to one percent in ~200 ps. To address these limits, we are deploying a fast point detector and acquire the full waveform generated by the synchrotron on the detector over ~100 ms. Using a field programming gate array (FPGA) the arrival time as well as the height of each x-ray pulses will be recorded, while at the same time the sample is exposed to a synchronized excitation. This will allow to directly correlate the excitation of the sample to its time-resolved XAS from pico- to milliseconds with 10s of picosecond time resolution. In this contribution we will first demonstrate the power of such an approach by reviewing results obtained using a simplified setup and then describe the upgrades planned using state of the art FPGA hardware.

IPD-03. Square-Wave Inverter Excitation for Magnetic Nanoparticle Tomography. *K. Higashino*[1], N. Okamura[1], T. Sasayama[1] and T. Yoshida[1] *1. Kyushu University, Fukuoka, Japan*

The imaging of magnetic nanoparticle (MNP) distributions is a promising biomedical imaging technique for detecting cancers [1]. A method is magnetic nanoparticle tomography (MNT), in which multiple magnetic sensors are used to detect the harmonic signal of MNPs [2] [3]. In our previous study [2] [3], a linear amplifier power supply with low power efficiency was used to generate the excitation magnetic field. In this study, a square-wave inverter was alternatively used to provide high efficiency. However, the third harmonic excitation field was generated by the general square-wave inverter excitation, degrading the imaging performance. Therefore, we developed a method to suppress the third harmonic by shifting the switching phase of the inverter. The experimental setup is shown in Fig. 1. A full-bridge inverter was used to generate a square excitation voltage. Generally, a square-wave voltage was generated by shifting the switching phase of the left- and right-arms by 180°. The square voltage generated using this method contained the third harmonic. We developed a method to suppress the third harmonic by shifting the switching phase by 120°. In this case, the third harmonic does not appear theoretically. The Resovist MNP sample (500 mg-Fe / 150 mg) was arranged and magnetized by an alternating-current magnetic field in the Z-axis using an excitation coil. The sample moved on the *x*-*y* plane, and the third harmonic signal of the MNPs was obtained using 16 detection coils. The distance between the excitation coil and the sample was set to 35 mm. Figs. 2(a) and (b) show the third harmonic signal distribution from MNPs using 180° and 120° shifts, respectively, detected by a detection coil. The signal from the MNPs was masked by the excitation field noise (Fig. 2(a)). In contrast, the peak and trough were visible. The results show that the proposed method increases the feasibility of MNT using a square wave inverter excitation. This study was supported by the Japan Society for the Promotion of Science (JSPS) KAKENHI (Grant Number JP21H01342).

[1] T. Knopp and T. M. Buzug, "Magnetic Particle Imaging—An Introduction to Imaging Principles and Scanner Instrumentation," Springer, 2012. [2] T. Sasayama, T. Yoshida, and K. Enpuku, "Two-dimensional magnetic nanoparticle imaging using multiple magnetic sensors based on amplitude modulation," *J. Magn. Magn. Mater.*, Vol. 505, Jul. 2020, Art. No.166765. [3] T. Sasayama, N. Okamura, and T. Yoshida, "Sensitivity improvement of magnetic nanoparticle imaging by compensation with digital-to-analog converter," *IEEE Trans. Magn*, Vol. 57, No.2, Feb. 2021, Art. No.5300605.

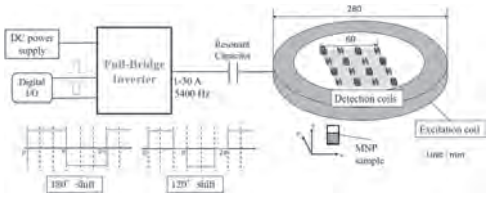

Fig.1. Experimental setup

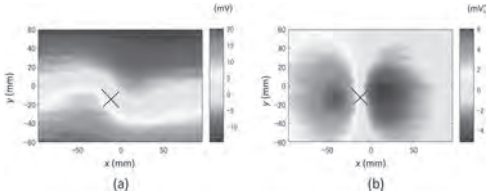

Fig. 2. Third harmonic signal distributions of MNPs using (a) 180° and (b) 120° shifts (The cross mark indicates the position of a detection coil.)

IPD-04. Dependency of magnetorelaxometry on the temperature of magnetic nanoparticles. *S. Arsalani*[1], P. Radon[1], M. Liebl[1], U. Steinhoff[1] and F. Wiekhorst[1] *1. Metrologie Magnetischer Nanopartikel, Physikalisch-Technische Bundesanstalt, Berlin, Germany*

Magnetic nanoparticles (MNPs) show a high potential in several biomedical applications such as hyperthermia and drug targeting. It is crucial for these applications to quantify and localize the MNPs in the body before cancer treatment. Our group in PTB has demonstrated the high capability of magnetorelaxometry (MRX) to quantify MNP distributions at room temperature in vitro and in animal models [1]. The typical MRX measurement starts with magnetizing the MNP by applying a moderate magnetic field. Then, after switching off the magnetic field the decay of the magnetic net moment is measured by sensitive magnetic field sensors such as a superconducting interference device (SQUID), fluxgate or optical magnetometer (OPM). The initial amplitude of the relaxation signal is a direct measure of the net magnetic moment of the magnetized sample, and it depends on the size, concentration, magnetic properties of MNPs and applied magnetic field. Since we are developing an MRX system for human application we need to investigate the effect of temperature (more than room temperature such as body temperature 37 C) on the MNP relaxation. In this work, the relaxation behavior at elevated temperatures from 27 C to 75 C of 8 sample types (iron oxide cores, hydrodynamic sizes from 70 nm to 250 nm) has been investigated using our 6 channel MRX device applying 4 mT magnetizing field. All the MNP systems showed a significant decrease of their relaxation amplitude with increasing temperature where the thermal fluctuations are speeding up the MNP relaxation. Figure1 exemplifies the MRX amplitude for Perimag (Micromod, Germany) MNP at different temperatures and Figure 2 shows the relaxation amplitude (ΔB) as a function of temperature (T). As an outlook, these results could be very useful for estimating relative temperature changes of tumor region right after magnetic heating treatments (magnetic hyperthermia).

F. Wiekhorst, U. Steinhoff and D. Eberbeck, Pharm Res., 29:1189–1202 (2012).

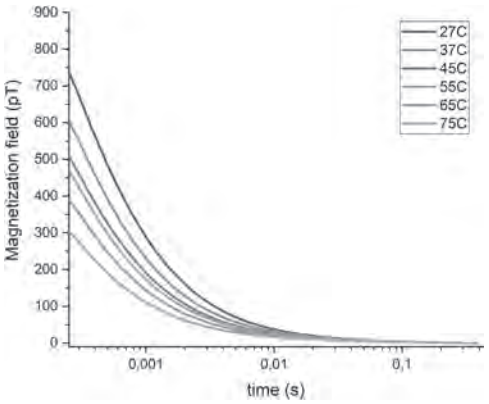

Fig. 1 The relaxation curves of Perimag MNP at different temperatures.

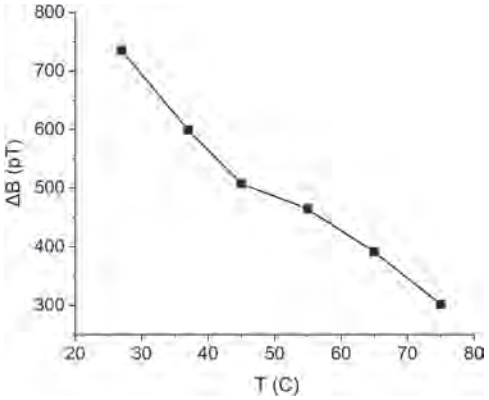

Fig. 2 The relaxation amplitude (ΔB) as a function of temperature (T).

IPD-05. Withdrawn

IPD-06. Static and Dynamic Magnetic Property Characterizations on Self-assembled Magnetic Nanoparticle Chains. *S. Liang*[1], V.K. Chugh[2], R. Saha[2], K. Wu[2], J. Liu[2], V.D. Krishna[3], M.C. Cheeran[3] and J. Wang[1,2] *1. Department of Chemical Engineering and Materials Science, University of Minnesota, Minneapolis, MN, United States; 2. Department of Electrical and Computer Engineering, University of Minnesota, Minneapolis, MN, United States; 3. Department of Veterinary Population Medicine, University of Minnesota, Minneapolis, MN, United States*

Magnetic nanoparticles (MNPs) can form chain structures in the presence of a static magnetic field (fixation field), as a result of dipolar interactions.[1, 2] These self-assembled MNP chains with tunable magnetic properties can be tailored for different applications and thus have attracted broad research interests.[1,3,4] However, the research on the physical parameters of the MNP chains and the influence of these parameters on the magnetic properties of the chains are limited. Herein, we investigated the effects of magnetic anisotropy and concentration of MNPs on static and dynamic magnetic properties of chains through magnetic particle spectrometer (MPS) and vibrating sample magnetometer (VSM). In this work, different concentrations of 18 nm γ-Fe_2O_3 MNPs in agarose solution are solidified at room temperature and form chains under a fixation field B_{fix} of 1500 G. The chain structure is visualized and confirmed by optical microscope as shown in Fig.1 (a)-(f). MNP chains are fixed with different angles to the detection field B_{det} in MPS and VSM systems. The dynamic magnetic responses of MNP chains in the form of the 5th harmonics are recorded from MPS system and plotted in Fig.1 (g)-(i). The results indicate strong angular dependence of the dynamic magnetic properties of MNP chains. In addition, the static magnetic responses of these MNP chains are characterized and the MH curves are compared. The dipolar interactions of MNPs in different chain structures and

relative angles between chains and detection fields are theoretically studied by micromagnetic simulations on mumax[3]. This observation will facilitate future design and application of MNP chains structures.

[1] E. Myrovali, et al., ACS Applied Materials & Interfaces., Vol. 13(18), P. 21602-21612 (2021) [2] J. A. De Toro, et al., The Journal of Physical Chemistry C., Vol. 117(19), P.10213-10219 (2013) [3] M. Tadic, et al., Applied Surface Science., Vol. 476, P. 641-646 (2019) [4] G. Diguet, et al., Journal of Magnetism and Magnetic Materials., Vol. 481, P. 39-49(2019)

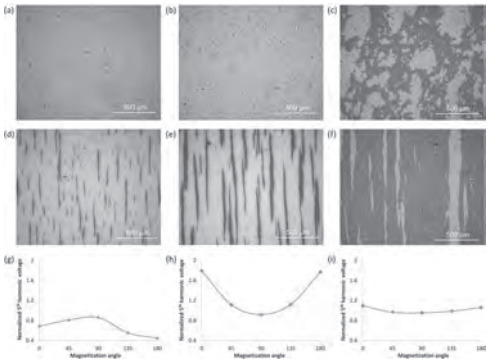

Fig.1: (a), (d) show the optical images of 0.5 mg/ml MNP sample fixed in agarose matrix in absence and in presence of an external magnetic field. (b), (e) show the optical images for 1 mg/ml sample whereas images for 4 mg/ml sample are shown in (c), (f). (g), (h), and (i) represent the normalized 5th harmonic voltage of MPS spectra w.r.t. the angle of applied field used to set the MNPs for concentrations of 0.5, 1, and 4 mg/ml, respectively. The harmonic voltages are normalized to the MPS spectra of sample fixed in agarose in absence of external field.

IPD-07. In situ observation of magnetic vortex in amorphous and nanocrystalline ribbon. *S. Zuo*[1], Y. Zhang[2], T. Zhao[2] and B. Shen[2] *1. Beihang University, Beijing, China; 2. Institute of Physics, Chinese Academy of Science, Beijing, China*

Noncollinear or noncoplanar spin textures, such as magnetic vortex, nontrivial bubble, and skyrmion, have attracted significant research interest because of the underlying fundamental applications as basic units of spintronic devices [1]. Magnetic vortex usually appear in the materials with weak magnetic anisotropy such as permalloy. Previous research reveals that magnetic vortices can spontaneous form in amorphous CeFeB ribbon and can be easily manipulated by external fields [2], which is important to the potential applications. The present work aims to study the magnetic vortices in amorphous and nanocrystalline ribbon by means of Lorentz TEM to reveal the key factors influencing magnetic vortex nucleation. Magnetic vortices and tree-like domain walls are observed in the $Ce_{14}Fe_{80}B_6$ amorphous ribbon (Figure 1). When the amorphous ribbon become nanocrystalline ribbon after suitable annealing, the magnetic vortex will appear in the grains with size about 30~150 nm and will not be stable if the grains are too large or too small (Figure 2), indicating the formation of magnetic vortices is closely related to shape limitation and defects. Magnetic vortices have also been observed in other amorphous materials such as $Fe_{78}Si_9B_{13}$, which may mean that magnetic vortices are the intrinsic magnetic domains in the amorphous alloys due to their weak magnetic anisotropy. Physics related to the magnetic vortex formation is discussed for present system, which probably stimulate further exploration of the universal phenomenon and mechanism.

[1] S.S.P. Parkin, M. Hayashi, L. Thomas, Magnetic domain-wall racetrack memory, Science 320 (2008) 190-194. [2] S. Zuo, M. Zhang, R. Li, Y. Zhang, L. Peng, J. Xiong, D. Liu, T. Zhao, F. Hu, B. Shen, J. Sun, Acta Materialia 140 (2017) 465-471.

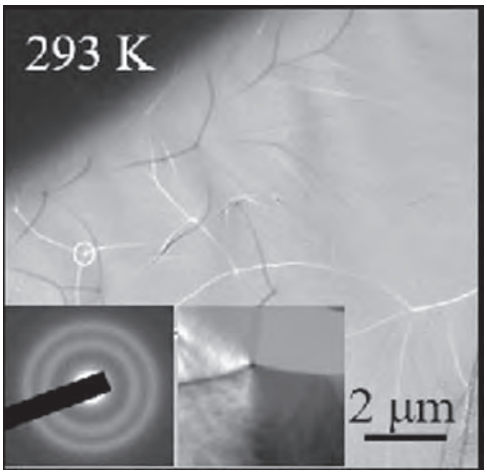

Figure 1 Lorentz TEM image of magnetic domains in $Ce_{14}Fe_{80}B_6$ amorphous ribbon, the insets showing the selected area electron diffraction and the lateral magnetization distribution of a magnetic vortex.

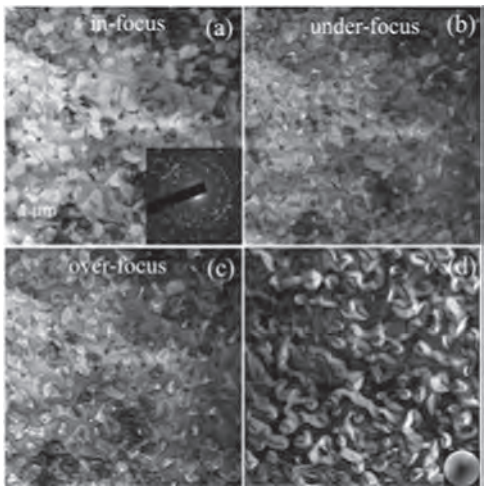

Figure 2 Lorentz TEM images of the annealed sample and corresponding lateral magnetization distribution, the inset showing selected area electron diffraction.

IPD-08. Spin-polarized scanning tunneling microscopy on Co-Fe alloy nanoislands. *H. Yang*[1,2], C. Hsu[3], W. Lin[3] and Y. Hasegawa[1] *1. The University of Tokyo, Kashiwa, Japan; 2. Karlsruhe Institute of Technology, Karlsruhe, Germany; 3. National Taiwan Normal University, Teipei, Taiwan*

$Co_{1-x}Fe_x$ bi-layer nanomagnets formed on a Cu(111) substrate with the alloy composition of x = 0, 0.2, 0.5, 0.8, and 1 were investigated using spin-averaged and spin-polarized scanning tunneling microscopy. At x = 0.2, the nano-sized island structures exhibit a similar triangular shape and an upward shift in the energy level of electronic states as compared to those of pure Co. On the other hand, at x = 0.5, the appearance of the nano-islands evolves from triangular to a round shape, and the peak energy of electronic states distributes irregularly within the islands. The hexagonal shape and inhomogeneous electronic states similar to pure Fe islands are found on the x = 0.8 islands. Spin-polarized conductance maps reveal that the perpendicular magnetization of the $Co_{1-x}Fe_x$ nanomagnets at x= 0, 0.2, and 0.5.

IPD-09. Magnetic properties and domain imaging of IrMn (5 nm)/Fe_2 CoSi (5 nm) bilayer. *A.K. Jana*[1], M. Raja[2], C. Arout[2] and J. Suryanaryana[1]
1. Physics, IIT Hyderabad, Hyderabad, India; 2. Magnetic Group, DMRL, Hyderabad, India

Thin films based on Heusler alloy (HA) have been attained great interest due to their multi-functional properties apart from their applications in spintronic devices due to half-metallic in nature [1]. In this manuscript, we investigate magnetic properties and domain imaging of IrMn (5 nm)/Fe_2CoSi (5 nm) bilayer. Structural properties of bilayer films were studied by grazing incidence X-ray diffraction (GI – XRD). Magnetic properties were carried out by vibrating sample magnetometer (VSM) Lakeshore 8600. Domain imaging and magnetization reversal were recorded with longitudinal magneto-optical Kerr effect (L-MOKE). Fig. 1 (a) shows in-plane and out of plane magnetization (M) vs. magnetic field (H) graphs for IrMn (5nm)/Fe_2CoSi (5 nm) bilayer with a coercivity (H_C) of 25 Oe. It is evident that the bilayer consists of in-plane magnetization. Fig. 1(b) depicts the azimuthal angle variation of coercivity (Hc), which demonstrates that this bilayer consists of uniaxial anisotropy along with four-fold anisotropy. The existence of four-fold anisotropy is consistent with the earlier reports [2,3]. In addition, we also tried to fit the H_C variation with an azimuthal angle with a four-fold anisotropy equation, $H_C = a\ Sin^2(\theta+b) + c\ Sin^2(\theta+e)\ Cos^2(\theta+e)$, where θ is azimuthal angle and a, b, c, and e are fitting parameters. Fig. 2 represents the M vs. H loop and corresponding domain images along the easy axis, which were measured with L – MOKE at 0º. It is evident that domain wall motion with saw tooth patterns governs the magnetization reversal process with increasing the field. The presence of saw tooth domains can be attributed to the existence of strong uniaxial anisotropy to reduce the magnetic charge density [4–6]. The decrease in the number of teeth in the domain images with the field could be due to the dominating Zeeman energy over the magnetostatic energy

[1] H. Luo, Z. Zhu, L. Ma, S. Xu, H. Liu, J. Qu, Y. Li, G. Wu, Electronic structure and magnetic properties of Fe $_2$ YSi (Y = Cr, Mn, Fe, Co, Ni) Heusler alloys: a theoretical and experimental study, J. Phys. D: Appl. Phys. 40 (2007) 7121–7127. https://doi.org/10.1088/0022-3727/40/22/039. [2] A.K. Jana, M.M. Raja, J.A. Chelvane, P. Ghosal, S.N. Jammalamadaka, Thickness dependent domain wall dynamics in Fe2CoSi thin films, Journal of Magnetism and Magnetic Materials. 521 (2021) 167528. https://doi.org/10.1016/j.jmmm.2020.167528. [3] A.N. Pogorily, A.F. Kravets, V.V. Nevdacha, D.Y. Podyalovskiy, S.M. Ryabchenko, V.M. Kalita, M.M. Kulik, A.F. Lozenko, A.Ya. Vovk, M. Godinho, L. Maurel, J.A. Pardo, C. Magen, V. Korenivski, Magnetic anisotropy of epitaxial Co $_2$ Fe-Ge Heusler alloy films on MgO (100) substrates, AIP Advances. 7 (2017) 055831. https://doi.org/10.1063/1.4978209. [4] M. Tortarolo, L. Thevenard, H.J. von Bardeleben, M. Cubukcu, V. Etgens, M. Eddrief, C. Gourdon, Fast domain wall dynamics in MnAs/GaAs films, Appl. Phys. Lett. 101 (2012) 072408. https://doi.org/10.1063/1.4746381. [5] K.-S. Ryu, S.-C. Shin, H. Akinaga, T. Manago, Real-time direct observation of temperature-dependent domain reversal behavior in epitaxial MnAs film on GaAs(001), Appl. Phys. Lett. 88 (2006) 122509. https://doi.org/10.1063/1.2189016. [6] A. Hubert, R. Schäfer, Magnetic domains: the analysis of magnetic microstructures, Softcover reprint of the hardcover 1st ed. 1998, corrected print. 2000, Springer, Berlin, 2014.

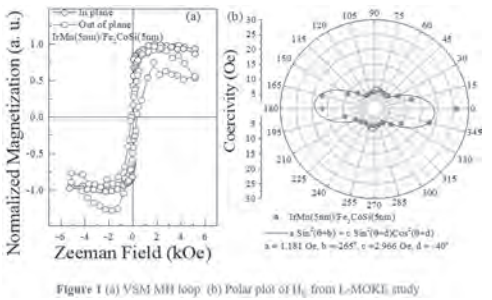

Figure 1 (a) VSM MH loop (b) Polar plot of H_C from L-MOKE study

Figure 1 (a) VSM MH loop (b) Polar plot of H_C from L-MOKE study.

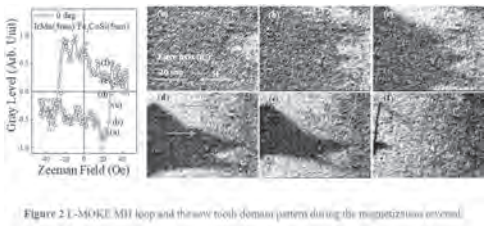

Figure 2 L-MOKE MH loop and the saw tooth domain pattern during the magnetization reversal

Figure 2 L-MOKE MH loop and the saw tooth domain pattern during the magnetization reversal.

IPD-10. Eddy Current Microscopy Utilizing CoPt Coated Probes. *Y. Yang*[1], A. Sokolov[2], X. Yin[3], Y. Liu[1,2], J. Trujillo[4] and S. Liou[1,2]
1. Department of Physics and Astronomy, University of Nebraska-Lincoln, Lincoln, NE, United States; 2. Nebraska Center for Materials and Nanoscience, University of Nebraska-Lincoln, Lincoln, NE, United States; 3. Western Digital Corporation, Fremont, CA, United States; 4. Department of Energy's National Security Campus, Kansas City, MO, United States

Eddy current microscopy (ECM) that utilizes magnetic probes is a nondestructive evaluation technique based on magnetic force microscopy (MFM) and is effective for mapping the electrical conductivity on the surface or in a shallow depth of a specimen [1-3]. In this study, it is demonstrated that MFM based ECM can be realized utilizing CoPt coated probes and this technique has the potential to visualize embedded details. A CoPt coating layer was deposited on commercially available atomic force microscope probes by magnetron sputtering and similar to previous work [4,5], treated with rapid thermal annealing to achieve high coercivity. The high coercivity leads to a well-defined magnetization direction, which is good for the resolution. The CoPt coating became granular after thermal annealing. As shown in Fig. 1, a CoPt granule of which the size is between 200 nm and 300 nm is at the tip of a probe. As the specimen, circular films made of Ru were deposited on a thermally oxidized silicon substrate using photolithography and magnetron sputtering. The thickness of the circular films is about 30 nm, and the diameter is 6 μm. The topographic image of a circle by tapping mode atomic force microscopy (AFM) with a nonmagnetic probe is shown in Fig. 2(a), while the lift mode scan in Fig. 2(b) with the nonmagnetic probe provides no visible imaging of the circle. As shown in Figs. 2(c) & 2(d), lift mode images by ECM utilizing a CoPt coated probe clearly map the metal circle with the lift height being 5 nm and 100 nm respectively. The contrast of the ECM images is valid in the wide range of lift height from 5 nm to 100 nm, and the range may extend further due to the long-range nature of magnetic interactions and the well-defined magnetization direction and large stray field of the CoPt coated probes, indicating that possibly embedded details in a specimen can also be visualized with ECM.

[1] B. Hoffmann, R. Houbertz, and U. Hartmann, Appl Phys A 66, S409–S413 (1998). [2] M. A. Lantz, S. P. Jarvis, and H. Tokumoto, Appl. Phys. Lett. 78, 383 (2001). [3] V. Nalladega, S. Sathish, K. V. Jata, and M. P. Blodgett, Rev. Sci. Instrum. 79, 073705 (2008). [4] L. Gao, L. P. Yue, T. Yokota, R. Skomski, S. H. Liou, H. Takahoshi, H. Saito, and S. Ishio, IEEE Transactions on Magnetics, vol. 40, no. 4, pp. 2194-2196, July 2004. [5] S. H. Liou, S. Huang, E. Klimek, R. D. Kirby, and Y. D. Yao, Journal of Applied Physics 85, 4334 (1999).

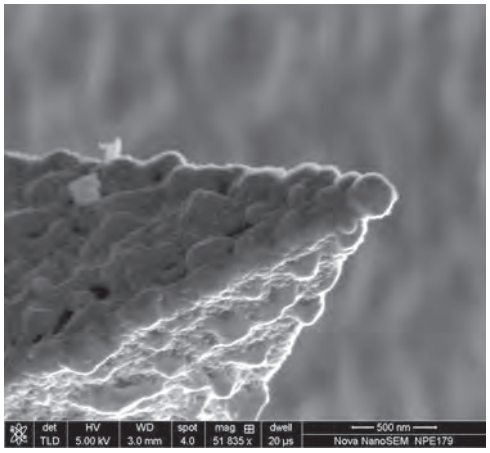

Fig. 1. An SEM image of the CoPt coated probes after thermal annealing.

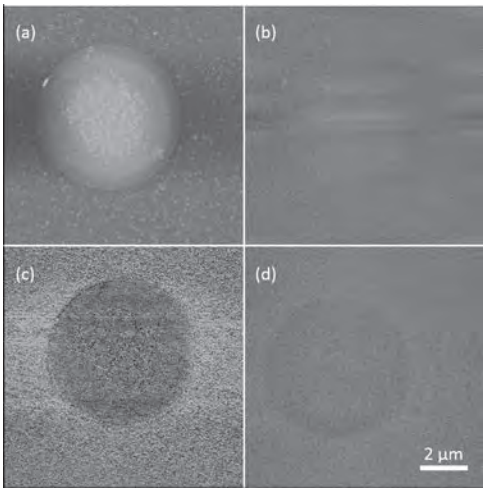

Fig. 2. (a) The topographic image of a circular film by tapping mode AFM with a nonmagnetic probe. (b) The lift mode scan of the circle with the nonmagnetic probe. (c) The ECM image at a lift height of 5 nm. (d) The ECM image at a lift height of 100 nm.

IPD-11. Asymmetric magnetic domain wall motion in a quasi-perpendicularly magnetized with interfacial Dzyaloshinskii-Moriya interaction. *S. Maji*[1], A. Mukhopadhyay[1] and P. Kumar[1] *1. Department of Physics, Indian Institute of Science, Bangalore, Bangalore, India*

Interfacial Dzyaloshinskii-Moriya interaction (iDMI) [1,2] along with perpendicular magnetic anisotropy (PMA) [3,4] in the ultrathin ferromagnetic material/heavy metal (FM/HM) interface has garnered significant attention in recent studies [5,6]. Field-induced domain wall motion has been observed in quasi-perpendicularly magnetized Pt/Co/Pt trilayers with interfacial Dzyaloshinskii-Moriya interaction (iDMI) using differential Kerr microscopy method in the creep regime (shown in Fig.1). Vineeth et al. [7] reported a quasi-PMA system whose magnetic easy axis is tilted with respect to the z-axis. An oblique angle sputter deposition technique had introduced a thickness gradient in one of the layers of a trilayer, results in a small tilt of magnetic anisotropy from the film normal. The tilt angle has been estimated in each trilayer by determining the shift in the out-of-plane magnetization hysteresis measurements under a bias magnetic field applied along with various in-plane directions. The effective in-plane field at the domain wall due to iDMI has been determined by decomposing the symmetric and asymmetric contributions of the domain wall motion. Furthermore, the asymmetric contribution has been decomposed into two contributions due to the tilted magnetic anisotropy and the exponentially decaying chiral damping. The nature of the asymmetric contribution owing to the tilted anisotropy was studied by the collective coordinate model (shown in Fig.2) and a functional form of the total asymmetric contribution has been determined and used to fit the asymmetric contribution [8].

[1] I.E. Dzyaloshinskii, J. Expt. Theor. Phys. (U.S.S.R.) Vol. 32, p.1547 (1957). [2] T. Moriya, Phys. Rev., Vol. 120 p.91 (1960). [3] P. F. Carcia, A. D. Meinhaldt, and A. Suna, Applied Physics Letters, Vol. 47, p. 178–180 (1985). [4] P. Li, T. Liu and M. Z. Wu, Nature Communications, Vol. 7, p.12688 (2016). [5] S. Hashimoto, Y. Ochiai, and K. Aso, Journal of Applied Physics, Vol. 66, p.4909–4916 (1989). [6] G. Q. Yu, P. Upadhyaya and K. L. Wang, Nature Nanotechnology, Vol. 9, p.548–554 (2014). [7] V. M. Parakkat, K. R. Ganesh, and P. S. A. Kumar, Phys. Rev. B, Vol. 96, p.104412 (2017). [8] A. Mukhopadhyay, S. Maji and P. S. Anil Kumar, J. Magn. Magn. Mater., Vol. 537, p.168125 (2021).

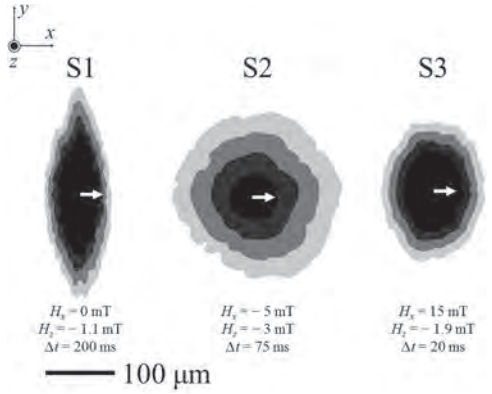

Fig.1: Field-induced domain wall motion for all the trilayers obtained using differential polar Kerr microscopy technique. Corresponding applied H_x and pulsed H_z with the pulse-width Δt are mentioned under the images. Azimuthal orientation of the tilted magnetic anisotropy has been shown using a white arrow for each trilayer.

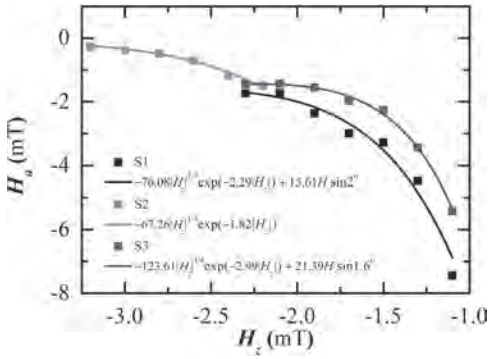

Fig.2: Dependence of asymmetric contribution, H_a on H_z have been shown for azimuthal orientation along the *x*-axis for all the trilayers. All the solid lines through the data points validate the CCM.

IPD-12. Observing 360 domain wall switching behavior in submicron permalloy rings. *K. Lai*[1], D. Shiu[1], R. Cao[2] and L. Horng[1] *1. Physics, National Changhua University of Education, Changhua, Taiwan; 2. Electrical Engineering, Feng Chia University, Taichung, Taiwan*

Two variables of permalloy ring was different width and thickness. Simulation results of OOMMF discovered the generation field of 360DW associated with thickness. The 360DW generated about thickness less than 10 nm, 11 nm thick above are not generated. Depending on the width and thickness can be divided into five blocks. We found the area about 360DW and vortex states were both generated, but there will not be this phenomenon in the narrow width of the ring, final the 360DW were not generation again in more thickness. In the minor loop, the ring had two difference states in zero field. In simulation, we employ one ring to generate one 360DW. This study

used the Object Oriented MicroMagnetic Framework (OOMMF) software to analyze different inner and outer diameter to exploit the magnetic state of the film with different thickness6. The parameters were saturation magnetization Ms= A/m, crystalline anisotropy 0, exchange constant A= J/m, Damping constant =0.5 and Cell Size 5nm. We fixed the outer diameter (Do) of ring was 1200 nm and explored separately the magnitude of inner diameter (Di) and thickness. In experiment, we used E-beam lithography define the graph and magnetrons sputtering fabricate our samples. The deposit parameters were 10 watt and 2mtorr. Hysteresis loop measure by magneto optical Kerr effect microscopy. Because of shadow caused a lot of noise in MOKE images. We used magnetic force microscopy to observing the domain structures. We have studied the effect of magnetic moment states for different film thickness. The OOMMF simulation predicts that the moment state change by film thickness varied from 5 to 30 nm. The 360DW state is generated for thickness form 5 to 10 nm, and disappears for thickness of 11 to 30 nm. The transverse domain wall state was replaced by vortex state in thickness above 22 nm. The sample with Do = 1200 nm, Di = 600 nm, and t = 10 nm as an example shown in Fig.1. We found two TDWs form onion state change into 360DW in B to E. Then from point D to E, the 360DW change into vortex state. The fig.2 was measure by magneto optical Kerr effect microscopy. It had similar curve to simulation.

X. H. Wang, W. K. Peng, and W. S. Lew. Journal of Appl. Phys., 106, 043905. (2009). E. Saitoh, M. Kawabata, K. Harii, H. Miyajima, and T. Yamaoka. Journal of Applied Physics, 95, 1986. (2004). Yu-feng Hou and Kannan M. Journal of Applied Physics, 111, 07B905. (2012). Meng Zhu, Christoph Mathieu, Werner Scholz, Sridhar Dubbaka, and Michael Kautzky, Journal of Applied Physics, 113, 17B905. (2013). Chia-Jung Hsu, etc. IEEE Transactions on Magnetics, vol. 50, no. 1. (2014).

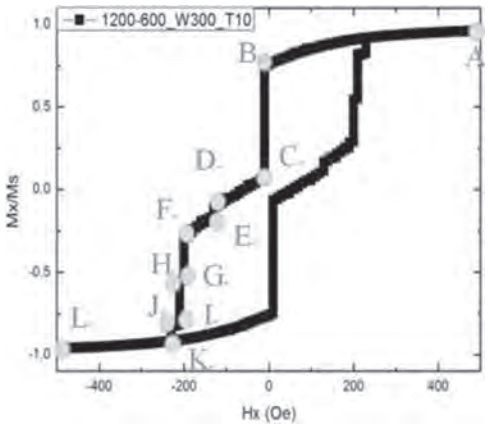

Figure 1. Simulation Magnetic hysteresis loop

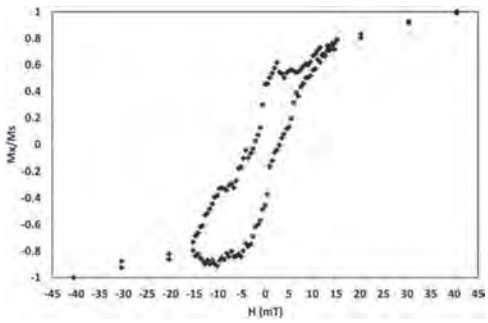

Figure 2. Experiment loop of t = 10 nm

IPD-13. Comparison of Driving Methods by SAMR for Amorphous Ribbons Magnetostriction Measurement. *V. Petrucha*[1] and M. Butta[1]
1. Faculty of Electrical Engineering, Czech Technical University in Prague, Prague, Czechia

Measurement of magneto-mechanical properties of soft magnetic materials (e.g. magnetostriction) provides useful information for typical applications of the materials in sensors and actuators. Measurement methods are developed continually, with emphasis on accuracy and repeatability as the magnetostriction coefficient approaches very low values e.g. for Co-based amorphous ribbons. While the coefficient can be influenced by material processing (e.g. thermomagnetic treatment) it is extremely useful for sensors with state-of-the-art parameters (ultra-low noise) to have the possibility to monitor the value or its change. A classic, indirect method of magnetostriction measurement is SAMR (Small Angle Magnetization Rotation) presented by Narita. The method uses a set of three coils which are used to saturate the sample with a DC field in the direction of the ribbon, to AC drive the magnetization vector by a small angle in the plane of the ribbon and finally to pick-up resulting second harmonic signal. Similar method is used for measurement of magnetic microwires where the driving coil is replaced by injecting current directly into the sample, where it creates the driving magnetic field. We present a novel comparison of these two drive principles for the ribbon samples where the injected driving significantly simplifies the construction of the instrument. Our preliminary results made with Metglas 2714A (2.5 mm wide ribbon, 20um thickness) show that the sensitivity with the injected current is much higher (see Fig.1), however the slope of the curves (magnetoelastic effect compensation field vs. applied strain) differs a bit. We will provide FEM simulation of the driving field in the ribbon to evaluate how the injected driving promotes measurement of surface magnetostriction with respect to bulk measurement in the case of the external coil drive where the high demagnetization factor can play a significant role.

K. Narita, J. Yamasaki, H. Fukunaga, IEEE Trans. On Magnetics, Vol. Mag-16, No. 2 (1980) A. Hernando, M. Vazquez, V. Madurga etc, Journal of Magnetism and Magnetic Materials 61, 39-47 (1986) L. Kraus, J. Phys. E: Sci. Instrum. 22, pp. 943-947 (1989) V. de Manuel, R. P. del Real, J. Alonso, and H. Guerrero Rev. Sci. Instrum. 78, 095104 (2007) Y. Le Bras, A. Lasheras, J. Gutierrez etc, Rev. Sci. Instrum. 84, 043904 (2013) Kwang-Eun Kim, and Chan-Ho Yang, AIP Advances 8, 105125 (2018) S. Gudoshnikov et al., Actuators 10, 93, (2021)

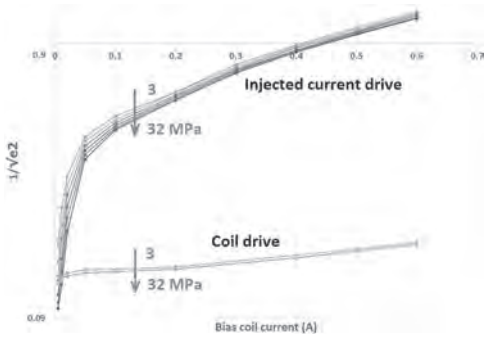

One over the square root of the second harmonic voltage induced in the pick-up coil for perpendicular coil and injected drive for different applied strains

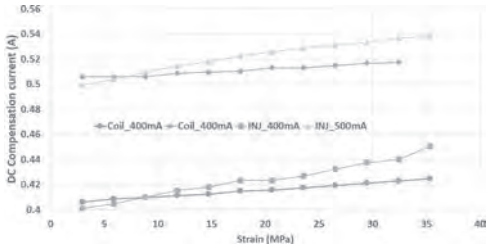

Compensation current needed to keep induced second harmonic constant for different strains (for two DC bias current values)

IPD-14. Magnetic measurement for various types of iron steel thickness using magnetic sensor and the effect of their electromagnetic characteristics. *K. Tsukada*[1], M. Hayashi[1], T. Kawakami[1], S. Adachi[1], K. Sakai[1], T. Kiwa[1], T. Ishikawa[2], M. Saari[3], K. Hori[4], K. Hisazumi[5] and T. Tominaga[5] *1. Okayama University, Okayama, Japan; 2. Kansai University, Suita, Japan; 3. Universiti Malaysia Pahang, Pekan, Malaysia; 4. Nippon Steel Metal Products Co., Ltd, Kanda, Japan; 5. Nippon Steel Corp, Futtsu, Japan*

The diagnosis and prevention of iron-steel infrastructure deterioration have become critical issues in recent years. To detect steel corrosion, a preliminary study of thickness measurement (extremely low-frequency eddy current testing : ELECT) using a magnetic sensor at extremely low-frequency ranges has been previously reported [1]. Iron-steel materials exhibit large variations in electromagnetic characteristics. In this study, the effect of electromagnetic characteristics on the magnetic thickness measurement was investigated to improve the thickness estimation. Four types of iron-steel plates (SS400, SM400A, SM490A, SMA400AW) with thickness ranging from 1 mm to 20 mm were measured via ELECT. The detected magnetic signal, consisting of a real and an imaginary component at each frequency, was plotted to obtain the magnetic spectrum. The differential magnetic vector between two appropriate frequencies is extracted from the magnetic spectrum, and the plate thickness is then estimated from the phase of the differential magnetic vector. For instance, the linearity of the calibration curves between the phase and thickness for each type of steel plate was obtained in the thickness range of 6–12 mm using a differential vector, which was obtained by subtracting the 3 Hz vector from the 5 Hz vector. However, the calibration curves for each type of steel plate did not coincide. To analyze the phase shift phenomenon, the electromagnetic characteristics (the permeability μ, the obtained magnetization curve, and the conductivity σ) of each type of steel plate were measured. The $\mu\sigma$ magnitude relationship for each type of steel is as follows: SM400 > SMA400AW > SS400 > SM490A. The parameter of $\sigma\mu$ was correlated in each calibration curve shift, and the linearity region in the curve was shifted to the low-thickness region according to the increment of frequency. Therefore, the difference in calibration curve for each type of iron-steel could be explained by the difference in $\sigma\mu$ parameter. In summary, this study clarified the relationship between the electromagnetic properties of various types of iron steel and the phase of detected magnetic signal in the thickness measurement.

[1]K. Tsukada, et al., “Detection of Inner Corrosion of Steel Construction Using Magnetic Resistance Sensor and Magnetic Spectroscopy Analysis”, IEEE Transactions on Magnetics, Vol. 52, No. 7,6201504 (2016)

Session IPE
MAGNETIC BIODETECTION AND THERAPY II
(Poster Session)

Anirudh Sharma, Co-Chair
Johns Hopkins University School of Medicine, Baltimore, MD, United States
Ravi L. Hadimani, Co-Chair
Virginia Commonwealth University, Richmond, VA, United States
Anna Guller, Co-Chair
Macquarie University, Sydney, Macquarie Park, NSW, Australia

IPE-01. The Modeling of Magnetic Detection of Iron Oxide Nanoparticles in the Stream of Patient-Specific Coronary Artery with Stenotic Lesion: the Effects of Vessel Geometry and Particle Concentration. *N.V. Kozlov*[1], S. Volchkov[1], F. Blyakhman[1,2], V. Chestukhin[3] and G.V. Kurlyandskaya[1,4] *1. Ural Federal University, Yekaterinburg, Russian Federation; 2. Ural State Medical University, Yekaterinburg, Russian Federation; 3. Research Institute of Emergency Care, Moscow, Russian Federation; 4. University of the Basque Country UPV/EHU, Leioa, Spain*

Magnetic nanoparticles (MNPs) prepared as a stable colloidal suspension dispersed in water have attracted special interest for different applications in theranostics [1]. MNPs of maghemite obtained by a laser target evaporation (LTE) were shown to be excellent candidates for this purpose [2]. Magnetic suspension flowing through the blood vessel creates magnetic fields which can be detected by giant magnetoimpedance magnetic field sensor (GMI) [3]. In this work, we develop a computer model for calculation of the distribution of blood flow velocity V and magnetic fields H in the area of a blood vessel with stenosis. Finite element model (FEM) is used to analyze the properties of the model system reconstructed from the image obtained during routine examination of a patient using angiography. Figures show selected results of the studies. It was shown that the relative change of the magnetic field strength in the area inside the blood vessel doesn't depend on the value of the external magnetic field H_e and the value of additional magnetic field connected to the blood flow is proportional to the concentration of MNPs. To describe the results obtained for a model of a real vessel, a model of a vessel in the form of a cylinder with different radius of curvature and thickness was studied. The results of calculations the flow of MNPs in the vessel showed that at 1.5 wt % of MNPs concentration (c=1.5 wt %) the relative change in the magnetic field in the area of stenosis is 0.43%, and in the area before stenosis is 0.33%. According to experimental data, the observed difference in the distribution of magnetic fields at a concentration of LTE MNPs from 0 to 2% can be measured using a thin-film detector of small magnetic fields GMI. This study was supported by the Ministry of Science and Higher Education of the Russian Federation (project No. FEUZ -2020-0051).

1. A. G. Roca, R. Costo, A. F. Rebolledo, S. Veintemillas-Verdaguer, P. Tartaj, T. González-Carreño, M.P. Morales, C.J. Serna, J. Phys. D Appl. Phys. 42, 224002 (2009). 2. N. A. Buznikov, A. P. Safronov, I. Orue, E. V. Golubeva, V. N. Lepalovskij, A. V. Svalov, A. A. Chlenova and G. V. Kurlyandskaya, Biosensors and Bioelectronics 117, 366-372 (2018). 3. G. V. Kurlyandskaya, M. L. Sánchez, B. Hernando, V. M. Prida, P. Gorria and M. Tejedor, M. Appl. Phys. Lett. 82, 3053–3056 (2003).

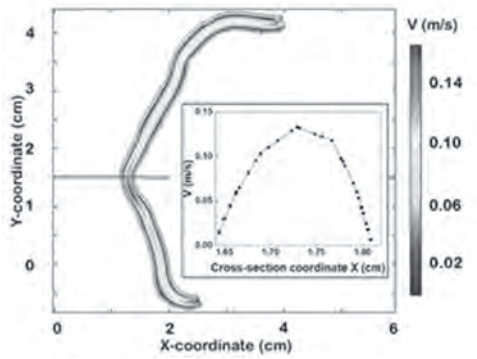

Fig.1. Velocity distribution in a blood vessel with stenosis. The inset shows the value along the cross-section indicated by horizontal red line.

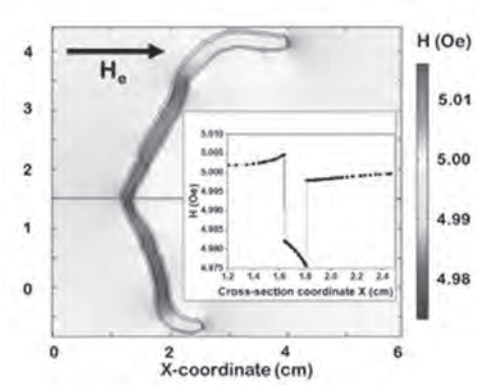

Fig.2. Magnetic field (H) distribution in a blood vessel with stenosis. The inset shows the value along the cross-section indicated by horizontal red line. H_e = 5 Oe and is directed from left to right, c=1.5 wt %.

IPE-02. Withdrawn

IPE-03. Magnetic Nanoparticle-based Fast and Reliable SARS-CoV-2 Detection Method. M.N. Bozkurt[1], *L. Doganturk*[1], S. Ozunlu[1], N. Gunduz Akdogan[2,3] and O. Akdogan[1,3] *1. Bahcesehir University, Istanbul, Turkey; 2. Piri Reis University, Istanbul, Turkey; 3. Nanoterial Technology Corporation, Istanbul, Turkey*

The COVID-19 disease, which was declared a pandemic worldwide by the World Health Organization(WHO) on March 11, 2020, has become a global problem for nearly two years. Currently, used methods like RT-PCR and antibody tests have largely maintained epidemic control but have also yielded unreliable results. Despite showing signs of Atypical Pneumonia

according to the CT result and clinic observations, the presence of patients with negative PCR tests reduces the confidence in PCR tests with false-negative probability. Other methods like antibody tests are considered more reliable after first week of the viral infection which shows that early diagnosis is still problematic. In that context, a new viral diagnostic kit is needed for fast, reliable, and accessible viral detection to decrease the rate of transmission. The novel technique relies on the specific interaction between modified magnetic iron nanoparticles and viral nucleic acid. In this study, Fe nanoparticles were synthesized by a salt-reduction technique using a Y-junction setup under Ar/H2 gas flow. XRD data of the particles corresponds to BCC Fe and the room temperature hysteresis loop reveals a soft ferromagnetic response (Figure.1). Bright Field TEM image (Figure.2) shows a narrow size distribution with an average size of 90nm. As particles were coated with silica followed by multiple modification steps for APTES attachment to increase SARS-CoV-2 RNA binding affinity. Precisely, the negative load of the nanoparticles was increased by the addition of a poly carboxyl tail on APTES which was attached to the silica layer of the modified nanoparticles. To test the adequacy and success of the modifications applied to nanoparticles, PCR analysis was considered to detect the presence of bonding between particles and viral RNA. In the experiments continued with PCR analysis, promising results related to viral RNA capture of synthesized nanoparticles have been achieved.

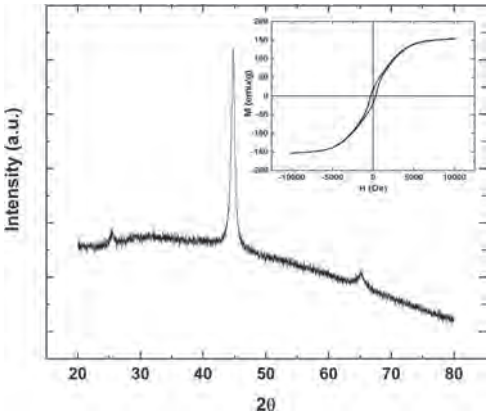

Figure.1 XRD data of the particles corresponds to BCC Fe and the room temperature hysteresis loop results shown reveals a soft ferromagnetic response.

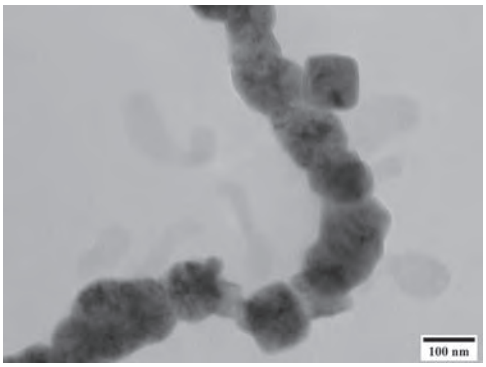

Figure.2 TEM image shows a narrow size distribution with an average size of 90nm.

IPE-04. Movable magnetically shielded room with 9-layers of permalloy for biomedical applications. *A. Kuwahata*[1,2], T. Yamaguchi[3], M. Fushimi[2], S. Chikaki[2], Y. Niwa[3] and M. Sekino[2] *1. Tohoku University, Sendai, Japan; 2. The University of Tokyo, Tokyo, Japan; 3. Ishida Ironwork's Co., Ltd., Mie, Japan*

The sensing of bio-magnetic fields originated from biological tissues, such as the brain and heart, enables to elucidate activities of humans and animals. However, due to the very-weak signal of bio-magnetic fields (10^{-14} Tesla) compared with geomagnetic fields (10^{-5} Tesla), a magnetically shielded room (MSR) [1] and active magnetic cancelling coils are required to reduce environmental magnetic noises [2,3]. In this study, we developed a movable MSR with 9-layers of permalloy and achieved the shielding factor of 10^8 which is the highest in the world as far as we know. Figure 1 shows the developed movable with 9-layers. The outside and inside dimensions of the cubic-shaped MSR are 1250 and 250 mm for biomedical applications with small animals such as rats. For the measurement of the magnetic fields, we utilized two kinds of highly sensitive magnetic sensors, Fluxgate sensor (502A, APPLIED PHYSICS SYSTEMS) and OPM (optically pumped magnetometer, QZFM-Gen2) to cover the wide dynamic range, from fT to mT. Under the application of the external AC magnetic fields (40 mT) with various frequencies (0.01-50 Hz), we evaluated the shielding factor (the ratio of magnetic field strength inside to outside MSR). Figure 2 shows the shielding factor of various combinations of MSRs. We achieved 2×10^8 of the shielding factor at 1 Hz. Furthermore, especially, at the low frequency range (<1 Hz), the shielding factor was 5×10^7. In contrast, at a higher frequency range (>10 Hz), the shielding factor decreases with increasing frequency due to the lack of aluminum layers. In summary, we developed the MSR with ultra-high performance to reduce environmental magnetic noise toward biomedical applications. The highest shielding factor is 2×10^8 at 1 Hz, which is the world record. As future works, we demonstrate high accuracy measurements of bio-magnetic fields such as magnetoencephalography and magnetocardiography in animal experiments.

[1] T. J. Sumner *et al.*, J. Phys. D: Appl. Phys. (1987). [2] E. Boto *et al., Nature* (2018). [3] K. Harakawa *et al.*, IEEE Trans. Magn. (1996).

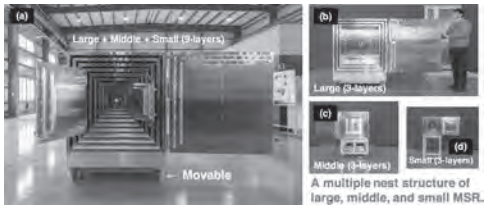

(a) Developed movable magnetically shielded room (MSR) with 9-layers of permalloy: (b) Large, (c) middle, and (d) small MSRs.

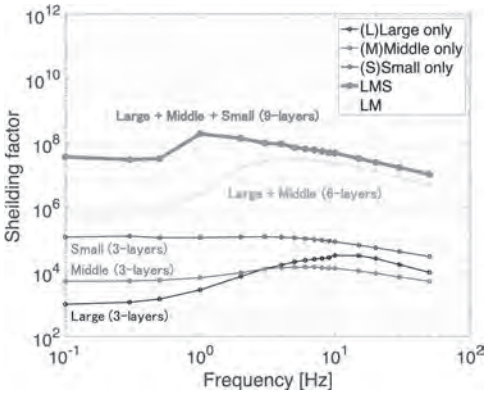

Shielding factor vs. frequency for various combinations of MSRs. Shielding factor of 2×10^8 is the highest value in the world as far as we know.

IPE-05. Synthesis and characterization of CTAB coated $Ni_xFe_{3-x}O_4$ magnetic nanoparticles for magnetic particle imaging (MPI).

N. Dogan[1], M. Irfan[2], N. Diktas[3], B. Mansuroglu[4] and G. Akbas[4] *1. Physics, Gebze Technical University, Gebze, Turkey; 2. Electronics Engineering, Gebze Technical University, Gebze, Turkey; 3. Material Engineering, Gebze Technical Univeristy, Gebze, Turkey; 4. Genetic and Molecular Biology, Yildiz Technical University, Besiktas, Turkey*

The advancement of nanotechnology has rapidly increased the research on nano-sized magnetic materials for biomedical applications [1-3]. Magnetic nanoparticles, which are used as contrast agents in Magnetic resonance imaging (MRI), draw attention with their use as tracer materials in magnetic particle imaging (MPI) systems. In this study, the Fe_3O_4 with different nickel doped samples coated with hexadecyltrimethylammonium bromide (CTAB) for medical imaging was investigated. Superparamagnetic behavior of the nanoparticles is inevitable for novel tracer agents for MPI applications. This behavior of the synthesized nanoparticles was evaluated with a vibration sample magnetometer (VSM). Dynamic response of the tracer agents to the alternating magnetic fields was also determined with magnetic particle spectroscopy (MPS) and their characteristics [4] are given in Table 1. Spatial resolution (mT) and relaxation time (μs) of the synthesized magnetic nanoparticles are quite close to commercially available Vivotrox (Magnetic Insight, USA) and Saynomag (Micromod GmbH, Germany). Five different doped samples of nickel ferrite (x=0, 0.25, 0.50, 0.75, 1) were synthesized, however, the results of the x=1 sample were in good agreement as compared to other tracer agents. Furthermore, the structural properties of the CTAB coated nickel ferrites were successfully characterized by fourier transformed infrared spectroscopy (FTIR), x-ray diffraction (XRD), and dynamic light scattering (DLS). The particles size achieved with DLS and XRD techniques was compatible with in-vivo movement. Toxicity analyzes have huge importance for in vivo applications. L929 mouse fibroblast cells were exposed to nanoparticles at different sample concentrations from 0.01 μM to 5 μM for 24 to 48 hours. Cell viability was investigated by MTT (3-(4,5-dimethyltriazol-2-yl)-2,5-diphenyltetrazolium bromide) method and presented in Fig. 1. Cell viability consistent behavior even at high concentrations promises image feasibility with increased spatial resolution.

[1] R.Hachani, M.Lowdell, M.Birchall, and et al. "Polyol synthesis, functionalisation, and biocompatibility studies of superparamagnetic iron oxide nanoparticles as potential MRI contrast agents*"*, Nanoscale, vol. 8, pp. 3278-3287, 2016. [2] K. Khoshnevisan, M. Barkhi, D. Zare, D. Davoodi, and M. Tabatabaei, "Preparation and Characterization of CTAB-Coated Fe_3O_4 Nanoparticles", Synthesis and Reactivity in Inorganic, Metal-Organic, and Nano-Metal Chemistry, vol. 42:5, pp. 644-648, 2012. [3] S. Sagadevan, Z. Zaman Chowdhury, and R. F. Rafique, "Preparation and Characterization of Nickel ferrite Nanoparticles via Co- precipitation Method", Materials Research, Vol. 21(2), 2018. [4] M. Irfan, N. Dogan, T. Sapmaz, A. Bingolbali, "Development of MPI Relaxometer for characterization of Superparamagnetic nanoparticles", J. Magn. Magn. Mater., Article 168082, 2021.

Sample	FWHM (mT)	Relaxation Time (us)	(5^{th} /3^{rd}) ratio
Vivotrax	8,64	4,56	0,44
Saynomag	7,54	6,44	0,57
$NiFe_2O_4$@CTAB	9,35	2,46	0,42

Comparison of the CTAB coated nanoparticle with MPI tracer agents.

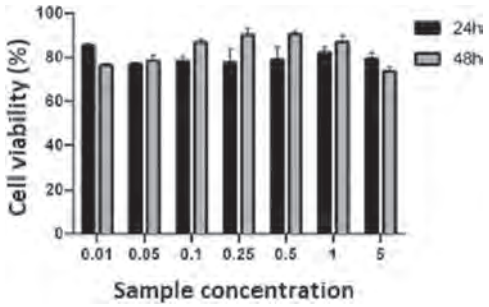

Cell viability at different sample concentrations.

IPE-06. Adhesion and differentiation of stem cells regulated by tuning of nano-ligand frequencies and sequences using barcode nanowires.

Y. Jeon[1], S. Min[2], H. Jung[3,4], C. Khatua[2], N. Li[2], G. Bae[2], H. Choi[2], H. Hong[2], J. Shin[2], M. Ko[2], H. Ko[2], I. Jun[5], *H. Fu*[2], S. Kim[2], R. Thangam[2], J. Song[5], V. Dravid[3,4], H. Kang[2,6] and Y. Kim[2,6] *1. Institute of Engineering Research, Korea University, Seoul, The Republic of Korea; 2. Department of Materials Science and Engineering, Korea University, Seoul, The Republic of Korea; 3. Department of Materials Science and Engineering, Northwestern University, Evanston, IL, United States; 4. International Institute for Nanotechnology, Evanston, IL, United States; 5. Department of Otorhinolaryngology-Head and Neck Surgery, Korea University, Seoul, The Republic of Korea; 6. Department of Biomicrosystem Technology, Korea University, Seoul, The Republic of Korea*

Barcode nanowire (BNW), also called multilayered nanowire has aroused enormous interests of researchers to apply them to bioengineered nanostructures such as cell imaging [1], interacting with regenerative cells [2,3] and biosensors [4]. Because they can be synthesized by pulsed electrodeposition method and this method can easily design and regulate the morphological features and their corresponding materials for the further chemical modification. Meanwhile, native extracellular matrix (ECM) can interact with stem cells by periodically presenting ligand. In this study, we devise an Fe-Au BNWs based ECM-emulator, which composed of RGD-coated Au and ligand-free Fe sequences. Fe-Au BNWs were electrodeposited by adjusting the two types of the current densities which corresponds to the reduction potential of each material. In addition, we regulated elapsed time of each current density to control the lengths of the Fe and Au segments. The prepared samples are composed of 4 types of frequencies dependent samples as $(Fe_{30nm}Au_{30nm})_{10repeats}$, $(Fe_{75}Au_{75})_4$, $(Fe_{150}Au_{150})_2$, and $(Fe_{300}Au_{300})$, and 2 types of sequences dependent samples as $(Fe_{75}Au_{150}Fe_{75})_2$, and $(Fe_{150}Au_{300}Fe_{150})$. Their morphological and microstructural properties were evaluated by electron microscopy and X-ray diffraction. Subsequently, we selectively modified Au surface with RGD and Fe surface with 6-amino-uncaproic acid without the changes of RGD densities between all groups. Fourier transform infrared spectroscopy confirmed the surface functionalization. Finally, BNWs facilitated the focal adhesion and mechanosensing of stem cells, which were estimated both in vitro and in vivo for the inducement of the differentiation. Moreover, they did not exhibit any toxicity to the cells and organs. Therefore, we believe that these findings can be applied to the strategies as a novel biomaterial presenting various style of barcoded ligand to stimulate adhesion and regulation of diverse cell functions.

[1] Son et al., ACS Nano 2013, 7, 9771 [2] S. Min et al., Adv. Mater. 2020, 32, 2004300 [3] Y. S. Jeon et al., ACS appl. Mater. Interfaces 2019, 11, 23901 [4] S. Min et al., Nano Lett. 20, 7272

IPE-07. Effect of Fiber Tracts on Resting Motor Thresholds During Transcranial Magnetic Stimulation. *C.J. Lewis*[1], N. Mittal[1], C.B. Hodges[2], B. Thakkar[3], Y. Cho[1], A. Andrade[4], B. Nevadomski[1], K. Li[1], C. Peterson[1] and R.L. Hadimani[1,5] *1. Biomedical Engineering, Virginia Commonwealth University, Richmond, VA, United States; 2. Physical Medicine and Rehabilitation, Virginia Commonwealth University, Richmond, VA, United States; 3. Physical Therapy, Virginia Commonwealth University, Richmond, VA, United States; 4. College of Humanities and Sciences, Virginia Commonwealth University, Richmond, VA, United States; 5. Mechanical and Nuclear Engineering, Virginia Commonwealth University, Richmond, VA, United States*

Introduction: Simulation based transcranial magnetic stimulation (TMS) studies have demonstrated the importance of anatomical variations in TMS treatments [1]. Most of the studies use magnetic resonance image (MRI) derived heterogeneous head models but lack anisotropy in their electrical and magnetic properties. Our objective was to use modeling and simulation techniques to determine the effect of neuroanatomy on resting motor thresholds (RMT) recorded from the first dorsal interosseous (FDI). Experimental Details: TMS was performed on 10 healthy patients using a Magstim BiStim2 and 70mm figure-of-eight coil and RMT values were collected using electromyography signals as a percentage of the maximum stimulator output (%MSO) [2]. MRI scans including diffusion tensor imaging (DTI) were used for fiber tract extraction (Fig 1), where individual fiber tract surface areas and tract fiber counts for the FDI were determined. T1 and T2 weighted images were taken from the MRI scans for segmentation and creation of anatomically accurate head models using SimNIBS pipeline [1]. Brain scalp distance (BSD) was measured at the point of stimulation in the models. TMS of the head models was simulated using finite element analysis to calculate cortical peak electric fields using Sim4Life (Fig 2) [3]. A linear mixed effects model was used to assess the effects of these parameters on RMT. Results: Peak induced electric fields were in the range of 90.5-147 V/m with a mean of 118.9 V/m at the cortical hotspot. Electric field and RMT are correlated, dependent on fiber tract surface area ($p = 0.036$) and tract fiber count ($p = 0.004$), but not on BSD ($p = 0.423$). Conclusion: The relationship between RMT and electric field intensity depended on both fiber tract surface area and tract count, emphasizing the effect of site-specific cortical architecture. The induced electric field at the hotspot region of the grey matter depended on the stimulator output (i.e. current in the coil). We found that MRI modeling techniques relate to the empirically collected data, suggesting an MRI based approach may be predictive of dosage determination and TMS outcomes.

[1] F Syeda, K Holloway, A A El-Genday, et. al, AIP Advances., Vol 7(5), (2017). [2] H C Smith, N J Davis, G Savic, et. al, Journal of Neurology, Neurosurgery, & Psychiatry., Vol 68(4), p.516-520 (2000). [3] Zurich Med Tech, Zurich, Switzerland, Sim4life (Version 6.2.1), 2021. [4] Fang-cheng Yeh. (2021, May 15). DSI Studio (Version 2021 May). Zenodo.

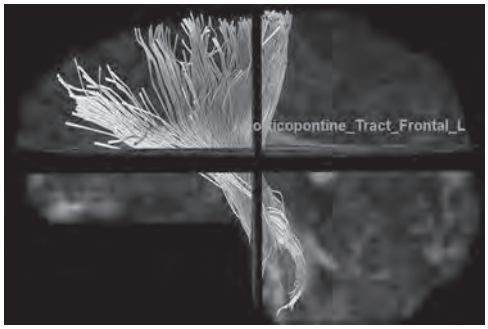

Fig. 1 Fiber tracts extracted from DTI [4].

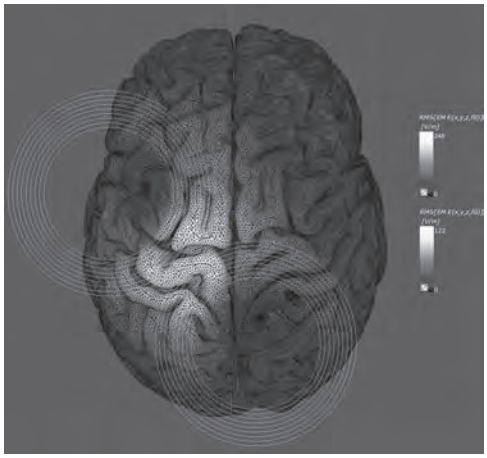

Fig. 2 M1 region peak electric field intensity.

IPE-08. Temperature Dependence of DC and AC Magnetization of Magnetic Particles with Low Curie Temperature for Magnetic Hyperthermia. *L. Ton That*[1] and S. Yabukami[1] *1. Tohoku University, Sendai, Japan*

Magnetic hyperthermia is a promising cancer therapy gaining great interest in recent years using heat generation ascribed to magnetic particles subjected to a high-frequency magnetic field. In previous studies, we developed thermosensitive magnetic micro/nanoparticles with high heating efficiency and considerable permeability change around the therapeutic temperature range of 43-45°C using a self-regulating ferromagnetic implant with low Curie temperature (FILCT) [1,2]. Using the developed magnetic particles, we also proposed contactless temperature measurement [3] and position detection methods for magnetic hyperthermia [4]. There have been several studies on the temperature dependence of magnetic properties of magnetic nanoparticles with high Curie temperature in the literature [5], whereas there is little on magnetic particles with low Curie temperature. In this study, the temperature dependence of DC and AC magnetization of the FILCT were measured using a commercial Quantum Design MPMS3 SQUID magnetometer. The FILCT was a soft magnetic material composed of Fe_2O_3:CuO:ZnO:MgO = 49:7:30:14 mol% with a Curie point of 45°C and an average particle size of 83.6 μm. In Fig. 1(a), under an external DC magnetic field of 70 kOe, the magnetization steadily decreased with increasing temperature, and the magnetization versus temperature curve could be fitted by the Bloch law $M_s(T) = M_s(0)(1-B_0T^{\alpha})$, where $M_s(0)$ is the saturation magnetization at zero temperature ($M_s(0)$=132.6 emu/g, α=1, B_o=2.07x10^{-3}K). On the other hand, in Fig. 1(b) under an AC magnetic field of 3 Oe, the ac susceptibility reached a plateau below the Curie temperature of 45°C and decreased significantly above the Curie temperature. By utilizing the magnetization versus temperature characteristic around the therapeutic temperature, we also have been developing a contactless temperature measurement for magnetic hyperthermia using pickup coils [1,2,3]. Currently, we are also measuring the temperature dependence of DC and AC magnetic properties of other Curie temperatures of FILCT and the synthesized magnetic nanoparticles to compare with the result of the FILCT above.

[1] L. Tonthat, Y. Yamamoto, F. Aki et al., IEEE Trans. Magn., Vol. 54, p.5400506 (2018) [2] L. Tonthat, Y. Yamamoto, K. Mitobe et al., AIP Advances, Vol. 10, p.125324 (2020) [3] F. Aki, L. Tonthat, H. Saito et al., Electron. Comm. Jpn., Vol. 101, p.58-66 (2018) [4] L. Tonthat, K. Mitobe, S. Yabukami, IEEE Trans. Magn., Vol. 57, p.5300205 (2021) [5] G. F. Goya, T. S. Berquó, F. C. Fonseca, J. Appl. Phys, Vol. 94, p.3520-3528 (2003)

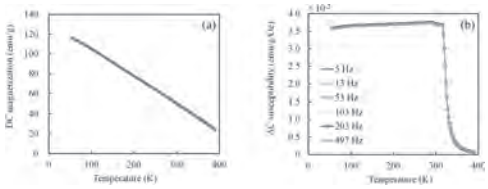

Fig. 1 Temperature dependence of (a) dc magnetization and (b) ac magnetic susceptibility.

IPE-09. Simplified fabrication of magnetic nanoparticles with directly adsorbed antibodies for bacteria detection. *T. Yoneyama*[1], T. Murayama[2], L. Ton That[1], A. Kuwahata[1], S. Yabukami[1], Y. Sato[3], Y. Teramura[4], W. Ikeda-Ohtsubo[5] and T. Ogawa[1] *1. Engineering, Tohoku University, Sendai, Japan; 2. Tohoku Gakuin University, Sendai, Japan; 3. The University of Tokyo, Bunkyo, Japan; 4. National Institute of Advanced Industrial Science and Technology, Tsukuba, Japan; 5. Agricultural Science, Tohoku University, Sendai, Japan*

1. Introduction Antigen-antibody reactions with conjugated magnetic nanoparticles (MNPs) are widely used for detecting viruses, bacteria, and proteins(1). In this study, we developed a novel method for adsorbing antibodies directly on the surface of MNPs that are not coated with protein. 2. Experiments MNPs (Fe_3O_4; average size 4 nm) were synthesized by a thermal decomposition method using oleylamine as a surfactant. The antibodies (anti-*Bifidobacterium longum*) were adsorbed to MNPs by using a rotary shaker during 30 min reaction. Nine samples were prepared in PBS at concentrations of 1.0, 0.5, and 0.1 mg/mL for MNPs and 10, 1.0, and 0.1 mg/mL for antibodies. To quantify the amount of antibody adsorbed on MNPs, the Micro BCA method (Dual-Range BCA Protein Assay Kit, VISUAL PROTEIN) was used. The amount of antibody was evaluated by the absorbance (wavelength 560 nm) measured with a microplate reader (MULTISKAN FC, Thermo Scientific). To confirm the occurrence of antigen-antibody reaction, *B. longum* bound to the antibody-MNPs was stained with DAPI and observed by an inverted microscope (CKX53, OLYMPUS) after 30 min antibody-antigen reaction using a rotary shaker. 3.Results Figure 1 shows the normalized amount of antibody adsorbed per mg of MNPs for each sample. We found that 15 μg/mg of antibody at least adsorbed to MNPs for all samples, and the amount of antibody adsorbed was independent of the concentration of MNPs, except for one sample (0.1/10). Figure 2 shows the microscope image of antibody-MNPs with stained *B. longum*. The fluorescence of DAPI bound to the DNA of *B. longum* was observed under UV light. This result indicates that *B. longum* is bound to the antibody-MNP. 4. Conclusion We established a novel method that *B. longum* antibodies directly adsorb on the surface of MNPs. We will quantify the amount of antigen that binds to the antibody-MNPs and demonstrate the detection of bacteria. Acknowledgment This work was supported by JST COI, JST ASTEP, and Grant-in-Aid for Scientific Research C (21K04090).

(1) Y. Teramura, Y. Arima, H. Iwata, *Analytical Biochemistry*, Vol. 357, pp. 208-215 (2006)

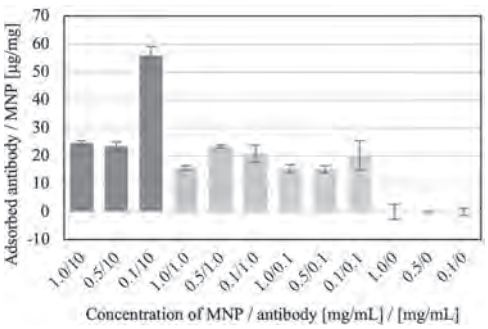

Fig. 1. Amount of Antibody adsorbed to MNPs.

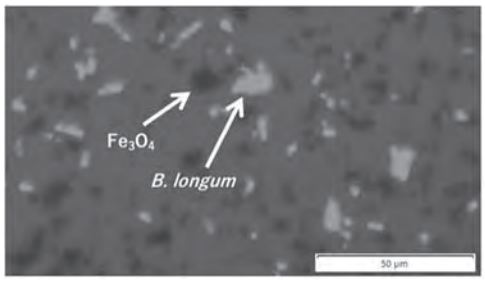

Fig. 2. Microscope image (x400, black: Fe_3O_4, white: B. longum) after antigen-antibody reaction and DAPI staining.

IPE-10. A Study on the Locomotive Advantages of a Multi-Modular Helical Magnetic Millirobot in Curved and Narrow Blood Vessels. *D. Lee*[1], H. Lee[1], D. Yang[1], K. Lee[1] and S. Jeon[1] *1. Mechanical and Automotive Engineering, Kongju National University, Cheonan, The Republic of Korea*

Various magnetic robots have been widely investigated as a possible means to replace conventional biomedical technologies [1, 2]. The use of multi-modular helical magnetic millirobots (MHMMs), such as the one shown in Fig. 1, has especially attracted attention since an MHMM can increase the number of modules by simply attaching additional modules along the longitudinal direction of the body without changing their radial dimensions [3]. Thus, an MHMM may employ multiple functional modules to perform complex tasks within a confined tubular environment such as the human blood vessel. In this research, we analytically and experimentally investigated the locomotive characteristics of the MHMM with respect to a different number of modules. It was seen that the MHMM becomes geometrically more suitable to navigate in a curved and narrow tube as the number of modules increases, even when the overall length of the MHMM does not change. We established a condition to calculate the least required number of modules to make the MHMM navigate in a given tubular condition. It was also seen that the nonlinear characteristics of the MHMM's rotational movement transmission derived from the universal joint mechanism used to connect modules decreases as the number of modules increases. Therefore, an MHMM composed of a large number of modules can navigate in a tube with a relatively harsh condition in a steady manner. In this research, we constructed prototype MHMMs with a different number of modules, as shown in Fig. 2, and demonstrated various navigating motions to show the validity of the proposed structure. Results showed that the MHMM composed of the largest number of modules (5) can navigate in a more confined tubular environment (high curvature and small diameter) compared to other MHMMs. This research can contribute to the development of multi-functional intravascular robots with high locomotive characteristics for various biomedical applications.

[1] K. E. Peyer, S. Tottori, F. Qiu, L. Zhang, and B. J. Nelson, "Magnetic helical micromachines," Chemistry, vol. 19, no. 1, pp. 28–38, 2013. [2] S. M. Jeon, G. H. Jang, H. C. Choi, S. H. Park, and J. O. Park, "Magnetic navigation system for the precise helical and translational motions of a microrobot in human blood vessels," J. Appl. Phys., vol. 111, no. 7, pp. 07E702, 2012. [3] S. M. Jeon, "A multi-modular helical magnetic millirobot navigating in curved tubular environments," AIP Advances vol. 7, no. 3, pp. 056721, 2017.

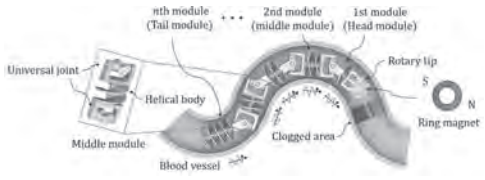

Fig. 1 Schematic view of the proposed MHMM navigating in a curved and narrow blood vessel.

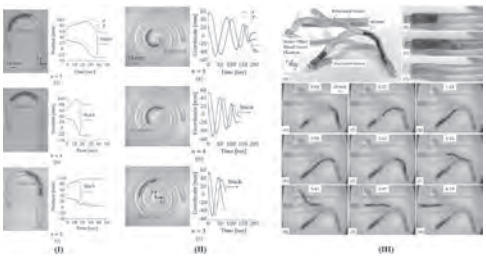

Fig. 2 Experimental results of the MHMMs' locomotion in different tubular conditions. (I. Decreasing diameter, II. Increasing curvature, III. Complex phantom)

IPE-11. 3D Printed Electromagnetics Micropump for Implantable Drug Delivery. *H. Lu*[1], S. Amara[1] and H. Fariborzi[1] *1. CEMSE, King Abdullah University of Science and Technology, Jeddah, Saudi Arabia*

Implantable drug delivery system is a prevailing approach for the drug administration [1]. The main challenge of implantable drug delivery systems is reliable implementation of a low power actuation device and a micropump with an accurate flow rate. Here we introduce a low flow rate implantable micropump fabricated using 3D printing, based on a low-power electromagnetic actuating system. We have designed the micropump structure shown in Fig. 1(a), made from polydimethylsiloxane (PDMS). The top membrane, which is 100 μm thick, was created using the spin coating. The cylindrical NdFeB magnet was placed on the membrane. The micropump structure and the membrane were bonded by 20 s of oxygen plasma. A solenoid with 2000 turns was applied as the actuator for the micropump, and it was located 2mm above the micropump as Fig. 1(b) depicts. Fig. 1(c) shows how we use the diffuser-nozzle element to achieve valveless one-direction flow. The electromagnetically actuated field could provide a periodic force on the membrane, so this top layer could deflect downward and upward. During the upward motion, negative relative pressure would be created inside the chamber and there will be more liquid drawn into the pump chamber through the inlet. On the contrary, during the membrane's downward motion, the pressure inside the chamber rises thus more liquid exit through the nozzle than the diffuser. Therefore, a net volume of liquid would be transferred from the diffuser to the nozzle for every period [2]. Under the actuation of a varying magnetic field generated by the electromagnet, micropump can produce a flow rate of 6±0.21 μl/s, which is close to previously simulated work [3]. The fabricated micropump is shown in Fig. 1(d). In summary, we successfully designed and fabricated an implantable drug delivery system, with high precision drug release [4]. The valveless unidirectional flow is achieved by using the diffuser-nozzle structure. More studies will be performed to implement a miniaturized, fully automatic and comfortable system for daily injection applications.

[1]. Ali, M. "A Survey on the Applications of Implantable Micropump Systems in Drug Delivery", *Current Drug Delivery* 2014; 11(1). [2]. Kumar N, George D, Sajeesh P, et al. Development of a solenoid actuated planar valveless micropump with single and multiple inlet–outlet arrangements. *Journal of Micromechanics & Microengineering*, 2016, 26(7):075013. [3]. Gidde, R.R., Pawar, P.M., Ronge, B.P. *et al.* Design optimization of an electromagnetic actuation based valveless micropump for drug delivery application. *Microsyst Technol* 25, 509–519 (2019). [4]. N. Elman, U. Upadhyay, Medical applications of implantable drug delivery micro-devices based on MEMS (Micro-Electro-Mechanical-Systems), *Curr. Pharm. Biotechnol*. 11 (2010) 398–403.

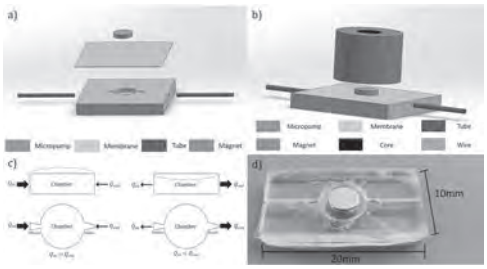

Fig. 1: (a) Implementation of the micropump structure. (b) Micropump with electromagnetic actuator. (c) Working principle of diffuser-nozzle. (d) Fabricated micropump.

IPE-12. Is it possible to use transcranial magnetic stimulation for multi-focus deep brain stimulation? *S. Liu*[1] and M. Sekino[1] *1. Department of Electrical Engineering and Information Systems, Graduate School of Engineering, The University of Tokyo, Tokyo, Japan*

Introduction: Transcranial magnetic stimulation (TMS) is extensively used in research and clinical applications pertaining to psychiatric and neurological disorders [1]. The current TMS treatments are all single-focus treatments. To satisfy the requirements of clinical treatment and improve the understanding of the synergies among different brain regions [2,3], researchers are investigating TMS that can stimulate multi brain regions. However, it is not clear whether the TMS can also develop multiple stimulation focal points in the deep brain region. Purpose: The purpose of this study is to investigate whether is it possible to use TMS for multi-focus deep brain stimulation Methods: We first established a mathematical relationship between the multi-focus electric field distribution and the winding of the TMS coil, thereby realizing the stream-function-based inverse design algorithm that can automatically generate the TMS coil winding pattern by setting the target E-field. Thereafter, we fixed the offset distance between the two-focal points of target electric fields and generated the corresponding coils by setting the focal points at different depths, thereby verifying whether the TMS coil can achieve multi-focus E-field to the deep target. Results: When the distance between the two focal points was set to 5 cm, through different depth settings and appropriate parameter selection, we theoretically found that the TMS coil can be developed for a depth that is several times the distance between the two focal points. Moreover, after further verification of the electric field generated by these coils, we found that they all meet the conditions for generating multiple focal points in the deep brain regions. Therefore, we theoretically confirmed that it is possible to use TMS for multi-focus deep brain stimulation.

[1] Lefaucheur, J. P., et., al, "Evidence-based guidelines on the therapeutic use of repetitive transcranial magnetic stimulation (rTMS).", (2014). [2] Buch, E. R., etl., al "Noninvasive associative plasticity induction in a corticocortical pathway of the human brain" (2011). [3] Arai, N., et., al, "State-dependent and timing-dependent bidirectional associative plasticity in the human SMA-M1 network"(2011)

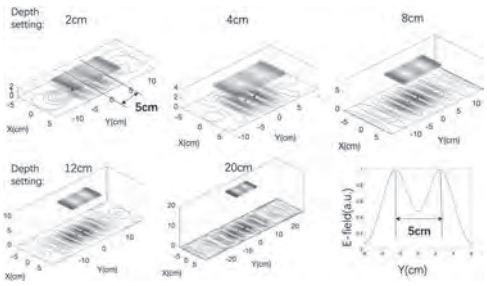

Fig.1 Generation of multi-focus TMS winding when the distance between the two focal points is fixed at 5 cm and are at different depths.

IPE-13. Implantable Magnetic Microcoils (μcoils) for Neuromodulation.
R. Saha[1], S. Faramarzi[2], R. Bloom[1], K. Wu[1], S. Liang[3], W. Low[4], S. Keirstead[4], T. Netoff[2] and J. Wang[1] *1. Electrical & Computer Engineering, University of Minnesota, Minneapolis, MN, United States; 2. Biomedical Engineering, University of Minnesota, Minneapolis, MN, United States; 3. Chemical Engineering and Material Science, University of Minnesota, Minneapolis, MN, United States; 4. Neurosurgery, University of Minnesota, Minneapolis, MN, United States*

Electrical and magnetic stimulation are used for neuromodulator therapies. Electrical stimulation is applied through an electrode in the brain, which is very focal while magnetic stimulation done transcranially, is non-invasive, highly permeable through tissues but not focal. Implantable micromagnetic stimulation (μMS) was pioneered by Bonmassar *et al.*[1] in 2012 by using commercially available sub-mm sized μcoils to stimulate neurons. As per Faraday's law of electromagnetic induction, a time-varying magnetic field induces an electric field which is spatially asymmetric. This induced electric field supports selective activation of neurons. Therefore, focal stimulation with magnetic fields may activate different populations of neurons than electrical stimulation and has the advantage that it doesn't require an electrochemical interface. This creates many safety limitations in the waveforms that can be applied to drive these devices. In this work, we have studied the neuromodulation with solenoidal μcoils of dimensions 1 mm × 0.5 mm × 0.6 mm with 21 turns. By solving a modified version of T-Ω formulation of Maxwell's equations on ANSYS-Maxwell software, the electromagnetic (EM) field calculations were then integrated to a NEURON model reported by Pashut *et al.*[2] to detect any possible elicitation of neuron response. Our results indicate that solenoidal μcoils can trigger action potential in neurons locally. Furthermore, excitatory post synaptic (EPSP) experiments performed on rat hippocampal slices for the same μcoils further corroborates our modeling results. This technology, despite its unique advantages is still in its infancy which is in ardent need of a protocol. Hence to fill this research gap, we further validated the EPSPs if they were biological, using a neurotoxin, named tetrodotoxin (TTX) which blocks the sodium channels on the neurons. We have successfully shown that on application of TTX to slices, we see no neuron response to magnetic stimulation; whereas, on washing out TTX, the neuron response from magnetic stimulation reappears.

[1] G. Bonmassar, S. W. Lee, D. K. Freeman *et al.*, "Microscopic magnetic stimulation of neural tissue," *Nat. Commun.*, vol. 3, p. 921, 2012. [2] T. Pashut *et al.*, "Mechanisms of magnetic stimulation of central nervous system neurons," *PLoS Comput Biol*, vol. 7, no. 3, p. e1002022, 2011.

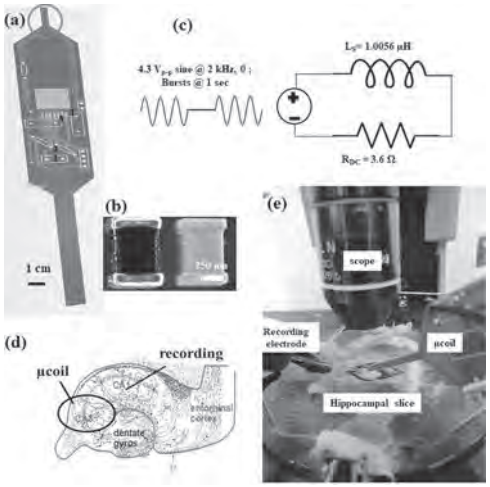

(a) The μcoil set-up (b) Image of sub-mm sized μcoils (c) The schematic of the driving circuitry (d) Schematic of the rat hippocampal slice (e) The neuron recording set-up.

IPE-14. Fe-Co magnetic nanowires for cancer cell destruction by magneto-mechanical actuation.
H. Chiriac[1], *A.E. Minuti*[1,2], A. Ghemes[1], D. Herea[1], L. Labusca[1], G. Stoian[1] and N. Lupu[1] *1. Magnetic Materials and Devices, National Institute of Research and Development for Technical Physics, Iasi, Romania; 2. Faculty of Physics, "Alexandru Ioan Cuza" University, Iasi, Romania*

Magnetic field actuation of magnetic particles causes the destruction of cancer cells by magnetomechanical effect [1]. High values of saturation magnetization at low magnetic field, along with magnetic anisotropy are the basic elements for increased values of the magnetomechanical effect. In this paper we present a new type of FeCo nanowires (NWs) that can induce cancer cell death by magnetomechanical effect, with large anisotropy (K) and high saturation magnetization (M_s) [2]. We prepared $Fe_{64.5}Co_{35.5}$ NWs with lengths of 30, 4 and 2 μm by electrolytic deposition in alumina membranes, with pores diameter of 200 nm and M_s of 146 Am^2/kg. We studied the effect of magnetic actuation in rotating magnetic field, with frequency of 10 Hz and intensity of 800 A/m, on the viability of human osteosarcoma cells (HOS). We used NWs concentrations of 0.1 and 0.2 mg/ml and time periods for the magnetic actuation of 20 and 40 min., applied 24 h after the introduction of the NWs into cell culture media. We found that Fe-Co NWs are biocompatible *in vitro*. Fig. 1 shows SEM images, highlighting that NWs are on and inside the cell membranes. Quantitative assessment of Fe content - ferrozine assay - shows that the concentration of the NWs inside cells and on their membrane is of 0.2 pg/cell. MTT assay shows that cell viability decreases after magnetic actuation down to 4%, for Fe-Co NWs shorter than 4 μm (Fig. 2). This strong effect is due to the destruction of cells by the actuation of NWs inside the cells, but also by the destruction of the membrane by action from the outside. The destruction of cancer cells using this type of NWs is stronger than the one caused by magnetic particles or other types of NWs [3], and it is due to their high magnetization and shape magnetic anisotropy. Moreover, the reduced value of the required magnetic field allows wide space maneuver, features that open significant perspectives in cancer therapy based on the magnetomechanical effect. *Acknowledgements - Work supported by (UEFISCDI) Contract no. PCE20/2021 (PN-III-P4-ID-PCE-2020-2381).*

[1] C. Naud, C. Thebault, M. Carriere, Y.X. Hou, R. Morel, F. Berger, B. Dieny and H. Joisten, *Cancer treatment by magneto-mechanical effect of particles, a review*, Nanoscale Adv., 2020, 2, 3632. [2] A. Ghemes, O. Dragos-Pinzaru, H. Chiriac, N. Lupu, M. Grigoras, D. Shore, B. Stadler and I. Tabakovic, *Controlled electrodeposition and magnetic properties of $Co_{35}Fe_{65}$ nanowires with high saturation magnetization*, J. Electrochem. Soc., 2017, 164, D13. [3] H. Chiriac, E. Radu, M. Tibu, G. Stoian, G. Ababei, L. Labusca, D.D. Herea, N. Lupu, *Fe-Cr-Nb-B ferromagnetic particles with shape anisotropy for cancer cell destruction by magneto-mechanical actuation*, Sci. Rep., 2018, 8, 11538.

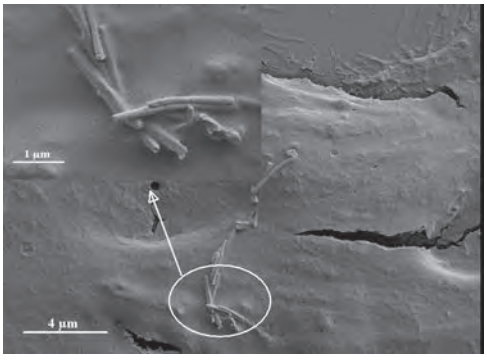

Fig 1. SEM image with HOS and NW.

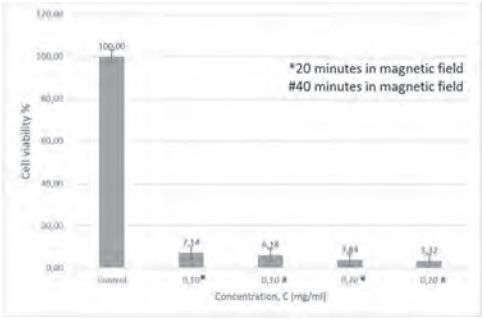

Fig 2. Cell viability after magnetomechanical actuation using two NWs concentrations (0.1 and 0.2 mg/ml).

IPE-15. A rapid magnetic serological test for COVID-19. *M. Salvador*[1], J. Marqués[1], F. Brero[2], F. da Silva[4], J. Martinez-Garcia[1], M. Mariani[2], A. Lascialfari[2], V. Pilati[3], C. Kern[3], F. Orsini[5], J. Depeyrot[4] and M. Rivas[1] *1. Department of Physics, University of Oviedo, Gijón, Spain; 2. Physics Department, University of Pavia, Pavia, Italy; 3. Laboratory for Environmental and Applied Nanoscience, Universidade de Brasilia, Brasilia, Brazil; 4. Institute of Physics, Universidade de Brasilia, Brasilia, Brazil; 5. Physics Department, University of Milan, Milan, Italy*

The COVID-19 pandemic has hit and drastically changed the world during the last months. The severe consequences reveal the necessity of new tools and procedures to reduce the impact of future emergencies. Lateral flow immunoassays (LFA), better known as "rapid tests", have been used to detect the infection. Now, when vaccination is the goal, they can be used to detect the body's immune response. Both immunoglobulin M (IgM) and immunoglobulin G (IgG) antibodies are produced against protein S, one of COVID-19 antigens. IgM is produced in the early stages of the infection whereas IgG takes longer but is more durable and could be the key to lasting immunity (Figure 1A-B). In this work, we propose a magnetic rapid serological test to detect and quantify the COVID-19 IgM and IgG antibodies in the blood (Figure 1C). Two different LFA have been designed to separate the antibodies against the RBD (a fragment of protein S). We tagged anti-human IgM and anti-human IgG with magnetic nanoclusters based on ferrite nanoparticles to make them detectable. These will produce a signal in the inductive sensor, specially designed to read LFA out [1][2]. The mapping technique uses an impedance analyzer synchronized with a micropositioner. The microstructural properties of the magnetic nanoparticles have been investigated by XRD, TEM, and AFM techniques while the magnetic properties have been assessed through NMR measurements and SQUID magnetometry. The detection and quantification of IgG and IgM are promising not only to identify exposed individuals but to generate quick data for rapid decision making. The authors would like to thank IEEE Magnetics Society for funding.

[1] A. Moyano, E. Serrano-Pertierra, M. Salvador, J. C. Martínez-García, M. Rivas and M. C. Blanco-López, Diagnostics, 2020, 10, 288. [2] D. Lago-Cachón, M. Oliveira-Rodríguez, M. Rivas, M. C. Blanco-López, J. C. Martínez García, A. Moyano, M. Salvador and J. A. García, IEEE Magnetics Letters, 2017, 8, 1-5.

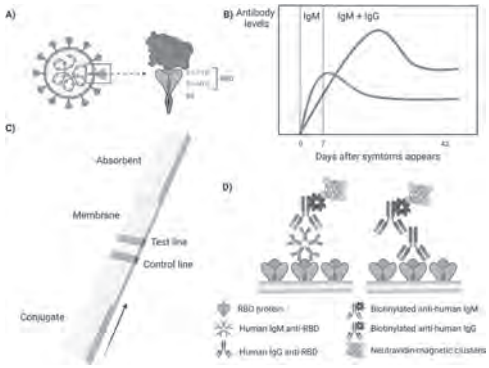

Figure 1. A) SARS-COVID-2 structure and amplification of protein S. B) Serology response: IgM and IgG production. C) Schematic LFA with its components. D) Schematic configuration of the tests designed to quantify the IgM (left) and IgG (right). Created with BioRender.com.

Figure 2. Inductive measurement setup to accurately quantify the IgG and IgM.

IPE-16. A detection system for Fusobacterium utilizing changes in the magnetic properties of magnetic nanoparticles-antibody-antigen aggregates. *S. Yabukami*[1], T. Murayama[2], S. Takahashi[1], J. Washio[1] and N. Takahashi[1] *1. Tohoku University, Sendai, Japan; 2. Tohoku Gakuin University, Sendai, Japan*

It has been pointed out that *Fusobacterium* species correlate with colorectal cancer, periodontal disease, Lemierre's syndrome, topical skin ulcers, etc. A quick and easy method to detect *Fusobacterium* species will be beneficial for point-of-care testing in various situations. We have already developed a bacteria-detection system that utilizes the magnetic response of magnetic nanoparticles applied by switching magnetic fields [1]. In the present study, the magnetic nanoparticles and *Fusobacterium* species were bound by an antigen-antibody reaction and aggregated into a spherical shape using a needle-shaped magnetic yoke. We can detect the bacterium based on the fact that the magnetic properties change depending on the number of magnetic nanoparticles and bacterium in the aggregate. The magnetic field application can separate the aggregation of the magnetic nanoparticle-antigen-antibody complex from other materials. Therefore, the bacterium can be detected without the washing process. In addition, the aggregation of magnetic nanoparticles improves the signal-to-noise ratio to detect the bacterium. *Fusobacterium nucleatum* ATCC 25586 were cultured and bound to protein A-coated magnetic nanoparticles (Nanomag-D, 0.5 μmf) via primary antibody (rabbit *Fusobacterium nucleatum* ANT0084). Fig. 1 shows the magnetic nanoparticles-antibody-antigen aggregation's magnetic response when the switching magnetic field was applied (about 10^6 CFU/ml). The magnetization was reversed when the applied field was switched.

Fig. 2 shows the magnetization when the magnetic flux density increased. The magnetization was evaluated as an integral of the waveform in Fig. 1. Compared with and without the bacterium, a strong magnetic field was necessary to reverse magnetization as the bacterium number increased. These results indicate that the concentration of *Fusobacterium nucleatum* can be estimated through the change of reversal magnetization.

[1] L. Tonthat et al., AIP Advances, vol.9, no. 12, 125325 (2019).

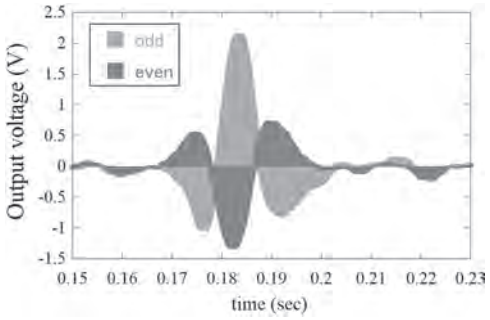

Fig 1. A magnetic response of the magnetic nanoparticles-antibody-antigen aggregation when the switching magnetic field was applied.

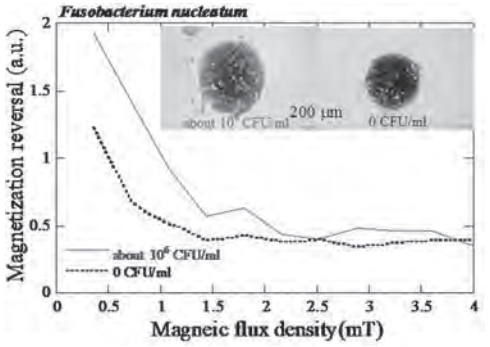

Fig. 2 Magnetization reversal as a function of switching magnetic flux density. In the photo of the aggregation, bacterium's amount was larger than that without the bacterium.

IPE-17. Development of Biocompatible Ni-ferrite Nanoparticles for Magnetic Hyperthermia. K. Ohara[1], K. Kodama[3], S. Hamada[1], K. Nashimoto[1], K. Aoki[3], K. Nakazawa[3] and *Y. Ichiyanagi*[1,2] *1. Physics, Yokohama National University, Yokohama, Japan; 2. Osaka University, Osaka, Japan; 3. Yokohama National University, Yokohama, Japan*

Magnetic nanoparticles have been drawn much attention and discussion for their biomedical applications. Previously, we reported the relationship between AC magnetic susceptibilities and significant hyperthermia effect of several kind of magnetic nanoparticles [1,2]. However, in order to utilize biomedical treatment, biocompatibility and dispersibility are important factors. In this study, we prepared Ni-ferrite nanoparticles with diameter between 3 nm and 17 nm when magnetic properties were first investigated. Then several sizes of polyethylene glycol (PEG) were modified to magnetic nanoparticles to solve the above problems. Effective heat dissipation for magnetic hyperthermia treatment in AC field depends on the magnetic relaxation parameters. AC magnetic measurements were performed in order to estimate the heating effect of MNPs for hyperthermia treatment. The particle size of the samples were varied and examined. Fig.1 shows the temperature increase of PEGylated Ni-ferrite nanoparticles in a 150 Oe, 15 kHz field. As expected by magnetic measurements, the 17 nm- sample showed significant heating effect than other samples. The temperature rose to more than 42.5 degrees Celsius, a temperature at which cancer cells are greatly supressed. Using human breast cancer cells, toxicity of PEGylated magnetic nanoparticles and without modified particles was investigated. The PEGylated samples showed a 30% increase in cell viability, confirming the improved biocompatibility of PEG modification. Furthermore, PEG has hydrophilic property, and the hydrodynamic diameter in water was measured to be about one order of magnitude smaller (Fig.2). Thus, the improvement of dispersibility in water was confirmed. Thus, we successfully developed highly biocompatible and dispersible magnetic Ni-ferrite nanoparticles and these particles were expected to be agents for hyperthermia treatment.

[1] Shigeoka, D., Yamazaki, T., Ishikawa, T., Miike, K., Fujiwara, K., Ide, T., Oshima, A., Hashimoto, T., Aihara, D., Kanda, K., Usui, A., Hosokai, Y., Saito, H. and Ichiyanagi, Y., 2018. Functionalization and magnetic relaxation of ferrite nanoparticles for theranostics. IEEE Transactions on Magnetics, 54(11), p.6100707. [2] Oshima, A., Kanda, K., Fujiwara, K., Ide, T., Takano-Kasuya, M., and Ichiyanagi, Y., 2020. PEGylation of CoZn Ferrite Nanoparticles for Theranostics. Journal of Nanoscience and Nanotechnology, 20(12). Pp.7255–7262.

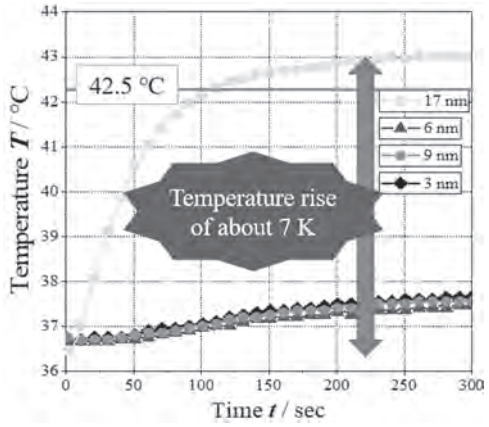

Fig1. Increase in temperature of various particle sizes of PEGylated Ni-ferrite nanoparticles.

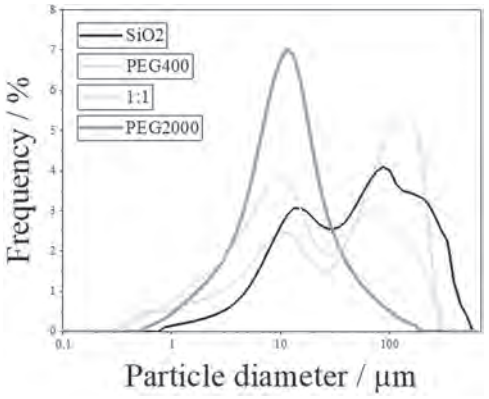

Fig.2 Water dispersibility of samples with varying amounts of PEG modification.

IPE-18. Handheld Magnetic Particle Spectroscopy (MPS) for Rapid, One-step, Wash-free Detection of SARS-CoV-2 Spike and Nucleocapsid Proteins in Liquid Phase. *K. Wu*[1], V.K. Chugh[1], V.D. Krishna[2], A. di Girolamo[1], Y. Wang[3], R. Saha[1], S. Liang[4], T.D. Gordon[5], P. Keady[5], M.C. Cheeran[2] and J. Wang[1,4] *1. Department of Electrical and Computer Engineering, University of Minnesota, Minneapolis, MN, United States; 2. Department of Veterinary Population Medicine, University of Minnesota, St. Paul, MN, United States; 3. Ocean Nano Tech LLC, San Diego, CA, United States; 4. Department of Chemical Engineering and Material Science, University of Minnesota, Minneapolis, MN, United States; 5. Aerosol Devices Inc., Fort Collins, CO, United States*

With the ongoing global pandemic of coronavirus disease 2019 (COVID-19), there is an increasing quest for more accessible, easy-to-use, rapid, inexpensive, and high accuracy diagnostic tools. Traditional disease diagnostic methods such as qRT-PCR (quantitative reverse transcription-PCR)

and ELISA (enzyme-linked immunosorbent assay) require multiple steps, trained technicians, and long turnaround time that may worsen the disease surveillance and pandemic control. In sight of this situation, a rapid, one-step, easy-to-use, and high accuracy diagnostic platform will be valuable for future epidemic control especially for regions with scarce medical resources. Herein, we report a magnetic particle spectroscopy (MPS, see Fig.1) platform for detection of SARS-CoV-2 biomarkers: spike and nucleocapsid proteins.[1]This technique monitors the dynamic magnetic responses of magnetic nanoparticles (MNPs) and uses their higher harmonics as a measure of the nanoparticles' binding states.[2,3] By anchoring polyclonal antibodies (pAbs) onto MNP surfaces, these nanoparticles function as nanoprobes to specifically bind to target analytes (SARS-CoV-2 spike and nucleocapsid proteins in this work) and form nanoparticle clusters. This binding event causes detectable changes in higher harmonics and allows for quantitative and qualitative detection of target analytes in liquid phase.[4] We have achieved detection limits of 1.56 nM (equivalent to 125 fmole) and 3.13 nM (equivalent to 250 fmole) for detecting SARS-CoV-2 spike and nucleocapsid proteins, respectively, as shown in Fig.2. This MPS platform combined with one-step, wash-free, nanoparticle clustering-based assay method is intrinsically versatile and allows for the detection of a variety of other disease biomarkers by simply changing the surface functional groups on MNPs.

[1] Wu, Kai, et al. *ACS Applied Materials & Interfaces* 13.7 (2021): 7966-7976. [2] Zhong, Jing, et al. *ACS sensors* 6.3 (2021): 976-984. [3] Wu, Kai, et al. *ACS applied materials & interfaces* 12.12 (2020): 13686-13697. [4] Wu, Kai, et al. *ACS applied materials & interfaces* 11.26 (2019): 22979-22986.

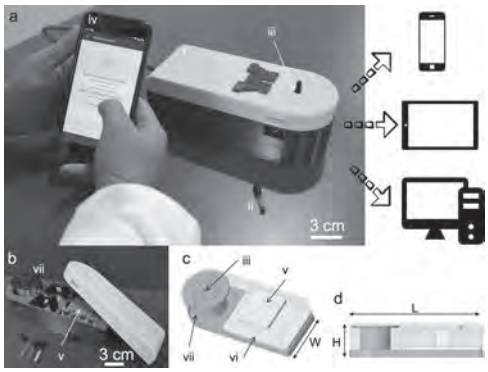

Fig.1. (a) Photograph of the MPS portable device with a smartphone application. The overall dimensions of device are 212 mm (L) × 84 mm (W) × 72 mm (H). (b) Photograph of the internal structures of the MPS device. (c) and (d) are the 3D models of the device.

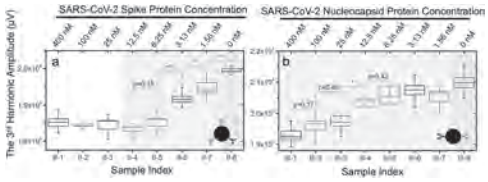

Fig.2. Concentration-response profiles of SARS-CoV-2 (a) spike and (b) nucleocapsid proteins.

IPE-19. Temporal Interference for Dual Site Transcranial Magnetic Stimulation. *Z. Higgs*[1], J. Boldrey[1] and D. Jiles[1] *1. Electrical and Computer Engineering, Iowa State University, Ames, IA, United States*

Transcranial Magnetic Stimulation (TMS) coils often are specific to deep brain or focal stimulation. A new technique is used which allows for deep and focal stimulation using temporal interference (TI). TI is a method that allows for steerability, focality, and depth of penetration. TI TMS operates based on the frequency difference of two different electric fields [1]. The TI stimulation frequencies would be in at 10kHz and is filtered by the brain's inherent lowpass [4] behavior [2]. The frequency difference between the two induced electric fields results in an envelope which allows for a more focal stimulation. By using a coil assembly with several coils (as seen in figure 1), two areas of the brain could be selected and stimulated, focally for use in dual site TMS. Dual site TMS allows for the stimulation of two parts of the brain, which enforces or interferes with brain signals. Dual site TMS stimulation is currently done with two independent coils which are placed on the head and allows for error when placing [3]. The use of a single TI TMS coil for dual site stimulation could allow for a more focused and consistent stimulation for use with dual site TMS.

[1] M. Zaeimbashi, A. Khalifa, C. Dong, Y. Wei, S. Cash, and N. Sun, "Magnetic Temporal Interference For Noninvasive, High-resolution, and Localized Deep Brain Stimulation: Concept Validation," 2020. [2] M. M. Sorkhabi, K. Wendt, and T. Denison, "Temporally Interfering TMS: Focal and Dynamic Stimulation Location," *2020 42nd Annual International Conference of the IEEE Engineering in Medicine & Biology Society (EMBC)*, 2020. [3] R. Sparing, D. Buelte, I. G. Meister, T. Pauš, and G. R. Fink, "Transcranial magnetic stimulation and the challenge of coil placement: A comparison of conventional and stereotaxic neuronavigational strategies," *Human Brain Mapping*, vol. 29, no. 1, pp. 82–96, 2007. [4] B. Hutcheon and Y. Yarom, "Resonance, oscillation and the intrinsic frequency preferences of neurons," *Trends in Neurosciences*, vol. 23, no. 5, pp. 216–222, 2000.

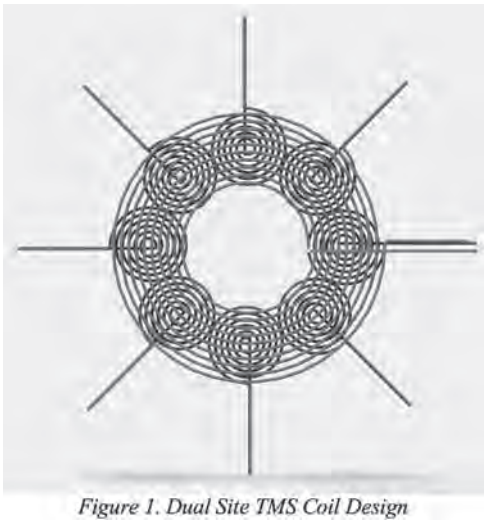

Figure 1. Dual Site TMS Coil Design

Figure 1

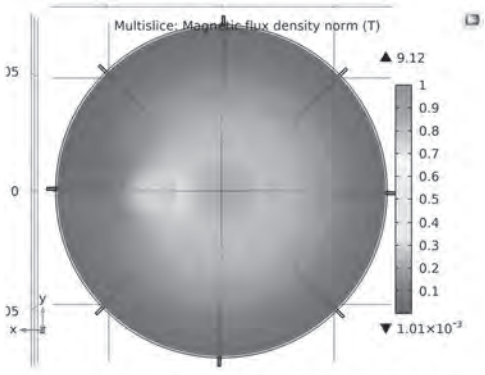

Figure 2. COMSOL Simulation of Dual Site TMS Coil

Figure 2

IPE-20. Combinational effects of GDNF, Aβ42, and pulsed magnetic stimulation on N27 neuronal cells. *J. Boldrey*[1], R. Yang[1], L. Que[1], I. Schneider[3], R.L. Hadimani[2] and D. Jiles[1] *1. Electrical and Computer Engineering, Iowa State University, Ames, IA, United States; 2. Mechanical and Nuclear Engineering, Virginia Commonwealth University, Richmond, VA, United States; 3. Chemical and Biological Engineering, Iowa State University, Ames, IA, United States*

Transcranial Magnetic Stimulation (TMS) has proven in recent years to be an effective method for neuromodulation without surgical interventions. Such non-invasive stimulation treatment has been approved by the U.S. Food and Drug Administration (FDA) for treating major depressive disorder (MDD), obsessive compulsive disorder (OCD) and certain types of migraine headaches [1]. Ongoing research is investigating the use of TMS for treating Alzheimer's Disease, Parkinson's Disease, and Post-Traumatic Stress Disorder (PTSD) [2][3][4]. Glial cell-derived neurotrophic factor (GDNF) is a protein that provides a protective effect for dopaminergic neurons [5,6]. GDNF can be secreted from different types of cells including the N27 dopaminergic neural cell line that is well-established *in vitro* model for neurodegenerative disease research. Pulsed magnetic stimulation from a commercial TMS system has shown to increase GDNF secretion in N27 cells [7]. Amyloid β 1-42 (Aβ42) is a beta amyloid peptide that is harmful to neural cells. Research has shown that Aβ42 play a crucial role in the onset of Alzheimer's Disease and Parkinson's Disease [8,9]. Our current research is investigating the combinational effects of GDNF, Aβ42, and pulsed magnetic stimulation on N27 cells. The stimulator used is a commercial TMS system commonly used in research studies on human subjects. The magnetic stimulation protocol used is the same that produced an increase in proliferation and GDNF secretion in N27 cells. Our results of the effects of Aβ42 on N27 cells show that the harmful effects are not directly correlated to the concentration of Aβ42. Concentrations lower than 22 x 10^{-8} M show little harmful effect, while concentrations between 22 x10^{-9} M and 22 x 10^{-12} M show large scale apoptosis, and concentrations above 22 x 10^{-12} M show low or no apoptosis. These results agree with Aβ42 research on humans. Current trials involve introducing GDNF, with and without magnetic stimulation, to determine the beneficial effects of stimulation on N27 cells against Aβ42.

[1] "FDA permits marketing of transcranial magnetic stimulation for treatment of obsessive compulsive disorder | FDA." [Online]. Available: https://www.fda.gov/news-events/press-announcements/fda-permits-marketing-transcranial-magnetic-stimulation-treatment-obsessive-compulsive-disorder. [Accessed: 010-Jun-2020]. [2] Sabbagh M, Sadowsky C, Tousi B, Agronin ME, Alva G, Armon C, Bernick C, Keegan AP, Karantzoulis S, Baror E, Ploznik M, Pascual-Leone A. Effects of a combined transcranial magnetic stimulation (TMS) and cognitive training intervention in patients with Alzheimer's disease. Alzheimers Dement. 2020 Apr;16(4):641-650. doi: 10.1016/j.jalz.2019.08.197. Epub 2020 Jan 16. PMID: 31879235. [3] C. Fricke et al., "Dual-Site Transcranial Magnetic Stimulation for the Treatment of Parkinson's Disease," Front. Neurol., vol. 10, no. March, pp. 1–9, 2019, doi: 10.3389/fneur.2019.00174. [4] R. J. Koek et al., "Neuromodulatory treatments for post-traumatic stress disorder (PTSD)," Prog. Neuro-Psychopharmacology Biol. Psychiatry, vol. 92, no. December 2018, pp. 148–160, 2019, doi: 10.1016/j.pnpbp.2019.01.004. [5] Gao, J., Kang, Xy., Sun, S. et al. Transcription factor Six2 mediates the protection of GDNF on 6-OHDA lesioned dopaminergic neurons by regulating Smurf1 expression. Cell Death Dis 7, e2217 (2016). https://doi.org/10.1038/cddis.2016.120 [6] B. J. Hoffer et al., "Glial cell line-derived neurotrophic factor reverses toxin-induced injury to midbrain dopaminergic neurons in vivo," Neurosci. Lett., vol. 182, no. 1, pp. 107–111, Nov. 1994, doi: 10.1016/0304-3940(94)90218-6. [7] Zhong, Xiaojing & Luo, Jie Daniel & Rastogi, Priyam & Kanthasamy, Anumantha & Jiles, David. (2018). Transcranial magnetic stimulation promotes the proliferation of dopaminergic neuronal cells in vitro. AIP Advances. 8. 056709. 10.1063/1.5007677. [8] JiSoo Park, *et al.* Three-dimensional brain-on-a-chip with an interstitial level of flow and its application as an in vitro model of Alzheimer's disease. *Lab Chip*, 2015, 15, 141. [9] Ba, M., Yu, G., Kong, M. *et al.* CSF $A\beta_{1-42}$ level is associated with cognitive decline in early Parkinson's disease with rapid eye movement sleep behavior disorder. *Transl Neurodegener* 7, 22 (2018). https://doi.org/10.1186/s40035-018-0129-5

IPE-21. Investigation of magnetic relaxation of intratumor magnetic nanoparticles for hyperthermia. *K. Honda*[1], K. Shimizu[2], H. Hirano[3], M. Futagawa[3], Y. Takemura[4] and S. Ota[3] *1. Electrical and Electronic Engineering Course, Graduate School of Integrated Science and Technology, Shizuoka University, Hamamatsu, Japan; 2. Department of Molecular Imaging, Institute for Medical Photonics Research, Hamamatsu University School of Medicine, Hamamatsu, Japan; 3. Department of Electrical and Electronic Engineering, Shizuoka University, Hamamatsu, Japan; 4. Department of Electrical and Computer Engineering, Yokohama National University, Yokohama, Japan*

Hyperthermia using magnetic nanoparticles (MNPs) is a cancer treatment technique that is expected to result in fewer physical burdens and side effects. The evaluation of the magnetization dynamics of MNPs to produce enough heat dissipation is important for their application in cancer therapy. The magnetization properties were measured with respect to MNPs that are injected into a tumor isolated from an animal's body during the measurement [1]. In the present study, the magnetization dynamics of intratumor MNPs in a tumor-bearing mouse were investigated. The commercially available instrument Resovist® (FUJIFILM Toyama Chemical Co., Ltd., γ-Fe_2O_3 nanoparticles) was used in this study. The particles were dispersed in diluted water, fixed with epoxy resin, and injected into the tumor, which were prepared as a liquid, solid, and intratumor samples, respectively. The concentration of all samples was 530 μg-Fe/mL. The magnetization dynamics under an alternating current (AC) magnetic field were evaluated by measuring the AC magnetization curves for each sample. The imaginary part of the susceptibility, χ'', was estimated from the area of the AC magnetization curves [2]. The amplitude and frequencies of the applied magnetic field were 4 kA/m and 10-10^4 Hz, respectively. Figure 1 displays the frequency dependence of χ'' for the liquid and solid samples. A local maximum was observed at 5 kHz in the liquid sample only; no maxima were observed in the solid sample. This maximum is due to the physical rotation of the particles along the magnetic easy axis, which is a result of Brownian relaxation. In the solid sample, the rotation of the particles was inhibited; therefore, only Néel relaxation due to magnetization rotation was occurred. In conclusion, we constructed a system to measure the AC magnetization curves of low concentrations of intratumor MNPs at low frequencies, where the signal from the magnetization was considerably low. Magnetization dynamics due to Brownian relaxation in the liquid sample were clearly observed. In the presentation, the frequency dependence of χ'' in the intratumor sample will also be shown.

[1] S. Dutz, M. Kettering, I. Hilger, R. Miiller, M. Zeisberger, "Magnetic multicore nanoparticles for hyperthermia-influence of particle immobilization in tumour tissue on magnetic properties", *Nanotechnology*., 22, 265102, (2011). [2] S. Ota, S. B. Trisnanto, S. Takeuchi, J. Wu, Y. Cheng, and Y. Takemura, "Quantitation method of loss powers using commercial magnetic nanoparticles based on superparamagnetic behavior influenced by anisotropy for hyperthermia", *J. Magn. Magn. Mater*., 538, 168313 (2021).

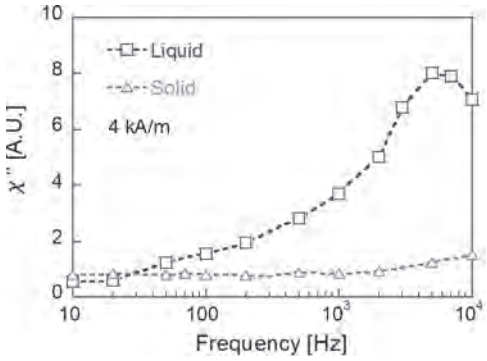

Frequency dependence of the imaginary component of susceptibility, χ''.

Session IPF
GEOMAGNETISM, BIOMAGNETISM, MAGNETIC FLUIDS, AND OTHER EMERGING TOPICS (Poster Session)

Tomoyuki Ogawa, Co-Chair
Tohoku University, Sendai, Japan
Mariana P Proenca, Co-Chair
IFIMUP (Portugal) and ISOM-UPM (Spain), Porto, Portugal

IPF-01. Conceptual Design for Microplastic Collection Device from Seawater with High Field HTS Magnet. *T. Mato*[1] and S. Nogushi[1]
1. Hokkaido University, Sapporo, Japan

Microplastics (MPs) in ocean environment are a kind of environmental pollution. Many papers have reported potential influences on the ocean and even terrestrial environment [1], [2]. MPs are plastic fragments with diameter smaller than 5 mm. Since chemicals easily stick to MPs, MPs work as a carrier of harmful substances such as Poly Chlorinated Biphenyl (PCB). Small fish or crustaceans eat the polluted MPs, and this may result in bad digestion or deterioration of health conditions. Since the number of MPs has been increasing [3], the development of MP collection method from the ocean is an urgent task towards the United Nations (UN) Sustainable Development Goals (SDGs) [4]. Several methods for MP collection have been proposed, such as collections by floatation, ultrasonic, and filter. However, these methods are not capable of processing a large amount of seawater, and the collection is intermittently conducted. One promising solution is using a strong magnetic field and its high gradient, *i.e*., a magnetic separation [5]. When a strong magnetic field with high gradient is applied to water including MPs, MPs experience a large magnetic force compared to water. Meanwhile, recently, the performances of high-temperature superconducting (HTS) magnets have been increasing. Currently, >15-T class magnets are easily available, and they can be applied to MP collectors from ocean. In this research, we propose a conceptual idea of MP collector from ocean environment using a high field HTS magnet. Fig. 1(a) shows the schematic view of the proposed MP collector. To evaluate the performance, we developed a fluid simulation code based on a particle method, coupled with magnetic field analysis. Fig. 1(b) shows one simulation case where the magnetic field with constant gradient of 12.5 T/m was applied to the tank of MP collector. As shown in Fig. 2, the proposed device gathers approximately 90 percent of the injected MPs. The details related to the optimal magnetic field or force acting on the magnets are presented at the conference.

[1] J. A. Sul and M. F. Costa, *Environ. Pollut.*, vol. 185, p. 352 (2014) [2] M. C. Rillig, A. Lehmann, A. A. Machado, *New Phytol.*, vol. 223, p. 1066 (2019) [3] A. Isobe, S. Iwasaki, K. Uchida, *Nat. Commun.*, vol. 10, Art. no. 417 (2019) [4] https://sdgs.un.org/goals [5] Y. Ueda, F. Mishima, Y. Akiyama, *Proceedings of Cryogenics and Superconductivity Society of Japan*, vol. 88, 2B–a03 (2013)

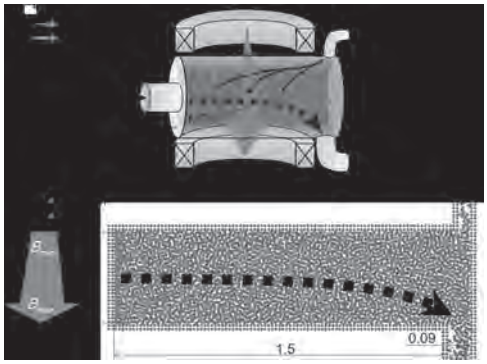

(a) Schematic view of proposed microplastic collector and (b) simulation result.

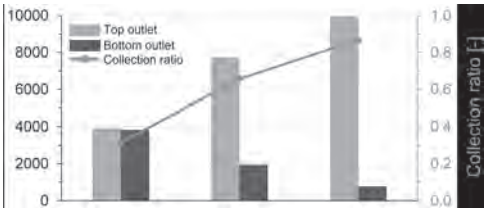

Simulated MP concentration and collection ratio.

IPF-02. An adaptive alternating magnetic interference suppression (AAIS) algorithm for geomagnetic vector measurement. *W. Wang*[1], K. Li[1], Z. Yang[1], J. Chen[1], L. Miao[1], J. Ou-Yang[1] and X. Yang[1]
1. Huazhong University of Science and Technology, Wuhan, China

When the electrical equipment on the carrier is running stably, its alternating magnetic interference can be equivalent to the hybridization of multiple narrowband noises [1]. How to overcome this narrowband magnetic interference is one of the key questions to achieve high-precision vector measurement of the geomagnetic field [2-4]. This paper proposes an adaptive alternating magnetic interference suppression (AAIS) algorithm as shown in Fig. 1. We used triaxial fluxgate sensor to collect the magnetic field data. Through short-time Fourier transform and wavelet transform analysis, the time-frequency diagram of the total magnetic field was obtained. Moreover, the time and frequency of alternating magnetic interference were analyzed. Next, the triaxial adaptive notch filter is utilized to suppress the three-component related magnetic interference. Thus, the measurement accuracy of the geomagnetic vector is effectively improved. The effectiveness of the algorithm is verified by the alternating magnetic field leaked by the motor. When the motor is running stably and the geomagnetic background is constant, a time interval of 10 seconds is used to quantify the compensation result of the AAIS algorithm. As shown in Fig. 2, the standard deviation (STD) of the x component is reduced from 3.63 nT to 0.42 nT, which is a reduction of 88.4%. The STD of the y component is reduced from 1.83 nT to 0.6 nT, which is a reduction of 67.2%. The STD of the z component is reduced from 7.31 nT to 0.54 nT, which is a reduction of 92.6%. These

results have fully confirmed the effectiveness of the algorithm. We highlight the benefit of AAIF considering it does not need a reference sensor. Through the influence of the alternating magnetic interference on the total magnetic field, AAIS can realize the error compensation of the geomagnetic vector measurement. This effectively improves the measurement accuracy of the three components of the geomagnetic field. Our work has practical implications in airborne, vehicle-mounted, and shipborne geomagnetic vector detection.

[1] E. I. Chernov, N. E. Sobolev, and A. A. Bondarchuk, the 2021 10th Mediterranean Conference on Embedded Computing (MECO), 2021. [2] L. Chen, P. Wu, and W. Zhu, Sensors, vol. 18, p. 6(2018). [3] D. Liu et al., Measurement Science and Technology, vol. 26, p. 1 (2015). [4] S. Bagha, D. P. Das, and S. K. Behera, IEEE/ACM Transactions on Audio, Speech, and Language Processing, vol. 28, p. 2084-2094 (2020).

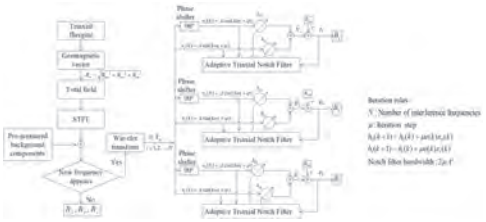

Fig. 1. AAIS algorithm principle diagram.

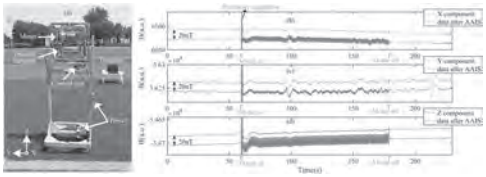

Fig. 2. Experimental setup and results.

IPF-03. Simulating the Heating of a Magnetic Fluid with Coupled Molecular Dynamics and Micromagnetics. *S. Helbig*[1], C. Abert[1], P. Sanchez[1], S. Kantorovich[1] and D. Suess[1] *1. Faculty of Physics, University of Vienna, Vienna, Austria*

Magnetic fluids have versatile properties, that make them very attractive for applications in biomedicine, e.g. in contrast agents, drug targeting and hyperthermia [1]. The magnetic characteristics of the fluid are given by the suspended magnetic single-domain nano-particles. Depending on the requirements of a specific application the material properties have to be chosen carefully and the field parameters need to be tuned for optimal control and efficiency. For magnetically induced hyperthermia as cancer treatment the requirement is to generate as much heat as necessary to destroy cancer tissue. In this case, a magnetic AC-field is used to stimulate the magnetic particles inside the carrier fluid. The heat induced inside by a magnetic AC-field is explained by two processes, the Brownian relaxation and Neel relaxation [2], and is generated by surface friction and flipping of the magnetization respectively. Both processes occur simultaneously and this can be simulated in our novel simulation model with a single-domain nano-particle in a viscous fluid. By analysing the energy losses due to friction and the hysteresis curves the heating of the fluid can be quantified. The combined power dissipation is then composed of both contributions, see Fig. 1. We could also identify the two steady state regimes by varying the field strength and frequency for which the particle favours either the flipping of the magnetic moment or rotating with the magnetic moment as a whole, see Fig. 2. Interestingly, depending on the initial angle between easy axis of the particle and the axis of the AC-field there are also some combinations of field parameters that potentially allow for both steady states to exist for different particles in a fluid due to resonances with the applied field. With this approach we hope to provide the groundwork necessary to facilitate the search for materials and the optimal settings for the AC-field to be used in hyperthermia.

[1] Q. A. Pankhurst, et al., J. Phys. D: Appl. Phys., Vol. 42, 224001 (2009)
[2] W. F. Brown, Micromagnetics, Interscience Publ. (1963)

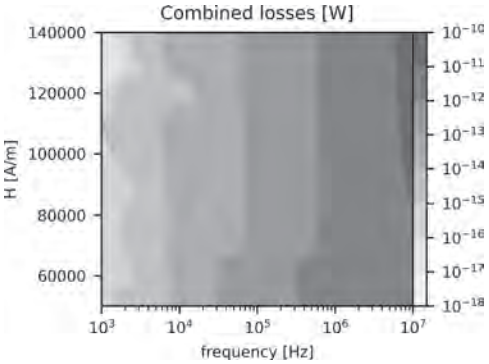

The combined losses from friction and hysteretic losses for one single-domain particle depending on the frequency and strength of the field.

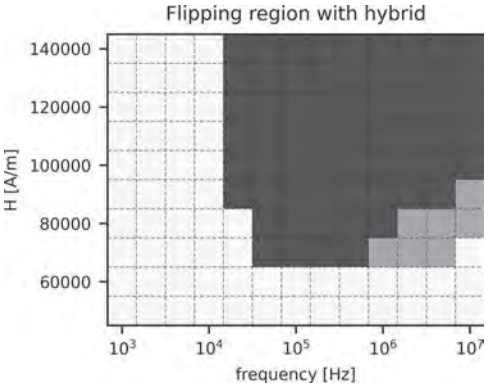

The flipping domain (dark red) with the initial angle-dependent hybrid region in light red, where flipping and rotating steady states are possible.

IPF-04. Coherent Compensation Method for Non-model Interference of Aeromagnetic Vector. *L. Miao*[1], W. Wang[1], Z. Yang[1], J. Ou-Yang[1] and X. Yang[1] *1. Huazhong University of Science and Technology, Wuhan, China*

Aeromagnetic interference is the main factor affecting the accuracy of aeromagnetic measurement. At present, there have been many researches on interference compensation for aeromagnetic scalar measurement, but relatively few researches on aeromagnetic vector compensation. Researchers have migrated the fixed, induced and eddy current magnetic interference models in aeromagnetic scalar compensation to vector compensation, and achieved better compensation results. However, there are still many non-model interferences in the actual aeromagnetic system, which are mainly caused by factors such as airborne electronic equipment and geomagnetic gradients. This paper proposes a coherent compensation method for non-model interference based on dual sensors. First, the classical aeromagnetic vector compensation model is used to compensate the magnetic field data, and there is still some residual interference in the compensation result. The analysis shows that the residual aeromagnetic vector interference of the two sensors has a strong correlation in most frequency bands, which means that the non-model interference of the two vector sensors has a linear relationship in the frequency domain. Assuming that the real geomagnetic signals measured by the two sensors are completely consistent, the transfer function of the interference signal can be calculated based on the self-spectrum and cross-spectrum of the signal in the frequency domain, and then the real geomagnetic signal can be obtained, so as to achieve suppression on the remaining non-model interference. This paper verifies the effectiveness of the algorithm in actual flight experiments. The three-axis root mean square error of the original uncompensated data in the experiment is 486.89nT, 342.97nT and 674.31nT. After being compensated by the classical model, the

root mean square error of the three components drops to 57.53nT, 59.07nT and 36.01nT. After the non-model interference is coherently compensated, the root mean square error of the three components is further reduced to 28.61nT, 33.35nT and 19.74nT, which are reduced by 50.27%, 43.54% and 45.18% respectively compared with the pure model method.

[1] Zhang, Q, Pang, H and Wan, C, Magnetic interference compensation method for geomagnetic field vector measurement, *Measurement*, Vol.91, p.628-633(2016) [2] Pang H, Pan M and Qu W, et al. The application of attitude change information in magnetic interference component suppression, Measurement, Vol.160, p.107841(2020) [3] Chen L, Wu P and Zhu W, et al. A Novel Strategy for Improving the Aeromagnetic Compensation Performance of Helicopters, Sensors (Basel, Switzerland), Vol.18(6), p.1846(2018)

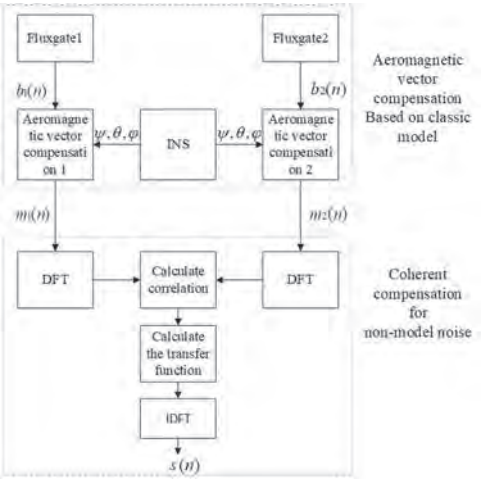

Fig.1 Algorithm flowchart

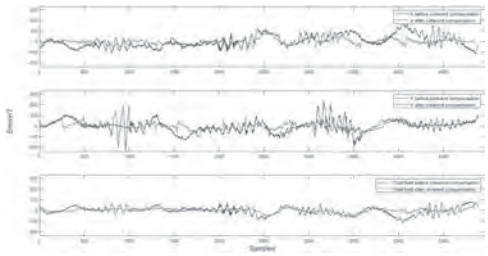

Comparison of compensation results

IPF-05. Dynamics of nonmagnetic inclusions in a microchannel with a magnetic fluid in an inhomogeneous magnetic field. P. Ryapolov[1], *E. Sokolov*[1], A. Vasilyeva[1] and D. Kalyuzhnaya[1] *1. SouthWest State University, Kursk, Russian Federation*

In previous works, we presented the results of the dynamics of the air-magnetic fluid interface under the influence of a non-uniform magnetic field of the moving ring magnet [1, 2]. A distinctive feature of the used magnetic systems is the presence of the magnetic levitation area, with the help of which it becomes possible to control the dynamics of non-magnetic inclusions in the magnetic fluid. This work presents the results of further studies, in which the experiments were performed in microchannels of various configurations with injection of a non-magnetic phase using the syringe pump. In addition to the dynamics of gas inclusions in a magnetic fluid in an inhomogeneous magnetic field, the behavior of non-magnetic droplets of various liquids is presented. The influence of the parameters of the magnetic field and the properties of a magnetic fluid on the dynamics of non-magnetic inclusions and the size of detached bubbles and drops is investigated. It was found that the feed rate of non-magnetic inclusions and external hydrostatic pressure do not affect the size of gas bubbles and non-magnetic drops detached from the levitating main volume. The ability to control the size of non-magnetic inclusions is shown using an external magnetic field and concentration of the magnetic fluid. The results presented in the work can be used to develop microfluidic counters and controlled dispensers of non-magnetic inclusions. The investigation was carried out with the support of part of the implementation of the state task for 2020 (No 0851-2020-0035).

1. P. A.Ryapolov, E. A.Sokolov, V. G. Bashtovoi, A. G. Reks, & E. B. Postnikov, AIP Advances, Vol. 11(1), P. 015206 (2021) 2. P. A. Ryapolov, V. M. Polunin, E. B. Postnikov, V. G.Bashtovoi, A. G.Reks, E. A. Sokolov, Journal of Magnetism and Magnetic Materials, Vol. 497, P. 165925 (2020)

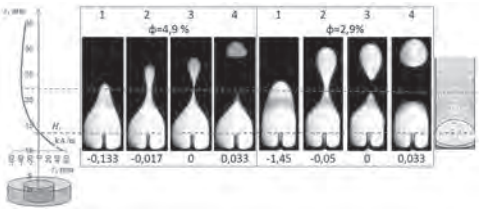

Data of video recording of the position of the interphase boundary of the volume of a nonmagnetic fluid in a magnetic fluid before, at and after the detachment of a nonmagnetic drop from it in an inhomogeneous magnetic field of a ring magnet

IPF-06. Random Number Generation from Different Types of Magnetic Domain Images. *S. Yoshida*[3], T. Kawashima[1], I. Nakamura[1], K. Yamada[2], H. Uchida[1] and S. Mito[3] *1. Toyohashi Univercity of technology, Toyohashi, Japan; 2. Utsunomiya University, Utsunomiya, Japan; 3. National Institute of Technology, Tokyo College, Hachioji, Japan*

1. Introduction Random numbers are an important resource in a science and engineering, such as numerical simulations, cryptography and machine learning. A Faster and simpler true random number generators (TRNG), which employs physical phenomena as a noise source, is needed. However, the TRNGs that is compact and faster than GHz is not realized yet. We focused on the magnetic-domain patterns in magnetic garnets as a noise source for TRNG. The magnetic domain can be generated repeatedly and chaotically, and converted to digital value at few Gbit/s by image sensors. The random numbers that generated from the labyrinth magnetic-domain patterns were passed the statistic randomness test (NIST SP800-22) [1]. In this study, other types of magnetic domains were investigated as the noise source. 2. Experimental Sputtered-polycrystalline bismuth substituted yttrium iron garnet (Bi:YIG) films on glass and gadolinium gallium garnet (GGG) substrates, and liquid phase epitaxy (LPE) holmium iron garnet (HoIG) film were investigated. About 3,000 magnetic domain images of each garnet were captured using a polarized light microscope, as shown in Fig. 1. The obtained images were processed to random sequence. The data process was composed of binarization, stable-pattern removal, bit-shift, and XOR. A hundred of the 10 Mbit sequences were generated and evaluated by the randomness test (NIST SP800-22) [2]. 3. Result and discussion A hundred of the 10 Mbit sequences were generated and tested. The results of the randomness test is shown in table 1. The NIST SP800-22 includes 15 periodicity tests. The p-value more than 0.01 indicates that the sequence is non-periodic (random). The pass rates on the table 1 is a ratio of the statistically random sequence. The pass rate more than 0.97 is passed the randomness test. The all samples passed almost of all tests. The low-score with the FFT test could be improved by optimization of the data processing. These results suggest that the random sequences could be generated from many types of magnetic domains.

[1] Takuya Kawashima, Shinichiro Mito, Random number generation using magnetic domain images of magneto-optic materials, Jpn. J. Appl. Phys. 59 SEEA07 (2020) [2] A. Rukhin, J. Soto, J. Nechvatal, M. Smid, E. Barker, S. Leigh, M. Levenson, M. Vangel, D. Banks, A. Heckert, J. Dray, and S. Vo, NIST Special Publication 800-22 Revision 1a (2010).

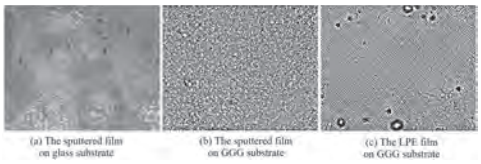

Fig. 1 Polarized microscope image of the garnet films

Test name	Sputtering(Glass)		Sputtering(GGG)		LPE(GGG)	
	P-Value sig.	Pass rate	P-Value sig.	Pass rate	P-Value sig.	Pass rate
Frequency	0.06	1.00	0.66	0.98	0.01	0.99
Block frequency	0.13	0.99	0.44	0.99	0.03	1.00
Runs	0.29	1.00	0.00	0.95	0.00	0.88
Longest run	0.69	0.98	0.72	1.00	0.03	0.99
Rank	0.32	1.00	0.78	0.99	0.05	1.00
FFT	0.00	0.41	0.00	0.84	0.09	0.99
Non-overlapping template	0.43	0.99	0.52	0.99	0.37	0.99
Overlapping template	0.06	0.98	0.00	0.93	0.02	0.97
Universal	0.90	0.99	0.24	0.99	0.32	0.99
Linear complexity	0.29	0.98	0.97	0.96	0.16	0.99
Serial	0.66	0.99	0.29	0.99	0.01	0.99
Approximate entropy	0.14	0.98	0.98	0.99	0.08	0.98
Cumulative sums	0.16	1.00	0.46	0.99	0.37	0.99
Random excursions	0.43	0.99	0.47	0.99	0.35	0.99
Random excursions variant	0.43	0.99	0.41	0.99	0.49	0.99

Table. 1 Result of SP800-22 for 100×10Mbit sequences

IPF-07. Adaptively Tunable Magnetorheological Elastomer-Based Vibration Absorber for a Propeller Aircraft Seat. *Y. Choi*[1] and N. Wereley[1] *1. Department of Aerospace Engineering, University of Maryland, College Park, MD, United States*

Aircraft propellers are a constant source producing excessive vibrations and noise due to aerodynamic loads imposed in flight. Such vibrations are transmitted to the cockpit and aircrews are inevitably exposed to the high levels of vibrations during flight. The prolonged exposure to severe vibrations due to extended missions can cause the discomfort and fatigue of the occupants, reducing the ability to make correct judgement and appropriate actions during the flight. One of effective way to provide comfortable work environment to occupants is to design a seat equipped with vibration absorbers that can isolate or reduce the unwanted vibration transmitted from the cockpit floor to occupant body. In this study, the adaptively tunable magnetorheological elastomer (MRE)-based vibration absorber was proposed for achieving better vibration reduction performance of a propeller aircraft seat. Since MREs are one of smart materials that can change their key physical properties by external stimuli, MRE-based vibration absorbers can provide both variable stiffness and damping by adjusting the magnetic field. As a result, MRE-based vibration absorbers have an adaptively tunable capability working at wider frequency range that can overcome the narrow operating frequency limitation of passive vibration absorbers. In this study, the simple but effective design of the MRE-based vibration absorber for a propeller aircraft seat was presented (Figure 1). In order to effectively concentrate the magnetic field generated from the electromagnet into the MRE pad areas, the electromagnetic analysis was also conducted by using a finite element method. Based on this analysis, the MRE-based vibration absorber was fabricated. The damper force characteristics of the MRE-based vibration absorber was experimentally evaluated by using an Instron material testing device. In order to confirm the tunability of the MRE-based vibration absorber, the frequency responses with respect to applied current inputs was experimentally obtained (Figure 2).

1. Z. Ilic, B. Rasuo, M. Jovanovic, S. Jovicic, L. Tomic, M. Jankovic, D. Petrasinovic, "The Efficiency of Passive Vibration Damping on the Pilot Seat of Piston Propeller Aircraft," Measurement 95, 2017, pp. 22-32. 2. S.D. Smith, "Human Vibration Assessment and Mitigation in Military Propeller-Driven Aircraft," the RTO AVT Symposium on Habitability of Combat and Transport Vehicles: Noise, Vibration and Motion, Prague, Czech Republic, 4-7 October 2004, RTO-MT-AVT-110.

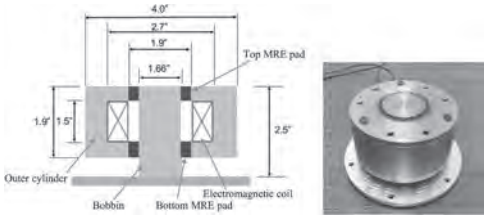

Figure 1. MRE-based vibration absorber for a propeller aircraft seat

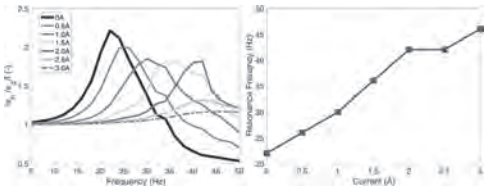

Figure 2. Frequency responses of the MRE-based vibration absorber

IPF-08. Cyclic Adhesion and Differentiation of Stem Cells by Reversible Stretching of Ligand-presenting Nanocoils. M. Ko[1], S. Min[1], H. Jung[2], W. Kim[3], S. Han[4], Y. Kim[1], G. Bae[1], S. Lee[1], R. Thangam[1], N. Li[5], Y. Jeon[1], H. Park[1], *Y. Kim*[1], U.K. Sukumar[6], J. Song[5], S. Park[7], S. Yu[8], Y. Kang[1], K. Lee[9], Q. Wei[10], D. Kim[4], S. Han[3], R. Paulmurugan[6], H. Kang[1] and Y. Kim[1] *1. Department of Materials Science and Engineering, Korea Univeristy, Seoul, The Republic of Korea; 2. Department of Materials Science and Engineering, Northwestern University, Evanston, IL, United States; 3. Department of Materials Science and Engineering, Korea Advanced Institute of Science and Technology, Daejeon, The Republic of Korea; 4. KU-KIST Graduate School of Converging Science and Technology, Korea University, Seoul, The Republic of Korea; 5. Department of Oto-rhinolaryngology-Head and Neck Surgery, Korea University, Seoul, The Republic of Korea; 6. Department of Radiology, Stanford University School of Medicine, Palo Alto, CA, United States; 7. Department of Advanced Materials Engineering, Chung-Ang University, Anseong, The Republic of Korea; 8. Department ofDepartment of Chemical and Biological Engineering, Korea University, Seoul, The Republic of Korea; 9. Department of Chemistry and Chemical Biology, Rutgers University, Piscataway, NJ, United States; 10. College of Polymer Science and Engineering, Sichuan University, Chengdu, China*

Cyclic nanoscale stretching and shrinking of ligands in the native extracellular matrix (ECM) can regulate complex cell-material interactions. [1] Ligand-presenting magnetic nanomaterials can imitate ECM dynamicity to control the cellular adhesion by *in situ* and cyclic control of changes in intrinsic ligand pitch. [2] Magnetic nanocoils offer remote, real-time, cyclic, and mechanical stretching ("ON") and shrinking ("OFF") of cell-adhesive Arg-Gly-Asp (RGD) ligand on a material surface in five repeated cycles (Fig. 1). The ligand pitch is independently regulated while maintaining the ligand-presenting surface area per nanocoil. We demonstrated that switching "ON" (ligand nanostretching) promotes time-regulated integrin ligation, focal adhesion, spreading, YAP/TAZ mechanosensing, and differentiation of viable stem cells, both *in vitro* and *in vivo*. The *in situ* reversible switching from "ON" (ligand-stretching) to "OFF" (shrinking) of the nanocoils in the mouse is confirmed by fluorescence resonance energy transfer (FRET) imaging, which is sensitive to the distance between donor and acceptor dyes. We also analyzed the shape-, length-dependent cellular adhesion by modifying the condition of electrodeposition. Our works provide novel insight for designing nanostructures with connected ligands to express nano-spaced declustering (increasing ligand nanocoil pitch), which is ineffective in nanowires to facilitate cell adhesion. This remote, real-time, cyclic, and cytocompatible control of the ligand pitch offers an effective strategy for improving the host cell adhesion and mechanosensing-mediated differentiation of stem cells *in vivo*.

[1] C. H. Turner, Bone 1998, 23, 399. [2] M. J. Dalby, N. Gadegaard, R. O. C. Oreffo, Nat. Mater. 2014, 13, 558

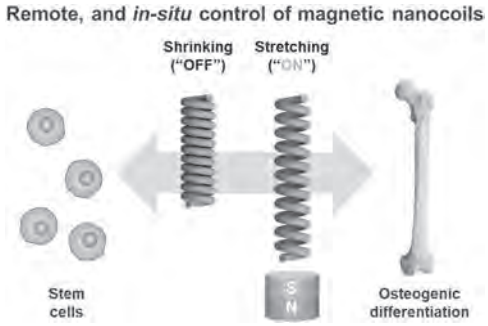

Fig. 1. Schematic diagram of remote, and in situ stretching and shrinking of ligand-presenting nanocoils.

IPF-09. Magnetic Moment Direction Estimation Method Based on Full Magnetic Gradient Orthonormal Basis Function. *Y. Qin*[1], M. Li[1], K. Li[1], J. Chen[1], Y. Pan[1], X. Yang[1] and J. Ou-Yang[1] *1. Huazhong University of Science and Technology, Wuhan, China*

Magnetic anomaly detection (MAD) is an important means of detecting the existence and localization of magnetic targets [1-2]. With the improvement of magnetic sensor technology, MAD has very large application prospects [3]. The traditional magnetic signal processing method cannot greatly improve the SNR (signal-to-noise ratio) while also restoring the target's characteristic [4]. Our research about Full Magnetic Gradient Orthonormal Basis Function [5] solves the problems of the low SNR of the magnetic anomaly signal, the influence of the sway of the magnetic gradiometer platform. But it can only detect the existence of the target and cannot obtain the characteristics of the target. In this paper, based on the full magnetic gradient tensor which contains huge spatial magnetic field information, we analyze the factor of each component in the target magnetic abnormal signal. A target's moment direction estimation method has been proposed, the flowchart is shown in Fig. 1(a). This method can estimate the target magnetic moment direction in 3-D Cartesian coordinates with a resolution of 30°. We have simulated 100 sets of targets with different magnetic moment sizes and distances, and the accuracy of the estimation of the target magnetic moment direction is 100% (Fig.1 (b)). The SNR is increased by 25.8 times on average (Fig.1 (c)). We put the magnetic moment of the target in 6 different directions and conducted 10 experiments in each direction (Fig.2 (a)). The original signal and the processed signal are shown in Fig. 2(b). The accuracy of the target magnetic moment estimation and the improvement of the SNR are shown in Fig. 2(c). Compared with the traditional signal processing method, the proposed method can estimate the magnetic moment direction of the target while greatly improving the SNR and the performance is not affected by the shaking of the sensor carrier. These are very helpful properties for the fast and large-scale detection of magnetic anomalies, such as aeromagnetic prospecting, medical micro-robot positioning.

[1]X. Chen, Road Vehicle Detection and Classification Using Magnetic Field Measurement, *IEEE Access*, vol. 7 p. 52622 (2019). [2]Y. Sui, Error Analysis and Correction of a Downhole Rotating Magnetic Full-Tensor Gradiometer, IEEE Access, vol. 8 (2020). [3]K. Kim, Magnetic Anomaly Detection Using Continuous Angle Alignment of Three-Axis Magnetic Signal, IEEE Sensors Journal, vol. 19, p. 743-750 (2019). [4]H. Jin, Magnetic Anomaly Detection and Localization Using Orthogonal Basis of Magnetic Tensor Contraction, IEEE Transactions on Geoscience and Remote Sensing, vol. 58, p. 5944-5954 (2020). [5]Y. Qin, Magnetic Anomaly Detection Using Full Magnetic Gradient Orthonormal Basis Function, IEEE Sensors Journal, vol. 20, p. 12928-12940 (2020).

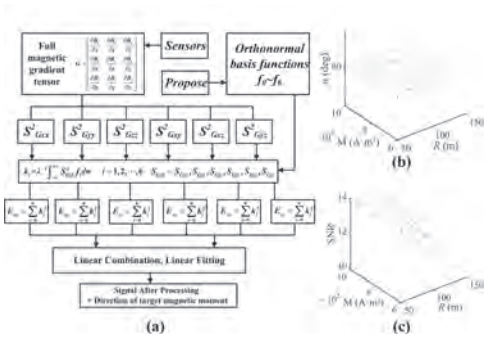

Fig.1. (a) Flowchart. (b) Accuracy of simulation experiment. (c) SNR after processing

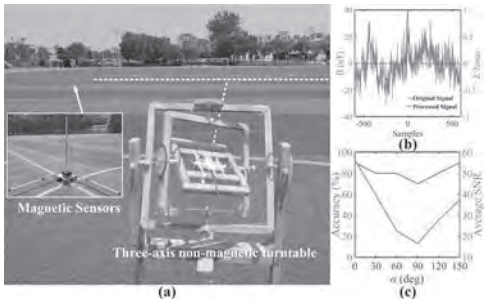

Fig.2. (a) Experimental device. (b) Original and processed signal. (c) Result of field experiment.

IPF-10. Chirality Induced Spin Selectivity in a 2D Chiral Channel. *N. Pandey*[1], A. Saha[1], D. Saha[1] and S. Ganguly[1] *1. Electrical Engineering, IIT Bombay, Mumbai, India*

Chiral molecules are the building blocks of most biomolecules and underlie many biochemical processes. A novel phenomenon called Chirality Induced Spin Selectivity (CISS) has emerged in recent times wherein electron polarization in chiral molecules translates to spin polarization [1]. It has been observed in DNA, proteins etc.[2]. Due to lack of inversion symmetry in chiral molecules a Rashba type spin orbit coupling (SOC) arises, which causes spin-filtering in chiral molecules. Here, we seek to model CISS in a 2-D channel material with a square lattice within the NEGF formalism, by adding an imaginary component originating from SOC to the Hamiltonian. This is motivated by the idea of chiral artificial receptors for enantioselective electronic noise sensors, capable of distinguishing between enantiomers [3]. The channel, assumed to be chiral, has a chiral electric field from the atoms present, the direction of which is used to probe the chirality of the channel. The chiral molecules break structure inversion symmetry but preserve time reversal symmetry, and so to break the degeneracy of the electrons a direction of propagation must be chosen [4]. The results in Fig. 2 show us that on selecting a direction of propagation by applying a bias we do get a particular spin polarization. The polarization gets reversed on changing the chirality of the channel. The spin polarization in the 2-D channel attests to its chiral nature, which can be utilized to sense chiral molecules. In an attempt to explore CISS in another work, we have included CISS into electron-phonon coupling and studied its effect on inelastic electron tunneling.

[1] Anup Kumara, Eyal Capua and Manoj K. Kesharwani, PNAS, vol. 114, no. 10, pp. 2474–2478 (2017). [2] Martin Sebastian Zöllner, Solmar Varela and Ernesto Medina, ChemRxiv. Preprint (2019). [3] Ashutosh Samal, Nidhi Pandey and Swaroop Ganguly, IEEE Sensors 2021 (submitted). [4] Ernesto Medina, Luis A. González-Arraga and Daniel Finkelstein-Shapiro J. Chem. Phys. 142, 194308 (2015).

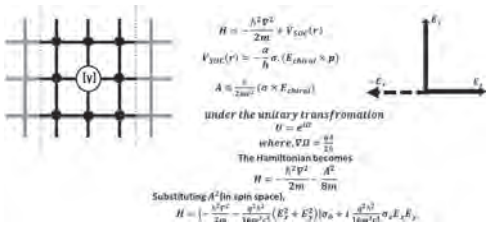

Fig. 1(a) A 2D channel with the spin-orbit coupling; γ is the on-site energy β_x, β_y are the nearest neighbour coupling in x and y direction respectively. (b) The mirror image of the chiral field used to probe the chirality in the channel.

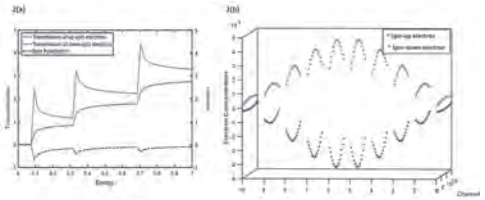

Fig. 2(a) The transmission of up-spin and down-spin electrons in the channel of right-handedness. The spin polarization in the channel due to difference in the up-spin and down-spin transmission, P= $(T_{up} - T_{down})/(T_{up} + T_{down})$, P reverses on changing the chirality.(b) The plot of electron concentration in the channel (sign implies the spin of the electron).

IPF-11. All-Optical Study of the Hard Magnetic Anisotropic Strontium Hexaferrite Nanoparticles Dynamics in Viscous Media. *V.V. Korolev*[1], A. Eliseev[1], E.O. Anokhin[1] and L. Trusov[1,2] *1. Lomonosov Moscow State University, Moscow, Russian Federation; 2. Shenzhen MSU-BIT University, Shenzhen, China*

Hard magnetic anisotropic nanoparticles ensembles attracted sizeable attention in the last years. Unique combination of magnetocrystalline and shape anisotropy paves the way for new exotic magnetic phenomena in colloidal systems: structural phase transitions in ferrofluids, pronounced linear dichroism and magnetorheological effects. Such particles may also act as multifunctional nanomagnet probes. Applications in cancer magnetomechanical therapy were previously shown. Most of these applications require the knowledge of the nanoparticle dynamics in media and the most common method is AC magnetometry. At the same time suspensions of the anisotropic nanoparticles demonstrate linear dichroism: effect of the nanoparticles orientation on the optical properties of the suspension. Colloidal solutions of the strontium hexaferrite $SrFe_{12}O_{19}$ nanoplates demonstrate one of the most prominent dichroic effect upon the application of the moderate magnetic field (up to hundred Oersteds), changing its optical density on the order of tens of percents. In the present work we show that this effect can be used to study Brownian relaxation of the nanoparticles under application of the alternating magnetic field. The relaxation data provides the information about viscous and elastic properties of the colloidal media. This could be readily applied to hundred-microliter-scale all optical *in situ* viscosity measurements using $SrFe_{12}O_{19}$ nanoparticles as probes. Dynamical behavior of the magnetic nanoplates under application of the AC magnetic field was studied by the means of numerical modelling as well as experimentally. Fokker-Planck based model was developed to describe the optical density modulation under the applied magnetic field. Model accounts for the size distribution of the nanoparticles in real system and gives qualitative explanation of the obtained data. This work was funded by the Russian Science Foundation, Grant No. 20-73-10129.

IPF-12. ELF Magnetic Regulation of Amphibian Metamorphosis: A qualitative Control of Following Salamanded Axolotl. *H. Nakagawa*[1], M. Fujimoto[2], S. Fujiwara[2] and T. Tadokoro[1] *1. Tokyo Denki University, Tokyo, Japan; 2. CPCC, Tokyo, Japan*

With a full understanding of a commercialized power frequency of 50/60 Hz, considerations for details in the competing situation between extremely low frequency (ELF)-field effects and biological adaptive responses to the magnetic forces in a living body are of great importance. The purpose of this study is to investigate ELF magnetic effects with different exposure timings on the forced metamorphosis of Mexican axolotls, which is induced by a function of thyroxine (T_4). One hundred and forty axolotls (about 5 months old, approximately 80 mm) were individually kept in appropriate square boxes containing a dechlorinated water without aeration. Following a soak with T_4 for 60 h, the T_4 solution was displaced by a dechlorinated water, employing an original water-renewing system [1]. Exposures of T_4-administrated axolotls to ELF fields (5.0 mT at 10 Hz) were performed using an air-cored coil system. The water temperature was strictly controlled at 24°C. The morphological changes and the survival rates of the axolotls affected by the prestimulation of the T_4 were monitored every day. In consequence, we discovered that the initiation timings of ELF field exposure did influence the speed of the morphological changes, as well as the survival rates of the following salamanded axolotls. As a point worthy of special mention, there was a close connection between the T_4-corresponding survival rates and serious indigestion/anorexia in the salamanded bodies. Our data could prove to be helpful for future reference with respect to a magnetic control study of tissue-regeneration.

1) H. Nakagawa and M. Ohuchi, IEEE Trans. Magn. 54, 5000405 (2018).

Session JOA
INDUCTION MACHINE AND SPECIAL MACHINE I

Mohammad Sedigh Toulabi, Chair
University of Windsor, Windsor, ON, Canada

CONTRIBUTED PAPERS

JOA-01. Coupled Numerical and Circuit Model Considering Stator and Field Winding Flux Linkage for Loss Minimization Control of Wound Field Synchronous Machines. A. Balamurali[1], *A. Kundu*[1], V. Kurramsetty[1], L. Iyer[2] and N. Kar[1] *1. University of Windsor, Windsor, ON, Canada; 2. Magna International Inc., Troy, MI, United States*

I. INTRODUCTION Wound field synchronous machines (WFSM) are becoming popular for traction applications due to permanent magnet–free design and additional controllability using field current [1], [2]. However, WFSMs have asymmetric cross-coupling between the field and *d*-axis, in addition to the *d*- and *q*-axis saturation and cross saturation. Thus, it is vital to consider losses [3], non–linear effects and the influence of the cross–saturation towards developing advanced control techniques. In [4], a dead-beat direct torque and flux control was developed for WFSMs. However, the influence of loss minimization (LM) control with non–linear effects is not studied. Thus, it is essential to develop an LM control with comprehensive mathematical model to study the influence of the parameter variations, inverter harmonics and current magnitudes on the losses. This paper proposes a novel coupled numerical and circuit WFSM model considering the mutual effects of field and stator windings. Additionally, an observer based LM control is used to compensate the non–linear voltage disturbances for improved performance. II. MODELING, IMPLEMENTATION AND RESULTS A coupled numerical and circuit model has been developed to include the saturation and cross–coupling effects in the test WFSM, fed from an IGBT inverter. The flowchart of the developed method to consider non–linear effects is given in Fig. 1. Rotor loss minimization (RLM) and total loss minimization (TLM) control methods were used to provide optimal stator and rotor current commands. The proposed model was used to analyze the impacts of varying *dq*– and field axis currents on the stator and rotor flux linkages. Figure 2(a) shows the comparison of calculated and actual measured torques. The conventional model does not include non–linear effects and the proposed coupled model includes all non–linear effects. The model is very accurate in representing the WFSM motor with saturation effects. Fig 2(b) shows the difference in total motor losses between the TLM and RLM methods derived using the proposed model. The TLM method improved the overall efficiency. The full paper will show the modeling procedure, further analysis of the effects of inverter harmonics, loss and efficiency maps.

[1]. Chunhua Liu, “Emerging Electric Machines and Drives — An Overview”, *IEEE Transactions on Energy Conversion*, vol. 33, no. 4, pp. 2270-2280, 2018. [2]. M. Ayub, et.al., “Brushless Operation of a Wound-Field Synchronous Machine Using a Novel Winding Scheme,” *IEEE Trans. Magn.*, vol. 54, pp. 1-4, 2019. [3]. P. Rasilo *et.al*., “Importance of Iron-Loss Modeling in Simulation of Wound-Field Synchronous Machines,” *IEEE Trans. Magn*, vol. 48, no. 9, pp. 2495-2504, 2012. [4]. Y. Nie et al., “Deadbeat-Direct Torque and Flux Control of Wound Field Synchronous Machine at Low Sampling to Fundamental Frequency Ratios,” *IEEE Trans. Ind. Appli.*, vol. 55, pp. 3813-3822, 2019.

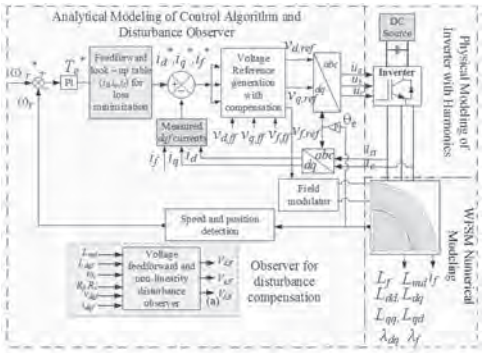

Fig. 1. Flowchart of developed method considering stator and field winding flux linkage and non-linear effects.

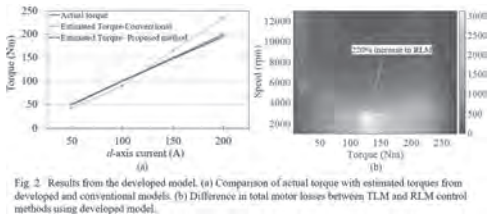

Fig. 2. Results from the developed model. (a) Comparison of actual torque with estimated torques from developed and conventional models. (b) Difference in total motor losses between TLM and RLM control methods using developed model.

JOA-02. The Outer Solid Rotor Induction Motor as an Alternative for Electric Vehicle Traction Applications. T. Abdo[1] and *A. Adly*[1] *1. Cairo University, Giza, Egypt*

Electric Vehicle (EV) industry share in the auto market has been recently surging [1]. So far, Permanent Magnet (PM) hub motors have emerged as the optimum choice for EV applications due to their high efficiency and power density capabilities [2]. Nevertheless, PM costs increse suggests that economic feasibility might impede EV dominance in different parts of the globe. Moreover, possible time degradation of a PM magnetiztion could also affect the expected feasibility of such usage [3]. In the quest to investigate a feasible alternative, this paper revisits the possibility of utilizing outer solid rotor induction motors. Among their advantages are the widespread relevant high expertise availability, the ease of manufacture in many factories all over the world, the relative low cost, and the possibility to be rigorously analyzed electromagnetically using the transmission line modeling (TLM) technique ([4]-[7]). In order to demonstrate this point analysis has been performed on a solid outer rotor induction motor whose inner stater data is identical with that of a PM hub motor given in [8]. Both TLM and finite element analysis (FEA) were caried out for the machine under consideration for different solid rotor conducting zone materials (Cu/Al) as well as for different air-gap lengths (0.5/1.0/1.5 mm). Fig. 1 demonstrates a high-level cross section of the machine as well as the micro-T circuit used to represent every zone in the TLM approach. Sample analytical normalized torque-speed curve results are given in Fig. 2 while being operated at the variable frequencies of 50 Hz and 25 Hz. While starting torque of solid rotor induction motors is relatively low, this may be ratified by means of frequency reduction through

an inverter which is a standard unit in any EV driver system. More details of the approach and comparisons with typical PM hub motors from the performance and cost perspectives are given in the full paper.

[1] P. Hertzke, N. Müller and S. Schenk, McKinsey & Company, 2017. [2] X. Sun, Z. Shi, Y. Cai, G. Lei, Y. Guo and J. Zhu, IEEE Trans. Transportation Electrification, Vol. 6, No. 3, pp. 1115-1125, 2020. [3] A.A. Adly and A. Huzayyin, Journal of Advanced Research, Vol. 17, pp. 103-108, 2019. [4] A.L. Cullen and T.H. Barton, Proc. of the IET, Vol. 105, No. 8, pp. 331 – 336, 1958, [5] A.A. Adly, IEEE Trans. Mag., Vol. 37, No. 4, pp. 2800-2802, 2001. [6] L. Qaseer, F. de León, and S. Purushothaman, ACES Journal, Vol. 26, No. 7, pp. 551-560, 2011. [7] J.F. Gieras and J. Saari, IEEE Trans. Ind. Electronics, Vol. 59, No. 6, pp. 2689-2700, 2012. [8] Z. Shi, X. Sun, G. Lei, Z. Yang, Y. Guo, and J. Zhu, IEEE Trans. Mag., Vol. 56, No. 2, p. 7508804, 2020.

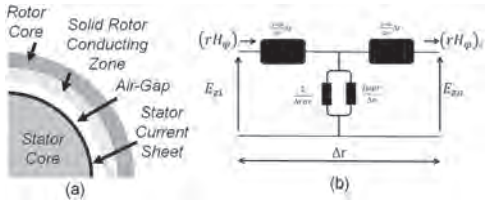

Fig. 1. (a) Outer solid rotor IM configuration, and (b) Micros-T circuit used in the TLM.

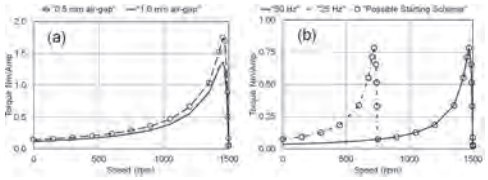

Fig. 2. (a) T-n curves for Al solid rotor corresponding to different air-gap lengths, and (b) T-n curves for Cu solid rotor and 0.5 mm air-gap lengths corresponding to different operational frequencies.

JOA-03. Winding Function-Based Analytical Modeling of Core Loss in an Induction Machine Considering Slotting Effects and the Frequency Dependent B-H Curve Characteristics. *B. Guruwatta Vidanalage*[1], M. Toulabi[1], T. Stachl[1], A. Lombardi[2], J. Tjong[3] and N. Kar[1] *1. Electrical and Computer Engineering, University of Windsor, Windsor, ON, Canada; 2. Nemak, Windsor, ON, Canada; 3. Mechanical Automotive and Materials Engineering, University of Windsor, Windsor, ON, Canada*

Analytical modeling is a computationally efficient method to predict the performance of induction machines (IMs). Conventional winding function-based (WFB) models are already available in literature [1]. For core loss prediction, the Bertotti core loss function [2] can be supported by conventional WFB model via providing the flux density distribution of the IM. However, in this analytical core loss prediction, flux density variation in the different sections of the magnetic core and the effect of the excitation frequency on the B-H curve are ignored [3], [4]. In this paper, using an extended WFB model, the neglected effects are considered to develop a computationally efficient improved core loss model to enhance the analytical core loss prediction. First the air-gap flux density (AGFD) of the IM is calculated using the proposed extended WFB model including slotting effects and magneto-motive-force (MMF) drops in the core areas considering the frequency-dependent B-H characteristics, then the machine core is sectionized into teeth and yoke sections so that the flux and core loss densities of each section can be analytically calculated. In Fig. 1(a), the AGFD distribution prediction using the proposed WFB model, under each stator tooth area over half of the machine's circumference at the rated operating point of a laboratory 11 kW IM is compared with the results from finite element analysis (FEA) for verification. The flux density distribution using FEA for the same operating condition is highlighted in Fig. 1(b) to visually authenticate the calculations of Fig. 1(a). Table I shows the core losses at the rated operating condition of the machine using FEA, conventional WFB model and the extended WFB model. By considering FEA as the reference target, the error in total core loss is reduced from 22.6% by conventional WFB model to 4.7% using the proposed WFB model. Detailed analytical calculations of core loss through the proposed WFB model and the additional loss results for various operating points will be provided in the final paper.

[1] A. Marfoli, L. Papini, P. Bolognesi and C. Gerada, IEEE Transactions on Energy Conversion, Vol. 36, p. 421-430 (2021). [2] X. Yu, Y. Li, Q. Yang, et al., IEEE Transactions on Magnetics, Vol. 55, p. 1-4 (2019). [3] H. Zhao, et al., IEEE Transactions on Magnetics, Vol. 53, p. 1-4 (2017). [4] D. Zhang, T. Liu, H. Zhao and T. Wu, IEEE Transactions on Industrial Electronics, Vol. 66, p. 9194-9204 (2019).

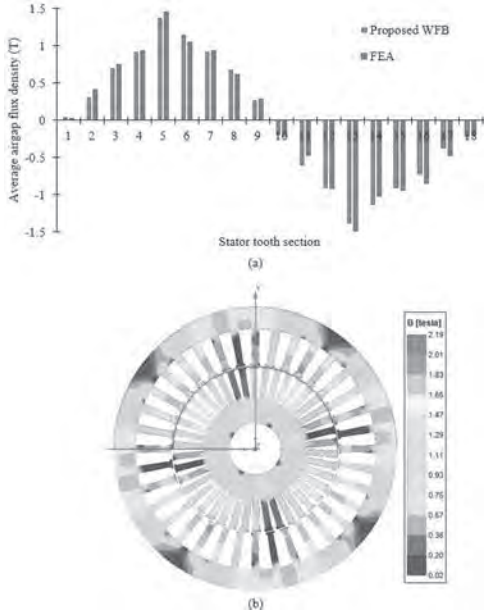

Fig. 1. Airgap flux density distribution. (a) Under the stator teeth. (b) In core using FEA.

	Stator losses (W)		Rotor losses (W)		Total iron loss (W)	Error (%)
	Hysteresis	Eddy current	Hysteresis	Eddy current		
FEA	49.68	19.68	1.89	4.36	75.5	
Conventional WFB	52.74	12.6	12.32	5.334	92.99	22.6
Proposed WFB	47.4	16.15	11.4	4.464	79.38	4.7

Table I. Comparison of the core loss predictions by different models at the rated conditions.

JOA-04. Validation of Standstill Magnetization Strategy of a Single Pole Pair FeCrCo-based Memory Motor. *F.D. de Sousa*[1], A. Battiston[1], F. Meibody-Tabar[2] and S. Pierfederici[2] *1. Mobility and Systems, IFP Energies nouvelles - Institut Carnot IFPEN Transports Energie, Rueil-Malmaison, France; 2. LEMTA Laboratory - Université de Lorraine, Vandoeuvre-Les-Nancy, France*

Concerns related to the commercial scenario of rare-earth magnets (REMs), the environmental damages caused by their use and extraction[1] and the generally required use of flux-weakening strategies for operations over the base speed [2],[3] have been affecting the interest in permanent magnet synchronous machines (PMSMs) for electrified systems. Variable Flux Memory Machines (VFMMs) [4] emerge in this context as an option for more sustainable mobility systems operating in a wider torque-speed range. Based on the use of low coercive force (LCF) magnets, these machines present as major feature an additional degree of freedom for control [5], defined by the regulation of their magnetic flux density. For this, short-time currents are injected in the stator windings. The use of AlNiCo alloys as LCF magnets in these machines has been often discussed due to the high remanent flux density and good thermal proprieties [1],[6] of these magnets.

However, similar materials as FeCrCo are still little explored. Even so, characteristics as their high working temperature and their mechanical resistance can be interesting for electrical machines. Therefore, this study presents a methodology for a standstill magnetization of a non-salient single pole pair FeCrCo-based VFMM for high-speed applications in the transportation electrification field. The rotor is designed as a solid cylinder for an easy adaptability to other stator geometries. A mathematical modeling defining the working point placement on the hysteresis curves of the magnet is developed and validated by Finite-Element Analysis. Experimental tests are carried out proposing an inverter in DC/DC mode for regulating the magnetization level of the FeCrCo. The armature reaction is then studied, highlighting the interaction between both the magnet and stator fields. Due to the singular magnetic behavior of the FeCrCo used, a methodology for validation of results obtained by experimental tests is developed by the estimation of the remanence in terms of the excitation field for characterizing the internal recoil lines.

[1]R. Jayarajan, N. Fernando and I. U. Nutkani, *IEEE Access*, vol. 7, pp. 70141-70156 (2019). [2] A. M. Aljehaimi and P. Pillay, *IEEE Transactions on Transportation Electrification*, vol. 4, no. 3, pp. 707-719 (2018). [3] H. Hua, Z. Q. Zhu, A. Pride, R. Deodhar and T. Sasaki, *IEEE Transactions on Industry Applications*, vol. 55, no. 2, pp. 1408-1419 (2019). [5] V. Ostovic, *IEEE Industry Applications Magazine*, vol. 9, no. 1, pp. 52-61 (2003). [6] C. Yu, S. Niu, S. L. Ho, W. Fu and L. Li, *IEEE Transactions on Magnetics*, vol. 51, no. 3, pp. 1-4 (2015)

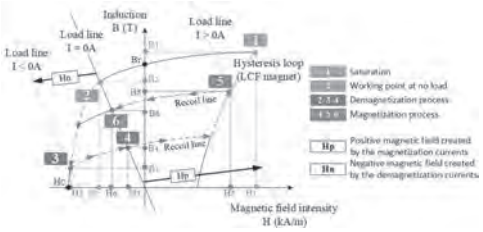

Fig.1. Theoretical regulation of the working point placement in a VFMM

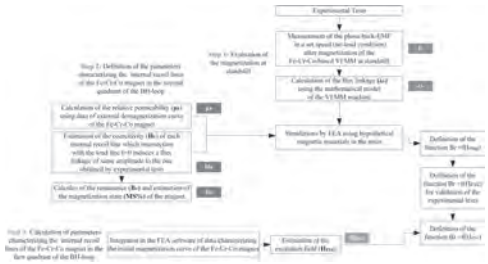

Fig.2. Methodology for validation of the working point placement of the FeCrCo

JOA-05. Characteristics Analysis and Comparison of Conventional and Segmental Rotor Type 12/8 Double Stator Bearingless Switched Reluctance Motors. *Z. Xu*[1], Z. Fan[1], Z. Zhou[1], Y. Qi[1] and F. Zhang[1]
1. Shenyang University of Technology, Shenyang, China

Bearingless switched reluctance motor (BSRM) not only has the advantages of bearingless motor, but also inherits the excellent characteristics of switched reluctance motor (SRM), and could reduce the vibration and noise of SRM, which is more suitable for high-speed driving fields [1]. Hence, many scholars studied on BSRMs [2]-[8] in recent years. To improve the output torque density and further weaken the coupling degree between torque and suspending force control, a novel segmental rotor type 12/8 DSBSRM is proposed in Fig. 1. The proposed structure includes three parts: outer stator, inner stator, and hybrid rotor. The outer stator has two types of stator poles: exciting and auxiliary poles. The torque windings are only wound on the exciting poles, and there are no windings on the auxiliary poles. The inner stator has four identical stator poles. The suspending force windings are wound on each inner stator pole. The hybrid rotor is composed of rotor segments, nonmagnetic isolator and toroidal core. The rotor segments and toroidal core are embedded in the outside and inside of the nonmagnetic isolator, respectively. Due to the special structure, the proposed motor operates in short flux paths, and the magnetic flux paths of the inner and outer stator are independent from each other. Therefore, compared with conventional DSBSRMs, the proposed DSBSRM not only improves the output torque density, but also has better decoupling characteristics between torque and suspending force control. To verify the proposed structure, finite element method (FEM) is employed to get the characteristics of the proposed structure. Meanwhile, a conventional 12/8 DSBSRM is also analyzed for comparison. Fig. 2 shows the average torque of conventional and proposed DSBSRMs. With the same current, the average torque produced by the proposed DSBSRM is higher than that of the conventional one at all current levels. Due to space constraints, comparison of other characteristics will be present in the final paper. Furthermore, test results will also be presented and analyzed to verify the validity of comparison results with FEM.

[1] Z. Xu, D. Lee and J. Ahn, IEEE Transactions on Industry Applications, vol. 51, no. 1, pp. 733-743 (2015). [2] T. Zhang, J. Chen and W. Zhu, IEEE Transactions on Magnetics, vol. 57, no. 6, pp. 1-4 (2021). [3] H. Wang, J. Bao, B. Xue, etc., IEEE Transactions on Industrial Electronics, vol. 62, no. 7, pp. 4298-4306 (2015). [4] Y. Huang, F. Huang, Y. Yuan, etc., IEEE Access, vol. 7, pp. 94342-94349 (2019). [5] C. Sun, J. Li, H. Ding, etc., IEEE Access, vol. 9, pp. 38626-38635 (2021). [6] H. Wang and F. Li, IEEE Transactions on Industrial Electronics, vol. 67, no. 6, pp. 4326-4337 (2020). [7] Z. Hao, X. Cao, X. Deng, etc., IEEE Transactions on Energy Conversion, vol. 35, no. 3, pp. 1278-1288 (2020). [8] J. Zhang, H. Wang, L. Chen, etc., IEEE Transactions on Magnetics, vol. 54, no. 1, pp. 1-13 (2018).

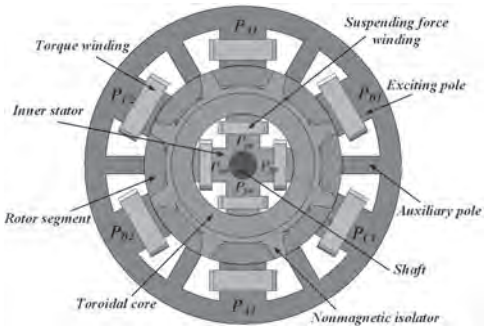

Fig. 1 Structure of the proposed DSBSRM

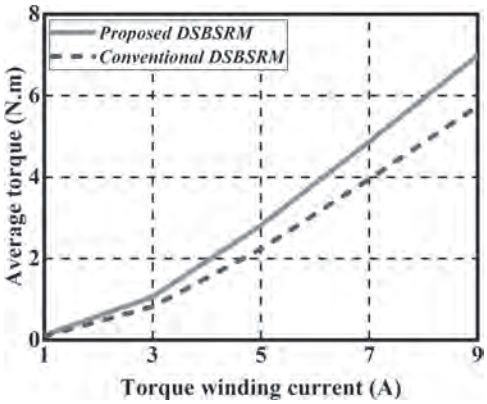

Fig. 2 Average torque of conventional and proposed DSBSRMs

JOA-06. Research on Magnetic Field Analytical Model of Annular Linear Induction Electromagnetic Pump. *T. Mei*[1], G. Liu[1], Z. Xu[1], S. Jin[1] and F. Zhang[1] *1. School of Electrical Engineering, Shenyang University of Technology, Shenyang, China*

As a clean and efficient new energy, nuclear energy is an inevitable choice to achieve sustainable energy development, and sodium cold fast reactor is one of the developing reactors of the 4th generation nuclear power system. To transport liquid metal, the electromagnetic pump has the advantages of no mechanical rotating parts, good sealing, low noise and high reliability. Compared with other types of electromagnetic pumps, ALIEP has a large flow rate and a high head, making it an ideal type of pump for the cooling system of large nuclear power equipment. The structure of ALIEP is shown in Fig1. However, using finite element to simulate the magnetic field of ALIEP is a heavy workload with a high cost of error. As the complex structure, and the influence of magneto-fluid mechanics on the electromagnetic field, it is difficult to establish analytical models. So we reduced the complex 3D magnetic field distribution to two 2D analytical models. In the 2D axial analytical model, we got the transfer matrix between two adjacent layers of electromagnetic field. $[B_{\rho n}\ B_{zn}]=[ch(\gamma_n s_n),\ iksh(\gamma_n s_n)/\gamma_n\ \gamma_n sh(\gamma_n s_n)/ik, ch(\gamma_n s_n)]\ [B_{\rho n-1}\ B_{zn-1}]$ Considering the longitudinal end effect of ALIEP, we introduce an empirical coefficient k_l, which can be understood as the existence of the end core weakens the average radial magnetic in the ideal case. The expressions of the electromagnetic force are $F_z=-\sigma_f(v_s-v_f)B_{\rho 2}{}^2 L c k_l$. The results are shown in Fig2. ALIEP usually uses separated outer stators, which will lead to uneven distribution of magnetic field along the circumferential direction. Therefore, we summarized the effects of the arrangement of the outer core on the distribution of the circumferential magnetic field. Combined with the 2D axial model, the electromagnetic force of liquid metal can be calculated. Based on the electromagnetic force of liquid metal as the index, the analytical model of ALIEP is established and used in the preliminary design, then combined with the finite element software in the later stage, which greatly reduces the design period, and ensures the calculation accuracy.

[1]Ruijie Zhao. Three-Dimensional Transient Characteristics and Unstable Flow Mechanism of ALIP Electromagnetic Pump[J].Journal of Drainage and Irrigation Machinery Enginerring,2019,37(10):841-847. [2]Electromagnetic pump Group, Institute of Mechanics, Chinese Academy of Sciences. Liquid Metal Electromagnetic Pump[M].Beiijng:Science Press,1979.

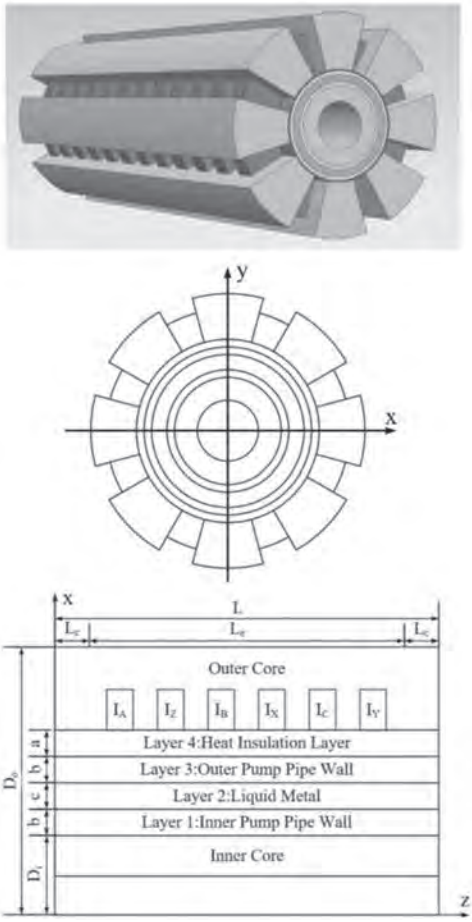

Fig1. 3D structure diagram and 2D analytical model of ALIEP

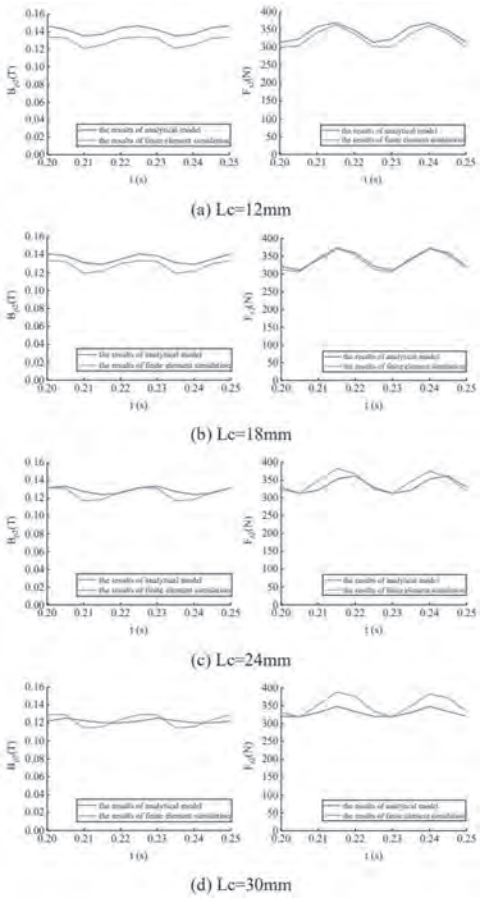

Fig.2. The finite element simulation validation of ALIEP axial analytical model

JOA-07. Power capability of shifted inductances axes permanent magnet machines. *H. Diab*[1], S. Asfirane[1] and Y. Amara[1] *1. GREAH, Université Le Havre Normandie, Le Havre, France*

In this contribution the power capability of shifted inductances axes permanent magnet machines (SIAPMM) is studied. Both low speed (maximum torque) and high speed (flux weakening) operations are analyzed. The goal is to start from a common ground already defined in some contributions dedicated to power capability of synchronous machines [1-3], and extend it to SIAPMM. The concept of SIAPMM have been introduced recently [4-8]. These machines can be regarded as the combination of non-salient PM rotor and a variable reluctance (VR) rotor under the same stator [Fig. 1(a)]. Two Park's referential frames can be then defined [Fig. 1(b)], one for the PM rotor part, and a second for the VR rotor part, shifted by an angle β [Fig. 1(b)]. The maximum torque can be increased by adequately choosing angle β. Instead of computing the "armature current / EMF" phase shift ψ maximizing the torque, as classically done, for SIAPMM the starting point consists of imposing the optimal angle value ψ = 0, and determining the optimal β angle [Figs. 1(c) and 1(d)]. It can be shown that β = π/4, if ρ < 1, and β = -π/4, if ρ > 1, where ρ is the saliency ratio (= Lq/Ld). Fig. 2(a) shows the percentage of "maximum torque" increase in the (Ldn, ρ) plane, of the SIAPM machines as compared to classical PM machines having the same ρ, and PM excitation flux linkage ΦPM. Ldn is the normalized value of d axis inductance, defined as (Ld×Imax/ΦPM), where Imax is the maximum armature current. The percentage increase is computed as (TSIAPM-TPM)×100/TPM. Fig. 2(b) compares power capabilities of a SIAPMM, and a classical PM machine, with (Ldn = 2.5, ρ = 1.5). The SIAPMM have a better power capability as compared to classical PM machine. In the full version, the power capability of SIAPMM is studied in the entire (Ldn, ρ) plane. The optimal flux weakening strategies to be adopted considering the values of Ldn and ρ will be defined.

[1] R. F. Schiferl and T. A. Lipo, "Power capability of salient pole permanent magnet synchronous motors in variable speed drive applications," *IEEE Trans. Ind. Appl.*, vol. 26, no. 1, pp. 115–123, Jan./Feb. 1990. [2] W. L. Soong and T. J. E. Miller, "Field-weakening performance of brushless synchronous AC motor drives," *IEE Proc. Electr. Power Appl.*, vol. 141, no. 6, pp. 331–340, Nov. 1994. [3] Y. Amara, S. Hlioui, H. Ben Ahmed, and M. Gabsi, "Power capability of hybrid excited synchronous motors in variable speed drives applications," *IEEE Trans. Magn.*, vol. 55, no. 8, 8204312, August 2019. [4] W. Zhao, T. A.Lipo, and B.-I. Kwon, "Optimal design of a novel asymmetrical rotor structure to obtain torque and efficiency improvement in surface inset PM motors," *IEEE Trans. Magn.*, vol. 51, no. 3, 8100704, March 2015. [5] W. Zhao, D. Chen, T. A. Lipo, and B.-I. Kwon, "Performance improvement of ferrite-assisted synchronous reluctance machines using asymmetrical rotor configurations," *IEEE Trans. Magn.*, vol. 51, no. 11, 8108504, Nov. 2015. [6] H. Yang, Y. Li, H. Lin, Z. Q.Zhu, S. Lyu, H. Wang, S. Fang, and Y. Huang, "Novel reluctance axis shifted machines with hybrid rotors," In Proceedings of the 2017 IEEE Energy Conversion Congress and Exposition (ECCE), Cincinnati, OH, USA, 1–5 October 2017. [7] T. Takahashi, Y. Miyama, M. Nakano, K. Yamane, *Permanent Magnet Rotating Electric Machine*, Japan PCT Patent Appl. WO 2019/064801 A1, 4 April 2019. [8] Z. Q. Zhu, and Y. Xiao, "Novel magnetic-field-shifting techniques in asymmetric rotor pole interior PM machines with enhanced torque density," *IEEE Trans. Magn.*, Early Access, 2021.

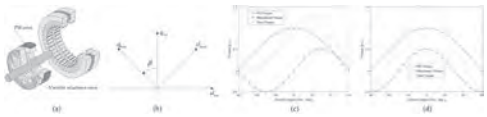

Fig. 1. SIAPM machines principal. (a) Structure of a SIAPM machine. (b) Park's referential frame definition. (c) Classical PM machine (β = 0). (d) SIAPM machine (β = π/4).

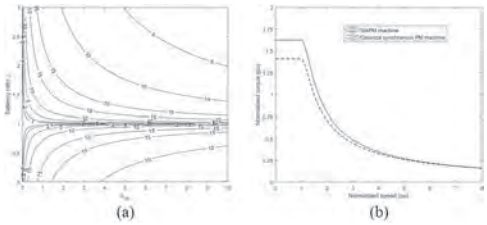

Fig. 2. Power capabilities of SIAPM machines. (a) Torque increase (low speed operation). (b) Operation over a large speed range (Ldn = 2.5, ρ = 1.5).

JOA-08. Withdrawn

JOA-09. Design and Testing of a Novel, Dual Wound, Magnetically Geared, Power-split Device. *J.G. Birchall*[1] and G. Cooke[1]
1. Magnomatics Limited, Sheffield, United Kingdom

A prototype MAGSPLIT3 machine has been designed, built and tested. This machine extends the functionality of the previous MAGPLIT machines by addition of a second motor winding in the stator, bringing new possibilities for novel powertrain arrangements. One such opportunity would be mild-hybridisation of vehicles involving non-electric ancillary components, improving both vehicle powertrain efficiency and efficiency of engine driven ancillary devices. MAGSPLIT3 uses the same magnetically geared

arrangement of a MAGSPLIT2, with the new winding enabling only a single set of rotors to act as a full power-split driveline offering previously unavailable functionality to ancillary devices such as air conditioning compressors. Allowing removal of alternators, operation of ancillary systems in the most efficient manner by freely selecting operating speeds independent from engine speed, and all-electric operation of the ancillary devices for when the internal combustion engine is turned off. This paper will explore design challenges faced, and will cover the testing of the machine, documenting how the efficiency behaviour changes across operating modes. A cross section of the prototyped machine is given in Fig.1 showing the dual rotors and dual windings of the MAGSPLIT3 machine. Two conceptually separate machines both utilising the same physical space leads to some interesting trade-offs when optimising. Initial dimensioning for a given set of requirements will be shown utilising standard approaches but highlighting how the additional design degrees of freedom have been handled. Some choices in the electromagnetic design space are discussed, such as split of copper between windings. Also discussed are design details that are shared, but have affects on each machine independently, such as the stator tooth widths. Lastly, the testing plan will be discussed together with the test setup and results. The testing was conducted on a fully instrumented dual dynamometer. Fig.2 shows the two shaft lines of the dynamometer, representing the crank of an internal combustion engine and the drive shaft of an air conditioning compressor, which can be seen complete with torque transducers and the drive belts of the target vehicle.

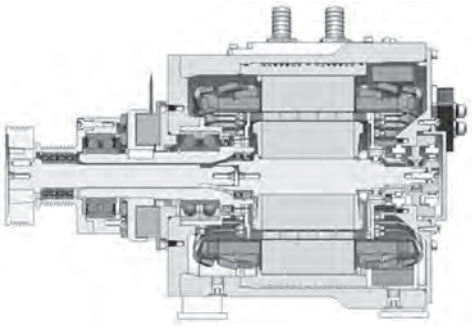

Fig.1

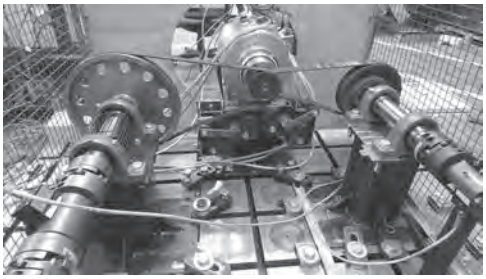

Fig.2

Session JOB
HIGH SPEED AND SPECIAL ROTATING ELECTRICAL MACHINES I

Wenlong Li, Chair
Nanjing University of Science and Technology, Nanjing, China

CONTRIBUTED PAPERS

JOB-01. Design and Analysis of a Novel Brushless Double-Fed Generator with Series Cage Bar Assisted Magnetic Barrier Rotor.
S. Yu[1], P. Tian[1], Z. Diao[1] and F. Zhang[1] *1. Shenyang University of Technology, Shenyang, China*

Brushless doubly fed generator (BDFG) is particularly suitable for wind power generation due to its inherent characteristics, such as no brush, small required inverter capacity and adjustable power factor[1-2]. There are two sets of stator windings with different pole numbers in the stator core and they are no direct coupling relationship. The electromechanical energy conversion of the generator is realized by magnetic field modulation of the special structure rotor[3-4]. In order to improve the magnetic field modulation ability of the rotor, thereby improving the energy conversion efficiency of the generator, a new hybrid rotor structure is proposed as shown in Fig.1. It can be seen that the proposed rotor is composed by series cage bars and radial magnetic barrier laminations. The assisted cage bars can more standardize the magnetic flux path, thereby increasing the rotor salient pole ratio and enhancing the rotor magnetic field modulation effect. Besides, the series cage bar can better regulate the magnetic flux path and induce a more sinusoidal magnetomotive force, which can reduce the content of ineffective harmonics and improve the effect of magnetic field modulation. The design of the proposed rotor is great difficult due to the numerous structural parameters and the interaction between cage bar and magnetic barrier. Therefore, a magnetic performance calculation model considering the mutual coupling action of the magnetic barrier and the series cage bar is constructed and the mapping law between the rotor magnetic field modulation ability and various structural parameters is studied. Based on research results, the design method of the proposed BDFG are analyzed and summarized. Furthermore, an 8+4 pole BDFG with the proposed new hybrid rotor is designed and analyzed by finite element method. Fig.2 shows the magnetic field modulation effect of the new rotor hybrid structure and the traditional magnetic barrier rotor structure under the same conditions. Through comparison, it can be seen that the proposed new hybrid rotor can effectively enhance the magnetic field modulation ability, thereby improving the energy conversion efficiency of the BDFG.

1. Y. Cheng, B. Yu, C. Kan and X. Wang, “Design and Performance Study of a Brushless Doubly Fed Generator Based on Differential Modulation,” IEEE Transactions on Industrial Electronics, vol. 67, no. 12, pp. 10024-10034, Dec. 2020. 2. J. Zhang, Y. Jiang, X. Hu and S. Xu, “A Brushless Doubly Fed Generator Based on Permanent Magnet Field Modulation,” IEEE Transactions on Industrial Electronics, vol. 67, no. 5, pp. 3505-3516, May 2020. 3. F. Zhang, S. Yu, Y. Wang, et al. “Design and Performance Comparisons of Brushless Doubly-Fed Generators with Different Rotor Structures,” IEEE Transactions on Industrial Electronics, vol. 66, no. 1, pp. 631-640. Jan. 2019. 4. A. Oraee, R. McMahon, E. Abdi, S. Abdi and S. Ademi, “Influence of Pole-Pair Combinations on the Characteristics of the Brushless Doubly Fed Induction Generator,” IEEE Transactions on Energy Conversion, vol. 35, no. 3, pp. 1151-1159, Sept. 2020

Diagram of hybrid rotor

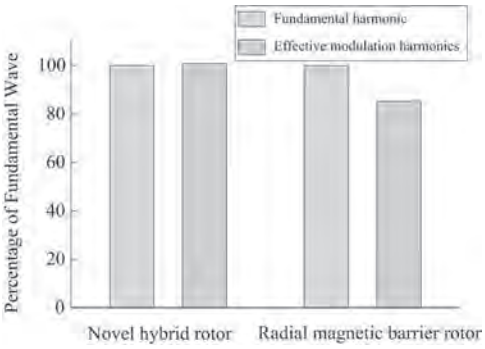

Modulation ability of different rotors

JOB-02. A Novel Dual-Rotor Hybrid-Excited Axial Flux Permanent Magnet Machine with Yokeless and Segmented Armature.
L. Jia[1], M. Lin[1], W. Le[1], A. Yang[1] and K. Lin[2] *1. School of Electrical Engineering, Southeast University, Nanjing, China; 2. Hohai University, Nanjing, China*

I. Introduction. The axial flux permanent magnet (PM) machine with yokeless and segmented armature (YASA) features the configuration of yokeless stator core, which shortens the flux path, suppresses the core loss and reduces the weight of the stator [1]. However, the YASA machine suffers from limited constant power speed range (CPSR) due to the large effective air-gap when equipped with surface-mounted PM rotors [2]. Conventionally, flux-adjustable methods of PM machines have mainly consisted of four aspects, i.e., increasement the inductance of d-axis, mechanical flux-weakening methods, hybrid-excited windings and memory machines [3]-[6]. This paper proposes a new dual-rotor hybrid-excited YASA machine (HEYASAM) with unequal teeth to adjust the air-gap flux density, which makes the advantageous features in aspect of wide CPSR and large torque output. The electromagnetic performances of the HEYASAM under different DC excitations are analyzed and validated using the FEA. II. Machine Topology. As shown in Fig. 1, the DC field windings (DCFWs) and the armature windings (AWs) are alternately mounted on the segmental stator cores, and the two rotors with consequent-pole PMs (CPMs) are positioned on both sides of the stator. In order to enlarge the area of the stator slots and mitigate the saturation of the stator teeth, the teeth widths are optimized to be unequal, i.e., large teeth with AW and small teeth with DCFW. The working principle of the flux adjustment of the HEYASAM is based on the variable magnetoresistance behavior. Fig. 2 (a) shows that although the coil flux linkage (FL) of each phase is unipolar, the resultant phase FL turns out to be

bipolar due to the DC bias and even-order harmonics offset in the coil FL. III. FEA Results. The phase FL under different DC excitations are compared in Fig. 2 (c). It is obvious that the DCFW can adjust the amplitude of the phase FL effectively, i.e., from 0.042Wb to 0.053Wb. Fig. 2 (d) shows the different phase current angles verse to the average torques under the rated current. The optimal current angle is not 0 due to the salient rotor. And the growth rate of the torque decreases gradually during the linear increase of the DC current because of the local saturation.

[1] A. El-Refaie and M. Osama, "High Specific Power Electrical Machines: A System Perspective," *China Electrotechnical Society Transactions on Electrical Machines and Systems,* vol. 3, no. 1, pp. 88-93, 2019. [2] Z. Q. Zhu and D. Howe, "Electrical Machines and Drives for Electric, Hybrid, and Fuel Cell Vehicles," *Proceedings of the IEEE,* vol. 95, no. 4, pp. 746-765, 2007. [3] X. Y. Wang, S. J. Xu, C. P. Li, and X. Li, "Field-Weakening Performance Improvement of the Yokeless and Segmented Armature Axial Flux Motor for Electric Vehicles," *Energies,* vol. 10, no. 10, Oct 2017, Art no. 1492. [4] M. Kasim and J. Fletcher, "Mechanical Field Weakening Techniques for an Axial Flux Machine," in *2019 International Conference on Sustainable Energy Engineering and Application (ICSEEA)*, 23-24 Oct. 2019 2019, pp. 7-15. [5] D. Xu, M. Lin, X. Fu, L. Hao, W. Zhang, and N. Li, "Cogging Torque Reduction of a Hybrid Axial Field Flux-Switching Permanent-Magnet Machine With Three Methods," *IEEE Transactions on Applied Superconductivity,* vol. 26, no. 4, pp. 1-5, 2016. [6] N. Li, J. Zhu, M. Lin, G. Yang, Y. Kong, and L. Hao, "Analysis of Axial Field Flux-Switching Memory Machine Based on 3-D Magnetic Equivalent Circuit Network Considering Magnetic Hysteresis," *IEEE Transactions on Magnetics,* vol. 55, no. 6, pp. 1-4, 2019.

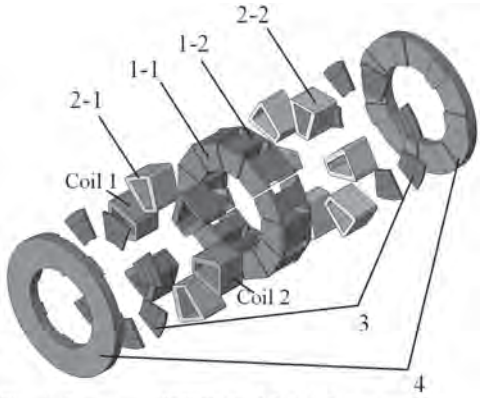

Fig. 1. Structure of HEYASAM. 1-1 Stator module with large teeth. 1-2 Stator module with small teeth. 2-1 AWs. 2-2 DCFWs. 3- PMs. 4-Rotor core.

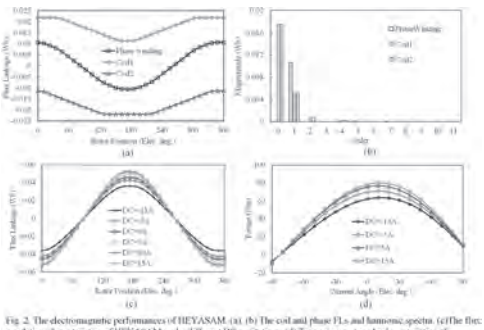

Fig. 2. The electromagnetic performances of HEYASAM. (a), (b) The coil and phase FLs and harmonic spectra. (c)The flux regulation characteristics of HEYASAM under different DC excitations. (d) Torque-current angle characteristics of HEYASAM under different DC excitations.

JOB-03. Ultra-Lightweight Motors for Urban Air Mobility Propulsion. *S. Duggan*[1], G. Cooke[1], D.J. Powell[1] and S.D. Calverley[1] *1. Magnomatics Ltd, Sheffield, United Kingdom*

Urban air mobility is expected to play a large part in future transportation, where conventional aircraft will be superseded by thousands of highly connected automated airborne vehicles [1]. One of the key barriers to success is the development of reliable lightweight propulsion motors. The conventional method of light-weighting motors uses mechanical gearing to increase motor speed and reduce torque output, however, in this sector the relatively low reliability of the gearbox and potential for catastrophic failure by jamming preclude this method. This paper describes the advances behind a special dual rotor, magnetically geared motor [2] designed for urban air mobility applications. The mechanical gearbox is replaced by a magnetic gearbox that is mechanically and magnetically integrated into the motor itself. The main motor operates at high speed and benefits from the low torque and low motor mass, the integrated magnetic gear reduces output rotor speed and provides a corresponding increase in output torque created by virtue of the extremely high airgap magnetic shear stress available. The magnetic design of this integrated motor is discussed and an exemplar 370Nm, 212mm OD machine is presented. The corresponding thermal design is discussed and loss models linking this with the electromagnetic design are detailed. The design is complimented with advances in mixed material structural design where composites are used within the non-magnetic structural parts. By combining the light-weighting gear effect without the adverse effect on reliability an air-cooled motor with a specific continuous torque density >30Nm/kg is created which is ~30% improvement on the leading competing technology.

[1] The Future of Vertical Mobility. Porsche Consulting, 2018. [2] Atallah, K. et al. "A novel 'pseudo2 direct-drive brushless permanent magnet machine", Proc. of IEEE Intermag, 4-8th May 2008, Madrid, Spain

JOB-04. Rotating Permanent Magnet Disc for Wireless Charging Autonomouns Guided Vehicles. *E. de Melo Henriques*[1], J. Lu[1] and S. Stegen[1] *1. School of Engineering, Griffith University, Brisbane, QLD, Australia*

Autonomous Guided Vehicles (AGVs) have been implemented in modern warehouse aiming for a full automation environment[1]. As any other electric vehicle, AGV requires fast charging of batteries to maintain the workflow on busy warehouses[2], especially when online sales have increased during the pandemic. Wireless charging systems (WCS) can be applied to recharge AGV with low maintenance cost while guarantying the safety of the workforce[3, 4]. However, wireless power transfer (WPT) loss efficiency on large air gaps due to leakage magnetic flux and to the increase of impedance on primary side[5], which require to apply a compensation circuit to optimize the power transfer[6]. This project proposes a novel model for WPT utilizing a DC motor of 2750 RPM and 300 W to spin a disc that has surface mounted permanent magnets (PMs), Figure 1. This disc is composed by 12 square and 12 circular PM, placed in pairs in the disc radius line, with the square PM near the end of the disc and the circular PM 5 mm from the square PM. The adjacent PM pairs have opposite polarity, so that when a coil is placed near this spinning PM disc, the magnetic field will oscillate inducing current on the receiver coil. An investigation on how much current can be harvest through this model is being conducted, also correlating the air gap between PM disc and receiver coils. In addition, the rotation of the PM disc and the induced current on receiver is being evaluated and an analysis of the optimum RPM speed for WPT is being conducted. Finite Element Method (FEM) simulations are being executed and analyzed, currently, a 2D model simulates the movement of the PMs over the coil, which resulted in an alternating induced current of 9A (peak). The main advantage of this model is utilizing the existing magnetic field of PM material, discarding the necessity of applying power to the transmitter, thus eliminating the parasite impedance losses. The system efficiency is expected to be improved in relation to existing WCS.

[1] P. R. Wurman, R. D'Andrea, and M. Mountz, "Coordinating hundreds of cooperative, autonomous vehicles in warehouses," The AI magazine, vol. 29, no. 1, pp. 9-19, 2008. [2] M. M. Oliveira, J. P. M. Galdames, K. T. Vivaldini, D. V. Magalhaes, and M. Becker, "Battery state estimation for applications in intelligent warehouses," in 2011 IEEE International Conference on Robotics and Automation, 2011, no. Conference Proceedings: IEEE, pp. 5511-5516, doi: 10.1109/ICRA.2011.5980548. [3] T. Bouanou, H. E. Fadil, and A. Lassioui, "Analysis and Design of Circular Coil Transformer in a Wireless Power Transfer System for Electric Vehicle Charging Application," in 2020 International Conference on Electrical and Information Technologies (ICEIT), 2020, no. Conference Proceedings: IEEE, pp. 1-6, doi: 10.1109/ICEIT48248.2020.9113190. [4] C. Panchal, S. Stegen, and J. Lu, "Review of static and dynamic wireless electric vehicle charging system," Engineering science and technology, an international journal, vol. 21, no. 5, pp. 922-937, 2018, doi: 10.1016/j.jestch.2018.06.015. [5] E. D. M. H. J. L. S. Stegen, "Wireless-power transfer for AGVs: a comparison between ferrite and amorphous core " presented at the Australasian Universities Power Engineering Conference, Tasmania, Australia, 2020. [6] W. Zhang, S.-C. Wong, C. K. Tse, and Q. Chen, "Design for Efficiency Optimization and Voltage Controllability of Series-Series Compensated Inductive Power Transfer Systems," IEEE transactions on power electronics, vol. 29, no. 1, pp. 191-200, 2014, doi: 10.1109/TPEL.2013.2249112.

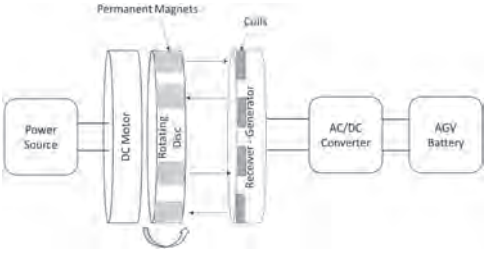

Schematic of proposed Rotating Wireless Power Transfer, utilizing a DC motor with a surface mounted magnetic disc coupled to the shaft.

JOB-05. Research on Interturn Short-circuit Characteristic of the High-speed Permanent-magnet Machine with Gramme-ring Windings.

N. Meng[1], Y. Wan[1], L. Zhu[1] and Y. Jia[2] *1. Nanjing University of Science and Technology, Nanjing, China; 2. AVIC Nanjing Engineering Institute of Aircraft System, Nanjing, China*

Due to the merits of high power density and efficiency, surface-mounted high-speed permanent-magnet machine (HSPMM) is regarded as a competitive candidate for high-speed application of aviation. However, the rotor flux cannot be disengaged when a short circuit (SC) is initiated, so a large interturn SC current of more than ten times of the rated current is usually generated, which seriously threatens the reliability of motor[1]. Recently, numerous studies have been reported concerning the interturn SC fault suppression methods for concentrated winding fault-tolerance PMM[2]. The arrangement sequence of wires was optimized to make the back potential of each coil the same, so that the influence of the position of shorted turns on the value of interturn SC current was eliminated[3]. With use of a new vertical strip windings, the interturn SC current was restrained near rated current[4]. Besides, the typical control methods of injecting flux-weakening current and shorting winding terminals are also investigated to limit the interturn SC current[5]. However, the healthy windings will be sacrificed and a large phase SC current may also be introduced, if shorting all the winding terminals. And the effectiveness of injecting flux-weakening current is extremely dependent on the high-accuracy and rapid detection technology, which is also a great challenge for HSPMM[6,7]. This paper found the characteristic of strong interturn SC fault tolerance of the Gramme-ring-winding HSPMM, providing a solution for HSPMM to high-reliability application. The shorted turns wound around the stator yoke have a very large inductance, so the interturn SC current can be tremendously decreased. For this motor, the analytical models of the interturn SC current and inductance are established. And the principles for characteristic of strong interturn SC fault tolerance is revealed. Then the influences of the position and turns of interturn shorted coil are studied. The analytical models are finally verified by finite-element method. The figures show the cross section of Gramme-ring-winding HSPMSM with one turn of shorted coil and the waveform of winding current. As can been, the interturn SC current is just little higher than rated current.

[1] J. Urresty, J. Riba, L. Romeral and H. Saavedra, "Analysis of demagnetization faults in surface-mounted permanent magnet synchronous with inter-turns and phase-to-ground short-circuits," 2012 XXth International Conference on Electrical Machines, 2012, pp. 2384-2389. [2] Y. Xu, Z. Zhang, Y. Jiang, J. Huang and W. Jiang, "Numerical Analysis of Turn-to-Turn Short Circuit Current Mitigation for Concentrated Winding Permanent Magnet Machines With Series and Parallel Connected Windings," IEEE Transactions on Industrial Electronics, vol. 67, no. 11, pp. 9101-9111, Nov. 2020. [3] Z. Sun, J. Wang, D. Howe and G. Jewell, "Analytical Prediction of the Short-Circuit Current in Fault-Tolerant Permanent-Magnet Machines," IEEE Transactions on Industrial Electronics, vol. 55, no. 12, pp. 4210-4217, Dec. 2008. [4] P. Arumugam, T. Hamiti, C. Brunson and C. Gerada, "Analysis of Vertical Strip Wound Fault-Tolerant Permanent Magnet Synchronous Machines," IEEE Transactions on Industrial Electronics, vol. 61, no. 3, pp. 1158-1168, March 2014. [5] G. Choi and T. M. Jahns, "PM Synchronous Machine Drive Response to Asymmetrical Short-Circuit Faults," IEEE Transactions on Industry Applications, vol. 52, no. 3, pp. 2176-2185, May-June 2016. [6] A. J. Mitcham, G. Antonopoulos, and J. J. A. Cullen, "Implications of shorted turn faults in bar wound PM machines," IEE Proceedings - Electric Power Applications, vol. 151, pp.651-657, 2004. [7] J. G. Cintron-Rivera, S. N. Foster and E. G. Strangas, "Mitigation of turn-to-turn faults in fault tolerant permanent magnet synchronous motors," IEEE Transactions on Energy Conversion, vol. 30, no. 2, pp. 465-475, June 2015.

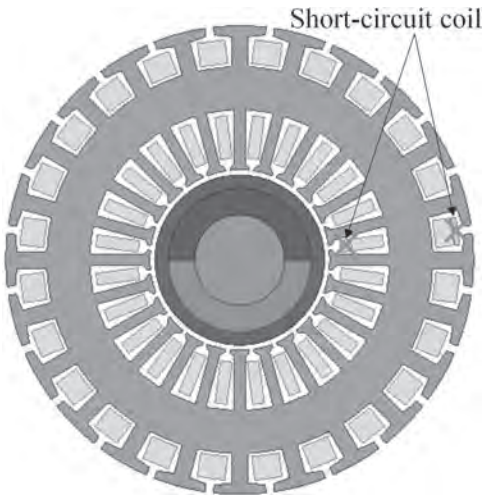

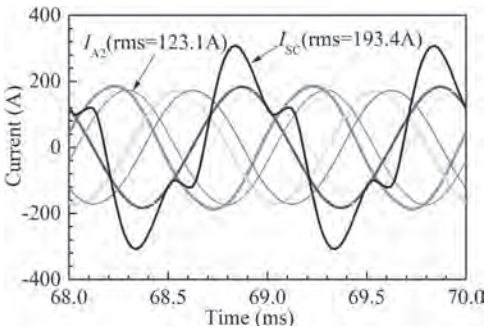

JOB-06. Research on Optimization Design of Low Speed and High Torque Motor with Single Hybrid Rotor and Double Stator Based on Surrogate Models. Z. Zhang[1,2], *S. Yu*[1], X. Li[1] and F. Zhang[1] *1. Shenyang University of Technology, Shenyang, China; 2. Dalian SMART DRIVE Co., Ltd., Dalian, China*

Low-speed and high-torque motors (LSHTMs) are widely used in many fields and become one of the current research hotspots of scholars at home and abroad [1-2]. In order to make full use of the internal space and increase the torque density of the traditional LSHTM, a new structure with double stator is proposed. The schematic diagram of the proposed motor structure is shown in Fig.1. It can be known that a hybrid structure of permanent magnet and reluctance is used for the rotor. In addition, in order to avoid the magnetic coupling of the inner and outer unit motors, a magnetic isolation ring is added between the permanent magnet rotor and the reluctance rotor, which brings great convenience to the control of the motor. The stator windings of the inner and outer unit motors are connected in parallel, and can be operated as an individual or a whole according to different load requirements. The structure parameters of this kind of motor are numerous and affect each other, which increases the difficulty of motor optimization design. This paper takes the improvement of average torque and the reduction of torque ripple as the optimization goals, and studies deeply on the optimization design of this kind of motor. Firstly, the sensitivity analysis of the key parameters of the motor is carried out by using the Latin hypercube design and the analysis of variance method to determine the optimization design variables of the motor. On this basis, a high-precision surrogate model of this kind of motor is constructed and simplified by dynamic surrogate model technology. Then, an optimization algorithm combining genetic algorithm and sequential subspace optimization method is proposed in order to improve the optimization accuracy and reduce the optimization cycle, the flow chart of the optimization algorithm is shown in Fig.2. Finally, based on the surrogate model and optimization algorithm, the motor is designed and optimized, and the correctness and effectiveness of the theoretical research method in this paper are verified by comparing the results before and after optimization.

1. M. Onsal, B. Cumhur, Y. Demir, E. Yolacan and M. Aydin, "Rotor Design Optimization of a New Flux-Assisted Consequent Pole Spoke-Type Permanent Magnet Torque Motor for Low-Speed Applications," IEEE Transactions on Magnetics, vol. 54, no. 11, pp. 1-5, Nov. 2018. 2. C. Xia, B. Ji and Y. Yan, "Smooth Speed Control for Low-Speed High-Torque Permanent-Magnet Synchronous Motor Using Proportional–Integral–Resonant Controller," IEEE Transactions on Industrial Electronics, vol. 62, no. 4, pp. 2123-2134, April 2015.

Schematic diagram of the proposed LSHTM with single hybrid rotor and double stator

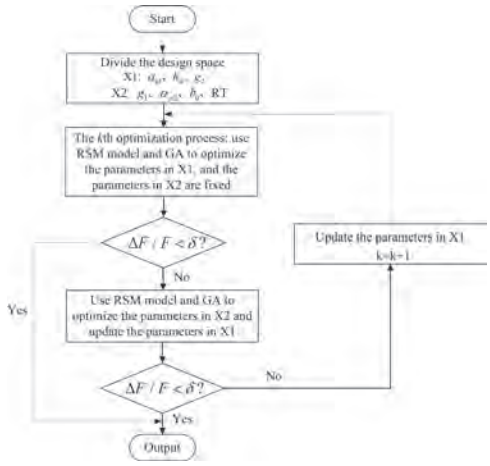

Flow chart of optimization design

JOB-07. Full Bridge Converter Control of a PM-SRM with Extended Conduction Strategy. *F. Kucuk*[1,2] and T. Nakamura[1] *1. Electrical Engineering, Kyoto University, Kyoto, Japan; 2. Electrical and Mechanical System Eng., Kyoto University of Advanced Science, Kyoto, Japan*

1. Introduction An Asymmetric Half Bridge (AHB) converter is a traditional converter topology for Switched Reluctance Motors (SRMs) but it has not been commercialized so far because of its limited use. A Full Bridge (FB) converter is a commercialized one and is widely used in AC motor control. FB control of the SRM was investigated in [1]–[4] and some torque control strategies were also presented in [5], [6]. However, torque control in these works were not effective because the FB converter was used with a limited conduction angle to avoid a short-circuit. Recently, a PM-SRM has been introduced to increase the SRM efficiency without losing much from low-cost feature [7]. However, the AHB converter is still an issue as mentioned above. In this study, a 6/4 PM-SRM has been controlled with a 3-phase FB converter while applying an extended conduction strategy to improve torque control performance. 2. FB control of PM-SRM Hysteresis controller is used for the torque control, whose input is defined by the error between PI controller and estimated motor torque (Fig 1a). A modified delta connection is required for the FB converter to achieve independent phase control as in the AHB converter (Fig. 1b). The dashed line in the figure displays current flow of ph A when T_1 and T_4 are made ON. Unlike the AHB converter, the FB converter normally cannot operate with a phase conduction over 30° and thus it is insufficient to suppress torque ripples in most cases. This can be overcome by shifting conduction period of upper switches and lower switches in such a way that total phase conduction is extended beyond the limitation. For the analysis, the conduction period of FB converter is set 10°-40° for upper switch (T_1) and is set 5°-35° for lower switch (T_4) whereas other phases are obtained by shifting conduction period of ph A by ±30°. Fig 2 displays the results of both converter cases for a reference speed of 500 rpm and a load of 10 Nm. As seen in the figure, torque ripples are properly suppressed with FB converter as in the AHB converter.

[1] A. C. Clothier and B. C. Mecrow, IEE Conf. Publication, no. 444, pp. 351–355, (1997). [2] J. W. Ahn and S. G. Oh, IEEE Trans. Ind. Appl., vol. 35, no. 5, pp. 1067–1075, (1999). [3] Y. C. Kim, Y. H. Yoon, and B. K. Lee, IEEE Annu. Power Electron. Spec. Conf., (2006). [4] P. Somsiri and K. Tungpimonrut, Int. Conf. Electr. Mach. Syst., pp. 1563–1568, (2007). [5] K. Tungpimolrut and S. Kachapornkul, 15th Int. Conf. Electr. Mach. Syst., pp. 1–5, (2012). [6] M. Elamin and Y. Yasa, IEEE Int. Electr. Mach. Drives Conf., pp. 1–7, (2017). [7] F. Kucuk and T. Nakamura, 13th Int. Conf. on Electr. Mach., pp. 2318–2322, (2018).

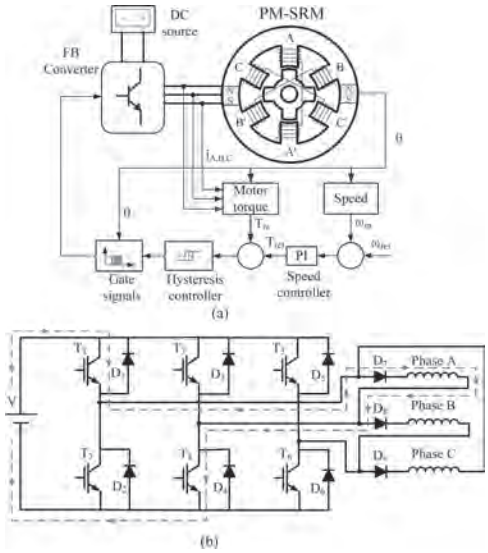

Fig 1. PM-SRM drive. a) Speed and torque control, b) FB converter and modified delta winding.

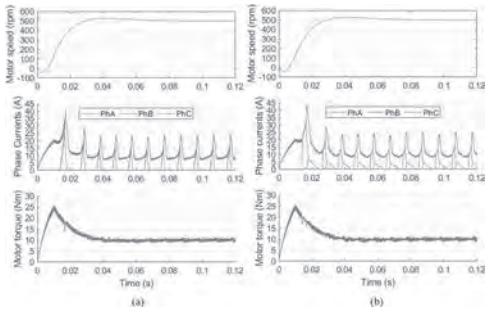

Fig 2. Analysis results for PM-SRM drive. a) with AHB converter, b) with FB converter.

JOB-08. Design of Litz Wires for a Slotless High-speed Permanent Magnet Motor with Gramme-ring Windings. *L. Zhu*[1], N. Meng[1], Y. Wan[1] and Q. Li[1] *1. Nanjing University of Science and Technology, Nanjing, China*

Recently an increasing demand emerges for high-speed permanent magnet motor (HSPMM) in fuel cell compressor application. Overheating is thought as one of the biggest causes for the failure of HSPMM. This paper presents a slotless Gramme-ring-winding HSPMM, so as to reduce the rotor eddy-current loss caused by stator slotting. Besides, it is convenient to fix the slotless windings. However, exposed to the alternating magnetic field of airgap, large AC loss will be generated in the slotless windings. Litz wire, with a high number of individually insulated, small gauge strands separated into bundles and continuously transposed, is employed to control the AC losses associated with high-frequency operation in this paper. Considering the influence of magnetic field of airgap, the analytical model for losses of the litz wire was built based on an external-rotor motor [1]. The components of the losses for litz wire was analyzed in an air-core pulsed alternator, and the diameter was optimized to minimize the loss[2]. Besides, the pitch of litz wire was thought has a great influence on the loss, and the design method of pitch was provided[3]. In addition, the impacts of the litz wire strand shape, such as circular, square and rectangular, were compared on AC copper loss of the HSPMM[4]. Due to the complex structure of litz wire, the calculation method of the equivalent thermal conductivity was given, based on the Gasar porous metal materials. This paper first analyzes the loss of the litz-wire gramme-ring winding based on the FEA methods, considering the different magnetic field of airgap and the outer slots of stator. Then the analytical model for the loss of litz-wire gramme-ring winding is established, and the diameter and shape are optimized to minimize the loss. After that, the thermal analysis model of the litz-wire gramme-ring winding is investigated, and the temperature rise is calculated. Moreover, the influence of diameter and shape of litz wire is also studied. Through the above studies, the design of litz wire is finally provided for the slotless gramme-ring-winding HSPMSM. Fig.1 shows the configuration of the studied motor, and Fig.2 is the distribution of current density in litz wires on different positions.

[1] Martin J, Yoon A, Jin A and Haran K. S, "High-Frequency Litz "Air-Gap" Windings for High-Power Density Electrical Machines". *Elect. Power Compon. Syst.*, vol. 45, pp. 798–805, May 2017. [2] W. Zhao, X. Wang, S. Wu, S. Cui, C. Gerada and H. Yan, "Eddy Current Losses Analysis and Optimization Design of Litz-Wire Windings for Air-Core Compulsators," *IEEE Trans. Plasma Sci.*, vol. 47, no. 5, pp. 2532–2538, May 2019. [3] Xu Tang and C. R. Sullivan, "Stranded wire with uninsulated strands as a low-cost alternative to litz wire," *in IEEE Power Electron. Specialists Conf. (PESC)*, 2003, pp. 289–295. [4] M. S. C. Pechlivanidou and A. G. Kladas, "Litz Wire Strand Shape Impact Analysis on AC Losses of High-Speed Permanent Magnet Synchronous Motors," *in Proc. IEEE Workshop Elect. Mach. Design, Control Diagnosis*, 2021, pp. 95-100. [5] X. Liu, D. Gerada, Z. Xu, M. Corfield, C. Gerada and H. Yu, "Effective Thermal Conductivity Calculation and Measurement of Litz Wire Based on the Porous Metal Materials Structure," *IEEE Trans. Ind. Electron.*, vol. 67, no. 4, pp. 2667-2677, April 2020.

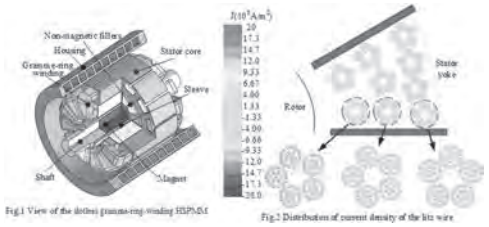

Fig.1 View of the slotless gramme-ring winding HSPMM

Fig.2 Distribution of current density of the litz wire

JOB-09. Performance Anaysis of Semi-Cloased C-Core Permanent Magnet Transverse Flux Generator. A. Muhammad[1], F. Khan[1], *B. Ullah*[1], M. Yousuf[1] and S. Hussain[1] *1. Electrical and Computer Engineering, COMSATS University Islamabad, Abbottabad Campus, Abbottabad, Pakistan*

Transverse flux machines (TFMs) are made up of armature coils that are wound in the circular direction and surrounded by armature cores. This configuration enables machines to be designed for multi-pole structures while maintaining a simple coil geometry regardless of the pole count. As a result, they generate more torque and power density than most machines with windings wound around teeth and inserted into slots [1]. However, TFMs continue to face manufacturing difficulties with their multi-pole rotor assembly due to the small and numerous permanent magnets (PM). Thus, a PM transverse flux generator is developed with less number of magnets on the rotor in comparison with conventional surface-mounted magnet rotor [2] while generating nearly the same power density at the same size and excitation conditions. This topology consists of 8 semi-closed stator cores having pole shoe to enhance flux linkage. Using viable space in stator cores, double coil is used in armature winding to enhance back-emf and make it fault-tolerant. The rotor consists of only PMs, 16 in number, placed in aluminum housing shown in Fig. 1a. Production complexity and rotor mass are reduced, resulting in a greater active power density. A three-dimensional finite-element model is created to validate the design's feasibility, and its electromagnetic performance is evaluated. No-load flux linkage, cogging torque, and back-emf are computed using 3-D FEM. Meanwhile, for load analysis, output current, output power, losses, efficiency and power density at various loads are investigated. FEM analysis indicates that by using this topology, 1.5 times better power density can be achieved by reducing stator cores and rotor magnets by 33%. Furthermore, leakage flux from inactive magnets in the proposed machine is significantly lower than in conventional and gives better efficiency as shown in Fig. 1b. Fabricated parts of PM

transverse flux generator is shown in Fig. 2a while Fig. 2b shows the back-emf waveform for both tested and simulated. The experimental results for back- emf validate the FEM analysis previews well.

[1] R. Kumar et al., “A Review on Transverse Flux Permanent Magnet Machines for Wind Power Applications”, IEEE Access, vol. 8, pp. 216543-216565, 2020. [2] A. Pourmoosa and M. Mirsalim, “A Transverse Flux Generator with a Single Row of Permanent Magnets: Analytical Design and Performance Evaluation”, IEEE Transactions on Industrial Electronics, vol. 66, no. 1, pp. 152-161, 2019.

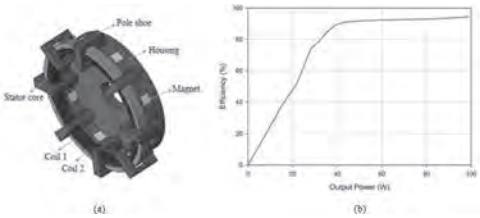

Figure 1 8/16 PMTFG with Double Coil (a) Simulated Model (b) Efficiency Verses Output Power

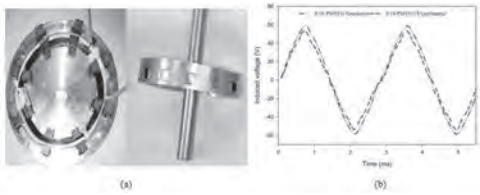

Figure 2 Construction of Prototype (a) Hardware Parts (b) Back EMF

Session JOC
LINEAR MOTORS, ENERGY HARVESTING AND VIBRATION ANALYSIS

Amr Adly, Chair
Cairo University, Giza, Egypt

CONTRIBUTED PAPERS

JOC-01. Design Optimization and Performance Investigation of a Novel Permanent-Magnet Synchronous Linear Motor with Traveling Magnetic Electromagnetic Halbach Array. *W. Qin[1] 1. School of Electrical Engineering, Beijing Jiaotong University, Beijing, China*

I. INTRODUCTION Linear permanent-magnet synchronous motors (LPMSMs) offer many advantages over rotary motors in some special applications, such as railway transportation and robotic systems [1-3]. However, the slotted topologies of LPMSMs suffer from the slot and end effects. A solution is to use ironless topologies of LPMSMs due to its unique features such as high dynamic performance and zero cogging force [4-6]. Although air-core LPMSMs are widely used in precision applications, they basically suffer from low developed thrust and thrust ripple, of which lead to undesirable performance [7, 8]. In order to increase the thrust density and decrease the force ripple, a novel air-cored primary named traveling magnetic electromagnetic Halbach array (TMEHA) was proposed for LPMSM. II. MACHINE TOPOLOGIES The configuration of the LPMSM with TMEHA is shown in Fig. 1(a). The main structure of this air-cored LPMSM includes one mover and one stator. The TMEHA was proposed to LPMSM as the primary windings, of which is composed of three-phase windings. Three phase coils are displaced symmetrically at every 120 electrical angle and the current waveform in the phases is a 120 wave. Each phase winding consists of two coils and the coils are divided into two general arrangements, i.e., vertical-piece and horizontal-piece arrangements. By placing the primary windings as TMEHA, the higher flux density and more sinusoidal magnetic field in the air-gap can get as possible than rectangular coil forms, so that the thrust density is increased and ripple decreased. III. RESULTS AND VALIDATION By using Space Harmonics method and 2D-FEA, the parameter optimization design of the proposed LPMSM is conducted, and the performance comparison with a rectangle coils is also carried out to prove the TMEHA superiority of the proposed design, shown as in Fig.2. Currently, we have designed and established a PMLSM with TMEHA prototype in laboratory, shown as in Fig.1 (b), the FEA and analytical results will be validated by the experiment results. The full paper will provide a more in-depth analysis and optimize parameters that affect performance in forces and ripple values.

[1] M. Wang, L. Li, and D. Pan, IEEE Transactions on Industrial Electronics, vol. 62, no. 11, pp. 6845-6854(2015). [2] F. Cui, Z. Sun, W. Xu and Y. Liu, CES Transactions on Electrical Machines and Systems, vol. 4, no. 2, pp. 142-150(2020). [3] K. Shin, H. Cho and S. Lee, IEEE Transactions on Magnetics, vol. 53, no. 6, pp. 1-4(2017). [4] S. G. Min, B. Sarlioglu, IEEE Transactions on Industrial Electronics, vol. 65, no. 2, pp. 1855-1864 (2018). [5] Z. Yao, J. Zhao and J. Song, IEEE Transactions on Industrial Electronics, pp. 1-1(2020). [6] A. Mohammadpour, A. Gandhi and L. Parsa, IET Electric Power Applications, vol. 6, no. 5, pp. 253-259(2012). [7] J. Seok-Myeong, L. Sung-Ho, IEEE Transactions on Magnetics, vol. 38, no. 5, pp. 3264-3266(2002). [8] Y. Shen, Q. Lu and H. Li, IEEE Transactions on Industrial Electronics, vol. 65, no. 2, pp. 1837-1845(2018).

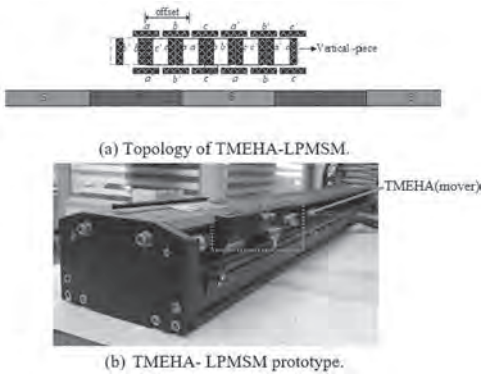

Fig.1 Proposed LPMSM with TMEHA configuration

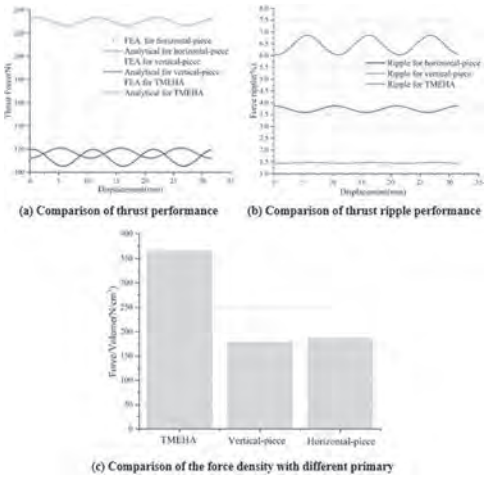

Fig.2. Comparison of the performances

JOC-02. Withdrawn

JOC-03. Key steps in designing a micro thermomagnetic generator. *M. Almanza*[1], N. Belkadi[4], E. Fontana[3], D. Nguyen Ba[1,2], T. Devillers[3], L. Becerra[2], N. Dempsey[3], M. Marangolo[2], F. Parrain[4] and M. LoBue[1] *1. Université Paris-Saclay, ENS Paris-Saclay, CNRS, SATIE, Gif-Sur-Yvette, France; 2. Sorbonne Université, CNRS, Institut des NanoSciences de Paris, Paris, France; 3. Université Grenoble Alpes, CNRS, Grenoble INP, Institut Néel, Grenoble, France; 4. Université Paris-Saclay, CNRS, Centre de Nanosciences et de Nanotechnologies, Palaiseau, France*

Internet of Things devices prompt a rising demand for autonomous and compact power supply generators to sustain low-power wireless sensor nodes. Due to the ubiquity of waste heat in buildings and urban environments, low-grade heat sources are very attractive for applications. Thermomagnetic

generators (TMG) can be small and autonomous. Ahmim's TMG [1] produces 4.2 μW (0.24 mW/cm^3 over a 35°C temperature difference. While this device exploits direct thermal contact with both reservoirs, a key element of a thermal device [2], the output power is penalized by a sub-Hertz working frequency. Khol's TMG [3] produces 118 mW/cm^3 at 84 Hz but over a larger temperature difference of 138°C. Their use of 5 μm thick Heusler Alloy films, compared to a 250 μm thick plate of LaFeSi by Ahmim, is an important factor to explain the different in the working frequency. We aim to explore the possibility to use thin films in Ahmim's TMG while keeping its low temperature difference capability. Ahmim's TMG has specific characteristics. Firstly, it needs to have a freestanding magnetocaloric film of several micrometers. Our recent work on Gd film deposition has shown a 17 μm film with significant magnetocaloric effect [4]. Secondly, it needs to have a magnetic field source that gives a maximum field variation but also confines the magnetic field in order to reduce the film displacement. By combining Gd films and high performance NdFeB micro-magnets [5], [6] with our design experience on macro devices (Fig.1), we will discuss the key steps of the design, e.g., the spring characteristics to achieve self-oscillating micro-devices. Several parameters need to be optimized, such as the micro-magnet pattern, the air gap and Gd film thickness. 3D numerical simulations of the magnetic force as a function of the material position and temperature (Fig. 2), which are being used to optimize the system design, will be discussed in detail. With our proposed design, if we assume a 50 Hz working frequency, there is 5mW of mechanical energy available.

[1] S. Ahmim, M. Almanza*, M. LoBue*, *IEEE Trans. Magn.*, pp. 1–1, (2020), [2] K. Klinar, T. Swoboda, and A. Kitanovski, *Adv. Electron. Mater.*, vol. 7, no. 3, p. 2000623, (2021), [3] M. Gueltig, F. Wendler, *M. Kohl.*, *Adv. Energy Mater.*, vol. 7, no. 5, p. 1601879, (2017), [4] D. Nguyen Ba, Y. Zheng, M. LoBue, *Phys. Rev. Appl.*, vol. 15, no. 6, p. 064045, (2021), [5] N. M. Dempsey, A. Walther, O. Gutfleisch, *Appl. Phys. Lett.*, vol. 90, no. 9, p. 092509, (2007), [6] F.O. Keller *et al.*, "Batch fabrication of 50 μm thick anisotropic Nd-Fe-B micromagnets," submitted.

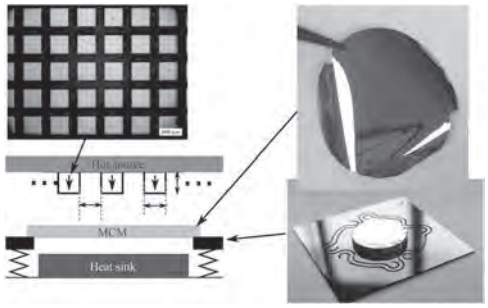

Fig. 1 Assembly of a TMG with NdFeB micro-magnets and a free standing gadolimium film mounted on the spring

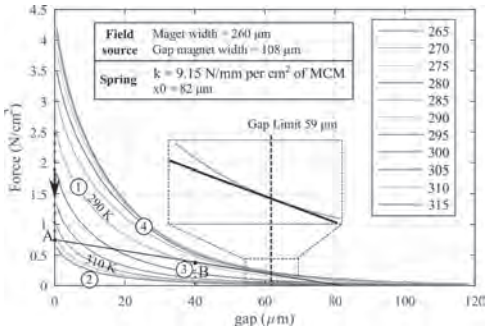

Fig. 2 Simulation of the magnetic force, spring recall force (black line), targeted cycle (dots)

JOC-04. Research on vibration reduction method of switched reluctance motor with amorphous alloy cores based on inverse-magnetostriction effect. T. Ben[1,2], *J. Wang*[1], L. Chen[1] and H. Nie[1]
1. College of Electrical Engineering and New Energy, China Three Gorges University, Yichang, China; 2. State Key Laboratory of Reliability and Intelligence of Electrical Equipment, Hebei University of Technology, Tianjin, China

I Introduction Due to the high-power density, simple structure and low cost, switched reluctance motors with amorphous alloy cores (SRMA) are widely applied in electric vehicles [1]. However, its development is limited by the vibration causing by the radial electromagnetic force. This paper proposes a new method to reduce the vibration of SRMA based on the inverse-magnetostriction effect. II Vibration reduction method based on inverse-magnetostriction effect The research in amorphous alloy motor is mainly about the evaluation of core loss and the literature involves vibration is rare [2]. The vibration mechanism of amorphous stator core was revealed through considering the Maxwell stress and magnetostriction stress [3]. However, the effective damping methods have not been involved and the inverse-magnetostriction effect was neglected. A method of vibration reduction for the SRMA is propose in this paper. First, compressive stress in the radial direction is applied to the stator teeth, because the magnetic permeability of the magnetic material will decrease under the action of compressive stress in the same direction. Then, the magnetic permeability is calculated by the nonlinear relationship with the stress. After the definition of the relative permeability of the stator core, the magnetic field distribution inside the motor is obtained. Second, the magneto-mechanical coupling model is established by combining the electromagnetic stiffness matrix and mechanical stiffness matrix to calculate the stress distribution of the stator core as shown in Fig.1(a-b). Third, the vibration reduction effect of the model is verified by the finite element simulation. III Results and discussion The simulation results of the sampling point of the stator teeth is calculated as shown in Fig.1(c-d). And the radial flux density of air gap (B_n) and radial electromagnetic force (F_n) is reduced by 13% and 20% respectively, which shows that the method can effectively reduce the radial electromagnetic force and has a certain damping effect.

[1]Bostanci E, Moallem M, Parsapour A, et al. Opportunities and Challenges of Switched Reluctance Motor Drives for Electric Propulsion: A Comparative Study[J]. Transportation Electrification IEEE Transactions on, 2017, 3(1):58-75. [2]S. Kahourzade, N. Ertuhrul, W. Soong, Loss analysis and efficiency improvement of an axial-flux PM amorphous magnetic material machine, IEEE Trans. Ind. Electron. 65 (7) (2018)5376–5383. [3]Xu X, Han Q, Qin Z, et al. Analytical methods for the radial electromagnetic vibration of stator in permanent magnet motors with an amorphous alloy core[J]. Mechanical Systems and Signal Processing, 2020, 145(3):106909.

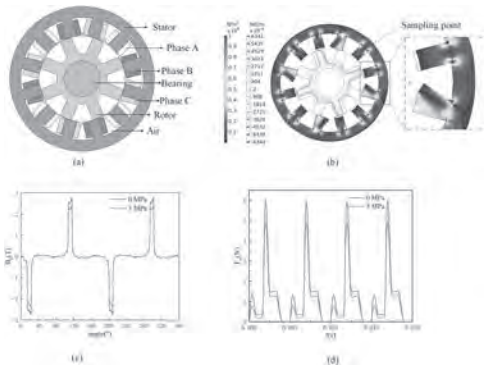

Fig.1. (a) Schematic diagram of the model, (b) Deformation of the stator core,(c) Distribution of radial flux density in air gap,(d) Radial electromagnetic force under different stresses.

JOC-05. Design and Analysis of Modular C-core Moving Magnet Linear Oscillating Actuator for Miniature Compressor Application.
S. Khalid[1], F. Khan[1], Z. Ahmad[2] and *B. Ullah*[1] *1. Electrical and Computer Engineering, COMSATS University Islamabad, Abbottabad Campus, Abbottabad, Pakistan; 2. Electrical, School of Electrical Engineering, Southeast University, Nanjing, China*

Tubular linear oscillating actuators (LOAs) which perform a linear reciprocating motion with a certain working stroke are widely applied to compressors, artificial hearts, and robotic arms, etc., due to their high power density and high efficiency. However, the LOAs have disadvantages of high flux leakage, low thrust force density, and complex fabrication which degrade the performance as well as increase the cost. To overcome these aforementioned demerits, a miniature tubular moving magnet linear oscillating actuator (MT-MMLOA) that operates on the principle of electromagnetic actuation is proposed. The proposed LOA consruction comprises two main parts: the stator and the mover as shown in Fig. 1(a). In this topology, the stator assembly is composed of a modular C-core structure along with a separator to prevent flux cancellation, and the axially magnetized permanent magnets (PMs) are accommodated by the mover assembly that contributes to high thrust force generation and presents a less costly actuator compared to the conventional actuator design. The CAD model of the proposed topology is shown in Fig. 1(b). The fabricated model of MT-MMLOA is displayed in Fig. 1(c). The finite element analysis is performed and validated experimentally as illustrated in Fig. 2(a). The experimental findings are under the tolerance of 5% relative to the simulation-based results. Electromagnetic performance comparison with different topologies proposed earlier in literature is carried out to prove the performance superiority of the proposed design. The results show that the motor constant, which is the performance parameter, is significantly increased from the conventional design shown in Fig. 2(b). The PM volume is reduced, which is cost-effective. The overall volume of the LOA is also reduced due to the reduction in PM volume, which is advantageous for compactness. Furthermore, the proposed topology is simple in structure, inexpensive, and easy to fabricate.

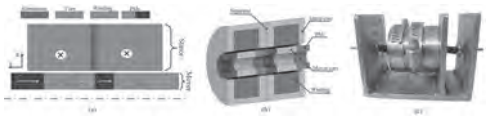

Fig. 1: Different views of proposed MT-MMLOA topology (a) 2D-axisymmetric view (b) Cross-sectional view of the CAD model (c) Experimental setup.

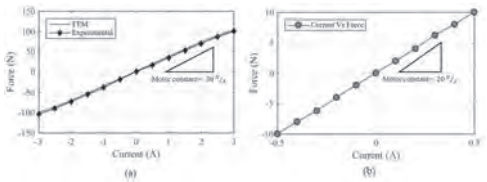

Fig. 2: Thrust force at different values of DC (Performance metrics) (a) Proposed LOA topology (b) Conventional LOA topology.

JOC-06. An Experimental Comparison Between an Ironless and a Traditional Permanent Magnet Linear Generator. *M. Trapanese*[1], V. Franzitta[1], D. Curto[1], C. Nevoloso[1], F. Raimondi[1] and R. Miceli[1] *1. Dipartimento di Ingegneria, Palermo University, Palermo, Italy*

Permanent Magnet Linear Generators (PMLG) are currently studied as a main solution for the conversion of the energy contained in sea waves. Typically, a PMLG consists of an iron-made armature and a moving shaft. Magnets are usually installed on the shaft and the coils on the armature. The moving shaft generates an electromotive force in the coils. Such a machine suffers from a high level of cogging force due to the interfaces between air and iron impairing its overall performance. However, the function of iron in Permanent Magnet (PM) based machines is simply that of driving the flux along a predesigned path. No amplification of the magnetic flux is generated by iron because the flux is generated by the permanent magnet. As a result, a well-tailored design of a PM generator could avoid the use of iron avoiding any permeability difference along with its magnetic circuits and therefore cogging force is completely suppressed. Several questions remain open: how much is the performance of an ironless generator affected by the absence of iron? Which is the comparison between a traditional and an ironless generator? In this paper, we try to address experimentally these questions. We have built two prototypes of PM linear generators that share the same geometry: one of the two is a traditional generator the other is an ironless generator. At first, we have characterized the two machines by measuring the main electrical and mechanical parameters: resistance, reactance, mass, magnetic fields. Secondly, we have performed several open circuit measurements, by measuring cogging force, vibrations, electromotive force when the slider is moving at some given conditions. Finally, we have performed several load tests by measuring cogging force, vibrations, output voltage, current, and output power when the slider is moving at some given conditions. The comparison reported in the paper shows that the performance of the traditional machine is slightly superior in comparison with the ironless one, but an ironless machine does not present any cogging force and is lighter than the traditional one. These features can be a great advantage in the field of sea-wave energy conversion.

JOC-07. Design and Analysis of Parallel Hybrid-Excited Superconducting Linear Motor for High Speed EMS Maglev. *X. Shi*[1], Y. Shen[1], T. Shi[1] and C. Xia[1] *1. College of Electrical Engineering, Zhejiang University, Hangzhou, China*

I Introduction After decades of development, electromagnetic suspension (EMS) maglev plays an important role in high-speed public transportation. The existing EMS maglev always operates with a small air gap (<10 mm), which puts forward very high requirement to railway construction. Besides, the excitation loss on electromagnets is very high, which causes undesirable temperature raise. In order to reduce to excitation loss meanwhile increasing the air gap, this paper proposes a parallel hybrid-excited superconducting linear motor for high-speed EMS maglev. Some of the electromagnets are replaced by high-temperature superconductor (HTS) to realize parallel excitation[1-3]. Compared with the conventional electromagnets, the excitation magnetomotive force (MMF) is much stronger while the excitation loss is almost zero in HTS magnets. II Topology and Results Fig. 1 shows the topology of parallel hybrid-excited superconducting linear motor (PHESLM). The secondary consists of 2 end poles, and 10 main poles which are divided into 3 HTS ones and 7 normal conducting ones. The HTS coils are energized by large constant currents and provide most excitation MMF, while the normal coils are used to control the maglev suspension height by small varying currents. Table.1 shows the FEM results. Taking common EMS with 10mm air gap as the benchmark, PHESLM provides 29.8% larger suspension force under the same condition, with only 42.4% excitation loss. With 20mm and 30mm air gap (but the same stator current), PHESLM provides 96.2% and 76.2% of benchmark suspension force with much suppressed ripples, while common EMS absolutely fails to levitate the maglev. Traction and suspension force can further increase when stator current increases. III Conclusion This paper proposes PHESLM to increase air gap width and reduce excitation loss. Based on FEM results, PHESLM provides enough traction and suspension force compared with common EMS, and implements an excitation loss reduction. Besides, PHESLM operating with large air gap contributes to railway building and improves ride comfort, which performs great potential in high speed maglev.

[1] Lee C Y,Jo J M,Lee J H,et al. Development of superconducting-hybrid magnetic levitation system for high-speed EMS maglev[C]. Electrical Machines and Systems (ICEMS),2013 International Conference on. IEEE,2013. [2] Xu J,Li J,Li G,et al. Design and Preliminary Prototype Test of a High Temperature Superconducting Suspension Electromagnet[J]. IEEE Transactions on Applied Superconductivity,2015,25(2) : 1-6.

[3] Gu C,Liu M,Xing H,et al. Design, construction and performance of an EMS-based HTS maglev vehicle[J]. Physica C Superconductivity & Its Applications,2005,423(1-2) : 37-44.

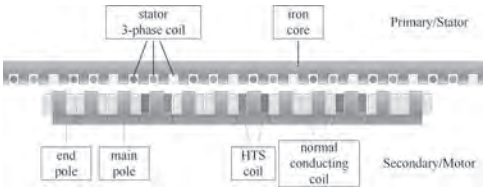

Fig. 1. Topology of PHESLM

	Air Gap Width (mm)	Total Excitation Loss (W)	Suspension Force		Traction Force (N)	
			Mean (N)	Ripple (%)	Mean (N)	Ripple (%)
Common EMS	10	3410.2	37065	0.59	2729	3.3
	20	3410.2	10642	0.25	1973	1.20
PHESLM	10	1948	48143	0.41	2733	4.1
	20	2665.1	35648	0.20	3310	1.3
	30	2799.3	28237	0.11	2064	1.1

Table.1 FEM results of PHESLM under different conditions

JOC-08. A Novel Electromagnetic Energy Harvester Based on Unbalanced Magnetic Compressing and Releasing Mechanism.

Y. Shen[1] and *X. Li*[1] *1. Aalborg University, Aalborg, Denmark*

Electromagnetic and piezoelectric mechanisms, as two main methods to transform the mechanical energy into electrical energy, have been applied widely. However, the output voltage is too low to drive the load in both mechanisms, when the devices are working in low frequency environments [1-2]. Although the cantilever mechanism can increase the frequency for serval to dozens of times, its structure is not compact and may require a large space for placing the cantilever, which would decrease the system power density dramatically and limit the application [3-5]. Compared to the existing energy harvesters with frequency up-mechanisms, the new Electromagnetic Energy Harvester (EMEH) based on unbalanced magnetic compressing and releasing mechanism is compact in its design and is easy to be realized. The proposed EMEH is aimed to solve the low power density and low output voltage problems from low vibration frequency sources. The basic structure of the proposed EMEH is shown in Fig.1. This harvester consists of a vibrated structure based on magnetic levitation and an axially magnetizing ring magnet, which is to be attached to the energy source. The main working principle can be divided into three stages. The first stage in left represents the oscillating magnet is pushed by the magnetic force between itself and the external ring magnet, which is driven by the force from the external vibration source. Continuing this movement, the relative axial distance between the oscillating magnet and the external driving ring magnet would finally reach 0, due to the opposite propelling force between the oscillating magnet and the magnet fixed in the bottom. After passing this breaking point, both the bottom magnet and the external ring magnet will produce force on the oscillating magnet to the opposite direction. Due to this large force and the sudden release mechanism, the oscillating magnet will be oscillating in a high speed between the top magnet and the external ring magnet. Fig.2 shows the open-circuit voltage from figure trigging of the prototype, which indicates a great performance of proposed EMEH.

[1] Kim, H.S., Kim, J.H. and Kim, J., *International journal of precision engineering and manufacturing*, Vol *12*, p.1129-1141 (2011). [2] Tan, Y., Dong, Y. and Wang, X., *Journal of Microelectromechanical Systems*, Vol. *26*, p.1-16 (2017). [3] Zorlu, Ö., Topal, E.T. and Kulah, H., *IEEE Sensors Journal*, Vol. *11*, p.481-488 (2011). [4] Zurbuchen, A., Haeberlin, A. and Pfenniger, A., *IEEE transactions on biomedical circuits and systems*, Vol. *11*, p.78-86 (2017). [5] Li, W., Chau, K.T. and Jiang, *IEEE Transactions on Magnetics*, Vol.*47*, p.2624-2627 (2011).

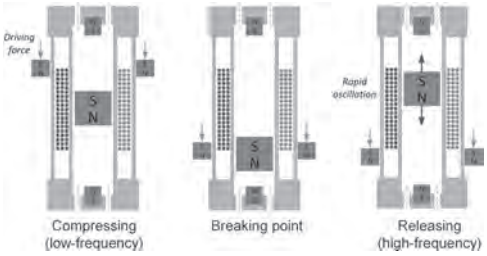

Schematic and working principle of proposed energy harvester

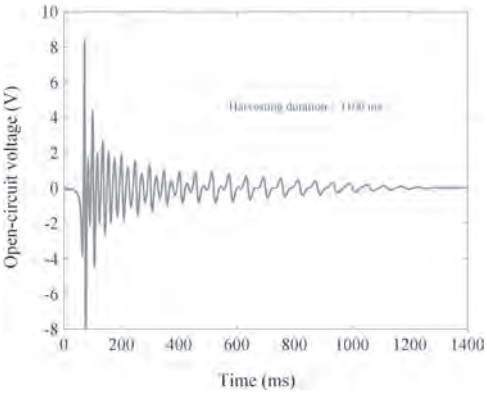

Open-circuit voltage

Session JOD
MAGNETICALLY GEARED, VARIABLE FLUX AND RELUCTANCE MACHINES

Siavash Pakdelian, Chair
University of Massachusetts Lowell, Lowell, MA, United States

CONTRIBUTED PAPERS

JOD-01. Cogging Torque Reduction of Integer Gear Ratio Axial-flux Magnetic Gear for Wind-Power Generation Application by Using Two New Types of Pole-Pieces. *B. Dai*[1], K. Nakamura[1], Y. Suzuki[2], Y. Tachiya[2] and K. Kuritani[2] *1. Graduate School of Engineering, Tohoku University, Sendai, Japan; 2. Prospine Co., Ltd., Osaki, Japan*

Introduction - Flux-modulated type magnetic gears are expected to be applied as step-up gears for wind-power generation because of their advantages, including high torque density and maintenance-free operation [1]. Among them, an axial-flux magnetic gear (AFMG) has attracted great attention recently since it has a smaller axial length and is easy to assemble. In some cases, magnetic gears are required to have an integer gear ratio based on design requirements of the entire system, which results in larger cogging torque in the high-speed rotor that causes vibration and startup error. In addition, the conventional skew rotor structure is complicated and poor in assembling [2]. To solve the problems described above, this paper proposes two new types of pole-pieces, one is an unequal-width-type, another is an unequal-spacing-type. Two new types of pole-pieces – Fig. 1(a) shows the AFMG [3] investigated in this paper, while the (b) and (c) are the proposed unequal-width-type and unequal-spacing-type pole-pieces, respectively. The gear ratio of this AFMG is an integer of 10 given by the number of pole pairs of the high-speed and the low-speed rotors of 3 and 30, respectively. As shown in Fig. 1(b), pole-pieces with three different circumferential width ratios, which are 0.3, 0.8, and 0.7, are combined in the unequal-width-type, while as shown in Fig. 1(c), the relative position of the pole-pieces is adjusted which leads to an unequal interval structure. Both types are aimed at canceling the cogging torque. The cogging torque is calculated by the three-dimensional finite element method (3D-FEM). Fig. 2 shows the results of the high-speed rotor cogging torque of the two proposed new types, where (a) is of the unequal-width-type and (b) is of the unequal-spacing-type, respectively. As shown in the figure, it is clear that both proposed types can reduce the cogging torque significantly. This work was supported in part by the WISE Program for AI Electronics, Tohoku University.

[1] K. Atallah and D. Howe, IEEE Trans. Magn., Vol. 37, pp. 2844-2846 (2001). [2] S. Ahmadreza Afsari, H. Heydari, and B. Dianati, IEEE Trans. Magn., Vol. 51, pp. 1-11 (2015) [3] B. Dai, K. Nakamura et al., ICEMS 2020, LS8H-2 (2020)

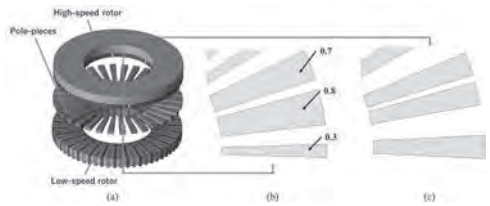

Fig. 1 The investigated AFMG and the proposed two types of pole-pieces; (b) unequal width, (c) unequal spacing.

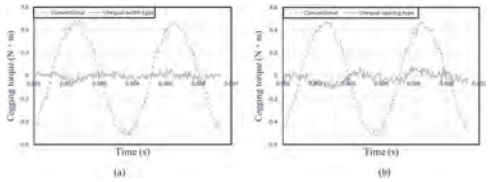

Fig. 2 The calculated high-speed rotor cogging torque of the two types of pole-pieces; (a) unequal width, (b) unequal spacing.

JOD-02. Optimizations of Rotating Cylinder Planetary Gear for High Torque Capability. Y. Zhan[1], *Z. Zhang*[1], X. Yuan[1], G. Xu[1] and N. Ding[2] *1. School of Electrical and Electronic Engineering, North China Electric Power University, Beijing, China; 2. Key Laboratory of Cleaner Production and Integrated Resource Utilization of China National Light Industry, Beijing Technology and Business University, Beijing, China*

A rotating cylinder planetary gear (RCPG) is a novel magnetic planetary gear with high torque density. The RCPG borrows the topology of the conventional flux-modulated magnetic gear, but it replaces the ferromagnetic blocks with the free-spinning magnetized cylinders called planet gears [1], [2], as shown in Fig. 1 (a). A cylinder is composed of a shaft made of magnet stainless steel and a magnet ring with one pair of poles. The high torque capability of RCPG relies on the large number of permanent magnets mounted on the rotors and planet gears. This abstract presents the optimization of the configuration of the magnets mounted on the cylinder shafts and rotors. The following steps are performed for the optimization. Step 1: the thicknesses of the inner, outer and planet gear magnets are optimized for the largest torque (design B-1) and the largest torque per volume of magnets (design B-2), respectively. The outer diameter of the outer back iron, the inner diameter of the inner back iron, the radial position of the planet gears, the diameter of the planet gear shafts and the lengths of air gaps are kept constant in the optimization. Step 2: design B-2 is further improved by adjusting the ratios of pole arc to pole pitch at the rotors, for the largest torque. This step ends up with design C. The above optimizations are carried out with multi-group genetic algorithm, and the torques are calculated by finite element method. The designs from the above steps are shown in Fig. 1. Table I details the configurations of the magnets in designs A, B-1, B-2 and C. The stall torque of design B-1 is increased by 47.5% than that of design A, however, at 73.1% more cost of magnets. Design B-2 which has higher performance cost ratio is chosen as the benchmark for the further improvement. In comparison to that of design B-2, the stall torque per volume of magnets of design C is increased by 9.7% though the stall torque is just slightly increased. The full paper will present a design of RCPG with Halbach magnet array on the rotors for further improvement of torque capability.

[1] K. Davey, T. Hutson, L. McDonald, *et al.* IEEE Transactions on Industry Applications, Vol. 52, p. 2253 (2016). [2] R. Wang, A. Matthee, S. Gerber *et al.* IEEE Magnetics Letters, Vol. 7, Art. no. 1303805 (2016).

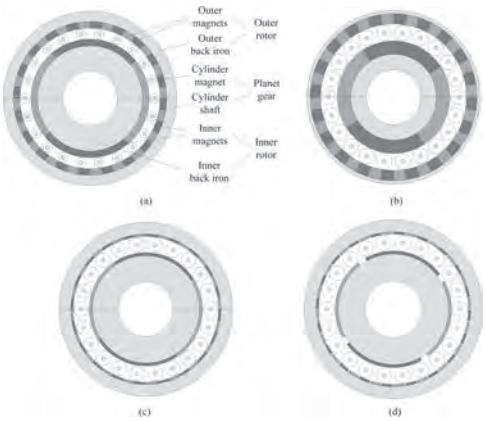

Fig. 1. RCPGs. (a) Design A (original). (b) Design B-1. (c) Design B-2. (d) Design C.

Parameters	Design A	Design B-1	Design B-2	Design C
Thickness of outer back iron (mm)	7.5	2.5	8.7	8.7
Thickness of inner back iron (mm)	18.8	11.5	19.6	19.6
Thickness of outer magnets (mm)	5	7.8	1.9	1.9
Thickness of inner magnets (mm)	5	10.1	2.3	2.3
Pole-arc-to-pole-pitch ratio of outer rotor (%)	100	100	100	90.8
Pole-arc-to-pole-pitch ratio of inner rotor (%)	100	100	100	91.1
Thickness of planet gear magnets (mm)	2	4.2	3.9	3.9
Total volume of permanent magnets (cm^3)	122.90	212.72	53.66	49.10
Stall torque (N·m)	86.51	127.61	82.03	82.36
Torque per unit volume of magnet (N·m/cm^3)	0.704	0.600	1.529	1.677
Torque density (N·m/L)	162.94	240.35	154.50	155.12

Table I Different Configurations of Magnets

JOD-03. Design of Bridged Flux Modulators in Coaxial Magnetic Gear. Y. Zhan[1], *K. Wang*[1], G. Xu[1] and N. Ding[2] *1. School of Electrical and Electronic Engineering, North China Electric Power University, Beijing, China; 2. Key Laboratory of Cleaner Production and Integrated Resource Utilization of China National Light Industry, Beijing Technology and Business University, Beijing, China*

In a coaxial magnetic gear, the modulating ring with bridges that integrate the steel pieces into a whole laminated ring, as shown in Fig. 1, can greatly save the assembly efforts than the conventional modulating ring composed of separate steel pieces [1]. The thickness of bridge (d), the ratio of pole arc to pole pitch (δ) and the number of clamping rods (n_c) should be carefully designed for the bridged modulating ring considering the tradeoff between torque capability, mechanical strength and cost. By using three-dimensional finite element method, this abstract investigates the effect of d and δ on the torque capability and the effect of d, δ and n_c on the mechanical stress of the modulating ring, as shown in Table I. The mechanical stresses of different designs are evaluated at approximately equal load condition. The calculated results suggest that smaller d is preferred in the magnetic design for high torque capability while larger d is preferred in the mechanical design for high strength. For the magnetic gear in this abstract, the increase of n_c up to 7 greatly reduces the stress in the modulating ring, but this effect is quickly saturated for n_c that is over 7. Within a large vicinity (0.333 to 0.583) of the optimal δ corresponding to the maximum pull-out torque, the variation of δ does not significantly deviate the pull-out torque from the maximum. This feature provides opportunities of further reducing the stress in the modulating ring by adjusting the value of δ, without downgrading the torque capability. The design procedure of bridged modulating ring should start with choosing a combination of d and n_c for acceptable levels of torque capability and mechanical strength. The designer should not choose very large n_c as that increases the cost as well as the eddy-current loss of the modulating ring and may not significantly reduce the stress. In addition to the appropriate value of n_c, the value of δ can be adjusted as the second step, to further reduce the stress and to keep the pull-out torque almost constant.

[1] D. Z. Abdelhamid and A. M. Knight, IEEE Transactions on Magnetics, Vol. 53, Art. no. 8112804 (2017).

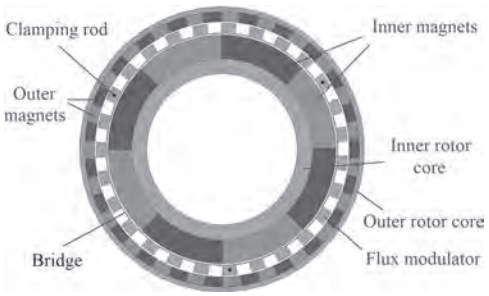

Fig. 1. Magnetic gear with bridged modulating ring.

Designs	d (mm)	δ	n_c	Outer rotor pull-out torque (N·m)	Under equal load condition	
					Mean outer torque (N·m)	Maximum stress (MPa)
1	1.0	0.500	3	15.70	13.66	121.12
2	0.8	0.500	3	16.24	13.53	198.19
3	0.8	0.500	4	16.24	13.65	115.16
4	0.8	0.500	5	16.24	13.67	73.88
5	0.8	0.500	6	16.24	13.66	55.84
6	0.8	0.500	7	16.24	13.65	36.11
7	0.8	0.500	8	16.24	13.70	35.46
8	0.8	0.500	9	16.24	13.68	27.19
9	0.8	0.333	3	16.00	13.67	149.41
10	0.8	0.375	3	16.33	13.60	153.21
11	0.8	0.417	3	16.44	13.55	179.69
12	0.8	0.458	3	16.53	13.62	196.78
13	0.8	0.583	3	15.11	13.71	162.95
14	0.8	0.333	7	16.00	13.62	40.43
15	0.8	0.375	7	16.33	13.60	36.30
16	0.8	0.417	7	16.44	13.66	37.21
17	0.8	0.458	7	16.53	13.65	38.38

TABLE I Pull-Out Torques, Load Torques and Stresses of Different Modulating Ring Designs

JOD-04. Vector Control for 12/10 Switched Reluctance Motor Using a 9-Switch Inverter. *N. Takemura*[1], K. Hirata[1], N. Niguchi[1] and H. Suzuki[1] *1. Osaka University, Suita, Japan*

1. Introduction Currently, permanent magnet synchronous motors (PMSMs) are commonly used as EV traction motors. However, there are some problems such as the cost of permanent magnets and the stable supply of rare earth resources. On the other hand, switched reluctance motors (SRMs) have simple, robust and inexpensive structure, but have problems such as large torque ripple, noise and vibration. In order to solve these problems, vector control for a 12/10 SRM using a 6-phase inverter has been proposed [1]. However, the number of switching devices for a 6-phase inverter is larger than that of a conventional 3-phase asymmetric inverter. In this paper, we propose a vector control for a 12/10 SRM using a 9-switch inverter and clarify its effectiveness. 2. Motor and Inverter The configuration diagram of the proposed 12/10 SRM and 9-switch inverter is shown in Fig. 1. The stator has 6-phase coils from A to F phases, and 2 coils of each phase are connected in series. The proposed 9-switch inverter has 3 bridges, and each bridge has 3 switching devices in series. The A-, C-, and E-phase coils are connected between the upper and middle switching devices, and the B-, D-, and F-phase coils are connected between lower and middle switching devices. 3. Analysis Result The proposed 9-switch inverter and a conventional 6-phase inverter are compared when a 12/10 SRM is driven under vector control. FEM analysis is coupled with Matlab/Simulink, where the rotation speed of the SRM is 1182 rpm, and the DC voltage is 36 V. The torque and current waveforms are shown in Fig. 2. The torque and current waveforms are almost the same with each other, and the little difference is thought to be due to the forward voltage drop of the diodes. 4. Conclusion The vector control for a 12/10 SRM using a 9-switch inverter was proposed and compared with the

conventional 6-phase inverter. The torque and current waveforms of both inverters under vector control were almost the same with each other. In this way, the effectiveness of the proposed vector control was clarified.

[1] Akira Kohara, Katsuhiro Hirata, Noboru Niguchi, Yuki Ohno, "Finite-Element Analysis and Experiment of Current Superimposition Variable Flux Machine Using Permanent Magnet," IEEE Trans. Magn., Vol. 52, No. 9, 8107807.

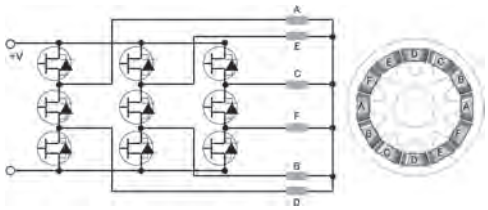

Fig.1 Configuration of proposed SRM and Inverter

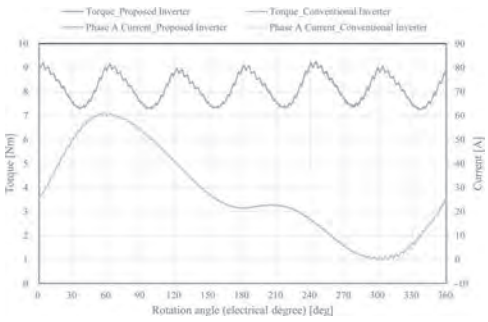

Fig.2 Torque and current waveforms of FEM analysis result

JOD-05. Design and Analysis of a Novel 2-Phase 4/3 FSPMM with Chamfering and Flange Rotor Poles. *B. Li*[1], J. Zhu[2], C. Liu[1] and Y. Li[1]
1. Hebei University of Technology, Tianjin, China; 2. University of Sydney, Sydney, NSW, Australia

I. Introduction Stator-permanent magnet (PM) electrical machines are potential for developing as high-speed (HS) electrical machines, due to their advantages of high torque density and robust rotor structure. As one of the most promising stator-PM machines, flux-switching permanent magnet machine (FSPMM) has comparable torque density with the rotor-PM machines and easy thermal dissipation. However, the high fundamental frequency of conventional FSPMM is inevitable, making it difficult to be driven by the power electronics device. In this paper, a novel dual-step 2-phase 4/3 FSPMM is proposed and analyzed. Compared with the traditional FSPMM with the odd number of rotor poles, the proposed structure has good flux linkage waveform, non-UMF and high torque density. II. Design and Performance of the Proposed 4/3 FSPM Machine Fig. 1(a) shows the structure of the novel dual-step 4/3 FSPM machine. With using this structure, it can achieve the least number of rotor poles. The PMs have the same magnetization direction, whereas the winding directions are inverse, as shown in Fig. 1(b) and (c). The two set of windings can be connected in series, therefore it is convenient to drive the machine. The rear rotor is offset by 60° mechanically with respect to the corresponding front rotor. An appropriate gap distance between two stators is necessary to accommodate the end of inverse windings and avoid excessive magnet flux leakage. The flange and chamfering rotor is designed to reduce the cogging torque, as shown in Fig.2 (a). The performance of the novel 4/3 FSPM is obtained by using the finite element method and the parameters optimization method. Fig. 2(b) shows that the UMF of the proposed machine. It can be seen that the UMF of the proposed machine is relatively small. The peak-to-peak value of the cogging torque which varies with width of rotor flange is drawn in Fig.2 (c). The designed machine can obtain minimum cogging torque of 360.71 mNm.

[1] H. Chen, A. M. EL-Refaie and N. A. O. Demerdash, "Flux-Switching Permanent Magnet Machines: A Review of Opportunities and Challenges-Part II: Design Aspects, Control, and Emerging Trends," in IEEE Transactions on Energy Conversion, vol. 35, no. 2, pp. 699-713, June 2020, doi: 10.1109/TEC.2019.2956565. [2] D. Ishak, Z. Q. Zhu and D. Howe, "Unbalanced magnetic forces in permanent magnet brushless machines with diametrically asymmetric phase windings," Fourtieth IAS Annual Meeting. Conference Record of the 2005 Industry Applications Conference, 2005., 2005, pp. 1037-1043 Vol. 2, doi: 10.1109/IAS.2005.1518484. X. Zhu, W. Hua, Z. Wu, W. Huang, H. Zhang and M. Cheng, "Analytical Approach for Cogging Torque Reduction in Flux-Switching Permanent Magnet Machines Based on Magnetomotive Force-Permeance Model," in IEEE Transactions on Industrial Electronics, vol. 65, no. 3, pp. 1965-1979, March 2018, doi: 10.1109/TIE.2017.2739688.

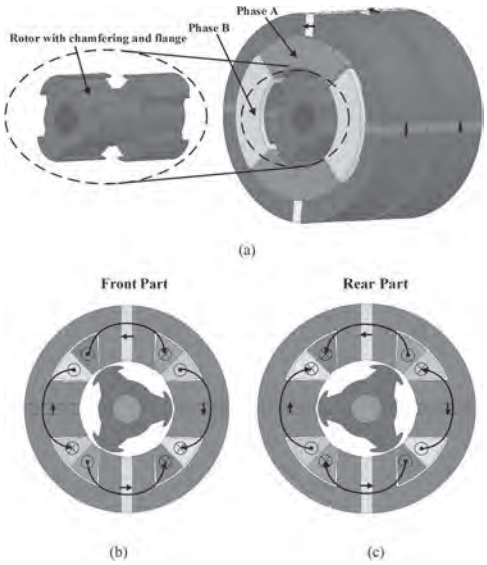

Fig. 1. (a) Topology of the proposed 4/3 FSPM machine. (b) Cross-section view of the front part. (b) Cross-section view of the rear part.

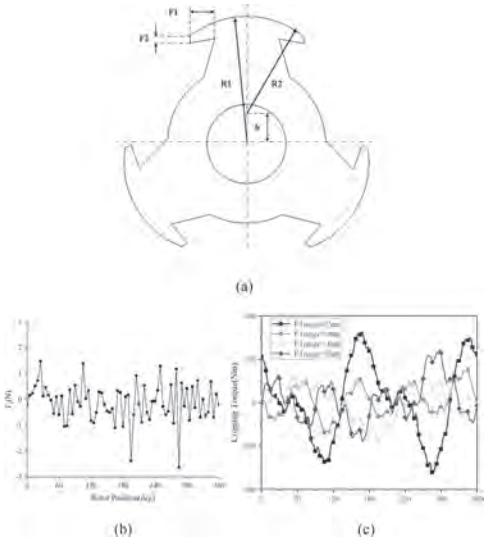

Fig. 2 (a) Chamfering and flange rotor. (b) Radial magnetic force of proposed machine. (c) Cogging torque with different width of flange

JOD-06. Torque Ripple Suppression of Doubly Salient Brushless DC Machine With Even-order Current Harmonic Injection. *Y. Sun*[1], Z. Zhang[1], X. Chen[1] and L. Yu[1] *1. Nanjing University of Aeronautics and Astronautics, Nanjing, China*

Doubly salient brushless DC (DSBLDC) machine has been attracting much attention for aviation and vehicular applications, owing to its simple structure, adjustable flux, and reliability. Despite those merits, the torque ripple of DSBLDC machine limits its applications at medium-and-low speeds. The current harmonic injection (CHI) method has been proposed to reduce torque ripple, dealing with the subsequent issue, such as vibrations, acoustic noise, even starting failure. The traditional CHI choice of odd order harmonics to limit torque ripple is almost useless for the 3-phase 12/8-pole DSBLDC machine, due to the excitation and armature winding configurations, which generate its unique magnetic circuit and inductance characteristics. Firstly, A new instantaneous torque model from the perspective of harmonics has been derived. The main components of the excitation inductance are the 1st, 2nd and 4th harmonics. Only the armature current harmonics interact with the same-order inductance harmonics can contribute to the average torque, otherwise it will lead to torque harmonics. Thus, a harmonic injection algorithm based on the 2nd and 4th current harmonics is proposed to reduce the torque ripple. Fig.1(a) shows the topology of the DSBLDC machine, which is marked by the concentrated stator-field-winding and the absence of rotor excitation. Experiment platform is shown in Fig. 1(b). The instantaneous torque as shown in Fig. 1(c) can be divided into two parts: average torque and torque ripple, which is used to solve the current amplitude and phase parameters of injected current as shown in Fig.2(a). Fig.2 shows the solution based on the harmonic injection algorithm. Case I contains only the fundamental wave. The 2nd harmonic is added into Case II. Case III contains the 1st, 2nd and 4th harmonics, reducing the torque ripple from 54.84% to 44.28%. The torque waveform and its FFT results are shown in Fig. 2(b) and Fig. 2(c). Using the system diagram in Fig. 2(d) can experimentally validate the foregoing simulation, the partial result about Case I is given in Fig. 2(e).

[1] X. Chen, Z. Zhang, L. Yu and Z. Bian, "An Improved Direct Instantaneous Torque Control of Doubly Salient Electromagnetic Machine for Torque Ripple Reduction," *IEEE Trans. Ind. Electron.*, vol. 68, no. 8, pp. 6481-6492, Aug. 2021. [2] G. J. Li, K. Zhang, Z. Q. Zhu and G. W. Jewell, "Comparative Studies of Torque Performance Improvement for Different Doubly Salient Synchronous Reluctance Machines by Current Harmonic Injection," *IEEE Trans. Energy Convers.*, vol. 34, no. 2, pp. 1094-1104, June 2019.

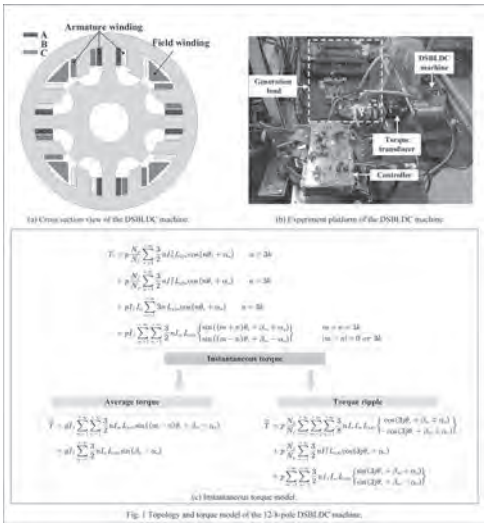

Fig.1 topology and torque model of the 12/8-pole DSBLDC machine.

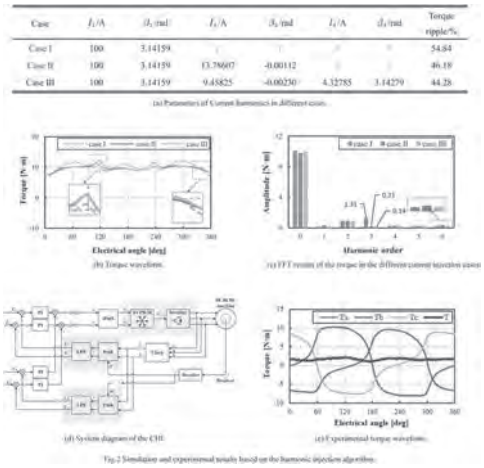

Fig.2 simulation and experimental results based on the harmonic injection algorithm.

JOD-07. Analytical Model of Radial Magnetic Force in Switched Reluctance Machines with Consideration of Magnetic Saturations. H. Hua[1], W. Hua[2], G. Zhao[3] and *Z. Zhou*[1] *1. Department of Electrical Engineering, Shanghai Jiao Tong University, Shanghai, China; 2. School of Electrical Engineering, Southeast University, Nanjing, China; 3. School of Electrical and Automation Engineering, Nanjing Normal University, Nanjing, China*

INTRODUCTION The structure of doubly salient laminations and concentrated windings as well as the operation with unipolar rectangle currents and pulsating torques result in the significant radial magnetic force (RMF) in switched reluctance machines (SRMs), which contributes to the vibration and acoustic noise [1][2]. The analysis of the RMF plays an essential role in SRMs, in which the analytical method (AM) featuring with fast calculation and low computing loading, is helpful in the initial design. However, due to the severe nonlinearity of SRMs, it is of challenge to analytically predict the RMF [3]. Based on magneto-motive force (MMF)-permeance model [4], an AM is developed in this paper, and the saturations are considered via a rotor-position-independent magnetic equivalent circuit (MEC). The AM predictions will be validated by the finite element (FE) results and a prototype SRM. ANALYTICAL MODEL and RMF RESULTS The overall flowchart is shown in Fig. 1. The MMF distribution along air-gap periphery originated from the winding function and excitation, together with the air-gap permeance considering both stator/rotor saliency, are employed to predict the air-gap radial flux density. Then the RMF is calculated with Maxwell stress tensor. The magnetic saturation effect is included via a simplified MEC. The calculated RMFs along the air-gap periphery at one rotor position with single-phase excited are shown in Fig. 2(a), where both the linear and saturated conditions are included, and FE results are presented for the validation. The AM calculations agree well with FE results. Moreover, the AM-RMF waveform along the half air-gap periphery during one electric period is shown in Fig. 2(b). CONCLUSION An AM has been developed for predicting the RMF of SRMs, considering doubly salient laminations, unipolar rectangle currents and magnetic saturations. The calculation results are validated by the FE predictions. In the coming full paper, the details of the method, the flux tube of MEC and saturation factor, the validations on various SRMs with different excitations including overlapped currents, will be presented. A prototype SRM is to be tested.

[1] C. Edrington, D. Kaluvagunta, J. Joddar, and B. Fahimi, "Investigation of electromagnetic force components in SRM under single and multiphase excitation," *IEEE Trans. Ind. Appl.*, vol. 41, no. 4, pp. 978-988, Jul./Aug. 2005. [2] A. Callegaro, B. Bilgin, and A. Emadi, "Radial force shaping for acoustic noise reduction in switched reluctance machines," *IEEE Trans. Power. Electron.*, vol. 34, no. 10, pp. 9866-9878, Oct. 2019. [3] M. Anwar and I. Husain, "Radial force calculation and acoustic noise prediction in

switched reluctance machines," *IEEE Trans. Ind. Appl.*, vol. 36, no. 6, pp. 1589-1597, Nov./Dec. 2000. [4] H. Hua, W. Hua, G. Zhao, and M. Cheng, "Torque production mechanism of switched reluctance machines with air-gap field modulation principle," *IEEE Trans. Energy Convers.*, vol. 35, no. 3, pp. 1617–1627, Sep. 2020.

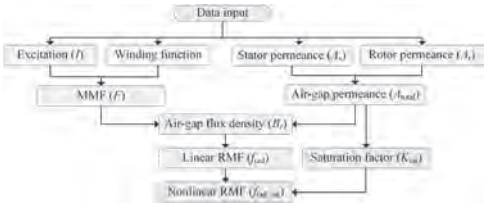

Fig. 1 Flowchart of AM of RMF.

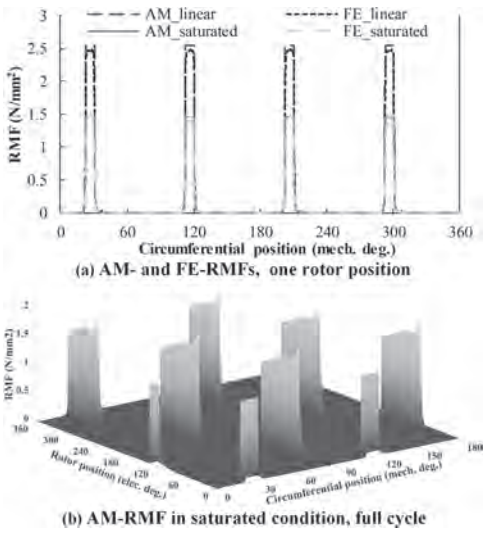

Fig. 2 RMF results along air-gap periphery.

JOD-08. Ultra-light Fault Tolerant Magnetically Geared Motor for Aerospace Pitch Control Actuation. *R.S. Dragan*[1], S. Duggan[1], D.J. Powell[1], G. Wilson[1] and R. Kinghorn[1] *1. Magnomatics Limited, Sheffield, United Kingdom*

The open rotor engine offers significant efficiency benefits over high bypass aero-engines (~15%). To realize maximum efficiency, the rotor blade pitch must be constantly adjusted in flight. With no possibility to lock out the actuator, operation at high torque is required for most of the flight. This paper discusses the design of a fault tolerant magnetically geared motor for the role of prime mover. The actuation system comprises mechanical linkages between the blades and nut, a screw and the drive motor. The gearing provided by the mechanical components results in a thermally rated motor specification requirement of 500Nm at 460rpm whilst the keep-in-zone for the actuator places limits on diameter and length and total actuator mass must remain <250kg. Magnetically geared machines are a magnetic and mechanical integration of a permanent magnet motor and magnetic gear. They exhibit very high shear stress (>100kPa) on a continuous basis. For this high temperature application, SmCo magnets have been selected and Vacoflux50 CoFe has been selected for weight reduction. A 2x3-phase fault tolerant winding architecture [1,2,3] has been chosen as it results in the lowest hazard rate compared with multiple phase machines. Such a winding requires particular combinations of stator slot/ magnet pole number. 12-slot designs with 6, 8 and 10 poles have been investigated and compared over a range of magnetic gear ratios in terms of shear stress, inertia, losses, torque ripple and Unbalanced Magnetic Pull (UMP). See Fig.1 for 12-slot, 8-pole results and Fig.2 for 12-slot, 8-pole flux plot. The active/active 2-channel fault tolerant design approach is reported, including no-load, on-load, short-circuit (SC) analysis, demagnetization analysis under SC conditions and thermal analysis in a faulted winding situation. The fault tolerant motor active mass has been reduced through iterative design and has an extremely high active torque density of 17.7Nm/kg, considering it is designed for air-cooled continuous duty, carries redundant windings and employs relatively low energy density SmCo magnets.

[1] B. C. Mecrow, A. G. Jack, J. A. Haylock, "Fault-tolerant permanent magnet machine drives," *IEE Proc. - Electr. Power Appl.*, vol. 143, no. 6, p. 437 (1996). [2] J. A. Haylock, B. C. Mecrow, A. G. Jack, "Operation of a fault tolerant PM drive for an aerospace fuel pump application," *Eighth International Conference on Electrical Machines and Drives, Conf. Publ. No. 444*, pp. 133–137 (1997). [3] *R. Dragan, R. E. Clark, E. K. Hussain, "Pseudo Direct Drive Electrical Machines for Flight Control Surface Actuation", 8th IET International Conference on Power Electronics, Machines and Drives (2016).*

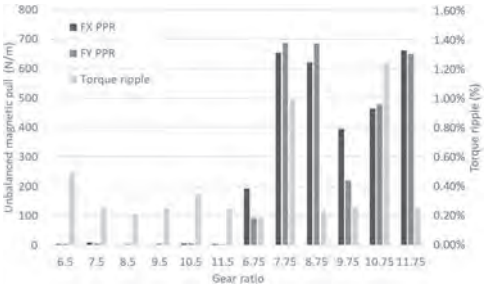

Fig.1 Torque ripple and UMP for a 12-slot, 8-pole machine.

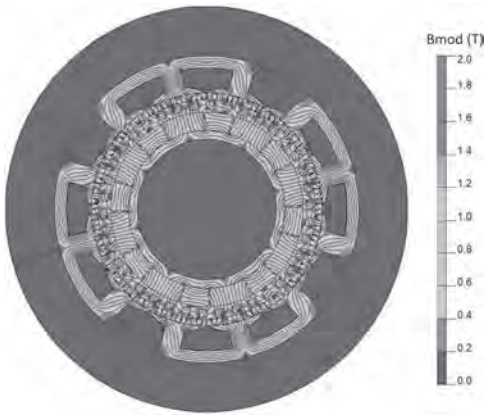

Fig.2 Flux density and flux lines in a 12-slot, 8-pole machine.

JOD-09. Investigation on Low Coercive Force Magnets in Variable Flux Memory Machines for Traction Applications. *Z. Zhou*[1], H. Hua[1], B. Zhang[1] and L. Zhu[1] *1. Department of Electrical Engineering, Shanghai Jiao Tong University, Shanghai, China*

I. INTRODUCTION Variable flux memory (VFM) machines were proposed to address the constant air-gap flux and thus sacrificed efficiency in high-speed operations of conventional permanent magnet (PM) machines [1]. The magnetization state (MS) of low coercive force (LCF) PMs can be intentional regulated by d-axis current pulses [2]. The properties and dimensions of LCF PMs are essential in VFM machines, which straightforwardly affect the intentional MS manipulation, torque density and unintentional demagnetization (UD) withstanding [3]. Two VFM machines with different LCF PMs, i.e. SmCo (Hc=335kA/m) and AlNiCo (Hc=112kA/m), are investigated and the guideline of PM design in VFM machines for EV tractions is proposed. II. MACHINE TOPOLOGY and PERFORMANCE Fig. 1 shows the VFM machine cross section, whose outline dimension is inherited from Prius2010 traction machine [4]. Two machine cases employing SmCo and AlNiCo as LCF PMs respectively, together with NdFeB PM to realize hybrid PM configuration for torque improvement, are presented. The NdFeB

PM volumes are identical in the two cases while the LCF PM thickness is 4mm for the SmCo case but 12mm for the AlNiCo case, which guarantees an equal PM MMF. As magnetization characteristics shown in Fig. 2, the MS range is 55.11% in the AlNiCo case with the limitation of rated current (236A), which is much higher than 23.15% in the SmCo machine. However, with 2 p.u. current limitation, the MS range of the SmCo case increases to 54.07%, which is close to the AlNiCo case. In addition, the torque of the SmCo case is higher than the AlNiCo case by >10%. III. CONCLUSION Although the identical initial PM MMFs are presented, the AlNiCo machine always requires lower de/re-magnetizing currents than the SmCo case. Nevertheless, the MS ranges are similar in both cases with 2 p.u. current limitation, while the SmCo machine exhibits a higher torque density. More details of the electromagnetic characteristics, LCF PM optimization, operation condition effects, and experimental validation will be demonstrated in the coming full paper.

[1] V. Ostovic, "Memory motors," *IEEE Ind. Appl. Mag.*, vol. 9, no. 1, pp. 52-61, Jan./Feb. 2003. [2] H. Yang, H. Zheng, Z.Q. Zhu *et al.*, "A novel variable flux dual-layer hybrid magnet memory machine with bypass airspace barriers," in *Proc. Inter. Conf. Electri. Mach. Drives (IEMDC)*, San Diego, USA, May 2019, pp. 2259-2264. [3] H. Yang, H. Lin, E. Zhuang *et al.*, "Investigation of design methodology for non-rare-earth variable-flux switched-flux memory machines," *IET Electr. Power Appl.*, vol. 10, Iss. 8, pp. 744-756, 2016. [4] H. Hua, Z. Q. Zhu, A. Pride *et al.*, "A novel variable flux memory machine with series hybrid magnets," *IEEE Trans. Ind. Appl.*, vol. 53, no. 5, pp. 4396-4405, Sep./Oct. 2017.

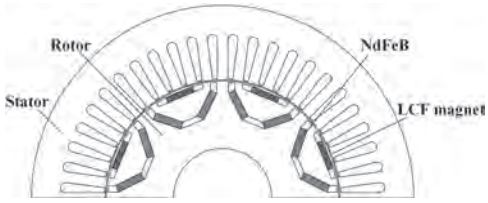

Fig. 1 Cross section of VFM machine.

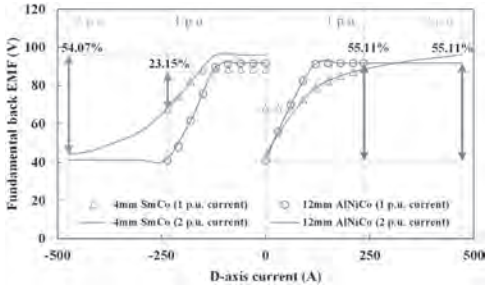

Fig. 2 Fundamental phase back-EMFs at 1500 r/min after different *d*-axis excitations.

Session JOE
SURFACE AND INTERIOR MOUNTED PERMANENT MAGNET ELECTRICAL MACHINES I

Ebrahim Amiri, Chair
The University of New Orleans, New Orleans, LA, United States

CONTRIBUTED PAPERS

JOE-01. Withdrawn

JOE-02. Noise and Vibration Prediction of a Six-Phase IPMSM in a Single Open-Phase Failure Under a Negative Sequence Current Compensated Fault Tolerant Control Mode. *P. Song*[1], W. Li[1], Z. Li[1], M. Toulabi[1] and N. Kar[1] *1. Department of Electrical & Computer Engineering, University of Windsor, Windsor, ON, Canada*

Open-phase failure is typical in multiphase machines [1]. During the open-phase faults and to support the desired developed torque in a six-phase interior permanent magnet motor (IPMSM), various fault tolerant control (FTC) methods have been proposed [2]-[3]. Although the degraded torque of a faulty IPMSM can be compensated via FTC, the noise and vibration (NV) behavior of the machine may still be affected. NV characteristics of healthy and open-phase IPMSMs have been studied before [4]-[6]. However, these characteristics have not been studied in FTC mode for an open-phase IPMSM. This paper, thus, predicts the NV performance of a laboratory six-phase IPMSM in a single open-phase fault under a negative sequence current compensated FTC mode, and the results are compared with the ones under healthy condition. The IPMSM is analyzed using finite element analysis (FEA) software and the single phase fault is remedied by FTC algorithm [2]. Fig. 1(a) shows the IPMSM and its section cut. The currents in healthy and faulty conditions are shown in Fig. 1(b) while phase A is open in faulty condition. Torque comparison is shown in Fig. 1(c). As seen, an average torque of 12.5 Nm is produced under both conditions. However, as presented in Fig. 2(a), radial electromagnetic force density under faulty condition is larger than the one under healthy condition. The acceleration and deformation in Figs. 2(b) and (c) show that the largest difference between the accelerations under two conditions happens at 6,800 Hz causing the sound pressure level (SPL) of the faulty IPMSM to be 14.1% larger than the healthy IPMSM as in Fig. 2(d). Furthermore, the maximum deformation under fault is 11.8% larger than the one under healthy condition. As demonstrated, although the IPMSM under faulty condition with FTC can produce comparable torque as healthy IPMSM, machine NV aspects need attentions. Experimental results and detailed NV analysis including modal analysis will be provided in the full paper.

[1] A. Salem and M. Narimani, "A review on multiphase drives for automotive traction applications," *IEEE Trans. Trans. Electrification*, vol. 5, no. 4, pp. 1329-1348, Dec. 2019. [2] W. Li, G. Feng, Z. Li, J. Tjong, and N. C. Kar, "Multireference frame based open-phase fault modeling and control for asymmetrical six-phase interior permanent magnet motors," *IEEE Trans. Power Electronics*, vol. 36, no. 10, pp. 11712-11725, Oct. 2021. [3] G. Feng, C. Lai, W. Li, J. Tjong, and N. C. Kar, "Open-phase fault modeling and optimized fault tolerant control of dual three-phase permanent magnet synchronous machines," *IEEE Trans. Power Electronics*, vol. 34, no. 11, pp. 11116–11127, Nov. 2019. [4] S. Yu and R. Tang, "Electromagnetic and mechanical characterizations of noise and vibration in permanent magnet synchronous machines," *IEEE Trans. Magnetics*, vol. 42, no. 4, pp. 1335-1338, April 2006. [5] W. Li *et al.*, "Structural analysis of single-sided axial-flux permanent magnet machines with different magnetic materials," *IEEE Trans. Magnetics*, vol. 57, no. 2, pp. 1-5, Feb. 2021. [6] Z. Song, Y. Yu, F. Chai, and Y. Tang, "Radial force and vibration calculation for modular permanent magnet synchronous machine with symmetrical and asymmetrical open-circuit faults," *IEEE Trans. Magnetics*, vol. 54, no. 11, pp. 1-5, Nov. 2018.

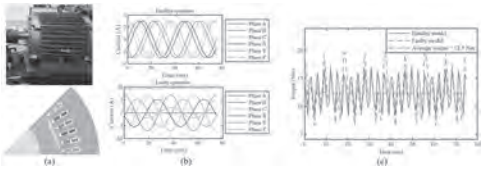

Fig. 1. IPMSM characteristics. (a) The investigated IPMSM and its section cut. (b) Input six phase currents. (c) Torque under two conditions.

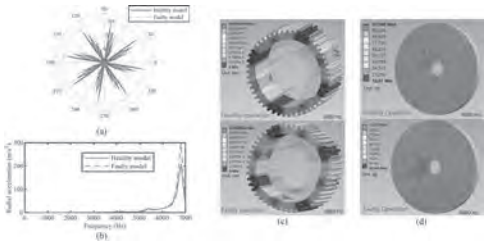

Fig. 2. NV performance. (a) Radial EM force density. (b) Radial acceleration. (c) Deformed housings. (d) SPL.

JOE-03. Decoupled Estimation Scheme for PMSMs Towards Accurate Inductance Modelling. Z. Li[2], W. Li[2], *P. Song*[2], D. O'donnell[2], J. Tjong[1] and N. Kar[2] *1. Department of Mechanical, Automotive and Materials Engineering, University of Windsor, Windsor, ON, Canada; 2. Department of Electrical & Computer Engineering, University of Windsor, Windsor, ON, Canada*

Comprehensive parameter identification and analysis are critical to develop accurate machine model. As reported in [1],[2], only two parameters can be estimated properly at the same time since the rank of the machine model is 2. However, in real-time application, machine parameters vary nonlinearly due to the change in operating conditions [3]–[5]. Therefore, more accurate knowledge of motor parameters requires more undetermined coefficients in machine modelling, which results in severer rank deficiency problem. To overcome the rank deficiency and achieve a better estimation accuracy of dq-axis inductance modelling, this paper designs an experimentally testing pattern illustrated in Fig. 1 for PMSM and proposes a decoupled estimation scheme in (1) considering system uncertainties including magnetic saturation, core loss, temperature effect and voltage source inverter nonlinearity. $(U_qI_d-U_dI_q)/\omega_e+(D_dI_s\cos(\theta)+D_qI_s\sin(\theta))\Delta V/\omega_e=I_qI_qL_q+I_d(\Lambda+L_dI_d)+I_qI_qL_q\Lambda/R_i$ (1) where variables I, U, L, λ, D with subscript 'd' and 'q' are current, voltage, inductances, flux linkage and distorted coefficients on dq-axis frame accordingly. Λ and ΔV are PM flux linkage and distorted voltage drop due to dead time effect of voltage source inverter. R_i is the core loss resistance. As mentioned previously, the proposed estimation approach takes core loss effect into account. Therefore, given different speed conditions

in (1), the differential model can be achieved by subtracting (1) at the first speed condition denoted as subscript 1 from the one at the second speed condition denoted as subscript 2, which contains the information of iron loss. In the full paper, an efficient least square method incorporating decoupled estimation scheme is employed to converge the undetermined coefficients in the proposed estimation model. The machine parameters including resistance, PM flux linkage and inductances will be estimated and reported. The estimated inductances illustrated in Fig. 2 will be validated through virtual signal injection based MTPA control and more experimental results will be presented to demonstrate the effectiveness of the proposed method.

[1] Y. Yu *et al.*, "Full parameters estimation for permanent magnet synchronous motors," *IEEE Trans Ind. Electron*, early access, May 2021 doi: 10.1109/TIE.2021.3078391. [2] C. Lai, G. Feng, Z. Li, and N. C. Kar, "Computation-efficient decoupled multiparameter estimation of PMSMs from massive redundant measurements," *IEEE Trans. Power Electron*, vol. 35, no. 10, pp. 10729-10740, Oct. 2020. [3] Y.-S. Han, J.-S. Choi, and Y.-S. Kim, "Sensorless PMSM drive with a sliding mode control based adaptive speed and stator resistance estimator," *IEEE Trans. Magn.*, vol. 36, no. 5, pp. 3588–3591, Sep. 2000. [4] G. Feng, C. Lai, and N. C. Kar, "A novel current injection-based online parameter estimation method for PMSMs considering magnetic saturation," *IEEE Trans. Magn.*, vol. 52, no. 7, pp. 1–4, Jul. 2016. [5] S.-J. Kim *et al.*, "Torque ripple improvement for interior permanent magnet synchronous motor considering parameters with magnetic saturation," *IEEE Trans. Magn.*, vol. 45, no. 10, pp. 4720–4723, Oct. 2009.

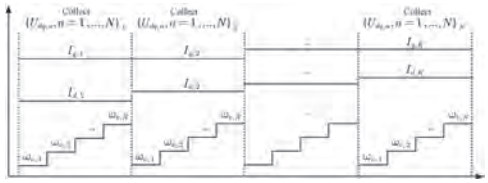

Fig.1. Illustration of experimental data collection

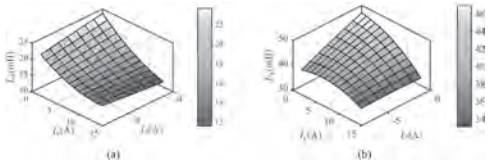

Fig.2. Estimated inductance maps. (a) d-axis (b) q-axis

JOE-04. Performance Evaluation of Hybrid Spoke-type Ferrite-NdFeB Permanent Magnet Motor. *H. Won*[1], Y. Hong[1], M. Choi[1], S. Li[1], H. Yoon[2], T. Haskew[1], J. Lee[3], T. Lee[3] and T. Lim[3] *1. Department of Electrical and Computer Engineering, The University of Alabama, Tuscaloosa, AL, United States; 2. Department of Mechanical Engineering, The University of Alabama, Tuscaloosa, AL, United States; 3. Institute of Fundamental and Advanced Technology (IFAT), Hyundai Motor Company, Uiwang, The Republic of Korea*

Recently, Ma *et al.* reported a hybrid rare-earth and ferrite permanent magnet (PM)-based spoke-type motor that can generate a comparable torque to the motor used in Prius 2010 with 60% lower cost [1]. However, the paper investigated only the motor having 10% NdFeB PM in the total PM volume on the top of the ferrite when the motor employs 3-phase integrated slot distributed winding (ISDW). This paper investigated the effect of the NdFeB PM position with different volume ratios for 3 different windings, including 3-phase (3Φ) ISDW, 3Φ fractional slot concentrated winding (FSCW), and 6Φ FSCW, on the motor performance using ANSYS Maxwell 2D. Fig. 1 shows the layout of 3 windings and 2 rotors: one with NdFeB PM on the top of the ferrite (M_{Top}) and the other with NdFeB PM on the bottom (M_{Bot}). Fig. 2 shows a change in the maximum torque (T_m) and torque ripple (T_{rip}) of the motor with 3 windings and 2 rotors with the height (H_m) of the NdFeB PM. The T_m of both M_{Top} and M_{Bot} decreases as the H_m decreases for all windings. This is because the T_m is proportional to the PM volume. On the contrary, a decreasing trend of T_{rip} with respect to an increase in the H_m is observed for both rotor types and windings except for 3Φ ISDW. Further, for the negative H_m, both T_m and T_{rip} of the M_{Top} and M_{Bot} show no difference for all windings. On the other hand, for the positive H_m, the M_{Bot} shows 0-100 Nm higher T_m but 0.57-18 % lower T_{rip} than the M_{Top} for all windings. These results suggest bottom NdFeB PM for high T_m and the top NdFeB PM for low T_{rip}. We will discuss performance metrics such as irreversible demagnetization, mechanical analysis, and maximum speed in this paper. This work was supported in part by the NSF-I/UCRC for EV-STS under Grant number 1650564.

[1] Q. Ma, A. El-Refaie, and B. Lequesne, *IEEE Transactions on Industry Applications*, vol. 56, no. 2, pp. 1452-1463 (2020)

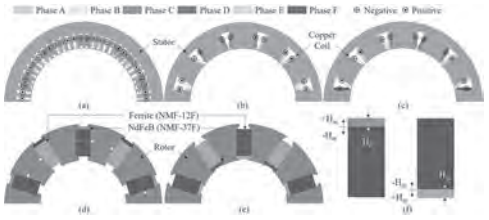

Fig. 1. Stator view: (a) 3Φ ISDW, (b) 3Φ FSCW, and (c) 6Φ FSCW; Rotor view with (d) M_{Top} and (e) M_{Bot} with (f) detailed description of the magnet.

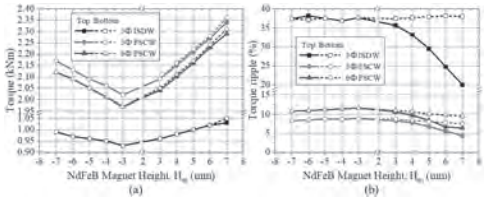

Fig. 2. (a) Maximum torque and (b) torque ripple of motor having 3Φ ISDW, 3Φ FSCW, and 6Φ FSCW and NdFeB top and bottom on the ferrite.

JOE-05. Design and Analysis of Novel Axial Flux Interior Permanent Magnet Machines with Yokeless and Segmented Armature. *L. Jia*[1], K. Lin[2], M. Lin[1], W. Le[1] and A. Yang[1] *1. School of Electrical Engineering, Southeast University, Nanjing, China; 2. College of Energy and Electrical Engineering, Hohai University, Nanjing, China*

I. Introduction. The disc shape of axial flux PM machine has opened up many configuration possibilities including the yokeless and segmented armature (YASA), which is regarded as a strong competitor of the new generation of high-power density and efficiency machines [1]. Owing to the absence of the stator yoke and the equipment of the non-overlapping concentrated winding, the YASA structure facilitates high slot fill factor and low stator iron loss [2]. However, the surface-mounted PM is usually used as the rotors of the YASA machine to ensure sufficient compactness and facilitation, which limits the output torque and the flux-weakening capability at the given volume of PM because of the low inductance [3]. This paper proposes a novel YASA structure with modular spoke-type PM (STPM) rotors to improve the torque characteristics. The close slot-pole combinations are applied and the four machines are compared to investigate the performances of winding factor (WF), back-EMF and torque output using 3-D FEA. II. Machine structure. As shown in Fig.1, the proposed YASA machine features one stator, two outer rotors with modular STPMs which circumferentially magnetized in the same directions. The magnetization directions of the PMs on the two rotors are opposite. Each piece of PMs is sandwiched by two rotor teeth to form a rotor module, which is fixed by a non-magnetic support plant. The operation principle can be expressed as the flux-switching between the PMs and stator core that embraces two typical situations [4]. III. Analysis and comparisons. The stator slot-opening, slot depth, PM and tooth width

of the rotor are optimized by parameter scanning method simultaneously to achieve the maximum torque. Fig. 2 (a) illustrates the back-EMF of the investigated machines, where the machines with 22- and 26- poles hold the higher amplitude since the higher WF. And the machine with 26-pole has highest torque output and the lowest torque ripple in Fig. 2 (b). More details of the machines are compared in Table I. Furthermore, modular design of the stator and rotor makes the production facilitation. And the larger inductance of d-axis expands the flux-weakening region and reduces the risk of irreversible demagnetization.

[1] A. El-Refaie and M. Osama, "High Specific Power Electrical Machines: A System Perspective," *China Electrotechnical Society Transactions on Electrical Machines and Systems,* vol. 3, no. 1, pp. 88-93, 2019. [2] N. Taran, V. Rallabandi, G. Heins, and D. M. Ionel, "Systematically Exploring the Effects of Pole Count on the Performance and Cost Limits of UltraHigh Efficiency Fractional hp Axial Flux PM Machines," *IEEE Transactions on Industry Applications,* vol. 56, no. 1, pp. 117-127, 2020. [3] L. Jia, K. Lin, M. Lin, W. Le, and S. Wang, "Comparative Analysis of Dual-rotor Modular Stator Axial-Flux Permanent Magnet Machines with Different Rotor Topologies," *IEEE Transactions on Applied Superconductivity,* pp. 1-1, 2021. [4] P. Su, W. Hua, Z. Wu, Z. Chen, G. Zhang, and M. Cheng, "Comprehensive Comparison of Rotor Permanent Magnet and Stator Permanent Magnet Flux-Switching Machines," *IEEE Transactions on Industrial Electronics,* vol. 66, no. 8, pp. 5862-5871, 2019.

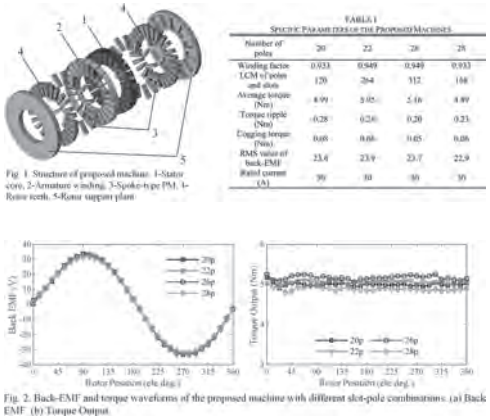

Fig. 1. Structure of proposed machine. 1-Stator core, 2-Armature winding, 3-Spoke-type PM, 4-Rotor teeth, 5-Rotor support plate.

TABLE I
SPECIFIC PARAMETERS OF THE PROPOSED MACHINES

Number of poles	20	22	26	28
Winding factor	0.933	0.949	0.949	0.933
LCM of poles and slots	120	264	312	168
Average torque (Nm)	4.99	5.05	5.16	4.89
Torque ripple (Nm)	0.28	0.24	0.20	0.23
Cogging torque (Nm)	0.05	0.04	0.05	0.06
RMS value of back-EMF	23.6	23.9	23.7	22.9
Rated current (A)	30	30	30	30

Fig. 2. Back-EMF and torque waveforms of the proposed machine with different slot-pole combinations. (a) Back EMF. (b) Torque Output.

JOE-06. A Nonuniform Step Skew Method for Cogging Torque Reduction in Permanent Magnet Synchronous Motor. Y. Cheng[1], *Y. Shen*[1], Y. Yan[1] and T. Shi[1] *1. College of Electrical Engineering, Zhejiang University, Hangzhou, China*

1 INTRODUCTION Permanent magnet synchronous motors (PMSMs) are increasingly popular in various industrial applications due to their high power density and high efficiency. In high performance servo applications, it is essential to reduce the cogging torque to improve the positional accuracy. One of the most widely used methods is step skewing with uniform magnets. However, it suffers from unbalanced axial electromagnetic force[1]. Herringbone skew method can eliminate the unbalanced axial electromagnetic force because of the symmetrical structure, while it leads to higher cogging torque and torque ripple than the conventional step skew method[2]. In this paper, a nonuniform step skew method is proposed. The PMs of the nonuniform step skew motor have various thicknesses and various skew angles, and show an axisymmetric distribution meanwhile. The proposed method not only reduces the cogging torque to a greater extent than the uniform skew method, but also completely eliminates the unbalanced axial electromagnetic forces. 2 THE METHOD AND RESULTS Fig. 1 shows the rotor structure of the nonuniform step skew method. The 3D structure of motor with nonuniform step skew is shown in Fig. 1(a), and Fig. 1(b) shows the nonuniform distribution of magnet poles. Fig. 2 shows the FEM analysis results of cogging torque and output torque. Compared to the conventional, the uniform step skew and the herringbone skew motors, cogging torque of the nonuniform step skew motor is reduced by 86%, 44%, 80% and the torque ripple is reduced by 45%,15%,18%, without additional reduction in output torque. In addition, due to the symmetrical structure of PMs, the unbalanced axial electromagnetic force can be eliminated. 3 CONCLUSION This paper has proposed a nonuniform step skew method for cogging torque reduction in PMSMs. Based on FEM analysis results, the motor with nonuniform step skew has less cogging torque and torque ripple than the conventional, the skew and the herringbone skew motors, without more sacrifice of torque density. Moreover, the unbalanced axial electromagnetic force can be completely eliminated with the symmetrical structure.

[1] M. Lukaniszyn, M. JagieLa, and R. Wrobel, Optimization of permanent magnet shape for minimum cogging torque using a genetic algorithm, *IEEE Trans. Magn.*, Vol. 40, no. 2, p.1228–1231(2004) [2] W. Fei and Z. Q. Zhu, Comparison of Cogging Torque Reduction in Permanent Magnet Brushless Machines by Conventional and Herringbone Skewing Techniques, *IEEE Trans. on Energy Conversion*, Vol. 28, no. 3, p.664–674(2013)

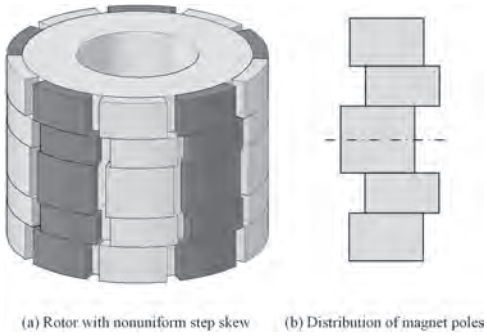

(a) Rotor with nonuniform step skew (b) Distribution of magnet poles

Fig. 1. Rotor structure of the nonuniform step skew motor

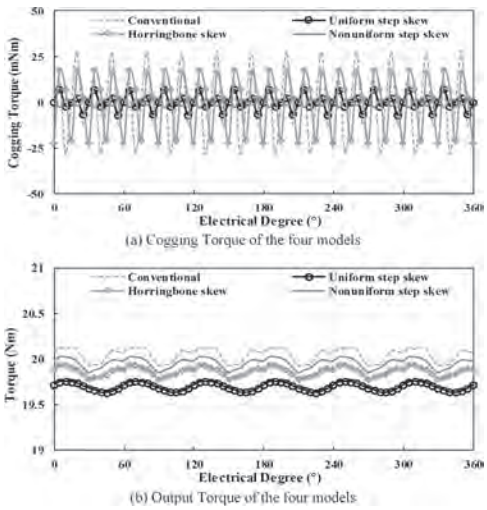

(a) Cogging Torque of the four models

(b) Output Torque of the four models

Fig. 2. Cogging torque and output torque

Session JOF
(SEMI)-ANALYTICAL AND NUMERICAL TECHNIQUES FOR DESIGN

Pierre-Daniel Pfister, Chair
Zhejiang University, Hangzhou, China

CONTRIBUTED PAPERS

JOF-01. General 2-D Analaytical Framework for Interior Permanent Magnet Machines. V.Z. Faradonbeh[1], A. Rahideh[1], *E. Amiri*[2] and G.A. Markadeh[3] *1. Department of Electrical and Electronics Engineering, Shiraz University of Technology, Shiraz, The Islamic Republic of Iran; 2. Electrical and Computer Engineering, University of New Orleans, New Orleans, LA, United States; 3. Engineering Department, Shahrekord University, Shahrekord, The Islamic Republic of Iran*

Among different analytical models, those that are capable of accounting for both radial and tangential flux components are preferred. The underlying principle of 2-D models is based on solving Maxwell's equations. However, applying 2-D boundary conditions in IPM machines is quite challenging since more than one variables exist at the boundaries between PMs and iron core. This limits the application of 2-D subdomain model in the family of IPM machines. In [1], the number boundary variables is reduced to one by segmenting magnets into multiple pieces, but the computational volume increases proportional to the number of segments. It is noted that iron bridges in IPM machines are always saturated and typically operate in the nonlinear region of the *B-H* curve [2]-[4]. Solving non-linear relations would require numerical methods, which further complicates the solution. In this paper, two solutions are proposed for enabling the 2-D modeling of IPM machines. The case study examined in this paper is a 9-slot/8-pole fractional-slot concentrated winding (FSCW) IPM machine (Fig. 1a). For this purpose, original interior PMs (Fig. 1a) are removed and modeled via a) virtual permanent magnets (VPM) (Fig. 1b), and b) virtual volume current (VVC) on the surface of the rotor body (Fig. 1c), and the 2-D Maxwell's equations are solved in each of the two transformed machines. Meanwhile, stator slotting effect is modeled via surface currents on the stator teeth lateral side (Fig. 1d). In other words, the radial and tangential flux components of the original IPM machine of Fig. 1a is equal to the sum of flux density of either Figs. 1b and 1d, or Figs 1c and 1d. The value and specification of the virtual magnets of Fig. 1b and virtual volume current of Fig. 1c are calculated subject to a condition that they produce the same radial flux density as the original interior magnets. Fig. 2 presents the calculated radial and tangential flux profiles. Analytical results are verified via finite element.

[1] M. Nakhli, A. Rahideh, M. Mardaneh, *IEEE Trans. Energy Conv*, vol. 33, no. 1, pp. 373-382. (2018). [2] B. Guo, Y. Huang, *IEEE Trans. Industrial Electronics*, vol. 66, no. 7, pp.5015-5024, (2019). [3] Y. Hu, Sh. Zhu, Ch. Liu, *IEEE Trans. Energy Conversion*, vol. 33, no. 1, pp.199-208, (2018). [4] J. Ou, Y. Liu, M. Doppelbauer, *IEEE Trans. Industrial Electronics*, Early Access, DOI.10.1109/TIE.2020.3026305.

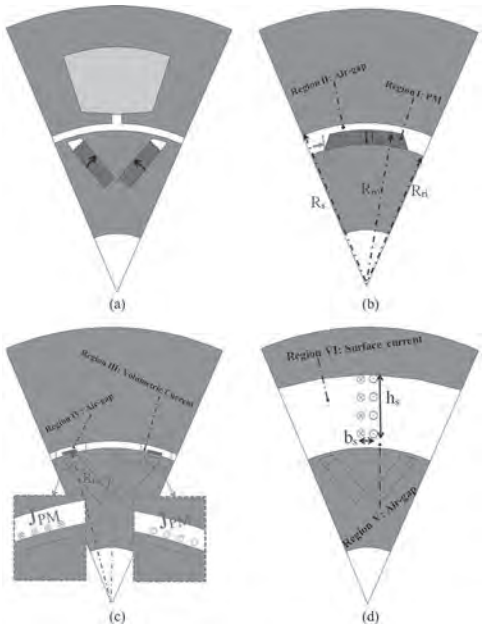

Fig. 1. Visual illustration of the modeling process, a) original IPM machine, b) VPM model, c) VVC model, d) modeling stator slotting effect.

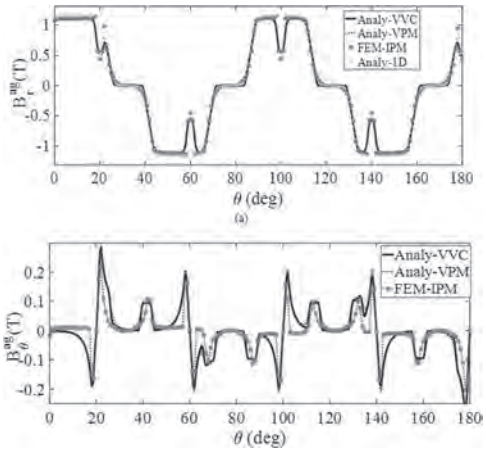

Fig. 2: Airgap flux density distribution with stator slotting effect, a) radial, b) tangential.

JOF-02. A Domain Decomposition Finite Element Method for the Magneto-Thermal Field Analysis of Electric Machines. Y. Zhang[1], X. Yang[2], W. Miao[1], Q. Zhou[1], *Z. Qiao*[1] and W. Fu[3] *1. Department of Electrical Engineering, Shanghai University, Shanghai, China; 2. State Key Laboratory of Reliability and Intelligence of Electrical Equipment, Hebei University of Technology, Tianjin, China; 3. Shenzhen Institutes of Advanced Technology, Chinese Academy of Sciences, Shenzhen, China*

The thermal design or thermal management of electric machines (EMs) has attracted intense attentions along with the increasing requirement for the power density [1]. Numerical model based magneto-thermal field analysis tools have been widely used in the evaluation of EMs [2]. However, the analysis process, involving magnetic field analysis, data mapping, and thermal field analysis, is time consuming, which fails to fulfill the demand of rapid design. In this paper, a domain decomposition finite element method is proposed for the magneto-thermal field analysis of EMs, in which these three key procedures are computed in parallel, hence the analysis efficiency is expected to be improved dramatically. The additive Schwarz domain decomposition finite element method is developed to solve the magnetic field and thermal field. In order to average the computation burden among processors, the computational domain is decomposed into several subdomains according to the discretized mesh. The formulated equations for subdomains, which are coupled by the interface unknowns are solved in parallel. The Krylov subspace method combined with preconditioning operator is employed to solve the generated algebraic system to improve the computation efficiency and avoid potential convergence problems. Since the discretized meshes of magnetic field and thermal field are not consistent, mesh mapping is required for the data transfer between these two fields. The advantage of decomposed domains could be utilized to simplify this mapping process in the proposed method. In addition, subdomain could adopt different mapping algorithms according to characteristic, which increases the flexibility of coupled analysis. A 24-slot/8-pole surface-mounted permanent magnet synchronous machine (PMSM) is analyzed using the proposed method. As shown in Fig.1, the discretized mesh, involving 11788 triangles and 5970 degree-of-freedoms, are decomposed into 15 subdomains. Results derived from the decomposed mesh are exhibited with the contours of magnetic potential (see Fig. 2). More results of the magneto-thermal analysis of this PMSM will be covered in the full paper.

[1] W. Wu, J. B. Dunlop, S. J. Collocott, and B. A. Kalan, IEEE Trans. Magn., vol. 39, no. 5, pp. 3334–3336 (2003) [2] Y. Zhang, X. Liu, H. Wu, S. Ho and W. Fu, IEEE Trans. Magn., vol. 56, no. 3, pp. 1-4 (2020)

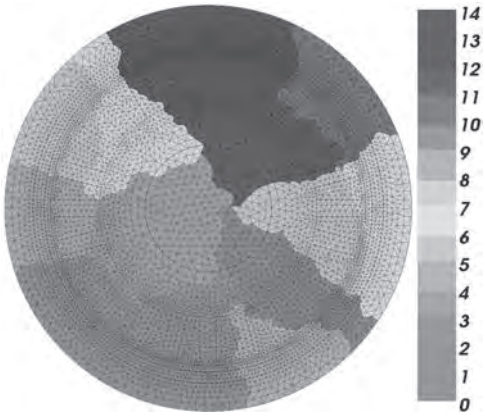

Fig. 1 The mesh and decomposed domains of the PMSM.

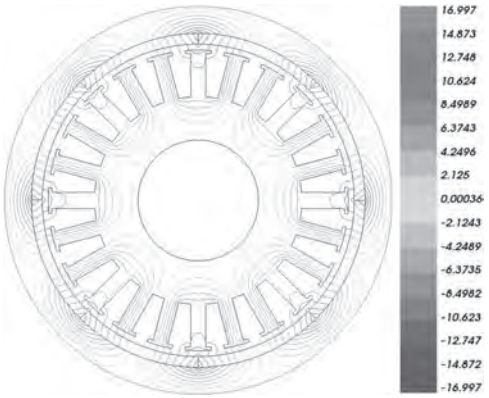

Fig. 2 The contours of magnetic potential.

JOF-03. Withdrawn

JOF-04. A Novel Reluctance Network Analysis Applicable for Open Magnetic Circuits. *Y. Hane*[1], K. Sugahara[2] and K. Nakamura[3] *1. Department of Electrical Engineering, Tohoku University, Sendai, Japan; 2. Faculty of Science and Engineering, KindainUniversity, Higashiosaka, Japan; 3. Department of Management Science and Technology, Tohoku University, Sendai, Japan*

A finite element method (FEM) is widely used in electromagnetic design and analysis, though a long calculation time and a large computer capacity are generally required. To overcome this issue, the authors proposed a reluctance network analysis (RNA) [1], which is suitable for fast calculation of various electric machines' characteristics, including transformers and motors. However, previous researches on the RNA were limited to closed magnetic circuits. To expand the application scope of the RNA for a wireless power transfer (WPT) and a particle accelerator, which have open magnetic circuits, this paper presents a novel RNA model for open magnetic circuits with the concept of the Kelvin transformation [2], [3], which has been utilized in the open boundary problems in the FEM. Fig. 1(a) – (c) show the proposed RNA model for open magnetic circuits in case of 2-D and 3-D axisymmetric analysis. As shown in Fig. 1(a), an analytical region including the point at infinity is separated into interior and exterior regions. Then, both regions are divided into multiple elements represented by unit magnetic circuits as shown in Fig. 1(b) and (c). Each reluctance can be determined by dimensions of the element and permeability of the material. In the quadrant regions, dimensions of an element l_r, l_q, l_z, l_j, l_r', l_q', l_z', and l_j' can be expressed by the following equations: $l_r = |r_1\text{-}r_2|$ (1) $l_q = r_1|q_1\text{-}q_3| = r_3|q_1\text{-}q_3|$ (2) l_z = const. (3) $l_j = p(r_1+ r_2)\sin(|q_1+q_3|/2)$ (4) $l_r' = |a^2/r_1' - a^2/r_2'|$ (5) $l_q' = a^2/r_1'|q_1'\text{-}q_3'| = a^2/r_3'|q_1'\text{-}q_3'|$ (6) l_z' = const. (7) $l_j' = p(r_1' + r_2')\sin(|q_1'+q_3'|/2)$ (8) On the other hand, in the rectangular regions, dimensions of an element are l_x, l_y, l_z, l_j, l_x', l_y', l_z', and l_j'. Among them, l_x and l_x' can be expressed by the following equations: $l_x = |x_1\text{-}x_2| = |r_1\text{-}r_2|$ (9) $l_x' = |x_1'\text{-}x_2'| = |a^2/r_1' - a^2/r_2'|$ (10) Fig. 2(a) - (c) show specifications of an analytical object and simulation results, respectively. Here, flowing flux density on a red solid line is compared. It is understood that calculated values of the RNA and FEM are in good agreement. Also, the RNA results hardly change even if the value of a changes within the range of the necessary and sufficient spatial resolution.

[1] K. Nakamura and O. Ichinokura, "Reluctance Network Based Dynamic Analysis in Power Magnetics", *IEEJ Trans. FM*, Vol.128, No.8, pp. 506-510 (2008). [2] S. H. Wong and I. R. Ciric, "Method of Conformal Transformation for the Finite-Element Solution of Axisymmetric Exterior-Field Problems", *COMPEL*, Vol. 4, No. 3, pp. 123-135 (1985). [3] I. R. Ciric and S. H. Wong, "Inversion Transformation for the Finite-Element Solution of Three-Dimensional Exterior-Field Problems", *COMPEL*, Vol. 5, No. 2, pp. 109-119 (1986).

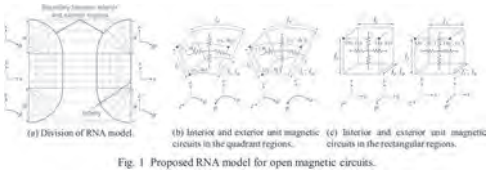

Fig. 1 Proposed RNA model for open magnetic circuits.

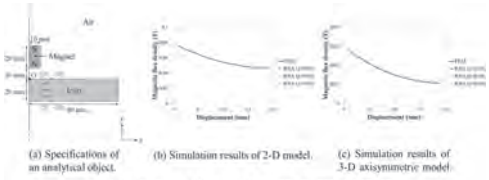

Fig. 2 Proposed RNA model for open magnetic circuits.

JOF-05. Magnetic Field Leakage Canceller Based on Loop Antenna Theory for Inductive Power Transfer. *Y. Narusue*[1] and H. Morikawa[1]
1. The University of Tokyo, Bunkyo, Japan

The reactive shielding [1] effectively weakens the magnetic field intensity around the vicinity of an IPT system. According to the CISPR guideline, however, the magnetic field intensity not only at the vicinity but also at 3-m or 10-m far from an IPT system needs to be weakened. In this study, we propose a passive magnetic field leakage canceller based on loop antenna theory as shown in Fig.1. Due to page limitations, only H_θ is discussed and detailed derivation is omitted in this abstract. According to the loop antenna theory, the magnetic field leaked from the loop current I with the radius a is proportional to $a^2 I$ [2]. Because the magnetic field leaked from a multiple turns coil is proportional to $\sum a_i^2 I$, the magnetic field leaked from the IPT system can be approximated as $H_\theta = M \sin\theta/(4r^3)$, where M is defined as $\sum a_i^2 I_{TX} + \sum a_j^2 I_{RX}$. The canceller's function is to generate $-H_\theta$ by using induced voltage. The induced voltage V_{ind} at the canceller loop can be calculated as $j\mu_0\pi\omega M/(2A)$, where A is the radius of the canceller loop. Because $M = A^2 I_{loop}$ needs to be satisfied for cancellation, the impedance Z of the canceller loop is formulated as $Z = j\mu_0\pi\omega A/2$ via $I_{loop} = M/A^2 = j\mu_0\pi\omega M/(2A)/Z$. Since the impedance Z does not depend on M, the leaked magnetic field can be canceled independently of a source. We conduct electromagnetic field simulations to evaluate the proposed canceller. Their parameters of coils are the same as in [3] and the displacement between them is 20 cm and the load impedance is set as maximizing the transfer efficiency. The canceller's radius is set to 1 m and a capacitor of 483 nF is connected considering the inductance of the canceller loop is 9.23μH. As shown in Fig.2, The proposed canceller can suppress the magnetic field intensity by about 17 dB at 10-m far in the y (horizontal) direction from the center of the transmitting coil although the difference of transfer efficiency is only 0.6 %. The reduction of 17 dB means that transmitting power can be increased 50 times under the same leakage level.

[1] J. Kim, J. Kim, S. Kong, et al., "Coil design and shielding methods for a magnetic resonant wireless power transfer system," Proceedings of the IEEE, vol. 101, no. 6, pp. 1332–1342, 2013. [2] C. A. Balanis, Antenna theory: analysis and design. John Wiley & Sons, 2012. [3] Y. Narusue, and H. Morikawa, "Magnetic energy minimization for suppressing magnetic field intensity of inductive power transfer systems," IEEE Transactions on Magnetics, June 2021 (Early Access).

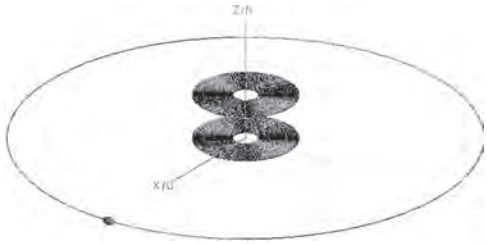

Structure of the proposed loop canceller and its simulation setup.

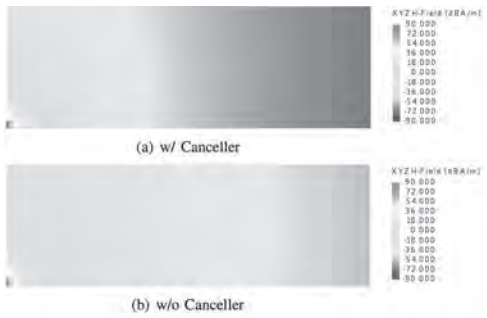

Comparison of magnetic field strength with 3kW transmission. The y-z dimension is from (0,0) to (15,5).

JOF-06. Full Analytical Solution for the Magnetic Field of Uniformly Magnetized Cylinder Tiles. *F. Slanovc*[1], M. Ortner[2], C. Abert[1] and D. Suess[1] *1. Faculty of Physics, University of Vienna, Vienna, Austria; 2. Silicon Austria Labs, Villach, Austria*

In this work, we present an analytical solution of the magnetic field for a uniformly magnetized cylinder tile (= cylinder volume element, see Fig. 1). The derivation is based on the method of magnetic surface charge densities for arbitrary Cartesian magnetization directions and cylinder tile geometries. In contrast to previous works [1,2], all resulting expressions have been reduced to analytical forms containing only elementary operations, trigonometric functions and elliptic integrals. All special cases (singularities and indefinite expressions) are discussed, allowing an exact evaluation of the magnetic field (up to numerical errors) at any point in space. The results are validated by comparison with finite elements solutions and numerical integration. It is further demonstrated how vectorized implementation of all special functions enables effective computational times in few tens of microseconds on simple mobile CPUs (e.g. Intel i5-8365U). An efficient implementation has been integrated in version 4 of the open-source Python-package Magpylib [3]. Possible applications of the derivations are the analytical study of the Halbach cylinder [4] (see Fig. 2), rotary encoder geometries [5,6], electrical machines [7], or any other magnetic geometry consisting at least partially of cylinder tiles. Furthermore, since a full cylinder can be completely subdivided into cylinder tiles, it allows the study of demagnetization effects while maintaining the rotational symmetry using the magnetostatic moment method [8].

[1] R. Ravaud and G. Lemarquand, Progress In Electromagnetics Research B., Vol. 24, p.17–32 (2010) [2] K.K. Nielsen and R. Bjørk, Journal of Magnetism and Magnetic Materials., Vol. 507, p.166799 (2020) [3] M. Ortner and L. G. C. Bandeira, SoftwareX., Vol. 11, p.100466 (2020) [4] K. Turek and P. Liszkowski, Journal of Magnetic Resonance., Vol. 238, p.52–62 (2014) [5] U. Ausserlechner, Progress In Electromagnetics Research B., Vol. 38, p.71-105 (2012) [6] S. Huber, J.-W. Burssens, N. Dupré et al., Multidisciplinary Digital Publishing Institute Proceedings., Vol. 2, p.809 (2018) [7] M. Galea, L. Papini, H. Zhang et al., IEEE Transactions on Magnetics., Vol. 51, p.8107309 (2015) [8] O. Chadebec, J.-L. Coulomb and F. Janet, IEEE Transactions on Magnetics., Vol. 42, p.515–520 (2006)

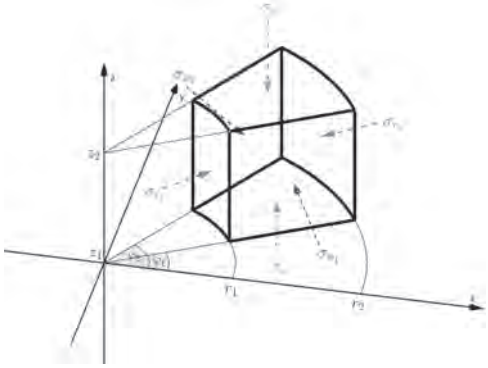

Geometry of cylinder tile with parametrization in cylindrical coordinates. Six surfaces contribute to the magnetic field.

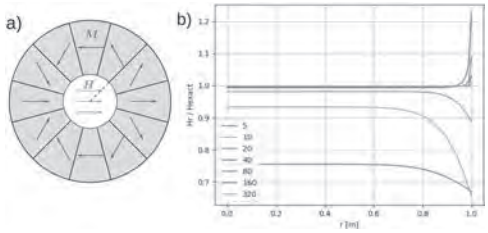

a) Cross-section through a Halbach cylinder array consisting of twelve cylinder tiles with different magnetization directions. The magnetic field is evaluated along the dashed blue line. b) Field for different numbers of subdivided cylinder tiles as a function of the radial coordinate r.

JOF-07. Particular Multi-Objective Permanent Magnet Machine Optimization for Ship Propulsion Applications. E. Karamanis[1] and *A.G. Kladas*[1] *1. Electrical and Computer Engineering, National Technical University of Athens, Athens, Greece*

Permanent magnet machines necessitating no rotor excitation and providing higher efficiency and power density than the induction motor rivals constitute a favored selection for electric ship propulsion applications. Alternative permanent magnet configurations enable handling of the main machine characteristics of weight, construction cost, efficiency and reliability [1]. Moreover, direct propeller traction is effective by adopting multipole electric machine structure [2] while multi phase winding configurations can provide performance improvements and harmonic distortion reduction [3]. Meanwhile, this enables implementation of independent inverter leg drive with reduced voltage and current specifications involving low cost power semiconductors by adopting adequate modular drive techniques [4] providing increased redundancy and fault tolerance. Another important feature of the target application is that the drive is operating usually at lower loading than the nominal one in order to achieve energy consumption reduction, which must be taken into account at the motor design stage. The present paper develops a genetic algorithm governing a multi-objective design approach coupled with a finite element model including consistent design constraints and drive cycle characteristics [5]. The novelty of the proposed technique resides on the overall calculation cases reduction by introducing orthogonal search and convergence criterion based on hypervolume evaluation of pareto front distribution. The proposed methodology is implemented in a particular ship application involving 500 kW and 350 rpm rated power. A five phase winding motor has resulted as optimum configuration and the respective field distribution under nominal operating conditions is shown in Fig. 1. The optimization procedure of multi-objective approach introduced resulted in the pareto front representation shown in Fig. 2. It may be noted that the proposed optimum five phase motor presents substantially reduced torque ripple and EMF THD than the optimum three phase one.

[1] A. Kasha, R. Lin, S. Sudhoff, 2017 IEEE Electric Ship Technologies Symposium, p. 437 (2017) [2] P. Thullen, T. Keim, J. Minervini, IEEE Transactions on Magnetics, vol. 11, no 2, p. 653, (1975) [3] Y. Sun, W. Zhao, J. Ji, IEEE Transactions on Vehicular Technology, vol. 69, no 9, p. 6901, (2020) [4] D. Ronanki, S. Williamson, IEEE Transactions on Transportation Electrification, vol. 5, no 1, p. 335, (2019) [5] X. Liu, C. Hu, X. Li, IEEE Transactions on Magnetics, vol. 57, no 7, (2021)

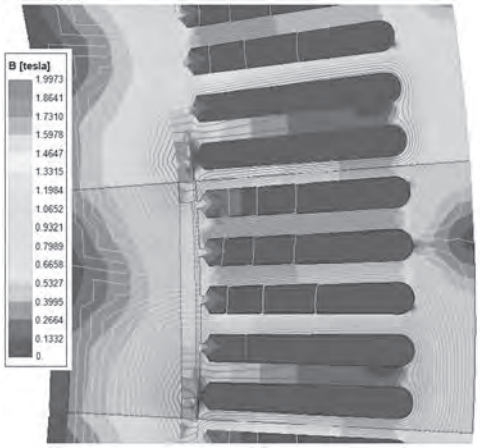

Fig. 1. Magnetic field representation in the five-phase optimal motor configuration

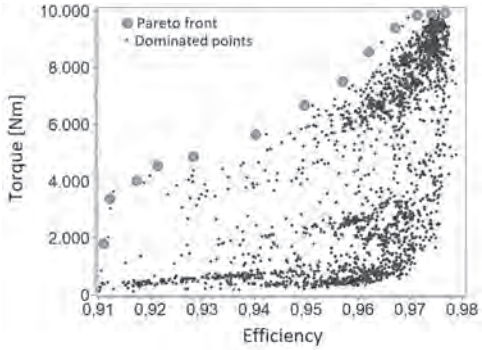

Fig. 2. Pareto front representation for the developed multi-objective optimization methodology

JOF-08. Current Loop Off Axis field Approximations with Excellent Accuracy and Low Computational Cost. *G.H. Chapman*[1] and D.E. Carleton[1] *1. School of Eng Sciece, Simon Fraser University, Burnaby, BC, Canada*

The current loop is a fundamental building block of cylindrically symmetric magnetic calculations. However the off axis field magnetic involves the subtraction of elliptical integrals and second kind which is computationally expensive, hard to manipulate in equations and difficult to visualize. By doing a different binomial series expansion on the original loop integral a series solution is created, which can be simplified to a set of approximations with useful characteristics: exactly correct at along the axis, and at distance, while at the current loop itself the relative error is limited, computational simple, easy to visualize the behavior and symmetry. Figure 1 shows for the radial field the first and second order fits where the parameters are optimized to give minimize the relative peak error. Note the symmetry that occurs by expressing as function of W, allowing maximum relative errors of 0.025 for 1st order and 2.9E-4 for second order (Figure 2 shows 2nd order relative error in all space). For axial field (Figure 1) the first order, due to the subtraction the accuracy is only modest but the 2nd order has a 9E-4 maximum relative error along, with zero error at the loop on the z=0 plane. The axial field

relative error stays low within the loop but outside does, and stays low for any h until it falls to 1% of the z=0 plane value, then lose accuracy as z is near where the field direction reverses sign due to slight differences in the zero crossing predicated coordinate, increasing again in accuracy as z further from the reveal. Higher order approximations add more W terms and see increasing accuracy – for radial 3rd order 1.8E-5, 4th 2,3E-6, 5th 4.9E-7, while axil goes as 3rd 4.6E-5, 4th 6E-6. Note that the simplicity of these functions suggests new ways combining loops to optimize such things as field uniformity. The final paper will show how these approximations are created, plus more details on the error distributions of these and higher orders

a=loop radius, h= radial field position, z= axial field position, I= current

$$W = \frac{4a^2h^2}{(h^2+a^2+z^2)}$$

Radial approximations

$$1^{st}\text{ order } B_{R\hat{a}1} \cong \frac{i\mu_0 I}{4}\frac{2\hbar a^2}{(h^2+a^2+z^2)^{5/2}}\left[3 + A_{R1}\left(\frac{W}{1-W}\right)\right] \quad A_{R1} = 3.50979812472990$$

$$2^{nd}\text{ order } B_{R\hat{a}2} \cong \frac{i\mu_0 I}{4}\frac{2\hbar a^2}{(h^2+a^2+z^2)^{5/2}}\left[3 + A_{R1}\left(\frac{W}{1-W}\right) + A_{R2}\left(\frac{ln(1-W)}{W}+1\right)\right]$$

$$A_{R1} = \frac{8\sqrt{2}}{\pi} \quad A_{R2} = 0.6495541988815$$

Axial 2nd order approximation

$$B_{\hat{A}z2} \cong \frac{\mu_0 I}{4}\frac{1}{(h^2+a^2+z^2)^{1/2}}\left[\frac{2a^2}{(h^2+a^2+z^2)}B_z - \frac{W}{4}A_z\right]$$

$$A_z = \left[3 + A_{z1}\left(\frac{W}{1-W}\right) + A_{z2}\left(\frac{ln(1-W)}{W}+1\right)\right]$$

$$B_z = \left[1 + B_{z1}\left(\frac{W}{1-W}\right) + B_{z2}\left(\frac{ln(1-W)}{W}+1\right)\right]$$

A_{z1}=3.60100981620484 A_{z2}=0.6506161246956

B_{z1}=0.900300245405 12 B_{z2}=-0.0675136749143

Figure 1: Current loop off axis field approximations of order 1 and 2

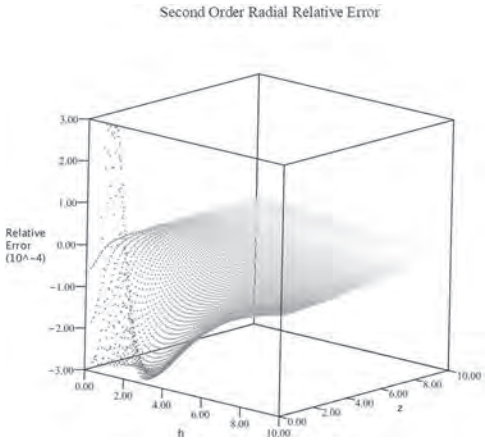

Figure 2: Radial field 2nd order approximation relative error

JOF-09. Analytical Modeling and Optimization of High Temperature Superconducting Single-sided Linear Induction Motor. *W. Qin*[1]

1. School of Electrical Engineering, Beijing Jiaotong University, Beijing, China

I. INTRODUCTION Single-sided linear induction motors (SLIMs) are widely applied in urban transportation system[1-3]. In order to increase the output power as well as to reduce the size of a machine, high temperature superconducting (HTS) SLIM, which is able to make the motor lighter and more compact while keeping large thrust to propel the traditional train or Maglev vehicle[4,5], has been developed successfully, shown as in Fig.1. However, the structure of HTS SLIM is very different from conventional LIM, and the material properties as the electrical conductivity and the magnetic permeability are more complicated than the conventional materials. To evaluate the performance of the HTS SLIM, the traditional analysis methods should be modified by considering the material properties of the HTS. This paper presents an improved analytical subdomain model for predicting the magnetic field and the and structural parameters on performance in HTS SLIM with semi-closed slots where the finite length of primary iron core and the electromagnetic state of the superconductor is taken into account. II. MACHINE TOPOLOGIES The configuration of the HTS SLIM is shown in Fig. 1. The main structure of this SLIM includes one mover (primary) and one stator (secondary). The developed HTS SLIM is composed of Bi-2223/Ag HTS coils cooled by liquid neon. Fig.1(a) shows the prototype of motor, where HTS primary coils consist of 15 double-pancakes with racetrack shape. The primary coils are arranged in 32 slots made of silicon steel. The primary of HTS SLIM, including the core and the coils, is placed in the cryostat filled with liquid neon. III. RESULTS AND VALIDATION In this paper, the HTS SLIM has been analytically modeled based on accurate subdomain with considering the slot parameters, critical current and end effects and so all, shown as in Fig.1(d). The flux density and force created by this analytical model are compared with FEM and experimental measurement shown as in Fig.2 and Tab.1, respectively. The implementation of analytical method and the influence of structural parameters on performance in the HTS LIM will also be discussed in the full paper.

[1]I. Boldea, CRC Press, U.K: London, pp. 55–128(2013). [2]Lv, G., Zeng, D. and Zhou, T. IEEE Trans. Ind. Electron., Vol, 64 (6), pp. 4382–4390(2017). [3]Boldea, I., Tutelea, and L.N., IEEE Trans. Ind. Electron., Vol, 65 (9), pp. 7504–7515(2018). [4]J. Zhao, T.Q. Zheng,., Physica. C., Vol, 471, pp. 1474-1478(2011). [5]Dong Li, Weili Li and Jin Fang., IEEE Trans. Appl. Supercond, Vol, 24, no.5, pp. 3600710(2014).

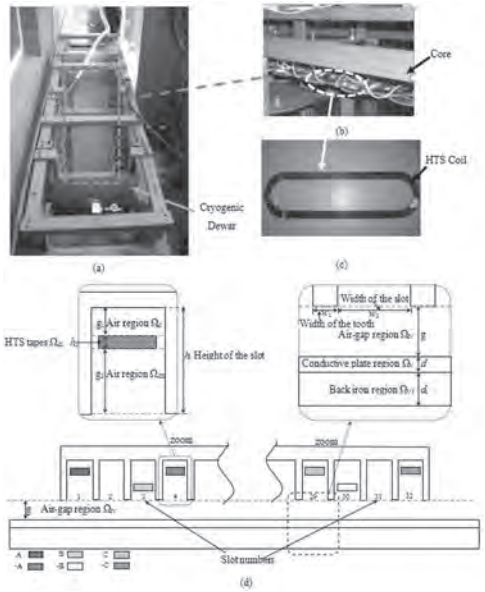

Fig.1 The configuration of the HTS SLIM

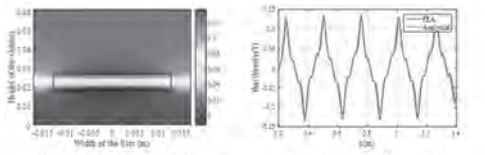

Fig.2 magnetic flux in slot and air-gap

Table .1 The thrust force comparision between analtical, FEM and experimental measurement

Phase Current	frequency	speed	Analytical	FEA	Measurement
13.7A	10Hz	0.968m/s	272N	275N	208N
18.0A	10Hz	0.671m/s	533N	540N	410N
22.0A	8Hz	0.597m/s	627N	630N	493N
25.7A	6Hz	0.254m/s	1090N	1080N	786N
28.6A	5Hz	0.246m/s	1117N	1130N	839N
33.1A	4Hz	0.287m/s	1140N	1156N	861N

Fig.2 and Table 1 Feild and Forces Results

JOF-10. Design and Analytical Magnetic Modeling of a Spherical Motion Generator with Multi-dof Electromagnetic Actuation.
X. Li[1] and S. Bai[1] *1. Department of Materials and Production, Aalborg University, Aalborg, Denmark*

A spherical motion generator (SMG) is a kind of mechanism or actuators that can obtain multi-degree-of-freedom (multi-dof) spherical motion [1,2]. SMGs such as permanent magnet spherical motors are driven by the interaction between spatially distributed permanent magnets (PMs) and air-core coils [3]. However, this type of SMGs have very limited torque outputs and confined tilting motion. To overcome these limitations, this paper proposes a novel design of SMG with integration of 3-dof actuation. The multi-dof actuation is implemented by the driving principle of spherical motors instead of attached motors and gears which increase the weight and cause hysteresis errors [4]. As shown in Fig. 1, the design of integrated SMG is mainly constructed by two parts: a spherical parallel manipulator (SPM) with infinite torsional motion and 3-dof electromagnetic actuation structure. The SPM composes a mobile platform and three slide units that are connected with each other by three identical links [5,6]. The slide units can move separately around the circular guide. Iron-core coils attached with the slide units are the rotors of the actuation structure, and the rotors are surrounded by evenly distributed PMs. Additionally, a passive spherical joint is integrated with the SPM design for position detection [7]. In this design, the air-core coils are replaced by iron cores to obtain an improvement in torque output, and the PM stator is skewed to reduce the cogging torque. In the paper, the design and working principle of this special SMG is introduced. The magnetic field distribution of SMG is studied by using the equivalent magnetic charge method. The analytical results of the magnetic flux density are validated by FEM with reasonable accuracy. In addition, an analytical cogging torque model is established. By discussing the skewing of the outer PM stator, the cogging torque can be minimized as shown in Fig. 2. The reduction of cogging torque helps to avoid mechanical vibration and obtain smooth rotation without changing the operating torque or output power. The analytical model can be used for further modeling, elimination of cogging torque and the optimization of design parameters.

[1] S. Bai, X. Li, and J. Angeles, Mechanism and Machine Theory, Vol. 140, p. 377-388 (2019). [2] F. Chai, L. Gan and Y. Pei, IEEE Transactions on Industry Applications, Vol. 56, p. 6338-6347 (2020). [3] D. Kang and J. Lee, IEEE Transactions on Magnetics, vol. 50, p. 785-788 (2014). [4] J. Enferadi and A. Shahi, Robotics and Computer-Integrated Manufacturing, Vol. 37, p. 151 – 161 (2016). [5] C. M. Gosselin and J. F. Hamel, 1994 IEEE International Conference on Robotics and Automation, Vol. 1, p. 781-786 (1994). [6] I. Tursynbek and A. Shintemirov, IEEE/ASME International Conference on Advanced Intelligent Mechatronics, p. 1780-1785 (2020). [7] J. Liu, H. Deng and C. Hu, Aerospace Science and Technology, Vol. 67, p. 62-71 (2017). [8] X. Li, J. Liu and W. Chen, Journal of Magnetism and Magnetic Materials, Vol. 493, p. 165707 1-11 (2020).

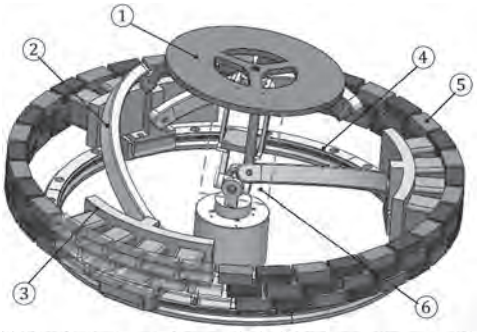

① Mobile platform; ②Curved link; ③Slide unit (Rotor coils); ④Circular guide; ⑤Stator PMs; ⑥ Passive spherical joint (Position detection unit)

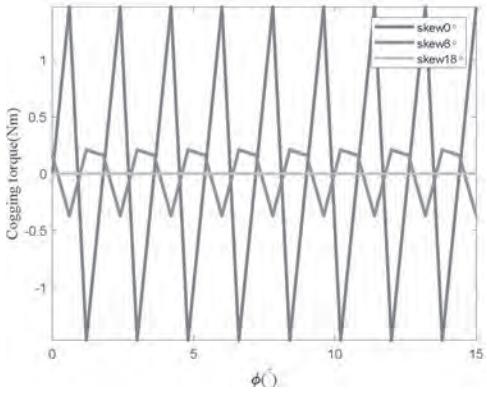

JOF-11. Efficient Modeling Framework for the Synthesis of a Novel Magnet Array for Planar Motors. A. Casado Ramoneda[1], *M. Kleijer*[1], D. Krop[1] and E. Lomonova[1] *1. Electrical Engineering, Eindhoven University of Technology, Eindhoven, Netherlands*

INTRODUCTION Nowadays, given the rapid growth of industry electronification, there is a huge demand for microchips [1,2]. Therefore, the lithography industry has a necessity to improve the wafer positioning systems such that the throughput of the lithography machine is increased. To reduce the mass and to remove the cable slabs of the traditional double stroke wafer positioning system [3,4], a single stage system has been proposed in [5], consisting of two vertically attached stationary coils and a moving magnet array. A 2D schematic of this Dual Layer Planar Motor (DLPM) is shown in Fig. 1. The employed Halbach array does not utilize the entire available space. Furthermore, the magnet-to-magnet force within the array results in an undesired mover bending. This paper presents a framework to evaluate different novel magnet array architectures for the DLPM. Different configurations are analysed such that the secondary magnetization patterns of the Halbach array fully utilize the available space. Furthermore, an optimization is performed to enhance the thrust and levitation forces, while curtailing the magnet array bending. *METHOD* The presented tool is semi-analytical: the magnet flux densities are obtained analytically based on the Magnetic Charge Modeling method and the coil bed flux densities through the evaluation of the Biot-Savart's law for a current carrying volume. The electromagnetic forces are derived numerically utilizing the Maxwell Stress Tensor. *CONCLUSION* The proposed analytical modeling method presents a framework for fast and accurate optimization of the DLPM. The model has been verified with Finite Element Modeling (FEM). Moreover, the approach improves the computation time compared to FEM in a maximum of a factor of 20. The optimization achieves a higher levitation force to weight ratio, even with the added magnet mass, according to Fig. 2. This releases stress from the power supply design as a lower heat dissipation requirement suffices. In the full paper the modeling approach will be elaborated on and the optimization for the thrust force is going to be addressed.

[1] P. Galloway, "Personal computers, microhistory, and shared authority: Documenting the inventor-early adopter dialectic," IEEE Annals of the History of Computing, vol. 33, no. 2, pp. 60–74, 2011. [2] S. Greenstein, "Shortages of integrated circuits," IEEE Micro, vol. 41, no. 4, pp. 86–88, 2021. [3] I. J. Compter, "Electro-dynamic planar motor," Precision Engineering, vol. 28, no. 2, pp. 171–180, 2004. [4] J. de Boeij, E. Lomonova, and J. Duarte, "Contactless planar actuator with manipulator: A motion system without cables and physical contact between the mover and the fixed world," IEEE Transactions on Industry Applications, vol. 45, no. 6, pp. 1930–1938, 2009. [5] J. Rovers, J. Jansen, and E. Lomonova, "Design and measurements of the double layer planar motor," International Electric Machines Drives Conference, 2013, pp. 204–211.

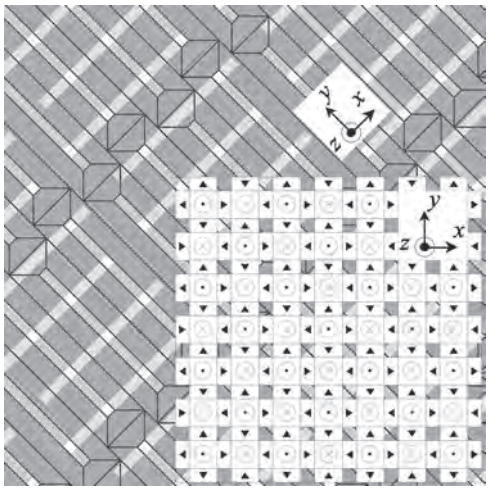

Fig. 1: Overhead view schematic of the DLPM.

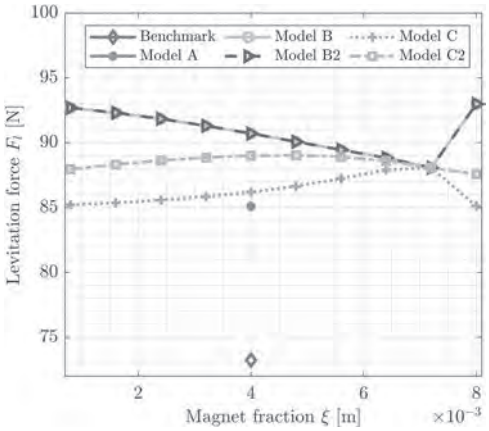

Fig. 2: Levitation force optimization results given different secondary magnetization expansions.

JOF-12. 3-D Analytical Magnetic Field Analysis of Axial Flux Coreless Permanent-Magnet Machine. *W. Qin*[1] and Y. Ma[2] *1. School of Electrical Engineering, Beijing Jiaotong University, Beijing, China; 2. Taiyuan Institute of China Coal Technology and Engineering Group, Taiyuan, China*

I. INTRODUCTION Coreless axial-flux permanent-magnet synchronous machines (AFPMSMs) have many advantages such as high power density, simple structure, high overload capability, no cogging torque and so on. It has been used more and more widely in many applications, such as flywheel energy storage systems, wind energy power generation, electric vehicles, and ultra-precision positioning and processing areas [1-3]. However, it is difficulty to accurate modeling of AFPMSM as 3D electromagnetic problems, such as the curvature effect and fringing effect[4-5]. To solve this problem, a three-dimensional analytical magnetic field analysis of the coreless AFPMSM based on based on the volume integral method is presented. II. ANALYTICAL MODEL The 3-D geometric model of the coreless AFPMSM is shown in Fig. 1 (a). This coreless AFPMSM consisting of one stator with ironless winding and two rotors with Halbach magnet array mounted on nonmagnetic supports. The Biot-Savart's law and volume integral approach is used to compute the magnetic field produced for the coils and PMs. The Halbach rotor modeled using equivalent current sheets. The 3-D analytical model for coils, axial magnetized magnets and shunt magnets are shown in Fig. 1(b),(c)and(d). The calculation of the magnetic field using the integral equations is obtained in very short times thanks to the use of particular volumetric basis elements for which the solution is obtained analytically. III. RESULTS AND VALIDATION The distribution waveforms of the z-component flux density at the central of the air gap under no-load condition are calculated by the proposed analytical method and FEM. As could be seen from Fig. 2 (a)and (b), the two waveforms match each other very well. The B_z at the average radius and outer radius calculated by the proposed model and 3D FEM are shown in Fig. 2(c) and (d), with a discrepancy of less than 4%. This is due to the difference in permeability between the proposed model and 3D FEM. More in-depth analysis and results will be present in the full paper.

[1] Z. Kohari, Z. Nadudvari, L. Szlama, M. Keresztesi, and I. Csaki, IEEE Trans. Appl. Supercond., vol. 21, no. 3, pp. 1497–1501. (2011). [2] T. F. Chan, L. L. Lai, IEEE Trans. Energy Convers., vol. 22, no. 1, pp. 86–94. (2007). [3] N. Taran, V. Rallabandi, G. Heins, and D. M. Ionel, IEEE Trans. Ind. Appl., vol. 54, no. 6, pp. 5907–5917. (2018). [4] Xu L, Xu Y, Gong J.. IEEE Transactions on Magnetics, vol. 54, no. 11, pp. 1-5.(2018). [5] Daghigh A, Javadi H, Torkaman H. IEEE Transactions on Magnetics, vol.52, no.9.(2016).

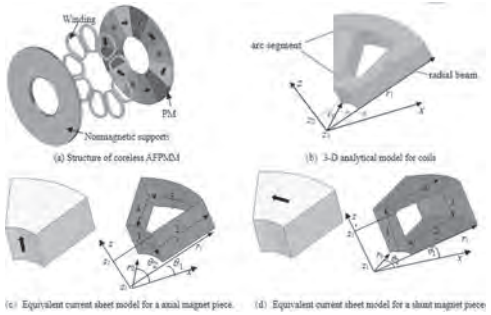

Fig.1 3-D schematic and analytical model of AFPMSM.

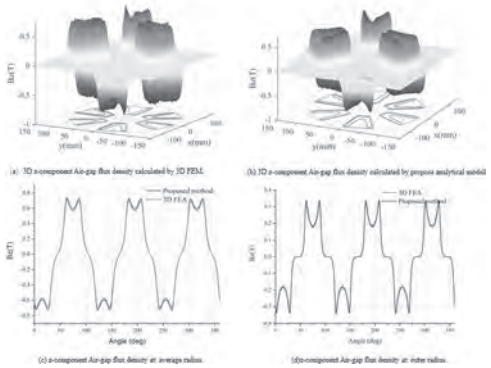

Fig.2 Z-component magnetic flux density comparison between a FEA model and analytic model along

JOF-13. Reduced Order Modeling Based on Multiport Cauer Ladder Network for Space Harmonics of Air-gap Flux Density in Cage Induction Motor. *Y. Takahashi*[1], K. Fujiwara[1], K. Sugahara[3] and T. Matsuo[2] *1. Department of Electrical Engineering, Doshisha University, Kyoto, Japan; 2. Graduate School of Engineering, Kyoto University, Kyoto, Japan; 3. Faculty of Science and Engineering, Kindai University, Osaka, Japan*

Because the direct coupling of a finite-element method (FEM) with circuit simulation of motors under speed/torque control generally requires huge computational costs, various model order reduction (MOR) techniques [1], [2] are frequently adopted for a current- and position-dependent motor model. As one of the hopeful MOR methods for a cage induction motor (IM), the Cauer ladder network (CLN) method [3] has been reported [4]. In this method, first, the Cauer circuit representations for the stator and rotor domains are constructed separately. Then, the Cauer circuit corresponding to each domain is connected based on the boundary conditions which the space harmonics (SHs) of an air-gap flux density waveform satisfy. However,

how to select the dominant components of the SHs has not been discussed. Because the increase in the number of SHs leads to a large computational cost, it is desired to apply as few components as possible to formulate the multiport CLN method. This paper proposes the method to select the appropriate number of SHs based on time and space harmonics analysis of the air-gap flux density waveform [5]. The dominant SHs, which are greater than p % of the fundamental, are extracted when the slip is 1. Furthermore, the procedure to derive circuit parameters in the Cauer circuit is modified to satisfy the condition that the sum of bar currents in the rotor domain is always zero [6]. Fig. 1 compares the flux lines given by the existing and the improved CLN methods. The proposed procedure enables us to obtain reasonable flux lines. Finally, the developed motor model is applied to the circuit simulation of a cage IM under speed control. Fig. 2 compares the time variation of a torque obtained from the FEM and the CLN method at $p = 1$ or $p = 5$. The numerical results are in good agreement even when using the CLN method at $p = 5$. The computation time of the FEM is about 2 h. In contrast, the CLN method at $p = 1$ and at $p = 5$ require about 60 s and about 23 s, respectively, which indicates the effectiveness of the proposed method. The detail of the proposed approach and more numerical results will be included in the full paper.

[1] T. Henneron and S. Clénet, *Int. J. Numer. Model.*, vol. 27, pp. 485-494, Feb. 2014. [2] T. Shimotani, Y. Sato, T. Sato, et al., *IEEE Trans. Magn.*, vol. 52, no. 3, Mar. 2016, Art. no. 7207004. [3] A. Kameari, H. Ebrahimi, K. Sugahara, et al., *IEEE Trans. Magn.*, vol. 54, no. 3, Mar. 2018, Art. no. 7201804. [4] T. Matsuo, K. Sugahara, A. Kameari, et al., *IEEE Trans. Magn.*, vol. 56, no. 3, Mar. 2020, Art no. 7514704. [5] H. Mikami, K. Ide, M. Takahashi, et al., *IEEE Trans. Energy Convers.*, vol. 14, no. 3, pp. 464-470, Sept. 1999. [6] H. Ebrahimi, K. Sugaraha, T. Matsuo, et al., *IEEE Trans. Magn.*, vol. 56, no. 3, 7513004, Mar. 2020.

Fig. 1. Comparison of flux lines.

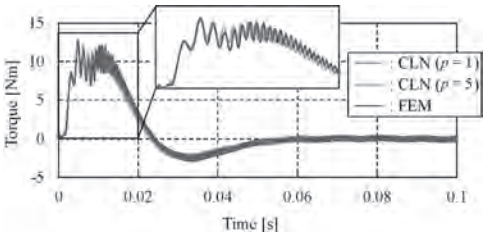

Fig. 2. Circuit simulation coupled with control system.

JOF-14. Comparaison Between Analytical and Reluctance Network Models in the Sizing Optimization of Permanent Magnet Synchronous Generator for Large Wind Turbine. *A. Bensalah*[1], G. Barakat[1] and Y. Amara[1] *1. Université Le Havre Normandie, Le Havre, France*

Reducing the time of the pre-design phase is an arduous task since the relationships between the different parameters and performances of the electrical machines are mostly nonlinear and highly complex. In the last decade a large number of methods has been proposed to predicted the magnetic field in electric machines. Few studies have focused on the comparison of those design models for high-power level machines. This paper presents a comparative study, for early-stage design, of three modeling techniques used on the design optimization of Permanent Magnet Synchronous Generators (PMSG) (See Fig.1) in order to determine the suitable candidate at Multi-MegaWatts (15 MW) rating. The first section exposes the multi-physical models of the selected machines. Two 2D (two-dimensional) magnetic models are presented. The first one is based on an analytical model, considering the direct solution of Maxwell equations using separation of variable technique. However, the second is issued from reluctance network using mesh-based formulation. In order to ensure optimum design and construction of the generator, a lumped network model is used to analyze the thermal behavior of the machine. These models are presented along with their relative advantages and drawbacks (accuracy, computation time). In the second section, multi-objectives optimization using genetic algorithm (NSGA-II) coupled with the already developed multiphysics model is applied to optimize the rare-earth permanent magnet mass within the generator. The obtained Pareto fronts corresponding to each of the two models optimization are then compared in terms of precision and computation time. Even if analytical model is less precise than reluctance network one, it appears clearly that the former is suitable for the early stages of the design process because it allows fast computation in case of large geometrical dimension variations which could be highly time consuming with the meshed (RN or FE) models. At the preliminary design stage an air-gap width of 20 mm, 42 pole and 420 slots has been adopted, with respect to a torque ≥ 1.8e6 MNm and T_{max}<125 °C in the slot. Fig.2 presents the preliminary results for the single stage geared PMSGs.

[1] H. Polinder, F. F. A. van der Pijl, G. -. de Vilder and P. J. Tavner, "Comparison of direct-drive and geared generator concepts for wind turbines," in IEEE Transactions on Energy Conversion, vol. 21, no. 3, pp. 725-733, Sept. 2006. [2] T. Huguette, A. Yacine and G. Barakat, "Overview of analytical models of permanent magnet electrical machines for analysis and design purposes". Mathematics and Computers in Simulation. 90. 162–177. [3] M.A. Benhamida, H. Ennassiri, Y. Amara, "Reluctance network lumped mechanical & thermal models for the modeling and predesign of concentrated flux synchronous machine". Open Physics. 16. 692-705.

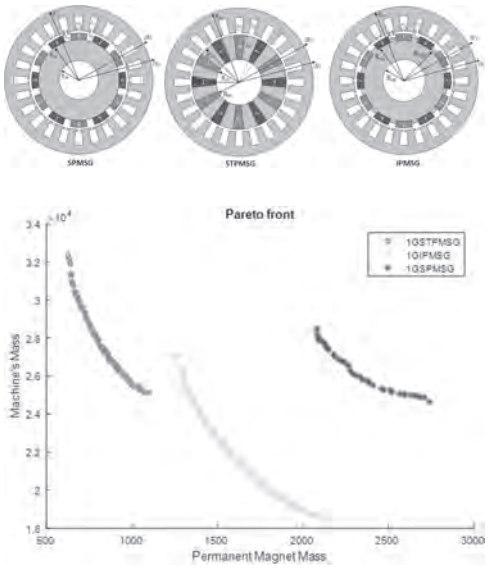

JOF-15. 3D Permeance Network Modeling for an Axial Field Flux Focusing Magnetic Gear. *H. Diab*[1], Y. Amara[1] and G. Barakat[1] *1. Université Le Havre Normandie, GREAH, Le Havre, France*

Magnetic gears (MGs) have emerged in the last 20 years with promising torque densities [1]-[5]. Some of their potential advantages are reduced maintenance and improved reliability. Axial field MGs offer multiple possible advantages over radial field configurations [6]. However, modeling axial field structures requires a 3D geometrical model to properly represent its performance. The purpose of this work is to present a 3D permeance network modeling technique for axial field flux focusing magnetic gears. Permeance network (PN) is a very well-known modeling technique. It's based on the concept of flux tubes where the geometry is divided into blocks with a central node, and then the network equations are generated using Gauss's law, which states that the sum of all fluxes into a node must be zero [7][8]. The unknowns to be solved then are magnetic scalar potential

values at every node. The nodes are connected through a lumped component which can be permeance or a source. Figure 1 shows the MG structure to be modeled with the elementary permeance block. It consists of three parts, a high-speed rotor (HSR), a low-speed rotor (LSR), and a stationary part. The versatility of the model will be demonstrated by changing multiple variables and calculating different quantities. Figure 2 compares the magnetic induction components calculated using the 3D PN model and a mean radius 2D finite element method model (FEM). The calculated components are at the LSR air gap side. The permanent magnets and the ferromagnetic materials were considered in their linear case with μ_{rf} = 10000, μ_{rpm} = 1, and B_r = 1.25T. The differences between the 2D model and the proposed 3D model are visible, where we can see a difference in the amplitudes and shapes which demonstrates the importance of the radial component in the axial field structures. The full work will demonstrate more the potential of the proposed model by performing linear and non-linear calculations and showing how this model can be very suitable for early design stages.

[1] K. Atallah and D. Howe, in IEEE Transactions on Magnetics, vol. 37, no. 4, pp. 2844-2846, (2001) [2] K. Atallah, J. Wang, and D. Howe, Journal of Applied Physics, vol. 97, no. 10, p. 10N516, (2005) [3] S. Mezani, K. Atallah, and D. Howe, Journal of Applied Physics, vol. 99, no. 8, p. 08R303, (2006) [4] V. M. Acharya, M. Calvin and J. Z. Bird, 7th IET International Conference on Power Electronics, Machines and Drives, pp. 1-6, (2014) [5] P. O. Rasmussen, T. O. Andersen, F. T. Joergensen and O. Nielsen, 38th IAS, pp. 1696-1702 vol.3, (2003) [6] M. Johnson, A. Shapoury and P. Boghrat, 2014 IEEE Energy Conversion Congress and Exposition (ECCE), pp. 5893-5900, (2014) [7] V. Ostović, Dynamics of Saturated Electric Machines. New York, NY: Springer New York, 1989. doi: 10.1007/978-1-4613-8933-0. [8] M. Amrhein and P. T. Krein, IEEE Trans. Energy Convers., vol. 24, no. 2, pp. 397–405, (2009)

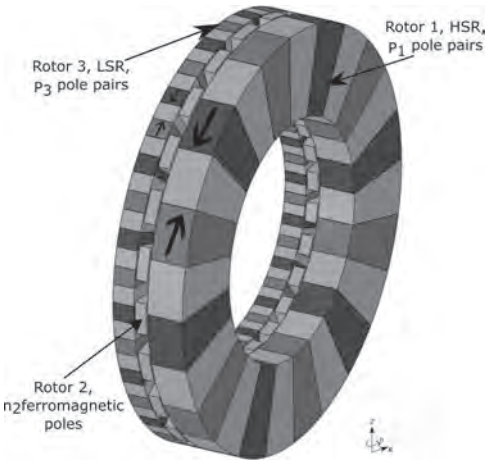

Fig.1 Flux focusing axial field magnetic gear with p1=6, n2=24, and p3=18 pole-pairs.

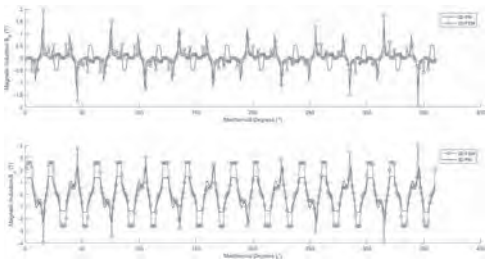

Fig.2 Axial and radial magnetic induction components calculated using the 3D PN and a 2D FEM model at the LSR airgap side.

Session JOG
DESIGN OPTIMIZATION, LOSS AND THERMAL MODELLINGS, MEASUREMENT OF ELECTRICAL MACHINES

Kyung-Hun Shin, Chair
Chonnam National University, Yeosu, The Republic of Korea

INVITED PAPER

JOG-01. From Backstage to Center Stage: Auxiliary Automotive Drives. *A. Mütze*[1] *1. Electric Drives and Machines Institute, Graz University of Technology, Graz, Austria*

While the important role of electric machnes on transportation electrification has risen to the foreground on many fronts, the millions of auxiliary drives used in automotive application have continued to remain one of the industry's best kept secrets hidden under the hood. With more than 100 of such auxiliary drives in typical mid-size and large executive cars, their role in enabling today's modern car's performances is of exceptional importance. Given the additional design freedom and performance spaces opened up by the use of power electronics, the number of such small electric drives in automotive applications has at least doubled over the course of the past two decades. Performance, safety, and comfort related drives become distinguished, and interest has spiked in terms of energy conversion efficiency, size, and cost, as well as when it comes to electromagnetic emission, noise, and fault tolerance. In this talk, we will discuss how these seemingly unnoticed small drives have been completely revolutionized within the recent years, where the beauty and power often emerge in rediscovering simplicity itself. Some examples explored in this talk include a simple drive re-design that can be considered during manufacturing, experimental determination of these drives' cogging torque, which are in the sub-milli Newtonmeter range, as well as increasing drive efficiency by reducing the control to its essence.

CONTRIBUTED PAPERS

JOG-02. A boundary topology optimization approach for lightweighting electric machines inspired by additive manufacturing. *L. Sethuraman*[1] and G. Vijayakumar[1] *1. National Wind Technology Center, National Renewable Energy Laboratory, Golden, CO, United States*

Minimizing the mass in electric machines while maintaining superior performance has become a new requirement for the advancement of drive trains used in wind energy and electric mobility. Topology Optimization (TO) for light-weighting electric machines using traditional approaches typically explore a restricted design space allowed by standard parameterizable geometry and manufacturing, while advanced methods like cell-based density approaches[1] suffer from a lack of robust manufacturability constraints during the optimization process. To overcome these drawbacks and identify best designs in terms of material reduction, we explore a grid-independent, boundary TO [2] where the outer boundary shape of the magnet is parameterized using Bezier curves. This approach will allow us to explore a large design space of free-form magnet shapes using fewer variables compared to cell-based TO methods while ensuring smooth boundaries for additive manufacturing. We conduct a design of experiments (DOE) to study the effect of different magnet shapes on machine performance by varying the control points on the Bezier curves. Each resulting topology in the DOE is imported into a parametric 2-dimensional CAD environment to build solid models with magnets distributed in the region bounded by the curves and analyzed using magnetostatic finite element analysis (FEA). A machine-learning based surrogate model is constructed using the data from the DOE to quantify the relationship between the control points, air-gap torque and mass. The control points are then optimized to maximize the torque density. The final paper will demonstrate this approach for minimizing the electrical steel mass in the IEA-15MW radial flux direct-drive wind turbine generator [4]. Free-from boundary TO resulted in a smooth shape with up to 20 ton reduction in electrical steel mass.

[1] L.Sethuraman, G.Vijayakumar, S. Ananthan *et al. Forsch Ingenieurwes* 85, 287–311 (2021). [2] D. Kim, S.Lee, B. Kwank *et al. IEEE Transactions on Magnetics*, 44,1002-1005 (2008). [3] LaunchPoint Technologies 7.5" Dual Halbach Motor Specifications, Available online athttps://cdn2.hubspot.net/hubfs/53140/DHA-075-6-75-1-4T3PY%20Housed%20LP%20motor%20data%20sheet%20v3p11-1.pdf [4] E.Gaertner, J. Rinker, L.Sethuraman et al. 2020. National Renewable Energy Laboratory. NREL/TP-5000-75698.

JOG-03. Influence of magnetization fixture winding parameters on airgap flux profile and performance of isotropic bonded NdFeB motor. *N.K. Sheth*[1], R.C. Angara[1], K.W. Hsu[1], N.E. Onal[1] and P. Villar[1] *1. Research and Development, Neo Performance Materials Pte Ltd, Singapore, Singapore*

Isotropic bonded NdFeB magnets are used extensively in various automotive, office automation and home appliance motors. Due to their superior magnetic properties over ferrite magnet, better motor efficiency and increased power density can be achieved. The magnetizing fixture winding configuration is critical in achieving the desired magnet flux profile[1] and motor performance[2]. In this paper the effect of various fixture winding configurations on resultant magnet flux profile and motor performance is presented for a 4-pole automotive accessory motor. Magnetizing fixtures are designed using different sizes of round conductors to achieve 3T magnetizing field on the magnet. It is observed that when the number of turns is kept the same, 29% reduction in conductor diameter made magnetization profile more radial. When this magnetized magnet is used in a motor, peak to peak cogging torque increased by 20%. Using two-dimensional (2D) finite element analysis (FEA), magnetization fixtures are designed for six different winding configurations. Figure 1 shows four of the winding configurations evaluated using 2D FEA, to arrive at magnetized magnet profile and corresponding motor performance. Table I summarizes the flux integral of magnetized magnet profile and corresponding motor performance. From this table it is observed that for a 4-pole magnet, the '1-column' conductor arrangement where-in the conductors are arranged along the radial direction in slot resulted in radial flux profile and highest flux integral per pole, resulting in higher back-emf and cogging torque. On the other side the flux integral per pole is minimum and flux profile becomes more sinusoidal for '1 row' arrangement in which the conductors are arranged along a concentric arc from fixture core surface. This arrangement results in wider transition zone, and in lowest back-emf and cogging torque. All the designed magnetization fixtures were built, and performance of motors with magnetized magnets is evaluated. The experimental results are in good agreement with the simulation results.

1. Y. N. Zhilichev, "Precise Multipole Magnetization of Disc Magnet for Sensor Application", IEEE Trans on Magnetics, Vol. 39, Issue 5, pp 3301-3303, Sep 2003. 2. Seok-Myeong Jang, Han-Wook Cho, Sung-Ho Lee, Hyun-Sup Yang, and Yeon-Ho Jeong, "The Influence of Magnetization Pattern on the Rotor Losses of Permanent Magnet High-Speed Machines", IEEE Trans on Magnetics, Vol. 40, Issue 4, pp 2062-2064, Jul 2004.

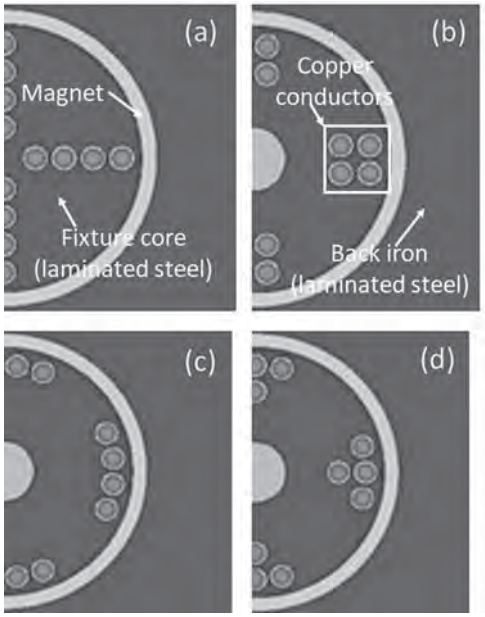

Fig.1. Various conductor arrangements (a) 1 column (b) 2 column (c) 1 row (d) Delta

Conductor configuration in the fixture slot	Flux Integral per pole ($T\text{-}^{n}$mech)	Motor back-emf integral ($V\text{-}^{n}$mech)	Peak-to-peak cogging torque (mN-m)
1 column	27.32	330	48
2 column	25.12	323	11
1 row	21.91	293	10
Delta	24.28	311	10

Table I Effect of conductor configuration on magnet flux and motor performance

JOG-04. A Novel Spoke-type PM Rotor with Hybrid Radial and Axial Flux Concentration for Reduction of Interpolar Leakage Flux.

J. Wang[2,1], W. Geng[2,1], Q. Li[2,1] and L. Li[2,1] *1. School of Automation, Naijing, China; 2. Nanjing University of Science and Technology, Naijing, China*

The flux leakages at axial end and radial inner side on the flux-concentrating rotor are more likely to generate, as shown in Fig.1, and therefore reduces the motor performance and degrades the utilization efficiency of PMs [1]-[3]. According to Table I, the modeling of the machines are carried out. Fig. 2 is the 2-D model. Fig. 3 shows the leakage flux by 3-D spoke type model. In Fig. 4, the air gap flux density, back electromotive forces (EMFs) and torque from the 2-D and 3-D analyses indicate a difference of approximately 10.33%, 5.88 % and 9.45%, respectively. Fig. 5 shows the rotor prototype and the test platform. The errors are 9.78% and 5.21% compared with the experiment respectively which indicates that the 3-D model is closer to the actual result than the 2-D model because the 3-D model takes leakage flux into account. The motor with novel rotors are shown in Fig. 6 and Fig. 7 which consumes the same weight of PMs with spoke-type model. The principle of reduction axial end leakage flux in Model 1 is shown in Fig. 6 (b). The details on the rotor of Model 2 is shown in Fig. 7 (b). The model in Fig. 6 is called Model 1. The model in Fig.7 is Model 2. Fig. 8 and Fig. 9 compare the rotor-end and rotor-interior leakage flux of two new structures and spoke-type motor under no-load. In the spoke type model the leakage flux is large, up to 0.9 T and 1.0 T. But it is only 0.38 T and 0.29 T in Model 1 and Model 2. The electromagnetic characteristics are compared in Fig. 10. Model 2 can further improve the air-gap flux density, back-EMF and torque, up to 1.499 T, 512.4 V and 68.7 Nm. In this paper, a novel rotor with hybrid radial and axial flux concentration considering leakage flux is designed. The 3-D models of concentrated winding PM motors with different rotors are built to analyze the leakage flux and electromagnetic performance. A 12-slot 10-pole motor with spoke type PM rotor is manufactured and experimented to verfy the significance of 3-D FEA takeing into account flux leakages. The 3-D FEA results of novel flux-concentrating PM rotors shows the axial leakage flux and rotor-interior leakage flux are decreased by 58.1% and 61.7%. The electromagnetic torque can be improved by 5.48% with phase current of 30 A.

REFERENCES S.-Il Kim, S. Park, T. Park, J. Cho, W. Kim, and S. Lim, "Investigation and experimental verification of a novel spoke-type ferrite-magnet motor for electric-vehicle traction drive applications," *IEEE Trans. Ind. Electron.*, vol. 61, no. 10, pp. 5763–5770, Feb. 2014. S. J. Galioto, P. B. Reddy, A. M. EL- Refaie, and J. P. Alexander, "Effect of magnet types on performance of high-speed spoke interior-permanent-magnet machines designed for traction applications," *IEEE Trans. Ind. Appl.*, vol. 51, no. 3, pp. 2148–2160, Dec. 2014. M. E.-R. Ayman et al., "Advanced high-power-density interior permanent magnet motor for traction applications," *IEEE Trans. Ind. Appl.*, vol. 50, no. 5, pp. 3235–3248, Feb. 2014.

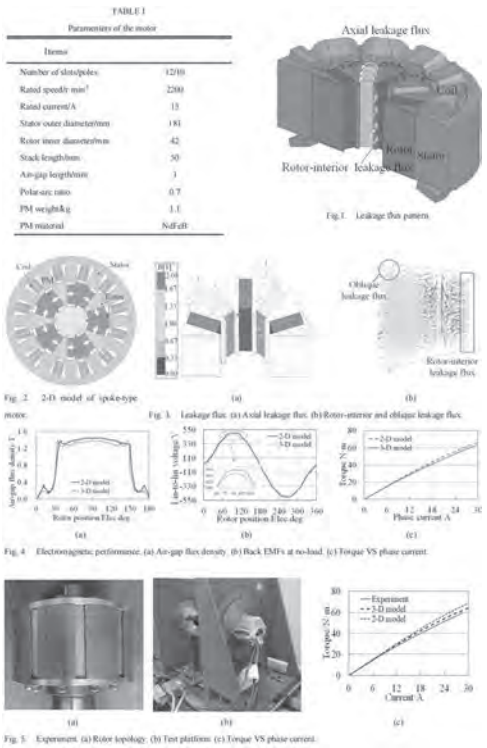

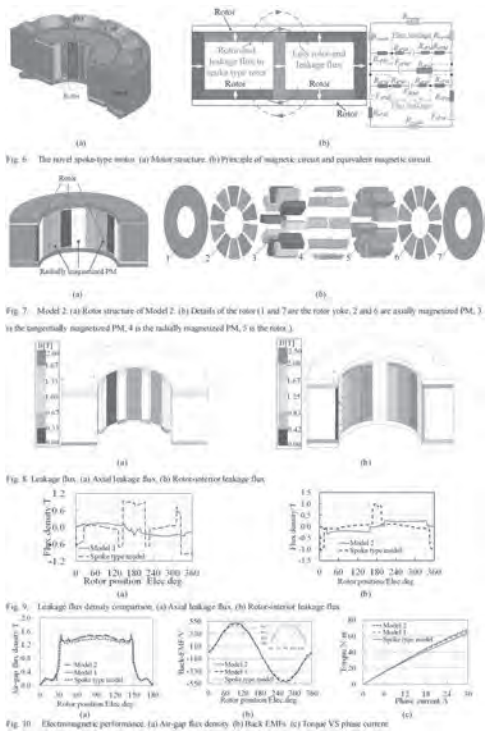

JOG-05. Iron Loss Calculation Method of Interior Permanent Magnet Motor Taking Carrier Harmonics into Account Based on Reluctance Network Analysis Representing Dynamic Hysteresis Characteristics. *Y. Hane*[1], Y. Uchiyama[2] and K. Nakamura[2] *1. Department of Electrical Engineering, Tohoku University, Sendai, Japan; 2. Department of Management Science and Technology, Tohoku University, Sendai, Japan*

It is necessary to accurately estimate iron loss including magnetic hysteresis behavior to develop high-efficiency electric machines. In a previous paper, a novel magnetic circuit model incorporating the play model [1] and Cauer circuit theory [2] was proposed. The play model is one of phenomenological models of the dc hysteresis characteristic. The Cauer circuit theory can simply express the skin effect by formulating the frequency characteristic of the complex permeability. Its calculation accuracy was proved by comparing the measured and calculated results of hysteresis loops and iron loss under PWM excitation by using simple-shaped ring cores. This paper presents that the above model is extended a reluctance network analysis (RNA) model to analyze devices with more complicated shapes such as motors. The proposed method is experimentally validated by using an IPM motor, which is generally driven by a PWM converter, as an object of discussion. Fig. 1(a) and (b) show the proposed RNA model of the IPM motor. In the stator core, each reluctance expresses the dc hysteresis characteristic and classical and anomalous eddy current losses. The dc hysteresis characteristic is represented by the play model, the classical eddy current loss is represented by the Cauer circuit theory, and the anomalous eddy current loss is represented by a simple controlled source element, respectively. On the other hand, each reluctance in an air gap and a rotor is determined by dimensions of each element and permeability of the materials, and each MMF generated from winding currents and permanent magnets is concentrated as a form of controlled source. Fig. 2(a) - (c) show the measured and calculated characteristics of torque, iron loss, and efficiency, respectively. Here, the theoretically infinite number of stages of the ladder circuit part which denotes classical eddy current loss is truncated at 3rd stage for practical use. From these figures, it is understood that both results are in good agreement. Besides, as shown in Fig. 2(d), the proposed method can draw the local hysteresis loop in a certain divided element, which is generally difficult to measure and calculate, though its calculation accuracy should be experimentally verified.

[1] S. Bobbio, G. Miano, C. Serpico, and C. Visone, "Models of Magnetic Hysteresis Based on Play and Stop Hysteresis", *IEEE Trans. Magn.*, Vol. 33, No. 6, pp. 4417-4426 (1997). [2] Y. Shindo and O. Noro, "Simple Circuit Simulation Models for the Eddy Current in Magnetic Sheets and Wires", *IEEJ Trans. FM*, Vol. 134, No. 4, pp.173-181 (2014). [3] K. Nakamura and O. Ichinokura, "Reluctance Network Based Dynamic Analysis in Power Magnetics," *IEEJ Trans. FM*, Vol.128, No.8, pp. 506-510 (2008).

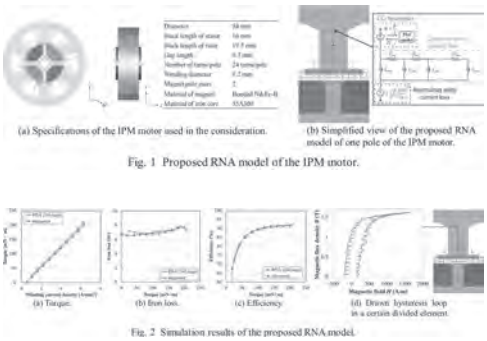

JOG-06. A Spoke Supported Superconducting Rotor with Rotating Cryocooler. *J. Xiao*[1], A. Samarakoon[1], T. Balachandran[1] and K. Haran[1] *1. University of Illinois at Urbana Champaign, Champaign, IL, United States*

This paper presents the design of a superconducting rotor with a spoke supported structure that minimizes the heat loss and enables the motor to be cooled by one cryocooler. The main challenge with the superconducting machines is the need to maintain the superconducting coils at cryogenic temperatures. Though usually placed in the vacuum, the cryogenic coils still receive a large amount of heat through the conduction of the torque tube which connects to the ambient temperature. The heat flown into the system exceeds the cooling capacity of a cryocooler and requires the boiling of cryogen, which comes with a more complicated and bulky hardware system[1][2]. The superconducting rotor proposed in this paper uses a spoke system to support the cryogenic windings. Connecting the windings to the shaft, the flexible spokes with low thermal conductivities transfer the torque from the windings to the shaft. The spoke system has much lower thermal conductivity than a traditional torque tube. Preliminary results show that with the ambient temperature 293K and the cryogenic temperature at 40K, the total heat transfer rate from the ambient environment to the cryogenic environment is about 4W, within the capability of a cryocooler that can be mounted on the rotor[3]. The cryocooler is arranged concentrically with the shaft of the rotor. Thermal straps connecting the cold end of the cryocooler to the windings to conduct the heat. An analytical thermal model is built for the rotor. The rotor's mechanical property and its thermal behavior are analyzed jointly so that the spoke system is optimized for high stress and lightweight. A physical model is also built to test the cryocooler performance in the rotational environment. A previous studies shows that the sterling-cycle cryocooler performance has not deteriorated at 1800rpm at the temperature of 100K[4][5]. The proposed design involves a lower operating temperature at 40K and a high vacuum environment surrounding the cold head.

[1] T. Balachandran, A. Yoon and D. Lee, "Ultra-High-Field, High-Efficiency Superconducting Machines for Offshore Wind Turbines," *IEEE Transactions on Magnetics*, doi: 10.1109/TMAG.2021.3094163. [2] B. -C. Kim and D. -W. Kang, "A Study on the Novel Design to Improve Efficiency of Wound Field Synchronous Machine, "*IEEE Transactions on Magnetics*, vol. 57, no. 2, pp. 1-6 (2021) [3] P. Tixador, Y. Brunet and P. Vedrine, "Electrical tests on a fully superconducting synchronous machine," *IEEE Transactions on Magnetics*, vol. 27, no. 2, pp. 2256-2259 (1991) [4] J. Ko, S. Jeong and H.Kim, "Rotating Cryocooler for Superconducting Motor," AIP Conference Proceedings 823, 653-660 (2006) [5] R. W. Dyson, R. H. Jansen and K. P. Duffy, "High Efficiency Megawatt Machine Rotating Cryocooler Conceptual Design," 2019 AIAA/IEEE Electric Aircraft Technologies Symposium (EATS), pp. 1-15 (2019)

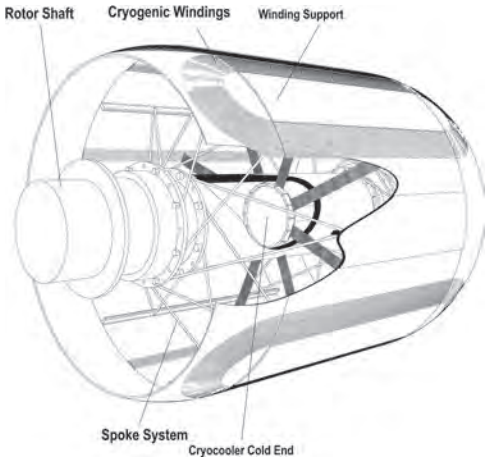

Figure1: The Drive End Cut-away Figure of the Superconducting Rotor

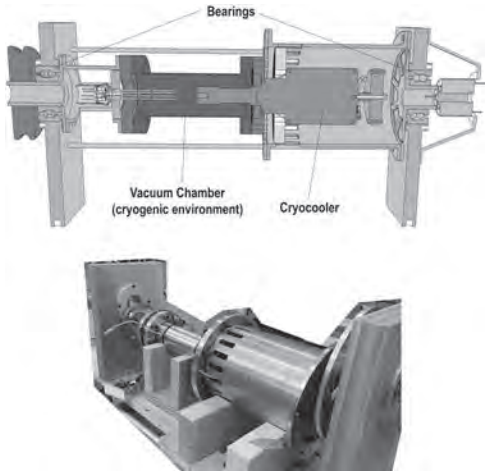

Figure2: Rotating Cryocooler Test Setup CAD Model and Physical Apparatus

JOG-07. Withdrawn

JOG-08. Analytical Investigation and Optimization of Surface Mounted Permanent Machines With Hybrid Magnetic Structure.
B. Poudel[1] and E. Amiri[1] *1. Department of Electrical and Electronics Engineering, University of New Orleans, New Orleans, LA, United States*

Due to the high cost of high energy rare earth (RE) magnetic material, design and analysis of motor topologies with low RE magnetic volume has become the subject of interest in many industrial applications [1]. The reduction of RE magnetic volume can be realized by replacing a portion of RE magnets with Ferrite magnets, referred to as hybrid structure (Fig. 1a) [2]. However, this should be accompanied by a systematic optimization to ensure the two types of magnets operate in a perfect harmony, and avoid undermining the overall performance of the machine. Finite element method (FEM) is a precise tool for designing and analyzing the performance of the machine but is computationally inefficient, particularly in optimization phase where it involves multiple iterative analysis loops [3]. Alternatively, the analysis can be carried analytically to avoid excessive computations. For this purpose, this paper presents an analytical modeling based on the airgap field modulation theory [4] to investigate and compare the response of the surface-mounted hybrid PM machines (Fig. 1a) against its baseline RE-PM counterpart (Fig. 1b). Next, we make use of the established analytical model for achieving the optimized design. The primitive magneto-motive force (MMF) generated by the rotor magnets is modulated by the stator teeth. As a result, the effective MMF is calculated by multiplying the primitive MMF of the rotor magnets with the permeance function (Fig. 2). Given that the permeability of RE and Ferrite magnets is different, the armature reaction field is also modulated by the salient rotor, despite the smooth structure of the round rotor core. The modulated armature reaction MMF of the hybrid structure will result in higher harmonics which will be extensively analyzed in torque production mechanism of the machine. Next, the machine structure is optimized using Genetic Algorithm (GA). The GA is chosen to exploit the crossover functionality and mutation feature of the algorithm.

B. Poudel, E. Amiri, P. Rastgoufard, *IEEE Transactions on Magnetics*, (2021) Q. Chen, G. Liu, W. Zhao, *IEEE Trans on Magnetics*, vol. 50, no. 12, pp. 1-10, Art no. 8207010, (2014). M. Ghahfarokhi, S.T. Boroujeni, A. D. Aliabad, *IET Electric Power Applications*, Vol. 14, Issue. 3, pp. 398-408, (2020). M. Cheng, P. Han and W. Hua, *IEEE Trans on Industrial Electronics*, vol. 64, no. 8, pp. 6063-6074, (2017).

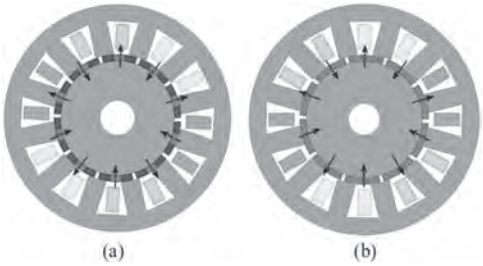

Fig. 1. SPM machine structure of (a) hybrid structure (b) baseline structure.

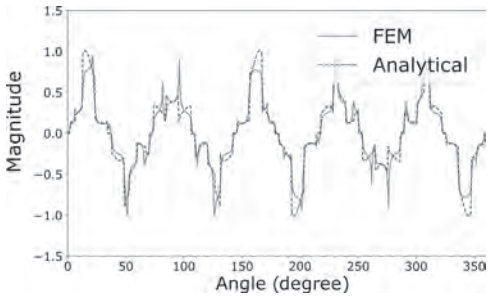

Fig. 2. The distribution of the Rotor PM MMF modulated by salient stator.

JOG-09. Reactor Vibration Reduction Using Global Topology Optimization Algorithms.
T. Ben[1,2], *P. Zhang*[1], L. Chen[1,2] and L. Hou[1] *1. College of Electrical Engineering and New Energy, China Three Gorges University, Yichang, China; 2. State Key Laboratory of Reliability and Intelligence of Electrical Equipment, Hebei University of Technology, Tianjin, China*

I Introduction Reactors have been widely used to ensure the stability of the power system by limiting short-circuit current, suppressing harmonic and compensating reactive power. There are some methods realize the vibration reduction of the reactor from the angle of the material filled at the air gap[1-2]. However, in order to improve this serious noise problem of the reactor, it is necessary to study the vibration reduction from the source of reactor vibration. Therefore, an optimization method based on topology optimization and GA(genetic algorithm) is proposed in this paper to reduce the segmented core reactor's vibration. II Topology Optimization of the Reactor This paper adopts the method of active vibration reduction and proposes a global topology optimization algorithm to get a novel design of the reactor. First, the electromagnetic-mechanical coupling model of the reactor is established to analyze the vibration and deformation of the reactor, which are shown in Fig1.(a-c). Second, the optimization problem is defined to obtain optimal configuration that minimum the vibration displacement of the

reactor under a minimum bound of the total volume. Then, by introducing a SIMP(Solid Isotropic Material with Penalization) function into the definition of the permeability of the reactor's air gap part materials, the distribution of ferromagnetic material is represented. Meanwhile, the inductance value of the reactor can be kept stable in the optimization process through the joint GA. Finally, a novel reactor structure is obtained as shown in Fig2.(a) and the finite element numerical method is used to calculate the optimized parameter values before and after the optimization to verify the excellence of the design. III Conclusion The calculation result at sampling point A is shown in the Fig.2(b). It can be seen that the vibration displacement after optimization is reduced by about 15%, which verifies the effectiveness of the proposed method in this paper.

[1]Gao Y, Nagata M, Muramatsu K, et al. Noise Reduction of a Three-Phase Reactor by Optimization of Gaps Between Cores Considering Electromagnetism and Magnetostriction[J]. IEEE Transactions on Magnetics, 2011, 47(10):2772-2775. [2]Rossi M, Besnerais J L. Vibration Reduction of Inductors Under Magnetostrictive and Maxwell Forces Excitation[J]. IEEE Transactions on Magnetics, 2015, 51(12):1-6.

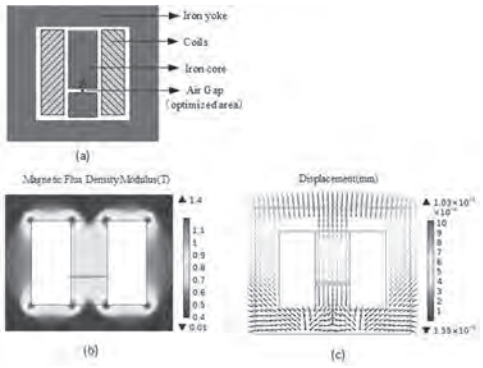

Fig.1. (a) Schematic diagram of the reactor,(b) Magnetic flux density modulus distribution nephogram,(c) Displacement distribution nephogram.

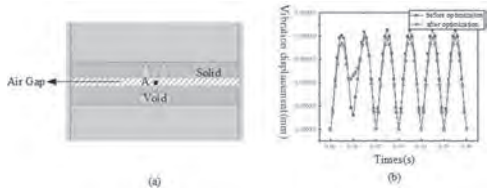

Fig.2. (a) Value distribution of control variable p,(b) Comparison of vibration displacement at sampling point a.

Session JPA
INDUCTION MACHINE AND SPECIAL MACHINE II
(Poster Session)

Po-Wei Huang, Co-Chair
National Cheng Kung University, Tainan, Taiwan
Thanh Anh Huynh, Co-Chair
National Cheng Kung University, Tainan, Taiwan

JPA-01. Investigation of Hybrid Magnet Arrangements in Dual-Layer PM Variable Flux Memory Machines. *W. Liu*[1], H. Yang[1] and H. Lin[1]
1. School of electrical engineering, Southeast University, Nanjing, China

I. Introduction Conventional series hybrid PM variable flux memory machines (VFMMs) normally suffer from limited flux regulation range and high magnetization current level [1]-[2]. Thus, the dual-layer VFMMs (DL-VFMMs) [3]-[4] by spatially separating low-coercive-force (LCF) and high-coercive-force (HCF) magnets are developed to address the foregoing drawbacks. However, it is a challenging issue to reasonably arrange hybrid PMs in the DL structure to achieve wide flux regulation range and excellent torque performance simultaneously. Therefore, the different hybrid PM arrangements in DL-VFMM are investigated and compared to reveal a utility magnet design guideline for DL-VFMM. II. Machine Topologies The investigated DL-VFMMs with different magnet configurations are developed as illustrated in Fig. 1, which are commonly characterized by a DL magnet arrangement with U- and V-shaped PMs, respectively. According to the magnetic circuit type, Model I and Model II can be regarded as series structures, while Model III and Model IV are characterized by a parallel-series magnetic circuit structure. In addition, the hysteresis models of HCF and LCF PMs are shown in Fig. 1(b), wherein the working point of LCF magnet can be flexibly adjusted within four *B-H* quadrants by a transient current pulse. III. Electromagnetic Performance The electromagnetic characteristics of the DL-VFMMs are shown in Fig. 2. Compared with the series types, the hybrid types show excellent flux regulation range while ensuring the torque performance under flux-weakened state. Specifically, the working point stabilizing effect from two HCF magnets make Model I shows the narrowest flux regulation range and maximum output torque. However, Model II exhibits widest flux regulation range, which benefits from more LCF magnets consumption. Finally, the test results of magnetization characteristics on the Model III prototype agree well with the finite-element (FE) predictions, which confirms the feasibility of the above analyses.

[1] A. Athavale, K. Sasaki, B. S. Gagas, T. Kato, and R. D. Lorenz, "Variable flux permanent magnet synchronous machine (VF-PMSM) design methodologies to meet electric vehicle traction requirements with reduced losses", *IEEE Trans. Ind. Appl.,* vol. 53, no. 5, pp. 4318- 4326, Sep./Oct. 2017. [2] Y. H. Kim, S. S. Lee, and J. H. Lee, "A study of flux control for high-efficiency speed control of variable flux permanent magnet motor," *AIP Advances*, vol. 8, no. 5, p. 056632, May 2018. [3] H. Yang, S. Lyu, H. Lin, Z. Q. Zhu, H. Zheng, and T. Wang, "A novel hybrid-magnetic-circuit variable flux memory machine," *IEEE Trans. Ind. Electron.*, vol. 67, no. 7, pp. 5258-5268, July 2020. [4] H. Yang, H. Zheng, H. Lin, Z. Q. Zhu and S. Lyu, "A novel variable flux dual-layer hybrid magnet memory machine with bypass airspace barriers," in *Proc. IEEE Int. Elect. Mach. and Drives Conf., (IEMDC)*, San Diego, USA, 2019, pp. 2259-2264.

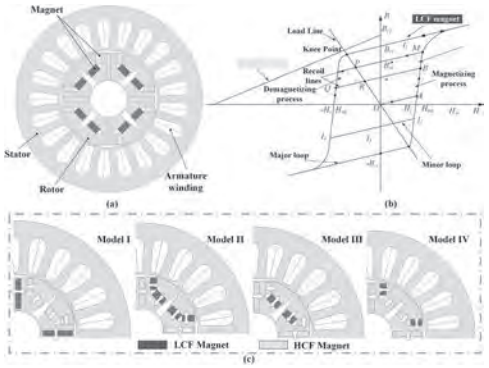

Fig. 1. (a) Cross sections of the investigated DL-VFMMs. (b) Hysteresis model. (c) Configurations of different magnet designs.

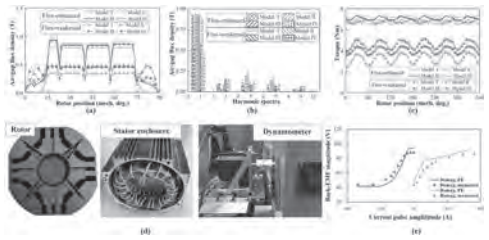

Fig. 2. (a) Air-gap flux density. (b) Harmonic spectrum. (c) Torque waveforms. (d) Prototype. (e) Test results.

JPA-02. Flux Analytical Calculation in the E-shape Stator Pole of Linear Rotary Permanent Magnet Motor. *K. Guo*[1] *1. Anhui University of Science and Technology, Huainan, China*

Abstract—Since the circumferential and axial widths of permanent magnet (PM) pole and stator pole are very sensitive to the back electromotive force (EMF) of linear rotary PM motor with E-shape stator, it is difficult to obtain the optimization value by the traditional design method. The flux calculated model is built and the main flux and side flux variation laws of stator pole are derived by the Schwarz Christoffel method. The analyzed results are consistent with the results analyzed by 3-D finite element method. I. Introduction The calculation of the magnetic field distribution is very important in the motor design. The subdomain method and separation of variables method can be used to calculate the magnetic flux density of slotless segmented-Halbach permanent magnet (PM) synchronous machine and single-cage induction machines [1][2], respectively. The flux calculation model of a linear rotary PM machine (LRPMM) with E-type stator (ES) structure is built by Schwarz Christoffel method (SCM), which can consider the side flux of the stator pole in circumferential and axial directions. II. Flux Calculation in the E-shape Stator pole of ES-LRPMM Fig. 1 shows the topology of ES-LRPMM. SCM is used to obtain the main flux and side flux of the stator pole by building finite-depth and infinite-depth stator slot models of the E-shape stator. Then the flux variation laws of stator pole are derived. Fig. 2 shows the main flux and side flux waveforms. It is seen that the angular

velocity of the flux is equal to the angular velocity of the mover while it works in rotary motion, and it is equal to three times of the angular velocity of the mover when it works in linear motion. III. Conclusion In order to reduce the difficulty of the optimization of ES-LRPMM, the flux in the E-shape stator section is analyzed by SCM and the variation law of the flux is deduced and concluded. Taking the cogging torque, detent force, torque and thrust as the optimization objectives, the optimum value of the motor structure is obtained.

[1]Z. Song, C. Liu, K. Feng, H. Zhao, and J. Yu, "Field prediction and validation of a slotless segmented-Halbach permanent magnet synchronous machine for more electric aircraft," *IEEE Trans. Trans. Electrif.*, vol. 6, no. 4, pp. 1577-1591, Dec. 2020. [2]A. Mollaeian, E. Ghosh, H. Dhulipati, J. Tjong, and N. C. Kar, "3-D sub-domain analytical model to calculate magnetic flux density in induction machines with semiclosed slots under no-load condition," *IEEE Trans. Magn.*, vol. 53, no. 6, pp. 1-5, June 2017.

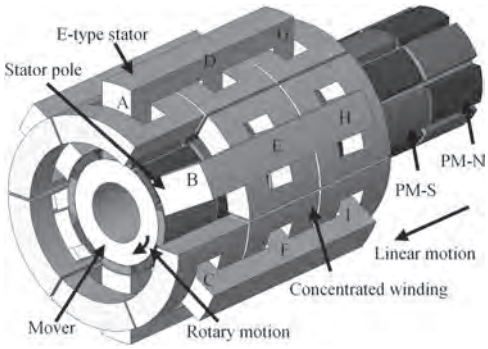

Fig. 1. Topology of ES-LRPMM

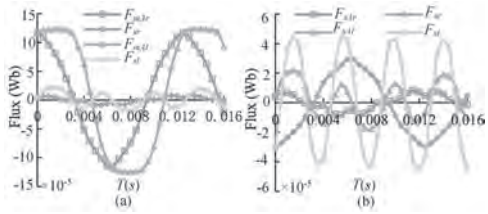

Fig. 2. Main and side flux waveforms, (a) main flux, and (b) side flux of phase *A* compared with the sum of phase *A*, *D*, *G* stator side flux when it works in rotary or linear motion.

JPA-03. Impact of End-Winding Regions for Air-Core Fully Superconducting Machines. *D. Lee*[1], N. Salk[1] and K. Haran[2] *1. Hinetics, LLC, Champaign, IL, United States; 2. Department of Electric and Computer engineering, University of Illinois, Urbana, IL, United States*

This paper presents MgB2 fully superconducting (SC) generators considering end-winding regions for improving accuracy to achieve high power density [1]. They enable size reduction by high current density without dc copper losses. However, ac losses are generated according to frequency, the magnitude of flux, and current [2-4]. Also, since the flux at the steel core is highly saturated around 3~5 T, iron losses at the steel core are high. To solve these problems, the proposed machine is an air-core fully superconducting generator [5]. Meanwhile, the impact of the end winding at the design step is neglected in conventional generators because its effect on torque production is small. However, in the case of SC generators, since the permeability of active parts under high saturation of flux density is getting similar to that of the end-winding region, it highly affects torque production. In particular, an air-core SC generator without a steel core should consider the impact of the end winding region. As a result, the end winding region can increase torque production by more than 50 %. Due to the complexity of 3D modeling and a longer computation time, the end-winding effect on torque production is generally avoided in fully superconducting machine design. Preliminary studies conducted on race-rack winding machines showed that additional 30% torque production could be obtained from the end winding of 3D simulation [6]. In addition to the torque production, the end winding also impacts inductance, ac loss, other electrical and mechanical parameters of the machine. In this paper, the impact of the end-winding region is solved based on an analytical method for reducing the computation time which is validated to be compared with 3D modeling. Finally, an optimal design is applied to a 10MW fully SC machine. Fig. 1 shows 3-D modeling for a fully superconducting generator. Fig. 2 shows comparison results of 2-D and 3-D analysis according to air-gap and stack length.

[1] F. Lin and R. Qu, IEEE Transactions on Applied Superconductivity, Vol. 28, No.3, (2018) [2] W. J. Carr, AC Loss and Macroscopic Theory of Superconductors Second Edition (Taylor and Francis Inc), (2001) [3] Z. Zhang and L. Ren, IEEE Transactions on Magnetics, Vol. 54, No.11, (2018) [4] G. Escamez and F. Sirois, IEEE Transactions on Magnetics, Vol. 52, No.3, (2016) [5] D. Lee and K. Haran, IEEE Transactions on Magnetics, Vol. 55, No.7, (2019) [6] J. H. J. Potgieter and M. J. Kamper, IEEE Transactions on Industry Applications, Vol. 50, pp. 2458-2466 (2014)

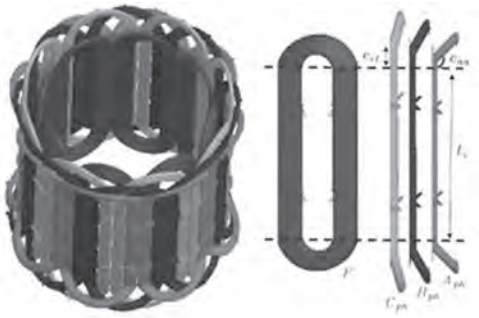

Fig 1. 3-D analytical modeling parameters for a fully SC machine.

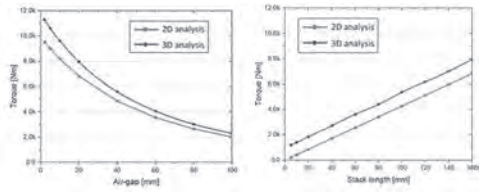

Fig 2. Comparison torque results of 2-D and 3-D analysis

JPA-04. Modeling and Analysis of Force Characteristics for Hybrid Excited Electrodynamic Wheels for Maglev Transportation. *W. Qin*[1], Y. Ma[2] and S. Tanzil[1] *1. School of Electrical Engineering, Beijing Jiaotong University, Beijing, China; 2. Taiyuan Institute of China Coal Technology and Engineering Group, Taiyuan, China*

I. INTRODUCTION The Maglev train has received renewed interest as of numerous advantages over the conventional wheel-on-rail system, such as less maintenance costs and lower noise and vibration[1,2]. The disadvantages of maglev systems are their higher initial capital cost and increased guideway complexity compared to conventional rail systems. A very low cost maglev methodology which is still in a research phase is called electrodynamic wheel (EDW) maglev[3,4]. However, the EDW system is easy to produce vertical oscillation and the constant air-gap flux generated by the PMs brings a challenge for controlling the forces actively[5]. To increase the active damping and realize control actively, a novel hybrid excited axial electrodynamic wheel(HEAEDW) is presented that tries to create thrust force with a constant airgap and realize control of the levitation force. II. MACHINE TOPOLOGIES A 3D schematic of a single proposed HEAEDW is shown in Fig. 1(a) and schematic of such vehicle is shown in Fig. 1(b). It has a simple and completely flat guideway, which could potentially be as low cost as high-speed rail. Its primary consists of primary core, three isolated phase windings and axial flux magnets. The PMs with different polarities are spatially mounted in symmetrically circumferentially on the surface of the tooth. The three phase concentrated windings, shown as in Fig.1(c)., are

wounded alternately on the primary core and supplied by AC currents in the phases with120° wave. III. RESULTS AND VALIDATION In this paper, a three-dimensional analytical approach, based on and second order vector potential (SOVP), is developed to calculate the HEAEDW's steady-state performances. In order to verify the accuracy of the analytical model, the finite element method is applied to calculate the forces characteristic, shown as in Fig.2(a). A comparison of the forces between FEA Model and SOVP model, a very good match was obtained shown as in Fig.2(b). Currently, we have designed and established a HEAEDW prototype in laboratory, The FEA and proposed approach results will be validated by the experiment results. More in-depth analysis and results will be present in the full paper.

[1] L. Hyung-Woo, K. Ki-Chan, and L. Ju, *IEEE Transactions on Magnetics,* vol. 42, no. 7, pp. 1917-1925(2006). [2] J. Z. Bird, *2019 12th International Symposium on Linear Drives for Industry Applications (LDIA)*, pp. 1-6(2019) [3] J. Bird, and T. A. Lipo, *IEEE Transactions on Magnetics,* vol. 45, no. 9, pp. 3233-3242, (2009). [4] N. Fujii, G. Hayashi, and Y. Sakamoto, *2000 IEEE Industry Applications Conference.*, vol. 1, pp. 257-262(2000). [5] R. F. Post, D. D. Ryutov, *IEEE Transactions on Applied Superconductivity,* vol. 10, no. 1, pp. 901-904(2000).

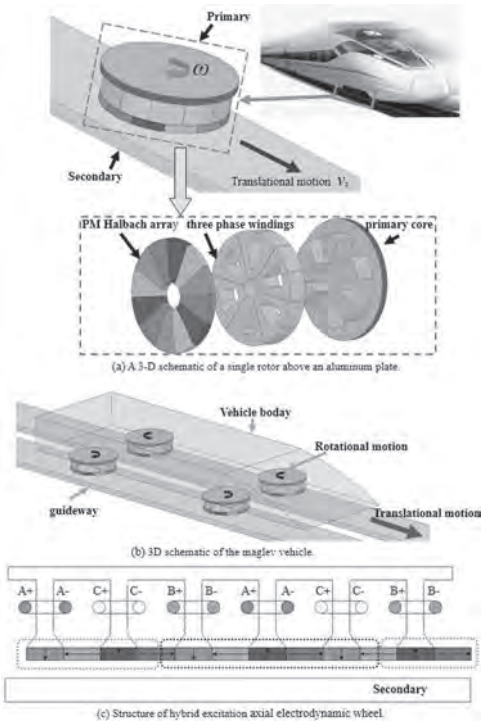

Fig.1. The schematic of HEAEDW.

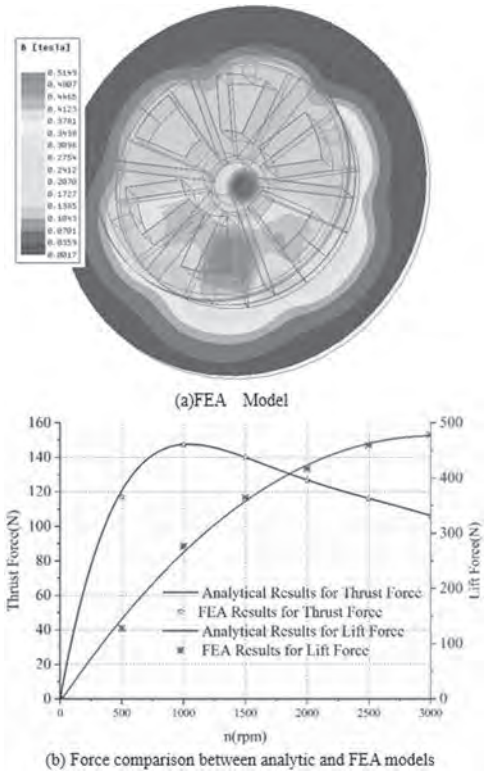

Fig.2 Calculation Results

JPA-05. Electromagnetic Analysis of the Eddy Current Effect to Impedance Performance of a Balanced Armature Receiver. *D. Xu*[1,2], X. Zhu[1], Y. Jiang[3], C. Wang[1,2] and S. Hwang[3] *1. Dept. of Precision Mechanical Engineering, Shanghai University, Shanghai, China; 2. Science and Technology on Near-surface Detection Laboratory, Wuxi, China; 3. School of Mechanical Engineering, Pusan National University, Busan, The Republic of Korea*

Balanced armature (BA) receiver is widely used in hearing aid, earphone and wearable devices because of its tiny size and good performance. Usually researchers do not consider the effect of eddy currents [1-3] for the performance of dynamic microspeaker because concentrating the performance at very high frequencies is not necessary for microspeakers. But for a BA receiver, which has a good high frequency performance and the performance should be simulated until 20 kHz. What's more, the effect of eddy currents in a BA receiver is much more notable because the soft magnetic materials in a BA receiver including armature and magnetic housing (as shown in Fig.1) are made by significantly higher relative permeability materials comparing of that in microspeaker. Electromagnetic transient analyses considering eddy currents by the 3D FEM are performed to obtain the nonlinear magnetic characteristics distribution in terms of frequency The current density distribution with and without considering eddy current in the electromagnetic analysis is shown in Fig.1, and we can know that the current density in the conductors is not uniformly distributed and is significantly higher in the armature inner surface than other places. Compared with the current without considering eddy currents, the current in the coil increases if eddy currents are considered. The added The resistance gap and inductance gap in the full frequency range can be obtained in the transient electromagnetic analysis by with and without considering eddy current, which can be used to supplement the Electromagnetic-Mechanical (E-M) coupling [4-7] not only in terms of vibration displacement, current, but also in terms of frequency. To compare the effect of eddy current, the displacement and impedance are measured using the Klippel setup, as shown in Fig.2, the impedance has already improved considering the effect of eddy currents at high frequencies.

[1] J. Jensen, F. T. Agerkvist, and J. M. Harte,"*Journal of the Audio Engineering Society*, vol. 59, no. 3, pp. 91–101, (2011). [2] Jensen, J. Diss. Ph. D. thesis, Technical University of Denmark, Kgs. Lyngby, Denmark, 2014. [3] Tsai, Yu-Ting, and Jin H. Huang. *Electroacoustics and Actuators A: Physical* 203 (2013): 324-334. [4] Xu Dan-Ping, Lu Han-Wen, Jiang Yuan-Wu, Kim Hyung-Kyu, Kwon Joong-Hak, & Hwang Sang-Moon, IEEE Access 5 (2017): 8930-8939. [5] Xu Dan-Ping, Jiang Yuan-Wu, Kwon Joong-Hak, & Hwang Sang-Moon, IEEE Transactions on Magnetics, 53(6), 1-4, 2017. [6] Xu Dan-Ping, Ph.D. Dissertation, "Analysis of a Balanced Armature Receiver Performances Considering Eddy Current, and Electromagnetic, Mechanical and Acoustic Coupling Effects," Pusan National University, Korea, 2018. [7] Dan-Ping Xu, Yuan-Wu Jiang, and Sang-Moon Hwang*. "Analysis of the magnetization effect of permanent magnets on the nonlinear magnetic characteristic distributions of a balanced armature receiver." *IEEE Transactions on Magnetics*, 2019, 55 (2): 1-5.

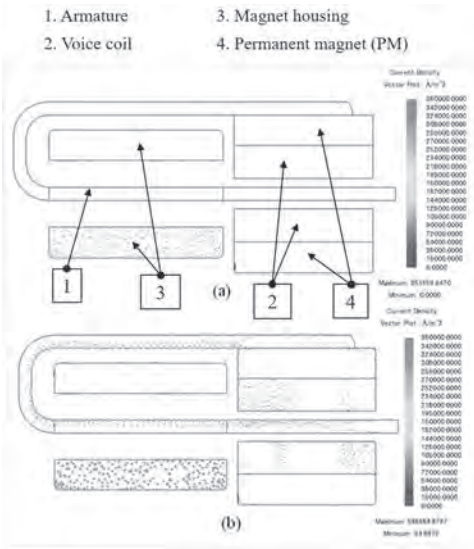

Fig.1 Current density distribution in the last step when f=5 kHz (a) Without eddy current and (b) with eddy current.

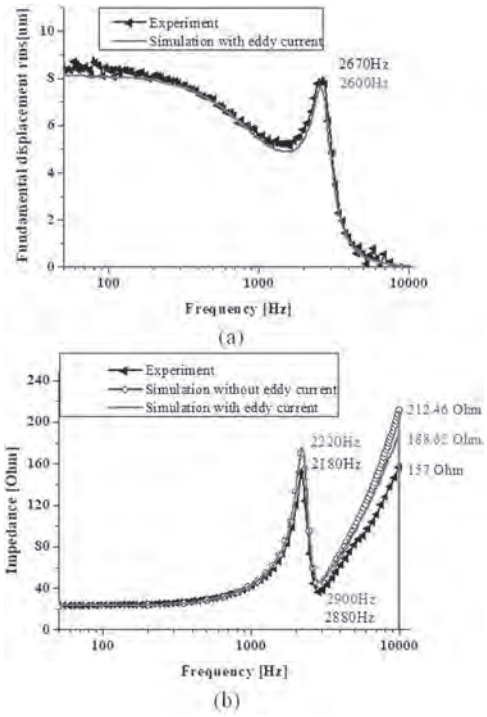

Fig.2 Comparison of experimental and simulated results in opened front cover and opened back hole case (a) Fundamental displacement magnitude and (b) impedance magnitude.

JPA-06. Study on the dynamic characteristics of an electromagnetic brake during power-loss braking. *X. Zhang*[1], L. Wang[2] and R. Pei[1]
1. Electrical Engineering, Shenyang University of Technology, Shenyang, China; 2. Suzhou InnMag New Energy,. Ltd, Suzhou, China

The form of power loss of an electromagnetic brake is closely related to the braking characteristics of the brake, which has a direct impact on the dynamic voltage, current, and braking torque, and has an important impact on the braking effect. This paper mainly studies the dynamic braking characteristics of the brake effect by directly disconnecting the main working circuit of the contactor. In order to reduce the high impulse voltage, it is necessary to release the energy by parallel discharge resistance on the side of the brake coil. In order to analyze the performance changes of the brake during the braking process, this paper deduces the magnetic circuit equation, circuit equation and motion equation theoretically, and analyzes their changes in the process. Based on the finite element simulation platform, the dynamic characteristics of the brake are simulated and analyzed. The study was based on a brake with a braking torque of 100Nm, coil resistance of 11Ω, coil voltage of 28V. Under different air gaps, the static electromagnetic suction force of electromagnetic brake is calculated, meanwhile the relationship between the voltage, current and braking moment at both ends of the brake coil with time was solved. Experiments show that the response time of the brake can be improved by increasing the discharge resistance value, but the reverse impulse voltage is also improved. Therefore, the discharge resistance should be increased as much as possible under the voltage withstand value of the contactor contacts. The higher the proportion of resistance increase, the shorter the time for braking torque to reach the rated value, but the smaller the proportion of brake response time increase.

[1] Cui You, Li Yong, Lu Yongping. Simulation analysis of thermal field in a high speed electromagnetic brake[C]. IMECS, HongKong, 2007: 1763-1766. [2] Bai Zhihong, Zhou Yuhu. Dynamic simulation and analysis of electromagnetic sctuator[J]. Journal of Electric Power, 2004, 19(3): 200-204. [3] Liu Tongjuan, Jin Nengqiang. Simulation analysis and study on transient property of electromagnet[J]. Low Voltage Apparatus, 2005, 6: 14-17.

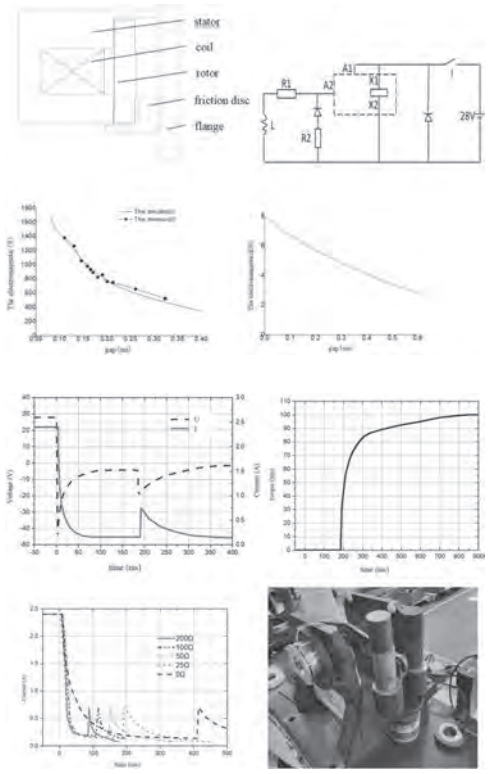

JPA-07. Analytical Model of Wound Rotor Synchronous Machine for Electric Vehicle Traction. *R. Hamidouche*[1,2], S. Mezani[1], T. Lubin[1] and T. Hamiti[2] *1. GREEN, Université de Lorraine, Nancy, France; 2. Nidec PSA emotors, Carrières-sous-Poissy, France*

The wound rotor synchronous machine (WRSM) constitutes a good alternative to PM synchronous machines for electric vehicles propulsion [1,2]. In the design optimization of electric vehicle traction motors a variety of operating points are required when considering the whole vehicle driving cycles [3]. To decrease the CPU time of such an optimization, we present a 2D analytical electromagnetic model of a WRSM capable of predicting airgap field harmonics in order to consider cost functions such as torque ripple and radial force harmonics. This paper proposes: 1 - A linear analytical method for magnetic field calculation in the air gap of WRSM including rotor slotting effect. The analytical method is based on the resolution of Laplace's and Poisson's equations in polar coordinates by separation of variables in low permeability subdomains [4]. A magnetic vector potential formulation is adopted. A 2D view of the model is shown in Figure 1 where the stator is represented by an equivalent current sheet. The iron material has an infinite permeability, so the PDEs are solved in the slot carrying a dc coil (region I), the slot opening (region II) and the air gap (region III). In each subdomain, the solution is written as a Fourier series whose coefficients are calculated using boundary conditions and continuity conditions between the different subdomains (normal flux density and tangential magnetic field). 2- A comparison between the analytical and the finite element [5] radial flux density distribution along a circle in the middle of the air gap under load condition and with the same assumptions is shown in Figure 2. The agreement is very good. The analytical computation takes 40 ms while the finite element solution requires 1.3 s. Hence, the analytical model is a very efficient tool to perform WRSM optimization on a driving cycle. In the extended paper, more details regarding the electromagnetic model, further comparison with FE results and the model limit with respect to magnetic saturation, will be given. Furthermore, a thermal model of the machine will serve to evaluate the winding temperatures. Hence, a coupled magneto-thermal optimization on a driving cycle will be presented and largely analyzed.

[1] P. Ramesh and N. C. Lenin, *IEEE Trans. on Magn.,* Vol. 55, no. 11, Nov. 2019. [2] J. D. Widmer, R. Martin, and M. Kimiabeigi, *Sustain. Mater. Technol.,* vol. 3, pp. 7–13, 2015. [3] P. H. Nguyen, E. Hoang, and M. Gabsi, *IEEE Trans. Veh. Technol.,* vol. 60, no. 5, pp. 1991–1998, 2011. [4] T. Lubin, S. Mezani and A. Rezzoug, *IEEE Trans. on Magn.*, vol. 46, no 4, pp. 1092-1099, April 2010. [5] D. C. Meeker, Finite Element Method Magnetics, Version 4.2 (19Apr2019 Build), https://www.femm.info

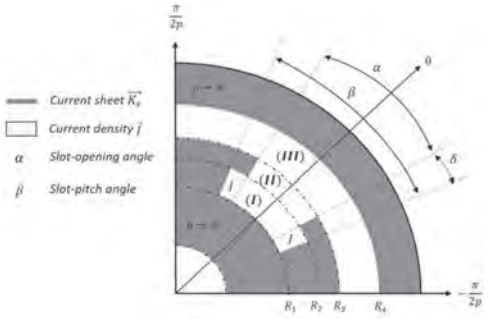

Fig.1. 2D view of the machine showing the different subdomains

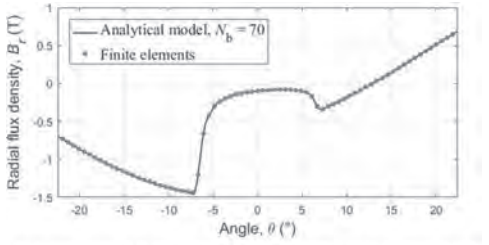

Fig.2. Comparison of air gap radial flux density distribution under a pole pitch (p=4)

JPA-08. Influence of Different Rotor Slot Structure on Electromagnetic Characteristics of Dual-Excited Synchronous Generator. G. Xu[1], *R. Li*[1], Y. Zhan[1] and H. Zhao[1] *1. North China Electric Power University, Beijing, China*

Traditional Synchronous Generator (TSG) has a field winding placed in the d-axis. This feature determines that the steady-state stability of TSG is limited to 90° in terms of power angle. The Dual-Excited Synchronous Generator (DESG) is provided with the d- and q-axis field windings, so that the direction of excitation mmf can be oriented in any direction by implementing different d-and q-axis direct currents[1]. Thus the stability of DESG is not restricted by the power angle limit, which enables the stable operation throughout the whole range of operating conditions. In addition the ability of DESG to consume the reactive power is stronger than that of TSG since the DESG is not restricted by the under-excitation limit [2]. The DESG can be used to solve the problems of the transient overvoltage in the convertor station of the Ultra-High VoltageDirect Current (UHVDC). A DESG has two field winding, thus there are no large teeth in the rotor of the DESG relative to that of the TSG, shown as in Fig.1. In this condition, the flux density on the rotor teeth of th DESG is easy to saturated. Such structures of DESG are expected to enhance the stability and ability of absorbing reactive power, and give the better electromagnetic characteristics. Therefore, it is neccessary to study the optimal rotor structure of the DESG. In this paper, three kinds of rotor slot structures are proposed as shown in Fig.1, and stator and rotor saturations, the air-gap flux densities and rotor losses of the DESG are compared. Case 1 is the rotor trapezoidal tooth, case 2 is the rotor rectangular tooth, and case 3 is the half trapezoidal tooth and half rectangular tooth. The comparison of the flux densities in each rotor tooth of DESG is shown in Fig.2. It can be seen from Fig.2 that the flux densities of the rotor small teeth are decreased in case 2 and 3 under single- and dual-axis excitation mode. A 7.5-kW DESG is developped to verified the correctness of the simulation. The results can provide theoretic support for the design and manufacture of the large DESG.

[1]Xu G, Wang Z, Liu B, et al. "Finite element calculation of electromagnetic characteristics and steady state stability of dual excited synchronous generator," IET Electr. Power Appl., pp.1–14, (2021), early access. [2] Shakaryan, Y., Sokur, P., "Experience in the development and operation of asynchronised turbogenerators and condensers in the Russian power system," Arch. Electr. Eng. Vol.64, no.1, pp. 7–15, (2015).

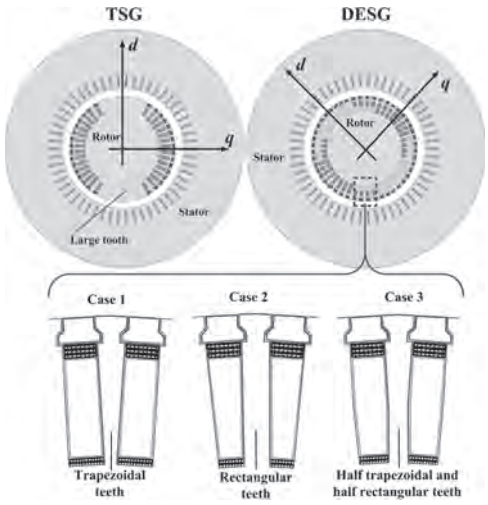

Fig.1 TSG and DESG with three rotor slot structures

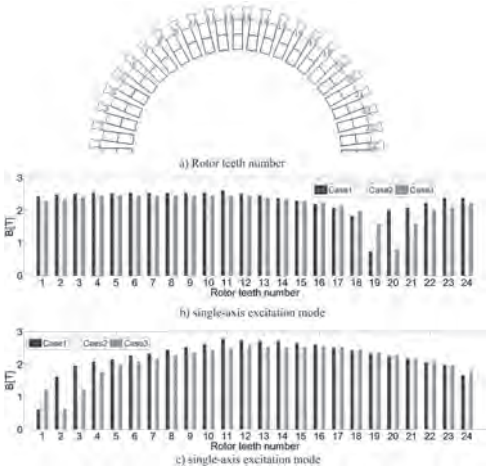

Fig.2 Comparison of flux densities in each rotor tooth of DESG with three rotor slot structures

JPA-09. Magnetic Field Analysis and Operating Characteristics of a Brushless Electrical Excitation Synchronous Generator with DC Excitation. *S. Zhu*[1], J. Yu[1], C. Liu[1] and K. Wang[1] *1. Nanjing University of Aeronautics and Astronautics, Nanjing, China*

1. Introduction The realization of the brushless excitation of the machine is important for the industrial application[1,2]. In this paper, a Brushless Electrical Excitation Synchronous Generator will be studied. The rotor coils are divided into two parts: The induction coils (Ci) and rotor excitation winding (Wr). They are connected by a half –wave rectifier which only has four diodes. Ci not only can induce the magnetic field produced by stator excitation current (Is), but also can take part in the induction of the stator armature. However, the magnetic distribution of the generator is not symmetrical as the conventional EESG. The magnetic field is studied by the frozen permeance method. A 1.5kVA prototype was fabricated to verify the correctness of the theoretical analysis and Finite Element Analysis. 2. Magnetic field distribution of DEESG The magnetic field distribution of DEESG under the no-load condition when I_s is 0.8A at 160ms is as shown in Fig.1. The reason for theasymmetry of the magnetic field distribution is studied. It also can be seen that because all the magnetic flux passes through the air gap, the magnetic flux density of air gap is also not symmetrical as shown in Fig.2. 3. Magnetic field Analysis Excited by Different Currents The frozen permeability method can be used to decompose the magnetic field which is excited by rotor excitation current I_r, Is and the currents of Ci respectively. The magnetic field distribution of DEESG when I_s is taken as the example to do analysis. The magnetic field which is only excited by I_r utilizing the frozen permeability method. The magnetic field distribution which is generated by the currents of Ci will also be studied. The function of Is will also be studied. It can demonstrate that the magnetic field produced by ac component of the currents of Ci can weaken the magnetic field produced by I_s. 4. Experiment A 1.5kVA prototype was fabricated to test the operating characteristics of DEESG. The magntic field can not be tested directly. The output voltage will be tested to demonstrate the magnetic field distribution of DEESG.

[1]F. Yao, Q. An, X. Gao, L. Sun, and T. A. Lipo, "Principle of Operation and Performance of a Synchronous Machine Employing a New Harmonic Excitation Scheme," *IEEE Trans. Appl. Ind.*, vol. 51, no. 5, pp. 3890–3898, Sep. 2015. [2]F.Bu, W. Huang, Y. Hu, et al. "An Integrated AC and DC Hybrid Generation System Using Dual-Stator-Winding Induction Generator With Static Excitation Controller," *IEEE Trans. Ener. Conv.*, vol.27, no.3, pp:810-812, July 2012.

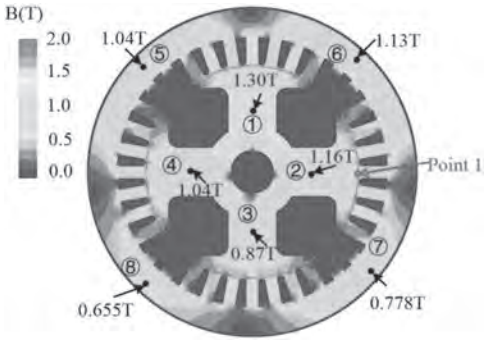

Fig.1 Field distribution of DEESG at the rated speed.

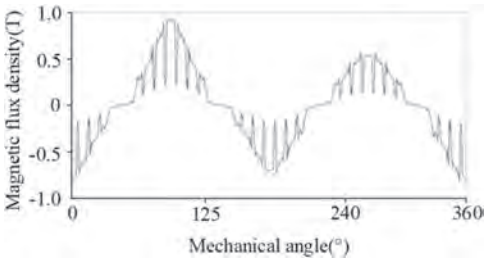

Fig.2. Magnetic flux density of air gap.

JPA-10. Three-phase Brushless Synchronous Generator Topology Without an Exciter with Experimental Verification. A. Arif[1], *M. Ayub*[3], N. Baloch[2], F. Arif[1] and B. Kwon[2] *1. Electrical Engineering, GIKI Topi KPK, Swabi, Pakistan; 2. Hanyang University, Ansan, The Republic of Korea; 3. Electronic Engineering, BUITEMS, Quetta, Pakistan*

Abstract— This abstract proposes a three-phase brushless synchronous generator topology without an exciter with experiment results. The proposed excitation topology uses different number of turns of armature winding in each phase to generate additional MMF harmonic for rotor field winding excitation. The propose excitation topology eliminates the utilization of external exciter and brushes and slip rings assembly. In specific, each phase of the machine is divided into series connected four coils, A1, A2, A3, and A4, wherein, coils A2 and A4 are wound with half of the coils turns compared to A1 and A3. On the rotor side, additional harmonic is placed beside field winding. Initially, DC current is supplied to rotor field winding

which starts induction on the armature winding as a conventional synchronous generator. After load connectivity on the generator, the current flows in the armature winding, whereas, the armature winding regions with coils A2 and A4 produce half magnitude of the stator MMF compared to the region with coils A1 and A3 due to change in coil turns. The change in MMF magnitudes in different regions produces additional sub-harmonic alongside fundamental harmonic in the machine airgap. This additional sub-harmonic induces voltage in the rotor harmonic winding and after rectification dc current starts to energize rotor field winding. Meanwhile, the dc source of the rotor is disconnected and the machine completely works as a brushless synchronous generator. 2D finite element analysis in FEM commercial software is performed and electromagnetic performance of the proposed topology is evaluated. A prototype machine is then manufactured to validate the operation of the proposed brushless generator. I. Proposed Brushless Self-excited Generator Topology Reference is made from available brushless machine topologies [1] – [3]. The proposed topology is shown in Fig. 1. Where stator and rotor winding connections are shown. Induced current in rotor harmonic and field winding is achieved and induced torque was observed. Detail electromagnetic performace analysis and experimental result will be discussed in full paper.

[1] Q. Ali, T. A. Lipo and B. Kwon, "Design and Analysis of a Novel Brushless Wound Rotor Synchronous Machine," in IEEE Transactions on Magnetics, vol. 51, no. 11, pp. 1-4, Nov. 2015, Art no. 8109804. [2] Hussain, A.; Kwon, B. A new brushless wound rotor synchronous machine using a special stator winding arrangement. Electr. Eng. 2017. 1-8. [3] M. Ayub, S.S.H. Bukhari, G. Jawad "Brushless wound field synchronous machine with third-harmonic field excitation using a single inverter" Electrical Engineering (2019)

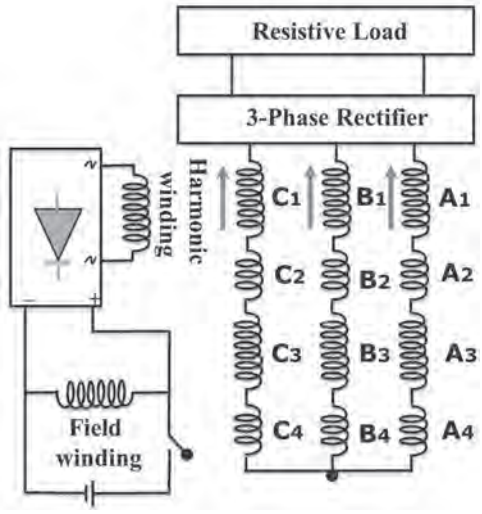

Fig. 1. Proposed topology

JPA-11. Fault Tolerant Performance and Open Circuit Compensation Strategy of Six-phase Permanent Magnet Synchronous Motor for All-electric Aircraft. Y. Li[1], *L. Chen*[1] and Z. Yu[1] *1. Shenyang University of Technology, Shenyang, China*

Abatract:Multi-phase permanent magnet synchronous motor(PMSM) is widely used in high power and high precision fields. The fault-tolerant performance of the drive motor is of great significance for all-electric aircraft applications, and it will be related to the safe operation of the whole machine. In this paper, a 100kW six-phase external rotor permanent magnet synchronous motor is designed, and its electromagnetic performance is analyzed by finite element method(FEM). And meanwhile the output torque ability of the motor under different open-circuit faults is analyzed in detail. Aiming at the reduction of output torque and torque fluctuation under one-phase and two-phase open circuit, different fault compensation measures are proposed based on the principle of magnetomotive force invariance and the principle of eliminating negative sequence components. And the parametric method is used to analyze and compare them. The analysis results show that the compensation strategy based on the magnetomotive force constant can keep the output torque of the motor unchanged and the torque fluctuation is small, and the compensation strategy is simple. After the open circuit of the drive motor, if the external environment of the aircraft cannot be forced to drop urgently, this compensation strategy can be adopted. The compensation strategy based on eliminating negative sequence sequence component starting from reducing torque fluctuation is more flexible.

Li L, Zhang J, Zhang C, et al. Research on electromagnetic and thermal issue of high-efficiency and high-power-density outer-rotor motor[J]. IEEE Transactions on Applied Superconductivity, 2016, 26(4): 1-5. Chen J, Nayar C V, Xu L. Design and finite-element analysis of an outer-rotor permanent-magnet generator for directly coupled wind turbines[J]. IEEE transactions on magnetics, 2000, 36(5): 3802-3809. Schmidt E, Susie M. Design studies on an external rotor permanent magnet synchronous machine for a position sensorless control—Comparison of Y-and Δ-connected stator winding[C]//CCECE 2010. IEEE, 2010: 1-5.

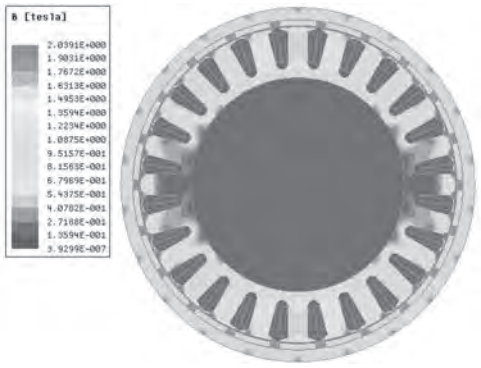

The distribution of no-load magnetic density

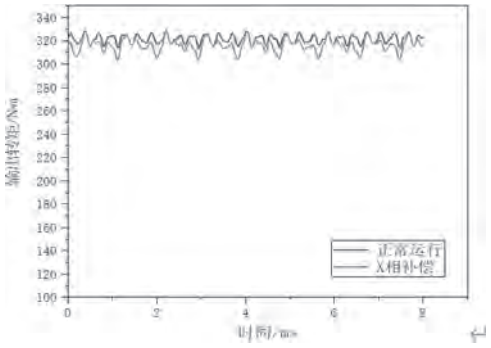

The torque curve under X phase compensation

JPA-12. Withdrawn

JPA-13. Bearing Fault Numerical Model for the Closed-slot Rotor Submersible Motor. *Z. Ke*[1], C. Di[1], X. Bao[1], B. Guan[2] and J. Yan[1] *1. School of Electrical Engineering and Automation, Hefei University of Technology, Hefei, China; 2. Department of Electrical and Computer Engineering, The Ohio State University, Columbus, OH, United States*

The submersible motor is common equipment used in the water supply and drainage systems. However, the bearing fault is a critical issue in submersible motors. It is an effective method to analyze the vibration signal of the motor end cover for bearing fault diagnosis [1]. But the submersible motor runs underwater, and the vibration signal will be easily disturbed by the flowing water. It is a feasible bearing fault diagnosis method to analyze the variation of the electromagnetic properties (such as the stator current) of

the motor [2]. Nevertheless, there is a lack of an available fault model which is capable of reflecting the electromagnetic response of the motor under the bearing fault. In this paper, a single point fault model of a closed-slot rotor submersible motor is established for bearing fault diagnosis. The heathy submersible motor model is established by the Finite Element Method (FEM). In the model, two relative permeability variation regions are created in the rotor edge and air gap. Because the bearing fault will lead to the periodic eccentricity (static eccentricity) of the shaft, the influence of the bearing fault on the motor performance can be considered by periodically changing the relative permeability of these regions. The model of the bearing fault submersible motor is shown in Fig.1. The relative permeability variation regions (black regions) are determined by the non-coincidence regions of the healthy and static eccentric rotors and are marked as regions 1 and 2. When the motor is running without the fault, the relative permeability in region 1 is set as the vacuum permeability, and region 2 is set as the silicon steel sheet permeability. In case of bearing fault, the setting is the opposite. Fig.2 shows the stator current and its spectrum diagram of the bearing fault model. It can be seen in Fig.2 (a) that the stator current is slightly distorted, which is marked in the red circle. Meanwhile, the characteristic frequency of the fault is shown in Fig.2 (b).

[1] T. Wang, Z. Liu, and G. Lu, *IEEE Transactions on Industrial Electronics*, vol. 68, no. 3, pp. 2598-2607 (2021) [2] M. Blodt, P. Granjon, and B. Raison, *IEEE Transactions on Industrial Electronics*, vol. 55, no. 4, pp. 1813-1822 (2008)

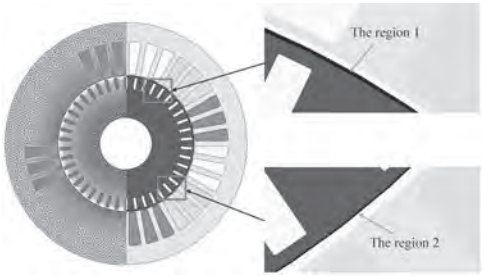

Fig. 1 The model of bearing fault submersible motor.

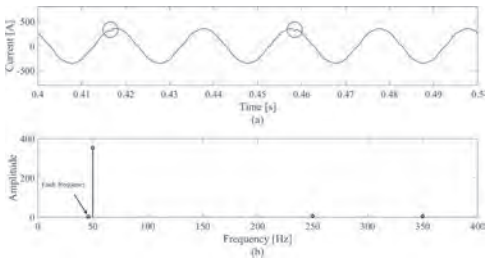

Fig. 2 The stator current and its spectrum diagram of the bearing fault model. (a) Stator current waveform. (b) Spectrum diagram of the stator current.

JPA-14. An Efficient Air-Gap Flux Density Analysis Method for the Design of Induction Machines. *J. Liu*[1], C. Di[1] and X. Bao[1] *1. School of Electrical Engineering and Automation, Hefei University of Technology, He Fei, China*

Air-gap flux density can be directly used in calculating the main electric machine parameters during the design process. Analytical methods are found to be an efficient option to characterize its waveform accurately in a simpler and less time-consuming way than the FEM does. However, it is a challenging question to find a well-performed method that applies to the induction machine, for the complicated rotor reaction and pulsations given by slots opening need special consideration. Some analytical methods can get a result close to the FEM one under the no-load state, but the methods have not been verified under load conditions [1-2]. In this paper, an improved analytical method is proposed to give quick and relatively accurate information on the air-gap flux density under different load cases. The proposed model, which is based on the product of the current linkage waveform and the permeance waveform, contains two improvements. First, the amplitude and the phase shift of the waveforms can be approached accurately from the equivalent circuit and the phasor diagram. Second, the variation of the permeance caused by the slots opening is represented by a series of rectangular pulses, of which the width and the height are calculated specifically using the geometry data of the machine. Many other factors that affect the distribution are all integrated into the model. The waveforms of the nominal-load air-gap flux density obtained by the analytical method and the FEM can be seen in Fig. 1 (a), while the corresponding amplitude spectrums are shown in Fig. 1 (b). The accuracy of the analytical results can be evaluated by calculating the Total Harmonic Distortion (THD) of the analytical waveform and comparing it to the FEA one. The curves in Fig. 2 show the THD value as a function of the slip. The two figures indicate that the analytical results agree well with the FEM results under different load cases. More results and discussions will be given in the entire paper.

[1] J. Laksar, J. Sobra and L. Veg, *2017 18th International Scientific Conference on Electric Power Engineering (EPE)*, pp. 1-6 (2017). [2] A. Mollaeian, E. Ghosh, and H. Dhulipati, *IEEE Transactions on Magnetics*, vol. 53, no. 6, pp. 1-5 (2017)

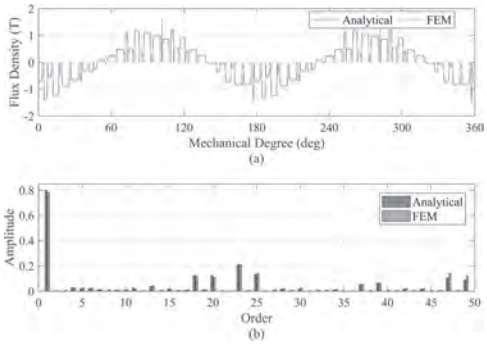

Fig. 1. Results obtained by the analytical method and the FEM (under nominal load). (a) Waveforms of the air-gap flux density. (b) Amplitude spectrums of the waveforms.

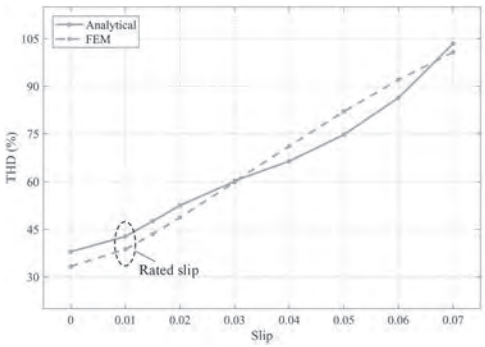

Fig. 2. Comparison of the THD values as a function of the slip.

JPA-15. A Comprehensive Effect Analysis of the Rotor Auxiliary Slot Geometry for the Water-filled Submersible Induction Motors. *J. Li*[1], C. Di[1] and X. Bao[1] *1. School of Electrical Engineering and Automation, Hefei University of Technology, He Fei, China*

Induction motors have been widely used in various fields because of economy and reliability. Its' secondary winding harmonic losses are always a problem that scholars devote themselves to solve. Zhao Haisen et. eliminated the slot harmonic, which is caused by slot opening, by using asymmetrical rotor slots[1]. Lin Qifang et. improved the efficiency of the motor by using split teeth on stator[2]. The auxiliary slots on the rotor side can weaken the first-order tooth harmonic of the rotor by changing the air-gap

magnetic permeability. In higher power ranges of the water-filled submersible induction motors, the rotor widely employs copper bar rotor with closed slots. Opening the auxiliary slots on the rotor surface will increase the water friction loss, so this paper chooses to open auxiliary slots inside the rotor between the rotor teeth. As shown in Fig.1, to simplify the analysis and modeling process, using α_1, α_2, and l_1 as the variable to express the width and the length of the auxiliary slot. The effects of the width and height of the auxiliary slot on harmonic reduction were studied by controlling variables. Taking into account the actual size of the motor, the value range of α_2 is 0.5°- 1.5°, and the value range of l_1 is 2.7- 18.7 mm. The initial distance between the top of the auxiliary groove and the outer circle of the rotor is the same as the height of the slot bridge, which affects harmonic content and motor performance will also be analyzed in this paper. As shown in Fig.2, the harmonic content of the first-order teeth harmonic of the rotor decreases with the increase of the size of the auxiliary slot while the second-order teeth harmonic keeps almost remain. The weakening effect is more obvious when the width of the auxiliary slot is increased. At the same time, the saturation of tooth magnetic density is more serious. The losses reduced by the auxiliary slot and the harmonics introduced will be analyzed in detail in this paper.

[1]Z. Haisen, Z. Jian and W. Xiangyu, IEEE Transactions on Magnetics, vol. 50, no. 2, pp. 769-772(2014). [2]Q. Lin, S. Niu and F. Cai, IEEE Transactions on Vehicular Technology, vol. 69, no. 12, pp. 14391-14400 (2020).

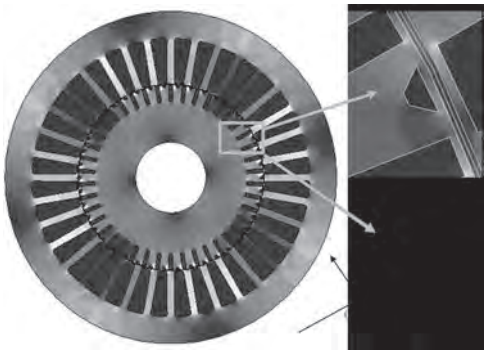

Fig. 1 Diagram of Auxiliary Slot.

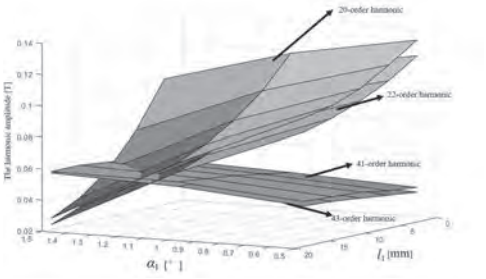

Fig. 2 Tooth Harmonic Amplitude Change Diagram.

JPA-16. Identification of magnetizing inductance of squirrel cage induction machine using FEM. Y. Djouadi[1], *A. Tounzi*[3], S. Taibi[2] and K. Idjdarene[1] *1. Laboratoire LTII, University of Bejaia, Bejaia, Algeria; 2. University of Batna 2, Batna, Algeria; 3. Univ. Lille, Arts et Metiers Institute of Technology, Centrale Lille, Junia, Villeneuve d'Ascq, France*

Squirrel cage induction machine (SQIM) is widely used and is well known for its saturation effect due to the weak air gap length. Therefore, to control it in an efficient way, this effect is generally taken into account through the magnetizing inductance L_m which is function of the magnetizing current I_m [1]. In case of a real machine, the waveform of the latter is determined from no load tests while supplying stator windings at different voltage magnitudes to take into account the whole saturation effect [2,3]. In the case of a virtual prototype, the same procedure is used on the basis of time step FEA. This is time consuming as only the variable values at steady state are of interest. The present paper deals with the identification of the waveform of the magnetizing inductance vs stator current amplitude on the basis of calculations using DC current supply. The proposed approach is used at standstill and the conductivity of the rotor bars is set equal to zero. Therefore, no rotor currents can be induced which is almost similar to no load operating. Then, phase A is supplied by I_A= I while phase B and C are supplied by I_B=I_C=(-1/2)I. I can be considered as the maximal value of three phase sinusoidal supply in case of no load running but at the same time, it represents I_d/1.5; I_d being the current along the d axis since the angle between stator and rotor reference axes can be considered equal to zero. This current is also the magnetizing current I_m. From the magnetic linkage fluxes of the 3 phases for different current amplitudes, the flux along d axis can be determined such as: Φ_m = sqrt (2/3)(φ_A - 0,5 φ_B -0,5 φ_C) and the magnetizing inductance by L_m= Φ_m / I_m. The proposed approach is applied in the case of a three phase SQIM of 5.5 kW, 230V, 50hz with 4 pole pairs. Both classical no load voltage tests and the proposed approach are used to determine $L_m(I_m)$. Fig. 1 shows the magnetic field distribution in the cross section of the studied machine when supplied by I_A=1A and I_B=I_C=-0,5A while Fig. 2 presents the comparison of $L_m(I_m)$ obtained by both approaches. In the final paper, more details about the proposed approach will be given and the results frm FEA will be compared to measurements.

[1] E. Levi, 'Impact of cross-saturation on accuracy of saturated induction machine models', IEEE Trans. on Energy Conversion, vol. 12, n° 3, 1997, pp 211-214. [2] A.V. Stankovic; E.L. Benedict; V. John; T.A. Lipo, "A novel method for measuring induction machine magnetizing inductances," in *IEEE Transactions on Industry Applications*, vol. 39, no. 5, pp. 1257 - 1263, Sep. 2003. [3] B. Rezaeealam, "Calculation of magnetizing and leakage inductances of induction machine using finite element method," Electrical engineering 103, pp: 315-323, 2021.

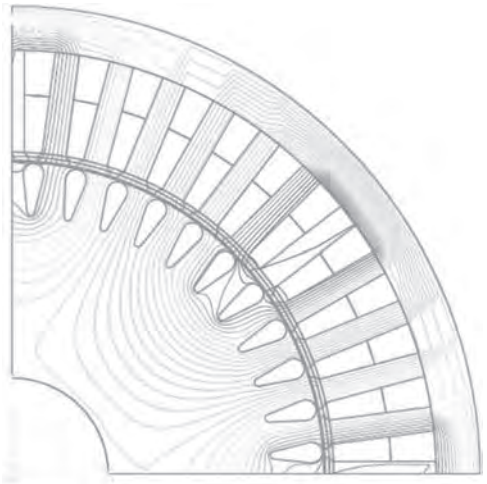

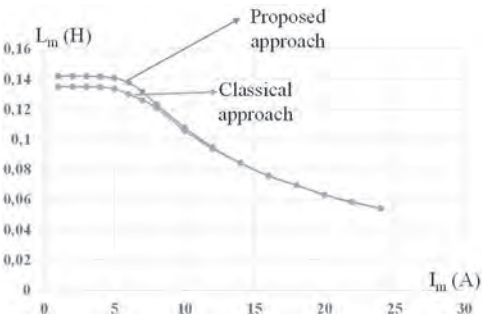

JPA-17. A Study on the Characteristics of Al/Cu Dissimilar Materials Applied to the Rotor Bar of IE4 Class Induction Motor. *M. Kim*[1,2], J. Park[1], K. Lee[1], S. Lee[1] and J. Choi[2] *1. Automotive material & Components R&D Group, Korea institute of Industrial Technology, Gwang-ju, The Republic of Korea; 2. Chungnam National University, Dae-jeon, The Republic of Korea*

In this paper, the characteristics of an induction motor using Al/Cu dissimilar materials for the rotor bar were analyzed. In general, an aluminum die-casting rotor have a problem in that the machine size increases when the efficiency is improved. Copper die-casting rotors with improve efficiency for the same machine size have a problem decreased starting torque, decreased power factor, low mass production, increased manufacturing cost Compared to aluminum die-casting rotor. Three-phase squirrel cage induction motors must satisfy price competitiveness while improving efficiency[1-2]. Al/Cu rotors can improve the problems of conventional aluminum and copper rotors. Al/Cu rotor is an alternative solution to improve the IE3 induction motors towards the IE4 class. It can be applied to an induction motor installed in a modern industry simply with low-cost than a copper die-casting rotor. The Al/Cu rotor size and material ratio were determined through electromagnetic field and thermal analysis in consideration of efficiency, starting torque, and power factor. The shaft dimensions and bearing spacing of the Al/Cu rotor were determined through mechanical and statistical analysis in consideration of critical speed, rotor center displacement, and bearing life. The mechanical properties were analyzed through the samples bonded to aluminum and copper. The Al/Cu rotor was die-cast considering the casting process conditions. The Al/Cu rotor is manufactured in precision grade by KS C 4202. The final model was subjected to loss and parameter separation tests according to IEC60034-2-1, K C IEC 60034-28. The validity of the proposed Al/Cu rotor is compared by multi-physics analysis results and experimental results.

[1] C. Lin and C. Hwang, IEEE Transactions on Magnetics, Vol. 52, No.7 (2016) [2] F. Ferreira, B. Leprettre, and A. Almeida, IEEE Transaction on Industry Applications, Vol. 52, No. 4, pp. 3603-3610(2016).

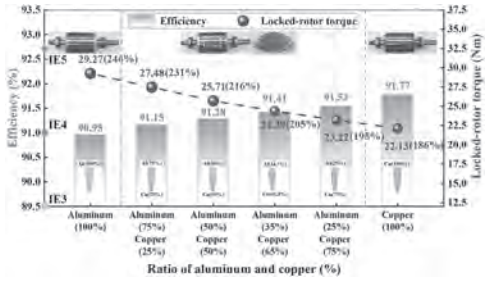

Fig. 1. Characteristics according to the combination ratio of Al/Cu Dissimilar Materials

Session JPB
HIGH SPEED AND SPECIAL ROTATING ELECTRICAL MACHINES II (Poster Session)

Hui Yang, Co-Chair
Southeast University, Nanjing, China
Qian Chen, Co-Chair
Jiangsu University, Zhenjiang, China

JPB-01. Study of Charging and Discharging of Regenerative Electric Energy of Direct Drive Generator on Electric Vehicle. *C. Hsu*[3], C. Fung[1] and J. Liu[2] *1. Mechanical Engineering, Oriental Institute of Technology, Banqiao District, Taiwan; 2. Digital Multimedia Design, Kainan University, Lu-Zhou, Taiwan; 3. Asia Eastern University of Science and Technology, New Taipei, Taiwan*

1. Study Objective This research develops a method for the design and implementation of a magnetic sensor constructed with super capacitor electromagnetic device for fast charging of the smart vehicles, which realizes the magnetic motor functional with Internet of Things (IoT) [1,2]. To establish and design the proto type machines for the electric vehicles, it is mainly to meet the sustainable energy manufacturing and lower cost for electric vehicles. 2. Method This study, it used an axial permanent magnet generator to generate direct current (DC) power. The process of charging and discharging the super capacitor system is developed. This system is integrated the fractional-order proportional-integral-derivative (FOPID) controllers with neural network (NN) to consider parameters in interception, calculation, and evaluation of the best solution to provide the maximum value of the electric vehicle, as shown in Figure 1. 3. Experiment Result and Discussion The magnetic sensor and generator signal uses the embedded system (fog computing) platform to detect the sensing signal, included as electric vehicle of the motor and image recognition function. The intercepted image signal and the sensing signal thorough NN and FOPID controller to feedforward signal, which are transmitted signal to the cloud server and provide sustainable power for electric vehicles, as shown in Figure 2. This study is to establish a fast electromagnetic charging device with fog computing controller, which is used to quickly process the electromagnetic energy generated by the generator, and intercept the voltage and current signals, and then perform data collection and storage operations. Among of them, a larger number of electromagnetic and electrical signals are collected, and its stability and operating characteristics of IoT are calculated and controlled to provide the electric vehicle quickly charging performance. The process of integration and experimentation for the motor and generator device can be obtained.

[1]Chang-Hung Hsu and Yi-Mei Huang, "Performance of the Noise and Vibration of the AC/DC Signal for a Permanent Magnetic DC Motor," IEEE Transactions on Magnetics, Early Access Articles. Accepted Publishing on the web 28 July 2020. [2]Chang-Hung Hsu, "Fractional Order PID Control for Reduction of Vibration and Noise on Induction Motor," IEEE Trans. on Magnetics, vol. 55, no. 11, pp. 6700507-1-7, 2019.

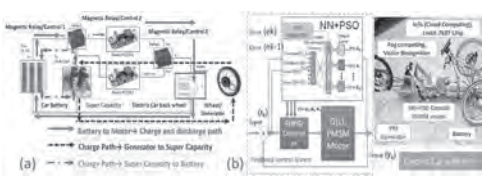

Figure 1 The structure of the charging and discharging system: (a) PMSM with super capacitor system, (b) PMSM control by with NN+PSO.

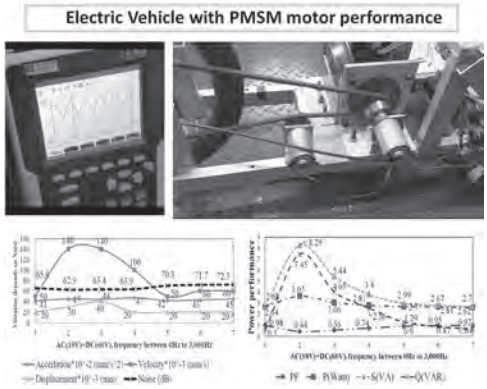

Figure 2 The IoTs system detects motor power, vibration and electric vehicle image recognition.

JPB-02. Withdrawn

JPB-03. A Novel Dual-layer Variable Flux Memory Machine with Segmented PM Design. *W. Liu*[1], H. Yang[1] and H. Lin[1] *1. School of electrical engineering, Southeast University, Nanjing, China*

I. INTRODUCTION Variable flux memory machine (VFMM) [1]-[2] equipped with low-coercive-force (LCF) PM is regarded as an enabling solution to realize the air-gap flux adjustment, which is competent for automotive applications. Moreover, the conventional series VFMMs [3] limited flux regulation range prevents it from fully utilizing the merits of VFMM in terms of efficiency improvement. Therefore, this paper proposes a novel design of dual-layer (DL) VFMM to address the foregoing drawbacks, which combines segmented LCF magnets and series magnet circuit to obtain the wide flux regulation range. II. TOPOLOGICAL DECOMPOSITION AND MACHINE TOPOLOGY The topology decomposition of the proposed DL-VFMM is shown in Fig. 1(a). Furthermore, the configurations of conventional series VFMM and the proposed machine are illustrated in Fig. 1(b) and (c). For the proposed machine, it is characterized by a DL magnet arrangement with U- and V-shaped PMs, in which the V-shaped PMs are composed of multiple segmented LCF magnets. The segmented LCF PM design makes the magnetic flux of the HCF PMs follow the *q*-axis LCF PMs to reach the *d*-axis LCF PMs under flux-weakened state, thus realizing large magnetic fluxes short-circuited within the rotor core, which leads to the expansion of flux regulation range. III. PRELIMINARY ELECTROMAGNETIC PERFORMANCE The electromagnetic characteristics of the two VFMMs are shown in Fig. 2. Compared with the conventional series VFMM, the proposed machine exhibits a wider flux regulation range. Besides, the torque waveforms of two machines under different MSs are illustrated in Fig. 2 (b). The torque amplitude of the proposed machine is similar to that of the conventional series VFMM under the flux-enhanced state. In addition, the efficiency maps of two machines are investigated in Fig. 2(c) and (d). The proposed machine exhibits higher efficiency under the flux-weakened state compare with the convention one.

[1] A. Athavale, K. Sasaki, B. S. Gagas, T. Kato, and R. D. Lorenz, *IEEE Trans. Ind. Appl.,* vol. 53, no. 5, pp. 4318- 4326, Sep./Oct. 2017. [2] Y. H. Kim, S. S. Lee, and J. H. Lee, *AIP Advances*, vol. 8, no. 5, p. 056632, May 2018. [3] H. Yang, H. Zheng, H. Lin, Z. Q. Zhu and S. Lyu, in *Proc. IEEE Int. Elect. Mach. and Drives Conf., (IEMDC)*, San Diego, USA, 2019, pp. 2259-2264.

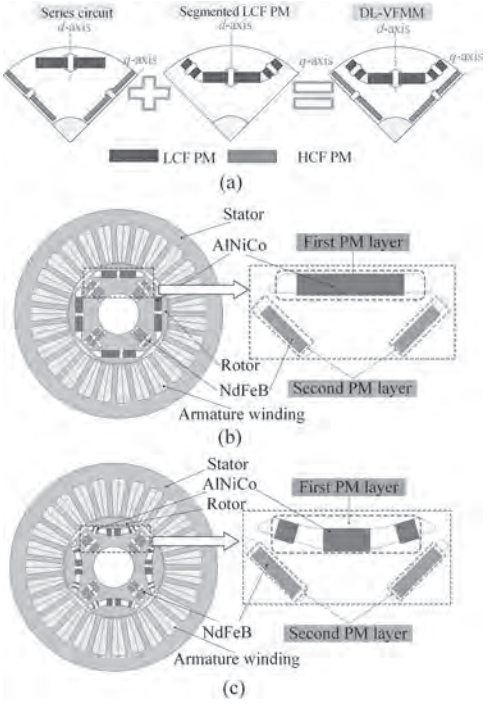

Fig. 1. Machine Topology. (a) Topology decomposition. (b) Conventional series VFMM. (c) Proposed DL-VFMM.

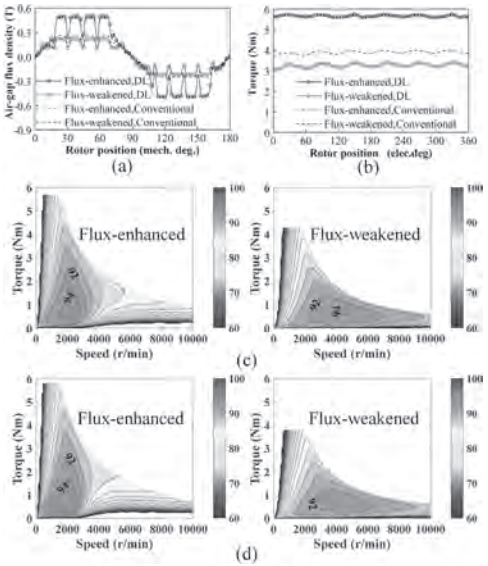

Fig. 2. (a) Air-gap flux density. (b) Torque waveforms. Efficiency maps of (c) proposed DL-VFMM and (d) conventional series VFMM.

JPB-04. Influence of Low-Coercive-Force Magnet Property on Electromagnetic Performance of Variable Flux Memory Machines. *W. Liu*[1], H. Yang[1] and H. Lin[1] *1. School of Electrical Engineering, Southeast University, Nanjing, China*

I. Introduction Variable flux memory machines (VFMMs) [1]-[2] equipped with low-coercive-force (LCF) PMs are competent for automotive applications. The magnetization states (MSs) of the LCF PMs can be flexibly varied by a current pulse, which can achieve an excellent flux adjustability with negligible additional copper loss [3]. Nevertheless, the magnetic properties of the LCF PMs, i.e., remanent flux density (*Br*) and coercivity (*Hc*), are closely related to the magnetization characteristics of VFMMs, which are unreported in detail. Thus, the influences of different LCF PM materials in hybrid-magnetic-circuit VFMMs (HMC-VFMMs) are investigated in this paper [4], which aims to provide a generic guideline for the LCF magnet grade selection. II. Machine Topology The investigated HMC-VFMM configuration is illustrated in Fig. 1(a), in which both series and parallel magnetic circuits are combined to achieve high torque density and excellent flux adjustability. Neodymium-iron-boron is selected as high-coercive-force (HCF) magnet, while the LCF magnet candidates have three choices in this case. The hysteresis curves of different LCF material candidates are shown in Fig. 1(b), in which AlNiCo exhibits the lowest *Hc*, followed by Ferrite and SmCo magnets, respectively. Ferrite shows the lowest *Br*, which implies that lower torque performance will be obtained under flux-enhanced state. III. Electromagnetic Performance The electromagnetic characteristics of the HMC-VFMMs equipped with different LCF magnets are shown in Fig. 2. SmCo-based model presents the widest flux regulation range, which benefits from highest coercivity amongst the three candidates. Ferrite-based model shows the lowest flux regulation range due to the low remanent flux density. Furthermore, AlNiCo-based model exhibits the minimum required magnetization current. Finally, the measured torque results of the investigated HMC-VFMM equipped with AlNiCo and NdFeB PMs agree well with the finite-element (FE) results, which confirms the feasibility of the proposed analysis.

[1] V. Ostovic, "Memory motors," *IEEE Ind. Appl. Mag.*, vol. 9, no. 1, pp. 52–61, Jan. 2003. [2] H. Hua, Z. Q. Zhu, A. Pride, R. P. Deodhar, and T. Sasaki, "A novel variable flux memory machine with series hybrid magnets", *IEEE Trans. Ind. Appl.*, vol. 53, no. 5, pp. 4396-4405, Sep./Oct. 2017. [3] F. Liu, L. Cheng, M. Wang, G. Qiao, P. Zheng, and H. Yang, "Comparative study of hybrid-PM variable-flux machines with different series PM configurations," *AIP Advances*, vol. 9, no. 12, p. 125241, Dec. 2019. [4] H. Yang, S. Lyu, H. Lin, Z. Q. Zhu, H. Zheng, and T. Wang, "A novel hybrid-magnetic-circuit variable flux memory machine," *IEEE Trans. Ind. Electron.*, vol. 67, no. 7, pp. 5258-5268, July 2020.

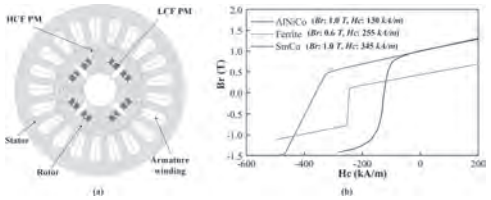

Fig. 1. (a) Cross section of the HMC-VFMM. (b) B-H Hysteresis curves.

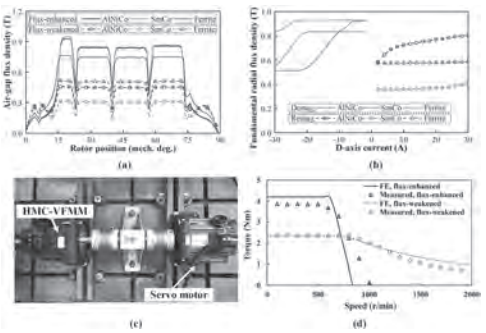

Fig. 2. (a) Air-gap flux density. (b) Magnetization characteristics. (c) Prototype. (d) Measured torque versus speed curves.

JPB-05. Classical and Mutually Coupled Winding Configuration Comparison for the Axial-Field Switched Reluctance Machine with Segmented Rotor. *S. Asfirane*[1], M. Hatoum[1], G. Barakat[1] and Y. Amara[1] *1. GREAH, Université Le Havre Normandie, Le Havre, France*

This paper deals with a 24-pole segmented rotor in a 3-phase, 36-slot per stator topology of an axial-field double stator switched reluctance machine (AFDSSRM). An axial-field segmental rotor switched reluctance motor with single stator and tooth winding is investigated in [1] acheiving higher torque density than the radial SRM. A double stator design of the same motor is presented in [2] to counter the unbalenced force due to the one sided excitation in the single stator version. For radial-field SRM, the mutually coupled winding configuration is compared to the conventional one in a number of works [3], [4] but it has never been investigated in the case of an AFDSSRM. Fig.1 (a) shows the classical winding (+A--B++C--A++B--C+) and (b) shows the mutually coupled one (+A-+B-+C-+A-+B-+C-). The topology of the AFDSSRM is made of 2 stators connected is series and a segmented rotor in between. Each stator tooth holds one coil dedicated to one phase. In this paper, The AFDSSRM is modeled using 2D finite element model (FEM). The 2D-FEM is established at the mean radius of the machine with the hypothesis of radial invariance of local quantities [5]. It is used to achieve calculations of self and mutal inductances, flux-linkage and torque for three different current distributions. The motor is first fed with 3-phase step current in unipolar and bipolar mode. Then a 3-phase sinusoidal current is used. Fig.2 illustrates the variation of self and mutual inductance for both winding configurations. It appears that in the case of the classical winding, the mutual inductance can be neglected and the self-inductance is up to 2.5 times higher than the mutually coupled one (10 Amp-current). For the mutually coupled configuration, the self and mutual inductance variations follow the same trend with regards to current and they are of the same order of magnitude. At the end, the results will be confirmed using a Full 3D-FEM for both configurations.

[1] W. Sun, Q. Li, L. Sun, L. Zhu and L. Li, "Electromagnetic Analysis on Novel Rotor-Segmented Axial-Field SRM Based on Dynamic Magnetic Equivalent Circuit," in *IEEE Transactions on Magnetics*, vol. 55, no. 6, pp. 1-5, June 2019, Art no. 8103105, doi: 10.1109/TMAG.2019.2901002. [2] B. Wang, D. Lee and J. Ahn, "Characteristic analysis of a novel segmental rotor axial field switched reluctance motor with single teeth winding," *2014 IEEE International Conference on Industrial Technology (ICIT)*, 2014, pp. 175-180, doi: 10.1109/ICIT.2014.6894934. [3] G. J. Li, X. Ojeda, S. Hlioui, E. Hoang, M. Gabsi and C. Balpe, "Comparative study of Switched Reluctance Motors performances for two current distributions and excitation modes," *2009 35th Annual Conference of IEEE Industrial Electronics*, 2009, pp. 4047-4052, doi: 10.1109/IECON.2009.5415318. [4] X. Liang, G. Li, J. Ojeda, M. Gabsi and Z. Ren, "Comparative Study of Classical and Mutually Coupled Switched Reluctance Motors Using Multiphysics Finite-Element Modeling," in *IEEE Transactions on Industrial Electronics*, vol. 61, no. 9, pp. 5066-5074, Sept. 2014, doi: 10.1109/TIE.2013.2282907. [5] H. Tiegna, Y. Amara and G. Barakat, "A New Quasi-3-D Analytical Model of Axial Flux Permanent Magnet Machines," in *IEEE Transactions on Magnetics*, vol. 50, no. 2, pp. 817-820, Feb. 2014, Art no. 7020204, doi: 10.1109/TMAG.2013.2285739.

Fig.1 Winding configuration of the AFDSSRM, a) Classical winding, b) Mutually coupled.

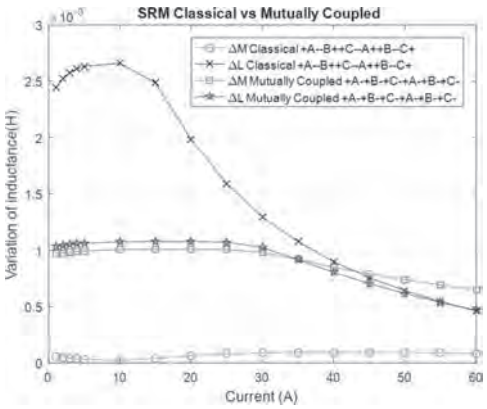

Fig 2. Variation of self and mutual inductance versus current for both winding configuration (Classical and Mutually Coupled)

JPB-06. Withdrawn

JPB-07. An Axial Flux Permanent Magnet Motor with Magnetorheological Fluid Brake Structure. *Y. Hu*[1] and W. Xu[1] *1. School of Electrical Engineering, Southeast University, Nanjing, China*

1. Introduction Magnetorheological fluid (MRF) is a material whose viscous and plastic rheological property can be changed sharply under an external magnetic field [1]. The brake based on MRF characteristics has the advantages of simple structure, fast response and convenient control compared with traditional brakes [2-3]. However, the current studies on MRF brake mostly use an independent structure [4-5] connecting in series with motor to form joint module, which has the defect of large axial length. It greatly limits the space of joint modules. In this paper, an axial flux permanent magnet motor (AFPMM) with MRF brake structure is proposed to obtain the small axial size and fast braking response. 2. Machine topology Fig.1(a) shows the top view of an AFPMM with MRF brake structure (no rotating seal cap for easy viewing), which has two working modes: rotation and brake mode. Fig.1(b) shows the front cutaway view of the proposed machine. Fig.1(c) shows 2D radial flux circuit of MRF brake structure. When the MRF is magnetized and thus the viscous force of MRF is rapidly increased, the large shear stress is produced to brake the AFPMM. 3. FE analysis In this paper, the speed and the maximum current density of the AFPMM are set to 1200 r/min and 8A/mm^2 respectively. Fig.2(a) shows the variation of motor torque under different axial excitation currents. Fig.2(b) shows radial component distribution of magnetic flux density in MRF along axial direction under two working modes. It can be found that the axial flux in rotation mode does not magnetize the MRF to produce brake torque. Based on Bingham model, the brake torque formula of MRF is shown in Fig.2(c). Fig.2(d) shows the variation of MRF brake torque under different radial excitation currents. It can be seen that the brake torque under the brake mode is enough to get an effective braking.

[1] J. Rabinow Magnetic fluid torque and forcetransmitting device. U.S. Patent Number 2575360, 1951. [2] J. Blake and H. B. Gurocak, "Haptic glove with MR brakes for virtual reality," *IEEE/ASME Trans. Mechatronics.*, vol. 14, no. 5, pp. 606-615, Oct. 2009. [3] S. Suzuki, Y. Kawase, T. Yamaguchi, K. Hirata and Y. Okaue, "Dynamic Response Analysis of

Shear-Type Compact MR Brake Using Finite Element Method," *IEEE Trans. Magn*, vol. 45, no. 3, pp. 1728-1731, March. 2009. [4] C. Rossa, A. Jaegy, J. Lozada and A. Micaelli, "Design Considerations for Magnetorheological Brakes," *IEEE/ASME Trans. Mechatronics*., vol. 19, no. 5, pp. 1669-1680, Oct. 2014. [5] N. Kobayashi, K. Kawase, S. Sato and T. Nakagawa, "Experimental Verification of Effects in an Emergency Stop by Installation of Magnetorheological Fluid Damper to an Elevator," *IEEE Trans. Magn*., vol. 53, no. 11, pp. 1-4, Nov. 2017.

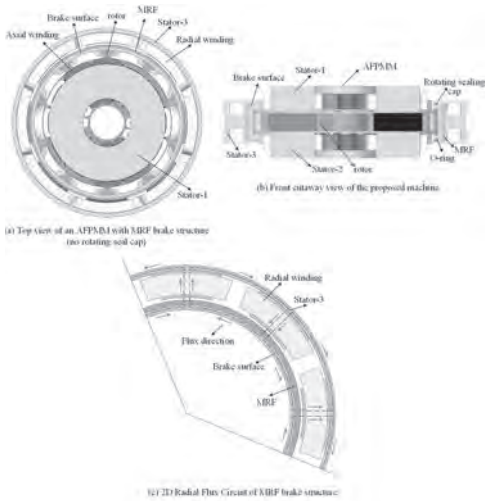

Fig.1 Machine topology

Fig.1 Machine topology

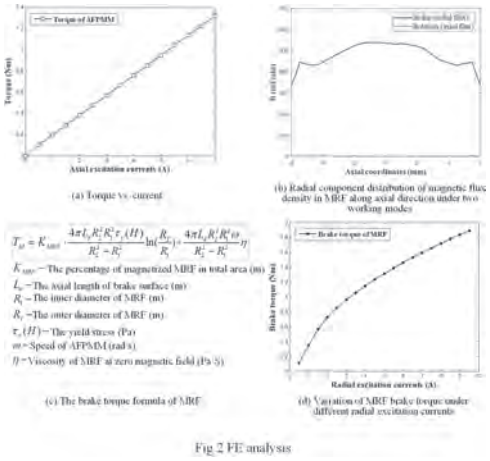

Fig.2 FE analysis

Fig.2 FE analysis

JPB-08. Increment of the linkage flux to the HTS by improved magnetic circuit in the HTS magnetic bearing. *R. Taniguchi*[1], S. Ishida[1], M. Minamitani[1] and S. Ohashi[1] *1. Electrical and Electronic Engineering, Kansai University, Suita, Japan*

Magnetic levitation using the pinning force of a high-temperature superconductors (HTS) has the advantage which is stable levitation without control [1], [2]. This paper studies the Increment of the linkage flux to the HTS by improved magnetic circuit in the HTS magnetic bearing. The rotor is levitated by the pinning force of the HTS. The two-layer ring- type rotor comprises a cylindrical and a ring-type permanent magnet, and the flux at the top side dose not interlink sufficiently with the HTS[3]-[5]. Fig.1 shows the structure and flux line of the two-layer ring-type rotor. A yoke-equipped ring-type rotor is introduced to study the improvement of the flux-use rate to use the flux at the top side. Fig.2 shows the yoke-equipped ring-type rotor. The rotor improves flux-use rate by equipping the yoke to the ring-type permanent magnet and the flux of this rotor is focused on the outer side of the HTS. By concentrating the flux of the rotor on the HTS, the pinning force of this rotor increases. The permanent magnet volumes of the two-layer ring-type rotor and the yoke-equipped ring-type rotor are almost the same. Furthermore, when the levitation gap is g = 10[mm], the total flux of the yoke-equipped ring -type rotor interlinked with the HTS surface increases by 68.4% compared with that of the two-layer ring-type rotor. The levitation force improves by 24.8% compared with that of the two-layer ring-type rotor. The guidance force improves by 62.6% compared with that one. In terms of its rotational characteristics, the maximum amplitude at the resonance point of the yoke-equipped ring- type rotor decrease by 59.1% compared with that one. This is because by concentrating the flux on the outer side of the HTS, the force that suppresses vibration during resonance has increased. In designing the magnetic circuit of the rotors, the flux interlinked with the HTS surface increased and focused to the outer side of the HTS. In this way, the levitation force, the guidance force, and the rotational characteristics of the yoke-equipped ring- type rotor are improved. As the result, the stability of the rotor has improved.

[1] F. C. MOON, "SUPERCONDUCTING LEVITATION", JOHN WILEY & SONS, NEW YORK, (1994) [2] J. Hull, M. Murakami, "Appications of bulk high temperture superconductors", in Proc of IEEE, vol. 92, no. 10, October 2004, pp1705-1718 [3] S. Sakai, K. Oguni, S. Ohashi, "Effect of the magnetic configuration on the rotational motion in the attractive type HTS-permanent magnet hybrid bearing", IEEE Trans on Applied Superconductivity, vol. 26, no.4, 3601204, June 2016. [4] T. Minami, S. Sakai, S. Ohashi, "Improvement of stability against vibration at the mechanical resonance in attractive type HTS permanent hybrid magnet bearing.", 2016 IEEE Region 10 Conference (TENCON2016), 16657805, 2016, pp3294-3297. [5] S. Takimura, T. Arai., T. Minami, S. Ohashi, "Basic characteristics of the yoke equipped rotors in the magnetic bearing using HTS pinning effect", IEEE Xplore Digital Library IEEE, 12th International Symposium on Linear Dives for Industry Applications (LDIA2019), 8770991, 2019.

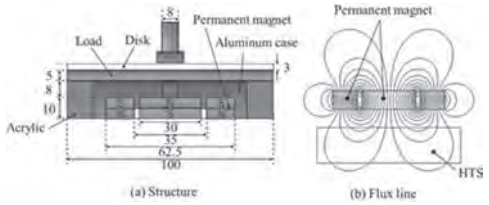

Fig. 1 Two-layer ring-type rotor

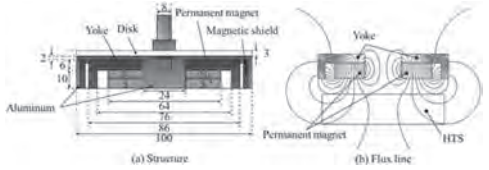

Fig. 2 Yoke-equipped ring-type rotor

JPB-09. Open-phase fault modeling for dual three-phase PMSM using vector space decomposition and negative sequence components. W. LI[1], *P. Song*[1], Q. Li[2], Z. Li[1] and N. Kar[1] *1. University of Windsor, Windsor, ON, Canada; 2. Nanjing University of Science and Technology, Nanjing, China*

The dual three-phase permanent magnet synchronous motors (DTP-PMSMs) possess two sets of three-phase winding exhibiting the high capability in fault-tolerant operations [1]. The open-phase fault is one typical fault and various research has been conducted on open-phase fault modeling and control of the DTP-PMSMs [2], [3]. Recently, a dynamic fault modeling and control for six-phase PMSMs based on multireference frame has been proposed [4]. In this paper, other than using the multireference frame, the fault modeling is based on the existing vector space decomposition (VSD) for DTP-PMSMs, and the open-phase fault is regarded as a combination of positive and negative sequence components. Therefore, the number of current regulators is reduced and dynamic performance is improved.

By using VSD, currents of the dual three-phase winding are projected into three orthogonal subspaces, namely αβ plane (torque-producing plane) and xy plane (non–torque–producing plane). Fig. 1(b) shows the current waveforms under open-phase fault, which can be represented by positive sequence currents (healthy operation) and negative sequence currents. The positive sequence currents are projected to αβ plane and the negative sequence currents are projected to xy plane. As shown in Fig. 2(a), in the αβ plane, the projected faulty currents are the dc currents as the projected positive sequence currents, and while in the xy plane, the projected faulty currents are the ac currents with the same dc components as the projected negative sequence currents. Since the torque only generated in the αβ plane, the torque generated under open-phase fault is stable as that under healthy operation. Fig. 2(b) compares the torque waveforms under the proposed fault modeling in this paper and the modeling based on a multireference frame. Since the harmonic components can be suppressed using VSD, the torque ripple is about 10% lower by using the proposed method. The detailed modeling and experimental verification will be presented in the full paper.

[1] Y. Demir and M. Aydin, "A novel asymmetric and unconventional stator winding configuration and placement for a dual three-phase surface PM motor," IEEE Trans. Magn., vol. 53, no. 11, pp. 1–5, 2017. [2] X. Wang, Z. Wang, Z. Xu, M. Cheng, W. Wang, and Y. Hu, "Comprehensive diagnosis and tolerance strategies for electrical faults and sensor faults in dual three-phase PMSM drives," IEEE Trans. Power Electron., vol. 34, no. 7, pp. 6669–6684, 2018. [3] L. Xiao, L. Zhang, F. Gao, and J. Qian, "Robust fault-tolerant synergetic control for dual three-phase PMSM drives considering speed sensor fault," IEEE Access, vol. 8, pp. 78912–78922, 2020. [4] W. Li, G. Feng, Z. Li, J. Tjong, and N. Kar, "Multireference frame based open-phase fault modeling and control for asymmetrical six-phase interior permanent magnet motors," IEEE Trans. Power Electron., 2021.

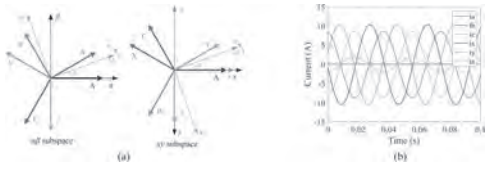

Fig. 1 (a) Vector space decomposition. (b) Dual three-phase current waveforms under open-phase fault.

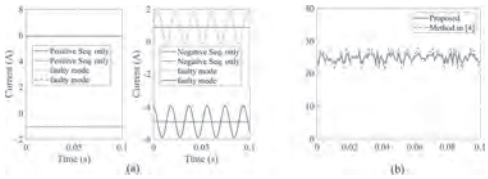

Fig. 2. (a) Current waveforms in different planes using VSD. (b) Torque waveforms comparison.

JPB-10. A Design of 3kW E-booster and Motor Drive with 12V and 48V System Comparison. *E. Park*[1] and Y. Kim[2] *1. Faculty of Smart Vehicle System Engineering, Chosun university, Gwangju, The Republic of Korea; 2. The Department of Electrical and Computer Engineering, Chosun university, Gwangju, The Republic of Korea*

I. Abstract As the number of motors used in vehicles increases, the battery voltage of the vehicle is also being proposed from the conventional 12V to 48V. Most of the electric superchargers that boost the engine efficiency of the vehicle use 12V and rotate at ultra-high-speed. However, when 12V is used, there is a problem of loss due to high current and ultra-high-speed. Therefore, in this paper, we compared the characteristics by designing a conventional 12V ultra high speed electric supercharger and geared 48V high speed electric supercharger. We also analyzed the controller as well as the motor, and showed that the proposed model is superior in terms of integrated size and efficiency. II. Introduction Current 12V batteries in automobiles are a voltage that the electric supercharger is not enough to generate useful boost pressure. As a solution to this problem, the 48V mild hybrid system is beginning to surface. Since the high output is required to match the rated speed of the ultra-high-speed motor used in the compressor for supercharging, a large amount of current flows to use at a low voltage of 12V, and the development of the technology has been stopped due to problems such as coil thickness and heat generation [1-4]. When changing from the existing 12V to 48V voltage system, the same power can be sent with only a quarter current, which reduces the cost and weight of the existing wire and reduces the load on the engine [5-8]. IiI. Design of 12V and 48V Ultra-high-speed Electric Supercharger Fig. 1 shows the design results of 12V and 48V ultra-high-speed electric supercharger. It shows higher power density and efficiency in the motor using 48V than when using 12V. IV. Design of High-speed Motor Fig. 2 shows the temperature of the motor driver. The results show that the 48V, 17.5krpm motor and drive show low operating temperature and high efficiency. Based on this data, we predicted the integrated size of the controller and the motor. As a result, when the 48V is used, the volume can be reduced to 1/10 of the inverter size from 12V and the motor size can be reduced by 33%.

[1] Y. Yamashita, S. Ibaraki, K. Sumida, M. Ebisu, B. An, and H. Ogita, "Development of electric supercharger to facilitate the downsizing of automobile engines," *Mitsubishi Heavy Ind. Tech. Rev.*, vol. 47, no. 4, pp. 1–6, Dec. 2010. [2] T. Noguchi, Y. Takata, Y. Yamashita, S. Ibaraki, "160,000 r/min, 2.7-kW Electric Drive of Supercharger for Automobiles," *2005 International Conference on Power Electronics and Drives Systems*, 2015. [3] T. Noguchi, M. Kano, "Development of 150000 r/min, 1.5 kW Permanent Magnet Motor for Automotive Supercharger," *2007 7th International Conference on Power Electronics and Drive Systems*, 2007. [4] T. Noguchi, Y. Takata, "2-kW permanent Magnet Motor Drive for Turbocharger" [5] S. Ibaraki, Y. Yamashita, K. Sumida, H. Ogita, and Y. Jinnai, "Development of the 'hybrid turbo,' an electrically assisted turbocharger," *Mitsubishi Heavy Ind. Tech. Rev.*, vol. 43, no. 3, pp. 1–5, Sep. 2006. [6] H. Breitbach, D. Metz, S. Weiske, and G. Spinner, "Application and design of the eBooster from BorgWarner," *BorgWarner Knowl. Library, Auburn Hills*, MI, USA, Tech. Rep., 2015. [7] S. Biwersi, S. Tavernier, and S. Equoy, "Electric compressor with highspeed brushless DC motor," *MTZ Worldwide*, vol. 73, no. 12, pp. 50–53, Dec. 2012. [8] C. Zwyssig, J. Kolar, S. Round, "fficiency Optimization of a 100W, 500,000rpm Permanent Magnet Machine Including Air Friction Losses," *Mechatronics, IEEE/ASME Trnas.*, vol. 14, no. 5, pp. 564-574, 2009.

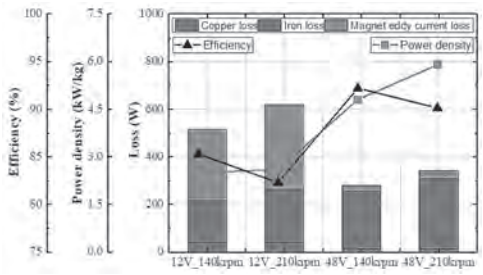

Fig. 1. Characteristics of 12V and 48V motor.

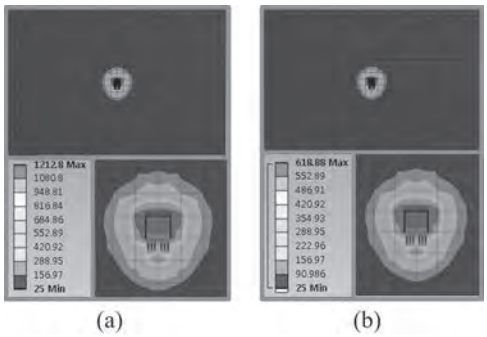

Fig. 2. Motor drive temperature (a) using 12V, (b) using 48V.

JPB-11. Electromagnetic characteristic analysis according to PAM-PWM inverter system of high-speed permanent magnet motor. *J. Woo*[1], T. Bang[1], J. Lee[1] and J. Choi[1] *1. Electrical Engineering, Chungnam-National University, Yuseong-gu, The Republic of Korea*

Recently, the demand for turbo compressors, one of the oil-free compressor, to reduce carbon dioxide emissions and energy consumption in the automobile industry has increased significantly, resulting in increasing research on this issue. The turbo compressor is applied with a high-speed permanent magnet(PM) motor because high-speed rotation is necessary in order to achieve the required pressure [1]. Generally, these PM motors are driven by a pulse width modulation (PWM) voltage source inverter for vector control. However, when the PWM control method controls in the low-speed range, the armature current is distorted, and torque is generated, thereby causing the performance to deteriorate [2]. In the case of pulse amplitude modulation (PAM), however, the DC link voltage required for motor control is generated, ensuring stable performance at both low and high speeds [3]. In this study, the effect of current harmonics, resulting from the carrier harmonics of the inverter generated when driving the motor according to these two control methods, are analyzed. By dividing the core of the motor, the magnetic behavior of the magnetic flux density was analyzed to derive the electromagnetic loss according to each control method [4-5]. As a result, an optimal method under motor driving conditions was found through comparison and analysis. Fig. 1(a) shows the 3D structure and manufacturing model of the high-speed motor. Fig. 1(b) shows the electromagnetic loss distribution according to the current. When compared with the sinusoidal current, the harmonic current of PWM has a significant effect on the eddy current loss of the rotor. Fig. 1(c) shows the line-to-line voltage under a no-load condition. Fig. 2 shows a dynamic simulation block diagram of the PWM and PAM control methods. An electromagnetic characteristics comparative analysis was performed through this dynamic simulation for each control method. A more detailed comparison of the results according to each control method will be provided in the full paper.

1. Seok-Myeong Jang, Jang-Young Choi, Kyoung-Jin Ko, Il-Jung Kim, Ho-Kyung Sung, “Performance analysis of permanent magnet machines considering magentic losses based on analytical parameter estimation”, 11th International Conference on Electrical Machines and Systems, pp.3152-3157, 2008. 2. Chen Liangliang, Xiao Lan, Hu Wenbin, Yan Yangguang, “Application of coupled inductors in parallel inverter system”, Electrical Machines and System, 2003. ICEMS 2003. Sixth International Conf. Vol. 1, pp. 398-401, 2003, Nov. 3. L. Schwager, A. Tuysuz, C. Zwyssig and J. W. Kolar, “Modeling and Comparison of Machine and Converter Losses for PWM and PAM in High- Speed Drives”, *IEEE Transactions on Industry Applications*, vol. 3, no. 2, pp. 995-1006, March/April 2014. 4. Cheol Han, Jang-Young Choi, Ji-Hun Ahn, Ji-Hwan Choi and Seok-Myeong Jang, “The harmonics influence and efficiency improvement in high-speed permanent magnet synchronous motor using 2-d finite element method“ IEEE INTERMAG CONFERENCE 2012, Vancouver, Canada, May 7-11, 2012 5. L. Ma, M. Sanada, S. Morimoto and Y. Takeda, “Iron Loss Prediction Considering the Rotational Field and Flux Density Harmonics in IPMSM and SynRM”, IEE Proc.-Electr. Power Appl, Vol.150, No.6, Nov., 2003.

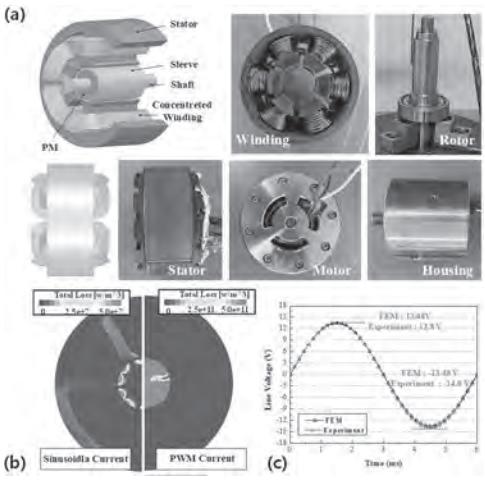

(a) 3D structure and Manufactured model of high speed motor, (b) Electromagnetic loss distribution and (c) Line voltage at no-load condition

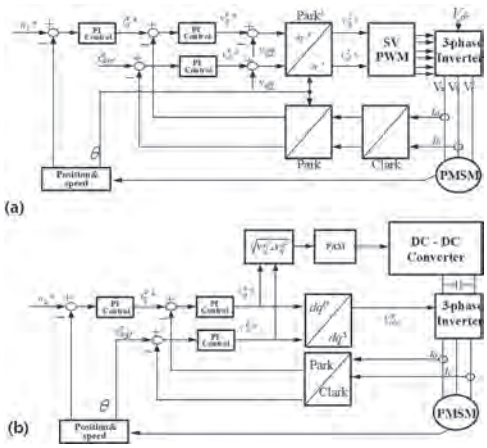

Dynamic simulation block diagram of (a) PWM and (b) PAM controls

JPB-12. A Study on the Reduction of Eddy Current Loss through Sleeve Design and the Improvement of Torque Density through Ferrofluid. *S. Song*[1], D. Kim[1] and W. Kim[2] *1. Department of Electrical Engineering, Hanyang University, Seoul, Kuwait; 2. Department of Electrical Engineering, Gachon University, Seong-Nam, The Republic of Korea*

High-speed PM motors are characterized to have the advantage of high power density. However, the loss density is also much higher than that of a costant speed motor, which can lead to excessive temperature rise. Surface-attached PM structures are the most common topology for these motors. Rotor retaining sleeves are also commonly used to prevent scattering of magnets. In surface-mounted PM motors, the retaining sleeve is directly exposed to a magnetic field. The eddy current losses induced by the harmonic magnetic field are large in the retaining sleeve. Since the rotor is located inside, it is difficult to emit heat. Therefore, the eddy current loss generated in the retaining sleeve can lead to an unbearable temperature rise in the rotor, which can have catastrophic effects such as irreversible demagnetization of PMs and reduced efficiency. Therefore, it is important to reduce the rotor eddy current loss while designing a high-speed PM motor. In general, the retaining sleeve uses a non-magnetic material. This is because, when magnetic material is used, the magnetic flux generated from the magnet is greatly leaked along the sleeve, resulting in performance degradation. Therefore, a non-magnetic material should be used. However, since the permeability of the non-magnetic material is the same as that of the airgap, the airgap increases as much as the sleeve thickness, causing performance degradation. Therefore, in this paper, eddy current loss is reduced by digging a groove in the retaining sleeve, and inserting a ferrofluid into

the groove to satisfy high power density and high efficiency. Ferrofluid refers to water or oil mixed with ultrafine powder. The magnetic fluid image observed by transmission electron microscopy (TEM) is shown in Fig. 1 (a). Ferrofluid does not have magnetism when there is no magnetic field, but it becomes magnetized when an external magnetic field is applied with a magnet. Materials with this property are called supermagnetic.

[1] Thirupathi, G.; Singh, R. Study of magnetoviscosity of ferromagnetic MnZn-ferrite ferrofluid. IEEE Trans. Magn. 2015, 51, 3–6. [CrossRef] [2] E. C. Lovelace, T. M. Jahns, T. A. Keim, and J. H. Lang, "Mechanical design considerations for conventionally laminated, high-speed, interior PM synchronous machine rotors," IEEE Trans. Ind. Appl., vol. 40, no. 3, [3] I.-J. Yang, S.-W. Song, D.-H. Kim, K.-S. Kim and W.-H. Kim, "Improvement in torque density by Ferrofluid injection into magnet tolerance of interior permanent magnet synchronous motor," J. Energies., vol. 14, no. 6, pp. 1736, Mar 2021.

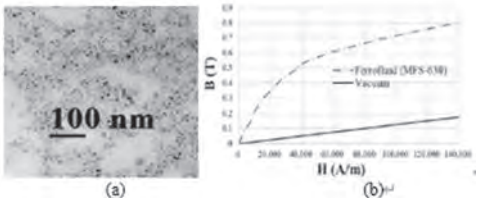

Fig. 1 TEM image of Mn0.75Zn0.25Fe2O4 (MZF) ferrofluid(a) and B-H curves of vacuum and ferrofluid(b).

Fig. 2 Magnetic flux line before(a) and after(b) ferrofluid injection of multiple groove type model

JPB-13. Novel Dual-Stator Single Rotor Consequent Pole PM Machine. J. Yang[1], *Z. Wang*[1] and S. Huang[1] *1. College of Electrical and Information Engineering, Hunan University, Changsha, China*

A novel dual-stator single-rotor consequent pole permanent magnet machine (DSCP-PMM) is proposed. The electromagnetic performance indexes including the air-gap flux density, back-EMF, and output toque are evaluated. It indicates that the proposed DSCP-PMM2 has higher toque density and lower torque ripple. I. Introduction Consequent pole permanent magnet machines (CP-PMMs) have attracted attention due to its high efficient utilization ratio of PM materials and low cost [1]. While the power density of CP-PMM would be lower than that of the conventional surface-mounted PM (SPM) machine. Meanwhile, the toque ripple would be deteriorated by the even-order harmonic components of phase back electromotive force (back-EMF) [2]. Addressing those issues, a novel dual-stator single-rotor CP-PMM (DSCP-PMM) is proposed and investigated in this paper. II. Structure and Operation Principle To improve the power density of CP-PMM, a dual-stator single-rotor consequent pole PM machine (DSCP-PMM) with N-iron-N-iron poles is proposed, as shown in Fig. 1(a), which is defined as DSCP-PMM1. To reduce the torque ripple, the rotor structure of DSCP-PMM is further improved, as shown in Fig. 1(b) and defined as DSCP-PMM2. Its rotor consists of two layers, one layer is N-iron-N-iron, and the other is iron-S-iron-S. The armature windings on the inner and outer stator of DSCP-PMM2 are connected to counteract the even-order harmonic component of the phase back-EMF. III. Performance Comparison The back-EMF waveforms and harmonic components of both machines are shown in Fig. 2(a) and 2(b), respectively. The back-EMF of DSCP-PMM1 contains even-order harmonic components, while the DSCP-PMM2 only consists of odd-order harmonic components. Fig. 3 shows the output torques of both machines. The average torques of DSCP-PMM1 and DSCP-PMM2 are 3.65 Nm and 3.81Nm, and the torque ripples of both machines are 79.6% and 21.8%, respectively. Thus, higher toque density and lower torque ripple could be obtained by the DSCP-PMM2. IV. Conclusion A novel dual-stator single-rotor consequent pole permanent magnetic machine (DSCP-PMMs) is proposed in this paper. Relevant results indicate that the proposed DSCP-PMM2 has higher toque density and lower torque ripple.

[1]S. U. Chung, H. J. Lee, B. C. Woo, J. W. Kim, J. Y. Lee, S. R. Moon and S. M. Hwang, "A feasibility study on a new doubly salient permanent magnet linear synchronous machine," *IEEE Trans. Magn.*, vol. 46, no. 6, pp. 1572–1575, Jun. 2010. [2]J. Li, K. Wang, F. Li, S. S. Zhu and C. Liu, "Elimination of Even-order-Order Harmonics and Unipolar Leakage Flux in Consequent-Pole PM Machines by Employing N-S-Iron–S-N-Iron Rotor," *IEEE Trans. Ind. Electron*., vol. 66, no. 3, pp. 1736-1747, Mar. 2019.

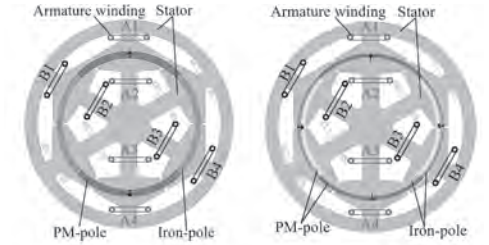

Fig. 1. Topologies of 6-slot/4-pole DSCP-PMM with different rotors. (a) DSCP-PMM1. (b) DSCP-PMM2.

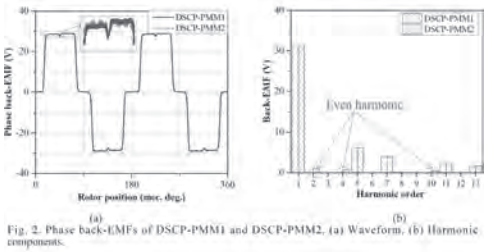

Fig. 2. Phase back-EMFs of DSCP-PMM1 and DSCP-PMM2. (a) Waveform. (b) Harmonic components.

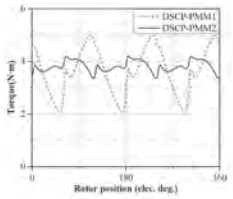

Fig. 3. Output torques of DSCP-PMM1 and DSCP-PMM2.

JPB-14. Design of an Integrated Pump and Axial Flux Switching Permanent Magnet Motor Based on Magnetic 3D Printing. *P. Huang*[1], T. Chang[1], C. Chang[1], C.U. Ubadigha[2], I. Jiang[1], M. Hsieh[3] and M. Tsai[2] *1. Electrical Motor Technology Research Center, National Cheng Kung University, Tainan, Taiwan; 2. Mechanical Engineering, National Cheng Kung University, Tainan, Taiwan; 3. Electrical Engineering, National Cheng Kung University, Tainan, Taiwan*

With the recent Covid-19 pandemic, the machine which is effectively isolated and secured from suspected contaminated space but capable of keeping continuous air exchange has become an important issue. The axial flux-switching permanent magnet motor (AFSPM) which combined the centrifugal pumps' fan blade and its motor rotor [1][2] could be a possible solution for that can eliminate the need for the drive shaft connecting the rotor and the impeller. Also, the shaft sealing mechanism of the centrifugal pump can be omitted and still achieve a leakless pump. However, achieving this is difficult since the magnets are expected to have the complicated shape of an impeller, which of course is hard to fabricate and also that the effective flux would be significantly decreased. In this study, an AFSPM with a centrifugal pump rotor is designed and a prototype based on high permeability

additive manufacture process is made to verify the design performance. Fig. 1 shows the structure and flux distribution by FEA software for the 6 slots and 7 poles AFSPM designed in this paper. The operated voltage is 12 V and the rated output speed is 1000 rpm. For the proposed integration model to perform the functions of motor rotor and impellers, the rotor salient poles are designed with a special skew which is able to interact with the stator excited magnetic field and also allow air to flow through. Fig. 2 (a) shows the components of the AFSPM which includes the magnetic metal 3D printed stator and rotor as well as the wire-cutting magnets; likewise, Fig. 2 (b) shows the Back-emf at the rated speed, which is measured as 0.19 V, and found to agree with the simulation result at 0.18 V. This paper presents the design and fabrication of a AFSPM with an integrated impeller rotor. With the proposed impeller shaped rotor design, the AFSPM could be applied for medical use to synchronically achieve the functions of complete isolation and air exchange between different spaces. The design is verified using FEA simulation, as well as a prototype and experimental results based on magnetic 3D printing method were also provided.

[1] H. Ding, Y. Li, S. G. Min and B. Sarlioglu, "Electromagnetic and thermodynamic design of a novel integrated flux-switching motor-compressor with airfoil-shaped rotor," *2017 IEEE Energy Conversion Congress and Exposition (ECCE)*, 2017, pp. 5409-5416, doi: 10.1109/ECCE.2017.8096905.
[2] S. -T. Wu, P. -W. Huang, T. -W. Chang, I. -H. Jiang and M. -C. Tsai, "Application of Magnetic Metal 3-D Printing on the Integration of Axial-Flow Impeller Fan Motor Design," in *IEEE Transactions on Magnetics*, vol. 57, no. 2, pp. 1-5, Feb. 2021, Art no. 8201205, doi: 10.1109/TMAG.2020.3014651.

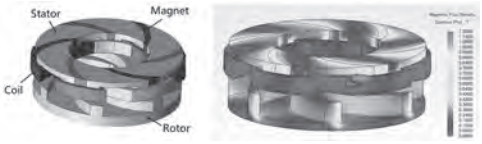

Fig. 1. Structure diagram of AFSPM

Fig. 2. (a) Components of AFSPM, (b) Back-emf at 1000 rpm

JPB-15. Structure and Design of a Novel AC Six-Pole Hybrid Magnetic Bearing. *T. Zhang*[1], Z. Wang[1] and X. Ye[1] *1. Faculty of Automation, Huaiyin Institute of Technology, Huaian, China*

The AC six-pole hybrid magnetic bearing (HMB) has the advantages of symmetrical structure, small force coupling[1]. However, the six-pole HMB is often made into homopolar HMB, which results in low levitation force density and low critical speed. Therefore, a novel AC 6-pole heteropolar HMB is proposed. It has the characteristics that the permanent magnets are installed in the radial space and the double air gaps are adopted. The structure of the proposed HMB is illustrated in Fig. 1. Six poles A, a, B, b, C and c are evenly distributed on the outer stator. The poles a, b and c extend inward and are connected with core X, Y and Z by six permanent magnets to form a circular inner stator. There are six inner air gaps under poles *a*, *b*, and *c*, X, Y, Z and three outer air gaps under poles *A*, *B*, and *C*. The levitation windings, marked as W_1, W_2, W_3, W_4, W_5, and W_6, are wound on the poles *A*, *a*, *B*, *b*, *C*, and *c*. The dotted lines describe the bias flux. One part of the bias fluxes passes through the outer air gaps, the other parts pass through the inner air gap. The coils of poles *A* and *b*, *B* and *c*, *C* and *a*, are respectively connected in series. Then the coils of poles *A*, *B*, and *C*, the coils of poles *a*, *b*, and *c*, are respectively connected in parallel as three phase control winding. The three-phase winding is electrified by one three-phase inverter. The equivalent magnetic circuit method is used to deduce the force-current relationships. The design methods of main parameters such as turn numbers of the windings and air gap lengths are given. The electromagnetic performances, such as flux distributions, air gap flux densities, force-current relationships, are calculated and analyzed to verify the structure, levitation mechanism and design method. The air gap flux densities waveforms and force-current relationships are shown in Fig.2.

[1] H. Eryong and L. Kun, "A novel structure for low-loss radial hybrid magnetic bearing," *IEEE Trans. Magn.*, vol. 47, no. 12, pp. 4725–4733, Dec. 2011.

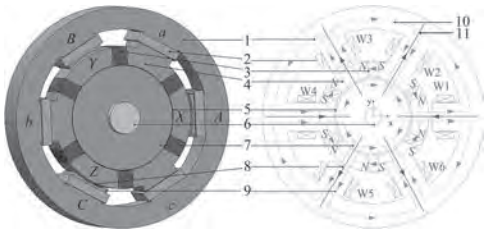

Fig. 1. Structure of novel AC 6-pole RHMB. 1-external stator core, 2-control windings, 3-permanent magnet, 4-internal stator core, 5-inner air gap, 6-shaft, 7-rotor core, 8-outer air gap, 9-stator levitation pole, 10-bias flux, 11-levitation flux.

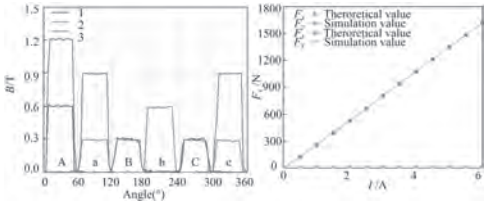

Fig. 2. Air gap flux densities waveforms and force-current relationships.

JPB-16. Broadening Design and Optimization of High Efficiency Region for a Dual-Mechanical Port Flux-Switching Permanent Magnet Motor. Z. Xiang[1], *J. Ren*[1] and L. Quan[1] *1. Jiangsu University, Zhenjiang, China*

Nowadays, the urgent energy crisis and serious environment pollution problem still represent two major challenges of the world. The development of vehicle industry is evolving toward the strategy of electric vehicles (EVs). For the modern EVs, the driving range in single charge is becoming one of key evaluation indicators which received a lot of attention [1]. The vehicle operation condition is usually compound and complex, including the frequent acceleration and deacceleration, sudden starting and stop, high-speed cruise, and heavy load climbing. Given this, a study on multi-mode optimization of PM motor is presented in [2], where the key is to consider multiple operation points into the optimization process. But for a traction motor, there is a high efficiency region for driving operation. When facing with the diverse operation conditions, the characteristics of high efficiency region are essentially the key factor to achieving the efficient operation of motor. Thus, how to consider the characteristic of efficiency region into the process of motor optimization is one of focus issues for traction motors. In this paper, the investigation of broadening design and optimization of high efficiency region is presented for a dual-mechanical port flux-switching PM (DMP-FSPM) motor, where the motor topology is shown in Fig. 1. To facilitate the design and optimization of high efficiency region, the region boundary is fit according to the theoretical analysis, as depicted in Fig. 2. Then, sensitivity analysis method is purposely utilized for obtaining the parameters which are relatively sensitive to the motor efficiency. The sensitivity results are given in Fig. 3. Six parameters are chosen as the design variables for optimization. Based on optimization, the iron loss of inner and outer motors of DMP-FSPM motor is reduced, as can be seen in Fig. 4 (a) and (b). In addition, for better presentation of the broadening optimization of high efficiency region, the efficiency map is also investigated, as shown in Fig. 5. Obviously, the high efficiency region is broadened effectively based

on optimization. Finally, more theoretical analysis, simulation study, and experimental results are given in the full paper.

[1] Jean-Michel Clairand, Javier Rodríguez-García, Carlos Álvarez-Bel, "Assessment of Technical and Economic Impacts of EV User Behavior on EV Aggregator Smart Charging," *JOURNAL OF MODERN POWER SYSTEMS AND CLEAN ENERGY*, vol. 8, no. 2, Mar. 2020. [2] Zixuan Xiang, Xiaoyong Zhu, Li Quan, Yi Du, Chao Zhang, Deyang Fan, "Multi-level Design Optimization and Operation of a Brushless Double Mechanical Port Flux-Switching Permanent-Magnet Motor," *IEEE Trans. Ind. Electron*., Vol. 63, no. 10, Oct. 2016.

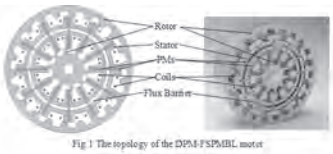

Fig.1 The topology of the DPM-FSPMBL motor

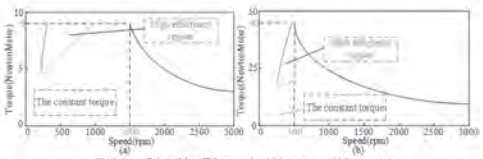

Fig.2 Curve fitting of the efficiency region.(a) Inner motor. (b) Outer motor.

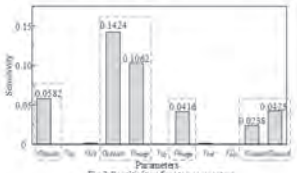

Fig.3 Sensitivity of motor parameters

TABLE
OPTIMAL RESULTS

Objectives	Initial	Optimal	Objectives	Initial	Optimal
	8deg	7.5deg		4.98deg	4deg
	7deg	6.5deg		4.24deg	3.6deg
	3.3deg	4deg		2.6	4deg

Efficiency	Motor	Rated condition	Initial	Optimal
	Inner	(1500rpm,9Nm)	0.918	0.922
	Outer	(720rpm,45Nm)	0.933	0.960

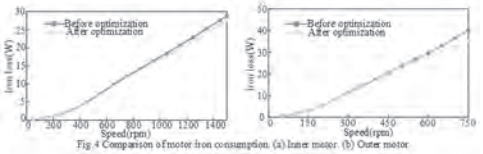

Fig.4 Comparison of motor iron consumption. (a) Inner motor. (b) Outer motor

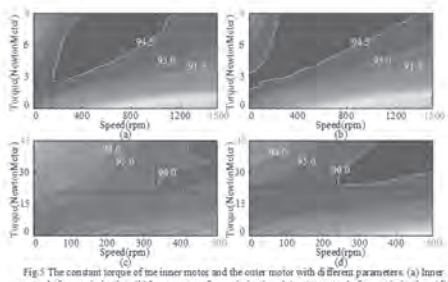

Fig.5 The constant torque of the inner motor and the outer motor with different parameters. (a) Inner motor before optimization. (b) Inner motor after optimization. (c) outer motor before optimization. (d) outer motor after optimization.

JPB-17. Novel Steel-Bar Starting Cage Line-Start Permanent Magnet Machine with Spoke Type Insulation Layers. *L. Li*[1], W. Fu[2] and S. Niu[1]
1. Electrical Engineering, Hong Kong Polytechnic University, Hong Kong, Hong Kong; 2. Shenzhen Institutes of Advanced Technology, Chinese Academy of Sciences, Shenzhen, China

Due to its excellent performances like high efficiency and high power factor[1], line-start permanent magnet (LSPM) machine is widely used in long-time operated applications, i.e., textile, pump, fan [1]. LSPM machine with squirrel cage doesn't need inverter to start, thus it has advantages of lower cost and smaller volume[2]. However, The rotor of LSPM machine just combine one interior permanent magnet (IPM) rotor and one induction rotor together into a whole rotor, thus the two rotor would compete the limited space when designing the rotor. Also, the aluminum-bar induction winding in the rotor only works in starting process, and it will occupy the limited magnet path of the rotor, which would be the extra burden to the machine because aluminum has permeability similar as air. Hence, a novel steel-bar starting cage line-start permanent magnet machine is proposed to solve this paradox. Low carbon steel 1010[3] is selected as rotor cage material to allow magnet flux pass through at steady state. Steel 1010 has high permeability but lower conductivity compared with aluminum and copper, the proposed machine shown in Fig.1 shows that steel-bar rotor could still start easily without the help of inverter, and has better performance at steady state as is shown in Fig.2. The spoke type insulation layers of the steel-bar is meant to reduce the core loss, but simulation results show that the starting process is also shorten. Besides, the torque ripple at steady state is also lower with the help of insulation layers. A LSPM machine with aluminum-bar cage is also designed to compare in Fig.2. The steel-bar is of larger cross area because steel-bar doesn't occupy magnetic path, which is a main advantage of steel bar. However, steel-bar is like closed opening slot when induced current flows through, so the steel-bar should be saturated before it produces flux to airgap, which is why steel-bar rotor has lower starting torque. But for pump load which requires low torque at low speed, proposed machine shows dominant advantages.

[1] Y. Zhou, K. Huang, P. Sun, IEEE Transactions on Power Electronics, Vol. 36, No.4(2021) [2] M. Lin, D. Li, X. Ren, IEEE Transactions on Industrial Electronics, Vol. 68, No.5(2021) [3] S. Maximov, R Escarela-Perez, S Magdaleno-Adame, IEEE Transactions on Magnetics, Vol. 51, No.6(2015)

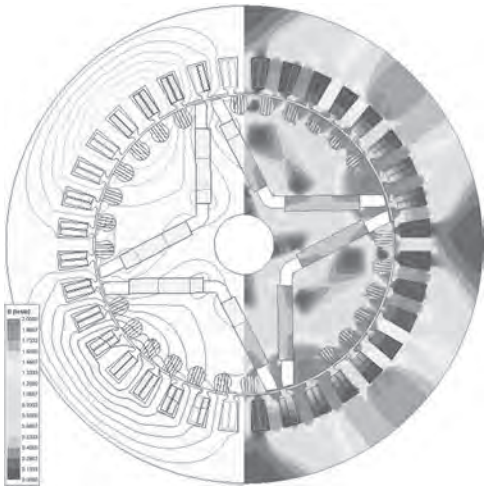

Fig.1 Proposed Steel-Bar Starting Cage Line-start PM Machine with Spoke Type Insulation Layers

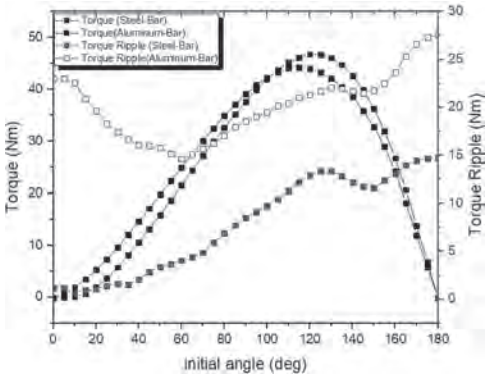

Fig.2 Torque and Torque Ripple vs Current Angle Curve of Proposed Machine and Traditional Aluminum-Bar Machine

JPB-18. Proposal of a Two-DOF Actively Controlled Consequent-Pole Bearingless IPM Motor. *Y. Fujii*[1] and A. Chiba[1] *1. Tokyo Institute of Technology, Tokyo, Japan*

Bearingless motor can suspend the rotor in a non-contact manner during generating torque, and solve challenges related to mechanical bearings. To simplify the system, two-degree-of-freedom (DOF) actively controlled consequent-pole bearingless permanent magnet motors (CPM) have previously been developed [1], [2]. The radial positions (x, y) are actively controlled by providing three-phase suspension currents with the suspension winding, and the remaining positions (z, θ_x, θ_y) are passively stabilized by an attractive force owing to the magnetic coupling of PM. In contrast, the torque is generated by providing three-phase motor currents with the motor winding. Uniquely, consequent-pole type bearingless motor needs no detection of the rotational angle for the regulation of the suspension force. This paper proposes a consequent-pole bearingless interior permanent magnet motor (CP-IPM). The CP-IPM uses the rectangular-shaped PMs, which are a lower cost compared with the arc-shaped PMs of CPM. Furthermore, the design freedom of the PMs arrangement in the rotor core is expanded, for example straight-, V-, and delta-shaped arrangement. The proposed CP-IPM is a novel bearingless machine as far as the author knows and has the potential to enhance the suspension and motor performance as well as reduction of the PMs cost. Fig. 1 shows the proposed CP-IPM used in the finite element analysis (FEA). The CP-IPM has an 8-pole/24 slot structure. The distributed winding generating two-pole magnetic field for the suspension and eight-pole magnetic field for the torque is wound in the slots, respectively. The two neodymium PMs with parallel magnetized, which are arranged in V-shape, generate N-pole. Consequently, the rotor core parts of between V-shaped arrangements no having the PMs, are magnetized to S-pole. Fig. 2 shows the torque and suspension force results by 3D-FEA when providing only motor current and when providing only suspension current to generate the suspension force in the x-direction, respectively. The results demonstrate that the proposed CP-IPM generate the torque and suspension force.

[1] J. Asama, D. Kanehara and A. Chiba, IEEE Trans. IAS., Vol. 50, No. 1, pp. 288-295 (2014) [2] J. Amemiya, A. Chiba, et. al., IEEE Trans. Magnetics, Vol. 41, No. 1, pp. 82-89 (2005)

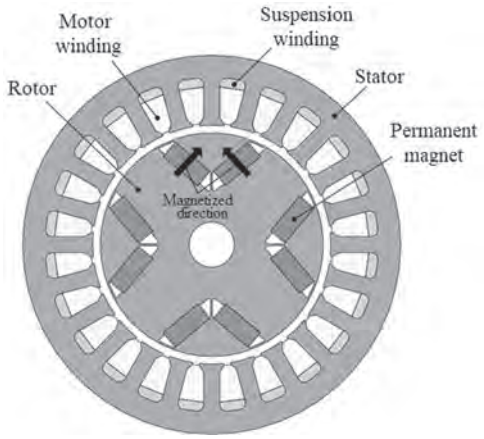

Proposed CP-IPM used in the finite element analysis

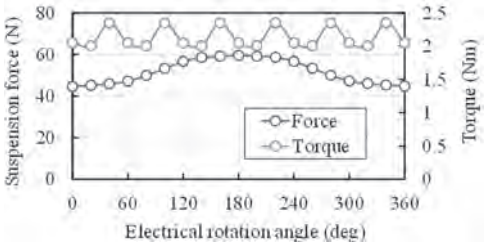

Torque and suspension force results by 3D-FEA

JPB-19. Withdrawn

JPB-20. Withdrawn

Session JPC
LINEAR MACHINES AND LINEAR ACTUATORS
(Poster Session)

Mi-Ching Tsai, Co-Chair
National Cheng Kung University, Tainan, Taiwan
Chinweze U. Ubadigha, Co-Chair
National Cheng Kung University, Tainan, Taiwan

JPC-01. Force Ripple Minimization Design for Consequent Pole Permanent Magnet Linear Synchronous Motor. *Y. Yue*[1], S. Jia[1], D. Liang[1] and Y. Liang[1] *1. Xi'an Jiaotong University, Xi'an, China*

Abstract—This paper focuses on the force ripple minimization of consequent pole permanent magnet linear synchronous motor (CP-PMLSM). By using arc teeth without tooth shoe, CP-PMLSM is investigated in detail by extensive finite element analysis (FEA). With Taguchi parameters method, the geometry of end teeth and auxiliary teeth is optimized to reduce the force ripple, and the optimal combination of parameters can be obtained. the contrasting result between the initial and the optimized PMLSM shows that the force ripple is suppressed to a quite low value in all load conditions by the aforesaid procedure. *Keywords*—Force ripple, finite element analysis, consequent pole, permanent magnet linear synchronous motor (PMLSM). I. Introduction Recently, Permanent Magnet Synchronous Linear Motors (PMSLMs) have been widely used in industry applications owing to their outstanding performance. However, as the magnetic circuit is disconnected at the end of the primary core, the distorted magnetic field makes the motor high force ripple. The addition of the auxiliary teeth and teeth notching are employed to reduce the detent force[1]. The geometry of end-teeth is optimized to reduce the force ripple in all load conditions [2]. High-order harmonic components can be suppressed by the optimal skewed PM design, and a discrete-time linearization observer is utilized to compensate low-order harmonic ones [3]. In this paper, arc teeth without tooth shoe is optimized to reduce the force ripple by extensive finite element analysis (FEA). The dimensions of end teeth and auxiliary teeth is optimized by Taguchi method to obtain the optimal combination of parameters. The contrasting result shows that the force ripple is suppressed to a quite low value in all load conditions by the aforesaid procedure. II. Electromagnetic Performance Evaluation The simulation results of flux density, back-EMF, and electromagnetic torque are analyzed by the finite element analysis (FEA). The load flux distribution is shown in Fig. 2. The Comparison of force wave and back-EMF in no-load and load between the initial and the optimized is shown in Fig. 3. The back-EMF and electromagnetic torque with various excitation modes are shown in Fig. 3.

[1] K. Shin, K. Kim, K. Hong, and J. Choi, "Detent Force Minimization of Permanent Magnet Linear Synchronous Machines Using Subdomain Analytical Method Considering Auxiliary Teeth Configuration," IEEE Trans. Magn., vol. 53, no. 6, pp. 1-4, 2017. [2] X. Xu, Z. Sun, B. Du, H. Feng, H. Du, and J. Lu, "Magnetic Unbalance and Thrust Ripple Reduction Design for Novel PMLSM with Halbach Consequent Pole." pp. 1-5. [3] M. Wang, L. Li, and D. Pan, "Detent Force Compensation for PMLSM Systems Based on Structural Design and Control Method Combination," IEEE Trans. Ind. Electron., vol. 62, no. 11, pp. 6845-6854, 2015.

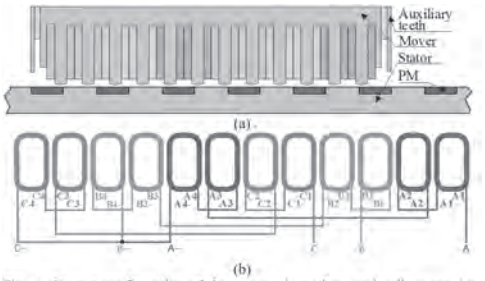

Fig. 1. Current configuration of the proposed topology and coil connection. (a) Motor topology (b) Primary winding connection.

Fig. 1.

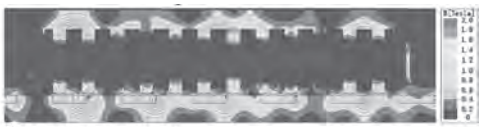

Fig. 2. load flux distributions.

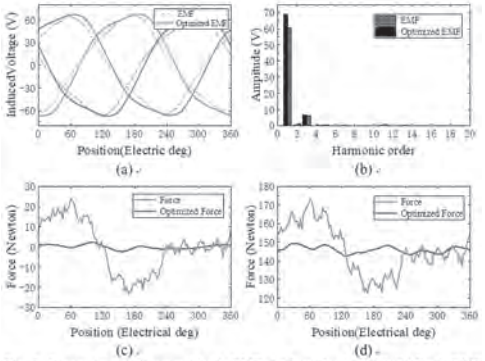

Fig. 3. Comparison of force and back-EMF. (a) Load back-EMF. (b) Back-EMF harmonics. (c) no-load force. (d) Load force.

Fig. 2. & Fig. 3.

JPC-02. Back-to-back Ω Stator Transverse Flux Permanent Magnet Linear Machine. *Z. Jia*[1], S. Peng[1], W. He[1], L. Yu[1], Y. Cao[1] and H. Jia[1] *1. Jiangsu Collaborative Innovation Center of Atmospheric Environment and Equipment Technology (CICAEET), Nanjing University of Information Science and Technology, Nanjing, China*

Transverse flux permanent magnet (TFPM) machine owns the characteristics of large torque and high efficiency[1]. Many new TFPM structures such as double C-hoop stator and double Ω-hoop stator machines have been proposed[2][3]. Accordingly, the new structure of back-to-back Ω-type stator TFPMLM is proposed to improve the stator space utilization based on the above mentioned previous machines. Owning to the better utilized stator space and the mutual decoupled electrical and magnetic loads the machine achieves better performances on higher peak force and thrust-weight ratio which is suitable for the application of urban rail transit. The distinguishing feature of the proposed machine is that one pair stator hoops share the same

winding to achieve more compact space utilization. Fig. 1(a) shows the schematic diagram of the fabricated prototype, which has pairs of back-to-back Ω-type stator hoops and a mover composited by cores and PMs. The stator hoops fixed in the non-ferromagnetic stationary pedestal and the mover cores and flux-concentrated PMs are screwed independently onto two non-ferromagnetic mover brackets. A linear guide rail contacts the stationary pedestal and the mover bracket. The sliding rail is lapped on head-end of the pedestal while the slide block is screwed onto the bracket. The armature winding binding each stator hoop pairs to form two half magnetic circuits twining round the stator hoops and the mover cores which are laminated by facile silicon-steel. Fig. 1 (b) shows the 3D-FEM magnetic field distributions with maximum flux density of 0.7T. Fig. 2 (a) shows the flux density with optimum value as 0.6 around to achieve the best performance. The flux linkage and the measured back-EMF waveforms with amplitudes of 70mWb and 30V respectively at rated moving speed of 1.5m/s are shown in Fig. 2 (b). The positioning force is obtained and optimized also to verify the analyses and feasibility of the structure design. A prototype with 120N peak force is fabricated and some experiments are conducted.

1) H. Weh and H. May, "New permanent magnet excited synchronous machine with high efficiency at low speed," Proc. ICEM, Pisa, 35-40, (1988). 2) Z. Jia, H. Lin, S. Fang, and et al. Cogging torque optimization of novel transverse flux permanent magnet generator with double C-hoop stator[J]. IEEE Transactions on Magnetics, 51(11): 8208104, (2015). 3) Z. Jia, W. Chen, L. Yu, and et al. A novel transverse-flux PM linear machine with double Ω-hoop stator. IEEE Transactions on Applied Superconductivity, 26(7): 1-4, (2016).

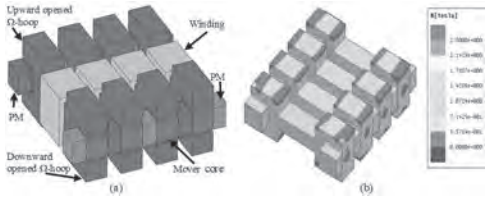

Fig. 1 The schematic diagram and the magnetic field distributions.

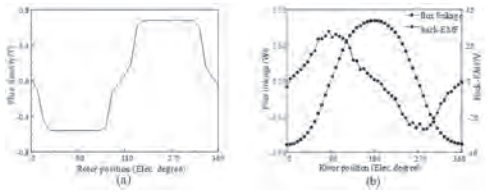

Fig. 2 Flux linkage and measured back-EMF waveforms.

JPC-03. Eddy Current Loss Analysis in Permanent Magnet Linear Gear Using Analytical Method. *J. Lee*[1], T. Bang[1], H. Lee[1], J. Woo[1], G. Jang[2] and J. Choi[1] *1. Chungnam National University, Daejeon, The Republic of Korea; 2. Korea Electric Power Research Institute, Daejeon, The Republic of Korea*

Gears are useful mechanical devices that transmit power. However, owing to physical contact mechanical gear have short lifespans [1]. Therefore, research on magnetic gear using permanent magnets (PM) is in progress [2]. Fig.1 shows the linear magnetic gear fabricated for this study. The magnetic gear has a flux-modulation fixed-pole between the high and low-speed movers [3]. Hence, magnetic flux is modulated and has the characteristics of a gear. However, the air-gap magnetic flux density waveform is distorted. Distorted air-gap magnetic flux density causes eddy current losses in the PM. The eddy current analysis of PM machines uses finite element method (FEM). But, FEM takes a long time to analyze [4]. In this study, we propose a method to calculate the eddy current loss using an analytical method. This method is very advantageous for initial designs where design parameters are frequently changed because of the fast analysis time. As shown in Fig. 2(a), the air-gap magnetic flux density was calculated using analytical method for a simplified two-dimensional linear magnetic gear. And Fig. 2(b) shows an analytical model for calculating the eddy current density induced by the PM of each mover using the superposition principle. Fig. 2(c) shows the comparison results of the air-gap flux density and eddy current density of each mover derived through the analytical method and FEM. Fig. 2(d) shows the eddy current loss distribution of the analytical model. The validity of the proposed method is proved by the analysis results, and the results were very similar to FEM. Therefore, the proposed method for calculating the eddy current loss is considered to be very useful. The analysis results, equations and measurements of the eddy current losses of the linear magnetic gear will be presented in more detail in the final paper.

[1] L. Shah, A. Cruden and B. W. Wiliams, "A Variable Speed Magnetic Gear Box Using Contra-Rotating Input Shafts", *IEEE Trans. Magn.*, vol. 47, no. 2, pp. 431-438, 2011. [2] B. McHilton, R. Crozier and M. Mueller, "Optimisation procedure for designing a Magnetic Gear", *The Journal of Engineering,* vol. 2017, no. 13, pp. 840-843, 2017. [3] J. Y. Lee and J. H. Chang, "Analysis of the Vibration Characteristics of Coaxial Magnetic Gear", *IEEE Trans. Magn.*, vol. 53, no. 6, Art. no.8105704, 2017. [4] T. Okitsu, D. Matsuhashi, Y. Gao and K. Muramatsu, "Coupled 2-D and 3-D Eddy Current Analyses for Evaluating Eddy Current Loss of a Permanent Magnet in Surface PM Motors," *IEEE Trans. Magn.*, vol. 48, no. 11, pp. 3100-3103, Nov. 2012.

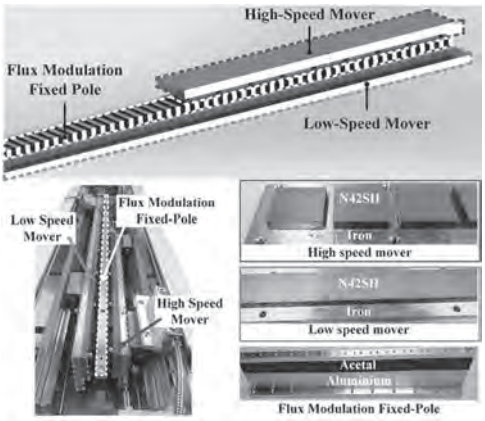

Fig. 1. Fabrication parts and test bed of linear magnetic gear.

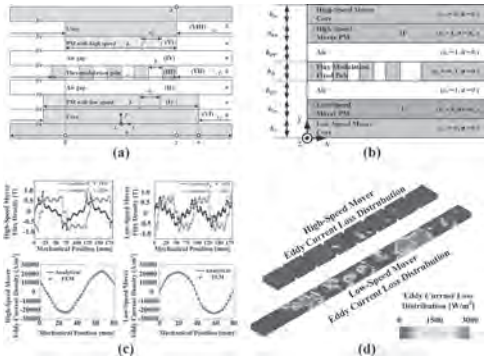

Fig. 2. (a) Simplified analytical model of the linear magnetic gear for magnetic field analysis (b) Analysis model for the prediction of eddy current density (c) Comparison results of air-gap magnetic flux density and eddy current density between analytical method and FEM (d) Eddy current loss distribution of linear magnetic gear using FEM.

JPC-04. Design and Analysis of a Linear-Rotary PM Actuator with Consequent-Pole Staggered Mover. *G. Jiang*[1], H. Zhou[1], W. Tao[1] and Q. Chen[1] *1. College of Electrical Information Engineering, Jiangsu University, Zhenjiang, China*

With the development of drive system, the linear-rotary (LR) actuators have been applied in robotics due to its multiple freedom degree characteristic [1]. Rare-earth permanent magnet (PM) materials, such as NdFeB, have high remanence density and coercivity, which can provide high energy density. Hence, the LR PM actuator has been widely used in the drive systems due to simple structure and small volume. In this paper, a LR PM actuator which involves linear, rotary and spiral motions is proposed for the application of multiple freedom degree robotics. The proposed actuator is composed of unique single stator with two sets of independent windings and consequent-pole staggered (CPS) PM mover, as shown in Fig. 1. The novelty is that one CPS PM mover is specially designed to generate radial and axial magnetic field, and to reduce PM consumption. Combined with it, two sets of independent orthogonal non-overlapping concentrated armature windings are employed to generate enough torque, thrust force and to achieve the decoupling operation of linear and rotary motions. The CPS mover is composed of several step-staggered parts. The magnetized direction of PMs in the adjacent step-staggered parts is opposite. The staggered degree of adjacent parts is π/Pr, where Pr is PMs pole pairs along the circumferential direction. Thus, the even-order harmonics of no-load back-electromotive force are eliminated by the CPS mover, which greatly reduce the torque ripple. To reduce the axial leakage flux, there is axial flux barrier between the step-staggered parts. Furthermore, the fault-tolerance (FT) teeth and armature teeth are alternately arranged on the stator to enhance FT performance. The electromagnetic performance of the proposed machine is predicted by finite-element method. Fig. 2 shows the output characteristic of proposed actuator. The average values of torque and thrust force are 6Nm and 158N, respectively. The torque ripple and thrust force ripple are 0.97% and 33%, respectively. More details and optimization will be discussed in the full paper.

[1] L. Xie, J. Si, and Z. Wang, "Overview of 2-Degree-of-Freedom Rotary-Linear Motors Focusing on Coupling Effect," in IEEE Trans. Magn., Vol. 55, p.1-11 (2019) [2] D. Dong, W. Huang, and Q. Wang, "Modeling and Optimization of a Tubular Permanent Magnet Linear Motor Using Transverse-Flux Flux-Reversal Topology," in IEEE Trans. Ind. Appl., Vol. 55, p.1382-1391 (2019) [3] J. Li, K. Wang and F. Li, "Reduction of Torque Ripple in Consequent-Pole Permanent Magnet Machines Using Staggered Rotor," in IEEE Trans. Energy Convers., Vol. 34, p.643-651 (2019)

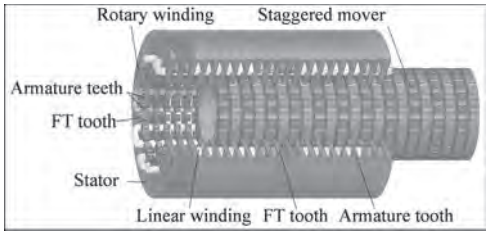

Fig. 1 Structure of proposed LR PM actuator.

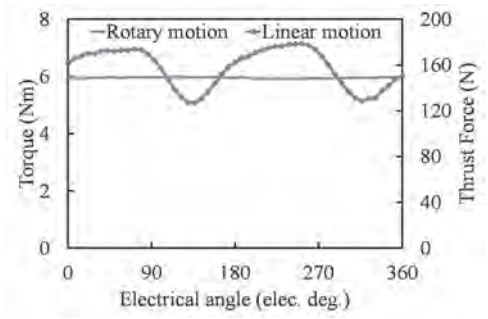

Fig. 2 Output characteristic of proposed LR PM actuator.

JPC-05. Electromagnetic Design of Single-Phase Permanent Magnet Linear Oscillation Actuator Considering Detent Force Minimum. *H. Zhang*[1], L. Jin[1], H. Yu[1], Z. Xu[1], J. Leng[1] and X. Zhu[1] *1. Southeast University, Nanjing, China*

Single-phase permanent magnet linear oscillating actuators (SP-PMLOA) have widely used in the application field of short-stroke and high frequency linear reciprocating, because of simple mechanical structure, without the rotary-to-linear conversion, low maintenance costs and fast dynamic response. In the design of SP-PMLOA, the detent force was seldom paid attention by scholars. Due to the unique assembly structure and the operation mode of the LOA, the detent force, which changes linearly in the stroke, can be equivalent to a magnetic resistance spring, and its effect on the electromagnetic performance can be ignored. However, the consequence of ignoring the detent force is that the power density of the SP-PMLOA becomes very low or the axial length of the SP-PMLOA is increased. Therefore, the principle of end force generation is introduced, and a new method to reduce end force and alveolar force is proposed in this paper. Generally, the detent force is the superposition of end force and cogging force, both of which are caused by the interaction between the permanent magnets in the mover and the stator core. Therefore, according to the principle of cogging force and end force generation, when the cogging force gradually increases, end force gradually decreases. The cogging force and the end force can be offset by changing the position of the permanent magnet. Fig.1 shows the structure of the novel SP-PMLOA, which adopts double-sided stators and one active mover. Three permanent magnets are arranged on the non-magnetizing back iron. The thickness of the middle permanent magnet is larger than that of the permanent magnets on both sides, which can effectively reduce the detent force. The detent force comparison of three models is shown in Fig.3. as can be seen, the maximum detent force of the improved model is slightly greater than that of one PM model, but smaller than that of the traditional three PMs model. In this paper, the detent force generation principle of SP-PMLOA has been analyzed. it has been validated that the proposed model can effectively reduce detent force and the amount of PMs used.

X. Chen, Z. Q. Zhu, D. Howe"Comparative study of alternative permanent magnet linear oscillating actuators," in Proc. Int. Conf. Elect. Mach. Syst., 2008, pp. 2826–2831. T. Ibrahim, J. Wang and D. Howe, "Analysis and Experimental Verification of a Single-Phase, Quasi-Halbach Magnetized Tubular Permanent Magnet Motor With Non-Ferromagnetic Support Tube," in *IEEE Transactions on Magnetics*, vol. 44, no. 11, pp. 4361-4364, Nov. 2008.

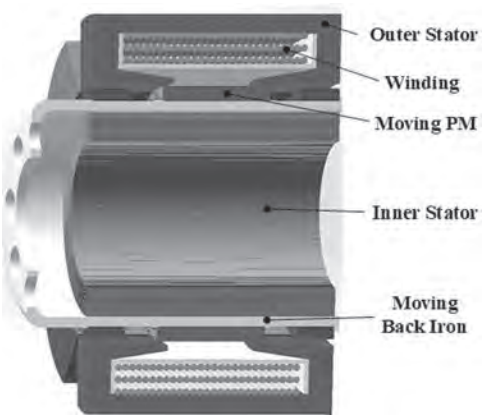

Structure of the SP-PMLOA

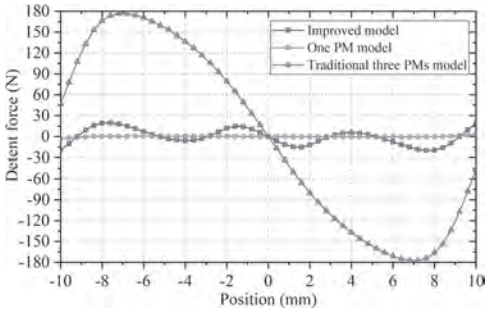

Detent force

JPC-06. Design optimization and Analysis of a Novel High Force Density Magnetic Lead Screw with Discretized PMs and Different Magnetized Directions. *Y. Liu*[1], H. Yu[1], Y. Wang[1] and Q. Zhang[1] *1. College of Electrical Engineering, Southeast University, Nanjing, China*

The magnetic lead screw (MLS) is a new linear actuator with a high force density that enables contactless energy transfer. Improving the force density and reducing the installation error of the approximate helical type permanent magnets (PM) are the key challenges to realize the MLS. In this paper, based on the study of several existing PMs shapes and magnetization methods for MLS, a new MLS based on a combination of PM structures and magnetization directions is proposed. it not only reduces the mounting error by approaching the helical pole in a simpler way, but also increases the force density of the MLS. The results show that in addition to the air gap and the sizes of the PM having a significant effect on the force density, the effect of backiron saturation on it also needs to be considered. Finally, the performance of the proposed structure is compared with several existing structures and it is concluded that the force density is increased by nearly 60% for the same MLS volume and amount of PMs. Index Terms — MLS, magnetization direction, structure, PM, force density. The three common structures of MLS are shown in Fig. 1. (a) is the traditional model of radial magnetization for PMs, (b) is the halbach model of PMs with halbach magnetization, (c) is the salient model of radial magnetization for PMs. (d) is the proposed model, which adopts halbach magnetization, the salient pole shape adopts the radial magnetization, and the rectangular shape adopts the axial magnetization, and the salient pole PM can fix the rectangular PM, which is easy to install. The operation principle and others will be detailed in the full text. The structure proposed in this paper is shown in Fig. 1(d), and the detailed design process will be described in the full text. At present, there are two kinds of processing and installation structures to simulate helical PM as shown in Fig. 2: half skew ring and discrete. This paper also makes a comparison of these two PM structures, so that a PM structure with simple processing and installation and high force density are given. Finally, the comparison of these structures is detailed in the full text.

[1] R. K. Holm, N. I. Berg, M. Walkusch, P. O. Rasmussen and R. H. Hansen, "Design of a Magnetic Lead Screw for Wave Energy Conversion," in IEEE Transactions on Industry Applications, vol. 49, no. 6, pp. 2699-2708, Nov.-Dec. 2013. [2] N. I. Berg, R. K. Holm and P. O. Rasmussen, "Theoretical and Experimental Loss and Efficiency Studies of a Magnetic Lead Screw," in IEEE Transactions on Industry Applications, vol. 51, no. 2, pp. 1438-1445, March-April 2015. [3] J. Ji, Z. Ling, J. Wang, W. Zhao, G. Liu and T. Zeng, "Design and Analysis of a Halbach Magnetized Magnetic Screw for Artificial Heart," in IEEE Transactions on Magnetics, vol. 51, no. 11, pp. 1-4, Nov. 2015, Art no. 8108604. [4] Z. Ling, J. Ji, J. Wang and W. Zhao, "Design Optimization and Test of a Radially Magnetized Magnetic Screw with Discretized PMs," in IEEE Transactions on Industrial Electronics, vol. 65, no. 9, pp. 7536-7547, Sept. 2018.

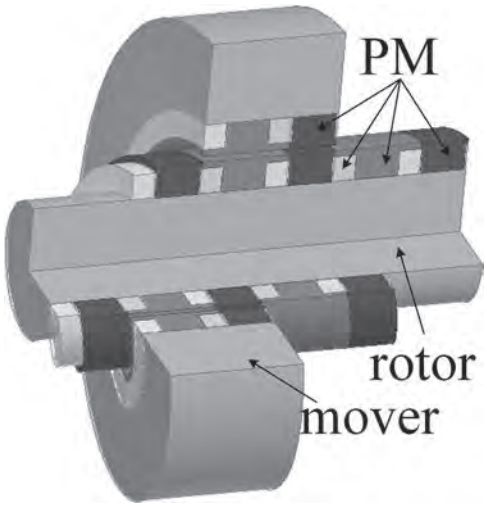

proposed model

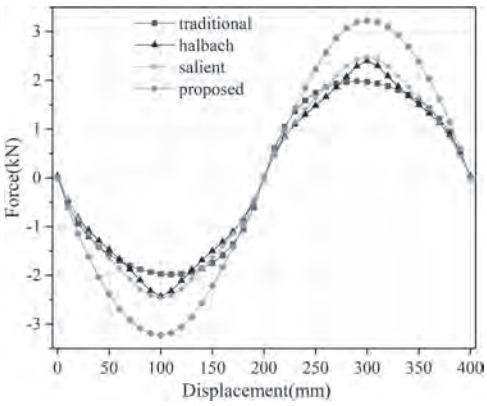

Performance comparison of four models

JPC-07. Design and Analysis of Novel Double-sided Flux Concentrated Permanent Magnet Linear Machines with Saturation Relieving Effect. *Y. Shen*[1], T. Shi[1] and C. Xia[1] *1. College of Electrical Engineering, Zhejiang University, Hangzhou, China*

In recent years, novel primary-excited PMLMs (PE-PMLMs) attract more and more attention with the merits of high thrust force density and low cost in long stroke application [1]. Different from the conventional PMLMs, PE-PMLMs integrate both the armature winding and PMs in the short primary, while the long secondary only consists of salient iron core [2]-[4]. The total cost can be greatly reduced thanks to this simple structure. However, PE-PMLMs still suffers from several key issues: 1) Severe saturation problem in the primary core. 2) Low overload capability due to the saturation problem. 3) Low mechanical reliability due to the influence of normal force on the primary. To solve these drawbacks in PE-PMLMs, this paper proposes a double-sided flux concentrated permanent magnet linear machines (DS-FCPMLMs) with saturation relieving effect. The utilized dual PMs in the primary yoke and slot opening can significantly improve the force density while relieving the saturation. Fig. 1(a) shows the topology of DS-FCPMLMs. Cross-shaped modular primary segments can be used to reduce the cost and enhance the extendibility of primary. Each primary module consists of one cross-shaped primary tooth and two coils. Then, PMs are employed in both the primary yoke and slot opening between two modules. The basic operation principle of this machine is shown in Fig. 1(b). The PM flux switches among four coils of the same phase at different secondary position. Hence, sinusoidal bipolar phase flux linkage can be obtained. Fig. 2 shows the electromagnetic performances of DS-FCPMLMs compared with DS-BFPMLMs that only has yoke PMs. Due to the flux concentrated effect, the back-EMF of DS-FCPMLMs can be

enhanced by 48% compared with DS-BFPMLMs. Besides, DS-FCPMLMs can provide the average force of 338 N, which is increased by 52% compared with DS-BFPMLMs. Moreover, the magnetic saturation can be relieved in DS-FCPMLMs with the effect of slot PMs. Therefore, the proposed DS-FCPMLMs have the potential to provide direct drive propulsion for long stroke application.

[1] Yiming Shen, Qinfen Lu, "Overview of Permanent Magnet Linear Machines with Primary Excitation," *Transactions of China Electrotechnical Society*, vol. 36, no. 11, pp. 2325-2343, Jun. 2021. [2] D. Wu, J. T. Shi, Z. Q. Zhu and X. Liu, "Electromagnetic Performance of Novel Synchronous Machines With Permanent Magnets in Stator Yoke," *IEEE Trans. Magn.*, vol. 50, no. 9, pp. 1-9, Sep. 2014. [3] M. Yuan and S. Niu, "Design and Analysis of a Novel Modular Linear Double-Stator Biased Flux Machine," *IEEE Trans. Magn.*, vol. 54, no. 11, pp. 1-5, Nov. 2018. [4] Y. Shen, Z. Zeng, Q. Lu and Y. Li, "Investigation of a Modular Linear Doubly Salient Machine With Dual-PM in Primary Yoke and Slot Openings," *IEEE Trans. Magn.*, vol. 55, no. 6, pp. 1-6, Jun. 2019.

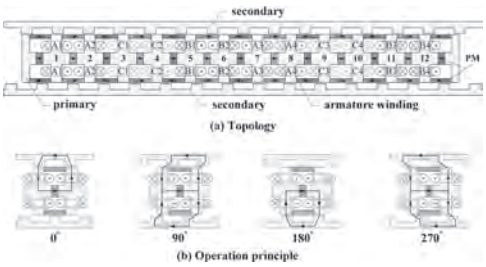

Fig. 1. The topology and operation principle of DS-FCPMLMs.

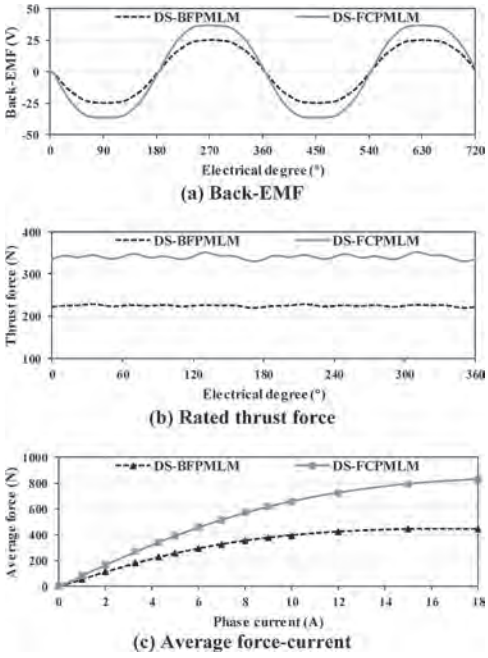

Fig. 2. The electromagnetic performances of DS-FCPMLMs.

JPC-08. Design and Analysis of a Novel Tubular High-PM-Utilization Transverse-Flux Linear Machine. *B. Liu*[1], J. Bai[1], G. Qiao[1], G. Liu[1], Y. Liu[1] and P. Zheng[1] *1. School of Electrical Engineering & Automation, Harbin Institute of Technology, Harbin, China*

Owing to the low PM utilization in conventional transverse-flux machines, a novel tubular high-PM-utilization transverse-flux linear machine (HPMU-TFLM) is proposed in this paper. Theoretically, the proposed machine has not only 100% PM utilization, but also has higher power factor and force density. First, the basic configuration and operation principle of HPMU-TFLM are introduced. Then, electromagnetic performance of the HPMU-TFLM is investigated and compared with other typical TFLMs. Fig.1(a) shows three-phase HPMU-TFLM configuration. There are 6 flux-concentrating teeth arranged in a single primary core, which are designed to fully concentrate the secondary PM flux. The PMs in the secondary side are alternately mounted along the moving direction. The axial distance between two adjacent PMs is equal to one pole pitch. Each phase is staggered by 2/3 pole pitch along the axial direction, namely phase difference in 120 electrical angles. Fig.1 (b) and (c) show the main magnetic flux direction in the axially adjacent primary cores is opposite. As the mover moves, the main magnetic flux direction alternates, and the back EMF in the armature coil is generated. Then three-phase alternating current is generated due to the mechanical phase difference. Fig.2 shows the 3D equivalent reluctance network of the HPMU-TFLM. The influence of leading parameters on force density and power factor is investigated. The ratio of axial flux-concentrating boot length to pole distance is defined as $W_{boot\_length.}$ Fig.3 (a) and (b) show respectively the force density and power factor distribution of the HPMU-TFLM versus PM magnetization length and W_{boot_length}. As the PM magnetization length increases, force density increases firstly and then decreases, but power factor continually increases. As the W_{boot_length} increases, force density increases firstly and then decreases, but power factor continually decreases. The performance comparison between the HPMU-TFLM and other typical TFLMs is presented in the Table.1 based on the same conditions. The results show the HPMU-TFLM has higher force density and power factor.

[1] Y. Sui, Z Yin and P. Zheng, "A tubular staggered-teeth transverse-flux PMLM with circumferentially distributed three-phase windings," IEEE Transactions on Industrial Electronics. vol. 66, no. 6, pp. 4837-4848, Jun. 2019. [2] X. Zhao, and S. Niu, "Development of a novel transverse flux tubular linear machine with parallel and complementary PM magnetic circuit for precision industrial processing," IEEE Transactions on Industrial Electronics. vol. 66, no. 6, pp. 4945-4955, Jun. 2019.

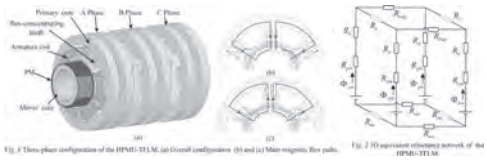

Basic configuration and equivalent reluctance network of the HPMU-TFLM

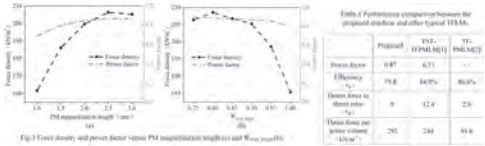

Analysis and comparison of electromagnetic performance

JPC-09. Analysis and Experimental Comparison of Detent and Static Force of a 3 kW Single-Phase Linear Permanent Magnet Generator for Stirling Engines. *K. Lee*[1], S. Lee[1], J. Park[1] and J. Choi[2] *1. Korea Institute of Industrial Technology, Gwang, The Republic of Korea; 2. Chungnam National University, Daejeon, The Republic of Korea*

The single-phase linear permanent magnet generator (SPLPMG), which is applied to the free piston Stirling engine (FPSE), has a simple structure and robust topology. The SPLPMG can easily drive the motor operation with a simple single-phase power supply for initial operation of the Stirling engine. Despite these advantages, the SPLPMG has the disadvantage that it is very difficult to evaluate due to its reciprocating linear motion [1]. Therefore, the detent force, the restoring force of the spring magnet, and the static thrust force of the SPLPMG are analyzed. An evaluation system for evaluating the detent force and the static thrust force is also proposed. The SPLPMGs must be designed to have a minimizing the detent force in the stroke section for smooth operation [2], [3]. In addition, the spring magnet pushes the position of the mover within the stroke section using the restoring force of the spring

magnet when the mover of the SPLPMG leaves the stroke section. Fig. 1(a) shows the shape of an SPLPMG for a Stirling engine. The capacity of the manufactured SPLPMG is 3 kW, the stroke interval is 11 mm, and the operation frequency is 60 Hz. To evaluate the detent force and the restoring force of the spring magnet in the stroke section of the manufactured SPLPMG, an experimental evaluation set was constructed as shown in Fig. 1(b). Based on the developed evaluation system, the detent force of the mover and the restoring force by the spring magnet will be evaluated and compared with the analysis results. In the case of linear generators, it is difficult to evaluate the thrust force for the input power when evaluating the load. Therefore, the load rated current will be applied while the mover is fixed, to evaluate the static thrust force. Fig. 2 shows the analysis results of the restoring force by the spring magnet, and the detent force. Based on the results of this analysis, the final paper will give a detailed comparison of the results of the analysis and experimental evaluation of the detent force, the restoring force of the spring magnet, and the static thrust force.

[1] Kyu-Seok Lee, Sung-Ho Lee and Jung-Hyung Park, IEEE TRANSACTIONS ON MAGNETICS, VOL. 54, NO. 11 (2018). [2] M. Inoue and K. Sato, IEEE TRANSACTIONS ON MAGNETICS, VOL. 36, NO. 4 (2000). [3] Mingna Ma, Liyi Li and Jiangpeng Zhang, IEEE TRANSACTIONS ON MAGNETICS, VOL. 51, No. 11 (2015)

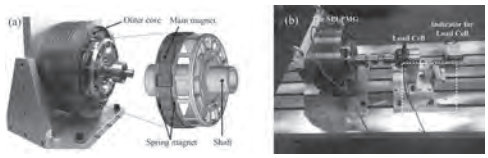

Fig. 1. (a) The SPLPMG topology. (b) Evaluation system.

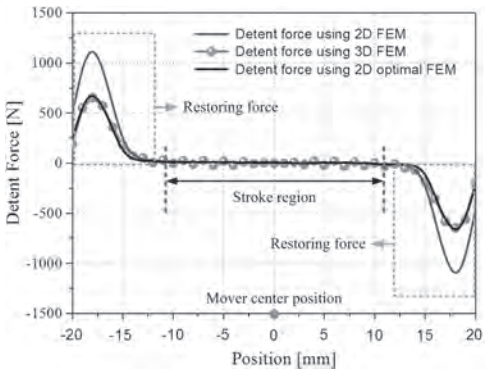

Fig. 2. The analysis results of the detent and restoring force.

JPC-10. Design of a Novel Hybrid-Excited Transverse-Flux Tubular Linear Machine with Complementary Structure. *Z. Li*[1] and S. Niu[1]
1. The Hong Kong Polytechnic University, Hong Kong, Hong Kong

Introduction Transverse flux tubular linear machine (TF-TLM) has merits of high torque density and low side force and is suitable for wave energy conversion (WEC) application. However, excited by permanent magnets (PM), it is hard for TF-TLM to adjust the air gap magnetic field and keep the terminal voltage constant at different operation speed [1]. In this paper, a hybrid-excitation transverse-flux tubular linear machine (HE-TF-TLM) excited by consequent-pole permanent magnet (CP-PM) and DC windings in parallel is proposed. The 3D FEA results have proved that the voltage regulation ratio of HE-TF-LM reaches 87.36%, and thrust density of the machine is not compromised, which is calculated as 155kN/m^3. Operation Principle Fig.1 (a1), (b1) (c1) illustrate the flux distribution of the generator of Phase A under condition of i_{dc}=0A, 6A and -6A respectively. Fig.1 (a2), (b2) and (c2) presents the magnetic field distribution via 3D FEA calculation. After applying DC current i_{dc}>0A, due to the large reluctance of PM, φ_{DCa} travels through A2 and A6 to form the magnetic route. Therefore, flux linkages in A2 and A6 are enhanced by φ_{DCa} and φ_{PMa} together. After applying DC current i_{dc}<0A, flux linkages in A2 and A6 are cancelled by φ_{DCa} and φ_{PMa}. However, as φ_{DCa} and φ_{PMa} join together in the field teeth, the saturation in the field teeth is inevitable under this condition. Results Analysis Fig.2 (a) presents the no-load back emf under different DC excitation (i_{dc}=0A, 6 A, -6A, N_{dc}=55). The 3D FEA results reveal that the back emf can be altered from 96mV/turn to 253mV/turn at unit speed. And the voltage regulation reaches 87.36%. Fig.2 (b) calculates the induced voltage under different working speed (0.5m/s, 1m/s and 2m/s). It is perceived that by altering the excitation current, the output voltage of the generator can keep constant. Fig.2 (c) presents the output thrust force of the machine under different DC excitations (i_{dc}=0A, 6 A, -6A). According to the FEA results, output thrust force reaches 279.14N, and the thrust density of the proposed machine can be effectively improved to 155 kN/m^3 at rated excitation (i_{dc}=6A). Meanwhile, the output thrust force can be effectively changed by altering DC current.

[1] X. Zhao and S. Niu, "Development of a Novel Transverse Flux Tubular Linear Machine With Parallel and Complementary PM Magnetic Circuit for Precision Industrial Processing," IEEE Transactions on Industrial Electronics, vol. 66, no. 6, pp. 4945-4955, 2019.

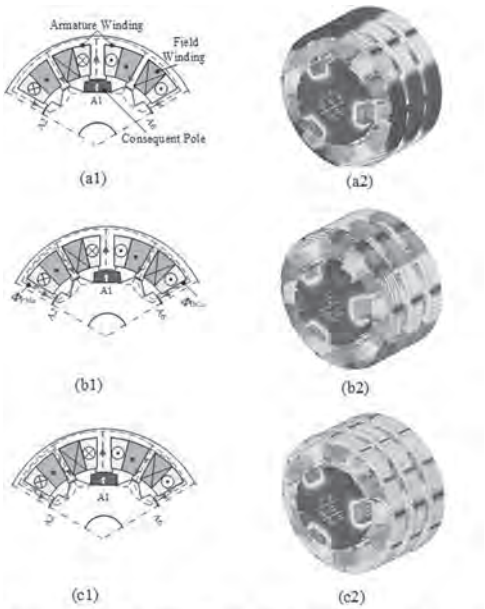

Fig.1 Flux distribution of the proposed machine. *(a1) Flux distribution under i_{dc}=0A. (a2) Flux distribution of 3D FEA under i_{dc}=0A. (b1) Flux distribution under i_{dc}=6A. (b2) Flux distribution of 3D FEA under i_{dc}=6A. (c1) Flux distribution under i_{dc}=-6A. (c2) Flux distribution of 3D FEA under i_{dc}=-6A.*

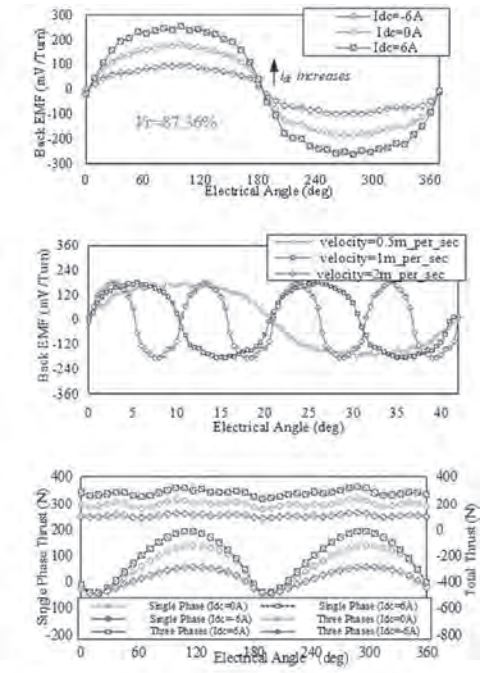

Fig.2 Performance of HE-TF-TLM *(a) Induced voltage under different* i_d. (b) *Induced voltage under different working speed. (c) Output thrust of single phase and three phases.*

JPC-11. Axial Flux Generator with Consequent-Pole PM Stator for Direct Drive Wave Energy Conversion. *Y. Li*[1], L. Huang[1], M. Chen[1], P. Tan[1] and M. Hu[1] *1. Department of Electrical Engineering, Southeast University, Nanjing, China*

I. Introduction Direct drive wave energy conversion (DDWEC) has attracted wide attention [1]. Various ways have been employed to further reduce the cost of wave energy conversion and promote the commercialization process, including the application of permanent magnets (PMs). PM generator has better electromagnetic performance for its high energy density [2,3]. The configuration of DDWEC proposed in this paper is combining the axial flux generator (AFG) and magnetic lead screw (MLS). However, the extensive use of PM will increase the manufacturing cost. For reducing the PM cost in DDWEC, a modified consequent-pole PM AFG (CPM-AFG) is proposed in this paper. By changing one side of PMs into iron-cores, which is called iron-pole, the volume of PM can be reduced. II. Generator Topology The whole configuration of the DDWEC system is that AFG located inside of the MLS is connected softly to the buoy when the screw and nut of MLS is connected directly to the buoy and rotor, respectively, as is shown in Fig. 1. Through MLS, the linear reciprocating motion of the wave can be transformed into the rotational motion of nut. When the buoy moves up and down, the rotor composed of modulation teeth in AFG rotate to generate energy. The rotor's angular velocity can be expressed as: $\omega=Gv=\pi v/\tau$ where G is defined as gear ratio of MLS, v is screw's linear velocity and τ is the pole width of MLS. Similar to magnetic gear, the pole pairs of armature windings p_{aw}, the pole pairs of PM p_{PM} and the iron pieces of rotor N_i should satisfy: $N_i = p_{aw} + p_{PM}$ Fig. 1 III. Results The simulation result shown in Fig. 2 indicates that although the volume of PM in the CPM-AFG is reduced by half, the flux linkage and torque are not reduced to half compared with the conventional surface-mounted PM axial flux generator (SPM-AFG). The amplitudes of SPM-AFG and CPM-AFG are 0.14Wb and 0.11Wb, respectively. The average electromagnetic torques of them are 23.2 Nm and 19.1 Nm, respectively. Fig. 2 IV. Conclusion Simulation results shown that the proposed CPM-AFG is suitable for DDWEC which can reduce the consumption of PM, reduce the cost of manufacture and improves the utilization ratio of PM.

[1] T. Xia, H. Yu, Z. Chen, L. Huang, X. Liu, and M. Hu, "Design and Analysis of a Field-Modulated Tubular Linear Permanent Magnet Generator for Direct-Drive Wave Energy Conversion," *IEEE Transactions on Magnetics,* vol. 53, no. 6, Jun 2017. [2] H. Dhulipati, S. Mukundan, Z. Li, E. Ghosh, J. Tjong and N. C. Kar, "Torque Performance Enhancement in Consequent Pole PMSM Based on Magnet Pole Shape Optimization for Direct-Drive EV," in *IEEE Transactions on Magnetics*, vol. 57, no. 2, pp. 1-7, Feb 2021. [3] Z. Z. Wu and Z. Q. Zhu, "Comparative Analysis of End Effect in Partitioned Stator Flux Reversal Machines Having Surface-Mounted and Consequent Pole Permanent Magnets," in *IEEE Transactions on Magnetics*, vol. 52, no. 7, pp. 1-4, July 2016.

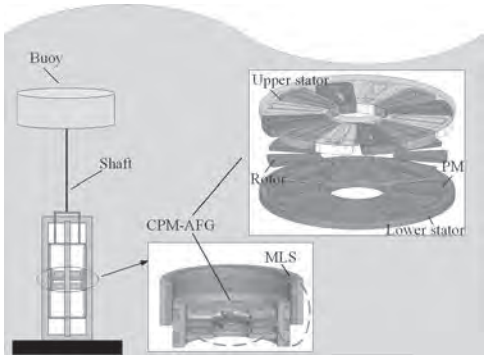

Fig. 1

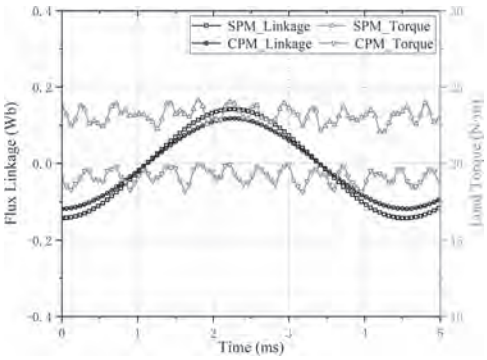

Fig. 2

JPC-12. Magnetic Flux Control Based on Magnetic Convergence or Divergence. *S. Park*[1], M.D. Noh[2] and Y. Park[2] *1. Graduate School, Chungnam National University, Daejeon, The Republic of Korea; 2. Mechatronics Engineering, Chungnam National University, Daejeon, The Republic of Korea*

Permanent magnet (PM) is the source of the magnetic flux, and the magnetic interaction occurs if the multiple PMs are used. The magnetic flux control (MFC) may be used to position an actuator precisely or to ensure the stability of the wall climbing robot. Thus, the focus of this study is to use the MFC not interfering with unwanted sensors and/or devices. To this end, the MFC based on magnetic convergence or divergence is proposed. The concept of the proposed MFC consists of a disk-type PM in the center of a cylinder-type PM. The MFC is caused by rotating the disk-type PM. For simulation purpose, the flux paths and a ferromagnetic plate are linked to the MFC, which completes the magnetic circuit. The cylinder and central PMs are assumed to be Alnico 5 with a respective diameter of 15 mm and 7 mm. A freeware FEMM 4.2 is used to conduct the magnetic simulations. Fig. 1 shows the simulation result of the divergence of MFC. Inset in Fig. 1 is the concept of MFC while two PMs align the poles parallel. The magnetic field from each PM diverges to form a strong magnetic field. The magnetic flux density to the plate is estimated to be about 1T. The state of MFC is changed from the divergence to the convergence by rotating the disk-type PM. Fig. 2 shows the simulation result of the convergence of MFC. Inset in Fig. 2

is the concept of MFC while two PMs align the poles anti-parallel. When the cylinder PM and the central PM provides the similar magnetic field, the magnetic field to the outside converges to zero. For the verification of conceptual design, the mathematical modeling is performed. The mathematical modeling includes geometric analysis with magnetic vector potential and Lorentz's force. The simulations are implemented for demonstration of the model. Through this process, the interaction of the PMs can be analyzed to verify the possibility of the model and to certify the suitability of the concept. It is expected that this model can be used in applications where multiple magnets are used without affecting other components.

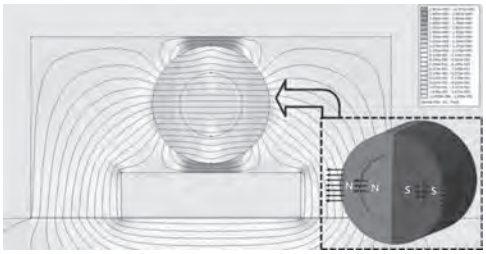

Fig. 1 Magnetic divergence of MFC

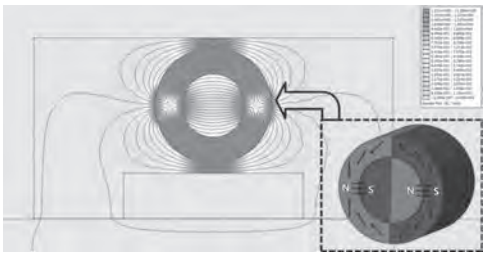

Fig. 2 Magnetic convergence of MFC

Session JPD
VIBRATION ANALYSIS AND ENERGY HARVESTING MAGNETIC DEVICES (Poster Session)

Jonathan Bird, Co-Chair
Portland State University, Portland, OR, United States
Xuerong Li, Co-Chair
Aalborg University, Aalborg, Denmark

JPD-01. Effects of Unequal-tooth Widths on Electromagnetic Vibration Source of Permanent Magnet Motors. *Z. Wu*[1] and Y. Fan[1] *1. Southeast Univeristy, Nanjing, China*

I Introduction Fractional-slot concentrated winding permanent magnet motor (FSCW-PM) has attracted much attention in many fields, due to its high efficiency, high power/torque density etc. However, the FSCW-PMs generally suffer from the large vibration, which limits the application. As known, the cogging torque and radial force will cause motor vibration. To reduce cogging torque, the unequal-tooth width design is proposed[1]. However, the cogging torque is increased when the unequal-tooth is used[2],[3]. Although, the effect of unequal-tooth on cogging torque is analyzed, the FSCW-PMs suitable for the unequal-tooth to reduce cogging torque is not described[4]. Moreover, the unequal-tooth is used to reduce the motor vibration[5]. Aiming to the unequal-tooth design, the researches on cogging torque and radial force are relatively independent. The effects of unequal-tooth on cogging torque and radial force are not clearly described for FSCW-PMs with different slot/pole combinations. II Cogging Torque According to theoretical analysis, the unequal-tooth can reduce cogging torque only for FSCW-PMs with specific slot/pole combinations. To validate the results, the cogging torques of FSCW-PMs with different slot/pole combinations are analyzed. When the unequal-tooth is used, the cogging torque is increased in Fig. 1(a), while the minimum cogging torque can be obtained in Fig. 1(b). Thus, the general rule derived analytically is verified. III Radial Force The effect of unequal-tooth on radial force of FSCW-PMs with different slot/pole combinations are analyzed. When the unequal-tooth is used, the 2rd harmonic is reduced in Fig. 2(a), while the 2rd harmonic is increased in Fig. 2(b), which are contrary to the cogging torque. Thus, the cogging torque and radial force should be tradeoff when using the unequal-tooth design. IV Conclusion In this paper, the effects of unequal-tooth on cogging torque and radial force are analyzed. The general rule for FSCW-PMs that suitable to reduce cogging torque by the unequal-tooth is revealed. Correspondingly, the effect of unequal-tooth on radial force is described. The research contributes to the design and optimization of the low-vibration FSCW-PMs.

V References [1] S. Hwang, J. Eom, G. Hwang, et al. "Cogging torque and acoustic noise reduction in permanent magnet motors by teeth pairing," *IEEE Trans. Magn*., vol. 36, no. 5, pp. 3144-3146, Sep. 2000. [2] D. Ishak, Z. Q. Zhu, D. Howe, "Permanent-magnet brushless machines with unequal-tooth widths and similar slot and pole numbers," *IEEE Trans. Ind. Appl.*, vol. 41, no. 2, pp. 584-590, Mar./Apr. 2005. [3] I. Petrov, P. Ponomarev, Y. Alexandrova and J. Pyrhönen, "Unequal teeth widths for torque ripple reduction in permanent magnet synchronous machines with fractional-slot non-overlapping windings," *IEEE Trans. on Magn.*, vol. 51, no. 2, pp. 1-9, Feb. 2015, [4] X. Tang, X. Wang, M. Tian, et al. "Study of reduction methods of cogging torque in line-start permanent magnet synchronous motor by changing the parameters of stator teeth and slots," *Transactions of China Electrotechnical Society*, vol. 31, no. 23, pp. 1-8, Dec. 2016. [5] W. Zhao, S. Zhu, J. Ji, G. Liu and Y. Mao, "Analysis and Reduction of Electromagnetic Vibration in Fractional-Slot Concentrated-Windings PM Machines," *IEEE Trans. Ind. Electron.* doi: 10.1109/TIE.2021.3071701.

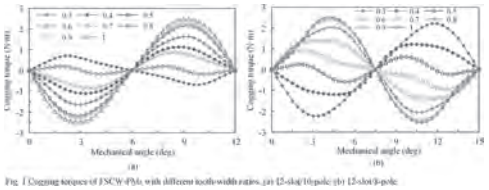

Fig. 1 Cogging torque

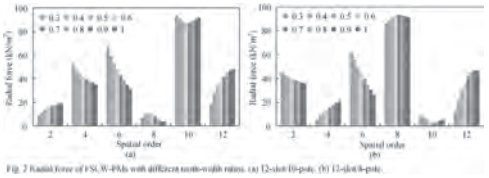

Fig. 2 Radial force

JPD-02. Design and Analysis of Omnidirectional Power Extender for Long-Range Underwater Wireless Power Transfer System. *X. Tian*[1], K. Chau[1], W. Liu[1] and H. Pang[1] *1. Department of EEE, The University of Hong Kong, Hong Kong*

Wireless power transfer (WPT) technology is being applied to many industrial applications [1]. It brings convenience and safety especially for undermine or underwater operation scenarios [1-2]. However, in those working scenarios, such as wireless charging for underwater robots or sensor networks, the system usually requires at least meter-range transmission distance, which is several times of the transmitter coil radius [2-3]. For traditional 2-coil-coupler system, the long-range operation will easily lead to unacceptable power loss and efficiency drop. Also, the traditional single-pad repeater is not suitable for underwater environment since the water flow will cause large and unstable angular misalignment. The variance of the mutual inductance between the coils can be very sensitive to the position relationships and the fluctuation may cause a system failure. To solve this problem, this paper presents an omnidirectional power extender for long-range underwater WPT systems. The proposed system configuration can be shown in Fig. 1. The power extender consists of two identical coils which are orthogonal and thus decoupled to each other [4]. The two coils are compensated separately for independent operation. Under the condition of the same internal resistances, the magnetic field generated by the two coils can be compensated by each other at arbitrary angles and the effect of the water flow can be effectively reduced. Thus, the system can have a relatively stable high output. Finite element analysis (FEA) has been conducted for a 100:1 scale-down system with the extender under the angular misalignment ranges from -90° to 90°. The simulated results of the output power are shown in Fig. 2. The system can reach over 70% efficiency for the transmission distance over 2 times the transmitter coil radius. The output power can be maintained over 35% even at the worst angular positions, which validates the effectiveness of the proposed system.

[1] W. Liu, K. T. Chau, C. H. T. Lee, L. Cao and W. Han, "Wireless power and drive transfer for piping network," *IEEE Transactions on Industrial Electronics*, doi: 10.1109/TIE.2021.3068675. [2] T. Kan, R. Mai, P. P. Mercier and C. C. Mi, "Design and analysis of a three-phase wireless charging system for lightweight autonomous underwater vehicles," *IEEE Transactions on Power Electronics*, vol. 33, no. 8, pp. 6622-6632, Aug. 2018. [3] Z. Yan, B. Song, Y. Zhang, K. Zhang, Z. Mao and Y. Hu, "A rotation-free wireless power transfer system with stable output power and efficiency for autonomous underwater vehicles," *IEEE Transactions on Power Electronics*, vol. 34, no. 5, pp. 4005-4008, May 2019. [4] X. Tian, K. T. Chau, W. Liu and C. H. T. Lee, "Analysis of multi-coil omnidirectional energy harvester," *IEEE Transactions on Magnetics*, vol. 57, no. 2, pp. 1-6, Feb. 2021.

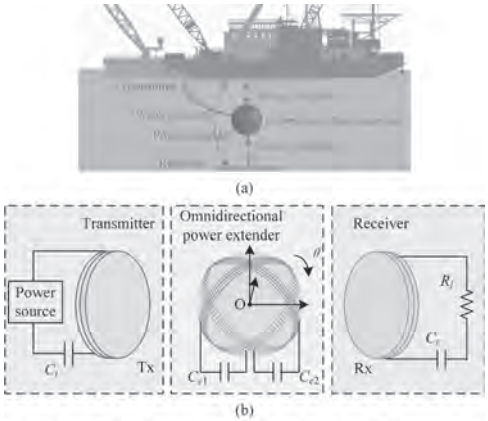

Fig. 1. Proposed omnidirectional power extender. (a) Application for underwater WPT system. (b) System configuration.

Fig. 1. Proposed omnidirectional power extender. (a) Application for underwater WPT system (b) System configuration

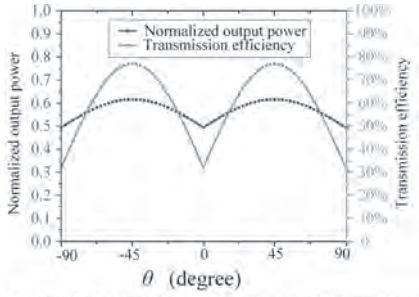

Fig. 2. Simulated output power versus angular misalignment.

Fig. 2 Simulated output power versus angular misalignment

JPD-03. Magnetic actuator capable of movement in all directions by the phase control of vibration components. *H. Yaguchi*[1] and S. Yamori[1] *1. Tohoku Gakuin University, Tagajo, Japan*

In the present study, a new principle of operation for the magnetic actuator capable of movement by controlling the phase of five vibration components has been considered. Fig. 1 shows a new magnetic actuator that can move 360 degrees in all directions. This magnetic actuator is composed of five vibration components A, B, C, D and E having the same specifications, an acrylic frame and plate, and two rubber permanent magnets. Five rubber permanent magnets were attached to the bottom of the acrylic frame to hold the actuator on the magnetic substance. One is a main rubber permanent magnet for holding the actuator on a magnetic substance. Another four sub rubber permanent magnets were attached to achieve stable movement. As shown in the Fig. 3, the forces generated by the vibration components A, B, C, D and E are F_A, F_B, F_C, F_D and F_E, respectively. As shown in Table 1, this magnetic actuator can move 360 degrees in all directions by controlling the phases of the other four vibration components based on the vibration of the vibration component A. Theoretical analysis is described in full paper. Fig. 4 shows the relationship between the phase difference in the vibration components A and B, C and the movement speed. The input current to the electromagnet in all vibration components was varied to 80, 100 mA. The movement speed shows the maximum value when the phase difference is 0 degree and 180 degrees. As an example, the movement characteristics of the magnetic actuator on a vertical plane are shown below. Fig. 5 shows the change in movement speed when the input current to the vibration components A, B, and C is fixed at 100 mA and the input current to the vibration components D and E is changed from 100 mA to 200 mA. Fig. 6 shows the change in the movement angle of the magnetic actuator under the above conditions. In both figures, the solid line shows the theoretical result and the plot shows the experimental result, and they are in good agreement. Fig. 7 shows the relationship between the load mass and the vertical upward speed when currents of 100 mA, 150 mA, and 200 mA are passed through the vibration components A and B, C. It was shown that the maximum traction force of this magnetic actuator was 2.2 N.

[1] Hiroyuki Yaguchi and Shun Sakuma : Improvement of a Magnetic Actuator Capable of Movement on a Magnetic Substance, *IEEE Transactions on Magnetics*, Vol. 52, No. 7, DOI:10.1109/TMAG.2016.2533433 (2016).

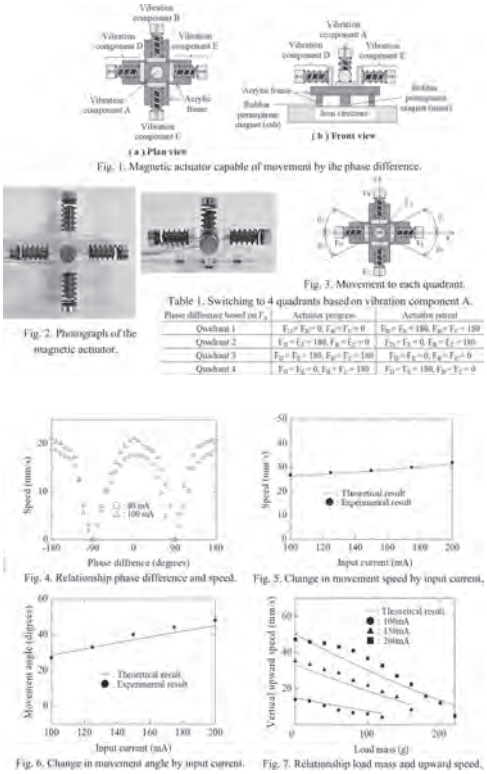

Fig. 1. Magnetic actuator capable of movement by the phase difference.

Fig. 2. Photograph of the magnetic actuator.

Fig. 3. Movement to each quadrant.

Table 1. Switching to 4 quadrants based on vibration component A.

Phase difference based on F_A	Actuation progress	Actuation retreat
Quadrant 1	$F_B=F_E=0$, $F_C=F_D=0$	$F_B=F_E=180$, $F_C=F_D=180$
Quadrant 2	$F_B=F_D=180$, $F_C=F_E=0$	$F_D=F_E=0$, $F_B=F_C=180$
Quadrant 3	$F_C=F_E=180$, $F_B=F_D=180$	$F_C=F_E=0$, $F_B=F_D=0$
Quadrant 4	$F_C=F_B=0$, $F_D=F_E=180$	$F_D=F_E=180$, $F_B=F_C=0$

Fig. 4. Relationship phase difference and speed.

Fig. 5. Change in movement speed by input current.

Fig. 6. Change in movement angle by input current.

Fig. 7. Relationship load mass and upward speed.

JPD-04. Control of Large Oscillation by Switching the Damping Mode of the Damper Coils in Electrodynamic Suspension System. *R. Betsunoh*[1], R. Yamamoto[1] and S. Ohashi[1] *1. Graduate School of Science and Engineering, Kansai University, Suita, Japan*

The electrodynamic suspension system (EDS) is used for levitation and guidance of the high speed magnetically levitation system[1]. The principle of the EDS system is electromagnetic induction, and this system has the advantage of stable levitation without gap control[2]. However, results of numerical simulations show that the damping factor of the EDS system is small. In this paper, levitation system of the JR Maglev is studied as the application of the EDS system, and to improve the damping factor, damper coil system is installed[3][4]. The damper coil current changes delayed by its self-inductance against the oscillation of the bogie. Thus, there are the periods that the force of the damper coil increases the oscillation. To solve this problem, the semi-active damper system is introduced. The damper coils are switched according to the oscillation velocity of the bogie and

the magnetic force generated by the damper coils. The damping factor is improved. When the bogie passes the vertical displacement z = 0.07[m] at the velocity v = 120[m/s], the oscillation in the semi-active damper system converges sooner than that in the passive damper system. But the maximum amplitude in the semi-active damper system is larger than that in the passive system. In the case that the oscillation is large, the period that the damper coil works becomes short caused by the pitching oscillation, and the damping factor becomes small. Therefore, the passive damper system is effective at large oscillation, and the semi-active damper system is effective at small oscillation. Therefore, the damping when the bogie passes the large displacement using the switching method switched the passive and semi-active damper system in the bogie running was considered. As a result of switching at t = 2.67[s], the oscillation becomes about 20% smaller than the semi-active damper system. And, the convergence time is 5.2% shorter than the semi-active damper system, and about 50% shorter than the passive damper system. In conclusion, by switching the damper system, the damping factor is improved, and the convergence time of the oscillation becomes short. Thus, the combined switching is effective to decrease the large oscillation efficiently.

[1] S.Ohashi, K. Higashi, H. Osaki, and E. Masada, "Running simulation of the superconductive magnetically levitated system," in *Proc. EPE,* vol. 3, 1995, pp. 650-655. [2] A. Seki, J.Kitano and S.Miyamoto, "Dynamics of the bogie of a maglev system with guideway irregularities", *IEEE Trans. on Magnetics* vol.32, No.5, pp5043-5045, 1996. [3] D.M.Rote, "Passive Damping In EDS Maglev Systems", in Proceedings of the 17th International Conference on Magnetically Levitated Systems and Linear Drives (Maglev'2002), 2002, PP01104. [4] S. Ohashi, "Weight Reduction of the Damper Coils in the Superconducting Magnetically Levitated Bogie", *IEEE Trans. on Magn.* Vol. 54, no. 11, 2018.

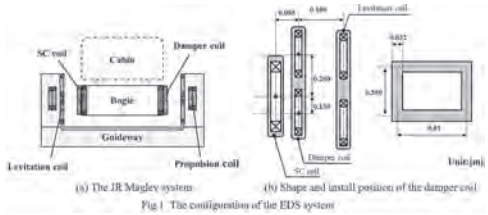

Fig.1 The configuration of the EDS system

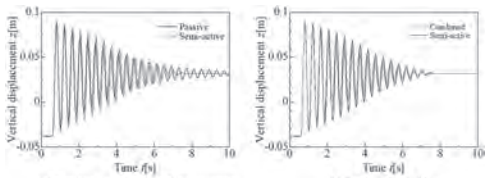

Fig.2 Running simulation at z = 0.07[m]

JPD-05. Withdrawn

JPD-06. Feature Extraction and State Identification of Transformer DC Bias Vibration Based on HHT-SVM. Z. Liang[1], *J. Li*[1], L. Li[1], Y. Qi[1], G. Li[1], N. Zheng[2] and Z. Wang[2] *1. School of Electrical Engineering, Dalian University of Technology, Dalian, China; 2. R & D, LUTE Electric Co., Ltd, Jining, China*

ABSTRACT Aiming at the problem of feature extraction and state identification of transformer DC bias vibration in HVDC transmission, the principle of transformer DC bias and the vibration mechanism of core and windings are studied and analyzed. Based on the dynamic simulation experiment platform, the vibration signals of transformer under different operating conditions are collected and carried out by the statistical calculation and Hilbert-Huang Transform (HHT). Then, the characteristic parameters and vibration law are obtained and explored. Taking the statistical parameters and HHT data of transformer as feature vectors, the DC bias state of transformer is identified by support vector machine (SVM) classification method, which provides a new idea and auxiliary decision-making means for DC bias fault diagnosis of transformer. The results showed that the ratio of windings vibration in 300 Hz frequency band increases under DC bias, while that of core vibration signal in 300 ~ 600 Hz frequency band increases. Through the SVM classification method, the mean identification rate of transformer DC bias state reaches 96.8%, which can accurately identify the problem of transformer DC bias. *CONTENT* This paper is organized as follows. In Section II, the mechanism of transformer vibration under HVDC bias magnetic state is described. In Section III, a identification method of HHT-SVM vibration signal is introduced. In Section IV, the vibration signal acquisition and result analysis based on HHT-SVM are presented and discussed in detail. *CONCLUSION* The vibration signals of transformer windings and core are affected by the distortion of excitation current and core saturation under the condition of DC bias magnetic field. Among them, the winding vibration signal changes little, but the amplitude of the 300 Hz frequency band increases, and the core vibration signal changes greatly, and the signal gradually shifts to the middle frequency band. By collecting vibration signals and combining with HHT-SVM identification method, the status of transformer DC magnetic bias can be effectively identified, which provides a new research idea and auxiliary decision-making means for transformer DC magnetic bias fault diagnosis.

[1] P. L. Jiang, *et al.*, Electrical Measurement & Instrumentation, Vol. 58, p. 25 (2021) [2] S. Q. Zhang, *et al.*, Proceeding of the CSEE, Vol. 39, p. 4334 (2019) [3] Z. Z. Wang, *et al.*, Transactions of China Electrotechnical Society, Vol. 36, p. 2801 (2021) [4] Y. P. Liu, *et al.*, Proceeding of the CSEE, Vol. 40, p. 4681 (2020) [5] C. Pan, S. Y. Yi, H. Su, IET Electric Power Applications, Vol. 13, p. 410 (2019) [6] M. R. Patel, IEEE Transactions on Power Apparatus and Systems, Vol. PAS-92, p. 1558 (1973) [7] N. E. Huang, Proceedings of Royal Society of London, p. 454 (1998) [8] J. Y. Wang, *et al.*, Transactions of China Electrotechnical Society, Vol. 30, p. 56 (2015)

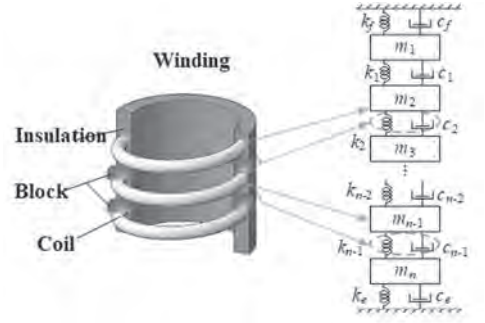

Fig. 1. Axial vibration model of transformer.

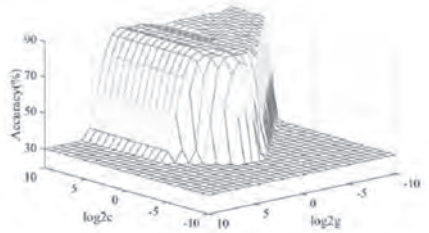

Fig. 2. SVM identification accuracy curve optimized by GSA.

JPD-07. Measurement and Frequency Characteristics Analysis of 500 kV Transformer Surface Vibration Signals. Z. Liang[1], *J. Li*[1,2], L. Li[1], Y. Qi[1], G. Li[1], N. Zheng[2] and Z. Wang[2] *1. School of Electrical Engineering, Dalian University of Technology, Dalian, China; 2. R & D, LUTE Electric Co., Ltd, Jining, China*

ABSTRACT The surface vibration signals of 500 kV autotransformer with different structures are measured, and the frequency domain characteristics of which are analyzed in this paper. Firstly, the surface vibration signal measuring points are set according to the specific arrangement of the core and windings of the transformer. Secondly, the vibration signals at different transformer measuring points under the same load and different loads are measured respectively. Finally, the frequency characteristics of the measured vibration signals are compared and analyzed. Then, use adaptive blind source separation algorithm (ABSSA) for transformer surface vibration signal processing, the two signals obtained are close to the vibration characteristics of core and windings respectively, and the same is true of the separated signals. It is proved that the accurate vibration signals of core and windings can be obtained by blind source separation, and is helpful for further analysis of the operation state of the transformer core and windings. *CONTENT* This paper is organized as follows. In Section II, the vibration mechanism of transformer ontology is introduced and analyzed. In Section III, the selection of vibration measuring points on transformer surface is described. In Section IV, the measurement of vibration signals on transformer surface is presented, and the comparison and analysis of the results are discussed in detail. *CONCLUSION* Combined with the structure of the transformer, the vibration signals of different measuring points on the surface of the 500 kV autotransformer with two different structures in actual operation were measured, and the ABSSA based on the classical least mean square algorithm (LMSA) was used to process the vibration signals on the surface of the transformer, and the two source signals were obtained, which are close to the signals of the blind source separation of the transformer. It is necessary to take into account the correlation between the vibration of the core and the windings, as well as the non-linearity of the vibration signal transmission process. This will be more conducive to transformer fault signal extraction and fault diagnosis.

[1] M. Mizokami and Y. Kurosaki, Journal of Magnetism and Magnetic Materials, Vol. 381, p. 208 (2015) [2] S. C. Ji, *et al.*, High Voltage Apparatus, Vol. 55, p. 1 (2019) [3] Y. J. Xia, *et al.*, Electrical Measurement & Instrumentation, Vol. 54, p. 7 (2017) [4] L. Zhang, *et al.*, Proceedings of the CSEE, Vol. 36, p. 3990 (2016) [5] J. Guo, *et al.*, Transactions of China Eletrotechnical Society, Vol. 27, p. 68 (2012) [6] S. C. Ji, *et al.*, High Voltage Engineering, Vol. 46, p. 257 (2020) [7] K. Chen Kai, *et al.*, Proceedings of the Chinese Society of Universities for Electric Power System and its Automation, Vol. 25, p. 56 (2013) [8] F. Zhang, *et al.*, Proceedings of the CSEE, Vol. 38, p. 2790 (2018)

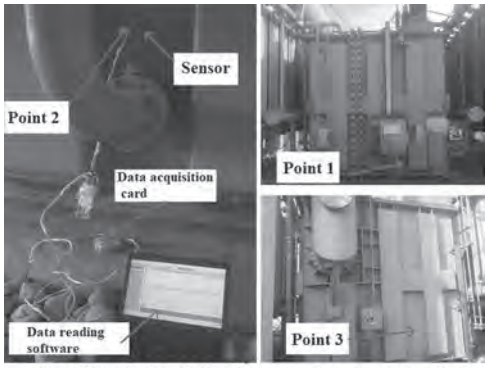

Fig. 1 Distribution of vibration measuring points of single phase transformer.

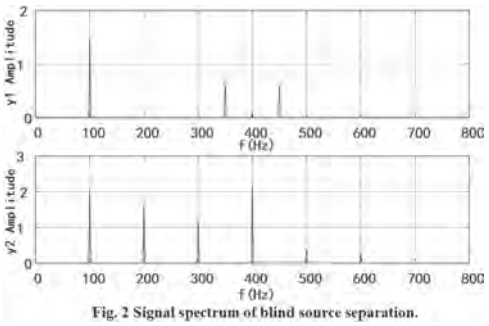

Fig. 2 Signal spectrum of blind source separation.

JPD-08. Design of Battery-less Wireless Switch that Share Coils in Common Using Electromagnetic Induction Energy Harversting Mechanism. S. Yang[1], M. Jeong[1], J. Bea[2] and *W. Kim*[1] *1. Gachon University, Gyeonggido, The Republic of Korea; 2. Dongyang Mirae University, Seoul, The Republic of Korea*

Wireless Sensor Network (WSN) node communication, which is used to gather information on a wide range of sensors, uses wireless communication that does not require wiring, but power is supplied via wired or battery[1]. In order to manufacture many small switches as battery-less, an economical self-powered generating application excluding additional elements such as piezoelectric elements are required. In addition, small electromagnetic induction studies are required because mechanical kinetic energy must be converted into electrical energy in a small spatial structure including push-buttons[2]-[4]. This paper proposes a self-powered generating apparatus applicable to two-gang wireless switches. The electromagnetic induction phenomenon follows Faraday's law, which generates induced voltage when the magnetic field passing through the coil changes at time. Electromagnetic induction self-powered generating apparatus require magnets and conductors that generate electromotive force to create magnetic fields. Figure 1 shows the proposed new two-gang switch structure and magnetic flux flow. The right side of the Conventional one-gang switch magnetic material 2 was opened and magnet 2 and magnetic material 4 were added. The coil is in common use and is assumed to have the same winding resistance and inductance for comparison with the conventional one-gang switch. The no-load back Electromotive Force(EMF) waveforms of the convolutional one-gang switch and the proposed two-gang switch are shown in Figure 2. In the two-gang switch, when the switch lever 1 and 2 are operated, the no-load back EMF waveform is divided into a positive direction and a reverse direction. Therefore, the switch can be miniaturized because sensors are not required to distinguish each push operation. And the performance has been improved to the induced voltage ratio 84% of the one-gang switch. Later, the mechanism of the proposed two-gang switch will be described in full paper to compared with the existing one-gang switch mechanism, and optimum design according to the detailed shape will also be added.

[1] Y. Choi, A Study on the Characteristic of Energy Harvesting Mechanism for Batteryless Wireless Switch., Journal of the Korea Academia-Industrial cooperation Society, Vol. 15, pp. 3114-3120 (2014) [2] J. Yang, M. Lee and M. Park, A 2.5-V, 160-μJ-output piezoelectric energy harvester and power management IC for batteryless wireless switch (BWS) applications., 2015 Symposium on VLSI Circuits (VLSI Circuits), pp. C282-C283 (2015) [3] J. Paradiso, T. Starner, Energy Scavenging for Mobile and Wireless Electronics., IEEE Pervasive computing., Vol. 4, pp. 18-27 (2005) [4] M. Kim, "Piezoelectric Mechanical Vibration Energy Harvesting", Journal of the Korean Society for Nondestructive Testing, Vol. 32, pp. 603-610 (2012)

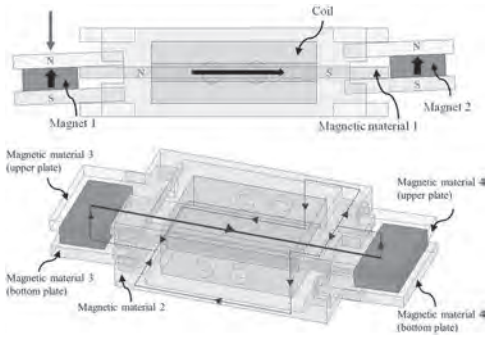

3-D view of Magnetic flux flow by conventional two-gang switch when the switch lever 1 is tilted down

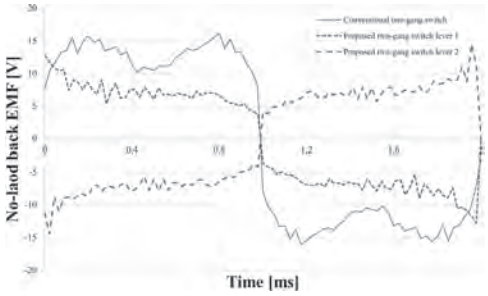

Comparisons of no-load back EMF

JPD-09. The Effect of Magnetism and Magnetic field on Locomotion of Hydrogen and Hydrogen Production Efficiency. Y. Chen[1], *Y. Li*[2,1] and C. Chen[1] *1. Mechanical Engineering, National Yang Ming Chiao Tung University, Hsinchu, Taiwan; 2. Mechanical and Aerospace Engineering, Chung-Cheng Institute of Technology, National Defense University, Taoyuan, Taiwan*

Hydrogen is considered as a potential energy carrier, because there is no greenhouse polluting gas (such as carbon dioxide) generated during the energy releasing process. Water electrolysis is the best way to obtain pure hydrogen, but its low energy efficiency greatly limits its wide application. Hydrogen is a diamagnetic substance that can be manipulated by an external field. The various locomotion behaviors of the hydrogen bubbles under different magnetism are first shown in Fig.1. Fig. 1(a) shows that hydrogen bubbles move upward from the surface of the graphite electrode when the voltage of 150V is applied. Fig1. (b) shows that hydrogen bubbles evolving from graphite electrode slightly move towards the upper right when the magnet S-pole is faced with the cathode. This motion indicates that the magnetic field may help detach the bubbles from the surface of graphite electrode because of the micro-magnetohydrodynamic (MHD) effect. Fig.1 (c) shows that hydrogen bubbles move towards the right more significantly when the graphite electrode is changed to a platinum electrode, which is a paramagnetic material with a higher magnetic susceptibility than graphite. This result shows that the paramagnetic property will further enhance the locomotion of the bubbles and detach bubbles from the electrode more quickly. Figs. 2(a) and 2(b) respectively show a platinum electrode faced with a magnet generates a greater increase in the current density and conductivity of the water under the same applied voltage. In this paper, electrodes with different magnetism are adapted to hydrogen production in water electrolysis. The various moving behaviors of the bubbles under the different magnetism of electrode and the field conditions will be demonstrated in the full paper and the effects of working parameters related to magnetism and water electrolysis are discussed as well.

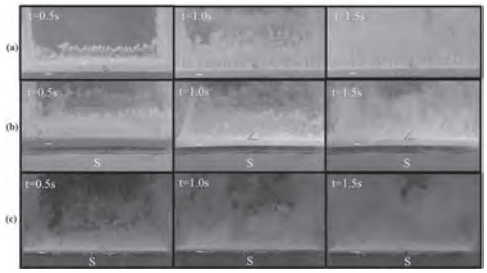

Fig.1 The sequential images of hydrogen bubbles detached from (a) graphite electrode without magnet (b) graphite electrode faced with the magnet S-pole (c) platinum electrode faced with the magnet S-pole.

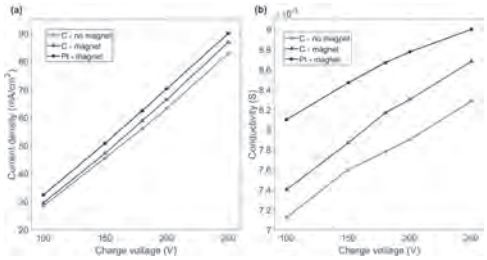

Fig.2 (a) Current density vs. Charging voltage (b) Conductivity vs. Charging voltage for the different electrodes with and without the effect of magnetic field.

JPD-10. Study on Vibration and Acoustic Noise of Anode Saturable Reactor under Sinusoidal and Non-sinusoidal Excitation. *C. Zhang*[1], T. Chen[1], Y. Li[1] and Q. Yang[1] *1. School of Electrical Engineering, Hebei University of Technology, Tianjin, China*

With power electronics technology applied widely, the Extra-high Voltage Direct Current (EHVDC) transmission which has lower loss and larger capacity than alternating current transmission performs a significant part of the power system. Anode saturable reactor (ASR) made of ultra-thin silicon steel plays an indispensable role in protecting the thyristor and the EHVDC converter valve. However, the magneto-strictive properties of ultra-thin silicon steel cause intensive vibration and acoustic noise of ASR during magnetization, which will reduce its service life and pollute the surrounding environment [1]. With frequency increases, the intensity of vibration and noise change obviously, especially the frequency when magneto-mechanical resonance occurs [2]. Further, the harmonic components existing in power grid aggravate the intensity of vibration and noise [3]. The influence of material properties and geometric shape of magnetic core on acoustic noise have been studied in [4]. But the vibration and noise distribution characteristics of ASR under sinusoidal and non-sinusoidal excitation have not been studied. In order to analyze the performance of ASR under practical operating conditions qualitatively and quantitatively, a core of ASR is measured under different excitations. The setup for vibration and acoustic noise measurement and data acquisition under sinusoidal and non-sinusoidal excitation are shown in Fig.1. The magnetization curve and loss curve of the core are obtained. The vibration acceleration and sound pressure are measured by accelerometer and microphone, respectively. The time domain waveform and frequency domain waveform of vibration and noise of the core under sinusoidal excitation without harmonic feedback are shown in Fig.2. The measured results are significative for the design of ASR to reduce the vibration and acoustic noise.

[1] P. N. Zhang, L. Li, & Juanjuan Z, et al. Vibration and noise reduction of HVDC anode saturable reactor by polyurethane damping elastomer. *International Journal of Electromagnetics and Mechanics*, vol. 58, no. 2, pp. 261-273, Nov. 2018, doi: 10.3233/JAE-180050. [2] X. G. Yao, T. P. P. Phway, A. J. Moses and F. Anayi, "Magneto-Mechanical Resonance in a Model 3-Phase 3-Limb Transformer Core Under Sinusoidal and PWM Voltage Excitation," *IEEE Transactions on Magnetics*, vol. 44, no. 11,

pp. 4111-4114, Nov. 2008, doi: 10.1109/TMAG.2008.2002790. [3] P. N. Zhang, L. Li. Vibration and noise characteristics of high-frequency amorphous transformer under sinusoidal and non-sinusoidal voltage excitation. *International Journal of Electrical Power & Energy Systems*, vol. 123, Dec. 2020, doi: 10.1016/j.ijepes.2020.106298. [4] S. Peng, B. Juergen. Influence of Material Properties and Geometric Shape of Magnetic Cores on Acoustic Noise Emission of Medium Frequency Transformers. *IEEE Transactions on Power Electronics*, vol. 32, no. 10, pp. 7916-7931, Oct. 2016, doi: 10.1109/TPEL.2016.2636572.

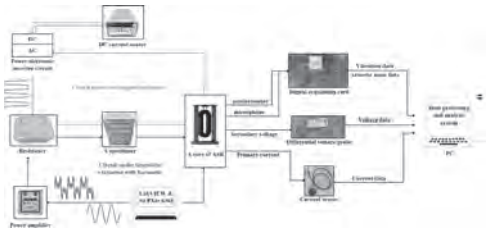

Fig.1. Setup for vibration and acoustic noise measurement and data acquisition under sinusoidal and non-sinusoidal excitation.

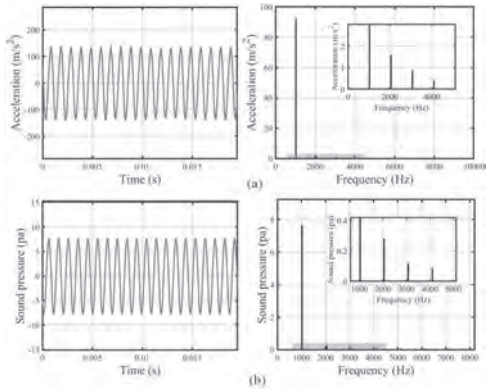

Fig.2. Time domain waveform and frequency domain waveform of vibration and noise of the core under sinusoidal excitation without harmonic feedback at 1.0 T and 500 Hz: (a) Vibration acceleration, (b) Sound pressure.

JPD-11. Vibration Analysis of Variable Flux Machines Considering the Memory Effect. *F. Liu*[1], P. Zheng[1], M. Wang[1] and G. Qiao[1] *1. Harbin Institute of Technology, Harbin, China*

Owing to high power density and high efficiency, permanent-magnet (PM) synchronous machines (PMSMs) are widely used in people involved areas [1]. The concomitant electromagnetic vibration and noise have aroused attention to comfort. However, the un-adjustable air-gap flux of the conventional rare-earth PM machine leads to limited constant-power speed range, and the efficiency is lower at high speed region which results from the inescapable flux-weakening current. In order to make the PM flux controllable, the variable flux machine (VFM) is proposed by employing the low-coercive-force (LCF) magnet [2]. The air-gap flux can be changed by applying *d*-axis current pulse to re/demagnetize the LCF magnet. The magnetization states of the LCF magnet can be 'memorized' depending on the amplitude of the current pulse. After the LCF magnet is demagnetized, the harmonic component of the PM magnetic field is changed, and the machine can operate at high speed. Therefore, the vibration characteristic of the VFM will be changed as the magnetization state of the LCF magnet is changed. However, the vibration characteristic analysis of VFMs considering the memory effect are not covered in the existing articles. In this paper, the vibration analysis of VFMs considering the memory effect are studied for a 27-slot/6-pole reverse-salient VFM. The first-order shear deformation laminated theory are adopted to calculate the modal frequency of the stator assembly, as shown in Fig.1. Based on the complex air-gap relative permeance method, the distribution of the PM magnetic field are calculated at different magnetization state. The unevenly re/demagnetization is also considered. If the VFM is re/demagnetized unevenly, the magnetic motive force of PM contains much even harmonic components, which will seriously deteriorate the vibration characteristic of the VFM. By using the Maxwell stress tensor method, the electromagnetic force waves are calculated, and Fig 2 shows the electromagnetic force of one magnetization state. Then the vibration are analyzed based on the above analysis, and the result is compared with the finite element method.

[1] Y. Qin, C. He and X. Shao, *J. Sound Vib.*, vol. 419, p. 249–267, (2018) [2] Z. Q. Zhu, H. Hua and A. Pride, IEEE Trans. on Magn., Vol. 53(11), 1-4 (2017)

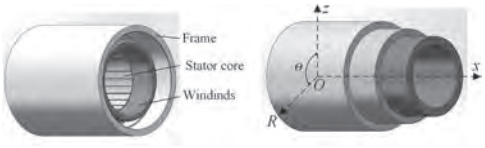

Fig. 1 The modal frequency calculation method

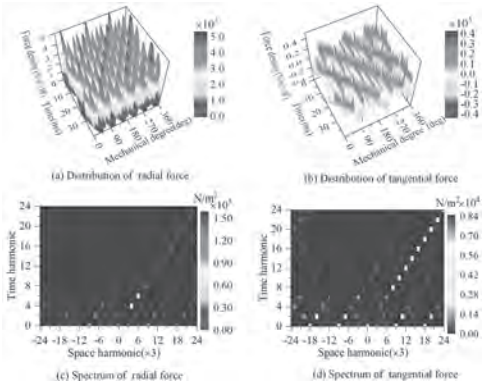

Fig. 2 The harmonic distribution of the electromagnetic force

Session JPE
MAGNETICALLY GEARED MACHINES AND RELUCTANCE MACHINES (Poster Session)

Kais Atallah, Chair
University of Sheffield, Sheffield, United Kingdom

JPE-01. Comparative Study of New Dual-Stator Consequent Pole Flux Reversal Arc Permanent Magnet Machines. *Y. Meng*[1], S. Fang[1], Z. Pan[1] and L. Qin[1] *1. School of Electrical Engineering, Southeast University, Nanjing, China*

I. Introduction Arc permanent magnet (PM) machines (APMMs) can directly connect the load without auxiliary devices, which are promising in large telescope drives [1] [2]. However, the conventional APMM with rotor PM suffers from a low PM utilization. In this paper, two new dual-stator consequent pole flux reversal APMMs (DS-CPFRAPMMs) are proposed and studied. The topologies and operation principles of the proposed machines are described. The electromagnetic performances of machines are analyzed by finite element analysis. II. Machine Topology and Operation Principle Fig. 1 shows the topologies of the proposed DS-CPFRAPMMs, which are named as machines I and II, respectively. It can be seen that both machines consists of two stators and one rotor, and each stator is composed of three modules. The three-phase concentrated windings are wound on the teeth of stator, which can offer the merits of short end length and low copper loss. Besides, the alternatively PMs and iron poles are placed on the top of stator teeth, which forms a consequent pole PM arrangement. The polarities of PMs on the inner and outer stators are opposite for machine I, while those are the same for machine II. Moreover, the rotor structures of machines I and II are also different. For machine I, the iron-only rotor is designed with double-sided salient poles. However, for machine II, the rotor is made up of separated iron poles. For both machines, each stator module and rotor forms a 12 stator-slot/11 rotor-pole combination. The operation principles of DS-CPFRAPMMs are based on the flux modulation effect, and the torque of machines are generated by taking advantage of the modulated air-gap field harmonics. III. Electromagnetic Performance Evaluation As shown in Fig. 2 (a) and (b), machine II has higher no-load phase flux linkage and back-EMF than machine I. According to Fig.2 (c), the average torque of machine II is 20.7% higher than that of machine I. However, machine I has a relatively low cogging torque. In addition, compared with machine II, machine I has a better over-load torque capability. More detailed design considerations and electromagnetic performance comparison results will be presented in the full paper.

[1] B. Li, J. Zhao and X. Liu, "Detent force reduction of an arc-linear permanent-magnet synchronous motor by using compensation windings,"*IEEE Trans. Ind. Electron.*, vol. 64, no. 4, pp. 3001–3011 (2017). [2] C. J. Jian, W. L. Ma and Y. K. Fan, "New methods for arc permanent magnet linear synchronous motor to decrease torque ripple,"*IEEE Trans. Magn*., vol. 48, no. 10, pp. 2659–2663 (2012).

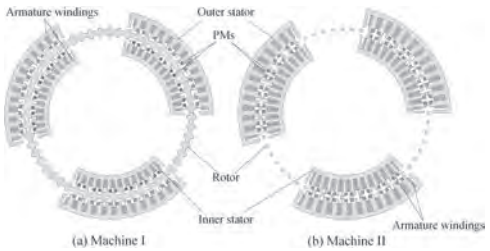

Fig. 1

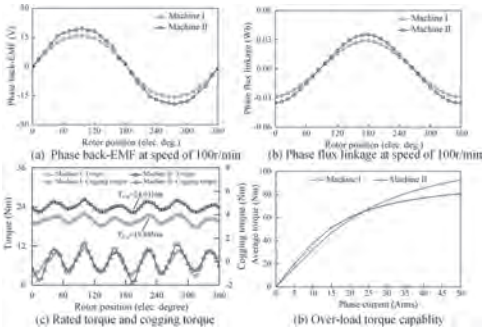

Fig. 2

JPE-02. Electromagnetic Characteristic Analysis of an Axial-Flux Magnetic-Geared Double-Rotor Machine with Interior-Modulating-Rotor. *J. Lang*[1], C. Tong[1], J. Bai[1], P. Zheng[1], J. Liu[1] and G. Liu[1] *1. Department of Electrical Engineering, Harbin Institute of Technology, Harbin, China*

Axial-flux magnetic-geared double-rotor machines (AMGDRMs) are verified a promising candidate for power splitting in hybrid electric vehicles (HEVs) [1]. However, in conventional AMGDRM, as can be seen in Fig. 1. (a), the modulating rotor is set in middle of stator and the permanent magnet (PM) rotor. Hence, the modulating rotor suffers from high axial magnetic force from the side of the PM rotor, resulting in low mechanical strength. In this paper, a new AMGDRM with interior-modulating-rotor is proposed to solve the problem of low mechanical strength. As shown in Fig. 1. (b)-(d), the PM rotor is set in middle of stator and the modulating rotor in proposed AMGDRM. Owing to that the PM rotor suffers from reverse axial magnetic forces from both sides simultaneously, the total axial magnetic force is dramatically reduced. The 3-D finite element analysis (FEA) simulation results shown in Fig. 1. (e) and (f) verify the low axial magnetic force property of proposed AMGDRM. Based on the magnetic-field modulating principle, the operating principle of proposed AMGDRM is investigated, and the speed and torque characteristics are also given. For the pole-pair configuration with p_s=3, p_{pm}=20, p_m=23, the simulated magnetic field distribution and its spectrum verify the operating principle, as shown in Fig. 2. (a) and (b). As shown in Fig. 2. (c) and (d), the no load back electromagnetic force (EMF) verifies the speed characteristic. Fig. 2. (e) and (f) show that the torques of stator, the modulating rotor and the PM rotor are always in direct proportion, validating the torque characteristic. A simplified analytical model, as shown in Fig. 2. (g), is proposed to investigate the influence of geometry parameters. Based on it, the analytical description of the magnetic field is deduced by magnetomotive force (MMF) and permeability functions. The influences of ferromagnetic pole-piece and PM on torque output are investigated. Fig. 2. (h) shows that the optimal pole-arc coefficient is about 0.3 at any thickness of ferromagnetic pole-piece, which agrees well with the proposed analytical model. As shown in Fig. 2. (i), the optimal thickness of PM is about 3mm and torque output rises with the pole-arc coefficient of PM increasing.

[1] M. Wang, C. Tong and Z. Song, *IEEE Trans. Ind. Electron.,* Vol. 66, p. 806-817(2019).

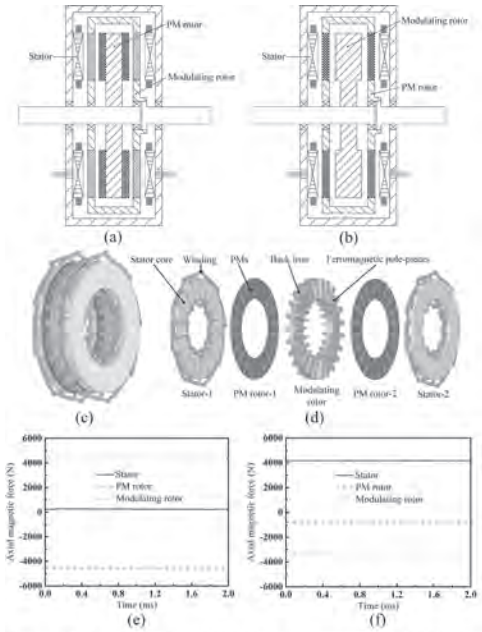

Fig. 1. (a) Conventional AMGDRM. (b) Proposed AMGDRM. (c) Overall view of proposed AMGDRM. (d) Exploded view of proposed AMGDRM. (e) Axial magnetic force in conventional AMGDRM. (f) Axial magnetic force in proposed AMGDRM.

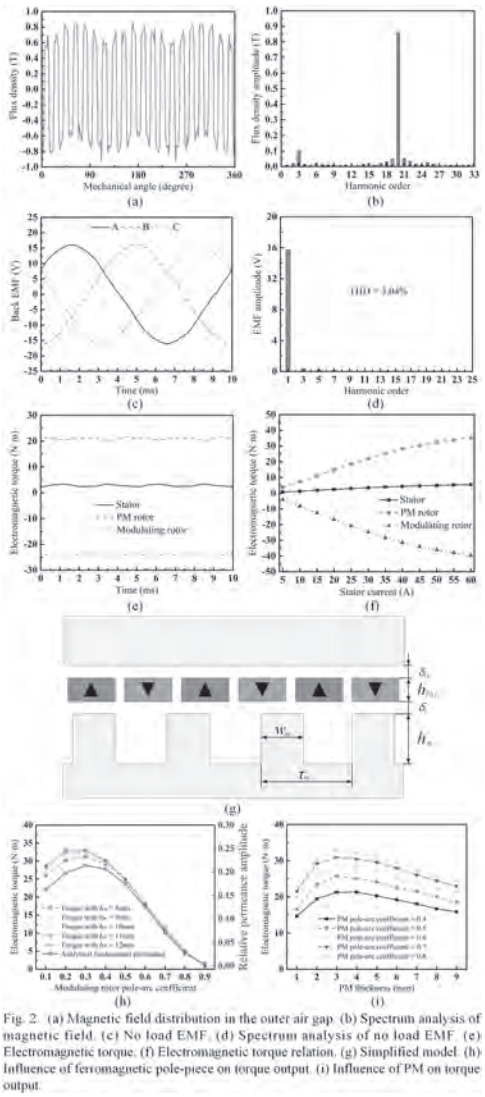

Fig. 2. (a) Magnetic field distribution in the outer air gap. (b) Spectrum analysis of magnetic field. (c) No load EMF. (d) Spectrum analysis of no load EMF. (e) Electromagnetic torque. (f) Electromagnetic torque relation. (g) Simplified model. (h) Influence of ferromagnetic pole-piece on torque output. (i) Influence of PM on torque output.

JPE-03. Investigation of a Transversely-Dislocated Brushless Double-Rotor Machine Based on Magnetic-Field Modulation. *Y. Wang*[1], Y. Sui[1], J. Liu[1], G. Liu[1] and P. Zheng[1] *1. Harbin Institute of Technology, Harbin, China*

The contra-rotating propeller (CRP) can be used for applications like unmanned underwater vehicles, wind power generations and aero propulsions [1]. The CRP system requires two output shafts with equal and opposite torques. Nowadays, that the contra-rotating machines (CRMs) directly drive the CRP is the most competitive choice in the CRP applications due to the advantages of high efficiency, low noise and compact volume. However, the main CRM schemes [2] exist rotating windings, which brings several inevitable problems like decreasing reliability, difficult dynamic balance and heat dissipation. In this paper, a transversely-dislocated magnetic-field modulated brushless double-rotor machine (TDMFM-BDRM), which has no rotating windings and no end winding, is proposed for the CRP system to solve the above problems. The TDMFM-BDRM is composed of a stator, a permanent-magnet (PM) rotor and a transversely-dislocated modulating (TDM) rotor, as shown in Fig. 1. The stator employs ring winding configuration distributed along the axial direction, which is similar to that of the tubular linear machine. The spoke-type PMs of the PM rotor are distributed along the circumferential direction. The TDM rotor is composed of the magnetic blocks and non-magnetic support. The three-dimensional magnetic-field modulated theory and the operating principle are investigated. The magnetic field distribution law in the air gap, the back electromotive force,

and the torque performance of the TDMFM-BDRM are investigated. The TDMFM-BDRM and the conventional CRM [2] are compared in many aspects like torque, torque ripple, loss, efficiency, and so on, as shown in Fig. 2. Both the TDMFM-BDRM and the conventional CRM employ water-cooled mode, but the TDMFM-BDRM can employ higher current density due to its stator is next to the frame. Fig. 2 indicates that the equal and opposite torques can be produced inherently by the TDMFM-BDRM, which can meet the needs of the CRP system. And the TDMFM-BDRM has higher torque density except the previously mentioned structural advantages compared with the conventional CRM.

[1] H. Shin, J. Chang, and D. Hong, "Axial-flux permanent-magnet dual-rotor generator for a counter-rotating wind turbine," *Energies*, vol. 13, no. 11, p. 2833 (2020) [2] J. Qiu, C. Shi and M. Jin, "Counter-rotating permanent magnet brushless DC motor for underwater propulsion," *2006 CES/IEEE 5th Int. Power Electron. and Motion Control Conf.*, Shanghai, China, vol. 2, pp. 1-5 (2006)

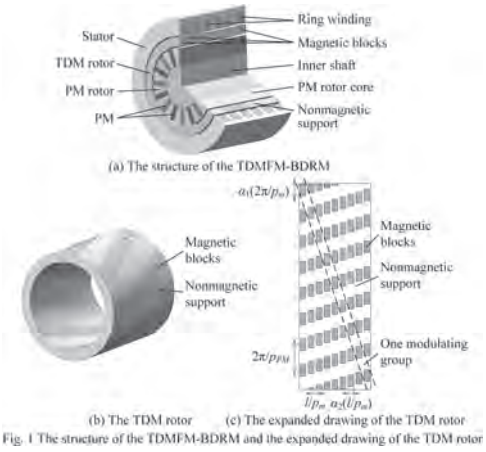

Fig. 1 The structure of the TDMFM-BDRM and the expanded drawing of the TDM rotor

Parameter	Value	
	The TDMFM-BDRM	The CRM
Outer diameter of the stator	202 mm	202 mm
Axial length	132 mm	132 mm
Radial length of the outer / inner air gap	1 mm	1mm
Pole-pair number of the stator	1	8
Pole-pair number of the PM rotor	8	8
Magnetic blocks number of one modulating group	9	-
Rotating speed	±1600 rpm	±1600 rpm
Torque of the outer rotor	91.4 N·m	60.6 N·m
Torque ripple of the outer rotor	7.48%	5.85%
Torque of the inner rotor	91.3 N·m	59.6 N·m
Torque ripple of the inner rotor	8.71%	6.46%
Core loss	625.1 W	376.3 W
Copper loss	1.09 kW	119.7 W
Eddy loss of PM	56.8 W	375.3 W
Efficiency	94.5%	94.9%

Fig. 2 The parameter comparison of two machines

Fig. 2 The parameter comparison of two machines

JPE-04. A Novel Coaxial Magnetic Gear with Convex Halbach Arrays and Spoke Structure. L. Jing[1] and *W. Liu*[1] *1. College of Electrical Engineering and New Energy, China Three Gorges University, Yichang, China*

Coaxial magnetic gear (CMG) is a novel transmission device, which is widely used in the field of low speed and high torque transmission. In order to improve the output torque of CMG, a novel CMG with convex Halbach arrays and Spoke structure is proposed in this paper. The permanent magnets of the inner rotor are Convex-T alternating arrangements. The PMs of the outer rotor are combination of Spoke structure and Halbach arrays. The Spoke part is magnetized along the tangential direction, and the Halbach part is magnetized along the radial direction. Using the unilateral effect of Halbach arrays, the air gap side magnetic field is strengthened and the yoke side magnetic field is weakened. In order to reduce the amount of iron, it is considered to slot on the outer rotor. The topological structure of CMG with 4 inner and 17 outer poles is established. The proposed CMG has the same volume size as the conventional CMG and the same amount of permanent magnets. The two-dimensional finite element method is used for simulating the proposed CMG. The magnetic field and electromagnetic torque of the CMG are calculated. Compared with the conventional CMG, the results show that the proposed CMG can effectively enhance the air gap flux density, reduce the non-working harmonic in the air gap, and the output torque is increased by 41.78%. This is of great significance to improve the torque density of the CMG.

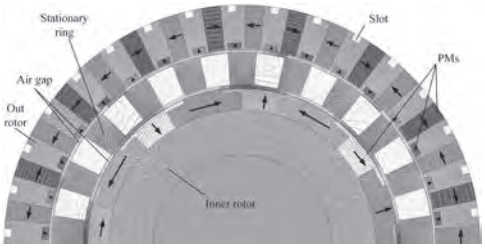

Fig. 1 The topology of the proposed CMG

Compared with the conventional CMG, the results of two models are listed in Table I:

Table 1. Torque comparison

	Type	T_{max}/(N·m)	T_{min}/(N·m)	T_{avg}/(N·m)
Inner torque	I	-56.425	-58.244	-57.361
	II	-81.067	-81.569	-81.293
Outer torque	I	343.607	244.206	243.851
	II	345.095	346.653	345.725

I: Conventional CMG. II: Proposed CMG. T_{max}, T_{min} and T_{avg} are the maximum, minimum and average value of the output torque respectively.

Table 1. Torque comparison

JPE-05. Gear ratio combination analysis and optimization for high torque density of dual magnetic gear. *E. Park*[1] and Y. Kim[2] *1. Faculty of Smart Vehicle System Engineering, Chosun University, Gwangju, The Republic of Korea; 2. The Department of Electrical and Computer Engineering, Chosun University, Gwangju, The Republic of Korea*

I. Introduction Dual magnetic gears are two magnetic gears connected in series. Unlike mechanical gears, magnetic gears have a characteristic that the higher the gear ratio, the lower the torque density. Table I shows the torque density according to the gear ratio [1-14]. Therefore, dual magnetic gear is used to show high torque density even at high gear ratio by using two low gear ratios with high torque density. This study targets a gear ratio of 90:1, and the number of possible dual combinations is 60. When various design parameters for optimization are applied here, the model to be reviewed increases exponentially. In this paper, an optimal design was first carried out for the reference model, a 90:1 single magnetic gear. Then, only the pole number analysis and basic design of the inner and outer rotors were performed for 60 combinations of dual magnetic gears, and the combination showing the highest torque density was selected. For the selected model, major design parameters were optimized. The main design parameters were analyzed for inner and outer yokes, inner and outer permanent magnet thickness, and pole piece length. Air gaps of inner and outer were fixed. II. Result As a result of analyzing the gear ratio combination, when the number of inner rotor poles was 4 and the number of outer rotor poles was 4 to 10, high torque density was shown. As a result of optimizing the main design parameters, the primary gear of the dual showed a torque density of 89kNm/m^3 and the secondary gear showed a torque density of 170kNm/m^3. When the two gears were combined, a torque density of 129kNm/m^3 was shown, which was 7.8 times higher than the torque density of 16.4kNm/m^3 of a 90:1 single magnetic gear, and the efficiency was improved by 31.5%p. One of the torque density analysis graph is shown in Fig. 1. Acknowledgment: This research was supported by Korea Electric Power Corporation. (Grant number: R19XO01-34)

[1] K. Atallah and D. Howe, "A novel high-performance magnetic gear," *IEEE Trans. Magn.,* vol. 37, no. 4, pp. 2844-2846, July. 2001. [2] K. Atallah, S. D. Calverley, and D. Howe, "Design, analysis and realisation of a

high-performance magnetic gear," *IEE Proceedings - Electric Power Applications*, vol. 151, no. 2, pp. 135-143, 2004. [3] Y. Wu, c. Chan, "A novel bicycle rear hub transmission with a magnetic gear mechanism," *Advances in Mechanical Engineering*, vol. 10, no. 7, pp. 1-9, 2018. [4] M. Desvaux, B. Traulle, R. Latimier, S. Sire, B. Multon, H. Ahmed, "Computation Time Analysis of the Magnetic Gear Analytical Model," *IEEE Trans. Magn*., vol. 53, no. 5, pp. 7000409, 2017. [5] M. Kowol, J. Kolodziej, M. Jagiela, M. Lukaniszyn, "Impact of Modulator Designs and Materials on Efficiency and Losses in Radial Passive Magnetic Gear," *IEEE Trans. Energy Conversion*, vol. 34, no. 1, pp. 147-154, 2019. [6] H. Shin, J. Chang, "Comparison of the Characteristics in the Surface Mounted Permanent Magnet and Flux Concentrating Coaxial Magnetic Gears Having the Solid Cores," *J. Electr. Eng. Technol.*, vol. 13, no. 3, pp. 1275-1284, 2018. [7] Y. Chen, W. Fu, S. Ho, H. Liu, "A Quantitative Comparison Analysis of Radial-Flux, Transverse-Flux, and Axial-Flux Magnetic Gears," *IEEE Trans. Magn*., vol. 50, no. 11, pp. 8104604, 2014. [8] D. Jang, J. Chang, "Effect of Stationary Pole Pieces with Bridges on Electromagnetic and Mechanical Performance of a Coaxial Magnetic Gear," *Journal of Magnetics*, vol. 18, no. 2, pp. 207-211, 2013. [9] X. Zhang, X. Liu, Z. Chen, "A Novel Coaxial Magnetic Gear and Its Integration With Permanent-Magnet Brushless Motor," *IEEE Trans. Magn*., vol. 52, no. 7, pp. 8203304, 2016. [10] X. Liu, Y. Zhao, X. Zhang, J. Gao, S. Huang, "Investigation of the Dynamic Characteristics of a Coaxial Magnetic Gear under Loading Condition Based on Analytical Model," *International conference on electrical machines and systems*, 2017. [11] M. Filippini, P, Alotto, "An optimization tool for coaxial magnetic gears," *The international journal for computation and mathematics in electrical and electronic engineering*, vol. 36, no. 5, pp. 1526-1539, 2017. [12] O. Molokanov. P. Dergachev, V. Kiruhin, P. Kurbatov, "Analyses and Experimental Validation of Coaxial Magnetic Planetary Gear," *International symposium on electrical apparatus and technologies*, 2014. [13] E. Gobl, G. Jungmayr, E. Marth, W. Amrhein, "Optimization and Comparison of Coaxial Magnetic Gears With and Without Back Iron," *IEEE Trans. Magn*., vol. 54, no. 11, pp. 8001604, 2018. [14] G. Jungmayr, J. Loeffler, B. Winter, F. Jeske, W. Amrhein, "Magnetic Gear: Radial Force, Cogging Torque, Skewing, and Optimization," *IEEE Trans. Industry Applications*, vol. 52, no. 5, pp. 3822-3830, 2016.

Reference	Gear ratio	Torque density (kNm/m³)
2018, Y. Wu et al.	2.6:1	120.1
2017, M. Desvaux et al.	3.5:1	102.3
2019, M. Kowol et al.	4:1	140.3
2018, H. Shin et al.	5.5:1	103.8
2014, Y. Chen et al.	5.5:1	117.7
2013, D. Jang et al.	5.5:1	93.2
2001, K. Atallah et al.	5.5:1	100.6
2016, X. Zhang et al.	5.75:1	91.1
2017, X. Liu et al.	5.75:1	87.9
2004, K. Atallah et al.	5.75:1	103.9
2017, M. Filippini et al.	8.33:1	78.8
2014, O. Molokanov et al.	11.5:1	70.2
2018, E. Gobl et al.	18:1	70
2016, G. Jungmayr et al.	21:1	56.1

Table I. Torque density according to the gear ratio

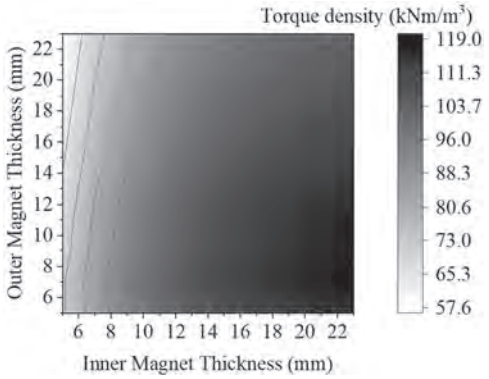

Fig. 1. Torque density analysis

JPE-06. Loss Analysis of Magnetic Gear with Halbach Arrays and Copper Bar. L. Jing[1] and *T. Wang*[1] *1. College of Electrical Engineering and New Energy, China Three Gorges University, Yichang, China*

Due to the magnetic field modulation of the modulating ring, a large number of harmonics can generate in the air gap. These harmonics act on the permanent magnet and magnetic ring, resulting in large eddy current losses and iron losses. In order to improve the harmonics in the air gap and reduce the losses, a novel magnetic gear with Halbach and copper bar is proposed in this paper. The permanent magnets (PMs) of the inner rotor adopted Halbach arrays. The iron yoke of outer rotor is slotted and add copper bar. The air gap flux density, output torque and loss of the magnetic are compared by finite element method. Compared with conventional magnetic gear, the results show that the proposed magnetic gear not only improves the air gap magnetic density and weakens the unworked harmonics, but also increases the output torque from 140.07Nm to 142.64Nm, reduces the eddy current loss by 32.24% and the iron loss by 16%. This model provides a new idea for loss analysis and optimization of coaxial modulated magnetic gear.

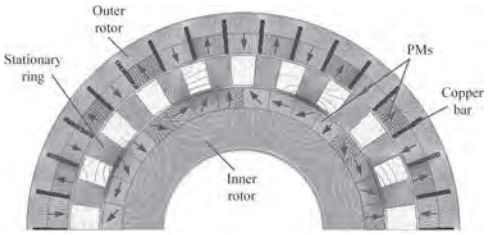

Fig. 1 CMG topology

A is defined as the torque ripple coefficient to represent the torque ripple. The specific formula is as follows:

$$\sigma = \frac{T_{max} - T_{min}}{T_{ave}} \quad (1)$$

Where, T_{max} is the maximum output torque; T_{min} is the minimum output torque. T_{ave} is the average output torque.

Table I Torque ripple

	type	T_{max}/(N·m)	T_{min}/(N·m)	T_{ave}/(N·m)	σ
Inner rotor	I	32.71	33.45	33.08	2.24
	II	33.28	33.67	33.45	1.17
Outer rotor	I	139.77	140.26	139.98	0.35
	II	142.50	142.82	142.64	0.22

I. conventional; II. proposed

Table I Torque ripple

JPE-07. A Novel Ironless Stator Magnetic-Geared Double-Rotor Machine. C. Tong[1], *J. Lang*[1], J. Bai[1], P. Zheng[1], J. Liu[1] and C. Ge[1] *1. Department of Electrical Engineering, Harbin Institute of Technology, Harbin, China*

Magnetic-geared double-rotor machines (MGDRMs) are verified a promising candidate for power split application [1]. However, there remains undesired torque ripple in conventional MGDRM. A new MGDRM with ironless stator, as shown in Fig. 1. (a), is proposed. The ironless stator structure can

eliminate stator slot effect and enable a more flexible winding configuration, resulting in low torque ripple. The simplified model of the proposed machine, as shown in Fig. 1. (b), is proposed. Thus, based on the magnetic-field modulating principle, the operating principle is investigated, and the speed and torque characteristics are also deduced. For the pole-pair configuration with p_s=3, p_{pm}=20, p_m=23, the simulated magnetic field distribution and its spectrum verify the operating principle, as shown in Fig. 1. (c) and (d). As shown in Fig. 2. (a) and (b), the no load back electromagnetic force (EMF) with low distortion verifies the speed characteristic. Fig. 2. (c) shows that the torque ripple of the proposed machine is 0.18%, validating the low torque ripple property. Furthermore, the torque ratio equals the theoretical value (i.e. pole-pair ratio). Fig. 2. (d) shows that the torques of stator, the modulating rotor and the PM rotor are always in direct proportion, validating the torque characteristic. Based on the simplified model shown in Fig. 1. (b), the analytical model consisting of magnetomotive force (MMF) and permeability functions is deduced to investigate the influence of key geometry parameters. The influences of ferromagnetic pole-piece and PM on torque output are investigated. Fig. 2. (e) shows that the optimal pole-arc coefficient of the modulating rotor is about 0.2, which approximately agrees with the proposed analytical model. It can be seen in Fig. 2. (f) that the torque output rises with the increment of ferromagnetic pole-piece thickness in the beginning and remains approximately unchanged when thickness is larger than 7mm. As shown in Fig. 2. (g) and (h), torque output rises with the pole-arc coefficient of PM increasing and the optimal thickness of PM is about 3mm, respectively. The trends of all above simulated results can be explained by the analytical model, validating the proposed model.

[1] J. Bai, P. Zheng and C. Tong, *IEEE Trans. Ind. Electron.,* Vol. 62, p. 4023-4033 (2015).

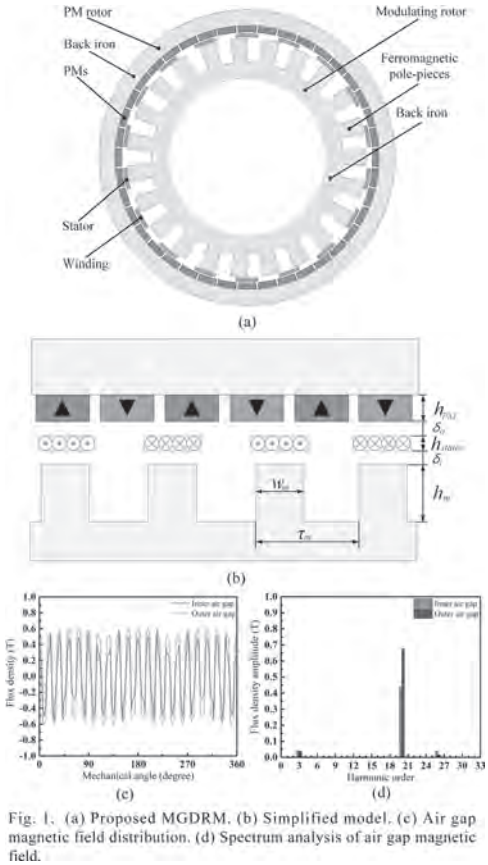

Fig. 1. (a) Proposed MGDRM. (b) Simplified model. (c) Air gap magnetic field distribution. (d) Spectrum analysis of air gap magnetic field.

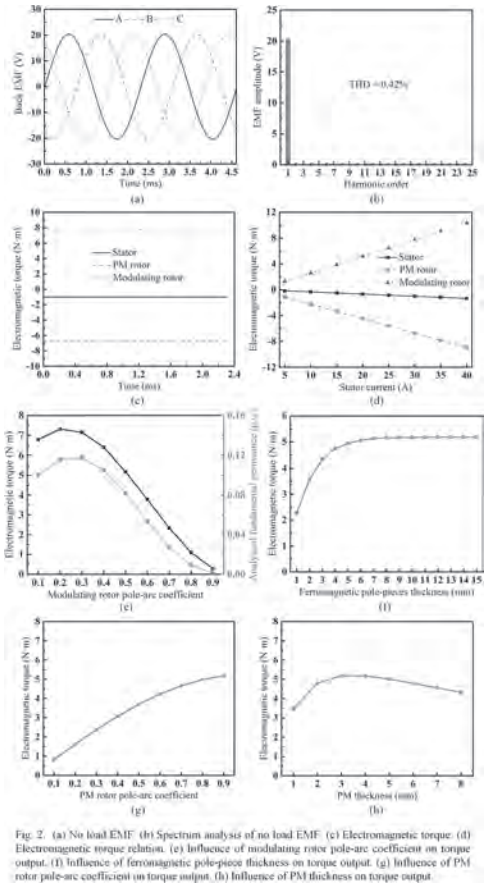

Fig. 2. (a) No load EMF. (b) Spectrum analysis of no load EMF. (c) Electromagnetic torque. (d) Electromagnetic torque relation. (e) Influence of modulating rotor pole-arc coefficient on torque output. (f) Influence of ferromagnetic pole-piece thickness on torque output. (g) Influence of PM rotor pole-arc coefficient on torque output. (h) Influence of PM thickness on torque output.

JPE-08. Topology Optimization of the Reluctance Magnetic Gear.

R. Safarpour[1] and *S. Pakdelian*[1] *1. Electrical and Computer Engineering, University of Massachusetts Lowell, Lowell, MA, United States*

This paper applies topology optimization (TO) to the reluctance magnetic gear (RMG) and achieves novel topologies with higher gravimetric torque density (GTD) and lower eddy current losses compared to the conventional RMG. Fig. 1a shows the conventional coaxial magnetic gear (MG). This configuration consists of two permanent magnet (PM) rotors and ferromagnetic pole pieces that serve as the flux modulator. This gear configuration has been mostly investigated for low speed applications. Challenges such as large eddy current losses in PM poles and the need for a retaining sleeve for the high speed rotor hinder the adoption of this gear configuration in high speed applications. As such, the RMG is proposed for such applications [1]-[3]. Fig. 1b shows the conventional RMG in which the inner rotor has a variable reluctance structure. A thorough comparison of the conventional RMG with the conventional PM MG has revealed that the RMG offers a drastically lower GTD and PM utilization compared to the PM MG [4]. In this paper, TO is used to enhance the RMG performance. In TO, the design region is divided into small elements such that each element can assume a set of pre-defined materials such as air, iron or PM. An optimization algorithm is then employed to determine the optimum distribution of pre-defined materials over the design region. Recently, a TO method based on the Normalized Gaussian Network is introduced [5]. The method is incorporated in JMAG-Designer software, employed in this paper for TO of the RMG. The design region of the TO of the RMG is the variable reluctance rotor (Fig. 2a). The TO algorithm has converged to rectangular iron teeth and non-ferromagnetic material core (Fig. 2b). Compared to the optimized conventional RMG, the new topology offers 5% increase in the volumetric torque density, 25% increase in GTD, and 20% decrease in eddy current losses. The full paper will include TO for RMG with different gear ratios as well as a comparison between the new topology and the conventional topology in terms of GTD, PM utilization and efficiency.

[1] K. Aiso, K. Akatsu and Y. Aoyama, "A Novel Reluctance Magnetic Gear for High-Speed Motor," IEEE Transactions on Industry Applications, vol. 55, no. 3, pp. 2690-2699, May-June 2019, doi: 10.1109/TIA.2019.2900205. [2] S. A. Afsari Kashani, "Design and Optimization of Coaxial Reluctance Magnetic Gear with Different Rotor Topologies," IEEE Transactions on Industrial Electronics, doi: 10.1109/TIE.2021.3053886. [3] K. Li, Z. Zhu and P. Wu, "A Reluctance Magnetic Gear for High Speed and Vibration Motor Systems," in Proc. 2018 25th International Conference on Mechatronics and Machine Vision in Practice (M2VIP), 2018, pp. 1-5, doi: 10.1109/M2VIP.2018.8600905. [4] S. Hasanpour, M. C. Gardner, M. Johnson and H. A. Toliyat, "Comparison of Reluctance and Surface Permanent Magnet Coaxial Magnetic Gears," in Proc. 2020 IEEE Energy Conversion Congress and Exposition (ECCE), 2020, pp. 307-314, doi: 10.1109/ECCE44975.2020.9236066. [5] T. Sato, K. Watanabe and H. Igarashi, "Multimaterial TO of electric machines based on normalized Gaussian network," IEEE Transactions on Magnetics, vol. 51, no. 3, pp. 1-4, March 2015, Art no. 7202604, doi: 10.1109/TMAG.2014.2359972.

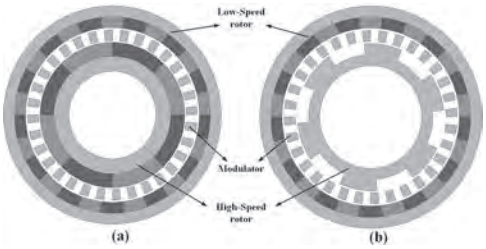

Fig. 1. (a) PM MG; (b) Conventional RMG.

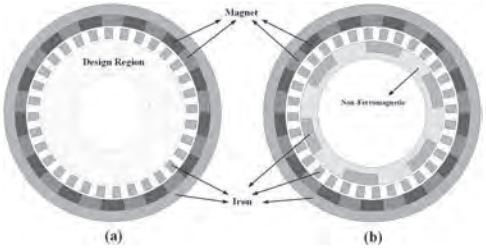

Fig. 2. (a) TO model of the conventional RMG; (b) Optimum topology.

JPE-09. 12/10 Switched Reluctance Motor with a Hex Connection.
H. Suzuki[1], K. Hirata[1], N. Niguchi[1] and N. Takemura[1] *1. Graduate School of Engineering, Osaka University, Osaka, Japan*

1. Introduction A 12-slot-8-pole switched reluctance motor (SRM) has benefits in many applications due to no permanent magnet, low-cost, and simple and robust rotor structure [1]-[4]. However, noises and vibrations of the 12/8 SRM are large due to its large torque ripple. In order to solve this problem, a 12/10 SRM with a star connection has been proposed, which has less torque ripple [5], [6]. In this paper, we propose a 12/10 SRM with a hex connection. The hex connection does not need a neutral point, and the stator has a short coil end height. Therefore, the size of the motor with the hex connection becomes smaller. The characteristics of the hex connection was compared with the star connection through 2D finite element analysis. 2. Comparison Fig. 1 shows a 12/10 SRM, inverter, hex and star connections. The stator has a 6-phase concentrated winding from A-phase to F-phase, and the in-phase coils are connected in series. The torque ripple and efficiency of the 12/10 SRM with hex and star connections are compared, where the voltage application timing is adjusted to satisfy an output power of 1 kW. Figs. 2 (a), (b) and (d) show the torque and current waveforms, and efficiency, respectively. Fig. 2 (c) shows the ratio of each harmonic component against the fundamental component in the coil current. From Fig. 2 (a), the torque ripple ratio of the hex connection model is less than that of the star connection model. This is because, from Fig. 2 (c), the coil current of the hex connection model has the third harmonic components. From Fig. 2 (d), the efficiency of the hex connection model is larger than that of the star connection model. This is because, from Fig. 2 (c), the ratio of the DC and fundamental components in the coil current is different between the hex and star connection models. 3. Conclusion A 12/10 SRM with the proposed hex connection is superior to that with the conventional star connection in terms of a torque ripple and efficiency. In the final paper, the difference between hex and star connections is theoretically described using a mathematical model. Furthermore, their load characteristics are compared by carrying out measurements on a prototype.

[1] J. Li, X. Song, Y. Cho, "Comparison of 12/8 and 6/4 Switched Reluctance Motor: Noise and Vibration Aspects," IEEE Trans. Magn., vol. 44, no.11, pp. 4131 - 4134, Nov. 2008. [2] C. Moron, A. Garcia; E. Tremps, J. A. Somolinos, "Torque Control of Switched Reluctance Motors," IEEE Trans. Magn., vol. 48, no.4, pp. 1661-1664, April. 2012. [3] G. J. Li; X. Y. Ma; G. W. Jewell; Z. Q. Zhu; P. L. Xu, "Influence of Conduction Angles on Single-Layer Switched Reluctance Machines," IEEE Trans. Magn., vol. 52, no.12, pp. 1-11, Dec. 2016. [4] Q. Sun, J. Wu, C. Gan, "Optimized Direct Instantaneous Torque Control for SRMs With Efficiency Improvement," IEEE Trans. Ind. Electron., vol. 68, no.3, pp. 2072 - 2082, March. 2021. [5] A. Kohara, K. Hirata, N. Niguchi, Y. Ohno, "Finite-Element Analysis and Experiment of Current Superimposition Variable Flux Machine Using Permanent Magnet," IEEE Trans. Magn., vol. 57, no.9, pp. 1-7, Sept. 2016. [6] A. Kohara, K. Hirata, N. Niguchi, "Vibration Comparison of Current Superimposition Variable Flux Machine and Switched Reluctance Machine," IEEE ICEM, Greece, AF-004677, pp.2337-2342, Sept. 2018.

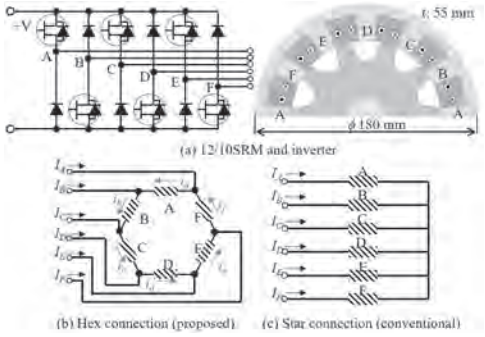

Fig. 1 Our proposed 12/10 SRM.

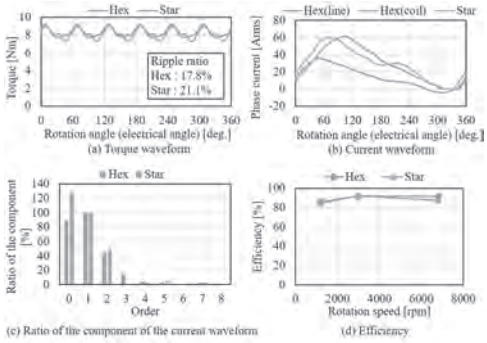

Fig. 2 Analysis result.

JPE-10. Torque Characteristic of Switched Reluctance Motor with Hybrid Excitation Segmented Rotor.
L. Jing[1] and *Y. Rao*[1] *1. College of Electrical Engineering and New Energy, China Three Gorges University, Yichang, China*

Switched reluctance motor (SRM) is a kind of doubly salient variable reluctance motor, which has the advantages of simple structure, reliable operation and large starting torque. The motor has the problem of large torque ripple, which causes vibration and noise during operation. In order to reduce torque ripple, a switched reluctance motor with hybrid excitation segmented rotor (HESSRM) is presented in this paper. Firstly, in HESSRM, aluminum block is used instead of silicon steel sheet rotor, the fan-shaped rotor core is

embedded into the non-magnetic aluminum block, and stator has full pitch three phase windings. The permanent magnet is embedded in the stator tooth and its magnetization direction is consistent with the excitation direction of the winding. Secondly, in order to further reduce the torque ripple, the switch-on and switch-off angles of the power converter should be optimized. Finally, a three-phase 12/8 pole HESSRM model is established. Through parametric simulation, the optimal position and size of the permanent magnet are obtained, and the electromagnetic properties of the motor such as flux linkage, air gap magnetic field and torque are calculated. Compared with the conventional SRM, the average output torque of the proposed HESSRM is increased by 36.49% and the torque ripple is reduced by 36.41%.

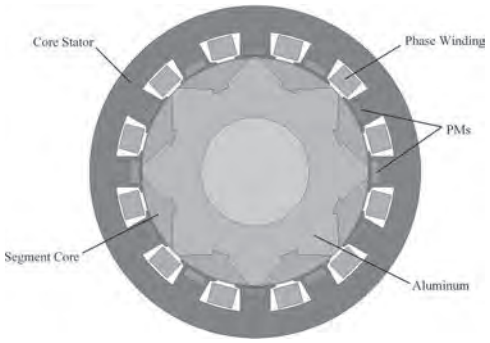

Topology of HESSRM

To illustrate the torque ripple, the Tripple parameter is defined as follows

$$T_{ripple} = (T_{max} - T_{min}) / T_{avg}$$

where T_{max} , T_{min} and T_{avg} are the maximum, minimum and average value of the output torque, respectively.

Compared with the conventional SRM, The results of two models are listed in Table 1:

Table 1. Torque comparison

	T_{min} (N·m)	T_{max} (N·m)	T_{avg} (N·m)	T_{ripple}
SRM	55.28	213.80	163.86	96.74%
HESSRM	162.60	300.18	223.65	61.52%

Torque comparison

JPE-11. Modeling and Simulation of Switched Reluctance Machine with Less and More Input Data: An Experimental Investigation.
A. Memon[1], K. Abro[1], *S. Bukhari*[3,2] and J. Ro[2] *1. Mehran University of Engineering and Technology Jamshoro, Jamshoro, Pakistan; 2. Chung-Ang University, Seoul, The Republic of Korea; 3. Sukkur IBA University, Sukkur, Pakistan*

A MATLAB environment-based mathematical model of a 4-phase Switched Reluctance Machine (SRM) with variable input data samples that were directly obtained from experimental data of flux linkage and static torque respectively is presented. The main objective of this research is to investigate the performance of the machine with less experimental data that is only possible with measuring instruments within accuracy and precision and extended data obtained through simulation. Firstly, the necessary experimental input data are discussed. Then, these data points are extended for a range of current and rotor positions. The accuracy of the results is verified by comparing the simulated current and torque profile of the machine with an experimental current profile. Experimental Data Experimental data of flux linkage $\psi(\theta, i)$ and static torque $T(\theta, i)$ in graphical form is shown in Fig. 1. The performance investigation of SRM under single-pulse mode operation relies on the following idea: 1) Extended data with more data samples through simulation by using interpolation methods. 2) Experimental data with fewer samples, which constitute the novel idea of this study. Previous studies [1-2] produced results through the inclusion of extended input data tables alone through interpolation. ■ The experimental and less simulated data matching to experimental data samples of flux linkage and static torque were included in the mathematical model. ■ The extended data of flux linkage and static torque obtained through simulation using interpolation were included in the mathematical model. ■ Switch on = –37°, Switch off = –7°, Resistance = 3.37 Ω, Speed = 312 rpm Fig.2 (a) shows simulations of applied voltage, flux, current, and torque profile for extended data and Fig 2(b) depicts the same with reduced data (experimental and simulated with fewer samples). Fig. 2(c) is an ample view of the experimental current profile for validation purpose. It can be seen from these figures that Fig. 2(a) matches with Fig.2(c) and there is a significant mismatch in Fig.2(b). Conclusion This research has experimentally investigated the performance of SRM with fewer and more data. The trend of results has shown accuracy with more data and mismatch with fewer data.

1. Memon, Ali Asghar, Syed Sabir Hussain Bukhari, and Jong-Suk Ro. "Experimental Determination of Equivalent Iron Loss Resistance for Prediction of Iron Losses in a Switched Reluctance Machine." *IEEE Transactions on Magnetics* (2021). 2. Diao, Kaikai, Xiaodong Sun, Gang Lei, Youguang Guo, and Jianguo Zhu. "Multiobjective system-level optimization method for switched reluctance motor drive systems using finite-element model." *IEEE Transactions on Industrial Electronics* 67, no. 12 (2020): 10055-10064.

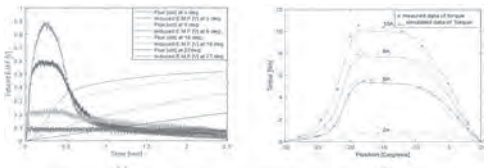

Fig. 1. Experimental data of: (a) E.M.F and computed data of flux, and (b) Static torque.

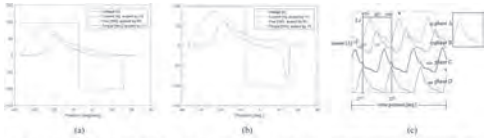

Fig. 2. simulations of applied voltage, flux, current and torque profile (a) with extended more data, (b) with experimental data, and (c) experimental current waveform.

JPE-12. A Study on High Efficiency Design by Reducing Rotor Iron-Loss of Synchronous Reluctance Motor.
J. Lee[1], K. Lee[1] and D. Jung[2] *1. Korea Electronics Technology Institute, Bucheon, The Republic of Korea; 2. School of Smart Mobility, Halla University, Wonju, The Republic of Korea*

1. Introduction Synchronous reluctance motor (SynRM) is a typical non-rare earth motor that generates reluctance torque by using the inductance difference that occurs due to the shape of a segment composed of a barrier and iron core composed of air gaps inside the rotor. Synchronous reluctance motor is composed of laminated core and copper, has a simpler structure and manufacturing process than induction motor, and does not generate secondary copper loss, so it is attracting attention as a motor that can secure IE4 or higher efficiency by replacing induction motor. In this paper, a detailed analysis of the iron loss occurring in the rotor was conducted and a reduction method was proposed. 2. *A study on the cause and improvement of rotor iron loss through harmonic analysis* Synchronous reluctance motor, a significant amount of rotor iron loss occurs. The causes of rotor iron loss were analyzed. Figure 1(a) shows the rotor shape. In order to confirm the distribution of iron loss inside the rotor, detailed analysis was conducted by dividing the rotor into segments and outer parts including ribs. Figure 1(b) is the result showing the percentage of iron loss by rotor element, and it can be seen that nearly 80% of the total iron loss occurring in the rotor occurs outside the rib structure. Figure 2 shows the magnetic flux change according to the movement of the rotor, and the cause of the iron loss was analyzed to be due to the spatial harmonics caused by the slot shape of the rotor and the stator, and a reduction method was studied. [1] - [2] 3. Conclusion In this paper, a method for high-efficiency design of SynRM was studied. It was confirmed that the saturation and release of magnetic flux were repeated when the rotor of SynRM passed through the slot of the stator at the lip according to the rotation. The factors were studied in detail through harmonic analysis, and a method for reducing iron loss through improvement of rib shape was proposed. In the full paper, the validity of this study was verified through the details of the study and actual production and testing.

[1] K. Yamazaki and Y. Seto, "Iron Loss Analysis of Interior Permanent-Magnet Synchronous Motors—Variation of Main Loss Factors Due to Driving Condition," *IEEE Trans. Ind. Appl.*, vol. 42, no. 4, pp. 1045-1052, 2006. [2] K. Yamazaki, Y. Fukushima and M. Sato, "Loss Analysis of Permanent-Magnet Motors With Concentrated Windings—Variation of Magnet Eddy-Current Loss Due to Stator and Rotor Shapes," *IEEE Trans. Ind. Appl.*, vol. 45, no. 4, pp. 1334-1342, 2009.

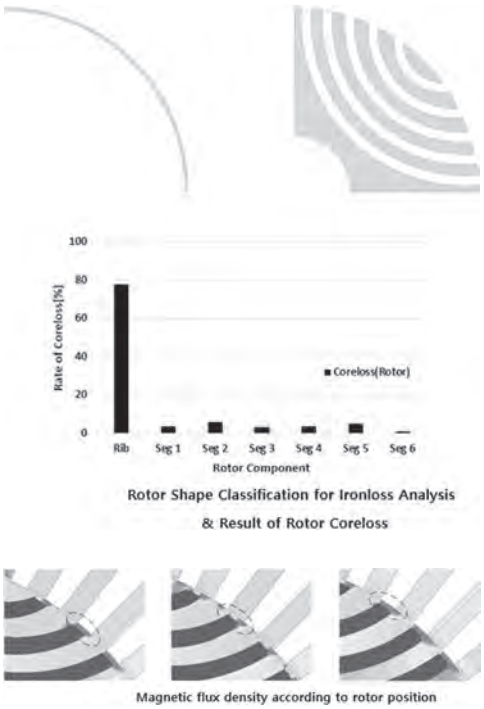

JPE-13. Core Loss Analysis of Switched Reluctance Motor Considering Hysteresis Effect. L. Chen[1,2], *Z. Zou*[1] and T. Ben[1] *1. College of Electrical Engineering and New Energy, China Three Gorges University, Yichang, China; 2. State Key Laboratory of Reliability and Intelligence of Electrical Equipment, Hebei University of Technology, Tianjin, China*

The magnetic circuit of switched reluctance motor(SRM) has a non-sinusoidal structure, and the switching performance of the control circuit changes with the period, resulting in complex electromagnetic performance, therefore, it is difficult to accurately calculate the core loss of SRM. Considering that SRM is affected by both alternating magnetization and rotational magnetization, an improved vector Play model is proposed for finite element analysis. This model not only satisfies the rotational hysteresis loss property but also improves the calculation accuracy of the core loss in the alternating field[1]. The traditional loss separation model can get accurate results for core loss calculation of motor under sinusoidal excitation, but this method can not be fully applied to the SRM under non-sinusoidal excitation. To verify the accuracy of the finite element simulation results, the magnetic flux density of stator and rotor core of SRM is decomposed into radial component and tangential component, The finite element model of SRM and the flux density waveform of typical points are shown in fig.1 and fig.2 respectively. For eddy current loss and excess loss, Fourier decomposition method is used to decompose the radial component and tangential component flux density of the motor into a series of sinusoidal magnetic density waveform, which is calculated by accumulation. For hysteresis loss, the equivalent elliptic loop(EEL) method was used to model the hysteresis loop in time domain[2]. This model divides the magnetic field intensity into reversible component and irreversible component, therefore, the calculation accuracy of dynamic hysteresis loss is improved. The accuracy of the improved vector Play model can be verified by comparing the results of core loss calculation with the finite element simulation results.

[1]D. Lin, P. Zhou and A. Bergqvist, "Improved Vector Play Model and Parameter Identification for Magnetic Hysteresis Materials," in *IEEE Transactions on Magnetics*, vol. 50, no. 2, pp. 357-360, Feb. 2014, Art no. 7008704, doi: 10.1109/TMAG.2013.2281567. [2]D. Lin, P. Zhou, W. N. Fu, Z. Badics and Z. J. Cendes, "A dynamic core loss model for soft ferromagnetic and power ferrite materials in transient finite element analysis," in *IEEE Transactions on Magnetics*, vol. 40, no. 2, pp. 1318-1321, March 2004, doi: 10.1109/TMAG.2004.825025.

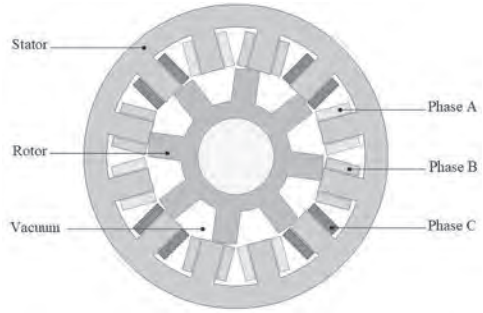

Fig.1 A two-dimensional model of a 12/8 structure switched reluctance motor

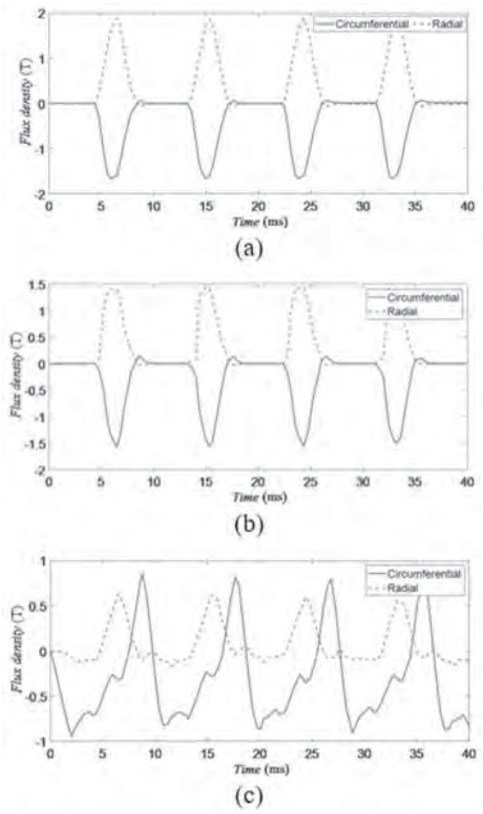

Fig.2 (a) Magnetic flux density waveform of stator pole (b) magnetic flux density waveform of rotor pole (c) magnetic flux density waveform of rotor yoke

JPE-14. A Novel Slot-PM-assisted Consequent-pole-PM Doubly-salient Machine with Hybrid Magnets of Ferrite PMs and Rare-earth PMs. *J. Jiang*[1] and S. Niu[1] *1. Electrical engineering department, The Hong Kong Polytechnic University, Hong Kong, Hong Kong*

Introduction Doubly-Salient machines (DSMs) have simple structure which provides high mechanical robustness and control flexibility, thus are suitable for wind power application [1-2]. However, due to the shortage of rare-earth

resources, the rare-earth PM material becomes more and more expensive. In order to reduce the machine cost, decreasing the usage of rare-earth PMs without sacrificing steady torque becomes a hot topic. Consequent pole concept, which uses only half of the PMs with the same magnetization direction, is proposed to save the dosage of PMs [3-4]. Furthermore, rare-earth PMs are replaced with ferrite PMs to avoid the usage of rare earth resources. In this paper, slot-PM-assisted consequent-pole-PM doubly-salient machine (SPMA-CPM-DSM) is proposed. The key is that the consequent-pole ferrite PMs are employed in the stator yoke to reduce the cost and small amount of tangential magnetized rare-earth PMs is placed in the slot opening to improve the torque production. This proposed hybrid magnet design can greatly enhance the PM utilization ratio and reduce PM cost without sacrificing the steady torque. Machine configuration Fig. 1 shows the configuration of three machines. For the conventional DSM, the polarity of yoke ferrite PMs alternates around the circle. For CPM-DSM, the yoke ferrite PMs of one polarity remain while the yoke ferrite PMs of another polarity are replaced with iron core. For SPMA-CPM-DSM, based on the structure of CPM-DSM, tangential magnetized slot rare-earth PMs are added to further enhance the steady torque. Electromagnetic performance Fig. 2 shows the electromagnetic performance of three machines. It can be seen that the flux linkage amplitude, back-EMF amplitude, as well as average torque of CPM-DSM is almost the same as that of conventional DSM. Since the PM usage of CPM-DSM is half of that of conventional DSM, consequent pole structure can reduce the ferrite PM usage without sacrificing the electromagnetic performance of the machine. In addition, with the employment of slot rare-earth PMs, the flux linkage amplitude, back-EMF amplitude, as well as average torque of SPMA-CPM-DSM is 79% higher than that of CPM-DSM, denoting the torque enhancing ability of slot PMs.

[1] Y. Zhao, D. Teng, and D. Li, "Comparative Research on Four-Phase Dual Armature-Winding Wound-Field Doubly Salient Generator with Distributed Field Magnetomotive Forces for High-Reliability Application," *IEEE Access*, vol. 9, pp. 12579-12591, 2021. [2] C. Shi, H. Wang and W. Liu, "Sensorless Control Method for Wound-Field Doubly Salient Starter/Generator with Two-section Interlaced-Rotor Structure," 2019 IEEE International Electric Machines & Drives Conference (IEMDC), 2019, pp. 254-259. [3] Consequent-Pole Vernier Machine With Hybrid Excitation and DC-Biased Sinusoidal Current," *IEEE Trans. Magn.*, vol. 53, no. 6, pp. 1-4, June 2017. [4] Y. Li, H. Yang, and H. Lin, "Investigation of Double-Side Field Modulation Mechanism in Consequent-Pole PM Machines with Concentrated Windings," *IEEE Trans. Energy Convers.*, pp.1-1, Dec. 2020.

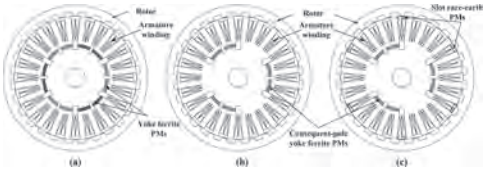

Fig. 1

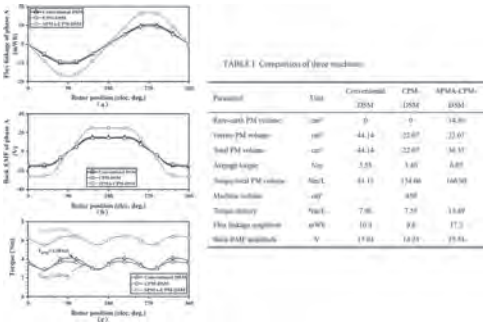

TABLE I Comparison of three machines

Parameter	Unit	Conventional DSM	CPM-DSM	SPMA-CPM-DSM
Rare-earth PM volume	cm^3	0	0	14.86
Ferrite PM volume	cm^3	44.14	22.07	22.07
Total PM volume	cm^3	44.14	22.07	36.93
Airgap length	l_{ag}	5.55	5.45	5.65
Torque/total PM volume	Nm/L	61.11	134.66	160.50
Machine volume	cm^3		650	
Torque density	Nm/L	7.08	7.55	13.69
Flux linkage amplitude	mWb	10.1	9.8	17.3
Back-EMF amplitude	V	17.01	14.21	25.51

Fig. 2

Session JPF
VERNIER MACHINES
(Poster Session)

Shuangxia Niu, Chair
The Hong Kong Polytechnic University, Kowloon, Hong Kong

JPF-01. A Magnetic Variable Speed Permanent Magnet Vernier Motor with Unequal Halbach Array and Non-uniform Air Gap. L. Jing[1] and *W. Tang*[1] *1. College of Electrical Engineering and New Energy, China Three Gorges University, Yi chang, China*

Aiming at the problems of high cost and high operational risk of traditional direct-drive motors at low speed and large torque output, an unequal Halbach array non-uniform air gap magnetic variable speed permanent magnet vernier motor is proposed in this paper, which makes full use of the internal space in coaxial magnetic gear, the coaxial magnetic gear and the bilateral permanent magnet excitation vernier motor are combined. Two sets of permanent magnets were placed on the stator and outer rotor respectively, and the permanent magnet magnetic field could be modulated to effective harmonic magnetic field components with a low pole-pair number and high speed by the dual-modulation effect of stator and outer rotor teeth. Then the armature winding was designed according to the effective harmonic magnetic fields to achieve the coupling between the magnetic fields excited by two sets of permanent magnets and armature windings. According to the principle of magnetic field modulation and unilateral magnetization effect, the unequal Halbach arrays could augment the magnetic field in the inner air gap. Moreover, the permanent magnets of the eccentric structure could obtain a non-uniform air gap, which is helpful to enhance the flux-modulation effect. The structural parameters such as the circumferential width and the radial height of the stator teeth that affect the performance of the motor are optimized. A two-dimensional model of the motor was established, and its output torque, no-load back-EMF, and air gap magnetic density were analyzed by the finite element method. The simulation results verified the correctness of the theoretical analysis.

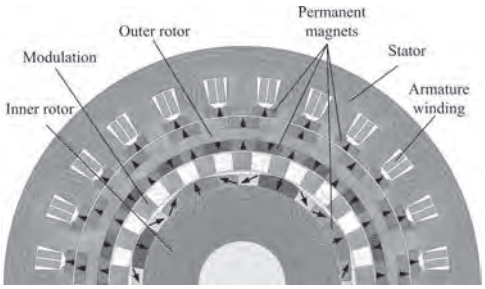

Fig. 1 The topology of an unequal Halbach array non-uniform air gap magnetic variable speed permanent magnet vernier motor

Table 1. Torque

	T_{max}/(N·m)	T_{min}/(N·m)	T_{ave}/(N·m)	K_T
Inner torque	60.75	61.28	61.03	0.87%
Outer torque	195.01	204.83	200.17	4.91%

T_{max}, T_{min}, T_{ave} are the maximum, minimum, average value of the output torque ripple respectively and K_T is torque ripple.

Table.1 Torque

JPF-02. A Novel Stator-PM Consequent-pole Dual Stator/Rotor Armature Winding Flux Modulated Machine for Multi-Torque Components. S. Jia[1], *S. Feng*[1], D. Liang[1] and X. Dong[1] *1. Xi'an Jiaotong University, Xi'an, China*

Abstract—This paper proposes a novel stator-PM consequent-pole dual stator/rotor armature winding flux modulated machine with the dc-biased current. Due to both armature windings and consequent-pole stator-PM interact with each other, this proposed machine contains six torque components. Compared with traditional stator permanent magnet machines and flux modulated machines, this machine makes full use of the space in the rotor cavity and giving full play to the flux modulation effect. *Keywords*—Hybrid excitation, DC-biased current, dual armature winding vernier machine. I. Introduction Recently, stator permanent magnet machines are gaining more and more research attention for their benefit of a robust rotor structure[1]. In the meantime, the flux modulated machines due to the natural high torque density characteristic are gaining more research interest, too [2]. Combining the advantages of both machines, the DC-biased hybrid excitation stator PM vernier machines (HEPMVMs) are proposed [3]. Compared with the stator PM machines, the DC-biased HEPMVMs improve the shortcomings of the inherent limited magnetic field adjustment ability, meanwhile, improve the torque density. However, these machines don't make full use of the space in the rotor cavity, and the reliability of torque output is poor, due to only contain stator armature winding. In this paper, the topology of DC-biased hybrid excitation consequent-pole stator-PM dual stator/rotor armature winding vernier machine (DAWVM) is proposed. As shown In Fig. 1, the stator has two-phase DC-biased winding and the teeth located PMs alternately, the rotor has three-phase winding. Therefore, high torque will be generated. The drive circuit, operation principle, and electromagnetic characteristics will be illustrated in the full paper. II. Electromagnetic Performance Evaluation The simulation results of flux density, back-EMF, and electromagnetic torque are analyzed by finite element analysis (FEA). The no-load flux distribution is shown in Fig. 2. The back-EMF and electromagnetic torque with various excitation modes are shown in Fig. 3. This machine exhibits larger torque due to containing six torque components, which will be illustrated in the full paper.

[1] Z. Zhu, H. Hua, D. Wu, J. Shi, and Z. Wu, *IEEE Trans. Ind. Appl*., vol. 52, no. 1, pp. 199–208, Jan./Feb. 2016. [2] S. Jia, R. Qu, W. Kong, D. Li, and J. Li, *IEEE Trans. Ind. App.*, vol. 54, no.2, Jul./Aug., pp:3187-3196, 2018. [3] S. Jia et al., *IEEE Trans. Ind. Appl.*, vol. 54, no. 2, pp. 1339-1348, March-April 2018.

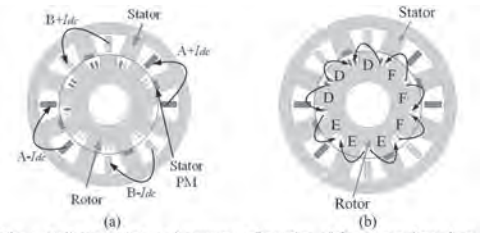

Fig. 1. Coil connections and current configuration of the proposed topology. (a) Stator part winding connection. (b) Rotor part winding connection.

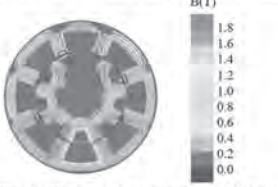

Fig. 2. No-load flux distributions when the stator DC/AC current is 14/0 A, rotor current is 0A.

Fig. 1 & Fig. 2

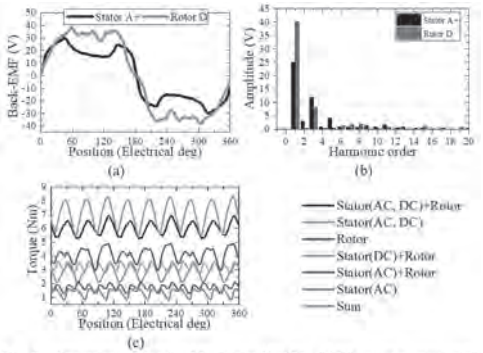

Fig. 3. Comparison of back-EMF (stator DC/AC: 14/0A, rotor current: 0A) and electromagnetic torque (stator DC/AC: 14/14A, rotor current: 15A). (a) back-EMF waveforms. (b) back-EMF harmonics. (c) Torque waveforms with various excitation modes.

Fig. 3

JPF-03. A Dual Armature Winding Vernier Reluctance Machine with Stator Five-phase DC-biased Current. S. Jia[1], *S. Feng*[1], Z. Liu[1] and D. Liang[1] *1. Xi'an Jiaotong University, Xi'an, China*

Abstract—This paper proposes a novel dual armature winding vernier reluctance machine (DAWVRM) with stator five-phase DC-biased current. Due to the dual stator/rotor armature winding, this proposed machine can produce four different torque components which make the machine has a larger torque density and high fault-tolerant. Meanwhile, due to the five-phase DC-biased current of the stator winding, the fault-tolerant ability of the machine is further improved. *Index Terms*—Dual armature winding, Five-phase DC-biased current, Multi-torque components, Vernier reluctance machine. I. Introduction To improve the torque density and realize better rotor space utilization, flux reversal machines (FRM) with armature windings wound on both stator and rotor teeth were proposed in [1], [2]. Compared with conventional FRM, that machine can yield 60% higher torque density. Meanwhile, the three-phase DC-biased current vernier reluctance machine (DC-biased VRM) is proposed and studied due to the higher torque density compared with the conventional VRM [3]. To satisfy both the high torque density and high fault-tolerant, the method of multi-torque components output can be adopted. In this paper, the topology of DAWVRM with stator five-phase DC-biased current is proposed. As shown In Fig. 1, the stator has five-phase DC-biased winding and the rotor has three-phase winding. As a result, four different torque components will be generated. The operation principle and electromagnetic analysis will be illustrated in the full paper. II. Electromagnetic Performance Evaluation The electromagnetic performance of the machine is predicted by FEA. The no-load flux distribution is shown in Fig. 2, and the maximum magnetic density in the yoke is 1.4T. The back-EMF of stator and rotor windings are shown in Fig. 3, and the output torque is shown in Fig. 4. When the stator rotor windings are excited simultaneously, the output torque (torque ripple) is 5.42Nm (0.116). When the stator/rotor is excited separately, the output torque is 1.61Nm/1.55Nm. This machine exhibits a larger torque density and high fault-tolerant due to containing four torque components, which will be illustrated in the full paper.

[1] Y. Zheng et al., *IEEE Trans. Magn.*, vol. 57, no. 2, pp. 1-6, Feb. 2021 [2] L. Wu et al., *IEEE Trans. Ind. Electron.*, vol. 68, no. 6, pp. 4780-4789, June 2021. [3] S. Jia et al., *IEEE Trans. Ind. App.*, vol. 54, no.2, Jul./Aug., pp:3187-3196, 2018.

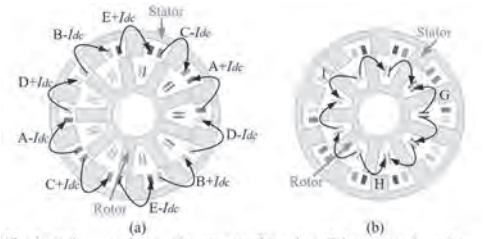

Fig. 1. Coil connections and current configuration of the proposed topology. (a) Stator part winding connection. (b) Rotor part winding connection.

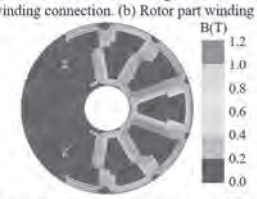

Fig. 2. No-load flux distributions when the stator DC/AC current is 8/0 A, rotor current is 0A.

Fig. 1 & Fig. 2

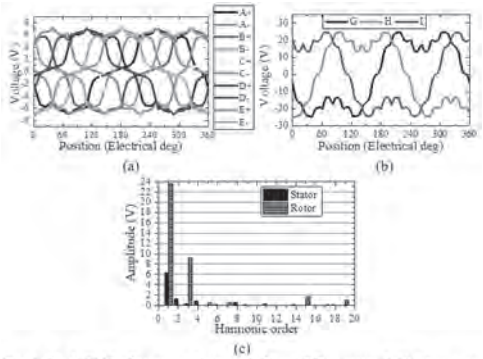

Fig. 3. Back-EMF of stator and rotor windings (When stator DC/AC current: 8/0A, rotor current: 0A). (a) Stator back-EMF waveforms. (b) Rotor back-EMF waveforms. (c) Back-EMF harmonics.

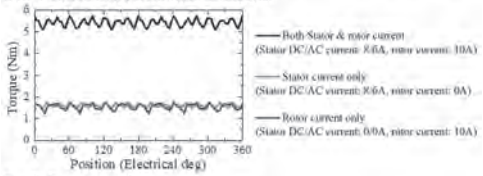

Fig. 4. Torque waveforms.

Fig. 3 & Fig. 4

JPF-04. A New Staggered Dual Stator Field Modulation Machine with O-Shape Permanent Magnet Excitation. H. Wang[1], *H. Zhu*[1], Z. Li[1], S. Chen[1] and S. Ding[1] *1. Nanjing Normal University, Nanjing, China*

In field modulation machine (FMM), the high speed armature magnetic field is modulated to couple with a low speed magnetic field generated by rotor with multiple pole-pair number of permanent magnets (PMs) for high output torque [1]. In order to increase torque production furtherly, dual stator FMM (DSFMM) is proposed, which can fully utilize space and PMs [2]. Another approach to enhance torque production is to increase airgap flux density by

using interior PM (IPM) or bilateral PM (BPM) arrangements in DSFMMs [3]. However, DSFMM excited by IPM or BPM alone can not achieve high sinusoidal airgap magnetic field. This paper proposes a new staggered DSFMM with O-shape PM arrangement (ODSFMM), which provides high sinusoidal airgap magnetic field for high quality torque production. Two radially magnetized PMs with opposite polarity are sandwiched between two tangentially magnetized PMs with opposite polarity, which forms the proposed O-shape PM arrangement for high sinusoidal airgap magnetic field with high flux density. The inner stator is rotated along shaft to form staggered DS structure for flux leakage reduction. The angle between the central axes of inner and outer stator teeth (α) is 15°. The open stator teeth play the role of modulation poles to modulate the magnetic field excited by O-shape PMs. The stator of the proposed machine employs three-phase 12-slot/2-pole single layer integral-slot distributed windings for high slot utilization and back electromotive force (EMF). To verify the merits of the proposed ODSFMM that is simply referred as Model I, the DSFMM with BPM excitation (simply referred as Model II) and with unrotated inner stator (simply referred as Model III) are designed, which share identical key design parameters, such as the volume of PM, outer radius, airgap length, and active stack length. The back-EMF, cogging torque, steady torque at rated state and steady torque at different current angles of the proposed designs are analyzed using finite element analysis (FEA). The FEA-predicted results show that the proposed ODSFMM can provide high sinusoidal back-EMF waveforms with high amplitude and high torque production with low torque ripple, which is desirable for accuracy operation applications.

[1] K. T. Chau, C. C. Chan, and C. Liu, "Overview of permanent-magnet brushless drives for electric and hybrid electric vehicles," *IEEE Trans. Ind. Electron.*, vol. 55, no. 6, pp. 2246-2257, Jun. 2008. [2] J. Kwon, and B. Kwon, "Investigation of dual-stator spoke-type vernier machine for EV application", *IEEE Trans. Magn.*, vol. 54, no. 11, pp. 1-5, Nov. 2018. [3] D. Li, R. Qu, and Z. Zhu, "Comparison of Halbach and dual-side vernier permanent magnet machines," *IEEE Trans. Magn.*, vol. 50, no. 2, pp. 801-804, Feb. 2014.

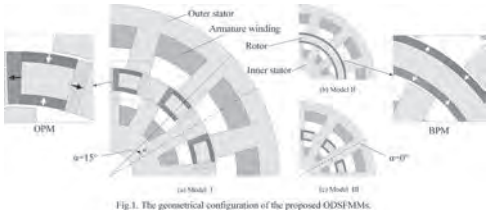

Fig.1. The geometrical configuration of the proposed ODSFMMs.

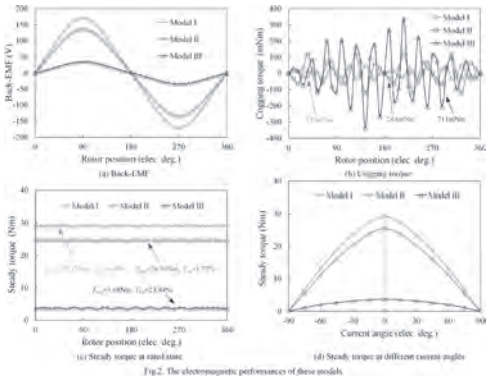

Fig.2. The electromagnetic performances of these models.

JPF-05. Withdrawn

JPF-06. A New Hybrid Magnet Dual Stator Field Modulation Machine With Different Split Ratios of Stators. H. Wang[1], *H. Zhu*[1], C. Wu[1], Z. Wei[1] and S. Ding[1] *1. Nanjing Normal University, Nanjing, China*

Field modulation machine (FMM) operates based on magnetic gear effect, which has the merit of high torque production at low operating speed [1]. Thus, FMM is suitable in direct-drive applications such as astronomical telescope and robot arms [2]. Hybrid magnet dual stator FMM (HMDSFMM) is developed for increasing output torque furtherly and obtaining high power factor [3]. Generally, the multiple-tooth stator is employed to increase split ratio for high torque density [4]. Nevertheless, the existing DSFMM with the same split ratio of inner and outer stators can not achieve the best electromagnetic performances. This paper proposes a new HMDSFMM with different split ratios of stators (DSR-HMDSFMM), which can achieve high quality torque production. The split tooth numbers of the outer and inner stators of the proposed DSR-HMDSFMM are designed as 2 and 3, respectively, which is expressed as K_1=[2,3]. The inner and outer stators using different split ratios take the advantage of reducing flux leakage and increasing torque quality. The total tooth numbers of inner stator is equal to that of outer stator because the same armature windings and PM excitation are used. The consequent pole rotor with NdFeB magnets establishes the main magnetic circuit for high PM utilization. Ferrite magnets are embedded between split teeth, which aim to enhance the airgap flux density and suppress the harmonic distortion. In order to find out the optimal combination of split ratios of stators, the proposed DSR-HMDSFMMs with K_2=[1,2], K_3=[1,3] and K_4=[2,2] are analyzed, which are simply referred as Model II, III, IV, respectively. Both of the inner and outer stators employ the three-phase 12-slot/2-pole integral-slot distributed double layer windings which can fully utilize slot space and high back electromagnetic force (EMF). The electromagnetic performances of proposed designs are analyzed by finite element analysis, including back-EMF, cogging torque, steady torque at rated condition and steady torque characteristics against current angle. The calculated results show that the proposed DSR-HMDSFMM with K_1=[2,3] exhibits the highest back-EMF and high quality torque production, which is suitable for the accuracy operation applications.

[1] A. Toba, and T. A. Lipo, "Generic torque-maximizing design methodology of surface permanent-magnet vernier machine," *IEEE Trans. Ind. Appl*., vol. 36, no. 6, pp. 1539-1546, Nov. 2000. [2] H. Wang, and S. Fang, "Design of new dual-stator field modulation machines," *IEEE Trans. Ind. Electron*., vol. 67, no. 7, pp. 5626-5636, Jul. 2020. [3] J. Kwon, and B. Kwon, "Investigation of dual-stator spoke-type vernier machine for EV application," *IEEE Trans. Magn.*, vol. 54, no. 11, pp. 1-5, Nov. 2018. [4] H. Wang, S. Fang, H. Yang, H. Lin, D. Wang, Y. Li, and C. Jiu, "A novel consequent-pole hybrid excited vernier machine," *IEEE Trans. Magn.*, vol. 53, no. 11, pp. 1-4, Nov. 2017.

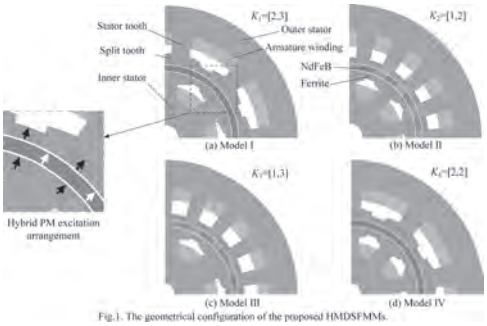

Fig.1. The geometrical configuration of the proposed HMDSFMMs.

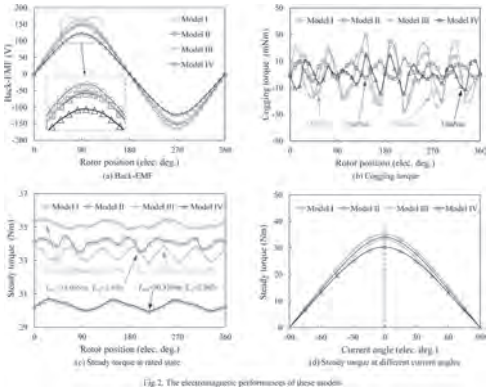

Fig. 2. The electromagnetic performances of these models

JPF-07. Torque Performances Improvement Method of Double-Stator Permanent Magnet Motor by Compensating Harmonic Torque.
D. Fan[1], L. Quan[1] and X. Zhu[1] *1. Jiangsu University, Zhenjiang, China*

Rare-earth permanent magnet motors have attracted considerable attention in the research field of electric vehicles (EVs), due to merits of high torque/power density, high efficiency. Nowadays, with the development of EVs, it poses critical design requirements for motors, like high torque and low torque ripple. In order to enhance motor torque density, V-shaped PM topology is adopted in [2]. In [3], multi-objective optimization is utilized to increase torque output and reduce torque ripple. It is noted that current research mainly focused on proposing novel motor topologies and utilizing motor optimization, while torque production mechanism is seldom considered. Consequently, it is necessary and important to improve motor torque performances based on motor operation principle. In this paper, based on flux modulation theory, a new torque performance improvement method is proposed for double stator permanent magnet (DS-FMPM) motor. In the proposed method, relationship between harmonic torque and output torque characteristics is investigated in detail. Then, by on optimization of motor design parameters, harmonic torque can be compensated purposefully, and enhanced output torque and reduced torque ripple can be realized simultaneously. Fig. 1 illustrates configuration of the investigated DS-FMPM motor. Fig. 2 shows the proposed torque performances improvement method by compensating harmonic torque. Fig. 3 shows contribution of different airgap flux harmonics for torque performances. It is observed that 14th airgap flux harmonic contributes to most of average torque, while 26th airgap flux harmonics result in torque ripple. Then, based on harmonic torque characteristics, multi-objective optimization is utilized to obtain optimal motor design, as shown in Fig. 4. Optimization results are obtained in Fig. 5 and Table I. It is observed that, by the compensation of harmonic torque of inner and outer motors, motor output torque is increased and torque ripple is decreased simultaneously, which verify the effectiveness of proposed torque performance improvement method. More detailed electromagnetic performance and experimental results will be presented in full paper.

[1] C. Liu, K. T. Chau, C. H. T. Lee, and Z. Song, "A critical review of advanced electric machines and control strategies for electric vehicles," *Proceedings of the IEEE*, doi: 10.1109/JPROC.2020.3041417. [2] W. Zhao, F. Zhao, T. A. Lipo, and B. Kwon, "Optimal design of a novel V-type interior permanent magnet motor with assisted barriers for the improvement of torque characteristics," *IEEE Trans. Magn.*, vol. 50, no. 11, Art. no: 8104504, Nov. 2014. [3] M. Seo, T. Lee, J. Kim, Y. Kim, and S. Jung, "Principal component optimization with mesh adaptive direct search for optimal design of IPMSM," *IEEE Trans. Magn.*, vol. 53, no. 6, Art. no: 8105604, Jun. 2017.

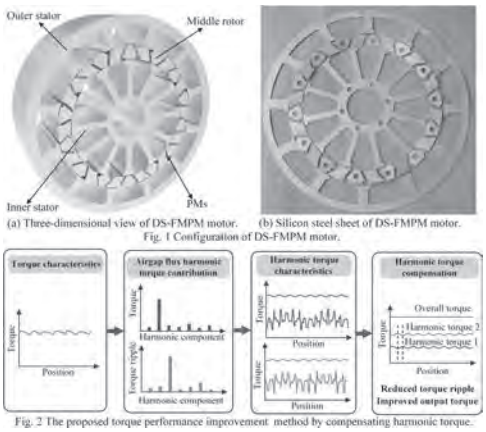

(a) Three-dimensional view of DS-FMPM motor. (b) Silicon steel sheet of DS-FMPM motor.

Fig. 1 Configuration of DS-FMPM motor.

Fig. 2 The proposed torque performance improvement method by compensating harmonic torque.

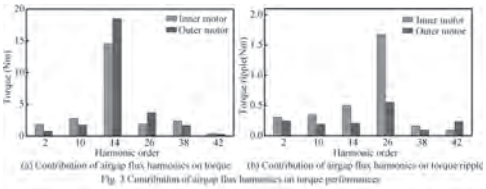

(a) Contribution of airgap flux harmonics on torque (b) Contribution of airgap flux harmonics on torque ripple

Fig. 3 Contribution of airgap flux harmonics on torque performances

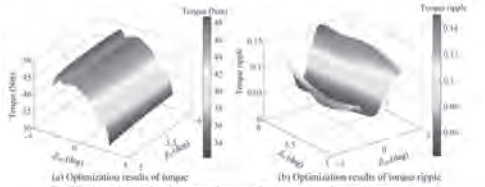

(a) Optimization results of torque (b) Optimization results of torque ripple

Fig. 4 Optimization results of torque performances by compensating harmonic torque

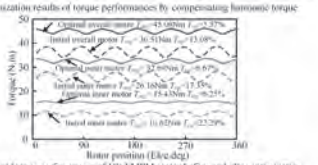

Fig. 5 Output torque performances of DS-FMPM motor before and after optimization.

TABLE I

COMPARISONS OF TORQUE PERFORMANCES BEFORE AND AFTER OPTIMIZATION

Average torque/Torque ripple		Before optimization	After optimization
28th Harmonic torque	Inner motor	8.72Nm/15.02%	4.64Nm/9.6%
	Outer motor	1.94Nm/28.63%	1.68Nm/26.45%
	Overall motor	5.67Nm/27.80%	6.32Nm/24.94%
Original torque	Inner motor	10.62Nm/22.29%	15.43Nm/6.25%
	Outer motor	26.16Nm/17.85%	32.69Nm/6.67%
	Overall motor	36.51Nm/13.08%	45.06Nm/5.57%

JPF-08. A New Hybrid Model for Copper Loss Analysis of Vernier Motor With Multi-Layer Winding. *Q. Chen*[1], Y. Fan[1] and Y. Lei[1]
1. School of Electrical Engineering, Southeast University, Nanjing, China

I. Introduction In the analysis of motor loss, the serious AC loss on the armature winding is caused by higher electric frequency, and this part of the loss is aggravated due to the end effect of the distributed winding, resulting in high-temperature rise, reducing motor efficiency and harming permanent magnet demagnetization [1-2]. Therefore, in the initial stage of design, the prediction of motor winding loss is particularly important. II. Analytical model In the calculation of active loss, due to the diversity of stator slot structures and the long span of distributed windings, the calculation is inconvenient. According to the principle of layering and area equivalence of windings, any stator slot model is equivalent to a semi-open rectangular slot, as shown in Fig. 1. The disorderly resistance in the slot is divided into n layers rectangles with equal height and width. Then, the boundary condition of the winding is used to solve the loss of the conductor in the slot. III. Hybrid loss computing model After calculating the loss of active winding, due to the difference of stator radius and winding span, the length of end passive winding is hard to calculate. so the analytical method is not accurate, and the 3-D FEM calculation is time-consuming. Therefore, the analytical method is not accurate, and the 3-D FEM calculation is time-consuming. Therefore, the end compensation winding is added to the analytical formula,

and the results obtained by the analytical method and the finite element method are iterated to obtain the compensation winding under the span, and the compensation windings with different spans are fitted. IV. Experimental verification To verify the above analysis, a double-layer short pitch winding vernier motor and platform are fabricated, as shown in Fig. 2. The loss of the motor is analyzed based on the power analyzer, and the experimental results are compared with the new calculation model. V. Conclusion The conductor loss in the slot can be predicted more accurately by layering the slot winding. For the end winding loss calculation, the FEM is added to form a hybrid calculation model, which makes the efficiency prediction more accurate.

[1] X. Xu, Z. Q. Deng and Z. M. Zhang. "Approximate Analytical Modeling and Verification of AC Loss in Stator Single Slot Windings of High-Speed Motor." Proceedings of the CSEE, 2021, 41(12): 4306-4315. [2] A. Lehikoinen, N. Chiodetto and E. Lantto. "Monte Carlo Analysis of Circulating Currents in Random-Wound Electrical Machines." IEEE Transactions on Magnetics, 2016, 52(8): 1-12.

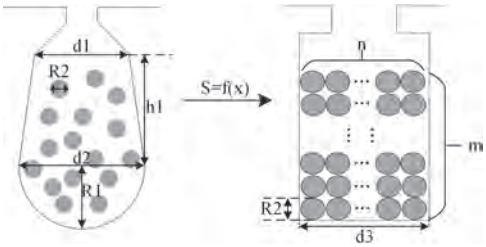

Fig.1 Slot geometry transformation

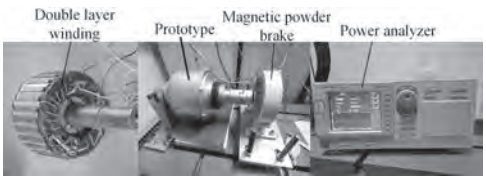

Fig.2 Experimental platform

JPF-09. Accurate Analytical Calculation of Magnetic Field of Permanent Magnet Vernier Motor. *B. Guo*[1], Y. Du[2], F. Peng[2], J. Dong[3], X. Qiu[1] and Y. Huang[2] *1. School of Electrical and Automation Engineering, Nanjing Normal University, NanJing, China; 2. School of Electrical Engineering, Southeast University, NanJing, China; 3. Faculty of Electrical Engineering, Delft University of Technology, Delft, Netherlands*

Permanent magnet vernier machine (PMVM), as one novel embranchment of low speed large torque permanent magnet synchronous machine (PMSM) based on flux modulation principle, which has broad application prospects in wind power generation, electric vehicles and other fields [1]. The flux modulation pole (FMP) is introduced into the stator tooth of the magnetic gear motor as the magnetic modulation ring in the magnetic gear motor [2], which makes the motor structure more complex, as shown in Fig. 1(a). Although the finite element method (FEM) has the advantages of high calculation accuracy, the modeling of complex geometric structure of the motor is time-consuming, and the solution speed is slow [3]. Fast and accurate calculation of the magnetic field of the PMVM, which is conducive to the rapid initial design and optimization of the PMVM. This paper proposes a sub-domain model for accurate calculation of PMVM magnetic field, which based on Schwarz-Christoffel mapping technique. Schwarz-Christoffel mapping is the transformation of a continuous line segment on the real axis of the w plane to the boundary of a polygon in the z plane and the upper half plane of the w plane to the interior of the polygon [4]. Through twice Schwarz-Christoffel mapping to get regular magnetic field graphics. Firstly, the z plane is transformed into the w plane; then the w plane is transformed to the t plane by the logarithmic transformation. The z-w-t plane correspondence is shown in Fig.2. The detailed derivation process will be presented in the full paper. In order to verify the correctness of the proposed PMVM magnetic field accurate subdomain model, the magnetic field calculation results of the FEM and the analytical model are compared. Fig.3 shows the FEM results of the radial component of air gap flux density under no-load and load conditions. The complete calculation results of the accurate subdomain model will be given in the full paper.

A. Toba, T. A. Lipo. Generic torque-maximizing design methodology of surface permanent-magnet vernier machine[J]. IEEE Transactions on Industry Applications, 2000, 36(6): 1539-1546. Zhang Yang. Study on Design and Analysis of Novel Permanent Magnet Vernier Wind Generator[D]. Southeast University, 2016. B. Guo, Y. Huang, F. Peng and J. Dong, "A New Hybrid Method for Magnetic Field Calculation in IPMSM Accounting for Any Rotor Configuration," in IEEE Transactions on Industrial Electronics, vol. 66, no. 7, pp. 5015-5024, July 2019, doi: 10.1109/TIE.2018.2868252. T. C. O'Connell and P. T. Krein, "A Schwarz–Christoffel-Based Analytical Method for Electric Machine Field Analysis," in IEEE Transactions on Energy Conversion, vol. 24, no. 3, pp. 565-577, Sept. 2009, doi: 10.1109/TEC.2009.2025412.

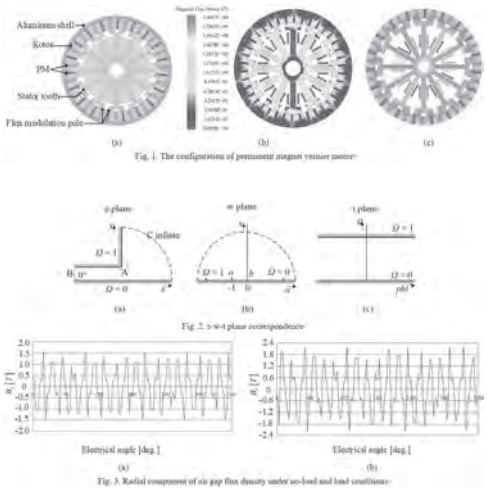

JPF-10. Torque Ripple Suppression of the Permanent Magnet Vernier Motor With Shifted Permeance Design. *T. Wang*[1], X. Zhu[1] and Z. Xiang[1] *1. Jiangsu University, Zhenjiang, China*

Due to the advantage of the high torque at low speed, the permanent magnet vernier motor (PMVM) has become an excellent candidate for low-speed direct-drive applications [1], such as electric vehicle, wind power generation and ship propulsion. To further improve the torque of the PMVM, a V-shaped PMVM (V-PMVM) is proposed in [2], which reveals that the high torque capability of the V-PMVM is resulted from the effective reduction of the flux leakage. However, because of the stator salient structure, the high torque ripple is still a major drawback for the V-PMVM. And, it is noted that, the large cogging torque is the main factor leading to torque ripple. Actually, with the development of magnetic field modulation (MFM) theory [3], the cogging torque of the PMVM can be explained by the MFM principle, where the cogging torque is essentially the result of the interaction of several air gap magnetic fields and cogging torque amplitude is proportional to the amplitude of the permeance. Thus, based on the MFM principle, a shifted permeance V-shaped PMVM (SPV-PMVM) is proposed to decrease the cogging torque and torque ripple in this paper. The topology of the SPV-PMVM with shifted permeance and its comparative structures are presented in Fig. 1(a). Fig. 1(b) shows the production process of the cogging torque of the PMVM. Then, based on the PM-MMF-shifted permeance model in Figs. 1(e) and (f), the theoretical calculation angles for cogging torque minimization are obtained and marked in Fig. 2(a). Further, the electromagnetic performances of these three motors are compared in Figs. 2(b)-(g). The SPV-PMVM has the largest back-EMF fundamental and the lowest THD. Meanwhile, compared to the V-PMVM, the cogging torque and torque ripple of the SPV-PMVM is reduced by 75% and 50%, with a slight increase in output torque. Compared to the S-PMVM, the output torque of

the SPV-PMVM is improved by 16.6%, while the torque ripple is kept in a similar level. Therefore, the SPV-PMVM cannot only effectively reduce the cogging torque and the torque ripple, but also make the back-EMF waveform more sinusoidal and the average output torque higher. More detailed theoretical analysis and simulation results will be presented in the full paper.

[1] Y. Ma and W. Fu, "Design and comparison of vernier permanent-magnet machines with different winding types based on fractional-slot windings," *IEEE Trans on Magn*, vol. 57, no. 6, pp. 1-5, Jun. 2021, Art no. 8105105. [2] D. Fan, L. Quan, X. Zhu, Z. Xiang, and H. Que, "Airgap-harmonic-based multi-level design and optimization of a double-stator flux-modulated permanent magnet motor," *IEEE Trans. Ind. Electron*., DOI: 10.1109/TIE.2020.3039207. [3] M. Cheng, P. Han, and W. Hua, "General airgap field modulation theory for electrical machines," *IEEE Trans. Ind. Electron.*, vol. 64, no. 8, pp. 6063-6074, Aug. 2017.

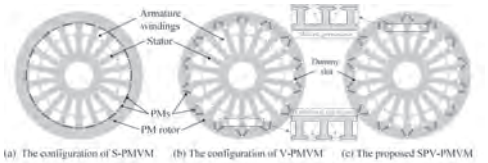

(a) The configuration of S-PMVM (b) The configuration of V-PMVM (c) The proposed SPV-PMVM

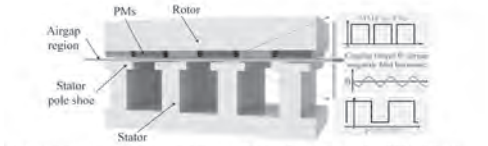

(d) The generation process of the cogging torque of PMVM based on magnetic field modulation principle

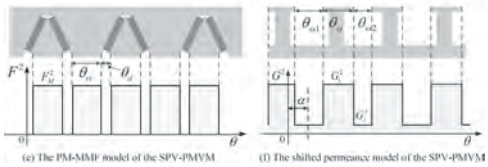
(e) The PM-MMF model of the SPV-PMVM (f) The shifted permeance model of the SPV-PMVM

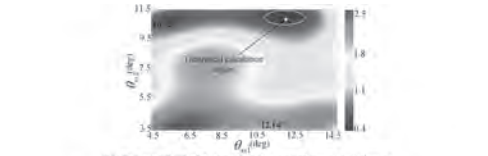
(a) Theoretical calculation angles of cogging torque minimization and cogging torque versus θ_{o1} and θ_{o2} by FEM

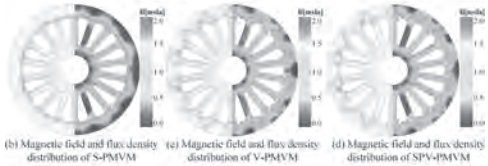
(b) Magnetic field and flux density distribution of S-PMVM (c) Magnetic field and flux density distribution of V-PMVM (d) Magnetic field and flux density distribution of SPV-PMVM

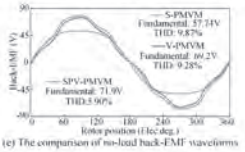

(e) The comparison of no-load back-EMF waveforms

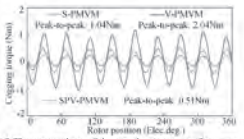

(f) The comparison of the cogging torque performance

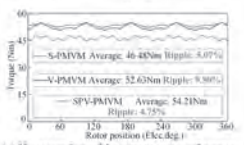

(g) The comparison of the output torque performance

JPF-11. Optimization Design and Investigation of a Vernier Permanent Magnet Machine with Improved Power Factor Based on Flux Modulation Theory. *J. Zhou*[1], X. Zhu[1] and D. Fan[1] *1. Jiangsu university, Zhenjiang, China*

Vernier permanent magnet (VPM) machines have attracted increasing attention because of high torque at low speed [1]. However, VPM machines generally suffer from relatively low power factor due to the increase of number of PM poles and flux leakage, which will result in the increase of power rating of inverters. Hence, it is very necessary to improve power factor of VPM. In [2], design principle of double stator is introduced for VPM, so reduced flux leakage and improved power factor are realized. In [3], hybrid-excited VPM is proposed to improve power factor, while motor copper loss and control difficulty is inevitably increased. It is noted that current research mainly focuses on proposing novel motor structure [4], while power factor mechanism is seldom considered. In this paper, based on flux modulation theory, a new power factor improvement method is proposed. A V-shaped VPM machine is selected as an optimization design example. In the proposed method, relationship between power factor and magnetic field is investigated detailed. Then, the correlation designs are achieved among the power factor, structure parameters and airgap harmonics. Fig. 1 shows configuration and corresponding design parameter of investigated V-shaped VPM machine. Fig. 2 shows the production mechanism of power factor. Fig. 3 shows the flux distribution and airgap flux density respectively. It can be seen that flux density of permanent magnetic field is larger than that of armature magnetic field. Therefore, the power factor of the motor is mainly determined by the permanent magnetic field. Then, from the perspective of harmonic modulation, THD of permanent magnet flux linkage is utilized to reflect flux linkage change and corresponding power factor. Fig. 5 shows comparison of flux linkage of main harmonics before and after optimization. Fig. 6 shows power factor before and after the optimization of the motor. It is indicated, by the proposed power factor improvement method, power factor of the motor can be improved effectively, which provides a potential research path for the increase of power factor of VPM. More detailed analysis and experimental results will be presented in the full paper.

[1] W. N. Fu, and S. L. Ho, "A quantitative comparative analysis of a novel flux-modulated permanent-magnet motor for low-speed drive," *IEEE Trans. Magn.,* vol. 46, no. 1, pp. 127–134, Jan. 2010. [2] Y. Shi and T. W. Ching, "Power factor analysis of Dual-Stator permanent magnet vernier motor with consideration on Turn-Number assignment of inner and outer stator windings," *IEEE Trans. Magn.,* vol. 57, no. 2, pp. 1-5, Feb. 2021. [3] T. W. Ching, K. T. Chau and W. Li, "Power factor improvement of a linear vernier Permanent-Magnet machine using auxiliary DC field excitation," *IEEE Trans. Magn.*, vol. 52, no. [4] Y. Liu, H. Li, and Z. Zhu, "A high-power factor vernier machine with coil pitch of two slot pitches," *IEEE Trans. Magn.*, vol. 54, no. 11, Nov. 2018.

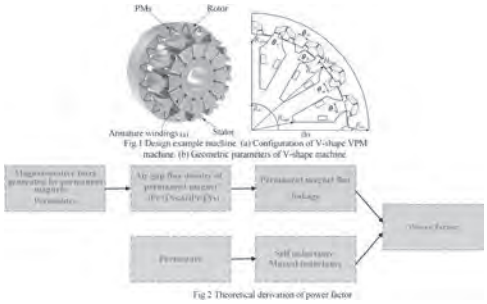

Fig.1 Design example machine. (a) Configuration of V-shape VPM machine. (b) Geometric parameters of V-shape machine

Fig.2 Theoretical derivation of power factor

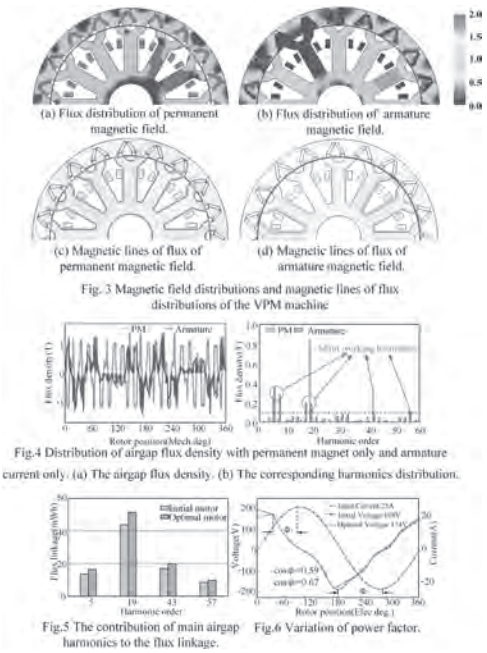

Fig. 3 Magnetic field distributions and magnetic lines of flux distributions of the VPM machine

Fig.4 Distribution of airgap flux density with permanent magnet only and armature current only. (a) The airgap flux density. (b) The corresponding harmonics distribution.

Fig.5 The contribution of main airgap harmonics to the flux linkage.

Fig.6 Variation of power factor.

JPF-12. Stator Core Loss Analysis and Investigation of Flux-Modulated Permanent Magnet Machine from Perspective of Harmonic Group Modulation. Z. Xiang[1], *J. Wei*[1] and X. Zhu[1] *1. Jiangsu University, Zhenjiang, China*

Flux-modulated permanent magnet (FMPM) machines receive more and more attention because of their outstanding advantages of excellent low-speed large-torque capability and high torque density. It is worth noting that, although the airgap harmonics possess the contribution on torque production, they are simultaneously the main source of increase of loss. In this paper, the stator loss is analyzed and investigated for the FMPM machine with two types of PM rotor topologies. Underlying the in-depth analysis of flux modulation principle, the concept of harmonic group modulation is proposed. The study of this paper indicates that the enhancement of modulation effect of harmonic group contributes to realizing the reduction of stator loss and improvement of output torque. In Fig. 1 (a) and (b), including the spoke-type PM to surface-insert PM. Fig. 2 depicts the derivation of the modulated-PM air-gap flux density, which can be seen that there are rich harmonic contents in the airgap magnetic field. Then, the airgap flux density is illustrated in Fig. 3 (a). And, the corresponding space-time harmonic distribution is presented in Fig. 3 (b), where the harmonics are classified as three groups according to the characteristics of frequency and amplitude. The relationships between the harmonic groups and stator core loss are also evaluated, as can be seen in Fig. 4. Obviously, compared with the surface-insert FMPM machine, the loss of spoke-type FMPM machine caused by harmonic group II is decreased effectively. It means that the stator core loss of spoke-type FMPM machine is lower than that of surface-insert FMPM machine. As expected, the conclusion is verified in Fig. 5 and Fig. 6. In addition, the back-EMF and output torque are also analyzed, as shown in Fig. 7 (a) and (b), respectively. More detailed electromagnetic performance and experimental results will be given in full paper.

[1] Z. Q. Zhu and Y. Liu, "Analysis of Air-Gap Field Modulation and Magnetic Gearing Effect in Fractional-Slot Concentrated-Winding Permanent-Magnet Synchronous Machines," in *IEEE Transactions on Industrial Electronics*, vol. 65, no. 5, pp. 3688-3698, May 2018. [2] X. Zhu, M. Jiang, Z. Xiang, L. Quan, W. Hua and M. Cheng, "Design and Optimization of a Flux-Modulated Permanent Magnet Motor Based on an Airgap-Harmonic-Orientated Design Methodology," in *IEEE Transactions on Industrial Electronics*, vol. 67, no. 7, pp. 5337-5348, July 2020. [3] K. Yamazaki and H. Ishigami, "Rotor-Shape Optimization of Interior-Permanent-Magnet Motors to Reduce Harmonic Iron Losses," in *IEEE Transactions on Industrial Electronics*, vol. 57, no. 1, pp. 61-69, Jan. 2010.

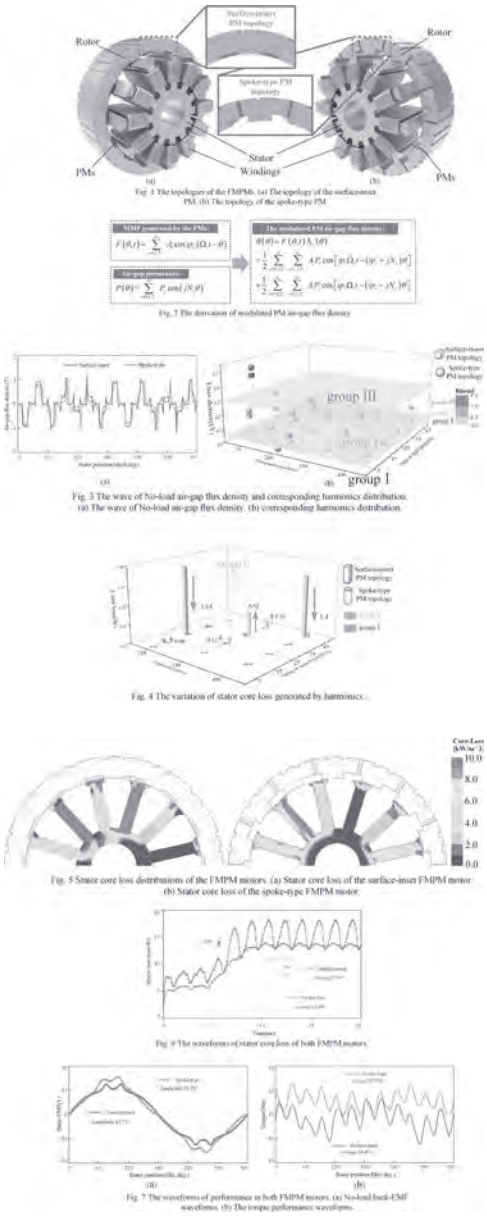

Fig. 1 The topologies of the FMPMs. (a) The topology of the surface-inset PM. (b) The topology of the spoke-type PM.

Fig. 2 The derivation of modulated PM air-gap flux density.

Fig. 3 The wave of No-load air-gap flux density and corresponding harmonics distribution. (a) The wave of No-load air-gap flux density. (b) corresponding harmonics distribution.

Fig. 4 The variation of stator core loss generated by harmonics.

Fig. 5 Stator core loss destributions of the FMPM motors. (a) Stator core loss of the surface-inset FMPM motor. (b) Stator core loss of the spoke-type FMPM motor.

Fig. 6 The waveforms of stator core loss of both FMPM motors.

Fig. 7 The waveforms of performance in both FMPM motors. (a) No-load back-EMF waveforms. (b) The torque performance waveforms.

JPF-13. Withdrawn

Session JPG
VARIABLE FLUX MACHINES
(Poster Session)

Xing Zhao, Chair
The Hong Kong Polytechnic University, Hong Kong, Hong Kong

JPG-01. A New Partitioned Stator Hybrid Excitation Machine with Internal Magnetic Ring. X. Zhu[1] and *L. Xu*[1] *1. Jiangsu University, Zhenjiang, China*

I. INTRODUCTION In recent years, partitioned stator switched flux permanent magnet machines have been extensively investigated thanks to their high torque and simple rotor structure, while suffering from poor flux adjustment capability [1]-[3]. Thus, partitioned stator hybrid excitation (PSHE) machines were proposed to enhance their flux adjustment capability [4]. However, the topological structure of the PSHE machine also suffer from a disadvantage that the internal stator reluctance weakens the strength of the working magnetic field. This disadvantage limits the improvement of torque density of the PSHE machine. In order to solve this problem, a novel internal magnetic ring stator partition hybrid excitation (IMR-PSHE) machine is proposed in this paper. The topological structure and performance analysis of this machine will be carried out below. II. BASIC TOPOLOGY AND RESULTS The proposed IMR-PSHE machine is illustrated in Fig. 1(a). Compared with the conventional PSHE machine shown in Fig. 1(b), the magnetic ring structure is added on inner stator of the proposed machine. The magnetic ring can provide low reluctance magnetic circuit for the low order working magnetic field harmonics. Fig. 2 shows the no-load back-EMF of the proposed IMR-PSHE and conventional PSHE machines at 400r/min. It can be seen from Fig. 2 (a) that the no-load back-EMF amplitude of the IMR-PSHE machine is significantly enhanced as compared to the PSHE machine. Also, as shown in Fig. 2(b), the no-load back-EMF primary harmonic of the IMR-PSHE machine is 63% higher than that of the PSHE machine. Fig. 3 shows the phase back-EMF waveforms with different field excitations. The label of Js in Fig. 3 represents the current density of the excitation windings. As shown, the range of regulation of no-load back-EMF of the IMR-PSHE machine is wider than that of the PSHE one. Fig. 4 shows torque comparison between IMR-PSHE and PSHE machines when the armature current is 7A. It can be found that the torque of the IMR-PSHE machine is 44% higher than the PSHE machine. More detailed results and analyses will be presented in the full paper.

[1] D. J. Evans and Z. Q. Zhu, IEEE Trans. Magn., Vol. 51, Art no. 8100114(2015). [2] D. Fan, L. Quan and X. Zhu, AIP Advances, Vol. 7, Art no. 056636 (2017). [3] Y. Du, J. Zhao and F. Xiao, IEEE Trans. Veh. Technol., vol. 70, p. 3187(2021). [4] H. Hua and Z. Q. Zhu, IEEE Trans. Energy Convers., Vol. 32, p. 495(2017).

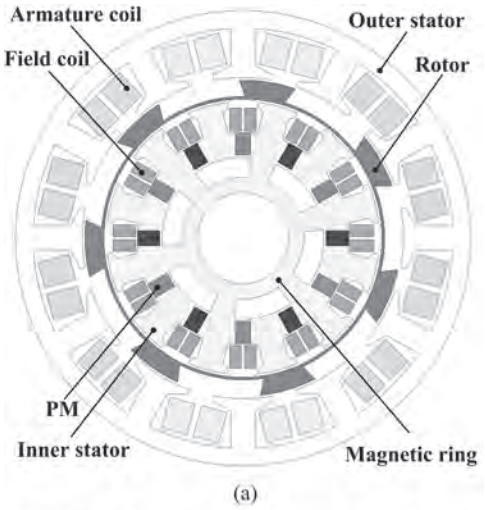

Fig. 1. Topologies of proposed 12-stator-slot/7-rotor-pole IMR-PSHE machine and conventional PSHE machine. (a) Proposed IMR-PSHE machine. (b) Conventional PSHE machine.

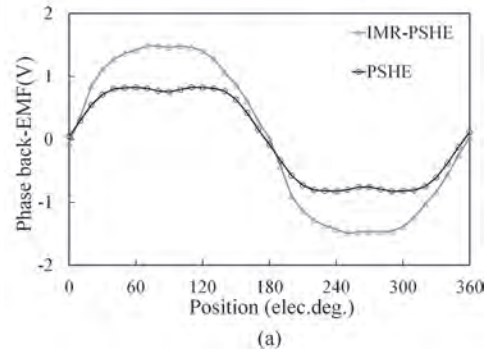

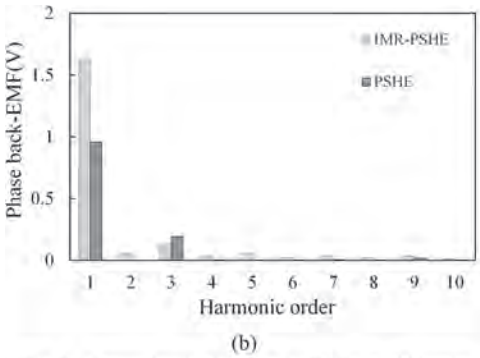

Fig. 2. Open-circuit phase back-EMFs at 400 r/min without field current. (a) Waveforms. (b) Spectra.

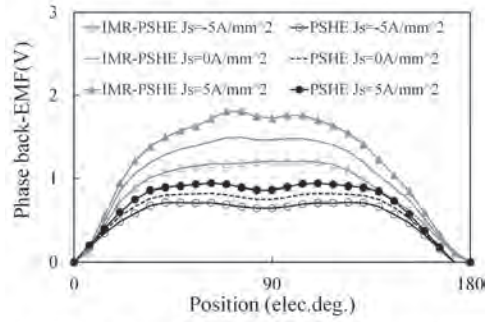

Fig. 3. Phase back-EMF waveforms at 400r/min with different field excitations.

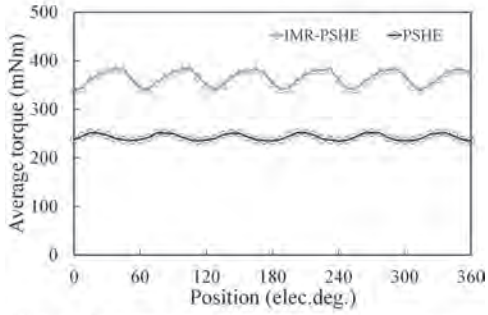

Fig. 4. Comparison of electromagnetic torque when the armature current is 7A.

JPG-02. Design and Analysis of a Reverse-Salient Hybrid-PM Variable-Flux Machine with Flux Bypass Path. *F. Liu*[1], P. Zheng[1], M. Wang[1] and G. Qiao[1] *1. School of Electrical Engineering & Automation, Harbin Institute of Technology, Harbin, China*

Due to the high power density and efficiency, permanent magnet (PM) synchronous machines are widely used. However, the unchangeable PM magnetic field results in the limited constant-power speed range, and the flux-weakening control inevitably increases copper loss. To reduce the PM flux and copper loss, hybrid-PM variable-flux machines (HP-VFMs) are proposed [1-4]. Although the PM flux variation range of the parallel-configuration HP-VFM is wider, the low coercive force (LCF) magnet is easily demagnetized by *q*-axis armature reaction [1, 2]. The series configuration possesses well on-load unintentional demagnetization withstand capability, but the normal demagnetization is more difficult [3, 4]. In order to address the aforementioned issues, a reverse-salient HP-VFM with flux bypass path is proposed by synergizing the advantages of parallel and series configuration. Since the maximum torque of the reverse-salient machine is produced by positive *d*-axis current, the unintentional demagnetization can be alleviated. Therefore, three topologies of reverse-salient HM-VFMs with series and parallel PM configuration are proposed, as shown in Fig. 1. The blue and the green blocks are the low and high coercive force (HCF) magnets, and *q*-axis flux barriers are designed to reduce L_q. The types and grades of the LCF magnet are determined by considering the reverse-salient ratio, power density and flux variation range of the three proposed machines. Because the HCF magnets are placed in both *d* and *q* axes of topology II and III, the L_q is further decreased. The ratio between parallel and series path is analyzed by changing flux bypass path, which is the distance of two HCF magnets near the LCF magnet. When the distance increases from 3.5mm to 8mm, the magnitude of no-load back EMF only decreases 8.8%, and the variation range of PM flux changes from 57% to 90%, which greatly increases the speed-expansion range, as shown in Fig 2. The proposed machine possesses wide air-gap flux variation range and well on-load demagnetization withstand capability, and can operate with high efficiency over the whole torque-speed range.

[1] M. Ge, J. Li and Qu, R. IEEE Transactions on Applied Superconductivity, Vol. 28(3), 1-5 (2018) [2] H. Yang, Z. Q. Zhu and H. Lin, IEEE Transactions on Magnetics, Vol. 53(6), 1-4 (2017) [3] A. Athavale, K. Sasaki and B. S. Gagas, IEEE Transactions on Industry Applications, Vol. 53(5), 4318-4326 (2017) [4] Z. Q. Zhu, H. Hua and A. Pride, IEEE Transactions on Magnetics, Vol. 53(11), 1-4 (2017)

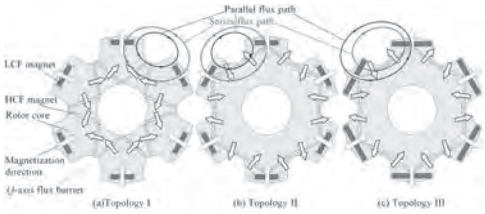

Fig. 1 Topologies of the proposed HPM-VFM

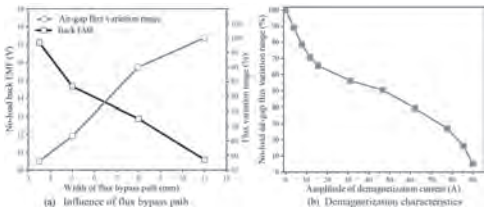

Fig. 2 Influence of flux bypass path and demagnetization characteristics

JPG-03. A Novel Series Hybrid Magnet Separated Variable Flux Memory Machine with Wide Flux Regulation Range. *X. Zhao*[1] and H. Lin[1] *1. Southeast University, Nanjing, China*

I. Introduction Variable flux memory machines (VFMMs) can dynamically adjust the air-gap magnetic field by changing the magnetization states (MSs) of low corrective force permanent magnets (LCF PMs), which solves the problem of flux-weakening difficulty of traditional PM machines [1]. In addition, in order to make the VFMMs have higher torque and excellent on-load demagnetization withstand capability, high corrective force PMs (HCF PMs) and LCF PMs are usually arranged in series to form a series hybrid magnet VFMM (SHM-VFMM) [2-3], as shown in Fig. 1(b). However, in the demagnetization state of traditional SHM-VFMM, LCP PMs are reversely protected by HCP PMs, which limits its flux regulation range. In order to broaden the flux regulation range of traditional SHM-VFMM, a novel series hybrid magnet separated VFMM (SHMS-VFMM) is proposed. II. Machine Topology Fig. 1 shows the topologies of the existing SHM-VFMM and the proposed SHMS-VFMM. In the proposed configuration, because HCF PMs and LCF PMs are separated and placed at an angle from each other, the magnetization effect of HCF PMs on LCF PMs can be weakened. Besides, some *q*-axis barriers are added to stabilize the MSs of LCF PMs under rated load [4]. III. Performance Comparison The proposed SHMS-VFMM topology is optimized by using multi-mode field circuit coupling model and multi-objective genetic algorithm. The optimal topology is shown in

Fig. 1(c). In order to ensure the fairness, the investigated two machines use the same stator and PMs amount. Fig. 2 compares the electromagnetic characteristics of the investigated two machines. The results show that the proposed SHMS-VFMM has similar torque, lower torque ripple and wider flux regulation range. It is worth mentioning that the flux regulation range of the proposed SHMS-VFMM is 2.2, which is 40% higher than that of the traditional SHM-VFMM. More performance comparison will be shown in detail in the full paper.

[1] V. Ostovic, *Proc. 36th IAS Annu. Meeting IEEE Ind. Appl. Conf.*, vol. 4, p. 2577–2584 (2001) [2] S. Zhang, P. Zheng and T. M. Jahns, *IEEE Trans. Magn.*, vol. 54 (11), p. 1-5 (2018) [3] H. Hua, Z. Q. Zhu and A. Pride, *IEEE Trans. on Ind. Appl.*, vol. 55 (2), p. 1408-1419 (2019) [4] Hui Yang, Hao Zheng and Heyun Lin, *IEEE Trans. Ind. Appl.*, vol. 57 (1), p. 340-351 (2021)

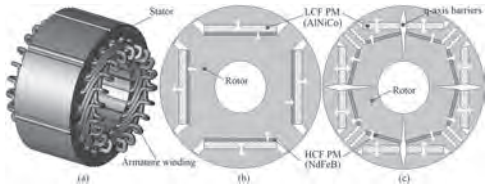

Fig. 1 Topologies of the investigated machines. (a) Stator (b) Traditional SHM-VFMM (c) Proposed SHMS-VFMM

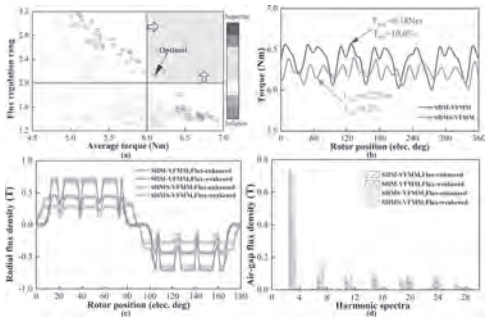

Fig. 2 Electromagnetic characteristics of the investigated machines. (a) Optimized result (b) Steady-state torque (c) and (d) Waveforms and harmonic spectra of open-circuit air-gap flux density.

JPG-04. Influence of Inverter Open-Circuit Fault on Variable Flux Memory Machine. *X. Zhao*[1] and H. Lin[1] *1. Southeast University, Nanjing, China*

I. Introduction Variable flux memory machines (VFMMs) can adjust the air-gap magnetic field by changing the magnetization states (MSs) of low corrective force (LCF) permanent magnet (PM), which makes VFMMs suitable for the traction machine of EVs [1]. As a traction machine of EVs, VFMMs need to be connected with inverter. However, the inverter open-circuit (OC) fault will affect the MS of LCF PM, which will affect safety of EVs. In addition, the inverter working principle determine that its IGBT needs to be frequently switched, which greatly increases the probability of inverter OC fault. It is worth mentioning that most research on VFMMs focuses on the topology innovation and most research on inverter focuses on its fault diagnosis [2-5]. However, because the LCF PM is easy to demagnetize, the research on the effect of inverter OC fault on VFMM performance has not been found. II. Model The inverter OC fault is realized by field-circuit coupling method. Fig. 1 shows the Field-circuit coupling model and VFMM topology. III. Research Results Fig. 2 shows the research results. After fault, the positive half wave of A-phase current will become 0. The DC component appears in 3-phase current, which makes them unbalanced and phase angle changed. Due to the change of phase angle, there will be a moment when 3-phase currents are 0 at the same time, which is called Zero-point. Before Zero-point (after Zero-point until A-phase current occur), the armature magnetic field decreases (increases) due to the decrease (increase) of B-phase and C-phase current. After fault, due to the change of armature magnetic field, LCF PM working point is lower when VFMM operates on no-load. It means that load demagnetization of LCF PM happened. In addition, at Zero-point, without the armature magnetic field torque is 0. Compared with normal operation, the torque is reduced by 29.5% and torque ripple is increased by 7.8 times when inverter operates in OC fault. It can be seen that the influence of inverter OC fault on VFMM performance is significant, and further study is necessary. This will be shown in detail in the full paper.

[1] V. Ostovic, *Proc. 36th IAS Annu. Meeting IEEE Ind. Appl. Conf.*, vol. 4, p. 2577–2584 (2001) [2] H. Hua, Z. Q. Zhu and A. Pride, *IEEE Trans. Ind. Appl*, vol. 53 (5), p. 4396-4405 (2017) [3] R. Tsunata, M. Takemoto and S. Ogasawara, *IEEE Trans. Ind. Appl.,* doi: 10.1109/TIA.2021.3068329 (2021). [4] M. Trabelsi, E. Semail and N. K. Nguyen, *IEEE J. Emerg. Sel. Topics Power Electron.*, vol. 6 (1), p. 339-351(2018) [5] H. Yan, Y. Xu and F. Cai, IEEE Trans. Power Electron., vol. 34 (1), p. 759-768 (2019)

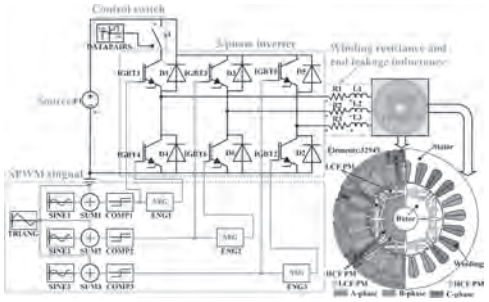

Fig. 1 Field-circuit coupling model

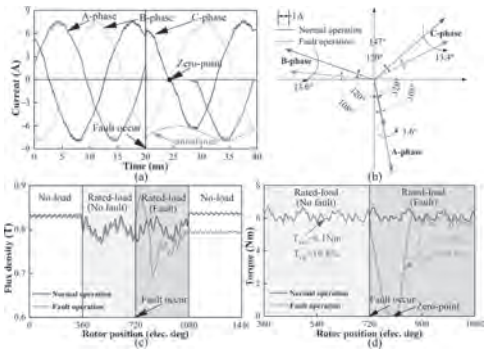

Fig. 2 Research results. (a) Current (b) Phase angle (c) LCF PM working point (d) Torque

JPG-05. Study on Variable Flux Memory Machine with Inter Turn Short Circuit Fault. *X. Zhao*[1] and H. Lin[1] *1. Southeast University, Nanjing, China*

I. Introduction Variable flux memory machines (VFMMs) can adjust the air-gap magnetic field by changing the magnetization states (MSs) of low corrective force (LCF) permanent magnet (PM), which solves the problem of flux-weakening difficulty of traditional PM machine and makes it suitable for the traction machine of electric vehicles (EVs) [1]. In addition, inter-turn short-circuit (ITSC) fault is the most common and dangerous fault [2]. The pulsating magnetic field produced by the loop current (LC) in ITSC fault will affect the MSs of LCF PM, which will affect the safety of EVs. It is worth mentioning that most of the research on VFMM focuses on the topology innovation [3-5]. However, because LCF PM is easy to demagnetize, the research on the effect of ITSC fault on VFMM performance has not been found. II. Model Fig. 1 shows the ITSC fault model. The VFMM employs a fractional slot distributed winding, and the number of the conductors in per layer is 32. The high corrective force (HCF) PM and LCF PM are placed in series. i_f is the LC. III. Research Results Fig. 2 shows the research results. After ITSC fault with LC, the pulsating magnetic field produced by LC can

enhance and weaken the armature magnetic field, which makes the LCF PM working point changed. Therefore, after fault, the LCF PM working point is lower when VFMM operation on open-circuit. It means that load demagnetization of LCF PM happened. However, when VFMM operates normally and in ITSC fault without LC, the LCF PM working point pre-and post-load doesn't change. In addition, compared with VFMM under normal operation, the torque is only reduced by 0.08 Nm and the torque ripple is only increased by 2.6% when LC is not considered. However, the torque is reduced by 14.3% and the torque ripple is increased by 3.6 times when LC is considered. The variation of the LCF PM working point in fault is the main reason. It can be seen that the influence of LC on VFMM performance is significant. It is necessary to further reveal the fault mechanism and explore new methods of fault identification. This will be shown in detail in the full paper.

[1] V. Ostovic, *Proc. 36th IAS Annu. Meeting IEEE Ind. Appl. Conf.*, vol. 4, p. 2577–2584 (2001) [2] A. Berzoy, A. A. S. Mohamed and O. Mohammed, *IEEE Trans. Magn.*, vol. 53 (6), Art no. 8105504, p. 1-4(2017) [3] H. Hua, Z. Q. Zhu and A. Pride, *IEEE Trans. Ind. Appl*, vol. 53 (5), p. 4396-4405 (2017) [4] R. Tsunata, M. Takemoto and S. Ogasawara, *IEEE Trans. Ind. Appl.*, doi: 10.1109/TIA.2021.3068329 (2021) [5] Hui Yang, Hao Zheng and Heyun Lin, *IEEE Trans. Ind. Appl.*, vol. 57 (1), p. 340-351 (2021)

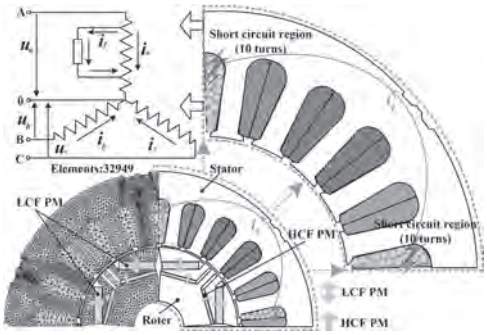

Fig. 1 The ITSC fault model

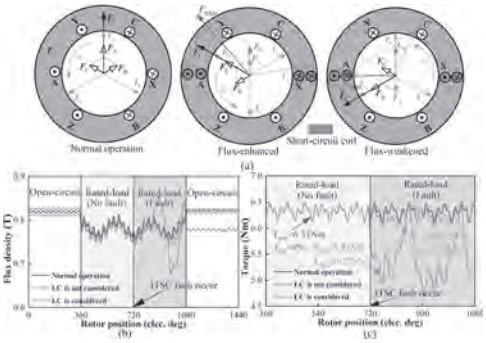

Fig. 2 Research results (a) Magnetomotive force variation (b) LCF PM working point (c) Torque

JPG-06. Investigation of an Axial Flux Switched Flux Hybrid Permanent Magnet Memory Machine. *L. Qin*[1], H. Yang[1], S. Fang[1], Z. Pan[1] and Y. Meng[1] *1. Southeast University, Nanjing, China*

I. Introduction Axial-flux permanent-magnet machine (AFPMM) has gained growing research interests due to its structural compactness, high torque and power density[1-2]. However, the non-adjustable magnetic fields produced by NdFeB PMs result in limited speed range of conventional AFPMM. Thus, the concept of memory machine is proposed to flexibly adjust air-gap flux [3-4]. Thus, in order to obtain high torque density and excellent flux adjustment capability in AFPMM, this paper proposes a new axial-flux switched flux hybrid PM memory machine (AF-SFMM). Besides, this paper develops a computationally efficient analytical method by combing quasi-3D finite element analysis (FEA) and magnetomotive force (MMF) permeance-based model to predict the electromagnetic performance of the proposed machine. The machine topology and operating principles are described, respectively. The back electromotive force (EMF) is investigated by the analytical and FEA. II. Topology and Analytical Model The topology and working principle of the AF-SFMM are shown in Fig. 1. The proposed machine is geometrically characterized by a dual-rotor and middle-stator configuration. The magnetization states (MSs) of the low coercive force (LCF) PM can be changed through a DC current pulse in the magnetizing windings. The NdFeB PMs fields will be either enhanced to pass through the air gap or short-circuited within the stator to obtain flexible online flux control. Two different MSs are defined as follows: flux-strengthened and flux-weakened. As shown in Fig. 2a, several circumferential planes at a certain radius are chosen from the real 3D model, which can be transformed into the equivalent radial-flux SFMM in a polar coordinate system. Subsequently, based on the MMF-Permeance model shown in Fig. 2b, the back-EMF is predicted. Fig. 2(c) shows the back-EMF at different MSs calculated by FEA and the analytical model. It can be observed that the slight mismatch between the analytical and FEA results is mainly caused by ignoring the fringing effect in teeth in the analytical model. The results show the excellent flux-adjusting ability of the proposed AF-SFMM.

[1] D. L. Patterson et.al. A comparison of radial and axial flux structures in electrical machines. *Proc. IEEE International Electric Machines & Drives Conference - IEMDC 2009*. pp.1029-1035.2009. [2] A. Parviainen, M. Niemela, and J. Pyrhonen, "Modeling of axial flux permanent magnet machines", *IEEE Trans. Ind Appl.*, vol. 40, no. 5, pp. 1333-1340, Sep./Oct. 2004. [3] V. Ostovic. "Memory motors," *IEEE Ind. Appl. Mag.*, vol.1, no. 9, pp.52-61, Jan. / Feb. 2003. [4] H. Yang, H. Lin, Y. Li, S. Fang, and Y. Huang. "Analytical modeling of switched flux memory machine," *IEEE Trans. Magn.,* vol. 54, no. 3, Jun. 2018.

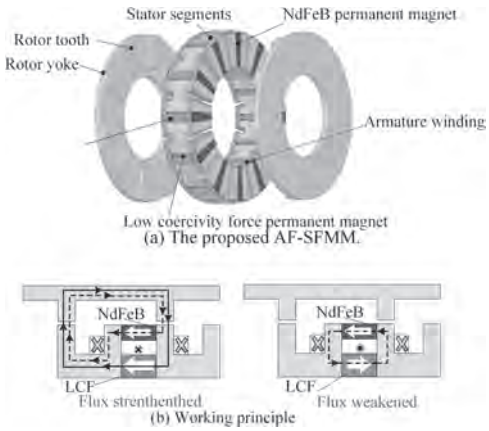

Fig.1 Topology and working principle

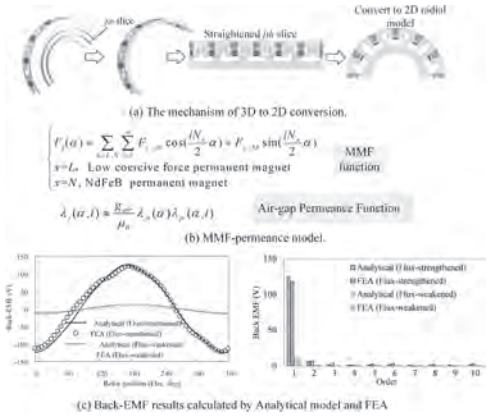

Fig. 2 The mechanism of 3D to 2D conversion and the back-EMF

JPG-07. A New Hybrid-Excited Partitioned Stator Flux Modulated Machine With Dual-PM. *Y. Meng*[1], S. Fang[1], Z. Pan[1] and L. Qin[1]
1. School of Electrical Engineering, Southeast University, Nanjing, China

I. Introduction Recently, flux modulated permanent magnet machines (FMPMMs) have attracted considerable attention due to the high torque density [1] [2]. However, the constant power speed range of FMPMMs is limited because of the uncontrollable PM flux, which restricts their applications. To solve the problem, this paper proposes a new hybrid-excited partitioned stator flux modulated machine with dual-PM (HE-PSFM-DPMM). The proposed machine employs the PMs on both the inner stator and rotor to enhance the torque capability. Meanwhile, the field windings are placed in the inner stator to achieve the flux regulation. II. Machine Topology and Operation Principle Fig. 1 shows the topology of the proposed HE-PSFMDPMM, in which a rotor is sandwiched by the inner and outer stators. The non-overlapping concentrated armature windings and field windings are wound on the teeth of outer and inner stators, respectively, which provide the advantages of short end length and low copper loss. Besides, the PMs and iron poles are alternatively placed on the top of inner stator teeth, which composes a consequent-pole PM configuration. The rotor of HE-PSFMDPMM is simply made up of the alternatively PMs and iron poles, and the PMs on the rotor are arranged as the Halbach array. The magnetization directions of PMs on the inner stator and rotor are marked in Fig. 1. The operation principle of the proposed HE-PSFMDPMM is based on the flux modulation effect [1], and the torque of machine is generated by taking advantage of the modulated air-gap field harmonics. III. Electromagnetic Performance Evaluation As shown in Fig. 2 (b) and (c), compared with using stator-PM only and rotor-PM only, the use of dual-PM can enjoy more abundant air-gap flux density working harmonics, which contributes to a high flux linkage. As shown in Fig. 2 (d), the maximum average torque is obtained when the dual-PM is used. According to Fig. 2 (e), the phase flux linkage can be effectively regulated by changing dc current density (J_{dc}). Moreover, the average torque increases with the increase of J_{dc}, as illustrated in Fig. 2(f). More detailed design considerations and electromagnetic performance analysis results will be presented in the full paper.

[1] M. Cheng, P. Han, and W. Hua, "General airgap field modulation theory for electrical machines," *IEEE Trans. Ind. Electron.*, vol. 64, no. 8, pp. 6063-6074 (2017). [2] Z. Z. Wu and Z. Q. Zhu, "Analysis of air-gap field modulation and magnetic gearing effects in switched flux permanent magnet machines," *IEEE Trans. Magn.*, vol. 51, no. 5, pp. 1–12 (2015).

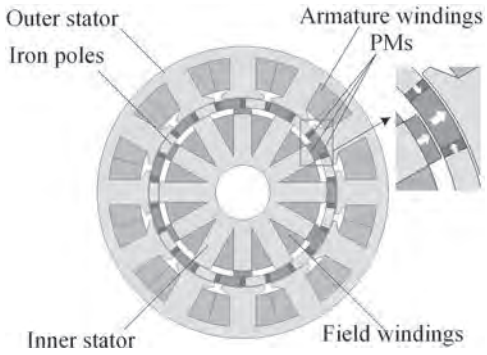

Fig. 1

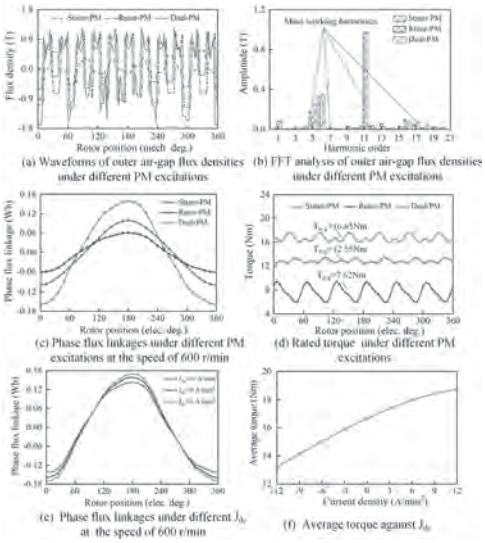

Fig. 2

JPG-08. A Novel Slot-PM-assisted Hybrid Magnet Memory Machine for Wind Power Generation. *J. Jiang*[1] and S. Niu[1] *1. Electrical Engineering Department, The Hong Kong Polytechnic University, Hong Kong, Hong Kong*

Nowadays, permanent magnet synchronous machine (PMSM) has attracted more and more attention in wind power application with its inherent merits such as high-torque density and high efficiency [1-2]. However, with the fixed PM excitation, it is not easy for the PMSM to provide controllable airgap flux and extend speed range to capture more wind energy [3-4]. To extend the constant-power speed range and improve the machine efficiency, a new slot-PM-assisted hybrid magnet memory machine (SPMA-HMMM) is proposed, in which hybrid PMs, namely high coercive force (HCF) PMs and low coercive force (LCF) are artificially combined and inset into both stator yoke and slot opening. Especially, one pole of yoke PMs are made of HCF PMs, and the other pole of yoke PMs are composed of LCF PMs with flexible flux regulation ability. LCF PMs can be freely magnetized or demagnetized through DC current pulses supplied by the DC magnetizing coils wound on the LCF PMs. Therefore, during the high-speed operation, high efficiency of machine can be achieved with negligible field excitation loss. In addition, the HCF slot PMs can further enhance the torque/power density of machine with parallel excitation. Machine configuration Fig. 1 shows the configuration of SPMA-HMMM. It is composed of 28-pole outer rotor and 24-slot inner stator as denoted in Fig. 1. The rotor consists of only iron core, hence providing mechanical robustness. The stator comprises all excitation sources, including 3 pole-pair slot PMs, 3 pole-pair yoke PMs, armature winding and DC magnetizing coils. It is worth noting that the yoke PMs are formed by both HCF PMs and LCF PMs. Electromagnetic performance Fig. 2 shows electromagnetic performance of proposed SPMA-HMMM. As denoted in Fig. 2(a) and Fig. 2(b), the open-circuit flux-linkage and back-EMF can be effectively enhanced or weakened at different magnetization states via different DC magnetizing current pulses applying to LCF yoke PMs. Therefore, flexible flux regulation can be realized. As shown in Fig. 2(c), with the employment of slot PMs, the average torque is enhanced by 30.9% under flux-enhancing magnetization state.

[1] T. Sheng, and S. Niu, "A novel design method for the electrical mahines with biased DC excitation flux Linkage," *IEEE Trans. Magn*, vol. 53, no. 6, pp. 1-4, Jun. 2017. [2] S. Niu, Y. Luo, W. Fu and X. Zhang, "An Indirect Reference Vector-Based Model Predictive Control for a Three-Phase PMSM Motor," *IEEE Access*, vol. 8, pp. 29435-29445, 2020. [3] H. Yang, H. Lin, Z. Q. Zhu, S. Niu, S. Lyu and H. Zheng, "A Novel Stator Spoke-Type Hybrid Magnet Memory Machine," 2019 IEEE International Electric Machines & Drives Conference (IEMDC), 2019, pp. 1576-1580, doi:

10.1109/IEMDC.2019.8785325. [4] H. Yang, S. Lyu, and H. Lin, "A Novel Hybrid-Magnetic-Circuit Variable Flux Memory Machine," *IEEE Trans. Ind. Electro.*, vol. 67, no. 7, pp. 5258-5268, July 2020.

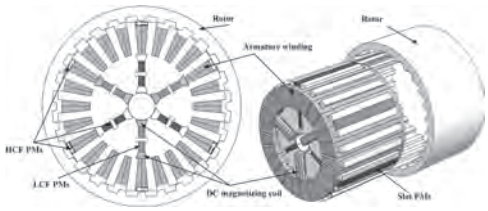

Fig. 1. Configuration of SPMA-HMMM.

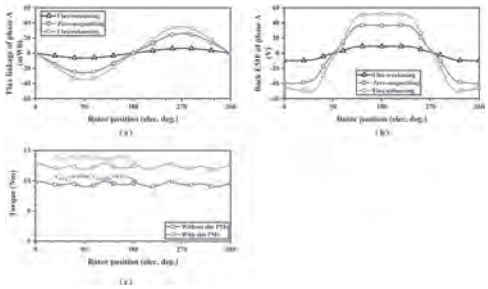

Fig. 2. Electromagnetic performance of SPMA-HMMM.

JPG-09. Analysis of a Variable Reluctance Field-modulated Transverse Flux Linear Generator. *M. Chen*[1], L. Huang[1], T. Xia[2], Y. Li[1], P. Tan[1], G. Ahmad[1] and M. Hu[1] *1. Electrical Engineering, Southeast University, Nanjing, China; 2. Nanjing Institute of Technology, Nanjing, China*

I. Introduction Recently, a variety of wave energy converters have been proposed with increasing concerns on low carbon electricity, of which direct drive wave energy converter (DD-WEC) requires fewer moving parts since the translator of the generator is coupled with the wave energy converter directly [1]. Permanent magnet linear generator (PMLG) is widely used for DD-WEC and permanent magnet transverse flux linear machine is a member of the variable reluctance PM linear machines family which are known to achieve high thrust density. So permanent magnet transverse flux linear generator (PMTFLG) is a good candidate in DD-WEC which is a typical low-speed high thrust application. Also, the air-gap flux can be adjusted by variable reluctance to extend the working range. Hence, in order to balance between extending the working range and achieving high thrust, more research should be done on PM positioning, number and shape of PMs and magnet material [2]. In this paper, a field-modulated transverse flux linear generator is proposed. By adjusting the machine topology and PM position, the generator can operate in a wide working range without sacrificing too much thrust density. II. Machine Topology and Operation Principle As shown in Fig. 1, the generator consists of outer stator, inner stator and moving translator. Some PMs and direct current field coils are placed in the inner stator, while the armature coils are placed in the outer stator slot and some PMs are inserted between the adjacent outer stator shoes. The moving part of the generator is translator and the moving direction is along z-axis. Silicon steel sheets and nonmagnetic sheets are arranged in the moving translator. The PMs which are inserted between the adjacent outer stator shoes can reduce the harmonics of back electromotive force (EMF). Fig. 1 III. Results Fig. 2 IV.conclusion Simulation results show that the air-gap flux can be adjusted by variable reluctance to extend the working range. The generator can operate in a wide working range without sacrificing too much thrust density.

[1] N. J. Baker, M. A. H. Raihan and A. A. Almoraya, "A Cylindrical Linear Permanent Magnet Vernier Hybrid Machine for Wave Energy," in *IEEE Transactions on Energy Conversion*, vol. 34, no. 2, pp. 691-700, June 2019. [2] R. Jayarajan, N. Fernando and I. U. Nutkani, "A Review on Variable Flux Machine Technology: Topologies, Control Strategies and Magnetic Materials," in *IEEE Access*, vol. 7, pp. 70141-70156, 2019.

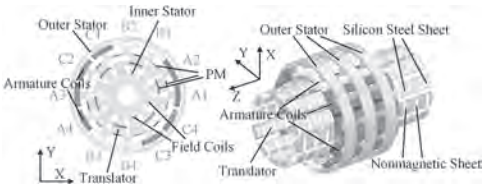

Fig. 1. Configuration of the proposed PMTFLG.

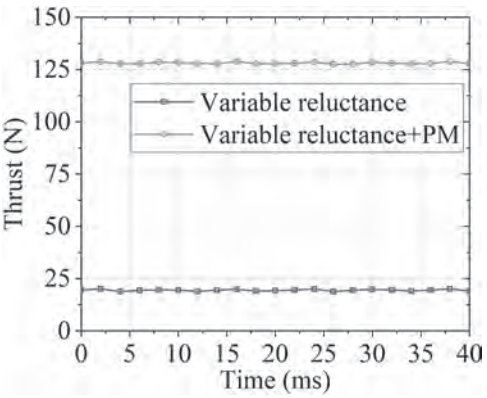

Fig. 2. Thrust of variable reluctance and variable reluctance and PM.

JPG-10. A New Variable Reluctance Memory Machine with DC Bias Magnetization Capability. *L. Qin*[1], H. Yang[1], S. Fang[1], Z. Pan[1] and Y. Meng[1] *1. Southeast University, Nanjing, China*

I. Introduction Memory machine (MM) has gained growing research interests due to its excellent flux adjustable capability with negligible excitation loss. The *d*-axis current pulse is applied to re/demagnetize the low coercivity force (LCF) permanent magnet (PM) [1]. However, it is a high requirement for the rotor position estimation when the magnetization level of the LCF PMs needs to be adjusted. Thus, the stator-PM MMs are proposed [2-3] which exhibit convenient online magnetization control and better rotor robustness. However, the stator-PM MM has a relatively low torque density due to the additional DC magnetization winding. Therefore, this paper proposes a new variable reluctance memory machine (VRMM) with DC bias magnetization capability. The proposed machine utilizes an open-winding configuration to generate a zero-sequence magnetizing current pulse to change the magnetization state (MS) of the LCF PMs. The machine configurations and operating principles will be described, respectively. The electromagnetic characteristics of the machines are systematically investigated. II. Machine Topology and Electromagnetic Performance Fig. 1 shows the topology and open-circuit field distribution of the VRMM. The stator and rotor cores have simple structures which facilitate modular manufacturing. The NdFeB PMs are tangentially magnetized, and the LCF PMs are radially magnetized. When the MS of LCF PMs can be changed by injecting DC bias pulse in the two armature windings adjacent to the LCF PMs. In this paper, three different MSs are defined, i.e., enhanced flux (EF), non-magnetized LCF (NM) and weakened flux (WF). As shown in Fig. 1b, the flux generated by LCF and NdFeB PMs pass through the armature winding together at EF level. A majority of magnetic fluxes do not pass through the armature winding, which becomes leakage flux in WF level. Fig. 2 shows the no-load and load performance of the proposed VFMM under different MSs. The electromagnetic performance under different MSs indicates that the proposed VFMM has excellent flux adjustment capability. The detail will be shown in the full paper.

[1] V. Ostovic, "Memory motors," IEEE Industry Applications Magazine, vol. 9, no. 1, pp. 52-61, Jan./Feb. 2003. [2] H. Yang, H. Lin, Y. Li, S. Fang, and Y. Huang. "Analytical modeling of switched flux memory machine," *IEEE Trans. Magn.,* vol. 54, no. 3, Jun. 2018. [3] H. Yang, L. Qin, H. Lin, and Z. Q. Zhu. "Investigation of torque characteristics of switched flux hybrid magnet memory machine by a coupled solution", IEEE Transactions

on Magnetics, vol. 56, no. 6, pp. 7515205, Apr. 2020. [4] S. Jia, R. Qu, and W. Kong. "Hybrid excitation stator PM vernier machines with novel dc-biased sinusoidal armature current", IEEE Transactions on Industry Applications, vol. 54, no. 2, pp. 1339-1347, Apr. 2018.

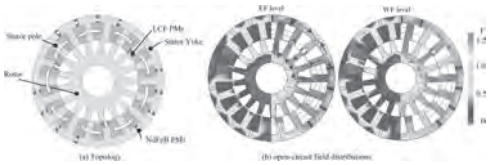

Fig. 1 The topology and open-circuit field distributions.

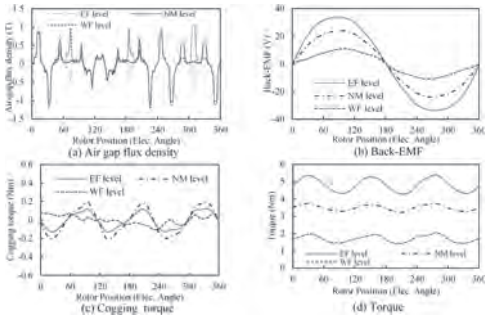

Fig. 2 Electrical performances.

JPG-11. Design Method of the Variable Flux Machines for Improving Torque Density. *F. Liu*[1], P. Zheng[1], M. Wang[1] and G. Qiao[1] *1. Harbin Institute of Technology, Harbin, China*

Due to high efficiency and good speed-extension capability, the variable-flux machine (VFM) is became one of the good candidates in the fields requiring wide speed range [1]. In order to make the permanent magnet flux controllable, the low-coercive-force (LCF) magnet are employed. For conventional permanent magnet synchronous machines (PMSMs), the high-coercive-force (HCF) magnets such as NdFeB and SmCo are used, and the coercive force of the HCF magnets are usually large than 800kA/m. To meet the flux variation requirement, the coercive force of the LCF magnet less than 120kA/m is preferred [2-4]. By replacing the LCF magnets in the VFM with the HCF magnet, the amplitude of the no-load air-gap flux density is changed from 0.6T to 1T, as shown Fig. 1. Therefore, the torque density of the VFM is usually less than 60% of the conventional PMSM. However, the reason why the torque density is lower and the general design method to increase the torque density are not covered in the existing articles. In this paper, the design method of the VFMs for improving the torque density is investigated. The PM flux variation range, re/demagnetization difficulty and torque density are comprehensively considered. Because there three-type PM configuration of the VFMs, parallel configuration, series configuration and hybrid configuration, which are all considered in the analysis method. Based on the magnetic circuit method, the re-magnetization is studied considering the saturation effect of the silicon sheet, magnetization current density and ascending branch of the hysteresis loop of the LCF magnet. In order to simplify the circuit model, all the non-linear effects are equivalent to piecewise straight line. The hysteresis loop of the LCF magnet is shown in Fig.2. The effect of the relative permeability, knee point and coercive force of descending branch of the hysteresis loop of the LCF magnet on the torque density are analyzed. By combine the ascending and descending branches, the ideal hysteresis loop of the LCF magnet is obtained, and the method to improve the torque density of the VFM is given.

[1] M. Ge, J. Li and Qu, R. IEEE Transactions on Applied Superconductivity, Vol. 28(3), 1-5 (2018) [2] H. Yang, Z. Q. Zhu and H. Lin, IEEE Transactions on Magnetics, Vol. 53(6), 1-4 (2017) [3] A. Athavale, K. Sasaki and B. S. Gagas, IEEE Transactions on Industry Applications, Vol. 53(5), 4318-4326 (2017) [4] Z. Q. Zhu, H. Hua and A. Pride, IEEE Transactions on Magnetics, Vol. 53(11), 1-4 (2017)

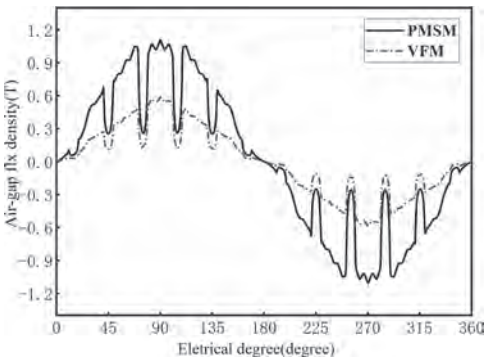

Fig. 1 Comparison of the no-load air-gap flux density

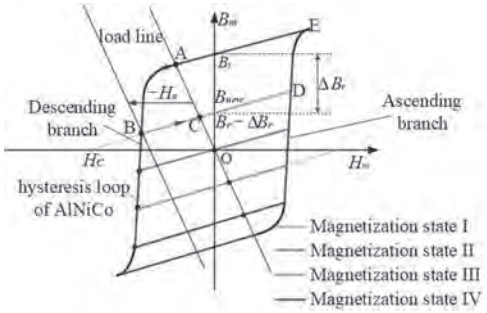

Fig. 2 The hysteresis loop of the LCF magnet

JPG-12. Comparative Study on Two DC Exicited Multitooth Flux-Switching Machines. *Z. Li*[1], G. Zhao[1], W. Hua[2], H. Hua[3] and X. Jiang[1] *1. Nanjing Normal University, Nanjing, China; 2. Southeast University, Nanjing, China; 3. Shanghai Jiao Tong University, Shanghai, China*

I. Introduction In recent years, dc excited multitooth flux-switching machines (DC-MFSMs) have attracted wide attention due to their excellent flux regulation capability and high reliability [1]. In this paper, a novel DC-MFSM is proposed by changing the winding configuration of the existing machine in literature [2]. Fig. 1 shows the topologies of the proposed and the existing DC-MFSMs, called model I and model II. The field winding of model I and model II employ concentrated winding on the same and adjacent stator, respectively. Corresponding, the magnetic polarities due to field windings of model I and model II close to the air gap can be respectively regarded as "N-S-S-N" and "N-N-S-S". The two models are the same except for the configuration of field windings. II. Performance comparisons Fig. 2(a) and (b) present no-load back electromotive force (back-EMF) of two DC-MFSMs at the speed of 1500N/min and the corresponding finite-element analysis (FFT) results. It can be seen that the amplitude of fundamental back-EMFs of the model I is nearly 78% higher than that of model II. In terms of the total harmonic distortion (THD) of the back-EMF waveform, the model I is slightly larger than model II. Furthermore, Fig. 2(c) shows the torque waveforms when the armature current density (J_a) and excitation current density (J_f) of the two machines are both 5A/mm^2. It can be observed that the average torque of model I and model II are 2.43 Nm and 2.29 Nm, respectively. Meanwhile, the torque ripple of model I is smaller. Due to unequal multitoothed distribution is adopted in model II during optimization, the peak-to-peak amplitude of model I (0.15Nm) is greater than that of model II (0.025 Nm), as shown in Fig. 2(d). Overall, the proposed novel DC-MFSM is superior to the conventional one since it exhibits much higher no-load back EMF and average torque, smaller torque ripple, and lower copper loss. The other performance, such as winding inductance, and efficiency, will be shown in the full paper.

[1] Y. Tang, J. J. H. Paulides and E. A. Lomonova, "Energy Conversion in DC Excited Flux-Switching Machines," *IEEE Transactions on Magnetics*, vol. 50, no. 11, pp. 1-4, Nov. 2014. [2] G. Zhao and W. Hua, "Comparative

Study Between a Novel Multi-Tooth and a V-Shaped Flux-Switching Permanent Magnet Machines," *IEEE Transactions on Magnetics*, vol. 55, no. 7, pp. 1-8, July 2019.

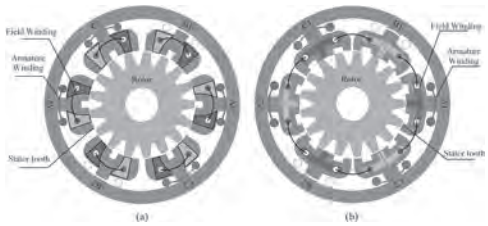

Fig.1. Topology of two dc excited MFSMs. (a) model I. (b) model II.

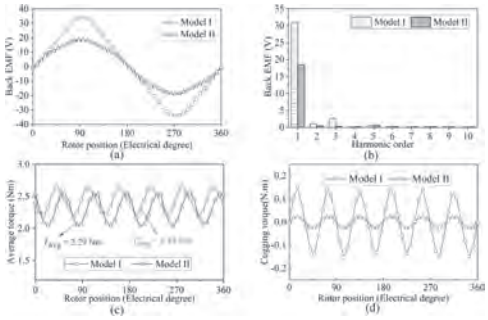

Fig.2. Performance comparisons of two models. (a) Back-EMF waveforms at 1500r/min. (b) Harmonics of back-EMF. (c) Average torque. (d) Cogging torque.

Session JPH
SURFACE AND INTERIOR MOUNTED PERMANENT MAGNET ELECTRICAL MACHINES II (Poster Session)

Metin Aydin, Co-Chair
Kocaeli University, Umuttepe, Izmit, Turkey
Chunhua Liu, Co-Chair
City University of Hong Kong, Hong Kong

JPH-01. Machine learning for fault detection in permanent magnet synchronous machines. *M. Hsieh*[1] and K. Shih[1] *1. National Cheng Kung University, Tainan, Taiwan*

This work presents an approach to detect the inter-turn short circuit (ITSC) and demagnetization faults of permanent magnet synchronous machines (PMSMs) using maching learning. PMSMs possess advantages such as compact size, lightweight, high efficiency, high power density, and easy control. Therefore, they are a popular choice for traction motors of modern electric vehicles (EVs) and many high-performance industrial applications. With the widespread applications of PMSMs, their development should not be only focused on efficiency enhancement but also on fault detection to secure operation safety and cost. Therefore, preventive detection of motor failures is key to improve reliability and reduce damage or maintenance costs. Based on the research of Industry Applications Society (IAS) [1], the stator fault of electric motors is taking up to 37% of all sorts of faults, where ITSC fault occurs the most commonly. Demagnetization is also one of the major fault types in PMSMs. Taking EVs as an example, the high-power density and stochastic load conditions would risk the traction motors in potential ITSC or demagnetization. Among the previous studies regarding fault detection systems for PMSMs, the most frequently applied methods are mathematical modeling combined with the measurement of current or voltage signals. The drawback of these methods is that they are often not able to identify minor variations precisely and classify fault types and levels. Machine learning can be a good tool to improve fault classification capability. With the help of machine learning [2], this work is capable of detecting faults of ITSC and demagnetization in a preventive way so that the system can be ensured in healthy operation. Thus, the motors or components can be replaced before any collapses occur. The proposed algorithm has been trained with both simulation and test data (Fig. 1) with data collected from around 10000 tests. The effectiveness has also been tested with experimental data, and the results show a 97% - 99% accuracy (Fig 2).

[1] M. O. Mustafa, G. Nikolakopoulos and T. Gustafsson, "Faults Classification Scheme for Three Phase Induction Motor," International Journal of System Dynamics Applications, vol. 3, no.1, Jan. 2014. [2] I. Kao, W. Wang, Y. Lai and J. Perng, "Analysis of Permanent Magnet Synchronous Motor Fault Diagnosis Based on Learning," IEEE Transactions on Instrumentation and Measurement, vol. 68, no. 2, pp. 310-324, Feb. 2019.

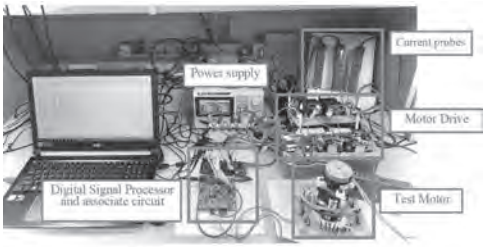

Fig. 1 Experimental Setup

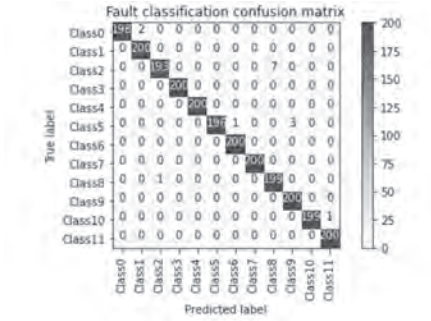

Training Set (no. images)		Test Set (no. images)	Accuracy	
Training	Verification			
9600	2400	2400	Max.	99.37%
			Min.	97.62%
			Mean	98.20%

Fig. 2 Classification results and Accuracy

JPH-02. A Study on Reducing Cogging Torque and Torque Ripple by Applying Rotating Tapering. *S. Lee*[1], I. Yang[2] and W. Kim[1] *1. Electrical Engineering, Gachon University, Seongnam, The Republic of Korea; 2. Electrical Engineering, Hanyang University, Seoul, The Republic of Korea*

The Interior Permanent Magnet Synchronous Motor (IPMSM) has cogging torque and torque ripple in its structure. Cogging torque and torque ripple reduction are important factors in motor design. Various studies have been conducted to reduce these factors. In most studies, the cogging torque reduction method is to reduce the peak-to-peak torque by dividing the d-axis of each stage by applying a skew. A method of applying a skew is effective to reduce cogging torque and torque ripple, but there is a difficulty in manufacturing due to the division of the permanent magnet. Also, unlike SPMSM, since permanent magnets are inserted into the rotor core, IPMSM cannot divide many stages due to manufacturability when skew is applied. Another method is to apply tapering to the rotor. Applying tapering to the rotor increases the air gap length, which reduces the change in reluctance. However, the larger the tapering, the more limited the shape of the permanent magnet, and the need to insert the magnet deep inside the rotor, so there is a risk of reduced output. In this paper, propose a Rotating Tapering method that combines skew and tapering. Rotating Tapering is a method of reducing the peaks of cogging torque and torque ripple by having the front and back cores have the same shape and thus have a symmetrical magnetic flux path. It maintains the advantages of rotor tapering and skew, improves manufacturability by not splitting the permanent magnet. For comparison with the Rotating Tapering application model, the basic model, the tapering application model, and the 2-step skew application model were comparatively analyzed. The validity of this paper was verified through 3D finite element analysis (FEA).

[1] K. Kim, "A Novel Method for Minimization of Cogging Torque and Torque Ripple for Interior Permanent Magnet Synchronous Motor," in IEEE Transactions on Magnetics, vol. 50, no. 2, pp. 793-796, Feb. 2014, Art no.

7019604, doi: 10.1109/TMAG.2013.2285234. [2] P. T. Luu, J. Lee, W. Hwang and B. Woo, "Cogging Torque Reduction Technique by Considering Step-Skew Rotor in Permanent Magnet Synchronous Motor," 2018 21st International Conference on Electrical Machines and Systems (ICEMS), 2018, pp. 219-223, doi: 10.23919/ICEMS.2018.8549086

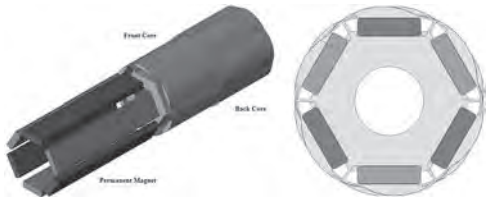

Rotating Tapering Rotor Shape

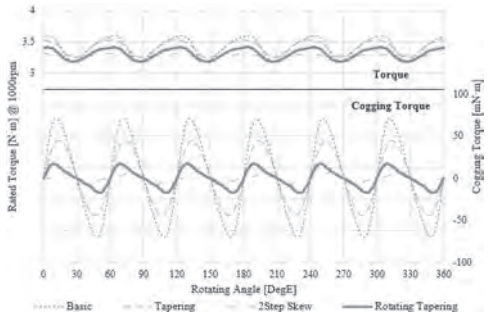

Rated Torque and Cogging Torque Analysis

JPH-03. Study and Experiments of Permanent Magnet Assembly in 10MW-class Permanent Magnet Synchronous Generator for Offshore Wind Turbine Using Analytical Method to Calculate the Magnetic Force. *H. Shin*[1] and J. Choi[1] *1. Chungnam National University, Daejeon, The Republic of Korea*

Offshore wind power generation has garnered interest as a promising renewable energy source owing to high wind speeds and not being scale-limited, and permanent magnet synchronous generators (PMSGs) are commonly used for generators [1]. Since the size of the PM increases with the machine size increasing, the PM should be manufactured in segments for convenient assembly. However, the magnetic force between magnet segments and the force of the magnet on the rotor core can cause it difficulties in assembling magnets. Although several studies have calculated the magnetic forces by using analytical method for immediate calculation, few studies have focused on performing magnetic force calculations for PM assembly. Therefore, in this study, the magnetic forces were calculated via Fourier analysis and Maxwell stress tensor (MST) in the process of PM assembly. The analysis model is a 10MW-class outer-rotor type PMSG, shown in Fig. 1. (a). The PM is axially segmented, as shown in Fig. 1. (b). The segmented PM is inserted and a steel plate was used to cancel out the magnetic force between the PM and rotor yoke, as shown in Fig. 1. (c). Since the analysis model has multipolar structures, the simplified model can be assumed to be a linear structure, as shown in Fig. 1. (d). The permeability of rotor yoke and steel plate was assumed to be infinite to ignore the saturation effect. The permeability of the PM was assumed to be the same as that of air [2, 3]. Fig. 2. (a) and (b) show the finite element method (FEM) and analytical results of the flux density and the magnetic force according to the radial distance, respectively. Owing to PM offset, there is a little difference in results. The radial distance can be selected in various assembly cases based on the analytical solution. The analysis model will be manufactured, and experimental results of the magnetic force will be compared with the analytical solutions. More detailed discussions and results will be provided in the final paper.

[1] W. Gul, Q. Gao, and W. Lenwari, "Optimal Design of a 5-MW Double-Stator Single-Rotor PMSG for Offshore Direct Drive Wind Turbines," *IEEE Trans. on Industry Applications,* vo1.56, no.1, pp.216-225, Jan, 2020. [2] S.-M. Jang, H.-J Park, J.-H. Choi, C. Han, and M.-S. Choi, "Analysis on the Magnetic Force Characteristics of Segmented Magnet Used in Large Permanent-Magnet Wind Power Generator," *IEEE Trans. on Magnetics*, vol.49, no. 7, pp.3981-3984, July, 2013. [3] Z. Q. Zhu, Z. P. Xia, L. J. Wu, and G. W. Jewell, "Analytical Modelling and Finite Element Computation of Radial Vibration Force in Fractional-Slot Permanent Magnet Brushless Machines," *IEEE Trans. on Industry Applications*, vol.45, no. 5, pp.1908-1918, July, 2010.

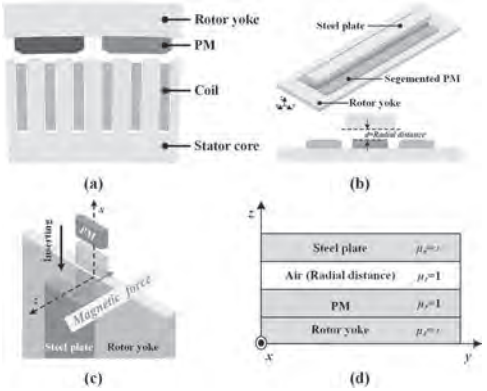

(a) Analysis model (b) Analysis model for the magnetic force (c) The process of inserting PM (d) Simplified model for analytical analysis

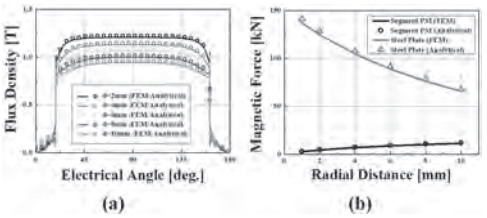

Analytical and FEM results in y direction: (a) Air-gap flux density (b) Magnetic force

JPH-04. Design of a Circulatory Assistance Actuator Applied to an Artificial Lung. *A. Sahnoune*[1,2], M. Hage Hassan[1], G. Krebs[1], C. Marchand[1], P. Dessante[1], O. Mercier[2] and J. Guihaire[2] *1. Paris-Saclay University, Centrale Supélec, CNRS, Laboratory of Electrical and Electronic Engineering of Paris, Gif sur-Yvette, France; 2. Preclinical Research Unit, Marie Lannelongue Hospital, Groupe Hospitalier Paris Saint Joseph, Paris Saclay University, Le Plessis-Robinson, France*

1. Introduction The ANR RHU BioArt-Lung 2020 project aims to develop an extracorporeal artificial lung with reduced size and mass. An essential element of the system is its circulatory assist centrifugal pump, which ensures blood circulation. Our work focuses on this pump's electric motor. Several papers present this medical technology [1-2]. In this article, we outline the electrical motor's specifications and then present an initial dimensioning using a Design of Experiments. We then analyse the chosen structure using both 2D and 3D finite element (FE) methods. A prototype is then manufactured, and performance tests carried out. 2. Specifications and design The motor design should, therefore, be compact (adapted to the pump Fig.1 (a)). It must respect several medical, electrical, and mechanical constraints. The motor design specifications are provided in Table 1. The chosen structure is a radial flux motor with surface permanent magnets (Fig. 1 (b)). Two pairs of poles and its stator contains twelve slots with a concentrated winding. To study several structures, a method based on a Design of Experiments [3] is used. Effects of the variables (dimensions, geometrics) on the outputs: cost functions (torque, mass, efficiency) and constraints (current density, voltage level) are analysed. 3. Performance analysis The PMSM is modelled by both 2D and 3D Finite Element (FE) methods in FEMM and Comsol® Fig.1 (b). Both no-load and on-load analyses are performed. The machine can deliver torque under load with an average value of 60.9 mNm. The amplitude of the torque ripples remains

acceptable (8%). The efficiency max of the PMSM is estimated to 85 %. Using iron loss model [4]. 4. PMSM prototype The prototype of the PMSM has been manufactured to test performance. Fig.1 (c) shows the active part of the engine prototype. In the final paper, a comparison will be presented to validate the simulation results. 5. Conclusion This article explores the design of a PMSM for the development of a portable artificial lung. Its pre-dimensioning is carried out using the Design of Experiments method. Details of the analysis and comparison will be described in the full paper.

[1] J. Asama, T. Oiwa, T. Shinshi, Experimental Evaluation for Core Loss Reduction of a Consequent-Pole Bearingless Disk Motor Using Soft Magnetic Composites., IEEE Transactions On Energy Conversion., VOL. 33, NO. 1 (2018) [2] J. Asama, T. Shinshi, H.Hoshi, A new Design for a compact Centrifugal Blood Pump with a Magnetically levitated Rotor., ASAIO Journal, (2004) [3] T. Ishikawa, S. Sato, S. Takeguchi, Design of a DC Motor Made of Soft Magnetic Composite Core by the Experimental Design Method., IEEE Transactions On Magnetics, VOL. 43, NO. 6, (2007) [4] A. Boglietti, Predicting Iron Losses in Soft Magnetic Materials With Arbitrary Voltage Supply: An Engineering Approach., IEEE Transactions On Magnetics., Vol. 39, No. 2 (2003)

Table 1 Machine parameter

Parameter	Value
Speed (rpm)	[2000 – 10 000] Avoid the risk of hemolysis and thrombosis
Flow (l/min)	[2 - 2.5]
Voltage max of the battery (V)	12.6
Current max of the battery (A)	10
Autonomy (min)	180
Rated torque (mNm)	20
Motor outer diameter (mm)	25
Stack length (mm)	30

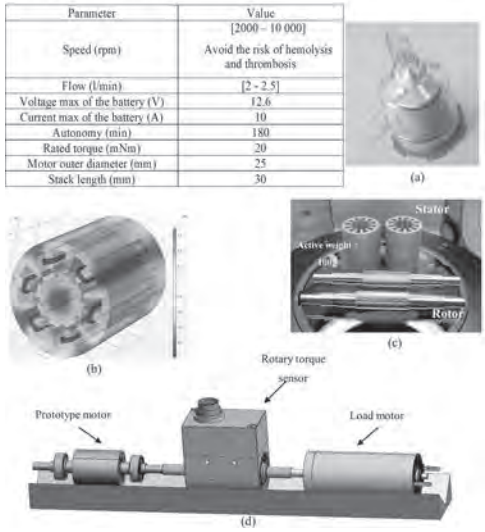

Fig.1 Pump (a), Flux density distribution (b), Prototype (c), Test bench (d)

JPH-05. A New Partitioned Stator Machine Based on Flux Modulation Effect. *H. Wang*[1], H. Zhu[1], S. Ding[1], Z. Wei[1] and C. Wu[1] *1. Nanjing Normal University, Nanjing, China*

The flux switching machine (FSM) and flux reversal machine (FRM) attract great attention because of simple structure of rotor, excellent heat dissipation and high reliability [1]. But both of the permanent magnets (PMs) and the armature windings placed in stator may decrease the space utilization, which limits the further torque production improvement [2]. Thus, the partitioned stator machines (PSMs) are developed, in which the armature windings and PMs are allocated in outer and inner stators to achieve high electromagnetic performances, respectively [3]. However, the existing PSMs with conventional PM arrays evolved from FSM or FRM can not provide high quality torque production. This paper proposes a new PSM with H-shape PM array (HPMPSM), which operates based on flux modulation effect and can offer high quality torque output and space utilization. In addition, the evolution process from conventional FSM and FRM to existing partitioned stator machines that operate based on flux modulation effect are described. H-shape PM (HPM) can be regarded as the combination of the interior PM array (IPM) in FSM and the surface mounted PM array in FRM, which could reduce the flux leakage and improve the flux density in airgaps effectively. HPM is composed of two tangentially magnetized PMs with opposite polarity and one radially magnetized PM. The polarity of the adjacent PMs in radial magnetization are opposite to form one-pole-pair PM excitation. The concentrated windings are adopted on outer stators for high efficiency, and the iron-pieces rotor is sandwiched between stators and has the merit of simple structure and high robustness. FSM, PSM with IPM, FRM, and PSM with surface mounted PM are designed and analyzed, which are simply referred as Models I, II, III, IV and V, respectively. By using finite element analysis (FEA), the electromagnetic performances of proposed HPMPSM are analyzed, containing back electromotive force (EMF), cogging torque, steady torque at rated condition and steady torque characteristics against current angle. The FEA-calculated result shows that the proposed HPMPSM can provide high back-EMF and high torque production with lowest torque ripple, which is desirable for electric vehicle application.

[1] X. Zhu, and C. H. T. Lee, "Overview of flux-modulation machines based on flux-modulation principle: topology, theory, and development prospects," *IEEE Trans. Transp. Electrification*, vol. 6, no. 2, pp. 612-624, Jun. 2020. [2] Z. Q. Zhu, and H. Hua, "Comparative study of partitioned stator machines with different PM excitation stators," *IEEE Trans. Ind. Appl*., vol. 52, no. 1, pp. 199-208, Jan.-Feb. 2016. [3] Z. Wu, and Z. Q. Zhu, "Comparative analysis of partitioned stator flux reversal PM machine and magnetically geared machine operating in stator-PM and rotor-PM modes," *IEEE Trans. Energy Convers*., vol. 32, no. 3, pp. 903-917, Sept. 2017.

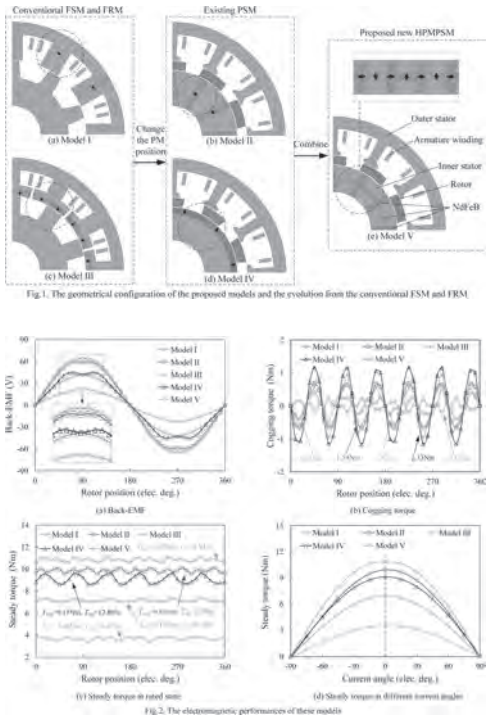

JPH-06. Application Analysis of Self-bonded Silicon Steel Sheet in High Power Density SPMSM. *Z. Yu*[1], Y. Li[1], Y. Jing[1] and J. Wang[1] *1. Shenyang University of Technology, Shenyang, China*

With the development of economy and social progress, people have higher requirements for environmental protection, travel comfort, energy saving and efficiency, so all-electric aircraft technology has been rapidly developed [1-4]. All-electric aircraft is powered by motor, and its performance requirements are higher than conventional motor. To be specific, the driving motor has the advantages of high power density, high torque overload capacity, and so on, which results in an extreme state of magnetic load and electrical load. Therefore, it is particularly important to research the accurate calculation and suppression technology of motor loss. In order to prevent stator core loss, B35A230 self-bonded silicon steel sheet is used as core material, which is a novel with the adhesive coating on the surface of the adhesive electrician ferromagnetic materials, and the coating on the surface of laminate is bonded together under a certain pressure and heat. The processed core can reduce the effect of the processing method on core loss, and the processed ring

specimen is shown in Fig. 1. Conventional stator cores require to be welded on the outside and inside of the core to fix, as shown in Fig. 2, which makes the core loss worse. At the same time, the influence of core axial welding on iron loss is difficult to be calculated by theoretical analysis and finite element simulation. Therefore, the magnetic property of B35A230 ring core with and without weld path is experimentally tested by ring specimen method in this paper. The experimental test system is shown in Fig. 3. The ratio-loss curves at different frequency and different flux density, and the influence law of weld path on core loss are obtained. According to the experimental results of ring specimen method, the loss calculation model is adopted to improve the accuracy, considering processing factors, alternating and rotating magnetization modes and harmonic magnetic fields.

[1] J. Serafini, *et al.*, "Conceptual All-Electric Retrofit of Helicopters: Review, Technological Outlook, and a Sample Design," *IEEE Trans. Transport. Electrific.*, vol. 5, no. 3, pp. 782-794, Sept. 2019. [2] S. Gunter, *et al.*, "Load Control for the DC Electrical Power Distribution System of the More Electric Aircraft," *IEEE Trans. Power Electron.*, vol. 34, no. 4, pp. 3937-3947, Apr. 2019. [3] T. Zhao, S. Wu, and S. Cui, "Multiphase PMSM with asymmetric windings for more electric aircraft," *IEEE Trans. Transport. Electrific*., vol. 6, no. 4, pp. 1592–1602, Dec. 2020. [4] Y. Wang et al., "Partial Discharge Investigation of Form-Wound Electric Machine Winding for Electric Aircraft Propulsion," *IEEE Trans. Transport. Electrific*., vol. 7, no. 1, pp. 78-90, March 2021.

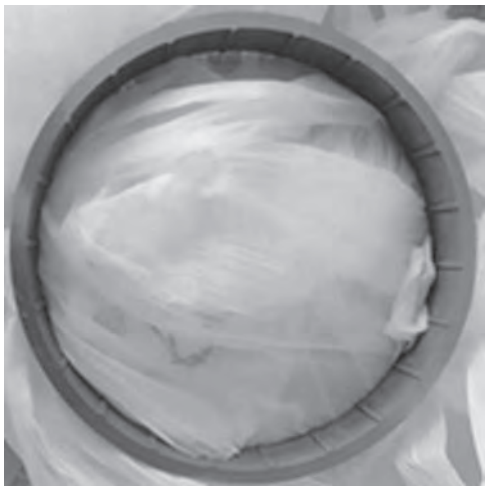

Fig. 1 Ring sample of B35A230 self-bonded silicon steel sheet

Fig. 2 Fixing process of conventional core

JPH-07. Withdrawn

JPH-08. All in one Magnetic Bearing in Permanent Magnet Synchronous Motor by Halbach Array. *I. Yang*[1], S. Lee[2], J. Lee[1], W. Kim[2] and D. Jung[3] *1. Electrical Engineering, Hanyang University, Seoul, The Republic of Korea; 2. Electrical Engineering, Gachon University, Seongnam, The Republic of Korea; 3. Smart Mobility, Halla University, Wonju, The Republic of Korea*

Ultra-high-speed permanent magnet motor is considered a key element to meet the ever-increasing technological demands. For high-speed motors, it is important to secure structural stability as well as electromagnetic design technology. A lot of research on bearings has been actively carried out to reduce friction in the mechanical part and increase efficiency [1], [2]. Magnetic bearings are non-contact bearings using the principle of magnetic levitation, and there is no friction and abrasion [3]-[6]. Magnetic bearings can compensate for the disadvantages of contact bearings. Despite the advantages of magnetic bearings, there are many difficulties in commercializing magnetic bearings. Increase of size and cost is the biggest difficulty in the use of magnetic bearings. If the motor design includes the existing magnetic bearing, the magnetic bearing is a separate structure that controls the shaft from the outside of the rotor and dramatically increases the size of the motor. As the size of the system increases, there are problems with mechanical limitations. Therefore, commercially available magnetic bearings are only possible in limited industrial fields. In this paper, through the halbach arrangement, an all in one magnetic bearing controlled inside the rotor is proposed. The 2D coupled model is shown in Fig. 1 and a 3D decomposition model is shown in Fig. 2. The halbach arrangement refers to a structure in which permanent magnets with different magnetization directions are combined. The halbach arrangement increases the magnetic field on one side and cancels the magnetic field on the other side. Therefore, in the case of a rotor to which the halbach arrangement is applied, the magnetic fields inside the permanent magnets cancel each other and disappear, and the rotor back yoke can be removed. If the rotor back yoke is removed and a hollow shaft is used, it is possible to secure the space inside the rotor, and the existing separate magnetic bearing inserted inside the rotor. Since all in one magnetic bearing does not need to include a bearing structure outside the rotor, it is possible to miniaturize the entire system.

[1] A. Jones, H. Mitterhofer and W. Gruber, *IEEE Trans. Ind. Electron*., vol. 61, no. 6, pp. 3119–3126 (2014) [2] S. Silber, J. Sloupensky and P. Dirnberger, *IEEE Trans. Ind. Electron*., vol. 61, no. 6, pp. 2990–2997 (2014) [3] Y. Le, J. Sun and B. Han, *IEEE Trans on Ind. Electron*., vol. 63, no. 6, pp. 3656–3665 (2016) [4] B. Han, Q. Xu and Q. Yuan, *IEEE Trans on Ind. Electron*., vol. 63, no. 4, pp. 2284–2293 (2016) [5] J. Sun, Z. Ju and C. Peng, *IEEE Trans on Ind. Electron*., vol. 64, no. 3, pp. 2196–2204 (2017) [6] Z. Xu, L. Xu and H. Bangcheng, *IET Electric Power Applications*., vol. 12, no. 8, pp. 1082–1089 (2018)

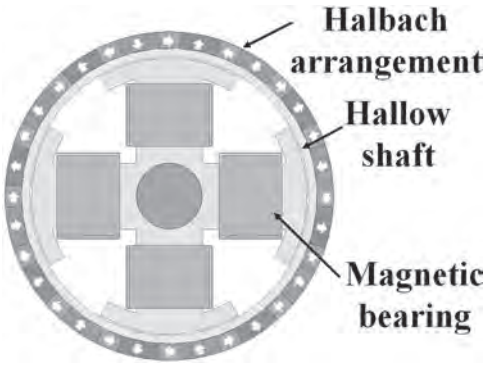

Fig. 1. 2D coupled model.

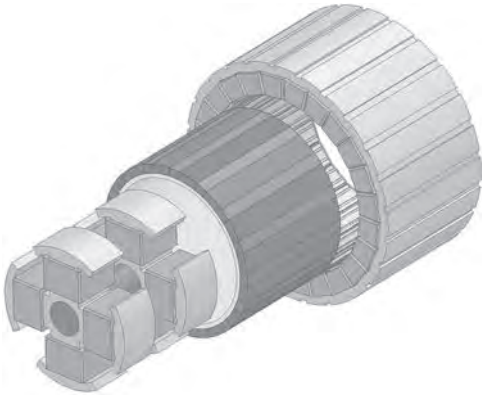

Fig. 2. 3D decomposition model.

JPH-09. Design and Analysis of a Novel Hybrid-Flux Consequent-Pole Permanent Magnet Memory Machine with Transverse Field Excitation. *M. Jiang*[1] and S. Niu[1] *1. Department of Electrical Engineering, The Hong Kong Polytechnic University, Kowloon, Hong Kong*

A new hybrid flux consequent-pole permanent magnet memory Machine (CPPM-MM) with transverse field excitation is presented in Fig.1(a). Compared to conventional designs, the novel design has the following merits: (a) The machine can control the field with DC excitation pulses by using Alnico-PM's characteristics of low coercivity and high remanence, which improves the field regulation capability and enhances the efficiency. (b) With the unique configuration design, the Alnico-PM excitation flux is transverse to the main flux path, thus having minimum interferences with the main flux. The Alnico-PM is axially magnetized and artificially placed in the middle of the solid rotor yoke. A circumferential DC field winding is placed in the middle of the laminated stator yoke, inside the solid stator yoke, and outside the AC winding. The solid stator yoke and solid rotor yoke enable the axial excitation flux to turn into radial flux and flow to the rotor through the stator teeth. Fig.1(b) shows the demagnetizing mode. The Alnico-PM will be excited by the DC excitation pulse, making the iron poles adjacent to NdFeB-PMs in tangential direction have the same polarity. The main flux will path through the stator yoke and rotor yoke radially and axially. Because the field generated by the rotor remains constant, armature windings cannot have flux linkage with the rotor, thus realizing the flux weakening. Fig.1(c) shows the magnetizing mode. The iron pole adjacent to NdFeB-PMs in the axial direction will have the same polarity at this state. The main flux path will pass the stator yoke and rotor yoke tangentially. The machine in this state is like a normal PMSM. A 3-phase 30-slot 4-pole-pair model is designed and analyzed in ANSYS Maxwell 3D. The air gap flux distribution in the states of non-magnetized, fully-demagnetized, and fully-magnetized is shown in Fig.2(a) to Fig.2(c), and their back EMF comparison is shown in Fig.2(d). The results show that the machine has relatively outstanding field controllability.

[1] J. A. Tapia, F. Leonardi and T. A. Lipo, "Consequent-pole permanent-magnet machine with extended field-weakening capability," *in IEEE Transactions on Industry Applications,* vol. 39, no. 6, pp. 1704-1709, Nov.-Dec. 2003. [2] Y. Gong, K. T. Chau, J. Z. Jiang, C. Yu and W. Li, "Analysis of Doubly Salient Memory Motors Using Preisach Theory," *in IEEE Transactions on Magnetics,* vol. 45, no. 10, pp. 4676-4679, Oct. 2009.

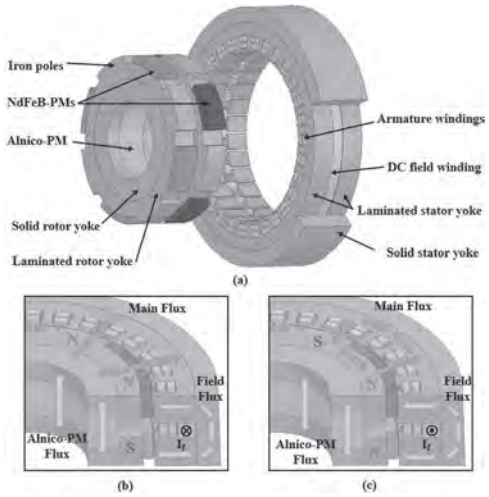

Fig. 1. Structure and different magnetizing modes of CPPM-MM.

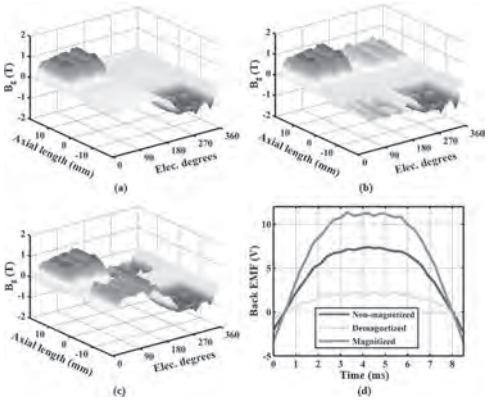

Fig.2. Air gap flux distribution and back EMF comparison of three magnetization states.

JPH-10. Accurate Demagnetization Analysis of Outer Rotor In-wheel Motor Under Braking Condition. *D. Jiang*[1], X. Huang[1], Z. Li[1] and Z. Liu[1] *1. Zhejiang University, Hangzhou, China*

I. Introduction With the development of electric vehicles and automatic driving technology, the outer rotor in-wheel motor has broad prospects in the field of unmanned vehicles for logistics due to its simple structure and large output torque. In order to remove mechanical brake device for compact structure, the large brake torque is essential. Consequently, q-axis current which is dozens of times the rated current will be inevitable. It dramatically increases the risk of demagnetization [1]-[3]. Therefore, the demagnetization of the permanent magnet (PM) motor considering the braking process,

PWM frequency, and control strategy is evaluated. II. Method To improve the analysis efficiency, a decoupling demagnetization analysis method is proposed, which considering the effect of thermal field, electromagnetic field and control circuit simultaneously. Firstly, the thermal circuit is used to obtain the maximum steady-state temperature of the PM motor at the largest current. Then the nonlinear motor model derived from the finite element analysis (FEA) replaces the Simulink motor in the control circuit. The braking current considering the control strategy (id=0 control) and PMW effect is obtained from Simulink. Finally, both current and speed under braking condition are input in the FEA software to calculate the max demagnetization ratio (MDR). III. Discussion and conslusion In Fig. 1(a), the ideal sinusoidal braking current was used in FEA to analyze the demagnetization. In Fig. 1(b), the supply current derived from the Simulink model was exported to the FEA software to consider the PWM effect and control strategy. They all lead to underestimation of the demagnetization. In Fig. 1(c), the proposed method is applied. It shows that the MDR decreases with the increase of PWM frequency because the harmonic amplitude of current is smaller at high PWM frequency. For motor control strategies, the current loop is often set slightly overshoot to improve the dynamic response. In Fig 2, it can be seen that reducing current overshoot can significantly reduce the demagnetization under different loads. Compared to the direct co-simulation model, the calculation time is greatly reduced using the proposed method. Acknowledgement: This work was supported by the National Key R&D Program of China (2019YFE0123500).

[1] S. Ruoho, J. Kolehmainen, and J. Ikaheimo, “Interdependence of Demagnetization, Loading, and Temperature Rise in a Permanent-Magnet Synchronous Motor,” IEEE Trans. Magn., vol. 46, no. 3, pp. 949–953, Mar. 2010. [2] H.-K. Kim and J. Hur, “Magnetic Field Analysis of Irreversible Demagnetization in Brushless DC Motor According to the Dynamic and Static Characteristic,” IEEE Trans. Magn., vol. 51, no. 11, pp. 1–4, Nov. 2015. [3] M.-K. Seo, T.-Y. Lee, and Y.-Y. Ko, “Irreversible Demagnetization Analysis with Respect to Winding Connection and Current Ripple in Brushless DC Motor,” IEEE Trans. Appl. Supercond., vol. 28, no. 3, pp. 1–4, Apr. 2018.

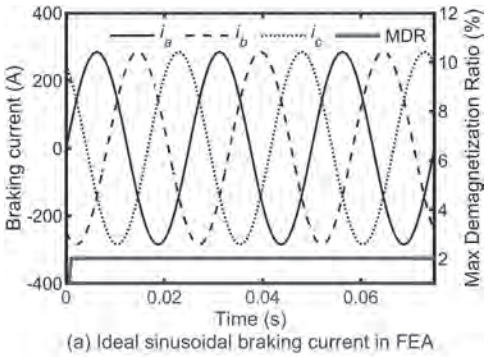

(a) Ideal sinusoidal braking current in FEA

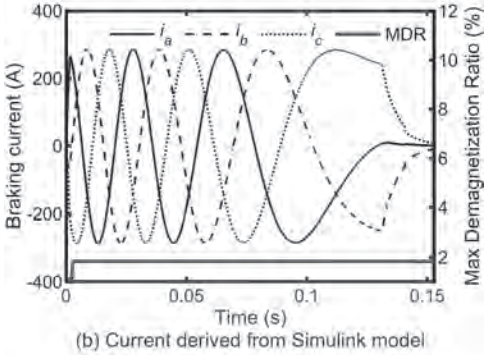

(b) Current derived from Simulink model

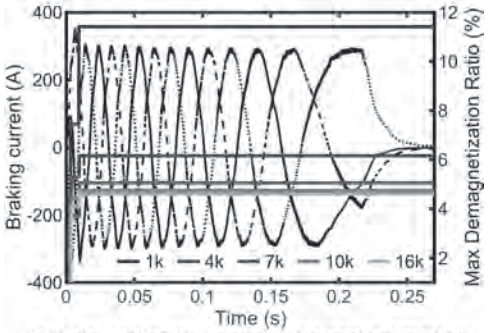

(c) A decoupling demagnetization analysis method considering different PWM frequencies

Fig. 1 Comparison among three methods.

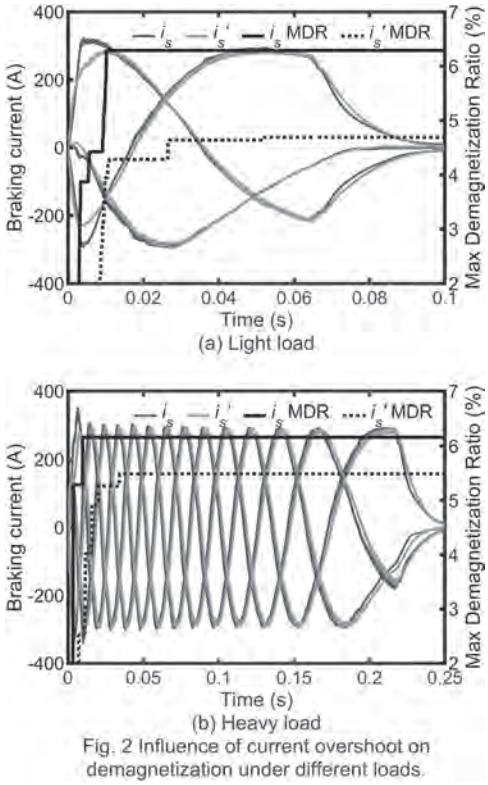

Fig. 2 Influence of current overshoot on demagnetization under different loads.

JPH-11. Novle Spoke-type Permanent Magnet Synchronous Generator Design considering the Characteristics of Wind Power Generator.

D. Kim[1], S. Kim[2], I. Yang[1], J. Lee[1] and W. Kim[3] *1. Hanyang University, Seongnam, The Republic of Korea; 2. Korea Electronics Technology Institute, Gwangju, The Republic of Korea; 3. Gachon University, Seongnam, The Republic of Korea*

Currently, among many new and renewable energies, research on wind power generators is being actively conducted. This is because wind power is more environmentally friendly and economical than other renewable energies. A variety of generator types are used for wind power generators, and among them, permanent magnet synchronous generators with excellent output density are widely used. Among the types of permanent magnets, heavy rare earth permanent magnets have an imbalanced supply and demand and high prices, so research using ferrite magnets has been actively conducted recently. However, there are not many studies on spoke-type wind power generators of 1kW or higher, and although the structure is the same as that of a motor, a design considering the characteristics of the wind turbine must be performed[1,2]. Typical characteristics to be considered are voltage fluctuation rate and cogging torque. This is because the voltage is reduced by resistance and inductance during power generation, and the starting performance of a wind power generator is directly related to the starting torque of the generator. In this paper, we propose a hybrid spoke type permanent magnet synchronous generator design considering the characteristics of a wind turbine. We analyzed the existing spoke type permanent magnet generator using a 3kW class wind power generator as a model, and proposed a hybrid spoke model in which the inner and outer bridges were alternately removed as shown in the Fig.1. And compare the performance of the conventional model and the proposed model through FEM. 3D analysis was performed to confirm the accurate performance considering the 3D effect, and the cause of the higher voltage fluctuation rate than the 2D analysis was analyzed. And to improve this, the rotor overhang structure was applied, and the optimal model was selected by comparing the tendency according to the number of stator slots and the overhang length. The performance of the final model was checked through FEM, a prototype was manufactured, and the results of the performance test were compared in Table.1, and the validity of the design was verified through this

[1] Xu Yang, Dean Patterson, Jerry Hudgins, 'Permanent magnet generator design and control for large wind turbines', 2012 IEEE Power Electronics and Machines in Wind Applications, 2012. [2] Sung Gu Lee, Won-Ho Kim, "A study on the axial leakage magnetic flux in a spoke type permanent magnet synchronous motor", 2017 IEEE International Electric Machines and Drives Conference, May. 2017.

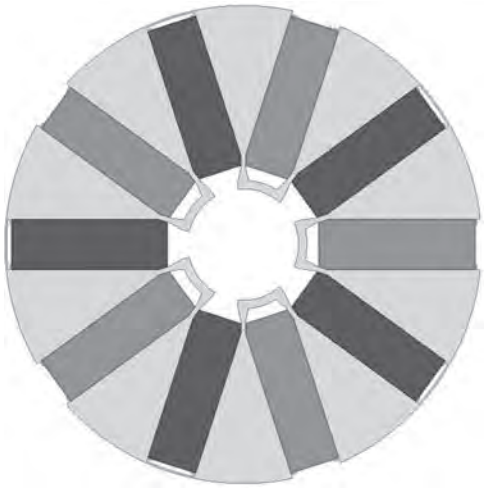

Fig.1 Cross section of Hybrid spoke-type rotor

COMPARISON OF TEST RESULTS AND FEA RESULTS

	Parameter	FEA Result	Test	Unit
No-Load	Line Voltage	232.10	230.99	V_{rms}
	Cogging Torque	2.7	2.5	Nm
Load	Line Voltage	218.17	212.79	V_{rms}
	Current	7.92	8.66	A_{rms}
	Torque	103.64	107.31	Nm
	Voltage fluctuation rate	6.38	8.43	%
	Output Power	2998.42	3160	W
	Efficiency	93.8	93.6	%

Table.1 Comparison of FEA and Test results

JPH-12. A Study on motor control technology through a new concept flux-torque control look up table based on electromagnetic flux.

H. Pyo[1], D. Nam[1], G. Park[2], W. Kim[1] and Y. Hwang[2] *1. Electrical Engineering, Gachon University, Gyeonggido, The Republic of Korea; 2. Electric System Development Team, Hyundai-Wia, Gyeonggido, The Republic of Korea*

Interior Permanent Magnet Synchronous Motor(IPMSM) is mainly used for EV driving motors because it can use reluctance torque, so it has high output, and can operate in a wide speed range through field weakening control. IPMSM drive uses the Maximum Torque Per Ampere(MTPA) control to generate the maximum torque per unit current in the constant torque region, and the field weakening control method to generate the torque in the constant output region[1]–[3]. In order to control torque using this control method, inductance, magnetic flux, and loss that change according to current and speed must be analyzed and reflected in torque characteristics. In general, to compensate for these shortcomings, a look-up table for d, q-axis current or magnetic flux and torque at a specific speed is prepared and used for control. When using a look-up table, loss, inductance, and saturation characteristics of magnetic flux are reflected, so that it is strong against variable changes, but it is difficult to accurately analyze the changing variables. In addition, there is a disadvantage in that the method of creating the look up table is complicated and the mapping time is long due to the rise of motor temperature. In this paper, a magnetic flux-based flux-torque control look up table was created based on the electromagnetic field design of IPMSM, and a look up table model based on the motor electromagnetic field design was devised to compensate through a test. When the designed electromagnetic field design-based look up table model is used, the torque operating point can be analyzed without actually manufacturing the motor, so the electromagnetic field design can be optimized. In general, the look up table used

for torque control of IPMSM is divided into a speed based look up table and a magnetic flux based look up table. Figure 1 (a) and (b) shows speed-torque control and flux-torque control look up table diagram. Figure 2 (a) and (b) shows comparison of test data and flux-torque control data.

[1] J. Alsawalhi and S. Sudhoff, "Design optimization of asymmetric salient permanent magnet synchronous machines*", IEEE Trans. Energy Convers*., vol. 31, no. 4, pp. 1315-1324, Dec. 2016. [2] Xinan Zhang, Gilbert Hock Beng Foo, Muhammed Faz Rahman, "A Robust Field-Weakening Approach for Direct Torque and Flux Controlled Reluctance Synchronous Motors With Extended Constant Power Speed Region", *Industrial Electronics IEEE Transactions on*, vol. 67, no. 3, pp. 1813-1823, 2020. [3] N. Bianchi, S. Bolognani, E. Carraro, M. Castiello, and E. Fornasiero, "Electric vehicle traction based on synchronous reluctance motors," *IEEE Trans. Ind. Appl*., vol. 52, no. 6, pp. 4762–4769, Jul./Aug. 2016.

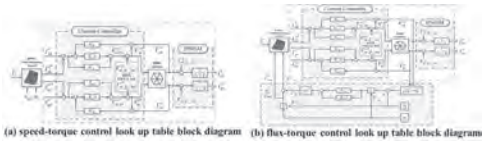

Fig. 1(a) Speed-torque control (b) Flux-torque control look up table block diagram

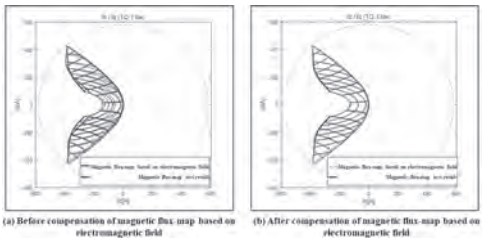

Fig. 2 (a)Before (b)After compensation of magnetic flux torque control look up table based on electromagnetic field and test graph comparison

JPH-13. Study on inductance parameter curve fitting method for flux-torque control of IPMSM. *H. Pyo*[1], D. Kim[2], M. Jeong[1], I. Yang[2], S. Song[2] and W. Kim[1] *1. Electrical Engineering, Gachon University, Gyeonggido, The Republic of Korea; 2. Electrical Engineering, Hanyang University, Seoul, The Republic of Korea*

In the case of speed-torque control, which is widely used in the existing current control, it has the advantage of excellent torque control characteristics by creating a current-map for each rotation speed and voltage of the motor [1] – [4]. However, in the case of speed-torque control, since it is a method made from DC voltage, it requires a lot of testing after production to extract data for each voltage in order to control it in consideration of voltage fluctuations. However, in the case of flux-torque control, unlike the principle of speed-torque control, there is no need to prepare a current-map for each voltage, so it does not take much time for testing. However, there is a disadvantage in that the value of the flux estimator needs to be adjusted, so that it is necessary to properly respond to voltage fluctuations for each driving area. In this paper, flux-torque control was performed based on the magnetic flux extracted from the electromagnetic analysis value. In this paper, a method of interpolating of inductance values, an important factor, was proposed to create a flux-torque control look-up table. In the case of inductance, it is difficult to measure because it is a result value that changes depending on the applied current and the saturation of the iron core. Therefore, in this paper research was conducted on the inductance interpolating method. Figure 1 is the comparison result data of flux linkage obtained through the interpolated data and actual test data. Figure 2 shows the comparison result data of d-q axis voltage graph through the interpolated data and actual test data. Based on the flux linkage data extracted from FEM, the nonlinear inductance was interpolated with the above mentioned formula. In the case of inductance interpolating proposed in this paper, it was confirmed that there is almost no error when comparing and analyzing the flux linkage of the actual test data. Therefore, it has accurate flux linkage data through FEM data, which is advantageous for motor flux-torque control.

[1] J. Alsawalhi and S. Sudhoff, "Design optimization of asymmetric salient permanent magnet synchronous machines", IEEE Trans. Energy Convers., vol. 31, no. 4, pp. 1315-1324, Dec. 2016. [2] Xinan Zhang, Gilbert Hock Beng Foo, Muhammed Faz Rahman, "A Robust Field-Weakening Approach for Direct Torque and Flux Controlled Reluctance Synchronous Motors With Extended Constant Power Speed Region", Industrial Electronics IEEE Transactions on, vol. 67, no. 3, pp. 1813-1823, 2020. [3] N. Bianchi, S. Bolognani, E. Carraro, M. Castiello, and E. Fornasiero, "Electric vehicle traction based on synchronous reluctance motors," IEEE Trans. Ind. Appl., vol. 52, no. 6, pp. 4762–4769, Jul./Aug. 2016. [4] S. K. Sahoo and T. Bhattacharya, "Field weakening strategy for a vector controlled induction motor drive near the six-step mode of operation," IEEE Trans. Power Electron., vol. 31, no. 4, pp. 3043–3051, Apr. 2016.

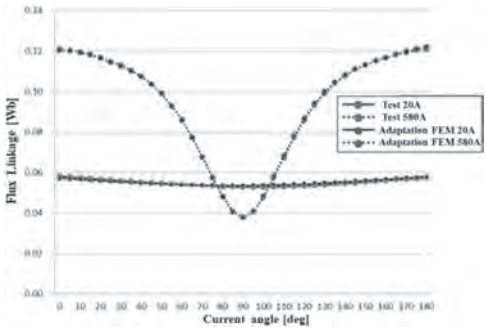

Fig. 1. Flux linkage/Current angle degree curve comparison of test data and after interpolated FEM result

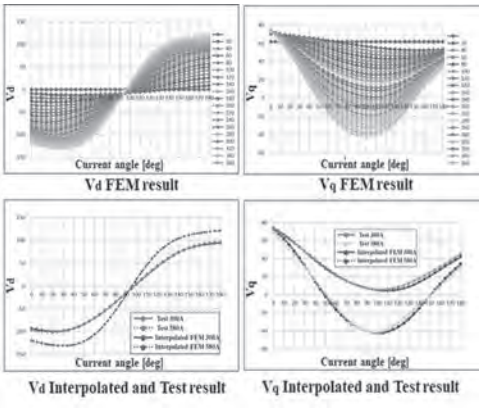

Fig. 2. D-Q axis voltage comparison of test data and after interpolated FEM result

JPH-14. Combined electromagnetic and mechanical optimisation of an interior permanent magnet rotor. *G. Zhang*[1] and G.W. Jewell[1] *1. Electronic and Electrical Engineering, University of Sheffield, Sheffield, United Kingdom*

In high-speed electrical machines, centrifugal forces within the rotor can be first-order constraints on electromagnetic optimisation. This can be particularly acute, even at modest speeds, in interior permanent magnet (IPM) machines in which magnets are retained entirely by the rotor core with no additional mechanical containment. A close-up of one such IPM is shown in Figure 1 with key dimensions defined. The magnets, which are profiled to reduce stress concentrations, act as dead-weights which must be resisted by the single-piece core. The electromagnetic and mechanical design pinch-points are the thickness of the outer rib that closes off the magnet slot (h_1) and the separation between magnets (h_2). Increasing h_1 or h_2 enhances mechanical

support but at the expense of greater leakage flux. A combined mechanical-electromagnetic optimisation was undertaken using 2D finite element analysis (FEA) to establish an optimal combination of rotor diameter, h_1 and h_2 to maximise torque density in an 8-pole, 100kW PM machine with a base speed of 4,000rpm and an extended speed range up to 12,000rpm. A maximum localised core stress limit of 240MPa was specified, this being 60% of the yield strength for NO20 alloy. The optimisation was done by systematic consideration of the design space rather than by formal optimisation methods. Rotor diameters from 120mm to 180mm in 15mm increments were considered, and for each diameter values of h_1 and h_2 which meet the mamximum stress limit at 12,000rpm were identified by structural FEA. For viable combinations of h_1 and h_2, torque was calculated by FEA for both 30 and 24 slot stators using FLUX2D. The axial length was then scaled to produce rated torque of 239Nm allowing the torque density to be calculated. The optimised rotor design diameter is 165mm and is 103mm long with a fractional-slot winding in a 30 slot stator. The overall machine has an active mass of 40.8kg with corresponds to ~2.5kW/kg. The paper described this optimisation study in detail and draws on the results to explore the nature of the design trade-offs in such rotors and impact of core properties.

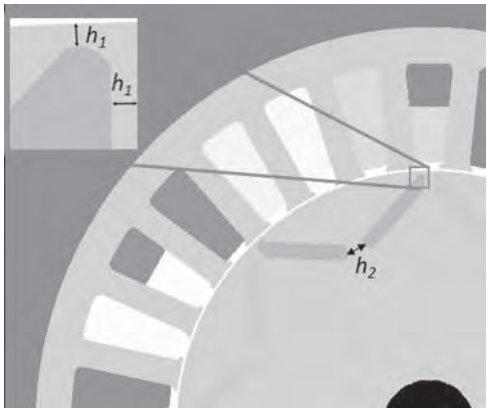

Figure 1 - Close up cross-section of the IPM machine type

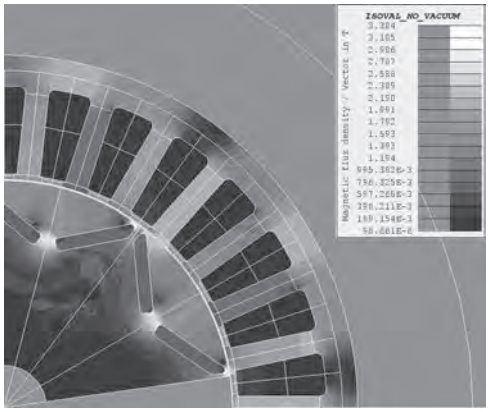

Figure 2 - Finite element predicted flux density at full-load

Session JPI
SURFACE AND INTERIOR MOUNTED PERMANENT MAGNET ELECTRICAL MACHINES III (Poster Session)

Oleksandr Dobzhanskyi, Co-Chair
Point Park University, Pittsburgh, PA, United States
Narayan Kar, Co-Chair
University of Windsor, Windsor, ON, Canada

JPI-01. Reducing Zero-Mode Vibration for Permanent Magnet Synchronous Machines through Changing Phases of Concentrated Forces.
Y. Xu[1] and *Z. Xu*[1] *1. School of Electrical Engineering and Automation, Harbin Institute of Technology, Harbin, China*

Introduction When permanent magnet synchronous machines (PMSMs) are running, electromagnetic forces acting on stator teeth excite vibrations. The electromagnetic forces can be decomposed into concentrated forces at different frequencies by FFT. If phase differences between the concentrated force are zero, zero-mode vibrations are excited. The zero-mode vibrations are generally dominant in PMSMs. Some approaches on optimizing the structure have been proposed for reducing the zero-mode vibrations. In addition, injecting harmonic currents into windings is also effective. However, almost existing methods aims to decrease the amplitude of concentrated forces. This study investigated the method of changing the phase difference between concentrated forces to transform zero-mode vibrations to nonzero-mode vibrations. Methodology The investigation used a finite-element model of surface mounted PMSM with 12 poles 36 slots. Its permanent magnets were optimized for decreasing the amplitude of concentrated forces. The main frequency of the zero-mode vibration of the model is 6 times fundamental frequency. So different 5^{th} harmonic currents were injected into windings for changing phases of concentrated forces. Then, concentrated forces before and after the injection were calculated respectively, and its phase differences were analyzed. Finally, the validity of the injection was verified by calculating vibrations. Result The phase difference between concentrated force was changed from 0 degree to 120 degree after the harmonic injection. Fig.1 shows the vibration before the harmonic injection, and Fig. 2 shows the vibration after the harmonic injection. The zero-mode vibration became the nonzero-mode vibration after harmonic injection and its amplitude was reduced. Conclusion Combining the optimization and the harmonic injection not only reduced the amplitude of the concentrated force, but also changed the phase difference between them. Thus, zero-mode of vibrations can be transformed into nonzero-mode vibrations, and their amplitudes are reduced significantly.

Fig.1 Acceleration of the core surface without harmonics

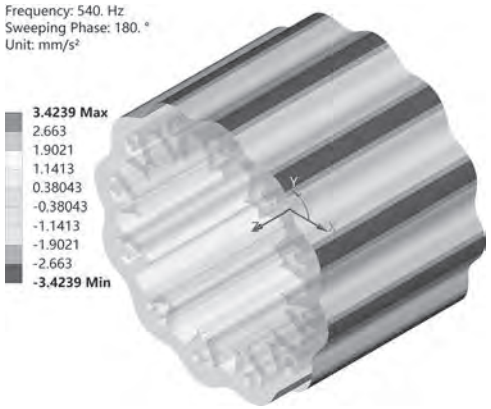

Fig.2 Acceleration of the core surface with harmonics

JPI-02. Suppression of Torque Ripple in a New Consequent-Pole Permanent Magnet Machine by Segmented Structure.
G. Qu[1], Y. Fan[1] and *Q. Chen*[1] *1. School of Electrical Engineering, Southeast University, Nanjing, China*

I. INTRODUCTION Due to their advantages of low permanent magnet (PM) cost and high torque density, consequent-pole PM (CPM) machines have drawn wide attention in some variable speed applications, such as electric vehicles [1]. However, CPM machines suffer from higher torque ripples than the traditional PM machines [2]. The traditional torque ripple suppression techniques introduced in [3-4] may result in some loss of the output torque. Therefore, a new CPM machine with segmented structure/unequal teeth (SU-CPM machine), which can decrease the torque ripple and increase the output torque, is proposed in this paper. II. MACHINE TOPOLOGY The SU-CPM machine is shown in Fig. 1(a). The V-type PMs and the iron cores in the rotor are arranged as the sequence of S-iron-S-N-iron-N. The stator teeth are subdivided into two types. The five-phase winding located in the stator is the fractional-slot concentrated winding, which is helpful to improve the fault-tolerant capability of PM machines. The conventional CPM machine with unsegmented structure/equal teeth (UE-CPM machine) is shown in Fig. 1(b). Compared with the UE-CPM machine, the stator of the SU-CPM machine is divided into three parts with different initial phase angles. In Fig. 1(c), the flux paths in the SU-CPM machine include two parts. The first flux path is composed of two PMs with opposite polarities. The second flux path is composed of one iron core and one PM. III. ELECTROMAGNETIC ANALYSIS The electromagnetic characteristics of this proposed machine are analyzed by the finite element method. The back electromotive force (back-EMF) waveforms are shown in Fig. 2(a). The output torque waveforms are shown in Fig. 2(b). It can be seen that the torque ripple of the SU-CPM machine is quite low (0.6%), compared with that (12.6%) of the UE-CPM machine. The cogging torque waveforms are shown in Fig. 2(c). IV. CONCLUSION A new SU-CPM machine is introduced and analyzed in this paper. It can be concluded that the SU-CPM machine can exhibit better electromagnetic properties than the UE-CPM machine.

[1] H. Hua, Z. Q. Zhu and H. Zhan, "Novel Consequent-Pole Hybrid Excited Machine With Separated Excitation Stator," *IEEE Trans. Ind. Electron.*, vol. 63, no. 8, pp. 4718-4728, Aug. 2016. [2] J. Li, K. Wang and C. Liu, "Comparative Study of Consequent-Pole and Hybrid-Pole Permanent Magnet Machines," *IEEE Trans. Energy Convers.*, vol. 34, no. 2, pp. 701-711, Jun. 2019. [3] X. Zhu and W. Hua, "An Improved Configuration for Cogging Torque Reduction in Flux-Reversal Permanent Magnet Machines," *IEEE Trans. Magn.*, vol. 53, no. 6, pp. 1-4, Jun. 2017. [4] Y. Pang, Z. Q. Zhu and Z. J. Feng, "Cogging Torque in Cost-Effective Surface-Mounted Permanent-Magnet Machines," *IEEE Trans. Magn.*, vol. 47, no. 9, pp. 2269-2276, Sep. 2011.

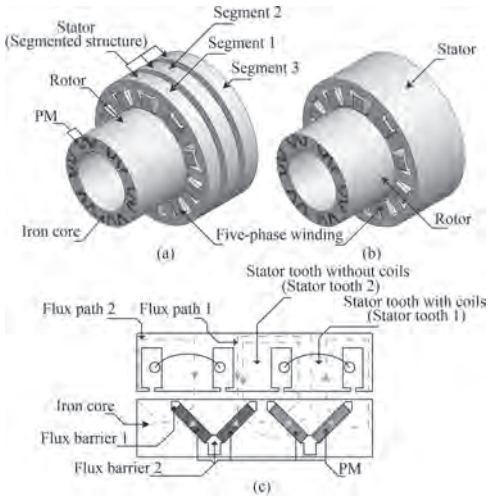

Fig. 1. Machine topologies. (a) SU-CPM machine. (b) UE-CPM machine. (c) Magnetic paths.

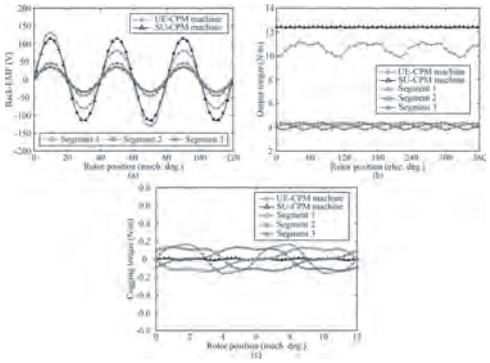

Fig. 2. Electromagnetic field analysis. (a) Back-EMFs. (b) Output torques. (c) Cogging torques.

JPI-03. Spoke-type Permanent Magnet Synchronous Generator Design to Improve Magnetizing and Cogging Torque Performance. *D. Kim*[1], I. Yang[1], S. Song[1], J. Lee[1] and W. Kim[2] *1. Hanyang University, Seoul, The Republic of Korea; 2. Gachon University, Seongnam, The Republic of Korea*

In this paper, a spoke-type permanent magnet synchronous generator (PMSG) rotor design was proposed considering the magnetization performance and cogging torque using a 500W class wind power generator as a model. The spoke-type PMSG is designed to have a structure in which a permanent magnet (PM) is vertically inserted into the rotor, which is unfavorable to magnetization [1.2]. Since the magnetization performance of PM is directly related to the demagnetization performance and mass productivity of PM, a design considering this is necessary. First, factors affecting the magnetization performance during magnetization of the spoke-type rotor were analyzed. Considering this, the rotor design was performed and the magnetization performance of the existing model and the proposed model was compared in Fig.1 through FEM. The magnetization conditions and PM usage of both models are the same. However, it can be confirmed that the proposed model has fewer non-magnetized and demagnetized areas than the existing model, and is fully magnetized. The design for reducing the cogging torque, which is directly related to the starting performance of the wind power generator, was additionally carried out. In general, the cogging torque is reduced by applying a skew to the rotor, but this has the disadvantage of poor performance and mass productivity. Therefore, a rotor shape in which the barrier is designed asymmetrically and then cross-laminated is proposed. The proposed shape has better mass productivity than the existing skew method, and it can be confirmed that the cogging torque is reduced by the effect as shown in the Fig.2. In the case of the proposed model, the line-to-line voltage was reduced by about 6.9% compared to the general spoke type. However, it was confirmed that the cogging torque was reduced by about 25.9% compared to the previous model, and the THD was improved by 2.43%P. Finally, the design of the spoke model with improved magnetization and cogging torque performance compared to the existing model was completed, and the satisfaction of the target specifications and design feasibility were verified through simulation.

[1] S. G. Lee, J. Bae and W. Kim, "Design Process of Spoke-Type Permanent Magnet Synchronous Motor Considering Magnetization Performance," in *IEEE Transactions on Applied Superconductivity*, vol. 30, no. 4, pp. 1-6, June 2020 [2] S. G. Lee, J. Bae, M. Kim and W. Kim, "Study on the Improvement of the Correction Coefficient Considering the 3-D Effect of Spoke-Type Permanent-Magnet Synchronous Motor," in *IEEE Transactions on Magnetics*, vol. 56, no. 3, pp. 1-5, March 2020

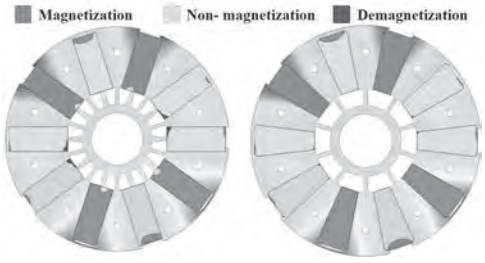

Fig.1 Comparison of magnetization analysis results

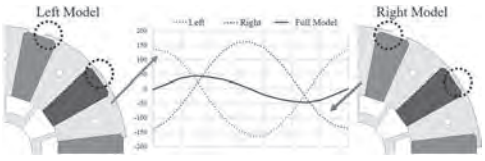

Fig.2 Rotor shape and cogging torque waveform

JPI-04. Characteristics Analysis and Design of Permanent Magnet Synchronous Motor Considering Cryogenic Environment. *D. Kim*[1], I. Yang[1], S. Song[1], D. Kim[2] and W. Kim[2] *1. Hanyang University, Seoul, The Republic of Korea; 2. Gachon University, Seongnam, The Republic of Korea*

Recently, Liquefied Natural Gas(LNG) has been widely used due to several advantages. To efficiently load LNG, a submersible pump as shown in the Fig.1 is used. A motor is contained in the submersible pump, and this motor is immersed in LNG fuel at a very low temperature(-193C). Therefore, it is necessary to use a motor that considers the cryogenic environment unlike the conventional motor. Induction motors are usually used in such a cryogenic environment. This is because, unlike general induction motors, due to the cryogenic environment, current density is high and resistance is low, so the same output can be satisfied even in a smaller size than general induction motors. However, in the case of a cryogenic motor, it is operated at a partial load other than the rated load. Since an induction motor is usually designed in consideration of only one operating point and the rated load, the efficiency is very low during partial load operation. In this paper, a characterization and design of a Permanent Magnet Synchronous Motor

(PMSM) considering a cryogenic environment is proposed. First, the target specifications of the conventional 15kw class cryogenic induction motor are shown in Table.1. The PMSM was designed in consideration of the target specifications, and the electromagnetic performance according to the magnet material (Nd, SmCo) and the mechanical stress in the cryogenic environment were compared together. Although the motor is mainly operated at cryogenic temperature, it is exposed to room temperature in the absence of fuel. Considering this, the electromagnetic performance and mechanical rigidity of the ring magnet type and the full magnet type were compared. A PMSM that satisfies the target specification was designed by analyzing the electromagnetic performance and mechanical performance according to the material and structure of the magnet through FEM and considering the partial load. Finally, the efficiency and mechanical characteristics of the existing induction motor and the final model at rated load and partial load were compared through FEM and the design feasibility was verified.

[1] H. M. Kim, K. W. Lee, D. G. Kim, J. H. Park and G. S. Park, "Design of Cryogenic Induction Motor Submerged in Liquefied Natural Gas," in *IEEE Transactions on Magnetics*, vol. 54, no. 3, pp. 1-4, March 2018 [2] C. Ai, Y. Huang and H. Wang, "Coupled Electromagnetic and Thermal Analysis of a 15kW Cryogenic Induction Motor for Submerged Liquefied Natural Gas Pumps," *2020 23rd International Conference on Electrical Machines and Systems (ICEMS)*, 2020, pp. 745-748

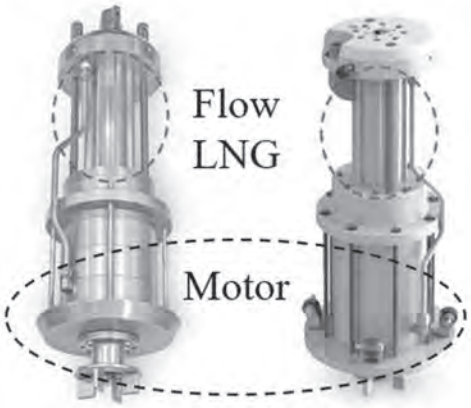

Fig.1 A submerged LNG pump with cryogenic motor

TABLE I MOTOR SPECIFICATION

Parameter	Value	Unit
Rated Power	15	kW
Speed @ rated power	10000	rpm
Partial Load Power	6	kW
Stator Outer Diameter	163	mm
Rotor Outer Diameter	96.6	mm
Stack length	110	mm
Efficiency	88	%

Table.1 Motor Specification

JPI-05. Stator Design of Interior PMSM for Reduction Shaft Voltage Considering the Electromagnetic Characteristics. *H. Yoon*[1], S. Jun[1], C. Kim[1], T. Ji[1], Y. Kim[2] and S. Jung[1] *1. Department of Electrical and Computer Engineering, Sungkyunkwan University, Suwon, The Republic of Korea; 2. Department of Electrical Engineering, Chosun University, Gwangju, The Republic of Korea*

Propulsion motors for electric vehicles (EVs) are driven by pulse width modulation (PWM) which generates a common-mode voltage (CMV) because the summation value of all phase voltages is not zero by PWM switching harmonics. The CMV and parasitic capacitances(Caps) in the motors cause shaft voltage (SV), which is the main factor for bearing failure. To overcome this issue, many articles have been presented, in which they proposed the methods such as the usage of the insulated rotor, ceramic bearing, and ground ring. However, since these methods increase manufacturing costs and require additional work, it is not reasonable to reduce the SV with the solutions [1-3]. Therefore, in this paper, we propose a novel design methodology for reducing SV of the propulsion motors based on the stator configuration considering electromagnetic characteristics. To do this, the bearing voltage ratio (BVR) defined as the ratio between the CMV and SV should be suppressed. Thus, the stator-rotor Cap (Csr) and the winding-rotor Cap (Cwr) should increase and decrease respectively when assuming the identical bearing Cap (Cb), since BVR is calculated as Cwr/(Cwr+Csr+Cb). The design variables of the interior permanent magnet synchronous motor (IPMSM) are defined as shown in Fig. 1. Wopen and Wcoil are changed to the width that is possible to manufacture and with the equal area respectively. Also, when Lcr is varying, the length of the slot is changing with the same value. The BVR is analyzed according to the variables for reducing SV. Moreover, AC copper loss is not negligible in the case of the hairpin winding model, which has a relationship with the coil shape and position that also affect the BVR. Hence, we analyze the BVR and efficiency considering AC copper loss as depicted in Fig. 2 [4]. In the manuscript, optimization applying particle swarm optimization (PSO) algorithm for reducing SV and maintaining efficiency taking into account AC copper loss will be carried out at low- and high-speed regions. Furthermore, the analysis method of the SV employing the electric discharge machining (EDM) effect will be proposed in detail [5].

[1] Umar Tabrez shami, Hirofumi Akagi, *IEEE Transactions on Power Electronics*, vol. 25, no. 6, pp. 1615-1625 (2010) [2] S. Lee, Hur, *IEEE Transactions on Industry Applications*, vol. 55, no. 2, pp. 1430-1436 (2019) [3] J. Park, T. R. Wellawatta, *IEEE Transactions on Industry Applications*, vol. 53, no. 5, pp. 4441-4449 (2017) [4] S. Wang, D. G. Dorrell, *IEEE Transactions on Magnetics*, vol. 51, no. 11, pp. 1-4, (2015) [5] J. Kalaiselvi, S. Srinivas, *IEEE Transactions on Industrial Electronics*, vol. 62, no. 1, pp. 144-152 (2015)

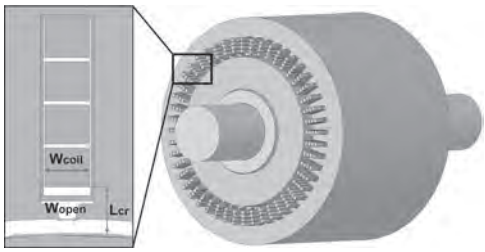

Fig.1. The design variables of the IPMSM

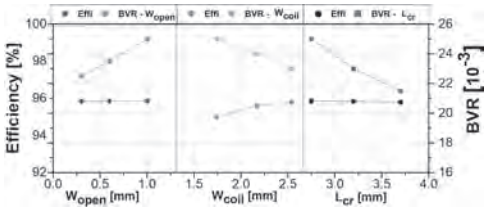

Fig.2. The BVR and efficiency depending on the variables

JPI-06. Segmented Asymmetrical Stator of PMSM for Torque Ripple Reduction. *C. Liu*[1], J. Zou[1], Y. Xu[1], G. Yu[1] and L. Zhuo[1] *1. Harbin Institution of Technology, Harbin, China*

I. Introduction PMSM is widely used in industrial fields because of the advantages of high power density and high efficiency [1-3]. However, torque ripple of PMSM can cause vibration and noise, which are not conducive to the smooth operation of the motor. Consequently, this paper proposes segmented asymmetrical stator design, which can reduce torque ripple without significant drop of average torque. II. Segmented Asymmetrical

Stator Design A 6-pole 9-slot PMSM is carried out to analyze the proposed stator design. Then segmented asymmetrical design is carried out to optimize the stator. The main parameters are θ and *W*. θ is the degree from the middle of teeth to the middle of slot opening. W is the width of the slot opening. From the FEA analysis, it's easy to find two torques which have opposite ripple phases. The first section is that when θ is 14° and *W* is 1.2 mm, and the second section is the mirroring of the first. The shapes of the sections and the torques are shown as Fig.1. According to the FFT analysis, the phases of sixth ripples of two sections are 65.9° and -109.3°, and the amplitudes are 0.1961Nm and 0.0763Nm. Adjusting the length ratio of the two sections to 2:5, then the amplitudes of sixth ripples are 0.056Nm and 0.0545Nm. The sixth ripples generated by two sections have the opposite phases and similar amplitudes, so the torque ripple of the whole motor can be decreased. The schematic of segmented asymmetrical stator and the torque waveforms are shown as Fig.2. III. Conclusion This paper proposes a segmented asymmetric stator structure. By optimizing the design parameters and adjusting the length of two stator segments, two torques with opposite ripple phases and similar ripple amplitudes can be obtained, so the two ripples can offset each other thus decreasing the torque ripple of the whole motor. This method doesn't require PM shape optimization, so the average torque will not decrease significantly.

Fig.1 Schematics of stator sections and waveform of torques

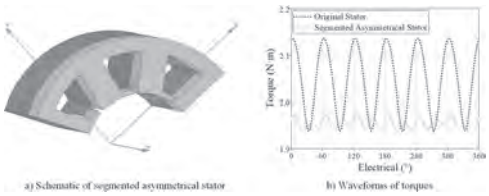

Fig.2 Schematic of segmented asymmetrical stator and waveform of torques

JPI-07. Design of Five-Phase PMSM with Hybrid Single/Double Layer Fractional Slot Winding for Torque Improvement under Third Harmonic Current Injection. *J. Huang*[1], Y. Sui[1], Z. Yin[1], Z. Yuan[1] and P. Zheng[1] *1. Harbin Institute of Technology, Harbin, China*

Five-phase permanent magnet synchronous machine (PMSM) can achieve torque improvement while keeping copper loss unchanged, when injecting 3rd harmonic current under the constraint of constant RMS value of phase current. Since torque of constant RMS harmonic injection (C_RMS) is proportional to the 1st and 3rd harmonic in back EMF (E_1 and E_3) of 5-phase PMSM, many researches aiming to enhance torque under C_RMS focus on improving E_1 and E_3 by optimizing winding arrangement or stator structure of PMSM [1-3]. In this paper, a novel 60-slot/22-pole 5-phase PMSM with hybrid single/double layer fractional slot winding (HLFSW) is proposed, which not only improves torque under C_RMS, but also has the advantage of lower space harmonic content in magnetomotive force (MMF). The proposed PMSM (M2) is compared with 20-slot/22-pole PMSM (M1), as shown in Fig. 1. M1 adopting fractional slot concentrated winding contains many harmonics in MMF, so to suppress non-working harmonics in MMF, M2 combines two sets of M1 windings with 99° difference in space. Besides, coil-pitch of M2 is optimized to 15.75° to improve E_1 and E_3, so as to further enhance torque under C_RMS. Since coil-pitch of M2 is shorter than that of M1 (18°), double-layer slots in M1 containing coils from different phases are separated to single-layer slots. Conversely, double-layer slots containing coils from the same phase remain unchanged, and that is why M2 adopts HLFSW. Comparing harmonic analysis of MMF and back EMF of M1 and M2 as shown in Fig. 2(a) and (b), the 9th harmonic is mainly suppressed, and E_1 and E_3 of M2 are higher than M1. Torque and losses of M1 and M2 under C_RMS are shown in Fig. 2(c) and (d), with phase current expressed below: $I_1=\{1/[1+(E_3/E_1)^2]\}^{0.5}*I_0$ $I_3=(E_3/E_1)*I_1$ where I_1 and I_3 are the amplitude of the 1st and 3rd harmonic current; I_0 is the amplitude of phase current before harmonic injection. Torque of M2 is always higher than M1 when I_0 increases, although with higher ripple. PM loss of M2 is much lower than M1 due to low space harmonics design, and the sum of PM loss and core loss of M2 is lower than M1.

[1] M. Farshadnia, M. A. Masood Cheema, A. Pouramin, R. Dutta and J. E. Fletcher, "Design of Optimal Winding Configurations for Symmetrical Multiphase Concentrated-Wound Surface-Mount PMSMs to Achieve Maximum Torque Density Under Current Harmonic Injection," in IEEE Transactions on Industrial Electronics, vol. 65, no. 2, pp. 1751-1761, Feb. 2018. [2] Z. Y. Gu, K. Wang, Z. Q. Zhu, Z. Z. Wu, C. Liu and R. W. Cao, "Torque Improvement in Five-Phase Unequal Tooth SPM Machine by Injecting Third Harmonic Current," in IEEE Transactions on Vehicular Technology, vol. 67, no. 1, pp. 206-215, Jan. 2018. [3] J. Huang, P. Zheng, Y. Sui, J. Zheng, Z. Yin and L. Cheng, "Third Harmonic Current Injection in Different Operating Stages of Five-Phase PMSM With Hybrid Single/Double Layer Fractional-Slot Concentrated Winding," in IEEE Access, vol. 9, pp. 15670-15685, 2021.

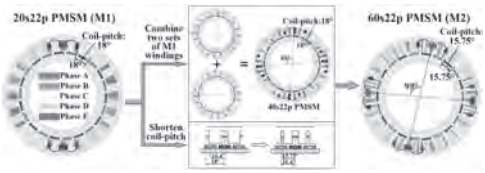

Fig. 1 Machine structure comparison.

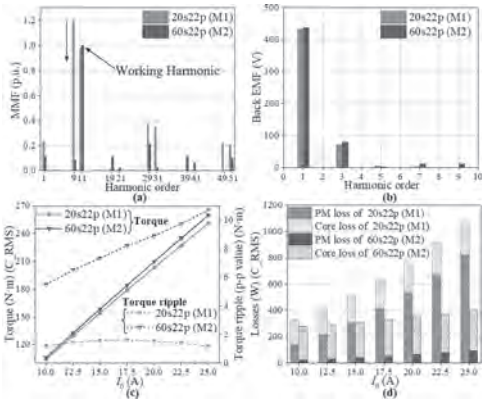

Fig. 2 Performance comparison. (a) Back EMF. (b) MMF. (c) Torque of C_RMS. (d) Losses of C_RMS.

JPI-08. A Novel High Torque Density Dual Three-Phase PMSM with Low Space Harmonic Content. *J. Huang*[1], Y. Sui[1], Z. Yin[1], Z. Yuan[1] and P. Zheng[1] *1. Harbin Institute of Technology, Harbin, China*

Permanent magnet synchronous machine (PMSM) with fractional slot concentrated winding (FSCW) is popular for short winding-end and easy assembly; however, many harmonics are contained in magnetomotive force (MMF) of PMSMs adopting FSCW, which causes high core loss and eddy current loss in PMs (PM loss). Most methods proposed to suppress non-working harmonics in MMF of FSCW decrease the working harmonic inevitably, which leads to torque decrease and is unfavorable in applications requiring high torque density [1-3]. Thus, a 36-slot/14-pole dual 3-phase PMSM with hybrid single and double layer fractional slot winding is proposed to reduce harmonics in MMF and improve torque simultaneously. The proposed PMSM (M3) is compared with 12-slot/14-pole and 24-slot/14-pole dual 3-phase PMSM (M1 and M2), as shown in Fig. 1(a). All machines are designed under the same specifications to ensure a fair comparison. The angle between two sets of 3-phase windings, namely Phase-A, B, C and Phase-D, E, F, is 30° for M1, but 15° for M2 and M3. All machines eliminate

certain non-working harmonic in MMF by the superposition of MMF generated by two sets of 3-phase windings. Superior to M1 and M2 with only 1st or 5th harmonic cancelled, both 1st and 5th harmonics are cancelled in M3, as shown in Fig. 2(b). It is because M3 adopts unequal-turn coils, with N1 turns of one side and N2 turns of the other side, which satisfies N2/N1=0.9, e.g. N1=20, N2=18, as shown in Fig. 2(a). Besides, working harmonic (the 7th harmonic) of M3 is improved and higher than M1 and M2, since coil-pitch of M3 is optimized to be 26.25°, shorter than that of M1 and M2 (30°). Thus, when injecting same phase current, torque of M3 is 6.44% and 7.16% higher than M1 and M2, as shown in Fig. 2(c). PM loss of M3 is lower than M1 and M2 due to lower space harmonic content, whereas core loss of M3 is slightly higher, as shown in Fig. 2(d). Flux density distributions of M1, M2, and M3 at the aforementioned operating point are shown in Fig. 1(b).

[1] G. Dajaku, W. Xie and D. Gerling, "Reduction of Low Space Harmonics for the Fractional Slot Concentrated Windings Using a Novel Stator Design," in IEEE Transactions on Magnetics, vol. 50, no. 5, pp. 1-12, May 2014. [2] G. Liu, F. Zhai, Q. Chen and G. Xu, "Torque Pulsation Reduction in Fractional-Slot Concentrated-Windings IPM Motors by Lowering Sub-Harmonics," in IEEE Transactions on Energy Conversion, vol. 34, no. 4, pp. 2084-2095, Dec. 2019. [3] V. I. Patel, J. Wang, W. Wang and X. Chen, "Six-Phase Fractional-Slot-per-Pole-per-Phase Permanent-Magnet Machines With Low Space Harmonics for Electric Vehicle Application," in IEEE Transactions on Industry Applications, vol. 50, no. 4, pp. 2554-2563, July-Aug. 2014.

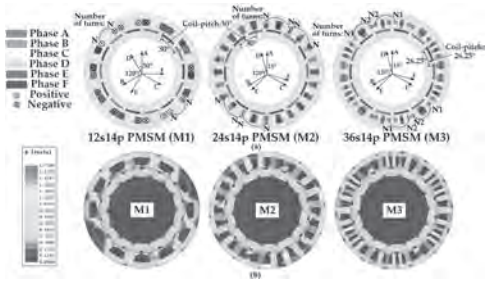

Fig. 1 (a) Structure of different machines. (b) Flux density distributions of machines.

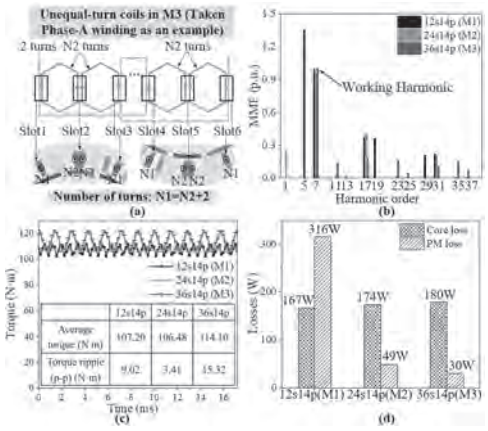

Fig. 2 (a) Winding layout of Phase-A in M3. (b) Harmonic analysis of MMF of different machines. (c) Torque comparison. (d) Losses comparison.

JPI-09. Effects of Harmonic and Power of Single-Phase Two-Pole Permanent Magnet Synchronous Generator. *C. Hsu*[3], J. Liu[2] and C. Fung[1]
1. Mechanical Engineering, Oriental Institute of Technology, Banqiao District, Taiwan; 2. Digital Multimedia Design, Kainan University, Lu-Zhou, Taiwan; 3. Asia Eastern University of Science and Technology, New Taipei, Taiwan

1. Study and Objective This research proposes a single-phase tow pole N-S stator core alternator, which uses a neural network algorithm (NNA) to predict the harmonic and power characteristics. This study, the generator is composited with a two-pole N-S rotor and a dual-coil which is defined as surface mounted permanent magnet synchronous motor (PMSM) structure [1,2]. This generator, it is driven by an external motor to generate single phase power. The prediction and comparison of power and harmonic analyzed by the NNA method with sensor and single chip, can be obtained. 2. Theory and Method This research uses a small 2-pole synchronous alternator, as shown in Figure 1. The synchronous generator is need to be driven by the synchronous speed by an external motor. The internal magnetic flux distribution of the synchronous generator is not a regular sine wave. The induced potential of the armature winding is a distorted sine wave. This research proposes recurrent neural network (RNN) to observe as performance of the generator, as shown in the Figure 2. The dynamic storage tank has internal weights, which define the internal circulation connection, and link to the dynamic library of the output layer through the output weights. The input is the parameters of voltage (V), current (A), real power (P), apparent power (Q), reactive power (S), etc. as the neuron weights to the output [3]. 3. Experimental discussion and conclusion This research is a single-phase two-pole alternator, which produces an average AC voltage of 37V, current of 0.11A, power factor of 0.99, P of 4.11 watts, Q of 0.48VAR, and S of 4.14VA during operation. This research focuses on learning the trained neural network system with a recursive state neural network. From the perspective of THD (Total harmonic distortion) performance, the third, fifth, and seventh harmonic have the most serious impact on the generator, and the harmonic situation of the motor can be predicted through the neural-like recognition system.

[1]W. Xu, X. Liu, and Y. Liu, "An investigation on the validity of power direction method for harmonic source determination," IEEE Trans. Power Del., vol. 18, no. 1, pp. 214–219, Jan. 2003. [2]C. Li, W. Xu, and T. Tayjasanant, "A critical impedance based method for identifying harmonic sources," IEEE Trans. Power Del., vol. 19, no. 2, pp. 671–678, Apr. 2004. [3]Chang-Hung Hsu, " Fractional Order PID Control for Reduction of Vibration and Noise on Induction Motor, IEEE Transactions on Magnetics, vol. 55, no. 11, pp. 6700507-1-7, 2019.

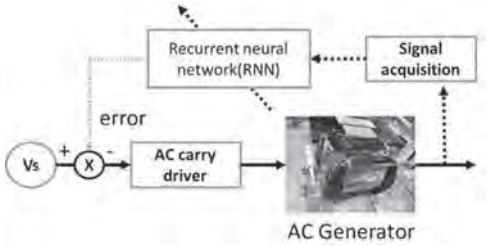

Figure 1 The two pole single phase generator harmonic performance detection by NN method

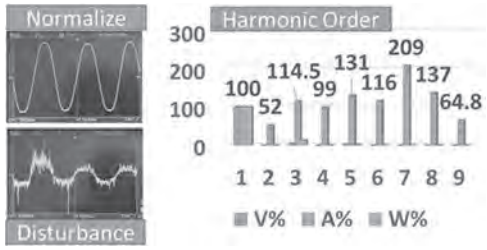

Figure 2 Harmonic measurement and power factor performance

JPI-10. Novel Method of Deriving Torque and Speed Curve of the Permanent Magnet Synchronous Motor Using Initial State Finite Element Analysis. *J. Son*[1] and D. Lim[1] *1. Department of Electrical, Electronic, and Computer Engineering, University of Ulsan, Ulsan, The Republic of Korea*

Motors are replacing conventional internal combustion engines in many applications to deal with fossil fuel crises and to reduce carbon emissions, and permanent magnet synchronous motors (PMSMs) are widely used in many fields due to their advantages such as a high power and high efficiency [1]-[4]. The torque and speed curve (TN curve) can be obtained by performing repetitive time-consuming finite element analysis (FEA) for each current phase angle. Therefore, this paper proposes initial state FEA (ISF) to derive the TN curve of the PMSMs that can reduce the analysis time and guarantee satisfactory accuracy. The average torque of the PMSMs can be calculated using the average flux linkage of each phase coil and input current. For the ISA, to reduce the calculation burden, the FEA is conducted at the initial rotor position, which means the number of the step is one, and the TN curve of the PMSM can be calculated using the flux linkage value of the ISF. Fig. 1 shows the *d* and *q* axis transformed flux linkage waveform obtained by the ISF and full period FEA (FPF) when the number of the step is 120 and the application is surface-mounted PMSM. The ISF result is marked with pink circle and located on the point, where the electrical angle is zero. The *d* and *q* axis flux linkages obtained by the ISF have 0.38% and 0.09% error compared with average FPF result. Using the flux linkage and input current, torque can be calculated. Fig. 2 show the torque according to the current phase angle calculated with the ISF and FPF. The maximum error rate was 0.37% and occurred at zero electrical degree, and the average error rate of the torque according to the current phase was 0.33%. Considering the calculation time of the ISF was 83% reduced compared with the FPF, the accuracy of the ISF is acceptable. The detailed explanation of TN curve deriving process of various types of PMSMs and verification of the ISF will be described at the full paper.

[1] S. Amamra and J. Marco, *IEEE Access*, vol. 7, pp. 178528-178538 (2019) [2] X. Ding, Z. Wang, L. Zhang and C. Wang, *IEEE Trans. Vehicular Technology*, vol. 69, no. 11, pp. 12797-12806 (2020) [3] Z. Liu, Y. Hu, J. Wu, B. Zhang and G. Feng, *IEEE Access*, vol. 9, pp. 19947-19959 (2021) [4] K. Yang, F. Zhao and Y. Wang, *IEEE Trans. Magnetics*, vol. 57, no. 2, pp. 1-5 (2021) [5] J. -G. Lee, D. -K. Lim and H. -K. Jung, *IEEE Trans. Magnetics*, vol. 55, no. 10, pp. 1-4 (2019)

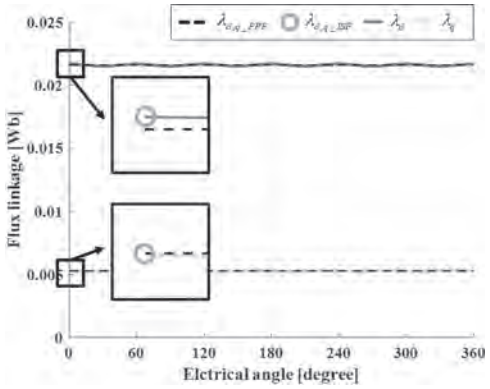

Fig. 1. Comparison of the *d* and *q* axis flux linkage obtained by the ISF and FPF.

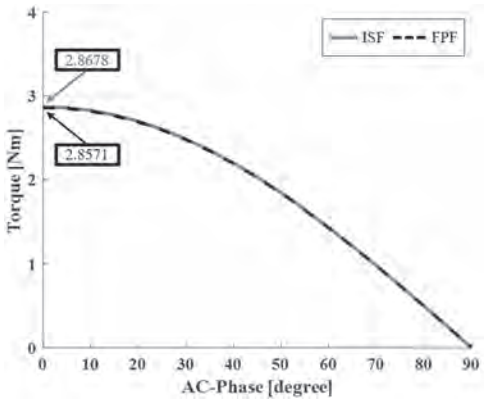

Fig. 2. Comparison of the calculated torque according to the current phase angle using the ISF and FPF.

JPI-11. Research on Cogging Torque and Radial Magnetic Force in Surface-Mounted Permanent Magnet Synchronous Motor with Dynamic Eccentricity. *L. Feng*[1], F. Zhang[1] and S. Yu[1] *1. Shenyang University of Technology, Shenyang, China*

In the actual production, the manufacturing and assembly error will inevitably lead to rotor eccentricity, which leads to different degrees of uneven air gap of the motor. When the motor is eccentric, the distortion of air gap waveform will produce significant low-order unbalanced magnetic pull (UMP) [1]. When the frequency and order of the low-order UMP with larger amplitude are close to the order and frequency of the natural mode of the motor, resonance is easy to occur, and the vibration and noise of the motor will increase significantly [2-3]. Therefore, in order to study the influence of dynamic eccentricity on the vibration and noise of motor, we report on an investigation into the frequency, order and amplitude of radial magnetic force. In this paper, surface-mounted permanent magnet synchronous motor (SPMSM) is taken as the research object, and the influence of rotor dynamic eccentricity on cogging torque and radial magnetic force is quantitatively analyzed by combining the exact analytical method (EAM) with the finite element method (FEM). The analytical model of radial magnetic force is established by magnetic conductance function method. Combined with spatio-temporal fourier decomposition, the distribution of radial magnetic force frequency, order and amplitude in the motor with dynamic eccentricity is obtained. The results show that the distortion rate of cogging torque decreases slightly with the increase of dynamic eccentricity, and the influence of dynamic eccentricity on cogging torque depends on the slot matching of motor. The motor will generate force waves with the same frequency and different order on the basis of the original magnetic force wave in the dynamic eccentricity. The amplitude of force and eccentricity are positively correlated. The new low-order force wave have a great influence on the vibration noise. Fig. 1 shows the relationship between cogging torque and eccentricity. Fig. 2 shows the frequency and order of radial magnetic force density. The full paper will present the detailed calculation procedure and analysis.

[1] DING Shuye, JIANG Shan, WANG Mengqi, et al. Influence of rotor eccentricity on magnetic density and core loss for induction motors[C]. International Conference on Applied Superconductivity and Electromagnetic Devices (ASEMD), 2015 IEEE. [2] TÍMÁR P L. Noise and Vibration of Electrical Machines [M]. Amsterdam: Elsevier,1989 [3] YU Y, BI C, HLA P N, et al. Incline unbanlanced magnetic pull Induced by misalignment rotor in PMSM[J]. IEEE Transactions on Magnetics, 2013, 49(6): 2709-2714.

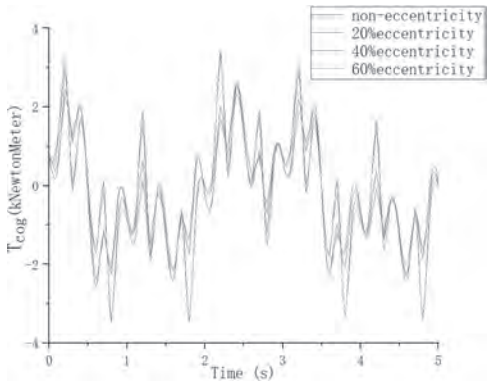

Fig.1 Cogging torque with different eccentricity

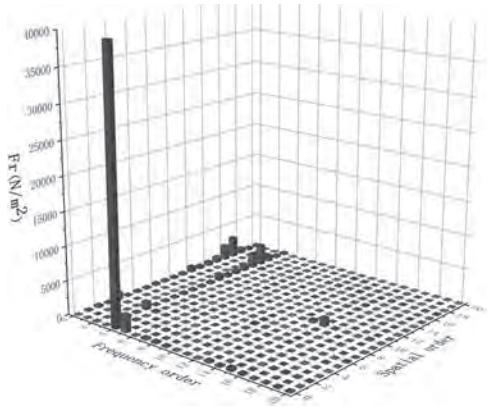

Fig.2 the frequency and order of radial magnetic force density

JPI-12. A Study on the Design Methodology of Spoke-type Motor with Overhang. *J. Jung*[1], J. Lee[2], D. Jung[3] and J. Lee[1] *1. Hanyang University, Seoul, The Republic of Korea; 2. Korea Electronics Technology Institute, Bucheon, The Republic of Korea; 3. Halla University, Wonju, The Republic of Korea*

1. Introduction High efficiency is important for home appliance motors. In this paper, we propose a magnetic flux-intensive structure for maximizing effective magnetic flux density in the air gap as a method for high efficiency of motors. For the miniaturization and efficiency of motors, the application of O/H structures as well as magnetic-concentrated structures was considered. A study was also conducted on the increase of unsaturated landings and harmonics, which are side effects that occur when applying O/H structures. 2. Methodology proposal for converting SPMSM to Spoke Type Motor In this paper, we propose a self-sustaining focused structure with O/H, a specification that can achieve high efficiency, miniaturization, and material cost reduction while considering mass production. We propose a methodology for the design of rotators and starters that should be considered for one-time landing after assembly, the biggest factor in the mass production of spoke-type motors. Furthermore, key design variables were derived to improve noise vibration characteristics, and improved noise characteristics were obtained compared to conventional models through radial force optimization. To improve efficiency and power density, we propose a design method for preventing axial leakage between permanent magnets and cores with O/H and a design method for minimizing magnetic flux leakage by improving the rotor. In this paper, we propose an overall methodology for design and testing to convert Inner-SPM motors to Spoke-type motors and demonstrate their validity through fabrication, testing and mass production review. 3. Conclusion This paper has studied the overall methodology for converting SPMSM into a Spoke-type motor. The results of improved mass production, power density, and efficiency were derived. Experiments with the manufacture of motors and landing yoke confirmed that the volume of motors decreased by more than 15%, resulting in material cost savings and efficiency at rated loads increased by more than 2%p. In full paper, it is planning to propose a development algorithm to convert SPMSM into a spoke type motor and conduct detailed analysis on improved characteristics.

M. Kimiabeigi, J. D. Widmer, R. Long, Y. Gao, J. Goss, R. Martin, T. Lisle, J. M. Soler Vizan, "High-Performance Low-Cost Electric Motor for Electric Vehicles Using Ferrite Magnets" IEEE Transactions on Industrial Electronics (Volume: 63, Issue: 1, Jan. 2016)

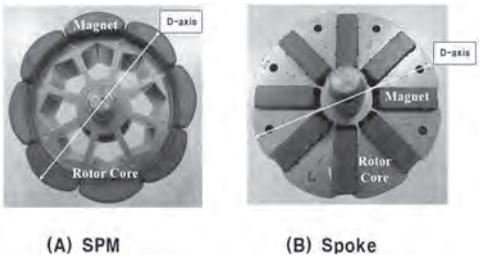

Fig 1

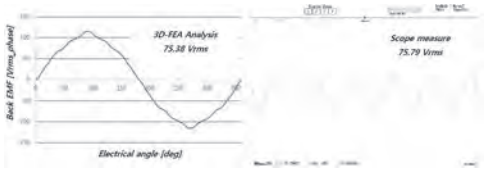

Fig 2

JPI-13. Improvement of No-Load Back EMF through Ferrofluid Pipe in Airgap of SPMSM. *I. Yang*[1], D. Shin[2], S. Lee[2], W. Kim[2] and K. Kim[3] *1. Electrical Engineering, Hanyang University, Seoul, The Republic of Korea; 2. Electrical Engineering, Gachon University, Seongnam, The Republic of Korea; 3. Smart Mobility, Halla University, Wonju, The Republic of Korea*

In this paper, the increase and decrease of the no-load back electro motive force (EMF) was confirmed by inserting a ferrofluid into the airgap of a surface permanent magnet synchronous motor (SPMSM). Ferrofluid is a black liquid that is strongly magnetized in the presence of a magnetic field [1]-[4]. Ferrofluid is a colloidal liquid composed of nanoscale ferromagnetic, usually made of organic solvents or water [1]-[4]. When an external magnetic field is applied to the ferrofluid, it has a high permeability value compared to vacuum, and it is possible for the ferrofluid to act as a core [5]. Therefore, placing the ferrofluid in the airgap can decrease the reluctance and increase the no-load back EMF [5]. Since ferrofluid is a liquid, a pipe that can contain ferrofluid is required to place the ferrofluid in the airgap of SPMSM. After injecting the ferrofluid into the pipe, it is possible to place the ferrofluid in the airgap by attaching glass plates on both sides. If ferrofluid is injected inside the pipe and the pipe is fixed inside the stator with a bond, the pipe cannot be separated after the experiment. If a pipe that can be detachably fixed to the stator side is made, it is possible to test various types of ferrofluid through another pipe after the test. To this end, in this paper, a structure in which the pipe is made into a protrusion shape and the protrusion is inserted into the slot opening is proposed. By attaching pins to both ends of the protrusion in the axial direction, the pipe can be fixed and separated from the stator side. An analysis model was selected as SPMSM for hairdryer with 2-poles and 3-slots. The coupled model is shown in Fig. 1 and the decomposition model is shown in Fig. 2. The no-load line voltage according to the capacity of ferrofluid was analyzed through finite element analysis (FEA). Then, a ferrofluid pipe was inserted into the actual prototype and compared with the results of FEA.

[1] S. Islam, M. Zubair and A. Tassaddiq, *IEEE Access.*, vol. 8, pp. 138551–138562 (2020) [2] A. O. Ivanov and O. B. Kuznetsova, *J. Magn. Magn. Mater.*, vol. 252, pp. 135–137 (2002) [3] N. Gautam, G. Thirupathi, and R. Singh, *IEEE Trans. Magn.*, vol. 52, no. 7, pp. 0–3 (2016) [4] G. Thirupathi and R. Singh, *IEEE Trans. Magn.*, vol. 51, no. 11, pp. 3–6 (2015)

[5] I.-J. Yang, S.-W. Song and D.-H. Kim, *J. Energies*., vol. 14, no. 6, pp. 1736 (2021) [6] S. Engelmann, A. Nethe, T. Scholz and H. D. Stahlmann, *J. Magn. Magn. Mater.*, vol. 293, pp. 685–689 (2005) [7] S. Engelmann, A. Nethe, T. Scholz and H. D. Stahlmann, *J. Magn. Magn. Mater.*, vol. 272–276, pp. 2345–2347 (2004) [8] G. Zeng *et al. IEEE Trans. Magn.*, vol. 56, no. 1, pp. 55–58 (2020)

Fig.1. Coupled model.

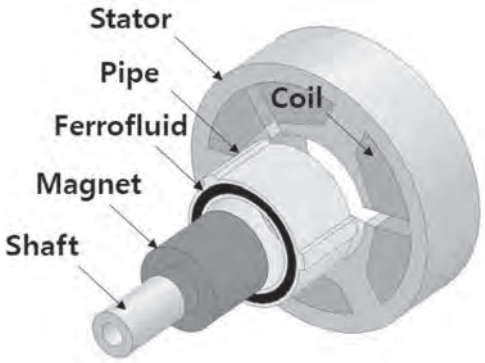

Fig.2. Decomposition model.

Session JPJ
(SEMI)-ANALYTICAL AND NUMERICAL TECHNIQUES FOR THE OPTIMAL DESIGN OF ELECTROMAGNETIC DEVICES
(Poster Session)

Jean-Philippe Lecointe, Chair
Univ. Artois, UR 4025, Laboratoire Systèmes Electrotechniques et Environnement (LSEE), Béthune, France

JPJ-01. Rotor Yoke Optimization of the Axial-Transverse Hybrid Flux Permanent-Magnet Machine Considering Magnetic Saturation. *P. Ma*[1], Q. Wang[1] and Y. Li[1] *1. Harbin Institute of Technology, Harbin, China*

Abstract : This paper presents an analytical subdomain model for the axial-transverse hybrid flux permanent-magnet machine (ATHFPMM) rotor yoke considering magnetic saturation. The two new methods are proposed to consider the influence of saturation. Compared with the finite element method (FEM), the analytical subdomain models with new methods have high accuracy. The proposed models are of reference value for the analysis and design of machines with magnetic saturation. 1. Introduction To achieve the higher power density of the ATHFPMM, the rotor yoke saturation is a problem need to consider [1]-[2]. The subdomain method is convenient to model without considering the magnetic saturation [3]. The equivalent air gap method is applied to the subdomain model to analyze the magnetic saturation in [4], while it has limitations. Thus, the two new methods are proposed to correct the subdomain model. Compared with the FEM, the results show that the new models have high accuracy. 2. Analytical model A. Subdomain model After simplification, the 3-D axial-transverse hybrid flux model can be equivalent to the 2-D model, as shown in Figure 1. The scalar magnetic potential in each region satisfies the Laplace equation, and the magnetic flux density can be obtained. B. The modified equivalent air gap method When the rotor yoke is saturated, the magnetic circuit in the yoke has a large reluctance, which will be equivalent to the virtual air-gap reluctance at point A. C. The average permeability method The permeability average value is taken as the entire rotor yoke region permeability. D. Methods comparison Taking a 20kW machine as an example, the models are compared. The results are shown in Figure 2. The h_j is the thickness of rotor yoke, and U_a is the phase voltage. 3. The ATHFPMM rotor yoke optimization A. Optimization design Based on the new model, genetic algorithm is used to optimize the ATHFPMM. B. Finite element verification The obtained scheme is analyzed by FEM, and the results are consistent with the design parameters. 4. Conclusion The two proposed methods for considering the magnetic saturation have high accuracy, and the proposed subdomain model can be conveniently applied to machine optimization.

Q. Yu, X. Wang and Y. Cheng, "Magnetic Modeling of Saliency Effect for Saturated Electrical Machines With a New Calculation Method," IEEE Transactions on Magnetics, vol. 52, no. 6, pp. 1-6, June 2016. G. Feng, C. Lai and N. C. Kar, "A Novel Current Injection-Based Online Parameter Estimation Method for PMSMs Considering Magnetic Saturation," IEEE Transactions on Magnetics, vol. 52, no. 7, pp. 1-4, July 2016 Z. Q. Zhu, L. J. Wu and Z. P. Xia, "An Accurate Subdomain Model for Magnetic Field Computation in Slotted Surface-Mounted Permanent-Magnet Machines," IEEE Transactions on Magnetics, vol. 46, no. 4, pp. 1100-1115, April 2010. P. Liang, F. Chai, Y. Li and Y. Pei, "Analytical Prediction of Magnetic Field Distribution in Spoke-Type Permanent-Magnet Synchronous Machines Accounting for Bridge Saturation and Magnet Shape," IEEE Transactions on Industrial Electronics, vol. 64, no. 5, pp. 3479-3488, May 2017.

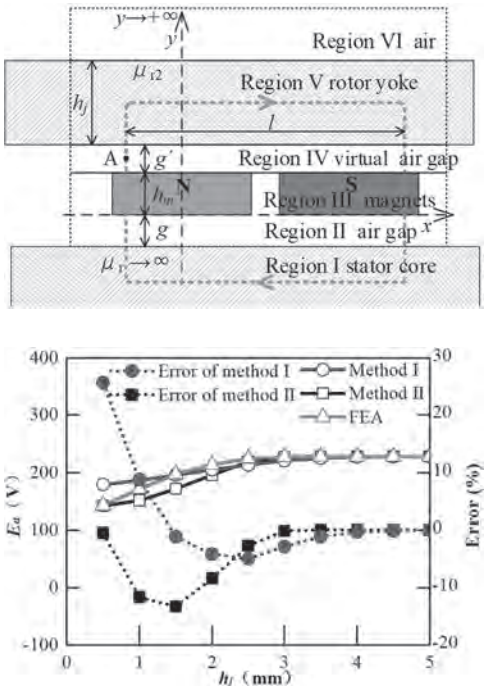

JPJ-02. Electromagnetic Analysis of the Saturation Effect of a Balanced Armature Receiver with Different Nonlinear Soft Magnetic Materials and Magnetizations. *D. Xu*[1,2], X. Zhu[1], Y. Jiang[3], C. Wang[1,2] and S. Hwang[3] *1. Dept. of Precision Mechanical Engineering, Shanghai University, Shanghai, China; 2. Science and Technology on Near-surface Detection Laboratory, Wuxi, China; 3. School of Mechanical Engineering, Pusan National University, Busan, The Republic of Korea*

The demands of balanced armature (BA) receiver are increasing in hearing aid, earphone and wearable devices because of its tiny size and good performance. The magnetic circuit of the electromagnetic field of a BA receiver includes an armature, a voice coil, two permanent magnets (PMs), and a magnet housing, as shown in Fig. 1. Among them, the armature and magnetic housing use nonlinear soft magnetic materials. In previous researches, the lumped parameter method (LPM) [1-5] and finite element method [6-7] are used to analyze the nonlinear magnetic characteristics distribution of the magnetic circuit. The extent of the nonlinear magnetic characteristics distribution is determined by the saturation of a magnetic circuit, as shown in Fig.1, a large amount of flux passes through the area of magnet housing, the armature wrapped by the coil and the U end. There are several reasons to affect the saturation for a magnetic circuit, such as the magnetization of PMs, the input current, the variant position of armature, the different soft magnetic materials and so on. In research [6], Xu has investigated the influence of magnetization of PMs on the nonlinear magnetic characteristics distribution by LPM. This study will continue the research method in [6-7], and investigate the saturation effect of the magnetic circuit using LPM with different permeability of nonlinear soft magnetic materials. Armature and magnet

housing use different types of alloy material. So as shown in Fig.2, total four alloy materials are used in this research: Alloy-1 and Alloy-2 materials with B-H curve will be used on armature and Alloy-3 and Alloy-4 materials with B-H curve will be used on magnet housing. The analyses will show that even with same magnetization of PMs, there are big differences on all of the nonlinear magnetic characteristics with different soft magnetic materials, especially in the situation of large vibration displacement and large input current. The distributions of other nonlinear magnetic characteristic and the analysis method will be shown in details in the full paper.

[1] Jensen, Joe, Finn T. Agerkvist, and James M. Harte. "Nonlinear time-domain modeling of balanced-armature receivers." Journal of the Audio Engineering Society 59.3 (2011): 91-101. [2] Jensen, Joe. Nonlinear distortion mechanisms and efficiency of miniature balanced-armature loudspeakers. Diss. Ph. D. thesis, Technical University of Denmark, Kgs. Lyngby, Denmark, 2014. [3] Tsai, Yu-Ting, and Jin H. Huang. "A study of nonlinear harmonic distortion in a balanced armature actuator with asymmetrical magnetic flux." Sensors and Actuators A: Physical 203 (2013): 324-334 [4] Dan-Ping Xu, Yuan-Wu Jiang, and Sang-Moon Hwang*. "Analysis of the magnetization effect of permanent magnets on the nonlinear magnetic characteristic distributions of a balanced armature receiver." IEEE Transactions on Magnetics, 2019, 55 (2): 1-5. [5] Dan-Ping Xu, Yuan-Wu Jiang, Hong-Li Zhang, and Sang-Moon Hwang*. "Fast electromagnetic analysis of a 3-D magnetic circuit in a balanced armature receiver." IEEE Transactions on Magnetics, 2019, 55 (2): 1-4. [6] Dan-Ping Xu, Han-Wen Lu, Yuan-Wu Jiang, Hyung-Kyu Kim, Joong-Hak Kwon, and Sang-Moon Hwang*. "Analysis of sound pressure level of a balanced armature receiver considering coupling effects." IEEE Access, 2017, 5: 8930-8939. [7] Dan-Ping Xu, Yuan-Wu Jiang, Joong-Hak Kwon, and Sang-Moon Hwang*. "Analysis of the effects of electromagnetic circuit variables on sound pressure level and total harmonic distortion in a balanced armature receiver." IEEE Transactions on Magnetics, 2017, 53(6): 8001504

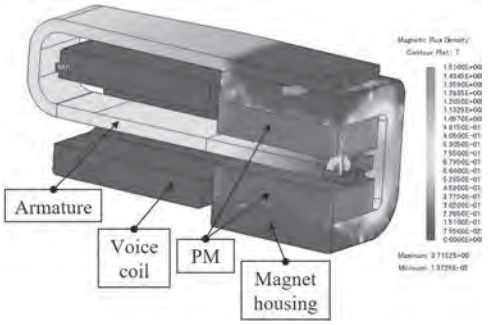

Fig.1 Contour plot of |B| when y=20 um and i=8 mA.

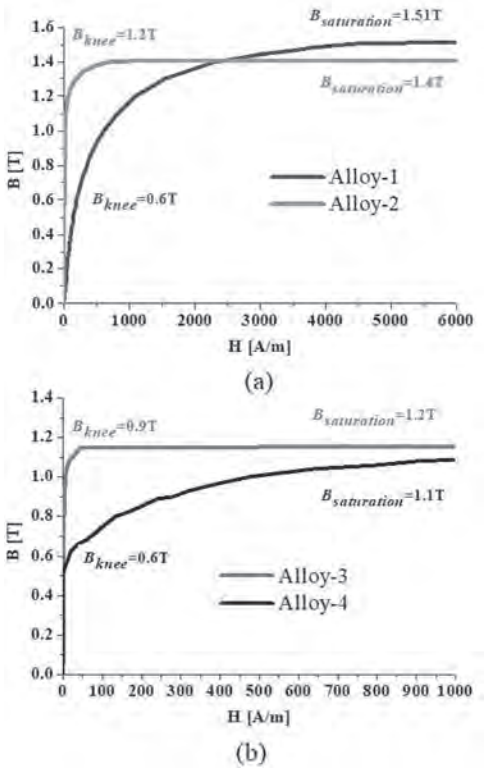

Fig.2 Different nonlinear material property of soft magnetic materials: (a) Armature (b) Magnet housing

JPJ-03. Withdrawn

JPJ-04. Multi-Objective Optimal design of SPMSM for Electric Compressor Using Analytical Method and NSGA-II Algorithm. *W. Kim*[1], C. Kim[2], K. Shin[3], T. Bang[1] and J. Choi[1] *1. Electrical Engineering, Chungnam National University, Daejeon, The Republic of Korea; 2. E&E Department, Hanon Systems, Daejeon, The Republic of Korea; 3. Power System Engineering, Chonnam National University, Jeonnam, The Republic of Korea*

In internal combustion engine vehicles, the compressor of the air conditioner is powered by the engine. However, the only source of power for electric vehicles (EVs) is the battery. Therefore, an EV uses electric compressors powered by batteries. Hence, lightweight and high efficiency of electric compressors is essential to increase the mileage of the EVs [1] [2]. Thus, optimal design of the surface permanent magnet synchronous motor (SPMSM) is required because it is the main component of an electric compressor. Recently, the Taguchi method, response surface method (RSM) and genetic algorithms (GAs) have been applied to the optimal design of motors for electric compressors [1][3]. However, those methods are disadvantages in terms of global optimization capability or time-consuming. This paper proposes a multi-objective optimal design method of SPMSMs for electric compressors. Non-dominated sorting GA (NSGA-II) was applied to find a Pareto front, and an analytical method was applied to solve the time-consuming problem of pareto-optimization. The validity of the proposed method was verified using the FEM and experiments of the initial model. Fig. 1(a) shows the flow chart of the proposed method for the optimal design of the SPMSM. The stator is designed using an analytical method according to the rotor selected by the NSGA-II algorithm. The Pareto front of the objective functions is generated according to the iteration. Fig. 1(b) shows the chosen optimal model and Pareto front of the THD, power density, efficiency, and magnet consumption. Fig.2 (a) shows the manufactured initial model. Fig. 2(b) shows the shape and size of the initial and the optimal

model. Fig. 2(c) shows a comparison of the objective function values of the initial and the optimal models. The THD and magnet consumption decreased by 31.8% and 42.2%, respectively, the power density increased by 20.2%, and the efficiency was maintained compare to the initial model.

[1] S. Cho, K. Jung and J. Choi, "Design Optimization of Interior Permanent Magnet Synchronous Motor for Electric Compressors of Air-Conditioning Systems Mounted on EVs and HEVs," in IEEE Transactions on Magnetics, vol. 54, no. 11, pp. 1-5, Nov. 2018 [2] S. Zhang, T. Zhang, W. Chen and H. Ji, "The Development Direction of Electric Air Compressor for Vehicle," 2020 3rd International Conference on Advanced Electronic Materials, Computers and Software Engineering (AEMCSE), 2020, pp. 720-722 [3] T. Raminosoa, B. Blunier, D. Fodorean and A. Miraoui, "Design and Optimization of a Switched Reluctance Motor Driving a Compressor for a PEM Fuel-Cell System for Automotive Applications," in IEEE Transactions on Industrial Electronics, vol. 57, no. 9, pp. 2988-2997, Sept. 2010

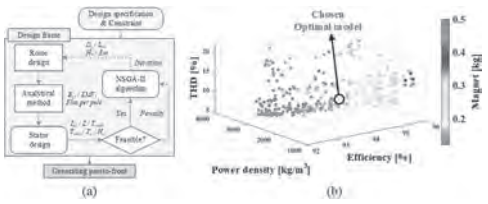

Fig. 1. (a) Proposed method flow chart (b) Pareto front of THD, Power density, Efficiency, Magnet consumption

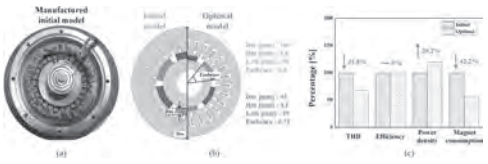

Fig. 2. (a) Manufactured initial model (b) Initial & Optimal model (c) Comparison between Initial & Optimal model

JPJ-05. A robust optimization design approach for hybrid PM motor considering manufacturing uncertainties of PMs. *J. Wu*[1], X. Zhu[1] and D. Fan[1] *1. Jiangsu University, Zhenjiang, China*

The rare-earth permanent magnet (PM) motor has been widely employed in various applications due to the merits of high-power density and high efficiency [1]. For this kind of motor, the Rare-earth PM is an essential component, which decides the performance of the motor. However, since the supply chain and price of the rare-earth PM material are unstable, the further large-scale application of rare-earth PM motor suffers limitations. To reduce the consumption of rare-earth PM, a type of hybrid PM motor has obtained much attention, where a large quantity of non-rare-earth PM is added as an assisted magnetic source to replace part of rare-earth PM [2]. For the hybrid PM motor, an outstanding problem is that there exist coupling effects between two PMs, resulting in the motor effective optimization design being difficult. Especially, during the actual manufacture stage, the existence of manufacturing tolerances and material imperfections on two PMs will exert more uncertain impacts on motor performance [3]. Thus, how to design the hybrid PM motor in an effective and reliable approach has attracted much attention. In this paper, a robust optimization design approach for hybrid PM motor is proposed, where two kinds of PM material manufacturing uncertainties are sufficiently considered. To better clarify the optimization method, a 12-slots/10-poles spoke-type hybrid PM motor is taken as a design example, which adopts NdFeB and Ferrite as co-excitation sources. Fig 1(a) shows the topology of the investigated hybrid PM motor, and Fig 1(b) illustrates the corresponding potential manufacture uncertainty factors of PM material, including magnetization direction, remanence, dimensions and assembling position. It is noted that as the PMs are manufactured and assembled separately, the uncertainties on each PM (1#~10# NdFeB and 1#~10# ferrite) are independent. During the research, the non-uniform uncertainties caused by these PMs will be comprehensively considered. Fig. 2 compared optimization results, which indicated that the proposed optimization method can not only improve the motor performance but guarantee the reliability of the design. More detailed designs and experiments will be presented in the full paper.

[1] A. Fatemi, D. M. Ionel, M. Popescu, Y. C. Chong and N. A. O. Demerdash, "Design optimization of a high torque density spoke-type pm motor for a formula e race drive cycle," IEEE Trans. Ind. Appl., vol. 54, no. 5, pp. 4343-4354, Sept.-Oct. 2018. [2] Z. S. Du and T. A. Lipo, "Cost-effective high torque density bi-magnet machines utilizing rare earth and ferrite permanent magnets," IEEE Tran. Energy Convers., vol. 35, no. 3, pp. 1577-1584, Sept. 2020. [3] Y. Yang, N. Bianchi, G. Bacco, S. Zhang and C. Zhang, "Methods to reduce the computational burden of robust optimization for permanent magnet motors," IEEE Tran. Energy Convers., vol. 35, no. 4, pp. 2116-2128, Dec. 2020.

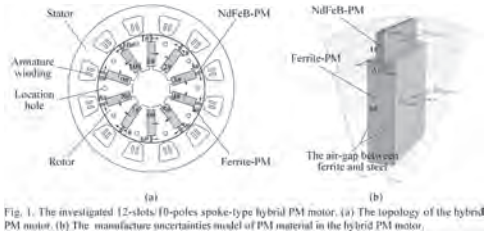

Fig. 1. The investigated 12-slots/10-poles spoke-type hybrid PM motor. (a) The topology of the hybrid PM motor. (b) The manufacture uncertainties model of PM material in the hybrid PM motor.

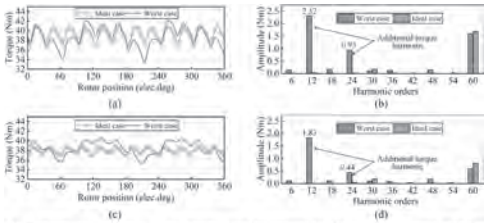

Fig. 2. The comparison of motor torque between initial and optimal. (a) The initial motor torque under the ideal case and the worst case. (b) Torque harmonic analysis for the ideal case and the worst case of the initial motor. (c) The optimized motor torque under the ideal case and the worst case. (d) Torque harmonic analysis for the ideal case and the worst case of the optimized motor.

JPJ-06. A Study on Performance Improvement by Reducing Axial Force of Double-Layer Spoke-type PMSM with Core Skew Structure. *D. Nam*[1], K. Lee[2], H. Pyo[1], M. Jeong[1] and W. Kim[1] *1. Electrical Engineering, Gachon University, SeongNam, The Republic of Korea; 2. Electrical Engineering, Michigan State University, East Lansing, MI, United States*

Double-Layer Spoke type PMSM can concentrate magnetic flux using a ferrite permanent magnet instead of a rare earth type permanent magnet similar to an conventional spoke type motor. In addition, the conventional spoke type permanent magnet motor did not utilize the reluctance torque properly because the d-axis and q-axis magnetoresistance were not large, but the Double-Layer Spoke type PMSM divides each permanent magnet into two. By inserting an iron core to reduce the q-axis magnetoresistance, the difference with the d-axis magnetoresistance is increased, and a high reluctance torque can be used. However, as the magnetoresistance difference between the d-axis and the q-axis increases, factors, such as cogging torque and torque ripple, increase, which adversely affects the operation of the motor. This will soon cause performance degradation, such as vibration, noise, and poor position and speed control. In order to compensate for this, in general, the method of applying a skew structure is most widely used, but it is also difficult to manufacture and sometimes increases the torque ripple, so it is not a good solution. Therefore, in [1], a study was conducted to improve manufacturability by applying core skew and to reduce cogging torque and torque ripple. In this paper, it was confirmed that the cogging torque, torque ripple in the high-speed operation area, and no-load THD were significantly reduced. However, it was confirmed that this core skew also increases the torque ripple in the low-speed operation area. There are many factors that affect the torque ripple, but as shown in Fig. 1, it can be confirmed that the axial force has some effect on the torque ripple. In addition, the axial force continuously transmits a mechanical load to the bearing connected to the

motor, causing vibration and noise, and shortening the life of the motor. Since the target model of this paper uses sensorless control, the torque ripple that affects the back electromotive force used for detection must be reduced.

[1] D. -W. Nam, K. -B. Lee, and W. -H. Kim, "A study on Core Skew considering manufacturability of double-layer spoke-type PMSM," Energies 2021, 14, 610, Jan. 2021. [2] G. -J. Park, Y. -J. Kim, and S. -Y. Jung, "Design of IPMSM applying v-shape skew considering Axial Force distribution and performance characteristics according to the rotating direction," IEEE Trans. Appl. Supercond., vol. 26, no. 4, Jun. 2016, Art. ID 7021404.

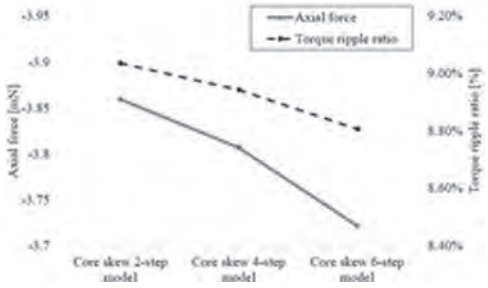

Fig. 1. Comparison of torque ripple and axial force according to the number of steps.

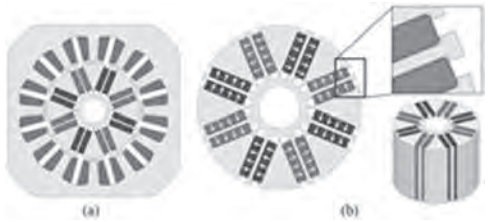

Fig. 2. Conventional model. (a) Stator and rotor; (b) rotor structure.

JPJ-07. Analysis of Unbalanced Magnetic Pull in Flux-Reversal Permanent Magnet Machines. *X. Zhu*[1] *1. Nanjing Normal University, Nanjing, China*

Abstract—The main purpose of this paper is to model and discuss the unbalanced magnetic pull (UMP) in flux-reversal permanent magnet (FRPM) machines and hence propose the corresponding reduction techniques. The magneto-motive-force (MMF)-permeance model is employed to derive the analytical expression of UMP in FRPM machine without rotor eccentricity. According to this analytical model, the UMP due to PM and armature reaction field can be obtained separately. Then, the influence of machine parameters on UMP is further investigated and verified by finite element analysis (FEA), including stator slot/rotor pole-pair (slot/pole) combination, winding layer, magnetization method and load condition, which can guide an engineer to choose the reasonable slot/pole combination to avoid the UMP in FRPM machines. Analytical Equation of Unbalanced Magnetic Pull According to magneto-motive-force (MMF)-permeance model [1], the air-gap flux density in FRPM machine is firstly obtained as shown in equation (1). Then, combined with the local force density at an arbitrary position θ, the UMP of the resultant global magnetic force that acts on the rotor due to the asymmetric air-gap field distribution is given as (3): $B(\theta,\alpha)=F_{pm}(\theta)\Lambda(\theta,\alpha)(\theta,\alpha)$ (1) $p_r(\theta,\alpha)=B^2(\theta,\alpha)/2\mu_0$ (2) $P_x(\theta,\alpha)=\int p_r(\theta,\alpha)\cos(\theta)\,d\theta$ (3) Definitions of the elements in equations (1) to (3), and the deriving process and more details will be given in the full paper. It should be noted that the final expression of UMP takes the machine parameters into consideration. According to the derived model, the stator slot/rotor pole-pair combinations exhibiting the UMP are summarized in Tab. I and Fig. 1. It should be noted that the UMP of the cases caused by armature reaction field and PM field are highlighted by grey shadow and red shadow, respectively. More details will be further discussed in the full paper.

[1] C. Bi, N. Aung, H. Phyu, Q. Jiang, and S. Lin, "Unbalanced magnetic pull induced by driven current in PM-BLDC motor operation," in *Proc. of ICEMS 2007*, Seoul, South Korea, Oct. 2007, pp. 780-785. [2] X. Zhu, W. Hua, Z. Wu, W. Huang, H. Zhang, and M. Cheng, "Analytical approach for cogging torque reduction in flux-switching permanent magnet machines based on magneto motive force-permeance model," *IEEE Trans. Ind. Electron.,* vol. 65, no. 3, pp. 1965-1979, Mar. 2018.

TABLE I Stator Slot/Rotor Pole-Pair Combinations *vs.* UMP

N_r	3	6	9	12	15	18	3	6	9	12	15	18
No. of rotor slots N_r												
										14		
										-	-	15
										16		16
		8									20	20
				10								21
												22
			12									

TABLE I Stator Slot/Rotor Pole-Pair Combinations *vs.* UMP

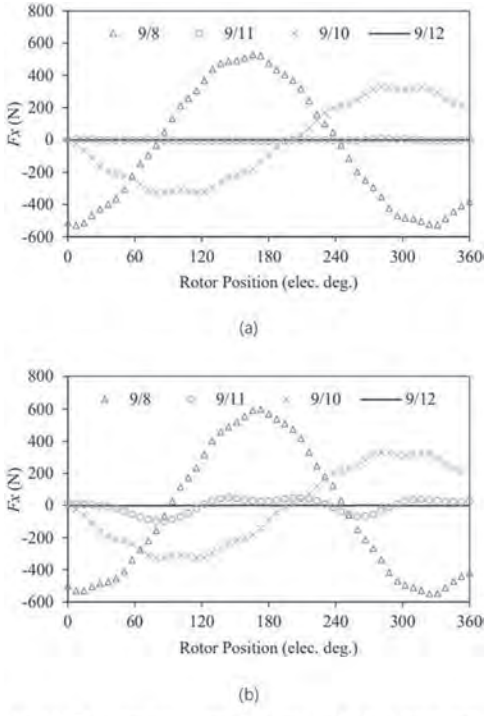

Fig.1 UMP *vs.* slot/pole combinations (m1). (a) No load. (b) On load.

Fig.1 UMP *vs.* slot/pole combinations (m1). (a) No load. (b) On load.

JPJ-08. High-Speed Motor Design through PWM Voltage Source Analysis and Harmony Search Algorithm. *I. Yang*[1], J. Lee[1], Z. Geem[2] and W. Kim[2] *1. Electrical Engineering, Hanyang University, Seoul, The Republic of Korea; 2. Electrical Engineering, Gachon University, Seongnam, The Republic of Korea*

For the design of a high-speed interior permanent magnet synchronous motor (IPMSM), the point M, which is the center of the voltage limiting source, is generally close to or included in the current limiting source. However, as the point M moves toward the center of the current limiting circle, the efficiency decreases at low speed and the torque ripple increases. This means that high-speed and low-speed performance must be considered

simultaneously in designing a high-speed motor, and there are several target functions. Accordingly, an optimal design is essential, and in this paper, the optimal solution was found using the harmony search (HS) algorithm. The HS algorithm was applied to optimization problems in various fields and showed superior performance compared to other algorithms [1],[2]. The HS algorithm is an optimization algorithm that uses the method of finding better harmony in order for players to find the optimal harmony in improvisation [3],[4]. The HS algorithm creates variables in the harmony memory, a space where randomly generated variables are stored. And the HS algorithm finds the optimal solution by generating a new solution and updating it through performance comparison with the existing solution. In this paper, by adding PWM voltage source analysis to the improved model derived through the HS algorithm, the accuracy of the high-speed IPMSM analysis was increased. In the case of high-speed motors, in general, a concentrated winding with better field-weakening performance compared to the distribution winding is selected. In the case of the distributed winding, the no-load back EMF is close to a sine wave compared to the concentrated winding, and the inverter can control the actual current close to a sine wave. The concentrated winding contains harmonics in the actual current relatively, so the actual current has an error with the simulation of applying a sinusoidal current. When analyzing the PWM voltage source, it is possible to reduce the error between the simulation and the actual test value.

[1] Z. W. Geem, "Optimal Cost Design of Water Distribution Networks Using Harmony Search," Engineering Optimization, vol. 38, no. 3, pp. 259-280 (2006) [2] Z. W. Geem, "Particle-Swarm Harmony Search for Water Network Design," Engineering Optimization, vol. 41, no. 4, pp. 297–311 (2009) [3] Z. W. Geem, Music-Inspired Harmony Search Algorithm: Theory and Applications, Springer, Berlin (2009) [4] Z. W. Geem, "Music-Inspired Harmony Search Algorithm and Its Experience-Based Derivative," New Physics: Sae Mulli, vol. 67, no. 5, pp. 608-614 (2017)

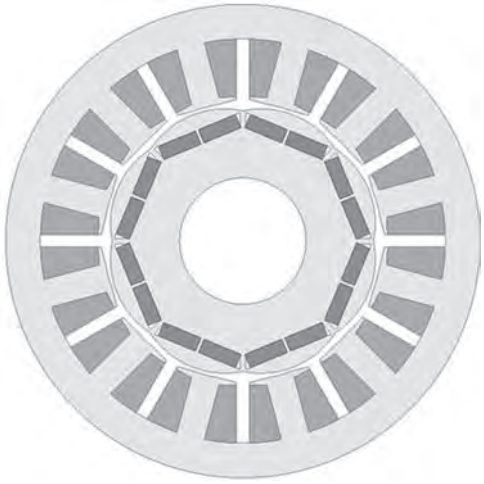

Fig. 1. 2D cross section of proposed model.

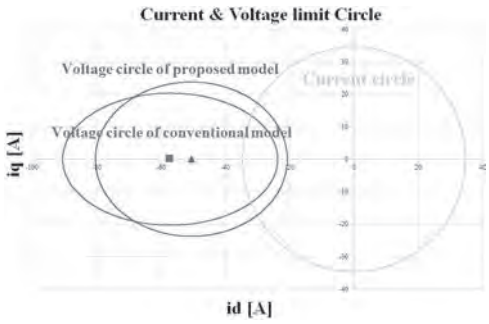

Fig. 2. Current and voltage limit circle.

JPJ-09. Random walk algorithm and semi 3D magnetic equivalent circuit based SPMSM design method. *S. Kim*[1], W. Kim[1], T. Bang[1] and J. Choi[1] *1. Electrical Engineering, Chungnam National University, Daejeon, The Republic of Korea*

Permanent magnet synchronous motors (PMSMs) often use magnet overhang structures to increase their power density and compensate for the leakage flux caused by the end effect [1][2]. If a PMSM has an overhang structure, 3D analysis is required for accurate evaluation. However, this is a time-consuming approach as it requires many modifications of the design parameters during the initial design of the PMSM. Recently, to solve this problem, 2D equivalent analysis methods that account for magnet overhang have been presented [3][4]. This paper proposes a design technique involving a semi 3D magnetic equivalent circuit (Semi 3D MEC) and a random walk algorithm (RWA). This technique incorporates the previously presented 2D equivalent analysis method. Magnetic equivalent circuits (MECs) exhibit the advantage of facilitating rapid analyses even if design parameters are modified during initial design. Consequently, a semi 3D MEC can rapidly analyze PMSMs with overhang structures. The RWA method uses a random number function to search for the minimum value of the global optimal solution. According to the rotor shape obtained by RWA iteration, the specific objective function and the PMSM volume can be optimized. The Semi 3D MEC in conjunction with RWA is regarded as a useful design method for PMSMs with overhang structures. This design method was validated by comparing with the analysis results of 3D finite element method. Fig.1(a) illustrates the process of iterating the RWA from the initial point to the optimal point and the convergence to the global optimum solution of the test function. Fig.1(b) shows the demagnetization curve of a permanent magnet. The magnetic flux density B_m and magnetic field intensity H_m are increased to compensate for the increase in magnetic energy according to the overhang structure in the 2D analysis. Fig.2(a) depicts the shape of the optimal model obtained by the proposed method. Fig.2(b) shows the volume of a surface permanent magnet synchronous motor (SPMSM) minimized via RWA iteration.

J.M Seo, I.S Jung, H.K Jung, and J.S Ro, IEEE TRANSACTIONS ON MAGNETICS, VOL. 50, NO. 5 (MAY 2014) D.K Woo, D.K Lim, H.K Yeo, J.S Ro, IEEE TRANSACTIONS ON MAGNETICS, VOL. 49, NO. 8 (AUGUST 2013) H.S Shin, K.H Shin, G.H Jang, IEEE TRANSACTIONS ON APPLIED SUPERCONDUCTIVITY, VOL. 30, NO. 4 (JUNE 2020) H.K Yeo, D.K Lim, and H.K Jung, IEEE TRANSACTIONS ON MAGNETICS, VOL. 55, NO. 6 (JUNE 2019)

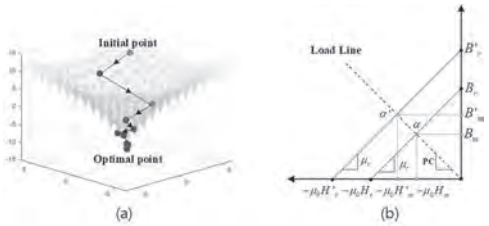

Fig.1(a) Random Walk Optimization of Test Function. (b) Demagnetization Characteristic of Permanent Magnet.

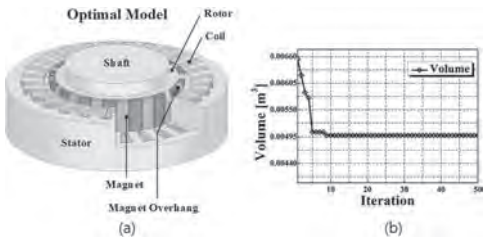

Fig.2(a) Optimal Model with PM Overhang. (b) SPMSM Volume Optimization result according to iteration.

JPJ-10. Design and Selection of Optimum Slot Parameters for SMPMSM Saturation Saliency with BP Net Approach. *H. Wang*[1]
1. School of Electrical Engineering, Southeast University, Nanjing, China

I. Introduction The saliency is essential using the method of high-frequency injection-based sensorless control[1]. The saliency in the spatial impedance is built by the spatial saturation on the leakage flux paths in for the structurally symmetrical ac machines. In [2], the stator or rotor bridge is inserted to generate saliency but the performance of torque is not considered. This paper investigates that the design of slot builds up the saliency for the surface mounted permanent magnet machine (SMPMSM) and parameters of design can be guaranteed the performance of torque by the Back Propagation network (BP net). II. Design method for SMPMSM Saliency Considering the saturation of flux AC machine makes the difference of d- and q- axes leakage inductances so that the saliency is acquired. Lots of flux linkages penetrate stator slots from the flux distributions of SMPMSM in Fig. 1. Because of leakage linkages, the saliency is acquired but it will bring the deterioration of performance of torque. To guarantee the performance of torque, the approach of optimum design needs to be investigated. The parameters of structure of the slot are shown in Fig.2. III. BP net for optimal parameters The approach of BP net is used in order that parameters are optimum for the set of average torque and the saliency level. The design steps are shown in the followed flowchart in Fig.3. After 7463 samples being trained, the results of regressions of the designed BP net are shown in Fig.4. The optimum parameters are selected according to the minimum of absolute error between FEM and BP predict results. Herein, 18 sets of data are tested and the results are listed in TABLE 1. The assumption is that the excepted salient ratio is equal to 1.2, and the optimum scheme is the17th because that the error of $(T/I)_{aver}$ for the 17th scheme is minimum as shown in TABLE 1.

[1] Jung-Ik Ha and Seung-Ki Sul, "Physical understanding of high frequency injection method to sensorless drives of an induction machine," in *Conference Record of the 2000 IEEE Industry Applications Conference. Thirty-Fifth IAS Annual Meeting and World Conference on Industrial Applications of Electrical Energy (Cat. No.00CH37129)*, Rome, Italy, 2000, vol. 3, pp. 1802–1808. [2] Jung-Ik Ha, M. Ohto, Ji-Hoon Jang, and Seung-Ki Sul, "Design and selection of AC machines for saliency-based sensorless control," in *Conference Record of the 2002 IEEE Industry Applications Conference. 37th IAS Annual Meeting (Cat. No.02CH37344)*, Pittsburgh, PA, USA, 2002, vol. 2, pp. 1155–1162.

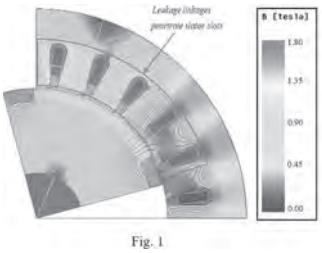

Fig. 1

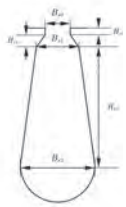

Fig. 2

Fig.1. Flux distribution of SMPMSM Fig.2. Diagram of structure of the slot

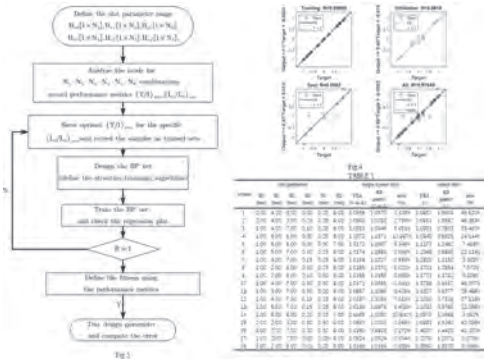

Fig.3. Flowchart for design of parameter using the BP net approach Fig.4. The regression result of designed BP net TABLE 1 The results of torque current ratio and salient ratio by the FEM and BP predict

JPJ-11. Experimental and Comparative Study of NVH of Permanent Magnet Machines According to Rotor Eccentricity with Fractional Pole/Slot Combinations. *T. Bang*[1], K. Shin[2], J. Lee[1], H. Lee[1], H. Cho[3] and J. Choi[1] *1. Electrical Engineering, Chungnam National University, Daejeon, The Republic of Korea; 2. Power System Engineering, Chonnam National University, Yeosu, The Republic of Korea; 3. Electro. Electric. and Comm. Eng. Education, Chungnam National Univeristy, Daejeon, The Republic of Korea*

Recently, permanent magnet synchronous motors (PMSMs) have been widely used in the industry owing to their various advantages such as high-speed operation, high efficiency, and compact design. However, PMSMs have the drawbacks of noise and vibration caused by the interaction between the stator and rotor magnets having high magnetic energy, significantly affecting the machine performance. The vibration and noise cause problems such as eccentricity, bearing fault, and misalignment of the PMSM. Therefore, it is important to determine electromagnetic vibration sources that actually affect vibration and noise. There are a few studies on the UMF of the PM machines. Therefore, to analyze the influence of each source, we proposed the design of PMSM with fractional pole/slot combination and equal characteristic performance, derived the dominant model of the pole slot combination for each electromagnetic vibration source through a finite element analysis, and carried out a comparative analysis of the results of the electromagnetic characteristic analysis. The derived pole-slot combination of the model is 8pole12slot. Thus, we analyzed the influence of each vibration source by conducting experiments and electro-mechanical coupled analysis using FEM, and then compared the results with fractional pole/slot combinations. Thus, in this study, to analyze the influence of each source, we derived the pole slot combination that is the dominant model for each electromagnetic vibration source. The analysis and prototype model used for the electromagnetic excitation analysis are shown in Fig. 1. The derived pole-slot combination is the 8pole 12slot and flow chart of NVH analysis. Figs. 2 show the electro-mechanical characteristic analysis results according to the eccentricity. This indicates that eccentricity significantly influences the NVH of the PMSMs. Therefore, the influence on each source could be analyzed. Detailed analysis and measurement results are discussed in the full paper.

[1] J. Zou, H. Lan, Y. Xu, and B. Zhao, "Analysis of Global and Local Force Harmonics and Their Effects on Vibration in Permanent Magnet Synchronous Machines," IEEE Trans. Energy convers., vol. 32, no. 4, pp.1523-1532, Dec. 2017. [2] D. Torregrossa, F. Peyraut, B. Fahimi, J. MBoua, and A. Miraoui, "Multiphysics finite-element modeling for vibration and acoustic analysis of permanent magnet synchronous machine," IEEE Trans. Energy Convers., vol. 26, no. 2, pp. 490–500, Jun. 2011. [3] H. Yang and Y. Chen, "Influence of radial force harmonics with low mode number on electromagnetic vibration of PMSM," IEEE Trans. Energy Convers., vol. 29, no. 1, pp. 38–45, Mar. 2014. [4] P. Beccue, J. Neely, S. Pekarek, and D. Stutts, "Measurement and control of torque ripple-induced frame torsional vibration in a surface mount permanent magnet machine," IEEE Trans. Power

Electron., vol. 20, no. 1, pp. 182–191, Jan. 2005. [5] Z. Q. Zhu, Y. Liu, and D. Howe, “Minimizing the influence of cogging torque on vibration of PM brushless machines by direct torque control,” IEEE Trans. Magn., vol. 42, no. 10, pp. 3512–3514, Oct. 2006. [6] D. Y. Kim, M. R. Park, J. H. Sim, and J. P. Hong, “Advanced Method of Selecting Number of Poles and Slots for Low-frequency Vibration Reduction of Traction Motor for Elevator,” IEEE/ASME Trans. Mechatro., vol. 22, no. 4, pp. 1554-1562, Aug. 2017. [7] J. F. Cieras, C. Wang, and J. C. Lai, Noise of Poly-phase Electric Motors. New York, NY, USA: Taylor & Francis, 2006.

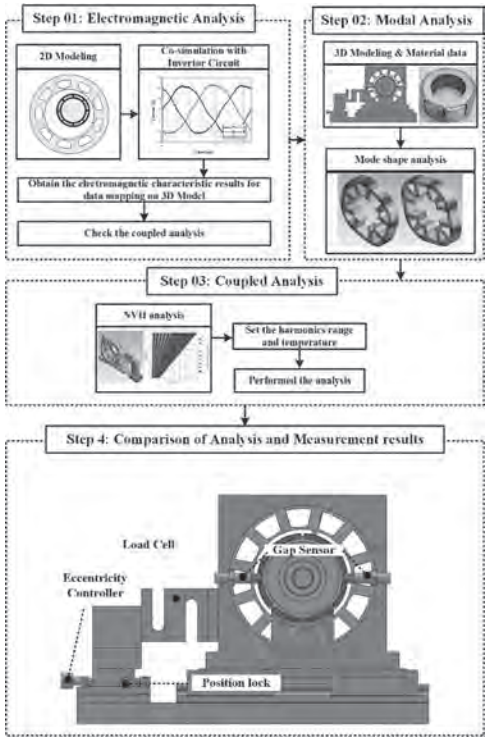

Figure 1. Flowchart of nvh analysis through co-analysis.

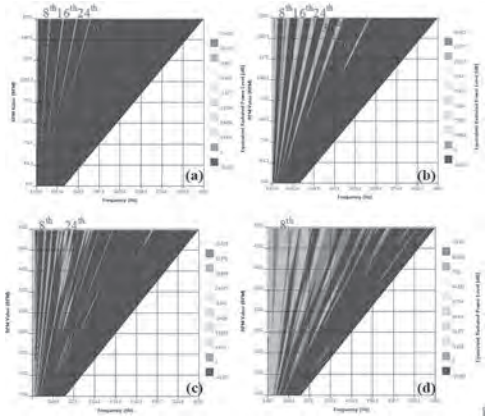

Figure 2 Analysis results of NVH: (a) 9slot healthy conditions (b) 9slot eccentricity conditions (c) 12slot healthy conditions (d) 12slot eccentricity conditions

Session JPK
(SEMI)-ANALYTICAL AND NUMERICAL TECHNIQUES FOR THE MODELING OF ELECTROMAGNETIC DEVICES (Poster Session)

Yacine Amara, Chair
University of Le Havre, Le Havre, France

JPK-01. Equivalent Analytical Calculation Theory of Inner Rotor and Outer Rotor Permanent Magnet Motor. *B. Guo*[1], Y. Du[2], F. Peng[2], J. Shi[1], X. Qiu[1] and Y. Huang[2] *1. School of Electrical and Automation Engineering, Nanjing Normal University, NanJing, China; 2. School of Electrical Engineering, Southeast University, NanJing, China*

Although the inner rotor permanent magnet (IRPM) motor and the outer rotor permanent magnet (ORPM) motor have different rotor structures, the analysis method of magnetic field is the same. An analytical method for calculating the no-load magnetic field of ORPM motor in the stator static coordinate and the rotor motion coordinate is presented in [1], this analysis method is based on the transformation of coordinate system, and does not consider the change of rotor structure. The magnetic field distribution calculation method of surface mounted permanent magnet motor is presented in [2], but unified inner/outer rotor structural permanent magnetic motor magnetic field calculation method is not given. Equivalent calculation of IRPM motor and ORPM motor with the same structure size is of great significance for motor design and performance analysis. In this paper, an equivalent analytical calculation theory of IRPM motor and ORPM motor is presented. The IRPM motor and ORPM motor with the same geometric size are established, as shown in Figure 1. The effects of curvature effects on magnetic field calculation is considered [3], and establish a unified calculation model. The complete unified computational theory derivation will be presented in the full paper. In order to verify the correctness of the equivalent calculation theory proposed in this paper, the finite element method (FEM) model and equivalent calculation model of the two motors are established according to Fig. 1. The FEM results and equivalent model results of air gap flux density component, output torque and other electromagnetic performance are compared. The comparison results show that the unified calculation model established in this paper is correct and has high calculation accuracy. Fig. 2 shows the comparison between the FEM results of the normal and tangential components of no-load air gap magnetic flux density and the equivalent calculation model. The complete electromagnetic performance comparison results will be given in the full paper.

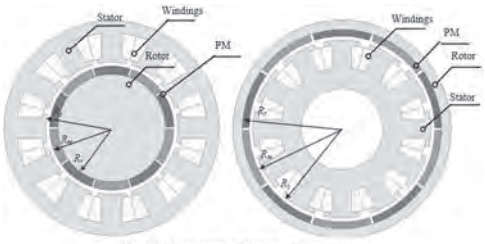

Fig. 1. The structure of inner and outer rotor

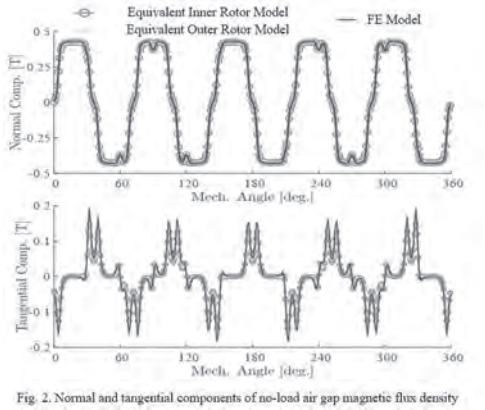

Fig. 2. Normal and tangential components of no-load air gap magnetic flux density

1) C. Ma et al., "Analytical Calculation of No-Load Magnetic Field of External Rotor Permanent Magnet Brushless Direct Current Motor Used as In-Wheel Motor of Electric Vehicle," in IEEE Transactions on Magnetics, vol. 54, no. 4, pp. 1-6, April 2018, Art no. 8103106, doi: 10.1109/TMAG.2017.2779861. 2) Z. Q. Zhu, D. Howe and C. C. Chan, "Improved analytical model for predicting the magnetic field distribution in brushless permanent-magnet machines," in IEEE Transactions on Magnetics, vol. 38, no. 1, pp. 229-238, Jan. 2002, doi: 10.1109/20.990112. 3) K. ATALLAH, Z. Q. ZHU, J. K. MITCHELL & D. HOWE (1994) CURVATURE EFFECTS IN RADIAL-FIELD PERMANENT MAGNET MACHINES, Electric Machines & Power Systems, 22:4, 511-520, DOI: 10.1080/07313569408955583 4) N. Boules, "Two-Dimensional Field Analysis of Cylindrical Machines with Permanent Magnet Excitation," in IEEE Transactions on Industry Applications, vol. IA-20, no. 5, pp. 1267-1277, Sept. 1984, doi: 10.1109/TIA.1984.4504593. 5) S. Asfirane, S. Hlioui, Y. Amara, and M. Gabsi, "Study of a Hybrid Excitation Synchronous Machine: Modeling and Experimental Validation," *Mathematical and Computational Applications*, vol. 24, no. 2, p. 34, Mar. 2019.

JPK-02. Withdrawn

JPK-03. An Improved Hybrid Method for Magnetic Field Calculation in Spoke PM machine. *B. Guo*[1], Y. Du[2], F. Peng[2], J. Dong[3] and Y. Huang[2] *1. School of Electrical and Automation Engineering, Nanjing Normal University, Nanjing, China; 2. School of Electrical Engineering, Southeast University, Nanjing, China; 3. Faculty of Electrical Engineering, Delft University of Technology, Delft, Netherlands*

With the advantages of high efficiency, high power density and wide constant power speed range, interior permanent magnet synchronous motor (IPMSM) is widely used in industrial, home applications, electric vehicles and other fields [1]. The magnetic equivalent circuit (MEC) model and finite element model (FEM) have been widely used in motor design. However, the MEC model has the disadvantage of low calculation accuracy, and the FEM model has the shortcomings of calculation time and occupy more computational resources [2]. The subdomain model is an optimal method for the initial design and optimization of the motor, which achieves a good compromise between the precision and the time of the magnetic field calculation [3]. In this paper, a hybrid model for magnetic field calculation considering rotor slots effect is proposed, which is improved the method in [3]. To take armature reaction into account, the IPMSM rotor is usually assumed to be a toothless model to simplify calculations [3], as shown in Fig.1. However, this simplified analytical model is difficult to accurately consider the armature reaction magnetic field. Considering that the relative permeability of the permanent magnet, a simplified and improved model of rotor structure

is presented in this paper. The rotor is equivalent to a slotted rotor, when solving armature reaction magnetic field, the permanent magnet is equivalent to air. In order to verify the correctness of the subdomain model proposed in this paper, the analytical calculation results and the FEM results of the air gap magnetic flux density of the general simplified model and the simplified model in this paper are compared. The results show that the accurate subdomain model proposed in this paper has better accuracy. On the other hand, the computation time of the proposed subdomain model and FEM are compared. This paper proposed an improved simplified subdomain model, which reduced the computation time remarkably while maintaining high accuracy. The complete analytical method derivation will be presented in the full paper.

1) J. Mun, G. Park, S. Seo, D. kim, Y. Kim and S. Jung, "Design Characteristics of IPMSM With Wide Constant Power Speed Range for EV Traction," in IEEE Transactions on Magnetics, vol. 53, no. 6, pp. 1-4, June 2017, Art no. 8105104, doi: 10.1109/TMAG.2017.2664859. 2) J.-M. Jin, The Finite Element Method in Electromagnetics, 2nd ed. New York, NY, USA: Wiley, 2002. 3) B. Guo, Y. Huang, F. Peng and J. Dong, "A New Hybrid Method for Magnetic Field Calculation in IPMSM Accounting for Any Rotor Configuration," in IEEE Transactions on Industrial Electronics, vol. 66, no. 7, pp. 5015-5024, July 2019, doi: 10.1109/TIE.2018.2868252.

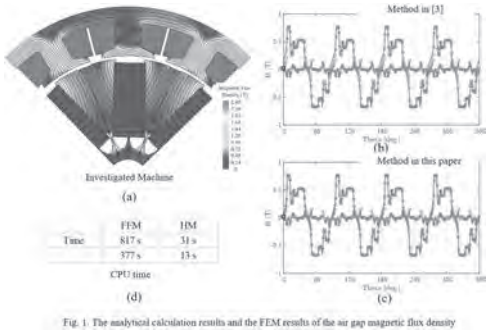

Fig. 1. The analytical calculation results and the FEM results of the air gap magnetic flux density

JPK-04. 2-D Analytical Modeling of Surface Mounted Permanent Magnet Machines With External Rotor Core. V.Z. Faradonbeh[1], A. Rahideh[1] and *E. Amiri*[2] *1. Department of Electrical and Electronics Engineering, Shiraz University of Technology, Shiraz, The Islamic Republic of Iran; 2. Department of Electrical and Computer Engineering, University of New Orleans, New Orleans, LA, United States*

External rotor machines are designed with the stator housed inside the rotor. Thanks to their extended rotor diameter, external rotor machines are capable of delivering higher torque under the same electrical loading. The enhanced torque delivery feature along with the robust mechanical structure have made external rotor PM machines an attractive choice for electric bike [1] and electric vehicle industry [2]. It is noted that numerical based analysis tools such as finite element (FE) may result in excessive computations at the early design phase and thus, analytical modeling is preferred. Among different analytical methods, subdomain model [3] is ranked in tier one. Despite excellent accuracy, the computational time of the subdomain model increases in proportion with the number of subdomains. It has been proven that the virtual current method [4] is significantly faster, with acceptable precision [5]. However, to this date the virtual current method has not been reported/applied to any class of SPM machines with external rotor. For this purpose, the virtual current method is extended and applied to a SPM machine with external rotor (Fig. 1a). The stator slots are modeled by injecting proper amount of magnetization current on the stator teeth lateral side $J_s(\varphi)$ (Fig. 1c). As a result, the flux distribution of the original slotted machine in Fig. 1a is equivalent to the sum of the flux distributions of two slotless machines (Fig. 1b and Fig. 1c). To simplify the model, by using Ampere's law, the injected surface currents in Fig. 1c is mapped/transferred to the surface of the slot opening area $J'_s(\varphi)$ as shown in Fig. 1d. Likewise, the armature current is also modeled via a magnetization current on the inner surface of the stator bore $J_{ar}(\varphi)$. Finally, the air-gap flux distribution is calculated by solving Maxwell's relations and applying boundary conditions and plotted in Fig. 2. Analytical results are verified by FE simulation.

[1] D. Lim, Yong-S. Cho, J. Ro, *IEEE Trans on Magnetics,* vol. 52, no, 3, (2016). [2] X. Guo, G. Liu, N. Shirazee, *IET Elec Systems in Transportation*, vol. 8, no. 2, pp. 95-100, (2018). [3] L. Wu, M. Zhu, D. Wang, *IEEE Trans. Magnetics*, vol. 55, no. 8, pp. 3949–3951, (2019). [4] V. Z. Faradonbeh, A. Rahideh, M. M. Ghahfarokhi, *IEEE Trans. Magnetics*, vol. 57, no. 1, (2021). [5] V.Z. Faradonbeh, A. Rahideh, G.A. Markadeh, *IET Electric Power Applications*, (2020).

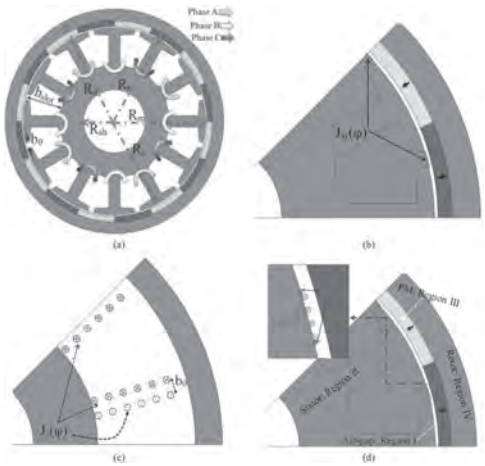

Fig. 1: a) Original slotted machine, b) slotless machine # 1, c) slotless machine # 2, d) final model.

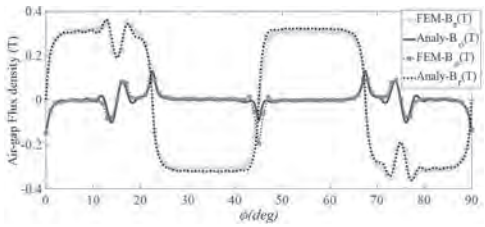

Fig. 2: Airgap PM flux density distribution along radial and tangential directions versus stator reference frame.

JPK-05. Withdrawn

JPK-06. Dynamic Modeling of Multi Disks Rotor System of Maglev Turbomachineries. *C. Wu*[1], Z. Su[1], D. Wang[1] and H. Jiang[1] *1. Naval University of Engineering, Wuhan, China*

For non-contact, low-loss and controllable support, active magnetic bearings (AMB) are increasingly used in turbomachineries, continuously improving the operating speed and power density of turbomachineries [1,2]. However, as an active support system, improper design of the AMB controller may arouse modal resonance of the rotor-AMB system and lead to poor system performance. It is necessary to analyze the dynamic characteristics of the rotor-AMB system for the AMB controller design [3]. With disk structure, the rotor-AMB system has coupling vibration modes between the disks and the shaft. Traditional analytical modeling methods of rotor dynamics can hardly analyze the dynamics characteristics of the multi disks rotor-AMB system. To solve the dynamic modeling problem, this paper establishes the dynamic model of the multi disks rotor-AMB system of maglev turbomachineries using the two-dimensional finite element method based on Euler Bernoulli beam theory. As shown in Fig. 1, four virtual spring dampers are introduced in the radial direction to connect the disk and the shaft. The

connection characteristics of the spring dampers are described by the angular stiffness and angular damping coefficient. The partition coefficient determines the radial relative position of the spring dampers and distributes the mass and inertia between the disk and the shaft, and the coupling model of the disks and the shaft is established. The angular stiffness and angular damping coefficients are identified from the system modes test data, and the division coefficient is obtained using multi-objective genetic optimization algorithm. Finally, a test rig is built as shown in Fig. 2(a) and the effectiveness of the proposed dynamic modeling method of the multi disks rotor-AMB system is verified through experiments as shown in Fig. 2(b).

[1] S. E. Mushi, Z. Lin and P. E. Allaire, "Design, Construction, and Modeling of a Flexible Rotor Active Magnetic Bearing Test Rig," in IEEE/ASME Transactions on Mechatronics, vol. 17, no. 6, pp. 1170-1182, Dec. 2012, doi: 10.1109/TMECH.2011.2160456. [2] J. Denk, D. Stoiber, H. Kopken and H. Walter, "Industrialization of AMB Systems With Standard Drive Technology," in IEEE Transactions on Industry Applications, vol. 49, no. 2, pp. 791-798, March-April 2013, doi: 10.1109/TIA.2013.2242426. [3] R. P. Jastrzebski, E. Kurvinen and O. Pyrhönen, "Design, Modelling and Control of MIMO AMB System with 3 Radial Bearing Planes for Megawatt-Range High-Speed Rotor," 2019 IEEE International Electric Machines & Drives Conference (IEMDC), 2019, pp. 805-811, doi: 10.1109/IEMDC.2019.8785378.

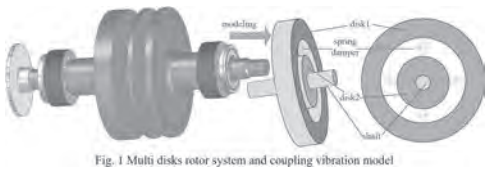

Fig. 1 Multi disks rotor system and coupling vibration model

Fig.1 Multi disks rotor system and coupling vibration model

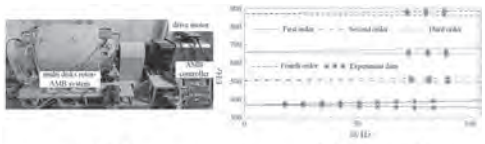

(a) Test rig (b) Experiment results

Fig. 2 Test rig and comparison between dynamic model results and experiments

Fig.2 Test rig and comparison between dynamic model results and experiments

JPK-07. Experimental Verification and Characteristic Analysis of a Permanent Magnet Synchronous Generator Using the Subdomain Method. *H. Lee*[1], T. Bang[1], J. Lee[1], J. Woo[1] and J. Choi[1] *1. Chungnam National University, Daejeon, The Republic of Korea*

Electromagnetic analyses of electric machines are widely classified into two methods: finite element methods and analytical methods. Finite element methods (FEMs) provide accurate results with an account of the saturation; however, they are time consuming to perform. In contrast, analytical methods provide fast analysis times and insights on the effect of the design parameters on the machine. [1] Analytical methods were studied as slotless models initially, and the permeance method, conformal mapping method, and subdomain method have been proposed to consider the slotting effect. Of these three, the subdomain method has the highest accuracy. [2]-[4] Therefore, this study deals with the characteristic analysis and experimental verification of a permanent magnet synchronous generator using the subdomain method. The governing equations were derived in each analysis region, and a magnetic field analysis was performed using the subdomain method. The circuit parameters such as the inductance, resistance, and induced voltage constant of the analysis model were calculated using the results of the subdomain method. Therefore, the calculated circuit parameters were applied to the equivalent circuit of the generator, and the output characteristics were derived. Fig. 1 shows the manufactured model and the experimental set. A no-load and a load test were performed through the back-to-back system. Fig. 2(a) shows a simplified analysis model for applying the subdomain method. The analysis region is divided into a permanent magnet, air gap, slot opening, and slot. Therefore, four governing equations and general solutions can be derived using the appropriate boundary conditions for each region. Fig. 2(b) shows the magnetic field density at the air gap. Fig. 2(c) and (d) indicates the induced voltage on the no-load condition and the output characteristics on the load condition. It can be confirmed that the results of the analytical model agree well with those of the FEM. More detailed results, discussions, and desired effects will be presented in the full paper.

[1] Z. Zhu, D. Howe and C. Chan, "Improved analytical model for predicting the magnetic field distribution in brushless permanent-magnet machine", IEEE Trans Magn., vol. 38, no. 1, pp.229-238, 2002. [2] Thierry Lubin, Smail Menani, Abderrzak Rezzoug, "Exact analytical method for magnetic field computation in the air gap of cylindrical electrical machines considering slotting effects", IEEE Trans Magn., vol. 46, pp. 1092-1099, 2009. [3] Z. J. Liu J. T. Li "Analytical solution of air-gap field in permanent magnet motors taking into account the effect of pole transition over slots" IEEE Trans. Magn. vol. 43 no. 10 pp. 3872-3882 Oct. 2007. [4] Z. J. Liu J. T. Li "Accurate prediction of magnetic field and magnetic forces in permanent magnet motor using an analytical solution" IEEE Trans. Energy. Convers. vol. 23 no. 3 pp. 717-726 Sep. 2008.

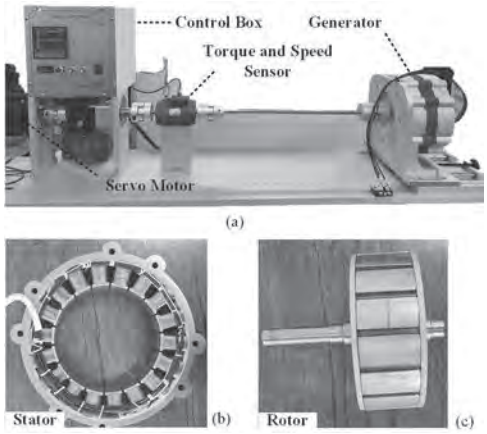

Fig. 1. (a) Experimental set, (b) stator, and rotor.

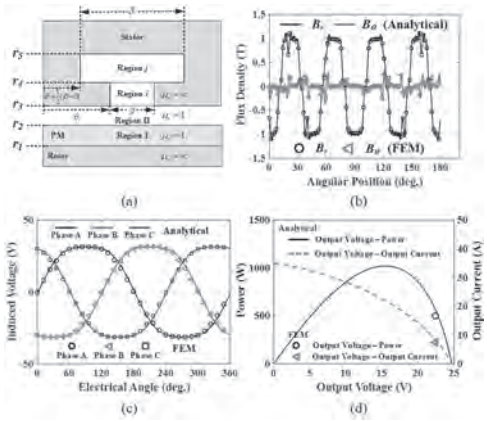

Fig. 2 (a) Simplified analytical model, (b) flux density, (c) induced voltage, and (d) performance characteristics.

JPK-08. Semi 3D Analysis of a Permanent Magnet Synchronous Generator Considering Overhang Structure Using 2D Finite Element Analysis and Equivalent Magnetic Circuit. *J. Hong*[1], H. Lee[1], J. Lee[1] and J. Choi[1] *1. Chungnam National University, Daejeon, The Republic of Korea*

Sleeve or bolting is applied to a permanent magnet synchronous generator (PMSG) to prevent defects caused by shattering. Bolting is more useful than the sleeve in manufacturing processes; however, the magnetic flux is reduced by the material characteristics of bolting. In addition, permanent magnet machines exhibit an overhang structure because the end effect causes leakage flux. Therefore, the axial length of the rotor must be considered in 3D analysis according to the overhang structure. However, the analysis is time-intensive for the 3D model with diverse and complex design variables. In this study, we performed a semi-3D analysis of a PMSG considering the bolting and overhang structure. The analysis time of a PMSG must be reduced because of the complex structure. Hence, we propose a semi-3D analysis for the 2D model by considering the operating point of the magnet in the 3D analysis. The operating point of the permanent magnet was calculated using magnetic energy analyses of the 2D and 3D models. Variations in the operating point were applied to the 2D analysis models, which were separated according to the permanent magnets and bolting regions. Then, a circuit parameter was derived using the semi-3D analysis and applied to the equivalent circuit of the generator. Characteristic analysis was performed using the superposition method. The results of the semi-3D model analysis were compared with those of the 3D model analysis. Figs. 1(a), (b), and (c) show the manufactured model. Fig. 2(a) shows the analysis model. Fig. 2(b) shows the variation in the operating point of the permanent magnet. Figs. 2(c) shows the output characteristic results from the comparison between the 3D and semi-3D models. We confirmed that the results of the semi-3D and 3D model analyses are congruent. Detailed data and experimental data is presented in the full paper.

Sung-Won Seo, Min-Mo Koo, Jang-Young Choi, Key-Yong Hong, “Characteristics Analysis of Permanent Magnet Linear Generator for small Scale Wave Energy Converter” KIEE, pp. 60-62, 2016 Kyung-Hun Shin, Jang-Young Choi, Kyong-Hwan Kim, Keyyong Hong. “Electromagnetic Analysis of Permanent Magnet Synchronous Generator Considering Permanent Magnet Bolting” KOSMEE, pp. 154-154, 2018 Phuong Thi Luu, Ji-Young Lee, Ji-Heon Lee, Byung-Chul Woo, “Design and Analysis of a Permanent Magnet Synchronous Motor Considering Axial Asymmetric Position of Rotor to Stator” ICEMS, pp. 37-40, 2018.

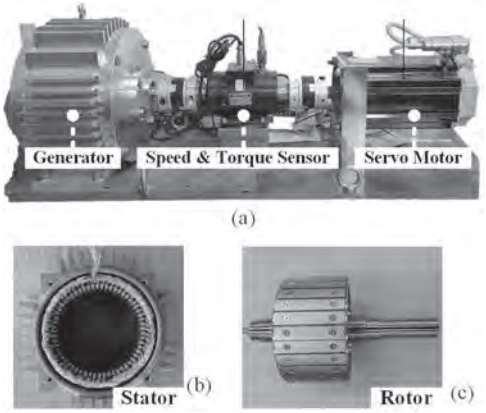

Figs. 1. Manufactured model: (a) experimental set, (b) stator, (c) rotor

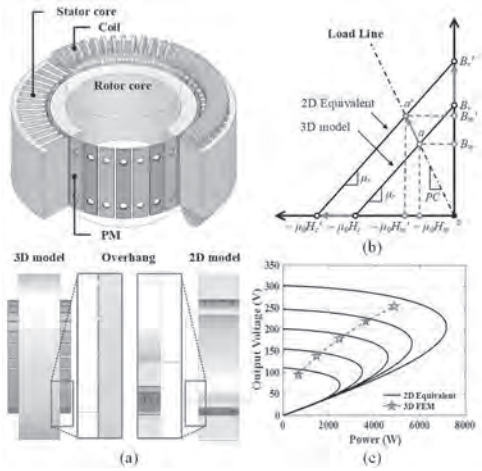

Figs. 2. (a) Analysis model, (b) demagnetization curve, and load power characteristic curve: (c) power-voltage curve

JPK-09. Mathematical Modeling of Wound Field Flux-switching Machines Considering Magnetic Saturation. X. Jiang[1], G. Zhao[1], W. Hua[2], H. Hua[3] and *Z. Li*[1] *1. Nanjing Normal University, Nanjing, China; 2. Southeast University, Nanjing, China; 3. Shanghai Jiao Tong University, Shanghai, China*

I. Introduction and Machine Modeling Fig. 1 shows the topology of a 6/5 wound field flux-switching machine (WFFSM), which is simple and reliable [1],[2]. However, the armature reaction and the excitation magnetic field are seriously coupled in WFFSM, resulting in a complicated mathematical model. To solve this problem, the mathematical model of 6/5 WFFSM is derived based on the precise inductance parameters considering magnetic saturation calculated by the frozen permeability method in this paper. The average electromagnetic torque equation is as follows: $T_{e(av)} = 3/2[P_r M_f I_m i_f \cos(\beta - \theta_{mb})] - 9/4[P_r L_{m1} I_m^2 \sin(2\beta - \theta_{b(2)})]$ (1) In this equation, $T_{e(av)}$ is composed of constant components of the excitation torque and the reluctance torque, which are related to the current parameters I_m, i_f, β, and the inductance parameters M_f, θ_{mb}, L_{m1}, $\theta_{b(2)}$. II. Verification of Mathematical Model Results Fig. 2(a) and (b) show the comparisons of the derived torque model and finite-element analysis (FEA) results under different current densities and different electrical angles, respectively. It can be seen that the derived model results are in good agreement with the FEA results. Fig. 2(c) shows the error between the model and FEA results in average electromagnetic torque. In most areas, the error is within 0.2%. When the current density is 10 A/mm^2, the error reaches a maximum of 0.42% due to magnetic saturation. Fig. 2(d) shows the comparison between the model and the finite-element interpolation of the maximum electromagnetic torque. The error between them is no more than 0.45%. More derivations and verifications of the mathematical model of 6/5 WFFSM will be shown in the full paper.

[1] Pollock and M. Wallace, “The flux switching motor, a DC motor without magnets or brushes,” *Conference Record of the 1999 IEEE Industry Applications Conference. Thirty-Forth IAS Annual Meeting (Cat. No.99CH36370)*, pp. 1980-1987 vol.3, 1999. [2] Y. Tang, J. J. H. Paulides and E. A. Lomonova, “Energy Conversion in DC Excited Flux-Switching Machines,” in *IEEE Transactions on Magnetics*, vol. 50, no. 11, pp. 1-4, Nov. 2014.

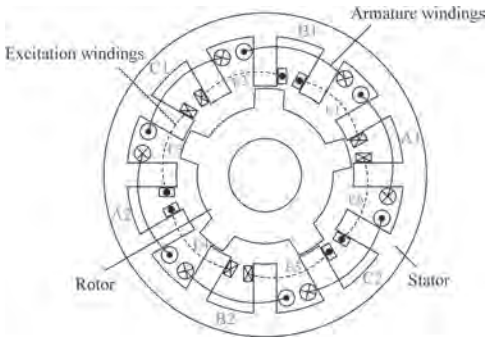

Fig. 1. Topology of a 6/5 WFFSM.

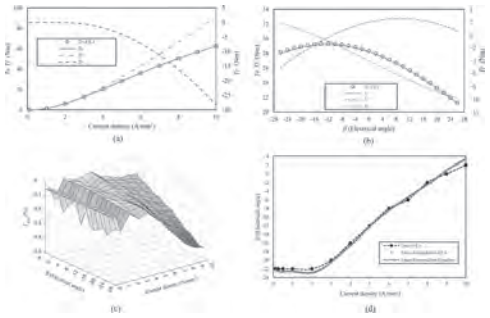

Fig. 2. Verification of mathematical model results. (a) The torque under different current densities when β=0°. (b) The torque at different electrical angles when the current density is 5A/mm². (c) The error between the model and FEA results in average electromagnetic torque under normal operation. (d) The electrical angle of maximum electromagnetic torque under different current densities.

JPK-10. Electromagnetic Analysis and Experimental Verification of Permanent Magnet Synchronous Machine Considering Axial Leakage Flux Using Subdomain Method. *K. Shin*[1], H. Park[2], H. Cho[3] and J. Choi[3] *1. Chonnam National University, Yeosu, The Republic of Korea; 2. Hyundai Mobis, Yongin, The Republic of Korea; 3. Chungnam National University, Daejeon, The Republic of Korea*

The electromagnetic design of permanent magnet synchronous machine (PMSM) is required to have a high-power per unit volume to improve system performances and to satisfy the maximum voltage limit under rated conditions. However, since the 2D analysis cannot consider the axial leakage magnetic flux, it is difficult to accurately predict the machine performance under the rated condition. Therefore, in this study, the electromagnetic analysis of PMSM considering axial flux leakage is proposed using a 2D subdomain analytical method. Fig. 1(a) shows the structure of PMSM with slotted structure and PM rotor. The leakage modeling of coil and stator to consider the effect of leakage by the end is shown in Figs. 1(b) and 1(c). Fig. 1(d) shows a 2D subdomain analytical model considering 3D axial leakage flux. To consider the axial flux leakage and end winding flux leakage [1], a proposed analytical model is defined that applies corrected permeability to slot and slot-opening regions. The governing equation in all subdomains can be solved, and the field distribution can be obtained by applying the boundary conditions on the interfaces between the subdomains [2], [3]. Based on these solutions, the electromagnetic performances such as back-EMF, inductance, electromagnetic torque, and torque-speed curve can also be determined analytically. The magnetic field and the electromagnetic performance obtained using the proposed analytical method were compared with those obtained using the finite element (FE) analysis, and experimental measurement in this paper. To measure the operating characteristics, a back-to-back system with a prototype and load generator is constructed as shown in Fig. 2(a). Fig. 2(b) compares torque-speed characteristics from the proposed analytical method with the conventional 2D FE and experimental results. The analytical approach, analysis, and experimental results will be presented in more detail in the full paper.

[1] J. Jung, H. Park, J. Hong, and B. Lee, "A novel approach for 2-D electromagnetic field analysis of surface-mounted permanent magnet synchronous motor taking into account axial end leakage flux," IEEE Trans. Magn., vol. 53, no. 11, Nov. 2017, Art. no. 8208104. [2] K.-H. Shin, H. I. Park, H.-W. Cho, and J.-Y. Choi, "Analytical calculation and experimental verification of cogging torque and optimal point in permanent magnet synchronous motors," IEEE Trans. Magn., vol. 53, no. 6, Jun. 2017, Art. no. 8106204. [3] T. Lubin, S. Mezani, and A. Rezzoug, "Two-dimensional analytical calculation of magnetic field and electromagnetic torque for surface inset permanent-magnet motors," IEEE Trans. Magn., vol. 48, no. 6, pp. 2080–2091, Jun. 2012.

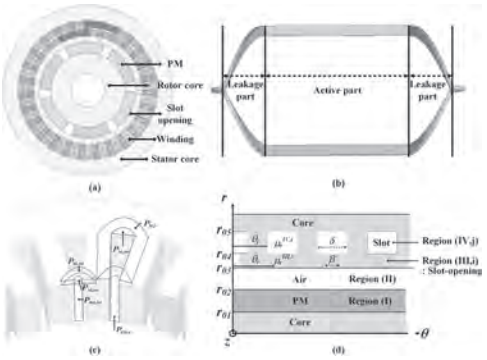

Fig. 1. Structure of PMSM: (a) analysis model, (b) winding with active and leakage part, (c) stator with permeances and (d) simplified analytical model.

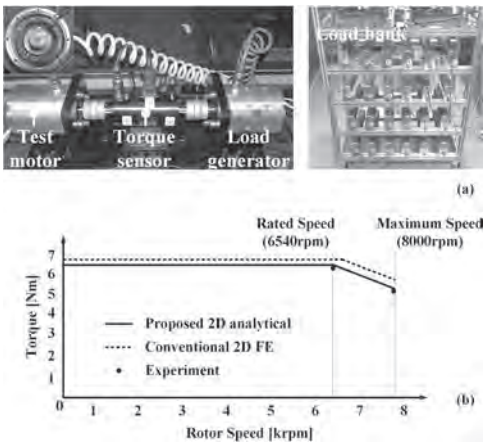

Fig. 2. (a) Experimental setup and (b) torque-speed curve obtained by 2D FE analysis, analytical and experimental results.

JPK-11. Magnetic Circuit Analysis of a New Radial-Axial Hybrid Excitation Machine. X. Wang[1], Y. Fan[1], Q. Chen[1] and *Z. Wu*[1] *1. Southeast University, Nanjing, China*

1. Introduction The hybrid excitation machine combines the permanent magnet(PM) and electric excitation to produce the magnetic field and realize the adjustment of the air gap magnetic field [1]. The two flux paths are coupled with each other, the electromagnetic characteristics are complex, and the magnetic field is often distributed in 3-D. The 3-D magnetic field is transformed into 2-D magnetic circuit, which reduces the amount of calculation and cost. It is of great significance to the initial parameter modeling and magnetic circuit analysis of the machine. 2. Topology A new radial axial hybrid excitation machine(RAHEM) is proposed, as shown in Fig. 1. The radial stator is wound with armature winding, and the axial stator with AC excitation winding is placed on the rotor side. The rotor core pole protrudes along the axial direction to form the axial magnetic pole to adjust the radial air gap magnetic field [2]. The N-S alternating pole is adopted, the two sides of the core pole are PMs with the same polarity, and the V-type is adopted

to increase the magnetic concentrating effect. 3. Magnetic circuit analysis The equivalent 2-D magnetic circuit model is established to analysis the flux distribution in different excitation magnetomotive forces(MMFs). The adjacent PMs form a group to produce the main air gap flux. The magnetic flux generated by the PMs at the core pole can be divided into radial core pole flux and axial core pole flux. If the excitation MMFs are positive, the axial flux decreases and the radial core pole flux increases. The magnetic density of the radial core pole varies greatly in different positive MMFs, which indicates that the RAHEM has good magnetic field regulation ability, as shown in Fig. 2. If the negative excitation MMFs are applied, the analysis will be shown in the full paper. 4. Conclusion A new RAHEM is proposed, and its equivalent 2-D magnetic circuit model is established, which can quickly analyze the magnetic field. The analysis results show that the RAHEM has good magnetic field regulation ability.

[1] Y. Fan, G. Y. Qu, C. Tan, et al. "Design and Analysis of a New Five-Phase Dual-Stator Consequent-Pole Brushless Hybrid Excitation Machine," IEEE Transactions on Magnetics, vol. 55, no.1, pp. 4353 – 4356. (2019) [2] D. Wang, D. Zhang, D. Xue, et al. "A New Hybrid Excitation Permanent Magnet Machine With an Independent AC Excitation Port,"IEEE Transactions on Industrial Electronics, vol. 66, no. 8, pp. 5872-5882. (2019)

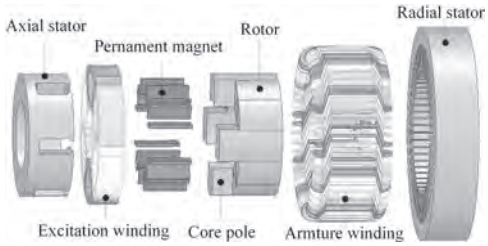

Fig.1. The structure of the RAHEM

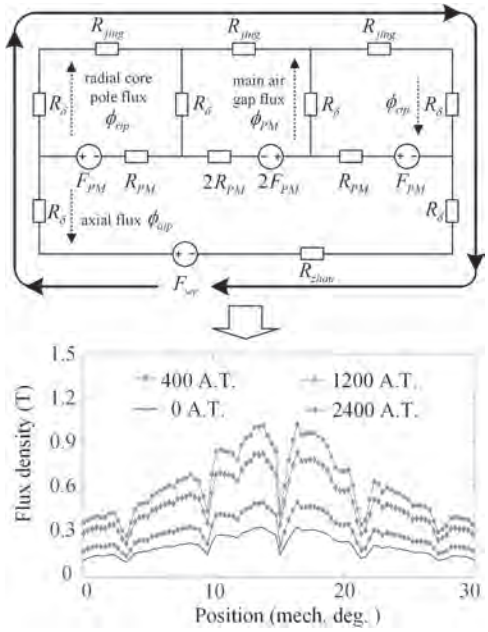

Fig.2. Magnetic circuit model and air gap flux density distribution in positive MMFs

JPK-12. Circuit Conversion Technique for Decomposition by Power Supplies of Combined Equivalent Circuit Based on Cauer Ladder Network Method. *H. Kaimori*[1], T. Matsuo[2] and H. Eskandari[2] *1. Science Solutions International Laboratory, Inc., Tokyo, Japan; 2. Kyoto University, Kyoto, Japan*

When considering an equivalent circuit that includes magnetic saturation of iron cores or bulk conductors, its effect depends on the sum of the primary and secondary coil currents. To express both effects in an equivalent circuit of two-port problem of transformer, it is reasonable to construct a combined equivalent circuit expressed with the sum of the coil currents as one power supply input [Fig. 1 (a)]. Therefore, this paper proposes a new effective conversion technique of combined equivalent circuits for multi-port problem including magnetic cores and bulk conductors. The presenting technique constructs a combined equivalent Cauer ladder circuit reduced by the CLN method based on the finite element (FE) eddy-current analysis [1~3], which is fed by the actual primary and secondary currents (no need to be unit currents). Then the combined equivalent circuit elements are decomposed into the primary and secondary side elements by converting the resistances and inductances to the normalized ones per unit current [Fig. 1 (b)]. In that case, the conversion depends on the ratio of the primary and secondary currents. To demonstrate the accuracy of the proposed conversion technique based on the CLN method, a sample eddy-current problem is analyzed. A transformer for power electronic devices has an iron core and two-port coils. The relative permeability of the magnetic core is 1000 and the conductivity of the core and two coils are $1*10^5$ S/m and $4*10^7$ S/m, respectively. Fig. 2 shows the impedance characteristics when the primary and secondary coils are excited with 2A and -3A, respectively. The results are in good agreement with those by the AC FE analysis, even when the primary and secondary currents are different. In addition, the impedances of the primary and secondary sides precisely exhibit the influence of the magnetic coupling and proximity effect including the conductive core. In the full paper a rigorous derivation and practical applications will be presented.

[1] A. Kameari, H. Ebrahimi, K. Sugahara, Y. Shindo, and T. Matsuo, IEEE Trans. Magn. vol. 54, no. 3, March (2018), Art. no. 7201804. [2] H. Ebrahimi, K. Sugahara, T. Matsuo, H. Kaimori, and A. Kameari, IEEE Trans. Magn. vol. 56, no. 3, March (2020), Art. no. 7513004. [3] S. Hiruma and H. Igarashi, IEEE Trans. Magn. vol. 56, no. 3, March (2020), Art. no. 7400608.

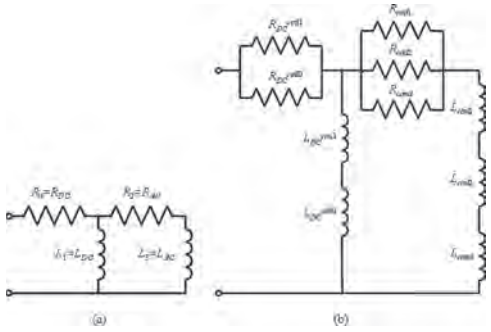

Fig.1 Circuit representation: (a) Conventional Cauer circuit, (b) Combined Cauer circuit

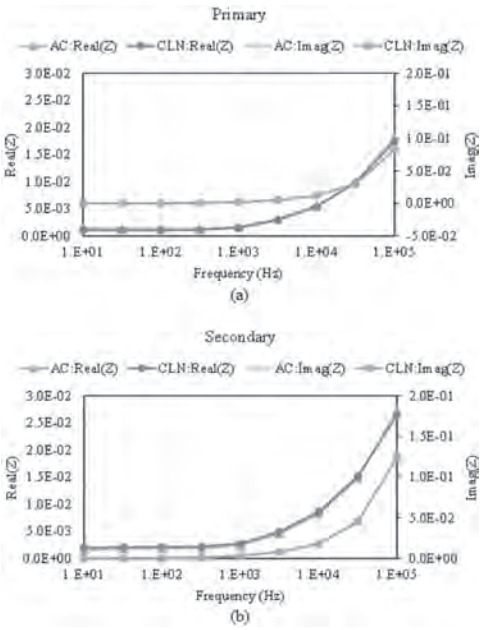

Eddy-current analysis for transformer model, (a) impedance characteristics of the primary side, (b) impedance characteristics of the secondary side.

JPK-13. An Improved Subdomain and Magnetic Circuit Hybrid Model for SPM Machines Accounting for Iron Saturation. *l. Wu*[1] and J. Li[1]
1. Zhejiang University, Hang Zhou, China

The hybrid model is applied increasingly for field prediction in surface-mounted permanent-magnet (SPM) machine with iron saturation[1][2]. The equivalent current sheet can be introduced to represent for iron saturation effect [2]. The hybrid model in [2] puts visual current on the inwall of slot (J_1, J_2 and J_3 in Fig. 1(a)) in subdomain for considering iron saturation. Therefore, the boundary condition along the slot inwall is changed. The vector potential in stator slot should be derived again according to the new boundary, which increases the complexity of subdomain model. For both simplifying model complexity and obtaining accurate magnetic field, this article presents an improved nonlinear subdomain and magnetic circuit (MC) hybrid model for SPM machines. As seen in Fig. 1(a), the equivalent surface current in loop 1 (J_4) is introduced creatively for predicting accurate magnetic field under iron saturation. In the improved model, the general expression of each subdomain and all boundary conditions keep unchangeable compared to traditional subdomain. Similar to loop 2 to 4, the Ampere law is applied along loop 1, the J_4 should satisfy $\oint J_4 \mathrm{d}s = -F_{yoke} - F_{tooth1} - F_{tooth2}$ (1) where the 'F ' denotes the magnetic potential drop. The surface current density (J_4) is calculated by equation (2) according to the MC model in Fig. 1(b). $J_4 = -(V_b - V_a)/S\mathrm{slot}$ (2) where 'V 'denotes the node magnetic potential and S_{slot} is the slot area. The air gap flux density of an 18-slots 10-poles SPM machine is predicted by the finite element analysis and the improved hybrid model as shown in Fig. 2. There is heavy saturation effect, therefore, the linear subdomain model overestimates drastically the magnetic flux density. The accuracy of the improved hybrid model is verified. The Newton Raphson method is applied for the convergence of MC model. For calculating the magnetostatic field, the original model in [2] and the improved model take 0.89 s and 0.51 s, respectively. The improved hybrid model can reduce the computation time by 43% in field prediction.

[1] A. Hanic, D. Zarko, D. Kuhinek, "On-load Analysis of Saturated Surface Permanent Magnet Machines Using Conformal Mapping and Magnetic Equivalent Circuits, " IEEE Trans. Energy Convers., vol. 33, no. 3, pp. 915–924, Sep. 2018. [2]L. Wu, H. Yin, D. Wang, "A Nonlinear Subdomain and Magnetic Circuit Hybrid Model for Open-Circuit Field Prediction in Surface-Mounted PM Machines," IEEE Trans. on Energy. Convers., vol. 34, no. 3, pp. 1485-1495, Sep. 2019.

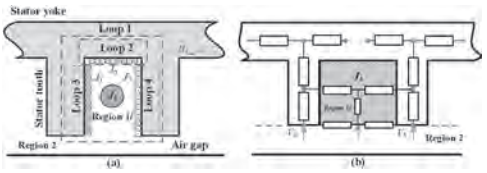

Fig.1 Equivalent transformation (a) ideal iron model with equivalent current (b) improved hybrid model

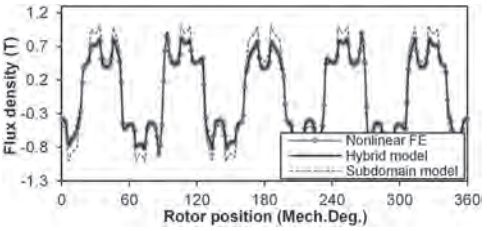

Fig.2 Comparison of radial air gap flux density results from subdomain, hybrid and FE model.

Session JPL
LOSS AND THERMAL MODELLING OF ELECTRICAL MACHINES, MAGNETIC BEARING (Poster Session)

Yanhui Gao, Chair
Oita University, Oita, Japan

JPL-01. Iron Losses Model for Induction Machines Considering the Influence of Rotational Iron Losses. *J. Yan*[1], C. Di[1] and X. Bao[1] *1. School of Electrical Engineering and Automation, Hefei University of Technology, Hefei, China*

Iron losses attract lots of attention because of the large proportion in the total losses of induction machines (IMs) [1]. However, the conventional iron losses estimation method is not precise enough, and an empirical coefficient is always needed in practical applications to further fix the iron losses. To predict the iron losses more accurately, modified iron losses models are proposed in this paper considering the non-sinusoidal magnetic field effects and the rotational iron losses. The maximum error between the losses estimated by the alternate iron loss model (AILM) with constant loss coefficients and Epstein test values is larger than 50% as shown in Fig. 1(a), where the AILM equation is also exhibited. The variable coefficients alternate iron loss model (VCAILM)'s loss coefficients vary with the frequency and the amplitude of the magnetic flux density, which makes the error much smaller (the maximum relative error is about 11%) as shown in Fig. 1(b). Based on the VCAILM, an elliptical iron loss model (EILM) is established to take the rotational losses into account, resulted from the time-varying instantaneous value of the rotational magnetic flied density in the lamination. Utilizing the major (Bmaj) and minor axes (Bmin) of the elliptical magnetic flux density shown in Fig. 2(a), the proposed EILM is capable of considering two situations, to be more specific the unsaturation and saturation cases, because the iron losses caused by a rotational field drop rapidly and approach zero at saturation [2]. Compared with the measured no-load iron losses according to IEEE 112B method, the AILM and proposed EILM estimate the no-load iron losses for the cases that the voltage ranges from 0.4 per unit (pu) to 0.9 pu (the base value is 10 kV). The corresponding comparative losses are displayed in Fig. 2(b), where the relative errors between the predicted and the tested results exceed 60% solved by the AILM and the errors are less than 17.7% solved by the EILM.

[1] W. Su, S. M, and P. Wang, *IEEE Trans. Magn.,* Vol. 55, p. 1-8 (2019)
[2] Y. Huang, J. Dong, J. Zhu, and Y. Guo, *IEEE Trans. Magn.,* Vol. 48, p. 1023-1026 (2012)

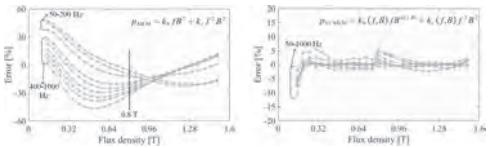

Fig. 1 The errors between iron loss model and Epstein tests. (a) AILM. (b) VCAILM.

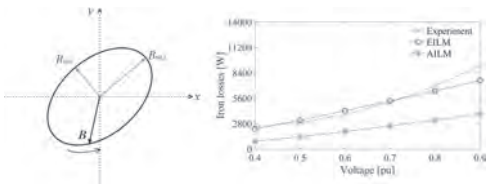

Fig. 2 EILM magnetic flux density and losses. (a) Elliptical locus of the magnetic flux density in the lamination. (b) Comparison of no-load iron losses.

JPL-02. Iron Loss Prediction in SPMSM by Using Deeping Learning Approach. *B. Guo*[1], Y. Du[2], J. Shi[1], X. Qiu[1], F. Peng[2] and Y. Huang[2] *1. School of Electrical and Automation Engineering, Nanjing Normal University, NanJing, China; 2. School of Electrical Engineering, Southeast University, NanJing, China*

Accurately simulating the magnetic field of electric machines is valuable in many industries and applications [1]. Various techniques are used to model a system. One of the most commonly used approaches is the finite element method (FEM), which is often the first type of model one learns in an introductory physics or engineering course [1]. however, the time of simulation time if often used hours or days when the geometry is complex. Researchers have been conducted on the modeling for a better trade-off between accuracy and CPU time. Each of the methods has its own advantages/disadvantages, but the overall issue common to all methods is that computation time significantly increases for complex structures [2]. In this paper, we proposed a Neural Network model is developed to predict the iron loss, hence, to deduce the higher computation time. The image transfer technique is applied in this task. In fIg. 1, we can see that the input/output data structure is based on the FEM model. The training data can be traded as image and used for learning. In the fourth column, the generative adversarial network (GAN) is introduced in order to overcome the blur effect. In fig.1, two networks, viz., generator and the discriminator, are fighting against each other and during the process of training, they trained in an alternating fashion. Detailed information can be found in the full paper. The test is done on a surface permanent magnet mounted machine, and the results show that the proposed method in 24 times faster than that of FEM model, while the accuracy is maintained as the same as FEM. This approximation model can be applied as the sample filter prior to the FEM in the optimization framework.

[1] I. H. Kao, W. J. Wang, Y. H. Lai, and J. W. Perng, "Analysis of Permanent Magnet Synchronous Motor Fault Diagnosis Based on Learning," *IEEE Trans. Instrum. Meas.*, pp. 1–15, 2018, doi: 10.1109/TIM.2018.2847800.
[2] A. Khan, V. Ghorbanian, and D. Lowther, "Deep Learning for Magnetic Field Estimation," *IEEE Trans. Magn.*, vol. 55, no. 6, pp. 1–4, Jun. 2019, doi: 10.1109/TMAG.2019.2899304.

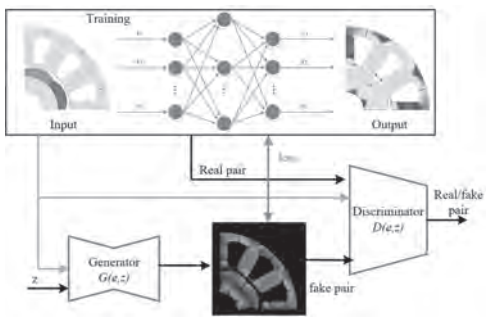

JPL-03. Characteristic Analysis and Experimental Verification of Electromagnetic Losses Considering Current Harmonics in High-Speed Permanent Magnet Synchronous Motors. K. Shin[1], H. Cho[2], J. Choi[2] and *T. Bang*[2] *1. Chonnam National University, Yeosu, The Republic of Korea; 2. Chungnam National University, Daejeon, The Republic of Korea*

High-speed permanent magnet synchronous motors (HPMSMs) are developed in direct-drive applications such as centrifugal compressors and vacuum pumps because of the advantages of compact size and high efficiency [1]. However, due to the small size, it has a high loss density and a limited heat dissipation surface, which causes difficulties in cooling [2]. Therefore, the accurate prediction of electromagnetic losses is very important in the design stage of HPMSM. In this study, electromagnetic analysis considering pulse width modulation (PWM) inverter and effective three-dimensional (3D) electromagnetic structure is proposed for predicting accurate electromagnetic losses of HPMSM. Fig. 1 shows the 3D structure and side view of the HPMSM and the evaluation system of the prototype. To accurately predict the applied current, it is necessary to derive the back EMF constant, resistance, and inductance using the 3D finite element method. Using the dynamic model based on the derived machine constants, it is possible to predict the applied PWM current similar to the experimental results as shown in Figs. 2(a) and (b). As shown in Fig.2(c), mechanical losses according to speed can be calculated by subtracting the core losses calculated from FEM from the measured no-load losses. Using the proposed effective 3D model, accurate electromagnetic losses such as AC and DC copper losses, core loss, and rotor loss can be predicted. Considering mechanical losses, the error between the proposed electromagnetic loss analysis and the experiment is within 3% according to the operating condition as shown in Fig. 2 (d). The analysis, discussions, and measurements of HPMSM will be explained in more detail in the full paper.

[1] D. Gerada, A. Mebarki, N. L. Brown, C. Gerada, A. Cavagnino, and A. Boglietti, "High-speed electrical machines: Technologies, trends, and developments," IEEE Trans. Ind. Electron., vol. 61, no. 6, pp. 2946–2959, Jun. 2014. [2] D.-K. Hong, B.-C. Woo, and D.-H. Koo, "Ultra High Speed Motor Supported by Air Foil Bearings for Air Blower Cooling Fuel Cells," IEEE Trans. Magn., Vol. 48, No. 2, pp. 871–874, 2012.

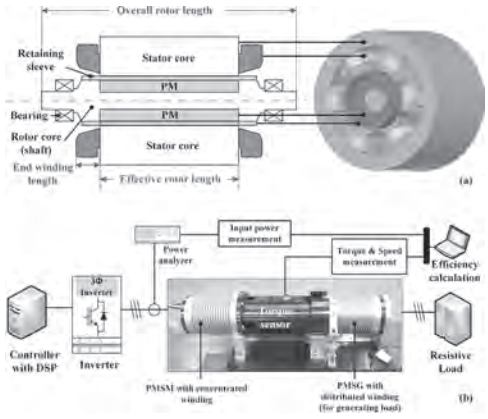

Fig. 1. (a) Structure of HPMSM with concentrated winding and (b) performance evaluation system.

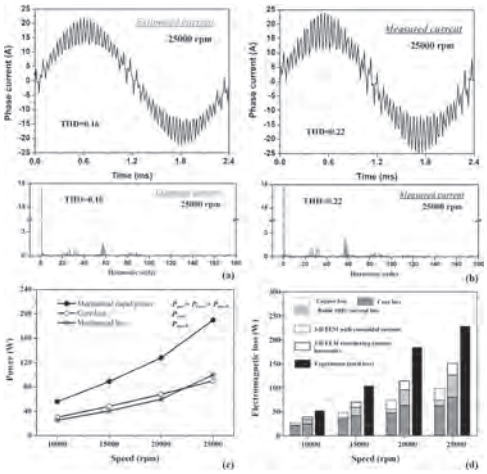

Fig. 2. Comparison with analysis and experimental results: (a) estimated, (b) measured phase current, (c) measured mechanical loss, and (d) electromagnetic losses.

JPL-04. Nonlinear Analytical Model for Predicting Magnet Loss in Surface-Mounted Permanent-Magnet Motors. Z. Li[1], X. Huang[1], Z. Chen[1], *X. Xu*[1] and T. Shi[1] *1. Zhejiang University, Hangzhou, China*

I. Introduction The eddy-current effect plays an important role in the loss analysis of high-speed motors due to high-frequency current. Conformal mapping model or subdomain model was proposed to calculate the magnet loss [1]-[3]. In this paper, a nonlinear analytical model (NAM) is proposed to predict the magnet loss considering slotting effect and nonlinearity effect. The equivalent current representing PM, winding current and iron nonlinearity is introduced to calculate the vector magnetic potential in the PM region using conformal mapping and Hague's equation. The influence of iron nonlinearity on the magnet loss is investigated in a 8-pole/9-slot motor to validate the proposed model. II. Nonlinear Analytical Field Model The linear relationship between the magnetic vector potential distribution and the equivalent current distribution is proposed to calculate the magnetic field in the PM region based on conformal mapping. The equivalent current including PM and winding is obtained based on the linear analytical model [1]. According to Ampere's law, the equivalent nonlinear current located in the slot is calculated from the magnetic circuit model of iron. Based on the nonlinear analytical solution of PM region, the eddy current in the magnet is calculated using $J_{eddy}=-\sigma(\partial As/\partial t)+C_{PM}(t)$ The total eddy current in each piece of PM should be equal to zero and therefore C_{PM} can be obtained. Then the instantaneous magnet loss in each piece of magnet can be obtained as $p_e=l_{ef}/\sigma\iint J_{eddy}{}^2 r dr d\alpha$ II. Discussion and Conclusion Fig. 1 shows the comparison of magnetic field prediction in PM region at rated load. The proposed model can accurately obtain the flux density in the PM region, which is key for accurate prediction of magnet loss. Fig.2 shows that the magnet loss is greatly affected by the load condition considering iron saturation. The NAM still achieves high accuracy compared with nonlinear FEM results. If the iron nonlinearity is neglected, the analytical model (LAM) will significantly overestimate the magnet loss for both motors. Hence, the high accuracy of NAM for predicting magnet loss is validated by the FEM. Acknowledgement : This work was supported by the National Key R&D Program of China (2019YFE0123500).

[1] N. Chiodetto, N. Bianchi, and L. Alberti, "Improved analytical estimation of rotor losses in high-speed surface-mounted PM synchronous machines," *IEEE Trans. Ind. App.*, Vol. 53, p.3548–3556 (2017). [2] L. J. Wu, Z. Q. Zhu, D. Staton, etc., "Analytical model for predicting magnet loss of surface-mounted permanent magnet machines accounting for slotting effect and load," *IEEE Trans. Magn.,* Vol. 48, p. 107–117 (2012). [3] P. D. Pfister, X. Yin, and Y. Fang, "Slotted permanent-magnet machines: general analytical model of magnetic fields, torque, eddy currents, and permanent-magnet power losses including the diffusion effect," *IEEE Trans. Magn.*, Vol. 52, p. 1–13, (2016).

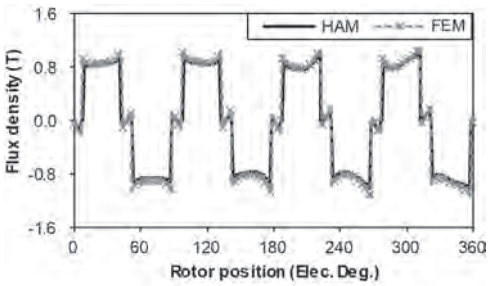

(a) radial component

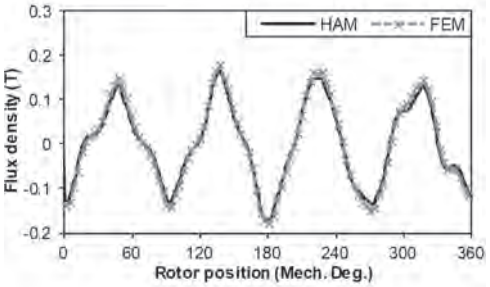

(b) tangential component

Fig. 1 The air-gap field along the middle PM for 8-pole/9-slot motor.

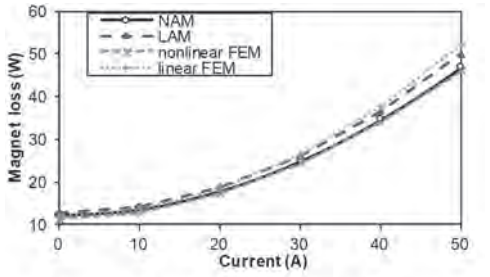

Fig. 2 The variation of magnet loss to load current for 8-pole/9-slot motor.

JPL-05. AC Loss Calculation and Analysis of Hollow Conductor for Doubly Salient Brushless DC Generator. J. Zhang[1], *Y. Xia*[1] and Z. Zhang[1] *1. Nanjing University of Aeronautics and Astronautics, Nanjing, China*

The doubly salient brushless DC generator (DSBLDCG) is suitable for aviation generator due to its simple and robust structure, and adjustable magnetic field [1]. The harsh environment of aviation operation puts forward a high demand on the thermal design of the generator winding. Hollow conductor with good heat dissipation performance can be used to replace conventional solid conductor in generator for winding cooling [2][3]. The harmonic content of the magnetic field in the slot of DSBLDCG is high and the radial component also exists, which makes its AC loss characteristics complex. Therefore, it is necessary to calculate the AC loss of the hollow conductor for DSBLDCG, analyze the influence of the conductor structural parameters on AC loss and optimize the structure of hollow conductor, so as to reduce the copper loss of the generator and facilitate the further cooling design. Fig. 1 shows the 2D finite element 1/2 section diagram of the 12-stator-pole/8-rotor-pole (12/8) DSBLDCG with hollow conductor. There are no windings or permanent magnets on the rotor, and the stator is wound with armature windings made of hollow conductors. Fig. 2 shows the magnetic flux density waveforms at different positions in the slot. The magnetic flux density can be decomposed into B_x in the x direction and B_y in the y direction. As the distance from the slot opening position increases, the amplitude of B_x decreases gradually, and B_y is mainly concentrated near the slot opening position. As shown in Fig. 3, the hollow conductor can be decomposed into four parts for the calculation of AC loss. The calculation formulas are shown as Equations (1) to (3). Fig. 4 shows the AC loss of hollow conductors at position I, II, III, and IV. It can be seen that as the distance from the slot opening position increases, the AC loss of the hollow conductor decreases. Take the hollow conductor at position I closest to the slot opening position as an example, the effect of conductor thickness on AC loss is compared and analyzed, as shown in Fig. 5. Considering the copper loss and cooling design of the generator comprehensively, 0.3mm section thickness of hollow conductor is more appropriate.

[1] Z. Zhang, L. Yu, Y. Wang, Y. Wang and Y. Yan, "Overview and design methodology of doubly salient brushless dc generators with stator-field winding," *IET Electr. Power Appl*., vol. 11, no. 2, pp. 197-211, Feb., 2017. [2] X. Chen, J. B. Wang, A. Griffo, and A. Spagnolo, "Thermal Modelling of Hollow Conductors for Direct Cooling of Electrical Machines," *IEEE Transactions on Industrial Electronics*, vol. 67, no. 2, pp.895-905, Feb., 2020. [3] F. Wu, A. E. Refaie, A. Al-Qarni. "Additively Manufactured Hollow Conductors Integrated with Heat Pipes: Design Tradeoffs and Hardware Demonstration," *IEEE Transactions on Industry Applications*, vol. 57, no. 4, pp.3632-3642, July/Aug., 2021.

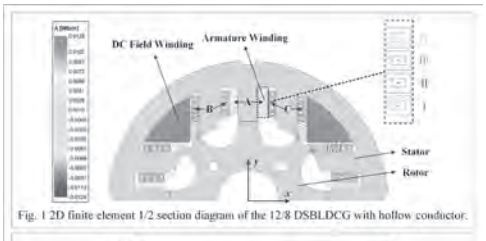

Fig. 1 2D finite element 1/2 section diagram of the 12/8 DSBLDCG with hollow conductor.

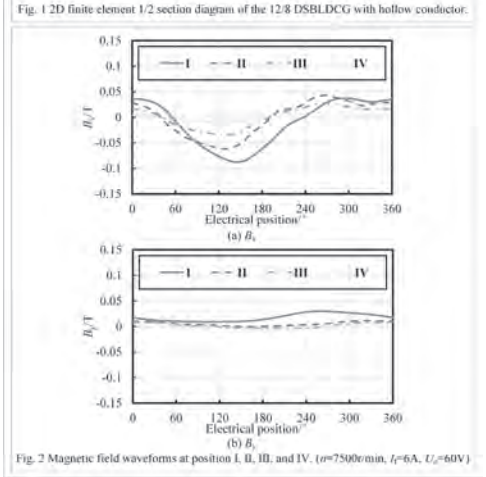

Fig. 2 Magnetic field waveforms at position I, II, III, and IV. (n=7500r/min, I_f=6A, U_d=60V)

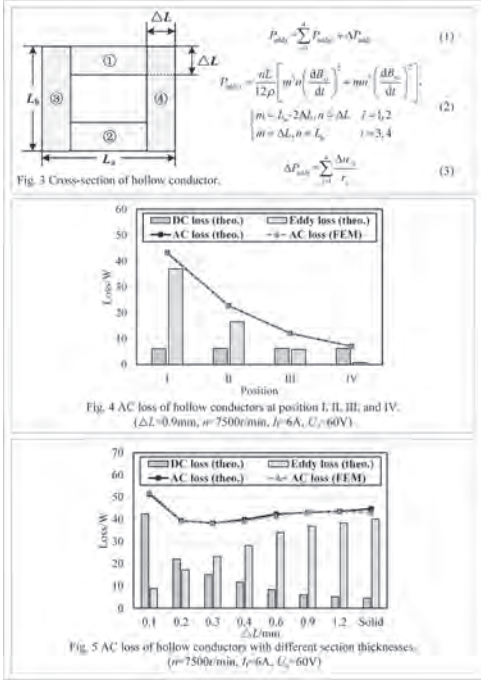

Fig. 3 Cross-section of hollow conductor.

Fig. 4 AC loss of hollow conductors at position I, II, III, and IV. (ΔL=0.9mm, n=7500r/min, I_f=6A, U_c=60V)

Fig. 5 AC loss of hollow conductors with different section thicknesses. (n=7500r/min, I_f=6A, U_c=60V)

JPL-06. Electromagnetic Simulation of Current and Temperature Distribution in Railgun Based on Moving Contact Resistance Model. C. Zhang[1], *S. Guan*[1], Y. Li[1] and Q. Yang[2] *1. Hebei University of Technology, Tianjin, China; 2. Tiangong University, Tianjin, China*

Sliding electrical contact (SEC) exists extensively in the electromagnetic (EM) launchers (e.g., railguns). In an EM railgun, the armature slides on the rails at hypervelocity, and the real contact interface is never perfectly smooth. Due to the elevations and depressions of the contact interface, the sliding pair only contacts at discrete asperities, called 'a-spots' by Holm, at microscale [1]. The contact microscopic morphology of the armature and the rail is shown in Fig. 1. The fact that the current is only flowing through the a-spots results in larger electrical resistance in the contact zone than bulk electrical resistance and the generation of separation force due to current constriction effects [2]. Thus, it is crucially important to build a detailed model of SEC considering contact resistance to compute the interfacial current density and temperature distributions accurately. A 2-D EM railgun with a C-type armature model is simulated by the multiphysics coupling finite element method. The calculation method of contact resistance is based on Holm's electric contact theory to simulate the real contact zone. Due to symmetry, only a half of the model is modeled, whose finite element mesh on the rail and armature is shown in Fig. 2. The copper rail and aluminum armature are used in the simulation. The driving current waveform is with a peak current of 100 kA and a rising time of 0.5 ms. An initial contact pressure of 10 MPa is applied on the apparent contact area. The armature is initially stationary and then accelerated up to 1000 m/s. The start-up behavior of the railgun is modeled to study the distribution of initial contact pressure, and then to analyze the influence of the unevenly distributed contact pressure on the interface current and temperature distributions. In this paper, the current and temperature distributions in an EM raligun have been studied by a theoretical analysis and numerical simulation. As the result shows, the skin effect and the influence of contact resistance is quite obvious when velocity is high, which provide a guidance for reducing the wear and damage of the contact surface.

[1]R. Holm, "Electric contacts handbook," Springer-Verlag (1958) [2] Bok-Ki Kim, Kuo-Ta Hsieh and F. X. Bostick, "A three-dimensional finite element model for thermal effect of imperfect electric contacts," IEEE Transactions on Magnetics, vol. 35, no. 1, pp. 170-174 (1999)

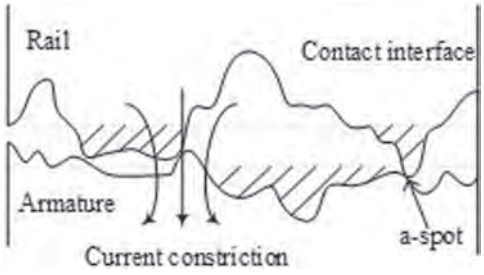

Fig. 1. Contact interface at the microscopic scale.

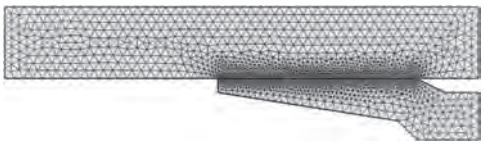

Fig. 2. Finite element mesh of the rail and armature.

JPL-07. Integrated Magnetics, Insulation and Cooling Architecture for Slotless Electric Machines. *D. Lee*[1], N. Salk[1] and K. Haran[2] *1. Hinetics, LLC, Champaign, IL, United States; 2. Department of Electric and Computer Engineering, University of Illinois, Urbana, IL, United States*

Electric vertical takeoff and landing (eVTOL) aircraft require compact, high power, high reliability electric motors and drives. Power demand on the electric propulsion system during take-off and landing can be up to 3-10x cruise power [1,2], and copper loss during these flight phases rises due to increased current density. As a result, the temperature in the conducting region can grow quickly to levels which may cause insulation failure. This paper presents an embedded cooling architecture that enhances heat transfer from the coils to the heatsink and prevents excessive temperatures [3]. The proposed machine topology is a slotless PMSM outrunner which achieves high electrical loading by extending the armature cross-section into area traditionally occupied by iron teeth [4, 5], making it suitable for the operating profiles of eVTOL aircraft. The slotless structure trades magnetic loading and associated iron loss for electrical loading and associated copper loss. To address the high loss concentration in the form-wound coils of a slotless stator, thin copper sheets are interleaved within the iron lamination stack to provide a thermal shunt from coils to heatsink. Additionally, a ceramic coil holder enhances both the side-wall thermal path and electrical insulation [6]. Figure 1 shows the cross-sectional configuration of one stator slot. Motor performance is gauged in terms of torque production, flux density, eddy current loss in the copper sheets, and equivalent thermal resistance as a function of the lamination stack copper fill factor as shown in Figure 2. Results show that the equivalent thermal resistance from conductor to heatsink is decreased by 40% at 20% copper lamination stack factor without ceramics, while torque production is reduced by 1%. Including ceramics in the analysis, an additional 10% reduction in equivalent thermal resistance is observed. A full paper presents the proposed motor's performance, load profiles for take-off and landing and includes eddy current loss, flux fringing, optimal heatsink design, thermal analysis and experimental test results.

[1] J. Xiao, N. Salk, and K. S. Haran, 2020 IEEE Power and Energy Conference at Illinois (PECI), pp. 1-8 (2020) [2] M. S. Islam, R. Mikail and I. Husain, in *IEEE Transactions on Industry Applications*, vol. 55, pp. 5789-5799 (2019) [3] Hyunkyu Moon, Nenad Miljkovic and William P. King, in International Journal of Heat and Mass Transfer, Vol. 153, pp.1-10 (2020) [4] D. Lee, A. Jin and K. Haran, in IET Electric Power Applications, vol. 12, pp. 1075-1081 (2018) [5] Fabio Luise, Alberto Tessarolo and Matteo De Martin, in *IEEE Industry Applications Magazine*, vol. 22, pp. 19-32(2016) [6] Z. Chen, Z. Li and Y. He, Elsevier Journal of the European Ceramic Society, vol. 39, pp. 661-687 (2019)

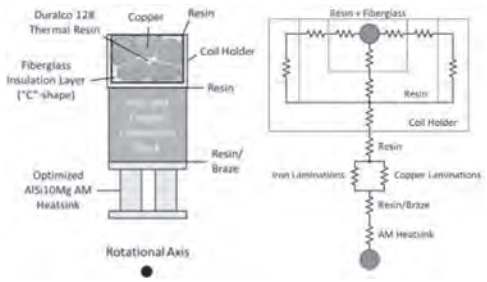

Figure 1. Slot configuration and thermal equivalent circuit

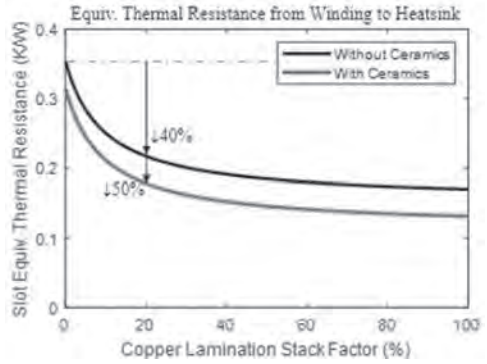

Figure 2. Thermal resistance versus copper lamination stack factor

JPL-08. Electromagnetic Thermal Coupling Optimization of Concentrated Winding PM Motor with Auxiliary Teeth for Electric Vehicle.

T. Zhu[1], W. Geng[1] and L. Li[1] *1. Nanjing University of Science and Technology, Naijing, China*

The hybrid electric vehicle composed of diesel engine and generator can greatly alleviate the "range anxiety" problem [1]. The concentrated winding PM motor with high power and small volume is adopted for the large transport or mining machinery vehicles. In order to solve the heat dissipation problem of concentrated winding PM motor and realize efficient cooling, the heat dissipation structure of stator core with auxiliary teeth without any additional facilities is introduced [1-4]. In this paper, the influence of auxiliary teeth in stator core on concentrated winding PM motor is studied from electromagnetic and thermal aspects. It can be used as an effective scheme for the thermal design of concentrated winding PM motor. Different from the slot type of general motors, a part of the stator core is extended into the slot to form the auxiliary teeth, as shown in Fig. 1. The purpose of adding the auxiliary teeth is to make the heat inside the slot winding have more paths to transfer to the outside. The stator core is mainly divided into three structures, as shown in Fig. 2. Fig. 5 shows the waveforms of the air-gap flux density. Fig. 7 shows the back EMF. The cogging torques are shown in Fig. 8. Fig. 9 shows the flux density contour. Fig. 10 shows a comparison of the torques of the three models. It can be seen the loss change from Fig. 11 and Fig. 12. Fig. 13 shows the change of torque from model 2 to model 3. Fig. 14 and Fig. 15 show the loss changes from model 2 to model 3. Fig. 16 shows the temperature distribution under the rated condition. The actual stator core with auxiliary teeth (Model 2) is shown in Fig. 17(a). In this paper, the influence of the size of stator core auxiliary teeth on concentrated winding PM motor is studied from electromagnetic and thermal aspects. The results show that the auxiliary teeth will weaken the performance of the motor and make the stator temperature drop and the rotor temperature rise. The auxiliary cooling teeth of stator core provide a new guide for the thermal design of concentrated winding PM motor.

REFERENCES [1] W. W. Geng, T Zhu, Q Li, et al. Windings Indirect Liquid Cooling Method for a Compact Outer-Rotor PM Starter/Generator with Concentrated Windings[J]. IEEE Transactions on Energy Conversion, 2021. [2] F Y Zhang, David G, Z Y Xu, et al. Back-Iron Extension Thermal Benefits for Electrical Machines With Concentrated Windings[J]. IEEE Transactions on Industrial Electronics, 2020, 67(3): 1728-1738. [3] Rafal W, Ahmed H. A. Feasibility Study of Additively Manufactured Heat Guides for Enhanced Heat Transfer in Electrical Machines[J]. IEEE Transactions on Industry Applications, 2020, 56(1): 205-215. [4] Michael G, Giampaolo B, Lee E, et al. Design of a High-Force-Density Tubular Motor[J]. IEEE Transactions on Industry Applications, 2014, 50(4): 2523-2531. [5] W. W. Geng, Z. R. Zhang, and Q. Li. High torque density fractional-slot concentrated-winding axial-flux permanent-magnet machine with modular smc stator, IEEE Transactions on Industry Applications, vol. 56 no 4, pp. 3691-3699, 2020.

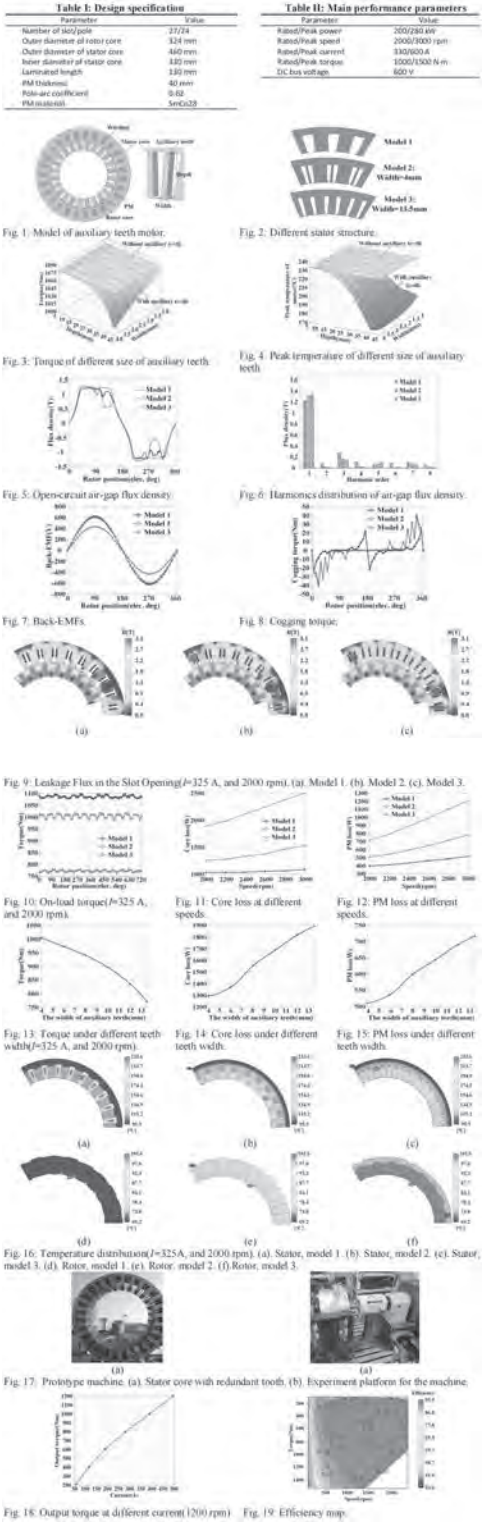

JPL-09. Asymmetrical Axial Magnetic Bearings for Turbomachineries.
H. Jiang[1], Z. Su[1], D. Wang[1], C. Wu[1] and Z. Li[1] *1. Naval University of Engineering, Wuhan, China*

Turbomachineries have large single-unit power and high efficiency, they play an important role in many areas, such as ship propulsion and thermal power generation and so on [1]. With the increase in demand, high power is an important development direction for turbomachineries in the future. However, now mechanical bearings are most used in turbomachineries, and the wear and loss at high speed severely restrict the speed. For this reason, the magnetic bearing (MB) is chosen to support the rotor to overcome the problems caused by the direct contact with the rotor [2]. However, limited by the operating principle of the steam turbine, the axial magnetic bearing (AMB) needs to overcome the large axial thrust generated by the steam flowing in turbomachineries. The traditional topology and design methods will cause the AMB to be too large to be integrated with the steam turbine. Therefore, this paper proposes an asymmetric axial magnetic bearing (AAMB) topology with large bearing capacity in a single direction. As shown in Fig. 1(a), the AAMB has a pair of stators of differential bearing and a stator of unidirectional bearing, both of which are fixed on the bearing seat and share a thrust plate. In normal operation, the unidirectional bearing works in the saturation zone of the material, it generate force and overcome the main axial thrust generated by steam. The differential bearing works in the linear region of the material, it is used to adjust the bearing capacity and overcome the remaining thrust. As shown in Fig. 1(b), The reluctance network method is used to establish the magnetic circuit model of the AAMB. And then the load capacity, dimensions and other constraints are considered, the shortest axial length is taken as the optimization object to design the AAMB, and the design scheme is obtained, and compared with the traditional differential bearing scheme, the main parameters of AAMB are shown in Fig. 2(a). Finally, The finite element model is built as shown in Fig. 2(b), the bearing capacity of the AAMB is verified by finite element method (FEM). The results show that the AAMB meets the bearing capacity requirements, and the overall axial length is less than half of the traditional design scheme.

[1]M. Altosole, U. Campora and S. Savio, "Improvements of the Ship Energy Efficiency by a Steam Powered Turbogenerator in LNG Propulsion Applications," 2018 International Symposium on Power Electronics, Electrical Drives, Automation and Motion (SPEEDAM), 2018, pp. 449-455. [2] H. B. Karayaka, A. Keyhani, B. L. Agrawal, D. A. Selin and G. T. Heydt, "Identification of armature, field, and saturated parameters of a large steam turbine-generator from operating data," in IEEE Transactions on Energy Conversion, vol. 15, no. 2, pp. 181-187, June 2000. [3]K. Kalista, "A proposal of the methodology for dynamic force coefficients identification of labyrinth seal with use of active magnetic bearings," 2018 18th International Conference on Mechatronics - Mechatronika (ME), 2018, pp. 1-5.

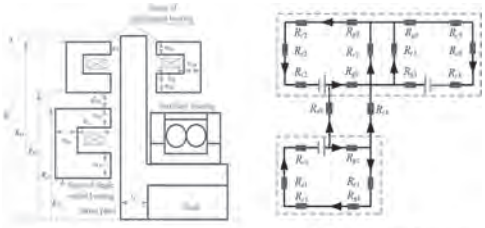

(a) Topology (b) Magnetic circuit model

Fig. 1 The topology and magnetic circuit model of the AAMB

Fig.1

Parameters	AAMB		Traditional differential bearing
	Differential bearing	Unidirectional bearing	
Air gap(mm)	0.5	0.5	0.5
Inner diameter of rotor(mm)	105	50	50
Outer diameter of rotor(mm)	130.0	99.7	150
Inner pole width(mm)	7.3	18.8	42.0
Outer pole width(mm)	6.2	11.9	25.4
Width of rotor yoke(mm)	7.1	19.0	42
Slot width(mm)	11.5	19.9	12.7
Slot height(mm)	22.0	33.5	25.0
Thickness of thrust plate (mm)	10		50
Outer diameter of thrust plate(mm)	131.5		131.5
Axial length(mm)	91.4		185.0
Maximum current(A)	14.84	12.50	12.56
Number of turns	51	101	51

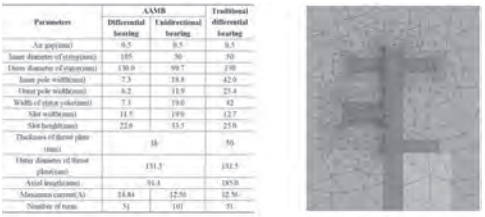

(a) Main parameters of AAMB (b) Finite element model

Fig. 2 The main parameters and finite element model of the AAMB

Fig.2

JPL-10. Withdrawn

JPL-11. Principle and Implementation of a Novel Double-stator Hybrid Magnetic Bearing.
X. Ye[1] and Z. Wang[1] *1. Faculty of Automation, Huaiyin Institute of Technology, Huaian, China*

Hybrid magnetic bearing (HMB) is a new electromagnetic device, which can levitate the rotor by magnetic forces with no mechanical contact. Thus, the machines equipped with HMBs can easily obtain the higher speed and power. However, the traditional HMBs is often composed of one rotor and one stator, and the levitation force is only generated on the inner or outer surfaces of rotor [1]. Therefore, the levitation force density of traditional HMB is low. To solve this drawback, a novel double-stator hybrid magnetic bearing (DSHMB), as shown in Fig.1, is proposed. The DSHMB consist of outer stator, rotor and inner stator. The rotor of DSHMB is divided into two parts by magnetic isolation material. Each outer and inner stator has four levitation poles. Two axial magnetized permanent magnet rings are inserted between the outer and inner stators. The levitation windings are wound on each pole of the inner and outer stator. Two bipolar switching power amplifiers are adopted to control the levitation windings to realize the stable levitation of the rotor. In addition, the levitation force mathematical models are deduced using equivalent magnetic circuit method. Then, the design of the main parameters is discussed. Three-dimensional finite element analysis is carried out to calculate the flux distributions, air gap flux densities waveforms and force-current relationships. The flux distribution and the air gap flux densities are shown in Fig.2. Furthermore, the coupling relationships of the two-degree-of-freedom levitation forces and force-displacement are analyzed. Finally, the experimental platform is constructed. The experiments are tested to verify the structure, models and design method.

[1] Z. Jin, X. Sun, Y. Cai, J. Zhu, G. Lei, and Y. Guo, "Comprehensive sensitivity and cross-factor variance analysis-based multi-objective design optimization of a 3-DOF hybrid magnetic bearing," *IEEE Trans. Magn.*, vol. 57, no. 2, Feb. 2021.

Fig.1 Structure of the proposed DSHMB.

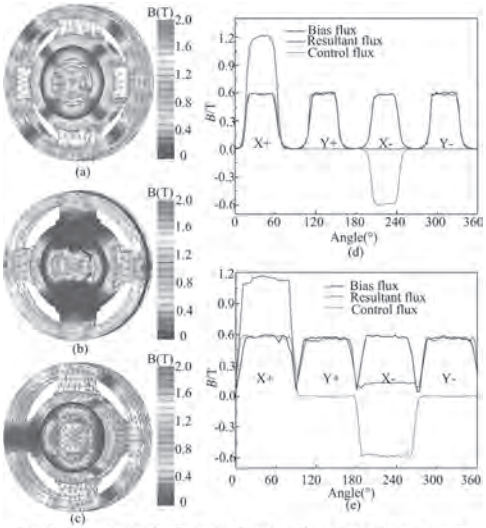

Fig. 2. Flux density distribution.(a) Bias flux distribution. (b) Levitation flux distribution to get F_{+xmax}. (c) Resultant flux distribution to get F_{+xmax}. (d) Waveform of air gap flux density of inner stator. (e) Waveform of air gap flux density of outer stator.

Fig. 2. Flux density distribution.(a) Bias flux distribution. (b) Levitation flux distribution to get F_{+xmax}. (c) Resultant flux distribution to get F_{+xmax}. (d) Waveform of air gap flux density of inner stator. (e) Waveform of air gap flux density of outer stator.

Session JPM
DESIGN OPTIMIZATION OF ELECTRICAL MACHINES
(Poster Session)

Weimin Guan, Chair
Wuhan University, Wuhan, China

JPM-01. Rapid multi-material discrete topology optimization for the design of electrical machines. *M. Hage Hassan*[1], T. Guillemot[1], X. Mininger[1], G. Krebs[1], A. Boumesbah[1] and P. Dessante[1] *1. Université Paris-Saclay, CentraleSupélec, CNRS, Laboratoire de Génie Electrique et Electronique de Paris, Gif-sur-Yvette, France*

This work paper presents a methodology based on discrete multi-material topology optimization (TO) for the design of electrical machine cores using finite element analysis. Our methodology is based on the Bi-directional Evolutionary Structural Optimization (BESO) heuristics to remove inefficient elements [1] or add magnets from a meshed model based on how they increase the magnetic energy. Determining the average torque with the calculation of its instantaneous values can be very expensive. The proposed methodology improves the average torque density while formulating cost function on calculated energy difference in the d-axis and q-axis. While usual multi-material topology optimization is formulated using a density-based method [2], this paper determines magnets distribution discretely. The magnetization magnitude can be considered as a discrete variable, and the challenge is to determine its direction. Thus, we deduce magnetization direction from the flux density distribution in the rotor; the magnet magnetization direction is chosen to be normal to B. The main advantage of the proposed methodology is that no "gray" materials are created, and the manufacturing of the machine with the proposed distribution of magnets can be realistically considered. The optimization problem is formulated in order to maximize the magnetic energy difference subject to $x_e = 0$ or 1, $x_m = 1$ or 0, $\sum(x_e.V_e)\text{-}V_{iron0} \leq 0$ and $\sum(x_m.V_m)\text{-}V_{magnets0} \leq 0$ where, x_e, V_e are the iron presence and volume of an iron element e, and x_m, V_m have the same definitions for the magnets. V_{iron0}, $V_{magnets0}$ are the constraints on volumes. The basic diagram is presented in the figure below. The methodology is applied to design several stator structures as given in Fig. 1. The final optimization design of each structure is a classical synchro-reluctant machine with inserted magnets is presented in Fig. 2. The computation time is less than 10 min with 8640 mesh elements.

[1] M. Garibaldi, C. Gerada, I. Ashcroft, and R. Hague, (March 13, 2019). "Free-Form Design of Electrical Machine Rotor Cores for Production Using Additive Manufacturing." ASME. J. Mech. Des. July 2019; 141(7): 071401
[2] T. Jung, J. Lee and J. Lee, "Design and Fabrication of Magnetic System Using Multi-Material Topology Optimization," in IEEE Access, vol. 9, pp. 8649-8658, 2021

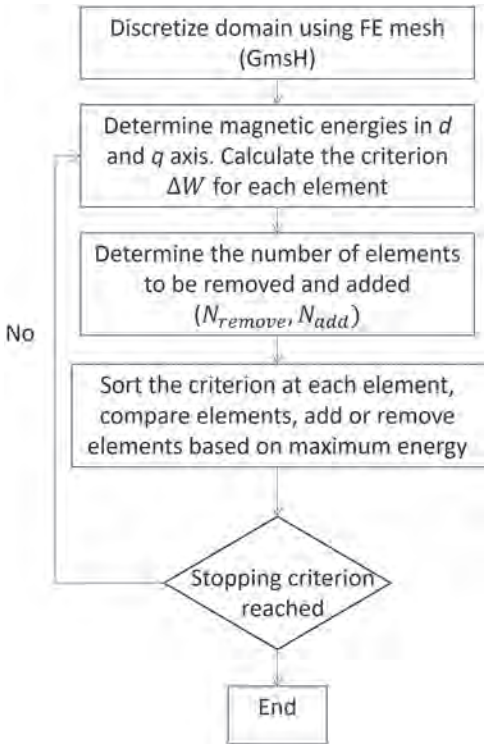

Figure 1. Methodology chart

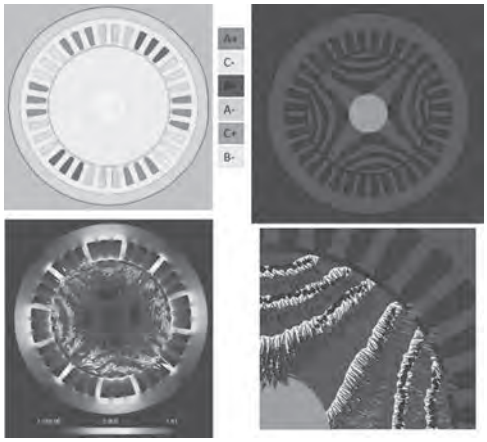

Figure 2. Optimized 36 slots electrical machines, flux density distribution and vectors in the flux barriers, magnets distribution

JPM-02. Comparative Study on Three Novel Hybrid Excited Multi-tooth Flux-switching Permanent Magnet Machines. *Z. Jin*[1], X. Zhu[1], S. Ding[1], S. Chen[1] and Z. Li[1] *1. Nanjing Normal Univercity, Nanjing, China*

I. Introduction Hybrid excited machines have attracted wide attention due to several advantages, such as easy adjustment of air gap magnetic field, high power density and high efficiency in wide speed range [1]. Nowadays, hybrid excited multitooth flux-switching permanent magnet (HE-MFSPM) machines have become a research hotspot [2]. Based on the literature [3], three novel HE-MFSPM machines are proposed in this paper. Fig. 1 shows the topologies of the proposed three HE-MFSPM machines, called Model I, Model II and Model III respectively. The three models are basically the same except that PM with radial magnetization is added in each dummy slot in Model II, while a fault tolerant tooth is employed and wound with field winding in Model III. Significantly, the amount of PM of the Model I is the least, and the amount of PM of Model II is equal to that of Model III. II. Performance comparisons Fig. 2 (a) presents the overload capability of three proposed HE-MFSPM machines supplied with the same excitation current density (J_f), i.e., 5A/mm^2. It can be seen that when the current density of armature winding (J_a) increases from 2A/mm^2 to 10A/mm^2, the torque of Model III increases the most, showing the best saturation characteristics. Fig. 2 (b) shows the speed range of the three proposed HE-MFSPM machines. It should be noted that all the three structures run at the same speed and the same rated voltage, i.e., 700r/min and 380V. It can be observed that Model III has the highest average torque in the constant torque region and has the widest speed range in the constant power region. Overall, all the proposed three HE-MFSPM machines exhibit good ability of flux regulation. But Model III is superior to Model I and Model II since it exhibits best overload capability, highest average torque and widest speed range. Moreover, fault-tolerant ability and modularity exist in Model III because of the existence of fault-tolerant teeth. The other performance, such as back-EMF, cogging torque and electromagnetic torque, will be further discussed in the full paper.

[1] Y. Wang and Z. Deng, "Hybrid excitation topologies and control strategies of stator permanent magnet machines for DC power system," *IEEE Trans. Ind. Electron*, vol. 59, no. 12, pp. 4601-4616, Dec. 2012. [2] Z. Zhu and S. Cai, "Hybrid Excited Permanent Magnet Machines for Electric and Hybrid Electric Vehicles," *CES Transactions on Electrical Machines and Systems*, vol. 3 no. 3, pp. 233-247, Sep. 2019. [3] G. Zhao and W. Hua, "Comparative Study Between a Novel Multi-Tooth and a V-Shaped Flux-Switching Permanent Magnet Machines," *IEEE Transactions on Magnetics*, vol. 55, no. 7, pp. 1-8, July. 2019.

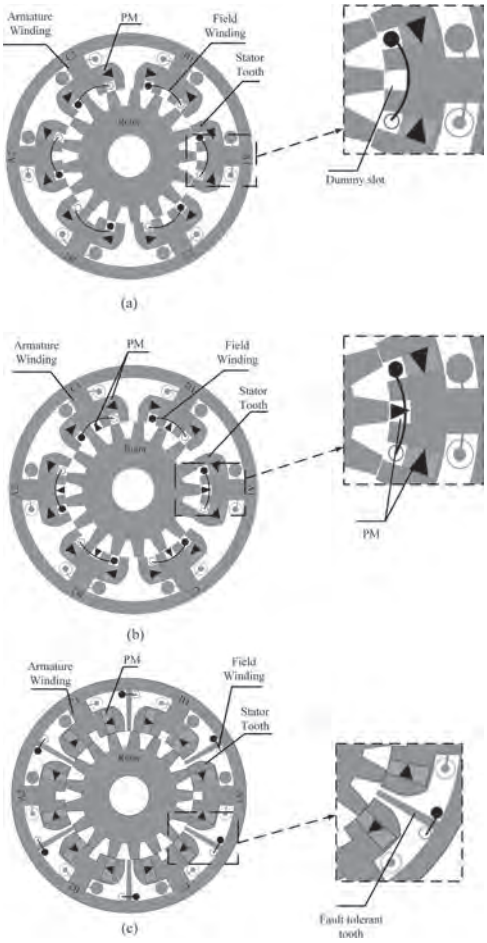

Fig.1. Topologies of three HE-MFSPM machines. (a) Model I. (b) Model II. (c) Model III.

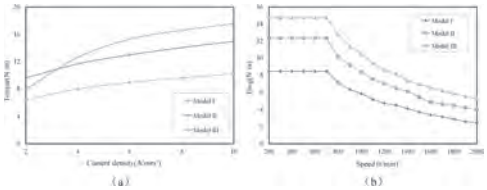

Fig.2. Performance comparisons of three models. (a)Overload capability. (b) Speed range

JPM-03. Withdrawn

JPM-04. An efficient decoupling approach for reliability-based design optimization of electrical machines. B. Ma[1], *J. Zheng*[1] and J. Zhu[2] *1. Hunan University, Changsha, China; 2. University of Sydney, Sydney, NSW, Australia*

Introduction: Considering the unavoidable uncertainties related to material properties, manufacturing errors, etc., the reliability constraints have been incorporated into the design optimization process in order to achieve the high reliability requirements of electrical machines [1]. The reliability-based design optimization (RBDO) is a double-loop optimization problem, since the reliability assessment which is generally an iterative procedure needs to be implemented at every iterative of the design optimization [2]. This work proposed an efficient decoupled RBDO framework for electrical machines based on the sequential optimization and reliability assessment (SORA) method [3] to avoid the heavy computational cost in the traditional

double-loop process. The proposed method: Fig. 1 illustrates the optimization procedure of the proposed method. Based on the SORA scheme, the optimization and the reliability analysis are decoupled in a sequential manner. That is to say, the reliability analysis is no longer required in each iterative of the optimization. In one sequential cycle, the deterministic optimization is formulated based on the most probable point information from the reliability analysis, and the reliability analysis is then performed after the deterministic optimization. Numerical example: A BLDC motor optimization benchmark problem is investigated to verify the effectiveness of the proposed method. Fig. 2 (a) shows the topology and Fig. 2 (b) presents the convergent history of the objective function in which different cycles are clearly shown. Each cycle consists of a reliability analysis and a deterministic design optimization. It is shown that only after a few cycles, the optimization converges while the reliability constraints can be satisfied at the same time. To verify the efficiency of the proposed method, the traditional double loop optimization is also implemented for comparison. The number of the performance function calls of the double loop method is 1807 for reaching the similar optimized solution which is much larger than the function calls of the proposed SORA-based method. Hence, the proposed optimization strategy shows very good computational efficiency for the motor design.

1 Ren Z, Zhang D, Koh C S. Investigation of reliability analysis algorithms for effective reliability-based optimal design of electrical machines. IET Science, Measurement & Technology, 2016, 10(1): 44-49. 2 Valdebenito M A, Schuëller G I. A survey on approaches for reliability-based optimization. Structural and Multidisciplinary Optimization, 2010, 42(5): 645-663. 3 Du X, Chen W. Sequential optimization and reliability assessment method for efficient probabilistic design. J. Mech. Des., 2004, 126(2): 225-233.

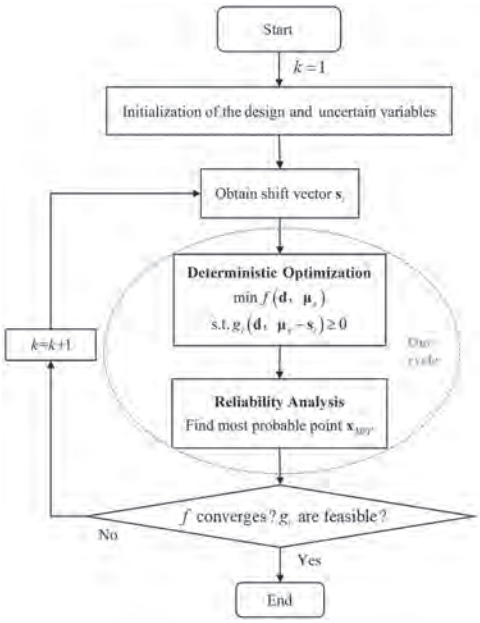

Fig.1

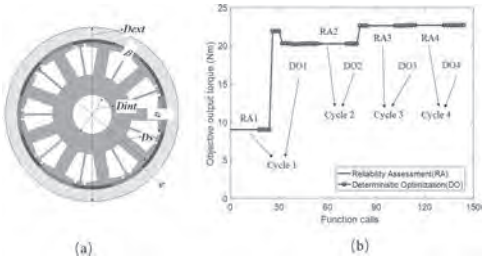

Fig.2

JPM-05. Field-Regulation Capability Research of Dual-Direction Hybrid Excitation Synchronous Generator. *J. Yu*[1], S. Zhu[1] and C. Liu[1]
1. Nanjing University of Aeronautics & Astronautics, Nanjing, China

Abstract —A dual-direction hybrid excitation synchronous generator (D-HESG) is presented for High voltage DC power system,and field-regulation capability is discussed. Theoretically, based on the configuration and operation principle, the flux path is analyzed and the equivalent magnetic circuit model is established. Then, the no-load and external characteristics are compared in three cases which are without axial excitation, single ended and double ended excitation. In addition, the flux density of key parameters under different field currents are compared and studied through simulation analysis. Finally, a 10kW prototype is tested to verify the simulation. I. Introduction In order to realize the brushless excitation technology, the method is adding the magnetic parts, and the axial field path is provided for the field winding. The reliability is high. II. Structure and Operating Principle Fig.1 shows the structure of D-HESG with dual-direction field windings. In addition to ordinary radial flux path, the generator exists another axial flux path. The equivalent magnetic circuit model is established, it can obtain the main parameters affecting the D-HESG performance. III. Field-regulation Capability Analysis By establishing non axial excitation model, single and double ended excitation model, the no-load and external characteristics are compared and analyzed. According to the equivalent magnetic circuit, the main air gap, additional air gap and the rotor yoke thickness have impact on the field-regulation performance. So, the influence of parameters change on the regulation multiple (Fig.2) is simulated and analyzed to determine the most appropriate parameters. IV. Experimental Verification A 10kW prototype is developed, and an test platform is built. The output voltage is adjusted by 27% with the field current. V. Conclusions In this paper, the operation principle of the D-HESG has been studied. And the field-regulation capability has been investigated. By adding axial magnetic circuit and double ended excitation, the D-HESG realizes convenient field-regulation and has a wide field-regulation range.

[1] W. Geng, Z. Zhang, K. Jiang, and Y. Yan, "A new parallel hybrid excitation machine: permanent-magnet/variable reluctance machine with bidirectional field regulating capability," IEEE Trans. Ind. Electron., vol. 62, no. 3, pp. 1372–1381, March. 2015. [2] C. Ye, Y. Du, J. Yang, X. Liang, F. Xiong, and W. Xu, "Research of an axial flux stator partition hybrid excitation brushless synchronous generator," IEEE Trans. Magn., vol. 54, no. 11, November. 2018.

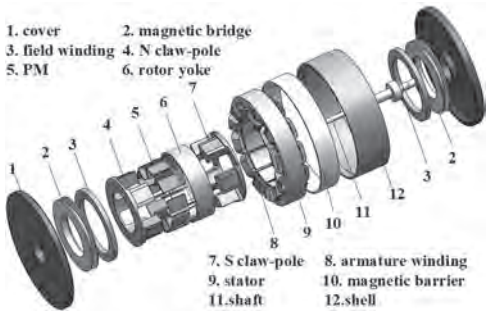

Fig. 1. Configuration of the D-HESG

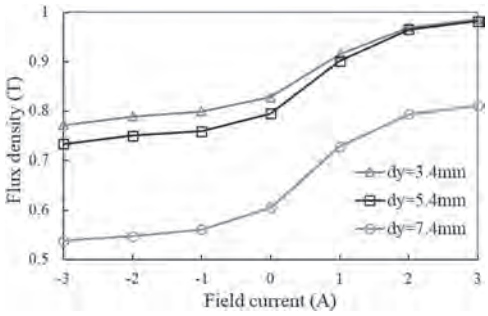

Fig. 2. Influence of field-regulation capability under different rotor yoke thickness

JPM-06. Design and Investigation of a New Variable Flux Memory Machine with Self-Flux Leakage Path. *X. Zeng*[1] and H. Lin[1] *1. Southeast University, Nanjing, China*

Variable flux memory machines (VFMM) has promising application prospect in electric vehicles (EVs) due to its wide speed range and high efficiency, which are brought about by the feature that its magnetization state (MS) can be flexibly adjusted by applying a short-time current pulse [1-3]. However, it is difficult for VFMM to balance the torque output capacity and the air gap flux adjustment ability. In this paper, a new VFMM with self-flux leakage paths is proposed to improve the torque density and extend the magnetic flux adjustment range simultaneously. The fact that the self-flux leakage paths work only in the demagnetization state is conducive to further expanding the speed range. Fig. 1 shows the configuration of the proposed VFMM. The rotor employs hybrid high and low coercive force (HCF and LCF) permanent magnets (PMs), where self-flux leakage paths are set between the adjacent circumferential PMs. In the constant torque region, the armature magnetic field forces the PM fluxes to pass through the nearby circumferential PMs, reducing the fluxes leakage and thus increasing the torque density of the machine. In the constant power region, the armature magnetic field weakens the PM field, making more fluxes leakage occur at the ends of radial HCF PMs. As a result, the air gap flux density of the machine is reduced, and the speed adjustment range is further broadened. Figs. 2(a) and (b) show the air gap flux densities under the highest and lowest MSs and the torque-speed curve of the proposed machines. It can be found that the air gap flux adjustment ratio and the speed expending range of the machine are up to 2.2 and 4.67 respectively, which indicates that the proposed VFMM has excellent comprehensive performance.

[1] V. Ostovic, "Memory motors," in *IEEE Ind. Appl. Mag*., Jan./Feb. 2003, vol. 9, no. 1, pp. 52–61. [2] X. Zhu, L. Quan, D. Chen, M. Cheng, Z. Wang, and W. Li, "Design and analysis of a new flux memory doubly salient motor capable of online flux control," *IEEE Trans. Magn*., vol. 47, no. 10, pp. 3220–3223, Oct. 2011. [3] H. Yang, S. Lyu, H. Lin, Z. Zhu, H. Zheng, and T. Wang, "A novel hybrid-magnetic-circuit variable flux memory machine," *IEEE Trans. Ind. Electron*., vol. 67, no. 7, pp. 5258-5268, July 2020.

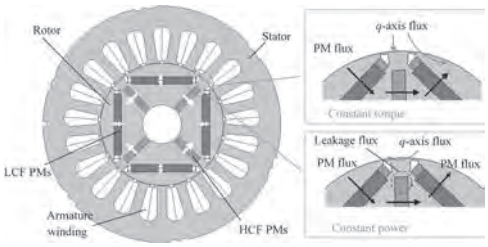

Fig. 1. Topology of the proposed VFMM machine.

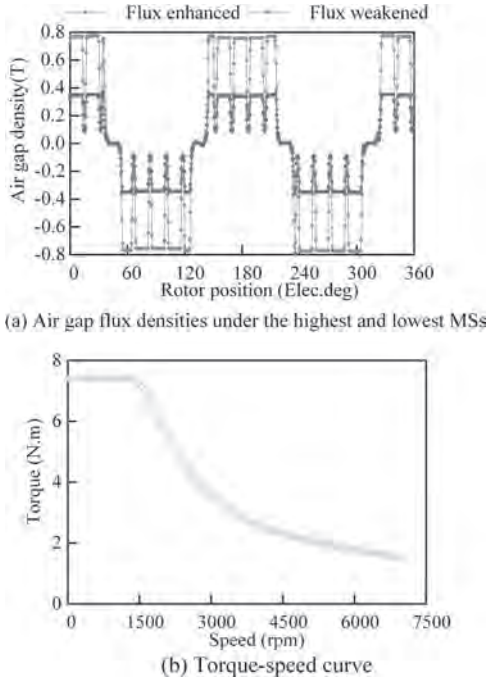

Fig. 2 Electromagnetic characteristics of the proposed VFMM.

JPM-07. Improvement of Torque Density by Rotor Structure of IPMSM with Dy-free Rare-Earth Magnet for Servo Motor. *D. Jang*[1], Y. Hwang[1], S. Lee[1], S. Kang[1] and S. Jung[1] *1. Department of Electrical and Computer Engineering, SungKyunKwan University, Suwon, The Republic of Korea*

The servo motor system applied to the robot joint for the machining requires the high controllability and output power density, and the operation efficiency. For this reason, servo motors have been designed with SPMSM (Surface mounted Permanent Magnet Synchronous Motor). SPMSM has the strength in the high efficiency, size reduction compared to the DC motor used in before 1990s. However, as shown in Figure 1, it is difficult to collect materials due to the increase the price of rare earth magnets recently. So low grade magnets are used, the size is increased or high current is used to satisfy the target performance, resulting in a situation in which PMSMS strengths such as miniaturization and high torque density are weaken. In this case, the heat generation and the heat displacement of the core parts due to the high current density reduce precision of motor. The applied current acts as friction heat to the bearing and is transmitted to the machine structure. In this case, position error of up to 80um occurs. In this paper, propose a IPMSM design using DY Free Bonded magnet for servo motor. IPMSM is applied to prevent the reduction of the torque density due to the using DY free. Generally, IPMSM is not applied to the servo motor due to the low controllability and high torque ripple. So, applying the rotor notch structure to reduce torque ripple and maximizes the reluctance torque. The harmonics of the 6th 12th component of the reference model are removed through the rotor notch structure. It can improve ripple, cogging and utilize effective reluctance torque through changes in the q axis flux path. Reluctance torque can reduce the current density and improve demagnetization characteristics and low heat resistance that act as a problem in DY FREE. In addition, the size reduction according to the improvement of output density minimizes the bending load on machine, thereby improving torque transferability, controllability. Variable of The DY content will be classified as 6%, 5.8%, 3.2%. Dy free model compared with reference model by demagnetization and heat resistance. Sensitivity of The torque and torque ripple, weight and power density, and thermal saturation of each model analyzed to FEM.

1) Performance Comparison between PMASynRM with Dy-Free Bonded Magnets and IPMSM with Sintered Magnets for Automotive Applications[Marika Kobayashi, Shigeo Morimoto, Masayuki Sanada, and Yukinori

Inoue Osaka Prefecture University] 2) Improvement of Demagnetization by Rotor Structure of IPMSM with Dy-free Rare-Earth Magnet [Keigo Imamura*, Masayuki Sanada*, Shigeo Morimoto* and Yukinori Inoue*]

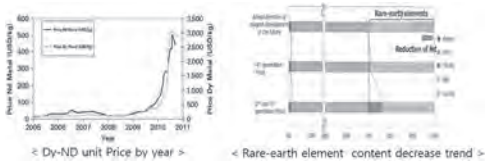

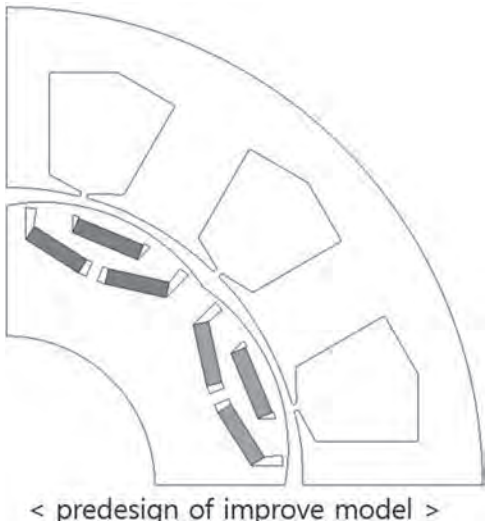

JPM-08. Detent Force Optimization in Linear Oscillatory Generator with Assisted Permanent Magnet and Semi-3D Effect for Stirling Engines Using Subdomain Analytical Method. *K. Shin*[1], J. Choi[2], H. Cho[2], K. Lee[3] and S. Lee[3] *1. Chonnam National University, Yeosu, The Republic of Korea; 2. Chungnam National University, Daejeon, The Republic of Korea; 3. Korea institute of Industrial Technology, Gwangju, The Republic of Korea*

A single-phase linear oscillatory generator (LOG) is widely used in direct-drive systems such as the Stirling engine system due to its advantages such as high transmission efficiency and simple structure as shown in Fig. 1 [1], [2]. However, one of their drawbacks is the generation of detent force caused by the attraction between the permanent magnet (PM) and the iron core. A large detent force causes thrust ripples and noise, which results in poor positioning accuracy [3]. Therefore, the prediction of the detent force is an important factor to be considered in the design of the LOG with PM mover. To solve these problems, this study proposes an electromagnetic analysis using an analytical method to optimize the detent force by applying spring PM to the PM mover [1]. This paper derives analytical solutions in terms of magnetic vector potential based on the subdomain model as shown in Figs 1 (b) and (c). From the analytical solution, the electromagnetic force is derived using the Maxwell stress tensor. The validity of the proposed method is verified through comparison with the results of finite element analysis as shown in Figs. 2 (a) and (b). Fig. 2 (c) shows the analysis result of the detent force according to the width of the spring PM at a minimum position of the stroke. Therefore, positive values of the detent force are generated to use restoring force. Fig. 2 (d) shows the comparison between the detent force with and without spring PM. It is observed that the direction of the detent force changes in the spring PM model and the force is hardly generated in the stroke region. The analytical technique, analysis results, discussions, and measurements of the LOG will be presented in more detail in the full paper.

[1] J. M. Kim, J. Y. Choi, K. S. Lee, and S. H. Lee, "Design and Analysis of Linear Oscillatory Single-Phase Permanent Magnet Generator for Free-Piston Stirling Engine Systems", AIP adv., vol. 7, no. 5, May 2017, Art. no. 056667. [2] K. H. Shin, K. H. Kim, K. Hong, and J. Y. Choi, "Detent Force Minimization of Permanent Magnet Linear Synchronous Machines Using Subdomain Analytical Method Considering Auxiliary Teeth Configuration", IEEE Trans. Magn., vol. 53, no. 6, June 2017, Art. no. 8104504. [3] K. H. Shin and J. Y. Choi, "Electromagnetic Analysis of Single-Phase Linear Oscillatory Actuator Based on Subdomain Analytical Model with End and Stacking Effects", IEEE Trans. Magn., vol. 57, no. 2, Feb. 2021, Art. no. 8000505.

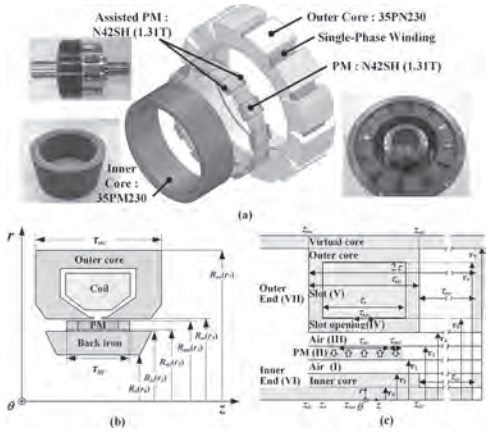

Fig. 1. Structure of LOG with PM: (a) main structure with a prototype, (b) analysis model, and (c) simplified analytical model.

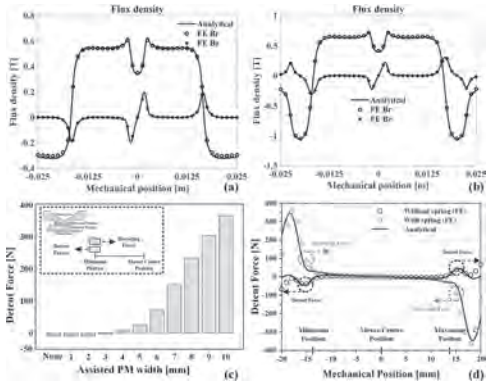

Fig. 2. Comparison of analysis results obtained by analytical model and 2D FE analysis: (a) flux density without assisted PMs, (b) flux density with assisted PMs, (c) detent forces according to a width of assisted PM, and (d) detent forces with initial and optimal models.

JPM-09. Electromagnetic Analysis and Vibration Reducing of Segmented Skew Rotor for Built-in U-shaped Permanent Magnet Motor. *Q. Li*[1], Q. Li[1] and W. Geng[1] *1. Nanjing University of Science and Technology, Naijing, China*

Torque ripple is the main cause of noise and vibration [1]. Mutual electromagnetic torque ripple is produced by a mismatch between excitation current and the shape of back-EMF [2]. So far, the most popular technology to reduce the cogging torque and torque ripple is skewing, including skewing of stator slots or magnet poles [3]. Based on the above analysis, this paper proposes a segment-skew U-shaped permanent magnet motor. The PMSM rotor topology used for vibration and noise research in this paper is shown in Fig. 1. PMSM parameters are shown in Table 1. Table 2 shows the torque ripple of the motor under different number of skew pole segments and angles. The data are the maximum and minimum values of torque ripple at peak current. According to Table 2, we choose a scheme with 5 segments and 5 degrees of skew angle in this paper. The spatial order of electromagnetic force is shown in Table 3. Only the major force wave orders are listed in the Table 3. Where is v the harmonic frequency of armature reaction

magnetic field; is harmonic frequency of rotor permanent magnetic field. Fig. 2 compares the torque ripple at the optimum Angle under different segments of the rotor under peak current. Fig. 3 compares the cogging torque of the rotor with and without segmented skew. Fig. 4 compares the line back electromotive force (EMF). Fig. 5 compares the torque ripple of the rotor at rated current and peak current. Fig. 6 compares the torque current curves of the rotor under MTPA and Id=0 control. Fig. 7 compares the external characteristic curves of the motor. Fig. 8 compares the torque ripple under the magnetic weakening characteristics. Fig. 9 compares the radial electromagnetic force harmonics of rotors. Fig. 10 shows the comparison of noise harmonic response curves of the motor at 5000rpm. Fig 11 and Fig 12 show the experimental equipment and results. In this paper, the characteristics of segmented skew and non-segmented skew rotor motors are studied. It is proved that the segmented skew rotor can make the Back-EMF curve more close to the sine wave, suppress the torque ripple, reduce the electromagnetic force generated by the first order tooth harmonics, and reduce the electromagnetic noise.

REFERENCES S. M. Hwang and D. K. Lieu, “Reduction of torque ripple in brushless DC motors,” Magnetics, IEEE Transactions on, vol. 31, pp. 3737-3739, D. C. Hanselman, “Eflect of skew, pole count and slot count on brushless motor radial force, cogging torque and back EMF,” *Electric Power Applications, lEE Proceedings* -, vol. 144, pp. 325-330, 1997-01-01 1997. G. Zhenhong, C. Liuchen and X. Yaosuo, “Cogging torque of permanent magnet electric machiens: An overview,” *in Electrical and Computer Engineering, 2009. CCECE ‘09. Canadian Conference on*,2009, pp.

Fig. 1 The proposed structure. (a) Motor simulation model(b) The rotor topology

Tab. I Parameters

Parameter	Value
Rated current/A	250
Peak current/A	500
Rated power/kW	90
Peak power/kW	180
Rated voltage/V	540
Magnet poles/Stator slots	6/54
Rotor outer diameter/mm	168
Rotor inner diameter/mm	80
Stator outer diameter/mm	290
Stack length/mm	150

Tab. II Torque ripple

Angle / Number	1	2	3	4	5	6	7
2	359.7/317.9	352.6/322.9	341.9/331.4	343.9/327.4	350.9/319.2	351.8/313.7	353.7/313.7
3	360.5/317.4	355.7/320.8	348.6/326.7	341.8/332.5	340.8/331.2	342.6/328.2	341.9/327.2
4	360.7/317.2	356.8/320.0	350.8/324.7	344.2/330.2	339.2/334.5	340.2/331.0	341.9/328.7
5	360.9/317.2	360.6/319.7	351.8/323.9	345.6/328.9	340.1/333.6	339.6/332.2	340.7/329.6
6	361.0/317.1	357.6/319.4	352.5/323.4	346.6/328.1	340.9/332.8	339.1/333.1	340.4/330.3

Tab. III Spatial order of electromagnetic force

n / P	3	-15	21	-33	39	-51	57
3	0						
9		6					
15		0	6				
21		6	0				
27			6				
33							
39							
45							
51						0(180)	6(180)
57						6(180)	0(180)

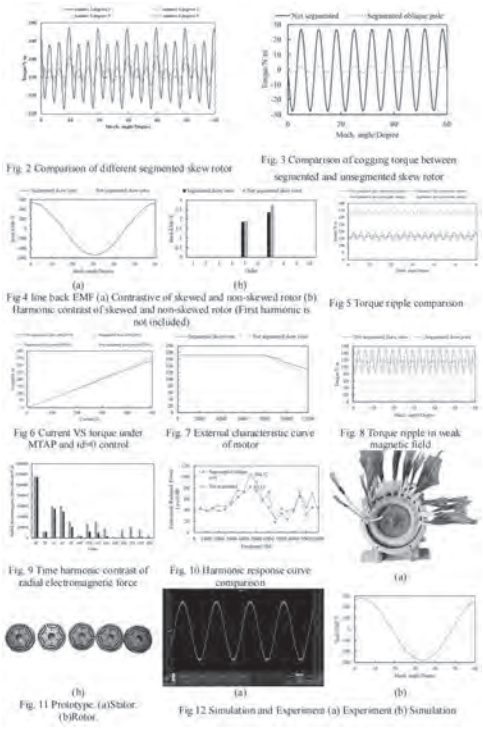

Fig. 2 Comparison of different segmented skew rotor

Fig. 3 Comparison of cogging torque between segmented and unsegmented skew rotor

Fig 4 line back EMF (a) Contrastive of skewed and non-skewed rotor (b) Harmonic contrast of skewed and non-skewed rotor (First harmonic is not included)

Fig 5 Torque ripple comparsion

Fig 6 Current VS torque under MTAP and id=0 control

Fig. 7 External characteristic curve of motor

Fig. 8 Torque ripple in weak magnetic field

Fig. 9 Time harmonic contrast of radial electromagnetic force

Fig. 10 Harmonic response curve comparesion

Fig. 11 Prototype. (a)Stator. (b)Rotor.

Fig 12 Simulation and Experiment (a) Experiment (b) Simulation

JPM-10. A Study on Design of Variable Power Electronic Brake Design for Semiconductor Manufacturing Process. *J. Lee*[1], R. Kim[1], J. Seo[1] and D. Jung[2] *1. Korea Electronics Technology Institute, Bucheon, The Republic of Korea; 2. Halla University, Wonju, The Republic of Korea*

1. Introduction In the case of the conventional wafer transfer robot for atmospheric environments, a robot system including a traveling axis to move the robot was applied, but the role of the traveling axis was changed to the form of a 5-axis horizontal articulated robot in which the role of the traveling axis was added to the robot, so that the work of multiple LPMs was reduced. transformed into possible forms. To implement this, the robot must have at least 5 independent axes. In order to drive the corresponding shaft, it is driven using an electromagnetic brake, and a stopping force is generated through the suction force of the permanent magnet located at the lower end. During operation, current is applied to the winding located at the center of the brake to cancel the attraction of the permanent magnet. *2. A study on the Design of Variable Power Electronic Brake* In order to calculate the suction force for achieving the target stopping force of the brake, it is derived using the friction coefficient according to the material condition of the effective area of the brake with the inner and outer diameters of the brake and the grounding boundary, as shown in Fig. 1. [1] Fig.1. shows the structural and flux density of the brake for semiconductor process designed through the formula when current input or not. The permanent magnet and the core are located on the lower part, and the rotor is positioned on the upper part of the brake pad. Table 1 shows the design results, and in the case of the friction coefficient, 0.4, which is the friction coefficient between the core and the brake pad, was assumed and applied *3. Conclusion* In this paper, the design of the electronic brake for semiconductor process was studied through the brake design method, and the structure of the brake was dealt with. Permanent magnets are arranged to satisfy the required force derived from the equation, and windings are arranged to offset them. Full Paper intends to verify the validity of the paper through the production and test results of the proposed model.

[1] H. Heisler “Advanced Vehicle Technology (Second Edition)”, pp.450-509, 2002. [2] Engineering ToolBox, (2001). [online] Available at: https://www.engineeringtoolbox.com [Accessed 28 May. 2021]

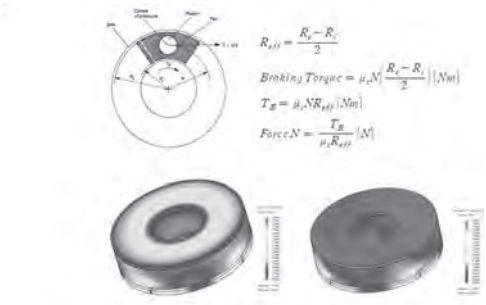

$$R_{eff} = \frac{R_o - R_i}{2}$$

$$Braking\ Torque = \mu_s N\left(\frac{R_o - R_i}{2}\right)[Nm]$$

$$T_B = \mu_s N R_{eff}[Nm]$$

$$Force N = \frac{T_B}{\mu_s R_{eff}}[N]$$

Clamping torque calculation method & Shape of Electrical Brake

Structure of Electrical Brake

- A -

*Best student presentation award finalist

- B -

*Best student presentation award finalist

*Best student presentation award finalist

*Best student presentation award finalist

- C -

*Best student presentation award finalist

*Best student presentation award finalist

- D -

*Best student presentation award finalist

- E -

*Best student presentation award finalist

- F -

*Best student presentation award finalist

- G -

*Best student presentation award finalist

*Best student presentation award finalist

- H -

*Best student presentation award finalist

*Best student presentation award finalist

- I -

*Best student presentation award finalist

- J -

*Best student presentation award finalist

- K -

*Best student presentation award finalist

*Best student presentation award finalist

*Best student presentation award finalist

- L -

*Best student presentation award finalist

*Best student presentation award finalist

*Best student presentation award finalist

- M -

*Best student presentation award finalist

*Best student presentation award finalist

*Best student presentation award finalist

- N -

*Best student presentation award finalist

- O -

*Best student presentation award finalist

- P -

*Best student presentation award finalist

- Q -

*Best student presentation award finalist

- R -

*Best student presentation award finalist

- S -

*Best student presentation award finalist

*Best student presentation award finalist

*Best student presentation award finalist

*Best student presentation award finalist

- T -

*Best student presentation award finalist

- U -

- V -

*Best student presentation award finalist

- W -

*Best student presentation award finalist

- X -

*Best student presentation award finalist

- Y -

*Best student presentation award finalist

- Z -

*Best student presentation award finalist

*Best student presentation award finalist